5th INTERNATIONAL FEZA conference

Valencia
Spain
2011
July 3-7

ABSTRACTS

First Edition, 2011 (electronic)

This editorial is member of the UNE, which guarantees the diffusion and commercialization of its publications at national and international level.

© of the present edition:
Editorial Universitat Politècnica de València
www.editorial.upv.es

© All commercial names, brands, or distinctive marks of any kind included in this piece of work are protected by law.

© Edited by:
Enrique Sastre
Teresa Blasco

ISBN: 978-84-8363-722-7 (electronic)
Ref. editorial: 6029

Any unauthorized copying, distribution, marketing, editing, and in general any other exploitation, for whatever reason, of this piece of work or any part thereof, is strictly prohibited without the authors' expressed and written permission.

5th International FEZA Conference, FEZA 2011

COMMITTEES

Chair	Avelino Corma, ITQ, Valencia
Co-Chair	Fernando Rey, ITQ. Valencia
Secretary	Teresa Blasco, ITQ, Valencia
Treasurer	Germán Sastre, ITQ, Valencia
Paper Selection Committee-Chairs	Antoine Gédéon, UPMC, Paris, France
	Mª José Díaz Cabañas, ITQ, Valencia
	Francisco Melo, ITQ, Valencia
	Enrique Sastre, ICP, Madrid
	David P. Serrano, URJC and IMDEA Energía, Madrid
Publications	Antonio Chica , ITQ, Valencia
	Mª José Franco, Cepsa, Madrid
	César Jiménez-Sanchidrián, UCO, Córdoba
	José M. López-Nieto, ITQ, Valencia
	María A. Uguina, UCM, Madrid
Post Conference School	Girolamo Giordano, University of Calabria, Italy
	Cristina Martínez, ITQ, Valencia
	Joaquín Perez-Pariente, ICP, Madrid
	Javier Pérez-Ramírez, ETH, Zürich, Switzerland
	Francesco Di Renzo, ICGM, Montpellier, France
Chairs Local Organizing Committee	Mercedes Boronat, ITQ, Valencia
	Pablo Botella, ITQ, Valencia
	Sofía Calero, UPO, Sevilla
	Juan M. Campelo, UCO, Córdoba
	Patricia Concepción, ITQ, Valencia
	Joaquín Coronas, UNIZAR, Zaragoza
	Urbano Díaz, ITQ, Valencia
	Isabel Díaz, ICP, Madrid
	Marcelo E. Domine, ITQ, Valencia
	José L. Jordá, ITQ, Valencia
	Jesús Lázaro, Cepsa, Madrid
	Francesc X. Llabrés i Xamena, ITQ, Valencia
	Carlos Márquez, ICP, Madrid
	Agustín Martínez, ITQ, Valencia

	Joaquín Martínez, ITQ, Valencia
	Pedro Martínez, Repsol, Madrid
	Michael Renz, ITQ, Valencia
	Enrique Rodríguez-Castellón, UMA, Málaga
	Mª José Sabater, ITQ, Valencia
	Susana Valencia, ITQ, Valencia
	José. L. Valverde, UCLM, Ciudad Real

CONTENT

FOREWORD **5**

PLENARY **7**

KEYNOTES **19**

ORAL COMUNICATIONS **35**

Synthesis and characterization of porous solids (SC) 37

Development of new materials (NM) 89

Modeling and theoretical studies (TH) 107

Petrochemical and environmental catalytic applications (PE) 121

Catalysis for fine chemicals and pharmaceuticals (FC) 137

Separations (SM) 157

Advanced technological applications (TA) 181

POSTERS **197**

Synthesis and characterization of porous solids (SC) 199

Development of new materials (NM) 457

Modeling and theoretical studies (TH) 567

Petrochemical and environmental catalytic applications (PE) 639

Catalysis for fine chemicals and pharmaceuticals (FC) 769

Separations (SM) 881

Advanced technological applications (TA) 967

Recent Research Reports (RRR) 1023

INDEX OF AUTHORS **1095**

FOREWORD

It is a great pleasure to present the Book of Abstracts of the 5th Conference of the Federation of European Zeolite Associations (FEZA), FEZA 2011, held in Valencia (Spain), from 3rd to 7th July, 2011. This is the first time that the Extended Abstracts of a FEZA Conference are edited only in electronic format, while keeping the Short Abstracts as paper form. This has been done according to the FEZA board decision of shortening as much as possible the time between the deadline for abstract submission and the presentation of accepted communications at the Conference. We hope that this policy will increase the novelty and quality of communications, as it will permit to publish the scientific results as articles in paper-printed periodic Journals.

In this Conference, we have approached an unusual referee process aiming the reduction of time delays, by building a pyramid of referees with different levels of involvement in the paper selection. We have asked to more than 100 recognized researchers working in porous solids to participate in this selection process. The work done by these evaluators has been outstanding in quality and time, rigorously reviewing more than 600 communications in 45 days. The work of the referees was harmonized by 26 coordinators who are experts in each Conference Topic. The whole process, elaboration of expert panels, evaluations, etc. have been tracked through the Web page of the Conference (www.FEZA2011.com). The Paper Selection and the Organizing Committees are deeply acknowledged to all experts involved (coordinators, evaluators and chairs of Paper Selection Committee) since the high level of this Conference could not have been reached without their input.

We also want to thank the support of industrial, academic and governmental entities that has been vital for the celebration of this event.

Finally, the Book of Abstracts you have on your hands include 513 communications, including Recent Research Reports, that have been distributed in seven main topics, 5 Plenary and 7 Keynotes Lectures delivered along the FEZA 2011 Conference.

We believe that these Abstracts are relevant because they present the main achievements on Zeolites and related fields in the last three years, as the result of continuous efforts invested in research. The oral and poster contributions have been classified in the main seven topics of the Conference:

- Synthesis and characterization of porous solids.
- Developments of new materials.
- Modeling and theoretical studies.
- Petrochemical and environmental catalytic applications.
- Catalysis for fine chemicals and pharmaceuticals.
- Separations.
- Advanced technological applications.

We hope that this Book of Abstract will show the important advances reached since the last edition of the FEZA Conference held in Paris in 2008 and, more importantly, this collection of different contributions from all around the world will serve as inspiration of researchers for further achievements in the field of zeolites and porous materials.

Valencia, 14th June, 2011

On behalf of the Organizing Committee

Avelino Corma

PLENARY

FEZA 2011

Directing Zeolite Structures into Hierarchically Nanoporous Architectures

Ryong Ryoo
Center for Functional Nanomaterials, Department of Chemistry, and Graduate School of Nanoscience and Technology (WCU), KAIST, Daejeon 305-701, Korea. E-mail: rryoo@kaist.ac.kr

Tremendous efforts were made in recent years to prepare mesoporous materials with microporous crystalline frameworks, using soft templates or hard templates. A new, exciting method is just emerging from surfactants that are functionalized with zeolite-structure-directing (ZSD) groups. The surfactant molecules contain one or two long alkyl tails that are joined with a ZSD multi-quaternary ammonium head group. Depending on the detailed structures, the head group can function as a ZSD agent for MFI, MTW or β zeolite. A large number of surfactant molecules can self-assemble into a lamellar, disordered or ordered mesoporous structure while their head groups act as ZSD agent for a crystalline microporous zeolite in aqueous solution. The use of these surfactants results in the generation of ultrathin zeolite nanosheets, zeolite nanosponges, or hierarchically mesoporous-microporous zeolites. The mesopore diameters of the hierarchically porous zeolites can be controlled by the length of the surfactant tails, and also by the addition of a pore swelling agent like trimethylbenzene. The thickness of the mesopore walls (or nanosheets) is controlled by the number of ammonium in head group, which can be rationally designed. The zeolite synthesis using this type of surfactants is expected to open a new field of nanomorphic zeolites or hierarchically nanoporous zeolitic materials. These zeolites would find new opportunities as adsorbents and solid acid catalysts for organic reactions involving large molecules.

Zeolite particles by disassembly and uses in thin films

Michael Tsapatsis

Department of Chemical Engineering and Materials Science, University of Minnesota, Minneapolis, MN 55455, USA

tsapatsis@umn.edu

As energy conservation continuously rises in importance, the necessity also increases to explore potential alternatives to many established thermally-driven processes such as distillation and crystallization. High-resolution molecular separations membranes have been reported based on preferential adsorption and/or minute size and shape differences. Among the candidates for selective separation, zeolite materials have been explored due to their molecular sieving potential predicted from intrinsic crystalline properties[1,2].

It has long been recognized that polycrystalline zeolite thin films can be used in a membrane or membrane reactor configuration to achieve improvements in separation and reaction process efficiency and operating cost savings. Supported polycrystalline zeolite membranes show serious promise for gas, vapor, and liquid separations including hydrocarbon mixtures, biofuel/water, and hydrogen/carbon dioxide separation for energy-efficient clean refineries, biorefineries, and zero emission power plants, respectively.

Although the first reports on zeolite membranes can be traced back to the 1940's, it is only since the 1990's that renewed research efforts were devoted to achieve this goal. To manufacture highly selective supported zeolite membranes, a deposition process to form crack-free, compact, polycrystalline zeolite thin films on porous substrates is essential. Despite the promising proof-of-concept demonstrations, commercial implementation is lagging behind because cost-effective, reliable and environmentally benign thin film deposition methods that can be scaled up to produce commercially relevant film quantities do not exist. Zeolite membrane technology for industrial-scale operations depends on reliable manufacturing that can generate hundreds to thousands of square meters of membrane area and achieve essential membrane characteristics: continuity with low defect density, appropriate out-of-plane orientation, and thin membrane thickness[3,4].

I will describe an emerging potentially scalable zeolite membrane fabrication method based on the combination of three recent enabling developments:

I. Films from zeolite nanosheets This concept was introduced about a decade ago[5-7] and is based on materials with structures intermediate between those of crystalline zeolite frameworks and typical layered materials, such as clay minerals. In contrast to typical clays, in these "layered zeolites", each layer includes a porous network (similar to zeolites), while the gallery between layers (as in clays) provides the ability for intercalation and exfoliation. Layers with 6^8, 8^{5-7}, 10^9 and larger member ring apertures[10] are available, and recent progress in exfoliation techniques[11] is enabling the synthesis of nanosheet suspensions for coatings.

II. Secondary growth methods Nanosized defects that could form in-between the zeolite layers during and after coating create non-selective pathways for transport which reduce

selectivity. They should be reduced or eliminated. However, non-zeolitic pathway closure should be accomplished without excessive deposition which would increase the membrane thickness and reduce flux without a corresponding gain in selectivity. Secondary hydrothermal growth in the presence of certain structure directing agents and crystal shape modifiers can achieve compact molecular sieve films with minimal thickness[12-13].

III. Rapid thermal processing methods After the zeolite membrane is made, it has to be activated at high temperature to remove molecules occluded in the zeolite micropores. Moreover, zeolite membranes often should be activated after fouling during operation. These necessary calcination processes often create cracks and other grain boundary defects with detrimental consequences in membrane selectivity. Furthermore, conventional calcination is a time-consuming and energy-intensive process that contributes significantly to the zeolite membrane fabrication cost while it creates a bottleneck for large-scale production. A calcination technique using lamp-based rapid thermal processing avoids defect formation and cuts processing time and cost significantly[14-15].

Recent progress in this front will be described.

1. Lin, Y. S.; Kumakiri, I.; Nair, B. N.; Alsyouri, H. Microporous inorganic membranes. Sep. Purif. Methods 2002, 31, 229-379.
2. Caro, J.; Noack, M.; Koelsch, P. Zeolite membranes: from the laboratory scale to technical applications. Adsorption 2005, 11, 215-227.
3. Morigami, Y.; Kondo, M.; Abe, J.; Kita, H.; Okamoto, K. The first large-scale pervaporation plant using tubular-type module with zeolite NaA membrane. Sep. Purif. Technol. 2001, 25, 251-260.
4. Caro, J.; Noack, M. Zeolite membranes – Recent developments and progress. Micropor. Mesopor. Mater. 2008, 115, 215-233.
5. Jeong, H.-K.; Nair, S.; Vogt, T.; Dickinson, L.C.; Tsapatsis, M. A highly crystalline layered silicate with three-dimensionally microporous layers. Nature Mater. 2003, 2, 53-58.
6. "Layered Silicate Material and Applications of Layered Silicates with Porous Layers" Tsapatsis M., Nair S. and Jeong H.W. U.S. Patent 6, 863, 983 B2 (2006).
7. "Layered Silicate Material and Applications of Layered Silicates with Porous Layers" Tsapatsis M., Nair S. and Jeong H.W. U.S. Patent 7, 087, 288 B2 (2006).
8. Corma, A.; Fornes, V.; Pergher, S.B.; Maesen, T.L.M.; Buglass, J.G. Delaminated zeolite precursors as selective acidic catalysts Nature 1998, 396, 353-356.
9. Choi, M.; Na, K.; Kim, J.; Sakamoto, Y.; Terasaki, O.; Ryoo, R. Stable single-unit-cell nanosheets of zeolite MFI as active and long-lived catalysts. Nature 2009, 461, 246-249.
10. Wei, B.; Yu, J.H.; Shi, Z.; Qiu, S.L.; Li J.Y. A new layered aluminophosphate [Al2P4O16] [C6H22N4][C2H10N2] with 4.12-net porous sheets. *J Chem Soc. Faraday Trans*. **2000**, *13*, 1979-1980
11. Maheshwari, S.; Jordan, E.; Kumar, S.; Bates, F.S.; Penn, R.L.; Shantz, D.F; Tsapatsis, M. Layer structure preservation during swelling, pillaring, and exfoliation of a zeolite precursor. J. Am. Chem. Soc. 2008, 130, 1507–1516.
12. Lai, Z.; Bonilla, G.; Diaz, I.; Nery, J. G.; Sujaoti, K.; Amat, M. A.; Kokkoli, E.; Terasaki, O.; Thompson, R. W.; Tsapatsis, M.; Vlachos, D. G. Microstructural optimization of a zeolite membrane for organic vapor separation. Science 2003, 300, 456-460.
13. "Crystalline Membranes" Tsapatsis, M. and Lai, Z. U.S. Patent 7, 357, 836 B2 (2008).
14. Choi, J.; Jeong, H. K.; Snyder, M. A.; Stoeger, J. A.; Masel, R. I.; Tsapatsis, M. Grain boundary defect elimination in a zeolite membrane by rapid thermal processing. Science 2009, 325, 590-593.
15. "Molecular Sieve Membranes and Thermal Treatment Methods for Making the Same" Tsapatsis M., Choi J. and Jeong H.K. U.S. Patent Application

Funding was provided by the National Science Foundation, the Department of Energy and ADMIRE.

High-valence transition metals Metal Organic Frameworks : from synthesis to applications

C. SERRE

Institut Lavoisier de Versailles, UMR 8180 CNRS- Université de Versailles Saint-Quentin, 45 avenue des E.U., 78305 Versailles, France ; Email : serre@chimie.uvsq.fr

Most MOFs are based on divalent cations (Cu, Zn, Co…) or Lanthanides.[1] This is due both to the easier synthesis of single crystals for structure determination purposes as well as less chemical constraints compared to those of higher valence metals. For higher charge density metals such as Ti, Zr and to a lesser extent Fe or Al, coordination between the linker and the metal comes in direct competition with the formation of metal oxide or hydroxide. However, if one excepts metal imidazolate solids, most MOFs usually exhibit a poor moisture stability which might restrict their use for some practical applications (separation, catalysis…). Recent studies have shown that the hydrothermal stability of MOFs is strongly related to the strength of the metal-oxygen (or nitrogen) bonds, increasing thus for a given coordination number, with the charge of the metal.[2] MOFs based on tri- or tetravalent transition metals (Fe, Ti, Zr), offer thus a better water stability. We will report here the synthesis of trivalent metal polycarboxylates (M= Fe, Al…) either rigid or highly flexible,[3] as well as a few zirconium(IV) and titanium dicarboxylate MOFs.[4,5] On the contrary, for drug delivery applications, degradability represents an advantage to avoid accumulation within the body of exogeneous species. However, a (too) fast degradability will induce a burst release of the cargo and thus a sufficient stability of the MOF, over a few hours or days in physiological conditions, is required. Finally, in addition to the discovery of new high valence metals based MOFs and the study of their stability,[6,7] we will report here some of their properties in the field of adsorption, separation and biomedicine.[8]

[1] Themed issue: Metal-organic frameworks, *Chem. Soc. Rev.*, **2009**, p. 1201
[2] J. J. Low, A. I. Benin, P. Jakubczak, J. F. Abrahamian, S. A. Faheem, and R. R. Willis *J. Am. Chem. Soc*. **2009**, *131*, 15834–15842
[3] G. Férey, *Chem. Soc. Rev*., 2008, **37**, 191-214
[4] J. H Cavka, S. Jakobsen, U. Olsbye, N. Guillou, C. Lamberti, S. Bordiga, K. P. Lillerud, *J. Am. Chem. Soc.* **2008**, *130*, 13850
[5] M. Dan-Hardi, C. Serre, T. Frot, L. Rozes, G. Maurin, C. Sanchez and G. Férey : *J. Am. Chem. Soc.*, 131, **2009**, 10857
[6] V. Guillerm, S. Gross, C. Serre, T. Devic, M. Bauer, G. Férey : *Chem. Comm*., **2010**, 46, 767
[7] V. Guillerm, M .Dan-Hardi, A. Vittadini, S. Gross, T. Devic, G. Férey, C. Serre *submitted*
[8] P. Horcajada, T. Chalati, C. Serre, B. Gillet, C. Sebrie, T. Baati, J. F. Eubank, D. Heurtaux, P. Clayette, C. Kreuz, J.-S. Chang, Y. K. Hwang, P.-N. Bories, L. Cynober, S. Gil, G. Férey, P. Couvreur, R. Gref, *Nat. Mater*., **2010**, 9, 172

selectivity. They should be reduced or eliminated. However, non-zeolitic pathway closure should be accomplished without excessive deposition which would increase the membrane thickness and reduce flux without a corresponding gain in selectivity. Secondary hydrothermal growth in the presence of certain structure directing agents and crystal shape modifiers can achieve compact molecular sieve films with minimal thickness[12-13].

III. Rapid thermal processing methods After the zeolite membrane is made, it has to be activated at high temperature to remove molecules occluded in the zeolite micropores. Moreover, zeolite membranes often should be activated after fouling during operation. These necessary calcination processes often create cracks and other grain boundary defects with detrimental consequences in membrane selectivity. Furthermore, conventional calcination is a time-consuming and energy-intensive process that contributes significantly to the zeolite membrane fabrication cost while it creates a bottleneck for large-scale production. A calcination technique using lamp-based rapid thermal processing avoids defect formation and cuts processing time and cost significantly[14-15].

Recent progress in this front will be described.

1. Lin, Y. S.; Kumakiri, I.; Nair, B. N.; Alsyouri, H. Microporous inorganic membranes. Sep. Purif. Methods 2002, 31, 229-379.
2. Caro, J.; Noack, M.; Koelsch, P. Zeolite membranes: from the laboratory scale to technical applications. Adsorption 2005, 11, 215-227.
3. Morigami, Y.; Kondo, M.; Abe, J.; Kita, H.; Okamoto, K. The first large-scale pervaporation plant using tubular-type module with zeolite NaA membrane. Sep. Purif. Technol. 2001, 25, 251-260.
4. Caro, J.; Noack, M. Zeolite membranes – Recent developments and progress. Micropor. Mesopor. Mater. 2008, 115, 215-233.
5. Jeong, H.-K.; Nair, S.; Vogt, T.; Dickinson, L.C.; Tsapatsis, M. A highly crystalline layered silicate with three-dimensionally microporous layers. Nature Mater. 2003, 2, 53-58.
6. "Layered Silicate Material and Applications of Layered Silicates with Porous Layers" Tsapatsis M., Nair S. and Jeong H.W. U.S. Patent 6, 863, 983 B2 (2006).
7. "Layered Silicate Material and Applications of Layered Silicates with Porous Layers" Tsapatsis M., Nair S. and Jeong H.W. U.S. Patent 7, 087, 288 B2 (2006).
8. Corma, A.; Fornes, V.; Pergher, S.B.; Maesen, T.L.M.; Buglass, J.G. Delaminated zeolite precursors as selective acidic catalysts Nature 1998, 396, 353-356.
9. Choi, M.; Na, K.; Kim, J.; Sakamoto, Y.; Terasaki, O.; Ryoo, R. Stable single-unit-cell nanosheets of zeolite MFI as active and long-lived catalysts. Nature 2009, 461, 246-249.
10. Wei, B.; Yu, J.H.; Shi, Z.; Qiu, S.L.; Li J.Y. A new layered aluminophosphate [Al2P4O16] [C6H22N4][C2H10N2] with 4.12-net porous sheets. *J Chem Soc. Faraday Trans*. **2000**, *13*, 1979-1980
11. Maheshwari, S.; Jordan, E.; Kumar, S.; Bates, F.S.; Penn, R.L.; Shantz, D.F; Tsapatsis, M. Layer structure preservation during swelling, pillaring, and exfoliation of a zeolite precursor. J. Am. Chem. Soc. 2008, 130, 1507–1516.
12. Lai, Z.; Bonilla, G.; Diaz, I.; Nery, J. G.; Sujaoti, K.; Amat, M. A.; Kokkoli, E.; Terasaki, O.; Thompson, R. W.; Tsapatsis, M.; Vlachos, D. G. Microstructural optimization of a zeolite membrane for organic vapor separation. Science 2003, 300, 456-460.
13. "Crystalline Membranes" Tsapatsis, M. and Lai, Z. U.S. Patent 7, 357, 836 B2 (2008).
14. Choi, J.; Jeong, H. K.; Snyder, M. A.; Stoeger, J. A.; Masel, R. I.; Tsapatsis, M. Grain boundary defect elimination in a zeolite membrane by rapid thermal processing. Science 2009, 325, 590-593.
15. "Molecular Sieve Membranes and Thermal Treatment Methods for Making the Same" Tsapatsis M., Choi J. and Jeong H.K. U.S. Patent Application

Funding was provided by the National Science Foundation, the Department of Energy and ADMIRE.

Needs and Trends in Rational Synthesis of Zeolitic Materials

Zhuopeng Wang, Jihong Yu* and Ruren Xu

State Key Laboratory of Inorganic Synthesis and Preparative Chemistry, College of Chemistry, Jilin University, Changchun 130012, P. R. China
Corresponding author: jihong@jlu.edu.cn

In this work, we will discuss the relationship between the geometric structures and catalytic properties of zeolitic materials, and highlight recent efforts and progress toward the designed synthesis of zeolitic materials. The future developing trends in this area has been prospected as well.

Introduction

The great importance and increasing needs for zeolites in adsorption and catalysis have become the driving force for developing new zeolitic materials with high catalytic activity and selectivity [1]. The superior catalytic properties of zeolites are closely related to their unique porous framework structures, as well as compositions and morphologies [2, 3]. Therefore, how to design desired zeolite structures based on practical catalytic requirements, and to achieve the rational synthesis of target zeolite materials is of great academic and industrial interest [4]. In this work, the needs and trends in rational synthesis of zeolitic materials will be discussed.

The relationships between geometric structures and catalytic properties

Zeolite catalysts can be considered as molecular reactors since their uniform channels or cavities of molecular dimension can accommodate molecules and allow catalytic reactions to take place inside. The most attractive property of zeolites which makes them distinct from other solid catalysts is the shape selectivity. Several types of shape selectivity have been proposed such as reactant shape selectivity, product shape selectivity and transition-state selectivity. The geometric characteristics such as the size of pore opening, shape of channel or cavity, channel dimension, and pore topology significantly affect the performance of zeolites in adsorption and catalysis. In this section, Studies on the geometric effect of zeolite structures on catalytic performances are reviewed, which may provide useful guidance for synthetic chemists to synthesize, modify, or tailor new zeolitic catalysts with desired structures.

Strategies toward designed synthesis

Rational synthesis of zeolites with desired structures remains great challenge for the synthetic chemists unless the complex formation mechanism is fully revealed. In the most recent decade, with the advances of our understanding on the fundamental of zeolite synthesis, many research efforts have been made toward the syntheses of tailor-made zeolitic materials with specific structures. In this section, some novel strategies toward the designed synthesis of new zeolite structures are highlighted, including designing novel OSDAs, introducing alternative framework elements directing specific building units, and 2D-3D topotactic condensation, etc.

Computer-assisted design and synthesis

Computational simulations have become an important tool in assisting in the design of zeolites with specific structures and properties [5]. By means of computational simulations, hypothetical zeolitic frameworks can be enumerated or even designed on purpose. In addition, molecular mechanical and quantum mechanical techniques are introduced to assist the studies of many aspects in zeolite field, such as predicting the structure directing effect in zeolite synthesis, simulating the adsorption and diffusion behaviors of guest molecules and active sites for catalysis. Data mining technique was employed to guide the synthesis of zeolitic materials as well. These works pave the way toward the ab initio synthesis of new zeolite materials.

Conclusions

We have discussed the relationships between catalytic properties and geometric structures of zeolites, and described recent progress that has been made in the aspect of the rational synthesis. The map to direct the rational synthesis of target materials with desired functions and structures can be drawn based on the understanding of the relationship of function-structure-synthesis. It should be pointed out that the most direct and final solution for rationalization of the synthesis of zeolites depends on a full understanding of the crystallization mechanism thus will allow us to chemically control the formation of zeolitic materials with predictable functions and structures.

Acknowledgements

This work is supported by the National Basic Research Program of China (2011CB808703) and the National Natural Science Foundation of China.

References

[1] Zones, S. I., Translating new materials discoveries in zeolite research to commercial manufacture, Microporous Mesoporous Mater., DOI: 10.1016/j.micromeso.2011.03.039.
[2] Corma, A., State of the art and future challenges of zeolites as catalysts, J. Catal., 216 (2003), 298-312.
[3] Cejka, J. and Wichterlova, B., Acid-catalyzed synthesis of mono- and dialkyl benzenes over zeolites: Active sites, zeolite topology, and reaction mechanisms, Catal. Rev.-Sci. Eng., 44 (2002), 375-421.
[4] Yu, J. and Xu, R., Rational Approaches toward the Design and Synthesis of Zeolitic Inorganic Open-Framework Materials, Acc. Chem. Res., 43 (2010), 1195-1204.
[5] Catlow, R., Bell, R., Cora, F. and Slater, B., in Introduction to Zeolite Science and Practice, eds. Cejka, J., van Bekkum, H., Corma, A. and Schuth, F., Elsevier, Amsterdam, 3rd revised ed edn., vol. Studies in Surface Science and Catalysis 168, 2007, pp. 659-700.

The formation of zeolites from solution - analysis by mass-spectrometry

Ferdi Schüth

Max-Planck-Institut für Kohlenforschung, Kaiser-Wilhelm-Platz 1, 45470 Mülheim

Introduction

The mechanism of zeolite formation from solution is one of the most elusive problems in zeolite science. Although substantial insight has been obtained by a variety of different experimental and theoretical methods, a deep understanding is still lacking. The nature and the dynamics of silicate and heteroatom-containing silicate species in solution is not well known – at least for the larger units -, and the elementary processes leading to the formation of specific zeolite structures are highly disputed. Electrospray ionization mass spectrometry (ESI-MS) is a powerful tool for the analysis of silicate solutions. It allows the elucidation of masses of species present, and by using MS-MS experiments, also structural information can be obtained.

Experimental Configurations

Depending on the specific question, different experimental configurations are used for the MS-analysis of zeolite synthesis solutions. For slow reactions proceeding on a time scale of hours, batch experiments are performed and samples are withdrawn periodically and injected into the inlet system of the mass spectrometer. For intermediate time scales, reaction solutions can be placed directly in a syringe and injected continuously from the syringe into the mass spec. Short times scales on the order of minutes are analyzed by using a tubular reactor with a split. After mixing the reagents, the reaction time is determined by the length of the tube and the flow rate of the solution. After the desired tube length, a split is used to collect most of the solution, but a small fraction is fed into the mass spec for analysis. Different systems are used, which can be heated as well, to allow reactions at different temperatures.
Different types of mass spectrometer and sprayer geometries have been evaluated for the analysis of pre-nucleating and nucleating zeolite solutions[1]. Off-axis sprayer geometries were found to be advantageous, since they prevent incrustations on the apertures and avoid memory effects.

Pre-nucleating Solutions

Several pre-nucleating systems have been studied with different goals. The hydrolysis of alkoxysilanes is important as the first step in the formation of zeolites from clear solution. MS analysis shows that depending on an organic additive (tetramethylammonium or tetraethylammonium) the system develops towards different oligomers, i.e. the cubic octamer or the trigonal prismatic hexamer, over a time period of several hours, if one starts with tetraethylorthosilicate (TEOS) as the silicate source[2]. While at the end of the reaction, either the octamer or the hexamer prevails, depending on the alkylammonium ion, both species are present at intermediate stages of the reaction. The temporal development of the system is highly dependent on the nature of the silicate source. The longer the alkyl chains of the alkoxy groups are, the slower is the hydrolysis and thus the development of the system. From methoxy over ethoxy to propoxy the time to reach the final species distribution increases by about one order of magnitude for each carbon atom in the alkyl chain.
However, the system is not static after reaching the final oligomer distribution. Using isotope labelling with ^{29}Si, it could be shown that the cubic octamer and the prismatic hexamer exchange silicon atoms also under steady state conditions on time scales of minutes to hours,

depending on temperature. This exchange proceeds in a concerted manner, i.e. it is not single silicon atoms which are exchanged, but complete faces of the oligomeric polyhedra[3].

Nucleating Solutions

The analysis of nucleating solutions by mass spectrometry poses special problems, since severe incrustation and clogging of the injector often accompany the experiments, because they are run under conditions, under which solid can form. Nevertheless, in most cases experiments could be performed for several hours before such problems occurred.

After the start of a zeolite synthesis, in all systems studied, first a population of small oligomers exists. These species grow in time, until, after solid is formed, rather smaller oligomers reappear, probably caused by the lower effective silicate concentration in solution. Experiments for three different zeolite systems, MFI, LTA and BEC, revealed that immediately before particles are detected by light scattering, structural elements of the zeolite structure to be formed are already present in solution, i.e. five-ring species in the case of MFI, cubic octamers linked directly via corners for LTA, and cubic octamers linked via a silicate tetrahedron for BEC[4]. This does not necessarily imply that the respective zeolite is formed by direct assembly of such oligomers, but does suggest, that the solution conditions favor the formation of specific structural elements, as they are also found in the later zeolite structure.

The evolution of specific oligomers were studied in more detail for the MFI system. MS-MS experiments were used to discriminate precisely between different oligomeric structures. Using this technique, it was possible to obtain insight into the processes occurrring during the induction period for MFI-formation. Initially, different cubic octamer species are predominant, but over time, the fraction of double five-ring species increases on the expense of double four-rings. If the ratio of the signal intensity of double four-rings over double five rings reaches approximately ten, MFI starts to form. This takes approximately 6 h at 170°C, 13 h at 100°C and over 400 h at 40°C. Thus, the induction time is required for a sufficient concentration of species to form which seem to be required for nucleation[5].

Incorporation of Heteroelements

Mass spectrometry is also highly suitable to analyze the incorporation of heteroelements into zeolites. Several different systems have been studied, including aluminum, germanium, gallium and titanium. ESI-MS confirms that germanium prefers sites in four-rings and double four-rings, while gallium was found to be located preferably in positions bridging closed ring species[6]. Aluminum incorporation is more difficult to study, since replacing silicon by aluminum (which requires an additional proton for charge balancing) leads to species with almost identical mass. Nevertheless, high resolution MS experiments and experiments with ^{29}Si allowed to also study such systems. Interestingly, clear proof was found that in solution species exist which violate Loewenstein's rule, something rarely found in solid state structures.

---

[1] S.A. Pelster, F. Schüth, W. Schrader, Anal.Chem. 79, 6005 (2007)
[2] S.A. Pelster, W. Schrader, F. Schüth. J.Am.Chem.Soc. 128, 4310 (2006)
[3] S.A. Pelster, B. Weimann, B.B. Schaack, W. Schrader, F. Schüth, Angew.Chem.Int.Ed. 46, 6674 (2007)
[4] B.B. Schaach, W. Schrader, F. Schüth, Angew.Chem.Int.Ed. 47, 9092 (2008)
[5] B.B. Schaack, I.H. Lim, W. Schrader, F. Schüth, unpublished
[6] B.B. Schaack, W. Schrader, F. Schüth, J.Phys.Chem.B 113, 11240 (2009)

KEYNOTES

FEZA 2011

In-situ spectroscopy of zeolite materials at the single particle level

Bert M. Weckhuysen

Debye Institute for Nanomaterials Science, Utrecht University, Universiteitsweg 99, 3584 CG Utrecht, The Netherlands; e-mail b.m.weckhuysen@uu.nl

Introduction

Heterogeneous catalysis is a fascinating, multidisciplinary science, which is core business to our energy, chemical and pharmaceutical industries as most reactions are catalyzed by at least one catalyst containing a multitude of distinct active sites. Although tremendous progress has been made in our understanding of catalytic solids, their functioning under realistic reaction conditions still represents a scientific challenge to both academia and industrial scientists. Deep mechanistic insight in the fundamentals of heterogeneous catalysis can only be acquired by using advanced characterization methods, often in combination with theory, as well as by the use of proper in-situ reaction cells and related measurement protocols.

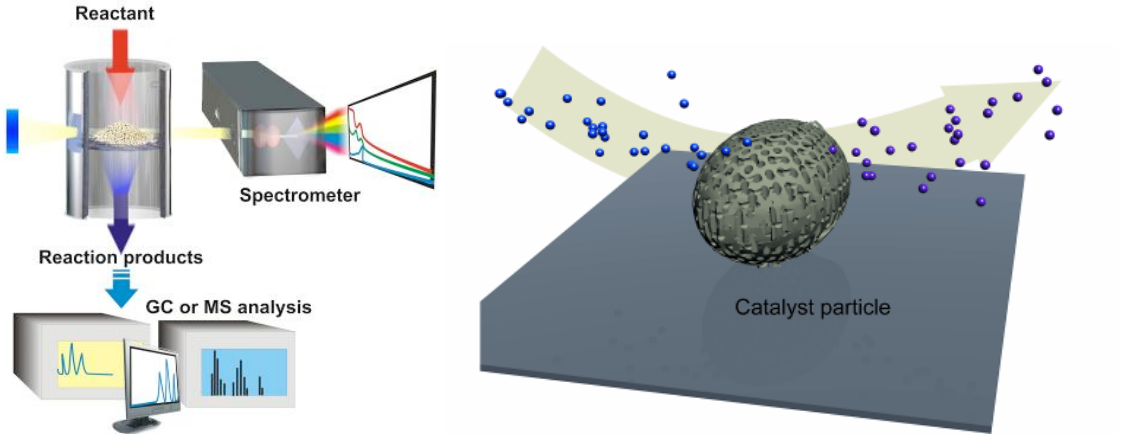

Figure 1. Schematics of the in-situ approach as applied to powdered catalyst materials (left) and the in-situ single molecule-single particle characterization approach (right).

In recent years we have seen the development of space-resolved in-situ characterization approaches, ultimately allowing performing single molecule-single catalyst particle studies, as illustrated in Figure 1. In this lecture, our work on the spatiotemporal characterization of individual zeolite catalyst particles at the micron- and nano-scale will be presented.

Results and Discussion

Three examples will be discussed: The first one relates to characterization methods, in particularly Electron Back-Scattering Diffraction (EBSD), UV-Vis micro-spectroscopy, confocal fluorescence microscopy and synchrotron-based IR, to shed insight in the presence of molecular diffusion barriers within large zeolite crystals and how they can be understood in relation to their morphology (Figure 2). As a showcase micron-sized ZSM-5 zeolite crystals will be discussed and in this manner the effect of dealumination processes on the removal of these diffusion barriers will be presented. In a second part of the lecture a thorough investigation of fluid catalytic cracking (FCC) particles will be discussed, in which intra- and inter-particle heterogeneities as a function of different deactivation protocols are elucidated. For this purpose, the styrene oligomerization in combination with fluorescence

micro-spectroscopy is used to compose changing Brønsted acidity maps. A final part of the lecture relates to the use of Scanning Transmission X-ray Microscopy (STXM) to unravel dealumination processes as well as coking profiles during methanol-to-olefin catalysis within industrial relevant ZSM-5 zeolite crystals at the nanoscale.

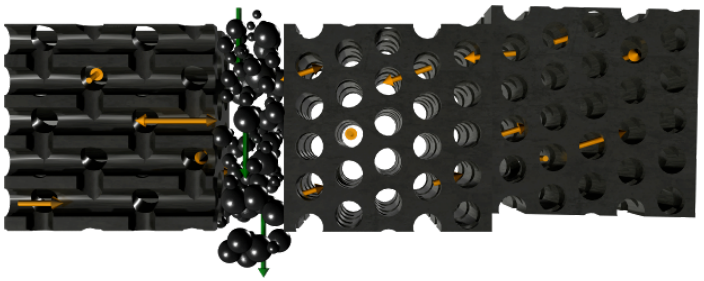

Figure 2. Schematic of molecular diffusion barriers occurring in micron-sized H-ZSM-5 crystals leading to spatiotemporal distributions of reaction products during catalysis.

Outlook

The characterization toolbox of catalyst scientists for investigating zeolite materials under realistic reaction conditions has been significantly expanded in the last decade. It is now possible to obtain within a 'single shot' (a) multiple in-situ characterization data, which are highly complementary; (b) 1-D, 2-D and 3-D chemical information of a zeolite catalyst as a function of reaction time down to microns and nanometers; and (c) single molecule and single active site information, providing insight in the catalyst dynamics. As more laboratories, including stations at synchrotron radiation facilities, are equipped with in-situ measurement facilities it should be clear that the future looks bright for scientists aiming to unravel mechanistic insights in the working and deactivation principles of zeolite materials. Based on such insights new and/or improved catalyst formulations can be developed.

Microporous Heteropolyhedra Framework Silicates: From Light Emission to NO Drug Delivery

João Rocha
Department of Chemistry, CICECO, University of Aveiro, 3810-193 Aveiro, Portugal, rocha@ua.pt

The frameworks of zeolites and related crystalline microporous oxides, such as aluminophosphates (AlPOs), are built up of tetrahedrally coordinated (Si, Al, P) atoms. Materials possessing mixed octahedral-pentahedral-tetrahedral microporous oxide frameworks (OPT solids) have been comprehensively studied since the early 1990s, and encompass silicates of Ti, Zr, Nb, V, Cu, Sn, Ca [1]. Owing to its wide-pore nature, fascinating structure and thermal stability titanosilicate ETS-10 is one of the most important OPT microporous material prepared so far. OPT materials display topologies and compositions unknown in the realms of zeolites and AlPOs. By the turn of the last century, the constituent elements of heteropolyhedral silicates were extended to lanthanides and, thus, important properties, such as photoluminescence (PL), became available [2].
Here, I shall review some of the main achievements in the field of OPT materials in the last fifteen years or so, encompassing new topologies [1], processing (membranes production) [3] and less 'conventional' zeolitic properties, in particular light emission (photoluminescence), slow release of drug gases (NO) [4], and magnetic resonance contrast agents [5].

Photoluminescent materials

One of the most important properties of OPT materials is light emission. PL materials, or phosphors, find applications in cathode ray tubes, projection televisions, fluorescent tubes and X-ray detectors. Lanthanide (Ln^{3+})-doped materials are of great interest for a wide range of other photonic applications, such as tunable lasers, light-emitting diodes, low-energy scintillators, amplifiers for optical communications and optical storage.
One of the grand challenges in the field of materials engineering of luminescent centres is to develop multifunctional systems combining light emission with other properties, including porosity. Clearly, OPT materials may help to effectively meet this aim.
Some milestones of the work in the field photoluminescent microporous OPT materials are:
a) $Na_4K_2Tb_2Si_{16}O_{38}\cdot 10H_2O$ (AV-9) [2] is the first example of a microporous X-ray scintillator (emitting light upon excitation with CuKα excitation).
b) An intriguing chiral system, $Na_3[(Y,Ln)Si_3O_9]\cdot 3H_2O$, for which it was shown that Eu^{3+} photoluminescence spectroscopy with excitation by unpolarised light in the absence of an external magnetic field is able to identify enantiomeric domains in chiral frameworks [6]; and c) $K_7Eu_3Si_{12}O_{32}\cdot 3H_2O$, the first silicate possessing Eu^{3+}-O-Eu^{3+} dimers (inter-Eu distance *ca.* 3.9 Å), *i.e.*, two edge-sharing $\{LnO_6\}$ octahedral embedded in a crystalline matrix [7]. The dimers exhibit a remarkably long emission $^5D_0$ lifetime of 10.29 ms at 12 K.

Slow release of NO

In the human body, NO is extremely important in vasodilatation, prevention of platelet aggregation and thrombus formation, neurotransmission, and wound repair. Only a few papers report on the biological activity of NO-releasing zeolites. Generally, in dehydrated zeolites, NO binds to extra-framework cations and is released after the materials contact with water and cations hydrate. We have developed a novel approach to design NO storage

and releasing microporous agents based on very stable OPT materials possessing *unsaturated* transition-metal centers (*e.g.* pentacoordinated Ti^{4+} in ETS-4) in the framework, rather than in the pores (Fig. 1) [4]. The capacity of ETS-4 to release NO in biologically-relevant amounts has been assessed experimentally using the oxyhemoglobin method.

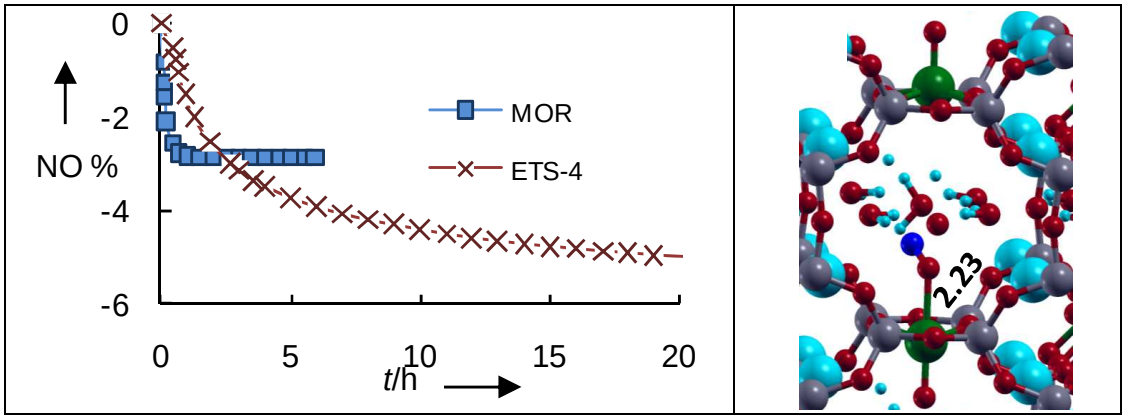

Fig. 1 – Left: Kinetic profiles of NO desorption on titanosilicate ETS-4 and zeolite mordenite, in high vacuum at 25 °C, after adsorption at 80 kPa. **Right:** interaction of the NO molecule with the pentacoordinated Ti^{4+} atom gives ETS-4 exceptional storing and releasing properties for nitric oxide delivery. The presence of water molecules helps to stabilize the NO adsorbed species.

MRI Contrast agents

The use of magnetic resonance in molecular imaging (MRI) applications is often limited by the low sensitivity of this technique, despite its high spatial resolution (μm). The investigation of molecular events at the cellular level requires a relatively large local concentration of contrast agent (CA) in order to achieve an observable contrast enhancement. Zeolites have already been explored as CAs in MRI, usually with Ln^{3+} introduced via ion-exchange of extra-framework cations. OPT materials have the advantage over zeolites that the Ln^{3+} ions are embedded in the framework in stoichiometric amounts and, thus, leaching of the metal is very much reduced. We have investigated aqueous suspensions of Ln-AV-9 crystals and found negligible water ^1H longitudinal relaxivities (r_1) for all Ln^{3+} ions studied and quite large transverse relaxivities (r_2) [5].

Acknowledgements

I am grateful to Fundação para a Ciência e a Tecnologia for financial support.

References

[1] Rocha, J. and Anderson, M. W., Eur. J. Inorg. Chem., (2000), 801-818; Rocha, J., Lin, Z., in Micro- and Mesoporous Mineral Phases, Reviews in Mineralogy and Geochemistry, Ferraris G. and Merlino S. (eds.), Mineralogical Society of America, Geochemical Society, 2005, Vol 57, Chapter 6, 173.

[2] Ananias, D., Ferreira, A., Rocha, J., Ferreira, P., Rainho, J. P., Morais, C., Carlos, L. D., J. Am. Chem. Soc., 123 (2001) 5735-5742.

[3] Sebastián, V., Lin, Z., Rocha, J, Téllez, C., Santamaria, J., Coronas, J., Chem. Commun., (2005) 3036-3037-

[4] Pinto, M. L., Rocha, J., Gomes, J. R. B., Pires, J., J. Am. Chem. Soc., in press.

[5] Pereira, G. A., Norek, M., Peters, J. A., Ananias, D., Rocha, J., Geraldes, C. F. G. C., Dalton Trans., (2008) 2241-2247.

[6] Ananias, A., Paz, F.A.A., Carlos, L.D., Geraldes, F.G.C., Rocha, J., Angew. Chem. Int. Ed., 45 (2006), 7938.

[7] Ananias, D., Kostova, M., Paz, F. A. A., Neto, A. N. C., DE Mora, R. T., Malta, O. L., Carlos, L. D., Rocha, J., J. Am. Chem. Soc., 131 (2009), 8620-8626.

KL-3

Zeolites and Related Mesoporous Materials for Multi-talented Environmental Solutions.

C. Perego, R. Bagatin, M. Tagliabue, R. Vignola.
eni S.p.A., Research Center for Unconventional Energies, v. G. Fauser 4, 28100, Novara, ITALY.
E-mail: carlo.perego@eni.com

Despite of over 25 years of intensive technological effort, sub-surface environment cleanup still remains a challenge. Traditional technologies have succeeded in reducing immediate threats of contaminated sites, while their ability to get further quality water improvements have been severely hampered by site-to-site variability, contaminant properties and inadequate design/implementation of remediation systems. Undoubted difficulties have been met in presence of heavy contaminations and within this framework, reliable and economical methodologies are still sought. Biological treatments are suitable mainly when few contaminants are present or low contaminant concentration allows microbial activities. In more complex situations, physical-chemical treatments are preferred. Among them, adsorption technologies are considered simple and effective for water treatment: the challenge is finding adsorbents able to operate in situations involving natural interfering species (*e.g.* humic substances or inorganic ions). Nanomaterials and membranes could provide a technological breakthrough in this field. Ideal adsorbents should have excellent adsorptive capacity, fast adsorption/desorption kinetics, long service life and stability under operating conditions. Activated Carbons (ACs) are typical ones. Unfortunately, ACs suffers of fire risk, pore clogging, hygroscopicity and lack of regenerability when used for the removal of Volatile Organic Compounds (VOCs).
Zeolites and related mesoporous materials have been investigated as alternative adsorbents because of their high adsorption capacity, reliable desorption performances and excellent chemical stability. In this paper we describe their use as versatile materials for environmental protection: natural zeolites for removal of heavy metals by ion exchange, hydrophobic zeolites in case of organic/oil contamination and silica-alumina mesoporous materials in case of massive organic/oil contamination. Finally, zeolite membranes are proposed for situations where use of adsorbents is improper (*i.e.* in presence of very high concentrations of mixed organic contaminants).
Natural zeolites for environmental applications are still gaining interests mainly due to their properties and significant worldwide occurrence. Specifically, their ion-exchange capacity for cations (*i.e.* ammonium and heavy metal) has been largely demonstrated.
Recently, natural zeolites and their modified forms have also been reported for removal of anions and organics from water systems. One of the purposes of this paper is updating recent research results on inorganic cation adsorption using natural zeolites as well as on modified zeolites for removal of anions and organic compounds. Application of synthetic (hydrophobic) zeolites for groundwater treatment deserves a special attention. Traditionally, remediation is performed using Pump & Treat (P&T) technology, involving extraction (*pump*) and the aboveground treatment (*treat*) of the groundwater before its re-injection. This technology needs adsorbents characterised by very fast adsorption/desorption kinetics. Use of Permeable Reactive Barriers (PRBs) represents a further innovative approach: the remediation is operated directly on the groundwater without the need of pumping on the ground. Adsorbent employed should have both high permeability and ability to front interfering effects able to reduce process efficiency. Hydrophobic zeolites have been proposed in both methodologies, as improvement to Granular Activated Carbons (GACs) exploiting both their high kinetics and selectivity. Furthermore, metal-doped zeolites have been claimed as

catalysts for organic contaminant decomposition in PRBs (*e.g.* halogenated compunds). We describe performances and advantages of using zeolites in field trials in both P&T and PRB applications: results have been obtained in gasoline refuelling stations (P&T) and in a coastal petrol refinery (PRB) respectively [1–3]. Successful experiences with zeolites have demonstrated their excellent adsorption capacity, inertness toward high molecular weight substances (*e.g.* humic acids) and inorganic cations, structure stability after prolonged immersion in water and finally, complete regenerability by simple thermal treatments. It has to be pointed out that advantage of using the same zeolite lot in subsequent cycles compensates the higher costs of these adsorbents with respect to conventional ones (*e.g.* GACs). On the other hand, zeolites, due to their structural limits, underperform in situations where huge hydrocarbon concentrations, dispersed oil and different types of heavy metals are present at the same time (*e.g.* produced waters from oil extraction). Recent works have shown that mesoporous materials can have larger adsorption capacity, good selectivity and improved recoverability for the removal of toxic compounds from aqueous solutions. The preparation of silica-based adsorbents has generated considerable interest due to their unique large specific surface area, regular pore structure and modified surface properties. Moreover, they can also be regenerated for many times after saturation. Mesoporous Silica-Alumina adsorbents (MSA) have been tested at eni laboratories for the removal of large amounts of organic compounds, (benzene and toluene at concentrations higher than 200 ppm) and dispersed oil. The need of contemporary removal of heavy metals, often present as cations and anions, and organic compounds has stimulated the synthesis of functionalised mesoporous silica, originating families of adsorbents specific for toxic cations or anions. Functional groups are anchored on the surface or inside the pores of the mesoporous silica. As a result, the adsorption capacity is partially influenced by metal-ligand concentrations. In general, removal of very high concentrations of contaminants can not be managed by adsorption. In this case, membrane separation systems could be the most practical choice.

Characterizations and applications of zeolite membranes have been extensively investigated since the mid of 1990s, owing to their potential molecular sieving action, controlled host–guest interactions and high thermal and chemical stability. The advantages of inorganic membranes compared with organic ones mainly refer to possibilities of high pressure application, steam cleaning and back flushing to remove fouling. The uniformity of zeolite micropore size is a key factor in comparison with amorphous membranes, where control of pore size distribution is difficult. There are a number of factors which control the separation properties of zeolite membranes: pore size, Si/Al-ratio and type of counter ions are among the most important. Furthermore, morphology, size and arrangement of zeolite crystals in a layer strongly affect permeation and separation characteristics, so that zeolite membrane technology, although very promising, presents difficulty in commercial diffusion.

As a conclusion, experiences presented and results obtained demonstrate that zeolites and related mesoporous materials could provide effective solutions for environmental remediation with particular reference to complex situations.

References

[1] R. Vignola, U. Cova, F. Fabiani, G. Grillo, R. Sbardellati, R. Sisto, Removal of MTBE and Hydrocarbons from Groundwater Using Specific Zeolites in Full-scale Pump & Treat and Demonstrative Permeable Reactive Barrier, Proceedings of the 4th International FEZA Conference, Paris, France (2008).

[2] R. Vignola, G. Grillo, R. Sisto, G. Capotorti, P. Cesti, M. Molinari, Synthetic Zeolites as Sorbent Material for Permeable Reactive Barriers at Industrially Contaminated Sites, Proceedings of the International Symposium on Permeable Reactive Barriers, Belfast, Northern Ireland (2004).

[3] R. Vignola, R. Bagatin, A. De Folly D'Auris, C. Flego, E. Previde Massara, M. Nalli, R. Sisto, Zeolite Performance and Longevity in a Permeable Reactive Barriers: one Year of Field Experience in a Refinery's Groundwater: Part 1 : the Performance, Micropor. Mesopor. Mater. (in press).

Applications of Automated electron Diffraction Tomography (ADT) on nanoporous materials

Ute Kolb, Enrico Mugnaioli
Institute of Physical Chemistry, Johannes Gutenberg-University, Mainz, Germany

Structural characterization of nano particles is often problematic for X-ray powder diffraction due to peak broadening. The impact of this effect is enhanced for large cell structures and phase mixtures. In these cases transmission electron microscopy (TEM), allowing to use imaging and diffraction on the same nano volume, is able to deliver significantly more information. Nevertheless, high resolution TEM, where structural features can be visualized directly at atomic resolution, demands high electron dose. This causes beam damage, from structural changes to complete amorphization, in most materials, either organic or inorganic, and is of high importance for frameworked and hydrated inorganic materials (like zeolites). In contrast, electron diffraction needs only a fraction of this electron dose and provides structural data with even higher resolution.
For a complete structure solution, three-dimensional experimental data are needed. Traditionally, this data is collected via a tilt of a pre-oriented nano-crystal around a low index crystallographic axis. The resulting diffraction patterns, which are oriented along low index zones, cover only a limited amount of reflections and are moreover affected by strong dynamical effects. Data quantity and quality are the key to a successful ab-initio structure solution and there is a strong need to improve both [1].

Automated electron Diffraction Tomography (ADT) is a recently developed approach for electron diffraction acquisition and analysis [2, 3]. The core idea is to collect not-oriented diffraction patterns in a tilt sequence around an arbitrary axis with fixed tilt steps. In such a way the totality of the accessible reciprocal space can be scanned inside the tilt range of the microscope goniometer.
ADT data sets have been collected with a FISCHIONE tomography holder and a cooled GATAN single-tilt holder on a Tecnai F30 S-TWIN transmission electron microscope equipped with a field emission gun working at 300 kV. STEM images, for crystal tracking, were collected by a FISCHIONE high angular annular dark field detector (HAADF). Nano electron diffraction patterns were acquired with a CCD camera (14-bit GATAN 794MSC). A mild illumination setting resulting in an electron dose rate of 10 - 15 e/Å^{2}s was used. Nano electron diffraction was performed employing a 10 μm C2 condenser aperture with a 100-50 nm beam on the sample. The above described equipment is not mandatory for ADT data collection. It has been shown that most standard TEMs are capable to be set up for this technique [4].
The resulting diffraction patterns can not be analysed manually any more, thus a dedicated software was programmed (ADT3D) which, after some geometrical corrections, reconstructs the three-dimensional reciprocal space. From this volume cell parameters can be determined using clustering-routines. Based on that, spots can be indexed and intensities integrated which are used without any further correction so far. The three-dimensional reciprocal space reconstruction provides additionally the chance to inspect the volume by eye and detect crystallographic specialities such as disorder, twinning or other individuals.
Data sets collected by ADT proved to be of higher quality than the ones collected by conventional electron diffraction based on oriented patterns. Dynamical effects are reduced such that a standard kinematic approach (intensities proportional to F_{hkl}^2) delivers ab-initio the complete structural model (direct methods implemented in SIR2008, included in the package

Il Milione [5]). A further improvement in reflection intensity collection was achieved by coupling ADT with precession electron diffraction (PED) [6] in order to improve the spot integration. PED was performed using the SpinningStar unit NanoMEGAS. The precession angle was kept at 1.2° which is significantly lower than angles used for the measurement of precessed in-zone diffraction patterns.
Based on ADT and ADT/PED data it was possible to solve about 30 structures in the last two years, some originating from single nanocrystals down to 30 nm [7]. Remarkably, large cell porous minerals [8], zeolites [9] and beam-sensitive metal-organic frameworks [10] have been solved in the last year by direct methods implemented in the same software used in X-ray crystallography. Examples of recently solved porous material structures will be proposed, including large cavities and doped zeolites and other porous frameworks.

References

[1] Mugnaioli, E., Gorelik, T., Kolb, U., Ab initio"structure solution from electron diffraction data obtained by a combination of automated electron diffraction tomography and precession technique. Ultramicroscopy, 109, (2009) 758-765.
[2] Kolb, U., Gorelik, T., Kübel, C., Otten, M.T., Hubert, D., Towards automated diffraction tomography: Part I–Data acquisition, Ultramicroscopy, 107 (2007), 507-513
[3] Kolb, U., Gorelik, T., Otten, M.T., Towards automated diffraction tomography. Part II - Cell parameter determination, Ultramicroscopy, 108 (2008), 763-772
[4] Gorelik, T.E., Stewart, A.A., Kolb, U., Structure solution with automated electron diffraction tomography data: different instrumental approaches, Journal of Microscopy, submitted (2011)
[5] Burla, M.C., Caliandro, R., Camalli, M., Carrozzini, B., Cascarano, G. L., De Caro, L., Giacovazzo, C., Polidori, G., Siliqi, D. & Spagna, R., IL MILIONE: a suite of computer programs for crystal strucutre solution of proteins, Journal of Applied Crystallography, 40 (2007), 609-613
[6] Vincent, R., Midgley, P.A., Double conical beam-rocking system for measurement of integrated electron diffraction intensities, Ultramicroscopy, 53 (1994), 271-282
[7] Birkel, C.S., Mugnaioli, E., Gorelik, T., Kolb, U., Panthöfer, M., Tremel, W., Solution Synthesis of a New Thermoelectric $Zn_{1+x}Sb$ Nanophase and Its Structure Determination Using Automated Electron Diffraction Tomography, Journal of the American Chemical Society, 132 (2010), 9881-9889
[8] Rozhdestvenskaya, I., Mugnaioli, E., Czank, M., Depmeier, W., Kolb, U., Reinholdt, A., Weirich, T., The structure of charoite, $(K,Sr,Ba,Mn)_{15-16}(Ca,Na)_{32}[(Si_{70}(O,OH)_{180})](OH,F)_{4.0} * nH_2O$, solved by conventional and automated electron diffraction, Mineralogical Magazine, 74 (2010), 159-177
[9] Mugnaioli, E., Gorelik, T., Stewart, A., Kolb, U., "Ab-initio" structure solution of nano-crystalline minerals and synthetic materials by automated electron tomography, in Krivovichev S.V., Minerals as Advanced Materials II, Springer, Berlin Heidelberg, in print (2011)
[10] Denysenko, D., Grzywa, M., Tonigold, M., Streppel, B., Krkljus, I., Hirscher, M., Mugnaioli, E., Kolb, U., Hanss, J., Volkmer, D., Elucidating Gating Effects for Hydrogen Sorption in MFU-4 Type Triazolate-Based Metal-Organic Frameworks Featuring Different Pore Sizes, Chemistry - A European Journal, 17 (2011), 1837-1848

Advanced Light Microscopic Techniques for Zeolite Characterization - Catalytic Exploration of new Zeolite Materials

Dirk De Vos, co-workers and collaborators*
Centre for Surface Chemistry and Catalysis, Katholieke Universiteit Leuven, Belgium
Dirk.devos@biw.kuleuven.be

The lecture will discuss new characterization techniques for zeolite materials, as well as recent catalytic results with new types of zeolite materials.

Second Harmonic Generation Microscopy and other Light Microscopic Techniques in zeolite characterization

In a first part of the talk, we'll focus on developments in light microscopy as applied to zeolite characterization. We'll first briefly review some of our achievements in *fluorescence microscopy*, and the efforts that have been made to improve the *spatial resolution*, e.g. by time-resolved, stochastic observation of catalytic sites. We'll also show how this technique can reveal diffusional limitations in catalyst particles, *e.g.* for the epoxidation of olefins in mesoporous Ti-containing catalysts [1].

As a complementary technique, we have recently introduced Second Harmonic Generation. SHG is a second-order nonlinear optical phenomenon which, within the electric dipole approximation, is forbidden for centrosymmetric systems. This means that only molecules adsorbed on surfaces give a SHG-signal, while the surrounding liquid phases do not generate a signal. This makes SHG ideally suited to study adsorption processes in the liquid phase *in situ*. Moreover, as a second-order process, SHG is very sensitive to symmetry, and can thus be used to unravel molecular organization. Until recently SHG-work on zeolites was limited to studies in which the zeolites were filled with dyes outside the SHG-apparatus or in which the signal was averaged over one or more crystals. We here will show how to use SHG to follow adsorption and diffusion processes on zeolitic materials in the liquid phase in real-time [2,3]

Recently we expanded our approach to second-harmonic generation microscopy (SHGM). SHGM has mainly emerged in the last decade for the visualization of biological systems, but has hardly been used so far in materials science. Herein we present the first SHGM studies on microporous materials. A study of *p*-nitroaniline in SAPO-5 crystals reveals that the tool can be used to map the organization of guest molecules. The study revealed the extent of the cooperative behaviour of PNA in SAPO-5 [4]. For ZSM-5 crystals it is shown that the organization of the guest molecules can be used to determine the crystallographic orientation of the different intergrown crystal parts [5]. The extent of dipolar chains in ZSM-5 moreover pointed towards a specific diffusion behaviour which has been further unravelled *in situ* with SHGM in the liquid phase. New studies in which SHGM is applied to other nanoporous materials are under way.

Catalytic use of zeolites derived from layered silicate precursors

A high-potential route to new zeolite materials is the topotactic condensation of layered materials. MCM-22 is probably one of the best known examples. In a collaborative effort[6], we have studied materials derived from precursors such as the layered silicates RUB-39, or RUB-36. Condensation of these materials results respectively in the three-dimensional zeolites RUB-41 (with RRO topology) and RUB-37 (with CDO topology). In early adsorption studies, the specific separation capabilities of RUB-41, with its 8-MR and distorted 10-MR channels were already revealed [7,8]. In a next step, Al was inserted succesfully into the

materials. Specifically, we will demonstrate that the constrained pores of Al-RUB-41 make it a suitable methanol amination catalyst, with a selectivity for monomethylamine and dimethylamine that is clearly enhanced because of product shape selectivity [9, 10]. In a next evolution, the space available in the pores can be enhanced by interlayer silylation of the material with compounds like dichlorodimethylsilane (DCDMS) or hexamethyldisiloxane. After calcination of a DCDMS expanded RUB-39, a new ordered material, named COE-2 is obtained [11]. A detailed catalytic study, with the decane hydrocracking as the test reaction, revealed that the pores of this COE-2 material are considerably more spatious than in the related RUB-41 material [12].

Catalytic application of zeolites with MEI topology

ZSM-18 is a microporous aluminosilicate with MEI framework. This zeolite structure was just recently obtained in its template-free form from an economically accessible synthesis and can thus be considered new [13]. Relevant characteristics are one-dimensional 12 MR (6.9 x 6.9 Å) pores and unique 3 membered Si-O rings. Presenting a rather Al-rich structure (Si/Al = 5.6), it is not immediately obvious for which reactions ZSM-18 might be a suitable catalyst. We will show data on the use of ZSM-18 as a catalyst for a series of test reactions. In addition, surface and structural effects of the catalyst will be investigated. Furthermore, the effect of dealumination will be assessed.

[1] Roeffaers et al., Angew. Chem. Int. Ed., 2009, 9285. De Cremer et al. , Angew. Chem. Int. Ed., 2010, 908.
[2] Van der Veen et al., Langmuir, 2009, 4256.
[3] Van der Veen et al., ChemPhysChem 2010, 870.
[4] Van der Veen et al., PCCP 2010, 10688.
[5] Van der Veen et al., JACS 2010, 6630.
[6] The work on the layered RUB-type of materials is a collective effort, headed by BASF (Dr. U. Müller, Dr. B. Yilmaz) in the INCOE project, together with H. Gies, F. Xiao, T. Tatsumi and X. Bao.
[7] Wang, Müller, Gies et al., Chem. Mater. 2005, 43.
[8] Tijsebaert et al., Chem. Commun. 2008, 2480.
[9] Yilmaz et al., Chem. Commun. 2011,
[10] Tijsebaert et al., J. Catal. 278 (2011) 246.
[11] Gies et al., Chem. Mater. 2011, 2545.
[12] Tijsebaert et al., J. Catal. in press, 2011.
[13] Gies et al., Microp. Mesoporous Mat. 132 (2010) 43.

Acknowledgements. We are grateful to BASF for support in the frame of the INCOE project on new zeolite materials.

* We are deeply indebted to our collaborators in this work: Dr. U. Müller, Dr. B. Yilmaz, Dr. M. Feyen, Profs. H. Gies, T. Tatsumi, X. Bao, F. Xiao. We also thank our sponsors: the Belgian Federal Government (IAP 6/27 – FS2), FWO (for fellowships and projects), the EU (Macademia project) and IWT.

* DDV is very grateful to all colleagues and co-workers who have contributed to the research: P. Jacobs, M. Van der Veen, B. Tijsebaert, M. Henry, G. Majano, T. Verbiest, J. Hofkens, B. Sels, G. Decremer, M. Roeffaers.

Design of inorganic nanoparticles for *in vivo* applications

Etienne Duguet
Institut de Chimie de la Matière Condensée de Bordeaux, CNRS, Univ. Bordeaux, France
duguet@icmcb-bordeaux.cnrs.fr

The aim of this communication is to present potential advantages of functionalized magnetic nanoparticles for diagnosis and therapy through (i) an overview of their potentialities, not only for MRI contrast enhancement, such as the commercial « (Ultrasmall)SuperParamagnetic Iron Oxide » or (U)SPIO, but also for magnetic fluid hyperthermia in oncology and remote-triggered drug release, (ii) an understanding of the problems involved as soon as nanoparticles are injected in the blood-compartment, such as the reaction of the mononuclear phagocyte system, the opsonization process and the parameters affecting the nanoparticle biodistribution and (iii) the possibilities for resolving them: surface modification for long-circulating or macrophage-evading nanoparticles, ligand grafting for active targeting of specific organs or tumour cells… Illustrations will be given from examples of the literature or derived from our current research efforts.

In vivo fate of invading nanoparticles

As soon as bare particles are, intentionally or not, injected in the blood compartment, they are subjected to the action of the mononuclear phagocyte system (MPS). The first step of the clearance mechanism is the opsonization process. Opsonins are circulating plasma proteins, which adsorb themselves spontaneously onto the surface of particles, and are capable of interacting with the specialized plasma membrane receptors on MPS cells. The second step consists in the endocytosis/phagocytosis of the particles by these cells, leading to their elimination from circulation and their simultaneous concentration in organs with high phagocytic activity. Therefore, particles are cleared up within minutes from the bloodstream; their typical final biodistribution is 80-90 % in the liver, 5-8 % in the spleen and 1-2 % in the bone marrow.

The design of long-circulating particles consists in minimizing their hydrodynamic radii and making their surface uncharged and hydrophilic in order to prevent/delay the opsonin adsorption. Moreover, if a definite tissue or cell type is targeted, specific ligands shall be grafted onto the particle surface in order to create affinity with the cell receptors (active targeting strategy).

Current and expected applications of magnetic nanoparticles (MNPs)

MNPs are more and more relevant in medicine because of the penetrability of magnetic fields into human tissues and the absence of endogenous magnetic entities.

Therefore, MNPs may be towed in magnetic gradients and concentrated in areas of medical interest (physical targeting strategy). The development of magnetic drug carriers has been attempted but it necessitates robust drug/MNPs conjugates capable to withstand blood flow dynamics and therefore large and highly-magnetised particles.

MNPs are able to alter the ^{1}H relaxation and hence to be used as contrast agents in magnetic resonance imaging (MRI). Commercial « (Ultrasmall) SuperParamagnetic Iron Oxide » or (U)SPIOare made of 3 to 10-nm crystals of maghemite/magnetite embedded in a dextran corona, which ensures their steric stabilisation and later their stealthiness. SPIO (hydrodynamic diameter of 50-100 nm) are easily phagocytised by the Kupffer cells and are used for liver MR imaging. Due to their smaller hydrodynamic diameter (20 nm), the plasma

half-life of USPIOmay reach 20 hours, making some MNPs capable to leak to the interstitium, where they are cleared by the macrophages of the lymphatic system or drained via the lymphatic system and subsequently accumulated in the lymph nodes (MR lymphography). Next MRI developments consist in moving from anatomical imaging to molecular imaging implying that dextran corona shall beefficiently derivatised with specific ligands.

Lastly, heat is released when MNPs are subjected to *ac* magnetic fields making them useful for oncology hyperthermia treatments. The control of the specific absorption rate (SAR) of magnetic aqueous dispersion is crucial for calculating the administration dose. In the literature, SAR values vary from 20 to 600 $W.g^{-1}$ (of magnetic element), but remain difficult to compare and poorly correlated to physical theories. The SAR improvement routes are based on a maximal dispersion state (single MNPs *vs.* aggregates), surface and core chemistry optimisation, and narrow size distribution of MNPs. Moreover, the control of *in vivo* temperature is equally crucial, because on the one hand heat conduction and energy adsorption *in vivo* are widely unknown and on the other hand local overheating may damage safe tissue. The ideal hyperthermia mediators should be self-regulating by stopping to heat as soon as the therapeutic temperature is reached. They should avoid overheating due to agglomerates and achieve a more uniform temperature distribution. For that purpose, ferromagnetic MNPs with an adjustable Curie temperature are of special interest.

Towards multifunctional platforms

It is now expected that the next developments will also concern multifunctional platforms which will enable to target specific organs, tissues, cells or sub-cellular compartments, to be monitored by MRI, to carry drug and release it at the right place and time. Thermoresponsive polymers / MNPs / drug reservoirs conjugates are being developed taking advantage of the MNPs heating in *ac* magnetic fields to trigger the drug release.

References

E. Duguet, S. Mornet, S. Vasseur, and J. M. Devoisselle, *Nanomed.*, 2006, **1**, 157-168.

Q. He, and J. Shi, *J. Mater. Chem.*, 2011, **21**, 5845-5855.

A.H. Lu, E.L. Salabas, and F. Schüth, *Angew. Chem. Int. Ed.*, 2007, **46**, 1224-1244.

Q.A. Pankhurst, N.K.T. Thanh, S.K. Jones, and J. Dobson, *J. Phys. D: Appl. Phys.*, 2009, **42**, 224001 (15pp).

E. Pollert, K. Knížek, M. Maryško, P. Kašpar, S. Vasseur, and E. Duguet, *J. Magn. Magn.Mater.*, 2007, **316**, 122-125.

A.G. Roca, R. Costo, A.F. Rebolledo, S. Veintemillas-Verdaguer, P. Tartaj, T. González-Carreño, M.P. Morales and C.J. Serna, *J. Phys. D: Appl. Phys.*, 2009, **42**, 224002 (11pp).

A.M. Schmidt, *Colloid Polym. Sci.*, 2007, **285**, 953-966.

F. Sonvico, C. Dubernet, P. Colombo, and P. Couvreur, *Curr. Pharm. Des.*, 2005, **11**, 2091-2105.

Coordination of extra-framework metal cations: effects on adsorption and catalytic properties of zeolites

Petr Nachtigall
Department of Physical and Macromolecular Chemistry, Faculty of Natural Sciences, Charles University, Albertov 2030, 128 40 Prague 2, Czech Republic.
petr.nachtigall@molecular.cz

Introduction

Zeolites are currently used in number of technological applications and the potential use of metal-exchange zeolites in wide range of technological fields, including adsorption, separation, and catalysis, is evident. While there is a fairly good understanding of most of these processes taking place in metal-exchange zeolites, a significant improvement of practical applications can be achieved by increased understanding of little details at the atomistic level. Assuming that the active site is accessible for adsorbate, the catalytic and adsorption activity of extra-framework metal cations in zeolites depends primarily on the metal cation coordination. Understanding of the effect of the extra-framework metal cation coordination in zeolites on their adsorption and catalytic activity is discussed based on the extensive reconciliation of experimental and theoretical results.

Results and discussion

The metal cation coordination in zeolites depends on (i) metal cation itself (size, charge, coordination preferences) and (ii) on zeolite topology and chemical composition (including aluminum distribution). The framework flexibility, that also affects the cation coordination, is determined by zeolite topology and composition.

A simple example of CO adsorption on Na-FER and Li-FER is shown in Fig. 1. Small Li^+ cation fits perfectly inside the 6R while Na^+ cation is located slightly above the 6R plane; as a consequence, CO adsorption on Na^+ in 6R is stronger than on Li^+ in 6R. On the contrary, the coordination of both Na^+ and Li^+ cations is similar in the 8R site on the channel intersection and, consequently, the CO adsorption is stronger on small Li^+ in 8R than on Na^+ in 8R.

Similar examples relevant for adsorption in alkali metal cation exchanged zeolites are discussed, including zeolites FER, MFI, LTA, FAU and various small molecules. The coordination of divalent cations in zeolites is also discussed, in particular, CO and CO_2 adsorption on Mg^{2+} and Ca^+ exchanged zeolites [1].

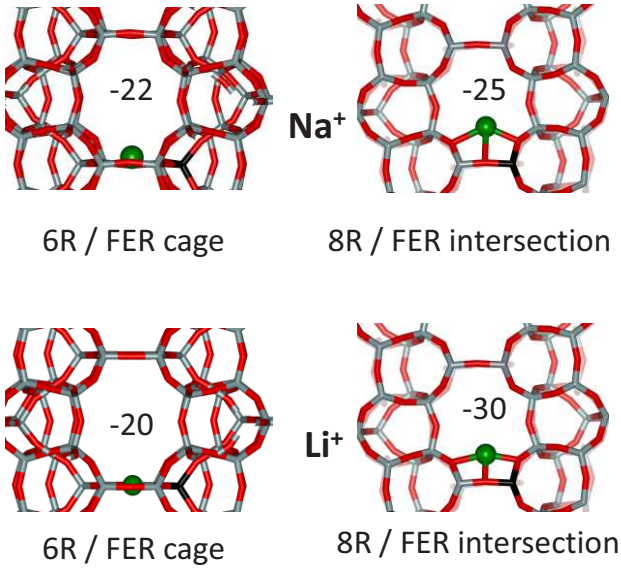

Figure 1. Calculated interaction energies (in kJ/mol) of CO with Li^+ and Na^+ cations located in 6R separating two FER cages and in 8R on the intersection of main and perpendicular channels in FER.

The effect of extra-framework cation coordination on the stability and structure of adsorption complexes is also very important for transition metal extra-framework cations. While the coordination of alkali metals or alkaline earth metals does not change much upon the interaction with adsorbate, the coordination of transition metal cations may change significantly upon the interaction with adsorbate. Adsorption enthalpies can differ as much as 50 kJ/mol depending on the extra-framework cation coordination with the framework [2]. The cation coordination also strongly affects the energies of reaction intermediates and transition states [3]. Examples of the role of the extra-framework metal cation coordination on the reaction path are discussed.

While the understanding of the effects of cation coordination on both adsorption and catalytic properties is mostly based on the results of systematic computational investigation, it is essential to compare the results with available experimental data. Therefore, a number of connections between experimental and theoretical work is drawn for both, adsorption and catalysis.

Conclusions

The better is the cation coordination with the framework the weaker is the cation interaction with adsorbate. A strong interplay of experiment and theory can help in understanding of effects of the cation coordination on adsorption and catalytic properties. The adsorption and catalytic properties of zeolites containing a particular extra-framework cation can be modified by an appropriate choice of zeolite topology and composition [4].

References

[1] R. Bulanek, I. Voleska, E. Ivanova, K. Hadjiivanov and P. Nachtigall, J. Phys. Chem. C, 113 (2009) 11066.
[2] A. Pulido and P. Nachtigall, Phys. Chem. Chem. Phys., 11 (2009) 1447.
[3] A. Pulido and P. Nachtigall, ChemCatChem, 1 (2009) 449.
[4] A. Zukal, A. Pulido, B. Gil, P. Nachtigall, O. Bludsky, M. Rubes and J. Cejka, Phys. Chem. Chem. Phys., 12 (2010) 6413.

ORAL COMMUNICATIONS

FEZA 2011

Synthesis and characterization of porous solids

FEZA 2011

Zeolite hybrid coating on aluminum substrates

Natacha LAURIDANT,[1] T. Jean DAOU,[1] Gilles ARNOLD,[2] Michel SOULARD,[1] Joël PATARIN,[1] Delphine FAYE[3]
1-Equipe Matériaux à Porosité Contrôlée (MPC), Institut de Science des Matériaux de Mulhouse (IS2M), LRC CNRS-7228, Université de Haute-Alsace, ENSCMu 3, rue Alfred Werner 68093 MULHOUSE Cedex, France
2-Equipe Mécanique, Matériaux et Procédés de Fabrication (MMPF), Laboratoire de Physique et Mécanique Textile (LPMT), CNRS-EAC 7189, IUT de Mulhouse, 61 rue Albert Camus, 68093, Mulhouse Cedex, France.
3-Service Laboratoires et Expertise, Centre National d'Etudes Spatiales (CNES),18 avenue Edouard Belin, 31401 Toulouse Cedex 9, France
jean.daou@uha.fr

Introduction

Due to the manifold applications of crystalline zeolites, such as in molecular sieving, ion exchange, selective adsorption, catalysis and microelectronic devices, increasing attention worldwide has been paid to the preparation of zeolites in forms suitable for practical utilization and to the development of methods for producing bilayer zeolites films with controllable thickness. This zeolite hybrid coating has great utility and its function and application can be easily tuned by changing the zeolite species used to generate it. Aluminum alloys are relevant for aerospace applications due to their many attractive properties such as: light weight, high mechanical strength and high heat conductivity. In order to solve the corrosion problems encountered on aluminum alloy, Yan et al. have developed a new class of zeolite corrosion-resistant coating using high-silica zeolites (MTW, *BEA, and MFI) [1,2]. Unfortunately, all attempts to combine low-silica-zeolite (LSZ) and aluminum substrates have met with great difficulty. Problems arise when attempting to synthesize LSZ coatings on aluminum substrates. LSZ synthesis solutions are known to have a very high pH, often greater than 14. This pH is very corrosive and dissolves the aluminum substrate during synthesis. This work is dedicated to the development of methods to produce low and high-silica-zeolites hybrid film on aluminum alloys substrates with desirable thickness for space decontamination applications.

Experimental

The bottom layer was prepared by in-situ crystallisation of the ZSM-5 zeolite according to the procedure described by Yan et al. [1]. EMC-1 zeolite (FAU structure-type) top layer was synthesized on the above protected substrate using secondary growth method. In a first step, faujasite seed crystals were prepared from a clear solution of molar composition $0.35Na_2O$:9TEAOH:$0.5Al_2O_3$:$25SiO_2$:$295H_2O$ as described by Jakob et al. [3]. The resulting solution was purified by centrifugation. In a second step, the aluminum substrates (AA-6061 and AA-7075) coated by ZSM-5 zeolite were placed in a 1 wt % aqueous solution of cationic polymer poly(diallydimethylammonium chloride) and immersed in the faujasite seed crystals colloidal suspension prepared above. Once the seeds had been adsorbed, 4 vertically fixed seeded substrate were immersed into a 48 mL autoclave containing a gel of molar composition 2.1 Na_2O:10 SiO_2:1 Al_2O_3:0.5 (15-crown-5):100 H_2O and hydrothermally treated at 110°C for 10 days. After the synthesis the so-obtained films were cleaned by ultrasonic bath to remove the loosely attached crystals, rinsed with water, dried and calcined at 550°C

with a plateau at 380°C and a low temperature ramp of 1°C per minute to avoid cracks in films.

Results and discussion

XRD pattern recorded on the bilayer film are presented in figure 1a. All detected diffraction peaks can be indexed to ZSM-5 and EMC-1 zeolites structures, apart the peaks between 38.47° and 44.72° which correspond to the aluminum substrate. Additional evidence for the existence of both zeolites types is provided by surface SEM images as shown in figure 1c by the presence of pyramidal shape crystals, typical of EMC-1 zeolite morphology. The bilayer film thickness was evaluated by cross-sectional SEM observations to be 10 µm while the thickness of EMC-1 zeolite top layer is approximately 1.5 µm. Proportions of the two types of zeolites in the bilayer film were also estimated by nitrogen sorption measurement using the method of mass assessment. The bilayer film seems to be composed of 15% (w/w) of EMC-1 zeolite and 85% (w/w) of ZSM-5 zeolite. This result is in perfect concordance with SEM observations of film thickness and calculations of deposited mass obtained thanks to volume of coated zeolites and zeolite density.
The strong adhesion of ZSM-5 zeolite coating to aluminum substrates as well as between the two zeolites layers were confirmed by scratch technique.

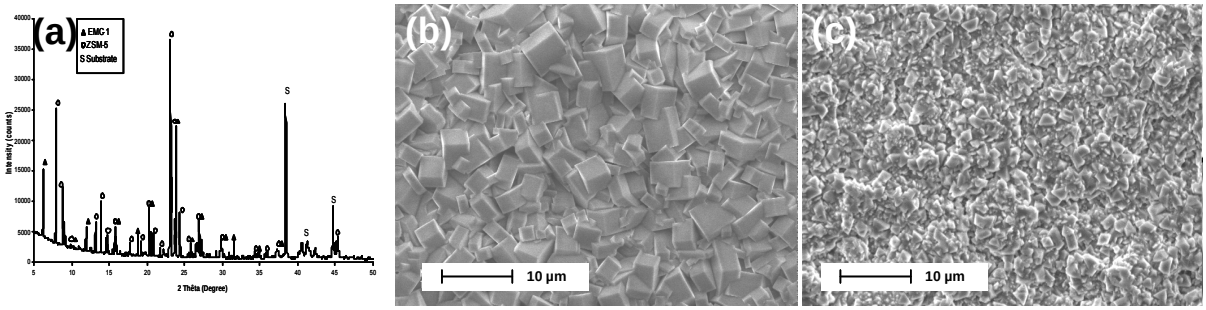

Figure 1. XRD pattern of the bilayer film of ZSM-5/EMC-1 zeolites on aluminum substrates (a) and SEM images of ZSM-5 zeolite film (b) and the bilayer film of ZSM-5/EMC-1(c) on aluminum substrates.

Conclusions

Zeolites hybrid bilayer film composed of a bottom layer of zeolite ZSM-5 and a top layer of zeolite EMC-1 was synthesized on aluminum alloys using secondary growth method. SEM and XRD results clearly indicate a homogeneous, highly crystallized and intergrown coating.

Acknowledgements

The authors would like to thank the CNES (Centre National d'Etudes Spatiales) and the CNRS (Centre National de la Recherche Scientifique) for financial support.

References

[1] Cheng, X., Wang, Z., Yan, Y., Corrosion-resistant zeolite coatings by in situ crystallization, Electrochemical and Solide-State Letters, 4 (2001), B23-B26
[2] Mitra, A., Wang, Z., Cao, T., Wang, H., Huang, L., Yan, Y., Synthesis and corrosion resistance of high-silica zeolite MTW, BEA, and MFI coatings on steel and aluminum, Journal of The Electrochemical Society, 149 (2002), B472-B478
[3] Jakob, A., Valtchev, V., Soulard, M., Faye, D., Syntheses of zeolite beta films in fluoride media and investigation of their sorption properties, langmuir, 25 (2009), 3549-3555

Zeolite Beta Mechanisms of Nucleation and Growth

Nathan D. Hould* and Raul F. Lobo*
Center for Neutron Science and Catalysis Center for Energy Innovation, University of Delaware, USA. nhould@udel.edu and lobo@udel.edu.

Introduction

Zeolite beta [1] is a model material to study the effects of Al and B heteroatom substitutions and structure directing agents (SDA) on zeolite nucleation and growth rates because it can be synthesized with Si to heteroatom ratios from 3 to ∞ [2-4]. The broad heteroatom synthesis concentration range is due to the variety of SDAs available to crystallize zeolite beta. In addition to charge, these SDAs range from inorganic (e.g., Na^+) to organic, the latter group containing one or two quaternary ammonium groups in addition to moieties such as benzyl groups, heterocyclic amines and ammonium groups, methylene chains, and methyl groups.

A significant number of investigations of zeolite nucleation and growth have been reported [5, 6]. The proposed nucleation mechanisms vary from classical [7] to complex mechanisms wherein an amorphous phase changes to become crystalline by internal Si-O-Si rearrangements [8]. There are also disagreements regarding zeolite growth mechanisms, commonly attributed to either colloidal aggregation [9] or monomer addition [10]. To test the validity of these models we have previously investigated zeolite beta formation in dilute solutions. Three populations of particles were observed during crystallization [11, 12]. Initially at room temperature supersaturated silica self-assembles into primary particles (< 3 nm). Upon heating the primary particles to 120°C, the least colloidally stable ones aggregate into secondary particles. The secondary particles have a density and composition similar to zeolite beta, change structurally over time to become zeolite beta nuclei, and aggregate into tertiary particles (zeolite beta) that subsequently ripen into well-ordered crystals exhibiting a well-defined morphology. Based on these observations a two-step model was proposed to describe zeolite beta nucleation. In this model the density and composition of the secondary particles becomes similar to zeolite beta upon heating and afterwards, a slower evolution of the secondary particle structure occurs to complete nucleation.

Experimental

Synthesis solutions at two concentrations were investigated. The molar composition of the dilute set of solutions was 1 $Si(OCH_2CH_3)_4$ / 80 H_2O / X NaOH / Y TEAOH / 0.02 $NaAlO_2$ where $X + Y = 0.6$ and X was 0 or 0.1. The dilute solutions were prepared as described in reference [12]. The molar composition of the concentrated set of solutions was 1 $Si(OCH_2CH_3)_4$ / 20 H_2O / X NaOH / Y TEAOH / L $Al(OCH_2CH_3)_3$ where $X + Y = 0.5$, X was 0 or 0.1, and $0.01 < L < 0.18$.

Synthesis solutions were investigated using dynamic light scattering (DLS) and small angle X-ray scattering (SAXS). The experimental setup is described elsewhere [11, 12]. Solids separated by centrifugation were analyzed using scanning electron microscopy (SEM, JEOL 7400F), thermal gravimetric analysis (TGA, Mettler Toledo TGA/DSC 1 STARe System), and Cu K_α powder X-ray diffraction (PXRD, Philips X'Pert X-ray diffractometer). The TGA program used was heating from 25 to 900°C at 3°C/min in 50 ml/min of air flow.

Results and discussion

The rates of zeolite beta nucleation and growth have been investigated in dilute synthesis solutions using DLS and SAXS. It was determined that the growth rate of zeolite beta is affected by the steric colloidal stability of the secondary particle population in the synthesis solution which, in turn, can be decreased by exchanging some sodium cations for TEA^+. This exchange also retards nucleation of zeolite beta at low Al concentrations ($L < 0.08$ in the concentrated synthesis solutions). Herein we have suggested that this is due to formation of internal $[[AlO_2]^- Na^+]$ ion pairs and the short-range excluded volume interactions of sodium cations that optimize T-atom voids in the secondary particles that are not the size of the pores in zeolite beta.

In more concentrated synthesis solutions the nucleation, growth, and solid solution chemistry have been investigated using DLS, SAXS, XRD, ICP-AES, SEM, and TGA. In the absence of sodium cations the crystallization process proceeds through the formation of primary, then secondary, and then tertiary particles as observed in the dilute solution. Using this knowledge we were able to synthesize nearly monodisperse zeolite beta particles with sizes between 100 and 500 nm by simultaneously changing concentrations of $Al(OCH_2CH_3)_3$, NaOH, and TEAOH in the synthesis solution to retain nucleation selectivity to zeolite beta while varying the relative rate of its nucleation to growth.

A mechanism of exchange of $[[\equiv SiO]^- TEA^+]$, $[[AlO_2]^- TEA^+]$, and $[[AlO_2]^- Na^+]$ ion pairs inside of zeolite beta has been identified using TGA. The exchange of these units enables the qualitative description of the free energy of the zeolite beta products and in turn this enables fitting of the observation of surface roughening into a model of growth analogous to well-established models in protein crystal growth. Identification of the limits of the number of SDAs occluded inside of zeolite beta enabled an approximation of the end-state diagram of the synthesis solutions using the T-atom framework density of zeolite beta and the volume to charge ratio of Na^+ and TEA^+. This is encouraging for future prediction of zeolite end-state diagrams.

Acknowledgements

N. D. H. thanks the Chevron Internship Program for sponsoring a summer internship at the Chevron Energy Technology Company where the concentrated solution syntheses were completed. This manuscript was prepared under cooperative agreement 70NANB7H6178 from NIST, U.S. Department of Commerce.

References

[1] J.M. Newsam, M.M.J. Treacy, W.T. Koetsier and C.B.D. Gruyter, Proc. Royal Soc. London. Ser. A, Math. Phys. Sci., 420 (1988) 375.
[2] K. Tsuji and M.E. Davis, Microporous Mater., 11 (1997) 53.
[3] K. Na, M. Choi and R. Ryoo, J. Mater. Chem., 19 (2009) 6713.
[4] S.I. Zones and S.-J. Hwang, Microporous Mesoporous Mater., 58 (2003) 263.
[5] C.S. Cundy and P.A. Cox, Microporous Mesoporous Mater., 82 (2005) 1.
[6] V. Nikolakis, D.G. Vlachos and M. Tsapatsis, J. Chem. Phys., 111 (1999) 2143.
[7] C.E.A. Kirschhock, R. Ravishankar, P.A. Jacobs and J.A. Martens, J. Phys. Chem. B, 103 (1999) 11021.
[8] W.H. Dokter, H.F. Vangarderen, T.P.M. Beelen, R.A. Vansanten and W. Bras, Angew. Chem., Int. Ed., 34 (1995) 73.
[9] T.M. Davis, T.O. Drews, H. Ramanan, C. He, Jingshan Dong, H. Schnablegger, M.A. Katsoulakis, E. Kokkoli, A.V. McCormick, R.L. Penn and M. Tsapatsis, Nature, 5 (2006).
[10] J.D. Rimer, D.D. Kragten, M. Tsapatsis, R.F. Lobo and D.G. Vlachos, Recent Advances in the Science and Technology of Zeolites and Related Materials: Proceedings of the 14th International Zeolite Conference, Cape Town, South Africa, 2004.
[11] N.D. Hould, S. Kumar, M. Tsapatsis, V. Nikolakis and R.F. Lobo, Langmuir, 26 (2010) 1260.
[12] N.D. Hould and R.F. Lobo, Chem. Mater., 20 (2008) 5807.

Local Structure Links in Zeolite Frameworks prepared following the F and OH-based Routes

Xiaolong Liu[1], Ugo Ravon[1,2], Alain Tuel[1]*
[1]*IRCELYON, UMR 5256 CNRS-Université de Lyon, 2 Ave A. Einstein, 69626 Villeurbanne Cedex, France.*
[2]*KAUST Catalysis Center (KCC), 4700 King Abdullah University of Science and Technology, Thuwal 23955 – 6900, Kingdom of Saudi Arabia.*
Corresponding author: alain.tuel@irtcelyon.univ-lyon1.fr

Introduction

Zeolites are generally prepared under hydrothermal conditions following two different routes: the "basic route", which leads to relatively small crystals with many structural defects, and the fluoride route, which provides zeolites with large and almost defect-free crystals, as evidenced by ^{1}H and ^{29}Si NMR [1]. The introduction of the fluoride route offered a significant number of new structures, particularly those containing D4R units, which could not be obtained in basic media [2]. Interestingly, many zeolites like **ZSM-5** and **ZSM-48** can be prepared in both media. For such zeolites, the question remains whether the two synthesis methods have some connections or not. If they have, those connections should shed light on the mechanism of formation of the corresponding zeolites. In the present work, we will show how **as-made** [F]-zeolites (such as ZSM-5 and ZSM-48) can be reversibly converted to [OH]-zeolites without any dissolution/recrystallization of the framework. The [F] ↔ [OH] "exchange" will also be investigated on less standard zeolites like **ITQ-13**, prepared in fluoride medium and containing D4R units in the structure. The influence of the location of F/OH anions in the framework will be discussed.

Experimental

Pure silica ZSM-5 and ZSM-48 were prepared using conventional synthesis routes. ITQ-13 was prepared following ref. [3] using hexamethonium cations as template. Treatments were performed under hydrothermal conditions using NH_4F or NH_4OH solutions. NMR spectra were obtained on a Bruker DSX 400 spectrometer and TEM was performed on a Jeol 2010.

Results and discussion

The morphology of pure silica ZSM-5 crystals synthesized through the OH-mediated route does not change upon treatment with NH_4F but significant modifications are observed in the corresponding ^{19}F and ^{29}Si NMR spectra (Fig. 1). The presence of an intense ^{19}F signal around -60 ppm after treatment suggests that F anions have been incorporated in the framework and occupy a $[4^15^26^2]$ cage, as it is the case for ZSM-5 prepared in the fluoride medium. Moreover, the ^{29}Si NMR spectrum looks better resolved and characterizes a less defective framework. The opposite situation is observed upon treating a zeolite prepared in the fluoride medium with a basic solution. The large crystals are preserved and the ^{19}F NMR signal, present on the original zeolite, disappears upon treatment. The resolution of the ^{29}Si NMR spectrum is partially lost, which reflects the presence of defect silanol groups. The complete disappearance of ^{19}F NMR signal indicates that the process is not limited to the surface but affects the whole crystal. Very similar results have been obtained on ZSM-48. In both zeolites, it has been reported that F ions are located in $[4^15^26^2]$ cages. Our experimental observations suggest an exchange between F and OH anions in the framework.

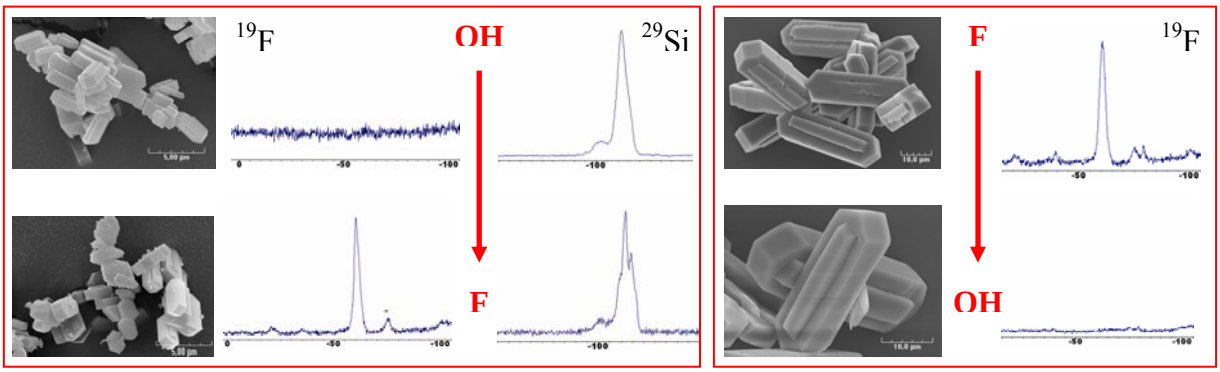

Figure 1: TEM pictures and NMR characterization of pure-silica ZSM-5 zeolites

In ITQ-13, F anions occupy 2 different positions in the framework: one is located at the center of D4R and the other is close to the 4MR window shared by two fused $[4^15^26^2]$ cages. ^{19}F MAS NMR spectra of pure silica ITQ-13 clearly show that F^- ions in $[4^15^26^2]$ cages can be exchanged for OH^- whereas those in D4R units cannot.

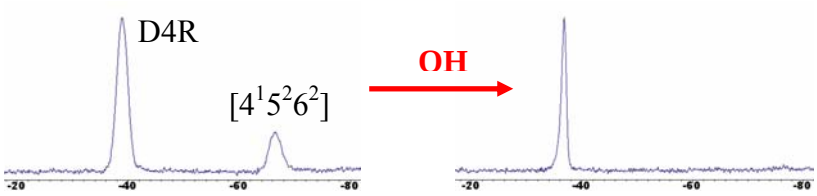

Figure 2: ^{19}F NMR spectra of [F] (left) and [F,OH] (right) pure silica ITQ-13

The mechanism of exchange will be discussed for a series of as-made zeolites with various compositions and framework topologies. Moreover, it will be clearly demonstrated that the process occurs without dissolution/recrystallization of the zeolite.

Conclusions

The easy exchange between F and OH in zeolite frameworks implies that anions could occupy similar positions in the framework and, consequently, could play a similar role in zeolite crystallization (stabilization of 4MRs). Exchange is possible in $[4^15^26^2]$ cages by migration of anions through 5MR or 6MR units. However, preliminary results show that a partial exchange is not possible in D4R units, probably because anions cannot pass through the narrow 4-ring windows or because these units are not stable in the absence of fluoride. Moreover, the possibility to tune the composition and framework defect concentration in zeolites opens new opportunities in the preparation of materials with controlled properties.

Acknowledgements

This presentation is based on work supported by Award No. UK-C0017, made by King Abdullah University of Science and Technology (KAUST)

References

[1] P. Caullet, J.L. Paillaud, A. Simon-Masseron, M. Soulard, J. Patarin, C.R. Chimie 8 (2005) 245.
[2] A. Corma, "Towards a rationalization of Zeolites and Zeolitic Materials", Proc. 14th International Zeolite Conference, Cape-Town, South Africa, Plenary Lecture, 2004.
[3] J.A. Vidal-Moya, T. Blasco, F. Rey, A. Corma, M. Puche, Chem. Mater. 15 (2003) 3961.

Heterogeneity of Al sites in a low silica KFI aluminosilicate synthesized by a novel method

Yannick Lorgouilloux, Yanliang Xiong, Christine E.A. Kirschhock, Johan A. Martens
Centre for Surface Chemistry and Catalysis, K.U. Leuven, Kasteelpark Arenberg 23, B-3001 Heverlee, BELGIUM, yannick.lorgouilloux@biw.kuleuven.be

Introduction

Cage-based zeolites are of advantage for a score of applications. In particular this is true for LTA, which for example can serve as host for unique metal clusters. For example K, AgI and Ag clusters in LTA zeolite exhibit specific magnetic[1], light-absorption[2] and luminescent properties[3]. LTA and KFI topologies have in common that both contain the same cavity called α or *lta*-cage. In both zeolites the α cages are accessible through eight-membered rings (8MRs). But while in LTA the α-cages are directly connected, in the KFI structure they are spaced by paulingite cages (*pau*), which makes KFI an interesting host topology.
KFI materials have been synthesized with several different protocols[4,5,6,7,8]. The majority of the obtained KFI zeolites have a Si/Al ratio higher than 2. Here we report a novel synthesis method for low-silica KFI type zeolite. The new method involves the use of an organic structure directing agent, *viz.* the tetramethylammonium cation, next to three alkali cations: lithium, sodium and potassium. A parametric study was conducted in order to determine the boundaries of the synthesis field of the KFI phase and some samples were cation exchanged by Ca^{2+} and K^{+}. Characterization of the samples showed that the very high Al content caused a symmetry reduction from cubic to rhombohedral due to an ordering of Al sites in the framework.

Experimental

The chemical composition of a typical starting gel for KFI synthesis was 4 SiO_2 : Al_2O_3 : 3 LiCl : 3.3 TMAOH : 0.2 NaCl : 0.4 KCl : 400 H_2O. The synthesis procedure was as follows: aluminum isopropoxide was dissolved in a solution of tetramethylammonium hydroxide (TMAOH), sodium chloride (NaCl) and potassium chloride (KCl) by heating at 90 °C until the solution was clear. After cooling down to 40 °C, tetramethyl orthosilicate (TMOS) dissolved in the same volume of methanol was added. Alcohols added and formed by the hydrolysis were boiled off. The amount of deionized water was adjusted and lithium chloride was added just before transferring the gel to a polypropylene bottle that was then treated at 90 °C for 7 days.
A synthesis parametrical study revealed the composition limits of the synthesis field. Ion exchange was carried out on some samples (three times at 60 °C) with either $Ca(NO_3)_2$ or KNO_3. As-synthesized and exchanged zeolite samples were characterized by several techniques including XRD, SEM, ^{7}Li, ^{13}C, ^{27}Al and ^{29}Si MAS NMR spectroscopy, TGA and chemical analyses.
PXRD revealed a symmetry reduction from Im3m to R3c. Before Rietveld refinement with GSAS[9] the lattice coordinates with Al inserted in 3 of the 8 T sites was relaxed using the Catlow library[10] and Gulp[11] with a charge neutralising background.

Results and discussion

The described synthesis led to phase pure KFI type zeolite. The parametrical study showed that the KFI synthesis field in the present system is very narrow, and that KFI is in competition with zeolites of the CHA, OFF and EDI types. TGA and chemical analyses

determined the composition of the new KFI material as: $|Li_{22.0}Na_{1.4}K_{2.7}((CH_3)_4N)_{5.6}|[Si_{60.2}Al_{35.8}O_{192}].68\ H_2O$

^{29}Si MAS NMR resulted in a Si/Al ratio of 1.66 confirming the very low value determined by chemical analysis (1.68).

The XRD powder patterns of the as-synthesized and exchanged samples showed that the high aluminum content caused a symmetry reduction from cubic to rhombohedral. From the eight, originally symmetrically equivalent, double six-rings (D6Rs) in the cubic system, two symmetrically different D6Rs were found in the lowered symmetry. Two were of type 1, and contained 6 Al each, while the remaining six D6Rs of type 2 contained 4 Al each. In total this resulted in 36 Al per original unit cell, matching perfectly the measured 35.8 Al. The resulting different charges of the D6Rs also affected the position of the charge compensating cations. Fig.1 illustrates the situation in the Ca-exchanged form . The two D6Rs of type 1 each have 2 Ca^{2+} in front of their six-rings, while type 2 D6Rs have Ca^{2+} positioned off centre.

To the best of our knowledge, this is the first time such a crystallographic ordering of Al sites led to a symmetry reduction in zeolites with a Si/Al ratio higher than 1.

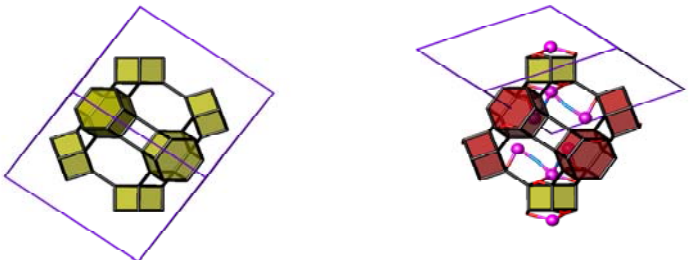

Figure 1. Representation of the 8 symmetrically equivalent D6MRs in the cubic KFI structure (Im3m, left) and of the new KFI rhombohedral structure (R3c, right), in which Ca^{2+} cations can be seen next to the type 1 yellow D6MRs (6Al) and the type 2 red D6MRs (4Al).

Conclusions

A new synthesis method for a zeolite with KFI framework, with tetramethylammonium, lithium, sodium, and potassium cations, was discovered. A parametrical study was conducted, which showed that in this compositional field other zeolite materials such as EDI, CHA and OFF are in competition with the KFI. The new KFI material showed a very high Al content (Si/Al ~ 1.7). A previously unseen crystallographic ordering of Al sites in the framework led to charge anisotropy in the cavities which may be exploited in novel applications.

Acknowledgements

JAM and CEAK acknowledge financial support by the Flemish Government for long-term structural funding (Methusalem), the Belgian Prodex office and ESA.

References

[1] Nozue Y., Kodaira T., Ohwashi S., Goto T., Terasaki O., Phys. Rev. B 48 (1993) 12253
[2] Kodaira T., Ikeda T., Takeo H., Chem. Phys. Lett. 300 (1999) 499
[3] De Cremer G., Antoku Y., Roeffaers M.B.J., Sliwa M., Van Noyen J., Smout S., Hofkens J., De Vos D.E., Sels B.F., Vosch T., Angew. Chem. Int. Ed. 47 (2008) 2813
[4] Barrer R.M., J. Chem. Soc. (1948) 127
[5] Kerr G.T., Science 140 (1963) 1412
[6] Robson H.E., US Patent 3,720,753 (1973)
[7] Verduijn J.P., US Patent 4,994,249 (1991)
[8] Shubaeva M.A., Zhdanov S.P., Russian Patent SU1,155,564 (1985)
[9] Larson A.C., Von Dreele R.B., Los Alamos National Laboratory Report LAUR 86-748 (2000)
[10] Schroder K.P., Sauer J., Leslie M., Catlow C.R.A., Thomas J.M., Chem. Phys. Lett. 188 (1992) 320
[11] Gale J.D., J. Chem. Soc., Faraday Trans 93 (1997) 629

Synthesized of microporous crystals of titanosilite (TS-1) along *b*-orientation assisted by organic Additives

Xiangju Meng[1]*, Zhichao Shan,[2] Hong Wang,[3] Liang Wang,[2] James P. Lewis,[3] and Feng-Shou Xiao[1]*
Department of Chemistry, Zhejiang University (XiXi Campus). Hangzhou 310028 P.R. China
E-mail: mengxj@zju.edu.cn; fsxiao@mail.jlu.edu.cn
Colloge of Chemistry,Jilin University, Changchun 130012, China.
Department of Mechanical and Aerospace Engineering, West Virginia University, Morgantown, West Virginia 26506-6106.

Introduction

Zeolites are regarded as one of the most important catalysts in industry because of their large surface area, high adsorption capacity, uniform and intricate channels, high thermal and hydrothermal stabilities, and well-defined micropores with excellent shape-selectivity in catalysis.[1] As example, titanosilicate TS-1 with a MFI-type framework are considered a milestone in catalytic oxidation due to its excellent performances in a series of oxidations using H_2O_2 as a clean oxidant.[2] MFI-type zeolite possesses an anisotropic framework with two intersecting 10-membered ring channels including straight channels (5.3×5.6 Å) parallel to *b*-axis and zig-zag channels (5.1×5.5 Å) parallel to *a*-axis.[3-5] Thus, by controlling crystalline length along *b*-axis, catalytic properties in oxidations and adsorption selectivities over TS-1 crystals could be significantly adjusted.

We have investigated the energy of three MFI orientations (001, 010, and 101) using *ab initio* DFT calculations, and the results indicate that (010) surface is the most energetic favorable orientation of the three candidates. This surface is potentially favorable for adsorption of organic additives due to the orientation and coordination of the exposed Si/O atoms on this particular surface. Thus, we proposed that as the different additives interact with this surface during the early crystallization period, the growth of MFI crystals along the *b*-orientation would be controlled.[6]

Experimental

Sheet-like TS-1 crystals (TS-1-S) were hydrothermally synthesized from starting titanosilicate gels with molar ratios of SiO_2/0.02 TBOT/0.3 TPAOH/40 H_2O/0.33 IPA/0.074-0.368 urea. Typically, (1) 0.154 g of TBOT was dissolved in 0.448 g of IPA, followed by addition of 10.26 mL of TPAOH (12.6 % wt.), 6 mL of water, and 5 mL of TEOS; (2) After stirring at room temperature for overnight, 0.5 g of urea was introduced into the gel; (3) After stirring for 4-5 h, the gel was transferred into an autoclave to crystallize at 180 °C for 24 h; (4) After filtrating at room temperature, drying at about 80 °C, calcining at 550 °C for 4 h, sheet-like TS-1 crystals (TS-1-S1) were obtained.

Chain-like TS-1 crystals (TS-1-C) were hydrothermally synthesized from starting titanosilicate gels with molar ratios of SiO_2/0.02 TBOT/0.3 TPAOH/40 H_2O/0.33 IPA/0.024-0.084 flurocarbon surfactant (FC-4). For comparison, normal TS-1 crystals were synthesized from a starting titanosilicate gel with a molar ratio of SiO_2/0.02 TBOT/0.3 TPAOH/40 H_2O/0.33 IPA.

Results and discussion

Fig. 1 shows SEM images for TS-1-S and TS-1-C crystals. TS-1-S samples synthesized in the presence of urea exhibit typical sheet-like morphology. Particularly, TS-1-S1 synthesized from molar ratio of urea with silica at 0.368 gives uniform crystals with *b*-axis

at *ca*. 80 nm and *a*-axis at *ca*. 400 nm. In contrast, TS-1-C2 samples prepared using FC-4 shows a chain-like morphology with *b*-axis at *ca*. 5 μm and *a*-axis at *ca*. 0.5 μm, which are reasonably attributed to the stack of TS-1 crystals along *b*-axis, confirmed by a high-resolution TEM image. Interestingly, TS-1-C2 crystals are mechanically stable even after ultrasonic treatment for 2 h, indicating that this chain morphology is not a result of physical aggregation but of strong interactions between the crystals.

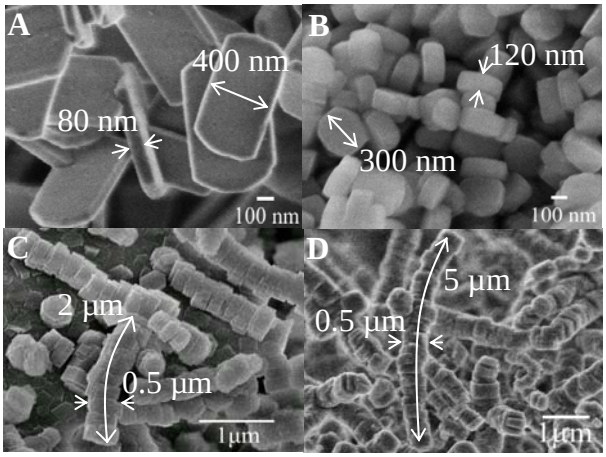

Fig.1 SEM images for (A) TS-1-S1, (B) TS-1-S2, (C) TS-1-C1 and (D) TS-1-C2 samples

It is worth noting that both urea and FC-4 play important role for the formation of sheet-like and chain-like TS-1 crystals. When these organic additives are absent in the starting titanosilicate gels, the morphology of TS-1 crystals are normal, in good agreement with those reported previously. When the starting gels have different molar ratios of the additive to silica, TS-1 crystals with distinguishable *b*-oriented length have been successfully obtained. These results have demonstrated that TS-1 crystalline morphology could be adjusted and controlled by the amount of urea and FC-4 in the starting gels. Notably, both urea and FC-4 exist during the synthesis period of TS-1 crystallization at 2-4 h, and these additives are also suitable for applications of the other zeolites. *e.g*. silicalite-I zeolite with sheet-like morphology is successfully synthesized in the presence of urea additive.

As a standard reaction benchmark, Beckmann rearrangement of cyclohexanone oxime shows that the catalytic activities are strongly dependent on *b*-oriented length of TS-1 crystals. TS-1-S catalysts with very short *b*-axis-length (*b*-axis of 80 and 120 nm and *a*-axis of 400 and 300 nm) are very active and stable. In contrast, TS-1-C catalysts with long *b*-axis-length (*b*-axis of 2 and 5 μm and *a*-axis of 0.5 μm) exhibit relatively low conversion. These results are attributed to the fact that the short *b*-axis-length of TS-1 crystals is favorable for the diffusion and conversion in Beckmann rearrangement of cyclohexanone oxime. On the other hand, TS-1-C2 exhibits high ratio of *p*-/*o*-xylene at 3.8 in adsorptive test of xylenes, which is potentially important for industrial production of *p*-xylene. On the contrary, TS-1-S1 gives the ratio at 1.2, indicating almost no difference for the adsorption of *p*-xylene and *o*-xylene.

Acknowledgements

This work is supported by the State Basic Research Project of China (2009CB623507), National Natural Science Foundation of China (21003107) and Fundamental Research Funds for the Central Universities (2010QNA3035).

References

[1] Corma, A., Chem. Rev. 95 (1995) 559-614.
[2] Taramasso, M., Perego, G., Notari, B., US Patent (1983) 4410501.
[3] Notari, B., Adv. Catal. 41 (1996) 253.
[4] Cundy, C. S., Cox, P. A., Chem. Rev. 103 (2003) 663-701.
[5] Corma, A., J. Catal. 216 (2003) 298-312.
[6] Shan, Z., Wang, H., Meng, X., Liu, S., Wang, L., Wang, C., Li, F., Lewis, J.P., Xiao, F.-S., Chem. Commun. 47 (2011) 1048-1050.

Spontaneous *t*-stilbene ionization in medium pore zeolites: Effects of spatial constraints on the charge transfers.

Matthieu Hureau, Alain Moissette, Hervé Vezin and Claude Brémard
Laboratoire de Spectrochimie Infrarouge et Raman UMR-CNRS 8516, Bât. C5 Université Lille 1 Sciences et Technologies, 59655 Villeneuve d'Ascq cedex, France.
E-mail : alain.moissette@univ-lille1.fr

Introduction

The observation of long-lived charge separated states within the zeolite internal void space is well-known [1-3]. However, most of the parameters stabilizing the charge separated states have to be clearly elucidated. In that context, the fate of the ejected electron is still a matter of debate and the influence of the framework topology has to be thoroughly understood. Therefore, we have used the *t*-stilbene probe molecule to follow the sorption course into Brønsted acidic zeolites with ferrierite (H-FER), H-ZSM-5 and mordenite (H-MOR) topologies and analogous Si/Al ratio. We have used continuous wave and pulsed EPR, diffuse reflectance UV-visible absorption (DRUVv) and Raman scattering to monitor the direct exposure of *t*-St crystals to dehydrated zeolites in the absence of solvent and under inert gas.

Experimental

Prior to sorption, weighed amounts of zeolite (ZSM-5 Si/Al = 13.5; H-FER Si/Al=10; H-MOR Si/Al=10) were freshly dehydrated by a calcination procedure up to 723 K under argon. Weighed amounts of dry *t*-stilbene (*t*-St, $C_{14}H_{12}$) were introduced into the cell under dry argon. The DRUVv spectra of the powdered samples were recorded using Cary 6000i spectrometer. The instrument was equipped with an external integrating sphere to study the powder zeolite samples through diffuse reflectance. A Bruker RFS 100/S instrument was used as a near-IR FT-Raman spectrometer (λ_{ex}=1064 nm). The CW EPR measurements were performed on a Bruker ELEXYS E580E spectrometer operating at X-band (~9 GHz). All measurements were made at room temperature or at 4.2 K. HYSCORE spectra were recorded at 4.2 K using the four pulse sequence $\pi/2$-τ-$\pi/2$-t_1-π-t_2-$\pi/2$-τ-echo.

Results and discussion

The spectral data show evidence of simultaneous *t*-St spontaneous ionization and the formation of long lived radical cation-electron and electron-hole pairs. The very long lifetimes of the transient species generated in zeolite (several months) allow their characterization with respect to the electronic and vibrational properties. The experimental data show clearly that the kinetics of *t*-St sorption, charge separation, and charge transfers depend dramatically upon the zeolite structure. The ionization rates and ionization yield values demonstrate that a strong synergy exists between the H^+ polarization energy and spatial constraints imposed by the channel topology. Different charge transfer behaviours are reported as a function of the zeolite structure. After ionization, the *t*-$St^{\bullet+}$ radical cations are stabilized for months in the narrow pores of H-FER (figures 1 and 2, left). In contrast, a competitive reaction mechanism is observed in H-ZSM-5 where *t*-$St^{\bullet+}$ evolve progressively to stable electron-hole pairs (*t*-St@H-ZSM-$5^{\bullet-\bullet+}$) through hole transfer (figures 1 and 2, right). The created charge transfer complex is characterized by an intense and broad absorption band in the visible spectral range [2,3]. The compartmentalization of the ejected electrons trapped away from the initial site of *t*-St ionization hinders probably charge recombination. Within the larger pores of H-MOR, the hole transfer is very fast and the radical cation-electron pair is not clearly detected but its formation constitutes indubitably the first stage of the electron transfer.

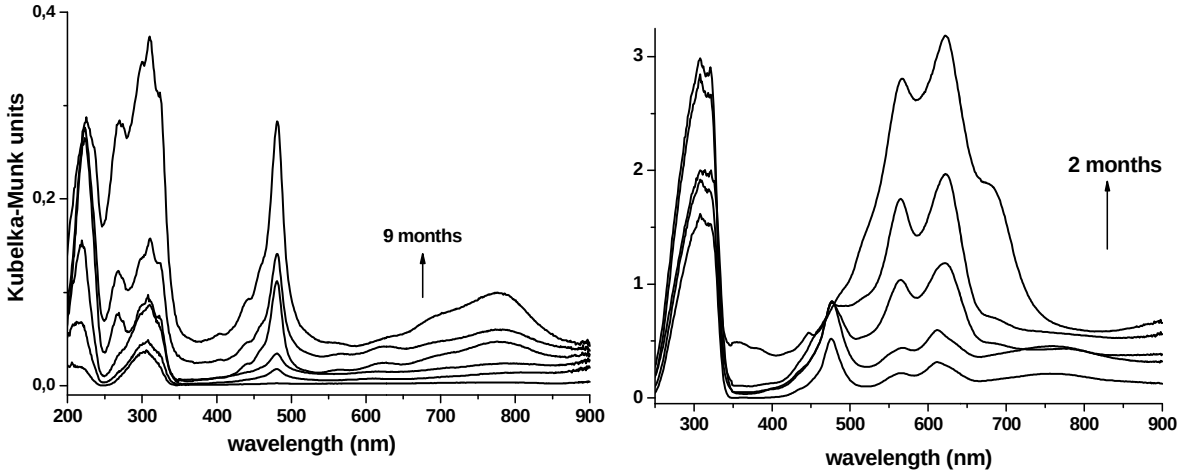

Figure 1. (Left): Diffuse reflectance UV-visible absorption spectra recorded for 9 months after the mixing of solid *t*-St and H-FER dehydrated at 723 K under argon. (Right): Diffuse reflectance UV-visible absorption spectra recorded for 2 months after the mixing of solid *t*-St and H-ZSM-5 dehydrated at 723 K under argon.

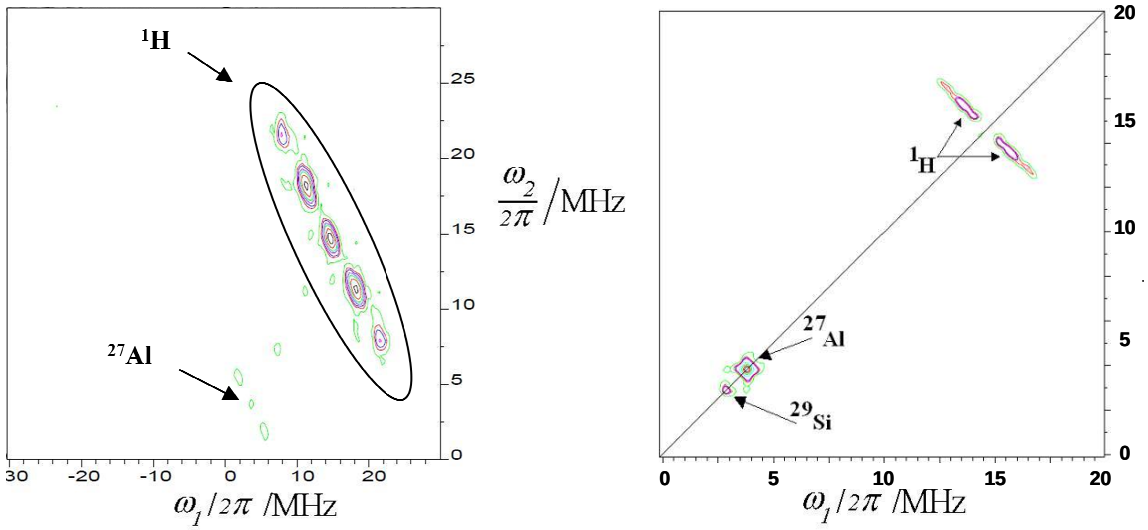

Figure 2. 2D-HYSCORE patterns recorded at 4.2 K after the mixing of solid *t*-St and dehydrated zeolite. (Left) *t*-St$^{\bullet+}$@H-FER$^{\bullet-}$ recorded 6 months after the mixing of t-St and H-FER. (Right) *t*-St$^{\bullet+}$@H-ZSM-5$^{\bullet-\bullet+}$ electron-hole pair recorded 2.5 months after the mixing of t-St and H-ZSM-5.

These features might tentatively be explained by using the non adiabatic electron transfer theory. The low reorganization energy in the narrow channels of H-FER might explain the strong stabilization of t-St$^{\bullet+}$ through a very slow hole transfer rate. In the less constrained H-ZSM-5 and H-MOR, the higher reorganization energy might explain the striking increase of the hole transfer rate to form charge transfer complexes. Thus, the charge transfers occurring within the channels of zeolites are largely controlled by the close match between *t*-St and the pores and by the field gradient that is considerably enhanced by confinement.

References

[1] Garcia H., Roth H.D., Chemistry Reviews, 102 (2002), 3947-4007.
[2] Vezin H., Moissette A., Hureau M. Brémard C., ChemPhysChem, 7 (2006), 2474-2477
[3] Moissette A., Brémard C., Hureau M., Vezin H., J. Phys. Chem. C, 111 (2007), 2310-2317.

Probing the active site during methane conversion over Cu-MOR with XAS

E.M.C. Alayon[a,b], M. Nachtegaal[a], E. Kleymenov[a], J.A. van Bokhoven[a,b]
[a]*Paul Scherrer Institute, 5232 Villigen, Switzerland*
[b]*Institute of Chemical and Bioengineering,ETH Zurich, 8093 Zurich, Switzerland*
evalyn.alayon@psi.ch

Introduction

In the last decade, Groothaert et al. showed that methane can be converted to a methanol-like species at mild conditions using Cu-exchanged zeolites [1]. However, the product strongly sorbed to the surface and the process was not catalytic. To successfully activate methane by partially oxidation to a methanol derivative one must understand the reaction mechanism. This necessitates knowing the structure of the Cu sites that participate in the reaction by determining them during the different reaction conditions. This poses a challenge, since there might be different Cu sites present and not all might participate in the reaction. High energy resolved fluorescence detected X-ray absorption spectroscopy (HERFD XAS) and time resolved XAS (QuickXAS) were explored to monitor the structure of the Cu atoms under different gas feeds.

Experimental

The Cu-zeolite catalyst was synthesized by aqueous ion exchange of the Na-form of mordenite (MOR) with copper acetate. Zeolite framework structure was characterized by X-ray diffraction (XRD) and N_2 physisorption (BET). The sizes of the copper aggregates were probed by TEM. The in situ XAS measurements at the Cu K-edge were performed at the SuperXAS beamline of the Swiss Light Source in Villigen, Switzerland. The HERFD XAS spectra were collected using a Johann-type spectrometer with a spherically bent Si(444) crystal [2]. Accuracy of the incident and emitted photon energy calibration was better than 0.2 eV. The QuickXAS measurements were in transmission geometry with the Si-111 channel-cut monochromator oscillating at 0.1 Hz (5-s resolution per spectrum). A copper foil absorption spectrum was simultaneously measured for internal energy calibration.
For the QuickXAS and HERFD XAS experiments, the catalyst was mounted inside a 3-mm diameter fixed bed quartz reactor heated with a hot air blower. Feed gases were introduced by a mass flow controlled gas mixing panel and the product gases monitored by a quadrupole mass spectrometer. The catalyst was activated in 50 mL/min of oxygen at 450°C, cooled down to room temperature in oxygen, reacted with methane at 150°C, and heated 5°C/min in 30 mL/min of helium. Standard data reduction of the XAS spectra was performed with XDAP [3]. HERFD XAS spectra of the catalyst were compared to those of Cu reference compounds.

Results and discussion

XRD and BET showed that the MOR topology was kept intact after ion exchange and the absence of crystalline copper particles greater than 3 nm. TEM micrographs of calcined Cu-MOR showed copper particles of 0.5-2 nm. After activation with oxygen and interaction with methane, the mass spectrometer detected CO_2 starting at 225°C during heating in helium, indicating that a reaction product from methane had sorbed on the catalyst surface, which has been previously reported by UV-vis measurement and GC analysis (after extraction) to be methanol [1]. Fig. 1 shows the HERFD XAS spectra of Cu-MOR under the different reaction steps and includes a spectrum of activated Cu-MOR dosed with methanol. For comparison, spectra of Cu reference compounds are also shown. The weak pre-edge feature at 8977 eV is the quadrupole allowed 1s→3d transition indicative of the Cu^{2+} state. The rising edge features above 8979 eV are assigned to 1s→4p transitions plus ligand-to-metal-charge-transfer

shakedown. The edge shifts to higher energy with oxidation state due to increased effective nuclear charge but is also influenced by ligand environment and symmetry. The absorption maximum is due to multiple scattering and is dependent on the local geometric structure [4].
The spectrum after calcination showed the pre-edge feature and the rising edge at 8985 eV, indicative of Cu^{2+} character. After cooling, flushing out excess oxygen, and interaction with methane at 150°C, the rising edge shifted to 8982 eV, the 8985 eV feature maintained, and the pre-edge feature lowered to half intensity. This could be an indication of mixed Cu^{2+}/Cu^{+} states under methane and reflects the added ligand environment. In comparison, the spectrum of Cu-MOR dosed with methanol does not have a pre-edge, has the similar rising edge at 8982 eV, and has an added feature at 8988 eV, which shows combination of reduced Cu state and strong ligand effects. A mixture of Cu states present could not be excluded and requires quantitative modeling. After heating in helium, the rising edge feature at 8982 eV significantly lost intensity, indicating loss of sorbed species, which is supported by the CO_2 signal in the MS trace. The pre-edge and edge features returned to almost similar shape as the starting Cu^{2+} state, showing re-oxidation. QuickXAS spectra indicated a stable first shell configuration during stages in the reaction run.

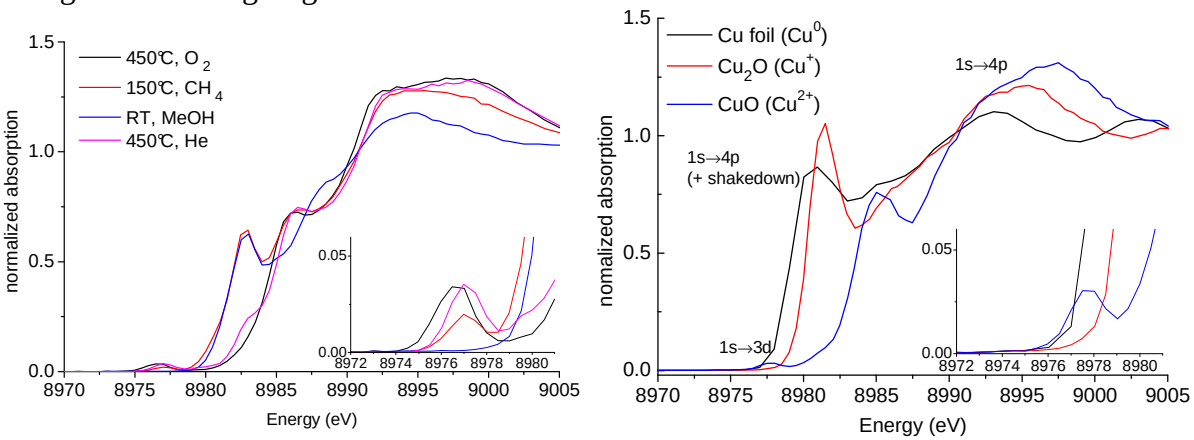

Figure 1. HERFD XANES spectra of Cu-MOR under different reaction conditions, with the pre-edge region emphasized in the inset (left) and the spectra of copper reference compounds (right).

Conclusions

In situ XAS showed the changes from Cu^{2+} after oxygen activation to a mixture of Cu^{2+} and Cu^{+} states of the copper particles in Cu-MOR upon methane conversion, similar to the reduction of Cu after methanol interaction.

Acknowledgements

We thank Dr. Frank Krumeich for TEM measurements, and Christian König, Min Wei Tew, Zhiqiang Ma, Long Qi, Renata Bessa-Duarte, and Jagdeep Singh for participating in the XAS measurements.

References

[1] Groothaert, M.H., Smeets, P.J., Sels, B.F., Jacobs, P.A., Schoonheydt, R., Selective oxidation of methane by the bis(u-oxo)dicopper core stabilized on ZSM-5 and mordenite zeolites, Journal of the American Chemical Society, 127 (2005), 1394-1395.

[2] Kleimenov, E., Bergamaschi, A., van Bokhoven, J., Janousch, M., Schmitt, B., Nachtegaal, M., High-resolution hard-x-ray fluorescence spectrometer, Journal of Physics, 190 (2009) 12035-12040

[3] Vaarkamp, M., Linders, J.C., Koningsberger, D.C., A new method for parametrization of phase shift and backscattering amplitude, Phyisica B, 208/209 (1995) 159-160.

[4] DuBois, J.L., Mukherjee, P., Stack, T.D.P., Hedman, B., Solomon, E.I., Hodgson, K.O., A systematic K-edge x-ray absorption spectroscopy study of the Cu(III) sites, Journal of the American Chemical Society, 122 (2000) 5775-5787.

A Co-templating Route to Cu SAPO STA-7, an Active Catalyst for the Selective Catalytic Reduction of NO with NH_3

Paul A. Wright,[1,*] A. Lorena Picone,[1] Stewart J. Warrender,[1] Alexandra M. Z. Slawin,[1] Lucia Gaberova,[2] Philip L. Llewellyn,[2] Beatrice Moulin,[3] Alexandre Vimont,[3] Sam Kyung Sung,[4] In-Sik Nam,[4] Min Bum Park[4] and Suk Bong Hong[4]

[1] School of Chemistry, University of St Andrews, Purdie Building, North Haugh, St. Andrews, Fife, UK. KY16 9ST; [2] Aix Marseille Univ. - CNRS, Lab Chim Provence, UMR 6264, F-13331 Marseille 3, France, [3] Univ Caen, CNRS, ENISCAEN, Catalyse & Spectrochim Lab, F-14050 Caen, France, [4] POSTECH, Dept Chem Engn, Pohang 790784, South Korea
Email: paw2@st-andrews.ac.uk

Introduction

The high temperature combustion of fossil fuels in stationary and mobile power sources gives rise to nitrogen oxides, NO_x, which are serious atmospheric pollutants. For engines operating under lean burn conditions and also in stationary power sources there is an excess of oxygen over fuel in the inlet mixture, so that selective catalytic reduction (SCR) of NO_x is required. One reductant that can be added to the exhaust gas is ammonia, and NH_3-SCR is a well-established approach to NO_x removal. Copper-exchanged ZSM-5 zeolite was reported in 1986 to be a good catalyst for direct SCR of NOx with hydrocarbons in vehicle emissions[1] and has since been studied extensively for this reaction and also for SCR with NH_3. Copper-exchanged zeolites with the chabazite structure have also been shown to be active catalysts for NH_3 SCR of NO [2]. Structural studies of chabazite Cu-SSZ-13 have located Cu^{2+} ions occupying 3-fold (6MR) sites[3]. Furthermore, copper-exchanged forms of the silicoaluminophosphate (SAPO) analogue of chabazite (Cu-SAPO-34) have been shown to be active for the SCR of NO with hydrocarbons such as propene and with NH_3.[4] Here we report the synthesis and characterisation of copper-containing SAPO STA-7 [5], (Cu-STA-7) prepared using a copper-cyclam complex (cyclam = 1,4,8,11-tetra azacyclotetradecane) as a co-template. Calcination of the as-prepared solid liberates Cu^{2+} from the complex, resulting in microporous Cu,H-STA-7. This preparation route has the advantage of avoiding the additional aqueous Cu^{2+} exchange and drying steps previously used to give Cu-SAPO catalysts, and also reduces the negative effects of hydrolysis of the structure associated with this process. In addition, Cu,H-STA-7 has been shown to be active in the SCR of NO in the presence of propene or ammonia, with particularly promising results achieved for NH_3 SCR in the presence or absence of H_2O.

Experimental

Cu-STAS-7 was prepared hydrothermally, and characterized by single crystal diffraction, synchrotron powder X-ray diffraction, SEM, EDX, TGA, ESR and UV-visible spectroscopy. Cu,H-STA-7 was prepared by calcination at temperatrures between 400 and 550 C, and characterised by adsorption, single x-ray diffraction, synchrotron powder diffraction (at 25 – 400 C) and NMR, IR, ESR and UV-visible spectroscopy, and the accessibility of the copper cations was probed by IR in combination with the stepwise adsorption of CO and NO as probe molecules. Catalytic experiments were conducted at atmospheric pressure in a conventional continuous-flow microreactor. Around 1 g of the catalyst was sieved to a mesh size of 20/30 to minimize the mass transfer limitations. Before the evaluation of activity, the catalyst was pre-treated in situ with a total flow of 3300 cm^3 min^{-1} containing 79% N_2 and 21% O_2 or 100% N_2 at 500 ^oC for 1.5 h and then cooled to room temperature. A reaction gas

mixture consisting of 500 ppm NO, 500 ppm NH_3 or 2000 ppm C_3H_6, and 5% O_2 with or without 10% H_2O in N_2 balance was fed into the reactor system. A total flow rate of 3300 cm^3 min^{-1} (100000 h^{-1} GHSV) was mainly used for the catalyst activity testing. The inlet and outlet gas compositions were monitored by a Nicolet 6700 FT-IR spectrometer.

Results and discussion

Copper cyclam is included as a co-template during the crystallization of SAPO STA-7, where it acts to partially balance the negative charge of the framework. Single crystal diffraction locates it within the large cages of the STA-7 structure, and the complex is confirmed to be intact by ESR and UV-visible spectroscopy. Calcination in oxygen liberates Cu^{2+} cations from the complex, and they are determined by Rietveld refinement of X-ray powder diffraction to partially occupy four crystallographically-distinct sites in the structure. IR spectroscopy with chemisorbed NO molecules supports this site distribution. The resulting Cu,H-SAPO STA-7 shows high activity for the SCR of NO with NH_3 in the presence and absence of admixed water vapour, and over the temperature range of 200 to 450 °C. The material is active for SCR with propene, but gives lower conversion than for Cu ZSM-5, which may be attributed to its smaller pore size.

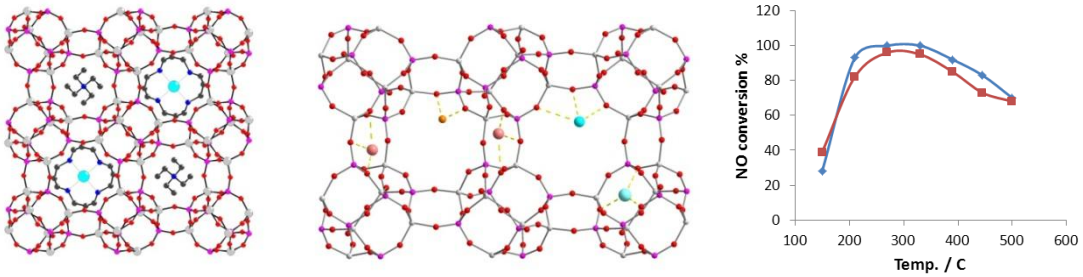

Figure (left) as-prepared Cu STA-7, (center) calcined Cu STA-7 and (right) NO SCR conversion with NH_3

Conclusions

Direct synthesis of SAPO STA-7 is possible using copper cyclam as a co-template. Upon calcination this liberates Cu^{2+} ions that occupy at least 4 different sites. The calcined solid is highly active for NH_3 SCR of NO. This approach can be generalized to the synthesis of other $AlPO_4$-based catalysts

We acknowledge Dr. Stephen P. Thompson at Diamond Light Source for help in collection of synchrotron data and Dr. Sharon Ashbrook and Mr Daniel Dawson for NMR spectra.

References

[1] M. Iwamoto, H. Furukawa, Y. Mine, F. Uemura, S. I. Mikuriya and S. Kagawa, J. Chem. Soc. Chem. Commun. (1986) 1272-1273.
[2] P. J. Anderson, J. E. Baillie, J. L. Casci,H.-Y. Chen, J. M. Fedeyko, R. K S. Foo and R. R, Rajam, US Pat. 132452 A2, 2008; I. Bull, R. S. Samuel, W. M. Jaglowski, G. S. Koermer, A. Moini, J. A. Patchett, J. C. Dettling and M. T. Caudle US Pat. 0285737 A1, 2009
[3] (a) D. W. Fickel and R. F. Lobo, J. Phys. Chem. C, 114 (2010) 1633-1640; (b) S. T. Korhonen, D. W. Fickel, R. F. Lobo, B. M. Weykhuysen and A. M. Beale, Chem. Commun. 47 (2011) 800-802.
[4] T. Ishihara, M. Kagawa, F. Hadama and Y. Takita, J. Catal. 169 (1997) 93-102
[5] M. Castro, R. Garcia, S.J. Warrender, P.A Wright, P.A. Cox, A. Fecant, C. Mellot-Draznieks and N. Bats, Chem. Commun., (2007) 3470-3472

Measuring silicon average connectivity by ^{29}Si NMR : the missing constraint to understand oligomers, nanoparticles and zeolite formation.

Francis Taulelle, Mohamed Haouas
Tectospin, Institut Lavoisier, University of Versailles Saint-Quentin en Yvelines, France ,
taulelle@chimie.uvsq.fr

Introduction

The synthesis of zeolites is still today a very challenging subject because many non consistent schemes exist, without a general consensus among them. One often believes that silicalite « clear sol » represents a simple enough system with the possibility of proving or disproving the existence of secondary building units in solution. This belief has been thinning due to more characterization of the nanoparticles present in what was believed to be "solutions" appear as stable sols. Actually, the silicalite precursor can be prepared out of silica or of TEOS mixed with tetra-alkyl-ammonium hydroxide (TAAOH) and water. The composition expressed as a SiO_2/TEOS:TAAOH:H_2O. The different objects present in the precursor apart from water, are the soluble species, from the monomer to high nuclearity oligomers, particles with various names, sub-colloidal or colloidal particles, the size of which varies from about 0.8 nm to several tens of nm. Actually, the evolution of silicon from the initial source to the different species under which it incarnates, would be defined by different states of silicon connectivity. Succeeding quantifying by NMR, the connectivity of silicon under its different state, oligomers, nanoparticles or crystals has been achieved, despite the many negatives previous attempts. It is the aim of this contribution to show off the role of the reduced parameter <n> in understanding where the control of zeolite selectivity lies.

Results and discussion

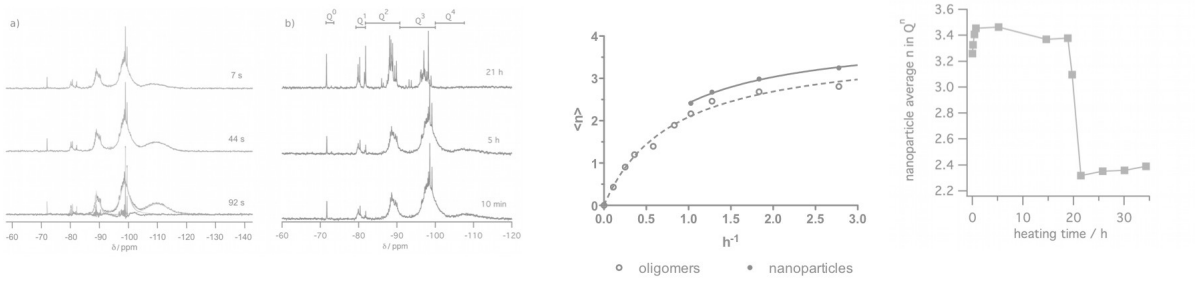

The results obtained provide for precursors solutions the evolution of the average connectivity with the degree of hydrolysis. For the precursor heat treated samples, the connectivity changes with the time of heating. The figure 2 displays the evolution of connectivity for the precursor, and figure 3 the connectivity of nanoparticles in the heat treated solution.
Figure 1 Figure 2 Figure 3
Nanoparticles must be divided into two categories, the nano-aggregates of 2-5 nm formed during hydrolysis with an average connectivity of about 3.2, and "intermediates particles" with much larger size 20-100 nm. When crystallization takes places, Bragg lines appears. With the average connectivity, possible models for describing the crystallization of zeolites can be checked for consistency with this critical data set. During crystallization the global connectivity does not change much, indicating a redistribution of bonds created during hydrolysis. Templating takes therefore place during the first "aging" period of heating for

crystallization. A model consistent with the global connectivity constancy during heating is displayed figure 4.

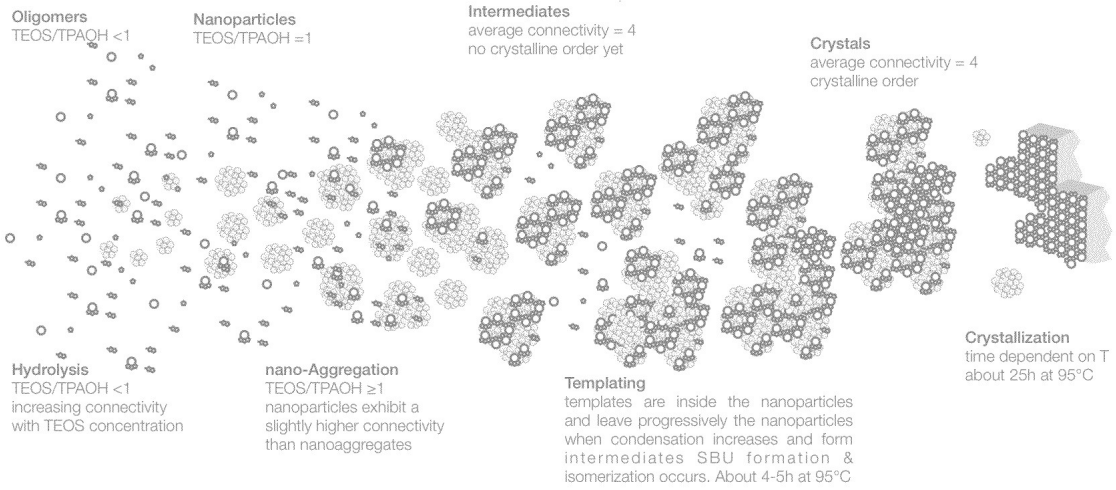

Figure 4. Crystallization mode.

Conclusions

By studying the average connectivity of silicon all along the paths from TEOS hydrolysis to synthesis of silicalite by heat treatment,[1-4] one can observe a invariant number of connectivity that is just redistributed among the silicon objects and sites. No new connectivity is globally created during synthesis. Most of the control of zeolite synthesis is achieved at the precursor formation and the first heating period where the templating effect takes place.

Acknowledgements

The "Leuven group", Pr. Johan Martens, Pr. Christine Kirschhock, Dr. Alexander Aerts, Dr. Lana Follens, Dr. Pieter Verlooy are thanked for their cooperation. The Nanogrowth consortium directed by Pr. M. Anderson in Manchester is also thanked as well as Dr. David Petry. Pr. K. P. Lillerud from Oslo University is thanked for his collaboration, and Einar Eilersten specifically on Chabazite and aluminum connectivity evolution.

References

[1] Investigation of the Mechanism of Colloidal Silicalite-1 Crystallization by Using DLS, SAXS, and ^{29}Si NMR Spectroscopy Alexander Aerts, Mohamed Haouas, Tom P. Caremans, Lana R.A. Follens Titus S. van Erp, Francis Taulelle, Jan Vermant, Johan A. Martens and Christine E.A. Kirschhock *Chemistry a European Journal*, (2010) 16, 2764

[2] Combined MS and NMR: attractive route to future understanding of the first stages of nucleation of nanoporous materials Petry, David P.; Wong, Stephen C. C.; Haouas, Mohamed; Taulelle, Francis; Gaskell, Simon J.; Anderson, Michael W. *Studies in Surface Science and Catalysis* (2008), 174 B (Zeolites and Related Materials), 941

[3] Characterization of nanoparticles in diluted clear solutions for Silicalite-1 zeolite synthesis using liquid ^{29}Si NMR, SAXS and DLS Follens, L. R. A.; Aerts, A.; Haouas, M.; Caremans, T. P.; Loppinet, B.; Goderis, B.; Vermant, J.; Taulelle, F.; Martens, J. A.; Kirschhock, C. E. A. *Physical Chemistry Chemical Physics* (2008), 10, 5574.

[4] Combined NMR, SAXS, and DLS Study of Concentrated Clear Solutions Used in Silicalite-1 Zeolite Synthesis Aerts, Alexander; Follens, Lana R. A.; Haouas, Mohamed; Caremans, Tom P.; Delsuc, Marc-Andre; Loppinet, Benoit; Vermant, Jan; Goderis, Bart; Taulelle, Francis; Martens, Johan A.; *Chemistry of Materials* (2007), 19, 3448.

Characterization of acidic zeolite catalysts by thermodesorption and cracking of *n*-nonane

Wacław Makowski, Kinga Mlekodaj
Faculty of Chemistry, Jagiellonian University, makowski@chemia.uj.edu.pl

Introduction

Acidic zeolites are highly active catalysts in cracking and isomerization of hydrocarbons. These reactions are usually followed by deposition of coke in the micropores that may affect both acidity and porosity of the catalysts, leading to their deactivation. The aim of this work was a complementary study on activity, deactivation and regeneration of zeolite catalysts in cracking of *n*-nonane. This hydrocarbon was selected as a probe because its thermodesorption has been found a good method for characterization of porosity of zeolites [1,2], mesoporous silicas [2-4] and their carbon replicas [4], allowing determination of the micro- and mesopore volume. Positions of the peaks in the thermodesorption profiles of nonane are directly related to the pore size. The mesopore size distributions determined from the quasi-equilibrated thermodesorption profiles of nonane show very good agreement with those obtained from N_2 desorption isotherms [3].

Experimental

The studied materials were commercial zeolites, differing in the pore size and connectivity as well as in acidity: H-USY (Si/Al=4.5, Linde), HY (Si/Al=15, Zeolyst), HZSM-5 (Si/Al=15, Zeolyst), HMOR (Si/Al=5.7, Bitterfeld Chemie AG, prepared from Na form).

All catalytic and thermodesorption experiments were performed using the catalytic microreactor system CATLAB (Hiden Analytical) equipped with the QMS detector and thermostated saturator for adding vapors to the carrier gas. Prior the experiments a sample of zeolite (25 mg, 0.4-0.5 mm particles) was activated by heating at 10°C/min to 500°C in He flow. Catalytic cracking of nonane was performed by heating the sample at 10°C/min to 500°C and stabilizing this temperature for 5h. Helium saturated with vapor of nonane (at 20°C, 0.43 % mol) was used as reaction mixture. In order to remove the coke formed during the cracking and regenerate the catalyst the temperature programmed oxidation (TPO) at 10°C/min to 700°C was performed using of 5% O_2/He mixture. For probing changes in porosity of the catalyst, temperature programmed desorption (TPD) of nonane was performed before and after the catalytic test and after the TPO: after preadsorption of nonane at 50°C for 1h followed by purging out excess, the molecules adsorbed in the micropores were desorbed by heating the sample in a flow of He at 10°C/min to 400°C.

The most intensive fragmentation mass 43 (C_3H_7) was selected as a measure of the concentration of nonane. For monitoring the cracking products the mass 28 (C_2H_4) was chosen. In the TPO of coke the masses 18 (H_2O), 28 (CO) 44 (CO_2) were also recorded.

Results and discussion

Result of the catalytic tests (Fig. 1) show that studied zeolites differ considerably in the catalytic activity: from 29% conversion for HY (Si/Al=15) to 82% for HZSM-5 (Si/Al=15). These two zeolites exhibit good stability, but for H-USY and HMOR quite fast deactivation is observed. The TPO profiles measured after the catalytic tests confirm that formation of coke is negligible on the stable catalysts. However, despite similar activity and deactivation rate much larger content of coke was found for H-USY than for HMOR.

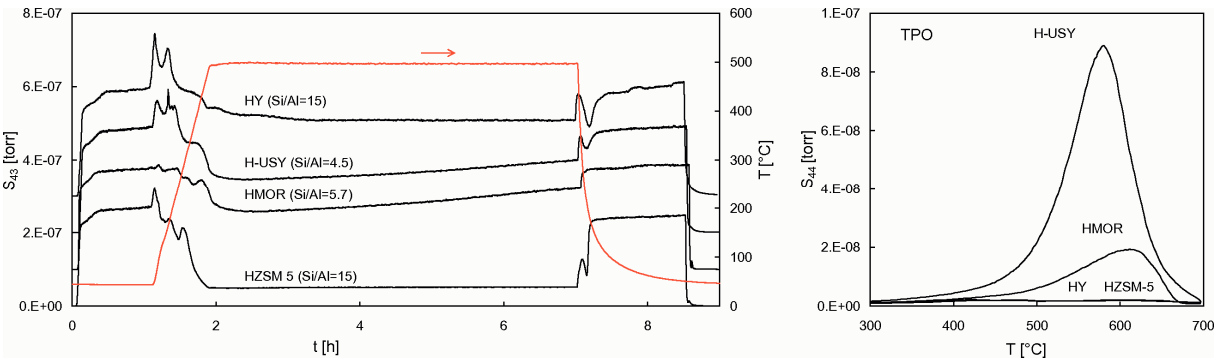

Figure 1. Left: Concentration profiles of nonane in the catalytic tests (the profiles for HMOR, H-USY and HY were shifted up by 1, 2 or $3 \cdot 10^{-7}$, respectively). Right: TPO profiles of the coke formed during the catalytic tests.

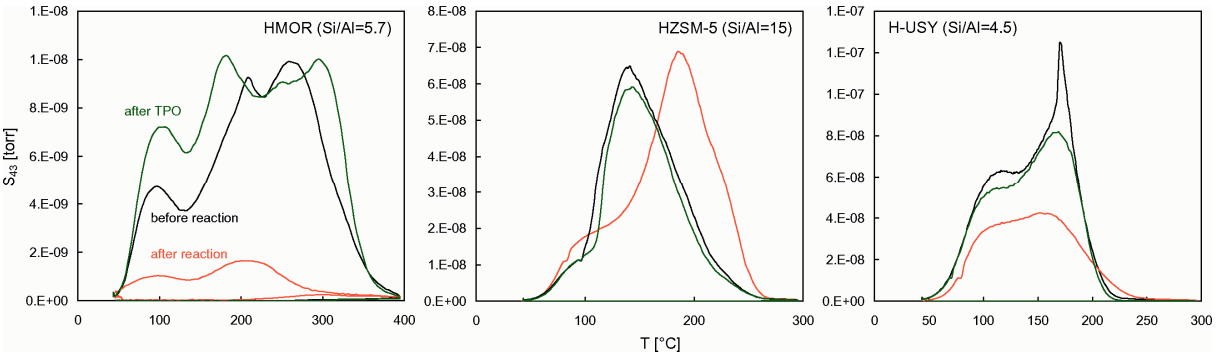

Figure 2. TPD profiles of nonane before and after the catalytic test and after the TPO of coke.

The initial parts of the catalytic tests, recorded for the increasing temperature, are similar to the quasi-equilibrated thermodesorption (QE-TPD) experiments [1]. For the least acidic zeolite HY (Si/Al=15) the QE-TPD profile is not affected by the catalytic reactions of desorbing molecules and contains two peaks: the low temperature one (84°C) corresponding to desorption from the mesopores and the micropore-related high temperature one (191°C). Additional peak observed for the more acidic H-USY (169°C) may result from desorption of the molecules chemisorbed on the strong acid sites. For HMOR and HZSM-5 cracking of the molecules desorbing from the micropores occurs.

The TPD profiles show changes in adsorption of nonane in the zeolites' micropores resulting from the coke deposition and its further oxidation (Fig. 2). Large decrease in micropore volume due to coking and its increase after TPO was found for HMOR and H-USY. For the coking-resistant HZSM-5 the corresponding changes are much smaller. Differences in the TPD profiles before the reaction and after TPO observed for HMOR and H-USY may indicate structural changes during oxidation at high temperature (700°C).

Conclusions

The use of nonane for probing both adsorptive and catalytic properties of zeolites provides an insight into origin of their activity, indicating that their catalytic performance depends not only on their acidity, but also on the pore size controlling adsorption degree of the substrate. These findings shall be compared with the standard porosity and acidity characterization of the zeolites obtained by means of N_2 adsorption and NH_3 thermodesorption.

References

[1] W. Makowski, B. Gil, D. Majda, Catal. Lett., 120 (2008) 154
[2] W. Makowski, P. Kuśtrowski, Micropor. Mesopor. Mater.,102 (2007) 283
[3] W. Makowski, L. Chmielarz, P. Kustrowski, Micropor. Mesopor. Mater., 120 (2009) 257
[4] M. Manko, B. Gil, R. Janus, P. Kustrowski, W. Makowski, Thermochim. Acta, 511 (2010) 82

Structure refinement of ordered mesoporous carbon materials from X-ray diffraction data

Wolfgang Schmidt
Max-Planck-Institut für Kohlenforschung, Mülheim an der Ruhr, Germany
schmidt@kofo.mpg.de

Introduction

At present, the majority of structural information of ordered mesoporous solids is usually provided by electron microscopy. Transmission electron micrographs as well as high resolution scanning micrographs reveal structural features such as pore geometry, pore size distributions, pore arrangements, and pore wall thicknesses. Much information from such micrographs usually can be assessed directly from the images. The information is completed by electron diffraction data. Far less commonly, structural information that exceeds mere lattice constant or symmetry determination is derived from X-ray diffraction patterns [e.g. 1-3].

However, lots of information can be deduced from a detailed analysis of diffraction data but unfortunately the information is not directly accessible. In contrast to normal crystal structure analysis, ordered mesoporous solids consist of periodically ordered pores that are enclosed by amorphous pore walls for most materials. The periodicity that causes the diffraction pattern is not due to periodic arrangements of atoms but to periodic variation of electron densities between pores and pore walls. Structural information can be accessed by different methods. Here, two approaches will be discussed. Fourier transformation of structure factors as derived from diffraction patterns as the first method and structure refinement via fitting of calculated XRD patterns of model structures to measured XRD patterns as the second method will be discussed on diffraction data of ordered mesoporous carbons.

Experimental

Ordered mesoporous carbons of type CMK-3 and CMK-5 were provided by Jörg-Joachim Nitz and Anhui Lu. They have been synthesized using SBA-15 silica as hard template with furfuryl alcohol, dissolved in trimethyl benzene, as the carbon source and oxalic acid as polymerization catalyst. After deposition of the carbon precursor, carbonization was achieved by heating at 850°C under protective atmosphere. XRD patterns have been measured at the SAXS beamline of the IBN (Graz, Austria) at the Elettra Synchrotron radiation source in Trieste, Italy. The powder samples were measured in 2 mm quartz capillaries. Integrated intensities of the individual reflections have been obtained with a multi-peak fitting routine of the Igor Pro 6.2 software package (WaveMetrics).

From the derived intensities then structure factors for individual reflections have been calculated taking Lorentz polarization factors into account. The obtained structure factors then have been used for direct calculation of electron density distribution maps via Fourier transformation.

Structures models have been obtained by distributing certain electron densities in a hexagonal unit cell in a manner that it describes the periodicity of the pore walls. From the distribution of the electron densities in the unit cell, theoretical diffraction patterns have been calculated and compared to measured XRD patterns. By modification of the structural parameters, such as lattice constant, rod/tube diameter, wall thickness, and electron density distribution between rods/tubes, differences between measured and calculated diffraction patterns could be minimized which resulted in refined structure models.

Results and discussion

A typical result of a direct calculation of electron density distribution from measured XRD intensities is illustrated in Figure 1. Using correct phases, quite reasonable electron density maps can be derived. However, using incorrect phases results in substantially wrong electron density distributions as shown on the right.

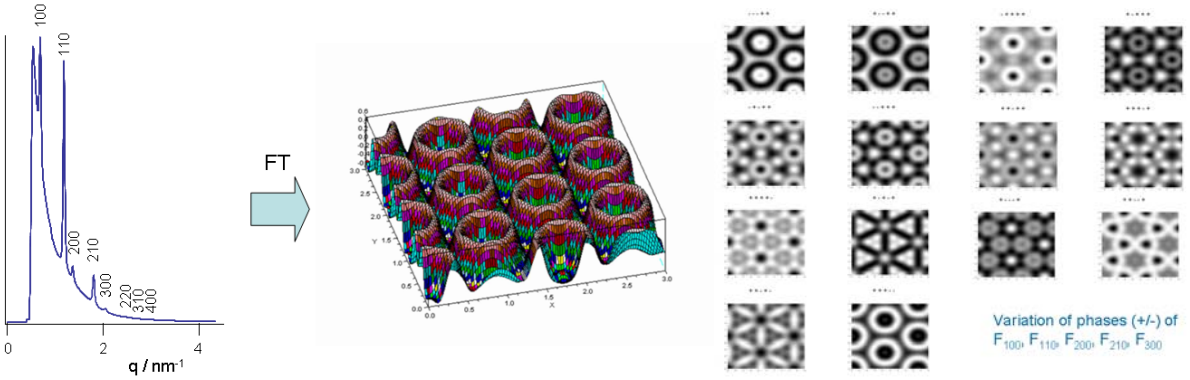

Figure 1. XRD pattern (left) and electron density distribution for CMK-5 (middle) as calculated via Fourier transformation of structure factors that have been derived from the XRD pattern. Projections of electron density maps applying different phases (right).

The phase for each reflection has to be known for a correct calculation. Unfortunately, the phase changes with different pore diameters and/or pore wall thicknesses. This problem can be overcome using the second approach. Building appropriate models allows not only refinement of the pore wall topology by searching for the best fit of calculated and measured XRD patterns. It also provides correct phases which then in turn can be used for the calculation of the electron density maps which allows easy verification or falsification of the structure model.

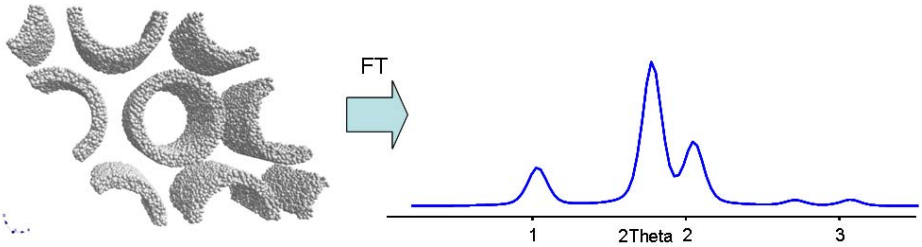

Figure 2. Structure model (left) and theoretical XRD pattern (right) as calculated using the electron density distribution of the structure model.

Variance of pore wall thickness and pore diameter allows for further refinement of the structure as well as consideration of electron density between adjacent rods or tubes.

Acknowledgements

Thanks to Jörg-Joachim Nitz and Anhui Lu for providing CMK-3 and CMK-5 samples and Heinz Amenitsch for support at the SAXS beamline at Sincrotrone Trieste, Italy.

References

[1] K.J. Edler, P.A. Reynolds, J.W. White, D. Cookson, J. Chem. Soc., Faraday Trans. 93 (1997) 199-202.
[2] L.A. Solovyov, S.D. Kirik, A.N. Shmakov, V.N. Romannikov, Adv. X-ray Anal.44 (2001)110-115
[3] D. Müter, S. Jähnert, J.W.C. Dunlop, G.H. Findenegg, Oskar Paris, J. Phys. Chem. C 113 (2009) 15211–15217

New insights into the resolution and connectivities between spin ½ and quadrupolar nuclei: application to the advanced-characterization of phosphate materials

L. Delevoye, O. Mentré, G. Tricot, L. Montagne, J. Trébosc, O. Lafon, J-P. Amoureux
Unité de Catalyse et Chimie du Solide, CNRS UMR8181, laurent.delevoye@ensc-lille.fr

Introduction

Solid-State NMR is one of the most used techniques for advanced characterization of the local environment in a large number of materials, such as zeolites, ordered porous solids, organic-inorganics hybrids, but also glasses, ceramics, crystalline or gels. For the last decades, the technique benefited from numerous improvements on different aspects, which can be classified into 3 categories: resolution, sensitivity and development of pulse sequences to highlight connectivities. On the latter case, a lot of these methodological developments have a focus on quadrupolar nuclei of spin number I>1/2, which constitute a majority of the nuclei found in the previously mentioned materials. In the present contribution, we will illustrate the progress in solid-state NMR, through the detection of spatial proximities and bonded connectivities between spin ½ and quadrupolar nuclei provided by Heteronuclear Multiple-Quantum Coherence (HMQC)-type pulse sequences. In this case, the advantage (higher sensitivity, better robustness) of the HMQC will be given by comparison with popular Cross-Polarization (CP) approach. All methodological developments will be applied to the advanced characterization of aluminophopshate molecular sieves, crystalline and amorphous phosphates.

Results and discussion

Amongst many advantages of *D*-HMQC method [1,2] over the CP technique,[3] the correlation can be obtained either through the evolution of scalar couplings between the heteronuclei or using dipolar recoupling techniques. In the latter case, we have demonstrated recently that SFAM [4] sequences provide higher efficiency and robustness to radio frequency (rf) inhomogeneity and resonance offset than the other recoupling sequences such as REDOR or R^3. We will show that the *D*-HMQC technique is little sensitive to rf-field, spinning speed fluctuations, offset and C_Q values, and it exhibits a very good efficiency that allows the detection of nuclei only present in minor proportions. The main conclusions will first be illustrated for model chemical systems, such as the molecular sieves $AlPO_4$-14 (*cf*. Fig. 1-a) or crystalline compounds. Then, the structures of various phosphate-based inorganic systems (*cf*. Fig. 1-b) will be investigated by S-{^{31}P} *D*-HMQC techniques where $S = {}^{27}$Al, ^{11}B and ^{51}V.[5]

In particular, the efficiency of *D*-HMQC will be demonstrated through the characterization of phosphate compound with less than 3% phosphorous content.

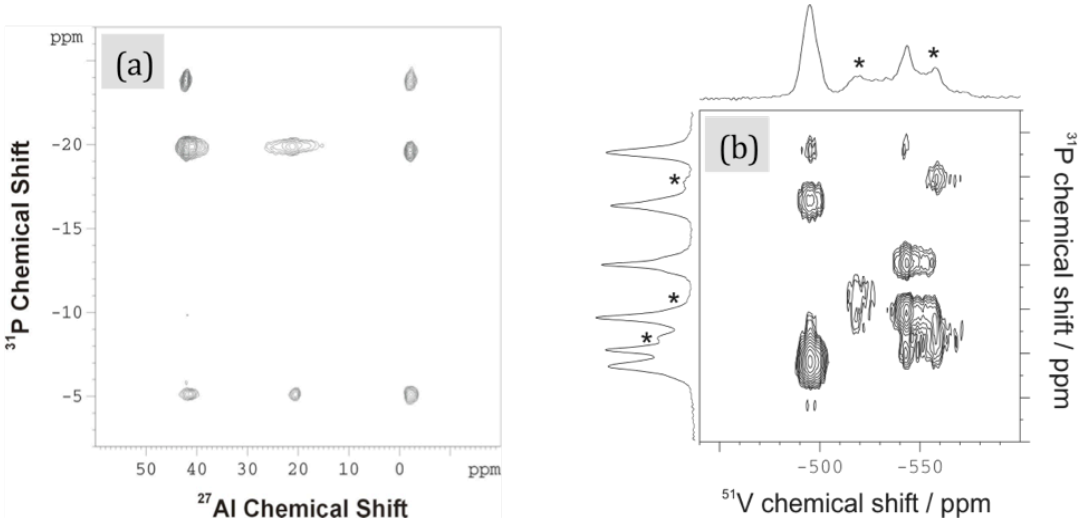

Figure 1. (a) *D*-HMQC MAS 2D spectrum of aluminophophate molecular sieves $AlPO_4$-14 highlighting proximities between aluminium and phosphorous sites. The experimental time was less than 7 hours. (b) *D*-HMQC MAS spectrum of vanadophosphate compound. Stars are used to denote impurities.

Conclusions

We will show that valuable and unreported information on the structure of porous phosphate materials can be obtained using *D*-HMQC sequence. The *D*-HQMC method alleviates the main limitations of the cross-polarization technique. In particular, it does not require complicated and time-consuming optimization procedures. Moreover, even if all examples given here refer to phosphate samples, it is obvious that this sequence can also be applied to probe spatial proximities between other spin-1/2 isotopes (^{29}Si, ^{1}H, ^{19}F…) and quadrupolar nuclei.

Acknowledgements
The authors are grateful for funding provided by the Region Nord/Pas de Calais, Europe (FEDER), CNRS, French Minister of Science, USTL, ENSCL and Bruker Biospin. Financial support from the TGIR RMN THC (FR-3050) for conducting the research is also gratefully acknowledged.

References

[1] Z. Gan *J. Magn. Reson.* 184 (2007) 39
[2] B. Hu, J. Trebosc, J.P. Amoureux, *J. Magn. Reson*. 192 (2008) 112-122.
[3] S. R. Hartmann, E. L. Hahn, *Phys. Rev*. 128 (1962) 2042
[4] O. Lafon, Q. Wang, B. Hu, F. Vasconcelos, J. Trébsoc, S. Cristol, F. Deng, J.-P. Amoureux *J. Phys. Chem. A* 113 (2009) 12864
[5] G. Tricot, O. Mentré, L. Delevoye, in preparation

AN IN-SITU STUDY OF Co AND Cu BASED ZEOLITES FOR THE SELECTIVE CATALYTIC REDUCTION OF NOx. NEW POSSIBILITIES FOR IN-SITU CATALYSIS AT ALBA SYNCHROTRON.

I. Peral, G. Guilera and C. Alonso-Escobar
Alba Synchrotron, Crta. BP 1413, Km 3.3, 08290 Cerdanyola del Vallès, Spain, iperal@cells.es

Introduction

ALBA synchrotron will soon open its doors to users. Such an important topic as is catalysis and chemical reactions under operando conditions has not gone unnoticed. The wide range of applications of zeolites makes them particularly interesting for industrial purposes. To improve their properties one needs to understand their structural changes in time at an atomic level while the reaction takes place. In this sense synchrotron techniques are very attractive to scientist working in this research field. This approach allows to relate structure, activity and functionality in a direct manner.
There are two beamlines at ALBA that will dedicate part or most of their time to carry out in-situ experiments; namely CLÆSS (Core Level Absorption&Emission Spectroscopies) devoted to X-ray Absorption Spectroscopy, and MSPD (Materials Science Powder Diffraction) devoted to High Resolution X-ray Powder Diffraction.
In this communication we will present the facilities and capabilities related to catalysis of both CLÆSS and MSPD beamlines and will give some illustrative examples of recent results performed with zeolite-based catalysts.

Experimental

2.5 wt% Co-TNU9 and 2.5 wt% Cu-TNU9 zeolite were synthesized following the ion exchange procedure [1] and calcined at 550 ^{o}C for 3h.
The zeolites were measured via X-ray Absorption Spectroscopy at the Co and Cu K-edges (7709 and 8979 eV, respectively) at Super-XAS beamline (SLS) and SpLine (CRG-ESRF) under real catalytic conditions in the standard catalytic cell described in the next section. In-situ reactions were carried out in 0.3% NO, 0.5%C_3H_8 and different percentages of O_2 (0%, 0.65%. 1.95% and 11.4%) and using a total flow of 100 mL/min. The measurements were done at ambient pressures and at different given temperatures ranging from rT up to 550 ^{o}C.
X-ray Powder Diffraction was carried out at SpLine (CRG-ESRF) under the same reaction conditions.

Results and Discussion

Two in-situ catalytic cells have been designed and built within the framework of a collabotration between the Instituto de Tecnología Químico – Valencia (ITQ) and ALBA synchrotron to carry out solid-gas catalytic experiments in both CLÆSS and MSPD beamlines. The first of the cells is a multi-purpose cell that allows to perform standard experiments where solid-gas reactions take place and different measurement configurations and combination of ancillary techniques are possible. The second cell instead, is intended to carry out time-resolved studies via either absorption or diffraction techniques. These cells are

able to work at temperatures up to 700 ^{o}C and pressures up to 20 bars. Both are highly reliable, robust and easy to use, which makes them ideal to be employed in synchrotrons. These two cells are a valuable asset to ALBA and will be available for the entire user community.
The first tests with the cells and control unit have already been performed in different synchrotrons. Those have shown to be highly reliable, robust and easy to use which makes them ideal for frequent and intensive usage.
The selective reduction of NOx in the presence of propane and O_2 by Co and Cu zeolites (TNU9, IM5 and BEA) has been investigated by XAS at the Co and Cu K-edges and XRD, in-situ, under catalytic conditions. This is an important method that enables to reduce NOx emissions in modern or diesel automobiles that work under lean conditions [2]. These zeolites appear to be highly active in converting NOx to N_2 at temperatures between 450 and 550 ^{o}C; especially the Co-based zeolite that is much more stable at high temperatures and in the presence of steam that typically comes out from the exhaust of a car.
No long range changes on the zeolite structures could be appreciated by XRD but it was found by XAS that the overall electronic density around the transition metal atom in the zeolite was important for the activity and stability of this catalytic reaction.

Conclusions

In this experiment we could conclude that the existence of the redox couple Co^{2+}/Co^{3+} and Cu^{+}/Cu^{2+} in the right amount was critical for the catalytic activity of the zeolite. In other words, the unique existence of one single oxidation state was unable to catalyze the reaction. Furthermore, the intrinsic pore structure appears to be also decisive for the activity of the Co,Cu-zeolites.

Acknowledgements

We would like to acknowledge the 'Ministerio de Ciencia e Innovación' (MICINN) for providing the ICTS-2008-18 grant that allowed to built the reactor cells. We are also especially grateful to Juan José Cortés, who worked with us thanks to the above mentioned program. He has been exceptionally valuable in the construction and manipulation of these cells.

References

[1] A. E. Palomares, J. G. Prato, A. Corma, Ind. Eng. Chem. Res. 42 (2003) 1538.
[2] M. W. Twigg, Appl. Cat. B-Environment. 70 (2007) 2.

Improved Stability of SSZ-13 for MTO: Mesopore Generation through Diquaternary Ammonium-Type Surfactants

Leilei Wu, Volkan Degirmenci, Pieter Magusin, Emiel J.M. Hensen*
Schuit Institute of Catalysis, Eindhoven University of Technology, P.O. Box 513, 5600 MB, Eindhoven, The Netherlands,
E-mail: E.J.M.Hensen@tue.nl

Introduction

SSZ-13 with the chabazite (CHA) topology is a promising catalyst for the methanol to olefins (MTO) reaction due to its high selectivity towards olefins (up to 87 wt %) [1]. Its silicoaluminophosphate (SAPO) analogue SAPO-34 is the commercially preferred catalyst because it leads to less coke formation. Both types of catalysts suffer from comparatively fast deactivation due to coke deposition in the microporous CHA framework, blocking the reactants' access to the acid sites and regeneration cycles remain crucial. One way to cope with catalyst deactivation due to coking appears to be the introduction of substantial mesoporosity. Desilication is a straightforward method to arrive at mesoporous zeolites Olsbye et al. reported mesopore generation in SSZ-13 by desilication with NaOH [2]. Despite the presence of mesoporosity, catalyst stability was not improved compared to the parent SSZ-13, possibly due to a lack of interconnectivity of the micro- and mesopore systems. Recently, Ryoo et al. have explored the use of diquaternary ammonium-type surfactants to prepare nanosheets of MFI zeolites [3]. Here, we investigate the synthesis of mesoporous SSZ-13 using $[C_{22}H_{45}\text{-}N^{+}(CH_3)_2\text{-}C_4H_8\text{-}N^{+}(CH_3)_2\text{-}C_4H_9]Br_2$ (denoted as $C_{22\text{-}4\text{-}4}Br_2$) as the mesoporogen. The zeolites were characterized by XRD, SEM, TEM, ICP-AES, Ar-physisorption, ^{1}H MAS NMR, CO FTIR and applied as catalysts for the MTO reaction.

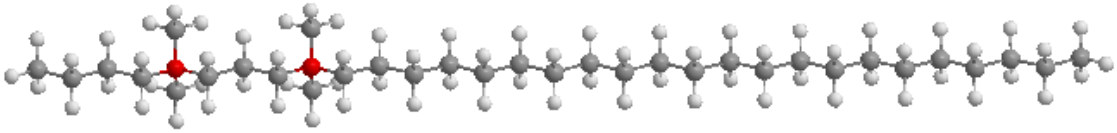

Scheme 1. Structure of $[C_{22}H_{45}\text{-}N^{+}(CH_3)_2\text{-}C_4H_8\text{-}N^{+}(CH_3)_2\text{-}C_4H_9]Br_2$.

Experimental

Mesoporous SSZ-13 was synthesized by using N, N, N,-trimethyl-1-adamantammonium hydroxide (TMAdOH) and $C_{22\text{-}4\text{-}4}Br_2$ as templates. The initial gel was subjected to crystallization in a Telflon-lined stainless-steel autoclave at 160°C for 6 days. After the crystallization, the solid product was collected by filtration, washed with deionized water and dried at 110°C. As-synthesized zeolite was calcined in air at 550°C for 6 h and ion-exchanged three times with 1.0 M NH_4NO_3 solutions followed by calcination at 550°C for 6 h in order to obtain its proton form.
Methanol conversion into olefins was tested in a fixed-bed reactor at 350°C at a WHSV of 0.8 g $g^{-1}h^{-1}$. In a typical experiment, the catalyst was pretreated in air at 550°C for 2 h prior to reaction. The products were analyzed by online gas chromatography.

Results and discussion

XRD patterns evidence the formation of zeolites with the CHA structure in all cases. Figure 1 shows SEM pictures of SSZ-13 and a representative mesoporous SSZ-13. Whereas the former sample clearly consists of large cubic crystalline particles, the latter particle is made up from very small crystals formed by limited zeolite growth. The SEM image suggests the presence of a network of mesopores integrated into the microporous crystal. The mesopore volume

determined by Ar physisorption is 0.21 g/cm^3 with a Langmuir surface area of 1032 m^2/g. Corresponding values are 0.01 g/cm^3 and 664 m^2/g for SSZ-13. The micropore volume of both samples is 0.18 and 0.21 g/cm^3 for SSZ-13 and mesoporous SSZ-13, respectively.

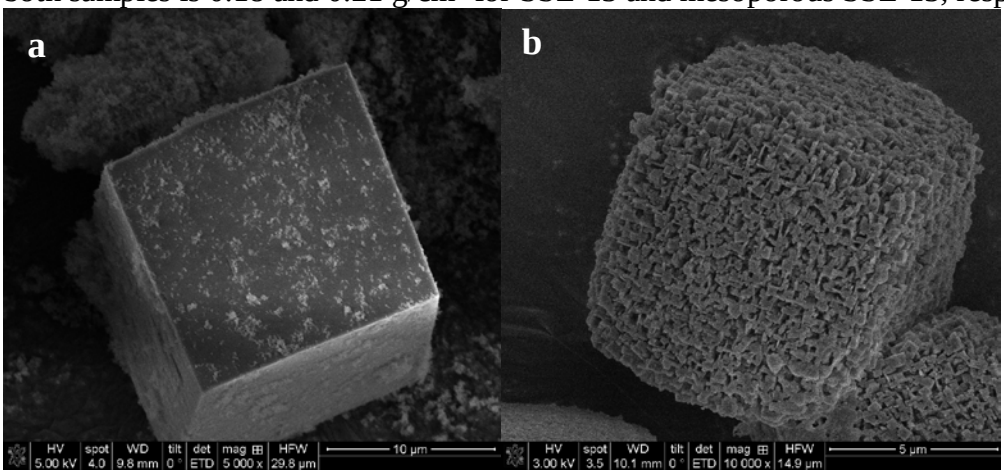

Figure 1. SEM images of a) SSZ-13 and b) mesoporous SSZ-13.

These samples were applied as catalysts in the MTO. As shown in Figure 3, the initial methanol conversion for both zeolites is 100%. Deactivation is expressed as the time needed to obtain a conversion of 50%. This was about 3 h for SSZ-13 and 7 h for the mesoporous zeolite. Both catalysts produce more than 90% olefins with a slight preference for propylene for the mesoporous SSZ-13 catalyst. Further optimization of the amount of mesoporogen has led us to obtain a catalyst with a life time of more than 20 h.

Conclusions

Mesoporous SSZ-13 was synthesized by use of a diquaternary ammonium-type surfactant, which limits the crystal growth to small zeolite domains. Catalytic tests for the MTO reaction revealed that mesoporous SSZ-13 can cope with more coke than SSZ-13, leading to improved catalyst stability.

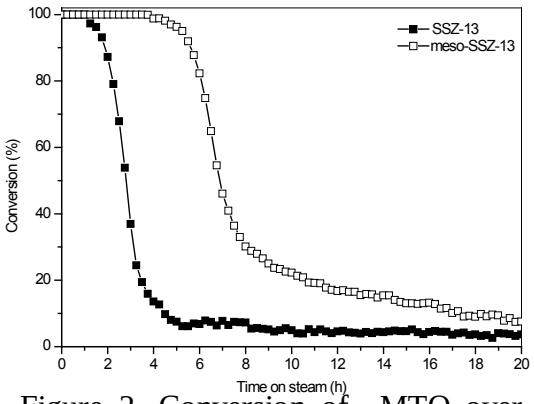

Figure 2. Conversion of MTO over SSZ-13 and mesoporous SSZ-13.

Acknowledgements

The authors thank the Technology Foundation STW of the Netherlands Organization for Scientific Research (NWO) for financial support.

References

[1] Yuen L-T., Zones S.I.,Harris T.V., Gallegos E.J., Auroux A., Product selectivity in methanol to hydrocarbon conversion for isostructural compositions of AFI and CHA molecular sieves, Micropor Mater, 2 (1994) 105-117.

[2] Sommer L., Mores D., Svelle S., Stöcker M., Weckhuysen B.M., Olsbye U., Mesopore formation in zeolite H-SSZ-13 by desilication with NaOH, Micropor Mesopor Mater 132 (2010) 384-394

[3] Choi M., Na K., Kim J., Sakamoto Y., Terasaki O., Ryoo R., Stable single-unit-cell nanosheets of zeolite MFI as active and long-lived catalysts, Nature 461(2009) 246-249.

Synthesis of Well-Structured Ultra Small Mesostructured Porous Silica Nanoparticles

Feifei Gao[1], Belén Albela[1], Sandra Casale[2], Laurent Bonneviot[1]*

[1] *Laboratoire de Chimie, UMR 5182 CNRS, Ecole Normale Supérieure de Lyon, Université de Lyon, 46 allée d'Italie, 69364 Lyon Cedex 07, France.*
[2] *Service de Microscopie Electronique de l'UFR de Chimie, Laboratoire Réactivité de Surface, UMR-7609 CNRS, Université Pierre et Marie Curie, 4 Place de Jussieu, 75252 Paris, France.*
**Corresponding author, e-mail: laurent.bonneviot@ens-lyon.fr*

Introduction

Nanosized porous materials can be applied as building units to create hierarchically structured porosity to minimize internal molecular diffusion for the design of adsorbents and catalysts. As stable colloidal suspension, they have been envisioned and tested as nanocargo for imaging and drug delivery in medical diagnosis and therapy. Monodispersion and size calibration are key points for a better structural control and toxicity problems. In addition, as nanocargo, their size should be smaller than 100 nm to avoid capillary plugging (embolism) in living systems. It remains a challenge particularly to obtain particles smaller than 50 nm particularly when monodispersity and shape control are targeted. The first report by Mann et *al.* was based on supersaturation control using dilution to quenching of the nucleation step followed by a neutralization meant to quenched the growth [1]. A "double surfactant system" was later proposed without supersaturation control and using instead an additional surfactant to the cationic surfactant, which is of non-ionic type and claimed to act as grain growth suppressant [2].

Here, a robust synthetic route for well-structured ultra small porous nanoparticles of less than 20 nm is obtained by combining the double quenching method of Mann et al. with the double surfactant approach cited above where the final pH quenching is performed at slightly acidic pH (5.5) and where the presence of a nonionic surfactant required in the initial stage apparently affects mainly the very first nucleation step rather than the growth step.

Experimental

Mesoporous silica nanoparticles were synthesized via a quenching method with two surfactants, cetyltrimethylammonium bromide (CTAB) and nonionic surfactant triblock copolymer Pluronic F127. The typical molar ratio in the reaction solution was 1 SiO_2 : 0.5 NaOH : 0.12 CTAB : 0.0048 F127 : 130 H_2O. The surfactants were dissolved in a basic solution with NaOH and distilled H_2O at RT under continuous stirring. A short time (40 s) after silica source (tetraethoxysilane (TEOS)) was added, the reaction solution was 6 times diluted using distilled water for the nucleation quenching. 4 min later, the pH of the solution was adjusted to 5.5 by HCl (2M). After stirring for 3 h, NaOH was added to achieve a very weak acidic or neutral condition (pH~6.5 to 7). The stirring was stopped after another 2 h, and the suspension was then kept in static solution at RT. A solid sample can by extracted by centrifugation. Surfactants were removed by calcination at 550 °C for 6 h.

Results and discussion

High-resolution transmission electron microscopy (HRTEM) image (Fig. 1a) shows spherical nanoparticles with homogeneous morphology and size (about 20 nm). X-ray diffraction (XRD) patterns (in Fig. 1b) exhibit rather intense broad peak with obvious though unresolved secondary peaks consistent with very small ordered domains. Assuming an hexagonal array of channels, the d_{100} would be ca. 5.3 nm consistent with the HRTEM observations. Notably, the XRD pattern increases in intensity but remains as broad consistent with a preserved monodomain size and ordering after removal of the surfactant molecules, as usually observed for bulk material where the surfactant removal leads to a better density contrast between the wall and the channel. Dynamic light scattering (DLS) measurement of the synthetic solution (not presented here) shows that the colloidal objects are distributed in size between 26 to 42 nm, while after dilution and ultrasonication treatment the primary particle size is monomodal at 18 nm (Fig. 1c). Despite the obvious aggregation of the primary particles in the synthetic conditions, the colloidal solution is stable at RT and can be kept for more than half a year at pH~6.5 to 7. The equilibrium between aggregates and primary particles slowly evolves in favor of the latter progressively increasing the amount of particles that can be harvested by ultracentrifugation. After 1 month, a yield about 60 % can be estimated from centrifugation. A typical mesoporous type adsorption-desorption with hysteretic loop suggesting large textural porosity was recorded. At high relative pressure, the N_2-adsorption volume reaches 1335 cm^3 g^{-1}, which indicates a large macropore volume consistent with a hierarchical porosity due to poorly dense packing. Several trial show that the non ionic template has to be present at the beginning of the process and affects mainly the nucleation step.

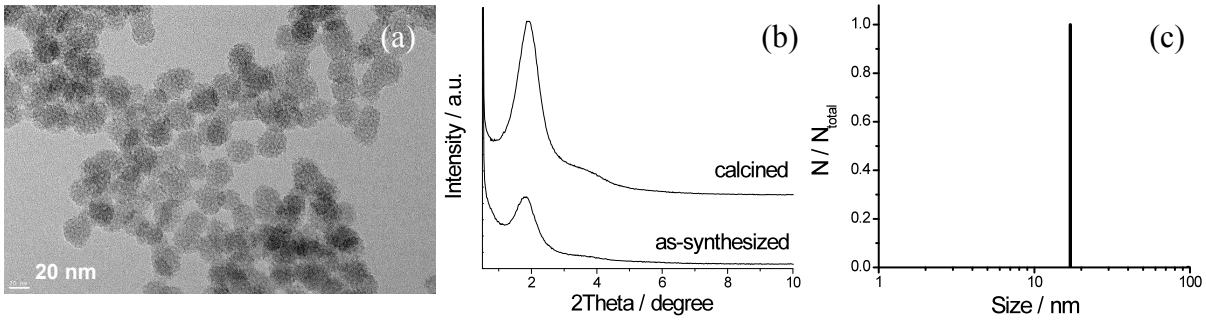

Figure 1. HRTEM image (a), XRD patterns (b), and DLS after ultrasonication (c) of mesoporous silica nanoparticles.

Conclusions

In summary, this work presents the synthesis of well-structured homogeneous mesoporous silica of less than 20 nm in size where two key steps are the use of a secondary surfactant and a rapid pH quenching at pH 5.5-6 before neutralization.

Acknowledgements: This work was supported by Award No. UK-C0017 of KAUST.

References

[1] a)Fowler, C. E.; Khushalani, D.; Lebeau, B.; Mann, S. Adv. Mater. 13 (2001), 649-652; b) Sadasivan, S.; Khushalani, D.; Mann, S. J. Mater. Chem. 13 (2003), 1023-1029; c) Sadasivan, S.; Fowler, C. E.; Khushalani, D.; Mann, S. Angew. Chem., Int. Ed. 41 (2002), 2151-2153.
[2] a) Suzuki, K; Ikari, K; Imai, H. J. Am. Chem. Soc. 126 (2004) 462-463; b) Suzuki, K; Ikari, K; Imai, H. Langmuir 22 (2006) 802-806.

Improvement of the hierarchical TS-1 properties by silanization of protozeolitic units in presence of alcohols

D. P. Serrano[1,2], R. Sanz[1], P. Pizarro[1], A. Peral[1], I. Moreno[1]
[1]*Department of Chemical and Energetic Technology, ESCET, Rey Juan Carlos University,*
[2]*Madrid Institute for Advanced Studies on Energy, IMDEA Energía,*
david.serrano@imdea.org

Introduction

Hierarchical zeolites have become one of the most promising ways to overcome the diffusion limitations in microporous catalysis. For this reason, the development of new strategies for the synthesis of hierarchical zeolites has attracted much attention in the last decade. In this context, organosilanes compounds have been employed as soft templates to prepare zeolitic materials with intracrystalline tunable porosity. One of these procedures is the zeolite crystallization from organofunctionalized seeds, which has proven to be applicable to the syntheses of a variety of zeolites (ZSM-5, Beta, TS-1…) [1-3]. The silanization agent prevents the total aggregation of the zeolitic nanounits, previously formed in a precrystallization step, into larger crystals during the subsequent hydrothermal treatment. We have found that when a high proportion of organosilane is introduced into the synthesis medium (>8 mol %, regarding to the total silica content of the gel) a viscous gel is formed, which hinders the diffusion of the organosilane in the gel and its anchoring onto the zeolitic seeds. In order to improve the silanization process in these conditions, in the present work, a variety of alcohols have been tested as solvent in the synthesis of hierarchical TS-1 zeolite, their influence in the physicochemical, textural and catalytic properties of the materials obtained being discussed.

Experimental

TS-1 synthesis gel was prepared following the procedure described by Taramasso et al [4]. This gel was precrystallized in a reflux system at 90 °C for 24 h. Then, the resulting solution was functionalized with an organosilane compound (phenylaminopropyltrimethoxysilane, 12 mol% regarding to the total silica content of the gel) at 90 ºC for 24 h, with or without the presence of an alcohol in the synthesis medium. After that, the alcohols were removed from the synthesis medium using a rota-evaporator. Finally, crystallization was carried out under autogenous pressure at 170 °C for 8 h using microwave heating radiation. For comparison purposes, a reference TS-1 zeolite was also prepared using the same synthesis route but omitting the precrystallization and silanization steps. The catalytic activity of these zeolites was evaluated in 1-octene epoxidation reactions using TBHP as oxidant.

Results and discussion

Hierarchical TS-1 zeolites synthesized using different alcohols as solvent have been denoted TS-1 (x, y), were “x” indicates the %mol of organosilane used and “y” references the alcohol employed. The reference TS-1 zeolite was designed as TS-1(0 %). XRD analyses indicate that all the samples prepared are well crystallized, as denoted the presence of sharp reflection lines at the characteristic 2θ positions of MFI structure. Likewise, the DR UV-Vis spectra evidenced the presence of isolated Ti^{4+} atoms incorporated into the zeolite framework in tetrahedral coordination, whereas extraframework TiO_2 phases were not detected. Physicochemical and textural properties corresponding to these samples are included in Table 1. All synthesized catalysts have significant Ti amounts, which are close to 1 %wt. On the other hand, it can be clearly observed that seed silanized samples possess significantly higher BET areas than the reference TS-1, which come from a higher contribution of the secondary

porosity, as it is indicated by the corresponding surface area (S_{SP}) and pore volume (V_{SP}) values. This increment of the textural properties assigned to the secondary porosity is higher when the synthesis gel in the silanization stage is diluted with alcohols (except for the sample prepared with 1-propanol). This effect is especially remarkable for the sample synthesized with ethanol, which achieve S_{BET} and S_{SP} values of 709 m^2/g and 521 m^2/g, respectively, keeping a high crystallinity degree and Ti atoms in a tetrahedral environment. The catalytic activity of hierarchical TS-1 zeolites was quite higher than that obtained with reference zeolite, due a higher proportion of more accessible titanium sites. Moreover, it is noteworthy that a reasonable correlation exists between the catalytic activity and the surface attributed to the secondary porosity. This is a clear indication that the catalytic activity of TS-1 zeolites with TBHP occurs within the secondary porosity, with negligible contribution of the Ti sites located within the zeolitic micropores. Finally, it is important to point out that the epoxide selectivity was 100 % and TBHP efficiency was higher than 88% in all cases.

Table 1. Ti content, textural properties and catalytic activity of TS-1 samples

Sample	Ti (wt%)	S_{BET} (m^2/g)	S_{MZ}[a] (m^2/g)	S_{SP}[a] (m^2/g)	V_{SP}[a] (cm^3/g)	X_{OCTENE}[b] (%)	TOF[b] (h^{-1})
TS-1 (0%)	1.16	446	362	84	0.075	6.7	11.9
TS-1 (12%, -)	1.21	628	256	373	0.337	27.1	37.9
TS-1 (12%, methanol)	1.16	664	245	420	0.293	31.6	47.0
TS-1 (12%, ethanol)	1.15	709	188	521	0.352	38.3	57.9
TS-1 (12%, 1-propanol)	0.95	579	247	332	0.201	16.3	29.9
TS-1 (12%, 2-propanol)	1.00	656	235	421	0.272	24.1	43.3

ZM: Zeolitic micropores, SP: Secondary Porosity. [a]Determined by applying the NLDFT method/ [b]Reaction conditions: 100ºC, 3 h, $(1\text{-octene/TBHP})_{MOLAR}$= 1.25, 0.2 g catalyst.

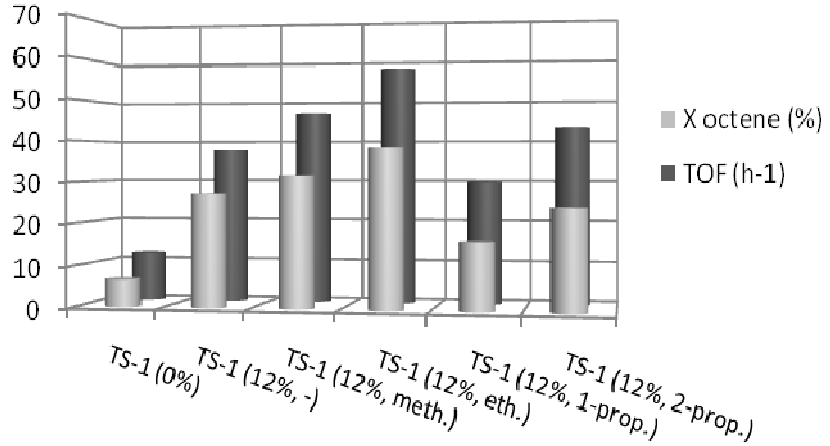

Figure 1. Catalytic activity of TS-1 samples in 1-octene epoxidation with TBHP.

Conclusions

In this work, we probed that, in the hierarchical TS-1 zeolites preparation, the dilution of the synthesis medium with alcohols improves the silanization step and, consequently, an increment in the values of the textural properties, such as S_{BET}, S_{SP} and V_{SP} is produced. Likewise, a good correlation between the catalytic activity and the proportion of this secondary porosity is observed.

References

[1] D. P. Serrano, J. Aguado, J. M. Escola, J. M.Rodríguez, A. Peral, Chem. Mater. 8 (2006) 2462.
[2] J. Aguado, D.P. Serrano, J.M. Rodriguez, Microporous and Mesoporous Mater. 115 (2008) 504.
[3] D. P. Serrano, R. Sanz, P. Pizarro, I. Moreno, Chem. Commun. (2009) 1407.
[4] M. Taramasso, G. Perego, B. Notari, U.S. Patent Nº 4410501.

Surfactant-Templated Mesoporous Zeolites

A.I. Carrillo,[a] J. García-Martínez[a,b,c*] M.Johnson[b], J. Valla[b], K. Li[b], J. Y. Ying*[c,d]
[a]*Molecular Nanotechnology Lab, Inorganic Chemistry Department University of Alicante, Aptdo. 99 – E-03080 Alicante (Spain) e-mail: j.garcia@ua.es*
[b]*Rive Technology, Inc., 1 Deer Park Drive, Suite A, Monmouth Junction, NJ 08852, USA*
[c]*Department of Chemical Engineering, Massachusetts Institute of Technology, Cambridge, MA 02139, USA*
[d] *Institute of Bioengineering and Nanotech., 31 Biopolis Way, The Nanos, Singapore 138669*

Introduction

A technique that can introduce controlled mesoporosity directly into crystalline zeolites would be highly desirable and will have great impact to catalytic processes, such as fluid catalytic cracking.[1] Herein, we describe a new surfactant-based technique that allows for precisely controlled mesoporosity to be introduced within a wide range of zeolite crystals (i.e. mesostructuring), e.g. FAU, MOR and MFI of various Si/Al ratios, while maintaining the chemical and physical properties of the zeolites (i.e. microporosity, crystallinity, acidity, etc.).[2] Testing of FCC catalysts made with mesostructured zeolite Y showed significantly improved selectivity in product yields (more transportation fuels and less coke, dry gas and uncracked bottoms).

Experimental

In a typical synthesis, 1.00 g of a zeolite in 64 mL of a 0.37 M solution of NH_4OH containing 0.70 g of cetyltrimethyl ammonium bromide (CTAB) was stirred for 20 min. The mixture was next heated at 80°C under autogenous pressure for 24 h. The solid was filtered, washed, and dried. Close to 100% recovery was observed, and there was no significant leaching of Si or Al species into the filtrate. Alternatively, other bases such as NaOH, Na_2CO_3 or tetrapropylammonium hydroxide (TPAOH) could be used. The pH of the reaction mixture was maintained at ~ 9–11 to avoid desilication.

Results and discussion

The method described allows for the controlled homogenous introduction of intracrystalline mesoporosity while maintaining the original zeolite crystals (Figure 1a) without the formation of any amorphous phase. This method does not modify the initial Si/Al of the zeolite and it can be applied to a wide variety of zeolites with a broad range of Si/Al ratios. Mesostructured zeolites show of the properties of conventional zeolites including crystallinity, microporosity, strong acidity and hydrothermal stability. The changes in the micropore volume of the mesostructured zeolite Y during the severe hydrothermal treatment steps described herein were similar in trend as those for conventional zeolite Y, but the mesoporosity is preserved even after deactivation (see Figure 1b). Mesostructured zeolites were also formulated with various matrix compositions into FCC microspheres (of ~ 70 micron in size) by spray drying. The catalysts, after being properly deactivated (e.g. at 788°C under 100% steam for 4 h), were tested on a fixed fluidized bed ACE testing unit with different feedstocks. The catalysts made from mesostructured zeolites produced significantly more gasoline and light cycle oil (transportation fuels), and less bottoms and coke. The improved product selectivity could be attributed to the mesostructure introduced into the zeolites that eased the diffusion limitation in the conventional zeolites.

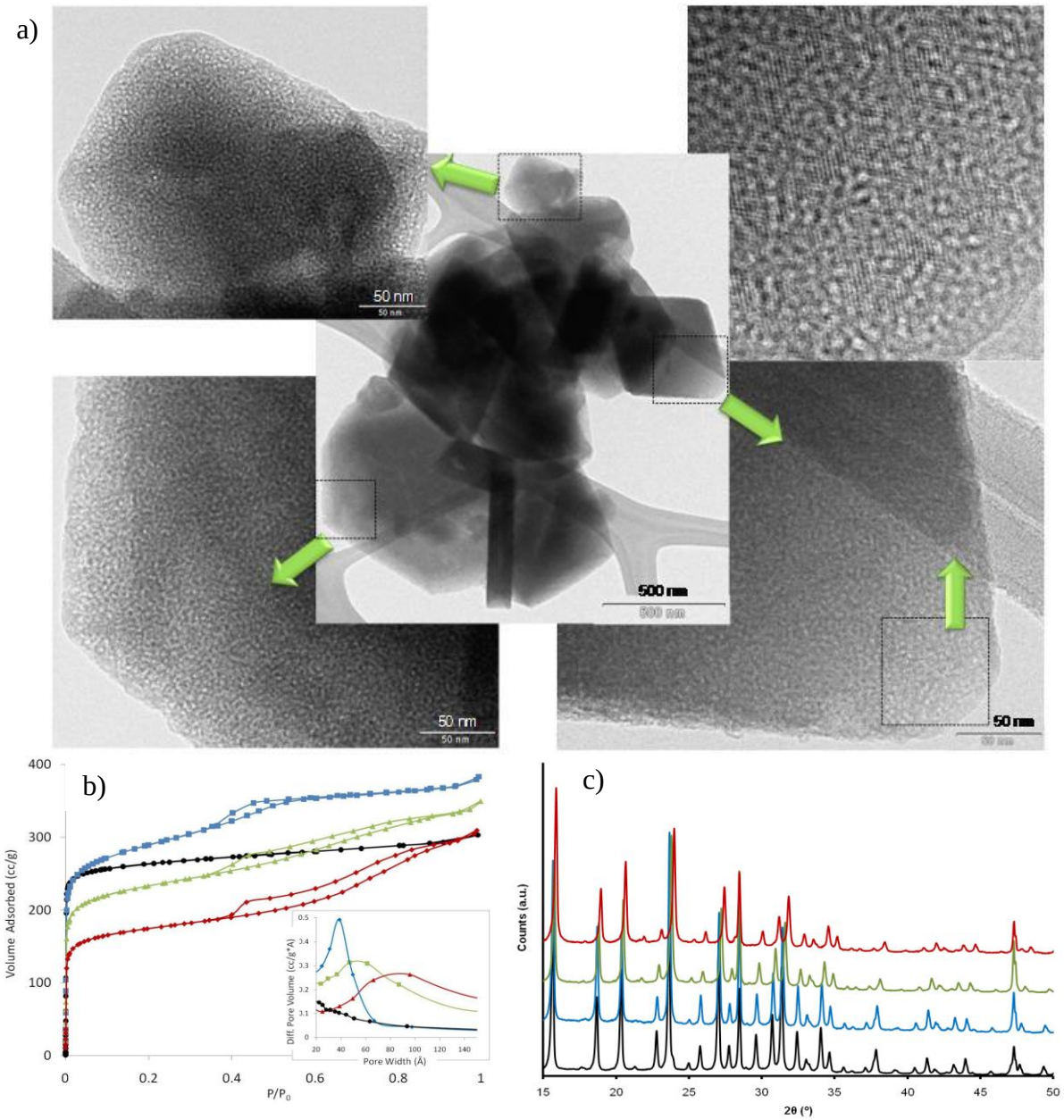

Figure 1. a) TEM micrographs of mesostructured type Y zeolite showing intracrystalline mesoporosity and b) Ar adsorption isotherms and c) X-ray diffraction patterns of NH_4Y (black), mesostructured Y (blue), and mesostructured USY before (green) and after (red) deactivation at 788 °C in 100% steam for 4 hours.

Conclusions

Zeolite Y with well-controlled intracrystalline mesoporosity has been prepared via a surfactant-assisted synthesis. The mesostructured zeolite Y demonstrated excellent hydrothermal stability. Testing of FCC catalysts made with mesostructured zeolite Y showed significantly improved selectivity in product yields, more transportation fuels and less coke, dry gas and uncracked bottoms.

References

[1] a) J. Weitkamp, L. Puppe, in *Catalysis and Zeolites: Fundamentals and Applications*, Springer, Berlin, Germany, **1999**, b) A. Corma, *Chem. Rev.* **1997**, *97*, 2373–241, c) J. Čejka, A. Corma, S. I. Zones, in *Zeolites and Catalysis: Synthesis, Reactions and Applications*, Wiley-VCH, Weinheim, Germany, **2010**.

[2] J. Y. Ying, J. García-Martínez, US Patent 7,589,041 B2, **2009**. J. García-Martínez, M. Johnson, US 20080138274, **2008**. J. García-Martínez, M. Johnson, US 20100021321, **2010**. L. Dight, J. García-Martínez, J. Valla, M. Johnson, US 20100190632, **2010**.

Delamination of Layered Zeolite Precursors under Mild Conditions

Isao Ogino[1], Einar A. Eilertsen[2], Michael M. Nigra[1], Sonjong Hwang[3], Jeong-Myeong Ha[1], Thomas Rea[4], Stacey I. Zones[1,4]*, Alexander Katz[1]*
[1]*Department of Chemical and Biomolecular Engineering, University of California Berkeley, Berkeley, California 94720*
[2]*University of Oslo, Department of Chemistry, Box 1033 Blindern, NO-0315 Oslo, Norway*
[3]*California Institute of Technology, Pasadena, California 91125*
[4]*Chevron Energy Technology Company, Richmond, California 94804*
**askatz@berkeley.edu, sizo@chevron.com*

Introduction

The emergence of a new class of catalysts consisting of delaminated zeolite precursors expands the range of reactions that zeolites catalyze by providing access for larger reactant molecules [1,2]. ITQ-2 represents the first example of such a material, which has been shown to be more active for the cracking of bulky molecules due to its more open micropore space [1]. The synthesis of ITQ-2 and other delaminated zeolite precursors typically requires a high pH medium during precursor material swelling, typically in the pH range of 13.5 – 13.8 [3,4], which is known to lead to partial amorphization of the zeolite layers during delamination [3,4]. Here, we demonstrate the synthesis of a new class of delaminated zeolite precursor materials, UCB-1, formed by delamination of MCM-22 (P) under mild conditions. We provide evidence of delamination by powder X-ray diffraction (PXRD), transmission electron microscopy (TEM), and nitrogen gas adsorption characterization of the synthesized material, and compare the results for those for ITQ-2. We report results from 29Si MAS NMR characterization of UCB-1 and ITQ-2, and highlight the high structural integrity of UCB-1. We also show the first results of catalytic performance tests, comparing the materials in model acid-catalyzed hydrocarbon conversions.

Materials and Methods

Reagents used in the synthesis of UCB-1 are all reagent grade without further purification. For comparison synthesis of ITQ-2 was performed as described previously [1].

Results and Discussion

PXRD characterization of as-made UCB-1 (pattern C) is shown alongside data for zeolites MCM-22 (P) (pattern A) and ITQ-2 (pattern B), which match literature [1], in Figure 1. This data demonstrates a similar powder pattern for UCB-1 relative to what was previously reported for ITQ-2 zeolite. The 001 (3.3°, ≈ 27 Å) and 002 (6.7°, ≈ 13 Å) peaks are significantly diminished in intensity after the treatment by the new method (Figure 1C), indicating loss of long range order in the direction perpendicular to the layer; thus, the results indicate that the new method delaminates MCM-22 (P). UCB-1 has a stronger 310 (26.0°) peak intensity than ITQ-2. This suggests preservation of a greater degree of long-range order in the direction parallel to the sheet for the material synthesized by the new method. TEM image characterization of MCM-22 (P) shows a rectilinear morphology, as reported in the literature, which is in stark contrast to the curved layers shown in Figure 2A for as-made material UCB-1. A closer examination of as-made UCB-1 via TEM shows single-layers of 2.5 nm thickness as well, indicating that MCM-22 (P) is delaminated efficiently.

Conclusions

The new delamination method for layered zeolite precursors presents several advantages over the conventional method, which are demonstrated using MCM-22 (P) as an example. The promising results encourage the application of the new method for delamination of other layered zeolite precursors.

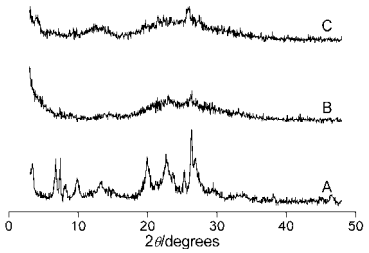

Figure 1. PXRD patterns characterizing as-made zeolites (A) MCM-22 (P), (B) ITQ-2, and (C) UCB-1.

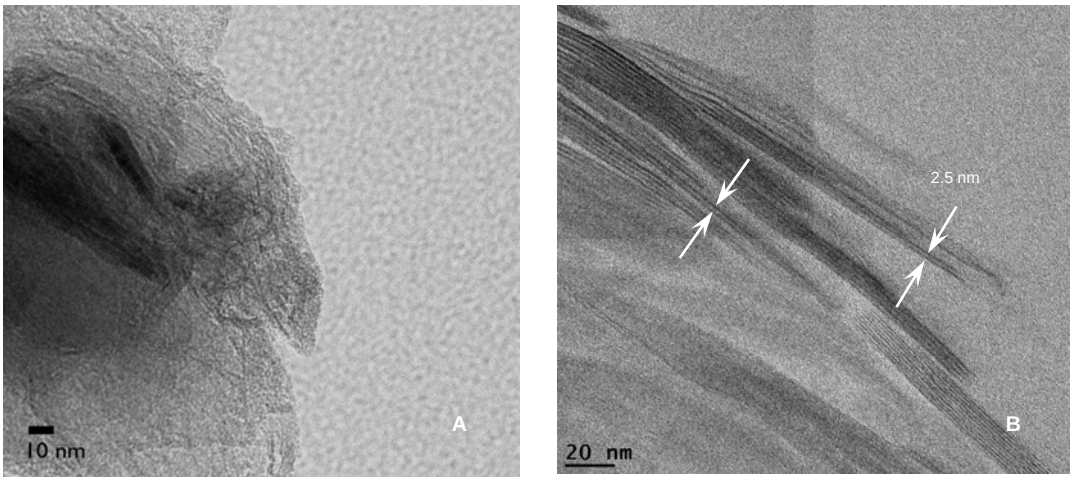

Figure 2. TEM images characterizing as-made UCB-1. The arrows in B indicate single layers.

Acknowledgements

The authors are grateful to the Management and Transfer of Hydrogen via Catalysis Program funded by Chevron Corporation for financial support.

References

[1] Corma, A., Fornes, V., Pergher, S. B., Maesen, T. L. M., Buglass, J. G., Delaminated zeolite precursors as selective acidic catalysts, Nature 396 (1998), 353-356

[2] Corma, A., Diaz, U., Domine, M. E., Fornes, V. J., New Aluminosilicate and Titanosilicate Delaminated Materials Active for Acid Catalysis, and Oxidation Reactions Using H_2O_2, Am. Chem. Soc. 122 (2000), 2804–2809

[3] Schenkel, R., Barth, J. O., Kornatowski, J., Lercher, J., Chemical and structural aspects of the transformation of the MCM-22 precursor into ITQ-2, Stud. Surf. Sci. Catal., 142 (2002), 69-76

[4] Maheshwari, S., Jordan, E., Kumar, S., Bates, F. S., Penn, R. L., Shantz, D. F., Tsapatsis, M., Layer Structure Preservation during Swelling, Pillaring, and Exfoliation of a Zeolite Precursor , J. Am. Chem. Soc. 130 (2008), 1507–1516

The first post-synthesis transformation of a 3-dimensional framework into a lamellar zeolite with modifiable architecture.

Wieslaw J. Roth*, Oleksiy V. Shvets[€], Mariya Shamzhy[€], Pavla Chlubná*, Martin Kubů*, Petr Nachtigall[¥], and Jiří Čejka*
**J. Heyrovský Institute of Physical Chemistry, Academy of Sciences of Czech Republic, v.v.i., Dolejškova 3, 182 23 Prague 8, Czech Republic,*
[€]L.V. Pisarzhevskiy Institute of Physical Chemistry, National Academy of Sciences of Ukraine,31 pr. Nauky, Kyiv 03028, Ukraine,
[¥]Department of Physical and Macromolecular Chemistry, Faculty of Natural Sciences, Charles University, Albertov 2030, 128 40 Prague 2, Czech Republic

Introduction

The large pore 14x12-ring UTL framework was discovered to undergo structural change in aqueous environment that is consistent with conversion into a lamellar material by degradation of the D4R units originally supporting its dense layer regions. This is diagnosed using X-ray powder diffraction characterization (XRD). Subsequent changes upon various treatments developed previously for investigation of layered zeolites such as calcination, stabilization and swelling further support the lamellar structure of the product (denoted IPC-1P; calcined form IPC-1; IPC = Institute of Physical Chemistry) and its potential for structural modification. The behavior of IPC-1P matches that of well-established layered zeolite derivatives like MCM-22 family, however, it provides completely new mode of preparation, i.e. from 3D framework. The demonstrated IPC-1P conversion into IPC-2, the iterlamellar expanded zeolite (IEZ), represents a reverse 2-D into 3-D process, albeit with different interlayer bridges. Additional characterizations including nitrogen sorption, TEM and powder pattern simulations, support the conclusions about structural transformations derived from XRD. This is the first example of the conversion of 3D zeolitic framework into a 2D material, which can be further modified structurally.

Experimental

Synthesis of B-UTL: Preparation of the B-UTL-15(X) zeolites was carried out using the method similar to that published elsewhere [1,2] with replacement of the part of silica source for H_3BO_3. Molar composition of reaction mixtures was $0.692–0.764SiO_2$:$0.036–0.108H_3BO_3$:$0.4GeO_2$:$0.6–0.7ROH/Br$:$30H_2O$. Typically, boric acid was dissolved in water with variable concentrations of SDA and hydroxide/bromide ratios. Crystalline germanium oxide was added and the mixture was stirred at room temperature producing clear solution. After this, silica (Aerosil 300) was added into obtained solution and the mixture was stirred at room temperature for 30 min. The resulting fluid gel was charged into 25 ml Teflon-lined autoclaves and heated at 175 °C for 9 – 15 days with agitation (~ 25 rpm). Usually, for appropriate mixing of the reaction mixture, a small Teflon cylinder was placed in an autoclave. Solid products obtained after preset synthesis times were recovered by filtration, washed with distilled water and dried overnight at 95 °C. To remove the SDA, the as-synthesized zeolites were calcined in a stream of air at 550 °C for 6 h with a temperature ramp of 1 °C/min.
Treatment of UTL and derivative samples: Hydrolysis was carried out in distilled water or 0.1 M HCl solution with liquid to solid ratio from 100-200 to 1 w/w, at temperatures from ambient to 100ºC, typically for overnight. Calcinations were carried out in air at 540 ºC for 4-6 h. Stabilization (IEZ synthesis) involved reacting 0.5 g of solid in 10 ml of 1 M HNO3

solution containing 0.1 g of $Si(CH_3)_2(OCH_2CH_3)_2$ at 170ºC for 16 h. The product was isolated by centrifugation, washed and calcined. Swelling was carried out by mixing a 25% solution of hexadecyltrimethylammonium chloride in water with 40% tetrapropylammonium hydroxide, w/w ratio 9/1, mixing with the solid , ratio at least 10:1 w/w and heating at 100 ºC for overnight. The solid was isolated by centrifugation, washed with small amount of water and dried at 50 ºC till dry. Typical weight gain was 60-100%. Swellings were also performed at room temperature.

Results and discussion

In this contribution we report on the discovery that the originally 3D structure of UTL zeolite in its porous form is unstable and can be post-synthetically transformed in aqueous environment into a lamellar solid, apparently with preservation of the structural integrity of the layers. We established this initially using X-ray powder diffraction and further validated with TEM electron microscopy, simulations and porosity measurements. Furthermore, we carried out various treatments conducive to modification of interlayer separation similar to those developed with layered zeolite precursors, like MCM-22P [1]. These treatments included calcination giving a contraction producing new microporous material IPC-1 (Figure 1), intercalation of cationic surfactants with swelling and stabilization referred to as producing interlamellar expanded zeolite (IEZ; denoted here IPC-2). The results support the postulated lamellar architecture that can be modified by intercalation and related treatments. This finding represents the first example of conversion of a 3D zeolite framework into a layered zeolite derivative (3D to 2D transformation). This contrasts the behavior of zeolite layered precursors [2], which convert into 3D frameworks by condensation of layers (2D to 3D transformation), recognized to date as irreversible. Of course, in the case of UTL the reverse process, i.e. restoration of the original D4R bridge is highly improbable, but one may consider the preparation of IPC-2 as the 2-D into 3-D transformation.

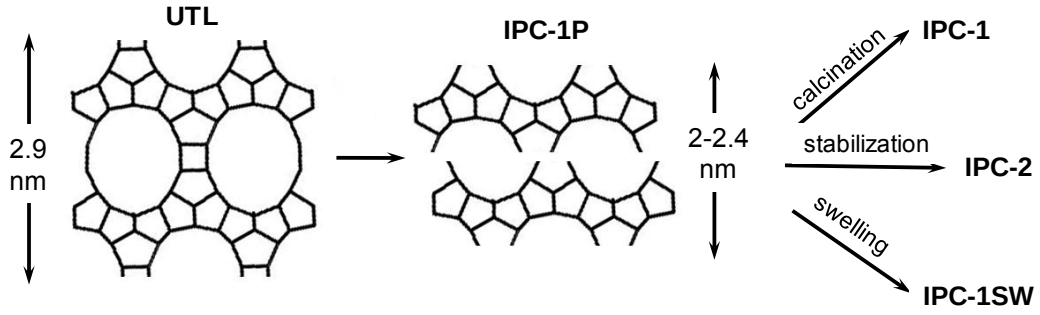

Figure 1. Transformation of UTL into layered zeolite (ICP-1P); its calcined (ICP-1), stabilized (IPC-2) and the swollen form (ICP-1SW).

References

[1]W.J. Roth, D. L. Dorset, *Microp. Mesopor. Mater.* **2011**, in press, 10.1016/j.micromeso.2010.11.007.

[2]W. J. Roth, in *Introduction to Zeolite Science and Practice, 3rd edition, Stud. Surf. Sci. Catal.*, Vol. 168 (Eds.: J. Čejka, H. van Bekkum, A. Corma, F. Schüth (eds.), Elsevier, Amsterdam, 2007, pp. 221-239.

The impact of coadsorbed molecules on the redox properties of Co^{2+} ions in zeolite CoZSM-5

Kinga Góra-Marek

Faculty of Chemistry, Jagiellonian University, Ingardena 3, 30-060 Krakow, Poland

Corresponding author: Kinga Góra-Marek, e-mail: gorak@chemia.uj.edu.pl

Introduction

Cobalt containing zeolites were subject of numerous studies because of their activity in denox processes and in reaction of some organic molecules. IR studies of the nature of the cobalt sites in the pentasil-type zeolites revealed the presence both Co^{3+} and Co^{2+} sites. Co^{2+} can exists in the form of the exchange cations, the bulk CoO, and in the form of an oxide-like clusters. The zeolites CoZSM-5 of higher Si/Al, i.e. of long distances between AlO_4^-, contains low amount of Co^{3+} and most of Co^{2+} takes the form of CoO and oxide-like clusters. The zeolites of low Si/Al are characterized by high contribution both of Co^{3+} and Co^{2+} in the exchange positions. Our earlier studies exhibited that the Co^{3+} species are supposed to exist in the oxide forms.

The exchangeable cations can be modified by the interaction either with framework oxygens or with molecules of different electron donor properties. The modification of the properties of the Co^{2+} cations in CoZSM-5 by the interaction with ammonia and pyridine molecules, being a strong electron donors, as well as with CO acting as an electron acceptor ligand is the subject of present study. The ability of the Co^{2+} cations to activate the NO molecule in the presence of the preadsorbed NH_3, pyridine and CO has been also investigated.

Keywords: CoZSM-5, NO adsorption, IR spectroscopy

Experimental

Zeolite CoZSM-5 (Si/Al=15, Co/Al=0.18) was obtained by an ionic exchange of a parent HZSM-5 in $Co(NO_3)_2$ solution at 350 K. Before the IR experiments the wafers of zeolites were activated *in situ* in an IR cell at 620 K at vacuum for 1 h. The measured doses of CO were sorbed in CoZSM-5 at 130 K, whereas the sorption of the other probe molecules (NO, ammonia,and pyridine) was performed at room temperature.

Results and discussion

The sorption of NO in zeolite CoZSM-5 at r.t. results in the formation of the set of bands of $Co^{2+}(NO)_2$ dinitrosyls as the most stable species (IR bands at 1810 and 1895 cm^{-1}). The presence of $Co^{2+}NO$ mononitrosyls was reported when the sorption of NO was performed at high temperature *ca.* 620 K [1-3]. The stretching frequency of NO molecule in $Co^{2+}NO$ mononitrosyls (1850 cm^{-1}) is similar as in gaseous NO (1875 cm^{-1}) pointing to the weak activation of the N-O bond by Co^{2+} cations neutralized only by the framework oxygens.

An important NO activation was observed when NO was sorbed in CoZSM-5 with preadsorbed molecules. What is interesting, the sorption of NO at r.t. in CoZSM-5 with preadsorbed NH_3, pyridine and CO molecules results in the formation of $Co^{2+}NO$ mononitrosyls. As mentioned before, this band is not detected when NO is sorbed in CoZSM-5 without preadsorbed molecules.

The presence of NH_3 and pyridine strongly influences the N-O stretching frequency in mononitrosyls adducts. Both for the $Co^{2+}(NH_3)_nNO$ and $Co^{2+}PyNO$ adducts the N-O frequency (1750 and 1800 cm^{-1}, resp.) is definitely lower than for NO in $Co^{2+}NO$

mononitrosyls without preadsorbed molecules (1850 cm^{-1}) indicating an important N-O bond activation. This N-O bond weakening is supposed to be realized by the electron transfer from a electron donor molecules to antibonding π^* orbital of NO.

At high NH_3 loadings the $Co^{2+}(NH_3)_{m\ (m\ =\ 5,\ 6)}$ complexes are formed. The interaction of NO with the ammonia rich complexes $Co^{2+}(NH_3)_m$ results in the formation of the NO species characterized by 1330 and 1660 cm^{-1} IR bands. The red shift from the position of gaseous NO (1875 cm^{-1}) evidences a vital weakening of the N-O bond. These bands are supposed to originate from the hyponitrites $[O\text{-}N{=}N\text{-}O]^{2-}$ species [4]. The hyponitrites $[O\text{-}N{=}N\text{-}O]^{2-}$ could be formed in the reaction of mononitrosyls $Co^{3+}(NH_3)_m(NO)^-$ with NO molecule from gas phase. It is reported that in the $Co^{3+}(NH_3)_m(NO)^-$ mononitrosyls the electron transfer from $Co(NH_3)_m$ to NO takes place [4]. In consequence, the cobalt becomes trivalent and NO gets negative charge (NO^-). The N-O stretching frequency (1330 cm^{-1}) is similar to that reported for NO^- (1146-1305 cm^{-1}). The hyponitrites $[O\text{-}N{=}N\text{-}O]^{2-}$ are believed to be precursors for the N_2O formation, which leads to N_2 in denox pathway. In CoZSM-5 with complexes $Co^{2+}(NH_3)_m$ the hyponitrites $[O\text{-}N{=}N\text{-}O]^{2-}$ are transformed into N_2O. The N_2O bands at 2224 and 1280 cm^{-1} develops simultaneously with the disappearance of the hyponitrites bands at 1330 and 1660 cm^{-1}. Therefore, the electron transfer from a basic ammonia molecules to NO in $Co^{3+}(NH_3)_m(NO)^-$ complexes plays an important role in the N-O bond activation.

The mechanism of the modification of the Co^{2+} cation properties by the coadsorbed CO molecules is different than for ammonia and pyridine. Contrary to ammonia and pyridine, CO acts as a strong electron acceptor. The flow of electron density from antibonding π^* orbitals of NO *via* Co^{2+} towards antibonding π^* orbitals of CO results in the strengthening of N-O bond (a blue shift of NO band) and in the weakening of C≡O band (a red shift of CO band).

Conclusions

The properties of NO interacting with Co^{2+} ions in zeolite CoZSM-5 exhibit the significant dependence on the kind of the coadsorbed molecules. As reported by various authors, in the pentasil-type zeolites *e.g.* CoZSM-5 and CoMOR without preadsorbed molecules nitrogen monoxide acts as reducer: Co^{3+} is reduced to Co^{2+} whereas NO is oxidized to NO^+ [3,4].
In the presence of ammonia, the electron transfer from the ammonia molecules to antibonding π^* orbital of NO influences the redox properties of nitrogen monoxide and NO acts as oxidant. The Co^{2+} cations are oxidized to Co^{3+} while NO is reduced to NO^- species, which are transformed into N_2O.
On the other hand, CO acts as the electron acceptor. The flow of electron density from antibonding π^* orbitals of NO *via* Co^{2+} towards antibonding π^* orbitals of CO results in the strengthening of N-O bond and in the weakening of C≡O bond.

Acknowledgements

This study was sponsored by the Ministry of Science and Higher Education, Warsaw, Poland (project no N N204 017039).

References

[1] K. Hadjiivanov, Catal. Rev.-Sci. Eng., 42 (1&2) (2000) 71-144.

[2] K. Hadjiivanov, E. Ivanowa, M. Daturi, J. Saussey, J.-C. Lavalley, Chem. Phys. Lett. 370 (2003) 712.

[3] K. Góra-Marek, B. Gil, M. Śliwa, J. Datka, Appl. Catal. A, General 330 (2007) 33.

[4] Encyclopedia of inorganic chemistry, editor-in-chief: R. BruceKing, 2 (1994) 723-731.

Application of solid-state electrochemistry techniques to polyfunctional organic-inorganic hybrid materials: the Maya Blue problem

Antonio Doménech*[a], María Teresa Doménech-Carbó[b], Noemí Montoya[c]

a: Departament de Química Analítica. Universitat de València. Dr. Moliner, 50, 46100 Burjassot (València) Spain. b: Institut de Restauració del Patrimoni, Universitat Politécnica de València. Camí de Vera 14, 46022, València, Spain. a: Departament de Química Inorgànica. Universitat de València. Dr. Moliner, 50, 46100 Burjassot (València) Spain.

Introduction

Maya Blue (MB), a famous pigment widely used in murals, pottery, codices and sculptures by the ancient Mayas and other people in Mesoamerica has claimed considerable attention because of its peculiar palette, ranging from a bright turquoise to a dark greenish blue, and its enormous stability. The interest paid to the chemistry of MB has been considerably reinforced in recent years because of its unique combination of organic and inorganic components at the molecular level [1]. Maya Blue can be described as a hybrid organic-inorganic material resulting from the attachment of indigo, a blue dye extracted from leaves of *Indigofera suffruticosa* and other species to the clay matrix of palygorskite, a fibrous phyllosilicate. The location of indigo molecules in the palygorskite framework, the nature of the indigo-palygorskite association in Maya Blue and the reasons for its peculiar hue still remain controversial [2]. In all these aspects, the voltammetry of microparticles (VMP) [3] has provided significant information; in particular, permitted to document the most ancient use of MB (Substructure IIC of Calakmul, Late Postclassical period) and suggested that dehydroindigo, the oxidized form of indigo, accompanies this dye in the palygorskite framework [4]. The dehydroindigo/indigo ration could be varied by varying the temperature of thermal treatment during MB preparation, thus resulting in different hues for the resulting pigment [4,5]. Chemometric analysis of Maya Blue samples from different sites suggested that the preparation procedure of Maya Blue probably changed along time following a ramified pattern [5,6].

Experimental

VMP experiments on MB specimens prepared from indigo (1% w/w) plus palygorskite mixtures as previously described [7] were performed upon abrasive attachment of few nanograms of sample to the surface of a paraffin-impregnated graphite electrode. 0.50 M sodium acetate buffer (pH 4.75) were used as electrolyte. Instrumentation and experimental details has been already described [4,5]. Series of kinetic experiments were performed by extracting aliquots of the MB specimens at different times during their isothermal heating at temperatures between 130 and 180 ºC.

Results and discussion

Figure 1 shows a typical voltammetric response for MB samples. Analysis of the variation of peak potentials and the relative height for signals corresponding to the dehydroindigo/indigo

and indigo/leucoindigo couples at different temperatures permits to establish thermochemical parameters for the dye/palygorskite attachment and determine the dehydorindigo/indigo ratio[4]. Voltammetric and chronoamperometric data leads to estimate the variation of the abundance of dye molecules with the deep within the crystals of palygorskite [6] and the coexistence of different topological redox isomers so that MB can be recognized as a polyfunctional hybrid material [7]. Remarkably, VMP analysis leads to establish the kinetics of solid-state processes involved in the preparation of MB.

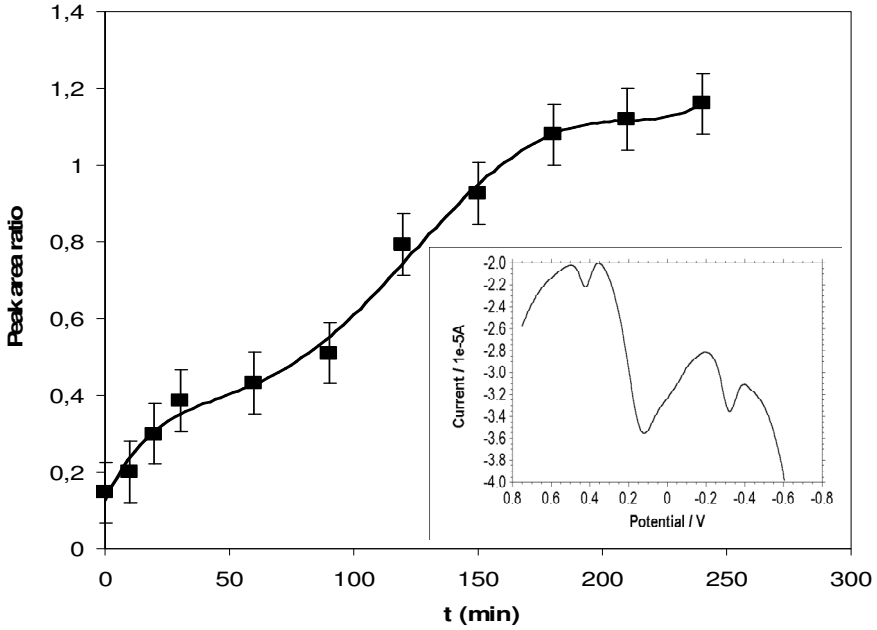

Figure 1. Time variation of the intensity of indigo oxidation peak relative to the background during heating at 130 ºC, representative of the kinetics of water loss of palygorskite coupled with indigo attachment to the clay matrix. Inset: typical square wave voltammogram for paraffin-impregnated graphite electrode modified with a MB specimen immersed into 0.50 M HAc/NaAc (pH 4.75). Conditions as in ref. [7].

References

[1] Gómez-Romero, P.; Sánchez, C., Hybrid materials. Functional properties. From Maya Blue to 21st century materials, *New Journal of Chemistry* 29 (2005) 57-58.

[2] Doménech, A.; Doménech, M.T.; Sánchez, M.; Vázquez, M.L.; Lima, E., Maya Blue as a nanostructured polyfunctional hybrid organic-inorganic material: the need to change paradigms, *New Journal of Chemistry* 33 (2009) 2371-2379.

[3] Scholz, F.; Schröder, U.; Gulabowski, R., *Electrochemistry of Immobilized Particles and Droplets*. Springer, Berlin, 2005.

[4] Doménech, A.; Doménech, M.T.; Vázquez, M.L., Dehydroindigo: a New Piece into the Maya Blue Puzzle from the Voltammetry of Microparticles Approach. *Journal of Physical Chemistry B* 110 (2006) 6027-6039.

[5] Doménech, A.; Doménech, M.T.; Vázquez, M.L., Chemometric Study of Maya Blue from the Voltammetry of Microparticles Approach. *Anaytical. Chemistry* 79 (2007) 2812-2821.

[6] Doménech, A.; Doménech, M.T.; Vázquez, M.L., Correlation between spectral, SEM/EDX and electrochemical properties of Maya Blue. A chemometric study. *Archaeometry* 51 (2009) 1015-1034.

[7] Doménech, A.; Doménech, M.T.; Sánchez, M.; Goberna, S.; Lima, E., Evidence of Topological Indigo/Dehydroindigo Isomers in Maya Blue-Like Complexes Prepared from Palygorskite and Sepiolite. *Journal of Physical Chemistry C* 113 (2009) 12118-12131.

Synthesis of Al-containing interlayer-expanded-MWW zeolite with high catalytic performance under neutral conditions

Toshiyuki Yokoi, Shun Mizuno, Hiroyuki Imai, Junko N. Kondo, Takashi Tasumi*
*Chemical Resources Laboratory, Tokyo Institute of Technology, 4259 Nagatsuta, Midori-ku, Yokohama 226-8503, Japan, *Corresponding author.ttatsumi@cat.res.titech.ac.jp*

Introduction

Treatment of the zeolitic layered precursor of Al-MWW, so-called Al-MWW(P), with diethoxydimethylsilane (DEDMS) in an acidic media leads to the formation of an aluminosilicate-type interlayer-expanded zeolite MWW (Al-IEZ-MWW) with expanded 12-membered ring (12-MR) micropores [1, 2]. Al-IEZ-MWW can serve as a useful acid catalyst for large molecules. In the silylation, the presence of the acid, *e.g.*, HNO_3, enhances the extraction of the structure-directing agent (SDA) in the interlayer, the hydrolysis of the silylating agent and the condensation reaction of the silylating agent and the interlayer-silanol groups. However, the silylation process under acidic conditions simultaneously causes dealumination from the **MWW** framework, resulting in the decrease in the acid amount [3].

Here we report a method for preparing the Al-IEZ-MWW without leaching of the Al species. The strategy is to conduct the silylation under neutral conditions; the silylation was conducted in the aqueous solution of ammonium salt, NH_4Cl, instead of HNO_3. The resultant Al-IEZ-MWW sample exhibited a high catalytic performance in the acylation of anisole.

Experimental

The layered precursor of the **MWW** aluminosilicate, Al-MWW(P), was hydrothermally synthesized from fumed silica according to the literature [1]. The Si/Al ratio of the Al-MWW(P) was found to be 27. The interlayer silylation of Al-MWW(P) was performed using diethoxydimethylsilane ($Si(OEt)_2Me_2$, DEDMS) as a silylation agent in aqueous solution of 1.0 M HNO_3 and NH_4Cl under reflux conditions for 24 h. After the silylation, the solid was recovered by filtration and rinsing with distilled water, and then dried at 100 ºC. The silylated products were calcined at 550 ºC for 6 h to give the Al-IEZ-MWW samples. Thus obtained products were denoted as *e.g.*, Al-IEZ-MWW (NH_4Cl). Conventional **MWW**-type aluminosilicate, Al-MWW, was also synthesized by calcination of Al-MWW (P).

To examine catalytic properties of the Al-IEZ-MWW samples, the Friedel-Crafts acylation of anisole with acetic anhydride was carried out at 60 ºC in an oil bath with stirring.

Results and discussion

Figure 1 shows the XRD patterns of Al-MWW (P), Al-MWW, Al-IEZ MWW (HNO_3) and Al-IEZMWW (NH_4Cl). The 002 reflection due to the layered structure along the c direction was observed in the XRD patterns of the products obtained through the interlayer-silylation in the aqueous solutions of HNO_3, NH_4NO_3, NH_4Cl and CH_3COONH_4, revealing

that Al-IEZ-MWW was successfully obtained even through the interlayer-silylation in the aqueous solutions of the ammonium salt. As a control, the silylation in the only water was unsuccessful.

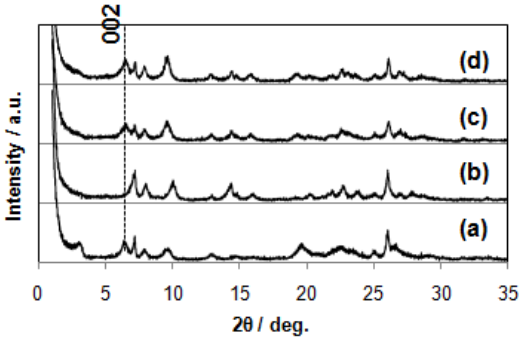

Figure 1 XRD patterns of (a) Al-MWW (P), (b) Al-MWW, (c) Al-IEZ MWW (HNO_3) and (d) Al-IEZMWW (NH_4Cl).

The BET surface areas of Al-IEZ-MWW (NH_4Cl) and Al-IEZ-MWW (HNO_3) were found to be 490 and 407 $m^2 \cdot g^{-1}$, respectively. Judging from the relative peak area of the D peak ($\underline{Si}Me_2(OH)_{2-n}(OSi)_n$) in the ^{29}Si MAS NMR spectra, the silylation degree of Al-IEZ-MWW (NH_4Cl) was higher than that of Al-IEZ-MWW (HNO_3). The neutral conditions would be more effective for the silylation reaction than the acidic conditions.

The silylation process in the aqueous solution of HNO_3 resulted in the dealumination from the **MWW** framework; the Si/Al ratio of the Al-IEZ-MWW (HNO_3) was found to be 35. Note that the leaching of Al species was not observed in the interlayer-silylation in the aqueous solution of NH_4Cl. The ^{27}Al MAS NMR spectra revealed that Al-MWW(P) has only tetrahedrally-coordinated Al species, while they were partially transformed into octahedrally-coordinated ones through the interlayer-silylation in the aqueous solution of NH_4Cl followed by the calcination.

The catalytic activity of Al-IEZ-MWW (NH_4Cl) for acylation of anisole was higher than conventional Al-MWW, but lower than Al-IEZ-MWW (HNO_3). This is due to the presence of octahedrally-coordinated Al species in the sample. Therefore, the effect of the acid treatment using HNO_3 of Al-IEZ-MWW (NH_4Cl) was investigated with the pH of the acid-treatment solution varied ranging from 0 to 2. The acid treatment with the pH of 0.5 led to the decrease in the Al amount (Si/Al = ca.54) but the catalytic activity was improved. The acid treatment with pH below 0.5 caused the leaching of tetrahedrally-coordinated Al species as well as octahedrally-coordinated ones, resulting in low catalytic activity.

Conclusions

A method for preparing the Al-IEZ-MWW without leaching of the Al species has been developed; the silylation was conducted in the aqueous solution of the ammonium salt. Furthermore, the use of ammonium salt improved the silylation degree. Thus prepared the Al-IEZ-MWW exhibited a high catalytic performance even after the acid treatment.

References

[1] Wu, P., Ruan, J., Wang, L., Wu, L., Wang, Y., Liu, Y., Fan, W., He, M., Terasaki, O., Tatsumi, T., J. Am. Chem. Soc., 130 (2008) 8178-8187.
[2] Inagaki, S., Tatsumi, T., Chem. Commun., (2009) 2583-2585.
[3] Inagaki, S., Imai, H., Tsujiuchi, S., Yakushiji, H., Yokoi, T., Tatsumi, T., Micropor. Mesopor. Mater. in press.

Atomic distribution of silver in silver-containing zeolite A revealed by Cs corrected scanning transmission electron microscopy

Alvaro Mayoral[1]*, Thomas Carey[2], Paul A. Anderson[2], Isabel Díaz[3]
[1] *Laboratorio de Microscopías Avanzadas (LMA), Instituto de Nanociencia de Aragón (INA), Universidad de Zaragoza, C/ Mariano Esquillor, Edificio I+D, 50018 Zaragoza, SPAIN*
Email: amayoral@unizar.es
[2] *School of Chemistry, University of Birmingham, Edgbaston, Birmingham B15 2TT, UK*
[3] *Instituto de Catálisis y Petroleoquímica, CSIC. c/Marie Curie 2, 28049 Madrid, Spain*

Introduction

Considering the good crystallinity of zeolites and the large structural parameters that they commonly present; it would be expected that they would provide excellent materials for transmission electron microscopic analysis. However, their stability under the electron beam has been the main drawback regarding a deep structural analysis with this technique. The first electron micrograph was recorded 1958[1], where two lattice fringes of {111} planes from natural faujasite (FAU) were observed. Following that work, electron microscopy was mostly applied to study the structure by electron diffraction analysis, as small impurities were more easily detectable through this method rather than X-ray powder diffraction. It was not until the late 70's when the first high resolution electron micrograph was recorded[2].

It has been widely accepted that the sensitivity of zeolites depends on ionization due to radiolytic damage[3-5]. The crucial factor in limiting the lifetime of the zeolites under the electron beam has been found to be the Si/Al ratio. A Si-rich zeolite is more stable than one with a low Si/Al ratio. The water content is a direct consequence of this ratio and the ionization of water is believed to be a critical factor regarding the stability of zeolites under electron irradiation.

High resolution transmission electron microscopy (HRTEM) has been the method employed for fine structure determination[6-8]. Unfortunately, with this technique, imaging guest materials as metals is not so straight forward and a complete characterization for these catalysts still remains a challenge. For this purpose, high-resolution scanning transmission electron microscopy (STEM) combined with a high angle annular dark field detector (HAADF) is a more convenient approach as the images are formed with high incoherent electrons giving a contrast that is strongly dependent on the atomic number Z of the observed atoms.

In the present work, we have combined this technique in a spherical aberration (Cs) corrected electron microscope, which allows reaching a resolution down to 0.8 Å to characterize silver ion-exchanged zeolite A (LTA).

Experimental

8 g. of lab-prepared NaA were stirred in a 0.1 M solution of $AgNO_3$ (Sigma Aldrich, 99%), for 16 h at room temperature. The solution obtained was then filtered and washed with 1 l of deionized water. After that, it was dehydrated at 425 ◦C for 12 h under 1×10^{-6} mbar, observing a colour change from white to brick orange.

For electron microscopy analysis the powder was deeply crushed using a mortar and pestle, dispersed in ethanol and finally placed onto a lacey carbon copper grid. Images were recorded in a FEI TITAN, operated at 300 kV. The spherical aberrations were corrected using a dodecapole corrector (CEOS) for the electron probe.

Results and discussion

One of the advantages of using STEM respect to TEM is that the electron beam is converged into a very fine spot, which is raster over the selected area leaving the rest of the material intact. In order to minimize the beam damage, the beam current was manually decreased until a minimum value where the zeolite was still visible. Fig.1a shows the low magnification of the well structured AgA. Large nanoparticles of 5 nm can be observed formed as a result of the silver mobility in the presence of air during manipulation. These nanoparticles, which commonly adopted icosahedral morphology, are too big to be formed inside the zeolite cages and must remain on the outer surface of the zeolite crystals. However, a closer observation revealed the presence of Ag atoms (white spots) and clusters within the zeolite cages, Fig. 1b and 1c (see inset, NaA, for comparison) display the atomic resolution images recorded along the [001] and [110] orientations respectively.
Due to the heavier atomic weight of Ag respect to Si, Al and O, these atoms and/or clusters appear much brighter than the zeolite framework making them easily identified.

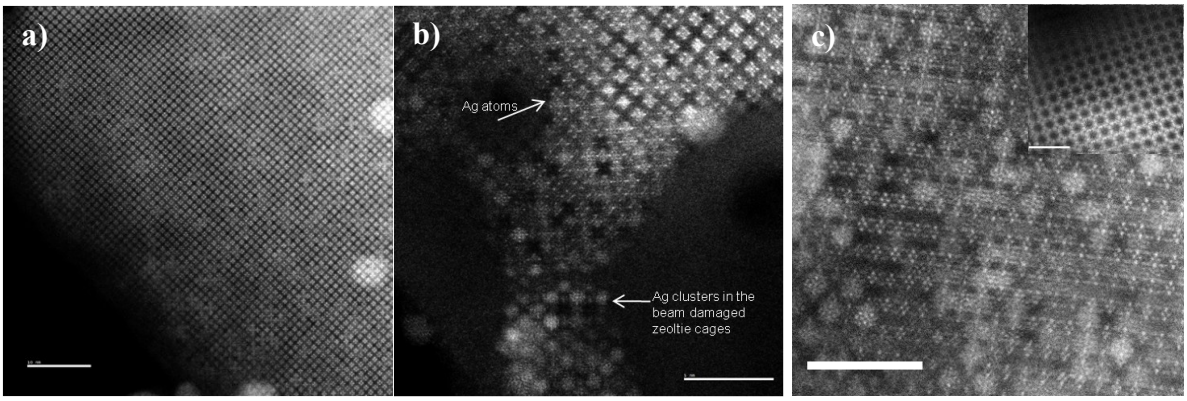

Figure 1 a) Cs corrected of AgA, scale bar 10 nm. b) High resolution image recorded along the [001] orientation and c) image recorded along the [110] orientation. Scale bars 5nm.

Conclusions

In the present study we have successfully applied aberration corrected STEM technique for the characterization of silver exchanged zeolite A. The silver distribution within the zeolite framework has been observed for the first time together with the formation of metal clusters inside the zeolite cages.

Acknowledgements

The authors would like to thank the University of Zaragoza, the Spanish government and the EPSRC for funding.

References

[1] Menter, J. W. Adv. Phys. (1958), 299.
[2] Sanders, J. V. Physics of Materials (1978).
[3] Treacey, M. M. J.; Newsam, J. M. Ultramicroscopy 23 (1987), 411.
[4] Csencsits, R.; Gronsky, R. Ultramicroscopy (1987), 421.
[5] Bursill, L. A.; Lodge, E. A.; Thomas, J. M. Nature (1980), 111.
[6] Díaz, I.; Kokkoli, E.; Terasaki, O.; Tsapatsis, M. Chem. Mater. 16 (2004), 5226.
[7] Villaescusa, L. A.; Díaz, I.; Barrett, P. A.; LLoris-Cormano, J. M.; Martínez-Mañez, R.; Tsapatsis, M.; Liu, Z.; Terasaki, O.; Camblor, M. A. Chem. Mater. 19 (2007), 1601.
[8] Readman, J. E.; Barker, P. D.; Gameson, I.; Hriljac, J. A.; Zhou, W.; Edwards, P. P.; Anderson, P. A. Chem. Commun. (2004), 736.

Referees comments

The work definitively shows some novelty in the sens that it uses advanced techniques (STEM/HAADF combined to Cs-correction) to precisely identify and locate isolated and clustered Ag species in zeolite crystals. Nevertheless, the interpretation of images (all white spots being attributed to silver) present some weakness, due especially i) to the lack of images of Ag-free A material (are they indeed the same as those presented here except for the white spots ?) and ii) to the absence of indication on Ag content (what is the expected level after exchange? what was the volume of 0.1M AgNO3 solution used for exchange of 8g of powder? is the Ag content in line with the high density of white spots seen on Fig. 1b and 1c?). These aspects need to be considered.

Due to the lack of space in the submission template some issues were not addressed but they were intended to be presented at the conference. Free Ag zeolite was also "imaged" to unambiguously attributed those white spots to silver (inset image, fig.2). The levels of exchange in that particular reaction were 100%. This yield have been tested several times through thermal gravimetrical analysis, X-ray diffraction, and EDX-TEM. See for example:

Dalton Trans.2006, 2368-2373

Nanotechnology 18, 2007,165708

Adv. Mater. 2001, 13, 1608

The solution was 250 mL 0.1 M which assure the excess of silver and therefore the 100% of exchange. And for that reason the materials was washed several times.In addition, We are currently developing STEM_HAADF simulations to confirm the atomic position and contrast observed in the images based on X-ray diffraction analysis in combination with Rietvield refinement.

Considering that the application of this technique to zeolites represents a novelty and that the location of "guest" atoms could have an enormous impact on the zeolitic and catalitycal fields we would like that the present manuscript would be reconsidered as oral presentation.

Inelastic neutron scattering for the study of hydrogen adsorption on porous solids

A.J. (Timmy) Ramirez-Cuesta
ISIS Facility, Rutherford Appleton Laboratory, STFC, Chilton, Didcot, OX11 0QX, United Kingdom, timmy.ramirez-cuesta@stfc.ac.uk

Introduction

Inelastic Neutron Scattering (INS) spectroscopy is an ideal tool to study hydrogen containing materials, since the incoherent scattering cross section of hydrogen is almost 20 times larger than any other element [1]. It is also very easy to establish comparison between experimental data and theoretical calculations, allowing a straightforward comparison and interpretation of the data when DFT calculations are available [2].

Theory

The rotational spectra of molecular hydrogen, does also fall within the range of the TOSCA spectrometer at ISIS. Therefore, it can also be used to study adsorption of molecular hydrogen in porous materials [1,3].
The rotational energy levels of the hydrogen molecule, in solid hydrogen (very weak interaction), are given by:

$$E_{JM} = J(J+1)B$$

where J and M are the angular quantum numbers. For hydrogen, the value of B is 7.35 meV. INS spectroscopy can measure the sharp para $\rightarrow$ ortho hydrogen transition, in particular the J 1$\leftarrow$0 transition, that corresponds to an energy transfer of 2B. The value of the constant B is determined by the moment of inertia of the hydrogen molecule. When the hydrogen molecule interacts with a surface the energy spectrum is more complex, and the nature of the spectrum will depend on the intensity and, in particular, characteristics of the interaction with the surface.

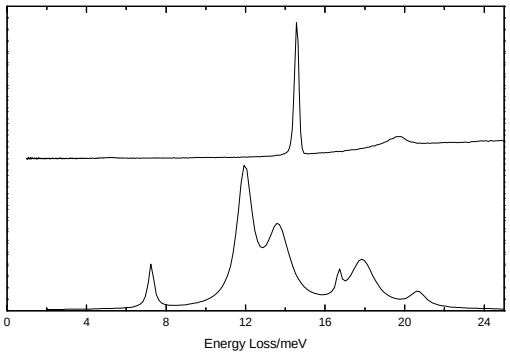

Figure 1. Top, spectrum of solid hydrogen (no interactions); bottom hydrogen on CoALPO (strong interaction)

The results show that the interaction of molecular hydrogen with carbons is very low and gives rise to a small shift of the rotational levels. On the other hand the zeolites, aluminophosphates and MOF show very large interactions between the hydrogen molecule and the substrate [4-7]. See figure 1.

H_2 in MOF

The adsorption of molecular hydrogen in Cu BTC has been studied using INS, the sample was loaded sequentially with an increased amount of para-hydrogen, see figure 2. The appearance of different rotational features as function of loading clearly show the different adsorption sites, by integrating the area under the peaks a very clear site by site adsorption isotherm can be produced.

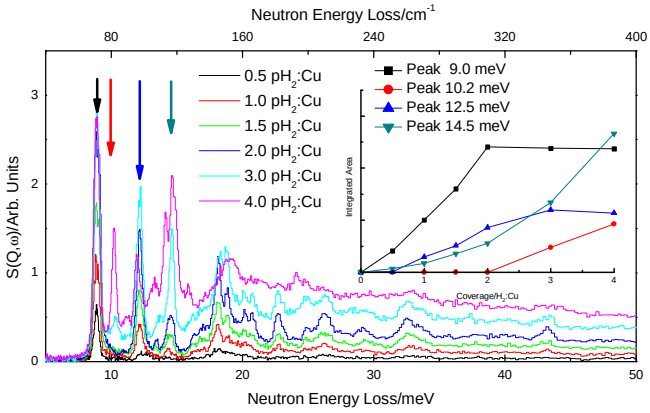

Figure 2. The INS spectra of hydrogen in CuBTC as function of loading, 4 different sites are apparent (arrows); the population is monitored by the area of each peak.

Effects of the cation charge in the adsorption of hydrogen in X-zeolite

The rotational-vibrational spectrum of H_2 was observed at low energy transfer (below *ca* 25 meV, 202 cm^{-1}); the vibration is that of the H_2 molecule against the binding site (H_2—X, not H—H). The vibration frequency is proportional to the polarising power of the cation (Na^+ < Ca^{2+} < Zn^{2+}). Polarisation of the H_2 molecule dominates the interaction of H_2 with this binding site [5-7]. The study of the translational modes of hydrogen is usually also applied to hydrogen clathrates [6,7].

Conclusions

INS is a very useful technique to study hydrogen containing materials and can be used to effectively study the interaction of molecular hydrogen with high surface area materials.

References

[1] PCH Mitchell, SF Parker, AJ Ramirez-Cuesta and J Tomkinson in “Vibrational Spectroscopy with Neutrons” World Scientific, London, (2005).
[2] A J Ramirez-Cuesta, Comp Phys Commun **157** 226-238 (2004).
[3] A J Ramirez-Cuesta, PCH Mitchell, S F Parker, P A Barrett Chem Commun 1257 (2000)
[4] Ramirez-Cuesta, AJ;et al; *Journal Of Materials* Chemistry, 17: 2533 (2007)
[5] Ulivi, L; Celli, M; Giannasi, A; Ramirez-Cuesta, AJ; Bull, DJ; Zoppi, M, PRB, 76: 161401 (2007)
[6] Ramirez-Cuesta, A. J.; Mitchell, P. C. H. Catalysis Today 2007, 120 (3-4), 368-373.
[7] AJ Ramirez-Cuesta, MO Jones, WIF David, Materials Today, 12, 2009, 54-61.

Development of new materials

FEZA 2011

Seed-directed Synthesis of Zeolites with Enhanced Performance in the Absence of Organic Templates

Bin Xie,[2] Haiyan Zhang,[2] Chengguang Yang,[2] Siyu Liu,[2] Limin Ren,[2] Lin Zhang,[2] Xiangju Meng,[1] Bilge Yilmaz,[3] Ulrich Müller,[3] and Feng-Shou Xiao[1]*
[1] *Department of Chemistry, Zhejiang University (XiXi Campus), Hangzhou 310028 P.R. China E-mail: fsxiao@mail.jlu.edu.cn*
[2] *Colloge of Chemistry, Jilin University, Changchun 130012, China.*
[3] *BASF SE, Ludwigshafen 67056, Germany.*

Introduction

Zeolites with intricate micropores have been extensively studied for a long time as an important class of industrial porous materials in different areas of chemical industry such as gas adsorption and separation, ion exchange, shape selective catalysis.[1] Earlier work on the synthesis of low silica zeolites normally used hydrated alkali cations as "templates" for the formation of the zeolite structural sub-units, and typical examples are A, X, Y, and L zeolites.[2] Latter, organic quaternary ammonium cations are introduced into aluminosilicate gels, leading to the discovery of the high silica zeolites,[3-6] and typical examples are ZSM-5,[3] Beta,[4] ITQ-21,[5] RUB-50,[6] where these organic cations direct the assembly pathway and fill the pore space. Herein, we have shown a novel route, seed-directed synthesis of Beta, Levyne, and Heulandite zeolites in the absence of organic templates, where zeolite seeds play similar roles to "organic templates" that direct crystallization of zeolites from the amorphous aluminosilicate gels.

Experimental

Seed-directed syntheses of Beta, Levyne, and Heulandite zeolites were performed from the starting aluminosilicate gel with molar ratios of SiO_2:1/40Al_2O_3:0.036Na_2O:35-41H_2O in the presence of Beta, RUB-50, and HEU seed, respectively. As a typical run for seed-directed synthesis of Beta (Beta-SDS) at 140°C, (1) 0.07 g of $NaAlO_2$ and 0.312 g of NaOH were dissolved in 8.64 ml of H_2O, followed by addition of 0.72 g of fumed silica; (2) After stirring for 10 min, 0.086 g of Beta zeolite seeds (Si/Al=10.2, 10.3%), was introduced into the gel; (3) The gel mixture with molar ratio of SiO_2:1/40Al_2O_3:0.036Na_2O:40.3H_2O was transferred into an autoclave to crystallize at 140°C for 18.5 h; (4) After filtration at room temperature and drying at about 80°C, crystalline products were obtained. Beta-SDS synthesized at 140 °C for 18.5 h in the presence of 10.3 % Beta seeds (Si/Al=10.2) was designated as 100 % crystallinity.

Results and discussion

Figure 1 shows XRD patterns of the samples synthesized in the same aluminosilicate gel without or with zeolite seeds of Beta, RUB-50 (LEV structure), and Heulandite in the absence of organic templates. Generally, Beta and RUB-50 are templated from tetraethylammonium (TEA^+) and Quinuclidine cations at 140-150°C, and Heulandite is synthesized in the presence of Li^+ cations at 250-300°C. Notably, when the aluminosilicate gel is absent of zeolite seeds, there is no crystalline product. However, when zeolite seeds of Beta, RUB-50, and Heulandite are introduced, Beta-SDS,[7-9] Levyne-SDS, and Heulandite-SDS zeolites are obtained at 120-140°C, respectively. These results indicate that the seeds play directing role for the crystallization of zeolites. This new synthesis methodology has been quickly scaled up by BASF (Ludwigshafen, Germany) and several hundreds of

kilograms of zeolite (Beta-SDS and Levyne-SDS) have already been produced following this novel route. It is worth noting that this approach represents an organotemplate-free and thus considerably low-cost route since in conventional industrial zeolite production organic template is typically the main cost driver. Organotemplate-free production of zeolites completely avoids the energy intensive high-temperature calcination step normally carried out for the removal of the templates. This also eliminates the formation of harmful gases due to the combustion of the organic component. In addition, the organotemplate-free route allows the utilization of simpler low-pressure vessels, which translates into significant cost savings in capital investment in industrial zeolite production. All in all, with the new cost structure made possible by organotemplate-free route, even the zeolite types that were previously considered to be too expensive for utilization in refinery applications such as fluid catalytic cracking, can now be employed in this field, which constitutes more than 95% of the zeolite catalyst demand worldwide.

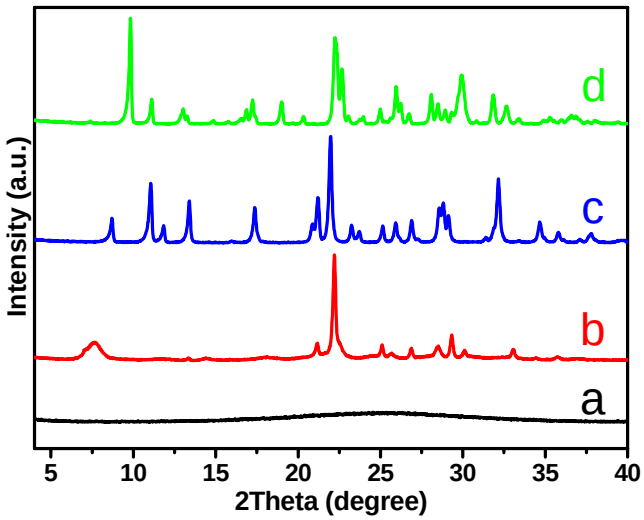

Fig. 1 XRD patterns of the samples synthesized in the aluminosilicate gel (a) without, with zeolite seeds of (b) Beta, (c) RUB-50, and (d) Heulandite in the absence of templates.

As a typical example, Beta-SDS was characterized by a series of mordern techniques. N_2 isotherms show that Beta-SDS exhibits BET micropore surface area at 632 m^2/g, which is much higher than that (BET micropore surface area at 452 m^2/g) of calcined Beta synthesized from using organic template of TEAOH (Beta-TEA). After calcination experiments (to test thermal stability) at 550 °C for 4 h, Beta-SDS still have high crystallinity and pure 4-coordinated Al species, while Beta-TEA remarkably reduce the crystallinity and produce partial 6-coordinated Al sites. Furthermore, after 100% steaming treatment at 750 °C for 8 h, Beta-SDS remains its crystallinity, but Beta-TEA obviously reduces its crystallinity. NH_3-TPD tests demonstrate that Beta-SDS has a significantly high density of acid sites compared to Beta-TEA. As a result, Beta-SDS shows much higher catalytic activity in cumene cracking than the conventional Beta-TEA and Y zeolites.

Acknowledgements

This work was supported by NSFC (20973079) and BASF foundation.

References

[1] Breck, D. W., Zeolite Molecular Sieves, Krieger, Malabar, 1984.
[2] van Bekkum, H., Flanigen, E. M., Jacobs, P. A., Jansen, J. C. Introdcution to Zeolite Science and Practice, Elsevier, Amsterdam, 2001.
[3] Kokotailo, G. T., Lawton, S. L., Olson, D. H., Meier, W. M. Nature, 272 (1978) 437-438.
[4] Treacy, M. M. J., Newsam, J. M. Nature, 332 (1988) 249-251.
[5] Corma, A., Díaz-Cabañas, M. J., Martínez-Triguero, J., Rey, F., Rius, J. Nature, 418 (2002) 514-517.
[6] Gruenewald-Lueke, A., Gies, H. Micropor. Mater., 3 (1994) 159-164.
[7] Cundy, C. S., Cox, P. A., Chem. Rev. 103 (2003) 663-701.
[8] Xie, B., et al., Chem. Mater. 20 (2008) 4533-4535.
[9] Majano, G., et al., Chem. Mater., 21 (2009) 4184-4191.
[10] Kamimura, Y., et al., Chem. Asian J., 5 (2010) 2182-2191; J. Phys. Chem. C., DOI: 10.1021/jp1098975.

Novel Macroporous Core@ Ordered Mesoporous Shell Structure: Catalytically Stable and Active Nanoreactor

Xiao-Yu Yang [1, 2], Li Yu [1, 2], Guastaaf Van Tendeloo [3], and Bao-Lian Su [1, 2 a *]
[1] *State Key Laboratory of Advanced Technology for Material Synthesis and Processing, Wuhan University of Technology, Luoshi Road 122, Wuhan 430070, P.R. China Laboratory of*
[2] *Inorganic Materials Chemistry (CMI), University of Namur (FUNDP), 61, rue de Bruxelles, B-5000 Namur, Belgium*
[3]*EMAT, University of Antwerp, Groenenborgerlaan 171, B-2020 Antwerpen, Belgium*
Corresponding author: bao-lian.su@fundp.ac.be

Introduction

Core-shell structures of nanoporous materials have received a lot of attention in recent years owing to the great versatility of the combined functionalities of cores and shells and their potential application in drug and biomolecule-delivery, separation science and confined-space catalysis.[1] There have been many successful examples, such as colloidal templating. Recent tendencies have centred on the replacement of the amorphous disordered core with say, ordered porous cores such as mesoporous materials and zeolites. However, direct synthesis of a hierarchically bimodal nanoporous core-shell structure is still a great challenge. Here we present the synthesis of spherical nanoparticles with a hierarchically macroporous core inside an ordered mesoporous shell via a one-pot reaction and its application in nanoreactor by in-situ encapsulation of metal oxide nanoparticles inside the core-shell structure [1].

Experimental

The typical synthesis of macroporous core@ mesoporous shell Aluminosilicates: (1) the mixture of 6 g Di-s-butoxyaluminoxytriethoxysilane and 6g TMOS were introduced into the solution (2.2 g of CTAB dissolved in 56 g of aqueous ammonia (pH = 11)) under stirring. (2) After stirring for 24 h, the solution was transferred to autoclaves and aged for 72 h at 80 °C. (3) After filtered, the product was calcined at 500 °C for 4 h to remove the organic templates.

Results and discussion

SEM images of the as-synthesized sample show that the spheres are homogeneously sized with a diameter of around 500 nm (Fig. 1a). Interestingly, foam-like hierarchically macroporous cages, of sizes 50-80 nm are observed inside these spheres by TEM studies (Fig. 1 b-d). A higher magnification image (Fig. 1d and insert) shows a ordered 2-D hexagonal (*P6mm)* mesostructure covering the foam-like macroporous cores. More importantly, the TEM image shows that the macroporous cages are inter-connected with uniformly ordered mesopores. The present core-shell structure provides a unique system for investigating nanoreactors, with the shell for designed for a better diffusion of reactants and products, and the core for encapsulation of active sites such as metallic nanoparticles. As an example of the introduction of the catalytically active sites into internal macroporous cores, the above synthesis strategy has been employed in the presence of an iron ions complex solution (Fig. 2). An aluminosilicate ester and TMOS, with a defined ratio, were added to an aqueous solution of $(NH_4)_3[Fe(CN)_6]$ and CTMAB (pH=11). The almuminosilicate ester and TMOS instantaneously created a foam-like macroporous core [2] containing iron species and a denser, ordered mesoporous shell as discussed above. After

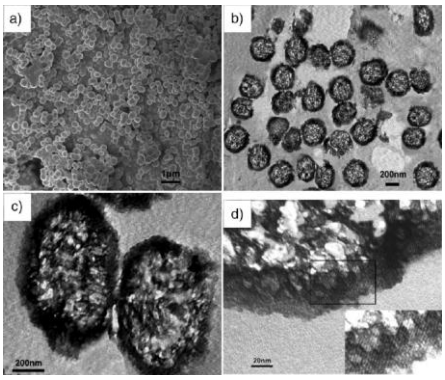

Figure 1. SEM image of as-synthesized (a) and TEM images of calcined sample (b-d).

calcination, the encapsulated iron species aggregate to Fe_2O_3 nanoparticles and the organic templates were removed, resulting in the formation of a nanoreactor with an ordered mesoporous shell and the macroporous core containing active Fe_2O_3 nanoparticles.

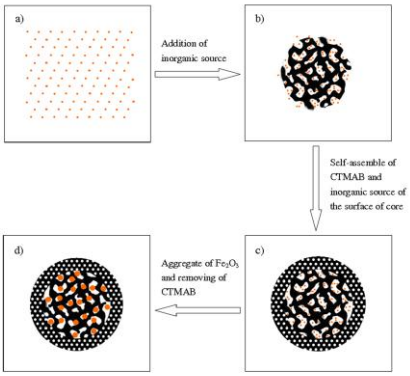

Figure 2. Proposed structure for the formation of the sample. (a) the aqueous solution containing iron species, (b) formation of foam-like macroporous core containing iron species, (c) formation of mesoporous shell in surface of macroporous core, and (d) nanoreactor with Fe_2O_3 nanoparticles.

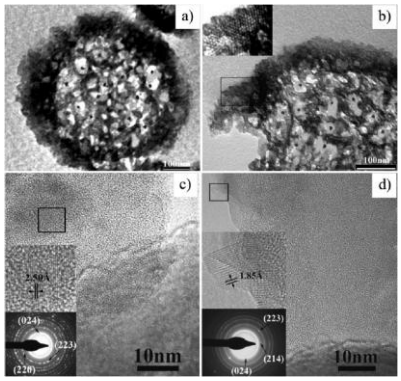

Figure 3. TEM and HRTEM images of calcined encapsulated Fe_2O_3 particles synthesized by various concentration of iron species (Figure 5a and 5c, Fe/CTAB = 10 and Figure 5b and 5d, Fe/CTAB = 5, molar rate).

The successful entrapment of Fe_2O_3 nanoparticles into the macroporous core was shown in Figure 3. The Fe_2O_3 nanoparticles exhibited a uniform size of 8-12 nm (Fig. 3a and 3b). Being larger than the entrance of mesoporous channels indicates that the nanoreactors can effectively prevent leaching of the active sites. Furthermore, these HRTEM images clearly exhibit that the sizes of Fe_2O_3 nanoparticles are gradually reduced with decreasing the concentration of iron species in the initial mixture of reactants. This indicates that the size of Fe_2O_3 nanoparticles by controlling the concentration of iron species in the initial mixture of reactants. Catalytic tests show that encapsulated Fe_2O_3 nanoparticles are very active for the catalytic conversion of phenol (22.5%). It is also noteworthy that recycled, encapsulated Fe_2O_3 nanoparticles still show comparable activities to that of the initial encapsulated Fe_2O_3 nanoparticles. For example, after 5 cycles, the encapsulated Fe_2O_3 still exhibits 90% of the initial activity.

Conclusions

The high activity and stability, and excellent recycling behavior of the encapsulated nanoparticles in the samples should directly be attributed to the unique core-shell synthesis of nanoporous materials with integral macro and mesoporosity. We believe that this method may open an exciting avenue for the preparation of hierarchically bimodal nanoporous materials with core-shell structures and for the design of nanoreactors with combined functionalities in the cores and the shells.

Acknowledgements: This work was supported by the Belgian Federal Government (Belspo PAI-IAP project, INANOMAT, P6/17), and Belgium-Viet Nam bilateral cooperation project, BL/13/V11). XYYang thanks FNRS for a “Chargé de recherche” position. BL Su thanks the China Education Ministry for “Changjiang chair visiting scholar” position at Wuhan University of Technology and Chinese central government for a position as “expert of the state” in the frame of “Thousand talents program”.

References

[1] X.-Y.Yang, Y. Li, G. Van Tendeloo, B.-L. Su, *Adv. Mater.* 21, 1368 (2009)
[2] X.-Y. Yang, A. Vantomme, A. Lemaire, F. Xiao , B.-L. Su, *Adv. Mater.* 18, 2117 (2006)

Incorporation of semiconductive polymer into mesoporous SBA-15 platelets: towards new luminescent hybrid systems

F. Cucinotta,[a] F. Carniato,[a] G. Paul,[a] S. Bracco,[b] C. Bisio,[a] S. Caldarelli[c] and L. Marchese[a]
[a]*DISTA and Nano-SiSTeMI Interdisciplinary Centre, Universitá del Piemonte Orientale A. Avogadro, Viale T. Michel 11, I-15121 Alessandria, Italy.*
[b]*Department of Materials Science, University of Milano-Bicocca, via R. Cozzi 53, Milan, Italy*
[c]*Aix Marseille Université, ISm2 UMR 6263, Campus de Saint Jérôme, Service 511 F-13013 Marseille*

Introduction

Organic optoelectronic devices are becoming commercially important in several fields, ranging from light-emitting diodes (OLEDs) to photovoltaic cells.[1] OLEDs based on semiconductive polymers are much cheaper to produce than their inorganic counterparts, can be operated with low voltages and their emissive color can be modulated. Although many progresses have been made in improving the semi-conductive performances of organic polymers, there are still drawbacks associated with the application of these materials, such as reduced fluorescence quantum yields and the tendency to photobleach in the presence of molecular oxygen. In order to circumvent these problems and increase both chemical and thermal stability of organic polymers, the design of hybrid structures containing an inorganic porous host represents a valid solution.[2] In this contest, this work presents a new hybrid luminescent system consisting of an electroluminescent polyphenylenevinylene (PPV) derivative, the Super Yellow copolymer (SY), incorporated into a plate-shaped mesoporous silica SBA-15. The physico-chemical behavior of the obtained hybrid material (named SY/SBA-15) (Fig. 1) will be also presented.

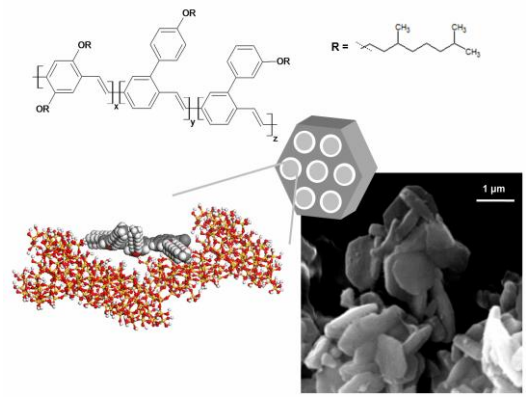

Fig. 1. Schematic view of the confinement of Super Yellow polymer into the nanochannels of SBA-15 platelets.

Experimental

The inclusion of Super Yellow copolymer (from Merck) into the channels of platelet SBA-15 crystals, prepared according to a formerly published procedure,[3] was performed by impregnation. Typically, 200 mg of SBA-15 powder were dispersed in 3 mL of anhydrous toluene and 1 mL of concentrated Super Yellow solution (6 mg × mL^{-1} in toluene) was added. The suspension was stirred at 50 °C under gentle nitrogen stream until solvent evaporation and the obtained material was washed with fresh toluene in order to remove the physisorbed copolymer.

Results and discussion

The physico-chemical properties of the SY/SBA-15 hybrid material were deeply investigated and compared with those of platelet SBA-15. The new hybrid composite reveals a decreased pore volume and size in comparison to the pure silica, confirming SY inclusion into the pores. Photoluminescence spectra of the hybrid system in isopropanol dispersion display red-shifted $\pi^* \leftarrow \pi$ transitions, respect to a pure SY solution. The emission of the composite broadens, peaking at 536 nm, and loses its vibrational structure, indicating that SY emissive and ground states are more distorted to each other than in solution, probably due to aggregation phenomena between the polymer chains within the mesoporous matrix. However, the chain aggregation is strongly reduced in comparison with a pure polymer film. Furthermore, the emission of the hybrid material is less sensitive to the presence of molecular oxygen and water than SY emission, as a consequence of a shielding effect of the SBA-15 channels. Photodegradation of SY in SBA-15 is strongly reduced (ca. 70%), respect to the bleaching a polymer film undergoes (ca. 25%) after 3 hours of light irradiation, confirming that oxygen diffusion into the mesoporous silica is significantly slowed (Fig. 2). Host-guest interactions involving SBA-15 silanols and aromatic rings of the polymer were studied by SS-NMR and IR spectroscopy.

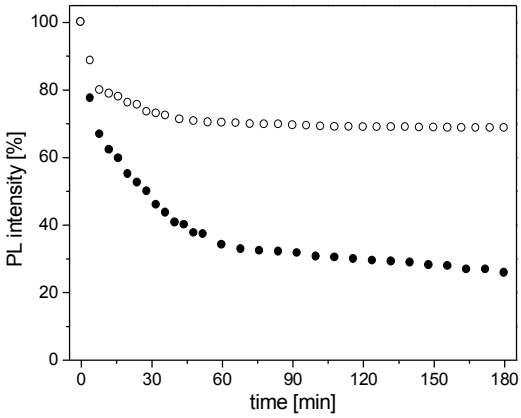

Fig. 2. Photoluminescence stability tests, carried out by irradiating at λ_{exc} = 400 nm a SY film (black dots) and a SY/SBA-15 film (white dots).

Conclusions

The new hybrid composite SY/SBA-15 displays decreased pore volume and size respect to pure platelet SBA-15 and the luminescence properties are consistent with a reduced aggregation in comparison with SY film. The material shows also remarkably increased photostability in comparison with pure organic film, which makes the hybrid composite a good candidate for the fabrication of LEDs with higher stability and operation lifetimes.

Acknowledgements

The financial support of the Regione Piemonte (CIPE 2006 Project, "Novel Nanostructured Materials for Light Emitting Devices and Application to Automotive Displays") is gratefully acknowledged. The authors thank Dr. Luca Bertinetti for the HRTEM analyses and Dr. Angiolina Comotti for her scientific support in the NMR results interpretation

References

[1] Sekitami, T. and Someya, T. Adv. Mater. 2010, 22, 2228.
[2] Angelos, S.; Johansson, E.; Stoddart, J. F. And Zink, J. I. Adv. Funct. Mater. 2007, 17, 2261.
[3] Chen, S.-Y.; Tang, C.-Y.; Chuang, W.-T.; Lee, J.-J.; Tsai, Y.-L.; Chan, J. C. C.; Lin, C.-Y.; Liu, Y.-C. and Cheng, S. Chem. Mater. 2008, 20, 3906.

Combinatorial synthesis of multifunctional MOF via a generic post-functionalization route. Application to acid/base catalysis.

M. Savonnet[1, 2], D. Bazer-Bachi[2], N. Bats[2], V. Lecocq[2], C.Pinel[1], D.Farrusseng[1]
[1]*Université Lyon 1, IRCELYON UMR 5256 CNRS; 2 avenue Albert Einstein; F-69626 Villeurbanne Cedex, France,* [2]*IFP Energies nouvelles Lyon, BP n°3, 69360, Solaize,France, david.farrusseng@ircelyon.univ-lyon1.fr*

Introduction

It is acknowledged that ultimately MOFs could mimic "enzymes" using "molecular recognition" concept to allow high chemio-, regio-, enantio-selectivity. We could indeed anticipate MOFs as potential "artificial enzymes" that can combine several properties at the nanometer scale in a concerted fashion. However to date, the number of MOFs with more than one reactive "catalytic" function is rather scarce. A key to address advanced MOF materials suitable for more sophisticated applications is to add functionalities of greater complexity in a controlled manner. The ability to modify the chemical environment of the cavities within MOFs would allow tuning of the interactions with guest species, and serve as a route to tailor the chemical reactivity of the framework. However, the introduction of reactive chemical functions by self-assembly methods is not a trivial task.
The post-synthetic modification (PSM) using covalent type grafting methods has seen outstanding evolution in the recent months. Nevertheless, methods developed so far are not very generic since they can be applied either to the most robust MOF due to relative harsh conditions or to linear or ramified alkyl (non functional) chains.

Experimental

We have recently reported an original PSM method starting from amino derived MOFs [1]. The first step consists in converting the amino group into azide (N_3). Without isolation nor purification, the desired functionalized material is obtained by grafting the corresponding alkyne using "Clik Chemistry".

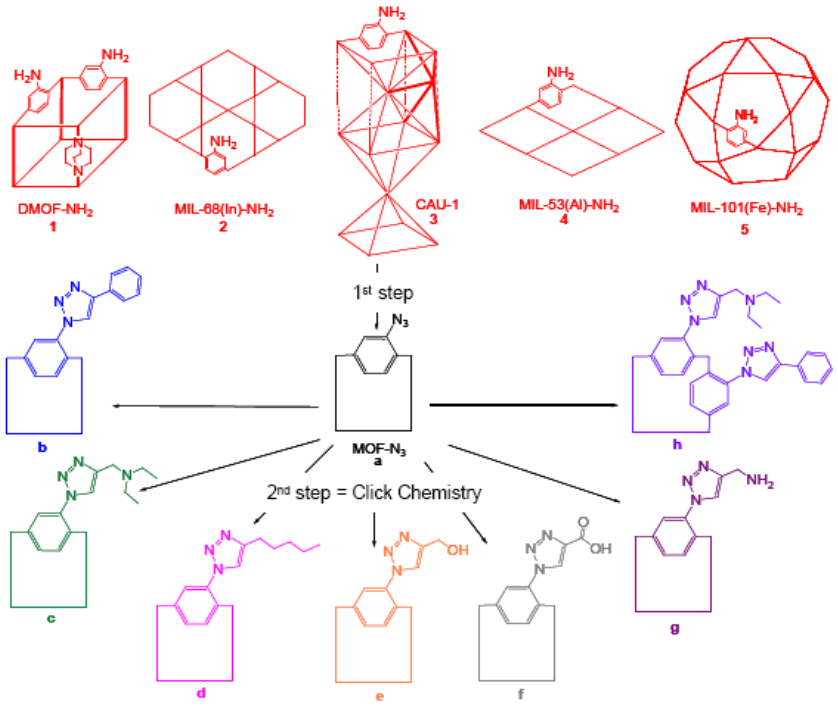

Figure 1.Strategy for the generalization of functionalized MOFs

Results and discussion

In this contribution, we show that our method can be applied to all kind of MOFs with respect to pore size range (micro to meso), chemical stability (low to high) and different degree of - structural flexibility and to all kind of grafted chemical functions (acid, coordinative, base, aromatic, aliphatic, hydrophilic). A diverse library of 48 original MOFs was synthesized and characterized.

- To the best of our knowledge, this work reports for the first time the synthesis of two dimensional combinatorial library of functionalized MOFs.
- We also show that we can control the grafting rate from 10 to 100%.
- For the first time, we report the effect of the grafting rate on the porous volume of the host MOF
- This method was also used to engineer catalytic MOFs for the transesterification of ethyldecanoate with methanol. Results show the linear increase of conversion with the increase of the degree of modification. The best performances are obtained for a multi-functionalized MOF which combined an optimum basicity/hydrophoby balance.
- Finally, new solutions to engineer catalytic site isolation will be presented.

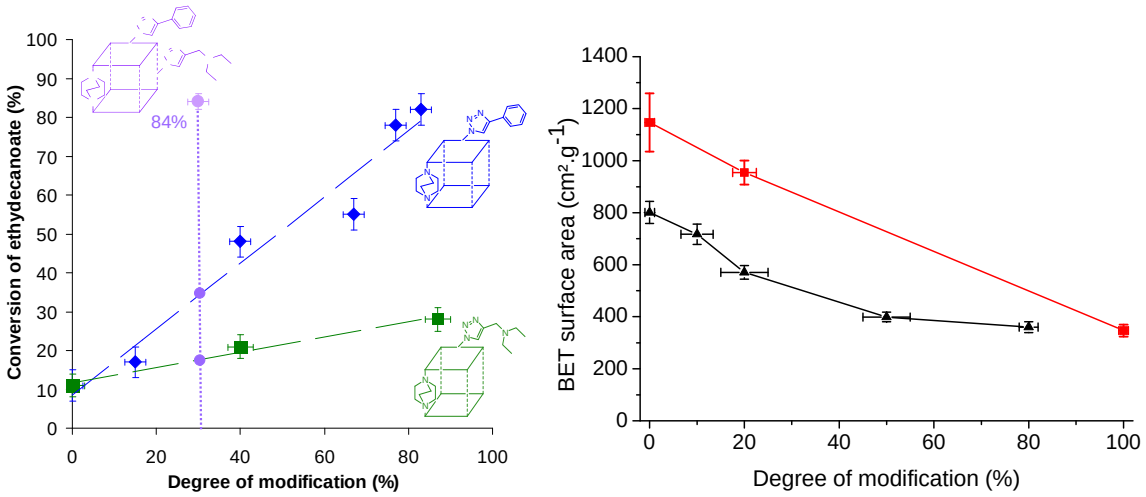

Figure 2.Effect of the degree of functionalization on ethyldecanoate conversion with methanol at 130°C after 20 h (left) and on BET (right)

Conclusions

In conclusion, this original PSM technique provides a high level of control for the engineering of tailor-made and powerful catalysts. Based on this study, we believe that the knowhow and knowledge developed in Polymer Science (“Click-Chemistry”) [2] will open new doors for the design of multifunctional catalysts.

Acknowledgements

We thank Aurélie Camarata for the technical work, along with IRCELYON and IFP Energies nouvelles.

References

[1] Savonnet, M. et al, Journal of the American Chemical Society, 132 (2010), 132, 4518-4519
[2] Hoogenboom, R., Meier, M. A. R., Schubert, U. S., Macromolecular Rapid Communications **2003**, *24*, 16-32

High-Throughput Study of Highly Porous Al-based MOFs

N. Stock, T. Ahnfeldt and H. Reinsch
Christian-Albrechts-Universität zu Kiel, Germany, stock@ac.uni-kiel.de

Introduction

Porous metal-organic frameworks built up from Al^{3+} ions and aromatic polycarboxylate linkers are well known as materials with high specific surfaces and noteworthy thermal stabilities. Prominent examples are the compounds Al-MIL-53, -69, -96, -100, and -110 [1, 2]. The synthesis of these compounds was previously achieved using aqueous reaction media. We have recently started a systematic study on the use of other solvents employing our high-throughput (HT) set-up comprising conventional as well as microwave heating [3-5]. In addition to the discovery of new phases containing new inorganic bricks, we were interested in the synthesis of isoreticular compounds of the well known Al-based MILs, i.e. incorporating larger organic or functionalized organic linker molecules. The latter should permit post-synthetic modification reactions. Here, we present the results on the HT investigation of Al^{3+} containing metal carboxylates.

Experimental

For the discovery and synthesis optimization in house developed high-throughput methods have been used to systematically investigate the parameter space [6]. Multiclaves containing 24 and 48 parallel reactor with a maximum volume of ca. 2.5 ml and 300 µl were used and the starting materials manually weighed in or dispensed. Automated characterization was carried out employing a high-throughput X-ray powder diffractometer system. Synthesis scale up was accomplished for selected systems up to the gram scale.

Results and discussion

The systems Al^{3+} / arylcarboxylic acid / solvent / base with solvent = H_2O, methanol, ethanol, isopropanol, acetonitrile or DMF were investigated in detail. In addition to terephthalic acid or trimesic acid, larger organic acids (naphthalenedicarboxylic acid or benzenetribenzoic acid) as well as functionalized organic acids were employed. The choice of methanol as solvent led to two new families of aluminium carboxylates $[Al_8(OH)_4(OCH_3)_8(BDC)_6]\cdot xH_2O$, CAU-1, and $[Al_2(OCH_3)_4BDC]\cdot xH_2O$, CAU-3, respectively (CAU = Christian-Albrechts-Universität) [3]. The structure of these compounds was determined from X-ray powder diffraction data. They contain unprecedented octameric (Fig. 1a) and dodecameric (Fig. 1b) Al-containing bricks, respectively, which are connected through the dicarboxylate ions to twelvefold-connected nets. The systematic investigation of the phase space using high-throughput methods allowed the synthesis of isoreticular compounds of CAU-1 and CAU-3 containing larger and/or functionalized linker molecules. Thus the porosity, i.e. the micropore volume and the specific surface, as well as the pore chemistry, e.g. the hydrophobicity, could be varied. Amino-functionalized CAU-1 was also used for post-synthetic modification reactions.

Changing the solvent to DMF and using the tritopic linker molecule benzenetribenzoic acid (H_3BTB), $[Al(BTB)]\cdot xH_2O$, named CAU-4, was also discovered. The synthesis was optimized changing chemical and process parameters and the final synthesis procedure was scaled up to the gram scale. CAU-4 is thermally stable up to 400 °C in air and exhibits an apparent specific BET-surface of 1520 m^2/g and a micropore volume of 0.61 cm^3/g. A

structural model was developed using the Universal Force Field as implemented in Materials Studio. The framework structure consists of isolated [AlO_6]-octahedra, which are bridged by carboxylate groups of the BTB-linker. These chains are connected by the tritopic aromatic building blocks, to form one-dimensional hexagonal channels with a diameter of ca. 10 Å.

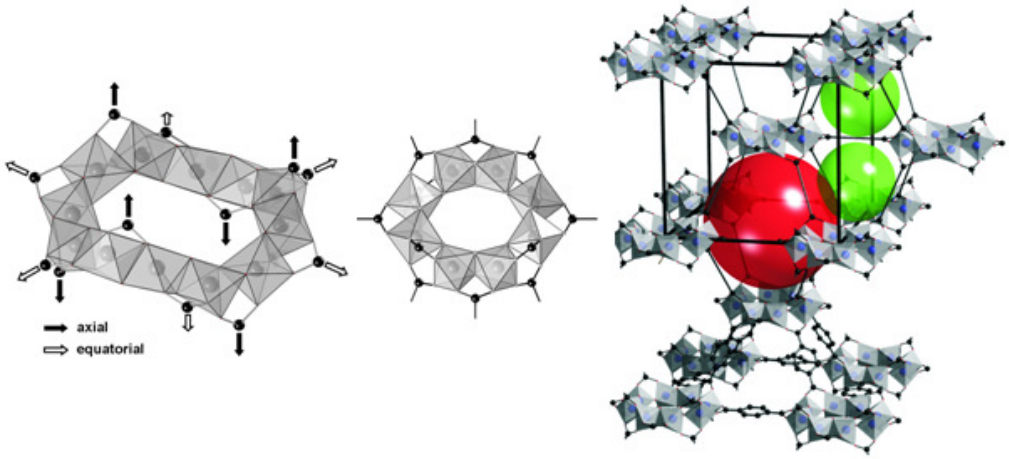

Figure 1. Al-containing bricks observed in CAU-3 (left) and CAU-1 (middle) and structure of CAU-1 (right). The octameric bricks are connected to 12 other units through the aminoterephthalate linker. Thus, distorted octahedral (red) and tetrahedral (green) cages are formed. For clarity some of the phenyl rings are replaced by a straight line.

Conclusions

The solvent employed in the systematic investigation of Al-containing MOFs has a profound influence on the structure formation. New Al-O clusters can be observed that lead to unprecedented open-framework structures with accessible porosity.

Acknowledgements

The work has been supported by the DFG (SPP 1362). The research leading to these results has received funding from the European Community's Seventh Framework Programme (FP7/2007-20013) under grant agreement n° 228862".

References

[1] C. Volkringer, D. Popov, T. Loiseau, G. Ferey, M. Burghammer, C. Riekel, M. Haouas, F. Taulelle, *Chem. Mater.* **2009**, *21*, 5695.
[2] C. Volkringer, T. Loiseau, M. Haouas, F. Taulelle, D. Popov, M. Burghammer, C. Riekel, C. Zlotea, F. Cuevas, M. Latroche, D. Phanon, C. Knöfelv, P.L. Llewellyn, G. Ferey, *Chem. Mater.* **2009**, *21*, 5783.
[3] T. Ahnfeldt, N. Guillou, D. Gunzelmann, I. Margiolaki, T. Loiseau, G. Ferey, J. Senker, N. Stock, *Angew. Chem.* **2009**, *121*, 5265.
[4] T. Ahnfeldt, D. Gunzelmann, T. Loiseau, D. Hirsemann, G. Férey, J. Senker, N. Stock, *Inorg. Chem.* **2009**, 48, 3057-3064.
[5] S. Bauer, C. Serre, T. Devic, P. Horcajada, J. Marrot, G. Férey, N. Stock, Inorg. Chem. **47** (2008) 7568.
[6] N. Stock, *Micropor. Mesopor. Mater.* **2010**, *129*, 287.

The role of the solvent on the dimensionality of the Mg-MOF investigated by NMR spectroscopy

Mojca Rangus[1], Matjaž Mazaj[1], Gregor Mali[1], Tadeja Birsa Čelič[1] and Venčeslav Kaučič[1,2]
[1]*National Institute of Chemistry, Hajdrihova 19, SI-1000 Ljubljana, Slovenia;* [2]*Faculty of chemistry and chemical technology, University of Ljubljana, Aškerčeva 5, SI-1000 Ljubljana, Slovenia;* mojca.rangus@ki.si

Introduction

Hybrid inorganic-organic coordination polymers or metal-organic framework (MOF) materials represent an extensive group of materials where inorganic building units are interconnected through rigid organic molecules (typically polycarboxylates) forming crystalline structure [1,2]. In the last decade they have been growing increasingly popular because of their vast potential in a variety of applications [3] such as heterogeneous catalysis, ion exchange, gas separation and storage, heat storage and drug delivery. In an attempt to synthesise new structures, the emphasis was also put on the variation of the solvent. The influence the solvent has on the structure and dimensionality was studied previously [4] and it was determined that the solvent can play an important role in the structure formation.
In this work we discuss the role of the solvent on the structure and formation of some new magnesium tricarboxylate phases.

Experimental

The synthesis of all compounds was carried out with constant ratios of magnesium acetate tetrahydrate ($Mg(ac)_2.4H_2O$, 99%, Fluka) and 1,3,5-benzenetricarboxylic acid (BTC, 95%, Aldrich), while the molar ratios of ethanol (EtOH, 99%, Aldrich) and deionised water varied. The components were mixed in a glass beaker and the white gel was then transferred to Teflon-lined stainless-steel autoclaves and solvothermally treated at 423 K for 24 h. Depending on the H_2O:EtOH ratio we obtained mononuclear complex (0D) $[Mg(H_2O)_4(BTC\text{-}H_2)_2]$, one- (1D) $[Mg_3(BTC)_2(H_2O)_{12}]$, two- (2D) $[Mg_2(H\text{-}BTC)(OH)_2(H_2O)_2]$ or three-dimensional (3D) Mg tricarboxylate structure [Mg(H-BTC)]. The structures of all four final materials were solved from single-crystal X-ray diffraction data collected on Nonius Kappa diffractometer with MoKα radiation (λ = 0.71073 Å). Mononuclear complex was proven to be isostructural to the $[Fe(H_2O)_4(BTC\text{-}H_2)_2]$ [5].
^1H, ^{13}C and ^{25}Mg NMR measurements were done on a Varian VNMRS 600 MHz (14.1 T) spectrometer equipped with a 3.2 mm T3 MAS solids probe.
The size and morphology of the crystals in the product were studied with scanning electron microscope Zeiss Supra™ 3VP.

Results and discussion

We used ^1H, ^{13}C and ^{25}Mg liquid and solid-state NMR spectroscopy to observe the framework formation and crystal growth of Mg MOF materials. We were able to observe the assembly of individual building blocks into coordination polymers during the synthesis procedure. Four distinct magnesium-based trimesates with different dimensionalities synthesised at different reaction conditions described in experimental section, were studied (Figure 1).

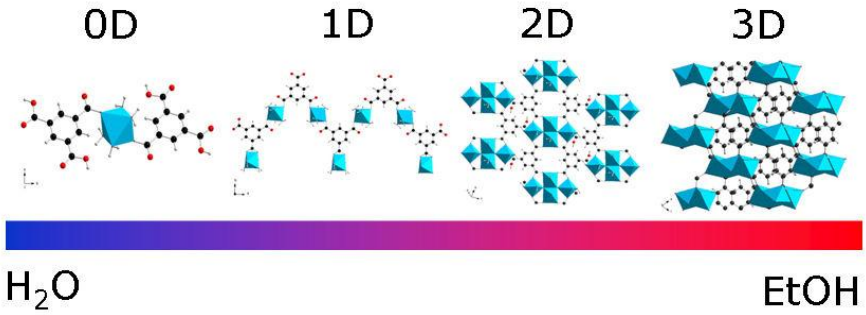

Figure 1. The dimensionality of the magnesium tricarboxylate framework depends solely on the molar ratio between water and ethanol in the solvent.

We were able to determine that the crucial difference in the framework formation takes place already in the initial mixture of the reagents, before heating. 1,3,5-benzenetricarboxylic acid reacts with Mg ions and forms an unordered structure that closely resembles the final crystalline product.
^{25}Mg NMR spectroscopy of Mg acetate dissolved in different H_2O:EtOH mixtures showed that the crucial factor determining the dimensionality of the final crystallite is the interaction between the solvent and the magnesium ions. Magnesium acetate dissolves well in water and Mg ions in the solution are very mobile which results in narrow signals in ^{25}Mg NMR spectra. Dissolution of $Mg(CH_3COO)_2$ in the solvent with higher ratios of ethanol is lower and the signals in NMR spectra are broadened. We believe that the same magnesium clusters or complexes that are present in the final compounds are formed, which broadens the ^{25}Mg NMR signals.

Conclusions

The solvent composition of the synthesis gel influences the dimensionality of the obtained crystalline MgMOF system. More precisely, as shown by ^{25}Mg NMR spectroscopy, the dimensionality of the system is determined by the interaction of magnesium ions with the solvent. By understanding the principles behind the framework formation we can tailor the structure of MOFs.

Acknowledgements

This work was supported by the Slovenian Research Agency research programme P1-0021.

References

[1] Férey, G., Hybrid porous solids: past, present, future, Chemical Society Review, 37 (2008), 191-214
[2] Kitagawa, S., Kitaura, R. and Shin-ichiro, N., Functional porous coordination polymers, Angewandte Chemie International Edition, 48 (2004), 2334-2375
[3] Cheetham, A.K., Rao, C.N.R. and Feller, R.K., Structural diversity and chemical trends in hybrid inorganic–organic framework materials, Chemical Communications, (2006), 4780-4795
[4] Fu, A.-Y., Jiang, Y.-L., Wang, Y.-Y., Gao, X.-N., Yang, G.-P., Hou, L., Shi, Q.-Z., DMF/H_2O Volume Ratio Controls the Syntheses and Transformations of a Series of Cobalt Complexes Constructed Using a Rigid Angular Multitopic Ligand, Inorganic Chemistry, 49 (2010), 5495-5502
[5] Riou-Cavellec, M., Albinet, C., Greneche, J.-M., Ferey, G., Study of the iron/trimesic acid system for the hydrothermal synthesis of hybrid materials, Journal of Materials Chemistry, 11 (2001), 3166-3171

Preparation of mesoporous organosilicas containing Tröger base builders. Textural and catalytic implications.

Estíbaliz Merino, Evelyne Poli, Urbano Díaz, Daniel Brunel, Avelino Corma
Instituto de Tecnología Química (CSIC-UPV) Universidad Politécnica de Valencia, Av. De los Naranjos s/n, 46022-Valencia, Spain, e-mail: acorma@itq.upv.es

Introduction

There are different strategies to covalently incorporate organic groups in the silica network of the nanoporous materials like to anchor the organacatalyst onto previously synthesized mesoporous materials by post-synthesis grafting methods and co-condensation processes in one-pot synthesis from mono-silylated precursors. However, the hybrid grafted samples may present important drawbacks for the partial blockage of pores and the undesired site-site interactions. There is a third route to obtain organic-inorganic hybrid materials that allows preparing less ordered mesoporous hybrid materials. The soft synthesis conditions together with the higher flexibility exhibited by the network associated to the non-ordered organization may encompass some of the mean problems entailed by the grafted materials or by the periodic mesoporous systems.

Experimental

The bis-silylated Tröger-base precursor was synthesized in two steps from 4-iodoaniline with formaldehyde and rhodium-catalyzed disilylation of the diodo derivative with triethoxysilane:

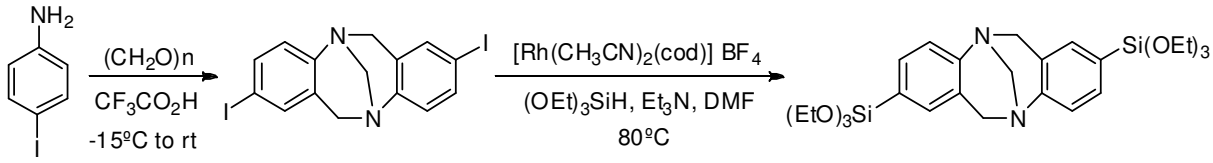

In Table 1 the chemical composition of the synthesized hybrid porous materials studied is shown.

Sample	Elemental analysis molar N/C exp[a]	Organic content[b] TB mmol/g $_{hybrid}$ (TB mmol/g $_{SiO2}$)	Thermogravimetric analysis TB mmol/g $_{hybrid}$ (TB mmol/g $_{SiO2}$)	Solid NMR T/T+Q (TB mmol/g$_{SiO2}$)
SBA15-TBG	0.10	0.62 (0.8)	1.08 (1.35)[c]	0.08 (0.6)
Si-TB-50A	0.14	1.75 (3.1)	2.33 (4.15)	0.30 (2.5)
Si-TB-50F	0.12	1.74 (3.0)	2.17 (3.7)	0.32 (2.7)

[a] Theoretical molar N/C ratio 0.13. [b] Determined by elemental analysis (N% and C%) considering dry sample (or pure silica content). [c] corresponding to 0.93 molecules per nm^2

Table 1. Chemical composition of the hybrid materials

Results and discussion

Here we prepared mesoporous organosilica hybrid materials based on Tröger base (TB) units, using first by a post-synthesis grafting method[1] and secondly through two one-pot sol-gel route in presence[2] or not of structure directing agents (SDAs) molecules.[3] These as-synthesized materials corresponds to three different types of nanostructured solids: (a) Troger's base-tethered SBA-15 silica resulting from mesoporous silica surface grafted with bis-silylated TB, (b) periodic mesoporous organosilicas featuring hexagonal type structure with rigid walls through self-assembling process, and (c) high surface orderedless mesoporous materials with flexible structure obtained by NH_4F sol-gel route in soft conditions, *i. e.* neutral pH and low temperature.[3] These hybrid mesoporous materials were extensively characterized, and the catalytic performance for a base catalyzed Knoevenagel reaction has been correlated with their physicochemical characteristics.[4]

Entry	Catalyst	Conversion %			Yield %	TON 2 h
		1 h	2 h	8 h		
1	TB	52.5	73.7	100	75.8	42.5
2	Si-TB-50F	40.5	71.6	99.9	99.9	41.4
3	Si-TB-50A	38.4	60.5	99.8	99.0	35.1
4	SBA15-TB-G	27.6	43.3	91.0	99.1	24.9

Table 2. Catalytic activity of the synthesized materials for the Knoevenagel reaction.

Conclusions

Tröger-base units have been covalently incorporated into mesoporous organosilicas framework for the first time. The incorporation of this organic builder into the structure was done through different synthetic processes from the bridged silylated precursor. The activity of these materials was tested in Knoevenagel reaction. The disordered hybrid materials obtained through the fluoride-assisted sol-gel method show the best performance. The hybrid mesoporous organosilica materials containing Troger´s base show a remarkable stability as catalyst during their recycles.

Acknowledgements

We are thankful financial support by Consolider- Ingenio 2010 (MULTICAT project). E.M. thanks Ministerio de Ciencia y Innovación by the support through Juan de la Cierva contract.

References

[1] Martin, T.; Galarneau, A.; Brunel, D.; Izard, V.; Hulea, V.; Blanc, A.C. Abramson, S.; Di Renzo, F.; Fajula, F., Sud. Surf. Sci. Catal., 2001, 135, 4621-4628.
[2] Mokaya, R., Jones, W., J. Mater. Chem. 1998, 8, 2819-2826.
[3] Díaz, U., García, T., Velty, A., Corma, A., J. Mater. Chem., 2009, 19, 5970-5979.
[4] Poly, E., Merino, E., Díaz, U., Brunel, D., Corma, D., J. Phys. Chem. C, submitted.

Mesopores Generation in ZSM-5 Crystals by Nuclear Tracks Imprinting

V. Valtchev,[a*] E. Balanzat,[b] V. Mavrodinova,[c] I. Diaz,[d] J. El Fallah,[a] J.-M. Goupil[a]

[a] *Laboratoire Catalyse & Spectrochimie, ENSICAEN, Université de Caen, CNRS, 6 boulevard du Maréchal Juin, 14050 Caen, France; E-mail: valtchev@ensicaen.fr*
[b] *CIMAP Centre de recherche sur les Ions les Matériaux et la Photonique, UMR 6252 CEA/CNRS/ENSICAEN, BP 5133 14070 CAEN, France*
[c] *Institute of Organic Chemistry, Bulgarian Academy of Sciences, Acad. Bonchev str., Sofia 1113, Bulgaria*
[d] *Instituto de Catálisis y Petroleoquímica, CSIC, C/Marie Curie 2, Cantoblanco, 28049 Madrid, Spain*

Introduction

Extraordinary selectivity of zeolites is often coupled with undesirable effects as diffusion limitation, pore blocking and catalysts deactivation. Two major avenues are considered in order to circumvent these drawbacks and fully explore the potential of zeolitic materials, namely synthesis of nanocrystals and preparation of conventional micron-sized zeolite crystals comprising larger (meso-)pores. Thermal and chemical stability of zeolite nanocrystals is not always comparable of their micron-sized counterparts. In addition, zeolite nanoparticles are still not readily available. Consequently, a lot of research was dedicated to the control formation of mesopores in zeolite crystals. The different approaches used to generate mesopores in zeolite crystals can be classified into two groups: i) bottom-up: sacrificial templates are incorporated in zeolite crystal during crystallization process and eliminated by post-synthesis treatment; and ii) top-down: wet chemical etching is used to "drill" mesopores. None of these approaches allows the generation of controlled in pore size and pore density network of mesopores ensuring access to the entire micropore volume of a zeolite crystal.

The present study reports on the use of a combination of a physical and a chemical approach that provide hierarchical zeolite crystals with ordered system of mesopores.

Experimental

ZSM-5 crystals were prepared in fluoride containing system from a gel with composition: $0.2(C_3H_7)_4NBr{:}0.07Al_2O_3{:}1.0SiO_2{:}\ 0.58NH_4F{:}15H_2O$ at 170°C for 10 days.

Latent track formed upon ^{238}U irradiation (GANIL,Caen) were developed by 0.5 wt. % HF acid treatment at room temperature for 5 min. The liquid:solid ratio was 50:1. As-synthesized and treated materials were characterization by X-ray diffraction (X'Pert Pro, PANalytical) scanning (TESCAN) and transmission (JEOL JEM 2000FX) electron microscopy, N_2 adsorption (Micromeritics 2010 ASAP). The catalytic tests were carried out in a fixed-bed flow reactor at atmospheric pressure and reaction temperature of 623 K. N_2 carrier gas was passed through a saturator filled with m-xylene and equilibrated at 293.2 K so as reactant partial pressure of 0.9 kPa to be attained. On-line analysis of the reaction products has been performed using HP-GC with 25m FFAP capillary column.

Results and discussion

The new preparation method reported here is based on the preferential etchability of latent nuclear tracks. More precisely the preparation of mesopores in zeolite crystals includes two stages: i) exposing zeolite crystals to a flow of high energy ions for inducing nuclear tracks; and ii) etching the nuclear tracks to create mesopores. An important feature of the technique is that one single particle is sufficient to create a damaged zone in zeolite crystal, which is characterized with high free energy. Substantially different etching velocity of the ion track

and the intact part of the crystals allows pore formation to be controlled. Thus, the physical treatment tracks down the pore formation during the following wet chemical treatment.
The method is exemplified by the formation of mesopores in ZSM-5 crystals. The formation of mesopores of heavily intergrown aggregates is difficult to be studied. Consequently, well shaped single crystals grown in fluoride media were employed in order to clearly visualize the mesopores issued from the nuclear track imprinting. The size of the crystals was about 5 µm along the *c* axis. Zeolite crystals were exposed to ^{238}U ion beam with fluencies corresponding to an average distance between ion impacts of 230, 700 and 1400 nm. The irritated samples were then etched with diluted HF acid and thoroughly washed with distilled water. XRD patterns of etched samples did not show any differences with the parent as-synthesized sample. The transmission electron microscopy (TEM) investigation revealed that the mesopores diameter is constant along the crystal length (Figure 1A,B). The formation of parallel mesopores of similar size crossing the entire zeolite crystals is a sound prove for the decisive effect of the ion beam treatment on the following chemical extraction step.
After calcination the resultant materials with average distance between pores of 230, 700 and 1400 nm were subjected to catalytic tests in the reaction of m-xylene conversion. The catalytic performance of the material with average mesopore distance of 230 nm shows much higher m-xylene conversion in respect to the initial non-treated ZSM-5 catalysts and the two materials with less mesopores per unit zeolite volume. Obviously, the procedure applied to develop denser inter-crystalline mesoporosity has had more beneficial effect on the catalytic behavior (Figure 1C).

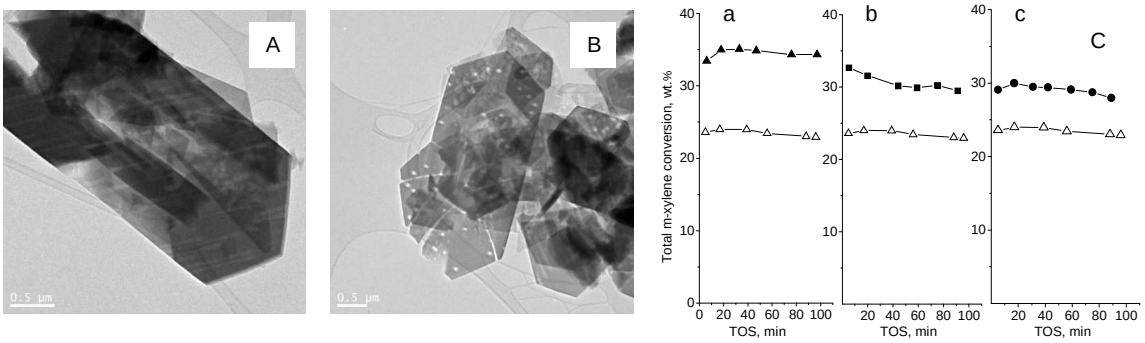

Figure 1. TEM micrographs of ZSM-5 crystals with ordered systems of mesopores parallel to 010 (A) and 100 (B) obtained by ^{238}U irradiation followed by diluted HF acid treatment; (C) Total m-xylene conversion as a function of the time on stream over the initial ZSM-5 sample (empty triangles) and the mesoporous zeolites with an average distance between the secondary pore system of 230 nm (a), 700 nm (b) and 1400 nm (c).

Conclusions

In conclusion, the presented study proved the possibility to form uniform parallel mesopores in zeolite crystals. The mesopore formation was pre-determined by creation of defect zones in the crystals vulnerable to chemical attack. High energy ^{238}U ion beam was employed to form latent track in the crystals, which were further subjected to attack with diluted HF solution and thus developed to uniform in size mesopores.
At present, the most evident application of hierarchical zeolites is in the area of heterogeneous catalysis where crystalline microporous solids with ordered system of mesopores can be used as model materials. Besides in the area of heterogeneous catalysis such materials are expected to show superior performance as detection media of sensors and electrodes.

Acknowledgements

V.V acknowledges the financial support from the program ANR – HiZiCOKE (contract No. 723).
V.V and I.D. are thankful for the financial support in the framework of France - Spanish bilateral program PICASSO (Spanish Ministry of Science and Innovation - projects CTQ2006-06282 and HF-2008-0066).

Modeling and theoretical studies

FEZA 2011

Effect of fluorine on the self-aggregation behaviour of aromatic molecules in the synthesis of microporous aluminophosphates

Luis Gómez-Hortigüela[*a,b], Fernando López-Arbeloa[c], Furio Corà[b], Joaquín Pérez-Pariente[a]

[a] *Instituto de Catálisis y Petroleoquímica-CSIC, c/ Marie Curie 2, 28049, Cantoblanco, Madrid, Spain.* [b] *Department of Chemistry, 20 Gordon Street, University College London, WC1H 0AJ, London, United Kingdom.* [c] *Departamento de Química-Física, Universidad del País Vasco-EHU, Apartado 644, 48080 Bilbao, Spain. Email: lhortiguela@icp.csic.es*

Introduction

The synthesis of crystalline microporous materials usually requires the presence of organic molecules that act as structure-directing agents (SDAs). To date, a large number of organic molecules of different sizes and shapes has been successfully used as SDAs. However, their structure-directing action has been invariably based on single molecular units; supramolecular chemistry has only rarely been mentioned, in contrast to the wide use of supramolecular arrangements in the synthesis of ordered mesoporous materials.

In recent years, a new concept in structure direction has been proposed [1,2], which uses the supramolecular chemistry of aromatic molecules, able to self-assemble through π-π type interactions, in order to get larger supramolecular structure-direction entities in a search for large-pore microporous structures. In particular, we have studied the structure direction behaviour of benzylpyrrolidine (BP) and (S)-N-benzylpyrrolidine-2-methanol (BPM) in the synthesis of aluminophosphates. Through a combined study based on fluorescence spectroscopy and molecular simulations, we observed that although both molecules self-assemble during the synthesis, only BPM forms supramolecular entities able to accommodate within the one-dimensional pores of AlPO-5; instead, BP forms differently oriented dimers whose dimensions are too large to enter the AlPO-5 porous network. We now study the effect of fluorine on the supramolecular behaviour of BP and BPM during the synthesis of AlPO-5.

Experimental

Hydrothermal synthesis of AlPO-5 materials was carried out with using BP or BPM and their corresponding ortho- or meta-fluorinated derivatives as SDAs. The obtained solids were characterized by XRD, TGA, elemental analysis and fluorescence spectroscopy. A computational study based on molecular mechanics of the aggregation behaviour of the molecules in solution was performed in order to understand the experimental observations.

Results and discussion

All the SDA molecules studied directed the crystallization of AlPO-5 (AFI). Fluorescence spectroscopy results showed no notable differences in the aggregation behaviour of the BP derivatives as a function of the fluorine presence. A low concentration of self-assembled dimers are found within the AlPO-5 structure regardless of the fluorine presence and position, indicating that F in BP is not able to modify its aggregation behaviour I : BP tends to form dimers with the pyrrolidine rings oriented in the same side in aqueous solution, unable to accommodate within the AFI channels, thus resulting in a major incorporation of monomers. However, an important difference is observed with the BPM fluorinated derivatives. BPM tends to incorporate as dimers within the AFI structure since these molecules self-assemble with the pyrrolidine rings in opposite sides due to the hydrophilic nature of their hydroxylated rings. Interestingly, fluorine dramatically changes this aggregation behaviour: the presence of fluorine, both in meta- and ortho- positions, leads to a notable decrease of the incorporation of dimers within the AFI structure. A computational study showed that meta-F tends to form larger (non-dimeric) aggregates of BPM due to a strong interaction between F atoms of different molecules, which are too large to be incorporated within the AFI channels; instead, ortho-F tends to decrease the self-assembling of BPM in solution. Both observations result in a preferential inclusion of monomers within the AlPO-5, explaining the experimental results.

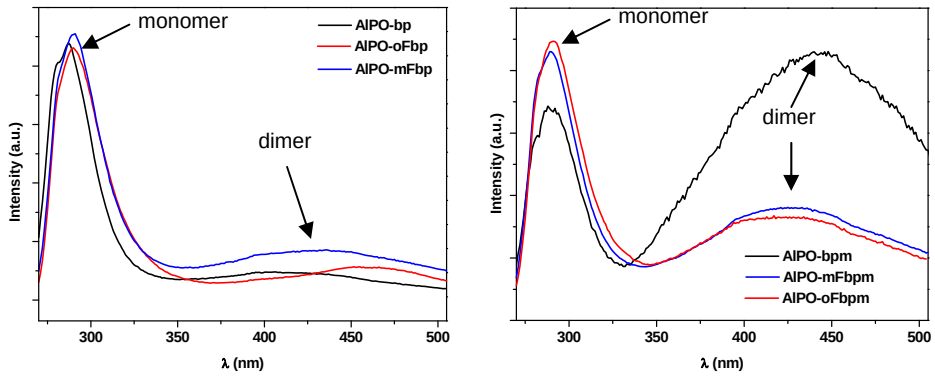

Figure 1. Fluorescence emission spectra (λ_{exc}=260 nm) of BP (left) and BPM derivatives (right) (non-fluorinated: black line; ortho-F SDA: red line; meta-F SDA: blue line).

Acknowledgements

Financial support of the Spanish Ministry of Education and Science (project CTQ2006-06282) is acknowledged. We thank Accelrys for providing their software and Centro Técnico de Informática-CSIC for running the calculations.

References

[1] Gómez-Hortigüela, L., Hamad, S., López-Arbeloa, F., Pinar, A.B., Pérez-Pariente, J., Corà, F., Molecular insights into the self-aggregation of aromatic molecules in the synthesis of nanoporous aluminophosphates: a multilevel approach, J. Am. Chem. Soc. 131 (2009), 16509-16524.

[2] Corma, A., Rey, F., Rius, J., Sabater, M.J., Valencia, S., Supramolecular self-assembled molecules as organic directing agent for synthesis of zeolites, Nature 431 (2004), 287-290.

Computational Design and Synthesis of Electroactive Poly Oxo Metalate Organic Frameworks (POMOFs); Towards new catalysts for H_2 production

L. M. Rodriguez Albelo,[a] R. Ruiz-Salvador,[a] R. Ngo Biboum,[b] L. Nadjo,[b] B. Nohra,[c] H. El Moll,[c] P. Mialane,[c] B. Keita,[b,*] A. Dolbecq[c,*] C. Mellot-Draznieks[d,*]

[a] *Zeolite Engineering Laboratory, Institute of Materials Research and Engineering (IMRE), University of Havana, Havana, 10400, Cuba.*
[b] *Laboratoire de Chimie Physique, Groupe d'Electrochimie et de Photoélectrochimie, UMR 8000, CNRS, Université Paris-Sud, Bâtiment 350, 91405 Orsay cedex, France.*
[c] *Institut Lavoisier de Versailles, UMR 8180, Université de Versailles Saint-Quentin en Yvelines, 45 Avenue des Etats-Unis, 78035 Versailles cedex, France*
[d] *Department of Chemistry, University College London, 20 Gordon St., London, WC1H 0AJ, UK.*

Introduction

The last decade has seen an unparalleled development of the rational design of MOFs that originates in reticular chemistry concepts.[1] In this very active context of hybrid framework materials or metal organic frameworks (MOFs),[2] polyoxometalates (POMs), a large family of soluble anionic metal oxide clusters of *d*-block transition metals in high oxidation states, constitute ideal building blocks for targeting new multifunctional materials due to their wide range of magnetic,[3] redox,[4] and catalytic properties. [5] In particular, the redox properties of POMs together with their ability to form metal organic frameworks as POMOFs with a variety of organic linkers provides a unique impetus for the synthesis of electroactive open-framework materials,[6] a research area still scarcely explored. Here, we sought to combine the flexibility with which MOFs may be computationally designed with the extensive electrochemical activity of POMs that may be exploited when they are retained in a robust framework. Our general philosophy is to use the ε-Keggin ion as an inorganic building block to (i) computationally explore its supramolecular assembly with various organic linkers, (ii) achieve the synthesis of stable architectures and (iii) finally explore the electroactivity of as-synthesized structures.

Computational and experimental methods

Computational method: We use here the ε-Keggin POM $\{\varepsilon\text{-}PMo^{V}_{8}Mo^{VI}_{4}O_{40-x}(OH)_xZn_4\}$ as the inorganic building blocks capped by four Zn^{2+} metallic ions. Its tetrahedral symmetry allows its combination with bidendate linkers such as 1,4 benzene dicarboxylic acid (**bdc**) or imidazolate (**im**), to target 4-connected networks analogues to zeolites or dense minerals (coesite, cristobalite, quartz). Alternatively, the choice of a tridentate linker such as 1,3,5 benzene tricarboxylic acid (**btc**) allows the construction of new (3,4) connected nets. Lattice energy minimizations allow us to explore the energy landscape of polymorphs in each {linker/ε-Keggin} system and identify the most stable topologies.
Experimental methods: Hydrothermal syntheses were carried out in 23 mL polytetrafluoroethylene lined stainless steel containers under autogenous pressure. The mixture (an aqueous solution of $(NH_4)_6Mo_7O_{24}{\cdot}4H_2O$, molybdenum powder, H_3PO_3, $ZnCl_2$, tetrabutylammonium hydroxide with **bdc**, **btc** or **im**) was heated to 180°C over a period of 1h, kept at 180°C for 40h and cooled down to room temperature over a period of 88h. The products were isolated by filtration and washed with ethanol. X-ray diffraction were carried out with a Siemens SMART three-circle or a Bruker Nonius X8 APEX 2 diffractometer, both

equipped with a CCD bi-dimensional detector using the monochromatized wavelength λ (Mo Kα) = 0.71073 Å. Finally, cyclic voltametry (CV) analyses were performed using a number of different modified electrodes techniques using the as-synthesized POMOFs.

Results and discussion

We show how the prediction of polymorphs in each {linker/ε-Keggin} system is performed with their energy ranking. The diamond-like **bdc**-based POMOF was predicted as the most thermodynamically stable one among a series of polymorphs, and was further successfully synthesized, exhibiting enhanced electrocatalytic reduction activity compared to the molecular precursors. Using **btc** as a linker, we discoved a new family of open-framework POMOFs (Figure 1) and synthesized a couple of new structures more active than platinum for hydrogene evolution reaction.

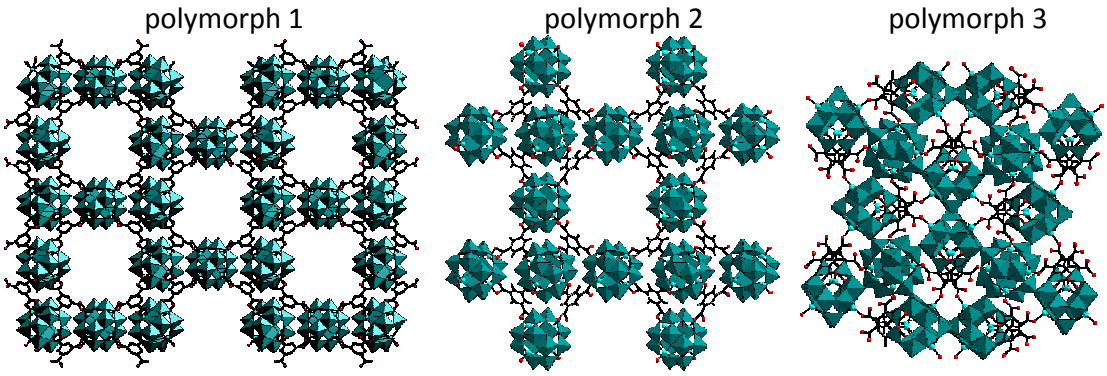

Figure 1. Crystal structures of three {btc/ε-Keggin} POMOFs polymorphs.

Conclusions

This work confirms that the {ε-$PMo^{V}_{8}Mo^{VI}_{4}O_{36}(OH)_{4}Zn_{4}$} POM is a versatile and powerful building block for the construction and synthesis of new POMOFs structures. A rationale for the stabilization of a number of structures over alternative polymorphs is proposed, highlighting a structure directing role of TBA in the assembly of the POMs. Also, this unique feature of POMOFs to allow the stabilization of electroactive POMs in MOF-type scaffold opens up promising perspectives for the conception of more efficient catalysts for HER.

References

[1] Ockwig, N. W.; Delgado-Friedrichs, O.; O'Keeffe, M.; Yaghi, O. M. *Acc. Chem. Res.* 38 (2005) 176.
[2] (a) *Chem. Soc. Rev.* 38 (2009) 1201-1508, Special Issue: Metal Organic Frameworks. (b) Rao, C.N.R.; Cheetham, A. K.; A. Thirumurugan, *J. Phys.: Condens. Matter.* 20 (2008) 083202.
[3] (a) Clemente-Juan, J. M.; Coronado, E. *Coord. Chem. Rev*. 193-195 (1999) 361. (b) Kortz, U.; Müller, A.; van Slageren, J.; Schnacke, J.; Dalal, N. S.; Dressel, M. *Coord. Chem. Rev*. 253 (2009) 2315. (c) Mialane, P.; Dolbecq, A.; Sécheresse, F. *Chem. Commun*. (2006) 3477.
[4] Keita, B.; Nadjo, L. *Electrochemistry of Polyoxometalates*, Encyclopedia of Electrochemistry, Vol. 7 (Eds.: Bard, A. J.; Stratmann, M.), Wiley-VCH, (2006) 607.
[5] Special issue on polyoxometalates, ed. Hill, C. L.: *J. Mol. Catal. A.* 262 (2007) 1-242.
[6] Rodriguez-Albelo, L. M.; Ruiz-Salvador, A. R.; Sampieri, A.; Lewis, D. W.; Gómez, A.; Nohra, B.; Mialane, P.; Marrot, J.; Sécheresse, F.; Mellot-Draznieks, C.; Ngo Biboum, R.; Keita, B.; Nadjo, L.; Dolbecq, A. *J. Am. Chem. Soc.* **2009**, *131*, 16078.

External Surface Adsorption on Silicalite-1 Zeolite Studied by Molecular Simulation

S.K. Schnell[‡,*], E. García-Pérez[#], J.M. Castillo[†], S. Calero[#], S. Kjelstrup[§] and T.J.H. Vlugt[‡]

‡ *Process & Energy Laboratory, Delft University of Technology, Leeghwaterstraat 44, 2628CA Delft, The Netherlands*
 # Department of Physical Chemical, and Natural Systems, University Pablo de Olavide, Ctra. Utrera km. 1. 41013 Seville, Spain
† Institut für Technische Thermodynamik und Termische Verfahrenstechnich, University of Stuttgart, Pfaffenwaldrig 9, 7059 Stuttgart, Germany
§ Department of Chemistry, Norwegian University of Science and Technology, 7491 Trondheim, Norway
∗ Corresponding author: s.k.schnell@tudelft.nl

Introduction

Molecular simulations are a powerful tool to study the adsorption of guest molecules inside zeolite crystals. However, adsorption of molecules on external zeolite surfaces has received far less attention. Surface adsorption and resistivities are of particular importance for a correct description of mass transport through a zeolite membrane. Here, we studied the adsorption of ethane, propane, and their equimolar mixture on the external surface of silicalite-1. Pure component and mixture isotherms at 308K are obtained from molecular simulations. The Ideal Adsorbed Solution Theory (IAST) of Myers and Prausnitz [1] correctly predicts competitive adsorption on the external surface.

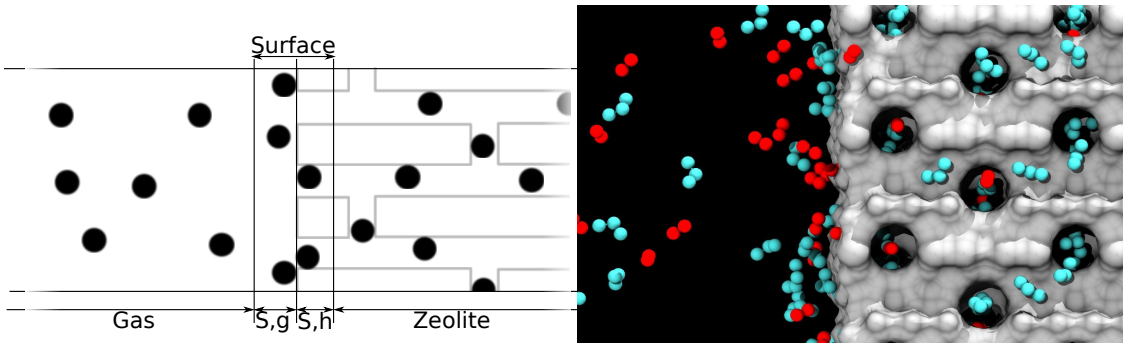

(a) (b)

Figure 1: (*a*) Schematic representation of the zeolite and the external surface. The external surface can be split into two parts; the gas part, S,g, and the host part, S,h. The crystallographic surface is selected as the dividing surface. (*b*) Typical snapshot from simulations showing the external surface of silicalite-1 with ethane and propane adsorbed. The red molecules are ethane, and cyan are propane.

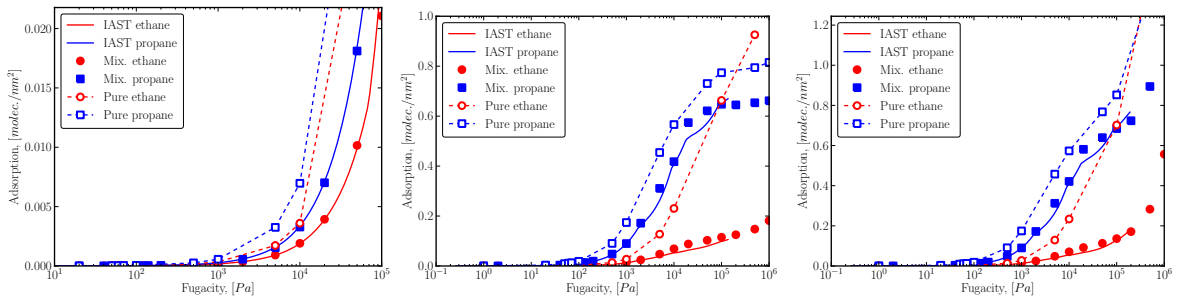

(a) (b) (c)

Figure 2: (*a*) The adsorption on the gas side of the surface. (*b*) The adsorption on the host side of the surface. (*c*) The surface adsorption on the surface as a total. The results from Ideal Adsorbed Solution Theory are plotted as the solid lines, while the closed symbols are from simulations with ethane and propane in an equimolar mixture.

Method

Configurational-bias Monte Carlo simulations in the grand-canonical ensemble are used to obtain the loading in the different parts of the zeolite as a function of the fugacity. For details on the simulations, we refer the reader to Refs. [2-3]. Simulations were performed with a zeolite, a gas phase, and a zeolite with two adjoining gas phases, see Fig 1.

The extent of the external surface, both on the gas side and host side of the crystallographic surface, is determined from changes in the local density. The bulk zeolite and gas phase are used as a reference. The surface is considered as a Gibbs-surface [4]. Fig. 2 shows the adsorption of ethane and propane on the silicalite-1 surface, both for pure component systems and mixtures. It is clear that for the gas side of the surface (Fig. 2a) the predicted values using IAST are in very good agreement with simulations, up until the fugacity approaches 10^5 Pa. At this point the surface loading starts increasing rapidly, indicating that condensation on the surface takes place. As for the host side of the surface (Fig. 2b), we also have a very good correspondence between values predicted from IAST and from simulation.

Conclusion

The IAST is able to predict the adsorption of ethane, propane and their mixture on the surface of silicalite-1. The gas-side of the surface give good predictions until condensations become important. For the host side, as well as for the total surface, IAST predicts the mixture composition well up till high pressures. In future studies, we will focus on the competitive adsorption of polar molecules on zeolite surfaces.

References

[1] Myers, A.L., Prausnitz, J.M.; Thermodynamics of mixed gas adsorption, AIChE J., 11 (1965) 121–130.
[2] Frenkel, D., Smit, B.; Understanding Molecular Simulations, Academic press, 2002.
[3] Vlugt, T.J.H., Zhu, W., Kaptaijn, F., Moulijn, J., Smit, B., Krishna, R.; Adsorption of Linear and Branched Alkanes in the Zeolite Silicalite-1, J. Am. Chem. Soc., 120 (1998) 5599–5600.
[4] Kjelstrup, S., Bedeaux, D.; Non-equilibrium thermodynamics of heterogeneous systems, World Scientific, 2008.

Adsorption of Short Alkanes in Chabazite - Modeling van der Waals Interactions

Florian Göltl, Jürgen Hafner
Universität Wien, Fakultät für Physik, Center for Computational Materials Science, Sensengasse 8/12, 1090 Vienna, Austria; florian.goeltl@univie.ac.at

Introduction

To model alkane adsorption in zeolites is a big challenge for density functional calculations. In these systems the strength of adsorption depends on two components: (i) the chemical interaction between the alkane and the adsorption site and (ii) the van der Waals (vdW) interactions between the alkane and the zeolite framework. While the specific interaction with the active site is well described by Density Functional Theory (DFT), the dispersion forces, which mediate the interactions with the framework go beyond DFT. In this work we test the performance of recently developed post DFT methods to describe the adsorption of methane, ethane and propane in protonated and Na-exchanged chabazite [1].

Theoretical

We calculated adsorption energies at different levels of theory: (i) semilocal gradient corrected functionals proposed by Perdew et al. (PBE, [2]), (ii) including dispersion corrections via semi-empirical pair potentials proposed by Grimme (PBE-d, [3]), (iii) using a non-local correlation functional designed to describe vdW interactions (vdW-DF, [4]), (iv) the adiabatic connection fluctuation-dissipation theorem in its random phase approximation (RPA, RPA-HF, [5,6]) and (v) second order Møller-Plesset perturbation theory for periodic systems (MP2, [7]). PBE, PBE-d and vdW-DF calculations were performed selfconsistently, including the optimization of the geometry of the adsorption complex, RPA and MP2 calculations were performed non-selfconsistently for geometries optimized at the PBE, PBE-d or vdW-DF levels. All calculations were performed using the Vienna Ab-Initio Simulation Package (VASP)[8].

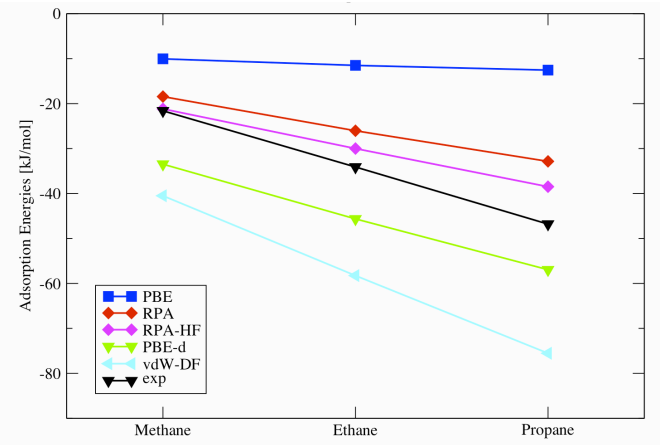

Figure 1: Adsorption energies in Na-exchanged Chabazite

Results and Discussion

Results for the adsorption energies of short alkanes in Na-exchanged and protonated chabazite are compiled in Figs 1 and 2. The calculated adsorption energies increase in the sequence PBE<RPA<RPA-HF<MP2<PBE-d<vdW-DF, the increment per additional CH_2 group is almost zero for PBE, similar for PBE-d, RPA and RPA-HF and largest for vdW-DF and MP2. Comparison with experiment at finite temperatures is not straightforward. Recent ab-initio MD simulations [9] have shown that due to the weakness of the adsorptive interaction, even at 300K only about 2/3 of the molecules adsorbed in the zeolite are bound to the acid site, 1/3 of the molecules move freely in the cavity and experience only vdW-interactions with the framework. Comparison with experiment should therefore use adsorption energies calculated for acid and purely siliceous chabazite averaged in a ratio 2:1. With these corrections best agreement with experiment in Na-chabazite [10] is found at the RPA-HF-level.

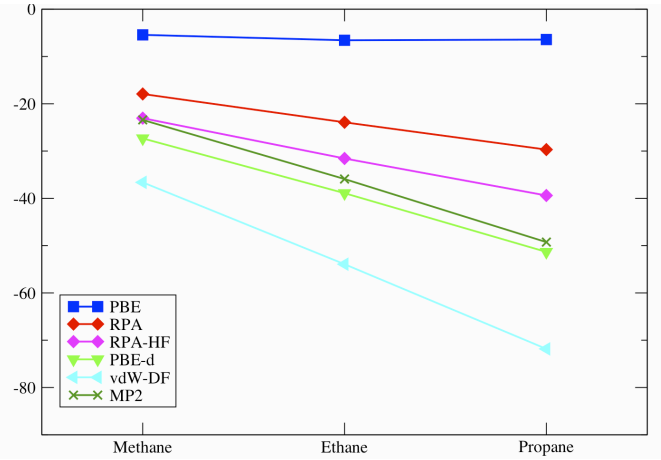

Figure 2: Adsorption energies in protonated chabazite

Conclusion and Outlook

We tested the performance of different methods to describe the adsorption of short alkanes in chabazite. Sadly none of these methods was ideal. MP2, the only method which seems to give results which are at least close to chemical accuracy, is limited by its computational effort and scaling behavior to smaller system sizes. Therefore a lot of work has to be invested to find a electronic structure method suitable for these applications.

References

[1] F. Göltl, J. Hafner, J. Chem Phys, 134, 064102, (2011)
[2] J.P. Perdew, K. Burke, M. Ernzerhof, Phys. Rev. Lett., 77, 3865 (1996)
[3] S. Grimme, J. Comput. Chem., 27, 1787-1799 (2006)
[4] M. Dion, H. Rydberg, E. Schröder, D.C. Langreth, B.I. Lundqvist, Phys. Rev. Lett., 92, 246401 (2004)
[5] J. Harl, G. Kresse, Phys. Rev. B, 77, 045136 (2008)
[6] X. Ren, A. Tkatchenko, P. Rinke, M. Scheffler, arXiv: 1011:2742v1, submitted to Phys. Rev. Lett. (2010)
[7] M. Marsman, A. Grüneis, J. Paier, G. Kresse, J. Chem. Phys. 130, 184103 (2009)
[8] G.Kresse, J. Hafner, Phys.Rev.B 48, 13115 (1993); G. Kresse, J. Furthmüller, Comput.Mat.Sci. 6, 15 (1996)
[9] T. Bučko, L. Benco, J. Hafner, J.G. Àngyàn, "Monomolecular cracking of propane over acidic chabazite: An ab initio molecular dynamics and transition path sampling study", submitted to J. Catal
[10] J.F.M. Denayer. et al. J.Phys.Chem C 112, 16593 (2008)

N_2O Decomposition in the absence of NO. Why does Fe-ferrierite have a superior activity with respect to Fe-ZSM-5 and Fe-beta? A combined DFT and multi-spectroscopic study

Stepan Sklenak and Zdenek Sobalik
J. Heyrovsky Institute of Physical Chemistry of the Academy of Sciences of the Czech Republic, Dolejskova 3, Prague 18223, Czech Republic
stepan.sklenak@jh-inst.cas.cz

Introduction

In the past ten years, attention was drawn to development of methods for the abatement of N_2O. Transition metal exchanged silicon rich zeolites are excellent candidates for the decomposition of nitrous oxide to nitrogen and oxygen. Fe-ZSM-5 was studied the most both experimentally and theoretically but Fe-ferrierite as well as Fe-beta were also investigated. Our recent study [1] showed that Fe-zeolite samples prepared by Fe(III) precipitation using organic solvent represent promising catalytic systems with a high and stable activity under conditions of nitrous acid plants. The catalytic activity of Fe-ferrierite in the absence of NO was found to be superior with respect to Fe-beta and Fe-ZSM-5 (ferrierite >> the beta zeolite > ZSM-5). On the other hand, all the three zeolites have similar activities in the presence of NO. We suggested that a collaboration of two Fe(II) cations accommodated in two adjacent sites located on the opposite sides of the eight-membered ring channel can explain for the superior performance of Fe-ferrierite. In this contribution, we focus on the investigation and description of (1) plausible active sites of Fe-ferrierite and their structures [2, 3], (2) the origin of the distinct reactivity of Fe-ferrierite, Fe-ZSM-5, and Fe-beta [2], and (3) a description of the mechanism of the N_2O decomposition on (a) two collaborating Fe(II) cations accommodated in two adjacent sites and (b) isolated Fe(II) cations [4].

Computational details

Five ferrierite double unit cell models were employed to investigate five distinct possible arrangements of the active sites in ferrierite. The first three models represent three distinct isolated cationic sites while the other two models feature two cooperating adjacent Fe(II) cationic sites. Spin polarized periodic DFT calculations (molecular dynamics and subsequent optimizations) were carried out employing the VASP code. The exchange-correlation energy was described by the PW91 generalized gradient approximation (GGA) functional. Brillouin zone sampling was restricted to the Γ-point. The plane-wave cutoff of 400 eV was utilized for geometry optimizations while a smaller cutoff of 300 eV was used for the molecular dynamics simulations.

Results and discussion

Our investigations [2] provided evidence based on our multiple spectroscopy results, DFT calculations, and structural models that two Fe(II) cations coordinated in two adjacent β sites of Fe-ferrierite most likely form the active site responsible for the superior activity of this catalyst in the N_2O decomposition in the low temperature region. The calculated Fe – Fe distance of the active site is 7.4 Å. The formation of the active sites results from a combination of (1) a suitable topology of the ferrierite framework and (2) an appropriate distribution of Al in the distinguishable T sites of the ferrierite framework as well as concentration of Al in these T sites. Both six-membered rings forming the two neighboring β sites must contain two Al atoms each (four Al atoms in total). Two adjacent β sites of Fe-beta can also form an active site with two collaborating Fe(II) cations. However, there are significant differences with respect to ferrierite. The Fe – Fe distance is somewhat longer and, more importantly, the distribution and concentration of Al in the rings with the geometry of the β site lead to a very low probability of occurrence of the active sites with two cooperating Fe(II) cations. This is responsible for the superior activity of Fe-ferrierite relative to Fe-beta. Two close α sites of the Fe(II) exchanged ZSM-5 zeolite coordinating two collaborating Fe(II) cations can compose the active site. However, the geometrical arrangement of two adjacent α sites is very distant from that of two adjacent β sites in ferrierite. Also the probability of a formation of these active sites is low due to an unfavorable Al distribution and Al concentration in the rings forming the α sites. Our study further reveals detailed mechanisms of the N_2O decomposition on both two collaborating Fe(II) cations accommodated in two adjacent sites and isolated Fe(II) cations [4]. The main feature of the former active site is the oxidation of FER-Fe-NO_2 to yield FER-Fe-NO_3 and subsequently release O_2(g).

Conclusions

The results of our investigations of the N_2O decomposition explain the order of the catalytic activity of Fe(II) exchanged zeolites (Fe-ferrierite >> Fe-beta > Fe-ZSM-5) and reveal the active sites of Fe-ferrierite and their structures and the catalytic mechanisms.

References

[1] K. Jisa, J. Novakova, M. Schwarze, A. Vondrova, S. Sklenak, Z. Sobalik, J. Catal. 262 (2009) 27.
[2] S. Sklenak, P. C. Andrikopoulos, B. Boekfa, B. Jansang, J. Novakova, L. Benco, T. Bucko, J. Hafner, J. Dedecek, Z. Sobalik, J. Catal. 272 (2010) 262.
[3] Z. Sobalik, P. C. Andrikopoulos, J. Novakova, P. Sazama, B. Bernauer, S. Sklenak, J. Catal. (2011), submitted.
[4] P. C. Andrikopoulos, Z. Sobalik, S. Sklenak, J. Catal. (2011), to be submitted.

Formation of zeolite like structure in template hydration layers

Alan J. W. Lobo[1], Keith T. Butler[2], Ben Slater,[1] Dewi W. Lewis[1]
[1] *Department of Chemistry, University College London, 20 Gordon St, London WC1H 0AJ,* UK
[2] *Dept. Materials Science and Engineering, University of Sheffield, Sir Robert Hadfield Building, Mappin Street, Sheffield, S1 3JD, UK*
email: a.lobo@ucl.ac.uk

Introduction

The role of the structure directing agent (SDA) has been the subject of many years of research however its role is still not full understood. It was proposed by Chang et al [1] that the hydration layer around the SDA forms a structure isomorphic to the final zeolite product. Such water is then replaced by silica to form a nucleation species[2,3,4]. Here we demonstrate how computational methods can be used to investigate the formation of such hydration layers around SDAs and their structure. *Ab inito* molecular dynamics (AIMD) simulations are used to generate trajectories which are then analysed for the presence of rings within the hydration layer around the SDA.

Experimental

Molecular dynamics (MD) simulations were carried out using the CP2K[5] code using the BLYP functional with DZVP basis set and GTH pseudopotentials. The energy cutoff was set to 280 Ry. SDAs were hydrated using our code then the cell volume equilibrated by running MD in an NPT ensemble at 350 K for 3 ps with a timestep of 1 fs. Trajectories were analysed to determine the formation of specific water structures and their lifetime.

Results and discussion

Our simulations of TMA (Figure 1) clearly reveal the formation of sodalite-like structures. An analysis of the lifetime of these structural motifs reveals that they are longer lived than in pure water. The number of rings found in the hydration layers of protonated and neutral aminoadamantane and piperidine and methylpiperidine, compared to pure water, was also analysed. Of note is that five and six-membered rings are more prevalent in the presence of the adamantanes than in pure water, whilst the number of four rings is diminished. A similar situation is found for both piperidine and methyl piperidine. Figure 2 shows the number of rings within 5Å of the nitrogen atom in each of the SDAs considered. A further striking feature of this analysis is the effect of protonation on the water structure (in the simulations of amino adamantane): far fewer rings form in the vicinity of the $–NH_3^+$ group than the neutral NH_2. This may be due to the fact that the hydrogens on the charged group participate directly in hydrogen bonding with the water, thus disrupting the (water-water) network, or due to a stabilizing effect of the lone pair, which is lost upon protonation, on rings.

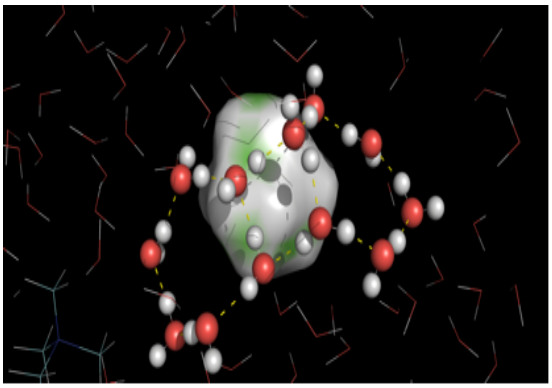

Figure 1: Formation of “sodalite-structured” water around TMA.

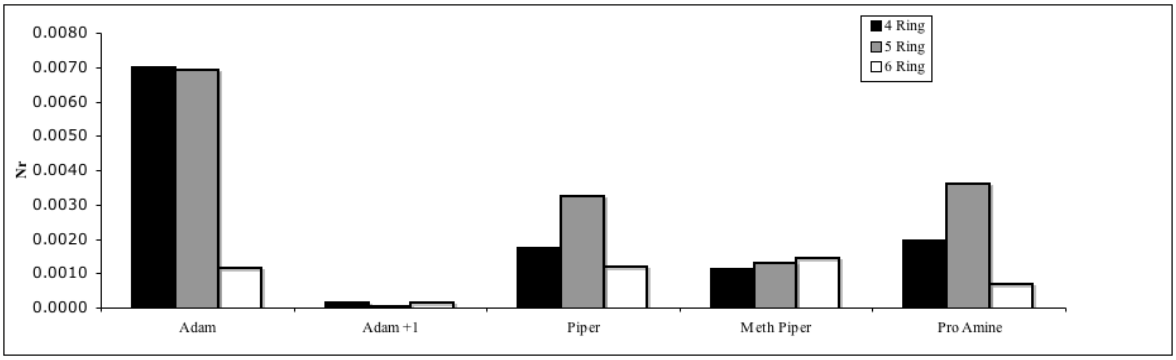

Figure 2: Normalised number of rings within 5 Å of the SDA.

Conclusions

QM molecular dynamics simulations show that a number of factors affect the size and lifetime of the rings within the water hydration layer around a SDA. All SDAs increase the occurrence of 5 and 6 member rings over those present in pure water. We will discuss further the agglomeration of silica to the water-SDA interface.

Acknowledgements

The authors would like to thank the EPSRC and ExxonMobil Research and Engineering for funding.

References

[1] Chang C. D., Bell, A. T., *Cat. Lett.*, **1991**, 8, 305
[2] Mootz, D., Seidel, J., *J. Incl. Phenom*, **1990**. 8, 139
[3] Cox, P. A., Casci, J. L., *J. Chem. Soc*, **1994**, 106, 473
[4] Szyja, B., Jansen, A., Verstaelen, T., van Santen, R., *PCCP*, **2009**, 11, 7605
[5] VandeVondele, J., Mohamed, M. K. F., Parrinello, M., Chassaing, T., Hutter, J., *Comp. Phys. Com.*, **2005**, 103, 167

Petrochemical and environmental catalytic applications

FEZA 2011

Insight into the nature of the active site in Cu-CHA for NH_3-SCR

Upakul Deka [a,b], Satu T. Korhonen [a,b], Bert M. Weckhuysen [b] and Andrew M. Beale[b]*
[a]*Materials Innovation Institute (M2i), Delft, The Netherlands;* [b]*Inorganic Chemistry and Catalysis, Utrecht University, The Netherlands; *a.m.beale@uu.nl*

Introduction

NH_3-Selective Catalytic Reduction (NH_3-SCR) is a widely used technology for NO_x reduction in the exhaust of heavy duty diesel vehicles. Recently, it has been reported that Cu containing chabazite (Cu-CHA) shows both exceptional activity and hydrothermal stability as compared to other available zeolite supports for such purposes [1, 2]. Owing to its structure, CHA possesses one ion exchange site for Cu in the zeolite [3, 4] and thus simplifies active site interrogation. In this work, we examine the origin of SCR activity of Cu-CHA as evidenced from a combination of laboratory spectroscopic and synchrotron based X-ray techniques.

Experimental

The catalysts were prepared by conventional wet ion exchange of $CuSO_4 \cdot 5H_2O$ with CHA (with varying Si/Al ratios). The SCR of NO over Cu-CHA catalysts was studied under plug flow conditions with feed concentrations of 1000 ppm NO, 1000 ppm NH_3 and 5% O_2 (with He as the carrier gas) at a GSHV 90000h^{-1}. The outlet gases were analyzed simultaneously by FTIR and MS. The fresh and spent catalysts were characterized by UV-Vis and XRD. *In situ* UV-Vis was used to study changes during catalytic reactions. Synchrotron based *operando* XAFS/XRD measurements were further used to provide complementary information on the local copper environment and long range order, respectively, under NH_3-SCR conditions.

Results and discussion

Catalytic tests done on Cu-CHA catalyst under plug flow SCR conditions showed excellent NO conversion with a very high selectivity towards N_2 (Figure 1, right).

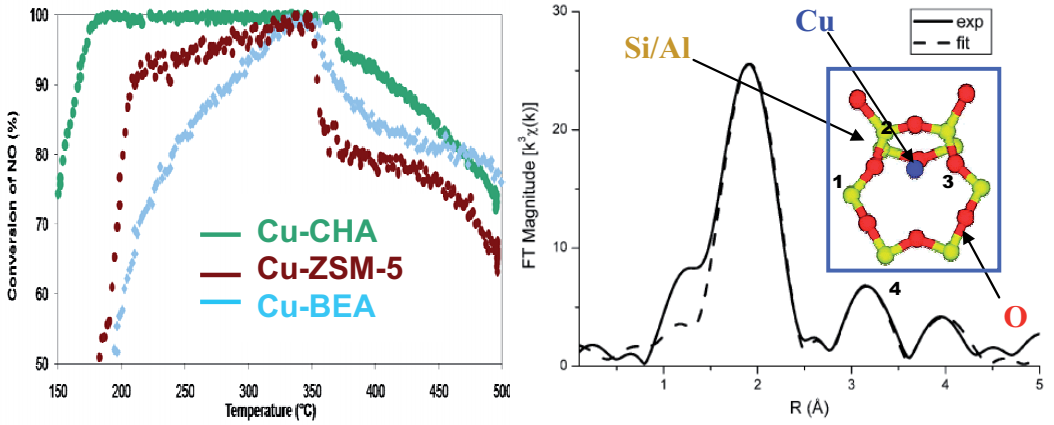

Figure 1: SCR activity comparison of different Cu-zeolites (left) and Fourier transform of $k^3\chi(k)$ EXAFS data (right) for Cu-CHA after calcination at 500°C (solid line) with the best fit (dash). Right inset: proposed model of Cu^{2+} in CHA as per EXAFS. Oxygens 1-3 (labeled) form the first near neighbours at 1.93 Å, while O4 is at 3.13 Å.

Irrespective of the Si/Al ratios tested in this study, the catalysts show only isolated Cu^{2+} species in the *ex situ* UV-Vis spectra (*d–d transition ~12000 cm^{-1} and CT (O-Cu) ~45000 cm^{-1}*). Pre-characterization studies using EXAFS (Figure 1) confirmed the presence of isolated Cu^{2+} in the CHA structure [4]. The Cu ion gets slightly distorted from the 6-oxygen ring resulting in a local distortion of the framework. *In situ* UV-Vis spectra recorded during SCR ramps further disregard the presence of species other than isolated Cu^{2+} ions in these systems under SCR conditions (Figure 2). However, upon introducing a Cu-CHA catalyst to a reducing atmosphere (5 % H_2), additional UV-Vis bands appeared as seen by a rising absorption edge at ~18000 cm^{-1}. This indicates the formation of Cu^{+} species, similar to that of Cu_2O (*CTLM Cu_2O ~18000-23000 cm^{-1} and ~32000 cm^{-1}*), which could further imply the possibility of the system to possess redox functionality.

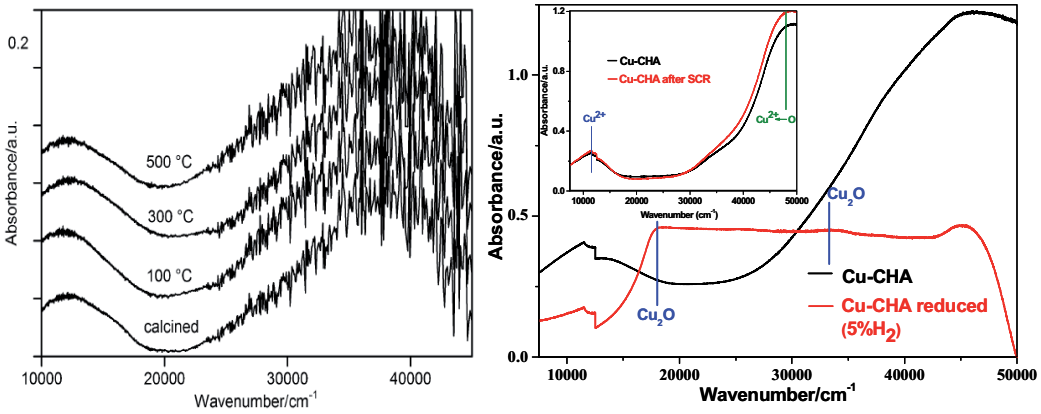

Figure 2: *In situ* UV-Vis for Cu-CHA under SCR conditions (left) and *ex situ* UV-Vis spectra of changing copper species during pre-reduction treatments (right). Right inset: *Ex situ* UV-Vis of Cu-CHA before and after SCR treatments.

Although upon exposure to highly reducing atmospheres, different Cu^{+} type species may be formed, under SCR conditions these species are not present or these transient species are readily oxidized. The importance of mononuclear Cu^{2+} species under SCR conditions is further investigated using combined XAFS/ XRD measurements under *operando* conditions and will be discussed further.

Conclusion

The extraordinary performance of Cu-CHA catalysts for NH_3-SCR has been investigated in terms of understanding the structure of the active Cu species within the zeolite and their behaviour under reaction conditions allowing us to obtain important insight into the relationship between the local structure and deNO_x activity.

References

[1] I. Bull, W.-M. Xue, P. Burk, R. S. Boorse, W. M. Jaglowski, G. S. Koermer, A. Moini, J. A. Patchett, J. C. Dettling and M. T. Caudle, US Patent 0285737 A1, 2009.
[2] J. H. Kwak, R. G. Tonkyn, D. H. Kim, J. Szanyi and C. H. F. Peden, *J. Catal.*, 275, (2010), 187.
[3] D. W. Fickel, R. F. Lobo, *J. Phys. Chem. C*, 114, (2010) 1633.
[4] S. T. Korhonen, D.W.Fickel, R.F.Lobo, B.M.Weckhuysen, A.M.Beale, *Chem. Comm.*, 47, (2011), 800.

An *operando* IR Study of the Effect of Unburnt HC and NO/NO_x Ratio on the NH_3-SCR Efficiency of a Commercial Automotive Fe-Zeolite Catalyst.

Olivier Marie[a], Irene Malpartida[a], Philippe Bazin[a], Marco Daturi[a] and Xavier Jeandel[b]

[a]*Laboratoire Catalyse et Spectrochimie, ENSICAEN, Université de Caen, CNRS, 6 Bd. Maréchal Juin, F-14050, Caen*
[b] *Renault SAS, DAPEM - P&I - Sce 66123, API : FR CTL L47 2 61, 1 allée Cornuel, F- 91510 Lardy*

Introduction

The growing environmental regulations have forced the development of lean-burn engines that offer, as Diesel engines, a reduction in fuel consumption and in CO_2 emissions. In these conditions of oxygen excess, the ammonia based selective catalytic reduction (SCR) permits the NOx abatement, particularly when Fe-containing zeolites are applied [1-3].
This work indeed aims at providing chemical data obtained at the laboratory scale for a simulation platform enabling a fast and reliable evaluation of the catalyst efficiency.
The chemical data useful for any reliable simulation cover a very broad range: in classical studies, only the gas phase analysis feeds the simulation with both the nature and amount of various molecules at the inlet and the outlet of the catalytic system. On the contrary, our approach consists in the application of a unique spectroscopic tool enabling to perform precise gas analyses while observing the catalytic system in working conditions (*operando*) and thus to provide the simulation with:

i) the nature of adsorbed species (either spectators, poisons or intermediates).
ii) the candidates for the active sites.
iii) more details on elemental steps and when relevant on the deactivation path.

Experimental

The investigated catalysts are powders obtained from scratching monoliths (either fresh or aged) wash-coated with Fe-ZSM5 and provided by Renault.
The samples were tested by the *operando* methodology, using Quadrupole Mass Spectrometry (Balzers TCP 121) and FTIR spectroscopy for both surface and gas analysis. A home-made low volume transmission IR reactor cell fitted with KBr windows was used [3]. Feed compositions similar to those occurring in exhaust gases of a Diesel engine were applied: 14% of O_2, 4% of CO_2, 1% of H_2O, 300 ppm of CO, 150 ppm of NO_x and 150 to 180 ppm of NH_3 in argon, at a space velocity of 120.000 h^{-1}. The impact of 85 ppm of HC was studied, either added solely to the flow or using a mixture of decane, toluene and propene. Different temperatures were tested between 160 and 400 ºC.

Results and discussion

When no HCs was present in the flow, we observed that NOx conversion increased with the temperature, reaching the maximum value (around 70%) at 400ºC. The NH_3-conversion was higher than the NO_x conversion in the whole temperature range which implies that NH_3 is partly oxidized by O_2 to yield N_2 (as checked by complementary studies). At high temperature, this parallel reaction account for about 30% of converted NH_3 not involved to reduce NO_x. Furthermore, the gas IR data do not provide ant N_2O evidence, confirming the high selectivity of the SCR reaction to dinitrogen.
When 85 ppm of HC was added to the flow, new trends were observed. The NOx conversion greatly decreased when lowering the temperature from 300 to 200ºC, especially in the

presence of $C_{10}H_{22}$ or C_7H_8. Whatever the HC nature, the parallel NH_3 oxidation by O_2 decreased because the oxidation sites are also involved in HC's conversion (as evidenced by CO production). From the IR surface data, the deposit of C-species was observed at 400°C with a stable amount remaining for all temperatures. As expected, the band intensities relative to adsorbed NH_3 and hydrocarbons increases when the temperature decreases. Specifically, adsorbed decane (without any further transformation) amount was quite high at T below 300°C. Regarding adsorbed toluene, it was hardly detected and only at the lowest T, whereas propene was never observed on the surface. Since the amount of available ammonium species (detected by IR under reaction flow) correlates with the SCR activity, the fact that HCs and NH_3 compete for the same adsorption sites (OH acidic Brønsted sites) explains the decrease of the SCR efficiency.

The NO/NO_x ratio effect was also investigated in realistic conditions. Pure NO_2 was shown to favour the SCR especially in the low temperature region. We indeed did not observed the best SCR efficiency for the expected $NO:NO_2 = 1$ ratio (fast SCR) and we assign this phenomenon to the presence of CO. Furthermore, the *operando* methodology allowed the clear evidence of ammonium nitrate formation at 165°C whose accumulation leads to a loss of activity for the NO_x reduction associated to the microporous system obstruction (fig.1)

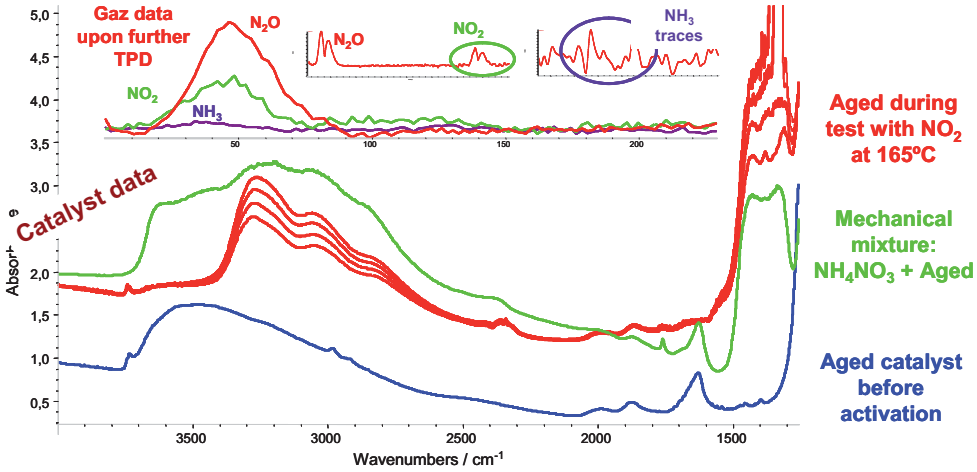

Figure 1. IR spectra of catalyst during the test at 165ºC (red), catalyst before activation and reaction (blue) and a mechanical mixture of NH_4NO_3 and catalyst (green).

Conclusions

Several parameters (unburnt hydrocarbon speciation, NO/NO_x ratio…) were studied regarding their impact on the SCR efficiency. Thanks to our *operando* system, we were able to conclude that among several HC residues, decane was the main poisoning agent, especially at intermediate reaction temperatures (T<300°C) due to its competitive adsorption (regarding NH_3) on active acidic sites. Furthermore, changing the NO/NO_x ratio enabled us to evidence an unexpected positive effect of pure NO_2 on the SCR efficiency in the whole temperature range which is related to the presence of CO. Finally, the catalyst deactivation upon ammonium nitrate deposit at temperature as low as 165°C was clearly evidenced by mean of the *operando* methodology.

References

[1] M. Santhosh Kumar, M. Schwidder, W. Grünert, U. Bentrup, and A. Brückner, J. Catal. 239 (2006) 173-186.
[2] S. Brandenberger, O. Kröcher, A. Tissler, and R. Althoff, Appl. Catal. B. 95 (2010) 348-357.
[3] I. Malpartida, E. Ivanova, M. Mihaylov, K. Hadjiivanov, V.B. Aubé, O. Marie, and M. Daturi, Catal. Today 149 (2010) 295–303

Heterogeneous oligomerization of ethylene on Ni-Beta catalysts

A. Martínez, M.A. Arribas, P. Concepción
Instituto de Tecnología Química, UPV-CSIC, Avda. de los Naranjos s/n, 46022, Valencia, Spain, amart@itq.upv.es.

Introduction

Oligomerization of ethylene is an important catalytic route for the synthesis of higher olefins used in the manufacture of valuable chemicals and clean fuels. Apart from oil refining, it can be produced from alternative energy resources such as natural gas (NG), coal or lignocellulosic biomass *via* syngas directly (Fischer-Tropsch) or indirectly by converting syngas to methanol followed by methanol-to-olefins (MTO) processes. Oxidative coupling of methane is another appealing source of ethylene to take profit of small NG reservoirs. In recent years, researches have been focused on developing efficient heterogeneous catalysts as an alternative to the current environmentally unfriendly technologies relying on homogeneous (mostly Ni complexes) systems. In this respect, Ni loaded on acidic mesoporous carriers such as silica-alumina, MCM-41 (and related mesostructures) as well as on zeolites (Y, MCM-22, MCM-36) have shown good prospects for ethylene oligomerization under mild conditions [1-3]. Main factors affecting the oligomerization performance of Ni-loaded catalysts are the amount and type of Ni species, amount and strength of acid sites, the Ni/acid sites ratio, and the support porosity. Severe deactivation, however, is usually observed for Ni-zeolite catalysts mostly due to blocking of the micropores by heavy (branched) oligomers. Here we address, for the first time, the catalytic behavior of Ni loaded on nanosized Beta zeolite for the oligomerization of ethylene. Ni speciation in Ni-Beta and reference Ni-USY was studied by in situ FTIR-CO in an attempt to gain insights into the origin of the distinct behavior.

Experimental

Two Ni-Beta samples with different Ni loadings and a Ni-USY catalyst were prepared by submitting commercial zeolites from Zeolyst Int. (name for commercial samples given in Table 1) to consecutive ionic exchanges with an aq. solution of $Ni(NO_3)_2$ at 70ºC for 4 h with intermediate washing and drying steps and final calcination at 550ºC for 3 h in flowing air. Materials were characterized by ICP-OES, XRD, N_2 physisorption, SEM, and FTIR-pyridine. Ni speciation in freshly activated selected Ni-Beta and Ni-USY catalysts and upon reaction with ethylene at the applied oligomerization temperature (120ºC) was studied by FTIR of adsorbed CO at RT. Ethylene oligomerization was carried out in a bench-scale fixed-bed reactor at 120ºC, P_{total}= 35 bar ($P_{C2=}$= 26 bar, Ar as balance), and WHSV= 2.2 h^{-1} after in situ activation of the catalysts under flowing N_2 at atmospheric pressure and 300ºC overnight.

Results and discussion

The nomenclature, parent zeolite (from Zeolyst Int.), and main properties of calcined Ni-zeolite catalysts are given in Table 1. Mean crystallite sizes derived from SEM images for Beta and USY zeolites were ca. 25 nm and 700 nm, respectively. As shown in Fig. 1, the two NiBeta catalysts displayed a stable activity with time-on-stream (TOS) during the gas-phase oligomerization of ethylene, in contrast to the severe deactivation observed for NiUSY. In the case of NiBeta, higher oligomerization activity and selectivity to liquid (C_{5+}) oligomers (45 wt%, Table 1) was attained over NiB-2 catalyst loaded with a higher amount of Ni. The activity, however, was not proportional to the Ni loading, indicating that not all the Ni species are probably involved in the oligomerization reaction. Moreover, the presence of a higher amount of cationic Ni^{2+} and Ni^{+} species (active for ethylene oligomerization) observed by FTIR-CO on freshly activated NiB-1 as compared to NiUSY (Fig. 2, spectra a and b,

respectively) might account for the higher catalytic activity of the former. After reaction with ethylene at 120ºC for 1 h, Ni^{2+} was completely reduced to Ni^{+} in NiB-1 while both Ni^{+} and Ni^{0} were detected in NiUSY (Fig. 2, spectra c and d, respectively). The formation of inactive Ni^{0} species would, at least partially, account for the loss of activity with time in NiUSY. Furthermore, analysis of the carbonaceous residues in spent catalysts (TG-DTGA) indicated a higher amount of high-temperature burning coke (T> 450ºC) in NiUSY, suggesting the formation of heavier oligomers trapped in the large supercages of the FAU structure as an additional cause of deactivation. Finally, worth mentioning that the nanocrystalline nature of Beta zeolite might help in facilitating the diffusion of the oligomers out of the crystallites thus contributing to the stability of NiBeta catalysts during the catalytic reaction.

Table 1. Main properties of Ni-Beta and Ni-USY catalysts.

Catalyst	Commercial zeolite	Bulk Si/Al ratio	Ni (wt%)	BET (m^2/g)	MPV (cm^3/g)	Acidity[a] (μmol/g) BAS	LAS	Oligomers distrib. (wt%) C_{3-4}	C_{5-9}	C_{10+}
NiBeta-1	CP811	12	1.7	601	0.19	70	137	77	21	2
NiBeta-2	CP811	12	2.6	589	0.18	55	143	55	26	19
NiUSY	CBV712	5.5[b]	1.8	607	0.25	148	79	80	18	2

[a] From FTIR-pyridine after desorbing the base at 250ºC. [b] Framework Si/Al ratio= 17 (from XRD).

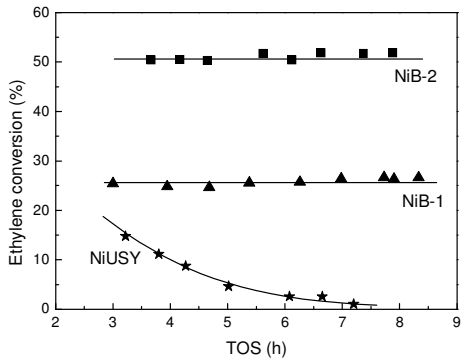

Fig. 1. Ethylene conversion as a function of time-on-stream (TOS) for NiBeta and NiUSY catalysts.

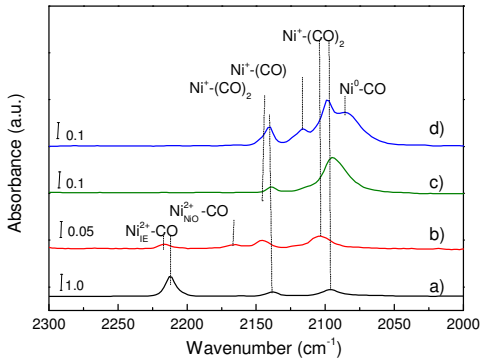

Fig. 2. IR spectra of CO adsorption on NiB-1 (a, c) and Ni-USY-1 (b, d) catalysts after pretreatment in N_2 at 300ºC for 3h (a, b) and after reaction with ethylene at 120ºC for 1h (c, d).

Conclusions

Ni loaded on nanosized Beta displays, in contrast to Ni-USY, a stable activity during ethylene oligomerization. FTIR-CO and TG-DTG analysis of spent catalysts suggest that deactivation in NiUSY is related to the formation of inactive Ni^{0} species by the reductant ethylene at the reaction temperature and by retention of heavier oligomers inside the large supercages.

Acknowledgements

Thanks are due to EU Commission for financial support through the project OCMOL (7^{th} FP, GA nº 228953). Further information about OCMOL can be found in http://www.ocmol.eu.

References

[1] Heveling, J., Nicolaides, C.P., Scurrell, M.S., Appl. Catal. A 173 (1998), 1-9.
[2] Hulea, V, Fajula, F., J. Catal. 225 (2004) 213-222.
[3] Lallemand, M., Rusu, O.A., Dumitriu, E., Finiels, A., Fajula, F., Hulea, V., Appl. Catal. A 338 (2008) 37-43.

Hydrocraking of long chain alkanes over Y zeolite with trimodal porosity

Régine Kenmogne[1], Annie Finiels[1], Vasile Hulea[1], Jovana Zečević[2], Heiner Friedrich[2], Petra E. de Jongh[2], Krijn P. de Jong[2], Sander van Donk[3], François Fajula[1*]
[1] *Institut Charles Gerhardt, UMR 5253 UM2-ENSCM-UMI-CNRS, 8 rue de l'Ecole Normale, 34296 Montpellier (France) * francois.fajula@enscm.fr*
[2]*Inorganic Chemistry and Catalysis,Utrecht University, Utrecht (The Netherlands)*
[3]*Total Research Center Feluy, Feluy (Belgium)*

Introduction

Zeolite catalyts featuring an interconnected network of mesopores demonstrate improved performance in a number of conversion processes compared to their purely microporous counterparts due to enhanced accessibility and transport of reagents and products to and from the active sites [1]. In recent years, a huge amount of research work has been paid to elaborate methods for producing bimodal micro-mesoporous materials, among which treatment of high silica zeolites with alkaline solution emerges as a most versatile, cost-effective and scalable procedure [2]. In this work, controlled desilication of a dealuminated Y zeolite by NaOH has been applied to optimize the selectivity of hydrocracking catalysts towards the production of middle distillates. A unique material, characterized by an intracrystalline trimodal discrete distribution of pore sizes and remarkable hydrocracking performance has been produced.

Experimental

The starting material was a commercially available steamed and acid leached zeolite H-Y (CBV760, Zeolyst, Si/Al = 30, 0.5-1µm, 0.31 meq H^+/g, hereafter HY-30). This material was base leached using 0.05 M or 0.10 M NaOH solution for 15 min at room temperature followed by NH_4^+ ion exchange and calcination to obtain HY-A (Si/Al = 25, 0.29 meq H^+/g) and HY-B (Si/Al= 20, 0.30 meq H^+/g), respectively. Catalytic performances of the Pt-loaded (0.3 wt% Pt) parent and desilicated zeolite samples were investigated for hydrocracking of n-hexadecane and squalane (fixed-bed down-flow reactor, catalyst grain size 180-425 µm, WHSV 1-3 h^{-1}, H_2/Hc = 4 mol/mol, total pressure 20 bar, 180-300°C).

Results and discussion

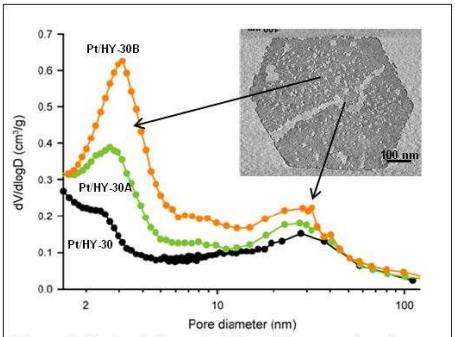

Figure 1: Textural characteristics of the parent and desilicated zeolites

The unique textural properties of the desilicated zeolites are depicted in Figure 1showing the (meso)pore size distribution derived from N_2 physisorption and a typical 3D-reconstruction image generated by electron tomography [3]. Besides structural micropores, two distinct networks of mesopores with small (~ 3 nm) and large (~ 30 nm) sizes are evidenced. While the later mesopores have been generated by steam dealumination, it appears clearly that the creation of the small mesopores is associated with the desilication process, generating a true intracrystalline trimodal porosity.

In the hydrocracking of n-hexadecane, rate constants calculated at 240°C appeared to be more than 4 times higher over the two desilicated zeolites compared to the reference HY-30 material indicating an improved catalyst effectiveness upon generation of the secondary network

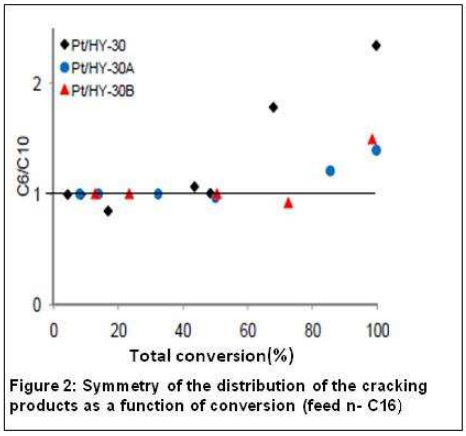

Figure 2: Symmetry of the distribution of the cracking products as a function of conversion (feed n- C16)

of small mesopores. More important, the distribution of the cracking products remained highly symmetrical up to high conversions as illustrated in Figure 2 by the evolution of the molar ratio between C6 and C10 products as a function of conversion. Actually, this ratio remains close to unity up to a conversion of *ca* 80% after desilication, showing the absence of secondary cracking, while a significant deviation is observed above a conversion of 40% in the case of the reference catalyst.

In the conversion of the more reactive squalane (branched C30 alkane) similar activities were obtained on the three catalysts. However, here again, a clear influence of the textural characteristics was noticed (Fig.3). At 75% conversion a symmetrical distribution of products, typical for a primary cracking, was obtained over HY-30A resulting in maximization of the C11-C19 fraction.

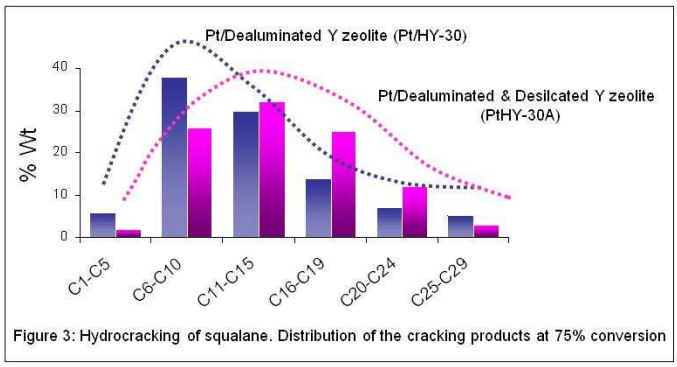

Figure 3: Hydrocracking of squalane. Distribution of the cracking products at 75% conversion

Conclusions

Alkaline leaching of traditional steam and acid washed dealumianted zeolite Y (exhibiting a Si/Al ratio of 30 and a network of mesopores 30 nm in size) under controlled conditions leads to the creation of a worm like network of smaller mesopores, with an average diameter of 3 nm. The desilicated materials preserve a high acidity and demonstrate improved activity in the hydrocracking of model long chain alkanes. Product selectivities show that these materials with intracrystalline trimodal porosity behave as ideal hydroconversion catalysts, preventing secondary cracking of reaction products and leading therefore to enhanced yields in median hydrocarbon fractions.

Acknowledgements

The authors thank Metin Bulut for assistance in the analysis of the squalane reaction mixture.

References

[1] For a recent review: Pérez-Ramírez J., Christensen C.H., Egeblad K., Christensen C.H., Groen J.C., Chem. Soc. Rev. 37 (2008) 2530.
[2] Groen J.C., Moulijn J.A., Pérez-Ramírez J., J. Mater. Chem. 16 (2006) 2121
[3] Friedrich, H., de Jongh, P.E., Verkleij, A.J., de Jong, K.P. Chem. Rev. 109, 1613 (2009).

BEA zeolite nano-crystals dispersed over alumina for n-hexadecane hydroisomerization

N. Batalha[1,2], S. Morisset[1] , L. Pinard[1], J.L. Lemberton[1], F. Lemos[2], P. Magnoux[2], F.R. Ribeiro[2]

[1]*Laboratoire de Catalyse en Chimie Organique, Université de Poitiers, UMR CNRS 6503, Faculté des Sciences, 40 avenue du Recteur Pineau, 86022 Poitiers Cedex, France.*

[2]*IBB, Institute for Biotechnology and Bioengineering, Centre for Biological and Chemical Engineering, Instituto Superior Técnico, UTL, Av. Rovisco Pais, 1041-001 Lisboa, Portugal.*

Email: ludovic.pinard@univ-poitiers.fr

Introduction

The cold properties (pour point) of Fisher-Tropsch waxes can be enhanced by changing the n-paraffins into iso-paraffins. This can be achieved using a hydroisomerization process, but this latter also produces cracking products. The hydroisomerization reaction requires a bifunctional catalyst which should have a strong hydrogenation function accompanied by a mild acid function in order to minimize the formation of cracking products [1]. A noble metal (i.e. platinum) supported on zeolite (i.e. ZSM-22 or BEA) is often used for this purpose [1-3].

The zeolites morphology often affects their catalytic performances. The ZSM-22 zeolite, in particular, avoids the cracking of the long chain paraffin, even at high hydroisomerization conversion. This is due to the small pore size and shape characteristics of this zeolite. In this case, the reaction occurs through a key-lock catalysis mechanism which favors isomerization [3]. Consequently, the ZSM-22 based catalysts are highly selective in slightly branched isomers (mainly monobranced) which are not too sensitive to cracking. Unfortunately, the activity of the ZSM-22 based catalysts catalytic is very weak due to the small monodimensional pore size structure characteristic of this zeolite.

A new strategy is proposed to increase the catalytic activity while keeping high isomerization selectivity. The use of large pore zeolite nano-crystals, such as the BEA zeolite ones, would reduce the diffusional limitations inside the zeolite crystals, which would allow the isomers to leave the catalyst before they crack. However, the BEA nano-crystals agglomerate after calcination increasing the diffusion limitations. Therefore, we carried out the direct germination of the BEA crystals over alpha alumina particles, which would prevent agglomeration.

Experimental

The BEA zeolite synthesis was carried out *in situ* on α-Al_2O_3 particles (0.2-0.4 mm), obtained by crushing and sieving α-Al_2O_3 extrudates. The molar composition of the starting gel was $23.6SiO_2 : 1.0Al_2O_3 : 1.9NaO_2 : 1.9TEA_2O : 235H_2O$. All the BEA zeolite based catalysts were prepared from the same gel. The characteristics of the BEA catalysts are presented in Table 1, as well as those of the HZSM-22 zeolite used as a comparison.

Table 1. Catalysts characteristics.

Catalyst	Zeolite loading (wt.%)	$V_{mesopore}$ (cm^3/g)	S_{BET} (m_2/g)	Si/Al	Brønsted acidity[1] (µmol/g)	Crystal size[2] (nm)
HZSM-22	100	0.183	595.0	30	278	1000
β	100	0.103	718.7	15.7	296	50
β/Al_2O_3 (1)	18.7	0.018	89.0	14.1	54	43
β/Al_2O_3 (2)	19.2	0.031	120.3	17.7	59	44
β/Al_2O_3 (3)	57.4	0.031	270.5	13.0	229	43

[1] determined by pyridine adsorption followed by IR.

[2] obtained using the Scherrer formula.

All the catalysts contained 1 wt.% platinum introduced through ion exchange with $[Pt(NH_3)_4]^{2+}$.

The catalytic tests were carried out in a fixed bed stainless steel reactor using n-hexadecane (10 mol.%) diluted in n-hexane under the following conditions: T=220ºC, P_{total}=30bar, H_2/n-C_{16} molar ratio=20.

Results and discussion

On all the catalysts, n-hexadecane transformed into isomerization products (monobranched M and multibranched B) and into cracking products, but the catalytic performances were quite different.

The HZSM-22 based catalyst exhibited the best isomerization selectivity (Table 2) due to its key-lock catalytic properties which favor the monobranched isomers formation (high M/B ratio). However, the activity of this catalyst was very low compared to the activity of the β zeolite based catalyst (5 versus 120, Table 2), but the latter catalyst exhibited a weak isomerization selectivity due to its large pore structure associated to the nanocrystallite agglomeration. On the other hand, as expected, the direct germination of the β zeolite over an alumina surface decreased the zeolite mesoporosity (Table 1) indicating the nanocrystallite aggregation decrease, reducing the molecule residence time inside the catalyst. Owing to the consecutive nature of the reaction mechanism, the isomerized molecules can exit the zeolite before they crack, which significantly increased the isomerization selectivity, and also provoked a neat increase in the M/B ratio. This phenomenon was all the less significant as the β zeolite content on the alumina surface increased. The β+Al_2O_3 (1) catalyst exhibited an isomerization selectivity similar to that of the HZSM-22 catalyst, but a much higher catalytic activity.

Table 2. Catalytic test results.

Catalyst	TOF (h^{-1})	M/B ratio[1]	$x_{max\text{-}isomer}$ (%)[2] (conv.%)
HZSM-22	5	8.8	87 (96)
β	120	0.6	55 (66)
β+Al_2O_3 (1)	81	1.8	80 (92)
β+Al_2O_3 (2)	133	1.1	72 (84)
β+Al_2O_3 (3)	110	1.0	65 (83)

[1]ratio between monobranched and multibranched isomers at 20% isomerisation yield.
[2]maximum isomerisation yield.

Conclusions

The direct germination of a β zeolite over alumina improves the zeolite hydroisomerization properties. The resulting catalyst presents at the same time the high activity of the β zeolite and an isomerization selectivity close to that of the HZSM-22 zeolite.

Acknowledgements

N. Batalha thanks the Fundação para a Ciência e Tecnologia (ref.SFRH/BD/43551/2008).

References

[1] Bouchy,C., Hastoy, G., Guillon, E., Martens, J.A., Ficscher-Tropsch waxes Upgrading via hydrocracking and selective hydrosiomerisation, Oil & Gas Science and Technology – Rev. IFP, 64 (2009) 91-112

[2] Martens, J.A., Tielen, M., Jacobs P.A., Relation between paraffin isomerisation capability and pore architecture of large-pore bifunctional zeolites, Studies in Surface Science and Catalysis, 46 (1989) 49-60

[3] Martens, J.A., Vanbutsele, G. Jacobs, P.A., Denayer, J., Ocakoglu, R. Baron, G. Arroyo, J.A.M., Thybaut, J., Marin, G.B., Evidences for pore mouth and key-lock catalysis in hydroisomerisation of long n-alkanes over 10-ring tubular pore bifunctional zeolites, Catalysis Today, 65 (2001) 111-116

Design of Ru-Zeolites for Hydrogen-free Production of Conjugate Linoleic Acids and Conjugated Oils.

An Philippaerts[1], Steven Goossens[1], Jan Geboers[1], Moniek Tromp[2], Stuart Turner[3], Gustaaf Van Tendeloo[3], Pierre Jacobs[1], Bert Sels[1*]
[1]Centre of Surface Chemistry and Catalysis, K.U.Leuven, Heverlee, Belgium; [2]Technische Universitat Munchen, Garching, Germany; [3]EMAT, University of Antwerp, Antwerp, Belgium
[*]bert.sels@biw.kuleuven.be

Introduction

Conjugated linoleic acids (CLAs) and conjugated vegetable oils are interesting compounds in the coatings, paints and polymer industries as well as in the food industry. As conjugated oils "dry" or polymerize more quickly than non-conjugated oils, they are very valuable for use in paints, inks and coatings[1]. Conjugated oils are also very reactive monomers for manufacturing of "bio-plastics"[2]. Finally, CLAs are also interesting from a nutritional point of view. Plenty of literature is available, describing the health benefits of CLAs[3]. While the isomer distribution is not important for the industrial applications (drying oils and bio-plastics), the type of CLA isomer is crucial for their beneficial effects on physiological properties. In particular two isomers have been known for their health effects, *viz. c*9,*t*11 and *t*10,*c*12, while recent research indicates that *t*9,*t*11 CLA also exerts beneficial health effects[4]. Today, CLAs are synthesized in free fatty acid form from vegetable oils rich in linoleic acid using soluble base catalysts[5]. Besides the ecological drawbacks, competitive hydrolysis of the ester linkages is the major limitation of the commercial process. The use of heterogeneous metal catalysts seems a more attractive route for industrial production of CLAs and conjugated oils. However, it does not seem easy to design a catalyst with high CLA selectivity as the competing hydrogenation reaction limits the CLA yield. Moreover, obtained productivity generally is low[6]. This contribution presents the direct production of CLAs over Ru supported on hierargical zeolites.

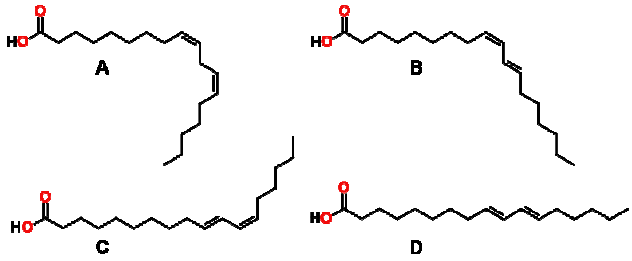

Figure 1. Structure of linoleic acid (C18:2 *c*9,*c*12; A) and three CLA isomers, *c*9,*t*11 (B), *t*10,*c*12 (C) and *t*9,*t*11 CLA (D).

Experimental

Different zeolite supports were loaded with 0.5 wt% Ru by ion-exchange using $Ru(III)(NH_3)_6Cl_3$ as Ru precursor. Prior to metal loading, the zeolite powder was changed from the proton to the NH_4-form by slurrying in an ammonia aqueous solution. Activation was conducted in a flow reactor under flowing nitrogen to 350 °C. Optionally, a reduction step at 400 °C under flowing hydrogen was performed. Catalysts were characterized with SEM, TEM, EXAFS, CO-chemisorption, N_2 physisorption and XRD. Isomerization of methyl linoleate and safflower oil at 165 - 180 °C was carried out in a 100 mL Parr-autoclave with sampling device and under 3.5 bar of N_2 under constant stirring (500 rpm). The fatty acid methyl esters were analyzed with GC.

Results and discussion

Different zeolite supports, varying in topology (ZSM-5, Y, BETA), Si/Al ratio and counter cation (H^+, Na^+, Cs^+) were tested for the conjugation of methyl linoleate. Ru/Cs-USY having a Si/Al ratio of 40 was identified as the most active and selective catalyst for isomerisation of

methyl linoleate to CLA at 165 °C[7]. Interestingly, no hydrogen pre-treatment of the catalyst or addition of H-donors is required to achieve industrially relevant isomerisation productivities. Moreover, the biologically most active CLA isomers, *viz.* *c*9,*t*11, *t*10,*c*12 and *t*9,*t*11, were the main products, especially at low catalyst concentration. Catalyst characterization with CO-chemisorption, EXAFS measurements, TEM analysis and TPO, reveals highly dispersed RuO_2 species in Ru/Cs-USY(40). It is assumed that such clusters in reaction conditions are transformed into highly dispersed Ru metal clusters via a reaction of autoxidation of methyl linoleate by Ru-O. Conjugation seems to be performed by means of hydrogen transfer between the fatty acids and the active Ru metal clusters on the catalyst, i.e. according to a classical Horiuti-Polanyi mechanism, since *cis,trans* CLAs at positions 9,11 and 10, 12 were shown to be primary products converted consecutively into *trans,trans* isomers with double bonds at the same and finally other positions.
Finally, the Ru/USY(40) catalysts were also tested in the isomerization of pure vegetable oils[8]. Because of the particular synthesis procedure, extra mesopores are created in the USY support, facilitating transport of the bulky triglyceride molecules to the active centres of the catalyst. We found a new method for the creation of small mesopores (2-5 nm) in commercially available USY zeolites, which show already some large mesopores (20-30 nm), caused by a steaming process. This is achieved, using only a diluted aqueous NH_3 treatment at room temperature. The degree of mesopore formation can be tuned by the concentration of NH_3 and by the counter cation (H^+<Na^+<Cs^+). Surprisingly, comparison of the Ru-dispersions, as measured by CO-chemisorption, reveals that the Ru dispersion increases with increase of mesopore formation. The mesoporous Ru/Cs-USY(40) catalyst performs excellent in the conjugation of vegetable oils. As an example, the isomerization of safflower oil at 180 °C under N_2, yielded after 2 hours 75 mg CLA/g oil with a very high specific yield, *viz.* 377 g(CLA)/(g(metal).h), pointing to a very efficient process. The level of the desirable *c*9,*t*11 and *t*10,*c*12 isomers at this point was almost 55 mg CLA/g oil. Moreover, as no H_2 or another H-donor is used in the catalytic process, almost no hydrogenation was observed and only very low amounts of undersirable C18:1 *trans* were analyzed in the product mixture.

Conclusions

A mesoporous Ru/Cs-USY(40) catalysts, containing highly dispersed Ru particles, performs excellent in the conjugation of methyl linoleate and vegetable oils. Because of the very high productivities obtained, this process can be a major breakthrough in the production of bio-based drying oils, paints and plastics. Moreover, as the beneficial CLA isomers are the main products with the Ru/Cs-USY catalyst and almost no C18:1 *trans* products are formed, this research may also accelerate the development of CLA enriched functional foods.

Acknowledgements

A.P. acknowledges F.W.O.-Vlaanderen (Research Foundation – Flanders) for a doctoral fellowship. The authors are grateful to the Flemish government for long term sponsoring (Methusalem, CASAS).

References

[1] a) T.F. Bradley, *US 2350583*, 1944; b) R.T. Sleeter, *US 5719301*, 1998; [2] Lu, Y., Larock, R.C., *ChemSusChem* 2, 136 (2009); [3] a) Bhattacharya, A. *et al., J. Nutr. Biochem.* 17, 789 (2006); b) Pariza, M.W. *et al., Progress in Lipid Research* 40, 283 (2001); [4] a) Coakley, M. *et al., Nutr. Cancer* 56, 95 (2006); b) Lee, Y., Vanden Heuvel, J.P., *J. Nutr. Biochem.* 21, 490 (2010); c) Ecker, J. *et al., Biochem. Biophes. Res. Co.*, 388, 660 (2009); [5] a) Saebo, A. *et al., US 6410761 B1* (2002); b) Westfechtel, A. *et al., US 20060106238 A1* (2006); [6] Philippaerts, A., *et al.* (submitted); [7] Philippaerts, A. *et al., ChemSusChem* (2011) (accepted); [8] Philippaerts, A. *et al.* (submitted).

Effects of the synthesis route on the catalytic behaviour of CeO_2 supported on H-ZSM-5 for gas-phase oxidation of 1,2-dichloroethane

C. Sampedro, B. de Rivas, R. López-Fonseca, M.A. Gutiérrez-Ortiz and J.I. Gutiérrez-Ortiz*
*Department of Chemical Engineering, Faculty of Science and Technology, Universidad del País Vasco/EHU, PO Box 644, E-48080, Bilbao, Spain, *joseignacio.gutierrez@ehu.es*

Introduction

Chlorine-containing volatile organic compounds (CVOCs) are widely used in the industry. Their release to the atmosphere involves a considerable environmental impact mainly related to the photochemical smog formation and to the depletion of the ozone layer in the stratosphere. In contrast with thermal incineration catalytic oxidation results more attractive for controlling CVOC emissions since it requires less severe conditions and it is more efficient and economically advantageous for the destruction of low concentrations of pollutants. The major challenge of this technology is to find an appropriate catalyst in terms of efficiency and cost.

In our previous studies we found that the pure cerium oxide, CeO_2, exhibited a promising potential for this environmental application owing to its high oxygen-storage capacity and facile redox cycle of Ce^{4+}/Ce^{3+} [1]. Thus, in order to improve its catalytic behaviour the idea of increasing the surface area of the active CeO_2 phase was explored by spreading CeO_2 at the surface of a support oxide. In this work, the H-ZSM-5 zeolite was particularly selected as a high-surface support. Additionally, it is expected that its notable acid properties may help in promoting the performance of the resulting bifunctional catalyst. Therefore the purpose of this study was to examine several methods for preparing CeO_2/H-ZSM-5 catalysts so as to find useful guidelines to design catalysts with a comparable activity to that exhibited by traditional noble metals and transition metal oxides. The performance of the synthesised catalysts was evaluated for the deep oxidation of 1,000 ppm of 1,2-dichloroethane (DCE). DCE is typically encountered in waste streams from chemical plants (PVC production) and dry-cleaning applications.

Experimental

Cerium nitrate was used as a cerium precursor. The HZSM-5 zeolite (Si/Al=27.3) was supplied by Zeolyst Corp. Four different methods were employed for obtaining CeO_2(10wt.%)/H-ZSM-5 catalysts: impregnation in aqueous solution (10CeIMw) and in organic solution (10CeIMe), precipitation with ammonium hydroxide (10CePP) and ion exchange (10CeEX). The samples (0.3-0.5 mm) were calcined in air at 550 ºC for 4 h. Then, they were characterised using various techniques, in an effort to understand the possible surface and structural characteristics that may contribute to the differences in performance for chlorinated VOC oxidation. Catalytic tests were performed in a bench-scale fixed bed reactor (150-550 ºC, 0.85 g, 500 ml min^{-1}) operated at atmospheric pressure and fully monitored by computer.

Results and discussion

XRD analysis showed that in all cases, cerium oxide was deposited over the zeolite with a fluorite-like structure. In addition TEM images showed that CeO_2 was deposited on the external surface of the zeolitic support [2]. On the other hand it was noted that the surface area was at around 370 m^2 g^{-1} irrespective of the synthesis route. Nevertheless, the preparation method did have a marked influence on the mean diameter of the CeO_2 crystallites [3]. Table 1 shows that smaller crystallites (3 nm) were obtained when the supported catalyst was prepared by impregnation with ethanol. This procedure led to a sample with a better ceria

dispersion, which entailed a promoted cerium reduction as revealed by the larger hydrogen consumption. On the other hand, the zeolite, apart from having a high surface area, expectedly presented a high surface acidity. The acid properties of the bifunctional catalysts were even slightly increased when ceria was incorporated with the 10CeIMe sample exhibiting the highest surface acidity.

Table 1. Physico-chemical properties of the bifunctional CeO_2/H-ZSM-5 catalysts.

Catalyst	Ce, wt%	S_{BET}, $m^2\ g^{-1}$	$dCeO_2$, nm	Total acidity, μmol $NH_3\ g^{-1}$	H_2 uptake (650 ºC), μmol $H_2\ g^{-1}$
H-ZSM-5	---	407	---	732	---
10CeIMw	11	372	8	742	260
10CeIMe	13	374	3	788	586
10CePP	13	374	4	659	441
10CeEX	5	373	-	664	177
CeO_2	100	99	10	112	340

Figure 1 shows the light-off curves of the prepared catalysts. For comparative purposes the activity data from pure CeO_2 and protonic zeolite are included. Interestingly, in all cases CeO_2 supported catalysts presented a promoted activity in relation to the reference bulk oxides. The following activity pattern was found: 10CeIMe>10CeIMw>10CePP>10CeEX>H-ZSM-5>> CeO_2. T_{50} values were in the 200-250 ºC range. Activity was thus found to be governed by a suitable combination of a notable surface acidity accompanied by an easy reduction of ceria crystallites. This observation was consistent with the best behaviour of 10CeIMe. Moreover, a higher crystallite size (7.6 nm) can be compensated by a larger acidity (742 μmol $NH_3\ g^{-1}$). This is the case corresponding to 10CeIMw which is more active than 10CePP with a crystallite size of 4 nm.

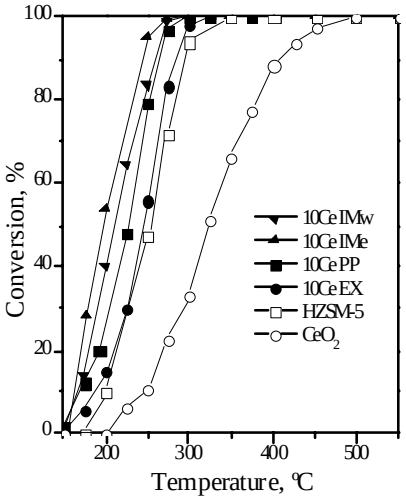

Figure 1. Light-off curves of the oxidation of DCE.

Also the product distribution of DCE oxidation was investigated. On one hand, H-ZSM-5 gave rise to notable amounts of vinyl chloride and CO as by-products. However, the CeO_2 supported catalysts were markedly more selective to CO_2 with a significantly reduced formation of the chlorinated by-product. CeO_2 also showed a certain activity for the Deacon reaction (oxidation of HCl to Cl_2) that led to the generation of appreciable quantities of molecular chlorine.

Acknowledgements

The authors wish to thank the UPV/EHU-Gobierno Vasco (SAIOTEK S-PE09UN23) for the financial support.

References

[1] de Rivas, B., López-Fonseca, R., Gutiérrez-Ortiz, M.A., Gutiérrez-Ortiz J.I., Structural characterisation of $Ce_{0.5}Zr_{0.5}O_2$ modified by redox treatments and evaluation for chlorinated VOC oxidation, Applied Catalysis B: Environmental, 101 (2011) 317-325.

[2] Sugi, Y., Kubota, Y., Komura, K., Sugiyama, N., Hayashi, M., Kim, J.-H., Seo, G., Shape-selective alkylation and related reactions of mononuclear aromatic hydrocarbons over HZSM-5 zeolites modified with lanthanum and cerium oxides, Applied Catalysis A: General, 299 (2006) 157-166.

[3] Song, H., Ozkan, U.S., The role of impregnation medium on the activity of ceria-supported cobalt catalysts for ethanol stream reforming, Journal of Molecular Catalysis A: Chemical, 318 (2010) 21-29.

Catalysis for fine chemicals and pharmaceuticals

FEZA 2011

Catalytic Activity of Lipase Immobilized in Novel Cage-like Mesoporous Organosilicas

Zhou Zhou, Simon Kullmann, Martin Hartmann (Martin.Hartmann@ecrc.uni-erlangen.de), Erlangen Catalysis Resource Center (ECRC), Friedrich-Alexander-Universität Erlangen-Nürnberg, Germany*
Robin N. Klupp Taylor, Huixin Bao, Institute of Particle Technology, Friedrich-Alexander-Universität Erlangen-Nürnberg, Germany

Introduction

In recent years, one of the most promising and rapidly growing areas is the utilization of enzymatic catalysis in the field of green and sustainable chemistry. Enzymes possess high activities as well as high chemo-, regio-, and stereo-selectivities under mild reaction conditions. However, the application of enzymes in industry is often hampered by their low operational stability (denaturation and deactivation), as well as the difficulties in recovery and recycling [1]. Thus, immobilization of enzymes onto solid supports attracts a lot of attention. Previous studies have shown that the ordered mesoporous silicas are promising candidates for the adsorption of enzymes [2]. As a consequence, interest has grown in the use of periodic mesoporous organosilicas as supports. Here, lipase from thermomyces lanuginosus (TLL) was chosen as model enzyme because it is a noticeably thermostable enzyme, which has been employed as biocatalyst in a variety of synthetic and industrial applications [3].

Experimental

The cage-like PMOs were synthesized by using TMB as a swelling agent and the block copolymer P123 as template under hydrothermal condition. For the immobilization of lipase, 10 mg of support was added to 1 mL of a TLL buffer solution by standard Bradford method before and after the sorption experiment. The hydrolysis activity was determined using 4-nitrophenyl palmitate (*p*NPP) as substrate; one unit is defined as the amount of lipase that liberates 1 µmol *p*-nitrophenol per minute. The transesterification activity of the immobilized lipase was tested by acylation of alcohols with vinyl propionate.

Results and discussion

In the present work, a group of hierarchically ordered PMOs with large cage-like pores were prepared with various organosilica units (ethylene, ethenylene, and phenylene bridged silanes). For the first time, TLL was physically adsorbed on these PMOs materials. The resulting biocatalysts were applied in hydrolysis and transesterification reactions. It turns out that the amount of lipase adsorption is significantly influenced by the organosilica units in the framework of the materials. All the PMOs exhibit higher adsorption capacity in comparison to pure silica supports (**Figure 1a**). Using phenylene-PMO as support, the total amount of lipase was adsorbed from buffer solution within one hour (Figure 1a **$LP_{benzene}$**). Moreover, we found that lipase immobilized on this series of materials showed much higher stability (**Figure 1b**) compared to lipase immobilized on pure silica materials. Lipase immobilized on PMOs exhibits relative activities of up to 500 % compared to the free lipase in the hydrolysis of *p*NPP. Furthermore, these novel catalysts were tested in the catalytic transesterification of vinylpropionate with 1-butanol in hexane. A butylpropionate yield of 80% was obtained at 40 ^{o}C with immobilized lipase on phenylene-PMO (**Figure 2** and **Table 1**). By increasing the reaction temperature to 60 ^{o}C, the product yield can be further improved. Meanwhile, the catalysts with the most hydrophobic surface (**$LP_{benzene}$**) preserves a high activity in the recycling runs. On the contrary **LP_{silica}** lost most of its activity after the first run.

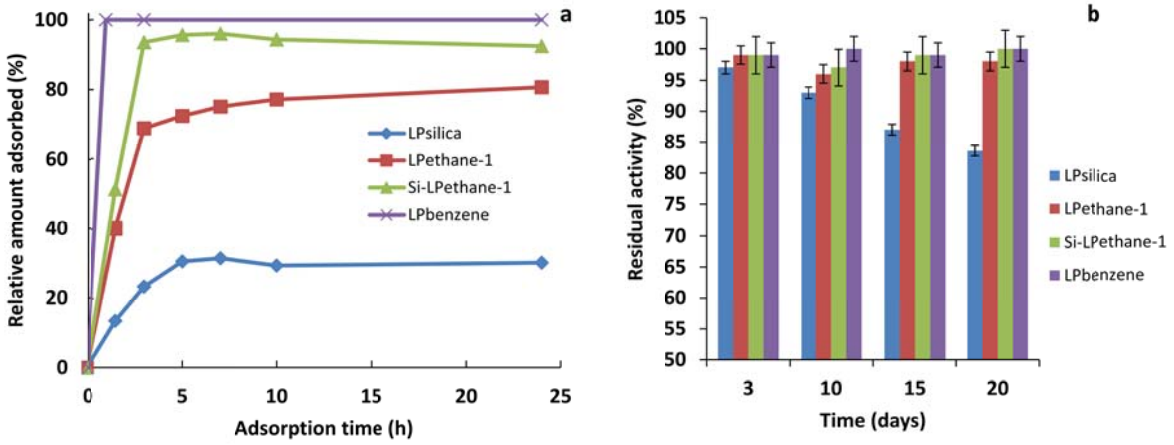

Figure 1. (a) Adsorption kinetics of lipase at 298 K (in a TLL/buffer solution, C = 0.24 g /L), and (b) Stability of immobilized TLL in buffer solution at room temperature.

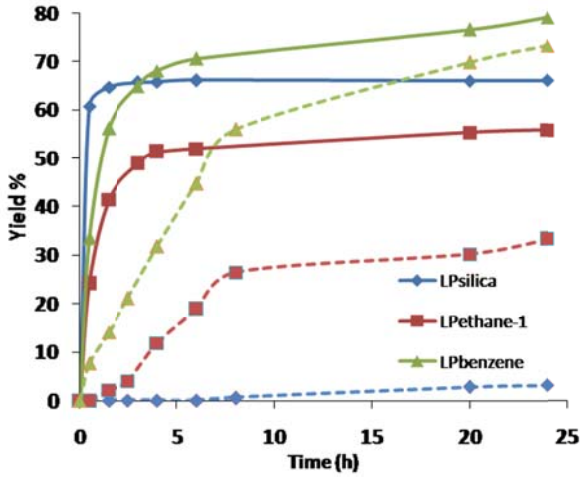

Table 1. The results of immobilized lipase catalyzed transesterification reaction.

Catalyst	T °C	Yield (%)[a]	Yield (%)[b]
LP_{silica}	40	66.0	3.0
	60	72.6	4.1
$LP_{ethane-1}$	40	55.9	33.2
	60	70.1	40.5
$LP_{benzene}$	40	80.0	73.3
	60	96.2	85.7

[a] first run after 24h; [b] recycle run after 24h. Yield was determined by GC with internal standard.

Figure 2. Transesterification of vinylpropionate with 1-butanol (1:1 molar ratio) over lipase immobilized on different supports in hexane using 10 wt% of immobilized lipase at 40 °C under stirring (500 rmp); (solid lines) first run; (dash lines) second run.

Conclusions

In conclusion, we have prepared a series of large-pore hierarchically ordered mesocellular cage-like organosilicas. Owing to the unique structure and hydrophobic surface property, the materials show an unprecedented high enzyme loading without mass-transfer limitations. Due to the inorganic-organic hybrid nature and the structure of these materials, they are superior supports which protect the immobilized lipase and enhance its catalytic activity.

Acknowledgements

We thank Alexandra Inayat for performing the argon adsorption experiments. The authors gratefully acknowledge the support of the Cluster of Excellence 'Engineering of Advanced Materials' at the University of Erlangen-Nürnberg.

References

[1] (a) V. V. Mozhaev, M. V. Sergeeva, A. B. Belova, Y. L. Khmelnitsky, Biotechnol. Bioeng. 35 (1990), 653. (b) S. G. Burton, D. A. Cowan, J. M. Woodley, Nat. Biotechnol. 20 (2002), 37.
[2] (a) M. Hartmann, D. Jung, J. Mater. Chem. 2010, 20, 844. (b) M. Hartmann, Chem. Mater. 17 (2005), 4577. (c) D. Jung, M. Paradiso, D. Wallacher, A. Brandt, M. Hartmann, ChemSusChem 2 (2009) , 161.
[3] R. Fernandez-Laffuente, J. Mol. Catal. B: Enzym. 62 (2009), 197.

Deciphering Support-Catalyst Interfaces within Heterogeneous Bio-derived Frameworks

David Xuereb, Joanna Dzierzak, Robert Raja*.
*School of Chemistry, University of Southampton, UK, SO17 1BJ. *Corresponding Author: R.Raja@soton.ac.uk; Presenting Author: djx1e08@soton.ac.uk*

Introduction

Heterogenizing bio-inspired organocatalysts and transition-metal complexes on a diverse range of porous supports provide practical alternatives to current methods and catalysts used in industrially significant processes. Solid phase bio-derived frameworks facilitate demanding chemical transformations in an environmentally benign and more sustainable manner. In light of the apparent advantages heterogeneous catalysts offer over homogeneous analogues, such as improvement in recycling, ease of recovery and stability, more appreciable consequences have become perceptible especially in terms of activity and selectivity. Previously [1] it has been established that deliberate restrictions of space inside the pore of a support, particularly in the vicinity of a tethered active site, induces chirality in a target molecule. Understanding this effect and the influence the support can have mechanistically on the stereo-chemical outcome of catalysis can be a great asset in being able to predict product distribution and stereomeric excesses. Moreover, the appreciation of the support-catalyst relationship provides avenues for not only optimising reaction conditions but to specifically tailor the support for desired outcomes in selectivity.

Well-characterized transition-metal complexes, which mimic the catalytic function of the active centres in metalloenzymes, can be anchored in a site-isolated fashion on to inorganic supports, giving rise to highly active and selective heterogeneous catalysts [2] (Fig 1). Using similar methods, amino acids that act as organocatalysts can also by immobilized and utilized in fundamental organic reactions such as the asymmetric aldol reaction, which is of great value when carried out with high selectivity, especially in the synthesis of complex drug molecules and fine chemicals.

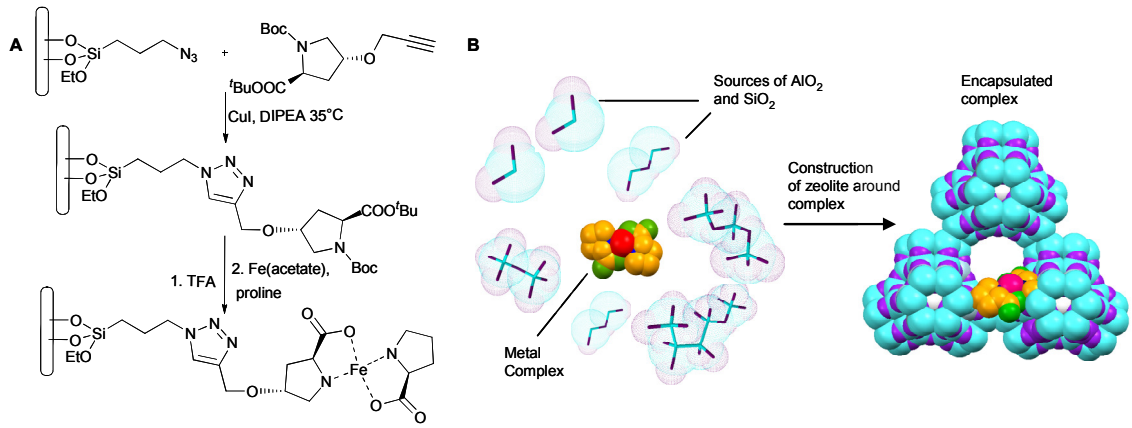

Figure 1: Covalent anchoring to mesoporous silica (A) and encapsulation within a zeolite (B).

Experimental

Metal amino acid complexes were encapsulated in zeolite X using a 'zeolite synthesis method' [3]. Heterogenization of the complexes onto mesoporous silica was achieved by covalent anchoring an amino acid through 'click chemistry' methods or by functionalizing the side chain with a tether before grafting, followed by coordination to the metal centre. Benzyl alcohol oxidation with O_2 was performed under a high-pressure and reaction products analysed by GC. Asymmetric aldol reactions were carried out in anhydrous conditions with ee's calculated using HPLC.

Results and discussion

Varying the support type, immobilization procedure and support properties of the bio-derived frameworks whilst concurrently measuring the direct effect on the catalysis can provide valuable information on the relationship between support and active site. In the presence of Fe-Proline complex benzyl alcohol can be selectively oxidised to benzaldehyde and the activity of the catalyst increases upon heterogenization due to the isolated single-site nature of the catalytic complex (Fig 2 right). More strikingly, turnover-numbers are significantly improved with immobilization on mesoporous silica in comparison to that of encapsulation within aluminosilicates. Understanding the reasons for this affords vital information about the mechanistic pathway, therefore providing opportunities to optimize catalysis. The same notion can be applied to covalently anchored organocatalysts on mesoporous silica. Results show (Fig 2 left) the ee of the aldol reaction is dependent on the pore diameter of the support. The pore aperture establishes the extent of the support-catalyst interaction and therefore the magnitude to which it affects the transition states in the mechanistic pathway that determine stereoselectivity. Rationalizing this interaction can be used to predict unexplored trends in catalyst behaviour (blue and orange sectors in Fig 2 left).

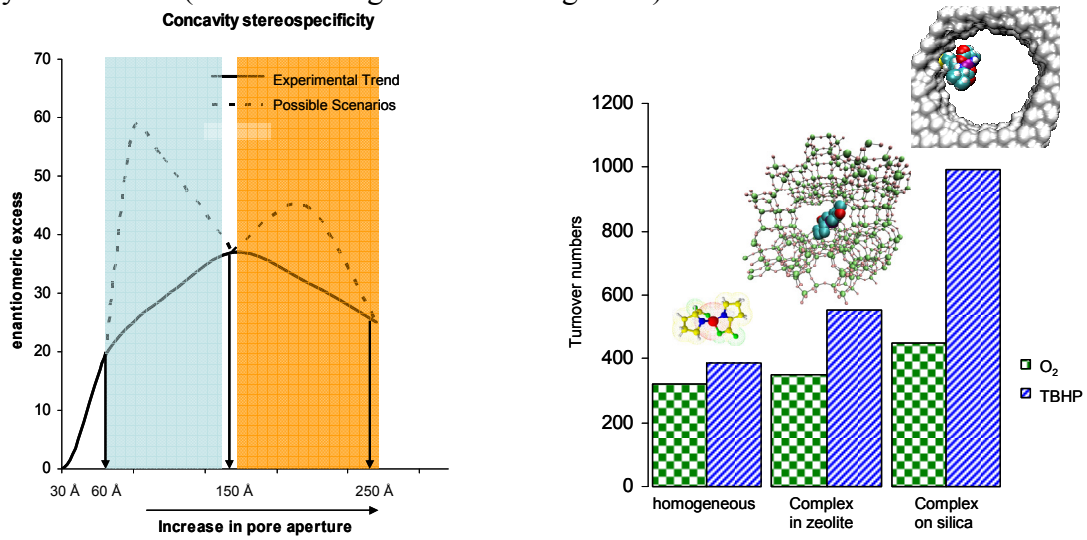

Figure 2. Support pore aperture affect on ee in the aldol reaction (left). Changes in activity of Fe-Proline catalyst in the oxidation of benzyl alcohol depending on support type (right).

Conclusions

Developing the insight into the relationship between the surface and the active-site creates novel approaches towards the rational design and optimisation in heterogeneous catalysis through support tuning and modification.

Acknowledgements

We would like to thank the EPRSC UK and the British-Italian Partnership for funding.

References

[1] (a) Thomas, J. M., Raja, R., Exploiting nanospace for asymmetric catalysis: confinement of immobilized, single-site chiral catalysts enhances enantioselectivity, accounts of chemical research, 41 (2008), 708-720 (b) Jones, M. D., Raja, R., Thomas, J. M., Johnson, B. F. G., Lewis, D. W., Rouzaud J., Harris, K. D. M., Enhancing the enantioselectivity of novel homogeneous organometallic hydrogenation catalysts, Angewandte Chemie-International Edition, 42, (2003), 4326-4331

[2] Dzierzak, J., Bottinelli, E., Berlier, G., Gianotti, E., Stulz, E., Kowalczyk R. M., Raja, R., The role of isolated active centres in high-performance bioinspired selective oxidation catalysts, Chemical Communications 46, (2010), 2805-2807

[3] Raja, R., Ratnasamy, P., Oxidation of cyclohexane over copper phthalocyanines encapsulated in zeolites, Catalysis Letters, 48, (1997), 1-10

Ionic liquids supported on SBA-15 as catalysts for chemical fixation of carbon dioxide: a high-throughput study in $scCO_2$.

C. Aprile,[a,b] F. Giacalone,[c] L. Liotta,[c] J. A. Martens,[b] P. P. Pescarmona,[b] M. Gruttadauria.[c]

[a] *Unité de Chimie des Nanomatériaux, FUNDP, Rue de Bruxeles 61, 5000, Namur, Belgium*
E-mail: carmela.aprile@fundp.ac.be
[b] *COK, K.U.Leuven, Kasteelpark Arenberg 23, 3001 Heverlee, Belgium*
[c] *Università degli Studi di Palermo, Viale delle Scienze, Pad. 17, 90128, Palermo, Italy.*

Introduction

The distinctive characteristics of mesoporous materials make them ideal scaffolds for hosting functional guests, including catalytically active species. Herein we report the synthesis of a new class of materials consisting of an ionic liquid phase supported on SBA-15, and their catalytic application in the cycloaddition of carbon dioxide to epoxides to yield cyclic carbonates. The chemical fixation of carbon dioxide is an attractive topic due to possibility of both recycling the greenhouse gas CO_2 and, at the same time, converting it into valuable products such as cyclic carbonates.[1] Recently, simple supported ionic liquids with halides counter-ions have been successfully employed as catalysts for the chemical fixation of carbon dioxide.[2] Our new class of catalysts is generated by the cross-linking and anchoring of multilayers of bis-vinylimidazolium salts on mercaptoalkyl-modified SBA-15. The combination of the activity of the ionic liquid with the characteristics of the porous matrix leads to excellent catalytic results.

Experimental

The experimental conditions used for the synthesis of cyclic carbonates are listed in Table 1. In all cases supercritical CO_2 was used with the double role of reagent and solvent. The experiments were performed using an innovative high-throughput reaction block.

Table 1. Reaction conditions for the synthesis of cyclic carbonates.

Catalysts[(a)]	Temperature (°C)	Pressure (bar)	Time(h)
SBA-15- ClA	150	100	3
SBA-15-ClB	150	100	3
SBA-15-BrB	150	100, 80[(b)]	3,1[(b)]
PS-ClA	150	100	3
PS-BrA	150	100	3

high-throughput reaction block

(a) Two different reactions conditions for the anchoring of the imidazolium salt were used: mechanical stirring (catalysts A) and magnetical stirring (catalysts B).
(b) Reaction performed in a visualization reactor (non high-throughput)

Results and discussion

Ordered mesoporous SBA-15 silica functionalized with mercaptopropyl groups was used as support for imidazolium catalysts bearing different counter ion (SBA-15-X). The synthesis was performed by reacting the thiol functionalized porous matrix with a bis-vinylimidazolium salt. Since the ionic liquid is added in excess relatively to the amount of -

SH groups, a newtwork of cross-linked imidazolium was obtained through self-addition reaction of the double bonds. The multilayered ionic liquid phase was generated through this oligomerization.

The materials were tested for the synthesis of cyclic carbonates and their activity was compared with ionic liquid supported on polystyrene (PS) prepared with the same approach. In order to investigate the versatility of our catalysts, three different epoxides were selected as substrates for the reaction with CO_2: a monosubstituted aliphatic epoxide such as propylene oxide, a monosubstituted aromatic compound like styrene oxide and the disubstituted cyclohexene oxide. The results evidenced a better catalytic activity of the SBA-15 supported ionic liquids (Fig. 1). The best of our catalysts, SBA-15-Br-B, displays a very high catalytic activity: after 1h reaction at 80 bar it gives a very good styrene carbonate yield (close to 75%) and reaches 90% epoxide conversion after 3h reaction, in all cases with a complete selectivity towards the cyclic carbonate product.

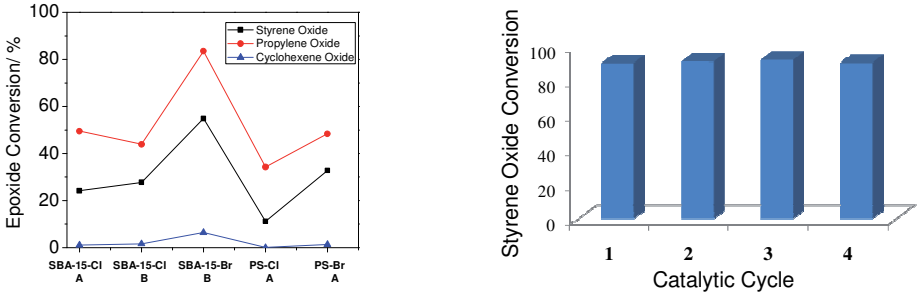

Figure 1. Cycloaddition of carbon dioxide to different epoxides (left) and recycling experiments of SBA-15-Br-B for the synthesis of styrene carbonate.

Thanks to its multilayered structure, SBA-15-Br-B achieves higher productivity (g of product per gram of catalyst) compared with other supported ionic liquid reported in the literature. The observed high productivity is an important feature from an industrial point of view, since a reduced amount of catalyst in a process would result in easier working up procedures and lower costs.

Conclusions

New multilayered ionic liquids supported on SBA-15 were synthesized and the materials were tested as catalysts for the chemical fixation of carbon dioxide. The best catalyst (SBA-15-BrB) achieved very high conversion and selectivity in the reaction with propylene and styrene oxides and displayed improved productivity compared to known supported ionic liquid catalysts. The catalyst can be easily recovered and recycled in consecutive catalytic runs without loss of activity. Rapid screening and reliable comparison of the catalytic behaviour of the materials was made possible by the use of a novel, unique high-throughput experimentation unit for studying reactions under supercritical carbon dioxide.

References

[1] D. H. Gibson, *Chem. Rev.*, 1996, **96**, 2063
[2] J. Sun, W. G. Cheng, W. Fan, Y. H. Wang, Z. Y. Meng and S. J. Zhang, *Catal. Today*, 2009, **148**, 361

Influence of defective sites of Silicalite-1 surface materials on the catalytic etherification reaction of 5-hydoxymethylfurfural

P. Lanzafame[a,*], D. M. Temi[a], S. Perathoner[a], G. Centi[a], A. Macario[b], A. Aloise[b] and G. Giordano[b]
[a] *Department of Industrial Chemistry and Engineering of Materials and CASPE-INSTM, Univ. of Messina, 98166Messina, Italy*
[b] *Department of Chemical Engineering and Materials, Univ. of Calabria, Rende, 87030 Cosenza, Italy*
[*] *corresponding author: planzafame@ingegneria.unime.it*

Introduction

The interest in renewable resources as chemical feedstocks for fuels and chemicals is considerably growing. For example, 5-hydroxymethylfurfural (5-HMF), the main product in the acid-catalyzed conversion of ligno-cellulosic biowastes, is a key platform molecule for the production of energy products, monomers for polymers and valuable fine chemicals [1].
In an our previous study, we have demonstrated that it is possible to obtain valuable components for biofuels [2] selectively, such as 5-(ethoxymethyl)furan-2-carbaldehyde (EMF), 1,1-dietoxy ethane (DE) and the ethyl 4-oxopentanoate (EOP) , by tuning the acidity of the catalyst surface in the etherification reaction of 5-HMF with ethanol [3].
As a consequence of these first results, we have better investigated the role played by the zeolitic defective sites on the catalytic behavior of Silicalite-1 in the etherification by ethanol of 5-HMF. In order to tune the hydroxyl population of the Silicalite-1 surface, different post-synthesis treatments have been carried out on the as-made catalysts. As function of the thermal treatment, the pH value of the ionic-exchange and the silylation procedure, the study on the catalytic behavior of the Silicalite-1 materials, in the above mentioned reaction, has been carried out. ^{29}Si-NMR, NH_3-TPD and IR analyses have been used as usual techniques in order to characterize the activated catalysts. The Amberlyst®15 catalyst has been used as referring solid acid catalyst, with strong Brönsted acidity.

Experimental

The Silicalite-1 materials have been prepared starting form a gel having the following molar composition: $1SiO_2$ –0.08 NaOH - 0.08 TPABr - $20H_2O$. All samples have been calcined at 450°C in air flow. After the calcinations procedure, the samples have been submitted to ionic exchange procedures by ammonium salt (in order to obtain the NH_4^+-form) and to a second thermal treatment at 450°C (in order to obtain the catalysts in H-form). The ionic exchanges have been performed at two different pH values = 5.5 or 10.5. Moreover, Silicalite-1 type material in H-form, has been silylated by hexamethildisilazane (HDMS) as organo-silane. Catalytic tests have been performed in a Teflon lined steal autoclave and carried out at 413 K for 5 hours. After the reaction the products were collected and analyzed using a Finnigan Trace GC Ultra with FID detector.

Results and discussion

Table 1 summarizes, as function of the post-synthesis treatments, the amount of the defective sites of the catalysts, measured by ^{29}Si NMR spectroscopy. It is possible to notice that the post-synthesis treatments strongly affect the hydroxyl population of the catalyst surface. As it can be expected, the calcination procedure drastically reduce the silanol groups of as made sample. Moreover, the ionic-exchange at low pH leads to the formation of the geminal silanols $Si(OH)_2$, while the silylation procedure allows to obtain a Silicalite-1 catalyst surface with the lowest silanol groups content.

Table 1. Post-synthesis treatments and amount of defect groups of the prepared catalysts.

Code Name	Characteristics of the catalyst surface	pH[#]	nr. SiOH/c.u. [§]	$Si(OH)_2$*
Na-Silicalite-1	As made	-	22	No
Na-S	Silicalite-1 in Na-form (after calcination)	-	4.8	No
S-NH_4^+-A	Silicalite-1 in NH_4^+-form	5.5	5.2	Very few
S-H-A	Silicalite-1 in H-form	5.5	4.7	few
S-NH_4^+-B	Silicalite-1 in NH_4^+-form	10.5	4.4	No
S-H-B	Silicalite-1 in H-form	10.5	5	No
S-HMS	S-H-B after silylation treatment	10.5	1.3	No

 # pH value of the ionic-exchange procedure
§ number of difective sites for cell unit
** geminal silanols estimated by ^{29}Si-NMR spectra*

The data obtained by catalytic tests evidence that the yields are closely related with the amount and the typology of hydroxyl groups in the Silicalite-1 materials (Fig. 1). When the number of silanols on the catalyst is low, the main reaction product is EOP, but when the number of silanols groups is increased the formation of DE is favored with respect to those of EOP. Increasing the number of defects on the Silicalite-1, indeed, the strength of Brönsted acid sites, responsible for the formation of EOP, is decreased.
The formation of EMF is also observed.

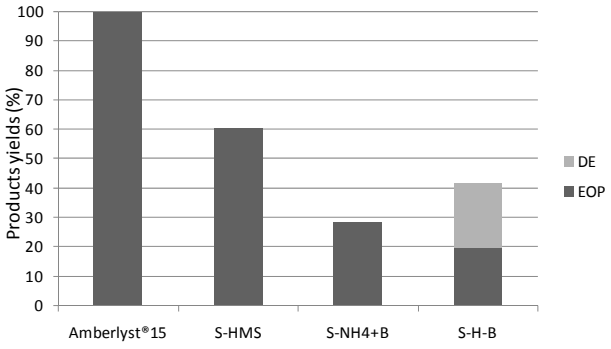

Figure 1. Main products yield from 5-HMF and ethanol

Conclusions

It was shown how the post-synthesis treatments affect the presence of defects on Silicalite -1 materials and how the presence of these defects plays an important role on the selectivity in the etherification of 5-HMF with ethanol to products of interest for biofuels and chemicals production. Further investigations are in progress to better understand the influence of the presence of these defects sites on the reaction mechanism.

Acknowledgements

This study was realized in the frame of the activities of Italian PRIN08 project "Catalytic upgrading of the fraction C5 in ligno-cellulosic biorefineries".

References

[1] Centi, G., Lanzafame, P., Perathoner, S., Analysis of the alternative routes in the catalytic transformation of lignocellulosic materials Catal. Today (2011),doi:10.1016/j.cattod.2010.10.099
[2] Gruter, G.J.M., Dautzenberg, F., Eur. Patent EP 1834950 (2007).
[3] Lanzafame, P., Temi, D.M., Perathoner, S., Centi, G., Macario, A., Aloise, A., Giordano, G., Etherification of 5-Hydroxymethyl-2-furfural (HMF) with ethanol to biodiesel components using mesoporous solid acidic catalysts, submitted to Catalysis Today

A Novel ITQ-2/TUD-1 Micro-Mesoporous Composite: *In-situ* Delamination as a Tool for the Preparation of Innovative Materials

Cindy C. Aquino, [a] Heloise O. Pastore, [b] Anthony F. Masters [a] and Thomas Maschmeyer [*,a]

[a] *Laboratory of Advanced Catalysis for Sustainability School of Chemistry, The University of Sydney , NSW 2006 Australia,* [b] *Micro- and Mesoporous Molecular Sieves Group, Instituto de Química, University of Campinas, SP Brazil.* [*]*E-mail: th.maschmeyer@chem.usyd.edu.au*

Introduction

Here, we report a new, one-pot method to prepare a highly active and yet selective as well as stable acidic micro-mesoporous zeolite catalyst composite for the conversion of bulky substrates (acetylisation of aldehydes). The process involves generating highly dispersed zeolitic sheets (ITQ-2) inside the synthesis gel of a mesoporous host structure (siliceous TUD-1) by the *in-situ* delamination of the zeolite MCM-22(P).

The active sites of zeolites reside mostly inside the microporous system. This spatial constraint imparts selectivity (substrate, product and transition state),[1] but at the cost of increased diffusion barriers. Our new methodology for the *in-situ* preparation of micro-mesoporous composites aims to address such issues and will be contrasted with the more established dispersion of pre-formed zeolite nanocrystals inside a mesoporous host.[2-4]

Experimental

Synthesis: The synthesies of MCM-22(P) and of TUD-1 were based on previously published procedures.[5-6] MCM 22(P) was swollen and delaminated according to Corma *et al.*[7] A typical example of the *in-situ* swelling and delamination of MCM-22(P) inside a TUD-1 synthesis gel to form the ITQ-2/TUD-1 composite is as follows: CTA^+ swollen MCM 22(P) was combined with triethanolamine (TEA, 7.2 g) and stirred at room temperature for 20 h. Then TEOS (10 g) was added dropwise and the bi-phasic mixture stirred for 40 min. Subsequently, it was exposed to ultrasonic treatment for 2.5 h, after which 5.3 g of a 40 wt % aqueous solution of TEAOH was added dropwise over a period of 5 min., followed by the drop-wise addition of distilled water (6.3 g) also over a period of 5 min. The mixture was then stirred for 24 h at room temperature after which time a cloudy solution/suspension had formed, which was dried at 100 °C overnight and transferred to a Teflon lined autoclave, where it was heated at 180 °C for 16 h. The material was extracted with ethanol and then calcined at 600 °C for 10h to produce *in-situ* ITQ-2/TUD-1 as a white powder.

Catalysis: All reaction steps were performed using Schlenk techniques. With all the materials tested, the total molar amount of aluminium was held constant (determined by ICP), assuming that every aluminium centre gives rise to an active site. For the acetalyzation of the aldehydes the reaction mixture also comprised trimethyl orthoformate, TMOF (14.1 mmol) in dichloromethane (2 mL) as solvent to achieve a single organic phase. The resulting catalyst suspensions were stirred at 40 °C under a N_2 atmosphere. Samples were taken at intervals (over 45 min.) and the reaction progress was analysed with gas chromatography, GC, and combined GC/MS (mass spectroscopy). All mass balances were +95%.

Results and Discussion

To determine if the *in-situ* delaminated material possesses advantages over the *ex-situ* ITQ-2/TUD-1 composite or the pure zeolite ITQ-2, the catalytic performance of these materials was tested and compared. The aldehydes screened are (in order of increasing bulkiness) heptaldehyde (I), 2 phenylpropionaldehyde (II) and diphenylacetaldehyde (III). The results are summarised in Table 1 and Figure 1. As expected, for all three substrates

TUD-1 alone shows no activity and there is no difference between ITQ-2's activity on its own and when part of a physical mixture with TUD-1.

Table 1. Summary of the rate constants for the acetalyzation reactions performed at 40°C, assuming a pseudo first-order reaction rate (SiO_2/Al_2O_3 of starting MCM-22(P) = 50).

Material	Rate Constant k ($*10^{-5}$ (s^{-1}))		
	(I)	(II)	(III)
TUD-1	-	-	-
ITQ-2	13	3.7	3.2
Physical mixture: ITQ-2/TUD-1	13	3.5	3.1
Composite: *Ex-situ* ITQ-2/TUD-1	11	7.5	6.9
Composite: *In-situ* ITQ-2/TUD-1	21	11	7.3

For the heptaldehyde (I), the relatively low steric demand of the substrate renders the differences between ITQ-2 and *ex-situ* ITQ-2/TUD-1 to be minimal. However, *in-situ* ITQ-2/TUD-1 displays much higher activities, consistent with the hypothesised better accessibility of the substrates to the composite's active sites due to the *in-situ* rather than *ex-situ* preparation method and also consistent with the mesoporous support acting as a 'sponge', pre-concentrating the substrate (as observed previously by Lercher *et al.*[8,9]) – an effect not available for unsupported ITQ-2. A more bulky substrate should accentuate these differences and this is, indeed, what can be observed. When 2 phenylpropionaldehyde (II) is tested there are now clear differences in the rates observed for ITQ-2 and those of the composite materials (ITQ-2 < *ex-situ* ITQ 2/TUD-1 < *in-situ* ITQ-2/TUD-1).

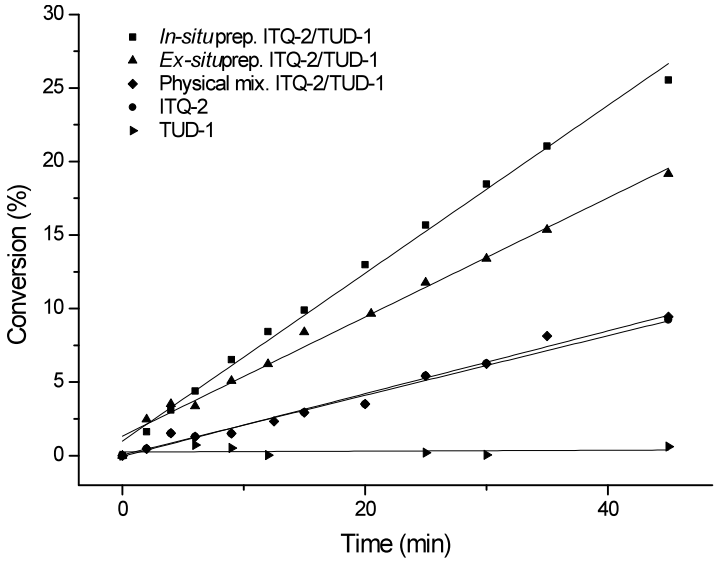

Figure 1. Conversion of 2-phenylpropionaldehyde to its diacetal over catalysts synthesised from MCM-22(P) with SiO_2/Al_2O_3 = 50 as a function of time.

Conclusions

Thus, the *in-situ* delamination preparation offers a novel and facile approach for the generation of micro-mesoporous nanocomposite materials, where layered zeolitic materials can be incorporated into the mesoporous structure and enhance the zeolite's reactivity.

References

[1] S. van Donk, A. H. Janssen, J. H. Bitter, K. P. de Jong, *Catal. Rev.* **2003**, *45*, 297-319.
[2] J. Čejka, S. Mintova, *Catal. Rev.* **2007**, *49*, 457-509.
[3] P. Waller, Z. Shan, L. Marchese, W. Zhou, T. Maschmeyer, *et al., Chem. Eur. J.* **2004**, *10*, 4970-4976.
[4] S. Lima, M. Pillinger, M. F. Ribeiro, A. A. Valente, *et al., App. Catal. A.* **2010**, *388*, 141-148.
[5] J. C. Jansen, Z. Shan, L. Marchese, W. Zhou, N. v. d. Puil, T. Maschmeyer, *Chem. Commun.* **2001**, 713-714.
[6] A. L. Santos Marques, J. L. J. L. Fontes Monteiro, H. O. Pastore, *Micro. Meso. Mater.* **1999**, *32*, 131-145.
[7] A. Corma, V. Fornes, S. B. Pergher, T. L. M. Maesen, J. G. Buglass, *Nature* **1998**, *396*, 353-356.
[8] A. Jentys, R. R. Mukti, J. A. Lercher, *J. Phys. Chem. B* **2006**, *110*, 17691-17693.
[9] A. Jentys, H. Tanaka, J. A. Lercher, *J. Phys. Chem. B* **2005**, *109*, 2254-2261.

2-Butyne-1,4-diol hydrogenation over palladium supported on Zn^{2+}-based MOF and host-guest MOF/calix[4]arene materials

V. I. Isaeva[1], O. P. Tkachenko[1], E. V. Afonina[1], L. M. Kozlova[1], G. I. Kapustin[1], W. Grünert[2], and L. M. Kustov[1]

[1]N. D. Zelinsky Institute of Organic Chemistry RAS, Moscow, 119991, Russia, tel.704991358991, fax 704991355328, sharf@ioc.ac.ru, LMK@ioc.a.ru,

[2]Lehrstuhl für Technische Chemie, Ruhr-University Bochum, D-44780 Bochum, Germany

Introduction

Metal-organic frameworks are microporous and mesoporous crystalline coordination polymers that may have perspective application for gas separation, catalysis and ion exchange. In particular, MOFs have attracted interest as novel support materials for heterogeneous catalysts [1]. From this point of view, MOFs are regarded as very interesting systems characterized by a number of variable parameters: network topology, surface area, porosity, crystalline phase uniformity, functionality responsible for donor-acceptor interactions of a substrate and a support surface, dispersion and localization of the catalytically active supported metal. The structure sensitivity is of great interest in heterogeneous catalysis, and Pd catalyzed hydrogenation of acetylenic alcohols is known as a structure-sensitive reaction. Our investigation aims at the elucidation of the main characteristics of metal organic frameworks as supports for palladium in the liquid–phase selective hydrogenation of 2-butyne-1,4-diol. On the other hand, the hydrogenation product, cis-2-butene-1,4-diol, is a valuable product since it is an intermediate in the production of endosulfan, vitamins A and B6, and is used in the paper, textile and polymer industries. The reaction yields a number of byproducts and thus the study of the influence of the Pd particle size and the support texture and functionality on both activity and selectivity is of major importance. 3D-metal-organic frameworks MOF-5 ($Zn_4O(BDC)_3$, BDC = benzene-1,4-dicarboxylate), IRMOF-3 ($Zn_4O(ABDC)_3$, ABDC = aminobenzene-1,4-dicarboxylate), 1D-metal-organic coordination polymer (MOCP) [$Zn(pz25dc)(DMF)_2$] (where pz25dc = pyrazine-2,5-dicarboxylate), and a host-guest material, e.g. MOF-5 containing encapsulated calix[4]arene were utilized for Pd deposition.

The synthesized Pd-containing metal organic framework systems were carefully characterized by a number of physicochemical methods: XRD, DRIFTS, XAS, SEM, and volumetric N_2 adsorption/desorption. In addition, the alkylation of toluene over synthesized MOFs was studied to characterize framework Lewis acid sites.

Experimental

Syntheses of MOF-5 samples were performed by the "direct mixing" method developed by Huang [2] (Sample **I**) and Yaghi [3] (Sample **II**). Synthesis of IRMOF-3 (Sample **III**) was performed according to Corma [4]. Calix[4]arene (10 wt. %) was encapsulated during the MOF-5 synthesis (Sample **IV**). The heteroaromatic MOCP (sample **V)** was synthesized starting from Zn^{2+} and pyrazine-2,5-dicarboxylic acid. N_2 adsorption data were obtained at 78 K. The powder XRD patterns were measured in a transmission mode using a Huber G670 Guinier camera diffractometer ($CuK_{\alpha 1}$ radiation, λ=1.54059 Å) at 295 K. Zn and Pd K edge X-ray absorption spectra were measured at the Hasylab (DESY, Hamburg). DRIFTS data were obtained by NICOLET "Protege" 460. SEM was performed by using a LEO 1455 VP with XR microanalyzer (Carl Zeiss). Palladium (0.5 – 5 wt. %) was introduced into MOF

samples *via* incipient wetness impregnation from a $Pd(OAc)_2$ solution followed by reduction in a hydrogen flow at 423 K. The hydrogenation of 2-butyne-1,4-diol was carried out in methanol (293 K, P_{H2} 1atm).

Results and discussion

In contrast with the non-active 0.5%Pd/C, Pd/MOFs (including low-loaded samples) showed a high activity and selectivity in 2-butyne-1,4-diol hydrogenation. The main product of 2-butyne-1,4-diol hydrogenation was cis-2-butene-1,4-diol. Simultaneously, the parallel reaction of 1,4-butenediol hydrogenation as well as cis-trans transformation took place at the second stage. Unlike the hydrogenation over 1-5%Pd/C, the first stage of acetylenic alcohol hydrogenation proceeded much faster on N-containing MOF-based catalysts (Pd/**III**, Pd/**V**), than the second stage - 2-butene-1,4-diol hydrogenation. It suggests a donor-acceptor interaction of the network surface sites with acetylenic alcohol. The calix[4]arene encapsulation in the MOF-5 porous structure leads to some activity and selectivity increase of 0.5-5% Pd/MOF-5/calix[4]arene as compared with Pd on parent MOF-5.
DRIFT spectroscopy of adsorbed CO indicated the presence of highly dispersed Pd in MOF. XAS shows that the supported Pd particles size and localization are strongly affected by the support nature. Treatment in a spherical particle approximation yielded an extremely small average diameter of Pd particle of ~ 5.5 Å for 3D-metal organic framework MOF-5, and of ~ 7 Å for Pd on host-guest material MOF-5/calix[4]arene. Most studies on size effects for alkyne hydrogenation have shown that an increase in the metal dispersion decreased the turnover frequency [5]. Actually, a higher activity and selectivity was achieved on heteroaromatic MOCP (**V**) containing the larger Pd particles (~ 12 Å).
Additional tests on toluene alkylation with *tert*-butylchloride were carried out. These tests in combination with DRIFTS of adsorbed acetonitrile-d_3 demonstrated the presence of Lewis acid sites in the support. Their strength depends remarkably on the network nature. Such acid sites affected significantly the side reaction of butanol and γ-oxybutyraldehyde formation in the case of the Pd/MOF-5 samples. The surface area does not influence the hydrogenation activity, which indicates the localization of Pd mainly at the outer surface of MOF microcrystals, i.e. all Pd species are accessible to the substrate.

Conclusions

The activity and selectivity of 2-butyne-1,4-diol hydrogenation depend significantly on the network topology, host-guest properties and organic ligand nature that control donor-acceptor interaction with the substrate, Lewis acidity and Pd dispersion. A higher activity and selectivity for the heteroaromatic Pd/MOCP as compared to conventional Pd/C was found.

References

[1] Esken, D., Zhang, X., Lebedev, O.I., Schröder, F., Fischer, R. A., J. Mater. Chem., 19 (2009), 1314-1319
[2] Huang, L., Wang, H., Chen, J., Wang, Z., Sun, J., Zhao, D., Yan, Y. Microporous and Mesoporous Materials 58 (2003), 105-114
[3] Tranchemontagne, D.J., Hunt, J.R., Yaghi, O.M., Tetrahedron, 64 *(*2008), 8553-8557
[4] Zhang, X., Llabres i Xamena, F.X., Corma, A., J. Catal., 265 (2009), 155-160
[5] Molnar, A., Sarkany, A., Varga, M., J. Mol. Catal. A, 173 (2001), 185-221

The electronic effects of ligand substitution on Lewis acid catalysis with MOFs

Frederik Vermoortele, Ben Van de Voorde, Rob Ameloot, Dirk De Vos
Center for Surface Chemistry and Catalysis, Katholieke Universiteit Leuven, Kasteelpark Arenberg 23, B-3001 Leuven, Belgium; tel. +32 163 214 69, frederik.vermoortele@biw.kuleuven.be

Introduction

Metal-organic frameworks (MOFs) are hybrid porous materials, which have been increasingly studied during the last years [1]. They are built up from metal ion nodes linked together by organic polydentate ligands. Because of their extremely high internal surface area and pores of molecular dimensions, MOFs show great potential for applications in adsorption and catalysis. The great variety in ligands offers the possibility to modify MOFs with either more electron withdrawing or electrondonating groups. These substituents, which all have different electronic properties, are likely to influence the electronic properties of the nodal points. Recently, we demonstrated the catalytic activity of UiO-66, a Zr-terephthalate, and its amino modified analogue [2].
In this work we demonstrate the correlation of the catalytic activity and the electronic properties of various substituted ligands in a series of UiO-66 analogues in the cyclization of citronellal.

Experimental

A series of UiO-66 analogues was prepared from a zirconium salt and terephthalic acid bearing different substituents (BDC-X in which X=F, Cl, Br, OCH_3, CH_3, NH_2, NO_2, H), by slightly adjusting synthesis conditions from literature [2,3]. 13.5 mmol $ZrCl_4$, 13.5 mmol substituted terephthalic acid and 13.5 mmol H_2O were dissolved in 6 mol *N*,*N*-dimethylformamide (DMF) at room temperature. Crystallization was carried out in a 1 L Schott bottle under static conditions in a preheated oven at 100 °C overnight. The resulting solid was filtered and repeatedly washed with DMF to remove unreacted ligand. Crystallinity and porosity were confirmed using XRD and nitrogen physisorption. The samples were activated by dehydration at elevated temperature (200-300 °C depending on the substituent) under deep vacuum.
Catalytic experiments were carried out in 10 ml crimp cap vials loaded with 75 mg of MOF catalyst and 5 ml of solvent. The cyclization of citronellal was carried out in toluene at 100 °C with a substrate to Zr ratio of 10.

Results and discussion

We probed the potential of the substitued UiO-66 materials for citronellal cyclization reactions (Table1).

Table 1. Conversions and selectivities of the citronellal cyclization using substitued UiO-66 MOFs after 24 h.

Catalyst	Conversion (%)	Selectivity (%)
UiO-66	31	76
UiO-66-Br	100	76,6
UiO-66-Cl	98	78,8
UiO-66-CH_3	77	75,4
UiO-66-NH_2	70	73,0
UiO-66-NO_2	100	80,7
UiO-66-F	77	78,0

The substituent has a pronounced influence on the conversion of citronellal. Conversion and selectivity of citronellal is remarkably higher in the presence of UiO-66 analogues bearing electron withdrawing (Cl, Br, F, NO_2) substituents. This result indicates an increased acidity of the nodal points. On the other hand, the selectivity drops when electron donating groups are used, as would be expected from the resulting decrease in acidity.

The altered activity in different UiO-66 analogues can be correlated to the electron withdrawing or donating properties of the substituents using the Hammett equation ($\text{Log } k_x/k_H = \sigma \rho$). With this method the initial reaction rate is correlated to the electronic effects (both resonance and field) of the substituent as shown in Fig. 1.

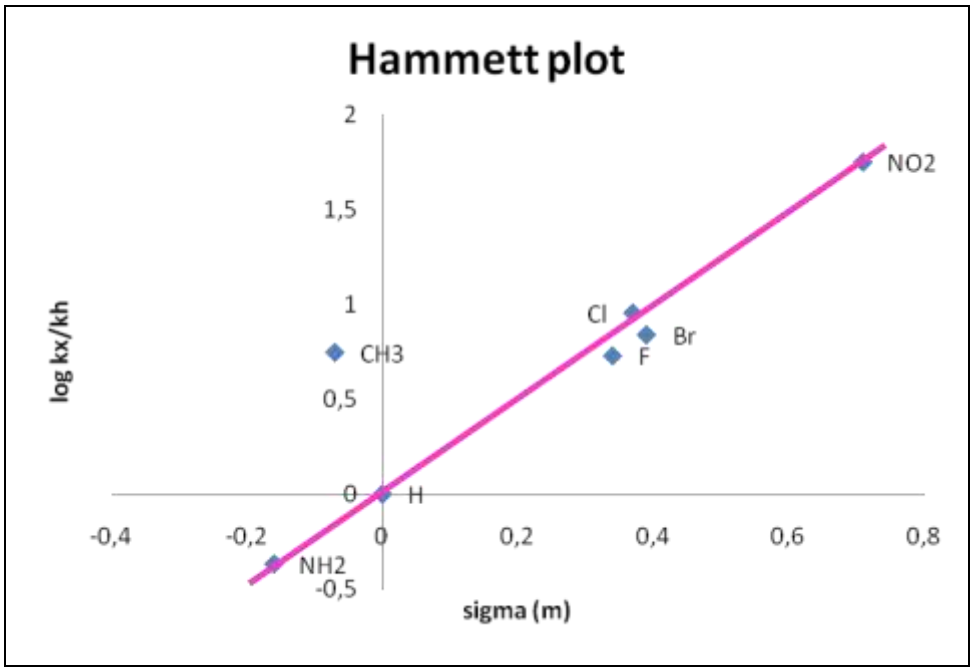

Fig. 1: Hammett plot with the correlation between the acivity and σ_m of the substituents.

The Hammett plot shows a nice correlation between σ_m and the activity, only the CH_3 substituted material has higher activity than expected.

Currently the research is broadened to other reactions (e.g. Oppenauer oxidation) and additional experiments are performed to gain more insight in the catalytic mechanism for instance by assessing the influence of the particle size,... Infrared measurements are performed to investigate the activation process.

Conclusions

We showed that ligand substituents have an electronic influence on the nodal points of the MOFs, using the Hammett-equation, we demonstrated. Using the appropriate ligand substitution, it is possible to tune the acidity of the MOFs.

References

[1] D. Farrusseng, S. Aguado and C. Pinel, Angew. Chem.-Int. Edit., 48 (2009), 7502-7513
[2] F. Vermoortele, R. Ameloot, A. Vimont, C. Serre and D. De Vos, Chem. Commun., 47(2011), 1521 - 1523
[3] J. H. Cavka, S. Jakobsen, U. Olsbye, N. Guillou, C. Lamberti, S. Bordiga and K. P. Lillerud, J. Am. Chem. Soc., 130(2008), 13850-13851

Catalytic Activity of Pure Germanosilicate UTL zeolite in Decane Test Reaction

Nataliia Kasian[a,b], Gina Vanbutsele[a], Kristof Houthoofd[a], Tamas I. Koranyi[a], Elke Verheyen[a], Johan A. Martens[a] and Christine E. A. Kirschhock
[a] *Centre for Surface Chemistry and Catalysis, K.U. Leuven, Kasteelpark Arenberg 23, B-3001 Heverlee, Belgium Fax: 32 16321998; Tel: 32 16321610;*
[b] *L.V. Pisarzhevsky Institute of Physical Chemistry, National Academy of Sciences of Ukraine, Pr. Nauky 31, 03028, Kyiv, Ukraine. Fax: 38 0445256216; Tel: 38 0445251190*
E-mail: natakasian@ukr.net

Introduction.
Germanosilicate extra-large pore zeolites are highly promising for application in catalysis especially in the field of oil refining and fine chemicals [1]. However there is a main limitation for their practical use: low hydrothermal stability. In the present work germanosilicate zeolite UTL was converted into a bifunctional catalyst and tested for hydroconversion of n-decane. To access the stability of framework three different strategies of the catalyst preparation were used.

Experimental.
The UTL samples were transformed into bifunctional catalysts (0.5 wt.% Pt) by three different manners. Pt was introduced by incipient wetness impregnation with $Pt(NH_3)_4Cl_2$ solution to as-made (as-made + Pt) and freshly calcined (calc + Pt) UTL samples and physical mixing of calcined UTL with Pt-containing amorphous silica (calc + Pt/silica). The catalytic activity of the Pt-silica gel in the decane hydroconversion was found to be negligible in the temperature range of interest. Decane hydroconversion was performed in a unit with 15 parallel reactor tubes, loaded with fixed beds of 50 mg catalyst. The H_2/decane molar ratio was 214. The contact time was 1400 $kg^{-1} \cdot s^{-1}$.

Results and discussion
FT-IR of germanosilicate UTL showed signals at 3730 and 3640 cm^{-1} in the hydroxyl region that were assigned to the presence of terminal Si-OH and Ge-OH groups, respectively. The temperature dependent desorption profiles of pyridine on UTL zeolite indicated presence of sites with medium acid strength - Brönsted acid centers (IR bands at 1543 and 1636 cm^{-1}) and Lewis acid sites (IR bands at 1454 and 1620 cm^{-1}). Calculated numbers of Brönsted and Lewis acid sites per unit cell was 0.21 and 0.07 respectively [3].

The presence of acidity in the UTL structure made testing its hydroconversion activity feasible. All three samples showed catalytic activity but to very different degrees. The conversion of n-decane on as-made + Pt started about 180 ºC and the activity increased much more rapidly with T compared with calc + Pt and calc + Pt/silica (Fig. 1).

The maximum yield of total isomers was about 42% on as-made + Pt (Fig. 2) compared to ca. 60% on Y samples. For both calc + Pt and calc + Pt/silica samples isomerization yield was very small (up to 10%) and cracking was the prevailing reaction. XRD and NMR indicated loss of cristallinity for calc + Pt, but preservation of structure for as-made + Pt sample even after 3 runs of testing.

The n-decane test served to reliably assess pore architecture of zeolites for a long time. Up to now almost every tested zeolite framework with 12-membered rings or smaller pores confirmed the trend of increasing ethyloctane vs. methylnonane selectivity with increasing pore width. The amount of EC8 formed on as-made + Pt (15.9%, Fig. 2) clearly exceeded EC8 for known zeolites (for example, the high EC8 amount 12.5 and 13.2% on FAU and MAZ respectively [2]).

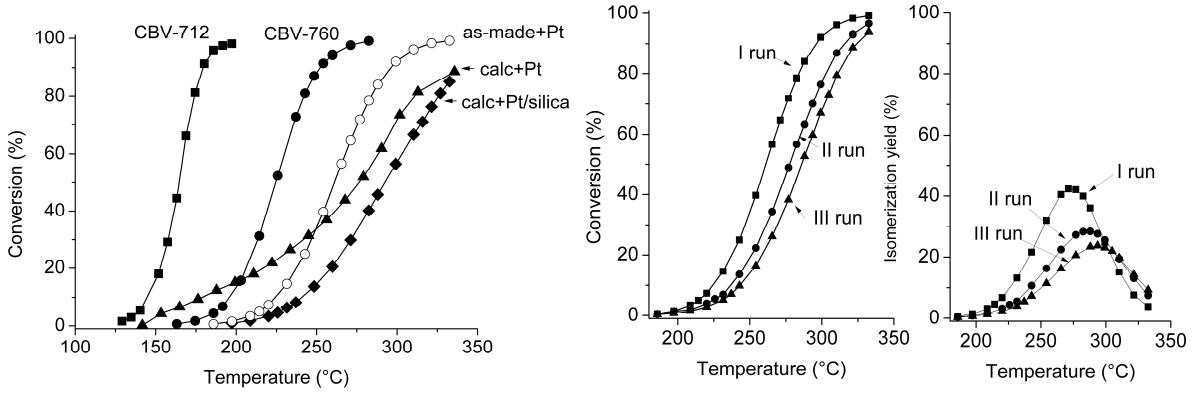

Figure 1. Decane conversion vs. T (left) and yield of sceletal isomerization on as-made + Pt (right) [3].

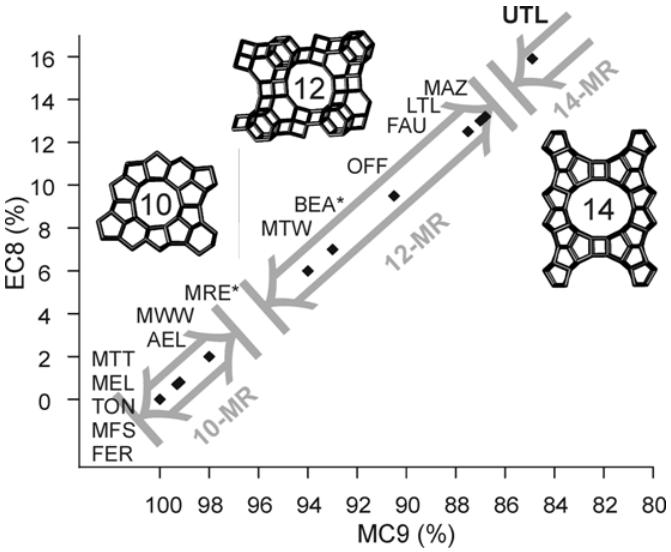

Figure 2. Content of EC8 against methylnonane (MC9) isomers in monobranched isodecane reaction product fraction on as-made+Pt sample, obtained at 5% n-decane isomerization conversion [4].

Conclusions

The results showed that preparation of bifunctional catalysts by classical wetness impregnation of Pt on calcined samples is not suitable for Ge-containing zeolites. Using the as-made sample in following catalyst pretreatment can preserve the UTL structure. Sample prepared this way presented sufficient activity for bifunctional catalysis and was stable after 3 runs of testing. The bi-directional channel of with extra-large pores allowed the formation of bulky ethyloctane molecules in larger proportions than in the widest 12-MR zeolites.

Acknowledgements

N.K. acknowledges the BELSPO for the Research Fellowship. C.E.A.K. and J.A.M. acknowledge financial support by ESA and the Belgian Prodex office. The work was supported by the Belgian government through the IAP–PAI network and by the Flemish government through long term structural funding to J.A.M. (Methusalem).

References

[1] J.Jiang, J. Yu, A. Corma, Angew. Chem. Int. Ed., 49(2010), 3120-3145.
[2] W. Vermeiren, J.-P. Gilson, Top. Catal., 52 (2009), 1131-1161.
[3] N. Kasian, T. I. Koranyi, G. Vanbutsele, K. Houthoofd, J. A. Martens, C. E. A. Kirschhock, Topics in Catalysis, 53 (2010), 1374-1380.
[4] N. Kasian, G. Vanbutsele, K. Houthoofd, T. I. Koranyi, J. A. Martens, C. E. A. Kirschhock, Catalysis Science and Technology, DOI: 10.1039/c0cy00043d.

Evidence for "Carbene-like" Intermediate in the Reaction of Methoxy Species with Light Alkenes on H-ZSM-5

Junko N. Kondo*, Hiroshi Yamazaki, Hiroyuki Imai, Toshiyuki Yokoi, and Takashi Tatsumi
Chemical Resources Laboratory, Tokyo Institute of Technology,
4259-R1-10 Nagatsuta-cho, Midori-ku, Yokohama 226-8503, Japan
*jnomura@res.titech.ac.jp**

Introduction

Methanol-to-olefin (MTO) reaction has been intensively studied because of the increasing demands for light olefins. One of the main reaction mechanism is made on the structure of hydrocarbons formed in zeolite channels, so-called "hydrocarbon pool (HCP)" [1, 2]. On the other hand, less research and discussion have been carried out on the initial C-C bond formation from the starting C_1 compound, methanol [3].

MTO and/or MTHC reactions start with the activation of methanol. The formation of methoxy species on zeolite upon exposure to methanol can be observed by infrared (IR) spectroscopy. Hunger *et al.* have recently been energetically studying the reactivity of methoxy species and has claimed that methoxy groups are active species in the MTO and/or MTHC reaction [3]. Here we closely investigated the reactivity of methoxy species on H-ZSM-5 by IR spectroscopy using isotopes.

Experimental

H-ZSM-5 (JRC-Z5-90H, Catalysis Society of Japan, Si/Al = 45) was pressed into a self-supporting disk (20 mm diameter, 60 mg) and placed in an IR cell attached to a vacuum system. The sample was pretreated by evacuation at 773 K with a liquid nitrogen trap for 1 h. IR spectra were obtained at a resolution of 4 cm^{-1} using a Jasco 4100 FT-IR spectrometer equipped with an MCT detector.

Results and discussion

Methanol molecules adsorb on the acidic OH groups of the ZSM-5 zeolite by strong hydrogen-bonding interactions, followed by dehydration to methoxy groups and water at temperatures above 473 K. Upon introduction of ethene, the decrease in the bands of methoxy groups and the recovery of the band of the acidic OH groups are clearly observed, indicating that methoxy groups on the sites of the acidic OH groups are consumed by the reaction with ethene. Neither methoxy species nor ethene molecules react individually at 523 K. In contrast, methoxy species react with ethene first to propene, and carbon chain elongation seems to proceed in the time course as revealed by GC analysis: thus, methoxy groups are regarded as methylation reagents of light alkenes.

To gain insight into the reaction mechanism, deuterated methoxy groups are produced from d_3-methanol (CD_3OH) and allowed to react with light olefins. On ethene introduction,

CD stretching bands decrease in intensity accompanied with appearance and the increase in intensity of the acidic OD band at 2655 cm^{-1}. It should be noted that only the acidic OD groups recover, while the acidic OH band at 3600 cm^{-1} is negligible in the subtracted spectrum. This indicates that the hydrogen of the acidic hydroxy groups can be only provided by methoxy groups but no possibility to be given from ethene molecules. In other words, C-C bond formation between d_3-methoxy groups and ethene molecules does not proceed with the CD_3 unit. Only two deuterium atoms are included in the product as CD_2 group, leaving one deuterium atom as an acidic OD group.

The methoxy groups were supposed to migrate as in the form of methyl cations in a similar manner to the motion of protons of acidic OH groups. Assuming the carbenium cation mechanism for the reaction observed in this study, where d_3-methoxy species react with ethene as CD_3^+ groups, 2-propyl cation ($CD_3CH^+CH_3$) would be present as an intermediate. For the conversion of 2-propyl cation to propene and Brönsted acid site, two possible pathways exist; one results in the formation of $CD_3CH=CH_2$ and an OH group, and the other $CD_2=CHCH_3$ and OD. The absence of the recovery of the acidic OH groups cannot be explained by the carbenium cation mechanism for the reaction. Thus, the methyl carbenium cation mechanism is not applicable in any cases.

Thus, the presence of carbene-like intermediate is the most likely, since deuterium originally present in the d_3-methoxy group is the source of the recovered Brönsted acid site (Figure 1). This reaction probably proceeds in a concerted manner as proposed by Hunger et al [3]. This reaction mechanism is also experimentally evidenced on various zeolites with other topologies as well as H-ZSM-5 samples with different aluminum contents.

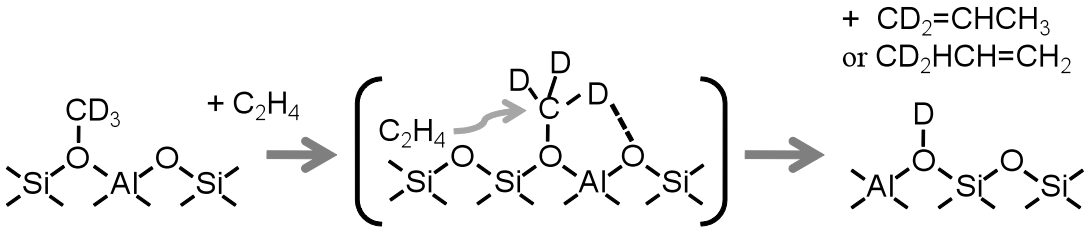

Figure 1. Proposed mechanism of the reaction of methoxy group with ethene to propene via carbene-like species.

Conclusions

We have clearly revealed the fashion of the addition of methoxy species to ethene via carbene-like species on acidic zeolites.

References

[1] M. Bjørgen, F. Joensen, K.-P. Lillerud, U. Olsbye, S. Svelle, Catal. Today 142, 90 (2009).
[2] D. M. McCann, D. Lesthaeghe, P. W. Kletnieks, D. R. Guenther, M. J. Hayman, V. Van Speybroeck, M. Waroquier, J. F. Haw, *Angew. Chem. Int. Ed.* 47, 5179 (2008).
[3] W. Wang, M. Hunger, Acc. Chem. Res. 41, 8, 895 (2008).

Separations

FEZA 2011

Interplay of metal connector and amine functionality in flexible MIL-53 MOFs: repercussion on CO_2 separation

Pablo Serra-Crespo[1], Elena Gobechiya[2], Jana Juan-Alcaniz[1], Alberto Martinez-Joaristi[1], Yaroslav Filinchuk[3,4], Christine E. A. Kirschhock[2], Jorge Gascon[1] and Freek Kapteijn[1]
[1]*Catalysis Engineering, ChemE-TUDelft, Julianalaan 136, 2628 BL Delft, The Netherlands*
[2] *Centre for Surface Chemistry and Catalysis, K.U. Leuven, Kasteelparck Arenberg 23-2461, B-3001 Heverlee, Belgium*
[3] *IMCN,UCL, pl. L. Pasteur 1, 1348 Louvain-la-Neuve, Belgium*
[4] *SNBL, ESRF, BP-220, 38043 Grenoble, France*
P.SerraCrespo@tudelft.nl

Introduction

Flexibility is a property rarely observed in classical crystalline microporous materials such as zeolites or other molecular sieves. In contrast, in the case of porous crystalline hybrids, the Metal Organic Frameworks (MOFs), where the entire framework is supported by coordination bonds and/or other weak cooperative interactions such as H-bonding, π–π stacking or Van der Waals interactions, many series exhibit a notable transformation in their structure during adsorption/desorption. This property, when understood and controlled, may give one more degree of freedom in the design of adsorption based separation processes [1].
Recently we reported the excellent performance of the flexible NH_2-MIL-53(Al) in the separation of CO_2/CH_4 mixtures [2, 3]. The enhanced performance of the material was attributed to its specific flexibility. The adsorption properties and separation ability of the NH_2-MIL-53(Al) are mostly due to a delicate interplay of weak dispersion forces controlling the flexibility of the framework [4]. In the current work, the research is extended to a series of NH_2-MIL-53 (X) frameworks based on group III elements (X= Al, Ga, In, Sc). After studying the influence of the metal on the structural transformation and the separation behavior of the different materials we are now able to identify the specific phenomena that strongly determine the performance of the adsorbents.

Experimental

A series of NH_2-MIL-53 (X) (where X= Al, Ga, In, Sc) has been synthesized hydrothermally using 2-amino terephthalic acid as a linker.
The thorough characterization of the whole series of materials includes *in situ* X-ray synchrotron diffraction under high pressure of CO_2, CH_4 and their mixtures, thermo-gravimetric analysis, *in situ* DRIFT, nitrogen adsorption and SEM. In addition, adsorption isotherms of carbon dioxide and methane have been determined at pressures up to 3 MPa at different temperatures and the results are complemented with breakthrough separation experiments in the presence of CO_2/CH_4 mixtures at different concentrations and pressures.

Results and discussion

In situ XRD results (Figure 1) demonstrate that in the case of the amino functionalized frameworks, in every case the narrow pore, *np* form of the framework is preferred after solvent removal, in contrast to the parent unfunctionalized MIL-53. This is due to the interaction between the amine moieties and the [XO_6] connectors via hydrogen bonding. This fact has very interesting consequences for separation, since starting from an *np* form allows to efficiently accommodate adsorbed molecules of a certain size (CO_2) while hampering the adsorption of bigger molecules (CH_4, N_2). In addition, the gas pressure needed for the *np*→*lp* transition of the framework varies among the different metal connectors, opening the door to further tuning the flexibility of the framework.

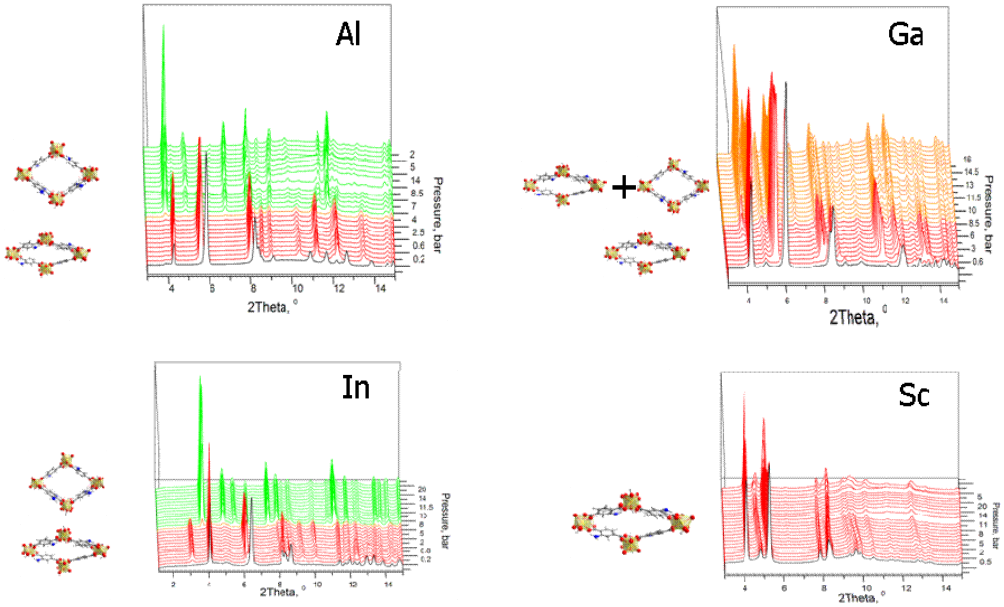

Figure 1 XRD *in situ* measurements in the samples NH_2-MIL-53 (Al, Ga. In, Sc) during CO_2 adsorption at 253 K over a pressure range of 0-20 bar.

Conclusions

The synthesis of four amino functionalized MIL-53 materials (where the metals are Al, Ga, In, Sc) has been achieved. Combining carbon dioxide adsorption and *in situ* XRD it has been demonstrated that the metal plays an important role in the flexibility of the framework.

References

1. Ferey, G. and C. Serre, Large breathing effects in three-dimensional porous hybrid matter: facts, analyses, rules and consequences. Chemical Society Reviews, 2009. **38**(5): p. 1380-1399.
2. Couck, S., et al., An Amine-Functionalized MIL-53 Metal Organic Framework with Large Separation Power for CO_2 and CH_4. Journal of the American Chemical Society, 2009. **131**(18): p. 6326-6327.
3. Boutin, A., et al., Thermodynamic analysis of the breathing of amino-functionalized MIL-53(Al) upon CO_2 adsorption. Microporous and Mesoporous Materials, 2011. **140**(1-3): p. 108-113.
4. Stavitski, E., et al., Induced shape selectivity through breathing modulation: Complexity behind CO_2 capture on NH_2-MIL-53 (Al). Langmuir. (*Submitted*).

Mixed Matrix Membranes comprising Functional Flexible Metal Organic frameworks for gas separation

Beatriz Zornoza[1*], Alberto Martinez-Joaristi[2], Pablo Serra-Crespo[2], Carlos Tellez[1], Joaquin Coronas[1], Jorge Gascon[2] and Freek Kapteijn[2]
[1] *Chemical and Environmental Engineering Department and Nanoscience Institute of Aragon, Universidad de Zaragoza, C/ Mariano Esquillor s/n 50018 Zaragoza, Spain*
[2] *Chemical Engineering Department, Catalysis Engineering, Delft University of Technology, Julianalaan 136, 2628 BL Delft, The Netherlands*
**bzornoza@unizar.es*

Introduction

Membrane processes have received significant attention as a promising technology for the separation of both gas and liquid mixtures. Concerning gas purification processes, over the last decade, various polymers have been modified with the incorporation of inorganic fillers (such as zeolites, carbon nanotubes, ordered mesoporous silica [1], metal-organic frameworks [2, 3], etc.) to produce mixed matrix membranes (MMMs). The advent of inorganic-organic hybrid membranes combines the superior gas transport properties of the inorganic materials and the desirable mechanical properties and good processability of polymers.

Experimental

The objective of this work is the fabrication of mixed matrix membranes from flexible, amino functionalized metal-organic frameworks (NH_2-MIL-53) for CO_2/CH_4 mixed gas separation. The extraordinary behavior of this material comprises: (1) the presence of amine functionalized groups able to adsorb strongly towards CO_2, and (2) the adsorption-induced structural transitions (breathing effect) giving rise to a pore widening under certain temperatures and pressures (Figure 1a) [4, 5]. Thus, gas separation measurements were performed at different pressures and temperatures to explore the effect of the flexible amino MOFs within the polymer matrix (polysulfone Udel®). The synthesized materials and membranes were also characterized by different techniques, including SEM, XRD, FTIR, TGA and nitrogen adsorption.

Results and discussion

SEM image (Figure 1b) reveals good and homogeneous dispersion of the particles (loading of NH_2-MIL-53 40 wt %) within the polymer matrix. Polymer membrane, Amino MIL-53 material, and mixed matrix membranes were tested at high CO_2 adsorption-desorption pressure showing a clear retarded pore opening when the MOF is embedded (Amino MIL-53 Al at -10ºC presents a CO_2 uptake at pressures higher than 8 bar). Moreover, the gas permeation performance (CO_2 permeabilities and CO_2/CH_4 real selectivities) of mixed matrix membranes with loadings of about 8, 16, 25 and 40 wt % was studied at different temperatures and pressures. Changes of structural pore flexibility of NH_2-MIL-53 within the polymer matrix were noticed when using lower temperatures (< 0ºC) and higher pressures (>7 bar) giving to a considerable increase in selectivity. Mixed matrix membranes with increasing NH_2-MIL-53 loadings (from 0 to 40 wt %) exhibited both higher CO_2 permeabilities and selectivities than the bare polysulfone matrix, with an optimum in performance for membranes containing a 25 % wt of MOF.

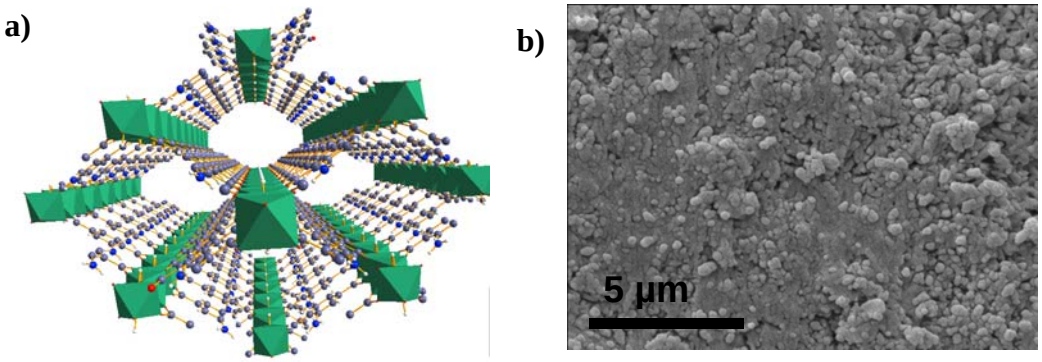

Figure 1. Structure of a) the synthesized Amino MIL-53 (Al); b) MMM prepared with Amino MIL-53 (Al) and polysulfone.

Conclusions

High quality of MMMs with flexible functionalized MOFs (NH_2-MIL-53 (Al)) and glassy polymer (polysulfone) with enhancing permeation and CO_2/CH_4 selectivity were prepared. Although the flexibility of the Metal Organic Framework is affected by the presence of the polymer, it can be used to increase CO_2 fluxes at high pressures while maintaining a high selectivity for CO_2.

Acknowledgements

Financial support from the Spanish Ministry of Science and Innovation (MAT2010-15870) and the Aragon Government (PI035/09) is gratefully acknowledged. B.Z. also acknowledges the funding from the Spanish FPU program. J.G. gratefully acknowledges the Netherlands National Science Foundation (NWO) for financial support through the VENI program.

References

[1] Zornoza, B., Téllez, C., Coronas, C.; Mixed matrix membranes comprising glassy polymers and dispersed mesoporous silica spheres for gas separation, Journal of Membrane Science, 368 (2011) 100–109.
[2] Perez, EV., Balkus, KJ., Ferraris, JP., Musselman, IH., Mixed-matrix membranes containing MOF-5 for gas separations, Journal of Membrane Science, 328 (2009) 165–173.
[3] Adams, R., Carson, C., Ward, J., Tannenbaum, R., Koros, WJ., Metal organic framework mixed matrix membranes for gas separations, Microporous and Mesoporous Materials, 131 (2010) 13–20.
[4] Gascon, J., Aktay, U., Hernandez-Alonso, MD., Van Klink, GMP., Kapteijn, F., Amino-based metal-organic frameworks as stable, highly active basic catalysts, Journal of Catalysis, 261 (2009) 75-87.
[5] Couck, S., Denayer, JFM., Baron, GV., Remy, T., Gascon, J., Kapteijn, F., An Amine-Functionalized MIL-53 Metal Organic Framework with Large Separation Power for CO2 and CH,. J. Am. Chem. Soc., 131 (2009) 6326-6327.

Liquid phase adsorption of organic compounds onto Metal Organic Frameworks (MOFs) studied by microcalorimetry

Mohammed Boulhout, Isabelle Beurroies, Philip.Llewellyn, Mickaël. Maes, Dirk De Vos, Renaud Denoyel.
Laboratoire Chimie Provence (UMR 6264), Marseille, France
mohammed.boulhout@etu.univ-provence.fr

Introduction:

Metal Organic Frameworks (MOF's) are a class of porous material which consists of hybrid crystalline compounds made up of clusters (or chains of metal ions) coordinated by organic linkers to form three dimensional structures. These innovative materials with promising capacities of adsorption have frequently been investigated for the development of gas storage and separation, whereas adsorption from solution has been much less studied. The separation of C_8 aromatic alkyl isomers [1] from the liquid phase is a real challenge for the petrochemical industry. Distillation is not effective for separating these isomers because of the proximity of their boiling points. Another challenge in which MOFs are expected to bring a breakthrough is the removal of refractory S and N compounds from fossil fuels [2]. Indeed, catalytic hydrodesulphurization (HDS) is increasingly difficult as the S level needs to be decreased below 10 ppm to obey environmental legislation. In the present work, we propose a thermodynamic study of adsorption from solution based on the determination of adsorption isotherms and adsorption enthalpies by microcalorimetry. The aim of this work is to give a better understanding of the influence of the structure and surface chemistry of MOF on their ability to separate different organic compounds.

Experiments and results

When adsorption from an organic phase is studied, the pretreatment conditions of the sample are very important to eliminate the competition with water. So, we have studied this influence of sample activation on MOF adsorption capacities. Different MOFs have been tested: UiO-66, MIL-53(Fe,Al) , for C_8 separation (Ethylbenzene and the 3 xylene isomers) and MIL-100(Fe) in the case of N and S recovery (Thiophene, N-methlcarbazole, dibenzothiophene, indole, and 1,2 dimethyindole).

- C_8 aromatic alkyls isomers single adsorption on MIL-53(Fe)

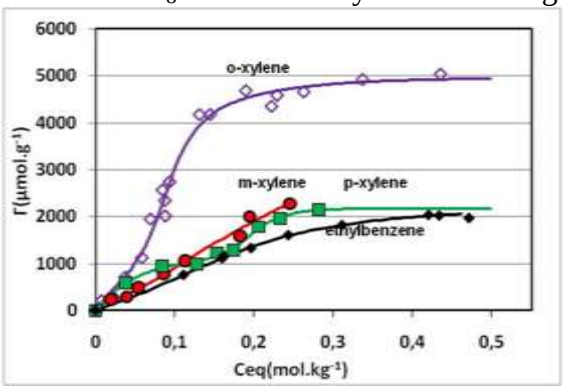

Figure1

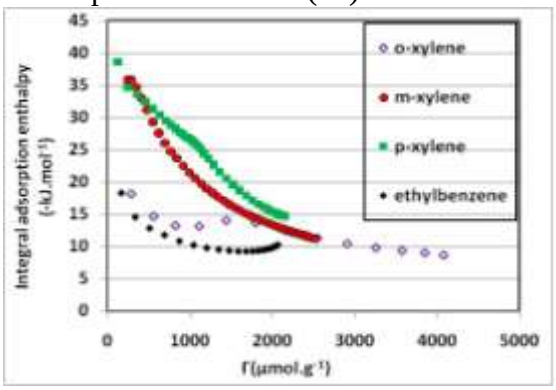

Figure2

Large differences of affinities (Figure 1) towards the MIL-53(Fe) are observed between the different C_8 compounds, which are not directly correlated with the adsorption enthalpies (Figure2). This adsorbent has a pronounced preference for ortho xylene isomer. The inversion between the affinity and the measured enthalpies illustrates the importance of entropic phenomena related to the molecules conformation in the pores. The same behaviour is observed with the other MOF tested (UiO-66 and MIL-53 (Al)).

❖ N and S compounds single adsorption on MIL-100(Fe)

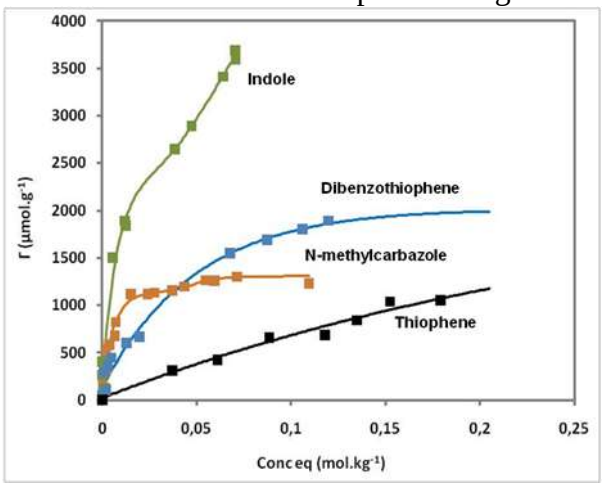

Figure3

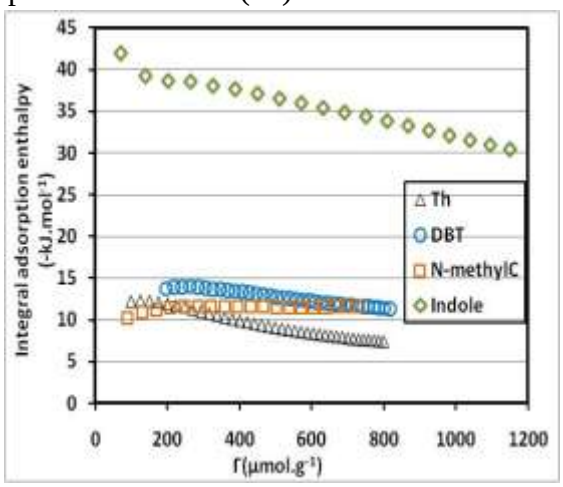

Figure4

The affinity obtained with the N-compounds is larger than for S-compounds (Figure3). Thiophene has a low affinity for MIL-100(Fe) in comparison with other compounds .The enthalpy values (Figure4) are in agreement with the affinity observed on the adsorption isotherm. .

Conclusion:

These results show a large influence of entropic contribution and molecular conformation during the displacement of the solvent (heptane) by the C_8 alkyls aromatic. The MIL-100(Fe) has a high adsorption capacity for selective removal of heteroatomic N compounds.

Acknowledgements

This study was supported by the European project FP7 MACADEMIA «MOF's As Catalysts and Adsorbents: Discovery and Engineering of Materials for Industrial Applications »coordinated by Total (Contract N CP –IP-228862-2). Thanks to the Institute Lavoisier of Versailles for supplying the samples.

References

[1] L.Alaerts, C.E.A.Kirschhock, M. Maes, M. A. van der Veen, V. Finsy, A. Depla, J.A. Martens, G. V. Baron, P.A. Jacobs, J. F. M. Denayer and D. E. De Vos. Angew. Chem. 2007, 119, 4371 –4375.

[2] Z.Varga, J.Hancsok, Petroleum &Coal, 2003, 45,135

Zeolite pervaporation membranes on hollow fiber supports

Zhengbao Wang[1]*, Qinqin Ge[1], Jia Shao[1], Yushan Yan[1, 2]
[1]Department of Chemical and Biological Engineering, Zhejiang University, Hangzhou, Zhejiang 310027, PR China. [2]Department of Chemical and Environmental Engineering, University of California, Riverside, CA 92521, USA. zbwang@zju.edu.cn*

Introduction

The hydrophilic zeolite NaA membrane is extremely selective for removal of water from organic solutions by pervaporation and can be used, therefore, for the production of water-free ethanol for biofuel application. Kita et al. [1] first reported that a water flux of 2.15 kg/m^{2}h and a water/ethanol separation factor of 10000 from a 90 wt.% ethanol solution at 75^{o}C. This separation performance was much better than that of polymeric membranes, e.g. polyvinyl alcohol (PVA) membrane commercially available from GFT of Germany. Mitsui Engineering and Shipbuilding Co. Ltd. in Japan adopted Kita group's technology and developed the first large scale pervaporation plant in 1998 using tubular (OD 12 mm) NaA membranes for dehydration of organic solvents. In 2003, Bussan Nanotech Research Institute Inc. (BNRI), a 100% subsidiary of Mitsui & Co. Ltd. Japan, tested successfully the dehydration of bioethanol in a pilot scale by using NaA membranes on alumina tubular support with 16 mm outer diameter and 1 m length for vapor permeation in Piracicaba, Sao Paulo State, Brazil. BNRI [2] reported that in pervaporation of a 90 wt.% ethanol solution at 75 ^{o}C the water flux was 5.6 kg/m^{2}h and the separation factor was ~10000. Despite their excellent water/ethanol separation factor and reasonable flux, the critical drawback shared by the two NaA membranes mentioned above is the large diameter of their tubular supports (i.e., 12 and 16 mm, respectively). This large diameter translates into low membrane area per unit volume, which in turn leads to large inefficient modules. It is also highly desirable to increase the water flux so that the module volume can be further reduced. We are interested in making zeolite membranes on hollow fiber supports, because of their high packing density (membrane surface area/volume ratio >1,000 m^2/m^3, if the outer diameter is smaller than 4 mm). Another goal of our work is to increase the water flux. The influences of seed size and concentration of seed suspension on the properties of zeolite membranes on alumina hollow fibers are investigated. The effects of the synthesis composition are studied using polymer-zeolite composite hollow fibers as supports, because there are uniform zeolite crystals as seeds on the surface of the supports.

Experimental

Two types of hollow fibers were used in this study. One is an alumina ceramic hollow fiber (HF) (OD 1.2 mm); another one is a PES-NaA composite hollow fiber (CHF) (OD 2 mm). They were cut into ~10 cm long, and mullite tubes (OD 12 mm) were cut into 5 cm for use. Alumina hollow fibers and mullite tubes were then coated with seeds by dip-coating zeolite LTA seed aqueous suspension (1-4 wt.%) using seeds with different size. The seed-coated supports were then dried at 60 ^{o}C and wiped. Zeolite seeds (average size: 0.8 μm) were from Mizusawa Chemical Co. Ltd., Japan.

The synthesis mixture with molar ratio of xNa_2O: $2SiO_2$: Al_2O_3: $155H_2O$ was made by mixing sodium metasilicate nonahydrate (sodium silicate or silica sol), sodium aluminate (Wako) and deionized water. The synthesis mixture was poured into a Teflon-lined stainless steel autoclave after stirring at room temperature for 30 min, and then supports were immersed into the synthesis mixture. The autoclave was put into a convectional oven preheated to 100 ^{o}C for 2-5 h. Zeolite membranes obtained on supports were taken out from the autoclave, and dried at 60 ^{o}C after washed with deionized water.

Pervaporation performance of zeolite membranes obtained was carried out using the homemade setup. Zeolite membranes on the hollow fiber (8-9 cm long) or tube (4-5 cm long) supports were pasted into a stainless steel tube, and then connected to the vacuum system. An ethanol/water solution of 90 wt.% in a flask was stirred and heated keeping at 75 ^{o}C. The permeate was collected in a trap after vacuuming for 15-20 min.

Results and discussion

We have successfully prepared NaA membranes on ceramic HF supports by seeded growth method. The seed layer was deposited by dip-coating of 0.8 μm seed suspension followed by wiping. XRD patterns of membranes obtained were consistent to zeolite LTA type, although the peak intensities were weak because of the thin coatings on one single hollow fiber support. XRD patterns of the powders from the same autoclave also confirm that zeolite LTA was the only crystalline phase formed during the synthesis. The zeolite membrane is smooth and the crystals are well intergrown in the continuous layer. The thickness of the dense layer of the zeolite NaA membranes is ca. 3-4 μm. There were no crystals found on the inner wall of the supports, because two sides of the supports were closed prior to the hydrothermal synthesis. Zeolite NaA membranes on HF supports showed higher flux (5.0 kg/m^{2}h) than on mullite tubes (1.9 kg/m^{2}h) when they have the same porosity (35%). The flux of LTA membrane on the mullite tube is similar to what is previously reported [1]. The flux of 9.0 kg/m^{2}h was obtained when the hollow fiber support with the porosity of 50% was used [3]. It is found that in order to prepare dense NaA membranes with high separation performance using dip-coating method, for seeds smaller than 100 nm and 200 nm, the optimal concentrations are 1 wt.% and 3 wt.%, respectively; while for large-sized seeds (>1500 nm), membranes obtained using the seed suspension with 4 wt.% seed concentration still have defects.

The separation factor of zeolite NaA membranes after 4 h synthesis on PES-NaA CHF supports were very high (α>10,000), indicating that zeolite NaA membranes on CHF support prepared by one single in-situ hydrothermal synthesis were continuous and well intergrown. The flux of zeolite membrane on CHF supports were 8.0-9.0 kg/m^{2}h, much higher than the results reported in literatures. Also all three zeolite membranes on the CHF supports after the 4 h synthesis showed the similar high PV selectivity (α>10,000), indicating the high reproducibility of the synthesis of zeolite membranes on CHF supports [4]. This shows the advantage of uniform imbedded zeolite crystals in polymer HF supports. It is found difficult to obtain high PV performance membranes on CHF supports using sodium metasilicate nonahydrate as silica source. Continuous zeolite membranes can be well synthesized using silica sol or sodium silicate as silica source. The reason of these differences is further explored.

Acknowledgements

We thank the National Natural Science Foundation of China (20876133 and 21028002), Science and Technology Department of Zhejiang Province (2009R50020) and Qianjiang Rencai (2008R10016) for financial supports. Y.Y. thanks the Chinese Ministry of Education for the Visiting Changjiang Scholar Professorship.

References

[1] Okamoto K., Kita H., Horii K., Tanaka K., Kondo M., *Ind. Eng. Chem. Res.* **40**, 163-175 (2001).
[2] Sato K., Nakane T., *J. Membr. Sci.* **301**, 151-161 (2007).
[3] Wang Z. B., Ge Q. Q., Shao J., Yan Y. S., *J. Am. Chem. Soc.* **131**, 6910-6911 (2009).
[4] Ge Q. Q., Wang Z. B., Yan Y. S., *J. Am. Chem. Soc.* **131**, 17056-17057 (2009).

Preparation and Characterization of Zeolitic Imidazolate Framework Molecular Sieve Membranes

H. Bux,[1] A. Feldhoff,[1] A. Huang,[1] Y.-S. Li,[2] J. Cravillon,[3] M. Wiebcke,[3] C. Chmelik,[4] J. Kärger,[4] M. Knauth,[5] S. Fritzsche,[5] T. Remsungnen,[6] and J. Caro[1]

[1]Leibniz University Hannover, Institute of Physical Chemistry and Electrochemistry, Germany; [2]Dalian Institute of Chemical Physics, Chinese Academy of Sciences, China; [3]Leibniz University Hannover, Institute of Inorganic Chemistry, Germany; [4]Leipzig University, Institute for Experimental Physics, Germany; [5]Leipzig University, Institute for Theoretical Physics, Germany; [6]Department of Mathematics, Faculty of Science, Khon Kaen University, Thailand;
Email; helge.bux@pci.uni-hannover.de

Introduction

Molecular sieve membranes in general represent a highly cost and energy effective solution to separate one species of molecules from another. However, high demands are made on porous membrane materials. Porous metal-organic frameworks (MOFs) are organic-inorganic hybrid materials which offer a unique customizability concerning pore sizes and adsorption affinities.[1] MOFs consist of metal cations or clusters bridged by organic ligand molecules, which can be modified with functional groups or replaced by derivatives, while the framework topology is retained.[2] Zeolitic imidazolate frameworks (ZIFs) are a sub type of MOFs, in which metal cations are tetrahedrally coordinated and connected by bidentate imidazolate ligands.[3] They frequently crystalize in zeolite-like structures, e.g. ZIF-7 (pore entrance size 3.0 Å) and ZIF-8 (pore entrance size 3.4 Å) in SOD topology. A number of ZIFs show an exceptional thermal and chemical stability, e.g. thermal decomposition points > 350 °C under air and resistance in boiling water, which appoints them as ideal membrane material.

Experimental

ZIF-7 and ZIF-8 membranes were prepared under solvothermal conditions by either in-situ crystallizations or by secondary growth of nanocrystalline seeds on-top of porous ceramic supports.[4,5] Scanning electron microcopy (SEM) and transmission electron microscopy (TEM) were performed to investigate the microstructure of the membranes. Permeation measurements were carried out by a modified Wicke-Kallenbach technique with different light gases and short chain hydrocarbons as pure gas and in mixture. The permeation results were compared with adsorption and diffusion data from IR microscopy (IRM) on large crystals.[6] In addition, molecular dynamics (MD) simulations including framework flexibility were used to understand the permeation results on molecular level.[7]

Results and discussion

In Figure 1 (left side) the cross-section of an oriented ZIF-8 layer obtained from secondary growth on-top of the ceramic supports is shown. Permeation measurements on the oriented ZIF-8 membrane show an increased performance in comparison with much thicker and non-oriented membranes prepared by in-situ crystallization (Figure 1, right). The separation performance of the ZIF-8 membrane can be estimated by a simple model from adsorption and diffusion data obtained by IRM. The prediction fits very well with the experimental measured membrane performance.[8]

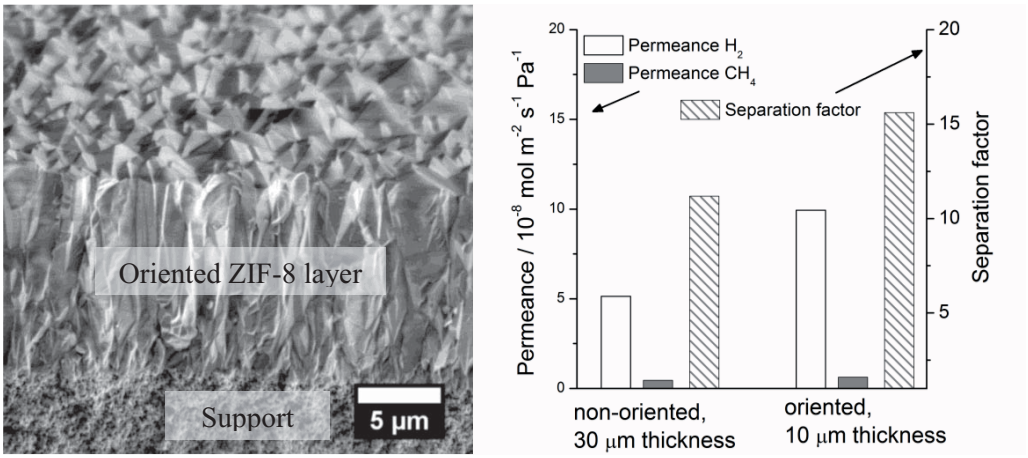

Conclusions

ZIF membranes can generally be prepared by different techniques. The measured moderate separation factors for light gases could be verified by IRM and are primary not result of undefined mass transport e.g. through grain boundaries. MD simulations show flexibility of the pore openings has major impact on the separation performance.

Acknowledgements

This work is part of the DFG Priority Program SPP 1362 “Porous Metal–Organic Frameworks”, organized by S. Kaskel. The financial support is gratefully acknowledged.

References

[1] G. Ferey, *Chemical Society Reviews* **2008**, *37*, 191.
[2] M. Eddaoudi, J. Kim, N. Rosi, D. Vodak, J. Wachter, M. O'Keeffe, O. M. Yaghi, *Science* **2002**, *295*, 469.
[3] A. Phan, C. J. Doonan, F. J. Uribe-Romo, C. B. Knobler, M. O'Keeffe, O. M. Yaghi, *Acc. of Chem. Res.* **2010**, *43*, 58.
[4] J. Cravillon, S. Munzer, S. J. Lohmeier, A. Feldhoff, K. Huber, M. Wiebcke, *Chem. Mater.* **2009**, *21*, 1410.
[5] a) Y. S. Li, F. Y. Liang, H. Bux, A. Feldhoff, W. S. Yang, J. Caro, *Angew. Chem. Int. Ed.* **2010**, *49*, 548; b) H. Bux, F. Y. Liang, Y. S. Li, J. Cravillon, M. Wiebcke, J. Caro, *J. Am. Chem. Soc.* **2009**, *131*, 16000.
[6] C. Chmelik, H. Bux, J. Caro, L. Heinke, F. Hibbe, T. Titze, J. Kaerger, *Physical Review Letters* **2010**, *104*.
[7] L. Hertag, H. Bux, J. Caro, C. Chmelik, T. Remsungnen, M. Knauth, S. Fritzsche, *J. Membr. Sci.*, *In Press, doi:10.1016/j.memsci.2011.01.019*.
[8] a) H. Bux, C. Chmelik, J. M. van Baten, R. Krishna, J. Caro, *Adv. Mater.* **2010**, *22*, 4741; b) H. Bux, C. Chmelik, R. Krishna, J. Caro, *J. .Membr. Sci.*, *In Press, doi:10.1016/j.memsci.2010.12.001*.

Separation of Alcohols on Chabazite and SAPO-34

T. Remy[1], J. Cousin Saint Remy[1], P.A. Webley[2], R. Singh[2] and J.F.M. Denayer[1]
[1]Department of Chemical Engineering, Vrije Universiteit Brussel, Pleinlaan 2, B-1050Brussel
[2]Department of Chemical Engineering, Monash University, Clayton Victoria, 3800, Australia
Tel.: + 32 2 629 32 62, Fax: + 32 2 629 32 48, Email: tom.remy@vub.ac.be

Introduction

Recently, the unusual adsorptive behaviour of n-alkanes on Chabazite (CHA) and SAPO-34 has been revealed [1]. CHA has a three-dimensional pore system with ellipsoidal shaped cages of 6.7 x 10 $Å^2$, which are interconnected via 8-membered ring windows with pore apertures of 3.8 x 3.8 $Å^2$. SAPO-34 is a silicon-, aluminum-, and phosphorus-based molecular sieve with the CHA topology. This material has excellent catalytic properties for the methanol-to-olefin (MTO) process [2]. A whole body of literature has already been devoted to the kinetics of the MTO process while only few studies have been undertaken to investigate the fundamental adsorption characteristics of SAPO-34 and CHA.

Experimental

Vapour phase adsorption isotherms of methanol, ethanol and propanol at 343K were measured using the gravimetric technique. Liquid phase adsorption capacities of 1-alcohols (methanol – octanol), n-alkanes (pentane – octane) and n-alkenes (pentene – hexene) were determined via batch adsorption at 298 K. To assess dynamic separation potential, breakthrough experiments for ethanol/hexanol and ethanol/propanol mixtures were carried out at different flowrates (0.1 – 4.0 ml/min) and temperatures (T = 298 – 473 K).

Results and discussion

Vapour phase adsorption isotherms of methanol and ethanol on SAPO-34 are of type I with almost equal saturation capacities for both alcohols: 18 wt% for methanol and 16 wt% for ethanol. Equilibration times are relatively small for these alcohols, i.e. always less than 30 minutes. Uptake kinetics of 1-propanol differ significantly from those of methanol and ethanol. The equilibration time for 1-propanol after a step in partial pressure from 0 mbar to 1.2 mbar is not in the order of minutes, but in the order of days.

Figure 1a shows the adsorbed amounts of the different C1–C8 1-alcohols in the liquid phase on SAPO-34 at room temperature after 3 hours. Methanol and ethanol are adsorbed in far larger quantities than propanol and the other longer 1-alcohols. The strong dependency of adsorption capacity on chain length is displayed in figure 1b. Small chain alcohols such as ethanol and methanol are able to completely fill the pores of the adsorbent. With increasing chain length of the 1-alcohols, the adsorption capacity decreases significantly. SAPO-34 can still hold one 1-propanol molecule per supercage but alcohols larger than 1-butanol are almost fully excluded from the micropores and adsorb only in very small amounts (< 9% of the available pore space on SAPO-34). The obtained results are in line with the liquid phase adsorption data of Daems et al. where a similar chain length dependent adsorption behaviour on the isostructural K-CHA was found (see also figure 1b for the K-CHA results) [3]. The results can be interpreted by comparing the size of the adsorbent cages and the length of the adsorbates. The lightest alcohols, methanol and ethanol, are small enough to align their main carbon chain perpendicular to the axis of the cage, allowing efficient filling of the pore volume. The main carbon chain of 1-propanol has to align along the longitudinal axis of the cage, leading to a much lower packing density. Moreover, this also results in much slower diffusion. Both effects lie at the basis of the cut-off in the C2-C3 region for the 1-alcohols.

The chain length of butanol ($L_{butanol}$ = 8.8 Å) also enables this molecule to reside inside the cages along the longitudinal axis. On the other hand, 1-pentanol has a chain length of 10 Å which renders it impossible for this molecule and the higher 1-alcohols to fit inside a single cage in a stretched configuration. As a result, a second cut-off in the C4-C5 region is observed for the 1-alcohols. It is clear that the hindered diffusion of pentanol and the higher 1-alcohols causes the extremely low adsorption capacity for these components.

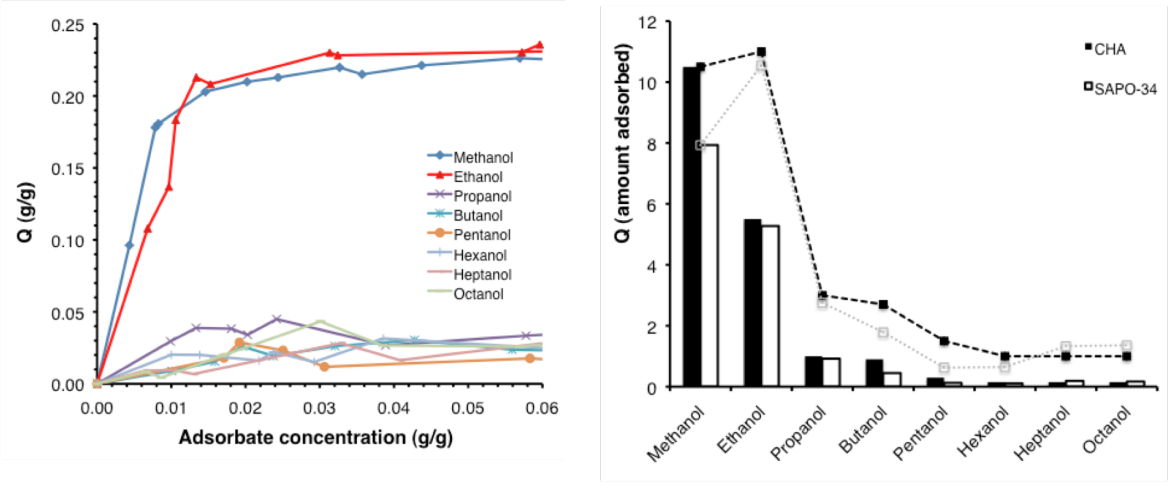

Figure 1: a) Liquid phase adsorbed amounts for C1-C8 1-alcohols on SAPO-34 at 298 K after 3h. b) Adsorption capacities of 1-alcohols on Na-CHA and SAPO-34 in liquid phase at room temperature. The bars and line graphs give the number of molecules and number of C-atoms adsorbed per supercage respectively.

Breakthrough separation experiments demonstrated the selective removal of ethanol from hexanol under all experimental flow rates and temperatures. SAPO-34 could separate ethanol from propanol at 298K however with low selectivity. Since, contrarily to hexanol, propanol is able to diffuse into the SAPO-34 cages (figure 1) it is able hinder the adsorption of ethanol. The obstructed ethanol diffusion results in a broad breakthrough profile and thus reduced selectivity. However a sharp breakthrough profile and higher selectivity is obtained for ethanol at higher temperature (348 K). The temperature rise increases the ethanol and propanol diffusivity causing ethanol to suffer less from the diffusional constraints imposed by pre-adsorbed propanol molecules. Preliminary tests have shown that ethanol could selectivity be removed from a mixture of C1-C4 alcohols.

Conclusions

SAPO-34 shows remarkable properties in the adsorption of short chain alcohols. As a result of its small cages connected via even smaller windows, it preferentially adsorbs short chain alcohol molecules with respect to their longer counterparts. Contrarily to typical zeolites with tubular pores, which have higher adsorption affinity for longer molecules, SAPO-34 and CHA show an inverse chain length dependent selectivity. This effect can be used to selectively separate short chain molecules from longer chain ones. Examples include the separation of butanol from shorter alcohols (ethanol/methanol), which could be relevant for the production of bio-butanol.

References

[1] Denayer, J.F.M., Couck, S., Ranjeet, S., *J. Phys. Chem. C.* 112 (2008), 16593-16599.
[2] Chen, J.Q., Bozzano, A., Glover, B., *Catal. Today* 106 (2005), 103-107.
[3] Daems, I., Singh, R., Baron, G.V., Denayer, J.F.M. *Chem. Commun.* 2007, 1316–1318.

Novel silicalite-1/PIM-1 hybrid nanocomposite membranes for gas separation: preparation and characterization

M. G. Buonomenna,[1] G. Golemme,[1,3]* P. M. Budd,[2] C. R. Mason,[2] P. Bernardo,[3] F. Bazzarelli,[3] J. C. Jansen[3]

[1]*Dipartimento di Ingegneria Chimica e dei Materiali, Università della Calabria; and Consorzio INSTM; Via Pietro Bucci 45A, I-87030 Rende, Italy <ggolemme@unical.it>.*

[2] *School of Chemistry, The University of Manchester, Manchester M13 9PL, UK.*

[3]*ITM-CNR, Istituto per la Tecnologia delle Membrane; I-87030 Rende, Italy.*

Introduction

Budd *et al.* and McKeown *et al.* were the first to report about a new class of rigid ladder-type polydioxanes containing highly contorted chains defined as polymers of intrinsic microporosity (PIM) [1,2]. Among these novel materials, PIM-1 is drawing attention due to a combination of outstanding permeability with moderate selectivity which defines the Robeson's upper bound line [3] for the O_2/N_2 and the CO_2/CH_4 gas pairs. Guiver *et al.* [4] reported that non-porous fumed silica is able to loosen the inherent polymer chain packing of PIM-1 in hybrid membranes. In the present work, for the first time silicalite-1 (MFI) crystals have been incorporated into PIM-1 and the gas permeation properties of the novel mixed matrix membranes (MMMs) have been investigated.

Experimental

Silicalite-1 (MFI) crystals of 0.35 μm size have been synthesized, calcined and functionalized with $(CH_2)_2Ph$ moieties to improve their compatibility with the PIM-1 polymeric matrix. N_2 sorption isotherms at 77 K have been carried on the MFI samples (Micromeritics, TriStar II 3020). A certain amount of MFI (35% v/v on a dry base) was suspended in a PIM-1/$CHCl_3$ solution, and the suspension was poured into a steel ring on a leveled glass surface, covered with a watch glass to reduce the evaporation rate. After solvent evaporation the resulting films were detached and conditioned by soaking in methanol. One film (PIM-001) was stored in methanol, left drying in air for 1h, dried under vacuum to remove the residual methanol and then tested in gas permeation experiments. Another film (PIM-003) was treated in the same way, but was aged at room temperature in air for 5 months before characterization. The permeability of pure gases (He, H_2, N_2, O_2, CH_4, CO_2; Δp = 1 bar) through the membranes was measured at 25°C.

Results and discussion

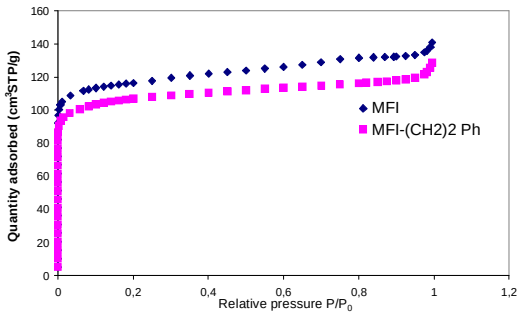

Figure 1. N_2 sorption isotherms at 77K of as-made and functionalized silicalite-1 crystals.

The N_2 sorption isotherms of as-made and phenethyl functionalized silicalite-1 crystals (Fig. 1) indicate that the surface functionalization does not obstruct the pores of the zeolite. The MFI crystals are well dispersed in the glassy PIM-1 matrix (Fig. 2). The pure gas permeability of the MFI/PIM-1 MMMs (Table 1) indicate that the composite membranes are defect free.

The permeability of the freshly prepared PIM1-001 membrane is much higher than the values displayed by PIM-1 soaked in methanol (PIM-1 $_{MEOH}$, [5]) and by the PIM-1/fumed silica MMM prepared by Guiver and co-workers [4], yet more selective than the latter. A strong ageing effect reduces the gas permeability of more than one order of magnitude, but yields the high selectivity observed with pure PIM-1 as well. The gas permeation data of the MMMs will be discussed in relation with the gas transport properties (diffusion, solubility) of gases in pure PIM-1 and silicalite-1.

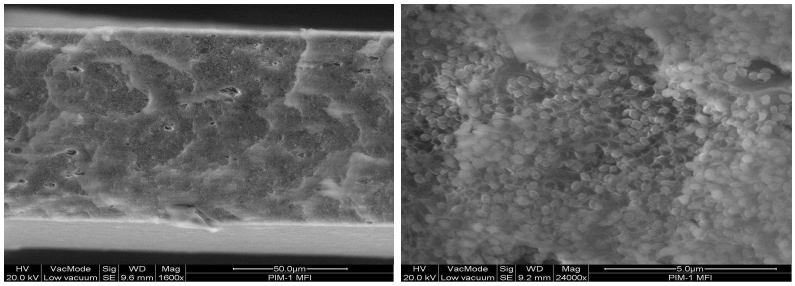

Figure 2. Cross sections of the aged silicalite-1/PIM-1 MMM (PIM003) at different magnifications (ESEM FEG Quanta 200).

Table 1. Gas permeability of MMMs silicalite-1/PIM-1 and PIM-1 membranes

Membrane	Gas permeability, Barrer*						Selectivity		
	He	H_2	O_2	N_2	CH_4	CO_2	O_2/N_2	CO_2/N_2	Ref.
PIM-001	5500	13970	6650	2370	6450	39770	2.8	17	This work
PIM-003	-	894	351	83	183	2530	4.3	31	This work
PIM-1	760	1630	580	180	310	4390	3.2	21	[5]
PIM-1 $_{MEOH}$	-	-	1610	500	740	12600	3.2	25	[5]
PIM-1/FS†	2940	7190	3730	1800	-	13400	2.1	7.5	[4]

*Barrer $\equiv 10^{-10}$ cm^3(STP) cm cm^{-2} sec^{-1} $cmHg^{-1}$. Fumed silica, 23.5 v%.

Acknowledgements

The work leading to these results has received funding from the European Community's Seventh Framework Programme (FP7/2007-2013) under grant agreement no. NMP3-SL-2009-228631, project DoubleNanoMem. We are grateful to Dr. Orazio Russo of Micromeritics Italia for his helpful support.

References

[1] N.B. McKeown, P.M. Budd, K. Msayib, B. Ghanem, Microporous polymer material, Int. Pat. WO05012397 (2005).
[2] P. M. Budd *et al.*, J. Membrane Sci. 251 (2005) 263.
[3] L. M. Robeson, J. Membrane Sci. 320 (2008) 390.
[4] J. Ahn *et al.*, J. Membrane Sci. 346 (2010) 280.
[5] P. M. Budd, *et al.*, J. Membrane Sci. 325 (2008) 851.

Natural Gas Sweetening by Adsorption on Silica-alumina

G. Bellussi[*], F. Bazzano[*], P. Broccia[+], A. Carati[*], E.F. Gambarotta[*], R. Millini[*], P. Pollesel[*], C. Rizzo[*], M. Tagliabue[§]
**) eni S.p.A., Refining & Marketing Division, v. F. Maritano 26, 20097, San Donato M.se, ITALY.*
+) eni S.p.A., Exploration & Production Division, v. Emilia 1, 20097, San Donato M.se, ITALY.
§) eni S.p.A., Research Center for Unconventional Energies, v. G. Fauser 4, 28100, Novara, ITALY.
E-mail: angela.carati@eni.com

Introduction

Natural Gas (NG) is got from reservoirs as mixture to be treated before transmission to downstream processors. H_2S and CO_2 are among the most common contaminants and when present in relevant amounts both bulk removal and polishing units have to be coupled to get final specifications [1]. Scrubbing by selective solvents, cryogenics and membranes have been proposed for bulk removal operations.
Pressure Swing Adsorption (PSA) technology has recently drawn NG industry attention because of its flexibility, eco-compatibility (absence of chemicals) and relatively low energy intensity. It is based on porous materials able to capture certain species at relatively high pressure P_{MAX} and to release them at a lower pressure P_{MIN} [2].
Applicability of PSA systems to bulk removal of H_2S and CO_2 from NG were studied at eni (no PSA processes are presently available for the bulk removal of H_2S). Aim of the activity was seeking for adsorbents able to get selectively large quantities of contaminants and to release them promptly by depressurisation.
Silica-alumina and silica were considered, due to their large apparent specific surface area (A-SSA), pore volume (V_P) and moderate heat of adsorption. Effect of their chemical composition and textural properties on key separation performances were evaluated by carrying out experiments both with single gases and with mixtures.

Experimental

Home-made microporous (ERS-8 type) and (micro)mesoporous (MSA type) silica-alumina were considered [3]. Furthermore, commercial microporous silica was added for comparison.
Each sample was characterised in term of elemental composition (ICP-AES, gravimetric analysis) and textural properties (N_2 adsorption at 77 K).
Single-gas (H_2S, CO_2, CH_4) adsorption isotherms were acquired at 303 K in the range from vacuum to 3000 kPa.
Most promising adsorbents were tested at 303 K over several adsorption-desorption cycles on a bench-scale fixed-bed adsorber (12.5 mm, ID; 1000 mm, L). Simulated sour NG (mixtures H_2S/CH_4 10/90 vol % or CO_2/CH_4 10/90 vol %) were adopted as feed.

Results and discussion

Sample	SiO_2/Al_2O_3 [mol/mol]	A-SSA [m^2/g]	V_P [cm^3/g]	d_P [nm]
MSA	276	900	0.74	3.2
ERS-8 (I)	82	705	0.31	1.2
ERS-8 (II)	246	1260	0.60	1.6
SILICA	Infinite	725	0.38	1.6

Table 1. Physical-chemical characteristics of silica-alumina and silica: SiO_2/Al_2O_3 molar ratio; BET apparent specific surface area, A-SSA; Gurvitsch specific pore volume, V_P; mean DFT pore diameter, d_P.

	CO_2				H_2S			
Sample	$\alpha_{CO2/CH4}$	Q_{MIN} [mmol/g]	Q_{MAX} [mmol/g]	ΔQ [mmol/g]	$\alpha_{H2S/CH4}$	Q_{MIN} [mmol/g]	Q_{MAX} [mmol/g]	ΔQ [mmol/g]
MSA	9	0.57	4.44	3.87	9	1.03	3.93	2.90
ERS-8 (I)	11	0.62	5.26	4.64	-	-	-	-
ERS-8 (II)	10	0.53	5.94	5.41	14	1.03	5.62	4.59
SILICA	8	0.45	4.07	3.62	11	0.80	3.79	2.99

Table 2. Performances of silica-alumina and silica in the separation X/CH_4 ($X = H_2S$, CO_2): Henry's selectivity, $\alpha_{X/CH4}$; X specific capacity, respectively, at P_{MIN} and P_{MAX}, Q; X working capacity from P_{MAX} to P_{MIN}, ΔQ. P_{MAX} = 1500 kPa has been adopted for CO_2; P_{MAX} = 500 kPa for H_2S; P_{MIN} = 50 kPa for both CO_2 and H_2S.

Data reported in Tables 1 and 2 show that at low pressure CO_2 specific capacity is quite low although favoured by polarity induced by the presence of aluminium. At higher pressures CO_2 specific capacity is maximised on microporous silica-alumina. Conversely, presence of mesopores gives a minor contribution to CO_2 specific capacity at high pressures. A similar behaviour is noticed also for H_2S adsorption. All considered adsorbents show selectivity and working capacity consistent with their application in PSA systems. Globally, ERS-8 (II) sample appears to be outstanding in term of high specific capacity, high working capacity and acceptable selectivity.
Bench-scale experiments carried out with simulated sour NG have confirmed the results obtained with single gases and have proved adsorbent stability over several PSA-type cycles.

Conclusions

Silica-alumina and silica have been evaluated as adsorbents for H_2S and CO_2 bulk removal from sour NG. A proprietary sample has been identified to be outstanding in term of specific capacity, working capacity and selectivity and suitable for the application in PSA systems [4]. This is a relevant result, considering that no PSA processes are presently available for the removal of huge quantities of H_2S from sour NG.

References

[1] R. Wagner, B. Judd, Fundamentals – Gas Sweetening, Proceedings of the 56th Laurance Reid Gas Conditioning Conference, Norman, OK (2006).
[2] D.M. Ruthven, S. Farouq, K.S. Knaebel, Pressure Swing Adsorption, Wiley – VCH, New York, NY (1994).
[3] C. Rizzo, A. Carati, M. Tagliabue, C. Perego, Stud. Surf. Sci. Catal., 128 (2000) 613.
[4] A. Carati, P. Broccia, C. Rizzo, L.G. Ciccarelli, M. Tagliabue, WO 2010/064121 A2 submitted by eni S.p.A.

The Adsorption of Salicylic Acid, Acetylsalicylic Acid and Atenolol from Aqueous Solutions onto Natural Zeolites and Clays: Clinoptilolite, Bentonite and Kaolin.

Vesna Rakić[1,4], Nevenka Rajić[2], Mina Jovanović[2], Aleksandra Daković[3], Aline Auroux[4]
[1]Faculty of Agriculture, Department of Chemistry, University of Belgrade, 11000 Belgrade, Serbia; [2]Faculty of Technology and Metallurgy, University of Belgrade, 11000 Belgrade, Serbia [3]Institute for Technology of Nuclear and Other Mineral Raw Materials, Belgrade, Serbia [4]Institut de Recherches sur la Catalyse et l'Environnement de Lyon (IRCELYON), UMR 5256 CNRS/Université Lyon1, 2 av. Albert Einstein, 69626 Villeurbanne Cedex, France
Corresponding author: vesna.rakic@ffh.bg.ac.rs

Introduction (Times New Roman, 12 pt, bold)

Pharmaceuticals have physiological effects on humans and animals in very low concentrations. The most important contamination of environment comes from pharmaceutical companies, but also from excretion from humans or animals [1]. Usually, they are designed in a way to be resistant to biological degradation. Being often polar compounds, they are soluble in water; therefore, during the production or use they arrive in soil, surface waters and eventually in ground and drinking water. Their detection, even in trace amounts, was enabled in recent years by development of very sensitive analytical techniques. Consequently, the investigations of their effects as well as the possibilities to remove them from the environment have received considerable attention. This study is devoted to assess the adsorption capacities of some natural minerals against chosen pharmaceuticals.

Experimental

Here, the possibilities to adsorb aqueous solution of salicylic acid, acetylsalicylic acid and atenolol (purchased from pharmaceutical company "Galenika", Belgrade, Serbia, concentrations of solution between 2 and 3 mmol/L) on clinoptilolite modified with sorbed Cu(II), Zn(II), Ni(II) or Mn(II) (2.9 % wt., 1.5% wt., 1% wt., and 0.9 % wt., respectively) have been probed. The procedure for metallic ion sorption has been published already [2,3]. Natural minerals (kaolin and bentonite, pure or ion-exchanged by octadecyldimethylbenzyl ammonium chloride, ODMBA-Cl, 25 – 90% of total exchange capacity) have been also probed as adsorbents. The adsorption was studied at 303 K, by titration microcalorimetry (Titrys from Setaram), employed to obtain the heats evolved as a result of adsorption. Adsorption experiments were performed under the same conditions, the equilibrium adsorbate concentrations were determined by fluorescence spectrophotometer (PTI 1609 from Photon Technology International). The crystallinities of adsorbents were checked by X-ray diffraction, before and after adsorption. The presence of other chemical species except initial

adsorbates has been probed in the liquid phase after adsorption, collecting ^{1}HNMR spectra (Bruker AVANCE 250 spectrometer) from the liquid state.

Results and discussion

The maximal adsorption capacities of investigated solids lie in the range of 10^{-5} – 10^{-6} mol/g. Modified clinoptilolite have shown higher capacities in comparison with natural mineral; the adsorption capacities are dependent on the type of metallic cation present in the structure. In the case of clays modified with organic cation, partial ion-exchange led to increase of adsorption capacity, while further increase in ODMBA-Cl content resulted in their decreasing. Figure 1 presents the results obtained for atenolol adsorption on modified clinoptilolite. Comparable results were obtained in the case of other investigated pharmaceuticals.

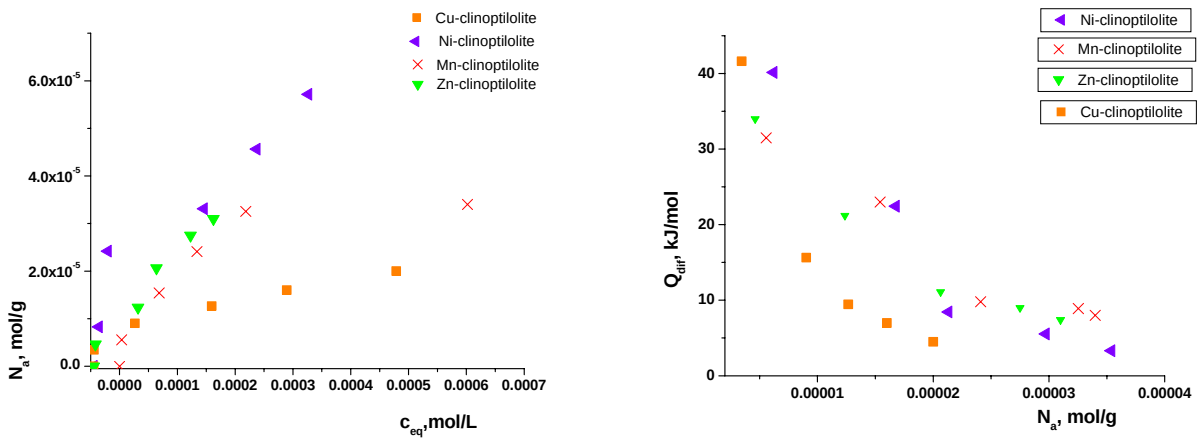

Figure 1. Adsorption isotherms (left); and differential heats of atenolol adsorption from aqueous solutions onto modified clinoptilolites (right).

Conclusions

The results obtained in this work show that natural materials can be used effectively in the removal of investigated pharmaceuticals by adsorption. Their adsorption capacities can be adjusted using different modification procedures.

References

[1] Klavarioti, M., Mantzavinos, D., Kassinos, D., Removal of pharmaceuticals from aqueous systems by advanced oxidation processes, Environment International 35 (2009) 402-417

[2] Stojaković, Dj., Hrenović, J., Mazaj, M., Rajić, N., On the zinc sorption by the Serbian natural clinoptilolite and the disinfecting ability and phosphate affinity of the exhausted sorbent, Journal of Hazardous Materials 185 (2011) 408–415

[3] Rajic, N., Stojakovic, Dj., Jevtic, S., Zabukovec Logar, N., Kovac, J., Kaucic, V., Removal of aqueous manganese using the natural zeolitic tuff from the Vranjska Banja deposit in Serbia, Journal of Hazardous Materials 172 (2009) 1450–1457.

Transport and separation properties of binary aromatic hydrocarbon mixtures in MFI powder, pellets and membranes

R. Kolvenbach[a], N. Al-Yassir[b], S.S. Al-Khattaf[b], O.C. Gobin[a], J.H. Ahn[a], A. Jentys[a], J.A. Lercher[a]
[a]Department of Chemistry, Catalysis Research Center, Technische Universität München, Lichtenbergstr. 4, 85748 Garching, Germany; [b]Center of Research Excellence in Petroleum Refining and Petrochemicals, King Fahd University of Petroleum & Minerals, Dharan, 31261, Saudi Arabia, Jentys@mytum.de

Introduction

The design of new zeolitic materials for shape selective reactions and separations for aromatic hydrocarbons such as xylenes is a challenging task in academic as well as industrial research. In this study we compare the transport processes of benzene and p-xylene in MFI particles, pressed pellets and crystalline membranes to describe the impact of compacting powder samples, which can serve as model for exudates, and of hierarchically structured materials on the transport properties.

Experimental

The Silicalite-1 membranes were produced by the Fraunhofer Institute for Ceramic Technologies and Systems (IKTS), with an average thickness of 30 to 60 μm. Scanning electron microscopy shows a texture composed of well-defined intergrown crystals of 50 μm diameter. The Silicalite-1 samples were supported on an asymmetric wafer made of titanium-dioxide with a minimum pore size of 30 nm. H-ZSM-5 powder with a Si/Al ratio of 45 composed of agglomerates with an average size of 360 (determined by SEM and DLS) and a primary particle size of 50-100 nm (measured by TEM and XRD) was used. The pressed pellets were produced by pressing the H-ZSM-5 powder. The thickness was varied between 0.5 and 1.5 mm.
The diffusion and separation of binary benzene/p-xylene mixtures of pressed H-ZSM-5 pellets and grown membranes were studied by the Wicke-Kallenbach method [1]. The transport/diffusion in isolated particles was examined by the pressure modulation frequency response method.

Results and discussion

The steady state permeability of p-xylene through a crystalline Silicalite-1 membrane was 5 times higher than of benzene and a separation factor between benzene and p-xylene of 0.2 was observed. The temperature dependency of the permeance is shown in Figure 1.
It is possible to obtain separation of p-xylene and benzene (separation factor of 5) if both substances were applied with the same partial pressure. The surface coverage of p-xylene was 6 to 7 times higher than of benzene according to the isotherms [2], which indicates that the transport through the membrane is controlled by diffusion inside the micropores.
In contrast, a separation of the binary mixture was not observed in the pressed pellets of H-ZSM-5. The overall permeability was two orders of magnitude higher than in the crystalline membrane, which indicates that the transport was controlled by Knudsen diffusion inside the mesopores.

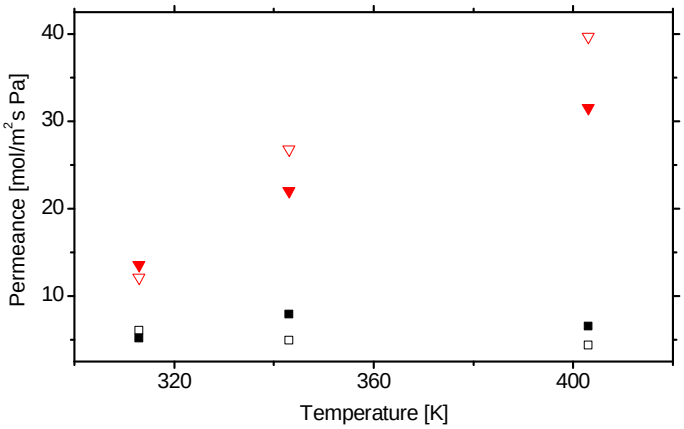

Figure 1: Transmission permeance as function of the temperature of benzene(■)/p-xylene(▼) (578.7 Pa/322.9 Pa) mixtures (filled symbols) compared to the single components (open symbols) in a Silicalite-1 membrane at 343, 373 and 403 K

In contrast to the crystalline membranes a faster diffusion of benzene compared to p-xylene was found in isolated H-ZSM-5 particles [3].
The differences between isolated particles and grown membranes can be understood in terms of the Stefan-Maxwell formalism, which describes the transport depending on the diffusion coefficient as well as the surface coverage and its gradient. Consequently, the p-xylene transport is enhanced through a membrane compared to benzene leading to an enrichment of p-xylene in the effluent stream.

Conclusions

The transport regime in H-ZSM-5 changes significantly from isolated particles to pressed pellets and crystalline membranes. In isolated particles the transport can be understood in terms of Fickian diffusion with a faster diffusion of benzene compared to p-xylene. In pressed pellets a similar steady state diffusion coefficient for benzene and p-xylene in the range of Knudsen diffusion was observed, indicating that the transport in the mesopores is rate limiting. The transport through a grown membrane was markedly influenced by the surface occupation of the diffusing substances resulting in a faster diffusion of p-xylene compared to benzene. Therefore, it is possible to separate p-xylene from a binary benzene/ p-xylene mixture with a separation factor of 2.6-5 depending on the temperature by using a Silicalite-1 membrane.

References

[1] Wicke, E.; Kallenbach, R.; Kolloid-Zeitschrift, 1941, 97, 135
[2] Song, L.; Rees, L.V.C., Microporous and Mesoporous Materials **2000**, *35-36*, 301
[3] Gobin, O. C.; Reitmeier, S. J.; Jentys, A.; Lercher, J. A., J. Phys. Chem. C, 2009, *113*, 20435.

High Pressure Calorimetry of Water Intrusion in Nanopores

Thomas Karbowiak, Christian Paulin and Jean-Pierre Bellat
Laboratoire Interdisciplinaire Carnot de Bourgogne, UMR 5209 CNRS-Université de Bourgogne, 9 Av. Savary, BP 47870, F-21078 Dijon, France
jean-pierre.bellat@u-bourgogne.fr

Introduction

Thermodynamic systems made of a hydrophobic porous solid and water as a non-wetting liquid have been considered as promising devices for energetic applications. Early works in this field started in the middle '90s on silica gels, and were then extended to functionalized organized mesoporous solids and pure silica zeolites (zeosils). Investigations were performed using an experimental approach to assess the intruded water volume along with the applied pressure, or by molecular simulation (Monte Carlo). According to phenomenon reversibility or irreversibility between intrusion and extrusion stages, the "water-zeosils" systems are able to restore, absorb or dissipate mechanical energy. Consequently, molecular spring, damper or shock-absorber behaviors can be observed.

Experimental

In order to measure thermal effects involved in the intrusion phenomenon of liquid water in a hydrophobic porous material, a specific high pressure calorimetric device, based on Setaram C80 Tian-Calvet calorimeter, has been designed [1]. This allows measurements of equilibrium thermal effects occurring during the intrusion of a fluid in a porous material in the high pressure range 0.1 to 400 MPa under isothermal conditions. The method used to obtain the corresponding thermal effect consists in applying a pressure increment or decrement, dp, on degassed liquid water in contact with the microporous solid placed in a high pressure calorimetric cell, at 298 K. The reference cell only contains liquid water maintained at the atmospheric pressure. The measured calorimetric heat is the result of two thermal effects: the heat due to the compression of the liquid bulk and the heat of intrusion. For each pressure step, to determine the differential intrusion heat per gram of zeolite $\delta Q/mdp$, it is necessary to subtract the compression heat of liquid water (determined experimentally) to the calorimetric heat. Finally the integral heat of intrusion can be calculated by integration of the differential intrusion heat in the pressure range of intrusion.

Results and discussion

This study particularly focuses on water intrusion in two pure silica zeolites: silicalite-1, which is a pure silica MFI-type zeolite, and chabazite. The use of this calorimetric device to measure thermal effects of liquid water intrusion, clearly depicts intrusion as an endothermic phenomenon occurring in the narrow range of pressure 90-95 MPa for silicalite-1, whereas it is exothermic for chabazite and in a lower pressure range 30-50 MPa (Figure 1). Intrusion-extrusion phenomenon appears to be irreversible. It is due in both cases to the creation of silanol defects in the material, as shown by FTIR and NMR spectroscopies [2,3,4]. Therefore, the thermal energy involved during the intrusion process does not correspond exclusively to the phase transition enthalpy from the bulk phase to the intruded phase, but also includes the energy involved in the formation of silanol defects and the interaction of water with them. The endothermicity or exothermicity would be related to coordination of water molecules inside the offered inner space: channels or cavities.

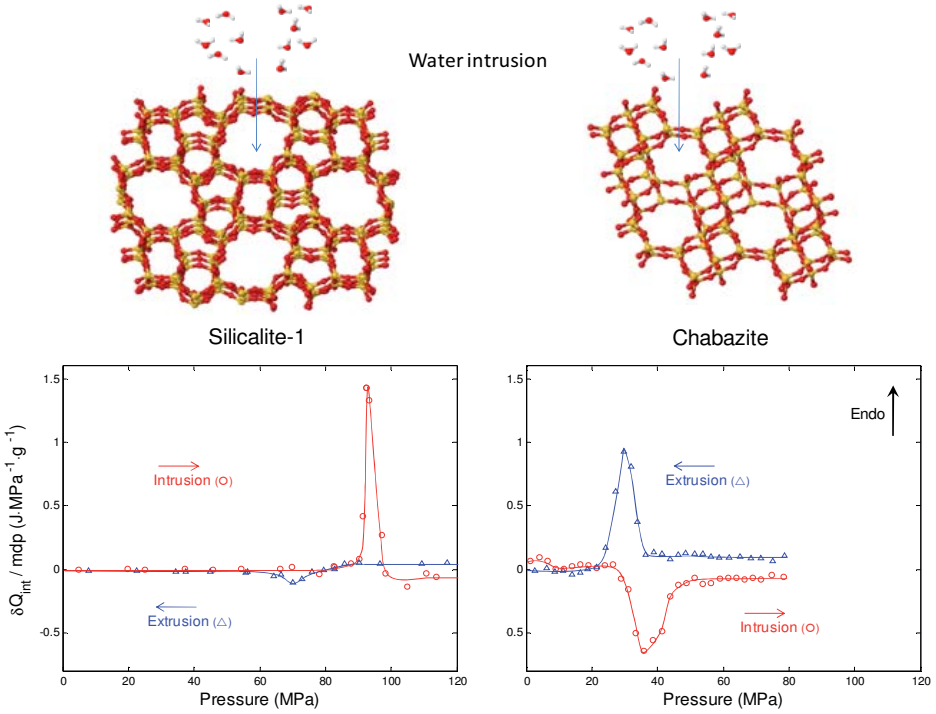

Figure 1. Thermal effects of water intrusion and extrusion in two pure silica zeolites: silicalite-1 (left) and chabazite (right).

Moreover, the successive intrusion-extrusion cycles of water in silicalite-1 and chabazite also display a decrease of the intrusion pressure between the first intrusion-extrusion cycle and the consecutive ones, whereas the extrusion pressures remain unchanged but lower than the intrusion pressure. After a "damper" behavior, these two materials really act as "molecular springs". If the first shift is attributed to the existence of silanol groups created during the first water intrusion, the hysteresis between intrusion and extrusion pressures seems to be in favor of the existence of a metastable intruded phase.

Conclusions

This original experimental approach allows thus to give better insights in the intrusion phenomenon of non-wetting liquids in hydrophobic porous solids.

Acknowledgements

This work was supported by the French Agence Nationale de la Recherche through the ANR program ''Heter-eau'', under Contract No. BLAN 06-3_144027.

References

[1] Karbowiak T., Paulin C., Bellat J.-P. Determination of water intrusion heat in hydrophobic microporous materials by high pressure calorimetry. Microporous Mesoporous Materials, 134 (2010), 8-15.

[2] Karbowiak T., Paulin C, Ballandras A., Weber G., Bellat J.-P. Thermal effects of water intrusion in hydrophobic nanoporous materials. Journal of the American Chemical Society, 131 (2009), 9898-9899.

[3] Trzpit M., Rigolet S., Paillaud J.-L., Marichal C., Soulard M., Patarin J. Pure silica chabazite molecular spring: a structural study on water intrusion-extrusion processes. Journal of Physical Chemistry B, 112 (2008), 7257-7266.

[4] Karbowiak T., Saada M., Rigolet S., Ballandras A., Weber G., Bezverkhyy I., Soulard M., Patarin J., Bellat J.-P. New insights in the formation of silanol defects in silicalite-1 by water intrusion under high pressure. Physical Chemistry Chemical Physics, 12 (2010), 11454-11466.

Advanced technological applications

FEZA 2011

Tri-functional MOFs and their potential use in drug delivery applications

Alistair C. McKinlay, Paul S. Wheatley and Russell E. Morris
EaSTChem School of Chemistry, University of St. Andrews, Purdie Building, St. Andrews, KY16 9ST, UK, acm14@st-andrews.ac.uk , rem1@st-andrews.ac.uk

Introduction

Metal organic frameworks (MOFs) have received significant interest in recent years owing to the potential use they may hold in many areas of industry. There is growing interest in the use of MOFs for biological and medicinal applications[1]. MOFs have already been shown to be able to store and controllably release large amounts of nitric oxide (NO)[2] (fig. 1). Until the early 1990s NO was known only as a highly toxic gas, however, interest in this free radical molecule has significantly increased due to its active role in human physiology[3]. It has been shown that exogenously applied NO leads to anti-thrombosis properties and promotion of wound healing[4]. MOFs have also recently been shown to be of real interest as storage and delivery vehicles for pharmaceuticals, in particular anti-cancer and anti-aids drugs as well as anti-inflammatory agents[5-7]. With a large number of antibiotics becoming less effective against bacteria which have increased resistance, the combination of a well-known antibiotic with NO and an appropriate metal could be extremely useful in keeping wounds clean and free of infection and also improve wound healing times. Metronidazole is an antibiotic drug commonly used in the treatment of *C difficile*[8]. However due to bacterial resistance (e.g. MRSA) it is now being used in combination with other more expensive drugs. This work aims to show that both biologically significant NO and pharmaceuticals can be simultaneously stored and released when triggered in a controlled manner that could have potential use in wound healing applications. Further to this, anti-bacterial testing shows that the MOFs display tri-functionality as the metal used in the chosen MOFs structure is also anti-bacterially active. This combination has been shown to be effective against a number of common hospital acquired infections (MRSA and *C difficile*). These results could form the platform for a new drug delivery method utilizing MOFs as the delivery vehicle.

Experimental

Both MOFs used in the experiments (Ni CPO-27 and HKUST-1) were synthesized and characterized according to the previously published procedures[9,10]. Metronidazole was adsorbed in the MOFs by dissolving the drug in anhydrous methanol before adding the previously dehydrated MOF and sealing with stirring for between 7 to 10 days. The resulting powder was washed filtered before being air-dried. UV measurements were carried out using a Perkin-Elmer Lambda 35 UV/VIS spectrometer with distilled H_2O as the background. NO adsorption and release measurements were carried out in the same manner as mentioned in previous publications[2,11] using a dehydration temperature of 80^{o}C to ensure no loss of drug.

Results and discussion

Metronidazole was successfully incorporated into two well-known MOFs (Ni CPO-27 and HKUST-1). Elemental analysis showed that the approximate metronidazole content was ~1 mmolg^{-1} in Ni CPO-27 and ~0.7 mmolg^{-1} in HKUST-1. UV spectroscopy was used to characterize the release of metronidazole from these MOFs in both powder and pellet form. Measurements taken over a number of days showed that the amount of metronidazole available for release from HKUST-1 was 0.7 mmolg^{-1} and for Ni CPO-27 was 0.3 mmolg^{-1} (fig. 2). NO adsorption and release measurements performed on the drug-loaded materials showed that although the metronidazole resides within the pores, it was still possible to store 3.5 mmolg^{-1} of NO within Ni CPO-27 and 1.7 mmolg^{-1} of NO in HKUST-1 (fig. 3). Release measurements were performed and the poor release of NO displayed by HKUST-1 was

expected as this has been observed before[11]. However the Ni CPO-27 metronidazole sample showed an almost total release of its stores (~3 mmolg^{-1} of NO) which again agrees with previously published results[2]. It was also shown that even after NO adsorption and release that it was possible to release the same amount of metronidazole that had been stored previously. Atomic adsorption spectroscopy was used to observe the release of the metal from the framework over time. This combination of drug delivery, NO and antibacterial metal release results in the MOFs displaying tri-functionality.

Conclusions

It has been shown that there is great potential for the use of MOFs as drug delivery vehicles as they can store and deliver biologically significant amounts of both metronidazole and NO simultaneously which has great implications for the future of wound healing therapies.

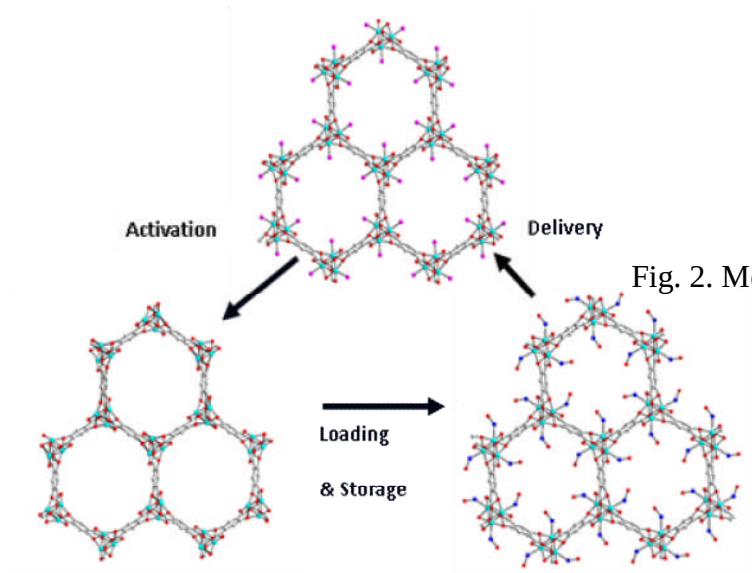

Fig. 1. The cycle of NO storage and release in MOFs

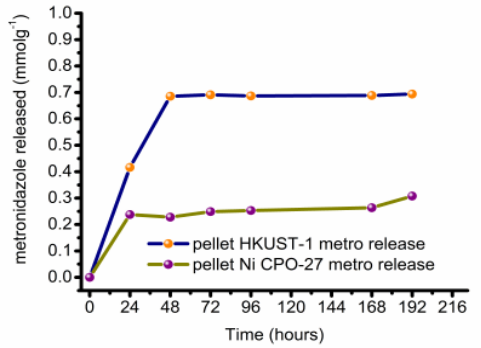

Fig. 2. Metronidazole released from different MOFs

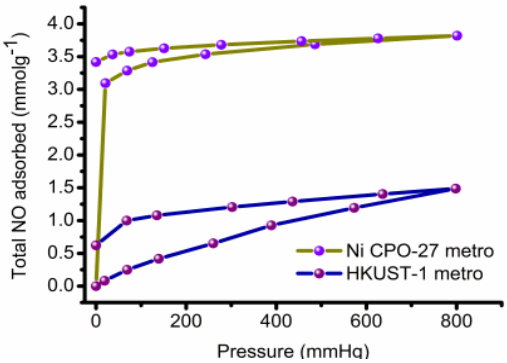

Fig. 3. NO adsorption in drug loaded MOFs

References

[1] McKinlay, A. C., Morris, R. E., Horcajada, P., Férey, G., Gref, R., Couvreur, P., Serre, C. Angew. Chem., Int. Ed. 49, (2010), 6260-6266.

[2] McKinlay, A. C., Xiao, B., Wragg, D. S., Wheatley, P. S., Megson, I. L., Morris, R. E. J. Am. Chem. Soc. 130, (2008), 10440-10444.

[3] Moncada, S., Palmer, R., Higgs, E. Pharmacol. Rev. 43, (1991), 109-142.

[4] Zhu, H., Ka, B., Murad, F. World J. Surg. 31, (2007), 624-631.

[5] Horcajada, P., Serre, C., Vallet-Regí, M., Sebban, M., Taulelle, F., Férey, G. Angew. Chem., Int. Ed. 45, (2006), 5974-5978.

[6] Horcajada, P., Serre, C., Maurin, G., Ramsahye, N. A., Balas, F., Vallet-Regi, M., Sebban, M., Taulelle, F., Férey, G. J. Am. Chem. Soc. 130, (2008), 6774-6780.

[7] Horcajada, P., Chalati, T., Serre, C., Gillet, B., Sebrie, C., Baati, T., Eubank, J. F., Heurtaux, D., Clayette, P., Kreuz, C., Chang, J.-S., Hwang, Y. K., Marsaud, V., Bories, P.-N., Cynober, L., Gil, S., Ferey, G., Couvreur, P., Gref, R. Nat. Mater. 9, (2010), 172-178.

[8] Freeman, C. D., Klutman, N. E., Lamp, K. C. Drugs 54, (1997), 679-708.

[9] Chui, S. S.-Y., Lo, S. M.-F., Charmant, J. P. H., Orpen, A. G., Williams, I. D. Science 283, (1999), 1148-1150.

[10] Dietzel, P. D. C., Georgiev, P. A., Eckert, J., Blom, R., Strassle, T., Unruh, T. Chem. Commun. 46, (2010), 4962-4964.

[11] Xiao, B., Wheatley, P. S., Zhao, X., Fletcher, A. J., Fox, S., Rossi, A. G., Megson, I. L., Bordiga, S., Regli, L., Thomas, K. M., Morris, R. E. J. Am. Chem. Soc. 129, (2007), 1203-1209.

Confined drugs in mesoporous silica for controlled release applications: a solid state NMR characterization

Thierry Azaïs[a], Nicolas Folliet[a], Daniela Aiello[b], Flaviano Testa[b], Flavien Guenneau[a], Andreï Nossov[a], Guillaume Laurent[a] and Florence Babonneau[a]

[a] *Université Pierre et Marie Curie-Paris6 and CNRS, UMR 7574, Laboratoire Chimie de la Matière Condensée de Paris, Collège de France, Paris, F-75005, France*

[b] *Department of Chemical Engineering and Materials, CR-INSTM, University of Calabria, 87036 Arcavacata di Rende (CS), Italy*

Introduction

Drug delivery systems are a new class of materials intensively studied in reason of their ability to increase the solubility of hydrophobic drugs in biological fluids. On a pharmaceutical point of view, it is of crucial importance to characterize the physical state of the encapsulated molecules as unexpected physical behaviours were observed due to strong confinement effect [1-2].

In this contribution we propose an overview of the solid-state NMR characterization of such systems. In particular, we show how variable temperature experiments can precisely characterize the physical state of drug-model molecules including ibuprofen (a nonsteroidal anti-inflammatory drug) and alendronate (a drug preventing osteoporosis) confined in mesoporous silica materials such as MCM-41 or SBA-15. Moreover, a multinuclear study was developed to identify the specific interactions that take place at the molecule/silica interface in such advanced drug delivery materials [3]. The experimental results are confronted to periodic DFT calculations including geometry optimisation and GIPAW calculations of NMR parameters. Finally, the homogeneity of the materials was investigated by an original method namely the hyperpolarized ^{129}Xe spectroscopy which allows building a precise model of the molecules partition in the mesoporous matrix.

Experimental

The method of encapsulation was the incipient wetness impregnation. The following drugs were encapsulated: ibuprofen (a nonsteroidal anti-inflammatory drug), lauric acid (an anti microbial fatty acid) and alendronate (a drug preventing osteoporosis). The following model molecules were also encapsulated: benzoic acid and phenylphosphonic acid. The silica mesoporous matrices used were MCM-41 and SBA-15 synthesized through standard protocol. Functionalized SBA-15 matrices were also used and synthesized through post-grafting of aminopropyl silane.

Results and discussion

The ^{1}H solid state NMR spectra of various samples are shown in **Fig. 1**.

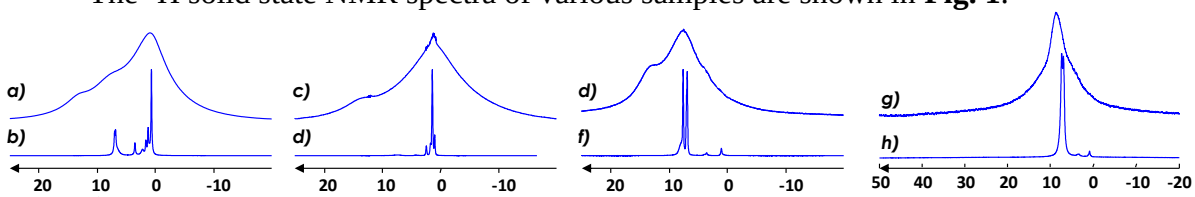

Fig. 1. *^{1}H solid state NMR of various molecules encapsulated in mesoporous silica matrices: b) ibuprofen, c) lauric acid, f) benzoic acid and i) phenyl phosphonic acid. The ^{1}H NMR spectra of the corresponding bulk substances are also shown for comparison on top (a, c, d and g).*

Encapsulated acids (carboxylic or phosphonic) exhibit very narrow ^{1}H resonances characteristic of a high dynamical behavior whereas the corresponding bulk substances display broad lines characteristic of rigid organic compounds due to ^{1}H homonuclear dipolar interaction. These experimental results are explained by the presence of confinement effect that drives the physical state of the encapsulated molecules which act as liquids at room temperature once entrapped. Confinement effects are now known to be responsible of the fast release kinetic profiles observed *in vitro* for mesoporous silica based drug release systems.

Confinement effects can be overcome by varying the chemical nature of the silica surface and by promoting molecules/walls attractive interactions. In the case of phenyl phosphonic acid encapsulated in aminopropyl modified SBA-15, attractive coulombian interactions $PO^{-}\ldots NH_3^{+}$ can explain the rigid nature of the organic framework. The proximity between the molecules and the walls can be investigated by the use of ^{1}H homonuclear dipolar interactions through the so-called double quantum (2Q) ^{1}H NMR experiments. **Fig. 2** displays the 2D ^{1}H 2Q experiment of phenyl phosphonic acid encapsulated in aminopropyl modified SBA-15. The cross peaks between the phenyl resonances and the propyl group proves unambiguously the proximities between the two species (d < 5-6 Å). A schematic representation of a possible phenylphosphonic acid/aminopropyl interaction can be seen on **Fig. 2**.

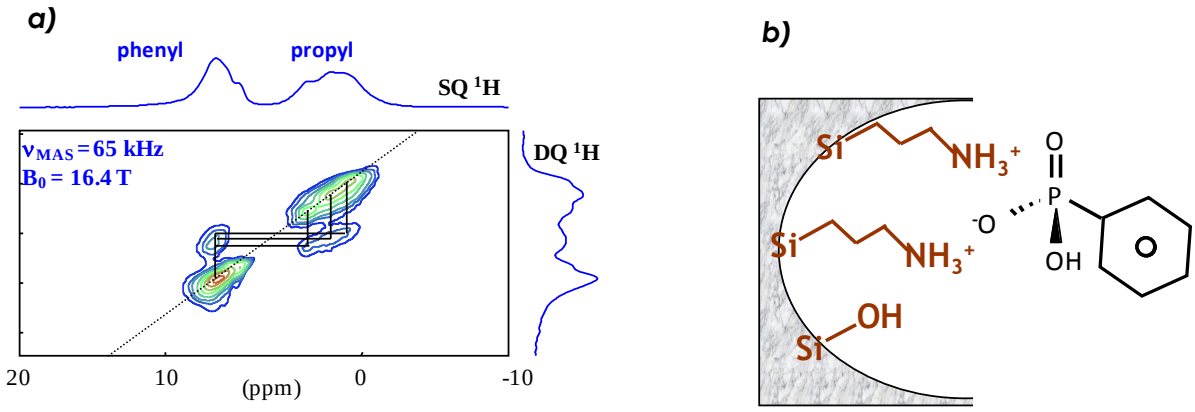

Fig. 2. a) 2D ^{1}H DQ spectrum of phenyl phosphonic acid encapsulated in aminopropyl modified SBA-15. b) Schematic representation of a possible phenylphosphonic acid/aminopropyl interaction

Conclusions

^{1}H solid state NMR is a very powerful tool to characterize drugs molecules and drug model molecules encapsulated in mesoporous silica materials. These species encapsulated in pure silica-based materials exhibit a very mobile behavior related to the presence of a strong confinement effect responsible of a depression of the thermodynamical parameters including melting temperatures. The modification of the chemical nature of the surface allows promoting strong host/guest interaction. Moreover, we demonstrate that the molecule/wall proximities can be easily investigated through ^{1}H DQ NMR experiments.

References

[1] T. Azaïs, C. Tourné-Péteilh, F. Aussenac, N. Baccile, C. Coelho, J-M. Devoisselle and F. Babonneau, *Chem. Mater.*, **2006**, 18, 6382-6390.

[2] T. Azaïs, G. Hartmeyer, S. Quignard, G. Laurent, C. Tourné-Péteilh, J-M. Devoisselle and F. Babonneau, *Pure and Applied Chemistry*, Vol. 81, No. 8, 1345–1355 (**2009**).

[3] Azais, T.; Hartmeyer, G.; Quignard, S.; Laurent, G.; Babonneau, F., *J. Phys. Chem. C*, ***2010***, *114 (19), 8884–8891*

Release Mechanisms for Bioactive Molecules from Mesoporous Silica

Thomas Bein[a]*, Axel Schlossbauer[a], Christian Dohmen[b], David Schaffert[b], Ernst Wagner[b]

[a]*Department of Chemistry and Center for Nanoscience, University of Munich (LMU), Butenandtstr. 5-13, Gerhardt-Ertl-Building, 81377 Munich, (Germany), Fax: (+49) 89-2180-77622, E-mail: bein@lmu.de*
[b]*Department of Pharmacy and Center for Nanoscience, Butenandtstr. 5-13 (D), 81377 Munich, (Germany)*

Introduction

Mesoporous silica systems are of great interest in novel concepts for targeted drug delivery. Their low toxicity combined with their high surface area and large accessible pore volumes make them suitable as transporters for anti-cancer drugs or other target-specific agents. An important aspect of such systems is the controlled release of compounds from the host material only at the desired location and at a specific time. To reach this goal, the porous host should respond to specific external triggers, such as changes in pH upon cell entrance, temperature changes or an increase of the redox potential of the environment.
Here we describe the pH-responsive release of acetal-linked mellitin from SBA-15 mesoporous silica, serving as an example for the above-mentioned release mechanisms. Mellitin, the active component of bee venom, is a small peptide containing 26 amino acids. It is widely investigated due to its lytic and apoptosis-inducing properties.

Experimental

As host material, large-pore SBA-15-type mesoporous silica was used. A mixture of Pluronic P123, cetyl-trimethylammonium bromide (CTAB), mesitylene, potassium chloride and hydrochloric acid was prepared to hydrolyze tetraethylorthosilicate (TEOS) and assemble the mesoporous structure. After calcination, the nitrogen sorption isotherm gave pore diameters of about 11 nm and a BET surface area of about 700 m^2/g [1]. The host was grafted with 3-mercaptopropyl-trimethoxysilane (MPTS) yielding sample SBA-SH. The thiol-containing host was reacted with acetal- or ether-containing linkers through maleimide coupling (see Figure; MK-linker (a) and BM-linker (b)), followed by reaction with cystein-terminated mellitin (samples SBA-MK-Mel and SBA-BM-Mel).

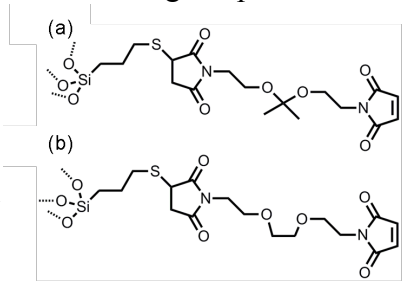

Results and discussion

The mellitin-conjugated SBA materials were exposed to solutions of PBS-buffer at either pH 7.4 or pH 5.5. These values represent the pH in extracellular fluid and in late endosomes after endocytosis, respectively. If triggered release can be achieved within this pH-range, the release mechanism offers a promising way for opening nanocarriers that have been internalized through endocytosis. A striking difference was found for the behavior of the two linkers and the resuling release of mellitin at the two pH values, as determined with a photometric method. At pH 7.4, the acetal-containing sample SBA-MK-Mel released almost no mellitin, while at pH 5.5, about 50% of the bound mellitin were released into the buffer within 60 minutes. For the following functional analysis of the released peptide, the samples were investigated in an erythrocyte lysis assay. Thus, the suspensions of the samples SBA-BM-Mel and SBA-MK-Mel were serially diluted in phosphate-buffered saline (PBS). A mouse erythrocyte solution was mixed with the respective sample suspension or free mellitin

solution as reference. The lysed fraction was determined photometrically. We observed that the MK linker remains stable at pH 7.4, preventing lysis even at the highest concentration tested. However, when the pH was lowered, the MK-linker was cleaved, resulting in the release of the encapsulated mellitin. In contrast, the BM-linker remained stable upon decreasing the pH, keeping mellitin covalently bound to the pore walls. Thus, the pH-sensitive cleavage of the acetal-mellitin bonds (at pH 5.5) and the effective release of mellitin from the mesoporous host could be clearly demonstrated in this study.

We will also discuss additional effective release mechanisms for colloidal mesoporous nanoparticles recently developed in our laboratory. For example, a novel DNA-based molecular valve offers a precisely programmable opening temperature.[1] The assembly of this multifunctional nano-device builds on a novel multifunctional core-shell colloidal mesoporous silica host, free available pore volume inside the host, selective functionalization of the pore mouths with a double-stranded DNA linker bearing two dyes for FRET monitoring, and biotin-avidin coupling for valve closure. The possibility to precisely program the opening temperature by varying the length and sequence of the double-stranded DNA linker makes this system unique and far more versatile compared to previously reported mechanisms.
Moreover, we will discuss a one-step assembly route where supported lipid bilayers (SLB) are deposited on functionalized colloidal mesoporous silica (CMS) nanoparticles, resulting in a core-shell hybrid system (SLB@CMS).[2] The supported membrane acts as an intact barrier against the escape of encapsulated dye molecules. These stable SLB@CMS particles loaded with the anticancer drug colchicine are readily taken up by cells and lead to the depolymerization of microtubules with remarkably enhanced efficiency as compared to the same dose of drug in solution.

Conclusions
Summarizing, we have developed several novel triggered release mechanisms for bioactive molecules from mesoporous silica. Such mechanisms form the basis for the evolution of complex multifunctional mesoporous silica agents for targeted drug release.

Acknowledgments
Support from DFG-SFB 486 and 749, from the NIM and CIPSM Excellence Clusters (LMU) and from CeNS is gratefully acknowledged.

References
(1) Schlossbauer, A., Warncke, S., Gramlich, P. M. E., Kecht, J., Manetto, A., Carell, T., Bein, T. *Angew. Chem., Int. Ed.* **49** (2010) 4734-4737.
(2) Cauda, V., Engelke, H., Sauer, A., Arcizet, D., Braeuchle, C., Raedler, J., Bein, T. *Nano Lett.* **10** (2010) 2484-2492.

Gold nanoclusters with mesoporous silica coating for combined chemotherapy and photothermal therapy of cancer cells

Manuel Quesada,[1] Ílida Ortega,[2,3] Carlos Muniesa,[1] Avelino Corma,[1] Eduardo Fernández,[2] Roque F. Madrigal,[4] Antonio Fimia[4] and Pablo Botella[1]

[1]Instituto de Tecnología Química, UPV-CSIC, Av. Los Naranjos s/n, 46022 Valencia, Spain; [2]Instituto de Bioingeniería, Universidad Miguel Hernández, Av. Universidad s/n, 03202 Elche, Spain; [3]Centro de Investigación Biomédica en Red (CIBER-BBN); [4]Departamento Ciencia de Materiales, Óptica y Tecnología Electrónica, Universidad Miguel Hernández, Elche, Spain

Introduction

Although the destruction of solid tumors by hyperthermia is valuable for cancer treatment, single heating techniques are not able to discriminate between tumor cells and neighboring healthy cells. One way to overcome this limitation is to perform a non invasive photothermal therapy using deep penetrating NIR lasers [1]. Here, the strong optical absorption in the Vis/NIR region of many Au nanostructures makes them attractive as photothermal agents for cancer therapy [2]. The absorption band of metal nanoparticles can be readily tuned by adjusting their shape and size [3] or by controlled assembly of gold nanoparticles [4]. Furthermore, the encapsulation of these gold nanoclusters in a biocompatible and multifunctional mesoporous silica scaffold provides high stability in biological fluids and allows simultaneous delivery of drugs. Here we present a novel hybrid nanoplatform for the *in vitro* destruction of cancer cells that combines the optical properties of a gold nanocluster core with the specific therapeutic activity of 20(S)-camptothecin (CPT) delivered within the regular pores of the silica shell.

Experimental

150-250 nm diameter nanoparticles with internal clusters of 5-9 gold nanoparticles and mesoporous silica coating (MSGC) were prepared according to a previous report [5]. CPT (0.8 wt%) was incorporated into the pores of the particles by soaking them in a DMSO solution and further washing with PBS. Materials were characterized by XRD, BET, DLS, TEM and UV-Vis/NIR. For the *in vitro* chemo and photothermal therapy test, 42-MG-BA human glioma cells were seeded with 100 µg/mL MSGC with or without CPT. A control group was also incubated with no nanoparticles. After 24 hours in culture, all samples were irradiated with a femtosecond pulsed Ti:Saphire laser (790 nm, 45 s, 76 W/cm^2). Immediately after NIR-light exposure, the medium was removed and cells were treated with Hoechst 33342 stain and/or acridine orange and fixed with paraformaldehyde in cacodydate buffer. Fluorescence was visualized with microscope equipped with specific set filters for UV and acridine orange, digital camera and computer-assisted image analysis program and a set of customized macros. Cell counts were performed manually on 15-20 randomly selected microscopic fields for each sample and statistically verified. Results on the combined chemo and photothermal therapy of cancer cells are shown in Table 1 and Figure 1.

Results and discussion

No effect on cell proliferation is observed in the control group after exposition at laser energy fluence of 76 W/cm^2 (n=5, p>0.05) (Figure 1a). Conversely, the internalization of MSGC in 42-MG-BA human glioma cells provokes a significant decrease in cell density and current mortality about 40% (Table 1, Figure 1b). Cell death is due not only to local heating effect but

Table 1. Cell density data after *in vitro* photothermal therapy on 42-MG-BA human glioma cells with MSGC (100 μg/mL) and the combined chemotherapy with CPT.

Sample	$D_{cluster}$ (nm)[a]	$D_{particles}$ (nm)[b]	Cell counts (cells/mm^2)
Control	---	---	1180 ± 35
MSGC	72.8 ± 6.5	150-250 (158 ± 33)	740 ± 72
MSGC+ CPT (0.8 wt%)	72.8 ± 6.5	150-250 (158 ± 33)	373 ± 64

[(a)] Hydrodynamic diameter (as determined by DLS).
[(b)] As determined from TEM images by measuring at least 200 particles: range (mean ± standard deviation).

also to mechanical stress and hydrodynamic pressure, which is produced by vapor microbubbles formation within the cytoplasm,thus, provoking the lysis of the somatic structure [6,7]. The mesoporous structure of the silica wall is crucial for the photothermal response of these materials, as generation of microbubbles is related with vaporization of water inside the pores. The incorporation of CPT into the pores also leads to a significant cytotoxic effect. Afterwards, laser irradiation destroys a significant amount of cells (Table 1, Figure 1c), and the combined action of chemo and photothermal therapy leads to almost 70% cell mortality. Moreover, CPT is expected to suppress tumor growth after irradiation [8].

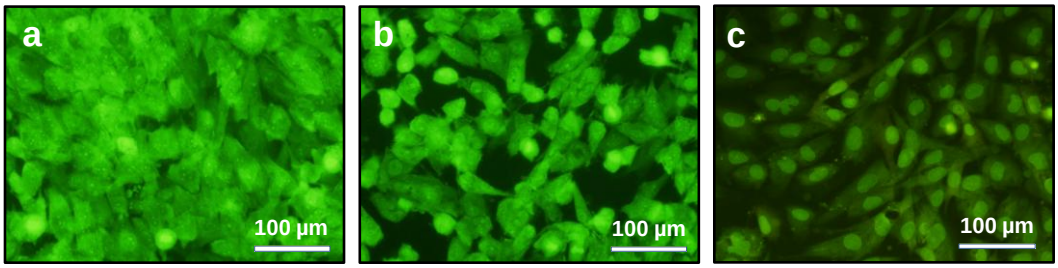

Figure 1. Fluorescence microscope images of 42-MG-BA human glioma cells after laser irradiation (76 W/cm^2). (a) Control with no nanoparticles. (b) Cells with 100 μg/mL of MSGC. (c) Cells with 100 μg/mL of MSGC loaded with 0.8 wt% CPT.

Conclusions

Nanoparticles with internal gold clusters and mesoporous silica coating are able to produce photothermolysis when internalized in 42-MG-BA human glioma cells and irradiated with a femtosecond pulse laser (790 nm). Cell death can take place through a thermal mechanism but especially by mechanical disruption of cellular components due to *in situ* generation of vapor microbubbles. The incorporation of CPT within the pores of the silica shell leads to a synergetic effect between the cytotoxicity of the drug and the photothermal activity, providing higher efficacy in the destruction of cancer cells than single laser irradiation.

Acknowledgements

This work was supported by projects FIS2006-09319 and MAT2006-14274-C02-01.

References

[1] Weissleder, R. *Nat. Biotechnol.* 21 (2001), 316-317.
[2] Pissuwan, D; Valenzuela, S.M.; Cortie, M.B. *Trends Biotechnol.* 24 (2004), 62-67.
[3] Sun, Y.; Xia, Y. *Science* 298 (2002), 2176-2179.
[4] Liz-Marzán, L.M. *Langmuir* 22 (2006), 32-41.
[5] Botella, P.; Corma, A. Navarro, M.T.; Quesada, M. *J. Mater. Chem.* 19 (2009), 3168-3175.
[6] Zharov, V.P.; Galitovsky, V.; Viegas, M. *Appl. Phys. Lett.* 83 (2003), 4897-4899.
[7] Lapotko, D.; Lukianova, E.; Potapnev, M.; Aleinikova, O.; Oraevsky, A. *Cancer Lett.* 239 (2006), 36-45.
[8] You, J.; Zhang, G.; Li, Chun. *ACS Nano* 4 (2010), 1033-1041.

Photoresponsive layered double hydroxides with controlable magnetic response

Gonzalo Abellán[a]*, Hermenegildo García[b], Eugenio Coronado[a], José Luis Jordá[b], Carlos Martí-Gastaldo[a], Antonio Ribera[a]
[a]*Instituto de Ciencia Molecular, Universidad de Valencia, Catedrático José Beltrán 2, 46980, Paterna, Valencia, Spain.* [b]*Instituto de Tecnología Química CSIC-UPV, Universidad Politécnica de Valencia, Avenida de los Naranjos s/n, 46022, Valencia, Spain.*
gonzalo.abellan@uv.es

Introduction

The development of magnetic materials whose properties can be controlled by means of an external stimulus can have potential applications for spintronics, information storage, sensoring, and other uses. One general strategy to develop this type of materials consists in modifying layered double hydroxides (LDHs) having magnetic properties by anionic exchange incorporating into the interlayer galleries a guest that can respond to the external input. In this context we have been interested in the preparation of magnetic LDH materials with photoresponse. Compared to other alternative inputs, light as external stimulus has the possibility of spatial and temporal resolution in the excitation, the absence of wasteful chemicals and the possibility to tune the response by selecting the appropriate wavelength.
Towards the general objective of the preparation of photoresponsive magnetic materials based on modified LDHs we have prepared a series of LDHs having Ni^{II} Al^{III}, Co^{II} Al^{III} and Zn^{II} Al^{III} in different atomic ratios. The presence of nickel and cobalt introduces magnetic response in the material while the combination of zinc and aluminum renders an LDH lacking magnetism that can be used as reference material. As photoresponsive components in the system we have selected azocompounds. Scheme 1 illustrates the structure of the three azo compounds that have been studied as well as a pictorial illustration of LDH incorporating azobenzenes. The selection of azobenzenes as photoresponsive components derives from the well studied reversible photoinduced *trans-cis* isomerization that causes a remarkable change in the dimension of the molecule that should be reflected in changes into the interlamellar separation of the LDH sheets [1].

Scheme 1. Structure of the three azocompounds and illustration of LDH-Azo compound.

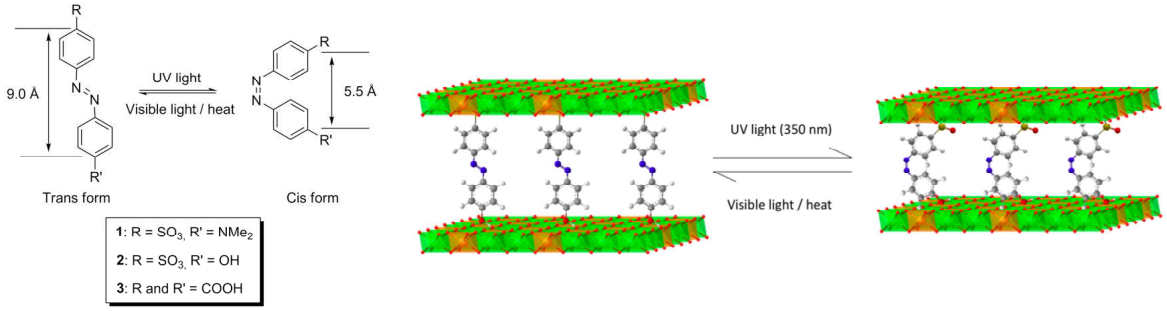

Methodology

One key step in the preparation of magnetic LDH containing azobenzenes is the process to incorporate photoactive aromatic azo compound. The target is to prepare a material in which the positive charges of the nanosheets are compensated by the negative azobenzenes in such a way that a highly crystalline solid is obtained. Incorporation of azobenzenes in LDH was achieved by anionic exchange and the progress of the intercalation can be followed by XRD

monitoring the shift in the position of the (003) peak. The crystallinity of the material can be determined by the number of counts of the (003) peak for a given amount of solid. Figure 1 shows representative XRD of some of the materials prepared showing the shift in the position of the (003) peak as well as the change in the intensity of the peak as consequence of the different level of crystallinity.

Results

Prior photophysical characterization of the properties of azobenzenes in solution has shown that azo compound **3** undergoes trans-cis isomerization reflected by the change in the optical spectrum that corresponds to a dissappearance of the visible band as 420 nm of the trans isomer and the growth of 360 nm band corresponding to the cis [2]. Observation of an isosbestic point shows that the two isomers interconvert one into the other. The cis isomer, once formed photochemically can revert thermally to the more stable trans isomer with a rate constant depending on the temperature. Figure 2 shows on UV-Vis spectra to illustrate these changes. With respect to the behaviour observed in solution, the photoresponse of LDH incorporated azobenzenes was significantly slower and less defined. The main problem is a uniform irradiation of the material that is probed spectroscopically and also the sufficient intensity of the light beam. Under optimal experimental conditions, evidence of the occurrence of cis-trans isomerization was obtained by XRD (shift in the (003) peaks) and optical spectroscopy (growth of the band corresponding to the cis isomer and decrease of the band corresponding to the trans isomer).

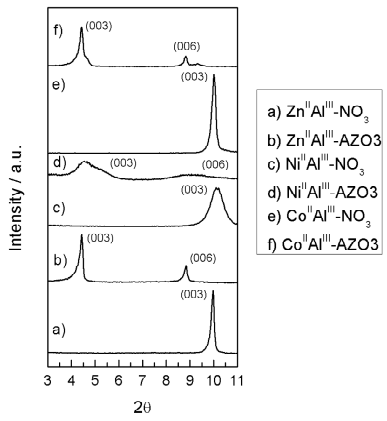

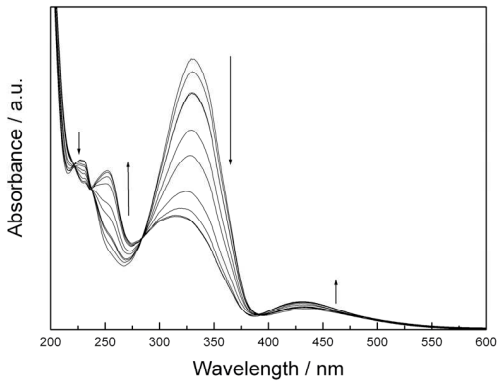

Figure 1. XRD spectra of some of the materials prepared. Figure 2. UV-Vis spectra of azocompound **3**.

Magnetization measurements using a SQUID magnetometer shows that the state of the material promoted by isomerization of the cis-trans is reflected in the magnetic properties of the solid that can be modulated varying the intensity of the light, the irradiation time and the nature of the metals and azobenzene of the LDH.
Further work in this field is aimed at the improvement of the photoresponse by selecting azobenzene with optimum photochemical response and by improvement of the preparation procedures.

References

[1] Ogawa, M. Photoisomerization of azobenzene in the interlayer space of magaidite, Journal of Materials Chemistry, 12 (11) (2002), 3304-3307

[2] Abellán, G., García, H., Gómez-García, C.J., Ribera, A., Photochemical behavior in azobenzene having acidic groups. Preparation of magnetic photoresponsive gels, Journal of Photochemistry and Photobiology A: Chemistry, 217 (1) (2011), 157-163

HYDROPHILIC ZEOLITE MEMBRANES ON SILICON SUBSTRATES FOR MONOLITH FABRICATION OF MICRODEVICES

Luaces, S.; Urbiztondo, M.; Mallada, R.; Pina, M.P.; Santamaria, J.
Nanoscience Institute of Aragon, University of Zaragoza, 50018 Zaragoza, Spain, jesus.santamaria@unizar.es

Introduction

In the chemical technology field, microfabrication concepts have found relatively few applications to date compared to the microelectronics industry, which is mainly due to the fact that production scenarios in the chemical industry usually involve the processing of high volume feeds, often containing impurities and foreign elements. In spite of this, several important developments in the realm of microdevices for the chemical and process industries have taken place during the last 15 years, mainly in the fields of microreactors and sensors. In particular, different 3D microstructures based on silicalite films [1-5] have already been developed by our group (see figure 1). Typically, the approach involves the preparation of a defect-freee zeolite thin layer onto the Si substrate followed by lithography and etching process for the zeolite micropatterning. As a matter of fact, the proof of concept has been demonstrated for Silicalite, which indeed exhibits limitations for practical applications. Therefore, the aim of this work is the synthesis of well-intergrowth hydrophilic zeolite membranes (i.e. NaA and NaY type zeolites) on silicon substrates for the monolith fabrication of microdevices. Herein, the main challenge relies on the chemical stability of Si wafers in the synthesis media (pH, time and temperature). Accounting from that, seeding stage, seeds size, gel composition for secondary growth, heating source, temperature and synthesis time have been carefully studied for both zeolites.

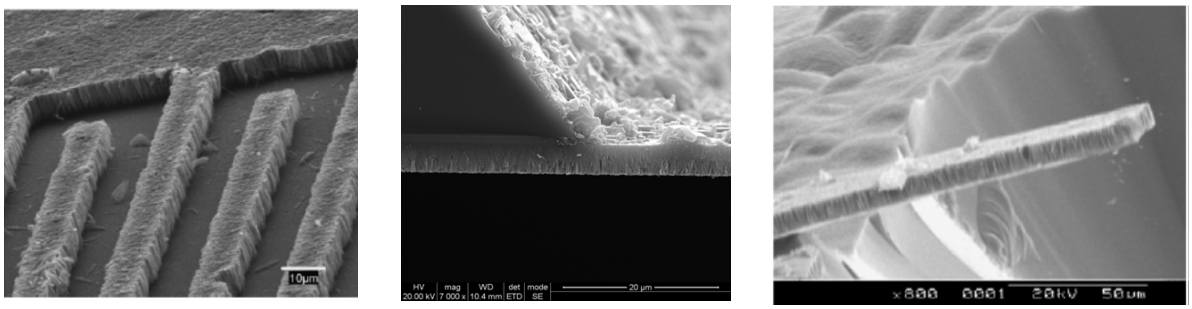

Figure 1. Silicalite-silicon based micro-devices a) microchannel type micro-reactor, b) micro-membrane and c) only-silicalite cantilever.

Experimental

Mostly, the secondary growth approach has been used for the preparation of supported NaA and NaY zeolite membranes. Thus, the following steps are involved: i) synthesis of colloidal zeolites for seeding; ii) 4” Si wafer seeding; iii) hydrothermal secondary growth (90º-100ºC); iv) template removal.

Results and conclusions

NaA and NaY well-intergrowth zeolite membranes have been successfully prepared over previously oxidized Si wafers (4" in diameter). In the case of LTA zeolite, layers 3 μm in thickness have been achieved after 7.5 hours of synthesis time at 90ºC. Similarly, 4.5 h are required for FAU counterparts (see Figure 2).

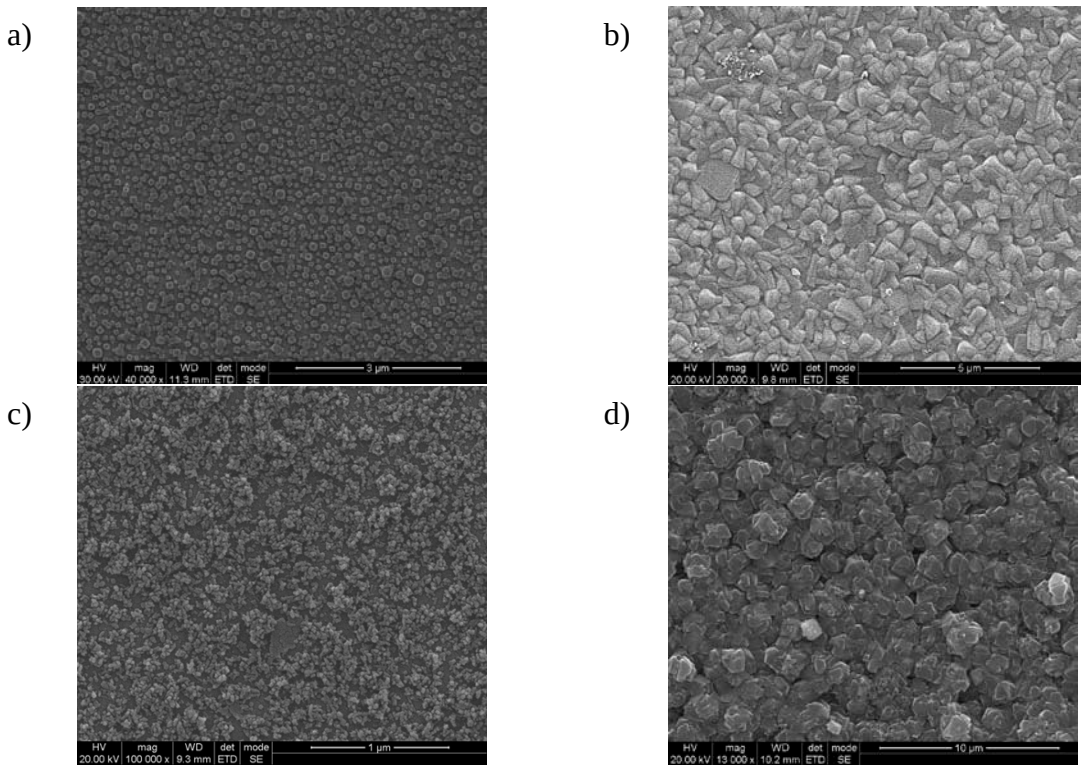

Figure 2. SEM pictures of: NaA (a) and NaY (c) top layer of single nano-crystals; and well-intergrowth NaA (b) and NaY membranes on Si wafers.

Accounting from that, it could be concluded that synthesis procedures for the fabrication of hydrophilic thin zeolite membranes onto Si wafers have been established. Our research efforts are now focused on the micropatterning of such zeolite layers for the development and testing of Si based microdevices. In particular, microchannel type reactors based on PtY zeolite for VOC combustion are under study.

References

[1] Development of microstructured zeolite films as highly accessible catalytic coatings for microreactors. M.A. Urbiztondo, E. Valera, T. Trifonov, R. Alcubilla, S. Irusta, M.P. Pina, A. Rodríguez, J. Santamaría. Journal of Catalysis, 2007, Vol. 250, pp. 190-194.

[2] Development of etching processes for the micropatterning of silicalite films. I. Pellejero, M. Urbiztondo, M. Villarroya, J. Sesé, M.P. Pina, J. Santamaría. Microporous and Mesoporous Materials, 2008, Vol. 114.

[3] Zeolite-modified cantilevers for the sensing of nitrotoluene vapors. M.A. Urbiztondo, I. Pellejero, M. Villarroya, J. Sesé, M.P. Pinaa, I. Dufour, J. Santamaría. Sensors and actuators, 2009, Vol. 137, pp. 608-616.

[4] Optical vibrometer for mechanical properties characterization of silicalite-only. J. Agustí, I. Pellejero , G. Abadal , G. Murillo , M.A. Urbiztondo , J. Sesé , M. Villarroya-Gaudó. Microelectronic Engineering, 2010, Vol. 87.

[5] Zeolite films and membranes: Emerging applications. M. Pina; R. Mallada, M. Arruebo, M. Urbiztondo, N. Navascués, O. Iglesia, J. Santamaría. Microporous and Mesoporous Materials. 2011. doi:10.1016/j.micromeso.2010.12.003.

Mesoporous Aluminosilica Monoliths Sensor for Selective Visualization of Toxic Metal Ions

Sherif A. El-Safty[1,2]
[1]*National Institute for Materials Science (NIMS, 1-2-1 Sengen, Tsukuba-shi, Ibaraki, 305-0047, JAPAN.E-mail: sherif.elsafty@nims.go.jp*
[2]*Graduate School for Advanced Science and Engineering, Waseda University, 3-4-1 Okubo, Shinjuku-ku, Tokyo 169-8555, Japan. E-mail: sherif@aoni.waseda.jp*

Introduction

Intense research activities have been focused on the synthesis, structural characterization, reactivity, and prospective applications of the mesoporous aluminosilica or alumina during the past decade [1]. If these molecular sieves could be prepared in 3D geometrical monoliths with uniformly-shaped pores, high acidity, structural integrity, thermal/hydrothermal stability via simple synthetic strategy, thus these materials would be expected to show widespread applications [2]. Although, the optical sensors and adsorbents based mesoporous powder/monolithic carriers recently became a hot packages for remarkably sensing and selective responses with respect to comparable indicator or probe molecules, the developments in the form of compact instrumental free ion-sensors are still under research level and currently being investigated using different techniques [3-5]. Here, we report optical aluminosilica sensors with high surface area and crystalline γ-Al_2O_3 alumina in framework for facile handling of signal read-out with visual detection of ultra-trace concentrations of organic and inorganic targets at the same frequency as the human eye.

Experimental

Ordered cubic Ia3d monolithic aluminosilica discs with low silica contents ($4 \leq Si/Al \leq 1$) that fabricated by using direct templating method of microemulsion liquid crystalline phase of P123 ($EO_{20}PO_{70}EO_{20}$) templates can be used as a miniaturized nano-membrane strips for anionic (TMPyP) dyes from aqueous solution at room temperature. Typically, aluminosilica monoliths were fabricated using microemulsion phases formed by addition of C_{12}-alkane (dodecane) to surfactant/(TMOS)/$AlCl_3$ mixture domains [2]. Moreover, in the basic laboratory sensing assays, we test the ability of the sensor dye-pellet to be used as an eco-friendly detection and removal of ultra-trace Hg(II) ions in aqueous solution. However, significant absorbance and color changes were observed with pH solution of 12.5.

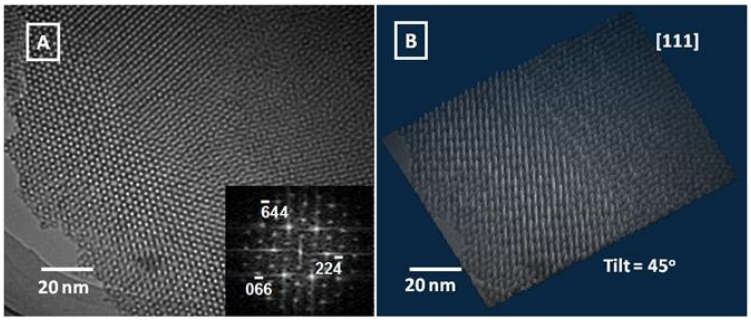

Fig. 1 *TEM, FTD and 3DTEM profiles of optical sensors for toxic metal ions based cubic Ia3d membranes.*

Results and discussion

TEM, FTD and 3DTEM profiles show evidence of retaining the high order of cubic Ia3d mesopores with fabrication of optical membrane sensor (Fig.1), which led to high flux and transport of organic TMPyP dye and inorganic Hg(II) analyte ions (in the order of minutes).

However, the surface acidity on the reactivity of aluminosilica pellets could result in significant effects on the overall adsorption capacity and affinity of anionic (2x 10^{-3} M) TMPyP probe. Strong ion-pair interactions between the TMPyP probe containing pyridinium ions and the negatively-charged (AlO_4^- units) γ Al_2O_3-rich silica host matrices led to retention of the sensor strips during the sensing assays of Hg(II) ions (Scheme 1). The amount uptake of TMPyP onto γ Al_2O_3-rich silica matrices were sufficient to create signal read-out "optical color change" as a response of the binding with toxic Hg(II) ions. Key to achieving design of optical sorbent strips is the dense accessibility and intrinsic mobility of the probe onto crystalline γ Al_2O_3 –silica framework matrices. Due to the probe accommodation into nanoscale membranes the sensitivity and binding response kinetics of hg(II) ions were significantly acheived. Thus, the membrane sensors would allowed simple preconcentration to yield high adsorption capacity of Hg(II) ions and simultaneously visual detection (Scheme 1).

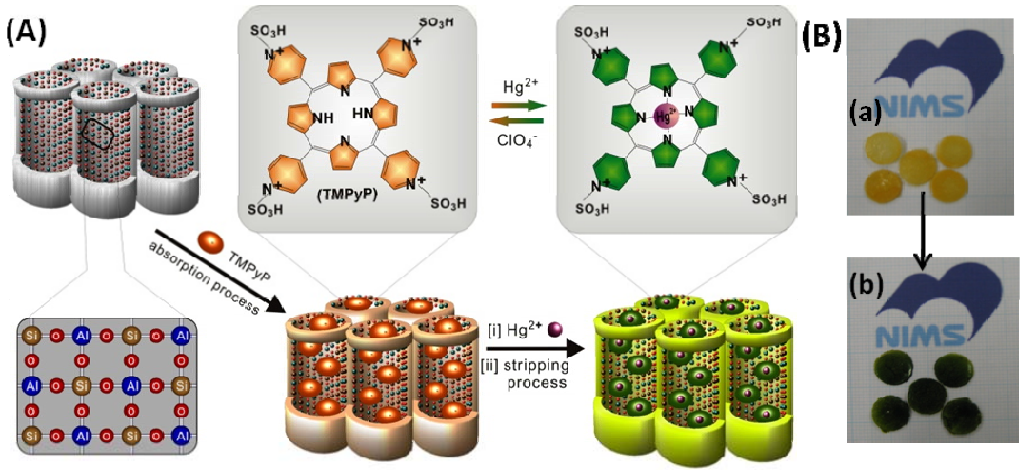

Scheme 1 *Design of optical membrane sensors (A) for removal of inorganic toxic pollutants. (B) Selectivity of Hg (ions) among all metals using TMPyP dyes at pH 12.5*

This simple recognition and removal of ultra-trace Hg(II) ion up to 10^{-11} M (detection limit) in real-world analysis, where basic UV-Vis. spectrometer could be effectively used. The reflectance spectra of the sensor strips exhibited a bathchromic shift from 410 nm to 450 during the recognition of Hg^{2+}, corresponding to the formation of the metal-chelate [Hg-TMPyP]$^{n+}$ complex. The portable sensor pellets were able to detect and complete removal of Hg(II) ions (in the order of 60 sec.), despite the presence of other interfering and toxic metal ions, for example Fe^{3+}, Ni^{2+}, Zn^{2+}, Cr^{6+}, Sb^{3+}, Bi^{3+}, Pb^{2+}, Cd^{2+}, Mn^{2+}, and Co^{2+}, as shown in Scheme 1B.

Conclusions

The current sensor design based on γ Al_2O_3-rich silica scaffolds in the form of highly mechanical stable pellet-like monoliths show advanced features to act as portable and storable strips. However, in addition to conventional recognition of Hg(II) ion at trace levels (~10^{-11} mol/dm^3), there is a further control of the sensing assay, governed by facile handling of signal read-out optical measurements with the same frequency of the human eyes.

References

[1] (a) Y. Lui, W. Zhang, T. J. Pinnavaia, *J. Am. Chem. Soc.* **2000,** *122*, 8791. (b) A. Corma, A. *Chem. Rev.* **1995**, 95, 559. (c) J. J. Chiu, D. J. Pine, S. T. Bishop, B. F. Chmelka *J. Cata.* **2004**, *221*, 400.
[2] S. A. El-Safty, et al. *Micro. Meso. Mater.* **2011,** 138, 51–62.
[3] (a) E. Coronado, et al. *J. Am. Chem. Soc.* **2005**, *127*, 12351.(b) J. V. Ros-Lis, et al. *Angew. Chem. Int. Ed.* **2005,** 44, 4405.
[5] (a) S. A. El-Safty, et al. *Angew. Chem. Int. Ed.* **2006**, *45*, 7202. (b) *Talanta* **2011**, *83*, 1341–1351. (c) *Adv. Funt. Mater.* ***2008***, 18, 1739- 1750. (d) *Adsorption*, **2009,** 15, 227-239.

POSTERS

FEZA 2011

Synthesis and characterization of porous solids

FEZA 2011

Could natural Serbian clinoptilolite efficiently remove metal ions from aqueous solutions and also be converted into a novel material after being metal-loaded?

Nevenka Rajic[1*], Djordje Stojakovic[2], Jasna Hrenovic[3] and Aleksander Recnik[4]
[1]*Faculty of Technology and Metallurgy, University of Belgrade, 11000 Belgrade, Serbia, nena@tmf.bg.ac.rs*
[2]*Innovation Centre of the Faculty of Technology and Metallurgy, University of Belgrade,*
[3]*Faculty of Science, University of Zagreb, Roosveltov trg 6, 10000 Zagreb, Croatia*
[4]*Jozef Stefan Institute, 1000 Ljubljana, Slovenia*

Introduction

Adsorption using natural adsorbents is generally considered to be the most suitable method for wastewater treatment. Clinoptilolite, as the most abundant natural zeolite, can therefore be regarded as a cost minimizing choice of the adsorbent for the developing countries. In Serbia, there are several zeolitic deposits with relatively high clinoptilolite content. A detailed spectroscopic and structural investigation of the sample from Vranjska Banja [1] showed that the zeolitic tuff contains three major mineral phases, the clinoptilolite being in the highest percentage (more than 70 wt. %). We have studied in detail kinetics and thermodynamics of the removal of Mn(II), Ni(II), Cu(II) and Zn(II) from aqueous solutions containing the metal ions in the concentration range of 50-400 mg dm^{-3} using this natural zeolitic tuff. Also, we have investigated whether the exhausted zeolite could possibly find applications as a novel material.

Experimental

The sorption isotherms and rate of sorption were determined at 298, 308, 318, 328 and 338 K using the batch method. 100.00 cm^3 of the solution were mixed with 1.0 g of zeolite sample (pretreated with a solution of NaCl) and the suspension was shaken for 24 h in a thermostated water bath. The solid was then recovered by filtration. All experiments were carried out at the original pH since preliminary investigations showed it to be optimal.
The samples of metal-loaded zeolite were thermally treated under air at 540 ^oC at a heating rate of 10 $^oC\ min^{-1}$. The obtained products were analyzed by the transmission electron microscopy (TEM).
A pure culture of *Acinetobacter junii* DSM 1532 has been used for testing the antibacterial activity of the Zn-containing samples. The *A. junii* was pregrown on the nutrient agar (Biolife, Italy) for 16 h at 30.0±0.1°C. Next, the biomass was suspended in sterile 0.05 mol dm^{-3} NaCl and inoculated into 100 cm^3 of autoclaved synthetic wastewater (composition in mg dm^{-3} of distilled water: Na-propionate 300; peptone 100; $MgSO_4 \cdot 7H_2O$ 10; $CaCl_2 \cdot 2H_2O$ 6; KCl 30; yeast extract 20; KH_2PO_4 88; pH=7.0±0.2). 1.00 g of the zinc-containing sample was added into the flask, while a control flask was left without the addition of the material. The flasks were incubated for 24 h at 30.0±0.5°C in a water bath. The concentration of phosphorous in wastewater was measured in a DR/2500 Hach spectrophotometer by the molybdovanadate method (Hach method 8114).

Results and discussion

The study shows that the Serbian natural zeolite can be used effectively in the removal of the Mn(II), Ni(II), Zn(II) and Cu(II) ions from aqueous solutions by adsorption. The removal efficiency (30-95 %) increases in order Ni < Mn ~Zn <Cu. The sorption capacity varies with the initial metal solution concentration and it increases with temperature for all the studied metals. The sorption isotherms are best represented by the Sips (Ni, Mn, Zn) and Freundlich (Cu) models and the sorption kinetics by the pseudo-second-order model. The sorption involves a combination of three processes: the film diffusion, the intra-particle diffusion, and a chemical cation–exchange between sodium ions of clinoptilolite lattice and the aqueous M^{2+} ions. The sorption was found to be endothermic and spontaneous in the 298–338 K range. Dehydration of the metal-loaded clinoptilolite at about 540 ^{o}C leads to the formation of crystalline NiO, ZnO and Cu_2O nano particles (2-5 nm) which are widespread over the clinoptilolite surface (Fig. 1).

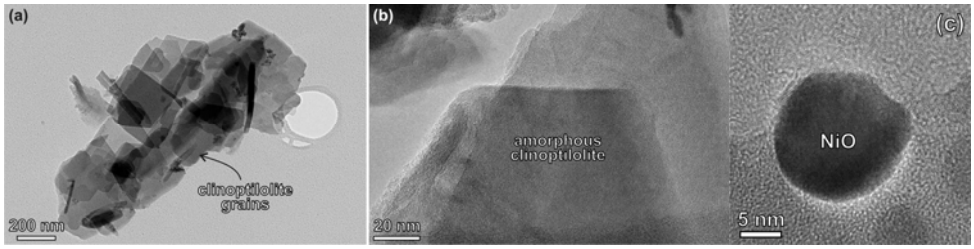

Figure 1. TEM image of the dehydrated manganese-loaded clinoptilolite (a). High-magnification image (b) shows a uniform surface of an amorphous clinoptilolite grain without any oxide nanoparticles. A NiO particle at the surface of nickal-loaded clinoptilolite (c).

Dehydration of the Mn-containing sample however does not lead to the formation of any oxide products and leads to disruption of the clinoptilolite lattice. The results concerning antibacterial activity suggest that zinc-loaded clinoptilolite exhibits an excellent antibacterial activity towards *A. junii* (99.99 %). It also effectively removes phosphate ions from solution (80 %).

Conclusions

This investigations show that the Serbian clinoptilolite can be used as sorbent for the removal Mn(II), Ni(II), Zn(II) and Cu(II) ions from aqueous solutions by adsorption The exhausted sorbent could find further application since oxide nanoparticles embedded in the zeolitic matrix have been known to exhibit catalytic activity for various reactions. Also, the Zn-containing clinoptilolite is a promising material for a final step in wastewater treatment, in which a simultaneous phosphate removal and disinfection can be achieved. These render the exhausted clinoptilolite a potential candidate for novel applications.

Acknowledgements

This work was supported by the Eureka project E!4208.

References

[1] Cerjan Stefanovic, S., Zabukovec Logar, N., Margeta K., Novak Tusar N., Arcon I., Maver K., Kovac J., Kaucic V., Structural investigation of Zn^{2+} sorption on clinoptilolite tuff from the Vranjska Banja deposit in Serbia, (2007) Micropor Mesopor Mater 105 (2007), 251-259.

Expanding the Concept of Zeolite Structures into a New Dimension Integrating 3-D Frameworks and Various Layered Forms

Wieslaw J. Roth[1*], Douglas L. Dorset[2], Jiří Čejka[3]
[1] *123 Boundbrook Ct., Sewell, NJ, 08080 (USA),* [2]*475 Ellis Road, Milford, NJ 08848 (USA),*
[3]*J. Heyrovsky Institute of Physical Chemistry, Academy of Sciences of the Czech Republic, Prague (Czech Republic); *wies.roth@gmail.com*

Introduction

We present the title concept as a new basic principle [1] and discuss its fundamental and practical significance and implications. The traditional, dominant concept defined idealized zeolite structures [2] as extended in 3-D periodic frameworks, built from 4-connected, corner-sharing tetrahedra, with each T-atom, except those on an external surface, having 4 different neighbors. It further implied formation of the frameworks by direct assembly in 3-D. This implication had a practical limiting consequence since, once formed, zeolite crystals and frameworks appeared to be immutable and not susceptible to a meaningful structural modification post-synthesis without some sort of degradation. This perspective presented structural variation of zeolites to be manifested *exclusively* by various framework types.

The discovery of layered zeolite precursors, first for MCM-22 [3][4] and then several other frameworks, demonstrated an unsuspected novel dimension to zeolite structures. The precursors were the first examples of at least two structural forms representing a framework that could be further modified, yielding additional novel representatives. The latter were exemplified by swollen-expanded, pillared, delaminated and other species. So far about ten frameworks have been recognized to have a layered precursor [5] but some of these frameworks were known for a long time as 3-D entities and only now have been prepared as layered derivatives. This suggests that still more zeolites, possibly all, may have some sort of layered precursor. Since it was demonstrated that layered zeolites can be structurally modified, zeolite frameworks became represented not only by their traditional 3-D networks but also by various assemblies of monolayers having analogous internal structure. In fact the former 3-D entities may be viewed as end-members, or a special case of layers fused congruently with vertical alignment, among diverse materials sharing common building layer.
.

Discussion

In this contribution the new concept is presented as an integrated 2-D scheme incorporating 3-D as well as various known lamellar forms of zeolite frameworks. It is shown in Figure 1. The proposed expanded concept of zeolite structures is best presented based on the MCM-22 zeolite family comprising the 3-D framework materials (MWW; MCM-22 and MCM-49) and lamellar forms like layered precursors (MCM-22P, EMM-10P), swollen MCM-22P, delaminated (MCMM-56, ITQ-2), pillared (MCM-36) and others (MWW-IEZ, EMM-13, EMM-12). This diversity is also reflected in the fact that the MWW framework has been synthesized directly in 4 distinct structural forms (identified in Figure 1). The individual members can be clearly identified and distinguished as various packing arrangements of MCM-22 monolayer using X-ray powder diffraction, which also allows structure assignment based on specific features observed in XRD patterns
.

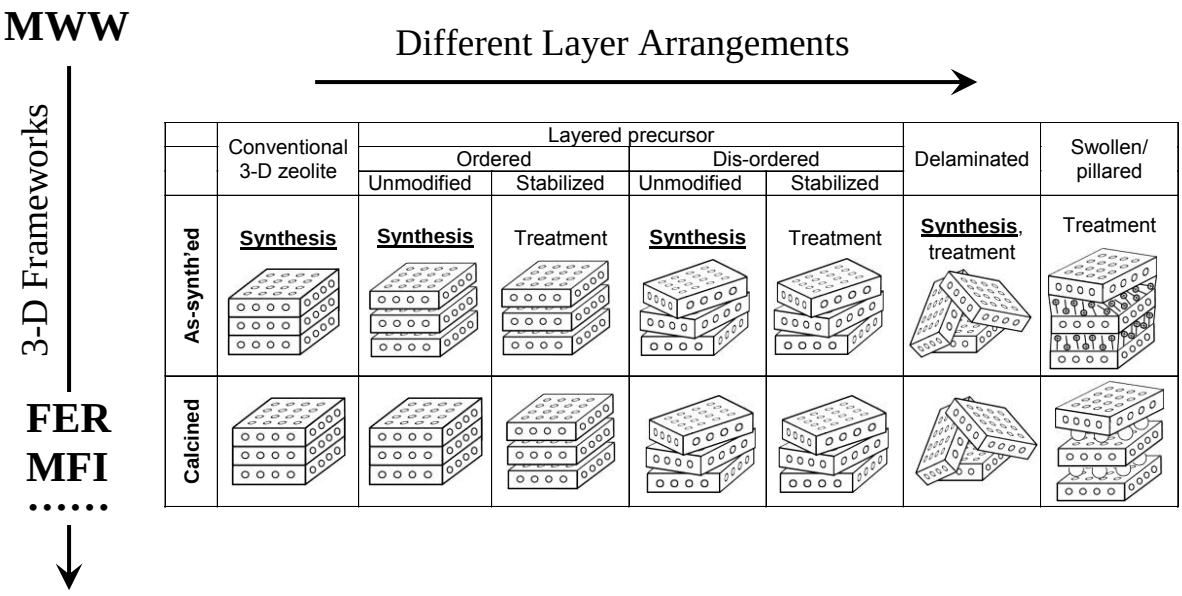

Figure 1. The integrated scheme incorporating 3-D frameworks and various known lamellar forms based on the MCM-22 family. The materials with different MWW layers arrangement obtained by direct synthesis, all containing the template, are labeled as **Synthesis**.

The additional MWW structures, such as expanded, delaminated, pillared, etc have been synthesized by chemical modification of the as-synthesized forms. These various materials are not only of fundamental interest but can demonstrate different catalytic behavior, including improvement in some regard compared to the conventional 3-D zeolite. Since these novel materials can be structurally modified post-synthesis, in contrast to the conventional 3-D frameworks, they offer infinite possibilities for tailored zeolite-based architectures.

As MCM-22 is the most thoroughly studied and developed system it can be a template for other frameworks and their precursors. This concerns not only the types of possible materials but provides a method for systematic approach to their identification by XRD, and subsequent characterization. In this context, the newly-discovered layered form of zeolite MFI [6] represents a remarkable development deserving full attention. It is very active catalytically, like MCM-22, and offers layers with perpendicular 10-ring pores enabling transport in the third dimension.

The presented expanded concept of zeolites structures provides a framework for systematic and formal treatment of layered zeolites that can be integrated with the traditional 3-D structures. It is open-ended process, enabling modification of structures with infinite possibilities. This, in turn, may call, in the long run, for selective approaches and judicious choice of materials to focus on, which will be also discussed.

As new fundamental insights and practical discoveries occur quite often in this field we will discuss the most recent and significant findings within the above proposed integrated system.

References

[1] Roth, W.J., Dorset, D.L., Microporous Mesoporous Mater., doi: 10.1016/j.micromeso.2010.10.052.
[2] Čejka, J., van Bekkum, H., Corma, A., Schuth, F., Stud. Surf. Sci. Catal., Vol.168, Elsevier, 2007.
[3] Leonowicz, M.E., Lawton, J.A., Lawton, S.L., Rubin, M.K.., Science, 264 (1994), 1910.
[4] Roth, W.J., Stud. Surf. Sci. Catal., Vol. 168, p. 221, Elsevier, 2007.
[5] Roth, W.J., Čejka, J., Catal. Sci.Technol., CY-PER-10-2010-000027.R1
[6] Choi, M., Na, K., Kim, J., Sakamoto, Y., Terasaki, O., Ryoo, R., Nature, 461, 2009), 246

Rapid Synthesis of Zeolitic Imidazolate Framework-8 (ZIF-8) Nanocrystals in Aqueous System

Yichang Pan and Zhiping Lai
Advanced Membrane and Porous Materials Center, King Abdullah University of Science and Technology, Thuwal, 23955-6900, Kingdom of Saudi Arabia., zhiping.lai@kaust.edu.sa

Introduction

Zeolitic imidazolate frameworks (ZIFs) are members of a new class of hybrid organic inorganic materials called metal-organic frameworks (MOFs).[1] Compared to other types of metal-organic framework materials, ZIFs often showed better thermal, hydrothermal and chemical stabilities, so they can be potentially applied many applications such as gas storage, separations, catalysis and chemical sensors.[2] Up to now, however, all ZIFs crystals reported so far were made in organic solvents such as dimethylformamide (DMF), diethylformamide (DEF) or methanol, etc. Attempts in aqueous solutions often ended up with 1D or non-porous materials.[3]

Here we report the first example of ZIFs, e.g. ZIF-8, synthesized in pure aqueous system at room temperature. The mean particle size of our products was ca. 85 nm, and the morphology is hexagonal. The yield of particle was ~80% based on the amount of zinc.

Experimental

Nanometer-sized ZIF-8 crystals with hexagonal shape were synthesized via rapid pouring an aqueous solution of $Zn(NO_3)_2 \cdot 6H_2O$ into an aqueous solution of 2-methylimidazole and the mixture was stirred at room temperature for 5 min. In addition, the two solutions were all filtered by filter paper before mixing. In a typical synthesis, 1.17 g of zinc nitrate (3.95 mmol) in 8 g DI water was added into a solution of 2-methylimidazole (22.70 g, 276.50 mmol) in 80 g DI water, and the molar ratio of 2-methylimidazole to zinc was 70:1. The product was collected by repeated centrifugation (6500 rpm, 30 min) and washed by DI water for three times, and was dried at 65 ^oC overnight in a drying oven.

Results and discussion

Fig. 1 shows the powder X-ray diffraction (XRD) patterns and the transmission electron microscope (TEM) images of the as-synthesized samples. Comparison of the sample XRD pattern to the pattern simulated from the ZIF-8 structure data indicates that the product is pure-phase ZIF-8 materials (Fig. 1 (a)). Peak broadening can be clearly observed from the sample XRD pattern, indicating the formation of nanosized crystals. From the Scherrer equation the crystallite size was calculated as ~70 nm. TEM pictures in Fig. 1(b) and (c) revealed that the particles were nanocrystals with sharp hexagonal facets. The mean particle size is ca. 85 nm. The polydispersity index is around 0.089 measured from dynamic light scattering. The electron diffraction pattern showed in the inset of Fig. 1(b) confirmed once again the product were high crystalline ZIF-8 crystals. The N_2 adsorption measurement indicates the BET and Langmuir surface areas of products are 1079 and 1173 m^2/g, respectively. This result is very close the value that was reported from ZIF-8 particles prepared in metanol.[4] In addition, the obtained nanoparticles can be well dispersed in methanol to form a stable suspension and can be kept for several weeks without settlement. Varying the molar ratio of 2-methylimidazole to zinc nitrate can further reduce the crystal size, but not much to the morphology. The crystal size was reduced from ~85 nm to ~50 nm when the ratio of 2-methylimidazole to zinc nitrate increased from 70 to 200.

An in-situ non-ambient XRD measurement was conducted in vacuum to illustrate the thermal stability of the product. The results showed that the sample could maintain the ZIF-8 framework structure even after 5 h heating at 450 oC, indicating that the release of the guest molecules didn't damage the framework structure. In addition, ZIF-8 nanocrystals are stable in boiling water for at least 5 days and in boiling methanol for 7 days, respectively. Furthermore, the crystal morphologies were also preserved very well.

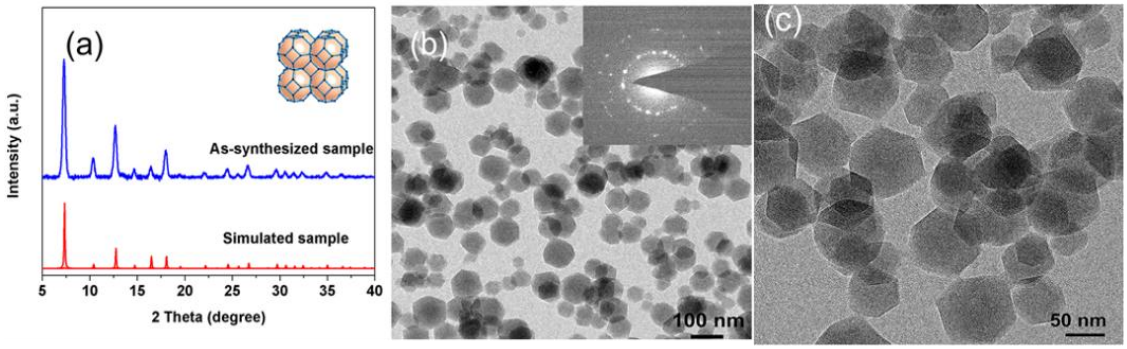

Figure 1 (a) XRD and (b, c) TEM pictures of as-synthesized ZIF-8 nanocrystals in pure aqueous solution.

Conclusions

The synthesis of ZIF-8 crystals in pure aqueous solution for the first time, and it is also the first example of ZIF materials synthesized in pure aqueous solutions. The synthesis method allowed us to make ZIF-8 nanocrystals in much shorter time with improved product yield compared to the synthesis processes developed in organic media. The product showed excellent thermal and chemical stabilities, and improved hydrothermal stability.

Acknowledgements

This work was supported by the faculty distribution fund from King Abdullah University of Science and Technology (KAUST).

References

[1] Phan, A., Doonan, C. J., Uribe-Romo, F. J., Knobler, C. B., O'Keeffe, M., Yaghi, O. M., Synthesis, Structure, and Carbon Dioxide Capture Properties of Zeolitic Imidazolate Frameworks, Accounts Chem Res, 43 (2010), 58-67.

[2] Banerjee, R., Phan, A., Wang, B., Knobler, C., Furukawa, H., O'Keeffe, M., Yaghi, O. M., High-throughput synthesis of zeolitic imidazolate frameworks and application to CO_2 capture, Science, 319 (2008), 939-943.

[3] Yaghi, O. M., Davis, C. E., Li, G. M., Li, H. L., Selective guest binding by tailored channels in a 3-D porous zinc(II)-benzenetricarboxylate network, J Am Chem Soc, 119 (1997), 2861-2868.

[4] Cravillon, J., Munzer, S., Lohmeier, S. J., Feldhoff, A., Huber, K., Wiebcke, M., Rapid Room-Temperature Synthesis and Characterization of Nanocrystals of a Prototypical Zeolitic Imidazolate Framework, Chem Mater, 21 (2009), 1410-1412.

IRMS-TPD study: Strong acid site of USY zeolite created by the post-treatment of NH_4NO_3 and its application

K. Okumura, T. Tomiyama, N. Katada, and M. Niwa
Department of Chemistry and Biotechnology, Graduate School of Engineering, Tottori University, miki.niwa@gmail.com

Introduction

Ultra-stable Y zeolite (USY) has been utilized for the petroleum refinery process, and therefore one of the most important industrial zeolite catalysts. However, due to the complex structure and acidity, the property and the catalytic function have not been sufficiently revealed yet. We have studied the acidity of Na_2H_2-EDTA treated USY [1] with an improved method of IRMS-TPD (Infrared/Mass spectroscopy-temperature programmed desorption) of ammonia to detect clearly the created strong Brønsted OH located at ca. 3600 cm^{-1}; and, it could be regarded as an active Brønsted site available for the alkane cracking [2]. Recently, we revealed an interesting finding that the post-treatment of USY by NH_4NO_3 effectively created the strong acid sites [3]. In the present study, therefore, the strong Brønsted OH in the USY has been studied in detail, and also the catalytic function of the Brønsted acid site, not only active for the cracking but also available for support of Pd in the cross-coupling reaction, will be studied.

Experimental

NaY (Tosoh, HSZ-320NAA, Si/Al_2 ratio 5.5) was ion-exchanged in a solution of NH_4NO_3, and the formed NH_4Y was treated by steaming usually at 823 K, followed by the post-treatment in a solution of NH_4NO_3 by varying the concentration. IRMS-TPD of ammonia was studied in a method previously reported [2]. Activity for the cracking of alkane was measured by a continuous-flow method. The activity of USY decreased small with time on stream, but it was recovered readily by the oxidation with oxygen. $Pd(NH_3)_4Cl_2$ was loaded on thus prepared USY, and used for Suzuki-Miyaura cross-coupling under the experimental conditions previously reported [4].

Table 1. Brønsted acidity of the USY prepared by the treatment in 0.5 to 7.5 M NH_4NO_3; Number A_0 ($molkg^{-1}$) and strength ΔH ($kJmol^{-1}$)

Brønsted OH	Super cage		Strong		Sodalite cage		D6R	
	A_0	ΔH	A_0	ΔH	A_0	ΔH	A_0	ΔH
H-Y	1.20	112	-		0.38	117	0.31	107
USY-0.5M	0.16	136	0.15	157	0.05	152	0.07	151
USY-2.3M	0.22	135	0.22	153	0.07	148	0.09	147
USY-7.5M	0.27	130	0.25	146	0.09	142	0.10	141

Results and discussion

Characterization of the USY acidity by an experiment of IRMS-TPD of ammonia

HY zeolite showed three kinds of Brønsted OH bands located in super cage (3635 cm^{-1}), sodalite cage (3556 cm^{-1}) and double 6 rings (D6R) (3532 cm^{-1}), and the solid acidity was characterized by the IRMS-TPD of ammonia experiment, as shown in Table 1. USY was prepared by the steaming, and it was found that the post-treatment of the steamed USY with NH_4NO_3 effectively created the strong Brønsted OH observed at 3598 cm^{-1}. The acidity of USY thus prepared by varying the concentration of NH_4NO_3 was measured, as shown in Table 1. The strength of the created strong Brønsted acid site (**Strong**) was *ca.* 150 kJ mol^{-1}, which was higher than those prepared by Na_2H_2-EDTA by 13 kJ mol^{-1} [1,2].

Cracking activity of the USY zeolite

Thus prepared USY had an excellent catalytic activity for cracking of such alkanes as octane and hexane. The activation energies for the octane cracking (E_a) on the USY were *ca.* 50 kJ mol^{-1}, as shown by marks in blue in Fig. 1, and these were the least values among the values previously observed [5]. When E_a and ΔH on HY and cation exchanged HY zeolite were summarized (Fig. 1), the E_a decreased with increasing the ΔH for the Brønsted OH. It was thus clearly revealed that the weak acidity of HY was enhanced by the addition of cation M^{2+} or by the preparation to USY, and the USY prepared by the post-treatment with NH_4NO_3 showed the excellent acidity and activity. The strong Brønsted acidity is, most probably, the origin of the activity of USY zeolite. The high activity of the USY thus prepared has already been reported, but the origin of the activity remained unsolved [6].

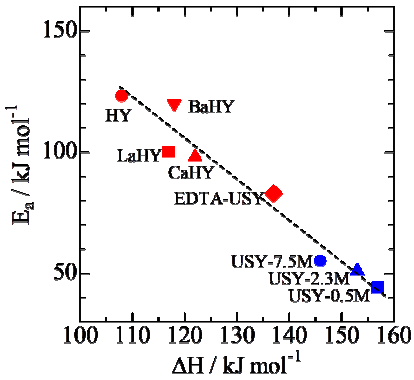

Fig. 1. Correlation between E_a and ΔH on HY and modified Y zeolites.

Activity of Pd/USY for the cross-coupling

Suzuki-Miyaura cross-coupling between aryl bromide and phenyl boric acid was studied using Pd loaded on the USY zeolite. By optimizing the experimental conditions, an extremely high catalytic activity was obtained [4]. Among the optimized conditions, the solid acidity of the USY zeolite had a strong effect on the catalytic activity. The USY was prepared by the steaming at different temperature, time and vapor concentration, followed by the post-treatment of 0.5 M NH_4NO_3 solution, and used as the support. When the acidity and the activity were compared, a strong relation between the amount of the created strong Brønsted acid site and the turn-over frequency of the cross-coupling was observed, as shown in Fig. 2. Thus, it was considered that the Pd loaded on the zeolite was activated by the strong Brønsted acidity to become the active catalytic site for the cross-coupling.

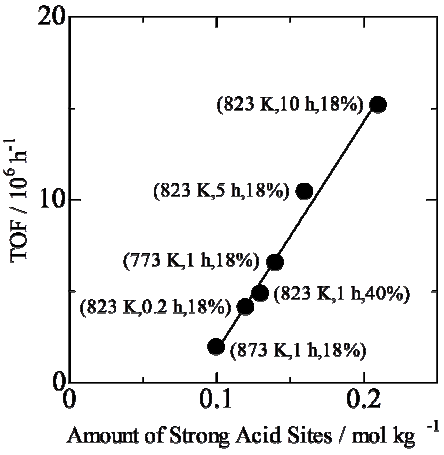

Fig. 2. Correlation between TOF and amount of strong Brønsted OH in USY prepared by the steaming at conditions (temp, time, and conc.), followed by the post-treatment.

Conclusions

The strong Brønsted acid site created by the post-treatment of USY with NH_4NO_3 was characterized to have the strength of acid site *ca.* 150 kJ mol^{-1} of ΔH. Due to the correlation between the strong acidity and catalytic activity, it is concluded that the created strong Brønsted OH plays the role of not only the active site for the cracking but also of the support to activate Pd for Suzuki-Miyaura cross coupling. Preparation, characterization, and catalytic function of the strong Brønsted acid site in USY were revealed.

References

[1] N. Katada, Y. Kageyama, K. Takahara, T. Kanai, H. A. Begum, M. Niwa, J. Mol. Catal., A, 211, 119 (2004).
[2] M. Niwa, K. Suzuki, K. Isamoto, N. Katada, J. Phys. Chem. B, 110, 264 (2006).
[3] K. Okumura, T. Tomiyama, M. Niwa, Chem. Lett., 40, 49 (2011).
[4] K. Okumura, T. Tomiyama, S. Okuda, H. Yoshida, M. Niwa, J. Catal., 273, 156 (2010).
[5] N. Katada, K. Suzuki, T. Noda, W. Miyatani, F. Taniguchi, M. Niwa, Appl. Catal., A: General, 373, 208 (2010).
[6] A. I. Biaglow, D. J. Parrillo, G. T. Kokotailo, R. J. Gorte, J. Catal., 148, 213 (1994).

Flash induction calcination: a powerful tool for total template removal and fine tuning of the hydrophobic/hydrophilic balance in silica-based mesoporous materials

Taissire Benamor, Laure Michelin, Bénédicte Lebeau* and Claire Marichal

Equipe Matériaux à Porosité Contrôlée (MPC), Institut de Science des Matériaux de Mulhouse (IS2M), LRC CNRS 7228, Université de Haute Alsace, ENSCMu, 3 rue Alfred Werner, 68093 Mulhouse Cedex, France.
**corresponding author e-mail: Benedicte.lebeau@uha.fr*

Introduction

Several methods have been suggested in the literature to remove the organic template occluded within the pores of Ordered Mesoporous Silica (OMS) materials[1] such as calcination[2,3] and/or chemical extraction by an organic solvent[4-7] microwave digestion[8] or UV radiation[9]. Chemical extraction is often incomplete and calcination modifies the hydrophilic/hydrophobic properties of the OMS since high temperature (typically ≥ 500°C) is required. Moreover, most of these process are lengthy and energy consumers. Consequently new method for template removal in OMS is highly desirable. The originality of this work is to use a rapid calcination method which is an energy saver process thanks to induction heating and can also be considered as a friendly environmental process because it avoids the use of solvent. This new method allows a complete removal of the surfactant (pluronic P123) in the case of SBA-15 type OMS at low temperature (300°C), fast heating rate and short calcination duration (15min). Furthermore it was observed that by varying the experimental parameters such as heating duration and/or heating temperature, a fine tuning of the hydrophilic/hydrophobic balance of SBA-15 materials is achievable. The induction calcination was also successfully applied to other type of mesoporous silica materials such as SBA-16 and MCM-41.

Experimental

A SBA-15 material was prepared following a typical procedure suggested in the literature by Zhao *et al* [1]. The starting molar ratio was: 1.0 TEOS: 0.017 P123: 5.6 HCl: 174 H_2O.
Calcination procedures: To liberate the porosity of the SBA-15, the as-synthesized samples were subjected to calcination at different temperatures and durations in a muffle furnace or in an induction furnace. In both cases, 100 mg of as-synthesized sample were put in a platinum crucible and calcination was performed between 300°C and 700°C for two short durations 5 and 15 min. For the short calcination time in the muffle furnace, the crucible was introduced in a preheated furnace at the desired temperature. For comparison the conventional long calcination duration was also performed, about 250 mg of the as-synthesized sample are placed in a porcelain crucible and put in the muffle furnace. The temperature is raised during 6 h to the desired temperature (300, 460, 500, 600 or 700°C), then holding at the same temperature for 4h.

Results and discussion

Whatever the calcination method, XRD diffractograms indicate a well ordered 2D hexagonal pore arrangement as expected for SBA-15 type materials. Consequently no collapse of the mesostructure is detected even at higher temperature and for longer calcination duration. In addition a significant broadening of the Bragg diffraction peaks reveals a less ordered 2D

hexagonal mesostructure. A framework contraction was also detected upon calcination that was closely related to the P123 decomposition [10].
The complete template removal was confirmed by TGA and ^{1}H-^{13}C CPMAS NMR analysis. An SBA-15 material free from surfactant was obtained after 15 min of induction calcination at only 300°C. For the short time muffle furnace calcination higher temperature is required (460°C for 5 min) to completely eliminate the surfactant. The removal of the template at such short time and low temperature is possible thanks to the fast induction heating rate and the rapid heat diffusion within the sample whereas in the case of the muffle furnace heating slower heat diffusion probably occurs.
This new calcination method provides an SBA-15 with higher textural and porosity characteristic (S_{BET}=1000 m^2g^{-1}, V_t=1.14 cm^3g^{-1} and V_m=0.20 cm^3g^{-1}) compared to the conventional calcination method (S_{BET}= 890 m^2g^{-1}, V_t=1.03 cm^3g^{-1} and V_m= 0.16 cm^3g^{-1}). Whatever the calcination process, these three porous characteristics in addition to the pore diameter slightly decrease with temperature increase. Increase of calcination duration up to 15 min at 700°C drastically affects these textural characteristics probably due to the network contraction observed by XRD.
To study the influence of such calcination methods on the silanol content of the samples ^{1}H decoupled ^{29}Si MAS NMR and TGA analyses were performed. The as-synthesized and calcined samples at 300°C exhibit roughly the same Q_2, Q_3 and Q_4 species distribution, while from 460°C to 700°C a concomitant increase of Q_4 and decrease of Q_3+Q_2 species is observed. This indicates that dehydroxylation occurs in this 460-700°C temperature range. These results are in agreement with XRD observations. For the conventional long time muffle furnace calcination the Q_4 increase and Q_3+Q_2 species decrease is more pronounced even at low temperature. Furthermore, the OH numbers determined by TGA and ^{29}Si MAS NMR analysis are in reasonable agreement. Above 300°C the number of silanol decreases significantly (from on average 3.8 to ~2 10^{-3} $mol.g^{-1}$ for 700°C).

Conclusions

Induction heating is the most suitable calcination process because it provides a SBA-15 material fully free of organic template with a high specific area, pore diameter and pore volume already at low temperature (300°C) for a very short time (15 min). Moreover, it was demonstrated that this calcination method can be applied to other OMS such as SBA-16 and MCM-41 materials. This method is rapid, easy to perform and ecofriendly since it is a one step and energy saving procedure avoiding the use of solvent. Moreover the hydrophobic/hydrophilic character can be modulated thanks to a judicious choice of temperature and duration of calcination. It was shown that samples with an important silanol content, which can be very attractive for post-synthesis grafting, can be prepared with a low induction calcination temperature, while hydrophobic samples require high induction calcination temperature.

References

[1] Zhao, D., Feng, J., Huo, Q., Melosh, N., Fredrickson, G. H., Chmelka, B. F.,Stucky, G.D, Science, 279 (1998), 548-552.
[2] Kleitz, F., Schmidt, W., Schüth, F, Micro. Meso. Mater, 65 (2003), 1-29.
[3] Berube, F., Kaliaguine, S, Micro. Meso. Mater, 115 (2008), 469-479.
[4] Yang. C-M., Zibrowius, B., Schmidt, W., Schuth, F, Chem. Mater, 16 (2004), 2918-2925.
[5] Grudzien, R. M., Grabicka, B. E., Jaroniec, M, Appl. Surf. Sci, 253 (2007), 5660-5665.
[6] Kurk, M., Jaroniec, M., Ko, H.C., Ryoo, R, Chem. Mater, 12 (2000), 1961-1968.
[7] Lang,N., Tuel, A, Chem. Mater, 16 (2004), 1961-1966.
[8] Tian, B., Liu, X., Yu, C., Gao, F. Luo, Q., Xie, S., Tu, B., Zhao, D, Chem. Commun, (2002), 1186-1187.
[9] Xiao, L., Li, J., Jin, H., Xu, R, Micro. Meso. Mater, 96 (2006), 413-418.
[10] Bagshaw. S. A., Bruce, I. J, Micro. Meso. Mater, 109 (2008), 199-209.

Preparation of Adjustable Metal Doping Aluminophosphate Molecular Sieves

Yanyan Wang, Lang Shao, Xu Li, Junbiao Wu, Jiyang Li*, Jihong Yu
†State Key Laboratory of Inorganic Synthesis and Preparative Chemistry, College of Chemistry, Jilin University, Changchun 130012, PR China, E-mail: lijiyang@jlu.edu.cn.

Introduction

Aluminophosphate molecular sieves ($AlPO_4$-*n*) with regular nanoporous void space have shown widespread applications in catalysis, ion exchange, and separation.[1] The partial substitution of the Al atoms in the framework by silicon or other metal elements results in the heteroatom containing aluminophosphate molecular sieves (MAPOs) with special properties in catalysis, photoluminescence, magnetism, and so forth. The content and location of heteroatom in the frameworks of MAPOs can be adjusted by the guest templates through the host-guest charge-density matching principle proposed by Stucky et al.[2] Besides organic amines as the guest templates, the F^- ions can also be employed in the synthesis to compensate the changes of the inorganic framework.[3]

In this work, three new iron aluminophosphates (Fe-ACO(**a**-**c**)) with ACO-zeotype structure and two magnesium aluminophosphate (Mg-LEV(**a**, **b**)) with LEV-zeotype structure have been synthesized. The M/Al (M=Fe, Mg) ratios in the frameworks can be effectively controlled by varying the amounts of hydrofluoric acid and organic templates in the initial reaction mixture.

Experimental

Syntheses of Fe-ACO(a-c). Aluminum triisopropoxide and the ferric oxalate were directly added to a 9 mL Teflon-lined stainless steel autoclave, followed by the addition of the diethylenetriamine (DETA), orthophosphoric acid (85 wt%) and hydrofluoric acid (40 wt %) successively without stirring. The reaction was carried out at 433K under autogenous pressure for 6 days. After filtered off, washed with deionized water, and dried at room temperature, the pure phases of these products were obtained. The yields of FeAPO-CJ66 (**a**-**c**) are 39, 28 and 32%, respectively.

Syntheses of Mg-LEV(a, b). Boehmite was dissolved into the distilled water with stirring, followed by the addition of magnesium acetate, organic amine and orthophosphoric acid. The organic amine used is 1,2-Diaminocyclohexane (DACH) for Mg-LEV(**a**) and N-methylpiperidine for Mg-LEV(**b**). The mixture was stirred thoroughly until the solid was completely dissolved, and the resultant gel was transferred into a 15 mL Teflon-lined stainless steel autoclave and heated at 180 °C for 3 days. After filtered off, washed with deionized water, and dried at room temperature, the pure phases of these products were obtained.

Table 1. Gel Compositions (Molar Ratio) for the Syntheses of Compounds.

Samples	Al_2O_3	P_2O_5	HF	Fe_2O_3/MgO	Templates	H_2O
Fe-ACO(**a**)	1.0	21.7	1.8	2.0	27.4	24.8
Fe-ACO(**b**)	1.0	21.7	4.1	2.0	27.4	28.7
Fe-ACO(**c**)	1.0	5.2	5.9	2.0	27.4	14.8
Mg-LEV(**a**)	1.0	8.0	0	2.0	4.0	1800
Mg-LEV(**b**)	1.0	3.0	0	1.0	4.4	548

* Al_2O_3 for Fe-ACO is $Al(OPr^i)_3$, and for Mg-LEV is boehmite.

Results and discussion

Fe-ACO(**a-c**) have been synthesized in the similar reaction system of Fe_2O_3-Al_2O_3-P_2O_5-DETA-HF-H_2O except that the amounts of orthophosphoric acid and hydrofluoric acid are different, in which ethylenediamine decomposed from DETA and F^- ions were used as the cotemplates. Mg-LEV(**a**, **b**) were prepared in hydrothermal system by using DACH or N-methylpiperidine as the template. The gel compositions for the syntheses of pure phases of these compounds are listed in Table 1.

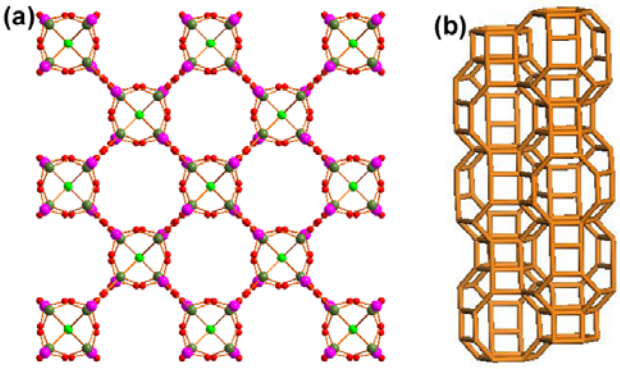

Figure 1. Structures of (a) Fe-ACO(**a-c**) and (b) Mg-LEV(**a**, **b**).

Single crystal analyses indicate that the structures of Fe-ACO(**a-c**) and Mg-LEV(a, b) are analogous to zeotype ACO and LEV, respectively (Fig.1). ICP analyses give rise to the Al/Fe ratios in Fe-ACO(**a-c**) are 1/3.9, 1/5.0, and 1/9.0. The F elemental analyses indicate that the content of F^- ions is close with that of Al atoms in the frameworks of Fe-ACO(**a-c**), which become smaller and smaller with the increase in the Fe contents in the frameworks. This reveals that the F^- ions can dramatically control the number of heteroatom incorporated into the framework. In the structures of Mg-LEV(**a**, **b**), the Mg/Al ratios are about 1/3 and 1/1.5, respectively, based on the ICP analyses. This maybe caused by the different organic templates, and it needs further study.

Conclusions

Three new members of zeolite ACO family, iron aluminophosphates Fe-ACO(**a-c**), have been successfully synthesized in the fluoride ion system by using F^- ions and ethylenediamine as the cotemplates. The Al/Fe ratios in the frameworks can be effectively controlled from1/9 to 1/5 to 1/3.9 through increasing the content of F^- ions in the synthesis. Two Mg doping aluminophosphates with LEV zeotype structure have been prepared by using different organic amines, DACH and N-methylpiperidine, as template. The Mg/Al ratios are about 1/3 and 1/1.5, respectively. This work indicates that organic template and F^- ions can adjust the content of heteroatom doped in the aluminophosphate.

Acknowledgements

This work is supported by the National Natural Science Foundation of China, the State Basic Research Project of China (grants 2007CB936402 and 2011CB808703), and the Major International Joint Research Project of China.

References

[1] Yu, J. H.; Xu, R. R. Chem. Soc. Rev. 35 (2006), 593–604.
[2] Liang, H. J.; Whited, G.; Nguyen, C.; Stucky, G. D. Proc. Natl. Acad. Sci. U.S.A. 104 (2007), 8212–8217.
[3] Lii, K. H.; Huang, Y. F.; Zima, V.; Huang, C. Y.; Lin, H. M.; Jiang, Y. C.; Liao, F. L.; Wang, S. L. Chem. Mater. 10 (1998), 2599–2609.

Hydrothermal Synthesis of Porous Beryllate Materials: Zeolite Inspired Frameworks

Benjamin T. R. Littlefield and Mark T. Weller
University of Southampton, SO17 1BJ, United Kingdom. M.T.Weller@soton.ac.uk

Introduction

Natural and synthetic zeolites have been the focus for extensive research owing to their many applications and huge potential number of new topologies. The majority of such materials are aluminosilicates, consisting of corner sharing TO_4 units, aluminate (AlO_4) and silicate (SiO_4) tetrahedra arranged in a framework. Many methods have been employed to form different topologies, and among these is the substitution of the T atom to form synthetic systems equivalent to zeolites, known as 'zeotypes'. Isomorphic heteroatom substitution at the Si and/or Al sites in 3-D structures is an effective method of framework modification with substituted elements including but not limited to; Mg, Al [1], Zn [2], Ge [3]and Zr [4]. Often the resulting zeotype has a different functionality from that of a traditional aluminosilicate and its structure can also be modified [5].

Research on frameworks incorporating the BeO_4 unit is sparse, a few rare minerals such as lovdarite, $K_2Na_6Be_4Si_{14}O_{36}•9H_2O$ and nabesite, $Na_2BeSi_4O_{10}•4H_2O$ are known, whereas synthetic Be containing frameworks are limited to several beryllosilicates, [6,7] beryllophosphates [8] and very few berylloarsenates [9].

Here we present the hydrothermal synthesis of several novel three dimensional and two dimensional berylloarsenate/phosphate frameworks including; three new potential zeolite topologies, BeAs-**MER** [10] and BeAs-**AFI** [11] topology analogues, the first synthetic equivalent of the **WEI** [12] topology as well as several interrupted frameworks. Of particular interest are the common structural features seen in these frameworks, such as the distortion of four rings leading to artificially increased framework density and the prevalence of the –OH unit bridging between Be-centred tetrahedra.

Experimental

All of the samples were prepared from commercially available materials of reagent grade that did not require further purification, a typical preparation is as follows:

Materials were synthesised *via* hydrothermal methods. The Be source, As source, solvent and organic template were stirred for 60 minutes before being transferred to a 23 mL Teflon^{TM}-lined Parr autoclave and heated at 413 – 473 K for 1 – 7 days. The reacted mixture was allowed to cool naturally to room temperature and the solid product removed from the remaining liquid by vacuum filtration. The product was then washed with H_2O (40 mL) and EtOH (20 mL) before being transferred to an oven to dry at 353 K for 12 hours.

Single crystals of each product were isolated for study via single crystal X-ray diffraction. Data were measured at 120 K on a Bruker Nonius KappaCCD diffractometers, using Mo-Kα (λ=0.71073 Å) radiation. Structures were solved using the WinGX package [13] by direct methods [14] using XPREP [15] and SHELXS-97 [16] and refined using SHELXL-97.

Results and discussion

Several new berylloarsenate and beryllophosphate structures will be presented including the interrupted three dimensional framework $[\{H\text{-pyridine}\}_2]^{2+}$

$\{Be_2[BeOH_2][AsO_4]_2[AsO_3OH]\}^{2-}$ (Fig. 1), its phosphate analogue and the fully connected three dimensional framework $[NH_4^+]_2\{Be_2[Be(OH)_2][AsO_4]_2\}^{2-}$.

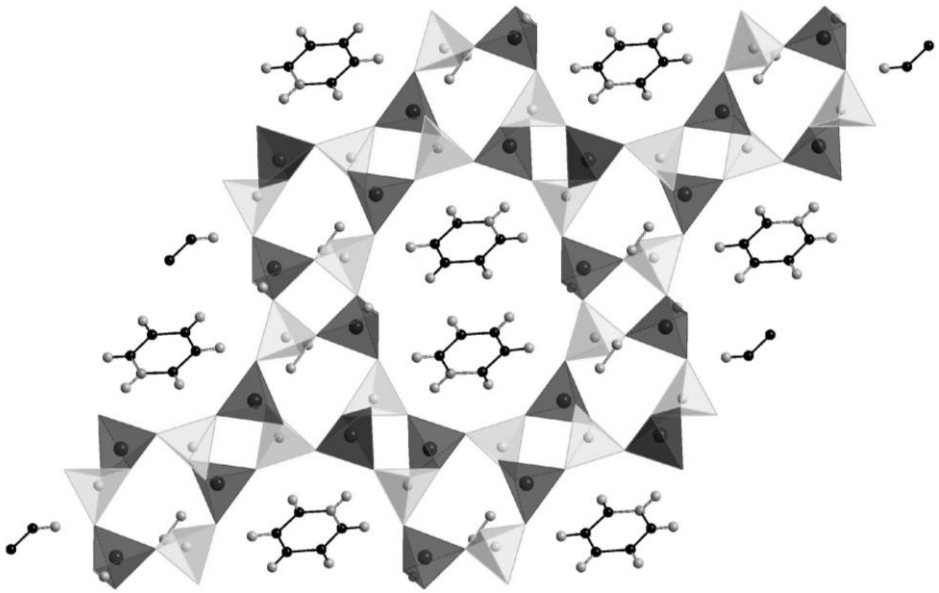

Figure 1. Viewed down *c*, Be and As centred tetrahedra are light and dark grey respectively; topology is related to AFI.

Conclusions

A family of new beryllium containing frameworks has been produced, sharing common building units and features but varying topologies providing further insight into framework modification.

Acknowledgements

We would like to acknowledge Jennifer Armstrong and Natalie Seaton for general assistance and contribution to the synthetic work respectively.

References

[1] J. T. Kloprogge, J. Porous Materials, 5 (1998), 5-41
[2] M. A. Camblor, R. F. Lobo, H. Koller, M. E. Davis, Chemistry of Materials, 6(11) (1994), 2193-2199
[3] H. Kosslick, V. A. Tuan, R. Fricke, C. Peuker, W. Pilz, W. Storek, J. Phys. Chem., 97 (1993), 5678-5684
[4] G. R. Wang, X. Q. Wang, X. S. Wang, S. X. Yu, Zeolites and Microporous crystals, 83 (1994), 67-74
[5] G. Sastre, A. Pulido, R. Castaeda, A. Corma, J. Phys. Chem., 108 (2004), 8830-8835
[6] J.A. Armstrong, M. T. Weller, Dalton Trans., (2006), 2998 – 3005
[7] J. A. Armstrong, M. T. Weller, J. Am. Chem. Soc., 132 (2010), 15679-15686
[8] W. T. A. Harrison, Acta Cryst., C57 (2001), 891-892
[9] T. E. Gier, G. D. Stucky, Acta Cryst., C51 (1995), 181-183
[10] E. Galli, G. Gottardi, D. Pongiluppi, Neues Jahrbuch fuer Mineralogie Monatsheft, (1979), 1-9
[11] J. M. Bennett, J. P. Cohen, E. M. Flanigen, J. J. Pluth, J. V. Smith, ACS Sym. Ser., 218 **(**1983), 109-118
[12] F. Walter, Eur. J. Mineral., 4 *(*1992), 1275-1283
[13] L. J. Farrugia, J. Appl. Crystallogr., 32 (1999), 837–838.
[14] G. M. Sheldrick, Acta Crystallogr., Sect. A: Found. Crystallogr., 46 (1990), 467–473.
[15] XPREP Bruker AXS Inc., Madison, Wisconsin, USA
[16] G. M. Sheldrick, University of Goettingen, Germany, *Release 97-2*, (1997).

Synthesis and characterization of novel late first-row transition metal fluorophosphate frameworks

Edward R. Williams, Jennifer A. Armstrong, Mark T. Weller
University of Southampton, Southampton, SO17 1BJ, UK, mtw@soton.ac.uk

Introduction

Porous metal framework materials have received significant research interest in recent years. Whilst zeolitic aluminosilicates are restricted to tetrahedral building units, the metal species within metal framework materials can form 3-, 4-, 5- and 6-coordinate polyhedra, depending on the metal. Indeed it is possible to have multiple metal polyhedra, as well as different metal oxidisation states within the same crystal structure. These units are typically combined with tetrahedral units (e.g. PO_4/AsO_4) to produce framework materials, which can have nanoporous structures. The structures produced are less rigid than the aluminosilcate zeolites, leading to important applications arising from ion-exchange. In addition, the structures can have useful magnetic properties coupled with the porosity, as well as potentially having redox catalytic properties. Examples of such materials include vanadium phosphates ($Cs[V_2(PO_4)(HPO_4)(H_2O)_2]$)[1] and zirconium arsenates ($[(enH_2)_{0.5}][Zr_2(PO_4)_2(HPO_4)F]\cdot H_2O$) [2].

Here we present the results of investigations into incorporating fluoride anions into late first-row transition metal phosphate frameworks, with the aim to hydrothermally produce frameworks consisting of metal polyhedra $[M(O,F)_n]$ (n=4-6) and phosphate tetrahedra $[P(O,F)_4]$. The use of metal fluorides (MF_x) as a source of both framework metal centres and fluoride has been shown as an excellent method for the production of metal fluorophosphate frameworks previously[3], and for this reason the same method was applied for this study.

Experimental

All products were produced by hydrothermal methods. A transition metal fluoride, phosphoric acid and counter cation or organic template were combined in a solvent and autoclaved at 398-498 K in a Parr 23 mL Teflon® lined autoclave for 2-18 days. The products were allowed to cool to room temperature before collecting by vacuum filtration and washed with 20 mL distilled water and 20 mL ethanol before drying.

Structures were determined by single crystal X-ray diffraction. Single crystal X-ray diffraction data for this report was collected on a Bruker-Nonius Kappa CCD diffractometer with an area detector. Molybdenum K_α radiation (λ=0.7107 Å) was used and the data collected at 120 K. The structure was determined using the WinGX package[4], with XPREP[5] used for the initial setup, SHELXS-97 used to solve the structure and refined further with SHELXL-97[6,7].

Results and discussion

A large number of late first-row transition metal fluorophosphate frameworks have been produced, with dimensionality ranging from discrete clusters to 3-dimensional porous structures. Perhaps the most interesting of these is a family of copper fluorophosphate 3D frameworks with large (11-12 Å diameter) channels (Fig. 1). The channels contain water, free anions such as phosphate groups and counter cations, resulting in a structure which could

have a large number of possible applications including ion-exchange materials as well as potentially catalytic properties.

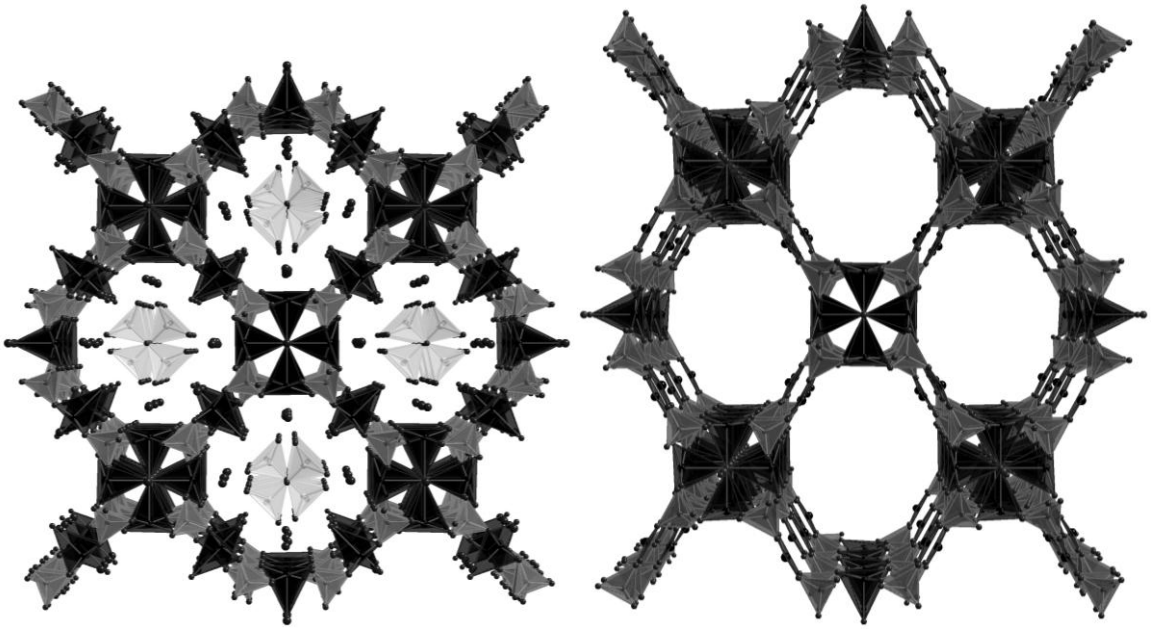

Fig. 1: Crystal structures of two copper fluorophosphates produced, showing the framework consisting of copper polyhedra (black) and phosphate tetrahedra (dark grey). Left: positions of free phosphate groups (light grey) and M'^{+} cations in the channels. Right: extra-framework species not shown to display porosity of the structure.

Conclusions

A large number of novel crystal structures have been produced, including several interesting 3D-porous structures. In general, a number of interesting structural features have been observed, including bridging (μ^2/μ^3) fluoride anions and the formation of fluorophosphate tetrahedra (PO_3F/PO_2F_2).

Acknowledgements

We would like to thank Sam Morris and Josh Treacher for showing the reproducibility of some structures produced.

References

[1] Haushalter, R. C., Wang, Z. W., Thompson, M. E., Zubieta, J., Inorg. Chem. 32 (1993), 3700-3704
[2] Kemnitz, E., Wloka, M., Trojanov, S., Stiewe, A., Angew. Chem. 35 (1996), 2677-2678
[3] Rouse, J., Redrup, K. V., Kotsapa, E. and Weller, M. T. Chemical Communications, (2009), 7209-7211.
[4] Farrugia, L. J., Journal of Applied Crystallography, 32 (1999), 837-838
[5] Sheldrick, G. M., XPREP. Space Group Determination and Reciprocal Space Plots, (1991)
[6] Sheldrick, G. M., Acta Crystallographica Section A, 46 (1990), 467-473
[7] Sheldrick, G. M., Release 97-2, University of Göttingen, Germany (1997)

Interzeolite conversion process of FAU type zeolite

Masaya Itakura, Yusuke Ide, Masahiro Sadakane, and Tsuneji Sano
Department of Applied Chemistry, Graduate School of Engineering, Hiroshima University, Higashi-Hiroshima 739-8527, Japan; E-mail: tsano@hiroshima-u.ac.jp

Introduction

Most of zeolite syntheses were carried out using amorphous aluminosilicate gels as starting materials in the presence of inorganic and/or organic structure-directing agents (SDAs). In the synthesis process, the formation of a zeolite phase proceeds often through the gradual transformation in sequence: amorphous phase → less stable zeolite → most stable zeolite [1]. As this phenomenon can be considered to be an alternative synthesis strategy for the hydrothermal conversion of one zeolite into another, i.e., interzeolite conversion, this method has attracted much attention.

We have also investigated the potential of the interzeolite conversion method, and already succeeded in synthesizing several types of zeolites from FAU and *BEA type zeolites [2,3]. In the conversion process, it is considered that the locally ordered aluminosilicate species (nanoparts) are produced by decomposition/dissolution of starting zeolite and then their assembly proceeds under a specific SDA, resulting in a fast crystallization rate and a high selectivity to a particular zeolite. However, we do not have enough data for understanding of nanoparts [4]. In this study, therefore, to get further information concerning nanoparts, we investigated both FAU–RUT and FAU–*BEA interzeolite conversion processes using several techniques such as XRD, NMR, and ESI-MS.

Experimental

The starting FAU type zeolite with various Si/Al ratios was prepared through dealumination treatment involving steaming and H_2SO_4 treatment. The dealuminated zeolite was added into an aqueous solution containing SDA (tetramethylammonium hydroxide: TMAOH or tetraethylammonium hydroxide: TEAOH), and then the mixture was placed into a 30 cm^3 Teflon-lined stainless steel autoclave. The molar composition of starting gel was SiO_2:0.02Al_2O_3:0.2SDA:5H_2O. The hydrothermal conversion was conducted at 140 °C for 2 h–7 d in the convection oven. The solid and solution parts were collected by centrifugation, and the solid product was washed thoroughly with deionized water. For comparison, the starting gels were also prepared using amorphous silica and γ-Al_2O_3 as Si and Al sources. Characterization of both solid and solution parts obtained were carried out by means of XRD, XRF, SEM, ^{27}Al NMR, ^{29}Si NMR, and ESI-MS.

Results and discussion

Fig. 1 shows XRD patterns of *BEA type zeolite obtained from FAU type zeolite and amorphous materials in the presence of TEAOH. As can be seen in Fig. 1A, the peaks corresponding to the starting FAU type zeolite completely disappeared at 2 h, and then pure and highly crystalline *BEA type zeolite was obtained after synthesis time of 2 d. On the other hand, prolonged synthesis time (7 d) was required in the case of amorphous materials (Fig. 1B). This indicates that the use of FAU type zeolite enhances the crystallization rate of *BEA type zeolite, namely the advantage of interzeolite conversion method. The fast crystallization of *BEA type zeolite from FAU type zeolite was also confirmed by ^{29}Si CP/MAS NMR (Fig. 2). The intensities of the peaks at –100 and –90 ppm corresponding to Q^3 and Q^2 species for the use of FAU type zeolite were larger than those for the use of amorphous materials. These results strongly suggest a difference in the chemical structure of nanoparts generated.

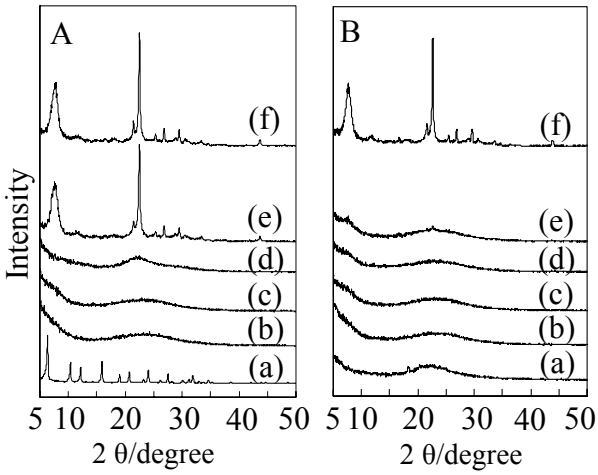

Fig. 1 XRD patterns of solids obtained from (A) FAU and (B) amorphous. Synthesis time: (a) 0 h, (b) 2 h, (c) 12 h, (d) 1 d, (e) 2 d, and (f) 7 d.

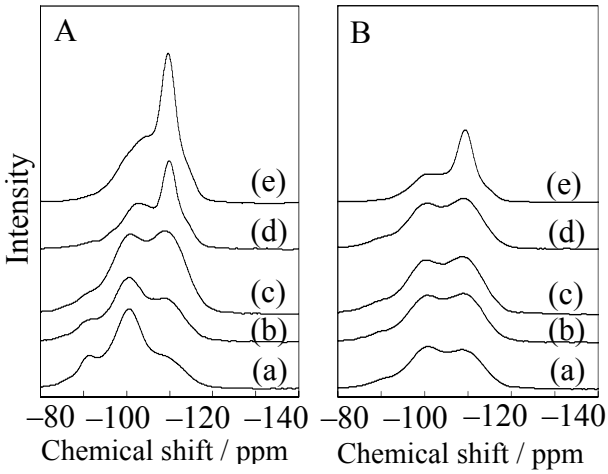

Fig. 2 ^{29}Si CP/MAS NMR spectra of solids obtained from (A) FAU and (B) amorphous. Synthesis time: (a) 2 h, (b) 12 h, (c) 1 d, (d) 2 d, and (e) 7 d.

Fig. 3 shows the ^{27}Al NMR spectra of aqueous parts obtained after synthesis time of 2 h. In the case of the synthesis of *BEA type zeolite from amorphous materials, there were no peaks. On the other hand, however, the peak assigned to tetrahedral coordinated aluminum species was observed at ca. 50 ppm for FAU–*BEA interzeolite conversion. The peak was also observed in FAU–RUT interzeolite conversion in the presence of TMAOH. In order to clarify the difference, the aqueous solutions obtained at the initial stage of hydrothermal conversion were analyzed by ESI-MS. In all negative-ion ESI-MS spectra, two types of species with various masses, clustered with and without SDA, were observed. Most species in FAU–RUT interzeolite conversion were assigned to the species clustered with SDA. Moreover, the species with higher masses were observed in the ESI-MS spectrum of FAU–*BEA interzeolite conversion as compared to the synthesis of *BEA type zeolite from amorphous materials.

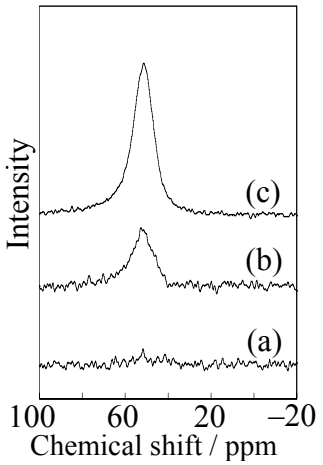

Fig. 3 ^{27}Al NMR spectra of aqueous solutions obtained after synthesis time of 2 h. (a) amorphous–*BEA, (b) FAU–*BEA, and (c) FAU–RUT.

Conclusions

The crystallization rate with FAU type zeolite as the starting material was better than that with amorphous aluminosilicate gel (the conventional synthesis). From the detail analyses of both solid and solution parts during the conversion process, the existence of species with different chemical structures was suggested.

Acknowledgements

We acknowledge Dr. H. Murata in Shimadzu Co. for ESI-MS measurements and valuable comments.

References

[1] Cundy, C.S., Cox, P.A., Micropor. Mesopor. Mater., 82 (2005), 1-78.
[2] Jon, H., Sasaki, H., Inoue, T., Itakura, M., Oumi, Y., Sano, T., Stud. Surf. Sci. Catal., 174 (2008), 229-232.
[3] Itakura, M., Ota, K., Shibata, S., Inoue, T., Ide, Y., Sadakane, M., Sano, T., J. Cryst. Growth, 314 (2011), 274-278.
[4] Jon, H., Ikawa, N., Oumi, Y., Sano, T., Chem. Mater., 20 (2008), 4135-4141.

Upgrading mesoporosity of ultrastable Y via sequential desilication and dealumination

Baojian Shen,*[a] Zhengxing Qin,[a] Xionghou Gao,[b] Qiaoxia Guo,[a] Baojie Wang[b]
[a]*State Key Laboratory of Heavy Oil Processing; the Key Laboratory of Catalysis of CNPC; and College of Chemical Engineering, China University of Petroleum, No. 18 Fuxue Road, Changping, Beijing 102249, PR China.* [b]*Lanzhou Petrochemical Center, Petrochemical Research Institute, PetroChina Company Limited, Lanzhou 730060, PR China.*
**baojian@cup.edu.cn*

Introduction

Steaming is the classical way to create mesopores into the framework of Y zeolite.[1] Removal of framework silicon provides another option for producing mesoporosity.[2] However, early experiment showed that the NaY zeolite did not possess more mesoporosity after desilication treatment.[3] Although it is well-accepted now it is because aluminum inhibits Si extraction, desilication remains as an important concept for Y zeolites, as shown in this work.

Experimental

Alkaline treatment of the parent NaY zeolite was conducted in aq. NaOH. Dealumination of the **a**lkaline **t**reated Na**Y** zeolite (ATY) and parent NaY zeolites were carried out via ion exchange and steaming. Product obtained via sequential desilication and steaming was named as USY_A. The reference sample prepared by steaming only was designated as USY.

Results and discussion

The framework Si/Al ratio of the NaY zeolite decreased from 3.1 to 2.8 after the alkaline treatment. The ^{29}Si-NMR spectra (Fig. 1A) show obviously that the relative intensity of peaks corresponding to Si(0Al) and Si(1Al) groups were decreased compared with that of the Si(2Al) and Si(3Al) units after the alkaline treatment. The ATY zeolite exhibited a micropore volume increment of 0.012 cm^3/g and a mesopore volume increment of 0.052 cm^3/g in comparison to its parent material. These changes in framework composition and in porosity properties inspired the proposal of the generation of the unrepairable hydroxyl nest shown in Fig. 1B. The USY_A zeolite shows similar Si/Al ratio and microporosity preservation compared with the USY zeolite (Table 1). On the other hand, The USY_A zeolite shows much higher amount of mesopore volume increment compared with its counterpart (Table 1), suggesting that the desilication treatment has greatly facilitated the mesopore development in ATY zeolite framework. Further data from NMR and IR supported this point on unique defect (Fig. 1B).

Table 1. Collection of Si/Al ratios and porosity data

Samples	Si/Al_{XRD}	V_{micro}[a]	V_{meso}[b]	V_{Hg}[c]
		cm^3/g		
Parent NaY	3.1	0.330	0.058	0.039
ATY	2.8	0.342	0.110	0.091
USY	7.9	0.336	0.176	0.133
USY_A	8.4	0.302	0.263	0.254

a: t-method; b: BJH method; c: cumulative mercury intrusion (6-100 nm)

TEM examination revealed that all parts of the crystal of the ATY zeolite exhibit uniform contrast under electron beams as its parent sample does (Fig. 2A, B), suggesting the neglectable destruction of framework in alkaline solution. The USY_A zeolite presents much higher density of mesopores observed as white contrast than the USY zeolite (Fig. 2C, D).

Moreover, a close examination of the TEM images revealed that the USY_A zeolite shows conspicuously increased grain boundary defects (Fig. 2D) than the USY zeolite (Fig. 2C), providing us with evident clue that the mesopores in the USY_A zeolite may be directly connected to the external surface of crystal particles. This was well supported by the obviously higher volume of mercury intrusion of the USY_A zeolite (Table 1, cumulative volume in pores with 6-100 nm aperture), and, especially, by the almost coincidence with the nitrogen adsorption data.

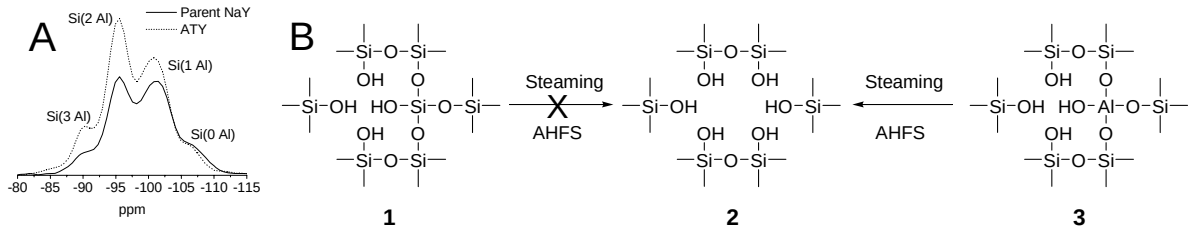

Fig. 1. ^{29}Si-NMR of the parent NaY and ATY zeolites (A); The conventional hydroxyl nest left by removal of framework aluminum or Si(0Al) (**1** in Fig. 1B), The unrepairable hydroxyl nest left by removal of framework aluminum (**2** in Fig. 1B), The unique hydroxyl nest in ATY zeolite left by removal of framework Si(1Al) (**3** in Fig. 1B)

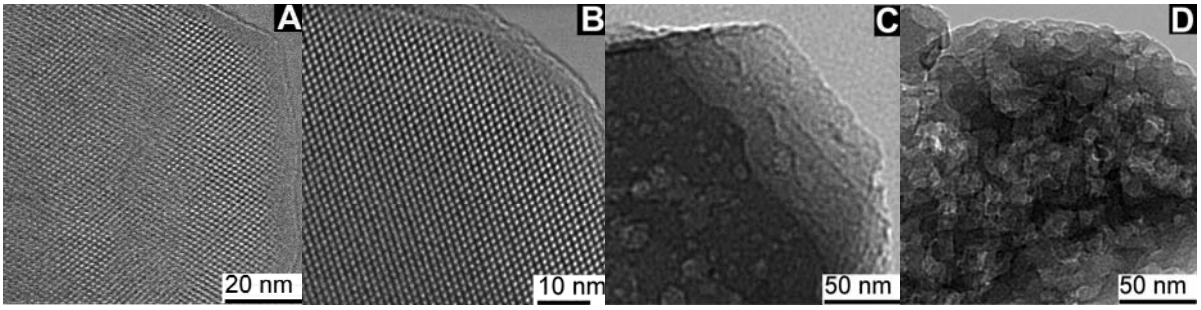

Fig. 2. TEM images of parent NaY (A), ATY (B), USY (C) and USY_A (D) zeolites.

Conclusions

Although both desilication and dealumination are utterly ordinary post-modification methods, they can act in excellent synergy in introducing mesopore into Y zeolite framework when combined in appropriate manner. By desilication, Si(0Al) and Si(1Al) atoms are selectively removed from the parent NaY zeolite, leaving its framework with a unique type of defects containing framework Al-OH. It is believed that these unique defects are unrepairable during dealumination due to its failure to receive the migrating silicate, hereby enables the consecutive desilication-dealumination a suitable route to highly mesoporous zeolites of modified accessibility and improved acidity.

Acknowledgements

The authors thank professor Xuanwen Li of Peking University for fruitful discussions, and acknowledge the funding of this project by MOST ‘‘973’’ Project of China (2010CB226904) and PetroChina.

References

[1] S. van Donk, A.H. Janssen, J.H. Bitter, K.P. de Jong, Generation, Characterization, and Impact of Mesopores in Zeolite Catalysts, Catalysis Reviews: Science and Engineering, 45 (2003) 297 - 319.

[2] J.C. Groen, T. Bach, U. Ziese, A.M. Paulaime-van Donk, K.P. de Jong, J.A. Moulijn, J. Pérez-Ramírez, Creation of Hollow Zeolite Architectures by Controlled Desilication of Al-Zoned ZSM-5 Crystals, Journal of the American Chemical Society, 127 (2005) 10792-10793.

[3] R. Le Van Mao, S. Xiao, A. Ramsaran, J. Yao, Selective removal of silicon from zeolite frameworks using sodium carbonate, Journal of Materials Chemistry, 4 (1994) 605 - 610.

Hydrothermal conversion of FAU zeolite in the absence of organic structure–directing agents

Ayako Yashiki, Ayumi Fujimoto, Shohei Shibata, Koutaro Honda, Yusuke Ide, Masahiro Sadakane and Tsuneji Sano
Department of Applied Chemistry, Graduate School of Engineering, Hiroshima University, Higashi -Hiroshima 739-8527, Japan. E-mail: tsano@hiroshima-u.ac.jp

Introduction

Generally, zeolites are synthesized by hydrothermal treatment of amorphous aluminosilicate gel as a starting material in the presence of organic structure-directing agents (OSDAs). However, the use of OSDAs is undesirable from a practical point of view because of their high cost as well as high environmental burdens. Therefore, the synthesis of zeolites from seed crystals without OSDAs has attracted considerable attention, and several research groups have already succeeded in the OSDA-free syntheses of ECR-1, ZSM-34, *BEA, RTH, and ZSM-12 zeolites. Recently we have investigated the potential of an alternative method for zeolite formation, i.e., the hydrothermal conversion of one zeolite type into another (interzeolite conversion), and succeeded in the synthesis of several types of zeolites from FAU zeolite as the starting material in the presence of various OSDAs. The crystallization rate with FAU zeolite in the presence of OSDAs is greater than that with aluminosilicate gel (the conventional synthesis). This is because the decomposition/dissolution of the starting zeolite generates locally ordered aluminosilicate species (nanoparts) that assemble and evolve into another type of zeolite.

In this study, therefore, we applied the interzeolite conversion method to the OSDA-free syntheses of *BEA, LEV and MAZ zeolites in the presence of correponding seed crystals.

Experimental

Starting FAU zeolites with various Si/Al ratios were prepared from NH_4-Y zeolite (Si/Al = 2.8, Tosoh Co., Japan) using a dealumination treatment involving a combination of steaming at 700 °C and H_2SO_4 (0.74 M) treatment at 75 °C for 4 h. The XRD pattern of the dealuminated zeolite showed no peaks other than those corresponding to the FAU structure. Hydrothermal conversion of FAU zeolite was carried out by adding the dealuminated FAU zeolite to an aqueous solution of NaOH; also, 5–33 wt% of non-calcined seed crystals were added on the basis of weight of silica. The seed crystalsof *BEA, LEV, and MAZ zeolites were synthesized from amorphous SiO_2 (Cab-o-sil M5)/γ-Al_2O_3 using TEAOH, choline hydroxide, and TMAOH as SDAs, respectively. The mixture was placed into a 30-cm^3 Teflon-lined stainless steel autoclave. Hydrothermal conversion was conducted at 70-125 °C for 24 h–14 days in a convection oven. The solid product was collected by centrifugation and washed thoroughly with deionized water. The obtained products were characterized by means of XRD, XRF, SEM, ^{13}C CP/MAS NMR, ^{27}Al MAS NMR, ^{29}Si MAS NMR, N_2 adsorption, and TG/DTA.

Results and discussion

Detailed synthesis conditions are listed in Table 1. We carried out the interzeolite conversion of FAU by changing $NaOH/SiO_2$ and H_2O/SiO_2 ratios as well as seed contents. Pure *BEA, LEV, and MAZ zeolites were obtained only with the higher alkalinity of the starting material and seed content. To our knowledge, this is the first report of FAU–*BEA, FAU-LEV, and FAU-MAZ interzeolite conversions although the yields were lower. The lower yield is probably due to the high alkalinity of the interzeolite conversion condition. When hydrothermal treatment was performed using calcined seed crystals, the interzeolite

conversion of FAU did not occur. For comparison, we attempted to synthesize *BEA, LEV, and MAZ zeolites by the conventional hydrothermal synthesis using $SiO_2/Al(OH)_3$ as the starting materials. However, pure zeolites were not obtained, thereby indicating the advantage of the interzeolite conversion method. Taking into account the fact that when calcined and non-calcined seed crystals (0.25 g) were treated with a 1.6 M NaOH aqueous solution (3.0 cm^3) at 125 °C for 2 h, a large different in hydrothermal stability was observed, namely non-calcined seed crystals did not decompose/dissolve, it proves that SDA cation containing seed crystals are more stable and consequently the crystal surfaces contribute to the crystal growth of *BEA, LEV, and MAZ zeolites.

Fig. 1 shows the XRD patterns for the FAU–*BEA interzeolite conversion process. It is clear that the FAU zeolite decomposed completely after hydrothermal treatment for 2 h. The intensities of the peaks corresponding to the *BEA zeolite increased with the hydrothermal treatment time, indicating the crystal growth of *BEA zeolite. Fig.2 shows SEM images of *BEA, LEV and MAZ zeolites obtained by the interzeolite conversion method.

Table 1 Interzeolite conversion conditions of FAU zeolite and products obtained.

Run No.	Synthesis conditions						Product		
	Si&Al source (Si/Al)	$NaOH/SiO_2$	H_2O/SiO_2	Seed (wt%)	Temp. (°C)	Time (days)	Phase	Yield (%)	Bulk Si/Al
1	FAU(22)	0.4	10	9.1	100	1	*BEA,Am.		
2	FAU(22)	0.6	10	9.1	100	1	*BEA	12	7.3
3	FAU(22)	0.6	20	33.3	125	1	*BEA	26	11
4	FAU(22)	0.6(KOH)	20	33.3	125	1	*BEA	34	11
5	FAU(22)	0.6	15	4.8	125	3	LEV	11	
6	FAU(25)	0.6	15	16.7	125	3	LEV	18	5.0
7	FAU(16)	0.6	20	33.3	70	28	MAZ	30	4.1

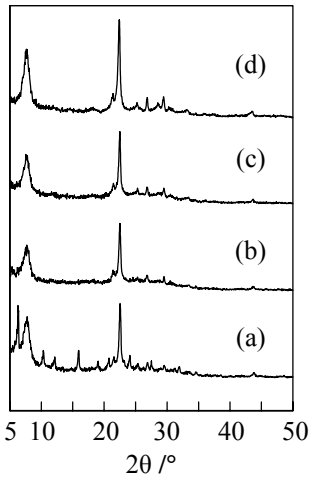

Fig. 1 XRD patterns of products obtained from FAU zeolite using NaOH and 9.1 wt% seed crystals at various crystallization times(100 °C) : (a) 0 h, (b) 2 h, (c) 12 h, and (d) 24 h.

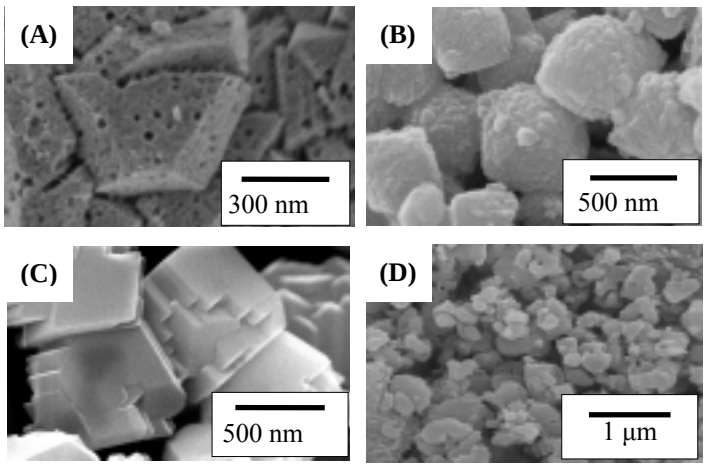

Fig. 2 SEM images of (A) starting FAU and the obtained zeolites of (B) *BEA (Run no. 3), (C) LEV (Run no. 6), and (D) MAZ (Run no. 7).

Conclusions

We successfully converted FAU zeolite into *BEA, LEV and MAZ zeolites using corresponding seed crystals in the absence of OSDAs. Our results strongly suggest the high possibility and potential of OSDA-free interzeolite conversions.

References

[1] Jon, H., Nakahata, K., Lu, B., Oumi, Y., Sano, T., Micropor. Mesopor. Mater., 96 (2006) 72-78.
[2] Inoue, T., Itakura, M., Jon, H., Takahashi, A., Fujitani, T., Oumi, Y., Sano, T., Micropor. Mesopor. Mater., 122 (2009) 149-154.

Boron in extra-large pore UTL zeolites: type, localization and strength of acid centers.

Oleksiy V. Shvets, Mariya V. Shamzhy, Pavel S. Yaremov, Vladimir N. Solomakha, Pavla Chlubná*, Jiří Čejka*.
*L.V. Pisarzhevskiy Institute of Physical Chemistry, National Academy of Sciences of Ukraine, 31 pr. Nauky, Kyiv 03028, Ukraine, *J. Heyrovský Institute of Physical Chemistry, Academy of Sciences of Czech Republic, v.v.i., Dolejškova 3, 182 23 Prague 8, Czech Republic, alexshvets@ukr.net.*

Introduction

Isomorphous introduction of boron into the framework of many zeolites was successful. In addition, some new zeolite topologies were discovered as borosilicates or borogermanosilicate [1]. Borosilicate zeolites display acid strength significantly lower than corresponding aluminosilicates but still being able to catalyze many reactions. In the present work we studied a direct introduction of boron into the framework of germanosilicate zeolites with UTL topology using several spiroazocompounds (SDAs, Fig. 1). The effects of SDA's nature, chemical composition and pH of the reaction mixture as well as duration of the synthesis on phase selectivity, limits of isomorphous introduction of boron into the framework, location and coordination of boron atoms, adsorption and acidic properties of prepared borogermanosilicates were investigated.

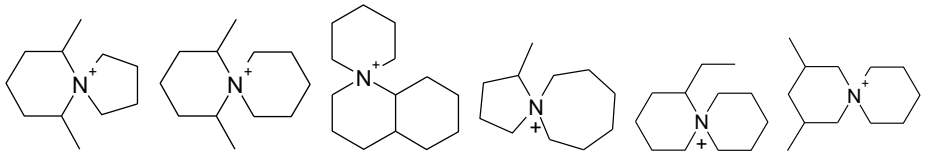

1 2 3 4 5 6

Figure 1. Prepared organic compounds used as SDAs

Experimental

Preparation of B-UTL samples was carried out using a method similar to that published in [2]. Molar composition of reaction mixtures was in the range $0.300–1.029SiO_2$:0.0–$0.156H_3BO_3$:0.171–$0.840GeO_2$:0.2–0.7ROH/Br:$30H_2O$. The solid products obtained after preset synthesis times were recovered by filtration, washed out with distilled water and dried overnight at 95 °C. To remove the SDA, the as-synthesized zeolites were calcined in a stream of air at 550 °C. X-ray powder diffraction, scanning electron microscopy, FTIR spectroscopy, adsorption of pyridine and 2,6-di-tert-butyl pyridine, argon and nitrogen adsorption at –196 °C, ^{1}H (300 MHz) NMR and solid state ^{11}B MAS NMR spectroscopy was used for investigation of prepared samples.

Results and discussion

Zeolites with UTL topology can crystallize from the reaction mixtures with a broad variability of chemical compositions. A detailed study of the peculiarities of crystallization of this zeolite phase shows that for B-free reaction mixture at pH ~ 11.0, the acceptable content of germanium and silicon is 0.167 – 0.750 and 0.833 – 0.250 respectively. Increasing boron content in the reaction medium narrows the fields of appropriate contents of silicon and germanium. The properties of SDAs strongly influence the upper limit of B content in the

reaction mixture, which still allow obtaining of pure UTL phase. Syntheses using SDA4, SDA5, and SDA6 resulted in the formation of a pure UTL phase in a wide range of B/(Si+Ge+B) ratios from 0.1 up to 11 pH boarders of UTL formation are equal to pH limits of region, where concentration of $Ge_8O_{15}(OH)_5^{3-}$ (D4R) in water is the highest. For series of samples prepared from the reaction mixtures with similar chemical composition and different pH values the B, Si and Ge contents in samples extremely depend on the pH value. While silicon content increases and germanium content predictably decreases with pH increment, boron content shows a local minimum at pH ~ 9. Boron content in UTL samples does not depend straightforwardly on its content in the reaction mixtures but silicon content substantially increases and germanium content decreases with increasing amount of boron in the reaction mixture. Consequently, there is a sharp enhancement of Si/Ge ratio for samples synthesized from boron-rich reaction gels. From ^{11}B MAS NMR data it follows that at rather low contents of boron in the structure of zeolites (prepared from reaction mixtures with relatively low pH = 8 – 9) the boron atoms are located mainly in T4 and T9 positions, in a smaller extent in position T6 (Fig. 2a). The increasing pH of the reaction mixture above 11 leads to a sharp increase in the Si/Ge ratio (and decrease in the concentration of Ge atoms in D4Rs) and favors additional introduction of boron atoms in T9 position. B-UTL zeolites exhibit predominantly Lewis acid sites and a small amount of the Brønsted acid sites (Fig. 2b). Only for samples prepared at pH lower than 8 the concentration of the Brønsted acid sites increases sharply.

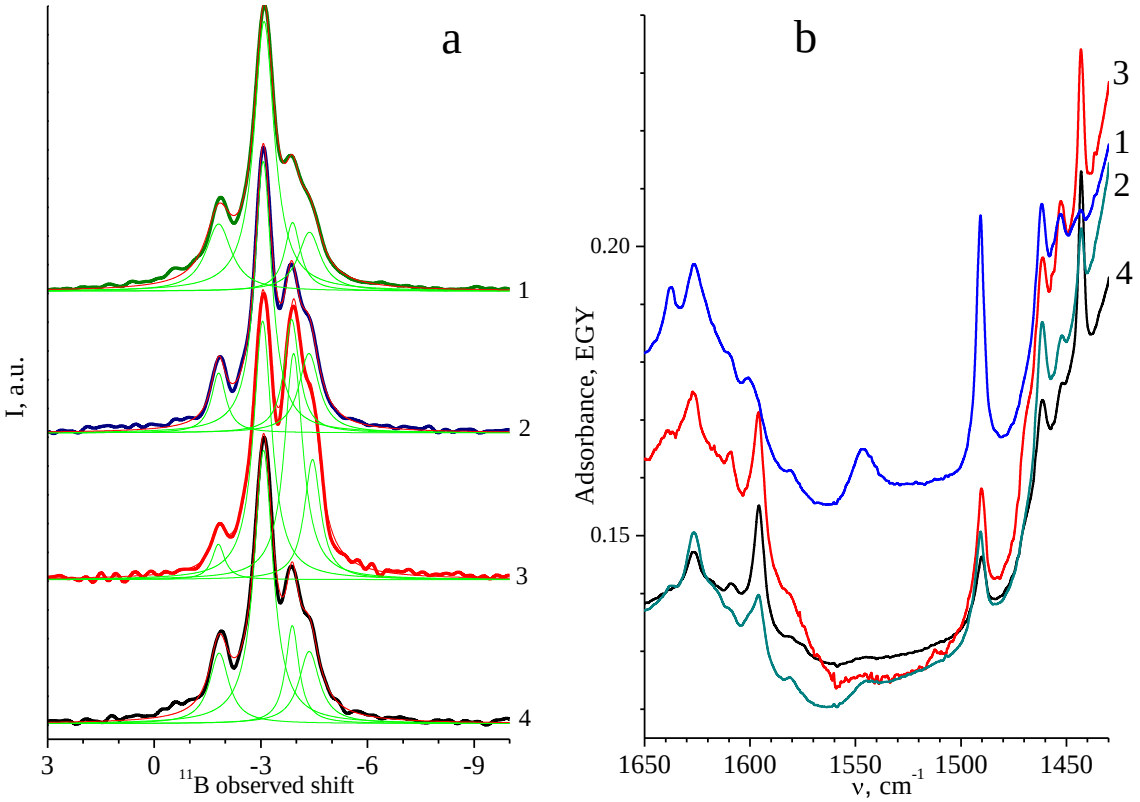

Figure 2. ^{11}B MAS NMR spectra of as-synthesized B-UTL zeolite samples (a) and FTIR spectra of pyridine adsorbed on B-UTL zeolite synthesized from reaction mixture of different composition (b).

References

[1] Cantín A., Corma A., Diaz-Cabanas M.J, Jordá J.L., Moliner M., J. Am. Chem. Soc., 128 (2006) 4216.
[2] Shvets O.V., Kasian N., Zukal A., Pinkas J., Čejka J., Chem. Mater., 22, (2010) 3482.

Thermodynamics of hydrogen adsorption on the metal-organic frameworks MIL-100(Cr) and MIL-101(Cr)

Gemma Turnes Palomino, Carlos Palomino Cabello and Carlos Otero Areán
Department of Chemistry, University of the Balearic Islands, 07122 Palma de Mallorca, Spain, g.turnes@uib.es.

Introduction

Metal-organic frameworks (MOFs) are among the porous solids currently more investigated as potential candidates for hydrogen storage by physical adsorption [1]. An advantage of MOFs is that in some of them unsaturated (open) metal cation centres can be generated by removal of the coordinated solvent molecules (which act as terminal ligands for the metal cations embedded in the porous framework) by thermal treatment under a vacuum. Following this strategy localized hydrogen adsorption centres (similar to those of zeolites) are created, and adsorption enthalpy is significantly increased; values in the range of 10-13 kJ mol^{-1} were reported [2]. While these relatively large ΔH^0 values are promising, one should keep in mind that the thermodynamics of hydrogen uptake and release is actually ruled by the combined effect of adsorption enthalpy and entropy, and not by ΔH^0 alone. With a view to gain further insight on the role of the correlation between stardard adsorption enthalpy and entropy, we report herein on a variable-temperature infrared (VTIR) [3] spectroscopic study on hydrogen adsorption on MIL-100(Cr) and MIL-101(Cr), which are MOFs having open metal (Cr^{III}) cations.

Experimental

The MIL-100(Cr) and MIL-101(Cr) samples used were synthesized at 493 K under hydrothermal conditions following the procedure described by Férey et al.[34], and checked by powder X-ray diffraction. Thermodynamics of hydrogen adsorption (at a low temperature) was studied by means of variable-temperature FTIR spectroscopy, following the VTIR method described elsewhere [4]. For IR spectroscopy, a thin self-supported wafer of the MOF sample was prepared and outgassed (at 400 K for 10 h followed by 5 h at 553 K) inside an IR cell which allowed in situ sample activation, hydrogen dosage and variable temperature IR spectroscopy to be carried out. Transmission IR spectra were recorded at 3 cm^{-1} resolution on a Bruker IFS66 instrument.

Results and discussion

Fig. 1 shows some selected FTIR spectra, in the H–H stretching region, of molecular hydrogen adsorbed on MIL-100 (Fig. 1a) and MIL-101(Fig. 1b); they were obtained, for a fixed dose of hydrogen, over a temperature range while simultaneously measuring IR absorbance, A, temperature, T, and hydrogen equilibrium pressure, p, inside the closed IR cell. From these spectra, the standard adsorption enthalpy, ΔH^o, and entropy, ΔS^o, were determined by following the VTIR method, which assumes Langmuir-type adsorption and validity of the (well known) integrated van't Hoff equation,

$$K(T) = \exp(-\Delta H^o/RT)\exp(\Delta S^o/R)$$

The linear van't Hoff plots of ln K versus the reciprocal of the temperature, obtained from spectra taken in the temperature range 79-105 K, gave the values of ΔH^0= -6.9 kJ mol^{-1} and ΔS^0= -80 J mol^{-1} K^{-1} for MIL-100, and ΔH^0= -9.5 kJ mol^{-1} and ΔS^0= -112 J mol^{-1} K^{-1} for MIL-101. Estimated error limits are ± 1 kJ mol^{-1} for enthalpy and ± 10 J mol^{-1} K^{-1} for entropy.

These values show a positive correlation between ΔH^0 and ΔS^0 similar to that reported for hydrogen adsorption on zeolites [5], and also found for the MOFs Mg-MOF-74 and Co-MOF-74 [6].The implications of such a correlation for hydrogen storage and delivery using MOFs will be discussed; and it will be shown that the optimum value of ΔH^0 for hydrogen delivery at room temperature (in the pressure range of 30 to 1.5 bar) is likely to be in the range of 22-25 kJ mol^{-1}; which is very significantly different from the often quoted value of ΔH^0_{opt}= -15.1 kJ mol^{-1}.

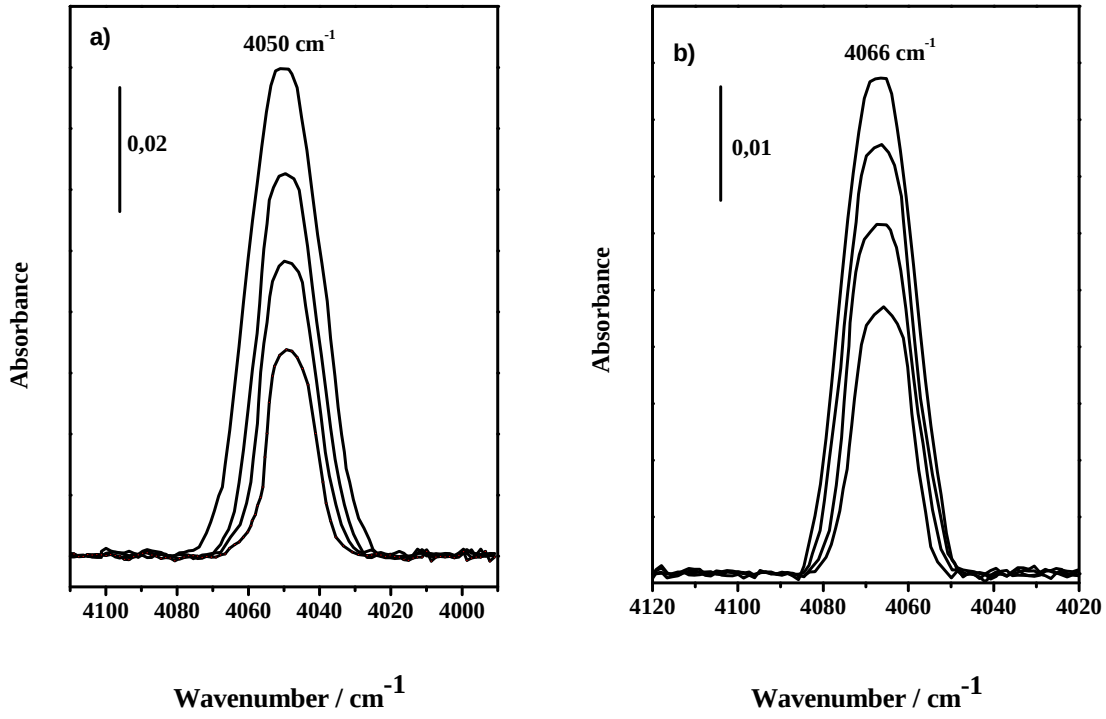

Figure 1. Representative VTIR spectra (MOF blank subtracted) of H_2 adsorbed on MIL-100 (a) and MIL-101 (b).

Acknowledgements

The Spanish Ministerio de Ciencia e Innovación (MICINN) and the European Funds for Regional Development (FEDER) are gratefully acknowledged for financial support (project MAT2008-00089). CPC acknowledges the support from the Ministerio de Educación y Ciencia (pre-doctoral fellowship).

References

[1] A. W. C. van den Berg, C. O. Areán, *Chem. Commun*. **2008**, 668-681.
[2] L.J. Murray, M. Dinca, J.R. Long, *Chem. Soc. Rev*. **2009**, *38*, 1294-1314.
[3] G. Férey, C. Mellot-Draznieks, C. Serre, F. Millange, J. Dutour, S. Surblé, I. Margiolaki, *Science* **2005**, *309*, 2040-2042.
[4] E. Garrone, C. O. Areán, *Chem. Soc. Rev*. **2005**, *34*, 846-857.
[5] E. Garrone, B. Bonelli, C. O. Areán, *Chem. Phys. Lett*. **2008**, *456*, 68-70.
[6] C. O. Areán, S. Chavan, C. P. Cabello, E. Garrone, G. T. Palomino, *ChemPhysChem* **2010**, *11*, 3237-3242.

Post-synthesis modifications of TUN zeolite

Martin Kubů, Naděžda Žilková, Jiří Čejka
J. Heyrovský Institute of Physical Chemistry, Academy of Sciences of the Czech Republic, v.v.i., Dolejškova 3, CZ-182 23 Prague 8, Czech Republic, martin.kubu@jh-inst.cas.cz

Introduction

Zeolites play an important role in numerous industrial applications as heterogeneous catalysts [1, 2]. However, their microporous structure often brings problems with limited diffusion and low accessibility of acid sites for bulkier molecules. One of the possible ways to overcome these problems represents hierarchical zeolites combining micropores and mesopores where the transport of bulky reactants and products proceeds with a higher efficiency [3, 4].
TUN is a new high-silica zeolite [5]. Its framework contains two distinct straight 10-ring channels. TUN crystallizes under hydrothermal conditions at the expense of a lamellar precursor over a very narrow range of Si/Al and $NaOH/SiO_2$ ratios in the presence of diquaternary ammonium structure directing-agent (SDA) 1,4-bis(N-methylpyrrolidinium) butane. The proton form of TUN exhibits high hydrothermal stability, strong acidity and unique shape selective properties in acid-catalyzed reactions of monoaromatic hydrocarbons.
This contribution focuses on the post-synthesis treatments of TUN zeolite via dealumination, desilication, and silylation. Textural, acidic, and catalytic properties of parent and modified TUN samples were investigated together with the relationship between acidity and catalytic activity in toluene disproportionation and its alkylation with isopropyl alcohol.

Experimental

TUN zeolite was synthesized according to Ref. [5]. The organic SDA cation was prepared according to the literature [6]. Detailed description of the synthesis conditions, post-synthesis treatments and characterization techniques applied to parent and post-synthetically modified TUN samples is given in [7]. Table 1 summarizes the abbreviations of all samples studied and the conditions of post-synthesis treatments applied.
The disproportionation and alkylation of toluene with isopropyl alcohol were investigated in a down-flow glass microreactor with a fixed bed of catalyst under atmospheric pressure. The reaction products were analyzed using an "on-line" gas chromatograph with flame ionization detector and a high-resolution capillary column. For more details see [7].

Table 1. Experimental conditions of post-synthesis treatment and textural properties.

marking	HNO_3 conc. (M)	NaOH conc. (M)	Si (wt. %)	time (h)	V_{mic} (cm^3/g)	V_{meso} (cm^3/g)	S_{BET} (m^2/g)	Δw (%)[a]
TUN	-	-	-	-	0.167	-	418	-
TUN/A	0.5	-	-	2	0.172	-	442	-
TUN/B	1.0	-	-	2	0.168	-	430	-
TUN/C	6.0	-	-	2	0.169	-	429	-
TUN/D	-	0.2	-	0.25	0.141	0.234	435	12.7
TUN/E	-	0.2	-	0.5	0.140	0.298	473	27.7
TUN/F	-	0.2	-	2	0.133	0.340	474	42.6
TUN/G	-	-	1.0[b]	-	0.160	-	406	-

[a] weight reduction after desilication, [b] TEOS

Results, discussion, conclusions

X-ray powder diffraction and scanning electron microscopy confirmed that TUN structure was preserved after all treatments. No significant changes were observed in the individual XRD patterns and in the shape and size of TUN crystals. Nitrogen adsorption isotherms

showed significant changes in the textural properties after desilication. With increasing time of the treatment with NaOH (Table 1) micropore volume decreased slightly, however, volume of mesopores and BET areas increased dramatically. Desilication resulted also in substantial changes in the concentration of acid sites, their location, and partially changed the type of acid sites. The concentration of Brønsted acid sites (c_B) decreased, the concentration of Lewis acid sites increased. The increase in c_B on the "external" surface of zeolites was determined by the adsorption of 2,6-di-tert-butyl pyridine. In toluene disproportionation, silylation provided a higher selectivity towards xylenes, higher xylene/benzene ratios and selectivity to *p*-xylene. In toluene alkylation with isopropyl alcohol, both dealumination and desilication decreased the selectivity to *p*-cymene. The highest selectivity to *p*-cymene of about 90% was achieved on silylated TUN with a simultaneous increase in selectivity to cymenes (Figure 1).

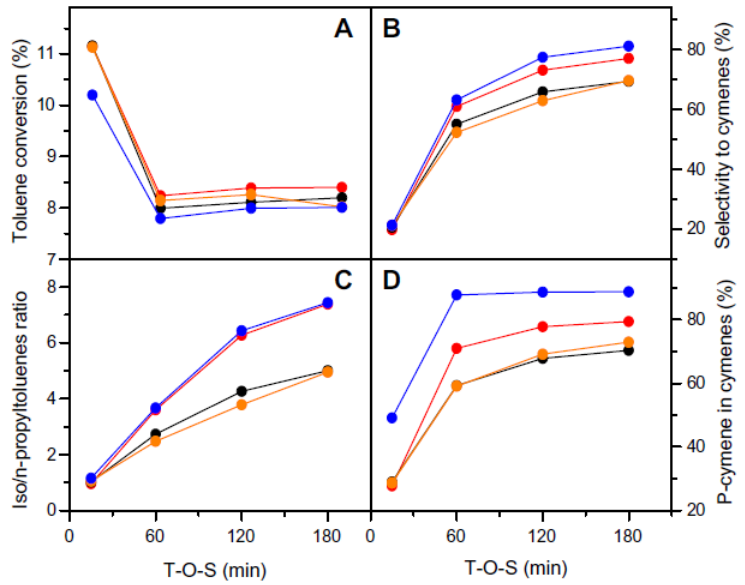

Figure 1. Time-on-stream dependence of toluene conversion (A), selectivity to cymenes (B), iso-/n-propyltoluene ratio (C) and *p*-cymene selectivity (D) in toluene alkylation with isopropyl alcohol at 250 °C for TUN (●), TUN/A (●), TUN/C (●) and TUN/G (●).

Obtained textural and catalytic results showed that TUN zeolite is very interesting for transformation of aromatic hydrocarbons with a potential for other reactions of aromatic hydrocarbons.

Acknowledgements

The authors thank the Academy of Sciences of the Czech Republic for the support and M.K. acknowledges the Grant Agency of the Czech Republic for financial support (106/11/0819 and 203/08/H032).

References

[1] Čejka, J., Corma, A., Zones, S.I. (Eds.), Zeolites and Catalysis: Synthesis, Reactions and Applications, Wiley-VCH, (2010), Weinheim

[2] Čejka, J., van Bekkum, H. (Eds.), Zeolites and Ordered Mesoporous Materials: Progress and Prospects, Studies in Surface Science and Catalysis, 157 (2005), Elsevier, Amsterdam

[3] Perez-Ramirez, J., Christensen, C.H., Egeblad, K., Christensen, C.H., Groen, J.C., Chemical Society Reviews, 37 (2008), 2530-2542

[4] Musilová-Pavlačková, Z., Zones, S.I., Čejka, J., Topics in Catalysis, 53 (2010), 273–282

[5] Hong, S.B., Min, H.K., Shin, C.H., Cox, P.A., Warrender, S.J., Wright, P.A., Journal of the American Chemical Society, 129 (2007), 10870-10885

[6] Kubů, M., Zones, S.I., Čejka, J., Topics in Catalysis, 53 (2010), 1330-1339

[7] Kubů, M., Žilková, N., Čejka, J., Catalysis Today, (2011), article in press

Interconnected mesopores and high accessibility in UVM-7-like silicas

Mónica Pérez-Cabero,[a] Ana B. Hungría, [b] José Manuel Morales, [a] Marta Tortajada, [c] Daniel Ramón, [c] Alaina Moragues,[a] Jamal El Haskouri,[ad] Daniel Beltrán [a] and Pedro Amorós [a*]
[a] Institut de Ciència dels Materials and [d] Fundació General, Universitat de València. P. O. Box 22085, 46071-Valencia (Spain), [b] Depart.de C. de Materiales, Ing. Metal. y Q. Inorg., Univ. de Cádiz, Campus Río San Pedro s/n 11510, Puerto Real, Cádiz (Spain), [c] Biópolis S. L., Polígono La Coma s/n, 46980-Paterna, Valencia (Spain). (*) pedro.amoros@uv.es

Introduction

The research on porous materials chemistry was boosted during the last decades by the discovery of the M41S silicas displaying regular pores in the meso range and the large number of real and potential applications affected [1]. However, it has been argued that its typical periodic and unimodal mesoporous structure could not offer specific advantages for certain applications requiring an enhanced accessibility to the active sites [2]. Hence, the presence of hierarchic pore systems structured at different length scales could offer significant advantages to overcome pore-blocking and related phenomena. One way to tackle the site accessibility problem is conceptually based on the decreasing (at the nanoparticle range) the particle size of the mesoporous material, shortening subsequently the mesopore length and increasing the texture volume. Based on this idea we synthesized bimodal porous silicas denoted as UVM-7 materials achieving a good control of pore sizes, particle dimensions and other parameters through chemical simple tools [3]. The intraparticle UVM-7 pore topology is worm-like but there is no evidence about the entangled or multiconected pore network. In this contribution we show the tridimensional nature of the mesopore network through direct and indirect probes.

Experimental

The synthesis of UVM-7 silicas has been carried out as previously described in detail [3]. The expansion of the mesopores has been realized by adding organic expansors such as TMB ($1 < TMB/CTAB < 8$). The isolation of UVM-7 carbon replicas has been performed through CVD, or by chemical methods (using furfuryl alcohol or sucrose for the pore filling) [4]. The incorporation of gold was realized by impregnation with $HAuCl_4$ solutions [5]. The adsorption of lysozime has been performed as described in ref. 6. The samples have been studied by XRD, N_2 adsorption-desorption isotherms, TEM, STEM and electron tomography.

Results and discussion

While in the case of MCM-41-like materials, even in the form of nanoparticles, it is evident from TEM images the presence of regular, unimodal and non-interconnected surfactant-generated mesopores (inset in Fig. 1a), a certain number of questions remains unclear from TEM or STEM images of UVM-7 partially disordered silicas. Hence, although the presence of a bimodal pore structure is evident according to the scheme in Fig. 1c, the possible tortuous or interconnected nature of the intra-nanoparticle mesoporous is not completely clear.

The electron tomography allows performing from TEM images recorded at different angles (Fig. 2a) a 3-D reconstruction of the mesostructure. From this analysis the textural-like meso/macro inter-particle pore (Fig. 2b) similar to the pores in xerogels is confirmed, as expected. On the other hand, the absence of hexagonal intra-particle mesopore arrays both at the surface and inside the particles (with the absence of coherence among consecutive cross sections, Fig. 2c-d) and a certain level of pore joining indicates not only the tortuous character typical of worm-like mesoporous system, but also the interconnection among mesopores.

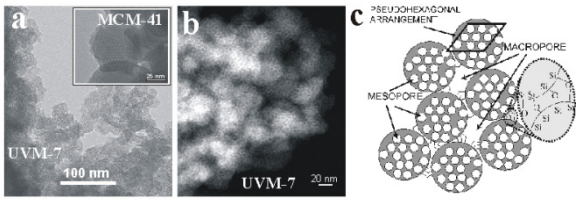

Figure 1. TEM (a),STEM (b) and scheme of UVM-7-like silicas.

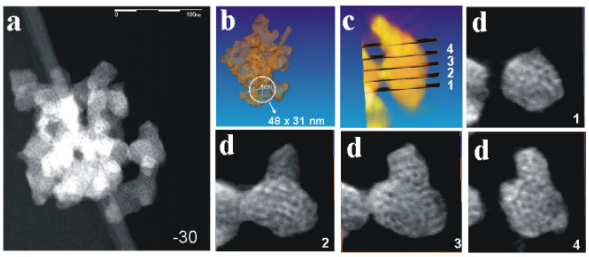

Figure 2. Electron tomography study of UVM-7.

The presence of at least entangled intra-particles mesopores (without discarding pore interconnection) is also supported through the isolation of self supported UVM-7 carbon replicas where the clustered organization of aggregated primary porous nanoparticles is preserved. Although a certain lost of order can be appreciated when compared to the silica parent material, the size and shape of the UVM-7 nanoparticles are clearly preserved in the carbon replica (Fig. 3a). An additional evidence of the pore connectivity is obtained by thermal treating gold impregnated UVM-7 silica. When samples were processed at T higher than the gold Tanmann temperature, mobility of the gold species occurs. The nucleation and growth of a centered single gold particle (*ca.* 1) inside each UVM-7 primary particle (Fig. 3b) could be accepted as an indirect probe of the existence of interconnectivity among mesoporous.

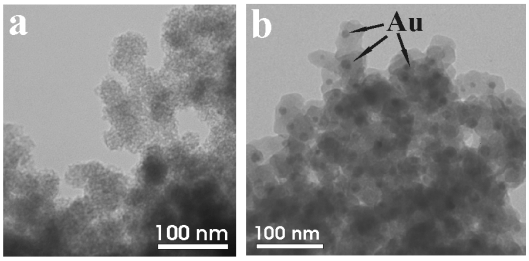

Figure 3. UVM-7 carbon replica (a). Au/UVM-7 treated at 700ºC (b).

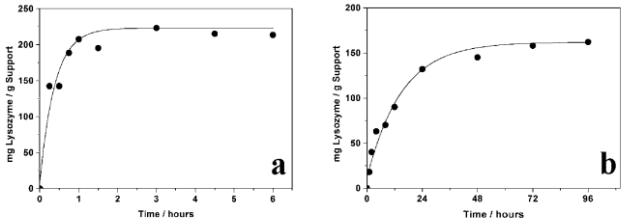

Figure 4. Lysozyme adsorption for (a) UVM-7 and (b) MCM-41

The resulting architecture, that allows overcoming usual problems as pore blocking, is the responsible for the enhanced accessibility achieved for UVM-7 silicas. As can be observed in Fig. 4, the adsorption of lysozyme (a globular enzyme with a hydrodynamic diameter of *ca.* 3 nm, slightly lower than the mesopore size), result extremely improved in UVM-7 silicas (Fig.4a) when compared to a conventional MCM-41 material (Fig. 4b). Both the adsorption rate as the loading level can be additionally enhanced by using UVM-7 materials with larger mesopores obtained through the use of TMB as swelling agent.

Conclusions

Following a remarkable parallelism with micellar systems, it is possible to prepare mesoporous silicas with topologies ranging from ordered, to disordered entangled and also to multi-connected and highly accessible pore arrays as occurs in UVM-7 materials.

Acknowledgements

We thank MEC (MAT2009-14564-C04-04) and GV (PROMETEO/2009/108) for support.

References

[1] Soler-Illia G. J. A. A., Sanchez C., Lebeau B., Patarin J., Chem. Rev. 102 (2002) 4093.
[2] Rolison D. R., Science 299 (2003) 1698.
[3] El Haskouri J., et al. Inorg. Chem. 47 (2008) 8267.
[4] Pérez-Cabero M., et al., Mat. Lett. 62 (2008) 2935.
[5] Pérez-Cabero M., et al.,J. Mater. Chem. 20 (2010) 6780.
[6] Tortajada M., et al., J. Mater. Chem. 15 (2005) 3859.

Embedded oxidic nanodomains inside mesoporous silicas: effective inorganic anchors for metal noble nanoparticles

Mónica Pérez-Cabero,[a] Jamal El Haskouri,[ab] Lorenzo Fernández,[a] Carmen Guillem,[a] Julio Latorre,[a] Aurelio Beltrán,[a] Benjamín Solsona,[c] Daniel Beltrán [a] and Pedro Amorós [a*]
[a] *Institut de Ciència dels Materials and* [b] *Fundació General, Universitat de València. P. O. Box 22085, 46071-Valencia (Spain),* [c] *Departament d´Enginyeria Química, Universitat de València, C/ Dr. Moliner 50, 46100 Burjassot, Valencia (Spain).* *(*) pedro.amoros@uv.es*

Introduction

Recent interest on metal noble nanoparticles includes a variety of areas such as biological markers, sensors, molecular recognition, and electronics [1]. This wide range of applications expands more classical activity related to catalysis [2]. Regardless of the specific application, the efficiency of these materials depends on two key factors: the nanoparticle size and dispersion and the particle fixing on different supports. In fact, the thermal stability constitutes a major drawback to any metal noble based nanomaterials. Hence, when Hüttig and Tamman temperatures are reached, atoms at defects and surfaces and at bulk level will become mobile. Moreover, these temperatures drastically drop down with the particle size [3]. Mesoporous silica-based materials could be considered as useful supports for nanoparticles because the expected nanosize confinement effect, but the null silica-noble metal affinity restricts drastically the temperature range of the catalytic processes [3]. Thus, even inside mesopores, the metal noble particles are able to migrate towards the outer surface under moderate temperature. The usual approach to minimize this problem is to modify the host surface with organic anchoring species. Although this strategy in general favours a better metal dispersion, the thermal stability usually does not result significantly improved due to the inherent instability of the organic groups used. The use of inorganic anchoring species constitutes a much better approach. In fact noble metal-MO_x materials are good catalysts for a variety of processes [4]. Here we describe how a wide family of MO_x-SiO_2 mesoporous nanocomposites, constructed from metal oxide nano-domains partially embedded inside silica walls (Figure 1), can be used as effective and extremely stable inorganic anchors favouring the nucleation, growth and stability of supported metal noble particles. This strategy constitutes a good and versatile preparative platform to design new noble metal-supported materials with a remarkable thermal stability.

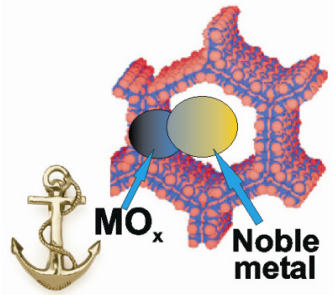

Figure 1. Scheme of inorganic anchors.

Experimental

The supports used for the gold deposition were MO_x-SiO_2 (M= transition metal) nanocomposites with unimodal (MCM-41 or UVM-11) and bimodal (UVM-7) pore structure. [5]. We used the one-pot atrane route, previously described in detail [5]. The gold inclusion was realized by impregnation with $HAuCl_4$ solutions and subsequent thermal treatments [6]. The samples were studied by XRD, N_2 adsorption-desorption isotherms, TEM, and spectroscopic, magnetic or optical techniques (depending of the MO_x nanodomains).

Results and discussion

Regardless the silica type (MCM-41, UVM-7 or the xerogel type UVM-11) [5] we have used the same preparative procedure to achieve an effective embodiment of the MO_x nanodomains.

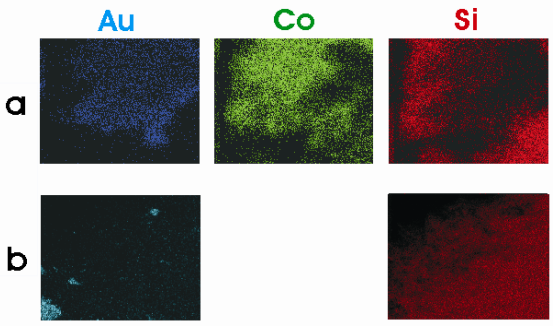

Figure 2. XEDS analysis of nanocomposites Au@-CoO_x-UVM-7 prepared by the atrane route (a) or impregnation (b).

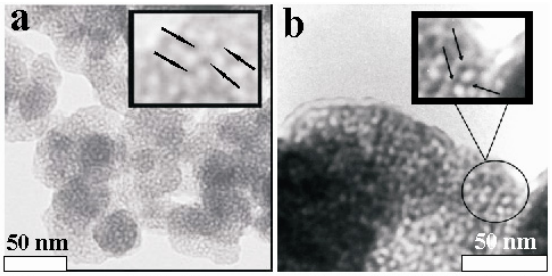

Figure 3. TEM images of (a) CoO_x-UVM-7 and (b) ZnO-MCM-41

Then, the success of the present approach in yielding MO_x-SiO_2 mesophases must be viewed as consequence of the coexistence of two non-interacting chemical systems: the nucleation and growth of MO_x particles and the formation of the silica mesophase. Hence, the rapid formation of the silica mesostructure strongly limits the growth of MO_x or the respective hidroxilated particles. Insofar as the reaction rates of the silica polymerization and mesophase growth are independent of the initial M content, similar nanoparticle sizes can be expected in all samples. The present strategy supplies materials with a high chemical homogeneity and a good control of the final composition (Figure 2). The presence of partially embedded MO_x nanodomains can be appreciated by TEM (Figure 3). Materials containing nanosegregated MO_x (M= Zn, Co, Ni, Ti, Zr, Sn ….) have been prepared [6,7]. Determination of the nanoparticle size has been realized trough magnetic, spectroscopic, TEM etc. depending on the nature of the M metal. Once fixed the MO_x anchors, these sites can be additionally modified to favor or not the surface hydroxylation. This point is a key aspect to adjust/modify the *zpc* of the MO_x anchors to favor the deposition (and subsequent nucleation and growth) of other metal species, in our case the noble metal complexes on these domains, instead of on the silica surface. The resulting homogeneity and dispersion of noble metal particles reflects just the achieved for MO_x sites (Figures 2a and 4). Moreover, the effective anchoring role of these domains together with the confinement inside mesopores induces a remarkable thermal stability.

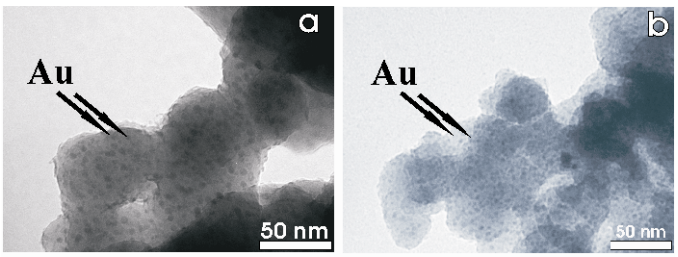

Figure 4. TEM images of Au@CoO_x-UVM-7 (a) as made and (b) after treatment at 773 K.

Conclusions

The described approach is very general and can be easily extended to the design of silica supported polymetallic nanoparticulated catalysts.

Acknowledgements

We thank MEC (MAT2009-14564-C04-04) and GV (PROMETEO/2009/108) for support.

References

[1] Daniel M.-C., Astruc D., Chem. Rev., 104 (2004) 293.
[2] Hutchings G. J., Chem. Commun., (2008) 1148. Corma A., García H., Chem. Soc. Rev., 37 (2008) 2096.
[3] Sun J., Bao X., Chem. Eur. J., 14 (2008) 7478.
[4] Comotti M., Li W. C., Spliethoff B., Schüth F., J. Amer. Chem. Soc., 128 (2006) 917.
[5] El Haskouri J., et al. Inorg. Chem. 47 (2008) 8267. Ortiz de Zárate D., et al., Sol. Stat. Sci., 10 (2008) 587.
[6] Pérez-Cabero M., et al.,J. Mater. Chem. 20 (2010) 6780.
[7] Fernandez L., et al. Nanotechnology 19 (2008) 225603. S. M., et al., J. Catal., 251 (2007) 388. Ortiz de Zárate D., et al., Eur. J. Inorg. Chem. (2006) 2572.

Connectivity analysis of aluminum and silicon in the clear sol precursor of SSZ-13 chabazite-type zeolite

Einar André Eilertsen,[a] Mohamed Haouas,[b*] Karl Petter Lillerud,[a] Francis Taulelle[b]
[a] *SMN/INGAP/Departement of chemistry, University of Oslo, Norway.*
[b]*Tectospin, Institut Lavoisier de Versailles, France.*
haouas@chimie.uvsq.fr.

Introduction

MFI-type silicalite-1 has served for a long time as a model system for studying zeolite synthesis mechanisms. The colloidal precursor route is of particular interest since it facilitates the characterization of the reactive medium. The initial stages of hydrolysis of tetraethyl orthosilicate (TEOS) in tetrapropylammonium hydroxide (TPAOH) solution for the preparation of silicalite-1 precursor were investigated by Petry et al. [1], and they showed that the nanoparticles present in the system had to be agglomerates of oligomers rather than real silica particles. In this work we studied, for the first time, the clear sol precursor for the chabazite zeolite in an attempt to explore the effect of another organocation, N,N,N-trimethyl-1-adamantammonium (TMAda), and the presence of Al on chemical composition, internal connectivity, and stability of nanoparticles as well as soluble species. The initial stages of the hydrolysis of TEOS in an aqueous solution of TMAdaOH were monitored by quantitative ^{29}Si and ^{27}Al NMR.

Experimental

Clear sols with the following composition: x SiO_2 – 0.02 Al_2O_3 – 0.6 TMAdaOH – 35 H_2O – 4x EtOH were prepared by adding the appropriate amount of TEOS to a solution of TMAdaOH, D_2O/H_2O and Al_2O_3 at room temperature. The resulting emulsion was vigorously stirred for 30 minutes before analysis with ^{29}Si and ^{27}Al NMR.

Results and discussion

The ^{29}Si NMR spectra of the clear sols at different stages of the hydrolysis with increasing Si/TMAdaOH ratio are shown in Figure 1. As shown in the figure with the progressive appearance of up-field signals, the connectivity of Si increases with the advancement of the hydrolysis. Formation of nanoparticles, as seen by broad resonances, appears when a Si/TMAdaOH ratio of one is reached. After that, more and more of the oligomers are converted into nanoparticles. This has also been observed with the silicalite-1 and silicalite-2 systems when TPAOH and TBAOH are used, and appears to be a general phenomenon for alkylammonium based silicate sols [1, 2]. As seen from the ^{27}Al NMR spectra in Figure 1, the connectivity of Al also increases with increasing Si/TMAdaOH ratio. After the nanoparticles are formed, the tetrahedrally coordinated Al is present mostly as being fully bound to four silicon atoms ($Al(OSi)_4$).

Figure 2 shows the average connectivity (T-O-T) for Si in the oligomers in solution and in the nanoparticles as well as for Al, calculated from the ^{29}Si and ^{27}Al ^{n}Q species distributions. The

connectivity of Si in the oligomers increases until the Si/TMAdaOH ratio equals one, when nanoparticles starts to form. After further hydrolysis, all oligomer ^{29}Si signals underwent line-narrowing as a result of incorporation of all aluminosilicates within the nanoparticles.

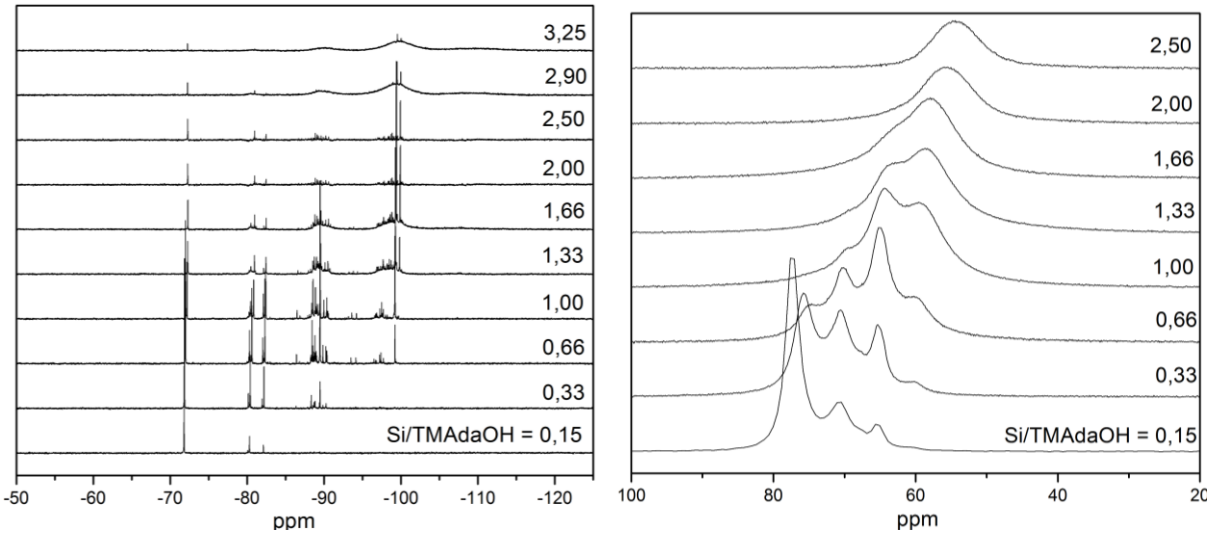

Figure 1: Evolution of ^{29}Si (left) and ^{27}Al (right) NMR spectra of clear sols with the progress of TEOS hydrolysis.

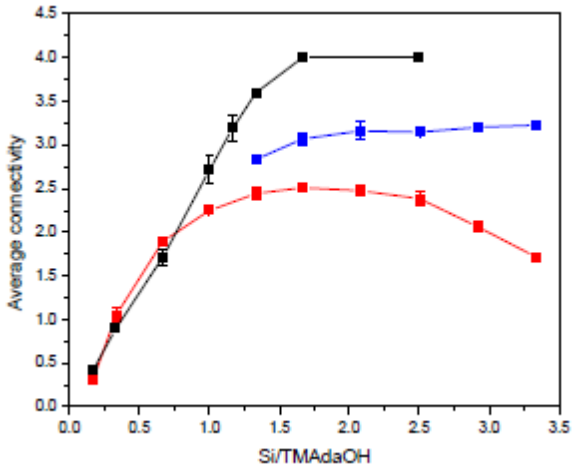

Figure 2. Average connectivity of Si in oligomers (red) and in nanoparticles (blue), and of Al (black) as function of TEOS hydrolysis progress.

Conclusions

The results showed similar behaviors of silicon connectivity and nanoparticles formation during TEOS hydrolysis to what has been seen for silicalite-1 and silicalite-2 [1, 2], confirming that is a general phenomenon independent on the nature of the organocation. It can also be seen that the Al is fully bound to four Si, and located exclusively in the nanoparticles.

References

[1] Petry, D., Haouas, M., Wong, S.C.C., Aerts, A., Kirschock, C.E.A., Martens, J.A., Gaskell, S.J., Anderson, M.W., Taulelle, F., J. Phys. Chem. C, 113 (2009), 20827-20836.
[2] Petry, D., Ph.d. thesis, University of Manchester (2009)

Particle manipulation during flow synthesis of mesoporous silica

Tsz Nok Ng, Xinqing Chen and King Lun Yeung
Department of Chemical and Biomolecular Engineering,
Hong Kong University of Science and Technology, Hong Kong, P.R. CHINA
Corresponding author: kekyeung@ust.hk

Introduction

Since early 1990s, the first mesoporous silica were discovered by scientists at Mobil Oil Company and by Kuroda and co-workers [1-3], it has attracted a lot of research interest regarding its size, structure, application, etc. A lot of efforts have been put on the size and morphology control of the silica because of the promising impact on the usage in different aspects. The relative hydrolysis and condensation rates of the silica precursor are the elemental factors that manipulate the size and morphology. The rates can be controlled by mean of changing the template material, pH, temperature and solvent. Microfluidics synthesis is a novel way in a highly controlled process offered by continuous process at small scale reactors such as reduced reaction volumes, faster heat and mass transfer, which is possible to prepare smaller particles with narrower particle size distribution, compared with the traditional reactors. In this project, microfluidic synthesis reactor was investigated to control the size of the mesoporos silica MCM-41 in a continuous microfluidic reactor. By introducing co-precursor synthesis condition, the size of the mesoporous silicate can be managed within the certain range. The targeting materials in this research are Tetraethyl orthosilicate (TEOS) and Tetramthyl orthosilicate (TMOS) different nano-scale mesoporous silica MCM-41 can be produced with different ratio of the two precursors.

Experimental

The nano-scale mesoporous silica MCM-41 was prepared using a microfluidic reactor setup. Structure directing agent Cetrimonium bromide (CTAB) was dissolved in DDI water with dissolved sodium hydroxide, in a molar ratio of 1 CATB: 10100 H_2O: 2.55 NaOH. The above solution was named as **solution A.** Then TEOS, TMOS and ethanol was mixed to give a **solution B** keeping the ratio of 1-χTEOS: χTMOS: 5.8(1-χ)+ 6.8χEthanol. The solution was set to mix in a T-mixer with a mixing volume ratio of **40 solution A: 1 solution B**. The final mixing ratio is 1 CTAB: 8.74 Si: 2.55 NaOH. Just after the mixing, nitrogen is pumped into the setup in another Tee-union to create a segment flow. The segmented flow was aged in an aging section made up of Teflon capillary for 5minutes at 80^{o}C. Sample was recovered by filtration in-situ.

Results and Discussion:

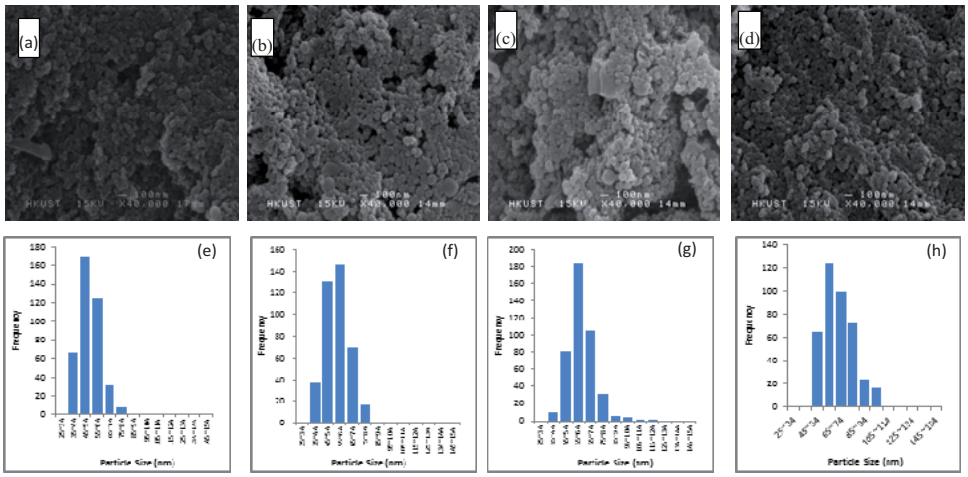

Figure 1. SEM image of sample with (a) 0% TMOS, (b) 5% TMOS, (c) 7.5% (d) 12.5% and the particle size distribution with (e) 0% TMOS, (f) 5% TMOS, (g) 7.5% (h) 12.5%

As the contents of the TMOS increase, the size of the particles also increase, this can be due to the difference in the hydrolysis rate of the precursors. The hydrolysis rate of TMOS is faster than that of TEOS by several orders. As the synthesis material involving the templating synthesis, the nucleation is followed the concentration of the structure directing agent, in this case the CTAB, with the same concentration of CTAB throughout all the operation. However the distribution becomes boarded as long as the contents of TMOS increase as shown in figure 2.

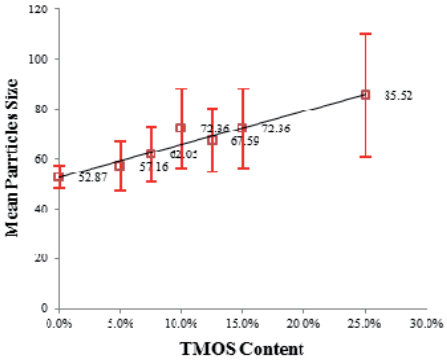

Figure 2. the means particle size with different TMOS content

Conclusions

This work shows a possible method to control the size of the mesoporus silica MCM-41 in a flow system. The hydrolysis rate can be increase by simply change the ratio of precursor and give a fine adjust on the particle size distribution.

References

[1] C.T. Kresge, M.E. Lenowicz, W. J. Roth, J. C. Bartuli and J. S. Beck, Nature, 1992, 359, 710-712

[2] J. S. Beck, J.C. Bartuli, W. J. Roth, M. E. Leonowicz, C. T. Kresge, K. D. Schmitt, C. T. W. Chu, D. H. Olson and E. W. Sheppard, et al, J. Am. Chem., 1992 114 10834-10843.

[3] S. Inagaki, Y. Fukushima, and K. Kuroda, J. Chem Soc., Chem Commmu., 1993, 680-682

The role of metal cations as templating species in chabazite framework formation

Leen Van Tendeloo, Elena Gobechiya, Johan Martens, Christine Kirschhock
Centre for Surface Chemistry and Catalysis, K.U. Leuven, Kasteelparck Arenberg 23-2461, B-3001 Heverlee, Belgium
Elena.Gobechiya@biw.kuleuven.be

Introduction

Quite a number of zeolite frameworks are formed in absence of any organic template. Experience taught the formation of a specific framework critically depends on conditions like gel composition, temperature and time. Small changes in pH or variation of the metal cation can entirely change the obtained topology from one type to another or prevent crystallization at all. The effect of the cations most probably lies in their direct interaction with and stabilisation of elemental aluminosilicate oligomers (AOs) and should depend on hardness, size and charge of the participating species, but virtually nothing is known about local interaction between metal ions and AOs. One strategy to increase insight into the stabilising role of metal ions on specific structural elements is detailed analysis of framework transformations. One example is the transformation of zeolite Y (FAU) into chabazite (CHA). Nominally, both topologies can be assembled exclusively from double six-rings(D6R). Bourgogne et al. [1] reported a synthesis which was verified by J. Warzywoda, by J. Cejka, and Liu Xinjin [2]. According to this work chabazite is formed through decomposition of the zeolite Y with Na/Al ratio below 0.17 in KOH solution with K/Al ratio 2 at 95° C in 96h. Exposure of a zeolite Y with Si/Al=2.6 and in absence of any Na ions led to quantitative formation of CHA with a framework composition $K_{11}Al_{11}Si_{25}O_{72}$. Based on this work the question arose if and how the structural information from the FAU framework is carried into the newly formed CHA topology. To gain more insight into the mechanism of transformation we varied Si/Al ratio, type and concentration of cations in the parent faujasite. We found that factors described as limiting in literature are not as stringent as reported.

Experimental

Chabazite was synthesized through decomposition of the zeolite Y in KOH solution at 95° C based on literature [1]. As initial compound for the framework transformation commercial zeolites Y with different Si/Al ratio and Na content were taken. To investigate the role of cations, ion-exchanged forms of zeolite Y (NH_4-, H-, Na-, K-, Ca-) were taken as a starting material for the framework transformation. Solid state ^{27}Al and ^{29}Si NMR, powder XRD, TGA and AAS were used for the characterization of the initial, intermediate and final materials.

Results and discussion

CHA and FAU topologies both contain double six rings (D6R) as a structural unit connected via edges, forming the sodalite cavity and supercage in FAU and chabazite cages in CHA. Like reported in literature simple exposure of a H-form of zeolite Y with Si/Al= 2.6 but with Na/Al ratio of .21 to aqueous solutions of KOH while heating indeed resulted in phase pure CHA after 96 hrs [1].
The original work on the CHA synthesis strongly advised the use of the H-form of zeolite Y. Especially the number of sodium ions in the starting material was described as limiting factor.

Faujasite usually is obtained as either pure Na- or mixed Na,K-form. So first the sodium needed to be exchanged by NH^{4+} before calcination and evacuation of NH3. Surprisingly, we observed the Na/Al ratio of the starting material is not as detrimental as thought [1]. The attempt to synthesize chabazite by decomposition of the Na-form of zeolite Y($Na_{52}Al_{52}Si_{140}O_{384}$) was as successful as the transformation of NH_4-, H-, or K- forms of this faujasite in KOH. At the same time the presence of Ca ions in the zeolite Y structure fully prevented this transformation. It has been observed that especially this cation has remarkable stabilising effect on the faujasite structure [3,4]. On the other hand, the presence of K^+ cations appeared as critical factor for chabazite framework formation. The attempt to use NaOH or CsOH solution for structure transformation of FAU to CHA did not succeed.
Our studies confirmed the Si/Al ratio has a strong influence on the system. For example faujasites with Si/Al ratio below 1 and above 6 resulted in low yields of crystalline CHA or even fully prevented formation of crystalline FAU under the same conditions.

Conclusions

Chabazite was synthesized from the decomposition of the zeolite Y in KOH according to the procedure reported by Bourgogne et al. [1]. As initial compound for the framework transformation commercial zeolites Y with different Si/Al ratio and Na content were taken as well as ion exchanged forms. Our investigations again revealed the crucial role the nature of the cations plays in interaction with aluminosilicate species involved in the formation of the final zeolite topology. A more detailed study currently is in progress to unravel the mechanism and the nature of the cation interaction in the crystallization process.

Acknowledgements

We acknowledge financial support by the Flemish Government for long-term structural funding (Methusalem), the Belgian Prodex office and ESA.

References

[1] M. Bourgogne, J.L. Guth, R. Wey, US Patent (1985) No 4,4503,024
[2] H. Robson, Verified Syntheses of Zeolitic Materials, Elsevier, 2001
[3] J.F.M. Denayer, et al., Micropor. Mesopor. Mater., 103 (2007) 1-10
[4] J.F.M. Denayer, et al., Micropor. Mesopor. Mater., 103 (2007) 11-19

Research of zeolites crystallization in the systems SiO_2-Al_2O_3-Na_2O-K_2O-TEA_2O

Golubeva O.Yu., Nikolaeva E.A.
Institute of Silicate Chemistry Russian Academy of Science, Russia, St.Petersburg, nab. Makarova d 2, e1ena_nikolaeva@mail.ruc

Introduction

Currently, more than 5 millions of hypothetical zeolite structures, which existence have been predicted on the basis of various methods of mathematical modeling, are described. A unified approach to the zeolites defined structures synthesis has not yet been developed. Only a few of hypothetical zeolites have been obtained in practice.

One of the hypothetical zeolites is a zeolite located in a series of type Y zeolites having alpha cages as components (see fig.1 A, B). Its existence was predicted on the basis of topological analysis and calculations based on the cellular automaton model [1, 2]. This hypotetical zeolite (ISC-1) is built of giant five-layer clusters containing 384 silicon atoms, with a cubic lattice and 25 Å unite cell size.

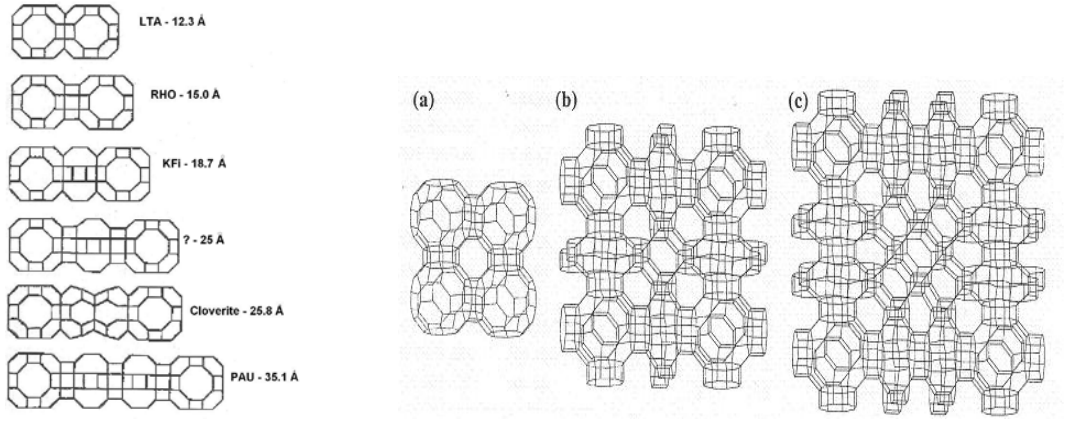

A) B)

Figure1. A)- Building units of zeolites having alpha cages as components. Only one these has nether been synthesized nor found in nature [1]. B)- Zeolites frameworks consisting of nanocomplexes formed as a result of paulingite Cellular Automaton: zeolite Rho: 0-cycle CA (a), hypothetical zeolite ISC-1: 1-cycle CA (b), paulingite: 2-cycle CA (c) [2].

The paulingite structure consists of 7 different cavities, 5 of them form the structure of zeolite predicted. Since the paulingite structure is the closest to the structure of ISC-1 zeolite, its synthesis conditions have been chosen as the base for the research. The aim of this research was to study the zeolites crystallization in the system SiO_2-Al_2O_3-Na_2O-K_2O-TEA_2O, where TEA_2O- tetraethylammonium oxide, in a wide range of SiO_2/Al_2O_3 ratios (from 5 to 19), in order to investigate the possible existence of new zeolites in this system.

Experimental

The following reagents were used for the synthesis: colloidal silica (40%), Sodium hydroxide (NaOH, 50% aqueous solution), potassium hydroxide (KOH, 40% aqueous solution), aluminum sulfate ($Al_2(SO_4)_3$*$18H_2O$, 98%), aluminum hydroxide ($Al(OH)_3$, 100%), tetraethylamonium hydroxide (TEAOH, 35% aqueous solution). The gel composition of the resulting mixture was $x$$SiO_2$:$Al_2O_3$:(0.067$x$)$Na_2O$:$y$$K_2O$:(0.2$x$-$y$)$TEA_2O$:0.3$Na_2SO_4$:15$x$$H_2O$, where x is varied between 5 and 19, y - between 0 and 1. After being kept at room temperature for 3 days, the synthesis mixture was charged into autoclaves and heated at 100^0C, 120^0C and 150^0C for 14-16 days. The samples synthesized were investigated by X-ray diffractometer type D-8 Advance «Bruker».

Results and discussion

Fig. 2 shows the phase variations in system studied as function of changing Si/Al ratio and potassium concentration. The diagrams obtained demonstrate the dependence of phase crystallization on synthesis temperature, Si/Al and K/Al ratios at following constansts: (TEA + K)/Si = 0.2, Na/Si = 0.067, H_2O/Si = 15.

It can be concluded that the studied area of compositions is the crystallization area of zeolites with paulingite, beta, phillipsite and merlinoite structures. Crystallization of these phases depends on the synthesis temperature. At 120^{0}C single-phase paulingite is the crystallization product at a ratio of initial components SiO_2/Al_2O_3=9 and K_2O/Al_2O_3=0.4. The areas of single-phase crystallization of beta and merlinoite are limited by the range of compositions with ratios SiO_2/Al_2O_3 from 6 to 8 and K_2O/Al_2O_3 from 0.6 to 1 for merlinoite and SiO_2/Al_2O_3 from 15 to 17 and K_2O/Al_2O_3 = 0.8 for beta. Increasing the temperature up to 150°C leads to the disappearance of the single-phased merlinoite, beta, paulingite crystallization areas.

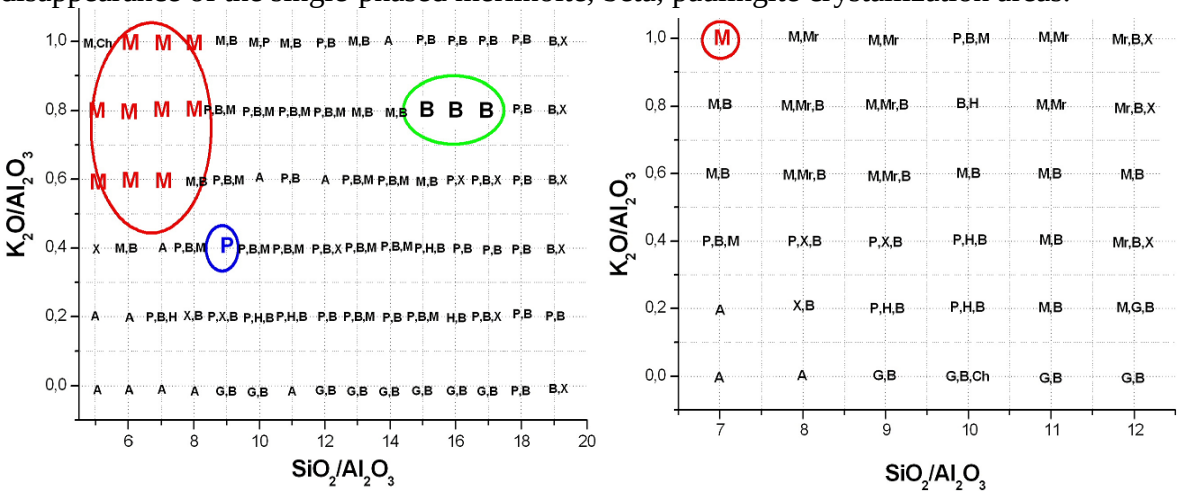

Figure 2. Fields of zeolites crystallization in the system SiO_2-Al_2O_3-Na_2O-K_2O-TEA_2O 120^{0}C (A), 150^{0}C (B). M - Merlinoite, B - Beta, G - Garronite, P - Paulingite, Mr - mordenite, H - phillipsite, Ch - chabazite, X - merlinoite = phillipsite, A - amorphous phase.

The results obtained can be explained by metastability of synthetic zeolites and their transitions to more stable forms depending on the different and often difficult to control factors. As can be seen from fig. 2 paulingite does not always reach a state of thermodynamic equilibrium, forming a mixture of merlinoite (phillipsite) and beta, that may be associated with structural similarity of merlinoite, phillipsite and paulingite and with the presence in them of identical cavities.

Conclusions

The study of zeolites crystallization in SiO_2-Al_2O_3-Na_2O-K_2O-TEA_2O system was made. The dependence of crystallization areas of different zeolite phases on the synthesis temperature SiO_2/Al_2O_3 and K_2O/Al_2O_3 ratios was found. It was establish that in studied area of compositions zeolites with paulingite, beta, phillipsite, merlinoite, mordenite and garonite structures can be crystallized.

Crystallization of these phases is largely determined by the temperature of synthesis. At 120°C single-phase paulingite, merlinoite and beta can be obtained. Increasing the temperature to 150°C leads to the disappearance of the single-phase merlinoite, beta and paulingite crystallization area and to mordenite appearance.

References

1.*Vaughan D., Strohmaier K.* Synthesis of ECR-18 – a synthetic analog of paulingite // Microporous and Mesoporous Materials. 1999. N. 28. p. 233-239.

2.*Shevchenko V., Krivovichev S.* Where are genes in paulingite? Mathematical principles of formation of inorganic materials on the atomic Level // Struct. Chem. 2008. V.19. N.4. p. 571-577.

Preparation of Sn-Beta by secondary methods

Christian Mårup Osmundsen[A,B], Kenny Ståhl[C], Esben Taarning[B]
[A] *Department of Physics, Technical University of Denmark, Anker Engelundsvej 1, 2800 Kgs. Lyngby, Denmark* [B] *Haldor Topsoe A/S, Nymøllevej 55, 2800 Kgs. Lyngby, Denmark*
[C] *Department of Chemistry, Technical University of Denmark, Anker Engelundsvej 1, 2800 Kgs. Lyngby, Denmark. E-mail: chmo@topsoe.dk*

Introduction

Incorporation of tin in a commercial sample of zeolite beta by secondary methods has been performed in order to prepare a Lewis acidic zeolite. These types of zeolites have recently been shown to be highly selective catalysts for a number of reactions, such as MPVO redox reactions [1] and retro-aldol condensations [2]. Especially Sn-Beta has been shown to be a very active and versatile catalyst. Because of the low solubility of tin in alkaline solutions, the catalysts are typically prepared by the fluoride synthesis route using long crystallisation times, typically in excess of two weeks [3]. This makes the preparation of the catalysts cumbersome and time consuming. Using post-synthesis treatment of zeolites it has previously been shown that it is possible to modify the metal composition of zeolites [4,5]. In this work a similar approach has been used to incorporate tin.

Experimental

Two approaches have been pursued to incorporate tin in a dealuminated commercial zeolite beta. In the first approach, the zeolite sample was heated under a flow of nitrogen, at which point a volume of gaseous $SnCl_4$ was slowly introduced into the nitrogen stream. The degree of incorporation was investigated as a function of reaction temperature.
The second approach consisted of performing a secondary crystallisation of zeolite beta by preparing a synthesis mixture resembling that used for the fluoride route [3], although using zeolite beta as the source of silicon. The mixture was crystallized at 140°C, typically for 48 hours. Conditions used for the preparations are shown in Table 1 along with the tin content of the finished catalyst as determined by ICP-OES. Samples G1 to G3 was prepared by the gas phase approach, while H1 to H3 was prepared by secondary crystallisation.

Table 1. Overview of prepared catalysts.

Catalyst	Comment	Tin content [μmol/g]
Sn-Beta	prepared by fluoride route	133
G1	reaction temp. 150°C	34
G2	reaction temp. 150°C	337
G3	reaction temp. 400°C	122
H1	contained 41 μmol/g Al	133
H2	-	216
H3	no template used.	15

The activity of the prepared catalysts were tested in the conversion of dihydroxyacetone, DHA, and sucrose to methyl lactate using previously reported procedures [1,2]. The results of the activity tests are given in Figure 1.

Results and discussion

By contacting dealuminated zeolite beta with $SnCl_4$ it is possible to insert large amounts of tin in the structure as shown by samples G2 and G3. Insertion in sample G1 did not occur to any significant degree; this sample had a lower initial defect concentration, indicating that the metal inserts into defects. Activity tests showed yields from the DHA conversion comparable to catalysts prepared by conventional methods indicating that isomorphous substitution does indeed take place.

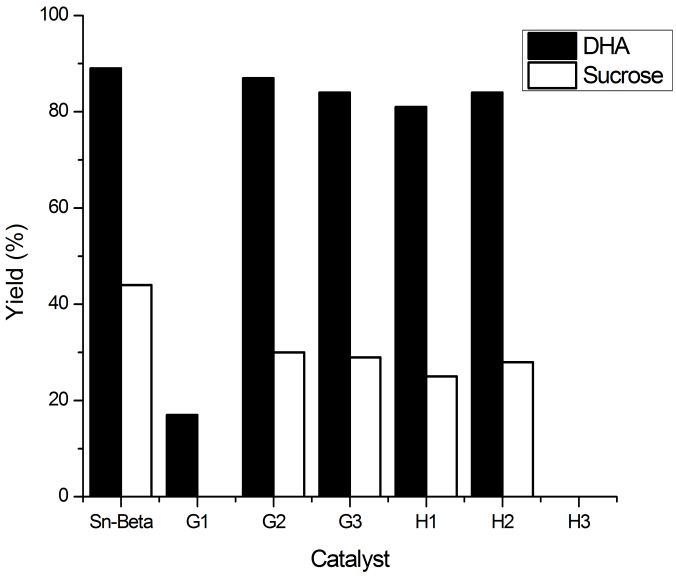

Figure 1: Yields of methyl lactate obtained with dihydroxyacetone, DHA, or sucrose as substrate.

By performing a secondary hydrothermal synthesis it was possible to obtain quantitative incoporation of tin in the sample. The only exception was H3, which was prepared without template. The need for the template to be present could indicate that the tin is incorporated by an Ostwald ripening mechanism. Catalyst H1 was prepared from a zeolite, which was used as recived and thus contained significant amounts of Al, however the expected decrease in methyl lactate yield from sucrose is not observed.

Conclusion

Preparation of Lewis acidic zeolites by traditional approaches is expensive hampering their industrial implementation. It has been demonstrated that secondary methods can be applied when preparring highly active Lewis acidic zeolites. The lower selectivity of these catalysts, as compared to conventionally prepared catalysts, for the production of methyl lactate is likely due to residual framework aluminum and a higher defect concentration. Using secondary methods both the synthesis time and the cost of the finished catalyst can be reduced. These results shows that secondary methods are applicable for incorporating metals with a wide range of ionic radii into zeolite structures, thereby allowing for faster screening of potential catalysts and faster implementation in large scale reactions.

Acknowledgements

The Catalysis for Sustainable Energy initiative is funded by the Danish Ministry of Science, Technology and Innovation

References

[1] Taarning, E. *et al. Chem. Sus. Chem.* **7**, 625–627 (2009).
[2] Holm, M. S., Saravanamurugan, S. & Taarning, E. *Science* **328**, 602–605 (2010).
[3] Renz, M. et al. Chem. Eur. J. 8, 4708–4717 (2002).
[4] Chang, C. D. US Patent No. 4,273,753 (1981).
[5] Krijnen, S. Ph.D. thesis, Technische Universiteit Eindhoven (1998).

Direct *in-situ* synthesis of preferentially *b*-oriented zeolite MFI layers

P. Hrabánek[1*], A. Zikánová[1], J. Drahokoupil[2], M. Matějková[1], I. Jirka[1], L. Brabec[1], V. Fíla[3], B. Bernauer[3], M. Kočiřík[1]

[1]*J. Heyrovský Institute of Physical Chemistry of the ASCR, v.v.i.; Dolejškova 2155/3, 18223 Prague 8, Czech Republic, pavel.hrabanek@jh-inst.cas.cz*
[2]*Institute of Physics of the ASCR, v.v.i.; Na Slovance 2, 18221 Prague 8, Czech Republic*
[3]*Institute of Chemical Technology Prague, Technická 5, 16628 Prague 6 Dejvice, Czech Republic*

Introduction

The optimization of synthesis procedures to prepare preferentially oriented zeolite MFI (ZSM-5 or silicalite-1) layers is a challenging topic. The oriented zeolite layers are attractive for possible applications in the field of membranes [1], microreactors [2], sensors [3] and optoelectronic devices [4]. A thin and fully intergrown *b*-oriented zeolite MFI membrane would exhibit higher fluxes due to an easy access to the straight channels in comparison with a random oriented membrane. It is also known that the orientation of zeolite MFI crystals essentially determines crack formation during template removal, where different expansion/shrinkage properties of silicalite-1 crystallographic axes are responsible. Due to the simplicity and possibility to easily coat the surface of complex geometrical objects such as grains, grids or monoliths, the one step direct *in-situ* hydrothermal synthesis of silicalite-1 layers was the primary focus of this work. The preferentially *b*-oriented silicalite-1 layers were synthesized on mercury surface, silicon wafer, non-porous and porous stainless steel (TRUMEM^{TM}) supports. The optimized synthesis procedures were based on the preparation of *b*-oriented zeolite MFI monolayer films [5]. The optimization was made by the addition of the second colloidal silica source (TOSIL/LUDOX) to promote preferred orientation and crystal intergrowth. The main factors that were observed after the synthesis of silicalite-1 layers included: (i) preferred crystal orientation, (ii) crystal intergrowth and (iii) layer compactness.

Experimental

Zeolite MFI (silicalite-1) crystal layers were hydrothermally synthesized on the surface of mercury, silicon wafer, non-porous, porous stainless steel (TRUMEM^{TM}) and ceramic supports. The optimized synthesis mixtures had a molar ratio of 1 SiO_2 : 0.32 TPAOH: 165 H_2O, where tetraethylorthosilicate and colloidal SiO_2 were used as silica sources in different ratios (TEOS/TOSIL, TEOS/LUDOX) and tetrapropylammonium hydroxide (TPAOH) as a structure directing agent. The synthesis solutions were aged for 4 hours. Particle size distribution of precursor species was measured by Dynamic Light Scattering (DLS) using Zetasizer Nano S. After the ageing, the solution was transferred to 100 ml Teflon-lined autoclaves. The crystallizations of silicalite-1 layers were performed at 165°C with duration of crystallization between 1 to 20 hours. The preferred crystal orientation, intergrowth and layer compactness were evaluated from Scanning Electron Microscopy (SEM, JEOL JSM 5500LV) and X-ray diffraction (XRD, PANalytical X`Pert diffractometer in Brag-Brentano geometry with Co radiation). Crystallographic Preferred Orientation (CPO) indexes were used for comparison between the samples.

Results and discussion

The synthesis solutions composed of two silica sources were optimized with respect to the preferred orientation of silicalite-1 crystals synthesized on different supports. Fig. 1 shows two examples of preferentially *b*-oriented silicalite-1 layer prepared on *P*-doped silica wafer (Fig. 1a) and fine-polished porous stainless steel support (Fig. 1b).

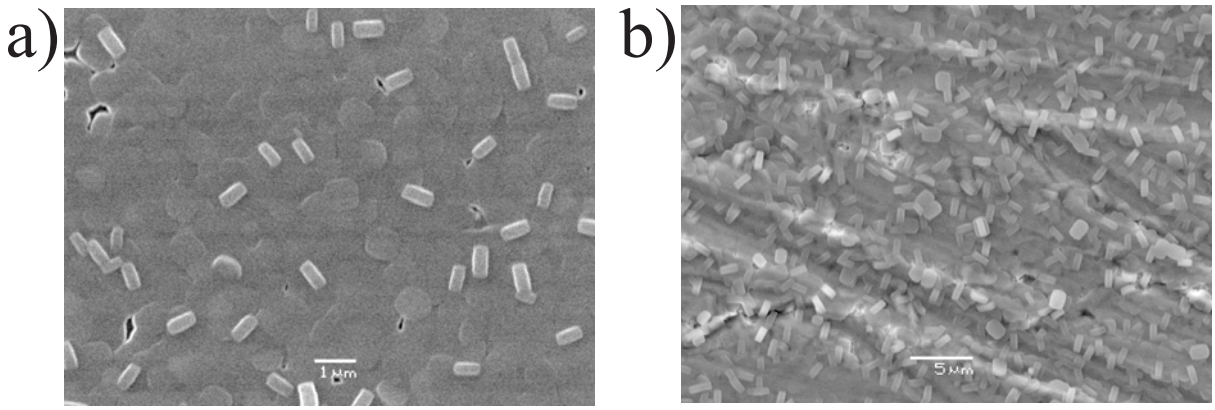

Figure 1. Preferentially *b*-oriented silicalite-1 layers synthesized on *a) P*-doped silica wafer, *b)* fine-polished porous stainless steel support.

The CPO indexes confirmed preferred orientation of zeolite MFI layers prepared on mercury, silica wafer, non-porous and fine-polished porous stainless steel supports.

Conclusions

The preferentially *b*-oriented silicalite-1 layers were prepared on mercury, silicon wafer, non-porous and fine-polished porous stainless steel supports. The synthesis solutions of two silica sources accelerated crystallization and promoted crystal intergrowth based on the observation of self-supported silicalite-1 layers.

Acknowledgements

The financial support by The Grant Agency of the AS CR via grants KAN 400720701 and IAA 400400909 is gratefully acknowledged.

References

[1] Z. Lai, G. Bonilla, I. Diaz, J.G. Nery, K. Sujaoti, M.A. Amat, E. Kokkoli, O. Terasaki, R.W. Thompson, M. Tsapatsis, D.G. Vlachos, Microstructural optimization of a zeolite membrane for organic vapor separation, Science, 300 (2003), 456-460.
[2] A. Eleta, P. Navarro, L. Costa, M. Montes, Deposition of zeolitic coatings onto Fecralloy microchannels: Washcoating vs. in situ growing, Microporous Mesoporous Materials, 123 (2009), 113-122.
[3] K. Sahner, G. Hagen, D. Schonauer, S. Reiss, R. Moos, Zeolites - Versatile materials for gas sensors, Solid State Ionics, 179 (2008), 2416-2423.
[4] G. Calzaferri, Zeolite microcrystals as hosts for supramolecular organization of dye molecules, CHIMIA, 52 (1998), 525-532.
[5] Z. Wang, Y. Yan, Oriented zeolite MFI monolayer films on metal substrates by in situ crystallization, Microporous Mesoporous Materials, 48 (2001), 229-238.

Direct synthesis and characterization of AlSBA-3

Ewa Janiszewska, Stanislaw Kowalak
Faculty of Chemistry, A. Mickiewicz University, Grunwaldzka 6, 60 780 Poznan, Poland,
eszym@amu.edu.pl

Introduction

SBA-type silica materials are ordered mesoporous molecular sieves with higher thermal stability than other MCM-type materials due to the much thicker walls and the contribution of micropores [1]. The microporosity of SBA-3 is more pronounced than those in SBA-15. Thermal and mechanical properties of SBA-3 are promising for their catalytic application [2]. For instance, NbSBA-3 was reported more effective catalyst for oxidative dehydrogenation of propane and oxidation of cyclohexene than the respective NbMCM-41 or NbSBA-15 catalysts [3]. The direct introduction of heteroatoms into the structure of SBA-type materials upon synthesis is very difficult because strongly acidic synthesis conditions [4] impede a formation of metal-O-Si bonds. For AlSBA-15 and AlSBA-1 both post-synthesis alumination and direct synthesis have been reported [5], while for AlSBA-3 only a post-synthesis method has been developed [6]. Here, we report the direct synthesis of AlSBA-3 containing tetrahedral Al and we demonstrate its catalytic activity for the propan-2-ol decomposition.

Experimental

The mesoporous aluminosilicates SBA-3 were prepared using cetyltrimethylammonium bromide (CTABr), tetraethyloorthosilicate (TEOS) and $Al(NO_3)_3 \cdot 9H_2O$ as main starting reagents. HCl was used for adjusting pH of the reaction mixture. CTABr was mixed with diluted HCl and then dissolved aluminium source was admitted. After 15 minutes, TEOS was added gradually (Si/Al = 50) with continuous stirring for next 30 min. and white precipitate was formed. The molar composition of the gel was 1 Si: 0.02Al: 0,27CTABr: 24HCl: 278 H_2O. The typical strongly acidic medium was used for preliminary syntheses. In further experiments pH of the suspension was adjusted to 2.2 or 3.1 value, respectively with aqueous ammonia. Stirring was continued for another 2 h and then the mixture was left at ambient, static condition for 22 h. The resulting precipitate was filtered, dried and calcined in air at 550 ^{o}C. For comparison the same procedure was used for Al-free SBA-3. The obtained samples were characterized by means of XRD, FTIR, elemental analysis ICP-AES, ^{27}Al MAS NMR, BET. The catalytic activity of the samples were examined in the propan-2-ol decomposition and cumene cracking.

Results and discussion

The low angle XRD patterns of the samples synthesized at pH<0 showed three distinct peaks characteristic of SBA-3 structure indicating high ordered mesopore system. The increase in pH of initial mixture resulted in a little lower intensity of XRD reflections and samples prepared at pH 3.1 indicated only one signal corresponding to 100 (hkl) index reflection which illustrated a feeble pore ordering. No distinct diffraction corresponding to any crystalline aluminium and/or silicon oxides are observed at higher angles. The ^{27}Al MAS NMR spectrum confirms the introduction of aluminium to the framework for samples synthesized at higher pH (Fig.1). The peak at 45.1 ppm is assigned to tetrahedrally coordinated Al. The lack of signal at ca. 0 ppm (from octahedral Al) confirms its exclusively tetrahedral coordination. Lack of any signal in the spectra of samples synthesized at pH<0

indicates the absence of any Al in these samples. The elemental analysis of samples synthesized at pH=2.2 indicate much lower Al content (Si/Al=303) than in starting gel. The same observations were reported for Al-bearing SBA-15 or SBA-1 [4,5]. The recorded nitrogen adsorption/desorption isotherms are a type of IV with inflection in the relative pressure range of 0.1-0.35. The surface area slightly decreases with growing pH of the synthesis mixture (regardless of the aluminium presence). The pH does not affect the pore diameter and volume for all silica samples, whereas Al introduced into the structure results in their increase.

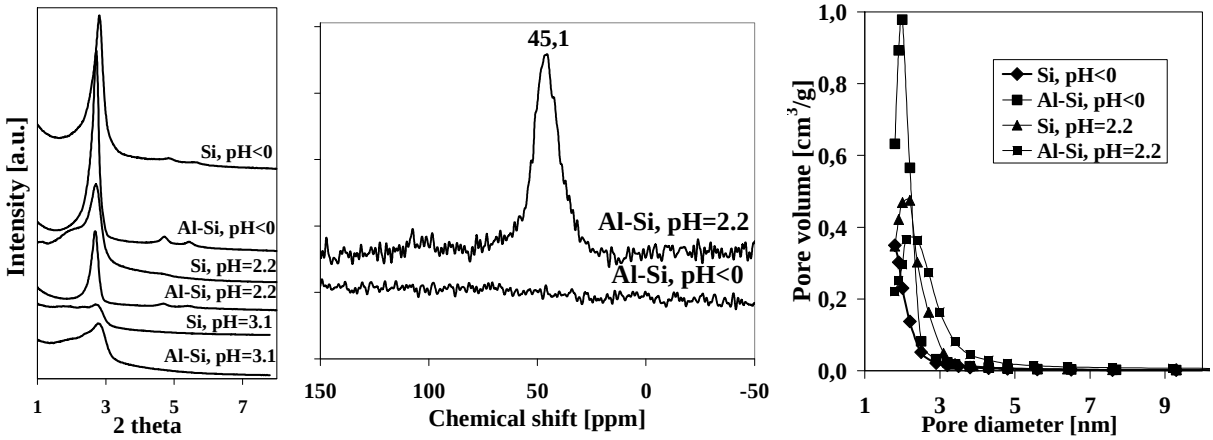

Figure 1. XRD patterns (left), ^{27}Al MAS NMR spectra (middle) and pore size distribution (right) for indicated samples.

The obtained aluminosilicate synthesized at elevated pH shows considerable activity in propan-2-ol dehydration (~60% at 230 ºC) which is in contrast to all silica samples. The activity in cumene cracking is negligible (~4,5%) suggesting the presence mainly weak active centers.

Conclusions

The direct synthesis of SBA-3 mesoporous materials at weaker acidic condition reduce slightly the ordering of mesopores and textural properties of the samples but certainly allows to introduce aluminium into the framework of mesoporous silica SBA-3 material. The ^{27}Al MAS NMR confirms the introduction of Al to the framework for sample synthesized at higher pH, which is reflected in a noticeable catalytic activity in reaction requiring acidic centers.

Acknowledgements

E. Janiszewska appreciates financial support from grant N N204 119238.

References

[1] Xu R., Pang W., Yu J., Huo Q., Chen J., Chemistry of Zeolites and Related Porous Materials: Synthesis and Structure, J. Wiley & Sons (Asia) Pte LTD, Singapore 2007
[2] Galarneau A., Desplantier-Giscard D., Di Renzo F., Fajula F., Catal. Today 68 (2001) 191-200
[3] Kilos B., Tuel A., Ziolek M., Volta J.C., Catal. Today 118 (2006) 416-424
[4] Vinu A., Murugesan V., Böhlmann W., Hartmann M., J. Phys. Chem. B 108 (2004) 11496-11505
[5] Hartmann M., Vinu A., Elangovan S.P., Murugesan V., Böhlmann W., Chem. Commun. 11 (2002) 1238-1239 and references therein
[6] Anunziata O.A., Martinez M.L., Costa M.G., Mater. Lett. 64 (2010) 545-548

FT-IR studies on FAU and MFI type protonic zeolites partially exchanged with alkali-metal cations

Gabriel Fiol Bibiloni, Montserrat Rodríguez Delgado and Carlos Otero Areán
Department of Chemistry, University of the Balearic Islands, E-07122 Palma de Mallorca, Spain. E-mail address: vdqugfb4@uib.es

Introduction

Brønsted acid zeolites constitute an important class of acid solids and they are currently used in a wide variety of industrial applications, mainly in the petrochemical sector and the production of fine chemicals. Brønsted acid strength of the bridging Si-O(H)-Al group is known to depend on several factors, paramount among them being Si:Al ratio of the zeolite framework, local configuration of the acid site and SiOAl angle [1]. Partial exchange of alkali-metal cations for protons is known to be a potential method to tune Brønsted acid strength [2], but the scarcity of systematic studies renders it difficult to attain the needed insight for establishing reliable trends. With a view to expand knowledge in this field, we report on detailed IR spectroscopic studies of FAU and MFI type protonic zeolites partially exchanged with Na^+ and K^+ cations.

Experimental

NH_4-Y (Si:Al = 2.6:1) and NH_4-ZSM-5 (Si:Al = 11.5:1) were used as parent materials. From them, partially alkali-metal exchanged samples were obtained by repetitive cation exchange with an aqueous solution of sodium or potassium nitrate. For IR spectroscopy, a thin self-supported wafer of each sample was prepared and heated under a dynamic vacuum at 650 K for 3h inside an IR cell. This thermal treatment leaves Brønsted acid OH groups (coming from NH_4^+) and simultaneously activates the zeolite. The effect of ion exchange on Brønsted acidity was tested by: (i) the blue-shift of the corresponding O–H stretching band of the unperturbed zeolite, and (ii) the red-shift of the same IR absorption band after interaction of the zeolite with CO (used as an IR probe molecule) at 100 K.

Results and discussion

Representative examples are shown in Fig. 1. In the case of (H,K)-Y, the non-exchanged zeolite (H-Y) shows the characteristic O–H stretching bands at 3644 and 3547 cm^{-1} (Fig. 1a), which correspond to Brønsted acid sites vibrating inside the supercage and inside the sodalite cage, respectively [3]. We will focus here on the band at 3644 cm^{-1}, which corresponds to the only Brønsted-acid OH groups easily accessible by adsorbed molecules. Spectra of partially K-exchanged samples show that this band shifts upwards as a function of K:H ratio, the blue-shift being more pronounced when K:H>0.7:0.3 (inset in Fig. 1a). Such a blue-shift testifies to a decreasing Brønsted-acid strength upon increasing K:H ratio, which was better quantified by the red-shift of the O–H stretching band after hydrogen-bonding interaction with adsorbed CO (shown in the bottom inset of Fig. 1a). Qualitatively, the same trend was found for partially K-exchanged H-ZSM-5 zeolites, as shown in Fig. 1b. Note that the IR spectrum of the purely protonic zeolite shows the Brønsted-acid OH band at 3611 cm^{-1}, while the smaller band seen at 3744 cm^{-1} corresponds to silanols. Corresponding spectra for a series of protonic

zeolites partially exchanged with sodium cations will also be shown. And the whole set of results will be analysed and discussed.

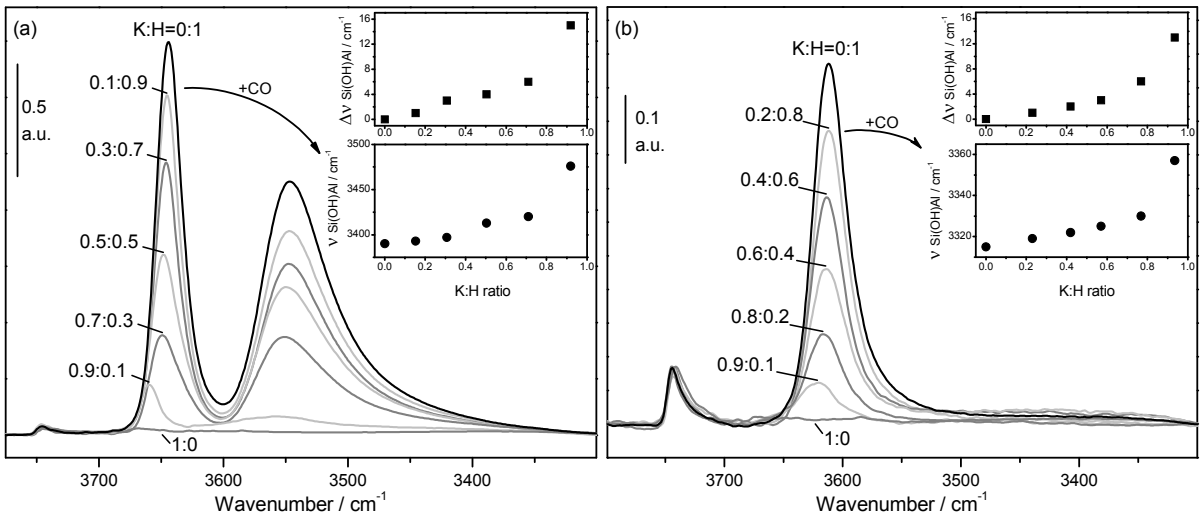

Figure 1. Representative IR spectra in the O–H stretching region of (a) (H,K)-Y and (b) (H,K)-ZSM-5 samples having different K:H ratios. Purely protonic zeolite spectra (H-Y and H-ZSM-5) shown in black. Top inset shows the blue-shift of the Brønsted-acid O–H stretching band versus K:H ratio. Bottom inset shows the red-shift of the Brønsted-acid O–H stretching band as a function of K:H ratio, derived from spectra obtained after adsorption of CO on the zeolite samples (not shown).

Acknowledgements

GFB acknowledges the support from the Conselleria d'Economia, Hisenda i Innovació del Govern de les Illes Balears (pre-doctoral fellowship).

References

[1] Grajciar, L., Arean, C.O., Pulido, A., Nachtigall, P., Periodic DFT investigation of the effect of aluminium content on the properties of the acid zeolite H-FER, Physical Chemistry Chemical Physics, 12 (2010), 1497-1506.

[2] Barthomeuf, D., Ohlmann, G., Pfeifer, H., Fricke, R., Acidity and basicity in zeolites, Studies in Surfaces Science and Catalysis, 65 (1991) 157-169.

[3] Gribov, E.N., Cocina, D., Spoto, G., Bordiga, S., Ricchiardi, G., Zecchina, A., Vibrational and thermodynamic properties of Ar, N_2, O_2, H_2 and CO adsorbed and condensed into (H,Na)-Y zeolite cages as studied by variable temperature IR spectroscopy, Physical Chemistry Chemical Physics, 8 (2006) 1186-1196.

Full compositional flexibility in the preparation of mesoporous zeolites by desilication

Danny Verboekend*, Maria Milina, Sharon J. Mitchell, and Javier Pérez-Ramírez
Institute for Chemical and Bioengineering, Department of Chemistry and Applied Biosciences, ETH Zurich, Wolfgang-Pauli-Strasse 10, CH-8093, Zurich, Switzerland.
**To whom correspondence should be addressed. E-mail:danny.verboekend@chem.ethz.ch.*

Introduction

The promising properties of hierarchical zeolites, *i.e.* zeolites with mesoporosity, have sparked intense effort to improve zeolite utilization in catalysis. Among the numerous methods available to prepare hierarchical zeolites, desilication by alkaline treatment is one of the most widely applied, emerging as a simple and effective approach. In the pore formation process, induced by alkaline treatment, framework aluminum has a regulatory effect, and was therefore labeled "pore directing agent" (PDA). Consequently, a confined molar framework Si/Al window (25-50) was identified leading to optimal introduction of intracrystalline mesoporosity.[1] However, the exact role of the PDA was not established, and the influence of both the Si/Al and NaOH concentration were never fully explored. Herein we demonstrate full compositional flexibility in the preparation of mesoporous zeolites by desilication. We introduce the 'desilication efficiency' to couple the developed mesopore surface area to the weight loss. It is demonstrated that the use of sequential alkaline-acid treatments or the inclusion of external PDAs leads to improved desilication efficiencies.

Experimental

MFI zeolites with Si/Al ratio 10 (Z10), 15 (Z15), 25 (Z25), 40 (Z40), and 1000 (Z1000) were used. Alkaline treatments of the parent zeolites in aqueous NaOH solutions were carried out at 338 K for 30 min with different NaOH concentrations (0.1-1.8 M). In case of silicalite-1 (Z1000), aluminum nitrate, gallium nitrate, or tetrapropyl ammonium hydroxide (TPAOH) was added to the alkaline solution prior to desilication. In the case of Z10 and Z15, some of the alkaline-treated zeolites were subsequently acid treated in 0.1 M HCl at 338 K for 6 h.

Results and discussion

An extended two-dimensional screening of desilication was performed as a function of NaOH concentration (0.1-1.8 M NaOH) and Si/Al ratio (10-1000), which enabled to introduce intracrystalline mesopores into zeolites of virtually all Si/Al ratios (Figure 1a). The introduction of additional mesoporosity (ΔS_{meso}) was evaluated as a function of weight loss, from which the 'desilication efficiency' was derived.[2] Figure 1b shows that the introduction of mesoporosity is optimal around Si/Al=40 and becomes less efficient for high-silica (Si/Al>200) and for high-alumina zeolites (Si/Al<15). Whereas the development of auxilary pores in high-alumina MFI is hampered due to excessive Al deposition (causing micro-and

mesopore blockage), the introduction of mesopores into silicalite-1 crystals is hampered due to the lack of Al (leading to the formation of large mesopores).[3]

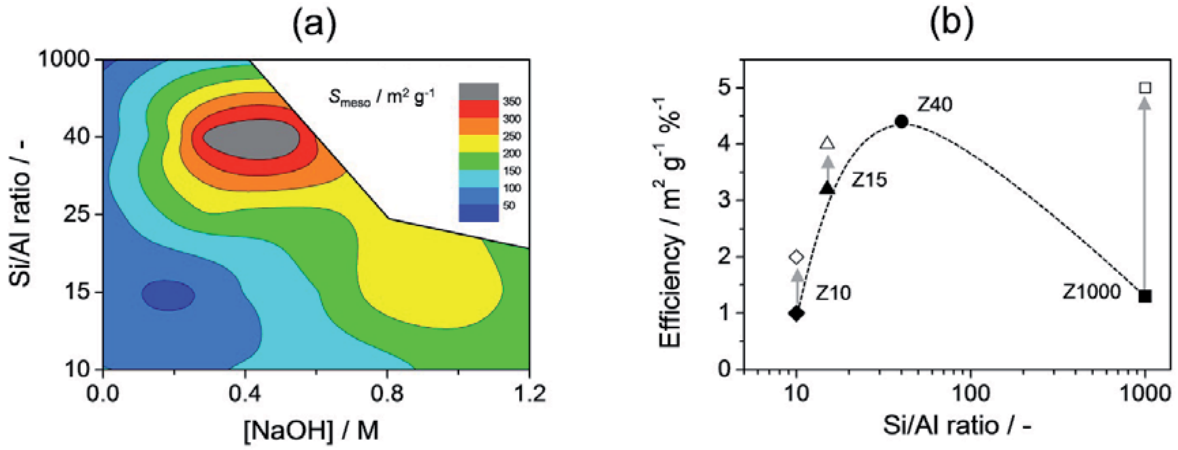

Figure 1. (a) Contour plot of the mesopore surface area obtained after two-dimensional screening of alkaline treatments on various ZSM-5 zeolites. The influence of Si/Al ratio is presented on the (*y*-axis) and the concentration NaOH of the alkaline solution is varied on the (*x*-axis). (b) The desilication efficiency plotted as a function of Si/Al ratio. The desilication efficiency is defined as mesopore surace area per percentage of weight loss (m^2 g^{-1} $\%^{-1}$). Open symbols indicate the increased desilication efficiency due to either an additional acid wash (Z10, Z15), or the use of external pore directing agents (Z1000).

A subsequent acid treatment performed on alkaline-treated high-alumina zeolites led to the removal of extra-framework aluminum, exposing all mesopores and fully restoring microporosity. On the other hand, the use of external PDAs, deliberately added to the alkaline solution, *e.g.* $Al(OH)_4^-$, $Ga(OH)_4^-$, or TPA^+, enabled to increase the efficiency of desilication of silicalite-1.[4] Figure 1b shows that thereby the desilication efficiency window is considerably enhanced. Moreover the use of external PDAs proved that the pore-directing role is not directly exerted by framework trivalent cations metals, but by species on the external surface of the zeolite.

Conclusions

Full compositional flexibility in the preparation of mesoporous zeolites by desilication was demonstrated. Alkaline treatment alone proved, most efficient in within a Si/Al ratio (15-200). In order to efficiently prepare mesoporous zeolites by desilication in the full range, the alkaline treatment should be either followed by an acid treatment (Si/Al<15) or the alkaline solution should be complemented with external PDAs (Si/Al>200).

References

[1] J. Pérez-Ramírez, C.H. Christensen, K. Egeblad, C.H. Christensen, J.C. Groen, *Chem. Soc. Rev.* 37 **2008** 2530.
[2] D. Verboekend, A.M. Chabaneix, K. Thomas, J.-P. Gilson, J. Pérez-Ramírez, *CrystEngCom* **2011** accepted.
[3] D. Verboekend, M. Milina, S.J. Mitchell, J.C. Groen, J. Pérez-Ramírez, *J. Phys. Chem. C* **2011** submitted.
[4] D. Verboekend, J. Pérez-Ramírez, *Chem. Eur. J.* 17 **2011** 1137.

Influence of the thermal treatment on the textural properties of hierarchically ordered porous alumina

Aline R. Passos, Leandro Martins*, Celso V. Santilli
*Institute of Chemistry, Universidade Estadual Paulista - UNESP, PO Box 355, 14800-900 Araraquara - SP, Brazil - * corresponding author: leandro@iq.unesp.br*

Introduction

Alumina is one of the most used inorganic materials in the chemical industry, widely used as adsorbents, catalysts or a catalyst support, and surface coatings in various industrial fields [1].

Significant interest has recently been directed toward the formation of hierarchical porous materials, which are defined as materials that contain a porous structure consisting of interconnected pores on different length scales [2]. Hierarchical porosity provides high surface areas and facilitates mass transport, which can improve a material's performance in many applications [3].

In this work we present a straightforward method of synthesizing porous aluminas through the conjugation of the sol–gel route as well as a dual soft template technique that consists of dispersed oil droplets and block copolymers micelles. By using this strategy, a series of aluminas with hierarchical macro–mesopores and high thermal stability are readily obtained.

Experimental

In a typical synthesis, 1.36 g of the Pluronic P123 surfactant was dissolved in 8.31 g of Milli-Q water at room temperature. After dissolution, 0.16 mL of n-pentanol was added as co-surfactant. Then 2.94 g of aluminum iso-propoxide was further added into the above solution under magnetic stirring followed by the addition of 2.10 g of HNO_3 to catalyze the hydrolysis of the alkoxide to produce aluminum hydroxide. The mixture was stirred at room temperature for 5 h. After the sol preparation, emulsification was performed by adding 22.75 g decahydronaphthalene under stirring. Gelation was induced by adding 1.31 mL of NH_4OH solution (29 wt.%). The gelated emulsions were drying at 50 °C for 2 days and calcined. The crystalline phases present in calcined samples were analyzed by X-ray diffraction powder (XRD). The pore size distribution was then determined from mercury intrusion porosimetry.

Results and discussion

Variation of XRD pattern with heat-treatment temperature is depicted in Fig. 1a. There are no clear reflections in the sample 500 °C, which confirms that the walls of alumina are in principle amorphous. Then the amorphous wall is converted to γ-Al_2O_3 after further treatment at a temperature of 600 °C. With the rise of temperature occurs an increase in the extent of crystallinity, the diffractogram of sample treated at 1000 °C exhibits a relatively high degree of crystallinity. When the heat-treatment is higher than 1000 °C, γ-Al_2O_3 phase diminishes, and instead, α- Al_2O_3 phase appears.

Fig. 1b demonstrates the pore size distributions measured for samples treated at different temperatures using mercury porosimetry. The macroporous structures are not significantly altered by the heat treatment. The median pore size, pore volume and BET surface area are summarized in Table 1. By heat treatment at temperature above 800 ºC, the BET surface area decreases. Simultaneously, the mesoporous volume decrease with increase in calcination temperature.

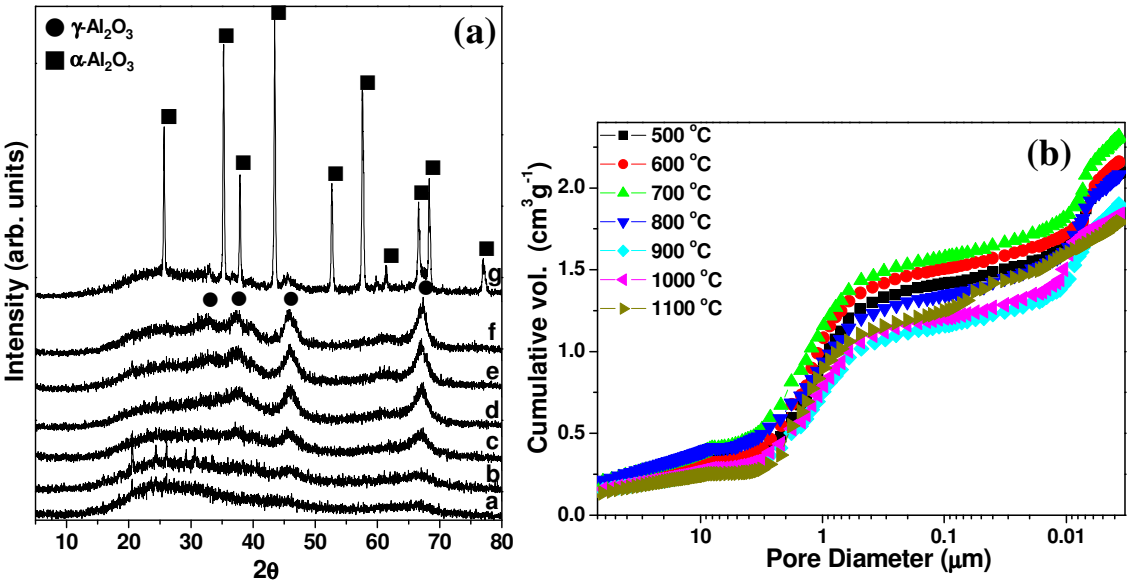

Figure 1. (a) Variation of XRD pattern with heat-treatment temperature, a) 500 °C; b) 600 °C; c) 700 °C; d) 800 °C; e) 900 °C; f) 1000 °C; g) 1100 °C; (b) pore size distribution and cumulative pore volume for samples treated at different temperatures.

Table 1. Pore volume of samples treated at different temperatures.

Heat-treated T(°C)	$D_{macropore}$ (μm)	$D_{mesopore}$ (nm)	$V_{mesopore}$ (cm^3/g)	$V_{macropore}$ (cm^3/g)	A_{BET} (m^2g^{-1})
500	1.3	7.8	0.66	1.05	372
600	1.3	7.3	0.64	1.16	337
700	1.4	8.4	0.74	1.14	346
800	1.2	8.4	0.72	0.91	360
900	1.3	6.4	0.74	0.86	167
1000	1.2	8	0.62	0.91	141
1100	1.4	50	0.51	0.97	22

Conclusions

Macro-mesoporous aluminas with hierarchical structure of pores were synthesized using one-pot pathway based on the dual templating process of pores by micelles and oil droplets. The synthetic technique as described here is very simple and reproducible. The macrostructure has high thermal stability up to a temperature as high as 1100 °C.

Acknowledgements

We are deeply grateful to CAPES, CNPq, and FAPESP for the financial support offered.

References

[1] Sun, Z. X., Zheng, T. T., Bo, Q. B., Du, M., Forsling, W., Effects of calcination temperature on the pore size and wall crystalline structure of mesoporous alumina J. Colloid Interface Sci., 319 (2008) 247-251

[2] Zhao, B., Collinson, M. M., Well-Defined Hierarchical Templates for Multimodal Porous Material Fabrication. Chem. Mater. 22 (2010), 4312–4319.

[3] Drisko, G. L., Zelcer, A., Luca, V., Caruso, R. A., Soler-Illia, G., One-Pot Synthesis of Hierarchically Structured Ceramic Monoliths with Adjustable Porosity. Chem. Mater. 22 (2010), 4379–4385.

Design of macro-mesopores in zirconia ceramics by emulsion templating

Marinalva A. Alves Rosa, Leandro Martins*, Sandra H. Pulcinelli, Celso V. Santilli
*Institute of Chemistry, Universidade Estadual Paulista - UNESP, PO Box 355, 14800-900 Araraquara - SP, Brazil - * corresponding author: leandro@iq.unesp.br*

Introduction

The use of templates to produce pores in materials has attracted the interest of several researchers overall the world. Thereby, emulsions and liquid foams are frequently used to create pores in materials like metals, polymers and ceramics. Surfactants are mostly applied to stabilize the interface liquid-liquid or air-liquid and to form pores in smaller scale of size [1]. When the surfactants are used in high concentration (up to critical micelle concentration, cmc) occurs the formation of micelles that may produce the mesopores (2<d<50nm), whenever they are only formed by surfactants molecules, and also micelles structures with oil or gas inside, forming the macropores (d>50nm) [1,2]. This hierarchical organization of the porous structure is a desirable characteristic for a number of applications, especially in catalysis.

The pores are usually produced by either the drying and thermal treatment of the emulsion and liquid foam that were formed or the solidification of the continuous phase [3]. The gelation of continuous phase around of the liquid droplets or air bubbles has been used to avoid the breakdown of the structure during the drying process. Therefore, the association of sol-gel process to these templates reaches extreme importance to maintain the formed structure [1,2].

Herein, we present a straightforward method to synthesize porous sulfated zirconium oxides through the conjugation of the sol-gel route and a soft template technique that consists of dispersed apolar phase and surfactants, producing an emulsion. With this strategy, a series of zirconium oxides presenting hierarchical macro-mesoporous structure were readily obtained.

Experimental

The sulfated zirconium hydrosol was prepared by mixing two solutions: 1.5 mol/L of $ZrOCl_2.8H_2O$ and 1.5 mol/L of aqueous sulfuric acid, in the 15:1 molar proportion of $Zr:SO_4$. The suspension was dialyzed against distilled water for 24 h. The zirconium concentration was increased from 0.5 to 3.5 mol/L by solvent evaporation. The resulting hydrosols were emulsified under constant stirring in the presence of 10 wt.% of block copolymer Pluronic F-127 ($H(OCH_2CH_2)_{106}(OCHCH_3CH_2)_{70}(OCH_2CH_2)_{106}OH$) as surfactant. The apolar phase used was the decahydronafatalen (DHN). During stirring the gelation was induced by adding sulfuric acid to the sol until reaching the 3:1 molar proportion of $Zr:SO_4$. Finally, the samples were aged for 9 days at room temperature, dried at 55 ºC for 48 h and calcined at 600ºC for 2h.

The samples porosity was measured by Dried-Fluid® picnometry (GeoPyc 1360, Micromeritics). The pore volume (P_{volume}) and the macropores size distribution was determined from mercury porosimetry, using the AUTOPORE III equipment (Micromeritics). BET surface areas (S_{BET}) and mesopore size distribution were estimated by nitrogen physisorption isotherms on equipment supplied by Micromeritics (ASAP 2010). The mesopores size distribution was calculated by BJH method (desorption branch of the isotherms). The scanning electron micrographs were recorded on Philips XL 30 equipment.

Results and discussion

The results are shown in the figure 1. It can observed that the evolution of the samples porosities (figure 1.a) were drastically increased when the surfactant is added and also after the apolar phase inner the system. The standard sample did not have surfactant or apolar phase, it was only the dried and thermal treated sulfated zirconia sol. Porosities up to 90% were obtained in these foams. The mesopores are around 3 and 9 nm (figure 1.b), with two families to samples

20 and 50 wt.% of DHN, due the instability of these emulsions used as template. That behavior is reinforced by the porosity and pore volume, smaller than others. Closed macropores were observed by SEM (figure 1.c) with the wall of the pores like fitted sheets.

The properties of porous zirconia ceramics are listed in table 1. The sample prepared with 60 wt.% of DHN showed high pore volume (1,48 cm^3g^{-1}) and surface area (127 m^2g^{-1}), with three families of macropores. The same behavior was observed for the samples with 30 and 40 wt.% of DHN, and the maximum of surface area to 40 wt.% (175 m^2g^{-1}). All these samples give us an idea about how the stability of the emulsion influences the final properties of the porous ceramics, since they were the most viscous and stable emulsion templates.

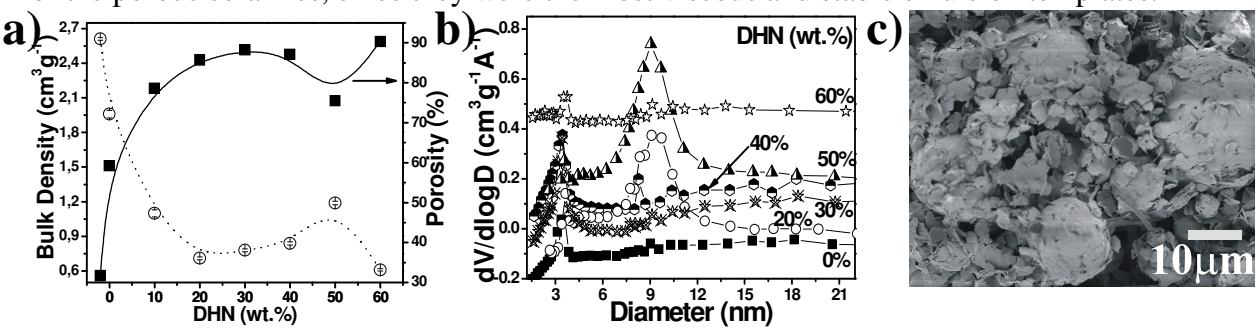

Figure 1. a) Evolution of bulk density and porosity of ceramic foams with the proportion of DHN; b) Mesopores size distribution obtained by N_2 adsorption; c) SEM of sample with 30 wt.% of DHN.

Table 1. Properties of zirconia ceramics.

Sample	P_{volume} (cm^3g^{-1})	S_{BET} (m^2g^{-1})	Pores diameters* (μm)
Standard	0.12	13	0.25
Sol+surfactant	0.30	119	20; 0.1
20 wt.% DHN	1.21	82	75
30 wt.% DHN	1.13	175	23; 1.8; 0.06
40 wt.% DHN	1.03	156	77; 1.8; 0.06
50 wt.% DHN	0.63	53	77; 1.8
60 wt.% DHN	1.48	127	77; 1.8; 0.1

* Macropores families obtained by Hg porosimetry.

Conclusions

Macro-mesoporous zirconium oxides were synthesized by one-pot pathway based on the emulsion templates and on the surfactant micelles templating. The macro-mesoporosity and porosity of such samples can be fine tuned by the proper choice of the apolar phase proportion on the emulsion.

Acknowledgements

We are grateful to CAPES/COFECUB, CNPq, and FAPESP for financial support.

References

[1] Backov, R. Combining soft matter and soft chemistry: integrative chemistry towards designing novel and complex multiscale architectures. Soft Matter, 2 (2006) 452-464.

[2] Martins, L.; Alves-Rosa, M. A.; Pulcinelli, S.H.; Santilli, C.V. Preparation of hierarchically structured porous aluminas by a dual soft template method. Microporous and Mesoporous Materials, 132 (2010) 268 –275, 201.

[3] Studart, A.R.; Gonsenbach, U.T.; Akartuna, I.; Tervoort, E.; Gauckler, L.J. Materials from foams and emulsions stabilized by colloidal particles. Journal of Materials Chemistry, 17 (2007) 3283-3289.

Synthesis, characterization and adsorption properties of functionalized SBA-16 nanoporous materials

Mariusz Barczak, Monika Oszust-Cieniuch, Andrzej Dąbrowski
Faculty of Chemistry, Maria Curie-Sklodowska University, M. Curie-Sklodowska Sq. 5, Lublin 20-031, POLAND, e mail: mbarczak@umcs.eu

Introduction

Nowadays, ordered nanoporous organosilicas constitute a very exciting field in materials chemistry and have numerous potential applications due to their high surface areas, large pore volumes of ordered mesopores and narrow pore size distributions [1,2]. Possibility of introduction of the organic and inorganic groups into the ordered structure of the final material during the synthesis is an additional invaluable advantage of the sol-gel processing of organosilicas [3-6].

In the present work, nanoporous SBA-16 organosilicas were synthesized via co-condensation of tetraethyl orthosilicate (TEOS) with functionalized alkoxysilanes bearing amine, thiol, vinyl, phenyl and cyano groups in the presence of Pluronic F127 as a template. Selected materials were tested as sorbents of bivalent metal ions such as Hg^{2+}, Pb^{2+}, Cu^{2+}, Cd^{2+}, and Zn^{2+}.

Experimental

The SBA-16 materials were obtained by method described in the literature [7]. The SBA-16 materials were characterized by FTIR and Raman Spectroscopy, X-ray diffractomentry, transmisiion ans scanning electron microscopy, thermogravimetry, elemental analysis and nitrogen sorption measurements. Batch adsorption experiment were performed from aquaous solution of metal ions – amounts adsorbed were determined by atomic absorption spectroscopy/UV-VIS spectroscopy/stripping voltamperometry.

Results and discussion

Obtained materials have well-developed ordered mesoporous structure - values of specific surface area are in the range 700-950 m^2/g and pore volumes 0.5-0.9cm^3/g. As it can be seen form the Fig. 1, the isotherms exhibit type IV with sharp capillary/evaporation steps and pronounced H2 hysteresis loops. The condensation step starts at a relative pressure of about 0.75, whereas the evaporation step ends suddenly at about 0.5, which is typical for mesoporous materials containing cage-like pores and narrow pore size distributions (PSDs). It was determined that structural and adsorption properties strongly depends on amounts of monomers co-condensing with TEOS.

The analysis of the XRD and TEM data confirms ordering of the samples while FT-IR/PAS data shows that co-condensation between TEOS and alkoxysilanes was successful and the final samples contain covalently bonded functional groups. The FT-IR/PAS testify to the presence in uncondensed silanol groups and traces of the Pluronic F127 in the final samples after extraction process.

The selected material have been tested as sorbents of Hg^{2+}, Pb^{2+}, Cu^{2+}, Cd^{2+}, and Zn^{2+} ions. Observed static sorption capacities testified to great usefulness of these materials towards effective and selective removal of these ions from wastewaters. Sorption capacities towards selected heavy metal ions are presented in Fig. 2.

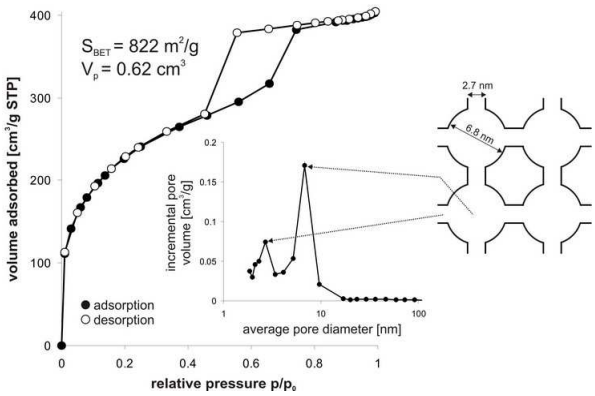

Fig. 1. Nitrogen sorption isotherm and PSD calculated from adsorption branch by BJH method (left), and porous structure of the materials studied (right).

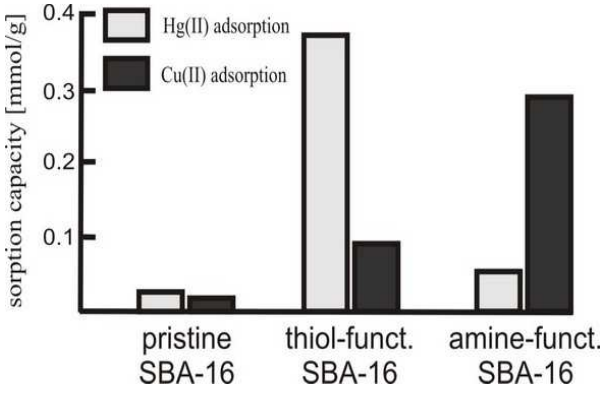

Fig. 2. Sorption capacities of the obtained materials towards selected heavy metal ions.

Conclusions

Highly ordered SBA-16 organosilicas functionalized with amine, thiol, vinyl, phenyl and cyano groups have been obtained by cocondensation of TEOS and proper monomers. These functionalities may be used for further chemical reactions or adsorption of different species. XRD, TEM and nitrogen adsorption/desorption data confirm high degree of ordering. The elemental analysis and FT-IR/PAS data shows that co-condensation between TEOS and alkoxysilanes was successful and the final samples contain covalently bonded functional groups. It was establish that synthesized SBA-16 functionalized with above-mentioned groups can be used as efficient sorbents of bivalent metal ions from liquid phase.

Acknowledgements

Authors thanks to Polish Ministry of Science and Higher Education for supporting the research under Grant No. N N204 111135.

References

[1] Zhao, D., Feng, J., Huo, Q., Melosh, N., Fredrickson, G.H., Chmelka, B.F., Stucky, G.D., Triblock copolymer syntheses of mesoporous silica with periodic 50 to 300 angstrom pores, Science, 279 (1998), 548-552
[2] Zhao, D., Huo Q., Feng J., Chmelka B.F., Stucky G.D., Nonionic Triblock and Star Diblock Copolymer and Oligomeric Surfactant Syntheses of Highly Ordered, Hydrothermally Stable, Mesoporous Silica Structures, J. Am. Chem. Soc., 120 (1998), 6024-6036
[3] Antochshuk, V., Olkhovyk O., Jaroniec M., Park I.-S., Ryoo R., Benzoylthiourea-Modified Mesoporous Silica for Mercury(II) Removal, Langmuir 19 (2003), 3031-3034
[4] Song, S.-W., Hidajat, K., Kawi, S., Functionalized SBA-15 materials as carriers for controlled drug delivery: Influence of surface properties on matrix-drug interactions, Langmuir, 21 (2005), 9568-9575
[5] Liu, A.M., Hidajat, K., Kawi, S., Zhao, D.Y., new class of hybrid mesoporous materials with functionalized organic monolayers for selective adsorption of heavy metal ions, Chem. Commun., 13 (2000), 1145-1146
[6] M. Barczak, E. Skwarek, W. Janusz, A. Dąbrowski, S. Pikus, Functionalized SBA-15 organosilicas as sorbents of zinc(II) ions, Applied Surface Science 256 (2010) 5370-5375
[7] Grudzien, R.M., Grabicka, B.E., Jaroniec, M., Adsorption and structural properties of channel-like and cage-like organosilicas, Adsorption, 12 (2006) 293-308

Effect of crystallization time on the particle size of beta nanozeolites

Saulo de Tarso Figueiredo Grecco[1*], Edilene Deise da Silva[2], Ernesto Antonio Urquieta-González[2] and Maria do Carmo Rangel[1]
[1]*Grupo de Estudos em Cinética e Catálise, Instituto de Química, Universidade Federal da Bahia, Federação. 40170-290. Salvador, Bahia, Brazil.*E-mail: grecco@ufba.br*
[2]*Departamento de Engenharia Química, Universidade Federal de São Carlos. 13565-905 São Carlos, São Paulo, Brazil*

Introduction

Zeolite-based catalysts have been successfully used in many industrial processes due to their special properties such as high specific surface area, high adsorption capacity, molecular dimensions of pores and high thermal and hydrothermal stability [1]. For some applications, their performances are affected by the particle size distribution and crystalline structure and then it is useful to prepare beta zeolite as discrete nano-sized crystals. In a previous work [2], it was reported that the sizes and pores of beta zeolite crystal could be tailored by addition of amphiphilic organosilane into the gel. In the present work, the effect of crystallization time on the size of beta zeolite nanocrystals, obtained through a gel containing amphiphilic organosilane, was studied. The catalysts were evaluated in cyclohexane cracking, as a model reaction.

Experimental

Nanocrystalline beta zeolites were prepared by adding 1.8355 g of [3-(trimethoxysilyl) propyl] octadecyldimethylammonium chloride (TPOAC) to the synthesis gel of conventional beta zeolite. The final molar gel composition was $1.5Na_2O$:Al_2O_3:$30SiO_2$:8.4TEAOH: 1.6TPOAC:$315H_2O$. The mixture was kept under hydrothermal treatment at 150 °C for 24, 48 or 96 h. Then the samples were centrifuged, the gel was washed with water and dried at 60 °C; the solid was calcined at 550 °C, for 6 h. The materials were submitted to three successive ion exchange with ammonium chloride solution 1 mol/L (50 mL/g of solid) at 80 °C, for 3 h. The solids were calcined at 550 °C, for 3 h, producing the beta nanozeolites in the acid form (HB_{TPOAC}-24, HB_{TPOAC}-48, HB_{TPOAC}-96). The catalysts were characterized by X-ray diffraction, nitrogen porosimetry and scanning electron microscopy and evaluated in the cyclohexane cracking at 400 °C and 1 atm.

Results and discussion

The formation of beta zeolite structure was confirmed by X-ray diffraction for all samples. It was also noted that the main peak of microporous structure ($2\theta \approx 22.4$ °) was getting broader and less intense as the crystallization time was decreased, indicating a decrease of the average crystal size. The particle sizes, calculated by Scherer equation, are shown in Table 1. The presence of organosilane led to a decrease of particle size. However, this effect depends on time crystallization; in a general tendency, the particle size decreased with this variable, in the presence of organosilane. These results are in accordance with the increase of the external area. The microporous and mesopores areas also increased due to the decrease of time crystallization. These results show that the decrease of time crystallization leads to a decrease of particle size with higher area of mesopores and micropores. Therefore the specific surface

Table 1. Specific surface area (Sg), area of micropores (Sg_m), external surface area (Sg_{ext}), area of mesopores (Sg_{mp}) and particle size (τ) of beta nanozeolites.

Samples	Sg ($m^2.g^{-1}$)	Sg_m ($m^2.g^{-1}$)	Sg_{ext} ($m^2.g^{-1}$)	Sg_{mp} ($m^2.g^{-1}$)	τ (nm)
HB-48	333	174	159	117	16
$HB_{TPOAC-24}$	467	302	165	108	12
$HB_{TPOAC-48}$	373	252	121	92	14
$HB_{TPOAC-96}$	314	219	95	68	15

area is related to both particle size and porosity. As a result, the highest time crystallization (96 h) led to a sample with the highest particle size and the lowest area of micropores and mesopores, producing the lowest specific surface area. It means that the organosilane is efficient in decreasing the particle size up to 48 h. After this time, the particles grow, regardless its presence. Type I isotherm, characteristic of microporous materials, was found for all samples. Also, the isotherms showed a narrow hysteresis loop of type H4, which is associated with the presence of secondary mesopores, among the particles. The images of scanning electron microscopy showed spherical agglomerates of small crystals with spongy morphology, with sizes close to 1 μm.

All catalysts were active in cyclohexane cracking. The addition of organosilane, during synthesis, caused an increase on conversion, a fact that was related to the decrease of particle size. The catalysts showed selectivity to products of cracking and isomerization reactions. They were selective to hydrocarbons in the following order: C5>C6>C4>C3 and were not selective to olefins. This is because 12-MR zeolites favored bimolecular hydride transfer pathways, which eventually increased the selectivity to light alkanes and to coke at the expense of ethylene and propylene.

Conclusions

The crystallization time (24, 48, 96 h) affects the particle size of beta zeolites, ranging from 12 to 15 nm, for samples prepared by the addition of an organosilane to synthesis gel. The organosilane is efficient in decreasing the particle size up to 48 h; after this time, the particles grow, regardless its presence. The micropores and mesopores areas also increased with decrease of crystallization time. All catalysts were active in cyclohexane cracking and selective to C3, C4, C5 and C6 hydrocarbons; the activity increased with the decrease of particle size.

Acknowledgements

STFG and EDS acknowledge CNPq for the scholarships. The authors thank CNPq and FINEP for the financial support.

References

[1] Corma, A., From microporous to mesoporous molecular sieve materials and their use in catalysis, Chemical Reviews, 97 (1997), 2373-2419.

[2] Venkatesan, C., Aoyama, K., Komura, K., Sugi, Y., A new synthesis route to nano-sized β-zeolite with organic silane containing surfactant, Studies in Surface Science and Catalysis, 174 (2008), 225-228.

Effects of Zeolite Cage Size on the Methanol-to-Olefins Reaction

Yashodhan Bhawe[1], Manuel Moliner-Marin[1], Yu Liu[2], Andre Malek[3], Beata Kilos[3], Mark E Davis[1]*

1California Institute of Technology, Pasadena, CA 91125
2 Hydrocarbon and Energy R&D, The Dow Chemical Company, Freeport, TX 77541
3Chemical Sciences, The Dow Chemical Company, Midland, MI 48640
**mdavis@cheme.caltech.edu*

Introduction

The Methanol-to-Olefins (MTO) reaction utilizes solid acid catalysts, such as silicoaluminates and silicoaluminophosphates, for the conversion of methanol to light olefins. This reaction can be used to obtain lower olefins from non-petroleum sources such as natural gas and coal (that are used to produce methanol). SAPO-34[1], a silicoaluminophosphate with the chabazite framework, has been investigated as a catalyst for this reaction and is the first catalyst to be commercialized. It has been suggested that cages are needed in the framework to promote selectivity to lower olefins[2]. Here, we investigate the effects of changing the size and shape of the cage on the conversion of methanol and the selectivity to ethylene and propylene in particular. The three solids that we studied were zeolites rather than SAPO's and contained contained cages from the LEV, CHA and AFX frameworks. All three cages have 8-membered ring windows, but are of different overall sizes and geometries as shown in Figure 1.

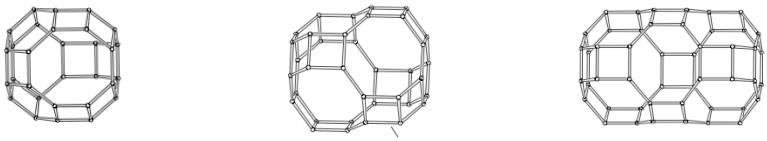

Figure 1: Cages from the LEV, CHA and AFX frameworks (left to right)

Experimental

The materials were synthesized to have similar Si/Al ratios. The compositions of the formed products were measured using an Oxford Inca Energy 300 EDS instrument.
Syntheses: Gels with the compositions shown in Table 1 were prepared and mixed at room temperature. The aluminium source for the CHA and the LEV materials was $Al(OH)_3$, but for the AFX material, it was Na-USY (Si/Al=12). The structure directing agents (SDA) were: N-methylquniclidinium hydroxide, N,N,N-trimethyladamantanamonnium hydroxide and 1,3-Bis(1-adamantyl)imidazolium hydroxide for LEV, CHA and AFX respectively. The syntheses were heated in a rotating oven at the specified temperature for the specified time.
Activation: The solids formed were washed with water, dried to $100^{O}C$, then calcined in air to $580^{O}C$. The structures were determined by XRD analysis and compositions by EDS analysis. The resulting solids were then exchanged with 1M NH_4NO_3.
Catalytic Testing: The zeolite powders were pelletized, crushed and supported on glass wool in a stainless steel flow reactor. The reactor effluent was analyzed on an Agilent 5390 GC/MS system. All tests were conducted with a methanol weight hourly space velocity of $1.3h^{-1}$, a feed concentration of 10% methanol in inert and a bed temperature of $400^{O}C$. The usual catalyst loading was 200 mg.

	Si	Al	NaOH	SDA	H_2O	T(^{O}C)	time
LEV	1	0.04	0.2	0.2	40	170	6 days
CHA	1	0.05	0.2	0.2	44	160	4.5 days
AFX	1	0.06	0.1	0.25	30	150	12 days

Table 1: Composition and reaction conditions for syntheses

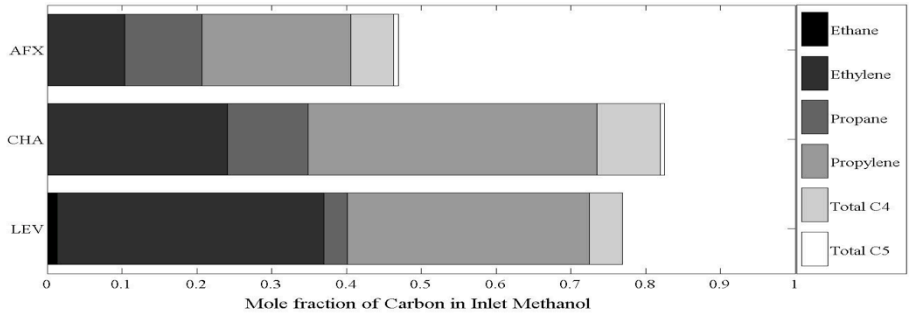

Figure 2: Selectivities after 90 mins. on stream

Results and discussion

The synthesis protocols yielded materials that had similar silicon to aluminium ratios; all materials had Si/Al of 13-16. Figure 2 shows a summary of the selectivities (all at 100% conversion) 90 minutes after the start of reactant flow. First, it can be seen that there is a much greater amount of light olefins and paraffins produced with the smaller cage materials. This is also reflected in the longer catalyst lifetime (3h52m, 4h10m and 1h15m for LEV, CHA, AFX respectively). Second, a trend can be observed with regards to increasing selectivity towards ethylene as the size of the cage gets smaller. Third, it can be seen that the propylene selectivity goes through a maximum at the CHA cage. It has been suggest that the cage geometry in CHA facilitates the formation of a hexamethyl benzenium intermediate[3] required for lower olefin formation in the MTO reaction. It is possible that cages either smaller or larger affect this intermediate. Fourth, the selectivity towards butylene seems to be unaffected by the size of the cage utilized in the reaction.

One possible explanation for the rapid deactivation and consequent low yield of lower olefins and paraffins for the AFX structure is that the coking of the smaller gme cage that is part of the AFX framework, but adjacent to the main aft cage (the rightmost cage in Fig. 1). Second, the larger cage could also rapidly form polycyclic aromatics, that are relatively inert and would not yield the desired products.

Conclusions

This work illustrates how cage size and geometry affect the selectivity for light olefins production from methanol when the size of the pore is not altered. Higher selectivities towards ethylene are obtained with smaller cages. These results suggest that it is the features of the cage with 8-membered ring pores that determine the light olefins selectivities.

Acknowledgements

We would like to thank the Dow Chemical Company for their support of this project.

References

1. B.V. Vora, et. al. in *Fourth Intl Nat Gas Conv Symp, Studies in Surf Sci and Cat*, vol. 107, Elsevier, Amsterdam, 1997, p. 87.
2. D. Chen, et. al. *Micro. and Meso. Mat. 29 (1999) pp 199-203*
3. Haw JF, Marcus DM, *Topics in Catal,* 34, 1-4, (2005) pp 41-48

The effect of the kind of organosilane on the properties of beta nanozeolite-based catalysts

Diego Rodrigues de Carvalho[1], Saulo de Tarso Figueiredo Grecco[1], Edilene Deise da Silva[2], Ernesto Antônio Urquieta-González[2] and Maria do Carmo Rangel[1*]
[1]*Grupo de Estudos em Cinética e Catálise, Instituto de Química, Universidade Federal da Bahia, Federação. 40170-290. Salvador, Bahia, Brazil.*E-mail: mcarmov@ufba.br*
[2]*Departamento de Engenharia Química, Universidade Federal de São Carlos. 13565-905 São Carlos, São Paulo, Brazil*

Introduction

In last years, nanozeolites have attracted much interest, especially for applications in petrochemical industries. By reducing the crystal size of zeolite to nanoscale, the diffusion restrictions of bulky molecules are decreased, besides the increase of specific surface area. These features improve their performance in catalysis, as compared to conventional zeolites. A promising procedure for preparing nanostructured zeolites is based on the functionalization of zeolite seeds with an organosilane, to prevent the growth of crystals during crystallization of zeolite. In a previous work [1], beta and ZSM-5 nanozeolites were successfully prepared using phenylaminopropyltrimethoxylane. In the present work, the influence of the kind of organosilane on the properties of beta nanozeolites was studied. The catalysts were evaluated in cyclohexane cracking, as a model reaction.

Experimental

All samples were synthesized with a molar composition of $30SiO_2/Al_2O_3/30TEAOH/1000\ H_2O$. The following organosilanes were used to functionalize the zeolite seeds: phenyltrimethoxysilane (PHTMS), aminopropyltriethoxysilane (APTES) and phenylaminopropyltrimethoxysilane (PHAPTMS) with a 5 % (mol) of total silicon in the precursor gel. During preparation, the gel was first crystallized at 140 °C, for 24 h; then, the organosilane was added to the gel, which was crystallized at 140 °C, for 48 h. The samples were centrifuged, washed with water and dried at 60 °C; then, they were calcined at 550 °C for 6 h, under air flow. The samples were characterized by X-ray diffraction, nitrogen porosimetry and scanning electron microscopy (SEM). The catalysts were evaluated in the cyclohexane cracking, using a tubular microreactor working at 400 °C, 1 atm and WHSV= 0.54 h^{-1}. The products were analyzed on line by a gas chromatograph.

Results and discussion

The solids showed the X-ray diffractograms typical of crystalline beta zeolite, with peaks at about $2\theta = 5$ and 22°. The presence of organosilane made the peaks broader and less intense, regardless its kind, indicating a decrease of crystal size of beta zeolite. The particle size, calculated by Scherrer equation, changed depending on the kind of organosilane, as shown in Table 1. It can be noted that the particles of the samples prepared with organosilane were smaller than that prepared without it (20 nm). Also, the length of organosilane chain plays a role in preventing the growth of the zeolite crystal. By comparing the NB-PHAPTMS and NB-PHTMS samples, one can see that the first one (higher chain) showed a smaller average crystal size. The hydrophilicity of organosilane also affects the crystal size, as we can see by comparing the NB-PHAPTMS and NB-APTES samples, which show similar particle sizes,

despite the different lengths of organosilane chain. In this case, both compounds have amino groups which are more hydrophilic than the phenyl group of the NB-PHTMS sample. Because of this, the seeds of the NB-PHAPTMS and NB-APTES samples were probably more dispersed, while the seeds of NB-PHTMS sample tend to form larger aggregates, in the aqueous precursor solution. From Table 1, one can see that there is no simple relationship between particle size and specific surface area, indicating the contribution of micropores. Therefore, the NB-PHAPTMS sample has the highest specific surface area because of the highest micropores area. All samples showed Type I isotherm, characteristic of microporous materials, with no significant hysteresis loop. The mesopore volume (Table 1) is mostly related to interparticles pores, typical of nanozeolites. From SEM, spherical agglomerates of small crystals with spongy morphology were detected, which are smaller than 500 nm. All samples were active in the catalytic cracking reaction of cyclohexane and showed. The initial conversion of cyclohexane varied between 40 and 45 % and stabilized at 15 %. The similar conversions can be related to the same SAR of the gel of zeolite seeds, leading to solids with similar acidities. In general, the conversion tends to increase with a decrease in particle size. The catalysts showed selectivity to products of cracking and isomerization reactions, in the following order: C5>C4>C6>C3 and were not selective to olefins, since 12-MR zeolites favor bimolecular hydride transfer pathways, increasing the selectivity to light alkanes and to coke.

Table 1. Specific surface area (Sg), area of micropores (Sg_m), external surface area (Sg_{ext}), micropore volume (V_m), mesopore volume (V_{mp}) and particle size (τ) of nanozeolites beta.

Amostras	Sg ($m^2.g^{-1}$)	Sg_m ($m^2.g^{-1}$)	Sg_{ext} ($m^2.g^{-1}$)	V_m ($cm^3.g^{-1}$)	V_{mp} ($cm^3.g^{-1}$)	T
NB- APTES	307	170	137	0.0852	0.2562	10
NB- PHAPTMS	586	390	196	0.1969	0.2566	12
NB- PHTMS	293	154	139	0.0773	0.2352	16

Conclusions

The kind of organosilane affects the textural properties of nanozeolites. Using phenyltrimethoxysilane (PHTMS), aminopropyltriethoxysilane (APTES) and phenylaminopropyltrimethoxysilane (PHAPTMS) to functionalize the zeolite seeds, in the crystallization step, one can obtain nanozeolites ranging from 10 to 16 nm, with specific surface area ranging from 293 to 586 m2/g. The different effects of organosilane in inhibiting the growing of seeds were related to its chain length as well as to its hydrophilicity. The nanozeolite with the lowest particle size (10 nm) was obtained by using APTES. All catalysts were active in the cracking reaction of cyclohexane and selectivity to hydrocarbons C3-C6.

Acknowledgements

DRC and STFG thank CAPES and CNPq for the scholarships. The authors thank CNPq and FINEP for the financial support.

References

[1] Serrano, D. P., Aguado, J., Escola, J. M., Rodríguez, J. M., Peral, A., Hierarchical zeolites with enhanced textural and catalytic properties synthesized from organofunctionalized seeds, Chemistry Materials, 18 (2006), 2462-2464.

Minimum layer thickness for characteristic zeolite behavior

Elke Verheyen[1], Changbum Jo[2], Johan A. Martens[1], Ryong Ryoo[2], Christine E.A. Kirschhock[1]
1.Center for Surface Chemistry and Catalysis, K.U. Leuven, Kasteelpark Arenberg 23, B-3001 Heverlee, BELGIUM
2. Center for Functional Nanomaterials, KAIST, Daejeon 305-701, KOREA
elke.verheyen@biw.kuleuven.be

Introduction

Intensive research and development have made zeolites a scientific, academic and industrial success-story. However, diffusion limitations due to large particle size often pose problems in many applications. Therefore, it is often not possible to exploit the full potential of zeolite catalysts. Reducing the thickness of zeolite crystals from micrometer to nanometer dimensions can partly eliminate this problem. An interesting question arises from the trend to continuously decrease particle size for applications. How far can the particle size be decreased without losing zeolitic character due to surface relaxation and pore termination? Recently, exceptionally thin sheets of ZSM-5 have been synthesized [1]. Comparison of the catalytic activity of such nanosheets with different thickness was performed to determine the minimum layer thickness for characteristic zeolite behavior.

Experimental

Nanosheet ZSM-5 was synthesized by the method described in literature [1]. Size and interlayer thickness was varied by adjusting the chain length of the structure directing agent (SDA). Using $[C_{22}H_{45}\text{-}N^{+}(CH_3)_2\text{-}C_6H_{12}\text{-}N^{+}(CH_3)_2\text{-}C_6H_{13}]Br_2$ as structure directing agent sample with layer thickness in b direction of 2 nanometer, further denoted as sample 22-66, was synthesized. This thickness corresponds to 1 unit cell along the straight channels of the MFI topology. Increasing the number of quaternary ammonium groups in the SDA to three and four gave rise to thicker layers, denoted as 22-666 and 22-6666 respectively. After calcination the individual layers were aggregated in disordered fashion.

Results and discussion

SAXS measurements of the samples confirmed the presence of disordered aggregates of ZSM-5 layers. Compared to bulk zeolite only the in-plain reflections [h0k] remained in the diffractogram. Due to the small framework thickness the inter-plain reflections along the b-axis were absent. The small angle region revealed broad signatures which related to characteristic distances between and within the layers. Nitrogen adsorption confirmed the presence of mesoporosity between the disordered layers. Structural characterization revealed the layer thickness of sample 22-666 and 22-6666 was very similar despite the different template lengths used for synthesis and for both range from 6 to 8 nanometer.
The acidity of the samples was estimated through pyridine adsorption followed by IR spectroscopy. With decreasing layer thickness a reduced number of Bronsted in favor of Lewis acid sites was observed. This indicates the aluminum on the surface preferably assumed Lewis character.
The catalytic performance was evaluated with the *n*-decane hydroisomerization/hydro-cracking reaction after loading the catalyst with 0,3% Pt. As reference served an industrial ZSM-5 with the same Si/Al ratio, CBV 8014. The conversions of *n*-decane are plotted against the reaction temperature in Figure 1. The layer thickness clearly influenced the catalytic performance. Nanosheets with a thickness ranging from 6 to 8 nm showed improved catalytic

activity due to significantly reduced diffusion limitation. But decreasing the thickness to unit cell dimensions lowered the catalytic conversion and the structure became even less active then the classic ZSM-5. Not only the absolute yield changed with layer thickness, but also the relative distribution of cracked products. ZSM-5 shows a typical symmetric product distribution, as illustrated in Figure 1 [2]. This M-shaped pattern was absent for the thinnest nanosheet. It can be concluded the single-unit-cell layer has lost the characteristics defining a ZSM-5 catalyst.

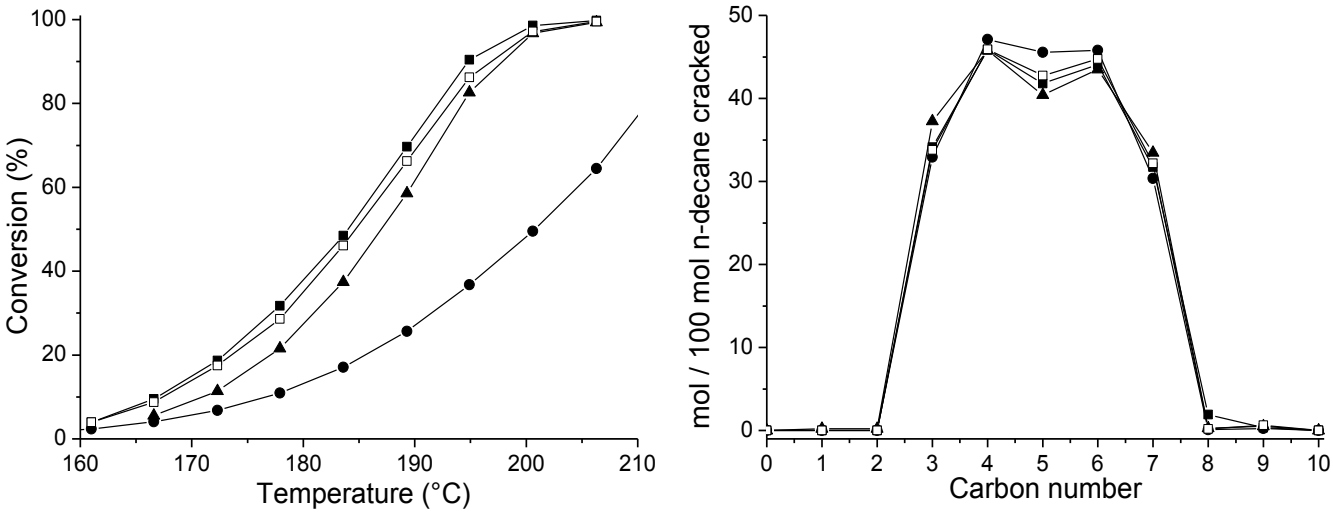

Figure 1 : *n*-decane conversion versus reaction temperature (left) and carbon number distribution of the cracked products of n-decane at 35% cracking yield (right) for the sample CBV 8014 (filled triangle), 22-66 (filled circle), 22-666 (filled square) and 22-6666 (open square).

Conclusions

Compared to bulk ZSM-5 zeolite layered nanosheets exceeding two unit cells in thickness showed increased catalytic activity in the *n*-decane hydroisomerization/hydrocracking reaction. However, a single-unit-cell nanosheet of MFI proved active to a lower degree. This led to the hypothesis that below a limiting size a zeolite loses its characteristic properties.

Acknowledgements

RR acknowledges the National Honor Scientist Program (20100029665) and the World Class University Program (R31-2010-000-10071-0) of the Ministry of Education, Science and Technology in Korea. JAM and CEAK acknowledge financial support by the Flemish Government for long-term structural funding (Methusalem), the Belgian Prodex office and ESA.

References

[1] Choi et al. Nature 461 (2009) 246-249

[2] Jacobs and Martens; Faraday Discuss. Chem. Soc. 72 (1981) 353-369

Study of the influence of basicity and borohydride -nitrate anionic composition in the synthesis of the cancrinite-sodalite system

Freddy Ocanto[1], Francys Torrealba[1], Carlos Felipe Linares[1], Caribay Urbina de Navarro[2]
1) Laboratorio de Catálisis y Metales de Transición. Facultad de Ciencias y Tecnología. Departamento de Química. Universidad de Carabobo. Valencia. Edo. Carabobo. Apartado Postal 3336.Venezuela. 2) Universidad Central de Venezuela, Facultad de Ciencias, Centro de Microscopía "Dr. Mitsuo Ogura", Caracas, Venezuela. ocantof@uc.edu.ve

Introduction

Cancrinites and sodalites are naturally occurring minerals that belong to the feldespathoid group, as well as the zeolite´s family. Both zeolites are comprised of the six ring stacking sequences: ABCABC for sodalite and ABAB for cancrinite. These zeolites can contain diverse anion into framework, which balancing the positive charge generated by structural cations [1]. Due to the structural similarity between both zeolites, they can be synthesized under similar reaction conditions. The formation of cancrinite or sodalite depends on present anion and the basicity of reaction medium during the synthesis process. Anions with threefold rotation axis, such as chromate or carbonate, generally direct the formation of the hexagonal cancrinite structure, while simple monatomic ions, e.g., Cl^-, Br^-, and those with lower symmetry, e.g., NO_2^- generate sodalite framework [2]. Likewise, the concentration of NaOH in reaction gel plays an important role in the synthesis of these zeolites: high concentrations (16 M NaOH) preferably produce sodalite, while medium NaOH concentrations (4 or 8 M) produce cancrinite [3]. This paper represents a contribution to the knowledge over the cancrinite-sodalite synthesis, using a combination of anions (nitrate and borohydride anions) at three different NaOH concentrations (3, 8 and 12 M)

Experimental

Synthesis of cancrinite-sodalite type zeolite system

The used methodology for the synthesis of cancrinite or sodalite was carried out according to the previously reported procedure [4]. Zeolite X, previously characterized (ZX, Strem Chemicals, Si/Al =1.3) was used as silicon and aluminum source. Subsequently, NaOH solutions of different concentrations: 3, 8 and 12 M were prepared. These solutions also contained mixture of nitrates and borohydride anions in different weight proportions: 0, 25, 50, 75 and 100% (nitrate). Then, one gram of zeolite X was impregnated with 10 mL of the before prepared NaOH solutions in Teflon reactor and placed in a convection oven at 80ºC for 24 h without agitation. After that, the solids were washed with abundant water until pH ≅ 7 and dried at 80ºC for 18 h. The solids were characterized by XRD, FT-IR spectroscopy and transmission electron microscopy (TEM).

Results and discussion

The FT-IR spectra of the solids for all NaOH concentrations show that pure nitrate cancrinite is obtained for 100% nitrate salt. Bands at (1424, 682, 622 and 574) cm^{-1} show that the cancrinite structure is obtained, and that nitrate anion is occluded into the solid framework. Similar results were also obtained for 100% borohydride. In that case, borohydride sodalite was produced. When, the nitrate concentration reaches a 50% (50% borohydride), nitrate cancrinite is also produced. For 25% nitrate (75% borohydride) and 3, 8 or 12M NaOH a mixture phases: nitrate cancrinite-borohydride sodalite is observed. This is an special condition where both phases are in competition. Results before mentioned, were also, corroborated by using powder-XRD. For 100% nitrate or 100% borohydride, pure nitrate cancrinite or pure borohydride is respectively obtained. These results were previously reported by FT-IR. On the other hand, nitrate cancrinite was also observed by XRD for a nitrate concentration between 0-50% of nitrate. For this range, does not exist any competition

between nitrate and borohydride anions; and the nitrate anion dominates the formation of nitrate cancrinite. The nitrate is a very strong template anion even in low NaOH concentrations and in presence of the other anions.
For 25% nitrate, XRD results were similar to FT-IR results. Cancrinite and sodalite phases were determined for 8 and 12M NaOH. However, for 3M NaOH and 25% nitrate was observed some traces of zeolite X together cancrinite and sodalite structures. The presence of zeolite X could be attributed to that NaOH was not enough to this zeolite completely reacted. (Fig. 1). TEM studies allowed observing the presence of the hexagonal phase characteristic of cancrinite and sodalite cubic phase. Figure 2 shows several hexagonal phase crystal.

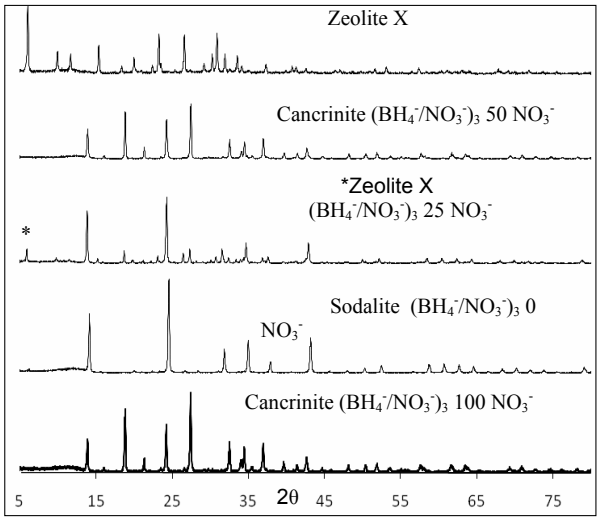

Figure 1. Diffractograms of samples synthesized at 3M NaOH solution and different BH_4^-/NO_3^- concentrations.

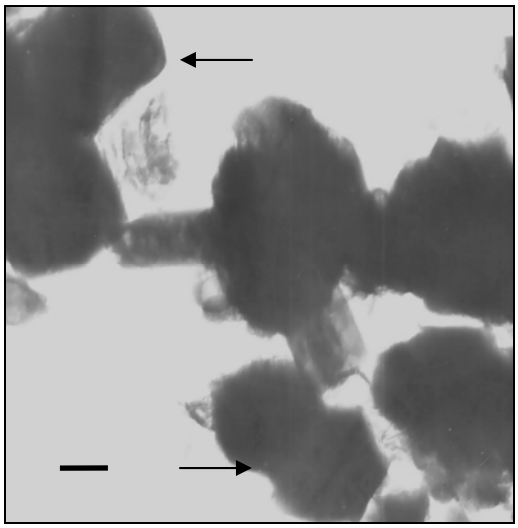

Figure 2. TEM image of sample synthesized at 12M NaOH solution and 50% BH_4^-/NO_3^- concentrations.

Conclusions

The nitrate is shown predominant toward the cancrinite formation until a concentration of 50% under all the used concentrations. For a 75% nitrate concentration and 3, 8 and 12 M NaOH seems to exist a competition between theses anions.

Acknowledgements

This research was supported by CDCH-UC and Project FONACIT Lab Nac 20010001442

References

[1] Barrer, R.; Cole, J.; Villiger, H. J. Chem. Soc. (A), 1516. (1970).
[2] Weller, M. J. Chem. Soc., Dalton Trans. 4227. (2000).
[3] Hermeler G, Buhl J-Ch, Hoffman W (1991) Catal Today 8:415
[4] Linares, C.; Madriz, S.; Goldwasser, M.; Urbina de Navarro, C. Studies in Surface Science and Catalysis. **135**, 331 (2001).

Preparation of Silicon (Oxy)Nitride with Various Regular Mesopore Structures thorough Nitridation of Silica with Ammonia

Fumitaka Hayashi, Ken-ichi Ishizu, Masakazu Iwamoto*
Chemical Resources Laboratory, Tokyo Institute of Technology, Yokohama, 226-8503, Japan
**Corresponding author: iwamoto@res.titech.ac.jp*

Introduction

Silicon nitride has attracted much attention because of its high temperature strength, low density, high dielectric constant, and basic property. Mesoporous silicon nitride (MSN) and oxynitride (MSON) appeared recently as a new class of non-oxide silicon-based mesoporous materials and might have great potentials in fields of catalysis, structural engineering, separation, chemical sensing, and electronics. MSN and MSON are generally prepared by the decomposition of nitrogen-containing silicon compounds, or the replacement of structural oxygen or carbon in mesoporous or mesostructured materials with nitrogen.[1] The previous investigations, however, could not overcome several disadvantages such as the insufficient regularity of mesopore structure and the low contents of nitrogen. Recently, we have developed the new and almost complete nitridation method of M41 with ammonia using a plug-flow reactor at 1273 K.[2,3] Herein, we applied our new preparation method to the nitridation of various mesoporous silicas.[4]

Experimental

The mother mesoporous silica M41-x, M48-x, SBA15 was prepared by hydrothermal treatment of a mixture of the silica source and surfactant, where x is the carbon number of main chain of surfactant used in the preparation. The parent silicas were heated in a flow of ammonia at 1273 K after mounted in a plug-flow reactor. The MSON obtained were named n-M41-x-A etc., where A is the total amount of ammonia per sample weight. The nitrogen contents were determined by a ion chromatography or an IR spectroscopy.

Results and discussion

We first examined the effect of pore diameter on the nitridation using various parent M41 samples (p-M41s) with different pore diameters. The nitrogen content increased monotonously at 0-2000 L_{NH3}/g, and it became constant above 2000. Figure 1 depicts the dependencies of the nitrogen contents of n-M41 samples on the total amount of NH_3 supplied at 1273 K. The maximum nitrogen contents were ca. 38 wt %, which was very close to 40 wt % of Si_3N_4, indicating almost complete nitridation. The figure shows that all of the experimental data on various p-M41s formed an excellent linear correlation line, indicating that the reaction rate of nitridation was independent of the pore size of p-M41.

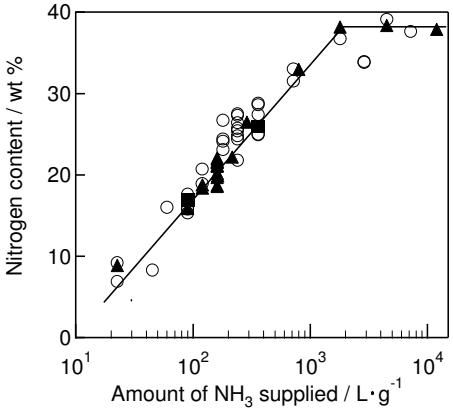

Figure 1. Dependencies of the nitrogen contents of n-M41-12 (open circle), n-M41-16 (closed triangle), and n-M41-22 (closed square) on the amount of NH_3 supplied per sample weight.

The effect of pore structure was then investigated. Two findings should be noted. Firstly, the linear correlations between the logarithmic amount of NH_3 supplied and the nitrogen content were again observed on these samples. Interestingly, the slopes of n-SBA15 and n-M48-16 were approximately the same as that of Figure 1. It follows that the nitridation mechanisms of mesoporous silicas would

be identical and independent of the pore size or the pore structure. The second point is that the maximum nitridation degrees of n-M41-16, n-SBA15, and n-M48-16 were 38, 35, and 39 wt %, respectively, at 2000-3600 L_{NH3}/g and almost the same.

The XRD patterns and the adsorption data of the nitrided samples revealed somewhat shrinkages of the lattices and the pore sizes and the maintenance of the hexagonal and cubic pore structures. The decrements in the lattice constants and the pore diameters through the nitridation were 0.8-1.8 nm and 0.9-2.2 nm. For example, the pore diameters and surface areas of almost completely nitrided n-M41-12, n-M48-16, and n-SBA15 were 529, 515, 363 m^2g^{-1}, and 1.9, 2.0, 8.1 nm. In this case, the thickness of pore walls are 1.2, 1.3, 1.8 nm, respectively, which values were larger by 0.4 nm than that of the respective parent silicas. The FE-SEM and TEM images of n-M41-12-720 and n-SBA15-3600 are shown in Figure 2 as typical examples. The figure clearly indicated preserving of the hexagonally-arranged channels. These results revealed that mesoporous silicas could be converted into mesoporous silicon (oxy)nitrides without essential loss of the regular pore structures.

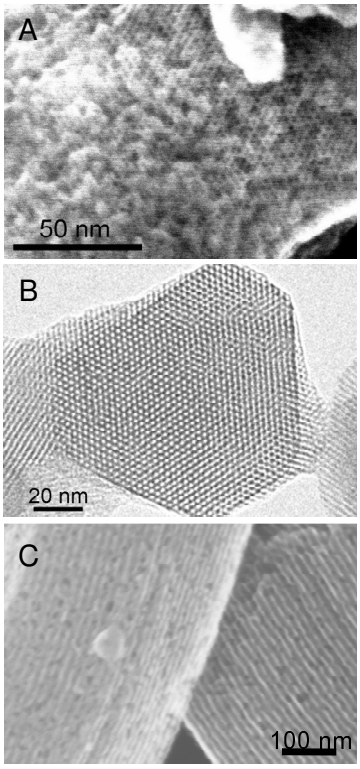

Figure 2. FE-SEM and TEM images of n-M41-12-720 (A, B) and n-SBA15-3600 (C).

At last, the local structures of Si in the nitrided samples were studied by a ^{29}Si MAS NMR spectroscopy. The mesoporous silicas heated at 1273 K in N_2 exhibited strong signals at -90 - -120 ppm. Upon the nitridation treatment, the signals gradually shifted to higher positions and finally got settled at around -50 ppm. The Q^4 species rapidly decreased upon the nitridation treatment and the reactivity of the Q^3 species was somewhat lower than that of Q4. On the other hand, the $SiO_3(NH_2$ or NH) species increased at the initial stage of the nitridation, was maximized at ca. 1 h, and then decreased, indicating the appearance as the intermediate. Similar phenomena were observed in the species, SiO_2N_2, $SiO_2N(NH_2$ or NH), $SiON_3$, and $SiON_2(NH_2$ or NH). Long-term treatment of M41 in ammonia finally yielded ca. 70% SiN_4 species, ca. 20% $SiN_3(NH_2$ or NH), and ca. 10% $SiON_2(NH_2$ or NH). The small amounts of oxygen remaining were consistent with the results of the above elemental analysis.

Conclusions

A family of mesoporous silicon (oxy)nitrides was successfully prepared by nitriding various mesoporous silicas with ammonia using a plug-flow reactor. The nitrogen contents were determined by the amount of NH_3 supplied per sample weight. The maximum nitrogen contents were 35-39 wt %. Characterization revealed the retention of regular pore structures and particle morphology. Since the precise control of pore size, pore structure, and particle morphology of mesoporous silica is well-established, the use of the present method would enable tailor-made synthesis of mesoporous silicon (oxy)nitrides through the conversion of silica into (oxy)nitride.

References

[1] For examples, S. Kaskel, K. Schlichte, *Phys. Chem. Chem. Phys*. 4 (2002) 1675.
[2] K. Ishizu, F. Hayashi, M. Iwamoto, *Chem. Lett*. 36 (2007) 1416.
[3] F. Hayashi, K. Ishizu, M. Iwamoto, *J. Am. Ceram. Soc*. 93 (2010) 104.
[4] F. Hayashi, K. Ishizu, M. Iwamoto, *Eur. J. Inorg. Chem*. 2010, 2235.

Synthesis and characterization of a family of beta zeotypes by an aging-drying method

Farlán Taborda [a *], Tom Willhammar [b], Consuelo Montes de C.[a], Xiaodong Zou [b]
[a] *Environmental Catalysis Research Group, Universidad de Antioquia, SIU, Cra. 53 No. 61-30 Medellín, Colombia.*
[b] *Berzelii Center EXSELENT on Porous materials and Inorganic and Structural Chemistry, Department of Materials and Environmental Chemistry, Stockholm University, SE-106 91 Stockholm, Sweden*
*efata020@udea.edu.co

Introduction

Zeolite beta draws attention because of its unique characteristics, in particular its three-dimensional pore channel system delimited by 12 TO_4 tetrahedral units, as well as, its acidity and acid catalysis. Zeolite beta is a highly faulted intergrowth of two polymorphs, A ($P4_122$ or $P4_322$) and B (C2/c), in a 40:60 ratio approximately [1]. Since polymorph A is chiral, a material enriched with this polymorph could have applications in asymmetric catalysis and chiral separations. In this contribution we report an aging-drying method for the synthesis of Si-beta, Si-Al-beta and Si-Ti-beta, aiming to increase polymorphic A enrichment.

Experimental

Si-beta was synthesized by adding tetraethylorthosilicate (TEOS) to a solution of tetraethylammonium hydroxide (TEAOH) and the mixture stirred at room temperature for a period of 6 to 18 h. Subsequently, hydrofluoric acid was dropwise added under continuous stirring. Ti-Si-beta and Al-Si-beta were synthesized following the above procedure but adding adequate amounts of TiF_4 or AlF_3, respectively, to TEAOH solution. The obtained gels were aged and dried at room temperature during one week. The gel compositions are listed in Table 1. Afterwards, gels were hydrothermally treated at 140 °C for 12 days. The products were filtered, washed with deionised water and dried at 85 °C overnight. The materials were then calcined at 560°C in air. PXRD of as-synthesized samples was carried out using Cu $K\alpha_1$ on a Panalytical MPD PRO X-ray powder diffractometer. A semi-quantitative approximation of the polymorphic A enrichment was ascertained by peak deconvolution of PXRD patterns in the low angle region by means of *X'Pert HighScore Plus 2.2a* software. ^{29}Si HPDEC MAS NMR spectra of calcined samples were recorded on a Bruker AVANCE-II 300 NMR spectrometer at 5 kHz spinning rate, 4 ms excitation pulse, 10 s recycle delay and resonance frequency of 59.63 MHz. FT-IR spectra of calcined samples were collected on a Perkin-Elmer Spectrum One by the KBr technique.

Table 1 Gel compositions and polymorphic A enrichment

Code	Molar batch composition of the starting mixtures	Aging-drying (days)	A/(A+B)% Peak Ratio
Si-12	SiO_2 : 0.54 TEAF: 1.75 H_2O	8	69
Ti-Si-12	SiO_2 : 0.54 TEAF: 1.65 H_2O : 0.02 TiF_4	8	69
Al-Si-12	SiO_2 : 0.54 TEAF: 1.50 H_2O : 0.02 AlF_3	7	64

Results and discussion

Pure and well crystallized beta phases were obtained after heating the aged-dried gels under autogenous pressure. PXRD of as-synthesized samples reveals that the first peak has a small shoulder or spur to the left, which is usually attributed to polymorph A enrichment. The first peak was separated into two peaks, centered around 7.2° and 7.8° 2θ, which could be

associated with polymorph B and A, respectively [2]. Polymorph A enrichment was estimated as the ratio A/(A+B) (Table 1). Additional experiments suggested a directing effect of loaded Al that led to a lower polymorphic A enrichment as could be seen in Table 1.
The ^{29}Si HPDEC MAS NMR spectra of selected samples (Fig. 1) exhibit three peaks at about -113, -114, and -117 ppm. These peaks are due to framework Si atoms in a $Si(OSi)_4$ environment (Q^4 species), located at different crystallographic sites [3]. No distinctive peaks around -100 ppm, which are usually attributed to Q^3 silicate species are observed. Thus, those materials appear to be free of framework defects with low Si connectivity (< 4). Also a significant band broadening was observed for Al-Si-12 zeolite in comparison with the other materials, most likely due to framework distortion by Al incorporation. Meanwhile, Si-12 and Ti-Si-12 NMR spectra are very similar, suggesting that Ti was not incorporated in the beta framework. This assumption is supported by the FT-IR spectrum of Ti-Si-12 sample (Fig. 2), since no band at 960 cm^{-1} is observed. This band is considered a fingerprint of framework Ti incorporation in zeotypes [4]. It could be observed that Si-12 and Ti-Si-12 FT-IR spectra are similar and their band vibrations are consistent with the five-ring pentasil building units of zeolite beta [1]. Regarding Al-Si-12 sample, the FT-IR spectrum confirms a defect-free structure, since it does not exhibit a band around 960 cm^{-1} [4].

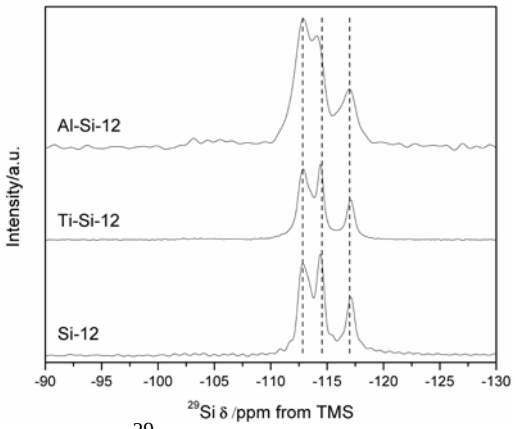

Figure 1. ^{29}Si HPDEC MAS NMR spectra

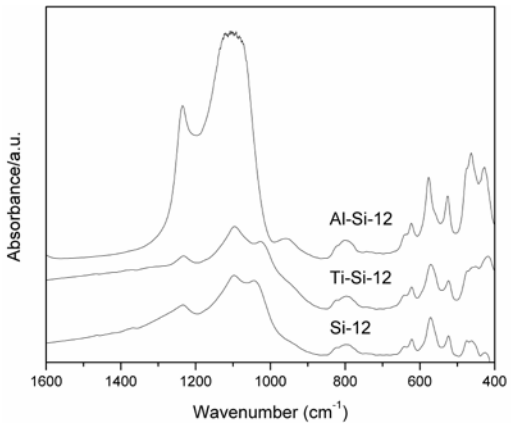

Figure 2. Framework vibration IR spectra

Conclusions

Well crystallized zeotypes with beta framework were obtained by the aging-drying method. Polymorphic A enrichments up to 69% were reached, though Al containing samples exhibited lower polymorphic A enrichement. Beta framework, Al incorporation could be proven whilst Ti incorporation was not accomplished by the synthesis method used in this work.

Acknowledgements

Financial support from Colciencias and UdeA, the Swedish Research Council (VR) and the Swedish Governmental Agency for Innovation Systems (VINNOVA) are grateful acknowledged. F.T. is grateful to Colciencias for a doctoral fellowship.

References

[1] Newsam, J.M., Treacy, M.M.J., Koetsier, W.T., Gruyter, C.B.D., Structural Characterization of Zeolite Beta, Proceedings of the Royal Society of London Series A, 420 (1988) 375.
[2] Takagi, Y., Komatsu, T., Kitabata, Y., Crystallization of zeolite beta in the presence of chiral amine or rhodium complex, Microporous and Mesoporous Materials, 109 (2008) 567.
[3] Fyfe, C.A., Strobl, H., Kokotailo, G.T., Pasztor, C.T., Barlow, G.E., Bradley, S., Correlations between lattice structures of zeolites and their ^{29}Si MAS NMR spectra: zeolites KZ-2, ZSM-12, and Beta, Zeolites, 8 (1988) 132.
[4] Camblor, M.A., Corma, A., Perez-Pariente, J., Infrared spectroscopic investigation of titanium in zeolites. A new assignment of the 960 cm^{-1} band Journal of the Chemical Society, Chemical Communications, (1993) 557.

Interlayer expanded Ti-MWW using different sylicating agents

F. Ferreira Madeira*, H. Imai, T. Yokoi, K. Nomura, T. Tatsumi
Chemical Resources Laboratory, Tokyo Institute of Technology, Japan
**madeira.f.aa@m.titech.ac.jp*

Introduction

Materials science plays a key role in the search for energy-efficient and waste-reducing process solutions. A way to increase the number of potential applications of lamellar materials, such as MWW, is post-modification treatments, such as metal incorporation, exfoliation, swelling, pillaring, etc… A structural change such as Interlayer expansion (IE) amplifies the possible uses of the material to a variety of molecules by allowing access to the active sites for bulky molecules. In this study we have explored the possibility of interlayer expansion for a titanium-containing MWW zeolite. Three different silycating agent were used: diethoxydimethylsilane (DEDMS), dimethoxymethylphenylsilane (DMMPS) and dimethoxydiphenylsilane (DMDPS). In this work, we will fully characterize and discuss the structural changes effected in the materials and its implications regarding their catalytic activity for the cyclohexene epoxidation reaction.

Experimental

Ti-MWW precursor was synthesized by post-synthesis through the reversible structural conversion [1]. Interlayer expansion was performed using 300 – 400 mg of sylicating agent per gram of catalyst under acid conditions using HNO_3 (50 mL per gram of catalyst), at 383 K, under reflux for 24h [2]. Titanium and silica content were measured by ICP. Ti was also characterized by UV-Vis. The insertion of silicating agents in the structure was characterized by IR, TG-DTA and NMR (^{29}Si, ^{13}C, ^{1}H). SEM images allowed us to verify the samples morphology. The materials were tested for the cyclohexene epoxidation reaction using H_2O_2 (in equimolar quantity) as oxidizing agent, at 333 K for 2 h (solvent CH_3CN).

Results and discussion

XRD patterns present low angle diffraction peaks characteristic of a lamellar structure along c-direction. Expansion was calculated from the XRD data (hkl=001) showing an increase of 2.8 (Ti-MWW(DEDMS)) - 3.4 Å (Ti-MWW(DMMPS), (DMDPS)). SEM analysis shows the existence of "thin flakes" and no apparent changes in the crystal morphology were detected after the interlayer expansion treatment (Figure 1). The ^{29}Si NMR analysis showed the shifting of the pure substances (sylicating agents) peaks when in the structure, confirming their incorporation. ^{13}C and ^{1}H NMR spectra confirmed the existence of these agents in the structure, as well as the molecules integrity. These findings were also supported by the IR spectra. More interestingly, IR spectra of the samples synthesized using DMMPS and DMDPS as silycating agents avowed these molecules integrity event at high temperature.

Evidence of the integrity of the aromatic groups was afforded even after treatment at 773 K, under air for 1 h.

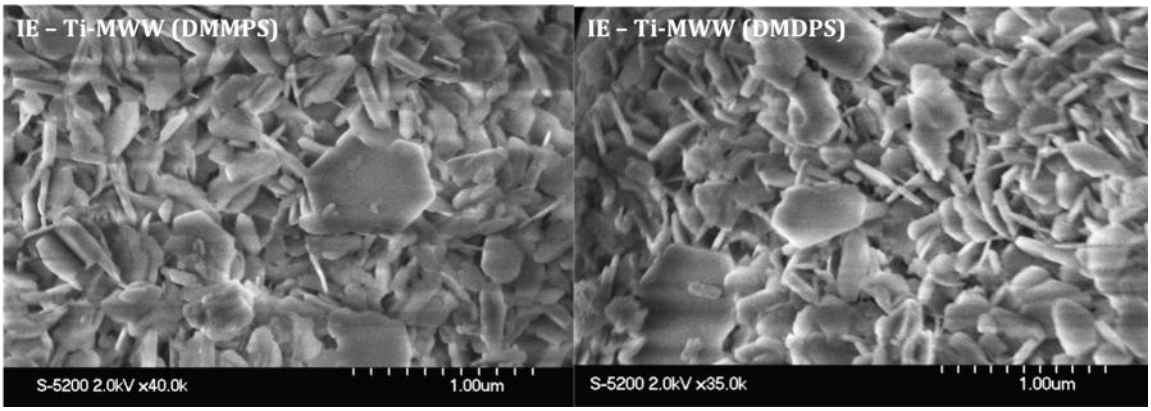

Figure 1. SEM images of interlayer expanded Ti-MWW using DMMPS and DMDPS

UV-Vis spectra allowed us to follow the changes in the state of Ti in the samples. Acid treatment alone removes some of the extra framework species, leaving mainly tetrahedrally coordinated Ti, however, when an interlayer expansion was performed, it appeared also a significant amount of octrahedrally coordinated Ti, and in some cases, a slight formation of anatase phase, which can be prejudicial to the catalytic activity. Nevertheless, the interlayer expanded samples had higher activity than Ti-MWW and excellent selectivity toward the epoxide product (~99%).

Conclusions

Interlayer expansion of titanium-containing MWW material was successfully achieved using DEDMS, DMMPS and DMDPS as sylicating agents. The incorporation of these agents, integrity of the molecules and its effects produced on the structure were fully characterized using XRD, IR, SEM, TG-DTA and NMR (^{29}Si, ^{13}C, ^{1}H) analysis. The catalytic results for cyclohexene epoxidation improved considerably by using the IE samples. All the interlayer expanded samples showed an almost exclusive selectivity towards the epoxide product. Since the active sites, for the epoxidation reaction, are thought to be tetrahedrally coordinated Ti, the results also show us that, in order to maintain a good catalytic activity, the interlayer expansion treatment, in the case of titanium containing MWW, must be optimized (total time of the treatment, acid concentration) in order to find the good balance between the successful insertion of the sylicating agent and a loss minimum of tetrahedrally coordinated Ti.

Acknowledgements

The authors would like to thank the Strategic Japanese-Spanish Cooperative Program for the project funding.

References

[1] Wu,P., Tatsumi, T., Chemical Communications 10 (2002) 1026-1027
[2] Wu,P, Ruan,J, Wang,L, Wu,L, Wang,Y, Liu,Y, Fan,W, He,M, Terasaki,O, Tatsumi,T, JACS 130 (2008) 8178-8187

Synthesis of RTH-type zeolites with various types of organic compounds and their catalytic properties as an acid catalyst

Hiroyuki Imai, Ming Liu, Masato Yoshioka, Toshiyuki Yokoi, Junko N. Kondo, Takashi Tatsumi
Chemical Resources Laboratory, Tokyo Institute of Technology,Yokohama 226-8503, Japan
ttatsumi@cat.res.titech.ac.jp

Introduction

Attention has been focused on the methanol-to-Olefins (MTO) reaction over zeolites such as ZSM-5 and SAPO-34 as one of the ways of producing propene for the recent decades. It has been found that pore sizes of zeolites influence a product distribution in the MTO reaction, and that zeolites with 8-membered ring pores are effective in producing light olefins [1]. Recently, we reported that **RTH**-type zeolites produced propene selectively in the MTO reaction [2]. We also reported the synthesis of the **RTH**-type zeolites in the absence of the structure-directing agents (SDA) [2]. Both of the zeolites synthesized in the presence and in the absence of SDA had apparently the same structures, morphologies and coordination states of introduced metals; however, they exhibited different catalytic properties [2]. SDA in the synthesis process of the zeolite seems to influence physicochemical and catalytic properties.
In this study, we synthesized the **RTH**-type zeolites with various types of SDA or in the absence of SDA, and conducted the MTO reaction over the zeolites to investigate the influence of SDA in the physicochemical and catalytic properties of the synthesized zeolites.

Experimental

RTH-type zeolites were synthesized by using 1,2,2,6,6-pentamethylpiperidine (PMP), 1-methylpiperidine (MP) and pyridine (PY) as a SDA with ethylenediamine (en) as a co-SDA; and in the absence of SDA [2]. The mixed gel containing the molar composition of 1 SiO_2 : 0.005 $Al_2(SO_4)_3$: 0.25 H_3BO_3 : 0.2 NaOH : 0.5 SDA : 2 en : 100 H_2O with 5 wt% calcined boron-containing RUB-13 (**RTH**) as a seed was hydrothermally treated at 170ºC for 7 days. The molar composition was 1 SiO_2 : 0.005 $Al_2(SO_4)_3$: 0.25 H_3BO_3 : 0.2 NaOH : 200 H_2O for the SDA-free synthesis. The obtained sample was calcined at 550ºC for 6 h. The **RTH**-type zeolites synthesized with PMP, MP, PY and in the absence of SDA are denoted by PMP-RUB-13, MP-RUB-13, PY-RUB-13 and TTZ-1, respectively.
The MTO reaction was carried out in the mixture of 5% MeOH and 95% He with the weight hourly space velocity (WHSV) of reactant of 0.9 h^{-1}.

Results and discussion

All samples showed the XRD patterns derived from **RTH** topology. The Si/Al ratios were 207, 190, 187 and 174 for PMP-RUB-13, MP-RUB-13, PY-RUB-13 and TTZ-1, respectively. The solid-state NMR measurement revealed that a peak attributed to tetrahedrally coordinated Al

species were observed on all samples, while no peak derived from octahedrally coordinated Al species was observed. A solid-state NMR with the high magnetic field (600 MHz) was utilized to investigate the environment of Al species in detail (Fig. 1). A peak around 56 ppm was observed on all samples, and another peak around 60 ppm was observed on TTZ-1 and PY-RUB-13 while a shoulder peak was observed around 60 ppm on PMP-RUB-13 and MP-RUB-13. These indicate that there are at least two types of Al species in the framework, and SDA influences the environment of Al species in the framework.

Fig. 2 shows the results of the MTO reaction over the zeolites at 400ºC. Conversion of methanol reached to 100% over three samples synthesized by using SDA at the initial stage of the reaction, and deactivation gradually progressed with the reaction time. Methanol conversion was below 100% even at the initial time of the reaction over TTZ-1. All samples produced selectively propene. On PMP-RUB-13, MP-RUB-13 and TTZ-1, the product distribution was almost retained during the reaction even though methanol conversion became below 100%. On PY-RUB-13, selectivity to propene was below 40% even at the beginning of the reaction and dimethyl ether became a main product after deactivation started. Research concerning the different catalytic behavior depending on the synthesis method is in progress.

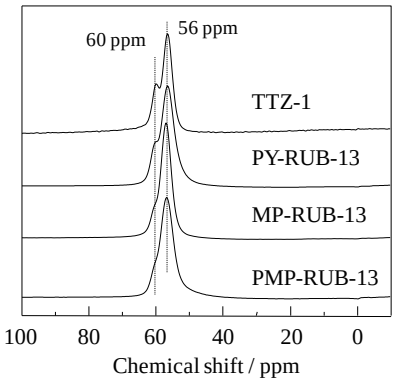

Figure 1. ^{27}Al MAS NMR spectra of the **RTH**-type zeolites (600MHz).

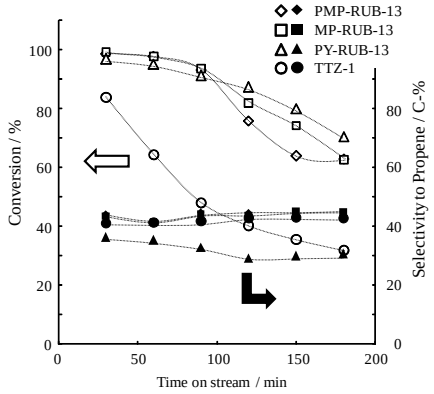

Figure 2. MTO reaction over the **RTH**-type zeolites at 400ºC.

Conclusions

RTH-type zeolites were successfully synthesized with various types of SDA and in the absence of SDA. SDA influenced the environment of Al species in the framework of the zeolites. All **RTH**-type zeolites produced propene selectively on the MTO reaction. However, the catalytic properties depended on the type of SDA used in the zeolite synthesis.

Acknowledgements

This work was partly supported by the green sustainable chemistry project of New Energy and Industrial Technology Development Organization (NEDO).

References

[1] Stöcker, M., Microporous Mesoporous Mater. 29 (1999) 3-48
[2] Yokoi, T., Yoshioka, M., Imai, H., Tatsumi, T., Angew. Chem. Int. Ed. 48 (2009) 9884-9887

OSDA-Free Synthesis of Zeolites: How can we broaden zeolite types?

Tatsuya Okubo*, Keiji Itabashi, Yoshihiro Kamimura, and Atsushi Shimojima
Department of Chemical System Engineering, The University of Tokyo, JAPAN
**okubo@chemsys.t.u-tokyo.ac.jp*

Introduction

Organic structure-directing agents (OSDAs) have enabled us to synthesize zeolites with novel framework types. The number of the framework types approved by the Structure Commission of IZC is more than 190. For the zeolites synthesized with OSDAs, calcination (or alternative process) is indispensable as post-treatment, which causes the increases of the production cost as well as energy consumption and environmental load. Practically, OSDA-free synthesis of zeolites has been one of the most important topics for the commercialization of zeolites. Thanks to the development of OSDA-free routes, several useful zeolites have been commercialized so far.

Recently, exciting topics were reported; several zeolites that had been believed that OSDAs must be used for the synthesis, such as *BEA [1, 2], RTH [3] and MTW [4] zeolites, could be synthesized without adding OSDAs but with seed crystals. We have investigated the OSDA-free synthesis of *BEA zeolite [5]. The synthesis region was further broadened although one synthesis point had been reported so far [1], and the influence of several parameters such as Si/Al ratios of seeds and heating time on the product was elucidated [5]. In the seed-free condition, the gel yielded MOR zeolite after long heating. More importantly, the "green" production was demonstrated by employing the product of the OSDA-free synthesis as seeds [5]. The formation process, especially the role of the seed crystals, was further investigated by carefully observing the intermediate products [6].

Now one of the most important questions is; which zeolites can be synthesized without OSDAs and how can we do so? In this presentation, our successes in broadening the zeolite types are reported, which is based on a working hypothesis with considering composite building units in zeolites.

Experimental

Formation region of *BEA zeolite with the corresponding seed crystals is shown in Fig. 1 [5]. MOR zeolite was formed when no seeds were added [5]. In place of *BEA, MEL or MFI or MOR zeolite crystals were added as seeds. MEL seed crystals were synthesized with an OSDA, which were removed by calcination before the use as seeds.

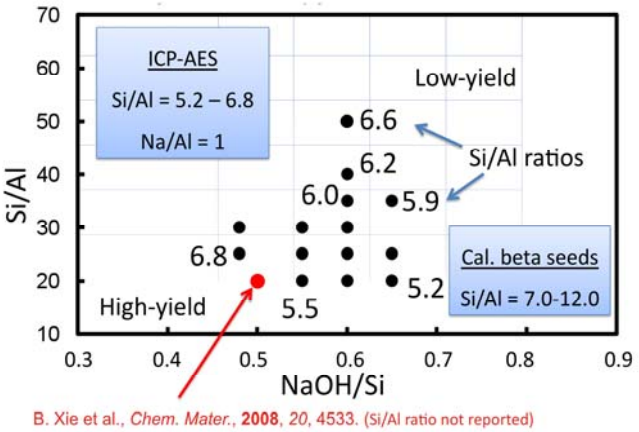

Figure 1 OSDA-free synthesis region of *BEA zeolite.

Results & discussion

XRD patterns for MEL and MFI zeolites are shown in Fig. 2 when each of them was added as seeds. An SEM image of MEL zeolite is shown in Fig. 3. MEL and MFI as well as MOR (not shown here) zeolites could be synthesized with the corresponding seeds from OSDA-free gel system. To the best of our knowledge, this is the first report on the OSDA-free synthesis of MEL zeolite. In the case of MOR zeolite, the crystallization rate was much faster than that of seed-free synthesis.

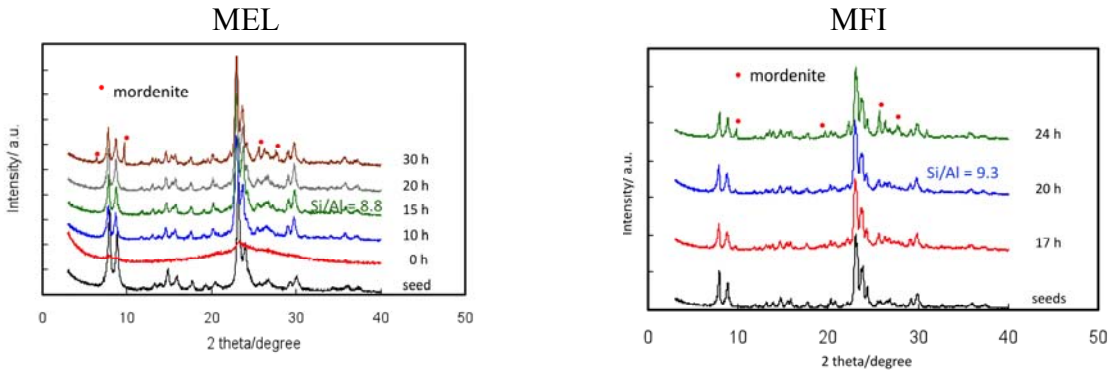

Figure 2 XRD patterns of MEL and MFI zeolites.

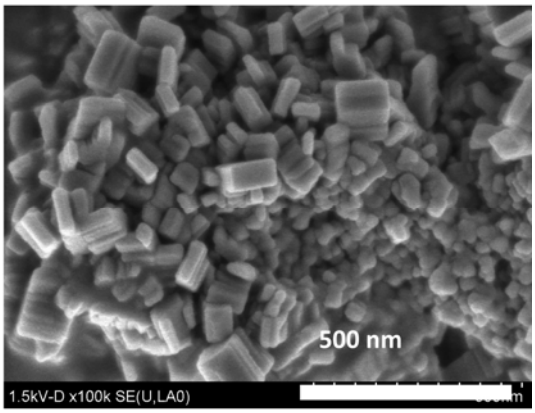

Figure 3 An SEM image of MEL zeolite.

What is common among MOR, *BEA, MFI and MEL zeolites? The structural properties were examined, and a significant feature was found not in the ring distribution level but in the composite building unit level. All the zeolites contain a common composite building unit. Based on this fact, we set a working hypothesis; for the OSDA-free synthesis, a target zeolite should be added as seeds to a gel that yield a zeolite containing a common composite building unit with the seeds when it is heated without seeds. This is a hypothesis to find out suitable synthesis condition, and we are not going to claim that such a composite building unit really exists in the gel prior to the crystallization. Thanks to this hypothesis, several OSDA-free routes have been found out; some of zeolites have never been synthesized without OSDAs.

Conclusions

OSDA-free synthesis of zeolites was successfully broadened from *BEA to other zeolites, and a working hypothesis to find out synthesis condition is proposed. Based on the hypothesis, the zeolite types were further broadened. Several examples not shown here will be introduced in the conference.

Acknowledgements

This work was supported by Grant-in-Aid for Scientific Research from the Japan Society for the Promotion of Science, and Nippon Chemical Industrial Co., Ltd.

References

[1] Xie, B.; Song, J.; Ren, L.; Ji, Y.; Li, J.; Xiao, F.-S. *Chem. Mater.* **2008**, *20*, 4533–4535.
[2] Majano, G.; Delmotte, L.; Valtchev, V.; Mintova, S. *Chem. Mater.* **2009**, *21*, 4184–4191.
[3] Yokoi, T.; Yoshioka, M.; Imai, H.; Tatsumi, T. *Angew. Chem., Int. Ed.* **2009**, *48*, 9884–9887.
[4] Iyoki, K.; Kamimura, Y.; Itabashi, K.; Shimojima, A.; Okubo, T. *Chem. Lett.* **2010**, *39*, 730–731.
[5] Kamimura, Y.; Chaikittisilp, W.; Itabashi, K.; Shimojima, A.; Okubo, T. *Chem. Asian J.* **2010**, *5*, 2182–2191.
[6] Kamimura, Y.; Tanahashi, S.; Itabashi, K.; Sugawara, A.; Wakihara, T.; Shimojima, A.; Okubo, T. *J. Phys. Chem. C* **2011**, *115*, 744–750.

Zeolite Y crystals with trimodal porosity - 3D imaging using electron tomography

Jovana Zečević[1], Heiner Friedrich[1], Cedric J. Gommes[2], Petra E. de Jongh[1], Metin Bulut[3], Sander van Donk[3], Régine Kenmogne[4], François Fajula[4] and Krijn P. de Jong[1]*
[1]*Inorganic Chemistry and Catalysis,Utrecht University, Utrecht (The Netherlands)*
[2]*Department of Chemical Engineering, University of Liège B6A, Liège (Belgium)*
[3]*Total Research Center Feluy, Feluy (Belgium)*
[4]*Ecole Nationale Supérieure de Chimie, Institut Charles Gerhardt, Montpellier (France)*
**k.p.dejong@uu.nl*

Introduction

Zeolite Y is the leading catalyst in various processes such as fluid catalytic cracking, hydrocracking and alkylation. Although the characteristic 3D micropore network of zeolite Y provides unique activity and shape selectivity, it may also induce slow mass transfer of reactants and products. Introduction of mesopores via commonly applied steaming and acid leaching of zeolite Y diminishes diffusion limitations, however those mesopores are relatively large and often present as cavities [1]. Ideal would be a hierarchical pore network, in which small mesopores would facilitate mass transfer from large mesopores into short micropores where catalysis takes place [2]. Here we report for the first time on a zeolite Y with intracrystalline trimodal porosity with micropores (~ 1 nm), small mesopores (~ 3 nm) and large mesopores (~ 30 nm), obtained by a combination of acid and base leaching [3].

Experimental

Starting material (to which we refer as HY-30) was commercially available steamed and acid leached zeolite H-Y (Zeolyst, CBV760). This material was base leached with 0.05 M or 0.10 M NaOH solution for 15 min at room temperature followed by NH^{4+}-ion exchange and calcination to obtain HY-A and HY-B samples respectively. N_2-physisorption isotherms were measured at liquid nitrogen temperature on a Micrometrics Tristar 3000. Electron tomography study (3D-TEM) was performed using a Tecnai 20 transmission electron microscope. Tilt series of images were acquired under bright-field imaging conditions for the angular range of about -75° to +75° with a tilt increment of 1° or 2° at a magnification of 19k or 29k.

Results and discussion

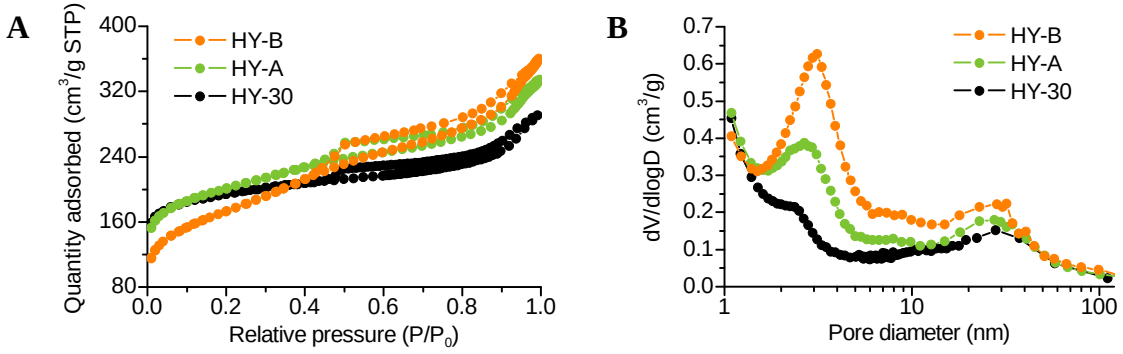

Figure 1. N_2-physisorption analysis of HY-30, HY-A and HY-B samples A) N_2 adsorption and desorption isotherms, B) BJH adsorption dV/dlogD pore size distribution.

N_2 adsorption and desorption isotherms indicate the presence of mesopores within all three samples, increase in total porosity by base leaching and decrease in microporosity for severely treated HY-B sample (Fig. 1a). BJH pore size distributions derived from the adsorption branches of the isotherms depict two distinct regions of small (~ 3 nm) and large mesopores (~ 30 nm), and show that the base leaching boosted predominantly the small mesopores while the volume of large ones increased only slightly (Fig. 1b).
Insight into the pore shape and connectivity was provided by electron tomography [4] yielding 3D-reconstructions of the internal morphology of particles on a nanometer scale (Fig. 2). For sample HY-30 we observed mainly channel-like mesopores with diameters of 20-30 nm. Base leaching slightly increased the diameter of these pores and roughened the surface. More importantly a whole new network of interconnected small mesopores (~3 nm) was observed. More severe base leaching further boosted these small mesopores, as was also clear from N_2-physisorption. In addition, XRD measurements showed that the crystallinity was preserved upon base leaching.

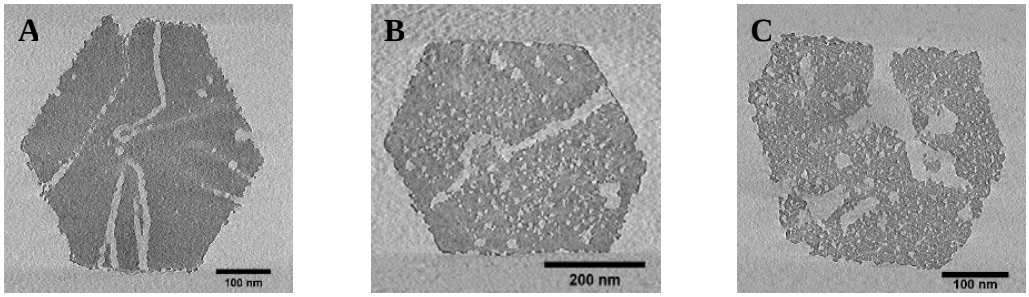

Figure 2. Virtual 0.5-0.8 nm thick cross-sections through 3D reconstructions of particles of A) HY-30 sample, B) HY-A sample, C) HY-B sample.

Conclusions

We have obtained zeolite Y crystals with micropores (~ 1 nm), small mesopores (~ 3 nm) and large mesopores (~ 30 nm) by base leaching of previously steamed and acid-leached material. These zeolite Y crystals with trimodal porosity displayed an improved hydrocracking performance.

Acknowledgements

H. Friedrich and K.P. de Jong acknowledge support from the National Research School Combination Catalysis (NRSCC) and from NWO-CW. P. E. de Jongh acknowledges NWO-Vidi for financial support.

References

[1] Janssen, A.H., Koster, A.J., and de Jong, K.P., On the Shape of the Mesopores in Zeolite Y: A Three Dimensional Transmission Electron Microscopy Study Combined with Texture Analysis, Journal of Physical Chemistry B, 106 (2002), 11905-11909
[2] Hartmann, M., Hierarchical Zeolites: A Proven Strategy to Combine Shape Selectivity with Efficient Mass Transport, Angewandte Chemie International Edition, 43 (2004), 5880-5882
[3] de Jong, K.P., Zečević, J., Friedrich, H., de Jongh, P.E., Bulut, M., van Donk, S., Kenmogne, R., Finiels, A., Hulea, V., Fajula, F., Zeolite Y crystals with trimodal porosity as ideal hydrocracking catalysts, Angewandte Chemie International Edition, 49 (2010), 10074-10078
[4] Friedrich, H., de Jongh, P.E., Verkleij, A.J., de Jong, K.P., Electron Tomography for Heterogeneous Catalysts and Related Nanostructured Materials, Chemical Reviews, 109 (2009), 1613-1629

The integral molar absorption coefficients of Cu^+ carbonyl complexes formed in zeolites

Karel Frolich, Eva Koudelkova, Eva Frydova, Roman Bulanek
Department of Physical Chemistry, Faculty of Chemical Technology, University of Pardubice, Studentska 573, CZ-53210, Pardubice, Czech Republic; karel.frolich@upce.cz

Introduction

Recently it was shown by combination of several experimental techniques and *per*DFT calculations, that after CO adsorption in Cu^+Me^+-FER zeolites (Me = H, Na, K, Cs) the formation of both isolated Cu^+-CO (2156 cm^{-1}) and bridged Cu^+-CO-Me^+ (2138 a 2112 cm^{-1}; Me = K, Cs) carbonyls takes place [1]. The population of bridged complexes formed on so called heterogeneous dual cationic sites, is higher for matrices with larger alkali-metal co-cations and higher Me^+/Cu^+ ratio. This contribution deals with the analysis of FTIR spectra of carbonyl complexes on FER zeolites with varying Cu^+ and co-cation ratio in order to check the validity of Beer-Lambert law (B-L law) in case of such zeolite systems and calculate the corresponding absorption coefficients and quantity of individual carbonyl types.

Experimental

Parent FER matrices with nominal Si/Al ratio 8.6 were calcined in the flow of oxygen and then the alkali metal forms were prepared by the one step ion exchange at 25 °C in 1M aqueous solution of NaCl, KCl, or CsCl. Na^+-FER, K^+-FER and Cs^+-FER samples were then contacted with 5.10^{-4} - 1.10^{-2} M aqueous solution of $CuCl_2$ or $CuAc_2$ (25 °C) to obtain the zeolite samples containing a required amount of Cu ions. The chemical compositions were determined by the WD XRF and correlated with data from H_2-TPR and adsorption of CO obtained from volumetric apparatus. FTIR spectra of carbonyls on CuMe-FER (after Cu^{2+} to Cu^+ *in situ* reduction at 450°C) were collected with resolution 2 cm^{-1} at RT and for comparison of individual samples they were normalized to unitary wafer surface density 7.4 mg/cm^2 (samples 6-11 mg/cm^2) using integral intensity of zeolite skeletal overtones as a benchmark.

Results and discussion

The obtained carbonyl spectra corresponding to monolayer coverage for Cu^+Na^+-FER, Cu^+K^+-FER and Cu^+Cs^+-FER systems are depicted in Fig.1A (the inset of Fig.1A contains spectra normalized to unitary absorbance). Cu^+Na^+-FER zeolites are characterized by formation IR band localized at 2156 cm^{-1} with shoulder at lower wavenumbers. This band reveals constant shape with varying Cu content (related to system Cu^+Na^+-MFI, Ref. [2]). For zeolites Cu^+K^+-FER and Cu^+Cs^+-FER, three spectral components at 2156, 2138 and 2112 cm^{-1} can be recognized, their population is dependent on Cu content in sample (see inset of Fig.1A). According to previous study [1], the high frequency band (2156 cm^{-1}) is due to isolated Cu^+-CO complexes and lower frequency bands (2138 and 2112 cm^{-1}) are ascribed to formation of bridged Cu^+-CO-Me^+ complexes. The overall integral intensity of carbonyl spectra was plotted as a function of adsorbed amount of carbon monoxide, taking to account Cu:CO ratio 1:1 (see Fig.1B). It can be seen, that this plot reveals clear linear relationship for whole range of concentration – Cu^+/Me^+ ratios (the exception is sample Cu^+K^+-FER with low Cu content (0.75E-4 g/mol) and high population of band at 2112 cm^{-1}). Based on this observation it can be concluded, that the ratio of molar absorption coefficients of isolated

Cu^+-CO and bridged Cu^+-CO-Me^+ complexes (with band at 2138 cm^{-1}) is nearly 1. The linear regression of A_{int} vs. n_{ACO} leads to the value of integral molar absorption coefficient ε = 338 (±6) km/mol. The potentialities of transmission IR spectroscopy to calculate the values of absorption coefficient of function groups and adsorbed species on zeolites and oxides was widely discussed in last two decades [3-5]. For similar systems it can reach satisfactory results and can be transferred from one to another. Our contribution extends this topic about the sensitivity of the IR response for carbonyl complexes formed in Cu^+-zeolitic systems and gives the outlook for analysis of the copper forming isolated and bridged complexes.

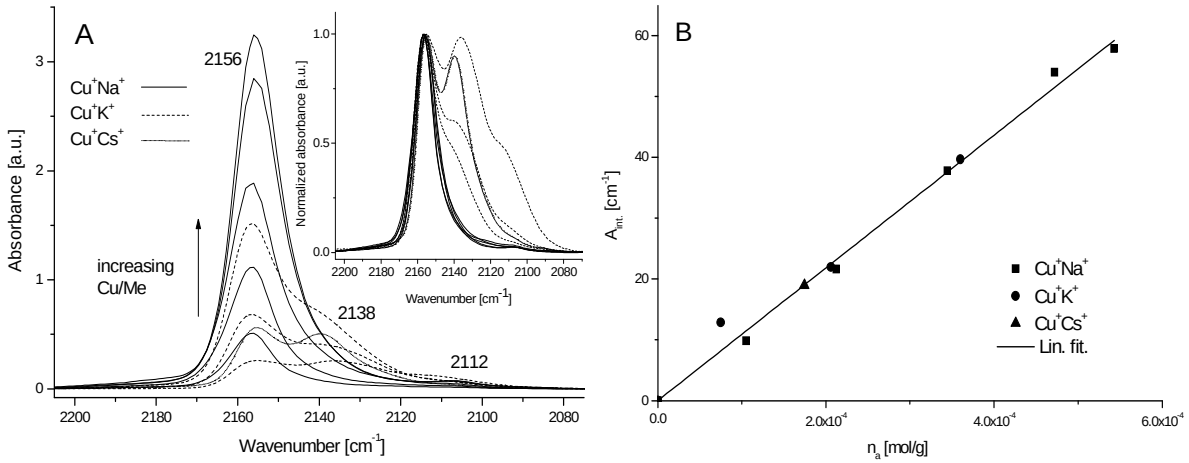

Figure 1. A) FTIR spectra of carbonyls in Cu^+Na^+-FER, Cu^+K^+-FER and Cu^+Cs^+-FER systems; B) Integral intensity of IR bands vs. adsorbed amount of CO

Conclusions

It was shown that the calculation of molar absorption coefficients of adsorbed species can be reasonable, when working with samples having very similar scattering features and comparable surface area and weight. The possibility to use the B-L equations was demonstrated for case of CO chemisorbed in zeolite systems with coordinated monovalent copper and alkali metal.

Acknowledgements

The Grant Agency of Czech Republic (projects No. P208/11/P276 and 203/09/0143) and Ministry of Education (project no. LC512) are acknowledged for financial support.

References

[1] R. Bulanek, K. Frolich, P. Cicmanec, D. Nachtigallova, A. Pulido, P. Nachtigall, J. Phys. Chem. C, submitted
[2] R. Bulanek, Phys. Chem. Chem. Phys., 6 (2004), 4208-4214
[3] E. Garrone, V. Bolis, B. Fubini, C. Morterra, Langmuir 5 (1989), 892.
[4] C. Morterra, G. Magnacca, V. Bolis, Catal. Today, 70 (2001)
[5] I.R. Subbotina, V.B. Kazansky, J. Krohnert, F.C. Jentoft, J. Phys. Chem A, 113 (2009), 839-844

Nb and Ta-FAU zeolites – the effect of preparation procedure on efficiency of metal incorporation and surface properties

Anna Wojtaszek[1,2,3], Maciej Trejda[1], Frederik Tielens[2,3], Maria Ziolek[1]

[1] *Adam Mickiewicz University, Faculty of Chemistry, Grunwaldzka 6, PL-60-780 Poznan, Poland; ziolek@amu.edi.pl*
[2] *UPMC Univ Paris 06, UMR 7197, Laboratoire de Réactivité de Surface - Casier 178, 4, Place Jussieu, F-75005 Paris, France*
[3] *CNRS, UMR 7197, Laboratoire de Réactivité de Surface, Casier 178, 4, Place Jussieu, F-75005 Paris, France*

Introduction

Substitution of zeolite silicon atoms by different metal ions, is of great importance because it can generate unique properties of the materials obtained. Recently Nb and Ta containing FAU zeolites have been successfully synthesised [1,2]. The large cavities in FAU structure and low Si/Al ratio as well as the synthesis without the use of organic template make the incorporation of group V metals relatively difficult. In this work we focus on two parameters in the synthesis route: i) nucleation type (primary or secondary) and ii) types of hydrothermal treatment (conventional or microwave heating). Moreover, we put our attention on the experimental and theoretical evidences for the generation of basicity by the introduction of group V elements into the zeolite.

Experimental

Preparation of Nb or Ta (denoted by X) containing materials of the FAU structure was based on the two-steps procedure (2S) including the mixing of seed and feedstock gels [1,2] and the one step method (1S) adapted from [3]. In the first procedure sodium silicate (Aldrich) was used as Si source, whereas in the second route colloidal silica (Aldrich) was applied. In both routes sodium aluminate (Riede-de Haën) and niobium or tantalum pentaethoxide (Aldrich) were the metal sources and Si/Al = 5 and Si/X = 32 or 64 were assumed in the gel. Hydrothermal treatment of the final gels was performed conventionally in oven or in Parr autoclave or by the use of microwave radiation (Milestone). The catalysts were characterized by XRD, UV-Vis, XRF, XPS techniques. Moreover, FTIR study in the vacuum cell was performed for the identification of hydroxyls on the zeolite surface and pyridine adsorption was used for the assessment of basic vs acidic properties of OH groups. The catalytic activity was tested in acetonylacetone cyclisation performed at 623 K in the gas phase.
In order to investigate the acid-base properties a zeolite model was constructed basing on sodalite. This model has been used with success in other related studies [4-7]. The sodalite unit cell contains one Al atom, one X (X = Nb or Ta) atom, and 10 Si atoms in the framework, and one sodium cation in the extra framework position. Basicity was probed by calculating different descriptors: the protonation energy and dehydroxylation energy. Group V elements were inserted into the zeolite framework in two different types of sites (X=O and X-OH) modelled by a three-dimensional sodalite framework containing Al and Na (counter ion).

Results and discussion

The efficiency of Nb and Ta incorporation into FAU skeleton strongly depends on both parameters studied, nucleation type and methods of hydrothermal treatment. Especially, one has to point out on the importance of the combination of both parameters. The application of two steps (2S) preparation of gel requires the hydrothermal treatment in the oven or autoclave for reaching the well crystallined Y type zeolite. High crystallinity of Y zeolite was also

obtained when the (1S) gel was heated at 373 K in a vessel lined with Teflon using a microwave digestion system. When the mixture of seed and feedstock gels (2S) was hydrothermally treated in the microwave at the same conditions as (1S) the zeolite structure was not formed.

Tantalum is easier included into the faujasite structure than niobium, independently of the methods of gel preparation and thermal treatment. The highest efficiency of Nb and Ta incorporation into Y zeolite skeleton was obtained when (2S) preparation procedure was used and the mixed gels were hydrothermally treated in the oven.

Table 1. Results of acetonylacetone cyclisation

Catalyst	Conversion, %	Selectivity, %	
		DMF	MCP
$Nb_{0.4}Al_{59.3}Si_{132.3}O_x$	23	33	67
$Nb_{1.8}Al_{57.6}Si_{132.6}O_x$	39	3	97
$Ta_{1.7}Al_{56.8}Si_{133.5}O_x$	19	7	93
$Ta_{2.9}Al_{57.5}Si_{131.6}O_x$	56	1	99
$Al_{54.2}Si_{137.8}O_x$	16	73	27

Catalyst – 0.05 g; Acetonylacetone volume – 0.5 cm^3; reaction time – 0.5 h; reaction temp. 623 K; DMF – 2,5- dimethylfuran; MCP – 3-methyl-2-cyclopentenone

Surface properties of NaY zeolites reflect the method of hydrothermal treatment. In case of Nb(Ta)NaY zeolites the catalytic activity and energy of electron charge transfer from oxygen to Nb(V) or Ta (V) in X-O-Si (UV-Vis results) are slightly dependant on the methods of gel preparation and hydrothermal treatment but they are influenced by the number of Nb or Ta introduced into the skeleton of Y zeolite. Nb and Ta incorporation enhances basicity of zeolites. The excess of local positive charge in the zeolite framework, in which Nb(V) or Ta(V) is located, is compensated by basic OH groups (observed in IR spectra). These groups were thought to be active in the formation of MCP in acetonylacetone cyclisation (Table 1). Selectivity to MCP is determined by the number of X atoms and their nature (Nb or Ta). The experimental results were confirmed by the calculation of the energy necessary for abstraction of protons from the reacted molecule (in this study – acetonylacetone) onto the zeolite surface. These calculations allowed us to define even more basic species than X-OH groups. The protonation energy which can be used as a descriptor for basicity is similar for Nb-OH or Ta-OH containing systems. When no aluminium is present in the framework the X-OH group is the most basic site, whereas in the presence of Al the bridging oxygen (Si-O-Al) site becomes the most basic.

Conclusions

The effect of Nb or Ta introduction into the Y zeolite skeleton depends on the methods of gel preparation and techniques of hydrtothermal treatment. The best efficiency was obtained by (2S) method and conventional hydrothermal treatment in the oven. The enhancement of basicity resulted from Nb and Ta incorporation is caused by X-OH formation and promoting effect of X on electron donating properties of bridging oxygen (Si-O-Al).

Acknowledgements

HPC resources from GENCI- [CCRT/CINES/IDRIS] (Grant 2010-[x2010082022]), the CCRE of Université Pierre et Marie Curie**.** COST action D36, WG No D36/0006/06, and Polish Ministry of Science and Education (grant No N N204 201140) are acknowledged for financial support.

References

[1] M. Trejda, A. Wojtaszek, A. Floch, R. Wojcieszak, E.M. Gaigneaux, M. Ziolek, Catal. Today 158 (2010) 170.
[2] M. Trejda, A. Wojtaszek, A. Floch, R. Wojcieszak, E.M. Gaigneaux, M. Ziolek, Stud. Surf. Sci. Catal. 175 (2010) 445.
[3] H. Katsuki, S. Furuta, S. Komarneni, J. Porous Mater. 8 (2001) 5.
[4] F. Tielens, S. Dzwigaj, Phys. Chem. Lett. 501 (2010) 59.
[5] A.E. Lewandowska, M.A. Banares, F. Tielens, M. Che, S. Dzwigaj, J. Phys. Chem. C 114 (2010) 19771.
[6] F. Tielens, T. Shishido, S. Dzwigaj, J. Phys. Chem. C 114 (2010) 9923
[7] F. Tielens, T. Shishido, S. Dzwigaj, J. Phys. Chem. C 114 (2010) 3141.

Preparation and in situ spectroscopic characterization of Cu-Clinoptilolite catalysts for the oxidative carbonylation of methanol

Roxana Pérez Vélez[a], María P. Elizalde Gonzáles[a], Ursula Bentrup[b]
[a]*Centro de Química de la Benemérita Universidad Autónoma de Puebla, Mexico*
[b]*Leibniz-Institut für Katalyse e.V. an der Universität Rostock, Germany*
ursula.bentrup@catalysis.de

Introduction

Clinoptilolite is the most abundant natural zeolite showing a framework structure with a two-dimensional channel system. Although clinoptilolite is a potential heterogeneous catalyst with a unique framework structure, only few studies concerning characterization of transition-metal-modified clinoptilolites and their application in heterogeneous catalyzed reactions have been reported. Otherwise, several Cu containing zeolite catalysts have been applied for dimethyl carbonate (DMC) synthesis finding promising results for Cu^{+}-Y zeolites [1-3]. DMC is an important gasoline additive and chemical, which is normally produced by phosgenation of methanol [4]. One alternative environmentally benign process could be the oxidative carbonylation of methanol to dimethyl carbonate, based on the catalytic gas phase reaction of methanol with carbon monoxide and oxygen.
Fore this reason, various Cu-modified natural and synthetic clinoptilolite samples were prepared and tested for DMC synthesis. The samples were comprehensively characterized by different spectroscopic methods mainly by *in situ* FTIR spectroscopy and *operando* DRIFTS/UV-vis-DRS/MS measurements.

Experimental

The raw clinoptilolite material (CH) was a pale white rock extracted from the mines at the San Luis Potosí Municipality from the San Luis Potosí State in Mexico. The synthetic clinoptilolite (SC) was purchased from a foreign laboratory (Prof. Craig Williams, University of Wolverhampton, UK). The Cu-containing samples with different Cu content were obtained by wetness impregnation and cation exchange. Impregnated and exchanged samples were calcined at 450°C under synthetic air flow during 12 hours.
The catalyst samples were characterized by XRD and several spectroscopic techniques (UV-vis, ATR). Mainly *in situ* FTIR spectroscopic investigations were made to study the adsorption of methanol (MeOH) and to evaluate the oxidation state of copper by using CO and NO as probe molecules.
To get knowledge about reaction intermediates and reaction products the catalytic reaction was studied under reaction-like conditions by *in situ* FTIR spectroscopic technique in transmission mode. Additionally, a multitechnique *operando* set up allowing simultaneous DRIFTS/UV-vis/MS measurements was applied to analyze reaction products, formation and changes of adsorbates as well as changes of the coordination sphere of the Cu cations

Results and discussion

By comparison of the ATR spectra and XRD pattern of the pure and Cu-loaded CH and SC samples it could be shown that the basic clinoptilolite structure remained even after the inclusion of Cu in both natural and synthetic catalysts independently of the loaded amount of Cu. At high Cu concentrations (10, 18 wt.%) crystalline CuO was additionally found by XRD.
Even after calcination procedure in air different Cu^{+} species were detected by adsorption of CO at room temperature indicated by several Cu^{+}–CO bands in the range 2170 - 2120 cm^{-1} in the FTIR spectra of the Cu-CH and Cu-SC samples. Band intensities and positions varied depending on the nature of the catalyst, the Cu content and the pretreatment procedure of the

samples. As detected by adsorption of NO, Cu^{2+} ions occupy different positions, too. There are Cu^{2+} ions at isolated (Cu^{2+}–NO band around 1900 cm^{-1}) and at strongly associated sites (band around 1880 cm^{-1}) occurring in CuO_x agglomerates, mainly in the impregnated samples. During the *in situ* FTIR experiments it was observed that Cu-CH and Cu-SC samples were able to oxidize CO as well as NO already at room temperature. Thus, gaseous and adsorbed CO_2 were detected. During NO adsorption NO_2, N_2O, N_2O_4 were formed in the gas phase while nitrato species adsorbed at the surface were additionally found.

The oxidative carbonylation of methanol was monitored by *in situ* FTIR and *operando* DRIFTS/UV-vis-DRS/MS. The spectra obtained during exposure of 4 wt.% Cu-SC and Cu-exchanged SC catalysts to the MeOH/CO/O_2 feed at 150°C are exemplarily shown in Fig.1.

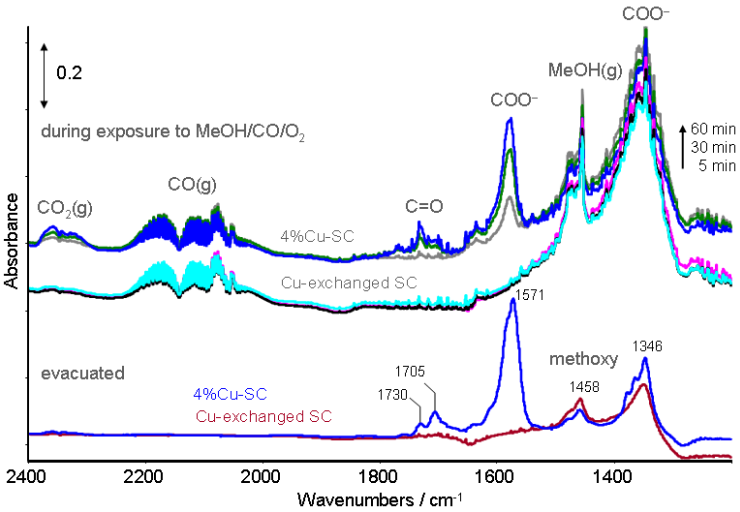

Figure 1. *In situ* FTIR spectra of Cu-SC catalysts obtained during exposure to MeOH/CO/O_2 feed at 150°C.

Whereas mainly methoxide is adsorbed on the exchanged catalyst, the formation of CO_2, carbonyl-containing species and formate (COO^-) was additionally detected on the 4 wt.% Cu-SC sample. The carbonyl bands result from formed methyl formate (MF) which was also found adsorbed at the catalyst surface after evacuation.

Furthermore, changes of the coordination sphere of the Cu^{2+} ions were observed in the UV-vis spectra obtained during *operando* DRIFTS/UV-vis/MS experiments. The main reaction products identified by MS analysis were dimethoxy methane (DMM) and MF, while no DMC formation could be detected. In contrast to the CuY system [1-3], Cu-clinoptilolite catalysts seem to be not suitable for DMC production.

Conclusions

In situ FTIR spectroscopic study of the adsorption of CO and NO as probe molecules provides comprehensive information in terms of nature, oxidation state and redox behaviour of Cu species being available in the investigated Cu-clinoptilolite samples. Exposure to MeOH/CO/O_2 feed gives DMM and MF as main oxidation products. In contrast to the Cu-Y catalyst system no DMC is formed. Obviously, the greater pore system of the Cu-Y zeolite compared to Cu-clinoptilolite combined with its essential higher surface area enhances the formation and dispersion of Cu^+ species which are able to fix CO. The latter is indispensable for an effective carbonylation reaction.

Acknowledgements

Financial support by the BMBF (MEX 08/005), Germany and CONACYT (I0110/127/08), Mexico is gratefully acknowledged.

References

[1] Y. Zhang, A.T. Bell, J. Catal. 255 (2008) 153-161.
[2] M. Richter, M.J.G. Fait, R. Eckelt, E. Schreier, M. Schneider, M.-M. Pohl, R. Fricke, App. Catal. B: Environmental 73 (2007) 269-281.
[3] J. Engeldinger, C. Domke, M. Richter, U. Bentrup, Appl. Catal. A: General 382 (2010) 303-311.
[4] D. Delledonne, F. Rivetti, U. Romano, Appl. Catal. A: General 221 (2001) 241-251.

A Design-Application Approach for Unravelling the Synergistic Active Sites in Solid Catalysts

R. Leithall,[a] A. Levy,[b] V. Shetti,[c] E. Gianotti,[c] S. Maurelli,[c] M. Chiesa,[c] and R. Raja.[a*]
[a]*School of Chemistry, University of Southampton, Southampton, SO17 1BJ, UK.*
[b]*Honeywell LLC, 101 Columbia Road, Morristown, New Jersey, 07962, USA.*
[c]*Universita Delgi Studi di Torino, Dipartimento di Chimica, I.F.M. Via Pietro Giuria, 7-10125, Torino, Italia.*
**Corresponding Author: R.Raja@soton.ac.uk (Presenting Author: rl705@soton.ac.uk)*

Introduction

Previous work has shown the successful synthesis and characterisation of a series of bimetallic and bifunctional aluminophosphate (AlPO) catalysts with tetrahedrally coordinated Co^{III} or Mn^{III} ions with simultaneous substitution with Ti^{IV} ions.[1] Aluminophosphates (AlPO) – formed from strictly alternating tetrahedral AlO_4 and PO_4 units – can produce effective catalysts by the substitution of either the aluminium(III) or phosphorus(V) sites by transition-metal ions. Metals such as cobalt, manganese or vanadium facilitate redox catalytic processes while the incorporation of magnesium or titanium leads to the formation of a Brønsted acid site.[2] It has been shown that $Co^{III}Ti^{IV}$AlPO-5 is particularly active for the epoxidation of cyclohexene[1] with a greater efficiency than the monometallic analogues (Co^{III}AlPO-5 and Ti^{IV}AlPO-5), highlighting a synergistic influence of the second metal in the framework.

Experimental

Simultaneous bimetallic substituted AlPO-5 catalysts – including CoCr, CoV, VTi, CrTi and CrV – were hydrothermally synthesised using N-methyldicyclohexylamine[3] as the structure directing agent. Powder x-ray diffraction confirmed phase-purity of the AFI structure, before calcination under a continuous flow of air at 550°C. Samples were characterized by BET surface area and ICP metal loading analysis. Oxidations of cyclohexene and benzyl alcohol were carried out at atmospheric pressure using acetyl peroxyborate (APB). The reaction components were analyzed by gas chromatography (Claurus 480 GC fitted with a flame ionization detector). Conversions were calculated from previously calibrated values against an internal standard, and turnover numbers (TON) obtained by 'moles of substrate converted per mole of metal'.

Results and Discussion

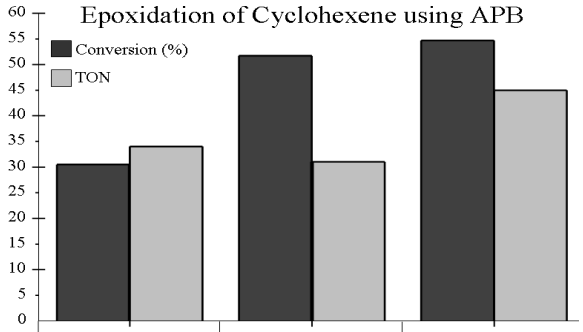

	CoTi	CrTi	VTi
DR UV/Vis Titanium Maxima /nm	230	250	235
Description	Defined	Shoulder at 295 nm	Defined
Moles of metal /100g of Catalyst (ICP)	4.92×10^{-2}	4.91×10^{-2}	3.72×10^{-2}

Figure 1: Relationship between the catalytic activity and the coordination geometry about the titanium active centre

Titanium-containing AlPO-5 catalysts (VTi, CrTi and CoTi) were tested for catalytic activity towards cyclohexene epoxidation, while DR UV/Vis spectroscopy was used to probe the coordination geometry of the titanium centre. Figure 1 shows the relationship between the catalytic activity of these catalysts and the tetrahedral nature of the active centre. CoTi and VTi combinations exhibit a defined maxima around 230nm (near the fingerprint region for tetrahedral titanium) and show greater conversions for the epoxidation reaction. However, the CrTi catalyst show a maxima which is shifted towards the octahedral coordination region with a shoulder appearing at 295nm, which is attributed to its reduced activity.

The most promising of these is the VTi combination, which has recently been studied by EPR and ESEEM. Correlation analysis confirms that vanadium is present in framework aluminium sites as vanadyl-type species (Figure 2). Early results indicate that titanium can be incorporated into the framework as Ti(III) at the aluminium site, as well as the phosphorus site, which has previously been suggested.[4]

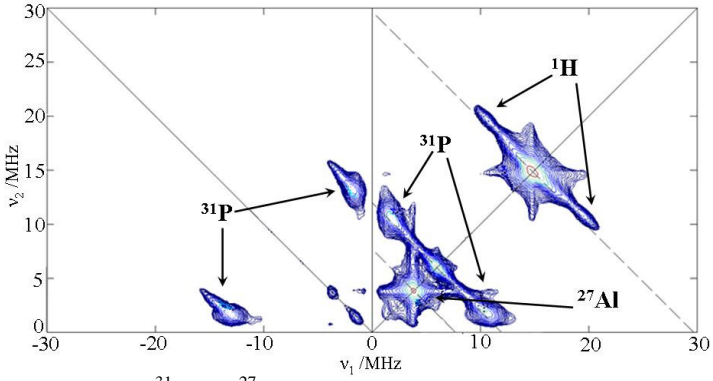

Figure 2: ^{31}P and ^{27}Al HYSCORE measurements provide evidence for framework incorporation of VO^{2+} in the VTiAlPO-5 structure at the aluminium site.

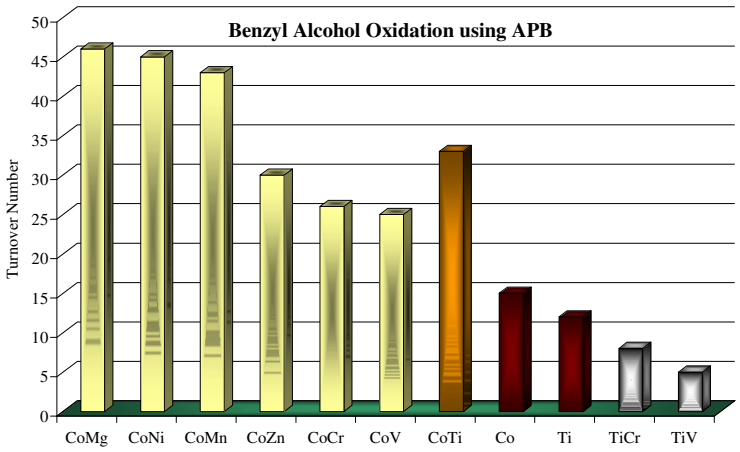

Figure 3: Catalytic activity of bimetallic AlPO-5 catalysts for the oxidation of benzyl alcohol, after 2 hours.

Combinations of bimetallic AlPO-5 catalysts were also screened for their activity for the oxidation of benzyl alcohol to benzaldehyde using APB as the oxidant. Interestingly, for this reaction it is the cobalt-containing catalysts, reported in figure 3, which show the most promising catalytic potential. In combination with a Brønsted acid functionality, this series of catalysts yield good conversion and turnover numbers.

Conclusions

From the results shown with the new series of catalysts it can be seen that the AlPO-5 framework can be optimised for the required reaction. For cyclohexene epoxidation, the titanium-containing catalysts were shown to be most active, while for the oxidation of benzyl alcohol, cobalt-containing catalysts with Brønsted acid functionality facilitate the reaction. This suggests that there are two contrasting mechanisms of reaction occurring, which can thus be optimised for each process, enabling the development of a new generation of highly active catalysts for industrially significant processes. The design-application approach of selecting the correct combination of metal centres to affect the required reaction, probing structure-property relationships, will be presented at the conference.

Acknowledgements

The authors would like to thank Honeywell LLC for their financial assistance and The British Italian Partnership for continually supporting our collaborations.

References

1. A. J. Paterson, M. E. Potter, E. Gianotti and R. Raja, *Chem. Commun.*, 2011, **47**, 517 - 519.
2. S. T. Wilson, B. M. Lok, C. A. Messina, T. R. Cannan and E. M. Flanigen, *J. Am. Chem. Soc.*, 1982, **104**, 1146 - 1147.
3. M. Sanchez-Sanchez, G. Sankar, A. Simperler, R. G. Bell, C. R. A. Catlow and J. M. Thomas, *Catalysis Letters*, 2003, **88**, 163 - 167.
4. A. M. Prakash, L. Kevan, M. H. Zahedi-Niaki and S. J. Kaliaguine, *J. Phys. Chem. B.*, 1999, **103**, 831 - 837.

Time resolved in-situ characterization of hexagonal and cubic silica/surfactant self-assembled systems

Florentin Michaux[1], Niki Baccile[1], Christel Gervais[1], Marianne Imperor-Clerc[2], Nicolas Folliet[1], Luca Malfatti[1], Florence Babonneau[1]

1- Laboratoire de Chimie de la Matière Condensée de Paris, UMR 7574, Université Pierre et Marie Curie-Paris 6 and CNRS, Collège de France, 11 Place M. Berthelot, 75005 Paris, France, Fax :+33 1 44 27 14 44; E-mail: florence.babonneau@upmc.fr
2- Laboratoire de Physique des Solides, UMR 8502, Université Paris Sud, 91405 Orsay, France, Fax: +33 1 69 15 60 86

Introduction

Surfactant templated mesoporous silica powders have been extensively studied in the past 15 years by exploiting the self-assembly properties of amphiphilic molecules or macromolecules in aqueous medium. The large success of these systems mainly relies on the apparent simplicity that enables to design porous networks with different architectures and pore sizes. However, a better control of the final nanostructures requires a deeper understanding of the interaction mechanisms between the templating agents and the network-forming species.
Previous studies on this topic have produced a lot of information on the cooperative self-assembly of these systems and much is now known about the mesostructure formation. Nevertheless, some information still lacks on the very initial moments of the process when it comes to comparing cubic and hexagonal systems obtained under highly acidic conditions with cationic surfactants and organically-modified silica precursors. Which is the shape of the micelles in solution prior to, during and after hydrolysis of the precursor? How does the nature of the inorganic precursor affect the micellar shape? How can we correlate the micellar geometry and the final msostructure? This work will show our latest experiments on the use of in-situ small angle x-ray scattering (SAXS) performed under a highly brilliant synchrotron radiation to follow the formation mechanism of templated silica powders in the presence of cationic surfactants with different polar head groups and organically-modified silica sources.

Experimental

Mesostructured silica powders are obtained in solution at room temperature using tetraethoxysilane and organically modified phenyl (PTES), vinyl (VTES) silanes. We used cationic surfactants with increasing polar head volumes (Cetyltri**methyl**ammonium bromide, Cetyltri**ethyl**ammonium bromide and cetyltri**propyl**ammonium bromide). SAXS studies were performed at the initial stage of the reaction when the alkoxide is added to the water/surfactant solution. SAXS experiments were performed at the SWING beamline of SOLEIL synchrotron (St. Aubin, France). Additional experimental details can be found in [1].

Results and discussion

In a recent work we used SAXS and Raman spectroscopy to perform a time resolved in situ study of three 2D hexagonal CTAB-templated samples as a function of the solution composition. Here, we show similar SAXS experiments performed on cubic silica system obtained with surfactants having larger polar head groups (CTEAB, CTPAB) or CTAB

combined with organically-modified silica precursors (VTES, PTES). These experiments were carried on very recently on the SWING beamline of the Soleil synchrotron, which offers a higher sensitivity under similar acquisition conditions with respect to our previous attempts at a different synchrotron facility. Fig.1 shows the SAXS pattern of a cubic system observed under two different synchrotron sources. In Fig.1.A, signal too noisy is of poor quality if compared to the acquisition done at SWING (Fig.1.B). This is easily verified by the presence of the high order peaks characteristic of the Pm3n space group of the cubic structure.

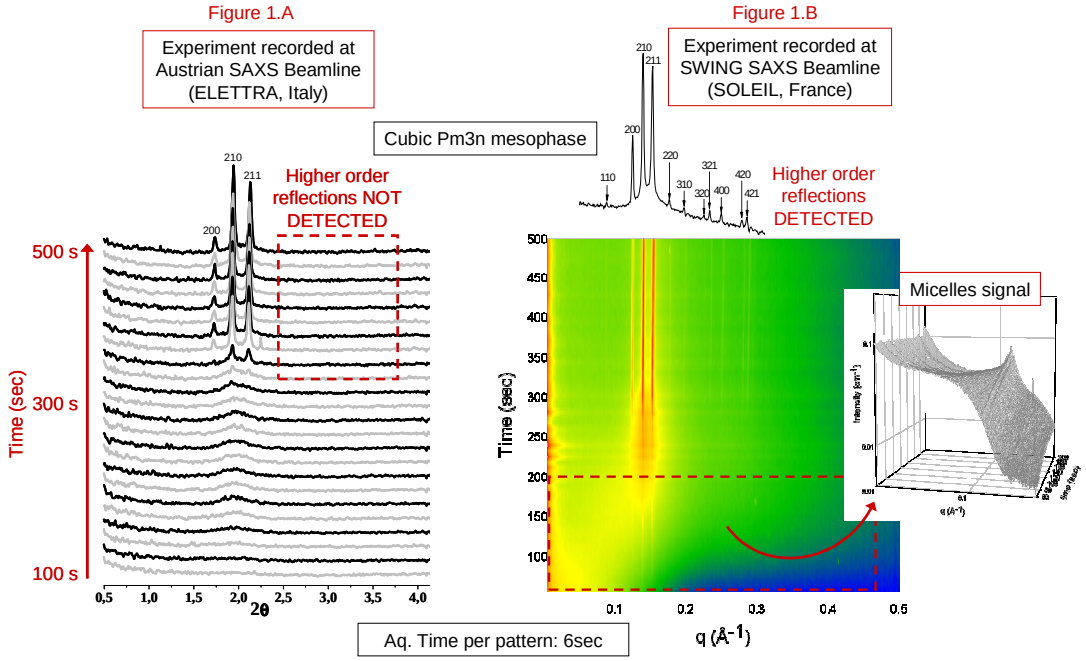

Figure 1. Time resolved SAXS data of the cubic Pm3n silica/surfactant system acquired under similar conditions at two different synchrotron facilities

Most interestingly, the micellar signal at low-q values can be easily detected. Its modelization with time will provide all the information concerning the shape and size of the micellar objects and their evolution. We notice the discrepancy between the SAXS pattern acquired for a cubic system (shown here) and the 2D hexagonal system (CTAB-templated) shown in [1]. In that case, the mesophase was formed directly without any appreciable scattering hump. When a cubic phase is formed instead, the micellar signal shown below evolves into a hump which systematically anticipates the formation of the cubic phase, as actually observed in hexagonal block copolymer templated systems [2]. A deeper (ongoing) analysis of these data will provide some straightforward answers to the questions introduced above.

Conclusions

This ongoing work aims at identifying the different mechanistic behaviors at the initial stage of self-assembling in surfactant-silica and organosilica cubic and 2D hexagonal systems. Very recent synchrotron studies performed under high brilliance conditions allow us to correlate the micellar geometry with the final mesophase.

References

[1] N. Baccile, C. V. Teixeira, H. Amenitsch, F. Villain, M. Lindén, F. Babonneau Chem. Mater., 2008, 20, 1161-1172
[2] V. Zholobenko, A. Y. Khodakov, Y. Andrei, M. Imperor-Clerc, D. Durand, I. Grillo, Isabelle, Adv. Coll. Interf . Sci., 142, 67-74

NaH nanoparticles encapsulated in amorphous silica

Peter P. Edwards[1], Asel Sartbaeva[1],
[1]*Department of Chemistry, University of Oxford, South Parks Road, Oxford, OX1 3QR, Great Britain*

Introduction

The large volume of void space within amorphous silica gels allow them to act as hosts for a wide variety of other functional materials. We report here the formation of crystalline nanoparticles of sodium hydride encapsulated in a host amorphous silica gel matrix [1]. These nanoparticles are formed by in situ hydrogenation of a precursor material - Na loaded silica gel - under mild conditions. The resulting material is considerably less pyrophoric and less air-sensitive than the bulk hydride. We anticipate that this formation method of in situ modification of reactive precursor material may have wide applications.

Experimental

Our starting material is silica gel loaded with sodium metal (32 wt%) provided by SiGNa Chem (this material is hereafter called Na-SG) [2]. The material is a coarse black powder and particulate sodium metal is dispersed in the nanoscale pores of the silica gel.
We have carried out both in situ hydrogenation and deuteration of Na-SG. The resulting material was characterised using Inelastic Neutron Spectroscopy (INS) and neutron diffraction on TOSCA and GEM instruments at ISIS (Chilton, UK), Rietveld analysis, High-Resolution Transmission Electron Microscopy (HRTEM) and Electron Paramagnetic Resonance spectroscopy (EPR).

Results and discussion

On exposure to H_2 gas the material reacts under mild conditions, visibly changing colour from black to brown. We attribute this change in colour to the conversion of metallic Na to ionic NaH dispersed in the silica matrix. Interestingly, the texture of the material did not significantly change, remaining a coarse powder, indicating that the silica gel matrix is not significantly disrupted by the reaction of the dispersed sodium metal with hydrogen/deuterium. This is understandable as the volume per sodium atom in the crystal structure of NaH is less than that in bulk metallic sodium, that is, formation of NaH leads to a volume contraction rather than expansion of the nanoparticulates. The material reacts vigorously with water, evolving hydrogen gas, and less vigorously with acetone. When this brown powder is exposed to air its colour slowly fades over several hours until the surface of the grains becomes almost white; it is not pyrophoric. We attribute this change in colour to the formation of NaOH, by a slow reaction with atmospheric moisture.

Conclusions

We find that a new phase of NaH, in the form of distinct crystalline NaH nanoparticles, can be readily formed within an amorphous silica gel matrix by in situ transformation of nanodisperse Na in the silica framework, by treatment with hydrogen gas under mild conditions. The formation of the nanoparticles appears to occur without significant disruption of the host silica gel matrix, so that nanoparticles remain encapsulated within the silica gel. We anticipate that our new approach of in situ transformation of a precursor material may have wide applicability to produce other reactive nanoparticles stabilized within a silica framework.

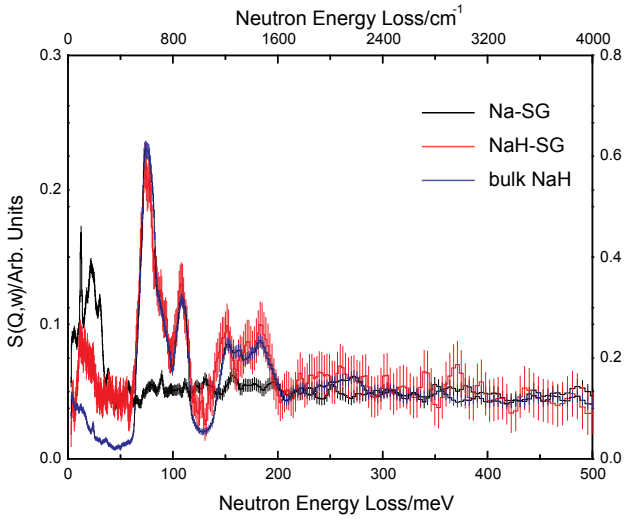

Figure 1: Inelastic Neutron Spectroscopy data on sodium SG (black), hydrogenated NaH-SG (red) and bulk sodium hydride (blue, scaled to match the maximum height of the red curve). The features around 100 meV are the optical modes, the ratio 2:1 due to LO-TO splitting, their presence indicates the existence of NaH crystallites that are least larger than 15 nm.

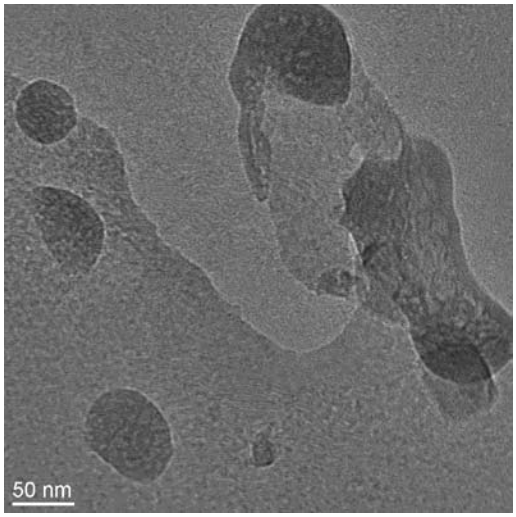

Figure 2: High Resolution Transmission Electron Microscopy image of NaH-SG sample showing three distinguishable NaH nanoparticles (on the left) of approximately 50nm in size. EDX was performed to confirm presence of Na.

Acknowledgements

AS would like to thank Glasstone Fellowship and Royal Soceity for funding.

References

[1] Sartbaeva A., Wells S.A., Sommariva M., Lodge M.M.J., Jones M.O., Ramirez-Cuesta A.J., Li G. and Edwards P.P., Formation of crystalline Sodium Hydride nanoparticles encapsulated within an amorphous framework, Journal of Cluster Science, 21, 543-549, 2010

[2] Dye, J.L., et al., Alkali metals plus silica gel: Powerful reducing agents and convenient hydrogen sources. Journal of the American Chemical Society, 127(26): 9338-9339, 2005.

[3] Shatnawi, M., et al., Structures of alkali metals in silica gel nanopores: New materials for chemical reductions and hydrogen production. Journal of the American Chemical Society, 2007. 129(5): 1386-1392, 2007

Effect of synthesis conditions on the structural properties of Ga-containing layered double hydroxides

Alba Álvarez, Raquel Trujillano and Vicente Rives*
GIR-QUESCAT, Departamento de Química Inorgánica, Universidad de Salamanca, Salamanca, Spain, vrives@usal.es

Introduction

Hydrotalcite-like compounds are layered double hydroxide (LDHs) with the formula $[M^{2+}_{1-x}M^{3+}x\ (OH)_2]^{n+}[A^{n-}_{x/n}].mH_2O$. Their structure is derived from that of brucite where some divalent cations are substituted by trivalent ones providing positive charged layers. The interlayer region is occupied by charge-balancing anions and water molecules.

There is a large variety of di- and trivalent cations able to form these compounds and also a large diversity of anions occupying the interlayer spacing. Hydrotalcites can be synthesized by a wide number of methods and are extensively used in industry as catalysts, catalyst precursors, adsorbents, drugs vehicles, polymer fillers, etc.

In particular, Mg^{2+}-Ga^{3+} hydrotalcites have been used for reduction of unsaturated aldehydes [1], as catalysts for the liquid-phase Friedel-Crafts alkylation of toluene by bencyl chloride, and in acylation reactions of aromatics [2]. Only very few studies about synthesis and structural characteristics of LDHs with Ga as trivalent cation have been reported [3] and, as far as we know, none about the synthesis of these solids by hydrothermal treatment under microwave irradiation.

We here report on the synthesis of different series of MgGa and NiGa hydrotalcites obtained by coprecipitation at pH=10 (NaOH 1M) or the urea hydrolysis method. The final mixture has been aged with and without hydrothermal treatment under microwave irradiation. Our goal was to find the precise synthesis parameters applicable to obtain solids with well defined particle size distribution and textural properties.

Experimental

Coprecipitation with Na_2CO_3 and NaOH

A portion of 25 ml of an aqueous solution containing Mg^{2+} or (Ni^{2+}) and Ga^{3+} nitrates (M/Ga molar ratio 3) was dropwise added to 75 ml of a water solution containing sodium carbonate at pH 10 (NaOH 1M). The obtained slurry was splitted in two parts, A and B. Portion A was stirred during 24 h in air, while portion B was treated in a microwave oven at 120 ºC for different periods of time. After the ageing treatments the suspensions were centrifuged, washed with distilled water and dried at 40 ºC in air. The ageing treatments tested were:

a) Stirring at room atmosphere for 8 h and then microwave irradiation for 2 h at 120 ºC.
b) Microwave irradiation for 2 h at 120 ºC.

Synthesis by the urea method

An aqueous solution of the cations with a M/Ga molar ratio 3 was added to 250 ml of an aqueous solution of urea. The Ga/urea molar ratios tested were 10 and 20. One portion of the solution was refluxed at 100 ºC for 25 h. The other one was directly submitted to hydrothermal treatment in a microwave oven at 120 ºC for different periods of time. The solids formed were separated by centrifugation, washed and dried at 40ºC under air atmosphere.

Results and discussion

The solids obtained were characterized by element chemical analysis, powder X-ray diffraction (PXRD), FT-IR and UV-Vis spectroscopies, thermal analyses (DTA and TG), particle size distribution analysis and specific surface area and porosity assessment.

All samples obtained by direct coprecipitation with NaOH showed PXRD patterns typical of the hydrotalcite structure, their crystallinity depending on the ageing treatment (with or without microwave irradiation) and the precise nature of the divalent cation. The nature of the solids synthesised by the urea method varied depending on the Ga/urea molar ratio and also on the ageing treatment. MgGa hydrotalcites prepared by the urea method with a Ga/urea molar ratio of 10 contained minor impurities, but when this ratio was increased to 20 only the hydrotalcite was formed. NiGa hydrotalcite was the only phase found whichever the Ga/urea molar ratio used. When the time under microwave irradiation was increased from 30 min to 2 h, it was found that the shorter time yielded the more crystalline sample. Impurities were segregated when the irradiation time was increased.

Particle size distribution results revealed a bi- or tri-modal distribution for solids with different phases. Microwave treatment and urea synthesis gave solids with a particle size ten times larger than those obtained without microwave treatment.

FT-IR spectra and thermal analysis results were in agreement with the results expected for the structure. UV-Vis spectroscopy revealed location of Ni^{2+} cations in octahedral sites.

Conclusions

Well crystallized layered double hydroxides with the hydrotalcite-like structure can be prepared by conventional precipitation and hydrothermal ageing, as well as by homogeneous precipitation by urea hydrolysis. Microwave ageing gives rise to better crystallized solids and minor segregation of co-phases, affecting as well to the particle size distribution.

The particle size distributions change deeply with the preparation procedure and the ageing treatment; so, narrower distributions are found for samples prepared through the urea method.

Acknowledgements

Authors acknowledge finantial support from ERDF and MICINN (grant 2009-08526); AA acknowledges a contract from JCyL.

References

[1] Aramendía,M.A., Borau, V., Jiménez, C., Marinas, J.M., Ruiz, J.R., Urbano, F., Influence of the preparation method on the structural and surface properties of various magnesium oxides and their catalytic activity in the Meerwein–Ponndorf–Verley reaction, Appl. Catal., A: General, 249 (2003) 207-215.
[2]] Choudary, V.R., Jana, S.K., Narkhede, V.S., Benzylation and benzoylation of substituted benzenes over solid catalysts containing Ga- and Mg-oxides and/or chlorides derived from Ga–Mg-hydrotalcite by its HCl pre-treatment or calcination, Appl. Catal A: General, 235 (2002) 207-215.
[3]Grand, L.M., Palmer, S.J., Frost, R.L., Synthesis and thermal stability of hydrotalcites based upon gallium. J. Therm. Anal. Calorim. 101 (2010) 195-198.

Hierarchical zeolites: IR studies of acid properties of zeolite ZSM-5 desilicated with NaOH and tetrabutylammonium hydroxide

Karolina Sadowska, Jolanta Sidor, Anna Wach, Piotr Kuśtrowski, Jerzy Datka
Faculty of Chemistry, Jagiellonian University, 30-060 Cracow, Ingardena 3, Poland
datka@chemia.uj.edu.pl

Introduction

Hierarchical zeolites obtained by the desilication process were the subject of numerous studies because of their interesting catalytic properties. Even though zeolites of various structures and composition were used and various bases were applied, the most frequently studied system was zeolite ZSM-5 desilicated with NaOH or NaOH and quaternary ammonium hydroxide mixtures. The process of Si extraction and pore system of desilicated zeolites were well defined, however the acid properties were not well characterized until now. As catalytic properties of zeolites depend strongly on their acidity, we undertook detailed IR studies of acid properties of zeolite ZSM-5 desilicated with NaOH solutions of various concentrations and with NaOH/tetrabutylammonium hydroxide (TBAOH) mixtures of various compositions. Various desilication time was also applied.

Our quantitative IR experiments of pyridine sorption provided information on the concentration of both Bronsted and Lewis acid sites. The experiments of pyridine desorption revealed, that two kinds of Bronsted sites exist: strongly acidic Si-OH-Al groups (IR band at 3610 cm^{-1}) and less acidic protonic sites not being those hydroxyls. The contribution of both kinds of protonic sites was determined. Low temperature experiments of CO sorption informed on two kinds of Lewis acid sites: extreframework Al species and sites formed by dehydroxylation. The IR experiments of pivalonitrile (tertbutylnitrile) sorption were also realized. Pivalonitrile being bulk molecule does not penetrate the channels of ZSM-5 and informs on the accessibility of sites to bulk reactant molecules.

Additionally to IR studies, ECSA measurements provided information on the composition of surface layers of zeolite crystals. Pore system was followed in porosimetric experiments and also by TEM microscopy.

Experimental

Parent zeolite ZSM-5 of Si/Al = 31.8 was used. Desilication was realized in 0.1, 0.2, 0.5 and 1.0 M NaOH solutions at 80^{o} C and in NaOH/TBAOH mixtures of various proportions. Desilication time varied from 0.5 to 5 h.

Results and discussion

The most important conclusions concerning desilication with NaOH only are following:

1. NaOH treatment resulted in Si/Al decrease from 31.8 to ca. 10 due to preferential Si extraction. According to ESCA results surface layer was more desilicated than the bulk.
2. Filtrate analysis showed, that NaOH dissolved partially zeolite, by extracting mostly Si, but also some Al. At higher NaOH concentration more zeolite was dissolved, higher was also the contribution of Al extracted (i.e. Si/Al in filtrate was lower).
3. Diluted NaOH (0.1 M) produced mesopores of diameters: of about 14 nm., more concentrated NaOH (0.2 and 0.5 M) produced mesopores of ca. 14 and 100 nm. The treatment with concetrated NaOH (1M) resulted in partial destruction of zeolites.
4. The mesopores formed by desilication are well seen in TEM pictures.

5. The analysis of IR spectra in hydroxyl region showed, that desilication increased the amount of isolated Si-OH on mesopore walls (the band at 3740 cm^{-1}) "parallel" to the increase of mesopores area (determined in porosimetric experiments). The internal Si-OH...O groups in "hydroxyl nests" (3500 and 3720 cm^{-1} bands) were removed indicating, that Si atoms connected to three other Si atoms were extracted first (before those connected with four other Si). The band of acidic Si-OH-Al hydroxyls (3610 cm^{-1}) increased upon mild desilication (0.1 and 0.2 M NaOH) due to the decrease of Si/Al. More severe desilication decreased Si-OH-Al band due to some zeolite destruction.
6. The concentration of protonic sites determined by quantitative experiments of pyridine sorption in parent zeolite was practically equal to the concentration of Al determined by chemical analysis (3.07/u.c. and 2.93/u.c. resp.).
7. The concentration of protonic sites increased upon mild desilication (0.1 and 0.2 M NaOH) "parallel" to decrease of Si/Al, but it decreased upon more severe desilication (with 0.5 and 1.0 M NaOH) due to some zeolite destruction.
8. In the zeolites desilicated in mild conditions (0.1 and 0.2 M NaOH) the concentration of protonic sites determined by IR was very close to the concentration of Al (determined by chemical analysis) indicating, that upon mild desilication all Al atoms are in framework positions and can form Si-OH-Al. Only upon desilication in severe conditions concentration of protonic sites was lower than of Al due to transfer of some Al from framework to extraframework positions.
9. IR studies of pyridine desorption revealed the presence of two kinds of protonic sites: strongly acidic Si-OH-Al and less acidic sites not being these hydroxyls (present mostly in zeolite desilicated with NaOH 0.5M).
10. IR studies of low temperature CO sorption revealed, that Lewis acis sites were formed mostly by dehydroxylation of protonic sites on mesopore walls.
11. The IR experiments of pivalonitrile (tertbutylnitrile), which does not penetrate the channels of ZSM-5 showed, that desilication increased the accessibility of acid sites inside zeolite pores, which were inaccessible to pivalonitrile in parent zeolite.

<u>The conclusions concerning desilication with NaOH and TBAOH mixtures are following:</u>

1. Desilication with NaOH/TBAOH mixtures is less effective than with NaOH itself, the decrease of Si/Al was less important than without TBA. ESCA results showed, that TBAOH protected surface layer against NaOH attack.
2. The analysis of filtrate showed, that addition of small amount of TBAOH to NaOH decreased the Al extraction from zeolite preventing the loss of acid sites.
3. The diameter of mesopores was smaller (7-11 nm) than with NaOH itself (14 and 100 nm). Mesopore diameter decreased with TBAOH concentration in the mixture.
4. The contribution of Si-OH on mesopores surfaces was bigger in the presence of TBAOH despite of some decrease of mesopores surface area.
5. The concentration of protonic sites was smaller than without TBAOH due to less effective desilication in the presence of TBAOH.
6. The concentration of Lewis acid sites is lower than without TBAOH, probably due to smaller extend of zeolite destruction and dehydroxylation.
7. The accessibility of acid sites (measured by pivalonitrile sorption) in zeolites desilicated with NaOH/TBAOH was better than for NaOH only.

Project operated within the Foundation for Polish Science MPD Programme co-financed by the EU European Regional Development Fund.

Mesoporous zeolite crystals with homogeneously distributed mesopores of controlled size induced by recyclable structuring agents

Robin Chal[1], Thomas Cacciaguerra[1], Delphine Minoux[2], Sander van Donk[2] and Corine Gérardin[1].
[1] *Institut Charles Gerhardt de Montpellier, France, robin.chal@enscm.fr, corine.gerardin@enscm.fr*
[2] *TOTAL research center, Feluy, Belgium.*

Introduction

Zeolites are widely used due to their microporous structure, strong acidity and ion exchange capacity. They possess catalytically active sites as well as uniformly sized and shaped micropores, which allow for their use as shape selective catalysts in refining and petrochemistry for instance. The growing demand for transportation fuels, resulting from over 99% of catalytic processes, pushes the refining industry to process heavier hydrocarbon sources in a near future. The use of conventional catalysts based on zeolites is then limited by the small size of the micropores that restrict the matter transport and prevents the large molecules from reaching the micropore volume. The development of new catalysts is thus essential and requires the optimization of active site accessibility for large molecules through the development of larger surface areas and larger pore volumes. For this, three approaches have been put forward involving the synthesis of zeolites with large pores (> 1 nm), the preparation of zeolite nanocrystals or the introduction of mesopores (2-50 nm) in zeolites [1].
Although today the industrially applied zeolite catalysts combining micro- and mesopores are synthesized by destructive dealumination or desilication pathways due to the low cost processes, the constructive approach permits a better control of pore size and distribution and has recently made significant progress in the synthesis of “hierarchical” pore systems. However, its application in industry is still limited because of cost issues, which is partially related to the high cost of the organic template. Indeed, once the material has been synthesized, the structuring agent is trapped inside the mesopores. In order to remove it, the material generally needs to be calcined, which decomposes the structuring agent and often has a detrimental effect, causing defects in the framework structure. Besides, calcination steps represent nearly 80% of the material cost and release gases that may cause environmental issues.
We study here a recent constructive method for preparing mesoporous zeolites resulting of the partial dissolution of the crystalline structure in basic medium to incorporate a mesopore structuring agent (CTAB) in the zeolite under hydrothermal conditions [2-4]. The influence of various parameters has been investigated such as concentration and nature of the structuring agent, the concentration and nature of the base, the duration of hydrothermal treatment or the Si/Al ratio of the starting zeolite. The objectives are to control the micropore and mesopore contributions and to elucidate the transformation mechanisms in this recrystallization route.

Experimental

Recrystallisation of HY zeolite in the presence of a secondary template: First, 1.67g of commercial zeolite HY powder (Zeolyst CBV-720, Si/Al=15) were added in 50mL of a 0.09M tetramethylammonium hydroxide (TMAOH, Sigma, 25% in water) solution. Then, 0.83g of hexadecyltrimethylammonium bromide (CTAB, Sigma, 98 %) was added and stirring continued for 30 min. The suspension was hydrothermally treated at 150°C for 20 hours in an autoclave. The solid was collected by filtration and washed with distilled water. The product was then dried at 80°C and calcined in air at 550°C for 8h with a ramp temperature of 1°C/min.

Results and discussion

In case of zeolite Y, this “recrystallization” yields a large mesoporous volume, a high surface area and a narrow pore size distribution centered at 4.2 nm by pseudomorphic transformation of the initial zeolite crystals. The pictures obtained by transmission electron microscopy show the coexistence of a microporous crystalline phase and a homogeneous vermicular mesoporous phase exhibiting a characteristic signal by X-ray diffraction.

N_2 adsorption isotherms reveal the presence of both micro- and mesopores in the material, with a high specific surface area of about 805 m^2/g and a mesopore size distribution centered at 4.2 nm. TEM images (Fig.1) show hexagonal zeolite Y crystals with a well organized mesoporous structure. At higher enlargement, a vermicular mesoporosity can be clearly observed inside these crystals along with a long range microporous crystalline structure from the initial zeolite.

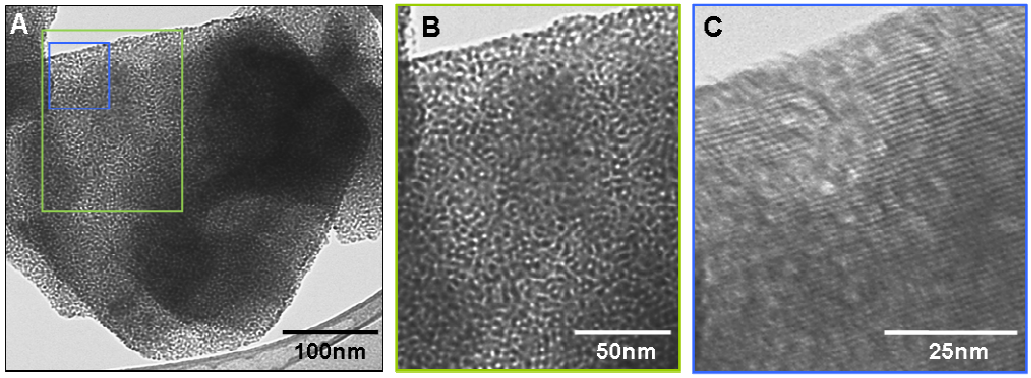

Figure 1. TEM images of zeolite HY recrystallized in the presence of CTAB and TMAOH, highlighting micro-and mesoporosity in the material at different magnifications and focuses.

However, industrial applications are limited by the use of a surfactant structuring agent such as CTAB, which imposes a calcination step or an extraction with organic solvents. Therefore we are currently adapting the preparation to the use of recyclable structuring agents, an environment friendly methodology developed in our laboratory for the preparation of amorphous mesoporous materials [4] and based on the use of new recyclable micelles resulting from the induced and reversible assembly of water-soluble polymers (double hydrophilic block copolymers or DHBC) under the action of a physicochemical stimulus. These polymers are then extracted from the material by washing with water, under mild conditions to release the porosity and can be reused for a new material synthesis.

Conclusions

Mesoporous zeolite Y crystals have been prepared hydrothermally from commercial zeolites in the presence of CTAB. They show a large specific surface area of 805 m^2/g and a narrow mesopore size distribution centered at 4.2 nm. Characterization results indicate that the material possesses a hierarchical structure with long range crystalline structure along with a homogeneous (in size and distribution) vermicular structure in the same crystals. We are now investigating the use of hydrosoluble structuring agents as mesopore-generating agents with our system in order to replace the classical surfactant templates.

References

[1] R. Chal, C. Gérardin, M. Bulut, S. van Donk, ChemCatChem 3 (2011) 67-81.
[2] Y. Goto, Y. Fukushima, P. Ratu, Y. Imada, Y. Kubota, Y. Sugi, M. Ogura, M. Matsukata, J. Porous Mater. 9 (2002) 43-48.
[3] I. I. Ivanova, A. S. Kuznetsov, V. V. Yuschenko, E. E. Knyazeva, Pure Appl. Chem. 76 (2004) 1647-1658.
[4] R. Chal, T. Cacciaguerra, S. van Donk, C. Gerardin, Chem. Commun. 46 (2010) 7840-7842.
[5] N. Baccile, J. Reboul, B. Blanc, B. Coq, P. Lacroix-Desmazes, M. In, C. Gerardin, Angew. Chem., Int. Ed. 47 (2008) 8433-8437.

Control of aluminum distribution in the framework of silicon rich zeolites - effect on catalytic properties

Zdenek Sobalik, Jiri Dedecek, Petr Sazama, Vendula Gabova, Blanka Wichterlova
J. Heyrovsky Institute of Physical Chemistry AS CR, Dolejskova 3, CZ 182 23, Prague 8, Czech Republic, zdenek.sobalik@jh-inst.cas.cz

Introduction

Low concentration of aluminum atoms in silicon rich zeolites (with Si/Al > 8) as ZSM-5, ferrierite, mordenite, MCM-22 or beta zeolite possesses a high variability of the arrangement of aluminum atoms in their frameworks. Aluminum atoms are present in silicon rich frameworks as isolated aluminum atoms and Al-O-(Si-O)$_2$-Al sequences, while Al-O-Si-O-Al sequences are not present.[1-3] The distribution of aluminum atoms can dramatically affect accommodation of transition metal ions in dehydrated materials. Bare divalent cations and/or other divalent cationic species can be supposed to be preferentially located in sites containing two Al atoms of an Al-O-(Si-O)$_2$-Al sequence. On the other side, monovalent cationic species are preferentially located in the vicinity of isolated Al atom. Thus, aluminum distribution can affect concentration and siting of metal ion species in zeolites and their properties which can be reflected in catalytic properties of metallozeolite based catalysts. Thus, the distribution of aluminum in the framework of silicon rich zeolite represents, together with the size and arrangement of the zeolite channel/cavity system a key parameter of the zeolite catalyst. It makes the preparation of the zeolite with controlled and defined concentration of isolated aluminum or Al-O-(Si-O)$_2$-Al sequences located in one ring are highly desirable. Such zeolites can represent an important and necessary step in the design of the new generation of highly active, selective and stable catalyst with properties individually tuned for specific reactions. In this paper, syntheses of industrially important zeolites with controlled concentration of isolated Al atoms or Al-O-(Si-O)$_2$-Al sequences is demonstrated. Moreover, parameters controlling aluminum distribution during the zeolite synthesis are discussed, as well as the effect of aluminum distribution on the catalytic activity of metallozeolite catalysts in various industrially important reactions.

Experimental

Ferrierite with Si/Al around 9 and ZSM-5 and beta zeolites with Si/Al 12 -15 were synthesized using different sources of aluminum and silica, with different templates and using precursors with different surface areas. All zeolites exhibited high crystallinity (according X-ray diffraction, FTIR experiments and SEM) with aluminum atoms exclusively in the framework (according ^{29}Si and ^{27}Al MAS NMR). Presence of Al-O-Si-O-Al sequences was excluded using ^{29}Si MAS NMR, the concentration of Al-O-(Si-O)$_2$-Al sequences was estimated using Co(II) ions as probes monitored in dehydrated maximum Co ion exchanged zeolite by UV-Vis-NIR diffuse-reflectance spectroscopy.[1-2]

Results and Discussion

Ferrierite, ZSM-5 and beta zeolites were prepared with or more than 90 % of isolates Al atoms or more 90 % of Al atoms in Al-O-(Si-O)$_2$-Al sequences located in one ring. It was found that variation of all parameters of the zeolite synthesis can affect the concentration of Al-O-(Si-O)$_2$-Al sequences in the zeolite. Cu-, Co- and Fe-zeolites prepared from parent matrices with different concentration of Al-O-(Si-O)$_2$-Al sequences (10 or 90 %) exhibited

dramatic differences in their catalytic activity in NOx-SCR by ammonia and hydrocarbons in the absence/presence of water vapor.

Conclusions

Industrially important silicon rich zeolites as ZSM-5, ferrierite and beta zeolite were synthesized or with highly prevailing (90 %) isolated aluminum atoms or with highly prevailing (90 %) Al-O-(Si-O)$_2$-Al sequences located in one ring. Different aluminum arrangement in the zeolite framework resulted in significantly different properties of transition metal ion species stabilized in these materials as it was demonstrated in dramatically different behavior of prepared metallozeolite catalysts in NOx abatement reactions. Thus, tuning of aluminum distribution in the zeolite opens the possibility for the optimization of properties of zeolite based industrial catalysts for specific reactions.

Acknowledgements

This work was financially supported by the Grant Agency of the Academy of Sciences of the Czech Republic (Project No. IAA400400904) and the Academy of Sciences of the Czech Republic (Project No. KAN100400702).

References

[1] Dedecek, J., Kaucky, D., Wichterlova, B., Chem. Commun. (2001) 970-971.
[2] Dedecek, J., Kaucky, D., Wichterlova, B., Gonsiorova, O., Phys. Chem. Chem. Phys. 21 (2002) 5406-5413.
[3] Takaishi, T., Kato, M., Itabashi, K., Zeolites 15 (1995) 21-32.

Characterization of Zeolite FAU-LTA Core-Shell Composites

Yifeng Yun[1], Zhengyang Wang[1], Wei Wan[1], Jie Su[1], Daniel Grüner[1,2], Wilder Carrillo-Cabrera[2], Xiaodong Zou[1*]
[1]*Berzelii Center EXSELENT on Porous Materials and Inorganic and Structural Chemistry, Department of Materials and Environmental Chemistry, Stockholm University, SE-106 91, Stockholm, Sweden*
[2]*Max-Planck-Institut für Chemische Physik fester Stoffe, D-01187, Dresden, Germany*
E-mail: Yifeng.Yun@mmk.su.se, xzou@mmk.su.se

Introduction

Zeolites are widely used as adsorbents, catalysts, ion exchangers, membranes and sensors.[1-3] Core-shell zeolite composites have attracted considerable attention due to their storage capability and chemical separation.[4] Here we present the synthesis of zeolite composites by epitaxial growth of zeolite A (LTA) shells on cores of zeolite X (FAU) cores of two different sizes. The growth rate and growth mechanism were studied by scanning electron microscopy (SEM) and powder X-ray diffraction (PXRD). Structures of the composites were studied by transmission electron microscopy (TEM).

Experimental

The X-A core-shell composites are prepared in two steps: synthesis of well-shaped core zeolite X crystals and epitaxial growth of zeolite A shell. Single crystals of zeolite X were synthesized from a gel with the following molar composition SiO_2 : 0.34 Al_2O_3 : 1.75 Na_2O : 237 H_2O. The gel was sealed in a Teflon-lined stainless steel autoclave and kept at 85 °C in static conditions for three days. The obtained solids were filtrated, washed with deionized water and dried at room temperature. The epitaxial growth of zeolite A on X was carried out according to the procedures described in Ref. [5]. The zeolite X core crystals and X-A core-shell composites were characterized by SEM (JEOL JSM-7000F), PXRD (PANalytical X'Pert PRO diffractometer using Cu $K_{\alpha 1}$ radiation) and TEM (JEOL-3010, operated at 300 kV). Cross-section samples for SEM studies were prepared by cross-section polisher (JEOL SM-09010) and those for TEM studies were made by focused ion beam (FIB, FEI Quanta 200 3D).

Results and discussion

Zeolite X single crystals with two different sizes, ca. 2 and 6 μm, were synthesized and used as the cores. The sizes and morphologies of the composites after different reaction times were studied using SEM. In order to understand the kinetics of epitaxial growth of zeolite A on X, the quantitative ratios between A and X in the core-shell composites after different reaction times were determined from the PXRD data by Rietveld refinement, as shown in Fig. 1. SEM observations of cross-sections of the composite crystals revealed the growth rate and quality of zeolite A; however, due to the un-uniform thickness of A around the core of zeolite X, no sound conclusions were drawn. TEM studies showed that zeolite A and X in the core-shell composites had a well-defined orientation relationship which can be summarized as $[110]_A//[110]_X$, $[-111]_A//[-11-1]_X$ and $[-11-2]_A//[1-1-2]_X$, as shown in Fig. 3. Three possible atomic structure models of the zeolite X-A interfaces are proposed, all with connected pores at the interfaces between zeolite X and A crystals, see Fig. 2.

Conclusions

Zeolite X-A core-shell composites with two different sizes of zeolite X cores have been synthesized by epitaxial growth. The growth rate and kinetics were studied by PXRD and SEM. Zeolites X and A in the core-shell composites have a well-defined orientation

relationship and the proposed atomic structures of the X-A interfaces suggest that the pores from the core and shell crystals are interconnected.

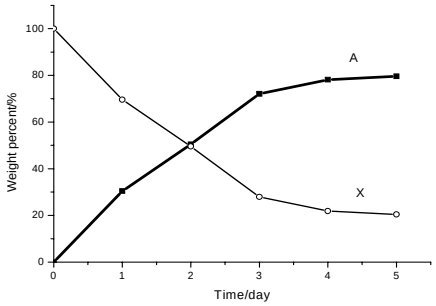

Fig. 1 Weight percent between A and X in core-shell composites after different reaction time.

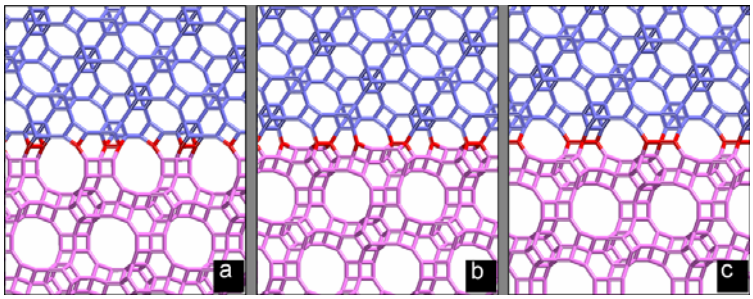

Fig. 2 Three possible atomic structure models for the X-A core-shell interface. (Above) zeolite A and (below) Zeolite X. The interface is in the middle.

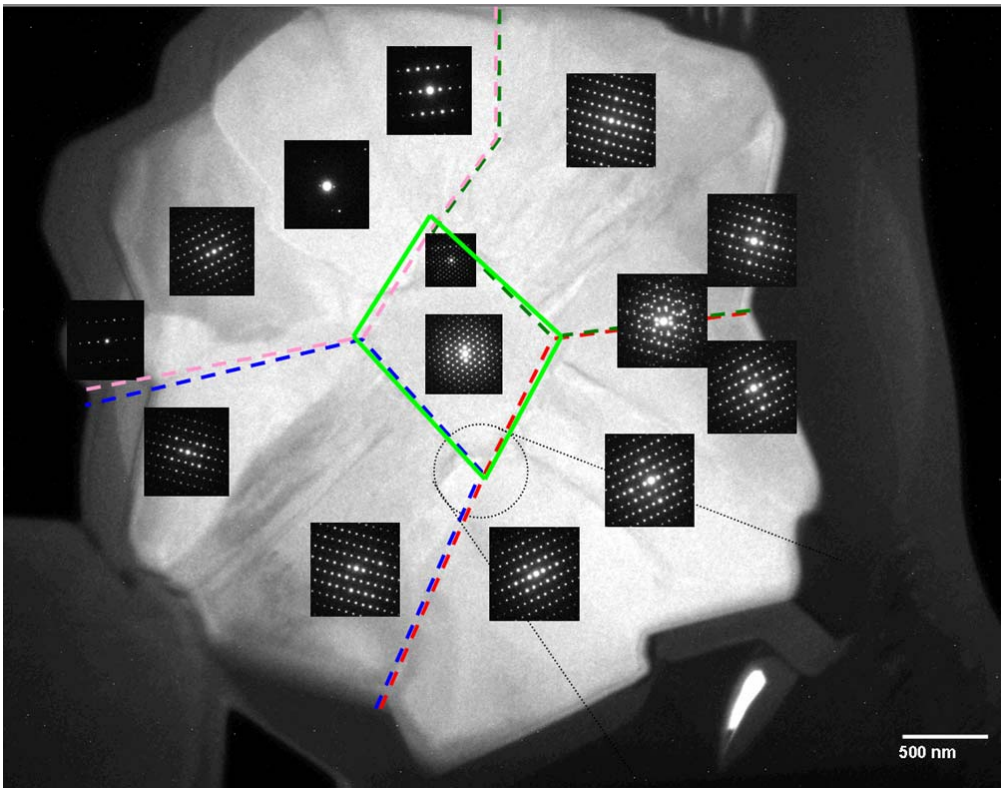

Fig. 3 Bright-field TEM image of an X-A composite crystal after 4-day growth of A on X. The zeolite X core in the middle of the image is marked by thick solid lines. The bright region around the zeolite X core is zeolite A shell, which is divided by different domains. Selected-area electron diffraction patterns were superimposed at the areas where they were taken.

References

[1] Davis, M. E., zeolites and molecular sieves: not just ordinary catalysts, Industrial and Engineering Chemistry Research, 30 (1991), 1675-1683.
[2] Davis, M. E., Ordered porous materials for emerging applications, Nature, 417 (2002), 813-821.
[3] Micheal T., Molecular sieves in the nanotechnology era, AIChE Journal, 4 (2002), 654-660.
[4] Bouizi, Y., Rouleau, L., Valtchev, V. P., Factors controlling the formation of core-shell zeolite-zeolite composites, Chemistry of Materials, 10 (2006), 4959-4966.
[5] Xiaoqin, Z., Ka-Lun, W., Sebastien, T., Till, H. M., Guangshan, Z., Valtchev, V., Svetlana, M., Platinum clusters confined in FAU–LTA hierarchical porous composite with a core–shell structure, Catalysis Today (2011) ASAP.

Synthesis with microwaves and characterization of mesoporous hectorites

Tatiana Sánchez, Pilar Salagre, Yolanda Cesteros.
Facultat de Química. Universitat Rovira i Virgili. C/Marcel·lí Domingo s/n 43007 Tarragona, Spain, tatiana.sanchez@urv.cat

Introduction

Hectorites are clays of the smectite group $Si_8Mg_{6-x}Li_xO_{20}(OH)_4]Xn_{x/n}.H_2O$, that present interesting applications in catalysis and in the preparation of composites [1]. Classical synthesis methods of these materials involve the use of high temperatures (>623K) or long times of heating at lower temperatures (393K). To solve these disadvantages, an interesting topic of research is the use of new technologies in the synthesis process. In hydrothermal treatments, the application of microwaves is a good alternative to reduce the synthesis time. Vicente et al reported a faster synthesis of hectorite by microwave-hydrothermal treatment at 393K in 8h instead of two week using conventional heating [2]. Another interesting technique is the ultrasounds to obtain an efficient reactant mixture [3]. An important disadvantage for hectorites application in catalysis is the collapse of their structure at relatively low temperatures. The introduction of pillars in interlamellar space or the delamination with mesopores layers aggregation can minimize this problem.

We describe the synthesis of mesoporous delaminated hectorite varying the pH of synthesis and employing microwaves and ultrasounds in the hydrothermal treatment and mixture of reagents stage respectively, to reduce the time of synthesis and increase crystallinity. These hectorites will be compared with silicate bearing hectorites, which present pillaring characteristics, also prepared with microwave or conventional heating.

Experimental

Delaminated Mesoporous Hectorites.

This type of hectorites was prepared following the method reported by Iwasaki et al [4]. An acidified sodium silicate solution was mixed with $MgCl_2$ and LiF. LiOH was then added for precipitation (to obtain pH=10 or 12). The molar ratio of reagents was Si:Mg:Li= 4,00:2,60:0,40. The resulting suspension was maintained 20 min in an ultrasound bath. Some experiments under ultrasounds were also performed at 40 min and 60 min to study the influence of this parameter. One sample was washed until pH=7 whereas the rest were washed maintaining the pH 10 and 12. Trimethyldodecylammonium chloride (AQ) was then added in molar ratio Li:AQ= 1:1. The hydrothermal treatment was performed by microwave irradiation at 453K for 1h or by conventional autoclave at 453K for 2h**.** All products were calcined at 893K for 75 min. The samples prepared were named as: $7HD_{20MW}$, $7HD_{40MW}$, $7HD_{60MW}$, $7HD_{20C}$, $7HD_{40C}$ and $7HD_{60C}$, $10HD_{20MW}$, $10HD_{20C}$, $12HD_{20MW}$. Each corresponds to pH, HD (delaminated hectorites), time of ultrasounds and type of thermal treatment (MW or C).

Silicate Bearing-Hectorites

Hectorites were prepared following the method reported by Torii et al [5]. First an acidified silicate solution was mixed with $MgCl_2$. NaOH was added until pH=10 to precipitate. The solution was washed, dried, and mixed with LiF. The molar ratio of reagents was Si:Mg:Li=4,00:2,70:0,30. The hydrothermal treatment was performed in two ways, one by laboratory microwave equipment at 453K for 1h ($10HB_{MW}$) and the other by conventional autoclave at 453K for 2h ($10HB_C$). Products were mixed with trimethyldodecylammonium chloride in molar ratio Li:AQ=1:1 and treated in reflux at 353K for 1h.

Samples were characterized by XRD, N_2 physisorption, TEM, NMR Si^{29}, ICP, XRF and determination of C.E.C.

Results and discussion

Table 1 summarizes the characteristics of the synthesized hectorites. XRD patterns of all samples were typical of clays materials and showed only one crystalline phase corresponding to hectorite (Fig 1). 001 reflection was not observed. This could be associated with delamination in HD hectorites, and with a very limited ordering in the c-axis for HB. At the same preparation conditions, the most crystalline delaminated hectorites were those prepared at pH=10 (higher crystallite size). The use of microwaves and the increase of ultrasounds time improved crystallization. The hectorite prepared at pH 12 was the most amorphous.

Table 1. Characterization of hectorites.

	BET area	CEC	XRD nm·	Si/ Mg	*Mg/ Alk		BET area	CEC	DRX nm·	Si/ Mg	*Mg /Alk
$7HD_{20MW}$	603	75,7	6,5	1,5	68,9	**$10HD_{20MW}$**	599	84,4	7,1	1,7	38,1
$7HD_{40MW}$	601	75,9	7,3	1,5	34,1	**$10HD_{20C}$**	590	73,1	6,3	2,2	56,4
$7HD_{60Mw}$	572	63,7	7,8	1,4	38,9	**$10HB_{MW}$**	262	39,0	11,9	1,4	7,2
$7HD_{20C}$	563	61,6	6,0	2,1	40,7	**$10HB_{C}$**	356	43,5	8,7	1,4	7,3
$7HD_{40C}$	561	53,0	6,5	2,2	14,6	**$12HD_{20MW}$**	353	39,0	5,7	1,1	52,9
$7HD_{60C}$	536	51,2	6,8	2,2	10,4						

*Alk= Alkalines ($Na^+ + Li^+$), · (006) crystallite size

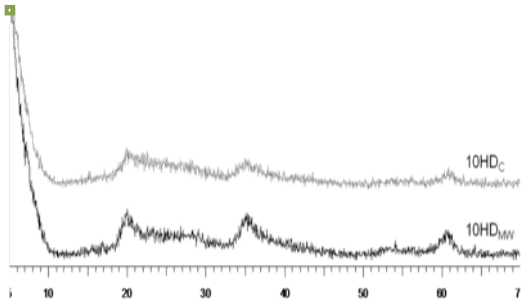

Figure 1. X-ray diffraction of $10HD_{20MW}$, $10HD_{20C}$.

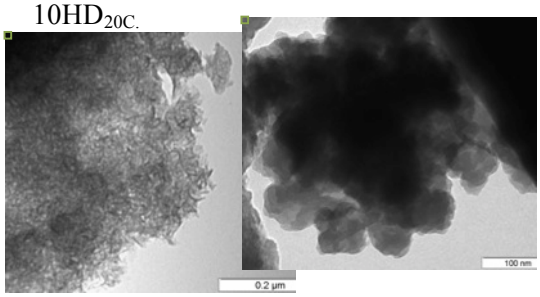

Figure 2. TEM images of $10HD_{MW}$ and $10HB_{MW}$

TEM images showed lamellar morphology for all samples (Fig 2). In delaminated hectorites we observed nano-sized layers aggregated to make mesoporous. In contrast, HB samples presented oriented layers. The BET area of delaminated hectorites of pH 7 and 10 when the synthesis was made with microwaves was higher (around 600 m^2/g table1.) than that prepared at higher pH. Besides, of these samples were more crystalline, and their CEC values were higher too. These characteristics can be related to the presence of alkaline (Li^+, Na^+) vacancies in the structure. The high Mg/Alk ratio and the shift to higher values of the peak corresponding to the Si^{4+} in the Td sheet (Si^{29} NMR) confirmed this fact.

HB hectorites were the most crystalline samples, but presented lowest areas and CECs, and not alkaline vacancies were observed.

Conclusions

Mesoporous delaminated hectorites synthesized by microwaves were more crystalline and presented higher areas and higher CECs than when conventional methods were used in the synthesis.

Acknowledgements

The authors are grateful for the financial support of the Ministerio de Educación y Ciencia of Spain and FEDER funds (CTQ2008-04433/PPQ).

References

[1] K. A. Carrado, Applied Clay Science 17, (2000) 1.

[2] I. Vicente, P. Salagre, Y. Cesteros, F. Guirado, F. Medina, J. E. Sueiras. Appl. Clay Science 43 (2009) 103

[3] S.P. Katdare, V. Ramaswamy, A.V. Ramaswamy, Microporous Mesoporous Materials 37 (2000) 329–336.

[4] T. Iwasaki, M. Reinikainen, Y. Onodera, H. Hayashi, T. Ebina, T. Nagase, K. Torii, K. Kataja, A. Chatterjee. Applied Surface Science. 130-132 (1998) 845

[5] K. Torii, T. Iwasaki, Y. Onodera, K. Hatakeda. Chemistry of Microporous Crystals. Kodansha and Elsevier. Tokyo, Japan (1991) 81.

Structural characterization of nanosized TiO_2 films inside SBA-15 pores

Juliana M. de Souza e Silva, Mathias Strauss, Camila M. Maroneze, Murilo P. Pereira, Yoshitaka Gushikem, Italo O Mazali.
Institute of Chemistry, University of Campinas, UNICAMP, P.O. Box 6154, 13083-970 Campinas, SP, Brazil mazali@iqm.unicamp.br

Introduction

Titanium dioxide has been proven to be versatile in the catalysis field, for example as support for metal and metal oxides[1] and as a catalyst itself for the photodegradation of organic pollutants.[2] For both listed applications, the use of TiO_2 on the nanometer scale is often employed because of nanoparticles high specific surface area and nanoparticles advantageous properties mainly attributed to quantum confinement effects.[2] However, the use of unsupported nanometric TiO_2 in solution is hindered by elevated costs for recovery and agglomeration or particle growth. To overcome these difficulties, nano-TiO_2 can be supported in high surface area supports, such as the rigid and thermally stable framework of mesoporous silica SBA-15. In this work, we present an effective method established in our research group for the controlled synthesis of nanometric TiO_2 inside SBA-15 pores by the impregnation, followed by the thermal decomposition, of titanium-based metallo-organic precursor.

Experimental

SBA-15 synthesis was based on procedure described elsewhere.[3] To obtain TiO_2@SBA-15, a solution of titanium (IV) di-(n-propoxy)-di-(2-ethylhexanoate) ($Ti(OnPr)_2(hex)_2$) was infiltrated in SBA-15 pores. Thereafter, the SBA-15 was filtered and copiously washed with hexane and thermally treated at 873 K. This procedure was named as one impregnation–decomposition cycle (IDC) and was repeated for 3, 5, 7 or 10 times, resulting in SBA-15/xTiO_2, with x corresponding to the IDC number.

Results and discussion

SAXS patterns of SBA-15 before and after IDC with $Ti(OnPr)_2(hex)_2$ (Fig 1 A) presented three characteristic (100), (110) and (200) signals, which result from the hexagonal ordering of the mesopores, and indicate that mesostructure is preserved even after 10 IDC. A shift in the reflections is observed after the first IDC and result from unit cell size a_0 contraction from 11.8 nm, for pure SBA-15, to 10.5 nm, for all SBA/xTiO_2 samples. N_2 adsorption-desorption isotherms (Fig 1 B) exhibited typical SBA-15 physisorption profile with type IV sorption isotherms with type H1 hysteresis loops. After seven successive IDC, one can observe a less steep adsorption step and a broader hysteresis loop, suggesting the formation of a

homogeneous layer of TiO_2 in the SBA-15 inner surface, causing progressive constriction in the pores width without their obstruction. DRS UV-Vis spectroscopy was used for the determination of the band gap variation upon IDC by extrapolation of the linear portion of the TiO_2 related band (Fig 1 C), since band-gap shift is a size induced effect observed for semiconductors nanoparticles, such as TiO_2.[2] IDC number increase resulted in band-gap shift to lower values, suggesting that TiO_2 in SBA-15 is under nanometric regime and increases in size after each IDC.

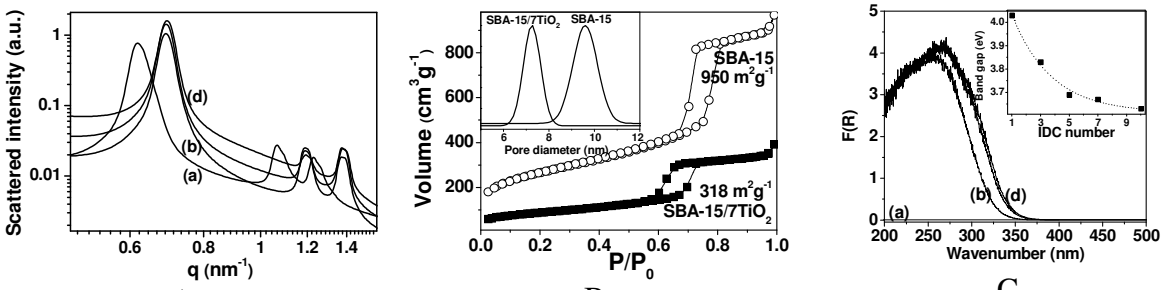

A B C

Figure 1. (A) SAXS patterns (B) N_2 physisorption isotherms (pore size distribution in detail) and (C) DRS UV-vis spectra (direct band-gap in detail) of (a) pure SBA-15 and (b), (c) and (d) for SBA-15/xTiO_2, with x = 3, 7 and 10, respectively.

Conclusions

SBA-15 with TiO_2 homogeneously distributed inside mesopores was prepared by the IDC methodology. Results presented show the ability to tune the size of TiO_2 inside SBA-15 mesopores, and therefore the capacity to control the band gap, the total pore size and the total surface area of the final material by only varying the number of infiltration-decomposition cycles.

Acknowledgements

The authors thank the National Institute of Science and Innovation in Complex Functional Materials (INOMAT), FAPESP, CNPq and CAPES for the fellowships and financial support. The Brazilian National Synchrotron Light Laboratory is acknowledged for SAXS experiments.

References

[1] Ulrike, D., The surface science of titanium dioxide, Surface Science Reports 48 (2003) 53-229.
[2] Strauss, M., Maroneze, C.M., de Souza e Silva, J.M., Sigoli, F.A., Gushikem, Y., Mazali, I.O., Annealing temperature effects on sol–gel nanostructured mesoporous TiO_2/SiO_2 and its photocatalytic activity, Materials Chemistry and Physics 126 (2011) 188–194.
[3] Yue, W., Xu, X., Irvine, J.T.S., Attidekou, P.S., Liu, C., He, H., Zhao, D., Zhou, W. Mesoporous Monocrystalline TiO_2 and Its Solid-State Electrochemical Properties Chemistry of Materials 21, (2009) 2540–2546.
[4] Ehrburger-Dolle, F., Morfin, I, Geissler, E., Bley, F., Livet, F., Vix-Guterl, C., Saadallah, S., Parmentier, J., Reda, M., Patarin, J., Iliescu, M., Werckmann, J., Small-Angle X-ray Scattering and Electron Microscopy Investigation of Silica and Carbon Replicas with Ordered Porosity, Langmuir 19 (2003) 4303-4308

Mechanically flexible silica thin films with high mesoporosity and tunable pore sizes

Sreeprasanth Pulinthanathu Sree[1], Jolien Dendooven[2], Annelore Schrauwen[3], Dries Smeets[3], André Vantomme[3], Kristiaan Temst[3], Kris Vanstreels[4], Mikhail Baklanov[4], Jin Won Seo[5], Jan D'Haen[6], Christophe Detavernier[2], Johan A. Martens*[1]

1. *Centre for Surface Chemistry and Catalysis, KU Leuven, Belgium*
2. *Department of Solid-State Physics, Ghent University, Belgium*
3. *Instituut voor Kern- en Stralingsfysica and INPAC, K.U. Leuven, Belgium*
4. *IMEC, Leuven, Belgium*
5. *Department MTM, Katholieke Universiteit Leueven, Belgium*
6. *Instituut voor Materiaalonderzoek (IMO) – IMOMEC, Universiteit Hasselt, Belgium*

***** *Corresponding author: E-mail: Johan.Martens@biw.kuleuven.be*

Introduction

Supported Mesoporous thin films with controlled accessible porosity are of great importance in the development of optical, electronic, sensor devices and catalytic surfaces. Pore size, pore volume and accessibility of the porosity are critical properties which qualify the films for various applications [1]. Here we report a facile and simple way of making mesoporous silica films with fully accessible porosity, tunable pore sizes and varying thicknesses. The synthesis of transparent and smooth silica thin films were realized via spin coating of a suspension of zeolitic nanoslabs and triblock copolymer on substrate, followed by hydrothermal annealing and calcination.

Experimental

The synthesis was inspired from that of 3 D ordered Zeotile-4 powder material [2, 3]. The zeolitic nanoslab suspension was combined with acidic triblock copolymer (P123). This mixture was diluted and spin coated over Clean Si wafers. The spin coated films were hydrothermally annealed by keeping them inside an autoclave at elevated temperatures (65-90°C) for 50-60 h, followed by drying and calcination. The calcined films were characterised with Ellipsometric porosimetry (EP), Atomic Force Microscopy (AFM), X-ray reflectometry (XRR), Transmission Electron microscopy (TEM), Rutherford Backscattering Spectroscopy (RBS) Grazing Incidence Small Angle X-ray Scattering (GISAXS) etc. Chemical functionalization of the films was realized via Atomic Layer Deposition (ALD).

Results and discussion

Ellipsometric porosimetry (EP) using toluene probe has been used as a convenient tool to determine the effective porosity of the films on their original support [4]. Films having porosity in the range of 70 to 90 vol%, Pore sizes of 5- 25 nm and thicknesses ranging from 100 to 500 nm were easily realized. AFM images revealed that the films had a very smooth surface (average surface roughness < 4nm). These transparent films processed very low refractive index (~ 1.08) and low density (~ 0.4 g/cm^3). From GISAXS it has been observed that the films had a disordered structure. The porous thin films exhibited a reversible shrinkage during adsorption-desorption of toluene. Shrinkage up to 30 % of its initial thickness as result of adsorption was observed, which is not very common in case of mesoporous silica films. The young modulus of these films measured by nano indentation was very low (0.9 GPa) which reasons its mechanical flexibility. Chemical functionalization of the pore walls of the film using Atomic Layer Deposition (ALD) [5] of TiO_2 confirmed the fully accessible porosity measured by EP. Ruther ford backscattering spectroscopy and TEM done after the ALD further confirmed the accessibility of the pores.

Conclusions

The mesoporous films we present have very high porosity which is fully accessible for organic as well as inorganic molecules. This fully accessible porosity was obtained by the random linking of nanoslabs. The adsorption of an organic molecule (toluene) and deposition of inorganic compounds (TiO_2) suggests the new films to be useful in all kinds of applications where accessibility of the porosity is critical. The adsorption induced shrinkage of the films also could be made useful in special applications such as nano actuators.

Acknowledgements

The authors acknowledge the Flemish IWT for financial support through an SBO-METACEL project. JAM acknowledges the Flemish government for long-term structural funding (Methusalem).

References

[1] E. K. Richman, T. Brezesinski and S. H. Tolbert, *Nat. Mater*. 2008, **7**, 712-717
[2] C. E. A. Kirschhock, S. P. B. Kremer, J. Vermant, G. Van Tendeloo, P. A. Jacobs, J. A. Martens, Chem. Eur. J. 11 (2005) 4306.
[3] S. Bals, K. J. Batenburg, D. Liang, O. Lebedev, G. V. Tendeloo, A. Aerts, J. A. Martens and C. E. A. Kirschhock, *J. Am. Chem. Soc*. 2009, **131**, 4769-4773.
[4] M. R. Baklanov, K. P. Mogilnikov, V. G. Polovinkin and F. N. Dultsev, *J. Vac. Sci. Technol. B*. 2000, **18**, 1385-1391
[5] S. M. George, *Chem. Rev*. 2010, **110**, 111-131.

Differences in hydrocarbons adsorption on PILCs of similar Zr (pillars) composition

J.M. Guil [a,*], S. Jatib Khatib [a], N.G. Almarza [a], A. Gallardo [a], J. Pires [b]
[a] *Instituto "Rocasolano", CSIC. Serrano, 119, 28006-Madrid (Spain)*
[b] *Departamento de Química e Bioquímica e CQB, Faculdade de Ciências, Universidade de Lisboa, Edifício C8,Campo Grande, 1749-016 Lisboa (Portugal)*
** J.M.Guil@iqfr.csic.es*

Introduction

Pillared interlayered clays (PILC) are being synthesized and studied to obtain materials with micropores larger than usual with controlled surface chemistry. They would be used in industrial processes in which reactant or product molecules are big. Limited success has been achieved getting adequate interlayer distances but stability under reaction conditions (temperature and humidity) is not sufficient yet. Research continues since it would be very interesting to produce low cost materials with those characteristics for adsorption and catalytic applications.
An important aspect of the studies is to characterize the pillars distribution in the interlayer space because it determines the microporous features once the pillar density and height have been fixed. To that end, we have applied our experience in studies of textural and molecular diffusion with zeolites and PILCs [1,2] by adsorption of hydrocarbons of different size and shape followed by volumetry and microcalorimetry. Information on surface energetics is also obtained. The experimental results will also be used in theoretical studies (modelling/simulation).

Experimental

PILCs were synthesized from two clays (Portosanto, Portugal, and Wyoming, USA). Table 1 shows Zr content and structural and textural properties of PILCs samples.

Tabla 1. Zr content and structural and textural properties of PILCs samples.

Sample		Zr mmol/g	pillars /nm^{-2}	h_{pillar}/ nm	V_{up} cm^3/g
PTS	**M6**	1,71	0,60	0,71	0,097
	M5	1,73	0,61	0,70	0,106
	M7	1,73	0,61	0,70	0,121
WYO	**M9**	1,71	0,60	0,85	0,101
	M8	1,87	0,67	0,85	0,103
	M10	2,01	0,73	0,78	0,077

Results and discussion

PILC(PTS) samples present the same pillar density and pillar height but micropore volumes are different. It must be due to a different distribution and grouping of pillars that produce larger micropore space although the mean dimension can be similar. In the case of PILC(WYO) the Zr content changes between samples. Equal and different pillar height and micropore volume were obtained.
Fig. 1 presents as an example volumetric isotherms of the used hydrocarbons on one of the samples. Total uptake depends on the molecular size and its facility of molecules to fit inside the microporous space.

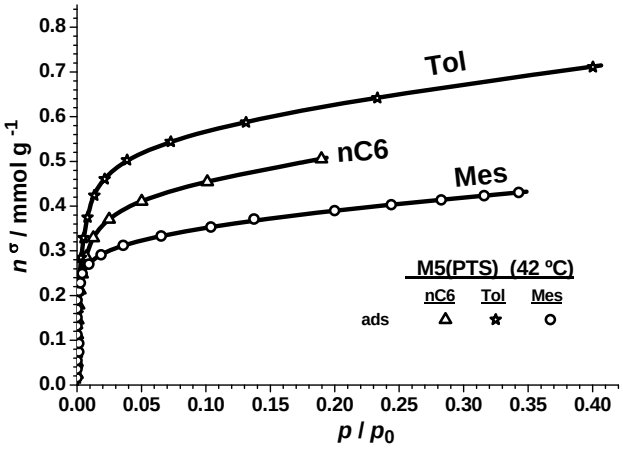

Fig.1. Adsorption on M5(PTS) sample.

Differential heats of adsorption vs. amount of adsorbed toluene on some of the PILCs are shown in Fig. 2. A large initial fall of the adsorption heat is apparent in all cases. It is due to the specific interaction of the aromatic ring with the acid centres on the pillars (Zr cations). Adsorption on the rest of the microporous volume follows. The increase of the heat afterwards in some cases is produced by lateral interactions; it unveils the existence of larger cavities. The final fall in the $q^{st,\sigma}$-n^{σ} curves marks the end of micropore filling ($n_{\mu p}$). The relative position of the calorimetric isotherms is related to the micropore size: the narrower produce somewhat higher heats of adsorption.

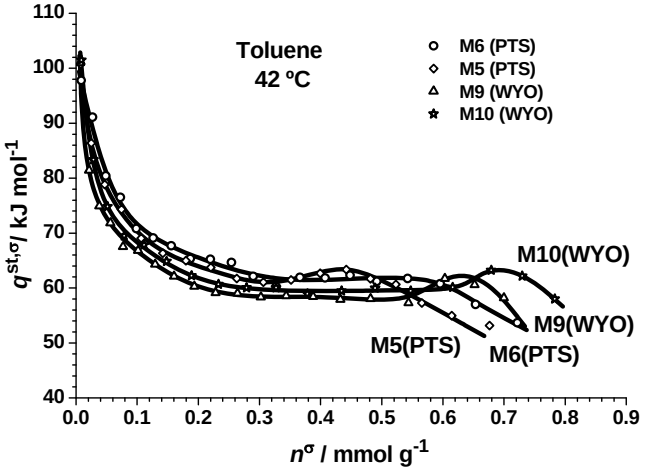

Fig. 2. Heat of toluene adsorption on PILCs.

Table 2 presents the results for the three adsorbates on the two families of PILCs. The packing density of the adsorbate inside the micropores, d_{pck}, and its percentage relative to the liquid density, $\%d_{pck} = 100 \cdot d_{pck}/d_{liq}$, gives an idea of the size of microporous cavities [1]. Percentage packing density, $\%d_{pck}$, of *n*-hexane and toluene on each PILC(PTS) sample are similar although micropore volumes are different. M9 and M8 WYO samples have similar micropore volume and pillar height; values of $\%d_{pck}$ are not so different. However, the M10(WYO) sample with lower pillar height and micropore volume presents the larger $\%d_{pck}$. We must conclude that it has a small number of cavities but of the largest dimensions.

Tabla 2. Hydrocarbons adsorption on PILCs samples

		n-Hexane			Toluene			Mesitylene		
		$n_{\mu p}$	d_{pck} *		$n_{\mu p}$	d_{pck} *		$n_{\mu p}$	d_{pck} *	
Sample		cm^3/g	mmol/cm^3	**$\%d_{pck}$**	cm^3/g	mmol/cm^3	**$\%d_{pck}$**	cm^3/g	mmol/cm^3	**$\%d_{pck}$**
PTS	**M6**	0,480	4,95	**67**	0,605	6,24	**68**	0,290	2,99	**38**
	M5	0,370	3,49	**47**	0,470	4,43	**48**	0,250	2,36	**30**
	M7	0,485	4,01	**54**	0,610	5,04	**55**			
WYO	**M9**	0,560	5,54	**75**	0,680	6,73	**73**	0,440	4,36	**55**
	M8	0,645	6,26	**84**	0,725	7,04	**77**	0,410	3,98	**50**
	M10	0,550	7,14	**96**	0,740	9,61	**105**	0,390	5,06	**64**

* $d_{pck} = n_{\mu p}$(microcalorimetry) / $V_{\mu p}$ ('*t*' method)

A similar analysis extended to all results, volumetric and calorimetric, allows us to get conclusions on the texture of these PILCs. Simulation studies with simple geometric models of the nanoscopic structure of the PILCs are being carried out. The goal is to determine how the distribution/grouping of pillars conditions the porosity and adsorption properties. The simulation of adsorption processes is carried out by Monte Carlo methods in the microcanonical ensemble.

Acknowledgements

Authors acknowledge the financial support from the Ministry of Science and Innovation, Spain (Project FIS2010-15502) and Madrid Autonomous Community (Project CM P2009/ESP-1691).

References

[1] J.M. Guil, R. Guil-López, J.A. Perdigón-Melón, A. Corma. "Determining the topology of zeolites by adsorption microcalorimetry of organic molecules ". *Micropor. Mesopor. Mat.*, 22 (1998) 269.

[2] J.M. Guil, J.A. Perdigón-Melón, M. Brotas de Carvalho, A.P. Carvalho, J. Pires. "Adsorption microcalorimetry of probe molecules of different size to characterize the microporosity of pillared clays". *Micropor. Mesopor. Mat.*, 51 (2002) 145.

Synthesis of Metallic Nanoparticles inside Organized Mesoporous Materials

Paulin Buchwalter,[1, 2, 3] Pierre Rabu,[2,*] Bénédicte Lebeau,[1] Jacky Rosé,[3] Pierre Braunstein,[3,*] Jean-Louis Paillaud.[1,*]

[1] *MPC-IS2M, LRC CNRS 7228, UHA, ENSCMu, 3 rue Alfred Werner, 68093 Mulhouse Cedex, France, *corresponding author: Jean-Louis.Paillaud@uha.fr*

[2] *IPCMS, UMR 7504 CNRS-UdS, 23 rue du Loess, BP43, 67034 Strasbourg cedex 2, France, *corresponding author: pierre.rabu@ipcms.u-strasbg.fr*

[3] *LCC, Institut de Chimie UMR 7177 CNRS-UdS, 4 rue Blaise Pascal, CS 90032, 67081 Strasbourg, France, *corresponding author: braunstein@chimie.u-strasbg.fr*

Introduction

The synthesis of nanoparticles inside mesoporous materials allows a better control of their size and dispersion. These properties are directly relevant to their use in catalysis. Recently, a range of metal phosphides have found applications in hydrodesulfurisation (HDS) [1] and hydrodenitrogenation (HDN) [2].
Moreover, mesoporous silica (SBA-15, SBA-16) show very reproducible and tunable characteristics: channel width, wall thickness and pore size distribution can all be controlled during the synthesis [3].
Here we describe an easy synthesis of cobalt phosphide nanoparticles, starting from molecular metal clusters. Following previous studies [4] and due to their stoichiometry, $Co_4(CO)_{10}(\mu\text{-dppa})$ (dppa = $Ph_2PNHPPh_2$) and $Co_4(CO)_8(\mu\text{-dppa})_2$ are shown to be excellent cobalt and phosphorous providers for the formation of Co_2P. In the present study, the cluster $Co_4(CO)_{10}(\mu_4\text{-PPh})_2$ presenting a square planar geometry of the four cobalt centers and a direct bond between them and both P atoms has also been used as precursor. Their impregnation inside mesoporous silica followed by calcination leads to confined Co_2P nanoparticles.

Experimental

The organometallic clusters and the mesoporous silica were synthesized according to the literature [5-7]. The clusters were characterized by IR, ^1H and ^{31}P NMR spectroscopies and then impregnated into the silica matrices by dipping into CH_2Cl_2 solutions. A thermal treatment under neutral or slightly reducing atmosphere at different temperatures gave the Co_2P nanoparticles (occluded and external). The structure and composition of the nanoparticles and of the matrices were studied by powder X-ray diffraction (PXRD), N_2 adsorption/desorption, transmission electron microscopy (TEM) and nanoprobe electron dispersive X-ray analysis (EDX).

Results and discussion

The combined studies of unsupported nanoparticles and of the impregnated silica matrices (namely PXRD, SEM, TEM) show that depending on the cluster precursor, different phases can be obtained: cubic Co, Co_2P and a P-rich amorphous phase. Metallic Co may be easily eliminated by dissolution from HCl solutions. PXRD were also collected as a function of temperature to follow the nanoparticle size growth. From Figure 1, the PXRD patterns prove that Co_2P is already formed at 500 °C. At this temperature, the particles are not directly observable by TEM but, using a replica technique [8] the difficulty is overcome.

Figure 1. Formation of nanoparticles as a function of temperature. The diffraction peaks from the alumina substrate have been removed for clarity (*).

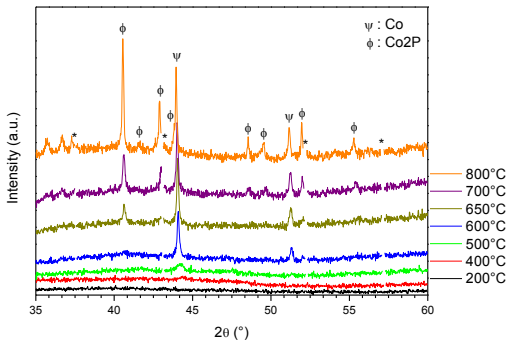

Figure 2. SEM (a) and TEM (b) images of Co_2P/SBA-15.

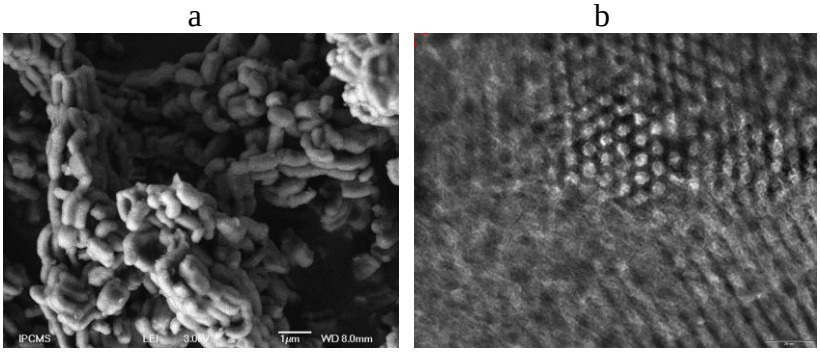

Conclusions

From well-defined molecular precursors with the suitable stoichiometry, confined Co_2P nanoparticles in organized mesoporous materials may be obtained at relatively low temperature. Catalytic tests in HDS and HDN will be performed.

Acknowledgements

We are grateful to the Région Alsace (Doctoral grant to P. Buchwalter) and the Centre National de la Recherche Scientifique and to the Ministère de la Recherche for support.

References

[1] J. A. Cecilia, A. Infantes-Molina, E. Rodriguez-Castellon, A. Jimenez-Lopez, Applied Catalysis B: Environmental, 92 (2009), 100–113.
[2] X. Duan, X. Li, A. Wang, Y. Teng, Y. Wang, Y. Hu, Catalysis Today, 149 (2010), 11–18.
[3] D. Zhao, Q. Huo, J. Feng, B. F. Chmelka, G. D. Stucky, J. Am. Chem. Soc., 120 (1998), 6024.
[4] F. Schweyer-Tihay, P. Braunstein, C. Estournès, J. L. Guille, B. Lebeau, J.-L. Paillaud, M. Richard-Plouet, J. Rosé, Chem. Mater., 15 (2003), 57-62.
[5] C. Moreno, M. J. Macazaga, M. L. Marcos, J. Gonzalez-Velasco, S. Delgado, J. Organomet. Chem., 452 (1993), 185-192.
[6] R. C. Ryan, L. F. Dahl, J. Am. Chem. Soc., 97:23 (1975), 6904–6906.
[7] D. Zhao, Q. Huo, J. Feng, B.F. Chmelka, G. D. Stucky, J. Am. Chem. Soc., 120 (1998), 6024-6036.
[8] G.Clavel, Y. Guari, J. Larionova, C. Guérin, New. J. Chem., 29 (2005), 275–279.

Effects of Surfactant Addition on Crystallinity and Yield of MFI Zeolites in OSDA-Free Synthesis

Teruoki Tago, Saori Fujiwara, Hiroki Konno, Yuta Nakasaka, and Takao Masuda
Division of Chemical Process Engineering, Faculty of Engineering, Hokkaido University, N13W8, Kita-Ku, Sapporo, Hokkaido, Japan, tago@eng.hokudai.ac.jp

Introduction

In hydrothermal synthesis of zeolites, organic-structure-directing agents (OSDA) are employed to form zeolite structure, in addition to alkali metals, and Si and Al sources. Recently, there has been growing interest in OSDA-free synthesis of zeolites, such as MFI and MOR. In the OSDA-free synthesis of zeolites, Si/Al ratio and concentration of alkali metals in the synthetic solution are important factors to form the zeolite structure. However, since formation of zeolite nuclei and crystals proceeds in a strong alkaline solution, nucleation/crystallization and resolution of zeolites simultaneously occurs, leading to low yield of zeolite and poor crystallinity due to deposition of amorphous silica.

In contrast, we successfully prepared MFI and MOR zeolite nanocrystals via hydrothermal synthesis in a water/surfactant/organic solvent [1–4], where the non-ionic surfactants adsorbed on the surface of the zeolite precursors likely induced the formation of zeolite nuclei. Moreover, it is considered that the adsorbed surfactant inhibit the zeolite nuclei and crystal from their resolution. Main objective of this study is development of OSDA-free synthesis of MFI zeolite at high zeolite yield. The effects of surfactant addition and Si/Al ratio on the crystallinity and yields of obtained MFI zeolites are investigated.

Experimental

Non-ionic surfactant (Polyoxyethylene(n)oleylether, $C_{18}H_{35}$-$(OC_2H_4)_n$-OH, n=2, 10, 15, 20, 50, defined as O-n hereafter) was employed in this study. A water solution containing Si and Al sources was obtained by hydrolyzing each metal alkoxide with an alkaline solution at room temperature. The molar ratio of Si to Al (Si/Al) were in the range of 12.5 to 200. Then, non-ionic surfactant, O-n, was added into the solution at constant concentrations of oxyethylene group 0.75 mol/L (e.g. O-10 and O-15 concentrations of 0.075 and 0.05 mol/L, respectively). The mixture was then placed in a Teflon sealed stainless steel bottle (100 cc bottle), heated to 423 K, and then held at this temperature for 48-72 h with stirring to yield MFI zeolite.

Results and discussion

In order to investigate the effect of surfactant properties on the crystallinity, OSDA-free MFI zeolite synthesis was carried out using the surfactants with different oxyethylene-chain length (O-n). It is well-known that HLB (Hydrophile-Lipophile Balance) value can be used to predict the surfactant hydrophilic/hydrophobic properties. As the hydrophobic property increases, the HLB value decreases, and vice versa. Accordingly, HLB values were used to

evaluate hydrophilic/hydrophobic properties of surfactants. Figure 1 shows the effects of HLB value on an amount of adsorbed N_2 within micropore, which was measured at relative pressure P/P_0 of 0.0 in N_2 adsorption isotherms. X-ray diffraction patterns of the samples in Fig. 1 showed the peaks corresponding to MFI zeolite. As shown in the figure, the addition of surfactant into the synthetic solution was effective in increasing the amount of adsorbed N_2 within micropore of MFI zeolite prepared in OSDA-free conditions. Moreover, the HLB vales of surfactant affected the amount of N_2 adsorbed on micropore, which reached to approximately 85-90 ml(STP)/g when using O-15. Since zeolites possess hydrophilic-hydrophobic properties on their surface, there exists the affinity between the zeolite surface and surfactant, depending on HLB values. Accordingly, the HLB values affected the development of micropore. Figure 2 shows the effect of Si/Al ratio on the yields of ZSM-5 zeolite, and FE-SEM images of the obtained samples. As compared with the sampel without surfactant, the yield of MFI zeolite at Si/Al=12.5 incresed from approximately 60 % to 90 % in OSDA-free synthesis using sufactant O-15. The high yield of zeolite in OSDA-free synthesis was ascribed to the adsorption of surfactant on the zeolite surface, where the resolution of Si and Al atoms in zeolite framework were inhibited. As shown in the FE-SEM images, the crystal sizes of MFI zeolite depended on Si/Al ratio, indicating that the Al ions in the solution enhanced the nucleation rate.

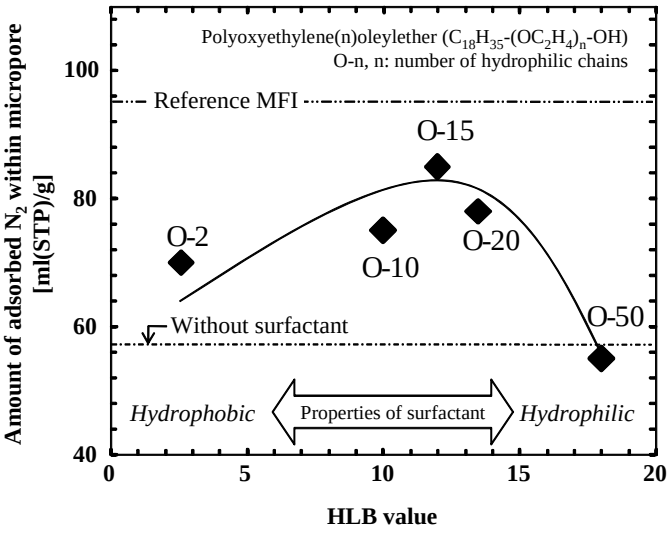

Fig. 1. Effects of HLB values of surfactant on an amount o f adsorbed N_2 within micropore.

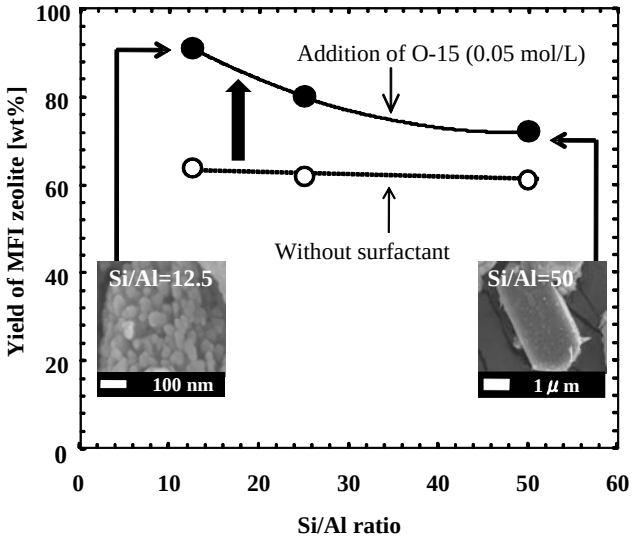

Fig. 2. Effects of Si/Al ratio and surfactant addition on yields of MFI zeolite.

Acknowledgements

This work was supported by the Research Grant Program from New Energy and Industrial Technology Development Organization (NEDO) of Japan.

References

[1] T. Tago, et al., Chem. Lett., 33, 1040-41 (2004)
[2] T. Tago, et al., J. Nanosci. Nanotechnol., 9, 612(2009)
[3] T. Tago, et al., Top. Catal., 52, 865(2009)
[4] K. Iwakai, et al., Micropor. Mesopor. Matt., in press

NMR studies of thermal stability of Zn-BTC

Tomaž Čendak[1], Tadeja Birsa Čelič[1], Mojca Rangus[1], Nataša Zabukovec Logar[1], Gregor Mali[1], Venčeslav Kaučič[1]
[1]*National Institute of Chemistry, Hajdrihova 19, 1000 Ljubljana, Slovenia; tomaz.cendak@ki.si*

Introduction

Metal Organic Frameworks (MOFs) are crystalline compounds built up from the metal atoms or clusters connected with the rigid multifunctional organic ligands (linkers). Known for their low density (down to 0.2 g cm^{-3}), high surface area (up to 5900 m^2 g^{-1}) and large pore volume (up to 2 cm^3 g^{-1}) [1], MOFs are suitable for gas storage, applications in heterogeneous catalysis and drug delivery [2]. Here we report on the solid-state NMR studies of thermal stability of porous zinc benzene-1,3,5-tricarboxylate (Zn-BTC).

Experimental

Zn-BTC used for the NMR studies was crystallized from the gel with molar ratios of reactants $Zn(ac)_2 \cdot 2H_2O$: BTC : 93.8 H_2O : 72.4 EtOH after solvothermal treatment at 448 K for 1 day in Teflon-lined autoclaves. ^1H-^{13}C CPMAS NMR spectra of the Zn-BTC powder have been recorded on a 600MHz Varian NMR system equipped with a Varian 3.2 mm MAS probe.

Results and discussion

Hydrothermal stability of Zn-BTC was evaluated by boiling in distilled water for different periods of time up to 16 hours under refluxing.

The reversibility of water sorption was first confirmed by XRD analysis. Zn-BTC samples were heated up to 200 °C and then allowed to rehydrate in humid air for 24 hours. The XRD patterns were collected using continuous scanning mode in 2θ range 5 - 70° with a scanning speed of 0.013° at a counting time of 100 s per step. The XRD pattern of as-synthesized Zn-BTC is shown in Figure 1a. Heating of the samples up to 200 °C (Figure 1b) causes the desorption of water from the pores and leads to a phase change. Dehydration is however reversible as shown by the XRD pattern of the rehydrated Zn-BTC (Figure 1c) which is equivalent to the pattern of the as-synthesized Zn-BTC.

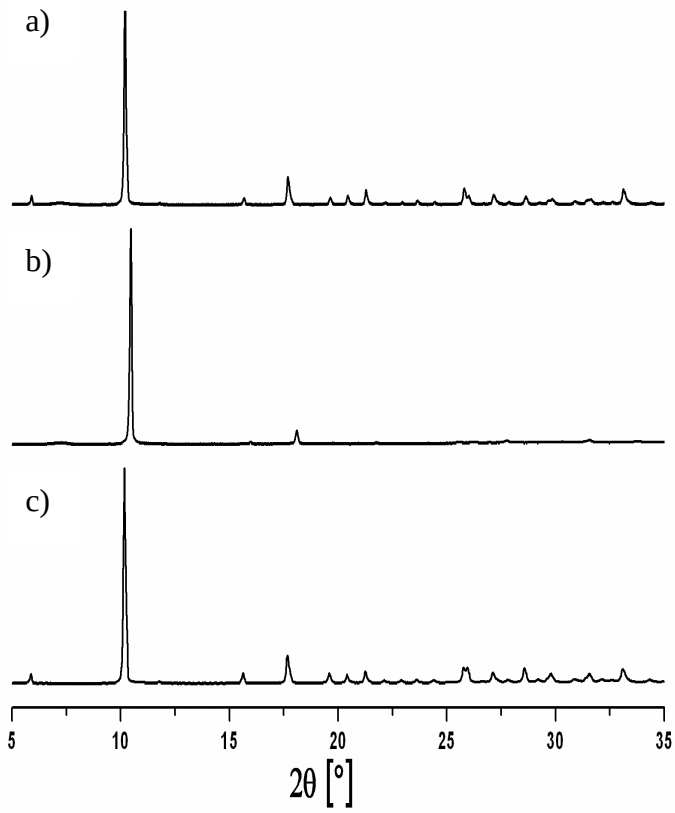

Figure 1: XRD patterns of a) as-synthesized Zn-BTC, b) a sample heated to 200 °C and c) a sample heated to 200 °C and rehydrated for a day.

Similar studies of thermal stability were then done using ^{13}C NMR spectroscopy. Carbon spectrum of powdered sample of as-synthesized Zn-BTC is shown in Figure 2a. Peaks corresponding to ^{13}C nucleus in aromatic rings (between 131 and 138 ppm) and carboxylic groups (between 174 and 178 ppm) are clearly visible. Samples of Zn-BTC were then heated in a flow of nitrogen. Heating up to 200 °C causes desorption of water from the pores and smaller framework modifications as seen by isotropic chemical shifts and broadening of peaks on the spectra (Figure 2b). Further heating collapses the structure as suggested by broad peaks in the NMR spectra (Figure 2c). Finally the reversibility of water sorption was studied. Zn-BTC sample was heated to 200 °C then left to cool down and rehydrate for three days. Comparing spectra of the rehydrated (Figure 2d) with the spectra of as-synthesized sample suggests that structure of Zn-BTC is re-formed after rehydration.

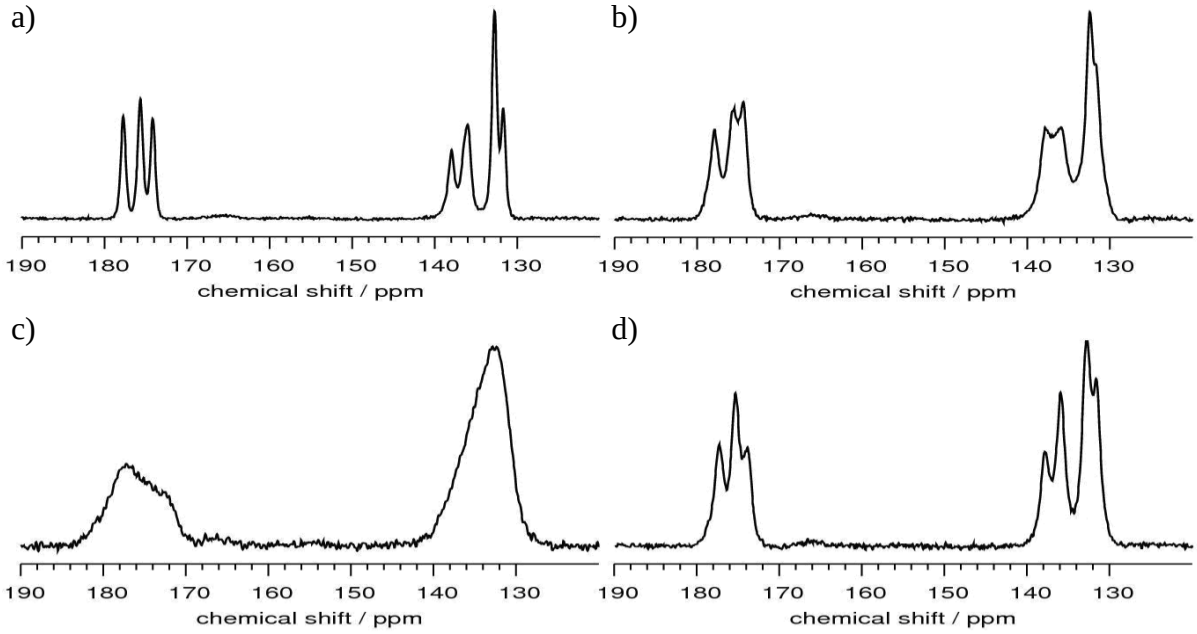

Figure 2: ^{1}H-^{13}C CPMAS NMR spectra of a) as-synthesized Zn-BTC, b) a sample heated to 200 °C, c) a sample heated to 300 °C and d) a sample heated to 200 °C then cooled and rehydrated for three days.

Conclusions

Solid-state NMR studies confirmed the thermal stability of Zn-BTC. For temperatures up to 200 °C structural changes of Zn-BTC framework are almost fully reversible if sample is allowed to rehydrate. If heated above 200 °C the framework irreversibly collapses.

Acknowledgements

The support of Slovenian Research Agency through the research programme P1-0021 is acknowledged.

References

[1] Ferey, G., Hybrid porous solids: past, present, future, Chemical Society Reviews, 37 (2008), 191-214
[2] Czaja, A. U., Trukhan, N., Müeller, U., Industrial applications of metal-organic frameworks, Chemical Society Reviews, 38 (2009), 1284-1293

Studies of the uptake and decomposition mechanisms of volatile metal carbonyls in zeolites

A. Shepherd and R.F Howe
University of Aberdeen, ashley.shepherd@abdn.ac.uk

Introduction

Molybdenum oxide based catalysts have significant importance for a variety of oxidation and hydrotreating reactions, as well as the much studied methane dehydroaromatization reaction. Catalysts are generally prepared from either the wetness impregnation of the zeolite with an aqueous solution of $(NH_4)_3Mo_7O_{24}$ or the physical mixing of MoO_3 with the zeolite. In both cases, MoO_3 crystallites on the surface can vapourise and migrate into the pores on calcination, however the extent of migration is unclear and many groups believe the vast majority of Mo species remain in large clusters on the surface.[1]

A potentially better method of preparing metal oxide/zeolite catalysts involves the room temperature sublimation and decarbonylation of $M(CO)_6$ (M = Mo, W).[2-5] This synthesis method has the potential to leave MO_3 in a highly dispersed state throughout the zeolite, leading in turn to a catalyst of higher intrinsic activity. However, the size of the $M(CO)_6$ molecule (greater than 7 Å) strongly restricts the choice of zeolite to those with larger pores. Furthermore, it can be difficult to control the weight loading of metal species in the catalyst.

Experimental

A selection Mo and W catalysts were prepared via this method, with the view of preparing catalysts of higher activity for the methane dehydroaromatization reaction. The zeolites selected included HUSY, HBeta, and HZSM-5. A variety of decarbonylation techniques were tested, including thermal decomposition (gradual and flash heating with and without the presence of O_2) and photodecarbonylation techniques (in the presence of O_2).[6] The catalyst weight loading was determined gravimetrically and verified using XPS. XPS also gave insight into the oxidation state of Mo species, as well as the extent to which Mo is oxidized by the zeolite protons after decarbonylation.

The resulting catalysts were characterized using a variety of techniques. XRD was used to verify structural integrity remains throughout the decomposition process. ^{27}Al Solid State NMR was used to investigate how the metal species interacts with the framework and IR spectroscopy was used to investigate the mechanism of decomposition of metal carbonyls within the zeolite pores.

Results and discussion

$Mo(CO)_6$ loaded well into zeolite HUSY and gave Mo weight loadings ranging from 3-12% depending on decarbonylation technique. Despite loading well into HBeta, Mo weight loadings varied from 0.7% - 9%. $Mo(CO)_6$ and $W(CO)_6$ do not load into HZSM-5 and only

surface weight loadings could be achieved. $W(CO)_6$ only weakly physisorbs into zeolites and weight loadings of W varied from 0-14% on HUSY and 0-9% on HBeta.

XPS analysis of as prepared catalysts before exposure to atmospheric air showed that the Mo metal remaining after $Mo(CO)_6$ decarbonylation is strongly oxidised by the zeolite protons leaving Mo in a high oxidation state.

XRD analysis showed that the decarbonylation and incorporation of Mo and W into all zeolites did not significantly effect the framework.

Analysis by IR showed that $Mo(CO)_6$ decarbonylates in stages to give a variety of different subcarbonyl species, first witnessed by Abdo *et al.*[2] The extent to which the various decarbonylation species are formed during gradual and flash heating methods can be compared.

The OH region of the IR spectrum is well known to give two peaks, corresponding to terminal silanol groups and Bronsted acid sites. In the case of HUSY, three peaks can be seen, corresponding to terminal silanols and the acid sites of both the sodalite cages and supercages. The extent to which acid sites are lost from the zeolite during decarbonylation, due to the anchoring of molybdenum on Al sites and the oxidation of Mo by zeolite protons could be monitored by analysing the areas of the corresponding peaks.

^{27}Al Solid State NMR confirmed the anchoring of Mo on Al sites in all zeolites and showed to which extent Al is extracted from the framework during this process.

Conclusions

The weight loading of Mo and W in zeolites can be controlled to some extent by choice of decarbonylation technique. A variety of characterization techniques were successfully employed to analyze these catalysts fully, in both the synthesis methods and the Mo species remaining after catalyst synthesis.

Acknowledgements

Acknowledgements to UOP and University of Aberdeen for funding this project.

References

[1] B. M Weckhuysen, D. Wang, M. P. Rosynek J. H. Lunsford, J Catal. 175 (1998) 338
[2] S. Abdo, R. F. Howe, J Phys. Chem. 87 (1983)1713
[3] P. Gallezot, G. Coudurier, M. Primet, B. Imeli, ACS. Symp. Ser. No. 40 (1997) 144
[4] Y. Okamoto, A. Maezawa, H. Kane, I. Mitsushima, T. Imanaka, J Chem. Soc., Faraday Trans. 1, 84 (1988) 851
[5] T. Komatsu, T. Yashima, J Mol. Catal., 40 (1987) 83
[6] G.A. Ozin, S. Ozkar, R.A. Prokopowicz, Acc. Chem. Res. 25 (1992) 553

Controlling structural properties in mesoporous materials with zeolitic features.

V. Meynen[1], J. Vernimmen[1], L. C. de Ménorval[2], M. Chiesa[3], S. Van Doorslaer[4], J. Kärger[5], F. Grinberg[6], M. Mertens[7], O.I. Lebedev[8,9], G. Van Tendeloo[9], P. Cool[1]
[1]*Laboratory of Adsorption and Catalysis, Department of Chemistry, University of Antwerpen, Universiteitsplein 1, B-2610 Wilrijk, Belgium*; vera.meynen@ua.ac.be
[2]*Agrégats, Interfaces et Matériaux pour l'Energie (AIME), ICG (UMR 5253 - CNRS), Université Montpellier II, 2 Place Eugène Bataillon, CC-1502, F-34095 Montpellier Cédex 5, France*
[3] *Department of Chemistry IFM, University of Torino and NIS, Via Giuria 7,I- 10125, Torino, Italy*
[4] *SIBAC, University of Antwerpen, Universiteitsplein 1, B-2610 Wilrijk, Belgium*
[5] *University of Leipzig, Fakultät für Physik und Geowissenschaften, Linnéstr. 5, D-04103 Leipzig, Germany*
[6] *Institute of Neuroscience and Medicine, Forschungszentrum Juelich GmbH, D-52425 Juelich, Germany*
[7] *VITO - Flemish Institute for Technological Research NV, Boeretang 200, B-2400 Mol, Belgium*
[8] *CRISMAT, UMR 6508, CNRS-ENSICAEN, 6 Bd Marechal Juin, 14050 Caen, France*
[9] *EMAT, University of Antwerp, Groenenborgerlaan 171, B-2020 Antwerpen, Belgium*

Introduction

Various synthesis methods exist for the introduction of zeolitic features in mesoporous materials. However, all methods have their specific benefits and drawbacks with respect to the structural control and properties of the obtained materials. Here, we show results on two different methodologies: (1) a one-pot synthesis approach in which part of the zeolite template (TPAOH) to prepare titanium-silicalite-1 is replaced by CTMABr for the templated induction of mesoporosity and (2) a post-synthesis impregnation of zeolitic nanoparticles in mesoporous supports [1]. Both methods are strongly divergent and have their benefits and drawbacks with respect to the mesoporosity, zeolitic features, diffusion and incorporation of hetero-elements.

Experimental

One-pot synthesis approach.

One-pot templated materials, denoted as meso-TSM, were prepared by an adjusted synthesis of the TS-1 zeolite [2], whereby part of the zeolite structure directing agent (TPAOH) was replaced by a mesopore templating agent (CTMABr). 1.4 g of CTMABr was dissolved in 13.5 mL of distilled water followed by the addition of 3.75 mL of TPAOH during stirring. Afterwards, 300 µL of TBOT and 5.6 mL of TEOS were added under vigorous stirring. After stirring for 1.5 hours at room temperature, the mixture was hydrothermally treated at 100, 125 or 150 °C with a variable duration (2, 4 or 7 days). After filtrating, washing and drying, the materials were calcined in ambient atmosphere at 550 °C for 6 h (heating rate 1 °C/min).

Post-synthesis impregnation of zeolitic nanoparticles.

A VS-1 nanoparticle solution was prepared as described in a previous article [1a]. The resulting clear solution containing the VS-1 nanoparticles was acidified with HCl with or without subsequent dilution. Different amounts and concentrations of the acidified VS-1 nanoparticle solution were impregnated on calcined SBA-15 by means of an incipient wetness impregnation. The ultimate product was dried and subsequently calcined up to 550 °C for 6 h in ambient atmosphere with a heating rate of 1 °C/min.

Results and discussion

One-pot synthesis approach.

Nitrogen-sorption and XRD show that the formation of the zeolitic phase is hampered in the presence of the mesotemplate CTMABr below 150°C. Hydrothermal treatment above 150°C results in the formation of a zeolitic phase but coincides with the decomposition of CTMABr resulting in a decrease of mesoporosity. The ratio of microtemplate/mesotemplate is found to be determining to tune the porosity characteristics of the resulting materials towards a dominant mesoporous structure or a pronounced zeolitic character. However, because of the competitive growth mechanism of the zeolitic phase and mesostructure, a trade-off remains between a high mesoporosity and a pronounced zeolitic character. In addition, HRTEM images clearly indicate that the obtained materials are composite materials with both phases closely intermingled rather than a true hierarchical structure.

Post-synthesis impregnation of zeolitic nanoparticles.

X-ray diffraction studies show that the material does not obtain any true long range zeolite character. Nevertheless, an increase in microporosity can be observed in N_2-sorption. Furthermore, N_2-sorption shows a clear control of the porosity characteristics in relation to the amount and concentration of the deposited zeolitic nanoparticles, allowing a good control on porous properties and consequently on diffusion. Since no true long range zeolite character was observed, spectroscopic studies were executed to reveal the chemical nature of the impregnated nanoparticles. EPR CW, pulse and HYSCORE experiments on uncalcined samples reveal differences between the chemical properties (hydrophilicity, local heterogeneity, interactions with gases) of the deposited VS nanoparticles and the full-grown zeolite caused by their small dimensions [3]. The observed differences in EPR suggest altered performance and stability of the nanoparticles in e.g. catalytic processes compared to the full-grown zeolite.

Conclusions

Although several methods can be applied to create bimodal materials, the structural properties and control is strongly divergent. One-pot synthesis approaches can be tuned to obtain both mesoporosity and true zeolitic character. However, no true hierarchical porosity can be achieved due to the trade-off between mesopores and zeolite formation. On the other hand, post-synthesis deposition methods allow for a much easier structural control but the zeolitic nanoparticles have strongly altered properties as compared to full grown zeolites. Nevertheless, both materials have interesting features, which could be beneficial in several applications.

Acknowledgements

J. Vernimmen is financially supported by the Fund for Scientific Research-Flanders (FWO). This work was done in the frame of the European NoE-FP6 project INSIDE POReS and a concerted research project (GOA) of the University of Antwerpen.

References

[1] (a)V. Meynen, P. Cool, E.F. Vansant, P. Kortunov, F. Grinberg, J. Kärger, O.I. Lebedev, G. Van Tendeloo, Micropor. Mesopor. Mater. 99 (1-2) (2007) 14-22; (b) D. Trong-On, A. Nossov, M.-A. Springuel-Huet, C. Schneider, J.L.Bretheron, C.A. Fyfe, S. Kaliaguine, J.Am. Chem. Soc. 126 (2004) 14324-14325

[2] X. Meng, D. Li, X. Yang, Y. Yu, S. Wu, Y. Han, Q. Yang, D. Jinag, F.-S. Xiao, J. Phys. Chem. B 107 (2003) 8972-8980

[3] (a) M. Chiesa, V. Meynen, S. Van Doorslaer, P. Cool, E.F. Vansant J. Am. Chem. Soc. 128 (2006) 8955-8963; (b) S. Zamani, M. Chiesa, V. Meynen, Y. Xiao, B. Prelot, J. Zajac, F. Verpoort, P. Cool, S. Van Doorslaer, J. Phys. Chem. C 114 (30) (2010) 12966-12975

Nanocomposite materials: synthesis and characterization of self-bonded pellets containing titano silicates and carbon nanotubes.

Pierantonio De Luca[1], Pietro Sergi[1], Danilo Vuono[2], Alfredo Aloise[2], Jànos B.Nagy[2]

1 Dipartimento of Pianificazione Territoriale. Università della Calabria. Arcavacata di Rende (CS)- 87030 Rende Italy. p.deluca@unical.it
2 Dipartimento di Ingegneria Chimica. Università della Calabria. Arcavacata di Rende (CS)- 87030- Rende Italy.

Introduction

In the last decade a variety of innovative materials has been developed for practical applications, challenges in developing aerospace, mechanical, bionic, medical and environmental. New achievements of materials that do not belong to conventional approaches offer great opportunities and challenges.
The ETS-10 and ETS-4 are microporous crystalline synthetic materials [1]. The different synthetic methods produce these materials as dust. Recently, ETS phases were synthesized in the pellets form directly by hydrothermal synthesis[2].
The carbon nanotubes were discovered fortuitously in 1991. In general, the nanotubes can be divided into two main families: single-walled nanotubes (single-walled nanotubes or SWNT) and multi-walled nanotubes (multi-walled nanotubes, or MWNT).
In this work was studied the possibility to combine the inherent characteristics of self-bonded microporous materials with the carbon nanotubes performance.
Self-bonded pellets composed of titanosilicate matrix-type and carbon nanotubes were synthesized. Studies and laboratory tests on samples to determine their constitution, properties and comparison with pellets titanosilicate matrix without nanotubes were carried out.

Experimental

Preparation of initial gels for the pellets was based on the following synthesis system expressed in moles:xNa_2O-0.6KF-$yTiO_2$-1.28xHCl-1.49SiO_2-39.5H_2O- with $1 \leq x < 2.5$, $0.1 \leq y \leq 0.3$ moles. Once prepared, the gel was dried at a temperature of 90° C for 24 hours.
The dried and pulverized gel was mixed with a precise amount of distilled water in the ratio dry gel/water=3.5, and were added varying amounts of carbon nanotubes (NT), specifically as 0.0%, 0.05% and 0.1% with respect to the amount of dry gel. It was obtained a paste that was preformed in a pelletizer at a pressure of 25bar/cm^2.
Then the pellets were inserted in Morey type autoclaves containing inside a teflon support with the aim of keeping the pellets raised by a few milliliters of water present in the autoclave. The autoclaves sealed were placed in an oven at 190° C for predetermined times.
The pellets obtained were then submitted to their chemical-physical characterization, in particular, the X-ray diffraction (XRD), thermal analysis (DSC, TG, DTG), compression tests, scanning electron microscopy (SEM). Furthermore, kinetic studies were performed to verify the influence of the amount of nanotubes on kinetic parameters.

Results and discussion

The data obtained showed that the pellets, irrespective of the phase obtained, are not formed for all systems studied, but their formation is dependent on the synthesis parameters used in the initial reaction system.
Initial systems containing Na_2O molar quantity greater than 2 and TiO_2 molar quantity greater than 0.2 lead to pellets with poor mechanical properties. For values that exceed these molar

amounts the product obtained is always in form of powder. It was observed that the pellets mechanical resistence depends primarily on three major parameters: % crystallinity, phase type and nanotubes percentage (tab.1).

Table 1-Examples of some samples obtained by the following reaction systems: xNa_2O-$0.6KF$-$yTiO_2$-$1.28xHCl$-$1.49SiO_2$-$39.5H_2O$-%NT with their mechanical resistance and % relative crystallinity.

Systems			**Obtained phase**	**%relative crystallinity**	**Mechanical resistance (Kp)**
x (mol.Na_2O)	y (mol.TiO_2)	%NT			
1.0	0.20	0.00	ETS-10 pellets	25	11.2
1.0	0.20	0.05	ETS-10 pellets	35	10.6
1.0	0.20	0.10	ETS-10 pellets	40	9.3
2.0	0.20	0.00	ETS-4 pellets	20	5.3
2.0	0.20	0.05	ETS-4 pellets	43	2
2.0	0.20	0.10	ETS-4 power	90	----

The % relative crystallinity has been obtained attributing a value of 100 to the sample with higher crystallinity and comparing the other samples crystallinity of same phase.
Pellets with high % relative crystallinity generally have lower mechanical resistence and it could be justified by the fact that to determine the pellets cohesion is the presence of a sufficient amount of amorphous phase.
The pellets of ETS-4 phase are generally less hard than those of ETS-10 pellets and it can be probably attributed to the different morphology of the crystals. In fact, the ETS-4 phase having a crystal morphology of the approximately cubic shape, it does not allow an adequate pellets compaction.
Since the mechanical resistence of pellets depends on parameters set out above, the addition of nanotubes does not always lead to a clear improvement in the mechanical properties of pellets. In pellets of ETS-4 phase it is evident that increasing the amount of nanotubes decreases the pellets mechanichal strength. Kinetic studies showed, for both ETS-4 and ETS-10 phases, a similar behavior. The induction time increases with increasing weight percentage of nanotubes in the system. This means that nanotubes delay the reaction initiation. The reaction rate, once the reaction is initiated, increases with increasing amount of nanotubes in the initial system.

Conclusion

It is possible to synthesize self-bonded pellets of ETS-4 and ETS-10 phase containing carbon nanotubes. The general trend is that increasing the amount of nanotubes decreases the mechanical strength and increases the crystallinity of the pellets, although it can still be obtained pellets containing carbon nanotubes with adequate mechanical strength.

References

[1] C.C. Pavel, D. Vuono, L. Catanzaro, P. De Luca, N. Bilba, A. Nastro, J. B.Nagy, Microporous and Mesoporous Materials, 56 (2002) 227-239
[2] D.Vuono, P. De Luca, J. B.Nagy, A. Nastro, Microporous and Mesoporous Materials, 109 (2008) 118-137

Post-synthesis modification of MIL-101(Fe) with nickel and magnesium cations for hydrogen sorption applications

Emanuela Žunkovič[1], Mojca Rangus[1], Matjaž Mazaj[1], Roman Gabrovšek[1], Venčeslav Kaučič[1,2,3], Nataša Zabukovec Logar[1,3,4]
[1]*National Institute of Chemistry, Hajdrihova 19, 1000 Ljubljana, emanuela.zunkovic@ki.si*
[2]*Faculty of Chemistry and Chemical Technology, University of Ljubljana, Aškerčeva cesta 5, 1000 Ljubljana*
[3]*CoE Low-Carbon Technologies, Hajdrihova 19, 1000 Ljubljana*
[4]*University of Nova Gorica, Vipavska 13, 5000 Nova Gorica*

Introduction

Hydrogen is an attractive alternative energy carrier of the future because of its high energy content and clean burning, but its storage is still a technological challenge [1, 2]. Porous Metal-Organic Framework materials (MOF) are considered as promising hydrogen storage materials, because their structures have low density, high surface area and large pore volume. The sorption process is quick and reversible, which is crucial for on-board applications; the disadvantage is that the process requires too low temperatures and too high pressure [3]. The incorporation of undercoordinated metal centres in MOFs by the impregnation of a given framework with excess metal ions shows the increase of hydrogen sorption at ambient temperature [4]. We report here on the impregnation of MIL-101(Fe) with nickel and magnesium cations and on the characterisation of the obtained products with the emphasis on the nature of metals in the structures.

Experimental

MIL-101(Fe) was synthesised by using $FeCl_3 \cdot 6H_2O$ (Aldrich, 99 %) and terephthalic acid H_2BDC as a ligand (Acros, 99 %) in N,N-dimethyl-formamide (Aldrich, 99,8 %) with molar ratios of 1.8 : 1 : 137, a slightly modified procedure for the preparation of amino-terephthalic analogue of MIL-101 [5]. After thermal treatment in Teflon-lined autoclaves (30 mL total volume) at 110 °C for 24 h, the final product (orange powder) was recovered by filtration, washed with DMF, and then dried at ambient conditions. MIL-101(Fe) was impregnated by stirring it for 4 hours at room temperature in either 0.5 M $Ni(NO_3)_2 \cdot 6H_2O$ (Kemika, 99 %) or 0.5 M $MgCl_2 \cdot 6H_2O$ (Aldrich, 99 %). The products MIL-101(Fe), Ni-MIL-101(Fe) and Mg-MIL-101(Fe) were initially characterised by X-ray powder diffraction and scanning electron microscopy. The amount of metal was detected by energy-dispersive X-ray spectroscopy (EDX). The thermal behaviour was investigated by thermogravimetric analysis and high-temperature XRD. X-ray absorption spectra (XAS) were measured in the transmission detection mode at C beamline of the HASYLAB synchrotron in Hamburg, Germany, to determine the local structure of the present metals. The porosity of structures was studied with N_2 adsorption isotherms.

Results and discussion

SEM images of octahedral crystals of MIL-101(Fe) show one-phase product (Fig. 1). The EDX analysis revealed up to 2 % of impregnated metals in the final products. The structural changes indicated by TG were also confirmed by HT-XRD indicating that the products were stable at least up to 300 °C (Fig. 2.a). Mass loss attributed to water desorption is enhanced after nickel and magnesium deposition in Ni-MIL-101(Fe) and Mg-MIL-101(Fe) suggesting

the presence of additional water sorption sites (Fig. 2.b, 2.c). N_2 adsorption isotherms of non modified nickel and magnesium modified MIL-101(Fe) show that nitrogen uptake is lower after grafting. The EXAFS analyses indicated the presence of well-distributed metal sites, i.e. the absence of NiO clusters in Ni-MIL-101(Fe) sample (Fig. 3).

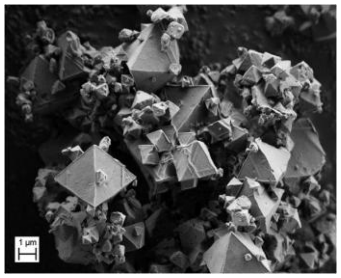

Figure 1. Octahedral crystals of MIL-101(Fe)

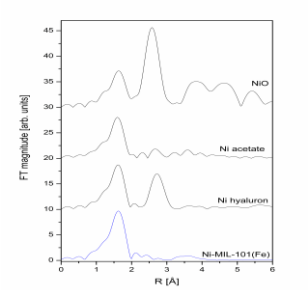

Figure 3. Fourier transformed XAFS spectra of Ni-MIL-101(Fe) sample compared with different reference compounds.

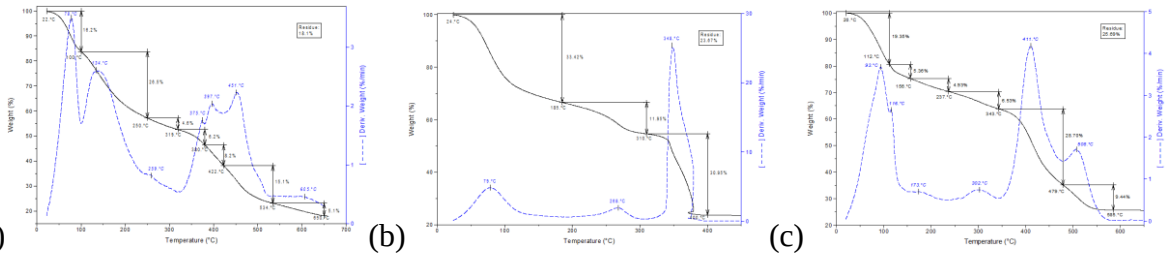

(a) (b) (c)

Figure 2. Thermal behaviour of (a) MIL-101(Fe), (b) Ni- and (c) Mg-MIL-101(Fe).

Conclusions

We synthesised highly-crystalline iron-terephthalate MIL-101(Fe) that was additionally grafted with nickel and magnesium. The initial material showed highly porous nature. Nickel and also magnesium impregnation of MIL-101(Fe) decreased the surface area of the products. Spectroscopic analyses indicated the absence of metal oxides within the pores. Hydrogen storage capacity measurements are in progress.

Acknowledgements

This work was supported by the Slovenian Research Agency research program P1-0021. We acknowledge the financial support by DESY and EU FP7/2007-2013 program ELISA (226716) and access to synchrotron radiation facilities of HASYLAB for XAS measurements.

References

[1] Morris, R.E., Wheatley, P.S., Gas Storage in Nanoporous Materials, Angewandte Chemie International Edition, 47 (2008), 4966-4981

[2] Ferey, G., Hybrid Porous Solids: Past, Present, Future, Chemical Society Reviews, 37 (2008), 191-214

[3] Lim, K.L., Kazemian, H., Yaakob, Z., Daud, W.R.W., Solid-State Materials and Methods for Hydrogen Storage: A Critical Review, Chemical Engineering & Technology, 33 (2010), 213-226

[4] Dincă, M., Long, J.R., Hydrogen Storage in Microporous Metal-Organic Frameworks with Exposed Metal Sites, Angewandte Chemie International Edition, 47 (2008), 6766-6779

[5] Bauer, S., Serre, C., Devic, T., Horcjada, P., Marrot, J., Férey, G., Stock, N., High-Throughput Assisted Rationalization of the Iron(III) Aminoterephthalate Solvothermal System, Inorganic Chemistry, 47 (2008), 7568-7576

An investigation of the role of acetone on the synthesis of two porous iron carboxylates

Tadeja Birsa Čelič[1], Nataša Zabukovec Logar[1], Mojca Rangus[1] and Venčeslav Kaučič[1,2]
[1]National Institute of Chemistry, Hajdrihova 19, 1000 Ljubljana, Slovenia; [2]Faculty of chemistry and chemical technology, University of Ljubljana, Aškerčeva 5, 1000 Ljubljana, Slovenia; tadeja.birsa@ki.si

Introduction

Metal-organic framework materials (MOFs) are currently attracting a tremendous amount of interest because of their unique chemical and structural characteristics, which enable a variety of applications [1]. Many researches have focused on the synthesis of new MOF materials and systematically investigated the role of pH, temperature, concentration, and time on their crystallisation [2]. Special emphasis has been recently put on the influence of the solvent properties, typically DMF, alcohols, ketones, alkanes, water and their mixtures, on the formation and structure transformations of MOFs [3]. Here we report on the controlling role of acetone in the syntheses of two iron benzene-1,3,5-tricarboxylates MIL-45(Fe) [4] and MIL-100(Fe) [5] from the same reagents.

Experimental

The syntheses were carried out from 3 to 7 days at 150 °C to 190 °C by using the constant $FeCl_3 \cdot 6H_2O$/benzene-1,3,5-tricarboxylic acid ratio, while the molar ratio of H_2O/acetone varied from 1:1.07 to 1:0.13. NaOH was added to the reaction mixtures to deprotonate the tricarboxylic acid. No hydrofluoric acid or any other mineralizing agent was used in the syntheses. The size and morphology of crystals in the product were studied with a scanning electron microscope Zeiss Supra™ 3VP. The crystal structures of obtained materials were confirmed with powder or single-crystal X-ray diffraction. Hydrothermal stability of the products was evaluated by boiling in distilled water for different periods of time up to 16 hours under refluxing. X-ray absorption (XAS) spectra of products and reference compounds were measured in the Fe K-edge energy region (7112 eV) in the transmission detection mode at XAFS beamline of the ELETTRA synchrotron facility in Basovizza, Italy in order to follow the changes in an average oxidation state and local structure of iron during formation and after hydrothermal treatment.

Results and discussion

The hydrothermal synthesis in the above mentioned time and temperature range always resulted in the formation of pure and highly crystalline large-pore MIL-100(Fe) structure. However, the addition of acetone into the same reaction mixture directed the crystallisation to the formation of MIL-45(Fe) material with smaller pores in the whole range of studied H_2O/acetone ratios and with slight variations in the crystallinity and phase purity of the obtained materials (Figure 1).
Test of hydrothermal stability revealed that MIL-100(Fe) retained its structure in boiling water for at least 16 hours, whereas MIL-45(Fe), which is thermally stable up to 400 °C, converted to MIL-100(Fe) already after a 15-minute treatment in water. The irreversible transformation was confirmed by XRD.
XANES study revealed that iron was in trivalent form in MIL-100(Fe) and divalent in MIL-45(Fe), which confirmed the reduction of Fe^{3+} to Fe^{2+} during the synthesis of MIL-45(Fe),

since Fe^{3+} was used as the starting iron source in all experiments. After the hydrothermal treatment the change in oxidation state from Fe^{2+} to Fe^{3+} was determined for MIL-45(Fe) sample, which is in accordance with its degradation to MIL-100(Fe).

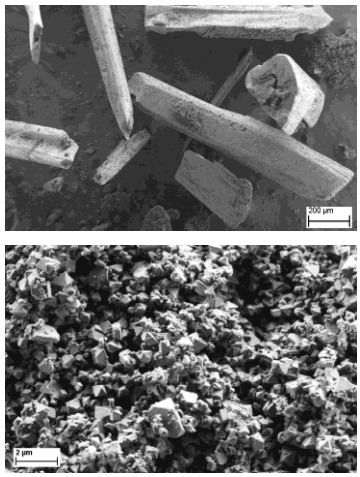

Figure 1. SEM images of MIL-45(Fe) obtained after 7 days at 190 °C with the molar ratio of H_2O/acetone 1:1.07 (top) and MIL-100(Fe) crystals obtained hydrothermally after 3 days at 150 °C (bottom).

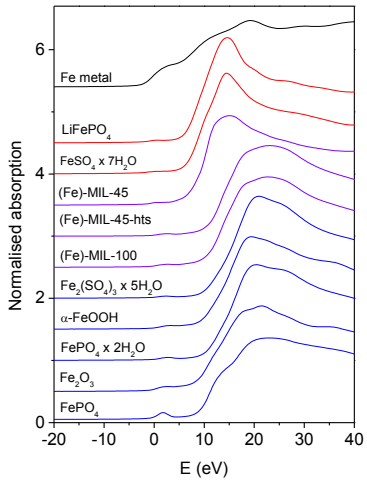

Figure 2. Fe K-edge XANES spectra of MIL-45(Fe), MIL-45(Fe)-hts, MIL-100(Fe) and standard Fe^{2+}, Fe^{3+} reference compounds. The spectra are displaced vertically for clarity.

Conclusions

The systematic investigation of the effect of variations in H_2O/acetone molar ratio on the reaction mixture revealed the controlling role of acetone in the formation of MIL-45(Fe) and MIL-100(Fe) structures through oxidation-reduction and solute-solvent interaction processes. The MIL-45(Fe) transformation to MIL-100(Fe) during hydrothermal treatment starts with a complete dissolution of the former structure in hot water.

Acknowledgements

This work was supported by the Slovenian Research Agency research programmes P1-0021. Access to SR facilities of ELETTRA (beamline XAFS, project 20085196) is acknowledged.

References

[1] Férey, G., Hybrid porous solids: past, present, future, Chemical Society Review, 37 (2008), 191-214
[2] Forster, P. M., Stock N., Cheetham A. K., A high-throughput investigation of the role of pH, temperature, concentration, and time on the synthesis of hybrid inorganic-organic materials, Angewandte Chemie International Edition, 44 (2005), 7608-7611
[3] Fu, A.-Y., Jiang, Y.-L., Wang, Y.-Y., Gao, X.-N., Yang, G.-P., Hou, L., Shi, Q.-Z., DMF/H_2O Volume Ratio Controls the Syntheses and Transformations of a Series of Cobalt Complexes Constructed Using a Rigid Angular Multitopic Ligand, Inorganic Chemistry, 49 (2010), 5495-5502
[4] Riou-Cavellec, M., Albinet, C., Livage, C., Guillou, N., Noguès, A., Grenèche, J.-M., Férey, G., Ferromagnetism of the hybrid open framework $K[M_3(BTC)_3]\cdot 5H_2O$ (M=Fe, Co) or MIL-45, Solid state sciences, 4 (2002), 267-270
[5] Horcajada, P., Surblé, S., Serre, C., Hong, D.-Y., Seo, Y.-K., Chang, J.-S., Grenèche, J.-M., Margiolaki, I., Férey, G., Synthesis and catalytic properties of MIL-100(Fe), an iron(III) carboxylate with large pores, Chemical Communications, 27 (2007), 2820-2822

Synthesis of Hierarchical ZSM-5 Zeolite from Silanized Seeds Employing Silylated Polymers as Organosilanes

T. J. Pinnavaia[1], D. P. Serrano[2,3], J. Aguado[4], S. S. Kim[1], A. Peral[2]

[1]Department of Chemistry, Michigan State University, East Lansing, MI 48823 (USA)
[2]Department of Chemical and Energetic Technology, ESCET, Rey Juan Carlos University, Móstoles 28933,Madrid (Spain), [3]Madrid Institute for Advanced Studies on Energy, IMDEA Energía, Móstoles 28933, Madrid (Spain), [4]Department of Chemical and Environmental Technology, ESCET, Rey Juan Carlos University, Móstoles 28933, Madrid (Spain),
david.serrano@imdea.org

Introduction

Zeolites with hierarchical porosity have attracted the attention in the last years [1]. In these materials, the presence of pores and channels of higher dimensions than the strictly zeolitic micropores has helped to overcome the mass-transfer limitations that conventional zeolites with micrometer crystal size show in some catalytic processes, mainly when voluminous molecules are involved in the reactions. Among the variety of methods that have been developed in order to introduce additional porosity into zeolitic structures, silylated polymers have been effectively employed as mesopore-directing agents in order to obtain zeolite single crystals with intracrystal porosity [2]. Zeolite crystallization from organofuntionalized seeds also has proven to be a versatile method applicable to the syntheses of a variety of hierarchical zeolites [3]. In this synthesis strategy organosilanes of the type $RSi(OR)_3$ are added over zeolitic nuclei previously formed, preventing the aggregation of the nanoparticles into larger crystals during the final hydrothermal treatment at high temperature. In this case, aggregated zeolite nanocrystals with intercrystal micro- and mesopores are attained. In this work, not a simple $RSi(OR)_3$ silane, but a silylated polymer is employed as organosilane in the synthesis of ZSM-5 zeolite from silanized seeds, and its influence in the textural and physicochemical properties of the materials synthesized is shown.

Experimental

A clear ZSM-5 precursor solutions was precrystallized at 90ºC for 20h [3]. Then, the zeolite seeds were functionalized with a silylated polymer [2] at 90ºC for 6h, the Si(polymer)/Si(precursor solution) ratio ranging from 0.0 to 0.15. The silylated polymer was formed by reaction of (3-glycidoxypropyl)trimethoxysilane (Aldrich) with a polypropylene oxide diamine (Jeffamine D-400, Huntsman) at a Si/NH ratio of 0.1. After the silanization stage, crystallization was carried out in Teflon-lined stainless-steel autoclaves at 150ºC and under autogeneous pressure for 8 days.

Results and discussion

XRD diffractograms of the calcined samples are displayed in Figure 1. The materials prepared employing a Si(silylated polymer)/Si(precursor solution) ratio ranging from 0.0 to 0.10 are clearly crystalline. Strong and sharp diffraction peaks are observed in these samples although slightly lower peak intensities are appreciated in their spectra when compared with the traditional nanocrystalline ZSM-5 (0.0). This fact could be attributed to the smaller crystalline domains present in these materials in regard to the reference sample. This effect is much more

important in the sample synthesized with a Si(pol.)/Si(gel) ratio = 0.12, in which low intensity signals corresponding to the main diffraction peaks of the ZSM-5 zeolite are appreciated and no trace of background signal characteristic of amorphous materials is observed. Finally, the sample synthesized employing the highest Si(pol.)/Si(gel) ratio in the silanization stage shows the diffraction pattern characteristic of a non-crystalline material.

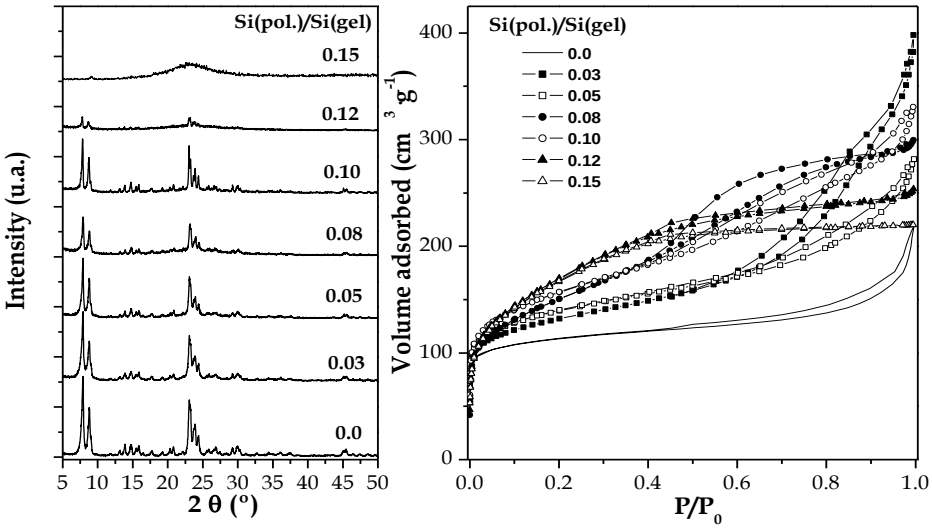

Figure 1. XRD diffractograms (left) and N_2 adsorpotion/desorption isotherms (right) of the calcined samples.

The zeolites synthesized from seeds organofunctionalized with the silylated polymer exhibit N_2 adsorption clearly higher than those of the reference nanocrystalline sample (Figure 1, right, and Table 1), denoting that these materials present improved textural properties, with enhanced porosity and higher values of BET and external surface area. At the same time, increasing the amount of Si-polymer incorporated in the silanization stage, the micropore volume diminishes (Table 1), corroborating that the size of the crystalline domains is reduced and the additional porosity is enhanced as the amount of Si-polymer employed increases. Silylated polymers are effective silanization agents in the synthesis of hierarchical zeolites by seed silanization and adjusting their proportion in the synthesis medium it is possible to control the pore size distribution (PSD) in the final materials (Table 1).

Table 1. Textural properties of the ZSM-5 materials synthesized.

Si(pol.)/Si(gel)	S_{BET} (m^2/g)	S_{EXT} (m^2/g)	V_{MIC} (cm^3/g)	PSD (nm)	Max.PSD (nm)
0.0	396	118	0.123	-	-
0.03	465	227	0.105	4-100	11
0.05	492	239	0.111	2-100	9
0.08	537	421	0.048	2-20	4
0.10	557	356	0.086	2-30	4
0.12	612	563	0.015	2-11	2
0.15	604	542	0.020	2-6	2

References

[1] K. Egeblad, C. H. Christensen, M. Kustova, C. H. Christensen, Chem. Mater. 20 (2008) 946
[2] H. Wang, T. J. Pinnavaia, Angew. Chem. Int. Ed. 45 (2006) 7603
[3] D. P. Serrano, J. Aguado, J. M. Escola, J. M. Rodríguez, A. Peral, Chem. Mater. 18 (2006) 2462

Influence of hydrogel "density" on synthesis of zeolite A

Ana Palčić, Josip Bronić, Boris Subotić
Ruđer Bošković Institute, Bijenička 54, 10000 Zagreb, Croatia,
Corresponding author's e-mail: josip.bronic@irb.hr

Introduction

Typical industrial synthesis of zeolite involves preparation of hydrogel by mixing of silicate and aluminate solutions (or sols), its hydrothermal treatment, and washing (NaOH removal) of the end crystalline product(s)[1,2]. In the starting mixture, the particles of precipitated amorphous aluminosilicate (gel) are dispersed in the liquid phase. Physico–chemical properties of hydrogels (consequently end product of synthesis) depend on the overall batch composition ($xMe_2O \times Al_2O_3 \times ySiO_2 \times zH_2O$) and the way of gel preparation (order of addition of silicate and aluminate solutions, mode and intensity of stirring of the reaction mixture, time and temperature of precipitation, etc.). Even small changes in mentioned processes (e.g., using of different silica sources, hydrogel ageing, template addition) [3,4] can give a different result with respect to the rate of crystallization, phase composition and to the particulate properties (particle size distribution, particle shape) of the crystals. Therefore, the objective of this work is to study the influence of the "density" of the starting hydrogel on kinetic parameters of transformation as well as on the final products' particulate properties.

Experimental

Starting alumino-silicate hydrogels were prepared by mixing of alkaline sodium silicate solution with sodium aluminate solution and homogenized by a disperser. Before hydrothermal treatment, prepared hydrogels were divided into needed number of HDPE reactors and heated under static conditions at 80 °C, in a convection oven. At predefined times, the samples were taken out, centrifuged, washed, dried and characterized using several methods (techniques) such as: powder X-ray diffraction for phase analysis, optical and scanning electron microscopy for determination of the crystal growth rate and morphology; and laser light scattering for crystal size distribution by volume and number.

Results and discussion

Different "density" of starting hydrogels was obtained using constant ratios Na_2O/H_2O and Al_2O_3/SiO_2 and decreasing SiO_2/H_2O ratio as shown in Table 1.

Table 1. Chemical composition (oxide form) of starting hydrogels and the size values of the end product, under which is 50% of particles by volume (L_{V50}) and by number (L_{N50}). L_{max} is the size of the largest crystals, determined by optical microscopy.

	Starting hydrogel composition (batch)				Particle size values		
	Na_2O	Al_2O_3	SiO_2	H_2O	L_{V50} / μm	L_{N50} / μm	L_{max} / μm
H1	3.2	1.400	2.667	250	10.045	0.776	11.752
H2	3.2	1.250	2.381	250	10.221	0.765	11.786
H3	3.2	1.050	2.000	250	9.315	0.786	10.763
H4	3.2	0.500	0.952	250	7.516	0.771	8.744
H5	3.2	0.300	0.571	250	7.930	0.769	9.093

From the size of the largest particles and L_{V50} is evident that high density of the starting hydrogel (H1 and H2) gives larger crystals at lower growth rate, while smaller crystals come from diluted systems (H4 and H5) at higher growth rate (Fig 1.). Due to the large number of

small particles in all systems (maxima around 1 μm, Fig 2.), L_{N50} value (Table 1.) is constant (the difference is within experimental error 0.773± 0.013 μm, about 1.7% of average value). Moreover, similar values for L_{V50} and L_{max} of dense (H1 and H2) and diluted (H4 and H5) systems show that the major changes in kinetics of transformation and final product particulate properties occur when SiO_2 batch concentration decreases from 2.381 to 0.952.

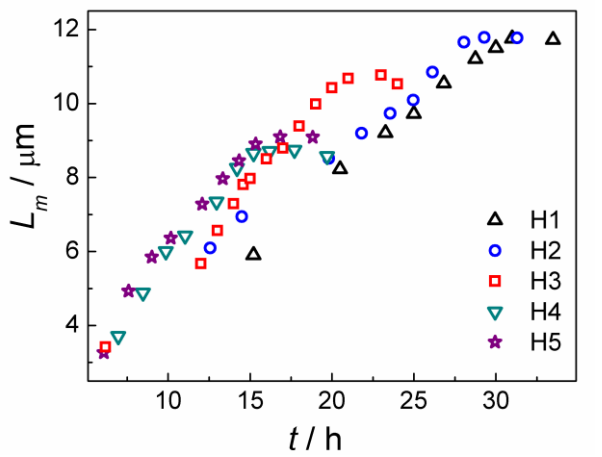

Figure 1. Growth of the largest crystals during reaction.

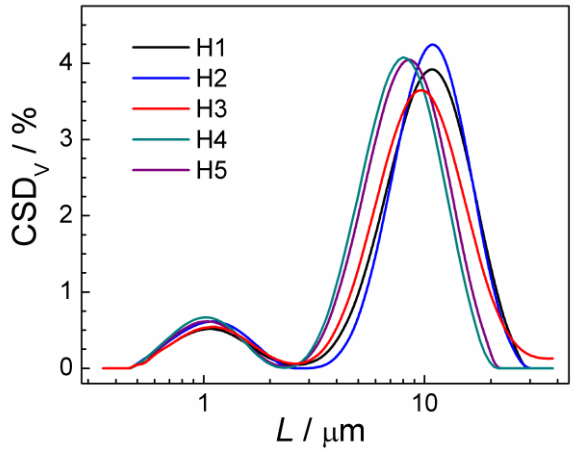

Figure 2. Crystal size distributions by volume of samples at the end of transformation.

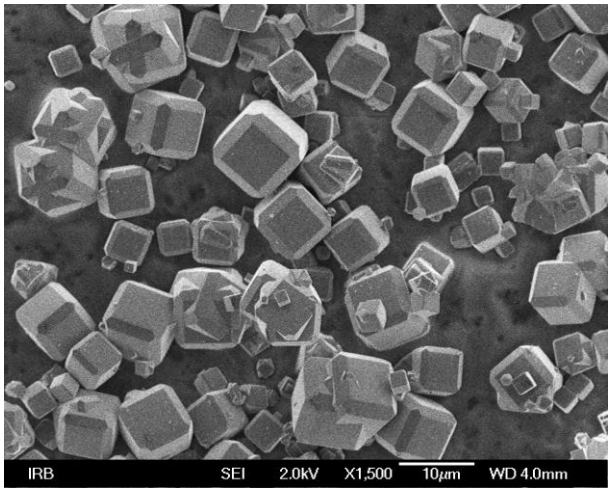

Figure 3. SEM photo (cubes with truncated edges and twin crystals) of the crystals at the end of crystallization of H3.

Conclusions

The end products of dense starting hydrogels have significantly larger crystals than from diluted systems. Particle size distributions by volume show bimodal distribution in all systems. Most of the changes in particulate properties come from the decrease in size of the population of larger particles with decreasing density of the starting system.

Acknowledgements

This work was supported by the Ministry of Science, Education and Sport of Republic of Croatia within basic project 098-0982904-2953.

References

[1] J. Bronić, A. Mužic, T. Antonić Jelić, J. Kontrec, B. Subotić, *J. Cryst. Growth*, **310** (2008) 4656-4665.
[2] C.-Y. Hsu, A.S.T. Chiang, R. Selvin, R.W. Thompson, *J. Phys. Chem. B*, **109** (2005) 18804-18814.
[3] A. Palčić, J. Bronić, Đ. Brlek, B. Subotić, *CrystEngComm*, **13** (2011) 1215-1220.
[4] S. Mintova, N.H. Olson, V. Valtchev, T. Bein, *Science*, **283** (1999) 958-960.

Synthesis of Highly Crystalline Nanosheets of MFI Zeolites under Static Conditions

Albert Machoke, Thangaraj Selvam & Wilhelm Schwieger
Chair of Chemical Reaction Engineering, University of Erlangen-Nürnberg
Egerlandstraße 3, 91058 Erlangen-Germany. *Albert.Machoke@crt.cbi.uni-erlangen.de*

Introduction

Multilamellar MFI zeolites are ultrathin nanosheets of MFI zeolites with a thickness of about 2 nm along the b-axis and an interlamellar spacing of about 4 nm [1-3]. This material has shown promising catalytic activities and longer catalytic life time mainly because of its hierarchical structure and nano dimensions [1]. Up to now, the synthesis of this material has been reported only under tumbling or rotation conditions and no attempts to obtain nanosheets of MFI under static conditions have been reported in the literature. Here, we present a systematic study on the synthesis and characterization of multilamellar MFI zeolites under static conditions.

Experimental

Highly crystalline nanosheets of MFI with different Si/Al ratios (50 - ∞) were synthesized under static conditions by using $C_{22}H_{45}{-}N^{+}(CH_3)_2{-}C_6H_{12}{-}N^{+}(CH_3)_2{-}C_6H_{13}$ as a template, TEOS as the silica source and $Al_2(SO_4)_3.18H_2O$ as the aluminium source. Prior to the actual synthesis of the zeolite, the template was synthesized by following the procedure of Choi et al [1]. Then, a starting gel with a molar composition of SiO_2 : 0.3 Na_2O : 0-0.01 Al_2O_3 : 0.1 template : 0.14-0.22 H_2SO_4 : $4C_2H_5OH$: 40 H_2O was prepared in accordance to the method of Choi et al. [1]. The final gel was transfered into 50 ml-teflon lined autoclaves and heated at different temperatures in a preheated oven over 20 days under static conditions. After the desired crystallization time, the autoclaves were quenched with cold water and the sedimented product was recovered by filtration. Finally the product was dried at 100 °C overnight and calcined in air at 550 °C for 4 hours.

Results and discussion

Figure 1 (a) shows the XRD patterns of the nanosheets of MFI synthesized at different crystallization times under static conditions at 150 °C. It can be seen that the formation of crystalline MFI starts already after 2 days and is completed within 4 days of time. No significant change in the MFI crystallinity as well as d-spacing was observed after 4 days. Furthermore, average pore diameter of 4.48 nm and BET surface area of 498 m^2g^{-1} have been measured by N_2-adsorption. The amount of organic material in the as-asynthesized product was about 40 % as detected by TG-MS (not shown). All the products were stable even after

calcination (550 °C) and further post-treatments. The high quality of these nanosheets has also been observed with SEM as shown in Figure 1 (b) (4 days synthesis time).

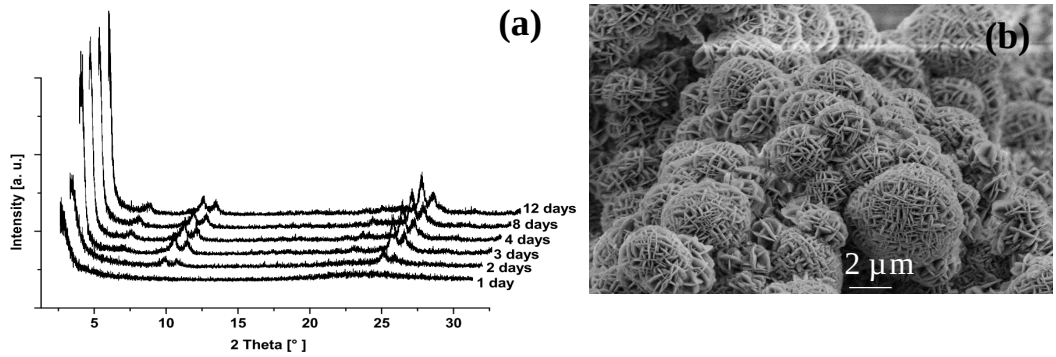

Figure 1: (a) XRD patterns and (b) SEM image of nanosheet of MFI zeolite synthesized under static conditions.

Conclusions

From the systematic studies of the synthesis of nanosheets of MFI zeolites, it is possible to synthesize this material in a wide range of crystallization parameters under static conditions. Further optimization of the synthesis procedure and catalytic testing are still in progress.

Acknowledgements

The authors are grateful to the cluster of excellence – engineering of advanced materials (EAM) for financing this work.

References

[1] Choi, M., Na, K., Kim, J., Sakamoto, Y., Terasaki, O., & Ryoo, R. Stable-single-unit-cell nanosheets of zeolite MFI as active and long lived catalysts, Nature, 461 (2009) 246-249
[2] Na, K., Choi, M., Park, W., Sakamoto, Y., Terasaki, O., Ryoo, R., Pillared MFI zeolite nanosheets of a single-unit-cell thickness, J. Am. Chem. Soc., 132 (2010) 4169-4177
[3] Schick, J., Daou, J., Caullet, P., Paillaud, J., Patarin, J., Mangold-Callarec, C., Surfactant-modified MFI nanosheets : a high capacity anion-exchanger, Chemical Communications, 47(3) (2011), 902-904

RUB-15 as layered precursor for 3-dimensional Interlayer Expanded Zeolites, IEZ

S. Grabowski, F. Heinrich, H. Gies

Institut für Geologie, Mineralogie und Geophysik, Ruhr-Universität Bochum, Germany
email: frances.heinrich@rub.de

Introduction

In the recent past two new strategies for synthesizing 3-dimensional microporous silicate frameworks were introduced, both starting from layered silicates as precursor materials. The topotactic condensation of silicate layers to microporous silicate zeolites proved to be an efficient and innovative route for the synthesis of new, medium pore materials with framework types such as CDO, RRO, RWR, or NIS, etc. Interlayer expansion of hydrous layer silicates introduced by Tatsumi and Wu recently links silicate layers in a condensation reaction with bridging silicate units, thus increasing pore size to large and extra large openings (1). In our contribution we would like to show that interlayer expansion is a versatile and more generally applicable technique by introducing the new, interlayer expanded zeolite material IEZ-RUB-15.

Experimental

RUB-15 as our layered precursor was synthesized using standard procedures described in literature employing tetramethylammonium cations as charge compensating cations (2). For layer expansion dried RUB-15 was treated hydrothermally at 170 °C in an aqueous solution of dimethyldichlorosilane, DMDCS, and acetic acid. The reaction was carried out in teflon lined stainless steel autoclaves heated in an oven for two days. The ratios of the starting materials were as follows:

ca. 200 mg RUB-15 641,6 mg H_2O 0,11 ml Dichlordimethylsilane 0,05 ml acetic acid conc.	170 °C	2 days

The product was recovered by filtration, washed and characterized with PXRD and SS NMR.

Results and Diskussion

The layer expansion using the silylating agent DMDCS leads, on the one hand, to significant changes in the layer spacing and, on the other hand, to the formation of a framework structure with bridges, constituting of - O - $Si(CH_3)_2$ - O groups. Whereas PXRD will show the new d-spacing after the reaction, SS MAS ^{29}Si NMR experiments reveal the connectivity of the tetrahedral centers and confirm the success of the reaction.
Fig.s 1a and b and 2a and b show the respective data of the diffraction- and NMR experiments of the as synthesized (Fig. 1) and interlayer expanded (Fig. 2) materials. The parent layer silicate is highly crystalline with perfect register of layers allowing for structure analysis in atomic resolution. The ^{29}Si NMR spectrum shows that Q^3 and Q^4-species are present in the layer in 2 : 1-ratio with a layer repeat of ~14 Å. Between neighbouring silicate layers 3 layers of water molecules are stacked forming a hydration shell for the tetramethylammonium cation. The removal of the hydrate water caused by the insertion and, synchronously, the formation of kovalent Si-O bonds connecting the layers leads to a slight shinkage of the interlayer distance. In addition, crystallinity is lost after the reaction (Fig. 2). However, SS MAS NMR results confirm that almost all Q^3 silicon has reacted

and, in addition, a new broad signal arises centered at -18 ppm.

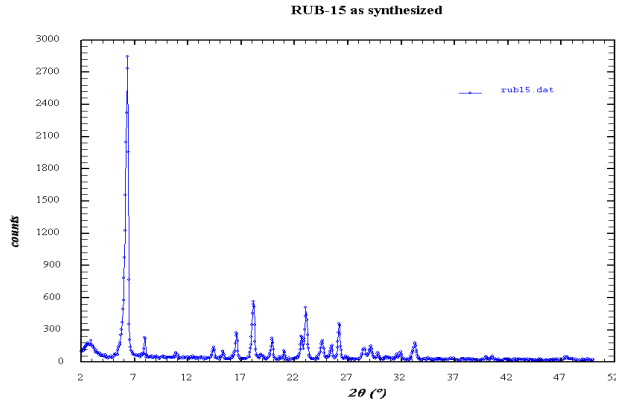

Fig. 1: a) PXRD of as synthesized RUB-15

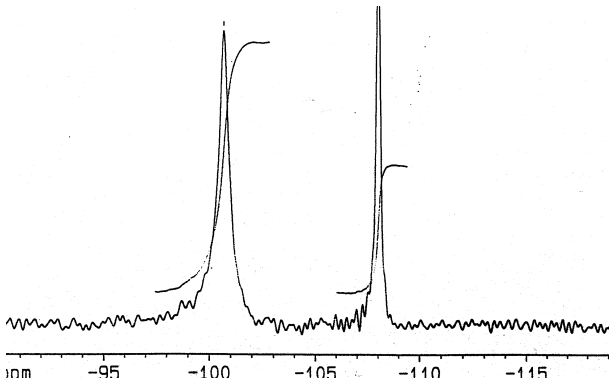

b) ^{29}Si NMR spectrum showing Q^3 and Q^4-Si with ratio 2:1.

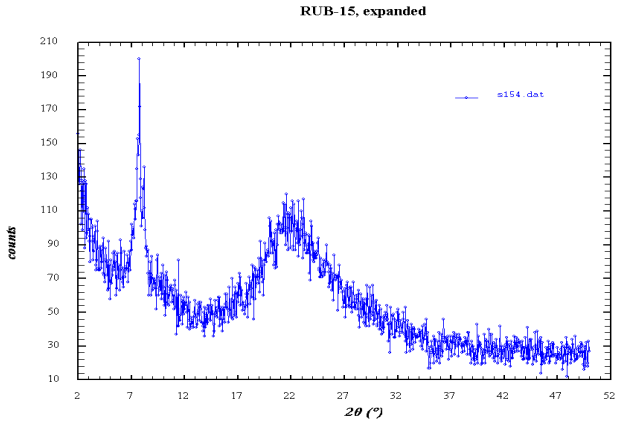

Fig. 2: a) PXRD of IEZ-RUB-15

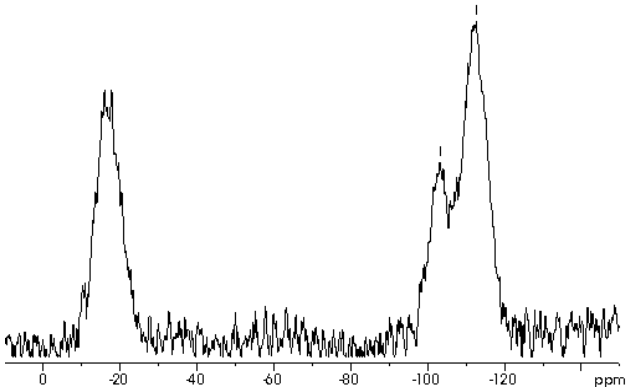

b) ^{29}Si NMR spectrum showing the bridging siloxane group (~-18 ppm) and signal of the silicate layer. CP increases the intensity of the bridging group.

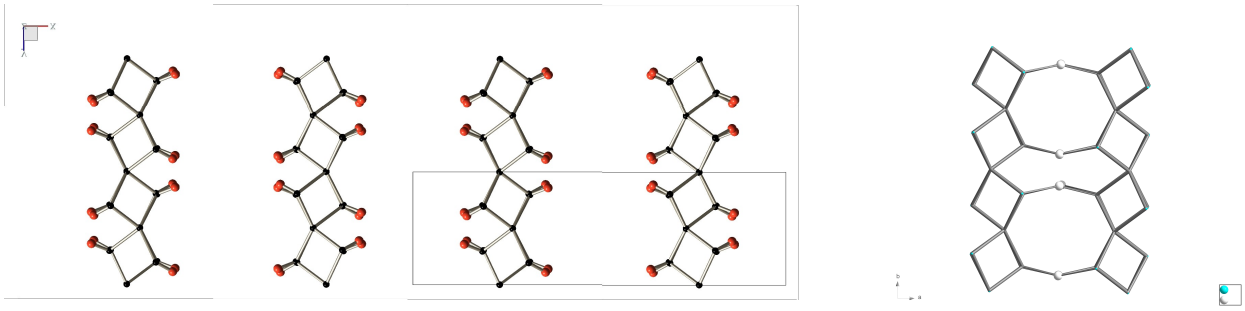

Fig. 3: a) Stack of RUB-15 layers before condensation b) IEZ-RUB-15 with O-Si$(CH_4)_2$-O link

Fig 3 shows the silicate layers stacked in the starting material (a) and siloxane-bridged expanded structure of IEZ-RUB-15.

LITERATURE:

(1) Wu, P. et al.: JACS **130,** 8178-8187 (2008).
(2) Oberhagemann, U., et al., Angew. Chem.Int . Ed. Engl.**35**, 2869-2872(1996).

IM-17: a new zeolite with an interrupted framework topology

Yannick Lorgouilloux,[1, 2] Mathias Dodin,[1] Jean-Louis Paillaud,[1*] Claire Marichal,[1] Philippe Caullet[1] and Nicolas Bats[3]
[1] *IS2M- MPC, LRC CNRS 7228, UHA, ENSCMu, 3 rue Alfred Werner, 68093 Mulhouse Cedex, France, Jean-Louis.Paillaud@uha.fr*
[2] *Katholieke Universiteit Leuven, Centrum voor Oppervlaktechemie en Katalyse, Kasteelpark Arenberg 23, 3001 Heverlee, Belgium*
[3] *IFP Energies Nouvelles, BP3, 69360 Solaize, France*

Introduction

The discovery of a new zeolite is always a challenge and several strategies have emerged in the past. One of them is the "high-throughput" synthesis illustrated by the use of hexamethonium as organic structure directing agent or SDA in hydroxide (OH^-) or fluoride (F^-) media. This strategy allowed the discovery of the 18- and 10-membered ring (10 MR) molecular sieve ITQ-33 [1] and more recently of ITQ-44, the first zeolitic structure possessing double 3 ring (*d3r*) units [2]. In our search for new large pore zeolites, we decided to engage decamethomium as SDA by varying several synthesis parameters in the (Si,Ge) system. This diquat has a longer chain than hexamethonium and is known to lead to the aluminosilicates Nu-87 (**NES**) [3] and ZSM-12 (**MTW**) [4] which are 10 and 12MR zeolites, respectively. Thus, in our investigations, a new molecular sieve, IM-17, was synthesized among known zeolites [5]. Here we present the synthesis, characterization, and structure of this new material.

Experimental

All hydrothermal syntheses were performed at 170°C in a homemade multi-autoclave containing sixteen 2 mLTeflon lined reactors. Gels were prepared both in OH^- and F^- media by mixing Aerosil 200 (>98% Degussa) or TEOS (>98%, Fluka), amorphous germanium oxide GeO_2 (>99.99%, Aldrich), HF acid (40%, Carlo Erba), distilled water, and decamethonium dihydroxide obtained from the bromide form (>98%, Fluka) by ion exchange in water (Dowex SBR LC NG, OH Form (Supelco)). A typical gel composition was 0.6 SiO_2 : 0.4 GeO_2 : 0.25 $R(OH)_2$: 10 H_2O, where R represents the decamethonium cation. The structure of IM-17 was solved from a powder X-ray diffraction pattern of the calcined product in space group *Cmmm* with a = 39.0721(6) Å, b = 22.2259(5) Å, c = 12.6846(3) Å. Solid state ^{29}Si MAS+DEC NMR experiments were also performed.

Results and discussion

In fluoride media the investigated gel compositions only led to EMM-1 (**BEC**) [6]. In OH^- media, **MFI**-type zeolite and/or IM-17 crystallized. It was shown that dilution, Si/Ge molar ratio and the source of silicon are important factors. Figure 1 summarizes some of the experiments performed for the IM-17 synthesis optimization. The best results were obtained in concentrated systems and with Aerosil 200 as the silica source. The asymmetric unit of IM-17 contains 14 crystallographic independent T sites, two of them having an occupancy factor of 0.5 and corresponding to disordered silanol groups. The chemical composition per unit cell of anhydrous calcined IM-17 after the Rietveld refinement is $[Si_{131.9}Ge_{44.1}O_{348}(OH)_8]$. IM-17 possesses a complex 3D pore system consisting of interconnected 12 and 10MR channels. The projection along the c-axis (Figure 2) shows two types of 12MRs, those with an ovoid

shape of dimensions 7.3 Å × 5.35 Å and those with a S shape supporting the silanol groups. At the intersection of the S shaped 12MR and two different 10MR channels, a [$4^4 5^8 6^4 10^4 12^2$] super cage is formed (Figure 3). This new topology contains six different composite building units (CBUs), namely *ats*, *bre*, *d4r*, *mel*, *lau* and *stf*.

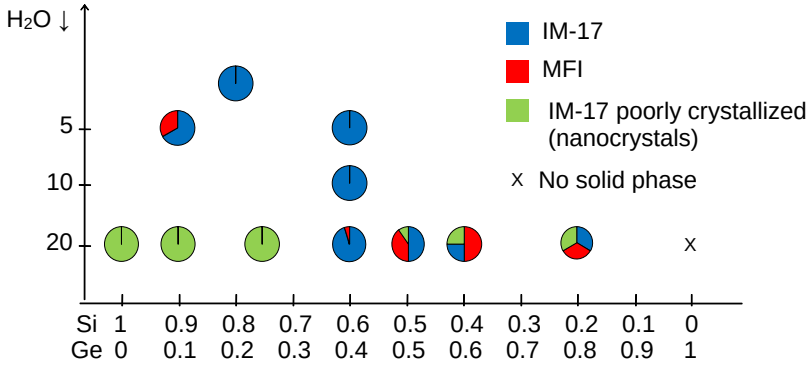

Figure 1. Reaction mixture dilution and Si/Ge molar ratio influence on the IM-17 synthesis.

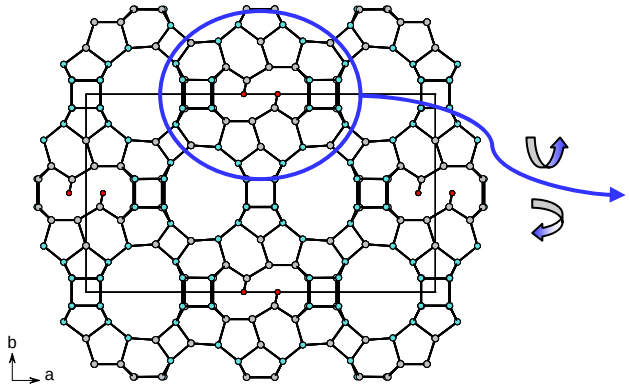

Figure 2. Projection of IM-17 down [001].

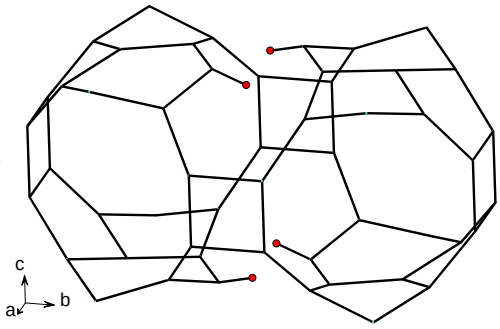

Figure 3. The [$4^4 5^8 6^4 10^4 12^2$] super cage present in IM-17 with its silanol groups.

Conclusions

Series of hydrothermal syntheses with decamethonium as SDA allowed the discovery of a new zeolite namely IM-17 in OH^- medium. This material with an interrupted framework possesses a large adsorption capacity (0.22 $cm^3.g^{-1}$) and a high potential in acid catalysis.

Acknowledgements

We are grateful to CNRS/IFP and Ministère de la Recherche for doctoral grants to Y. L and M. D., respectively.

References

[1] A. Corma, M.-J. Díaz-Cabanãs, J. L. Jordá, C. Martínez, M. Moliner, Nature. 443 (2006), 842-845.
[2] J. Jiang, J. L. Jordá, M.-J. Díaz-Cabanãs, J. Yu, A. Corma, Angew. Chem. 122 (2010), 5106-5108.
[3] M. D. Shannon, J. L. Casci, P. A. Cox, S. J. Andrews, Nature. 353 (1991), 417-420.
[4] A. Moini, E. Valyocsik, US Patent 5.192.521, 1993.
[5] Y. Lorgouilloux, J.-L. Paillaud, P. Caullet, J. Patarin, N. Bats, WO Patent 2009/090338-A1, 2009.
[6] A. W. Chester, S. S. Dhingra, US Patent 2003/0185751-A1, 2003.

BACTERICIDAL ACTION OF CANCRINITE AND A-TYPE ZEOLITES

C. Urbina de Navarro[1], F. Ocanto[2], C. F. Linares[2], M. Brikgi[2], D. Reyes[3], T. Rojas[4], C. Martinez[4]

1) Universidad Central de Venezuela, Facultad de Ciencias, Centro de Microscopía Electrónica "Dr. Mitsuo Ogura", Caracas, Venezuela. 2) Universidad de Carabobo, Facultad Experimental de Ciencias y Tecnología, Departamento de Química, Laboratorio de Catálisis y Metales de Transición. 3) Universidad de Carabobo, Facultad Experimental de Ciencias y Tecnología, Departamento de Biología.4) Universidad de Carabobo, Facultad de Ciencias de la Salud. Departamento de Microbiología Médica. caribay.urbina@ciens.ucv.ve

Introduction

When talking about zeolites, the first thing that comes to mind is their use as molecular sieve or catalyst support. However, in recent decades, these solids have successfully ventured into other areas like the pharmaceutical industry, being used as carriers of anti-diarrhea, anti-parasitic, etc [1,2,3]. These solids have been quite successful as a germicide. Our research group has used the cancrinite type zeolite as a carrier of metals for use as bactericides against bacteria from the soil, obtaining very interesting results [4]. It should be noted that the zeolite acts only as a carrier of the metal, and ion exchange properties determine the controlled release of metal. Although zeolites only serve as a support, their properties are important in the formulation of bactericides.

Experimental

In this paper we studied the bactericidal action of commercial A and synthesized cancrinite type zeolites, exchanged with Ag, Cu and Ag/Cu, against to *Escherichia coli (E. coli)* and *Pseudomonas aeruginosa (P. aeruginosa).* The synthesis of nitrated cancrinite zeolite was based on the impregnation of a X faujasite type zeolite with a solution of sodium nitrate and sodium hydroxide 5M [5]. Ion exchange of zeolites was carried out by placing the nitrated cancrinite zeolite or A zeolite in contact with the salt solution of the cation or cations described above (hydrothermal exchange.) Besides the type of zeolite and the cation exchanged, we studied the influence of the amount of modified zeolite on its bactericidal action [5].

Results and discussion

XRD and the IR studies of the solids obtained from X type zeolite; show that nitrated cancrinite type zeolites were obtained. These same studies carried out on both types of zeolites (A and cancrinite) exchanged with metals; indicate that structural integrity is maintained. Chemical analysis by ICP indicated that the amounts of metal exchanged on both types of zeolites are practically the same, allowing a better comparison of the bactericidal action of the studied solids. The effect of the mass of nitrated cancrinite and A type zeolites exchanged with silver, copper and a mixture of these metals, were carried out on the exponential phase of bacterial growth to ensure the vitality of both microorganisms. The results indicate that silver has a strong bactericidal action against *Escherichia coli*, even at low metal concentrations. In the case of copper, it did not show a good bactericidal effect on

any of the tested solid. By contrast, the results suggest that a low amount of this metal is essential for the development of these organisms acting as a trace element. Solids containing both metals have a lethal effect even in the presence of trace elements like copper. These results show the strong bactericidal action of silver, even in the presence of vital trace elements, not allowing the proliferation of organisms. With regard to the bactericidal action against *Pseudomonas aeruginosa* of the cancrinite type zeolites exchanged with silver, have the best bactericidal activity in comparison with the other solids studied. It was found that the minimum mass of the studied zeolite matrices, which have bactericidal activity against *Escherichia coli*, is 2.5 mg and 20 mg to *Pseudomonas aeruginosa*. Bactericidal effect was observed after 10 min and remains at least three hours

Conclusions

The antibacterial zeolites with Ag and Ag/Cu showed bactericidal activity against these microorganisms, silver ions have strong bactericidal action against Escherichia coli at low cation concentrations. Copper ions act as trace element for microorganisms. The cancrinite zeolite exchanged with silver, showed the highest bactericidal activity against *Pseudomonas aeruginosa*. The low weights required of zeolite with bactericidal action, represents a significant savings of reagents and a decrease in the quantity discharged of silver ions into the environment.

Table 1. - Bactericidal Action of cancrinite and A type zeolites against *Escherichia coli*

Solid	Bactericidal Action	Solid	Bactericidal Action
Can-Ag	Strong	A-Ag	Strong
Can-Cu	Very low	A-Cu	Very low
Can-Ag/Cu	Middle	A-Ag/Cu	Middle

Can: cancrinite type zeolite A: A type zeolite

Acknowledgements

This research was supported by Consejo de Desarrollo Científico y Humanístico CDCH 2385-2004 and Project FONACIT Lab Nac 20010001442

References

[1] Rivera, M.; Olguín, M.; García, I.; Alcántara, O.; Rodríguez Fuentes, G. Microporous and Mesoporous Mater. **39**, 431. (2000).
[2] Inoue, Y.; Hoshino, M.; Takahashi, H.; Noguchi, T.; Murata, Y.; Kanzaki, Y.; Hamashima, H.; Sasatsu. M. J. Inorg. Biochem. 92, 37. (2002).
[3] Matsumura, Y.; Yoshikata, K.; Kunisaki, S.; Tsuchido, T.; Appl. Enviro. Microbial. **69**, 4278. (2003).
[4] Brikgi; M. Thesis. Universidad de Carabobo, Venezuela. Dpto. de Química. (2003).
[5] Ocanto, F. PhD Thesis. Universidad Central de Venezuela. (2009)

Mesoporous ZSM-5 templated by an amphiphilic organosilane – Catalytic activity in the cyclohexane cracking

Edilene D. da Silva, Kele T. G. Carvalho, Saulo T. F. Grecco, Alexandre A. S. Gonçalves, Ernesto A. Urquieta-Gonzalez*
*Department of Chemical Engineering, Federal University of Sao Carlos, C. Postal 676, CEP 13.565-905, Sao Carlos-SP, Brazil,*urquieta@ufscar.br*

Introduction

A great number of zeolites and zeolitic structures are very known but only few of them have been so extensively applied in catalysis as ZSM-5 zeolites. Among other industrial applications, ZSM-5 zeolites (3D microporous system with diameters of about 0.55 nm) are used as additive in the Fluid Catalytic Cracking (FCC process), allowing to improve the octane number of the gasoline. ZSM-5 zeolites transform hydrocarbons with low octane number in light n-paraffins and olefins [1]. However, the ZSM-5 micropores limit the diffusion of heavy hydrocarbons not allowing their transformation inside the crystals. Intracrystalline diffusion of large molecules is critical during the cracking reactions. Several potential solutions have been explored with the most of them leading to interparticle mesopores. Nevertheless, the use of soft or hard templates together with the micropores organic template during the zeolite synthesis has been able to produce mesopores inside the zeolite crystals. An important advance in this research field was the use of amphiphilic organosilanes as soft mesopores template reported by R. Ryoo and co-workers [2].
In this work, it was used an amphiphilic organosilane to produce mesoporous ZSM-5 zeolites with the aim to verify their acid activity in the cyclohexane cracking and to compare them with the performance of a commercial ZSM-5 zeolite.

Experimental

ZSM-5 zeolites were synthesized using the organosilane [3-(trimethoxy-silyl)propyl] octadecyldimethylammoniumchloride, TPOAC, 72 wt% solution, Aldrich). The synthesis gel, adapted from [2], was $1Al_2O_3$:10TPABr:$10Na_2O$:$38SiO_2$:1.6TPOAC:$7200H_2O$. The mixture was stirred for 2h at 25 °C, then, the gel was transferred to a stainless-steel Teflon-coated autoclave and crystallized for 5 days at 130 °C (sample $Z_{TPOAC}130$) or 150 °C (sample $Z_{TPOAC}150$). The obtained solids were separated by filtration, washed, dried at 60 °C for 6h and calcined at 500 °C. The H-form of the zeolites was obtained by NH_4^+ ionic exchange with subsequent thermal treatment at 550 °C. Physical and chemical characterizations were done using XRD, SEM, AAS, NH_3-TPD and N_2 sorption measurements. The cyclohexane cracking on the studied zeolites was carried out at 400 °C and using a contact time of 0.54 h^{-1}.

Results and discussion

Fig. 1a shows the XRD patterns of the soft templated $Z_{TPOAC}130$ and $Z_{TPOAC}150$ samples and of a commercial H-ZSM-5. It can be seen that all samples are crystalline and contain exclusively diffraction peaks of the MFI type structure [3]. Coherently, the isotherms of the commercial H-ZSM-5 (Fig. 1b) are of type I (only micropores). On the other hand, $Z_{TPOAC}130$ and $Z_{TPOAC}150$ zeolites clearly show N_2 adsorption in micropores and in intracrystalline mesopores (isotherm of type IV) with H1 hysteresis. The mesopore size distributions are centered in 3.4 and 2.5 nm for $Z_{TPOAC}130$ and $Z_{TPOAC}150$, respectively (Fig. 1c). The textural properties of the mesoporous zeolites (Table 1) evidence lower mesopores formation at higher synthesis temperature with both samples having similar morphology (Fig. 2a and 2b). Fig. 2c shows that the TPOAC templated zeolites are active in the clyclohexane cracking with the

more crystalline $Z_{TPOAC}150$ (Fig. 1a), having more and similar conversion than the $Z_{TPOAC}130$ and the commercial H-ZSM-5, respectively. This behavior indicating that the use of an amphiphilic organosilane do not alter the ZSM-5 capability to develop its well known acid properties, as was verified by NH_3-TPD (not shown), with the mesopores formation and acid strength depending on the synthesis temperature.

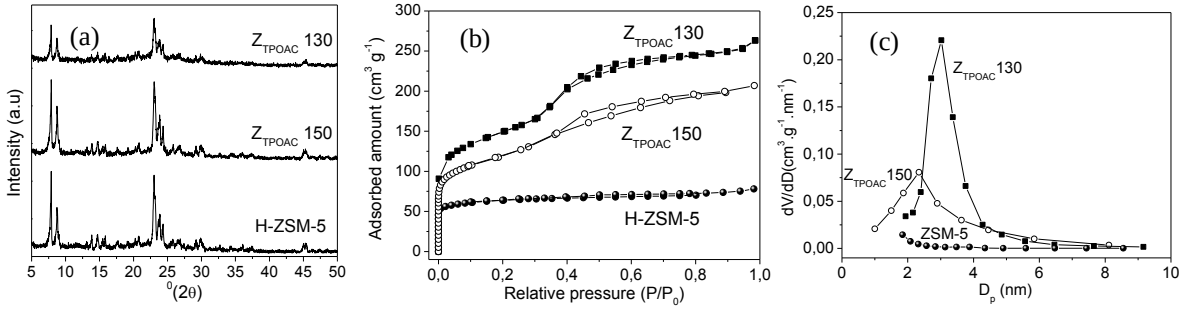

Figure 1. (a) XRD patterns; (b) N_2 adsorption-desorption isotherms; (c) pore size distributions of the soft templated zeolites and of the commercial H-ZSM-5.

Table 1. Si/Al ratio and textural properties of the studied zeolites.

Samples	Si/Al	S_{Ext} (m^2 g^{-1})	V_{Meso} (cm^3 g^{-1})	V_{Micro} (cm^3 g^{-1})
$Z_{TPOAC}130$	16.3	344	0.3268	0.0804
$Z_{TPOAC}150$	19.0	138	0.1505	0.1696
H-ZSM-5	24.0	90	-	0.1200

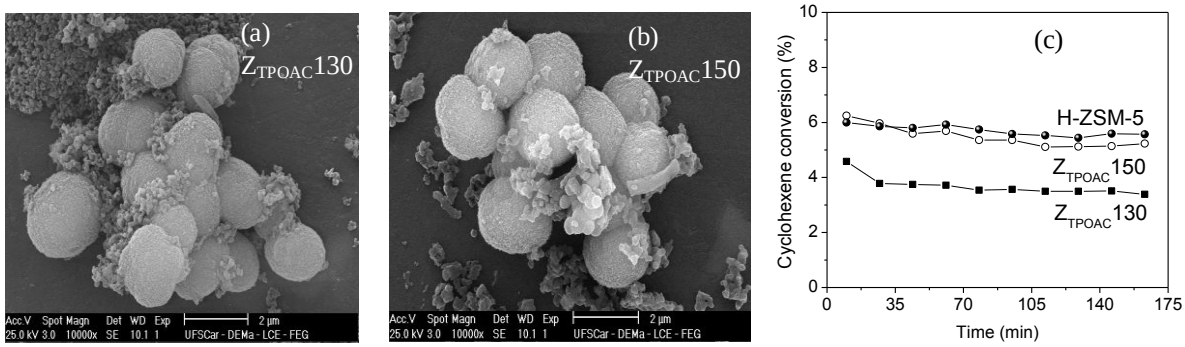

Figure 3. (a) and (b) SEM images and (c) conversion of cyclohexane on the ZSM-5 zeolites.

Conclusion

The use of TPOAC during the synthesis of ZSM-5 zeolites led to the formation of intracrystalline mesopores. The mesoporous zeolites were active in the cyclohexane cracking with the mesopores formation and acid strength depending on the synthesis temperature.

Acknowledgements

The authors gratefully acknowledge the financial support provided by CNPq-Brazil.

References

[1] Buchanan, J.S. The chemistry of olefins production by ZSM-5 addition to catalytic cracking units; Catal. Today 55 (2000) 207–212

[2] Choi, M., Cho, H. S., Srivastava, R., Venkatesan, C., Choi, D. H., Ryoo, R; Amphiphilic organosilane directed synthesis of crystalline zeolite with tunable mesoporosity, Nature Materials, 5 (2006), 718-723.

[3] Petushkov, A., Yoon S., Larsen**,** S. C; Synthesis of hierarchical nanocrystalline ZSM-5 with controlled particle size and mesoporosity, Microporous Mesoporous Materials, 137 (2011), 92-100.

Physicochemical characterization of CMK-1, CMK-3, and CMK-8 ordered mesoporous carbons modified with amino groups

M. Lezanska[*a], P. Pietrzyk[b]
[a] *Faculty of Chemistry, Nicolaus Copernicus University, Gagarina 7, 87-100 Torun, Poland,*
[b] *Faculty of Chemistry, Jagiellonian University, Ingardena 3, 30-060 Krakow, Poland*
Corresponding author: M. Lezanska, e-mail: miriam@chem.uni.torun.pl

Introduction

Amination is an important tool for modification of carbon surface. Introduction of amino groups onto the surface changes basicity of the latter and various compounds can be immobilized by the NH_2 groups, resulting in further modification of the surface. Functionalisation with the amine groups has been performed to develop an effective adsorbent for transition-metal ions like, e.g., Cu^{2+} [1]. The $-NH_2$ groups generated on the surface of mesoporous carbons, discussed in this work, are expected to play a role of reacting centers able to bind 5,10,15,20-tetrakis(4-carboxyphenyl)porphine, a complex the molecule of which contains the –COOH groups. This way, immobilization can occur. Interaction between the -COOH functional groups of the carbon surface, mediated by carbodiimide derivatives, and amino groups originating from ligands of complexes have already been reported [2].
The amination of mesoporous carbons is performed in a two -step process: 1) nitration and 2) reduction of the nitro groups. The porous structures of carbons and acidity were examined and the influence of the conditions of each step on the properties of modified replicas was evaluated.

Experimental

The processes of nitration and reduction were studied on ordered carbon replicas of the types of CMK-1 ($I4_1/a$) [3], CMK-3 (P6 mm) [4], and CMK-8. The materials were prepared from sucrose and synthesized in the pores of ordered silica matrices: MCM-48 ($Ia3d$), SBA-15 (P6 mm), and KIT-6 ($Ia3d$) [5], respectively.
The nitration reaction was carried out with a mixture of 70% nitric acid and concentrated sulfuric acid at 0°C. The reduction of nitrated carbons was proceeded in aqueous ammonia solution containing sodium hydrosulfite, similarly to the method described elsewhere [6]. The porous structures of replicas and matrices were characterized by the nitrogen adsorption. A variety of experimental techniques had been used to characterize functional groups of porous carbon, such as Boehm titration methods, XPS, elemental analysis, and TGA. The Raman spectra were recorded to estimate a level of graphitization.

Results and discussion

The aminated carbons contain up to 2.2 wt. % of N. The XPS N 1s main peak centered at 399.5 eV has shown that mainly the nitrogen bound to a carbon atom belonging to an aromatic entity C-N-H was created. Introduction of amino groups onto the carbon surface can be confirmed by an increase in the hydrogen content occurring after reduction as compared to that of nitrated samples.
The shape of the ad/desorption isotherms of nitrogen (type IV according to IUPAC) for carbon replicas and matrices indicates the presence of mostly mesopores and a small fraction of micropores. The nitration process caused the structure of the CMK-1 carbon to collapse partially, whereas a further decrease in sorption capacity was obtained due to

the reduction. The BET surface areas of the parent CMK-1, the nitrated sample, and of the amino-modified one were 1144, 727, and 616 m^2/g, respectively. Moreover, the pore volume of 0.5 cm^3/g of the parent replica diminished to 0.3 cm^3/g. The structure of CMK-8 carbon was less influenced by the oxidative/reductive treatment, as compared to that of CMK-1. The reason for that was possibly thicker walls of the CMK-8 material. The CMK-3 carbon replica was the best ordered one. The surface area of CMK-3 was equal to 1137 m^2/g and did not practically change after modifications. Its pore volume reached 1 cm^3/g and it diminished by half after amination. However, the external surface area and the area of primary mesopores developed because of functional groups that had been created on the surface. The pore size distribution after modification was still monomodal, though average pore size diminished from 3.5 to 2.1 nm. The highest amount of acidic functional groups has been created on the CMK-3 surface after nitration, as it was confirmed by the Boehm method. The whole acidity of CMK-3-NO_2, equal to 2.93 mmol/g, resulted from the phenolic groups, lactones, and carboxylic groups. The concentration of the latter prevailed. The obtained CMK-3-NH_2 material was able to immobilize ca. 10 wt. % of the TCCP ligand.

References

[1] W. Yantasee, Y. Lin, G. E. Fryxell, K. L. Alford, B. J. Busche, C. D. Johnson, Ind. Eng. Chem. Res. 43 (2004) 2759
[2] C. M. Elliott, R. W. Murray, Anal. Chem. 48 (1976) 1247
[3]. R. Ryoo, S. H. Joo, S. Jun, J. Phys. Chem. B 103 (1999) 7743
[4] S. Jun, S. H. Joo, R. Roo, M. Kruk, M. Jaroniec, Z. Liu, T. Ohsuna, O. Terasaki, J. Am. Soc. 122 (2000) 10712
[5] T-W. Kim, F. Kleitz, B. Paul, R. Ryoo, J. Am. Soc. 127 (2005) 7601
[6] M. Abe, K. Kawashima, K. Kozawa, H. Sakai, K. Kaneko, Langmuir 16 (2000) 5059

Direct Synthesis of Thiol-functionalized Micro/Mesoporous Zeolites

Ka-Lun Wong, Jean-Michel Goupil, Valérie Ruaux, Svetlana Mintova*

Laboratoire Catalyse et Spectrochimie, ENSICAEN-Université de Caen-CNRS, 6 Bd. Maréchal Juin, 14050 Caen, France

Introduction

The incorporation of organic moieties in the channels or anchoring on the surfaces of microporous (zeolites) and mesoporous molecular sieves (e.g. MCM- and SBA-type materials) has provided them with distinctive properties for a broad range of applications such as immobilization of enzymes, drug delivery carriers, encapsulation of metal nanoparticles, etc.

Nanoporous materials can be functionalized by different pathways, which are categorized in two groups: (i) post-synthesis and (ii) direct synthesis approaches. Post-synthesis methods involve treatment on the initially prepared porous materials, using grafting of organofunctional compounds onto the pore walls via covalent bonds. The grafting process is a reaction between suitable organic moieties with the surface silanol groups of the material. The direct synthesis method involves co-condensation of an organofunctional compound with inorganic precursors during synthesis in a single step.

In this study, the synthesis of micro/mesoporous pure silica molecular sieve functionalized with thiol groups by co-condensation method is reported. The 3-mercaptopropyl-trimethoxysilane (MPTS) with bifunctional groups was used as organofunctional compound and co-silica source.

Experimental

Thiol-functionalized micro/mesoporous materials (MPTS-silicalite-1) with different ratios of SiO_2 and MPTS are synthesized. For comparison, amorphous SiO_2 with MPTS (MPTS-SiO_2) and pure silicalite-1 (TPA-silicalite-1) samples are prepared. The samples were characterized with XRD, SEM, thermal analysis, elemental analysis, N_2 physisorption, NMR, IR and Raman spectroscopies.

Results and Discussion

Micro/mesoporous (MPTS-silicalite-1) structure with high crystallinity is obtained by co-condensation technique when appropriate amount of MPTS is used. The samples exhibit diffraction peaks characteristic of the microporous MFI-type zeolite and a broad peak at 1.8 °2θ, which correspond to the mesoporous structure. The co-condensation process occurring in the presence of MPTS is leading to a high degree of framework cross-linking between the zeolite silica framework and the organosiloxane resulting in the formation of both micro- and meso- pores. The organo-functionalized sample contains nanoparticles with a size below 50 nm which tend to form larger agglomerates. An evidence for the incorporation of MPTS in the sample is obtained by chemical analysis; about 2.1 mmol and 1.6 mmol MPTS per gram is present in the micro/mesoporous and amorphous silica, respectively. Besides, the incorporation of MPTS in the samples was confirmed by NMR spectroscopy. In addition to the Q^4 [$Si(OSi)_4$] and Q^3 [$Si(OSi)_3OH$] in the ^{29}Si NMR, two well-resolved peaks at -68 and -55 ppm were found for the MPTS-silicalite-1, which are attributed to T^3 [R-C-Si-$(OSi)_3$] and

T^2 [R-C-Si$(OSi)_2$OH] species, respectively. The T^2 and T^3 species confirm the presence of organosilane centers from the MPTS, and show that the Si–C bonds remain intact during the synthesis. This is an indication for the high degree of framework cross-linking between zeolite silica framework and the organosiloxane from the MPTS. To identify the organic moieties attached to the zeolite framework, the solid state ^{13}C CP-MAS NMR and Raman measurements were carried out. In addition to the resonance peaks at 62.7, 16.3, 11.3 and 10.1 ppm attributed to the ^{13}C sites from the TPAOH, additional peaks at 35.5, 34.7, 14.0 and 13.0 ppm, are observed in the MPTS-silicalite-1 (Figure 1A). Moreover, the Raman spectra show bands at 650 and 740 cm^{-1}, which are assigned to $\nu_{C\text{-}Si}$ and $\nu_{C\text{-}S}$ stretching mode of the MPTS compound. The bands at 1259 (doublet), 1302, and 1413 cm^{-1} are attributed to the C-H bending mode of the propyl chain of MPTS, and their slight shifting is proving that the MPTS is incorporated in the channels of the MPTS-silicalite-1 sample.

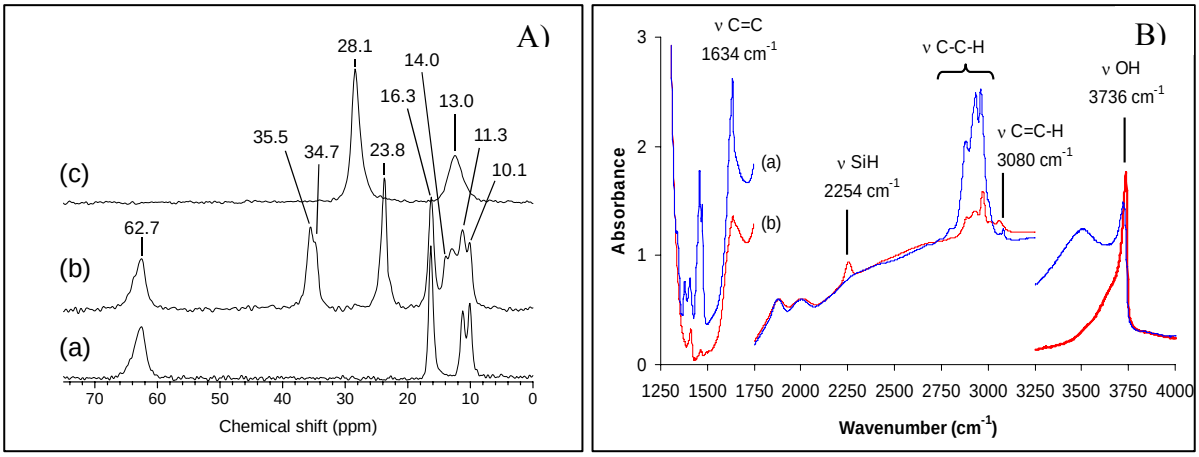

Figure 1. A) ^{13}C CP-MAS NMR spectra of (a) TPA-silicalite-1, (b) MPTS-silicalite-1, and (c) MPTS-SiO_2; B) IR spectra of MPTS-silicalite-1 thermally treated under vaccuum: (a) 673 K and (b) 823 K.

The modification of the MPTS-silicalite-1 thermally treated under vacuum is followed by IR spectroscopy (Figure 1B). At low temperature, the anchored propylthiol is evident, the bands at 2930 and 1430 cm^{-1} from the methylene vicinal to S atom are present. During the heating under vacuum, the intensities of both groups of ν(C-H) and δ (C-H) bands decrease and their pattern change, thus revealing the modification and elimination of organic moieties. Notably, the formation of sorbed ethene is evidenced. Above 723 K, further degradation of anchored species result in the formation of Si-H groups and free silanol groups.

Conclusions

In conclusion, micro/mesoporous material functionalized with thiol groups has been prepared by co-condensation method using 3-mercaptopropyltrimethoxysilane as organofunctional compound and co-silica source. During the synthesis, the methoxy groups of MPTS are hydrolyzed and the organosiloxane are cross-linked with the silica source thus forming a porous framework with micropores (silicalite-1) and ordered mesopores. Consequently, the thiol groups covalently tethered to the silicon atoms of MPTS are incorporated into the pure silica molecular sieve. The incorporation of MPTS is confirmed by chemical analysis, NMR, Raman and IR spectroscopies.

A MULTIFUNCTIONAL IRON TRIMESATE MOF

Jong-San Chang,[1*] Young Kyu Hwang,[1] Alexandre Vimont,[3] Marco Daturi,[3] Philip L. Llewellyn,[4] Jean Marc Grenèche,[5] P. Couvreur,[6] R. Gref,[6] Patricia Horcajada,[2] Gérard Férey,[2] Christian Serre[2]

[1] *Catalysis Centre for Molecular Engineering (CCME), Korea Research Institute of Chemical Technology (KRICT), Sinseongno 19, Yuseong-gu, 305-600 Daejon (South Korea), E-mail: jschang@krict.re.kr*

[2] *Institut Lavoisier, UMR CNRS 8180, Université de Versailles Saint Quentin, Versailles, France, E-mail: serre@chimie.uvsq.fr*

[3] *Laboratoire Catalyse et Spectrochimie, UMR CNRS/ENSICAEN 6505, Université de Caen Basse-Normandie, UNICITE, Caen, France*

[4] *Laboratoire Chimie Provence, Université de Provence - UMR CNRS 6121), Marseille, France*

[5] *Laboratoire de Physique de l'Etat Condensé, UMR CNRS 6087, Université du Maine, 72085 Le Mans, France*

[6] *UMR CNRS 8612 Faculté de Pharmacie Université Paris Sud, France*

Introduction

MOFs are the latest class of porous solids, and are built up from almost any metal centers from the periodic table and organic linkers bearing complexing groups (carboxylates, phosphonates imidazolates…), resulting in a wide range of structures, pore size and compositions. However, so far, no real application based on MOFs has been reported despite their promising properties in gas storage, separation or catalysis. Some of us have reported meanwhile the iron(III) trimesate MIL-100(Fe) (MIL stands for Materials from Institut Lavoisier) which exhibits oxo-centered trimers of Fe(III) octahedra, a cubic array of very large cages (25-29 Å) accessible through microporous windows (5-9 Å) with a large surface area and pore volume (2000 $m^2.g^{-1}$; 1.1 $g.cm^{-3}$).[1]

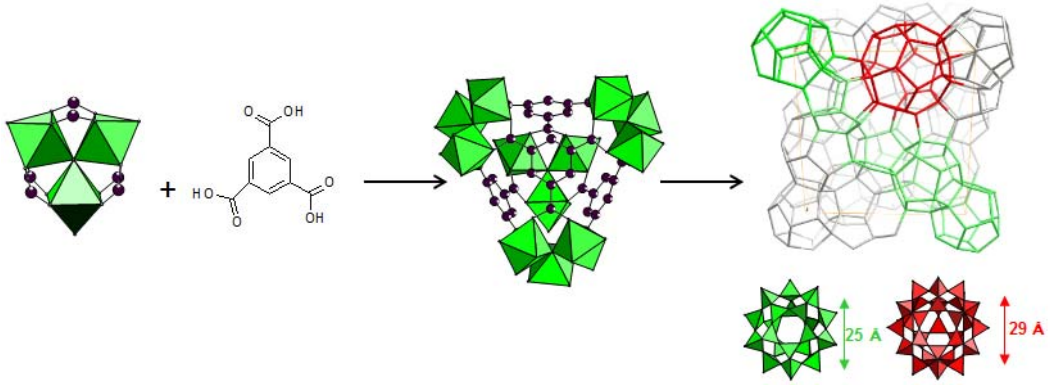

Figure 1 : oxocentered trimer of octahedron and BTC linker; hybrid supertetrahedron; hybrid structure of MIL-100(Fe) with the two types of mesoporous cages.

Experimental

Fe-MIL-100 was synthesized according to the previously reported conditions, using HF, Fe° and 1,3,5 BTC in water at 150°C. Activation was performed using hot water and KF treatment at 70°C in water. Samples prior to sorption tests were outgassed overnight at T=150-250°C while solids was dehydrated prior to encapsulation tests at 100°C.

Results and discussion

Oxidation state of MIL-100(Fe) can be tuned with a partial reduction of iron using heating and vacuum.[2] IR spectroscopy, Mossbauer analyses, microcalorimetry

experiments, breakthrough curves, indicates that the back donation effect of Fe(II) species formed by the controlled pre-activation is at the origin of the strong interaction between the metal site and unsaturated gas molecules. A significant propylene/propane selectivity (> 10) at low partial pressures (5 kPa) was evidenced, with the integrity of the framework kept upon partial reduction of iron(III), as well as a satisfactory regenerability and cyclability of the sorbent. This redox behavior can be further used for catalytic applications through the Friedel and Crafts Benzyl alkylation.[1] Secondly, MIL-100(Fe) exhibits a low toxicity, is biodegradable and can upload records amounts of antitumoral or anti-retroviral drugs and deliver it on a controlled manner under physiological conditions.[3] The hydrothermal stability of MIL-100(Fe) has also been also demonstrated. Finally, MIL-100(Fe) can be produced at large scale (Kg) under industrially relevant conditions.

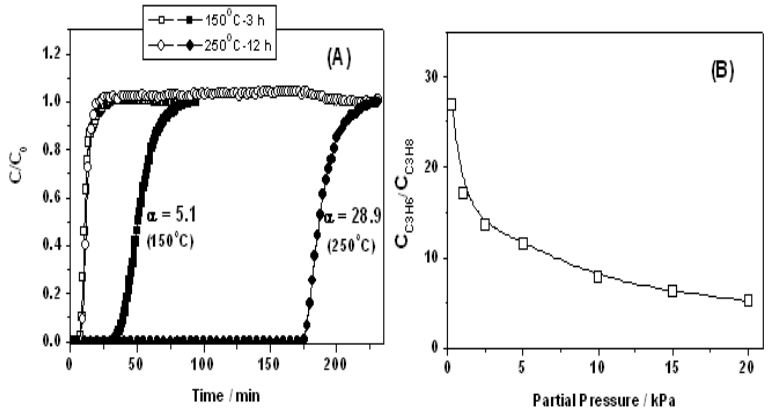

Figure 2 : (A) Breakthrough curves of an equimolar binary mixture of propane (open symbols) and propylene (closed symbols) in MIL-100(Fe) activated at 150°C for 3 h and 250°C for 12 h in He; (B) Separation factors (□) of propylene over propane obtained from breakthrough curves of MIL-100(Fe) depending on partial pressures. In breakthrough curves, partial pressure of equimolar mixture is 0.25 kPa. Measurement temperature is 40°C for (A) and (B).

Conclusion

The mesoporous iron trimesate MIL-100(Fe) sample combines many interesting features (large pore volume, non toxic, biodegradable, hydrothermal stability, synthesis at large scale, redox behavior, reducibility…) that makes it one of the most promising MOF candidate for a large scale application.

Acknowledgements

Y.-K. Seo, H. Leclerc, E. Bloch, T. Chalati, S. Surblé and I. Margiolaki are acknowledged for their participation to these results.

References

[1] P. Horcajada, S. Surblé, C. Serre, D.-Y. Hong, Y.-K. Seo, J.-S. Chang, J.-M. Grenèche, I. Margiolaki, and G. Férey, *Chem Comm*., 2820 (2007).

[2] J. W. Yoon, Y.-K. Seo, Y. K. Hwang, J.-S. Chang, H. Leclerc, S. Wuttke, P. Bazin, A. Vimont, M. Daturi, E. Bloch, P. L. Llewellyn, C. Serre, P. Horcajada, J.-M. Grenèche, A. E. Rodrigues, and G. Férey, *Angew. Chem. Int. Ed*. **2010**, 49, 5949 –5952

[3] (a) P. Horcajada, T. Chalati, C. Serre, B. Gillet, C. Sebrie, T. Baati, J. F. Eubank, D. Heurtaux, P. Clayette, C. Kreuz, J.-S. Chang, Y. K. Hwang, P.-N. Bories, L. Cynober, S. Gil, G. Férey, P. Couvreur, R. Gref, *Nat. Mater*., **2010**, 9, 172; (b) A. C. McKinlay, R. E. Morris, P. Horcajada, G. Férey and C. Serre, *Angew. Chem. Int Ed*., **2010,** *49*, 6260

Rational Design and Control of the Dimension of MOFs based on 4-hydroxyisophtalate ligand

Lei Wu[1,2], Gérald Chaplais[1], Bernd Marler[3], Angélique Simon-Masseron[1], Heribert Graetsch[3], Joël Patarin[1], Ming Xue[2], Guang-Shan Zhu[2], Shi-Lun Qiu[2]

[1] *Equipe Matériaux à Porosité Contrôlée (MPC), Institut de Science des Matériaux de Mulhouse (IS2M), LRC CNRS 7228, Université Haute Alsace, ENSCMu, 3 rue Alfred Werner, 68093, Mulhouse Cedex, France.*
[2] *State Key Laboratory of Inorganic Synthesis & Preparative Chemistry, Jilin University, Changchun 130012, China*
[3] *Institut für Geologie, Mineralogie und Geophysik, Ruhr-Universität Bochum, Universitätsstr. 150, D-44780 Bochum, Germany*

Introduction

Within the last fifteen years, the development of a new class of organic–inorganic hybrid compounds, mainly designated as coordination polymers or metal–organic frameworks (MOFs), has overwhelmingly increased. Own to their potential porous feature, MOFs constitute promising candidates for gas storage, separation, drug delivery, electronic and optical applications, sensing, magnetism and catalysis.[1,2] In this purpose, we aim to prepare new MOF type materials from carboxylate with or without nitrogen-based aromatic ligands for gas storage and separation.

Hereafter, we report the synthesis and description of five new structures prepared from 4-hydroxyisophtalic acid (H_3oip-4) and transition metals such as Cu, Cd, Zn (Fig. 1). In four cases, nitrogen-based aromatic ligands (4,4'-bipyridine: BPY, 1,2-di(4-pyridyl)ethylene: DPE and 1,2-bis(4-pyridyl)ethane: BPE) were added to the starting media. Mild or hydrothermal treatments led to Cu_2(OH)(DMF)(oip-4)·(DMF)(H_2O)$_2$ (**1**), Zn(Hoip-4)(BPY)·(DMF)(H_2O)$_2$ (**2**), Zn(Hoip-4)(DPE)·DMF (**3**), Cd(Hoip-4)(DPE)·(DMF)(H_2O) (**4**) and Zn_4(Hoip-4)$_4$(BPE) (**5**). In addition, the thermal behaviour of compounds **1-5** was investigated by thermogravimetric analysis (TGA).

Experiment

Synthesis. All reagents and solvents were used as received from commercial suppliers without further purification ($Cu(NO_3)_2$·3H_2O, Carlo Erba, 99.5%; $Cd(NO_3)_2$·4H_2O, Carlo Erba, 99.5%; $Zn(NO_3)_2$·4H_2O, Carlo Erba, 99.5%; H_3oip-4, $C_8H_6O_5$, TCI, 98%; BPY, $C_{10}H_8N_2$, Alfa Aesar, 98%; DPE, $C_{12}H_{10}N_2$, Aldrich, 97%; BPE, $C_{12}H_{12}N_2$, Aldrich, 99%; DMF, C_3H_7NO, Fluka, 99%).

Table 1. Synthesis conditions for compounds **1-5**

Compound	Temp. (°C)	Time (h)	Molar composition
1	90	24	Cu:H_3oip-4:**DMF**:**H_2O** = 1:2:**387:554**
2	70	96	Zn:H_3oip-4:BPY:**DMF**:**H_2O** = 2:1:1:**1033:1107**
3	70	96	Zn:H_3oip-4:DPE:**DMF**:**H_2O** = 2:1:1:**773:2214**
4	70	96	Cd:H_3oip-4:DPE:**DMF**:**H_2O**:**C_2H_5OH** = 2:1:1:**773**:**2214:69**
5	150	96	Zn:H_3oip-4:BPE:NaOH:**CH_3OH**:**H_2O** = 1:1:1:1:**500:3320**

Results and discussion

Description of the structure. The copper-containing MOF **1,** prepared without any nitrogen based aromatic ligand, exhibits a three-dimensional network with a distorted rutile-type topology. Conversely, the syntheses from BPY and DPE in the presence of Zn^{2+} or Cd^{2+} cations yield two-dimensional structures (**2-4**). The latter hybrid compounds display a similar ABAB stacking of (4,4) sheets. Unlike MOFs **2-4**, the structure of **5** consists of three-dimensional framework despite the involvement of BPE. The structural difference between **3** and **5** could be explained by the nature of the ligand, since BPE is more flexible than DPE.

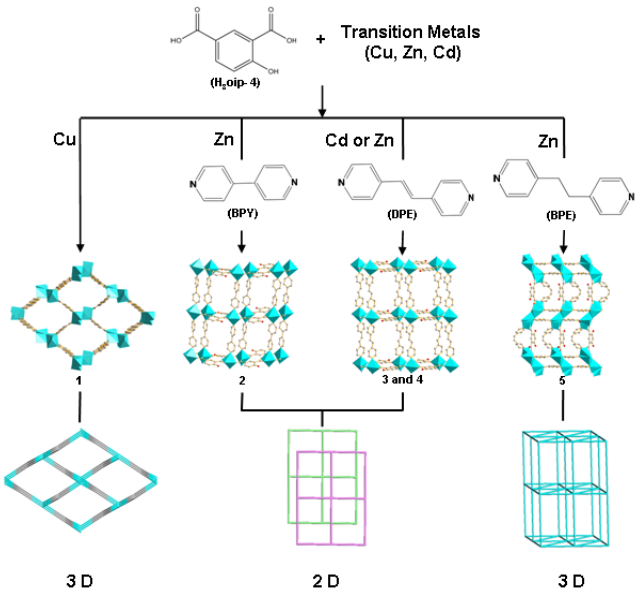

Figure 1 : Representations of the topologies for compounds **1-5**

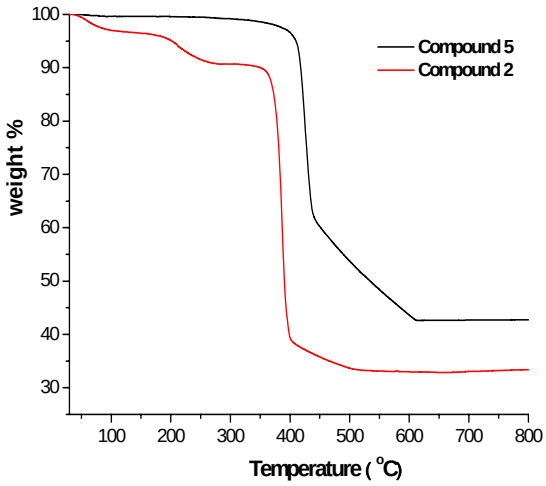

Figure 2 : TG curves of compounds **2** and **5**

Thermal stability. TGA of compounds **2** and **5,** performed in air with a heating rate of 10°C/min, are presented in Fig. 2. Further analyses (not shown) indicate that the thermal stability of compounds **1, 2, 3** and **4** is similar. Indeed, after the release of trapped water (except for **3,** without water) and DMF molecules (for **1, 2, 3 and 4**), the structures remain stable until 300-400°C. As for **5**, the TG curve shows no weight loss corresponding to guest molecules and the structure is also stable until 400°C before collapsing.

Conclusion

We have successfully synthesized five novel metal-organic frameworks (MOFs), built from transition metals and the H_3oip-4 ligand, which exhibit different topologies due to the absence or presence as well as the flexibility of nitrogen-based aromatic ligands (BPY, DPE, BPE).

Acknowledgements

This work was supported by the State Basic Research Project (2006CB806100), Outstanding Young Scientist Foundation of NSFC (20625102), NSFC (Grant nos. 20831D02, 20771041 and 20531030), and “111” program of Ministry of Education.

References

[1] S. T. Meek, J. A. Greathouse, M. Allendorf, Adv. Mater. 23 (2011) 249-267.

[2] J. Y. Lee, O. K. Farha, J. Roberts, K. A. Scheidt, S. T. Nguyen, J. T. Hupp, Chem. Soc. Rev. 38 (2009) 1450-1459.

Thermodesorption as a new tool to characterize hierarchical micro-/mesoporous materials

Maria Manko[1], Waclaw Makowski[1], Benoit Coasne[2], Anne Galarneau[2]

[1]Faculty of Chemistry, Jagiellonian University, Kraków, Poland. [2]Institut Charles Gerhardt Montpellier, UMR 5253 CNRS/UM2/ENSCM/UM1, ENSCM, 8 rue de l'Ecole Normale, 34296 Montpellier Cedex 5, France. e-mail: makowski@chemia.uj.edu.pl

Introduction

Zeolites are efficient catalysts but their use is often limited due to hindered internal diffusion. As a result, different strategies have been developed to improve the diffusivity of reactants by creating mesoporosity in zeolite crystals or creating zeolites in the walls of mesoporous silica [1]. The characterization of such complex materials with hierarchical micro/mesoporosities by standard N_2 adsorption technique is difficult. Here, we propose a new method, based on the adsorption/desorption of molecules in flow followed by thermodesorption, to better characterize these new materials. Such a new technique is fast (2-3 h) and requires low sample amounts (a few mg). In previous works, different probes (n-hexane, n-nonane, 1-butanol) were used in quasi-equilibrium temperature programmed desorption and adsorption (QE-TPDA) to characterize ordered mesoporous silica (MCM-41, SBA-15) [2] and zeolites (ZSM-5, FAU) [3]. QE-TPDA allows calculating the pore volume and the pore size distribution of mesoporous materials using the Kelvin equation (BJH method) [4]. Larger pore sizes induce lower desorption temperature: desorption of nonane is observed at 77, 190 and 240°C for MCM-41 (3.8 nm), FAU (0.78 nm) and ZSM-5 (0.51 nm), respectively. In the present work, we compare QE-TPDA with normal TPD obtained after outgasing the pores to distinguish the probes present in the pore volume and adsorbed at the surface of the materials, respectively. Two probes, n-nonane and water, and two mesoporous materials, MCM-41 (smooth surface) and SBA-15 [5-7] with microporosity, have been tested.

Experimental

Ordered mesoporous silicas were synthesized as following reference [5]. The calcined silicas were characterized by N_2 sorption at 77K. The thermodesorption experiments were performed using a TPD setup with a chromatographic TCD detector [2,3]. Silica samples (ca. 2-3 mg) were first activated to 500°C under He flow (10°C/min). After cooling to 25°C, nonane or water adsorption in the materials was performed from He saturated with the adsorbate. After complete adsorption, the materials were placed under He flow at 25°C for 90 min before TPD in pure He flow performed by heating (10°C/min) from 25 to 500°C. For the QE-TPDA, He saturated with the adsorbate was used instead of pure He. Heating and cooling cycles (2°C/min), which provide desorption and adsorption, were repeated several times.

Results and discussion

Fig.1 shows the N_2 sorption isotherms for MCM-41 and SBA-15 with pore diameters of 3.8 and 6.0 nm (BdB method [6]). While MCM-41 is formed of straight cylindrical pores, SBA-15 synthesized at 60°C exhibits additional micropores of 1x1 nm^2 size [5,7]. Nonane thermodesorption (Fig.1) obtained by QE-TPDA and TPD show differences between MCM-41 and SBA-15 materials. For MCM-41, nonane desorption temperature is the same for QE-TPDA and TPD (77°C), showing no difference in the adsorption energy for the molecules located within the mesopores or on the surface. In contrast, for SBA-15, a stronger interaction

of nonane molecules with the surface is evidenced by the higher desorption temperature of nonane (98 vs. 60°C) in TPD compared to QE-TPDA. This confirms the presence of micropores at the surface of SBA-15 leading to high affinity for nonane as in zeolites.

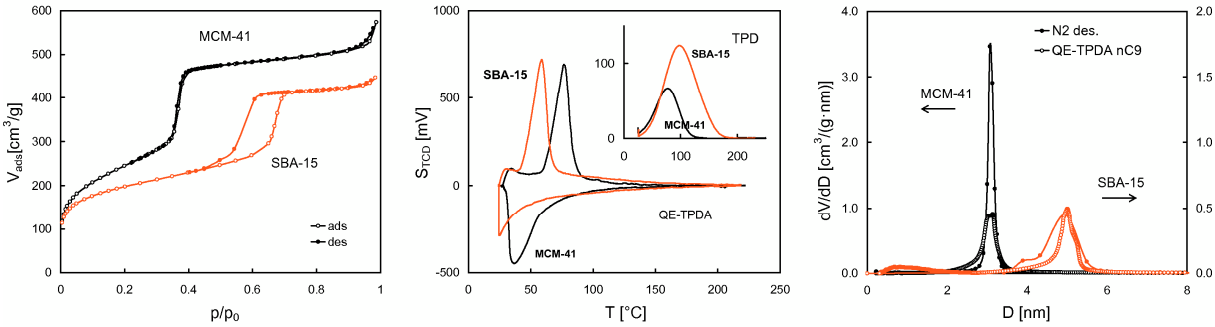

Figure 1. (left) Nitrogen sorption at 77K, (middle) QE-TPDA and TPD of nonane, (right) Pore size distribution determined by BJH methods from nitrogen isotherms and from QE-TPDA, for MCM-41 and SBA-15.

In QE-TPDA, the decrease in desorption temperature between MCM-41 and SBA-15 is in line with the increase of pore size. The pore size distribution calculated from QE-TPDA using the BJH method for nonane is in perfect accordance with the pore size distribution calculated by N_2 desorption (Fig.1). The pore size underestimation (3.1 and 5 nm, for MCM-41 and SBA-15, respectively) determined by BJH method is due to the fact that this method does not take into account the increase of surface tension as the pore size decreases, as in BdB method. The pore volume calculated by QE-TPDA for MCM-41 is in perfect accordance with the pore volume (0.66 mL/g - 3.74 mmol/g) evaluated from n-nonane adsorption isotherm [8] at 313 K, but is inferior to N_2 pore volume. Indeed the pore volume determined with large molecules decreases with the increase of the molecule size: $V_{molecule}/V_{N2}$ = 0.92, 0.86, 0.81 for CO_2, n-nonane, α-pinene, respectively [8] due to a non ideal packing of the molecules into the pores. For SBA-15, starting from the pore volume of nonane (QE-TPDA) probing the interior of the pore, the expected N_2 pore volume for SBA-15 should be 0.52 mL/g. As a value of 0.64 mL/g was found with nitrogen, a micropore volume of 0.12 mL/g is estimated for SBA-15 (20% of the pore volume). Smaller differences between MCM-41 and SBA-15 are observed by QE-TPDA or TPD when water is used as a probe; thus it seems not suitable for this technique.

Conclusions

Comparison of nonane QE-TPDA and TPD allows probing micropores in a hierarchical porous silica and assessing pore size distributions. Work is in progress to analyze complex hierachical structures and develop thermodesorption techniques as a characterization tool.

Acknowledgements. This work was supported by the International PhD-studies programme at the Faculty of Chemistry Jagiellonian University within the Foundation for Polish Science MPD Programme co-financed by the EU European Regional Development Fund.

References

[1] J. Perez-Ramirez et al., *Chem. Soc. Rev.*, 37 (2008) 2530.
[2] W. Makowski, B. Gil, D. Majda, Catal. Lett., 120 (2008) 154.
[3] M. Manko, B. Gil, R. Janus, P. Kustrowski, W. Makowski, Thermochim. Acta, 511 (2010) 82.
[4] W. Makowski, L. Chmielarz, P. Kustrowski, Microporous Mesoporous Mater., 120 (2009) 257.
[5] A. Galarneau, M. Nader, F. Guenneau, F. Di Renzo, A. Gedeon, J. Phys. Chem. C, 111 (2007) 8268.
[6] A. Galarneau, D. Desplantier, R. Dutartre, F. Di Renzo, Microporous Mesoporous Mater., 27 (1999) 297.
[7] A. Galarneau, H. Cambon, F. Di Renzo, R. Ryoo, M. Choi, F. Fajula, New J. Chem., 27 (2003) 73.
[8] A. Brenguer-Murcia, A. J. Fletcher, J. Garcia-Martinez, D. Cazorla-Amoros, A. Linares-Solano, K.M. Thomas, *J. Phys. Chem. B*, 107 (2003) 1012.

Silica/alumina-clay heterostructures

C. Belver[1,2], P. Aranda[1], E. Ruiz-Hitzky[1]
[1] *Instituto de Ciencia de Materiales de Madrid, CSIC, Cantoblanco, 28049 Madrid (Spain).*
[2] *Ing. Química, Universidad Autónoma de Madrid, Cantoblanco, 28049 Madrid (Spain).*
carolina.belver@uam.es

Introduction

Since long time ago, clay minerals have been considered as pristine systems to develop porous materials, being the development of optimum catalysts one of the main topics of interest. Pillared clays incorporating different metal oxides (alumina, iron oxides, titania, etc) or mixed metal oxides have been studied in this context [1]. Other synthetic approach, described by Pinnavaia et al. [2], achieved the creation of porous clay heterostructures (PCH) with modulate porosity. More recently, the development of new heterostructures based on layered silicates has been obtained by a soft chemical route based on sol-gel and heterocoagulation processes. The resulting materials described high surface areas because of the great exfoliation degrees of the clay layers [3-5]. This methodology has been extended to clays with a fibrous morphology, leading to the formation of nanoparticles on the surface of the silicate fibres [6]. In this communication, we have applied this innovative approach to synthesize porous silica/alumina-sepiolite heterostructures.

Experimental

The synthetic procedure use a commercial organosepiolite (Pangel B40, Tolsa) as pristine material. A homogenous dispersion of this organosepiolite is prepared in a butanol medium. The resultant suspension is treated at 50 ºC with a mixture of aluminium and silicon alkoxides (aluminium tri-sec-butoxide and tetramethyl orthosilicate), varying the molar ratio of Si:Al and controlling the hydrolysis by adding the stoichiometric amount of water. The mixture is kept at 50 ºC until the formation of a viscous gel that is dried overnight at 50 ºC. The silica/alumina mesophases generated are finally heating at 550 ºC under a control atmosphere to get the desired heterostructures.

Results and discussion

The incorporation of a silica/alumina network over sepiolite occurs through the sol-gel process described in Figure 1. The presence of alkylchains on sepiolite is responsible of the controlled hydrolysis and polycondensation of a mixture of silicon and aluminum alkoxides in the core of a sepiolite non-aqueous suspension. This procedure yields to the coagulation of the mixture, resulting in the formation of a homogenous gel. After a designed thermal treatment, the organic matter of the dried system is removed and the silica/alumina network consolidated.

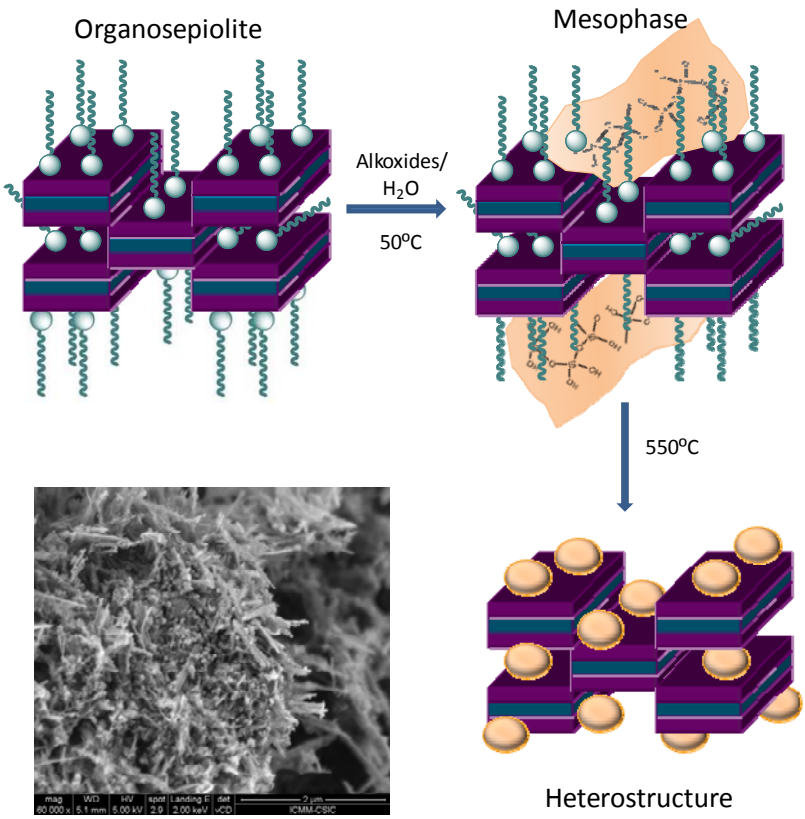

Figure 1. Mechanism of the synthesis approach and SEM photograph of a heterostructure.

The characterization of these systems reveals the formation of silica/alumina nanoparticles located around the sepiolite fibers (Fig.1) thanks to the silanol groups of the sepiolite. The presence of alkylchains favored the generation of small particles avoiding the creation of silica/alumina aggregates. These new heterostructures describes surface areas ca. to 250-300 m^2/g. The porosity of the resulting materials can be design depending on the oxide network generated. Thus, high silica contents generated microporous systems whereas the presence of alumina enhances the mesopous formation. The incorporation of a silica/alumina network on sepiolite also permits to tune its surface acidity, the values increase from 0.1 to 1.4 mmol acid sites per gram according to the aluminum amount.

Conclusions

Fibrous clays offer a good opportunity to develop a large number of heterostructures due to the presence of silanol groups in their external surface that facilitate their assembling to other particles. The anchoring of a silica/alumina network offers opportunities to develop novel porous clay heterostructures as a new class of acid catalysts. Compared to PILCs and other silica/alumina systems they exhibit advantages such as larger specific surface area, development of mesoporosity, and the possibility of tuning the acidity by varying the Si/Al ratio.

Acknowledgements

The authors acknowledge the financial support from CICYT (Spain; project MAT2009-09960). C.B. is indebted to MICINN for a Ramón y Cajal contract.

References

[1] A. Gil, S.A. Korili, R. Trujillano, M.A. Vicente Eds., *Pillared Clays and Related Catalysts*, Springer, New York, 2010. [2] A. Galarneau, A. Barodawalla and T.J. Pinnavaia, *Nature*, 373 (1995) 529–53. [3] S. Letaïef and E. Ruiz-Hitzky, *Chem. Commun.*, (2003) 2996-2997. [4] S. Letaïef, M. A. Martín-Luengo, P. Aranda and E. Ruiz-Hitzky, *Adv. Funct. Mater.*, 16 (2006) 401-409. [5] E. Manova, P. Aranda, M. A. Martín-Luengo, S. Letaïef and E. Ruiz-Hitzky, *Micropor. Mesopor. Mater.*, 131 (2010) 252-260. [6] P. Aranda, R. Kun, M. A. Martín-Luengo, S. Letaïef, I. Dékány and E. Ruiz-Hitzky, *Chem. Mater.*, 20 (2008) 84–91.

Mesopore evaluation of microporous zeolite from N_2 gas adsorption isotherm

Kazuyuki Nakai[1)], Masayuki Yoshida[1)], Hiromitsu Naono[1)], Kohtaro Ueda[2)], Yasushi Sekine[2)], Eiichi Kikuchi[2)] and Masahiko Matsukata[2)]
[1)] *R&D Group, BEL JAPAN Inc. 1-9-1, Haradanaka, Toyonaka, 561-0807 JAPAN*
[2)]*Department of Applied Chemistry, School of Advanced Science and Engineering, Waseda University, Okubo 3-4-1, Shinjuku, Tokyo 169-8555 JAPAN*
Corresponding author: kazu@nippon-bel.co.jp

Intorduction

Micropores of zeolite materials play key roles for gas separation; PSA and TSA and catalytic reaction. However, it is of vital importance for making process and kinetic performance improvement to know the relationship of mesopore and macropore to the micropore in industrial applications. Recently, nano-zeolite, mesoporous zeolite and zeolite membranes are focused on the possibility of the more effective improvement. TEM and SEM observations are available methods to check mesopore size, however are only a surface appearance measurement. Gas adsorption technology can evaluate these bulk mesoporosity by using these tiny molecular probes. We will report the mesopore evaluation method of mesoporous MFI zeolite crystal and zeolite membrane from gas adsorption isotherms.

Experimental

We synthesized two different zeolite materials; one type is an etched MFI zeolite particle which has mesopores in crystal by alkali etching from hydrothermal synthesis zeolite (NaOH MFI) and de-Boronated zeolite (B-MFI) the other type is a zeolite membrane which is ZSM-5 microcrystal supported on α-alumina porous support tube. These mesoporous zeolite material has been measured using TEM, SEM photograph and N_2 gas adsorption (BELSORP-max, BEL Japan, Inc.) at 77.4K.

Results and discussion

SEM image of alkali etched zeolite show surface roughness in Fig. 1 and 2.

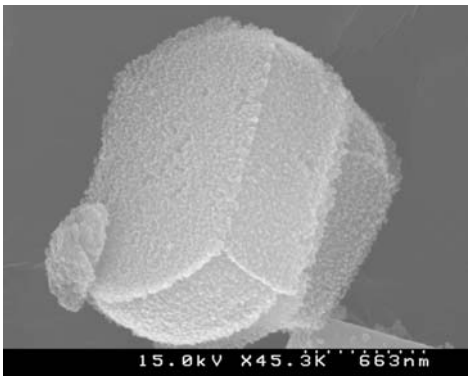

Fig. 1. MFI zeolite etched NaOH aq (1h)

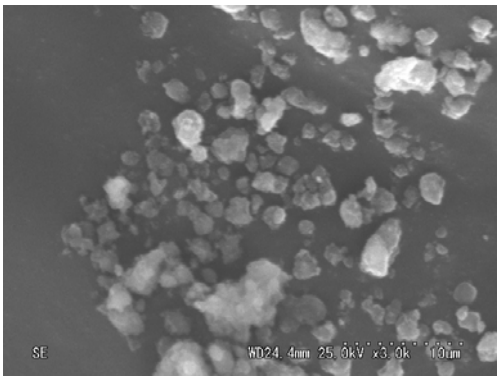

Fig. 2. De-Boronated MFI zeolite etched NaOH aq (5h)

High resolution N_2 adsorption isotherms at 77.4K of the MFI zeolite were measured from $P/P_0=10^{-8}$ to $P/P_0=0.997$. We made a large sample cell for zeolite membrane (10mmφ, L=30mm) without any break of sample. The result of adsorption isotherms and pore size distribution (PSD) by GCMC are shown in Fig.3, 4 and 5, respectively. All of their MFI have the micropore at around 0.5-0.6 nm from PSD. All of the isotherms show type I isotherm and

slightly include type IV isotherm which has different hysteresis. We evaluate surface area and micro and mesopore volume from BET and t-plot of desorption isotherm up to P/P_0=0.995 (8nm) in Table 1.

Table 1. Surface area and pore volume from BET and t-plots (desorption isotherms)

	Parent (Silicalite)	NaOH-MFI	B-MFI
Total SSA(BET)/m^2g^{-1}	435.6	397.3	399.0
External SSA/m^2g^{-1}	2.2	9.5	3.5
Micropore volume/cm^3g^{-1}	0.172	0.153	0.123
Mesopore volume/cm^3g^{-1}	0.035	0.151	0.122

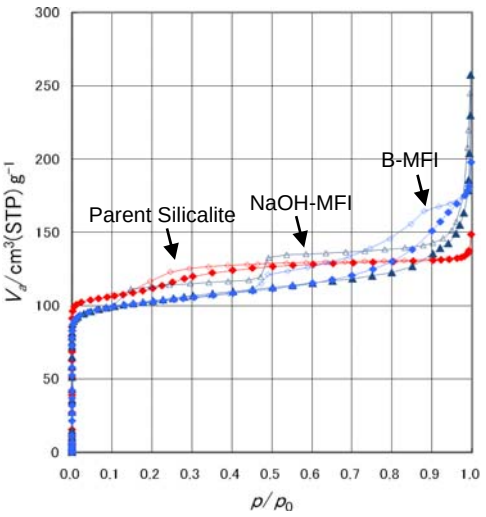

Figure 3. N_2 adsorption isotherm at 77K

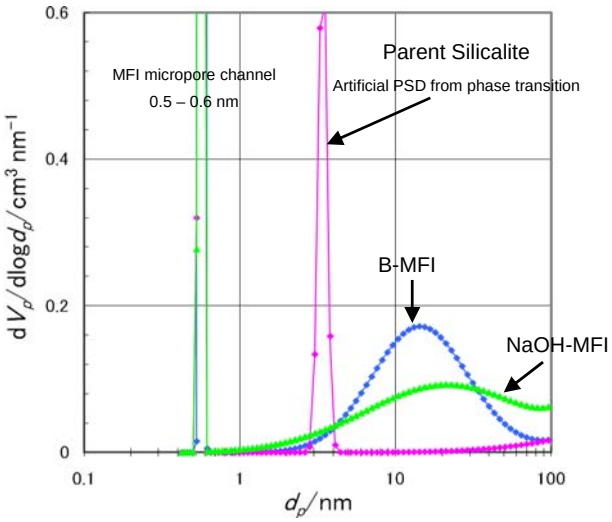

Figure 4. Pore size distribution by GCMC.

In the case of mesoporous zeolite, Parent silicalite has negligible mesopores although there is an artificial pore peak at 3~4nm produced by a phase transition which has been reported by Nakai, et al [1]. On the other side, NaOH-MFI and B-MFI have mesopores of around 15nm as well as micropore. Furthermore, the mesopores of B-MFI had an even sharper distribution than that from NaOH-MFI. From the t-plots of Parent and NaOH-MFI, we found increasing mesopore volume in spite of not so much change external surface area. We succeed to synthesize two type MFI zeolites with large mesopore volume.

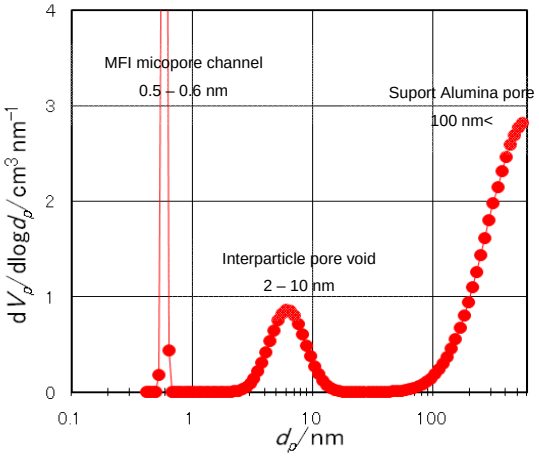

Figure 5. Pore size distribution of zeolite membrane from GCMC

In the case of zeolite membrane, PSD show three distributions which attribute zeolitic pore, interparticle pore of zeolite crystal and support alumina tube pore in respectively. This sample show H_2 permeation rate is 13 ml/min. We guess this high flow rate is coming from interparticle pore of zeolite crystal.

From these results, t-plot (desorption isotherm) and GCMC PSD from high resolution N_2 isotherm is very usuful for determine pore information of zeolite.

Reference

[1] K. Nakai et al., IZC-IMMS 2010, Sorrento July 4 -9, 2010.

Morphology-Control of Ordered Mesoporous Carbons with Extremely High Porosity

Jörg Schuster,[1] Benjamin Mandlmeier,[1] Andreas Keilbach,[1] Ralf Köhn,[2] Markus Döblinger,[1] Heinz Amenitsch,[3] Thilo Dörfler,[1] Teresa Dennenwaldt,[1] Thomas Bein[1]

[1]*Department of Chemistry and Center for NanoScience, University of Munich, Butenandtstr. 5-13 (E), 81377 Munich, Germany, bein@lmu.de*
[2]*Center for Free-Electron Laser Science, Notkestrasse 85, 22607 Hamburg, Germany*
[3]*Institute of Biophysics and Nanosystems Research, Austrian Academy of Sciences Schmiedlstraße 6, 8042 Graz, Austria*

Introduction

Ordered mesoporous carbons (OMCs) are of great interest based on their high surface areas, large pore volumes, chemical inertness and electrical conductivity. These qualities make them applicable for uses as electrode materials in batteries, supercapacitors and fuel cells, as adsorbents for separation and gas storage, and as catalyst supports, respectively.
Control of the OMC features in all three dimensions is challenging but critical for specific applications and for the improvement of their properties, i.e., (i) the chemical composition and structure of the walls determining the electronic properties and the reactivity, (ii) the mesoporous structure in terms of crystallographic symmetry, pore sizes, pore volumes and surface areas, and (iii) the OMC morphology at the microscale, such as powders, thin films, nanofibers or nanoparticles, determining molecular access to the pores. However, often the optimization of one parameter results in compromising other parameters, for example, high temperatures are needed for carbonization and good electrical conductivity but they can result in shrinkage or even collapse of the mesostructure. Herein we report on the synthesis of OMCs with controlled nano-morphologies, that is, thin films,[1] filaments encapsulated within anodic alumina membrane pores,[2] free nanofibers and spherical nanoparticles.

Experimental

For the synthesis of the OMCs, we use the confinement in pre-synthesized porous silica templates to create the desired OMC-morphologies during evaporation-induced self-assembly of precursor solutions. Ordered structures of organic templates were cast with silica precursor solutions to form inverse silica structures. The macroporous silica structures were then used as templates for the mesoporous carbon precursor solutions. Carbonization at 900 °C was followed by etching of the silica templates with hydrofluoric acid and OMCs with hierarchical porosity were formed.

Results and discussion

The 3D-confinement results in beneficial properties regarding the thermal stability and shrinkage behavior of OMCs. As a main result from this restricted shrinkage effect, the OMCs exhibit larger pores, higher pore volumes and greater surface areas compared to bulk materials from the same precursor solutions.[2] Figure 1 shows TEM micrographs of highly ordered spherical mesoporous carbon nanoparticles (left) and nanofibers (right), which both exhibit extremely high porosities above 2.0 cm^3/g and 2000 m^2/g, respectively. For mesoporous carbon nanoparticles, this porosity is one of the highest ever reported.

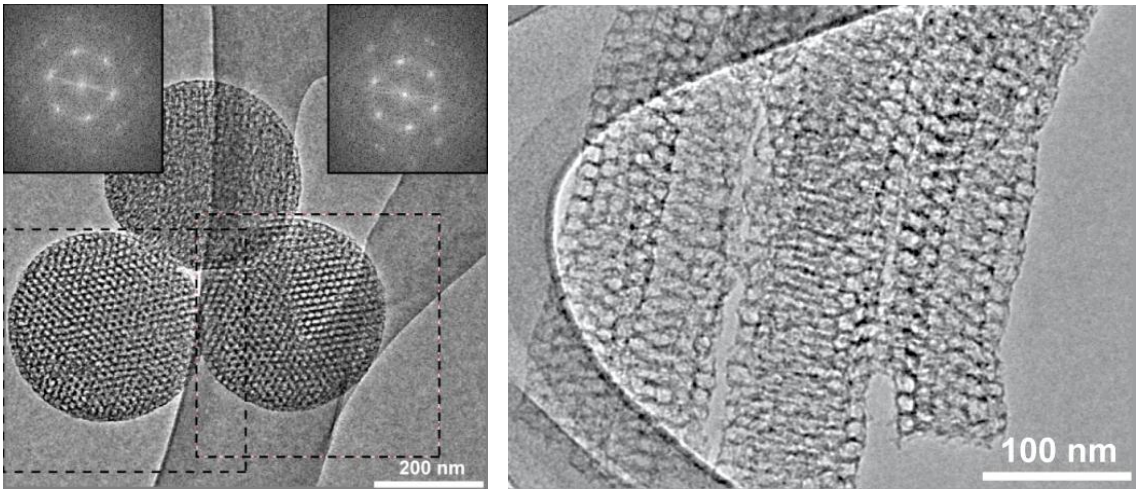

Figure 1: TEM micrographs of spherical OMC nanoparticles (left) and nanofibers (right).

The resulting morphologies have high potential in applications such as batteries, supercapacitors, as adsorbents for separation and gas storage, and as catalyst supports, respectively. The novel materials are being investigated in energy storage applications and the promising results will be discussed.

Conclusions

We have demonstrated 3D-morphology control in the synthesis of highly-ordered mesoporous carbon structures. For this purpose we used the confinement in pre-synthesized porous templates to create the desired OMC-morphologies. The 3D-confinement shows favorable effects regarding the thermal stability and shrinkage behavior of OMCs and thus on the resulting porosity. The OMC spheres and fibers are being investigated in energy storage applications due to their extremely high porosities above 2.0 cm^3/g and 2000 m^2/g, respectively.

Acknowledgements

The authors thank the Nanosystems Initiative Munich (NIM) and the DFG (SFB 486) for supporting this work.

References

1. Schuster, J.; Koehn, R.; Keilbach, A.; Doeblinger, M.; Amenitsch, H.; Bein, T., *Chem. Mater.* **2009,** *21* (24), 5754-5762.
2. Schuster, J.; Keilbach, A.; Koehn, R.; Doeblinger, M.; Doerfler, T.; Dennenwaldt, T.; Bein, T., *Chem. Eur. J.* **2011**, in press.

Influence of synthesis conditions on the generation of intercrystalline mesoporosity in CoAPO-5

Alicia Manjón-Sanz, Manuel Sánchez-Sánchez and Enrique Sastre
Instituto de Catálisis y Petroleoquímica, CSIC, Madrid, Spain
E-mail address: manuel.sanchez@icp.csic.es

Introduction

Paradoxically, the most severe restriction about the industrial applications of zeolites and zeotypes (i.e. reactants/products diffusion) is based on some properties allowing them to be unique and effective catalysts (confinement and shape-selectivity) [1]. In order to limit the diffusion problems of molecular sieves maintaining their catalytic properties relating to their porous nature, different synthesis strategies have been proposed and/or developed, including zeolitic materials with higher pores [2,3], severe reduction of crystal size [4], mesoporous materials with walls composed by microporous nanocrystals [5] or generation of both intra and/or intercrystalline mesoporosity in microporous materials. In a recent work [6], we reported the influence of heteroatom (Me) nature on the generation of intercrystalline mesoporosity in MeAPO-5, just using the highly specific structure-directing agent (SDA) N-methyldicyclohexylamine (MCHA) for AFI structure [7] and no extra agent to generate mesoporosity.
In this work, following the systematic studies to form these materials with this particular SDA, we study the influence of different synthesis variables (cobalt content, pH value of the starting gel, crystallization time and temperature) in the generated mesoporosity nature in CoAPO-5.

Experimental

CoAPO-5 materials were prepared by hydrothermal treatment (1-18 hours, 423-483 K) of gels with composition 1.0 P : (1-*x*) Al : *x* Co : *y* MCHA : 25 H_2O. *x* and *y* were systematically varied in ranges of 0-0.08 and 0.5-1.6, respectively. The resultant blue solids were characterized by XRD (phase identification and crystal size estimation by Scherrer equation), DRUV-visible, SEM, and N_2 adsorption/desorption isotherms at 77 K

Results and discussion

The excellent specificity of the SDA MCHA towards AFI-structured materials was again made clear by obtaining $AlPO_4$-5/CoAPO-5 as the unique crystalline phase in all the attempts irrespective of the synthesis conditions. The only exceptions were found when: i) very short crystallization times (for instance, one hour) and relatively low crystallization temperatures (423 K) were simultaneously used, as no crystalline phase could be detected, presumably for kinetic reasons; ii) crystallization temperature was as high as 483 K and crystallization times longer than 4 hours, since an unknown dense phase appears as impurity of the AFI material. In all CoAPO-5 samples, the right incorporation of Co^{2+} into the $AlPO_4$-5 framework was confirmed by DRUV-visible spectroscopy.
Figure 1A, 1B and 1C show the N_2 adsorption/desorption isotherms at 77 K, some representative SEM pictures and the evolution of the mesoporous volume (estimated by subtracting the microporous volume to the whole porous volume as determined by BJH method from adsorption branches) for three CoAPO-5 samples prepared under the same conditions with different amounts of Co. Systematic changes in N_2 adsorption/desorption behavior in the mesoporous region, in particle morphology and size, and in mesoporous volume with increasing Co content, are evident. Thus, the size of the particles (Figure 1B),

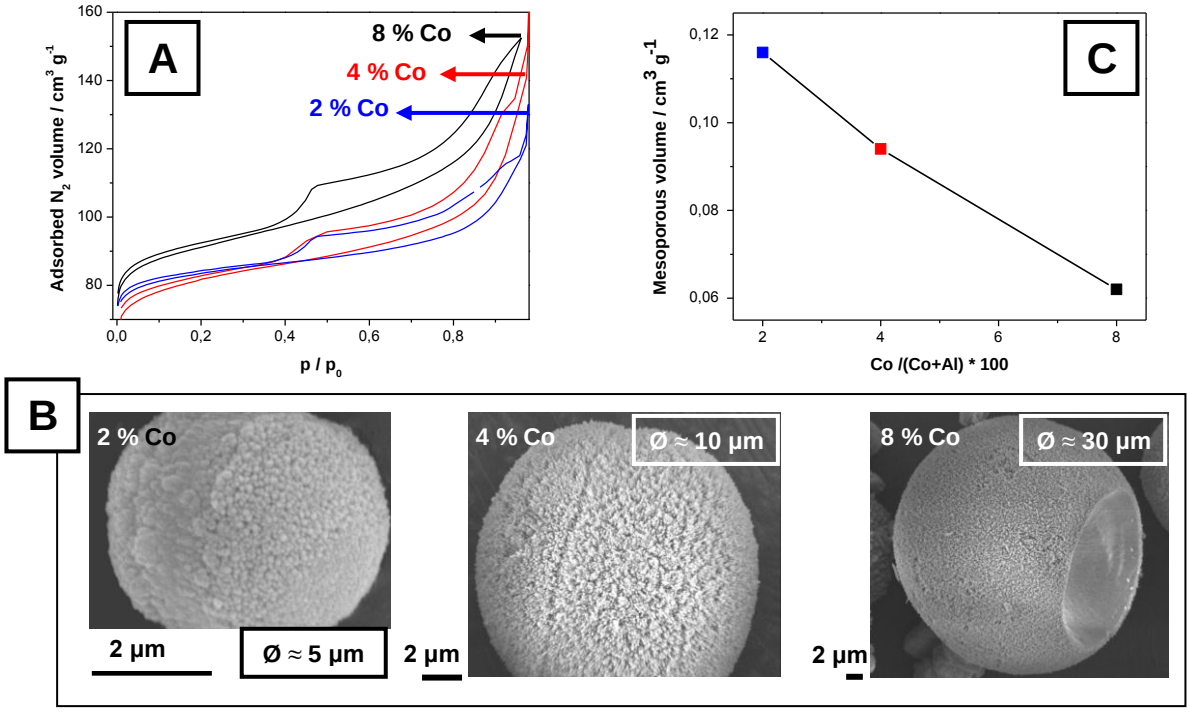

Figure 1. Characterization results of three CoAPO-5 prepared with Co/(Co+Al+P) ratio of 2, 4 and 8 %. A) N_2 adsorption/desorption isotherms at 77 K. B) SEM pictures showing representative agglomerates of nanocrystals. C) Plot of mesoporous volume *versus* Co content.

which are actually aggregates of hundreds of crystals, substantially grows as Co content in the gel increases. More directly related to our aims, the mesoporous volume both substantially and linearly decreases as Co content becomes richer.

Based on similar systematic characterization analyses, the magnitude of the intercrystalline mesoporosity in CoAPO-5 prepared with this SDA is higher when increasing the crystallization temperature, shortening the crystallization time or increasing the pH value of the starting gel (i.e. increasing *y*).

Conclusions

The extraordinary phase-specificity of MCHA towards $AlPO_4$-based AFI-structured materials as well as their ability to form nanocrystals highly ordered in aggregates containing inter-crystalline mesoporosity, have allowed us to establish that low Co content, high pH values of the starting gels, short crystallization time and high crystallization temperature favor the extent of generated mesoporosity in CoAPO-5 materials directed by this SDA.

Acknowledgements

Authors acknowledge Spanish Science and Innovation Ministry for financial support (MAT-2009-13569).

References

[1] J.C. Groen, L.A.A. Pffer, J. Perez-Ramirez, *Micropor. Mesopor. Mater.* 60 (2003) 1.
[2] M.E. Davis, C. Saldarriaga, C. Montes, J. Garces, C. Crowder, *Nature* 331 (1988) 698.
[3] J.L. Sun, C. Bonneau, A. Cantin, A. Corma, M.J. Diaz-Cabanas, M. Moliner, D.L. Zhang, M.R. Li, X.D. Zou, *Nature* 458 (2009) 1154.
[4] I. Shmidt, C. Madsen, C.J.H. Jacobsen, *Inorg. Chem.* 39 (2000) 2279.
[5] A. Karlsson, M. Stocker, R. Schmidt, *Micropor. Mesopor. Mater.* 27 (1999) 181.
[6] A. Manjón-Sanz, M. Sánchez-Sánchez, P. Muñoz-Gómez, R. García, E. Sastre, *Micropor. Mesopor. Mater.* 131 (2010) 331.
[7] M. Sánchez-Sánchez, G. Sankar, A. Simperler, R.G. Bell, C.R.A. Catlow, *Catal. Lett.* 88 (2003) 163.

Thermal behaviour of the hybrid organic-inorganic ECS-3 material: an *in situ* powder diffraction study

Stefano Zanardi, Roberto Millini, Erica Montanari
Eni S.p.A R&M Division, San Donato Milanese Research Center, Via F. Maritano 26, I-20097 San Donato Milanese (MI), Italy, stefano.zanardi@eni.com

Introduction

The introduction of organic moieties in the zeolite framework providing new materials with lipophilic/hydrophobic character has become a hot topic in the recent years [1-7]. A new class of microporous crystalline hybrid organic-inorganic aluminosilicates, referred to ECS, has been recently synthesized in eni laboratories [8]. One of these materials, ECS-3, showed a Type I nitrogen adsorption isotherm and interesting textural properties (specific surface area = 105 m^2/g, pore volume = 0.11 ml/g), due to intracrystalline porosity typical of microporous materials like zeolites. The crystal structure of ECS-3 has been recently solved by using Automatic Diffraction Tomography [9], it is monoclinic with space group Cc and unit cell parameter: a ~ 19.77, b ~ 28.33 and c ~ 9.76Å, β ~ 102.7°.
Analogously to zeolites, the understanding of the structure behaviour of microporous crystalline hybrid organic-inorganic aluminosilicates materials upon heating is of great importance for potential applications. As a matter of fact, due to the presence of organic moieties, the heating process can lead to a dramatic structural collapse or even to the total structural breakdown, hampering any possible catalytic application. Accordingly, in order to evaluate the thermal behaviour of ECS-3, an *in-situ* high temperature X-ray powder diffraction experiment was carried out. The structural information obtained by Rietveld refinements are here reported.

Experimental

ECS-3 was synthesized as reported elsewhere [8]. The *in-situ* high-temperature X-ray powder diffraction experiment were performed using a PANalytical X'PERT PRO diffractometer equipped with an Anton Paar HTK 1200 resistance heating chamber and a RTMS (real-time multiple strip) X-Celerator detector. Data were collected in continuous mode over $3° \leq \theta \leq 90°$ angular region, with an accumulation time of 400 s/step, using CuKα radiation (λ = 1.54178Å). Four scans were carried out and rebbinned at the end of the data collection in order to emphasize structural modification during the same. Data were collected at room temperature, 50, 75, 100, 125, 150 and 200ºC: the sample was heated with a heating rate of 2°C/min and maintained at the selected temperature for 3 hour, in order to keep it as close as possible to its thermodynamic equilibrium. The different temperatures were selected on the basis of the thermogravimetric analyses (TGA) performed with a Mettler M3 thermobalance. Data were collected from 25 to 900 °C, with a heating rate of 2 °C/min.

Results and discussion

XRD analysis indicates that ECS-3 maintains its crystallinity up to 150°C, whereas at 200°C a dramatic worsening of the quality of the diffraction pattern occurs, as a consequence of an incipient structural breakdown. Figure 1 shows the unit cell variations of ECS-3 as a function of the heating temperature. It should be noted that the unit cell contraction is almost isotropic with the exception of the parameter *a,* that seems to increase at 150°C. The unit cell volume contraction associated to the de-

hydration of the structure is equal to 3.5% at 150°C. Rietveld refinements indicate a continuous decreasing of the water molecules occupancy as the temperature increases. Interestingly, at 150°C water molecules are still present in the ECS-3 porosity.

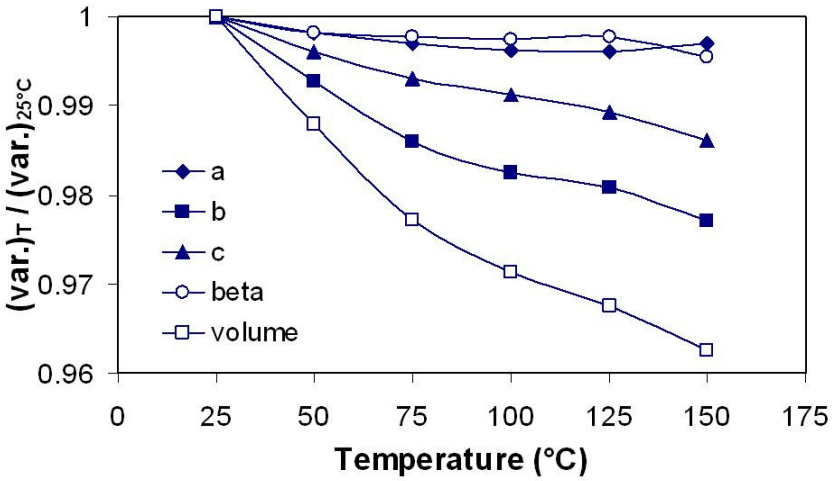

Figure 1. ECS-3 unit cell parameters variations normalized to the room temperature value.

Conclusions

The *in situ* X-ray powder diffraction analysis, performed after heating at 50, 75, 100, 150 and 200 °C showed that the ECS-3 structure is stable up to 150°C with amorphization starting after heating to 200 °C. During the heating process, only small variations were noted in the dimensions of the unit cell and the dehydration process is not completed at 150°C. Thus, the incipient amorphization observed at 200°C could be a cooperative result of the breaking of the Si-C bond and the re-organization of sodium and potassium ions after loss of the coordinated water molecules.

References

[1] Corma, A., Diaz, U., García, T., Sastre, G., Velty, A. JACS 132 (2010), 15011.
[2] Mochizuki, D., Kowata, S., Kuroda, K., Chem. Mater. 18 (2006), 5223.
[3] Yamamoto, K., Takahashi, Y., Tatsumi, T., Stud. Surf. Sci. Catal. 135 (2001), 299.
[4] Yamamoto, K., Sakata, Y., Nohara, Y., Takahashi, Y., Tatsumi, T., Science 300 (2003), 470.
[5] Yamamoto, Y., Nohara, Y., Domon, Y., Takahashi, K., Sakata, Y., Plévert, J., Tatsumi, T., Chem. Mater. 17 (2005), 3913.
[6] Yamamoto, K., Tatsumi, T., Chem Mater. 20 (2008), 972.
[7] Su, B.L., Roussel, M., Vause, K., Yang, X.Y., Gilles, F., Shi, L., Leonova, E., Edén, M., Zou, X. Micropor. Mesopor. Mater. 105 (2007), 49.
[8] Bellussi, G., Carati, A., Di Paola, E., Millini, R., Parker Jr., W.O., Rizzo, C., Zanardi, S.,Micropor. Mesopor. Mater. 113 (2008), 252.
[9] Zanardi, S., Montanari, E., Di Paola, E., Millini, R., Bellussi, G., Carati, A., Rizzo, C., Gemmi, M., Mugnaioli, E., Kolb, E., in Proceedings of 16th International Zeolite Conference joint with the 7th International Mesostructures Materials Symposium, Sorrento (Italy), 2010, 1708-1709.

DIVERSE MOBILITY OF D_2O MOLECULES IN FAUJASITE CAGES: A DEUTERON NMR INVESTIGATION

Z.T. Lalowicz[1], G. Stoch[1], A. Birczyński[1], K. Góra-Marek[2], J. Datka[2]
[1]*H. Niewodniczański Institute of Nuclear Physics PAS, Kraków, Poland*
[2]*Department of Chemistry, JagellonianUniversity,Kraków,Poland*
Zdzislaw.Lalowicz@ifj.edu.pl

Introduction

Studies of dynamic behavior of water molecules in zeolites is the main part of investigations aiming to elucidate eg. catalytic properties in relation to mechanism at molecular level. Here we apply deuteron NMR methods to study D_2O dynamics in faujasites in a wide range of temperatures. Similar research was performed in other microporous materials [1]. DRIFT spectroscopy and neutron powder diffraction were applied to study adsorption of D_2O in NaX [2]. Structure and coordination of water molecules derived there provides a good reference base for discussion of our results.

Experimental

Experimental procedures and sample preparation had been described before [3]. Amount of D_2O, related to sodium cation abundance, equals 100%, 200%, 300% and 500% in faujasite samples with Si/Al = 1.3, 1.8 and 2.4.

Results relaxation

Deuteron spin-lattice relaxation time was measured at temperatures above 220K. Activation energy was derived using the dependence of the correlation time $\tau_c = \tau_0 \exp(E_a/kT)$. Results are summarized in Table I. E_a = 12.5kJ/mol was obtained for NaX(1.3) 500%. Measurements performed below 217K disclose three time constants in the relaxation process. These may be related to separate spectral components, but that point is out of scope of the present report.

Table I. Activation energy values.

	100%	**200%**	**300%**
NaX (1.3)	E_a=12.5 kJ/mol	E_a=18.4 kJ/mol	E_a=10.5 kJ/mol
NaY (1.8)	E_a=9 kJ/mol	E_a=8.7 kJ/mol	E_a=14.3 kJ/mol
NaY (2.4)	E_a=4.5 kJ/mol	E_a=9 kJ/mol	E_a=23 kJ/mol

Results – spectra

Deuteron NMR spectra provide a direct evidence for the symmetry of deuteron mobility [1,3]. So called Pake doublets, with peak separation $3/4C_Q$, are observed for rigid deuterons and allow to measure the quadrupole coupling constant C_Q. The peak separation equals $1/4C_Q$ for deuterons rotating about a threefold axis. Twofold exchange of two deuterons in D_2O, called also π-jumps, results in so called pagoda shape [Fig.1]. Gaussian spectra, with decreasing width, represent reorientations approaching isotropic symmetry and increasing correlation frequency. There are two Gaussian components with different width in the spectra measured above 220K. Their width at room temperature increases with decreasing Si/Al for 300% loading. Contribution of the narrow line equals at room temperature 1/2N, N, 2N and 2.5N, for NaX samples with 100%, 200%, 300% and 500% loading, respectively, where N equals to the number of Na^+ ions per unit cell. The narrow component decays when temperature goes down. That dependence was fitted with a function 1–bexp(-aT) with a = 0.045/K for all samples. Both components broaden significantly, but retain Gaussian shape, when temperature approaches about 220K. A phase transition appears at slightly lower temperatures, eg. at 217K for NaX 500% sample, and shape of spectra changes drastically.

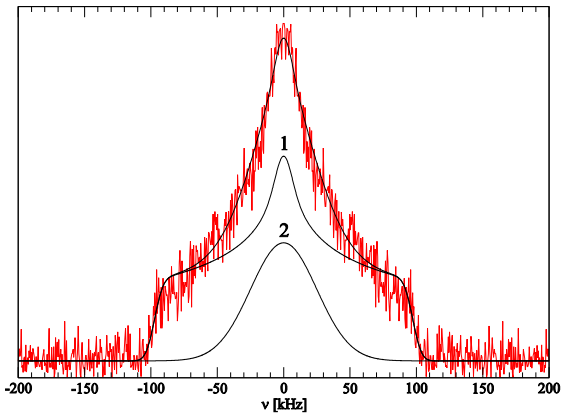

Fig.1. Deuteron NMR spectrum of NaX (1.3) 100% sample at 210K. Labels 1 and 2 refer to pagoda and Gaussian components, respectively.

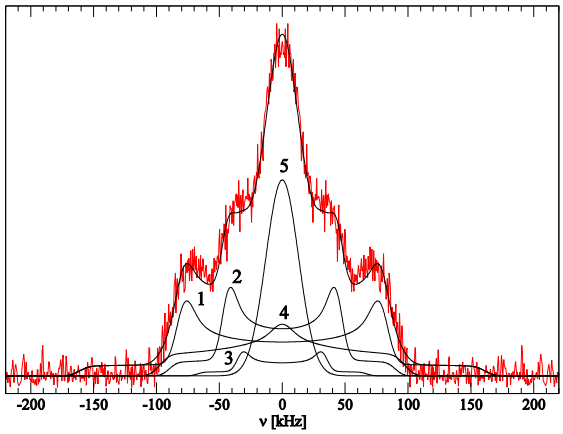

Fig.2. Deuteron NMR spectrum of NaY(2.4) 500% sample at 193K. Labels 1,2 and 3 - Pake doublets, 4 - pagoda, 5 – Gaussian.

At temperatures below 220K we have broad lines which can be decomposed into components with characteristic shapes [1,3]. Pake doublets, characteristic for immobile deuterons, dominate in the spectra for almost all samples at low temperatures. Only the spectrum of NaX(1.3) 100% sample shows dominating contribution of the pagoda component, accompanied by a broad Gaussian or Pake doublets at high (Fig.1) or low temperature limits, respectively. At higher water content in NaX samples there is a stepwise increase of the pagoda component on expense of Pake doublets in the range from 150K to 180K, depending on the loading. Contribution of the pagoda at a plateau decreases with increasing amount of water, remaining part comes mainly from a Gaussian broad line. Pake doublets dominate in the spectra of NaY(2.4) 300% sample in the whole temperature range. Even at 193K contributions amount 59%, 19% and 22% from Pake doublets, pagoda and broad Gaussian, respectively (Fig.2). Following quadrupole coupling constants had been obtained for the following spectral components in most cases: pagoda – 260kHz, Pake doublets – 120kHz, 180kHz, 220kHz and 260kHz.

Discussion

The fraction of freely rotating water molecules is related to Si/Al ratio. Translational freedom vanish at the phase transition. The nature of the phase transition is related to a spectroscopic window of NMR. Deuterons are observed as rigid, when the correlation time τ_c becomes longer than $(2\pi C_Q)^{-1}$. Molecules involved in double and single hydrogen bonds, attributed to pagoda and Gaussian components, respectively, dominate at lower loading. Formation of hexamers on increasing loading stabilizes the structure. Therefore most of deuterons are rigid at low temperatures, and pagoda appears only at high enough temperature. Pagoda dominates in the spectra of NaX samples. On the other hand, rigid deuterons dominate the spectrum of NaY(2.4)300%, what indicates on a role of sodium cations in water hexamer formation.

Acknowledgements

This project was generously supported during 2010-2013 by the Ministry of Science and Education, Poland, Grant no N N202 127 939.

References

[1] O'Hare B., Grutzek M.W., Kim S.H., Asay D.A., Benesi A.J., J. Magn. Reson.195 (2008) 85-102
[2] Hunger J., Beta I.A., Böling H., Ling C., Jobic H., Hunger B., J. Phys. Chem. B, 110 (2006) 342-353
[3] Lalowicz Z.T., Stoch G., Birczyński A., Punkkinen M., Krzystyniak M., Góra-Marek K., Datka J., Solid State Nucl. Magn. Reson., 37 (2010) 91-100

New modification strategy of MFI zeolite membrane in supercritical media

Martin Drobek[1], Julius Motuzas[1*], Véronique Durand[2], Audrey Hertz[2], Eric Louradour[3], Nadine Del Bianco[3] and Anne Julbe[1]
1-Institut Européen des Membranes (UMR 5635 CNRS), Université Montpellier 2, CC47, Place Eugène Bataillon, 34095 Montpellier Cedex 5, France. Julius.Motuzas@iemm.univ-montp2.fr
2-Commissariat à l'Energie Atomique et aux Energies Alternatives, DEN/DTCD/SPDE/ Laboratoire des Fluides Supercritiques et des Membranes, BP 17171, 30207 Bagnols sur Cèze, France.
3-Céramiques Techniques et Industrielles (CTI SA), 382 Avenue du Moulinas, La Resclause, 30340 Salindres, France.

Introduction

Due to unavoidable intercrystalline defects and poor molecular sieving properties of common zeolite membranes, there have been reported numerous physical and chemical strategies for their synthesis with a reduced number of defects, or with reduced channel size (application in gas or vapor separation) or with specific adsorption or catalytic properties.
The typical modification methods widely described in the literature include isomorphous substitutions of, e.g. Al, Fe, B, V, Ti or Ge in the structure, ion exchange, silylation, atomic layer deposition (ALD), chemical vapour deposition (CVD), selective coking, catalytic cracking and reactions with adsorption sites in the zeolite structure [1,2].
In the present work a new post-synthesis method has been investigated, which is based on on-stream modification of MFI membranes in supercritical CO_2 (SC-CO_2). Chosen because of its attractive transport properties and easily adjustable solvent power, SC-CO_2 acts as a solvent in which methyldiethoxysilane or other metal-organic and alkoxide precursors can easily be solubilized and then transported to the inorganic porous support where deposition occurs.

Experimental

MFI zeolite membranes were grown on α-Al_2O_3 commercial supports (Pall-Exekia) according to the procedure described in [1] using a microwave (Milestone ETHOS 1600) or a classical oven. Membranes were formed by secondary growth, observed by FE-SEM (Hitachi 4500) and their microstructure was analysed by XRD (PANalytical X'Pert Pro). The membrane modification was performed in on-stream high pressure reactor where SC-CO_2 with silica precursor (methyldiethoxysilane or tetraethoxysilane) passed through the zeolite membrane at a selected temperature and permeate flow rate. The observed increase of ΔP due to accumulation of the deposited material in/on the MFI membrane was recorded and served as an indication of the degree of membrane modification. The membrane quality and performances before and after modification were compared through single gas permeance measurements.

Results and discussions

The initial MFI zeolite membranes exhibited, before modification, a relatively high N_2 permeance in the range 1-4*10^{-6} mol.m^{-2}.s^{-1}.Pa^{-1} with N_2/SF_6 permselectivity in the range of 50-60 at room temperature and 0.5 bar transmembrane pressure. These membranes were directly subjected to on-stream modification process. The type and quantity of silica precursor, permeate flow rate and number of modification cycles were studied. The typical weight increase of the MFI membrane was very low (< 0.05%). Very first results are shown in

Fig. 1. The membranes properties in terms of N_2 permeance and corresponding N_2/SF_6 permselectivities were remarkably changed by the modification treatment. As expected a lower permeance and higher permselectivity were measured for the modified membranes.

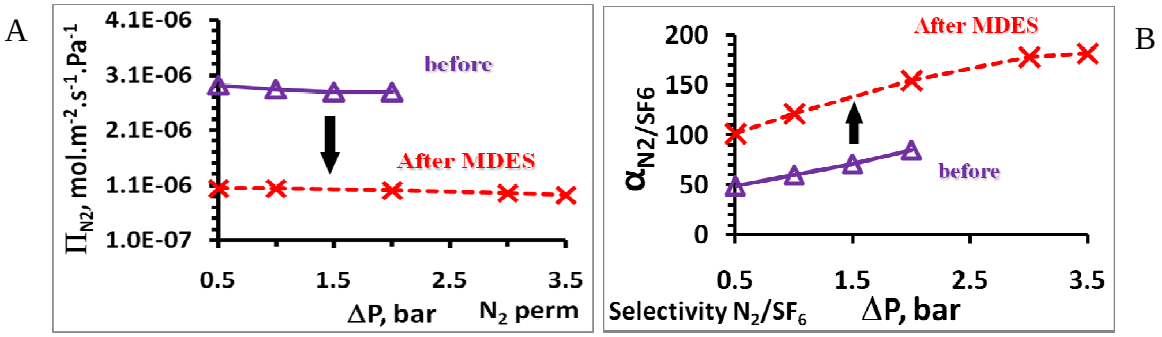

Figure 1. Typical evolution, vs. transmembrane pressure, of the N_2 permeance and N_2/SF_6 permselectivty at 25°C, for a MFI zeolite membrane before (A) and after (B) methyldiethoxysilane modification.

The observed decrease of the gas permeance proved the deposition of silica precursor in the membrane structure. Moreover, from the higher permselectivities there may be estimated that the deposition takes place not just on the membrane surface but as well inside the membrane pores (either zeolitic pores or non-zeolitic defects).

Conclusions

The on-stream modification of MFI zeolite membranes led to a decrease of N_2 permeance with the simultaneous improvement of their permselectivities. Further work is in progress to determine the exact location where the deposition of the silica precursor takes place (zeolite channels or non-zeolitic intercrystalline pathways) and thus better understand the resulting membranes structure. The specifically attractive properties of supercritical fluids open the way to a large range of (green) strategies for the controlled modification of zeolite membranes by using on-stream methods.

Acknowledgements

Part of research leading to these results has received funding from French FUI, the region of Languedoc-Roussillon and OSEO Innovation, under grant agreement N° 092906408 EJ N°5728 (MEGA project).

References

[1] A. Julbe, in “Introduction to Zeolite Science and Practice” Second edition , H. van Bekkum, J. Cejka, A. Corma, F. Schuth (Eds), Studies in Surf. Sci. and Catal., Elsevier, Amsterdam 2007, Chapter 6, pp 181.
[2] Z. Tang, J. Dong, T.M. Nenoff, Langmuir 2009, 25(9) 4848.
[3] J. Motuzas, A. Julbe, R.D. Noble, A. Van der Lee, Z.J. Beresnevicius, Rapid synthesis of oriented silicalite-1 membranes by microwave-assisted hydrothermal treatment, Microporous and Mesoporous Materials, 92 (2006) 259-269.

The stability of copper species on Cu, Au/SBA-3 mesoporous materials

Justyna Florek-Milewska, Maria Ziolek,
A. Mickiewicz University, Faculty of Chemistry, Grunwaldzka 6, 60-780 Poznań,
ziolek@amu.edu.pl

Introduction

Copper and gold particles have been for a long time used for similar purposes in heterogeneous catalysis [1]. Copper materials are usually used in hydrogenation and oxidation reactions [2,3]. The materials modified by gold are widely applied in selective oxidation processes [4,5]. If both metals are loaded on the support the interactions between them change the catalytic activity of the materials [6,7] and create very interesting properties.

The main point of this paper was the preparation of catalysts containing both, copper and gold species loaded on ordered mesoporous SBA-3 materials and characterisation of the stability of copper species. The focus was on the methods of sample modification by both metals (step by step or one-pot impregnation) and on the role of the nature of copper salt used for impregnation.

Experimental

SBA-3 mesoporous materials were synthesized according to the procedure described by Stucky et al. [8] and modified by different methods. As the first one the wetness impregnation with copper and gold was used. These metals were introduced into SBA-3 samples step by step (one after the other, first Cu and next Au) – the relevant sample is labelled as Au/Cu/SBA-3 or by one-pot mixture – labelled as Au&Cu/SBA-3. The second way involved modification with gold during the synthesis (the sample labelled as AuSBA-3) followed by post synthesis wetness modification by copper salt. Two different loadings of both metals were applied, 1 and 3 wt.%. For copper precursors ammonium tetrachlorocuprate dihydrate or copper II nitrate trihydrate were used. $HAuCl_4$ was applied as a gold source. The impregnated samples were dried at 373 K for 5 h and then calcined at 623 or 673 K for 3 h.

The physicochemical properties of the samples were investigated by XRD, N_2 adsorption-desorption, ICP, UV-Vis, and XPS techniques. The stability of copper species was investigated by thermal treatment in the range RT – 673 K under helium flow or vacuum.

Results and discussion

The diffractograms of all materials prepared in the small-angle range show that they have ordered hexagonal structure as indicated by the presence of the highest peak at $2\Theta = 2.7°$ and two smaller peaks at $2\Theta = (4\text{-}6)°$. Nitrogen adsorption isotherms are typical of SBA-3 and are of type IV according to the IUPAC classification. The textural parameters for selected materials are summarized in Table 1. The presence of metallic gold in all samples was indicated by UV-Vis spectra and XPS results.

In the wide angle range of the XRD patterns the peaks at $2\Theta = 38.1°$ and $2\Theta = 44.2°$ for gold-containing materials correspond to the metallic gold [9] and confirm the UV-Vis results. The samples with a higher copper loading (3wt % as assumed) exhibit more or less intense peaks assigned to CuO ($2\Theta = 35.5$ and $38.7°$) . Interestingly, the intensity of these reflexes strongly depends on the copper source used for the impregnation (it is much higher when Cu(II) nitrate is used instead of ammonium tetrachlorocuprate dihydrate) and on the impregnation procedure. It could be caused by the difference in CuO dispersion (the higher the dispersion the lower the intensity of XRD peaks), or by the presence of copper in the phase other than CuO or by the removal of a part of copper species during calcination of the material after impregnation. The introduction of gold after Cu loading (step by step impregnation) does not

change the CuO phase in XRD pattern. However, when a mixture of ammonium tetrachlorocuprate dihydrate and $HAuCl_4$ was used for the one-pot impregnation or copper was loaded on AuSBA-3 (where Au was introduced during the synthesis of SBA-3 material), the peaks assigned to CuO are absent in the XRD pattern. These results prompted us to study the stability of copper species on the mesoporous SBA-3 silica.

The ICP analyses indicate slight loss of copper species after calcination (the highest when the one-pot impregnation was applied). But more important is the stability of copper species under thermal treatment in the inert atmosphere (in helium flow or under vacuum). It is an important feature because the catalysts prepared are to be used in the catalytic reactions (PROX or CO oxidation) requiring activation under these conditions.

Results of the thermal treatment under vacuum indicate that for some samples a part of copper sublimates in the form of $CuCl_2$ (a blue species deposited on the glass cell). This phenomenon is observed only when ammonium tetrachlorocuprate dihydrate is used as a copper source and the assumed copper loading is 3 wt.%. It is not the case when the loading of Cu is lower (1 wt.%) and if Cu(II) nitrate is applied for the impregnation (even for the high Cu loading). Taking into account the temperature of sublimation one can order the stability of copper depending on the method of impregnation and the presence or absence of gold as a modifier. The lowest sublimation temperature (260 ºC) is observed for 3%Cu&3%Au/SBA-3 material (the sample prepared by one-pot impregnation with both metal sources containing chloride ions) and the highest (350 ºC) one for 3%Cu/SBA-3 (the sample containing only copper introduced from ammonium tetrachlorocuprate dihydrate).

Table 1. Texture parameters for selected samples.

Catalyst	Surface area BET (m^2g^{-1})	Average pore diameter BJH (nm)
3%Cu/3%AuSBA-3	1080	2.9
3%Cu/1%AuSBA-3	1061	2.9
3%Cu/3%Au/SBA-3	1005	2.5
3%Cu&3%Au/SBA-3	1106	2.3
1%Cu/1%Au/SBA-3	1103	2.7

Conclusions

Copper introduced by impregnation of SBA-3 and AuSBA-3 materials with the assumed loading of 3 wt.% and with ammonium tetrachlorocuprate dihydrate as a source of Cu is not stable under thermal treatment in vacuum. The sublimation of $CuCl_2$ which occurs under these conditions is caused by the presence of chloride ions in the Cu source and its deposition on the support. It is enhanced by the presence of gold species in the material.

Acknowledgements

Polish Ministry of Science (Grant No. N N204016539) is acknowledged for the financial support of this work.

References

[1] C.L. Bracey, P.R. Ellis, G.J. Hutchings, Chem. Soc. Rev.38 (2008) 2231.
[2] F-W. Chang, T-C. Ou, L.S. Roselin, W-S. Chen, S-C. Lai, H-M. Wu, J. Mol. Catal. A: Chem. 313 (2009) 55.
[3] P. Haider, J-D. Grunwaldt, A. Baiker, J. Catal., 248 (2007) 175
[4] E. Sacaliuc, A. M. Beale, B. M. Weckhuysen, T. A. Nijhuis, J. Catal., 248 (2007) 235.
[5] M. M. Schubert, S. Hackenberg, A. C. Veen, M. Muhler, V. Plazak, R. J. Behm, J. Catal., 197 (2001) 113.
[6] S. Scire, S. Minico, C. Crisafulli, S. Galvagno, Catal. Commun., 2 (2001) 229.
[7] X. Liu, A. Wang, X. Wang, C-y. Mou, T. Zhang, Chem. Commun., (2008) 3187.
[8] Q. Huo, D. Margolese, U. Ciesla, D. Demuth, P. Feng, T. Gier, P. Siegier, A. Firouzi, B. Chmelka, F. Schuth, G. D. Stucky, Chem. Mater. 6 (1994) 1176.
[9] I. Sobczak, Catal Today, 142 (2009) 258.

Investigation of Adsorption Properties of Natural Zeolite from Yavu Region, Sivas-Turkey

Onder Orhun[1], Sevket Caliskan[1]
[1]*Anadolu University Science Faculty Physics Department 26470 Eskisehir-Turkey,*
Corresponding Author: oorhun@anadolu.edu.tr

Introduction

Due to having microporous structure, natural zeolites have large surface area which is surface of channels through it. Diameters of these channels are approximately between 5 and 10 Å. Specific surface area is defined as surface area per gram natural zeolite.Because zeolites have capability of adsorption of all inorganic and organic molecules and ions, scientific and technological importance of natural zeolites will always increases. Natural zeolites can selectively adsorb from gas and vapour phases or liquid mixtures with multi components and ionic solutions. For this reason, natural zeolites take place among adsorptive materials. Specific surface area, mean pore diameter, adsorption isotherm type are main adsorption properties of natural zeolites. Adsorption properties could be determined by adsorption and desorption isotherms of nitrogen on natural zeolites at 77 K.
If adsorption properties of any natural zeolites were defined, it can be reply the question of on which application field this natural zeolite can be used. Aim of this study is to define adsorption properties of natural zeolite from Yavu region, Sivas-Turkey, main components which are clinoptilolite and mordenite, and consequently to help for decision of selection for application field.

Experimental

Adsorption isotherms of Yavu zeolite which dimension of powder is 63 μm, were obtained by high speed volumetric sorption analizor (Quantachrome, Nova 2200) which runs by B.E.T. method. Structural formulas of clinoptilolite and mordenite are $\mathbf{Na_6Al_6Si_{30}O_{72}24H_2O}$ and $\mathbf{Na_8Al_8Si_{40}O_{96}24H_2O}$ respectively [1],[2]. The mineral content of natural zeolite sample was calculated from x-ray diffractogram obtained by x-ray diffractometer (Bruker AXS, D8 Advance). The equation of mineral content is $W_i = (K_iI_i/\Sigma K_iI_i) \times 100$, where W_i is the percentage mineral in the sample, K_i is the approximate area of a given peak to the total peak area and I_i is the intensity of the basal peak [3],[4]. According to XRD analysis, natural zeolite sample includes clinoptilolite 15.2%, mordenite 81.5 %, and quarz 3.3 %. In this study, addition to natural zeolite, through the preparation of Ca^{2+} and K^+ modified forms, batch method was applied by using 1 M $CaCl_2$ and KCl solutions, respectively.

(a) (b)

Figure 1: (a)B.E.T. adsorption isotherm and (b) Langmuir adsorption isotherm of natural zeolite

Investigation of adsorption properties of natural, Ca^{2+} and K^{+} modified forms of zeolite was realized by High Speed Adsorption System (Quantachrome 2200). B.E.T. and Langmuir adsorption isotherms of natural zeolite could be seen in Figure 1 (a) and (b) respectively.Using lineer regions of these curves, specific surface areas of natural, Ca^{2+} and K^{+} modified forms of zeolite could be obtained. Beside of this, average pore diameters of these three forms could be obtained by B.J.H. method.

Results and Discussion

Table 1: Comparision of some adsorption properties of various forms of zeolite obtained from Yavu region, Sivas-Turkey.

Adsorption Property	Natural Form	Ca^{2+} Form	K^{+} Form
Specific Surface Area From B.E.T. Model (m^2/g)	23.95	8.97	18.82
Specific Surface Area From Langmuir Model (m^2/g)	45.70	16.33	35.12
Average Pore Diameter From B.J.H.Model (Å)	55.653	68.254	61.615

As shown in Table 1, because of exchanging of Ca^{2+} and K^{+} ions with cations on surfaces of channels through the structure, average pore diameters were increased and then naturally, specific surface areas were decreased. Ionic radii of Ca^{2+} and K^{+} cations are 1.80 Å and 2.20 Å respectively [5]. Therefore, because of increasing average pore diameter, cations which are bigger than Ca^{2+} and K^{+} ions leave structure of zeolite. Because K^{+} cation has bigger ionic radius than ionic radius of Ca^{2+} , average pore diameter of K^{+} form is smaller than average pore diameter of Ca^{2+} form. As average pore dimeter would decreased, specific surface area would increased. This situation could seen in Table 1.

References

[1] Dyer, A., An Introduction to Zeolite Molecular Sieves, John Wiley&Sons, (1988), 16-18.
[2] Korkuna,O,Leboda,R.,Skubiszewska, J.Z.,Vrubleska, T.,Gunko,V.M.,Ryczkowski,J., Structural and Physicochemical Properties of Natural Zeolites: Clinoptilolite and Mordenite, Microporous and Mesoporous Materials,(2006).
[3] Müller, G. ,Methods in Sedimentary Petrology, E. Schweizerbart'sche Verlagsbushhandlung,(1967), Stuttgart.
[4] Unaldi, T., Orhun, O, Kadir, S., Physicochemical Characterization of Natural and Na^{+}-, K^{+}-, Ca^{2+}- and Mg^{2+}-modified Clinoptilolite from Gördes (Manisa, Turkey), Adsorption Science&Technology, (2009), 27,6,615-631.
[5] Vainstein B.K., Fridkin V.M., Indenbom V.L., Modern Crystallography II, Springer Verlag (1982), p.85.

Keywords: Clinoptilolite, mordenite, adsorption.

Thermal Investigation of Natural Zeolite from Yavu Region, Sivas-Turkey

Sevket Caliskan[1], Onder Orhun[1]
[1]*Anadolu University Science Faculty Physics Department 26470 Eskisehir-Turkey,*
Corresponding Author: sevketcaliskan@anadolu.edu.tr

Introduction

Thermal analysis includes the methods in which any physical property of any natural zeolite was measured as a function of temperature or any heat which was adsorbed or liberated through any reaction was followed. Main methods of thermal analysis are thermogravimetric analysis (TGA) and differential thermal analysis (DTA). In thermogravimetric analysis (TGA) method, mass variation of natural zeolite are measured versus temperature increase. These curves of mass versus temperature are called as thermogram. Generally, the reason of these mass variation is absent from the microporous structure of natural zeolite of gas formed H_2O, S, N_2 and the other components or leave from the structure of natural zeolite of gases such as CO_2, SO_2 at the end of thermal decomposition of inorganic components such as metal carbonates, metal sulfates. On the method of differential thermal analysis (DTA), applying same heating program to two material which are sample of natural zeolite and inert reference material, temperature difference between two material was measured. Thermal curve was obtained as plotting temperature difference versus the temperature of natural zeolite. Investigating DTA curves can answer the question of "Are chemical reactions through the structure and phase transformation exothermic or endothermic?".
If thermal properties of any natural zeolites were defined, it can be reply the question of on which application field this natural zeolite can be used. Aim of this study is to define thermal properties of natural zeolite from Yavu region, Sivas-Turkey, main components of which are clinoptilolite and mordenite, and consequently, to help for decision of selection for application field.

Experimental

Thermal analysis of Yavu zeolite which dimension of powder is 63 μm, were obtained by TGA/DTA system (Setaram Setys Evolution 1750) which runs at N_2 atmosphere and heating rate of 10^oC/min and uses alumina (Al_2O_3) crucible. Structural formula of clinoptilolite is $\mathbf{Na_6Al_6Si_{30}O_{72}24H_2O}$ and its secondary building unit is **4-4-1**. Structural formula of mordenite is $\mathbf{Na_8Al_8Si_{40}O_{96}24H_2O}$ and its secondary building unit is **5-1** [1],[2]. The mineral content of natural zeolite sample was calculated from x-ray diffractogram obtained by x-ray diffractometer (Bruker AXS, D8 Advance). The equation of mineral content is $W_i = (K_iI_i/\Sigma K_iI_i) \times 100$, where W_i is the percentage of mineral in the sample, K_i is the approximate area of a given peak to the total peak area and I_i is the intensity of the basal peak [3],[4]. According to XRD analysis, natural zeolite sample includes clinoptilolite 15.2%, mordenite 81.5 %, and quarz 3.3 %. In this study, addition to natural zeolite, through the preparation of Ca^{2+} and K^+ modified forms, batch method was applied by using 1 M $CaCl_2$ and KCl solutions, respectively. TG and DTA curves of these three forms were obtained by thermal analysis system (Setaram, Setsys Evolution). In figure 1, as an example, TG and DTA curve of natural zeolite could be shown.

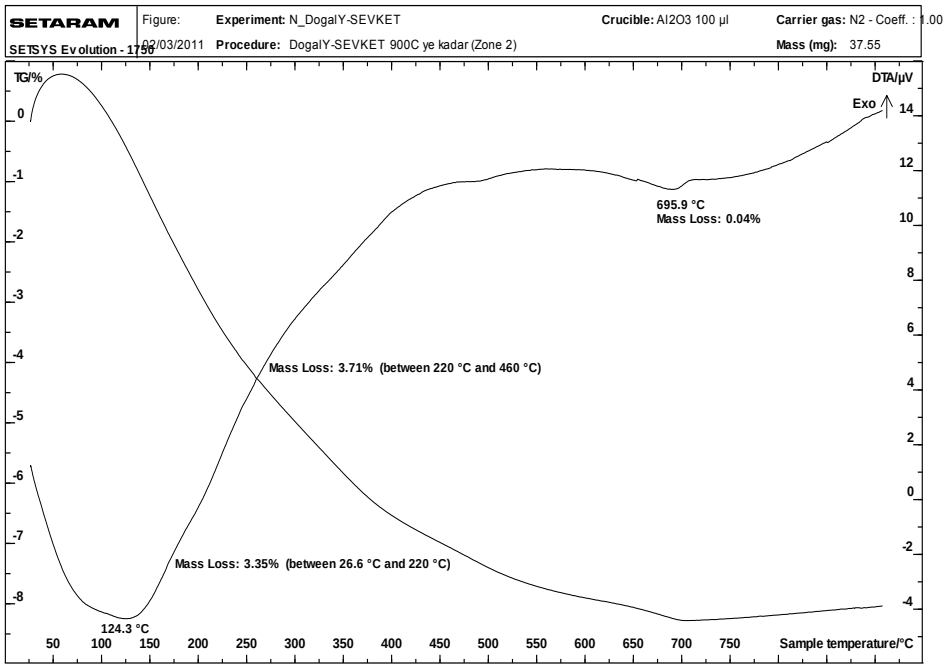

Figure 1: DTA and TG curves of natural zeolite.

Results and Discussion

Table 1: Comparision of natural zeolite obtained from Yavu region, Sivas-Turkey to its modified forms in terms of peaks on their DTA and TG curves

Information of peaks on DTA and TG curves	Natural Form	Ca^{2+} Form	K^{+} form
Minimal Temperature of Surface Water Desorption (^{o}C)	124.3	73.3	119.8
Mass Loss Percentages of Surface Water Desorption(%)	7.07 (between 26.6^{o}C and 460^{o}C)	5.82 (between 34^{o}C and 412^{o}C)	6.39 (between 26.5and 450^{o}C)
Temperature on Other Endothermic Peaks(^{o}C)	695.9	478	477.4
Mass Loss Percentages on Other Endothermic Peaks(%)	0.04	0.2	0.32

Comparision of natural zeolite to modified forms in terms of peaks on their DTA and TG curves could be shown in Table 1. Other endothermic peaks of natural, Ca^{2+}, K^{+} forms were due to structural modifications. After about 900^{o}C, structures of all three forms fall down. Because crystal water leaves structure. For this reason, to have a care, through various industrial applications, temperature must not exceed 900^{o}C.

References

[1] Dyer, A., An Introduction to Zeolite Molecular Sieves, John Wiley&Sons, (1988), 16-18.
[2] Korkuna,O,Leboda,R.,Skubiszewska, J.Z.,Vrubleska, T.,Gunko,V.M.,Ryczkowski,J., Structural and Physicochemical Properties of Natural Zeolites: Clinoptilolite and Mordenite, Microporous and Mesoporous Materials,(2006).
[3] Müller, G. ,Methods in Sedimentary Petrology, E. Schweizerbart'sche Verlagsbushhandlung,(1967), Stuttgart.
[4] Unaldi, T., Orhun, O, Kadir, S., Physicochemical Characterization of Natural and Na^{+}-, K^{+}-, Ca^{2+}- and Mg^{2+}-modified Clinoptilolite from Gördes (Manisa, Turkey), Adsorption Science&Technology, (2009), 27,6,615-631.

Keywords: Clinoptilolite, mordenite, thermal investigation

FRAMEWORK AND GRAFTED INCORPORATION OF CUBANE-TYPE Mo_3S_4 CLUSTER INTO MESOPOROUS SILICA MATERIALS

A. I. Carrillo,[a] I. Sorribes,[b] E. Serrano,[a] R. Llusar,[b] C. Vicent,[c] J. Garcia-Martinez[a*]
[a]*Molecular Nanotechnology Lab., Inorganic Chemistry Department, University of Alicante, Carretera San Vicente s/n, E-03690 Alicante,* [b]*Departament de Química Física i Analítica, Universitat Jaume I, 12071 Castelló,* [c]*Serveis Centrals d´Instrumentació Científica, Universitat Jaume I, 12071 Castelló.* ada.carrillo@ua.es

Introduction

Surfactant-templated silica materials show some remarkable properties such as large surface area and controllable pore volume and size distribution.[1-3] One of the limitations of these materials is their lack of active sites. Different strategies have been investigated to introduce catalytically active sites into mesoporous silicas including co-condensation of active species during mesoporous material synthesis or post-synthesis methods such as functionalization by grafting.[4] In this work, we present the incorporation of the cubane-type $[Mo_3S_4(dmpe)_3(MPTES)_3]PF_6$ cluster (dmpe = 1,2-Bis(dimethylphosphine)ethane; MPTES = (3-Mercaptopropyl)triethoxysilane) into mesoporous silica.

Experimental

Hybrid mesoporous materials have been synthesized by two different approaches to achieve the Mo_3S_4 cubane-type cluster incorporation into mesoporous silica via covalent attachment: i) a two-step approach, where mesoporous silica MCM-41 was firstly prepared and subsequently the cubane-type cluster was chemically grafted onto the surface of MCM-41 (grafting synthesis) and ii) a one-pot approach (*in-situ* synthesis) where the mesoporous material was prepared by co-condensation of both the functionalized molybdenum cluster (in ethanol solution) and tetraethylorthosilicate (TEOS). The molybdenum cluster concentration in the solids was varied between 1-5wt% nominal Mo:SiO_2. Samples was labeled as IS-cluster-x or G-cluster-x where IS and G stands for in situ or grafting incorporation respectively, *x* stands for the wt% nominal amount of the molybdenum into the material, *x* = 1, 3, and 5. The textural properties of the solids decrease, in all of the cases, with the increase in the amount of Mo_3S_4 cluster as shown in Table 1.

Results and discussion

Table 1. Structural parameters of samples prepared by the two different approaches with the highest and the lowest amount of Mo_3S_4 cluster into their framework.

Samples	d_p[a] (nm)	A_{BET}[b] (m^2/g)	V_p[c] (cm^3/g)	d_{100}[d] (nm)	Samples	d_p[a] (nm)	A_{BET}[b] (m^2/g)	V_p[c] (cm^3/g)	d_{100}[d] (nm)
G-cluster-1	3.0	745	0.75	4.40	IS-cluster-1	2.2	868	0.67	4.05
G-cluster-5	2.7	650	0.52	4.40	IS-cluster-5	1.9	693	0.63	4.47

[a]Average mesopore diameters were estimated from the adsorption branch of the nitrogen isotherm using the BJH method. [b] The BET surface area was estimated by using multipoint BET method using the adsorption data in the relative pressure (P/P_0) range of 0.05–0.30. [c] Mesopore volume measured at the plateau of the adsorption branch of the nitrogen isotherm ($P/P_0 = 0.8$). [d] Spacing d_{100}, from XRD spectra.

The morphology of hybrid mesoporous materials was investigated by transmission electron microscopy, see Figure 1. Solids prepare with the one-pot method present a non ordered structure due to the use of ethanol during the synthesis process. In the case of grafting materials the well-ordered hexagonal structure, typical of MCM-41 materials, is kept after the post-synthesis modification.

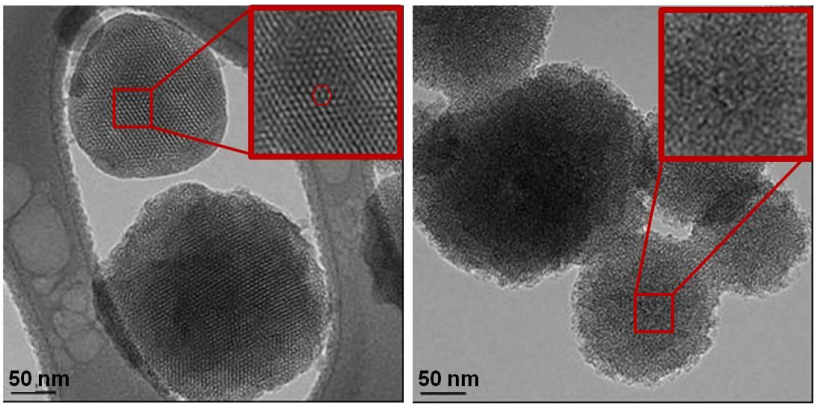

Figure 1. TEM images of two representative samples prepared by the post-grafting method and with the highest amount of cluster (left) and by the in-situ method and the lowest amount of cluster (right).

Conclusions

Two groups of mesoporous solids with Mo_3S_4 clusters into their framework were prepared. The one-pot synthesis produces a non-ordered materials whereas solids prepared using the post synthesis method show well-ordered structured. All of the materials prepared present good textural properties with surface areas and pore volumes in the order of 700 m^2/g and 0.6 cm^3/g, respectively.

Acknowledgements

This research has been funded by the Spanish Ministerio de Educación y Ciencia (CTQ2005–09385–C03–02, CTQ2008-02670 and CTQ2006-14909-C02-01), the Spanish Ministerio de Ciencia e Innovación (Fundació Bancaixa-UJI (research project P1.1B2007-12) and Generalitat Valenciana (ACOMP/2009/105 and Prometeo/2009/053). The authors would also like to thank the Technical Services of the Universities of Alicante the Universitat Jaume I. I.S. and E.S. thanks the Spanish Ministerio de Ciencia e Innovación (MICINN) for a doctoral fellowship (FPU) and the Juan de la Cierva Program (ref. JCI–2008–2165). Authors the Department of Applied Physics of the University of Alicante.

References

[1] Kresge, C.T., Leonowicz, M.E., Roth, W.J., Vartuli, J.C., Beck, J.S., Ordered mesoporous molecular sieves synthesized by a liquid-crystal template mechanism, Nature, 359 (1992), 710-712.
[2] Corma, A., Preparation and catalytic properties of new mesoporous materials, Topics in Catalysis, 4 (1997), 249-260.
[3] Jia, M., Seifert, A., Thiel, W.R., Mesoporous MCM-41 materials modified with oxodiperoxo molybdenum complexes: efficient catalysts for the epoxidation of cyclooctene, Chemistry of Materials, 15 (2003), 2174-2180.
[4] (a) Trong-On, D., Desplantier-Giscard, D., Danumah, C., Kaliaguine, S., Perspectives in catalytic applications of mesostructured materials, Applied Catalysis A: General, 222 (2001), 299-357. (b) Zhou, W.J., Albela, B., Ou, M., Perriat, P., He, M.Y., Bonneviot, L., Framework and grafted nickel ethylenediamine complexes in 2D hexagonal mesostructured template synthesis, Journal of Materials Chemistry, 19 (2009), 7308-7321.

Reduction of copper, supported on ZSM-5, studied by DRX, UV-Vis-DR, EPR, SEM-EDS and Raman spectroscopy

F. Chávez-Rivas[1,2,§,*], R. Zamorano-Ulloa[2], V. Petranovskii[3], and I. Rodríguez-Iznaga[4]
[1]*Department of Inorganic, Physical and Material Chemistry, University of Turin, Via P. Giuria 7, 10125 Torino, Italy; § On sabbatical leave, granted by ESFM-IPN, Mexico*
** fchavez@esfm.ipn.mx*
[2]*Departamento de Física, Escuela Superior de Física y Matemáticas del IPN, 07738, México D.F., México*
[3]*Universidad Nacional Autónoma de México, Centro de Nanociencias y Nanotecnología, Apdo. Postal 14, C.P. 22800, Ensenada, B.C., México*
[4]*Instituto de Ciencia y Tecnología de Materiales (IMRE), Universidad de La Habana, Zapata y G, s/n. Ciudad de La Habana 10400, Cuba*

Introduction

Copper-containing ZSM-5 zeolites are known as challenging catalysts for de-NOx reactions [1] among others important catalytic applications. In this report we present the results of versatile study of effects provoked by Cu reduction in hydrogen flow over Cu-ZSM-5 zeolites at temperatures of 150 and 350 ºC. A number of species of the ionic nature can be formed during the activation treatment; neutral small metal particles and few atomic clusters are possible products of copper ion transformations also. The effects due to the copper reduction by hydrogen were monitored using XRD, UV-Vis, EPR, SEM-EDS and Raman spectroscopy.

Experimental

Set of ZSM-5 samples with varied SiO_2/Al_2O_3 molar ratio (MR) was synthesized and generously supplied by Dr. Alireza Abbaspur, from Isfahan Technology University, Iran. Selected for this work samples have MR of 30 and 70. Copper ion exchange was carried out from 0.1 M $Cu(NO_3)_2$ aqueous solution for one day. Exchanged samples were dried, and reduced in H_2 flow at temperatures of 150 and 350 ^oC for 4 h. Scanning electron microscopy, as well as EDS (Energy Disperse Spectroscopy) spectra were performed with a Quanta 3D FEG beam (FOCUSED ION BEAM). EDS spectra were measured at specific spots with different size. Measurements showed approximately 1 wt % of Cu for all samples. Micrographs at various magnifications were obtained at 16 kV. Diffuse reflectance spectra (DRS) were collected on a Varian Cary 300 using a standard diffuse reflectance unit. EPR spectra of air-exposed hydrated samples were measured at 300 K with a JEOL JES-RE3X spectrometer at a frequency of 9 GHz, power of 1 mW and modulation frequency of 100 KHz. Raman spectroscopy and optical images were measured with a computer-model BX41 Olympus Micro-Raman HR800 whose sources were two laser excitation wavelengths of 633 and 785 nm. X-Ray diffraction measurements were done with a Philips X'Pert diffractometer, using Cu K_α radiation.

Results and discussion

XRD patterns of all the samples demonstrates typical for ZSM-5 zeolite structure, and were influenced neither by ion exchange, nor by reducing treatment. Diffuse reflectance UV-Vis spectra of Cu-ZSM-5-30 and Cu-ZSM-5-70 demonstrates how the peak of Cu^{2+} ions, centered at 850 nm, disappears during reduction treatment, in line with appearance of reduced copper species; in general similar to observed during reduction treatment of Cu-Mordenite [2].

EPR spectra of reduced Cu-ZSM-5-30 and Cu-ZSM-5-70 samples at room temperature are characterized by wide axial Cu^{2+} ions signals with week hyperfine absorption. These axial asymmetric signals are associated with two different hydrated Cu^{2+} ions sites. The spectra and EPR intensity show a slight but measurable dependence on the reduction treatment.

SEM micrographs of Cu-ZSM-5-30 and Cu-ZSM-5-70 reduced at 150 ºC present a sharp difference in morphology. The SEM micrographs of Cu-ZSM-5-30-150 sample at magnification of 500X and 1000X, (Figures 1A and 1B) show crystalline particles with irregularly shaped crystals of various sizes with apparent sides in the range from 50 to 1μm and prevailing crystal sizes less than 20 μm, meanwhile, the micrographs of Cu-ZSM-5-70-150 sample (not shown) show mainly spherical particles with prevailing diameters less than 30 μm. SEM images of Cu-ZSM-5-30-350 present the formation of new crystalline particles composed of domains with marked edge boundaries, that is, these new particles are formed during the reduction at 350 ºC. On the contrary the micrographs of Cu-ZSM-5-70-350 almost remain unchanged by the reduction treatment at 350 ºC.

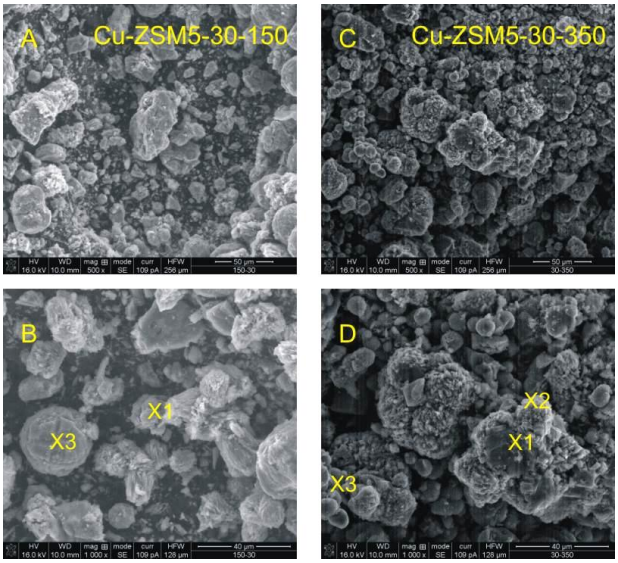

Figure 1. SEM micrographs of Cu-ZSM5-30 sample reduced at 150 ºC, (A and B), and reduced at 350 ºC (C and D).

Raman spectra of all reduced Cu-ZSM-5 samples are characterized by a band at 373 cm^{-1} and several weak peaks and shoulders when exited by the 785 nm line. These signals overlap to a strong photoluminescence background centered at 800 cm^{-1}. The 633 nm excitations generate two more weak peaks below 280 cm^{-1}. Probably the change observed in the photoluminescence background is related to reduction treatments.

Conclusions

Copper reduction in the zeolite matrix is influenced both by the temperature of reducing treatment and by the chemical composition of zeolite, that is by SiO_2/Al_2O_3 molar ratio. This influence is partly due to difference in copper ion sites in line with MR changing.

Acknowledgements

The authors acknowledge support of Assistant Director of the Center of Nanocience and Micro and Nanotechnology of IPN Dr. A. Rodriguez, and collaboration of Dr. Mayahuel Ortega Aviles, Dr. Hugo Martinez and M. in C. Luis Alberto Moreno in the SEM and Raman measurements. F. Chavez-Rivas and R. Zamorano-Ulloa acknowledge the support of COFAA-IPN. This research was supported by CONACYT, Mexico, through Project #102907.

References

[1] V.I. Parvulescu, P. Grange, B. Delmon, Catalytic removal of NO, Catalysis Today 46 (1998), 233-316

[2] V. Petranovskii, V. Gurin, N. Bogdanchikova, A. Licea-Claverie, Y. Sugi, E. Stoyanov, The effect of SiO_2/Al_2O_3 molar ratio in mordenite upon the optical appearance of reduced copper, Materials Science and Engineering: A, Structural Materials: Properties, Microstructure and Processing, 332 (2002), 174-183

Enzyme-containing Liposomes for stable biocatalysts preparation

A. Macario[a, *], U. Diaz[b], A. Corma[b], G. Giordano[a]
[a]*Dip. Ing. Chim. & Mat., Università della Calabria, via P. Bucci, 87036 Rende (CS), Italy*
[b]*Instituto de Tecnología Química (UPV-CSIC), Universidad Politécnica de Valencia, Avd. De los Naranjos s/n 46022 Valencia, Spain*
**corresponding author: email macario@unical.it, telephone number +39.0984.49.66.67*

Introduction

Enzyme-containing vesicles (or liposomes) are interesting systems in which a biocatalyst is immobilized noncovalently, with several advantages over the conventionally immobilized enzyme. First of all, the noncovalently entrapped enzyme retains its free and stable conformation in the biocompatible microenvironment inside the liposome membrane. The activity of the enzyme entrapped inside liposomes significantly depends on the substrate permeability across the liposome bilayers [1]. For this reason, the enzyme-containing vesicles could be used for bio-specific reactions, using substrate mixtures. Various enzyme have been encapsulated inside small and large unilamellar vesicles by various methods, such as the dry lipid film hydration, the freezing and thawing, the dehydration-rehydration and the extrusion [2]. The last one is the most characterized method because monodisperse and regular extrude liposome nanospheres can be obtained. However, the liposomes, but in general the organic system, are not thermally and chemically stable and, hence, the enzyme molecules can be denatured and/or released from the vesicles. Silica nanoparticles could be employed for storage of active biomolecules: their biocompatibility and stability towards external agents make them attractive systems to overcome the stability drawbacks of organic molecules. In this work we report the synthesis of organic-inorganic solid with spherical morphology where enzymes, as active compounds, are encapsulated. The nanospheres are composed of an organic internal liposomal-enzyme phase covered by an external self-assembled silica shell. In order to avoid the enzyme leaching, the porosity of the silica shell has been modulated using different silica sources and/or developing organic fragments on the silica shell in order to reduce the opening mouth of the pores.

Experimental

The synthesis of nanospheres was carried out using an emulsion of lecitine (as liposome sources) where enzyme has been added after solvent evaporation. The formation of inorganic silica shell, around the liposome/enzyme phase, was obtained by polymerization of the silicon precursor (TEOS or sodium silicate). For the organic-inorganic shell preparation, ester fragments have been covalently bonded to the silica units [3].

Results and discussion

The first encapsulated enzyme was the lipase from Rhizomucor miehei. Different samples were prepared in order to change the amount of encapsulated lipase (Table 1). The amount of

encapsulated enzyme was evaluated by UV-Visible method. When the initial enzyme concentration was 1M, the highest immobilization efficiency was obtained.

Table 1. Prepared samples starting from solutions with different enzyme concentrations

Sample Code	Initial Enzyme Concentration [M]*10^3	Amount of encaps. Enz. [mg]	% Immob.	Enz. Amount in the solid [%wt]
BL	0	0	0	0
LL1	0.5	14	95.8	3.9
LL2	1	29	98.3	7.6
LL3	2	54	96.5	9.4
LL4	3	80	95.1	15

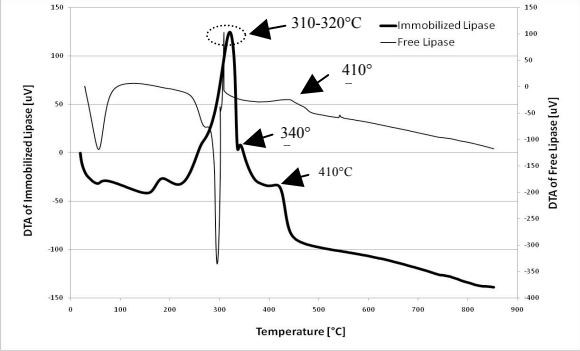

Figure 1. DTA curves of free lipase and of nanospheres, with purely siliceous external shell containing the enzyme (LL2)

The incorporation of internal organic liposome/lipase phase, into the external inorganic silica shell, is clearly corroborated by thermogravimetric analysis [3] (Fig. 1). Fig. 2 shows an isolated nanosphere containing lipase enzyme and liposomal phase (sample LL2).

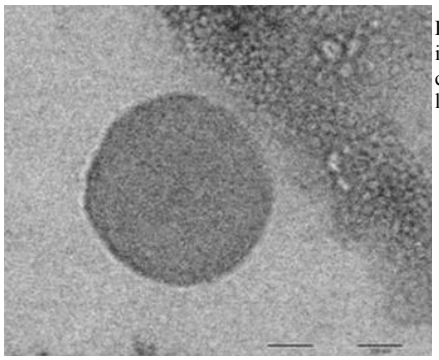

Figure 2. TEM image of isolated nanosphere containing lipase and liposome (LL2)

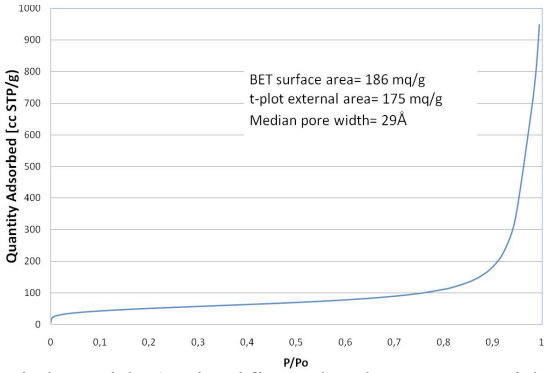

Figure 3. N_2 ads. isotherm of nanosphere containing lipase and liposome (LL2)

The activity of the enzyme (transesterification of triglycerides) significantly decreases with the increasing of the initial enzyme concentration (Fig. 4), meaning that, when the enzyme is encapsulated in large amount, it is less free to move and, then, to meet and catalyze the substrate.

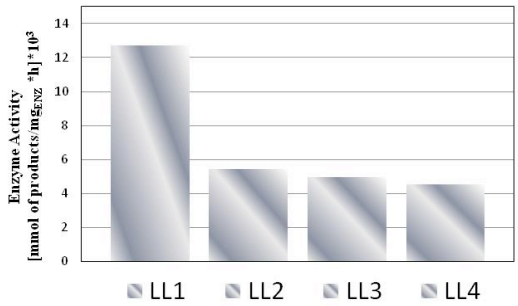

Figure 4. Lipase/Liposome nanospheres activity

The pore size of the external silica shell prepared by TEOS as silica precursor is 29 Å: this pore dimension does not avoid the leaching of the enzyme. Further investigations are in progress in order to reduce the pore size of external shell of nanospheres by changing the silica precursor and by attaching the organic fragments covalently to silica shell.

References

[1] Walde P, Marzetta B., 1998. Bilayer permeability-based substrate selectivity of an enzyme in liposomes. Biotechnol Bioeng 57:216–19.

[2] Walde P., Ichikawa, S., 2001. Enzymes Inside Lipid Vesicles. Preparation , Reactivity and Applications. Biomol.Eng.18:143-177.

[3] A. Corma, U. Diaz, M. Arrica, E. Fernandez, I. Ortega, Angew. Chem. Int. Ed. 48 (2009) 6247-6250.

Low temperature synthesis of nanosized LTA- and FAU-type zeolite crystals

L. Dimitrov[a], D. Nihtjanova[a], Y. Kalvachev [a], V. Valtchev[b]
[a] *Institute of Mineralogy and Crystallography, Bulgarian Academy of Sciences, Acad. G. Bonchev Str., bl. 107, 1113 Sofia, Bulgaria*
[b] *Laboratoire Catalyse & Spectrochimie, ENSICAEN, Université de Caen, CNRS, 6 boulevard du Maréchal Juin, 14050 Caen, France*

Introduction

The synthesis of zeolite nanocrystals in the form of stable colloidal suspensions was one of the important events in zeolite science during the past decade.[1] The synthesis of zeolite crystals with narrow particle size variation requires homogeneous distribution of the viable nuclei in the system. Therefore, the homogeneity of the starting system and simultaneity of the events leading to the formation of precursor gel particles, and their transformation into a crystalline product, are of primary importance for the synthesis of zeolite nanoparticles. In general, very diluted systems containing abundant amounts of tetraalkylammonium hydroxides are used in the synthesis of zeolite nanocrystals. The alkaline cation concentration in such systems has to be very limited in order to avoid the flocculation of the gel particles. All these factors together with the careful choice of the silica source allow the stabilization of "clear" starting solutions, where only discrete gel particles are present. A serious drawback, that has important economic and environmental impact, is the large amount of organic structure directing agents (OSDA) used in such preparations. In addition, the organic SDA requires high temperature calcination of the zeolite in order to open zeolite porosity, which leads to aggregation of the individual particles. Thus the synthesis of discrete zeolite crystals from organic SDA-free systems is highly desired since it would open an alternative route for preparation of nanozeolites. The present study reports on the synthesis of zeolite A (LTA-type) and zeolite X (FAU-type) nanocrystals from OSDA-free system at low temperatures.

Experimental

The low temperature syntheses of zeolites were performed from systems with the following compositions: LTA-type: 6.0 Na_2O : 0.505 Al_2O3 : 1.0 SiO_2 : 150 H_2O
FAU-type: 4.0 Na_2O : 0.2 Al_2O3 : 1.0 SiO_2 : 200 H_2O

The reactants used were: sodium silicate solution (Merck, 28 wt % SiO_2, 8 % Na_2O, 65 % H_2O), $NaAlO_2$ (Riedel de-Haën, 54.3 wt. % Al_2O_3, 43.4 wt. % Na_2O), NaOH (Merck, 98 wt. %) and distilled water. In a typical preparation, a clear sodium silicate and aluminate solutions were firstly prepared. The zeolite precursor mixture was produced by vigorous 60 min mixing of the clear alkaline silicate and aluminate solutions. The resultant gel was stored in an oil bath (T=35, 50 and 65°C) in sealed polypropylene bottles. Small aliquots of the mixtures were taken at different periods of time. Prior to taking aliquots, the samples were shaken in order to disperse the settled particles. After the synthesis, the solid was recovered by a series of high speed centrifugation and re-dispersion in water.

The ultimate zeolite product and the intermediates were analyzed by X-ray diffraction (D2 Phasor from Bruker) with CuKα radiation, working at acceleration 30 kV and current 10 mA., scanning (Philips SEM-515, at 30 kV) and transmission (JEOL 2100, at 200 kV) electron microscopy, nitrogen adsorption measurements Micromeritics ASAP 2020, dynamic light scattering (Malvern Zetasizer-Nano) and atomic absorption spectroscopy (AAS) (Varian Techtron AA6).

Results and discussion

The crystallization temperature has a pronounced effect on the ultimate zeolite crystal size. As a rule, lower temperatures lead to smaller particle sizes, however at the expense of a substantial decrease of the crystallization rate. In order to obtain zeolite A and zeolite X for a reasonable period of time under ambient conditions, a highly alkaline, very reactive initial systems were employed. Besides the temperature, the crystallization kinetics of any particular zeolite is affected by the alkalinity and the composition of the reaction mixture. The preliminary study showed that the silica source comprising low weight silica species yielded the smallest zeolite crystals. Further all components of the initial system were varied in order to optimize the crystallization time. The most promising results were obtained with the compositions provided in the experimental section. The crystal growth kinetics of LTA-type and FAU-type zeolites was studied at 35, 50 and 65°C in order to find a compromise between the size of zeolite nanoparticles and the duration of the synthesis process. Thus zeolite nanoparticles with size below 200 nm (Figure 1) were obtained for crystallization time ranging between 12 and 40 h.

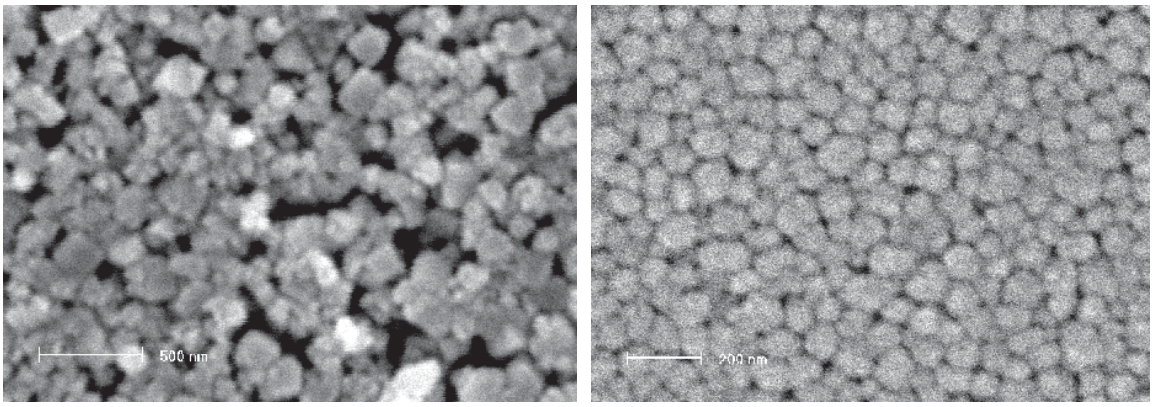

Figure 1. SEM micrographs of LTA-type (left) and FAU-type nanozeolite particles obtained at 35°C.

Conclusions

The present investigation has demonstrated that the use of very reactive hydrogel systems allow the formation of low silica zeolites for reasonable periods of time. The low temperature conditions favor the nucleation over the growth and thus nanozeolite crystals were obtained. The size of obtained crystalline aggregates vary between several tens and several hundred nanometers, while the individual crystal are much smaller in size.

The fraction of the silica converted into zeolite reaches 80 %, whereas the conversion of silica in organic-template-containing clear solutions yielding LTA- and FAU-type zeolites is usually below 10 %. Thus, the room temperature synthesis of zeolite nanoparticles from organic template free precursors offers an attractive alternative for the preparation of colloidal zeolite crystals.

Acknowledgements

The authors acknowledge the financial support from Bulgarian National Scientific Fund (contract No. 02/47).

References

[1] Tosheva, L., Valtchev, V., Nanozeolites: Synthesis, Crystallization Mechanism, and Application, Chem. Mater. 17 (2005) 2494-2513

Effect of preparation method on metal-support interactions in Ni/ZSM-5+Al_2O_3 catalysts

Aleksandra Masalska, Jolanta Grzechowiak, Karolina Jaroszewska, Włodzimierz Tylus
Wrocław University of Technology, Faculty of Chemistry, Poland,
Aleksandra.Masalska@pwr.wroc.pl

Introduction (Times New Roman, 12 pt, bold)

The method of metal incorporation is a contributing factor in the physicochemical properties of the catalyst (dispersion; metal crystallite distribution and size; acidity), as well as in the metal-support interactions. Metal may be incorporated into the support/components of the support before or after the stage of support forming. When the support is a composite, the method of combining its components also gains in importance. Addition of the active metal before catalyst formation provides a strong interaction between support and metal precursor, and produces catalysts of a high metal content and good dispersion. Strong metal-support interactions may favour a modification in metal and acid sites [1], but may as well induce the formation of compounds that are difficult to reduce [2]. This work attempts to ascertain how the method of zeolite combining/mixing with aluminium hydroxide and the method of nickel incorporation affect the surface properties and reducibility of the catalysts obtained.

Experimental

Catalyst preparation. Examined were Ni catalysts (8 wt.% NiO) supported on Al_2O_3+Ni,H-ZSM-5 (1:1) (Table 1). The preparation of series A catalysts involved aging of a mixture of zeolite and aluminium hydroxide powders in water followed by their peptisation (1% HNO_3). In the A_S method dry powders of zeolite and $Al(OH)_3$ were made subject to peptisation. The preparation of series E catalysts entailed a mixture of two pastes obtained separately: zeolite (with 1% HNO_3) and peptisate of aluminium hydroxide (with 1% HNO_3). In the E_P method, powdered zeolite was incorporated into peptised aluminium hydroxide. Nickel (nickel(II) nitrate(V)) was added before the stage of support forming (method F), by impregnation of the support already formed and calcined (method I), or by a two-stage method (F+I), where one-half of the metal was deposited before support forming, and one-half by impregnation. In series A catalysts, $Ni(NO_3)_2$ was added to aluminium hydroxide, and in series E catalysts to a zeolite and aluminium hydroxide mixture. Extrudates were dried and calcined (480^o C, 3 h).
Catalyst characterization. The catalysts were characterized by N_2 sorption (at 77 K), TPR (up to 850°C), ICP, XRD, SEM, TEM, H_2 chemisorption, XPS, NH_3-TPD and PY-IR. When use was made of H_2 chemisorption and XPS, the catalysts were reduced in H_2 at 500°C.

Results and discussion

The catalysts displayed an S_{BET} of 258–298 m^2/g, a pore volume of 0.28–0.36 cm^3/g and an average pore diameter of 4.5–5.5 nm (Table 1). Total acidity (determined by NH_3-TPD) varied from 0.82 to 0.89 mmol NH_3/g (with ammonia desorbed over the range of 300–450ºC accounting for 50%). Py-IR measurements show that in all of the catalysts Lewis acid sites were dominant (Brønsted/Lewis ratios varying from 0.24 to 0.28). The preparation method contributed to the extent of zeolite and alumina separation, as well as to the nickel distribution on the catalyst surface and along the extrudates' cross-section (SEM). In the catalyst prepared by the two-stage method (A/F+I) of metal deposition, the mean size of Ni particles is larger on the zeolite crystal surface (13−28 nm) than on the alumina surface (7−19 nm) (TEM).

Table 1. Preparation method and some physicochemical properties of the catalysts obtained.

Catalyst code	ZSM-5 &Al_2O_3 combining	NiO deposition	S_{BET} (m^2/g)	V_C (cm^3/g)	V_{MIK} (cm^3/g)	APD[a] (nm)	V_{H2}[b] (cm^3/g)	D[c] (%)	Relative amount of Ni[d] (at.%)		
									$NiAlO_4$*	NiO**	Ni^{o}***
A/F+I	A	F+I	269	0.35	0.039	5.2	0.404	3.7	46	40	14
A/F	A	F	298	0.36	0.028	5.0	0.103	0.9	51	40	9
E/I	E	I	283	0.35	0.029	5.0	0.267	2.2	41	41	18
E/F+I	E	F+I	258	0.35	0.032	5.5	0.310	2.6	43	46	11
E/F	E	F	269	0.33	0.041	4.9	0.181	1.5	52	41	7
E_P/F	E_P	F	284	0.30	0.033	4.7	0.151	1.3	49	42	9
A_S/F	A_S	F	281	0.28	0.024	4.5	0.241	2.0	50	40	10

[a]Average pore diameter (BHJ method). [b]Volume of H_2 adsorbed. [c]Dispersion. [d]by XPS; Ni $2p_{3/2}$: *BE = 857.9 eV. **BE = 855.3 eV. ***BE = 852.8 eV.

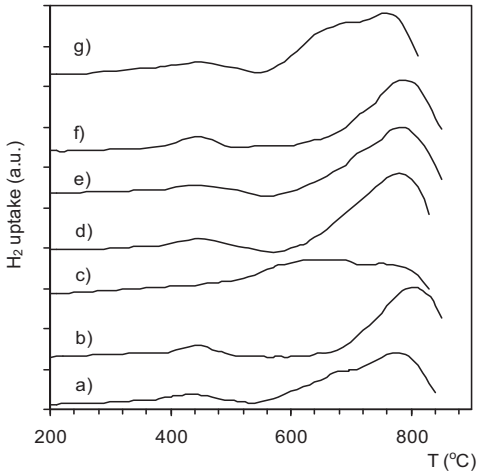

Fig. 1. TPR profiles of catalysts: A/F+I (a), A/F (b), E/I (c), E/F+I (d), E/F (e), E_P/F (f), A_S/F (g).

None of the catalysts tested has X-ray diffraction lines characteristic for nickel species (Ni, NiO and $NiAl_2O_4$) (not shown). All catalysts display a low reducibility, which is due to the strong Ni-support interactions. The formation of Ni−Al oxide spinels and Ni oxide species that are difficult to reduce is confirmed by TPR, and XPS experiments. All TPR profiles exhibit high-temperature reduction regions at 650−800°C (Fig.1). H_2 chemisorption measurements show that Ni dispersion (D) varies between 0.9 and 3.7%. Ni^0 proportion on the catalyst surface (at.% upon deconvolution of the Ni $2p_{3/2}$ region) does not exceed 20% (Table 1).

Conclusions

Regardless of the method used for combining zeolite and alumina or nickel incorporation, metal-support interactions in the catalysts obtained are strong. When the whole quantity of the nickel precursor was incorporated before catalyst formation, metal-support interactions were slightly stronger (D = 0.9−2.0%; 7−10 at.% Ni^0) than when the nickel precursor was deposited by the single-stage method involving impregnation of the support already formed and calcined, or by the two-stage method with one-half of the metal being incorporated before support formation, and one-half being introduced by impregnation of the catalyst formed (D = 2.2−3.7%; 11−18 at.% Ni^0). Catalysts prepared by the impregnation method displayed higher metal-to-acid ratios than those prepared by the single-stage method of nickel precursor incorporation before support forming.

References

[1] Minchev, C., Zubkov, S.A., Valtchev, V., et al. Appl. Catal. A:Gen., 119 (1994), 195-204
[2] Twigg, M.V., Richardson, J.T., Appl. Catal. A:Gen., 190 (2000), 61-72

Effect of different mesoporous networks on the catalytic activity of V-SBA-15 and V- MCF obtained by direct synthesis.

Marco Piumetti[1], Barbara Bonelli[1*], Pascale Massiani[2], Stanislaw Dzwigaj[2], Ilenia Rossetti[3], Yannick Millot[2], Marco Armandi[1], Edoardo Garrone[1]
[1]Dipartimento di Scienza dei Materiali ed Ingegneria Chimica and INSTM Unit of Politecnico di Torino, C.so Duca degli Abruzzi 24, 10129, Torino, Italy,[2]Laboratoire de Réactivité de Surface (CNRS-UMR 7197), Université Pierre et Marie Curie, Case 178, 4 place Jussieu, 75252, Paris, CEDEX 05, France.[3]Dipartimento CFE e ISTM-CNR, Università di Milano, via Golgi 19, 20133, Milano, Italy. Corresponding author: barbara.bonelli@polito.it

Introduction

SBA-15 and MCF silicas that are characterized by large and uniform pores size, thick walls and high surface area represent very interesting supports for V-active centers allowing a large concentration of accessible, isolated and well defined active sites. In this work, two V-SBA-15 [1] and V-MCF [2] systems (V content *ca.* 2.5 wt.%) prepared by direct synthesis were tested in both selective (ODH of propane to propene) and total oxidations (dichloromethane decomposition, the most stable chlorinated-alkane).Their physico-chemical and catalytic properties were compared with those of similar materials with the same V content [3], namely two mesoporous samples prepared by impregnation (V-SBA-15-i and V-MCF-i) and a non-porous one prepared by flame pyrolysis (V-SiO_2) [4].

Experimental

A V-SBA-15 sample was prepared by direct synthesis (V content *ca.* 2.5 wt. %) as reported in literature [1] Likewise, a V-MCF sample (V content *ca.* 2.5 wt. %) was obtained by a novel direct synthesis [2,3]. For comparison, two catalysts were synthesized by impregnation of SBA-15 and MCF supports (referred to as V-SBA-i and V-MCF-i, respectively). A non-porous catalyst (V-SiO_2) was prepared by flame pyrolysis (FP) [4]. Samples were characterized by powders XRD, FE-SEM and TEM microscopies, N_2 sorption isotherms at -196 °C, H_2-TPR, ^{51}V MAS NMR, DR UV-Vis, micro-Raman and FT-IR. Catalytic measurements were carried out in a fixed-bed reactor under aerobic conditions at different reaction temperatures (200-500 °C).

Results and Discussion

The samples directly synthesized exhibited higher specific surface areas (up to 820 m^2g^{-1} for V-SBA-15 and 925 m^2g^{-1} for V-MCF) as compared to impregnated ones. Raman spectroscopy of V-SBA-15 and V-MCF showed V=O stretching modes of isolated V species in tetrahedral coordination (ca. 1035 cm^{-1}), whereas typical bands of polymeric VO_x and micro-crystalline V_2O_5 were observed with both V-SBA-15-i and V-MCF-i samples. Likewise, TEM images revealed the presence of V-based clusters only at the surface of impregnated samples. IR spectroscopy showed that more abundant and acidic sites were obtained by impregnation. Better catalytic performances in both selective and total oxidation reactions were achieved with V-SBA-15 and V-MCF as compared to impregnated ones, as consequence of a better V dispersion. Interestingly, higher selectivity to propene (ODH of propane, Figure 1A) was obtained with V-MCF as compared to V-SBA-15, whereas better dichloromethane conversions (Figure 1B) were achieved with V-SBA-15 instead of V-MCF (a similar trend was observed with impregnated samples). Finally, a non-porous sample V-SiO_2 with comparable V content and V species well dispersed and incorporated into the silica framework [4] was tested in the same reactions, showing a lower catalytic activity than mesoporous samples in both cases.

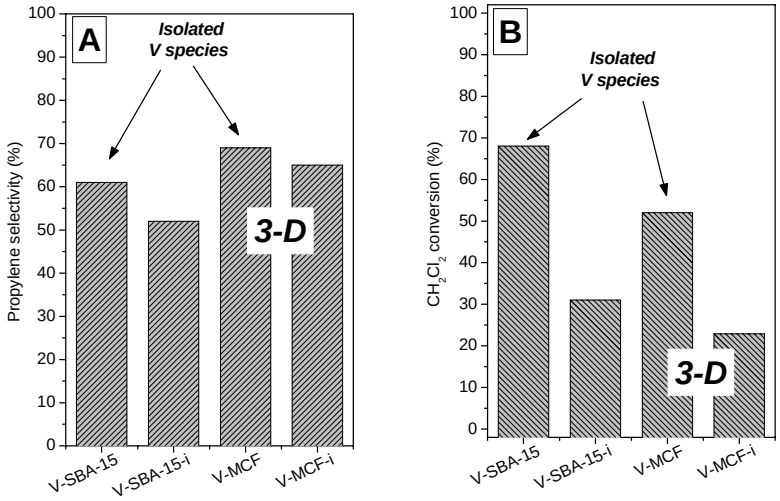

Figure 1. Catalytic results achieved with V-containing SBA-15 and MCF catalysts, the latter having a 3-D pores network: A) Selectivity to propene at iso-conversion (ODH of propane; ca. 4 % propane conv.) and B) dichloromethane conversions (total oxidation). V-contents: ca. 2.5 wt. %; aerobic conditions; TOS = 10 min.; T = 500 °C.

Conclusion

The catalytic behaviour of V-MCF and V-SBA-15 is assigned to the different porous network of the two systems. SBA-15 has monodimensional mesopores that may favour longer residence times of molecules, unlike the 3-D ultra-large pores of MCF and therefore deeper oxidations occur in SBA-15 systems. On the other hand, the lower activity of a non-porous sample (V-SiO_2) confirmed the important role of catalyst porosity in oxidation reactions.

References

[1] M. Piumetti, B. Bonelli, M. Armandi, L. Gaberova, S. Casale, P. Massiani, E. Garrone, Micropor. Mesopor. Mater. 133 (2010) 36-44.
[2] M. Piumetti, B. Bonelli, P. Massiani, S. Dzwigaj, M. Armandi, L. Gaberova, E. Garrone, Micropor. Mesopor. Mater. DOI: 10.1016/J.micromeso.2010.11.010 (2010).
[3] M. Piumetti, B. Bonelli, P. Massiani, S. Dzwigaj, I. Rossetti, S. Casale, L. Gaberova, M. Armandi, E. Garrone, Catal. Today DOI: 10.1616/j.cattod.2010.10.066 (2010).
[4] I. Rossetti, L. Fabbrini, N. Ballarini, F. Cavani, A. Cericola, B. Bonelli, M. Piumetti, E. Garrone, H. Dyrbeck, E. A. Blekkan, L. Forni, J. Catal. 256 (2008) 45-61.

Direct exfoliation of layered zeolite Nu-6(1)

P. Gorgojo[a], A. Galve[a], C. Téllez[a], J. Coronas[a]
[a]*Department of Chemical and Environmental Engineering and Nanoscience Institute of Aragon, Universidad de Zaragoza, 50018 Zaragoza, coronas@unizar.es*

Introduction

Layered materials have been investigated widely in the last years, and several materials have been delaminated as MCM-22P and PREFER obtaining ITQ-2[1] and ITQ-6[2]. There is interest in these materials because they may be good catalysts due to high surface area and easy access to pores and acid sites.
Usually delamination of layered materials is taken in two steps, first step is the swollen of the zeolite by intercalating surfactant cations between the layers, and then the second step is the extraction of the surfactant cations by ultrasounds or chemical treatment.
Nu-6(1) is a layered zeolite discovered in the beginning of the 80´s, by removing 4,4´ bipyridine template molecules Nu-6(2) is obtained. It has been reported that this zeolite can be swollen by exchanging 4,4´bipyridine by cetyltrimethylammoniun (CTA^+) or decyltrimethylammonium (DTA^+) and then extract the intercalated molecule to give the delaminated zeolite ITQ-18[3,4].

Experimental

Nu-6(1) was synthesized as described by Corma and coworkers[3]. The zeolite was synthesized with three different Si/Al ratios: 45, 90 and ∞. CTA-Nu-6(1)a was treated with CTA^+ and TPAOH at a range of pH of 9 and a temperature of 25-80ºC, afterwards it was sonicated and calcined at 580ºC. CTA-Nu-6(1)b was treated at pH 12 at room temperature, CTA-Nu-6(1)c, d and e were treated at pH 9 (given by an arginine buffer) and 80ºC. These samples were calcined at 580ºC. The conditions of the experiments are listed in Table 1.

Table 1. Exfoliation conditions for different Nu-6(1) samples.

Sample	Si/Al	Temperature (˚C)	pH	Time (h)
CTA-Nu-6(1)a	45	25-80	12.9	220
CTA-Nu-6(1)b	45	RT	12.0	16
CTA-Nu-6(1)c	45	80	8.6	26
CTA-Nu-6(1)d	77	80	9.0	26
CTA-Nu-6(1)e	352	80	9.0	26

Results and discussion

In order to know the success of the treatment with CTA^+ the degree of 4,4´bipyridine extraction was calculated for sample CTA-Nu-6(1)a being 3.9, 6.7, 13.3, and 33.7% at 40, 50, 65 and 80ºC, respectively. XRD showed a small peak at low angles indicating swelling of the material although the peak was small and that suggested a small percentage of swollen

material. The calcination of this material gave a material with a surface area of 302 m^2/g. Samples CTA-Nu-6(1)b and c did not show any peak at low angle XRD, after calcining these samples had a surface area of 292 and 272 m^2/g. This treatment did not swollen the Nu-6(1) material and the calcinations gave Nu-6(2) zeolite, this material was not exfoliated Nu-6(1) (ITQ-18) but exfoliated Nu-6(2). Conventional as-made Nu-6(2) has a surface area of 50 m^2/g [3], which suggests that the zeolite has directly been exfoliated during the treatment with CTA^+ carried out in this work. Figure 1 shows TEM pictures of exfoliated Nu-6(2).
In addition, the influence of aluminum was studied in three different Nu-6(1) samples prepared with different Si/Al ratio. This Si/Al ratio was determined by XRF being 45, 77 and 352. These samples were treated with the same process as sample CTA-Nu-6(1)c using CTA^+ giving rise to surface areas of 272, 128 and 35 m/g, respectively.

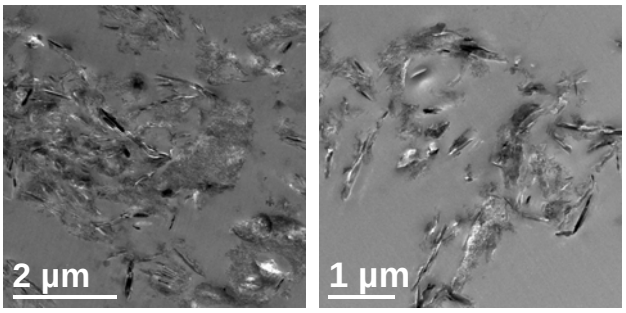

Figure 1. TEM pictures of exfoliated Nu-6(2)

Conclusions

The low bipyridine extraction observed in CTA^+ exchange at room temperature suggests that the process is controlled by the adsorption of surfactant CTA^+ and is consistent with a lack of swelling of the zeolite. Mild pH (around 9) and temperature (room temperature) conditions leading to the direct exfoliation of Nu-6(1) were identified. These exfoliation conditions produced neither the swelling of the material (since no low angle peak was observed by XRD) nor the amorphization of the solid (since upon exfoliation the calcined solid exhibited all the XRD and SAED features of Nu-6(2)). This is the reason why the obtained material, having a BET specific surface area of about 300 m^2/g, was denominated exfoliated Nu-6(2). Finally, there is a strong relationship between the exfoliation yield in terms of BET specific surface area and the Si/Al ratio of the precursor. The best results were obtained for the material with the lowest Si/Al ratio (45) which seems to favor the ion exchange interaction between the surfactant and the layered zeolite.

Acknowledgements

Financial support from the Spanish Science and Innovation Ministry (MAT2007-61028) is gratefully acknowledged. P.G. and A.G. also acknowledge their respective grants from the Spanish FPU and FPI programs.

References

[1] A. Corma, V. Fornes, S. B. Pergher, T. L. M. Maesen, J. G. Buglass, Nature 396 (1998) 353-356.
[2] A. Corma, U. Diaz, M. E. Domine, V. Fornes, J. Am. Chem. Soc. 122 (2000) 2804-2809
[3] A. Corma, V. Fornes, U. Diaz, Chem. Commun. 24 (2001) 2642-2643
[4] H. L. Zubowa, M. Schneider, E. Schreier, R. Eckelt, M. Richter, R. Fricke, Microporous Mesoporous Mater. 109 (2008) 317-326

Automated electron Diffraction Tomography (ADT) – a new technique for routine structure solution of nano-crystalline zeolites and porous materials

Enrico Mugnaioli, Ute Kolb
Institute of Physical Chemistry, Johannes Gutenberg-University, Mainz, Germany

Transmission electron microscope (TEM), providing imaging and diffraction information from the same volume, is a powerful tool to investigate nano materials where single crystal or powder X-ray diffraction fails. High resolution TEM can directly visualize structural features at atomic resolution, but demands high electron dose and may cause severe beam damage for frameworked and hydrated inorganic materials (like zeolites). In contrast, electron diffraction needs only a fraction of this electron dose and provides structural data with even higher resolution.
Normally, for a complete structure solution three-dimensional experimental data are needed. Traditionally the collection of three-dimensional diffraction data is performed by a tilt of a pre-oriented nano-crystal around a low index crystallographic axis. Diffraction patterns collected in such a way are oriented low index zones. This strongly limits the amount of accessible reflections and enhances dynamical effects, hampering the possibility of ab-initio structure solution.
Automated electron Diffraction Tomography (ADT) is a recently developed approach for electron diffraction acquisition and analysis [1, 2]. The idea is to sample the full reciprocal space inside the tilt range of the microscope goniometer avoiding in-zone patterns and using a mild illumination on the sample. The crystal is imaged and tracked during the tilt in scanning transmission mode (STEM) and nano electron diffraction (NED) patterns are collected sequentially.
Cell parameter determination, three-dimensional reconstruction of reciprocal space and intensity integration are performed automatically with the software ADT3D. Data sets collected by ADT proved to be of higher quality than the ones collected by conventional electron diffraction based on oriented patterns. Dynamical effects are so reduced that a standard kinematic approach normally delivers ab-initio the complete structural model. Coupling this technique with precession electron diffraction [3] in order to improve the spot integration, it was possible to solve complex structures from a single nanocrystal down to 50 nm in diameter [4]. Porous minerals [5], zeolites [6] and beam-sensitive metal-organic frameworks [7], even with large cells up to 30000 $Å^3$, have been solved in the last year (see Table 1) by direct methods implemented in the same software packages as used in X-ray crystallography. Examples of recently solved porous material structures will be proposed, including large cavities and doped zeolites and other porous frameworks.

Experimental

For TEM-ADT investigations samples were suspended in ethanol and sprayed onto carbon coated copper grid using a modified sonifier. The TEM work was carried out with a Tecnai F30 S-TWIN transmission electron microscope equipped with a field emission gun working at 300 kV. STEM images were collected by a FISCHIONE high angular annular dark field detector (HAADF). Nano electron diffraction patterns were acquired with a CCD camera (14-bit GATAN 794MSC).
ADT data acquisitions were performed with a FISCHIONE tomography holder and a cooled GATAN single-tilt holder. The ADT data acquisition was performed with the module

described in [1]. A mild illumination setting resulting in an electron dose rate of 10 - 15 e/Å^{2}s was used. Nano electron diffraction was performed employing a 10 μm C2 condenser aperture with a 100-50 nm beam on the sample. Precession of the beam was performed using the SpinningStar unit NanoMEGAS. The precession angle was kept at 1.2°.
The program ADT3D was used for the data processing, including 3D diffraction volume reconstruction, automated cell parameter determination, intensities integration procedures, and data visualization and validation. The ab-initio structure solution was performed by direct methods implemented in SIR2008, included in the package Il Milione [8]. A fully kinematical approach was used (intensities proportional to F_{hkl}^2), and no correction was applied to the intensity data.

Table 1. Examples of porous structures recently solved by ADT data.

Material	Space group	Cell lengths (Å)			Independent non-H atoms
		a	b	c	
Charoite-90	$P2_1/m$	32.0	19.6	7.1	90
Charoite-96	$P2_1/m$	32.1	19.8	7.2	87
Natrolite	Fdd2	18.3	18.6	6.6	10
ZSM-5	Pnma	20.1	19.9	13.4	39
ITQ-45	Ima2	17.9	22.4	13.9	41
MUF-4large	Fm3m	32.0	32.0	32.0	9
ECS-3	Cc	19.8	28.3	9.8	74

References

[1] Kolb, U., Gorelik, T., Kübel, C., Otten, M.T., Hubert, D., Towards automated diffraction tomography: Part I–Data acquisition, Ultramicroscopy, 107 (2007), 507-513
[2] Kolb, U., Gorelik, T., Otten, M.T., Towards automated diffraction tomography. Part II - Cell parameter determination, Ultramicroscopy, 108 (2008), 763-772
[3] Vincent, R., Midgley, P.A., Double conical beam-rocking system for measurement of integrated electron diffraction intensities, Ultramicroscopy, 53 (1994), 271-282
[4] Birkel, C.S., Mugnaioli, E., Gorelik, T., Kolb, U., Panthöfer, M., Tremel, W., Solution Synthesis of a New Thermoelectric $Zn_{1+x}Sb$ Nanophase and Its Structure Determination Using Automated Electron Diffraction Tomography, Journal of the American Chemical Society, 132 (2010), 9881-9889
[5] Rozhdestvenskaya, I., Mugnaioli, E., Czank, M., Depmeier, W., Kolb, U., Reinholdt, A., Weirich, T., The structure of charoite, $(K,Sr,Ba,Mn)_{15-16}(Ca,Na)_{32}[(Si_{70}(O,OH)_{180})](OH,F)_{4.0} * nH_2O$, solved by conventional and automated electron diffraction, Mineralogical Magazine, 74 (2010), 159-177
[6] Mugnaioli, E., Gorelik, T., Stewart, A., Kolb, U., "Ab-initio" structure solution of nano-crystalline minerals and synthetic materials by automated electron tomography, in Krivovichev S.V., Minerals as Advanced Materials II, Springer, Berlin Heidelberg, in print (2011)
[7] Denysenko, D., Grzywa, M., Tonigold, M., Streppel, B., Krkljus, I., Hirscher, M., Mugnaioli, E., Kolb, U., Hanss, J., Volkmer, D., Elucidating Gating Effects for Hydrogen Sorption in MFU-4 Type Triazolate-Based Metal-Organic Frameworks Featuring Different Pore Sizes, Chemistry - A European Journal, 17 (2011), 1837-1848
[8] Burla, M.C., Caliandro, R., Camalli, M., Carrozzini, B., Cascarano, G. L., De Caro, L., Giacovazzo, C., Polidori, G., Siliqi, D. & Spagna, R., IL MILIONE: a suite of computer programs for crystal strucutre solution of proteins, Journal of Applied Crystallography, 40 (2007), 609-613

n-Butene oligomerization over micro/mesoporous materials based on ferrierite

Yu.P Khitev[a]., Yu.G. Kolyagin[a], O.A. Ponomoreva[a], F.Fajula[b], I.I. Ivanova[a]
[a]*Department of Chemistry, Moscow State University, Moscow, Russia, iiivanova@phys.chem.msu.ru*
[b] *Institut Charles Gerhardt Montpellier, UMR 5253 CNRS, UM2, ENSCM, 8 Rue de l'Ecole Normale, 34296 Montpellier Cedex France*

Introduction

Oligomerization of n-butenes over solid acid catalysts is an attractive way to obtain higher olefins such as octenes. The branched octenes can be applied for gasoline blending, whereas the less branched ones can be used for the synthesis of alcohols. The latter can be further processed into diisononylphthalates, which are excellent polyvinyl chloride plasticizers. Zeolites with narrow pores (such as ferrierite) are among perspective catalysts for this processes [1]. The main drawbacks of these catalysts are rather low yield of target product and fast catalyst deactivation, which is due to intracrystalline diffusion limitations in zeolitic porous system. The aim of this contribution was to synthesize micro/mesoporous composite materials based on ferrierite, which will allow to increase the accessibility of the active sites and to increase the activity of the catalyst in this process.

Experimental

Micro/mesoporous materials with different contributions of micro- and mesoporosity were prepared by recrystallization of ferrierite with Si/Al = 34 in alkaline solution in the presence of cethyltrimethylammonium bromide following the procedure described in [2]. The materials were characterized by elemental analysis, XRD, FTIR, TEM, SEM, nitrogen adsorption-desorption, NH_3-TPD and IR spectroscopy of adsorbed pyridine.The n-butene conversion was carried out in a fixed bed reactor operated under steady state conditions at 200-300ºC and under high pressure (45 bar). The weight hourly space velocity of n-butene-1 was 2 h^{-1}. The nitrogen /n-butene-1 molar ratio was around 4.

Results and discussion

The main characteristics of the materials obtained are given in Table 1.

Table 1. Characteristics of recrystallized ferrierites

Samples	C_{NaOH} (M)	Si/Al	*Relative crystalinity**	a_{NH3}** (μmol/g)	V_{mic} (cm^3/g)	V_{total} (cm^3/g)	V_{mic}/V_{total}
H/FER	-	34	1.0	565	0.116	0.130	0.90
H/ReFER-0.8	0.43	31	1.1	670	0.106	0.131	0.81
H/ReFER-0.5	0.8	33	0.77	549	0.105	0.180	0.51
H/ReFER-0.3	1.2	31	0.70	466	0.066	0.226	0.29
H/ReFER-0.1	1.8	31	0.36	277	0.045	0.356	0.13

* - estimated from the intensity of the diffraction peak at 2θ of 9.44 using the parent ferrierite as a reference
** - concentration of acid sites determined by NH_3 TPD

The different degree of recrystallization was achieved by varying of NaOH concentration. The relative crystallinity increased slightly for the sample obtained after recrystallization under moderate alkalinity (Table 1). This effect was likely to be due to the dissolution of some amorphous phase contained in the parent ferrierite and/or to the recovery of some ferrierite phase due to the healing of defects in the zeolite framework. Further increase of the alkalinity led first to partial and then to complete transformation of ferrierite into MCM-41 followed by a gradual decrease of the amount and strength of the acid sites. At the same time, the accessibility of the Brønsted acid sites for pyridine increased drastically (Fig. 1). In the parent ferrierite only 22% of the total number of Brønsted acid sites was available for pyridine. The increase of the degree of recrystallization led to the increase of the accessibility up to 97% for H/ReFER-0.1.

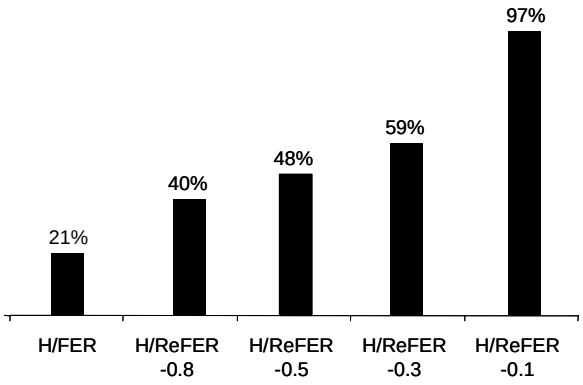

Figure 1. Contribution of Brønsted acid sites accessible for pyridine

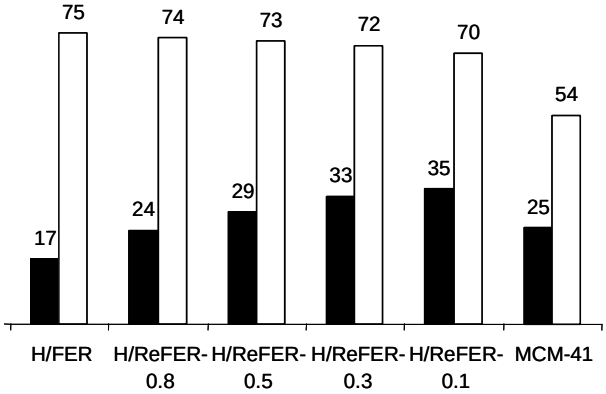

Figure 2. Conversion of n-butene ■ and selectivity to octenes □ at 250°C

The increase of the accesibility of the acid sites was followed by the gradual increase of the catalyst activity in n-butene oligomerization (Fig. 2). n-Butene conversion increased from 17% for parent ferrerite to 35% observed for H/ReFER-0.1 at 250°C. On the contrary, the selectivity to octenes did not change significantly. All recrystallized materials showed better catalytic performance with respect to both parent ferrierite and MCM-41 mesoporous material. However the best result was achieved over H/ReFER-0.1 with the most open porous structure.

Acknowledgements
The authors thank Total S.A. for the financial support. Yu. Khitev thanks Haldor Tøpsoe A.S. for PhD fellowship.

Conclusions
Micro/mesoporous materials obtained by recrystallization of ferrierite showed improved catalytic properties in n-butene oligomerization with respect to both parent ferrierite and MCM-41 mesoporous material. The effect is due to enhanced accessibility of the active sites and easier transport of bulky molecules provided by mesopores. The best catalytic performance was achieved on composite materials with high degree of recrystallyzation.

References
[1] Klepel, O., Loubentsov, A., Böhlmann, W., Papp, H., Oligomerization as an important step and side reaction for skeletal isomerization of linear butenes on H-ZSM-5. Applied Catalysis A: General 255 (2003) 349–354.
[2] Ordomsky, V.V., Murzin, V.Y., Monakhova, Yu.V., Zubavichus, Y.V., Knyazeva, E.E., Nesterenko, N.S., Ivanova, I.I., Nature, strength and accessibility of acid sites in micro/mesoporous catalysts obtained by recrystallization of zeolite BEA. Microporous and Mesoporous Materials 105 (2007) 101–110.

NMR studies on various cation forms of the natural zeolite natrolite with a complete degree of Si-Al order in hydrated and dehydrated states

Min Bum Park[(1)], Suk Bong Hong[(1)], Aurélie Vicente[(2)] and Christian Fernandez[(2)*]

(1) Department of Chemical Engineering and School of Environmental Science and Engineering, POSTECH, Pohang 790-784, Republic of Korea, sbhong@postech.ac.kr

*(1) Laboratoire Catalyse et Spectrochimie, Ensicaen, Université de Caen, CNRS, 6 bd du Maréchal Juin, 14050 Caen, France, email: *christian.fernandez@ensicaen.fr*

Introduction

Zeolites are microporous crystalline materials with wide variety of applications, *e.g.*, adsorption, ion exchange, catalysis... With natural zeolites being discovered more than 200 years ago, intensive research is nowadays aimed at developing new synthetic zeolites with tailored properties for specific task. In a given zeolite lattice, the replacement of tetravalent Si atoms by trivalent Al or Ga atoms places negative charges on the framework, which should be compensated by non-framework cations. These charge-compensating cations are loosely held in the pores of a zeolite and can be exchanged by other cations, making zeolites good cation exchangers. Therefore, zeolites are useful in water softening, nuclear wastes removal, and gas storage. Additionally, they can discriminate between molecules of different sizes and shapes. This ability legitimates their consideration as "molecular sieves" and has been the basis for many applications in current catalysis and separation technologies.

Natrolite is one of the first natural zeolites which have been reported in the literature by the early 1800's. It is also one of the first zeolites of which crystal structures have been established early on by 1930's by Pauling and Taylor. Nonetheless, its unique chemical and structural characteristics have continued to be discovered up to date, probably due to the flexible connectivity of the NAT topology. Pressure, as well as temperature, has been shown to alter the structure and the composition, in many cases, in unprecedented ways.
The aim of the work presented here is to gain detailed insights into the non-equivalent tetrahedral sites (T-sites) in hydrated and dehydrated forms of various extra-framework cation-exchanged natural natrolite to better understand the performance of these materials.

Results and discussion

Magic-angle-spinning (MAS) NMR spectroscopy of ^{27}Al and ^{29}Si has proven to be a powerful tool to reveal the chemical environment of the tetrahedral framework atoms in aluminosilicate zeolites. In this work, high resolution MAS NMR and 2D NMR correlation techniques have been used to determine the silicon-aluminum orderings in the zeolite framework. In particular, 2D multiple-quantum (MQ) and satellite (ST) MAS NMR spectroscopies strongly improve the resolution of the ^{27}Al NMR spectrum (fig 1f-g), due to the averaging of the second-order quadrupolar interaction effects. Additionally, these high-resolution MQMAS and STMAS techniques were also combined with ^{29}Si MAS NMR to produce highly resolved correlation spectra of the studied samples.

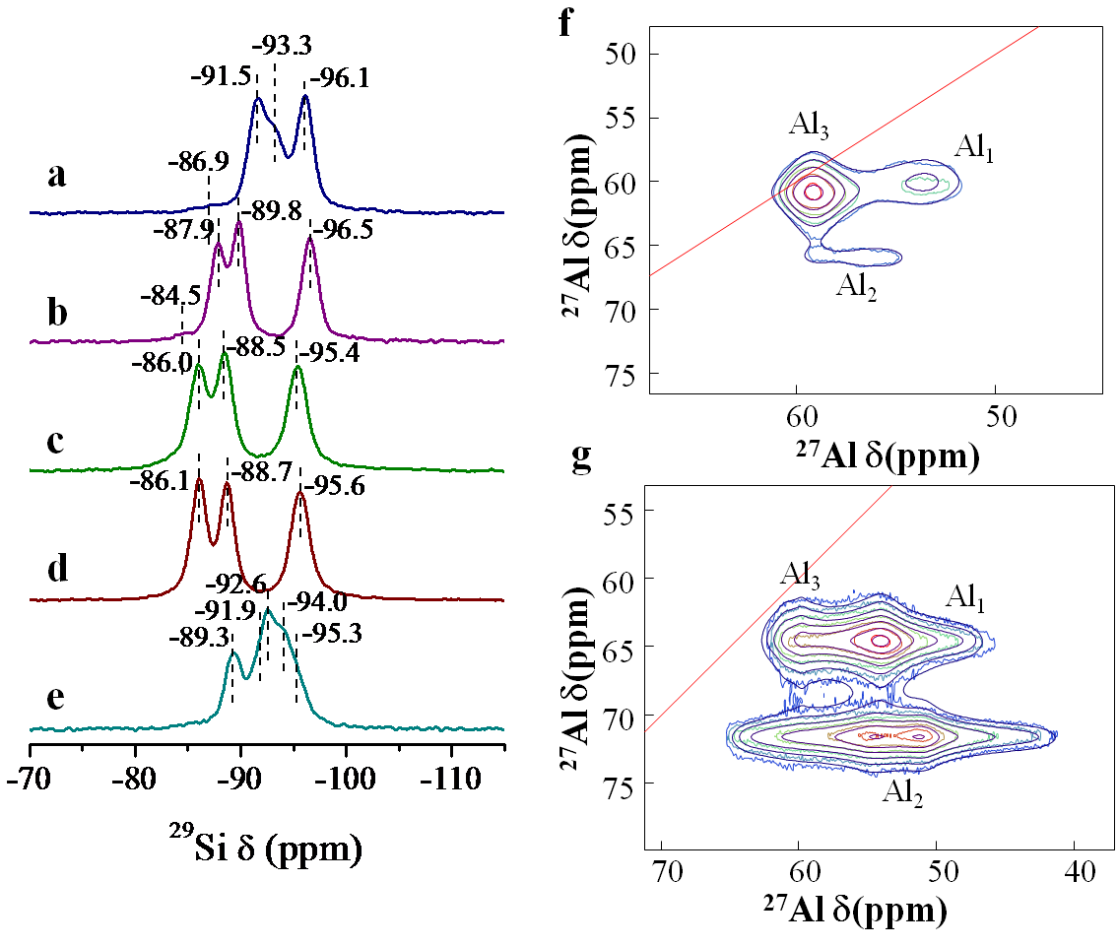

Figure 1: NMR spectra of hydrated samples : ^{29}Si MAS NMR of a)Ba-NAT, b) Sr-NAT, c) Ca-NAT, d) Scolecite, e) Mg-NAT, and ^{27}Al Double-Quantum Filtered-STMAS NMR of f) Ba-NAT and g) Ca-NAT

Conclusions

The results obtained by a combination of these NMR techniques, in comparison with XRD data, lead to very precise information to understand the arrangement of the various non-equivalent T atoms in the various exchanged samples.

Particular characteristics of Ag-exchanged LTL zeolite in K and H form

R. Bartolomeu[a,b], R. Bértolo[a], S. Casale[c], A. Fernandes[a], C. Henriques[a], P. Da Costa[b], M. F. Ribeiro[a]
[a]*Instituto Superior Técnico, Institute for Biotechnology and Bioengineering, Centre for Biological and Chemical Engineering, Av. Rovisco Pais, 1049-001 Lisboa, Portugal, filipa.ribeiro@ist.utl.pt*
[b]*Université Pierre et Marie Curie, CNRS UMR 7190, 78210 Saint Cyr l'École, France*
[c]*Université Pierre et Marie Curie, CNRS UMR 7197, 75252 Paris, France*

Introduction

Zeolite L possesses a LTL framework with characteristic one-dimensional 12-membered oxygen rings with a diameter of 7.1 Å. It has been extensively studied since the discovery of the remarkable selectivity of Pt/KL catalyst for hexane aromatization [1]. More recently, zeolite L has proven to be an ideal host material for the supramolecular organization of molecules, complexes and clusters [2].
On the other hand, Ag-exchanged zeolites have been reported to be active in the photocatalytic decomposition of NO or N_2O as well as in the *de*NO_x reaction [3]. They can also be used as antimicrobial agents [4] or in methane activation.
Two L zeolite samples, one in basic form (KL) and other in acid form (HL) were ion-exchanged with Ag in order to study the characteristics of silver particles and the effect of the presence of either H^+ or K^+ in the zeolite.

Experimental

Commercial KL zeolite with Si/Al = 3 was provided by *UOP*. HL zeolite was prepared by ion exchanging KL zeolite with a NH_4NO_3 solution and calcined under air at 500 ºC for 8 h.
Ag/HL and Ag/KL zeolites were prepared by ion-exchange with an $AgNO_3$ solution under standard conditions. Then, the samples were calcined as described above.
Zeolites were characterized by X-Ray Diffraction (XRD), Temperature Programmed Reduction (H_2-TPR), *in situ* diffuse reflectance UV-Vis at several temperatures under air and H_2, High Resolution Transmission Electron Microscopy and Temperature Programmed Desorption of NO (NO-TPD).

Results and discussion

Silver content in Ag/KL and in Ag/HL zeolites was determined by ICP analysis and was found to be 5.2 and 4.5 (wt.)%, respectively. XRD showed that both zeolites retained its crystallinity after ion-exchange with Ag.
H_2-TPR (Fig. 1) showed, contrarily to results reported in the literature for Ag-exchanged ZSM-5 zeolites [3], only one reduction peak for Ag/KL and Ag/HL. Moreover, the reduction peak of Ag/HL appears at a much higher temperature than that of Ag/KL.
DRS UV-Vis analysis (Fig. 1) revealed that after heating under air at 500 ºC both zeolites presented an absorption band around 225 nm, which corresponds to Ag^+ in the zeolite exchange sites, but Ag/KL had a large band from about 330 nm up to 800 nm which can be ascribed to Ag partially charged clusters ($Ag_n^{\delta+}$) and Ag metallic clusters (Ag_m). However, Ag absorptions in Ag-exchanged zeolites have only been reported up to 500 nm. On the other hand, after heating under H_2 at 500 ºC, although both zeolites presented absorption bands

above 330 nm, Ag/KL exhibited a much stronger absorption band than Ag/HL. This confirms the different reducibility of the Ag species present on both zeolites.

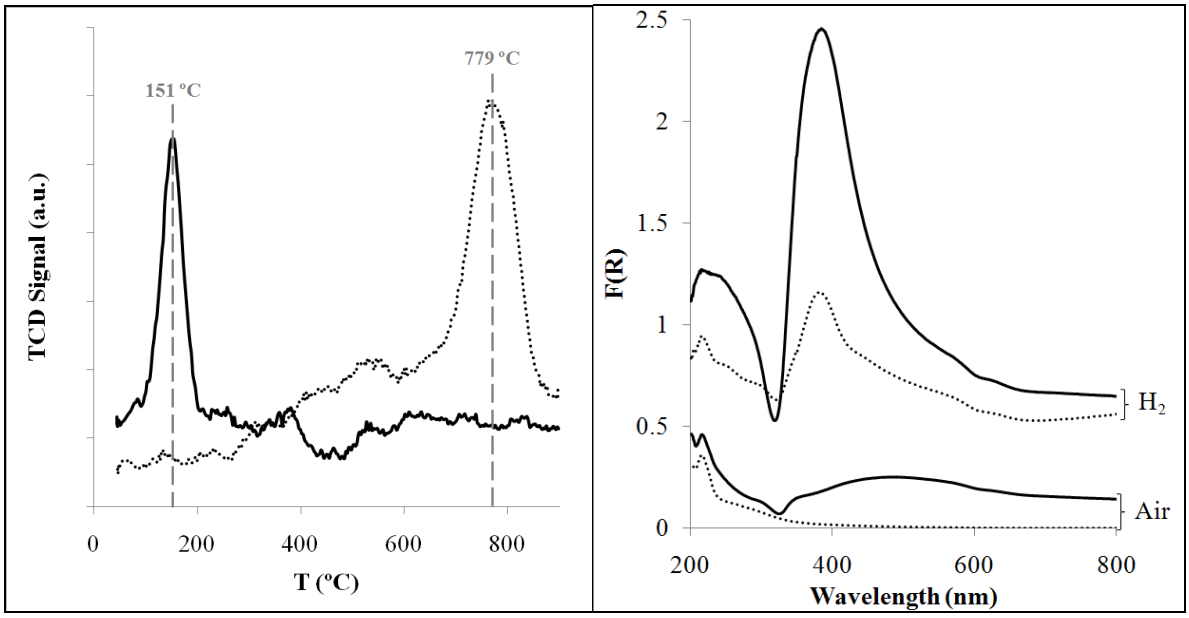

Figure 1. H_2-TPR profile (left) and UV-Vis spectra (right) of Ag/KL (—) and Ag/HL (.....).

HR-TEM showed the presence of Ag nanoparticles with a mean diameter of 2 ± 1 nm on Ag/KL and 4 ± 2 nm on Ag/HL. Therefore, the presence of K^+ instead of H^+ promotes the formation of smaller Ag particles. Inter-reticular plane measuring seems to indicate that these particles correspond to Ag^0. NO-TPD also evidenced striking differences between both zeolites concerning NO desorption peaks.

Conclusions

Ag-exchanged L zeolite presents different features when compared with other Ag-exchanged zeolites studied in the literature. Moreover, the presence of either K^+ or H^+ affects the type of Ag species and the size of Ag particles as showed by H_2-TPR, *in situ* diffuse reflectance UV-Vis and HR-TEM. Therefore, these two cations can be used to tune the Ag species present on Ag-exchanged L zeolites according to the desired application.

Acknowledgements

The authors wish to thank to FCT (Portugal) for financial support (grant number SFRH/BD/44108/2008 and project number PTDC/EQU-ERQ/102771/2008).

References

[1] Derouane, E.G., Vanderveken, D.J., Structural recognition and preorganization in zeolite catalysis: Direct aromatization of n-hexane on zeolite L-based catalysts, Applied Catalysis, 45 (1988), L15-L22
[2] Brühwiler D., Calzaferri G., Torres T., Ramm J.H., Gartmann, N., Dieu, L.-Q., López-Duarte, I., Martínez-Díaz, M.V., Nanochannels for supramolecular organization of luminescent guests, Journal of Materials Chemistry, 19 (2009), 8040-8067
[3] Shibata, J., Shimizu, K.-i., Takada, Y., Shichi, A., Yoshida, H., Satokawa, S., Satsuma, A., Hattori, T., Structure of active Ag clusters in Ag zeolites for SCR of NO by propane in the presence of hydrogen, Journal of Catalysis, 227 (2004), 367-374
[4] Rai, M., Yadaw, A., Gade, A., Silver nanoparticles as a new generation of antimicrobials, Biotechnology Advances, 27 (2009), 76-83

Development of porous carbon derived from polybenzoxazine and its application as an electrode for supercapacitors

Thanyalak Chaisuwan, Nuntiya Mahingsupan, and Sujitra Wongkasemjit
The Petroleum and Petrochemical College and the National Center of Excellence for Petroleum, Petrochemicals, and Advanced Materials, Chulalongkorn University, Bangkok 10300, Thailand, Corespondence Email: thanyalak.c@hotmail.com

Introduction

Novel porous carbon was prepared by using polybenzoxazine, a new type of phenolic resins, through a sol-gel process before carbonization in an inert atmosphere at 800°C. The BET surface area of the resulting porous carbon was approximately 360 m^2/g. The activation of this porous carbon was also investigated in order to compare the physical and electrochemical properties. The BET surface area of the activated porous carbon was increased more than twice in comparison with that of the unactivated porous carbon. The electrochemical behaviors were studied by cyclic voltammetry, galvanostatic charge-discharge, and electrochemical impedance spectroscopy. The results showed that the polybenzoxazine-based porous carbon exhibited good electrochemical performance. The best electrochemical behaviors with the specific capacitance of 109 F/g were obtained from the electrode prepared from porous carbon which underwent heat treatment at 300 °C in air.

Experimental

Porous polybenzoxazine was prepared through a sol-gel process by using bisphenol-A, formaldehyde, and triethylenetetramine (TETA) as a precursor for porous carbon. The porous carbon electrodes were fabricated and then heat treated at 300°C in air for 120 min to modify the electrode surface and to improve affinity with the electrolyte. Activated porous carbón was prepared by carbonization of as-prepared porous carbon with carbon dioxide at 900°C for 180 min.

Results and discussion

The surface characteristics of resulting porous carbons derived are listed as follows:

Parameter	Porous Carbon	Heat-treated Porous carbon	Activated Porous Carbon
BET surface area (m^2/g)	360	372	910
Total pore volume (cm^2/g)	0.24	0.25	0.54
Average pore size (nm)	2.69	2.65	2.40
*Mesoporosity (%)	54.2	44.0	31.5
*Microporosity (%)	58.3	64.0	74.1

*Mesoporosity = (mesopore volume/total pore volume) × 100

*Microporosity = (micropore volume/total pore volume) × 100

The activated porous carbon had large amount of micropores along with high surface area, gave higher specific capacitance than non-activated sample. The reason is that the polybenzoxazine derived porous carbon activated at 900 °C under carbon dioxide had the average pore diameter approximately of 2.40 nm, which was large enough to be accessible electrochemically for aqueous electrolyte to establish the electrical double layer. However, the heat-treated porous carbon at 300 °C in air yielded the highest specific capacitance caused by its low micropore fraction, suitable pore size for electrical double layer formation and its pseudocapacitive behavior, originated from surface functional group on carbon aerogel surface, which built up during the heat treatment at 300°C in air. Generally, the higher the specific surface area of the activated carbon, the higher the ability for charge accumulation, resulting in the higher the specific capacitance of the carbon electrodes. But in fact, it is much more complicated. The nature and the porosity of the precursor also play important roles for the charge accumulation.

Conclusions

Novel porous carbon was successfully synthesized via ambient drying by using polybenzoxazine as a precursor. All porous carbon electrodes showed good electro-chemical performances. The specific capacitance of the electrode fabricated from activated carbon porous carbon was higher than that derived from the non-activated one due to its high useable surface area for electrical double layer formation. However, the heat-treated porous carbon electrode showed the best specific capacitance due to its pseudocapacitive behaviors.

Acknowledgements

Authors would like to thank the assistance of the following funding agencies for financial supports.

· National Center of Excellence for Petroleum, Petrochemicals and Advanced Materials
· Thailand Research Fund
· The Rachadapisake Sompote Research Funds, Chulalongkorn University

References

[1] Lorjai, P., Chaisuwan, T., Wongkasemjit, S., Porous structure of polybenzoxazine-based organic aerogel prepared by sol–gel process and their carbon aerogels, Journal of Sol-Gel Science and Technology, 52 (2009), 56-64.

[2] Katanyoota, P., Chaisuwan, T., Wongchaisuwat, A., Wongkasemjit, S., Novel polybenzoxazine based-carbon aerogel electrode for supercapacitors, Material Science and Engineering B, 167 (2010), 36-42.

[3] Hwang, S.W. and Hyun, S.H. Capacitance control of carbon aerogel electrode, Journal of Non-Crystalline Solids, 347 (2004) , 238-245.

[4] Li, J., Wang, X., Wang, Y., Huang, Q., Dai, D., Gamboa, S., and Sebastian, P.J. Structure and electrochemical properties of carbon aerogels synthesized at ambient temperatures as supercapacitors., Journal of Non-Crystalline Solids, 354 (2008), 19-24.

Study of disordered zeolite structures by TEM

Tom Willhammar [a]*, Farlán Taborda [b], Peter Oleynikov [a], Xiaodong Zou [a]
[a] *Berzelii Center EXSELENT on Porous materials and Inorganic and Structural Chemistry, Department of Materials and Environmental Chemistry, Stockholm University, SE-106 91 Stockholm, Sweden*
[b] *Environmental Catalysis Research Group, Universidad de Antioquia, SIU, Cra. 53 No. 61-30, Medellín, Colombia*
** tom.willhammar@mmk.su.se*

Introduction

Zeolites have played a significant role in the development of the modern society. It has been widely used as catalysts, adsorbents, medium for gas separation etc. Knowledge about the structure is crucial in order to get better understand of the properties. A majority of the zeolites have ordered structures and can be solved by conventional methods. There are however numerous zeolites with disordered structures which demand more complex routes for structure solution. Transmission electron microscopy is an important technique for studying disorderd zeolite structures. Here we use the disordered zeolite beta structure as a type material [1, 2]

Results and discussion

Zeolite beta is heavily disordered and is built up of a mixture of two twin components stacked in a disordered manner throughout the crystal, see Figure 1a. When studied using diffraction techniques (such as X-ray or electron) the disorder gives rise to diffuse scattering. All spots with index *3n 3m l* stay sharp whereas other spots are broadened along the ***c****-axis and form streaks, see Figure 1b. High resolution electron microscopy (HRTEM) is very powerful technique especially when it comes to study disordered structures and defects. The images provide the possibility to study the local projected potential distribution. However, in contrast to diffraction data, it remains a technique for local information and will not reveal structure information representative for the whole crystal.

The intensity distribution along the diffusely scattered lines is related to the stacking sequence of the structure. By gaining more knowledge about this relationship, information about the disordered structure can be attained from the diffraction data. The first step of this study is to understand the diffuse scattering and its origin; this has been done by simulations of diffraction. The simulations have been made either with a kinematical approximation using the software DIFFaX [4] or by using the multislice method for calculations of dynamical electron diffraction.

Kinematical simulations for stacking sequences with different stacking sequences have different intensity distributions as can be seen in Figure 2. Most peaks coincide well with the experimental data from a sample of zeolite beta with an approximate content of 68% polymorph A type stacking, estimated from deconvolution of PXRD data. There is however one major peak in the experimental pattern that is not present in the simulated data, found at $l \approx \pm 3$. This peak is however present in the simulated diffraction pattern including dynamical scattering using multislice simulations, see Figure 1c. This indicates that the multislice simulations are well in accordance with the dynamical scattering and can be used for further analyses of the diffuse scattering.

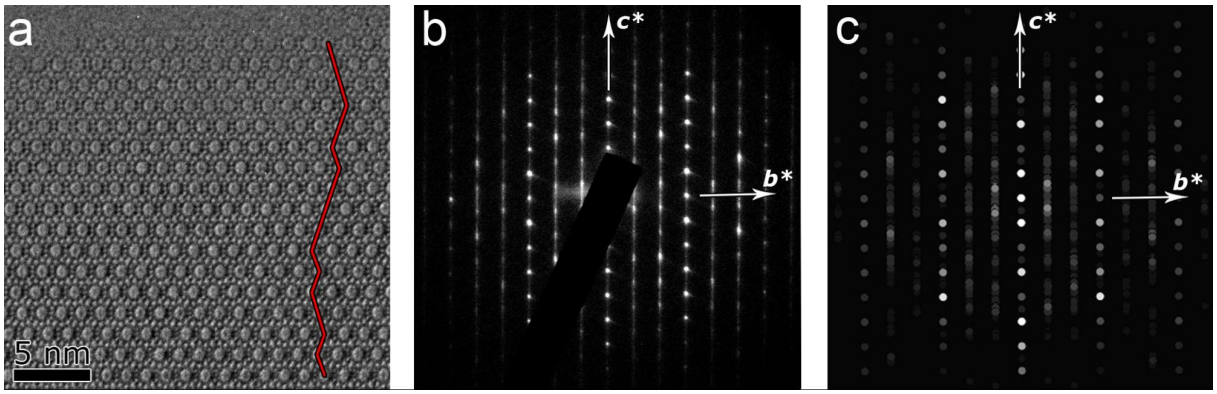

Figure 1. a) HRTEM image of zeolite beta taken along the $[100]_A$ direction. b) Selected area electron diffraction pattern taken along the same direction. c) Diffraction pattern simulated with the multislice method viewed along the $[100]_A$ direction.

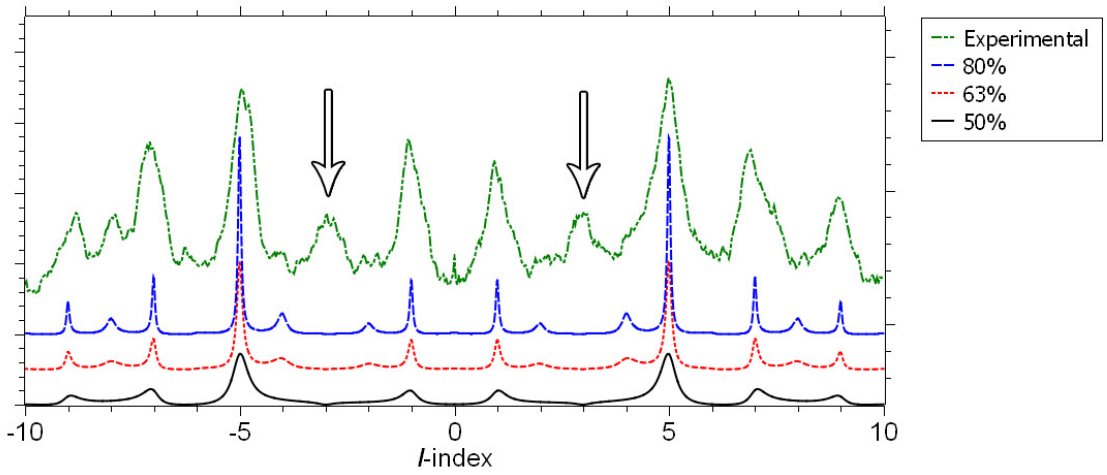

Figure 2. Electron diffraction intensity profiles simulated using DIFFaX. The intensity profles along the $(0\ 2\ l)_A$ line are plotted for stacking sequences with 50%, 68% and 80% polymorph A type stacking. Experimental data with an estimated content of 68% A-type stacking shown on top. Peaks assigned to the dynamical scattering are marked with arrows.

Conclusions

There are numerous of disordered zeolites that need a more detailed understanding. HRTEM and electron diffraction are important techniques for studying the disordered structures.. Gaining more knowledge about the diffuse scattering will help us in the study of these structures. In order to create a better understanding of the diffuse scattering, we have studied first which features of the scattered intensities that carries direct structural information and then the relationship between the structural features and the diffuse scattering.

References

[1] J.M. Newsam, M.M.J. Treacy, W.T. Koetsier and C.B.D. Gruyter, Structural characterization of zeolite beta, Proc. R. Soc. London, Ser. A, 420 (1988) 375.
[2] J.B. Higgins, R.B. LaPierre, J.L. Schlenker, A.C. Rohrman, J.D. Wood, G.T. Kerr and W.J. Rohrbaugh, The framework topology of zeolite beta, Zeolites, 8 (1988) 446.
[3] Treacy M.M.J.; Newsam J.M.; Deem M.W. A General Recursion Method for Calculating Diffracted Intensities from Crystals Containing Planar Faults Proc. R. Soc. London, Ser. A 433 (1991), 499-520

Selectivity of Pt catalysts containing AlSBA-15 in 1-methylnaphthalene hydrogenation

Karolina Jaroszewska[1]*, Jolanta R. Grzechowiak[1], Aleksnadra Masalska[1], Jacek Grams[2]
Wrocław University of Technology, Faculty of Chemistry, Gdańska 7/9, 50-344 Wrocław, Poland
2Technical University of Łódź, Institute of General & Ecological Chemistry, Żeromskiego 116, 90-924 Łódź, Poland
**Corresponding author: karolina.jaroszewska@pwr.wroc.pl*

Introduction

Considering the quality of diesel oil (low polyaromatics content, high cetane number), it is essential to improve the activity of the catalysts being elaborated not only for aromatic hydrocarbons hydrogenation but also for ring opening. In the case of 1-methylnaphtalene (1-MeN) conversion, it has been found that to maximize the cetane number, it is preferable to use catalysts with a high selectivity towards *cis*-decalins (thermodynamically less stable) [1]. Noble metals supported on MCM-41 mesoporous materials have been successfully tested in the naphthalene hydrogenation/hydrodecyclization [2]. Since SBA-15 stability is much higher than MCM-41 [3], there is an interest to investigate SBA-15 as a support for catalyst devoted to hydrotreating processes. Aluminium substituted SBA-15 materials could be chosen as a catalysts support for moderate acidic-catalyzed reactions. In this work, we report the application of Pt/AlSBA-15 for catalytic conversion of 1-MeN. Our study is focused on assessing the effect of Pt content on the selectivity towards *trans*- and *cis*-decalins. The results for Pt/AlSBA-15 are discussed and compared with those for Pt/Al_2O_3 which is used in the hydrogenation of aromatics.

Experimental

AlSBA-15 samples were synthesized by the methodology described elsewhere [4]. Mesostructured materials with the Si/Al=20 ratio were obtained using aluminium sulphate. The AlSBA-15 was mixed with a binder (20 wt.% of AlO(OH) – Pural KR-1), impregnated with the Pt precursor solution and then shaped into pellets. Platinum was incorporated by the incipient wetness method using an aqueous solution of $H_2PtCl_6.6H_2O$. Catalysts containing 1.2; 3.0 and 5.0 wt.% of platinum were denoted as Pt/AlSBA-15, 3Pt/AlSBA-15 and 5Pt/AlSBA-15, respectively.
X-ray diffraction (Siemens 5005 CuK_α), N_2 adsorption at 77 K (Autosorb-1C; Quantachrom), ^{29}Si MAS NMR (AC 200; Bruker), scanning electron microscopy (JEOL 1200 EX), TOF-SIMS, and IR-Py were used for catalysts characterization. Pt dispersion was determined by the H_2-O_2 titration method. Activity and selectivity of the Pt/AlSBA-15 catalysts were tested in the hydrogenation of 1-MeN in a fixed-bed lab-scale microreactor, at 200-350^{o}C, atmospheric pressure and W/F = 0.8 g·s/cm^3. Prior to catalytic tests, the sample was reduced in hydrogen flow at 350^{o}C (1 h) and 400^{o}C (0.5 h).

Results and discussion

XRD patterns show that the AlSBA-15 catalysts are characterized by a well ordered structure; the N_2 isotherm is typical of mesoporous structures (type IV). AlSBA-15 have a surface area of 875 m^2/g, a mean pore diameter (BJH method) of 1.3 nm, a pore volume of 1.26 cm^3/g, and a total acidity of 0.21 mmolNH_3/g. The physical properties of alumina are as follows: surface

area, 296 m^2/g; mean pore diameter (BJH method), 4.9 nm; pore volume, 0.39 cm^3/g, and total acidity, 0.39 mmolNH_3/g.
The results show that AlSBA-15-supported Pt catalysts are more active in 1-MeN hydrogenation than is the Pt/Al_2O_3 catalyst (Fig.1a). At lower reaction temperature, 1-MeN conversion over Pt/Al_2O_3 is by 15% lower than over Pt/AlSBA-15 (Fig. 1a). At higher temperature Pt/Al_2O_3 is almost inactive; over Pt/AlSBA-15, conversion totals 70%. The test also included 5Pt/AlSBA-15(results not shown). The results of catalysts selectivity at 200 and 240^{o}C are shown in Figs. 1b and 1c. The products obtained over Pt/Al_2O_3 contain methyltetralins. The yield of methyldecalins in the hydrogenation products obtained over Pt/AlSBA-15 increases with platinum content. The increase in the Pt amount, however, is concomitant with the decrease in the *cis-/trans*-methyldecalins ratio. The differences in the selectivity between the catalysts in the isomerization reaction decrease with the rise in reaction temperature, amounting to 0.60 and 0.30 for catalysts containing 1.2 wt.% and 3 wt.% Pt at 200^{o}C, respectively.

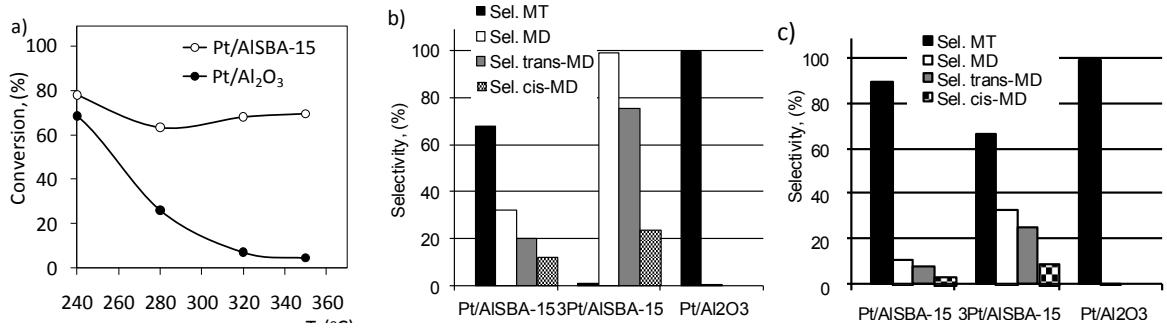

Figure 1. Catalyst activity in 1-MeN hydroconversion: conversion (a), selectivity at 200 ^{o}C (b), selectivity at 240 ^{o}C (c); (MD = methyldecalins, MT = methyltetralins).

Conclusions

Our results show that, at the low temperature (200 and 240^{o}C), regardless of the platinum amount, 1-MeN conversion over Pt/AlSBA-15 is higher than that over Pt/Al_2O_3. In contrast to Pt/SBA-15, the products obtained over Pt/Al_2O_3 contain a low amount of methyldecalins. The content of methyldecalins in the products of hydrogenation over Pt/AlSBA-15 increases with the increase in the Pt amount. However, the increase in the metal/acid ratio of the Pt/SBA-15 catalysts is concomitant with the decrease in the *cis-/trans*-methyldecalins ratio. One of the reasons for difference between activity of the Pt/SBA-15 and Pt/Al_2O_3 is the variety of Pt distribution.

Acknowledgements
The financial support by the Ministry of Science and Higher Education is gratefully acknowledged (1 T09B 073 30).

References

[1] Dokjampa, S., Rirksomboon, T., Osuwan, S., Jongpatiwut, S., Resasco, D.E., Comparative study of the hydrogenation of tetralin on supported Ni, Pt, and Pd catalysts, Catal. Today, 123 (2007), 218-223
[2] Jacquin, M., Jones, D.J., Roziere, J., Jimenez-Lopez, A., Rodríguez-Castellón E., Trejo-Menayo, J.M., Lenarda, M., Storaro, A., Vaccari, J., Cetane improvement of diesel with a novel bimetallic catalyst, J. Catal. 228 (2004), 447-459
[3] Zhao, E., Feng, J., Huo, Q., Melosh, N, Fredrickson, G.H., Chmelka, B.F., Stucky G.D., Triblock Copolymer Syntheses of Mesoporous Silica with Periodic 50 to 300 Angstrom Pores, Science, 279 (1998), 548-552
[4] Roth, W.J., Vartuli, J., Synthesis of mesoporous molecular sieves, Stud. Surf. Sci. Catal., 157 (2005), 91-110

Analysis of Si- and Al- related defects sites in micro- and micro-mesoporous high-silica zeolites. Effect on selectivity and durability in MTH

Petr Sazama[1*], Blanka Wichterlova[1], Jiri Dedecek[1], Zdenka Tvaruzkova[1], Luisa Palumbo[2]
[1]*J. Heyrovský Institute of Physical Chemistry, Academy of Sciences of the Czech Republic, CZ-182 23 Prague 8, Czech Republic, [*]email: petr.sazama@jh-inst.cas.cz*
[2]*Dipartimento Chimica IFM - NIS Centre of Excellence, Università di Torino, via P. Giuria 7, I-10125 Torino, and INSTM, Research Unit of Torino, Italy*

Introduction

The activity of high-silica zeolites related to highly acidic bridging groups and the shape selectivity effect enables processing of cracking reactions, isomerisation, alkylation, MTH etc. with high selectivity at high levels of conversion. Although, linear relationship has been found for concentration of strong acid sites and conversion, e.g. in cracking of paraffins, catalytic processes are of high complexity and others structural parameters participate in reactants transport, activation and transformation[1-4]. Both the commercial and those H-ZSM-5 synthesized in the laboratory, with highly regular XRD structure and well-developed micropore volume, often contain in the framework low concentration of Al- and Si-related defective sites. The Al-related defects form various Lewis sites, namely of the extra-framework and framework Al electron acceptor site types. Beside framework Si atoms in regular Td coordination, the Si-related defects represented by internal silanols form the less ordered environment compared to that of the ideal zeolite structure.

This study has attempted to analyse the local structures and the reasons for the "reversible" and "irreversible" formations of perturbation of the regular framework. The impact of the presence of Al atoms at various crystallographic sites and the local density of Al atoms in the framework (population of the [Al–O–(Si–O)$_n$–Al] sequences) is analysed in ZSM-5 and BEA zeolites[1,2]. Defect sites in micro-mesoporous ZSM-5 are analysed with respect to the various ways for introduction of mesopores into the micropore structure[4]. Recent progress in methodology has been employed in analysis of the structure of zeolite by high-resolution 2D (3Q) ^{27}Al MAS NMR, ^{29}Si MAS NMR and FTIR spectra of OH groups and molecular probes measured at low temperature (20 K). The effect of low concentration of Si- and Al- related framework perturbations (defects) in the regular framework of small crystals of microporous and micro-mesoporous H-ZSM-5 on their activity, selectivity and life-time is analysed in methanol transformation to hydrocarbons.

Experimental

The concentration of [Al–O–(Si–O)$_1$–Al] sequence in the framework and extra-framework Al were analysed by ^{29}Si MAS NMR high-power decoupling experiments. The concentration of [Al–O–(Si–O)$_2$–Al] and [Al–O–(Si–O)$_{n>2}$–Al] sequences in the framework was determined from the exchange capacity for Co(II) ions and quantitative analysis of d–d transitions of bare Co(II) ions in the UV-Vis spectra of the dehydrated CoNa-zeolites. Al siting in the T positions of the framework was analysed using high resolution ^{27}Al 3Q MAS NMR spectroscopy carried out on a Bruker Avance 500 MHz Wide Bore spectrometer. FTIR spectra of OH groups and C≡N groups of adsorbed d_3-acetonitrile and nitrogen sorption measurements were employed to identify the structure and content of Td Al atoms in the framework connected with structural Si-OH-Al groups, of perturbed framework Al atoms, Al-OH groups, Al-Lewis electron acceptor sites, and internal and external Si-OH groups in micro- and micro-mesoporous ZSM-5 and BEA zeolites. The methanol transformation was carried out in a fixed-bed through-flow reactor typically at 370°C and WHSV of 20 h^{-1}.

Results and discussion

The structure of ZSM-5 and BEA zeolites was analysed with an attempt to understand the stability of the framework and origin of the framework defects. The regularity of the framework and the formation of Al-OH and internal silanols, perturbed Td coordinated framework Al atoms and Lewis sites were analysed with respect to (i) the population of [Al–O–(Si–O)$_n$–Al] sequences in the framework, (ii) siting of Al atoms in the individual crystallographic sites and (iii) the procedures for incorporation of mesopores into the microporous structure.

(i) The effect of concentration of Al atoms in Al-O-(Si-O)$_2$-Al and Al-O-(Si-O)$_{n>2}$-Al sequences in the framework on stability of the framework of BEA zeolites with similar Si/Al ratios is demonstrated. The framework of BEA with high concentration of Al atoms in Al-O-(Si-O)$_2$-Al sequences exhibits higher stability compared to that with prevailing concentration of Al in the Al-O-(Si-O)$_{n>2}$-Al sequences. The Al-O-(Si-O)$_{n>2}$-Al sequences in the framework of BEA zeolites are easily perturbed already during detemplating and result in the formation of the framework Al Lewis sites and the extra-framework Al.

(ii) The analysis of the relation between perturbation of the framework and siting of Al atoms in the individual crystallographic sites of ZSM-5 zeolites shows that the Al siting represents a key parameter controlling formation of electron acceptor acid sites. This is the first experimental evidence that the Al siting in different crystallographic sites can affect properties of zeolite catalyst. As the Al siting in individual crystallographic sites of silicon rich zeolites can be varied by the conditions of zeolite synthesis, the results open a possibility to tune presence/absence of electron acceptor acid sites in zeolite catalysts.

(iii) The different procedures leading to hierarchic micro-mesopore structure were analysed with respect to the formation of defective sites. The formation of mesopores by zeolite desilication by alkaline treatment (removing a part of the zeolite containing internal silanols) and subsequent leaching of perturbed framework aluminium (Al-Lewis sites, Al-OH) by oxalic acid resulted in the non-defective highly regular micro-mesoporous structure.

A series of micro- and micro-mesoporous zeolites with highly regular and, on the other side, a defective framework were investigated in transformation of methanol to low olefins, aromatics and paraffins. It is shown that even low concentration of Al- and Si-related defective sites substantially affects the product composition and stability of conversion during methanol transformation to hydrocarbons. The low-defective highly ordered micro-mesoporous H-ZSM-5 favours formation of C_2 and C_3 olefins, and provides long life-time. On contrary, the zeolites with defective sites enhance hydrogen transfer reactions leading to higher selectivity to aromatics and paraffins and coke formation causing deactivation.

Conclusions

The findings of the relationships between the distribution of Al atoms in the framework and structural stability provide an insight into the origin and formation of defect sites in ZSM-5 and BEA zeolites. These findings point out on the way of preparation of catalysts with highly regular framework of micro-mesoporous H-ZSM-5 with enhanced durability and selectivity in methanol to olefin transformation.

References

[1] S. Sklenák, J. Dědeček, Ch. Li, B. Wichterlová, V. Gábová, M. Sierka, J. Sauer, Angewandte Chemie - International Edition 46 (2007) 7286.

[2] P. Sazama, J. Dědeček, V. Gábová, B. Wichterlová, G. Spoto, S. Bordiga, Journal of Catalysis 254 (2008) 180.

[3] O. Bortnovsky, P. Sazama, B. Wichterlová, Applied Catalysis A: General 287 (2005) 203.

[4] P. Sazama, B. Wichterlova, J. Dedecek, Z. Tvaruzkova, Z. Musilova, L. Palumbo, S. Sklenak, O. Gonsiorova, Microporous and Mesoporous Materials, in press.

Inert Gas Confinement in Sub-nano Alveoli Molecularly Imprinted into the surface of mesostructured porous silica

Younes Bouizi[1], Mohamad El Eter[3], Kun Zhang[2], Belen Albela[1], Ming-Yuan He[2], Marie-Anne Springel-Huet[4], Antoine Gédéon[4], Laurent Bonneviot[1]
[1]Laboratoire de Chimie, UMR 5182, ENS de Lyon, 46 allée d'Italie, 69364 Lyon Cedex 07, France; [2]Shanghai Key Laboratory of Green Chemistry and Chemical Process, East China Normal University, 3663, North Zhongshan Road, 200062, Shanghai, China; [3]KAUST Catalysis Center (KCC), King Abdullah University of Science and Technology, Thuwal, Kingdom of Saudi Arabia, [4]Laboratoire de Chimie de la Matière Condensée CNRS, UMR 7574, Univ. Paris 06, F-75252 Paris 05, France. Corresponding author e-mail : laurent.bonneviot@ens-lyon.fr

Introduction

Among the surfactant templated silicas, MCM-41 occupies a special place as the first discovered and also the most studied one. It is classically templated by a cationic surfactant, cethyltrimethylammonium ($CTMA^+$) and, possesses a hexagonal array of monodimensional channels. They are widely applied in fields as adsorption, separation, trapping, catalysis, microelectronics, medical imaging, vectorization and controlled release of therapeutic molecules owing to their unique narrow pore size distribution in the meso-scale range 2 to 30 nm, their large internal volume (~ 0.9 cm^3/g)) and their extended surface area (~ 1000 m^2/g). In fact, nitrogen or argon adsorption profiles of these materials exhibit at 77 K, in addition to the classical capillary condensation due to mesopores, a steep adsorption at low relative pressures, $P/P_0 < 0.1$, usually assigned to micropores of materials like zeolites. Since there is no such micropores in MCM-41, this strong uptake at low pressure is likely due to the surface roughness. The latter is assigned her to sub-nano alveoli imprinted by the surfactant heads.

Experimental

MCM-41 was prepared as described in previous papers [1,2] .The surfactants used are the alkylltrimethylammonium *p*-toluenesulfonate (alkyl = dodecyl (C_{12}-TATos) or cetyl (C_{16}-TATos)). BET surface area, Xe and Ar adsorption measurement were performed with BELSORP-max analyzer (BEL Japan, Inc.). ^{129}Xe-NMR spectra were acquired using a Bruker MSL 400 spectrometer operating at 100 MHz.

Results and discussion

The confinement of xenon atoms in the voids of the surface roughness of porous mesostructured silicas (C_{16}-MCM-41) is demonstrated for the first time by solid-state NMR of Xenon 129. This conclusion is inferred from a set of measurements made on materials in the presence or absence of a specific blocking micropore agent, namely the tetramethylammonium ion (TMA^+). This latter is characterized by a hydrated diameter of 0.67 nm and van der Walls diameter of 0.42 nm. The void size is first probed by hyperpolarized ^{129}Xe NMR at 298 K. The NMR signal associated with Xe in the mesopores appears at 58 ppm to 10 Torr and moves up to 40 ppm at 800 Torr. The signal of xenon in the subnano-alveoli appears only above 140 Torr at 70 ppm with a weak pressure dependence. This unusual behavior is characteristic of a dynamic confinement forced at high pressure into these alveoli. The volume and size of both microalveoli and mesopores correspond respectively to both hydrophilic head diameter and hydrophobic tail length of surfactant showing for the first time dual templating role of the surfactant. In order to further characterize the roughness, we realize a comparative gas uptake of Xe and Ar between 279 and 307 K over two mesoporous

silica, namely the C_{12}-MCM-41 and C_{16}-MCM-41, reminding that their Van der Waals diameter are 4.32Å and 3.76Å, respectively. The polar head of surfactant is the same in both cases (tri methyl), only the hydrophobic tail is different, which is C_{12} and C_{16}. These materials have a porous internal volume ($V_{(internal)}$) of 0.77 cm^3/g and 0.85 cm^3/g respectively (measured using N_2 adsorption at 77 K). Surprisingly, both argon and even more obviously xenon are retained in both MCM-41. If we normalize the volume of adsorbed xenon to the internal pore volume, it appears that the effect of gas retention is higher for the C_{12}-MCM-41 (Fig. 1 and 2).

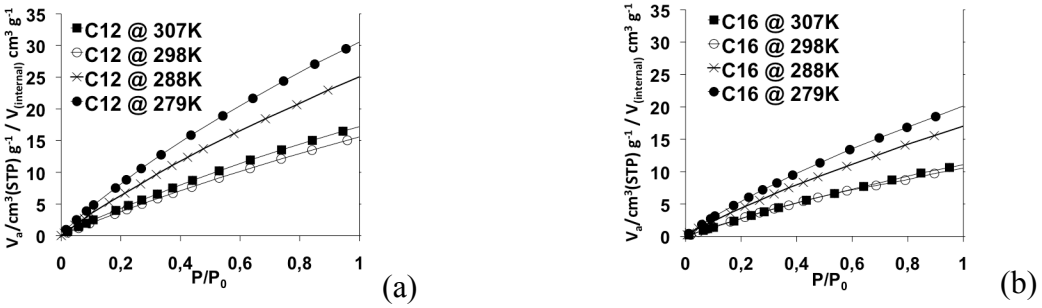

Figure 1: Xe adsorption isotherm at 279, 288, 298 and 307K of C_{12}-MCM-41 (a) and C_{16}-MCM-41 (b) (Volume Xe adsorbed / Internal pore volume Vs. P/P_0).

The remarkable uptake difference between both C_{12}- and C_{16}-MCM-41cannot be assigned to the change of the mesopore diameter only. This phenomenon can be better explained assuming the presence of alveoli coming from the imprint of the hydrated head of the surfactant during the material synthesis. The estimated diameter would therefore be close to 0.7 nm and larger than 0.42 nm. A mere geometrical model can lead to an estimation of the depth of these alveoli.

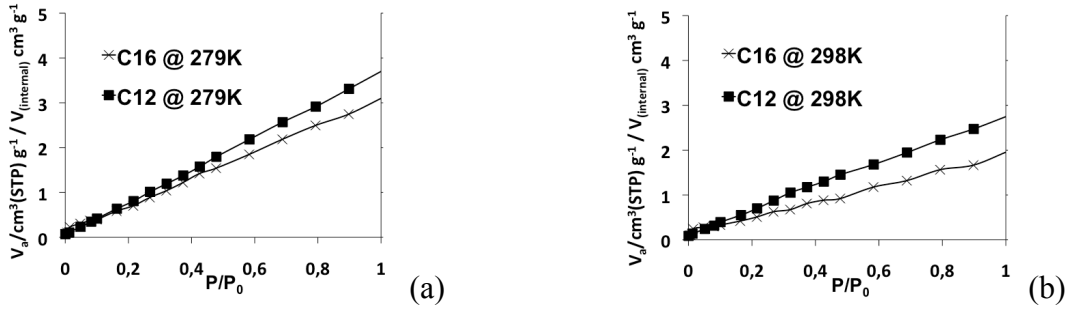

Figure 2: Ar adsorption isotherm at 279K (a) and 298K (b) of C_{12}-MCM-41 and C_{16}-MCM-41 (Volume Xe adsorbed / Internal pore volume Vs. P/P_0).

Conclusions

These silicas were synthesized in the presence of cationic surfactants used as a template for mesoporosity. We show in this work that mesopore surface roughness is not random but rather shaped by the imprint of the head of the cationic surfactant generating cells of about 0.7 nm in diameter.

Acknowledgements

This work was supported by CADENCED Project with King Abdullah University of Science and Technology (KAUST).

References

[1] Bonneviot, L.; Morin, M.; Badiei, A. Patent WO 01/55031 A1, 2001.

[2] Reinert, P.; Garcia, B.; Morin, C.; Badiei, A.; Perriat, P.; Tillement, O.; Bonneviot, L. Stud. Surf. Sci. Catal. 2003, 146, 133– 136

Meso-macroporous material for Acid Catalysis in Biorefinery

H. Ma, F. Baino, S. Fiorilli, R. Mortera, C. Vitale-Brovarone and B. Onida
Department of Materials Science and Chemical Engineering, Politecnico di Torino, Italy
barbara.onida@polito.it

Introduction

Conversions of wood-based biomass into fuels, power and chemicals (which take place in a biorefinery [1]) have attracted much interest due to the vast amount and the sustainment of the source. Materials with bimodal porosity, in particular meso-macroporous materials in which mesoporosity contains the catalytic sites and macroporosity favors mass diffusion, are promising catalysts to perform hydrolysis of wood-based biomass into smaller molecules.

We synthesized a meso-macroporous material containing Al-MCM-41, denoted hereafter as Al-MCM41-SCNA, and we tested its activity in hydrolysis reactions related to biomass conversions.

Experimental

The meso-macroporous catalysts, Al-MCM41-SCNA, were synthesized in two steps. First, a glass-ceramic scaffold containing SiO_2, CaO, Na_2O and Al_2O_3 in the ratio 57:34:6:3 (denoted SCNA) was prepared following reference [2]. Then, the SCNA scaffold was dipped in the Al-MCM-41 synthesis batch [3] for 12 min. After drying at room temperature overnight, the scaffold was calcined at 823K in nitrogen for 8 hours (heating rate 1 K/min). In order to increase the amount of incorporated Al-MCM-41 a second dipping was performed for one sample. Al-MCM-41 and MCM-41 in powder form were also prepared for comparison. The Al-MCM41-SCNA system was analyzed by scanning electron microscopy coupled with energy-dispersive spectroscopy (SEM/EDS), X-ray diffraction (XRD), N_2 sorption and thermal gravimetric analysis (TGA). Infrared spectroscopy of adsorbed basic probes provided information on sample acidity. Catalytic activity of the sample was tested in the hydrolysis of sucrose and starch. Al-MCM-41 powder and the powder pressed in a pellet form were also tested for comparison.

Results and discussion

The SCNA scaffold shows interconnected macropores, with a total porosity of about 50% in volume. SEM pictures of Al-MCM41-SCNA (Fig. 1) evidence the presence of Al-MCM41 particles inside macropores.

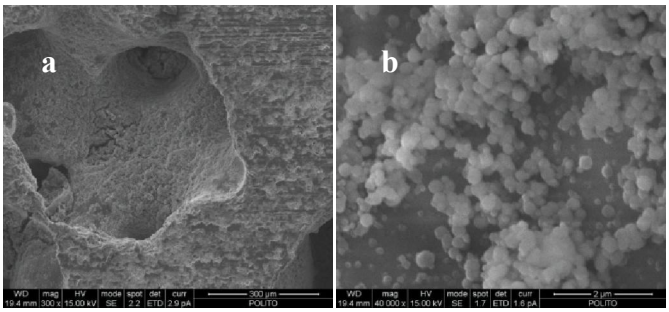

Fig. 1 SEM pictures of Al-MCM41-SCNA at low (a) and high (b) magnification.

N_2 sorption isotherms, as well as the pore size distribution and the XRD pattern of Al-MCM41-SCNA, are similar to that observed for Al-MCM-41 in powder form (fig. 2). The content of Al-MCM-41 inside the scaffold, as evaluated by the BET specific surface area, was about 1% w/w for the sample obtained after a single dipping, and 2% w/w for the sample obtained after two dipping steps. Further dipping does not increase the amount of incorporated Al-MCM-41.

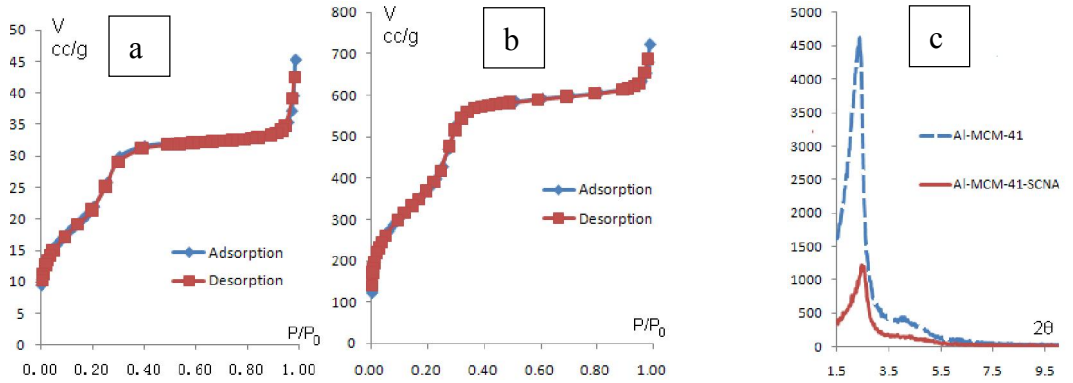

Fig. 2 Isotherms of a) Al-MCM41-SCNA (2% w/w), b) Al-MCM-41 in powder form, and c) XRD patterns of same materials

The activity of Al-MCM41-SCNA (1% w/w of Al-MCM-41) in hydrolysis reactions is close to that observed for Al-MCM-41 in powder form dispersed in the reaction batch (fig. 3a), which is definitely higher than that observed for the same sample pressed in pellet form (fig. 3b). This evidences that anchoring the catalyst particles inside the scaffold macropores is beneficial to the catalytic activity with respect to the powder pressed in pellet form.

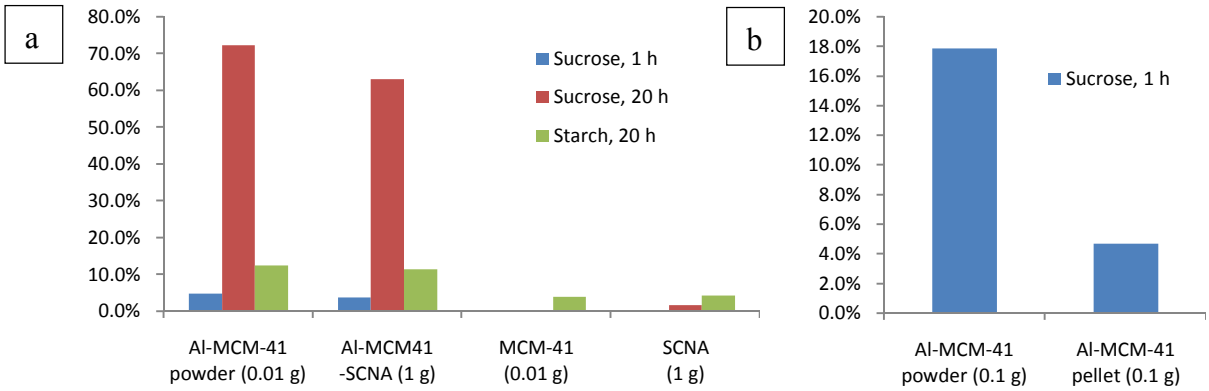

Fig. 3 Percentage amount of hydrolyzed sucrose and starch at different reaction time

Conclusions

A meso-macroporous catalyst was prepared, incorporating Al-MCM-41 inside a SCNA macroporous scaffold. The catalyst is active in the hydrolysis of sucrose. The catalytic tests evidence the benefit of using the meso-macroporous system compared to the mesoporous catalyst in pellet form.

References

[1] M. Stöcker, *Angew. Chem.*, 47 (2008) 9200-9211

[2] C. Vitale-Brovarone et al., *J Mater. Sci. Mater. Med.*, 20 (2009) 809-820

[3] R. Carrott et al., *Micropor. Mesopor. Mater.*, 92 (2006) 270-285

Different Kinds of Vanadium Species in Vanadium Containing Zeolites Evidenced by Experimental and Theoretical Investigations

Karolina Chalupka[1], Anna E. Lewandowska[2], Miguel A. Banares[2], Yannick Millot[3], Frederik Tielens[3], Michel Che[3], Stanislaw Dzwigaj[3]
[1]*Institute of General and Ecological Chemistry, Technical University of Lodz, Lodz, Poland,* [2]*Catalytic Spectroscopy Laboratory, Institute of Catalysis and Petroleum Chemistry, CSIC, Madrid, Spain,* [3]*Laboratoire de Réactivité de Surface, UPMC, CNRS, UMR 7197, Paris, France, Corresponding author: stanislaw.dzwigaj@upmc.fr*

Introduction

The nature and environment of vanadium(V) ions incorporated in dealuminated BEA zeolite (VSiBEA) by a two-step postsynthesis method were recently characterized using various techniques [1]. Because of the absence of d–d transitions in the range 600–800 nm in the DR UV-Vis spectra and V(IV) EPR signal, the diffuse reflectance (DR) UV–Visible bands observed at 270 and 340 nm for VSiBEA were assigned to oxygen-to-tetrahedral V(V) charge transfer transitions involving oxygen in bridging (V-O-Si) and terminal (V=O) positions. The presence of distorted tetrahedral V(V) species in VSiBEA zeolites has been confirmed by ^{51}V magic-angle spinning (MAS) NMR studies, which reveal a peak at -633 ppm [2]. In contrast with V species grafted onto a SiO_2 surface or introduced in mesoporous siliceous materials, it was shown that distorted tetrahedral V(V) species are stable in ambient moisture in VSiBEA zeolites, whereas on SiO_2 or mesoporous materials, vanadium changes spontaneously from tetrahedral to octahedral coordination. A particular environment of vanadium in the zeolite framework was suggested to be responsible for the higher tolerance to ambient moisture [3]. To obtain more precise information about nature of the framework and extra-framework V(V) species a comparative investigation by FTIR, RMN, Raman and DR UV-vis of V_xSiBEA, and by DFT calculations of vanadium in sodalite structure, related to different vanadium framework sites in V_xSiBEA, were performed in this work.

Experimental

V_xSiBEA zeolites (x = 0.05 - 4.0 V wt.%) were prepared by the two-step postsynthesis method reported earlier [1-3] using an aqueous solution of ammonium metavanadate in great excess with the low concentration (10^{-2} -10^{-3} mol.L^{-1}) and pH = 2.5. The suspension was left for 3 days at room temperature without any stirring. The solids were recovered by centrifugation and dried in air at 353 K overnight. V_xSiBEA zeolites (x = 0.05, 0.2, 0.3, 0.9, 1.0, 1.6, 2.0, 2.8 and 4.0 V wt.%) were prepared and labelled $V_{0.05}SiBEA$, $V_{0.2}SiBE$, $V_{0.3}SiBE$, $V_{0.9}SiBEA$ $V_{1.0}SiBEA$, $V_{1.6}SiBEA$, $V_{2.0}SiBEA$, $V_{2.8}SiBEA$ and $V_{4.0}SiBEA$, respectively.

Results and discussion

The combined use of DR UV-vis and Raman spectroscopies allows to evidence three kinds of tetrahedral V(V) with different structure in V_xSiBEA zeolite (Scheme) [4]. In all cases, vanadium species possess distorted tetrahedral configuration. At very low vanadium content (0.05 wt.%), the majority of tetrahedral V(V) species are strongly distorted and have a non-hydroxylated pyramidal structure $(SiO)_3V{=}O$ with V=O stretching at 1054 cm^{-1} whereas the remaining tetrahedral V(V) species are less distorted with a hydroxylated pyramidal structure $(SiO)_2(HO)V{=}O$ with V=O stretching at 1018 cm^{-1}.

In contrast, at higher vanadium contents (0.2 - 2 wt.%), the main distorted V(V) species possess a non-hydroxylated pyramidal structure $(SiO)_3V{=}O$ with V=O stretching at 1033-1036 cm^{-1}. Periodic DFT calculations confirm the presence of three different kinds of V site in V-containing zeolites. The experimental Raman bands recorded for V_xSiBEA with low and

high V content were confirmed on the basis of DFT calculations related to seven vanadium model sites. The difficulty to assign the vibrations in V-containing silica materials is due to the overlap of the different critical vibrational fingerprints (V=O, and Si-O-V vibration modes). At much higher vanadium contents (2.8 - 4 wt.%), the extra-framework octahedral V(V) species appears in the V_xSIBEA zeolite as evidenced by DR UV-vis and ^{51}V MAS NMR.

Three types of tetrahedral V(V) in zeolite framework

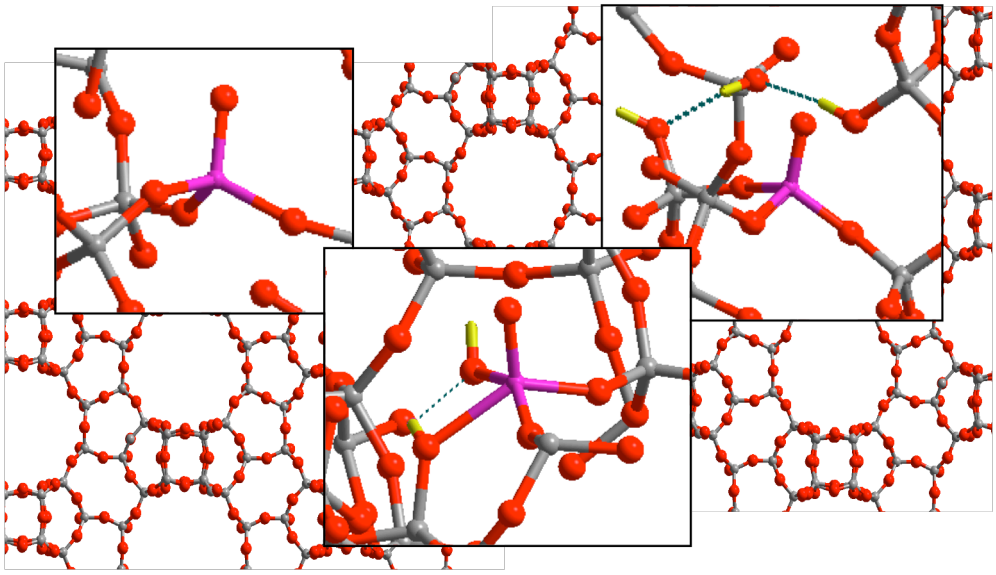

RAMAN/DFT Investigation

Conclusions

Three kinds of tetrahedral V(V) species have been evidenced in V_xSiBEA zeolite by combination use of DR-UV-vis and Raman spectroscopies. For very low V content (0.05 wt %), the majority of V(V) ions exhibits a strongly distorted tetrahedral structure with a non-hydroxylated pyramidal $(SiO)_3V{=}O$ structure with V=O stretching at 1054 cm^{-1}, whereas a minority adopts a distorted tetrahedral structure with hydroxylated pyramidal $(SiO)_2(HO)V{=}O$ structure with V=O stretching at 1018 cm^{-1}. In contrast, for higher V content (0.2 - 2 wt %), the main distorted V(V) species possesses a non-hydroxylated pyramidal $(SiO)_3V{=}O$ structure with V=O stretching at 1033-1036 cm^{-1}. Periodic DFT calculations confirm the presence of three different kinds of V site in V-containing zeolites.

References

[1] Dzwigaj, S. Peltre, M.J., Massiani, P., Davidson, A., Che, M., Sen, T., Sivasanker, S., Incorporation of vanadium species in a dealuminated β zeolite, Chem. Commun., (1998), 87-88.

[2] Dzwigaj, S., Matsuoka, M., Anpo, M., Che, M., A comparative study of V species in β zeolite by photoluminescence, diffuse reflectance UV-Visible and ^{51}V NMR spectroscopies, Catal. Lett. 72 (2001) 211-214.

[3] Dzwigaj, S., Massiani, P., Davidson, A., Che, M., Role of silanol groups in the incorporation of V in β zeolite, J. Mol. Catal. A, 155 (2000) 169.-182.

[4] Lewandowska, A.E., Banares, M. A., Tielens, F., Che, M., Dzwigaj, S., J. Phys. Chem. C 114 (2010) 19771-19776.

Characterization of Al and Ga substituted MCM-41

Manuel Díaz-García[1], Joaquín Pérez-Pariente[2], Enrique Sastre[2], Carlos Márquez-Álvarez[2], Gabriel Herrera-Pérez[3], Julia Aguilar-Pliego[1], Mirella Gutierrez [1]
[1]*Universidad Autónoma Metropolitana, Azcapotzalco, Mexico DF, Mexico.*
[2]*Instituto de Catálisis y Petroleoquímica, CSIC, Madrid, Spain.*
[3]*Instituto Tecnológico Superior de Irapuato, Guanajuato, Mexico.*
apj@correo.azc.uam.mx

Introduction

Mesoporous materials MCM (Mobil Composition of Matter) since its discovery in 1992, have been the subject of numerous investigations. Their applications as catalysts or catalyst supports have been one of the most studied fields. For this reason different methods have been proposed to try to increase the acidity of these mesoporous materials, one of which is substitution of silicon with trivalent metals [1]. In this paper we report on the modification of MCM-41 with Al^{3+} or Ga^{3+} to increase acidity. The results of characterization and test reactions how changes in acidity.

Experimental

The synthesis of the materials was made by the coprecipitation method, with: 250 mL of 30% NH_4OH, 1000 mL of distilled water, 5.6 g cetyltrimethylammonium bromide (CTAB), together with $Al(NO_3)_3$ or $Ga(NO_3)_3$ in different molar ratios Si/M^{3+}. The mixture was kept under stirring for 30 min and then 28 mL of tetraethylorthosilicate (TEOS) were added, drop wise. The mixture was left under constant stirring at room temperature for 24 h. The filtered solids were washed with distilled water, and then calcined at 550 °C with a flow of 10 mL/min of air.

X-ray diffraction was performed using a Phillis X-pert equipment using copper tube (CuKα). The surface area was determined with a Micromeritics ASAP-2020 surface area and porosity analyzer. Attenuated total reflectance IR spectra were recorded in the range of 4000 – 350 cm^{-1} using a Varian Excalibur FT-IR spectrophotometer with a Gladier ATR accessory. The morphology of the samples was studied by transmission electron microscopy (TEM) with a Carl Zeiss EM910 microscope using bright field technique. Elemental analysis was performed by ICP-OES using a Perkin Elmer Optima 3300 DV, equipment. Acidity was evaluated by pyridine adsorption followed by FTIR in the transmission mode using a Nicolet Nexus 670 FTIR spectrometer equipped with a MCT detector, and by means of the m-xylene isomerization reaction test 400 °C [2].

Results and discussion

The samples show the X-ray diffraction pattern exhibiting the (100), (110), (200) and (210) reflections characteristics of an ordered MCM-41 material. When the amount of Ga^{3+} or Al^{3+} increases in the synthesized materials the characteristic diffraction peaks become broader and less intense, indicating a progressive disorder in the ordered MCM-41 structures. This is also confirmed by TEM. The total amount of Al and/or Ga in the solids is measured by elemental analysis. It can be observed that the incorporation of gallium to the material is more effective than aluminum, and increases with increase of the corresponding metal in the synthesis gel (Table 1). The incorporation of metal ions in tetrahedral positions in the solid framework is assessed by infrared spectroscopy, ATR-FTIR. The IR spectrum of Si-MCM-41 shows two

characteristic bands at ~445 and 1059 cm^{-1} corresponding to the bending and the stretching O-Si bond respectively. These bands present a shift to lower frequencies in samples substituted with Ga and/or Al, indicating the incorporation of these elements to the framework.

Table 1. Elemental and Textural analyses of the different samples

Si/M^{3+} (synthesis gel)	Ga substituted			Al substituted		
	Si/Ga (solid)	Area (m^2/g)	Pore size (nm)	Si/Al (solid)	Area (m^2/g)	Pore size (nm)
5	16.6	876	3.5	3.6	763	3.1
10	8.3	835	3.6	6.8	669	3.4
15	15.4	977	3.8	9.8	728	3.9
20	18.6	1356	3.7	12.5	1071	3.1
25	25.4	918	3.7	15.8	965	3.1

The isomerization of m-xylene has been used as a test reaction to evaluate the Brönsted acidity of the different samples. Samples substituted with Ga are not active in this reaction, under the experimental conditions used in this work, probably due to their low number of Brönsted acid centers, while samples substituted with Al, with higher content of this kind of acidity show an appreciable activity in the reaction.

Conclusions

The incorporation of metal ions in the framework of MCM-41 increases the acidity of the resulting material Gallium substitution promotes predominantly Lewis acidity, while Aluminum substitution generates mainly Brönsted acid centers. This has been evidenced by FTIR and test reactions.

Acknowledgements

We are thankful for the financial support of the CSIC (Spain) and CONACYT (Mexico), project 2008MX0051.

References

[1] Kruk M., Jaroniec M., Sayari A., *"Application of large pore MCM-41 molecular sieves to improve pore size analysis using nitrogen adsorption measurements"*. Langmuir **13***(1997)* 6267-6273.

[2] Pérez-Pariente J., Sastre E., Corma A., *"Isomerization and disproportionation of m-xilene selectivities induced by the void structure of the zeolite framework"*. Applied Catalysis **45**(1988) 85-101.

[3] Luque R., Campelo J. M., Conesa T. D., Luna D., Marinas J. M., Romero A. A., *"Ga-MCM-41 synthesis and catalytic activity in the liquid-phase isomerisation of α-pinene"*. Microporous and Mesoporous Materials **103** (2007) 333-340.

[4] Emeis C.A.; *"Determination of integrated molar extinction coeficients for infrared adsorption bands of pyridine adsorbed on solid acid catalysts"*. Journal of Catalysis **141**(1993) 347-354.

[5] Fricke R., Kosslick H., Lischke G., Richte M.; *"Incorporation of gallium into zeolites: syntheses, properties and catalytic application"*. Chemical Reviews **100**(2000) 2303-2405

[6] Díaz García M., Aguilar-Pliego J., Herrera-Pérez G., Guzman L., Schachat P., Noreña-Franco L., Aguilar-Elguezabal A., Gutierrez-Arzaluz M. *"Isomerization of pinene with Al and Ga-modified MCM-41 mesoporous material"*. Advanced Materials Research **132**(2010) 162-173.

Synthesis of zeolites from coal fly ash using mine waters (circumneutral and acid mine drainage) as a substitute for pure water

Nicholas M. Musyoka[1*], Leslie F. Petrik[1], Richard Akinyeye[1], Godfrey Madzivire[1] and Eric Hums[2]
[1]*Environmental and Nano Science Research Group, Department of Chemistry, University of the Western Cape, Private Bag X17 Bellville, 7535, South Africa.* [2]*Consulting Environmental Catalysis, P.O. Box 1848, 91008 Erlangen, Germany *Corresponding author's e-mail: nmusyoka@uwc.ac.za, tel/fax: +27 021 959 3878*

Introduction

Coal fly ash and mine waters are two types of waste effluents that are produced from coal mining operations and coal combustion process respectively. These wastes are considered as an environmental liability [1]. Fly ash is a fine-grained inorganic spherical non-opaque glassy particulate residue which is derived from minerals included in coal during the combustion process. During and after the coal mining process, acidic or circumneutral mine water is generated depending on the geology of the bedrock in the coal mine. Such water poses environmental concern at mining sites and require expensive technologies to treat before it can be discharged in rivers or used for other applications. Acidic waters, acid mine drainage (AMD), are caused predominantly by pyrite oxidation while circumneutral mine waters (CMW), often referred to as either Ca–Mg or Na-rich waters, are produced when AMD undergoes partial neutralization due to the surrounding geology as the AMD flows past dolomite rich mineral [2]. The need to achieve zero effluent discharge in the mines and coal fired power stations has prompted scientist to search for new and innovative ways of recycling these wastes. Previous studies have shown that fly ash can be used in remediation of circumneutral and acid mine drainage waters [1-2]. Other investigations have also shown that zeolites can be synthesized from the fly ash and solid residues collected after the co-disposal reaction of fly ash and mine drainage [1, 3] The current study focuses on the synthesis of zeolites from fly ash and mine waters collected from Mpumalanga province in South Africa. The use of these two wastes in zeolite synthesis will not only offer a potentially capital savings option for disposal of these wastes but will also be advantageous to the coal mines and power stations since it will enable constructive use of the large volumes of waste that they generate. A modified classical hydrothermal synthesis process was used to produce zeolites in this study.

Experimental

Coal fly ash and two types of mine waters (acid and circumneutral) were collected from a coal combustion power plant and a coal mine respectively in Mpumalanga province in South Africa. The mine waters were applied as a substitute for ultrapure water in the synthesis of zeolites from fly ash. For comparative purposes, zeolites made using ultrapure water were synthesized using a known molar regime from a previous study [3]. Fly ash and sodium hydroxide in a mass ratio of 1:1 was dissolved in 100 ml of each mine water in a plastic 250 ml sealable bottle. A magnetic bar was added to the mixture and then placed on a magnetic stirrer. The speed of rotation was set at 800 rpm with the heater adjusted to a predetermined temperature of 48 ^{o}C which was controlled by a temperature probe inserted through the lid. The ageing reaction was allowed to proceed for 48 hours. After the ageing reaction time, 150 ml of mine water was added to the slurry while stirring and the resulting homogenous solution was transferred in aliquots of 10 ml into 23 ml Parr bombs which were sealed and later placed in a thermostated Memmert hot air oven for 48 hours at 140 °C in order to allow

crystallization to occur. X-ray diffraction (XRD) analysis of feedstock (Fly ash) and zeolitic products was performed using a Philips X-ray diffractometer. Multielement analysis (major oxides and trace elements) was conducted using Philips PW 1480 X-ray spectrometer. Hitachi X-650 scanning electron microanalyser was used for morphological analysis.

Results and discussion

The pH for circumneutral water and acid mine drainage was found to be 6.5 and 2.5 respectively. The elemental composition of the waters is shown in Table 1. The XRD analysis of fly ash revealed that it had quartz, mullite, hematite, magnetite and amorphous glassy phases as major phases (Figure 2). The synthesized zeolites showed disappearance of these phases due their consumption during the zeolitization process. When circumneutral mine water was used, an almost pure phase zeolite Na-P1 was obtained while hydroxy sodalte zeolite was obtained when acid mine drainage was used (Figure 2).

Fig. 1 Composition of the mine waters

Element (ppm)	Circum-neutral water	Acid mine water
Na	886.58	70.48
Ca	70.35	598.73
Mg	39.54	398.90
K	9.94	34.16
Mn	0.009	88.22
B	2.61	0.09
Sr	2.05	1.02
Fe	0.06	8158.20
SO_4^{2-}	1475.25	42 862
Cl	24	9.80

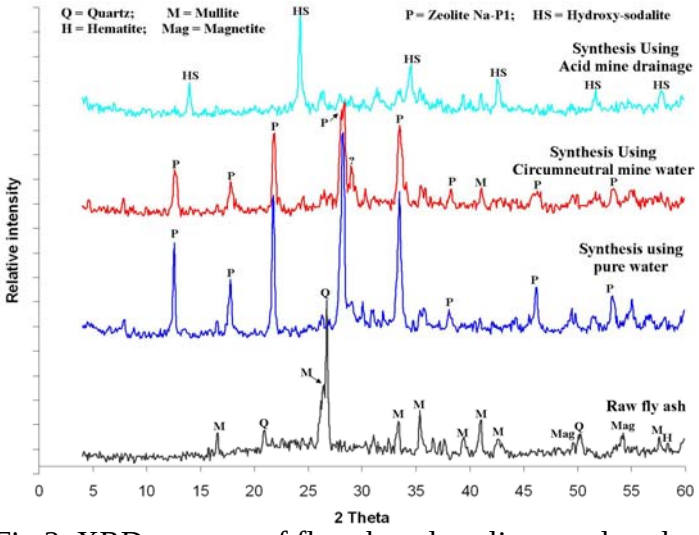

Fig 2. XRD patterns of fly ash and zeolites produced using ultrapure water, acidic and circumneutral water

Conclusions

The results from this study have proved that it is possible to synthesize zeolites using impure mine waters. Further investigations are underway to determine the major reasons for the differences in the type of zeolites produced.

Acknowledgements

The authors would like to acknowledge Eskom and National Research Foundation for providing the funds to make this study possible.

References

[1] Gitari, M.W., Petrik, L.F., Etchebers, O., Key, D.L., Iwuoha, E., Okujeni, C. Treatment of acid mine drainage with fly ash: removal of major contaminants and trace elements. Journal of Science Health A: Toxic Hazardous Substances 41 (2006), 1729–1747.

[2] Madzivire, G., Petrik L. F., Gitari W. M., Ojumu T. V., Balfour G. Application of coal fly ash to circumneutral mine waters for the removal of sulphates as gypsum and ettringite, Minerals Engineering 23 (2010) 252–257.

[3] Musyoka, N. M. Hydrothermal synthesis and optimisation of zeolite Na-P1 from South African coal fly ash. MSc thesis, University of the Western Cape, South Africa, 2009.

The induction period in MFI synthesis studied by ESI-MS spectrometry

B.B. Schaack, I.H. Lim, W. Schrader, F. Schüth
Max-Planck-Institut für Kohlenforschung, Kaiser-Wilhelm-Platz 1, 45470 Mülheim, Germany
schueth@mpi-muelheim.mpg.de

Introduction

During the synthesis of most zeolites, the first crystalline material is only observed with a certain time-lag after preparation of the synthesis solution or gel. This time-lag is often called the induction period. Various methods have been employed to obtain insight into the processes occurring during this induction period, but the phenomenon has remained rather elusive. Over the recent years, we have developed electrospray ionization mass spectrometry (ESI-MS) as a tool for the study of pre-nucleating and nucleating zeolite synthesis solutions. Due to the success achieved with this method for germanium-based systems, we decided to use ESI-MS also in order to elucidate the processes during MFI-nucleation.

Experimental

The aluminium containing zeolite ZSM-5 ([Al]ZSM-5) was obtained by dissolving silica (SiO_2) at 80 °C over night in a basic aqueous solution of the tetrapropylammonium cation (TPA^+), which was used as organic template. After the complete dissolution of silica the aluminium source (aluminum(III)-isopropylate) was added, leading to synthesis mixtures with the following overall molar compositions:

$$0.99\ SiO_2 : 0.0099\ Al(iPrO)_3 : 0.2\ TPAOH : 20\ H_2O.$$

Subsequently the reaction media were set to the required synthesis temperature and analyzed by means of ESI-MS, ESI-MS/MS as well as dynamic light scattering (DLS). The nucleation of [Al]ZSM-5 was studied at various synthesis temperatures starting from 40 to 170 °C. All syntheses above 100 °C were carried out in special designed stainless steel autoclaves. In order to study the incorporation of aluminum in the different oligomers, some experiments were carried out using isotopically enriched ^{29}Si.

All ESI mass spectra were recorded in negative mode using a Waters ZMD quadrupole mass spectrometer with Z-spray alignment. The ESI-MS/MS experiments were performed on a Bruker Esquire 3000 mass spectrometer with electric ion trap with an Agilent ESI source.

Results and discussion

The synthesis starts as a clear solution after complete dissolution of the silica, and thus mass spectra could be recorded from the start of the reaction. Directly after dissolution of the silica,

primarily monomeric species were observed. After addition of the aluminum source and heating up the mixture to 170°C, higher oligomers start to occur. Prominent species formed have masses which could either correspond to double four-rings (D4R) with two monomeric silicate units attached to the corners, or to double five-ring (D5R) species. A maximum of one aluminum atom was invariably found in these oligomeric species. After six hours, the concentration of the larger oligomers decreases again, at the same time, first particles are observed by dynamic light scattering. XRD revealed that the final solid was ZSM-5 with a Si/Al ratio of 120, as determined by EDX.

MS/MS experiments were used to determine the exact nature of the oligomers over the course of the synthesis. These studies revealed that in the beginning, the predominant solution species is the D4R, which is somewhat surprising, since this is not a structural element of the MFI-structure. However, with increasing reaction time, the oligomer distribution shifts more and more to the D5R-species. Immediately before the first particles are observed by light scattering, the ratio of D5R/D4R is around 10, i.e. the D5R is the predominant species. While D5R is not an SBU of the MFI structure, it at least contains the five-ring, which is a characteristic structural motif of MFI. Reactions were carried out at different synthesis temperature, and for each temperature, solid particles were observed after the D5R/D4R ratio reached a value of around 10 (Fig. 1).

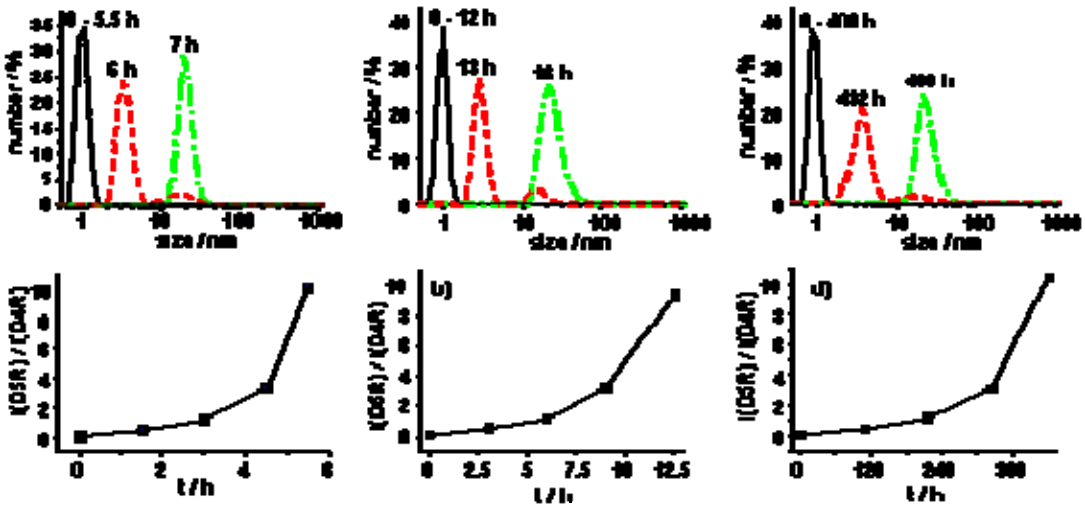

Fig. 1: Nucleation of Al-MFI at different temperatures (170°C left, 100 °C middle, 40 °C right). Top: particle size distribution determined by light scattering. Bottom: ratio between double-five ring silicate species and double-four ring silicate species over synthesis time determined by ESI MS.

Conclusions

ESI MS has revealed that during the induction period in MFI synthesis the silicate oligomer distribution develops towards D5R units. When the D5R/D4R ratio reaches approximately ten, MFI-structured solid forms, which suggests that solution species containing the five-ring are decisive for formation of this zeolite.

Structure and morphology of red pigments based on sepiolite

E. Atanes*, M. M. Vela, I. Carrillo, A. Cambra, F. Fernández-Martínez

evangelina.atanes@upm.es. Departamento de Química Industrial y Polímeros, E.U.I.T. Industrial, Universidad Politécnica de Madrid, C/. Ronda de Valencia, 3. 28012 Madrid

Introduction

The industrial manufacture of artificial ultramarine is currently quite common and cheap using kaolin, sulphur and soda as raw materials, as well as a simple thermal synthesis procedure. However, increasingly stringent environmental legislation has forced producers to reduce the volatile sulphur compounds in the flue gas of plants. This is the main reason for seeking alternative synthesis methods of coloured products analogous to ultramarine [1,2]. With this aim, a variety of zeolites both natural and synthetic have been tried being the sulphur anion-radicals chromophores encapsulated inside the zeolite structure [3]. The anion-radicals $S^{\cdot-}_3$ and $S^{\cdot-}_2$ are identified as blue and yellow chromophores, respectively. The red shade of some kinds of ultramarine is attributed sometimes to the anion-radicals $S^{\cdot-}_4$, although the literature data are scarce.
Sepiolite is a fibrous magnesia-silicate with molecular sized channels and groves which give them an important commercial value and a great number of applications [4]
The sepiolite has higher channels size than zeolite structures which are very suitable for the accommodation of sulphur radical anions bulkier than $S^{\cdot-}_3$ and $S^{\cdot-}_2$ in order to to obtain pigments with new colours. The encapsulation and stabilization of choromophore groups will be achieved during the folding of the sepiolite tridimensional structure by thermal treatment (Ruiz *et al.*, 1996; Frost, 2009).
The aim of this work was to synthesize pigments based on sulphur's cromophors encapsulated on sepiolite; in particular, we tried to synthesize analogues of ultramarine with red hues. The pigments obtained were characterized by colour analysis, Fourier infrared spectroscopy FTIR, X-ray diffraction and scanning electron microscopy.

Experimental

A mechanical mixture of natural sepiolite mineral from Vicalvaro-Vallecas (Madrid, Spain), sulphur and $Na_2S{\cdot}xH_2O$ as precursors of chromophores groups was heated in a reducing atmosphere to 800ºC. The S/Na_2S ratio was varied from 0.5 to 7, sulphur mass being 0.517g in all samples. The synthesis step was analyzed by thermogravimetric analysis. The colour of pigments was measured with CIELAB/LCH colour spaces. FTIR, X-ray diffraction and scanning electron microscopy was employed to analyze the structure and morphology of synthesized materials.

Results and discussion

Red coloured products were obtained by thermal treatment at S/Na_2S ratio of 1 and 0.5 (see Figure 1). These samples present a maximum of reflectance in the visible zone belonging to the red, with a maximum at 700 nm (S/Na_2S ratio = 1) and 670 nm (S/Na_2S ratio = 0.5). However at higher S/Na_2S ratios black and grey samples were obtained.
The thermogravimetric analysis, X-ray diffraction and FTIR analysis of samples reveals that as the content on Na_2S diminished, the structure is similar to sepiolite subjected to the same thermal treatment. The folding of the sepiolite structure and the introduction of chromophores

groups was also observed. The Na_2S or polysulphides (S_x^{2-}) are responsible for the red colour creating some bond with the external coordination water and Mg^{2+} of the sepiolite.

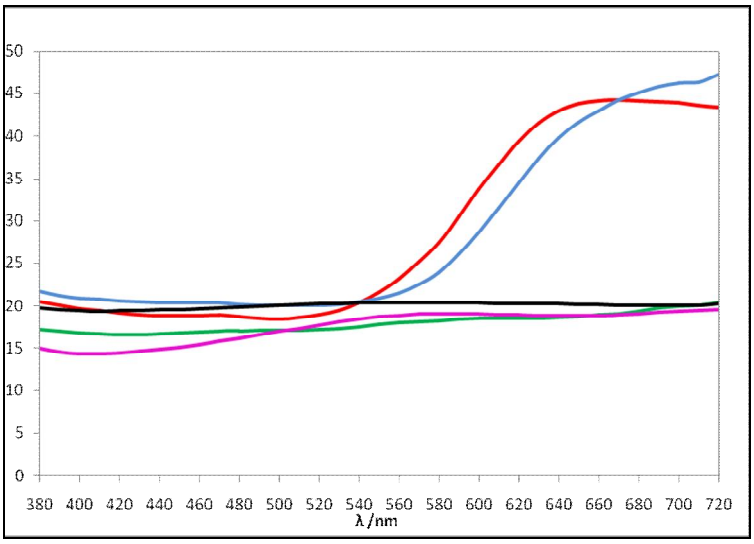

Figure 1. Spectral reflectance of samples between 380 and 720 nm.

S/Na_2S ratio = (----) 0,5, (----) 1, (----) 3, (----) 5 y (----) 7.

Acknowledgements

We gratefully acknowledge the company Tolsa (Madrid, Spain) for the samples of sepiolite and Ministerio de Ciencia e Innovación (project DGI MAT2010-19460) for the financial support.

References

[1] Kowalak, S., Jankowska, E., Mikołajska, A., Using of zeolite LOS for preparation of sulfur pigments, Micropor. Mesopor. Mater. 127 (2010) 126–132.
[2] Kowalak, S., Jankowska, A., Application of zeolites as matrices for pigments, Micropor. Mesopor. Mater., 61 (2003) 213-222.
[3] Jankowska, A., Kowalak, S., Synthesis of ultramarine analogs from erionite, Micropor. Mesopor. Mater., 110 (2008) 570-578.
[4] Valentín, J.L., López-Manchado, M.A., Rodríguez, A., Posadas, P., Ibarra, L., Novel anhydrous unfolded structure by heating of acid pre-treated sepiolite, Appl. Clay Sci., 36 (2007) 245-255
[5] Ruiz, R., del Moral, J. C., Pesquera, C., Benito, I., González, F. Reversible folding in sepiolite: study by thermal and textural analysis, Thermochim. Acta, 279 (1996) 103-110.
[6] Frost, R.L., Kristóf, J., Horváth, E., Controlled rate thermal analysis of sepiolite, J Therm. Anal. Calorim., 98 (2009) 749–755.

A sweeter route to titanium zeolite catalysts

Andy Smith and Gopinathan Sankar
University College London, Department of Chemistry
London WC1H 0AJ
andy.smith@ucl.ac.uk

Introduction

Since the invention of titanium silicalite-1 in the 1983[1], titanium containing zeolites have received much research interest as selective oxidation catalysts. The mode of action of these catalysts is assumed to depend on the titanium atoms being substituted into the framework, thus having tetrahedral coordination. Typical titanium sources for the synthesis of the materials are titanium alkoxides. Insertion of titanium atoms into the crystallising zeolite framework depends crucially on the rate of hydrolysis of the alkoxide ligands. Too fast and the titanium will tend to precipitate out of solution as TiO_2, and not be incorporated into the zeolite. To combat this tendency, we have investigated a water soluble titanium source, based on the reducing sugar, glucose.

Experimental

Titanium gluconate was prepared according to the method of Nelson[2], and further utilised in the synthesis of titanium MFI zeolite. Tetraethylorthosilicate was used as silica source and tetrapropylammonium hydroxide as a templating agent. The synthesis gel had composition 22.73 SiO_2: 2.273 TiO_2: 9 TPAOH: 500 H_2O. The gel was charged in to a Teflon-line steel autoclave and heated to 190°C for 96 hours. The product was recovered by filtration and washed with distilled water. Tests of the catalytic performance of this material are currently underway.

Results and discussion

Powder X-ray diffraction of the material (see Figure 1) shows it to be crystalline, phase pure, zeolite with the MFI framework. SEM images of the material (see Figure 2) show that the crystallites are of uniform size (ca 2 micron) and exhibit the coffin-shaped habit typical of MFI zeolites. EDS analysis (see Table 1) of the material shows that the silicon and titanium atomic percentages are 32.05 and 1.28 respectively, giving a Si/Ti ratio of 25.03. This compares favourably with high Ti-loading titanium silicalite materials synthesized by conventional methods[3].

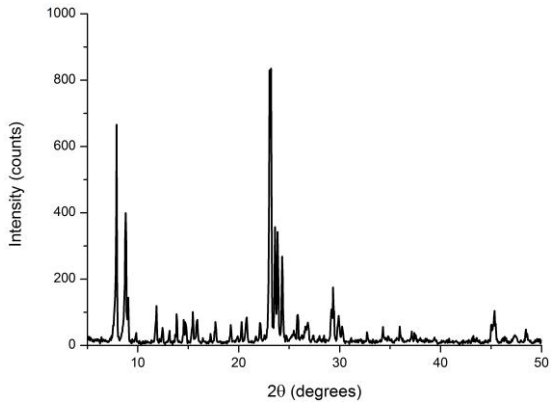

Figure 1: PXRD of Ti-MFI

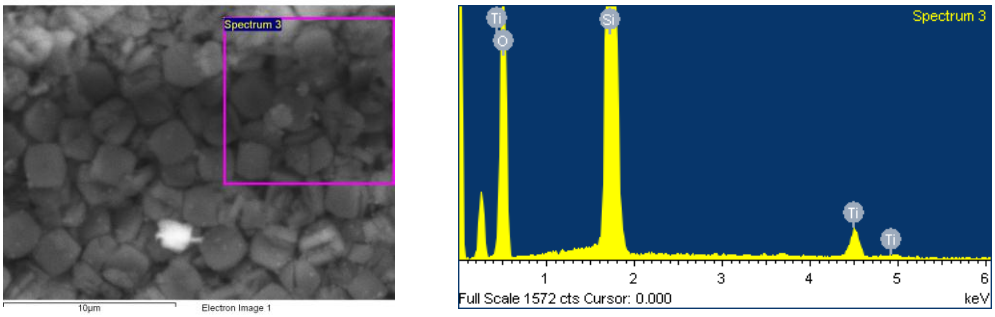

Figure 2: SEM image and EDS spectrum of Ti-MFI

Element	Weight%	Atomic%	Compd%	Formula
Si K	44.39	32.05	94.96	SiO2
Ti K	3.02	1.28	5.04	TiO2
O	52.59	66.67		
Totals	100.00			

Table 1: EDS analysis of Ti-MFI

Titanium edge XANES data were collected at the B18 beamline at Diamond Light Source (see Figure 3). The pre-edge feature in these spectra is a sensitive measure of the titanium environment with the material. It corresponds to an electronic transition that is forbidden for atoms in an octahedral environment and fully allowed for atoms in a tetrahedral environment. Tetrakis-triphenylsiloxy titanium, $[Ti(OSiPh_3)_4]$, is a model compound for tetrahedral titanium coordination in zeolite frameworks, and shows a large sharp pre-edge feature. For comparison the XANES spectrum of the starting material, titanium gluconate, is included in Figure 3. This material only has a weak pre-edge feature, indicating that the coordination of titanium is largely octahedral. Ti-MFI produced using titanium gluconate also shows a strong pre-edge feature, suggesting that a large proportion of titanium atoms present are in tetrahedral coordination. The titanium environment changes markedly between the gluconate and the crystalline Ti-MFI. Calcining Ti-MFI at 823K increases the pre-edge feature intensity. This is interpreted as the loss of framework water or template molecules that were creating a pseudo-octahedral environment around otherwise tetrahedral framework titanium atoms.

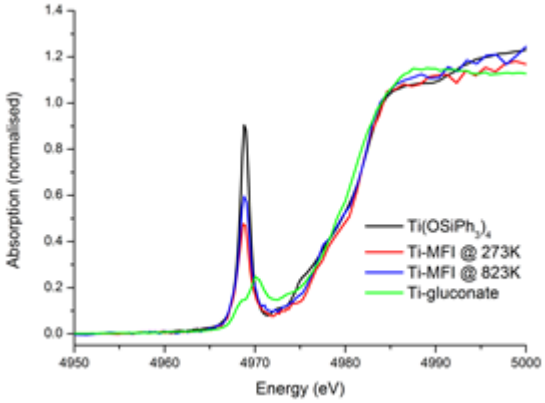

Figure 3: Ti edge XANES of Ti-MFI

Conclusions

We have demonstrated that water soluble titanium sources, based on carbohydrate chemistry, are a viable alternative to titanium alkoxides for the synthesis of titanium zeolites.

Acknowledgements

The authors would like to thank Diamond Light Source for the beamtime necessary to complete this study.

References

1. M. Taramasso, G. Perego and B. Notari, US Patent 4410501 (1983).
2. W.K. Nelson, US Patent 2227508 (1941).
3. WB. Fan, RG. Duan, T. Yokoi, P. Wu, Y. Kubota, T. Tatsumi, *J. Am. Chem. Soc.*, **130**, 10150-10164 (2008)

Platelets of zeolites with isometric structure formed by oriented aggregation of nanoparticles

R. Benabdallah[1,2], F. Hamidi[2], R. Arletti[3], A. Bengueddach[4], F. Di Renzo[1]
[1]*Institut Charles Gerhardt Montpellier, UMR 5253 CMRS-UM2-ENSCM-UM1, Matériaux Avancés pour la Catalyse et la Santé, Montpellier, France, direnzo@enscm.fr*
[2]*Département de Chimie, Université des Sciences et Technologie d'Oran, Oran, Algeria*
[3]*Dipartimento di Scienze Mineralogiche e Petrologiche, Università di Torino, Torino, Italy*
[4]*Laboratoire de Chimie des Matériaux, Université d'Oran Es-Senia, Oran, Algeria*

Introduction

The formation of single crystals by coalescence of aggregates of oriented nanoparticles has been initially suggested in biomineralization systems [1] and has been recently developed in the fast-growing field of mesocrystallization [2]. Bidirectional aggregation of nanoparticles can provide lath-like materials useful as gas barrier and polymer charge. Most instances of mesocrystallization, including examples from the seolite synthesis, occurs in the presence of organic moieties [3, 4]. In this communication, some examples of organic-free faujasite and sodalite morphologies are presented, which cannot be accounted for by differential growth rates of single-crystal faces and appear as likely instances of mesocrystallization.

Experimental

Faujasite crystals are formed from synthesis gels of composition 3.9 Na / 0.45 Al / SiO_2 / 35 H_2O. Sodalite crystals are coproducts of syntheses of zeolite LSX from gels of composition 5.8 Na / 1.2 K / 0.77 Al / SiO_2 / 70 H_2O.

Results and discussion

Sodalite and faujasite crystals formed at high alkalinity in the described synthesis conditions present a morphology of hexagonal platelets, as shown in Fig. 1.

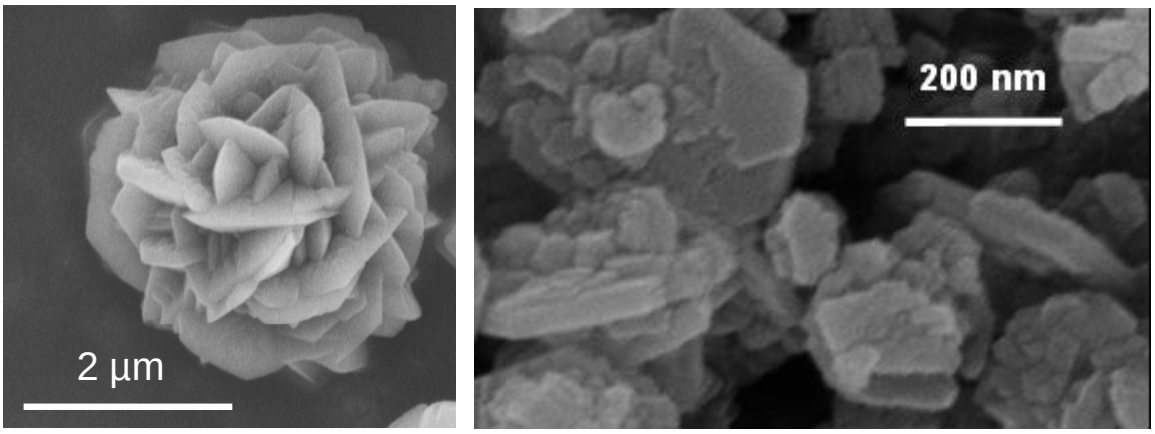

Figure 1. Flowerlike cluster of tabular crystals of hydroxysodalite (left) and lamellar crystals of faujasite (right).

The X-ray powder diffraction pattern of flat-crystal faujasite samples present unequal widths of the diffraction lines, suggesting unequal development of the crystals in different directions.

When the linewidths coresponding to defined sets of Miller indices are separately considered, it appears that the crystals are much shorter in the 111 direction of the triple axis than in the perpendicular hk0 directions. The application of the Scherer formula D = ? / ß cos? indicates a thickness of 15 nm and a lateral extension of 60 nm for the tabular crystals. The slopes of the Williamson-Hall plots, proportional to the periodicity disorder, indicate that the crystals are perfectly ordered in the 111 direction and significantly disordered in other directions. Analyses of the angles between crystalline planes indicates that tabular crystals are formed by cubic subunits bidirectionally aggregated on the 100 faces.

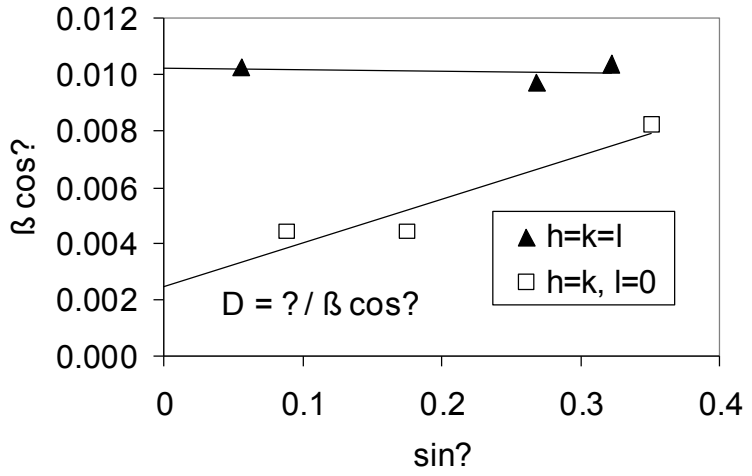

Figure 2: Williamson-Hall plot from the XRD powder pattern of lamellar faujasite nanocrystals. Linewidths are separated according to the crystallographical orientation.

A mechanism for the formation of lamellae independent from the crystal structure has been early proposed for the aggregation of surfactant-coated spheres of amorphous silica [4]. The charge of the surfactant bilayers around the silica particles creates a repulsive interaction. Unfrequent contacts between particles result from statistical collisions. Once aggregates of at least three particles are formed, any new particle approaching the face of the aggregate finds a collective electrostatic repulsion much stronger than the repulsion from the rim of the aggregate. As a consequence, the aggregate preferentially grows laterally and assumes a sheet morphology. In the case of the formation of flat zeolite crystals, the high surface charge expected for nanoparticles formed from alkaline solution [5] can account for a similar mechanism of oriented aggregation. The nature of the cation affects the aggregation behaviour, as the presence of tetramethylammonium cations favour the formation of usual octahedral faujasite crystals.

References

[1] S. Mann, Nature Mater. 8 (2009) 781.
[2] H. Cölfen, M. Antonietti, Mesocrystals and Nonclassical Crystallization, Wiley, Chichester 2008, 276 pp.
[3] C.E.A. Kirschhock, V. Buschmann, S. Kremer, R. Ravishankar, C.J.Y. Houssin, B.L. Mojet, B. L., R.A. van Santen, P.J. Grobert, PA. Jacobs, J.A. Martens, Angew. Chem., Int. Ed. 40 (2001) 2637.
[4] T.M. Davis, T.O. Drews, H. Ramanan, C. Hei, J. Dong, H. Schnablegger, M.A. Katsoulakis, E. Kokkoli, A.V. McCormick, R.L. Penn, M. Tsapatsis, Nature Mater. 5 (2006) 400.
[5] R.K. Iler, The Chemistry of Silica, Wiley, New York 1979, 390.
[6] J.P. Jolivet, C. Froidefond, A. Pottier, C. Chanéac, S. Cassaignon, E. Tronc, P. Euzen, J. Mater. Chem. 14 (2004) 3281.

A New Trend Predicting the Organic Template Effects in the Hydrothermal Synthesis of A-type Zeolite

Amir Enferadi Kerenkan*, Ali Akbar Babaluo, Behruz Bayati
Nanostructure Materials Research Center, Department of Chemical Engineering, Sahand University of Technology, Tabriz, I. R. Iran, P.O. Box 51335/1996.
a_enferadi @sut.ac.ir

Introduction

The choice of organic template is of crucial importance in the formation of a particular zeolite structure. Templating was defined as the phenomenon occurring during either the gelation or the nucleation process whereby the organic species organize oxide tetrahedra into a particular geometric topology around themselves and thus provide initial building blocks for a particular structure. The roles of organic guest molecules are summarized as follows based on the specificity of the inorganic host and organic guest: (i) space-filling species; (ii) SDAs; and (iii) templates [1].

Hydrophilic A-type (LTA or NaA) zeolite is one of the most important zeolite structures which has been reported as the first commercial zeolite membrane and proposed for a separation of several industrially important gases [2]. It has been reported that in the synthesis of A-type zeolite, using tetra methyl ammonium hydroxide (TMAOH) as the organic template decreases the seeds size dramatically [3], but the effects of increasing of TMAOH on the crystallinity, morphplogy and average particle size of the synthesized zeolite were not clearly discussed in the literatures. In this work, the variation trend of these parameters with addition of TMAOH in the synthesis of A-type zeolite was investigated and the optimum amount of organic template is proposed.

Experimental

The precursor gels were prepared in two steps. First, sodium hydroxide, aluminum foil and tetra methyl ammonium hydroxide were dissolved in deionized water and then silica sol was added to above prepared solution under stirring at high speed. The final molar composition of the gels was: $2SiO_2$: $1Al_2O_3$: $3Na_2O$: $x(TMA)_2O$: $200H_2O$ (x = 0, 1.5, 2.75, 4, 5.5 and 7). Then the mixture was transferred to a teflon-lined stainless steel autoclave and hydrothermally treated for 24 h in an oven at 60˚C. After the hydrothermal treatment, the products were recovered, thoroughly washed with deionized water and then dried at 80˚C for 4 h. Finally, in order to remove TMAOH, products were calcined in air at 550˚C for 3days. The experiments conditions and the results for various organic template contents were presented in Table 1.

The crystalline structure of the synthesized zeolite seeds was determined by X-ray diffraction (XRD) patterns and their crystallite sizes (S_c) were calculated using the standard Scherrer's formula [2]. Morphology, particle size (S_p) and Standard of deviation for S_p (SD) of the products were investigated by scanning electron microscopy (SEM) and image analyzer software.

Table 1. Experiments conditions and characteristics of the synthesized zeolite particles

Sample	x (Number of moles of $(TMA)_2O$ in the synthesis mixture)	Product size (nm)		
		S_c	S_p	SD
LTA-1	0	28	1290	350
LTA-2	1.5	37	580	120
LTA-3	2.75	35	620	140
LTA-4	4	41	770	200
LTA-5	5.5	-	-	-
LTA-6	7	-	-	-

Results and Discussion

Comparison of XRD patterns of the synthesized zeolites with standard A-type zeolite illustrated that LTA-1, LTA-2, LTA-3 and LTA-4 samples have the pure NaA zeolite structure. By increasing the organic template content, the purity of NaA zeolite phase decreased. At x=5.5, the presence of other picks confirmed that some side phases in NaA zeolite phase have been formed and at last, LTA-6 (x=7) could not be identified as A-type zeolite. As an example, XRD patterns of LTA-1 and LTA-6 samples and SEM micrographs of LTA-1 and LTA-2 samples are shown in Fig. 1 and Fig. 2, respectively. Analyzing the SEM micrographs of the samples showed that in the synthesis of LTA zeolite, particle size decreases dramatically with the addition of TMAOH and reach to minimum values at x=1.5. Further increasing the template amount up to x=4 causes to more uniform and cubic morphology of the crystals only (LTA-3 and LTA-4).

The great effect of template can be explained by the following reason: crystallization takes place in a nearly clear synthesis mixture. This solution must reach the necessary degree of supersaturation to start the nucleation step. The presence of TMAOH in the synthesis mixture accelerates reaching the necessary degree of supersaturation by increasing the concentration of the mineralizing agent OH^- and therefore increasing the solubility of the silicon and aluminum precursors. In this way, the organic template promotes the nucleation process. But after the formation of certain amounts of nuclei or even crystal, degree of supersaturation decreases due to reactants consumption. So, more nucleation is not possible because of the lack of initial material sources. This gives rise to this subject that the increasing of organic template did not have a strong effect on the average particle size and just leaded to higher crystallinity.

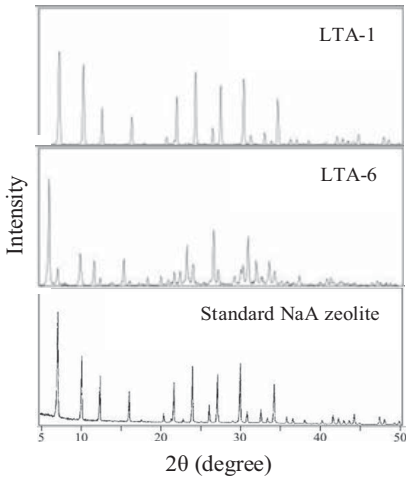

Fig. 1 XRD patterns of two samples in comparison with standard NaA zeolite

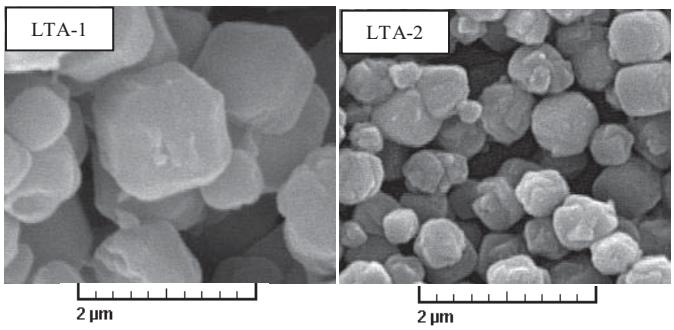

Fig. 2 SEM micrographs of two samples of the synthesized NaA zeolites

Conclusion

By addition of TMAOH to the synthesis mixture, a significant reduction is occurred in the average size of synthesized NaA zeolite particles. Also, increasing its amount leads to more crystallinity of the particles. But, this increase was only possible up to a specified value since high amount of TMAOH is not favorable for the formation of pure NaA zeolite phase.

References

[1] Yu J. Synthesis of Zeolites. in "Introduction to Zeolite Science and Practice" Studies in Surface Science and Catalysis, vol. 168, J. Čejka, H. van Bekkum, A. Corma and F. Schüth, Eds., Elsevier, Amsterdam (2007).

[2] Bayati B., Babaluo A.A. and Karimi R., Hydrothermal Synthesis of Nanostructure NaA Zeolite: The Effect of Synthesis Parameters on Zeolite Seed Size and Crystallinity, J. Europ. Ceramic Society, 28 (2008) 2653–2657.

[3] Schoeman B.J., Sterte J. and Otterstedt J.-E., Colloidal zeolite Suspensions, Zeolites, 14 (1994) 110–116.

New Insights on the Immobilization of TiO_2 on Porous Silicate Supports - an Efficient Photocatalytic System for Decomposition of VOC

Nataša Novak Tušar[a,b], Minoo Tasbihi[b], Venčeslav Kaučič[a,c] Urška Lavrenčič Štangar[b]
[a]*National Institute of Chemistry, Hajdrihova 19, SI-1001 Ljubljana, Slovenia;* [b]*University of Nova Gorica, Vipavska 13, SI-5000 Nova Gorica, Slovenia;* [c]*Faculty of Chemistry and Chemical Technology, University of Ljubljana, Aškerčeva 5, SI-1001 Ljubljana, Slovenia; e-mail: natasa.novak@ki.si*

Introduction

Air pollution by VOCs (Volatile Organic Compounds) is becoming nowadays a big environmental problem [1]. For air cleaning TiO_2 photocatalysis represents one of the very efficient AOP (Advanced Oxidation Methods) that can decompose chemically and microbiologically stable VOCs [1]. However, the photocatalytic activity of nanocrystalline TiO_2 powder can be significantly suppressed due to the agglomeration of particles to microsized aggregates, TiO_2 poor adsorption characteristics for organic compounds and its relatively low surface area lead to great limitations in exploiting the photocatalyst to the best of its photoefficiency. These problems can be solved by immobilization of nanocrystalline TiO_2 on the porous silicate supports [2]. In this work we discuss the advantages of immobilization of TiO_2 nanoparticles on ordered and disordered mesoporous silicates as high surface area supports in terms of efficiency of this photocatalytic system for decomposition of VOCs.

Experimental

Ordered (SBA-15) and disordered (KIL-2) silicate structures were prepared via procedures already reported in the literature [3,4]. Active anatas-TiO_2 nanoparticles in a form of aqueous sols were prepared using titanium tetrachloride ($TiCl_4$) as a precursor via sol-gel method using $HClO_4$ as peptizing mediator at low-temperature preparation conditions [5]. Ordered and disordered mesoporous silicates were impregnated via sol-gel impregnation methods with different amounts of low-temperature prepared TiO_2 sols. The Ti/Si molar ratio was adjusted to 1/2, 1/1 and 2/1. The catalytic powders prepared from SBA-15 and KIL-2 mesoporous silicate supports were denoted as TiSBA-15(x) Ti/KIL-2(x), respectively, where x means the Ti/Si nominal molar ratio. Characterization of prepared catalysts was performed using X-ray powder diffraction, N_2 sorption measurements, scanning electron microscopy (SEM), elemental analysis (EDAX), high-resolution transmission electron microscopy (HRTEM), UV and visible spectroscopy (UV-VIS) and Fourier transform infrared spectroscopy (FTIR). The photocatalytic degradation of toluene as a model VOC pollutant was carried out in a gaseous fluidized-bed photoreactor equipped with UVA light source and connected on-line to the GC-MS analyzer.

Results and discussion

The physico-chemical properties of the prepared photocatalytic powders characterized by different techniques (see Experimental part) are shown in Table 1. The influence of Ti/Si molar ratio and of the mesoporous silica structure was investigated toward the adsorption capacity and photocatalytic degradation of toluene (Table 1). The results showed that adsorption capacity and photocatalytic degradation kinetics were similar using photocatalysts with the same Ti/Si molar ratio and different mesoporous silicate structure. The adsorption

capacity was decreasing as a function of the increasing Ti/Si molar ratio in the case of both types of mesoporous silicate support. Similar band gap value and similar photocatalytic degradation of toluene if compared to the commercial reference Millenium PC500 (prepared at high-temperature procedure) was observed by Ti/SBA-15 and Ti/KIL-2 composites with molar ratio Ti/Si = 1/1 (Table 1) prepared at low-temperature procedure.

Table 1: Some physico-chemical characteristics, dark adsorption capacity and photocatalytic activity of the anatas-TiO_2-silicate powders prepared at low-temperature procedure.

Sample	Ti/Si molar ratio	The amount of TiO_2 in the powder (wt %)	Crystallite size (nm)	S_{BET} (m^2g^{-1})	Band gap (eV)	Dark adsorption capacity (% of adsorbed toluene)	Rate constant k (first order) (min^{-1})
SBA-15	-	-	-	589	-	53	-
Ti/SBA-15(1/2)	1/2	40	10	560	3.39	20	0.0043
Ti/SBA-15(1/1)	1/1	58	10	498	3.20	16	0.0121
Ti/SBA-15(2/1)	2/1	74	12	336	3.14	8	0.0067
KIL-2	-	-	-	504	-	49	-
Ti/KIL-2(1/2)	1/2	40	5	345	3.26	17	0.0031
Ti/KIL-2(1/1)	1/1	58	5	309	3.17	14	0.0096
Ti/KIL-2(2/1)	2/1	74	7	296	3.15	9	0.0064
Ti1	-	73	8	80	3.11	9	0.0006
Millennium PC500	-	100	5-10	300	3.20	19	0.0114

Ti1 –TiO_2 powder prepared at low-temperature procedure described in the reference [5] consists of 73% anatas-TiO_2 and 27% organic
Millennium PC500 – commercial TiO_2 powder prepared at high-temperature procedure consists of 100% anatas-TiO_2

Conclusions

The photocatalytic activity of immobilized TiO_2 nanoparticles (low-temperature preparation) on ordered and disordered mesoporous supports was considerably improved by using supported TiO_2-silicate catalyst than by using pure titania powder prepared from the same source. The results further demonstrate that the prepared TiO_2-silicate photocatalytic powders enable the decomposition of VOC at mild reaction conditions in gaseous reactor, therefore the system represents a promising photocatalytic system for air- cleaning process evaluation.

Acknowledgements

This work was financially supported by the Slovenian Research Agency (research programs P1-0021, P2-0377 and applied research project L2-1129).

References

[1] Wang, S., Ang, H.M., Tade, O.M., Volatile organic compounds in indoor environment and photocatalytic oxidation: State of the art, Environmental International 33 (2007) 694-705.
[2] Tasbihi, M., Lavrenčič Štangar, U., Černigoj, U., Jirkovsky, J., Bakardijeva, S., A., Novak Tušar, N., Photocatalytic oxidation of gaseous toluene on titania/mesoporous silica powders in a fluidized-bed reactor, Catalysis Today, doi: 10.1016/j.cattod.2010.08.015.
[3] Novak Tušar, N., Ristić, A., Mali, G., Mazaj, M., Arčon, I., Arčon, D., Kaučič, V., Zabukovec Logar, N. MnOx nanoparticles supported on a new mesostructured silicate with textural porosity, Chemistry – A European Journal, 16 (2010), 5783-5793.
[4] Mazaj, M. Stevens, W.J.J., Zabukovec Logar, N., Ristić, A., Novak Tušar, N., Arčon, I., Daneu, N., Meynen, V., Cool, P., Vansant, W.F., Kaučič, V., Synthesis and structural investigations on aluminium-free Ti-Beta/SBA-15 composite, Microporous and Mesoporous Materials 117 (2009) 458-465.
[5] Tasbihi, M., Lavrenčič Štangar, U., Černigoj, U., Kogej, K., Low-temperature syntesis and characterization on anatase TiO_2 powders from inorganic precursors, Photochemical & Photobiological Sciences 8 (2009) 719-725.

Lamellar silicates are still valid precursor to mesoporous materials with controlled pores sizes and distribution

Hipassia M. Moura, Fabio A. Bonk and Heloise O. Pastore*
Institute of Chemistry, University of Campinas
Rua Monteiro Lobato, 270, CP 6154 – Cep 13084-971 – Campinas/SP - Brasil.
** 055 19 35213017; gpmmm@iqm.unicamp.br*

Introduction

Surfactant-intercalated magadiite is used for the preparation of elastomeric polymer-layered silicate nanocomposites[1] that show improved tensile properties owing to the reinforcement effect of the silicate nanolayers. Magadiite isomorphously substituted by aluminum may be used to prepare pentasil zeolites as well as ferrierite.[2] It can also be used as a precursor to obtain PILCs (Pillared Interlayered Clays)[3] providing materials with high surface area and high catalytic potential. The pillaring process involves essentially the reaction between the layered material and an ionic species to swell the solid followed by fixation of the lamella position with silica-based pillars. Thus, the choice of swelling/spacing director allows obtaining materials with controllable interlayer distances according to the interest.

In this sense, this work shows that the use of varied cetyltrimethylammonium bromide (CTAB) concentration into the interlamellar space of magadiite and [Al]-magadiite during the PILCs synthesis brings significant changes in the product structure and on the interlayer space itself. These findings create new opportunities for synthesizing clay-based catalysts or adsorbents with designed pore structure, accessibility and activity.

Experimental

Cetyltrimethylammonium-Magadiites: To a suspension of magadiite or [Al]-magadiite (Si/Al=15) (synthesized as described by *Superti et al*[4]) in water (1 wt.%), CTAB was added and the mixture was kept under magnetic stirring for 4 h. In this step, different amounts of CTAB were used in relation to the exchangeable sodium ions. Considering the general formula of magadiite as $Na_2Si_{14}O_{29}.(5\text{-}10)H_2O$, CTA^+ was exchange with CTA/Na molar percentages equal to 25, 50, 75 and 100 were used. Finally, the material was washed with copious amounts of distilled water, until the end of foaming and dried in air. The samples were named CTA,Na-magaX and CTA,Na-[Al]-magaX (where X corresponds CTA/Na molar percentage).

Pillarization process: The pillaring occurred by the method proposed by *Zhu et al*.[3] The TEOS/CTA molar ratio was 160 for all the experiments. The materials were calcined at 500ºC for 10h. The samples were named PILC-magaX and PILC-[Al]-magaX (where X corresponds to CTA/Na molar percentage on the starting magadiite).

Results and discussion

The comparison of the X-ray diffractograms of samples prepared in this work (Figure 1) with the profiles from the literature[4] showed that magadiite and [Al]-magadiite have well crystallized structure. After the ion exchange process (Figure 1b), confirmed by C and N elemental analyses, a 1.6 nm increase in the interlayer space was observed in all the samples.

The TEOS/CTA molar ratio is an important factor for successful pillaring. When the pillaring agent is introduced (Figure 1c), TEOS produces silica-pillars that are firm enough to prop the expanded gallery after the removal of surfactants (Figure 1d).

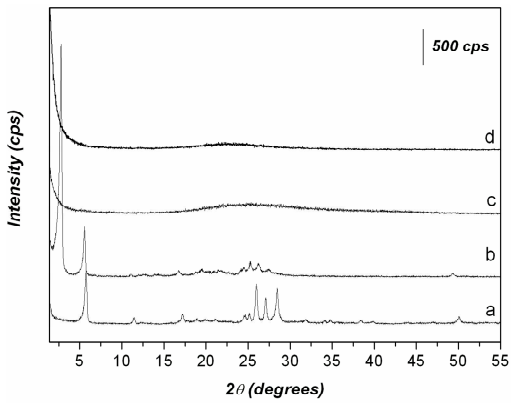

Figure 1. A) X-ray diffractograms of samples along the pillaring process. (a) [Al]-magadiite, (b) Na,CTA-[Al]-maga100, (c) pillared with TEOS and (d) after calcination for magadiite.
(Given the similarities in the diffraction behavior of the samples regardless of the precursor and CTA/Na molar ratios used in the synthesis, only results related to PILC-[Al]-maga100 are shown to illustrate.)

Through Fourier transformed infrared spectroscopy (FTIR) and solid state nuclear magnetic resonance (SS-NMR) techniques, the evolution of the structural order was probed showing that after organic surfactants have been eliminated the tetrahedra of TEOS are arranged into three-dimensional silica framework. The success of pillarizing process is confirmed by significant increases in the surface area and pore sizes of the PILCs-magadiites when diminishing the surfactant concentration.

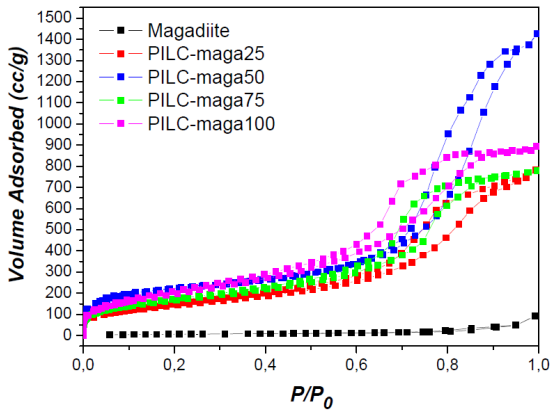

Figure 2. N_2 adsorption-desorption isotherms for PILCs derived from magadiite.

Table 1. Surface area, pore volume and pore diameter of magadiite and their pillared forms.

	Surface area[a] ($m^2.g^{-1}$)	Surface area[b] ($m^2.g^{-1}$)	Pore volume[b] ($cm^3.g^{-1}$)	Poro diameter[b] (nm)
Magadiite	25	23	0.1	13
PILC-maga25	512	482	1.1	9.4
PILC-maga50	764	879	2.3	9.0
PILC-maga75	599	831	1.3	6.9
PILC-maga100	663	627	0.6	3.7
PILC-[Al]-maga75	827	701	0.7	5.1
PILC-[Al]maga100	492	482	1.5	1.2

[a] MultiPoint BET; [b] DFT method

The N_2 adsorption-desorption isotherms of the PILCs magadiite are shown in Figure 2 while the data of surface area, pore volume and pore size are shown in Table 1. The PILCs-magadiites have a pronounced increase in porosity and surface area, and thus in adsorption, which is due to the fact that TEOS, as the pillaring precursors are converted to silica pillars, forming the rigid intercalated porous structure.

Conclusions

Monitoring the steps in the preparation of pillared materials enabled to design new porous materials with particular structures for particular applications in catalysis, adsorption processes and other.

Acknowledgements

The authors are grateful to PIBIC-SAE/UNICAMP and CAPES for the scholarships granted and to FAPESP for the financial support to this work.

References

[1] Wang, Z.; Lau T.; Pinnavaia T.J.; *Chemistry of Materials* 8, **1996**, 2200.
[2] Borbèly, G.P.; Beyer, H.K.; Kiyozumi Y.; Mizukami, E.; *Microporous Materials* 11, **1997**, 45.
[3] Zhu, H.Y.; Ding, Z.; Lu, C.Q.; Lu, G.Q.; *Applied Clay Science* 20, **2002**, 165.
[4] Superti, G.B.; Oliveira, E. C.; Pastore, H. O., Gatti, G. Marchese, L.; *Chemistry of Materials* 19, **2007**, 4300.

Surface and pore structure assessment of hierarchical zeolites by advanced water and argon sorption studies

Matthias Thommes[a*], Sharon Mitchell[b], Javier Pérez-Ramírez[b]
[a]*Quantachrome Instruments, 1900 Corporate Drive, Boynton Beach, Florida, 33426, USA.*
[b]*Institute for Chemical and Bioengineering, ETH Zurich, Wolfgang-Pauli-Strasse 10, CH-8093 Zurich, Switzerland.*
[*]*Corresponding author: Matthias.Thommes@quantachrome.com*

Introduction

Alkaline treatment is a widely-applied post synthesis method for the preparation of hierarchical zeolites. The selective dissolution of framework Si leads to the creation of intra-crystalline mesopores, which have proven to be highly beneficial in improving the zeolite utilization efficiency for catalytic applications [1]. Due to its lower solubility, the framework Al remains undissolved in basic solution, leading to a decrease in the Si/Al ratio of the mesoporous zeolites and possible modification of the surface properties. Desilicated zeolites are known to have increased Lewis acidity, which may be largely removed by subsequent acid washing, which is thought to restore the acidic properties of the parent zeolite [2]. Characterization methods which permit surface sensitivity will be advantageous in understanding the compositional alterations occurring in zeolites upon alkaline treatment. We report the combined use of Ar and H_2O adsorption to provide further insight into the pore and surface structure and properties of hierarchical zeolites prepared by desilication.

Experimental

Two ZSM-5 zeolites with nominal Si/Al ratios of 25 (Z25) and 40 (Z40) were obtained from Zeolyst International. Hierarchical ZSM-5 (Z40-A) was prepared by desilication of Z40 (1 g) in aqueous sodium hydroxide (0.2 M, 30 ml) for 30 min at 65°C, as described previously [3]. Washed hierarchical zeolite (Z40-AW) was obtained by treatment of Z40-A (1 g) with dilute HCl (0.1 M, 30 ml) for 6 h at 65°C [4]. Zeolites were characterized in their acidic form.
Ar 87 K sorption experiments were performed with manometric techniques (Quantachrome's Autosorb I MP, Autosorb IQ), and water sorption experiments were performed (at 298 K) with gravimetric and manometric sorpion analyzers (by using Quantachrome's Aquadyne and Hydrosorb). Prior to the sorption experiments the samples were outgassed for 12 hours under turbomolecular pump vacuum at 350°C. Advanced pore size analysis was performed by analyzing the argon 87 K data with a NLDFT method which assumes argon 87 K adsorption in the cylindrical siliceous zeolite pores in the micropore range and an amorphous silica pore model for the mesopore range [4]. In addition, the zeolite crystallinity was confirmed by X-ray diffraction, the mesopores were studied by transmission electron microscopy, and the bulk Si/Al ratio was determined by atomic absorption spectroscopy.

Results and discussion

Argon adsorption was used to characterize the pore structure of the zeolites studied. The isotherms of the microporous (Z25 and Z40) and of the mesoporous (Z40-A and Z40-AW) zeolites show very close agreement in the low pressure range (Figure 1a), despite differences in Si/Al ratio (Si/Al from 25-40), demonstrating the insensitivity of Ar to surface properties.

In contrast, clear differences in uptake are evident in the water adsorption isotherms of Z25 and Z40 (Figure 1b), which show greater uptake at low relative pressure for the hydrophilic Z25. Comparison of the H_2O and Ar adsorption isotherms of mesoporous Z40-A (Figure 1c) highlights the impact of compositional sensitivity on the respective adsorption behavior of the

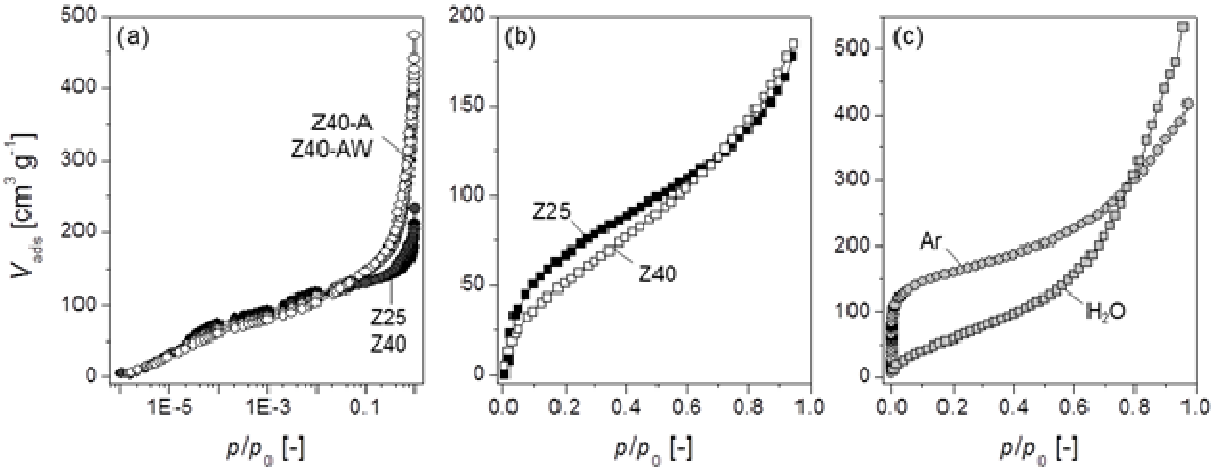

Figure 1. a) Semi-logarithmic Ar (87K) adsorption isotherms of the micro- and mesoporous zeolites, b) adsorption branch of the H_2O (298 K) adsorption isotherms of Z25 and Z40, c) comparison of the adsorption branch of H_2O and Ar isotherms of mesoporous Z40-A.

two adsorbates. Contrary to argon, which fills the ZSM5-pore at very low rel. pressures (See Figure 1a), micro-and mesopore filling with water adsorption is shifted significantly to higher rel. pressures indicating that water only partially wets the pore walls. Differences between the Z40-A and Z40-AW zeolites (not shown here) indicate that the surface of the acid washed sample has increased hydrophilicity, which is not expected from analysis of the bulk composition alone.

Conclusions

Assessment of the pore and surface properties of hierarchical zeolites is enhanced by the application of H_2O adsorption. Ar 87 K adsorption provides an accurate understanding of the pore structure, being insensitive to the surface chemistry. Further complimentary information with respect to the surface properties (e.g. hydrophobicity/hydrophilicity) is gained from the H_2O adsorption isotherms, which are found to be sensitive both to the Si/Al framework ratio and Al distribution of the zeolite. Our findings are not only important for a comprehensive surface and pore structural characterization of hierarchical zeolites in particular with regard to optimizing their application in catalysis, but also in general for further advancing the characterization of nanoporous materials.

References

[1] Pérez-Ramírez, J., Christensen, C.H., Egeblad, K., Christensen, C.H., Groen, J.C., Chem. Soc. Rev., 37 (2008), 2530-2542.
[2] Fernandez, C., Stan, I., Gilson, J.-P., Thomas, K., Bonilla, A., Pérez-Ramírez, J., Chem. Eur. J., 16 (2010), 6224-6233.
[3] Groen, J., Peffer, L.A.A., Moulijn, J.A., Pérez-Ramírez, J., Chem. Eur. J. 11 (2005), 318-334.
[4] Ravikovitch, P.I.,Neimark, A.V., Personal Communication (2001); Thommes; M., In: *Introduction to Zeolite Science and Practice* (3rd revised Edition), (Cejka, J., van Bekkum, H., Corma, A., Schüth, F., eds.), Stud. Surf. Sci. Catal.,**168** (2007), Chapter 15, pp.495-525, Elsevier.

The Structure and Properties of Micro/mesoporous Fe-silicalite-1/SBA-15 Composite Material

Márton Kollár[a], Zoltán Károly[b], Magdolna R. Mihályi[a], Károly Lázár[c], József Valyon[a]

[a]*Institute of Nanochemistry and Catalysis, Chemical Research Center, Hungarian Academy of Sciences, Pusztaszeri út 59-67, Budapest 1025, Hungary*
[b]*Institute of Materials and Environmental Chemistry, Chemical Research Center, Hungarian Academy of Sciences, Pusztaszeri út 59-67, Budapest 1025, Hungary*
[c]*Institute of Isotopes, Hungarian Academy of Sciences, Konkoly Thege Miklós út 29-33, Budapest H-1121, Hungary, lazar@iki.kfki.hu*

Introduction

Iron-containing mesoporous molecular sieves attract interest because they can be catalysts of various oxidation reactions. Several methods (mainly post-synthesis grafting [1]) were developed for incorporation of iron into SBA-type mesoporous silica materials. The introduction of iron-substituted zeolite seeds was also attempted [2].
The aim of this work was to prepare ferrisilicate materials, having bimodal porosity, by embedding of zeolite analogue Fe-silicalite-1(FeS-1) nanoclusters/crystals into SBA-15 and to get a closer insight into the structure of the material. Powder X-ray diffraction, electron microscopy, N_2 physisorption, UV-visible and Mössbauer spectroscopies were used to characterize the structure, morphology, and textural of the material, as well as the oxidation and coordination states of the iron. The FTIR spectra of adsorbed of nitric oxide was determined and analyzed to learn more about the iron sorption sites.

Experimental

A two-step synthesis procedure was applied [2]. First the FeS-1 seeds or microcrystals were synthesized in basic media. In the second step, the FeS-1 was added in different amounts (0.25-0.4 g) to the acidic synthesis solution of SBA-15, containing Pluronic P123 (2.4 g) structure-directing agent and tetraethyl orthosilicate (5.6 g) as Si source. The mixture was stirred at 40°C for 20 h, and then transferred into an autoclave for hydrothermal treatment at 100°C for 24 h. The products were washed with distilled water, dried in air and calcined at 450°C for 5 h.

Results and discussion

Table 1. The Fe content and textural properties of the calcined samples.

Sample	Si/Fe	Mesopore volume[a] (cm^3/g)	Micropore volume[a] (cm^3/g)	PSD maximum[b] (nm)
SBA-15	-	1.13	0.08	6.0
FeS-1(seed)/SBA-15	340	0.43	0.10	6.8
FeS-1(crystals)/SBA-15	270	0.63	0.10	4.5
FeS-1(crystals)/SBA-15	150	0.89	0.10	5.5

[a] Estimated from the alpha-s plots, [b] The pore size distribution (PSD) was calculated by the BJH method

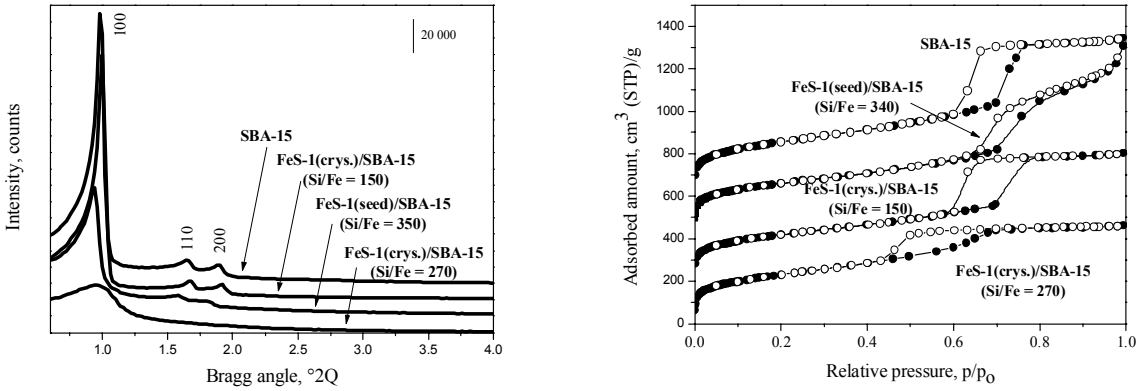

Figure 1. XRD patterns (A) and N_2 adsorption-desorption isotherms (B) of the calcined samples. Isotherms are offset for clarity.

The *100*, *110* and *200* reflections in the XRD pattern of the pure silica SBA-15 sample (Fig. 1A) indicate the long-range hexagonal ordering of parallel cylindrical mesopores. In the Fe-containing samples the intensity of the *100* reflection was lower (Fig. 1A), suggesting that the FeS-1 nanoclusters or crystals of μm size reduce the hexagonal ordering of tri-block copolymers micelles, serving as templates of the SBA-15 synthesis. These samples have mesopore volumes lower than that of the SBA-15 sample (Table 1). The reduction of mesoporosity, however, was not paralleled by the microporosity. The micropore volume showed even a slight increase (Table 1). This result suggests that the microporosity is originated from two sources: first from the SBA-15 component itself, and secondly, from the zeolite component. In the SBA-15 silica micropores were generated when the ethylene oxide chains of the copolymer template were removed from the silica walls of the mesopores.
Mössbauer data revealed that the location and coordination of some iron atoms changed upon reduction of the sample (H_2, 400 °C). Although most of the iron ions remained in its original position within the FeS-1 seeds, a small portion was relocated into the pore walls of the SBA-15. About 26 % of iron could participate in reversible $Fe^{2+} \Leftrightarrow Fe^{3+}$ redox processes. However, the ferric state remained the most prevailing.
Adsorption of NO on the reduced samples gave ν(NO) bands, assigned to the $Fe^{x+}(NO)_n$ nitrosyls (x=2, 3; n = 1, 2, 3).

Conclusions

The hydrothermal synthesis of mesoporous SBA-15 silica in the presence of nanoclusters or microcrystals of zeolite analogue Fe-silicalite-1 result in Fe-containing samples with micro/mesoporosity. Data suggest that the mesopore ordering of the composite is lower than that of the pure silica SBA-15. Mössbauer data indicates that iron is located in the framework of the clusters or crystals embedded into the silicate. Reduction with H_2 resulted in the formation of coordinatively unsaturated Fe^{2+} and Fe^{3+} sites.

Acknowledgements

The authors are grateful for the financial support of the Hungarian National Scientific Research Fund (OTKA Project No. K 68414).

References

[1] Nozaki, H., Lugmair, C., Bell, A.T., Tilley, T.D., Synthesis, characterization, and catalytic performance of single-site iron(III) centers on the surface of the SBA-15 silica, J. Am. Chem. Soc., 124 (2002), 13194-13203
[2] Han, Y., Meng, X., Guan, H., Yu, Y., Zhao, L., Xu, X., Yang, X., Wu, S., Li, N., Xiao, F.-S., Stable iron-incorporated mesoporous silica materials (MFS-9) prepared in strong acidic media, Microporous and Mesoporous Materials, 57 (2003), 191-198

Effect of pH on the mesopore structure and Al incorporation of disorder mesoporous materials

G.Gonzalez [a],[*], V.Sazo[b], M.E. Gomes[a]
[a]*Lab Materiales, Centro. Ing.Materiales y Nanotecnologia, Instituto Venezolano de Investigaciones Cientificas.*
[b] *Escuela de Quimica, Fac. Ciencias,Centro de Catálisis,Petróleo y Petroquímica, Universidad Central de Venezuela, Caracas 1020-A, Venezuela*
*[a] *Corresponding author: Fax:58-212 5041418 and e-mail:gemagonz@ivic.gob.ve*

Introduction

In the present work a detailed study of the effect of pH, in the range of 0 to 4.5, over the mesostructure of a disordered mesoporous material has been carried out. Also, the effect of hydrolysis on the Al incorporation at the different pH, was studied varying the order of addition of the aluminum salt, before and after hydrolysis. The materials were characterized by SEM, TEM, ICP and N_2 adsorption. Catalytic activity of 1-butene was performed . The materials showed a disordered mesostructure for all the pH range studied. A continuous increase in pore diameter and decrease in particle size with pH increase was observed. Al incorporation was favoured as pH increased; the highest incorporation was obtained at pH 4.5. An important effect of hydrolysis on Al incorporation was manifested on the location of the metal. Hydrolysis also had an effect on the distribution and strength of the acid sites. The materials that showed the highest skeletal isomerization selectivity were those synthesized at pH 4.5, with Al incorporated after hydrolysis.

Experimental

Nonilfenolpolietoxilado was used as surfactant. Tetraethoxysilane (TEOS), Aldrich and $Al(NO_3)_3$. $9H_2O$ from Fischer were used as silica and aluminium sources. The disordered mesoporos materials (SMIVIC) were synthesized with the following procedure, but modifying the pH of the synthesis gel from 0 to 4.5. The surfactant was dissolved in de-ionized water under continuous agitation for 12h at room temperature, acid solution of HCl (12 M) was added till pH zero was reached. TEOS was added under continuous agitation. Al incorporation was performed by adding a certain amount of $Al(NO_3)_3$. $9H_2O$ to the synthesis gel before TEOS hydrolysis (BH) or after TEOS hydrolysis (AH), to obtain a Si/Al ratio =30. The variation of pH (0-4.5) was carried out 1h after the silica hydrolysis began with NH_4OH solution. Hydrothermal synthesis was performed under continuous stirring for 48h at 363K in a closed bottle immerses into a thermostatic bath. The solid products obtained were filtered, thoroughly washed with distilled water and dried at 333K for 48h. Calcination was carried out at 793K for 10h under an air flux with a heating rate of 1K/min to remove the template.

Results and discussion

Fig. 1 shows the dramatic change of particle morphology by SEM for the different pH used. The formation of macropores and the reduction of particle size as pH increases can be observed.. There are several parameters that influence the hydrolysis and condensation reactions: activity of metal alkoxide, water/alkoxide ratio, solution pH, temperature and nature of the solvent and additive [1]. The microstructure and surface chemistry of materials are very sensitive to variation of these parameters. Fig. 2 show the N_2 adsorption isotherms and BJH pore size distribution of the materials synthesized at the different pH without The pore size distribution calculated by BJH model for each material is presented on the right hand side. The isotherms are type IV, except for pH 0 that shows a characteristic supramicroporous isotherm. The pore size and pore volume increase with the increase in pH

The incorporation of Al narrows and flattens up the desorption branches, becoming parallel to the adsorption branches similar to a H4 type, suggesting the presence of solids consisting of aggregates or agglomerates of particles forming slit shape pores with uniform shape. As pH is increased the condensation rate increases while the hydrolysis rate decreases [1]. However in the range of pH below 4, hydrolysis of TEOS is still high compared to its condensation rate. In this environment the Al species can interact with the surfactant through weak electrostatic interactions and this interaction will change the final location of the Al species if the process takes place before or after hydrolysis.

Conclusions

The variation of pH has a strong influence in the mesostructure. Increase pH increases pore volume, pore diameter and surface area. The particle size decreases with increase in pH, especially for pH 4.5. Increase pH also favors Al incorporation.
The hydrolysis condition determines the distribution of structural Aluminum in the materials.

References

[1] T C.J.Brinker and G.W.Scherrer, Sol-Gel Science, Academic Press, London, 1990,pp. 97-234

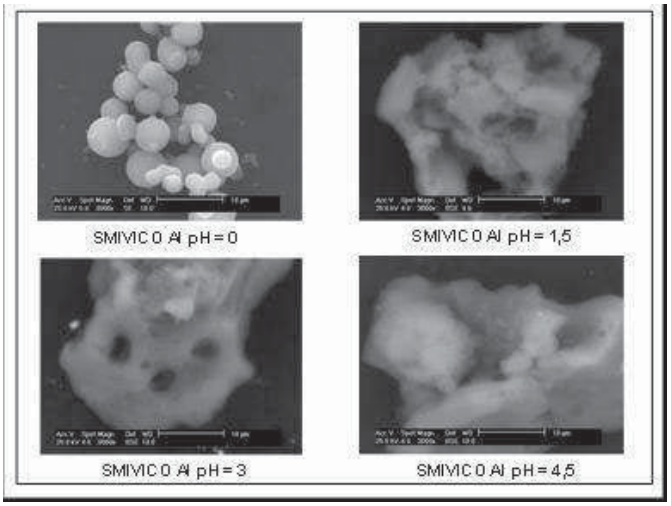

Fig. 1 SEM images of the materials synthesized at different pH

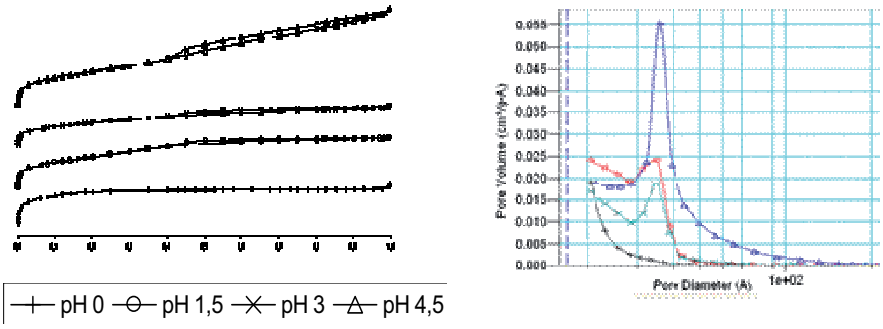

Fig. 2 N_2 adsorption isotherms of the materials synthesized at different pH

Insights on the pore topology of ITQ-28 zeolite by means of adsorption measurements and catalytic testing

Susana Valencia, Avelino Corma, Joaquín Martínez-Triguero, Miguel Palomino, Fernando Rey and M. José Sabater
Instituto de Tecnología Química (UPV-CSIC). Av. de los Naranjos s/n. 46022 Valencia. Spain
svalenci@itq.upv.es

Introduction

The availability of zeolitic structures with different pore topology makes them very useful materials as selective catalysts and adsorbents in a great variety of industrially interesting processes [1,2]. Once a new zeolite material is obtained, it is submitted to characterization measurements with the aim of finding out its structure and using it in the appropriated processes. However, in some cases the poor quality of the samples or the complexity of the structure makes difficult solving the structure and, therefore, an important number of zeolitic materials exist with unknown structure. The latter is the case ITQ-28 zeolite that was synthesized for the first time a few years ago [3]. In this work, we have shed light on the pore topology of ITQ-28 zeolite by means of characterization using adsorption measurements and catalytic testing.

Experimental

Zeolite ITQ-28 was synthesized in fluoride medium as aluminosilicate using the dicationic ammonium organic structure directing agent (R) obtained according to the following scheme:

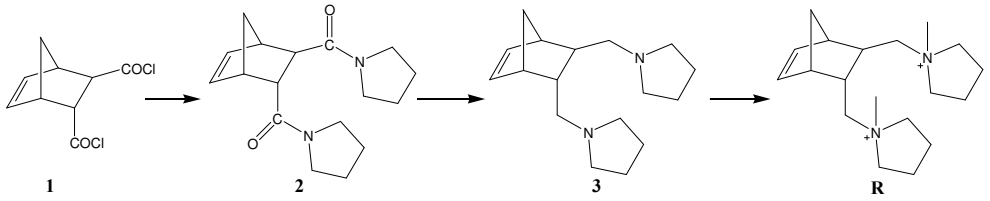

The appropriated amounts of reactants were mixed in order to obtain a gel of the following molar composition:
SiO_2 : 0.025 Al_2O_3 : 0.26 $R(OH)_2$: 0.52 HF : 7 H_2O
The sample obtained after crystallization at 175ºC under rotation for 14 days was calcined at 580ºC and submitted to different characterization measurements, including XRD, ^{27}Al MAS-NMR, IR spectroscopy, NH_3 TPD, and N_2 and Ar adsorption. Calcined ITQ-28 zeolite was submitted to adsorption experiments of butane and isobutene to asses its pore aperture and, it was also used as catalyst in the 1-hexene and 4-methyl-1-pentene cracking reactions.

Results and discussion

The XRD pattern obtained for zeolite ITQ-28 (Fig. 1a) is not coincident with any existing zeolite of the Database of Zeolite Structures of the IZA [4], confirming that this is a new zeolitic material. Zeolite ITQ-28 has a Si/Al ratio of 12, as shown by ICP analysis, indicating that Al has been incorporated in the solid, whereas ^{27}Al MAS NMR confirms that it is tetrahedrally coordinated in the framework and only a minor signal assigned to octahedral Al is observed after calcination. The IR spectrum in the hydroxyl region evidences the presence of OH groups at 3630 cm^{-1} that could have acidic properties but, when adsorbing pyridine as a

basic probe molecule, no interaction with these OH was observed, suggesting that pyridine is not able to access the porosity of this zeolite. On the other side, NH_3 TPD measurements carried out in the sample demonstrated its acidic character and allows us to hypothesize that ITQ-28 zeolite structure could be constituted by pore apertures of small pore dimensions.
From the N_2 and Ar adsorption isotherms, a BET surface area value of 385 m^2/g, a micropore volume of 0.17 cm^3/g and a mean pore diameter of 5.7Å were found for ITQ-28. These results indicate that it is probably a multidimensional pore zeolite with a medium pore aperture, contrarily to what has been discussed above. Nevertheless, the possibility of having small pore windows that give entrance to large cavities can not be discarded.

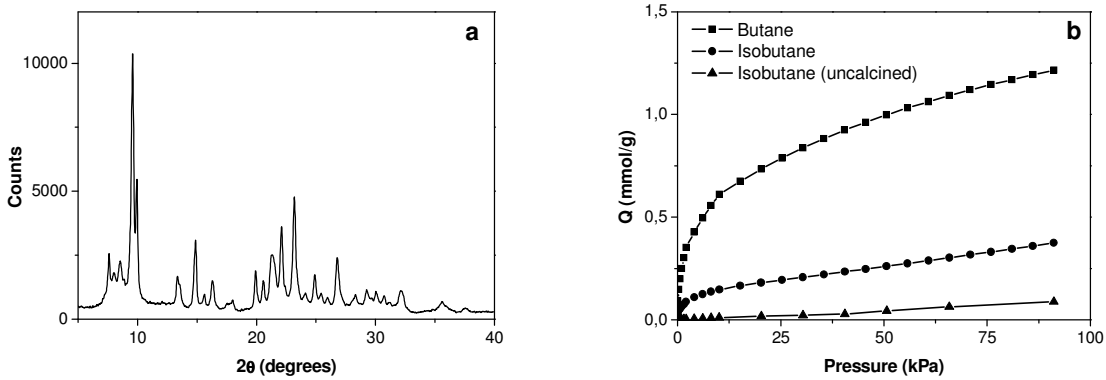

Figure 1. XRD pattern of calcined ITQ-28 zeolite (a) and, butane and isobutane adsorption isotherms at 25ºC (b).

In order to get more insight in the pore topology, adsorption of a linear and a branched hydrocarbon (butane and isobutane) was carried out, since branched molecules can not access the porosity of small pore zeolites. The results shown in Fig. 1b indicate that butane is adsorbed in much higher amount than isobutane, but the latter is not negligible as it should be for a small pore zeolite. With the aim of separating the contribution of adsorption in the external surface of the zeolite, an isotherm was performed in the non-calcined sample confirming that its contribution to the total adsorption is not as high as to justify the isobutane adsorption in the calcined zeolite (Fig. 1b).
From these results, it can be envisaged that ITQ-28 structure could be constituted by a bidimensional medium pore system with a non-circular aperture, resulting in a constrained pore opening.
Finally, the results obtained using ITQ-28 as catalyst in the cracking reaction of a linear and a branched olefin (1-hexene and 4-methyl-1-pentene) indicated that the selectivity and product distribution agree well with a microporous system as described above formed by constrained medium pore apertures.

Acknowledgements

Financial support by Spanish and regional institutions is gratefully acknowledged (MAT2009-14528-C02-01, CTQ2007-66614/PPQ, PAID-06-08:3279 and GV/2009/066).

References

[1] Corma, A., Martínez, A., *Stud. Surf. Sci. Catal.*, 157 (2005), 337-366.
[2] Barrer, R.M., in *Zeolite and Clay Minerals as Sorbents and Molecular Sieves*, Academic Press, London (1978).
[3] Corma, A., Sabater, M.J., Valencia, S., WO Patent 2005/030646 (2005).
[4] www.iza-structure.org/databases/

Ultrasound irradiation as suitable tool for the preparation of high active acid catalysts of HPA/Al-MCM-48 type

Michal Horňáček[1], Pavol Hudec[1], Narendra Kumar[2], Agáta Smiešková[1], Dmitry Yu. Murzin[2], Tapio Salmi[2].

[1] Department of Petroleum Technology of and Petrochemisty, Faculty of Chemical and Food Technology, Slovak University of Technology, Radlinského 9, 812 37 Bratislava, Slovak Republic
[2] Åbo Akademi University, Laboratory of Industrial Chemistry and Reaction Engineering, Process Chemistry Centre, Biskopsgatan 8, FIN-20500 Turku/Åbo, Finland

Introduction

MCM-48 is a member of the M41S family of mesoporous molecular sieves, disclosed in 1992 [1,2]. MCM-48 has a three-dimensional channel system, which consists of two interpenetrating pore systems separated by a continuous silica wall. These materials are characterized by a regular array of pores, in the 2.0 - 10.0 nm range, with uniform diameter, high specific surface area and pore volume.

Heteropoly acids (HPA) have proved to be the alternative of traditional acid catalysts, such as sulfuric acid and aluminium chloride, due to their strong acidity and environmental benignity. With the emergence of mesoporous molecular sieve materials [3], HPAs supported mesoporous materials have received much attention [4]. In such research, HPAs usually form finely dispersed species on the internal surface inside the pores of mesoporous materials. Moreover, higher catalytic activities for these samples than for the conventional catalysts were observed, meaning that the potential of the mesoporous material-supported HPAs are of significance in acid catalysis. In this paper we prepared HPAs supported catalysts by different loading methods including ultrasound and compared their textural, acid and catalytic properties.

Experimental

The mesoporous molecular sieve type's of Al-MCM-48 was synthesized according to Shih et al. [4]. 10 wt. % of HPW supported on mesoporous materials (denoted HPW/Al-MCM-48) were prepared by three different methods: 1) ultrasound irradiation (US), 2) impregnation (IMP) from water solution and 3) ion exchange (IE). The basic samples were exposed to an appropriate amount of a 0.02 molar aqueous solution of the acid to achieve a final loading of 10% wt. Ultrasound was executed at 30 kHz and 300 W. Impregnation was performed in a vacuum rotavapour. The sample was mixed with an appropriate amount of 0.02 molar aqueous solution of the acidfor 16 hours at room temperature. The slurries from both methods were evaporated to dryness under vacuum at 80°C. Ion exchange was realized in magnetic stirrer with an appropriate amount of a 0.02 molar aqueous solution of the acid to achieve a final loading of 10% for 24 hours at 60°C. Then the samples were filtered, dried and calcined at 170°C for 4 h.

The crystalline phase identification and structure purity determination of all samples was determined by X-ray powder diffraction. Surface characteristics were measured by adsorption of nitrogen at the temperature of -197 °C in ASAP 2400 (Micromeritics); adsorption data were treated by BET isotherm. The acidity of investigated samples was measured by infrared spectroscopy (ATI Mattson FTIR) by using pyridine (≥99.5%) as a probe molecule for qualitative and quantitative determination of both Brønsted and Lewis acid sites. The catalytic activity was tested by isomerization of o-xylene at 350 °C in atmospheric flow micro reactor on-line connected with a gas-chromatograph.

Results and discussion

XRD provides direct information of pore structure and phase purity of these materials. All calcined samples proved on XRD patterns typical of well-defined mesoporous structure and showed an intense diffraction peaks at low angle which are indexed as (2 1 1), (2 2 0), (3 2 1), and (4 2 0) reflection. After loading of HPW on Al-MCM-48 arises the decrease of intensity of mainly diffraction peak indexed as (2 1 1). These characteristics are consistent with a well-ordered cubic structure, which is typical for Al-MCM-48. Values of unit cell parameters and d-spacings of all tested samples are given in Table 1. The d-spacings are corresponding to cubic Ia3d space group of Al-MCM-48 as reported in literature [2].

In all adsorption isotherms of nitrogen up to three regions characteristics of this sort of isotherm can be distinguished: (1) formation of second adsorption layer on the surface (BET-range), (2) capillary condensation inside mesoporous and (3) multilayer adsorption on the externals surface. All materials exhibit a step rise commencing at 0.21 – 0.32 of relative pressure due to the capillary condensation of nitrogen in the mesopores. Afte the HPW loading on the support, both surface area and pore volume decreased, which seems logical as the impregnated HPW is dispersed and deposited on the support surface, decreasing consequently also the effective pore diameter (Table 1).

Table 1 Physico-chemical characteristics of Al-MCM-48 samples

Catalyst	d_{211} (nm)	a_0 (nm)	D_p (nm)	t (nm)	S_{BET} ($m^2.g^{-1}$)	V_p ($cm^3.g^{-1}$)	Acidity ($\mu mol.g^{-1}$)	BAS ($\mu mol.g^{-1}$)	LAS ($\mu mol.g^{-1}$)
Al-MCM-48	3.30	8.07	2.68	1.27	1079	1.015	180	58	122
HPW/Al-MCM-48(US)	3.22	7.90	2.15	1.48	705	0.522	271	125	146
HPW/Al-MCM-48(IMP)	3.35	8.20	2.08	1.61	722	0.542	201	93	112
HPW/Al-MCM-48(IE)	3.42	8.39	2.32	1.55	820	0.580	244	116	128

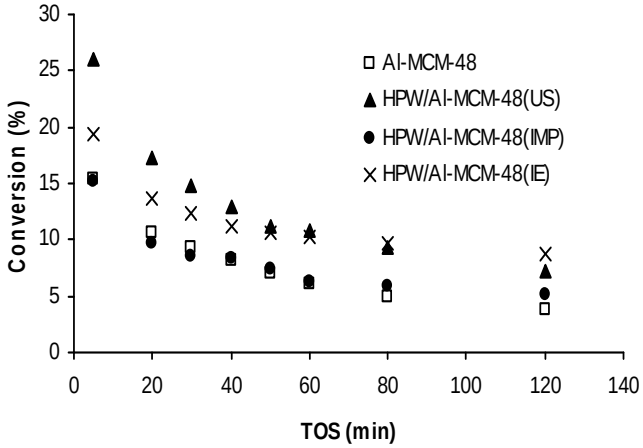

Fig.1 The comparison of catalytic activity in isomerization of o-xylene.

After HPW loading on the support the conversion increased together with Brønsted and Lewis acidity, but at the same quantity of loaded HPW the acidity depends on the way of loading. The catalytic activity was tested by isomerization of o-xylene in flow microreactor (Fig.1). The highest initial conversion achieved the sample with the highest acidity, prepared by the use of the ultrasound. The ultrasound loading seems to be the most suitable method for the HPA-loading to the carrier in comparison with the standard IE or IMP methods to prepare very active acid catalyst.

References

[1] C.T. Kresge, M.E. Leonowicz, W.J. Roth, J.C. Vartuli, J.S. Beck, Nature 359 (1992) 710.
[2] J.S. Beck, J.C. Vartuli, W.J. Roth, M.E. Leonowicz, C.T. Kresge, K.D. Schmitt, C.T.W. Chu, D.H. Olson, E.W. Sheppard, S.B. McCullen, J.B. Higgins, J.L. Schlenker, J. Am. Chem. Soc. 114 (1992) 10834.
[3] M.A. Schwegler, H. van Bekkum, N.A. de Munck, Appl. Catal. A: Gen. 74 (1991) 191.
[4] Y.Y. Liu, K. Murata, M. Inaba, N. Mimura, Catal. Commun. 4 (2003) 285.

Effect of washing on the properties of HZSM-5 zeolite modified with phosphoric acid

Miroslaw Derewinski[1], Priit Sarv[2]
[1]*Jerzy Haber Institute of Catalysis and Surface Chemistry, Polish Academy of Sciences, Krakow, Poland*
[2]*Priit Sarv, Institute of Physics and Biophysics, Estonian Academy of Sciences, Tallinn, Estonia*

Introduction

The post-synthesis modification of MFI (ZSM-5) type zeolites with phosphorous compounds is known method varying their catalytic performance [1, 2]. The PZSM-5 catalysts show high selectivity in the formation of *para*-substituted benzene derivatives which is the result of decrease of acidic properties of phosphorous modified zeolites and steric hindrance caused by formation of occluded extraframework species in the zeolitic channels. The aim of the present study has been to answer the following questions:
- what is a spatial distribution of phosphorous deposit in the ZSM-5 structure,
- what is a real reason for a decrease in number of the acid sites in H_3PO_4 modified zeolite samples,
- is the modification of ZSM-5 zeolite with H_3PO_4 an irreversible process?

Experimental

xPZSM-5 with different amounts of phosphorous (x=1, 2 and 5%) have been prepared by impregnating HZSM-5 (Si/Al=70) with water suspension of orthophosphoric acid (H_3PO_4) followed by calcination of impregnated samples at 550^{o}C. The subsequent washing with water at 80^{o}C followed by temperature treatment (550^{o}C) was performed to study if zeolite physicochemical properties, altered by deposition of phosphorous compounds, can be restored. ^{1}H, ^{27}Al, ^{29}Si and ^{31}P MAS NMR, SEM, EDAX and TPD of bases (ammonia, pyridine) were used to characterize the zeolites under study.

Results and discussion

EDAX analysis of xPZSM-5 showed that the phosphorous containing species are located mainly near the external surface of the zeolite crystals. Even for the highest P content (5wt %) no phosphorous compound were found outside the crystals. Non-uniform distribution of Al found in the parent sample can at least partially affect the phosphorous distribution in the P modified samples.
^{27}Al and ^{29}Si MAS NMR data showed that impregnation with H_3PO_4 followed by the calcination of impregnated samples at 550^{o}C, resulted in the dealumination of the framework [3]. Both ^{27}Al and ^{31}P MAS NMR revealed the presence of aluminum phosphate formed in the reaction of H_3PO_4 with dislodged aluminum species and polyphosphoric acids formed during the calcination of P modified samples. The introduced phosphorous decreased the concentration of strong Brønsted acid sites which was explained by the lattice dealumination rather than by a reaction of orthophosphoric acid with protonic acid sites [3].
Temperature programmed desorption (TPD) data of preadsorbed bases (ammonia, pyridine) confirmed a decrease in acidity of the samples under study, proportionally to the amount of

phosphorous introduced. 5%wt of P completely blocked access to pyridine to acid sites (some adsorption of ammonia on weak acid sites was still observed).

The applied washing procedure removed about 70% of P initially introduced into ZSM-5 structure. Temperature programmed activation spectra showed that for washed xPZSM-5 zeolites peaks of the water desorption, attributed to polyphosphate condensation (about 180°C) were not present.

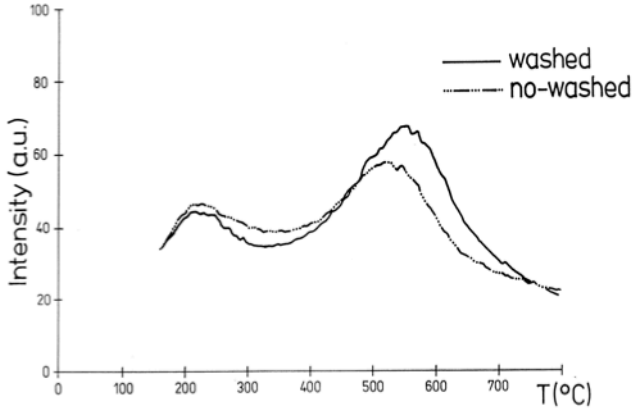

Figure 1. TPD of pyridine from fresh and washed 2%PZSM-5 samples.

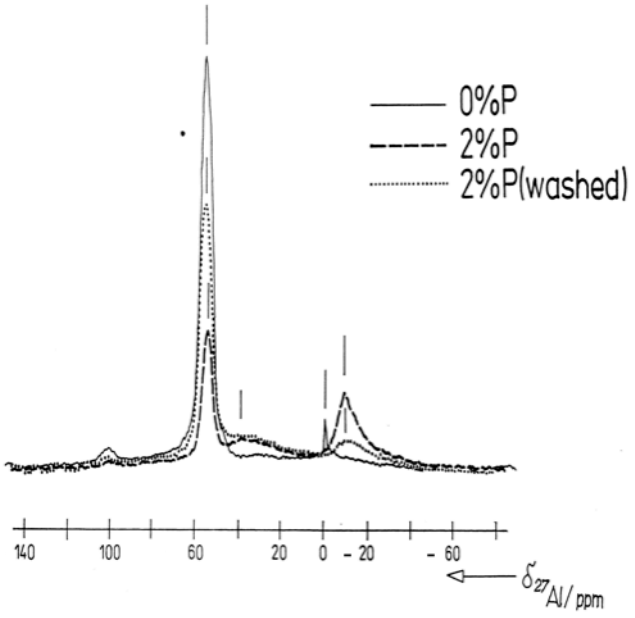

Figure 2. ^{27}Al MAS NMR spectra of parent HZSM-5, 2%PZSM-5 and washed samples

TPD of preadsorbed pyridine confirmed that at concentration of 1-2%wtP washing recovered to a certain extent strong Brønsted acid sites (Fig.1.). The strong acid sites recovered after washing the samples with smaller P loading, exhibited higher TPD maximum (gamma peak) than no washed samples. This can be caused by influence of the extralattice material upon the strength of bridging hydroxyls. ^{27}Al MAS NMR reveals that washing restores a part of the tetrahedrally coordinated framework Al. The remaining part is removed on washing, bringing about the irreversible dealumination of the framework (Fig. 2).

Conclusions

We report results of the study on washing the phosphorous impregnated ZSM-5 zeolite. The obtained data have shown partial reversibility of the dealumination process upon water treatment. Temperature programmed desorption (TPD) of bases (ammonia, pyridine) has proved the recovery of strong acid (Brønsted type) sites in the washed samples. Simultaneously, ^{27}Al and ^{31}P MAS NMR data have evidenced restoration of at least part of the framework Al^{IV} and removal of Al and P containing species from the channels of the zeolite crystals.

References

[1] W.W. Kaeding, S.A. Butter, U.S. Patent 3,911,041 (1975)
[2] W.W. Kaeding, C. Chu, L.B., Young, B. Weinstein, S.A. Butter, J. Catal. 67 (1981) 159
[3] J. Caro, M. Bulow, M. Derewinski, J. Haber, M. Hunger, J. Karger, H. Pfeifer, W. Storek, B. Zibrowius, J. Catal. 124 (1990) 367.

RTH-type aluminosilicate zeolites synthesized using phosphorous containing structure directing agents

J. A. Vidal-Moya, R. Simancas, M.Hernández-Rodríguez, M. T. Navarro, A. Cantín, D. Dari, N. Velamazán, J. L. Jordá, T. Blasco, F. Rey
Instituto de Tecnología Química (UPV-CSIC),Universidad Politécnica de Valencia. Consejo Superior de Investigaciones Científicas. Avda. De los Naranjos s/n, 46022-Valencia, Spain, tblasco@itq.upv.es,

Introduction

Zeolite RUB-13 possesses a RTH type structure consisting of a bidimensional eight member ring channels system with an aperture of 4.1x3.8 Å [1,2].

Here we report, the synthesis and characterization of pure silica and aluminosilicate RUB-13 zeolites with Si/Al framework molar ratio in the range 13-25, which were obtained through a novel route using phosphorous-containing organic moieties (shown in Scheme 1) instead of the classical quaternary amine cations as organic structure directing agents (OSDA). The characterization of the as synthesized and calcined RUB-13 zeolites was carried out by using a variety of techniques, and more especially solid state NMR spectroscopy.

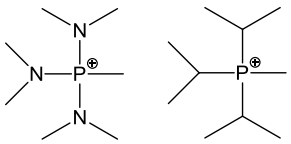

Scheme 1. OSDAs used in this study.

Experimental

Gels of chemical composition 0.5 SDA^+OH^- : (1-x) SiO_2 : x Al_2O_3 : 7 H_2O : 0.5 HF have been prepared in fluoride or in alkaline media using the phosphorous containing cations as SDA. A portion of sample was calcined at 1023 K for 5h. Zeolites with Si/Al molar ratio of 25, 18 and 13 are obtained from gels with a Si/Al=35, 25 and 15, indicating that more aluminum than silicon is incorporated into the final solid.

^{13}C, ^{19}F, ^{27}Al, ^{29}Si and ^{31}P have been recorded using a Bruker AV400 spectrometer with the sample spinning at the magic angle at rates between 5-25 kHz depending on the detected nucleus.

Results and discussion

The XRD data of the as synthesized material are characteristic of highly crystalline RUB-13 zeolite as pure phase. The zeolite structure is maintained after calcinating the samples at 1023 K during 5 h.

The positive charge of the phosphorous containing cations entrapped into pure silica RUB-13 zeolite were compensated by fluoride anions or structural defects, depending on the media employed for their syntheses. Trivalent aluminum atoms substituting for silicon atoms into the

zeolite framework introduces negative charges which compensate the phosphorous containing cations.

Figure 1 shows the ^{29}Si, ^{27}Al and ^{31}P MAS NMR spectra of RUB 13 zeolite with a Si/Al=18 as synthesized and calcined forms. The ^{29}Si spectrum of the original sample shows two peaks at -113.7 ppm of $Si(OSi)_4$ sites and at -106.9 ppm due to the contribution of $Si(OSi)_4$ and of $Si(OSi)_{4-n}(OAl)_n$ sites. The ^{27}Al MAS NMR spectra of Figure 1 indicate that all aluminum occupies framework sites in the original samples but calcination generates extraframework species (Al_{oct} at -13 ppm, and distorted Al sites and aluminophosphate at -32 ppm), so that only a small fraction remains at framework positions. The ^{31}P MAS NMR spectrum of the original sample shows a peak that correspond to the phosphonium species but upon calcinations a very broad band with several components in the range (-10) ppm – (-40) ppm which indicate the formation of phosphate-like species isolated and with various degrees of condensation as well as aluminum phosphate.

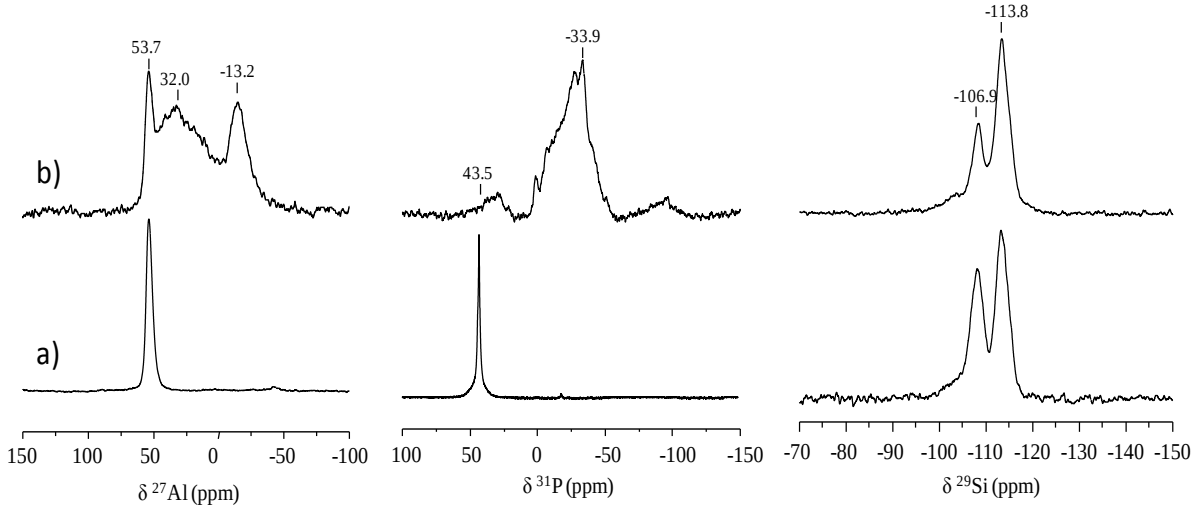

Figure 1. ^{27}Al, ^{31}P and ^{29}Si MAS NMR spectra of sample with Si/Al=18, a) as prepared, b) calcined sample.

Conclusions

The use of phosphorous containing cations as structure directing agent has allowed the crystallization in fluoride and alkaline media of pure silica and Al-containing RUB 13 zeolites of varying composition up to a Si/Al ratio of about Si/Al= 13. In the as-synthesized zeolites, all aluminum is incorporated into the structure and the occluded OSDA is fully preserved in the zeolite cavities. Upon calcinations, phosphorous containing moieties are transformed into phosphates species, and most aluminum atoms leave the framework sites. Some extraframework aluminum is involved in an aluminophosphate phase.

Acknowledgements

The authors acknowledge Spanish Government (projects MAT2009-14528-C02-01 and PLE2009-0054) for financial support. R.S., M.H.R. and N.V. thank to UPV, MICINN and CSIC for Predoctoral fellowships, respectively.

References

[1] Vortmann, S. et. al. *Microporous Materials,* **4** (1995), 111 - 121.
[2] Lee, G.S. *J. Solid State Chem.*, **167** (2002) 289 – 298.

New synthesis of Pure silica and Ge-containing SSZ-73 zeolites

M. Hernández-Rodríguez, J. A. Vidal, J. L. Jordá, T. Blasco, F. Rey
Instituto de Tecnología Química (UPV-CSIC), Avda. De los Naranjos s/n, 46022-Valencia, Spain, frey@itq.upv.es,

Introduction

Zeolite SSZ-73 (SAS) has been synthesized previously by Zones' group at Chevron [1] using a highly selective Organic Structure Directing Agent as pure silica zeolite. Its synthesis as pure phase was rather difficult because crystallization of RUB-13 (RTH) competes with SSZ-73 because different isomers of the same OSDA direct the synthesis to these two phases [1,2]. Then, the synthesis of pure SSZ-73 relays on the purity of the OSDA, which is not an easy task. Here, we report a convenient method for preparation of pure SSZ-73 zeolite as pure silica and as Germania-silica materials. Also, the preferential occupation of Ge of sites located at eight-ring has been demonstrated by means of X-Ray diffraction and Multi-Nuclei Solid State MAS-NMR spectroscopy.

Experimental

SSZ-73 zeolites were obtained from synthesis gels having the following chemical composition: *x* SiO_2 : *(1-x)* GeO_2 : *0.5* OSDA : *0.5* HF *7* H_2O, where *x* was varied from 1 to 0.667 (Si/Ge = ∞ - 2) and OSDA is the tri-tert-butyl-methyl-phosphonium hydroxide. The gels were heated in Teflon lined stain-less steel autoclaves at their autogenous pressure at temperatures in the range of 175 – 150ºC for 24 – 72 hours under continuous rotation (20 r.p.m.). The solids were collected by filtration and exhaustively washed with distilled water at 80ºC, and finally dried at 100ºC, overnight. The resulting zeolites were characterized by means of X-Ray diffraction and multi-nuclei MAS-NMR spectroscopy in the as-made form and as well as after submission to calcination 700ºC in dried air.

Results and discussion

Table 1 provides the Si/Ge ratio employed and the final chemical of the zeolites SSZ-73. There, it is evident that the final products posses nearly the same Si/Ge ratios than the original crystallization media, varying from pure silica to Si/Ge ratio of 3.5. Also, the Phosphorous contents in all the preparations of SSZ-73 are very close to 2, which is the expected value for one OSDA in each cavity of SSZ-73 structure and the same value than that obtained in previous zeolites SSZ-73 [1]. The crystallinity and purity of the zeolites SSZ-73 was very high as deduced from their corresponding X-Ray diffraction patterns shown in Figure 1.
The integrity of the occluded tetraalkylphosphonium in the as-made zeolites was confirmed by means of ^{31}P and ^{13}C-MAS-NMR spectroscopy.

Table 1. Chemical compositions of Zeolites SSZ-73

Sample	$(Si/Ge)_{gel}$	$(Si/Ge)_{solid}$	P (mol/U.C.)
3.5Ge-SAS	3.5	3.5	1.96
5Ge-SAS	5	4.6	1.99
10Ge-SAS	10	9.1	2.02
15Ge-SAS	15	13.2	2.01
Si-SAS	∞	∞	1.98

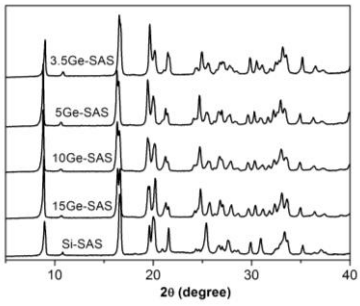

Figure 1. XRD patterns of zeolites SSZ-73

The SSZ-73 samples were submitted to 'in-situ' calcination and the resulting zeolites were analyzed by X-Ray Diffraction. The Rietveld analyses of the corresponding patterns permit to unambiguously calculate the Germanium occupation of the two crystallographic sites and the unit cell parameters of the SSZ-73 structures. The parameter *c* of the tetragonal cell linearly decreases as the Germanium content, while the parameter *a* increases, but there is no clear proportionality between the enlargement of the parameter *a* and the Germanium content of the zeolite. The calculated Unit Cell volumes of the SSZ-73 samples are not following any clear dependence with the Germanium content. Indeed, the Unit Cell volume decreases at low Germanium content, and subsequently increases from Si/Ge content lower than 5. These results suggest that there is a preferential sitting of Germanium in one of the two crystallographic sites. This has been confirmed from the Rietveld analyses of the X-Ray patterns, indicating that at low Germanium content only T1 is occupied by Ge, while above Germanium content higher than 3.2 Ge atoms per Unit Cell, also T2 starts to be occupied by Ge as it is shown in Figure 2. These results are fully consistent to those obtained from ^{19}F-MAS-NMR study of the as-made zeolites Ge-containing SSZ-73.

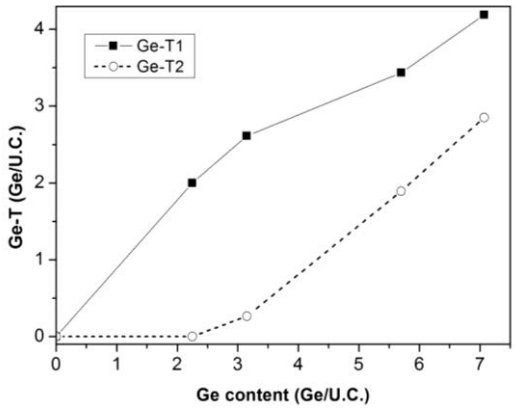

Figure 2. Crystallographic Ge occupation on SSZ-73 structure depending on the Ge content.

Since 8-memberd rings of the SAS structure is formed exclusively by T1 sites, it could be concluded that Ge preferentially occupies 8-ring at the SAS structure. The reason of this preferential occupation is still being studied.

Conclusions

Here we report the preferential occupation by germanium in sites located at the 8-ring of the SAS structure. To our knowledge, this is the first report of preferential sitting in zeolite structures of Germanium at structural positions different than those located at Double-Four-Rings.

Acknowledgements

The authors acknowledge Spanish Government (projects MAT2009-14528-C02-01 and PLE2009-0054) for financial support. M.H.R thanks to MICINN for Predoctoral fellowship.

References

1. D. S. Wragg et al., *Chem. Mater.* **19** (2007) 3924-3932.
2. C. Kim et al., *Micropor. Mesopor. Mater.* **116** (2008) 227–232.
3. A. Corma et al., *Angew. Chem. Int. Ed.* **49 (**2010) 3120 – 3145.

A New Phosphazene based Route for Synthesis of UTD-1

R. Simancas, M. T. Navarro, A. Cantín, D. Dari, N. Velamazán, J. A. Vidal-Moya, J. L. Jordá, T. Blasco, F. Rey
Instituto de Tecnología Química (UPV-CSIC), Universidad Politécnica de Valencia. Consejo Superior de Investigaciones Científicas. Avda. de los Naranjos s/n, 46022-Valencia, Spain, frey@itq.upv.es

Introduction

The first report on UTD-1 is dated on 1995 [1]. In that earlier report, the Structure Directing Agent (SDA) employed was not an organic cation, but the organometallic moiety: bis(pentamethyl-cyclopentadienyl)cobalt(III) cation. Later, UTD-1 was recognized as the first silica based extralarge zeolite with pore apertures formed by 14 tetrahedra [2], opening the possibility of processing large molecules by zeolite-based catalysts. However, one of the main drawbacks of this synthesis was the employment of $(Me_5Cp)_2Co^+$ as SDA, since its transformation into the hydroxide form, which is added to the synthesis gel is rather difficult, and upon calcination, Co species remains inside the channels and are difficultly remove. Up to our knowledge, there is no any report on an alternative route for synthesizing UTD-1 zeolites. Here, we report a new synthesis route for preparing UTD-1 based on the use of phosphazenes as structure directing agents, which can be easily completely removed by calcination and subsequent water washing. Also, we report the synthesis of B and Al containing UTD-1 materials, which are of interest for catalytic applications.

Experimental

UTD-1 zeolite was typically obtained from synthesis gels having the following chemical composition: SiO_2 : *x* B_2O_3 : *0.5* OSDA : 15 H_2O, where *x* was varied from 0 – 0.01 and OSDA is the 1,1,1,3,3,3-Hexakis(dimethylamine)diphosphazene hydroxide. The gels were heated in Teflon lined stain-less steel autoclaves at their autogenous pressure at temperatures at 135ºC for 15 – 50 days under continuous rotation (60 r.p.m.). The solids were collected by filtration and exhaustively washed with distilled water and dried at 100ºC, overnight. The resulting zeolites were characterized by means of X-Ray diffraction and multi-nuclei MAS-NMR spectroscopy in the as-made form and as well as after calcination 700ºC in dried air. Some of the solids were submitted to secondary treatments for removing the occluded phosphorous species or for incorporating Al sites instead of B centres.

Results and discussion

Figure 1 shows a typical X-Ray Diffraction pattern of UTD-1 zeolite in the as-made, calcined, Al-containing and washed materials and Table 1 provide the relevant chemical compositions of these samples.

Table 1. Chemical compositions of UTD-1 zeolites

Sample	Si/B	Si/P	Si/Al
As made	42	15.1	--
Si-DON	--	16.4	--
B-DON	48	16.5	--
Al-DON	>2000	134.1	36.2
Washed-DON	63	276.2	--

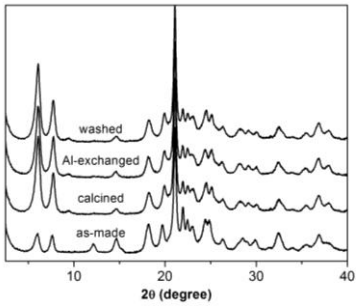

Figure 1. XRD patterns of UTD-1 samples

C/N and C/P ratios as well as the ^{13}C (signal at 37 ppm) and ^{31}P (signal at 17 ppm) MAS-NMR spectra of the as-made UTD-1 solids were in very good agreement with that of free phosphazene, concluding that the OSDA remains intact filling the pores of the UTD-1 zeolite.

The structure of UTD-1 has been confirmed by means of X-ray diffraction technique. Indeed, the XRD pattern of the calcined material was indexed according to a *Cmcm* unit cell with the following unit cell parameters: a = 18.943(3), b = 22.993(5), c = 8.459(1) Å. The BET surface area and total micropore volume of the calcined material (calculated from the N_2 adsorption isotherm by applying the *t*-plot method) were 224 m^2/g and 0.055 cm^3/g, respectively. The very low micropore volume is attributed to the presence of phosphorous debris produced upon calcination of the occluded phosphazene. This phosphorous species can be removed just by washing with an ammonium acetate (3M) aqueous solution, resulting in a solid of 346 m^2/g and 0.115 cm^3/g of surface area and micropore volume, respectively. The Horvath-Kawazoe formalism applied to the adsorption Ar isotherm shows an averaged pore diameter of 6.9 Å, which is close to the crystallographic 14R pore aperture of UTD-1.

^{11}B-MAS-NMR spectrum of calcined B-UTD-1 shows the typical lineshape of a mixture of tetrahedral and trigonal boron species, which are found in the hydrated zeolites. This result indicates that B is isomorphically incorporated into the UTD-1 framework.

The main goal of synthesizing UTD-1 zeolite was to study its acid properties, but B-UTD-1 shows very weak acidity precluding its catalytic use for many processes. Then, we have exchanged B(III) by Al(III) in order to increase the acidity of the zeolite. When this is done, Al-UTD-1 is obtained, which develops strong acidity able to retain pyridine even at 350ºC under vacuum. The presence of Al in tetrahedral coordination has been proved by ^{27}Al-MAS-NMR spectroscopy, and the Al-UTD-1 shows a main resonance at 55 ppm, whose presence is generally taken as an evidence of the incorporation of aluminium atoms in zeolite frameworks. This main signal is accompanied by a minor and narrow resonance at 0 ppm, due to the presence of a very minor proportion of extraframework aluminium .

Conclusions

This study has shown that is possible to synthesize pure silica and B-containing UTD-1 zeolites using phosphazenes as structure directing agent. Al exchange of B-UTD-1 and subsequent calcination can be successfully use for the preparation of Al-UTD-1 zeolite, which show strong acid properties and could be employed for catalytic purposes.

Acknowledgements

The authors acknowledge Spanish Government (projects MAT2009-14528-C02-01 and PLE2009-0054) for financial support. R.S. and N.V. thank to UPV and CSIC for Predoctoral fellowships, respectively.

References

1. K. J. Balkus et al., *Prepr. – A.C.S., Division Petroleum Chem.* **40** (1995) 296 – 297.
2. C. C. Freyhardt et al., *Nature* **318** (1996) 295 – 298.

A novel reliable route for Li-A [ABW] synthesis

P. Aprea[a], D. Caputo[a], N. Gargiulo[a], A. F. Gualtieri[b] C. Colella[a,*]
[a]*Dipartimento di Ingegneria dei Materiali e della Produzione, Università Federico II, Piazzale V. Tecchio 80, 80125 Napoli (Italy);* [b]*Dipartimento di Scienze della Terra, Università di Modena e Reggio Emilia, Via S. Eufemia 19, 41100 Modena (Italy)*
**Corresponding author: carmine.colella@unina.it*

Introduction

Li-A [ABW] (from now onwards Li-ABW) is a synthetic zeolite [1], characterized by high-density and strong anionic field (Si/Al ratio = 1). The framework of Li-ABW consists of a regular array of non-crossing channels, filled with Li^+ ions and H_2O molecules, which are hydrogen-bonded to each other in a very uncommon one-dimensional chain, parallel to the channels direction. Although, in general, Li-ABW is not considered suitable for technological applications, due to the small size of its pores, some investigations have been recently carried out to explore the possibility of employing this zeolite in hydrogen adsorption and storage processes [2]. This paper reports the characterization of a Li-ABW sample, obtained with a novel synthesis route which is reliable and easier than the usually adopted procedures [3, 4].

Experimental

Li-ABW was synthesized by hydrothermal treatment of an amorphous gel, obtained using, as reactants, Ludox HS 40 (silica source), $Al(OH)_3$ (Serva) and $LiOH \cdot H_2O$ (Carlo Erba).
Synthesis parameters, such as time and temperature, were preliminarily explored in the ranges 6-120 hours and 90-180°C, respectively. The best yield in terms of product amount and purity was obtained, reacting for 72 hours, at 140°C, a batch with the following molar composition: $4Li_2O \cdot Al_2O_3 \cdot 2SiO_2 \cdot 780H_2O$.
The synthesized product was characterized by SEM, XRPD (CuKα rad.), and chemical analyses. Cation exchange behaviour of Li-ABW towards Na^+ and K^+ was also evaluated.

Results and discussion

Chemical analysis. The chemical composition of the synthesized product turned out to be: Li_2O, 10.07%; Al_2O_3, 35.66%; SiO_2, 41.68%; H_2O, 12.70%, which gives the following formula unit $Li_{0.97}Al_{1.01}SiO_4 \cdot 1.02\ H_2O$, not very far from the theoretical one ($LiAlSiO_4 \cdot H_2O$). Accordingly, calculated cation exchange capacity (CEC) was equal to 6.71 meq/g, compared to the value of 6.94 meq/g of the theoretical formula.

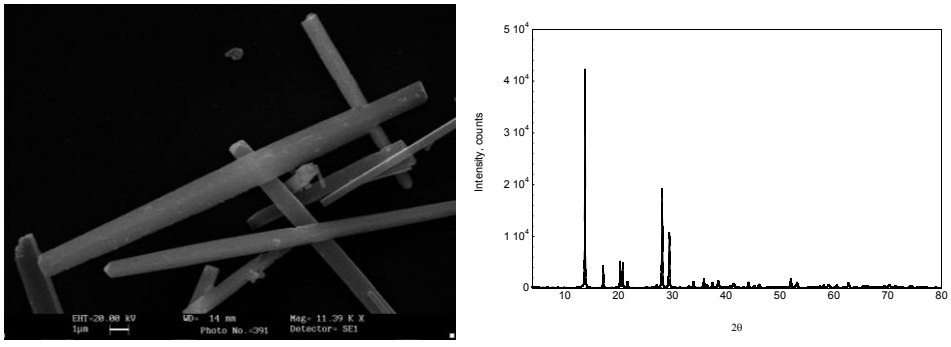

Fig. 1 - Scanning electron micrograph and XRPD pattern of the synthesized product.

Morphology and structural refinement. Figure 1 (left) reports a micrograph of the synthesized sample. The image shows a highly crystalline, extremely clean product, characterized by acicular crystals, about 30 μm long. No amorphous phase is apparently evident.
Figure 1 (right), showing the XRPD pattern of the obtained product, confirms the substantial purity of the sample, as no extra reflections were detected besides those of Li-ABW. RIR/Rietveld refinement resulted in an orthorhombic cell; space group $Pna2_1$; cell constants: a = 8.195 Å, b = 10.327 Å; c = 5.005 Å, in good agreement with the literature [5]. Crystallinity was evaluated indirectly through estimation of the amorphous content (internal standard NIST 676), which turned out to be 3.6 w%.

Ion exchange. ABW framework is compatible with large extraframework cations. Anhydrous silico-aluminate Rb-, Cs-, and Tl-ABW are known, apart from a number of analogous phases with isomorphous replacements of one or both framework cations. Considering that the above large cations were included in the framework during synthesis [6], it may be of interest to know if, and to which extent, Li-ABW can undergo cation exchange with medium-size cations, such as Na^+ and K^+. Figure 3 reports the isotherms of Na^+ and K^+ exchange for Li^+ in zeolite Li-ABW at 25.0°C and 0.10 total normality.

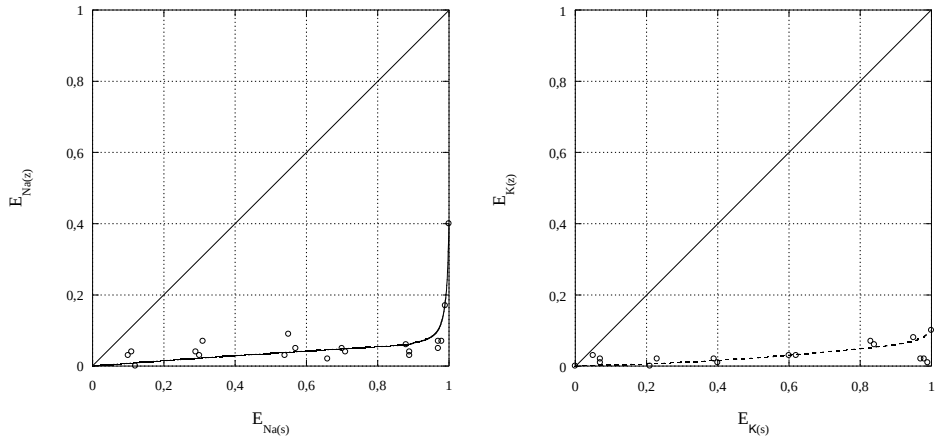

Fig. 2 - Cation exchange isotherms of Na^+ (left) and K^+ (right) for Li^+ at 25.0 °C and 0.10 N. $E_{Na(s)}$, $E_{K(s)}$ = equivalent fraction of the ingoing cation in solution, $E_{Na(z)}$, $E_{K(z)}$ = equivalent fraction of the ingoing cation in zeolite. Solid-to-liquid ratio: 1:100; time allowed for equilibrium: 8 days.

Inspecting Fig. 2, points out that cation exchange is not complete neither for Na^+ nor for K^+; in addition both isotherms denote a very unselective behavior. The maximum amount of exchange do not exceeds 40% of the CEC for Na^+ and about 10% for K^+, as expected considering the high density of the zeolite framework. It is concluded that large cations can enter the framework only during synthesis and have most likely a structure-directing role.

References

[1] Barrer, R.M.; White, E.A.D., J. Chem. Soc. (Lond) 1951, 1267.
[2] Dong, J; Wang, X; Xu, H; Zhao, Q; Li, J, International Journal of Hydrogen Energy, 32, 2007, 4998.
[3] Norby, P.; Nørlund Christensen, A; Krogh Andersen, I. G., Acta Chemica Scandinavica A40, 1986, 500.
[4] Liu, G.; Shi Q.; Liu, L.; Xu, H.; Li, J.; Dong, J., Studies in Surface Science and Catalysis 174, 2008, 185.
[5] Krogh Andersen, E.; Ploug-Sørensen, G., Z. Kristallogr., 176, 1986, 67.
[6] Krogh Andersen, I.G.; Krogh Andersen, E.; Norby, P.; Colella, C.; de' Gennaro, M., Zeolites, 11, 1991, 149.

Elaboration of Metallic Oxide Nanoparticles Prepared by the Hydrolytic Route using Maize Starch Stabilization

Hafedh Kochkar[1*], Gilles Berhault[2] and Abdelhamid Ghorbel[3]

[1] *Centre National de Recherches en Sciences des Matériaux, Technopôle de Borj-Cédria, 8027, B.P.73 Soliman, Tunisie.*
[2] *Institut de Recherches sur la Catalyse et l'Environnement de Lyon, UMR 5256 CNRS-Université de Lyon, 69100 Villeurbanne, France.*
[3] *Laboratoire de Chimie des Matériaux et Catalyse, Faculté des Sciences de Tunis, 2092, El-Manar-Tunisie.*
Corresponding author: email: h_kochkar@yahoo.fr

Introduction

Nanomaterials hold special features attracting the interest of a variety of industrial and applied activities such as electronics, medicine, catalytic support and cosmetic [1]. Some nanomaterials such as silica, titania, alumina, zirconia and iron oxide are already commercially available. This interest is due to the special properties of nanomaterials, resulting from the quantum size effects and the extremely high surface-to-volume ratio. Different methods have been proposed in order to obtain particles with high purity, homogeneity, stability and less than 100 nm in diameter. Some methods are: the sol-gel process, the reaction spray technique, the thermal plasma and the laser synthesis. Indeed, the preparation of stable nanometric objects is difficult, owing to surface energy minimization by coalescence to high-dimension particles. Particular organic polymers are currently proposed as surfactants and stabilizers [2], although they may react or contaminate final products.
Based on the above facts, we focused on the preparation of metal oxides nanomaterials using maize starch (essentially composed of amylose (20%) and amylopectin (80%)) as stabilizer. This approach benefits from many advantages related to the use of maize starch as stabilizer (readily availability; inexpensive, environmentally benign and easy to process compound). In this communication, we report that maize starch, behaves in cyclohexane solution as a non-ionic stabilizer in the preparation of oxide and hydroxide nanoparticles obtained from the hydrolysis of metal alkoxides.

Experimental

All the chemical reagents ($Ti(O^iPr)_4$, $Zr(O^iPr)_4$, $Al(OBu)_3$, $Si(OMe)_4$, maize starch and cyclohexane) are purchased from commercial sources (Aldrich and Acros) and used without further purification. In a typical preparation, diluted metal precursors (0.05 mol) in parent alcohol (10 ml) were added dropwise to cyclohexane solution (50 ml) under vigorous stirring at 60 °C. Next, 0.5 mol of water was added for hydrolysis step of metal alkoxide. Finally, starch is added to reach a final concentration of 33.6 g/L. The final gel was aged at the same temperature for 48 h. Starch removal from the inorganic matrix was carried out by calcination at 500 °C for ca. 2 h under air.
Samples were characterized by means of N_2 adsorption-desorption at 77K, X-ray Diffraction (XRD), TG-DTA, Scanning Electron Microscopy (SEM), Transmission Electron Microscopy (TEM) and ATR-FTIR spectroscopy.

Results and discussion

Prepared oxides are displayed in Table 1, with indication of main structural and morphological features.

Table 1: Metal oxides properties

Oxide	Precursor	Specific surface area ($m^2.g^{-1}$)	Average pore diameter (nm)	Crystalline phase	Particle diameter (nm)
TiO_2	$Ti(O^iPr)_4$	54	8	Anatase	60
ZrO_2	$Zr(O^iPr)_4$	29	15	Monoclinic	30
Al_2O_3	$Al(OBu)_3$	146	8	Amorphous	22
SiO_2	$Si(OMe)_4$	298	6	Amorphous	23
SiO_2‡	$Si(OMe)_4$	236	13	Amorphous	17

‡ Silicon precursor was added to the starch gel.

TGA curves of metal oxides (not shown here) under air flow show a weight loss occurring between 300 °C and 450 °C which can be attributed to starch removal. No significant weight loss was observed above 500 °C. The N_2 adsorption-desorption isotherms of the calcined metal oxides are of type IV characteristic of mesoporous materials with an H2 hysteresis-loop according to the IUPAC classification.

It was reported earlier [2] that in mesoporous metal oxides prepared through surfactant templating, the surfactant micelle is incorporated into the continuous oxide matrix, leaving mesopores after removal of the surfactant. However, starch polymer should not play any templating role. Mesoporous materials are in fact obtained here through the aggregation of small metal oxide particles that have been stabilized in solution by starch (inter-granular porosity). Moreover, no XRD features were observed at low 2θ angles. Metal oxides particle diameter ranges from 17 to 60 nm. Recently, Callone et al. [3] nicely demonstrated starch removal from inorganic metal oxides (TiO_2, In_2O_3, CeO_2) by using α-amylase and yeast leading to smaller particle diameter compared to those obtained by calcination.

The stabilization effect of starch was enhanced when silicon precursor is hydrolyzed first after starch addition. This shows a different interaction behavior between starch and oxide or hydroxide nanoparticles.

Conclusions

Our work demonstrates for the first time the possibility to prepare mesoporous metal oxides (TiO_2, ZrO_2, Al_2O_3 and SiO_2) in cyclohexane using a non-ionic starch as stabilizer and without any pH control. The stabilization at high starch concentration avoids any undesired precipitation. The pore characteristics of SiO_2 can be monitored and controlled by the stabilization of the oxide and/or the hydroxide nanoparticles obtained during the hydrolysis step of silicon alkoxide.

Acknowledgements

This work was financed by the Laboratoire de Chimie des Matériaux et Catalyse (LCMC) de la Faculté des Sciences de Tunis.

References

[1] Hill, J., Heriot, Y., Worsfold, O., Richardson, T.H., Fox, M.A., Bradley, D.D.C., Dynamics of Forster transfer in polyfluorene-based polymer blends and Langmuir-Blodgett nanostructures, Synthetic Met. 139 (2003), 787-790.

[2] Kresge, C.T., Leonowicz, M.E., Roth, WJ. Vartuli J.C, Beck, J.S., Ordered mesoporous molecular-sieves synthesized by a liquid-crystal template mechanism, Nature 359 (1992), 710-712.

[3] Callone, E., Carturan, G., Sicurelli, A., nanopowders of metallic oxides prepared by the hydrolytic route with starch stabilization and biological abetment, J. of Nanosciences and Nanotechnology 6(2006), 1-5.

Synthesis and characterization of vanadium incorporated Al-PILCs

Suna Balci, Aylin Tecimer
Gazi University, Chemical Engineering Department, Ankara, TURKEY
sunabalci@gazi.edu.tr

Introduction

Due to the impurity, limited pore sizes, lack of permanent porosity, structure and thermal stability and catalytic activity, clay minerals have limitations especially in the catalyst and catalyst support applications. By the pillaring, while preserving the crystal/layer structure by inserting the voluminous pillar agent between the clay layers followed by fixation by calcinations, thermally stable micro-meso porous samples, capable of molecular sieve property named as pillared intercalated clays (PILCs) are obtained. PILCs have the possibility of application both as catalyst support and adsorbent because of their own peculiar properties. For the pillared structure, stable structure, functional high surface area as well as the amount and distribution of catalytic active centers (metal/metal combinations) and acid centers (Lewis and Brönsted) are also important in reaction temperatures and they are potential environmental catalyst for air pollution control and organic conversion. These properties are easily arranged by the correct choice of pillar agent(s). Literature studies have shown that, thermal stability or catalytic activity is low for the pillared clays synthesized by the use of catalytic active components alone. The use of pillars of dual compounds with the appropriate selection caused increases both in catalytic activity/acid centers and thermal stability [1-5]. Al-pillared clays (Al-PILCs) synthesized by Al_{13} Keggin ion possess several advantages as the use of support. The Al-polyoxocation, i.e., Keggin ion-Al_{13} has a well-defined chemical composition, structure and charge, and it is thermally stable in PILCs [1-5]. The most common methods synthesizing this structure are forced hydrolysis by a base of an aluminum salt solution. Al-PILCs have surface area and basal spacing values up to 500 m^2/g and 2 nm respectively. They have bidisperse, (micro and meso) pore structure [1-3, 6-11]. Second metal incorporation by post-synthesis by ion exchange or impregnation and isomorphous replacement of aluminum in the Keggin ions were suggested by several authors to improve catalytic properties [2-4, 6, 8, 10-11]. Vanadium shows high activity especially for oxidation reactions and gives d-spacing above 2.0 nm. The studies related with the pillaring with vanadium and dual combination of vanadium and aluminum are rare and in those studied the detailed characterization studies for the investigation of both surface and catalytic properties are not to take into consideration [11-13].

Experimental

In this study, by using Hancili White (HW) bentonite from Middle Anatolian as the host and keeping the "base(OH)/metal(Al)" ratio as 2.0 Al-PILC was obtained as support. The phsicochemical and mineralogical properties of the host clay Al-PILC synthesis method were previously reported [6-8]. By use of vanadyl sulphate hydrate ($VOSO_4xH_2O$) or sodium metavanadate ($NaVO_3$), and wet impregnation, washing after wet impregnation and impregnation from solution methods, vanadium was loaded as active compound in two different amounts to the Al-pillared clay that was pre-calcined at 573 K. After then the samples were calcined at 573 K and 773 K. X-ray diffraction patterns with 2θ (Bragg angle) ranges of 4°–70°were obtained by using a Philips PW 1840. Pore size analysis were done by use of the nitrogen adsorption/desorption isotherms obtained from Quantochrome Autosorb 1C between $10^{-7} < P/P_0 < 1.0$. The samples were outgassed at 573 K for 4 h under high vacuum before the measurements. Scanning electron microscopy (SEM) and MAP images of some samples were taken by a JEOL-JSM-6060 with accelerating voltage of 25 kV. The near

surface compositions of metals and Si in the synthesized solids were determined using an energy dispersive X-ray spectroscopy (EDS) equipped in the electron microscope JEOL-JSM-6400 and the MAP images were also taken. The metal compositions are reported as in their oxide forms. By use of Quanto 400F Field Emission SEM, EDAX of one sample was taken for the comparison. Surface metal compositions to 5-7 nm depth were estimated from SPECS ESCA X-ray photoelectron spectroscopy (XPS). FTIR spectra of pyridine adsorbed and desorbed samples at different temperatures were also recorded to get an idea about the type/distribution of acid sites. Approximately 1 hour dwell time was allowed at each desorption temperature. Thermal behaviours of the samples were investigated by Setaram Simultaneous TG/DTA under air and nitrogen flows with a heating rate of 5^0C min^{-1}.

Results and discussion

Loading of vanadium caused decreases in the XRD peak intensity and the basal spacing belonging Al-PILC and vanadium incorporated samples with basal spacing values from 1.75 to 1.35 nm were obtained. The nitrogen adsorption/desorption study showed that, the highest surface area after support, was observed for $NaVO_3$ loaded by impregnation from solution and calcined at 300^0C and the lowest surface area was observed for $NaVO_3$ loaded by wet impregnation and calcined at 500^0C. The rise in, Al/Si ratio relative to raw clay was seen from EDS analysis. The $NaVO_3$ loading resulted higher V/Si ratio than the other vanadium source did. It was seen from XPS analysis vanadium was bonded with $2p_{3/2}$. XPS analysis showed that Al/Si ratio decreased from 0.46 down to 0.35 by vanadium impregnation. The layered structure of Al-PILC and the placement of vanadium particles between these layers and onto the clay particles' surface were observed in the TEM analyses. Fast dehydration till 300^0C temperature, then decreases in mass loss and solid-solid reaction with hydroxylation at 900º C were observed in TGA/DTA analyses of samples. A high endothermic peak below 150^0C and an exothermic peak above 800^0C were observed for all PILCs. The consistence of V-O-Al and V-O-Si bonds and Bronsted and Lewis acid centers were observed in FTIR results.

References

[1] Figueras, F., Pillared clays as catalyst. Catal. Rev. Sci. Eng. 30 (1998) 457–499.

[2] Kloprogge, J.T., Synthesis of smectites and porous pillared clay catalysts: a review. J. Porous Mater. 5 (1998) 5–41.

[3] Bergaya, F., Theng, B.K.G., Lagaly, G., Handbook of Clay Science. Elsevier, New York. (2006)

[4] Gil, A., Korili, S.A., Vicente,M.A., Recent advances in the control and characterization of the porous structure of pillared clay catalysts. Catal. Rev. 50 (2008) 153–171.

[5] Ding, Z., Kloprogge, J.T., Frost, R.L., Porous clays and pillared clays-based catalysts. Part 2: a review of the catalytic and molecular sieve applications. J. Porous Mater. 8 (2001) 273–293.

[6] Turgut Başoglu F., **Balci S.**, "Micro-mesopore analysis of Cu^{2+} and Ag^{+} containing Al-pillared bentonite", *Appl.Clay Sci.*, 50 (2010) 73-80.

[7] Turgut Başoglu, F., **Balcı, S.**, "Surface properties of metal incorporated Al-pillared clay catalysts analyzed by chemisorption and infrared analysis", *G.U.J.Sci.*, 22 (2009) 215-225

[8] **Balcı, S.**, Tomul, F., "Characterization of Al-, Cr-pillared clays and CO oxidation", *Appl.Clay Sci.*, 43 (2009) 13-20

[9] Tomul, F., **Balcı, S.**, "Synthesis and characterization of Al-pillared interlayered bentonites", *G.U.J.Sci.*, 21(2008) 21-31

[10] Oliveira, L.C.A., Lago, R.M., Fabris, J.D., Sapag, K., Catalytic oxidation of aromatic VOCs with Cr or Pd-impregnated Al-pillared bentonite: byproduct formation and deactivation studies. Appl. Clay Sci. 39 (2008) 218–222.

[11] Vicente, M.A., Belver, C., Trujillano, R., Banares-Munoz, M.A., Rives, V., Korili, S.A., Gil, A., Gandia, L.M., Lambert, J.F., Preparation and characterization of vanadium catalysts supported over alumina-pillared clays. Catal. Today 78 (2003) 181–190.

[12] Bahranowski, K., Serwicka, E., "ESR study of vanadium-doped alumina and titania-pillared montmorillonites ", ***Colloids and Surfaces,*** 72 (1993) 153-160.

[13] Boudali, L., K., Ghorbel, A., Grange, P., Figueras, F., " Selective catalytic reduction of NO with ammonia over V_2O_5 supported sulfated titanium-pillared clay catalysts: influence of V_2O_5 content " , ***Applied Catalysis,*** 59 (2005) 105-111

H_2S-Temperature Programmed Reduction and XRD studies for characterization of CoMo/γ-alumina+*x*AgY sulphided catalysts: influence of silver zeolite loading

Yamina Boukoberine [a], Boudjemaa Hamada [b]

Process Engineering Laboratory, UER of applied chemistry, EMP, BP 17, Bordj El Bahri, Algiers, Algeria; Email: boukabrine_yamina05@yahoo.fr

[b] *Petrochemical Synthesis Laboratory, Chemistry and Hydrocarbons Faculty, UMBB, 01. Independence Avenue, Boumerdes, Algeria*

Introduction

The US Clean Air Act Amendments of 1990 and the new regulations by the US Environmental Protection Agency (EPA), and government regulations in many countries call for the production and use of more environmentally friendly transportation fuels with lower contents of sulfur and aromatics [1, 2]. On bifunctional catalysts the first step of an alkane transformation is the dehydrogenation on the metal, followed by the isomerization or the cracking of the olefin on the acid sites, and lastly by the hydrogenation of the new olefin on the metallic sites [3]. The aim of the present work is study of the silver zeolites loading influence on the H_2S-Temperature Programmed Reduction and XRD for characterization of CoMo/γ-Al_2O_3+*x*AgY sulphided catalysts during hydrodesulfurization of thiophene.

Experimental

The materials used were an industrial CoMo/γ-Al_2O_3 catalyst which were provided by *Procatalyse* (S_{BET} = 210 m^2/g, V_P = 0,50 cm^3/g, MoO_3-CoO: 14 %-3 %), silver nitrate [$AgNO_3$] provided by Fluka (99,9 % purity) and NH_4Y zeolite of chemical form $Na_1 (NH_4)_{52.33} Al_{53.33} Si_{138.67} O_{384}$ (CBV500) provided by Zeolyst International Society. For catalytic tests, thiophene used was provided by Acros Organics with 99.5 % purity and 1,050 of density. In the present study, the series of CoMo/γ-Al_2O_3 + AgY*(x)* bifunctional catalysts, *x* being the wt % of loading AgY zeolite, were prepared by physically mixing of an industrial catalyst CoMo/γ-Al_2O_3 and the zeolite in different proportions. The AgHY adsorbent was prepared by solid-state ion-exchange method. The sulfidation mechanism was carried out by temperature-programmed sulfidation. The crystallinity of the zeolite and the possible formation of silver oxide were evaluated from the powder XRD patterns recorded on a Philips X'pert PRO diffractometer. The industrial CoMo/γ-Al_2O_3 catalyst and Ag- exchanged zeolite were characterized by hydrogen temperature-programmed reduction (H_2-TPR). These measurements were performed after pretreatment of the catalysts and the catalytic tests. The experiments for thiophene HDS are carried out at atmospheric pressure in a continuous flow fixed-bed reactor and at different temperatures (573, 593 and 613 K).

Results and discussion

The XRD analysis of the AgY zeolite forms before and after the sulfidation are displayed in Fig. 1. The XRD pattern of AgY zeolite (Fig. 1-b) showed the appearance of a significant diffraction lines at 2θ values of 38° and 44°. These results suggest the formation of a small amount Ag_2O species. The Fig. 1-c shows the XRD patterns of AgY zeolite calcined and sulfided. It is clear that the AgY zeolite structure were retained after the sulfidation treatment.

High crystallinity faujasite from fly ash – control of silica solubility by acid-base pretreatment as efficient tool determining zeolitization.

L.Titelman[1], O.Shein[1], M.V.Landau[1*], A.Metzger[2], M.Herskowitz[1]

[1] *Blechner Center for Applied Catalysis and Process Development, Chemical Engineering Department; Ben-Gurion University of the Negev, Beer-Sheva, 84105, Israel*
[2] *Israel Electric Company, Haifa, 31000, Israel*
[*] *corresponding author: mlandau@bgu.ac.il*

Introduction

Fly ash (FA) produced in large amounts at power stations represents an attractive feedstock for zeolites production [1,2]. It is cheap, contains more than 75 wt.% of SiO_2-Al_2O_3 and made as fine powder convenient for chemical treatments. Zeolitization of FA requires conversion of crystalline phases - quartz and mullite, to water soluble silicate-aluminate by fusion with NaOH. But this does not solve the problem of preparation of high crystallinity zeolite materials due to relatively low reactivity of existing in FA amorphous metalo-silicates containing Ca, Mg, Al, Fe, Ti and Cu which content reaches 20-30 wt.%. In the present work was demonstrated a direct dependence of the FA zeolitization ability on the content of water soluble silica. The amount of soluble silica in FA can be controlled by its pre-treatment mode including acid treatment before NaOH fusion. This yielded a faujasite material with 90% crystallinity at the zeolitization step.

Experimental

The FA supplied by Israeli Electric Co. according to X-ray phase analysis contained 8wt.% quartz, 25wt.% mullite ($Al_6Si_2O_{13}$) and a glassy amorphous phase represented by areas of pure silica (hallo at $2\theta=22^o$, 45wt.%) and areas where silica was partially substituted by other metals (hallo at $2\theta=30^o$, 21wt.%). Its chemical composition included (wt.%): SiO_2 (49.7); Al_2O_3 (23.8); Fe_2O_3 (7.9); CaO (7.0); P_2O_5(2.0); TiO_2 (1.9); MgO (1.0); CuO (0.5). The surface area was 5 m^2/g, particle size 1-20 μm, BD = 1.14 g/cm^3. The content of water-soluble silica in starting FA and after different chemical treatments was estimated based on weight loss and chemical analysis of pretreated FA after two-step water treatment at r.t. (60/1 w/w) and then at 90°C (100/1 w/w). The FA pretreatments included fusion with $NaHCO_3$ at 650°C, 1h; fusion with NaOH at 500°C, 1 h and treatments with concentrated H_2SO_4 or HNO_3 at 110°C, 120h followed by fusion with NaOH. Zeolitization was conducted in Teflon autoclave with composition of reaction suspension $20Na_2O$:SiO_2(FA);$460H_2O$ at temperature 104°C for 24 h.

Results and discussion

The zeolitized FA contained faujasite as main zeolite component and included different amounts of Sodalite, Zeolites A and NaP1, so that purity of faujasite phase (wt.% in zeolite fraction of zeolitized FA) ranged from 78 to 99%. Plotting the total zeolites crystallinity (wt.% of all zeolites in zeolitized FA) versus the content of soluble silica in fresh FA(1) and FA pretreated by fusion with $NaHCO_3$(2), fusion with NaOH(3) and two-step acid – NaOH treatments (4,5) (Fig.1) yielded a straight line that extrapolates to 20% zeolites crystallinity at

zero content soluble silica. This corresponds to the dependence of total zeolites content in zeolitized FA: $Z = A*[SiO_{2soluble}] + 20\%$, where $A \sim 1$. It means that in used FA only 20% of SiO_2 can be converted to zeolite phases by solid state zeolitization in alkaline medium, while 80% of silica require dissolution and formation of intermediate primary crystallization colloidal units.

The highest solubility of silica was after acid treatment followed by NaOH fusion. It increased the FA surface area to 18-44 m^2/g producing mesopores and reduces the content of metals raising the silica content to 61-66%. Fusion of fresh FA converts quartz and mullite to

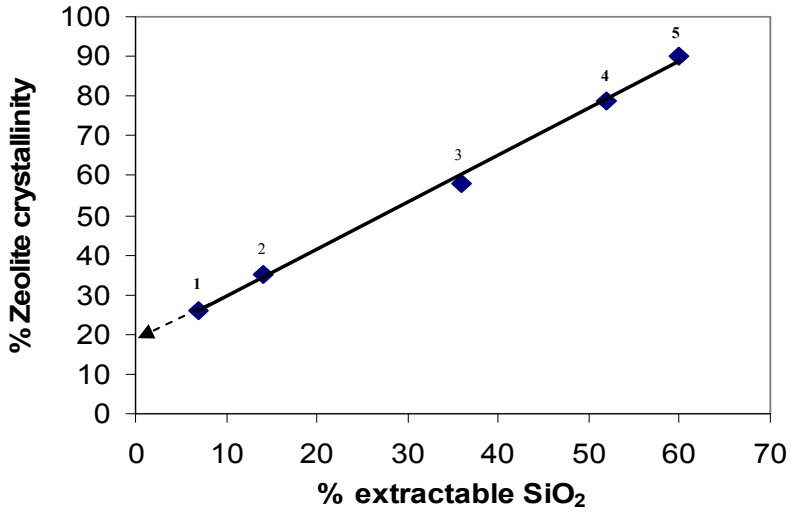

Figure 1. Effect of the amount of water-extractable silica on zeolitization of FA

Na_2SiO_3 and $NaAlO_2$ phases that disappeared after water-extraction leaving glassy SiO_2-phase with two amorphous areas. Zeolitization of FA after NaOH fusion yields material with about 60% total zeolites content and amorphous phase characterized by XRD hallo at $2\theta=30^o$. Acid treatment reduces the area of this XRD hallo in FA, so that after zeolitization the amount of amorphous glassy phase decreases significantly yielding zeolitic material with 90 wt.% content of faujasite and surface area of 615 m^2/g.

This material demonstrated ability for decreasing the content of Al, Co, Cr, Mn,P,Si,V and Zn in industrial wastewater containing all these elements at amounts 15-935 ppm by 90-99%. It displayed 4.1 mmol/g adsorption capacity for CO_2 at 25°C.

Conclusions

Acid handling of fly ash before fusion with NaOH strongly increases the solubility of silica component in water after this two-step pre-treatment. This increases the reactivity of fly ash at subsequent zeolitization step yielding a material containing 90 wt.% of zeolite faujasite phase with high ability for adsorption of heavy metals from wasdtewater and CO_2.

References

[1] X.Querol, N.Moreno, “Zeolites”, In "Combustion Residues", M.Cox, H. Nugteren, M.Janssen-Jurkovicova, Eds., John Wiley and Sons Ltd., 2008, 210.
[2] H.W.Nugteren, Coal Fly Ash: from Waste to Industrial Product. Part.Part.Syst.Charact., 24, 49, 2007.

A Study of Formation of SAPO-34 under Dry Gel Conversion Conditions

Lu Zhang, Yining Huang
Department of Chemistry, University of Western Ontario, London, Canada, yhuang@uwo.ca

Introduction

Silicoaluminophosphate (SAPO) based microporous materials are important acidic catalysts. SAPO-34 has a CHA framework topology containing chabazite cages with an eight-ring window. The framework is built upon double six-rings joined together by four-rings. SAPO-34 is used in industry as a catalyst in conversion of methanol to olefins (MTO). Although crystallization of SAPO-34 has been examined [1-3], the mechanism of crystallization is still not fully understood. Normally, SAPOs are normally prepared by hydrothermal synthesis (HTS). An alternative method is dry gel conversion (DGC) [4]. Specifically, the pre-dried gel powder containing structure directing agent (SDA) is separated from a small amount of pure water in an autoclave which is not in contact with the gel before heating and treating this reactive gel powder in water vapor at elevated temperature and pressure converts the gel to crystalline molecular sieves [5]. Since the initial "dry" gel actually contain significant amount of water, the fundamental mechanisms underlying the crystallization in hydrothermal synthesis and DGC may be similar. However, because bulk liquid is lacking, the mass transportation is limited. Therefore, the reaction can be slower, allowing the intermediates to be detected under favorable circumstances. Thus, examination of the evolution of the dry gel phase may assist in understanding the crystallization in conventional hydrothermal process. In this work we used DGC method to examine the formation of SAPO-34 using morpholine as SDA. The attention was also paid to the effect of HF on crystallization.

Experimental

The SAPO-34 initial dry gel samples were prepared according to the method described in ref. [6]. A series of intermediates was synthesized by placing 1.0 g of initial dry gel powder into small Teflon cups. Each cup was placed in a 23-ml Teflon-lined autoclave with 0.3 g (without HF) and 0.7 g (with HF) distilled water at the bottom and heated in an oven at 473 K. The reactions were quenched in cold water.

Results and discussion

Fig. 1A shows the PXRD patterns of the dry gel prepared with HF as a function of heating time. The initial dry gel has the layered structure (so called pre-phase [2]). After 1.5 h the layered phase starts being converted to triclinic SAPO-34. SAPO-34 with trigonal symmetry begins forming after 3 h. The final SAPO-34 product obtained is a mixture of triclinic and trigonal phases. The evolution of the dry gel is similar to that observed in HTS [2,3]. The situation for the gel made without HF is different (Fig. 2B). The initial gel is amorphous, but it immediately transforms to a layered phase upon heating. Interestingly, this crystalline phase further evolves into a semi-crystalline layered phase as indicated by PXRD, from which SAPO-34 eventually crystallize in a pure trigonal phase.

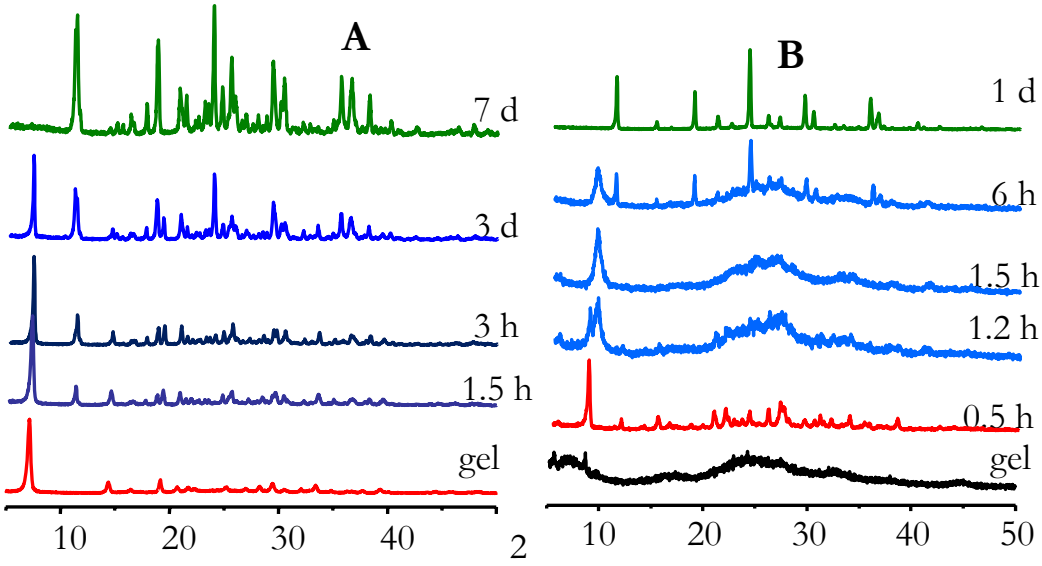

Fig. 1. PXRD patterns of the dry gel (A) with and (B) without HF heated at different times

Upon washing with water, PXRD patterns (not shown) indicate both crystalline and semi-crystalline intermediates produced from the initial gel without HF transform to amorphous materials, suggesting the structures of these intermediates are probably partially held by weak forces such as van der Waals forces or/and very weak hydrogen bonding. Washing, on the other hand, has no effect on the pre-phase with HF, implying that the pre-phase has fully developed covalent bonding. These observations explain why the crystallization time is much shorter for the system without HF because weak non-bonding in the intermediates allows reorganization of the local structure to proceed with ease towards the formation of the final product under the conditions where a bulk solution is lacking.

Solid-state ^{31}P and ^{27}Al MAS NMR spectra (not shown) provide crucial information on the local P and Al environments in various intermediates. In combination with EDX analysis, ^{29}Si NMR MAS and ^{1}H to ^{29}Si cross polarization spectra show that the Si incorporation is also affected by HF. For the system without HF, the crystalline layered phase is essentially AlPO in nature. The silica dispersed in the gel reacts with alumina to first form aluminosilicate species which are likely occluded between the layers. They are gradually incorporated into the semi-crystalline phase and, eventually, in SAPO-34. For the system with HF, ^{29}Si NMR data show that the pre-phase has no Si and Si atoms are incorporated into the framework as an isolated species Si(4Al)(9P) first and then several other Si environments gradually form in the framework at a longer crystallization time.

Acknowledgements

Y.H. thanks the NSERC of Canada for a research grant

References

[1] Xu, L., Du, A.P., Wei, X.Y., Wang, Y.L., Yu, XY, He, Y.L., Zhang, X.Z., Liu, Z.M., Microporous and Mesoporous Materials, 115 (2008) 332-337.
[2] Vistad, O.B., Akporiaye, D.E., Lillerud, K.P., Journal of Physical Chemistry. B, 105 (2001) 12437-12447
[3] Yan, Z., Chen, B.H., Huang, Y.N., Solid State Nuclear Magnetic Resonance, 35 (2009) 49-60
[4] Xu, W., Dong, J., Li, J., Wu, F., J. Chemical Communications (1990) 755.
[5] Rao, P.R.H.P., Matsukata, M. Chemical Communications (1996) 1441.
[6] Chen, B.H., Huang, Y.N., Microporous and Mesoporous Materials, 123 (2009) 71-77.

The Effects Of The Preparation Method On The Characteristic Properties Of The Al_2O_3/ZrO_2 Composed Co_3O_4, MnO_2, Ag and Ni Catalysts

Filiz Balikci Derekaya and Derya Mercan
University of Gazi, Institute of Science And Technology, Department of Advanced Technologies, filizb@gazi.edu.tr

Introduction

The aim of this study is to investigate the effects of the preparation methods on the characteristic properties of the catalysts. Recent years mostly surfactant assisted reagents have been used in the catalysts preparation. Surfactants were used in order to prepare catalysts in nanometer scale. According to the literature mostly cetyltrimetilamonyumbromid (CTAB) was used as a surfactant. According to these studies catalysts having average pore diameter in mesopore diameter scale were obtained [1-4]. For this aim four different catalysts namely $Co_3O_4/Al_2O_3/ZrO_2$, $MnO_2/Al_2O_3/ZrO_2$, $Ag/Al_2O_3/ZrO_2$ and $Ni/Al_2O_3/ZrO_2$ prepared.

Experimental

All catalysts were prepared by using three different methods which were co-precipitation, surfactant assisted co-precipitation and surfactant assisted co-precipitation with ultrasonic irradiation mixing. $ZrO(NO_3)_2.xH_2O$, $AgNO_3$, $MnN_2O_6.4H_2O$, $Ce(NO_3)_3.6H_2O$, $Co(NO_3)_2.6H_2O$ ve $Ni(NO_3)_2.6H_2O$ as precursors and CTAB as a surfactant were used in order to prepare catalysts. All catalysts were calcined at 550^oC for 3 h in air atmosphere.

Characteristic properties were determined by using different techniques. The phases in catalyst structure were determined by using X-Ray diffraction; surface areas, pore diameters, pore volumes were determined by using N_2 physisorption; the surface morphology was determined by SEM; the reduction temperature and adsorption properties determined by using temperature programmed methods (TPR-H_2, TPD-CH_4).

Results and discussion

The phases present in the catalysts were determined by the XRD studies. The phases determined by the XRD were changed with the catalyst composition. In general for CeO_2, ZrO_2, CeZroxide, MnO, Mn_2O_3, MnCeZroxide, Co_3O_4, CoO, NiO, metallic Ag phases were obtained in catalysts. The XRD diagram of the $Ni/Al_2O_3/ZrO_2$ catalyst was given in Figure1.

The surface area results of the catalysts are given in Table 1. The highest surface area was obtained for the $MnO_2/Al_2O_3/ZrO_2$ catalysts. All catalysts gave average pore diameter in the mesopore diameter scale. The average pore diameter curves of the $Ni/Al_2O_3/ZrO_2$ were shown in Figure 2. Except for the $Ag/Al_2O_3/ZrO_2$ catalysts which had Type III. adsorption/desorption isotherm in BDDT classifications, the N_2 adsorpstion/desorption isotherms of the other catalysts fit to the Type IV. and Type V. isotherm in the BDDT classifications.

Table 1. Surface areas of the catalysts.

Catalysts	Multipoint BET Surface Area m_2/g		
	Preparation Method		
	Co-precipitation C	Surfactant Assisted Co-precipitation S	Surfactant Assisted Co-precipitation with ultrasonic irradiation mixing U
$MnO_2/Al_2O_3/ZrO_2$	131.1	160.4	142.7
$Co_3O_4/Al_2O_3/ZrO_2$	82.67	94.33	92.33
$Ni/Al_2O_3/ZrO_2$	146	204.2	150.3
$Ag/Al_2O_3/ZrO_2$	55.44	23.75	5.5

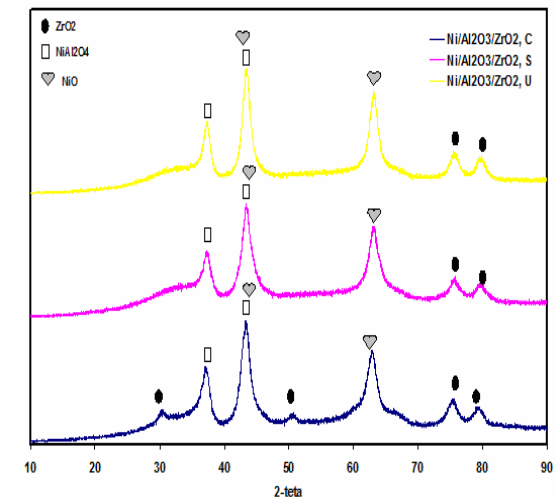

Figure 1. XRD diagram of the $Ni/Al_2O_3/ZrO_2$ catalysts.

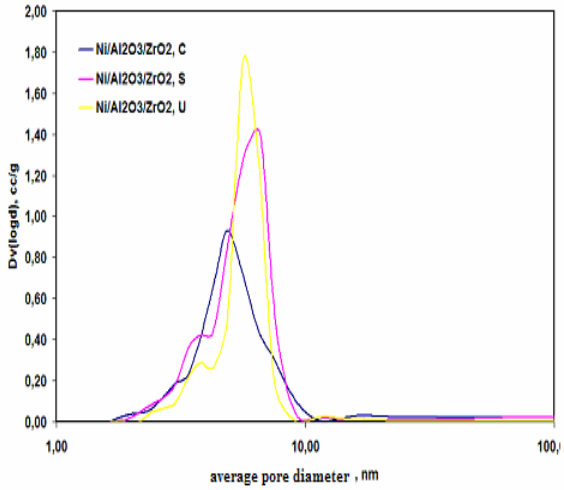

Figure 2. Average pore diameters of the $Ni/Al_2O_3/ZrO_2$ catalysts.

Conclusions

In this study the effects of the preparation method on the characteristic properties of the catalysts were investigated. The highest surface area was obtained for the catalysts prepared by the surfactant assisted co-precipitation method and the $MnO_2/Al_2O_3/ZrO_2$ catalysts. All catalysts gave average pore diameter in mesopore scale and the uniform (or single) average pore diameter results obtained from the catalysts prepared by the surfactant assisted method with ultrasonic irradiation mixing.

Acknowledgements

The authors gratefully acknowledged the financial support of the TUBITAK MAG 109M230 project. We are also grateful to Prof. Dr. Çiğdem Güldür for this help in providing equipment.

References

[1] Liu, H., Ma, Z., Chu, Y., Sun, W., Surfactant-assisted synthesis, characterization and catalytic properties of nanostructure porous WO_3/ZrO_2 solid acid, Colloids and Surfaces A: Physicochem. Eng. Aspects, 287 (2006), 10-15.

[2] Cao, J.L., Wang, Y., Yu, X.L., Wang, S.R., Wu, S.H., Yuan, Z.Y., Mesoprous CuO-Fe_2O_3 composite catalysts for low-temperature carbon monoxide oxidation, Applied Catalysis B: Environmental, 79 (2008), 26-34.

[3] Laosisipojana, N., Assabumrungrat, S., Charojrochkul, S., Steam reforming of ethanol with co-fed oxygen and hydrogen over Ni on high surface area ceria support, Applied Catalysis A. General, 327 (2007), 180-188.

[4] Fan, Y., Bao, X., Wang, H., Chen, C., Shi, G., A surfactant assisted hydrothermal deposition method for preparing highly dispersed W/γ-Al_2O_3 hydrodenitrogenation catalysts, Journal of Catalysis, 245 (2007), 477-481.

Stabilization of Y zeolites using NaCl during synthesis.

Héctor Armendáriz-Herrera[a], Salvador Ibarra[a], Francisco Hernández-Beltrán[b]*,
M. Lourdes Guzmán-Castillo[a], Patricia Pérez-Romo[a], José Fripiat[a], Jaime Sánchez-Valente[a]
[a] *Programa de Procesos de Transformación;* [b]*Dirección de Ingeniería de Proceso,*
Instituto Mexicano del Petróleo, E. Central L.Cárdenas 152, 07730, México D.F., México.
**corresponding author: fjhernan@imp.mx*

Introduction.

Improving properties of Y zeolites is of paramount interest due to their extended commercial use as adsorbents and catalysts. Properties of Y zeolites are strongly related to their synthesis conditions. In this paper we report on the effect of using a strong electrolyte such as NaCl on the synthesis and properties of Y zeolites.

Experimental.

Six zeolite samples were prepared through seeding by using crystals of a precrystallized Y zeolite added to a hydrogel of $4.3NaO:Al_2O_3:10SiO_2:180H_2O$ molar composition and further adding NaCl and/or TMAOH in variable relative amounts (table 1). The hydrogel was aged for 18 h at room temperature, then stirred and autoclaved at 95 °C for 5 h. The solids were recovered by filtration, washed with bidistillated water up to pH = 7, dried at 120 °C for 18 h and calcined at 500 °C for 4h. These as-synthesized zeolites were three folds ion-exchanged in a 1M NH_4NO_3 solution, filtered, dried and calcined at 500 °C. Samples were studied by XRD, N_2 adsorption for total and MSA (micropore surface area), FT-IR, ^{29}Si NMR and ^{23}Na NMR (performed on hydrated zeolites). The Na content was analyzed by AA. The SiO_2/Al_2O_3 ratio was calculated from ^{29}Si NMR. Solid (0.1 g) were tested in the cracking of n-hexane in a down flow reactor at 450°C, atmospheric pressure and 0.9 mol(nC_6) g^{-1} h^{-1} flow rate.

Results and discussion.

As-synthesized, zeolites were pure and highly crystalline showing MSA varying between 725-750 m^2/g. Upon ion exchange and calcination, zeolites prepared with NaCl comparatively showed higher stability. These zeolites retained higher MSA and crystallinity (C_R) but kept also a higher content of Na (table 1). The band at 573 cm^{-1}due to the double T6 ring (DT6R) of the FAU structure in the FTIR spectra (figure 1) was clearly visible in HF5 and HF9 but barely in HF1 and HF7. The destruction of this band corresponds to a structural collapse [2].
The width of the ^{23}Na MAS NMR spectra (figure 2) must be assigned to strong interactions of the hydrated Na^+ cation found in different locations of the zeolite structure and to the overlapping of the resonance bands. In order to have a better insight on the chemical environment and location of Na^+ cations deconvolution of the spectra was performed. The best fitting obtained from this analysis (figure 2 as dotted curves) shows bands attributable to Na^+ located in supercages (ca.+3 ppm), sodalite cages (-6 ppm) and hexagonal prisms (-0.5 ppm), the latter being absent in HF5 and HF9. Based on other reports [3,4], we attributed the lines at +5, +1.5/+2.0 ppm in samples HF5 and HF9 to $[Na_4Cl]^{3+}$ located in the sodalite cages and in the supercages respectively, and the broad shoulder in HF9 to a $[Na_x(NaCl)_y]^{x+}$ ($x \leq 4$ and $y \leq 10$) complex in supercages.^{29}Si NMR (not shown) gave also valuable information about the zeolite lattice ordering. The characteristic bands attributed to different environments of Si atom were clearly identified in samples HF1, HF5 and HF6. They overlapped in HF10 and were undistinguishable in HF1 and HF7.
The catalytic test showed that the initial nC_6 conversion varied between 17-57% mol depending on the zeolite, HF5 and HF9 being less active but much more stable. These results can be mainly explained by a lower acidity due to the higher Na content in such zeolites.

Table 1. Relative amounts of NaCl and TMAOH added into the synthesis gel and main properties of the ion-exchanged and calcined zeolite samples.

Parameter	HF1	HF5	HF6	HF7	HF9	HF10
$NaCl/SiO_2$ (mol/mol)	0	0.74	1.0	0	0.74	0.68
$TMAOH/SiO_2$ (mol/mol)	0	0	0	0.018	0.018	0.036
[a]C_R, %	70	87	97	30	94	92
SiO_2/Al_2O_3	4.2	3.6	3.9	5.1	3.6	4.1
Na (wt%)	0.63	4.54	--	0.57	4.49	2.81
[b]MSA (t-plot), m^2g^{-1}	384	614	563	207	592	551

[a] Relative crystallinity from XRD $=\Sigma I_c/(\Sigma I_c+\Sigma I_a)$ from reference [1]; [b] from the t-plot method.

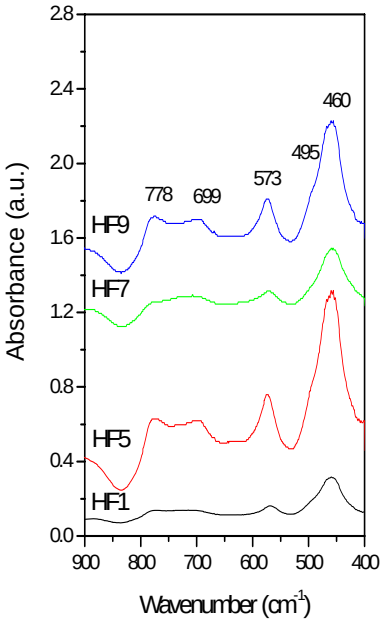

Figure 1. FTIR of zeolites.

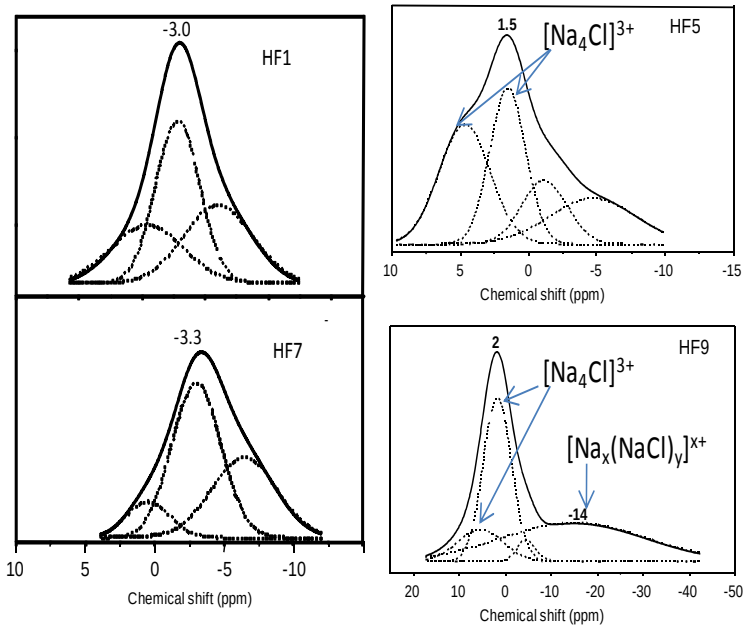

Figure 2. ^{23}Na MAS NMR spectra of zeolites.

Conclusions.

Zeolites synthesized in presence of NaCl were more stable to thermal and ion exchange treatments as evidenced by several techniques. However, the Na^+/NH_4^+ exchange in such zeolites was a boring process to carry on, thus producing less active but more stable cracking catalysts. Deconvolution of ^{23}Na NMR spectra may be interpreted by the presence of $[Na_4Cl]^{3+}$ or $[Na_x(NaCl)_y]^{x+}$ in the sodalite cages and in the supercages of the Faujasite structure. Such halide complexes could be the origin of the higher resistance to Na^+ exchange and of a higher stability.

References.

[1] Aouali, L., Teanjean, J. , Dereigne, A., Tougne, P., Delafosse D., Structural evolution of dealuminated Y zeolites during various chemical treatments, Zeolites, 8, 6 (1988) 517-522.

[2] Flanigen, E. M., Khatami, H., Szmanski, H. A., Infrared Structural Studies of Zeolite Frameworks, ch. 16 in Molecular Sieve Zeolites-I, E. M Flanigen, L.B. Sand (Eds.) ACS ser. 101, August 1, 1974, 201-229.

[3] Nielsen N. Chr., Bildsøe H., Jakobsen H. J. , Norby P., 7Li, 23Na, and 27Al quadrupolar interactions in some aluminosilicate sodalites from MAS n.m.r. spectra of satellite transitions , Zeolites 11, 6 (1991) 622-632.

[4] Seidel, A. Tracht U., Boddenberg, B., Study of the Dispersion of Sodium Chloride in Zeolite NaY, J. Phys. Chem. 100 (1996) 15917-15922.

Development of new materials

FEZA 2011

MOF-type Aluminum Pyromellitates MIL-118, MIL-120 and MIL-121: Solid-State NMR Characterization

Mohamed Haouas,[1] Francis Taulelle,[1] Christophe Volkringer,[2,3] Thierry Loiseau,[2,3] Gérard Férey[2]
[1]Tectospin & [2]Groupe Solide Poreux, Institut Lavoisier de Versailles, France. [3]Present address: Unité de Catalyse et Chimie du Solide, Université de Lille, France.
haouas@chimie.uvsq.fr

Introduction

Metal-organic frameworks (MOF) or coordination polymers exhibit structures based on the extended connection of organic linkers with metallic building units (also chains, or layers) generating infinite 3D topologies. In our study on the reactivity of trivalent cations, we focused our efforts in the elaboration of aluminum-based MOFs. MOF-type aluminum compounds are exclusively carboxylates-based materials. Very recently different teams described the synthesis and the properties of functionalized aluminum terephthalates of MIL-53 type. For instance, the occurrence of free carboxylic acid needs a perfect control of the reaction conditions to generate at the same time and on the same ligand, free -COOH and coordinated -COO carboxylate functions. The study of the phase diagram of the reactivity of the pyromellitate ligand (1,2,4,5-benzenetetracarboxylate) with aluminum allowed us to isolate three distinct phases, called MIL-118 [1], MIL-120 [2], and MIL-121 [3] (MIL-n stands for Materials Institut Lavoisier), by varying the reaction pH adjusted with NaOH. Here, this contribution deals with the solid state NMR characterization of these new three aluminum pyromellitates, $Al_2(OH)_2(H_2O)_2[C_{10}O_8H_2]$ (MIL-118A), $Al_2(OH)_2[C_{10}O_8H_2]$ (MIL-118B), $Al_2(OH)_2[C_{10}O_8H_2].3H_2O$ (MIL-118C), $Al_4(OH)_8[C_{10}O_8H_2].5H_2O$ (MIL-120), and $Al(OH)[C_{10}O_8H_4].2H_2O$ (MIL-121). Multinuclear MAS and multidimensional techniques were employed including ^{1}H-^{1}H DQ-SQ and SQ-SQ RFDR, ^{1}H-^{27}Al HETCOR, ^{27}Al 3QMAS, ^{13}C CPMAS, etc...

Experimental

^{27}Al and ^{1}H MAS NMR spectra were recorded with a Bruker Avance 500WB spectrometer operating at 11.7 T. The spinning frequency used was 30 kHz. Typical spectra were recorded at Larmor frequency of 130.315 MHz relative to an aqueous solution of $Al(NO_3)_3$ and 500.133 MHz relative to TMS for ^{27}Al and ^{1}H respectively. The high-resolution solid-state ^{13}C MAS NMR spectra were measured at 50.33 MHz, on a TecMag Apollo 200 NMR spectrometer, capable of high power ^{1}H-decoupling. The spinning rate used for ^{1}H-^{13}C cross-polarization and magic angle spinning experiments was 10 kHz at ambient temperature. The spectra were referenced to adamantane, which showed two peaks at 29.6 and 38.5 ppm with respect to standard TMS.

Results and discussion

The phase domains of MIL-118, MIL-120 and MIL-121 in the system aluminum-pyromellitate-NaOH-water were found to depend mainly on the synthesis pH. Regarding the connectivity of aluminum in the inorganic sub-network, low pH favors a connection via μ_2-OH corner (MIL-118 and MIL-121) of AlO_6 octahedra whereas for higher values of pH, the aluminum-centered octahedra are linked to each other with common edge corresponding to two μ_2-OH groups (MIL-120). On the organic part, the increase of the starting pH value induces a constant increase of the number of coordinating oxygen atoms per pyromellitate ligand. For MIL-121, MIL-118, and MIL-120 respectively 4, 6, and 8 carboxyl oxygen atoms are connected to Al cations. These observations are presented in Figure 1.

MOF-type Aluminum Pyromellitate	Oragnic ligand configuration	Inoragnic sub-network configuration	Starting pH value
MIL-120 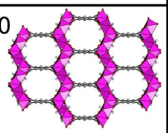	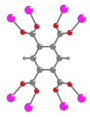	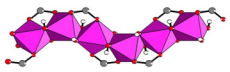	12.2
MIL-118 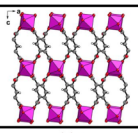	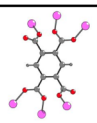	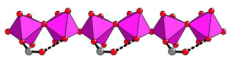	2.0
MIL-121 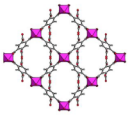	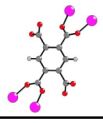	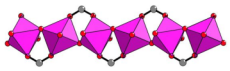	1.4

Figure 1. Influence of pH related to the formation of MOF-type aluminum pyromellitate frameworks.

The ^{27}Al, ^{1}H, and ^{13}C nuclei probe the local environment of the organic-inorganic network, and also the extra-framework species occluded within the channels systems as well as their mutual interaction as a function of the materials state, ie., as-synthesized, activated, and evacuated. The effect of these interactions within the pores on the structural change and evolution reversibly or not are also evidenced confirming the high flexibility of such porous solids.

Conclusions

Solid state NMR is shown to be a tool of choice for fine structural analysis at atomic level of aluminum based MOF materials and is complementary to XRD. Additional crucial information can be gained by this technique when detection of hydrogen network or disordered occluded species fails with conventional diffraction techniques.

References

[1] Volkringer, C., Loiseau, T., Guillou, N., Férey, G., Haouas, M., Taulelle, F., Audebrand, N., Margiolaki, I., Popov, D., Burghammer, M., Riekel, C., Crys. Growth Des., 9 (2009), 2927.
[2] Volkringer, C., Loiseau, T., Haouas, M., Taulelle, F., Popov, D., Burghammer, M., Riekel, C., Zlotea, C., Cuevas, F., Latroche, M., Phanon, D., Knoefelv, C., Llewellyn, P. L., Férey, G. Chem. Mater., 21 (2009), 5783.
[3] Volkringer, C., Loiseau, T., Guillou, N., Férey, G., Haouas, M., Taulelle, F., Elkaim, E., Stock, N., Inorg. Chem. 49 (2010), 9852.

Influence of the silica source to the ionic liquid templated zeolite synthesis

J.M. Martínez Blanes, S. Ivanova*, F. Romero Sarria, M. A. Centeno, J. A. Odriozola
Instituto de Ciencia de Materiales de Sevilla, Centro mixto CSIC-Universidad de Sevilla, Avda. Americo Vespucio 49, 41092 Sevilla, Spain, svetlana@icmse.csic.es

Introduction

Zeolites are known to possess a microporous structure with well-defined pore architecture and size. Zeolites can be loaded via ion-exchange by cations to suit requirements of a specific chemical transformation. However, a precise control of chemical composition and microstructure is insured by the synthesis procedure. The synthetic technologies for these materials usually involve the use of structure directing agents (SDA), bulky organic molecules which can be removed only by a high temperature treatment increasing the price of the final compound and sometimes damaging the inorganic structure[1, 2]. Recently, ionic liquids (ILs) have proved to be an excellent media for inorganic synthesis; in addition, they have attracted increasing attention as templates or solvents for the fabrication of zeolites or nanomaterials [3,4]. ILs possess tunable solvent properties through which they can easily interact with various surface and chemical reaction environments; moreover, ILs with hydrophobic regions and high directional polarizability can form extended hydrogen bond systems in the liquid state, resulting in a highly structured self-assembly [5].

In this study we report the synthesis of three different zeolite structures using the same ionic liquid as a structure directing agent in the same synthesis conditions, changing only the silica source. Depending on the later and on its degree of hydrolysis the zeolite self organization around the ionic liquid results in 8-, 10-, or 12 – membered ring zeolites.

Experimental

The chemicals used for the synthesis were the commercials, tetraethoxysilane (TEOS, 99% Alfa Aesar), SiO_2 Aerosil (Degussa), sodium metasilicate (Foret S.A.), 1-Butyl-3-methylimidazolium methane sulfonate (Bmim) synthesized as proposed by Cassol et al. [6], sodium hydroxide pellets (NaOH, Merck) and sodium aluminium oxide (Alfa Aesar).

In a typical synthesis the gel containing all the precursors (composition presented in Table 1) was aged for 4 hours at 35ºC and then placed in a sealed stainless steel autoclave. The hydrothermal synthesis was performed at 170ºC during 5 days. The similar molar ratios of the gel were reported by Mignoni et al. [7], but different ionic liquid was used.

Table 1. Molar composition (expressed in ratio) and silica source of the gel

	A	**B**	**C**
Si/Al	43	43	43
Si/OH	2	2	2
Bmim/Si	0.39	0.39	0.39
H_2O/Si	60	60	60
Si/Na	1.8	1.8	0.39
Si source	Aerosil	TEOS	Na_2SiO_5 $5H_2O$

Results and discussion

Our previous studies on the MFI type zeolite synthesis using 1-butyl, 3-methyl imidazolium methanesulfonate as a structure directing agent in water rich media show that the resulted zeolite like structure posses an interrupted framework character, thermally instable [3]. In this study we report the change of the synthesis condition from water rich to water poor highly basic environment, which results in zeolite structures with far better crystallinity (Figure 1). The use of diverse Si sources for which a different degree of hydrolysis and gelification was observed, results in three different zeolite families. When the Aerosil is used, high degree of Si hydrolysis and organization around the ionic liquid is obtained, thus producing a 12-

membered ring of the BEA type zeolite. The change to TEOS results in 10-membered MFI type zeolite structure, and the use of sodium metasilicate, as Si source for which the velocity of gelification is very low, result in 8-membered ANA type zeolite.

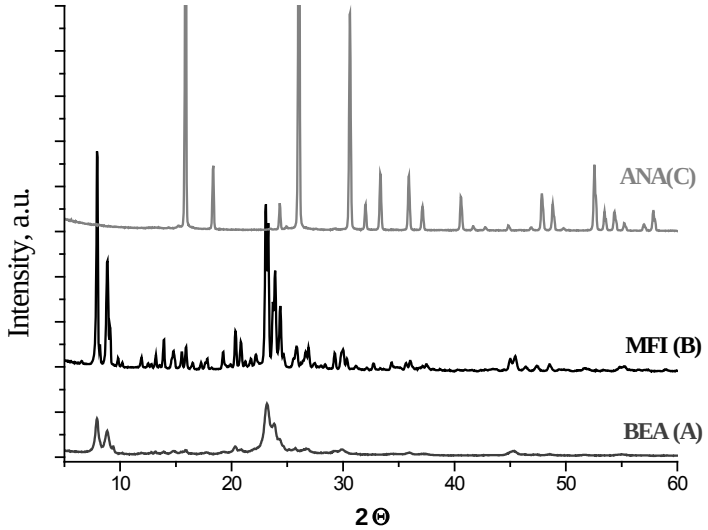

Fig.1.XR Diffrasctograms of the obtained solids in function of the Si source BEA(A)-Aerosil, MFI(B)-TEOS and ANA(C) – Na_2SiO_5

The use of the same ionic liquid as a structure directing agent for all the synthesis in the same conditions shows that the presence of different structure directing agent is not necessary for the organisation of the zeolite structure. More important seems to be the affinity of the template to the Si source, and its degree of hydrolysis. The influence of the temperature on the ionic liquid micelle organisation and on the hydrolysis of the Si source is also studied.

Conclusions

The use of one unique template (1-butyl, 3-methyl imidazolium methanesulfonate) for zeolite synthesis and its interaction with three different sources of Si is studied. The different degree of hydrolysis of the Si precursor and the different organization around the ionic liquid micelles results in three families of zeolites (8-, 10-, or 12 – membered ring).

Acknowledgements

Financial support for this work has been obtained from Junta de Andalucía (Plan Andaluz de Investigación, grupo TEP106). S. Ivanova and F. Romero-Sarria acknowledge MEC for their contract Ramón y Cajal.

References

[1] Cundy, C. S., Cox, P. A., The hydrothermal synthesis of zeolites: Precursors, intermediates and reaction mechanism, Microporous and Mesoporous Materials 82 (2005), 1-78

[2] Kuehl, J.H., Timken H.K.C., Acid sites in zeolite Beta: effects of ammonium exchange and steaming, Microporous and Mesoporous Materials, 35-36 (2000), 521-532.

[3] Morano, A., Ivanova S., Romero Sarria F., Centeno M.A., Odriozola J.A., Synthesis of ionic liquid templated zeolite like structures, Studies in Surface Science and Catalysis, Volume 175, 2010, Pages 597-600

[4] Avellaneda R. S., Ivanova S., Sanz O., ., Romero Sarria F., Centeno M.A., Odriozola J.A., Ionic liquid templated TiO_2 nanoparticles as a support in gold environmental catalysis, Applied Catalysis B: Environmental 93 (2009) 140–148

[5] Li, Z., Li, L., Yuan, Q., Feng, W., Xu, J., Sun, L., Song, W., Yan, C., Sustainable and Facile Route to Nearly Monodisperse Spherical Aggregates of CeO_2 Nanocrystals with Ionic Liquids and Their Catalytic Activities for CO Oxidation, Journal of Physical Chemistry C 112 (2008), 18405–18411.

[6] Cassol, C. C., Ebeling, G., Ferrera, B., Dupont, J., A Simple and Practical Method for the Preparation and Purity Determination of Halide-Free Imidazolium Ionic Liquids, Advanced Synthesis & Catalysis, 348 (2006), 243 – 248.

[7] Mignoni, M. L., de Souza, M. O., Pergher, S. B.C., de Souza, R. F., Bernardo-Gusmao, K., Nickel oligomerization catalysts heterogenized on zeolites obtained using ionic liquids as templates, Applied Catalysis A: General 374 (2010) 26–30

Enhanced Capacity of Li_2MnSiO_4 Cathode Material in Framework of Periodic Mesoporous Carbons

Takashi Kawase and Hideaki Yoshitake
Division of Materials Science and Chemical Engineering, Yokohama National University
yos@ynu.ac.jp

Introduction

Lithium metal-silicate (Li_2MSiO_4, M= Fe, Mn and Ni) has attracted considerable interest for a cathode material for lithium battery, since the oxide solid with a high surface area was successfully prepared by sol-gel method followed by the thermal decomposition under reducing conditions. Two Li^+ in the formula have been expected to be incorporated with the charged/discharged process to realize high capacities more than 330 mAh g^{-1}, though the experiments have provided much less capacities almost corresponding to electrochemical process with one Li^+. High capacities have recently been reported for the cathode composed of dispersed lithium metal-silicate particles coated with a carbon thin layer, which is probably carbonaceous “impurity” that is difficult to be removed in the preparation. Although the mechanism of the enhancement by coating with carbon has not been thoroughly elucidated, the optimization of the nanostructure of the carbon-Li_2MSiO_4 composite is highly desired in order to achieve the stoichiometric charge-discharge reactions. In this study, we develop Li_2MnSiO_4 particles in mesoporous carbon CMK-8 by nanocasting method. Since CMK-8 has a mesopore around 3.5 nm in a periodic structure, its framework is suitable to the support of nanoparticles and to provide the conductive media at the same time.

Experimental

Mesoporous carbon CMK-8 was prepared by the inverse replication using saturated aqueous solution of sucrose, sulfuric acid and mesoporous silica KIT-6 as a carbon source, the dehydration catalyst and the hard template, respectively. The mixture was dried and heated at 433 K for 6 h. The solid thus obtained was soaked with the same sucrose-sulfuric acid solution, dried and heated at 433 K for 6 h, followed by thermal decomposition at 1173 K for 5 h in vacuum. The KIT-6 template was removed with 5 wt HF. The first stage of the preparation of lithium manganese silicate was the incipient wetness of CMK-8 into an aqueous solution containing lithium acetate, manganese acetate, tetraethyl orthosilicate, citric acid and ethylene glycol. After the absorption of liquid, the solid was dried at 333 K, followed by thermal decomposition and reduction at 973 K for 12 h with 5% hydrogen. This impregnation-thermal decomposition/reduction process was repeated once or twice in several cases. The powdery solid was moulded into a disk electrode with 5 wt% PTFE, which was mounted in a two-electrode cell with a lithium counter electrode.

Results and discussion

The X-ray diffraction and the nitrogen adsorption were applied to characterize the structure of the carbon framework CMK-8. The peaks were found at the position assigned to the diffractions from the (211), (220), (420) and (332) in XRD. The nitrogen adsorption increased between p/p_0= 0.4 and 0.6, implying a well developed mesoporous structure with a pores around 3.4 nm. BET specific surface area and pore size were 1900 m^2 g^{-1} and 1.6 cm^3 g^{-1}, respectively. All these data indicate a successful synthesis of CMK-8. The XRD of the mesoporous carbon-Li_2MSiO_4 composite agreed with the pattern of Li_2MSiO_4, though it contained several peaks attributed to impurities. We confirmed nearly complete removal of silica by thermogravimetric measurement of this mesoporous carbon, where 99 % of the weight was lost until the temperature reached at 920 K.

The charge-discharge curves are shown in fig. 2. The specific capacity reaches at 360 mAh g^{-1}, which is larger than the theoretical value for two Li^+ insertion-desorption reaction: 330 mAh g^{-1}. However, as we considered that the capacitance of mesoporous carbon could be involved in this large capacitance, we measured the charge/discharge properties of CMK-8 and reduced the data from fig. 1 to obtain the net electrochemical property of Li_2MnSiO_4 particle in the CMK-8 framework. The data are shown in fig. 2. These curves approximately indicate the charge/discharge behaviour of Li_2MnSiO_4 in CMK-8, whose specific capacity is ca. 235 mAh g^{-1}, though irregular fluctuations are found in at the both ends of charge and discharge processes.

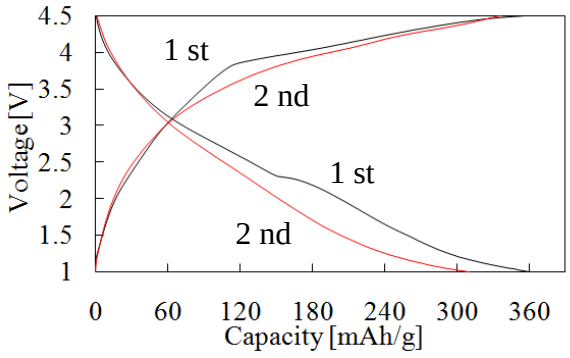

Figure 1. Charge-discharge curves of CMK-8- Li_2MnSiO_4 nanocomposite cathode.

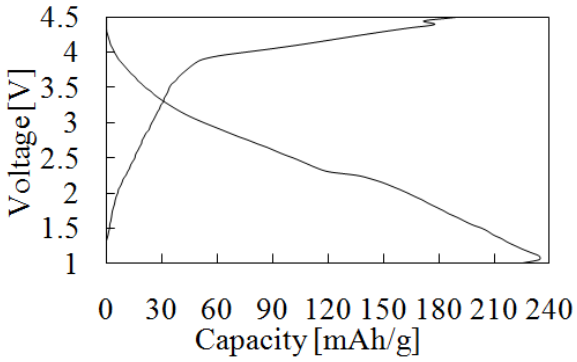

Figure 2. "Net" charge-discharge curves of Li_2MnSiO_4 nanoparticles in CMK-8.

Conclusions

Mesoporous carbon CMK-8 was used for the framework supporting Li_2MnSiO_4 nanoparticles and the electrochemical behaviour of this carbon-Li_2MnSiO_4 nanocomposite was investigated as a cathode material of Li-ion secondary battery. The net capacitance of Li_2MnSiO_4 in CMK-8 was 235 mAh g^{-1}, which was higher than that expected for one Li^+ process, 167 mAh g^{-1}.

Acknowledgements

The authors are grateful for the financial support by NEDO.

Sulfur containing Ethene Bridged PMOs as Adsorbent and Catalyst

Els De Canck and Pascal Van Der Voort
Centre for Ordered Materials, Organometallics and Catalysis (COMOC), Department of Inorganic and Physical Chemistry, Ghent University, Krijgslaan 281-S3, 9000 Ghent, Belgium. Els.DeCanck@UGent.be, Pascal.VanDerVoort@UGent.be

Introduction

Periodic Mesoporous Organosilicas (PMOs) [1] are promising materials and research in this area has expanded enormously. They are ordered materials with high specific surface areas (~1000 m^2/g), large pore volumes (~0.9 cm^3/g) and narrow pore size distributions with pores of approximately 7 nm. Furthermore they combine inorganic rigidity with organic chemical flexibility resulting in a stable material with many modification opportunities.
PMOs are synthesized using a template such as the non-ionic triblock copolymer P123 ($PEO_{20}PPO_{70}PEO_{20}$) and an organobissilane as precursor, in this contribution $(OEt)_3Si$-CH=CH-$Si(OEt)_3$ will be used. After removal of the template, a highly ordered mesoporous material is obtained which can be further functionalized and fine-tuned for one specific application. In this study, the synthesis and use of modified trans ethene bridged PMOs as mercury(II) ion adsorbents and as solid acid catalysts will be discussed. First, a thiol functionalized Periodic Mesoporous Organosilica (Fig. 1) will be presented which has been recently reported by our research group [2].

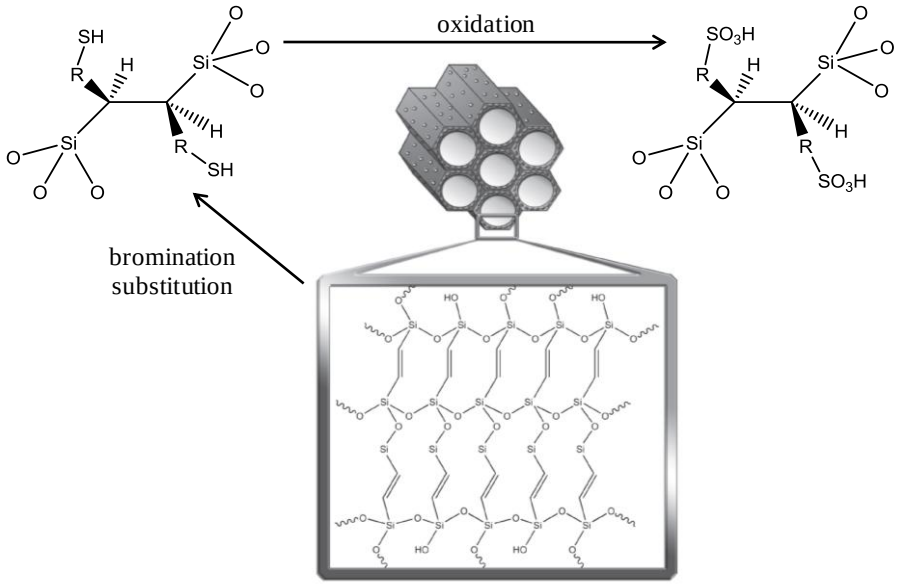

Figure 1. Transformation of the trans ethene bridged Periodic Mesoporous Organosilica in an adsorbent or catalyst. R is an alkyl or thioether group with variable chain lengths.

Secondly, the ethene bridged PMO material can be applied as a solid acid catalyst for liquid phase reactions when sulfonic acid groups are incorporated.

Experimental

The adsorbents can be prepared starting from a pure trans ethene bridged PMO. First, a bromination of the trans ethene bond occurs. Secondly, the bromine is successfully substituted by the Grignard reagent of 3-chloro-1-propanethiol (Fig. 2) [2]. Other reagents (also dithiols) with longer chains can be used in the substitution step (step 2; Fig. 2).

This results in an adsorbent with large specific surface area, narrow pore size distribution and 0.4 mmol of reachable thiol groups on the material. The thiol groups is subsequently oxidized to sulfonic acid groups, immediately converting the mercury(II) adsorbent in an acid catalyst.

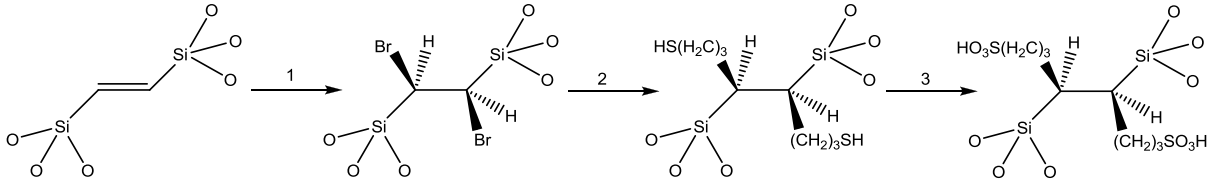

Figure 2. Functionalization of the PMO via a bromination of the ethene bond (1) and a subsequent substitution of the bromine (2). The thiol group is oxidized with the formation of a sulfonic acid group (3).

Results and discussion

The thiol containing adsorbent has been compared with several other thiol containing silica materials in the adsorption of mercury(II) ions in aqueous solution: SBA-15 grafted with propylthiol groups (post-synthetic route) and a silica material prepared via one-pot-synthesis [2]. The chemical and structural stability and adsorption behavior of these materials has been investigated in Hg(II) adsorption desorption experiments.

Whereas the silica grafted or co condensed adsorbents lose their structure or functionalities during several mercury(II) adsorption and desorption cycles in aqueous media, the thiol functionalized PMO completely maintains its structure and amount of functionalities. Next, the influence of the initial mercury(II) concentration on the adsorption behavior of the PMO adsorbent was investigated (Fig. 3). Further experiments were performed to determine the maximum adsorption capacity of the PMO adsorbent (64 mg Hg^{2+}/g) and implies thus a 1:1 ratio of Hg(II) towards thiol group.

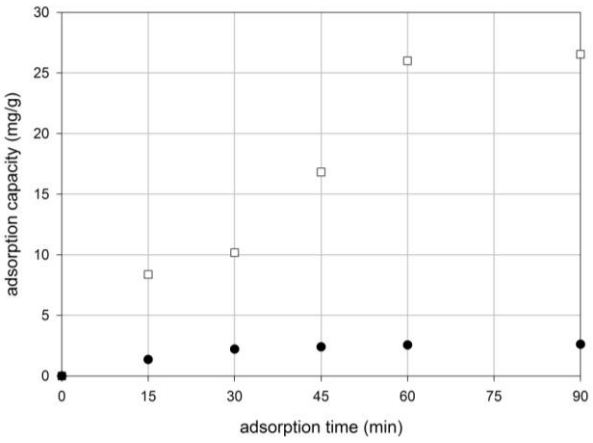

Figure 3. Investigation of the influence of the initial mercury(II) concentration on the adsorption time. The initial mercury(II) concentrations were 10 (•) and 100 (□) ppm.

The catalytic performance of the PMO containing sulfonic acid will be evaluated for esterification reactions and several catalytic runs will be performed. Also, the influence of the chain length of the sulfonic acid group on the catalytic activity will be discussed.

Acknowledgements

The authors thank Ghent University for financial support.

References

[1] Van Der Voort P., Vercaemst C., Schaubroeck D., Verpoort F., Ordered mesoporous materials at the beginning of the third millennium: new strategies to create hybrid and non-siliceous variants, Physical Chemistry Chemistry Physics, 10 (2008) 347-360.
[2] De Canck E., Lapeire L., De Clercq J., Verpoort F., Van Der Voort P., New Ultrastable Mesoporous Adsorbent for the Removal of Mercury Ions, Langmuir 26 (2010) 12, 10076-10083.

Entrapment of indigo and its derivatives into zeolite X, synthesis of new Maya Blue analogs

Anna Zywert, Małgorzata Łukarska, Stanisław Kowalak
Faculty of Chemistry, A. Mickiewicz University, Poznań, Poland,
zywert@amu.edu.pl

Introduction

Maya Blue pigment was manufactured in pre-Columbian Mesoamerica for almost thousand year and its bright blue or turquoise coloration and exceptional resistibility results from entrapment of indigo molecules into fibrous clay (palygorskite) tunnels [1]. The nature of strong interaction between dye and inorganic matrices remains still not quite clear [2]. It was found [3] that some zeolites can act as efficient matrices for encapsulation of indigo molecules, and moreover, they can alter their hue due to various cations introduced into zeolites. The following study is focused on faujasite (X) containing entrapped indigo (IN) and its derivatives such as thioindigo (TI), leuco-indigo (LI) and indigo carmine (IC). The dye molecules were introduced into zeolite cavities either by thermal (Maya) procedure or by crystallization of zeolites from the gels supplemented by respective dyes.

Experimental

Zeolites NaX as well as their modification with various cations (Na, Ca, Mg, K, Zn) were applied for entrapment of IN, TI, LI, IC. Two first dyes were ground with zeolite and then heated at elevated temperatures. The other two dissolved in water were used for impregnation of zeolites, followed by thermal treatment. Another series of syntheses comprised crystallization of zeolite X from gels containing mentioned dyes. The resulting products were sublimated or extracted (Soxhlet) with solvents (DMF, water, respectively) to check the efficiency of dye molecule entrapment. The properties of the resulted pigments were characterized by means of physicochemical techniques (UV-vis, IR, XRD, TG, DTA).

Results and discussion

The samples of zeolite NaX or KX ground with TI then heated at 100^{o}C show intense coloration whereas these with IN are rather pale and color and its intensity depends very much on treatment temperature. It is in contrast to other types of zeolites (L, mordenite, AlPO-5) and to other cationic forms of zeolite X, showing very intense and various colors already upon mild heating (Table1). The influence of zeolite cations is also very noticeable in pigments based on TI. Zeolite Na-X impregnated with aqueous solution of LI shows pale yellow color which turns blue upon exposure to air, particularly at elevated temperature, due to oxidation of dye towards IN. Incorporation of IC into NaX was unsuccessful and all dye was removed on washing. It was in contrast to AlPO-5 and ZSM-5 matrices which provided good stability of resulted pigments. It is likely that due to bulky sulfonic groups the IC molecules are too large to be accommodated in inner cavities.
The crystallization of zeolite X was conducted from gels accompanied by either aqueous solutions of LI and IC or by powder admixtures of IN and TI. It seems that last two dyes do not interfere crystallization. Contrary to Maya procedure the resulted IN X indicate intense color which might suggest different localization of dye in zeolite upon crystallization than during crushing. Solutions of dyes included into crystallization mixture (IC) do not affect the synthesis either (except for LI), although IC undergoes decomposition upon crystallization.

Table 1. Colors of the pigments prepared by introduction of indicated dyes into zeolite X.

Maya Blue procedure							Crystallization with dyes
Dye \ Zeolite		NaX	KX	CaX	MgX	ZnX	Color of products
IN	prepared	blue-grey	pale blue	blue	deep blue	i. blue	navy blue (FAU)
	sublimated	green-grey	yellow-green	turqu-oise	deep green	i. green	dark green
TI	prepared	light pink	violet	pink-violet	deep violet	pink-violet	pink (FAU)
	washed (DMF)	lilac	deep lilac	pink	pink-violet	light-violet	pale pink
LI	impregnate	yellow	—	blue	—	—	light blue (SOD/FAU)
	aged	blue	—	pale blue	—	—	pale blue
IC	prepared	light blue	—	—	—	—	white (FAU)
	washed	white	—	—	—	—	white

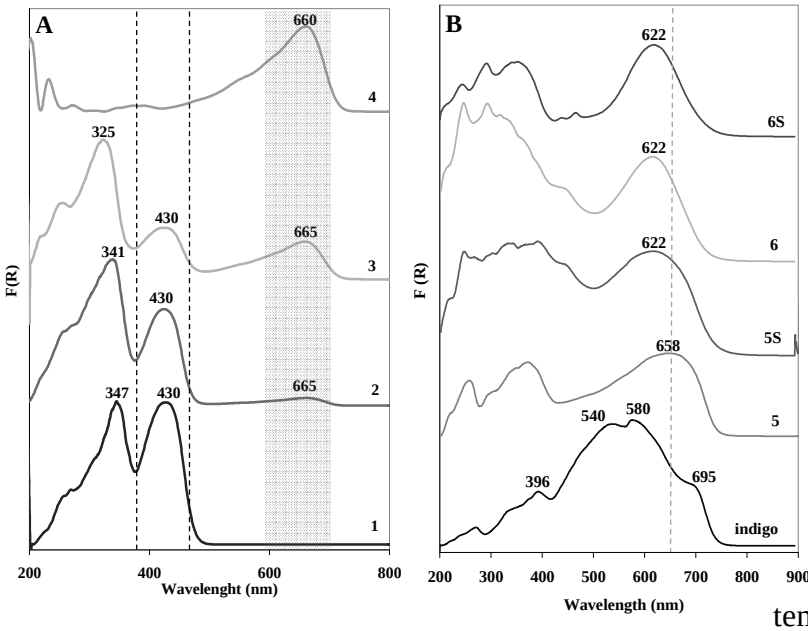

Figure 1. UV-vis spectra of selected pigments.
A. 1. X impregnated with LI
2. (1) after 10 minutes
3. (1) after 20 minutes
4. (1) after 24 hours
B. 5. NaX with IN
6. CaX with IN
S – after sublimation

Conclusions

The Maya procedure with NaX and KX and IN leads to products of pale coloration and only heating at higher temperature (e.g. upon sublimation) results in intense coloration. In the case of other cation modification the products attain deep colors already upon heating at 100^{o}C. Probably the alkaline cations inside the supercage impede a localization of indigo molecules in two adjacent cavities. The above effect is not seen for TI. The sample prepared by impregnation of NaX with LI is pale yellow and only after some time (mainly on heating) turns blue, which reminds the conventional vat dyeing of fabrics. Impregnation of NaX with IC does not lead to stable pigment, because the dye molecules are probably too large to occupy faujasite cavities. The presence of dyes in initial mixtures usually does not affect crystallization of zeolite X (except for LI). The IN localization in crystallized zeolite X is probably different than that in thermally entrapped.

Acknowledgements

Anna Zywert appreciates financial support under the grant N N204 021439.

References

[1] A.O Shepard, *Am. Antiq.* 27 (1962) 565-566
[2] A. Doménech, M.T. Doménech-Carbó, P. Váquez de Agredos, *J. Phys. Chem. B* 110 (2006) 6027-6039
[3] S. Kowalak, A. Zywert, G. Cruciani, , Zeolite L as Matrix for Zeolitic Maya Blue, 16-th IZA Conference, Sorrento 2010.

Niobium-doped titania nanoparticles and mesoporous films as transparent conductors

Yujing Liu,[a] Johann M. Szeifert,[a] Johann M. Feckl,[a] Benjamin Mandlmeier,[a] Jiri Rathousky,[b] Oliver Hayden,[c] Thomas Bein,[a] Dina Fattakhova-Rohlfing[a]
[a]*Department of Chemistry and Biochemistry, University of Munich (LMU), Butenandtstrasse 5-13, 81377 Munich, Germany, Dina.Fattakhova@cup.uni-muenchen.de*
[b]*J. Heyrovský Institute of Physical Chemistry, Academy of Sciences of the Czech Republic, Dolejškova 3, 182 23 Prague 8, Czech Republic*
[c]*Siemens AG, Corporate Technology, CT T DE HW3, Guenther-Scharowsky-Str. 1, 91050 Erlangen, Germany*

Nanoparticles and mesoporous films of transparent conducting oxides (TCOs) add new performance and functional properties to those exhibited by TCOs as thin dense films. While the TCO nanoparticles open a way to the low temperature fabrication of conducting composites or the printing of patterned electrodes, the periodic porous films of TCOs provide large surface area electrodes able to accommodate considerable amounts of functional guest molecules in electrochemical, electrocatalytical, photovoltaic and sensing applications.
Niobium-doped titanium dioxide (NTO) is a novel transparent conductor, a cheaper and chemically stable alternative to indium tin oxide (ITO) [1]. Conducting NTO materials have been so far obtained only by physical techniques (such as pulsed laser deposition) or high temperature solid state reactions [2], both approaches being unsuitable for the fabrication of nanostructured materials. Nanostructured NTO films prepared by chemical methods exhibited however only negligible or low conductivity, or their conductivity was not addressed [3].
In this communication we present a solvothermal synthesis of crystalline monodispersed niobium doped titania nanoparticles using *tert*-butanol as both a novel reaction medium and an oxide source [4], which has been recently reported a suitable solvent for the synthesis of ultrasmall and highly dispersible nanoparticles [5]. Furthermore, the ability of the obtained nanocrystals to self-assemble into complex 3D mesoporous nanostructures and the electrical conductivity of the nanoparticles and mesoporous films have been studied.

Experimental

For the synthesis of niobium-doped titania nanoparticles with 20 mo % Nb content, 0.16 ml (1.44 mmol) of $TiCl_4$ and 0.09 ml (0.36 mol) of $Nb(OEt)_5$ were added to *tert*-butanol (12 mL, 1.8 mmol). The clear solution was kept at 100 ^oC in in a Teflon-sealed autoclave for 4 h. For fabrication of mesoporous films, a solution of Pluronic F127 (0.07 g, 0.006 mmol) in THF (2 mL) was added to 0.2 g of non-washed particles previously separated by centrifugation (metal oxide content was 1.75 mmol as determined by TGA analysis), and stirred until the particles were redispersed. Conc. HCl (0.2 ml) was added to obtain a clear solution, which was dip coated on various substrates to obtain the mesoporous films. The films were heated in air at 300 ^oC for 2 hours and/or in N_2 at 500 ^oC for 2 hours, with a ramp speed of 0.5 $^oC\ min^{-1}$ for each heating step. The average thickness of the films after heating is around 200 nm.

Results and discussion

The developed solvothermal procedure in *tert*-butanol enables the preparation of crystalline doped and undoped non-agglomerated titania nanoparticles, whose size can be controlled in the range from 4 to 15 nm by changing the reaction temperature and time (Fig.1a). The

anatase lattice of these particles can incorporate more than 20 mol % of Nb ions without phase separation. The nanoparticles are easy to disperse at high concentrations in tetrahydrofurane and to assemble into periodic porous mesostructures, the assembly being directed by commercial Pluronic block-copolymers. The resulting mesoporous films show a regular mesostructure with crystalline pore walls, a d-spacing of 17 nm, a uniform pore size of 10 nm, a high porosity of 43 %, and a large surface area of 190 m^2/cm^3 (Fig. 1b).
Substitutional doping with niobium donates electrons into the conduction band of titanium dioxide and thus increases the charge carrier concentration, which drastically increases electrical conductivity of the titania particles. The electrical conductivity of as-prepared nanoparticles containing 20 mol % Nb is $2 \cdot 10^{-5}$ S/cm, rising to 0.25 S/cm due to a treatment at 600 ^{o}C in nitrogen (Fig. 1c). Time-domain terahertz spectroscopy and microwave impedance spectroscopy of the doped particles have revealed that electron hopping is the dominating contribution to the conductivity at terahertz frequencies.

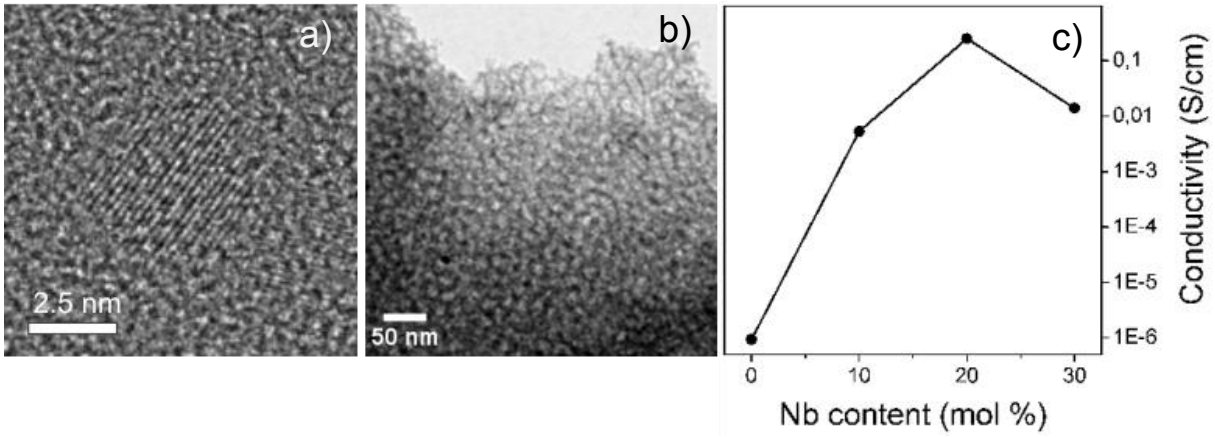

Figure 1: TEM image of: (a) NTO nanoparticles with 20 mol % Nb, (b) a mesoporous film assembled from nanoparticles, and (c) conductivity of nanoparticles annealed in N_2 at 600 ^{o}C.

Acknowledgements

The work was supported by the German Research Foundation (DFG, grant No. FA 839/1-1), Nanosystems Initiative Munich (NIM) and LMUexcellent funded by the DFG, and the Grant Agency of the Czech Republic (grant No. 104/08/0435-1). Y. L. is grateful to the Siemens/DAAD program for a postgraduate scholarship.

References

[1] Furubayashi, Y., Hitosugi, T., Yamamoto, Y., Inaba, K., Kinoda, G., Hirose, Y., Shimada, T., Hasegawa, T., A transparent metal: Nb-doped anatase TiO_2, Appl. Phys. Lett., 86 (2005), 252101-3.
[2] Zhang, S. X., Kundaliya, D. C., Yu, W., Dhar, S., Young, Y., Salamanca-Riba, L. G., Ogale, S. B., Vispute, R. D., Venkatesan, T., Niobium doped TiO_2: Intrinsic transparent metallic anatase versus highly resistive rutile phase, J. Appl. Phys., 102 (2007), 013701.
[3] Dros, A. B., Grosso, D., Boissiere, C., Soler-Ilia, G., Albouy, P. A., Amenitsch, H., Sanchez, C., Niobia-stabilised anatase TiO_2 highly porous mesostructured thin films, Microporous Mesoporous Mater., 94 (2006), 208-213.
[4] Liu, Y., Szeifert, J. M., Feckl, J. M., Mandlmeier, B., Rathousky, J., Hayden, O., Fattakhova-Rohlfing, D., Bein, T., Niobium doped titania nanoparticles: synthesis, assembly into mesoporous films and electrical conductivity, ACS Nano, 4 (2010), 5373–5381.
[5] Szeifert, J. M., Feckl, J. M., Fattakhova-Rohlfing, D., Liu, Y., Kalousek, V., Rathousky, V., Bein, T., Ultrasmall titania nanocrystals and their direct assembly into mesoporous structures showing fast lithium insertion, J. Amer. Chem. Soc., 132 (2010), 12605-12611.

ZIFs can breath !

Sonia Aguado[1], Gerard Bergeret[1], Marc Pera-Titus[1], Virginie Moizan[2], Carlos Nieto-Draghi[3], Nicolas Bats[2], David Farrusseng[1]

[1] IRCELYON, Institut de Recherches sur la Catalyse et l'Environnement de Lyon, Université Lyon 1, CNRS F-69626 Villeurbanne, France, E-mail: sonia.aguado@ircelyon.univ-lyon1.fr
[2] IFP Energies Nouvelles, Physics and Analysis division BP3, F-69360 Solaize, France
[3] IFP Energies Nouvelles, Department of Thermodynamics and Molecular Simulation, F-92852 Rueil-Malmaison, France

Soft porous crystals that exhibit dynamic frameworks upon external stimuli such as variations of pressure, temperature or electric field are the latest generation of porous solids. They are bi(multi)stable crystalline materials with long-range structural ordering that possess a structural transformability. The phase transformation can take place when a guest molecule is adsorbed or removed from the network. This property is very attractive for designing new generations of adsorbants or sensors using "gate-opening" features.

First porous Zinc imidazolates were discovered by Huang *et al*.[1] In these solids, tetrahedral Zn(II) are solely coordinated by nitrogen atoms of the imidazolate bridging ligand. These solids were reexamined by Yaghi and co-workers, who extended this class of porous coordination polymers to 90 novel structures by high throughput screening.[2] Because the Zn-im-Zn linkage is similar to the Si-O-Si linkages found in zeolites, the zinc imidazolate solids usually crystallize in the same topologies as do aluminosilicates. These structures are therefore referred to as Zeolite Metal-Organic Frameworks (ZMOF) [3] or, more frequently, as Zeolite Imidazolate Frameworks (ZIF).[2] Their high hydrothermal, chemical and thermal stability further reinforce their similarity to zeolites. ZIF materials are, however, not as rigid as zeolites. For example, Cheetham *et al*. reported that the sodalite cell of ZIF-8 can shrink or expand, to a limited extend, under pressure due to rotation of the linkers. More recently, the same team has shown that upon heating, ZIF-4 undergoes a reversible transformation from the crystal to the amorphous state.[4]

In this study, we show for the first time that ZIF-7 exhibits a reversible breathing effect upon changes in temperature or CO_2 partial pressure.[5] The thermodynamics of the process are studied in detail and compared to other reference flexible MOFs. We demonstrate that a reversible phase-to-phase transformation is responsible for this phenomenon. To the best of our knowledge, this constitutes the first example of a guest-induced gate-opening ZIF.

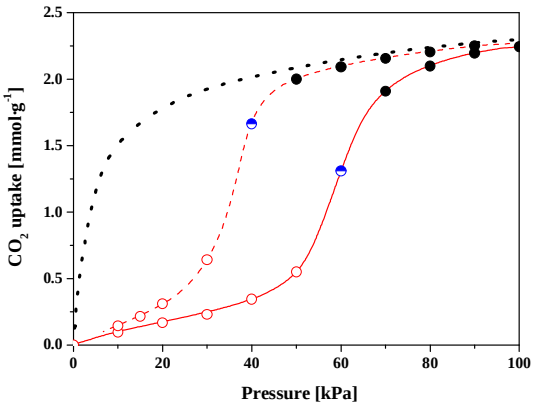

Figure 1. Match between XRPD pattern and CO_2 adsorption at 303 K. The symbols correspond to the labels of the different phases. The dashed line is the GCMC adsorption of the lp ZIF-7 phase

References

[1] (a) X. Huang, Y. Lin, J. Zhang, X. Chen, *Angew. Chem., Int. Ed.* **2006**, *45*, 1557; (b) X. Huang, J. Zhang, X. Chen, *Chin. Sci. Bull.* **2003**, *48*, 1531.

[2] K. S. Park, Z. Ni, A. P. Cote, J. Y. Choi, R. D. Huang, F. J. Uribe-Romo, H. K. Chae, M. O'Keeffe, O. M. Yaghi, *Proc. Natl. Acad. Sci. U. S. A.* **2006**, *103*, 10186.

[3] Y. Liu, V. C. Kravtsov, R. Larsen, M. Eddaoudi, *Chem. Comm.* **2006**, *14*, 1488.

[4] T. D. Bennett, A. L. Goodwin, M. T. Dove, D. A. Keen, M. G. Tucker, E. R. Barney, A. K. Soper, E. G. Bithell, J.-C. Tan, A. K. Cheetham, *Phys. Rev. Lett.* **2010**, *104*, 115503.

[5] S. Aguado, G. Bergeret, M. Pera-Titus, V. Moizan, V. Moizan-Baslé, C. Nieto-Draghi, N. Bats, D. Farrusseng, *New J. Chem.* **2011**, doi:10.1039/C0NJ00836B.

Enhancement of catalytic activity in one-pot oxidation using Pd/SiO_2@Ti containing mesoporous silica core-shell type catalyst

Shusuke Okada, Takashi Kamegawa, Kohsuke Mori and Hiromi Yamashita
Division of Materials and Manufacturing Science, Graduate School of Engineering, Osaka University, yamashita@mat.eng.osaka-u.ac.jp

Introduction

Hydrogen peroxide (H_2O_2) is one of the most attractive oxidizing agents from the view point of environmental, because the theoretical by-product is only water. Current production process via anthraquinone auto-oxidation processes involves many environmental adverse. Direct synthesis of H_2O_2 from H_2 and O_2 gases is one of the promising alternative technique. However, the catalyst for H_2O_2 synthesis also actives for H_2O_2 decomposition in this process. In order to overcome this thorny problem, one-pot synthesis to utilize in situ generated H_2O_2 for oxidation reaction is very attractive [1]. Here we designed a new core-shell type catalyst, based on this approach, to improve the catalytic efficiency for one-pot oxidation. It was found that the relative position between H_2O_2 generation site (Pd nanoparticle) and oxidation site (Ti-mesoporous silica) significantly affects on the catalytic performance.

Experimental

Two types of core-shell catalysts with different Pd site were prepared. One is Pd supported SiO_2 covered by Ti containing mesoporous silica shell (Pd/SiO_2@TiMSS) and the other is SiO_2 covered by Pd supported Ti containing mesoporous silica shell (SiO_2@ Pd/TiMSS). The schematics models of Pd/SiO_2@TiMSS and SiO_2@ Pd/TiMSS are shown in Figure 1. At first, Pd nanoparticle was loaded on SiO_2 sphere. Next, Ti containing mesoporous silica shell was created on the Pd loaded SiO_2 surface. Finally, it was calcined to remove structure directing agent (SDA) to obtain Pd/SiO_2@TiMSS. SiO_2@ Pd/TiMSS was obtained by the first coating of Ti containing mesoporous shell followed by the loading of Pd nanoparticle. Pd nanoparticles are located within the mesoporous structure in the Pd/SiO_2@TiMSS, while Pd nanoparticles are located on the outer surface of the mesopores in the SiO_2@ Pd/TiMSS.

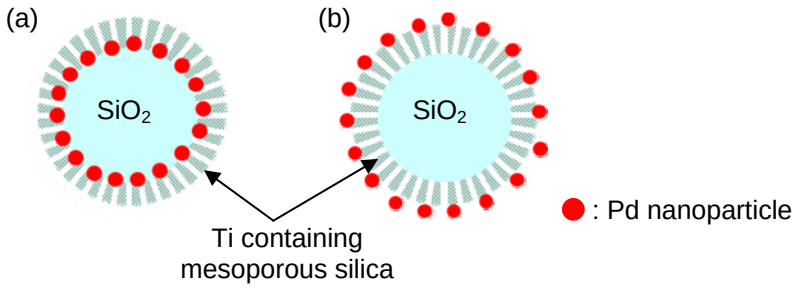

Figure 1. Schematics models of Pd/SiO_2@TiMSS (a) and SiO_2@ Pd/TiMSS(b).

Results and discussion

As shown in Figure 2, TEM images of Pd/SiO_2@TiMSS and SiO_2@Pd/TiMSS reveals these catalysts are core-shell structure and Pd nanoparticle deposited at the intended site. The thickness of the shell is about 30 nm. The UV-Vis spectra and XANES spectra exhibited Ti species in the Ti-mesoporous shell is tetrahedral coordination suitable for oxidation reaction using H_2O_2 as oxidizing agent. The pore structure was characterized by small angle XRD and N_2 adsorption and desorption. The XRD spectra shows clear peak centered around $2\theta = 2.4°$ and N_2 adsorption and desorption isotherm showed typically type IV isotherm. These results indicate the shell have mesoporous structure with uniform pores.

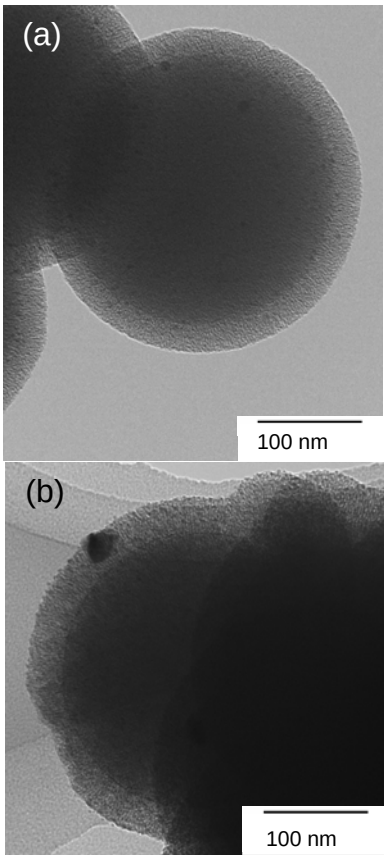

Figure 2. TEM image of Pd/SiO_2@TiMSS (a) and SiO_2@ Pd/TiMSS(b).

We explored the catalytic activity of these core-shell catalysts in the direct synthesis of H_2O_2 from H_2 and O_2 gases and one-pot oxidation reaction of methyl phenyl sulfide using in situ synthesised H_2O_2. The formation rate of methyl phenyl sulfoxide and methyl phenyl sulfone with these two catalyst are shown in Figure 3. Although the activity of these two catalysts for the generation of H_2O_2 from H_2 and O_2 gases were almost same, the activity for the one-pot oxidation of methyl phenyl sulfide using Pd/SiO_2@TiMSS is higher than that of SiO_2@Pd/TiMSS by a factor of three. Moreover, the selectivity of metyl phenyl sulfoxide is improved by using Pd/SiO_2@TiMSS than using SiO_2@Pd/TiMSS.

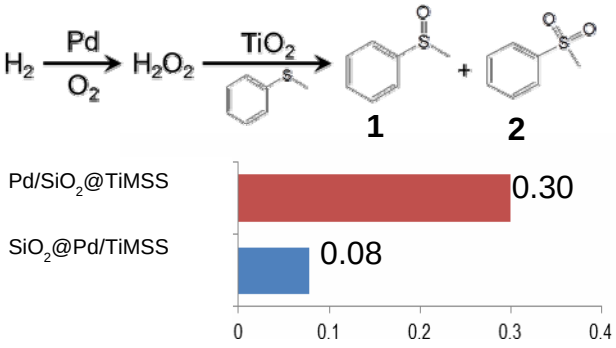

Figure 3. Formation rate in the one-pot synthesis.

Conclusions

Two type of core-shell catalysts with different Pd deposited positions were synthesized successfully. In the one-pot oxidation using in situ synthesized H_2O_2, it is revealed the relative position between H_2O_2 generation site and oxidation site significantly effect the catalytic activity.

References

[1] Kohsuke Mori, Yuki Miura, Sayoko Shironita, and Hiromi Yamashita, *Langmuir* **2009**, 25, 11180.

Formation of surface Diels-Alder adducts on ethenylene-bridged periodic mesoporous organosilicas

D. Esquivel[a], E. De Canck[b], C. Jiménez-Sanchidrián[a], P. Van der Voort[b], and F. J. Romero-Salguero[a]
[a]*Departamento de Química Orgánica, Facultad de Ciencias, Universidad de Córdoba, Campus de Rabanales, Edificio Marie Curie, Carretera Nacional IV-A, km. 396, 14014-Córdoba (España);*[b]*University of Ghent, Department of Inorganic and Physical Chemistry, Krijgslaan 281, B-9000 Ghent (Belgium). qo2rosaf@uco.es*

Introduction

Since the so-called periodic mesoporous organosilicas (PMOs) were reported [1], they have attracted a great interest as a novel class of hybrid materials with a homogeneous distribution of organic fragments. However, only a few studies dealing with their functionalization, particularly bromination and sulfonation, have been carried out. Recently, a new route of surface modification has been suggested by Diels-Alder reaction between the double bonds of an ethenylene-PMO and benzocyclobutene [2]. The generalization of this process to other more common dienes would lead to interesting materials with new pendant groups linked to the organic bridges of the framework.

Experimental

The starting material, a 100 % E-ethenylene-bridged PMO (e-PMO), was synthesized by a previously reported procedure by Van der Voort et al. [3]. The Diels-Alder reaction was carried out as follows: a mixture of the e-PMO and the diene (benzocyclobutane, dicyclopentadiene or anthracene) in 20 ml dodecane was aged in an autoclave at 200 ºC during several days. After filtering, the resulting solid was repeatedly washed with chloroform to assure the complete elimination of the unreacted diene. Subsequently, each material was functionalized with sulfonic acid groups by reaction with either chlorosulfonic acid or fumed sulfuric acid. Sulfonic acid functionalized mesoporous organosilicas were used as catalysts for the esterification of acetic acid with ethanol and their activities compared to that of Amberlyst-15.

All solids were exhaustively characterized by several techniques such as nitrogen adsorption, powder X-ray diffraction, thermal analysis, DRIFT and ^{13}C NMR, among others.

Results and discussion

XRD analyses showed that the ordered hexagonal mesostructure of e-PMO remained after the Diels-Alder reactions and the subsequent sulfonations. However, the (100) peaks were shifted to higher angles due to the structural contraction caused by the thermal treatment (200 ºC). All materials exhibited type IV isotherms with a step at relative pressures $0.4<P/P_0<0.8$ and narrow pore size distributions.

The formation of the surface Diels-Alder adducts was confirmed by DRIFT and ^{13}C NMR measurements. DRIFT spectra showed C-H stretching vibration bands above 3000 cm^{-1}. ^{13}C MAS NMR spectra (Figure 1) exhibited several peaks, besides that corresponding to the double bonds in the framework, which corroborated the existence of the surface adducts. For example, those with benzocyclobutene and anthracene had signals around 126 ppm attributed to the aromatic groups.

After sulfonation, the modified e-PMOs were used as catalysts for the esterification of acetic acid. They showed high conversions and reaction rates close to that of Amberlyst-15, thus confirming the application of these materials as solid acid catalysts.

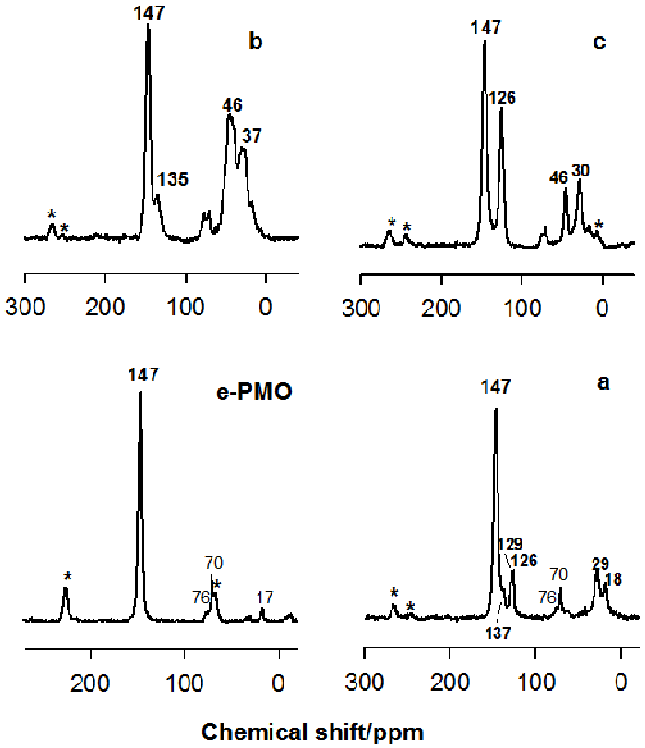

Figure 1. ^{13}C CP/MAS NMR of the ethenylene-bridged PMO before (e-PMO) and after the Diels-Alder reaction with benzocyclobutene (a), dicyclopentadiene (b) and anthracene (c).

Conclusions

The Diels-Alder reaction between the C=C bonds of an ethenylene-bridged PMO and different dienes seems to be a quite general route for the surface modification of these materials. In addition, these new pendant organic fragments can be further functionalized to introduce acid sites in the mesopores, thus enabling them to be used as catalysts.

Acknowledgements

The authors would like to thank Ministry of Science and Innovation of Spain (Project MAT2010-18778) and Junta de Andalucía (P06-FQM-01741) for financial support. D. E. acknowledges Ministry of Education and Science for a research and teaching fellowship.

References

[1] Inagaki S., Guan S., Fukusmina Y., Ohsuna T., Terasaki O., Novel mesoporous materials with a uniform distribution of organic groups and inorganic oxide in their frameworks, Journal of the American Chemical Society, 121 (1999) 9611-9614; Melde B. J., Holland B. T., Blandford C. F., Stein A., Mesoporous sieves with unified hybrid inorganic/organic frameworks, Chemistry of Materials, 11 (1999) 3302-3308; Asefa T., MacLachlan M. J., Coombs N. Ozin G. A., Periodic mesoporous organosilicas with organic groups inside the channel walls, Nature, 402 (1999) 867-871.

[2] Nakajima K., Tomita I., Hara M., Hayashi S., Domen K., Kondo J. N, A stable and highly active hybrid mesoporous solid acid catalyst, Advanced Materials, 17 (2005) 1842-1846.

[3] Vercaemst C., Ide M., Allaert B., Ledoux N., Verpoort F., Van der Voort P., Ultra-fast hydrothermal synthesis of diastereoselective pure ethenylene-bridged periodic mesoporous organosilicas, Chemical Communications, (2007) 2261-2263.

Synthesis of functionalized ordered mesoporous resins

Witold Bożejewicz, Jakub Dzitko, Stanisław Kowalak
Faculty of Chemistry, A. Mickiewicz University, Poznań, Poland
wektor@amu.edu.pl

Introduction

Recently sulfonated carbons obtained by incomplete carbonization of common natural product such as sugar showing catalytic acid sites have been reported [1]. However, the reported materials were nonporous and exhibited low surface area, which limited their potential catalytic activity due to restricted accessibility to acid active sites. The catalytic properties could be markedly improved by modification of preparation procedure in order to increase the surface area and to develop a uniform pore system. The attempts to introduce catalytically active groups to the resins by using respective derivatives of phenol were successful but the resulted products did not show ordered porosity [2]. Here, we report a new and easy method to synthesize sulfonic acid-functionalized ordered mesoporous polymers. The main aim of the study is a direct preparation of self-assembly phenol-formaldehyde resins with sulfonic groups.

Experimental

The preparation procedure was based on conventional synthesis of phenol-formaldehyde resins modified by adding the porogenous agents as well as sulfonated derivative of phenol. Phenol, formaldehyde and sodium 4-hydroxybenzenesulfonate were dissolved in NaOH solution and stirred at 70 °C for 30 min. Then the aqueous solution of Pluronic P123 was added. The heating under reflux with stirring was continued for 90 hours. The final products were filtered, washed with water and dried. The soft template (Pluronic P123) was removed by boiling with 48% sulfuric acid. Standard method to remove template, calcination at 360 °C in inert gas atmosphere, removed also sulfonic groups (Fig.2C). The products were characterized by means of XRD, IR, TG/DTA, TEM, N_2 adsorption/desorption.

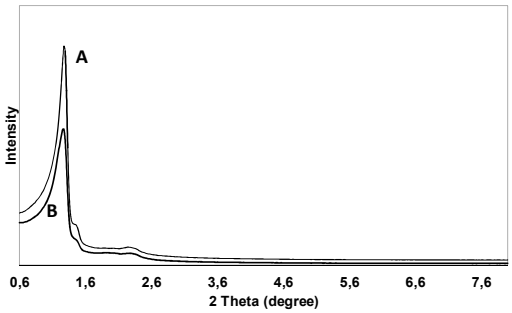

Fig.1. XRD pattern of mesoporous resins prepared with higher (A), and lower (B) 4-hydroxybenzenesulfonate content.

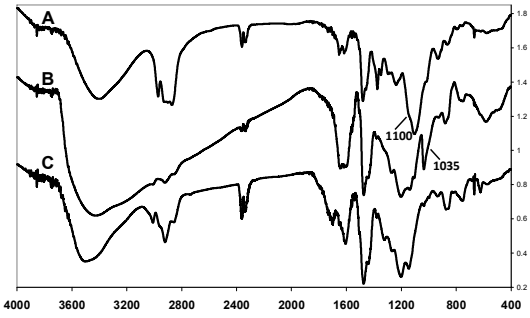

Fig.2. FTIR of mesoporous resins prepared with Pluronic (A), after removed template by sulfuric acid (B), and after removed template by calcination at 360 °C in N_2 atmophere (C).

Results and discussion

The products obtained upon phenol-formaldehyde condensation with Pluronic P123 after H_2SO_4 treatment show the low angle XRD patterns (Fig.1.) characteristic of well-ordered mesopore structure.

The incorporation of organic functional groups was confirmed by FTIR. Figure 2 shows the FTIR spectra of the mesoporous polymers prepared from phenol, sodium 4-hydroxybenzenesulfonate and

formaldehyde. Lack of absorbance at 1100 cm^{-1} (Fig.2.A) suggests that the template is completely removed after boiling with 48% sulfuric acid at 90°C. The absorbance bands at 3007 and 2934-2868 cm^{-1} are assigned to the –C–H and –CH2 stretching vibrations from the aromatic polymeric framework, respectively; while the absorbance at 1610 and 1481 cm^{-1} are assigned to the stretching bands from the benzene ring. More importantly, the absorbance at 1035 cm^{-1} attributed to the S=O symmetric stretching (Fig.2.B) prove the incorporation of $–SO_3H$ group within the polymer.

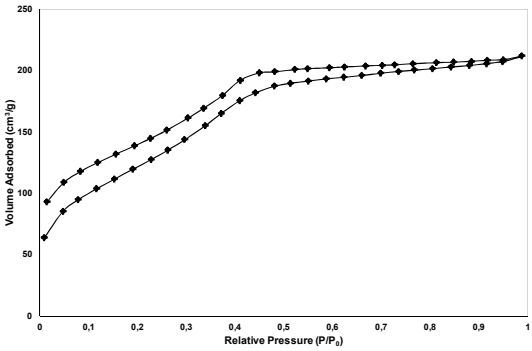

Fig.3. N_2 adsorption desorption isotherm of functional mesoporous polymers with $–SO_3H$ groups

The low temperature nitrogen adsorption on the sample prepared with Pluronic 123 show the isotherm (Fig.3) reminding the type IV, although the typical sharp uptake at p/p_o is not significant. The adsorption and desorption branches are not closed at low relative pressure, which is a typical sorption behavior of polymer materials. The estimated average pore size is ~ 2.8 nm, a BET surface area 464 m^2/g, and a pore volume 0.32 cm^3/g.

The sulfonated samples contrary to the non modified porous polymers indicate a noticeable catalytic activity for decomposition of propan-2-ol towards diisopropyl ether.

Conclusions

The presented results indicate a possibility to prepare the well ordered resin molecular sieves with aid of Pluronic or other porogeneous agents. It is also possible to obtain other novel ordered porous resins with phenol derivatives. The functionalized mesoporous polymers indicate activity in catalytic test reaction requiring the presence of acidic sites.

Acknowledgements

Witold Bożejewicz appreciates financial support under the grant N N204 137939.

References

[1] M. Toda, A. Takagaki, M. Okamura, J. N. Kondo, S. Hayashi, K. Domen and M. Hara, *Nature*, 2005, 438, 178.
[2] Z. Yang, J. Wang, K. Huang, J. Ma and Y. Lu, *Macromolecular Rapid Communications*, 2008, 29, 442-446.

Kaolinite-Polymer compounds: 2-hydroxyethyl methacrylate and 3-(trimethoxysilyl)propyl methacrylate grafted on kaolinite

Breno F. Ferreira[a], Paulo S. Calefi[a], Katia J. Ciuffi[a], Eduardo J. Nassar[a], Miguel A. Vicente[b], Raquel Trujillano[b] and Emerson H. de Faria[a]

[a] *Universidade de Franca, Av. Dr. Armando Salles Oliveira, Parque Universitário, 201, 14404-600, Franca, SP, Brazil,*
[b] *Departamento de Química Inorgánica, Universidad de Salamanca, Plaza de la Merced, S/N, 37008 Salamanca, Spain (Miguel A. Vicente: mavicente@usal.es)*

Introduction

Polymeric materials have usually been prepared including in their composition natural or synthetic inorganic compounds such as clays, talc, quartz, calcium carbonate or mica, in order to improve the properties and/or reduce the preparation cost of the final polymers[1]. In this context, the insertion of monomers in the interlayer space of clay minerals leads to materials combining functionalities of the organic ligand such as reactivity and flexibility, with the specific properties of the inorganic matrix, such as chemical and thermal stability, giving rise to new materials with high functionalities and unique properties [2-3]. Various inorganic matrices such as silica, zeolite, and titania have been employed in the development of hybrid organic-inorganic matrices. Several clay composites have been synthesized with particular thermo-mechanical and electrical properties. However insufficient attention has been paid to kaolinite, in spite that it is the most abundant clay and can give a rise of interesting clay-polymer composites and nanocomposites. Taking into consideration that clay-polymer nanocomposites have countless applications, and that their derivatives containing methacrylate groups are potentially applicable in various scientific and technological areas, we have carried out the functionalization of a kaolinite (Ka) from São Simão, Brazil, with 2-hydroxyethyl methacrylate (HEMA) and 3-(trimethoxysilyl)propyl methacrylate (TMSPM), by displacement of dimethylsulfoxide (DMSO). The materials resulting from the reaction between molten HEMA and TMSPM and Ka-DMSO solids were characterized by X-ray diffraction (XRD), thermal analysis, infrared absorption spectroscopy (IR) and transmission electronic microscopy (TEM).

Experimental

The nanocomposite materials were obtained by keeping a mass of the precursor (Ka-DMSO) in the presence of the monomers HEMA or TMSPM for 48 h. The molar ratios HEMA/Ka and TMSPM/Ka were 5:1. The reactions were carried out at 150 ºC. The resulting materials were washed with ethanol five times, oven-dried at 80ºC, and designated Ka-HEMA and Ka-TMSPM, respectively.

Results and discussion

Ka had a basal spacing of 7.14 Å, which increased up to 11.20 Å in the sample treated with DMSO. Thus, the expansion of the interlayer space produced by the incorporation of DMSO molecules was 4.06 Å, which agrees with literature data [2, 3]. The solids Ka-HEMA and Ka-TMSPM did not show great increases in the basal distance, which appeared in both solids at 11.45 Å. On the other hand, the diffraction effects not depending on the stacking of the layers in the *c*-dimension did not appear, due to the polymerization of amorphous polymer. The low crystallinity of these solids and the decrease of the peak corresponding to

the basal distance (001 reflection) of the hybrid compound compared to the peak of Ka can be attributed to the disorder in arrangement of the layers induced by the presence of HEMA and TMSPM molecules polymerized in the interlayer region. The grafted materials Ka-HEMA and Ka-TMSPM after washed once with toluene shows the complete amorphization of the solids, and the characteristic peak of the intercalated material at 11.45 Å disappears completely, which suggests that the treatment with toluene can induce the exfoliation of the grafted layers.

Ka-HEMA and Ka-TMSPM displayed bands at 3699 and 3618 cm^{-1}, characteristic of inter- and intralamellar hydroxyls, respectively. The other bands assigned to interlamellar hydroxyls (at 3668 and 3653 cm^{-1}) were not observed. The broad band at 3600 cm^{-1} in this region, assigned to the presence of hydroxyl groups or adsorbed water on hydrophilic polymers, confirmed the exfoliation for all composites. Bands characteristic of methacrylate groups were also observed at 2993, 1728 and 1192 cm^{-1} , assigned to C-H, C=O and α-CH_3 isotactic polyhydroxiethylmethacrylate (PHEMA) and at 1454, 1388 and 1242 cm^{-1} corresponding to δ-CH_2, α-CH_3 and C-O stretching of syndiotactic PHEMA [4]. The typical band of the interlamellar aluminol group at 938 cm^{-1} was absent for both samples, confirming the reaction between hydroxyl groups from kaolinite and hydroxyl or silanol groups from HEMA and TMSPM, respectively by condensation reactions. The displacement of the bands corresponding to interlamellar hydroxyls and the appearance of new bands in regions related to methacrylate groups evidence the entrance of methacrylate molecules from HEMA and TMSPM into the interlamellar space of kaolinite. At the same time, the absence of S=O vibrations in the spectra shows the total substitution of DMSO by methacrylate monomers.

Conclusions

HEMA and TMSPM effectively displaced DMSO molecules from kaolinite interlayer, giving rise to Al-O-C bonds, thereby characterizing formation of a hybrid organic-inorganic matrix. XRD revealed the incorporation of the organic molecules DMSO, and then HEMA and TMSPM into the interlayer space of kaolinite. Displacement of the bands due to interlayer hydroxyl groups in the infrared absorption spectra and the presence of vibrations due to methacrylate groups at 3349, 3331, 3290, and 1589 cm^{-1} also confirm the functionalization of kaolinite with the monomers. TEM micrographs confirm the partial exfoliation of kaolinite after insertion of HEMA and TMSPM monomers. These materials will be applied as support of catalyst to effective immobilization of ironporphyrins and phtalocyanines complexes, and also as adsorbent from wastewater.

Acknowledgements

Brazilian authors thank FAPESP, CNPq, and CAPES for financial support and Spanish authors acknowledge ERDF, MICINN (grants MAT2007-66439-C02 and MAT2010-21177-C02) and AECID (grant D/030161/10).

References

[1] Pavlidou, S.; Papaspyrides,C.D. A review on polymer–layered silicate nanocomposites. Progress in Polymer Science 33 (2008) 1119-1198.

[2] Tunney, J.J., Detellier, C., Interlamellar covalent grafting of organic units on kaolinite. Chemistry of Materials 5 (1993) 747-748.

[3] de Faria, E.H.; Ciuffi, K.J.; Nassar, E.J.; Vicente, M.A.; Trujillano, R.; Calefi, P.S. Novel reactive amino-compound: Tris(hydroxymethyl)aminomethane covalently grafted on kaolinite. Applied Clay Science 48 (2010) 516-521.

[4] Hassan, S.A.; Yehia, F.Z.; Hassan, H.A.; Sadek, S. A.; Darwish, A.S. Various characteristics and catalytic performance of iron (II) phthalocyanine immobilized onto titania- and vanadia-pillared bentonite clay in in situ polymerization of methyl methacrylate An attempt to synthesize novel polymer/iron phthalocyanine/pillared clay nanocomposites. Journal of Molecular Catalysis A: Chemical 332 (2010) 93-105.

Catalytic applications of microwave-assisted synthesized saponites

R. Trujillano[a] E. Rico[a], M.A. Vicente[a], V. Rives[a], K.J. Ciuffi[b], A. Cestari[b], A. Gil[c], S.A. Korili[c]

[a] *GIR-QUESCAT, Departamento de Química Inorgánica, Universidad de Salamanca, Plaza de la Merced S/N, 37008 Salamanca, Spain (Raquel Trujillano: rakel@usal.es)*
[b] *Universidade de Franca, Av. Dr. Armando Salles Oliveira, 201 Pq. Universitário CEP 14404600 – Franca, Sao Paulo, Brazil*
[c] *Departamento de Química Aplicada, Universidad Pública de Navarra, 31006 Pamplona, Spain*

Introduction

Natural expandable clays (smectites) are widely used in several applications, such as adsorption, catalysis, synthesis of nanomaterials, etc. The properties (for instance, chemical or mineralogical composition, particle size, specific surface area, etc.) of natural clays depend on the mineralogical origin, but these problems can be overcome by using synthetic clays usually prepared by hydrothermal procedures at high temperatures and pressures for long times. Microwave assisted synthesis offers an alternative route to obtain synthetic clays without using these severe conditions.

Saponite has the theoretical formula $[Si_{8-x}Al_x]^t\ [M^{2+}{}_6]^o\ O_{20}\ (OH)_4\ [M^{+}{}_x]\cdot nH_2O$, the divalent octahedral cation being mainly Mg^{2+} in natural samples. In this formula, it is possible to change the nature of the divalent octahedral cations (within a range of ionic radii), the nature of the exchangeable cations, and the degree of Si-Al isomorphous substitution in the octahedral sheet (even certain trivalent cations different from Al^{3+} can also substitute Si^{4+}).

The microwave-assisted synthesis of saponite with various different elements in their composition is reported here. The synthesis is combined with mechanical grinding in order to improve the properties of the solids. The catalytic activity of these solids in the epoxidation of (Z)-cyclooctene by hydrogen peroxide is evaluated, an environmentally-friendly reaction that can be considered a test reaction of the oxidation potential of a catalyst [1].

Experimental

Sodium silicate (aqueous solution, SiO_2 27 wt. %) and the chlorides of the divalent (Mg^{2+}, Ni^{2+}, or Fe^{2+}) and of the trivalent (Al^{3+} or Fe^{3+}) cations were used as source of these elements. The synthesis was carried out in strongly alkaline conditions, provided by NaOH and $NaHCO_3$. The targeted saponite formula was $[Si_7M^{III}{}_1][M^{II}{}_6]O_{20}(OH)_4[Na_1]\cdot nH_2O$. The gels obtained after mixture of the reagents were sealed in a 100-mL Teflon reactor and treated hydrothermally in a Milestone Ethos Plus microwave furnace at 180 °C, for 8 hours. The epoxidation of (Z)-cyclooctene was carried out in 4-mL vials, in which hydrogen peroxide, (Z)-cyclooctene, cyclohexanone (internal standard) and the catalysts were added, the solvent being a 1:1 mixture of 1,2-

dichloroethane/acetonitrile. The products of the reaction were analyzed by gas chromatography.

Results and discussion

Most of the solids synthesized were exclusively formed by saponite, except the solid with Fe^{2+} as the divalent cation, which was unpurified with Fe_2O_3 and analcime (Figure 1). Their specific surface areas were in the 200-470 m^2/g range. All of them were active for the epoxidation of (Z)-cyclooctene by hydrogen peroxide, the selectivity being always 100 % to the epoxide (cyloocteneoxide) and the conversion reached a maximum value of 7.7% after 24 h reaction (sample containing Fe^{3+} as tetrahedral cation and Mg^{2+} as octahedral one) and 8.8 % after 48 h of reaction (sample containing Al^{3+} as tetrahedral cation and Mg^{2+} and Ni^{2+} as octahedral cations).

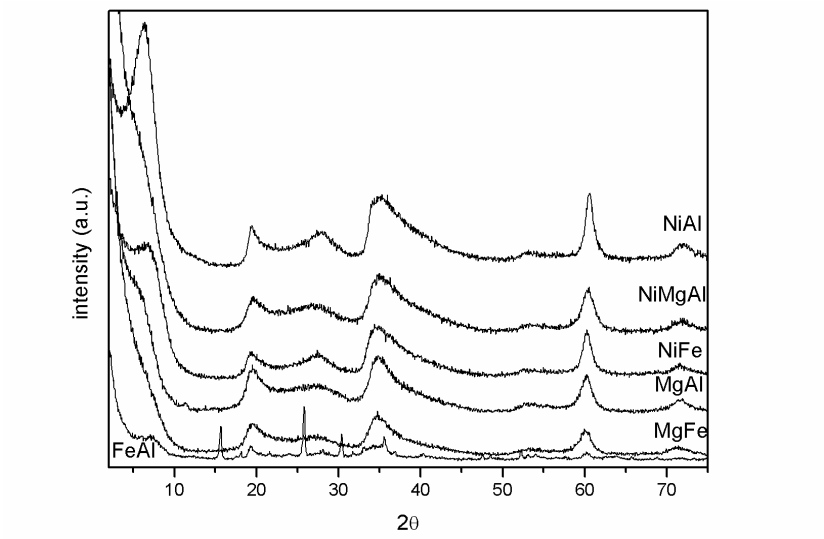

Figure 1. X-ray diffraction patterns of the prepared saponites. The notation of the samples refers to their divalent and trivalent cations.

Acknowledgments

Spanish authors acknowledge ERDF, MICINN (grants MAT2007-66439-C02 and MAT2010-21177-C02) and AECID (grant D/030161/10), and Brazilian authors thank FAPESP, CNPq, and CAPES for financial support.

References

[1] R. Trujillano, E. Rico, M.A. Vicente, V. Rives, K.J. Ciuffi, A. Cestari, A. Gil, S.A. Korili. Rapid microwave-assisted synthesis of saponites and their use as oxidation catalysts. Applied Clay Science, in press (doi: 10.1016/j.clay.2010.12.005).

Preparation of Antimicrobial Surfaces with Zeolites

Zeynep Ustaoğlu[a], Selami Demirci[b], Nurcan Baç[a], Fikrettin Şahin[b]
a-Department of Chemical Engineering, b Department of Genetics and Bioengineering
Yeditepe University Kayisdag cad. Atasehir 34755 Istanbul Turkey,
zeynep_ustaoglu@yahoo.com

Introduction

Microorganisms such as fungi, yeast, and bacteria can live almost everywhere on the earth and some of which may be primary and opportunistic pathogens causing clinically important diseases on human being, animals and plant in the world. The current technology available to control pathogenic microbial flora in *in vivo* and *in vitro* conditions based on use of antimicrobial agents such as antibiotics, antiseptics, disinfectants and synthetic drugs. Toxicity, increasing adverse drug reaction and the appearance of drug resistance forced the scientists to develop novel and safer antimicrobial agents for management of broad spectrum microorganisms [1]. So far, there is no a full-broad spectrum antimicrobial agent available for antimicrobial material production. Zeolites are composed of silicon, aluminium, and oxygen in a framework with cations, water within pores, and are basically nanoporous alumina silicates [2]. Silica is a neutral regular tetrahedron in which positive charge of silicon ion is balanced by oxygen. However, in alumina structure there is unbalanced negative charge. Therefore, the total structure of zeolite has a negative charge and this charge is balanced by cations (Na^+ or K^+) [3]. These positive ions can be exchanged for other desired ones in a contact solution. The aim of this study was to develop novel antimicrobial agents which can be combined with different materials used for manufacturing of antimicrobial surfaces. In the present study, silver nanoparticles or zeolites loaded with different concentrations and combinations of metal ions (copper, zinc, and silver) were synthesized and tested on different kinds of fungi and yeast species. The results showed that silver nanoparticles were not effective on fungi species tested. However, optimized concentration of silver zeolite formulation tested was found to be effective on all kinds of microorganisms tested. Combination of silver zeolite with liquid paint demonstrated the presence of excellent antimicrobial activity of metal surfaces covered with silver zeolite embedded paints. This is the first study demonstrated that the newly synthesized silver zeolite formulations can be used to develop antimicrobial materials and surfaces in the future.

Experimental

In this work, Zeolites A and X are synthesized using sodium aluminate, sodium metasilicate and soddium hydroxide under hydrothermal conditions. Compositions of ingredients vary according to the type of zeolite. The gel composition used for Zeolite A is in the range: 1.94-3.39 Na2O: Al2O3: 0.84-1.77 SiO2: 117-194 H2O; and for Zeolite X it changes to 6-17 Na2O: Al2O3: 3.5-8 SiO2: 300-670 H2O. The synthesis gel is vigorously shaken for the homogenization, and is placed into high density polyethylene (HDPE) bottles and placed into a convection oven at 90 ºC. After a predetermined cooking period bottles are taken and the zeolite product is filtered and dried. Preliminary characterization is done by SEM (Scanning Electron Microscope) images and X-Ray diffraction. The zeolites synthesized in sodium form are then ion exchanged with silver copper and zinc ions for antimicrobial activity. Then antimicrobial tests were performed for 50 types of microorganisms for each zeolite type which were ion exchanged at different concentration of solutions. Using these antimicrobial

zeolites paint mixtures are prepared, and applied to surfaces and microbial testes are performed.

Results and discussion

The antimicrobial activity starts as soon as silver, copper and zinc ions are released from the zeolite crystals into the system containing microorganisms. In this study we examined the antimicrobial activity of antimicrobial zeolites against *E- Coli*, *Pseudomonas aeruginosa*, *Candida albicans*, *Staphylococcus aureus* and 40 other microorganizms. Silver zeolite is effective for every microorganism. Using these zeolites antimicrobial paints and surfaces are developed.

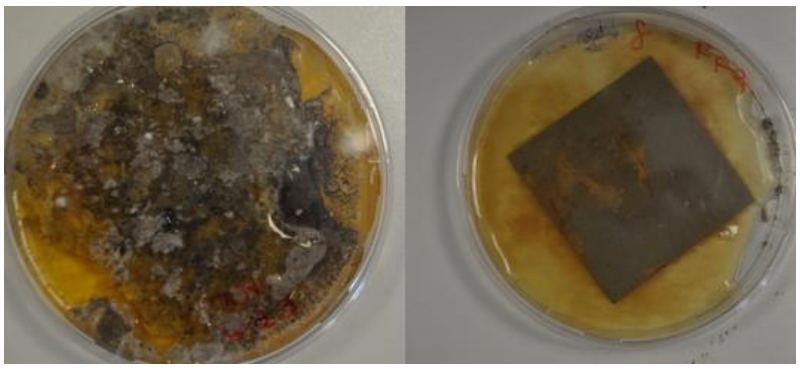

a b

Figure 1.a. Negative control for Aspergillus niger. Aspergillus niger was growth on the metal surface which was painted with paint ordinary paint. b. There is no fungus growth on the metal plate which was painted with paint includes antimicrobial zeolite.

Conclusions

The paints containing silver, cupper and zinc zeolites showed antimicrobial effect on bacterial strains, mold and yeast species tested. The most effective zeolite was silver ion-exchanged zeolite.

References

[1] McDonnell, G. and A. Russell, "Antiseptics and disinfectants: activity, action, and resistance", Clinical Microbiology Reviews, Vol. 12, No. 1, pp. 147, 1999.
[2] Sayari, A., "Recent advances and new horizons in zeolite science and technology", Studies in Surface Science and Catalysis, Vol. 102, pp. 1–47, 1996.
[3] Thongkasam, C., Dealumination study of zeolite Y, M. S. Report, Suranaree University of Technology, 2006.

A novel procedure for the preparation of mesoporous crystalline tin dioxide films with large pores and fully crystalline walls

Dina Fattakhova-Rohlfing[a], Jiri Rathousky[b]
[a]*Department of Chemistry and Biochemistry, University of Munich (LMU), Butenandtstrasse 5-13, 81377 Munich, Germany, Dina.Fattakhova@cup.uni-muenchen.de*
[b]*J. Heyrovsky Institute of Physical Chemistry, Academy of Sciences of the Czech Republic, Dolejskova 3, 182 23 Prague 8, Czech Republic, jiri.rathousky@jh-inst.cas.cz*

Tin oxide is a technologically important semiconducting material, which is widely used for sensors and catalysts due to the marked change in the electrical conductivity upon the interaction with reducing or oxidizing species. A well-developed porosity, controlled pore size distribution, large interface area and high crystallinity of the tin oxide films are very important for such applications.

Metal oxides with highly ordered periodic nanostructures are conventionally prepared by a spontaneous self-organization of inorganic building blocks (metal oxide precursors) and micelles of amphiphilic molecules (structure-directing agents) in an evaporation-induced self-assembly process. The mesostructure ordering of sol-gel derived tin oxide precursors requires the use of surfactants with a very strong hydrophilic-hydrophobic contrast such as small surfactants, which, however, provide mesostructures with only a small pore size, or a special type of amphiphilic polymers, which are not yet commercially available. [1,2] The preparation of crystalline mesoporous tin oxide films with a larger pore size using commercially available Pluronic polymers is far from straightforward due to the unfavorable interaction of its micelles with the precursor tin oxide species, so a rather elaborate and time-consuming post-synthesis treatment is needed. Therefore in the present communication we have aimed at the preparation of defined building blocks with suitable size and surface properties in order to gain more control over the self-assembly and the mesostructure of the formed films.

Experimental

These building blocks were prepared as follows. $SnCl_4$ was dissolved in ethanol, then distilled water was added. After stirring for about 5 minutes, ammonium hydroxide was added, pH after the ammonia addition equalling 1.32. The mixture was stirred for up to 20 h at 20 to 60 ^{o}C. Afterwards Pluronic F127 dissolved in butanol was added, the optimum Pluronic to tin oxide molar ratio being 0.8, followed by aging the solution for a certain time depending on temperature. The films were prepared by dip-coating glass or Si wafers with the prepared solution at a withdrawal rate of 1.8 mm/s. Finally the films were calcined at 300 to 400 °C.

Results and discussion

We have found that the weak mesostructuring ability of Pluronic polymers is due to an unfavorable interaction of its micelles with the precursor tin oxide species. [3] Therefore, we have optimized the interaction strength and the affinity to self-assemble by the variation of the size, charge and hydrophilicity of the tin oxide precursor. The key issue in the whole process is the sol-gel formation of suitable colloidal particles of tin oxide precursor, which act as the building units of the assembled mesostructures. Their formation was triggered by the addition of ammonium hydroxide and controlled by its amount and the reaction time. Despite the addition of hydroxide, the pH of the alcoholic solution is still very low of 1.2-1.4. The relative

concentration of ammonium hydroxide (the optimum OH/Sn molar ratio equalling 2.6) as well as duration and temperature of the hydrolysis reaction influence significantly the properties of hydrolyzed tin oxide species and the mesostructure assembled from them. We have found that species ca. 3 nm in size were formed shortly after the addition of the ammonium hydroxide to the tin tetrachloride solution. The size of the species continuously increased with the reaction time, reaching a maximum of 8 ± 3 nm after ca. 19 hours, i.e. the time of the precursor solution aging required for the mesostructure to be formed. Therefore, we suggest that the ca. 8 nm oligomers are important mesostructure precursors suitable for the self-assembly around the Pluronic micelles.

The films coated from such a solution were calcined in air at 300 to 400 ^{o}C in order to condense and crystallize the inorganic framework and to remove the template. They exhibit a well-developed worm-like porosity with a wall to wall distance of ca. 18 nm and a surface area of up to 50 cm^2/cm^2 (corresponding to 55 ± 5 m^2/g). The walls are completely crystalline, being composed of nanocrystals 2.5 - 3 nm and 3 – 3.5 nm for films calcined at 300 and 400 ^{o}C, respectively. (Fig. 1)

To sum up, we have developed a new facile procedure for manufacturing crystalline thin films of tin oxide with a uniform mesoporous architecture and full crystallinity of the walls. The developed protocol offers a practical advantage of a facile and fast preparation. The obtained films could be of a significant interest for applications where the high crystallinity, small crystal size, large pore size, accessible porosity and high surface area are of primary importance, such as in sensorics and catalysis.

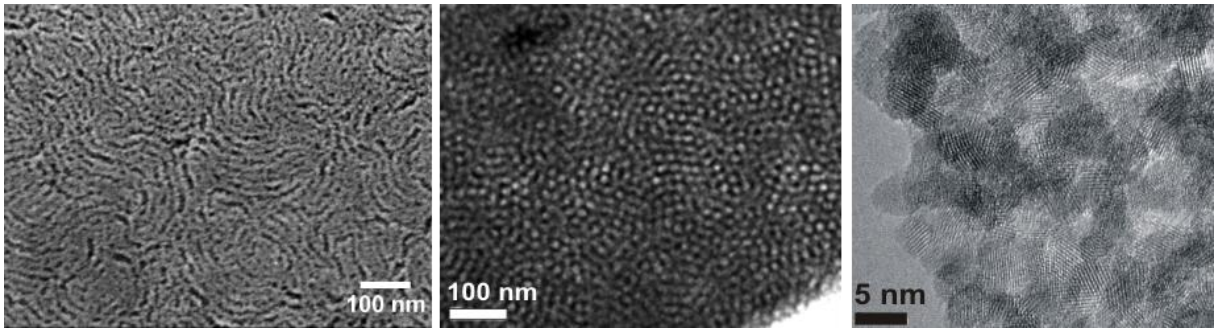

Figure 1. SEM (left), TEM (middle) and high resolution TEM (right) images of the mesoporous SnO_2 films calcined at 300 ^{o}C demonstrating their mesoporous structure and crystallinity.

Acknowledgements

The work was supported by the German Research Foundation (DFG, grant No. FA 839/1-1), Nanosystems Initiative Munich (NIM) and LMUexcellent funded by the DFG, and the Grant Agency of the Czech Republic (grant No. 104/08/0435-1).

References

[1] D. Grosso, C. Boissiere, B. Smarsly, T. Brezesinski, N. Pinna, P. A. Albouy, H. Amenitsch, M. Antonietti, C. Sanchez, Nat. Mater., 3 (2004) 787.
[2] A. Thomas, H. Schlaad, B. Smarsly, M. Antonietti, Langmuir, 19 (2003) 4455.
[3] D. I. Fried,.A. Ivanova, V. Müller, J. Rathousky, B. M. Smarsly , D. Fattakhova-Rohlfing, Nanoscale, (2011), DOI:10.1039/C0NR00872A.

Functional ordered mesoporous silica materials prepared with reversible and functionalizing micelles of hydrophilic block copolymers

J. Warnant [1,2], J. Reboul[1], G. Layrac[1], C. Jérome [2], P. Lacroix[1], M. In[3] and C. Gérardin[1].
1) Institut Charles Gerhardt, Montpellier, France, corine.gerardin@enscm.fr 2) CERM University of Liège, Belgium. 3) LCVN University of Montpellier, France.

Introduction

Here we intend to show that hydrophilic block copolymers represent green, innovative and functionalizing structure-directing agents for the controlled synthesis of functional ordered mesoporous silica materials.

A generation of structuring agents composed of the assemblies of amphiphilic non-ionic copolymers is discovered in the middle of the nineties. These copolymers are constituted of a water-insoluble block (poly(propylene oxide) PPO, poly(styrene) PS or poly(butadiene) PB, poly(isoprene) PI) and an hydrosoluble poly(ethylene oxide) PEO block able to interact with silica precursors in acidic aqueous medium. The (PEO-PPO-PEO) Pluronics polymers are well-known agents for preparing highly ordered 2D-hexagonal mesoporous silica structures (SBA-15) with tunable large and uniform pore sizes (up to 30 nm). The thick wall SBA-15 silica materials, in particular, exhibit greater hydrothermal stability than the thinner wall MCM-41 structures obtained with conventional cationic surfactants. Once the structuring agent is removed, these materials present a considerable interest because of the high specific surface areas and the possibility to control pore size distributions; these features have made them interesting candidates for applications in adsorption, catalysis, sensing or as host-guest materials. Nevertheless, very few applications of ordered mesoporous materials finally come into the market due to the limitations of the template removal processes. Indeed, usually, the template is removed either by calcination or by extraction in organic solvents, which is neither environment friendly nor energy saving.

Recently, we proposed a new synthesis strategy for preparing ordered mesoporous silica materials in soft conditions, which allows the recovery and recycling of the structuring agent in water at room temperature [1, 2]. The concept consists in replacing the classical amphiphilic template by an induced and reversible assembly of water-soluble block copolymers. The micellization process results from electrostatic interactions between two oppositely charged polymers in aqueous solution, a hydrophilic polyelectrolyte-neutral diblock copolymer and a homopolyelectrolyte. Electrostatic complexation leads to an associative phase separation, known as complex coacervation. The presence of the neutral block ensures that the insoluble electrostatic polyion complex is sterically stabilized in solution as a micellar assembly. A great advantage of such polyion complex (PIC) systems is that the phenomenon of micellization is tunable in water with parameters influencing the electrostatic interaction such as the ionic strength, the temperature and the pH. We have particularly studied the case of pH sensitive polyion complex micelles formed between polymers containing blocks, which are weak polyacids and polybases. We have shown that such micelles can be used as structuring agents of silica. Mesostructured hybrid polymer-silica materials were formed by precipitation in water at room temperature and under soft conditions, in a pH range corresponding to the domain of micelle stability. The final ordered porous systems are then simply obtained by a pH change of the material aqueous suspension, the pH variation inducing the PIC micelle dissociation process. The polymers recovered in water could then be recycled for other synthesis runs.

Experimental

Materials are obtained by precipitation in water according to a procedure similar to that used for preparing SBA-15 mesostructured silica. Double hydrophilic block copolymers, constituted of a linear or comb polyethyleneoxide (PEO, PAMPEO) block and a polyacrylic (PAA) or

polymethacrylic acid (PMAA) block, are first mixed with a weak polybase typically a polyamine like an oligochitosane, a polyetheleneimine, a poly(lysine). Electrostatic complexation between the PMAA block and the polyamine leads to the formation of PIC micelles. Hydrolysis and condensation of tetraethoxysilane in the presence of the micelles lead to precipitation of the materials, which are collected and characterized by TEM, XRD, N_2 adsorption/desorption isotherms.

Results and discussion

We first studied the case of polyion complex micelles constituted of polyacrylic acid-b-polyethyleneoxide double hydrophilic block copolymers (DHBC) and an oligochitosane. We showed that the micelles successfully act as structuring agents of silica, leading to 2D hexagonal hybrid silica-polymer mesostructured materials. This is achieved when asymmetric DHBC are used, such as PEO_{5000}-b-PAA_{1580}. Thus, we put into evidence for the first time that polyion complex micelles of DHBC are able to form mesophases, in a similar way as classical amphiphilic block copolymers. This lyotropic behaviour had never been observed before in the case of PIC micelles. The second key result is that a change of the asymmetry degree of the block copolymer can induce the formation of different hybrid mesostructures with varying micelle morphologies (Fig. 1). We evidenced that an increase of the PAA block length leads to the obtention of lamellar mesophases; this must be related to a change in the relative volume of the insoluble block comparatively to the soluble block, leading to a curvature change of the micelles. Thus, lamellar hybrid mesophases were obtained when the PAA block length was increased to PEO_{5000}-b-PAA_{2400}. These combined results reveal that the behaviour of polyion complex micelles presents some similarities with that of classical amphiphilic polymers. It should be noticed that a considerable advantage of PIC micelles compared to micelles of conventional amphiphilic polymers is that PIC micelles result from complexation between two entities, creating thus more versatile systems, whose properties may be varied by changing the nature of each polymer independently. We have then taken advantage of that property and we varied the nature of the polyamine. We studied the case of an oligochitosane, a polyethyleneimine, a polyallylamine, and a polylysine. We obtained structures with different degrees of organization, whose characteristics could be related to the properties of the respective complex micelles. We also studied the influence of the architecture of the neutral hydrosoluble block of the DHBC, the possibility to wash out the polymers and obtain ordered mesoporous materials and finally the possibility to directly functionalize silica pores with polymer chains by selectively releasing one of the two polymers.

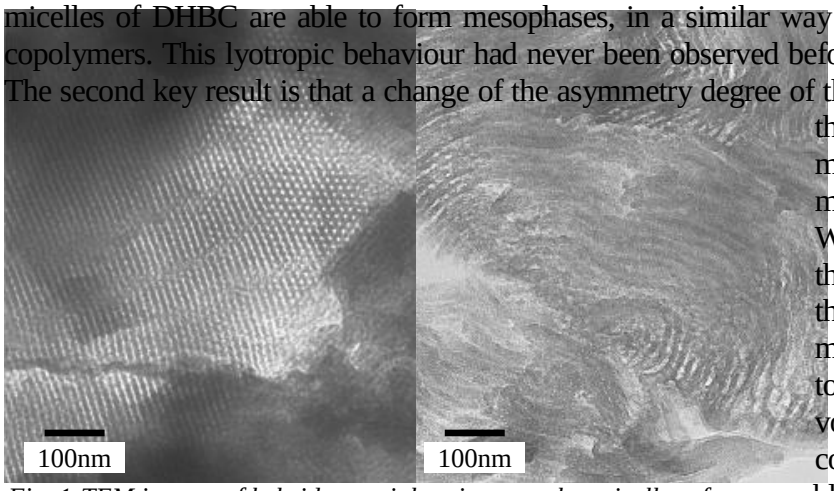

Fig. 1:TEM images of hybrid materials using complex micelles of oligochitosane with PEO_{5000}-b-PAA_{1580} (a) and PEO_{5000}-b-PAA_{2400} (b)

Conclusions

New structuring agents based on non-amphiphilic polymers were used for preparing mesoporous silica; they result from complexation between hydrosoluble polymers. We showed that they successfully induce the formation of mesostructured silica materials whose properties may be varied very conveniently just by varying the properties of one of the polymers constituting the new electrostatic polyion complex micelles.

References

[1] N. Baccile, J. Reboul et al, *Angew. Chem. Int. Ed.* 2008, 47, 8433 –8437.
[2] N. Baccile, M. In, C. In-Gérardin, F. Luck, J. Reboul, S. van Donk, Patent WO 2009/081000

Dual-Porogenic Surfactant-Driven Synthesis of Disordered Mesoporous Molecular Sieves Built with Microporous Zeolite Beta Framework

Kyungsu Na, Changbum Jo, Jeongnam Kim, Kanghee Cho, Jinhwan Jung, and Ryong Ryoo*

*Center for Functional Nanomaterials, Department of Chemistry, KAIST, Daejeon 305-701, Korea. Graduate School of Nanoscience and Technology (WCU), KAIST, Daejeon 305-701, Korea. *To whom correspondence should be addressed. E-mail: rryoo@kaist.ac.kr*

Introduction

Synthesis of mesoporous molecular sieves built with crystalline framework has been of great interest in nanoporous materials science and related industrial technology. Compared to solely microporous or solely mesoporous molecular sieves, the hierarchical coexistence of micropores and mesopores in a single solid porous structure can provide many advantages in various applications as a catalyst, an adsorbent and a separation medium. Various synthesis attempts for hierarchically porous zeolite molecular sieves have been reported to date.[1~4] Herein, we present a dual-porogenic surfactant-directed synthesis route for mesoporous molecular sieves built with a zeolite beta framework, using an organic surfactant functionalized with a specific zeolite structure-directing group. The resultant materials exhibit a disordered mesostructure with a uniform mesopore diameter, in which the thickness of the mesopore walls can be adjusted in the range of 2.9 ~ 5.1 nm according to the surfactant structure and where the mesopore diameter is also widely adjustable in the range of 3.5 ~ 21 nm with the addition of mesopore swelling-agent such as 1,3,5-trimethylbenzene (1,3,5-TMB).

Experimental

A series of dual-porogenic surfactants was synthesized by multi-step organic reactions. Synthesis of mesoporous molecular sieves was performed under the hydrothermal conditions used for conventional zeolites, except for the use of dual-porogenic surfactants. No conventional structure-directing agent (SDA) like quaternary ammonium salts was used. Without any of organic SDA, the synthesis conditions produced no zeolite structures.

Results and discussion

Mesoporous molecular sieves having crystalline zeolite framework were synthesized by using gemini-type organic surfactants with alternatively repeating quaternary ammoniums, phenylene and hexamethylene spacers. $C_{22}H_{45}$-$N^+(CH_3)_2$-C_6H_{12}-$N^+(CH_3)_2$-CH_2-(*p*-C_6H_4)-CH_2-$N^+(CH_3)_2$-C_6H_{12}-$N^+(CH_3)_2$-$C_{22}H_{45}$ (N_4-phe in short) was the bottom-most surfactant which can generate a disordered mesoporous assembly of a nanocrystalline zeolite beta framework. During the zeolite synthesis, inorganic precursors were crystallized around the hydrophilic region of the surfactant, while the self-assembly of surfactant micelles derived the disordered

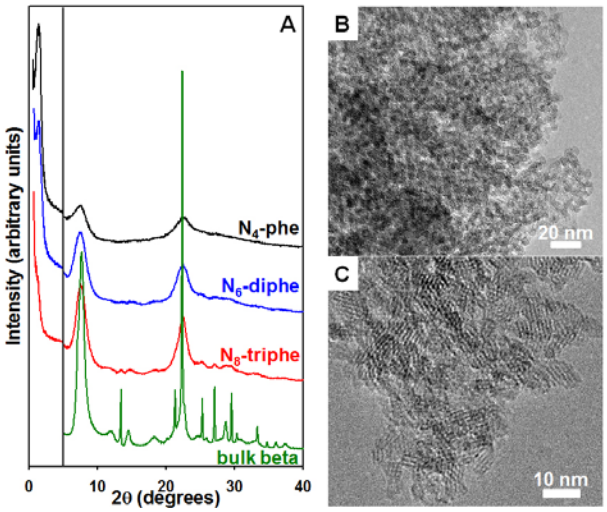

Figure 1. (A) XRD of disordered mesoporous molecular sieves built with a zeolite beta framework synthesized by N_4-phe, N_6-diphe and N_8-triphe surfactants. (B, C) TEM images of a disordered beta synthesized by N_6-diphe surfactant.

mesostructure.

'C_6-diphe' having 6 ammoniums with 2 phenylene spacers, and 'C_8-triphe' having 8 ammoniums with 3 phenylene spacer can be used for the synthesis of zeolites with different framework thickness (Fig. 1A). Figure 1A shows XRD patterns of the zeolite products obtained via three surfactants with different numbers of ammonium (4, 6 and 8) and phenylene spacers (1, 2 and 3), of which the XRD positions are consistent with that of bulk zeolite beta. The XRD result also indicates that the high-angle peak width is gradually sharpened as the number of ammonium and phenylene spacers in the surfactant increase, indicating that the mesopore wall (*i.e.*, the zeolite framework) is thickened. Carbon replication of the mesoporous framework (Fig. 2A) reveals that the framework thickness is gradually increased from 2.9 to 5.1 nm with high uniformity.

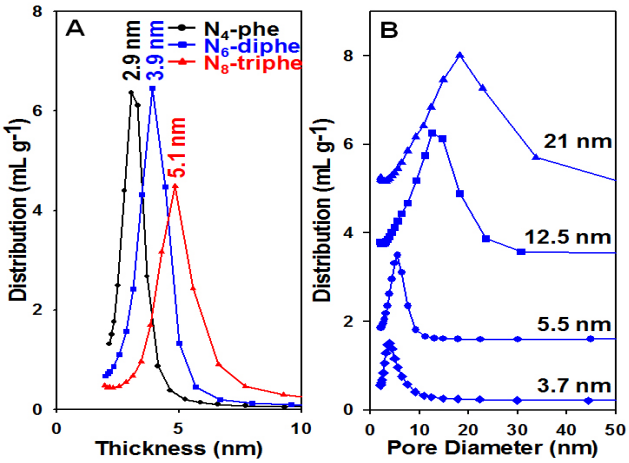

Figure 2. (A) Framework thickness distribution controlled by surfactant structures. (B) Expansion of mesopore diameter by the addition of swelling agent.

Fig. 1B and 1C show TEM images of the zeolite product obtained with N_6-diphe, which shows a typical disordered mesostructure with a highly nanocrystalline zeolite framework. The BET surface area and the total pore volume are 870 m^2g^{-1} and 1.14 cm^3g^{-1}, respectively. The mesopore diameter is very uniform at 3.7 nm. Remarkably, when 1,3,5-TMB was added to the synthesis gel as a mesopore-swelling agent, the mesopore diameter was systematically expanded to 21 nm as a function of the amount of 1,3,5-TMB (Fig. 2B).

Conclusion

Mesoporous molecular sieves built with a zeolite beta framework were synthesized via the dual-porogenic surfactant-driven synthesis route, in which zeolite crystallization occurred only around the hydrophilic ammonium region. Hence, the crystal thickness could be finely controlled (2.9 ~ 5.1 nm) in proportion to the number of ammonium and phenylene spacers in the surfactant. Additionally, the mesopore diameter could also be controlled over a wide range of mesopore regime (3.7 ~ 21 nm). These two remarkable features of the present synthesis strategy are unprecedented in zeolite science to date. As a further work, it would be necessary to find valuable applications utilizing the present materials with various framework thicknesses and mesopore diameters.

Acknowledgement

This work was supported by the National Honor Scientist Program (20100029665) and World Class University Program (R31-2010-000-10071-0) of the Ministry of Education, Science and Technology in Korea.

References

[1] S. van Donk, A. H. Janssen, J. H. Bitter, and K. P. de Jong, *Catal. Rev.* **2003**, 45, 297.
[2] B. T. Holland, L. Abrams, and A. Stein, *J. Am. Chem. Soc.* **1999**, 121, 4308.
[3] M. Choi, H. S. Cho, R. Srivastava, C. Venkatesan, D. -H. Choi, and R. Ryoo, *Nature Mater.* **2006**, *5*, 718.
[4] M. Choi, K. Na, J. Kim, Y. Sakamoto, O. Terasaki & R. Ryoo, *Nature* **2009**, 461, 246

Synthesis of porous clay heterostructures (PCH´s) formed from synthetic high charge mica: Effect of time on the synthesis.

A. C. Perdigón, A. Saavedra, B. Ortiz, F. González, C. Pesquera, C. Blanco
Dpto. Ingeniería Química y Química Inorgánica, E.T.S.I.I. y T., Universidad de Cantabria, carmen.pesquera@unican.es

Introduction

True micas are 2:1 layered aluminosilicates with charge density as high as 2 negative charge per unit cell, with non hydrated cations compensating the layer charge in the interlayer space. A new family of swelling synthetic micas has been successfully synthesized with an unusual cation exchange capacity -up to 468 meq/100g of clay in Na-4-mica- with up to four monovalent hydrated cations accommodated in the ditrigonal holes in the external surface of the tetrahedral layer [1]. Despite the large negative charge originated by isomorphic substitution of silicon by aluminum in the tetrahedral layer, high charge micas unlike brittle micas, exhibit unexpected structure stability.
Porous clay heterostructure (PCH) are a new class of solid acids firstly proposed by Pinnavaia et al. with pore sizes in the rarely observed supermicropore to small mesopore region [2]. They are formed by the surfactant-directed assembly of mesostructured silica within the two dimensional galleries of a moderate charged layered clay. Most of the silicates used for this application are smectite type with up to 1.2 negative charges per unit cell. Although several efforts have been made to increase the acidity of the PCH, the most popular methods involve tedious post- and pre-treatments [3]**.** Swelling high charge micas are ideal materials to be explored regarding this application; in first place due to the extraordinary number of intrinsic acidic places in their structure, attributed to the high level substitution of aluminum for silicon in the tetrahedral layer mentioned above, and in second place because synthetic micas, unlike smectites, have shown high thermal stability of the structure and the acidic places. In this work, we present the synthesis of Porous Clay Heterostructures (PCH) formed from two high charge micas with 2 and 4 charges per unit cell respectively, varying the interaction time of TEOS.

Experimental

High charge micas with 2 and 4 negative charges per unit cell have been synthesized following the "NaCl method" described elsewhere [4, 5]. The materials are referred as Na-M2 and Na-M4 respectively. PCH materials were synthesized as follow: In the first step the interlayer sodium cations were exchanged for organic hexadecyltrimethylammonium cations (CTA). The amount of organic cations used for exchange was two times the cation exchange capacity of the raw materials. The samples were added to an aqueous solution of CTABr and stirred at 50ºC for 9 and 29 days for Na-M2 and Na-M4 respectively. The excess of salt was removed by washing with desionized water and centrifugation. The resulting solid was air-dried and they were denominated as M2-9 and M4-29 respectively. In the next step neutral amine co-surfactant (decylamine) and TEOS were added to 0.5 g of M2-9 and M4-29 in the following organoclay/amine/TEOS ratio of 1/11/108 and 1/7/71 respectively. After, 24h for M2-9 and 72h for M4-29 sample, the interaction of the organoclay with the neutral amine at room temperature, TEOS was added to the mixture and under stirred at room temperature was during 4, 24 and 48h. The materials were recovered by filtration and leaving in an atmosphere

of 50% of humidity for 13 days. At the end the materials were calcined at 600ºC for 2h (heating rate 1ºC/min). The samples will be denoted M2-x and M4-x where "x" indicated the interaction time of the materials with TEOS.

Textural properties and distribution of the porosity of the PCH samples were determined by the N_2 adsorption-desorption technique. X-Ray Diffraction (XRD) technique has been used to characterize the long-range order of the synthesized samples in the different steps. The acidity was determined using cyclohexylamine chemisorption.

Results and discussion

The XRD patterns obtained from the M2-9 and M4-29 samples show a strong peak at 2.7º and 2.6º, 2θ respectively, which is attributed to the symmetrical basal [001] reflection with a basal spacing value of 32.7 and 34.0 Å respectively. This indicates that the exchange of sodium ions with the CTA in the samples has been successful because there is a displacement of the basal reflection from 7.4º for the original micas. The PCH samples synthesized present type IV adsorption isotherms with H3 hysteresis loop, characteristics of materials with slit-shaped pores. Porous solids have surface area of 601 m^2/g with a pore volume of 0.474 cm^3/g for M2-4 sample and 297 m^2/g with a pore volume of 0.307 cm^3/g for M4-4 sample. PCH materials exhibit a clear maximum at pore size of 2.0 nm and 2.5 nm for M2-4 and M4-4 samples respectively, obtained from the pore size distribution using the BJH model for the adsorption branch of the isotherm. The total acidity of the PCH samples increases from 0.11 mmol/g for the mica to 0.56 mmol/g for M2-4 sample. The acid sites detected are placed in the medium and strong acidic regions, with two desorption peaks centred at 350°C and 480°C, respectively. The samples obtained with higher interaction time of TEOS have lower results.

Conclusions

Porous clay heterostructures were synthesized by a surfactant-directed interaction of Si precursor with synthetic high charge micas. Formation of PCH structures leads to an increase of specific surface area, pore diameter and total acidity. The highest obtained results were with the lowest interaction time of Si precursor with the samples.

Acknowledgements

We gratefully acknowledge the Spanish Ministerio de Ciencia e Innovación (MICINN), project MAT2010-18862 for financial support, and A.C. Perdigón thanks the Spanish MEC for a Ramón y Cajal contract (RYC-2005-000625).

References

[1] Gregorkiewitz, M., Rausell-Colom, J.A., Characterization and properties of a new synthetic silicate with highly charged mica-type layers, American Mineralogist, 72 (1987), 515-527

[2] Galarneau, A., Barodawalla, A., Pinnavaia, T., Porous clay heterostructures formed by gallery-templated synthesis, Nature, 347 (1995), 529-531

[3] Picjowich, M, Mokaya, R., Porous clay heterostructures with enhanced acidity obtained from acid-activated clays, Chemical Communications, (2001), 2100-2101

[4] Park, M., Lee, D.H., Choi, C.L., Kim, S.S., Kim, K.S., Choi, J., Pure Na-4-mica: Synthesis and characterization, Chemical Materials, 14(6) (2002), 2582-2589

[5] Perdigón, A.C., González, F., Pesquera, C., Li, D., Blanco, C., Novel acidic solids from high charge Na-micas by mild hydrothermal treatment, Microporous and Mesoporous Materials, 133 (2010), 100-105.

Advances in the Synthesis of Permanently Porous Phosphonate MOFs Based on N,N'-piperazinebis(methylenephosphonate) and Related Linkers

Michael T Wharmby,[1] John P. S. Mowat,[1] Gordon M. Pearce,[1] Stuart R. Miller,[1] Norbert Stock,[2] Paul A. Wright[1]
[1] *School of Chemistry, University of St Andrews, UK;* [2] *Institut für Anorganische Chemie, University of Kiel, Germany; mtw8@st-andrews.ac.uk*

Since the discovery of carboxylate metal organic frameworks (MOFs) in the late 1990s there has been a considerable interest in the use of porous coordination polymers.[1] Porous metal phosphonate frameworks had been known for some time before the discovery of the first carboxylate MOFs, but their development has been slower. Nevertheless, phosphonate ligands display a range of coordination modes not available to carboxylates, making alternative network topologies possible. The ligand N,N'-piperazinebis(methylenephosphonic acid) (H_4**L**) and its derivatives (Fig. 1)[2] have proven similarly versatile to terephthalic acid, widely used in carboxylate MOF synthesis. H_4**L** may coordinate metal cations through one, two or three phosphonate O atoms. At high synthesis pH the piperazinyl N atom may also engage in coordination, whilst at low pH the protonated N atoms may engage in H-bonding to direct crystallisation.

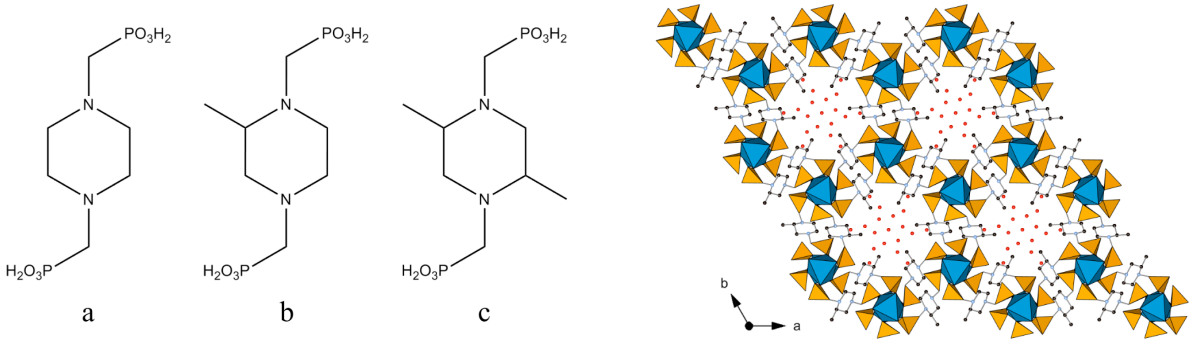

Figure 1: *Left* - Phosphonic acid ligands used in this work: a) H_4**L**; b) H_4**L'** c) H_4**L''**; *Right* – STA-13 viewed parallel to the channel axis.

Work with tri- and tetravalent transition metal cations yielded the first permanently porous phosphonate MOF, MIL-91.[3] Reaction of H_4**L** with the rare-earth cations yields a small pore structure, M_2(**L**H_2)$_3$·xH_2O, which may be reversibly dehydrated and rehydrated, but shows no porosity to other gases due to a strong contraction of the structure on dehydration, observed by X-ray crystallography. Using the racemic 2-methyl derivative, H_4**L'**, together with rare-earth cations, the permanently porous STA-13 structure is prepared.[4] Unlike the H_4**L**-based structure, this framework does not distort on dehydration, leaving pore openings of approx. 3 Å. We report here the results of computer simulations and experimental adsorption measurements on STA-13 for a range of fuel-related gases, including CO_2, CH_4 and C_2H_6, and also consider the factors determining the phase formed in the M^{3+}-**L'** system.

For divalent cations, the first reported phosphonates were non-porous. However at elevated synthesis pH the permanently porous, large pore STA-12(Ni) is obtained (Fig. 2).[5,6] Loss of chemisorbed water from this structure on dehydration causes a distortion of the structure to triclinic. The fully-dehydrated structure has pore widths of approximately 9 Å and also has accessible coordinatively unsaturated sites (CUS), providing Lewis acidic sites for catalysis. The adsorptive properties of STA-12(Ni) have already been reported.[6] A range of other metal forms of this material have been prepared and we report their synthesis, adsorptive properties, and preliminary magnetic measurements.

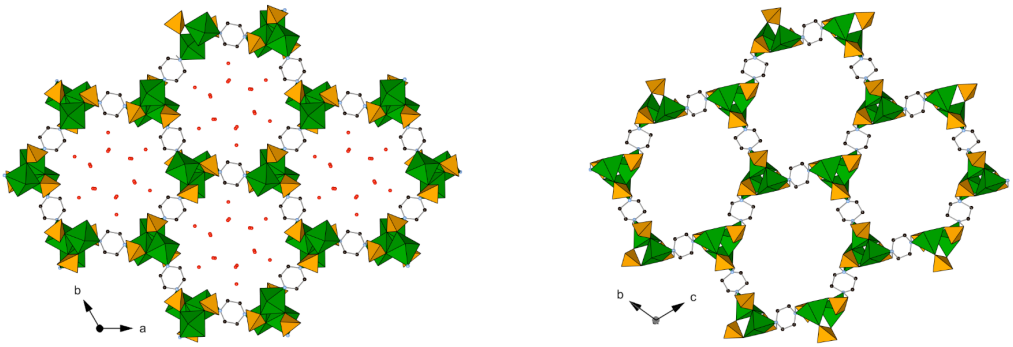

Figure 2: The structures of as-prepared (*left*) and fully-dehydrated STA-12 (right).

The preparation of framework materials with very large pore volumes is an important target for applications in gas storage and drug delivery. Unlike zeolites, which are limited by the constraints of the tetrahedral building unit, very large pore MOFs may be synthesised following the *isoreticular synthesis* approach, increasing the length of the organic linker whilst retaining its connectivity. Under suitable conditions, reaction of N,N'-4,4'-bipiperidinebis(methylenephosphonic acid), H_4**LL** (Fig. 3), topologically similar to H_4**L**, with Co^{2+} and Ni^{2+} yields STA-16,[7] an isoreticular analogue of STA-12. The structure of STA-16 has been determined by synchrotron X-ray powder diffraction. It has a channel diameter of 1.8 nm, determined both crystallographically and by N_2 adsorption data. STA-16 is the first porous phosphonate MOF prepared by isoreticular synthesis, and also has coordinatively unsaturated sites. The synthesis and properties of this remarkable new porous phosphonate MOF, in addition to other new phases formed with H_4**LL** and di-, tri- and tetravalent cations, will be discussed.

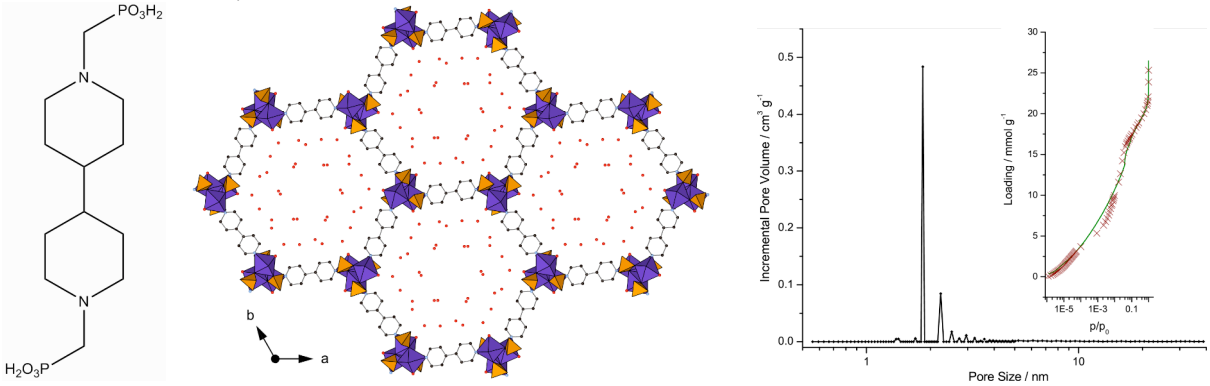

Figure 3: Ligand H_4**LL** (*left*) used in the preparation of STA-16. Structure of STA-16 (middle) with pore-size distribution (*right*) obtained from NLDFT and the fitted isotherm

References

1. J. R. Long and O. M. Yaghi, Eds., *Chem. Soc. Rev.*, 2009, **38**, 1201.
2. J. P. Mowat, J. A. Groves, M. T. Wharmby, S. R. Miller, Y. Li, P. Lightfoot and P. A. Wright, *J. Solid State Chem.*, 2009, **182**, 2769-2778.
3. C. Serre, J. A. Groves, P. Lightfoot, A. M. Z. Slawin, P. A. Wright, N. Stock, T. Bein, M. Haouas, F. Taulelle and G. Férey, *Chem. Mater.*, 2006, **18**, 1451-1457.
4. M. T. Wharmby, S. R. Miller, J. A. Groves, I. Margiolaki, S. E. Ashbrook and P. A. Wright, *Dalton Trans.*, 2010, **39**, 6389-6391.
5. J. A. Groves, S. R. Miller, S. J. Warrender, C. Mellot-Draznieks, P. Lightfoot and P. A. Wright, *Chem. Commun.*, 2006, 3305-3307.
6. S. R. Miller, G. M. Pearce, P. A. Wright, F. Bonino, S. Chavan, S. Bordiga, I. Margiolaki, N. Guillou, G. Férey, S. Bourrelly and P. L. Llewellyn, *J. Am. Chem. Soc.*, 2008, **130**, 15967-15981.
7. M. T. Wharmby, J. P. S. Mowat, S. P. Thompson and P. A. Wright, *J. Am. Chem. Soc.*, 2011. (on the web, DOI: 10.1021/ja1097995)

Synthesis and characterization of Ru supported on carbon nanofibers

Vicente Jiménez*, Paula Sánchez, José Luís Valverde, Amaya Romero[1]

*Facultad de Ciencias Químicas / Escuela Técnica Agrícola[1], Departamento de Ingeniería Química, Universidad de Castilla-La Mancha, 13071 Ciudad Real, Spain. *E-mail address: vicente.jimenez@uclm.es.*

Introduction

The properties of carbon nanofibers (CNFs) make them promising candidates as catalyst supports in heterogeneous catalysis due to their unique structures and potential applications. CNFs are usually classified into three types depending on how the graphene sheets line up with respect to the fiber axis [1]: platelet type CNFs (graphene sheets lined up perpendicular to the fiber axis), tubular type CNF (graphene sheets parallel to the fiber axis) and, fishbone type CNFs (graphene sheets inclined respect to the fiber axis).

Ruthenium has long been recognized as an efficient catalyst in both metallic and oxide forms in a large number of reactions of commercial and environmental importance [2]. Normally, this active phase is deposited on supports such as alumina, silica, activated carbon or graphite. Nevertheless, there are very few studies in which nanostructured carbon (e.g. CNFs) has been used as the support and even fewer using different types of these nanostructure supports.

Experimental

CNFs were grown at different temperatures at atmospheric pressure in a fixed-bed reactor located in a horizontal oven; synthesis temperatures were: 450 ºC to obtain mainly platelet type CNFs, 600 ºC to fishbone type CNFs and 850 ºC to tubular type CNFs according to the procedure described in ref. [3]. Ruthenium catalysts were prepared by the wet impregnation method using $Ru(NO)(NO_3)_3$ (Alfa Products) as the metal precursor salt. The resulting solid residue was dried at 110 ºC for 24 hours and then reduced at 400 ºC in a flow of H_2 for 2 hours. The metal loading of the catalysts thus prepared was 0.5 wt%. Both the supports and catalysts were characterized by the following techniques: N_2 adsorption-desorption, X-ray diffraction (XRD), transmission electron microscopy (TEM), temperature programmed oxidation (TPO), temperature programmed desorption (TPD), temperature programmed reduction (TPR), acid-base titrations and hydrogen pulse chemisorption.

Results and discussion

Table 1 shows the physicochemical properties of the CNFs and the reduced Ru catalysts. It could be observed that the graphitic character of CNFs (TPO and XRD analysis) increased in the following CNFs type order: platelet>fishbone>tubular. As expected, the most graphitic CNFs presented lower BET surface area in comparison with the other CNFs [3]. After the introduction of the metal, it is interesting to note the significant increase in the micropore area that occurred in tubular CNFs whereas it diminished in the other CNFs types. Moreover, the mesopore area decreased markedly after metal incorporation in the following order: platelet>fishbone>tubular. These results could be related with the position of the Ru particles on the different supports. Thus, the smaller surface areas of the catalysts based on Ru deposited on platelet and fishbone type CNFs was due to the occupation of the CNFs adsorptive sites by highly dispersed Ru nanoparticles. These results are in clear agreement with the determined metal dispersion values (Table 1) showing that, the highest Ru dispersion values were obtained with the platelet and fishbone type CNFs which is associated with a strong metal-support interaction between Ru and the graphitic edges of CNFs [4]. On the other hand, the micropore surface area increase that was observed in the case of the Ru deposited on tubular CNFs could be associated to the presence of additional oxygen containing groups and defects on the CNFs surface thet were created during the Ru deposition

treatment [5]. In Table 1 can be observed the increase of oxygen groups in the tubular type CNFs (note that the amount of NaOH needed to neutralize the surface acid groups was almost two times higher after Ru incorporation than before). In contrast, the amount of oxygen groups were almost the same after the Ru deposition on fishbone and platelet type CNFs (the amount of NaOH was almost the same both before and after Ru incorporation). The presence of these oxygen groups has been generally considered a requisite to increase the CNFs hydrophilicity and therefore, has a strong influence on the deposition of the metal precursor on the CNFs surface. It is interesting note that the presence of oxygen-containing groups seems to be in direct relation with the average Ru diameter, which decreased for higher amounts of acidic groups (Table 1).

	CNFs support			**Ru-based CNFs catalysts**		
	Platelet	**Fishbone**	**Tubular**	**Platelet**	**Fishbone**	**Tubular**
BET surface area (m^2/g)	286.0	202.0	68.0	183.6	175.9	93.9
Micropore area (m^2/g)	57.0	25.0	2.0	11.7	20.6	28.7
npg[1]	7.7	8.6	12.3	-	-	-
Weigh loss temperature range (ºC)[2]	380-585 (519)	430-618 (546)	545-715 (640)	-	-	-
NaOH added ($mmol \cdot g^{-1}$)	0.75	0.56	0.19	0.78	0.58	0.40
Ru dispersion (%)	-	-	-	67.7	63.5	58.5
$d_{Ru,}$ (TEM^3/H_2^4) (nm)	-	-	-	1.04/1.41	1.48/1.50	1.93/1.63

[1]npg: number of grapheme planes in the crystallites (Lc/d002) obtained by XRD
[2]In brackets: temperature at which the maximum of the oxidation temperature peak appears.
[3]Average diameter of Ru particles determined by counting around 200 particles on the TEM images.
[4]Average diameter of Ru particles measured using H_2 chemisorption technique.

Conclusions

Different types of carbon nanofibers (platelet, fishbone and tubular) were employed as supports to deposit ruthenium by wet impregnation. It was found that the textural properties and amount of acidic oxygen-containing groups in the supports are clearly dependent on the orientation of the graphitic sheets. This fact, in turn, determines the Ru particle size, its dispersion and its interaction with the support.

Acknowledgements

The authors gratefully acknowledge financial support from the Regional Government of Castilla-La Mancha (Projects PBI-08-038 and PCI-08-0020-1239).

References

[1] T. J. Zhao, D. Chen, Y. C. Dai, W. K. Yuan, A. Holmen. Synthesis of Dimethyl Oxalate from CO and CH3ONO on Carbon Nanofiber Supported Palladium Catalysts. Ind. Eng. Chem. Res. 43 (2004) 4595-4601.

[2] B. Coq, P.S. Kumbhar, C. Moreau, P. Moreau, M.G. Warawdekar, Liquid phase hydrogenation of cinnamaldehyde over supported ruthenium catalysts: Influence of particle size, bimetallics and nature of support. J. Mol. Catal. 85 (1993) 215-228.

[3] V. Jiménez, A. Nieto-Márquez, J. A. Díaz, R. Romero, P. Sánchez, J. L. Valverde, A. Romero. Pilot plant scale study of the influence of the operating conditions in the production of carbon nanofibers Ind. Eng. Chem. Res. 48 (2009) 8407-8417.

[4] C. Amorin, M. A. Keane. Palladium supported on structured and nonstructured carbon: A consideration of Pd particle size and the nature of reactive hydrogen. J. Colloid Inter. Sci. 322 (2008) 196-208

[5] V. Jiménez, P. Sánchez, J. L. Valverde, A. Romero. Influence of the nature of the metal hydroxide in the porosity development of carbon nanofibers. J. Colloid Inter. Sci. 336 (2009) 226-234

Structural transformation of polyacrylonitrile deposited on mesoporous silicas by precipitation polymerization

Rafał Janus[1], Piotr Kuśtrowski[1], Anna Wach[1], Marek Drozdek[1], Barbara Dudek[1], Zofia Piwowarska[1], Pegie Cool[2]
[1]*Faculty of Chemistry, Jagiellonian University, Ingardena 3, 30-060 Kraków, Poland, kustrows@chemia.uj.du.pl*
[2]*Department of Chemistry, University of Antwerpen, Universiteitsplein 1, B-2610 Wilrijk, Belgium*

Introduction

The polymer-derived porous carbons are interesting materials due to a large number of their potential applications in adsorption and catalytic processes. The properties of these materials are strongly depended on the structural transformations occurring during a heat treatment. The mechanism of the thermal decomposition of polyacrylonitrile (PAN), a raw material often used for the preparation of microporous activated carbon, has been widely described in literature [1]. The main stages of the PAN decomposition are presented in Fig. 1. This process begins at about 270°C when PAN is transformed into so called 'ladder form'. Higher temperatures induce dehydrogenation and the formation of the aromatic structure through the condensation of adjacent ladder species. Finally, above 600°C nitrogen loss corresponding to the deep dehydrogenation occurs and graphite-like structures are formed.

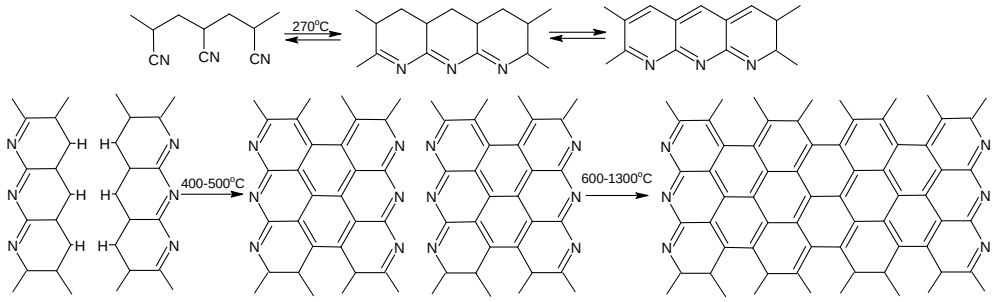

Figure 1. The mechanism of the thermal transformation of PAN [1].

In the presented work, the influence of silica support presence on the thermal stability of PAN layers deposited onto mesoporous silicas (wide pore silica gel as well as SBA-15 and MCM-41 molecular sieves) and the mechanism of polymer decomposition was studied.

Experimental

The PAN/silica hybrid materials were obtained by the introduction of polymer onto support surface [2]. Polymer was deposited on the silica surface by the precipitation polymerization of acrylonitrile in water slurry of an appropriate support. The polymer/support mass ratios were controlled by using the proper amounts of monomer. The obtained precursors were carbonized at 200–450°C in an oxygen-free atmosphere.
The samples were characterized using low-temperature adsorption of nitrogen (textural parameters), thermogravimetry (coating effectiveness, temperature ranges of PAN decomposition), SEM (morphology) and DRIFT, UV-vis-DRS and XPS (surface composition). Adsorption tests for the elimination of methyl-ethyl ketone (MEK) vapour were performed under dynamic conditions.

Results and discussion

Low-temperature N_2 adsorption showed that all used silica materials can be classified as mesoporous solids, however they differ significantly in surface areas, total pore volumes and pore size distributions. The deposition of PAN followed by carbonization resulted in a decrease in surface area and total pore volume. This fact confirms the successful coating of the silicas surface with carbonaceous species. It was found that the external and internal surface of the silica particles was homogeneously covered with polymer layers before carbonization. After the thermal treatment the highly dispersed carbon domains were formed on the surface.
The DRIFT spectra collected for the samples carbonized at increasing temperatures exhibited the presence of PAN forms recognized earlier in literature. Nevertheless, the temperature range of PAN transformations was strongly depended on the textural parameters of the used support. The higher specific surface area, the higher thermal stability of polymer was observed. This supports the existence of specific interactions between a silica surface and polymer layer. Such interactions are additionally confirmed by the differential DRIFT spectra recorded for the neat supports and PAN/support carbonizates, which displayed shifts between characteristic bands for the parent silica and the carbon-coated one. Changes in the surface composition of precursors and carbonizates were controlled by XPS analysis.
The sorption capacity in the elimination of methyl ethyl ketone (MEK) from gas phase depended strongly on the carbonization temperature. The highest capacity was found for the composites carbonized at 300°C.

Conclusions

The carbonization temperature plays an important role in the formation of surface carbonaceous species determining the adsorption properties of the obtained materials. The dependence between the dispersion of polyacrylonitrile layers on silica surface and the thermal decomposition of polymer was explained. The spectroscopic studies confirmed that the thermally induced transformations of PAN are influenced by the textural parameters of a silica support. A higher specific surface area results in a higher dispersion of polymer material and an improvement of its thermal stability. The MEK adsorption tests showed the highest sorption capacity for the samples containing the ladder form of PAN.

Acknowledgements

This work was supported by the Polish Ministry of Science and Higher Education under the grant no. N N507 553238. Rafał Janus wishes to thank the Foundation for Polish Science MPD Programme co-financed by the EU European Regional Development Fund for the financial support.

References

[1] Molenda, M., Dziembaj, R., Piwowarska, Z., Drozdek, M., A new method of coating of powdered supports with conductive carbon films, Journal of Thermal Analysis and Calorimetry, 88 (2007), 503-506
[2] Kuśtrowski, P., Janus, R., Kochanowski, A., Chmielarz, L., Dudek, B., Piwowarska, Z., Michalik, M., Adsorption properties of carbonized polyacrylonitrile deposited on γ-alumina and silica gel by precipitation polymerization, Materials Research Bulletin, 45 (2010), 787-793

Proton sponges in hybrid mesoporous materials for base catalysis

Enrica Gianotti*[1,2], Urbano Diaz[1], Avelino Corma[1]
[1]*Instituto de Tecnología Química (UPV-CSIC) Universidad Politécnica de Valencia. Consejo Superior de Investigaciones Científica, 46022 Valencia, Spain.*
[2]*Department of Chemistry IFM and NIS-Centre of Excellence, University of Turin, 10125 Turin, Italy.* gianotti@itq.upv.es

Introduction

The heterogenisation of organic molecules though their insertion into the network of inorganic matrixes has allowed to obtain organic-inorganic hybrid materials that cover a wide range of applications in different areas as optics, electronics, energy, environment, biology, medicine, catalysis [1,2]. In the field of heterogeneous catalysis, the organic-inorganic hybrids offer the advantage to merge the properties of inorganic materials (high mechanical, thermal and structural stability) and of organic moieties (flexibility and functionality). Moreover, the nature of the active sites that can be introduced in the inorganic catalysts is limited, whilst the organic molecules can be functionalised to catalyse a larger variety of reactions but suffer from their inability to be recycled. In this view, the production of new organic-inorganic materials may overcome these drawbacks allowing the structural insertion of the specific catalytic functions through the organic moieties, while the inorganic part allows heterogenizing the catalyst and increasing the stability. In this way, it should possible to design multifunctional materials [3]. In this contribution, the organic-inorganic mesoporous materials have been produced using a NH_4F-catalysed sol-gel process, at neutral pH and low temperatures, that avoids the use of structural directing agents (SDAs)[4]. Proton sponges have been used as the organic builder of the hybrids, while the inorganic part corresponds to silica tetrahedra. The proton sponges are diamines with neighboring atoms at short distance and aromatic frames, such as naphthalene and phenanthrene and exhibit high unusual basicity. The 1,8-bis(dimethylamino)naphthalene (DMAN)[5], the archetype of proton sponge, with pK_a=12.1 and 1,8-bis(tetramethylguanidino) naphthalene (TMGN) [6], a new organosuperbase, with pK_a= 25.1, have been heterogenized in a non-ordered mesoporous silica. The synthesised hybrids were studied as base catalysts in Knoevenagel condensation. Several recycling tests were also performed to evaluate the catalyst deactivation and reusability.

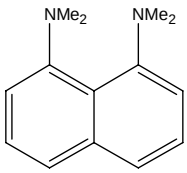

DMAN

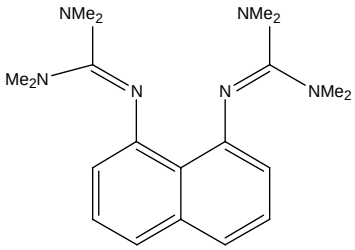

TMGN

Experimental

The DMAN and TMGN were functionalized by the insertion of nitro groups using a mixture of HNO_3 and H_2SO_4. Then, the nitro groups were reduced to the amino in H_2 using Pd/C as catalyst and finally, the amino-proton sponges were silylated using 3-(triethoxysilyl)propylisocyanate. The non–ordered hybrids were synthesised using an NH_4F co-condensation route [4]. Tetramethoxysilane (TMOS), used as silica precursor, and silylated-proton sponges (hereafter indicated as PS-Si) were mixed in CH_3OH at 298K. After dissolution of precursors, a water solution of NH_4F was added. The final reaction mixture has the following molar composition: 1-x SiO_2 : x PS-Si : 4 MeOH : 4 H_2O : 0.00313 NH_4F.

Several hybrids with different proton sponges loading, starting from x=0.001 to x= 0.1, were synthesized. All the hybrids were characterized by volumetric, thermogravimetric, elemental analysis, solid state MAS-NMR (^{13}C, ^{29}Si) and FTIR.

Results and discussion

Organic-inorganic materials based on the silylated-PS inserted into non-ordered mesoporous silica have been synthesized using NH_4F-catalyzed sol-gel route at neutral pH. These conditions allow binding covalently the functionalized proton sponges' fragments to the inorganic units of mesoporous silica, forming the framework of the silica materials. Elemental analysis (Table 1) confirms the presence of the organic moiety in the hybrids. More specifically, the presence of carbon evidences that organic units are present in the silica network, in fact SDAs were not used during the synthesis of these solids and consequently carbon atoms can only belong to the functionalized DMAN or TMGN species.

Table-1. Elemental analysis and textural properties of the DMAN/SiO_2 hybrids.

Samples	DMAN loading x	Organic content (EA)/%	SSA_{BET}/ m^2g^{-1}	Mean pore diameter / Å
	0.001	1.57	763	28
	0.002	2.3	752	28
DMAN/SiO_2	0.005	2.9	725	27
	0.01	3.6	600	26
	0.05	12.6	455	30
	0.1	16.4	329	30

Conclusions

Non ordered organic-inorganic mesoporous materials have been obtained by the insertion of proton sponges (DMAN or TMGN) fragments bonded to silica units. The absence of SDAs and the use of soft synthesis conditions are validated in this study, being possible to design functional hybrid materials which contain stable, isolated and active basic sites able to carry out condensation processes to form carbon-carbon bonds. The resultant materials are stable, active and selective base catalysts for Knoevenagel condensation, reactions that require strong basic sites.

Acknowledgements

The authors thank financial support by Consolider-Ingenio from Spanish Government.
EG thanks Marie Curie Fellowship (FP7-PEOPLE-2009-IEF) for financial support**.**

References

[1] Hoffmann, F., Cornelius, M., Morell, J., Fröba, M., *Angew. Chem. Int. Ed*., 45 (2006), 3216-3251.
[2] Sànchez, C., Rozes, L., Ribot, F., Laberty-Robert, C., Grosso, D., Sassoye, C., Boissiere, C., Nicole, L., *C.R. Chimie*, 13 (2010), 3-39.
[3] Wight, A.P., Davis, M.E., *Chem Rev*., 102 (2002), 3589-3614.
[4] Diaz, U., Garcia, T., Velty, A., Corma, A., *J. Mater. Chem*., 19 (2009), 5970-5979
[5] Alder, R.W., Bowman, P.S., Steele, W.R.S., Winterman, D.R., *Chem. Commun*., (1968), 723-724
[6] Raab, V., Kipke, J., Gschwind, R.M., Sundermyer, J., *Chem. Eur. J*., 8 (2002) 1682-1693
[7] Gianotti, E., Diaz, U., Coluccia, S., Corma, A., in preparation

Revealing the Molecular Assembly of Zeolitic Imidazolate Frameworks through Atomic Force Microscopy

Pablo Cubillas, Pak Y. Moh, Michael W. Anderson and Martin P. Attfield
Centre for Nanoporous Materials. School of Chemistry, The University of Manchester, Oxford Road, Manchester, M13 9PL, UK, Pablo.cubillas-gonzales@manchester.ac.uk

Introduction

Metal organic frameworks (MOFs) are one of the most important classes of nanoporous crystalline solid as they possess a wide range of pore sizes and the flexibility to tailor chemical properties by functionalisation of the organic linkers [1]. For these reasons, the potential applications of MOFs are far reaching. Understanding the fundamental aspects of the growth of MOFs is critical to develop better materials for new and enhanced applications. One of the most pressing questions related to the growth of nanoporous materials is the formation of the structure around the voids in the framework. Several possibilities can be envisioned involving different growth units and mechanisms for the assembly of these units to form the void-enclosed framework units. However, only direct observations at the nanoscale under growing conditions can reveal the answer to this problem. Atomic force microscopy (AFM) can provide this kind of detailed observations. In this paper we report results from in-situ AFM growth experiments in three different zeolitic imidazolate frameworks (ZIFs): ZIF-8, ZIF-67 and ZIF-76.

Experimental

Crystals of ZIF-8 were synthesized according to the method of Park [2]. ZIF-67 and ZIF-76 were grown following the recipe provided by Banerjee [3]. In all cases seed crystals were grown directly over glass substrates that could be fitted on the fluid cell of the AFM. Growth solutions were prepared by mixing a 2% DMF mother solution with 98% methanol in the case of ZIF-8. ZIF-67 and ZIF-76 growth was carried out on diluted DMF solutions containing the appropriate metal and organic linkers. AFM was carried out on a Nanowizard II from JPK A.G. Scanning was done in contact mode using low spring constant (<1 N/m) cantilevers.

Results and discussion

For all three systems studied growth was observed to take place by a “birth and spread” mechanism, spiral growth or a combination of the two. The shape of the terraces observed varied from system to system and also between different facets for the same type of crystal. In the case of ZIF-8 terraces on the {110} faces where observed to have a truncated rhombohedra morphology. This is consistent with the 2-fold symmetry of this face and shows that growth is faster on the <100> direction than in the <110>. In the case of ZIF-67 terraces growing on the {100} face possess a square shape, in accordance to the 4-fold symmetry of the facet. For ZIF-76, two different facets were studied; the {100} shows the formation of nearly isotropic terraces. On the contrary triangular terraces were observed on the {111} face, reflecting, again, its symmetry. In all cases, cross-sectional analysis of the terraces show that they possess a monolayer height equal to the plane spacing for that particular face, i.e. each monolayer is a unit cell high.

AFM observations at slow growth conditions allowed following in great detail the formation and development of 2-D nuclei, as shown in Fig. 1 for a ZIF-8 crystal. Cross-sectional analysis of the nuclei reveals a continuous increase of step heights, with measured values of 0.46, 0.60, 0.80, 0.91 and 1.07 ± 0.1 nm (Fig. 1, not all heights shown). The final step size corresponds to 1.2 nm or one monolayer in height which took 15.6 min. to grow after the

initial nucleation. These measured sub-step heights can be related to different surface terminations, as shown in Fig. 1. The 0.41 nm step height corresponds to a single $MeIm^-$ and implies, firstly, that the MOF's surface termination is not an $MeIm^-$ but rather a zinc cation with a weakly coordinated solvent species attached; and secondly that in order to achieve the formation of a localised surface island, some interaction and involvement of solvent molecules with the $MeIm^-$ molecules must exist, as the distance between each $MeIm^-$ molecule preclude the formation of strong coordinate bonds. Therefore solvent molecules will provide stabilising interactions to bridge the pores in the structure. The following measured step height (0.60 nm) would correspond to the attachment of Zn^{2+} and $MeIm^-$ ions to the surface tethered $MeIm^-$ ions. This demonstrates that the growth of ZIF-8 occurs by addition of individual ions and not by pre-assembled sub-units in solution. Further step heights follow through addition of individual metal or linker ions.

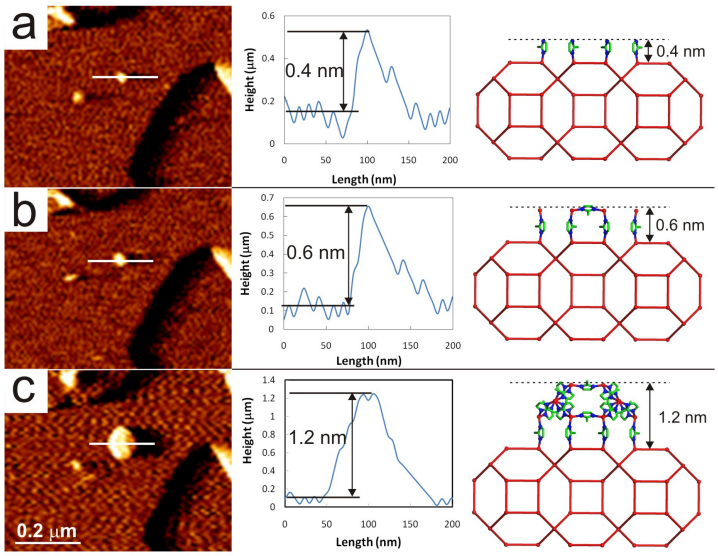

Figure 1. AFM deflection images (first column) showing the nucleation and growth of a ZIF-8 monolayer on the {110} face. Second column, associated cross-sections showing the varying heights at different stages of formation. Third column, simplified model showing the most probable surface termination for each stage.

Observations on both ZIF-67 and ZIF-76 give similar results, indicating that this mode of growth is pervasive in ZIFs, although is possible that it may also be the case for zeolites and zeotypes.

Conclusions

We have revealed that the growth of ZIFs at low supersaturation conditions takes place by the nucleation and spreading of successive metastable unenclosed sub-layers to eventually form the stable, enclosed framework structure. This process must be dependent on the presence of nonframework species that bridge the developing pores during growth. By means of AFM we have also identified some of the fundamental growth units involved in the process for the systems studied. These findings could instigate the development of improved synthesis methods to control the properties of these nanoporous materials.

Acknowledgements

The authors wish to acknowledge the Leverhulme Trust and the EPSRC for funding and the Malaysian government for provision of a studentship for P.Y.M.

References

[1] Ferey, G., Hybrid porous solids: past, present, future, Chemical Society Reviews, 37, (2008), 191-214.

[2] Park, J.S., Ni, Z., Cote, A.P., Choi, J.Y., Huang, R., Uribe-Romo, F.J., Chae, H.K., O'Keeffe, M., Yaghi, O.M. Exceptional chemical and thermal stability of zeolitic imidazole frameworks. Proceedings of the National Academy of Sciences, 27 (2006), 10186-10191.

[3] Banerjee, R., Phan, A., Wang, B., Knobler, C., Furukaw, H., O'Keeffe, M., Yaghi, O.M., High-Throughput Synthesis of Zeolitic Imidazolate Frameworks and Application to CO2 Capture, Science, 319 (2008), 939-943.

Catalytic activity of HKUST-1 coated on ceramic foam

T. Granato*, R. Olivo, F. Testa, A. Katović, R. Aiello
Departimento di Ingegneria Chimica e dei Materiali, Università della Calabria, 87030 Rende (CS), Italia. granato@unical.it

Introduction

Unit operations performed using materials with hierarchical porosity represents today an important challenge in chemical industry. Reactors or adsorption units with hierarchical porosity are prepared through coating with a micro-, meso- or micro/meso-porous material on a macro-porous inorganic support. Advantages are low pressure drop, improved heat and mass transports, easy assembly of reactors, catalyst coating amount that can be tuned [1,2].
Aim of this work is preparation, characterization and evaluation of a specific catalytic activity of the copper-bearing metal-organic framework HKUST-1 material supported on a macro-porous alumina-based ceramic foam (CF).

Experimental

The commercial CF, model VUKOPOR A (nominal size (d) 25 × (h) 15 mm, Lanik-Czech Republic) with a cell density of 30 PPI (Pores Per linear Inch), was used as support for the HKUST-1 deposition. The coating was obtained using the in-situ conventional one-step hydrothermal crystallization technique. In the standard synthesis [3,4], an 1.8M copper nitrate tri-hydrate aqueous solution was mixed with an 1.0M 1,3,5-benzene tri-carboxylic acid solution (ethanol solvent) for 30 minutes at 25°C. The obtained hydrogel was poured on the CF specimen, heated at 110°C for 18 hours in autoclave. The Cu-BTC-coated sample (HKUST-1/CF) was washed with distilled water and re-immersed in the same starting hydrogel for a second consecutive deposition cycle.
Hydrogen peroxide (HP) decomposition tests were carried out in a thermostated tubular reactor, nominal size ID=3.0mm and L=20mm. Six HKUST-1/CF samples were alternated with seven CF-as-made supports in the tubular reactor and kept at 70°C. The HP aqueous solution (0.1M) was fed to the reactor by a peristaltic pump at the same temperature. Three reaction tests were carried out for 120 minutes varying the flow rates at 0.80-1.50-2.25 ml/min (tests A, B, C), respectively. The reaction product was fed for 20 minutes to 20 ml of 0.01 M phenol solution in water at 70°C. Both the HP and phenol decompositions were monitored during all the experiments.

Results and discussion

The HKUST-1 coating amount after two consecutive deposition cycles was 19.8 wt.% and the corresponding specific surface area (BET method) 161.2 m^2/g. The X-Ray diffraction patterns of the coated and as-made powder HKUST-1 material showed that the sample is crystalline. The CF presence determined the lower peaks intensity in the HKUST-1/CF pattern with respect to powder. The SEM micrograph (Fig. 1) revealed the presence of HKUST-1 crystals ranging between 50-115 μm and some copper impurities on the CF surface [5]. In Figure 2 the reaction tests results are displayed. Phenol conversion (X_{ph}) increased, ranging between 62.3% (test A), 69.5% (test B), 93% (test C), with the increase of the volume of HP-decomposed fed. It occurred although the HP activation process efficiency decreased with the increase of flow rate, due to the lower residence time in the tubular reactor. We estimate the process efficiency as the ratio between the phenol and HP decomposed molar amount. These

values are 0.18 for the test A, 0.20 for the test B, 0.22 for the test C, showing that it is more convenient the highest flow rate.
The HKUST-1/CF catalysts were used for more than twenty consecutive reaction runs at different flow rates, showing an excellent stability. The HKUST-1/CF copper leaching was measured on the HP activated solution. The value was generally negligible and was attributed to the release of copper impurities deposited on the CF surface.

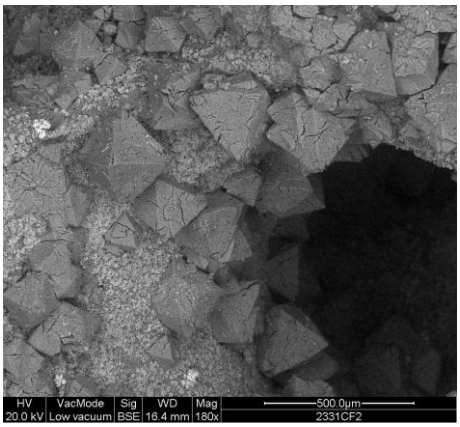

Figure 1. SEM micrograph of HKUST-1 coated.

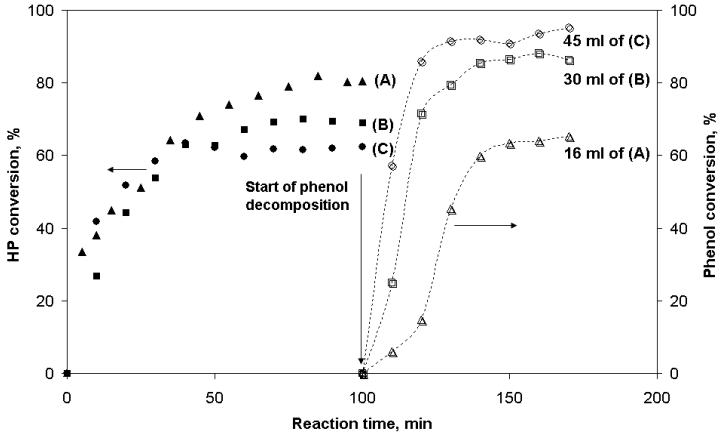

Figure 2. X_{HP} (%) @ 0.8(▲), 1.5(■), 2.25(●) ml/min. X_{ph} (%) @ (A)-16ml (Δ), (B)-30ml (□), (C)-45ml (○).

Conclusions

HKUST-1/CF samples were used in hydrogen peroxide decomposition tests in continuous conditions. The samples were able to activate the HP solution, in fact, the reaction product was added to a phenol solution promoting the organic molecule abatement with a conversion of 93% after 30 minutes. The results showed that the HKUST-1/CF samples have a high catalytic stability and that at the selected reaction conditions the efficiency of the process increases with the increase of the flow rate.

Acknowledgements

Financial support is acknowledged by authors from MIUR — Ministry of Instruction, University and Research (PRIN funding "Hierarchical porosity materials for gas adsorption and pollutants removal").

References

[1] Peng, H.X., Fan, Z., Evans, J.R.G., Busfield, J.J.C., Microstructure of ceramic foams, Journal of the European Ceramic Society, 20 (2000), 807-813
[2] Incera Garrido, G., Patcas, F.C., Lang, S., Kraushaar-Czarnetzki, B., Mass transfer and pressure drop in ceramic foams: a description for different pore sizes and porosities, Chemical Engineering Science, 63 (2008), 5202-5217
[3] Wang, Q.M., Shen, D., Bülow, M., Lau, M.L., Deng, S., Fitch, F.R., Lemcoff, N.O., Semanscin, J., Metallo-organic molecular sieve for gas separation and purification, Microporous Mesoporous Materials, 55 (2002), 217-230
[4] Chui, S.S.-Y., Lo, S.M.-F., Charmant, J.P.H., Orpen, A.G., Williams, I.D., A chemically functionalizable nanoporous material $[Cu_3(TMA)_2(H_2O)_3]_n$, Science, 283 (1999), 1148-1150
[5] Schlichte, K., Kratzke, T., Kaskel, S., Improved synthesis, thermal stability and catalytic properties of the metal-organic framework compound Cu3(BTC)2, Microporous Mesoporous Materials, 73 (2004), 81-88

Functional hybrid catalysts based in layered inorganic precursors pillared with bridged silsesquioxanes

T. García, U. Díaz, A. Velty, A. Corma.
Instituto de Tecnología Química, UPV-CSIC, Universidad Politécnica de Valencia, Avenida de los Naranjos s/n, E-46022 Valencia, Spain, tgarciaf@itq.upv.es

Introduction

The preparation of multifunctional materials with applications in nanotechnology and catalysis is a matter of much interest [1]. In this case, structured porous hybrid materials appear as useful nanosystems where organic and inorganic components interact covalently as building blocks at nanometric scale imparting de advantages of inorganic materials and organic molecules [2]. The use of layered inorganic precursors is one of the most efficient routes to obtain structured nanohybrids by introducing specific organic molecules into the interlayer space [3, 4]. One approach to this would involve the use of bridged silsesquioxanes (disilanes) precursors as intercalation agents. In this study, we have synthesized functional layered porous hybrid materials, one of these formed by magadiite and disilanes which contain disulfide (BTES), ethylendiamine (BTMN) and ethylene (BTEethy) groups, and the other formed by the layered precursor of MWW type-zeolite and 1,4-bis(triethoxysilyl)benzene (BTEB), this disilane being intercalated as pillars into the interlayer space [5]. These hybrids materials would be useful to carry out acid, basic or tandem catalytic processes.

Experimental

Magadiite and MWW precursor were obtained following the state-of-art [6].The layered silicate is swollen with n-hexylamine and the zeolitic precursor with cetyltrimethylammonium hidroxyde solution for 2 days at room temperature and for 16 hours at 353 K, respectively. Finally, into the mixture, disilanes (Figure 1) are introduced as pillaring agents together with n-hexane or dioxane solutions for 7 days at room temperature or 2 days at 353 K, respectively. The products were recovered by centrifugation and air-dried at 333 K. The swelling agents were removed using acid extraction processes.

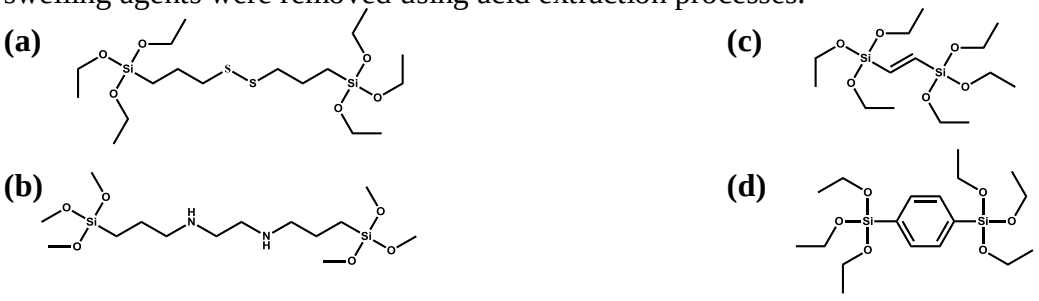

Figure 1. Bridged silsesquioxanes used as pillaring agents: (a) Bis(triethoxysilylpropyl)disulfide (BTES), (b) Bis(trimethoxysilylpropyl)ethylendiamine (BTMN), (c) Bis(triethoxysilyl)ethylene (BTEethy) and (d) 1,4-bis(triethoxysilyl)benzene (BTEB).

Results and discussion

Different experiments were carried out using disilanes as pillaring agents to obtain hybrid materials with layered characteristics. The organic linkers present in the initial organosilanes could be incorporated between the layers of lamellar silicic or zeolitic precursors, covalently bonded to surface of inorganic layers. The diffraction patterns confirm that disilane molecules are perpendicularly intercalated into the interlayer space of the precursors. C/N and C/S ratios for extracted samples confirm the presence of the organic molecules in the interlayer space being coincident with the theoretical ones. The hybrids are stables up to 400 ºC (TGA and DTA analyses), showing a higher hydrothermal stability when arylic groups (600 ºC) are intercalated in the interlayer space. The galleries formed between the MWW zeolitic precursor layers due to the presence of organic pillars exhibited pores of ~ 54 Å of diameter. In all synthetized materials, channels were generated. The ^{13}C CP/MAS NMR spectra of the organic-inorganic materials show, in all cases, a peak around ~ 0 ppm assigned to carbon species directly bonded to Si atoms. This fact confirms that the organic fragments remain intact as in the initial bridged silsesquioxane reagents. The ^{29}Si CP/MAS NMR spectra exhibit characteristic bands around ~60 ppm assigned to T-type silicon species, namely silicon species having Si-C bond. This fact confirms the presence of organic modified silicon species bonded to the layers in these materials.

The potentially of these materials as acid catalysts was corroborated by the generation of sulphonic groups (SO_3H) from disulfide linkers through reduction processes. The layered materials with BTMN fragments intercalated between magadiite layers were also employed as promising base catalysts for condensation reactions. On the other hand, the post-synthesis treatments of the zeolitic hybrids have allowed the functionalization of the organic counterpart with basic amino groups which combined with the acid sites due to tetrahedrally coordinated framework aluminums in the individual MWW layers, result in bifunctional acid-base catalysts. Their potential has been shown for acid-base two step cascade processes such as the synthesis of benzylidene malonitrile from malonitrile and benzaldehyde dimethylacetal.

Conclusions

Hybrid layered materials with well-defined porosity were prepared by pillaring lamellar inorganic precursors with bridged disilanes used as intercalation agents. The solids were used as bifunctional catalysts for consecutive catalytic processes.

Acknowledgements

Financial support by the Spanish Government (Consolider-Ingenio 2010 MUTICAT Project) is gratefully acknowledged. TG is gratefully by the JAE predoctoral fellowship from CSIC.

References

[1] Sánchez, C. C.; Julián, B.; Belleville, P.; Popall, M. J. Mater. Chem., 15 (2005), 3559.
[2] Hoffman, F.; Cornelius, M.; Morell, J.; Fröba, M. Angew. Chem., Int. Ed., 45 (2006), 3216.
[3] Ruiz-Hitzky, E.; Darder, M.; Aranda, P. J. Mater. Chem., 15 (2005), 3650
[4] Kwon, O.Y.; Shin, H. S.; Choi, S. W. Chem. Mater., 12 (2000), 1273.
[5] Diaz, U.; Cantín, A.; Corma, A. Chem. Mater., 19 (2007), 3686.
[6] Lagaly, G.; Beneke, K.; Weiss, A. American Mineralogist 60 (1975) 650; Leonowicz, M. E.; Lawton, S. L.; Lawton, J. A.; Rubin, M. K. Science, 264 (1994), 1910.

Luminescent mesostructured hybrid nanoparticles

Ivana Miletto[1], Emanuela Bottinelli[1], Giuseppe Caputo[2], Salvatore Coluccia[1] and Enrica Gianotti[1]
[1]*Department of Chemistry IPM and NIS - Centre of Excellence. University of Turin - Via Pietro Giuria, 7. 10125 Turin (Italy) ivana.miletto@unito.it*
[2]*Cyanine Technologies S.p.A. Turin, Italy*

Introduction

Ordered mesostructured porous materials have attracted increasing attention since their synthesis allows a precise control of the features and morphology. Mesoporous MCM-41 silicas have high specific surface area and pores with defined dimensions and uniform distribution. These features make mesoporous systems ideal candidates as host materials to guest organic molecules, producing organic-inorganic hybrid materials. Traditionally, these mesostructured materials were used as supports in heterogeneous catalysis and as molecular sieves. More recently, they have been exploited for hosting organic or inorganic fluorophores, in order to obtain a new class of hybrid materials with potential applications as solid lasers [1], photoinduced switching [2], optical sensors [3] and cellular imaging [4,5]. The confinement of a luminescent moiety within the pores and channels of mesoporous materials should result in the protection of the guest against both chemical and photochemical decomposition (e.g. photo-oxidation reaction for organic dyes) and thermal decomposition.
The immobilisation of the guest species inside the channels of the mesoporous materials can be achieved by physical adsorption, direct synthesis or post-synthesis grafting. In this contribution, synthesis and characterisation of photoluminescent hybrid organic-inorganic materials will be described. MCM-41-type mesoporous silica nanoparticles were used as host materials and indocyanine dyes and Ruthenium complexes [6,7] as guest species.

Experimental

MCM-41-type mesoporous silica nanoparticles were synthesized according to a slightly modified method of Radu et al. [8]. Two strongly luminescent ruthenium complexes (Scheme 1, structures I and II) were physically adsorbed within the MCM-41 nanoparticles channels.
Due to the different functional groups available on the structure of the fluorophore (Scheme 1, structures III and IV), in particular of terminal trimethoxysilane moieties, three different approaches were followed for the preparation of fluorescent cyanine-MCM-41 hybrids: *i)* post-synthesis adsorption, *ii)* post-synthesis grafting and *iii)* one-pot synthesis.
Morphological and structural characterization was carried out by XRD, UHRTEM, volumetric analysis and FTIR. The confinement effect within the mesopores on the photophysical properties of the guest molecules were investigated by DR-UV-Vis, photoluminescence spectroscopies and lifetime measurements. The redox properties of the ruthenium complexes-based hybrids have

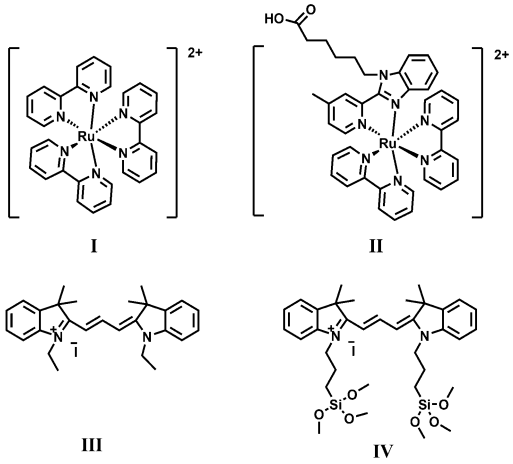

Scheme 1 Structures of the luminescent guests

been studied by cyclic voltammetry and the electrogenerated chemiluminescence (ECL) has been acquired in the presence of the co-reactant tri-n-propylamine.

Results and discussion

MCM-41-type mesoporous silica nanoparticles, with an average particle size of 100 nm, show a regular pore system consisting of a hexagonal array of unidimensional channels with a 22Å mean pores diameter and a Specific Surface Area of ca.1060 m^2/g (figure 1). Morphological and structural characterization revealed that the hybrid materials maintained the basic features of MCM-41 nanoparticles.

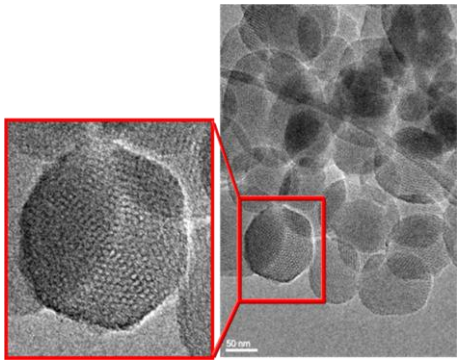

Figure 1 UHRTEM micrograph of MCM-41-type nanoparticles

DR-UV-Vis and photoluminescence spectroscopies, used to evaluate the influence of the encapsulation on the photoemission properties of the guests, showed for all the samples a beneficial effect on the stability and the overall brightness of the encapsulated guests with respect to the free molecules in solution. In addition, all the hybrids were characterized by two different lifetimes, suggesting the presence of two different silica microenvironments around indocyanine/Ruthenium complexes. The longer one can be attributed to the guests located inside the pores, whilst the molecules adsorbed on the external surface are responsible for the shorter one. With respect to the ruthenium based hybrids, it has to be noticed that ruthenium complexes encapsulated within the pores of MCM-41 nanoparticles maintained their high ECL efficiency.

Conclusions

Highly bright and stable luminescent hybrids have been prepared by the immobilization of indocyanine dyes and ruthenium complexes within the channels of MCM-41 nanoparticles.
The nanostructured spaces of the host material afford effective three-dimensional environments for orientation and immobilization of guest species, resulting in unique spectroscopic features of the final hybrids. The obtained materials have interesting potential applications as photoluminescent and electrochemiluminescent probes for diagnostics and imaging.

Acknowledgements

The authors are grateful to prof. Pierluigi Civera and prof. Danilo Demarchi research groups from Politecnico di Torino for the ECL characterization of the hybrids.
I.M. and E.B. thanks ASP, Piedmont Region and MIUR for financial support.

References

[1] Wu, S.; Zhu, C. *Opt. Mater.* 1999, *12*, 99.
[2] Wirnsberger, G. et al. *Adv.Mater.* 2000, *12*, 1450.
[3] Fiorilli, S. et al. *Sens. Actuators,B* 2004, *100*, 103.
[4] Lin, Y. S. et al. *Chem. Mater.* 2005, *17*, 4570.
[5] Gianotti, E. et al. *Appl. Mater. Interfaces*, 2009, 1 (3), 678.
[6] Bottinelli, E. et al. *Nuovo Cimento B* 2008, *123B(10-11)*, 1449.
[7] Bottinelli E. et al. *J. Fluoresc*. 2010 In Press DOI:10.1007/s10895-010-0605-5
[8] Radu, D.R. et al.. *J. Am. Chem. Soc.* 2004, *126*, 13216.

Computational study of the capability of transition metal exchanged zeolites for purification of hydrogen for fuel cell applications

Hristiyan A. Aleksandrov, Petko St. Petkov, and Georgi N. Vayssilov
Faculty of Chemistry, University of Sofia, 1126 Sofia, Bulgaria, e-mail: gnv@chem.uni-sofia.bg

Introduction

Fuel cells (FC) based on hydrogen are among the key components of the desired "hydrogen economy". Hydrogen feed industrially produced usually contains notable amount of CO, which hindrens the normal functioning of the FCs, and in particular of the proton-exchange membrane (PEM) FCs, due to poisoning of the noble metal catalyst on the electrode. Despite the progress in improving the resistance of the PEMFC electrodes towards CO poisoning, still the desired CO concentration in the feed is rather low, of the order of 10 ppm [1]. One of the possibilities for reduction of CO content in the hydrogen feed is the highly selective CO adsorption from the gas mixture at ambient conditions [2,3]. By this reason, in the present communication we present theoretical study which is based on thermodynamic analysis of competitive adsorption of CO and H_2 on specific adsorption sites in transition metal exchanged zeolites using data derived from state-of-the-art computational modeling.

Computational details

We carried out periodic DFT calculations with the PW91 exchange-correlation functional using Vienna ab initio simulation package (VASP) [5,6]. Ultrasoft pseudopotentials were used as implemented in the VASP package. Due to the large unit cell (see below) the Brillouin zone was sampled using only the Γ point. The valence wave functions were expanded in a plane-wave basis with a cutoff energy of 400 eV. The modeled cations and complexes were located at a six-membered ring in mordenite structure. The monoclinic unit cell of the zeolite framework was optimized for the pure silicate structure with dimensions a = b = 13.675 Å, c = 7.54 Å [7].

Results and discussion

From the calculated thermodynamic stability of the different complexes (assuming Boltzmann distribution) we calculated the concentrations of different surface species depending on the temperature and the mole fraction of the impurity gas in H_2 (considered at total pressure of 100 kPa). For the complexes with CO we presented in Fig. 1 the concentration of the metal sites which are not involved in M(CO) or $M(CO)_2$ complexes (in logarithmic scale, denoted as [1-$M(CO)_n$]) for different cations as a function of mole fraction of CO in the feed. This figure allows us to estimate down to what CO concentration the corresponding material can purify the feed. In order to use efficiently the adsorbent we may impose a requirement that no more than 10^{-5} of the metal ions participate in complexes different from di-carbonyls or monocarbonyls.

The results show that on rhodium, cobalt and iridium-exchanged zeolites one can purify hydrogen from CO to concentrations 2.6×10^{-10}, 5.9×10^{-9}, and 4.8×10^{-8}, respectively, via dicarbonyl complexes [8], thus using most efficiently the metal sites in the adsorbent (Fig. 1 – dashed red line for Co and full lines for Rh and Ir). However, in case of using Co^+, Ni^+, and Cu^+ exchanged zeolites, the monocarbonyl species are also sufficiently stable to contribute in the purification of H_2 from CO. As can be seen from the solid lines in Fig. 1, corresponding to the degree of purification of hydrogen when CO impurities are bound both in $M(CO)_2$ and M(CO) complexes, then much higher purification can be achieved, 7.7×10^{-17}, 1.9×10^{-15}, and 3.9×10^{-12}, for nickel, cobalt, and copper, respectively (Fig. 1). Thus, for essentially complete purification of hydrogen one can use Co^+ or Ni^+ exchanged zeolites, but also Cu^+ zeolite gives

degree of purification that is far beyond the value required currently for utilization of hydrogen in the PEMFC.
In a similar way we also modeled the purificaton of H_2 from N_2, NH_3 and H_2S.

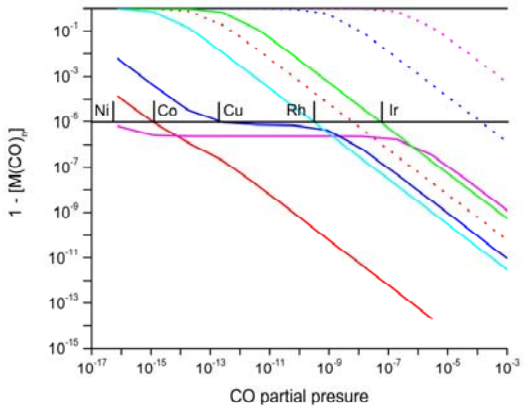

Figure 1. Concentration of the metal sites which are not involved in the complexes with the impurities for different cations as a function of mole fraction of the corresponding impurity in H_2 (10^5 Pa) at 298 K: $M(CO)_2$ (dotted lines) and $M(CO)_2$ + M(CO) (solid lines) (for Rh and Ir the dotted and solid lines coincide due to the low stability of the monocarbonyl complexes).

Conclusions

With respect to purification of hydrogen from CO we can summarize the following features of the different cationic forms of the zeolites:

- Ni^+ and Co^+ exchanged zeolites can provide the highest degree of purification of hydrogen from CO to CO concentrations below 10^{-15} – 10^{-16}, as in case of cobalt this purification can be accomplished via formation of dicarbonyls down to 10^{-8}, which provides twice higher efficiency of the adsorbent;
- Rh^+ and Ir^+ exchanged zeolites efficiently remove CO from hydrogen as dicarbonyls but their serious disadvantage is the high price of the metal; moreover, their performance as adsorbents can be achieved also with zeolites exchanged with other transition metal cations;
- Ag^+ is not relevant for purification of H_2, due to the low stability of its complexes with the impurity ligands;

The recommended adsorbent is Cu^+ exchanged zeolite since it can purify hydrogen down to CO concentrations of 10^{-12}, which is sufficient for practical applications; in particular two other advantages of copper should be taken into account: the weaker binding of CO compared to the other modeled cations (that will facilitate the regeneration of the adsorbent) and the low price of copper compared to the other metals.

Acknowledgements

This work was supported by the Bulgarian National Science Fund (Contracts DO02-82/08, D002-184/08 and the Center for supercomputer applications Super CA+).

References

[1] L. Shore, R. J. Farrauto, *Handbook of Fuel Cells: Fundamentals Technology and Application*, ed. W. Vielstich, A. Lamm, H. A. Gasteiger, John Wiley & Sons Ltd., West Sussex, 2003, vol. 3, p. 211.
[2] *Japan Pat.* JP2006342014-A, 2005.
[3] N. W. Ockwig, T. M. Nenoff, *Chem. Rev.*, 2007, **107**, 4078–4110.
[4] J. P. Perdew, Y. Wang, *Phys. Rev. B*, 1992, **45**, 13244–13249.
[5] G. Kresse, J. Hafner, *Phys. Rev. B*, 1994, **49**, 14251–14269.
[6] G. Kresse, J. Furthmüller, *Comput. Mater. Sci.*, 1996, **6**, 15–50.
[7] L. Benco, T. Bucko, J. Hafner, H. Toulhoat, *J. Phys. Chem. B*, 2005**, 109**, 22491–22501.
[8] K. I. Hadjiivanov, G. N. Vayssilov, *Adv. Catal.* 2002, **47**, 307-511.

High quality PMO materials with excellent stability via fast synthesis methods

G. Smeulders[1]*, A. Silvestre-Albero[2], M. Mertens[3], K. Houthoofd[4], O. I. Lebedev[5], G. Van Tendeloo[5], B. Maes[6], J. Martens[4], F. Rodriguez-Reinoso[2], P. Cool[1], V. Meynen[1]
*1 University of Antwerpen, Laboratory of Adsorption and Catalysis, Universiteitsplein 1, 2610 Wilrijk, Belgium, * geert.smeulders@ua.ac.be*
2 University of Alicante, Inorganic Chemistry, Ctra. San Vincente-Alicante s/n, 03080 Alicante Spain
3 VITO NV (Flemish Institute For Technological Research), Boeretang 200, 2400 Mol, Belgium
4 KULeuven, Centrum voor Oppervlaktechemie en Katalyse, Kasteelpark Arenberg 23, 3001 Heverlee, Belgium
5 University of Antwerpen, Organic synthesis, Groenenborgerlaan 171, 2020 Antwerpen, Belgium
6 University of Antwerpen, EMAT, Groenenborgerlaan 171, 2020 Antwerpen, Belgium

Introduction

Periodic mesoporous organosilicas (PMOs) are one of the latest innovations in the field of nanoporous materials. Similar to ordered mesoporous silica (OMS), the synthesis of PMOs is based on the use of organic templating molecules as structure directing agents (SDAs). In the case of PMOs however, the precursor contains an organic functional group (R) bridged between two silesquioxanes, which can be generally written as: $(R'O)_3SiRSi(OR')_3$. The amount of possible organic bridging groups is limited but can be further modified via post-synthesis methods making them extremely flexible nanoporous materials. They can be tuned for all kinds of applications, such as catalysis, sorption, k-low,… Of course it's of the outmost importance that the synthesis procedure is optimal to render a high quality and uniform material with excellent stability under the required circumstances.
In our work we examined the chemical, mechanical as well as the hydrothermal stability of PMO and compared them with their pure siliceous analogues. Secondly we were able to synthesize PMOs with a 20% higher surface area and pore volume in a much shorter synthesis time. The underlying mechanism responsible for the fast synthesis of high quality materials unravelled.

Results and discussion

Microwave-assisted synthesis has been applied for the preparation of various OMSs and recently also for PMO materials [1]. We found that each separate step of the PMO synthesis can be conducted under microwave conditions, drastically reducing the synthesis time. Next to the time reduction, the pore volume and the surface area have increased by more than 25%, without influencing the pore size or the ordering of the mesoporous structure. The hydrolysis (stirring) step can be shortened both under normal conditions and by applying microwave heating. Using microwave technology, the extraction procedure can be done in one single step of only 15 minutes.

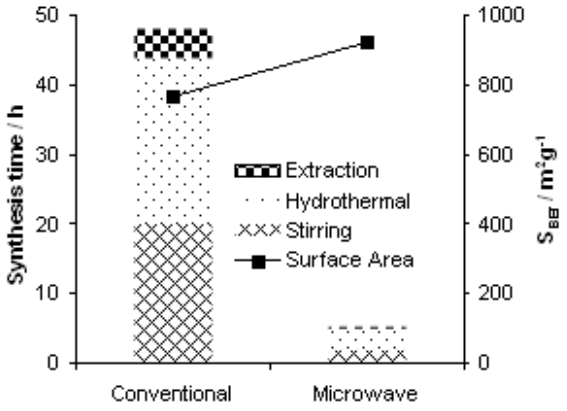

But the most important part in this process is the aging (hydrothermal) step. This step is not only responsible for the increase in volume and surface area, but also determines the final morphology of the PMOs. Comparing the heating ramps of conventional - and microwave synthesis, a large difference in ramp time to reach 100°C has been observed. We studied the influence of this ramping time on the synthesis of benzene bridged PMO's and found an effect on both porosity and morphlogy of these powders depending on the applied heating ramp.

This way it became clear that microwave heating during the aging step isn't a necessity to acquire high quality materials in a short time. It can also be obtained using classical synthesis methods by simply adopting a carefully chosen heating profile. Applying an alternative heating procedure on classical heating equipment (normal oven), allows us to obtain the above described 25% increase in porosity and morphology control in the same short time intervals as microwave. These altered heating ramps induced in conventional ovens allows for a cheaper and full alternative for microwave-assisted synthesis, which is not possible by simply reducing the aging time under normal synthesis conditions.

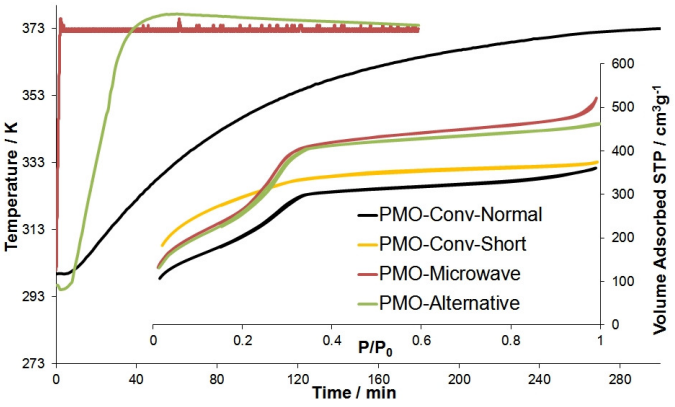

Next to the optimized synthesis procedure, we also examined the stability of these PMOs. A series of mechanical pressures and a number of hydrothermal conditions, variation of time and temperature were performed. The chemical stability of the different powders was evaluated by stirring 2 hours in an alkaline medium. The hydrothermal, mechanical as well as the chemical stability of the PMOs appeared to be more stable compared to their silica counterparts, e.g. MCM-41 and SBA as well as HMDS grafted MCM-41, under the "stress" conditions applied.

Conclusions

(1) The importance of carefully chosen heating ramps on the synthesis time and quality (high surface area and morphology) of PMO materials is shown. (2) The stability of PMO materials was found to be very high as compared to pure siliceous analogues and grafted MCM-41. This makes it an ideal candidate for further modification reactions and application as a catalyst or adsorbent.

Acknowledgements

This work was executed in the frame of the Fund for Scientific Research-Flanders (G.0294.10)

References

[1] G. Smeulders, V. Meynen , G. Van Baelen, M. Mertens, O. Lebedev, G. Van Tendeloo, B.U.W. Maes and P. Cool, J. Mater. Chem. (2009) 19 3042-3048

New zeolites COE-3 and COE-4 obtained by interlayer expansion of layered silicate RUB-36: Structure analysis.

Postalkoxysilylation of the layered silicate precursors to get new crystalline framework structures with expanded pore openings had been demonstrated using lamellar precursors of structure types MWW, FER and CDO. The reslting interlayer expanded zeolites were reported to be thermally and hydrothermally stable. Here we report the interlayer expansion of another layered silicate, RUB-36, using a variety of silylation agents (chlortrimethylsilane, ethoxytrimethylsilane, triethylsilane, triethylchlorosilane, dichlorordimethylsilane, hexamethyldisilane, hexamethylcyclotrisiloxane, 1,1,3,3-hetramethyldisiloxane, hecamethyltetrasiloxane and octamethyltrisiloxane) which results in new zeolitic materials called COE-3 (as) and COE-4 (calc). COE-3/COE-4 obtained with dichlorodimethylsilane was structurally investigated using X-ray powder diffraction and N_2 adsorption.

Powder X-ray diffraction shows the surprising periodicity of the expanded silicate framework. Indexing of the PXRD confirms that the ferrerite layer remained preserved (a = 7.372(2) Å, b = 13.951(2) Å, c = 12.179(6) Å, ß = 107.5(1)°). Since X-ray experiments characterize the entire sample, the framework and pore structure are uniform and define new zeolite materials. N_2 adsorption of the interlayered product confirms that the pores are thermally stable and can be accessed after calcination with typical values for the extended ring sizes (ca. 350 m²/g).

Alkaline metal exchange optimization of SOD-ZMOF materials for potentially improved hydrogen adsorption

Guillermo Calleja, Carmen Martos, J. Ángel Botas, Gisela Orcajo and José A. Villajos
Department of Chemical and Energy Technology, Universidad Rey Juan Carlos.
guillermo.calleja@urjc.es.

Introduction

Metal-Organic Framework materials (MOFs) have been presented since their discovery as a promising route to achieve DOE targets for hydrogen storage systems [1]. However, porous materials are not able to retain significant amounts of hydrogen at near-ambient conditions due to the weak interactions between hydrogen molecules and the potential adsorption sites of their surfaces. In this sense, zeolite-like imidazolate metal-organic framework (ZMOF) materials are interesting candidates to improve the interaction hydrogen-surface since their negative-charged structure can be potentially ion-exchanged, tuning the physico-chemical properties of their cavities. If this simple ion-exchange process is carried out with metal cations, the electric field inside the pores is expected to increase, and therefore the interaction with hydrogen molecules became also stronger [2]. In the case of SOD-ZMOF material (ZMOF with Sodalite zeolitic topology) the negative charge of the structure is compensated by imidazolium cations that also act as a structure directing-agent. In previous works, RHO-ZMOF (ZMOF with RHO zeolitic topology) has been targeted for metal cation exchange [2, 3, 4] and tested for hydrogen adsorption; however SOD-ZMOF, in spite of having smaller pores suitable for hydrogen molecules confinement compared to its homologue RHO-ZMOF, has not received the same attention in the literature and has been only studied by our group [4]. The aim of this contribution has been to incorporate alkali metal cations into the materials to enhance their hydrogen gas adsorption properties, a concept which has been frequently explored for other MOF systems. Specifically, ion-exchange procedure for SOD-ZMOF material with Li^+, Na^+, K^+ has been optimized, maximizing the ion exchange degree achieving near stoichiometric proportion, minimizing the contact time and keeping unaltered the structural and textural properties of the material.

Experimental

SOD-ZMOF material was prepared basically following the procedure published elsewhere [3], and the ion exchange procedure was carried out as follows: 30 mg of crystals previously washed with a mixture of ethanol/water were suspended into a 1 N metal nitrate solution in ethanol/water mixture for 24 h. Then, crystals were washed with the same solvent mixture seven times in order to remove the rest of non-compensating ions, and finally washed with acetonitrile for 1 day. Materials so obtained were analyzed by Powder-XRD, N_2 Adsorption-Desorption, TGA, ICP-AES and SEM-EDAX. Ion-exchanged materials were named Li-SOD_1d, Na-SOD_1d and K-SOD_1d, where nomenclature refers to "*metal ion-ZMOF type_exchanging time*".

Results and discussion

Figure 1 shows the PXRD patterns of optimized exchanged SOD-ZMOF materials together with the as-synthesized material. In all cases, reflections from pure SOD-ZMOF phase have been detected. Additionally, SEM image of K-SOD_1d taken with the Retro-Dispersed Detector shows homogeneous composition and similar crystal morphology after the ion-

exchange process, being these results better than those obtained by other procedures [4] where morphology was completely modified.

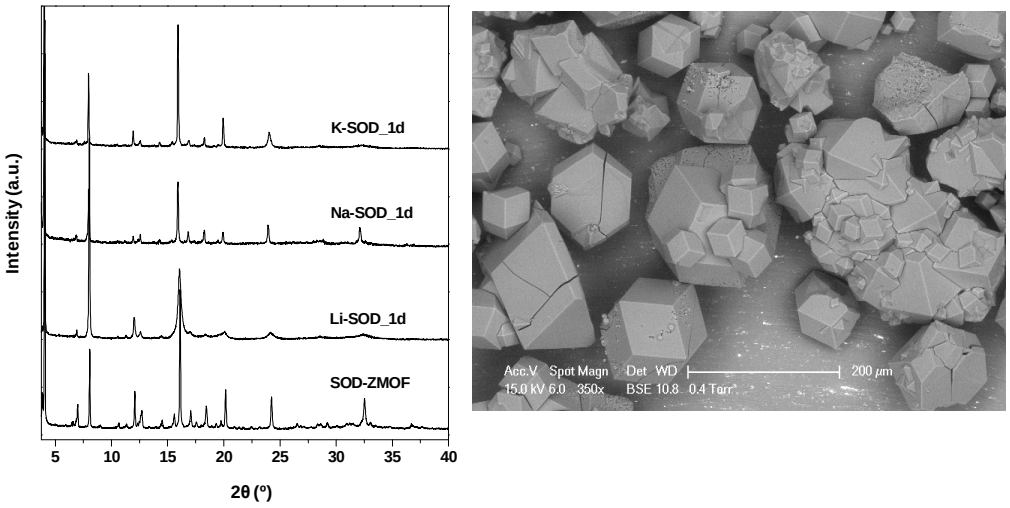

Figure 1. Left: PXRD of all SOD-ZMOF materials. Right: SEM image of K-SOD_1d.

Similar values of textural properties have been obtained for the exchanged materials compared to the original SOD-ZMOF, being BET surface area 600 m^2/g and pore volume 0.250 cm^3/g. A high ion-exchange degree near stoichiometric proportion has been reached for all the samples in just 1 day of treatment, compared to that obtained before [4]. The tendency observed was an increase of ion-exchange degree with the atomic number of the alkaline metal.

Conclusion

In summary, ion-exchange has been successfully carried out in SOD-ZMOF materials with some alkaline metal ions, reaching near stoichiometric proportions, while keeping unaltered the structural and textural properties. These materials are potentially good candidates for hydrogen storage applications, being able to exhibit higher hydrogen storage capacity than the SOD-ZMOF materials already reported [4].

Acknowledgement

The authors thank the ‘‘Comunidad de Madrid’’ and the Spanish Ministry of Science and Innovation for their financial support to the SOLGEMAC Project through the Program of Activities between Research Groups (S2009/ENE-1617) and CICYT (Project CTQ2009-11934), respectively.

References

[1] Furukawa H., Miller, M.A., Yaghi, O.M., Independent verification of the saturation hydrogen uptake in MOF–177 and establishment of a benchmark for hydrogen adsorption in Metal–Organic Frameworks, J. Mater. Chem., 17 (2007), 3197–3204.
[2] Nouar, F., Eckert, J., Eubank, J.F., Forster, P., Eddaoudi, M., Zeolite-*like* Metal–Organic Frameworks (ZMOFs) as hydrogen storage platform: lithium and magnesium ion–exchange and H_2–(*rho*–ZMOF) interaction studies, J. Am. Chem. Soc., 131 (2009), 2864–2870.
[3] Liu, Y., Kravtsov, V.C., Larsena, R., Eddaoudi, M., Molecular building blocks approach to the assembly of zeolite–like metal–organic frameworks (ZMOFs) with extra–large cavities, Chem. Comm., (2006), 1488–1490.
[4] Calleja, G., Botas, J.A., Sánchez-Sánchez, M., Orcajo, M.G., Hydrogen adsorption over zeolite–like MOF materials modified by ion exchange, International Journal of Hydrogen Energy, 35 (2010), 9916–9923.

Desilicated MOR zeolite as bifunctional catalyst in *n*-hexane hidroisomerization

R. Monteiro[a], V. Paixão[a], J. Rocha[b], A.P. Carvalho[c], A. Martins[a]
[a]*DEQ and CIEQB, ISEL, Rua Conselheiro Emídio Navarro, 1, 1959-007 Lisboa, Portugal*
[b]*Dep. Química and CICECO, Universidade de Aveiro, 3810-193, Aveiro, Portugal.*
[c]*DQB and CQB, FCUL, Campo Grande C8, 1749-016, Lisboa, Portugal.*
ana.carvalho@fc.ul.pt

Introduction

Zeolites have been widely used as catalysts as well as adsorbents in separation and purification processes, due to a unique combination of properties such as high surface area, well defined microporosity, high thermal stability and intrinsic acidity. Nevertheless, the purely microporous character of these materials often imposes limitations to some applications in the fields of petroleum refining, petrochemistry and fine chemical, due to restricted access to the active sites, especially when bulky reaction intermediates are involved. To overcome this limitation, several studies focused on the generation of mesoporosity through a controlled extraction of silicon from the framework in alkaline medium (desilication) have been carried out [1].
Hydroisomerisation of light naphta is an industrially important process for the production of high octane gasoline. This reaction is generally carried out over bifunctional catalysts Although Pt/HMOR is a commonly used catalyst in this reaction, the selectivity into the most valuable products, dibranched isomers, is considered medium. In this sense, modifications of the zeolite, such as desilication, can be performed in order to facilitate the formation of bulky dibranched isomers. In this work we studied the potentialities of desilicated HMOR zeolite as support for Pt deposition and the catalytic behavior of bifunctional Pt/HMOR in n-hexane hydroisomerisation.

Experimental

MOR zeolite, from Zeolyst (Si/Al = 10) was submitted to alkaline treatment at 85 ºC, for 2 h using NaOH in different concentrations (0.1 to 0.5 M), by preparing a suspension with a ratio NaOH/zeolite = 30. The solid was recovered by centrifugation and washed with distilled water. The alkaline-treated samples were converted into the H-form by three consecutive exchanges with 1 M NH_4NO_3 solution for 3 h at 80 ºC. The solid was dried overnight, and finally calcined in air flow at 500 ºC for 3 h. The samples were named: M/NaOH conc (M). Platinum (about 1% weight) was introduced by incipient wetness impregnation using $[Pt(NH_3)_4]^{2+}$ as metal precursor. The samples were named: PtM/NaOH conc (M). The characterization techniques used were powder X-ray diffraction, (Philips PW 1710 diffractometer), ^{27}Al and ^{29}Si MAS NMR (Bruker Avance III 400 NMR spectrometer) and N_2 adsorption at low temperature (ASAP2010). The catalytic tests were performed in a flow reactor under a total pressure of 1 bar. Samples were previously calcined under air flow at 300ºC for 5 h and reduced *in situ* under H_2 flow at 500 ºC for 3h. Toluene hydrogenation was carried out at 110 ºC, H_2/toluene molar ratio = 45 with toluene diluted in *n*-hexane (1:5 molar ratio) and WHSV= 100 h^{-1}. n-Hexane transformation was performed at 250 ºC with a molar ratio H_2/n-C_6 = 9, WHSV = 6.6 to 53.4 h^{-1}. The products were analyzed on-line by GC equipped with FID, using capillary columns (PONA for toluene hydrogenation and CP-SQUALANE for n-hexane hydroisomerization).

Results and discussion

The characterization of the samples by powder X-ray diffraction denotes some lost of crystalinity, more important in the case of sample M/0.5. The desilication of the structures was confirmed by the NMR results. The results of N_2 adsorption (Table 1) show that the treatments promoted the development of mesoporosity, which increases with the base concentration. The hydrogenating properties of Pt/MOR samples were evaluated by the model reaction of toluene hydrogenation. Table 2 shows the initial hydrogenating activities for parent and desilicated samples. Desilicated samples show higher activities when compared with PtM, increasing with the base concentration. This behavior can be explained attending to aneasier accessibility of the reactant to the metal sites dispersed inside the porous structure, as a consequence of the mesoporosity created by desilication treatment.

Table 1. Textural parameters of parent and desilicated samples.

Sample	V_{micro} (cm^3g^{-1})	$V_{ultramicro}$ (cm^3g^{-1})	$V_{supermicro}$ (cm^3g^{-1})	V_{meso} (cm^3g^{-1})
M	0.20	0.19	0.01	0.05
M/0.1	0.20	0.18	0.02	0.04
M/0.2	0.21	0.19	0.02	0.19
M/0.5	0.17	0.16	0.01	0.21

Table 2. Initial activity for toluene hydrogenation.

Sample	Initial Activity (mol $h^{-1}g^{-1}$)
PtM	0.70
PtM/0.1	0.80
PtM/0.2	2.44
PtM/0.5	3.41

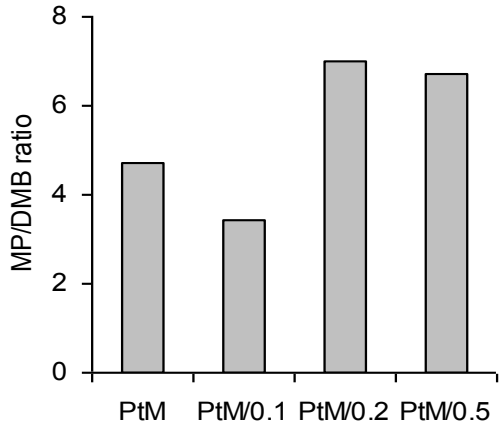

Figure 1. MP/DMB ratio for *n*-hexane hydroisomerization.

In the transformation of *n*-hexane the total conversion ranged from 5 to 40 %. The reaction products for all samples are isomerization products, mono-branched methylpentanes (2-MP and 3-MP) and di-branched dimethylbutanes (2,2-DMB and 2,3-DMB), methylcyclopentane, benzene and cracking products. Figure 1 shows the ratio between the mono-branched (MP) and di-branched (DMB) isomers. Only PtM/0.1 sample presents an increased selectivity in DMBs when compared with PtM sample. These results point out that, when a large volume of mesoporous is present the formation of DMB products is unflavoured. Instead oligomerization reactions occurred, as indicated by the presence of secondary cracking products.

Conclusions

The slight modification of textural properties of MOR zeolite improves the selectivity of bifunctional catalyst (PtM/0.1) into dibranched isomers. This study demonstrated that desilication treatments can be beneficial to catalytic purposes, nevertheless the desilication conditions need to be properly controlled, since high mesoporous volumes are not directly related to a better catalytic performance.

References

[1] Paixão, V., R., Carvalho, A.P., Rocha, J., Fernandes, A., Martins' A., Modification of MOR by desilication treatments: structural, textural and acidic characterization. Microporous and Mesoporous Materials, 131 (2010) 350-357.

Adsorption of α-tocopherol on clinoptilolite tuff from ethanol, ethyl acetate, n-hexane

S.U. Vasileva, E.V. Borodina, D.L. Kotova, V.F. Selemenev
Russia, Voronezh, Voronezh State University
sv_vasileva@mail.ru
evborodina@gmail.com

Introduction

Unique adsorption and ion exchange properties, mechanical and chemical resistance, high acid and radiation resistance of high-silicon of natural zeolites are causes their wide range of applications.

One of the important properties of zeolite tuff is their ability to sorption of biologically active substances aor example amino acids, vitamins and minerals. Fat-soluble vitamin E is a powerful antioxidant and it is essential to living organism. Vitamin E, fixed in the zeolite carrier, is potentially of the vitamin and mineral premixes and animal feeds. It is known from the literature data, the amount of adsorbed vitamin E on the adsorbents depends on the type of solvent [1, 2]. The aim of work is investigation of sorption α-tocopherol on clinoptilolite tuff from ethanol, ethyl acetate, n-hexane solutions.

Experimental

The sorption of vitamin E was studied on the zeolite tuff located in Ugra, Russian Federation. This type of zeolite represents a multiphase mixture. The main rock-forming mineral is clinoptilolite (68 %) [3].

Vitamin E (α-tocopherol) supplied by Sigma (Germany) was used. Structural formula of α-tocopherol is shown in Figure 1.

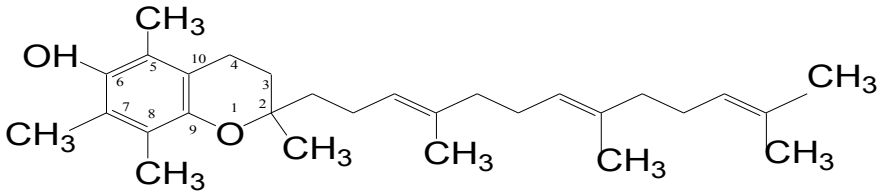

Fig. 1. Chemical formula of α-tocopherol

The pre-treatment of clinoptilolite tuff with 4.0 M HCl was carried out to for dealumination and increasing the sorption capacity. Sorption equilibrium between clinoptilolite tuff (fraction 0,02-0,06 mm) and α-tocopherol solution was studied at 295 ± 2 K in static conditions using variable concentrations [4].

Air-dry samples of clinoptilolite tuff placed in flat-bottomed flask with a solution of α-tocopherol 5.8 * 2.10 - 46 mmol / l. The mixtureswere kept under stirring at a given temperature for 24 hours to establish the equilibrium in the system. Equilibrium time was determined before from preliminary kinetic experiment. After the solutions were separated from zeolite by filtration and analyzed by UV-spectroscopy Shimadzu equipment. The quantity of adsorbed a-tocopherol–absorbed, converted to 1.0 g of sorbent was determined from the difference in the concentrations of initial solution and after contact with his clinoptilolite tuff.

Results and discussion

Sorption of α-tocopherol on native clinoptilolite tuff (fractions 0,02-0,06 mm) is low. The clinoptilolite tuff were modified by acid treatment to increase the sorption of

parameters The sorption of α-tocopherol on clinoptilolite tuff activated with 4.0 M HCl was investigated.

Interphase distribution between α-tocopherol and clinoptilolite tuff from different solvents (ethanol, ethyl acetate, hexane) were evaluated on the basis of sorption isotherms obtained at 295 K (Fig. 2). The experimental data indicate the strength of hydrophobicity of the solvent effect on the value of maximum sorption capacity clinoptilolite tuff.

The best sorption capacity of natural mineral was reached conducting sirption from ethanol. Adsorption of α-tocopherol is more favorable than the solvation in the volume of ethanol solution. Equilibrium sorption capacity of zeolite tuff in α-tocopherol from ethanol to 1.37 times greater than from ethyl acetate and to 1.72 times greater than from hexane.

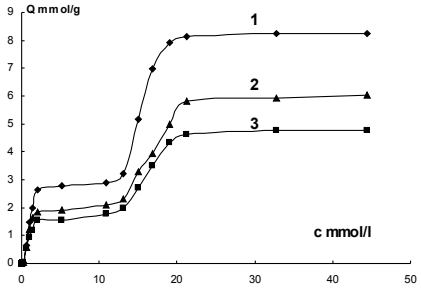

Figure 2 sorption isotherm :1-solvent is ethanol, 2-ethyl acetate solvent, 3 - solvent hexane

This fact can be explained by hydrophilicity of solvents. The strength of hydrophilicity of the solvents is changed in a series of ethanol> ethyl acetate> hexane. Contribution of hydrophobic interactions in adsoption of α-tocopherol on dealuminated clinoptilolite tuff is advantageous compared with the formation of adsorption complexes between vitamin E and the active basic and acidic centers of sorbent.

Conclusions

Thus, investigation sorption of α-tocopherol on dealuminated zeolite tuff from ethanol, ethyl acetate, hexane was done. It was determined the largest amount of α-tocopherol was adsorbed on clinoptilolite tuff from ethanol solution.

References

[1] G. Chandrasekar A. Vinu, V. Murugesan and M. Hartmann Adsorption of vitamin E on mesoporous silica molecular sieves / Studies in Surface Science and Catalysis, volume 158, (2005), p 1169-1176 /

[2] G. A. Kovalenko I and E. V. Kuznetsova Adsorbtion of antiseptics (furacilin, chlorhexidine) and vitamin E on carbon-containing enterosorbents / Pharmaceutical Chemist1T Journal Vol. 34, No. 6, (2000), p 45-49.

[3] Cherenkov Y., Kotova, DL Sorption and physico-chemical properties of the zeolite deposits of the Polar Urals Ugra / Sorption and chromatography. Processes. 2006. - V.8., Issue 2, s.314-319.

[4] Polyansky, NG, Gorbunov VG, Kazantsev, NL Methods for studying ion-exchange resins. -M.: Chemistry, 1976.-208p

Chiral ordered mesoporous silica obtained using amino acids

Susana Lacasta, Víctor Sebastián, Clara Casado, Álvaro Mayoral, Pilar Romero, Ángel Larrea, Eugenio Vispe, Pilar López-Ram-de-Viu, Santiago Uriel, Joaquín Coronas*
Departamento de Ingeniería Química y Tecnologías del Medio Ambiente and Instituto de Nanociencia de Aragón, Universidad de Zaragoza 50018 Zaragoza, Spain.
coronas@unizar.es

Introduction

The availability of an inexpensive and robust porous chiral silica-based solid could help the development of enantioselective adsorption separations as a feasible alternative to other existing approaches. Chiral microporous solids such as certain zeolites would not have pores large enough for treating molecules of relatively large size. Other chiral (helical) mesostructured materials recently reported exhibit chirality (in terms of the length of one complete helix turn) on a scale about two orders of magnitude larger than the mesopore size, and hence do not show chiral separation performance [1].
In the present work, chiral ordered mesoporous silica (COMS) has been prepared by hydrothermal synthesis at high pH, in the presence of the amino acids L-arginine, L-histidine, L-isoleucine and L-proline and quaternized aminosilane N-3[3-(trimethoxysilyl)propyl]-N-octadecyl-N,N-dimethylammonium chloride (C_{18}-TMS) and tetraethyl orthosilicate (TEOS) as silica sources, followed by calcinations [2]. This COMS has the same 2D hexagonal structure as MCM-41 ordered mesoporous silica prepared with cetyltrimethylammonium (CTA) surfactant 2. However, our COMS does not lose enantioselectivity upon calcination, in contrast to non-ordered enantioselective sol-gel materials. For instance, chiral sol-gel imprinted materials obtained with chiral cationic surfactant lose enantioselectivity upon calcinations [3].

Experimental

Silica mesoporous powders were prepared using tetraethyl orthosilicate as the main Si source and the quaternized silicon source, N-3[3-(trimethoxysilyl)propyl]-N-octadecyl-N,N-dimethylammonium chloride as initiator, in the presence of several amino acids: L-arginine, L-histidine and L-isoleucine, and L-proline. The molar composition was TEOS : C_{18}-TMS : amino acid : H_2O : NaOH = 6 : 1 : 2 : 1000. The resulting mixture was maintained at 80 ºC for 24 h. The organic material was removed by calcination at 650 ºC for 8 h. For comparison purposes, samples were prepared with DL-amino acids and with D-proline

Results and discussion

The charge-matching between organic surfactant and inorganic silicate components established in the case of the hydrothermal synthesis of MCM-41 and SBA-15 can also be applied to C_{18}-TMS and the corresponding amino acid. However, there are important differences between the conventional synthesis of MCM-41 using CTA cation [4] and the syntheses carried out here combining C_{18}-TMS surfactant and amino acids:
a) The possibility of condensation between hydrolyzed C_{18}-TMS surfactant molecules to produce dimers.
b) The possibility of organization of the aminosilane dimers into micelles where the amino acid molecules could electrostatically interact with the positively charged C_{18}-TMS dimers.

c) The reaction of hydrolyzed C_{18}-TMS surfactant molecules having silanol groups with silicate species via covalent bonds.
d) The micelle constituted by alternating C_{18}-TMS dimers and amino acids or negatively charged silica species makes possible the efficient transference of chirality to the ordered mesoporous silica in a mechanism where the amino acid leaves its molecular imprint in the silica.
The ordered mesoporous silica obtained possesses the MCM-41 hexagonal order (as seen by LA-XRD and TEM) and BJH pore sizes in the 2.8-3.3 nm range with BET specific surface areas as high as 1130 m^2/g. Calcined COMSs have been tested in enantioselective adsorption experiments. Samples of the four studied COMSs were stirred with the corresponding solutions of racemic Pro, Ile, His or Arg in their zwitterionic form and the solutions were then analyzed (see Figure 1). Other racemates of interest have successfully been addressed with these materials.

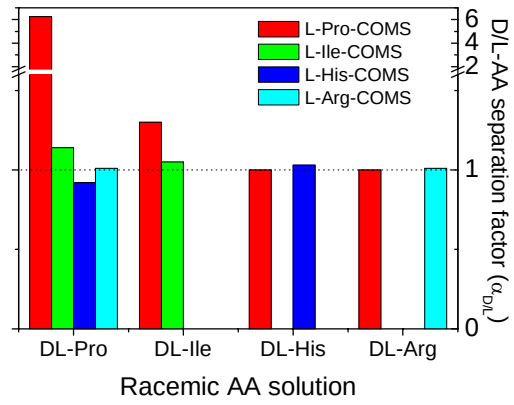

Figure 1. Enantiomeric separation factors resulting from shaking calcined L-AA-COMS with racemic AA solutions (AA refers to Arg, His, Ile and Pro). Racemic proline can clearly be resolved with L-Pro-COMS ($\alpha_{D/L}$= 6.26 ± 1.98) and, to a lesser extent, with L-Ile-COMS ($\alpha_{D/L}$ = 1.14 ± 0.01) and even with L-His-COMS, where a small degree of reverse enantiodiscrimination ($\alpha_{D/L}$ = 0.92) was observed.

Conclusions

Even though arginine, histidine, isoleucine and proline are different in terms of side chain polarity and hydropathy index, all of them give rise to ordered mesoporous silica. This suggests that the experimental procedure used in this research is flexible enough for probable application to most of the standard amino acids and to other kinds of chiral organic compounds as chirality inductors. This would open up new possibilities for a multitude of applications involving, among others, asymmetric catalysis and enantiomeric separation.

Acknowledgements

Financing from the Spanish Ministry of Science and Innovation and the Aragon Government is gratefully acknowledged.

References

[1] J. Fan, S.W. Boettcher, C.K. Tsung, Q. Shi, M. Schierhorn, G.D. Stucky, Chem. Mater. 20 (2008) 909.
[2] S. Lacasta, S. V., C. Casado, A. Mayoral, P. Romero, A. Larrea, M.P. Lopez-Ram-de-Viu, E. Vispe, S. Uriel, J. Coronas, Chem. Mater. 10.1021/cm1032546 (2011).
[3] S. Fireman-Shoresh, S. Marx, D. Avnir, Adv. Mater. 19 (2007) 2145.
[4] J.S. Beck, J.C. Vartuli, W.J. Roth, M.E. Leonowicz, C.T. Kresge, K.D. Schmitt, C.T.W. Chu, D.H. Olson, E.W. Sheppard, S.B. McCullen, J.B. Higgins, J.L. Schlenker, J. Am. Chem. Soc. 114 (1992) 10834.

Recycling of silicate waste from nanocasting into microporous zeolites

Jung Ho Kim, Yoon Kyung Kim, Song Min Young, Jin Sol Park, and Jong -Sung Yu*

Department of Advanced Materials Chemistry, Korea University, Jochiwon, ChungNam 339-700, Republic of Korea. E-mail: jsyu212@korea.ac.kr; Fax: (+81)-41-867-5396

Template nanocasting synthesis of porous carbon materials usually requires the selective removal of the template silica from carbon/silica composites, not only resulting in waste of chemicals, but also posing significant environmental concerns as well as waste treatment. In this work, recycling of etched silica waste released from such nanocasting synthesis is successfully performed to regenerate valuable microporous MFI type silica materials, which can help not only in saving chemicals, but also in decreasing chemical waste for better improvement of our environments.

KEYWORDS : silica waste, nanoporous carbon, waste recycling, mesoporous materials, nanocasting

Introduction

Porous carbon materials have attracted considerable attention because of their remarkable properties such as high specific surface areas, large pore volumes, chemical inertness, and good mechanical stability, which have great potentials in many areas of modern science and technology, including water and air purification, gas separation, catalysis, chromatography, energy storage, and electrode for battery, solar cell and fuel cell [1]. Formation of uniform and 3-dimensionally interconnected pores and specific morphologies in these nanostructured carbon materials is usually achieved by nanocasting of inorganic nanostructured materials as hard templates. The whole procedure of the nanocasting synthesis of mesoporous carbon usually involves pre-synthesis of a mesoporous silica host, infiltration of a carbon precursor into the mesoporous silica host, carbonization of the carbon precursor infiltrated into the silica host and then selective dissolution of the sacrificial silica host from the carbon–silica composite to generate silica-free mesoporous carbon replica [2].

However, the procedure in such silica-directed synthesis of the porous carbon usually requires the selective removal of the template silica from the carbon/silica composite by harmful hydrofluoric acid or NaOH, not only wasting valuable chemicals, but also posing significant environmental concerns as well as waste treatment. Although the removal of silica framework by dissolution in aqueous NaOH solution has been already documented, hydrofluoric acid is still largely used for the extraction of silica, in which case, a special reactor is also required with extra care. However, there is no report yet concerning the recycling of such etched silica waste into valuable functional silica materials. Here, we report an efficient recycling method of silica waste selectively etched in the nanocasting method for the formation of silica-free mesoporous carbon replica. The recycling process represents a regeneration of microporous silica materials by a hydrothermal process of silicate oligomers from the silica effluent and added structure directing agent. That is, the silica effluent is not wasted, but rather utilized to produce valuable microporous silica materials by this approach.

Experimental

Mesoporous carbon replica was prepared by a simple nanocasting method using a calcined SBA-15 host as a hard template using phenol and paraformaldehyde as carbon precursor. The silica template was then selectively dissolved by stirring the carbon/silica composite in ~3.5 M NaOH solution for 10 min and heating in oven at 353 K for overnight. The solid product was filtered, and washed with ethanol, and dried and identified as a CMK-3 mesoporous carbon by XRD. The first filtered effluent containing silica waste was secured for recycling and mixed with aqueous solution of 3.0×10^{-2} M $AlCl_3\cdot6H_2O$ so that the mixture has various Si/Al molar ratios. Either tetrapropylammonium hydroxide (TPAOH) or tetrapropyl-ammonium bromide (TPABr) was used as a template agent for the synthesis of ZSM-5 zeolite.

Results and discussion

A photograph of the first filtered effluent containing silica waste (Fig. 1a) confirms that the slightly turbid solution was retrieved from the silica-carbon composite. Figure 1b shows a composition ternary diagram of Na_2O-SiO_2-H_2O of three different etched silica effluents and commercial sodium silicate solutions from J. T. Baker and Aldrich. The etched silica waste as a silica source is considered to be a kind of new sodium silicate, which is different from well-defined commercial sodium silicate. So-obtained sodium silicate can have different structures and degrees of polymerization in addition to the difference in composition, viscosity and pH compared to commercial one, exhibiting different physical and chemical properties.

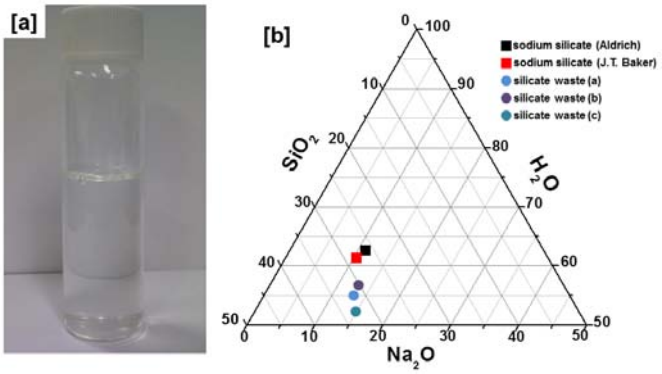

Figure 1. Photograph of an etched silica waste from SBA-15 template (a) and Na_2O-SiO_2-H_2O ternary diagram of three different etched silica wastes and commercial sodium silicates (b).

In a subsequent recrystallization process, the mixture with surfactant solution in alkaline condition was placed into the stainless autoclave, heated to 373 K, and held at that temperature for 24 h to have ZSM-5 zeolites, whose crystal structures were confirmed by XRD. All the diffraction patterns of the resulting zeolite prepared at different Si/Al molar ratios =∞, 40 and 30 in this study agreed well with that of typical ZSM -5 zeolite as previously reported [3]. The ZSM-5 crystalline structure starts to decrease when the Si/Al ratio in the synthesis medium decreases to 20, and completely disappears at Si/Al = 10, indicating that the Si/Al ratio is an important factor for the generation of the ZSM-5 crystals as well as their morphological shape. There were not significant differences in XRD patterns for the ZSM-5 prepared with either TPAOH or TPABr.

In summary, sacrificial silica waste released from typical template synthesis of nanostructured carbon was recycled to regenerate highly valuable microporous zeolite silica. This approach thus can improve cost effectiveness for the silica-directed nanocasting mass production of nanostructured carbon by better utilizing the otherwise silica waste into highly desirable valuable microporous silica.

References

[1] Fang, B., Kim, J. H., Kim, M. -S., Yu, J. -S., *Chem. Mater*. *21* (2009), 789-796.
[2] Yoon, S. B., Kim, J. Y., Kooli, F., Lee, C. W., Yu, J. -S., *Chem. Commun*. (2003), 1740-1741.
[3] Meier, W. M.; Olson, D. H. *Atlas of Zeolite Structure, 2nd revised ed.*; Butterworth: Cambridge, 1987.

Hybrid Biocatalysts: PMO as stabilizer for lipase in methanol

Beatriz González, Rosa M. Blanco, Isabel Díaz*
Instituto de Catálisis y Petroleoquímica, idiaz@icp.csic.es

Introduction

The industrial interest in selectivity of lipases and their application in stereoselective processes in pharmaceutical industry or regioselective nutraceuticals synthesis enlighten the relevance of the immobilization of these enzymes. The use of lipase has also been investigated in the production of biodiesel. By means of the enzymatic metanolisis of residual fats, the production of alkaline salts of fatty acids and soaps could be avoided. For this reason, there is still room for producing a biocatalyst based on lipase that is stable in methanol and therefore allows for massive industrial implantation of the enzymatic route in this process.

The hydrophobic domain of lipases has been largely used to anchor them on hydrophobic surfaces of insoluble supports [1,2]. Supports of different chemical nature have been used having always hydrophobic groups covering their surfaces to interact with this area of lipases. The use of Ordered Mesoporous Materials as supports offer a good connectivity between the pores so the substrates and/or products may diffuse more easily through the pores despite the small pore diameter. The small particle size of these materials also contributes to diminish diffusional restrictions. The discovery of periodic mesoporous organosilicas (PMO), with organic groups forming the pore walls, has provided new opportunities for enzyme immobilization. PMO based on ethane bridges has been tested as support for cytochrome c and xylanase with no improvement in enzyme loading/leaching in comparison with the pure silica SBA-15 support [3,4]. Further efforts on fabricating more hydrophobic walls to adsorb lysozyme implied the use of bifunctional mesoporous organosilicas with different fraction of diethylenebenzene and ethane groups [5], or mixtures of propylamine, benzene and biphenyl PMOs [6]. Recently, we have shown that there is an optimum of degree of hydrofobicity that leads to a higher performance of the lipase [7]. The high hydrophobicity of the PMO wall along with the confinement of the enzyme within the pores facilitates the formation of strong interactions enzyme-support. The intense interaction reduces the mobility of the protein, and therefore it slows down its denaturation. Like consequence, the stability increases. The obtained hybrid catalyst is more stable in the presence of methanol than a similar catalyst where lipase is anchored through octyl groups of an amorphous meso-macroporous silica OAS. This catalyst had proved highly active and stable in different incubation media [8].

Experimental

In the synthesis of PMO, 1.76 g of Pluronic P123 was dissolved in 69 g of water, 5.18 g of KCl, and 1.18 g of HCl at room temperature, after 10 min of vigorous stirring, 3.08 g of 1.2-bis(triethoxysilyl)ethane (BTEE) was added as silica source. The solution was kept at room temperature for 24 h, and then transferred into an autoclave and heated at 100 °C for 24 h. The solid was collected by filtration and dried at room temperature. Removal of the surfactant was made by extraction with an EtOH/HCl solution. Different amounts of a commercial extract of CaLB containing 4 mg protein per mL were dissolved in 50 mM phosphate buffer pH 7.0 up to a total volume of 10 mL. For a quick activity test, the hydrolysis of pNPA was assayed spectrophotometrically at 348 nm. The tributyrin hydrolysis activity assay was used to check the hydrolytic activity of the supported biocatalysts. For further details in these assays see reference [7]. For stability tests, the enzymatic suspensions are first prepared in the different media (data will be detailed) and sealed to avoid evaporation. The vials were shaken in a roller agitator at room temperature in order to have homogenous mixtures. Leaching, thermal stability and different MeOH/water ratios have been tested. In all the cases, the PMO

supported biocatalyst is compared with soluble free lipase and with an equivalent biocatalyst based on amorphous silica (Octyl Amorphous Silica, OAS) widely studied in our lab [8].

Results and discussion

The stability of PMO+Lipase catalyst was tested in different concentrations of methanol. The most relevant results are displayed in Fig. 1. In 100% of methanol lipase supported on PMO is most stable in the short term, maintaining 75% of activity after 1 hour whereas the other two catalysts already dropped to 30% within this time. In prolonged incubation the activities fall remarkably in the three cases due to the instability of lipase in this media. When the concentration of the dissolution is 50% of methanol, the stability of the catalyst PMO+Lipase remains very high for a day of incubation.

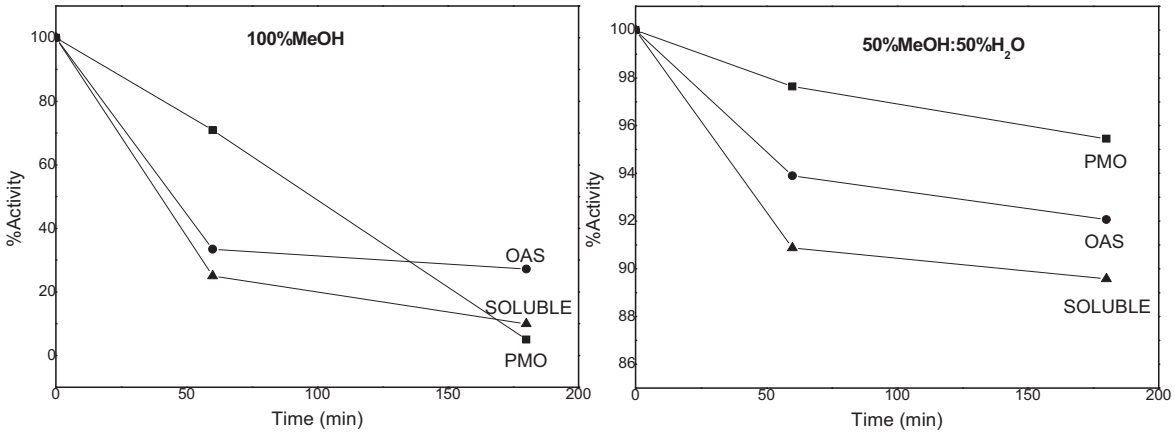

Figure 1. For both 100%MeOH and 50MeOH:50H_2O incubations 6 mg of PMO+lipasa/ml catalyst; 3 mg of OAS+lipasa/ml; and 2.510^{-3} mg of soluble lipase/ml were employed.

The stabilization that is obtained with the PMO is superior to the one of the octylated amorphous silica (OAS) with average pore diameter four fold higher than lipase dimensions. Consequently, the contact surface is not large despite the strength of the hydrophobic interaction of lipase with octyl groups. Oppositely, pore diameter of PMO is only slightly higher than lipase size so the enzyme contacts the inner surface of the channels all around. The presence of methanol promotes changes in hydrogen bonds inducing changes in tertiary structure. Hydrophobic side chains of amino acids that are usually buried within the structure of the protein in aqueous medium become re-oriented towards external surface of the protein. These "extra" hydrophobic groups on the protein surface can also interact with the hydrophobic wall of PMO so that new interactions are established. As a result the structure of the enzyme becomes more rigid and consequently, also more stable.

Acknowledgements

The Spanish Ministry of Education and Science is acknowledged for the financial support (MAT-2009-13569).

References

[1] T. Gitlesen, M. Bauer, P. Adlercreutz, Biochim. Biophys. Acta 1345 (1997) 188.
[2] M. T. Reetz, Adv. Mater. 9 (1997) 943.
[3] S. Z. Qiao, C. Z. Yu, W. Xing, Q. H. Hu, H. Djojoputro, G. Q. Lu, Chem. Mater. 17 (2005) 6172.
[4] S. Hudson, E. Magner, J. Cooney, B. K. Hodnett, J. Phys. Chem. B 109 (2005) 19496.
[5] C. Li, J. Liu, X. Shi, J. Yang, Q. Yang, J. Phys. Chem. C 111 (2007) 10948.
[6] M. Park, S. S. Park, M. Selvaraj, D. Zhao, C-S. Ha, Micropor. Mesopor. Mater. 124 (2009)
[7]E. Serra, E. Díez I. Díaz, R. M. Blanco, Micropor. Mesopor. Mater. 132 (2010) 487.
[8] R. M. Blanco, P. Terreros, M. Fernández-Pérez, C. Otero, G. Díaz-González, J Mol Catal B: Enzym. 30 (2004) 8.

Synthesis and Characterisations of Novel Alloy Supported Catalysts

R. Th. A. Al-rubaye[1], A. A. Garforth[2]
[1,2]*School of Chemical Engineering and Analytical Science, The University of Manchester, Uk,*
[1] *Rana.Al-Rubaye@postgrad.manchester.ac.uk,* [2] *arthur.garforth@manchester.ac.uk.*

Introduction

This work is aimed of the growth of Zeolite coatings (e.g. ZSM-5) onto a metal surface (Fecralloy) for catalytic application. Usually, zeolites are used in powder composite form (pellets) and are backed to form a fixed bed. Disadvantages are the pressure drop, diffusion problems, and hot and cold spots[1-2]. However, the structured catalysts with large channel guarantee low pressure drop and improve mass and heat transfer [3-4]. In addition, small zeolite crystals which are adhere on the metal surface and form thin layer, improved effectiveness, and faster diffusion. [5].

The supported catalysts have been characterised using X-ray diffraction (XRD), Electron microscopy (SEM), Energy Dispersive X-ray analysis (EDX), BET surface area, and Thermogravimetric Analysis (TGA).The structured catalysts have been tested by cracking of n-heptane at temperatures between 325-450°C. Briefly summarised, using TGA to measure the weight loss during the thermal cycle followed by SEM confirms the production of uniformly coated firmly attached ZSM-5 Layers on a metal alloy wire. The characterisation by SEM and XRD shows the transition from oxide on an alloy wires to zeolite hydrothermally synthesised zeolite coated surface. The zeolite coated wires compared favorably with the equivalent weight of pure ZSM-5 under identical reaction conditions.

Experimental

The synthesised coating method consisted of hydrothermal crystallisation of zeolite in the presence of metal alloy which was pre-treated (Figure 1). All the synthesis steps were carried out in stainless steel autoclaves with PTFE liners. The metal alloy wires used were pre-treated and oxidised for 4 hours at 1000°C, to form thin oxide layer on the wires surface. The wires were 0.5 mm diameter. The oxidised wires were immersed in ZSM-5 synthesis gel ($6.36Na_2O:1.86Al_2O_3:0.2TPAOH:60\ SiO_2:1864H_2O$) under hydrothermal conditions at 180 °C. The structured catalyst were calcined by heating from ambient temperature to 450/550 °C for 16 hours at 1 °C/min to remove the template. Then the calcined wires were ion-exchanged with 0.1M NH_4NO_3 at 70 °C under constant agitation for 4 h. The ion-exchanged wires were washed prior to repeating the ion-exchange process twice more. Additional calcination was applied to convert the NH_4-ZSM-5 form to HZSM-5 form.

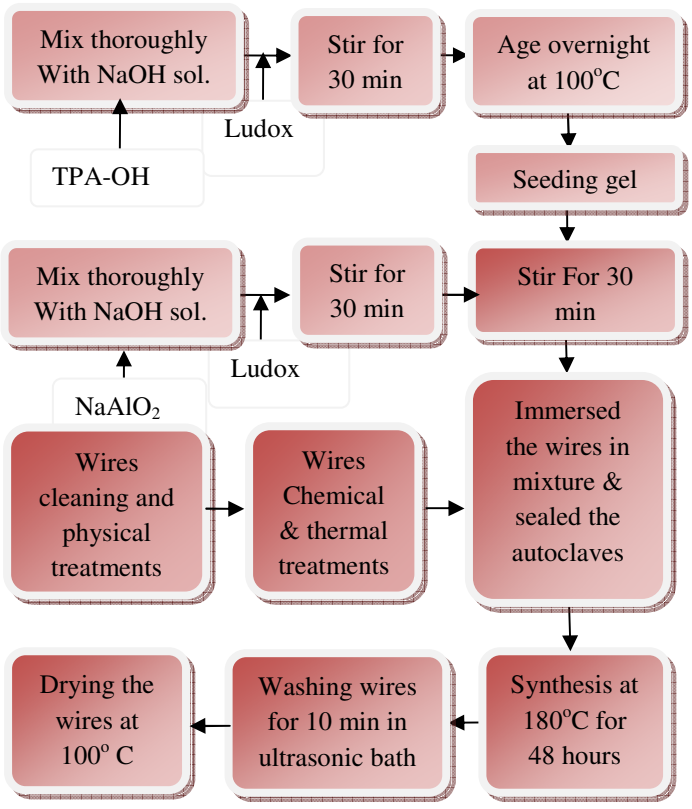

Figure 1. The schematic diagram for the zeolite coating synthesis.

The cracking of n-heptane was performed in a 4 mm i.d. Pyrex tubular microreactor loaded with 0.17 g catalyst coated on the surface of the wires. The deactivation and the selectivity of the structured catalyst were compared to the fixed bed of pelletized catalyst. The deactivation test was performed as function of time on fresh structured catalyst at fixed contact time. The selectivity tests were carried out, before and after the deactivation at different contact times at temperatures 325-450^{o}C.

Results and discussion

The SEM and XRD show the formation of the zeolite crystals covering the alloy wire. All wires were subject to ultrasonic to dislodge any lose material prior to catalyst testing (Figure 2&3). The SEM images revealed the wires were totally covered with ZSM-5 crystals with average crystal diameter 2.8µm and with Si/Al= 11.2. The conversion for the cracking of n-heptane on the wire surface coated with ZSM-5 is shown in Figure 4.

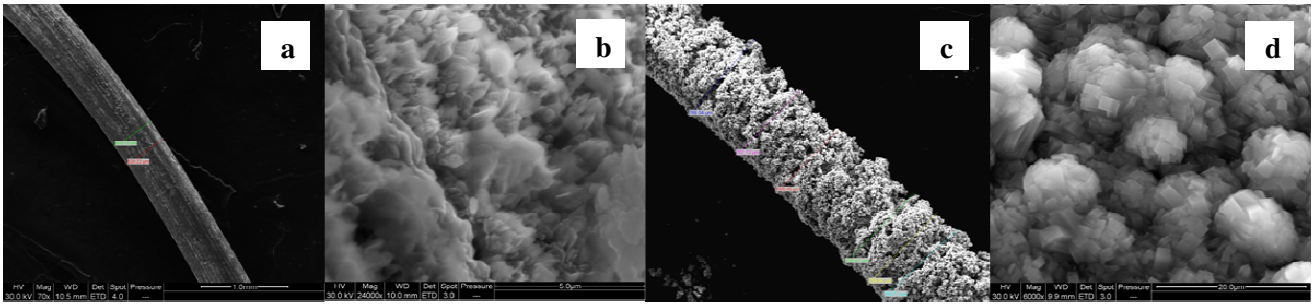

Figure 2.ESEMs for the alloy wire surface; (a) uncoated wire, (b) increased magnification of oxide layer on the wires surface, (c) coated wire with ZSM-5, (d) increased magnification of ZSM-5 on the surface.

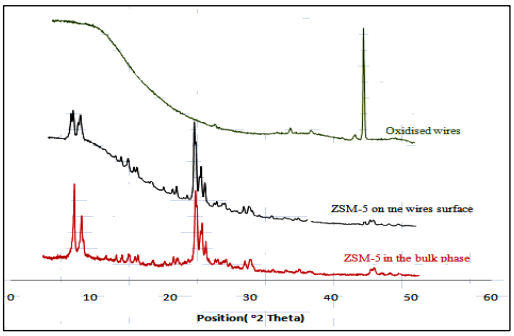

Figure 3.XRD patterns for oxidized and uncoated wires, coated wires and product ZSM-5

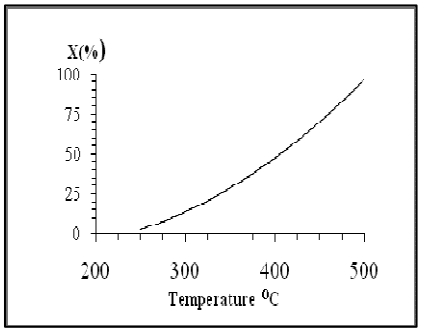

Figure 4. Conversion of cracking n-heptane over the structured catalyst at different temperatures.

Conclusions

This research demonstrates the production of uniformly coated firmly attached ZSM-5 Layers on a metal alloy wire. The characterisation by SEM and XRD shows the transition from oxide on an alloy wires to zeolite hydrothermally synthesised zeolite coated surface. The zeolite coated wires compared favorably with the equivalent weight of pure ZSM-5 under identical reaction conditions.

References

[1] Eleta, A., et al., Microporous and Mesoporous Materials 123 (1-3) (2009) 113-122.
[2] Kiwi-Minsker, L. and A. Renken, Catalysis Today 110 (1-2) (2005) 2-14.
[3] Clet, G., J.C. Jansen, and H. van Bekkum, Chemistry of Materials 11 (7) (1999) 1696-1702.
[4] Koroglu, H.J., et al., Journal of Crystal Growth 241 (4) (2002) 481-488.
[5] Di Renzo, F., Catalysis Today 41 (1-3) (1998) 37-40.

Synthesis and catalytic performance of CHA-type SAPO materials

T. Álvaro-Muñoz[1], I. Díaz[1], J. El Fallah[2], C. Márquez-Álvarez[1], V. Valtchev[2], E. Sastre[1]
[1] *Instituto de Catálisis y Petroleoquímica, CSIC, Madrid, Spain; esastre@icp.csic.es*
[2] *Laboratoire of Catalyse and Spectroscopy, ENSICAEN-Université de Caen -CNRS, Caen, France*

Introduction

The increasing demand of olefins has renewed the interest of methanol-to-olefins (MTO process) as a route to obtain these valuable petrochemicals from carbon sources alternative to petroleum. Methanol can be efficiently produced from syngas obtained by natural gas reforming or carbon gasification, and it might even provide an environmentally carbon neutral alternative to fossil carbon sources [1], if produced by chemical recycling of carbon dioxide via hydrogenation [2] or from syngas obtained by biomass gasification [3]. Small-pore silicoaluminophosphate SAPO-34 (chabazite type of structure) has been proven an efficient catalyst for MTO process, showing exceptionally high selectivity to lower olefins [4]. However, these catalysts undergo rapid deactivation due to deposition of high molecular weight hydrocarbons on the pore entrances [5,6] which completely blocks the internal channels of the SAPO-34 crystals. Extensive studies indicate that the morphology of these materials can affect their properties and applications. The catalytic adsorption may be strongly correlated with the particle size due to the diffusion limitations of the guest molecules in the micropores [7]. For large catalyst crystals, residence time for hydrocarbons is high because of the long diffusion path. Aromatic compounds cannot escape from the pores of SAPO-34 and successive polymerizations readily occur because of the long reaction time. Therefore, the control of the size of SAPO-34 crystals is a very important factor for improving the activity and lifetime of the catalyst. In the present work, we compare the performance of nano- and micron-sized crystals of SAPO-34 in MTO reaction.

Experimental

SAPO-34 was synthesized under hydrothermal conditions using tetraethylammonium hydroxide (TEAOH) to template the zeotype structure. Micron-sized SAPO-34 material crystallized at 423K from a synthesis gel with molar composition $1Al_2O_3$:$1P_2O_5$:$0.6SiO_2$:$30H_2O$:1TEAOH and nanocrystalline SAPO-34 was synthesized at 393, 423, and 443K from a synthesis gel with molar composition $x(TEA)_2O$:Al_2O_3:xP_2O_5:$0.6SiO_2$:yH_2O where x=2, 2.5 and 3 varying the silicon source, y=37x. The organic template was removed by calcination at 823 K. The solids were characterized by powder X-ray diffraction, thermogravimetric analysis, SEM, ICP-AES and N_2 adsorption. Methanol conversion to olefins was tested in a fixed-bed reactor at atmospheric pressure and 673 and 723 K. The reaction products were analyzed on-line by gas chromatography.

Results and discussion

All synthesis parameters were varied in order to obtain nanosized SAPO-34 crystals (structural type CHA). Besides gel composition the morphology of SAPO-34 crystals was influenced by the silica source. The employed colloidal silica provided plate-like crystals built of aligned rhombohedral crystallites. The size of the crystals ranged between 200 and 500 nm (Figure 1). Spherical particles with size of about 100 nm, built of much smaller crystals, were obtained when tetraethylorthosilicate was used as a silica source. The kinetics of crystal

growth has also been studied in order to find a compromise between the crystal size and synthesis duration.
All the catalysts exhibited a good activity and selectivity in the initial stage of the reaction. It has been observed an important influence of the crystal size on the activity, selectivity and life time of the different samples. Nano-sized SAPO-34 showed a remarkable stability in the MTO reaction (Figure 2), retaining high conversion (more than 80%) during thirteen hours time-on-stream, while for micron-sized SAPO-34 the activity dropped after seven hours.

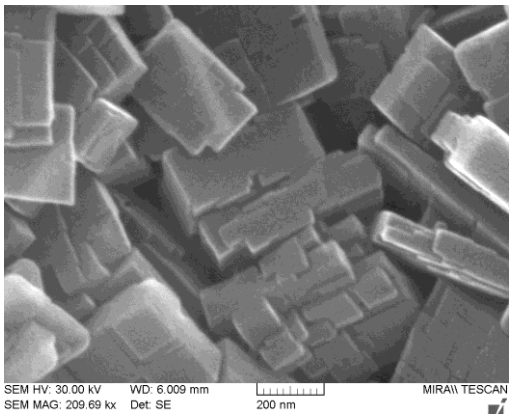

Figure 1. SEM image of nano-sized SAPO-34 crystals prepared with colloidal silica.

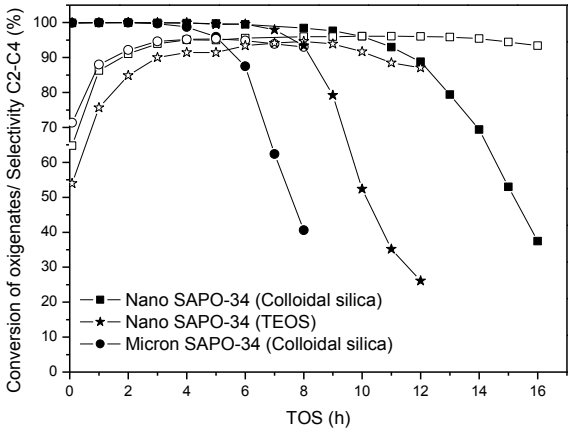

Figure 2. MTO reaction conversion (full symbols) and selectivity (open symbols). Test conditions: WHSV =1.2h^{-1}, T=673K, 1.0 g of catalyst.

Conclusions

SAPO-34 nanocrystals were successfully synthesized varying the chemical composition of the initial gel and synthesis conditions. The ratio phosphoric acid / template was found to be the most important parameter determining the crystal size of ultimate product. Nanosized SAPO-34 materials showed longer catalyst lifetime than the micron-sized counterpart.

Acknowledgements
We are thankful for the financial support of the Spanish Ministry of Science and Innovation, projects CTQ2006-06282 and HF-2008-0066. TAM acknowledges CSIC for a PhD grant. V. Valtchev and J. El Fallah acknowledge the financial support from the program ANR – HiZiCOKE (contract No. 723).

References
[1] G.A. Olah, A. Goeppert, G.K.S. Prakash, J. Org. Chem. 74 (2009) 487
[2] C. Song, Catal. Today 115 (2006) 2
[3] C.N. Hamelinck, A.P.C. Faaij, J. Power Sources 111 (2002) 1
[4] J. Liang, H.-Y. Li, S-Q. Zhao, W.-G. Guo, R.-H. Wang, M.-L. Uing, Appl. Catal. 64 (1990) 31
[5] D. Chen, K. Moljord, T. Fuglerud, A. Holmen, Microporous Mesoporous Mater. 29 (1999) 191
[6] S. Wilson, P. Barger, Microporous Mesoporous Mater. 29 (1999) 117
[7] Y. Hirota, K. Murata,M. Miyamoto, Catal. Lett 140 (2010) 22

Titanosilicate delaminated material UZAR-S2 obtained from AM-4

Clara Casado,[1,2] Diego Ambroj,[1,2] Álvaro Mayoral,[2] Eugenio Vispe,[3] Carlos Téllez,[1,2,*] Joaquín Coronas[1,2]

1 Chemical Engineering Department, Universidad de Zaragoza, 50018, Spain
2 Instituto de Nanociencia de Aragón, Universidad de Zaragoza, 50018, Spain
3 Organic Chemistry Department and Instituto Universitario de Catálisis Homogénea, University of Zaragoza, 50009, Spain

[*] *Corresponding author: ctellez@unizar.es*

Introduction

Exfoliated or delaminated materials obtained from layered silicates and zeolites, due to the fine particles produced, are useful for catalysis [1], for enhancing the permselectivity of polymer-zeolite nanocomposite membranes,[2,3] for the immobilization of enzymes on their highly hydroxylated and ordered external surface,[4] for the production of polymer-layered silicate nanocomposites with improved tensile properties [5] and so on.

AM-4 microporous titanosilicate belong to the so-called OPT family of mixed siliceous materials, where OPT refers to octahedral-pentahedral-tetrahedral frameworks. It is a monoclinic layered solid, with the molecular formula $Na_3(Na,H)Ti_2O_2(Si_2O_6)_2 \cdot 2H_2O$, built from TiO_6 octahedra and SiO_4 tetrahedra forming five-tier sandwiches $Si_T : Ti_O : Si_T : Ti_O : Si_T$ (T: tetrahedral; O: octahedral). It also contains intra- (in small cages within the layers) and interlayer Na^+ cations, and water molecules. In this work, a new material, UZAR-S2, has been obtained by swelling and exfoliation of the layered precursor microporous titanosilicate AM-4.

Experimental

AM-4 was obtained by a seeded-synthesis protocol to control the particle size of the precursor material [6]. The conditions of AM-4 synthesis are listed in Table 1. The smaller material, sample D, was protonated with acetic acid and swollen with nonylamine, which was therefore extracted in HCl/ethanol/water medium to obtain UZAR-S2. The procedure is analogous to that developed in our laboratory for the delamination of the microporous titanosilicate JDF-L1 to UZAR-S1 [3]. The delamination process was characterized by XRD, TGA, N_2 adsorption/desorption isotherms, ^{29}Si MAS NMR, FT-IR, UV-Vis, SEM and TEM.

Table 1. Synthesis conditions of the AM-4 crystals at 230 ºC and SEM pictures

	Ti source	Seeding	Time (h)	Size (μm)
A	Anatase (100-300 nm)	-	96	L: 6.9 ± 0.8 T: 0.6 ± 0.1
B	Anatase (< 25 nm)	-	96	L: 3.9 ± 0.5 T. 0.3 ± 0.1
C	Anatase (< 25 nm)	B	24	L: 2.7 ± 0.3 T: 0.2 ± 0.03
D	Anatase (< 25 nm)	B	12	L: 1.3 ± 0.2 T: 0.05 ± 0.02

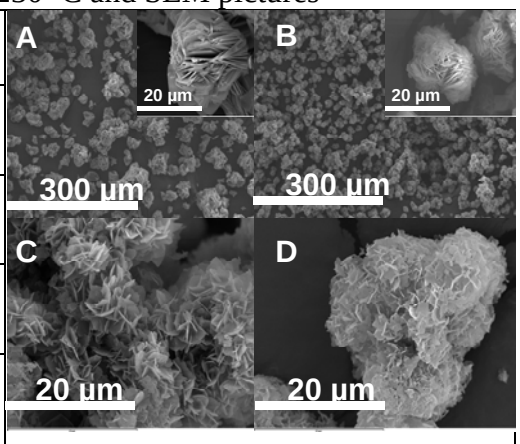

Results and discussion

The characterization carried out reveals that UZAR-S2 is a partially delaminated material composed of sheets about 13 nm thick, which contains 9 single layers of the precursor titanosilicate. AM-4 scarcely adsorbs N_2, and this is reflected by a BET specific surface area of only 7 m^2/g (sample D in table 1) and up-to date maximum BET surface area of 122 m^2/g was attained for UZAR-S2. The CO_2 adsorption capacity of UZAR-S2 is about 5 times higher than that of original AM-4, because the delaminated product has a higher specific surface area available than the layered precursor as it is shown in Figure 1.

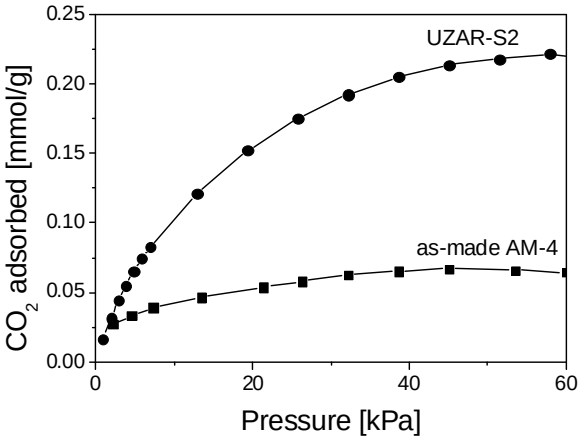

Figure 1. CO_2 adsorption isotherms in UZAR-S2 and as-made AM-4 (sample E in Table 1).

XRD, TEM, FTIR, NMR and DR-UV characterizations suggest a partial intercalation process that affects the material as a whole but preserves the layer structure. Furthermore, the Si/Ti atomic ratio in UZAR-S2 (6 because of leaching during the synthesis procedure) is higher than those corresponding to other titanosilicate delaminated materials obtained from layered Ti-zeolites. This predicts a good performance of UZAR-S2 in selective oxidation reactions.

Conclusions

The seeding procedure can help reducing the synthesis time of AM-4 crystals without compromising the purity of the crystalline phase. The size reduction allows swelling and delamination of the material. Characterization by several analytical techniques suggests that the intercalation process is successfully performed and partial exfoliation of the original material is obtained, providing a final product with more active sites available for adsorption.

Acknowledgements

Financial support from the Spanish Ministry of Science and Innovation (MAT2010-15870 and CIT-420000-2009-32) and the Government of Aragón (PI03/09) is gratefully acknowledged.

References

[1] Corma, A., Fornes, V., Pergher, S.B., Maesen, Th.L.M., Buglass, J.G., Delaminated zeolite precursors as selective acidic catalysts, Nature, 396 (1998), 353-356.
[2] Choi, S., Coronas, J., Jordan, E., Oh, W., Nair, S., Okamoto, F., Shantz, D.F. Tsapatsis, M., Layered Silicates by Swelling of AMH-3 and Nanocomposite Membranes, Angewandte Chemie International Edition, 47 (2008) 552-517.
[3] Rubio, C., Casado, C., Gorgojo, P., Etayo, F., Uriel, S., Téllez, C., Coronas, J., Exfoliated titanosilicate material UZAR-S1 obtained from JDF-L1, European Journal of Inorganic Chemistry, 2010 (2010) 159-163.
[4] Corma, A., Vornés, V., Jordá, J.L., Rey, F., Fernandez-Lafuente, R., Guisan, J.M., Mateo, C., Electrostatic and covalent immobilisation of enzymes on ITQ-6 delaminated zeolitic materials, Chemical Communications, 2006 (2006) 419-420.
[5] Wang Z., Pinnavaia, T.J., Hybrid organic-inorganic nanocomposites: Exfoliation of magadiite nanolayers in an elastomeric epoxy polymer, Chemistry of Materials, 10 (1998) 1820-1826.
[6] Rubio, C., Casado, C., Uriel, S., Téllez, C., Coronas, J., Seeded synthesis of layered titanosilicate JDF-L1, Materials Letters, 63 (2009) 113-115.

Quantitative and qualitative studies of MOFs properties by IR spectroscopy

Barbara Gil[1], Bartosz Marszalek[1], Florence Ragon[2], Thomas Devic[2], Christian Serre[2]

[1] *Faculty of Chemistry, Jagiellonian University, Ingardena 3, PL-30060 Kraków, Poland, gil@chemia.uj.edu.pl*
2 Institut Lavoisier, UMR CNRS 8180, Université de Versailles Saint-Quentin-en-Yvelines, 45 avenue des Etats-Unis, 78035 Versailles cedex, France

Introduction

The novel class of porous materials, metal-organic frameworks, MOFs, show very promising sorption properties. The characterization of sorption properties is very often carried out by IR spectroscopy, which is one of the most versatile tools for exploring the adsorbent-adsorbate mutual relation and changes in their structure and properties. Such guest-host interactions have been followed by IR with great success in the case of zeolites. However, it soon appeared that these experiences cannot be implicitly transferred to the investigation of the properties of MOFs.
In the present paper some peculiarities encountered during investigation of some of the MOF materials, MIL-53 and MIL-125 series, will be presented.

Experimental

The MOFs samples were placed on IR-transparent silicon discs from methanol solutions, put in an IR cell and pretreated in vacuum (10^{-3} mBa). IR spectra were measured using Mid-IR Bruker Tensor 27 spectrometer, at 2 cm^{-1} resolution.

Results and discussion

IR quantitative studies: absorption coefficients

The main problem one encounters upon quantitative investigation of IR data for solids is the Beer-Lambert law applicability [1]. For investigations of MOF properties additional practical problems need to be resolved. The classic IR bands of well known probe molecules are no longer useful for MOFs investigation because they are often masked by the adsorbent own vibrations. The only exception, acetonitrile maximum of the C≡N stretching, cannot also be taken as it is, because the frequencies and thus the absorption coefficients are different then for zeolites, and even more, they vary for different MOFs. For the purpose of determination of the concentration of coordinatively unsaturated metal sites (Lewis-type centers), the absorption coefficients of d_3-acetonitrile were determined for acetonitrile on CuBTC (band at 2270 cm^{-1}) as equal to ε=2.78 cm/μmol and for MIL-125 (2263 cm^{-1} band) ε = 0.56 cm/μmol. The position and the absorption coefficient of the band of coordinatively bonded pyridine at 1069 cm^{-1} seemed to be independent of the MOF used and equal to 0.042 cm/μmol.

H/D exchange: acidity vs availability problem

H/D isotopic exchange is a widely applied method when investigating (i) accessibility of the surface species and (ii) their relative acidity. Kinetics of H/D exchange was recently proposed as a measure of the acidity of hydroxyl groups in zeolites [2]. However it is essential to note that also non-acidic protons are exchanged for deuterium, at the same conditions as acidic

species. H/D exchange of MIL-125-NH_2 shows that not only the OH groups in the nearest neighborhood of the metallic centers are exchanged but also non-acidic NH_2 protons form organic linkers. The kinetics of their exchange is shown in Figure 1.

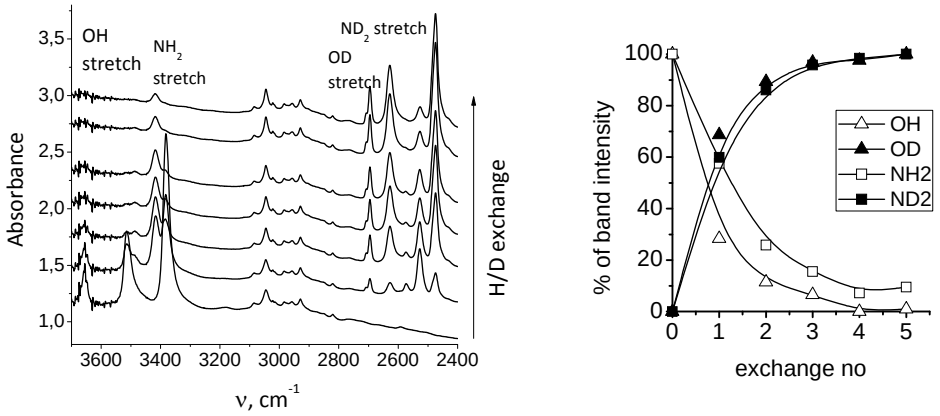

Figure 1. IR spectra of MIL-125-NH_2 during H/D exchange and the rate of the exchange.

Co-adsorption of probe molecules: probing the electron properties of metal centers

Co-adsorption of probe molecules can be used to probe heterogeneity of the metallic centers in MOFs – in terms of their oxidation and coordination state. One of the examples is co-adsorption of pyridine as electrondonor species and CO. Pyridine bonded to metallic centers is forwarding electrons and therefore lowering the frequency of co-adsorbed CO, depending on the initial oxidation state of copper. With the same base applied, the band of CO-Cu^{2+} is perturbed stronger than the CO-Cu^{+}. Therefore, two kinds of copper centers exist in CuBTC, differing significantly with their oxidation state. Cu^{2+} centers are readily available and most likely, easily changing their coordination state, thus being able to bond not only 'framework' oxygens from the paddlewheel structure but also pyridine and CO at the same time.

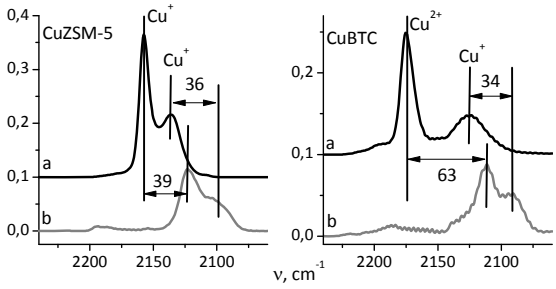

Figure 2. CO interaction with pyridine-free (a) and pyridine-loaded (b) CuZSM-5 and CuBTC.

This demonstrates that a systematic study of MOFs by IR spectrometry techniques may provide valuable insight into their properties and behavior.

Acknowledgements

Authors wish to thank European Project MACADEMIA for financial support.

References

[1] Morterra, C., Magnacca, G., Bolis, V., Catal. Today, 70 (2001) 43-58.

[2] Gabrienko, A.A., Arzumanov, S.S., Toktarev, A.V., Danilova, I.G., Freude, D., Stepanov, A.G. Phys. Chem. Chem. Phys. 12 (2010) 5149-5155

Alkylation of Benzene with propylene with zeolite membrane

Rayón A. R., Gutiérrez A. M., Aguilar P. J., Mugica A. V., Torres R. M.
Área de Química Aplicada, Universidad Autónoma Metropolitana, Av. San Pablo 180, México D.F., trm@correo.azc.uam.mx.

Introduction

Presently, most of the worldwide supply of cumene is used as a raw material for phenol production. Typically, cumene is produced either in the liquid or gas phases. The comercial technology of alkylation of benzene with propylene using sulphuric acid and phosphoric acid catalyst supported on kieselguhr suffered of corrosion problems and complicated neutralisation steps, also safe handling, [1, 2]. However, in recent years commercial production rapidily shift to processes which use zeolite catalysts. The zeolite-based routes offer benzene-to-cumene selectivity, high product purities and the ability to regenerate the catalyst, eliminating a waste disposal problem. Besides a high activity, the zeolite should have a high selectivity to cumene minimizing side effects for example, oligomers of propylene which can reduce the quality of final product. Slightly less important is the polyalkylation of benzene because the isopropylbenzene (DIPBs) and triisopropyl-benzene produced can be recovered by transalkylation with benzene to cumene [4]. In recent years the literature has reported the use of zeolite beta for cumene synthesis [2, 3] showing the best catalytic activity and selectivity features. Therefore this paper presents results of synthesis of beta zeolite membrane, molar ratio SiO_2/Al_2O_3=90 and results of alkylation of benzene with propylene in a membrane reactor at different reaction conditions.

Experimental

The beta zeolite membrane was synthesized using a tubular support commercial gama-alumina (Exekia T1-70) of 25 cm in length, 1.0 and 0.7 cm in diameter outer and inner. The gel precursor was prepared using aluminum metal (Merck) and silica powder (Merck) dissolved in a solution of sodium hydroxide (Mallinckrodt), the solution is added tetraethylammonium hydroxide (TEAOH, Aldrich 35%w) with potassium hydroxide (Merck). The crystallization of the gel was performed at a temperature of 170◦C. The synthesis was conducted in static mode and under autogenous pressure, the beta zeolite film was characterized by X-ray Diffraction and Scanning Electron Microscopy. The membrane was subjected to a study of permeation of nitrogen.

The alkylation of benzene with propylene was carried out in a membrane reactor using a feed of benzene and propylene at 99% purity. The reaction conditions were: constant pressure of mixture and reaction temperature varied in the range of 200 to 300°C. Propylene gas was fed in phase with a flow of 50 cm^3/min, which was passed through a saturator containing benzene at a temperature of 25°C. The gas flow was controlled using a fine adjustment valve. The analysis of reaction products was performed by gas chromatography in a Hewlett Packard 5890 series II coupled to a FID detector and a column PONA 50 m.

Results and discussion

Figure 1, shows the diffractogram of zeolite beta membrane, molar ratio SiO_2/Al_2O_3=90 where there are characteristic peaks of zeolite and a high crystallinity. The catalytic membrane reactor showed good thermal and mechanical stability. Low conversion of isobutene was observed at 300°C. However, when the temperature was raised at 200°C conversion was 42% and the selectivity to cumene 13.5%**.** The selectivity of the membrane reactor improves to 53.5% at 300°C, secondary product, was minimizing in the membrane reactor.

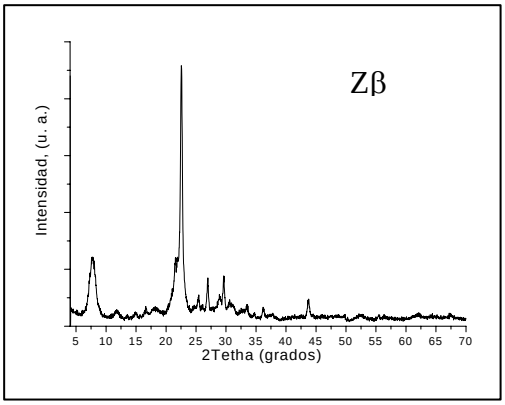

Figure 1. Diffractogram of zeolite beta membrane

Conclusions

X Ray Characterization of the membrane, show that a film was zeolite Beta on alumina support. The catalytic test show that the catalytic activity of zeolite beta membrane is active for the reaction of alkylation of benzene with propylene, reaching a maximum of 53.54% selectivity to cumene, with a total conversion of 18.9%. The reaction tests were maintained for 30 h and no notice of deactivation. The high activity showed can be attributed to the strong surface acidity of the catalyst. The catalytic membrane reactor shows better performance for this reaction in comparison with the fixed bed reactor, when they were tested at the same reaction conditions.

References

[1] Hydrocarbon Processing. March (2003) 88-89.
[2] G. Bellussi, G. Pazzuconi, C. Perego, G. Girotti, and G. Terzoni, J. Catal., 157 (1995), 227.
[3] K. Tanabe, W. F. Hölderich. Applied Catalysis A: General 181 (1999), 399-434
[4] Mavrodinova M. Popova, R. M. Mihályi, G. Pál-Borbély and Ch. Minchev. Applied Catalysis A: General 248 (2003), 197-209.

Selective Detection of Cs^+ in Water Solutions via One-Step Formation of a New Type of Struvite-Like Phosphate

Stanislav Ferdov[†] and Zhi Lin[§]
[†]*Department of Physics, University of Minho, 4800-058 Guimares, Portugal, sferdov@fisica.uminho.pt*
[§]*Department of Chemistry, CICECO, University of Aveiro, 3810-193 Aveiro, Portugal*

Introduction

To date, the main sensors of cesium ions are based on atomic absorption spectroscopy, [1] radioanalysis, [2,3] and ion-selective electrodes (ISEs) [4-6] which have a good sensitivity but require expensive instruments and/or controlled experimental conditions. More recently, different types of fluorescent molecular sensors are receiving an increasing attention because of their excellent selectivity to cesium ions, [7-12] but their applications are limited by the requirements for certain solubility and the right choice of the sensing ionophore for given conditions. [13] Here we report a new type of sensor, which is inorganic and it detects cesium ions via structure transformation of $Na_3MnH(P_{0.9}O_4)_2$ [14] to $CsMn(PO_4)\cdot 6H_2O$ at room temperature in presence of other competing alkaline ions. The detection of cesium is not spectroscopic and it is based on a collection of an ordinary powder X-ray diffraction pattern.

Experimental

The synthesis of $Na_3MnH(P_{0.9}O_4)_2$ was performed according to our previously reported recipe. Namely, a solution of 0.47 g of NaH_2PO_4 (Aldrich) in 8.67 g of distilled water was mixed with 13.28 g of MPMD (Du Pont). Then, 0.05 g of $MnSO_4\cdot H_2O$ (Aldrich) dissolved in 6.58 g of distilled water was added to the above solution. The crystallization was performed under static conditions at 150 °C for 6 days.

Results and discussion

Immersing $Na_3MnH(P_{0.9}O_4)_2$ in pure water or alkaline water solutions results in specific structural transformations that are sensitive to the presence or absence of cesium ions (Figure 1). In pure water, $Na_3MnH(P_{0.9}O_4)_2$ transforms to a phase whose majority of diffraction peaks coincide with the ones of the mineral switzerite ($Mn_3(PO_4)_2\cdot 7H_2O$) (Figure 2a,1). The same effect was observed when $Na_3MnH(P_{0.9}O_4)_2$ is immersed in 1 M solutions of KCl, LiCl or RbCl for 72 h at room temperature. This indicates that $Na_3MnH(P_{0.9}O_4)_2$ is indifferent to the used alkaline elements. However, adding small amounts of cesium ions (in form of CsCl) results in transformation of $Na_3MnH(P_{0.9}O_4)_2$ to a new type of struvite-like material $CsMn(PO_4)\cdot 6H_2O$. The estimated threshold of sensitivity of this transformation is 0.01 M of cesium ions (Figure 2b–d,2). Thus, when the concentration of cesium is 0.01 M the result is a mixture of $Mn_3(PO_4)_2\cdot 7H_2O$ and $CsMn(PO_4)\cdot 6H_2O$ (Figure 2d). Increasing the cesium concentration to 0.1 M the only phase that crystallizes is $CsMn(PO_4)\cdot 6H_2O$ and the same

effect is observed in concentration up to 1 M (Figure 2e). In concentrations of cesium ions less than 0.01 M it is formed only $Mn_3(PO_4)_2{\cdot}7H_2O$ (Figure 2b). When other alkaline ions (Li, K, Rb) with concentration of 1 M are used instead of cesium, the run product is indifferent to them and $Na_3MnH(P_{0.9}O_4)_2$ always transforms to $Mn_3(PO_4)_2{\cdot}7H_2O$ (Figure 3a–c,1). Within these experiments, the most noteworthy finding is that cesium can be also detected in multiple alkaline solutions. Thus, in mixture of 1 M solutions of NaCl, KCl, LiCl, and RbCl it can be detected 1 M concentration of cesium ions as $Na_3MnH(P_{0.9}O_4)_2$ transforms to $CsMn(PO_4){\cdot}6H_2O$ (Figure 3d, 2).

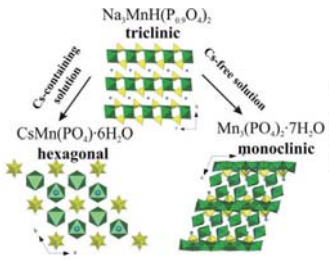

Figure 1. Schematic presentation of the way of detection of cesium ions via selective phase transformation of $Na_3MnH(P_{0.9}O_4)_2$ to $Mn_3(PO_4)_2{\cdot}7H_2O$ or $CsMn(PO_4){\cdot}6H_2O$.

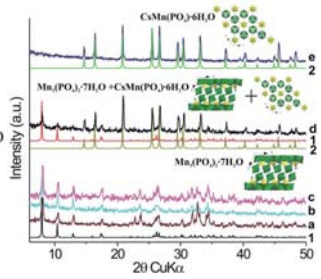

Figure 2. Powder XRD patterns showing the phases obtained after immersing $Na_3MnH(P_{0.9}O_4)_2$ in (a) pure water, (b) 0.001, (c) 0.003, (d) 0.01, and (e) 1 M solutions of CsCl. The obtained XRD patterns are compared with the calculated ones of the mineral switzerite $Mn_3(PO_4)_2{\cdot}7H_2O$ (1) and $CsMn(PO_4){\cdot}6H_2O$ (2).

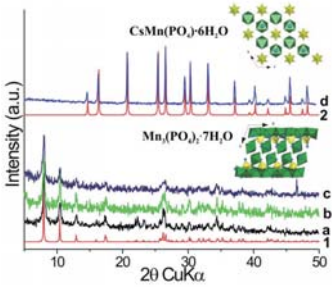

Figure 3. Powder XRD patterns showing the phases obtained after immersing $Na_3MnH(P_{0.9}O_4)_2$ in 1 M solutions of (a) LiCl, (b) KCl, (c) RbCl and (d) a mixture of 1 M solutions of LiCl, NaCl, KCl, RbCl, and CsCl. The obtained XRD patterns are compared with the calculated ones of the mineral switzerite $Mn_3(PO_4)_2{\cdot}7H_2O$ (1) and $CsMn(PO_4){\cdot}6H_2O$ (2).

Conclusions

A new cesium selective inorganic sensor that can work at room temperature in different types and concentrations of competing alkaline cations in water solutions was developed. The detection of the cesium ions is realized by an ordinary powder XRD pattern.

Acknowledgements

This work was supported by FCT, project PTDC/CTM/108953/2008.

References

[1] Vanhoe, H.; Vandecasteele, C.; Versieck, J.; Dams, R. Anal. Chem. 61 (1989) 1851.
[2] Theimer, K. H.; Krivan, V. Anal. Chem. 62 (1990) 2722.
[3] Van-Renterghem, D.; Cornelis, R.; Vanholder, R. Anal. Chim. Acta 257 (1992) 1.
[4] Saleh, M. B.; Hassan, S. S. M.; Abdel Gaber, A. A.; Abdel Kream, N. A. Anal. Lett. 36 (2003) 2367.
[5] Arida, H. A. M.; Aglan, R. F.; El-Reefy, S. A. Anal. Lett. 37 (2004) 21
[6] Radu, A.; Peper, S.; Gonczy, C.; Runde, W.; Diamond, D. Electroanalysis 18 (2006) 1379.
[7] Ji, H.-F.; Brown, G. M.; Dabestani, R. Chem. Commun. 1999, 609.
[8] Souchon, V.; Leray, I.; Valeur, B. Chem. Commun. 2006, 4224.
[9] Casnati, A.; Pochini, A.; Ungaro, R.; Ugozzoli, F.; Arnaud, F.; Fanni, S.; Schwing, M.-J.; Egberink, R. J. M.; de Jong, F.; Reinhoudt, D. N. J. Am. Chem. Soc. 117 (1995) 2767.
[10] Wintergerst, M. P.; Levitskaia, T. G.; Moyer, B. A.; Sessler, J. L.; Delmau, L. H. J. Am. Chem. Soc. 130 (2008) 4129.
[11] Webber, P. R. A.; Beer, P. D.; Chen, G. Z.; Felix, V.; Drew, M. G. B. J. Am. Chem. Soc. 125 (2003) 5774.
[12] Arnaud-Neu, F.; Asfari, Z.; Souley, B.; Vicens, J. New J. Chem. 20 (1996) 453.
[13] Lamare, V.; Dozol, J. F.; Fuangswasdi, S.; Arnaud-Neu, F.; Thuery, P.; Nierlich, M.; Asfari, Z.; Vicens, J. J. Chem. Soc., Perkin Trans. 2 (1999) 271.
[14] Ferdov, S.; Lopes, A. M. L.; Lin, Z.; Ferreira, R. A. S. Chem. Mater. 19 (2007) 6025.

Modified sulfonic acid-functionalised SBA-15 as robust catalyst for the processing of FFA/water-containing feedstocks for biodiesel production

L.F. Bautista[1,*], J.A. Melero[1], G. Morales[1], J. Iglesias[2], R. Sánchez-Vázquez[1]
[1]Department of Chemical and Environmental Technology and [2]Department of Chemical and Energy Technology. Universidad Rey Juan Carlos. C/ Tulipán s/n. E28933 Móstoles, Madrid, Spain. [*]fernando.bautista@urjc.es

Introduction

Biodiesel is one of the most industrially developed biofuels to allow a reduction in oil use and dependency of European countries as targeted by the EU Directive 2009/28/EU. However, first generation biodiesel has shown serious drawbacks and limitations relative to conventional diesel fuel due to high production costs, competition with the food market for raw materials and lack of availability of the refined edible oils as starting materials. Thus, to overcome the above mentioned problems expanding the number and type of oil sources towards cheaper, non-edible and readily available in larger amounts (second generation biodiesel), such as waste oils and fats, would be helpful. Nevertheless, waste oils and fats usually contain a high number of impurities, including free fatty acids (FFA) and water. Raw materials with these compounds cannot be processed by existing homogeneous base-catalyzed biodiesel processes –water leads to triglyceride hydrolysis and further neutralization of the resulting FFA seriously compromises the yield to biodiesel-. Within this work, we present a reliable and promising strategy for the design of a heterogeneous acid catalyst able to process FFA/water-containing feedstocks for biodiesel production in a very efficient manner.

Experimental

Sulfonic acid-functionalized SBA-15 materials were prepared following the co-condensation strategy using the appropriate organosilane for the synthesis of arenesulfonic acid SBA-15 (Ar-SBA-15) [1] and propylsulfonic acid SBA-15 (Pr-SBA-15) [2]. Surface hydrophobisation of SBA-15-type materials was accomplished by silanol end-capping through a chemical modification with (methoxytrimethyl)silane [3].

Catalytic runs were performed at previously optimised operating conditions (163ºC, 8.34 %wt catalyst, 28.4 methanol:oil molar ratio and 2000 rpm) [1] in a 25 mL stainless steel autoclave reactor by transesterification of crude palm oil (10.8 %wt FFA) with methanol in the presence of different amounts of water. Fatty acid methyl ester (FAME) yield was measured by ^{1}H-NMR analysis. Thorough textural, structural and chemical characterization of catalytic materials was performed by N_2 adsorption/desorption isotherms, X-ray diffraction, single pulse ^{29}Si solid state NMR, acid-base titration, thermogravimetric and elemental analysis.

Results and discussion

The addition of just 1 wt% of water to the reaction medium leads to a significant reduction on the yield of FAME both in Ar-SBA-15 and Pr-SBA-15. This activity decay seems to be related to the high avidity of the strongly hydrophilic sulfonic groups for water molecules, displacing the chemical reactions equilibria in the proximities of the catalytic sites. Thus, the hydrolysis of FAME or triglycerides, which competes with transesterification reactions, seems to be quite favoured in the presence of water molecules, significantly reducing the FAME yield. Silanol end-capping (hydrophobisation) leads to increased FAME yield by >7%, being insensitive to the addition of 1 wt% of water. This result suggests that the surface hydrophobisation is effective in avoiding the access of water molecules to the catalytic acid sites. A step forward was taken by removing the water molecules from the reaction medium (present in the starting oil and produced by the esterification of the free fatty acids) through

the addition of molecular sieves. This strategy proved to be efficient since the highest FAME yield was achieved when it was applied. The water generated during the esterification of FFA seems to be more relevant to the catalytic process than that coming from the raw materials, probably because the water molecules emerging from the esterification of FFA readily interact with the catalytic acid sites, remaining adsorbed thereon. Figure 1 shows the kinetics of the yield of FAME for different catalysts and amounts of water:

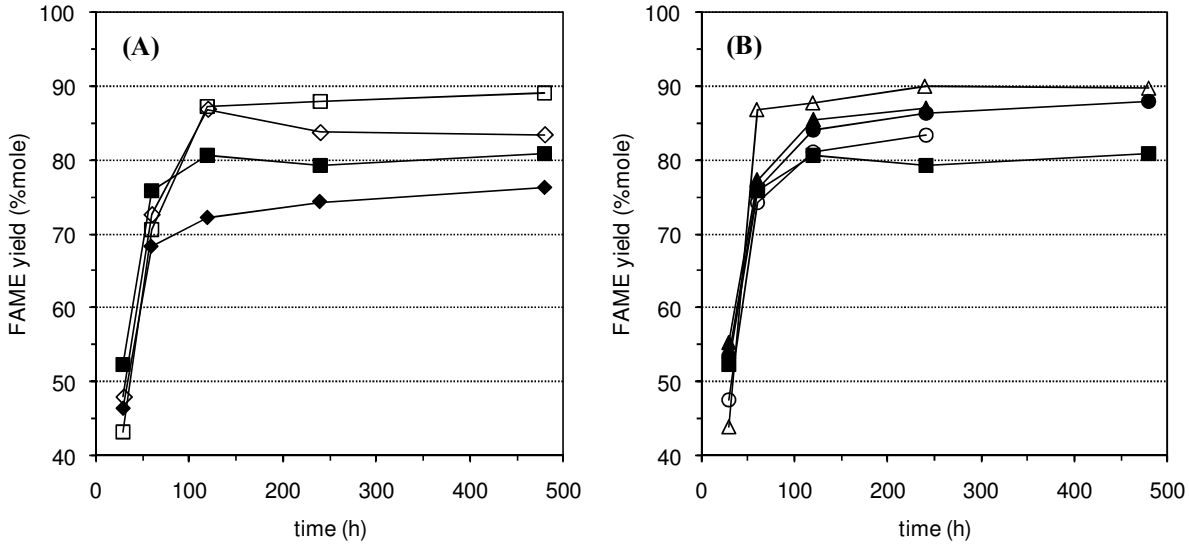

Figure 1. Yield of FAME for the transesterification of crude palm oil; A: (■ Ar-SBA-15, ◆ Ar-SBA-15 + water 1%wt, □ Pr-SBA-15, ◇ Pr-SBA-15 + water 1%wt); B: ((■ Ar-SBA-15, ● Capped Ar-SBA-15, ▲ Capped Ar-SBA-15 + water 1%wt, ○ Ar-SBA-15 + dried oil, △ Ar-SBA-15 + zeolite).

Conclusions

Sulfonic acid functionalised mesostructured silica materials have shown an important activity for the production of biodiesel from crude palm oil. However, the presence of water in the reaction medium significantly decreased the yield of FAME. The end-capping of the free silica surface created a hydrophobic environment around the catalytic acid sites, increasing the yield of FAME even if water was artificially added to the reaction. The addition of a water-sequestering molecular sieve, such as zeolite 3A, allowed processing FFA/water-containing raw materials over these catalysts, reaching high yields towards biodiesel.

Acknowledgements

Financial support from Ministerio de Ciencia e Innovación (Project CTQ2008-01396/PPQ) and Comunidad de Madrid (Project S2009ENE-1734) is kindly acknowledged. RSV gratefully acknowledges FPI grant award from the Spanish government.

References

[1] Melero, J.A., Bautista, L.F., Iglesias, J., Morales, G., Sánchez-Vázquez, R., Suárez-Marcos, I., Biodiesel production over arenesulfonic acid-modified mesostructured catalysts: Optimization of reaction parameters using response surface methodology,Topics in Catalysis, 53 (2010), 795-804.

[2] Melero, J.A., Bautista, L.F., Iglesias, J., Morales, G., Briones, D., Biodiesel production with heterogeneous sulfonic acid-functionalized mesostructured catalysts, Energy & Fuels, 23 (2009), 539-547.

[3] Melero, J.A., Bautista, L.F., Iglesias, J., Morales, G., Sánchez-Vázquez, R., Biodiesel production from crude palm oil using sulfonic acid-modified mesostructured catalysts, Chemical Engineering Journal, 161 (2010), 323-331.

Liquid phase allylic oxidation over Cu-containing MOFs

I. Luz, F. X. Llabrés i Xamena, A. Corma, M. Boronat, A. León
Instituto de Tecnología Química (UPV-CSIC), Universidad Politécnica de Valencia, Consejo Superior de Investigaciones Científicas, Avda. de los Naranjos, s/n 46022 Valencia, Spain

Introduction

We have recently reported [1] that a copper-containing MOF, $[Cu(2\text{-pymo})_2]$ (2-pymo = 2-hydroxypyrimidinolate) has interesting potential as heterogeneous catalyst for the liquid-phase aerobic oxidation of tetralin (T-H). However, this Cu-MOF showed some limitations, the most important being the high level of tetralinhydroperoxide (T-OOH) accumulated at the beginning of the reaction and a low selectivity to the ketone, α-tetralone (T=O). We have now extended our studies to another Cu-MOF, $[Cu(im)_2]$ (im = imidazolate), which has a related chemical composition and crystalline structure. As we will show, this material presents a better catalytic performance as compared to $[Cu(2\text{-pymo})_2]$ in terms of activity, maximum T-H conversion, selectivity to T=O and low T-OOH accumulation. The differences between both materials are rationalized with the help of DFT calculations. Besides tetralin, we have also studied the aerobic oxidation of other substrates: cumene (CM) and ethylbenzene (EB). These studies let us evaluate the general applicability of the Cu-MOFs as catalysts for paraffin oxidation.

Results and discussion

Figure 1 shows a comparison of T-H conversion and kinetic evolution of products obtained over the two Cu-MOF compounds studied, while selected data corresponding to the other substrates is summarized in Table 1.

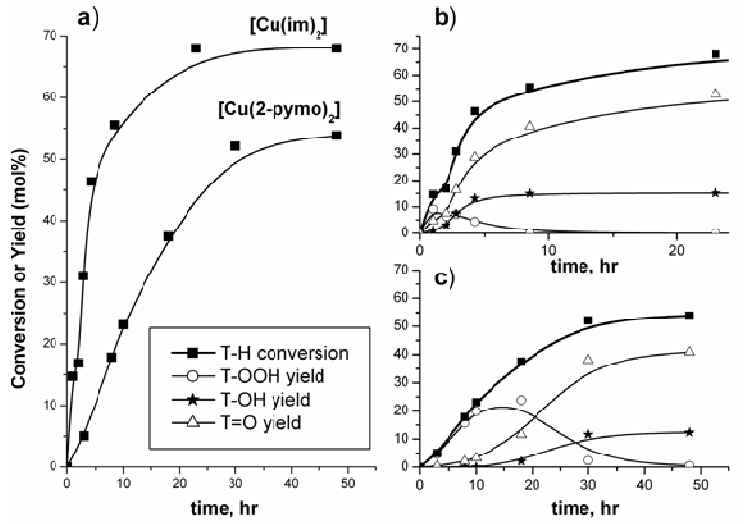

Figure 1. Conversion of T-H over $[Cu(im)_2]$ and $[Cu(2\text{-pymo})_2]$ (part a). Time conversion of T-H and time evolution of products over $[Cu(im)_2]$ and $[Cu(2\text{-pymo})_2]$ is also shown in parts b) and c), respectively.

Table 1. Selected kinetic data for the aerobic oxidation of various organic substrates over [Cu(2-pymo)$_2$] and [Cu(im)$_2$] MOF catalysts.

Tetralin (T-H)				
	Conv. 8 h	Conv. max	T=O/T-OH	[T-OOH]max
[Cu(im)$_2$]	55%	68% (22 h)	3.5	9% (1 h)
[Cu(2-pymo)$_2$]	18%	52% (48 h)	2.7	24% (18 h)
Cumene (CM)				
	Conv. max	Select. CM-OH	[CM-OOH]max	
[Cu(im)$_2$]	99% (23 h)	74%	2% (1.5 h)	
[Cu(2-pymo)$_2$]	87% (23 h)	64%	24% (8 h)	
Ethylbenzene (EB)				
	Conv. 5 h	Conv. max	Select. AP	
[Cu(im)$_2$]	23%	29% (40 h)	86%	
[Cu(2-pymo)$_2$]	6%	25% (40 h)	87%	

T-H: Tetralin; T-OOH: Tetralinhydroperoxide; T=O: α-tetralone; T-OH: α-tetralol; CM: Cumene; CM-OOH: cumene hydroperoxide (2-phenyl-2-propylhydroperoxide); CM-OH: cumene alcohol (2-phenyl-2-propanol); EB: Ethylbenzene; AP: Acetophenone.

Conclusions

As we have shown, MOFs having Cu^{2+} centers linked to 4 heterocyclic nitrogen atoms are active and reusable heterogeneous catalysts for aerobic liquid phase allylic oxidations. In general, copper imidazolate presents a better catalytic performance as compared to [Cu(2-pymo)$_2$], which results in higher alkane conversion, higher selectivity and low accumulation of alkylhydroperoxides in the reaction medium. In our opinion, the differences between the two catalysts may be related with the different coordination environment of the Cu^{2+} sites in both materials. While copper ions in [Cu(2-pymo)$_2$] are in square planar coordination, in [Cu(im)$_2$] these centers are displaced out of the plain, in a highly distorted tetrahedral coordination. Thus, the deformation energy needed for the addition of radical species to copper sites is probably lower in [Cu(im)$_2$]. Theoretic calculations to corroborate this hypothesis are currently under way. We have recently found that [Cu(2-pymo)$_2$] and [Cu(im)$_2$] follow a similar catalytic activity trend for 1,3-dipolar cycloaddition reactions [4], which do also imply ligand rearrangements undergone upon addition of a reactant molecule to the catalytic center.

References

[1] F. X. Llabrés i Xamena, O. Casanova, R. Galiasso Tailleur, H. Garcia and A. Corma, J. Catal., 2008, 255, 220-227.
[2] L. C. Tabares, J. A. R. Navarro and J. M. Salas, J. Am. Chem. Soc., 2001, 123, 383-387.
[3] N. Masciocchi, S. Bruni, E. Cariati, F. Cariati, S. Galli and A. Sironi, Inorg. Chem., 2001, 40, 5897-5905.
[4] I. Luz, F. X. Llabrés i Xamena and A. Corma, J. Catal., 2010, 276, 134-140.

Organic-bridged low silicon content Faujasite X zeolites ZOF-LSX

Kevin Vause[1], Xiao-Yu Yang[1,2] and Bao-Lian Su[1,2*]
[1]*Laboratory of Inorganic Materials Chemistry (CMI), University of Namur (FUNDP), 61, rue de Bruxelles, B-5000 Namur, Belgium*
[2] *State Key Laboratory of Advanced Technology for Material Synthesis and Processing, Wuhan University of Technology, Luoshi Road 122, Wuhan 430070, P.R. China*
* Corresponding author: bao-lian.su@fundp.ac.be

Introduction

Faujasite-type zeolites are the one of the most important classes of zeolitic materials and are largely used in industrial processes such as FCC, isomerisation, alkylation and organics and air separation due to their very interesting properties. In recent years, many modification methods have been developed to confer some new and advanced chemical functions into the pores of zeolites with organic groups. The surface functionalisation using organosilanes to graft some organic groups has been made and generally resulted either in the modification of primarily the external surface of the crystals or in organic groups covalently bound within the micropores. Although the organic groups could be used as catalytically active sites, this surface functionalisation induced often a blockage of pores and only high-silica zeolites were prepared (with Si:Al > 10). Recently, Tatsumi *et al* managed to synthesize new organic-inorganic hybrid zeolites, ZOL, in which certain oxygen atoms have been replaced by methylene groups [1]. Various types of hybrid materials with the LTA, MFI, and BEA structures have been obtained [2]. However, this work has attracted less attention and Faujasite type zeolites with organically bridged organic groups in the framework have still not been reported. The aim of the present work is to synthesize the low silicon content Faujasite LSX zeolites with organically bridged framework.

Experimental

Sodium aluminate and a mixture of sodium hydroxide and potassium hydroxide solutions were prepared and aged overnight, then mixed together. Into which the methylene-bridged bis[triethoxysilyl]methane white colloidal solution was added. The obtained mixture was aged for 3h at 70°C. It is worthy to note that the removal of ethanol from the gel was extremely crucial. The obtained gel with a chemical composition of $1SiO_{1.5}(CH_2)_{0.5} : aAl_2O_3 : bNa_2O : cK_2O : dH_2O$ (*a*: 0.25-0.33, b: 1.38-1.66, c: 0.11-0.15 and *d*: 13.90-33.60) was then crystallized in a Teflon-lined autoclave at 93°C from 7 to 13 days. After washing and drying, the obtained powders have been characterized with a series of techniques such as XRD, SEM-EDS, MAS NMR, FTIR, TG, N_2 adsorption and elemental analysis.

Results and discussion

X-ray diffraction pattern of ZOF-LSX zeolites have been compared with that of a traditional LSX zeolite. The unit cell parameters have been calculated by TREOR 90 program. Our materials belong to Faujasite LSX zeolite. The slightly higher unit cell parameters observed for ZOF-LSX could be due to the angle and larger distance of Si-CH_2-Si compared to Si-O-Si, demonstrating indirectly that the CH_2 groups are incorporated within the framework. **N_2 adsorption isotherm** of type I, typical microporous materials is observed. Even if its surface area (387 m^2/g) and its pore volume (0.23 cm^3/g) are slightly lower than those for the conventional X zeolite, this decrease could be due to the presence of methylene groups with two hydrogen atoms pointed towards the supercages.

FTIR spectroscopy revealed the presence of three vibration bands at 1450, 1405 and 1264 cm^{-1} that are not present in a conventional X zeolite and assigned respectively to the normal mode of bending vibration of CH_2 group, to the scissoring of Si-CH_2 and to the symmetric bending and the deformation of Si-CH_3. On the basis of these IR analyses, we can conclude that CH_2 groups were successfully introduced within the framework of X zeolites. **SEM** (Fig. 1) revealed a ball-like shape with a particle size twice larger than that of conventional LSX zeolite.

^{29}Si MAS NMR (Fig. 2) can prove, in a quantitative way, the presence of CH_2 groups within the framework. The strong and sharp signal at –85 ppm corresponds to a group of Si(4Al) and the small shoulder at –90 ppm to a group of Si(3Al, 1Si). The calculated Si/Al ratio is 1.03. A group of weak signals at around -62 ppm can be attributed to the organically functionalized silicon species: Si(1C, 3T). The percentage of Si-C bonds in the whole sample is 11.2 %.

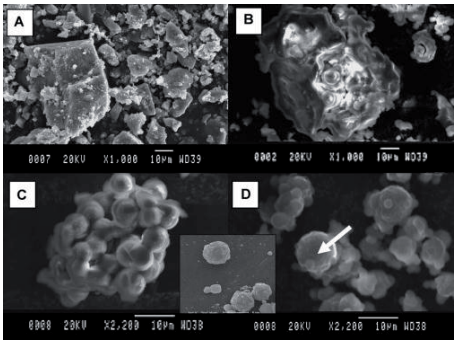

Fig. 1. SEM pictures of ZOF-1 samples at different crystallization times: (A) 7 days, (B) 9 days, (C) 11 days and (D) 13 days. (Inset is the SEM picture of the conventional X zeolite).

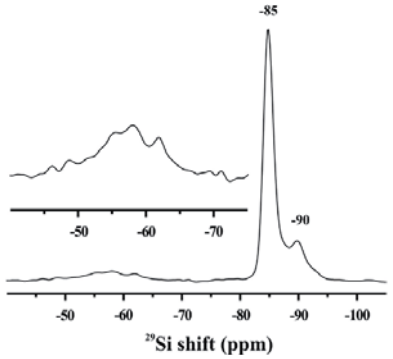

Fig. 2. ^{29}Si MAS NMR spectrum obtained from ZOF-9 at 9.4 T and 8.0 kHz spinning frequency. The inset spectrum displays a zoom over the signal region reflecting Si–C bonding.

Conclusions

Low silicon content and highly thermal stable Faujasite LSX zeolites with organic-bridged frameworks (ZOF-LSX) have been for the first time synthesized, in which oxygen atoms in the zeolite frameworks are partially superseded by methylene groups using methylene-bridged bis[triethoxysilyl]methane (BTESM) as a silicon source. Despite the incorporation of methylene groups in the framework (Si-CH_2-Si), the Si/Al ratio of the present materials attains to a very low value of 1.03. The presence and the amount of the methylene groups within the framework have been revealed by a series of techniques such as ^{29}Si and ^{13}C MAS XRD, NMR, SEM-EDS, FTIR, TG, N_2 adsorption and elemental analysis.

Acknowledgements

This work was supported by the Interuniversity Attraction Poles Program (P6/17)-Belgian State-Belgian Science Policy and the European Program of InterReg III (Programme France-Wallonie-Flandre, FW-2.1.5).

References

[1] K. Yamamoto, Y. Nohara, Y. Domon, Y. Takahashi, Y. Sakata, J. Plévert and T. Tatsumi, *Sciences*, **(2003)**, *300*, p470-472
[2] K. Yamamoto, Y. Nohara, Y. Domon, Y. Takahashi, Y. Sakata, J. Plévert and T. Tatsumi, *Chem. Mater.*, **(2005)** *17*, p3913-3920

Hierarchically Micro-Meso-MacroPorous Aluminosilicates Constructed from Zeolites Nanocrystals with Strong Acidity and Highly Catalytic activity

Xiao-Yu Yang,[1,2] Yu Li,[1,2] Arnaud Lemaire,[2] Ying-Xu Wei,[3] Zhong-Min Liu,[3] Guastaaf Van Tendeloo,[4] and Bao-Lian Su[1, 2, *]

[1] *Inorganic Materials Chemistry (CMI), University of Namur (FUNDP), 61, rue de Bruxelles, B-5000 Namur, Belgium.*

[2] *State Key Laboratory of Advanced Technology for Material Synthesis and Processing, Wuhan University of Technology, Luoshi Road 122, Wuhan 430070, P.R. China Laboratory of*

[3]*Dalian National Laboratory for Clean Energy, Dalian Institute of Chemical Physics, Chinese Academy of Sciences*

[4]*EMAT, University of Antwerp, Groenenborgerlaan 171, B-2020 Antwerpen, Belgium*

** Corresponding authors Email: bao-lian.su@fundp.ac.be*

Introduction

Solid acidic catalysts play a vital role in the development of the chemical industry and environmental pollution control.[1] Hierarchically porous zeolitic materials, displaying both micro-meso-macroporousity and strongly acidic sites are more desirable to increase efficiencies within industrial processes. Ideally, such catalysts should possess well-defined macropores, and interconnected mesopores in the macropore walls which have been constructed by tunable micropores units. More importantly, on all length scales, the larger pores should be connected from the smaller pores, yielding agreater range of wide applications such as the FCC process. Herein, we describe the preparation and characterization of hierarchically micro-meso-macro porous zeolitic materials via quasi-solid state crystallization process. These hierarchically porous materials were constructed from zeolites nanocrystals, and displayed strong acidity, which is a very important factor when used in catalytic reactions.

Experimental

The general synthesis procedure is illustrated in Figure 1. Meso-macro porous aluminosilicatos were mixed with tetrapropylammonium (TPA^+), and a supplementary silica source which facilitated the transformation of the amorphous phase of the meso-macroporous aluminosilicates to micro-meso-macroporous zeolite ZSM-5 architecture. The crystallization process was performed under quasi-solid state conditions using glycerol. This could prevent the mesoporous and macroporous structures being destroyed.

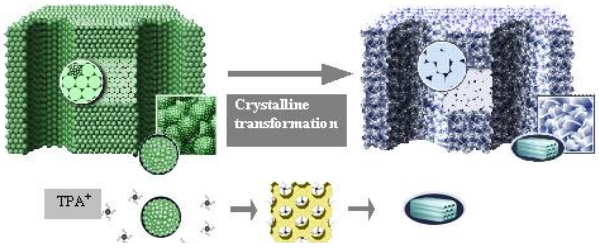

Figure 1. Schematic representation of synthesis of hierarchically micro-meso-macro porous aluminosilicates: (left) the initial meso-macro porous aluminosilicates constructed from amorphous particles (inset), (middle) the quasi-solid state crystallization process from amorphous frame to crystalline segment and crystalline frame using by structure director (TPA^+) and glycerol, and (right) the micro-meso-macro porous aluminosilicates constructed from zeolites nanocrystals (inset).

Results and discussion

SEM and TEM (Fig. 2 and Fig. 3) revealed that a well organized hierarchically micro-meso-macro porous architecture was formed under the quasi-solid state synthesis conditions at 130 ^oC over various reaction periods (initial, 1day, and 2days, designated as MMM(0), MMM(1) and MMM(2) respectively). The initial material had well-defined macropores, interconnected by worm-like mesopores. The macroporous walls had an amorphous framework (Fig. 2A). After 2 days at 130 ^oC, The zeolite MFI nanocrystals replaced the amorphous phase, and the mesoporosity and macroporosity were not affected (Fig. 2B). As

the reaction time proceeded (1 day), MFI particles in the material (MMM(1)) began to form around the macropores (Fig. 3A). The dark-field TEM image (Fig. 3B) was recorded on the same region as the bright-field TEM image (Fig. 3A). The bright spots in the image correspond to MFI nanocrystals (Fig. 3B). The nanocrystals centered around the macropores were disappeared and embedded within the continuous amorphous inorganic matrix to form crystalline structures while preserving the meso- and macro- porous structures (Fig. 3A, B and C). The highly crystalline zeolite MFI particles were subsequently obtained after 2 days, and were found within the frame of meso-macroporous aluminosilicates precursor (Fig. 3D, E and F). Notably, these images showed that the randomly oriented nanocrystals replaced the majority of the amorphous phase in the initial material, constructing a micro-meso-macroporous aluminosilicates structure. Catalytic activities of the cracking of 1,3,5-triisopropylbenzene (TIPB) show that the calcined MMM(2) yields the high activity (88.6%). This observation further confirm that MMM(2) has a strong acidity and high catalytic activity. MMM(2) is an excellent candidate for a catalyst in the industrial cracking for petroleum, particularly of the petroleum residues for which high reaction temperatures and large pore sizes are required.

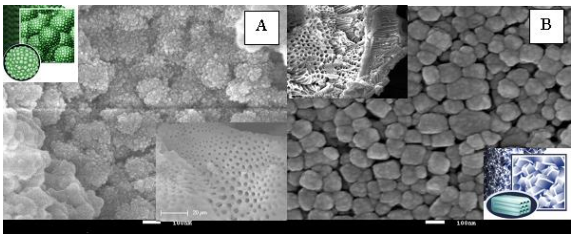

Figure 2. SEM investigation on the formation of micro-meso-macro porous aluminosilicate: (A) MMM(0), (B) MMM(2) and corresponding proposed schematic drawing (insets of A and B).

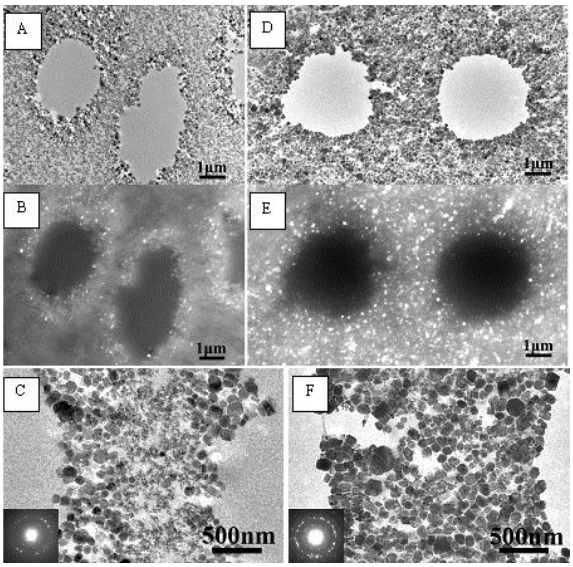

Figure 3. TEM investigation on the formation of micro-meso-macro porous aluminosilicate: Bright-field (A), dark-field (B) images of the same area of MMM(1) and the higher magnification image of MMM(1) (C) taken from (A); Bright-field (D), dark-field (E) images of the same area of MMM(2) and the higher magnification image of MMM(2) (F) taken from (D).

Conclusions

These materials constitute the first example of hierarchically micro-meso-macro porous zeolitic architecture with strong acidity. They lend two very important advances in the search for new catalysts. Firstly, our materials show a well-defined macroporous structure, which has a highly interconnected mesoporous system, in addition to the mesopores that were constructed by the crystallized microporous zeolites. Secondly, we could modulate zeolites types and their micropore size by a simple and clean method that could yield new insight into the synthesis of these hierarchically micro-meso-macroporous materials.

Acknowledgements

This work was supported by the Belgian Federal Government (Belspo PAI-IAP project, INANOMAT, P6/17), and Belgium-Viet Nam bilateral cooperation project, BL/13/V11). XYYang thanks FNRS (Fonds National de la Recherche Scientifique in Belgium) for a "Chargé de recherche" position. BL Su thanks the China Education Ministry for "Changjiang chair visiting scholar" position at Wuhan University of Technology and Chinese central government for a position as "expert of the state" in the frame of "Thousand talents program".

References

[1] X.-Y. Yang, A. Vantomme, A. Lemaire, F. Xiao , B.-L. Su, *Adv. Mater.* 18, 2117 (2006)

Hybrid organic/inorganic nanotubes of imogolite type

Cristina Zanzottera[1], Barbara Bonelli[1*], Edoardo Garrone[1], Christian Fernandez[2] and Aurelie Vicente[2]
[1]*Dipartimento di Scienza dei Materiali e Ingegneria Chimica, Politecnico di Torino, C.so Duca degli Abruzzi 24, I-10129, Torino, Italy;*
[2]Laboratoire Catalyse et Spectrochimie ENSICAEN, Université de Caen, CNRS, 6 bd du Maréchal Juin, 14050 CAEN, France;
**Corresponding author: barbara.bonelli@polito.it.*

Introduction

Besides well known nanoporous materials like zeolites and Metal-Organic Frameworks (MOFs), imogolite, a nanotubular alumino-silicate with chemical formula $(OH)_3Al_2O_3SiOH$ [1,2], exhibits interesting surface features and offers potential technological applications due to its intrinsic physic-chemical properties, *i.e.* an inner diameter of 1.0 nm and the presence of SiOHs and Al(OH)Al groups at the inner and outer surface, respectively.

Aim of this work is to fully characterize the structure and the chemical properties not only of proper imogolite, but also those of two hybrid imogolite-like materials obtained after functionalization of the inner and/or outer surface of imogolite nanotubes. Particularly, the introduction of methyl groups on the inner surface enhances CH_4 adsorption [3] and amino-groups at the outer surface should especially increase affinity for CO_2, that rapidly combines with amines to form carbamates [4].

Experimental

Proper imogolite (IMO) was synthesized as reported in ref. 2. An imogolite-like material with the inner surface covered by Si-CH_3 groups in place of silanols (Me-IMO), obtained according to ref. 5, was dried overnight at 100–110 °C under vacuum to remove moisture before the following functionalisation process: 0.052 mL of 3-APS (3-aminopropylsilane) was added under stirring to a suspension of 0.2 g Me-IMO in anhydrous toluene (60 mL) and refluxed at 100 °C for 12 h under inert atmosphere. The slurry was then cooled and washed with toluene, so obtaining the amminated product (Me-IMO-NH_2) that was filtered and dried at room temperature [6]. CO_2 uptake was measured by means of adsorption/desorption isotherms at 298 K (Quantacrome Autosorb 1C). Samples physico-chemical properties were characterized by means of XRD, FE-SEM, FT-IR, XPS, BET, TGA-Mass and MAS-NMR techniques.

Results and discussion

Figure 1a reports XRD patterns of the three materials studied, showing typical reflection peaks of the hexagonal structure in which nanotubes are aligned [2]. From the main peak, center-to-center distances (a) between two adjacent nanotubes were calculated, corresponding to 2.54 nm (IMO), 2.47 nm (Me-IMO) and 2.67 nm (Me-IMO-NH_2). The increase of (a) after grafting is probably due to some spacing effect by amino-propyl groups anchored at the external surface. With all materials, nanotubes form bundles, as seen in the FESEM picture reported in Figure 1b. The stability of functionalized surface was studied by recording IR spectra of samples outgassed at increasing temperatures. Particularly, Me-IMO-NH_2 presents the typical bands due to the bending $\delta(NH_2)$ modes of the amino group as well as the symmetric and asymmetric stretching modes of CH_2 groups, up to 300°C. TGA-Mass (25-500°C) measurements showed that Me-IMO-NH_2 is more stable with respect to the other samples and that the mass fragments leaving the surface are those proper of the aminopropyl chain. Me-IMO can uptake almost a double amount of CH_4 with respect to IMO, though its uptake capacity is lower with respect to that of other efficient materials (*e.g.* activated carbons

and 13X zeolite). CO_2 isotherms at 298 K are showed in Figure 2a. So far, these materials can not compete with industrial amine-based adsorbents.

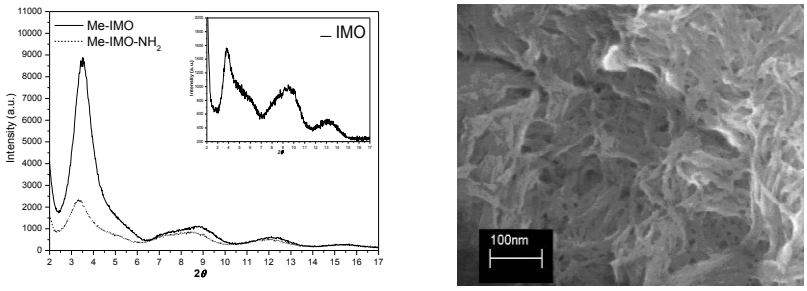

Figure 1: a) XRD patterns of IMO (inset), Me-IMO and Me-IMO-NH_2; b) FESEM picture of Me-IMO showing the occurrence of bundles.

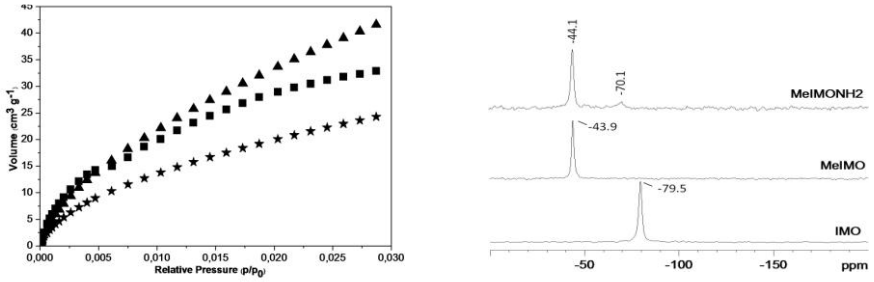

Figure 2: a) CO_2 isotherms IMO (square), MeIMO (triangle) and MeIMONH_2 (stars)
b) ^{29}Si MAS-NMR of IMO, Me-IMO and Me-IMO-NH_2

MAS-NMR results available confirmed the presence of methyl group on the inner surface [3] and the successful aminopropyl grafting on the outer surface, as recently reported [7]. Figure 2b shows the ^{29}Si MAS-NMR spectrum of imogolite samples: due to the functionalization of the inner surface the peak found in IMO at -79.5 ppm, due to the Si-OH bond, is shifted to *ca* -44 ppm (Me-IMO: -43.9 ppm; Me-IMO-NH_2: -44.1 ppm), confirming the presence of the new Si-CH_3 bond. Moreover, only the aminated sample presents a second peak that coherently confirmed the presence of the aminopropyl group, $\equiv O_3Si\text{-}CH_2\text{-}CH_2\text{-}CH_2NH_2$, on the outer surface at -70.1 ppm. The ratio between the two peaks of ^{29}Si confirms, also, the XPS results.

Conclusions

In this work, for the first time the structure of an aminated imogolite material and the chemical properties of hybrid imogolite-like structures were studied. Three different samples were analyzed: IMO (proper imogolite) nanotubes, with an inner hydrophilic surface covered by SiOH groups and an outer mildly basic surface; Me-IMO nanotubes, with an inner hydrophobic surface cover by methyl groups, able to absorb CO_2 reversibly at a low temperature; Me-IMO-NH_2, with an inner hydrophobic surface cover by methyl groups and an outer surface functionalized with amino-groups that resulted to be more stable with respect to the other samples.

References

[1] Yoshinaga N., Aomine A., Soil Sci. Plant Nutr. 8 (3) (1962) 22.
[2] Bonelli B., Bottero I., Ballarini N., Passeri S., Cavani F., Garrone E., J. Catal. 264 (2009) 15.
[3] Bottero I., Bonelli B., Ashbrook S.E., Wright P.A., Shou W., Tagliabue M., Armandi M.,Garrone E., Phys Chem Chem Phys 13(2) (2001) 744.
[4] Chang A.C.C., Chuang S.S.C., Gray McMahan, Soong Y., Energy & Fuels 17 (2003) 468.
[5] Bonelli B., Bottero I., Garrone E., IT Patent 0001380065.
[6] Qi X., Hyesun Y., Sang-Hyeup L., Juyoung Y, Sung-Jin K., J. of Ind. and Eng. C. 14 (2008) 136.
[7] Wang H., Huang J., Wu S., Xu C., Xing L., Xu L. and Kan Q., Materials Letters 60 (2006) 2662–2665.

Mesoporous Materials Containing Cu(II) and Ni(II) Complexes in Their Framework

N. Linares, A.I. Carrillo, E. Serrano, J. Garcia-Martinez*
Laboratorio de Nanotecnología Molecular, Departamento de Química Inorgánica, Universidad de Alicante, Carretera San Vicente s/n, E-03690, Alicante, Spain. E-mail: j.garcia@ua.es; Web: www.ua.es/grupo/nanolab

Introduction

The formation of anionic surfactant templated mesoporous silica (AMS) was first proposed by Yokoi *et al.* [1] in 2003. In this route, cationic functional groups are used as co-structure directing agents (CDSA) that, under appropriate synthetic conditions, interact electrostatically with the hydrophilic head of anionic surfactants, while their alkoxysilanes groups co-condense with TEOS to form the silica network. Coupled with the multitude of materials that can be prepared by the anionic synthetic route, one of the main advantages of this synthesis compared with neutral or cationic surfactants, is the prior existence of a high production of anionic salts (mainly for the detergent industry) getting a decrease in its cost.
In this work, we carried out the *in-situ* incorporation of cationic complexes in mesoporous siliceous structures using the anionic route. Whereas some studies have been reported regarding the incorporation of cationic complexes into the structure of mesoporous silica materials during their synthesis[2], their ability to act as co-structure directing agents by the anionic route has not been reported so far. The final goal is to ensure the incorporation of the complex in the mesopore of the solid. The method uses cationic complexes containing terminal triethoxysilane groups as ligands as CSDAs which interact electrostatically with the anionic surfactant on one hand and co–condense with TEOS on the other, inducing the precipitation of the silica around the micelles of surfactant, as shown the diagram in Fig 1.

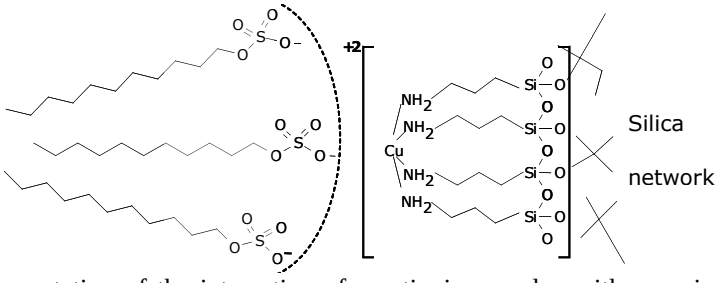

Fig. 1. Schematic representation of the interaction of a cationic complex with an anionic surfactant (sodium dodecyl sulfate) and the silica network.

Experimental

Cationic complexes formed by reaction of Cu(II) and Ni(II) with a primary amine ligand with terminal triethoxysilane groups, have been synthesized and incorporate to the hybrid materials using the anionic route for the synthesis of mesoporous silica materials. The electrostatic interaction of the cationic complexes and the anionic surfactant assures the location of the complexes into the pores of the material. In a typical synthesis, the anionic surfactant sodium dodecyl sulfate (SDS) or sodium dodecanoate (SD) was magnetically stirred (400 rpm) in a water:ethanol mixture at 60ºC. The metal precursor, copper chloride ($CuCl_2$) or nickel chloride ($NiCl_2 \cdot 6H_2O$), was dissolved in this surfactant solution. As silica sources, tetraethylorthosilicate (TEOS) and 3-aminopropyltriethoxysilane (APTES) were added over the previous solution. Immediately, the alkoxysilane APTES and the metal precursor, Cu(II) or Ni(II), react to give the cationic complexes used as CSDAs changing the colour of the suspension. The final molar ratio of the synthetic gel was XAPTES:(1-

X)TEOS:0.1Suf.:180:H_2O:20EtOH, this mixture was stirred 1h at 60 ºC and allowed to react at 60 ºC under static conditions during 48 h. The obtained solid was washed with water, ethanol and acetone in succession, filtered off, and air dried at 40 ºC. Finally, the surfactant was removed by an ion-exchange method.

Results and discussion

Hybrid mesoporous materials have been synthesized using Cu(II) and Ni(II) complexes as CSDAs in the anionic route of synthesis for mesoporous silica materials. After surfactant extraction, mesoporous materials with regular disordered porous (see Fig. 2.) and specific surface areas up to 400 m^2 g^{-1} were obtained. The proposed route can significantly increase the amount of complex incorporated into the material compared to post-synthetic techniques such as grafting functionalization (near to 9 wt% and 5 wt% for Cu(II) and Ni (II) complexes, respectively). The ion-exchange technique developed for the extraction of the anionic surfactant maintains the chemical integrity of the complexes.

a) b)

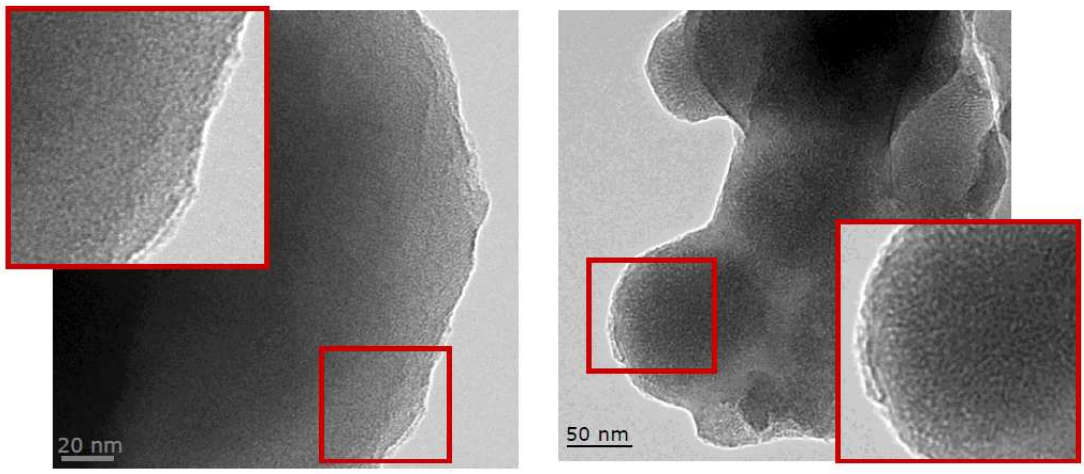

Fig. 2. TEM images of representative hybrid materials containing a) 9 wt% Cu/material and b) 5 wt% Ni/material prepared by the anionic route.

Conclusions

Mesoporous solids with cationic metal complexes in their framework were prepared by co-condensation of TEOS with metal complexes containing trialkoxysilane terminal groups in the presence of a surfactant. These materials show non-ordered mesoporosity, and surface areas and pore volumes in the order of 400 m^2/g and 0.55 cm^3/g respectively. The chemical integrity of the complexes after surfactant extraction was confirmed using spectroscopic techniques.

Acknowledgements

The authors thank the Spanish MICINN for financial support (Project CTQ2005-09385-C03-02), N.L. and E.S. for a doctoral fellowship FPI program (ref. BES-2006-13056) and the Juan de la Cierva Program (ref. JCI–2008–2165).

References

[1] a) T. Yokoi, H. Yoshitake, T. Tatsumi, *Chem. Mater.*, 15 (2003) 4536. b) S. Che, A.E. Garcia-Bennett, T. Yokoi, K. Sakamoto, H. Kunieda, O. Terasaki, T. Tatsumi, *Nature Materials*, 2 (2003) 801.

[2] (a) R.J.P. Corriu, A. Mehdi, C.Reyé, C. Thieleux, *Chem. Commun.*, 2003, 1564. (b) H.Zhu, D.J.Jones, J.Zajac, R.Dutartre, M.Rhomanri, J.Rozière, *Chem.Nater.*, 2002, **14**, 4886. (c) W–L.Zhou, B.Albela, M.Ou, P.Perriat, M–Y.He, L.Bonneviot, J. *Mater. Chem.*, 2009, **19**, 7308.

Structural transition of MIL-53 under pressure

Mohammed Boulhout, Isabelle Beurroies, Philip.Llewellyn, C.Serre, Renaud Denoyel. Bogdan Kuchta.
Laboratoire Chimie Provence (UMR 6264), Marseille, France
mohammed.boulhout@etu.univ-provence.fr

Introduction:

Metal Organic Frameworks (MOFs) are porous material which consists of hybrid crystalline compounds made up of clusters or chains of metal ions coordinated by organic linkers. This fascinating family of materials shows promise in several current strategic areas of application. One special property of some Metal Organic Framework (MOF) materials is their flexibility, which can be accompanied by large volume variations[1]. This flexibility often leads to a structural transition and may be induced by the adsorption of fluids. A clear structural transition is observed for the MIL-53 family under gas pressure[2]. Correlations have been established between the adsorption energy of the guest molecule and the occurrence of the transition. Nevertheless, these structural transitions are not only due to the guest-host interaction. A recent study showed that the structural transition between large pores (LP) and narrow pores (NP) can be observed for MIL-53 without the presence of any adsorbate but by simply varying the temperature[3].Surprisingly, there is no study to our knowledge about the effect of pressure on these structural changes, although it is expected that a transition from the LP to the NP phase would occur provided a high enough pressure was applied to the MOF crystal. This is why it is proposed here to use a mercury porosimetry apparatus to create an isostatic pressure around MIL-53(Cr) particles[4].

Experimental and results:

The mercury intrusion-extrusion experiments were performed with two MIL-53 samples: MIL53 (Cr) and MIL-53(Al). Before performing these experiments the MOF was pre-treated in order to have the open structure prior to mercury intrusion-extrusion.

- Mercury porosimetry analysis of MIL-53(Cr):

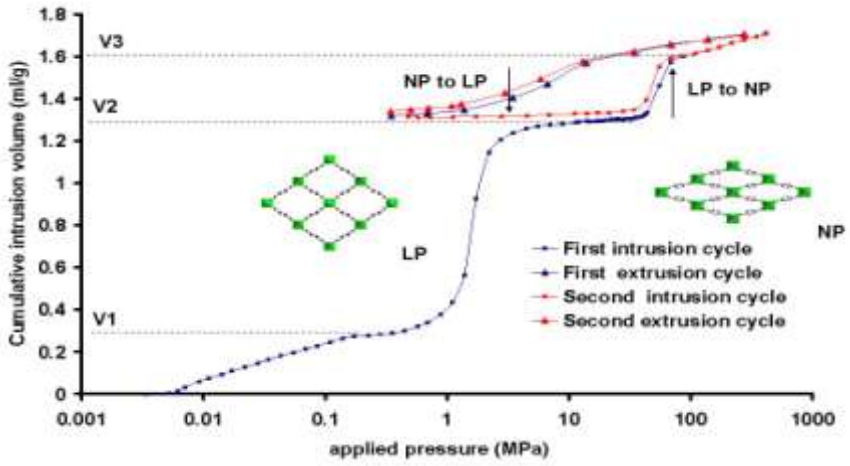

The clear step in the volume /pressure curve around 55MPa is interpreted as the LP to NP transition under the effect of pressure. The pressure induces a reversible transition but with hysteresis, as observed for the temperature induced transition.

A simple qualitative model is proposed to interpret this "breathing" transition. In this model, we consider two energetic contributions, one due to the attractive dispersion forces between ligands, and the other one due to the deformation of the bonds angle between the ligands and the metallic center. Quantitative estimations have been made using energetic parameters coming from ab initio calculations. The competition between the two energy terms stabilizes one of the two phases with an energy barrier between them. This leads to hysteresis when one phase is being transformed into the other, as observed experimentally. The range of values calculated with this model for the energy barrier is in agreement with the mechanical work calculated by mercury porosimetry.

Conclusion:

This study shows that the mechanical properties of flexible MOF materials can be observed directly using mercury porosimetry: the modulation of an external pressure gives energetic and volumetric information on the flexibility of MOF systems. It also shows that these systems may be potentially used in mechanical energy storage type applications.

References:

(1) (a) S. Kitagawa, R. Kitaura, S.-I. Noro, *Angew. Chem. Int. Ed*, **2004**, *43*, 2334; (b) G. Férey, C. Serre : *Chem. Soc. Rev.*, **2009**, 38(5) 1380-1399.

(2) C. Serre, F. Millange, C. Thouvenot, M. Noguès, G. Marsolier, D. Louer and G ;Férey. *J. Am. Chem; Soc* .**2002**, *124*, 13519–13526

(3) Y. Liu, J.-H. Her, A. Dailly, A.l J.Ramirez-Cuesta, D. A. Neumann and C. M.Brown. *J. Am. Chem; Soc.* **2008**, *130*, 11813–11818.

(4) I. Beurroies, M.Boulhout, P. L. Llewellyn, B. Kuchta, G.Férey, C.Serre and R.Denoyel. Angew. Chem. Int. Ed. 2010, 49, 7526 –7529

(5) Coudert and al. Chem.Soc.Rev.,2008 ,130,14294-14302

Dynamic behaviour of a new open framework calcium terephthalate

Nataša Zabukovec Logar[1,2], Matjaž Mazaj[1], Gregor Mali[1], Mojca Rangus[1] and Venčeslav Kaučič[1,2]
[1]National Institute of Chemistry, Hajdrihova 19, 1000 Ljubljana, Slovenia; [2]CoE Low-Carbon Technologies, Hajdrihova 19, 1000 Ljubljana; natasa.zabukovec@ki.si

Introduction

MOFs based on alkaline-earth metals raised great interest in the recent years. The use of inexpensive, non-toxic initial compounds and the simplicity of synthetic procedures (relatively low temperatures and short times of crystallization) in syntheses of magnesium and calcium polycarboxylates are in accordance with ecological trends of lower energy consumption and efforts for a cleaner environment [1-2]. Furthermore, low molecular masses of magnesium and calcium and consequent low densities of these materials enable higher w/w uptake of hosting molecules to adsorbent in comparison with already known transition-metal polycarboxylates in gas storage applications. In drug delivery applications, the most attractive property is their non-toxicity, which allows them to be used as nanocarriers for encapsulated active species in the pores or for controlled release of framework constituents (e.g. Ca ions or therapeutic organic molecules) by degradation in body fluids [3]. Systematic study of Ca-carboxylate system lead us to a new Ca-based terephthalate Ca(BDC)(H_2O)(DMF) with 3-dimensional open-framework structure and interesting structural changes upon heating and subsequent hydration/dehydration treatments.

Experimental

The material was synthesised solvothermally in the mixture of water and N,N'-dimethylformamide (DMF) using $Ca(NO_3)_2.4H_2O$ and terephthalic acid (BDC) as precursors. Crystal structure of the obtained material (Figure 1) was determined using laboratory single-crystal X-ray diffraction. The hydrothermal behaviour of the material was investigated by TG, high-temperature XRD and NMR analyses and porosity of the products with N_2 and CO_2 physisorption. X-ray absorption (XAS) spectra of materials together with reference compounds were measured in the Ca K-edge energy region in the transmission detection mode at XAFS beamline of the ELETTRA synchrotron facility to study the local structure of calcium at different temperatures and states of hydration.

Results and discussion

The as-synthesised Ca(BDC)(H_2O)(DMF) contains infinite chains of edge-sharing 8-fold Ca-polyhedra connected with terephthalate linkers (*Pmnb*, a = 6.7220(3) Å, b= 11.0171(4) Å, c = 18.5549(6) Å). A fraction of the 3-dimensional open framework structure with 1-dimensional channels along crystallographic a-axis is shown in Figure 2. Ca^{2+} centres in the structure are coordinated with 6 oxygen atoms from carboxylate groups and the remaining two coordinated oxygen atoms belong to water and DMF molecules, respectively. TG analysis of the as-synthesised material shows weight losses in three distinct steps, up to 150 ^{o}C (surface and coordinated water loss), up to 400 ^{o}C (DMF desorption) and up to 650 ^{o}C (decomposition of BDC linker). Calcination at 400 ^{o}C leads to a complete removal of DMF molecules as proven by NMR.

The removal of water and DMF molecules from the structure causes opening of the channels and changes in crystal symmetry as determined by N_2 sorption analysis and powder X-ray diffraction. Hydration of the calcined sample, which is fully reversible process, triggers additional changes in the crystal structure. The rearrangement of atoms in both the first and second coordination sphere of Ca during thermal treatment and hydration was confirmed by EXAFS analysis (Figure 3). The calcined structure is stable up to 500 ^{o}C (Figure 4).

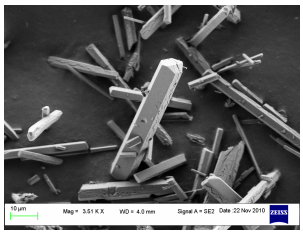

Figure 1. SEM of Ca(BDC)(H_2O)(DMF).

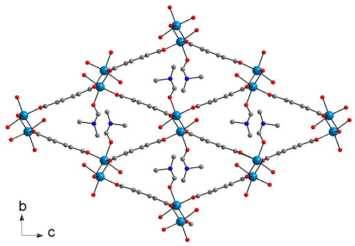

Figure 2. Structure of as-synthesized Ca(BDC)(H_2O)(DMF) (along *a* axis).

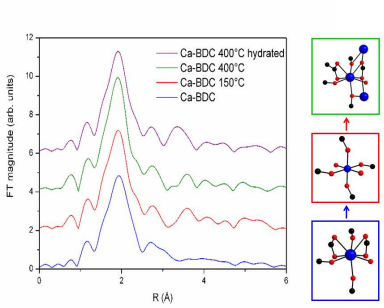

Figure 3. FT EXAFS spectra of the as-synthesized (Ca-BDC) and thermally treated/hydrated samples.

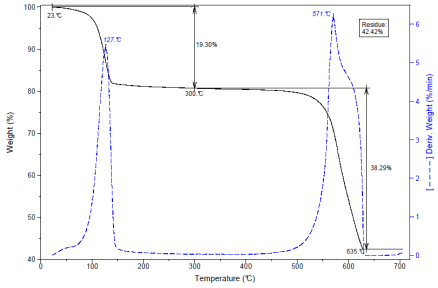

Figure 4. TG of calcined and rehydrated sample.

Conclusions

We have prepared a new calcium terephthalate, which exhibits porous structure after removal of solvent molecules from the pores and show reversible structural changes upon hydration/dehydration treatment.

Acknowledgements

This work was supported by the Slovenian Research Agency research programmes P1-0021. Access to SR facilities of ELETTRA (beamline XAFS, project 20085196) is acknowledged.

References

[1] Williams, C.A., Blake, A.J., Wilson, C., Hubberstey, P., Schroder, M., Novel Metal-Organic Frameworks from Group II Metal Cations and Aryldicarboxylate Anionic Ligands, Crystal Growth & Design, 8 (2008), 911-922

[2] Platero-Prats, A.E., de la Pena-O'Shea, V.A., Snejko, N., Monge, A., Gutierrez-Pueble, E., Dynamic Calcium Metal-Organic Framework Acts as a Selective Organic Solvent Sponge, Chemistry: A European Journal, 16 (2010), 11632-11640

[3] Miller, S.R., Horcajada, P., Serre, C., Small chemical causes drastic structural effects: the case of calcium glutarate, CrystEngComm, 13 (2011), 1894-1898

Incorporation of Titanium (IV) on a Partially Hydrophobized MCM-41 with a Dipodal Silane and Application to Cyclohexane Epoxidation

Lin FANG[a,b], Belén ALBELA[a], Peng WU[b], Ming-Yuan HE[b] and Laurent BONNEVIOT[a]
(a) Laboratoire de Chimie, Ecole Normale Supérieure de Lyon, Université de Lyon, (b) Shanghai Key Laboratory of Green Chemistry and Green Processes, East China Normal University, China

Introduction

The presence of hydrophobic functions is known to improve to the catalytic performance of Ti-MCM-41 materials for epoxidation reaction[1]. Usually, the hydrophobization of the surface is obtained in the last step of the catalysts synthesis by capping the surface silanol using chlorotrimethylsilane. Recently, some of us have developed an novel approach called Molecular Stencil Patterning (MSP) technique using using either cetyltrimethylammonium (CTA^+) or tetramethyl ammonium (TMA^+) ions as the surface protecting group during the capping sequence that leave free spaces to isolate catalytic metal ions in a subsequent grafting sequence [2]. Herein, MSP is applied to modify the surface of MCM-41 (LUS) with dipodal silane (Ethyl-1,2-bis(dimethylsilyl), EBDMS) as isolating hydrophobic function and Ti(IV) as catalytic centers tested here for epoxidation of cyclohexene. It is found that the grafting of dipodal EBDMS displaces the protecting ammonium molecular stencyl and does not lead to the same type of molecular patterning than the capping using monopodal trimethyl function.

Experimental

The synthesis scheme is described in the following scheme using recipes described in refs. 1 and 2. The LUS material is equivalent of a MCM-41 prepared from the tosylate salt of the templating CTA^+ ions. The latter are ion exchange for TMA^+ groups and, partially removed using HCl water-ethanol solution (1 H^+ for 1 TMA^+). Then, the surface is capped using the *ad hoc* silazane that leads to surface EBDMS grafting. After removal of the remaining TMA^+ ions and drying at 120°C, [$Ti(Oi\text{-}Pr)_4$] titanium alkoxydes diluted in cyclohexane is reacted in reflux for 16 h. The final product is thoroughly washed with cyclohexane and dried in air at 8O°C overnight. Materials obtained using 25, 50 and 75% TMA+ coverage where obtained and named LUS-Tn-TiPr where n = 25, 50, 75. The epoxidation of cyclohexene was run using typically 10 mmol cyclohexene, 10 mmol terbutyl hydroperoxyde (TBHP), 10ml acetonitrile at 333 K, for 2 h.

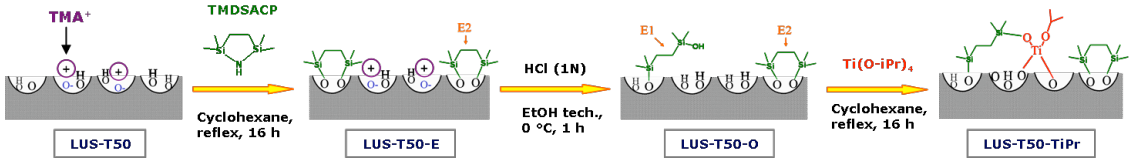

Results and discussion

The results are similar whatever the initial TMA+ coverage and therefore described here for 50% initial TMA^+ coverage only. Monitoring the retention of the EBDMS species using C-H stretching vibrations of the CH_2 groups typical (region 2800-3000 cm^{-1}), the retention then the removal of the TMA^+ ions using N-C stretching vibrations typical (1492 cm^{-1}) and the decrease of the remaining silanol groups (960 cm^{-1}), the grafting of EBDMS was proved

while TMA^+ was retained or subsequently removed without reversing the grafting by acid treatment. ^{29}Si MAS NMR spectra confirms in addition to Q_2, Q_3 and Q_4 of the silicon atoms of amorphous siliceous pore wall, the presence of ungrafted dimer or oligomers of EBDMS (less than 5%, narrow peak at 7 ppm), marginally monografted EBDMS revealed by small M_0 signal at 18 ppm) and , mainly double grafted EBDMS (80-95%, 13 ppm). The molar ratio, $EBDMS/Si_{inorg}$ calculated from ^{29}Si MAS NMR is remains constant at 0.21 ± 0.02 during after grafting, acid removal of TMA and Ti grafting, acid extraction produces only slight amount of monografted species. Same coverages were obtained for the other solids revealing that despite the retention of the TMA+ ions the EBDMS succeeds to graft both silanoxy groups and move the ammonium ions on top of it. Wit out EBDMS, UV visible spectra exhibits an adsorption at 300 nm (33 000cm-1) due to titanium clusters. In the presence of EBDMS, the hydrated Ti containing LUS exhibit a large signal fitted with four UV-vis gaussian peaks centered at 200 nm, 227 nm, 255 nm and 282 nm (Fig.1a). The former two are assigned to charge transfer bands of the Ti-OSi, Ti-OH bridges similar to the $[Ti-(OH)(OSi)_3]$ open sites of titanium silicalite-1. The 282 nm band is a typical of the $[Ti(OSi)_4]$ closed sites. The resonant Raman band at 1078 cm^{-1} (irradiation at 252 nm) is consistent with the UV data (Fig. 1b).

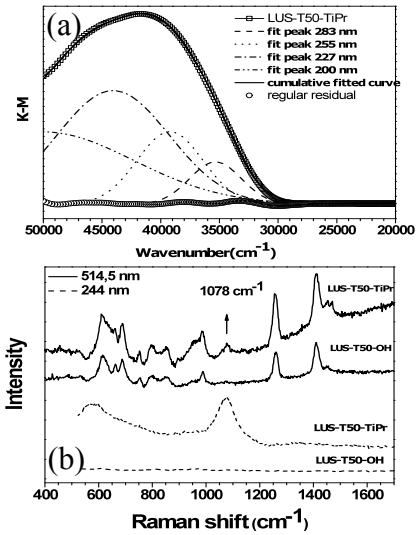

Figure 1 (a) UV-vis and (b) UV Raman spectra at RT for samples with EBDMS and after Ti grafting.

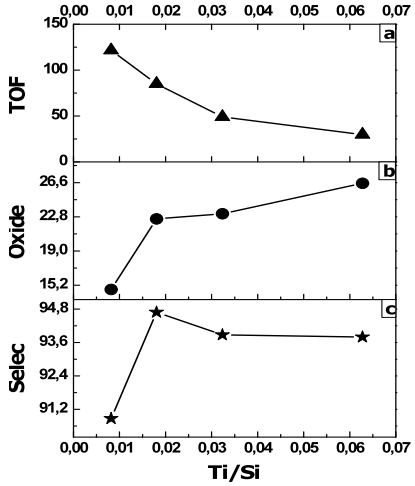

Figure 2 The (a) TOF, (b) oxide and (c) selectivity for epoxidation of cyclohexene on LUS-T50-TiPr with different Ti loading.

High selectivity in epoxidation of cyclohexene confirms the positive hydrophobic effect of EBDMS while low amount of Ti is preferred.

Conclusions

Dipodal EBDMS groups like trimethysilyl groups are efficient capping groups in presence of TMA^+ group partially covering the surface. Subsequent grafting of titanium leads mainly to isolated titanium species active in epoxidation of cyclohexene. Nonetheless, TMA^+ seems not as efficient as expected against EBDMS for MSP. Work is in progress concerning this point.

References

[1] Igarashi N., Hashimoto K., Tatsumi T., *Microporous Mesoporous Mater.,* 2007, **104**, 269.
[2] Zhang K., Albela B., He M., Wang Y., Bonneviot L., *Phys. Chem. Chem. Phys*., 2009, **11**, 2912.
[3] Abry S., Lux F., Albela B., Artigas-Miquel A., Nicolas S., Jarry B., Perriat P., Lemercier G. and Bonneviot L., Chem. Mater. 21, 2349, 2009

Carbon Nanotube Membranes by Templated Growth in Porous Media

Georgios N. Karanikolos*, Eleni C. Vermisoglou, Georgios Pilatos, Georgios E. Romanos, Nick K. Kanellopoulos
*Institute of Physical Chemistry, Demokritos National Research Center, Athens 153 10, Greece, *karanikolos@chem.demokritos.gr*

Introduction

Carbon nanotube (CNT) membranes have the potential to advance current performance of catalytic and separation processes, mainly owing to (1) the speculation that CNTs can exhibit extremely high permeability, as indicated by theoretical studies [1], owing to their smooth internal graphitic surface that provides nearly frictionless molecular transport or enables single file diffusion, and (2) recent studies showing that molecules and particles inside nanotubes behave drastically different than when they are in a non-restricted environment, due to the synergistic effect of confinement by the tube and interaction with the internal graphitic surfaces, which can have a direct favorable impact on the conversion of various molecules to useful products by catalysis-under-CNT-confinement. CNTs as catalyst supports distinguish themselves from other carbon materials, e.g. activated carbon and carbon nanofibers, in that they consist of well graphitized walls with semiconducting or metallic characteristics and a tubular morphology with well defined dimensions. Theoretical studies have shown that the electron density is shifted from the inside to the outside of CNT channels, and that inside gas molecules exhibit a binding energy different from those outside the tubes. The CNT restriction effect is also demonstrated by recent experimental evidence concerning tuning of the redox properties of iron and iron oxide nanoparticles by encapsulation within CNTs of varying inner diameters [2].

Experimental

CNT membranes were fabricated using porous templates, such anodized alumina, in a flow-though CVD reactor, and optimized using a variety of carbon precursors, catalysts, and growth conditions. In a particular growth experiment, a colloidal suspension of surfactant-coated iron oxide nanoparticles (ferrofluid) was introduced into the pores to function as a dual-action source for the formation of CNTs, i,e consisting of both the catalyst and the carbon provided by the organic stabilizing molecules, in order to trigger nanotube nucleation. At the CVD temperature (740 °C), an external feed of C_2H_4 in a flow-through-the-pores mode provided continuous carbon supply thus ensuring a uniform growth throughout the membrane thickness, and contributing to prevention of pore blocking. Under this mechanism, the graphene layers that segregate from the densely-deposited catalyst particles along the pores of the template merge with each other encapsulating the metal particles, which are rearranged upon growth, while confinement by the cylindrical pore directs structure roll-up yielding nanotube formation.

Results and discussion

The CNT pores of the resulting membranes exhibit three-fold monodispersity, i.e. in terms of diameter, thickness, and inter-tube separation distance, and high graphitic quality as indicated by Raman spectroscopy. The membranes were also doped with nanoparticles for added functionality. For instance, magnetic properties were induced to the CNT pores by in-situ inclusion of magnetic iron carbide nanocrystals inside the tube walls [3]. The stability of the

wall-encapsulated magnetic particles, which was confirmed by extended exposure of the CNT hybrids in highly oxidative conditions (concentrated nitric acid), prolongs material durability and extends the limits of application conditions without compromising functionality. The ferromagnetic composites consisting of monodisperse, aligned, and inherently open-ended CNTs can, among other applications, open up new prospects in high-flux magnetic separations and microfluidics, bio-capturing, and controlled drug delivery and release. The internal CNT morphology was evaluated by a combination of adsorption, single phase and relative permeability through the tubes providing insights of various crucial details of the overall internal surface and hollow space characteristics of the CNT pores [4].

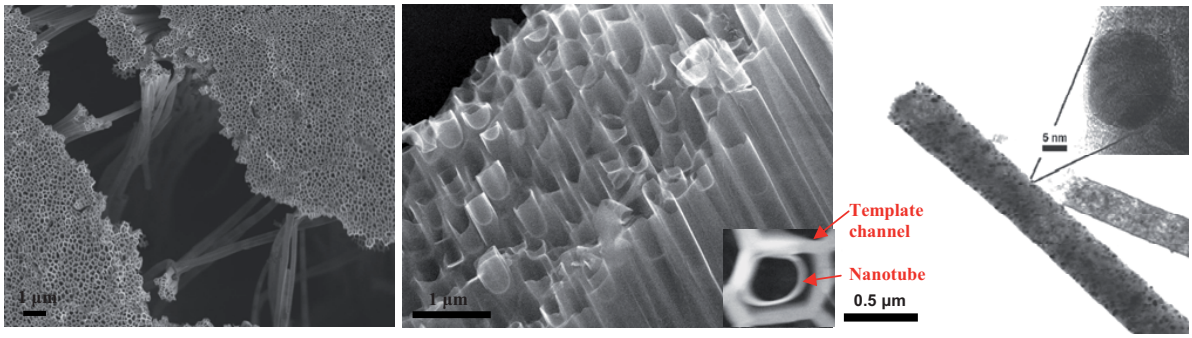

Figure 1. (left, middle) CNT membranes, (right) CNTs with Fe_3C particles encapsulated within their walls

References

[1] A. I. Skoulidas, D. M. Ackerman, J. K. Johnson, D. S. Sholl, Phys. Rev. Lett. **2002**, 89, 1859011
[2] W. Chen, X. Pan, X. Bao, J. Am. Chem. Soc. **2007**, 129, 7421.
[3] E. C. Vermisoglou, G. N. Karanikolos, G. Pilatos, E. Devlin, G. E. Romanos, C. M. Veziri, N. K. Kanellopoulos, Adv. Mater. **2010**, 22, 473.
[4] G. Pilatos, E. C. Vermisoglou, G. E. Romanos, G. N. Karanikolos, N. Boukos, V. Likodimos, N. K. Kanellopoulos, Adv. Funct. Mater. **2010**, 20, 2500.

ITQ-39: A new molecular sieve with a system of pores between those of ZSM-5 and Beta zeolite

Manuel Moliner[1], Jorge González[1,2], M. Teresa Portilla[1], Fernando Rey[1], Francisco J. Llopis[3], Avelino Corma[1]*
[1] *Instituto de Tecnología Química (UPV-CSIC), Universidad Politécnica de Valencia, Consejo Superior de Investigaciones Científicas, Valencia, Spain.* [2] *Escuela de Ciencias Químicas, Universidad de Colima, Colima, Mexico.* [3] *Departamento de Ingeniería Química, Universitat de Valencia, Valencia, Spain. * Corresponding author: acorma@itq.upv.es.*

Introduction

Despite the advances described in the structure elucidation of new materials, there are occasions where the real structure cannot be achieved. This is the case of the molecular sieve described here, named ITQ-39 [1]. In this situation, one may get an indirect way to clarify the pore topology and dimensions by considering that the selectivity towards a desired product in a chemical process will change depending on the shape and size of the channels of the zeolite. Then, the combination of adsorption studies with the reactivity of selected probe molecules can provide a good approximation to the pore topology [2], and consequently to predict its possibilities for the different industrially relevant catalytic processes. This molecular sieve, named ITQ-39, shows an extensively faulted structure, being the structure elucidation very difficult. For this reason, we will use a combination of characterization techniques, and a series of catalytic test reactions, such as *m*-xylene isomerization/disproportionation and benzene or toluene alkylation with ethanol or propanol [3], in order to approximate the pore structure of ITQ-39. Further knowledge is gained by comparing its catalytic behavior with other two zeolites, one medium pore size (ZSM-5) and one large pore size (Beta).

Experimental

New zeolite ITQ-39 was synthesized following the procedure described in [1]. For characterization and catalytic comparison, two commercial zeolites, ZSM-5 (MFI) and Beta (BEA) were supplied by Tricat GmbH and Zeolyst International respectively. Gas phase benzene and toluene alkylation and *m*-xylene isomerization reactions were carried out in a fixed bed down-flow reactor as previously reported in [3].

Results and discussion

The XRD patterns of ITQ-39 and Beta zeolite are compared in Figure 1. The results indicate certain similarities between them, but also significant differences. The principal differences between both diffractograms, among others, are the presence in the ITQ-39 of a peak in the 2θ angle close to 6.5, a peak at 7.5 that shows a pronounced shoulder and, finally, three consecutive peaks between 21 and 23 degrees.

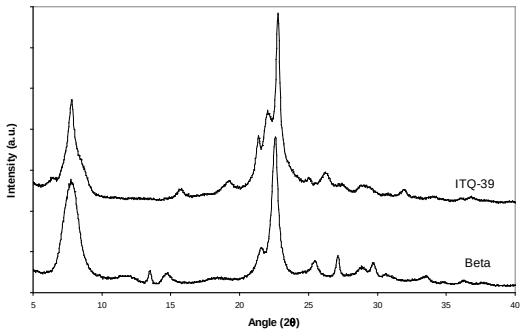

Figure 1. Powder XRD patterns for ITQ-39 and Beta zeolites

Chemical and textural properties of the three materials are summarized in Table 2. The N_2 and Ar adsorption isotherms reveal that the micropore volume and pore diameter for ITQ-39 lies in between Beta and ZSM-5.

Table 1. Chemical, textural and catalytic properties in *m*-xylene isomerization

Zeolite	Si/Al	S_{BET} (m^2/g)	$V_{Micropore}$ (cm^3/g)	Pore diameter (Å)	p/o [a]	i/d [b]	TMB [c] (normalized %)		
							1,3,5	1,2,4	1,2,3
ZSM-5	11	379	0.15	5.6	2.0	33.4	-	100.0	-
ITQ-39	13	547	0.18	6.1	1.2	3.6	15.8	77.8	6.4
Beta	13	586	0.21	6.5	1.1	2.9	26.4	65.8	7.9

[a] *Para/Ortho-xylene ratio (p/o),* [b] *isomerization/disproportionation ratio (i/d) and* [c] *trimethylbenzenes (TMB) distribution at 20% m-xylene conversion.*

The results of *m*-xylene isomerization/disproportionation as a reaction test (Table 1) indicates that the ITQ-39 zeolite presents a three-directional channel system with large pores (12-MR), with an effective pore diameter and internal void spaces in between that of Beta and ZSM-5 zeolite.

With respect to benzene or toluene alkylation with ethanol or isopropanol, the selectivity to monoalkylated products (cumene, ethyltoluene and cymene) is much larger over ITQ-39 than Beta or ZSM-5 (Figure 2). Furthermore, the formation of the undesired n-propylbenzene or n-propyltoluene is very low, as correspond to a large pore zeolite. These results can be of interest from an industrial point of view due to the high selectivity to main products and low selectivity to n-propylaromatics when ITQ-39 is used as catalyst.

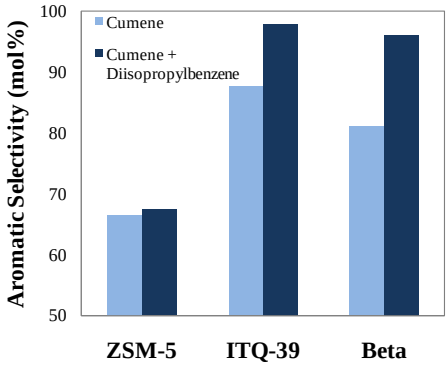

Figure 2. Aromatic Selectivity in benzene alkylation with isopropanol (X = 9 %)

Conclusions

A new molecular sieve, named ITQ-39, has been synthesized. This zeolite shows an extensively faulted structure with very small domains that make very complicated the structure elucidation. The characterization indicates that this structure could be related to Beta zeolite, but with lower pore diameter and pore volume. The use of test reactions, such as isomerization and disproportionation of *meta*-xylene, and benzene and toluene alkylation, adds further information on pore topology, indicating that the unresolved ITQ-39 zeolite presents a three-directional channel system with large pores (12-MR), with an effective pore diameter and internal void spaces in between that of Beta and ZSM-5 zeolite. The pore dimensions and topology of ITQ-39 result in very promising results for application of this zeolite to alkylation of aromatics with olefins.

Acknowledgements

Financial support by the Spanish MICINN (MAT2009-14528-C02-01) and Consolider Ingenio 2010-MULTICAT is gratefully acknowledged. Generalitat Valenciana is also thanked for funding through the Prometeo program. M.T. Portilla gratefully acknowledges CSIC for JAE fellowship.

References

[1] A. Corma, M. Moliner, F. Rey, J. González, WO2008/092984 A1 (2008).
[2] A. Corma, A. Chica, J.M. Guil, F.J. Llopis, G. Mabilon, J.A. Perdigon-Melon, S. Valencia, J. Catal. 189 (2000) 382.
[3] (a) A. Corma, C. Corell, F. Llopis, A. Martínez, J. Pérez-Pariente, Appl. Catal. A 115 (1994**)** 121, (b) A. Corma, V.L. Costa-Vaya, M.J. Díaz-Cabañas, F.J. Llopis, J. Catal. 207 (2002**)** 46, (c) F.J. Llopis, G. Sastre, A. Corma, J. Catal. 242 (2006**)**, 195.

Develop of new Ruthenium(II) Materials and Their Application in Selective Hydrogenation

Ismail Warad*, Zeid Al-Othman and Saud I Al-Resayes

Department of Chemistry, Science of College, P.O. Box 2455, King Saud University, Riyadh-11451, KSA. warad@ksu.edu.sa

Introduction

Phosphine ligands have been intensively used in coordination chemistry because of their electron-donating power [1]. Diphosphine ligands have received particular attention, because in general they form more stable complexes than their non-chelating phosphine analogues under the harsh reaction conditions required for catalysis. Novel diphosphine Ru(II) complex-based hybrid inorganic-organic materials immobilized via a diamine co-ligand site instead of the conventional diphosphine ligand have been prepared [2].

Experimental

General procedure for the preparation of the complex **2**

3-(2-Aminoethyl)aminopropyl]trimethoxysilane (0.035 mL, 0.55 mmol, 10% excess) was dissolved in dichloromethane (10 mL) and the solution was added dropwise to a stirred solution of **1** (500 mg, 0.50 mmol) in dichloromethane (10 mL) within 5 min. The mixture was stirred for ca. 2 h at room temperature while the color changed from brown to yellow. After removal of any turbidity by filtration (P4), the volume of the solution was concentrated to about 5 mL under reduced pressure. Addition of diethyl ether (40 mL) caused precipitation of a solid, which was filtered (P4). After recrystallization from dichloromethane/*n*-hexane, complex **2** was obtained in analytically pure form.

General procedure for sol–gel processing of xerogel **3**

Compound **2** (300 mg, 0.235 mmol) and $HSi(OMe)_3$ (10 equivalents) in methanol (10 mL) were mixed together. The sol–gel took place when a THF/water mixture (4 mL, 1:1 v/v) was added to the solution. After 24 h stirring at room temperature, the precipitated gel was washed with diethyl ether (50 mL of each), and petroleum ether (40 mL). Finally the xerogel was ground and dried under vacuum for 24 h to afford after workup 500 mg of **3** as a pale yellow powder.

General procedure for surface modified material **4**

Compound **2** (0.300 mg, 0.235 mmol) dissolved in CH2Cl2 (50 mL) was added dropwise to a suspension of ProntoSil 120-5 Si (5 mm) (0.5 g) in dry toluene (50 mL) and stirred at 25 °C for 2 h to allow the diffusion of the molecular precursor into the pore channels. The reaction mixture was then refluxed for 24 h. After filtration, the unreacted ruthenium precursor was removed by thoroughly washing the solid twice with toluene then CH2Cl2 (25 mL each). Finally, the resulting solid was dried *in vacuo* (~ 0.40 atm) at 30 °C to afford 620 mg of **4** as a pale white powder.

Results and discussion

These complexes were prepared by two different methods: sol-gel and surface modification techniques (Scheme 1). The structures of the desired materials were deduced by several available physical measurements like elemental analyses, infrared, FAB-MS and ^{1}H-, ^{13}C and ^{31}P-NMR spectroscopy. The structures of xerogel **3** and modified **4** were studied by solid state ^{13}C-, ^{29}Si- and ^{31}P-NMR spectroscopy, infrared spectroscopy and EXAFS. These materials were stable enough to serve as hydrogenation catalysts in homogenous and heterogonous

phases. Selective hydrogenation of functionalized carbonyls using these complexes was carried out under mild conditions (Scheme 2).

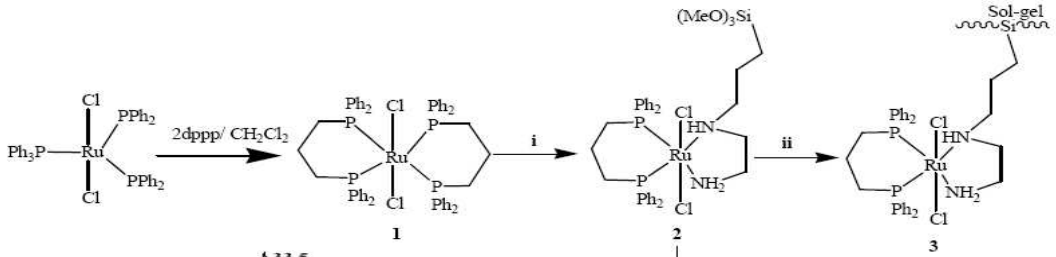

Scheme 1. The synhetic route used in the preparation of the hydrogenation catalyst **2**, the sol-gel xerogel **3**, and the modified **4**.

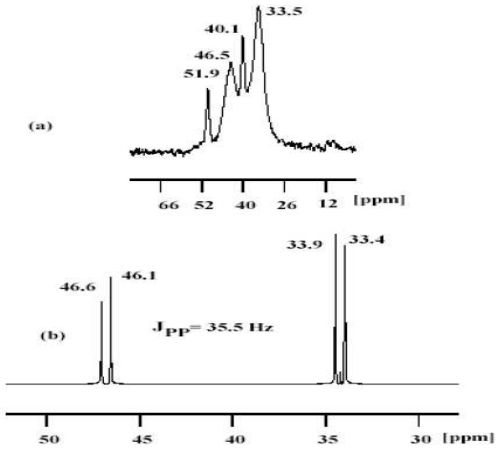

Figure 1. (a) ^{31}P-CP/MAS-NMR spectrum of the modified **4**, (b) ^{31}P{1H} of complex **2** in CD_2Cl_2

The structures of the desired materials were deduced by several available physical measurements like elemental analyses, infrared, FAB-MS and ^{1}H-, ^{13}C and ^{31}P-NMR spectroscopy. The structures of xerogel **3** and modified **4** were studied by solid state ^{13}C-, ^{29}Si- and ^{31}P-NMR spectroscopy, infrared spectroscopy and EXAFS. These materials were stable enough to serve as hydrogenation catalysts in homogenous and heterogonous phases. Selective hydrogenation of functionalized carbonyls using these complexes was carried out under mild conditions (Scheme 2).

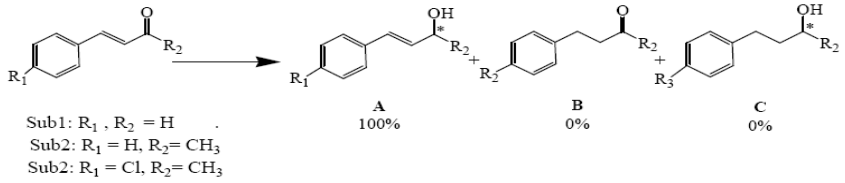

Scheme 2. Hydrogenation of unsaturated carbonyl compounds possibilities

Conclusions

Several polymeric Ruthenium(II) complexes were prepared and tested as catalysts for the hydrogenation of unsaturated ketones, they showed high degree of stability and activity as well as an excellent degree of carbonyl hydrogenation selectivity under mild conditions.

Acknowledgements

The authors would like to thank Sabic Company for the financial support through project no. SCI- 30-14, 2010.

References

[1] Lindner, E.; Al-Gharabli, S.; Warad, I.; Mayer, H. A.; Steinbrecher, S.; Plies, E.; Seiler, M.; Bertagnolli, H. Diaminediphosphineruthenium(II) interphase catalysts for the hydrogenation of unsaturated ketones. Z. Anorg. Allg. Chem 629. (2003), 161–171.

[2] Warad, I. Supported and non-supported ruthenium(II)/phosphine/[3-(2-aminoethyl) aminopropyl]trimethoxysilane complexes and their activities in the chemoselective hydrogenation of trans-4-phenyl-3-butene-2-al, Molecules 15 (2010), 4652-4669.

Copper-silver-zinc trimetallic system on mordenite: effect of order of ion-exchange on Cu^{2+} and Ag^{+} thermal reduction.

Inocente Rodríguez Iznaga[1,*], Vitalii Petranovskii[2,*], Eder Lugo-Medina[2,3], F. Chávez-Rivas[4,5,§,] and Felipe Castillón Barrasa[2]
[1]*Instituto de Ciencias y Tecnología de Materiales (IMRE) – Universidad de La Habana, Zapata y G, s/n, La Habana 10400, Cuba.*
[2]*Centro de Nanociencias y Nanotecnología (CNyN) – Universidad Nacional Autónoma de México, Ensenada, B.C., México.*
[3]*Departamento de Ingeniería Química, Instituto Tecnológico de Los Mochis, Blvd. Juan de Dios Bátiz y 20 de Noviembre, 81250 Los Mochis, Sinaloa, México*
[4]*Department of Inorganic, Physical and Material Chemistry, University of Turin, Via P. Giuria 7, 10125 Torino, Italy; § On sabbatical leave, granted by ESFM-IPN, Mexico*
[5]*Departamento de Física, Escuela Superior de Física y Matemáticas del IPN, 07738, México D.F., México*
Corresponding authors: inocente@fisica.uh.cu and vitalii@cnyn.unam.mx

Introduction

Zeolites modified with Cu, Zn and Ag species are of interest due to their catalytic and olygodynamic features [1,2]. Reports are mainly known for monometallic systems, while there are only few studies dedicated to multi-metallic systems. Significant differences in type and stability of the metal species are observed even in binary systems [3]. The aim of present work was to study the influence of preparation protocol on the thermal reduction of mixed trimetallic Cu^{2+}-Ag^{+}-Zn^{2+} system supported on mordenite.

Experimental

Synthetic Na-Mordenite with SiO_2/Al_2O_3 ratio equal to 13, supplied by Zeolyst International, was firstly exchanged with Cu^{2+}, Zn^{2+} or Ag^{+} from 0.1 M solutions of corresponding nitrates. Exchange was done during 24 h, with solid/solution ratio of 1g/5mL; the solutions were replaced after 12 hours. Cu^{2+} and Zn^{2+} exchange was performed at 100°C; Ag^{+} was exchanged at room temperature. To obtain trimetallic forms, CuMor and ZnMor were treated with mixed in 5:1 ratio $Zn(NO_3)_2/AgNO_3$ and $Cu(NO_3)_2/AgNO_3$ solutions, respectively, under the similar conditions at room temperature. The resulting samples are referred as AgCu_ZnMor and AgZn_CuMor. The Cu, Ag and Zn content in CuMor, AgMor and ZnMor samples was 3.9%, 13.8% and 1.8%, respectively; in AgZn_CuMor -- 3.2%, 0.7% and 0.9% and in AgCu_ZnMor -- 1.6%, 0.7% and 1.4%, respectively. These samples were subjected to reduction treatments:
1- *In tubular furnace*: Reduction in H_2 flow at 50 – 450°C, during 4 h. The samples before and after the reduction were studied by XRD and UV-vis diffuse reflectance spectroscopy.
2- *Temperature-Programmed Reduction (TPR-H_2):* Study was carried out in an Automated Chemisorption Analyzer – Quantachrome INSTRUMENTS from 20°C to 800°C (heating rate of 10°C/min), using a gas flow of 25 cm^3/min with 4% H_2 (v/v in N_2).

Results and discussion

The reduction profile of TPR-H_2 of the AgCu-ZnMor trimetallic sample shows three peaks with maxima centered at 49°C, 100°C and 230°C. The 49°C peak has been associated to the first step of Ag^{+} reduction, leading to small cluster formation. The 100°C peak was related

with reduction both of Ag^{+} and Cu^{2+}, resulting in formation of larger silver clusters and quasi-colloidal particles, and in formation of Cu^{+} and polinuclear charged copper aggregates. Finally, the 230°C peak was associated with reduction of all cationic species to the elemental state. The reductions profile of the AgZn_CuMor shows a first very low-intense peak at 85°C, and two other intense peaks at 260°C and 440°C, which are in line with the reduction profile of the CuMor. The 260°C peak is very intense and was associated with reduction both of Ag^{+} and Cu^{2+}, while the 440°C peak was related with final reduction of copper cationic-species. Thus, the reduction profiles and the peaks location for AgCu_ZnMor and AgZn_CuMor trimetallic samples are very different, which demonstrate that sequence of ion exchange used in the preparation protocol for these samples do influence subsequent reduction processes.
UV-Vis spectra of the reduced AgCu_ZnMor sample show that the 320 nm band, associated with Ag_8 clusters, appear starting from 100°C, while it isn't clearly observed for AgZn_CuMor sample. Additionally, a clear decrease of Cu^{2+} band (800-850nm) is observed in trimetallic samples at 100°C, which is not typical for CuMor reduced at this temperature. This decrease is more notable in AgCu_ZnMor sample than in the AgZn_CuMor, confirming the influence of exchange treatment sequence on the properties of the obtained samples. One can conclude that Cu^{2+} reduction in the trimetallic systems is favored, and that it is more feasible when Zn^{2+} is exchanged before Cu^{2+} and Ag^{+} incorporation. The intensity of the plasma resonance band at 550 nm that belongs to copper nanoparticles increases with the temperature. Starting from 300°C peaks of silver clusters and quasi-colloidal particles disappeared, and the optical properties of the samples start to be similar to the "metal blacks", that is finely dispersed metals with structureless absorption over UV-Vis range [4]. XRD patterns of the trimetallic samples reduced at 250°C-450°C show the peaks corresponding to metal silver and copper, indicating reduction and aggregation of both metals, which is consistent with UV-Vis and TPR data.

Conclusions

Thermal reduction in hydrogen of Cu^{2+}-Ag^{+}-Zn^{2+} trimetallic system in mordenite was studied. The Ag^{+} and Cu^{2+} reduction is sensitive to the order used to exchange the cations of this trimetallic system. The Cu^{2+} reduction in the trimetallic systems is favored, which is more feasible when Zn^{2+} is first incorporated than Cu^{2+} and Ag^{+}. The use of trimetallic system leads to the diversity in obtained reduced species both copper and silver and appears to be an alternative important to inside on the reduction temperature and formation of the resultant nanoparticles and clusters reduced.

Acknowledgements

Support of E. Aparicio, E. Flores, M. Vega, T. Kreztchmar and I. Gradilla is acknowledged. This research was granted by CONACYT 102907, CONACYT 50547-Q and "Program of international academic exchange of the scientific research coordination (2010) - UNAM".

References

[1] Pârvulescu V.I., Grange P., Delmon B., Catalytic removal of NO, Catalysis Today, 46 (1998), 233-316.
[2] Rivera-Garza M., Olguin M.T., Garcia-Sosa I., Alcántara D., Rodríguez-Fuentes G., Silver supported on natural Mexican zeolite as an antibacterial material, Microporous and Mesoporous Materials, 39 (2000), 431-444.
[3] Rodríguez-Iznaga I., Petranovskii V., Castillón F., Farias M.H., Effect of the Zn(II) on the reduction of Cu(II) in natural clinoptilolite, Optical Materials, 29 (2006), 105-109.
[4] Lysenko V.S., Mal'nev A.F., Optical characteristics of metal blacks, Journal of Applied Spectroscopy, 10 (1969), 566-570.

Hydrogen Storage on modified materials type Ni/Carbon

J. Salmones[1], C. P. Rueda Martínez[1], M. A. Valenzuela[1], B. Zeifert[2], J. L. Contreras-L.[3]
[1,*]*Laboratorio de Catálisis y Materiales, A. C., ESIQIE IPN, Av. IPN s/n Col. Lindavista, 07738, México D, F. México.email: jose_salmones@yahoo.com.mx.*
[2]*ESIQIE UPALM, IPN. Departamento de Metalurgía, Av. IPN s/n Col. Lindavista, 07738, México D, F. México.*
[3]*Universidad Autónoma Metropolitana Azcapotzalco, Av, San Pablo 180, Col. Reynosa, México D, F.*

ABSTRACT

Hydrogen newest interest is mostly to environment troubles by emission damages produced by fossil fuels. Also, the demand for more efficient energetic sources has increased different types of technologies interest, such as fuel cells using hydrogen. Microporous materials (e. g.. zeolites, activated carbons) have been used in a great variety of gases and catalytic separation process. Adsorption capacity from these materials have been strongly determined by their textural properties, such as inner surface, geometry and pore size distribution, and surface irregularity. In this work has been studied the hydrogen storage capacity in a porous system, which has been provided by activated carbon with different specific surfaces (600-1600m^2g^{-1}) and impregnated with 2.5, 5.0 and 10%w nickel concentrations to determine its effect on adsorption capacity.

Introduction

Hydrogen storage in carbon nanotubes at temperatures almost environment is based on a chemical reaction between carbon and hydrogen atoms (as opposed to the physical absorption of hydrogen molecules, which occurs at cryogenic temperatures). This requires breaking down the hydrogen-hydrogen bond in the H2 molecule, a process that can be catalyzed by the presence of metals such as palladium or platinum supported on carbon. In recent years, we have focused on the preparation of metal / catalyst, particularly in doped carbon nanotubes and to investigate the storage capacity when exposed to hydrogen gas with high pressure, with the purpose or effect would explain of catalysis in hydrogen storage.

Since carbon nanotubes are usually available only in small quantities, the history of hydrogen storage in carbon nanotubes had been affected by the experimental difficulties to measure the absorption and evolution of small amounts of hydrogen at high pressure conditions of hydrogenation process. Thus, a second aim of our study was to apply a technique capable of measuring changes of hydrogen from a fraction of a milligram at pressures up to 50 bar. Recent results of Nikitin and co-workers, show a large storage capacity of carbon nanotubes exposed to hydrogen atoms, and indicate that carbon nanotubes are promising as a means of storage if the H2 molecules can be dissociated [1]. Also been reported that the capacity can be increased by the addition of a metal catalyst [2-3]. These recent investigations and border have recently been published by several authors, perhaps the most significant works are: [4] K. M. Thomas and [5] Shangzhao Shi, Yang Jiann Hwang, [6] Ki-Joon Jeon, [7] M. Jorda, [8] Z. G. Huang and C. Rueda, [9].

EXPERIMENTAL

The catalysts used were synthesized from a solution of nickel chloride ($NiCl_2$). We used 3 different activated carbons were prepared 3 samples of each to 2.5% w, 5% w 10% w nickel concentration. For this process permeated by magnetic stirring for a period of 3 hours, which is the time required for the nickel is incorporated into activated carbon. After completion of stirring, the charcoal is put on the stove to evaporate the liquid phase. This was left to dry for 24 hours. Finally, the activated carbon was a tube furnace where it was calcined at 500 ° C

(using an inert atmosphere) to remove all impurities and residual chloride nickel chloride solution.

HYDRING/DEHYDRING

The fundamental principle of hydriding and dehydring of the samples is the detection of changes in weight, under conditions of controlled temperature and pressure in a balance PCTM-6000. In a first step, the total weight of the sample holder and the samples are recorded by the scale. The computer software determines the current to be imposed on the electromagnet base for the rod and the slide levitate. In a second step, the team recorded tare weight and imposes power of levitation. The differences in weight during the experiments correspond to changes in the sample.

TEXTURE

Measurements of specific surface area, volume and average pore diameter of solid materials degassed at 120 ° C and examined for this study were carried out in a Micromeritics ASAP-2600 Digisorb by nitrogen adsorption at -196 ° C. The specific area estimation was performed using the method of Langmuir and BET with pressures on (P / Po) of nitrogen according to ASTM-D-3663. The specific total pore volume was obtained from the volume of nitrogen adsorbed at a partial pressure of 0.98, using 0.2 to 0.4 g of sample. The data of average pore diameter were derived from pore volume distributions analyzed and calculated using the theoretical model of BET (Brunauer, Emmett and Teller).

RESULTS AND DISCUSSION

Experiments were conducted in the balance PCTM-6000, samples were previously activated by two cycles of hydriding / deshidruración at a temperature of 200 ° C, this will set a 3MPa pressure for hydriding and 0.01 MPa for dehydring. The results are presented in graphs of H_2 adsorbed against pressure.

Shows the scanning electron microscopy using a dual beam scanning electron microscope in high vacuum mode (FIB, Model Quanta 3D FEG, FEI, Netherlands). The results indicate that the hydrogen storage capacity is a function of metal content and dispersion.

Scanning electron microscopy was carried out an inspection of the surface morphology and elemental mapping carried out to determine the distribution of coal and nickel mainly. In samples MAS03 MAS01 and found that the carbon retains the typical morphology of activated carbon without heat treatment and lack of interconnected pores, however, smooth surfaces can be seen under the walls of mesoporous carbon, and rough surfaces at the edges of fractures of the larger particles.

CONCLUSIONS

The activity and selectivity of supported metal catalysts are strongly influenced by the amount of metal, the size of dispersed metal particles, the method, and composition of support. The amount of adsorbed hydrogen depends directly on the metal dispersion, active particle size and pore volume, as shown by measurements of surface area, pore size coupled with surface micrographs. The sample M-3 was the one with the best characteristics for hydrogen storage and was also presented by the size and distribution of activated carbon particles and homogeneous nickel. All this is summarized and concluded it is inherent in each sample

References [1] A. Nikitin, H. Ogasawara, D. Mann, R. Denecke, Z. Zhang, H. Dai, K. Cho, and A. Nilsson, *Phys. Rev. Lett*. **95**, (2005) 225507. [2] A. D. Lueking, and R. T. Yang, *Appl. Catal. A*, **265**, (2004) 259. [3] E. Yoo, L. Gao, T. Komatsu, N. Yagai, K. Arai, T. Yamazaki, K. Matsuishi, T. Matsumoto, and J. Nakamura, *J. Phys. Chem. B*, **108**, (2004) 18903. [4] K. M. Thomas, *Catalysis Today* **120**, (2007) 389-398. [5] Shangzhao Shi, Jiann Yang Hwang. *International Journal of Hydrogen Energy* **32** (2007) 224-228. [6] Ki –Joon Jeon, Alexandros Theodore, Chang –Yu Wu, Mei Cai *International Journal of Hydrogen Energy* **32** (2007) 1860-1868. [7] M. Jordá Beneyto, D. Lozano Castelló, F. Súarez García, D. Casorla-Amorós, A. Linares Solano *Microporous and Mesoporous Materials* **112**, (2008) 135-142. [8] Z. G. Huang, Z. P. Guo, A. Calka, D. Wexler, H. K. Liu, *Journal of alloys and Compounds* **427**, (2007) 94-100. [9] C. Rueda Martínez, Tesis Maestro en Ingeniería Química, ESIQIE, Instituto Politécnico Nacional, (2010).

Modeling and theoretical studies

FEZA 2011

Acidic Properties of Small Pore Zeolites with Different Framework Topologies and Their SAPO Analogues

Naonobu Katada[1]*, Kazuma Nouno[1], Jun Kyu Lee[2], Jiho Shin[2], Suk Bong Hong[2], and Miki Niwa[1]
[1]*Department of Chemistry and Biotechnology, Graduate School of Engineering, Tottori University, Japan,* [2]*Department of Chemical Engineering and School of Environmental Science and Engineering, POSTECH, Korea, katada@chem.tottori-u.ac.jp*

Introduction

Silicoaluminophosphate molecular sieves (SAPOs) are believed to have weak or moderate acidity compared to their aluminosilicate zeolite analogues, and this is a motive of application of SAPOs to such a catalytic reaction as MTO (methanol to olefin). As far as we know, however, no direct comparison has been made for the Brønsted acid strength between zeolites and SAPOs with the same framework topologies. We have developed a method of ammonia IRMS-TPD (infrared / mass spectroscopy temperature-programmed desorption) for measurement of number and strength of Brønsted and Lewis acid sites on a solid [1]. Application of this method to CHA zeolite (chabazite) and SAPO (SAPO-34) suggested the weaker acidity of SAPO [2]. Subsequently, we systematically compared the acidic properties of zeolites and SAPOs with AFX, RHO, CHA, ERI, LEV and LTA structures, i.e., cage-based and small pore frameworks.

Experimental

All zeolitic materials employed here were synthesized in Teflon-lined autoclave according to the reported procedures [3] and calcined in air at 823 K for 8 h. The aluminosilicate samples were then refluxed twice in 1.0 M NH_4NO_3 solutions (1.0 g solid / 100 cm^3 solution) for 4 h. About 7 mg of sample (NH_4 form of aluminosilicate or H form of SAPO) was compressed into a self-supporting disk (10 mm i.d.), and evacuated at 773 K. In a helium flow, IR spectra were collected with heating the sample from 373 to 773 K at every 10 K. Ammonia was then adsorbed at 373 K, and IR spectra were again collected with heating. Simultaneously, outlet gas was analyzed with mass spectrometer (MS). Numbers and ammonia desorption enthalpies of Brønsted and Lewis acid sites were calculated on the basis of the combined information from (1) decreasing rate of NH_4^+ bounded to Brønsted acid site (estimated from 1430 cm^{-1}-band in IR spectrum), (2) decreasing rate of NH_3 coordinated to Lewis acid site (estimated from 1250 cm^{-1}-band in IR) and (3) gaseous concentration of desorbed ammonia (quantified from MS), as described in our previous paper [1].

Results and discussion

All the synthesized samples showed high crystallinity. As shown in Table 1, the number of Lewis acid sites was negligible in most cases. The number of Brønsted acid sites of SAPO-17 was similar to the number of Si atoms incorporated, suggesting the stoichiometric generation of acid site by isomorphous substitution of P^{5+} with Si^{4+}. However, generally, the number of Brønsted acid sites was smaller than the Si content in SAPO or the Al content in zeolite.
The aluminosilicate zeolites with different framework types showed different Brønsted acid strengths, and even within one framework type (CHA), a difference in the Brønsted acid strength was found between SSZ-13 (highly siliceous) and chabazite (highly aluminated). It should be interesting to discuss the origin of such differences, but here we will concentrate on

the comparison of acid strength between zeolite and SAPO. The most important finding in Table 1 is that the Brønsted acid strength of SAPO was always weaker than that of aluminosilicate zeolite with the same framework type without any exception.
It is possible to discuss the difference between isolated Si and SiO_2 island in SAPO. The sample B of SAPO-34 showed higher acid strength than that of the sample A. The nuclear magnetic resonance (NMR) indicates that most of Si atoms were isolated to form $Si(OAl)_4$ in the sample A, while considerable amounts of $Si(OSi)_4$ (= SiO_2 islands), SiOH, AlOH and POH were present in the sample B [2]. We have calculated the ammonia desorption enthalpies of acid sites due to the isolated Si and the SiO_2 island in SAPO-34 using density functional theory (DFT) [2]. The observed enthalpies on the samples A and B are in good agreement with the calculated values for the isolated Si and the SiO_2 island, respectively. It is concluded that an isolated Si atom in SAPO framework generates a weak Brønsted acid site.

Table 1. Number and strength of acid site

Sample	IZA framework type code	Zeolite or SAPO	[Al] in zeolite or [Si] in SAPO / mol kg^{-1}	Number of Brønsted acid site / mol kg^{-1}	Ammonia desorption enthalpy of Brønsted acid site / kJ mol^{-1}	Number of Lewis acid site / mol kg^{-1}
SSZ-16	AFX	zeolite	2.4	0.30	144	0.06
SAPO-56	AFX	SAPO	1.6	0.78	131	0.00
Rho	RHO	zeolite	3.4	1.69	143	0.03
Rho-SAPO	RHO	SAPO	1.9		121*	
Levyne	LEV	zeolite	1.9	0.31	142	0.03
SAPO-35	LEV	SAPO	1.4	0.67	123	0.00
UZM-12	ERI	zeolite	2.5	0.41	139	0.10
SAPO-17	ERI	SAPO	0.3	0.41	113	0.00
UZM-9	LTA	zeolite	4.7	0.36	129	0.00
SAPO-42	LTA	SAPO	0.5	0.08	118	0.12
Chabazite	CHA	zeolite	5.6	2.07	136	0.00
SSZ-13	CHA	zeolite	2.8	0.63	149	0.40
SAPO-34, sample A	CHA	SAPO	1.6	0.86	121	0.00
SAPO-34, sample B	CHA	SAPO	1.5	0.37	133	0.00

*: Because of the weak intensity of IR spectrum, quantification of Brønsted and Lewis acid sites was impossible. The ammonia desorption enthalpy of total acid sites are shown.

Conclusion

Acid strength of SAPO is weaker than that of aluminosilicate zeolite with the same framework type.

References

[1] Niwa, M., Suzuki, K., Katada, N., Kanougi, T., Atoguchi, T., Ammonia IRMS-TPD study on the distribution of acid sites in mordenite, J. Phys. Chem., B, 109 (2005) 18749-18757.
[2] Suzuki, K., Nishio, T., Katada, N., Sastre, G., Niwa, M., Ammonia IRMS-TPD measurements on Brønsted acidity of proton-formed SAPO-34, Phys. Chem. Chem. Phys., in press.
[3] Baerlocher Ch., McCusker, L. B., http://www.iza-structure.org/database, and references therein.

Optimizing force field parameters for guest-zeolite interactions

T.J.H. Vlugt[1,*], E. Eggink[1], A. Garcia Sanchez[1,2], E. S. McGarrity[1], S. Calero[2]

[1]*Process & Energy Laboratory, Delft University of Technology, Leeghwaterstraat 44, 2628CA Delft, The Netherlands*
[2]*Department of Physical, Chemical and Natural Systems, University Pablo de Olavide, Ctra. de Utrera, Km. 1, 41013 Sevilla , Spain*

[*]*Corresponding author: t.j.h.vlugt@tudelft.nl*

Introduction

Molecular simulations are a powerful tool to study the adsorption behavior of small guest molecules in zeolites. The applicability of these molecular simulations critically depends on the quality of the force field used. Therefore, there is now a considerable interest in constructing transferable force fields that can be used for many zeolite framework types [1-3]. Unfortunately, fitting force fields for guest-zeolite interactions to experimental adsorption data requires excessive amounts of CPU time. In the present work, we propose a new fitting method by constructing a fast predictive model for the outcome of an adsorption simulation. The fitting of the force field can then be performed using the predictive model and therefore the number of molecular simulations is minimal. As this predictive model is orders of magnitude faster than conventional molecular simulations, the computational effort for fitting force field parameters is significantly reduced. As a proof of principle, we consider the adsorption of methane in all-silica zeolites (AFI, TON) .

Experimental

Classical molecular simulations are used to compute the Henry coefficients and heats of adsorption of methane in all-silica zeolites. Guest-host interactions are described with Lennard-Jones interactions, in which only the oxygen atoms of the framework are taken into account. For details about the methodology and the force field we refer the reader to Refs. [2,3]. Zeolite crystal structures were obtained from the IZA database [4]. A predictive model is constructed by approximating the zeolite channels as an infinitely long annulus. The interaction of guest molecules with the zeolite is modeled as an effective interaction with the interior surface of the annulus. This effective interaction is directly related to the force field parameters in molecular simulation [5]. The volume of the annulus represents the excluded volume of the zeolite. In this case, the Henry coefficient and the heat of adsorption can be obtained analytically resulting in a predictive model for how adsorption properties depend on the force field parameters in molecular simulation.

Results and Discussion

In Figure 1, we show the dependence of the heat of adsorption and Henry coefficient on the Lennard-Jones parameters for methane-host interactions, both from molecular simulation and the predictive model. When the Lennard-Jones size parameter σ is approximately equal to the channel diameter of the zeolite, the adsorption becomes less favorable. This is clearly observed for TON-type zeolite for $\sigma \approx 3.8$Å, both in molecular simulations and in our model. In all cases, the model correctly predicts how the results of molecular simulations depend on the Lennard-Jones parameters for the methane-host interactions.

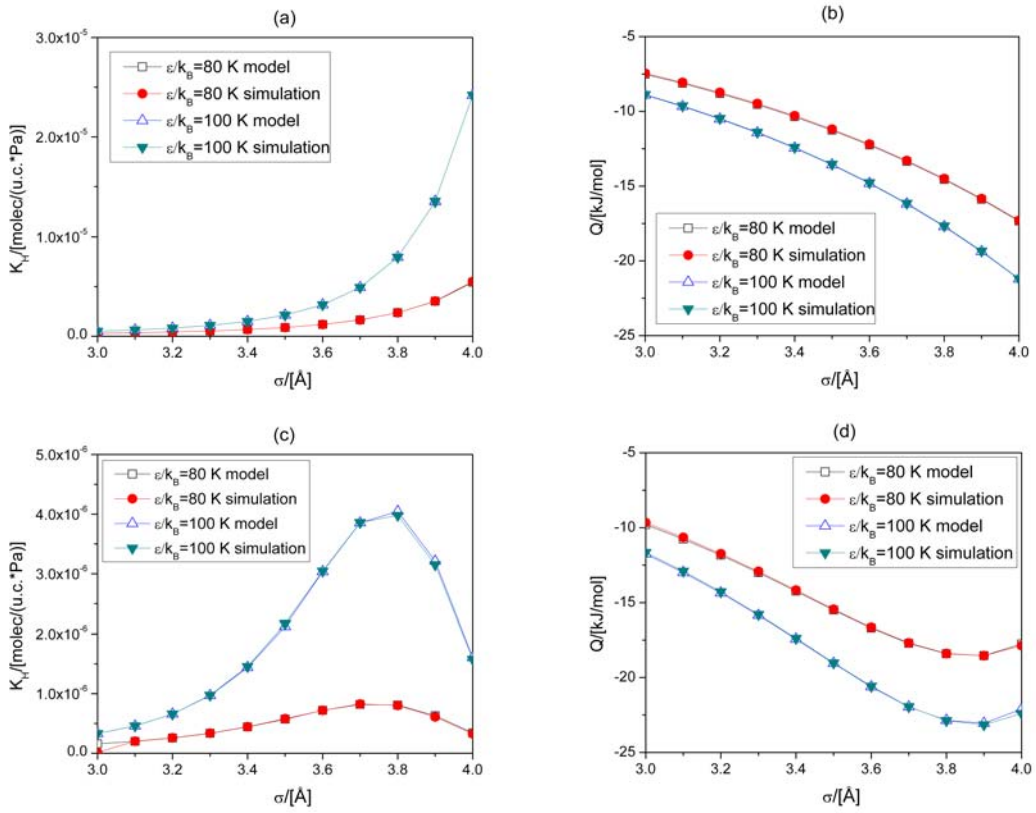

Figure 1. Henry coefficient (a) and heat of adsorption (b) for AFI-type zeolite. (c) and (d): similar but for TON-type zeolite.

In Refs. [2,3] it was shown that the adsorption of methane in all-silica zeolites is well described by ε/k_B=115K and σ=3.47Å. For AFI, this results in a Henry coefficient of K_H=3.62*10^{-6} molec./(u.c. Pa) and a heat of adsorption of Q=-14.9 kJ/mol. We now investigate if we can recover the values of ε and σ using only these values of K_H and Q. The adsorption is modeled using our predictive model, parameterized using 3 random combinations of ε and σ. A simplex optimization using our predictive model takes less than 0.1 second on a desktop computer and results in ε/k_B=114.0K and σ=3.478Å. Reparameterization of the model using simulation data around the first guess and a second simplex optimization results in ε/k_B=115.0K and σ=3.470Å. In summary, using our predictive model only 6 molecular simulations are needed for accurately fit parameters describing the guest-host interactions. We are currently working on extending the method to more complex molecules and interactions.

References

[1] García-Sánchez, A., Ania, C.O., Parra,J.B., Dubbeldam, D., Vlugt, T.J.H., Krishna, R., Calero, S., A Transferable force field for carbon dioxide adsorption in zeolites, J. Phys. Chem. C., 113 (2009), 8814-8820

[2] Dubbeldam, D., Calero, S., Vlugt, T.J.H., Krishna, R., Maesen, T.L.M., Smit, B., United atom force field for alkanes in nanoporous materials, J. Phys. Chem. B, 108 (2004), 12301-12313

[3] Dubbeldam, D., Calero, S., Vlugt, T.J.H., Krishna, R., Maesen, T.L.M., Beerdsen, E., Smit, B., Force field parameterization through fitting on inflection points in isotherms, Phys. Rev. Lett., 93 (2004), 088302.

[4] www.iza-structure.org/databases/

[5] Tjatjopoulos, G.J., Feke, G.J., Mann, J.A., Molecule-micropore interaction potentials, J. Phys. Chem., 92 (1988), 4006-4007.

Development and test of modified zeolite catalysts activity in oxidation reaction of n-propyl alcohol

D.B.Tagiyev[1], S.S.Fatullayeva[1], A.M.Aliyev[2], S.M.Mejidova[2], G.A.Ali-zadeh[2]
[1]Azerbaijan Medical University, 23, Bakikhanov str, Baku, 1022, Azerbaijan
[2]Institute of Chemical Problems, 29, H.Javid ave, Baku, 1143, Azerbaijan
Corresponding author: sevafatullayeva@hotmail.com

Introduction

The heterogeneous catalytic oxidative conversion of aliphatic alcohols is a highly perspective method of carboxylic acids preparation. Ion-exchanged properties, large internal surface, regulated distribution of acidic sites over surface, molecular-sieved selectivity in catalysis, crystal structure with homogeneous pores and thermal stability of zeolites create favourable conditions for creation of high-effective metalzeolite catalysts on their basis in presence of metals cations with known catalytic properties for multistage reactions of oxidative conversion of alcohols. Studies carried out over the catalysts, prepared on the basis of natural and synthetic zeolites with the different transition metals, in the oxidation reactions of ethyl, isopropyl, butyl, isoamyl alcohols have shown that these catalysts are the active catalytic systems for conversion of these alcohols into aldehydes, ketones, acids and esters [1-3]. Activity and selectivity of zeolites in these reactions is caused both oxidation-reduction properties of the elements and acidic-basic properties of zeolite contact itself.
The present paper is dedicated to the study on selection of active metalzeolite catalysts for the oxidative conversion reaction of n-propyl alcohol.

Experimental

Catalytic tests of activity of the synthesized samples of metalzeolite catalysts (synthetic zeolites of A, X, Y types and natural ones-clinoptilolite and mordenite) modified by ion-exchange method with the cations of Cu^{2+}, Pd^{2+}, Sn^{2+}, Zn^{2+} in the reaction of n-propyl alcohol oxidation were carried out on a flow installation with the fixed bed of catalyst at mole ratios of reagents $C_3H_7OH:O_2:N_2=1.0:(1.0\div7.0):(1.0\div15.0)$, space velocity 600-4500 h^{-1} and temperature interval 140-300^{0}C. The reaction products were analyzed by GC and IR-spectroscopy. Before studying catalysts were activated by air current at 723 K for 2 hours and then cooled up to the reaction temperature.

Results and discussion

Selection of active catalytic system was carried out on the basis of three groups of synthesized modified zeolite catalysts for n-propyl alcohol oxidation reaction into propionic aldehyde, propionic acid and propylpropiponate. The carried out tests have shown that proceeding of n-propyl alcohol oxidation reaction with preferred formation of propionic aldehyde, propionic acid and propylpropiponate depends on zeolite type, distribution of acidic sites over catalyst surface, concentration and nature of introducing cation and the conditions of the reaction as well. On the basis of the experimental data the total scheme of reaction proceeding of oxidation of n-propyl alcohol over metalzeolite catalyst can be depicted as:

$$C_3H_7OH \xrightarrow{+½O_2} CH_3CH_2CHO \xrightarrow{+½O_2} CH_3CH_2COOH \xrightarrow[-H_2O]{+C_3H_7OH} CH_3CH_2COOC_3H_7$$

It has been established that zeolites modified with Cu^{2+} and Pd^{2+} in comparison with another cations are more selective in the processes of lower aliphatic alcohols oxidation into aldehydes, carboxylic acids and esters of carboxylic acids. The ions of bivalent copper, palladium and also Brönsted acidic sites are catalytically active centers for the studied reactions. This circumstance and also the temperature proximity of these reactions create the favourable conditions for the development of catalytic systems for the preferred formation of one of the abovementioned oxygen-containing compounds.
The zeolites investigation of different types has shown that these samples reveal the various activity in the vapour-phase oxidation reaction of n-propyl alcohol (Table 1). As seen from the Table 1, catalysts prepared on the basis of zeolite A are highly more active in the reaction of direct oxidation of n-propyl alcohol into propionic acid. The differences in the activity and selectivity of catalysts appear to be connected with unequal acidity of zeolites on the basis of which catalysts have been synthesized, it being known that in it the ratio of number and strength of acidic sites play an important role.

Table 1. Activity of synthetic and natural zeolites modified with Cu^{2+}(0.5 wt.%) and Pd^{2+}(0.1 wt.%) in the oxidation reaction of n-propyl alcohol

Zeolites	Conversion of n-propyl alcohol, %	Yield, %		
		Propionic aldehyde	Propionic acid	Propyl-propionate
NaX	32.6	25.1	2.9	-
NaY	68.5	41.4	2.6	-
CaA	66.3	2.6	49.1	-
NaA	57.6	2.4	45.1	-
Clinoptilolite (89%)	32.7	2.1	4.8	16.1

Space velocity: 1400 h^{-1}; Mole ratio of alcohol:O_2:N_2=1.0:4.0:5.0;
Reaction temperature: 190^{0}C.

It has been established that in the case of the use of X and Y types zeolites as the catalysts for the oxidation of n-propyl alcohol these catalysts are more active for the oxidation reaction of n-propyl alcohol into propionic aldehyde. At the same time zeolite of clinoptilolite type shows activity in the one-stage synthesis of propylpropionate from n-propyl alcohol oxidation reaction.

Conclusions

The studies carried out over the catalysts, prepared on the basis of natural and synthetic zeolites modified by different metals cations, in the oxidation reactions of aliphatic alcohols have shown that these catalysts are the active catalytic systems for conversion of these alcohols into aldehydes, acids and esters. Activity and selectivity of zeolites in these reactions is caused both oxidation-reduction properties of the elements and acidic-basic properties of zeolite contact itself.

References

[1] L.Jinglin, L.Bin, L.Jiang and et al., J.Catal., 20 (1999) 429.
[2] K.I.Matiyev, A.M.Aliyev, C.M.Mejidova, Azerb. neftyanoye khozaystvo, 1 (1998) 40.
[3] T.N.Shakhtakhtinski, A.M.Aliyev, A.R.Kuliyev, C.M.Medjidova, M.Kh.Muradov, Dokl. AN Rossii, 343 (1995) 4, 496.

Catalysis by a non-functionalized Metal-Organic Framework: Acido-basicity at the external surface of ZIF-8

C. Chizallet, S. Lazare, D. Bazer-Bachi, F. Bonnier, V. Lecocq, E. Soyer, A. Quoineaud, N. Bats
IFP New Energy, BP3, 69360 Solaize, France, celine.chizallet@ifpenergiesnouvelles.fr

Introduction

The design of Metal-Organic Frameworks (MOF) for applications in catalysis is the object of a growing interest. The functionalization of the linker or crystallization of the structure with unsaturated nodes are widespread methods to reach competitive catalytic activities. ZIF-8 [2,3] should not be catalytically active, as the linker is not functionalized and as all nodes are saturated in the bulk structure. However in the present contribution, ZIF-8 is shown to be able to catalyze transesterification of vegetable oil with significant activity. Rationalization of this behavior at the atomic scale is provided by combining CO adsorption monitored by FTIR and DFT calculations. We demonstrate that the acido-basic sites are located at the external surface of the material or at defects, but not in the microporosity of ZIF-8. [4,5]

Experimental section and computational methods

The synthesis of ZIF-8 was carried out with slight modifications to the procedure reported by Huang et al,[2] upon reaction of 2-methylimidazole dissolved in methanol with a zinc hydroxide solution in aqueous ammonia. *In situ* infra-red spectra were recorded at 100 K after adsorption of pulses of CO, on the solid pre-treated in vacuum (10^{-6} mbar) at 473 K. Catalytic tests (transesterification of rapeseed oil by various alcohols, molar alcohol/oil ratio = 27.5) were performed in a stainless steel batch reactor at 473 K. Density Functional Theory calculations were performed within periodic (VASP program, PW91 functional) and cluster (Turbomole program, B3LYP functional) approaches.

Results and discussion

The transesterification of vegetable oil produces alkyl esters (when methanol is used, fatty acid methyl esters –FAME- are obtained and can be used as biodiesel), thanks to acido-basic catalysis. The reaction of rapeseed oil with methanol at 473 K, in the presence of ZIF-8 as a catalyst, led to nearly full conversion into alkyl esters in less than 2 h. This corresponds to a significant improvement in catalytic properties as compared to a conventional $ZnAl_2O_4$ heterogeneous catalyst (fig. 1-a). This improvement is confirmed for the reactions of vegetable oil with ethanol, 1-propanol and 1-butanol. The FTIR spectra obtained after adsorption of CO on ZIF-8 (fig. 1-b) are complex and suggest the existence of available Lewis, Brønsted acid and basic sites.
The nature of plausible active sites were studied by DFT calculations. The three following hypotheses were investigated: (i) the Zn node may be able to increase temporarily its coordination number to achieve Lewis acid type activation ; (ii) a node-to-linker bond may temporarily de-coordinates to activate the reactants by the Lewis acid moiety (unsaturated node) and/or the basic one (unsaturated linker) ; (iii) the active sites may be located at the external surface, or at structural defects of the MOF. Hypotheses (i) and (ii) were invalidated by periodic DFT calculations: both methanol and CO were indeed shown to be unable to be coordinated to the metal within the bulk of the ideal solid.

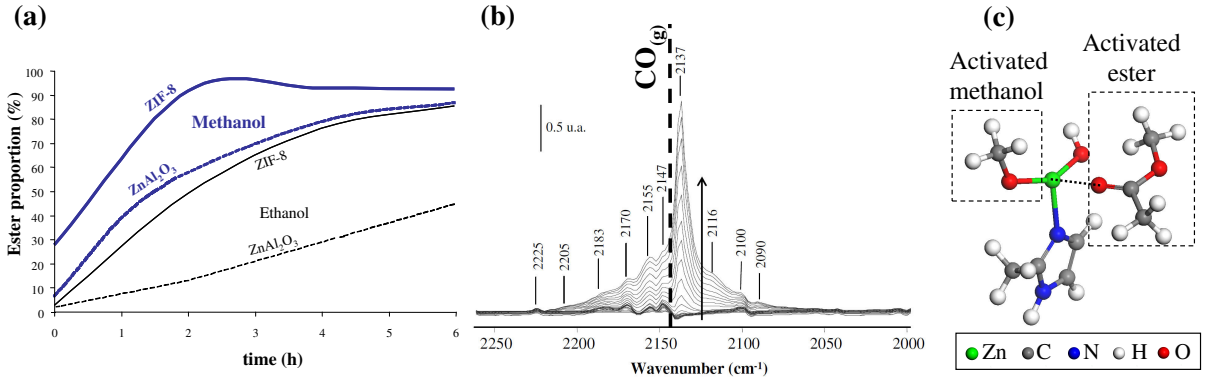

Figure 1. (a) Conversion of vegetable oil into alkyl esters by methanol and ethanol, catalyzed by ZIF-8 or $ZnAl_2O_4$. (b) FTIR difference spectra of ZIF-8 recorded after adsorption of CO, in the CO zone. (c) DFT result depicting the co-activation of methanol and an ester molecule in the vicinity of a Zn_{II} species.

Hypothesis (iii) was validated thanks to cluster calculations (pre-validated by some periodic benchmarks). Various coordination numbers for Zn ions were modelled by specific clusters. Their respective affinity for atmospheric water and CO_2 was calculated *ab initio*. A great variety of sites were thus found the surface: OH and NH groups, hydrogenocarbonates, low-coordinated Zn atoms, and free N^- moieties belonging to linkers. The stability of each kind of species as a function of the operating pressure and temperature was determined thanks a thermodynamic model. An assignment of the CO region of the FTIR spectra can thus be proposed, on the basis of frequency calculations of CO adsorbed on the various sites within various adsorption modes. The complex infrared spectrum is attributed to the coexistence of classical C-adducts of CO with acid sites and other modes on basic sites (O-adducts and side-on adducts). Adsorption energies and CO frequency shifts show that some strong Lewis sites exist (in particular Zn_{II} species), as well as strong Brønsted acid sites (NH groups), together with basic sites (OH groups and N^- moieties). By calculating the co-adsorption of a model ester (methyl acetate) and methanol (fig. 1-c), we show the prevailing role of Zn_{II} species as acid sites, combined with N^- moieties and OH groups as basic ones, in determining the catalytic properties of ZIF-8.

Conclusions

Combining catalytic, infra-red and computational techniques, we show that defects in non-functionalized MOFs and their external surface can play a prevailing role in catalytic applications. This work opens new perspectives on the use of MOFs in catalysis and, more generally, on the properties of their external surface.

References

[1] Farrusseng, D.; Aguado, S.; Pinel, C., *Angew. Chem. Int. Ed.*, **2009**, 48, 7502-7513; Corma, A.; Garcia, H.; Llabrés i Xamena, F. X., *Chem. Rev.*, **2010**, 110, 4606-4655
[2] Huang, X. C.; Lin, Y. Y.; Zhang, J. P.; Chen, X. M., *Angew. Chem. Int. Ed.*, **2006**, 45, 1557-1559.
[3] Parks, K. S.; Ni, Z.; Coté, B.; Choi, J. Y.; Huang, R. D.; Uribe-Romo, F. J.; Chae, H. K.; O'Keeffe, M.; Yaghi, O. M., *PNAS*, **2006**, 103, 10186-10191.
[4] Chizallet, C.; Bats, N., *J. Phys. Chem. Lett.*, **2010**, 1, 349-353
[5] Chizallet, C.; Lazare, S.; Bazer-Bachi, D.; Bonnier, F.; Lecocq, V.; Soyer, E.; Quoineaud, A. A.; Bats, N., *J. Am. Chem. Soc.*, **2010**, 132, 12365-12377

New Insights into Substrate Binding and Activation by Cationic Sites in Zeolites: ETS-NOCV Perspective

E. Broclawik[1*] J. Załucka[2], P. Kozyra[2], M. Mitoraj[2] and J. Datka[2]
[1] *Institute of Catalysis, Polish Academy of Sciences, Niezapominajek 8, 30-239 Krakow*
[2] *Faculty of Chemistry, Jagiellonian University, Ingardena 3, 30-060 Krakow, Poland*
**broclawi@chemia.uj.edu.pl*

Introduction

Electron transfer processes within the active site and a substrate, recognized already as the important factor in catalysis on zeolites [1] may result from individual processes of various symmetry and impact on the substrate bonding and activation. We use new theoretical tool for charge transfer analysis (ETS-NOCV) to decompose redistribution of electron density, accompanying fragments bonding, into independent electron transfer channels and estimate their importance. It allows to extract charge transfer types in systems without strict symmetry and may be used with flexible strategy of dividing multicomponent systems such as zeolitic active sites, into fragments. We have introduced two alternative fragmentation schemes of three-component embedded cluster models of Cu(I) and Ag(I) sites in zeolites hosting adsorbed molecules. They provided insight into electron transfers as well between the substrate and a site as between framework oxygens and a cation. [2-4]. In this contribution we present cross-analysis of charge transfers between the substrate, the cation and framework oxygens, with the focus on the influence of zeolite on donation/backdonation processes, tuning properties of embedded cation and thus activity of Me(I) sites.

Computational

Models of Me(I) cationic sites in ZSM-5 were obtained by combined QM/MM method, linking force field (GULP) treatment of periodic framework with DFT (Turbomole) calculation for a cluster model of the active site. ETS-NOCV analysis, linking the Extended Transition State (ETS) approach with the Natural Orbitals for Chemical Valence (NOCV) method was used to decompose electron density redistribution into independent density flow channels with corresponding contributions to orbital binding energy ΔE_{orb}^{i} (ADF) [5].

Results and discussion

Alternative fragmentations allowed to characterize electron transfer channels from framework oxygens to the cation of appropriate symmetry: opposing σ-donation of substrate bonding electrons and supporting π*-backdonation to substrate antibonding orbitals. While the second process enhances substrate activation (as measured by IR frequency red-shift), the first one weakens activation ability upon embedding transition metal cation in zeolite (see Fig. 1). Thus the activity of a cationic site must be viewed as resulting from framework effect on the sensitive balance between opposing electron transfer channels.

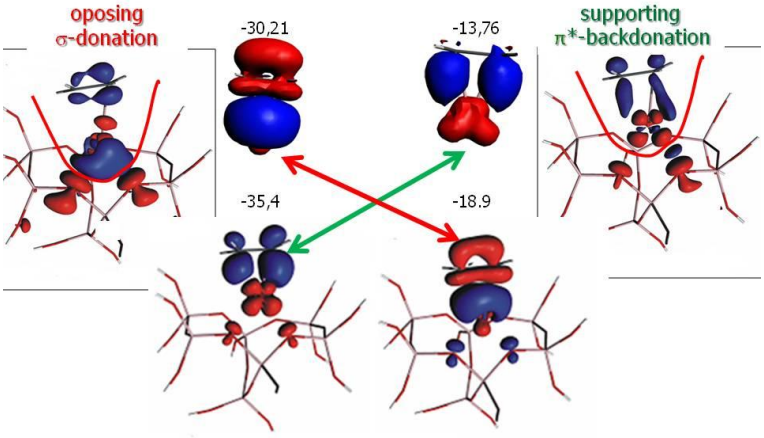

Figure 1 Electron transfers (ΔE_{orb}^{i} in kcal/mol) for ethene on Cu^{+}/Cu(I)-ZSM-5 (up/down) red/blue - electron outflow/inflow. Left/right insets represent charge flow from framework oxygens to cation, responsible for suppressing σ-donation and enhancing π*-backdonation.

.

Detailed analysis for ethene, ethyne and formaldehyde (FA) substrates (see Table 1) showed that activation decrease due to reduction of σ-donation was outweighed by the increase in π*-backdonation for Cu(I) but not for Ag(I) (except ethyne, due to very sensitive triple bond).

	ΔE_{orb}^{i} [kcal/mol]	ethene	ethyne	FA
Cu(I)	opposing σ-donation	-20.0	-21.2	-18.0
	supporting π^{*}-backdonation	-17.8	-17.3	-12.0
	$\Delta\Delta\nu_{calc}$ [cm^{-1}]	-8	-59	-3
Ag(I)	opposing σ-donation	-17.7	-17.8	-12.4
	supporting π^{*}-backdonation	-9.6	-9.8	-
	$\Delta\Delta\nu_{calc}$ [cm^{-1}]	+7	-33	+26

Table 1 Energetic importance of two dominant electron transfers from framework oxygens for Cu(I)- and Ag(I)-ZSM5 and impact on frequency red-shifts due to cation embedding.

Conclusions

Zeolitic framework regarded as an electron reservoir may either support (Cu^{+}) or impair (Ag^{+}) electronic processes underlying catalysis. Thus enhancing effective activity of cationic site requires fine tuning of as well σ-donation as π*- backdonation ability.

References

[1] D. Berthomieu, S. Krishnamurty, B. Coq, G. Delahay, A. Goursot, J. Phys. Chem. B 105 (2001) 1149
[2] E. Broclawik, J. Zalucka, P. Kozyra, M. Mitoraj, J. Datka, J. Phys. Chem. C 114 (2010) 9808
[3] E. Broclawik, J. Zalucka, P. Kozyra, M. Mitoraj, J. Datka, Cat. Tod. (2010) doi:10.1016/j.cattod.2010.08.020
[4] P. Rejmak, M. Mitoraj, E. Broclawik, PCCP 12 (2010) 2321
[5] A. Michalak, M. Mitoraj, T. Ziegler, J. Phys. Chem. A. 112 (2008) 1933

The Kinetic Monte Carlo Simulations Study of the Self-Diffusivity in the One-dimensional Lattice Gas Model with Two Non-equivalent Sites

Alexander Tarasenko and Lubomir Jastrabik
Institute of Physics, v.v.i., Academy of Sciences of the Czech Republic, Na Slovance 2, 182 21, Prague, Czech Republic, taras@fzu.cz

Introduction

Microporous carbons and various zeolites have found recent interest in many areas including chemistry, chemical engineering and materials science, due to their potential for use in catalysis, removal of toxic and odorous chemicals, separation and storage of gases like hydrogen, in the development of the hydrogen fuel cells to name but a few. There is a great interest in the elucidating the fundamental aspects of the adsorption, desorption and diffusion in these rather specific inhomogeneous structures.

In many cases, the efficiency of the application of these materials as molecular sieves or adsorbents decisively depends on the transport properties of the adsorbed molecules. The diffusive mass transfer controls the rates of many processes. Diffusion in porous materials has been studied extensively in model cylindrical pores by Hahn and Kärger [1,2] and Mon and Percus [3,4].

Model

We study the diffusion of guest particles by the kinetic Monte Carlo simulations in the framework of the lattice-gas formalism. The zeolite structure is modeled by one-dimensional lattice with deep and shallow sites. The one-dimensional lattice mimics structures of substances like microporous carbons and zeolites. From the general point of view there is a system of deep sites or traps (spherical chambers in zeolites, pores in carbons, etc.) connected by shallow sites -- easy migration pathways (channels) for the adsorbed particles.

Using simple ideas about the particle migration over such lattice we derive the approximate analytical expressions for the diffusion coefficients and compare the theoretical dependencies with the numerical data. It occurs that these expressions work fairly well in the case of weak lateral interaction between the adsorbed particles. They give qualitative and even semi-quantitative description of the particle migration in this heterogeneous lattice.

We used the kMC simulations for calculations of the tracer and jump diffusion coefficients, adsorption isotherms and isothermal susceptibility for some representative values of the lateral interaction between the adsorbed particles.

Results and discussion

The coverage dependencies for the self or tracer diffusion coefficient are shown in Fig.1. The diffusion coefficient describes diffusion of the tagged particles. The coverage dependencies have a maximum at the stoichiometric loading $\theta=0.5$. The deep adsorption sites act like traps for the migrating particles. As the particle concentration increases, the particles fill the traps and the effective length of the particle jump successions increases and reaches its maximum value at the stoichiometric loading when all deep sites are occupied and all shallow sites are empty. Than diffusion proceeds over the homogeneous quasi-one-dimensional lattice and diffusion coefficient decreases as the tracer diffusion coefficient is a monotonic decreasing

function of the particle concentration for the homogeneous lattice gas systems. Experimentally maxima in diffusion coefficients are known for molecular fluids migrating in zeolites [5]. Using different experimental techniques the authors measured diffusion of methanol in NaX zeolite crystals and obtained what they said: "*the somewhat unusual maximum in the trend of self-diffusivity with loading*." In another experiment they measured the diffusion of water in activated carbons [6]. There was a maximum of the tracer diffusion coefficient at θ=0.5. The experimental dependence is qualitatively the same as plotted in Fig.1 for the case φ=0. Really such behavior is not surprising at all and is universal for the inhomogeneous systems with deep sites and is independent on the symmetry of the lattice, and its dimensionality [7].

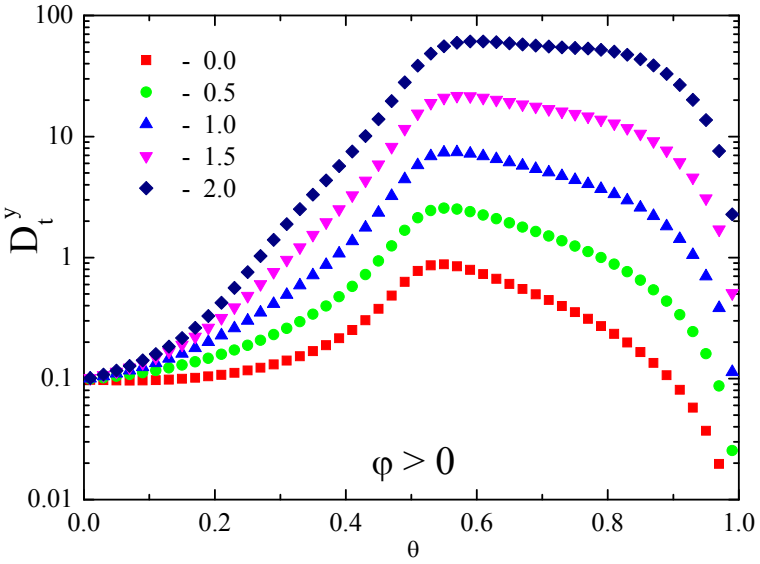

Figure 1. The kMC dependencies of the self diffusion coefficient for different values of the lateral interaction parameter φ as indicated.

Acknowledgements

This work has been supported by the projects KAN301370701 AV CR and 1M06002 of the MSMT CR.

References

[1] Hahn, K., Kärger, J., Kukla, V., Single-file diffusion observation, Phys. Rev. Lett. 76 (1996), 2762-2765

[2] Hahn, K., Kärger, J., Molecular dynamics simulation of single-file systems, J. Phys. Chem. 100 (1996), 316-326

[3] Mon K.K., Percus, J.K.,Self-diffusion of fluids in narrow cylindrical pores, J. Chem. Phys. 117 (2002), 2289-2292

[4] Mon, K.K., Percus, J.K., Pore-size dependence of quasi-one-dimensional single-file diffusion mobility, J. Phys. Chem. C 111 (2007), 15995-15997

[5] Brandani, S., Ruthven, D.M., Kärger, J., Concentration dependence of self-diffusivity of methanol in NaX zeolite crystals, Zeolites 15 (1995), 494-495

[6] Kärger, J., Pfeifer, H., Molecular self-diffusion in active carbons, Pure & Appl. Chern., 61, (1989), 1875-1880

[7] Tarasenko, A., Jastrabik, L., Diffusion of particles over heterogeneous lattices, Appl. Surf. Sci. 256 (2010), 5137-5144

Adsorption and diffusion phenomena of n-hexane within MFI-type zeolite in vapor phase

Yuta Nakasaka, Takahito Kawahara, Hiroki Konno, Teruoki Tago, Takao Masuda
Division of Chemical Process Engineering, Faculty of Engineering, Hokkaido University, N13W8, Kita-ku, Sapporo 060-8628, Japan
Corresponding author email: nakasaka@eng.hokudai.ac.jp

Introduction

Recently, demand for light olefin, especially propylene, which are raw materials of petrochemical industry, are increasing. Accordingly, development of new selective propylene synthesis process by catalytic cracking of naphtha over zeolite has been expected. However, pore diameter of zeolites is close to the molecular size of naphtha component. Therefore, information of diffusion and adsorption mechanism within zeolite are important for design of efficient zeolite catalyst. In this study, diffusivity and amount of adsorbed n-hexane, which was selected as model material of naphtha, within silicalite-1, H-ZSM-5 and H-ZSM-5 with coke was examined by using constant volumetric method and effect of the acid site and coke on the diffusivity and amount of adsorbed n-hexane were discussed.

Experimental

Silicalite-1(SL), H-ZSM-5 and H-ZSM-5 with 43wt% coke (coke-ZSM-5), which is obtained after catalytic cracking of n-hexane, were used as adsorbent. The structure and shape of the silicalite-1, H-ZSM-5 crystal were measured by using XRD and FE-SEM, respectively. The intracrystalline diffusivities (D_{ad}) of n-hexane within those adsorbents were measure by the conventional constant volumetric method at a temperature ranging from 373 K to 573 K and a pressure below 1.5 kPa. In this experiment, adsorption isotherm of n-hexane was also measured. The apparatus and procedure are the same as in our previous work [1]. Effective diffusivity (D_{eff}) which has been used for calculation of effective factor of porous catalyst was calculated by following equation

$$D_{eff} = H \times D_{ad} \quad (1)$$

where H is the partition factor which is obtained from adsorption isotherm.

Results and discussion

Adsorption potential (A) which means the change in free energy when gas component adsorbed on surface of catalyst is calculated as following equation.

$$A = RT \ln (P_0/P) \quad (2)$$

where P_0 is saturated vapor pressure, and P is equilibrium pressure.

Relationship between the adsorption potential, and an adsorbed volume calculated from the adsorption isotherm was correlated to a single line (denoted as characteristic curve [2]), regardless of adsorption temperature and pressure. Figure 1 shows the characteristic curve obtained in this study, and it is clear that the adsorption potentials could be correlated with each single curve against the adsorbed volume. In this figure, characteristic curve of coke-

ZSM-5 was close to that of SL. From this result, it is considered that condition of adsorption site of coke-ZSM-5 become similar to SL because of coke deposited on the acid site of H-ZSM-5. On the other hand, the curve of H-ZSM-5 was different with that of SL and coke-ZSM-5, because the amount of adsorbed n-hexane to H-ZSM-5 was larger than that of those adsorbents.

Figure 2 shows relationship between effective diffusivities of n-hexane within adsorbents and adsorption potential. It is clear that effective diffusivities of n-hexane within those adsorbents correlated with each single line regardless of adsorption temperature. Magnitude of effective diffusivity within H-ZSM-5 and coke-ZSM-5 were reduced to 1/100 of that within SL. In the case of H-ZSM-5, n-hexane molecule strongly adsorbed on the acid site of H-ZSM-5 and residence time of n-hexane on the site becomes long. On the other hand, in the case of coke-ZSM-5, the pore volume of coke-ZSM-5 become small because of deposited cokes on the acid site of H-ZSM-5, and it is considered that the cokes make n-hexane molecules difficult to diffuse within the pore of coke-ZSM-5. Accordingly, effective diffusivities of n-hexane molecules within coke-ZSM-5 were smaller than that in H-ZSM-5.

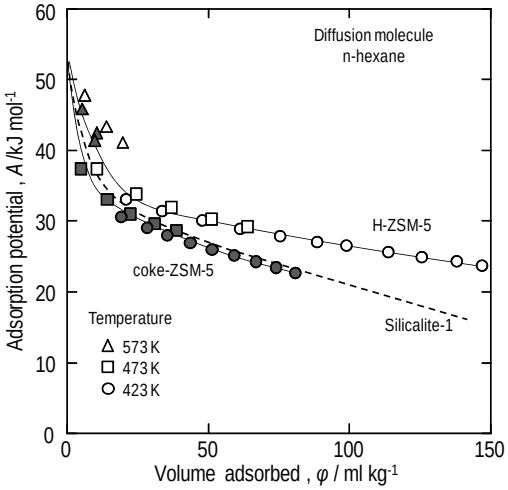

Fig.1 Relationship between adsorption potential and adsorbed volume of n-hexane to the adsorbents

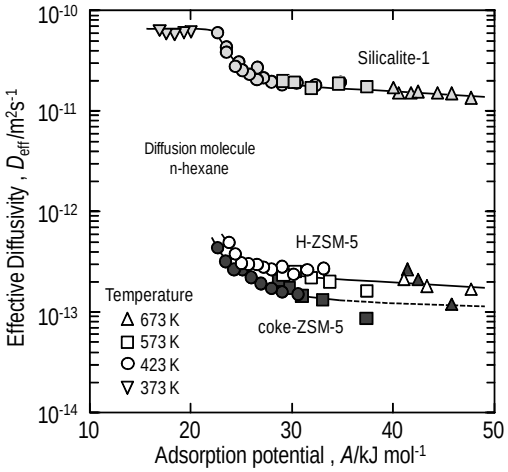

Fig.2 Relationship between effective diffusivity of n-hexane within SL, H-ZSM-5 and coke-ZSM-5 and adsorption potential.

Conclusion

Diffusivity and amount of adsorbed n-hexane within silicalite-1, H-ZSM-5 and coke-ZSM-5 have been measured. In this study, it is found that effective diffusivities of n-hexane within MFI-type zeolite and adsorption potential could be correlated with each single curve.

Acknowledgements

This work was supported by the Research Grant Program from New Energy and Industrial Technology Development Organization (NEDO) of Japan.

References

[1] T. Masuda, Diffusion mechanisms of zeolite catalysts, Catalysis Surveys from Asia, 7 (2003), 133-143

[2] T. Kei-i, Kyuchaku, by Kyoritsuzensho, 1965, Chap. 3, pp.39-42

Flexibility of ZIF-8 through experiments and simulations: swing effect of imidazolate rings in SOD topology

D. Fairen-Jimenez,[1] S. A. Moggach,[2] M. T. Wharmby,[3] P. A. Wright,[3] S. Parsons[2] and T. Düren[1]
[1]Institute for Materials and Processes, School of Engineering, The University of Edinburgh, UK. [2]School of Chemistry, The University of Edinburgh, UK. [3]School of Chemistry, University of St. Andrews, UK., David.Fairen@ed.ac.uk

Introduction

Zeolitic imidazolate frameworks (ZIFs) have emerged as a very promising family of MOFs. Their great stability, high porosity, framework diversity, transition metal centres and tailored linkers make them ideal candidates for gas separation and storage applications. Although many MOFs show the same adsorption behaviour as traditional rigid microporous materials, some of them exhibit structural changes in the framework during the adsorption process, leading to interesting selectivity properties. In the prototypical structure ZIF-8, we have observed experimentally that molecules which are theoretically too large to pass through the windows of the framework are adsorbed in the material. The adsorption of such large molecules implies flexibility, associated with a swing effect in the imidazolate linkers. However, a thorough understanding of this behaviour is a pre-requisite to exploit this phenomenon. In this work, we explore structural flexibility in ZIF-8 using different experimental techniques combined with molecular simulations.

Previous work demonstrated the effect of pressure up to 1.47 GPa on structural changes of ZIF-8.[1] Though this pressure is much higher than a typical adsorption pressure, it is essential to explore structural changes caused by the adsorption of fluid molecules. On applying high pressure to ZIF-8 (i.e. 1.47 GPa) a new phase was observed which we refer here as ZIF-8HP. In this work, we have used ZIF8-HP structure together with the structure of the conventional ZIF-8 to simulate N_2 adsorption using GCMC.

Experimental

ZIF-8 was prepared following the method described by Huang et al. in ref 1. N_2 adsorption isotherms were recorded at 77 K using a Micromeritics ASAP 2020 instrument. X-ray diffraction samples were introduced in quartz capillaries, and outgassed under high vacuum. Before being sealed, one of the samples was loaded with N_2 at a relative pressure of 0.4 P/P_0. *In-situ* XRD data were collected on station I11 at the Diamond light source. The adsorption of N_2 was investigated using grand canonical Monte Carlo (GCMC) method to model gas adsorption on a series of ZIFs using the multipurpose simulation code Music. The standard 12-6 Lennard-Jones (LJ) potential was used to model the dispersive interatomic interactions (UFF and TraPPE force fields) whereas the Ewald summation technique was used to calculate the electrostatic interactions between N_2 molecules.

Results and discussion

The experimental adsorption isotherm of N_2 at 77 K showed two steps occurring at 2×10^{-3} and 2×10^{-2} P/P_0 (Figure 1, left). However, in contrast with the experimental curve, no steps were found during the simulations on a rigid ZIF-8 structure obtained at ambient pressure. The isotherm simulated in this structure fits the experimental structure in the low pressure range of the isotherm very well, correctly describing the Henry constant, which is a direct measure of the strength of the interactions. However, the prediction deviates from the experimental data when the pressure is higher than 2×10^{-4} P/P_0. When running the simulations on the ZIF-8HP phase previously found at 1.47 GPa, the isotherm deviates from the experimental at low pressure, but predicts the step-shape of the experimental isotherm correctly. The combination of both simulated adsorption isotherms is able to match the experimental isotherm.

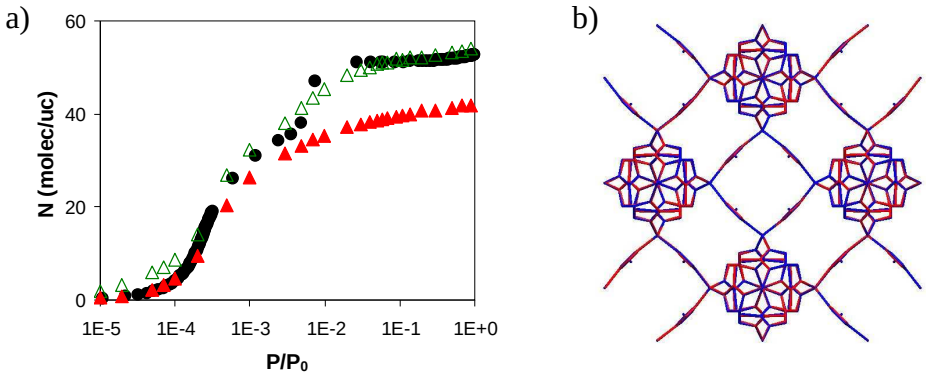

Figure 1. a) N_2 adsorption on ZIF-8 at 77 K: experimental, black circles; and simulated data on ambient pressure structure, ZIF-8, red closed triangles and high-pressure structure, ZIF-8HP, green open triangles. b) Overlay of ZIF-8 loaded with N_2 (blue) and ZIF-8HP (red).

In order to confirm that the ZIF-8HP structure is indeed observed at high nitrogen loadings, we measured in situ powder XRD measurements on ZIF-8 and a separate sample which was loaded with N_2. The comparison of the N_2-ZIF-8 structure with ZIF-8HP shows no difference, showing the same reorientation of the imidazolate linkers (Figure 2, right). This confirms the existence of a change in structure caused by a swing effect of the imidazolate linker.

We extended our research to study the influence of different functional groups on the swing of the imidazolate rings. We studied in detail the effect of the flexibility on the window sizes and therefore its effect on the mobility of molecules with different kinetic sizes through the ZIF frameworks. We have found that tuning the flexibility, i.e. choosing different functional groups in the imidazole linker, the swing effect can modify the diffusivity of fluids through the porous network. We propose that these new ideas provide an extra parameter in the design of new porous solids.

References

[1] Moggach, S., Bennett, T., Cheetham, A. Angewandte Chemie International Edition 48 (2009), 7087-7090.

Multi-scale simulations of structure directing effect in zeolite synthesis

B.M. Szyja, R.A. van Santen, E.J.M. Hensen
Inorganic Materials Chemistry, Department of Chemical Engineering and Chemistry, Eindhoven University of Technology, Den Dolech 2, 5612AZ Eindhoven, The Netherlands,
b.m.szyja@tue.nl

Introduction and description of the model

The scope of this work is the investigation of the structure direction effect in the pentasil zeolite synthesis. In our study we have followed the scheme of synthesis proposed by Kirschhock et al [1], where after initial stage if oligomerization, the structures having 11 silicon atoms in the form of 3 condensed 5-membered rings have been discovered to be stable. Subsequently three such oligomers would agglomerate to form Si_{33} precursor.

This is the earliest possible stage where the structure direction can take place, as the MFI and MEL type Si_{33} precursors have different structures – as opposed to Si_{11} oligomers, which geometry is identical for MFI and MEL. However, there are more stages where such an effect can be present – i.e. the agglomeration of the Si_{33} precursor into bigger units can also be influenced by the interaction with the template.

This work is focused on three different stages of the zeolite formation, which have been investigated using different scale methods. From the simultaneous analysis of all the results, we have concluded that the role of the template changes during the synthesis process and it is not limited to the simple lock-and-key model as believed previously.

Results and discussion

We have identified three possible connections between two Si_{11} units that distinguish the structures of MEL and MFI precursors. The MEL one have 4- and 6-membered rings in the structure, whereas the MFI precursors contain only 5-rings. In order to be consistent with experimental findings, we should expect that tetrabutylammonium interacts stronger with either 4- or 6-ring, and tetrapropylammonium stabilizes the 5-ring. This is indeed the case, it is confirmed by the results of DFT Molecular Dynamics simulations, gathered in Table 1.

Table 1. Interaction energy [eV] of templates located in the internal and external location with respect to the precursor.

	TPA (in)	TPA (out)	TBA (in)	TBA (out)
4-ring	-8.0	-3.6	-9.8	-5.8
5-ring	-6.9	-3.9	-7.8	-4.0
6-ring	-7.9	-3.9	-10.5	-4.8

The effect of the stabilization of the 4- and 6-rings is evident for the TBA located either in internal or external space. The interaction energy of TPA is also the strongest with 5-membered ring, when the template is located outside, however – from the inside, the interaction is weaker by approx. 1 eV.

The analysis of the next stage can provide the explanation of this finding. As soon as the initial channel in the precursor is fully formed, there is not enough room for the template cation inside the cavity, and its preferable position is outside, in the space that is equivalent to the channel intersection in the fully formed framework [2]. As soon as the TPA is pushed

outside, it cannot stabilize the internal part of the precursor, and only the external interaction can play a role. The relevant snapshots from classical MD simulations are shown in Figure 1.

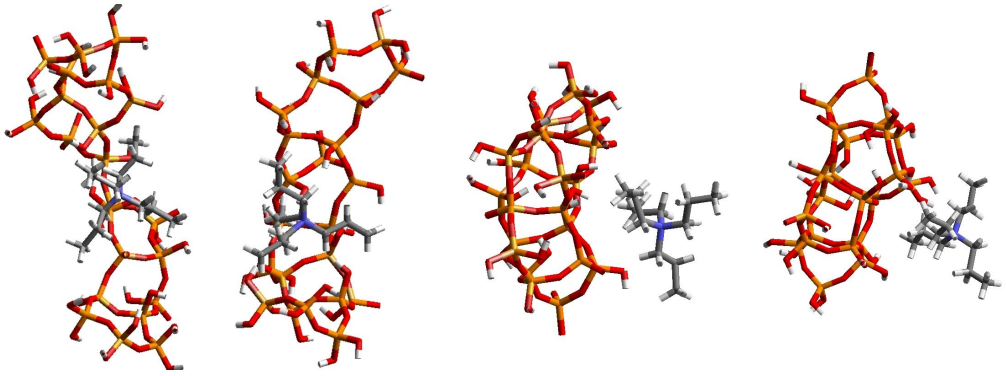

Figure 1. The position of the TPA with respect to the silicate during the channel formation.

Again, the results of the channel formation explain the interaction of the template/silicate system in the subsequent step of agglomeration of two Si_{33} units. The important factor in this step is the length of the carbon chain in the TAA cation. The chains of the TBA are too long and cause steric repulsion when the Si_{33} precursors are aligned in the same way as in the final MEL framework, and therefore not all intersections are occupied. As TPA has shorter chains – full occupation is possible for TPA/MFI system. However, the stronger interaction with TBA compensate this effect – the stabilization energies amount to -164 kcal/mol for TPA/MFI system and -170 kcal/mol for TBA/MEL. The results of the framework decomposition to the interacting species is shown in Figure 2.

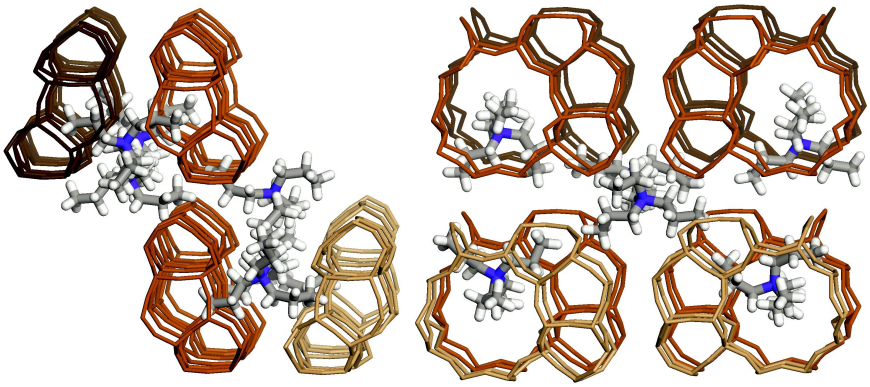

Figure 2. The proposed stable structure – the results of agglomeration of 8 Si_{33} precursors.

Conclusions

The role of the template molecules is not limited to any particular stage of the synthesis. Instead, it is a "multipurpose" molecule, its different properties are of importance in the steps of: (a) stabilization of the small ring silicate species, (b) keeping the shape of the channel intact and (c) alignment and stabilization of two Si_{33} precursors into a larger agglomerate.

References

[1] Kirschhock, C.E.A., Ravishankar, R., Verspeurt, R., Grobet, P.J., Jacobs, P.A., Martens, J.A., J. Phys. Chem. B, 103 (1999), 4965–4971.
[2] Szyja, B.M., Jansen, A.P.J., Verstraelen, T., van Santen, R.A., Phys. Chem. Chem. Phys., 11(35), 7605-7610.
[3] Szyja, B.M., Hensen E.J.M., van Santen, R.A., Catal. Today (2010), doi:10.1016/j.cattod.2010.08.018

Proton redistribution in silicon island of SAPO material

Mahsa Zokaie, Unni Olsbye, Karl Petter Lillerud and Ole Swang*
inGAP Centre for Research-Based Innovation/ Centre for Materials Science and Nanotechnology, Department of Chemistry, University of Oslo, P.O. Box 1033, Blindern, N-0315 Oslo, Norway. Email: Ole.Swang@kjemi.uio.no.

Introduction

SAPOs are crystalline microporous aluminophosphates in which some phosphorus atoms are replaced by silicon-proton pairs. SAPO-34 has the highly symmetric chabazite topology with only one symmetrically independent tetrahedral site (T-site) and four unique oxygen sites. The protons introduced to ensure charge neutrality after silicon inclusion may coordinate to one of the four different oxygens. The preferred position of the proton at isolated acid sites has been the subject of both experimental [1] and computational [2] studies. An interesting feature of SAPOs is the formation of so-called «silicon islands», which are formed when at least two adjacent T sites are occupied by silicon. Such islands have also been studied experimentally [3] and theoretically [4]. In the latter study, it was assumed that the protons necessary to keep the silicon island neutral would occupy the same positions as those preferred for solitary silicon atoms. Preliminary computational studies led us to doubt that assumption. In the present work, we have investigated the relative stabilities of different proton distributions around a 5-atom silicon island in SAPO-34 through periodic molecular mechanics energy minimization calculations, and we arrive at a number of criteria that a proton distribution must satisfy to be stable.

Methodology

A silicon island formed by replacing 4 Al and 1 P atom with Si was chosen for closer scrutiny. This is believed to be the smallest stable silicon island in SAPO-34 [4]. Three protons are needed to provide charge neutrality after substitution. The central Si atom is connected to four other Si atoms through oxygen bridges; hence we assume that no protons will bond to its associated oxygen atoms. The four remaining silicon atoms each have three oxygen atoms to which protons can bond. If we assume that each tetrahedron will accommodate only one proton, we arrive at 108 different possible structures, only differing in the proton positions. Each of these structures were optimized at constant pressure using the force field of Catlow [5] as implemented in the GULP program [6] as part of the Materials Studio 5.0 program system[7].

Results and discussion

The relative energies for the 108 structures are plotted in Figure 1e. The results indicate that the proton placement is critical for stability, as the limit deviation in our data set is as high as 90 kJ/mol. An attempt to make a simple correlation between stability and electrostatic repulsion between the three protons based on their mutual positions failed. Careful analysis of the different structures yielded the following criteria for excluding structures as unstable:

- Two protons connected to oxygen atoms in the same ring, disregarding ring size
- All three protons connected to oxygen atoms connected to silicon atoms in the same 6-ring

- At least one proton pointing towards large zeolite cavities or rings of larger than 8 T-atoms (Structures with proton on O(4))
- At least one proton connected to an oxygen atom in the O(2) positions

(O(4) is the common oxygen of one 4-ring and two 8-rings and O(2) is the oxygen which is shared by one 4-ring , one 6-ring and one 8-ring.)

Excluding all these structures, the remaining structures were all within 20 kJ/mol of the ground state (red points in Fig. 1e)

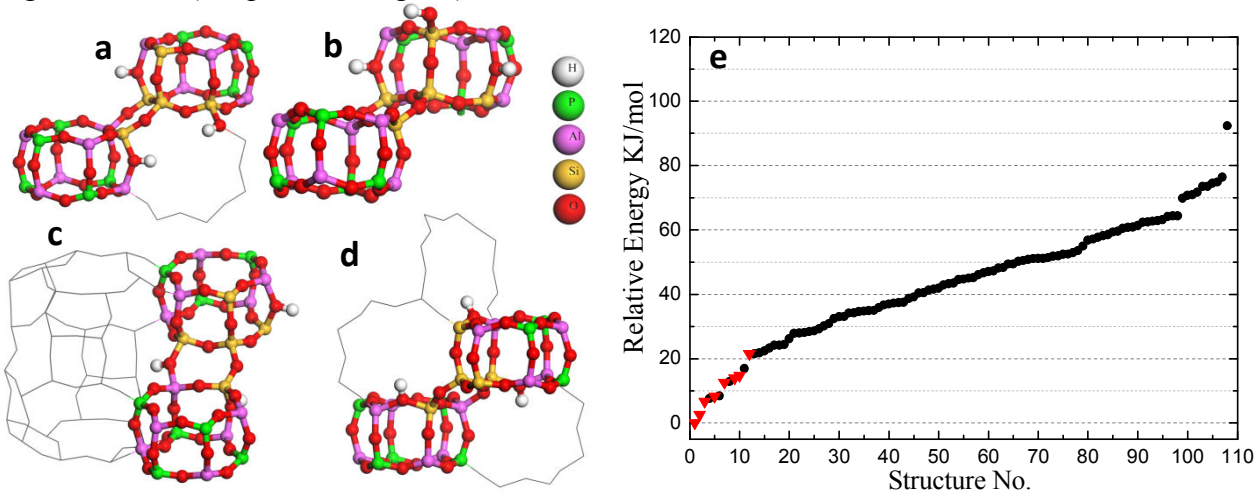

Figure 1.a-e: a-d) examples of unstable structure due to: a)Protons connected to oxygen atoms in the same ring, b)Protons connected to tetrahedra located in same double six ring, c)Proton pointing to open space (connected to O(4)) and d)Proton connected to O(2). e)Relative energy of different structures calculated by molecular mechanics. Black points are structures belonging to at least one of the abovementioned categories and red points are remaining stable structures.

Conclusions

Our calculation shows that the most stable configurations of protons around a silicon island cannot be predicted from the most stable proton coordination for a single silicon atom. This fact is borne out by the great energy difference of the possible proton configurations. We have established criteria for stability for the proton configuration around a 5-atom silicon island in SAPO-34. The transferability of finding to larger islands and other topologies, is presently under investigation in our group.

References

[1] Smith, L., A.K. Cheetham, R.E. Morris, L. Marchese, J.M. Thomas, P.A. Wright, J. Chen, On the Nature of Water Bound to a Solid Acid Catalyst, Science, 271 (1996), 799-802

[2] Shah, R., J. D. Gale, M. C. Payne, Comparing the acidities of zeolites and SAPOs from first principles, Chemical Communications, (1997), 131-132

[3] Derewinski, M., M.J. Peltre, M. Briend, D. Barthomeuf, P.P. Man, Solid-state transformation of SAPO-37 molecular sieve above 1100 K, Journal of the Chemical Society, Faraday Transactions, 89 (1993), 1823-1828

[4] Sastre, G., D.W. Lewis, C.R.A. Catlow, Modeling of Silicon Substitution in SAPO-5 and SAPO-34 Molecular Sieves, The Journal of Physical Chemistry B, 101 (1997), 5249-5262

[5] Schröder, K.-P., J. Sauer, M. Leslie, C. Richard, A. Catlow, J.M. Thomas, Bridging hydrodyl groups in zeolitic catalysts: a computer simulation of their structure, vibrational properties and acidity in protonated faujasites (H---Y zeolites), Chemical Physics Letters, 188 (1992), 320-325

[6] Gale, J.D., GULP: A computer program for the symmetry-adapted simulation of solids, J. Chem. Soc., Faraday T rans., 93 (1997), 629-637

[7] Materials Studio 5.0, Accelrys Software Inc., San Diego (http://www.accelrys.com).

Insigths Into Kinetically Driven Molecular Separations in 8-ring Zeolites from Molecular Dynamics

Aldo F. Combariza, German Sastre, and Avelino Corma
Instituto de Tecnología Química, Universidad Politécnica de Valencia, Consejo Superior de Investigaciones Científicas, Av de Los Naranjos S/N, 46022 Valencia, Spain
E-mail: afabri@itq.upv.es, gsastre@itq.upv.es, acorma@itq.upv.es

Introduction

Zeolites with cages and channels separated by 8-ring windows have been recognized as potential candidates for the entropic separation of hydrocarbons with sizes close to the 8-ring window aperture. Materials recently synthesized such as ITQ-3 [1], ITQ-29 [2], and ITQ-32 [3] allow the molecular sieving of hydrocarbons with similar kinetic diameters.

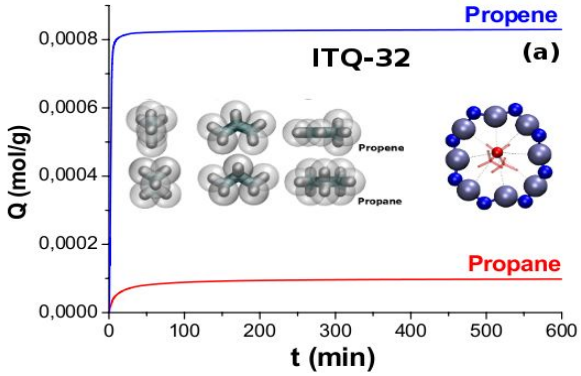

Fig. 1 Uptake of Propane and Propene in zeolite ITQ-32.

In the present communication, we report results from molecular dynamics (MD) on the behaviour of methane, ethane, propane, and propene adsorbed in three different all-silica 8-ring zeolites: LTA[1], ITE[2], and, IHW[3]. Our objective is twofold: to shed ligth on the kinetic character of the molecular sieving process, and to characterize the molecular motion of the guest according to the framework topology.

Methodology

To model the short and long-range interactions between atomic centers we have initially defined a potential energy surface taking into account three main terms: the zeolite potential energy (V_{zeo}), the guest potential energy (V_{guest}), and the intermolecular potential energy contribution, ($V_{zeo\text{-}Guest/Guest\text{-}Guest}$) [4]. We have used the NVE ensemble for the MD simulations and histogram sampling for the probability density calculations. Simulation cells are generated by appropriate scaling of the experimentally reported unit cells. The loading is set to four guest molecules per simulation cell for all systems, to ensure that guest intraintercage mobility is not controlled by adsorbate-adsorbate interactions. Intracrystalline self-diffusion constants were obtained from the Einstein relation, and occupation probability density relative to the center of mass of the guest molecules was determined from a history sampling procedure. From the self-diffusion coefficients obtained at different temperatures, it was possible to estimate the Arrhenius activation energy. Our calculations show that the linearity, and thus the validity of the Arrhenius behavior, is not comprehensive over the whole range of

temperatures, therefore the calculated values of activation energy should only be seen as a qualitative result (*Vide infra*).

Results

Table 1. Self-Diffusion coefficients and Arrhenius activation energies for adsorbates in pure silica 8-ring zeolites. Self-Diffusion coefficients for CH_4, C_2H_6, and C_3H_6, are reported at 600 K. Values for C_3H_6 and C_3H_8 are reported separately at 1200 K.

		Self-Diff. Coeff. D_s (m^2/s) **Activation Energy** *AE(kJ/mol)*				
Framework	**Critical Window Size**	**CH_4** D_s10^{-9}	**C_2H_6** D_s10^{-10}	**C_3H_6** D_s10^{-11}	**C_3H_6** D_s10^{-10}	**C_3H_8** D_s10^{-11}
Si-LTA	*4.1*	*6.1 – 2.5*	*4.3 – 2.9*	*5.6 – 7.6*	*1.5 – 7.6*	*3.8 – 21.8*
Si-ITE	*3.8*	*11 – 2.6*	*12 – 5.6*	*7 – 14.9*	*3.4 – 14.9*	*16 – 29.9*
Si-IHW	*3.5*	*3.9 – 7.1*	*1.1 – 7.4*	*0.82 – 12.3*	*0.56 – 12.3*	*1.5 – 54.1*

Discussion and Conclusions

Self-diffusion coefficients show a decreasing trend correlated with increasing guest kinetic diameter sizes and decreasing zeolite critical window size, confirming experimental measurements on the diffusion hindrance exerted by the eight-ring window present in the structure of the framework. Guest translational long-range motion is shown to be highly influenced for the topological features of the framework, with the dimensionality of the diffusion paths presented by the framework posing a noticeable influence. The influence of the eight-ring window size of the framework is clearly seen by comparing the diffusional coefficients of methane, ethane, and propene, giving larger values for the wider window opening of Si-LTA and lower for the somewhat elongated conformation of the Si- IHW zeolite. This trend is confirmed by looking at the activation energies, which also show an increasing tendency in the order Si-LTA, Si-ITE, and Si-IHW. Propane and propene inter- and intracage motion comparison allows one to see a somewhat different picture, with a higher intercage motion for propane in Si-ITE, which precludes the rationalization of the self-diffusion coefficient based on the critical size of the windows. Thus, the framework topology will dictate the diffusional behavior of the guest, which can be clearly appreciated by the differences in activation energies and self-diffusional constants calculated.

Acknowledgements

Funding through Ministerio de Ciencia e Innovación (Project MAT2007-64682) and computing time from Red Española de Supercomputación are gratefully acknowledged. A.F.C. thanks the Instituto de Tecnología Química UPV-CSIC for a Doctoral Research Fellowship.

References

[1] Corma, A.; Rey, F.; Rius, J.; Sabater, M. J.; Valencia, S. Nature 2004, 431, 287–290.
[2] Camblor, M. A.; Corma, A.; Lightfoot, P.; Villaescusa, L. A.; Wright, P. Angew. Chem., Int. Ed. 1997, 36, 2659–2661.
[3] Cantin, A.; Corma, A.; Leiva, S.; Rey, F.; Rius, J.; Valencia, S. J. Am. Chem. Soc. 2005, 127, 11560–11561.
[4] Combariza, A. F.; Sastre, G.; Corma, A. J. Phys. Chem. C 2009, 113, pp 11246–11253.
[5] Combariza, A. F.; Sastre, G.; Corma, A. J. Phys. Chem. C 2011, 115, pp 875–884.

Location of diphenyl-polyene within non acidic zeolites. A combined theoretical and spectroscopic study of the sorption sites

Matthieu Hureau, Alain Moissette, Claude Brémard
LASIR, UMR-CNRS 8516, Bât C5 Université de Lille 1 Sciences et Technologies, 59655 Villeneuve d'Ascq cedex, France E-mail: matthieu.hureau@univ-lille1.fr

Introduction

The internal porous void of the zeolite might induce high confinement and high electrostatic field. The combined effects of the tight fit of aromatic molecule in zeolite channel, high aluminum content and highly polarizing cation can generate spontaneously radical cation-electron pairs or can stabilize photoinduced charge separated states for long times. Although the observation of long-lived charge separated states within the zeolite internal void space is well-known, most of the parameters stabilizing these systems have to be clearly elucidated to develop potential applications. Particularly the influence of the framework topology, extraframework cation and aluminum content has to be carefully understood.
In that context, we have used diphenyl-polyene (DPP) molecules (**Figure 1**) (t-Stilbene, 1,4-diphenyl-1,3-butadiene, 1,6-diphenyl-1,3,5-hexatriene) as molecular probes to study the adsorption within three non-acidic medium pore zeolites (ferrierite *FER*, ZSM-5 and mordenite *MOR*) and to investigate the behavior of the occluded molecule as a function of zeolite structure, charge compensating cation and Si/Al ratio. We have used diffuse reflectance UV-visible absorption (DRUVv), Raman scattering and fluorescence spectroscopy to monitor the direct exposure of DPP crystals to dehydrated zeolites in the absence of solvent and under inert gas. We have also determined the preferred sorption site of the probe molecule by using Monte Carlo simulations.

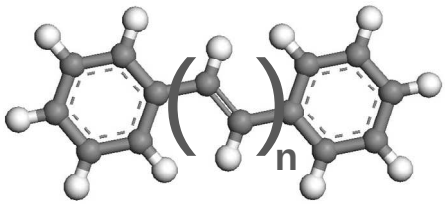

Figure 1: Diphenyl-polyene molecules (n= 1: *trans*-Stilbene, n= 2: 1,4-diphenyl-1,3-butadiene, n= 3: 1,6-diphenyl-1,3,5-hexatriene)

Results and discussion

Monte Carlo simulations and subsequent energy minimization procedures show that the molecules can penetrate into the void space of each zeolite. The calculations show evidence of the close interaction between the aromatic rings of the occluded molecule and the charge compensating cation. The theoretical data through the distribution of calculated energies show the presence of two different sorption sites depending on the cation size. Thus, for small Li^+, Na^+, K^+ cations, the molecule is facially coordinated to the cation while for Rb^+, Cs^+ cations, the molecule is not facially coordinated to the cation but is located in its the close vicinity as shown in **Figure 2**.

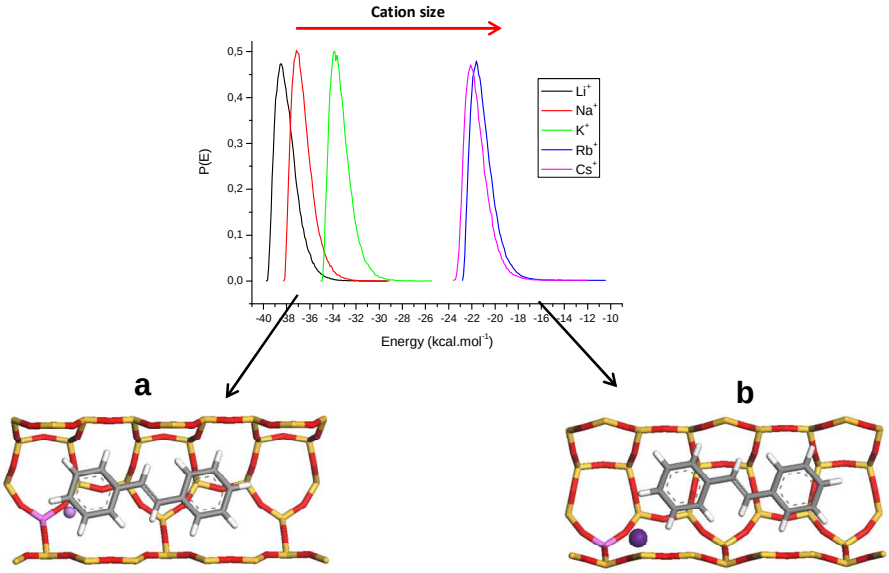

Figure 2: Distribution of calculated energies of *t*-Stilbene molecules occluded in M^+-exchanged ferrierite. **Picture a:** Predicted conformation and sorption site in ferrierite of *t*-Stilbene facially coordinated to the extraframework cation M^+ (M^+ = Li^+, Na^+ and K^+). **Picture b:** Predicted conformation and sorption site in ferrierite of *t*-Stilbene near the extraframework cation M^+ (M^+ = Rb^+ and Cs^+).

In order to corroborate the theoretical data, complementary experiments were carried out using DRUVv, fluorescence and Raman spectroscopies. The DRUVv spectra exhibit a red shift of the absorption band corresponding to the occluded molecule when the charge compensating cation size increases. The fluorescence spectra confirm these features by highlighting various environments for the adsorbed molecule depending upon the cation type. The Raman spectra show also evidence of a significant difference in the vibration spectra recorded according to the cation size (**Figure 3**).

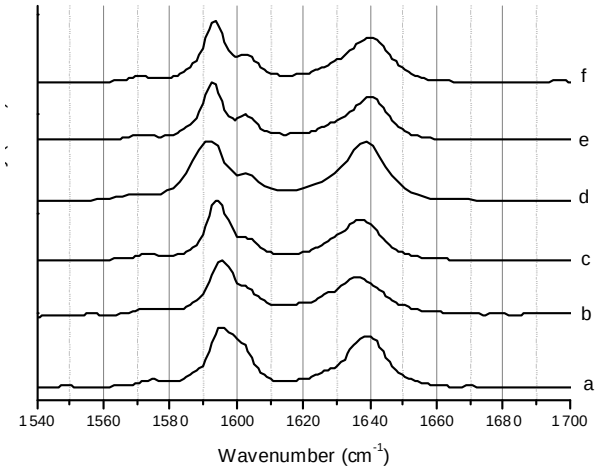

Figure 3: FT-Raman spectra in the 1540-1700 cm^{-1} range recorded at room temperature of *t*-Stilbene molecules occluded in: **a)** silicalite-1, **b)** TS-1, **c)** $Na_{6,6}$ZSM-5, **d)** $K_{6,6}$ZSM-5, **e)** $Rb_{6,6}$ZSM-5, **f)** $Cs_{6,6}$ZSM-5.

Influence of organic ligand functionalization on the adsorption properties of flexible MIL-53(Fe) materials: a study by experiments and computations

Naseem A. Ramsahye[1], Thuy Khuong Trung[1], Thomas Devic[2], Patricia Horcajada,[2] Pascal Yot[1], Christian Serre[2], François Fajula[1], Gérard Férey[2], Philippe Trens[1]
1 Institut Charles Gerhardt, UMR CNRS 5253, Ecole Nationale Supérieure de Chimie de Montpellier, 8 rue de l'Ecole Normale, 34296 Montpellier cedex 5, France
2 Institut Lavoisier, UMR CNRS 8180, Université Versailles Saint Quentin, 45 avenue des Etats-Unis, 78035 Versailles, France. philippe.trens@enscm.fr

Introduction

Certain MOFs, such as the MIL-*53(Al, Cr, Fe)* series, are flexible and undergo a structural transition between two or more phases during the adsorption of both polar and non-polar molecules.[1] In the case of MIL-53(Fe), 4 distinct phases have been observed during the adsorption of alkane molecules; a *very narrow* pore (*VNP*), two *intermediate* forms (*int1* and *int2*), and a *large* pore (LP) form.[2] The extent and the mechanism of this "breathing" depend on the identity of the metal centre, which is a parameter that may be varied in order to modify the properties of the material. A second way to modify the physicochemical properties of the material is the substitution of functional groups for one or more H atom on the organic linkers. The effect of this would be to provide new interaction sites, and in the case of flexible MOFs, can alter the flexibility of the framework. New intraframework interactions would change the chemical potential required to induce the phase transition, and a substitution on the aromatic rings can change the nature of the pi electron system, and thus any interaction between the aromatic rings that may stabilize certain phases. In this study, we have combined experimental and computational techniques to study and characterize the behavior of a series of modified MIL-53(Fe)-X materials (X=Cl, Br, CH_3, NH_2) upon adsorption of normal alkanes. The use of non-polar alkanes as adsorbates allows the study of the physical properties of the different frameworks without the presence of any specific interactions between the adsorbate and the framework.

Experimental

The isotherms for the adsorption of the normal alkane series *n*-hexane to *n*-nonane on the materials were obtained by manometric at 313K, and included kinetic measurements. The modified MIL-53(Fe) samples were synthesized following the procedures already published.[3] In their activated forms, these materials are all initially in a *VNP* form. In order to obtain further insight into the adsorption process at the molecular level, the isotherms and adsorption enthalpies were calculated using classical Grand Canonical Monte Carlo simulations and x-ray diffraction experiments (PXRD) enabling a complete study of the structure and changes during the process.

Results and discussion

Our results collectively show that functionalisation leads to a marked modification of the flexibility of the MIL-53(Fe)-X materials and their behaviour upon adsorption. The exact behaviour depends on the adsorbate and the analogue at hand. As per the other members of the MIL-53 family, the isotherms contain 2 regions separated by a substep (figure 1), corresponding to at least two different structures, *i.e.* more than one phase. The exception is

the MIL-53(Fe)-Cl case, where no features on the isotherms indicate a phase transition. However, the PXRD, the GCMC simulations and kinetic data show otherwise.

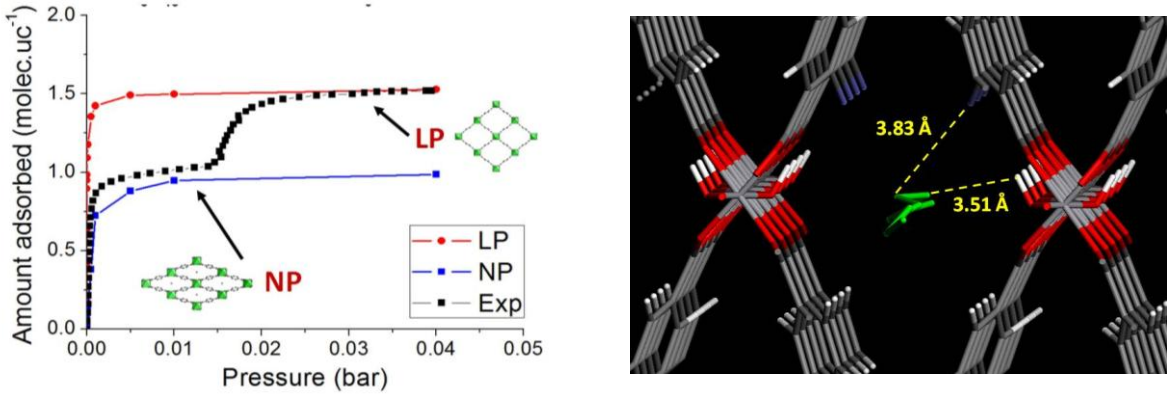

Figure 1: *Left:* Comparison of the experimental and the calculated isotherms in the NP and LP forms for *n*-octane molecule in MIL-53(Fe)-CH_3. *Right:* A typical configuration of n-nonane in MIL-53(Fe)-Br (*narrow pore*, *NP*), showing an interactions with the framework.

For the MIL-53(Fe)-Br and $–CH_3$ forms, the GCMC simulations confirm that the substeps are due to the presence of the NP and LP forms, although the story is more complex than the non-modified MIL-53(Cr, Al, Fe). The structural transition starts from the *VNP*, passes through the *NP* form and finishes at the *LP* form, thus differing from the non-modified MIL-53(Fe) material in that no intermediate *int1* pore form is observed. The pressures at which the transitions are increasingly lower as one increases the alkyl chain length of the adsorbate, an effect which is rationalised in terms of the adsorption enthalpy and the interactions that occur within the pores. These calculations demonstrate that the addition of a $–CH_2$ group on the adsorbate has an associated enthalpy, and that these alkanes have an enthalpy of adsorption that are at least as high as those measured with polar molecules (e.g. CO_2). This indicates that the breathing may be induced by non-specific van der Waals interactions. Our simulations also show that the orientations of the molecules within the pores play an important role in governing the amounts adsorbed than the conformation of the alkanes, but these factors do not determine the pressure at which the structural change occurs. Crystalline phase mixtures have been observed from our XRD data during the phase transitions, which may mean that the transitions are not necessarily homogenous.

Conclusions

This study characterizes the properties of a series of modified MOF materials by a combination of experimental and computational techniques showing that the behavior of the material upon adsorption is greatly influenced by the ligand modification. Our results have been further rationalized by a molecular level study by computational modeling, allowing the prediction of the isotherms, enthalpies and a molecular level mechanism of adsorption.

Acknowledgements

The authors are grateful for funding from the French ANR project “SAHFS”.

References

[1] Tanaka, D. *et. al., Angew. Chem. Int. Ed* **2008**, *47*, 3914
[2] Llewellyn, P. L. *et. al., J. Am. Chem. Soc.* **2009**, *131*, 13002
[3] Devic, T. *et. al., Journal of the American Chemical Society* **2010**, *132*, 112

Effect of linker substituents on the epoxidation performance of V-MIL-47

Matthias Vandichel[1], Karen Leus[2], Yingya Liu[2], Michel Waroquier[1], Pascal Van Der Voort[2] and Veronique Van Speybroeck[1]

[1] *Center for Molecular Modeling, Ghent University, Belgium*
[2] *Center for Ordered Materials, Organometallics and Catalysis, Department of Inorganic and Physical Chemistry, Ghent University, Belgium*
Matthias.Vandichel@Ugent.be

Introduction

Metal Organic Frameworks (MOFs) are crystalline porous solids composed of a three-dimensional network of metal ions held in place by multidentate organic molecules. In recent years, MOFs have received considerable attention as potentially valuable materials for gas storage and catalysis. Until now, most of the studies on the catalytic activity of MOFs are focused on structures that contain coordinative unsaturated metal sites, as it is often believed that the coordinative saturated MOFs will not be catalytically active. In this contribution we will discuss the catalytic performance of a completely saturated Metal Organic Framework, V-MIL-47 [1], for the oxidation of cyclohexene [2]. In this case, the catalytic activity need to be explained by accessible surface sites or internal defects. Furthermore, the influence of the amine and nitro functionalized MIL-47 on the oxidation of cyclohexene will be discussed theoretically and experimentally. These new MIL-47 analogues with extra electron donating or withdrawing groups will be compared to the conventional MIL-47 for the oxidation of cyclohexene. Moreover a catalytic cycle, based on molecular modeling on the non-substituted V-MIL-47 will be presented. Also, the effect of substituents on radical generation regeneration of the catalyst will be discussed.

Theoretical section

Geometry optimizations were first performed with the Gaussian03 package using the B3LYP hybrid functional. The double-zeta Pople basis set 6–31+G(d) was used for all the atoms except vanadium, for which the LANL2DZ effective core potential was applied. Even though this methodology was used for the calculation of the frequencies and the construction of Table 1, the energies will be refined by single point energy calculations at the b3lyp/6-311+g(3df,2p)-D3 level of theory. The fastest activated epoxidation mechanism via vanadium *tert*-butylperoxo complexes was taken from earlier results [2,3] and happens via a $V^{+IV}O(OOtBu)$ complex. To account for the substituent effect in this complex, the two linkers in the cluster model of MIL-47 (Figure 1) were modified. For clarity, only one out of four relevant orientations of the linker substituents is shown in Figure 1.

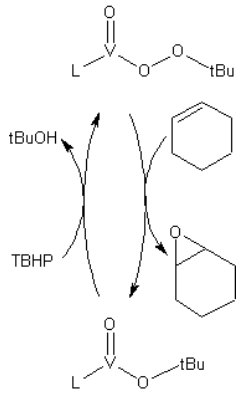

The calculation of kinetic parameters is done by an in-house developed software module TAMkin [4]. As the pre- and post-reactive complexes, immediately formed from the transition state are not discussed, only apparent energy differences will be discussed (no intrinsic barriers).

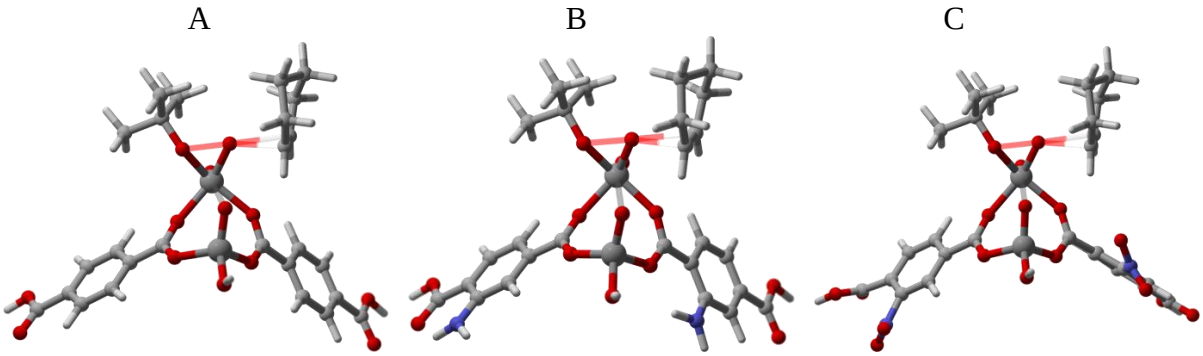

Figure 1: Examples of epoxidation transition states on a MIL-47 clusters with two terephtalic linkers: (A) normal MIL-47, (B) MIL-47(NH_2); (C) MIL-47(NO_2)

Results and discussion

Table 1 gives us an overview of the bimolecular kinetic parameters fitted between 273 and 373 K for model systems A, B and C (Figure 1). Those three systems can be ordered on the basis of the epoxidation rate: C > A > B.

Table 1. The pre-exponential factor (A_{fwd}, 1/s), the activation energy ($E_{a,fwd}$, kJ/mol), the kinetic rate coefficient at 323 K (k_{fwd}, mol m^{-3} s^{-1}) and the free energy barrier for the transition state at 323 K (ΔG_{323}, kJ/mol) are shown for the epoxidation reaction.

Cluster model	A_{fwd} (1/s)	$E_{a,fwd}$ (kJ/mol)	k_{fwd} (323K) (mol m^{-3} s^{-1})	ΔG_{323} (kJ/mol)
A	3.71E+04	61.9	3.58E-06	103.3
B	3.81E+03	61.0	5.11E-07	108.5
C	2.28E+04	57.1	1.29E-05	99.8

Conclusions

Various linker modifications of V-MIL-47 have been tested experminentally and theoretically for the epoxidation of cyclohexene with TBHP. In this contribution, theoretical calculations confirm how various linker substituents affect the epoxidation behavior. In summary, the epoxidation reaction accelerates with electron withdrawing substituents, while it decelerates with electron donating substituents.

Acknowledgements

This research is co-funded by the Ghent University, GOA grant nr. 01G00710 and Methusalem grant nr. 01M00409, BELSPO in the frame of IAP 6/27 and the European Research Council (FP7(2007-2013) ERC grant nr. 240483).

References

[1] Barthelet K, Marrot J., Riou D., Férey G., Angew. Chem. Int. Ed 41 (2002) 281.
[2] Leus K., Muylaert I., Vandichel M., Marin G. B., Waroquier M.,Van Speybroeck V., Van Der Voort P., Chem.Commun 46 (2010) 5085.
[3] Vandichel, M. et al., submitted to Journal of Catalysis.
[4] Ghysels, A.; Verstraelen, T.; Hemelsoet, K.; Waroquier, M.; Van Speybroeck, V. Journal of Chemical Information and Modeling 50 (2010) 1736.

Confinement Effects of H_2 Adsorption in MOFs

Diego A. Gomez, Aldo F. Combariza, German Sastre
Instituto de Tecnología Química, Universidad Politécnica de Valencia, Consejo Superior de Investigaciones Científicas, Av de Los Naranjos S/N, 46022 Valencia, Spain
E-mail: dagomez@itq.upv.es, afabri@itq.upv.es, gsastre@itq.upv.es

Introduction

Two of the main factors which favour the adsorption, or the gas retention, in a microporous solid are the affinity of the surface for the adsorbate and the confinement effects of the cavities. While the first factor relates directly with the composition of the solid and determine the strength and nature of the adsorbate-adsorbent interactions, the second one is mainly related to the crystal topology. As recently reviewed[1] there is a big group of MOFs which have been tested experimentally for hydrogen adsorption. Particularly, high gravimetric uptakes (%wt) at low pressure and temperature (1 bar and 77 K) have been reported for the MOFs presented in Table 1[2,3,4.]

Table 1. Experimental gravimetric adsorption (77K and 1 bar) and properties of some MOFs.

	wt%	Density (g/L)	M-atoms/Å^3	S. Area (BET)	Pore V. (cm^3/g)	Pore size (Å^3)
PCN-12	3.05	0.81	0.00196	1943	0.94	-
Cu2(QPTC) NOTT-103	2.56	0.987	0.00134	2929	1.28	8.0
Cu3(tdbb) NOTT-112	2.3	0.503	0.00092	3800	1.62	7.2/8.6/10.9/12.6/21

Molecular Dynamics (MD) simulations were performed with a general force field in order to gain insights on the influence of framework topology and metal-H_2 interaction strength in hydrogen adsorption in MOFs. The force field models a fixed MOF system, with parameters extracted from the general valence DREIDING force field, and intermolecular MOF-H_2 short-range Van der Waals interaction modeled via Lennad-Jones potentials[5,6]. The occupancy maps obtained from trajectories of H_2 molecules adsorbed within selected MOFs were analysed and compared against reported Inelastic Neutron Scattering (INS) images.

Results and discussion

Detailed determination of adsorption zones for adsorbed H_2 in MOFs is achieved through INS. To our knowledge this analysis has been achieved on a few MOFs such as MOF-5, MOF-74, HKUST-1, PCN-12 and MIL-53.

MD calculated occupancy maps show a good qualitative correlation with the INS data reported (Figure 1, top), despite the simplicity of the force field employed in the simulations. For instance, the MD results obtained for the MOF-74 show a set of well defined zones of adsorption over the MOF surface at high isovalues of occupancy (most occupied zones along the simulation). The occupancy map agrees with INS data reported for the stronger adsorption positions. At low isovalues of occupancy, less populated zones appear, which could correspond to a second layer of H_2 adsorbed.

On the other hand, the results for the HKUST-1 (Cu-BTC) indicate that at high isovalues of occupancy the molecules are retained mainly in the small cages of the framework (Fig. 1, bottom), despite that the strongest interaction of the H_2 molecules occur with the Cu atoms.

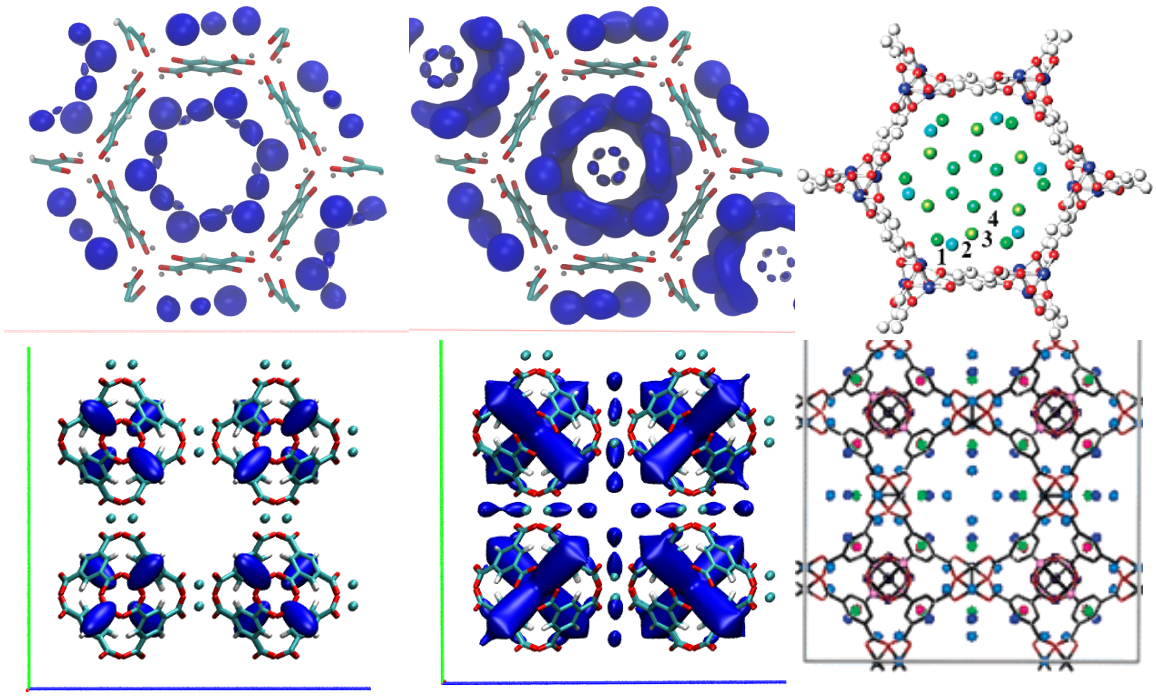

Figure 1. Occupancy maps at high and low isovalues and reported adsorption positions obtained from INS for MOF-74 (top) and HKUST-1(bottom).

The artificial increase of the Cu···H_2 interactive potential leads to similar results suggesting that the main factor of retention of the H_2 molecules into the pores correspond to a synergistic contribution of the confinement effects in the small cages and, with less influence, the attraction to the metal atoms.

This result could explain the favourable adsorption properties of the MOFs presented in Table 1, with different distributions of pore sizes and cages, and for which similar MD results were obtained.

Acknowledgements

D.G.H. acknowledges MICINN for a FPI scholarship. A.F.C. thanks Instituto de Tecnología Química UPV-CSIC for a Doctoral Research Fellowship. Funding through Ministerio de Ciencia e Innovación (Project MAT2007-64682) and computing time from Red Española de Supercomputación are gratefully acknowledged.

References

1. a. S. Ma and H.-C. Zhou, *Chemical Communications* 2010, 46, 44-53, b. D. Zhao, D. Yuan, and H.-C. Zhou, *Energy & Environmental Science,* 1 (2008), 222-235.
2. X.-S. Wang, S. Ma, P. M. Forster, D. Yuan, J. Eckert, J. J. López, B. J. Murphy, J. B. Parise, and H.-C. Zhou, *Angewandte Chemie*, 47 (2008), 7263-7266.
3. X. Lin, I. Telepeni, A. J. Blake, A. Dailly, C. M. Brown, J. M. Simmons, M. Zoppi, G. S. Walker, K. M. Thomas, T. J. Mays, P. Hubberstey, N. R. Champness, and M. Schröder, *Journal of the American Chemical Society*, 131(2009), 2159-2171.
4. Y. Yan, X. Lin, S. Yang, A. J. Blake, A. Dailly, N. R. Champness, P. Hubberstey, and M. Schröder, *Chemical Communications*, 2009, 1025-1027.
5. H. Frost and R. Q. Snurr, *Journal of Physical Chemistry C*, 2007, 111, 18794-18803.
6. S.L. Mayo, B. D. Olafson, W. A. Goddard, *Journal of physical Chemistry,* 1990, 94, 8897-8909.

First Principles Characterization of H_2 Adsorption in MOFs

Diego A. Gomez and German Sastre
Instituto de Tecnología Química, Universidad Politécnica de Valencia, Consejo Superior de Investigaciones Científicas, Av. de Los Naranjos S/N, 46022 Valencia, Spain
E-mail: dagomez@itq.upv.es, gsastre@itq.upv.es

Introduction

The need for a clean and sustainable energy source for on-board applications has increased the efforts to investigate the adsorption of hydrogen in Metal-Organic Frameworks. MOFs are the best candidates for H_2 storage by physisorption[1] (e.g. NOTT-112=7.07wt%, 50g/L at 77K and 40bar[2]) but further improvements are required to reach the proposed targets (5.5 wt%, 40g/L at ~235K and 5-40 bar for 2015).

Although uptake capacities are commonly measured experimentally there is a shortage of deeper characterization studies aimed to locate hydrogen based on INS or X-ray diffraction. In this work we have estimated H_2 uptake for some MOFs from first-principle calculations using as models small clusters of MOFs (e.g. Fig. 1), this allowing to estimate the strength and number of H_2 molecules that can be adsorbed on active sites of different topologies.

Results and discussion

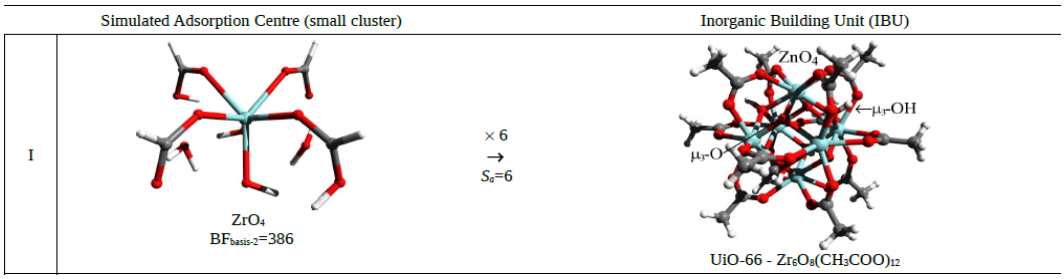

Figure 1. Cluster employed in the calculations and IBU extracted from the UiO-66.

The main results are presented in Table 1 in terms of adsorption energies, gravimetric ($x\%$) and volumetric uptakes (ρ_{H2}). Taken into account the different coordination environments of the metal atoms in the MOFs evaluated, it is interesting to observe that the average adsorption energy per adsorption centre (E_{ads}/n) are of similar values. However, not all the structures have similar hydrogen uptake per metal atom (see $'n'$ in Table 1), nor similar density of metal atoms (see 'm' in Table 1). These two newly defined parameters, as well as material density, ρ_{MOF}, allow to identify suitable structures for volumetric and gravimetric targets.

UiO-66 presents the adsorption centre with the highest 'n' (5) which explains the large uptakes ($x\%$ and ρ_{H2}) calculated. The similar gravimetric uptakes calculated for MOF-5 and MIL-88A(Pd) can be adscribed to: for MOF-5, to the high number of molecules adsorbed per metal atom (n=4) and for MIL-88A(Pd) to the high density of metal centres ('m'=0.0040).

Table 1. Average adsorption energies (E_{ads}/n), material (ρ_{MOF}) and metal atom (m) densities and gravimetric ($x\%$) and volumetric (ρ_{H2}) uptakes calculated.

	UiO-66	MIL-47	MFU-1b	MIL-88A(Pd)	MOF-5[19]
E_{ads}/n (kJ/mol) [a]	-2.20 (site 'a')	-2.42 (site 'a')	-2.12 (site 'a')	-2.51 (site 'a')	-2.38 (site 'a')
	-	-	-0.96 (site 'b')	-	-
m (M-atoms/Å^3)[b,g]	0.0027	0.0026	0.0010	0.0040	0.0019
ρ_{MOF} (g/cm^3)[c]	1.24	1.00	0.36	1.39	0.59
n (H_2/M-atom)[d,g]	5	2	3	4	4
x (gravimetric %)[e,g]	3.5	1.7	2.7	3.5	3.9
ρ_{H_2} (g/L)[f]	45.3	17.5	9.9	50.8	25.1

[a] Adsorption energy per H_2 molecule. Sites indicated in Figure 1. [b] Metal atoms per cubic Ångström. [c] MOF density. [d] H_2 molecules adsorbed per metal atom. [e] Gravimetric uptake (wt%). [f] Volumetric uptake (grams of hydrogen per litre of material).

Adsorption of less than 4 molecules per metal atom leads to low uptakes as observed for MIL-47 and MFU-1b. Figure 2 presents the gravimetric uptake (x) as a function of $'m{\cdot}n'$. From this, it is possible to identify the requirements in terms of ρ_{MOF}, $'m'$ and $'n'$, for a solid material with H_2 storage applications. For instance, to reach the 2015 proposed target (highlighted in Fig. 2), a material with a density of 0.8 g/cm³ should present a value of $'m{\cdot}n'$ 0.014.

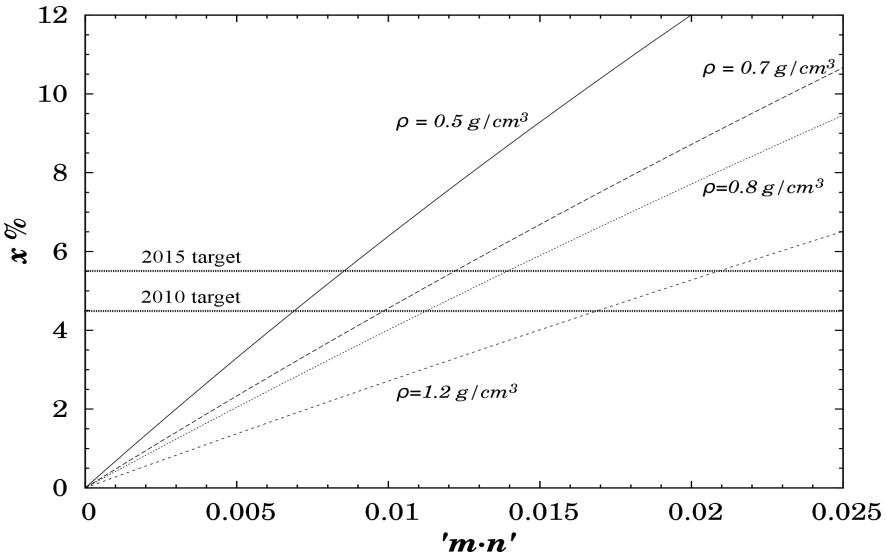

Figure 2. Gravimetric uptake (x) as a function of $'m{\cdot}n'$ for different values of material density. $'m'$ is density of metal atoms, $'n'$ is number of H_2 molecules adsorbed per metal atom.

Acknowledgements

D.G.H. acknowledges MICINN for a FPI scholarship. Funding through Ministerio de Ciencia e Innovación (Project MAT2007-64682) and computing time from Red Española de Supercomputación are gratefully acknowledged.

References

1. C. Liu, F. Li, L.-P. Ma, and H.-M. Cheng, *Advanced Energy Materials,* 22 (2010), E28-E62.
2. Y. Yan, X. Lin, S. Yang, A. J. Blake, A. Dailly, N. R. Champness, P. Hubberstey, and M. Schröder, *Chemical Communications,* (2009), 1025-1027.

Synthesis and tuning of bimodal materials with zeolitic features

Cynthia J. Van Oers[a], Myrjam Mertens[b], Vera Meynen[a], Pegie Cool[a]
[a] *Laboratory of Adsorption and Catalysis, Department of Chemistry, University of Antwerpen, Campus Drie Eiken, Universiteitsplein 1, B-2610 Wilrijk, Belgium, Tel.: + 32 3 265 23 79, Fax: + 32 3 265 23 74, cynthia.vanoers@ua.ac.be*
[b] *Flemish Institute for Technological Research, VITO N.V., Boeretang 200, B-2400 Mol, Belgium*

Introduction

Zeolites are widespread in the industrial world for sorption, separation and catalytic applications as a result of their good activity, selectivity and stability. Nevertheless, these microporous materials possess a limited use towards large, bulky molecules and viscous liquids, because of their narrow pore size distribution and small pores (∅ < 2 nm). On the other hand, mesoporous materials do possess larger pores (2 < ∅ < 50 nm), but exhibit a lower hydrothermal and mechanical stability due to the amorphous nature of their pore walls. A combination of both materials, i.e. a mesoporous structure with zeolitic features, would be ideal. Therefore, the research on this topic has been directed towards the tuning of combined mesoporous zeolitic materials possessing a wide range of different functionalities.

The presented work focuses on two different approaches to obtain bimodal micro- and mesoporous materials with tuneable zeolitic features, namely a mesotemplate-free synthesis procedure (1) and a post-synthetic impregnation method (2).

Experimental

(1) Mesotemplate-free synthesis

The mesotemplate-free synthesis procedure doesn't involve a structure directing agent for the mesopores. [1] Therefore, the method is not only short and facile, but also has extra benefits on an economic and environmental level by avoiding the use of often expensive and/or poisonous supramolecular or polymeric templates. Zeolite Beta nanoparticles solutions are used as silica-alumina source. The properties of the obtained bimodal materials can be altered by simple changes in the synthesis of the zeolite nanoparticles, like adapting the synthesis temperature. The schematic representation of the synthesis procedure is shown in figure 1.

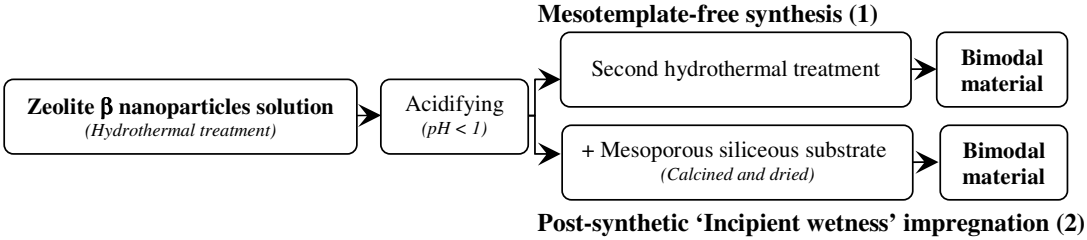

Figure 1: Schematic representation of the mesotemplate-free and post-synthetic synthesis

(2) Post-synthetic 'Incipient wetness' impregnation

The post-synthetic approach to synthesise bimodal zeolitic structures, involves incipient wetness impregnations of zeolite Beta nanoparticles (same as used in the mesotemplate-free synthesis) on different ordered amorphous siliceous substrates (i.e. SBA-15, MCF). Analogous to the former synthesis method, the porosity and the zeolitic properties can be altered by adjusting the synthesis of the zeolite Beta nanoparticles. Figure 1 gives a schematic representation of the synthesis method.

Results and discussion

The mesotemplate-free synthesis method and the post-synthetic impregnation have two important synthesis steps in common. First of all, the zeolite Beta nanoparticles used for the syntheses are in both cases prepared under the same conditions. This implicates that the characterisation of the impregnated samples can give us knowledge over the zeolite Beta nanoparticles, which can be correlated to the properties of the mesotemplate-free structures. The second resemblance between the two syntheses is the acidifying step. Especially for the mesotemplate-free method, the acidifying of the nanoparticles to a pH lower than 1 is indispensable. Most likely, the strong acidic environment causes the loss of a ligand of the micropore directing agent (i.e. TEAOH), similar to the observations made for TPAOH. [2] As a result, the zeolite nanoparticles are no longer able to grow further into a crystalline framework, but instead organise into a mesoporous structure via a sol-gel mechanism.

Although the first synthesis steps are identical in both methods, the structural properties of the obtained bimodal materials (mesotemplate-free synthesis vs. post-synthetic impregnation) differ strongly. The mesotemplate-free synthesised materials show a bimodal porosity. However, because of the lack of a structure directing agent for the mesopores, these materials do not have any ordering in their mesoporosity. On the other hand, the impregnated samples not only show bimodal porosity, also the ordering of the original substrate is preserved. Despite of these differences, the zeolitic features in both types of materials are very similar, due to the identical nanoparticles synthesis step. Therefore, both types of materials show microporosity in nitrogen sorption measurements (77K). Remarkable is the threshold in the tuning of the microporosity; in case of synthesising the nanoparticles at a temperature below or equal to 140°C (during 24h), only a small amount of micropores is obtained. In contrast, if the nanoparticles are synthesised at an elevated temperature (i.e. 150°C/24h), the micropore volume is more than doubled. This threshold is also visible in several techniques used to investigate the zeolitic features of the materials. In TGA/DTG spectra all the bimodal structures show zeolitic characteristics, but these are much more profound in the spectra of the materials based on nanoparticles synthesised at elevated temperatures (above 140°C). Similarly, higher synthesis temperatures (above 140°C) are needed during the preparation of the zeolite nanoparticles, in order to observe zeolitic features for the obtained bimodal structures in DRIFT and XRD.

Conclusions

Bimodal structures with zeolitic features have been synthesised using two different approaches, a mesotemplate-free and a post-synthetic impregnation. Both methods give rise to bimodal micro- and mesoporous materials, whereby the microporosity and the zeolitic features can be tuned by altering the synthesis temperature of the zeolite Beta nanoparticles.

Acknowledgements

Cynthia J. Van Oers thanks the Fund for Scientific Research – Flanders (FWO) for financial support.

References

[1] C. Van Oers, W. J. J. Stevens, E. Bruijn, V. Meynen, P. Cool and E. F. Vansant Micropor. Mesopor. Mater. 120 (2009) 29

[2] V. Meynen, P. Cool, E. F. Vansant, P. Kortunov, F. Grinberg, J. Kärger, M. Mertens, O. I. Lebedev, G. Van Tendeloo, Micropor. Mesopor. Mater. 99 (2007) 14

Population balance of seed-induced, SDA-free crystallization of sub-micrometer zeolite ZSM-5

Nan Ren[1], Josip Bronić[2] and Boris Subotić[2]
[1]*Department of chemistry, Shanghai Key Laboratory of Molecular Catalysis and Innovative Materials and Laboratory of Advanced Materials, Fudan University, Shanghai 200433, P.R.China* [2]*Division of Materials Chemistry, Laboratory for the Synthesis of New Materials, Ruđer Bošković Institute, Bijenička 54, 10000 Zagreb, Croatia*
Corresponding author: Boris Subotić, Subotic@irb.hr

Introduction

Taking into consideration the advantages of SDA-free synthesis and positive effects of seeding on the formation of zeolite ZSM-5 crystals [1-3], recently we reported a controllable and low-cost procedure for the synthesis of zeolite ZSM-5 with adjustable submicron crystal size and the specific structure with all-silica core and aluminum containing shell [1]. Post-synthesis alkaline treatment of the products resulted in dissolution of silica core and formation of hollow particles with the shell of zeolite ZSM-5 [1]. Due to increased surface area, such hollow ZSM-5 particles are potentially interesting as catalysts. Thus the prediction and control of both the size of hollow particles and the thickness of ZSM-5 shell through the control of crystallization pathway is important for potential applications of the hollow spheres in catalytic processes. From this reason, based on the proposed mechanism of crystallization [1], we created population balance model of crystallization which enables either the evaluation of the proposed mechanism and prediction of the particulate properties of products.

Experimental

The reaction mixture having the batch composition $1.0Al_2O_3/100SiO_2/28Na_2O/4000H_2O$ seeded with 4, 8, 16 and/or 32 wt. % of silicalite-1 seed crystals of different size (90 – 690 nm) was prepared as described previously [1]. The reaction mixture was divided among needed number of autoclaves and heated at 483 K for predetermined times t_c. After cooling, phase separation (filtration), washing and drying (at 353 for 1d), the solid products were calcined at 823 K for 6 h, before characterization. The XRD patterns were recorded on a Rigaku D/Max-rB 12 kW diffractometer (Cu Kα). Particles (crystals) size distribution (PSD) curves of the products of hydrothermal treatment were determined with a Malvern Mastersizer 2000 laser light-scattering (LLS) particle size analyzer.

Results and discussion

The population balance of the crystallization process is defined as [4]: $d(m_o)_j/dt_c = dN/dt_c = 0$ (1); $d(m_1)_j/dt_c = Q(m_o)_j$ (2); $d(m_2)_j/dt_c = 2Q(m_1)_j$ (3); $d(m_3)_j/dt_c = 3Q(m_2)_j$ (4); $Q = dD_j/dt_c$ (5), where $(m_i)_j$ (i = 0, 1, 2, and 3) are moments of the particle size distribution of zeolite crystals at crystallization time t_C, N_j is the number of crystals with size D_j at the crystallization time t_c and Q is the rate of crystal growth. The subscript j represents particular populations of the crystals having the size among 20 nm increments (see solid curve in Fig. 1A). Changes of the incremental size, $(D_p)_j = (D_s)_j + \int Q dD_j$, where $(D_s)_j$ is the incremental size of seed crystals and the mass $m_z = 3G\rho\sum(m_3)_j$ of the crystalline end products were calculated by

simultaneous solution of differential Eqs. (1) – (5) by fourth-order Runge-Kutta method, as explained previously [4].

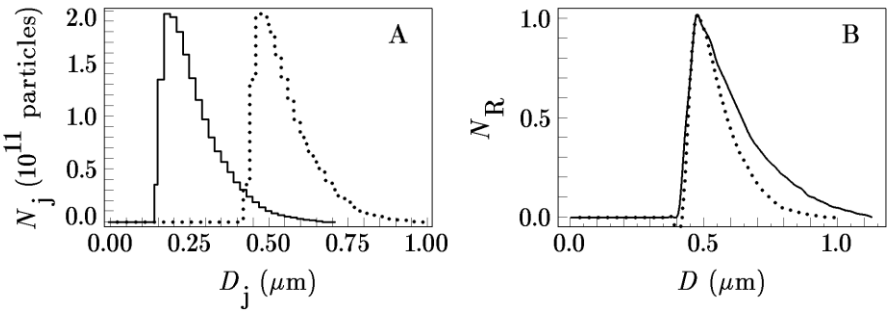

Figure 1. (A) Measured number, $N_j = (N_s)_j$, of crystals, in 4 g of silicalte-1 seed crystals (solid curve) and simulated (calculated) number, $N_j = (N_p)_j$, of crystals in 29.78 g of the crystalline end product (crystallized at 4 g of seeds; dotted curve), presented as functions of the crystal size $D_j = (D_s)_j$ (solid curve) and $D_j = (D_p)_j$. (B) Measured (solid curve) and calculated (simulated; dotted curve) relative number, N_R, having the size D.

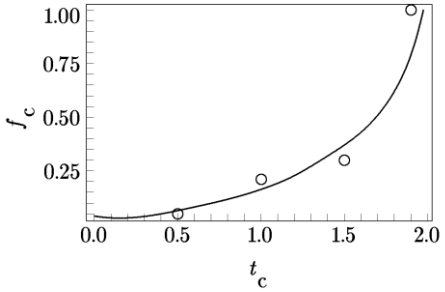

Figure 2. Measured (○) and calculated (simulated; curve) fractions of zeolite ZSM-5 crystallized by growth of 4 wt. % of seed crystals having the crystal size distribution shown by solid curve in Fig. 1A.

Fig. 1 shows that agreement between measured and calculated (simulated) crystal size distribution of the product is almost excellent for $D \leq 0.5$ μm, but that the product contains a portion of particles having the size larger than the predicted one. This diagreement can be simply explained by the formation of small fraction of crystal aggregates during the crystallization [5]. On the other hand, almost perfect correlation between measured and calculated kinetics of crystallization (see Fig. 2) shows that the formation of aggregates do not considerably influence the growth rate of zeolite ZSM-5 on silicalite-1 seed crystals. The well or almost perfect correlations between measured and calculated data shows that the SDA-free crystallization of zeolite ZSM-5 on nano-size silicalite-1 seeds takes place by a linear, size-independent growth of seed crystals and, at the same time, that the rate of crystallization and particulate properties of products can be predicted by population balance model.

References

[1] N. Ren, Z.-J. Yang, X.-C. Lv, J. Shi, Y.-H. Zhang, Y. Tang, Microporous Mesoporous Mater. 131 (2010) 103-
[2] M. Pan, J.S. Lin, Microporous Mesoporous Mater. 43 (2001) 319.
[3] M. Lassinatti, F. Jereman, J. Hedlund, D. Creaser, J. Sterte, Catal. Today 67 (2001) 109.
[4] T. Antonić Jelić, J. Bronić, M. Hadžija, B. Subotić, Microporous Mesoporous Mater. 105 (2007) 65-74.
[5] N. Ren, J. Bronić, B. Subotić, X.-C. Lv, Z.-J. Yang, Y. Tang, Microporous Mesoporous Mater. 139 (2011) 197-206.

A Simulation Study of Water and Hydrogen Sulfide in Cu-BTC

J.J. Gutiérrez-Sevillano[#], L. García-Montalbán, E. Caballero-Rivero, S. Hamad, A. Martín-Calvo, and S. Calero.

Department of Physical Chemical, and Natural Systems, University Pablo de Olavide, CTRA. Utrera km. 1. 41013 Seville
[#] jjgutierrez@upo.es

Introduction

We performed a systematic simulation study on the adsorption and diffusion behaviour of pure and binary mixtures of water and hydrogen sulfide in Cu-BTC metal-organic frameworks (MOFs). These structures are nanoporous materials made of metal ions linked together by organic ligands. They usually have a periodic composition with channels, big pores, and large surface areas. MOFs show a wide variety of linkers leading to very different type of frameworks with unique geometry and different properties. In Cu-BTC, copper ions are linked by benzene-1,3,5-tricarboxylate (BTC) giving a unit cell with eight octahedral side pockets.

Methods

We have performed Monte Carlo simulations in the μVT ensemble as well as Molecular Dynamics in the NVT ensemble to obtain the adsorption and diffusion properties. We have carried out *ab initio* calculations using VASP[1] and Gaussian03[2], in order to obtain the interaction energies between the guest molecules and the framework. The Cu-BTC framework was considered rigid, with Lennard-Jones parameters taken from the DREIDING[3] force field, except those for Cu, which were taken from the UFF[4] force field. Lorentz–Berthelot mixing rules were used to calculate mixed Lennard-Jones parameters and the atomic charges for the MOFs were taken from Castillo et al.[5] The crystal structure of Chui et al.[6] includes axial oxygen atoms weakly bonded to the Cu atoms, which correspond to water ligands. Our simulations have been performed on the dry Cu-BTC with these oxygen atoms removed. Water has been modeled using the Tip5pEw model proposed by Rick et al.[7] and for hydroge sulfide we used the model and force field parameters developed by Kristof and Liszi[8].

Results and discussion

The study was performed at 298K for the pure gases and binary mixtures of 10:90, 1:99, and 1:999 bulk concentrations of water and hydrogen sulfide. The adsorption isotherm of the 10:90 mixture shows a very high selectivity in favour of water. This selectivity disappear for the 1:99 mixture, and reverses in favour of hydrogen sulfide for the 1:999 mixture, where the adsorption of hydrogen sulfide is higher than the adsorption of water.

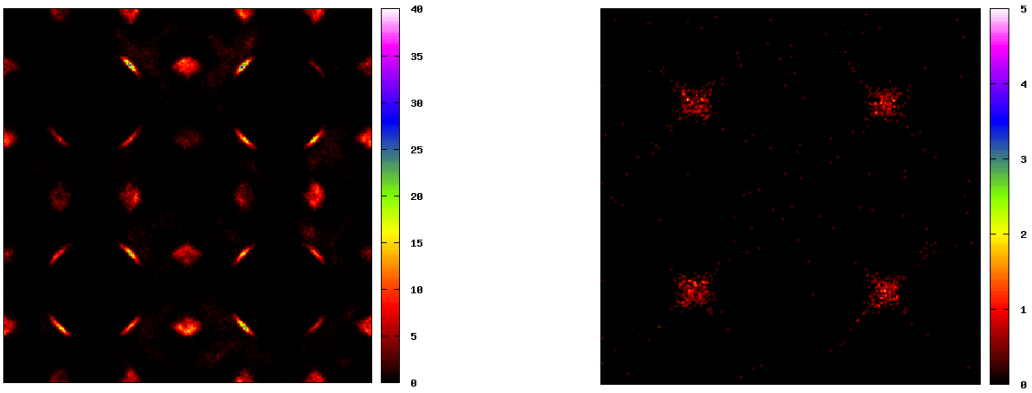

Figure 1. Water (left) and hydrogen sulfide (right) in Cu-BTC metal-organic framework. The snapshots were performed at 300Pa and 298K.

Based in our simulation results we were able to identify the preferential sites of adsorption in Cu-BTC for all the systems (Figure 1) proving that the molecules of water have large affinity for the metal center in Cu-BTC compared to the molecules of hydrogen sulfide.

Conclusions

We performed molecular simulations of binary mixtures containing water and hydrogen sulfide in Cu-BTC at 10:90, 1:99, and 1:999 bulk compositions. Our simulations show high selectivity in favor of water for the first bulk composition, no selectivity for the second, and a reverse in the selectivity for the third composition. The preferential adsorption of water and hydrogen sulfide occurs in different sites of Cu-BTC. The differences in adsorption make of this structure a potential interesting material to be used in the separation of water/hydrogen sulfide mixtures.

Acknowledgements

This work was supported by the Spanish MCINN (CTQ2007-63229 and MAT2009-14528-C02-01), and by the "Junta de Andalucía" (P07-FQM-02595). J.J. G-S thanks MCINN (CTQ2007-63229) for his predoctoral fellowship.

References

[1] G. Kresse and J. Furthmüller,Phys. Rev. B 54, (1996),11169 .
[2]Gaussian 03, Revision C.02, M. J. Frisch, et al., Gaussian, Inc., Wallingford CT, (2004).
[3]S.L. Mayo, B. D. Olafson, W.A. Goddard *J. Phys. Chem.*, 94, (1990), pp 8897–8909
[4] A. K. Rappe, C. J. Casewit, K. S. Colwell, W. A. Goddard III, W. M. Skiff *J. Am. Chem. Soc.*, (1992), 114 (25), pp 10024–10035
[5] J. M. Castillo, T. J. H. Vlugt, and S. Calero. J. Phys. Chem. C, 112, (2008), 41, 15934-15939
[6]S. S. Y. Chui, S. M. F. Lo, J. P. H. Charmant, A. G. Orpen and I. D. Williams, Science, 283, (1999), 1148-1150
[7] Rick, S. J. Chem. Phys. 120, (2004), 6085–6093
[8] Kristof, T.; Liszi, J. J. Phys. Chem. B,101, (1997), 5480

Flexibility Effect in Zeolites

R. Bueno-Pérez*[a], S. Calero[a], D. Dubbeldam[b] and P.J. Merkling[a]
[a] *Department of Physical, Chemical, and Natural Systems, University Pablo de Olavide, Ctra. Utrera km. 1,41013 Seville, Spain*
[b] *Van't Hoff Institute for Molecular Sciences, University of Amsterdam, Nieuwe Achtergracht 166, 1018 WV Amsterdam, The Netherlands*
** rbueper@upo.es*

Introduction

The adsorption, diffusion and structural characterization of a series of flexible siliceous zeolites have been undertaken by computer simulations. Flexibility affects some of the material properties strongly, while for others the benefit is negligible. Self-diffusion of guest molecules like argon or methane has been found to be greatly enhanced by modeling a flexible zeolite host. Adsorption is affected in a lesser and more subtle way [1]. By comparing several popular force fields for zeolites from the literature with a deliberately simplistic force field, the importance of accuracy of the force fields for reproducing flexibility is assessed [2].

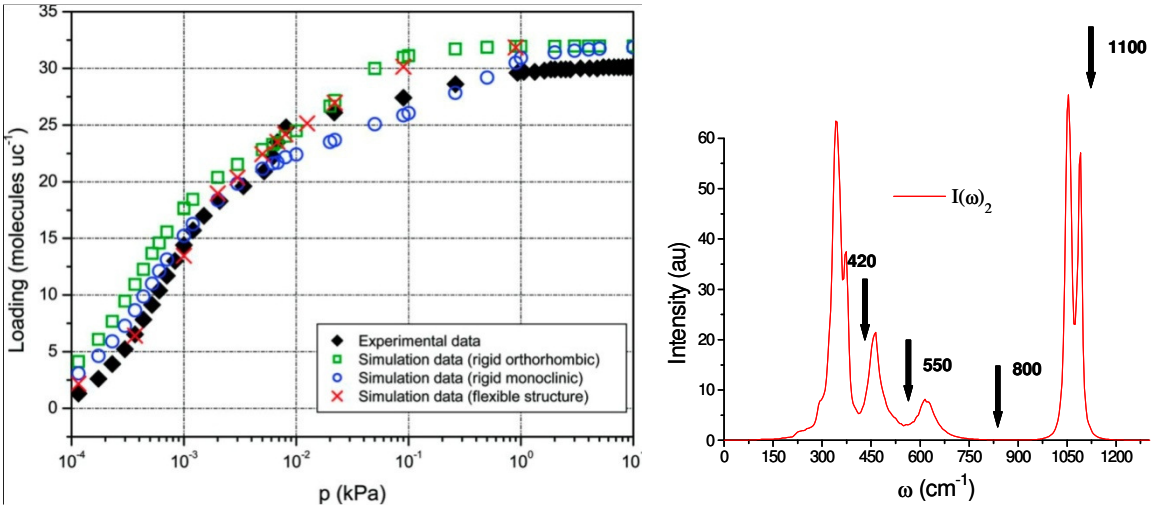

Figure 1. Computed adsorption isotherms for Argon in MFI at 77 K [1]. Using flexibility of the framework, adsorption properties were reproduced far better (left). Inrared spectrum of the MFI framework (right).

Methods

Three different popular force fields for zeolites obtained from the literature we compared: Nicholas et al. [3], Demontis et al. [4] and Hill&Sauer [5]. We reproduced the IR spectra obtained by the original authors, providing a valuable check on the reliability of our results.

IR spectra were calculated by Molecular Dynamics for several types of zeolites: sodalite, ITQ-29, orthorhombic and monoclinic silicalite (MFI), Aluminum free LTA, faujasite, mordenite, MEL, TON and FER.

Results and discussion

Within pure silica structures, the connectivity and secondary building units are responsible for substantial changes in the IR spectra. This was used as a testfield for three popular silicate force fields. Remarkable differences were found in the ability of the force fields to reproduce experimental IR spectra.

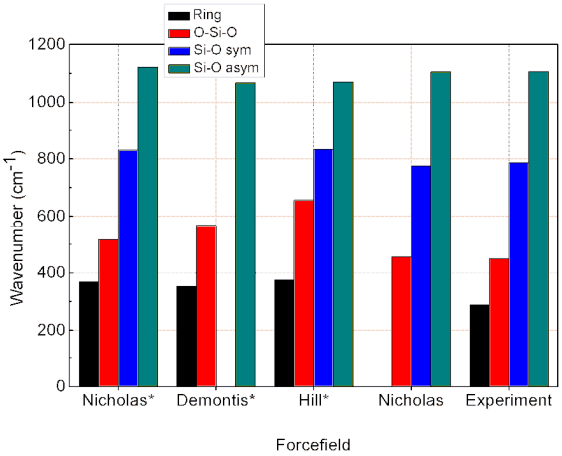

Figure 2. Comparison of the peaks in the IR spectra obtained by molecular simulation for the three popular force fields (*) and the IR spectra data obtained from the literature. The results labeled Nicholas without star belong to the IR spectra obtained by Nicholas.

Conclusions

The Demontis force field, the far simplest of the three force fields from the literature, provides flexibility, although a very inaccurate one. This is not enough to characterize the framework but it allows for the deformation of the structure, which is very important for the calculation of self-diffusion coefficients of bulky guests, and probably for adsorption properties.

On the other hand, both Nicholas and Hill force fields perform better, reproducing experimental spectra reasonably well. Of these, Nicholas force field is better suited to reproduce changes of structures.

Acknowledgements

This work is supported by the Spanish MCINN (CTQ2010-16077) and by the Junta de Andalucía (P07-FQM-02595).

References

[1] García-Pérez E., Parra J.B., Ania C.O., Dubbeldam D., Vlugt T.J.H., Castillo J.M., Merkling P.J., Calero S, Unraveling the Argon Adsorption Processes in MFI-Type Zeolite, Journal of Physical Chemistry C, 112, 9976 (2008).

[2] Bueno-Pérez R., Calero S., Dubbeldam D., Merkling P.J. in preparation.

[3] Nicholas J.B., Hopfinger A.J., Trouw F.R.,Iton L.E., Molecular Modeling of Zeolite Structure. 2. Structure and Dynamics of Silica Sodalite and Silicate Force Field, Journal of the American Chemical Society, 113, 4792 (1991).

[4] Demontis P., Suffritti G.B., Quartieri S., Fois E.S. and Gamba A., Molecular dynamics studies on zeolites. 3. Dehydrated zeolite A, Journal of Physical Chemistry, 92, 867 (1988).

[5] Hill J.R., Sauer J., A Molecular Mechanics Potential for Silica and Zeolite Catalysts Based on Ab Initio Calculations 2. Aluminosilicates, Journal of Physical Chemistry, 99, 9536 (1995).

The role and peculiar properties of α-sites in N_2O decomposition over FeMFI

L.Pirutko, V.Chernyavsky, E.Starokon, A.Kharitonov, G.Panov
Boreskov Institute of Catalysis SB RAS, Novosibirsk, Russia.
E-mail: pirutko@catalysis.ru

Introduction

Search for ways to effectively reduce nitrogen oxides in industrial emissions gives pulse to the study the Fe-containing zeolites (MFI, FER or BEA), which are highly active in SCR of nitrogen oxides with ammonia and hydrocarbons, and also in the N_2O decomposition [1,2]. The last reaction has been established to proceed [3,4] with participation of a particular form of reduced iron Fe^{2+}, stabilized in zeolite matrix, so called α-sites. It was shown only on the set of zeolites with iron introduced at the stage of hydrothermal synthesis. More opportunities to create effective catalysts open methods of introducing iron into a ready zeolite matrix [5]. The role of α-sites in catalytic activity of such systems is unclear and question is still debated. Here we make a systematic study of the role of iron and α-sites in the N_2O decomposition using the zeolites modified by iron after hydrothermal synthesis.

Experimental

The samples FeMFI and FeBEA differ with Fe content (the first digit in a sample code), the Al content (Si/Al - second figure), the activation procedures ("s" –steamed at 650 °C in 50% H_2O in He; "c" – calcined at 900 °C in He), HS- hydrothermal synthesis. Fe content were varied from 0.006 to 10 wt. %. The catalytic activity was measured at temperature-programmed decomposition (TPD) of N_2O (Fig. 1) in a helium flow with 55 mbar N_2O. The concentration of α-sites was measured in the vacuum set up [6].

Results and discussion

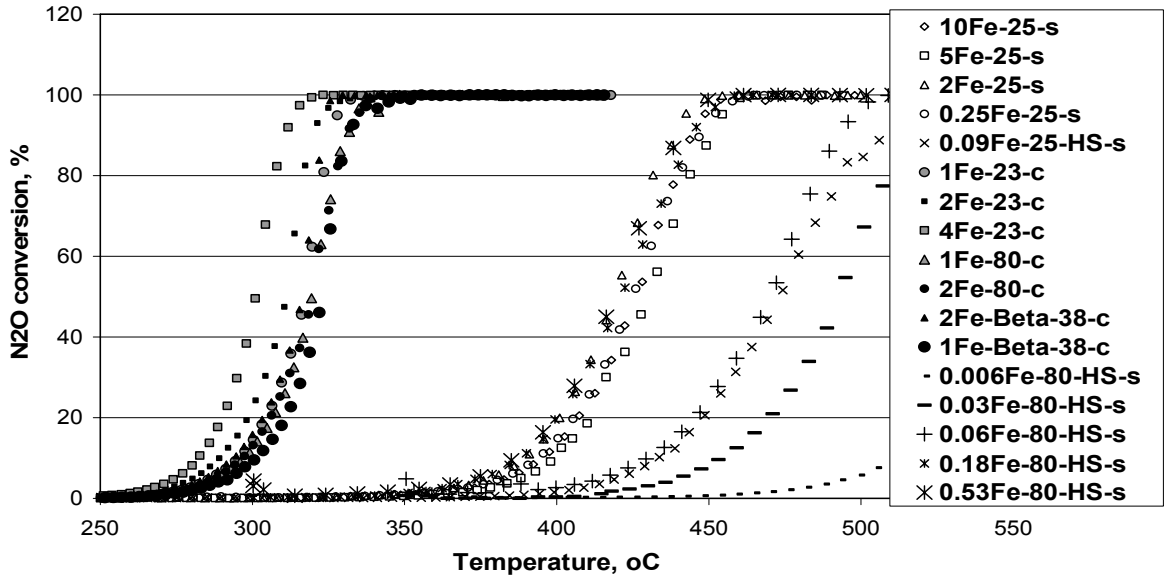

Figure 1. N_2O conversion vs. T for Fe-zeolites prepared by different ways.

Temperature dependences of N_2O conversion (Fig.1) show strong variation in the samples activity. Arrhenius plots (Fig. 2) for kα - reaction rate constant per mmole α-sites - merge into lines corresponding to value of activation energy E_a=52±4 kcal/mol for all samples. It is interesting that value of kα are grouped into two linear relationships, which includes the only samples activated in the same way. This means that the activity in N_2O decomposition is really determined by the presence of α-sites, whose activity does not depend on the composition of the zeolite matrix or the iron content. But the catalytic properties of α-sites are very strongly influenced by the activation procedure. The samples calcined at 900 °C, being very active even at 300-350 °C, show values of kα to 2 orders of magnitude larger than steamed samples demonstrate. To explain this fact the hypothesis of the participation of surface complexes [NO] in catalytic process is attracted. It is stated earlier [7] they are accumulated on the surface of the zeolite and considerably facilitate the desorption of surface oxygen into gas phase with the release of free α-site.

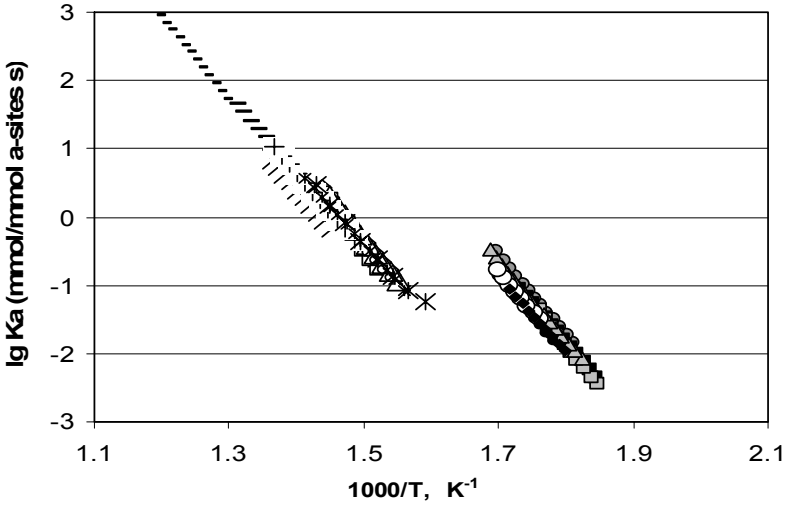

Figure 2. Arrenius plots of kα for Fe-zeolites prepared by different ways. Sample designation as in Fig.1.

Conclusions

Thus, Fe-containing zeolites, obtained by postsynthesis iron introduction, demonstrate high activity in N_2O decomposition. Their catalytic activity is determined by the presence of α-sites. Activity of these sites does not depend on the iron content, but it strongly is influenced by the activation procedure.

Acknowledgements

This work was supported by the Ministry of Education and Science of the Russian Federation (project No. 02.740.11.0147)

References

[1]. G. Centi, S. Perathoner, F. Vazzana, M. Marella, M. Tomaselli, M. Mantegazza, *Advances in Environmental Research* 2000, 4, 325-338.

[2]. J. Perez-Ramirez, F. Kapteijn, K. Schoffel, J. Moulijn, *Appl. Catal. B: Env.* 2003, 44, 117-151.

[3]. V. Chernyavsky, L.Pirutko, A.Uriarte, A.Kharitonov, G.Panov, *J. Catal.*, 2007, 245, 466-469.

[4]. L.V. Pirutko, V.S. Chernyavsky, E.V. Starokon, A.A. Ivanov, A.S. Kharitonov, G.I. Panov, *Applied Catalysis B: Env.*, 2009, 91, 174-179.

[5]. J. Perez-Ramirez, F. Kapteijn, J.C. Groen, A. Domenech, G. Mul, J.A. Moulijn, *J. Catal.,* 2003, 214 , 33-45.

[6]. G.I. Panov, A.K. Uriarte, M.A. Rodkin, V.I. Sobolev, *Catal. Today,* 1998, 41, 365-385.

[7]. D.A. Bulushev, A. Renken and L.Kiwi-Minsker, *J.Phys.Chem B,* 2006, 110, 305-312.

Flexibility window in zeolites: pressure behavior and phase transitions

Asel Sartbaeva[1], Stephen A. Wells[2], G. D. Gatta[3],
[1]*Department of Chemistry, University of Oxford, South Parks Road, Oxford, OX1 3QR, Great Britain*
[2]*Department of Physics and Centre for Scientific Computing, University of Warwick, Gibbet Hill Road, Coventry, UK CV4 7AL, Great Britain*
[3]*Dip. Scienze della Terra, Universita' degli Studi di Milano, Via Botticelli, 23, I-20133 Milano, Italy*

Introduction

We have recently discovered a new property of realizable zeolites – the flexibility window – which is a geometric property possessed by all natural and synthetic zeolite frameworks [1]. We find that it is connected both to the selection of hypothetical zeolite frameworks [2] and to the pressure behaviour of natural zeolites [3,4].

Results and discussion

The flexibility window in a zeolite structure can be identified by geometric simulation [5]. In this method the polyhedra of the framework are matched to the templates with ideal bond lengths and angles and the mismatch between the templates and atoms is minimised. If there exists some range of densities within which the mismatch can be reduced to zero, we call this range the "flexibility window" (Figure 1). It appears that all zeolites found in nature and all realizable synthetic zeolites possess a flexibility window. Critically, we conjecture that if no such window exists for a hypothetical tetrahedral structure, then the structure simply can not be realized as an aluminosilicate framework without placing an unacceptable strain on the bonds and angles within the tetrahedra. On figure 1 we show flexibility windows for several framework types and crystobalite, amorphous glass and quartz.

Since all synthetic and natural zeolites possess this property, but many hypothetical structures do not, the existence of a flexibility window can provide a valuable selection criterion when evaluating hypothetical zeolite framework structures as potential synthetic targets [2]. We are conducting a search to identify such hypothetical structures at the moment.

Furthermore, we find that the flexibility window is intimately connected to the pressure behaviour and pressure-induced phase transitions in natural zeolites [3,4]. In three natural zeolites with ANA-framework: analcime, wairakite and leucite, we found that phase transitions occur on compression when the structure is brought close to the edge of the flexibility window (Figure 2). It appears that the transition to a low-symmetry polymorph is triggered when a high-symmetry structure can no longer exist without inevitable distortions of the polyhedra.

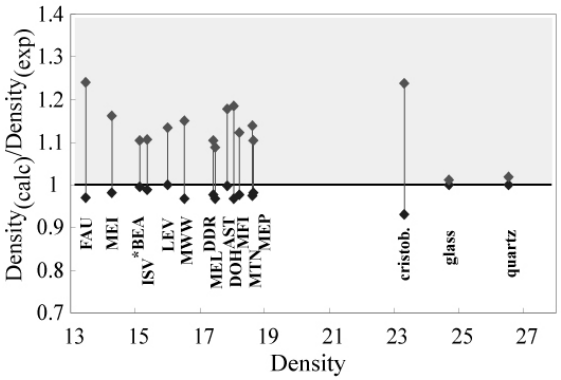

Figure 1 Flexibility windows for some pure-silica zeolites, denoted by their framework type, and denser silicates including cristobalite, quartz and amorphous silica glass.

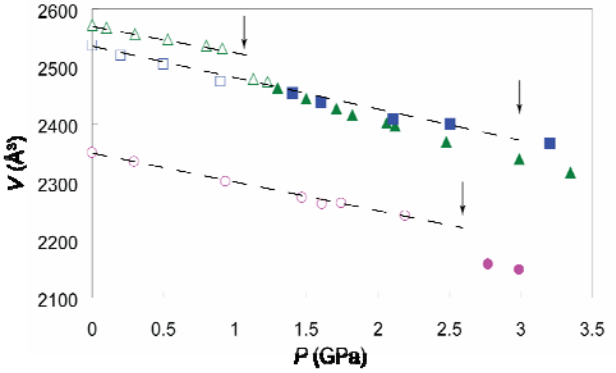

Figure 2 *P-V* data for ANA-framework materials: analcime (triangles), wairakite (squares) and leucite (circles). Open symbols - within flexibility window and closed where the framework is intrinsically distorted. Arrows indicate phase transitions.

Conclusions

Flexibility window is a new and important property of natural and synthetic zeolites. We conjecture that hypothetical zeolites, possessing this property, are realizable. We further found that flexibility window is connected with pressure behavior of zeolites. In analcime, wairakite and leucite, pressure-induced structural transitions occur at the edge of the flexibility window.

Acknowledgements

AS would like to thank Glasstone Fellowship and Royal Society for funding. SAW thanks Leverhulme Foundation for funding.

References

[1] A. Sartbaeva, S. A. Wells, M. M. J. Treacy and M. F. Thorpe, The flexibility window in zeolites, Nature Materials, 5 (2006) 962.
[2] M.M.J. Treacy, K.H. Randall, S. Rao, J.A. Perry and D.J. Chadi, Enumeration of periodic tetrahedral frameworks, Zeit. Fur Krist., 212 (1997) 768.
[3] G.D. Gatta, A. Sartbaeva, S.A. Wells, Compression behaviour and exibility window of the analcime-like feldspathoids: experimental and theoretical findings, European Journal of Mineral., 21 (2009) 571.
[4] A. Sartbaeva, G.D. Gatta and S.A. Wells, Flexibility window controls compression behavior in analcine zeolite framework, Europhysics Letters, 83 (2008) 26002.
[5] S. A. Wells, M. T. Dove and M. G. Tucker, Finding best-fit polyhedral rotations with geometric algebra, Journal of Physics Condenced Matter, 14 (2002) 4567.

Molecular Simulation of Adsorption of *n*-hexane and benzene in Na-MFI zeolites

García-Pérez, E. and Calero S.
Department of Physical Chemical, and Natural Systems, University Pablo de Olavide, Ctra. Utrera km. 1. 41013 Seville, Spain.
Corresponding author: egarper@upo.es

Introduction

We perform Configurational-bias Monte Carlo (CBMC) simulations to study low-coverage adsorption properties of hexane and benzene in MFI-type zeolites with different density of non-framework sodium cations. The effect of the concentration of sodium cations was systematically analyzed, and our results show that the position of these cations influences these properties.

Method

The Henry coefficients and enthalpies of adsorption were computed using Configurational Bias Monte Carlo in the NVT ensemble at 493.15 K. Benzene is modeled as a rigid molecule whereas *n*-hexane is defined as a flexible molecule and we grow test chains during the simulation using the Rosenbluth weight of the adsorbate. Detailed information about this method can be found elsewhere [1]. Both are described with a united atom model, in which CH_x groups are considered single interaction centers with their own effective potentials.

The MFI-type zeolite is a three-dimensional pore system characterized by two sets of interconnecting channels defined by 10-membered rings, with straight channels extending in the *y*-direction and zig-zag channels in the *x*-direction. This structure can be synthesized with a composition range $8 \leq Si/Al \leq \infty$ with 12 distinct crystallographic T-sites [2]. In our model cations can move freely.

The interactions between guest molecules (*n*-hexane, benzene, and sodium cations) with the zeolite host framework are modeled by Lennard-Jones and Coulombic potentials. We use a force field, where the density and mobility of the non-framework cation, the density of the framework aluminium, and all host-guest interactions are carefully taking into account.

Results and discussion

The simulated adsorption enthalpy of benzene is considerably lower than that of *n*-hexane for the same density of cations in the structure, for example, for five sodium cations in the T3-site

is 66.62 kJ mol^{-1} compared to 73.58 kJ mol^{-1}. For both components we find similar behaviour, the density of non-framework sodium cations provokes an increasing of the adsorption enthalpies. The enthalpy of adsorption dramatically increases up to four sodium cations per unit cell, the number of the intersections between the straight and zig-zag channels in a unit cell framework. These results are displayed in Figures 1 and 2.

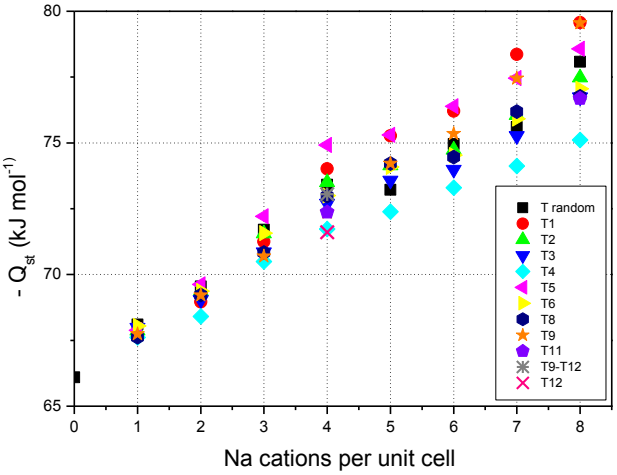

Figure 1. Heats of adsorption of *n*-hexane in Na-MFI zeolites at 493.15 K

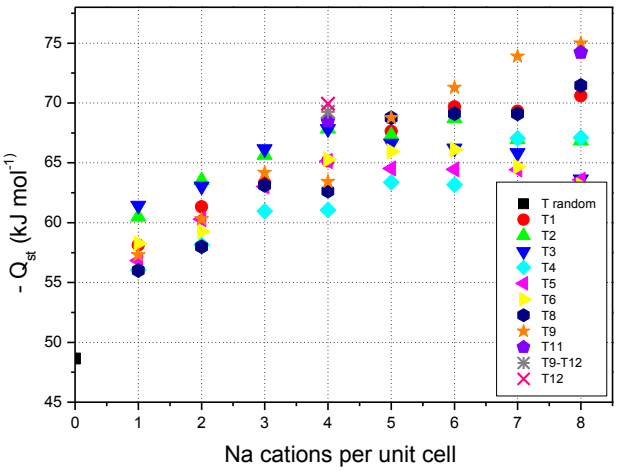

Figure 2. Heats of adsorption of benzene in Na-MFI zeolites at 493.15 K

Analysis of the occupancies of the individual adsorption sites (straight channels, zig-zag channels, and intersections) from the simulation data indicates that benzene adsorbs only in the intersections and *n*-hexane adsorbs preferentially in the intersections; straight and sinusoidal channels are also occupied but to a lower extent.

Conclusions

MFI-type zeolite is formed by two types of channels which intersect creating a bigger extra adsorption site; that is capable of adsorbing larger molecules. This feature could induce strong selectivity for this type of mixtures.

Acknowledgements

This work is supported by the Spanish MCINN (CTQ2010-16077) and by the Junta de Andalucía (P07-FQM-02595)

References

[1] Vlugt, T. J. H.; García-Pérez, E.; Dubbeldam, D.; Ban, S.; Calero, S. Computing the heat of adsorption using molecular simulations: The effect of strong Coulombic interactions, Journal of Chemical Theory and Computation 4 (2008), 1107-1118
[2] Baerlocher, C; Meier, W.M; Olson, D.H. Atlas of zeolite framework types. Elsevier, London, 2001

Molecular modeling of enantioselective catalysis in chiral MOFs

Thomas Bogaerts, [†]Matthias Vandichel, [†] Michel Waroquier, [†] Pascal Van Der Voort, [‡] Veronique Van Speybroeck, [†]

[†]*Center for Molecular Modeling, Ghent University, Technologiepark 903, B-9052 Zwijnaarde, Belgium. (thomas.bogaerts@ugent.be)*

[‡]*Centre for Ordered Materials, Organometallics and Catalysis, Ghent university, Krijgslaan 281 (S3), B-9000 Gent, Belgium*

Introduction

In recent years, metal-organic frameworks (MOFs) have been developed as a novel class of microporous materials. MOFs are crystalline hybrid materials consisting of metal ions and polyfunctional organic ligands.[1] They have attracted the attention of many research groups in both academia and industry, with over 1000 publications on an annual basis due to the exceptional promises for energy storage, catalysis and energy-related gas separations. Up to now, most focus has been lying on the development of new structures whereas their usage in specific applications remains still quite limited. Recently, MOFs have also been applied as heterogeneous catalysts.[2, 3] An active metal centre for catalysis applications can be present in many different ways, either within the metal building blocks or incorporated in the linker during a post modification process.

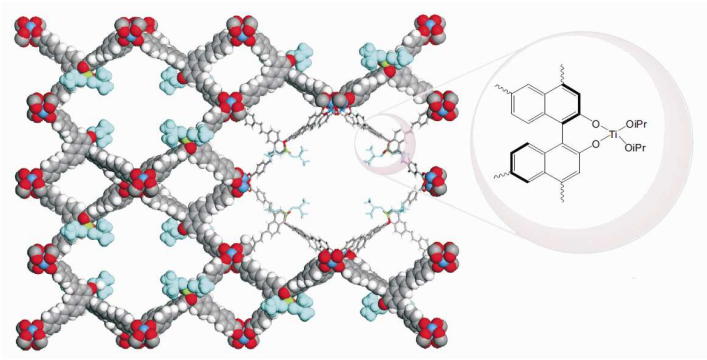

Figure 1: Detailed view of the internal structure and the incorporated active center.[4]

Goal and methodology

In 1980 Sharpless and Katsuki achieved a breakthrough in enantioselective epoxidation of allylic alcohols. They showed that in the presence of tert-butyl hydroperoxide (TBHP) and a complex of Titanium and a chiral tartrate ligand, an allylic alcohol could be converted into an epoxide with good yield and excellent enantioselectivity.[5] The goal of this study is designing a heterogeneous catalyst for this reaction by incorporating a titanium active center in a chiral MOF with a post modification process. BINOL-type linkers are ideally suited for this procedure (Figure 1). An analogous procedure was already utilised by Ma et al.[4] for other enantioselective reactions, for example the asymmetric diethylzinc and alkynylzinc additions. The goal of this research is to determine if this catalyst could also be used for the Sharpless enantioselective epoxidation. The enantioselectivity is studied by means of molecular modelling techniques. Hereby, a QM/QM oniom methodology is applied to evaluate the enantioselectivity of a chosen allylic alcohol within the surroundings of the catalyst. We used 2-penten-1-ol (Figure 2) as test substance for this study since it is a simple and easy to model compound that has limited options for side reactions.

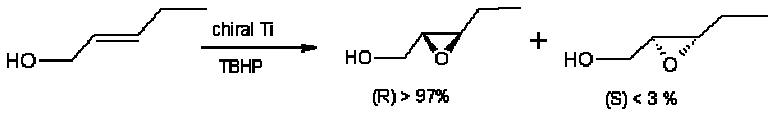

Figure 2: Enantioselective epoxidation with tert-butylhydroperoxide (TBHP)

Results and discussion

The staggered conformation of the naphthalene moieties in the BINOL linkers (Figure 1) and the bulky peroxide cause steric hindrance that lead to a preferred orientation in the transition state. That preferred orientation will, in turn be the cause of the enantioselectivity.

We have identified two possible pathways for the epoxidation of the allylic alcohol. The first is the one proposed by Sharpless *et al.*[6] In this mechanism the alcohol will first bind to the titanium and due to the sterical hindrance only one approach of the reactants is preferred which causes the final enantioselectivity.

A second mechanistic proposal consists of a bimolecular pathway. In this reaction scheme, the allylic alcohol does not bind directly to the titanium center. Depending on the transition state orientation of the reactant compared to the peroxide, a different enantiomer will be formed. Certain approach modes of the reactants are more preferred due to the occurrence of stabilizing hydrogen bridges. In this proposal, the most stable pathway gives the opposite enantioselectivity from the unimolecular pathway.

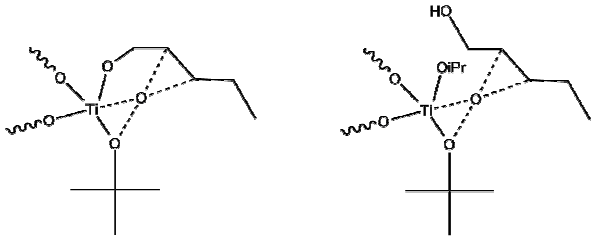

Figure 3: Schematic representation of the unimolecular (left) and bimolecular (right) transition states.

Our results indicate the unimolecular pathway as the most favorable, with a free energy for the transition state of 85.4 kJ/mole compared to 104.2 kJ/mole (both compared to the starting products).

Conclusions

Our molecular modeling results show that the postmodified chiral MOF with a titanium active site is a good candidate to use as a heterogeneous catalyst for the Sharpless asymmetric epoxidation as enantioselectivities over 90% are predicted.

Acknowledgement

This work is supported by the Fund for Scientific Research; Flanders (FWO), the Research Board of Ghent University (BOF), and BELSPO in the frame of IAP/6/27. Funding was also received from the European Research Council under the European Community's Seventh Framework Program [FP7(2007-2013) ERC grant agreement number 240483].

References

[1] J. R. Long, O. M. Yaghi, *Chemical Society Reviews* **2009**, *38*, 1213.
[2] A. Corma, H. Garcia, F. X. L. Xamena, *Chemical Reviews* **2010**, *110*, 4606.
[3] K. Leus, I. Muylaert, M. Vandichel, G. B. Marin, M. Waroquier, V. Van Speybroeck, P. Van der Voort, *Chemical Communications* **2010**, *46*, 5085.
[4] L. Ma, J. M. Falkowski, C. Abney, W. Lin, *Nat Chem* **2010**, *2*, 838.
[5] T. Katsuki, K. B. Sharpless, *Journal of the American Chemical Society* **1980**, *102*, 5974.
[6] K. B. Sharpless, S. S. Woodard, M. G. Finn, *Pure and Applied Chemistry* **1983**, *55*, 1823.

Ab initio study on the deactivation of zeolite and zeotype catalysts during the MTO process

Kristof De Wispelaere[1], Jeroen Van der Mynsbrugge, Bart De Sterck, Karen Hemelsoet, Michel Waroquier and Veronique Van Speybroeck
Center for Molecular Modeling, Ghent University, http://molmod.ugent.be/
[1]kristof.dewispelaere@ugent.be

Introduction

The depletion of oil reserves and the rapidly increasing demand for base chemicals such as ethylene and propylene initiated the quest for chemical processes based on alternative feedstock. Among these, the methanol-to-olefin process (MTO), using natural gas, coal or biomass as raw material, is one of the most important. MTO conversion occurs in acidic zeolites or zeotype catalysts. For industrial applications H-SAPO-34, which has a chabazite topology, shows the best performance and the highest selectivity toward light olefins.[1]

The generally accepted reaction mechanism for MTO is based on a hydrocarbon pool hypothesis, in which organic molecules (predominantly polymethylbenzenes) trapped within the anorganic zeolite framework act as co-catalysts. Methylation of the hydrocarbon pool species and subsequent olefin elimination are the key steps in the production of ethylene and propylene.[2] An important secondary effect of the presence of reactive methylbenzenes, is the formation of polycyclic aromatic compounds.[3] These large molecules are considered as coke, blocking the cages or channels, poisoning the active sites and finally deactivating the catalyst. Because the channels connecting the cages in chabazite topologies are narrow, polyaromatic molecules typically remain trapped inside the cages.[4] Coke formation increases with the acid strength of the catalyst, causing deactivation to occur faster in H-SSZ-13, the more acidic zeolite analogue of H-SAPO-34.[5]

Scope and results

In this contribution H-SSZ-13, H-SAPO-34 and H-ZSM-58 are considered. H-SSZ-13 and H-SAPO-34 have a chabazite topology whereas H-ZSM-58 is characterized by a DDR topology. Both topologies consist of cages connected by 8-membered ring windows through which only small molecules can pass.
By means of state of the art molecular modelling techniques the activities of benzene, naphthalene, and phenanthrene toward methylation by methanol are compared.[6] This allows the assessment of the influence of the acid strength and topology on the stability of these species and their tendency to lead to the formation of polyaromatics.

The unimolecular reaction rates for the methylation of benzene, naphthalene and phenanthrene increase in this order for the CHA topology whereas they decrease for DDR. The corresponding intrinsic forward reaction barriers are displayed in Figure 1. The effect of acid strength and the confined space in the different topologies can be clearly observed.
Additionally, a possible route for the formation of peri-fused bicyclic compounds via isobutene, a commonly formed side-product in the MTO process, is proposed in an effort to investigate its contribution to the formation of deactivating species. Isobutene can be formed during the

methanol conversion but it is too bulky to leave the cages of CHA or DDR catalysts. Therefore reaction between isobutene and aromatic species is expected likely to occur.

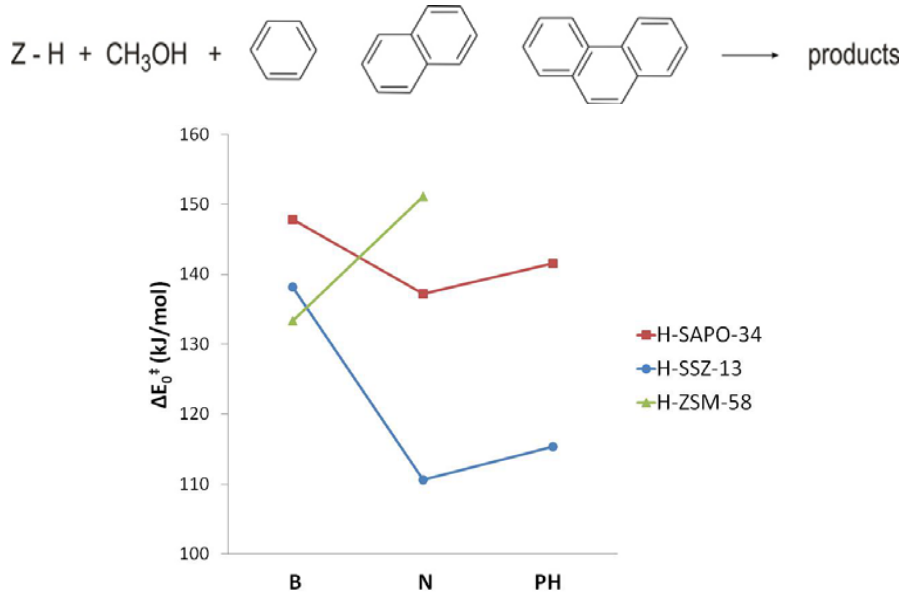

Figure 1: Forward reaction barriers for the methylation of benzene (B), naphthalene (N) and phenanthrene (PH) in H-SSZ-13, H-SAPO-34 and H-ZSM-58

This research also implies a tight cooperation with experimental, mainly spectroscopic data. Calculated IR spectra and experimentally obtained spectra are compared.[7] Theoretical spectra can ease the analysis of the complex experimental spectra whereas the experimental spectra can be a guideline for molecular modelling.

Acknowledgement

This work is supported by the Fund for Scientific Research; Flanders (FWO), the Research Board of Ghent University (BOF), and BELSPO in the frame of IAP/6/27. Funding was also received from the European Research Council under the European Community's Seventh Framework Program [FP7(2007-2013) ERC grant agreement number 240483].

References

[1] Chen, J.Q., Bozzano, A., Glover, B., Fuglerud, T. and Kvisle, S., Catal. Today 106 (2005) 103.

[2] McCann, D.M., Lesthaeghe, D., Kletnieks, P.W., Guenther, D.R., Hayman, M.J., Van Speybroeck, V., Waroquier, M. and Haw, J.F., Angew. Chem. Int. Ed. 47 (2008) 5179.

[3] Hemelsoet, K., Nollet, A., Vandichel, M., Lesthaeghe, D., Van Speybroeck, V. and Waroquier, M., ChemCatChem 1 (2009) 373.

[4] Mores, D., Stavitski, E., Kox, M.H.F., Kornatowski, J., Olsbye, U. and Weckhuysen, B.M., Chem. Eur. J. 14 (2008) 11320.

[5] Bleken, F., Björgen, M., Palumbo, L., Bordiga, S., Svelle, S., Lillerud, K.-P. and Olsbye, U., Top. Catal. 52 (2009) 218.

[6] Van Speybroeck, V., Van der Mynsbrugge, J., Vandichel, M., Hemelsoet, K., Lesthaeghe, D., Ghysels, A., Marin, G. B. and Waroquier, M., J. Am. Chem. Soc. 133 (2011) 888.

[7] Hemelsoet, K., Ghysels, A., Mores, D., De Wispelaere, K., Van Speybroeck, V., Weckhuysen, B. M. and Waroquier M., Catal. Today (2011), submitted

Red shift in CO IR-Spectra Evidencing Di- and Tri-carbonyl Capture on Microporous NaY Zeolite

Olivier Cairon and Hazar Guesmi*
UPPA-UFR S&T BP1155, 64013 Pau, France, UPMC-Université Pierre et Marie Curie, LRS, UMR 7197 CNRS, 4 place Jussieu, 75252 Paris, France. hazar.guesmi@upmc.fr

Introduction

IR spectroscopy is one of the more informative experimental techniques that allow at the nanoscale level a thorough understanding of the reversible physical adsorption of small guest molecules in microporous zeolites. Particularly, CO as a probe has been extensively used for characterizing many classes of zeolites containing various cations [1-6]. Distinguishable IR bands after CO introduction are the signature of relevant and specific CO/alkali metal interaction but their interpretation is far from being always so obvious. Recent developments on theoretical methods are supporting IR band attributions for adsorbed species [7]. Although NaY cationic Faujasite is one of the most widely used microporous materials for separation and purification processes, it has never been investigated by means of such combined approach. In this work we use both IR and DFT analysis to provide reliable description of weak solid-gas interactions supporting the formation of polycarbonyls in NaY zeolite [2-4] whose IR signatures are red-shifted in respect with the number of CO that bind Na^+ cation.

Experimental and theoretical details

In order to limit the IR signal saturation usually observed with high CO doses, we use a very thin pellet of NaY Faujasite. Details on the IR spectra resolution and experimental procedure can be found elsewhere [3, 4]. DFT/B3LYP study of the formation of polycarbonyl species in NaY faujasite was investigated considering a cluster model of 37-39 atoms which represents one of the six member rings (6MR) of the sodalite cages (see Figure 1).

Results and discussion

DFT optimized geometries of *n*-CO molecules interacting with a sodium cation located in a SII site of high aluminium loading six-ring, $Al_3Si_3Na_3O_{18}H_{12}$ cluster model, are reported in Figure 1. As depicted in Table 1, DFT harmonic calculations are found to fairly mirror the experimental results of νCO positions as a function of CO amounts. The mono-carbonyl species possess the most stable adsorption energy followed by di- and tri-carbonyl species. The νCO stretching mode for mono-carbonyls is predicted at 2170 cm^{-1} which is in a good agreement with the experimental average position observed at 2171.5 cm^{-1}. The two CO molecules forming the adsorbed di-carbonyl species vibrate at 2158 cm^{-1} and 2155 cm^{-1}. These calculated νCO stretching modes reproduce very well the red shift of about 10 cm^{-1} that is experimentally observed when the capture of two CO molecules occurs [3, 4]. Similarly, the assignment of the νCO position at 2148.5 cm^{-1} due to the formation of tri-carbonyls [3, 4] is also reproducible by calculation. Indeed, two of the three as-calculated νCO positions for tri-carbonyl species, Table 1, are found to vibrate at much lower positions compared to the mono and di-carbonyl species. Decrease of the vibrational frequencies of CO interacting with Na^+ sodium are the signature of Na^+-CO distance lengthening. In other words, the presence of

other CO in the vicinity as far as higher CO doses are concerned would favour polycarbonyls formation with Na^+-CO distance lengthening.

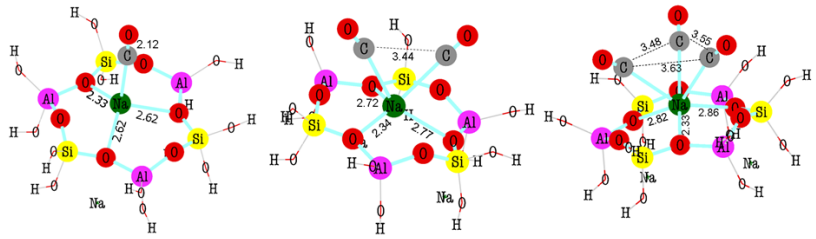

Figure 1: *n*CO molecules interacting with Na^+(SII): a) *n*=1, b) *n*=2 and c) *n*=3. Reported bonding length values are in Angstrom.

CO capture	Eads	dNa-CO	Calculated νCO[1]	Experimental νCO[2]
CO	-22	2.69	2170	2171.5
2CO	-17	2.81 2.91	2158 (as) 2155 (as)	2159.5
3CO	-14	2.78 3.07 3.19	2156 (as) 2151 (as) 2149 (as)	2148.5

Table 1: DFT adsorption energies (kJ/mol), dNa-CO distances (Å) and νCO (cm^{-1}) stretching frequencies of CO molecules (calculated and observed experimental positions) interacting with Na^+(SII). Symmetric, *(s)* and asymmetric, *(as)* νCO stretching frequencies are also reported for di- and tri-carbonyl species.

Conclusions

This first combined experimental and theoretical study of the CO capture in NaY Faujasite demonstrates that the different surfaces carbonyls species are resulting from the completion of the vacant coordination Na^+ sites as indicated by both their experimental and theorical insights. The red shift of about 10 cm^{-1} experimentally observed for the different νCO positions are reproduced well by our DFT calculations. Polycarbonyls formation is favoured for higher amounts of guest CO molecules.

References

[1] Ugliengo, P.; Garrone, E.; Ferrari, A.M.; Zecchina, A.; Otero Arean, C. J.Phys. Chem. B 103 (1999), 4839.
[2] Hadjiivanov, K.; Knözinger, H., Surf. Sci. 603 (2009), 1629.
[3] Cairon, O.; Loustaunau, A., J. Phys. Chem. C 112 *(* 2008), 18493.
[4] Cairon, O., Phys.Chem.Chem.Phys., 12 (2010), 14217-14226.
[5] Otero Areán, C.; Nachtigallová, D.; Nachtigall, P.; Bludsky, O.; Garrone, E.; Rodríguez Degado, M. Phys Chem. Chem. Phys. 9 (2007), 1421.
[6] Nour, Z., Petitjean, H., Berthomieu, D., *J Phys. Chem. C* 114 (2010), 17802.
[7] Nachtigall, P., Otero Arean, C. Phys. Chem. Chem. Phys. 12 (2010), 6307.

[1] Scaled values (scaling factor= 0.9659)
[2] Experimental average positions

Cu(II) sorption on natural clinoptilolite: experiments and kinetics modeling

Mina Jovanovic, Nevenka Rajic, Bojana Obradovic
Faculty of Technology and Metallurgy, University of Belgrade, Belgrade, Serbia,
mjovanovic@tmf.bg.ac.rs

Introduction

Natural zeolites have attracted a great attention due to their abundance, low-cost and excellent selectivity for a number of toxic heavy metal cations. The aim of this work was to experimentally investigate sorption kinetics of Cu(II) ions from aqueous solutions at different concentrations and temperatures using natural clinoptilolite and then to develop a kinetic model based on the sorption mechanism.

Experimental

Natural clinoptilolite (Vranjska Banja, Serbia, particle size: 60 – 120 μm) was pre-treated with NaCl (2.0 mol dm^{-3}). Hydrated salt $CuSO_4 \cdot 5H_2O$ (Zorka Pharma, Serbia) was dissolved in distilled water to yield following concentrations of Cu(II) ions: 100, 200 and 300 mg dm^{-3}. Series of batches with 1 g of the Na-modified clinoptilolite suspended in 0.1 dm^3 of Cu(II) ion solution were left over a period of time up to 24 h in a water bath at 25, 35 and 45 ºC. Concentration of Cu(II) in the solution was determined by an atomic absorption spectrophotometer (Varian SpectrAA 55B). At least five measurements were done for each determination.

Results and discussion

Natural clinoptilolite used in this work was shown to effectively remove Cu(II) ions from water solutions (Fig. 1). Experimental data were modeled by the Lagergren pseudo-second-order kinetics as:

$$\frac{dx}{dt} = k(x_e - x)^2 \qquad (1)$$

where x and x_e are the concentrations of sorbed Cu(II) at time t and at equilibrium, respectively, and k is the rate constant. By applying integrated linear form of the Eq. (1) on experimental data, rate constants and equilibrium concentrations of sorbed Cu(II) can be determined (Fig. 1a). The obtained values of model parameters are summarized in Table 1.

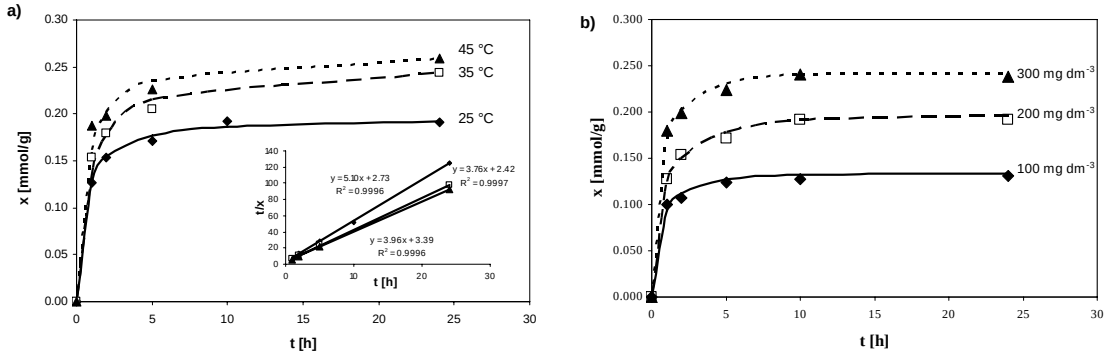

Figure 1. Sorption of Cu(II): experimental data (symbols) and model predictions (lines). a) Lagergren pseudo-second-order model (c_0=200 mg dm^{-3}); b) novel kinetic model (25 ^oC)

Although excellent agreements of model predictions with experimental data were obtained, kinetic rate constant values did not follow any consistent trend either with temperature or with Cu(II) concentration (Table 1). Similar findings were previously reported [1-3] indicating that the simple pseudo-second-order kinetic rate constant is actually a complex function and cannot be directly related to the ion exchange mechanism.

Table 1. Parameters of the Lagergren pseudo-second-order kinetic model (k [g mol^{-1} h^{-1}] and x_e [mmol g^{-1}]) at different initial solution concentrations (c_0 [mg dm^{-3}]).

	25 °C		35 °C		45 °C	
c_0	k	x_e	k	x_e	k	x_e
100	18415	0.133				
200	9525	0.196	4445	0.252	5715	0.266
300	12065	0.242	4445	0.291	3810	0.337

In order to get an insight in the mechanism of Cu(II) ion immobilization in zeolite, we have developed a novel kinetic model based on following reactions:

$$2Na_zP_{0.5} \underset{k_2}{\overset{k_1}{\rightleftarrows}} 2Na^+_{(aq)} + P \quad (2)$$

$$Cu^{2+}_{(aq)} + P \underset{k_4}{\overset{k_3}{\rightleftarrows}} Cu_zP \quad (3)$$

where k represents kinetic rate constant of each of the reactions and P is the free cation site in the zeolite lattice for binding of one Cu^{2+} ion. Index *0.5* in the Eq. (2) indicates that 2 sites occupied by Na^+ ions are closed to each other to provide 1 site (P) for Cu^{2+} ion. It is assumed that the concentration of free sites is low and constant over time. Thus, the differential equations for rates of free sites generation and Cu(II) ions sorption were associated to derive the final expression for Cu(II) sorption rate as:

$$\frac{dx}{dt} = k_1 \frac{(c_0 - x)(c_{BZ0} - 2x)^2 - 4K'x^3}{4k_2'x^2 + (c_0 - x)}; \qquad K' = \frac{k_2k_4}{k_1k_3} = \frac{(c_0 - x_e)(c_{BZ0} - 2x_e)^2}{4x_e^3} \quad (4)$$

where c_0 and c_{BZ0} are the initial concentrations of Cu(II) in solution and Na^+ ions in the zeolite lattice, respectively, and k_2' is the constant defined as $k_2' = k_2/k_3$. The constant K' is determined from the equilibrium. The Eq. (4) was solved numerically resulting in excellent agreements with experimental data (Fig. 1b) while values of the constant k_1 were found to increase with the increase in temperature as well as with Cu(II) concentrations (Table 2).

Table 2. Parameters of the novel kinetic model (k_1 [g mol^{-1} h^{-1}] and k_2' [g mol^{-1}]) and calculated constants K' [-] at different initial solution concentrations (c_0 [mg dm^{-3}]).

	25 °C			35 °C			45 °C		
c_0	k_1	k_2'	K'	k_1	k_2'	K'	k_1	k_2'	K'
100	209	10438	2.00						
200	418	25052	2.67	835	29228	0.48	5010	102296	0.30
300	1044	33403	2.20	2088	73069	0.75	6263	123173	0.27

Conclusions

In this work, we have investigated sorption kinetics of Cu(II) ions on natural clinoptilolite and derived a novel, mechanicistic kinetic model. The model predictions were in excellent agreement with experimental data indicating potentials for broader model applications to other toxic metal ions providing insights into the sorption mechanism.

Acknowledgements

This work was supported by the Ministry of Science, Serbia (Eureka 4208).

References

[1] Svilovic, S., Rusic, D., Stipisic, R., Journal of Hazardous Materials, 170(2009), 941-947
[2] Singh, S., Verma, L. K., Sambi, S. S., Sharma, S. K., Proceedings of the World Congress on Engineering and Computer Science 2008, WCECS 2008, October 22 - 24, 2008, San Francisco, USA
[3] Argun, M. E., Journal of Hazardous Materials 150(2008), 587-595

A theoretical and experimental spectroscopy study on methanol and ethanol conversion over H-SAPO-34

Karen Hemelsoet,[1,2] An Ghysels, [1] Davide Mores,[2] Kristof De Wispelaere, [1] Veronique Van Speybroeck,[1] Bert M. Weckhuysen,[2] Michel Waroquier[1]
Center for Molecular Modeling, Ghent University, Technologiepark 903, 9052 Zwijnaarde, Belgium[1] and Inorganic Chemistry and Catalysis, Debye Institute for NanoMaterials Science, Utrecht University, Sorbonnelaan 16, 3584 CA Utrecht, The Netherlands[2]
karen.hemelsoet@ugent.be

Introduction

The elucidation of the structure-activity relation of zeolites or zeotype materials remains very challenging. Recent advances in both theoretical and experimental techniques provide new opportunities to study these complex materials and any catalytic reaction occurring inside. Two recent computational studies investigated in detail methylation reactions on alkenes within an acidic ZSM-5 catalyst. It was shown that but enthalpy barriers [1] and rate coefficients [2] of individual reactions can now be calculated with "near chemical accuracy". In order to establish new active reaction routes, the knowledge of formed intermediates is crucial. The characterization of such intermediates can be done using a variety of spectroscopic techniques and in this contribution, IR and UV-VIS are applied. Methanol and ethanol conversion over H-SAPO-34 is investigated [3]. Two stages of the process are investigated: (1) the initial adsorption of the alcohols, (2) the formation of carbonaceous compound, which can be seen as both hydrocarbon pool species and coke precursors.

Computational Details

Large finite clusters are applied, the models are constructed using Zeobuilder [4]. A multi-layered method combining an ONIOM(B3LYP/dgtzvp:HF/dgtzvp)-D energy and ONIOM(B3LYP/dgtzvp: MNDO) geometry is used. The normal mode post-processing analysis is performed using the in-house developed software model TAMkin [5].

Results and discussion

Calculated adsorption energies of methanol and ethanol in a SAPO 44T cluster indicate that ethanol is absorbed more strongly compared to methanol by almost 14 kJ mol^{-1}. Dispersion effects are found to be crucial. IR spectra of the large finite clusters containing the adsorbed alcohols indicate that both alcohols behave in a similar way, which is in agreement with the experimental in situ DRIFT measurements. In addition, the clusters are loaded with singly methylated aromatic hydrocarbons, which are representative reaction intermediates of the alcohol conversion process. Computed IR spectra of these species adsorbed on H-SAPO-34 point out that the characteristic C=C vibrations of the larger aromatic compounds exhibit a peak with maximal intensity at 1610 cm^{-1}, experimental bands are observed at 1607 and 1600 cm^{-1} for methanol and ethanol, respectively.

To get more detailed information from the IR spectra, a detailed normal mode analysis (NMA) of the computed vibrational spectra is applied. A combined Partial Hessian Vibrational Analysis - Mobile Block Hessian (PHVA-MBH) is presented, in which groups of

atoms (such as the guest atoms in the zeolitic material) are considered as mobile blocks during the vibrational analysis [6]. This allows to separate the framework-guest vibrations and to visualize the induced peak shifts of the gas phase spectra upon adsorption in the heterogeneous catalyst.

Moreover, contemporary functionals such as CAM-B3LYP seem promising for the computation of UV-VIS spectra.

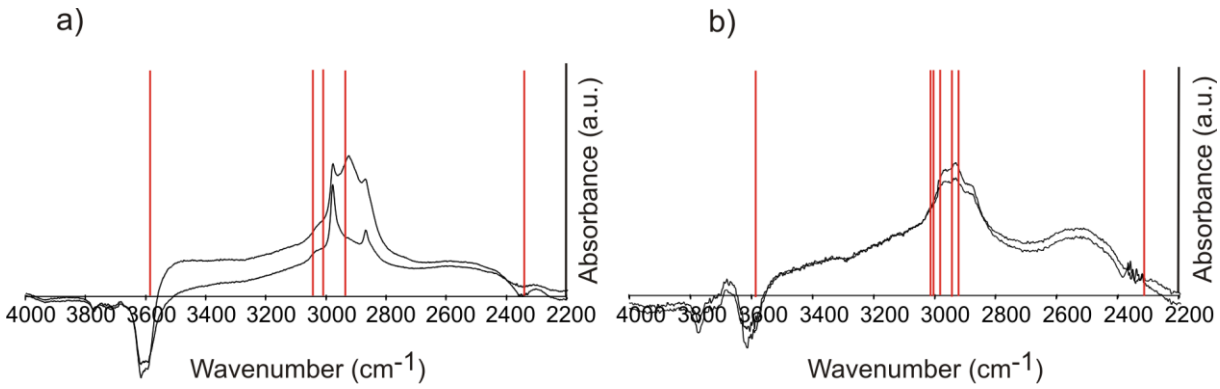

Figure 1. In situ DRIFT spectra (black) and computed IR peak locations of the early stage of methanol (a) and ethanol (b) conversion in H-SAPO-34.

Conclusions

A detailed normal mode analysis of calculated vibrational spectra of reactive intermediates in a SAPO-34 44T cluster provides a great help to unravel the complicated spectra. It is of general use in heterogeneous catalysis. In this contribution, the SAPO-34 framework vibrations could be separated from the vibrations of the guest molecules in the zeolitic pore and led to assignment of experimental peaks. Contemporary DFT functionals seem promising for the computation of UV-VIS spectra.

Acknowledgements

We wish to acknowledge the FWO - Flanders and the Research Board of Ghent University for continuous support. Computational resources and services used in this work were provided by Ghent University. This work was also supported by the Dutch National Science Foundation (NWO-CW VICI and TOP subsidies to B.M.W.).

References

[1] Svelle, S.; Tuma, C.; Rozanska, X.; Kerber, T.; Sauer, J. *J. Am. Chem. Soc.* **2009**, *131*, 816-825.
[2] Van Speybroeck, V.; Van der Mynsbrugge,J.; Vandichel, M.; Hemelsoet, K.; Lesthaeghe, D.; Ghysels, A.; Marin, G.B.; Waroquier,M. *J. Am. Chem. Soc.* **2011**, *133*, 888-899.
[3] Hemelsoet, K.; Ghysels, A.; Mores, D.; De Wispelaere, D.; Van Speybroeck, V.; Weckhuysen, B.M.; Waroquier, M. *Catal. Today* **2011**, submitted.
[4] Verstraelen, T.; Van Speybroeck, V.; Waroquier, M. J. Chem. Inf. Mod. 2008, 48, 1530-1541.
[5] Ghysels, A.; Verstraelen, T.; Hemelsoet, K.; Waroquier, M.; Van Speybroeck, V. *J. Chem. Inf. Model.* **2010**, *50*, 1736-1750.
[6] Ghysels, A.; Van Neck, D.; Van Speybroeck, V.; Verstraelen, T.; Waroquier, M. *J. Chem. Phys.* **2007**, *126*, 224102; Ghysels, A.; Van Speybroeck, V.; Pauwels, E.; Van Neck, D.; Brooks, B. R.; Waroquier, M. *J. Chem. Theor. Comp.* **2008**, *4*, 614-625

Computational study of zeolite dealumination and formation of silanol nests

Sami Malola, Francesca Bleken, Stian Svelle, Ole Swang
inGap Center of Research Based Innovation, Department of Chemistry, University of Oslo, P.O. Box 1033 Blindern, N-0315, Oslo, Norway, stian.svelle@kjemi.uio.no

Introduction

Zeolites are porous catalytic materials - marvelous for the needs of petrochemical industry. In zeolites, aluminum will form both framework Brønsted and extra-framework Lewis acid sites and is thus responsible for the catalytic behavior of the material. Importantly, the distribution and density of the acid sites can be guided by steaming at high temperature, under which hydration reactions weaken the bonding between aluminum and the framework, eventually leading to the detachment of atoms creating vacancies like silanol nests. This process is referred to as dealumination, and plays a pivotal role in the practical application of zeolites as catalysts. For example, zeolite Y, which is employed in the catalytic cracking of heavy oil fractions, is typically dealuminated by steaming to reduce the density of acid sites before application [1]. Herein, we present a detailed reaction mechanism for the dealumination process. The results are compared to the analogous process where silicon is removed from the framework (desilication).

Computational details

In this contribution, we use periodic density-functional theory (DFT) calculations as implemented in the code-package Quantum Espresso, which uses ultra-soft pseudo-potentials for electron-ion interactions and plane waves as a basis set. For xc-contribution we use the Perdew-Burke-Ernzerhof (PBE) GGA-functional. To calculate reaction paths and activation energies we have performed extensive nudged elastic band method (NEB) calculations. To ensure computational efficiency in NEB-calculations we have selected the 36 atom unit cell of chabazite to be our modeling structure. To further confirm our observations we have performed calculations for the double sized unit cell with Quantum Espresso and for the original unit cell with hybrid B3LYP-functional with DFT-code CASTEP in Materials Studio and also used the Grimme dispersion correction (DFT-D) to account for van der Waals interactions [2].

Results and discussion

The energetics of the reaction paths for the dealumination and desilication can be seen in Figure 1 and a scheme of the processes is shown in Figure 2. The upper lines in Figures 1a and 1b is based on assuming that additional water molecules are available without intermediate adsorption steps, whereas for the lower lines, the sequential adsorption of water molecules is explicitly taken into account. Both processes occur via stepwise hydrolysis, eventually leading to an $Al(OH)_3(H_2O)$ species for dealumination and $Si(OH)_4$ for desilication. These species have only weak interactions with the remaining zeolite framework and are thus expected to be mobile. A silanol nest, comprising four silanol hydroxyl groups, is formed in the zeolite framework as a consequence of both processes.

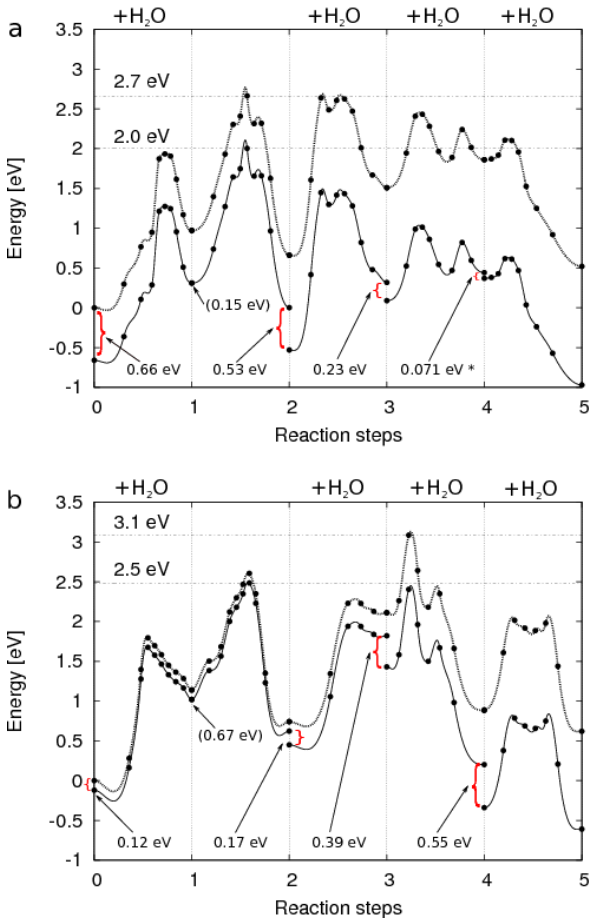

Figure 1. DFT paths for a) dealumination and b) desilication combined from 5 different NEB-paths. Effective barriers are labeled for both approaches separately in the upper left corner. Water adsorption energies are seen as discontinuous jumps in the lower curves.

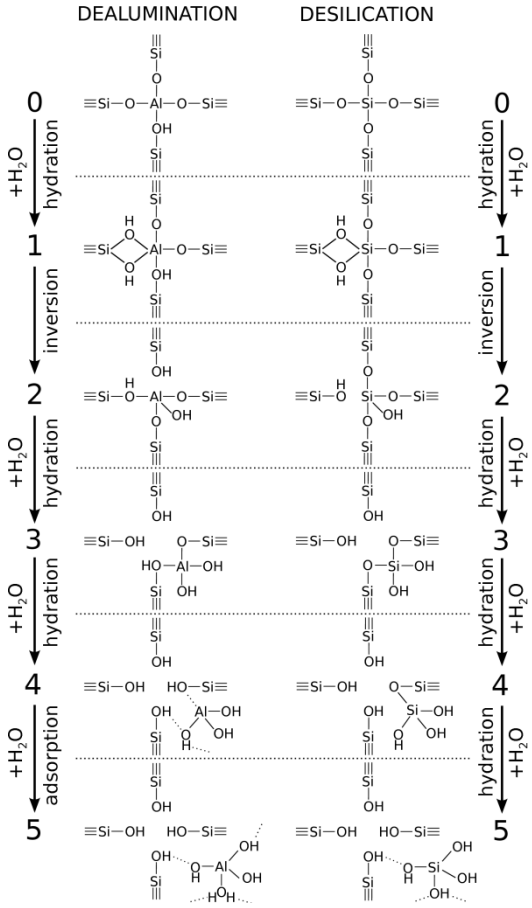

Figure 2. Reaction steps with intermediate configurations drawn in schemes for dealumination on the left and for desilication on the right. Solid lines denote covalent bonds and dotted hydrogen bonds.

Conclusions

A detailed mechanism has been described for the removal of both framework aluminum and silicon. Substantially lower barriers are encountered for dealumination compared to desilication, and our results thus agree the experimental observations.

Acknowledgements

This publication forms a part of the inGAP Center of Research-based Innovation, which receives financial support from the Research Council of Norway under contract no. 174893. S.M. acknowledges the KOSK II program of the Research Council of Norway for a postdoctoral scholarship.

References

[1] van Donk, S., Janssen, A.H., Bitter, J.H., de Jong, K.P. Catal. Rev. Sci. Eng. 45 (2003) 297-319.
[2] Grimme, S. J. Comp. Chem. 27 (2006) 1787-1799.

Dynamic Model of Breathing Transitions in MOF's

Carles Triguero*, Francois-Xavier Coudert*, Anne Boutin,** Alain H. Fuchs,* Alexander V. Neimark*,***
**Chimie ParisTech & CNRS, Paris, France; carlos-triguero@chimie-paristech.fr*
***École normale supérieure, Paris, France*
****Department of Chemical and Biochemical Engineering, Rutgers, The State University of New Jersey, USA.*

Phenomenon of adsorption-induced deformation attracted recently a considerable attention owing to its relevance to practical problems of mechanical stability and integrity of novel nanoporous materials. Micro- and mesoporous materials find numerous applications as selective adsorbents and catalysts, substrates for biosensors and drug delivery, membranes and films in various nanotechnologies, which involve fluids adsorbed or confined to nanoscale pores within rigid or compliant solid matrixes. Guest molecules adsorbed in pores cause a substantial stress in the host matrix leading to its contraction or swelling. Although various experimental manifestations of adsorption-induced deformation have been known for a long time, a rigorous theoretical description of this phenomenon is lacking. We present a general thermodynamic approach suggested for predicting adsorption stress and respective deformation in various microporous and mesoporous materials. The proposed method is based on the analysis of adsorption isotherms by means of molecular simulations, density functional theory, and empirical models.

Moreover, the recent discovery of reversible breathing transitions between open and closed pore structures (**lp** and **np** phases) in flexible metal-organic frameworks (MOF) brought about a new physical phenomenon that represents a challenging problem for the theorists. Breathing transitions in MOF's like MIL-53 occur in the process of adsorption of various guest molecules; as well as during variations of temperature, or external pressure. We present a dynamic network model of adsorption-driven breathing transitions, which takes into account a complex interplay of adsorption and elastic interactions. The proposed MC model is based on the Hamiltonian, which depends on the deformation strain *e* and adsorption loading *n* that may vary from sell to cell,

$$\Phi[\{e\},\{n\}] = \phi_{\mathrm{c}}[\{e\}] + \phi_{\mathrm{c-c}}[\{e\}] + \phi_{\mathrm{c-p}}[\{e\},\{n\}] + \Delta F_{\mathrm{h}}$$

The first term in the RHS of the Hamiltonian accounts for the elastic energy of the cell. The second term is the responsible of elastic cell-cell interactions. The third term describes the interaction between the adsorbed particles and the cell; it includes the adsorption energy and the adsorption strain. The forth term is the difference of free energies between reference lp and np cell in vacuum. The MC process involves two types of moves, insertion of guest molecules and change of cell identity between **lp** and **np**. The simulation implies the elastic relaxation of the network and the change of the elastic energy contributes into the probability of acceptance of MC moves. An example of simulation is given in the Figure. For certain conditions, there are, two consecutive **lp** → **np** → **lp** transitions associated with the sharp adsorption uptake and respective changes of the network volume. This example is purely illustrative; however it captures the main features of breathing phenomena observed experimentally.

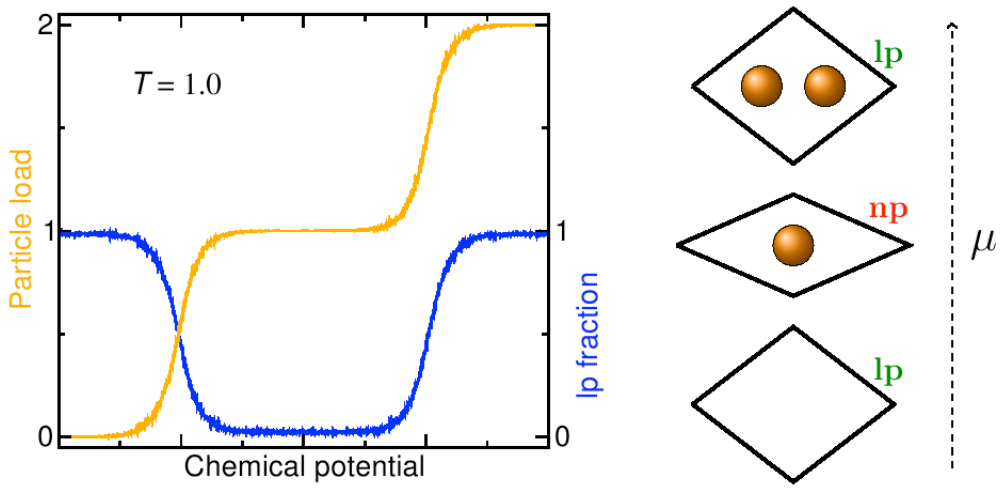

Fig. 1: Typical results of a breathing material as obtained from the dynamic model we developed. Upon increase of chemical potential, the host material contracts then swells.

References

[1] A. V. Neimark, F.X. Coudert, A. Boutin, and A. H. Fuchs, - Stress-based model for the breathing of metal–organic frameworks, *J. Phys. Chem. Lett.,* **2010**, 1, 445–449.
[2] A. V. Neimark, F.-X. Coudert, C. Triguero, A. Boutin, A. H. Fuchs, I. Beurroies and R. Denoyel, submitted for publication.

Molecular Simulation Characterization and Adsorption Studies of a Challenging New MOF

Marta De Toni[1,2], Pluton Pullumbi,[2] François-Xavier Coudert[1], Alain H. Fuchs[1],
1: Chimie ParisTech and CNRS, France; 2: Air Liquide, Paris, France

In this work we characterize a new nitrogen functionalized MOF that was synthesized in 2009 by the group of R. Guillard et al. [1]. It is built by cyclic triamines and carboxylate groups linking together zinc cations, and presents an extra-framework halogen anions [Fig.1]. It has a cubic symmetry and only a type of channels, interconnected two-by-two through windows [Fig.2].

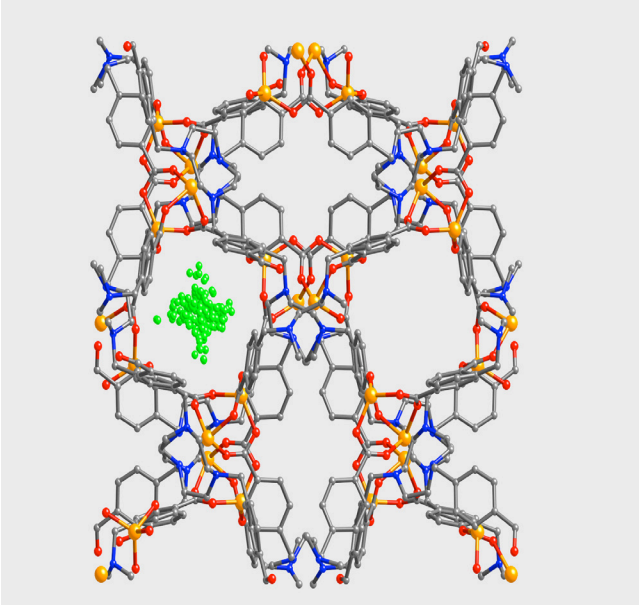

Fig.1. A view of the unit cell and the site occupied by Cl^-

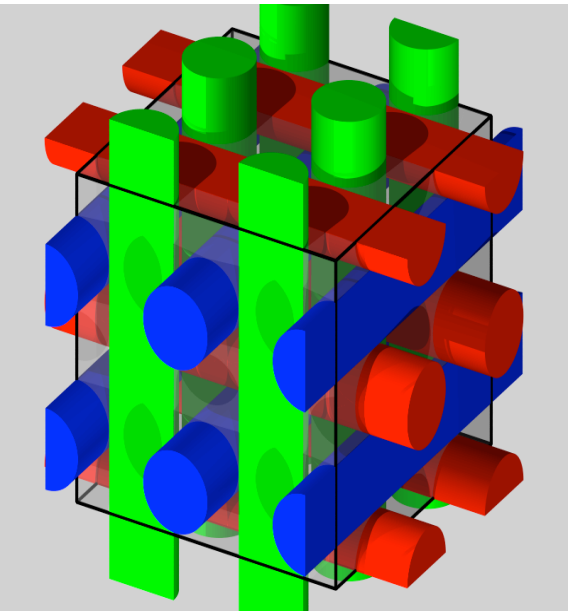

Fig.2. A schematic of the accessible channels

The molecular simulation of this new MOF was challenging because its includes tetraazamacrocyles, which are not typically featured in materials and whose atomistic description is an open question for molecular simulation. We used DFT calculations on clusters extracted from the large unit cell to determinate the partial atomic charges of the MOF. These were combined with existing potentials for the description of the adsorption fluid molecules (optimized for reproducing fluid phase equilibria).

Molecular simulation allowed to determine the location of halogen anions (Br^-, Cl^-, F^-) in the unit cell, which was not possible experimentally. Each ion is localized around a specific and well-defined site, with a spread varying with temperature (from 77 K to room temperature). The Br^- and Cl^- sites are similar, while the F^- site is slightly different and less mobile (as a harder anion).

After having characterized this MOF (porosity, connectivity and distribution of the anions), we calculated the CO_2 and H_2O adsorption isotherms at high pressure and at different

temperatures in the presence of each type of anions considered. We also investigated the coadsorption properties of this material at 300 K for mixtures of CO_2, CO, O_2, N_2 and CH_4 with different ratios. We find a high selectivity that decreases at high pressure.

References

[1] G. Ortiz, S. Brandes, Y. Rousselin, R. Guillard, submitted to Nature Materials (2011)

Understanding Type V Isotherms for H_2O and CO_2 Adsorption in MOFs

François-Xavier Coudert*, Selvarengan Paranthaman, Marta De Toni and Alain H. Fuchs.
Chimie ParisTech, CNRS and Univ. Pierre et Marie Curie, 11 rue Curie, 75005 Paris, France. Tel : +33 1 44 27 67 51. E-mail : fx.coudert@chimie-paristech.fr

Introduction

Nanoporous metal–organic frameworks (MOFs) are topical materials displaying a large range of crystal structures and host–guest properties. Among the proposed applications of MOFs, adsorptive storage and separation of strategic gases (H_2, CO_2, CH_4) are of particular importance and have gained a lot of attention in recent years.
Some MOFs, such as MOF-5 (also known as IRMOF-1), HKUST-1 and DUT-4, are unstable in the presence of water vapour. Others, however, are stable even when left in liquid water for long periods of time. A coherent, global understanding of the factors behind water stability of MOFs is still lacking and is hard to tackle. If only a few water adsorption (and desorption) isotherms in MOFs have been published, on the contrary water adsorption has been extensively studied in other porous materials from both experimental and theoretical points of view. The special case where the confining matrix is hydrophobic, in particular, has attracted a lot of interest in the past decade and many systems for which water adsorption in hydrophobic spaces is relevant, such as activated carbons and all-silica zeolites, functionalised or coated mesoporous materials were studied.[1]
We extended these investigations to hydrophobic MOFs, performing a molecular simulation study of water adsorption in Al(OH)(1,4-ndc) and its functionalised variants, and of CO_2 adsorption in IRMOF-*n* (*n* = 1, 10, 16). In both cases, type V isotherms were obtained, and we shed some light on the nature of the adsorption transition by exhibiting the effect of confinement on the phase diagram of the adsorbates. We also demonstrated the influence of pore size and functionalisation of the organic linker on the hydrophobicity (or "CO_2-phobicity") of the material.

Results and discussion

Partial atomic charges of material Al(OH)(1,4-ndc) were optimised in order to reproduce the experimental isotherms for water at 298 K. We used parameters from previous work by Snurr et al. that reproduces adequately experimental data for CO_2 adsorption in IRMOF-1 at different temperatures between 195 K and 273 K. For both phenomena a type V isotherm is obtained and this can be explained by considering the hydrophobic (and "CO_2-phobic") nature of the internal surface of the materials studied. The water-MOF and CO_2-MOF interactions are, in these cases, much smaller than water-water and CO_2-CO_2 interactions and thus the adsorption process at low pressure is unfavourable from a free energy point of view. Because interested on probing the water adsorption in a series of functionalised variants of the MOF family Al(OH)(1,4-ndc), we calculate, as shown in Fig.1, the adsorption and desorption isotherms for different degree of methylation (2, 4 and 8 respectively). It can be clearly seen that such a functionalisation of the material has an effect on the saturation uptake and the adsorption pressure. If the impact of methylation on saturation uptake can be simply explained as a steric effect, the influence on the adsorption pressure is a consequence of the changes of the chemical nature of the interior surface of the pores, the added apolar methyl groups shielding the more polar carboxylate groups from the adsorbate[2].

In order to better characterize the type V isotherm, observed for water adsorption in Al(OH)(1,4-ndc), we analysed it from the point of view of liquid–vapour phase transition under confinement. Studying the number of molecules adsorbed at the pressures corresponding of the transition, we notice the presence of intermediate thermodynamic states that means the adsorption observed is a continuous transition. From a microscopic point of view, such intermediate states correspond to situations where some channels are empty while others are completely filled. A cooperative mechanism among neighbouring pores leads the global transition for the material to be continuous and it is observed also for the methyl-fonctionnalised materials. In the case of water adsorbed in Al(OH)(1,4-ndc), and its methylated derivatives, thus, as confinement increases, the critical point shifts to lower temperature[2].

To characterize CO_2 adsorption in similar materials, we considered a family of isoreticular materials (IRMOF-*n* where *n* = 1, 10, 16) differing only in their organic linkers, and thus in porous volume. We calculated their adsorption isotherms at different temperatures, in good agreement with both experimental data and existing molecular simulations.[3] We found that when the temperature increases, the transition become continuous and the higher the internal volume the more important this effect. We were able to determine the transition pressure for each material at the temperatures studied. Reporting these data on the phase diagram showed in Fig. 2, we highlight the effect of confinement on the critical temperature for "CO_2-phobic" IRMOFs : when the porous volume increases, the temperature decreases[4].

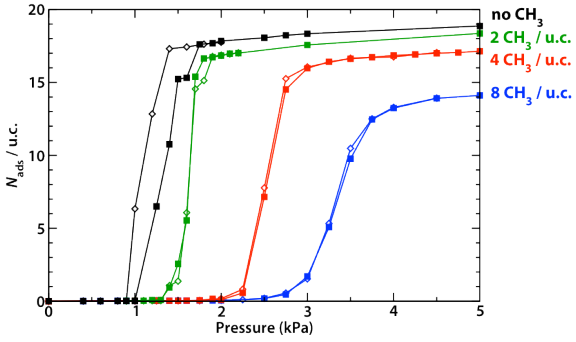

Fig. 1: Isotherms for adsorption (filled symbols) and desorption (open symbols) of water in Al(OH)(1,4-ndc) and derivates.

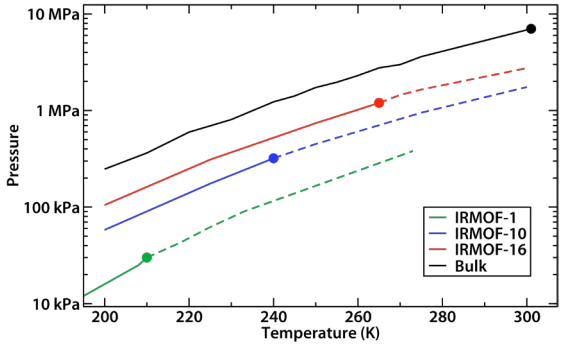

Fig. 2: Phase diagram of CO_2 in IRMOF-*n* (*n* = 1, 10, 16) and the confinement effect on the critical temperature.

Simulation techniques

The calculation of isotherms was performed using Grand Canonical Ensemble simulations. Water molecules are described by the TIP4P-Ew model and CO_2 molecules by a TraPPE model with three atomic charges; the dispersion and repulsion interactions are modeled by a 12-6 Lennard-Jones potential between all atoms.

References

[1] F-X. Coudert, F. Caillez, R. Vuilleumier, A. H. Fuchs and A. Boutin, *Faraday Discuss.*, **2009**, 141, 377
[2] S. Paranthaman, F-X. Coudert and A. H. Fuchs, submitted to *Phys. Chem. Chem. Phys.*
[3] K. S. Walton, A. R. Millward, D. Dubbeldam, H. Frost, J. J. Low, O. M. Yaghi and R. Q. Snurr, *J. Am.Chem. Soc.*, **2008**, 130, 406.
[4] M. De Toni, F.-X. Coudert, A. H. Fuchs, submitted to *Langmuir*.

Vibrational spectra of polysiloxane and bridged polysilsesquioxane xerogels – a theoretical investigation

Piotr Borowski, Mariusz Barczak, Karol Pilorz
Faculty of Chemistry, Maria Curie-Sklodowska University, M. Curie-Sklodowska Sq. 5, Lublin 20-031, POLAND, e mail: pibcio@vsop404.umcs.lublin.pl

Introduction

The silicon-containing porous materials are often characterized by means of the vibrational spectroscopy. The existence of some of the functional groups, which are present in the final materials obtained in the course of the sol-gel polycondensation process (see e.g. [1] and references therein; *cf.* Figure 1), can be confirmed by finding the relevant bands on the IR spectra. However, it frequently happens that the bands important from the point of view of the identification of the functional groups or some structural motifs are located close to, or even in the range of the spectrum, where the strong band corresponding to the Si–O stretching vibration appears. The interpretation of the spectra can be greatly facilitated by the quantum chemical calculations.

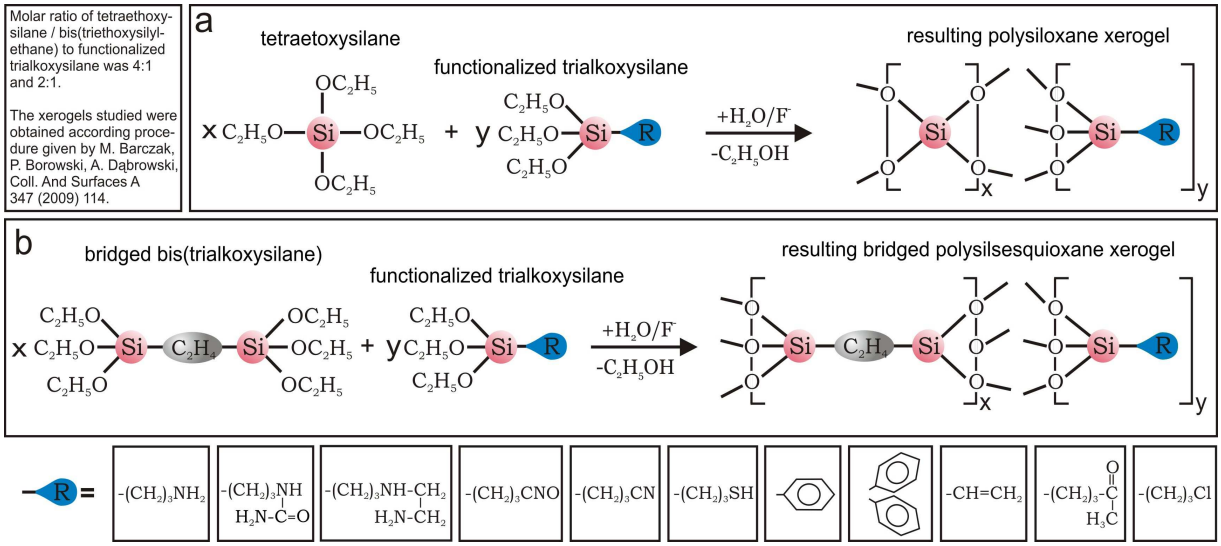

Figure 1. Scheme of the co-condensation route used for synthesis of the materials studied and functional groups introduced into silica framework

Results and discussion

It is well known that the harmonic frequencies (the only theoretical frequencies available for systems as large as the representative fragments of the macromolecules) obtained from a quadratic force field computed at *ab initio* or DFT levels of theory with the aid of the so-called Wilson-Decius-Cross method (see e.g. [2]) are typically too high compared with the fundamentals observed in the vibrational spectra. Much better agreement between the calculated and experimental frequencies is obtained using scaling methods such

as the so-called scaled quantum mechanical (SQM) force field method [3,4], or the recently proposed effective scaling frequency factor (ESFF) method [5]. It was shown [6] that in a general case of molecules with various structural motifs, the ESFF method renders the scaled frequencies somewhat lower than SQM. The application of the simulated spectra based on the SQM and ESFF scaled frequencies (calculated from B3LYP force fields of a representative fragments of macromolecules) in the interpretation of the experimental spectra of the final materials will be presented. In this simulation the band widths were allowed to vary, but the overall integral intensity was assumed to be equal to the computed at a given theoretical level. The predictive capabilities of the SQM and ESFF methods will be discussed.

Conclusions

Theoretical studies turned out to be very helpful in the interpretation of the vibrational spectra of the functionalized organosilica materials. The simulated bands based on the scaled frequencies obtained from the B3LYP force fields of the representative fragments of the final materials are in good agreement with the experimentally observed ones. Such simulation should be preferably carried out using a number of conformers of a given fragment, due to their presence in the bulk phase of the final material.

Acknowledgements

This study was partially supported by the European Community (FP7/2007-2013) under the Marie Curie International Research Staff Exchange Scheme (IRSES), Project No. 230790.

References

[1] M. Barczak, P. Borowski, A. Dąbrowski, Coll. And Surfaces A 347 (2009) 114.
[2] E. B. Wilson, Jr, J. C. Decius, P. C. Cross, Molecular Vibrations. The Theory of Infrared and Raman Vibrational Spectra, Dover Publications, Inc., New York, 1955.
[3] P. Pulay, G. Fogarasi, G. Pongor, J. E. Boggs, A. Vargha, J. Am. Chem. Soc. 105 (1983) 7037.
[4] J. Baker, A. A. Jarzecki, P. Pulay, J. Phys. Chem. 102 (1998) 1412.
[5] P. Borowski, M. Fernández-Gómez, M. P. Fernández-Liencres, T. Peña Ruiz, Chem. Phys. Letters 446 (2007) 191.
[6] P. Borowski, A. Drzewiecka, M. Fernández-Gómez, M. P. Fernández-Liencres, T. Peña Ruiz, Chem. Phys. Letters 465 (2008) 290.

Prediction of adsorption of odor compounds in zeolites by molecular modeling studies

Cristian Constantin Brunchi, Juan Manuel Castillo Sanchez, Thijs J.H. Vlugt, Herman J.M. Kramer

Process& Energy Laboratory, Delft University of Technology, NL-2628 CA Delft, The Netherlands
Corresponding author e-mail: c.c.brunchi@tudelft.nl

1. Introduction

This study is focused on the use of Monte Carlo simulations for the screening of potential zeolite adsorbents that can be used to remove VOC's present in ppm range in a toluene stream. Five compounds having different sizes and functional groups were chosen as model impurities: butanal, ethyl-hexenal, dimethyl-cyclohexanone, trimethyl-anisole and trimethyl-phenol.

Simulations have been performed at a temperature of 300 K to study the adsorption properties of these compounds in silicalite (MFI-type) and Na-Y zeolites. Single-component, binary-mixture and 6-mixture isotherms, as well as Henry coefficients and heats of adsorption have been computed. The zeolite is modeled as a rigid crystal as described by Kiselev and co-workers [1]. The cubic lattice parameter of the FAU u.c. is 25.028 Å and the u.c. composition is $M_{54}Si_{138}Al_{54}O_{348}$, where M denotes a monovalent cation. This corresponds to a Si/Al ratio of 3.55. The Na+ cation positions inside the FAU framework were obtained from an NVT – Monte Carlo simulation. The butanal, ethyl-hexenal, dimethyl-cyclohexanone and –CH3 alkyl groups in the substituted benzene rings are described using a united-atom model [2]. The non-bonded interactions between the molecules and between the molecules and the zeolite are described with a Lennard-Jones potential.

2. Results

The molecules were modelled using the TraPPE force-field [3-8]. However, because of the different sets of parameters used in our simulations, the Lennard-Jones parameters from the cited literature were further fitted to describe the vapour-liquid curve of the phase diagram. Fig. 1 presents the simulated toluene isotherms, obtained using the van Koningsveld [9] and Olson [10] model of MFI, in comparison with various experimental data from the literature [11-14]. Using the van Koningsveld model, the result is in resonable agreement with the experimental data available in the literature. The model also predicts the inflection at an adsorbate loading of 4 molecules/u.c. (63 mg/g).

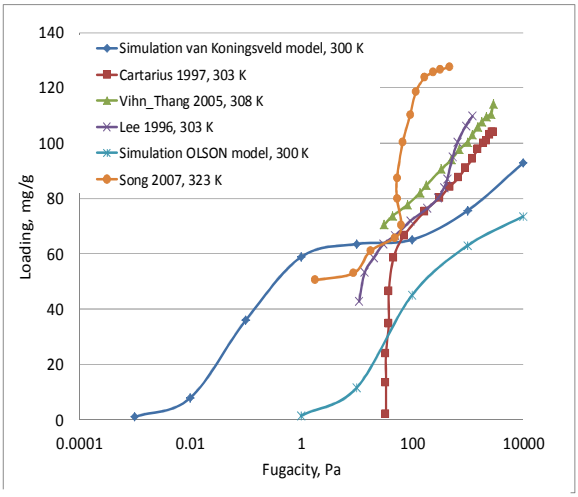

Fig. 1. Isotherms of toluene in silicalite (MFI-type). Comparison between simulated adsorption isotherm obtained in this work and several experimental results from the literature.

In Table 1 we present the Henry coefficients and the heats of adsorption in MFI and FAU, computed at zero coverage as described by Vlugt and co-workers [15]. At zero coverage it is safe to assume an ideal Langmuir behavior for the system and we can compute the binary selectivities as the ratios of Henry's constants. In MFI only toluene, butanal and ethyl-hexenal can diffuse/adsorb through the pores. Judging from the selectivities in FAU, all

compounds can adsorb very well from the binary mixture with toluene; however, when all compounds are present in the mixture, the competition between the species has a very strong influence on the final adsorption as can be seen in Fig. 2. Butanal is preferentially and strongly adsorbed in the whole concentration range, trimethyl-phenol and the di-substituted cyclohexanone show a weak adsorption capacity while the tri-substituted phenol and anisole hardly adsorb at all.

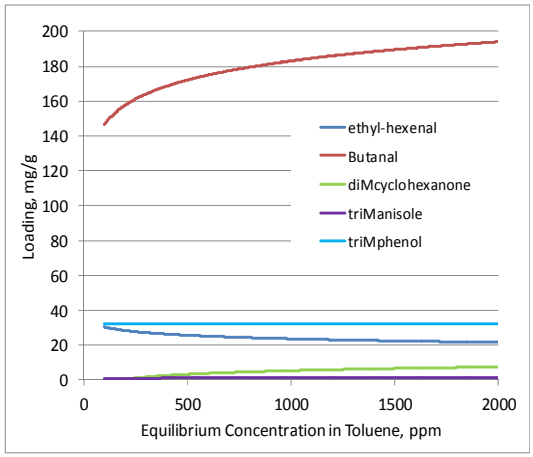

Fig. 2. Adsorption behaviour of the studied mixture in FAU. Simulation conditions: 5000 Pa, 300 K

The toluene heat of adsorption in MFI at around 300 K is reported in several literature studies [11-13, 16-20]. However there is no agreement amongst reported values. The average heat of adsorption of Toluene in FAU reported by Canet and co-workers [21] (-70 kJ/mol) is in very good agreement with the value obtained in our simulations. To the best of our knowledge, there is no data available for the other compounds in the literature.

Table 1. Computed Henry coefficients, selectivities and heats of adsorption at zero coverage.

Substance	K in MFI	K in FAU	Selectivity in MFI	Selectivity in FAU	ΔHads in MFI	ΔHads in FAU
	mol/kg/Pa	mol/kg/Pa			kJ/mol	kJ/mol
toluene	0.01	69	-	-	-56	-76
triMphenol	-	$4 \cdot 10^{10}$	-	$5.8 \cdot 10^{8}$	-	-138
triManisole	-	$6 \cdot 10^{7}$	-	$8.8 \cdot 10^{5}$	-	-118
diMcyclohexanone	-	$1 \cdot 10^{5}$	-	$1.5 \cdot 10^{3}$	-	-91
butanal	0.61	$1 \cdot 10^{6}$	49	$1.4 \cdot 10^{4}$	-67	-108
ethyl-hexenal	209	$1.7 \cdot 10^{9}$	$1.7 \cdot 10^{4}$	$2.4 \cdot 10^{7}$	-90	-135

3. Conclusion

A model to describe the adsorption behaviour of several VOC's was developed. Because the availability of experimental data is lacking, not all computed properties could be validated. Experiments in FAU are underway.

Acknowledgements: This is an ISPT project.

References

1. Kiselev, A.V., et al., J. Chem. Soc., Faraday Trans. 2, 1978. **74**: p. 367-379.
2. Ryckaert, J.-P. and A. Bellemans, Faraday Discuss., 1978. **66**: p. 95-106.
3. Siepmann, J.I., B. Chen, and J.J. Potoff, J. Phys. Chem. B, 2001. **105**(15): p. 3093-3104.
4. Siepmann, J.I. and M.G. Martin, J. Phys. Chem. B, 1999. **103**(21): p. 4508-4517.
5. Siepmann, J.I. and M.G. Martin, J. Phys. Chem. B, 1998. **102**(14): p. 2569-2577.
6. Siepmann, J.I. and N. Rai, J. Phys. Chem. B, 2007. **111**(36): p. 10790-10799.
7. Siepmann, J.I., J.M. Stubbs, and J.J. Potoff, J. Phys. Chem. B, 2004. **108**(45): p. 17596-17605.
8. Siepmann, J.I., C.D. Wick, and M.G. Martin, J. Phys. Chem. B, 2000. **104**(33): p. 8008-8016.
9. Vankoningsveld, H., H. Vanbekkum, and J.C. Jansen, Acta Crystallographica B, 1987. **43**: p. 127-132.
10. Olson, D.H., et al., J. Phys. Chem., 1981. **85**(15): p. 2238-2243.
11. Cartarius, R., H. Vogel, and J. Dembowski, Physical Chemistry Chemical Physics, 1997. **101**(2): p. 193-199.
12. Vinh-Thang, H., et al., Langmuir, 2005. **21**(11): p. 5094-5101.
13. Lee, C.K. and A.S.T. Chiang, J. Chem. Soc., Faraday Trans., 1996. **92**(18): p. 3445-3451.
14. Song, L., et al., Microporous and Mesoporous Materials, 2007. **104**(1-3): p. 115-128.
15. Vlugt, T.J.H., et al., Journal of Chemical Theory and Computation, 2008. **4**(7): p. 1107-1118.
16. Pope, C.G., J. Phys. Chem., 1986. **90**(5): p. 835-837.
17. Masuda, T., et al., Microporous and Mesoporous Materials, 1998. **23**(3-4): p. 157-167.
18. Mukti, R.R., A. Jentys, and J.A. Lercher, J. Phys. Chem. C, 2007. **111**(10): p. 3973-3980.
19. Talu, O., C.J. Guo, and D.T. Hayhurst, J. Phys. Chem., 1989. **93**(21): p. 7294-7298.
20. Thamm, H., J. Phys. Chem., 1987. **91**(1): p. 8-11.
21. Canet, X., J. Nokerman, and M. Frere, IAS Journal, 2005. **11**: p. 213-216.

Structural and dynamics properties of hydrogen confined phases in Silicalite-I zeolite.

J.P. Coulomb[a]*, N. Floquet[a] , P.L. Llewellyn[b] and G. André[c].
[a]*C.I.N.A.M. – CNRS, Campus de Luminy, Case 901,13288 Marseille Cedex 09, France.*
[b]*MADIREL – UMR 6121, Centre de S[t.] Jérome, 13397, Marseille Cedex 20, France.*
[c]*Laboratoire Léon Brillouin, CEA – Saclay, Saclay, France.*
** corresponding.author@email : coulomb@cinam.univ-mrs.fr*

Introduction

We have investigated the structural and dynamics properties of confined hydrogen phases in Silicalite-I zeolite by neutron diffraction (D_2 hydrogen isotope) and incoherence quasi-elastic neutron scattering (HD hydrogen isotope). Such a system, is particularly interesting due to the fact that hydrogen sorption isotherm in Silicalite-I presents a nice isotherm sub-step, characterized by a pronounced hysteresis loop. From the analysis of the neutron diffractograms and neutron spectrograms measured at different hydrogen loadings on both sides of the isotherm sub-step, we conclude to the existence of a phase transition from a H_2 confined fluid phase to a H_2 confined commensurate solid phase. Recall that we have studied in detail the thermodynamic and structural properties of a large number of simple gas (He, Ar, Kr, N_2, CO, O_2) confined in Silicalite-I and ZSM-5 zeolites [1-5], but hydrogen is the first one which is suited for dynamic properties analysis from incoherent neutron scattering.

Experimental

The Silicalite-I zeolite sample has been synthesized at the Prof. K. Unger Laboratory of Inorganic Chemistry (Mainz - RFA), while the neutron diffraction and the incoherent quasi-elastic neutron scattering experiments, have been performed at the Léon Brillouin Laboratoire (Saclay – France), on the G4-1 two axis diffract-tometer and MIBEMOL time of fly spectrometer, respectively. Detailed cali-bration sorption isotherms of confined hydrogen phase have been measured during the neutron scattering experiments to determined the host Silicalite-I hydrogen loadings of each neutron counts with great accuracy (as illustrated on **figure 1**).

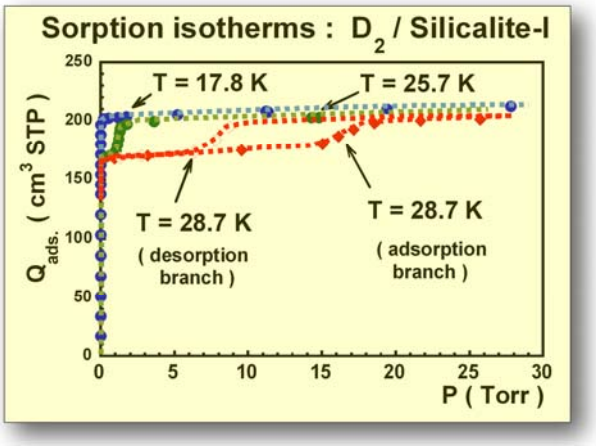

Figure 1 : Detailed calibration sorption isotherms of confined hydrogen in Silicalite-I zeolite, measured at different temperature (17.8 K, 25.7 K and 28.7 K), during the neutron diffraction experiment accomplished on the G4-1 two axis diffractometer. A pronounced hysteresis loop has been observed during the isotherm sub-step formation at T = 28.7 K.

Results and discussion

During the hydrogen sorption phenomenon in the Silicalite-I zeolite at T = 25.7 K, we have observed large modifications of the neutron diffractogram which characterizes the outgazed Silicate-I sample. In particular, the intensities, of the two main diffraction peaks located at low wave vector values (Q ≈ 0.6 $Å^{-1}$), greatly decrease and finally vanish (as shown on **figure 2**). On the other hand, the intensity of the diffraction peak located at 2.1 $Å^{-1}$ increases a little. After the isotherm sub-step formation, on the isotherm plateau (at 95% D_2 loading), the main diffractogram modifications concern the appearance of several narrow diffraction peaks in the wave vector range (1.8 < Q < 2.5 $Å^{-1}$). We interpret such extra diffraction peaks as the signature of a hydrogen confined phase solidification. The Rietveld analysis of such a neutron diffractogram is in progress (at the present time the Bragg reliability factor is still rather high around 20 %, we continue the D_2 confined phase structure refinement). We have represented schematically on the **figure 3**, the presently proposed confined hydrogen structure. Concerning the hydrogen (HD) molecular mobility D_t, we have measured by incoherent quasi-elastic neutron scattering, an abrupt change of D_t during the sub-step formation. Moreover D_t vanishes on the isotherm plateau. We interpret our result as a phase transition between a confined fluid phase and a confined solid phase.

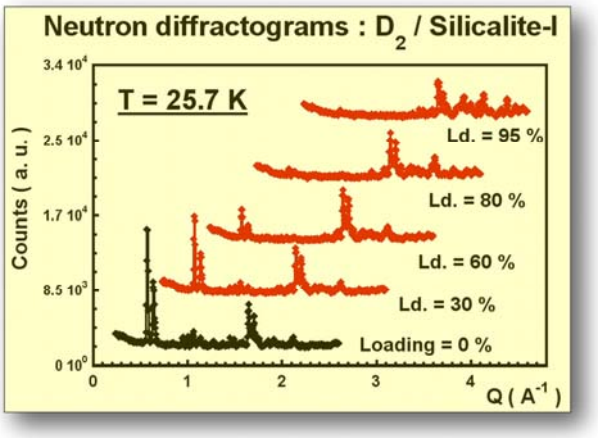

Figure 2 : Neutron diffractograms of the Silicalite-I zeolite measured at T = 25.7 K for different hydrogen (D_2) loadings (0 %, 30 %, 60 %, 80 % and 95 %).

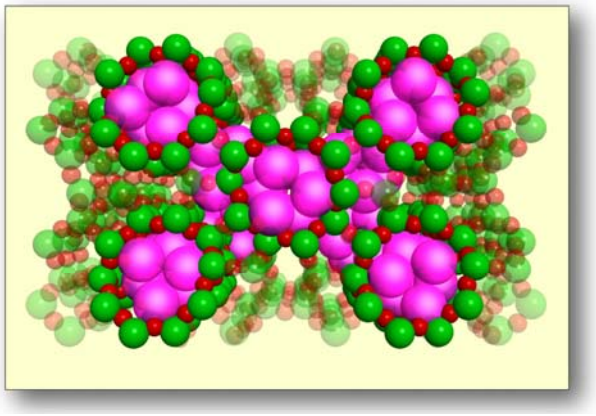

Figure 3 : Schematic representation of the structure of the confined hydrogen phase in Silicalite-I zeolite at full H_2 loading (44 molecules / u.c.).

Acknowledgements

The authors greatly acknowledge U. Müller and H. Reichert of the Prof. K. Unger Laboratory of Inorganic Chemistry (Maintz – RFA) for the Silicalite-I samples supplies.

References

[1] P.L. Llewellyn, J.P. Coulomb, Y. Grillet, J. Patarin, G. André and J. Rouquerol, Langmuir 9 (1993) 1846.
[2] P.L. Llewellyn, J.P. Coulomb, Y. Grillet, J. Patarin, G. André and J. Rouquerol, Langmuir 9 (1993) 1852
[3] J.P. Coulomb, C. Martin, P.L. Llewellyn and Y. Grillet, Studies in Surface Science and Catalysis, Vol. 105, (1997) 2355.
[4] J.P. Coulomb, N. Floquet, N. Dufau, P.L. Llewellyn and R. Khan, Microporous and Mesoporous Materials, 101 (2007) 271.
[5] N. Floquet, J.P. Coulomb, J.P. Bellat, J.M. Simon, G. Weber and G. André, J. Phys. Chem. C, 111 (2007) 18182.

Petrochemical and environmental catalytic applications

FEZA 2011

Methanol transformation in presence of ethylene.

Pieter Struelens*, Delphine Minoux**, Nikolay Nesterenko**, J.P. Dath** and Pierre Jacobs*

** Centre for Surface Chemistry and Catalysis, Katholieke Universiteit Leuven, Kasteelpark Arenberg 23 - bus 2461, 3001 Heverlee, Belgium, pieter.struelens@biw.kuleuven.be*
*** Total Petrochemicals Research Feluy, Zone Industrielle Feluy C, B-7181 Seneffe, Belgium*

Introduction

The conversion of methanol to hydrocarbons (MTH) over acidic zeolite catalysts has been the subject of widespread research since the reaction was discovered by Mobil researchers in the aftermath of the 1973 oil crisis. Originally intended to produce gasoline (Methanol To Gasoline, MTG), the research of the MTH reaction quickly narrowed towards the production of light olefins (Methanol To Olefins, MTO) and even to propylene (MTP).
The present work emphasizes on the MTP reaction. In particular, the reaction of methanol or dimethyl ether (DME) in presence of ethylene will be discussed, aiming at investigating the possibility of selective propylene production from ethylene and methanol. Medium pore zeolites were used with various Al content and different morphology. Catalysts were tested in a continuous flow reactor in a wide range of conditions, so as to determine the product reaction network, in terms of primary or subsequent events. In contrast to prior literature work [1-7] where labeled methanol was used, in this work a mechanistic study was performed with ^{13}C singly labeled ethylene.

Experimental

The experiments were carried out in a continuous quartz fixed bed reactor filled with 1 g of catalyst pellets with sizes ranging from 250 to 500 µm. The feed was composed of ethylene and dimethyl ether (DME). Nitrogen was used as a carrier gas.
Reactions were carried out in a 180-300°C temperature range in order to suppress secondary side reactions
The products leaving the reactor were sampled on-line, separated and analyzed using GC-FID. The analysis of the labeling experiments was carried out by a GC-MS system.
In order to verify the reaction network, potential product intermediates were also (co-)fed to the reactor, *viz.* propene, butane, diethylether.

Results and discussion

Different zeolite catalysts, mainly with MFI but also with CHA, MTT, FER, TON, MMW and MOR topology, were exposed to DME and/or ethylene feed at inlet reaction temperatures below 300°C. In such conditions 100% propylene selectivity can be achieved at low feed conversion. Co-feeding of ethylene has a positive effect on DME conversion, while pure ethylene (in absence of DME) favors oligomerization. Upon co-feeding DME and ethylene, a 'unique curve' for each catalyst topology between DME conversion and propylene selectivity was observed (fig 1). Generally, the experiments allow stating that at low reaction temperatures propylene selectivity is inversely proportional to the conversion and this phenomenon is governed only by catalyst topology, rather than by specific reaction conditions.

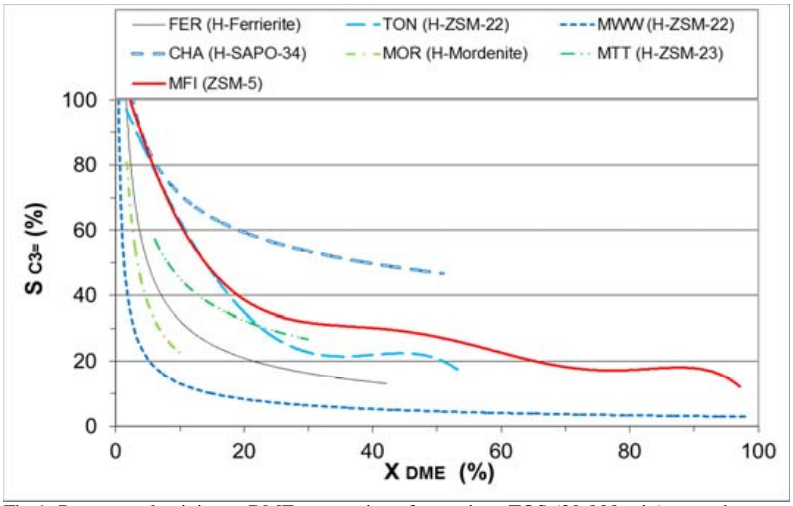

Fig 1: Propene selectivity vs DME conversion after various TOS (30-900 min) on various catalysts at various reaction temperatures.

The labeling experiments with singly labeled ethylene in presence of DME and in conditions where 100% propylene selectivity was achieved, indicate that propylene formation occurs nearly exclusively via methylation of ethylene. As the reaction temperature and the conversion rises, the degree of ethylene methylation diminishes, while the production of propylene is more and more the result of methanol propagation (results not shown).
An important observation is the fact that propylene can be formed by methanol propagation as well as ethylene methylation. Propylene selectivity is very high at low DME conversions as a result of the exclusive occurrence of ethylene methylation. The major reason for the decreasing selectivity at higher conversion is the faster propylene methylation (compared to ethylene) as well as its faster oligomerization rate (compared to ethylene). Moreover, in the latter conditions a new mechanism, *viz.* methanol methylation, is intervening yielding a variety of products.

Conclusion

In this work ethylene and DME have been co-fed to a flow reactor at low temperatures with different catalysts. The main goal of this work was to examine how and to what extent propylene molecules are formed over different types of catalysts. Low reaction temperatures invariably showed low conversions but very high propylene selectivity, irrespective of catalyst or condition used. At the low conversions, propylene is primarily formed by methylation of ethylene. The observation of a unique curve connecting DME conversion and propene selectivity, it is concluded that the reaction selectivity is topology dependent. As the reaction temperature and the conversion rises, the degree of methylation of ethylene diminishes and the production of propylene is increasingly governed by methanol propagation. As the reaction conversion rises at constant temperature, the degree of methylation of ethylene also diminishes. It follows that ethylene methylation is inversely proportional to the conversion of DME .

References

[1] M. Stöcker, Microporous and Mesoporous Materials 29 (1999) 3
[2] K.J. Chao, Proceedings 8th int. Congres on Catalysis, Verlag Chemie, Weinheim, 1984, p. V-667
[3] I.M. Dahl, S. Kolboe, Catal Letters 20 (1993) 329
[4] S. Kolboe, I.M. Dahl, Studies in Surface Science and Catalysis (1995) Vol 94 427-434
[5] M. Bjorgen et al. Journal of Catalysis 249 (2007) 195-207
[6] S. Svelle, Journal of Catalysis 224 (2004) 115-123
[7] S. Svelle, Journal of Catalysis234 (2005) 385-400

Liquid Fuels Via Zeolite-Supported Hybrid Fischer-Tropsch Catalysts

C. L. Kibby, K. Jothimurugesan, T. Das, R.J. Saxton*
Chevron Energy Technology Company, rsaxton@chevron.com

Introduction

Syngas conversion offers a potential alternative to flaring or reinjection for monetization of associated gas. However, certain deployment applications disfavor the hydroprocessing infrastructure required to upgrade the linear paraffin wax product for blending or transport. We describe here Chevron's *N*ext *G*eneration *S*yngas *C*onversion$_{TM}$ (NGSC$_{TM}$) technology, a commercially viable hybrid syngas conversion catalyst comprising both a Fischer-Tropsch active metal and a zeolite component that truncates the Anderson-Schultz-Flory (ASF) distribution to provide a liquid hydrocarbon product without the need for downstream hydroprocessing. This talk will focus on catalyst and process development including a discussion on the effect of zeolite properties on product specifications.

Experimental

Hybrid Fischer-Tropsch catalysts have been prepared by single, step non-aqueous impregnation of cobalt and ruthenium solutions onto commercially available 1/16" zeolite extrudates to give a typical catalyst composition of 7.5% Co/0.19% Ru/zeolite/Al_2O_3. The catalysts were then activated using a specific reduction-oxidation-reduction (ROR) procedure. Detailed catalyst preparation and characterization have been described [1]. Fischer-Tropsch activity was studied in fixed bed reactors at temperatures between 205°C and 235°C with a total pressure of 5-20 atm, H_2/CO ratios of 1.5 to 2.0 and a total gas flow rate of 2100-6000 cubic centimeters of gas (0°C, 1 atm) per gram of catalyst per hour.

Results and discussion

Hybrid or modified syngas conversion catalysts using an acidic component in some combination with a Fischer-Tropsch active metal have been known for many years [2]. It is believed that the acidic functionality, usually a zeolite, provides for oligomerization, cracking, and isomerization reactions of olefins on the Brønsted acid sites. These reactions serve to break the ASF hydrocarbon distribution and limit the yield of a separate solid wax phase and give a distribution of primarily liquid and gas products.

To date a majority of the reported hybrid catalysts have been either physically mixed solid particles of separate Fischer-Tropsch and zeolite catalysts or a zeolite powder onto which a Fischer-Tropsch metal has been directly impregnated or ion-exchanged. However, both of these approaches suffer relative disadvantages. In order to limit light-gas formation and obtain an acceptable yield of liquid product the Fischer-Tropsch metal and the acid functionality require close proximity to one another. For a physically mixed system this requires catalysts of small particle size leading to unreasonably high pressure drop over the length of a fixed bed reactor. Catalysts in which the Fischer-Tropsch metal is deposited directly on a zeolite powder result in unavoidable ion-exchange and neutralization of the acid sites as well as unacceptable pressure drops in commercial fixed bed operations.

We report here Chevron's *N*ext *G*eneration *S*yngas *C*onversion$_{TM}$ (NGSC$_{TM}$) technology, a syngas conversion process that provides for a high yield of a fungible, fully blendable liquid hydrocarbon product in a single reactor. No downstream hydroprocessing of a separate solid wax phase is necessary. The preparation and catalytic activity of commercially viable zeolite extrudate catalysts are described in which the Fischer-Tropsch metals reside exterior of the zeolite channels so as to provide for high activity of both the polymerization and isomerization/cracking reactions. Further, a significant effect of both zeolite morphology as well as process conditions on the resultant product slate will be demonstrated. For example, Figure 1 illustrates the difference in hydrocarbon distribution using catalysts prepared with ZSM-12, a single dimensional 12-MR zeolite, or ZSM-5, a multi-dimensional 10-MR zeolite.

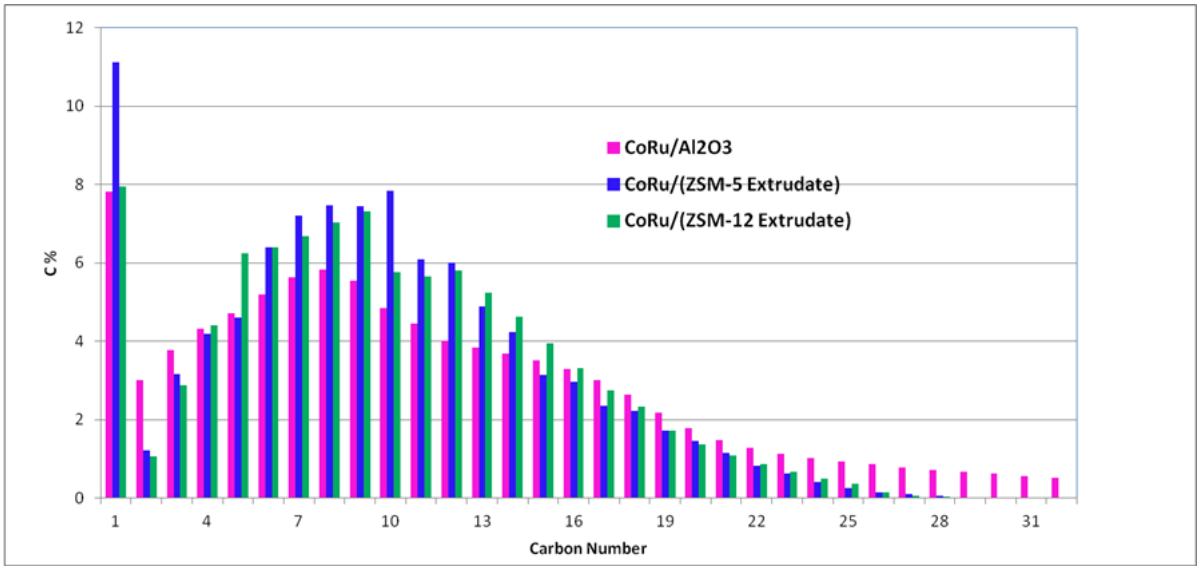

Figure 1. Comparison of hydrocarbon distribution using cobalt FTS catalyst (red) and NGSC catalysts based on ZSM-5 (blue) and ZSM-12 (green).

Conclusions

Chevron's *N*ext *G*eneration *S*yngas *C*onversion$_{TM}$ (NGSC$_{TM}$) technology, based on a novel, commercially viable hybrid Fischer-Tropsch catalyst, provides a liquid hydrocarbon product in high yield without the need for downstream hydroprocessing of a separate wax phase. The enhanced safety implications of this simplified process as well as the flexibility of catalyst composition allow for increased optionality in deployment options for monetizing associated or remote hydrocarbon assets.

Acknowledgements

Expert technical assistance from Jim Fox, Josh Lee and Mike Palad, valuable discussions with Rich Sasson, Anne Helgeson, Gordon Deppe and Stacey Zones and continued financial support from Chevron Energy Technology Company are gratefully acknowledged.

References

[1] See, for example, early Mobil patents 4,086,262, 4,207,248 and 4,304,871
[2] See US Patent 7825164 and publication numbers 20100160464 and 20100312030; technology also covered under US application numbers 12/478204, 12/780,672, 12/622972, 12/797439, 12/797773, 12/797801, 12/902915, 12/914713, 61/407773, 12/953042 and 12/953024.

Key Role of Zeolite Pore Structure for Selective Production Propylene from Pentene and Hexene

Toshihide Baba*, Yasuyoshi Iwase, To-ru Koyama, Hajime Munakata, Akimitsu Miyaji, and Ken Motokura
Department of Environmental Chemistry and Engineering, Tokyo Institute of Technology, Nagatsuda 4259, Midori-ku, Yokohama, Japan.

Introduction

We have proposed a mechanism for the production of C_3H_6 from C_2H_4 *via* carbenium cations intermediates in the initial stage. C_3H_6 could thus be produced *via* an oligomerization-cracking mechanism involving carbenium cations intermediates. In this mechanism, the selectivity for C_3H_6 should not depend on which olefin species are produced in the pores of zeolite. This would allow the possibility of controlling C_3H_6 selectivity by something other than the molecular sieve effect.

In this work, on the basis of the oligomerization-cracking mechanism for the production of C_3H_6 from C_2H_4, the cracking reactions of hexene and pentene olefins were examined using zeolites with 8-, 10-, and 12-menbered rings (MR) and various pore volumes. Highly selective production of C_3H_6 from olefins (pentenes and hexenes) can be accomplished by employing a new concept: adjusting the pore volume of a zeolite to accommodate the volume of an olefin and/or its carbenium cations, as opposed to a conventional molecular sieve approach.

Experimental

Various zeolites were prepared with the hydrothermal synthetic technique. The amounts of Si, Al, and P in silicoaluminophosphate molecular sieves and of Si, Al, and Na in aluminosilicate molecular sieves were determined by inductively coupled plasma atomic emission spectroscopy. For the aluminosilicate molecular sieves, the ratio of Si/Al in their framework was determined by ^{29}Si MAS NMR measurements.

The zeolite was packed in a continuous flow reactor (10 mm i.d. silica tubing) in a vertical furnace. After calcinations of the catalyst, the conversion of olefins such as C_5H_{10} was carried out using a continuous-flow reactor at atmospheric pressure. The hydrocarbon distributions are expressed on a carbon-number basis, exclusive of the coke remaining in the reactor.

The volumes of olefins and their carbenium cations were calculated with the density functional theory (DFT). To determine the pore volume of a part of the zeolites, the amount of adsorbed Ar was measured at 87 K.

Results and Discussion

1) Selective Conversion of 1-hexene to C_3H_6

The similarity of the volumes of olefins and their carbenium cations to the pore volumes of the zeolite catalysts for the conversion of C_2H_4 into C_3H_6 served as an important motivation. When olefins are used as reactants, the selective production of C_3H_6 could proceeds over zeolites, whose pore volumes are comparable to the volumes of the olefins and/or their carbenium cations generated by the reaction of the olefins with acidic protons. On the basis of our concept, we selected SAPO-31with 12-MR and ZSM-22 with 10-MR, since the pore volume of these zeolites can be estimated to be *ca.* 100 $Å^3$, which is close to the volume of 1-hexene carbenium cations estimated by DFT calculation. This indicates that the dimerization of hexenes, such as 1-hexene, cannot proceed in the pore of and SAPO-31 and ZSM-22, and that the unimolecular cracking reaction should proceed to produce C_3H_6. SAPO-31 gave C_3H_6 with 85% selectivity at 80% conversion of 1-hexene, while ZSM-22 gave C_3H_6 with 92 % selectivity at the same conversion of 1-hexene, as expected.

2) Selective Conversions of 2-methyl-2-butene and 2-pentene to C_3H_6 and C_2H_4

Considering the classical cracking mechanism *via* carbenium cations, it is difficult to believe that the cracking of pentene proceeds *via* a unimolecular cracking mechanism, because the three modes of β-scission of C_5 carbenium cations ($C_5H_{11}^+$) all involve a primary cations. If the selective production of C_3H_6 by the cracking of 1-hexene or 3-hexene can be controlled by the use of a pore, which can accommodate the molecular volume of hexyl cations, then it should be possible to convert 2methyl-2-butene and 2-pentene to both C_3H_6 and C_2H_4. In other words, if the unimolecular cracking of these pentenes can be controlled by the pore volume of a zeolite catalyst, it is possible that equal amounts of C_3H_6 and C_2H_4 are produced simultaneously when using zeolite catalysts. For example, a highly selective unimolecular cracking of 2-methyl-2butene into C_3H_6 and C_2H_4 proceeded over ZSM-22. Thus, C_3H_6 and C_2H_4 were produced with both 96% selectivity at nearly 100% conversion. The pore volumes ZSM-22(10-MR) was almost the same big as that of pentyl cations. The volumes of these cations were about 95 ~ 140 A^3.

When the conversion of 2-penetne was carried out by using ZSM-22, C_3H_6 and C_2H_4 were also produced with both 96% selectivity at 98% conversion.

Conclusion

Highly selective production of C_3H_6 from olefins can be accomplished by employing a new concept: adjusting the pore volume of a zeolite to accommodate the volume of an olefin and/or its carbenium cations, as opposed to a conventional molecular sieve approach.

A Very Efficient Process for the Transformation of Methyl Mercaptan to Hydrocarbons and H_2S on Solid Acid Catalysts

Edouard Huguet[a,b], Vasile Hulea[a], Robert Durand[a], Catherine Leroi[b], Renaud Cadours[b], Bernard Coq[a]

[a]*Institut Charles Gerhardt Montpellier - UMR 5253 CNRS-UM2-ENSCM-UM1, MACS, 8, rue de l'Ecole Normale, 34296 Montpellier cedex 5 (France).* [b]*TOTAL Petrochemicals France, Pôle Recherche et Développement Mont/Lacq, BP 4, 64170, Lacq (France). bernard.coq@enscm.fr.*

Introduction

Natural gas always contains contaminants including hydrogen sulfide, carbonyl sulfide, mercaptans, etc… . Conditioning natural gas for marketing requires the removal of these contaminants, which comprises several main operations. Usually, the treated gas still contains: 2% CO_2, 4 ppm H_2S and 20-50 ppm total sulfur. In view of both increasingly stringent environmental regulations, technical requirements for further catalytic processes and the discovery of new gas deposit with high mercaptans concentration, deeper desulfurization becomes in high demand. Thus, it is desirable for users of natural gas to have concentrations of mercaptans lowered to 1-5 ppmv. Modern processes for the deep removal of mercaptans and COS are generally based on fixed bed adsorption and chemical reactions. Deep mercaptans removal through chemical processes may include oxidation, alkaline treatment,[1] reaction with olefins[2] and hydrodesulfurisation.[3] The challenge is to discover new processes without addition of any reactants and producing low wastes.

To this end, this work describes for the first time the chemical transformation of methyl mercaptan to hydrocarbon (hereafter denominated M2TH) on acidic zeolites.[4] This transformation was evoked in a few sentences in only one report and some patents.[5]

Experimental

The M2TH is carried out on H-ZSM-5 (Si/Al: 15), H-Y (Si/Al: 15) and H-FER (Si/Al: 10) in a fixed-bed reactor with CH_3SH in N_2 stream (0.5/99.5, vol/vol) from 573 to 823 K. The mass of catalyst was 100 mg and the gas flow 50 mL min^{-1}.

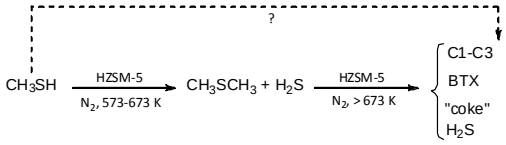

Catalytic transformation of CH_3SH into hydrocarbons on HZSM-5

Results and discussion

Figure 1 shows the conversion of CH_3SH as a function of temperature on HZSM-5. Below 673 K, CH_3SH is selectively converted into similar amounts of CH_3SCH_3 and H_2S according to the reaction: $2CH_3SH \rightarrow CH_3SCH_3 + H_2S$. From 573 to 673 K the CH_3SH conversion is 70-75%, which corresponds to the equilibrium conversion.[6] Above 673 K, the CH_3SH conversion reaches near full conversion at 823 K. The DMS decreases to the benefit of methane, ethane and propane (C1-C3), as well as benzene, toluene and xylene (BTX). Methane represents more than 90% amongst C1-C3. The direct

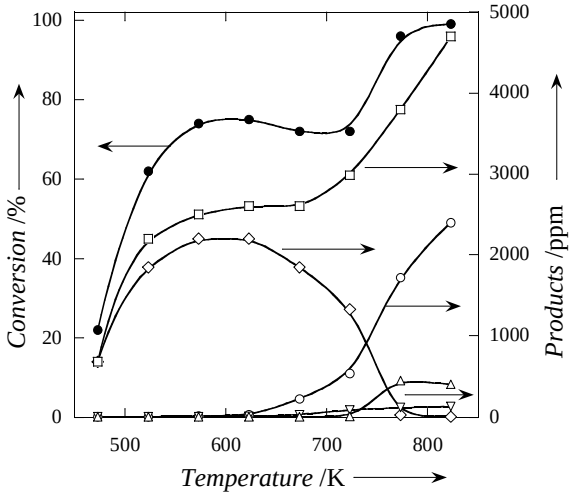

Figure 1. CH_3SH Conversion of as a function of temperature on HZSM-5; (●) conversion, (□) H_2S, (◇) DMS, (○) CH_4, (▽) C_2H_6, (△) BTX.

conversion of DMS (not shown) confirms that DMS is the intermediate in the M2TH.
At 823 K, a CH_3SH conversion ca 99-100% is maintained for 13 h before declining smoothly with the appearance of DMS. The deactivation process is due to coke deposition. The amount of coke on the catalyst was determined by thermogravimetric analysis. The amount of carbon transformed from CH_3SH, except DMS, as well as the amount of carbon found in the products formed (except DMS), were determined over the 13 h period. The carbon balance fits necely with the CH_3SH transformed (103%). The efficiency of a regeneration process was evaluated on the used HZSM-5, by air calcination at 823 K. The regenerated catalyst exhibits the same catalytic properties.

Table 2. Long lasting runs for the conversion of CH_3SH on HZSM-5, HY and H-FER at 823 K. Amounts of carbon transformed from CH_3SH into products after 13 h.

Catalyst	CH_3SH conversion[a]		DMS in effluent[b]	C in products /mg			C bal. /%	Selectivity /%		
	/%	C /mg	/ppm	C_1-C_3	BTX	coke		C_1-C_3	BTX	coke
HZSM-5	98	103	< 20	55	43	8.2	103	53.4	41.7	8.0
HY	67	50.5	380	29	4.1	14.8	96	60.8	8.5	30.5
H-FER	40	32	1050	19	2.0	11.5	100	57.8	6.3	35.9

[a]Conversion into the final products only: C1-C3, BTX, "coke"; average integrated value.
[b]Remaining DMS not fully converted to C1-C3, BTX and "coke", average integrated value.

Similar long-term experiments (13 h) were carried out at 823 K with HY and H-ferrierite. On the lasting period of 13 h, the CH_3SH conversion to the final products, C1-C3, BTX, coke, was about 99%, 67% and 40% on H-ZSM-5, HY and H-ferrierite, respectively (Table 1). Very clear differences of catalytic properties appear. Regarding activity, HZSM-5 is the most efficient catalyst with full CH_3SH conversion into C1-C3, BTX and coke. From TPD of NH_3, HZSM-5, HY and H-ferrierite exhibit 1.2, 0.9 and 1.8 mmol g^{-1} acid sites. One may anticipate that the activity of H-zeolite in the M2TH process is not dominated by the acidity of the zeolite, and that the zeolite topology is of importance. This is the same for selectivity; HY and H-ferrierite yield more alkanes, less aromatics and high coke amount. In contrast, HZSM-5 is less selective for producing coke but much more for aromatics. This behavior is similar to that observed in the MTO process.[7] The selectivity to coke formation is lower when a feed of $CH_3SH/H_2O/CH_4$ (0.5/1.5/98) was processed, 4% in comparison to 8% for a dry feed.

Conclusions

This work demonstrates for the first time that the selective conversion of CH_3SH into hydrocarbons and H_2S can be successfully achieved at high temperatures in the presence of protonic zeolites without addition of any reactant. One can thus contemplate that M2TH will be a very attractive new process for the deep removal of methylmercaptan from the industrial streams and gas deposits, as we claimed in a recent patent.[8]

References

[1] K. M. Brown, W. K. T. Gleim, P. Urban, *Oil & Gas Journal*, **1959**, *57*, 73-78; MEROX process: http://www.uop.com/refining/.
[2] P. Briot, R. Cadours, S. Drozdz, F. Lecomte, *US Patent* **2007**/0193925.
[3] A. Carlsson, G. J. van Heeringen, *US Patent* **2009**/00447201.
[4] E. Huguet, V. Hulea, R. Durand, C. Leroi, R. Cadours, B. Coq, *Angew. Chem. Inter. Ed*., submitted.
[5] C. D. Chang, A. J. Silvestri, J. Catal. 1977, 47, 249-259; S. A. Butter, A. T. Jurewicz, W. W. Kaeding *US Patent* **1975**, 3,894,107; J. E. Stauffer *US Patent* **2008** 7,381,847.
[6] A. V. Mashkina, V. R. Grunvald, V. I. Nasteka, B. P. Borodin, V. N. Yakovleva, L. N. Khairulina, *React. Kinet. Catal. Lett*. **1990**, *41*, 357-362.
[7] a) M. Stöcker, *Microporous Mesoporous Mater*. **1999**, *29*, 3-48; b) J. F. Haw, W. Song, D. M. Marcus, J. B. Nicholas, *Acc. Chem. Res*. **2003**, *36*, 317-326.
[8] Patent Total 2011.

Conversion of ethanol into light olefins over phosphorus-modified HZSM-5(Ga) zeolite

Yoshiyasu Furumoto, Yasumitsu Harada, Nao Tsunoji, Yusuke Ide, Masahiro Sadakane and Tsuneji Sano
Department of Applied Chemistry, Graduate School of Engineering, Hiroshima University, Higashi -Hiroshima 739-8527, Japan; E-mail: tsano@hiroshima-u.ac.jp

Introduction

Light olefins such as ethylene and propylene are essential raw materials for the petrochemical industry. Production of light olefins from bio-ethanol obtained by fermentation of biomass has attracted much attention. The production of light olefins from bio-ethanol is an example of the carbon neutral process. However, there are only a few reports concerning ethanol conversion to light olefins, especially propylene. Recently, we investigated the ethanol conversion over various ZSM-5 type zeolites and found that Ga-isomorphous subsituted ZSM-5 zeolite (HZSM-5(Ga)) also exhibits an excellent performance for ethanol conversion [1]. However, the catalytic activity and stability are insufficient for industrial processes. Very recently, Song et al. reported that modification of HZSM-5(Al) zeolite with phosphorous is very effective for improvement of the catalytic activity and stability [2]. From such viewpoints, in this study, we investigated an influence of phosphorous modification on the catalytic performace of HZSM-5(Ga) zeolite .

Experimental

ZSM-5(Ga) zeolite with a SiO_2/Ga_2O_3 ratio of ca.70 was synthesized as follows. Certain amounts of colloidal silica(Cataloid SI-30) and tetrapropylammonium bromide(TPABr) were added to a stirred mixture of gallium nitrate and sodium hydroxide in deionized water. The resultant hydrogel(SiO_2/Ga_2O_3=70, OH^-/SiO_2=0.1, $TPABr/SiO_2$=0.1, H_2O/SiO_2=40) was transferred into a 300 ml stainless-steal autoclave and stirred at 160^{o}C under autogenous pressure for 16 h. The precipitated crystals obtained were washed with deionized water, dried at 120^{o}C, and calcined at 500^{o}C for 10 h. The zeolite was protonated using a 0.6M HCl at room temperature, and calcined in air at 500^{o}C for 6 h. The bulk SiO_2/Ga_2O_3 ratio and the BET surface area of HZSM-5(Ga) were 69 and 389 m^2/g, respectively. The phosphorous-modified ZSM-5 zeolites(P/HZSM-5(Ga)) were prepated by an impregnation method with a 0.02M $(NH_4)_2HPO_4$. Characterization of samples prepared was carried out by XRD, XRF, SEM, FT-IR, N_2 adsorption and ^{71}Ga MAS NMR. Ethanol conversion was carried out by using an atmospheric-pressure flow reactor at 400-600 ^{o}C. The reaction gas fed in a composition of 50 mol% ethanol and 50 mol% N_2. The products obtained were analyzed by gas chromatography. The yields were calculated based on the concentration of N_2 as an internal standard.

Results and discussion

Figure 1 shows the relatioship between the P/Ga ratio of P/HZSM-5(Ga) and the light olefin yields at the reaction conditions of temp.=500^{o}C and W/F=0.03 g_{cat}/ml/min. The C_3H_6 and C_4H_8 yields slightly increased with an inrease in the P/Ga ratio and reached the maximum value at the P/Ga ratio of ca.0.3, while the C_2H_4 yield increased

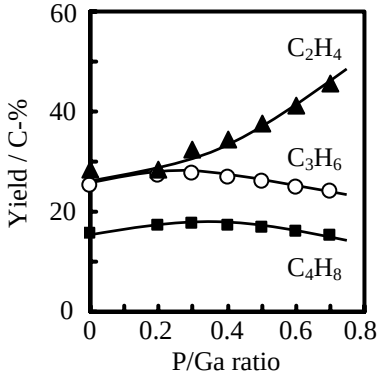

Fig. 1 Ethanol conversion over varios P/HZSM-5 (Ga). Temp.= 500˚C, W/F=0.03 g_{cat}/ml/min.

monotonously with the P/Ga ratio, indicating that oligomerization of ethylene produced by dehydration of ethanol is suppressed by the phosphorous modification, probably due to lower Brönstead acid sites. Figure 2 shows the time on stream of the C_3H_6 yield over P/HZSM-5(Ga) with a P/Ga ratio of 0.3. For comparison, the C_3H_6 yields over HZSM-5(Ga) and HZSM-5(Al, SiO_2/Al_2O_3 =74) were also shown. Because we wanted to keep the initial C_3H_6 yield similar, we set the W/F values to 0.03 g_{cat}/ml/min (P/HZSM-5(Ga) and HZSM-5(Ga)) and 0.0125 g_{cat}/ml/min(HZSM-5(Al)). The rapid decrease in the C_3H_6 yield was observed for HZSM-5(Al), while the gradual decrease for HZSM-5(Ga). On the other hand, however, the C_3H_6 yield over P/HZSM-5(Ga) hardly changed after the reaction for 8 h.

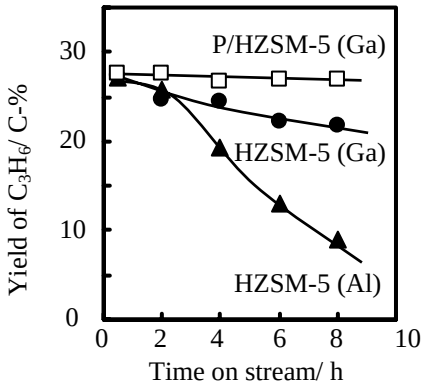

Fig. 2 Time on stream of C_3H_6 over P/HZSM-5 (Ga), HZSM-5 (Ga) and HZSM-5 (Al). Temp.= 500˚C, W/F=0.03 g_{cat}/ml/min (P/HZSM-5(Ga), HZSM-5(Ga)), W/F=0.0125 g_{cat}/ml/min (HZSM-5(Al)).

To clarify the difference in the catalytic stability among these zeolites, TG and ^{27}Al and ^{71}Ga MAS NMR measurements were carried out for fresh and used zeolite catalysts. Although there was a large difference in the W/F value between HZSM-5(Ga) and HZSM-5(Al), only small difference was observed in the amount of carbonaceous deposits after the reaction for 8 h, that is, 3.2 wt% for HZSM-5(Ga) and 4.7 wt% for HZSM-5(Al). On the other hand, the amount of carbonaceous deposits on P/HZSM-(Ga) was smaller (1.3 wt%). Figure 3 shows ^{71}Ga and ^{27}Al MAS NMR spectra of zeolite catalysts before and after the reaction for 8 h. In the ^{71}Ga MAS NMR spectra of both P/HZSM-5(Ga) and HZSM-5(Ga), the peak assigned to the terrahedrally coordinated framework galliums was observed at ca.160 ppm and the peak intensity hardly changed before and after the reaction, indicating the higher hydrothermal stability of HZSM-5(Ga) zeolite. On the other hand, in ^{27}Al MAS NMR spectra of HZSM-5(Al), there was a large difference in the intensity of the peak at ca.55 ppm assigned to the tetrahedrally coordinated framework aluminums. Namely, the considerable dealumination was observed for the used catalyst.

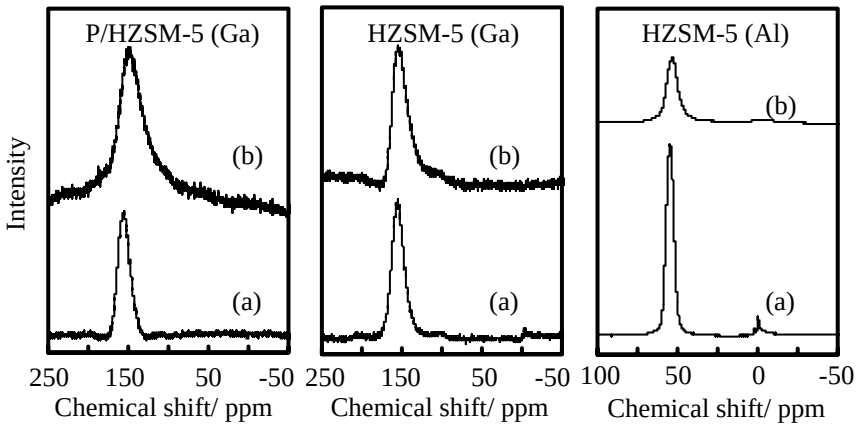

Fig. 3 ^{71}Ga and ^{27}Al MAS NMR spectra of P/HZSM-5 (Ga), HZSM-5 (Ga) and HZSM-5(Al) before (a) and after (b) reaction.

Conclusions

The C_3H_6 yield was strongly dependent upon the phosphorous content in the zeolite and the highest C_3H_6 yield (ca.27 C-%) was observed for the P/HZSM-5(Ga) with a P/Ga ratio of 0.3. The phosphorous modification also improved the catalytic stability.

References

[1] Goto, D., Harada, Y., Furumoto, Y., Takahashi, A., Fujitani, T., Oumi, Y., Sadakane, M., Sano, T., Appl. Catal. A 383 (2010), 89-95.
[2] Song, Z., Takahashi, A., Nakamura, I., Fujitani, T., Appl. Catal. A, 384 (2010), 201-205.

Tungstophosphoric Acid Incorporated Silicate Structured Nanocomposite Mesoporous Solid Acid Catalysts: Alcohol Dehydration Applications

Dilek Varisli[b], Aysegul Ciftci[a],, Gulsen Dogu[b], Timur Dogu[a]
[a] *Middle East Technical University, Department of Chemical Engineering, Ankara Turkey*
tdogu@metu.edu.tr
[b]*Gazi University, Ankara , Turkey.*

Introduction

Heteropolyacids (HPA), like tungstophosphoric acid (TPA) and silicotungstic acid (STA), with their very high Bronsted acidity and high proton mobility, have good potential as solid acid catalysts. Major disadvantages of these materials are their very low surface area and high solubility in polar solvents. In our recent studies, novel STA and Nafion incorporated silicate structured mesoporous nanocomposite solid acid catalysts were synthesized following hydrothermal procedures and tested in alcohol dehydration reactions [1-4].

Dehydration of ethanol yields ethylene, which is the main feedstock of petrochemical industry, and diethyl ether (DEE), which has excellent transportation fuel properties [2,3]. With its very high cetane number and clean burning properties, dimethyl ether (DME) is also a highly promising alternate/additive to diesel fuel and LPG and it can be produced by dehydration of methanol over solid acid catalysts [1]. In the present study, TPA incorporated mesoporous catalytic materials were synthesized following one-pot and impregnation procedures and catalytic performances of these materials were tested in dehydration reactions of ethanol and methanol.

Experimental

TPA incorporated silicate structured mesoporous nanocomposite solid acid catalysts were synthesized following one-pot hydrothermal and impregnation procedures, using cetyltrimethylammonium bromide as the surfactant. Hydrothermal synthesis was performed at 120^{o}C in a Teflon lined autoclave. In the case of one-pot procedure, the pH of the synthesis solution of TPA, TEOS and surfactants was lower than 0.5 and following the thermal analysis, calcination temperature of the synthesized material (TRC-W40) was decided as 400^{o}C. In the case of impregnated material (TPA@MCM-41), first MCM-41 was synthesized and then TPA with the desired composition was impregnated. Catalytic performances of the synthesized materials were tested in dehydration of ethanol and methanol, in a flow reactor at different temperatures, ranging between 150- 400^{o}C.

Results and Discussion

TPA incorporated materials prepared by the one-pot procedure were found to be highly stable and insoluble in polar solvents. XRD, and nitrogen adsorption analysis of the synthesized materials showed that the characteristic ordered pore structure of MCM-41 was partly deformed during one-pot synthesis and impregnation procedures. Characteristic Keggin structure of TPA is essentially conserved in TPA@MCM-41 (by XRD, FTIR). However, this structure was partly destroyed and WO_x clusters were formed in the mesoporous silicate lattice of the catalysts prepared by the one-pot procedure. Formation of WO_x nanorods and W nanoballs within the silicate structured mesoporous lattice was also reported in our earlier publications [2-4], in the case of of STA incorporated materials. STEM, EFTEM, XPS and EDX mapping analyses, indicated that HPA's were very well dispersed within the mesoporous amorphous silicate lattice of the synthesized materials. Some properties of the synthesized materials are reported in Table 1. DRIFTS analysis of the pyridine adsorbed

materials proved the presence of strong Bronsted as well as less strong Lewis acid sites in materials prepared by both TPA impregnation and one-pot procedures.

Table 1. Physical and chemical properties of the synthesized materials.

Sample ID	W/Si from EDS	S_{BET} (m^2/g)	Pore Volume (cm^3/g)	Av. pore diameter (nm)
MCM-41	-	1000	1.00	2.9
TRC-W40	0.52	263	0.51	5.6
TPA@MCM-41	0.18	183	0.15	1.4

Ethanol dehydration results yielded very high ethanol conversion values, approaching to 90% with TPA@MCM-41 and over 40% with TRC-W40 at 300°C and at a space time of 0.27 s.g.cm^{-3}. Ethylene selectivity values approached to 100% at this temperature, while DEE selectivity was much higher at lower temperatures (Fig. 2). In the case of methanol dehydration, DME selectivity was close to 100% at all temperatures. Results proved that materials prepared by the impregnation of TPA into MCM-41 were more active than the catalysts prepared by the one-pot procedure (TRC-W40), in dehydration of both methanol and ethanol. However, activity of TRC-W40 was highly stable even after repetitive washing with water and it gave higher DEE selectivity in ethanol dehydration reaction. Comparison of the results obtained with TPA incorporated catalysts with our previous results obtained with STA incorporated materials, indicated that STA incorporated catalysts were more active.

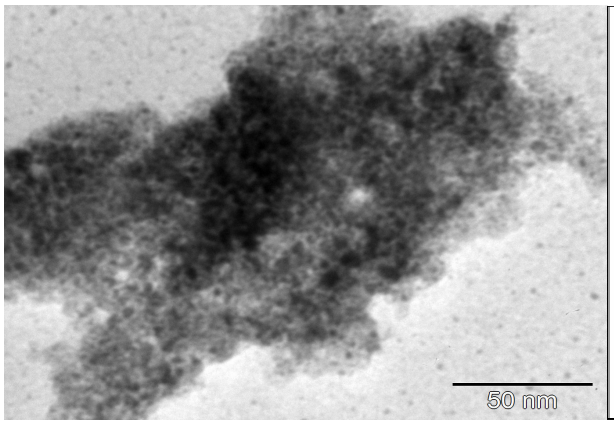

Figure 1. TEM image of TRC-40W

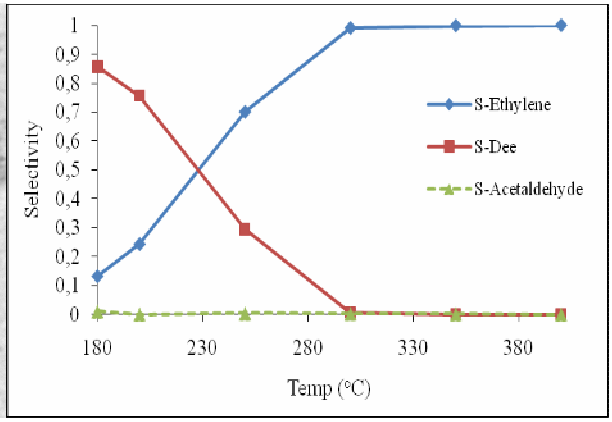

Figure 2. Ethylene and DEE selectivity values obtained with TPA@MCM-41 (space time: 0.27 s.g.cm^{-3})

Conclusions

TPA incorporated mesoporous catalytic materials, which were prepared by one-pot and impregnation procedures, were found to have partially ordered mesopores and relatively high surface area values. These materials were composed of well dispersed active compound within the amorphous silicate lattice and showed good catalytic performance in dehydration of ethanol or methanol to produce diethyl ether, ethylene or dimethyl ether, respectively. A major superiority of catalysts prepared by the one-pot procedure is their stable and high activity even after repetitive washing with polar solvents.

Acknowledgements

TUBITAK grants 106M073 & 105M571. Middle East Technical University.

References

[1] Ciftci A., Sezgi N.A., Dogu T., Ind. Eng. Chem. Res., 49, 6753, 2010.
[2] Varisli D., Dogu T., Dogu G., Ind. Eng. Chem. Res., 48, 9394, 2009.
[3] Varisli D., Dogu T., Dogu G., Chem. Eng. Sci., 65, 153, 2010.
[4] Ciftci A., Varisli D., Dogu T., Int. J. Chemical Reactor Eng., 8, A-45, 2010.

Conversion of Methanol to Diesel by Catalytic Cascade Reactions

Antoine Lacarriere[1,2*], Julien Robin[1], Dariusz Swierczynski[1], Annie Finiels[1], François Fajula[1], Vasile Hulea[1], Francis Luck[2]
[1]*Institut Charles Gerhardt, UMR 5253 UM2-ENSCM-UMI-CNRS, 8 rue de l'Ecole Normale, 34296 Montpellier (France).*
[2]*Total SA, Scientific Development Division, Catalysis & Process Engineering, 2 place Jean Millier, 92078 Paris La Défense Cedex (France).*
**Antoine.Lacarriere@enscm.fr*

Introduction

Methanol conversion into hydrocarbons (olefins, gasoline and diesel fuel) over zeolites is one of the most promising applications involving non-oil based sources (natural gas, coal, and biomass) [1, 2]. Depending on the catalyst and reaction conditions, the products may be light olefins (MTO process) or high octane gasoline (MTG process). To obtain diesel fuels (C_{12}^{+} hydrocarbons), the olefinic fraction from the MTO process can be converted over zeolites, such as HZSM-5 with the MOGD oligomerization process [3]. However, ethylene, which is the main product in the MTO technology, is only slightly involved in the oligomerization catalyzed by acidic zeolites. In this work, we design a three-step process, including MTO (over chabazite zeolite), ethylene oligomerization (over Ni-MCM-41) and olefins co-oligomerization (over H-MCM-41), as a potential route for methanol conversion into long-chain hydrocarbons.

Experimental

HSSZ-13 zeolite (Si/Al = 2.8), an aluminosilicate with chabazite topology, was prepared from Y type zeolite, by following the hydrothermal preparation procedure described elsewhere [4]. The methanol conversion was performed in a fixed bed reactor using 250 mg catalyst, with nitrogen as carrier gas. The effluent was analyzed by online GC-FID system. H-MCM-41 and Ni-MCM-41 (2 % Ni) were prepared using Na-AlMCM-41 (Si/Al = 10, pore size 9 nm) starting material, according to reference [5]. The catalytic ethylene oligomerization and olefins co-oligomerization were performed in a 0.3 L well-mixed gas-slurry reactor operating in semi-batch mode, in heptane, at 4 MPa and 150°C. The products were analyzed by GC.

Results and discussion

In order to optimize the catalytic performances and the reaction parameters, methanol conversion, ethylene oligomerization and olefins co-oligomerization were studied separately, and the representative results are briefly discussed hereafter.

Methanol to olefins. SSZ-13 zeolite, obtained under optimized conditions by alkaline treatment of the HY zeolite, was used as catalyst in the methanol conversion carried out at 450°C and $2h^{-1}$ WHSV. The catalytic behavior in the MTO process was typical of microporous solids with CHA topology, revealing a very high selectivity to light olefins (42% $C_2^{=}$ and 35% $C_3^{=}$) and a significant deactivation rate (Fig. 1).

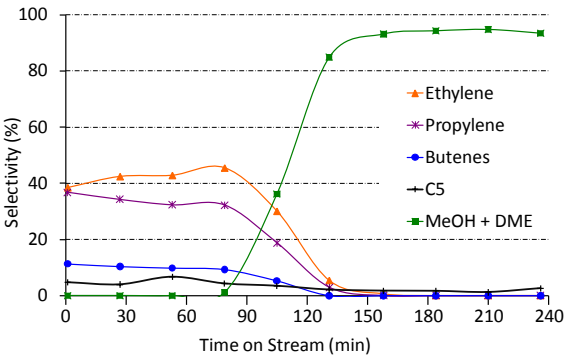

Figure 1. Selectivity in methanol conversion over SSZ-13 zeolite.

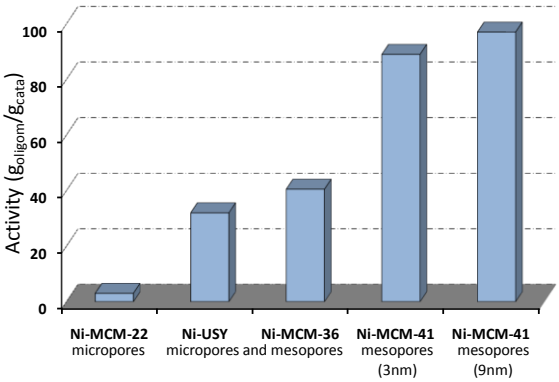

Figure 2. Oligomerization activities exhibited by different Ni-exchanged materials

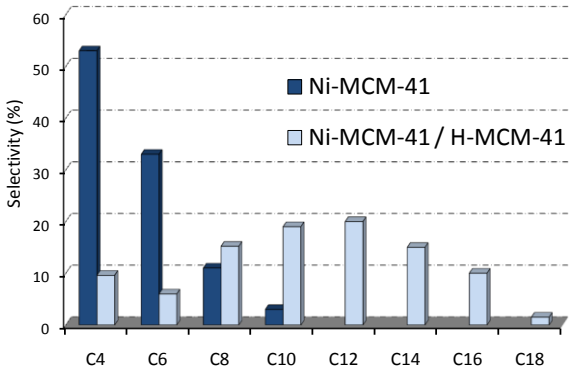

Figure 3. Product selectity in olefins oligomerization and co-oligomerization

Ethylene oligomerization. Figure 2 compares the excellent average activities obtained on Ni-MCM-41 mesoporous materials (pore size 3 and 9 nm) with those previously reported, obtained in the presence of Ni-exchanged zeolites with different topologies [6,7]. These results show that the catalytic activity is strongly dependent on the pore size: the larger the diameter, the higher the activity. In fact, the mesopores facilitate the diffusion of larger olefins obtained from the oligomerization process, which results in a low deactivation rate and high activity. The Ni-exchanged zeolites suffered severe deactivation, mainly due to micropores blockage by heavy products. Contrariwise, ethylene oligomerization catalyzed by Ni-MCM-41 was very selective, yielding almost exclusively olefins with an even number of carbon atoms, and presenting a near Schulz–Flory distribution: $C_4>>C_6>C_8>C_{10}^+$ (Fig. 3).

Olefins co-oligomerization. In order to obtain hydrocarbons with chains longer than 10 carbon atoms, the Ni-MCM-41 catalytic oligomerization was assisted by an acid catalysis. Bifunctional MCM-41 catalysts, containing both nickel and acid sites, exhibited a severe deactivation. Then, two methods were applied: (i) one-pot, Ni-MCM-41 and protonated H-MCM-41 were added in the reactor at the beginning of the ethylene oligomerization and (ii) ethylene oligomerization (Ni-MCM-41) and olefins co-oligomerization (H-MCM-41) were consecutive reactions, performed successively in the same reactor, in the same conditions. No significant difference between the performances of both processes was observed. The results, displayed in Fig. 3, show that after the co-oligomerization, most of products are C_{10}^+ hydrocarbons.

Conclusions

A three-stage strategy for converting methanol into long-chain hydrocarbons is proposed. SSZ-13 zeolite is an efficient catalyst for the first MTO step, while Ni-MCM-41 and H-MCM-41 reveal very interesting properties as catalysts for the oligomerization of light olefins under mild conditions.

References

[1] Froment, G.F., Dehertog, W.J.H., Marchi, A.J., Catalysis 9 (1992) 1-64
[2] Stöcker, M., Microporous Mesoporous Mater. 29 (1999) 3-48
[3] Keil, F.J., Microporous Mesoporous Mater. 29 (1999) 49-66
[4] Zones, S.I., U.S. Patent 4 544 538 (1985)
[5] Hulea,V., Fajula, F., J. Catal. 225 (2004) 213-222
[6] Lallemand, M., Finiels, A., Fajula, F., Hulea, V., Appl. Catal. A 301 (2006) 196-201
[7] Lallemand, M., Rusu, O., Dumitriu, E., Finiels, A., Fajula, F., Hulea, V., Appl. Catal. A 338 (2008) 37-43

Enhanced photoluminescence emission and photooxidation activity of the anchored Pt(II) pyridyl complex onto mesoporous silica

Kohsuke Mori, Kentaro Watanabe, Hiromi Yamashita
Division of Materials and Manufacturing Science, Graduate School of Engineering, Osaka University, mori@mat.eng.osaka-u.ac.jp.

Introduction

The incorporation of guest species into porous inorganic materials, such as clays, zeolites, and mesoporous materials, has been extensively studied with respect to synthesizing functional inorganic-organic supramolecular materials. The resulting materials exhibit unique physicochemical properties that are controlled by the state of the guest molecules, in addition to the nature of the functional groups on the host surface [1-3]. In this study, new luminescent inorganic-organic hybrid materials are developed by anchoring the chloro(2,2':6',2''-terpyridine)platinum(II) ([Pt(tpy)Cl]Cl) complex to different mesoporous silica hosts (MCM-41, SBA-15, and MCM-48) modified with (3-aminopropyl)trimethoxysilane (APTMS). The differences in the pore dimensions and structures of these materials make it possible to investigate the effect of nanoconfinement on anchored guest molecules. In addition, we herein report that the anchoring of this Pt complex enables selective photooxidation of styrene derivatives by molecular oxygen (O_2) [4].

Experimental

Anchoring of Pt complex: Chloroform solution of [Pt(tpy)Cl]Cl was stirred with APTMS-modified MCM-41 sample at room temperature for 24 h. The product was recovered by vacuum filtration, washed with chloroform, and dried under vacuum overnight to give Pt(tpy)/MCM-41 (Pt: 0.4 wt%). Pt(tpy)/SBA-15 (Pt: 0.4 wt%) and Pt(tpy)/MCM-48 (Pt: 0.4 wt%) were prepared by the same method using SBA-15 and MCM-48, respectively. In the case of MCM48, other samples with different Pt loadings (0.2, 0.8, and 1.2 wt%) were also prepared.

Photocatalytic liquid-phase oxidation: The powdered Pt catalyst (0.01 g), styrene (10.0 mmol), and acetonitrile (15 ml) were introduce into a quartz reaction vessel (30 ml). The resulting mixture was bubbled with oxygen for 30 min in dark conditions. Subsequently the sample was irradiated from a sideways direction using a 500 W Xe lamp for 24 h at ambient temperature. The resulting solution was analyzed by GC. The turnover number (TON) was defined as follows: TON = products [mol]/Pt atoms on catalyst [mol].

Results and discussion

[Pt(tpy)Cl]Cl complex was successfully anchored to a series of APTMS-modified mesoporous silica materials (MCM-41, SBA-15, and MCM-48). Pt L_{III}-edge X-ray absorption fine structure (XAFS) measurements reveal that the Pt complex reacts with amino groups anchored on the mesoporous silica to create a new Pt–N bond accompanied by elimination of the Pt–Cl bond (Scheme 1).

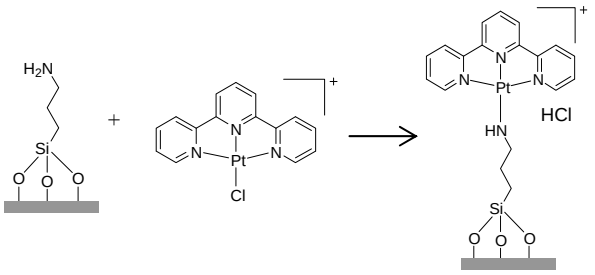

Scheme 1. Anchoring of $[Pt(tpy)Cl]^+$ onto the modified silica surface.

Upon anchoring, the non-emissive Pt(II) complex exhibits strong photoluminescence at room temperature, which is maximized near 530 nm due to ligand-centered (^{3}LC) and/or metal-to-ligand charge transfer (^{3}MLCT) transitions. The intensities of the emission increase in the order of MCM-41 < SBA-15 < MCM-48 (Fig. 1A). In the case of MCM-48, the emission intensity is the highest at 0.4 wt% Pt loading, while concentration quenching is observed accompanied with a new emission due to the metal-metal-to-ligand charge-transfer (^{3}MMLCT) transition at high Pt loading (Fig. 1B).

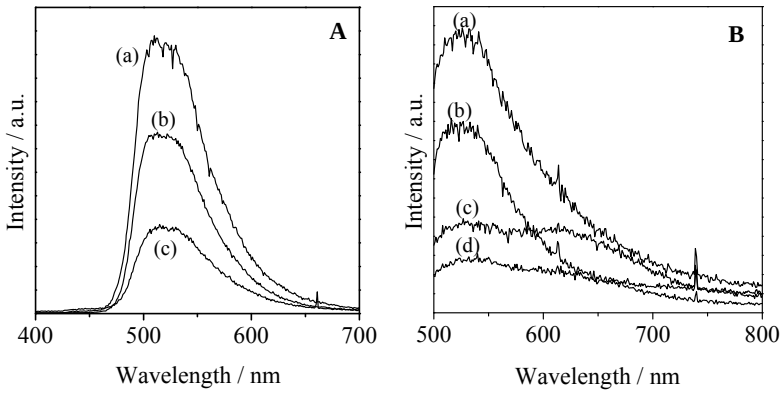

Figure 1. (A) Photoluminescence spectra of Pt(tpy)-anchored on silica samples: (a) Pt(tpy)/MCM-48 (0.4wt%), (b) Pt(tpy)/SBA-15 (0.4wt%), and (c) Pt(tpy)/MCM-48 (0.4wt%) at λ_{ex} = 330 nm. (B) Photoluminescence spectra of Pt(tpy)-anchored on MCM-48 at various Pt loadings at λ_{ex} = 450 nm: (a) 0.2 wt%, (b) 0.4 wt%, (c) 0.8 wt%, and (d) 1.2 wt%.

Anchoring of the [Pt(tpy)Cl]Cl complex to mesoporous silica results in a photocatalyst which allows highly selective transformation of styrene to benzaldehyde and styrene oxide in the presence of molecular oxygen at room temperature. Interestingly, the photocatalytic activity varies according to the type of mesoporous silica material and the loading amount. This tendency corresponds with the increasing intensity of the luminescence emission due to the ^{3}LC and/or ^{3}MLCT states. It can be supposed that the enhanced excitation rate and quantum efficiency of the anchored Pt complex, due to the differences in nanoconfinement, increase the energy and/or electron transfer to O_2, which ultimately enhances the photooxidation activity. The 3D-connected channel structure of the MCM-48 silica also accounts for the high photocatalytic activity, where the diffusion of O_2 toward the anchored Pt complex occurs smoothly compared to the one-dimensional MCM-41 and SBA-15 silicas, as demonstrated by the quenching rate constants obtained from Stern-Volmer plots.

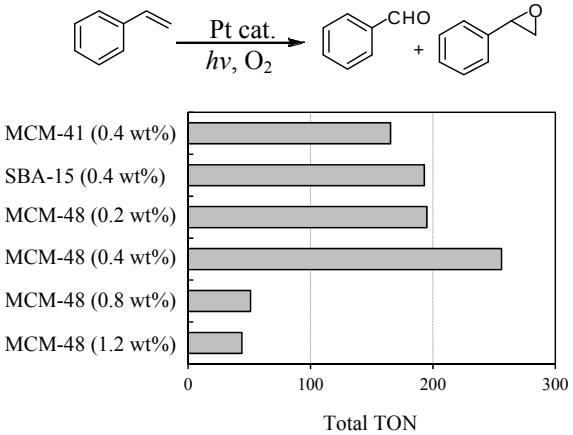

Figure 2. TON for the photocatalytic oxidation of styrene in the presence of O_2.

References

[1] K. Mori, K. Kagohara, H. Yamashita, *J. Phys. Chem. C*, **112**, 2593 (2008).
[2] K. Mori, M. Kawashima, K. Kagohara, H. Yamashita, *J. Phys. Chem. C*, **112**, 19449 (2008).
[3] K. Mori, M. Kawashima, M. Che, and H. Yamashita, *Angew. Chem. Inter. Ed.*, 49, 8598 (2010).
[4] K. Mori, K. Watanabe, M. Kawashima, M. Che, and H. Yamashita, *J. Phys. Chem. C*, in press.

Reversible NO_x storage on Ru zeolites

Steven Heylen†, Sylvia Smeekens†, Christine E. A. Kirschhock†, Johan A. Martens†

† Centre for Surface Chemistry and Catalysis, Katholieke Universiteit Leuven, Kasteelpark Arenberg 23, 3001 Leuven, Belgium

Corresponding author: johan.martens@biw.kuleuven.be

Introduction

Exhaust gases from motor vehicles are an important source of environmental pollution. Forthcoming EURO 6 legislation is triggering a renewed interest in deNO_x technologies. In earlier work we presented Na-Y zeolite as a sulfur tolerant NO_x adsorbent. However its applicability for NO_x-trapping is limited due to the relatively slow NO_x desorption and the requirement of a 1:1 NO:NO_2 stochiometry in the exhaust gas mixture [1-4]. To circumvent these drawbacks, we incorporated transition metals into the Na-Y zeolite. Out of a selection of metals, the loading of Na-Y with ruthenium resulted in a remarkable NO_x adsorption and rapid desorption behavior. The nature of the adsorption site for NO was revealed using ^{23}Na MAS NMR and XRD in combination with structure refinement [5-6].

Experimental

Zeolite Na-Y (Si/Al ratio 2.71) was loaded with variable amount of ruthenium (0,5 to 3wt%) by an ion exchange with $RuCl_3$. Lean-rich cyclic NO_x adsorption-desorption experiments were conducted in a quartz, fixed-bed reactor in the temperature range 230-315°C. Exhaust gas was simulated with the following feed gas compositions: lean, 1000 ppm NO, 3% H_2O, 5% O_2 and balance N_2; rich, 3% H_2O, 1% H_2 and balance N_2 at a GVSV between 15000 and 120000 h^{-1}. The gas composition at the reactor outlet was analyzed with a chemiluminescence detector (Ecophysics CLD 700 EL ht). X-ray diffraction was performed on a STOE STADI-P diffractometer in transmission mode using Cu-Kα1 radiation. Rietveld refinements and Difference Fourier Electron Density Analyses were performed using the GSAS/EXPGUI software package. ^{23}Na MAS NMR spectra were recorded on a Bruker Avance DSX400 spectrometer

Results and discussion

A representative NO_x adsorption-desorption cycle of the Ru/NaY NO_x adsorbent is shown in Figure 1.

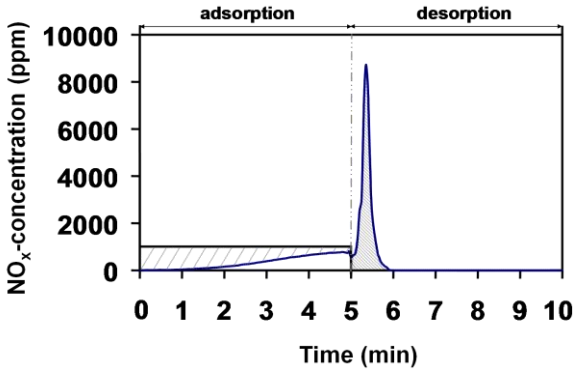

Figure 1. A detailed NO_x adsorption/desorption pattern recorded at the outlet of a Ru(3%)/Na-Y adsorbent bed at 250°C. Gas composition during lean phase was 1000ppm NO, 5% O_2, 3% H_2O and balance N_2. Regeneration of the adsorbernt was done with 1% H_2, 3% H_2O and balance N_2.

Significant NO_x uptake was observed during the first minutes of the adsorption phase. After switching to regeneration gas, rapid NO_x desorption was obtained which was completed within 1 minute. During this NO_x release, the peak NO_x concentration amounted 8000ppm. The NO_x adsorption capacity was 3.2 mg of NO_x/g. When H_2 was left out of the regeneration gas, regeneration of the Ru(3%)/Na-Y zeolite lasted more than 10 minutes, pointing out that the presence of H_2 was essential for obtaining fast release.

Ru/Na-Y samples after NO_x saturation and after regeneration were investigated with XRD. Decreasing the Ru loading increased the NO_x adsorption capacity. This suggested that NO_x adsorption did not occur on ruthenium. ^{23}Na MAS NMR experiments revealed a drastic change of the sodium cation distribution when regeneration was done in presence of H_2. The only species in the adsorbent which could be affected by a redox cycle was ruthenium. Therefore it was concluded that the reduction of ruthenium caused the dramatic change in Na^+ cation environments and destruction of the NO_x adsorption site. This hypothesis was confirmed by Rietveld refinement in combination with electron density maps. A schematic representation of the proposed mechanism is shown in Figure 2.

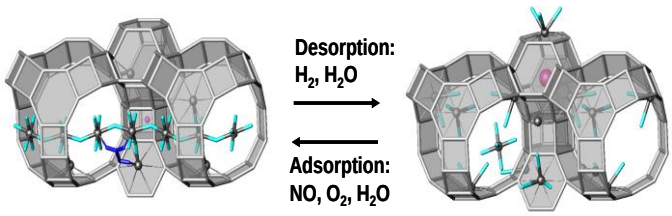

Figure 2. Schematic representation of the proposed NO_x adsorption/desorption mechanism of a Ru/Na-Y zeolite. The adsorbed N_2O_3 molecule is represented as the blue molecule in the Na-H_2O network The Ru atom, shown as the purple sphere, is situated in the hexagonal prism during lean phase and in the sodalite cage during rich phase.

To overcome the rather limited NO_x storage capacity of Ru/NaY based NO_x adsorbents, we incorporated different counter cations. The incorporation of barium led to the most promising results. Compared to the maximum NO_x uptake of the Ru(1%)/Na-Y zeolite (4.8 mg NO_x/g) the adsorption capacity in the barium exchanged material has tripled (16.1 mg NO_x/g) while the mechanism still is reversible and release easily could be triggered by switching to reducing conditions.

Conclusions

Ru loaded Y zeolite is a unique NO_x adsorbent in which NO_x is trapped as N_2O_3 in sodium-water networks extending in the supercages. Oxidation of NO into NO_2 using molecular oxygen is performed by extraneous ruthenium metal particles. The presence of a small amount of Ru atoms corresponding to about one atom per unit cell is crucial for obtaining reversible NO_x adsorption. The introduction of barium leads to a remarkable enhancement of the NO_x storage capacity.

Acknowledgements

J. M. acknowledges the Flemish Government for long-term structural funding (Methusalem). S.H. is grateful to FWO Vlaanderen for a research grant. The work is part of a concerted research action (GOA) and supported by Excellence funding (CECAT).

References

[1] Monticelli O., Loenders R., Jacobs P.A., Martens J.A., Catal. Today 21, 1999, 215-220.
[2] Sultana A., Loenders R., Monticelli O., Kirschhock C., Jacobs P.A., Martens J.A., Angew. Chem. Int. Ed. 39, 2000, 2934-2937.
[3] Brilhac J.F., Sultana A., Gilot P., Martens J.A., Environ. Sci. Technol. 36, 2002, 1136-1140.
[4] Sultana A., Habermacher D.D., Kirschhock C.E.A., Martens J.A., Appl. Catal. B 48, 2004, 65-76.
[5] Labaki M., Issa M., Smeekens S., Heylen S., Kirschhock C.EA., Villani K., Jeguirim H., Habermacher D., Brilhac J.F., Martens J.A. Appl. Catal. B 97, 2010, 13–20.
[6] Smeekens S., Heylen S., Villani K., Houthoofd K. , Godard E., Tromp M., Seo J.W., DeMarco M., Kirschhock C.E.A., Martens J.A., Chem. Sci. 1, 2010, 763-771.

Oxygen Precursor to the Reactive Intermediate in Methanol Synthesis by Cu-ZSM-5

Pieter Vanelderen[1], Pieter J. Smeets[1,2], Ryan G. Hadt[2], Julia S. Woertink[2], Robert A. Schoonheydt[1]*, Bert F. Sels[1] and Edward I. Solomon[2]
[1] *Center for Surface Chemistry and Catalysis, K.U.Leuven, Leuven, Belgium,[2] Department of Chemistry, Stanford University, Stanford, California 94305, bert.sels@biw.kuleuven.be; edward.solomon@stanford.edu*

Introduction

In scope of the declining oil production in the future, methane becomes an important alternative as an energy source and feedstock for the chemical industry. This requires the activation of C-H bonds, no simple task for an inert molecule like methane. One challenging way involves the direct conversion of methane into methanol with molecular oxygen. In nature mono-oxygenase enzymes are capable of selectively oxidizing methane into methanol. Fe (sMMO) and Cu (pMMO) dinuclear cores were put forward as plausible candidates of the active core. Inspired by nature, a Cu catalyst was designed in the pores of the ZSM-5 zeolite. In previous work, we showed that Cu-ZSM-5 is able to activate molecular oxygen. The active oxygen core has a characteristic absorption band (i.e. 22700 cm^{-1}) in the UV-vis spectrum, and we unambiguously assigned it to a mono (μ-oxo) dicopper core ($[Cu_2O]^{2+}$) [2]. Upon contacting this active core with methane, methanol is formed selectivity at low temperature. Despite this unique observation, a continuous catalytic cycle has not been demonstrated today for reasons of an unknown reaction mechanism [1]. More fundamental insight of the reaction mechanism is thus highly mandatory. This work reports the assignment of the oxygen precursor that leads to the active $[Cu_2O]^{2+}$.

Experimental

Na-ZSM-5 (VAW, Si/Al=12) samples were ion-exchanged with aqueous solutions of varied Cu(II)-acetate concentrations. The samples were initially calcined under O_2 at 450 °C for 2 h (5 °C/min, 50 mL/min), followed by a He flow overnight (50 mL/min). This treatment results in the autoreduction of the Cu sites in Cu-ZSM-5. Fiber optic UV-vis spectroscopy was used to monitor spectral changes of Cu-ZSM-5 at ambient and elevated temperatures, and resonance Raman measurements were performed to obtain the electronic and geometric structure information regarding the Cu/O_2 species in Cu-ZSM-5. MS was used to monitor the O-isotope distribution in O_2-TPD experiments.

Results and discussion

The new Cu precursor complex was discovered by activating O_2 with Cu-ZSM-5 at ambient temperatures. A characteristic absorption band in the UV-vis spectrum at 29000 cm^{-1} was observed, which transforms into the 22700 cm^{-1} band upon heating. Laser excitation into the 29000 cm^{-1} absorption feature yields a resonance Raman (rR) spectrum characterized by $^{18}O_2$ isotope sensitive and insensitive vibrations at 736 ($\Delta^{18}O_2$: 41 cm^{-1}) and 269 cm^{-1}, respectively (fig 1A). These vibrational frequencies and isotope perturbation pattern are characteristic of the μ-(η^2:η^2) peroxo dicopper(II) species, $[Cu_2(O_2)]^{2+}$. Thus, we assign the 736 and 269 cm^{-1} features to the O-O stretch (νO-O) and the Cu-Cu stretch (νCu-Cu) of the μ-(η^2:η^2) peroxo dicopper(II) moiety, respectively. The 29000 cm^{-1} absorption band is thus assigned as a peroxo π^*_σ to Cu(II) charge transfer (CT) transition. Upon heating the sample the μ-(η^2:η^2)

peroxo dicopper(II) precursor rR features disappear. In parallel, excitation at 457.9 nm (21834 cm^{-1}) during the heating experiment shows the enhancement of the vibrational features presented in fig 1B. These have been assigned in ref 2 as the isotope sensitive, intense symmetric (456 cm^{-1}) and weak anti-symmetric (870 cm^{-1}) stretching vibrations characteristic of the μ-oxo-bridged $[Cu_2O]^{2+}$ species. These results parallel the absorption changes (29000 cm^{-1} to 22700 cm^{-1}), and thus suggest the conversion of the side-on bridged peroxo dicopper(II) species into the $[Cu_2O]^{2+}$ species, reactive in the selective oxidation of methane to methanol. O_2-TPD experiments with $^{18}O_2$ show the incorporation of the second ^{18}O atom into the zeolite lattice during the transformation of $[Cu_2(O_2)]^{2+}$ into $[Cu_2O]^{2+}$.

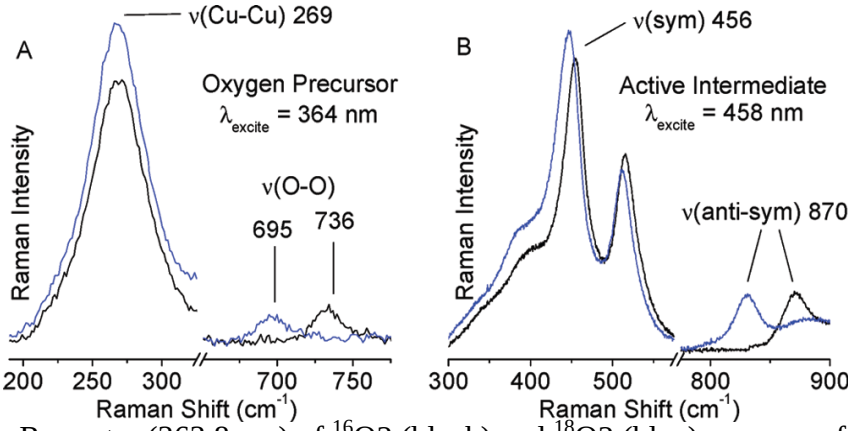

Figure 1.(A) rR spectra (363.8 nm) of $^{16}O2$ (black) and $^{18}O2$ (blue) precursor formed at RT; (B) rR spectra (457.9 nm) of reactive site formed by heating the O2 precursor rR samples [3].

Conclusions

The combined operando UV-vis and resonance Raman study allows the determination of the major species acting in the O_2 activation process using Cu-ZSM-5 and the final selective oxidation of methane into methanol [3]. The complete understanding of this methanol producing core will have a major contribution to different scientific disciplines. Cu-ZSM-5 could serve as a model for the design of active sites, as well as a tool to better understand the working mechanism of enzymes. Ultimately, the insight will pave the way to develop a catalytic cycle into the system, and catalytically convert methane to methanol.

Acknowledgements

This work was financially supported by FWO (G.0695.11). P.V. acknowledges K.U. Leuven for a doctoral fellowship, P.J.S. acknowledges the IWT, FWO, and K.U.Leuven for graduate and postdoctoral fellowships, and J.S.W. acknowledges the NIH for a traineeship. R.G.H. is a Gerhard Caspe Stanford Graduate Fellow.

References

[1]Groothaert, M. H.; Smeets, P. J.; Sels, B. F.; Jacobs, P. A.; Schoonheydt, R. A., Selective Oxidation of Methane by the Bis(μ-oxo)dicopper Core Stabilized on ZSM-5 and Mordenite Zeolites, J. Am. Chem. Soc., 127 (2005), 1394-1395

[2]Woertink, J. S.; Smeets, P. J.; Groothaert, M. H.; Vance, M. A.; Sels, B. F.;Schoonheydt, R. A.; Solomon, E. I., A $[Cu_2O]^{2+}$ core in Cu-ZSM-5, the active site in the oxidation of methane to methanol, Proc. Natl. Acad. Sci. U.S.A,. 106 (2009), 18908-18913

[3]Smeets, P. J.; Hadt, R. G.; Woertink, J. S.; Vanelderen, P.; Schoonheydt, R. A.; Sels, B. F.; Solomon, E. I., Oxygen Precursor to the Reactive Intermediate in Methanol Synthesis by Cu-ZSM-5, J. Am. Chem. Soc., 132 (2010), 14736-14738

Catalytic Behaviour and Adsorption Properties of Modified Mordenites for Low Temperature n-Butane Conversion

D.B. Tagiyev[1,2], S.I. Abasov[1], S.S. Fatullayeva[2], R.V. Starikov[1]
[1] *Institute of Petrochemical Processes of Azerbaijan NAS,* [2] *Azerbaijan Medical University*
dtagiyev@hotmail.com

Introduction

Metal containing zeolites and sulfated zirconia are both active catalysts for normal paraffins conversion to branched isomers. Mordenites are potential environmentally friendly catalysts for this reaction, however, show activity at relatively high temperatures. Dealumination and modification of mordenite increase its activity [1,2]. The aim of present contribution is an investigation of n-butane isomerization over dealuminated mordenites modified with zirconia, sulfate ions and cobalt, and comparison of these data with the Dubinin-Radushkevich adsorption isoterm parameters for the study of the modified mordenites microporous structure.

Experimental

Mordenite-zirconia catalysts have been prepared by impregnation of dealuminated mordenite with SiO_2/Al_2O_3 ratio 17 (sample HM_{17}) by solution of $ZrO(NO_3)_2 \cdot 2H_2O$ or by mixture of zeolite with washed hydroxide zirconia. Sulfate has been introduced by incipient wetness impregnation with 2M $(NH_4)_2SO_4$ solution. Samples were dried at 100-110˚C for 5 h, calcined at 600˚C for 3 h and stored in air. Catalysts were analyzed by XRD, DTA and UV-spectroscopy.
Isomerization of n-butane was studied at 175-250˚C. Catalytic tests have been performed through a fixed bed reactor operated at atmospheric pressure. Catalyst pellets (1.5 g) was activated at 500˚C for 2 hours in dry air current and cooled up to reaction temperature. Tests were carried out with pure n-butane with 5 ml min^{-1} rate or with hydrogen using as carrier gas (10 ml min^{-1}). Reaction products were analyzed by gas chromatography.
The adsorption of benzene vapors was gravimetrically determined in volumetric-vacuum unit at 20±0,1ºC within pressure range from zero to P/P_o=0.2-0.3. The isotherms obtained are satisfactorily described by Dubinin-Radushkevich equation.

$$\ln a = \ln W_o \rho - BRT \ln(P_o/P)^2$$

where, a – amount of the adsorbed compound; W_o – volume of adsorption space (cm^3/g) accessible for adsorption; B – isotherm angle of slope; P_o – adsorptive saturated vapours pressure; P – adsorptive vapour pressure.

Results and discussion

In contrast to non-dealuminated mordenite, being an active in n-butane conversion at temperatures 300-350˚C and showing low selectivity concerning isobutane, dealuminated HM_{17} sample shows higher selectivity at 250˚C. HM_{17} impregnation with $ZrO(NO_3)_2$ aqueous solution with following decomposition at 500˚C results in considerable increasing of activity and decreasing of reaction temperature. It should be noted that as distinct from HM_{17}, ZrO_2/HM_{17} sulfation still more increases catalysts activity at lower temperatures (Table 1).

Table 1. Conversion of n-butane over modified mordenites

Catalyst	Temperature (˚C)	n-Butane conversion, %	Isoparaffins yield,%
HM_{17}	250	28.0	18.6
4% SO_4^{2-}/ HM_{17}	250	28.2	19.1
5% ZrO_2/ HM_{17}	220	30.0	21.5
4%SO_4^{2-}/5%ZrO_2/ HM_{17}	220 190	37.7 34.5	28.1 25.3
Co/ SO_4^{2-}/ ZrO_2/ HM_{17}	190	43.0	30.8

XRD and TGA of HM_{17} and after its promoting with zirconia and sulfate ions do not show essential changes in crystal structure and samples thermal behavior. After promoting endothermic peak at 113˚C is displaced to 123˚C, and weak endothermic peak is appeared at 353˚C. These peaks are connected with dehydration and zirconia salt decomposition processes.

It is known that the mordenite microporous structure is characterized with the availability of two types of micropores having 12- and 8-membered oxygen windows with cross-section 0.67x0.7 and 0.29x0.57 nm. Within the framework of Micropores volumetric filling theory (MVFT) B change means the change of adsorption characteristic energy connected with the catalyst micropores effective radius. It was found that W_o and B values for catalysts HM_{17}, 5% ZrO_2/ HM_{17} and 4%SO_4^{2-}/5%ZrO_2/ HM_{17} are increased (Table 2).

Table 2. Adsorption parameters of n-butane conversion catalysts

Catalyst	W_o, cm^3/g	B
HM_{17}	0.07	0.03
5% ZrO_2/ HM_{17}	0.09	0.04
4%SO_4^{2-}/5%ZrO_2/ HM_{17}	0.11	0.08

Such regularity of W_o change corresponds to the arrangement of these zeolites in a row by their adsorption capacity and B by the sizes of inlet windows to the large channels. Hence, W_o and B parameters are the reflection of their microporous structure.

HM_{17} modification with simultaneously zirconium and sulfate ions leads to increase of B parameter and increase isoparaffins yield. Considering that isobutane is differed from n-butane and cracking products by critical diameter the reason of the observed differences in isoparaffin yields may be connected with the changes of diameters of the inlet window to the zeolite wide cavities.

Conclusions

It can be supposed that the modifying effect of zirconia and sulfate ions on the HM_{17} is connected with surface growth of samples, change of force and concentration of acid centers, and the other hand, with optimization of zeolite microporous structure.

References

[1] Ganizares P., de Lucas A, Dorado F., *n*-Butane isomerization over H-mordenite: role of the monomolecular mechanism, Applied Catalysis, A : General, 196 (2000) 225-231

[2] Tagiyev D.B., Starikov R.V., Rustamov M.I., Development of modified mordenite-zirconia catalysts active at low temperature n-butane isomerization . Studies of Surface Sciences and Catalysis, 174 (2008) 1223-1226

Isomerization of 1-alkenes on K-modified H-ZSM-5 zeolites

Inés Coleto,[a] Dolores Esquivel,[a] María I. López,[a] María A. Carmona,[a] Manuel Mora,[a] José R. Ruiz,[a] Rafael Roldán,[b] Juan P. Gómez,[b] César Jiménez-Sanchidrián,[a] Francisco J. Romero-Salguero[a]

[a] *Departamento de Química Orgánica, Universidad de Córdoba, Campus de Rabanales, Edificio Marie Curie, Ctra. Nnal. IV, km 396, 14014 Córdoba, Spain, qo1jisac@uco.es*

[b] *Centro de Tecnología de Repsol, Ctra. Nnal. V, km 18, 28631 Móstoles (Madrid), Spain*

Introduction

A high content of 1-alkenes in gasoline causes serious problems concerning both the emissions and the engines. In consequence, different alternatives have been posed to convert the abundant alkenes coming from FCC processes. Thus, they have been transformed into aromatics and/or isoalkanes to preserve the octane number of gasoline [1]. Also, it would be clearly advantageous to isomerize terminal and linear to internal and branched alkenes, especially multisubstituted ones, which are much more interesting for their direct use for blending in reformulated gasolines and as reactants in subsequent reactions (hydrogenation, etherification, alkylation, hydroformylation, metathesis, polymerization, etc.) leading to products of increased value as components of fuels or fine and intermediate chemicals [2,3].

Experimental

The parent zeolite (ZSM-5 with a SiO_2/Al_2O_3 ratio of 80) was purchased from Zeolyst Int. (reference CBV8014). Potassium was deposited into the protonic form of the zeolite by both impregnation to incipient wetness and ion exchange. Platinum was also incorporated to some samples. All catalysts were characterized by different techniques, such as X-ray diffraction analysis, nitrogen adsorption isotherms, temperature programmed desorption of ammonia (acid properties) and, in some case, temperature programmed reduction and H_2 chemisorption. The catalytic tests were performed in a fixed-bed continuous flow reactor (10 mm i.d.) connected by a thermostated pipe to a gas chromatograph. In this work, the transformations of two 1-alkenes (pent-1-ene and hex-1-ene) have been studied.

Results and discussion

At a WHSV of 33.3 h^{-1}, the HZSM-5 sample gave rise to conversions higher than 90% of pent-1-ene under hydrogen above 450 ºC. The major products were pent-2-enes with a *trans* to *cis* ratio around 2.5. Other compounds, mainly branched isomers, were also present in small amounts. The selectivity drastically changed upon increasing the temperature. Thus, at 500 ºC the main products came from the cracking and the skeletal isomerization (both alkanes and alkenes). The 2-methyl-but-2-ene isomer was predominat (11.6%). Also, a significant fraction of C6 and C7+ compounds was present. In addition, a yield to cycloalkanes and cycloalkenes (C5 + C6) of 5.4% was remarkable. At 550 ºC, the products from the cracking reactions markedly increased whereas the others decreased. Moreover, in comparison to the reactions at 450 and 500 ºC an enhancement of the yield to aromatic compounds, mainly alkylbenzenes, was observed.

At 350 ºC, but decreasing the WHSV to 10.0 h^{-1}, cracking was still very high (close to 50%), even though the proportion of skeletal isomers exceeded 30%, particularly isoalkenes. The reaction of Pt supported H-ZSM-5 zeolites gave rise to the hydrogenation of the alkene as

the main reaction. In order to tailor the acidity of the zeolite, potassium was incorporated to the zeolite. The higher the K content, the lower the amounts of cracking products and C6 and C7+ compounds and the higher the conversion to pent-2-enes (Figure 1). Moreover, as the K content was higher, the selectivity to skeletal isomers increased. Thus, the yields to the latter compounds were 55.1 and 33.1% for the zeolites with 2.5% and 0.7% K, respectively.

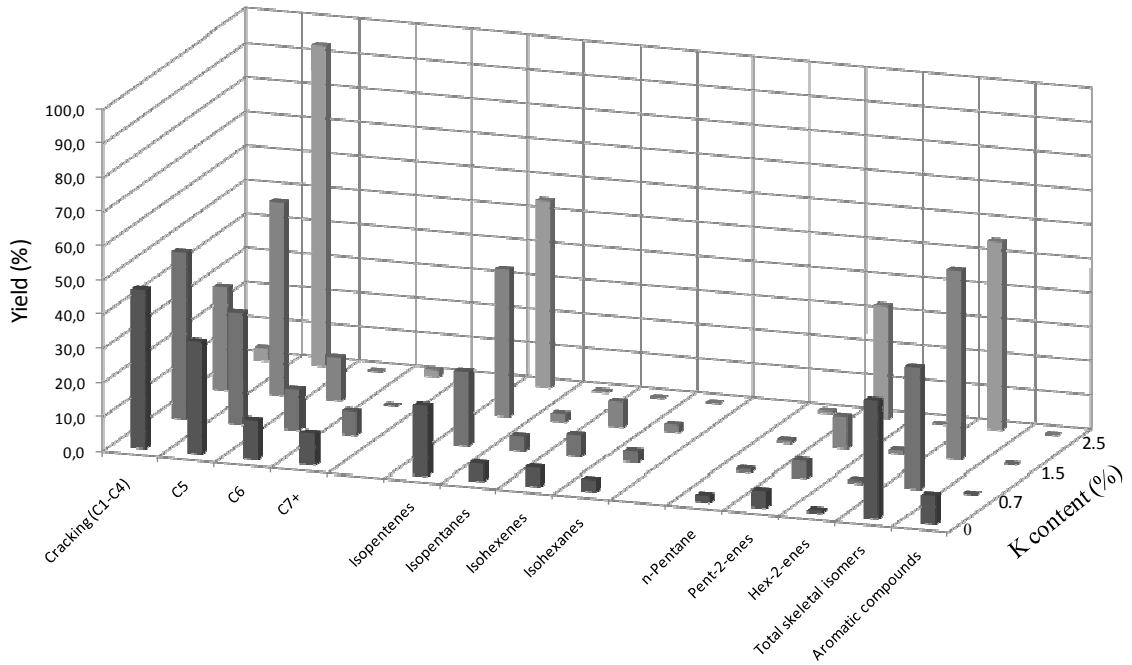

Figure 1. Products distribution in the transformation of pent-1-ene as a function of the potassium content in HZMS-5 zeolites.

The transformation of hex-1-ene has also been investigated on a ZSM-5 zeolite containing a 2.0% K and 0.5% Pt. The hydrogenating activity was high but also the conversion to position and particularly to skeletal isomers (both isoalkanes and isoalkenes). The latter exceeded 30% whereas the cracking was moderate.

Conclusions

The acid properties of ZSM-5 can be modulated by incorporation of potassium in order to increase the skeletal isomerization of 1-alkenes and minimize their cracking. The predominance of each process is related to the distribution of acid sites in the zeolite.

Acknowledgements

The authors wish to acknowledge funding of this research by Ministerio de Ciencia e Innovación (Project MAT2010-18778), Junta de Andalucía (group FQM-346) and Repsol.

References

[1] Long, H., Wang, X., Sun, W., Xiong, G., Wang, K., Effect of acidity on n-octene reaction over potassium modified nanoscale HZSM-5, Fuel 87 (2008) 3660-3663.
[2] Coleto, I., Roldán, R., Jiménez-Sanchidrián, C., Gómez, J.P., Romero-Salguero, F.J., Transformation of α-olefins over Pt–M (M = Re, Sn, Ge) supported chlorinated alumina, Fuel 86 (2007) 1000-1007.
[3] Coleto, I., Roldán, R., Jiménez-Sanchidrián, C., Gómez, J.P., Romero-Salguero, F.J., Valorization of α-olefins: Double bond shift and skeletal isomerization of 1-pentene and 1-hexene on zirconia-based catalysts, Catalysis Today 149 (2010) 275-280.

Hydroisomerization of benzene and n-heptane on platinum mordenite-alumina catalysts for production of the ecological fuels

Belopukhov E.A., Belyi A.S., Kiryanov D.I., Smolikov M.D.
Institute of Hydrocarbons Processing SB RAS, Omsk, Russia, eugebel@yandex.ru

Introduction

It is known that the technology of simultaneous processing of light straight run (C_5-C_6 alkanes) and light reformate can be used in order to reduce benzene level in a finished gasoline [1]. At the same time J.-K. Chen et al. [2] observed inhibition of paraffins isomerization in the presence of the benzene on Pt/zeolite catalysts. To date quite a number of researches deals with the increasing of the target reactions selectivity, e.g. investigations of A. Martínez et al. [3] or M.J. Ramos et al. [4].

Our main objectives are to determinate the optimal conditions for hydro-improvement of a benzene-containing fraction (either medium straight run 70-85°C or light reformate) without light straight run and to select the most appropriate catalysts for this process. Particularly in the report we consider influence of H-mordenite/alumina ratio on parameters of the model mixture conversion.

Experimental

The catalysts used in this work are platinum supported on mordenite-alumina. Carriers were prepared by peptization of NH_4-form of mordenite and pseudoboehmite by force of the treatment with acetic acid solution under stirring. Then extrudates of carrier were formatted and drying at 120°C. In order to convert NH_4MOR to HMOR and pseudoboehmite to alumina all carriers were calcined at 500°C. The NH_4-form of mordenite (ref. CBV-21A) with Si/Al ratio of 20 was purchased from Zeolyst International and pseudoboehmite (ref. PURAL SB1) was supplied by the SASOL Germany GmbH. Platinum (0.3 wt.%) was incorporated into the calcined carriers from a mixture of H_2PtCl_6 solution and dilute solution of acetic acid. Platinum loaded catalysts were dried at 120°C. Reduction was performed *in situ* in H_2 flow at 350°C. In this way following catalysts with the H-mordenite percentage of 5, 10, 20, 30, 50, 70 were obtained. For example platinum catalyst on 30% HMOR and 70% Al_2O_3 are named as Pt/A-MOR-30.

The acid properties of the carriers and the catalysts were characterized by NH_3-TPD on AutoChem II 2920 “Micrometrics” precision chemisorption analyzer.

Catalytic investigation was carried out for the model reactions with a binary mixture of 21 wt.% benzene and 79 wt.% n-heptane in a down-flow fixed-bed reactor under the following conditions: P = 15 bar, T = 200-320°C, LHSV (liquid hourly space velocity) = 2 h^{-1}, hydrogen/hydrocarbons molar ratio = 3.

Results and discussion

The reaction of benzene hydroisomerization includes the stage of hydrogenation of benzene to cyclohexane (CH) and the stage of isomerization of the latter to methylcyclopentan (MCP). Straight-chain heptane partly isomerizates to branched-chain one. The conversion of benzene was 100% in the whole range of temperatures on all catalysts.

The research of the effect of H-mordenite/alumina ratio on the model mixture conversion and hydroisomerization selectivity showed that the optimum mordenite percentage in the catalyst is about 20-30 wt%. At these contents, yield of MCP reach the close to equilibrium value at 280-310ºC. When the zeolite content is lower than 20%, the catalytic activity is shifted to not so thermodynamically favourable high temperature zone. In the case of the Pt/A-MOR-30 catalyst the conversion level of cyclohexane at 290-300°C is 77-82% when the selectivity of the MCP formation is near 100%. The MCP/CH ratios equal 3.08 and 4.05 respectively. The conversion of n-heptane at this temperatures reach 70% with selectivity to iso-heptanes above 70%.

The results of NH_3-TPD of the samples show that the acidity decreases with decreasing the content of mordenite in the carrier. The changing of acidity occurs additively and temperature shift of the acidity maximums are not observed. Comparison between the catalytic results and acidity data show that decreasing of catalysts activity directly correlate with lowering of catalyst acidity.

Conclusions

Thus, at the work the optimal conditions for hydro-improvement of a benzene-containing fraction were determinated. It is shown that optimized mordenite content in the catalyst makes it possible to reach the equilibrium yield of the MCP on the Pt/A-MOR catalysts with the selectivity of the MCP formation is near 100%.

Acknowledgements

The authors thank Gulyaeva T.I. and Ponomaryova G.A. for their participation in physicochemical studies of the samples as well as Udras I.E. and Tregubenko V.Yu. for discussing of catalysts preparation refinements.

References

[1] Hancsók, J., Magyar, S., Sloboszlai, Z., Kalló, D., Investigation of energy and feedstock saving production of gasoline blending components free of benzene, Fuel Processing Technology, 88 (2007), 393-399.
[2] Chen, J.-K., Martin, A.M., Kim, Y.G., John V.T., Competitive Reaction in Intrazeolitic Media, Industrial & Engineering Chemistry Research, 27 (1988), 401-409.
[3] Arribas, M.A., Martínez, A., Simultaneous isomerization of n-heptane and saturation of benzene over Pt/Beta catalysts, Catalysis Today, 65 (2001), 117-122.
[4] Ramos, M.J., de Lucas, A., Jiménez, V., Sánchez, P., Valverde, J.L., Hydroisomerization of different refinery naphtha streams by using a beta zeolite catalyst, Fuel Processing technology, 89 (2008), 721-727.

Perspective nanostructured SnO_2 materials as catalysts for VOCs elimination and hosts for lipases immobilization

M. Dimitrov[1]*, M. Guncheva[1], D. Zhiryakova[1], L. Mitsova[1], Tz. Lazarova[2], T. Tsoncheva[1]
[1]*Institute of Organic Chemistry with Centre of Phytochemistry, Bulgarian Academy of Sciences, 1113 Sofia, Bulgaria, e-mail: md2@orgchm.bas.bg*
[2] *Institute of General and Inorganic Chemistry, Bulgarian Academy of Sciences, 1113 Sofia*

Introduction

Tin dioxide is a potential candidate as catalyst in various redox processes since it comprises large numbers of crystal defects that ensure high mobility of lattice oxygen. Besides, its intrinsic non-stoichiometry could be used more efficiently if the SnO_2 particle size is decreased in the nanoscale due to the faster migration of the oxide ions within the SnO_2 to lattice positions and also the more likely higher exposure of defects due to increased surface to volume ratio. Additionally, the introduction of finely dispersed active metal/metal oxide component via grafting with metal complexes will further increase the surface non-stoichiometry of SnO_2, making it potential support for redox catalysts. Our previous results on pure nanostructured SnO_2 materials showed their potential as active, stable and selective catalysts to total oxidation of VOCs [1]. In addition, inorganic enzyme carriers in comparison with polymeric ones are structurally more stable, environmentally more acceptable and resistant to organic solvents and microbial attack in view of their use as biocatalysts. Generally, silica, alumina and iron oxide have been the main focus of the scientific investigations in this field. Nanostructured tin dioxide materials have not been tested as supports for enzyme immobilization yet. We expect that they will be effective carriers for lipases due to their large surface area and pores in the nanosize range, The present work deals with the comparison of the properties of nanosized SnO_2 powders prepared by sol-gel techniques from Sn(IV) *tert*-butoxide or $SnCl_4$ as tin sources and their modifications with Pt or Pd. The aim is to test the potential of metal supported nanostructured SnO_2 materials as catalysts for VOCs elimination. The efficiency of lipase immobilization on pure nanosized SnO_2 as well as the catalytic activity and stability of the obtained biocatalysts are also studied.

Experimental

The synthesis of the nanostructured SnO_2 materials was conducted as described in [1]. Two series of samples were prepared from $SnCl_4$ and Sn(IV) *tert*-butoxide and designated SnO_2-A and SnO_2-B, respectively. The grafting with 1 and 4 wt % Pt or Pd was done by using the molecular design dispersion method from the corresponding metal acetylacetonates. The samples were characterized by X-ray diffraction, N_2 physisorption, thermogravimetric temperature-programmed reduction in hydrogen (TG-TPR) and catalytic combustion of ethyl acetate (30 mg of catalyst, 0.59 % ethyl acetate in air, and WHSV of 335 h^{-1}). Lipases from *Candida rugosa*, *Rhizopus delemar* and porcine pancreas were immobilized on SnO_2-A via physical adsorption. The amount of protein adsorbed on the carriers after the immobilization procedure was determined using Lowry method and bovine serum albumin as standard protein for calibration. The activity and stability of the immobilized enzymes was estimated using titrimetric method and tributyrin as a substrate [2].

Results and discussion

The high specific surface area (70-200 m^2/g) and the small particle sizes (4-10 nm) of the prepared nanostructured SnO_2 materials favour the high dispersion and ubiquitous distribution

of the supported palladium and platinum through the tin dioxide as proven by the X-ray diffraction patterns (not shown). Only in the case of 4Pt/SnO_2-A and 4Pd/SnO_2-A small reflections due to metallic Pt and Pd were registered, respectively. All modified samples exhibit catalytic activity towards ethyl acetate oxidation above 470 K, while high catalytic conversion with almost complete selectivity to CO_2 was registered above 570 K. At this temperature, the pure SnO_2 shows very low catalytic activity that decreases with time on stream. Under isothermal conditions (T=575 K) all modified samples show stable catalytic activity (Fig. 1). The 4 wt. % samples have higher conversion rates with the exception of the samples from series A where bigger metallic particles were present (Fig 1a). The much higher

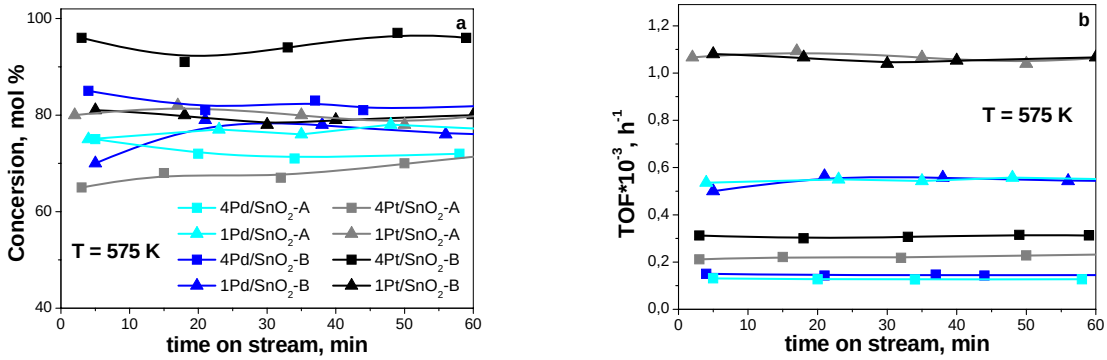

Figure 1. Total oxidation of ethyl acetate at 575 K presented as (a) conversion and (b) TOF, TOF are calculated as moles of ethyl acetate converted to CO_2 per mole of metal per hour.

turnover frequencies (TOF) values calculated for the samples containing 1 wt. % metal (Fig. 1b) could be due to the fact that the metal (Pt or Pd) additionally activates the lattice oxygen of the support, which is confirmed by the TG-TPR data showing much easier reduction of the SnO_2 in case of the modified samples.

We found that the efficiency of the lipase immobilization on SnO_2-A depends on the molecular size of the enzyme. The protein loading varies more than eight times within the three enzymes. The best results, protein loading of 24.7 $mg.g^{-1}$ carrier and activity of 760 Ug^{-1} carrier were obtained with the lipase from *Rhizopus delemar* (32 kDa). All immobilized biocatalysts enhance their thermal stability and tolerance toward the reaction medium.

Conclusion

Only a small amount very highly dispersed noble metal additive is sufficient to dramatically increase the oxidation ability of nanostructured SnO_2 at relatively low temperatures, which makes it a very perspective catalyst for VOCs elimination. Moreover, it was found that SnO_2 is a promising host material for lipase and has beneficial effect on lipase activity and stability.

Acknowledgements

The authors thank the National Science Fund of Bulgaria (project DMU 02/20) for the financial support.

References

[1] Dimitrov, M., Tsoncheva, T., Shao, S., Köhn, R., Novel preparation of nanosized mesoporous SnO_2 powders: Physicochemical and catalytic properties, Applied Catalysis B: Environmental, 94 (2010), 158-165.

[2] Rua, M.L., Schmidt-Dannert, C., Wahl, S., Sprauer, A., Schmid R., Thermoalkalophilic lipase of Bacillus thermocatenulatus. Large-scale production, purification and properties: aggregation behaviour and its effect on activity, Journal of Biotechnology, 56 (1997), 89–102.

Application of immobilized on tin dioxide lipase from *Bacillus stearothermophilus* MC7 in a wax-ester synthesis

Maya Guncheva*, Momtchil Dimitrov, Diana Zhiryakova

Institute of Organic Chemistry with Centre of Phytochemistry, Bulgarian Academy of Sciences, 1113 Sofia, Bulgaria e-mail: maiag@orgchm.bas.bg

Introduction

Wax esters are widely used as emulsifiers, emollients and drug carriers [1]. The conventional synthesis of wax-esters involves harsh reaction conditions (hazardous solvents, reduced pressure, high temperatures, and catalysts). Use of enzymes is alternative to the conventional synthesis. The utilization of lipases as catalysts in ester production makes the process more effective, selective and environmentally friendly, and decreases the cost of the product [2]. However, there are still obstacles to large scale application of biocatalysts such as their stability in the reaction conditions (medium, temperature, substrate inhibition, etc.) as well as multiple usage of the enzyme. These problems can be overcome by application of immobilized preparations.

Inorganic supports are structurally stable and resistant to oils which are the main substrates of lipases. Ordered mesoporous materials have been successfully used as carriers for lipases, trypsin, and penicillin acylase, etc. [3]. The support for enzyme immobilization, however, should be chosen carefully because it is able to alter the enzyme specificity. There is still a big demand for novel efficient enzyme supports.

Here we present the synthesis of a novel nanostructured tin dioxide (nano-SnO_2) and its application as a matrix for a lipase from *Bacillus stearothermophilus* MC7. The thermal and pH-stability of the novel biocatalyst was assayed. We examined the effectiveness of the immobilized MC7 lipase in stearyl stearate preparation in environmentally friendly medium (two ionic liquids and non-solvent system). The operational stability of the biocatalyst in several consecutive synthetic reactions was also tested.

Experimental

The lipase from *B. stearothermophilus* MC7 (lipase MC7) was gift from Dr. M. Kambourova [4]. The nanostructured tin dioxide was synthesized using $SnCl_4$ as a tin source and the triblockcopolymer Pluronic P 123 as structure directing reagent.

The physical adsorption of lipase MC7 on nano-SnO_2 was carried out at room temperature for 12 h, and then the preparation was dried under a flow of nitrogen. The activity of the free and the immobilized lipase was estimated spectrophotometrically [4]. The amount of protein loading on the carrier was evaluated as the difference in protein concentration of the lipase solution before and after immobilization according to Lowry et al. [5]. The lipase-catalyzed esterification of stearic acid and 1-octadecanol was carried out at 65ºC for 5h. The isolation and the analysis of the stearyl stearate have been previously described [6]

Results and discussion

The immobilization of lipase from *B. stearothermophilus* MC7 on tin dioxide (nano-SnO_2-MC7) yielded a protein loading of 15.3 mg/g carrier and the hydrolytic activity was 15,000 U/g carrier toward 4-nitrophenyl palmitate. We found that nano-SnO_2-MC7 carried out the synthesis of long chain esters twice more effectively than immobilized lipases from *C. antarctica*, *R. niveurs* and *A. niger* [7]. The synthetic activity of nano-SnO_2-MC7 was comparable to those described for immobilized lipases from *R. miehei C. rugosa* [6, 8]. The

preparation gave 75% yield of stearyl stearate for 5h at the optimal temperature (65ºC). The biocatalyst preserved up to 50% of its synthetic activity after five hours heating at 70ºC in solvent free system in presence only of the substrates. Recently ionic liquids have been extensively studied and used as green solvents in organic synthesis. They are not volatile and possess good chemical and thermal stability. The impact of the ionic liquids containing chloride anion on the lipase activity has not been extensively studied yet. We tested the effect of 3-methyl-1-octyl imidazolium chloride [OMIM][Cl] and methyl trioctyl ammonium chloride [TOMA][Cl] on nano-SnO_2-MC7 activity. The imidazolium derivative had a beneficial effect on the nano-SnO_2-MC7 activity. The synthetic reaction proceeded with higher rate and for 5 h almost a complete conversion of substrates was achieved. This made the performance of the biocatalyst 1.3 fold more effective than that in the solvent free system. The effect of media in this case was comparable to the effect of the activation of nano-SnO_2-MC7 by the non-ionic surfactant PEG1500. In presence of [OMIM][Cl] the enzyme preserved about 60% of its initial activity after 5h heating at 75^{o}C. The immobilized lipase MC7 was easily separated from the reaction media containing imidazolium chloride due to its lower-viscosity. As expected, it ensured higher operational stability of the biocatalyst. Our results showed that, nano-SnO_2-MC7 applied in the sysnthesis of stearyl stearate in solvent free system kept 47% of its activity at the 8th run, while in presence of [OMIM][Cl] it was 90% active . In our study we found that [TOMA][Cl] completely inactivated nano-SnO_2-MC7 lipase when added to the reaction mixture.

Conclusions

High activity of lipase nano-SnO_2-MC7 in the green solvent [OMIM][Cl] as well as operational stability of the immobilized preparations and their thermal stability in low-aqueous medium are characteristics of the enzyme which makes it applicable and sufficiently valuable in large scale production of wax-esters.

Acknowledgements

The authors thank the National Science Fund of Bulgaria (project DMU 02/20) for the financial support.

References

[1] Villalobos-Hernandez, J.R.; Muller-Goymann, C., In vitro erythemal UV-A protection factors of inorganic sunscreens distributed in aqueous media using carnauba wax–decyl oleate nanoparticles, European Journal of Pharmaceutics and Biopharmaceutics, 65 (2007), 122–125.

[2] Petersson, A.; Gustafsson, L.; Nordblad, M.; Borjesson, P.; Mattiasson, B.; Adlercreutz, P., Wax esters produced by solvent-free energy-efficient enzymatic synthesis and their applicability as wood coatings, Green Chemistry, 7 (2005), 837–843.

[3] Yiu H., Wright P., Enzymes supported on ordered mesoporous solids: a special case of an inorganic hybrid, Journal of Materials Chemistry, 15 (2005), 3690 – 3700.

[4] Kambourova, M., Kirilova, N., Mandeva, R., Derekova, A., Purification and properties of thermostable lipase from a thermophilic Bacillus stearothermophilus MC 7, Journal of Molecular Catalysis B: Enzym., 22 (2003) 307–313.

[5] Lowry, O., Rosebrough, N., Farr, A.L., Randall, R., Protein measurement with the folin phenol reagent. Journal of Biological Chemistry, 193 (1951), 265 – 275.

[6] Guncheva, M., Zhiryakova, D., High-yield synthesis of wax esters catalysed by modified Candida rugosa lipase, Biotechnology Letters, 30 (2008), 509–512.

[7] Gunawan, E., Basri, M., Rahman, M., Salleh, A., Rahman, R., Lipase-catalyzed synthesis of palm based wax-esters, Journal of Oleo Science, 53 (2004), 471 – 477.

[8] Rodrigues, R., and Fernandez-Lafuente, R., Lipase from Rhizomucor miehei as an industrial biocatalyst in chemical process, Journal of Molecular Catalysis B: Enzym., 64 (2010), 1–22.

PERFORMANCE OF TUNGSTOPHOSPHORIC ACID LOADED SBA-15 CATALYSTS IN DEGRADATION REACTION OF POLYETHYLENE

Buğçe Aydemir, Naime Aslı Sezgi, Timur Doğu
Middle East Technical University, 06531 Ankara/TURKEY, sezgi@metu.edu.tr

Introduction

Plastic materials are widely used throughout the world due to their low price, high capacity of production and simple processing techniques. These qualifications of plastic materials provide them a great potential of use in plenty of industrial applications. Plastic materials are generally non-biodegradable, in other words, incapable of decomposing biologically in the nature. This disability brings the problems of accumulation of plastics with an increasing trend and uncontrollable environmental pollution. In recent years, plastic materials are degraded into lower molecular weight liquid and gaseous products which are potential raw materials and fuels for petrochemical industry. The use of catalysts enhances the formation of more valuable hydrocarbons at lower reaction temperatures and residence times[1-3].

Experimental

In this study, tungstophosphoric acid (TPA) containing SBA-15 materials were synthesized by impregnation of TPA into hydrothermally synthesized SBA-15, to be used in catalytic degradation of polyethylene. TPA was incorporated to the porous framework of SBA-15 with different W/Si ratios, using tungstophosphoric acid hydrate as the acid source.

Non-catalytic and catalytic degradation experiments of polyethylene were performed in the degradation reaction system at different temperatures and TPA loadings. The polymer used in these experiments was polyethylene of M_n 1700, density 0.92 g/ml, polydispersity index 2.35. Liquid and non-condensed gaseous products were analyzed using a gas chromatograph.

Results and discussion

From XRD analysis, it was observed that introducing acidic compounds did not cause deformations in the regularity and by EDS analysis, it was found out that even at higher loadings, acidic compounds were introduced effectively to SBA-15 materials. Nitrogen adsorption-desorption isotherms showed that the synthesized materials exhibited type IV isotherms. SEM and TEM pictures (Figure 1) showed the hexagonal regularly ordered structure of SBA-15 materials. FTIR analysis of the pyridine adsorbed synthesized materials revealed the existence of Lewis and Brønsted acid sites in the synthesized materials.

From TGA analysis, it was observed that SBA-15 samples reduced activation energy of the reaction effectively. Also, a decrease in reaction temperature was observed when using TPA loaded SBA-15 materials.

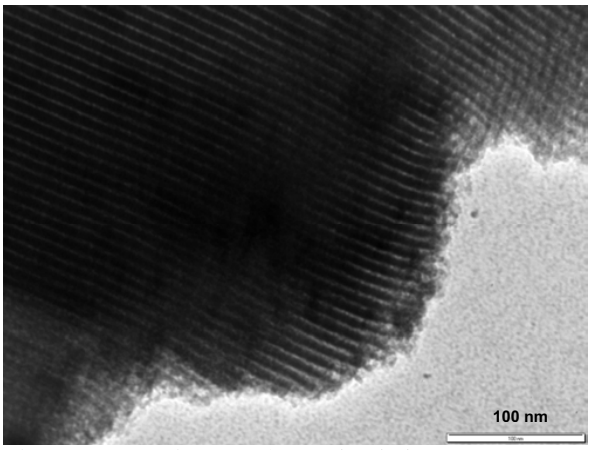

Figure 1. TEM image of TPA loaded SBA-15

In non-catalytic degradation reactions, selectivity of C3 and C4 hydrocarbon gases was high and in catalytic degradation reactions, selectivity of ethylene was significantly high. In the liquid analysis of non-catalytic degradation reactions, it was observed that the product distribution was mainly composed of hydrocarbons greater than C18. The use of TPA loaded SBA-15 materials resulted in a liquid product distribution in the range of C5-C14, which is the hydrocarbon range of gasoline fuel.

Conclusions

TPA loaded SBA-15 catalysts were synthesized successfully. These materials exhibited Type IV isotherms. Their average pore diameters were approximately 6.5 nm. With these catalysts, the liquid product distribution was shifted to a range of hydrocarbons lower than C18. They enhanced the production of gasoline range hydrocarbons.

Acknowledgements

The authors thank Middle East Technical University Research Fund (BAP-03-04-2008-08) for the financial support, Central Laboratory of Middle East Technical University for analyses. The authors also thank Dr. Lucian Barbu Tudoran for TEM analysis.

References

[1] Van Grieken, R., Serrano, D.P., Aguado, J., Garcia, R., Rojo, C., Thermal and catalytic cracking of polyethylene under mild conditions, Journal of Analytical and Applied Pyrolysis, 58-59 (2001), 127-142.
[2] Aguado, J., Serrano, D.P., San Miguel, G., Escola, J.M., Rodriguez, J.M., Catalytic activity of zeolitic and mesostructured catalysts in the cracking of pure and waste polyolefins, Journal of Analytical and Applied Pyrolysis, 78 (2007), 153-161.
[3] Mikulec, J., Vrbova, M., Catalytic and thermal cracking of selected polyolefins, Clean Technologies and Environmental Policy, 10 (2008), 121-130.

NiMo/SBA-15 catalysts prepared with citric acid: an interesting behavior in dibenzothiophene hydrodesulfurization

Diego Valencia, Óscar Pérez, Tatiana Klimova*
*Facultad de Química, Universidad Nacional Autónoma de México, Cd. Universitaria, Coyoacán, México D.F., 04510, México *klimova@servidor.unam.mx*

Introduction

Nowadays, the need to improve the removal of sulfur from gasoline and diesel oil by means of deep hydrodesulfurization (HDS) is driven by the new environmental legislations regarding fuel specifications [1]. Many efforts are aimed to design more active or selective HDS catalysts, depending on their particular application. Recently, different nanostructured materials have attracted attention as supports for deep HDS catalysts. Among them, well-ordered mesoporous molecular sieves of the SBA-15 type have already been tested as supports for HDS catalysts. In the present work, we report results from a comparison study of NiMo catalysts supported on SBA-15 prepared by co-impregnation of Ni and Mo active phases with and without the addition of a chelating agent (citric acid, CA). This study was undertaken to inquire on the effect that thermal treatment and the amount of CA have on the characteristics of NiMo/SBA-15 catalysts and their behavior in HDS of dibenzothiophene (DBT).

Experimental

NiMo catalysts were prepared by incipient wetness impregnation of SBA-15 with aqueous solutions of $(NH_4)_6Mo_7O_{24}•4H_2O$, $Ni(NO_3)_2•6H_2O$ and CA [2]. Ni:Mo:CA molar ratio was 1:2:X. Calcination temperature ($T_{calc.}$) of oxidic NiMo catalysts and amount of CA used (X) are showed in Table 1.

Table 1. Preparation conditions of NiMo catalyst soported on SBA-15.

Catalyst	$T_{calc.}$ (^oC)	Amount of CA (X)
NiMo (100)	100	-
NiMo (500)	500	-
NiMoCA2.7 (100)	100	2.7
NiMoCA2.7 (300)	300	2.7
NiMoCA2.7 (500)	500	2.7
NiMoCA4.2 (100)	100	4.2
NiMoCA6.3 (100)	100	6.3

Catalysts were characterized by TGA, nitrogen physisorption, small-angle and powder XRD, TPR, UV-vis DRS, and HRTEM. The DBT HDS activity tests were performed in a batch reactor at 300 ^oC and 7.3 MPa total pressure for 8 h. Prior to the catalytic activity evaluation, the catalysts were sulfided ex-situ at 400 ^oC for 4 h in a stream H_2S in H_2. The course of the reaction was followed by withdrawing aliquots each hour and analyzing them by GC.

Results and discussion

TGA results showed that CA was completely eliminated from uncalcined catalyst in air atmosphere at temperature between 100 and 500 °C. XRD characterization of NiMo/SBA-15

catalysts prepared without adding CA revealed poor dispersion of Ni and Mo oxide species. The signals of an Anderson heteropolymolybdate $(NH_4)_4[Ni(OH)_6Mo_6O_{18}]\bullet 4H_2O$ were observed after thermal treatment at 100 °C. This phase was transformed into $NiMoO_4$ at 500 °C. Formation of the above crystalline phases was avoided in the samples prepared with the addition of CA during impregnation. DRS and TPR characterization of the catalysts showed that CA significantly increases the dispersion and reducibility of octahedral Mo species. HRTEM of the sulfided NiMo/SBA-15 catalysts revealed that smaller and less stacked MoS_2 particles are formed when CA is used during the impregnation. In line with this, activity of the NiMoCA/SBA-15 catalysts was higher than that of the NiMo/SBA-15 ones and increased with the calcination temperature. An interesting and unexpected trend was observed for the selectivity of the NiMoCA catalysts with variation of the temperature of heat treatment. Thus, the catalysts calcined at low temperature (100 and 200 °C) showed high selectivity towards the direct desulfurization (DDS) of DBT (Table 2), whereas the samples calcined at higher temperature (300-500 ^oC) were more selective for the hydrogenation (HYD) route. Increase in the amount of citric acid used in the catalyst preparation resulted in more dispersed Mo species (HRTEM) and further improvement in the selectivity towards the DDS route of DBT HDS (Table 3). Catalysts prepared without a chelating agent (CA) almost did not change their activity and selectivity upon calcination.

Table 2. HDS activity and selectivity of NiMo/SBA-15 catalyst calcined at different temperatures.

Catalyst	DBT conversion		Selectivity
	4h	8h	BP/CHB* ratio
NiMo (100)	37	72	0.8
NiMo (500)	40	76	0.9
NiMoCA2.7 (100)	49	82	3.0
NiMoCA2.7 (300)	51	84	0.9
NiMoCA2.7 (500)	63	96	0.4

* at 50 % DBT conversion.

Table 3. HDS activity and selectivity of NiMo/SBA-15 catalyst prepared with different amounts of CA.

Catalyst	DBT conversion		Selectivity
	4h	8h	BP/CHB* ratio
NiMo (100)	37	72	0.8
NiMoCA2.7 (100)	49	82	3.0
NiMoCA4.2 (100)	48	81	4.2
NiMoCA6.3 (100)	39	74	8.5

Conclusions

NiMoCA/SBA-15 catalysts are outstanding catalytic systems that allow one to modify easily the selectivity towards DDS or HYD routes by varying calcination temperature or amount of CA added.

Acknowledgements

Financial support by CONACYT-Mexico (grant 100945) is gratefully acknowledged. The authors thank I. Puente Lee, C. Salcedo Luna, M. Aguilar Franco, M. Portilla and E. Reynoso for technical assistance with HRTEM, XRD and TGA/DTG/DTA characterizations

References

[1] Song, C., An overview of new approaches to deep desulfurization for ultra-clean gasoline, diesel fuel and jet fuel, Catalysis Today, 86 (2003) 211-263.

[2] Valencia, D., García-Cruz, I., Klimova, T., Effect of citrate addition in NiMo/SBA-15 catalysts on selectivity of DBT hydrodesulfurization, Studies in Surface Science and Catalysis, 175 (2010) 529-532.

The effect of alkali metals in gold-modified zeolites on the adsorptive-catalytic deodorization

Izabela Sobczak*, Michał Rydz, Maria Ziolek
A. Mickiewicz University, Faculty of Chemistry, Grunwaldzka 6, 60-780 Poznań, Poland
E-mail: sobiza@amu.edu.pl*

Introduction

Recently, in the area of environmental protection much attention has been paid to curb odours emissions. Among others, selective adsorption processes with on-site regeneration of the adsorbents are very promising to reduce the concentration of odour producing substances below odour threshold [1]. Presently, activated carbon with a very high-surface area because of extreme porosity has become the most common adsorbent for air pollution (odours) control applications. However, gold or gold and iron modified BETA and ZSM-5 zeolites have been also found to be able to adsorb high amount of odours from the air containing dibutyl sulphide (Bu_2S) with high selectivity [2]. Moreover, it has been shown in the literature [3] that modification of zeolites by alkali metal ions is one of the methods for improvement of electronic and catalytic characteristics of supported gold, mainly in oxidation processes.
The idea of this work was to get insight into the possible use of gold-modified zeolites (Beta and ZSM-5) treated with alkali metals for deodorisation of air by adsorption and catalytic transformation (mainly oxidation) of odours. Dibutyl sulphide (Bu_2S) was applied as a model compound for odours containing sulphur as heteroatom. Taking into account an improvement of oxidation of sulphide adsorbed, the modification of sorbents was performed with sodium and potassium, well known as electron-releasing modifier on different supports. The roles of the amount (wt.%) of alkali metals in Au/zeolite and anion in alkali salt were considered.

Experimental

H-Beta (Si/Al = 12.5, Süd Chemie) and H-ZSM-5 (Si/Al = 44.9, Süd Chemie) - types of zeolites were used for further modification. The gold catalysts were prepared by deposition-precipitation with $HAuCl_4$ (1 wt.%) [2]. Na and K -modified zeolites were obtained by two methods: 1) adsorption (treatment of Au-sample with 0.5 M $NaNO_3$ and KNO_3 or NaCl aqua solution for 24 h at 303 K) and 2) wetness impregnation (Au/Na(K) = 1:1). The materials prepared were calcined at 623 K.
The physicochemical properties of the samples prepared were characterized by the standard techniques, XRD, UV-Vis, TEM, test reactions and pyridine adsorption.
Adsorption of odour, dibutyl sulphide (Bu_2S), was performed at room temperature by the use of the balance scale with the sorbent in the glass box purged with air flow. In this box the appropriate odour was evaporated and the amount of adsorbed compounds was continuously weighed to plot the adsorption curves. The amount of Bu_2S adsorbed/desorbed was analysed by the elemental analysis.

Results and discussion

The results of odours adsorption presented in Table 1 show a significant influence of the alkali metal introduction into gold-zeolite on the amount of adsorbed sulphide and total amount of adsorbates. The wt.% of Na and K depends on the method of modification and is much higher for zeolites modified by the adsorption (1-2% for Na and 2-4% for K) than impregnation (0.05% for Na and 0.08% for K). The introduction of high content of alkali metal into gold-zeolites generates basicity of the surface indicated by the test reactions (AcoAc cyclisation and 2-propanol decomposition), whereas the low Na and K content does not change acidic character of Au-zeolites. It is important to note, that contrary to the results

obtained for Au/oxides [4], alkali cations in zeolites do not protect gold species from agglomeration and in consequence of Na or K modification the size of gold nanoparticles is bigger than in the gold zeolites without alkali metal treatment (the increase in average Au particle size from ca. 8 to 18 nm). The largest gold particles (70 nm except smaller one) are present on the surface of Na(Ads_Cl)/Au-Beta zeolite prepared using NaCl salt, because chloride ions promote mobility and agglomeration of gold species. Simultaneously, the removal of gold occurs as a result of Cl^- interaction with Au species. It indicates the important role of anion in the modifier and its influence on the content and properties of the final catalyst.

The amounts of Na and K determine the total sorption capacity and the amount of Bu_2S adsorbed on alkali metal modified Au/ZSM-5 and Au/Beta zeolites. The high content of Na and K (close or above 100% of cation exchange reached in the adsorption method) decreases the total sorption capacity of all adsorbates (Bu_2S, H_2O, CO_2 and others from air) because of the blockage effect. However, what is important, the amount of Bu_2S adsorbed is similar before and after modification with Na and K, especially for Beta type zeolite. That is why the selectivity of Bu_2S adsorption increases (Table 1).

Table 1. The amounts of Bu_2S adsorbed on examined materials

Catalyst	% wt of all adsorbates	% wt of Bu_2S	Sel., * %
Au-Beta	30.36	14.01	46
Na(Impr)/Au-Beta	30.77	13.95	45
Na(Ads)/Au-Beta	22.57	12.79	57
K(Ads)/Au-Beta	25.16	13.89	55
Au-ZSM-5	32.87	10.75	33
Na(Ads)/Au-ZSM-5	18.14	8.53	47

* Selectivity as the amount of Bu_2S in total amount of adsorbates

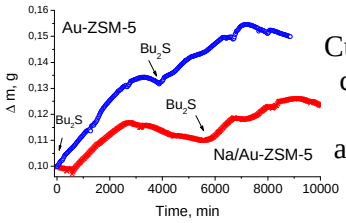

Figure.1 Curves of air containing Bu_2S adsorbed at RT

The most important finding from this work is the improvement of the oxidative properties of gold zeolites by the addition of Na and K. The shape of the adsorption curves (Fig.1 for ZSM-5 zeolites) show some periodic losses of mass which could be explained by the desorption of Bu_2S caused by its migration in straight channels and/or by the desorption of products of Bu_2S catalytic oxidation. The formation of SO_2 as the product of catalytic oxidation of Bu_2S with oxygen from the air was documented by UV-Vis spectra performed after adsorption of the odour. After introduction of alkali metal the desorption of SO_2 from the catalyst surface is faster, which allows easy regeneration of zeolite via cyclic catalytic oxidation of odour. The increase in oxidative properties of alkali modified Au-zeolites was confirmed also by CO to CO_2 oxidation reaction.

To conclude, the study performed indicated the attractiveness of ZSM-5 and Beta zeolites modified with gold and alkali metals for odour removal from the air, mainly because of the high selectivity to Bu_2S sorption and its easy transformation towards odourless oxides via catalytic oxidation.

Acknowledgements

Polish Ministry of Science (Grant No. N N204 032536) is acknowledged for the financial support of this work. Acknowledge is made also to Johnson Matthey (UK-USA) and Süd Chemie (Germany) for the supply of the $HAuCl_4$ and β and ZSM-5 zeolites, respectively.

References

[1] A. Callterieri, P.H. Thiesen, B. Niemeyer, Waste Management, 25 (2005) 985.
[2] I. Sobczak. H. Pawlowski, J. Chmielewski, M. Ziolek, J. Hazardous Mat. 179 (2010) 444-452.
[3] A. Simakov, I. Tuzovskaya, N. Bogdanchikova, A. Pestryakov, M. Avalos, M.H. Farias, E. Smolentseva, Catal. Communications 9 (2008) 1277–1281.
[4] Ch. Baatz, U. Pruße, Catal. Today 122 (2007) 325–329.

The structure effect of sulphonated SBA-15 and MCF on niobium incorporation and catalytic behaviour in glycerol esterification

K. Stawicka, M. Trejda, M. Ziolek

Adam Mickiewicz University, Faculty of Chemistry, Grunwaldzka 6, 60-780 Poznań, Poland, tmaciej@amu.edu.pl

Introduction

Bringing into play of waste glycerol became a new challenge since a global production of this alcohol significantly increased. This growth was determined by many regulations stimulating the biodiesel production. Biodiesel is mainly obtained through triglycerides transesterification with alcohols leading to fatty acids esters and glycerol. It seems to be reasonable turning waste alcohol into the product that can be also used as biofuel, which in consequence makes the most of renewable source. This goal can be reached by glycerol esterification with acetic acid, since triacetyloglycerol (triacetin), i.e. one of the esterification products, is known as valuable blending component of biodiesel. For this purpose different kinds of materials having strong Brønsted acidic centres were examined, e.g. zeolites, sulphonated resins or MCM-41 and SBA-15 samples containing oxidised MPTMS species, i.e. (3-mercaptopropyl)trimethoxysilane. Since the glycerol esterification involves rather bulky molecules in the liquid phase, the size and shape of pores in catalysts could determine the activity and selectivity in this process. Herein, we present detailed study on sulphonated mesoporous materials of SBA-15 and MCF type that contain niobium as a promoter. The impact of niobium and a kind of structure on the formation and stability of surface sulphonic species determining activity and selectivity in the glycerol esterification are examined.

Experimental

The SBA-15 and MCF materials having MPTMS species on the surface were prepared via modified hydrothermal synthesis procedure described previously in [1] and [2], respectively. Ammonium niobate(V) oxalate (Aldrich) was applied as a niobium source (Si/Nb = 32, 64). MPTMS (Aldrich) and H_2O_2 (Merck) were added into the solution. The gel was stirred at 313 K for 20 h and heated at 383 K for 24 h without stirring. For both kinds of materials the organic template was removed by constant extraction with ethanol for 24 h using the Soxhlet apparatus and finally dried at RT overnight.

Different characterisation techniques were used, i.e. XRD, N_2 adsorption/desorption, XRF, elemental and thermal analyses, FTIR, UV-Vis, FTIR + pyridine adsorption.

The reaction of glycerol and acetic acid was performed in a liquid phase in batch reactor without any solvents. The reaction was carried out under nitrogen atmosphere at 373, 398 and 423 K for 4 h using 100 mg of catalyst. Different molar ratios of glycerol to acetic acid were applied (1:3, 1:6, 1:9). Reuse of catalysts was performed. Products were analysed by a GC (Varian CP 3800) equipped with 60 m VF-5ms capillary column and FID detector.

Results and discussion

All materials prepared in this study showed mesoporous structure typical of SBA-15 or MCF samples as evidenced by standard characterisation techniques, i.e. XRD and N_2 adsorption/desorption measurements. The highest efficiency of niobium incorporation into the mesoporous silicate structure was observed for SBA-15 materials. It was found that the addition of niobium to the synthesis gel, during preparation of MCF sample, caused the formation of both phases, i.e. SBA-15 and MCF, as evidenced by SEM and TEM images. Interestingly, this was not observed when niobium was inserted into the gel together with

MPTMS. In this case pure MCF phase was detected, although, depending on niobium content, the defect holes in the material structure appeared. Similar defects have been previously observed in the literature for the mesoporous niobiosilicates of MCM-41 type [3]. The SBA-15 structure allowed incorporation of bigger amount of MPTMS species than MCF structure, however in both cases the positive effect of niobium on thiols oxidation to suphonic species was observed. Niobium was also found to preserve the oxidation of methoxy species originating form MPTMS, as evidenced by FTIR spectroscopy. This fact made the higher oxidation of thiol groups possible. The efficiency of sulphonic species formation was also found to be dependent on the kind of mesoporous structure. In spite of lower niobium concentration in the final MCF materials the effectiveness of sulphonic species formation was better for these samples. The abovementioned results allowed us to propose the different states of MPTMS species on silicate and niobiosilicate surfaces (Fig. 1) [4].

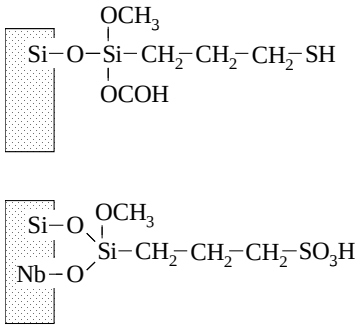

Fig. 1. Dependence of MPTMS bonding to the surface on the chemical composition of the solid

The acidic properties of mesoporous solids were examined in the glycerol esterification with acetic acid. The results obtained at optimised conditions are shown in Table 1. The highest glycerol conversion was reached for MCF samples. It can be notice that the conversion and selectivity to triacetin was determined by both, the mesoporous structure and effectiveness of thiol oxidation to sulphonic species. As it was presented above, the later aspect is dependent on niobium loading. This can explain why the samples containing niobium showed much higher yield of triacetin. The reuse tests proved the stability of sulpnonic species and gave similar catalytic results.

Table 1. Results of glycerol esterification with acetic acid carried out at 423K for 4h; glycerol to acetic acid ratio = 1:9

Catalyst	Conversion %	Selectivity / yield %		
		MAG	DAG	TAG
MP-SBA-15	54	26 / 14	58 / 31	16 / 9
MP-NbSBA-15-64	66	11 / 7	53 / 35	36 / 24
MP-NbSBA-15-32	73	10 / 7	49 / 36	41 / 30
MP-MCF	90	15 / 14	58 / 52	27 / 24
MP-NbMCF-64	89	11 / 10	51 / 45	38 / 34
MP-NbMCF-32	85	12 / 10	52 / 44	36 / 31

MAG – monoacetin; DAG - diacetin TAG – triacetin

Last number in niobiosilicate samples stands for Si/Nb ratio assumed

Conclusions

The most valuable finding of this work is determination of interplay between chemical composition and mesoporous structure having an impact on glycerol esterification with acetic acid. Materials obtained showed relatively high yield of triacetin formation, similar or higher than described in the previous literature data.

Acknowledgement

Polish Ministry of Science and Higher Education (grant 118/COS/2007/03) and COST D36/0006/06 are acknowledged for a financial support.

References

[1] D. Margolese, J.A. Melero, S.C. Christiansen, B.F. Chmelka, G.D. Stucky, Chem. Mater. 12 (2000) 2448-2459.

[2] P. Schmidt-Winkel, W.W. Lukens, D. Zhao, P. Yang, B.F. Chmelka, G.D. Stucky, J. Am. Chem. Soc. 121 (1999) 254-255

[3] B. Kilos, M. Aouine, I. Nowak, M. Ziolek, J.C. Volta, J. Catal. 224 (2004)314-325.

[4] M. Trejda, K. Stawicka, M. Ziolek, Appl. Catal. B: Environmental, (2011) submitted.

Watching the Methanol to Olefin Process with Time and Space Resolved X-ray Diffraction

David S. Wragg,[a] Matthew G. O'Brien,[b] Francesca Bleken,[a] Unni Olsbye,[a] Bert M. Weckhuysen[b] and Helmer Fjellvåg[a]
[a] *inGAP Centre for Research Based Innovation, Centre for Materials and Nanotechnology and Department of Chemistry, University of Oslo, 0315 Oslo, Norway.*
[b] *Department of Inorganic Chemistry and Catalysis, Debye Institute for Nanomaterials Science, University of Utrecht, Sorbonnelaan 16, 3584 CA Utrecht, Netherlands.*

Introduction

Methanol to olefin (MTO) conversion is a key step in the journey from natural gas and biomass to high value chemical products like plastics [1, 2]. SAPO-34, a model catalyst for this process, expands microscopically due to coke formation during the reaction [3]. We have used this feature of the crystallographic unit cell to track the progress of the reaction in a fixed bed reactor using time and space resolved high energy X-ray diffraction. The results allow us to make interesting observations concerning the origin of the "carbon pool" [4] which is believed to be the basis of the conversion process and also the driving force for the expansion of SAPO-34.

Experimental

SAPO-34 catalysts with 4 and 8 % silicon were pressed into pellets and sieved to a size of between 0.25 and 0.42 mm. 100 mg of the pellets were loaded into a fixed bed quartz tube reactor of 4 mm internal diameter with a quartz frit supporting the bed. Reaction gases (helium bubbled through methanol held at 19.5 °C) were fed upwards through the frit at rates between 30 and 50 ml min^{-1}. The reactor was heated with two Leister LE mini heat guns fitted with heat spreaders. The temperature profile in the centre of the reactor was measured using a thermocouple at 10 points from bottom to top of a loaded catalyst bed. It decreased from 346 °C at the bottom to 338 °C at the top. The product stream was analysed using a European Spectrometry Systems ecoSys-P Man-Portable mass spectrometer with a capillary inlet and heated inlet tube.

Powder XRD data were collected at beamline ID15 of the European Synchrotron Radiation Facility (ESRF) with a wavelength of 0.14257 Å (89.965 KeV), using a Pixium area detector at a sample - detector distance of 1473 mm. The reactor and heat guns were mounted on a Huber xyz stage capable of very fast translations in the z-direction, with a goniometer head for alignment. During data collection the reactor was moved down through the beam at a rate of 0.5 mm s^{-1} with diffractograms being acquired every second, the reactor was then moved back up in 1 second between scans with no data collection.

The data were reduced using DATASQUEEZE and analysed using parametric Rietveld refinements in TOPAS academic [5].

Results and discussion

We have previously demonstrated in a microreactor that the unit cell of SAPO-34 expands strongly in the c-axis direction during the MTO process [3]. Contour plots of the *c*-axis length during the scanning reaction allow us to see a reaction front moving up through the catalyst bed over time (figure 1).

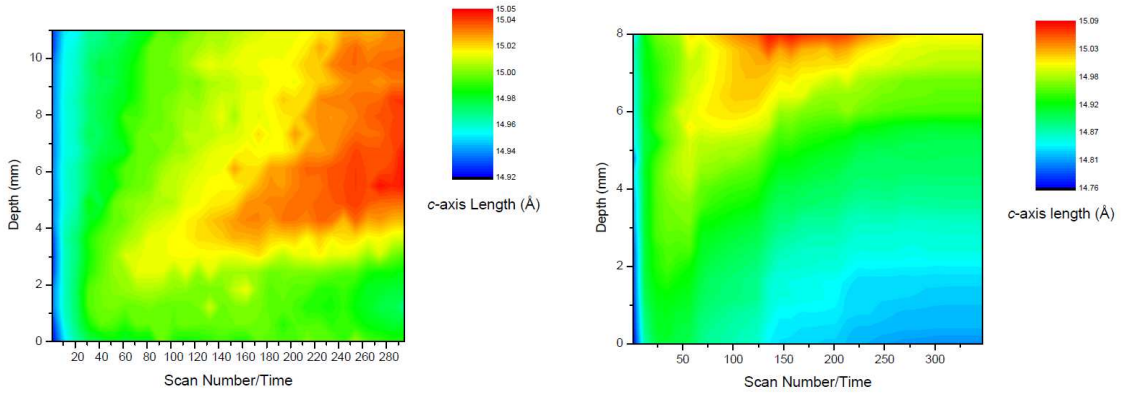

Figure 1. Contour plots of the SAPO-34 *c*-axis length during the MTO process versus position in reaction bed and time. Each numbered scan corresponds to a complete scan up the reactor bed, so that the scan number axis represents time. Left image = 30 ml min^{-1} methanol/He flow, Right image = 50 ml min^{-1} methanol/He flow switched to pure He after scan 125.

The expansion, reflecting build-up of coke inside the chabazite cages, begins at a point part-way up the catalyst bed before spreading upwards, supporting the theory of a critical amount of methanol to dimethyl ether conversion being required to establish the carbon pool of intermediates which produce olefins. The onset time of catalyst expansion varies depending on the flow rate through the reactor but more interestingly it appears that a decrease in the *c*-axis occurs at the base of the reactor later in the process at higher flow rates (50 ml min^{-1}). Switching from methanol to helium flow emphasises this effect with a significant portion of the bed returning to its initial *c*-axis size without oxidative regeneration (figure 1, right).

The expansion of SAPO-34 under MTO conditions has been attributed to the build up of reaction intermediates and coke in the pores which corresponds with reversible deactivation of the catalyst. Our mass spectrometry results suggest that the reactor was not fully deactivated during our experiments which is in agreement with the XRD results showing that some parts of the bed do not undergo significant expansion in the timescale of our tests.

Conclusions

We have used time and space resolved synchrotron powder XRD to show that a front of expanded catalyst spreads up through a fixed bed reactor during the MTO process. Even after several hours on stream we see significant differences in catalyst expansion across the bed which coincide with the beginning of deactivation as measured in mass spectra collected in parallel with the XRD data.

Acknowledgements

We thank SINTEF Oslo for catalyst samples and the ESRF for beamtime at ID15. This work was funded by inGAP and the Norwegian Research Council.

References

[1] M. Stöcker, Microporous Mesoporous Mater., 29, (1999), 3-48.
[2] M. E. Davis, Nature, 417, (2002), 813-821.
[3] D. S. Wragg, R. E. Johnsen, M. Balasundaram, P. Norby, H. Fjellvåg, A. Grønvold, T. Fuglerud, J. Hafizovic, Ø. B. Vistad, D. Akporiaye, J. Catal., 268, (2009), 290-296.
[4] U. Olsbye, M. Bjørgen, S. Svelle, K.-P. Lillerud, S. Kolboe, Catal. Today, 106, (2005), 108-111.
[5] A. A. Coelho, TOPAS V4.1, Bruker AXS, (2006).

Investigation of isomerization and hydrocracking of Fischer-Tropsch wax on Pt/AlSBA-15 and Pt/MCM-22 catalysts

György Pölczmann[1], József Valyon[2], Magdolna R. Mihályi[2], Márton Kollár[2], Zoltán Eller[1], Jenő Hancsók[1]
[1]*University of Pannonia, Department of Hydrocarbon and Coal Processing*
[2]*Chemical Research Center, Institute of Chemistry, Hungarian Academy of Sciences*
[*]*Corresponding e-mail: hancsokj@almos.uni-pannon.hu*

Introduction

Because of the problems of sustaining the environment and the crude oil supply the use of fuels and lubricants produced from renewable feedstocks have come to the front nowadays. In this respect it is very important to develop catalytic system that can be applied to produce a balanced mixture of gas oil and base oil from Fischer-Tropsch (FT) wax (mixture of mainly high molecular weight n-paraffins) produced from biomass-derived synthesis gas. Furthermore, it is important to find the proper catalysts and advantageous process parameters [1-3]. The high-molecular-weight n-paraffins can be effectively isomerized on bifunctional catalysts. There are only a few indications about the application of catalysts carrying active hydrogenation/dehydrogenation(HD/DHD) metal component on micelle-templated aluminosilicate (MTAS) materials, having ordered uniform mesoporous channels [4,5]. We studied a Pt-supporting Al-substituted silica SBA-15 material (Pt/AlSBA-15) as catalyst, not investigated in detail in this reaction yet. We compared it to a Pt/MCM-22 zeolite catalyst which has been recommended earlier for the isomerization of high molecular weight n-paraffins [4].

Experimental

The AlSBA-15 material was synthesized according to the procedure of Vinu et al. [6]. MCM-22 was hydrothermally synthesized from a synthesis gel of SiO_2 : 0.036 Al_2O_3 : 0.024 Na_2O : 0.265 Na_2SO_4 : 0.517 hexamethyleneimine : 42.6 H_2O at 145 °C for 10 days. The Brønsted acid site concentrations were determined by ammonia thermo-desorption experiments, using the NH_4-exchanged samples (0.65 mmol H^+/g for SBA-15 and 0.96 mmol H^+/g for MCM22). The analysis of the N_2 adsorption isotherm of the AlSBA-15 material gave pore diameter of 3.6 nm. In contrast, the active sites of the calcined zeolite MCM-22 are located in zeolite micropores (10-MR channels, supercages, having 0.7 nm x 1.8 nm main dimensions, and 12-MR cups of the outer surface of the crystals). 0.5 wt. % of Pt was loaded by incipient wetness impregnation method on both supports using tetraammineplatinum(II)hydroxide hydrate. The experiments were carried out in a high-pressure microreactor system in continuous operation and on a catalyst with steady-state activity. The main properties of the feedstock FT paraffin were: n-C_{18}-C_{57}): 97.4%, sulfur: < 5 mg/kg, pour point: 72 °C. The following reaction parameters were applied: T= 275-375 °C, P=40-80 bar, LHSV=1.0-3.0 h^{-1}, H_2/hydrocarbon ratio: 400-800 Nm^3/m^3. The composition of the products was determined by GC.

Results and discussion

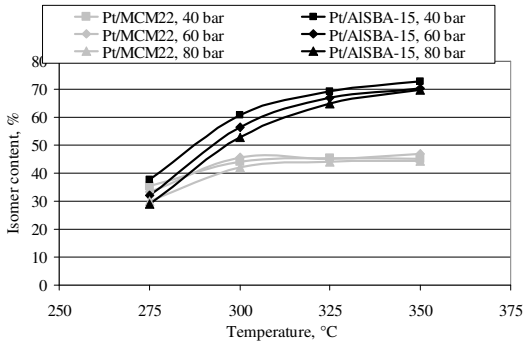

Figure 1. The effect of process parameters to the isomer contents of the liquid products

Our catalytic result showed that on the Pt/AlSBA-15 catalyst higher yield of liquid product (C_{5+}) could be reached than on the Pt/MCM-22 catalyst. On the Pt/MCM-22 catalyst the yield of light fraction (C_{5-}) increased significantly at reaction temperatures above 300 °C. Methane and ethane was formed only on the Pt/MCM-22 catalyst. In the C_{5-} products, obtained on both catalysts, mainly isobutane was identified, indicating that the cracking mostly followed the isomerization. It is important that the isomer content of the liquid products (C_{5+}) was significantly higher on the Pt/AlSBA-15 catalyst than on the other catalyst at the same process parameters (Figure 1). We found that using the Pt/AlSBA-15 catalyst at advantageous combinations of reaction parameters (T= 300-325 °C (C_{11}-C_{20})/ 275-300 °C (C_{21}-C_{30}), P=40-80 bar, LHSV=1.0-2.0 h^{-1}) we can obtain C_{11}-C_{20} and C_{21}-C_{30} fractions, having high isoparaffin contents (63.5-85.6% and 34.1-58.7%) and adequate yields (29.9-36.6% and 46.2-58.8%). We experienced that the gas oil fractions having the lowest pour point were obtained at the highest concentrations of 5-methyl isomers. The C_{21}-C_{30} fraction can be used as environmentally friendly, high viscosity index (VI ≥ 125) base oil. These fractions are virtually free of sulfur-, aromatics- and nitrogen. The activity and isomerization selectivity of the catalysts did not change after 240 hours time on stream.

Conclusions

Owing to the higher isomerization and lower cracking activity the mesoporous Pt/AlSBA-15 catalyst the gas oil and base oil fractions obtained from FT wax had higher isoparaffin content than the corresponding product obtained using microporous Pt/MCM-22 zeolite catalyst. The lower cracking activity comes from the weaker acidity and the shorter residence time of the reactants and the products in the pore system.

References

[1] C. Bouchy, G. Hastoy, E. Guillon, J.A. Martens: „Fischer-Tropsch Waxes Upgrading via Hydrocracking and Selective Hydroisomerization", Oil & Gas Science and Technology, **2009**, 64, 91-112.

[2] Gamba, S., Pellegrini, L.A., Calemma, V., Gambaro, C.: „Liquid fuels from Fischer–Tropsch wax hydrocracking: Isomer distribution", Catalysis Today, 2010, 156 (1-2), 58-64.

[3] Kobayashi, M., Saitoh, M., Togawa, S., Ishida, K.: „Branching Structure of Diesel and Lubricant Base Oils Prepared by Isomerization/Hydrocracking of Fischer-Tropsch Waxes and α-Olefins", Energy & Fuels, **2009**, 23, 513-518.

[4] Deldari, H.: „Suitable catalysts for hydroisomerization of long-chain normal paraffins", Applied Catalysis A: General, **2005**, 293, 1-10.

[5] Rosetti, I., Gambaro, C., Calemma, V.: „Hydrocracking of long chain linear paraffins", Chemical Engineering Journal, 2008, doi:10.1016/j.cej.2009.03.018

[6] Vinu, A., Murugesan, V., Böhlmann, W., Hartmann, M.: „An Optimized Procedure for the Synthesis of AlSBA-15 with Large Pore Diameter and High Aluminum Content**",** J. Phys. Chem. B, **2004**, 108, 11496-11505.

Vanadium species supported on inorganic oxides as catalysts for propene epoxidation

A. Held, J. Kowalska-Ku?, K. Nowi?ska.

A. Mickiewicz University, Pozna?, Poland

Propylene oxide (PO) is an important intermediate still produced mainly by means of wasteful chlorhydrine technology, although the manufacture with hydrogen peroxide application has been developed in last decade. Recently, a new, environmentally friendly method based on N_2O oxidant appeared to be very promising. Vanadium modified silica containing materials (SBA-3, SBA-15, MCM-41, amorphous silica) showed significant activity in epoxidation of propylene with N_2O as an oxidant. In contrary, non silica oxides (Al_2O_3, TiO_2, MgO, MgF_2) applied as supports did not result in formation of active vanadium catalysts (PO yield was below 0.5%). SBA-3 containing micropores (diameter ~1.7 nm) appeared the best silica support for active vanadium species. PO yield for V/SBA-3 samples (with vanadium concentration equal to 1-2 wt. %) reached almost 8%. The monolayer vanadium loading was the most advantageous for selective propylene oxidation. The UV-Vis and IR spectra of adsorbed NO confirmed the formation of isolated vanadium species on the support surface. The broad range of reduction peaks at TPR profiles (430 - 615ºC) for the vanadium samples with different supports clearly indicates substantial differences in vanadium – support interaction.

Insertion of extraframework Fe species into zeolite T positions under NH_3-SCR conditions

S.M. Maier [a], A. Jentys [a], M. Janousch [b], J.A. van Bokhoven [c], J.A. Lercher [a]
TU München, Department of Chemistry, Catalysis Research Center, 85748 Garching, Germany [a]
Paul Scherrer Insitut, Swiss Light Source, 5323 Villigen PSI, Switzerland [b]
ETH, Institute for Chemical and Bioengineering, CH-8093 Zurich, Switzerland [c]
johannes.lercher@ch.tum.de

Introduction

Diesel engines prove to be among the most fuel efficient technologies, however, the formation and emission of NO_x to the atmosphere still presents considerable concerns with respect to acid rain and greenhouse gas formation. Previous studies showed that Fe-zeolites are promising catalysts for the reduction of NO_x using NH_3 as reducing agent (e.g., via aqueous solutions of urea) [1]. A major challenge in the application of these catalysts is the presence of different Fe oxide species and their relation to the catalytic activity [2]. In the contribution presented we focus on the changes of the Fe species under NH_3-SCR conditions in the presence of steam by a detailed characterization of the zeolite matrix and the Fe species. This leads us to the conclusion that extraframework Fe can be inserted into zeolite T-atom positions resulting in the generation of new Brønsted acid sites under the conditions of the NH_3-SCR reaction.

Experimental

The FeBEA catalysts were prepared by a single-step wet-ion exchange of HBEA (Si/Al = 18) in acidic media using $FeSO_4 \cdot 7H_2O$ as precursor salt and heat treated at 480°C in nitrogen. Afterwards the samples were steam treated under NH_3-SCR conditions corresponding to 1000 ppm NO, 1000 ppm NH_3, 5 % O_2 and 5% H_2O balanced in N_2 at temperatures between 450°C and 600°C. The concentration of acid sites as well as the distribution of Al in the obtained zeolites were characterized by IR spectroscopy of adsorbed pyridine, temperature programmed desorption of NH_3 and Al XANES. The nature of the Fe species was analyzed by IR spectroscopy, XAFS and UV/Vis spectroscopy.
The activity of the catalysts for the reduction of NO_x with NH_3 was studied in a flow reactor system in combination with IR spectroscopic gas analysis.

Results and discussion

The wet-ion exchange resulted in a FeBEA catalyst with high activity containing mainly isolated Fe ions in ion-exchange positions, which is proven by UV/Vis and XAFS measurements. The steam treatment under NH_3-SCR conditions led to an increase of the concentration of Brønsted acid sites while the concentration of Lewis acid sites decreased

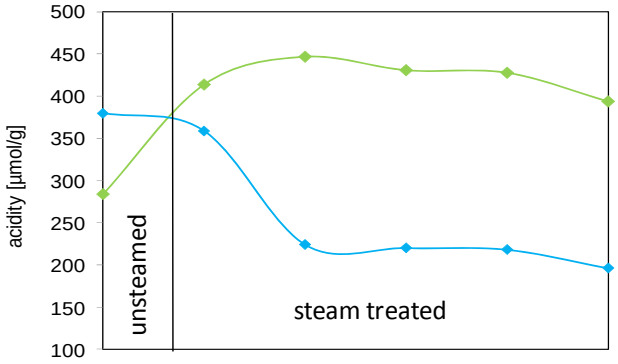

Figure 1: Concentration of Brønsted (green) and Lewis (blue) acid sites of the FeBEA samples.

by the same value. IR spectroscopy from adsorption of pyridine revealed that this decrease is mainly due to Lewis acid sites linked to Fe centers. The distribution of Al in the zeolite investigated by Al XANES showed that although the concentration of acid sites changed, the Al distribution remained constant throughout all steam treated samples.
UV/Vis spectroscopy indicated the formation of tetrahedral coordinated Fe species under the conditions of the NH_3-SCR reaction, which contradicts the expected aggregation of the Fe species to Fe_2O_3 clusters. This unexpected behavior could be explained by the insertion of extraframework Fe species into T atom positions of the zeolite framework. This can be understood in analogy to the insertion of Al into the zeolite framework under NH_3 atmosphere [3]. The analysis of the XAFS (at the Fe-edge) showed a decrease of the Fe-O distance from 2.15 Å for the untreated FeBEA samples to 1.86 Å for the steam treated sample. In addition, the NH_3-SCR treatment led to the increase of the pre-edge peak in Fe XANES, which is characteristic for Fe in tetrahedral coordination. The insertion of Fe species into framework positions could be further verified by IR spectroscopy, showing a transformation of the extraframework Fe-OH band at 3682 cm^{-1} to a band at 3627 cm^{-1} assigned to Fe-OH Brønsted acid sites. During this process, the concentration of silanol groups (3740 cm^{-1}) decreased due to the insertion of extraframework Fe into the silanol nests at structural defects.

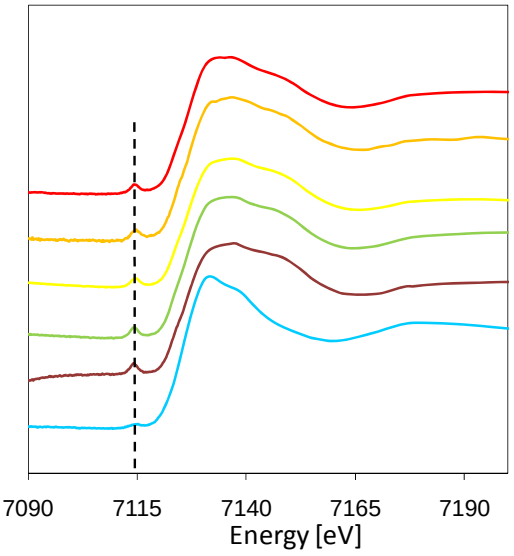

Figure 2: FeXANES of unsteamed (blue) and steamed FeBEA samples.

Conclusions

The influence of the reaction conditions of the NH_3-SCR reaction on FeBEA catalysts containing mainly isolated extraframework Fe ions was investigated. The Fe ions present at extraframework positions were incorporated into T atom positions in the zeolite framework which prevents the agglomeration of the Fe species to Fe_2O_3 clusters and also leads to the formation of additional Brønsted acid sites. These isomorphoursly substituted Fe atoms were found to be active in the NH_3-SCR reactions**.**

Acknowledgements

Portions of this research were carried out at the light source facility DORIS III at DESY, Hamburg, Germany. DESY is a member of the Helmholtz Association (HGF). We would like to thank Adam Webb in assistance in using beamline X1. Discussions in the framework of IDECAT are gratefully acknowledged. The project was funded by the Bayerisches Staatsministerium für Wissenschaft, Forschung und Kunst.

References

[1] R. Q. Long, R. T. Yang, J. Catal. 2000, 194, 80.
[2] M. Schwidder, M. Santhosh Kumar, U. Bentrup, J. Pérez-Ramírez, A. Brückner, W. Grünert, Microp. Mesop. Mater. 2008, 111, 124
[3] J. A. van Bokhoven; D. C. Koningsberger; P. Kunkeler; H. van Bekkum, *J. Catal.* **2002**, *211*, 540.

Desulfurization of FCC gasoline
Alkylation of 3-methylthiophene with olefins over acidic zeolites.

Benoit Dupuy, Frédéric Richard*, Sébastien Laforge, Patrick Magnoux.
Laboratoire de catalyse en chimie organique, UMR 6503 CNRS - Université de Poitiers, 40 Avenue du Recteur Pineau, 86022 Poitiers Cedex, France

E-mail: frederic.richard@univ-poitiers.fr

Introduction

Deep desulfurization of gasoline is an important research topic in order to reduce the sulfur content (less than 10 ppm since 2009 [1]). Indeed sulfur components lead to the formation of SOx, which are responsible of acidic rains, but also act as a poison affecting the activity of catalytic converters. About 90% of the sulfur in gasoline comes from FCC naphta, which represents more than 25 %vol. of the typical gasoline pool in Western Europe. Therefore, deep desulfurization of gasoline is needed to reduce the sulfur content in FCC naphta. In order to limit the consumption of olefins, which are responsible of the good octane number of gasoline cut, desulfurization of this feedstock can be possible by increasing the weight of the sulfur impurities through alkylation with olefins. Therefore, the alkylated sulfur compounds can be concentrated in the heavier fractions of gasoline streams and finally separated by distillation. This process, namely Olefinic Alkylation of Thiophenic Sulfur (OATS), has been developed by British Petroleum [2]. The catalysts could be used are supported phosphoric acid (SPA) [3], zeolites [4] and supported heteropolyacids [5].

The aim of the present contribution is to evaluate the activity and the selectivity of three acidic zeolites (HY, HBEA and HMCM-22) for the alkylation of 3-methylthiophene (3MT) with two olefins (hex-1-ene and 2-methylpent-1-ene) chosen as model molecules representative of sulfur and olefins compounds, respectively, likely to be present in the FCC naptha.

Experimental

The experiments were carried out at 120°C in a fixed bed reactor under atmospheric pressure. The molar ratio 3MT/olefins was kept constant and equal to 0.3. The weight of the catalysts was varied between 0.05 g and 0.2 g. Before each experiment, the zeolites were activated at 450°C under air flow. The reaction products were analyzed by gas chromatography.

After reaction, the products slightly adsorbed onto the catalysts were eliminated by a soxhlet extraction. The products strongly adsorbed or blocked in the zeolite pores were analyzed after dissolution of the zeolites in a hydrofluoric acid solution as described in literature [6].

Results and discussion

In a first time, pure reactant transformations were carried out over the three zeolites (HY, HBEA and HMCM-22) which present similar Brønsted acidities. In these conditions, 3MT was unreactive whereas hex-1-ene (H1N) and 2-methylpent-1-ene (2M1P) were totally converted initially. Nevertheless, a complete deactivation of all zeolites was observed after 6 hours on stream during the transformation of H1N. On the opposite, the catalysts were stable during the transformation of 2M1P. For both alkenes, double bond isomerization and

dimerization products were observed. In the case of H1N, the reaction products were essentially composed of hex-2-enes and hex-3-enes, whereas 2M1P mainly led to the formation of 2-methylpent-2-ene.

In the second time, the transformation of mixtures of 3MT and alkenes was carried out over the three zeolites. As expected, in presence of 2M1P, the alkylation of 3MT was more important than the one observed in presence of H1N whatever the zeolite, as shown in Fig. 1. These results can be explained by a different stability of the reaction intermediates involved. Indeed, the protonation of 2M1P leads to the formation of a tertiary carbocation which is more stable and reactive than the carbocations formed from H1N. In the case of the use of 2M1P as alkylating agent, HMCM-22 was the more active (Fig. 1), and HBEA was the more selective in monoalkylated products (Fig. 2). This could be related to the location of active sites in both zeolites. In the case of the HBEA zeolite, these sites are only inside the pores, allowing a good selectivity in monoalkylation due to steric constraints. Over HMCM-22, a significant proportion of sites is located on external surface [7] leading to a better activity but a lower selectivity in monoalkylation. Finally, HY seems to be as active as HBEA initially, but the deactivation of HY was the most significant. This can be explained by the formation of polyalkylated species, favoured by the presence of large pores in HY, which remained trapped inside the zeolite and inhibited the access to the active sites.

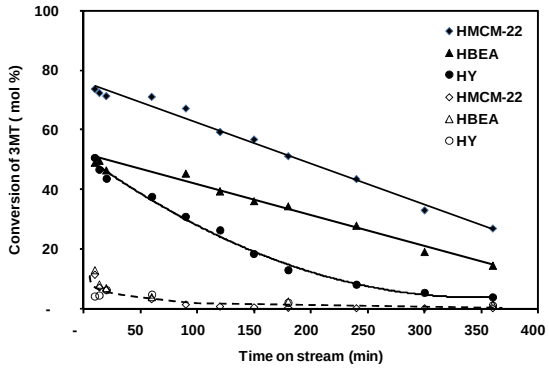

Figure 1: Conversion of 3MT in presence of H1N (empty symbol) and 2M1P (full symbol) over zeolites

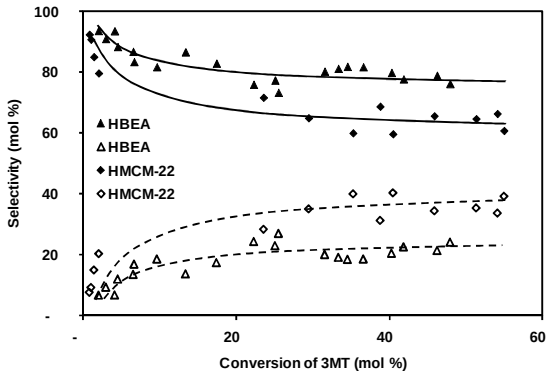

Figure 2: Selectivity of monoalkylated (solid line) and dialkylated (dotted line) products for the alkylation of 3MT by 2M1P

Conclusions

In this work, HBEA and HMCM-22 zeolites were shown to be active in alkylation of 3-methylthiophene by 2-methylpent-1-ene, HBEA being more selective in monoalkylated products which limit the olefins consumption. Nevertheless, whatever the zeolite, a very important deactivation was observed. The use of other acidic solids as heteropolyanions or sulfonic resins will be considered in further experiments.

Acknowledgements

Benoit Dupuy thanks the “Agence Nationale de la Recherche” for his PhD grant.

References

[1] Official Journal of the European Union 76 (2003) 10
[2] Wiltshire J., BP Technol. Mag. 32 (2000) 10
[3] Bellière V, Lorentz C., Geantet C., Yosimura Y., Laurenti D., Vrinat M., Appl. Catal. B 64 (2006) 254
[4] Zhang Z., Liu S., Zhu X., Wang Q., Xu L., Fuel Process. Tech. 89 (2008) 103-110
[5] Arias M., Laurenti D., Bellière V., Geantet C., Vrinat M., Yoshimura Y., Appl. Catal. A 348 (2008) 142
[6] Guisnet M. and Magnoux P., Appl. Catal. 54 (1989) 1
[7] Laforge S., Martin D., Guisnet M., Micropor. Mesopor. Mater. 67 (2004) 235

Beneficial effect of coke via radical formation for ethanol transformation into hydrocarbons

Karima Ben Tayeb[1], Ludovic Pinard[1*], Sébastien Laforge[1], Christine Canaff[1], Patrick Magnoux[1], Sylvie Maury[2], Nicolas Cadran[2], Olivier Delpoux[2], Hervé Vezin[3], Nadia Touati[3]
[1] *LACCO, UMR 6503, Université de Poitiers, 86022 Poitiers Cedex, France ;*
e-mail : Ludovic.pinard@univ-poitiers.fr
[2] *IFP-Lyon, Rond point de l'échangeur de Solaize, BP 3, 69390 Vernaison, France.*
[3] *LASIR, UMR 8516, Université des Sciences et Technologies de Lille, 59655 Villeneuve d'Ascq Cedex, France.*

Introduction

Due to the rise and instability of oil prices, the development of biofuels becomes primordial for all industrialized countries. Among all the alternatives, ethanol emerges as a viable source [1, 2]. Although it can be naturally added to the gasoline pool, its incorporation at high contents requires the modification of the motorisation systems, and so, its transformation becomes a more viable and realistic alternative.

In a previous study [3, 4], HZSM-5 zeolite was found to be a very stable catalyst for the ethanol transformation into hydrocarbons at 350°C and at high pressure (30 bar). After 24 hours of reaction, ethanol was still totally transformed into hydrocarbons in spite of a near total loss of Brønsted acidity, 92% loss of microporosity and high coke content inside its micropore volume. Experiments have shown that the hydrocarbons formation does not occur at the external surface but probably at the pore mouth of the channel. Ethanol conversion into hydrocarbons could proceed, as for the methanol transformation into hydrocarbons, either by the hydrocarbon pool mechanism or by a radical mechanism. Carbon centered radicals were detected by EPR-CW analysis after 24 hours of reaction indicating that a radical mechanism may occurs in pore mouth of the channel. Moreover, this mechanism can provide an explanation of the high conversion over HZSM-5 despite an important loss of its acidity and porosity. Nevertheless, it remains to be established whether these radical species actually do participate in the hydrocarbons formation and also to be determined when and how radicals are generated.

The goal of this work is to study the formation and the nature of the radical species responsible to the ethylene oligomerization.

Experimental

The ethanol transformation was carried at 350°C under nitrogen in a fixed bed reactor at a total pressure of 30 bar with a molar ratio N_2/ethanol of 4. A gas flow of 3.3L.h^{-1} was kept during the reaction and commercial ethanol (96%v/v) was fed at a GHSV of 5.3h^{-1}. The reaction products were analyzed by on-line gas chromatography equipped with a PONA capillary column, which allows the identification of all hydrocarbons. In addition to on-line analysis, the liquid is also recovered and analyzed by GC-MS spectroscopy.

The catalysts were characterized before and after reaction by different spectroscopy techniques, such as IR and EPR analysis. Coke deposit over the spent catalysts was extracted using HF/CH_2Cl_2 and analyzed by GC-MS.

Results and discussion

Under our operating conditions, ethanol was totally converted into ethylene, C_{3+} hydrocarbons, water and traces of diethyl ether. No deactivation for ethanol conversion was observed (even after 24h of running). During the first hour, the yield into ethylene decreases progressively coinciding with the C_{3+} hydrocarbons yield increase. The C_{3+} hydrocarbons are divided into three fractions according to the carbon number: C_3-C_4 (methane and ethane are produced in negligible amounts), C_5-C_{11} and C_{12+}; and also divided according to their chemical family: Paraffin, Olefin, Naphtene, and Aromatic (PONA). Table 1 reports the

fractions selectivity evolution versus the time-on-stream. The amount of C_3-C_4 fraction decreases with the increase of C_5-C_{11} and C_{12+} fractions. The products become more and more aromatics. This change in products selectivity with the TOS coincides with a change in the physico-chemical properties of the HZSM-5(40). As expected, the decrease of the micropore volume and the number of acid sites is due to the increase of the carbon deposit (coke) inside the catalyst (Table 2). The nature of the carbon deposit changes also with the TOS. Initially, it is composed only of highly alkylated mono aromatics which are then transformed into more condensed aromatics such as alkylated naphtalenes and molecules with 3 aromatic rings. Thus, the coke is both responsible for the poisoning of Brønsted acid sites and pore blockage, as well as the appearance of free radicals. Indeed, the CW-EPR measurements have shown, on the coked samples, a well-defined paramagnetic signal which is proportional to the carbon content. Moreover the width of the paramagnetic signal changes with TOS which suggests a change in the radical species nature as it was already observed with the coke composition evolution. The increase of the radical species amount could be responsible to the increase of ethanol aromatization with TOS.

Table 1. Evolution of the products selectivity with TOS.

TOS (min)	C_2H_4	C_3-C_4	C_5-C_{11}	C_{12+}	Paraffins	Aromatics
5	6.5	27.1	54.2	12.2	18	39
10	4	17.8	67.7	10.5	19	55
60	0	2.9	78.9	18.2	7	82

Table 2. Evolution of the physico-chemical properties on HZSM-5(40) zeolite with TOS.

TOS (min)	Brønsted acidity (µmol/g)	Micropore volume (cm^3/g)	Carbon content (wt%)	Amount of radical species (µmol/g)
0	297	0.177	0	0
5	265	0.132	1.4	0.3
10	213	0.120	1.5	0.6
60	241	0.098	2.3	1.1

Conclusion

HZSM-5 (40) zeolite is very stable for the ethanol transformation into hydrocarbons at 350°C and 30 bar total pressure in spite of a loss of Brønsted acidity and microporosity with time-on-stream by coke formation. The coke is composed of alkyl aromatic hydrocarbons which is occluded in the zeolite structure and generates long lived stable radical species. We suppose that radicals play an important role in the ethanol oligomerization (aromatization). Nevertheless, it remains to be established the importance of the radical reaction compared to the acid mechanism commonly admitted.

Acknowledgements

Karima Ben Tayeb thanks IFP Energies nouvelles for financial support.

References

[1] Aguayo, A.T., Gayubo, A. G., Study of operating variables in the transformation aqueous ethanol into hydrocarbons on an HZSM-5 zeolite, Journal of Chemical Technology and Biotechnology, 77 (2002), 211-216.
[2] Nguyen, T. M., Le Van Mao, R., Conversion of ethanol in aqueous solution over ZSM-5 zeolites. Study of the reaction network, Applied Catalysis, 58 (1990), 119-129.
[3] Ferreira Madeira, F., Gnep, N. S., Magnoux, P., Maury, S., Cadran, N., Ethanol transformation over HFAU, HBEA and HMFI zeolites presenting similar Brønsted acidity, Applied Catalysis. A, 367 (2009), 39-46.
[4] Ferreira Madeira, F., Gnep, N. S., Magnoux, P., Vezin, H., Maury, S., Cadran, N., Mechanistic insights on the ethanol transformation into hydrocarbons over HZSM-5 zeolite, Chemical Engineering Journal, 161 (2010), 403-408.

Scorpionate complexes supported in desilicated MOR zeolite. Catalytic oxidation of cyclohexane in heterogeneous medium

A. Martins[a,b*], R. Monteiro[a], M. Andrade[c], A.P. Carvalho[c], L.M.D.R.S. Martins[a,d], T.F.S. Silva[d], E.A.B. Alegria[a,d], A.J.L. Pombeiro[d]
[a]*ADEQ, ISEL, Rua Conselheiro Emídio Navarro, 1, 1959-007 Lisboa, Portugal*
[b]*CIEQB, ISEL, Rua Conselheiro Emídio Navarro, 1, 1959-007 Lisboa, Portugal*
[c]*DQB and CQB, FCUL, Campo Grande C8, 1749-016, Lisboa, Portugal.*
[d]*CQE, Complexo I, IST, Av. Rovisco Pais, 1049-001 Lisboa, Portugal*
[*]*amartins@deq.isel.ipl.pt*

Introduction

Nowadays the present environmental regulation led to significant modifications of industrial processes. In order to reduce or eliminate solvents several chemical reactions that occurred in the presence of homogeneous catalysts have been replaced by cleaner processes using heterogeneous ones. In this sense, one of the most used strategies is the immobilization of the catalysts in materials with high surface area that can behave as supports. Due to the intrinsic microporosity of zeolites it is often difficult to accommodate large molecules inside its porous structure. Recently a new methodology - desilication - was developed with the purpose of create larger pores (mesopores or larger micropores) in zeolite structures using an alkaline treatment.
C-scorpionate ligands *e.g.*, $HCpz_3$ (Tpm) and derivatives are undoubtedly among the most important face-capping, six-electron N-donor ligands in coordination chemistry, having applications in diverse fields ranging from catalysis to supramolecular chemistry. In fact, our recently prepared C-scorpionate metal transition complexes have shown their ability as catalysts in several industrial reactions such as the partial oxidation of gaseous and liquid alkanes.
The scope of this work is to study the potentialities of desilicated MOR zeolite as support for C-scorpionate complexes and to evaluate the behavior of the immobilized complexes as heterogeneous catalysts. The catalytic behavior is explored for the industrially significant peroxidative oxidation of cyclohexane to cyclohexanol and cyclohexanone, under mild conditions, as an alternative for the industrial process that uses homogeneous Co catalysts and dioxygen as oxidant, at a considerably high temperature of 150 ºC. The obtained results are compared to the ones obtained in homogeneous medium.

Experimental

MOR zeolite, from Zeolyst (Si/Al = 10) was submitted to alkaline treatment at 85ºC, for 2 h using NaOH 0.5M, according to the procedure described in the literature [1]. Hydrotris(pyrazolyl)methane complexes $[MCl_n\{HC(pz)_3\}]$ [M=V (**1**) or Re (**2**), n=3; M=Fe (**3**), n=2; pz=pyrazolyl] or C-functionalized derivatives $[CuCl_2\{HOCH_2C(pz)_3\}]$ (**4**) and $[VOCl_2(TpmPy)]$ [TpmPy=4-((tris-2,2,2-(pyrazol-1-yl)ethoxy)methyl)pyridine] (**5**) were prepared according to published methods [2].
The scorpionate complexes **1**-**5** were immobilized in parent and desilicated MOR zeolite supports, using the wet-impregnation method, using the same procedure reported in a previous study [3].
The supports and the heterogeneous catalysts were characterized by powder X-ray diffraction, (Philips PW 1710 diffractometer) and low temperature N_2 adsorption (ASAP2010). The oxidation reactions were carried out in Schlenk tubes and under N_2, according to a method

used for homogeneous scorpionate catalysts [2]. Products were analyzed by GC (internal standard method) at a FISONS Instruments GC 8000 series gas chromatograph with a FID detector and a DB-WAX capillary column. Blank experiments confirm that no cyclohexanol or cyclohexanone are formed without the metal catalyst.

Results and discussion

The characterization of the supports by powder X-ray diffraction denotes some lost of crystalinity of the zeolite upon desilication. However, after the immobilization of the complexes the crystalinity of the samples is practically unchanged. The results of N_2 adsorption on the supports demonstrate that the alkaline treatment promoted the generation of mesoporosity, according to the mesoporous volumes (V_{meso}), 0.05 $cm^3\ g^{-1}$ for MOR and 0.21 $cm^3\ g^{-1}$ for desilicated MOR.
Scorpionate complexes **1**-**5** are shown to act as catalysts or catalyst precursors for the partial oxidation of cyclohexane to the cyclohexanol and cyclohexanone mixture, at room temperature and using an aqueous solution of H_2O_2 as the oxidant, reaching TON values from 100 - 700. Concerning the metal center, their activity follows the sequence V, Cu, Re and Fe.
The heterogeneous systems exhibited a catalytic activity, under mild conditions, similar to that found for the homogeneous C-scorpionate complexes, with TONS up to 700. Studies of reproducibly, catalyst recycling and lixiviation are presented.

Conclusions

The generation of mesoporosity by desilication treatments revealed to be a good strategy to improve the anchorage of the scorpionate complexes on the zeolitic support.
The immobilized C-scorpionate complexes appear to be an improved way to achieve the oxidation of cyclohexane to the cyclohexanol and cyclohexanone mixture, under mild conditions.

Acknowledgements

This work has been partially supported by the Foundation for Science and Technology (FCT) and its PPCDT (FEDER funded) programme.

References

[1] Paixão, V., R., Carvalho, A.P., Rocha, J., Fernandes, A., Martins' A., Modification of MOR by desilication treatments: structural, textural and acidic characterization. Microporous and Mesoporous Materials, 131 (2010) 350-357.
[2] a) Wanke, R; Guedes da Silva, M.F.C. Lancianesi, S., Silva, T.F.S. Martins, L.M.D.R.S., Pettinari, C. Pombeiro, A.J.L., Synthesis and Coordination Chemistry of a new N_4-polidentate class of pyridyl-functionalized scorpionate ligands: complexes of Fe^{II}, Zn^{II}, Ni^{II}, V^{IV}, Pd^{II} and use for hetero-bimetallic systems, Inorg. Chem., 49 (2010) 7941-7952. b) Silva, T.F.S. Mishra, G.S. Guedes da Silva, M.F. Wanke, R; Martins, L.M.D.R.S. Pombeiro, A.J.L, Cu^{II} complexes bearing the 2,2,2-tris(1-pyrazolyl)ethanol or 2,2,2-tris(1-pyrazolyl)ethyl methanesulfonate scorpionates. X-ray structural characterization and application in the mild catalytic peroxidative oxidation of cyclohexane, Dalton Trans.(2009) 9207-9215 c) Silva, T.F.S., Alegria, C.B. Martins, L.M.D.R.S. Pombeiro, A.J.L, Scorpionate Vanadium, Iron and Copper Complexes as Selective Catalysts for the Peroxydative Oxidation of Cyclohexane under Mild Conditions, Adv. Synth. Cat., 350 (2008) 706-716. d) Alegria, E.C.B.A., Martins, L.M.D.R.S., Haukka, M., Pombeiro, A.J.L., Rhenium Complexes of Tris(pyrazolyl)methanes and Sulfonate Derivative, Dalton Trans. (2006) 4954-4961.
[3] Mishra, G.S., Alegria, C.B., Martins, L.M.D.R.S., Pombeiro, A.J.L, Cyclohexane oxidation with dioxigen catalysed by supported pyrazole rhenium complexes, J. Mol. Cat., A, 285 (2008) 92-100.

Catalytic cracking of hexane over MCM-68 zeolite

Yoshihiro Kubota,[a] Satoshi Inagaki,[a,b] Kazuyoshi Takechi,[a]
[a] *Division of Materials Science and Chemical Engineering, Yokohama National University, 79-5 Tokiwadai, Hodogaya-ku, Yokohama 240-8501, Japan. E-mail: kubota@ynu.ac.jp*
[b] *Interdisciplinary Research Center, Yokohama National University, 79-5 Tokiwadai, Hodogaya-ku, Yokohama 240-8501, Japan*

Introduction

MCM-68 zeolite (**MSE**) is a new type of three-dimensional zeolite with a 12×10×10-MR channel system that was reported by Mobil researchers [1,2]. The zeolite has a characteristic structure in which a 12-MR straight channel intersects with two independent tortuous 10-MR channels and has a super cage (18-MR×12-MR), which is accessible only through 10-MR channels [3]. The features of the MCM-68 zeolite are attracting attention [4-7] because there are only a handful of zeolites that contain three-dimensional channel systems with large pores.

In order to simplify the complicated aspects of the catalytic cracking of naphtha, the cracking of *n*-alkane, especially *n*-hexane, is often examined as a model reaction [8,9]. In this work, we have investigated the catalytic properties of Al-MCM-68 and dealuminated MCM-68 for hexane cracking, and in particular the selectivity for propylene, compared with other various zeolite catalysts [10].

Experimental

MCM-68 zeolite (**MSE**) was synthesized by known methods [3-5]. The calcined MCM-68 was treated with aqueous NH_4NO_3 solution to obtain NH_4^+-form MCM-68, which was calcined at 550 ºC for 6 h. The obtained H-MCM-68 (Si/Al = 13) was used as a catalyst in the cracking of hexane. The dealumination of the calcined MCM-68 (Si/Al = 13) was carried out by treating with 0.5*N* HNO_3 solution at 80 ºC for 2 h. The dealuminated MCM-68 (Si/Al = 51) was used in the catalytic reaction. ZSM-5 (**MFI**, JRC-Z5-90H, Si/Al = 45) and mordenite (**MOR**, JRC-Z-HM90, Si/Al = 45) were used without any pre-treatment. Dealuminated zeolite beta (***BEA**, Si/Al = 41) was prepared by the HNO_3 treatment of parent zeolite beta (HSZ-940 HOA, Tosoh, Si/Al = 19).

The cracking of hexane was performed under atmospheric pressure in a down-flow quartz-tube microreactor. Prior to running the reaction, 100 mg of catalyst pellets were packed in a fixed-bed of the reactor, and preheated at 650 ºC for 1 h in a stream of air. The reaction was performed at 450, 500, 550 and 600 ºC for 70 min at each temperature (W/F = 12.1 g-cat. h (mol-hexane)$^{-1}$). The reactants and products were separated by a capillary column and analyzed by using GC-14B (Shimadzu) with a flame-ionization detector. The conversion of hexane and the selectivity to each product are calculated on the carbon-basis of the initial amount of hexane.

Results and discussion

Figure 1 shows the product distributions for hexane cracking over various zeolite catalysts. In all the zeolite catalysts tested, selectivity to propylene was fairly constant, even after deactivation due to coking, and slight production of methane and benzene was observed at reaction temperatures higher than 550 ºC. Hereafter, the initial selectivity after 5 min of time on stream at each temperature is discussed with a focus on the propylene selectivity. MCM-68(13) had a lower selectivity of 22% to propylene at 450 ºC. As the reaction temperature increased, the selectivity to propylene catalyzed by MCM-68(13) gradually increased up to 39% at 600 ºC. It should be noted that the dealuminated MCM-68(51) had a higher

selectivity of 45–50% to propylene, at all the reaction temperatures examined, from 450 to 600 ºC. Such high propylene selectivity up to 45% was hardly observed in the other zeolite catalysts examined in this study, and the high propylene selectivity could be correlated to the characteristics of the pore systems as well as Al distribution of .the dealuminated MCM-68 catalyst.

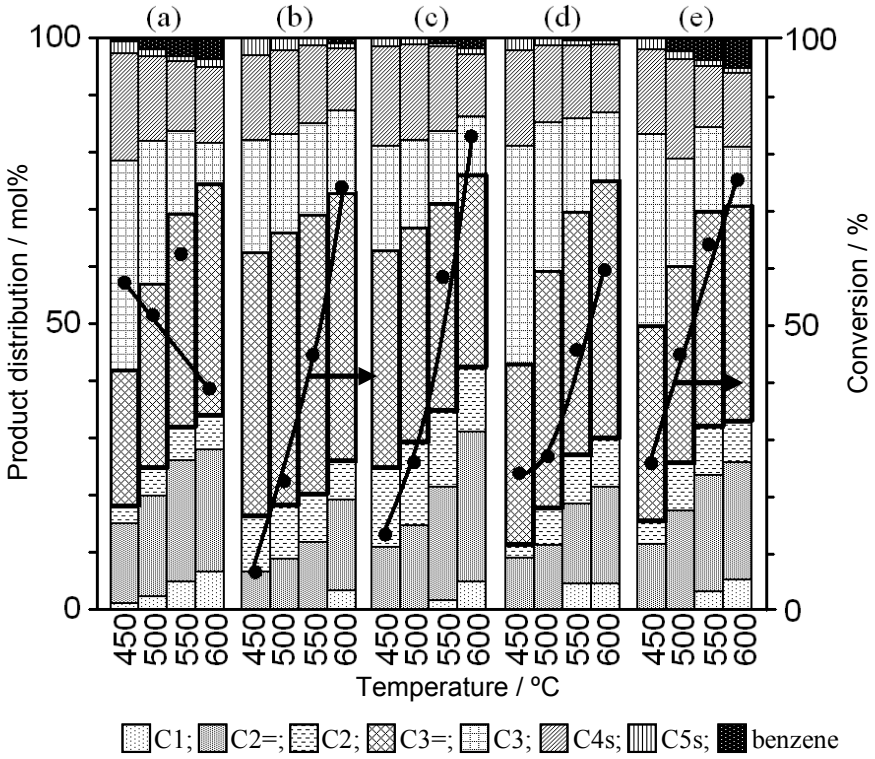

Figure 1 Hexane conversion and product distributions for hexane cracking over various zeolite catalysts after 5 min of time on stream.
(a) MCM-68(13), (b) dealuminated MCM-68(51), (c) ZSM-5(45), (d) morndenite(45) and (e) dealuminated beta(41).

Conclusions

Dealuminated MCM-68(51) exhibited sufficient catalytic activity and durability to coke formation for hexane cracking from 450 to 600 ºC, whereas significant deactivation due to coke formation was observed for Al-rich MCM-68(13). Dealuminated MCM-68(51) also had higher propylene selectivity of 45–50 % in comparison with ZSM-5(45) and other zeolite catalysts tested at the reaction temperatures of 450 to 600 ºC.

References

[1] Ch. Baerlocher, L. B. McCusker and D. H. Olson, Atlas of Zeolite Framework Types, Elsevier, Amsterdam, 6th edn, 2007, see also: http://www.iza-structure.org/databases/.
[2] D.C. Calabro, J.C. Cheng, R.A. Crane Jr., C.T. Kresge, S.S. Dhingra, M.A. Steckel, D.L. Stern, S.C. Weston, U.S. Pat., 2000, 6 049 018.
[3] D.L. Dorset, S.C.Weston, S.S. Dhingra, *J. Phys. Chem. B*, 110 (2006) 2045.
[4] T. Shibata, S. Suzuki, H. Kawagoe, K. Komura, Y. Kubota, Y. Sugi, J.-H. Kim, G. Seo, *Microporous Mesoporous Mater.,* 116 (2008) 216.
[5] T. Shibata, H. Kawagoe, H. Naiki, K. Komura, Y. Kubota, Y. Sugi, *J. Mol. Catal. A*, 297 (2009) 80.
[6] S. Ernst, S. P. Elangovan, M. Gerstner, M. Hartmann, S. Sauerbeck, *Abstr. 14th Int. Zeol. Conf.* 2004, 982.
[7] S. P. Elangovan, M. Ogura, S. Ernst, M. Hartmann, S. Tontisirin, M. E. Davis, T. Okubo, *Microporous Mesoporous Mater.*, 96 (2006) 210.
[8] S.M. Babitz, B.A. Williams, J.T. Miller, R.Q. Snurr, W.O. Haag, H.H. Kung, *Appl. Catal. A*, 179 (1999) 71.
[9] T.F. Narbeshuber, H. Vinek, J.A. Lercher, *J. Catal.*, 157 (1995) 388.
[10] S. Inagaki, K. Takechi, Y. Kubota, Chem. Commun., 46 (2010) 2662.

Oxygen mobility enhancement over ceria/zeolite hybrid catalysts: catalytic air pollution abatement application.

I. Maupin, J. Mijoin, J. Barbier Jr., N. Bion, T. Belin, P. Magnoux
Laboratoire de Catalyse en Chimie Organique, UMR CNRS 6503, Faculté des Sciences, Université de Poitiers, 40 avenue du Recteur Pineau, 86022 Poitiers Cedex, France,
irene.maupin@univ-poitiers.fr

Introduction

For several years, many conventions have tried to heighten public awareness of the danger that Volatile Organic Compounds (VOCs), harmful pollutants for environment and toxic for human, represent [1]. According to the nature and the concentration of the VOCs, thermal incineration, catalytic oxidation and various recovery methods are some of the used techniques. Catalytic oxidation presents the advantage of decreasing the working temperatures and consequently the costs, and limiting the nitrous oxides formation [1-2].
Among potential catalysts, ceria (CeO_2) is well-known for its efficiency in oxidation assigned to its strong oxygen mobility [3]. On another side, basic zeolites and particularly faujasites (NaX) ones proved their capacities in VOCs catalytic oxidation [4-5]. Thanks to high zeolites porosity, organic molecules to treat spend more time near active sites and catalysts efficiency can be improved.
The main part of this work was the preparation of hybrid catalysts with strong oxygen mobility - oxygen storage capacities and oxygen exchange - and high porosity. Keeping the zeolite regeneration capacity and its poisoning resistance were also taken into account.
Catalytic experiments were performed with isopropanol to check the mixture interest in oxidation.

Experimental

Hybrid catalysts were synthesized mixing ceria and zeolite in various mass ratios (10, 20, 35, 50, 65 and 80 wt% ceria). Several preparation method were tested: mechanical mixture (M), high temperature treatment preceded (HT) or not (C) by sieving and dry impregnations in oven (IE), under vacuum (IV) and in oven under vacuum (IEV).
Acidity was characterized by pyridine adsorption followed by FTIR spectroscopy. Pore sizes distribution, pore volumes and specific surface areas were determined by N_2-physisorption. Structure, crystallinity and particle sizes were calculated with reference to XRD analyses. Oxygen storage capacities were measured following carbon monoxide oxidation in transitory regime without oxygen in gas phase (Oxygen Storage Complete Capacity OSCC and Oxygen Storage Capacity in dynamic conditions OSC). Temperature-programmed isotopic exchange (TPIE) and isothermal isotopic exchange (IIE) of oxygen were followed by mass spectrometry.
The gaseous feed used for catalytic combustion experiments was composed of 1360 ppm of isopropanol in synthetic and wet air. After catalyst activation, the reaction was carried out at constant temperature (between 120 and 450°C) in a fixed bed reactor at atmospheric pressure and followed for 5 hours.

Results and discussion

The crystallographic structure of each compound does not seem to be affected by the preparation since significant peaks of ceria and faujasite are still visible in each XRD spectrum. The main part of ceria seems to be deposited on the zeolite external surface.

The presence of ceria even in low amount seems to enhance the average pore size, near the one of pure ceria, and the pore sizes distribution varies with the preparation method.
Moreover, the hybrid catalysts present higher oxygen storage capacities especially in dynamic conditions (Fig.1).

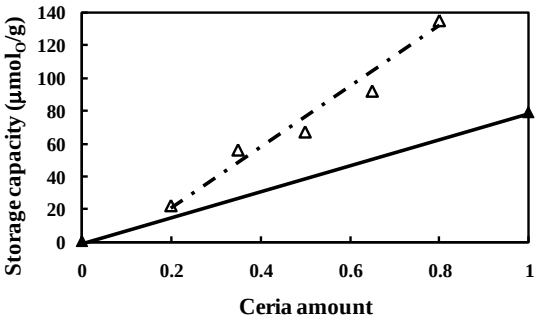

Figure 1: Interpolated values (▲) and experimental results (△) for OSC.

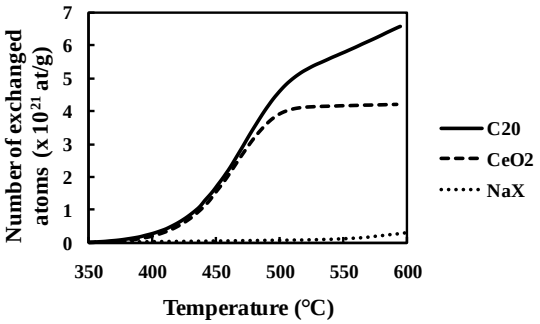

Figure 2: Ne determination in TPIE over ceria, NaX and one hybrid catalyst (C20).

Comparing the behavior of parent NaX zeolite and ceria samples to the one of C20 hybrid catalyst, it appears that the number of oxygen atoms exchanged (Ne) is largely superior to the expected one, considering the Ne addition in both ceria and NaX compounds (Fig.2), as corroborated by IIE experiments at 450 and 550°C. The oxygen exchange enhancement can be due to the ceria presence which could exalt the oxygen mobility of the zeolite skeleton like showed by Chang *and al.* on transition metal loaded zeolites [6]. Moreover, we compared the $^{16}O_2$ and $^{16}O^{18}O$ partial pressures ratio of ceria and C20. At low temperatures, it is below 1 for the two solids while it becomes superior to 1 for C20 at higher temperatures. This indicates a simple heteroexchange at low temperatures over both solids and a new mechanism (a multiple exchange) from 500°C over C20.
In addition, a synergy effect was observed over HT50 and C50 in isopropanol combustion with a significant T_{50} decrease (225 to 190°C) compared to CeO_2/SiO_2(1:1) catalyst, prepared by mechanical mixture in equal mass ratio. Unfortunately, CO_2 yields and lightoff temperatures do not present a logical trend in relation to ceria amount.

Conclusions

Several factors are involved in catalytic performances as oxygen storage capacity and oxygen mobility. Mixing ceria and zeolite properties led to high increasing of both parameters, probably due to a better mobility of NaX skeleton oxygen.
However this behavior is not sufficient to ensure efficient catalytic results. Further studies will be necessary to clarify the catalysts behavior.

References

[1] Le Cloirec, P., Les composes organiques volatils (COV) dans l'environnement, in P. Le Cloirec (Editor), Technique et Documentation, Paris, 1998, Chap.1
[2] Moretti, E. C., Reduce VOC and HAP emissions, Chemical Engineering Progress, 98 (2002) 30-40
[3] Dai, Q., Wang, X., Lu, G., Low-termperature catalytic destruction of chlorinated VOCs over cerium oxide, Catalysis Communications, 8 (2007) 1645-1649
[4] Beauchet, R., Magnoux, P., Mijoin, J., Catalytic oxidation of volatile organic compounds (VOCs) mixture (isopropanol/o-xylene) on zeolite catalysts, Catalysis Today, 124 (2007) 118-123
[5] Pinard, L., Magnoux, P., Ayrault, P., Guisnet, M., Oxidation of chlorinated hydrocarbons over zeolite catalysts 2. Comparative study of dichloromethane transformation over NaX and NaY zeolites, Journal of Catalysis, 221 (2004) 662-665
[6] Chang, Y.-F., Somorjai, G. A., Heinemann, H., An $^{18}O_2$ temperature-programmed isotope exchange study of transition-metal-containing ZSM-5 zeolites used for oxydehydrogenation of ethane, Journal of Catalysis, 154 (1995) 24-32

Mössbauer studies of the nature and redox properties of Fe species in iron ferrierite catalysts

Edyta Tabor[a*], Karel Závěta[b], Zdeňka Tvarůžková[a], Zdeněk Sobalík[a]

J. Heyrovský Institute of Physical Chemistry of the ASCR, v. v. i.,
Dolejškova 3, CZ-182 23 Prague 8, Czech Republic
[b]Joint Laboratory for Mössbauer Spectroscopy, Faculty of Mathematics and Physics,
Charles University in Prague, V Holešovičkách 2, CZ -180 00 Prague 8, Czech Republic
**Corresponding author. E-mail address: edyta.tabor@jh-inst.cas.cz*

Introduction

Due to their unique redox properties, iron zeolites exhibit high catalytic activity in several reactions as selective catalytic reduction of nitrogen oxide by hydrocarbons [1-3]. Among the zeolite family, ferrierites (FER) with low iron loading exhibited excellent catalytic properties in N_2O decomposition in the absence of NO. Nevertheless, the structure of the iron active sites playing curtail role in N_2O decomposition is still matter of discussion. Mössbauer spectroscopy is the excellent tool for characterization of iron species [4,5]. Using this method the oxidation state of iron as well as coordination around of iron species can be analyzed. The goal of this work was identification of the nature of iron species in Fe-FER with low iron loading and monitoring of their redox behavior under O_2 and N_2O treatment. This analysis could be the base for determination of the relationship between structure of the iron site in FER and their catalytic activity in N_2O decomposition.

Experimental

Iron ferrierites were prepared using synthesis method based on the impregnation of FER by acetylacetone solution of $^{57}FeCl_3$ [4]. In all syntheses, isotopically enriched $^{57}FeCl_3$ (prepared from iron oxide with ^{57}Fe enrichment over 96 %; Isoflex, U.S.) was used. The samples of iron ferrierite with Fe/Al molar ratio of 0.018, 0.036, 0.072 and 0.30 were denoted as Fe-$FER_{0.018}$, Fe-$FER_{0.036}$, Fe-$FER_{0.072}$, and Fe-$FER_{>0.30}$ respectively. The FTIR and UV-Vis spectroscopy was used to support the Mössbauer results. The N_2O decomposition was measured using fixed-bed plug flow-through micro-reactor in the temperature range 350 – 450 °C.

Results and discussion

Iron ferrierites with low iron lading Fe/Al = 0.018., 0.036, 0.072 were used as model catalyst for N_2O decomposition in the absence of NO. In spite of the low iron loading the investigated catalysts exhibited a high catalytic activity in N_2O; the results are displayed in Fig. 1. By FTIR and UV-Vis spectroscopy it was shown that iron atoms were located prevailingly in the cationic positions and that iron oxides were absent. Analysis of Mössbauer spectra of dehydrated samples confirmed that iron is located in α and β cationic positions [4]. Moreover, using Mössbauer spectroscopy distinguishing between β-1 and β-2 sites was possible. Sample Fe-$FER_{0.018}$ and Fe-$FER_{0.036}$ contained exclusively Fe(II). In the samples with Fe/Al 0.018 and 0.036 the population of β sites was 90 % and 75 %, respectively. Sample with Fe/Al = 0.072 containing not only Fe(II) (77 %) located in α and β cationic positions but also 33 % of Fe(III).

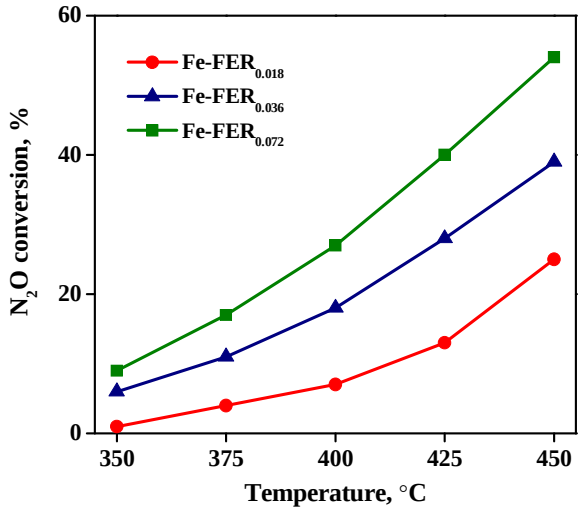

Figure 1. Temperature dependence of N_2O decomposition on Fe-$FER_{0.018}$, Fe-$FER_{0.036}$, and Fe-$FER_{0.072}$.

In all investigated samples O_2 treatment led to the oxidation of about the same proportion of the iron cations, i.e. presenting about 20% of the Fe(II) present in the samples. These results clearly suggest that only part of the iron located in cationic positions could be transformed into oxidized form by molecular oxygen. It further indicates lower resistance of α and β-2 sites to O_2 oxidation in comparison to β-1 site. On the other hand, nearly total transformation of Fe(II) to Fe(III) was observed after oxidation by N_2O.

Conclusions

Mössbauer studies of dehydrated Fe-$FER_{0.018}$, Fe-$FER_{0.036}$, and Fe-$FER_{0.072}$ supported by FTIR and UV-Vis results led to characterization of iron in different cationic position in FER. Moreover, two β sites in FER were experimentally distinguished by Mössbauer parameters. Mössbauer studies of redox properties of iron ferrierites combine with catalytic results of N_2O decomposition over Fe-$FER_{0.018}$, Fe-$FER_{0.036}$, and Fe-$FER_{0.072}$ shown that iron located in cationic positions played a decisive role in N_2O decomposition.

Acknowledgements

This work was financially supported by the Grant Agency of the Academy of Sciences of the Czech Republic (Project No. KAN100400702), the Grant Agency of the Czech Republic (Project No. 203/09/1627)

References

[1] L. Čapek, L. Vradman, P. Sazama, M. Herskowitz, B. Wichterlová, R. Zukerman, R. Brosius, J.A. Martens, Applied Catalysis B Environmental 70 (2007) 53-57
[2] A.M. Frey, S. Mert, J. Due-Hansen, R. Fehrmann, C.H. Christensen, Catalysis. Letters 130 (2009) 1-8
[3] L.V. Pirutko, V.S. Chernyavsky, A.K. Uriarte, G.I. Panov, Applied Catalysis A: General 227 (2002) 143-157
[4] K.A. Dubkov ., N.S. Ovanesyan, A.A. Shteinman, E.V. Starokon, G.I. Panov, Journal of Catalysis 207 (2002) 341-352
[5] E.Tabor, K. Závěta, .K. Shatu, Z. Tvarůžková, Y.Sobalík, Catalysis Today (2010) doi:10.1016/j.cattod.2010.09.017

Synthetic fuels from the new Fischer-Tropsch Co/SiC catalyst. Influence of alkali-earth promoter.

A.R. de la Osa, A. De Lucas, J.L. Valverde, A. Romero, J. Díaz-Maroto, P. Sánchez.
Affiliation: Chemical Engineering Deparment, Faculty of Chemistry, University of Castilla La Mancha, Avda. Camilo José Cela 12, 13071, Ciudad Real, Spain. AnaRaquel.Osa@uclm.es

Introduction

Synthetic fuels production from gasification of coal-biomass (10 wt. % exhausted olive husk) mixtures, in an IGCC (Integrated Gasification Combined Cycle) plant (ELCOGAS), is currently studying since no major differences have emerged in the shape of plant operation and emission values over the use of regular fuel. However, industrial processing has demonstrated that a Water Gas Shift unit may be needed in order to obtain a syngas composition that provides good performance in Fischer-Trospch synthesis (FTS) [1, 2].

Fischer-Tropsch process is capable of producing liquid hydrocarbon fuels from syngas and electricity and heat by cogeneration of the tail gas from the reactor. The use of cobalt based catalyst provides high activity, high selectivity to linear paraffins and stability toward deactivation by water [3]. Silicon carbide is a ceramic material with good chemical and thermomechanical properties that has been scarcely used as catalyst support [4]. In a recent paper the newer SiC has been demonstrated to be an excellent and promising support in such exothermic reaction as compared to the usually used alumina support [5]. It is important to note that Fischer-Tropsch selectivity is strongly influence by nature of support, particle size, metal loading, basicity and/or preparation method [6]. In this sense, the effect of basic promoters such as alkali-earth oxides supported on alumina was also studied, resulting in an important shift towards diesel fraction [7]. Thus, the aim of this work was to study the effect of Ca oxide as promoter of Co/SiC catalyst on the production and selectivity to synthetic fuels by FTS.

Experimental

A fixed bed reactor of 1 m length and 17.7 mm internal diameter was used (Fig.1). Experiments were carried out at: 20 bar, 220-300ºC, $H_2/CO=2$ with N_2 balance, gSiC/gcat=6 and gas hourly space velocity (GHSV) 6000 $Ncm^3/gcat.h$. Cobalt based catalyst using different calcium metal loading were prepared by multiple steps incipient wetness impregnation. The characterization of both support and catalysts was carried out in terms of Atomic Absorption (AA) and Inductively Couple Plasma (ICP), XRD patterns, Temperature Programmed Reduction (TPR), Pulse Oxidation and Acid-base Titrations.

Figure 1. Bench scale set-up.

Results and discussion

Some of the characterization results are displayed in Table 1. Cobalt dispersion was found to be enhanced by the use of calcium oxide as promoter. This fact has been attributed to the ability of alkali-earth oxide to favor a decrease in particle size of cobalt species. It implies a stronger metal-support interaction and then a lower degree of reduction. As a result, selectivity to synthetic fuels was significantly modified.

Table 1. Characterization results.

Co (wt. %)	Ca (wt. %)	dCo_3O_4 (nm) (XRD)	dCo^0 (nm) (XRD)	Degree of reduction (%)	HCl consumption (pKi ≤ 7) ($cm^3\ g^{-1}$)
5.0	0.0	36.6	27.5	34.0	-0.2
5.0	1.0	34.4	25.8	30.0	0.6
5.0	2.0	*	*	18.9	6.8

*Under detection limits

Acknowledgements

Financial Supports from the Ministerio de Ciencia e Innovación of Spain (CENIT-PiIBE project) and ELCOGAS S.A. are gratefully acknowledged.

References

[1] A. Demirbas, Prog. Energy Combust. Sci. 33 (2007) 1–18.

[2] Jornada Experiencia y futuro del carbón sostenible en la Central de Gasificación Integrada en ciclo combinado (GICC) de ELCOGAS, S.A. Madrid, 17 de Febrero 2010. Ed.: ELCOGAS, S.A.

[3] Ø. Borg, S. Eri, E.A. Blekkan, S. Stosater, H. Wigum, E. Rytter, A. Holmen, J. Catal. 248 (2007) 89–100.

[4] Y. Zheng**,** Y. Zheng, W.-P. Yu, R. Wang, K.-M**.** Wei. Chinese Journal of Inorganic Chemistry 24 (2008) 1007-1011**.**

[5] A.R. de la Osa, A. De Lucas, A. Romero, J.L. Valverde, P. Sánchez. Catal. Today (2011). doi:10.1016/j.cattod.2010.12.010.

[6] D.B. Bukur, X. Lang, D. Mukesh, W.H. Zimmerman, M.P. Rosynek, C. Li, Ind. Eng. Chem. Res. 29 (1990) 1588–1599.

[7] A.R. de la Osa, A. de Lucas, J.L. Valverde, A. Romero, I. Monteagudo, P. Coca, P. Sánchez. Catal. Today (2011). doi:10.1016/j.cattod.2010.11.064

Bifunctional catalytic conversion of cellulose into hexitols

Jan Geboers, Stijn Van de Vyver, Kevin Carpentier, Pierre Jacobs and Bert Sels

Centre of Surface Chemistry and Catalysis, Department of Molecular and Microbial Chemistry, Catholic University of Leuven, Kasteelpark Arenberg 23, 3001 Heverlee, Belgium. Fax: +32 16 32 1998; Tel: +32 16 32 14 63, E-mail: jan.geboers@biw.kuleuven.be

Introduction

Cellulose is the most abundant source of biomass. Unlike starch, it is insoluble in water and not digestible by humans because of the semicrystalline structure composed of β-1,4-glycoside bonded glucose monomers. One of the most promising routes for cellulose valorisation is inspired by reactions on starch, and relies on the one-pot dual catalytic conversion of cellulose into useful chemicals. Herein, cellulose is hydrolysed under action of an acid catalyst, followed by a fast metal-catalyzed hydrogenation of the formed glucose to hexitols. Hexitols, viz. sorbitol, mannitol and sorbitan, are important platform molecules, which are also used as precursors to renewable chemicals and fuels. A main advantage of the bifunctional catalytic approach is the fast removal of the unstable glucose, avoiding its degradation into caramel, tars, etc. Since the formed hexitols have a higher thermal stability than the corresponding hexoses, higher process temperatures and cellulose feed concentrations are feasible than in the classic cellulose hydrolysis. Several authors have recently reported on the bifunctional catalytic conversion of cellulose diluted in water (0.8-2 wt%) using catalyst loadings of 0.2 to 0.4 wt% achieving hexitol yields in the range of 30-73 %, typically within 24 h [1]. These results were recently reviewed [2]. However, the need remains for a catalytic system that is capable of more rapidly and selectively transforming more concentrated cellulose feeds into hexitols in high yields. In an effort to help address these issues, we have recently developed several systems that are capable of a fast and selective hydrolytic hydrogenation of concentrated cellulose feeds, achieving the highest hexitol yields and selectivities reported [3-5]. Here, we report on our most recent system, wherein cellulose is converted to hexitols over a Ru-loaded acid zeolite in presence of trace amounts of mineral acids [6]. The minute amount of acid (35 ppm *vs* 10^4 ppm indrustrially) avoids many problems with product neutralisation, acid recuperation and equipment corrosion that are ususally encountered when working with mineral acids at high reaction temperature.

Experimental

Ball milled cellulose (BMC; characterized in [3]) was used in all reactions. $Ru(NH_3)_6Cl_3$ was ion-exchanged onto zeolite carriers and reduction was performed in a quartz reactor under H_2 at 400°C. All experiments were performed in a batch autoclave at 190°C. When the reaction temperature was reached, the reactor was pressurized to 50bar H_2. Reaction mixture: 1g BMC, 0.5g Ru/zeolite, 50ml H_2O, 35ppm HCl.

Results and discussion

In a first phase of the research, zeolites were tested in reactions with a constant, low acid (HCl) amount, *viz.* 35 ppm, resulting in pH 3 in the mixture. The best results were achieved with mordenite and USY zeolite topologies with Si/Al ratios >15. An illustration of their

capacity to reductively split cellulose is given in the figure, showing hexitol yields above 50% within 24 h. Through optimisation of the acid-to-metal ratio, yields could be further increased to 86% in 24h for 35ppm HCl and a Ru(0.2)/USY zeolite. Increasing the acid amount to 106ppm yielded **80% hexitols in 3h**. By increasing the amount of all components in the mixture five-fold, **93% hexitols** were obtained **in 13h**, showing the systems ability to convert even concentrated feeds (10 wt%).

Based on the results of mechanistic experiments, we propose the following concept to rationalize the exceptional performance of the new system: depolymerisation of the cellulose chains happens under action of three different acid sources. Hot water is known to hydrolyze cellulose, chiefly to oligomers. In our system, hydrolysis is aided by HCl and the external zeolite acid sites, creating a pool of soluble cello-oligomers and glucose that is adsorbed into the zeolite pores, where the zeolite acid sites further depolymerize the oligomers to glucose. The adsorbed glucose is in close proximity to the Ru clusters in the zeolite. This essentially eliminates a considerable part of the diffusion path for glucose, favoring a highly selective and extremely active hydrogenation.

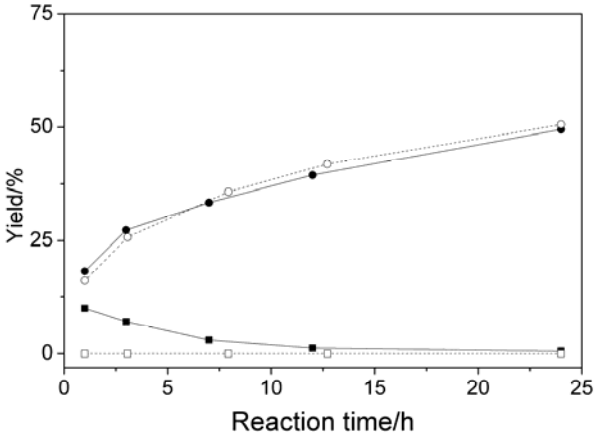

Fig. 1 Hydrolytic hydrogenation of cellulose with HCl & Ru(1.8)/H-USY (open); HCl & Ru(3)/MOR (filled). O: hexitol ; □: glucose.

Conclusions

We report that, contrary to what is claimed in literature, zeolites can be highly active and selective catalysts for biomass conversion. In fact, when combined with trace amounts of mineral acids, Ru/H-zeolites become one of the most performant catalytic systems for the hydrolytic hydrogenation of cellulose reported to date. Thanks to a 'conveyor belt' mechanism, the system takes advantage of the zeolite acid sites and its ability to adsorb cello-oligomers and depolymerize them to glucose. This results in full cellulose conversion with a minute acid amount. Up to 93% yield was achieved in 13h for a 10wt% feed.

References

[1] a) A.A. Balandin, N.A. Vasunina, S.V. Chepigo and G.S. Barysheva, Doklady Akademii Nauk SSSR, 1959, 128, 941-944; b) V. I. Sharkov, Angew. Chem. Int. Ed., 1963, 2, 405-409; c) P. Jacobs and H. Hinnekens (Synfina-Oleofina), EP0329923, 1989; d) A. Fukuoka, P. L. Dhepe, Angew. Chem., Int. Ed., 2006, 45, 5161; e) N. Ji, T. Zhang, M. Zheng, A. Wang, H. Wang, X. Wang, J. G. Chen, Angew. Chem., 2008, 120, 8638–8641; Angew. Chem. Int. Ed., 2008, 47, 8510–8513; f) N. Ji, T. Zhang, M. Zheng, A. Wang, H. Wang, X. Wang, Y. Shu, A. L. Stotllemyer, J. G. Chen, Catal. Today, 2009, 147, 77–85; g) M. Y. Zheng, A. Q. Wang , N. Ji, J. F. Pang, X. D. Wang, T. Zhang, ChemSusChem, 2010, 3, 63–66; h) R. Palkovits, K. Tajvidi, J. Procelewska, R. Rinaldi, A. Rupper, Green Chem. 2010, 12, 972-978; i) R. Palkovits, K. Tajvidi, A. Ruppert and J. Procelewska, Chem. Commun., 2010, 47(1), 576-578.

[2] S. Van de Vyver, J. Geboers, P. Jacobs and B. Sels, ChemCatChem, 2011, 3(1), 82-94.

[3] J. Geboers, S. Van de Vyver, K. Carpentier, K. de Blochouse, P. Jacobs, and B. Sels, Chem. Commun. (2010), 46, 3577-3579.

[4] S. Van de Vyver, J. Geboers, M. Dusselier, H. Schepers, T. Vosch, L. Zhang, G. Van Tendeloo, P. Jacobs, and B. Sels, ChemSusChem 3(6) (2010) 698-701;

[5] S. Van De Vyver, L. Peng, J. Geboers, H. Schepers, F. De Clippel, C. Gommes, B. Goderis, P. Jacobs and B. Sels, Green Chem., 2010, 12(9), 1560-1563.

[6] J. Geboers, S. Van de Vyver, K. Carpentier, P. Jacobs, and B. Sels, Chem. Commun. (2011), submitted.

Nickel-Zirconia Core-Shell Nanostructures for Dry Reforming Of Methane

Fatemeh Nouroozi, Andreas Peters, Roger Gläser*.
Institute of Chemical Technology, Universität Leipzig, Linnéstr. 3, D-04103 Leipzig, Germany

Introduction

Nickel catalysts for the dry reforming of methane use various supports such as SiO_2 [1], Al_2O_3 [2] and zeolite [3] as well as ZrO_2 [4]. However, there are several drawbacks associated with the rapid deactivation of supported nickel catalyst due to sintering of nickel particles at the high reaction temperature and coke formation [1,5,6]. An approach to avoid metal sintering is to encapsulate the catalyst within a shell of a mesoprous material. In the present work, this core-shell approach was applied to obtain a "nanoreactor" entailing nickel nanoparticles (NPs) inside zirconia shells. This was achieved by a layer by layer core-shell method [7]. The activity of the obtained catalysts was compared with that of zirconia hollow spheres impregnated with nickel.

Experimental

Nickel nanoparticles were synthesized based on literature reports [8], and used as main core for the synthesis of Ni@ZrO_2 hollow spheres. The core was coated with silica followed by coating with zirconium hydroxide using zirconium butoxide (0.90 mL, 80 wt.-% in butanol). Removal of the organics and crystallization of zirconia were achieved by calcination at 900 ^oC for 2h. The catalysts have been characterized with ICP-OES, TEM, SEM, XRD, XPS, TPR, and N_2 physisorption. Tests of the materials in catalytic reforming of methane with carbon dioxide reaction were carried out in a fixed-bed flow reactor. Typically, 50 mg of catalyst powder were reduced in an H_2 flow at 750 ^oC for 2 h prior to reaction. Then, an equimolar stream of argon, methane, and carbon dioxide with a total flow rate of 100 mL min^{-1} at 750 ^oC was passed over the catalyst for 20 h. The products were analyzed by gas chromatography with TCD detector.

Results and discussion

XRD patterns of both Ni@ZrO_2 and nickel-containing zirconia hollow spheres obtained by impregnation (Ni/ZrO_2) show the presence of tetragonal crystalline phases for Zirconia (t-ZrO_2, JCPDS 14-0534; Fig. 1a). The core-shell structure with a sphere diameter of ca. 90nm are visible in TEM images (Fig. 1b). Based on TEM and SEM images, shell thickness and sphere size is directly connected to the size of the core matterial. i.e., larger cores result in larger spheres with thinner shells. The textural properties of various Ni-containing catalysts as assessed by N_2 physisorption are shown in Table 1. Typically, Ni@ZrO_2 has a specific surface area of 182 m^2 g^{-1} and a specific pore volume of 0.25 cm^3 g^{-1}.

The catalytic reforming of methane with carbon dioxide test shows a methane conversion of 20 % with a coke deposition of < 1 wt.-% for Ni@ZrO_2, after 20 h on-stream. At contrast, the catalyst from impregnation of the zirconia hollow spheres with nickel is significantly less active (methane conversion of 14 %) and more affected by coking (15 wt.-% after 20 h).

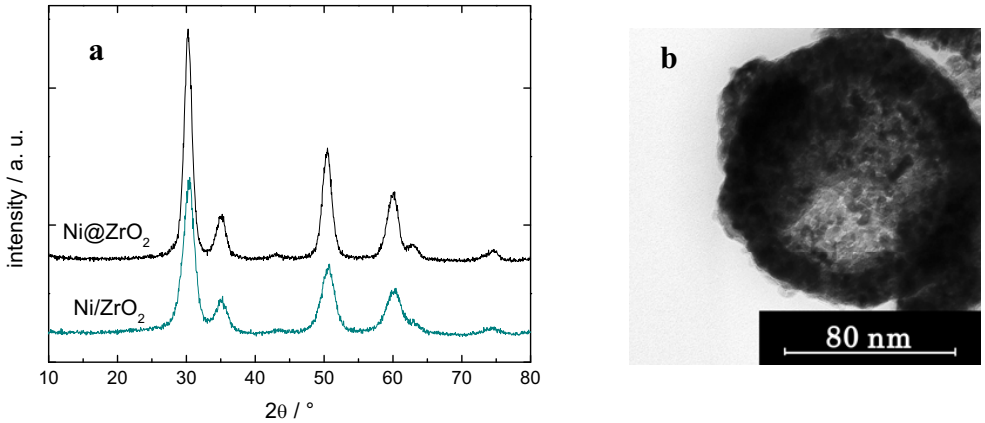

Figure 1. a) Wide angle XRD pattern for Nickel-containing hollow spheres (Ni@ZrO_2), and Ni/ZrO_2 b) TEM images for Ni@ZrO_2.

Table 1. Specific BET surface area, pore volume, and average pore diameter of two Ni on ZrO_2 (Ni@ZrO_2: Ni in hollow spheres; Ni/ZrO: impregnation of Ni onto hollow spheres).

Sample	S(BET) / (m^2 g^{-1})	V(BJH) / (cm^3 g^{-1})	d(BJH) / nm
Ni@ZrO_2	182	0.25	5.8
Ni/ZrO_2	191	0.14	14.7

Conclusions

Zirconia nanoreactors entailing Nickel nanoparticles were successfully synthesized and their catalytic activity for dry reforming of methane was proven. These catalysts show a continuous conversion rate of methane and carbon dioxide with a low coke deposition of < 1 wt.-% after 20 h on-stream. The typical size of the hollow spheres is 90 nm and specific surface area and pore volume are as high as 182 m^2 g^{-1} and 0.25 cm^3 g^{-1}, respectively. The up-scaling of the synthesis procedures will be a challenge to be solved in the near future.

References

[1] Pan, Y.X., Liu, C.J., Shi, P., J. Power Sources 176 (2008), 46–53
[2] Zhu, X.L., Huo, P.P., Zhang, Y.P., Cheng, D.G., Liu, C.J., Applied Catalysis B, 81 (2008), 132–140
[3] Rezaei, M., Alavi, S.M., Sahebdelfar, S., Bai, P., Liu X.M., Applied Catalysis B, 77 (2008), 346–354.
[4] Luengnaruemitchai, A., Kaengsilalai, A., Chemical Engineering Journal, 144 (2008), 96–102.
[5] Kroll, V.C.H., Swaan, H.M., Mirodatos, C., Journal of Catalysis, 161 (1996), 409–422.
[6] Pan, Y.X., Liu, C.J., , Cui, L., Catalysis Letters, 123 (2008), 96–101
[7] Arnal, P.M., Comotti, M., Schüth, F., Angewandte Chemie,118 (2006), 8404 –8407
[8] Winnischofer, H., Rocha, T. C. R., Nunes, W. C., Socolovsky, L. M., Knobel, M., Zanchet, D., ACS Nano, 2(2008), 1313–1319

Kinetic Study of Hydrogen Production by Catalytic Decomposition of Methane over Mesostructured Carbons

D.P. Serrano[1,2], J.A. Botas[1], P. Pizarro[1], G. Gómez[1] and J. Martín[1]
[1]*Department of Chemical and Energy Technology, ESCET, Universidad Rey Juan Carlos C/ Tulipán s/n, 28933, Móstoles (Madrid), Spain*
[2]*IMDEA Energía Institute, C/ Tulipán s/n, 28933, Móstoles (Madrid), Spain*
david.serrano@urjc.es

Introduction

Catalytic decomposition of methane has become a promising alternative for hydrogen production since it is free of CO/CO_2 emissions [1]. Although metal catalysts exhibit the highest initial activities, they are rapidly deactivated by deposition of carbon, which is the co-product of the reaction. Alternatively, the use of carbon materials as catalysts presents a number of advantages: a) high thermal stability; b) strong resistance to chemical deactivation; c) the reaction could be autocatalytic; d) regeneration step might be not needed, and e) the carbon produced might have different commercial applications [2]. Recently, we have reported that ordered mesoporous carbons (CMK type) exhibit excellent catalytic activity and deactivation resistance in methane decomposition reaction [3].
In this work we present a kinetic study of the CMK-type carbons (CMK-3 and CMK-5) for catalytic decomposition of methane. For comparison purposes, two black carbons (CB-bp and CB-v) and one mesoporous activated carbon (AC-meso) have been also studied.

Experimental

CMK-3 and CMK-5 carbons were synthesized using a nanocasting pathway with pure silica SBA-15 as hard template, according to the literature [3].
Methane decomposition reactions were performed on a simultaneous DSC-TGA thermobalance (TGA-DCS1, Mettler Toledo). Reactions were carried out under isothermal conditions at 965 ºC and using different compositions of reactive gas (10, 20 and 40 % of CH_4 in Ar). Hydrogen production was indirectly measured through the weight increase of the solid sample in the TGA during the reaction due to carbon deposition, according to the following reaction scheme:

$$CH_4\,(g) \rightarrow 2H_2\,(g) + C\,(s) \qquad (1)$$

Results and discussion

Table 1 summarizes the most important textural properties of the carbonaceous catalysts tested. All carbons are amorphous and exhibit BET surface areas above 1000 $m^2\ g^{-1}$, except for CB-v. Both CMK samples present a highly ordered mesoporous structure, resulting from the replication of the pure silica SBA-15 used as hard template during their synthesis. Moreover, CMK-5 has the highest BET surface area due to its bimodal pore structure.
Figure 1 shows the evolution of the carbon deposits weight relative to the initial catalyst amount (C_{dep}/C_0), together with the calculated hydrogen production from methane decomposition for all the carbonaceous catalysts, measured at different methane partial pressures. In all cases, the amount of both reaction products increases as the methane concentration in the reactive gas is higher. At long reaction times CB-bp and AC-meso are practically deactivated, whereas the activity of CB-v and both CMK-s show a significant and relatively stable activity. From Table 1, it can be observed that after 24 h of reaction, CMK-5 presents the highest reaction rate, close to twice the value of CB-v. Independently of the carbon nature, considering the rate equation $r_0 = k_P \cdot P_{CH_4}^n$, the reaction order was n=0.5. A

half-order reaction is often related with a dissociative mechanism where the reactant requires two surface-active sites to be anchored and converted.

Table 1. Textural properties and reaction rates at different times of the samples.

Catalyst	S_{BET} ($m^2 \cdot g^{-1}$)	S_{MESO} ($m^2 \cdot g^{-1}$)	S_{MICRO} ($m^2 \cdot g^{-1}$)	$r_{t=0}$ ($g_{Cdep}/g_{cat} \cdot h$)	$r_{t=6h}$ ($g_{Cdep}/g_{cat} \cdot h$)	$r_{t=24h}$ ($g_{Cdep}/g_{cat} \cdot h$)
CB-bp	1552	475	1077	2.062	0.054	0.034
CB-v	205	95	110	0.68	0.70	0.14
AC-meso	1392	396	996	3.080	0.043	0.045
CMK-3	1187	1187	-	5.20	0.17	0.15
CMK-5	1730	1730	-	6.058	0.32	0.27

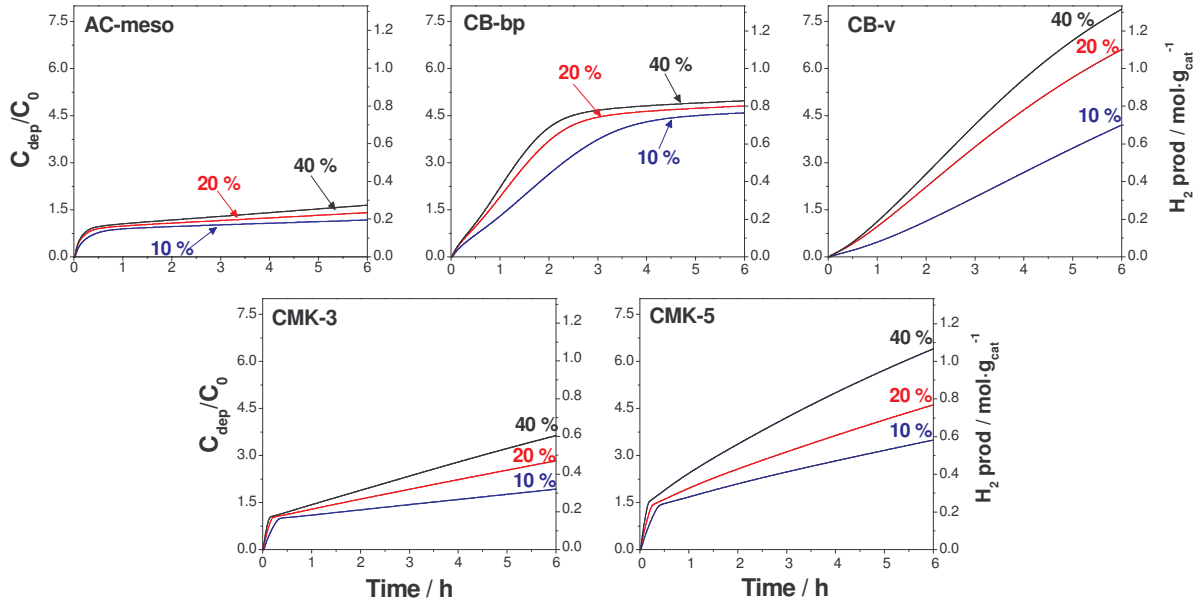

Figure 1. Evolution of the relative carbon gain and hydrogen production for the carbonaceous catalysts, measured at 965 ºC and using different reactive gas compositions.

Conclusions

A kinetic study of the catalytic decomposition of methane over different carbonaceous catalysts has been performed in a thermobalance. For all the samples, the reaction order was n=0.5. The comercial carbon black CB-v and both mesostructured carbons (CMK-3 and CMK-5) remain active at the end of the reaction while the rest of samples are practically deactivated whatever the methane concentration in the reactive gas is.

Acknowledgements

The authors thank to Spanish "Ministerio de Educación y Ciencia" for supporting this work through the Project ENE2008-05471/ALT.

References

[1] Abbas, H.A., Wan Daud, W.M.A., Hydrogen production by methane decomposition: A review, International Journal of Hydrogen Energy, 35 (2010), 1160-1190.

[2] Muradov, N., Smith, F., Raissi, A.T., Catalytic activity of carbons for methane decomposition reaction, Catalysis Today, 102-103 (2005) 225-233.

[3] Serrano D.P., Botas, J.A., Fierro J.L.G., Guil-López R., Pizarro P., Gómez G., Hydrogen production by methane decomposition: origin of the catalytic activity of carbon materials, Fuel, 89 (2010), 1241-1248.

Methanol conversion into olefins over silicoaluminophosphates with intergrown CHA/AEI structures

E.E. Knyazeva, I.L. Aranovich, S.V. Konnov, O.V. Shutkina, O.A. Ponomareva, I.I. Ivanova

A.V. Topchiev Institute of Petrochemical Synthesis of Russian Academy of Science,
ivanova_ii@ipc.ac.ru

Introduction

Silicoaluminophosphates with the CHA and AEI structure types are promising catalysts for the synthesis of light olefins from methanol. The CHA type materials (SAPO-34) have an advantage of high activity and selectivity to ethylene and propylene, while AEI type catalysts (SAPO-18) are more stable and have longer lifetime [1,2]. A possibility to obtain silicoaluminophosphates with intergrown CHA/AEI phases may allow to combine the benefits of the individual phases and to obtain catalysts with improved activity and selectivity. This idea is backed by the literature data pointing that CHA- and AEI-silicoaluminophosphates can be obtained from reaction mixtures having identical composition and the same template - tetraethylammonium hydroxide [3].

Experimental

Synthesis of silicoaluminophosphates with the pure CHA and AEI structural types was carried out using the procedures described in [3]. The formation silicoaluminophosphates with intergrown CHA/AEI phases was achieved by changing of pH of the reaction mixture during synthesis. After crystallization, washing and drying the samples was calcined at 500^{o}C for 2 hours to remove the template. The materials obtained were characterized by XRD, SEM, nitrogen adsorption, TG-DTA, and TPD of ammonia. They were also tested in methanol conversion into olefins at 400^{o}C and weight hourly space velocity (WHSV) of 2g/g*h.

Results and discussion

XRD data obtained over CHA, AEI and CHA/AEI samples are presented in Fig.1a. Samples CHA and AFI show reflexes typical for corresponding individual phases. In the case of CHA/AEI sample, the disappearance of the peak at 18,8 degr.2θ (Fig.1a,*) and arising of the peak at 17,1 degr. 2θ (Fig.1a,▼) gives an evidence for the formation of the intergrown CHA/AEI phase as it was claimed in [4].

The DTA curves of the freshly synthesized samples presented in Fig.1b also confirm the above conclusion, pointing to different temperatures of silicoaluminophosphates detemplating. The sample with the individual CHA framework type loses its template at 450^{o}C. In the case of AEI sample the template removal occurs at 340 ^{o}C. On the contrary, CHA/AEI sample shows two peaks, which are not typical for CHA and AFI.

The acidic properties of the samples were investigated by TPD NH_3. The content of the acidic centers in AEI and CHA/AEI samples was found to be 1300 μmol/g, while over CHA sample it reached 1600 μmol/g. The TPD profiles of AIE and CHA/AIE samples show the only peak at ~ 200^{o}C, indicating that these samples contain only weak acidic sites. On the contrary, CHA-sample is characterized by both weak and strong sited, as confirmed by the appearance of two peaks with the maxima at 200 and 400^{o}C, respectively. Thus, the acidic properties of CHA/AEI are closer to AEI than to CHA.

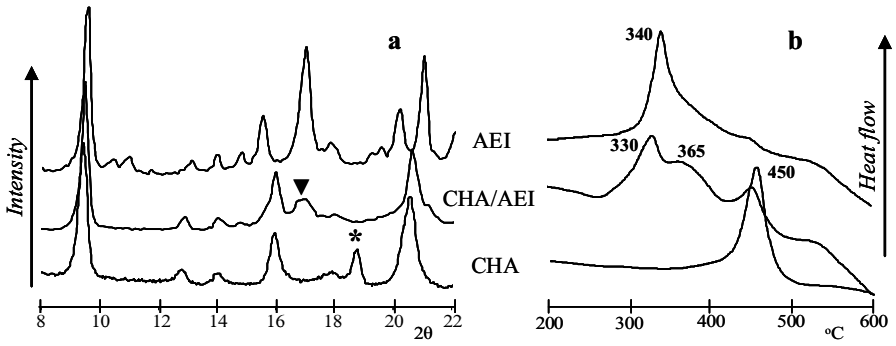

Figure1. XRD patterns (a) and DTA curves (b) of silicoaluminaphosphates

The catalytic data obtained over for CHA, AEI and CHA/AEI samples are shown in Table 1, The comparison of CHA and AEI samples points to higher selectivity to ethylene over CHA due to stronger confinement effects over this sample. On the contrary, AEI characterized by more open structure, shows higher selectivity to propene and butenes. Besides that, more methane, ethane and propane are formed on CHA as a consequence of stronger acidity over this catalyst. Silicoaluminophosphate with intergrown CHA/AEI phases shows superior catalytic properties with respect to both CHA and AEI samples. Besides higher selectivity to ethylene and propene it is characterized by higher stability of catalytic activity in time.

Table 1. Properties of silicoaluminophosphate in MTO process

Samples	Selectivity, % mol.						Time of 100% conversion retaining, h
	CH_4	C_2H_4	C_3H_6	C_4H_8	C_2H_6	C_3H_8	
CHA	5	43	37	9	1	1	4
AEI	1	33	44	16	0	0,5	5
CHA/AEI	1	46	38	11	0	0,2	8

Conclusions

It has been demonstrated that catalytic properties of silicoaluminophosphates with CHA and AEI structures in methanol conversion into olefins can be improved by synthesis of silicoaluminophosphates with intergrown CHA/AEI structures. These materials have higher selectivity to ethylene and propylene and higher stability of catalytic activity in time.

Acknowledgements

Financial support of Russian Foundation for Basic Research is gratefully acknowledged.

References

[1] Hereijgers, B.P.C., Bleken, F., Nilsen, M.H., Svelle, S., Lillerud, K.-P., Bjшrgen, M., Weckhuysen, B.M., Olsbye, U., Product shape selectivity dominates the Methanol-to-Olefins (MTO) reaction over H-SAPO-34 catalysts, Journal of Catalysis, 264 (2009), 77–87
[2] Gayubo, A.G., Vivanco, R., Alonso, A., Valle, B., Aguayo, A.T., Kinetic Behavior of the SAPO-18 Catalyst in the Transformation of Methanol into Olefins, Ind. Eng. Chem. Res., 44 (2005), 6605-6614
[3] Verified synthesis of zeolitic materials, Second revised Edition, H.Robson Editor, Elsevier, 2001
[4] Pat. WO 2005/103204 A2, 2005

Conversion of methanol over TNU-9, IM-5, ZSM-11 and ZSM-5. Intersection volumes of 10-ring influence selectivity towards coke and the importance of aromatics in the alkene-forming reaction mechanism[1].

Francesca Bleken[1], Wegard Skistad[1], Katia Barbera[2], Marina Kustova[3], Silvia Bordiga[2], Pablo Beato[3], Karl Petter Lillerud[1], Stian Svelle[1], Unni Olsbye[1]

[1] *inGAP Center of Research Based Innovation/Center for Materials Science and Nanotechnology (SMN), University of Oslo, Department of Chemistry, N-0315 Oslo, Norway*

[2] *Dipartimento di Chimica IFM-NIS Centre of Excellence, Università di Torino, Via P. Giuria 7, 10125 Turin, Italy*

[3] *Haldor Topsøe, Nymøllevej 55, DK-2800 Kgs. Lyngby, Denmark*

francesca.bleken@kjemi.uio.no

Introduction

Channel intersections in zeolites have profound effect on the product distribution of the methanol-to-hydrocarbons (MTH) process over zeolites with 10-ring channels. The 3D ZSM-5 product spectrum contains aromatics while the 1D ZSM-22 gives a much greater amount of branched and linear aliphatics[2]. In this study, the aim has been to further elucidate the role of these intersections on the reaction mechanism(s) and product distribution.

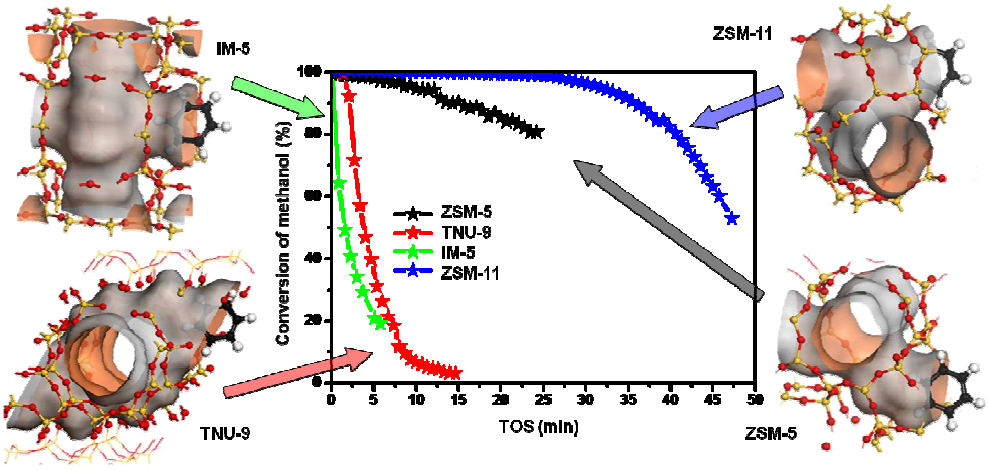

Figure 1. The 10-ring channels intersect differently in the four catalysts, giving rise to different volumes in which reactions can occur.

Experimental

Four zeolites with three dimensional 10-ring channels, were compared for the conversion of methanol: ZSM-5, ZSM-11, TNU-9 and IM-5. 40 mg of catalyst was tested in a tubular fixed bed reactor with i.d. 3 mm. He was used as carrier gas through a methanol evaporator kept at 20 °C, such that the WHSV was kept at 9 g MeOH/g cat/h. Catalyst temperature was 350 °C. Effluent analysis was performed with an on-line GC/FID. Spent catalyst was dissolved in HF acid and retained organic material was analyzed on a GC/MS after extraction with CH_2Cl_2.

Results and discussion

The materials consisted of crystals below 2 microns with Si/Al = 14-24 and the same acid strength as measured by CO-FTIR. The channel intersection sizes had little influence on the product spectrum of the effluent in the methanol conversion as seen in Figure 2 (left). However, the selectivity towards coke, and hence also the rate of deactivation due to coke varied tremendously over the four catalysts. Figure 2 (right) shows the retained material that

was extracted with CH_2Cl_2 after dissolution of the deactivated catalyst. It is evident that the two catalysts with the largest channel intersections, IM-5 and TNU-9, produced much larger aromatic compounds than ZSM-11 and ZSM-5. This separation into two "groups" is also evident in the life-time analyses (Figure 1). The two catalysts that formed the least amount of large hydrocarbons had a distinctly longer life-time.

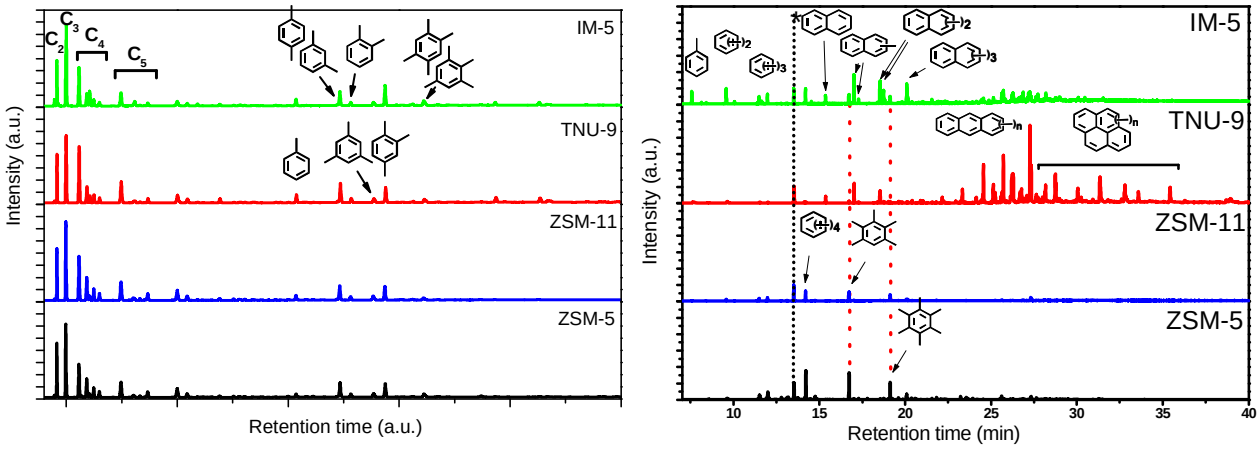

Figure 2. The effluent at full conversion (left) and retained soluble hydrocarbons after test (right) for IM-5, TNU-9, ZSM-11 and ZSM-5. WHSV = 9 g MeOH/g cat/ h at 350°C.

Analysis of the yield *versus* conversion plots (not shown) shows that the yield evolution with declining conversion was very similar for the four catalysts. Changes in intersection volumes influenced selectivities towards deactivating coke to a large degree, while effluent selectivities were very similar for the four catalysts. Penta- and hexamethyl benzene were observed in the effluent of TNU-9 and IM-5, but not ZSM-11 and ZSM-5. The yield in these highly methylated benzenes decreased at full methanol conversion, indicating that they were converted by other reactions than methylating reaction, as has been previously suggested for larger channel zeolite Beta[3]. This observation is in agreement with a larger degree of an aromatics-based cycle to form alkenes in the two catalysts with largest channel intersections, while an alkene-based cycle dominates alkene formation in ZSM-5 and ZSM-11.

Conclusions

Conversion of methanol over the 3D 10-ring zeolites ZSM-5, ZSM-11, TNU-9 and IM-5 shows very similar product distribution, but a large variation in selectivity towards coke. IM-5 and TNU-9 have the largest cavities and have much higher selectivities towards polyaromatics compared to ZSM-5 and ZSM-11. The high selectivity towards blocking coke is accompanied with a much faster rate of deactivation.

Acknowledgements

F.B. acknowledges the Norwegian Research Council through grant 171158 for financial support.

References

[1] F. Bleken, W. Skistad, K. Barbera, M. Kustova, S. Bordiga, P. Beato, K. P. Lillerud, S. Svelle, U. Olsbye, *Physical Chemistry Chemical Physics* **2011**, *13*, 2539-2549.

[2] S. Teketel, U. Olsbye, K.-P. Lillerud, P. Beato, S. Svelle, *Microporous Mesoporous Mater.* **2010**, *136*, 33-41.

[3] M. Bjørgen, U. Olsbye, D. Petersen, S. Kolboe, *J. Catal.* **2004**, *221*, 1-10.

The influence of Co content on the catalytic activity of Co_xSiBEA zeolites in CO oxidation

K. A. Chalupka[1,*], W. K. Jozwiak[1], S. Dzwigaj[2,*]

[1*] *Institute of General and Ecological Chemistry, Technical University of Lodz, Zeromskiego 116, 90 - 924 Łódź, Poland; Corresponding author: karolinachalupka@op.pl*

[2*] *Laboratoire de Reactivite de Surface,UPMC, CNRS, UMR 7197, 3 rue Galilée, 94200 Ivry–sur – Seine, France; Corresponding author: stanislaw.dzwigaj@upmc.fr*

Introduction:

During the last decades the development of catalytic carbon monoxide oxidation catalysts has became an important research topic [1]. The removal of CO is very important reaction and plays the huge part of environmental protection. Carbon monoxide oxidation has significance in gas purification in closed-cycle CO_2 lasers, CO gas sensors, air purification for respiratory, purification of hydrogen for fuel cells [2,3].

Heterogenous catalysts that can work at low temperature are useful in oxidation of CO. The both noble and other transition metals have been used as catalysts for CO oxidation. However the high cost of the noble metals and their sensitivity to sulfur poisoning are the reasons of the searching of new transition metals catalysts. In the last years, the zeolites have been widely used in various processes. Their high surface area and possibility of good dispersion of metals make zeolites useful in catalytic processes [1, 4].

In this work the influence of the Co content on the catalytic activity of Co_xSiBEA catalysts in CO oxidation was investigated. The state and nature of Co species were investigated by DR UV-vis, XPS, TPR-H_2 and CO.

Experimental:

Samples preparation: Series of Co_xSiBEA catalysts were prepared by two-step postsynthesis method described earlier [5]. Precursor of Co was aqueous solution of cobalt nitrate ($Co(NO_3)_3 \cdot 6H_2O$). This method allows controlling the introduction of Co ions in the zeolite framework or extra framework position. In the first step the TEABEA zeolite was treated in a 13 $mol \cdot L^{-1}$ HNO_3 solution (4 h, 80 °C) to obtain a dealuminated organic-free BEA. The resulting SiBEA (Si/Al > 1300) with vacant T-atom sites was recovered by centrifugation, washed with distilled water, and dried overnight at 80 °C. To introduce Co(II) ions in vacant T-atom sites (T = Al), SiBEA was stirred under aerobic conditions for 24 h at 25 °C in 200 mL of $Co(NO_3)_2 \cdot 6H_2O$ aqueous solution with different concentrations to obtain the Co_xSiBEA samples with various Co content (x = 0,5; 1,5; 3; 5; 20 wt. % of Co).

Methods of catalysts characterization: DR UV-vis spectra were recorded on a Varian Cary 5E spectrometer equipped with a double integrator with $BaSO_4$ as a reference. XPS experiments were performed on photoelectron spectrometer with hemispherical analyzer SES R4000 (Gammadata Scienta) using Al Kα (1486.6 eV) radiation. The vacuum in the XPS chamber was around 10^{-9} mbar. The power of the X-ray source was 400 W and the energy pass for analyzer was 10 eV, corresponding to FWHM of 0.9 eV for the Ag $3d_{5/2}$ peak. Binding energy (BE) for Si2p and Co2p was measured by taking the C1s peak at 284.5 eV as the internal standard. The TPR-H_2 measurements were carried out in automatic TPR system (AMI-1) in the temperature range 25 - 900°C with the linear heating rate 5-10°C/min. Samples (weight about 0,1 g) were reduced in hydrogen stream (5% H_2 - 95% Ar) with the gas volume velocity 40 cm^3 per minute. Hydrogen consumption was monitored by a thermal conductivity detector (TCD). The TPR-CO measurements were carried out in quartz reactor using a gas mixture 3%CO - 97%He in the temperature range 25˚C - 780˚C with the linear heating rate 7°C/min. Carbon monoxide consumption and carbon dioxide formation were recorded by MS detector.

Catalytic activity test: Carbon monoxide oxidation tests were carried out in a fixed bad reactor using a gas mixture of O_2 and CO with molar ratio 3 : 1 (total gas flow: 37 ml/min) and mass of catalyst 0,15 g. Process was carried out under atmospheric pressure at 25 - 500°C and reagents were analyzed by gas chromatograph. Before catalytic test the catalysts were pretreated in air at 500°C for 3h.

Results and discussion:

The TPR-H_2 and TPR-CO analysis of Co_xSiBEA samples show only one reduction peak at high temperature (680 - 800°C) for samples with low Co content (< 3 wt. % of Co). It indicates strong interaction of Co species with support and presence of isolated mononuclear Co species. For Co_xSiBEA samples with high Co content besides of the peak at about 750-785 °C corresponding to mononuclear Co species, two reduction peaks at lower temperature (315 and 415°C) were observed suggesting the appearance of polynuclear Co species. The presence of mononuclear and polynuclear Co species in Co_xSiBEA samples with high Co content was confirmed by DR UV-vis investigation. XPS mesurements exhibit for Co_xSiBEA samples with low Co content the core level BE of $Co2p_{3/2}$ at 783 eV. This value is very close to that reported elsewhere for Co^{2+} ions [6].

The catalytic tests showed that activity of Co_xSiBEA catalysts grows up with increasing of Co content. $Co_{0,5}SiBEA$ achieves CO conversion of 100% at temperature 470°C and $Co_{20}SiBEA$ achieves the same CO conversion at much lower temperature (200°C) (**Fig. 1**).

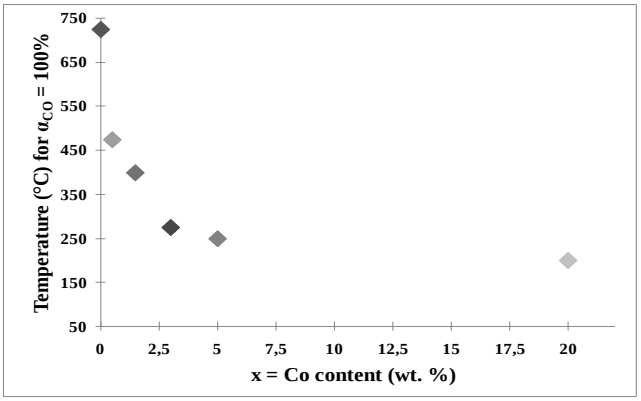

Fig. 1 The influence of Co content on the activity of Co_xSiBEA (x = 0,5; 1,5; 3; 5; 20 wt. % of Co) in CO oxidation

Conclusions:

The catalytic activity of Co_xSiBEA zeolites in CO oxidation increases with Co content. It seems that catalytic activity of Co_xSiBEA in CO oxidation is related to the presence of mononuclear Co species which amount increases with Co content up to 5 wt. % as evidenced by DR UV-vis and TPR method. At higher Co content ($Co_{20}SiBEA$) when lots of polynuclear Co species is formed, the catalytic activity of Co_xSiBEA is almost not changed, as shown by very similar temperature of 100% CO conversion for Co_5SiBEA and $Co_{20}SiBEA$.

References:

[1] Kang M., Song M. W., Lee C. H., Catalytic carbon monoxide oxidation over CoO*x*/CeO2 composite catalysts, Appl. Catal. A: General 251 (2003) 143 – 156

[2] Kang Y.-M., Wan B.-Z., Preparation of gold in Y-type zeolite for carbon monoxide oxidation, Appl. Catal. A: General 128 (1995) 53 – 60

[3] Bi Y., Lu G., Catalytic CO oxidation over palladium supported NaZSM-5 catalysts, Appl. Catal. B: Environmental 41 (2003) 279 – 286

[4] Corma A., State of the art and future challenges of zeolites as catalysts, J. Catal. 216 (2003) 298 – 312

[5] Dzwigaj S., Che M., Incorporation of Co(II) in Dealuminated BEA Zeolite at Lattice Tetrahedral Sites Evidenced by XRD, FTIR, Diffuse Reflectance UV-Vis, EPR, and TPR J. Phys. Chem. B 110 (2006) 12490 - 12493

[6] Moulder J.F., Syicle W.F., Sobol P.E., Bomben K.D., in: J. Chastain (Ed.), Handbook of X-Ray Photoelectron Spectroscopy: A Reference Book of Standard Spectra for Identification and Interpretation of XPS Data, Perkin-Elmer, Eden Prairie, MN, 1992, 82

Structure analysis of vanadium species in micro- and meso-porous catalysts

Š.Botková[1], Libor Čapek[1], P. Čičmanec[1], M. Pouzar[1], R. Bulánek[1], A.Zukal[2], J.Mayerová[2]

[1]*Department of Physical Chemistry, Faculty of chemical technology, University of Pardubice, Studentská 573, CZ 532 10 Pardubice, Czech Republic, libor.capek@upce.cz*
[2]*J. Heyrovsky Institute of Physical Chemistry Academy of Sciences of the Czech Republic, v.v.i., Dolejškova 2155/3, CZ 182 23 Prague 8, Czech Republic*

Introduction

The oxidative dehydrogenation (ODH) of light alkanes is an attractive way for the production of corresponding olefins. A large number of catalysts have been studied in the ODH of ethane. They encompass: (i) mixed oxide catalysts containing, for example, vanadium, molybdenum and niobium, and (ii) metal species such as vanadium and nickel supported on inorganic solids or micro- and mesoporous materials [1].
This work contributed to the analysis of the synthesis specimens by specifying the number of species present in the V-based catalysts (V-zeolites, V-MMT, V-mesoporous silicas, V-alumina). A combination of UV-Vis spectroscopy, H_2-TPR, N_2-adsorption, voltammetry of microparticles, Raman, XRD and SEM provided complex analytical information of the vandium species. The present contribution also deals with (i) the activity of single V-based catalysts in ODH of ethane and (ii) the relation between structure of vanadium species and their relation to the ODH of ethane.

Experimental

ZSM-5 (MFI) zeolites were supplied by Zeolyst. The silica mesoporous supports with various Si/Al ratio were synthesized from tetraethylorthosilicate as a silica precursor and various structure directing agent mentioned in literature [2]. Alumina and mesoporous alumina were supplied by Eurosupport and NanoScale, respectively. V-based catalysts were prepared by impregnation from H_2O/EtOH solution of vanadium acetylacetonate. The catalysts were dried for 24 h at RT. Finally the calcinations were performed for 8 h in air at 600, 700, 800 and 900°C. These procedures led to a different distribution of vanadium species.
The ODH of ethane was carried out in a quartz through-flow micro-reactor at 540-650 °C and atmospheric pressure, typically with 200 mg of the catalyst diluted with 1 cm^3 of silicon carbide inert. The reaction mixture (9 vol. % C_2H_6, 2.5 vol. % O_2 and the rest of helium) was kept at a total flow of 100 ml/min (W/F 0.12 $g_{cat}.s.ml^{-1}$).

Results and discussion

V-based catalysts were prepared with various vanadium contents (0-9 wt. % V), by various processes and by various thermal pretreatment. These processes led to different distributions of vanadium species (Fig.1). The complex analysis of vanadium species by the techniques discussed above evidenced the presence of the several types of vanadium species. The most important vanadium species on the catalyst supports are monomeric [VO_4] with tetrahedral coordination (O=V–(O-Sup)$_3$), vanadate dimeric or oligomeric chain- or sheet-like structures, polyvanadate anions, and 3-D nano- and microstructures of V_2O_5 at higher V-loadings. While,

the presence of monomeric and oligomeric tetrahedral vanadium species were dominant at low vanadium concentration, above 3.2 wt % V oxide-like species were formed [3]. Textural properties and structure of supporting materials were preserved after the impregnation of vanadium species. To achieve a high activity and selectivity in oxidative dehydrogenation of ethane, vanadium atoms should be highly dispersed up to vanadium content as high as possible. The optimum catalytic efficiency in ODH of ethane is achieved in V-loading between 2 and 4 wt.% V, when highly dispersed probably oligomeric V(V) species are prevailing. Adversely, the catalysts with high % of V_2O_5 (scherbinaite) has very poor both selectivity and conversion. The selectivity-conversion behavior of V-based catalysts is shown in Figure 2. The conversion of ethane 22 % and the selectivity to ethene 55 % was achieved with vanadium supported on hexagonal mesoporous silica at 600 °C. V-alumina was more active in comparison with V-HMS. V-alumina had the ethane conversion 28 % and the selectivity to ethene 60%. The activity of V-alumina was further improved by using mesoporous alumina support.

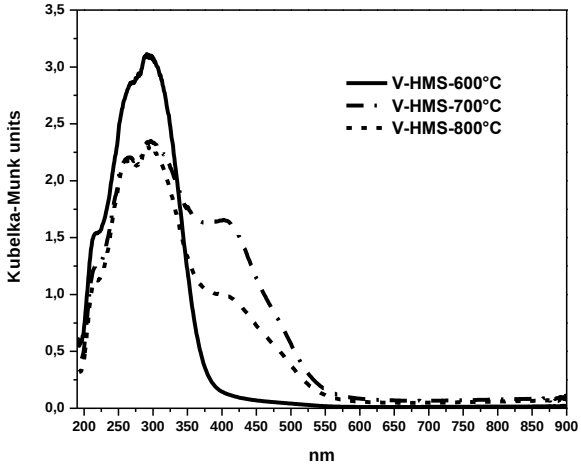

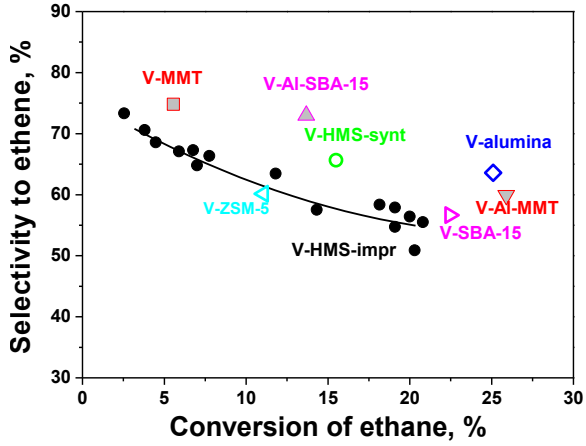

Figure 1. UV-Vis spectra of dehydrated V-HMS calcined at 600°C, 700°C, 800°C
Figure 2. Dependence of selectivity of ethene on conversion of ethane for V-based catalysts with different vanadium content and calcination temperature

Conclusions

The synthesis conditions, post-synthetic pre-treatment (steam and high- temperature calcinations) and concentration of vanadium influenced the distribution of vanadium species on the individual matrices and its catalytic activity.

Acknowledgements

The authors gratefully thank to the Grant Agency of Czech Republic for financial support (projects No. P106/10/0196) and Ministry of Education, Youth and Sports (MSM0021627501).

References

[1] Cavani , Ballarini N., Cericola A., Catalysis Today 127 (2007) 113-131
[2] Tanev P. T., Pinnavaia T. J., Science 267 (1995) 865.
[3] T. Grygar, L. Čapek, J. Adam, V. Machovič. , J. Electroanal. Chem. 633 (2009) 127-136.

BIOMIMETIC CATALITICAL OXIDATION METHANE TO METHANOL ON ZEOLITE NAM

I.T.Nagieva, T.M.Nagiev
Baku State University, Baku, Azerbaijan
E-mail: tnagiev@azeurotel.com; tnagiev@azeriland.com

Introduction

Lots of investigations in the field of active biomimics synthesis to mimic enzymatic functions [1] have been executed for the last decade. However, most synthesized catalysts function in the aqueous phase either in the medium of pure solvent - benzene, acetonitryl (reaction for propane oxidation with oxygen) as tetraphenylporphyrin complexes [2] or the latter are fixed on silicagel (reaction for cystein and hydroquinone oxidation with molecular oxygen) [3]. Herein, by ascertaining the fact of substrate oxidation, authors didn't present numerical values to characterize a catalytic activity of samples, their loading mass, process technological parameters. By presenting only selectivity value, the authors didn't present the other quantitative parameters (yield, conversion).

Experimental

In the synthesized biomimics NaM possessing acid-base properties plays role of peptide inorganic substitute in the native cytochrome P-450. The synthesis of $PPFe^{3+}OH$/ NaM was carried out by adsorption method. Hemin with Fe content as 8,6% ("BDH", England) was used as an active center to be immobilized. This hemin was dissolved in the aqueous-alcoholic solution (pH=9). Final samples contained 1,25 mg and 2 mg of an active mass by gram of carrier NaM. The catalase activity of $PPFe^{3+}OH$/NaM (1,25 mg/g) and components of its carrier - NaM compared to 5% H_2O_2 spontaneous homogeneous ^ decomposition (t_{exp}= 23°C, weight of samples = 0,5g, H_2O_2 = 20 ml) was studied.

Unlike the above-described works [2,3], the possibility (established by the authors) of $PPFe^{3+}OH$/NaM application in the gaseous phase allows to increase process efficiency, make it free of some technological difficulties, and, within temperature range as 110-180°C, leads to the formation of $PPFe^{3+}OOH$/NaM's intermediate to be responsible for monooxygenase oxidation. The process was carried out in the gaseous phase, in the quartz through-flow type reactor. Its reaction zone was loaded with biomimic granules and the reagents - CH_4 and 20% H_2O_2 were fed into respectively.

Results and discussion

It was found out that the catalase activity of NaM is 4 times higher than that of in case of H_2O_2 homogeneous decomposition, and is 1,5 times lower than that of $PPFe^{3+}OH$/NaM's. The volume of oxygen released for time unit is taken for the catalase activity. With the aim of activity increasing, biomimic samples were exposed to a thermal treatment at 300, 400, 500°C in the flow of inert gas - nitrogen for 1 h. Afterwards, these samples were tested for the catalase activity under condition close to the above-mentioned ones. It was found out that ail the thermally treated biomimic samples exceed the catalase activity of untreated one, and an increase in temperature causes an increase in the catalase activity for the thermally treated samples of $PPFe^{3+}OH$/NaM. As a result, the catalase activity of $PPFe^{3t}OH$/NaM sample treated at 500°C, was 10 times higher than that of untreated sample's, the catalase activity of the sample treated at

30O°C was 3 times higher than that of untreated one's. A positive effect of thermoactivation for biomimic immobilized on NaM was hereby concluded.
It was found out that biomimic $PPFe^{3+}OH/NaM$ possessed the monooxygenase activity from I10°C (sample with content as 2 n g/g), and the yield of CH_3OH made up 2% under 100% selectivity. This experiment was carried out for lh. and the last 30 min featured a decrease in the yield of CH_3OH. A twofold increase in H_2O_2 feed leads to a rapid decrease in the yield of CH_3OH (only its traces were observed)- On increasing a temperature of experiment to 180°C, the yield of CH_3OH decreased to 1,3% (sample - 1.25 mg/g) under 100% selectivity. Reaction system $PPFe^{3+}OH/NaM$ - H_2O: - H_3O - CH_4 is two-substrate, and both catalase and monooxygenase reactions run there.

$$PPFe^{3+}OH/NaM + H_2O_2 \xrightarrow{fast} PPFe^{3+}OOH/NaM + H_2O \xrightarrow{H_2O_2} PPFe^{3+}OH/NaM + O_2 + +H_2O$$

$$PPFe^{3+}OOH/NaM+CH_4 \xrightarrow{slow} PPFe^{3+}OH/NaM+CH_3OH$$

Number of catalytic turnovers for $PPFe^{3+}OH/NaM$ (with content as 1,25 mg/g) in the catalase reaction made up 175 h^{-1}, but in the monooxygenase reaction (t_{exp} =I80°C) - 4h^{-1}

Conclusion
The synthesized biomimic $PPFe^{J+}$0H/NaM in the hydroxylation of thermostable methane under the process mild conditions featured significant activity for the catalase reaction and insignificant activity for the monooxygenase reaction under 100% selectivity in the gaseous phase.

References.

1. T.M.Nagiev. Coherent Synchronized Oxidation Reactions by Hydrogen Peroxide. Elsevier. Amsterdam. 2007. p.325
2. Ellis P,E. (Ir), Lyons I.E. Effect of Fluorination of the Mesophenyl Groups on Selective Tetraphenylporphyrinato Iron (III) - Catalysed Reactions of Propane with Molecular Oxygen. J. Chem. Soc. Chem.Commun. N 18, 1989, pp. 1315-1316.
3. Kireyev S.G., Romanovsky B.V,, Journal of Physical Chemistry, Vol. LX, N 8, 1986, pp.2090-2091.

Pyrrole HDN by Tungsten Disulfide Catalysts

P. A. Luque[1,*], E. Lugo-Medina[2], A. Olivas[1]

[1]*Instituto Tecnológico de Los Mochis, Blvd. Juan de Dios Batiz y 20 de Noviembre. Los Mochis, Sin. 81250, México.*
[2]*Centro de Nanociencias y Nanotecnología, UNAM, Apdo. Postal 2681, Ensenada, B.C. 22800, México.*
**pluque@cnyn.unam.mx*

Introduction

Traditionally the sulfide based catalysts have been used for total hydrogenation [1,2]. Originally they were conceived to solve the problems of deactivation and sulfurated heterocompound poisoning [3] frequently present in raw materials however they also turned out to be resistant to carbonaceous deposits [4]. It was chosen pyrrole as a simple model molecule with the purpose of test the catalytic activity of WS_2, but another important reason of this study is that pyrrole and its derivatives are considered to be the strongest catalyst poison among heterocyclic compounds containing nitrogen [5]. This work reports the hydrogenation of pyrrole by WS_2. The catalysts were synthesized and characterized by several psychochemical techniques before reaction.

Experimental

Several methods exist for the preparation of thiosalt precursor [6-8]. Homogeneous sulfide precipitation (HSP) was used because the prepared catalysts for this method have the most exposed surface area and they achieve bigger uniformity regarding other methods. In this work the precursor $(NH_4)_2WS_4$ was obtained as in reference [9]. The ammonium thiotungstate (ATT) was first prepared with a water solution of ammonium metatungstate and ammonium hydroxide, and then it was bubbled with hydrogen sulfide for 4 h, afterwards the reaction vessel was kept in an ice bath to create yellow ammonium thiotungstate condensation. The obtained crystals were filtered and kept in sealed containers under argon to avoid contamination. Reduction of the samples was carried out exposing them to a gaseous flow of H_2S/H_2 to 20% in volume for 4 h at 673 K [10]. Afterward, the samples are once again sealed under argon.

Results and discussion

The surface area values determined of the synthesized catalyst were 16±0.5 m^2/g. These values of surface area are characteristic of ex situ synthesized catalysts [11]. By means of EDS analysis, an atomic relationship was observed of [W/S=0.33]. The diffraction pattern of the catalyst WS_2 showed one intense reflection characteristic of the catalyst in test is observed around 14.3°, in comparison with the reference it can indicate that the sample presents a low crystalinity. It is observed that the decomposition of pyrrole by hydrogen using our prepared catalyst is preferential toward butylamine in a range of 573 to 823 K. When the temperature was closed to 873 K the selectivity was preferable toward butane. Also in all the

measurements we had small amounts of secondary products originated by the different routes of decomposition of pyrrole. Morávek and coworkers studied the kinetic of the pyrrole hydrodenitrogenation (HDN) in presence of Ni-W/Al_2O_3 and the standard industrial Ni-Mo/Al_2O_3, they observed higher relative reactivity of pyrrolidine and 1-butylamine, to a one-step reaction: pyrrole→NH_3+C_4 hydrocarbons [12]. In those results the yield is butane and ammonia, but with WS_2 catalyst the selectivity is preferential to butylamine at the same temperature. In the study of the conversion of pyrrole we found that with our synthesized catalyst of WS_2 it was possible to obtain a conversion almost of 100 % in approximately 20 minutes at 523 K and atmospheric pressure. Also, in the whole analysis course (9 hours) the catalyst did not present deactivation. Hegedűs and co-workers [13] in acidic medium, at 6 bar and 353 K during 8 h, in presence of Pd/C obtained 100 % of conversion toward pyrrolidine. Nevertheless, the conversion percentage of our WS_2 catalyst was similar at conditions of less pressure and considerable time but toward butylamine and butane products. It could be possible to deduce that considering the selectivity the reaction pressure is a most important parameter than temperature.

Conclusions

Was synthesized and characterized an unsupported catalyst of WS_2. This was effective for the pyrrole decomposition to almost 100 %. According to the obtained products, the decomposition of pyrrole was carried out for three different routes that are: hydrogenation, hydrodenitrogenation and hydrogenolysis. The catalyst was selective mainly toward the butylamine in the range of 573 to 823 K that was caused by the hydrogenolysis of the C-N bond, but when arriving to 873 K change toward mainly the hydrodenitrogenation to the butane.

Acknowledgements

We thank to Eric Flores, Israel Gradilla, Eloísa Aparicio, Francisco Ruiz, Pedro Casillas, Jorge Palomares and Margot Sainz for their technical assistant in the realization of this work. To projects PAPIIT IN 107008 and CONACYT 14037y.

References

[1] Hamdy Farag Appl. Catal. 331 (2007) 51-59.
[2] P. Rayo, J. Ramírez, M. S. Rana, J. Ancheyta, A. Aguilar-Elguézabal, Ind. Eng. Chem. Res. 48 (2009) 1242-1248.
[3] Chun-e XIANG, Yong-ming CHAI, Yun-qi LIU, Chen-guang LIU, J Fuel Chem Technol. 36 (2008) 684-690.
[4] R.R. Chianelli, A.F. Ruppert, M.J. Yacaman, A. Vazquez-Zavala, Catal. Today. 23 (1995) 269-281.
[5] V. Háda, A. Tungler, L. Szepesy, Appl. Catal. A: General 210 (2001) 165-171.
[6] G. Hagenbach, P. Courty, B. Delmon, J. Catal. 31 (1973) 264-273.
[7] F. Pedraza, S. Fuentes, Catal. Lett. 65 (2000) 107-113.
[8] M. Zdražil, Catal. Today. 3 (1988) 269-365.
[9] A. Olivas, E.C. Samano, S. Fuentes, Appl. Catal., A. 220 (2001) 279-285.
[10] G. Alonso, V. Petranovskii, M. Del Valle, J. Cruz-Reyes, A. Licea-Claveríe, S. Fuentes, Appl. Catal., A. 197 (2000) 87-97.
[11] A. Olivas, D.H. Galván, G. Alonso, S. Fuentes, Appl. Catal., A. 352 (2009) 10-16.
[12] V. Morávek, J.C. Duchet, D. Cornet, Appl. Catal. 66 (1990) 257-266.
[13] L. Hegedűs, T. Máthé, A. Tungler, Appl. Catal., A. 152 (1997) 143-151.

Hydroreforming of the LDPE thermal cracking product over Ni supported hierarchical and commercial HZSM-5

J. Aguado[1*], D. P. Serrano[2], J. M. Escola[1], A. Garcia[1], A. Peral[2], L. Briones[1], R. Calvo[3], E. Fernandez[3]

[1]*Department of Chemical and Environmental Technology, ESCET, Universidad Rey Juan Carlos, c/ Tulipan s/n, 28933, Mostoles, Madrid (Spain)* jose.aguado@urjc.es

[2] *Department of Chemical and Energy Technology, ESCET, Universidad Rey Juan Carlos, c/ Tulipan s/n, 28933, Mostoles, Madrid (Spain)*

[3]*URBASER I + D + i, Av. Tenerife 4, 28703, San Sebastian de los Reyes, Madrid (Spain)*

Introduction

Waste plastics constitute a subject of deep environmental concern in western societies because around 50% of them end up in landfills (EU data, year 2007) [1]. Polyolefins (LDPE, LLDPE, HDPE, PP) are especially important wastes since their share accounts for more than 60 % of the total waste plastics. Among the different alternatives to deal with this problem, catalytic conversion treatments which convert plastic wastes towards fuels over solid acid catalysts has received increased attention due to valuable nature of the obtained products (gas, gasoline, gasoils) [2]. However, conventional catalytic cracking treatments with direct contact between the catalyst and the plastic show some disadvantages such as the fast deactivation of the catalyst by the impurities present as well as the formation of a great deal of olefins, which precludes its straight application as fuels. In this regard, two stages processes with an initial thermal cracking followed by catalytic hydroreforming of the obtained product appears as a good choice since no contact exists between the catalyst and the impurities. In addition, the catalytic hydroreforming enables to control the product distribution as well as to hydrogenate the olefins, improving the quality of the fuels. Among the different catalysts, hierarchical zeolites [3] show promising properties due to the presence of a secondary mesoporosity which allows faster diffusion of the bulky polymer macromolecule as well as to the possibility of depositing metal particles inside the formed mesopores.

In this work, the hydroreforming of the product resulting from LDPE thermal cracking at 400ºC was subjected to hydroreforming at 310 - 350ºC over two Ni supported bifunctional catalysts: a Ni supported hierarchical HZSM-5 (Ni–h-ZSM-5) material prepared by a seed silanization method and Ni supported over commercial HZSM-5 (Ni-c-ZSM-5) material. Henceforth, the results obtained are shown.

Experimental

Hierarchical HZSM-5 zeolite was prepared by a seed silanization method [3]. Both hierarchical and commercial HZSM-5 zeolites were impregnated with nickel nitrate, calcined and reduced with hydrogen at 500ºC. The theorical nickel content was 7 wt % while the Si/Al atomic ratio of the catalysts was of 30. The catalysts were characterized by conventional techniques: XRD, N_2 adsorption isotherm at 77 K, H_2 TPR, ICP and TEM. The hydroreforming experiments were performed in a batch reactor at 310 – 350ºC under a 20 bar hydrogen pressure for 45 min. The feed was the product obtained in the thermal cracking of LDPE at 400ºC, formed by a $C_2 – C_{35}$ hydrocarbon mixture. The gaseous and liquid products were analysed by GC. In addition, the bromine index and cetane number of the liquid products were also determined.

Results and discussion

The characterization data of both activated catalysts shows significant differences between them. BET surface area values for Ni-h-ZSM-5 and Ni-c-ZSM-5 were 458 and 336

m^2 g^{-1}, due to the presence of a secondary mesoporosity in the former created by the smaller size of its ZSM-5 constituing nanounits. H_2 TPR and TEM micrographs indicate only the presence of bulky nickel particles over the external surface of the Ni-c-ZSM-5, while a second population of smaller Ni particles is observed over Ni-h-ZSM-5. In this regard, the bromine index of the liquid fuels obtained in the hydroreforming at 350ºC over Ni-c-ZSM-5 and Ni-h-ZSM-5 was of 37.2 and 10.3 g Br_2 / 100 g, respectively, pointing out a higher hydrogenating activity over the hierarchical zeolite based catalyst.

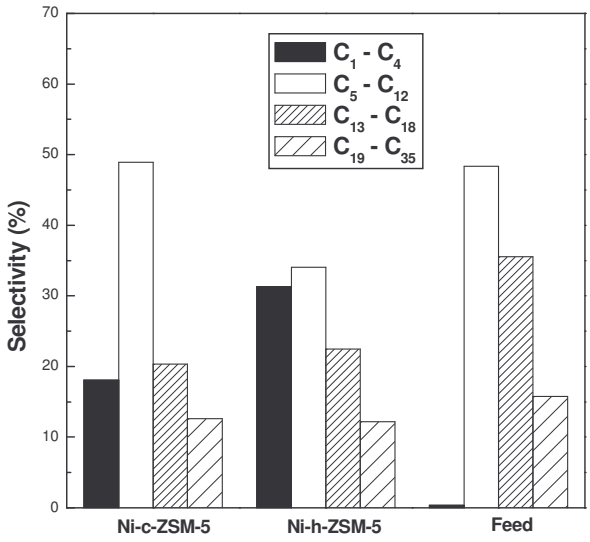

Figure 1. Hydroreforming results at 350ºC under 20 bar of H_2

The hydroreforming results at 350ºC are shown in figure 1. Higher hydroreforming activity is observed over Ni-h-ZSM-5 which leads towards higher selectivities towards gases (C_1 – C_4, 30%), mostly at the expense of gasolines (C_5 – C_{12}) and light diesel (C_{13} – C_{18}). In contrast, the hydroreforming of the heavy diesel fractions (C_{19} – C_{35}) is low over both catalysts, likely to its higher diffusional constraints.

Conclusions

Ni-h-ZSM-5 catalyst was more active than Ni-c-ZSM-5 catalyst leading towards high content in gaseous products (C_2 – C_4, 30%), because of its secondary mesoporosity. The liquid fuels also displayed lower bromine index, likely due to the presence of smaller Ni particles, more active for hydrogenation

Acknowledgements

The authors want to thank the company URBASER for their financial support to this research.

References

[1] Association of plastics manufacturers in Europe APME), The compelling facts about plastics 2007, www.plasticseurope.org, Brussels, 2008.
[2] J. Aguado, D. P. Serrano, J. M. Escola, Ind. Eng. Chem. Res. 47 (2008) 7982.
[3] D. P. Serrano, J. Aguado, J. M. Escola, J. M. Rodriguez, A. Peral, Chem. Mater. 18 (2006) 2462.

Framework Mn in Mesostructured Silicate as Catalyst for the Decomposition of Organic Dye

Darja Maučec[a], Nataša Novak Tušar[a,c], Magda Cotman[a], Albin Pintar[a,b], Venčeslav Kaučič[a,b]
[a]National Institute of Chemistry, Hajdrihova 19, SI-1001 Ljubljana, Slovenia; [b]Faculty of Chemistry and Chemical Technology, University of Ljubljana, Aškerčeva 5, SI-1001 Ljubljana, Slovenia; [c]University of Nova Gorica, Vipavska 13, SI-5000 Nova Gorica, Slovenia; e-mail: natasa.novak@ki.si

Introduction

Among a wide range of organic pollutants detected in industrial and municipal wastewater, dyes are an important group [1]. An attractive, sludge free alternative for the treatment of dyes in wastewater, is the use of advance oxidation processes (AOPs) [2]. Hydroxyl radicals ($^{\cdot}OH$), highly reactive species generated in sufficient quantities by AOPs, have ability to decompose dyes. Most of AOPs use a combination of strong oxidizing agents (*e.g.* H_2O_2, O_3) with catalysts (*e.g.* transition metal ions) and irradiation (*e.g.* ultraviolet and visible light).
The current study reports a green decomposition of methylene blue, in industry the most important basic cationic dye, by advanced oxidation method (AOP) using H_2O_2 as the oxidant and mesostructured silicate MnKIL-2 with framework manganese as heterogeneous catalyst. The KIL family is related to mesostructured silicate families with interparticle (textural) porosity (HMS, MSU, NBS) [3]. Manganese is known as one of the most intensively used elements to promote redox catalysis [4].

Experimental

Recently, we have developed the controlled two-step synthesis of the novel mesostructured KIL silicate family [3]. For this study, we stabilized manganese with Si/Mn molar rations from 0.005 to 0.05 via solvothermal synthesis into a new inorganic matrice from KIL family (KIL-2) and denoted the potential catalysts as 005MnKIL, 01MnKIL, 02MnKIL and 05MnKIL. Thorough characterization of prepared catalysts was performed using X-ray powder diffraction, N_2 sorption measurements, scanning electron microscopy (SEM), high-resolution transmission electron microscopy (HRTEM) and X-ray absorption spectroscopy (EXAFS and XANES) [3]. Catalytic wet peroxide oxidation studies were carried out in a 250-ml five-necked glass reactor equipped with a magnetic stirrer, heating jacket and a condenser. In a typical run, water containing methylene blue dye (c_0=50 mg/l) was transferred into the reactor and a known amount of a catalyst (100 mg) was added to the solution. The suspension was thermostated at T=25^{o} C under continuous stirring and sparging by means of pure nitrogen. Just prior starting the reaction, concentrated solutions of hydrogen peroxide were added. Representative aqueous-phase samples were withdrawn at periodic intervals and immediately filtered. Temporal concentration of dye in withdrawn samples was determined by means of UV/VIS spectrophotometry. The total amount of organic substances (*i.e.* unconverted model pollutant and intermediates) in withdrawn aqueous-phase samples was determined by measuring the total organic carbon (TOC). In all analyses, 3–4 repeated measurements were taken for each liquid sample, and the average value of TOC was reported. The error of analysis was never greater than ±0.5 %.

Results and discussion

Mesostructured manganese modified KIL-2 catalysts with various Mn/Si rations (from 0.005

to 0.05) were prepared and characterized. XRD, SEM and N_2 physisorption confirmed structural properties of the materials (not shown). From TEM, EXAFS and XANES analysis framework manganese (catalysts with Mn/Si rations 0.005 and 0.01) and extra-farmework manganese (catalysts with Mn/Si rations 0.02 and 0.05) incorporated into KIL-2 structure were determinated (not shown). Among catalysts containing various loadings of manganese, the lowest activity in the process of wet peroxide oxidation was observed over the catalysts with framework manganese with Mn/Si=0.05 (see Figure 1, 005MnKIL), while the highest activities for methylene blue decomposition were obtained in the presence of catalysts with extra-framework manganese (Figure 1, 02MnKIL and 05MnKIL). However, it was found out by a detailed examination of withdrawn aqueous-phase samples that catalysts with extra-framework manganese significantly promote simultaneous decomposition of hydrogen peroxide used as an oxidizing agent. With this respect, the catalyst with framework manganese and molar ratio Mn/Si=0.01 (Figure 1, 01MnKIL) was found as an optimal catalytic system, since it exhibits both activity for methylene blue oxidation comparable to catalysts with extra-framework manganese and low ability for H_2O_2 decomposition. The investigation of the wide range of operating and reaction conditions using 01MnKIL (Figure 1) as catalyst and the evaluation of the efficiency of this purification system is in progress.

Conclusions

Oxidative destruction of over 80 % of organic dye methylene blue was achieved in 30 minutes in preliminary studies by using prepared catalyst (mesostructured silicate MnKIL-2 with framework Mn, Mn/Si=0.01 and interparticle porosity) in the process of wet peroxide oxidation as one of AOP representatives. The results further demonstrate that the prepared solid enables deep oxidation of organic matter towards carbon dioxide at mild reaction conditions; therefore, it is a promising catalyst to facilitate the AOP wastewater treatment.

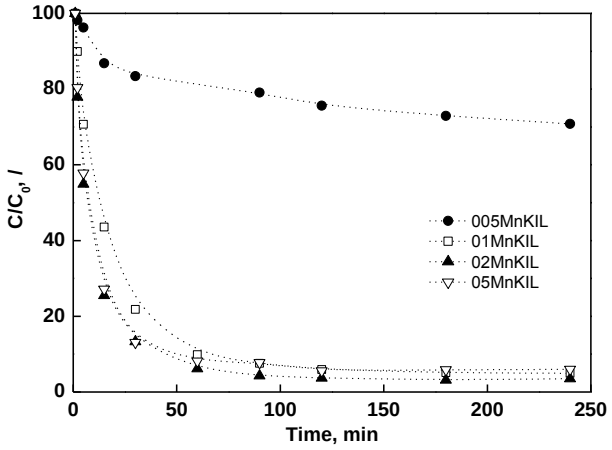

Figure 1. Relative concentration of methylene blue as a function of time obtained during the wet peroxide oxidation carried out at T=25^o C and atmospheric pressure in a batch slurry reactor in the presence of manganese modified porous silicate catalysts with Si/Mn molar rations 0.005 (denoted as 005MnKIL), 0.01 (denoted as 01MnKIL), 0.02 (denoted as 02MnKIL) and 0.05 (denoted as 05MnKIL).

Acknowledgements

This work was financially supported by the Slovenian Research Agency (research programs P1-0021 and P2-0150).

References

[1] Pirkanniemi, K., Sillanpää, M., Heterogeneous water phase catalysis as an environmental application: a review, Chemosphere, 48 (2002), 1047-1060

[2] Stasinakis, A.S., Use of selected advance oxidation processes (AOPs) for wastewater treatment – a mini review, Global NEST Journal, 10 (2008), 376-385

[3] Novak Tušar, N., Ristić, A., Mali, G., Mazaj, M., Arčon, I., Arčon, D., Kaučič, V., Zabukovec Logar, N. MnOx nanoparticles supported on a new mesostructured silicate with textural porosity, Chemistry – A European Journal, 16 (2010), 5783-5793

[4] Novak Tušar, N, Jank, S., Gläser, R., Manganese-containing Porous silicates: Synthesis, Structural Properties and Catalytic Applications, ChemCatChem, 3 (2011), 254-269

Methyl Mercaptan and Carbonyl Sulfide Traces Removal through Adsorption and Catalysis on Zeolites and Layered Double Hydroxides

Philippe Trens[a], Andrey Ryzhikov[a], Vasile Hulea[a], Didier Tichit[a], Catherine Leroi[b], Didier Anglerot[b], Bernard Coq[a]
[a]*Institut Charles Gerhard de Montpellier, UMR 5253 CNRS/ ENSCM / UM2 / UM1, "Matériaux Avancés pour la Catalyse et la Santé", 8 rue de l'Ecole Normale, 34296 Montpellier Cedex 5, France.* Corresponding author : philippe.trens@enscm.fr
[b]*TOTAL SA, Pôle Recherche et Développement Mont/Lacq, BP 47 – 64170, Lacq, France.*

Introduction

Natural gas always contains contaminants or other unacceptable substances including carbon dioxide, hydrogen sulfide, water, carbonyl sulfide, mercaptans, heavy hydrocarbons and mercury [1]. Conditioning natural gas for marketing generally requires the removal of these contaminants, which comprises several main operations among which deacidizing (CO_2 and H_2S removal, partial extraction of methyl-, ethyl- and propylmercaptan), dehydration, gasoline extraction. The deacidized gas usually contains 2% CO_2, 4 ppm H_2S and 20-50 ppm total sulfur (mercaptans and COS). In view of both increasingly stringent environmental regulations and technical requirements for further catalytic processes (e. g. syngas fabrication), deeper desulfurization becomes in high demand.
The most efficient adsorbents for mercaptans capture are metal-promoted zeolites [2] and active carbon [3]. However, even though active carbons exhibit larger adsorption capacities than zeolites, they are more sensitive to the regeneration process.
Regarding COS removal, the main purifying treatment is the catalytic hydrolysis leading to CO_2 and H_2S, which are in turn eliminated through classical deacidizing processes. Usually the COS hydrolysis is performed at temperature higher than 100 °C, but recent studies showed than the reaction can be effectively achieved under milder reaction conditions [4].
The adsorption of COS is much less documented. In the open literature, only few materials, including supported rhodium, activated carbon [5] and layered double hydroxides [6] have been reported as possible sorbents for COS. On that account, we present new results describing the highly efficient elimination of CH_3SH and COS traces in CH_4, in relation with adsorption and heterogeneous catalytic processes using original sorbents and catalysts.

Experimental

Metal exchanged zeolites and layered double hydroxides (LDH) were prepared according to conventional routes documented in the literature. Before use, the powdered materials were pressed, crushed and sieved to keep the grains size 150-350 μm.
The same experimental set up was used for both adsorption and catalytic experiments. It consists of a fixed bed reactor fed with two mass flow controllers for both reactant and activation gases. The detection was carried out by on line sampling of the outflowing gas to a gas chromatograph equipped with a flame photometric detector (Shimadzu GC 2014). The materials were activated in situ at 300 °C in flowing N_2 for 30 min.

Results and discussion

The affinity of both sulfur compounds for Me-zeolites was higher than that for LDHs. On the other hand, the affinity of COS was found lower in comparison with CH_3SH. Generally, for a

given zeolite structure, the global adsorption of CH_3SH for metal-exchanged zeolites was found to increase with the basicity and the valence of the cation. The catalytic hydrolysis of COS was performed on the same materials to compare the conversion of COS related to the affinity of COS species for the different materials.
COS conversions obtained at various temperature are listed in Table 1. In the case of Me-containing X zeolite, it can be observed that there are considerable differences of activity among the catalysts, indicating that the nature of the cations plays a major role. Thus, CsNaX and NaX are excellent and good catalysts, respectively, for COS hydrolysis, whereas CaX and MgNaX show insignificant activity. Based on these results, it is reasonable to consider that the catalytic activity of these materials can be related to their surface basicity. Indeed, the more basic NaX and CsNaX zeolites are by far the best catalysts.

Table 1. COS conversions (%) on calcined LDH-type materials (left) and Me-containing X zeolite (right); GHSV = 7000 h^{-1}

T / °C	50	100	150	200
Mg-Al (CO_3)	58	100		
Mg-Al (NO_3)	3	9		
Zn-Al (CO_3)	0	24		36
Zn-Al (NO_3)	0	12	32	48
Ni-Al (CO_3)	44	100		41
Ni-Al (NO_3)	12	100		
γ-Al_2O_3	26	100		

T / °C	50	100	150	200
CsNaX	10	85	100	
NaX	2	6	100	
BaNaX	1	3	12	100
CaNaX	1	2	4	5
MgNaX	1	2	4	5

LDHs with different composition (not shown here), as well as mixed oxides, derived from LDHs by calcination at 550°C, were also screened for their ability to catalyze the COS hydrolysis. Mixed oxides proved highly active catalyst in COS hydrolysis (table 1).
We suggest that the basic sites CO_3^{2-} ions at external surface can account for the reactivity of the LDH samples activated at 300 °C. Exchange of NO_3^- for CO_3^{2-} greatly decreases the basicity of the LDHs which become almost totally inactive. This confirms that CO_3^{2-} are the active sites, in agreement with the results reported for the reaction between formaldehyde and acetone with NO_3^-- and CO_3^{2-}-containing Mg/Al LDHs [7].

Conclusions

The sorption of CH_3SH and COS and the catalytic hydrolysis of the latter were tested with metal exchanged zeolites and LDH materials. The basicity of the catalysts was found to rule the hydrolysis. The LDH-based materials are far more active catalysts than the Me-zeolites. The CO_3^{2-}-containing mixed oxides exhibited outstanding catalytic activity for COS hydrolysis performed at temperatures lower than 100 °C

References

[1] A. Rojey, B. Durand, in "Le gaz naturel: production, traitement, transport", Publications de l'institut Français du Pétrole, Editions Technip, 1994, 7-19 and references therein.
[2] M. Ziolek, J. Czyzniewska, J. Lamotte, J. C. Lavalley, React. Kinet. Catal. Lett. 53 (1994) 339-46.
[3] S. Bashkova, A. Bagreev, T. Bandosz, J. Environ. Sci. Technol. 36 (2002) 2777-2782.
[4] B. Thomas, B.P. Williams, N. Young, C. Rhodes, G.J. Hutchings, Catal. Lett. 86 (2003) 201-205.
[5] M.L. Sattler, R.S. Rosenberk, J. Air Waste Manage. Assoc. 56 (2006) 219-224.
[6] D.E. Sparks *et al*, Appl. Catal. B: Environ. 82 (2008) 190-198.
[7] E. Suzuki, Y. Ono, Bull. Chem. Soc. Jpn, 61 (1988) 1008.

Catalytic performance of a CVD modified HZSM-5 for *p*-diethylbenzene production

J.L. Sotelo, A. Rodríguez, V.I. Águeda, P. Gómez
Chemical Engineering Department, Faculty of Chemistry, Complutense University of Madrid, Avenida Complutense s/n, 28040, Madrid, Spain.
Tel.: +34913944115, Fax.: +34913944114, e-mail: pilar.gomez@quim.ucm.es

Introduction

Disproportionation is an important reaction in the interconversion processes between aromatics, especially for producing dialkylbenzenes. Normally *p*-dialkylbenzenes are the isomers with more industrial applications. For example, *p*-diethylbenzene is a high-valued desorbent used in the *p*-xylene adsorptive separation process. ZSM-5-type zeolites are employed in ethylbenzene disproportionation processes [1] mainly due to its shape selectivity. Shape selective processes allow a reduction in the production cost and lower subproducts generation. These processes can be improved using different approaches such as external surface modification of the catalysts by techniques including the chemical deposition of silica in the liquid phase (CLD) or in the vapour phase (CVD) using various precursors [2, 3].
In the first place, a study of the variables in the CVD process employed for ZSM-5 modification, such as precursor, deposition time, flow rate and deposition temperature is presented. Secondly, a study of the catalytic performance of the modified zeolites in the ethylbenzene disproportionation under different reaction conditions is reported.

Experimental

The starting material was a HZSM-5-type zeolite with a Si/Al ratio of 13, supplied by Zeocat. The zeolite, after being agglomerated with alumina (final Si/Al ratio of 8.4) and calcined at 550 ºC, was packed in a fixed bed glass reactor. A flow of He saturated in the precursor (tetramethyl orthosilicate, TMOS or tetraethyl orthosilicate, TEOS) was fed to the bed, which was heated to the deposition temperature for a certain deposition time. Finally the zeolite was calcined for 5 hours at 550 ºC. The modified catalysts were characterized by FRX in order to determine the Si/Al ratio obtained after the silica deposition.
A modified catalyst was selected and used in the ethylbenzene disproportionation employing the experimental set-up previously described in detail [4]. Pure ethylbenzene was pumped at a flow rate of 0.5 $cm^3 \cdot min^{-1}$. Experiments were carried out at different temperatures and pressures ranging from 325 to 400 ºC and from 1 to 91 bar. Samples were analysed by a GC with a FID detector. After the experiments, catalysts were analyzed by thermogravimetry, in order to obtain their coke content.

Results and discussion

Among all the variables studied, the deposition temperature had the greatest effect. The Si/Al ratios obtained after the deposition process, carried out at different temperatures, are shown in Fig. 1, for the two precursors employed (TMOS and TEOS). As it can be seen in the figure, the temperature has a positive effect on deposition for both precursors. However, the deposition reached with TMOS is higher than that obtained employing TEOS at all the temperatures assayed. This is due to the higher reactivity of TMOS, so that a higher deposition time is necessary with TEOS to obtain similar Si/Al ratios to that obtained with TMOS.

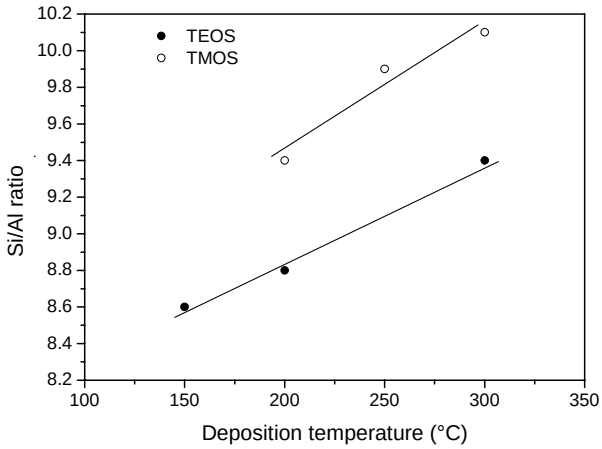

Figure 1. Effect of deposition temperature on the Si/Al ratio

The zeolite modified with TMOS at 300 ºC was selected for the catalytic study in the ethylbenzene disproportionation under different reaction conditions, and some significant results are shown in Fig. 2. The *p*-selectivities obtained at different conversions with the modified HZSM-5 are higher than the thermodynamic equilibrium *p*-selectivity obtained with the parent zeolite (Fig. 2.a). Moreover, at the same reaction conditions (Fig. 2.b), a lower conversion is obtained with the modified material, but this can be compensated for a higher *p*-selectivity reached, obtaining a *p*-diethylbenzene yield similar to the yield reached with the parent zeolite but reducing the amount of by-products. Furthermore, the material modification improves the selectivity to diethylbenzene, avoiding unwanted secondary reactions, and reduces the coke content of the catalysts.

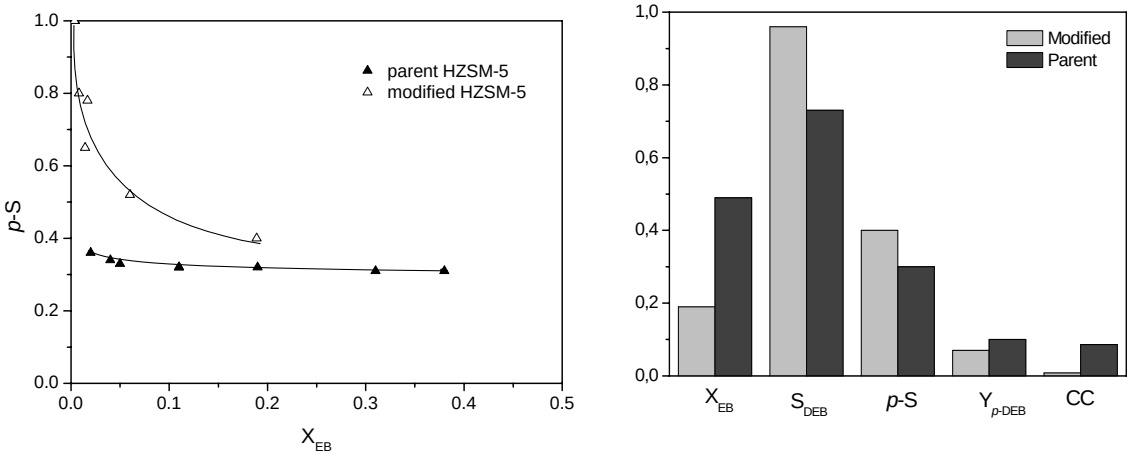

Figure 2. Comparison of the catalytic performance of the parent and the modified HZSM-5: (a) *p*-S at different reaction conditions and (b) catalytic results at 400ºC and 46 bar

References

[1] Beck, J. S., McCullen, S. B., Olson, D.H., Venkat, C.R. (Mobil Oil Corporation), US 5406015 (1995)
[2] Niwa, M., Kato, S., Hattori, T., Murakami, Y., Fine control of the pore-opening size of the zeolite mordenite by chemical vapour deposition of silicon alkoxide, Journal of the Chemical Society, Faraday Transactions I, 80 (1984), 3135-3145
[3] Zhu, Z., Chen, Q., Xie, Z., Yang, W., Kong, D., Li, C., Shape-selective disproportionation of ethylbenzene to para-diethylbenzene over ZSM-5 modified by chemical liquid deposition and MgO, Journal of Molecular Catalysis, 248 (2006), 152-158
[4] Sotelo, J.L., Rodríguez, A., Águeda, V.I., Gómez, P., Supercritical fluids as reaction media in the ethylbenzene disproportionation on ZSM-5, Journal of Supercritical Fluids, 55 (2010), 241-245

m-Xylene and mesitylene transformations over EUO zeolite: Effect of the sodium exchange and location of the active acid sites

J. Martins[a,b], S. Laforge[a,*], P. Magnoux[a], E. Guillon[c], F. Lemos[b], F. Ramôa Ribeiro[b]

[a] *Laboratoire de Catalyse en Chimie Organique, UMR 6503 CNRS - Université de Poitiers, 40 avenue du Recteur Pineau, 86022 Poitiers Cedex, France*
[b] *IBB–Institute for Biotechnology and Bioengineering, Centre for Biological and Chemical Engineering, Instituto Superior Técnico, UTL, Av. Rovisco Pais, 1049-001 Lisboa, Portugal*
[c] *IFP Energies nouvelles, Direction Catalyse et Séparation, Rond-point de l'échangeur de Solaize, BP 3, 69390 Vernaison, France*

[*] *Corresponding author: sebastien.laforge@univ-poitiers.fr (S. Laforge)*

Introduction

EU-1 is a medium-pore zeolite belonging to the EUO framework type. Its pore architecture is formed by a monodimensional system of 10-membered ring (10-MR) channels (5.8 × 4.1 Å), periodically interrupted by alternating 12-MR "side pockets" (6.8 × 5.8 × 8 Å). This pore structure leads to an original catalytic behaviour which is generally intermediate between large and medium-pore size zeolites [1-3]. The most promising results obtained with EU-1 zeolite concerned the bifunctional isomerisation of ethylbenzene to xylenes (C_8 aromatic cut) [4]. During this transformation carried out over mixtures of Pt-Al_2O_3 and H-EU-1 zeolite, the desired xylenes selectivity increases strongly with time-on-stream [5]. This fact was explained by a fast deactivation by "coke" deposits of the inner protonic sites of the zeolite, on which many side reactions (disproportionation, transalkylation) occurred whereas the protonic sites located at or near the external surface, on which only isomerisation occurs, remain active.
On the other hand, Moreau *et al.* showed that the partial exchange of the protonic sites of H-MOR zeolites by sodium cations allowed increasing the selectivity to xylene during ethylbenzene transformation over Pt/Al_2O_3-NaHMOR catalysts, due to a the strong decrease in the rates of the bimolecular side-reactions [6, 7]. The same authors also suggested that *m*–xylene transformation at 350°C can be used to check the effect of sodium exchange on the rates of isomerisation, disproportionation and transalkylation reactions.
In this work, *m*-xylene transformation at 350°C was used to evaluate the effect of sodium exchange on the physicochemical and catalytic properties of EU-1 zeolites. Furthermore, the location of the sodium cations will be discussed on the basis of the transformation of mesitylene (1,3,5-trimethylbenzene), a bulky reactant which can only react at or near the external surface of 10-MR zeolites.

Experimental

An as-synthesized EU-1 zeolite provided by IFP was calcined and exchanged in order to obtain a protonic H-EU-1 sample, using the procedure detailed in Ref.[1]. This sample was then exchanged at room temperature and for 4 hours with sodium nitrate solutions. Different exchange levels were obtained by varying the sodium nitrate concentration: 30, 60, 100, 200, 300 and 500 mol.% of the protonic acidity of the parent zeolite. The catalyst acidity was determined by pyridine adsorption followed by FTIR spectroscopy [1]. The *m*-xylene and mesitylene transformations were then carried out in a fixed-bed glass reactor at 350 °C and atmospheric pressure, using nitrogen as a carrier gas ($P_{N2}/P_{reactant}$ = 13). The products were collected at different time on stream (*TOS*) and analysed by gas chromatography.

Results and discussion

Fig. 1a and b show that, as expected, the sodium exchange rate increases with the $NaNO_3$ solution concentration whereas the total Brönsted acid sites concentration decreases.

Nevertheless, the introduction of the first cations seems to occur faster, which could be related to a very fast and easy exchange of the strongest acid sites, as previously proposed in the case of MOR zeolite [7].

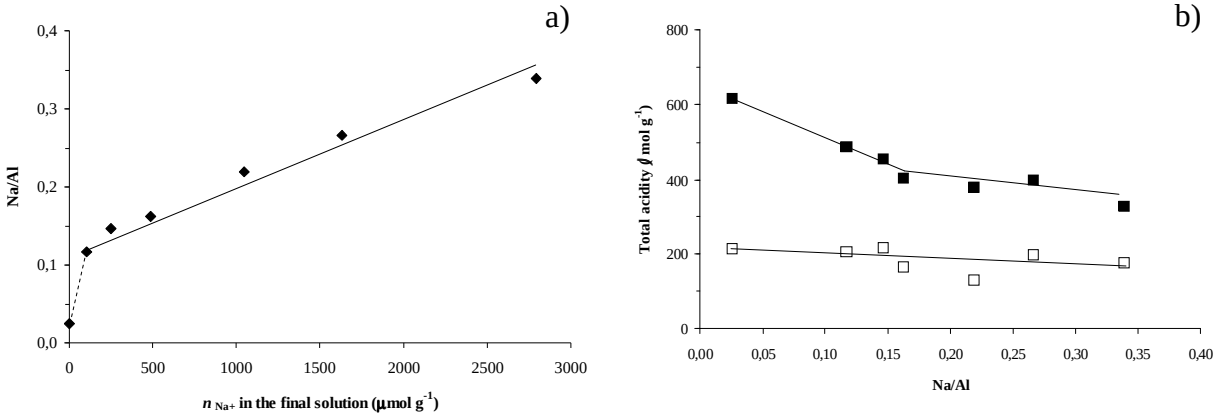

Fig. 1: Sodium exchange of the H-EU-1 zeolite sample. a) Effect of the sodium nitrate solution concentration on the exchange rate (molar Na/Al ratio). b) Evolution of the Brönsted (■) and Lewis (□) acidity as a function of the exchange rate.

This suggestion is supported by the evolution of the initial *TOF* values obtained in *m*-xylene transformation (Fig. 2a): fast decrease at low exchange rate (Na/Al < 0.15) and then quasi constant value. On the other hand, the same evolution of *TOF* can be observed when mesitylene is transformed on the various samples (Fig. 2b). According to the fact that this reactant is too bulky to enter the pores of EU-1 zeolites, the strong decrease in the *TOF* value might be attributed to a preferential exchange of the protonic sites located at or near the external surface of the EU-1 crystallites, and in particular those located in external side-pockets which are very active during ethylbenzene isomerisation [5].

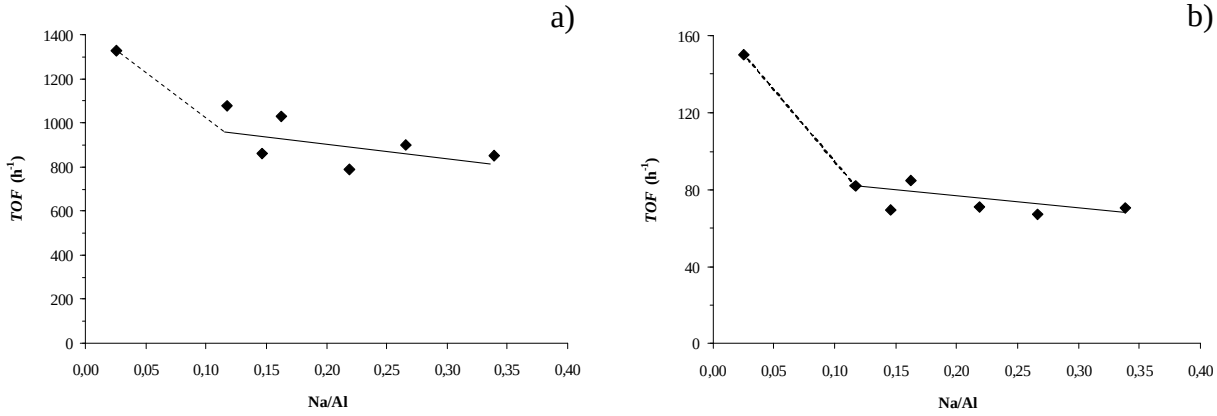

Fig. 2. Transformation of *m*-xylene (a) and mesitylene (b) at 350 °C. Turn-over frequency (*TOF*) taken as the ratio of the initial activity determined after 2 min of reaction to the Brönsted acid sites concentration) versus Na/Al ratio.

References

[1] P.C. Mihindou-Koumba, J.-D. Comparot, S. Laforge, P. Magnoux, *J. Catal.* 255 (2008), 324
[2] G.N. Rao, R. Kumar, P. Ratnasamy, *Appl. Catal.* 49 (1989), 307
[3] W. Souverijns, L. Rombouts, J.A. Martens, P.A. Jacobs, Micropor. Mater. 4 (1995), 123
[4] L. Rouleau, F. Kolenda, E. Merlen, F. Alario, US Pat. 0,051,757 A1, to Institut Français du Pétrole, 2001
[5] F. Moreau, P. Moreau, N.S. Gnep, P. Magnoux, S. Lacombe, M. Guisnet, *Microp.Mesop.Mat.* 90 (2006), 327
[6] F. Moreau, N.S. Gnep, S. Lacombe, E. Merlen, M. Guisnet, *Appl. Catal. A: General* 230 (2002), 253
[7] F. Moreau, P. Ayrault, N.S. Gnep, S. Lacombe, E. Merlen, M. Guisnet, *Microp. Mesop. Mat.* 51 (2002), 211

Use of microwaves for the synthesis of sulfonic acid-functionalized mesoporous silica. Application as catalyst in glycerol etherification.

María Dolores González, Yolanda Cesteros and Pilar Salagre
Departament de Química Física i Inorgànica. EMaS. Universitat Rovira i Virgili.
C/ Marcel·lí Domingo s/n, 43007 Tarragona, Spain, mdolores.gonzalez@urv.cat

Introduction

Nowadays biodiesel is an attractive and environmentally friendly alternative to petrodiesel fuel. During biodiesel manufacture, by transesterification of vegetable oils with methanol, glycerol is formed as by-product (10 wt % of the total product). The price of glycerol is falling (until 0.1 $/kg) as fast as biodiesel plants are being built. For this reason, an important research is currently starting in order to find new outlets for the surplus glycerol by converting it into high value-added products that improve the economy of the whole process [1-2].
One high interesting option is the catalytic etherification of glycerol (Fig. 1), in the presence of tert-butanol or isobutene, to obtain di- and tri- tertiary butyl ethers of glycerol (h-GTBE), which can be used as oxygenated fuels replacing the highly toxic to the environment, methyl tertiary butyl ether (MTBE), and reducing remarkably the emissions of particulate matter [2]. The best catalysts reported for glycerol etherification (with isobutene or tert-butanol) were strong acid ion-exchange resins (Amberlyst type). Mesoporous silicas functionalized with organosulfonic acid groups, introduced by conventional heating, have been tested as catalysts for the glycerol etherification with isobutene resulting in high conversion and moderate selectivity values to h-GTBE [3]. The use of microwaves for the synthesis and modification of materials is becoming an important tool to reduce the synthesis time (energy saving). However, there are not studies about the use of microwaves during sulfonation of mesoporous silicas instead of conventional heating. Also, we have not found references about the use of sulfonated mesoporous silicas as catalysts for the etherification of glycerol with tert-butanol.

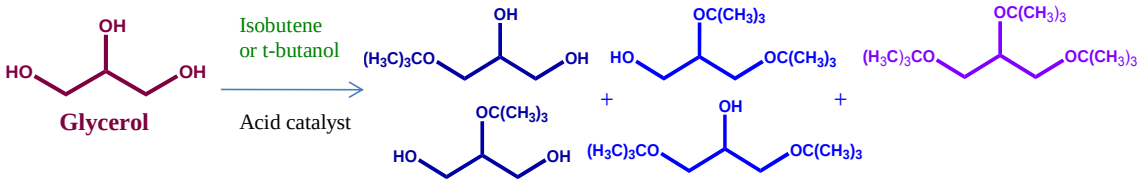

Figure 1. Glycerol etherification with isobutene or t-butanol.

In this work, we prepared two sulfonic acid-functionalized SBA-15 samples with microwaves and by conventional heating, respectively. These samples were used as catalysts for the etherification of glycerol with t-butanol or isobutene. Two non functionalized silicas with different surface characteristics were also tested for this reaction for comparison.

Experimental

SO_3H-SBA-15 samples were prepared by adding 4.0 g triblock copolymer poly(ethylene glycol)-block-poly(propylene glycol)-block-poly(ethylene glycol) ($EO_{20}PO_{20}EO_{20}$) to 125 ml of 2 M HCl at room temperature under stirring. Then, the solution was heated to 40 ºC and TEOS (9 g) was added dropwise. After 45 min, 2.8 g of 2-(4-chlorosulfonylphenyl) ethyltrimethoxysilane (CSPTMS) solution in methylene choride (50%, Gelest) was added dropwise (to prevent phase separation). After that, sample was heated under continuous stirring at 40 ºC for 24 h by traditional refluxing (sample SO_3H-C) or at 40 ºC for 2 h by refluxing under microwaves (sample SO_3H-MW). The reaction mixture was transferred to a Teflon-lined autoclave and heated at 100 ºC in a conventional oven for 24 h. The resulting

product was filtered, washed repeatedly with a large amount of water, and dried in air overnight. The surfactant template was removed by extraction with ethanol under reflux for 24 h, and later calcination in air at 200 ºC for 24 h. One commercial silica of low surface area ($2m^2/g$, Sigma-Aldrich), and a high-surface area pure silica SBA-15, prepared by the method previously explained without acid funcionalization, were also used (samples Silica and SBA-15, respectively). Catalysts were characterized by XRD, N_2 physisorption, desorption of cyclohexylamine by TGA, and FTIR techniques. Etherification of glycerol was carried out with t-butanol or isobutene (glycerol/t-butanol or isobutene = ¼) in a batch reactor under N_2 at 1 atm and 75ºC using 1 g of catalyst. Samples were analyzed by gas chromatography.

Results and discussion

From XRD, we observed that the three synthesized SBA-15 samples showed the typical hexagonal structure. The use of microwaves allowed us to introduce a higher number of sulfonic groups in the mesoporous silica at much shorter time, as confirmed by the lower surface area obtained by N_2 physisorption (Table 1) and by the higher number of acid centres observed by desorption of cyclohexylamine by TGA, and FTIR techniques for this sample.

After 24 h of reaction, pure silicas (Silica and SBA-15), with different surface area and porosity, did not show activity for the glycerol etherification (Table 1). This can be explained because of the low amount of acid centres of these samples. However, functionalized SBA-15 catalysts were active due to the presence of sulfonic acid groups. Interestingly, the sample functionalized with microwaves showed higher conversion and higher selectivity to di- and tri- tertiary butyl ethers of glycerol than that functionalized by conventional heating with similar selectivity to di- and tri-ethers to that obtained with the Amberlyst acid catalyst [4].

Table 1. Catalytic results for glycerol etherification after 24 h of reaction.

Catalyst	BET area (m^2/g)	Etherification with t-butanol			Etherification with isobutene		
		Conv (%)	$S_{monoethers}$ (%)	$S_{di- and triether}$ (%)[a]	Conv (%)	$S_{monoethers}$ (%)	$S_{di- and triether}$ (%)[a]
Silica	2	0	0	0	--	--	--
SBA-15	820	0	0	0	--	--	--
SO_3H-C	622	56	87	13 (traces)	99	15	85(28)
SO_3H-MW	559	68	70	29 (1)	100	9	91(39)

[a] In parenthesis, selectivity to triether (%).

Conclusions

The use of microwaves for sulfonic functionalization of mesoporous silica modified the properties of these materials resulting in higher conversion and higher selectivity to the desired products than those obtained with the catalyst functionalized by conventional heating. This has been explained by the higher number of sulfonic acid centres obtained for the microwave sample.

Acknowledgements

The authors are grateful for the financial support of the Ministerio de Ciencia e Innovación and FEDER funds (CTQ2008-04433/PPQ) and for the FPU grant (AP2007-03789).

References

[1] (a) Pagliaro, M., Ciriminna, R., Kimura, H., Rossi, M., Della Pina, C., Angew. Chem. Int. Ed. 46 (2007) 4434-4440; (b) Zhou, C.H., Beltramini, J.N., Fan, Y.X., Lu, G.Q., Chem. Soc. Rev. 37 (2008) 527-549.

[2] Behr, A., Eilting, J., Irawadi, K., Leschinski, J., Lindner, F., Green Chem. 10 (2008) 13-30.

[3] Melero, J.A., Vicente, G., Morales, G., Paniagua, M., Moreno, J.M., Roldán R., Esquerro, A., Pérez, C., Appl. Catal. A: Gen. 346 (2008) 44-51.

[4] Klepacova, K., Mravec, D., Bajus, M., Appl. Catal. A: Gen. 294 (2005) 141-47.

Pd-Co/HBEA catalysts with enhanced activity for the Selective Catalytic Reduction of NO_x with methane

Joana Pereira[a], Ana Paula Ferreira[b], Sandra Capela[c], Auguste Fernandes[a], Patrick da Costa[d], Filipa Ribeiro[a], Carlos Henriques[a]

[a]*Instituto Superior Técnico, Institute for Biotechnology and Bioengineering, Centre for Biological and Chemical Engineering, Av. Rovisco Pais 1049-001 Lisboa, Portugal,* carlos.henriques@ist.utl.pt

[b]*CiiEM, ISCSEM, Quinta Granja, Campus Universitário, 2829-511 Caparica, Portugal*

[c]*GDF SUEZ, Research and Innovation Division – CRIGEN, 361, Avenue du Président Wilson – BP 3393221 Saint Denis La Plaine Cedex, France*

[d]*Université Pierre et Marie Curie, Paris 6, Institut Jean Le Rond d'Alembert, CNRS UMR 7190, 2 Place de la Gare de Ceinture, 78210 Saint Cyr l'École, France*

Introduction

The practical application of metal exchanged zeolites for the abatement of NOx is nowadays limited by catalysts stability, namely due to the presence of water in the exhaust gases from both mobile and stationary sources [1].

Metal exchanged Co and Pd-Co zeolites have shown to be promising for the selective catalytic reduction of NO_x (SCR-NO_x) with methane, in oxidizing atmospheres [2].

A previous work [3] showed that hydrothermal treatments, performed over Pd/Co-HBEA catalysts, allow to increase significantly their stability as well as the activity and selectivity, under wet conditions.

In the present work, a detailed characterization and catalytic evaluation of hydrothermal treated Pd-Co-HBEA catalysts in the CH_4-SCRwas performed in order to emphasise the role of metal species re-distribution in the enhancement of catalysts performance, after hydrothermal treatments.

Experimental

Commercial BEA zeolite, with Si/Al = 12.5 was provided by Zeolyst International in the ammonium form. Co-zeolite catalyst with 2wt.% Co was prepared by ion-exchanging the ammonium form with a cobalt acetate solution, then calcined at 500ºC under air flow. Bimetallic Pd-Co catalysts were obtained by ion-exchanging the monometallic form with the required amount of palladium nitrate tetra-ammine solution, in order to obtain a 0.15 wt.%. Pd 2 wt.% Co/BEA catalyst. The exchange was followed by calcination at 450ºC under air flow.

Catalysts steaming was performed with a mixture of air and 10 vol.% water, at 450, 500 and 550ºC. Steaming was performed in different stages of catalyst preparation, i.e., before or after metallic exchange. Catalysts were characterized by X-Ray Diffraction (XRD), Temperature Programmed Reduction (H_2-TPR) and UV-Vis DRS performed at high temperature under gas flow. The reduction of NOx by methane, in the presence of oxygen excess, was carried out in a fix-bed flow reactor. Reactants mixture composition intends to simulate a natural gas lean burn engine exhaust: 150 ppm NO, 1500 ppm CH_4, 7% vol. O_2, 2% vol. H_2O in Ar, with a GHSV of 45000 h^{-1}.

Results and discussion

Bimetallic $Pd_{0.15}Co_2$ - HBEA catalyst shows low activity and selectivity values, when tested in the CH_4-SCR of NO under oxygen excess and 2% vol. H_2O.

Nevertheless, for PdCo-HBEA samples previously pretreated under steaming conditions at several temperatures, DeNOx activity increases when tested in the presence of water vapour. The sample steamed at 500ºC shows a global increase of NO conversion of about 20%, in all the studied temperature range (Fig. 1*A*), when compared to the unsteamed catalyst.

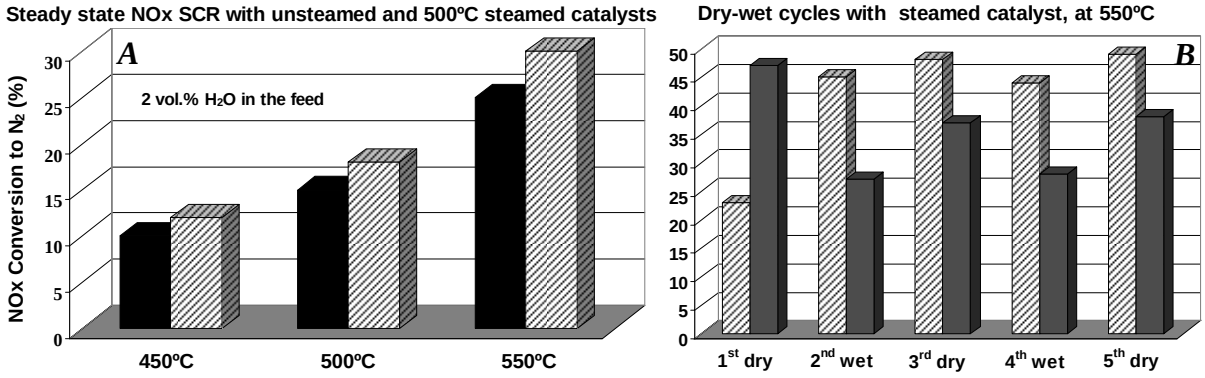

Figure 1: ***A*** - Steady-state NOx conversion with unsteamed■ and steamed▨ catalyst; ***B*** - Dry-wet (2 vol.% H_2O) cycles at 550ºC with steamed catalyst: NOx▨ and methane■ conversions

Dry-wet reaction cycles (Fig. 1*B*), performed with steamed catalyst shows a surprisingly improvement in activity, when water is introduced in the reaction mixture (2^{nd} wet), while CH_4 conversion decreases.

XRD analysis revealed no loss of crystallinity after steaming or catalytic tests. UV-Vis DRS shows that ion-exchanging Co-HBEA catalysts with palladium, followed by calcination or even by steaming treatments did not significantly perturb the Co^{2+} ions in exchange positions. On the contrary, H_2-TPR tests reveal the formation of considerable amounts of reducible metal species, at lower temperatures (between 100 and 300 ºC).

Conclusions

Results obtained in the present work shows that steaming of Pd/Co-HBEA catalysts can result in an increase of catalytic performances. The observed re-organization of cobalt species takes place without modifying the distribution of ion-exchanged Co cationic entities and constitutes a key factor for the increased activity and stability of these catalysts when tested under wet conditions.

The formation of cobalt species reducible at low temperatures seems to be a major factor resulting from hydrothermal treatments. The involvement of these species in the mechanism of reduction of NO, including the oxidation of NO to NO_2 at low temperatures has been reported as beneficial to the SCR of NO with CH_4: the interaction between Pd species and Co oxo-cations, with the possible formation of multi-metallic species has been suggested [3].

This global behaviour can be attributed to (i) the redistribution of metallic species on steamed catalysts (favouring, for instance, the formation of NO_2), (ii) to a synergetic effect between Co and Pd cations induced by steaming treatment or (iii) to some stabilization induced by extra-framework aluminium species.

References

[1] D. Kaucky, A. Vondrova, J. Dedecek, B. Wichterlova, J. Catal 194 (2000) 318-329.
[2] J.A.Z. Pieterse, H. Top, F. Vollink, K. Hoving, R.W. van den Brink, Chemical Engineering Journal 120 (2006) 17-23.
[3] A.P. Ferreira, C. Henriques, M.F. Ribeiro, F.R. Ribeiro, Catalysis Today 107–108 (2005) 181–191.

Characterization of Pd and In species in PdInH-mordenite for the SCR of NO_x with methane.

Hernán Decolatti[a*], Ferenc Lónyi[b], Hanna Solt[b], Eduardo Miró[a], Laura Gutierrez[a].
[a] *Instituto de Investigaciones en Catálisis y Petroquímica (FIQ,UNL-CONICET), Santiago del Estero 2829, 3000 Santa Fe, Argentina. * e-mail: herdeco@fiq.unl.edu.ar.*
[b] *Institute of Surface Science and Catalysis, Chemical Research Center, Hungarian Academy of Sciences,Pusztaszeriút 59-67, 1025 Budapest, Hungary.*

Introduction

The abatement of the NO_x emissions of small power plants or engines that use natural gas is a problem difficult to solve when working under lean conditions. In this sense, the proposed reduction of NO_x on zeolitic catalysts or oxides with methane has produced promising results [1]. Different metals exchanged in ZSM5 and ferrierite have been reported as active catalysts for this reaction[2]. It is usually accepted that the oxidation of NO to NO_2 is an important step in the reaction under study [3]. Moreover, on In-zeolite catalysts, InO^+ species are associated with a high NO_x adsorption capacity which in turn favors the reaction rate [4]. In this work we used several techniques to characterize the generated species when indium and palladium were exchanged in H-mordenite and the effect of the Pd/In ratio on the said species was investigated. We studied the activity of In-Hmordenite catalysts obtained by reductive solid-state ion exchange and the effect of the addition of Pd.

Experimental

Catalysts Preparation: H-mordenite (Süd Chemie AG, Si/Al = 6.7, BET area = 409m^2/g) and In_2O_3 were mixed applying intense co-grinding. By reductive solid state ion exchange, InH-mordenite (InHM) samples were prepared, reducing the In_2O_3/H-mordenite mixture in H_2 flow at 500 °C for 2 hours and then reoxidizing it in O_2 flow at 400 ºC for 1 hour. The In/Al molar ratio of the obtained mordenite catalysts were 1/6 and 1/3. Catalysts containing 0.5% Pd (PdInHM and PdHM) were prepared by impregnating the InHM and HM samples with a solution of $Pd(NH_3)_4(NO_3)_2$ and heating the samples in O_2 flow at 350 °C for 1 hour.
Catalysts Characterization: N_2 Adsorption: The nitrogen adsorptions were performed at 77 K using a Micromeritics ASAP 2020 instrument. BET and t-plot analyses were applied. Temperature-programmed reduction: An Okhura TP2002S instrument equipped with a TCD detector was used. The reducing gas was 5% H_2 in Ar and the heating rate was 10 °C/min. NO-TPD: It was conducted in a flow equipment with controlled gas flow and heating. The desorbed gases (NO, N_2O and NO_2) were monitored and quantified by FTIR using a gas cell.
Catalytic test: The powder catalysts were evaluated using the same flow reactor described in the NO-TPD experiments. The composition of the reagent stream was: NO = CH_4,4000 ppm and 2% O_2 (GHSV: 15000 h^{-1}). The reactor effluent composition was monitored for CH_4, CO, NO, N_2O and NO_2 by FTIR.

Results and Discussion

The InHM(1/3) and InHM(1/6) catalysts have a NO to N_2 conversion with the typical shape of a volcano, where the conversion decreases at a certain temperature because of the undesired methane combustion. The presence of Pd in PdInHM(1/3) leads to an increase of NO_x conversion at temperatures above 500 °C. This activation phenomenon is permanent and on a second test, the NO to N_2 conversion is greater in the temperature range studied. PdInHM(1/6) did not show the activation recorded in PdInHM(1/3). The BET surface area of the catalysts decreased with the indium exchange as a consequence of the presence of bulky InO^+ species inside the mordenite channels. The TPR of monometallic catalysts was carried out as reference. For the PdHM sample, a negative peak at 106°C is attributed to some hydrogen produced during the decomposition of the palladium hydride β phase [5]. A low temperature peak could relate to oxidized Pd species at the external surface of the zeolite as

these are likely the first ones to be reduced. It is well known that wet impregnation could result in larger PdO clusters deposited at the external surface of mordenite. For InHM and PdInHM solids, the main reduction peak is below 400°C suggesting the presence of $(InO)^+$ at zeolite exchange positions wich is associated with active species for the CH_4-SCR of NO_x [6]. No reduction peaks are observed at temperatures higher than 600 °C; therefore, it could be inferred that there is no highly crystalline In_2O_3 in the matrix. For all the catalysts studied in this work, the amount of hydrogen consumed during the TPR experiments decreased after their use under reaction conditions. This could be due to the presence of some Pd-In interaction that leads to a lower reducibility of indium exchanged species, or to a decrease in the amount of those. In NO-TPD experiments, NO_2 desorption besides NO were observed in all solids, at different rates depending on the Pd/In ratio and on whether the solids were fresh or used. The NO_2 formation is associated with the presence of adsorbed oxygen on the zeolite surface [7] or the oxidation of adsorbed NO on In associated species (InO^+ at exchange positions or In_xO_y species). An increase in the amount of NO_2 formed during the NO adsorption on the used PdInHM(1/3) catalyst suggests a greater amount of oxygen species associated with the network or the indium in the matrix. This increment of the active species could explain the increase in NO conversion observed in the reaction conditions. From the catalytic results and solids characterization by NO-TPD, it can be noted that there is clearly a correlation between the maximum catalytic activity obtained for each catalyst and the NO_2 and NO desorbed ratio. Figure 1 shows that when this ratio increases, the catalytic activity also enhances; so, we can say that it is influenced by the catalyst ability to form NO_2.

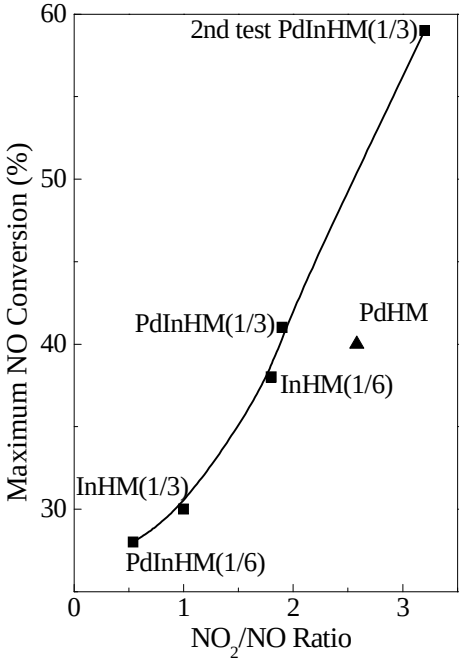

Figure 1: Desorbed NO_2/NO ratio

Conclusions

The proportion of indium in the catalyst is a predominant factor in the promoting effect of Pd for the SCR of NO. For higher In loading, PdInHM(1/3), the addition of Pd results in an increase in the catalytic activity which is more pronounced after certain time-on-stream at 500 °C. The TPR experiments indicate that the majority of In is under the form of $(InO)^+$ active sites. The Pd-In interactions in the bimetallic samples are interpreted in terms of the mobility of Pd, giving place to its migration towards sites of low accessibility in the case of the PdInHM(1/6) sample, and to the occurrence of Pd-In entities which are readily available to the reaction medium in the case of the PdInHM(1/3) sample. There was a clear correlation between the maximum catalytic activity of each catalyst and its ability to form NO_2 in the NO-TPD experiments.

Acknowledgements

The authors acknowledge the financial support received from UNL, CONICET and ANPCyT. Thanks are given to the Hungarian-Argentinean program that made this joint project possible.

References

[1] Y. Sato, H. Yu-u, N. Mizuno, M. Iwamoto, Appl. Catal. 70 (1991) L1-L5.
[2] L. J. Lobree, A. W. Aylor, J. A. Reimer, H. V Bell, 2nd World Congress on Env Catalysis, Miami, 1998.
[3] E. Kikuchi, M. Ogura, Cat Surv. Jpn 1 (1997) 227.
[4] T. Sowade, C. Scmidt, F.W. Schutze, H. Berndt, W. Grunert, J. Catal. 214 (1) (2003) 100-112.
[5] T. C. Chang, J.J. Chen, C. T. Yeh, J. Catal. 96 (1985) 51-57
[6] X. Zhou, Z. Xu, T. Zhang, L. Lin, J. Mol. Catal. A: Chemical 122 (1997) 125-129.
[7] M. A. Ulla, L. Gutierrez, E. A. Lombardo, F. Lónyi, J. Valyon, Appl. Catal. A. General 277 (2004) 227

AN INVESTIGATION OF ACTIVITIES AND SELECTIVITIES OF H-ZSM5 AND H-FERRIERITE ZEOLITES MODIFIED BY DIFFERENT METHODS IN N-BUTENE ISOMERIZATION

Emre Kılıç, Selahattin Yılmaz*
*Department of Chemical Engineering, Izmir Institute of Technology, Urla Izmir 35430, Turkey, * e-mail: emrekilic@iyte.edu.tr, e-mail: selahattinyilmaz@iyte.edu.tr*

Introduction

Skeletal isomerization of n-butene to isobutene has attracted much attention on all of the world to meet the demand for isobutene[1]. The pore structure and the acidity of the catalyst plays important role in selectivity to isobutene. Strong acidic catalysts cause cracking and oligomerization. On the other hand weak acidic catalysts cause double bond isomerization. So that catalyst must be at the optimum acid strength for isobutene formation [2]. Among the large number of catalysts, 10 membered ring zeolites (H-ZSM5, H-Ferrierite (H-FER), SAPO-11) are the most active, and stable catalysts since their pore sizes (between 4-5,5 A^o) are very suitable for isobutene formation[3, 4]. Although H-ZSM5 and H-FER catalysts are very active and stable catalysts, their selectivities are not sufficient to obtain high selectivity to isobutene. Modification of their acidity is an alternative way to increase their selectivity [5]. In this study different modifications methods were used to modify H-ZSM5 and H-FER acidity.

Experimental

Synthesized H-ZSM5 with Si/Al ratio of 77, commercial H-FER were used as parent catalysts. These zeolites were modified by chemical liquid deposition method using tetraethylorthosilicate (TEOS) and 3-aminopropyltriethoxysilane (3-amino) as modification agents. They were also modified by acid, alkali and ammonium hexafluorosilicate (AHFS) treatments using HCl, NaOH and AHFS, respectively. Before the HCl treatment, catalysts were treated with alkali solutions (Pre-alkali treatment). Crystallinity, morphology, acidity and textural properties were characterized using XRD, SEM, NH_3-TPD, FTIR and BET. A fixed bed reactor system was used for the testing of catalysts for 1-butene skeletal isomerization reaction. A feed gas contained 7 % 1-butene in N_2. The WHSV was 22 h^{-1}. The reactions were performed at 375 ^oC.

Results and Discussion

SEM and XRD results showed that crystal structure and morphology of the catalysts were preserved after modifications, only slight change on crystallinity was observed on acid and 3-amino treatment. Modifications affected H-ZSM5 and H-FER similarly, so only the results for H-ZSM5 were given in this abstract. Table 1 shows the textural properties and catalytic performance of H-ZSM5 catalyst. It was seen that except alkali treatment, modifications decreased the surface area of the parent catalysts. This decrease was more significant with 3-amino treatment which could be related to pore blockage and dealumination by 3-amino, so effective deposition occurred by this agent [6].

The acidity of H-ZSM5 and its modified forms were studied by NH_3-TPD. TEOS modification reduced acid sites slightly with some pore narrowing. On the other hand total number of acid sites decreased dramatically after 3-amino modification, because of the pore blockage and dealumination. Although total acidity did not change in alkali treatment, strong acid sites increased because of the extra-framework structures occurring during modification [7]. Selective modification was obtained by AHFS treatment which passivated unselective acid sites without narrowing pores and changing structure.

Activity and selectivity of the catalysts were also affected by modifications. Since most of the acid sites and pores were blocked, selectivity of the parent catalysts were reduced the most after 3-amino deposition. TEOS modification improved the selectivity of the parent catalysts since the surface area and total acid amount of the catalysts decreased slightly with this deposition agent. Alkali treatment caused desilications and increased the activity but decreased the selectivity of the catalyst. Pre-alkali-acid treatment reduced acid sites slightly, this caused an increase in selectivity and decrease in activity. The highest selectivities to isobutene were observed by AHFS treatment although activity of the catalysts decreased slightly. In this treatment, a thin layer was formed on the surface of zeolites and unselective sites were passivated. AHFS treatment also blocked the pores slightly. All of these let to higher isobutene selectivity.

Table 1. Textural properties and catalytic performance of H-ZSM5 and its modified samples

Catalysts	BET Surface Area (m^2/g)	H.K. Pore Diameter (Å)	Total Acidity (mmol NH_3/ gcat)	X*	S*	Si/Al Ratio
H-ZSM5	421.3	9.3	0.376	51.48	57.97	76.3
H-ZSM5 -TEOS	405.3	8.7	0.354	47.7	63.74	79.4
H-ZSM5-3amino	319.4	6.8	0.227	25.78	51.87	170.0
H-ZSM5-NaOH	427.0	9.1	0.365	64.48	52.09	78.4
H-ZSM5-NaOH-HCl	406.1	9.0	0.368	49.42	66.67	78.0
H-ZSM5-AHFS	411.4	9.3	0.364	47.36	75.37	85.1

***X:** Conversion of n-butene (%), **S: %** Selectivity to Isobutene (%)

Conclusion

It has been demonstrated that the acidity of the synthesized H-ZSM5 and commercial H-FER could be controlled by some modification methods. Some modifications blocked pores, some modificataions reduced the acid sites dramatically. TEOS modified catalysts acidity&pore size did not change much, it slightly improved selectivity to isobutene. 3-amino treatment blocked pores of the zeolite and caused some dealuminations. Alkali treatment affected surface area, acidity and caused desilications. The best results for selectivity to isobutene were obtained by AHFS treatment which modified the zeolites acidity &pores slightly.

References

[1] Y. Shang, P. Yang, M. Jia, W. Zhang, T. Wu ., Modification of MCM-22 zeolites with silylation agents: Acid properties and catalytic performance for the skeletal isomerization of n-butene, Catalysis Communications 9, (2008), 907–912.

[2] Cañizares, P.; Lucas, de A.; Dorado, F. & Pérez, D., Effect of zeolite pore geometry on isomerization of n-butane, Applied Catalysis A: General, 190:1-2, (2000), 233-239.

[3] Houzvicka, J., Hansildaar, S., Ponec, V., The Shape Selectivity in the Skeletal Isomerisation of n-Butene to Isobutene, Journal of Catalysis, Vol. 167, No. 1, (1997), 273-278.

[4] Suh, Y., Lee, J., Rhee, H., Skeletal isomerization of 1-butene over sulfate promoted zirconia with large surface area prepared by an atrane route, Applied Catalysis A: General, 274, (2004), 159–165.

[5] E. Kilic, S. Yilmaz., HZSM-5 and H-Ferrierite Acidity Modification by Silylation and Their Activities in n-butene Isomerisation, International Journal of Chemical Reactor Engineering, (2010), Vol. 8: A164

[6] W. Ding, G.D.Meitzner, E.Iglesia., The Effects of Silanation of External Acid Sites on the Structure and Catalytic Behavior of Mo/H-ZSM5, Journal of Catalysis, (2002), 206, 14-22.

[7] Y.Q.Song, Y.L. Feng, F. Liu, C.L. Kang, X.L. Zhou, L.Y. Xu, G.X. Yu., Effect of variations in pore structure and acidity of alkali treated ZSM-5 on the isomerization performance., Journal of Molecular Catalysis A: Chemical, (2009), 310, 130–137.

Development of template assistant one-pot synthesis Ni-ZrO_2composites for catalysis application

E.V.Golubina, A.O.Turakulova, T.P.Otorozhenko, E.S.Lokteva, M.V.Lobanov, V.V.Lunin
Department of Chemistry, M.V.Lomonosov Moscow State University, Moscow, Russia
golubina@kge.msu.ru

Introduction (Times New Roman, 12 pt, bold)

Porous ceramics (ZrO2, alumina etc.) are widely used as catalysts support. Synthesis of oxides with hierarchical porous structure is of great importance in order to provide the accessibility of active sites to reagents. To create mesoporous structure organic templates are widely used. Prepared oxide materials are then impregnated by active metal precursor followed by metal reduction.
In this paper one-pot synthesis of Ni-ZrO2 composites with citric acid or with wood templates are studied. Segregation of Ni particles is observed during Red-Ox treatment. Catalytic activity was tested in hydrodechlorination of chlorobenzenes and CO oxidation.

Experimental

Ni-ZrO2 composites (6 wt. % Ni) were prepared. Biomorphous Ni-ZrO2 composite (Ni-ZrO2_bio) was prepared by calcination of sawdust, impregnated by solutions of Ni(NO3)2 and ZrO(NO3)2. Calcination temperature was determined by DSC-TG.
Another method is sol-gel technique with citric acid as chelating agent. Solution of citric acid, Ni(NO3)2 and ZrO(NO3)2 was slowly evaporated at 80 C. Obtained precursor was calcinated at 600 C on air. This sample is denoted as Ni-ZrO2_s-g.
Textural properties were investigated by nitrogen adsorption/desorption on Quantachrome AUTOSORB. Samples morphology was studied by XRD (Rigaku Miniflex II diffractometer) and SEM-EDX (Olympus 3100, JEOL, Japan). Temperature programmed reduction was performed by H2 (5%) –Ar at liner heating. Hydrogen consumption were determined by thermal conductivity detector.
Hydrodechlorination of chlorobenzene was performed in flow-type reactor at temperatures 25 – 350 C as described in [1]. CO oxidation (2%CO + 1%O2 in He) was performed by a pulsed microcatalytic technique at temperature range of 150 – 400°C.

Results and discussion

Study of textural properties of prepared samples revealed mesoporous structure (Fig.1), BET surface area is 50 m2/g (Ni-ZrO2_bio) and 38 m2/g (Ni-ZrO2_s-g). Pore volume is 0,22 and

0,17 ml/g for biomorphous and sol-gel composites, correspondingly. Morphology of prepared samples were investigated by SEM. Microphotographs are presented on Fig.2.
Nickel is uniformly distributed in fresh samples according to mapping of elements (Ni, Zr, O) obtained by EDX analysis.

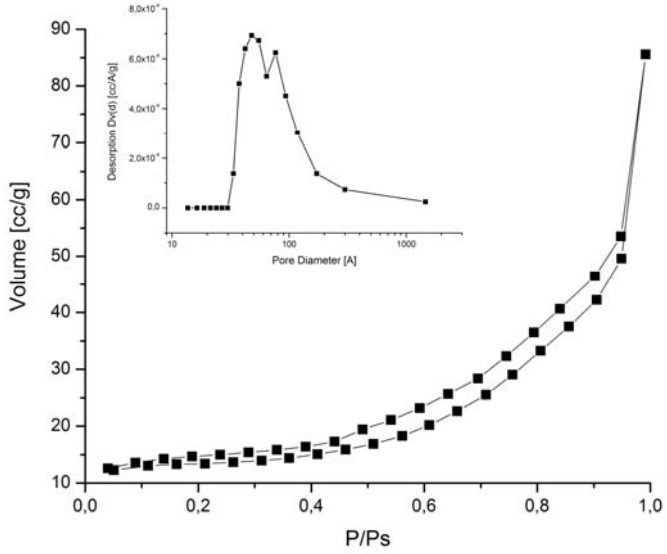

Fig. 1. N_2 adsorption-desorption isotherm and pore size distribution for biomorphous Ni-ZrO2

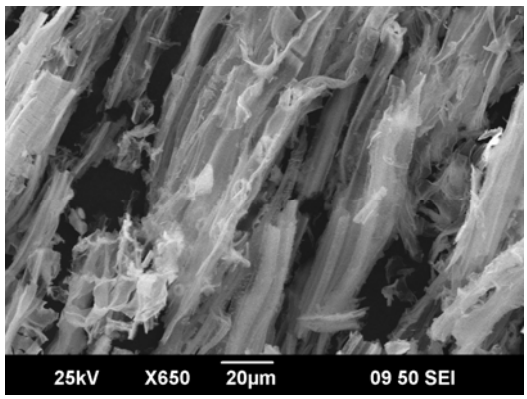

Fig. 1. SEM microphotograph of biomorphous Ni-ZrO2 composite

Reduction process were studied by temperature programmed reduction. Biomorphous zirconia is partially reduces at temperatures higher 600 C. ZrO2 is hardly reduced oxide, and reduction of biomorphous sample proceeds due to the presence of impurities form wood template. TPR spectra for fresh Ni-ZrO2_bio has two reduction peaks which are corresponded to reduction of two form of nickel: surface NiO species and Ni2+ incorporated into ZrO2 lattice. After TPR sample was oxidized on air at 600 C. Reduction behavior is significantly changes because of segregation of nickel to surface. Following oxidative treatment does not lead to changes in TPR profile. Similar reduction behavior was observed for Ni-ZrO2_s-g composite. But in this case 2 Red-Ox cycles are necessary for nickel segregation. Prepared Ni_ZrO2 composites shows high catalytic activity in reductive transformations of chlorobenzenes and CO oxidation.

Conclusions

Approaches for one-pot synthesis of mesoporous catalytically active Ni-ZrO2 composites is proposed.

Acknowledgements

Authors thank E.Nesterova for help in SEM-EDX study. This work is supported by Russian Ministry of education and science (State Contract #02.740.11.0026), RFBR (10-03-00372-a) and President RF grant for young scientists (МК-158.2010.3).

References

[1] E.V. Golubina, E.S. Lokteva, S.A. Kachevsky, A.O. Turakulova, V.V. Lunin // Studies in Surface Science and Catalysis, Volume 175, 2010, Pages 293-296

Ca^{2+}-exchanged ferrierite: an excellent catalyst for selective formation of light alkenes in catalytic cracking of *n*-octane

Lixia Wang*[1], Kenichi Ozawa*[1], Takayuki Komatsu*[1], Takuji Ikeda*[2]
Tokyo Institute of Technology, Japan[1]*
*National Institute of Advanced Industrial Science and Technology, Japan *[2]*
komatsu @cms.titech.ac.jp (Takayuki Komatsu)

Introduction

Light alkenes, especially ethylene and propylene, which are produced by thermal cracking of naphtha show more and more importance in chemical industry. Because the thermal cracking is an energy intensive process, catalytic cracking has now drawn much attention. In this study, the catalytic cracking of *n*-octane was used as a model reaction of naphtha cracking. Ca^{2+}-exchanged ferrierite showed high selectivity and stability in *n*-heptane cracking [1]. So we applied it in the cracking of *n*-octane and tried to clarify the effect of Ca^{2+}-exchange through the characterization.

Experimental

Na,K-ferrierite (Na,K-Fer) with Si/Al atomic ratio of 8.0 was hydrothermally synthesized [1]. Ca^{2+}-exchange was carried out with an aqueous solution of calcium chloride at 343 K. A fixed-bed flow reactor was used for the cracking of *n*-octane under atmospheric pressure at 823 K. W/F corresponded to 1.0–54 g h mol^{-1} with a constant helium/octane molar ratio of 9.0.

Results and discussion

Compared with other zeolites, such as H-Y, H-beta and H-MCM-22, both H-Fer and H-ZSM-5 showed high selectivity to ethylene and propylene. Fig. 1 shows the change in selectivity to ethylene and propylene with *n*-octane conversion. The selectivity increased in the order, H-Fer < H-ZSM-5 < Ca(68%),H-Fer. Ca^{2+}-exchange into H-ZSM-5 reduced the activity without obvious increase in selectivity to light alkenes. As to H-Fer, however, Ca^{2+}-exchange improved its selectivity to light alkenes. When the conversion of *n*-octane approached 100%, the selectivity increased for Ca(68%),H-Fer, while that of H-ZSM-5 and H-Fer decreased.

Ca^{2+}-exchange also improved the stability greatly. Fig. 2 shows the change in *n*-octane conversion with time on stream. The initial conversion decreased, but the stability increased after Ca^{2+}-exchange. The conversions of *n*-octane after 6.6 h on stream were 76% and 75% of the initial values on Ca(89%),H-Fer and Ca(68%),H-Fer, respectively, while that was only 14% on H-Fer. TG analysis showed that the amounts of coke formed in 6.6 h of the reaction were only 2.3% on Ca(89%),H-Fer, 3.7% on Ca(68%),H-Fer and 10.7% on H-Fer.

Ferrierite has two-dimensional pores consisting of 8- and 10-MR channels. Rietveld analysis of XRD and calculation by Maximum Entropy Method for Ca(89%),H-Fer showed that Ca^{2+} cations were mainly located at the center of 8-MR channels. The formation of coke and alkanes would be reduced by such Ca^{2+} cations because hydride transfer to form alkanes and coke precursors is a bimolecular reaction and needs larger space like intersections of 8- and 10-MR channels. NH_3-TPD showed that the Ca^{2+}-exchange decreased the amount of strong acid sites and the total amount of acid sites. It is known that strong acid sites accelerate the formation of coke and high acid density would increase the hydride transfer.

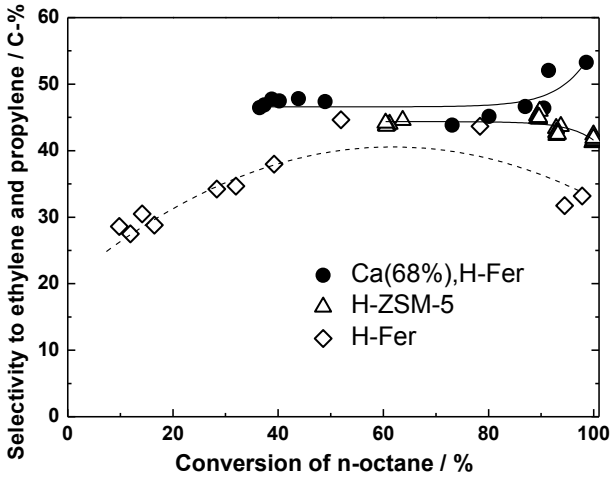

Figure 1. Change in selectivity to ethylene and propylene with *n*-octane conversion.

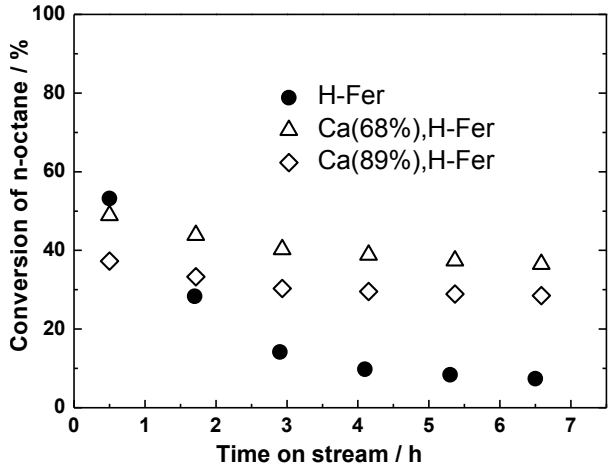

Figure 2. Change in *n*-octane conversion with time on stream.

Conclusions

Ca^{2+}-exchange into ferrierite can improve the stability and the selectivity to light alkenes through the blocking effect on 8-MR channels and the reduction of acid strength and density.

Acknowledgements

This work was financially supported by NEDO (New Energy and Industrial Technology Development Organization).

References

[1] Komatsu, T., Ishihara, H., Fukui, Y., Yashima, T., Selective formation of alkenes through the cracking of *n*-heptane on Ca^{2+}-exchanged ferrierite, Applied Catalysis A: General, 214 (2001), 103-109

Mesoporous, microporous and delaminated supports for Pd-Sn catalysts in the water nitrates hydrogenation

A. E. Palomares, C. Franch, A. Corma
Instituto Universitario Mixto de Tecnología Química (UPV-CSIC), Avenida de los Naranjos s.n., 46022-Valencia (Spain), apalomar@iqn.upv.es

Introduction

The concentration of nitrates in natural water has increased in the last years, mainly due to the use of fertilizers and to the animal excreta. In these areas an important number of water sources surpass the legal limit of 50 mg/L of nitrates. There are different techniques for the nitrate removal as reverse osmosis or biological processes. Nevertheless, these techniques present some problems as the effluent post-treatment or the exploitation costs. Another alternative is the catalytic removal of nitrates. It is based in the liquid phase nitrate hydrogenation on a catalyst containing noble metals. Typically, bimetallic catalysts containing Pd or Pt, and another metal, such as Cu, Sn or In, supported on alumina have been applied for this reaction [1, 2]. The inconvenient of this process is the formation of undesired products such as NO_2^- and NH_4^+. The formation of these products is probably related to mass transfer problems [3, 4]. The diffusion of the reactants towards the active centers is very influenced by the nature of the support, for this reason it is necessary an adequate selection of it in order to design an active catalyst.
In previous works we developed an active Pd-Sn catalyst supported on alumina [5]. In this work we study the activity of Pd-Sn catalysts supported on other micro and mesoporous supports for the catalytic reduction of the nitrates.

Experimental

The supports used in this work were the ITQ-2 zeolite, the ITQ-6 zeolite, the MCM-41, and the MCM-22 zeolite. The different micro and mesoporous materials are synthesized in our laboratory. The Si/Al ratio of these materials was between 25 and 30. Pd and Sn were added to the support by incipient wetness impregnation with the soluble salts of the desired metals in order to have a metal concentration of 5% of Pd and 2.5% of Sn. The sample was initially impregnated with $SnCl_4.H_2O$, dried at 423 K and calcined in air at 773 K for 1 h. After that, $Pd(NO_3)_2.H_2O$ was added and the catalyst was dried and calcined again at the same temperature. The catalysts were reduced with hydrogen at 773 K for 4 h before reaction. The surface areas of the Pd-Sn catalysts prepared were: 489 m^2/g for the Sn/Pd/ITQ-2, 402 m^2/g for the Sn/Pd/ITQ-6, 779 m^2/g for the Sn/Pd/MCM-41, and 422 m^2/g for the Sn/Pd/MCM-22.
The catalysts were tested in a continuous flow stirred tank reactor (600 mL), where the reactant solution was fed into the reactor at atmospheric pressure with a liquid flow rate of 5 mL/min. The mass of catalyst was 3 g and a mixture of CO_2 and H_2 (1:1) with a total flow of 500 cm^3/min was introduced into the reactor during the reaction. The experiments were carried out at 293 K, and the reactor was stirred at 900 rpm. The reaction progress was followed by taking, at defined periods, small aliquots for the photometric determination of nitrate, nitrite and ammonia concentration.

Results and discussion

In this work we have studied the activity in the catalytic reduction of nitrates of some Pd-Sn catalysts supported on two delaminated zeolites, as ITQ-2 and ITQ-6, on a mesoporous material, as MCM-41, and on a MCM-22 zeolite that is a medium porous size zeolite. The

results obtained are summarized in figure 1. As it can be seen, the best results were obtained with the catalysts supported on mesoporous and delaminated materials. The worst results were obtained with the catalyst supported on MCM-22, because the microporous of the zeolite are less accessible resulting in an increase of the mass transfer problems and in a decrease of the catalytic activity. The differences obtained when comparing the activity of the catalysts supported on delaminated zeolites, i.e. the Sn/Pd/ITQ-2 and the Sn/Pd/ITQ-6, could be explained by the different morphology of both materials. The ITQ-2 external surface is more accessible than that of ITQ-6 resulting in a slightly better activity for the catalyst supported on the ITQ-2 zolite. The comparison of the catalytic behavior of the Pd-Sn catalyst supported on the delaminated zeolites and that of the catalyst supported on a mesoporous material (MCM-41) shows that both catalysts present a similar activity, but a higher selectivity to nitrogen is obtained for the Pd-Sn catalysts supported on delaminated zeolites. In this way, the best results are obtained with the Pd-Sn catalysts supported on ITQ-2 zeolites because the structure of the ITQ-2 makes easy the access of the reactants to the active sites of the catalyst and it also favor the desorption of the products formed, improving the catalyst selectivity towards nitrogen.

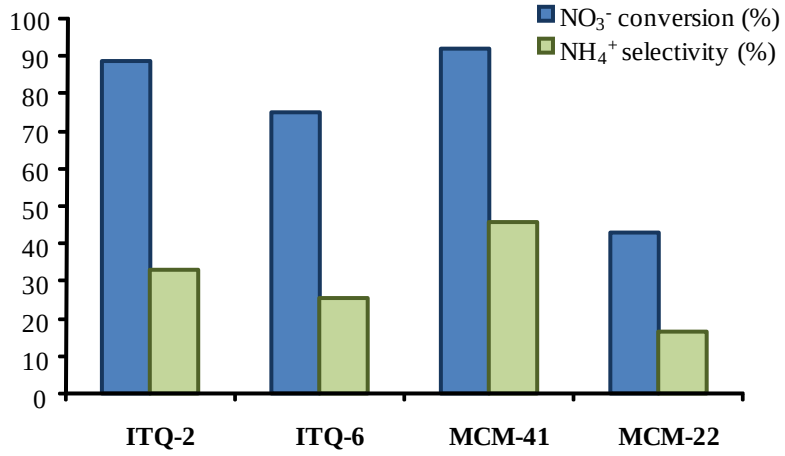

Figure 1. Activity of the 2.5%Sn and 5%Pd (weight) catalysts supported on ITQ-2, ITQ-6, MCM-22 zeolites and MCM-41.

Conclusions

It can be concluded that when using micro or mesoporous materials as supports for the Pd-Sn catalysts in the catalytic reduction of nitrates in water, the best results are obtained with the supports that present a high external surface area that minimize the mass transfer problems. In this way, the activity and selectivity of the catalyst used for this reaction is improved, being the delaminated zeolites, as ITQ-2 or ITQ-6, and the mesoporous materials, as MCM-41, the most adequate catalytic supports.

References

[1] S. Hörold, K. D. Vorlop, T. Tracke and M. Sell, Catalysis Today, 17 (1993) 21.
[2] A. Pintar, J. Batista, Catalysis Today 53 (1999) 35.
[3] U. Prüsse, K.D. Vorlop, Journal of Molecular Catalyst A, 173 (2001) 313.
[4] O.M. Ilnitch, L. V. Nosova, V.V. Gorodetskii, V.P. Ivanov, S.N: Trukhan, E.N. Gribov, S.V. Bogdanov, . F.P. Cuperus, Journal of Molecular Chemistry, 158 (2000) 237.
[5] A. E. Palomares, C. Franch, A. Corma, Catalysis Today, 149 (2010) 348.

Towards an Optimal Ethylene Oligomerization Catalyst based on Single-Event MicroKinetic Modelling

K. Toch, J.W. Thybaut*, G.B. Marin
Laboratory for Chemical Technology, Ghent University, Belgium, Joris.Thybaut@UGent.be

Introduction

As the worlds' crude oil reserves are declining, the global energy demand is rising and the environmental legislation is becoming more and more strict, the search for low-emission fuels and chemicals is evermore a hot topic. Alternative routes are being explored to valorize methane, e.g., via ethylene formation by oxidative coupling. At present, ethylene oligomerization using homogeneous catalysis is an established industrial process, resulting selectively in even carbon atom numbered alpha alkenes. Heterogeneous catalysis is preferred over homogeneous catalysis, among others, because of environmental reasons. Moreover, heterogeneous catalysis offers more opportunities to tune the product yields to the market demands, i.e., linear α-alkenes or a complex mixture to be used as high octane fuel blend [1].
The aim of this work is to contribute to the development of an active, stable and selective catalyst for ethylene oligomerization. This challenge is addressed via fundamental modeling using Single-Event MicroKinetics (SEMK) [2]. An intrinsic kinetic data set is being acquired on a bench mark catalyst and will be used for regression purposes, i.e., to determine the model parameters, which can be classified as kinetic and catalyst descriptors. In particular the latter descriptors can be varied through simulation, in order to identify the optimal catalyst behavior.

Procedures

Experiments are performed in a fixed bed plug-flow reactor on a bench-mark silica-alumina catalyst impregnated with 1.8 wt% Ni. The temperature was varied from 443 K to 503 K, i.e., the range in which acid catalyzed reactions are reflected in the product yields [1]. Total pressures between 1.0 and 3.5 MPa are used with a molar ethylene content in the feed of 60%. The space time was varied from 3.0 to 45.0 kg_{cat} s mol_{eth}^{-1}. Care is taken to avoid heat and mass transfer limitations.
A microkinetic model was constructed describing the intrinsic ethylene oligomerization kinetics according to the SEMK methodology [2]. The reaction network was limited to molecules with a maximum carbon number of 12 and consisted of over 3000 species and over 10000 elementary steps. Physical adsorption of the components inside the catalyst pores, prior to any chemical elementary step was included via a Langmuir isotherm.

Results and discussion

As reported in the literature [1, 3], the catalyst exhibited two regions of activity as function of the temperature, see Figure 1 (left). At low temperatures mainly linear α-alkenes are obtained as products resulting from a coordinated insertion mechanism of ethylene on an

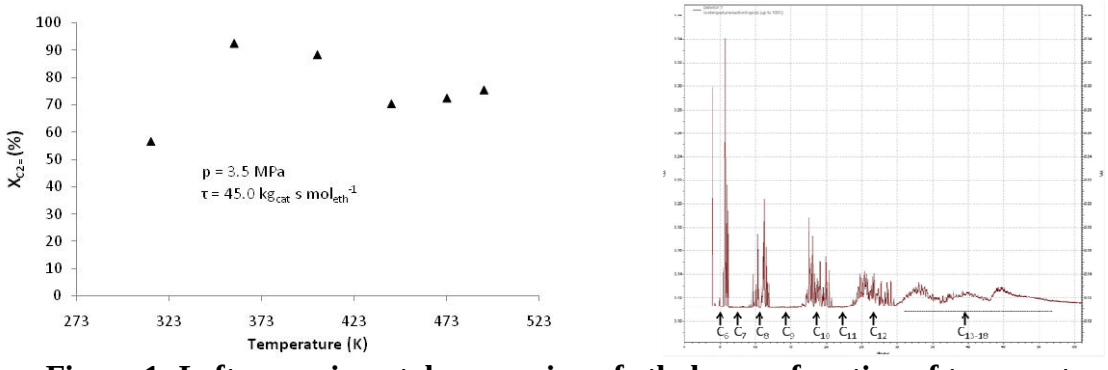

Figure 1: Left: experimental conversion of ethylene as function of temperature at 3.5MPa and 45.0 kg_{cat} s mol_{eth}^{-1}; Right: chromatogram of the collected liquid phase (C_6 to C_{18}) mixed for several experiments at different conditions.

active nickel cation site. Between 373 and 403 K, in the presence of ethylene, an irreversible transformation of Ni occurs leading to an activity loss of the catalyst below this temperature [1]. At higher temperatures, i.e., above 423 K, stable catalyst behavior was obtained for a time-on-stream up to 6 hours. The absence of odd carbon numbered alkenes in the product spectrum shows that no cracking occurred, see Figure 1 (right).

Because higher operating temperatures offer a wider range of possibilities for tuning the product yields, the corresponding data are assessed first using the microkinetic model. At present simulations have been performed using initial parameter values based on literature data [1] and have not been further optimized yet by regression. The metal-ion function is critical for ethylene dimerization to butene. In contrast to ethylene, which can only form primary carbenium ions, butenes can lead to more stable secondary carbenium ions that participate in acid catalyzed oligomerization reactions. While the C_4 fraction is entirely built up out of linear alkenes, C_6 and heavier fractions also contain branched isomers. Pure metal-ion catalyzed oligomerization results in an Anderson Schulz Flory distribution. The acid catalyzed oligomerization disturbs this ASF distribution, however, see Figure 2, left. This is more pronounced with increasing temperatures, see Figure 2 right. The decrease with the temperature of the linear alkene content in the C_8 fraction from 43.2 % at 443 K to 25.2 % at 503 K, also illustrates the increase of the relative importance of acid catalyzed reactions at higher temperatures.

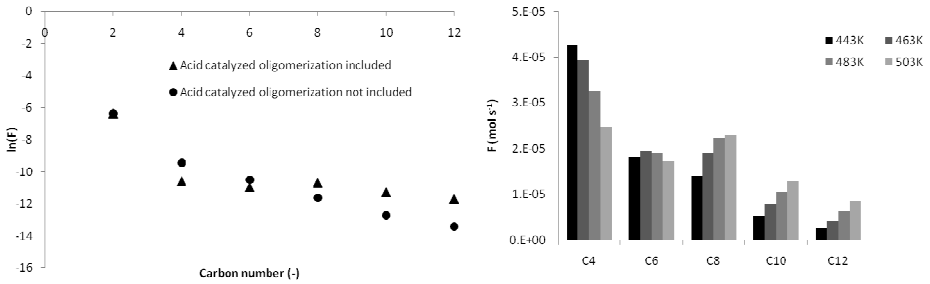

Figure 2: Left: natural logarithm of the molar outlet flow rates as function of the carbon number; Right: product distribution as function of temperature, acid catalyzed oligomerization included at 3.5 MPa and 6.7 kg_{cat} s mol_{eth}^{-1}.

Conclusions

A microkinetic model for ethylene oligomerization at higher temperatures is constructed and is able to qualitatively reproduce the experimental trends. The C_4 species formed all have a linear character because ethylene dimerization occurs on the metal-ion sites, while the C_6 to C_{12} species are mainly branched, due to the acid catalyzed reactions. Because of the acid catalyzed reactions, deviations from the Anderson Schulz Flory product distribution are obtained. No odd carbon numbered alkenes are present, indicating the absence of cracking. The kinetic and the catalyst descriptors in the Single-Event MicroKinetic model will be quantitatively determined by regression and optimal catalyst descriptor values will be identified.

Acknowledgements

The research leading to these results has received funding from the European Community's Seventh Framework Program FP7/2007-2013 under grant agreement n° 228953.

References

[1] Heveling, J., C.P. Nicolaides, and M.S. Scurrell, Applied Catalysis a-General, **173** (1998).

[2] Thybaut, J.W., I.R. Choudhury, J.F. Denayer, G.V. Baron, P.A. Jacobs, J.A. Martens, and G.B. Marin, Topics in Catalysis, **52** (2009).

[3] Sohn, J.R., Catalysis Surveys from Asia, **8** (2004).

Introduction of bioethanol in gasoline via alkylation reaction

R. Roldán, I. Ribas, J. P. Gómez
Centro de Tecnología de Repsol, rroldanm2@repsol.com

Introduction

European directive 2003/30/CE establishes minimum contents of bio-renewable compounds in transport fuels: a 5,75% of the energy content in gasoline and gasoil in 2010, and it is envisaged to increase up to 10% in 2020.

The strategy for some oil refiners for introducing bio-components in gasoline is the use of both ethanol and ethyl tertiarty butyl ether (ETBE). Bioethanol is etherified with isobutene to yield ETBE, but its production is limited by the availability of isobutene in each refinery. The total ETBE production is equivalent to 2% of the gasoline energy content, which involves that an additional source of biofuel must be put into play. One solution is to directly blend ethanol with gasoline. However, this choice presents several drawbacks, like the solubility in water of ethanol, its high vapor pressure and the potential incompatibility with the materials employed in the logistics of the product. It also involves an increase in the overall gasoline production, while the foreseen demand of gasoline is slightly declining in the near future.

In order to meet the biofuels content requirement, different routes for manufacturing biofuels with higher energy content, compatible with current fuel, logistics and engine requirements are needed. If possible, this alternative fuel should be manufactured in existing refineries, taking advantages of process units that have now more availability due to lower gasoline market demand in Europe.

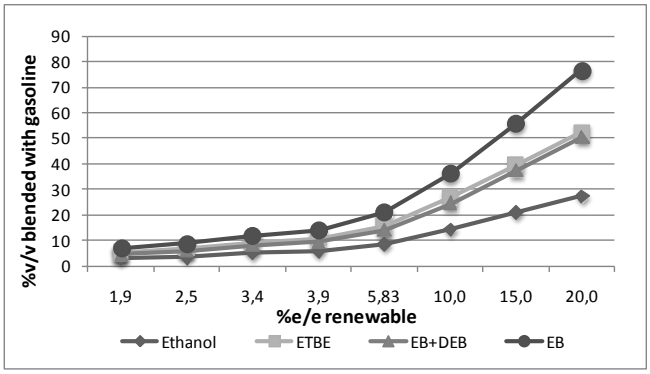

Figure 1. Content of biofuel required for specified energy content in gasoline

In this research, a different alternative for introducing bioethanol in the gasoline is explored. Ethanol is chemically converted by direct alkylation with benzene, producing ethylbenzenes. Practically, ethanol is reacted with a naphtha reformate. This approach entails several advantages. The ethylbenzenes formed present similar energy content to that of ETBE. They are oxygen free compounds, already existing in conventional gasoline. On the other hand, this

process reduces or eliminates benzene in gasoline, which is restricted to a level of 1% vol. in Europe. Hence, hydrogenating such benzene prior to elaborate the final gasoline blending, which requires hydrogen and energy consumption, might be no longer needed. In addition, non pure aqueous ethanol can be used.

Experimental

In this work the alkylation reaction of ethanol with benzene has been investigated on several zeolites, since these materials are reported to be catalytically active in this reaction [1, 2]. It has been carried out in a fixed bed reactor at temperatures of 200-400 ºC. Zeolites Beta (SiO_2/Al_2O_3 = 25), Y (2,5) and ZSM-5 (80) have been used as catalysts. Benzene has been added as component of a naphtha reformate. The influence of the temperature and type of naphtha feed has been studied, including the effect of naphthenes in the feed.

Results and discussion

It has been found that benzene conversion decays in a short time. When feeding heavy reformate, higher aromatic compounds than benzene are preferably alkylated.

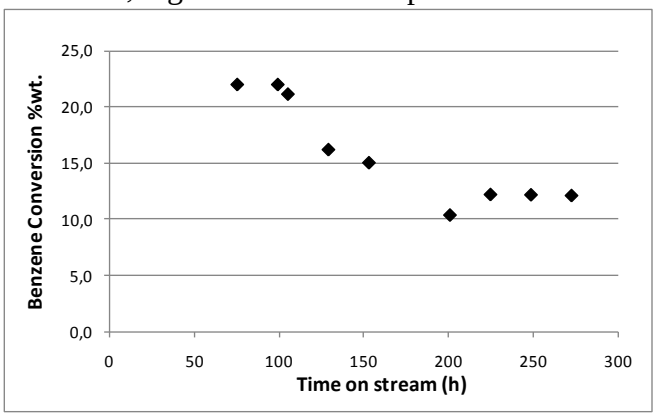

Figure 2. Benzene conversion.

Conclusions

Activity and stability in the test performed is not enough for obtaining the objective of benzene <1% in gasoline and further research must be done to make this process attractive.

References

[1] Corma, A., Llopis, F. J., Martínez, C., Sastre, G., Valencia, S., The benefit of multipore zeolites: Catalytic behaviour of zeolites with intersecting channels of different sizes for alkylation reactions, Journal of Catalysis, 268 (2009), 9-17.

[2] Yuan, J. J., Gevert, B. S., Alylation of benzene with aqueous solution of ethanol over ZSM-5 catalysts, Indian Journal of Chemical Technology, 13 (2006), 334-340.

Insights into the role of ZSM-5 acidity in the syngas-to-DME reaction

Andrés García-Trenco, Agustín Martínez.
Instituto de Tecnología Química,UPV-CSIC, Avenida de los Naranjos s/n, 46022 Valencia, Spain, amart@itq.upv.es.

Introduction

Major players in the transport sector are rekindling an interest in dimethyl ether (DME) as alternative to diesel fuel largely because it is relatively cheap, has high cetane number, and produces lower toxic emissions from combustion. This interest is promoting research in the one-step syngas-to-DME (STD) process as an alternative to the traditional two-step technology [1]. Particularly attractive is the carbon neutral bio-DME produced from biomass-derived syngas which might help in reducing greenhouse gas emissions. Catalysts employed for STD most commonly comprise physical mixtures of a Cu-based methanol synthesis catalyst (MSC) and an acid zeolite (typically H-ZSM-5) dehydration component. While it is generally consented that the acidity of H-ZSM-5 is of paramount significance in the context of STD, the previous literature is unclear regarding how the type (Brønsted, Lewis), density, and strength of the zeolite acid sites impact the performance of hybrid STD catalysts [1-3]. The present contribution intends to shed more light into the acid site requirements of H-ZSM-5 for both the methanol dehydration step and the overall STD process.

Experimental

A commercial H-ZSM-5 sample (CBV3020, Zeolyst Int, Si/Al= 16, denoted as HZ) was modified as follows in order to produce samples with different acid properties: a) partial ionic exchange with Na^+ (three exchange levels: Na/Al= 0.14, 0.27, 0.39), b) partial exchange with Co^{2+} (three exchange levels: Co/Al= 0.08, 0.15, 0.20), c) treatment with HCl (1M) at 100ºC for 12 h (sample HZA). A silicalite-1 (S-1) zeolite was synthesized and used as acid site-free reference dehydration component. A CuZnAl (abbreviated as CZA, Cu:Zn:Al atomic ratio of 6:3:1) methanol synthesis catalyst was prepared by coprecipitation from the respective metal nitrate precursors. Hybrid catalysts were produced by carefully milling the powders of CZA and zeolite components in a 2:1 weight ratio. Catalysts were characterized by ICP-OES, XRD, N_2 adsorption, ^{27}Al MAS NMR, FTIR-pyridine, and NH_3-TPD. Methanol dehydration tests were carried out in a fixed bed reactor at 260ºC (the applied STD temperature) and atmospheric pressure. STD reactions were performed in a fixed-bed reactor at 260ºC, 4.0 MPa, and 1700 $ml_{syngas}/(g_{cat} \cdot h)$ using a syngas of molar composition 66%H_2/30%CO/4%CO_2. Prior to feeding syngas the hybrid catalysts were pretreated in a 5%H_2/N_2 reductive gas stream at 245ºC for 10 h in order to bring the CZA component into its active state.

Results and discussion

The BET and $V_{\mu pore}$ values for the acid treated HZA sample were slightly lower than for the parent zeolite, while Na- and Co-exchanged samples showed a decreasing trend with increasing the degree of exchange due to partial blockage of micropores by the exchanged cations. As to the acidity, the parent HZ contained both Brønsted and Lewis acid sites (the later related to EFAL species) with predominance of the former (B/L ratio= 4.6). Partial exchange of H^+ in HZ with Na^+ or Co^{2+} produced an obvious decrease in the density of Brønsted acid sites (BAS). For both NaxHZ and CoxHZ series, the amount of BAS linearly decreased with the M/Al ratio (M= Na, Co). Furthermore, NH_3-TPD revealed that Na^+ preferentially neutralized the strongest acid sites. The effect of exchange on the Lewis acidity was less straightforward. Thus, a decrease in the amount of Lewis acid sites (LAS) was evidenced from FTIR-pyridine for the NaxHZ series with no apparent link to the Na amount.

This could be due to the exchange by Na^+ of some cationic-type EFAL species (contributing to Lewis acidity in HZ) and/or to the Lewis acidity of the exchanged Na^+ cations being too weak to coordinate pyridine even at the lowest desorption temperature applied (250ºC). For CoxHZ, the amount of LAS raised with the Co/Al ratio, with the newly formed Co^{2+}-related LAS being weaker than those associated to EFAL but stronger than those of Na^+. Finally, acid treatment of HZ hardly affected the amount and strength of the BAS but virtually suppressed the Lewis acidity (B/L=31.5) due to selective removal of EFAL (as seen by ^{27}Al MAS NMR).

The acid characteristics of the ZSM-5 samples profoundly impacted the methanol dehydration activity (no activity was detected for S-1 lacking acid sites). The best correlation between the dehydration activity and acidity was found when considering the strongest BAS (those retaining pyridine at 400ºC), as shown in Fig. 1. A closer look to the data in Fig. 1 reveals, however, that the acid treated HZA sample was less active than the parent HZ zeolite despite both displayed nearly the same amount of strong BAS, thus pointing towards an active role of EFAL-related strong LAS. By contrast, LAS of a lower strength associated to the exchanged Na^+ and Co^{2+} cations appear not to be involved in the dehydration reaction.

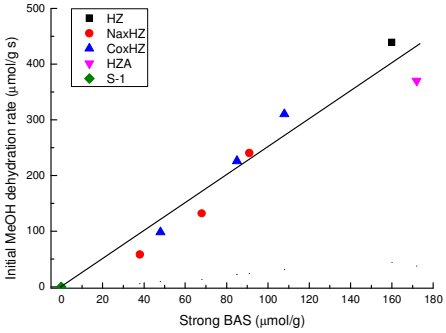

Fig. 1. Correlation between MeOH dehydration activity and zeolite acidity (S_{DME} > 99.95%).

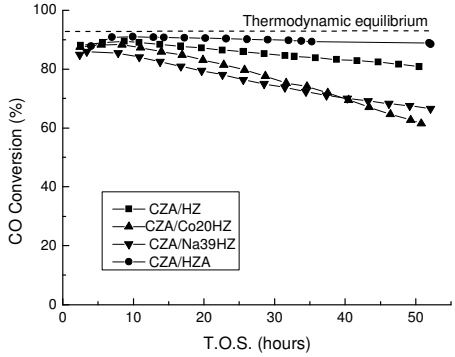

Fig. 2. CO conversion as a function of TOS for hybrid CZA/ZSM-5 (2:1) catalysts during STD.

As shown in Fig. 2, the hybrid catalysts displayed distinct deactivation behavior with TOS. Hybrids comprising zeolites with high amount of active dehydration sites (HZ and HZA) displayed the highest stability with TOS. In particular, that consisting of EFAL-free HZA showed the best performance during STD featuring high stability and DME selectivity (ca. 95% in a CO_2-free basis) with very minor formation of hydrocarbons (<0.3 wt%). Differences in stability between the hybrids can be related to both the density of active dehydration sites and detrimental CZA-zeolite interactions, the later being more relevant in catalysts comprising cation-exchanged zeolites.

Conclusions

The methanol dehydration activity of ZSM-5 is mostly driven by the density of strong BAS. Strong LAS associated to highly-dispersed EFAL species do also contribute to the overall dehydration activity but seem to have a negative effect on stability during STD.

Acknowledgements

Financial support by the CICYT of Spain through project CTQ2010-17988/PPQ is gratefully acknowledged. A.G.T. thanks the MICINN of Spain for an FPI Ph.D. scholarship.

References

[1] Ge, Q., Huang, Y., Qiu, F., Li, S., Appl. Catal. A 167 (1998), 23-30.
[2] Mao, D,. Yang, W., Xia, J., Zhang, B., Song, Q., Chen, Q., J. Catal. 230 (2005), 140-149.
[3] Kim, J.H., Park, M.J., Kim, S.J., Joo, O.S., Jung, K.D., Appl. Catal. A 264 (2004), 37-41.

Gasoline or diesel fuel production by the selective oligomerization of isobutene catalyzed by mesoporous MSU-S aluminosilicates

Dongho Park,[1,2] Seong-Su Kim,[1] Thomas J. Pinnavaia,[1] Francisco Tzompantzi,[2] Julia Prince,[3] Jaime S. Valente[*,3]

*[1] Department of Chemistry, Michigan State University, USA; [2]Department of Biomedicinal Chemistry, Inje University, Korea; [3]Universidad Autonoma Metropolitana-I, Departamento de Quimica, Mexico; [4]Instituto Mexicano del Petroleo, Mexico; *jsanchez@imp.mx.*

Introduction

The oligomerization of light (C_2-C_5) olefins, especially of the C_4 stream from FCC units, has received much attention in the past decades. Dimerization of isobutene yields $C_8^=$ branched olefins; after hydrogenation, a clean, high octane gasoline (RON=100, MON=100) is obtained [1]. The $C_{12}^=$ trimers may be used as diesel and jet fuel additives, amongst other things [2]. Owing to increasingly stringent environmental regulations on the use of MTBE, a surplus of isobutene is expected, as it is the main raw material for MTBE synthesis. In this context, catalytic isobutene oligomerization has acquired renewed importance.

There is an active search for an acid catalyst that may provide high $C_8^=$ and $C_{12}^=$ selectivity, while minimizing the formation of larger oligomers ($\geq C_{16}^=$). Many studies have focused on the use of zeolites, whose acidity enables acceptable conversions and selectivities. Nevertheless, GHSVs must remain low, and still they typically display fast deactivation rates. Extended oligomerization reactions generate high molecular weight oligomers that remain occluded in pore cavities, depositing as coke and deactivating the catalysts. Therefore, a suitable catalyst for this reaction must combine an acid strength comparable to that of zeolites with a meso-pore structure that facilitates diffusion of bulky oligomers.

The aforementioned requirements are not exclusive of oligomerization reactions; indeed, they may be applicable to a number of acid-catalyzed reactions. In this sense, the development of mesostructured aluminosilicates, denoted as MSU-S, may be considered a breakthrough. The success of the approach is due to the use of protozeolitic nanoclusters, or zeolite seeds, as framework precursors. Zeolitic subunits in framework walls confer the materials with exceptional hydrothermal stability and strong acidity [3, 4]. Furthermore, the mesoporosity, large specific surface areas and pore volumes displayed by these materials facilitates diffusion of bulky molecules. Thus, MSU-S solids possess all the required features for an effective oligomerization catalyst. Here we examine the catalytic activity, selectivity and stability of MSU-S_{BEA} for the oligomerization of isobutene. Commercial USY and BEA zeolites are also tested as a comparison.

Experimental

Zeolite Beta seeds with a nominal Si/Al ratio of 44 were prepared according to previously described methods [3,4] For the preparation of wormhole mesostructured aluminosilicate, MSU-S/W_{BEA}, the Beta seeds were added under stirring to a surfactant solution, containing tallow tetraamine, water and HCl, then heated. A non-mesostructured analog, denoted MSU-S/S_{BEA}, was synthesized by digestion of BEA seeds. The final products were recovered by filtration, dried, and calcined at 600 °C for 4 hours. As a comparison, we tested commercial BEA and USY zeolites with Si/Al ratios of 45 and 2.5, respectively, purchased from Zeolyst.

The catalytic activity for the isobutene oligomerization reaction was determined using a fixed bed glass reactor with a volume of 5 mL and using 0.2 g of catalyst. Catalysts were activated at 400 ºC for 12 h in flowing air. Afterwards, the temperature was lowered to 60 ºC and then a mixture of isobutane/isobutene was fed into the reactor at atmospheric pressure (gas phase). For the first reaction test, the GHSV was constant (32.8 h^{-1}), and a 50:50 (w/w) mixture of isobutane/isobutene was used, for 30 h of reaction. In the second reaction test, the GHSV value was varied at 32.8, 65.7 and 131.5 h^{-1} with a 70:30 (w/w) mixture of

isobutane/isobutene, for 30 h of reaction. The analysis of products was made with a Varian Star 3600 CX gas chromatographic equipped with a FID detector and a 24 ft 20% MBEA column coupled to the reactant system. The conversion is reported in terms of the fraction of isobutene depleted and the selectivity is reported as $C_8^=$ and $C_{12}^=$ mol fractions.

Results and discussion

The morphology, structure and properties of the MSU-S mesostructured aluminosilicates assembled from protozeolitic precursors, or zeolite seeds, have been the subject of several previous reports [3,4]. Pyridine adsorption studies revealed that mesostructured aluminosilicates have strong Lewis and Brönsted acid sites, comparable in strength to those of USY and BEA commercial zeolites.

During the first test reaction (*vide supra*), it was observed that, even though all catalysts present a significant deactivation during the first 5-6 h on stream, it is more pronounced in the commercial catalysts. USY drops from an initial conversion of 43% to only 5% after 6 h. The deactivation of zeolite BEA is slightly less in comparison to the USY catalyst; judged by a sustained 10% conversion over 30 h reaction time.

Notably, mesostructured MSU-S/W_{BEA} and MSU-S/S_{BEA} are significantly more active and stable, compared with the zeolites. Both catalysts show stable conversions above 30% for at least 30 h on stream. In particular, the wormhole-like mesostructure of MSU-S/W_{BEA} favors high conversions, as these materials provide three-dimensional mesoporosity that reduces pore length and diffusional rate limitations. The strong acidity of both mesostructured samples, promoted by the protozeolitic framework structure, also plays a determinant role. Reaction products at these conditions are mainly $C_8^=$ isomers, with selectivity $\geq$ 70% in all cases; the remaining fraction consists of $C_{12}^=$ isomers. High molecular weight oligomers ($C_{16}^=$ and higher) are not produced in any case.

Catalyst MSU-S/S_{BEA} was chosen to study the effect of space velocity and feed composition on selectivity and deactivation (second reaction test, *vide supra*). As expected, the highest conversion, around 80%, is obtained at the lowest GHSV; activity was maintained for up to 30 h on stream. An increase in GHSV to 65.7 h^{-1} decreases conversion slightly, due to added competition for active sites. With higher space velocities (131.5 h^{-1}), catalytic activity is lost rapidly, as is usually the case. Nevertheless, the lowest GHSV (32.8 h^{-1}) used in this work is still much higher in comparison to the GHSV/WHSV values used in previous studies of this reaction [1, 2]. The selectivity to $C_8^=$ and $C_{12}^=$ products for a 70:30 isobutane:isobutene feed is particularly noteworthy. In this case, the reaction is highly selective (~90%) towards $C_{12}^=$. Also, the selectivity is not dependent on space velocity, and undesirable high molecular weight oligomers ($C_{16}^=$ and higher) are not formed.

Conclusions

In summary, hydrothermally stable, strongly acidic, mesoporous MSU-S solids with large surface areas appear as excellent catalysts for isobutene oligomerization. The reactivity, selectivity and longevity of these catalysts are superior to commercial zeolite catalysts and to other acid catalysts that have been reported for isobutene oligomerization. Furthermore, selectivity to the dimeric and trimeric products of interest ($C_8^=$ or $C_{12}^=$) can be adjusted simply by changing the feed composition.

Acknowledgements

J. S. V. gratefully acknowledges the Mexican Academy of Science and the United States-Mexico Foundation for Science for a research grant.

References

[1] Mantilla, A.; Tzompantzi, F.; Ferrat, G.; Lopez-Ortega, A.; Alfaro, S.; Gomez, R.; Torres, M. Catal. Today 2005, 107, 707.
[2] Yoon, J. W.; Chang, J.-S.; Lee, H.-D.; Kim, T.-J.; Jhung, S. H. J. Catal. 2007, 245, 253.
[3] Liu, Y.; Pinnavaia, T. J. Chem. Mater. 2002, 14, 3.
[4] Liu, Y.; Pinnavaia, T. J. J. Mater. Chem. 2004, 14, 1099.

Hydrodeoxygenation of methyl esters over Ni-Beta zeolite with hierarchical porosity

Cristina Ochoa Hernández[1]; Yongxing Yang[1]; Juan M. Coronado[1]; Víctor A. de la Peña O'Shea[1]; David P. Serrano[1,2]

[1] *Thermochemical Processes Unit, Institute IMDEA Energy, c/ Tulipán s/n, 28933 Móstoles, Madrid, Spain, e-mail: cristina.ochoa@imdea.org*

[2]*Department of Chemical and Energy Technology, ESCET, Rey Juan Carlos University, 28933 Móstoles, Madrid, Spain*

Introduction

Biofuels constitute a potential alternative to replace part of the fossil-derived fuels. The European Union has set a 10% target for energy from renewable sources in transport by the year 2020 [1]. In this sense, pyrolysis integrated with upgrading processes is able to convert lignocellulosic biomass into liquid hydrocarbon fuels. Bio-oils, obtained from pyrolysis, are a complex mixture containing oxygen compounds (acids, esters, phenols, guaiacols...) which involve poor properties to be used directly in a conventional engine [2, 3]. Hydrodeoxygenation is a process for biofuel upgrading, which implies the removal of residual oxygen by reaction with H_2 to obtain water and saturated hydrocarbons. In this work, we focused on hydrodeoxygenation of methyl esters, as model compounds, using Ni supported over Beta zeolite with hierarchical porosity and conventional Beta zeolite. Improved textural properties of hierarchical zeolites have a positive effect in hydrodeoxygenation reactions of these bulky molecules.

Experimental

Catalyst preparation and characterization. Hierarchical Beta zeolite (Beta(PHAPTMS)) was prepared from a solution with a molar composition as follows: Al_2O_3 : 60SiO_2 : 15.5TEAOH : 1000 H_2O. The precursor solution was precrystallized in an autoclave under autogenous pressure at 135ºC for 3 days. The solid obtained was mixed with an aqueous solution containing phenylaminopropyltrimethoxysilane (PHAPTMS) and tetraethylammonium hydroxide (TEAOH). The resulting mixture was kept under reflux and stirring at 90ºC for 6h. The crystallization was completed by autoclave treatment at 135ºC for 7 days [4]. Conventional Beta zeolite (Beta(0)) for comparison purpose was also synthesized according with the same procedure but omitting the precrystallization and silanization stages. In both cases, the solid products obtained were dried overnight at 110ºC and calcined in air at 550ºC for 5h. Nickel was added to the supports by incipient wetness impregnation of an aqueous solution of $Ni(NO_3)_2{\cdot}6H_2O$ to obtain 5 wt% loadings. The solids impregnated were dried overnight at 110ºC and calcined at 550ºC for 5 h. All samples were characterized by X-ray diffraction (XRD), nitrogen and argon adsorption-desorption isotherms, ICP-AES and TPR/TPD.

Catalytic test. A mixture of esters with up to 70% of methyl oleate was diluted with n-heptane and used as feedstock. Hydrodeoxygenation assays were carried out under continuous flow in a fixed-bed tubular reactor. The reactor was loaded with 200 mg of catalysts. Before reaction, catalyst was in situ reduced with a flow of pure hydrogen at 550ºC for 5h. The reaction was carried out for 6 h with the following conditions: 350ºC, 30 bar of hydrogen and 20.4 h^{-1} (WHSV). The liquid and gaseous products were analyzed by gas chromatograph.

Results and discussion

XRD results confirm the formation of beta zeolite in all synthesized materials. Besides, samples with hierarchical porosity present broader peaks than those corresponding to the reference Beta zeolite, suggesting the existence of smaller crystals or a higher number of defects [4]. According to XRD patterns in figure 1a, nickel precursors have been converted completely into NiO during calcination. Significant differences are observed in the textural properties of these systems (figure 1b). Beta zeolite prepared from silanized seeds presents a high BET surface area compared to Beta(0) sample because of the presence of higher micro- and mesoporosity. This fact is evidenced in the figure 1c, where pore size distributions are obtained by applying NLDFT model. A shift in the maximum of the pore size distribution is observed in Beta(PHAPTMS) sample, which shows a microporous contribution centered at 6.1 Å (5.5 Å for Beta(0)) and a second maximum centered at 25 Å due to the presence of mesopores (absent in Beta(0)). A decrease of surface area is observed after Ni incorporation. Catalytic tests exhibit methyl oleate conversions up to 90% in nickel impregnated samples. Ni-Beta(PHAPTMS) shows changes in product distribution due to its improved textural properties.

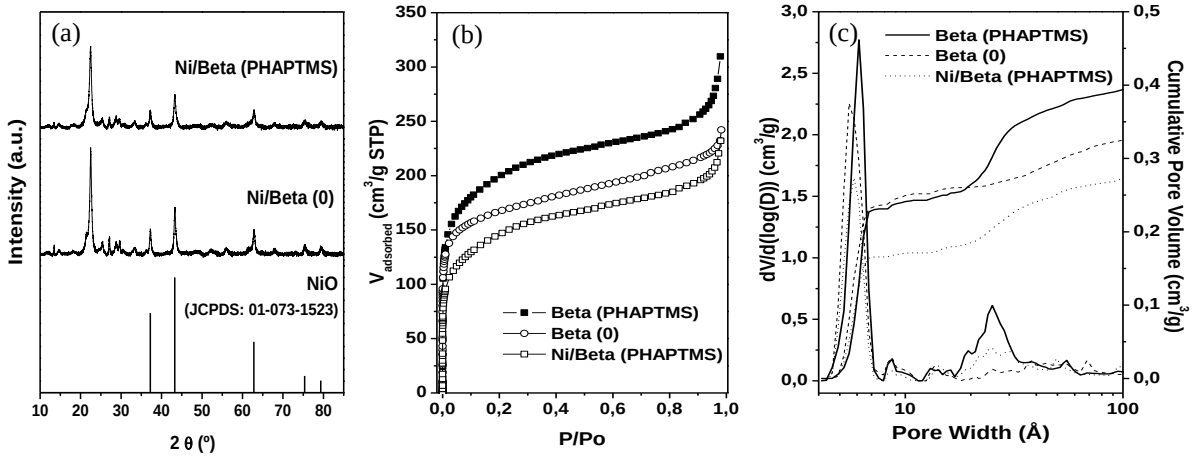

Figure 1. (a) XRD spectra of samples containing nickel (b) Ar adsorption isotherms at 87 K (c) Pore size distributions using NLDFT model.

Conclusions

Beta zeolite with hierarchical porosity has been impregnated with nickel and tested in HDO reactions of methyl esters showing high methyl oleate conversions and hydrocarbon distributions in diesel range.

Acknowledgements

This work has been supported by the regional government of Madrid through RESTOENE research project (Ref.: P2009/ENE-1743, Consejería de Educación de la Comunidad de Madrid).

References

[1] On the promotion of the use of energy from renewable sources, Directive 2009/28/EC, 23 April 2009.

[2] Huber, G.W., Corma, A., Synergies between bio- and oil refineries for the production of fuels from biomass, Angewandte Chemie International Edition, 46 (2007), 7184-7201.

[3] Serrano-Ruiz, J.C., Dumesic, J.A., Catalytic routes for the conversion of biomass into liquid hydrocarbon transportation fuels, Energy & Environmental Science, 4 (2011), 83-99.

[4] Serrano, D.P., Aguado, J., Escola, J.M., Rodríguez, J.M., Peral, A. Hierarchical zeolites with enhanced textural and catalytic properties synthesized from organofunctionalized seeds, Chemistry of Materials, 18 (2006), 2462-2464.

Oxygen Free Conversion of Natural Gas to Useful Hydrocarbons and Hydrogen using Monometallic Mo and Bimetallic Mo-Fe, Mo-Co or Mo-Ni/HZSM-5 Catalysts Prepared by Mechanical Mixing

Ahmed K. Aboul-Gheit [a], Mohamed S. El-Masry [b], Ahmed E. Awadallah [a,*]
[a] *Process Development Division, Egyptian Petroleum Research Institute, Cairo 11787, Egypt,*
[b] *Misr Fertilizer Production Co. (MOPOCO), Damietta, Egypt.*
** Corresponding author, e-mail: ahmedelsayed_epri@yahoo.com*

Introduction

Methane dehydroaromatization (MDA) under non-oxidative conditions, being considered as a promising route for direct conversion of methane into high value- added chemicals like benzene, toluene and naphthalene, has attracted increasing attention in the past several decades because of the current importance and industrial interest in effective utilization of natural gas [1–5].

In principle the conversion is an excellent way in which to convert methane directly to higher hydrocarbons and the hydrogen is, of course an extremely valuable co-product. It has been demonstrated that the performance Mo/ H-ZSM-5 can be improved by the addition of elements such as W, Ga, Ru, Cu Al, Co, Cu, Fe, Pt, Zn and Zr [3, 6–8], while V, Li and P on the other hand tend to decrease the activity [3,8].

This work aims to reach a compromise of the activities of Mo/HZSM-5 catalyst (well known highly active aromatization catalyst) after promotion with Fe, Co or Ni (well known active hydrogen producing metals) for hydrocarbons and hydrogen production.

Experimental

The metal oxides powders (MoO_3, Fe_2O_3, Co_2O_3 and Ni_2O_3) were obtained by calcining ammonium heptamolybdate, iron, cobalt or nickel nitrates in air at 550^{o}C for 4 h then deeply mechanically mixed with HZSM-5 zeolite powder to produce 6wt%Mo, 3wt%Mo+3wt%Fe, 3wt%Mo+3wt%Co and 3wt%Mo+3wt%Ni/H-ZSM-5 catalysts, respectively. Natural gas conversion was carried out under atmospheric pressure using a down-flow fixed bed reactor composed of a silica tube 1.5 mm ID charged with 0.5 g catalyst heated at 700^{o}C and a gas hourly space velocity (GHSV) of 1500 ml g^{-1} h^{-1} at a time-on-stream of 240 min. The hydrocarbon products were analyzed by Arnel Perkin Elmer-Claurs 500 Natural gas analyzer.

Results and discussion

It is evident from Fig. 1 that the overall conversion to hydrocarbons (ethylene and aromatics) is significantly higher on the monometallic Mo/H-ZSM-5 against the bimetallic Fe, Co or Ni-Mo/HZSM-5 catalysts at all time-on-stream values. The electronic structure

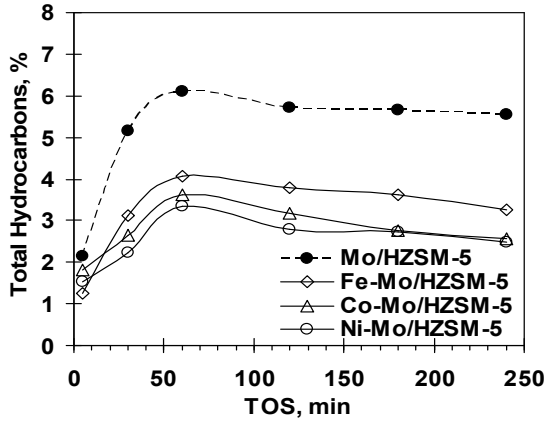

Fig. 1. Overall conversion of natural gas using Mo, Mo-Fe, Mo-Co and Mo-Ni/HZSM-5 catalysts.

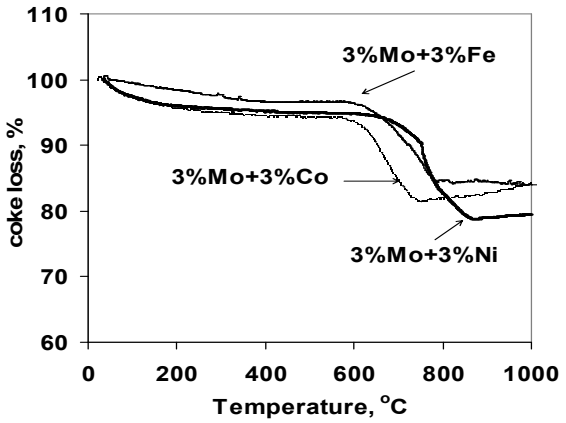

Fig. 2. TGA of Mo, Mo-Fe, Mo-Co and Mo-Ni/HZSM-5 catalysts.

play an important role in catalytic activity. In many cases a direct relationship has been found between the catalytic activities of transition metals and the electronic properties of the unfilled d-orbitals. Maximum reaction rates are found for metals with six to eight d- electron [9], i.e., Fe, Co or Ni which can be explained in terms of electronic effects. Moreover, the degree to which the d orbitals are filled with electrons has considerable influence on the chemisorption capability of metals. This would assist to strengthen the adsorption of CH_4 which increase the rate of coke formation as we move from Fe to Ni (Fig. 2).

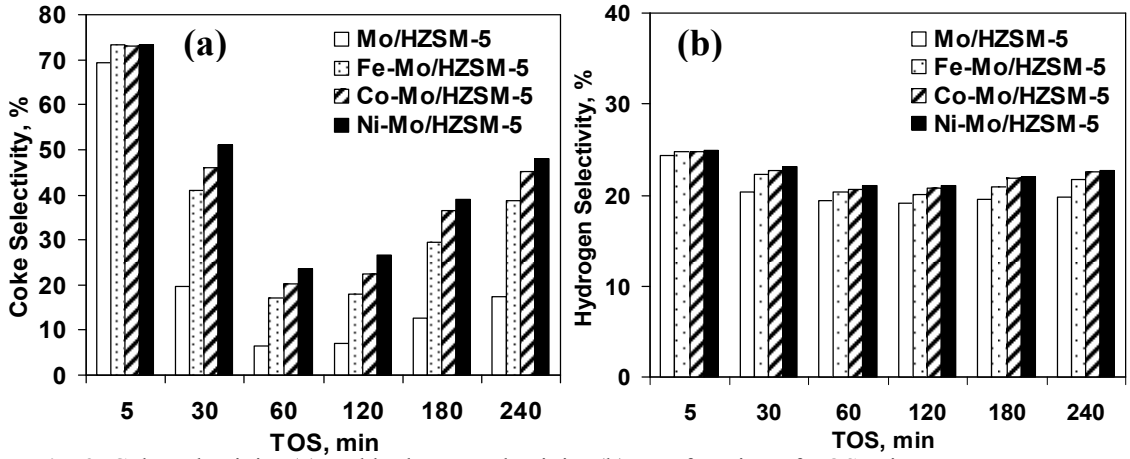

Fig. 3. Coke selectivity (a) and hydrogen selectivity (b) as a function of TOS using Mo, Mo-Fe, Mo-Co and Mo-Ni/HZSM-5 catalysts.

The electronegativity of the loaded metals can be summarized as follow: Fe (1.83), Co (1.88), and Ni (1.91). The susceptibility of interaction with the H^+ proton of HZSM-5 by metal species will increase with increasing electronegativity from Fe to Co then to Ni, where the metal oxide/carbide prefers to deposit on the strong acid sites of the HZSM-5 zeolite surface and channels, causing masking of a part of acid sites and decreasing in the H^+ proton repulsion, and consequently increases the zeolite acid strength, which finally increases the tendency to coke formation as well as hydrogen selectivity (Fig. 3) and hence a decrease of the aromatics yield.

It has been found using the four current catalysts, that the coke production selectivity and hydrogen production selectivity (Figure 3) at 5 min TOS, are ~72%and ~24%, respectively. A carbon level of 72% on each catalyst is equivalent to 6 carbon atoms, whereas a hydrogen level of 24% is equivalent to 24 hydrogen atoms, and hence, each carbon atom corresponds to four hydrogen atoms, which is the composition of methane (CH_4). This is, exactly the same finding occurred when using Pd, Ir, Cr or W promoted-Mo/HZSM-5 catalysts, as well as their unmodified Mo/H-ZSM-5 [10,11].

Reference

[1] Wang L., Huang J., Tao L., Xu Y., Xie M., Xu G., Catal. Lett. 21 (1993) 35.
[2] Solymosi F., Erdöhelyi A., A. Szöke, Catal. Lett. 32 (1995) 43.
[3] Xu Y., Lin L., Appl. Catal. A 188 (1999) 53.
[4] Xu Y., Bao X., Lin L., J. Catal. 216 (2003) 386.
[5] Hassan A., Sayari A., Appl. Catal. A 297 (2006) 159.
[6] Liu B., Yang Y., Sayari A., Appl. Catal., A 214 (2001) 95.
[7] Dong Q., Zhao X., Wang J., Ichikawa M., J. Nat. Gas Chem. 13 (2004) 36.
[8] Burns S., Hargreaves J.S.J., Pal P., Parida K.M., Parija S., Catal. Today 114 (2006) 383.
[9] Jens Hagen, Industrial Catalysis, Wiley-VCH Verlag GmbH&Co. KGaA., 1998.
[10] Aboul-Gheit A.K., Awadallah A.E., El-Kossy S.M., Mahmoud A.H., J. Nat. Gas Chem. 17 (2008) 337.
[11] Aboul-Gheit A.K., Awadallah A.E., J. Nat. Gas Chem. 18 (2009) 71.

STUDY OF PdIn-ZEOLITE CATALYSTS BY XPS AND TEM-EDX.

Hernán Decolatti[a*], Ferenc Lónyi[b], R. Magdolna Mihályi[b], József Valyon[b], Alicia Boix[a], Laura Gutierrez[a].
[a] *Instituto de Investigaciones en Catálisis y Petroquímica (FIQ,UNL-CONICET), Santiago del Estero 2829, 3000 Santa Fe, Argentina. * e-mail: herdeco@fiq.unl.edu.ar.*
[b] *Institute of Surface Science and Catalysis, Chemical Research Center, Hungarian Academy of Sciences,Pusztaszeriút 59-67, 1025 Budapest, Hungary.*

Introduction.

The selective catalytic reduction of NOx with methane in the presence of oxygen excess (NOx-SCR) is a promising method to reduce the NOx emission of power plants fuelled by natural gas [1]. The transition metals-zeolite catalysts are able to activate the relatively stable methane molecule for the reaction. Several studies suggest that indium-containing zeolites show significant activity in the NOx-SCR [2,3]. The catalytic activity is generally attributed to cationic indium species. On the other hand, Pd zeolites have also been reported as active catalysts for the mentioned reaction [4] but they deactivate due to the agglomeration of Pd cations into bulky PdO particles outside of the zeolite pore structure.
We recently achieved a significant improvement in catalytic activity using PdInHM catalysts [5]. To avoid the problems of pressure drop and improve the transfer of energy and mass, the powders are normally washcoated on monolithic supports. It is crucial to obtain structured catalysts with catalytic properties similar to the powders. In this work, monolithic PdInZeolite catalysts were prepared by washcoating. Fresh and used catalysts were characterized by XPS and TEM-EDX techniques to establish a relationship with the catalytic activity of solids.

Experimental

In,H-zeolite samples were prepared by the method of reductive solid state ion exchange (RSSIE). H-mordenite (H-M, Süd-Chemie AG; Si/Al = 6.7) and H-ZSM-5 (our synthetic product; Si/Al = 33.0) were mixed with In_2O_3 applying intense co-grinding. The obtained In_2O_3/H-zeolite mixtures were treated in H_2 flow at 773K for 1 h, then cooled down to room temperature in He flow and finally oxidized in O_2 flow at 673 K. The Al/In ratio of the obtained zeolitic catalysts was 3. Catalysts, having 0.5 wt% Pd content, were prepared by impregnating the InH-Zeolite samples with a $Pd(NH_3)_4(NO_3)_2$ solution and by heating the impregnated samples in O_2 flow at 623K for 4 h. The respective catalysts were designated as PdInHM and PdInHZSM5. The washcoating was performed by impregnating a suspension of the powder catalysts in deionized water, on a cordierite support with square-section cells to achieve the expected zeolite load (approximately 20% on dry basis). After each immersion, N_2 was blown to eliminate the excess liquid and achieve a homogeneously thick film on the walls. It was dried in a stove and afterwards treated in He flow at 400 ºC for 2 h.
XPS analyses were performed in a multi-technique system (SPECS) equipped with a dual Mg/Al X-ray source and a hemispherical PHOIBOS 150 analyzer operating in the fixed analyzer transmission (FAT) mode. The spectra were obtained with a pass energy of 30 eV; an Al Kα X-ray source was operated at 200W and 12 kV. Spectra were acquired in the In 3d, Pd 3d, O 1s, C 1s, Si 2p, Si 2s and Al 2p regions. The Si 2p peak at 102.7 eV binding energy (BE) was taken as internal reference. The splitting of In 3d5/2–In 3d3/2 XPS signals was considered 7.6 eV for the signal processing. All the peaks were fitted by a Gaussian–Lorentzian component wave-form in order to calculate the surface atomic ratio. The data processing and peaks deconvolution were performed using the Casa XPS software.
Transmission electron microscopy investigations were carried out using a JEOL 2000 FXII apparatus using an acceleration voltage of 200 kV.

Results and Discussion

In previous work, we found that the addition of 0.5% of Pd to InH-mordenite enhances the activity of the catalyst in the SCR of NO with methane. On the other hand, monoliths prepared by washcoating showed a catalytic behavior similar to that of the original powders.

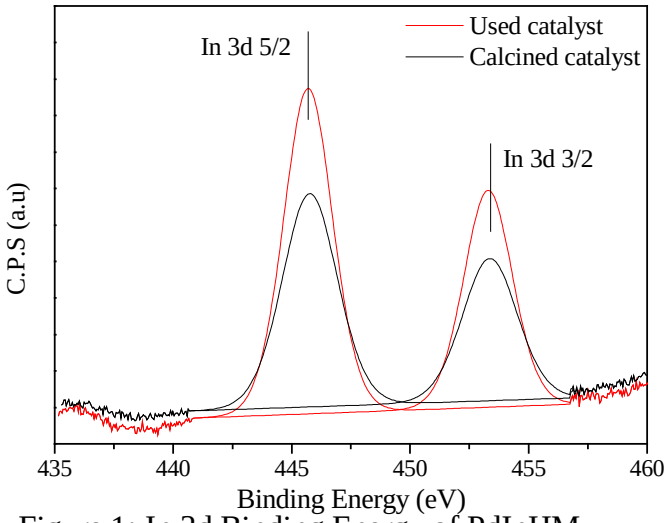

Figure 1**:** In 3d Binding Energy of PdInHM

We analyzed by XPS the Pd 3d and In 3d electronic levels, along with those of the zeolite structure. For all calcined samples (air at 400 º C) we found an In3d 5/2 binding energy value near 445.5 eV; this corresponds to the InO^+ species at exchange positions (Figure 1). This species is reported as active and selective for the above mentioned reaction. After being used in the SCR there was a shift of about 1 eV to a lower binding energy (BE) for the catalyst supported on HZSM5. However, for the HMOR the binding energy remained constant (Table I). On the other hand, the observed B.E for Pd 3d corresponds to PdO species. Probably there was a migration of indium from the channels of zeolite to the surface after the catalyst was used in SCR because the surface atomic In/Si ratio increased. The PdInHM catalyst was analyzed by TEM and EDX and we found that after the reaction there is an increase in the size of Pd particles (15 nm to 30 nm) and these remained homogeneously distributed on the matrix and we also found a segregation of indium (300 nm to less than 4 nm). These results correlate with the catalytic tests, which indicated that the activity of PdInHM increased after the first evaluation of the solid while the catalyst supported on HZSM5 (PdInHZSM5) did not show this effect.

Table I: XPS In 3d 5/2

Catalyst	**Binding Energy (eV)**	
	Calcined	Used
InHZSM5	445.5	444.5
PdInHZSM5	445.4	444.4
PdInHM	445.7	445.8

Conclusions

We observed that the activation of the PdInHM catalyst is due to a change of the interaction of particles of Pd and In under reaction conditions. It was also possible to obtain the same catalytic behavior as the powder catalyst when they were incorporated into monolithic structures using the washcoating technique.

Acknowledgements: The authors acknowledge the financial support received from UNL, CONICET and ANPCyT. Thanks are also given to Elsa Grimaldi for the English language editing and to the Hungarian-Argentine program NKTH-MINCYT wich made this joint project possible.

References

[1] V.I. Parvulescu, P. Grange, B. Delmon, Catal. Today 46 (1998) 233-316.
[2] F.G. Requejo, J.M. Ramallo-López, E.J. Lede, E.E. Miró, L.B. Pierella, Catal. Today 54 (1999) 553-558.
[3] J.M. Ramallo-López, L.B. Gutierrez, A.G. Bibiloni, F.G. Requejo, E.E. Miró, Catal. Lett. 82 (2002) 131-139.
[4] B. Wen, Q.Sun, W.M. H. Sachtler, J. Catal., 204[2](2001)314.
[5] F Lónyi, H. Solt, J. Valyon, H. Decolatti, L. Gutierrez, E. Miró. Appl Cat B 100 (2010).

Comparison of dealumination and desilication of mordenite in alkylation of benzene with 1-alkene

Hudec P., Horňáček M., Smiešková A., Jorík V.
Department of Petroleum Technology of and Petrochemisty, Institute of Organic Chemistry, Catalysis and Petrochemistry, Faculty of Chemical and Food Technology, Slovak University of Technology, Radlinského 9, 812 37 Bratislava, Slovak Republic

Introduction

The replacing of classic, liquid-phase FC-acid catalysts with suitable solid acids is one of the highest challenges of today's research in heterogeneous catalysis. One of the conditions of the successful replacing is the low reaction temperature for heterogeneous catalysts similar as for homogeneous is used. As solid acid catalysts, mainly zeolites are in the focus of interest. To approach the overall catalytic activity of heterogeneous zeolitic catalysts, the influence of internal diffusion is necessary to eliminate to the highest possible extent. The most known method have been for long time the dealumination, by which the strength of acid zeolitic sites increased together with the creation of a secondary mesoporous system. Another method for the creation of a secondary mesoporus and even macroporous system is desilication [1-3]. From this point of view the mordenite is one of the most studied zeolites.

One of the industrial processes where the great effort is made to replace the FC-catalyst with more environmentally friendly solid acid is the alkylation od benzene with 1-alkenes C_{10}-C_{12} or even longer as a method for the preparation of cationactive surfactants precursors. In this paper, the comparison between the dealumination and desilication as two different processes of the secondary mesoporous system creation was studied in the alkylation of benzene with 1-alkenes in liquid phase.

Experimental

Na-mordenite with Si/Al=6.4 was synthesized in Research Institute of Petroleum and Hydrocarbon Gases in Bratislava. Ammonium form (NH_4-M) was prepared by repeated treatment with NH_4NO_3. H-form was prepared by calcinations of ammonium form at 500 °C in the flow of air.

Dealuminated samples of mordenite were prepared by different combination of hydrothermal treatment in deep-bed conditions at 780 °C and acid dealumination with HCl. Desilication of mordenite was realized by the treatment of mordenite samples with 0.2-5 M solutions of NaOH at 80°C (MD-0.2 – MD-5 according to the NaOH concentration). Desilicated samples were ion exchanged with NH_4NO_3 solution and calcinated at 500 °C in the flow of air.

XRD diffraction and SEM was used to characterize the crystallinity and crystal size and morphology after desilication of mordenite. The formation of a secondary pore structure after dealmination and desilication was measured by physical adsorption of nitrogen at -196,5 °C with data treatment by BET, t-plot and BJH methods. Acidity was determined by TPDA.

Catalytic activity in alkylation of benzene with 1-dodecene was realized in a mixed batch reactor at 200 °C (Be:1-dodecene = 8.6:1 mol:mol, 2% wt. of catalyst).

Results and discussion

After dealumination, Si/Al ratio increased from 6.4 up to 45.5. As a result of dealumination, a secondary mesoporous system was created, increasing S_t from 13 to almost 150 m^2/g. At the same time the micropore volume stayed at high level of 0.170-0.200 cm3/g, and the acidity decreased from 1.82 mmol/g to 0.36 mmol/g [4]. The size of a secondary mesopores created was predominantly in the range of tens of nm.

By desilication of mordenite with NaOH solution up to 2M concentrations the XRD spectra confirmed the stability of mordenite structure [3]. Secondary porous structure formed was substantionally greater – up to action of 1M NaOH with the diameter of 200-500 nm, and after desilication with higher concentrated NaOH even in the range of macropores.

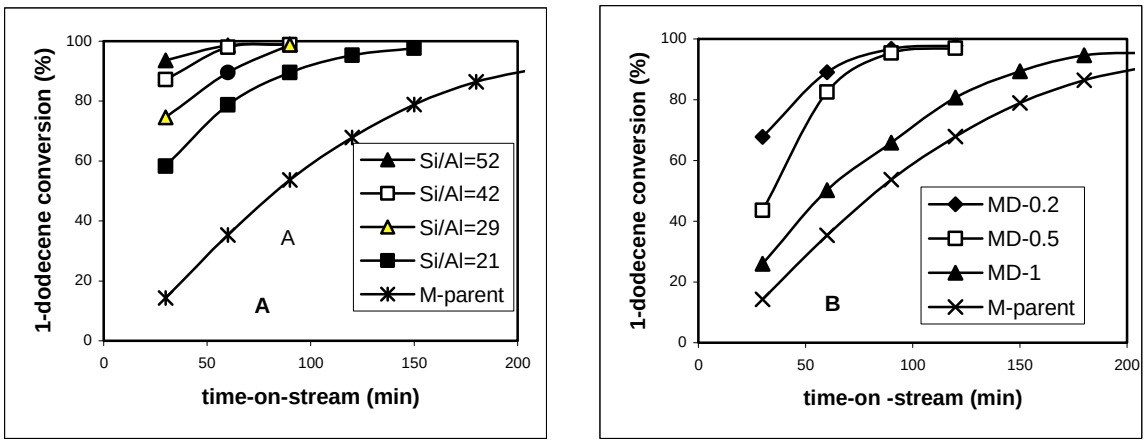

Fig.1 Conversion of 1-dodecene over dealuminated (A) and desilicated (B) mordenites

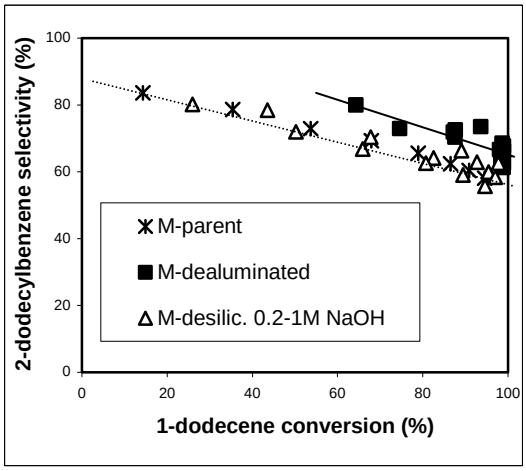

Fig. 2 Selectivity vs. conversion

The activity of mordenites after dealumination increased with the dealumination degree from Si/Al=6.4 to 52 and it seams that by further dealumination the activity could even increase- Fig. 1A. On the other side, the desilication seems to be positive for alkylation activity only at very low NaOH concentration – up to 0.2M, further desilication decrease the activity even if secondary pore system increased – Fig. 1B. The selectivity to 2-phenyl isomer of desilicated mordenites in comparison with the parent mordenite did nod changed, those of dealuminated samples even little increased – Fig.2

Conclusions

Dealumination of mordenite creates the secondary porous system in the range of small to middle mesopores, while desilication of mordenite creates a secondary porous system falling to great mesopores and even to macropores. Even if the acidity of mordenites samples after dealumination decreased, and the formation of a secondary porous system was in the range of tens of mesopores, their activity in alkylation of benzene with 1-dodecene in liquid phase was comparable and even higher than the activity of desilicated samples with higher total acidities and with secondary porous system in the range of great mesopores and macropores. The selectivity to 2-phenyldodecane for dealuminated mordenites was even little greater (about 70% at more than 95% conversion) than for parent mordenite and its desilicated forms.

References

[1] Groen J., Zhu W., Brouwer S., Huynink S.J., J. Am. Chem. Soc. 129 (2007), 355-360
[2] V.Paixao, A.P.Carvalho, J.Rocha, A.Fernandes, A.Martins. Micropor. Mesopor. Mater. 131 (2010) 350
[3] Hudec P., Hudá M., Horňáček M., Smiešková A., Proc. of the 10th Pannonian Int. Symp. On Catalysis, Krakow, Poland, Aug. 29-Sept.2 (2010). p.21-28
[4] P. Hudec, A. Nociar, A. Smiešková, T. Jakubík., Stud. Surf. Sci. Catal. 158B (2005), 1795–1802.

Brönsted acidic zeolites and molecular sieves for the synthesis of precursors for high quality diesel

Michael Renz, Olalla de la Torre, and Avelino Corma
Instituto de Tecnología Química (UPV-CSIC), Universidad Politécnica de Valencia – Consejo Superior de Investigaciones Científicas, Avda. de los Naranjos s/n, 46022 Valencia, Spain, mrenz@itq.upv.es

Introduction

Energy supply in the post-fossil era is one of the main concerns of Chemistry and a particular challenge when transportation fuels are considered. First generation biocarburants such as biodiesel (FAMEs) or ethanol from sugar cane or starch have been abandoned for competition with food production. Hence, second generation biocarburants should be obtained from non-edible biomass (waste) that is grown elsewhere but on crop land. A valuable contribution to the solution of this problem may be a process that has been presented recently [1]. Sylvan (2-methylfuran) is the key-intermediate of this process and two molecules are subsequently hydroxyalkylated with an aldehyde and alkylated with the resulting alcohol (see eq. 1). After hydrodeoxygenation of the produced difuran derivative an alkane mixture is obtained with a high cetane number (71).

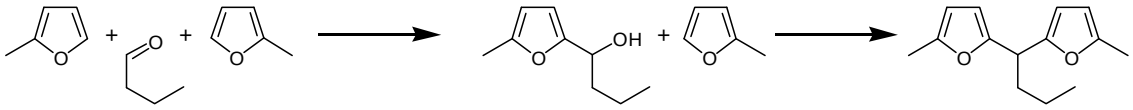

(eq. 1)

For the hydroxyalkylation/alkylation reactions Brönsted acidic resins have been employed [2, 3]. Herein, this reaction will be carried out with different catalysts involving zeolites and resins and *para*-toluenesulfonic acid for comparison reason. It will be shown that zeolites are interesting catalysts for this reaction and several hundreds of turnovers are achieved per catalytic site.

Experimental

The catalytic activity of the materials were tested in the following way: 1.30 g (18.0 mmol) of butanal were mixed with 3.00 g (36 mmol) of 2-methylfuran, a 50-mg sample of the catalyst was added and the reaction mixture stirred magnetically and heated to 50 ºC for 8 h. Aliquots were taken periodically and analyzed by gas chromatography.

Results and discussion

The reaction of Sylvan with butanal was carried out in the presence of USY and Beta zeolites. The USY samples were commercial zeolites (Zeolyst) with Si/Al ratios from 2.5 to 27.5. The Beta zeolites were synthesized in fluoride (Si/Al ratios from 13 to 103) and in alkaline medium (Si/Al ratio from 13 to 112) and characterized by X-Ray diffraction to confirm the zeolite structure and by ICP-EOS to determine the aluminium content. These samples were tested in batch mode and the best results for each series is displayed in Table 1. It can be seen that the highest conversion was achieved with zeolites involving a small range of Si/Al ratios from 13 to 20. With the synthesized Beta samples yields of up to 60% were obtained (cf. entries 3 and 4) and with a commercial sample 67% (entry 2). The yield was lower than the 90% achieved with the macroreticular resin Amberlyst 15 (entry 7), however, the unreacted substrates can be recovered easily by distillation due to their low boiling point of 66 and 75 ºC

for Sylvan and butanal, respectively. When the catalytic activity is compared with respect to the number of catalytic sites, i.e. the mol of product per mol of active sites (turnover number, TON), the zeolites were superior to the resin. A TON of up to 385 was observed with a zeolite Beta sample synthesized in fluoride medium (entry 4) whereas the resin resulted only a TON of 138 (entry 7). The mesoporous amorphous Al-MCM-41 showed also a high catalytic activity with a TON of 402 and a comparable yield as the zeolites although considerable amounts of the intermediary furfuryl alcohol derivative were observed (entry 6). With respect to the initial activity measured after 15 min reaction time the USY zeolite achieved a similar value as the macroreticular resin (cf. entries 5 and 7) whereas all zeolite Beta samples showed only one third of this initial activity. This was probably due to the smaller pore size of zeolite Beta that restricted the diffusion of the substrate and the diffusion out of the latter became rate determining.

Table 1. Catalytic activity of different catalysts for the reaction of Sylvan with butanal.

		Si/Al Ratio		Yield[b]	TON[c]
Entry	Catalyst	[mol/mol]	Initial Activity[a]	[%]	[mol/mol]
1	p-TosOH		1142	88	71
2	Beta (Zeolyst)	13	101	67	202
3	Beta (nanocrystalline)	15	111	59	199
4	Beta F^-	20	89	60	385
5	USY (Zeolyst)	20	331	53	241
6	MCM-41	30	92	60[d]	402
7	Amberlyst-15		314	90	138

[a] initial activity in mmol of product/g of catalyst/h; measured after 15 min reaction time. [b] of 2,2'-butylidenebis[5-methylfuran] with a purity of at least 93% after 8 h reaction time. [c] mol of product obtained per mol of Al. [d] only 88% of the obtained product was 2,2'-butylidenebis[5-methylfuran] and 7% was 2-(1-hydroxybutyl)-5-methylfuran.

Conclusions

Brönsted acidic Beta zeolites and mesoporous molecular sieves are interesting catalysts for the reaction of aldehydes with Sylvan to form Diesel precursors. The highest turnover numbers were achieved with these catalysts that also provide the possibility of regeneration by calcination in contrast to Brönsted acidic resins.

Acknowledgements

This work was supported by the CYCIT (MAT-2006-3798164 and Consolider Ingenio 2009 CDS 00050).

References

[1] Corma, A., de la Torre, O., Renz, M., Villandier, N., Production of high quality diesel from biomass waste products, Angewandte Chemie International Edition, 50 (2011), in press; DOI: 10.1002/anie.201007508.
[2] Iovel, I., Goldberg, Y., Shymanska, M., Hydroxymethylation of furan and its derivatives in the presence of cation-exchange resins, Journal of Molecular Catalysis, 57 (1989), 91-103.
[3] Riad, A., Mouloungui, Z., Delmas, M., Gaset, A., New synthesis of substituted difuryl or dithienyl methanes, Synthetic Communications, 19 (1989), 3169-3173.

Catalytic degradation of pure and waste polymers in the presence of zeolite and mesoporous catalysts

János Halász*

Department of Applied and Environmental Chemistry, University of Szeged
Rerrich tér 1, H-6720 Szeged, Hungary; halas@chem.u-szeged.hu

Introduction

The amount of plastic wastes generated by our society is growing rapidly. The low biodegradability of different plastics creates a serious environmental problem. Traditional thermal cracking can be applied to transform thermoplastics into gases, liquid hydrocarbons and solid residue. However, thermal cracking yields low value unstable hydrocarbons within a broad range of molecular weight. Catalytic degradation generally operates at lower temperature and can result products with better quality [1,2]. The objective of this work is to study the potential of modified ZSM5 zeolite, MCM41 mesoporous silica and hydrotalcites as catalysts for degradation of PE, PP, PS, PET and PVC using thermal analytical method and laboratory reactor experiments.

Experimental

Commercial plastics: PE, PP, PS and PVC in granule form have been used as model feed. The degradation of pure polymers was followed using either by utilizing of thermoanalytical method (*MOM Derivatograph Q, Hungary*) or in a laboratory batch reactor system with gaschromatographic product analysis (*Shimadzu GC2010, Japan*).
The synthesized Na-ZSM-5 zeolite was modified by conventional or solid state ion-exchange [3] to form H-, Fe-, Cu-, Ni- and Ti-ZSM5 samples, while the mesoporous catalysts (Fe- and Ti-MCM-41) were synthesized by isomorphous substitution [4], as well as the hydrotalcites containing Fe-, Cu-, Cr- or Ca-oxide in the Mg,Al-LDH structure. The fresh and used catalysts were characterized by XRD, TEM, N_2 adsorption and IR-spectroscopy.

Results and discussion

The TG analysis of PET proves a relatively sharp, one steep weightloss with a maximum in the DTG curve placed at 480 ^{o}C. This behavior corresponds with the thermal degradation of this polyester of narrow molecular mass distribution. On Fig. 1(a) the TG and DTG curves for PET/Ti-MCM41 catalyst mixture with 10 % catalyst content can be seen. The polymer degradation in the presence of catalyst takes place at a lower temperature, due to the catalytic cracking. The difference of the PET and the PVC in the catalytic degradation can be seen in Fig. 1(b). The decomposition of PVC takes place at least in two steps.

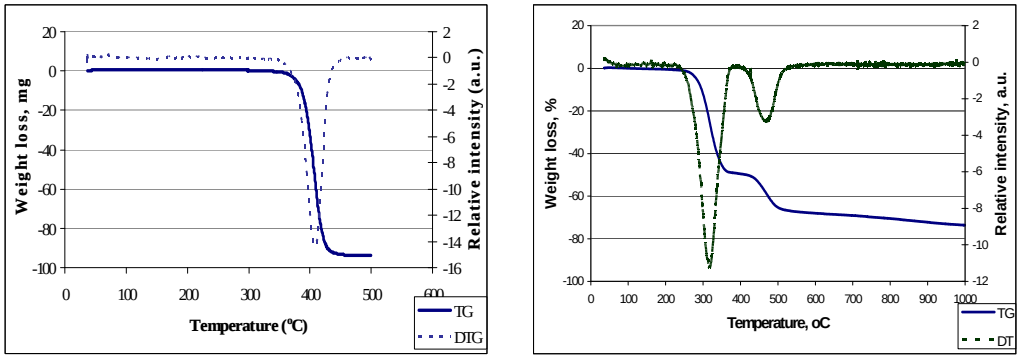

Fig. 1: Thermal analytical study of PET (a) and PVC (b) degradation over Ti-MCM41 catalyts

The laboratory reactor experiments proved that H-ZSM-5 catalyst possessing strong acid sites resulted in less liquid products and more gaseous components than the other, transition metal containing catalysts.
For PP degradation the non-acidic Ti-MCM41 and the Fe-ZSM-5 samples produced liquid hydrocarbons with yields about 90%, which is higher than that of non-catalytic thermal degradation. Similar results have been obtained for PS degradation, however, the activity of the catalyst with small pore sizes (ZSM-5) have had lower activity (no reaction observed below 350 ^{o}C).
The catalytic degradation of PVC takes place at least in two steps: the first one is the leaving of HCl. In this reaction the catalysts with basic character (CaO, $CaCO_3$, hydrotalcites and Mg-Al-mixed oxides) have high activity, due to the stabilization of the system by the reaction with the releasing HCl.

Conclusion

From the results obtained it can be concluded that not only the catalyst framework but also the polymer structure determinate the activity of porous materials in the catalytic degradation of plastic wastes. The polymer chain ends are able to penetrate into the pore system of the catalyst. reaching the active sites into the channel system**.**
Polymer with aromatic ring. i.e. PS and PET show lower activity in the case of catalysts with smaller pore sizes (ZSM-5). By other hand, the higher pore size resulted in higher initial reactivity, but the coke deposition was improved in the catalysts of large pores, can lead to a fast deactivation.

References

[1] S.C. Cardona and A. Corma, Appl. Catal. B: Environ., 25 (2000) 151.
[2] M. Azhar-Uddin, Y. Sakata, A. Muto, Y. Shiraga, K. Koizumi, Y. Kanada and K. Murata, Micropor. Mesopor. Mater., 21 (1998) 557.
[3] I.H. Metcan, A.R. Ozkan, R. Isler, J. Yanik, M. Saglam and M. Yuksel, Fuel. 84, (2005) 619.
[4] Q. Zhou,. C. Tang, Y-Z. Wang and L, Zheng, Fuel 83 (2004) , 1727.

Bioethanol Steam Reforming on Modified Mordenite zeolite

J.F. Da Costa-Serra, M.T. Navarro, F. Rey, A. Chica*
Instituto de Tecnolgía Química (UPV-CSIC), Universidad Politécnica de Valencia, Consejo Superior de Investigaciones Científicas, Avenida de los naranjos s/n, 46022 Valencia, Spain
(*) corr. author: achica@itq.upv.es Fax: +34 96 387 78 13 Tel: +34 96 387 70 00 ext: 78508

Introduction

The future scarcity of fossil fuels, the rising of their price, the pollution associated with their use and the potential environmental disasters due to their collection, make necessary to develop renewable and cleaned energy alternatives independent of fossil fuels. Hydrogen based fuels offer an attractive alternative to the hydrocarbon fuels currently used. But to realize the full benefits of a hydrogen economy-sustainability, increased energy security, diverse energy supply and reduced air pollution hydrogen must be produced from available renewable resources. Reforming of renewable biomass feedstocks [1], such as bioethanol, can be used for hydrogen production [2,3]. Catalysts for H_2 production from bioethanol steam reforming is under development. High activity and selectivity are the main catalytic behaviors for these materials. Besides selectivity and conversion, surface area of the support plays an important role in the preparation of highly active and selective bioethanol steam reforming catalysts. Zeolites have attracted much attention as catalysts and supports due to their high surface due and functional characteristics, such as adsorption, acidity, ion exchange and molecular sieve properties [4]. We have explored the activity, selectivity, and stability of Co supported over a modified commercial Mordenite in the steam reforming of bioethanol. Commercial Mordenite has been previously desilicated in order to generate mesoporosity and increase the external surface. A complete characterization of Co-based modified Mordenite catalyst has been carried out (XRD, BET area, TPR and TEM), which has allowed to establish interesting relationships between its catalytic performance and physico-chemical properties.

Experimental

Modification of Mordenite zeolite was carried out treating the commercial Mordenite (CBV20A from Zeolyst) with an alkaline solution. This treatment partially dissolves some Si and/or Al yielding to the formation of ‘holes’ in the zeolite particles. The presence of these ‘holes’ results in the development of mesoporosity in the zeolite. Co was incorporated by incipient wetness impregnation with an aqueous solution containing the required amount of $Co(NO_3)_2\ 6H_2O$ to achieve a nominal concentration of 20 wt% of metal in the final catalysts. The solid was further dried at room temperature for 16 h and after calcined in muffle oven at 873 K for 3 h. Catalytic test was carried out in a fully automated stainless steel fixed bed continuous reactor at different reaction temperatures (673-873 K), H_2O/Bioethanol of 13 and atmospheric pressure. Catalysts were reduced in situ in flow of pure H_2 before reaction. The materials were characterized by N_2 adsorption, XRD, TPR, and TEM in order to know their physico-chemical properties more relevant.

Results and discussion.

Characterization by XRD and N_2 adsorption shows that the modified MOR zeolite retains the most part of its original crystallinity, while mesoporosity are generated. Mesoporosity is confirmed by TEM, **Figure 1**. As it can be seen in these pictures there is no significant

modification of the crystal size upon alkaline treatment, but large 'holes' are created inside of the MOR particles.

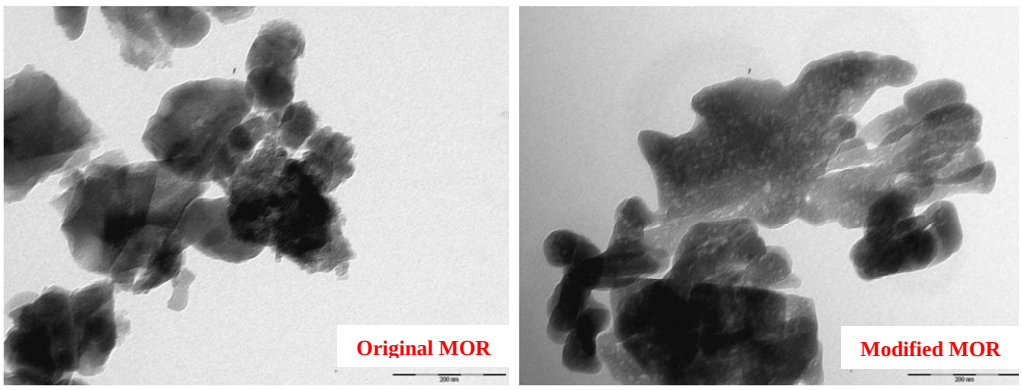

Figure 1. TEM microphotographs of original MOR and modified.

Modified MOR zeolite containing alkaline metals (Na) and Co exhibits the highest catalytic activity and hydrogen selectivity in the bioethanol steam reforming, **Table 1**. The presence of alkaline metals (Na) improves the H_2 selectivity and decreases the C_2H_4 production. Acid sites and metallic cations (cobalt cations), has been detected in the samples without Na (Co/mod-MOR, Co/MOR). It could explain the large amount of C_2H_4 produced by these samples since the presence of acid sites and metallic cations favor the dehydration of ethanol [2].

Table 1: Bioethanol conversion and products selectivity. Reaction conditions: 400ºC, atmospheric pressure, H_2O/EtOH of 13 and GHSV of 4700 h^{-1}.

Catalyst	EtOH Conv., mol %	Selectivity, mol %							
		CH_4	CO	CO_2	H_2	C_2H_4	C_3H_6	C_2H_4O	C_3H_6O
Co/MOR	92,00	4,70	6,29	7,21	28,23	46,92	0,07	6,57	0,01
Co/mod-MOR	79,57	10,26	12,10	9,64	36,22	18,98	0,16	12,62	0,03
Co/mod-MOR(Na)	98,24	15,47	18,87	12,03	46,02	0,24	0,02	7,31	0,04

Conclusions

The results show that catalytic steam reform of bioethanol can be carried using modified MOR zeolite containing alkaline metals (Na) and Co. Mesoporosity generated in the modified MOR seems to account for the best results obtained with this modified zeolite. The results here presented could be improved by removal the acid sites and metal cations within the zeolite.

Acknowledgements

Dr. Antonio Chica thanks to the UPV and the CSIC for funding. The doctoral Javier Francisco Da Costa Serra acknowledges the CSIC for granted the scholarship predoctoral-JAE-CSIC.

References

[1] G. Huber, S. Iborra, Corma, Chem Rev. 106 (2006) 4044-98.
[2] R.M. Navarro, M.A. Peña , J.L.G. Fierro, Chem. Rev 107(2007) 3952-91.
[3] A. Chica, S. Sayas, Catal. Today, 146 (2009) 37-43.
[4] J. Cejka, A. Corma, S. Zones, "Zeolites and Catalysis: Sythesis, Reactions and Aplications", Ed: Wiley-VCH, Weinheim, 1ª Edition, April 2010.
[5] Inokawa, H., Nishimoto, S., Kameshima, Y., Miyake, M., Inter J Hydrogen Energy 2010;35:11719-11724.

p-hydroxybenzoic acid degradation by CWAO over ruthenium supported on CeO_2-Al_2O_3 mixed oxides

Mohamed Triki[1,*], Zouhaier Ksibi[2], Abdelhamid Ghorbel[2], Francisco Medina[3]

[1] *Centre National de Recherches en Sciences des Matériaux (CNRSM), Pôle Technologique de Borj-Cédria, BP 73, 8027 Soliman, Tunisie*
[2] *Laboratoire de Chimie des Matériaux et Catalyse (LCMC), Faculté des Sciences de Tunis, Université de Tunis el Manar, Campus Universitaire, 2092 Tunis, Tunisie*
[3] *Departament d'Enginyeria Quimica, Universitat Rovira i Virgili, Campus sescelades, 43007 Tarragona, Spain*
[*] *Corresponding author: mhtriki@yahoo.fr*

Introduction

The Catalytic Wet Air Oxidation (CWAO) has become one of the most promising methods for the treatment of phenolic compounds especially found in wastewaters. In order to promote the efficiency of this technology, ruthenium supported catalysts have been used. In this light, several supports have been investigated [1, 2]. Herein, CeO_2-Al_2O_3 mixed oxides with different weight ratios have been prepared using the sol-gel method and used as supports for ruthenium catalysts. We study the catalytic behavior of 1%Ru/CeO_2-Al_2O_3 in the CWAO of p-hydroxybenzoic acid (p-HBZ) chosen as a model of phenolic compounds typically found in olive mill wastewaters.

Experimental

CeO_2 support was prepared by dissolving $Ce(NO_3)_3$•$6H_2O$ in absolute ethanol under vigorous stirring. Then, droplets of NH_4OH were added to obtain a precipitate. Al_2O_3 support was synthesized via the sol-gel process by using aluminium tri-sec-butoxide as precursor and sec-butanol as solvent. CeO_2-Al_2O_3 mixed oxides were elaborated as follows: $Ce(NO_3)_3$•$6H_2O$ was dissolved in sec-butanol. Ethylacetoacetate was then added into the solution to control the hydrolysis-condensation reactions. A solution of aluminium tri-sec-butoxide in sec-butanol was added in order to obtain 5, 10 and 20 as CeO_2/(CeO_2+Al_2O_3) weight ratio. Finally, an aqueous solution of HNO_3 (0.1M) was added to obtain a gel. All the samples were dried in supercritical conditions (P = 42 bars; T = 263°C) of the solvent to obtain aerogels which were calcined under oxygen at 500°C for 3h. The ruthenium catalysts (1 wt% Ru/support) were prepared by impregnation of the support with ethanolic solution of ruthenium(III) chloride. These catalysts were dried at 90 °C for 24 h and then reduced under hydrogen at 300°C for 2 h. Characterization of samples was performed by means of N_2 adsorption-desorption of nitrogen at 77 K, X-ray Diffraction (XRD), TPR, UV-Visible, Scanning Electron Microscopy (SEM) and Transmission Electron Microscopy (TEM). The CWAO of aqueous solutions of p-HBZ (10 mmol/L) has been carried out over the catalyst (500 mg) at 140°C and 50 bar air. The kinetic of the degradation of organic compounds was followed by HPLC.

Results and discussion

The textural properties and p-HBZ conversion after 7h of reaction over 1 wt% Ru/support catalysts are summarized in Table 1. The introduction of different amount of Ce into system increases the surface area of the pure supports. The high values of surface area of the Ru/Ce-Al catalysts indicate a high dispersion of the CeO_2 in the Ce-Al aerogels mixed oxides.

A-TYPE ZEOLITE MEMBRANE SYNTHESIS FOR PRODUCTION OF METHANOL WITH CO_2 HYDROGENATION

Tu?ba, Çelik [(1)]; Çi?dem , Güldür [(2)].

[(1)] Gazi UniversityAnkara, Turkey; [(2)] , .

Nowadays, one of the important problem that we face is the global warming and the increase of carbondioxide concentration in the atmosphere is the major cause of this problem. For this reason, to decrease the amount of CO_2 emitted during any chemical reaction and to convert CO_2 into feasable chemicals attracted the attention of the researchers. Methanol has gained great importance with its physical and chemical properties. Due to being used as a fuel; being converted into other alternative fuels, being converted into other chemicals, like formaldehyde, researches are carried out to find ways to produce methanol with high yields at moderate conditions.

Methanol synthesis reaction is limited by the equilibrium. A membrane reactor used to removed some reaction products from the reaction system. This work has the purpose of with zeolite membrane synthesis because, among inorganic materials, zeolite is a promising candidate for high performance membranes for industrial applications. An A-type zeolite membrane was formed by hydrothermal reaction. A porous α-alumina tube was used as the support for a zeolite membrane.Synthesis experiments were conducted for various synthesis times by using a reaction mixture compositon. Higly crystalline zeolite A could be synthesis from sodium silicate and sodium alüminate mixture with large synthesis times. When zeolite A membrane was formed by different sources of silicalite , particle size distrubiton of the product crystals were observed to change.

High activity of ruthenium supported catalysts in CWAO of p-HBZ was observed. We found that the optimal cerium content in the Al_2O_3 support was 20 wt%. The activity of the Ru/Al_2O_3 and Ru/CeO_2 was also tested for comparison. It was found that the addition of CeO_2 on the alumina support improves the activity of Ru catalysts. The activity of the samples decreases in the following order: Ru/Ce-Al (20) > Ru/Ce-Al (10) > Ru/Ce-Al (5) ≈ Ru/Al_2O_3 > Ru/CeO_2. This result is probably due to the fact that Ce-doping, with an optimum ratio, allows a better ceria dispersion showing high surface area that improves the reducibility of ceria and promotes the electronic properties and dispersion of the ruthenium particles.

Table 1 Textural properties and p-HBZ conversion after 7h of reaction over Ru catalysts

Catalyst	S_{BET} * ($m^2.g^{-1}$)	<Dp> (nm)	p-HBZ conversion (%)
Ru/Ce-Al (20)	*292 (*303*)*	14	88
Ru/Ce-Al (10)	298 *(306)*	15	77
Ru/Ce-Al (5)	259 *(262)*	21	60
Ru/Al_2O_3	*196 (*233*)*	23	62
Ru/CeO_2	40 *(40)*	13	53

* *The data in brackets are the S_{BET} of the supports before impregnation, <Dp>: average pore diameter*

The mixed oxide system plays a significant role to enhance the activity compared to the corresponding single oxide. In fact, this new system ultimately enhances the catalytic activity. The improvement of the activity could be attributed to the outstanding redox properties of ceria-alumina mixed oxides and the capacity for these supports to favour the oxygen transfer from the active site to the organic molecule.

Conclusions

Ruthenium catalysts supported on CeO_2-Al_2O_3 mixed oxides prepared via sol-gel method show high activity in CWAO of p-HBZ. The activity of 1%Ru/Ce-Al (20) is higher than that of Ru/Al_2O_3 and Ru/CeO_2 catalysts. This result is due to the synergy effect between ceria and alumina affecting the surface structural properties of Ce-Al support. The high dispersion of both the ruthenium particles and the CeO_2 on alumina improves the catalytic activity.

Acknowledgements

We are indebted to the European Union for financial support (code A/5927/06) "Novel oxidative catalytic technologies for olive oil mill wastewater"). Mercè Moncusi Mercadé and Mariana Stefanova Stankova from Universitat Rovira i Virgili (Spain) are gratefully acknowledged for the microscopy experiments.

References

[1] Triki, M., Pham Minh, D., Ksibi, Z., Ghorbel, A., Besson, M., Ruthenium catalysts supported on TiO_2 prepared by sol–gel way for *p*-hydroxybenzoic acid wet air oxidation, Journal of Sol-Gel Science and Technology (2008) 48, 344-349

[2] Triki, M., Ksibi, Z., Ghorbel, A., Medina, F., Preparation and characterization of CeO_2–TiO_2 support for Ru catalysts:Application in CWAO of p-hydroxybenzoic acid, Microporous and Mesoporous Materials (2009) 117, 431-435

Steam dealumination of MFI zeolite: Compensation effect

A. Corma [a], J. Mengual [b], P.J. Miguel [c]
[a] *Instituto de Tecnología Química, UPV-CSIC, Universidad Politécnica de Valencia, Avda. de Los Naranjos s/n, 46022 Valencia, Spain. Corresponding author: acorma@itq.upv.es*
[b] *I.U.I. de Ingeniería del Agua y Medio Ambiente, IIAMA, Universidad Politécnica de Valencia, Camino de Vera s/n, 46022 Valencia, Spain*
[c] *Departamento de Ingeniería Química, Universitat de València, Doctor Moliner 50, 46100 Valencia, Spain*

Introduction

In some refining operations the zeolite catalysts work at high temperatures in presence of steam. In these conditions zeolites suffer dealumination processes, i.e., extraction of framework aluminum, with consequent change in the number and distribution of active sites, causing a variation of zeolite activity and selectivity. Therefore, the study of these dealumination processes is very important, especially the effect they have over the properties of own catalyst and over its activity and selectivity.
In the following work we study the effect of dealumination degree on the cracking activity of MFI zeolite and the evolution of their active sites using cracking experiments.

Experimental

Cracking experiments were conducted using *n*-heptane as feed and He as carrier gas. MFI zeolite sample, with a Si/Al ratio of 15, was obtained from PQ Zeolyst. The experiments were carried out at atmospheric pressure. In all experiments the feed flow was constant. The products of reaction were analyzed in a online G.C.
Dealumination process, also at atmospheric pressure, was conducted at 923 K with a steam partial pressure of 36.2 kPa balanced with He until the specific dealumination time (t_{deal}).

Results and discussion

Firstly, we performed the experiments of catalytic cracking with non dealuminated zeolite. Results of these from Fig. 1A show a small decrease on activity during the first few seconds time on stream (*TOS*), followed by a very constant activity. This has been attributed to the low coking ability of MFI [1]. However, when the reaction is carried out with zeolite which will be progressively dealuminated with time (t_{deal}), the overall conversion (X) at the reactor outlet strongly and continuously decreases with *TOS* ($TOS \equiv t_{deal}$). Note that, as a reference, we have also included the purely thermal conversion (X_T). Dealumination process produces a loss of framework Al^{IV} with the corresponding loss of Brönsted acidity [2] and, consequently, a decrease on zeolite activity, more important than the slight fall of activity caused by the coke formation. It should be noticed that the dealumination process occurred without loss of crystallinity as indicated by the XRD and micropore volume of the sample.
Fig. 1B1 shows the Arrhenius plot at relatively high temperature for a family of catalysts derived from original MFI zeolite by treatment with steam at different times. The lines, in this figure, are not parallel for all dealumination times and the slope increases with time. Consequently, there is an increase of the apparent activation energy of the cracking process (E_C) when the catalyst becomes more dealuminated. This variation may suggest that there is a distribution of active sites with different acid strength. During the dealumination process, that results in a loss of those acid sites, the sites with high enthalpy of adsorption (with lower apparent activation energies) are the ones that are more rapidly depleted (or transform into

others with lower enthalpies). In this sense, Dědeček et al. [3] show that during MFI dealumination a change in the proportion of "Al pairs" to "single Al" occurs and even a change in the cationic site for those "Al pairs". This leaves a catalyst with a more homogeneous distribution of active sites, in where the stronger acid sites have been preferentially removed and the weaker ones are predominant.

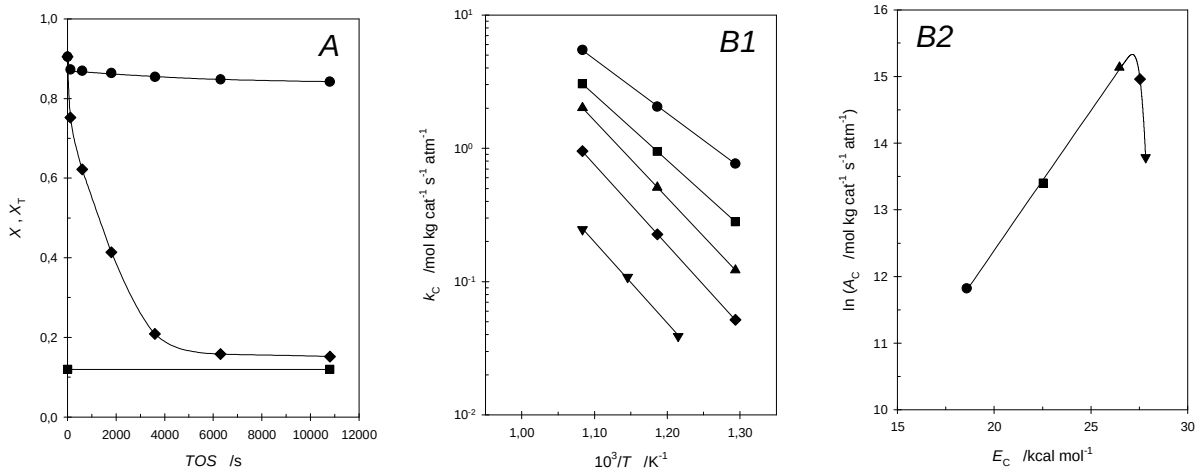

Figure 1. A: Overall (X) and thermal (X_T) conversion *vs.* *TOS* at 923 K. Non dealuminated zeolite (●); Dealuminated zeolite at $t_{deal} \equiv TOS$ (◆); Thermal conversion (■)
B: Compensation effect. t_{deal} /s: 0 (●); 120 (■); 600 (▲); 1800 (◆); 3600 (▼)

Figures 1B shows that for dealumination times beyond 600 s, the apparent activation energies remain constant tend to a limit value around 27.8 kcal mol^{-1}, indicating that the catalyst surface is quite homogeneous from the acid sites point of view. Nevertheless, the number of active sites continues to be removed during dealumination time, as it is indicated by a decrease in the apparent pre-exponential factor (A_C), expressed per mass of catalyst.
The increasing linear dependence between ln A_C and E_C shown in Fig. 1B2 is typical of processes in which there is a compensation effect [4]. This linear dependence, assuming that the intrinsic kinetic parameters remain practically constant, implies a linear correlation between the entropy and enthalpy of adsorption [5]. Therefore, the compensation effect observed could be explained taking into account that the modification of the zeolite by steam results in changes of the overall adsorption heats, while remaining constant the intrinsic parameters of active sites.

Conclusions

From this study we can highlight that the steam dealumination leads to decreased activity by loss of acid sites and as the catalyst is more dealuminated, the apparent activation energy increases until reaching a constant value. We have also observed a compensation effect, possibly due to the variation of adsorption parameters by a selective dealumination of different acid sites during that process.

References

[1] Corma, A., Miguel, P.J., Orchillés, A.V., Appl. Catal. A, 117 (1994), 29-40
[2] Beyer, H.K., Molecular Sieves - Science and Technology, 3 (2002), 203-255
[3] Dědeček, J., Gábová, V., Wichterlová, B., Stud. Surf. Sci. Catal., 142B (2002), 1817-1824
[4] Galwey, A.K., Adv. Catal., 26 (1977), 247-322
[5] Ramachandran, C.E., Williams, B.A., van Bokhoven, J.A., Miller, J.T., J. Catal., 233 (2005), 100-108

Catalysis for fine chemicals and pharmaceuticals

FEZA 2011

Exceptionally Highly Selective Bisphenol A Synthesis on Layered Silicates with Spatially Arranged Propyl Sulfonic Acid

Yusuke Ide, Noriko Kagawa, Masahiro Sadakane, Tsuneji Sano*
Department of Applied Chemistry, Graduate School of Engineering
1-4-1 Kagamiyama, Higashi-Hiroshima, 739-8527, Japan
tsano@hiroshima-u.ac.jp

Introduction

Solid materials that allow for molecular-level fine structural and compositional tuning have attracted increased attention to mimic enzyme reactions. Layered inorganic solids and the derivatives are the possible candidates due to the large surface area derived from well-defined nanostructures composed of ultrathin oxide layers (so called "nanosheets") and materials' diversity. Among them, the organic derivatives with silane coupling reagents have exhibited molecular recognition abilities, possibly due to spatially arranged one or multiple kinds of functional groups in the interlayer nanospace.[1] These reports motivate us to investigate stereo-, region-, and chemoselective syntheses of target organic compounds on silylated layered materials.

In the synthesis of bisphenol A from acid-catalyzed condensation between acetone and phenol, it is known that the selectivity of the desired *p,p'* isomer to the by-product *o,p'* one enhances when the reaction is conducted in the presence of thiol, accordingly, a lot of efforts has been done to design heterogeneous catalysts containing sulfonic acid and thiol groups.[2] In the present study, we have synthesized the silylated derivatives of a layered silicate, magadiite, modified only with propylsulfonic acid and interestingly found that the *p,p'* isomer formed with an extraordinary *p,p'*/*o,p'* isomer ratio (~ 1000) when the amount of the immobilized propylsulfonic acid, which directly correlates to the spatial distribution in the interlayer nanospace, was tuned.

Experimental

The immobilization of propylsulfonic acid group on a layered silicate, magadiite ($Na_2Si_{14}O_{29}$), was conducted on the basis of the reported method with slight modification.[3] The dodecyltrimethylammonium ion-exchanged form of magadiite (abbreviated as DTMA-mag) was mixed with a solution of 3-mercaptopropyltrimethoxysilane (MPS) in toluene and the solvent was evaporated from the mixture. The precipitation was reacted with a solution of of tris(2-carboxyethyl)phosphine hydrochloride in ethanol at room temperature for 72 h and the product was separated by filtration followed by washing with a mixture of ethanol and 0.1 mol L^{-1} of an aqueous hydrogen chloride solution, yielding the mercaptopropylsilylated derivative of magadiite (MPS_x-mag; *x* denotes the amount (groups) of the attached MPS per $Si_{14}O_{29}$ unit). The mercaptopropylsilylated derivative was mixed with 7 mol L^{-1} of an aqueous nitric acid solution and the mixture was stirred at room temperature for 6 h. The sulfonated product (SPS_y-mag; *y* denotes the amount (groups) of the attached MPS per $Si_{14}O_{29}$ unit) was separated by filtration, washed with water, and 0.1 mol L^{-1} of an aqueous hydrogen chloride solution. To control the amount of the attached propyl sulfonic acid (SPS), the added amount of MPS was tuned.

The synthesis of bisphenol A was conducted as follows: SPS_y-mag was added to vaial (50 mL) and dried under vacuum at 60 ^oC for 6 h. Phenol (2400 per H^+ in mole) and acetone (300 per H^+ in mole) were added, the vaial was sealed under argon, and the mixture was stirred at 90 ^oC for 48 h. The catalyst was removed by filtration ad washed with acetonitrile to a total filtrate volume of 100 mL, and the products were quantified by HPLC analysis.

Results and discussion

Fig. 1 shows the X-ray diffraction patterns of DTMA-mag, $MPS_{1.2}$-mag, and $SPS_{1.2}$-mag together with that of the parent magadiite. The basal spacing of magadiite, 1.4 nm, increased to 2.7 nm and then decreased to 1.8 nm during ion exchange and silylation processes, respectively. In the ^{29}Si MAS NMR spectrum of $MPS_{1.2}$-mag, the integral ratio of Q^3/Q^4, which reflects the amount of interlayer silanol groups, was much smaller than that of magadiite. These results indicate the attachment of MPS on the silicate sheet via Si-O-Si bond (Fig. 1 inset). The ^{13}C CP/MAS NMR spectra (Fig. 2) and compositions of $MPS_{1.2}$-mag before and after oxidation revealed that the attached thiol was quantitatively converted to sulfonic acid. Similar results on XRD patterns, NMR spectra, and elemental analyses were obtained when the amount of the added MPS was changed, indicating the formation of sulfonated magadiites with different amount of the attached SPS, which directly correlates to the spatial distribution in the interlayer space (Table 1).

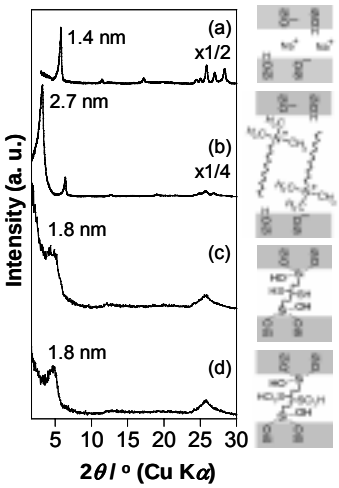

Figure 1. X-ray diffraction patterns of (a) magadiite, (b) DTMA-mag, (c) $MPS_{1.2}$-mag, and (d) $SPS_{1.2}$-mag. Inset shows the schematic structure of the products.

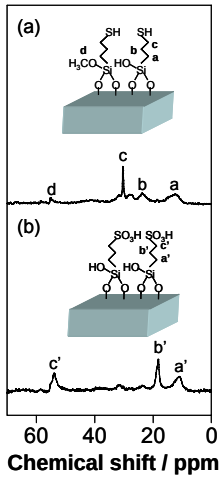

Figure 2. ^{13}C CP/MAS NMR spectra of (a) $MPS_{1.2}$-mag and (b) $SPS_{1.2}$-mag.

When all the obtained propylsulfonated materials were used for the synthesis of bisphenol A from acid-catalyzed condensation between acetone and phenol, *p,p'*-bisphenol A was preferentially formed. Higher selectivity was obtained when SPS_y-mag with larger amount of the attached SPS was used. Surprisingly, $SPS_{1.2}$-mag gave the best result with a *p,p'*/*o,p'* isomer ratio of ca. 1000 (Table 1), which was considerably larger than those reported for other heterogeneous catalysts; for example, *p,p'*/*o,p'* isomer ratio of 20 was obtained on a mesoporous silica modified with thiol and sulfonic acid.[2a] When the surface coverage with propyl sulfonic acid is higher, the size and geometry of the interlayer void is so matched with those of *p,p'*-bisphenol A that propyl and sulfonic acid groups attached on the catalyst surface cooperatively interact with phenyl and hydroxyl groups of the product (Fig. 3).

Table 1. Catalytic activities of materials tested.

Catalyst	Distance between adjacent silyl groups / nm	Activity / mmol per H^+ h	*p,p'*/*o,p'* isomer ratio
$SPS_{1.2}$-mag	0.64	0.15	943
$SPS_{0.70}$-mag	0.88	0.058	42
$SPS_{0.60}$-mag	0.91	0.037	28
$MPS_{1.2}$-mag	0.64	0	-
H_2-mag*	-	0	-

*Proton-exchanged form of magadiite.

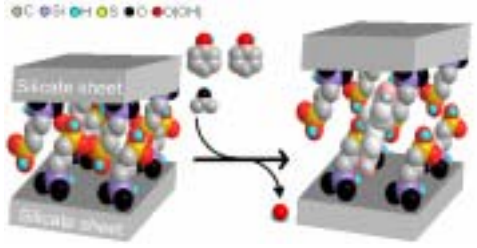

Figure 3. Schematic drawing of *p,p'*-bisphenol A formation in the SPS-mag bearing higher surface coverage with propyl sulfonic acid.

References

[1] a) Ogawa, M., Okutomo, S., Kuroda, K., J. Am. Chem. Soc., 120 (1998), 7361-7362; b) Ide, Y., Ogawa, M., Angew. Chem. Int. Ed., 46 (2007), 8449-8451; c) Ide, Y., Iwasaki, S., Ogawa, M., Langmuir, in press.

[2] a) Margelefsky, E. L., Bendjeriou, A., Zeidan, R. K., Dufaud, V., Davis, M. E, J. Am. Chem. Soc., 130 (2008), 13442-13449; b) Shimizu, K., Kontani, S., Yamada, S., Takahashi, G., Nishiyama, T., Satsuma, A., Appl. Catal. A, 380 (2010), 33-39.

[3] Ide, Y., Ozaki, G., Ogawa, M., Langmuir, 25 (2009), 5276-5281.

Catalytic activity of ionic Au^{3+} supported on mesoporous MgF_2 in the diastereoselective one-pot synthesis of (±) menthol from *rac*-citronellal

Alina Negoi[1], M. Tudorache[1], Stefan Wuttke[2], Erhard Kemnitz[2], Simona M. Coman[1], Vasile I. Parvulescu[1]
[1]*Department of Organic Chemistry, Biochemistry and Catalysis, Faculty of Chemistry, University of Bucharest, Regina Elisabeta Blvd., no. 4-12, Bucharest 030016, Romania;* [2]*Institut fur Chemie, Humboldt-Universitat zu Berlin, Brook-Taylor-Strasse 2, D-12489, Berlin, Germany*
Corresponding author: vasile.parvulescu@g.unibuc.ro

Introduction

One of the major industrial routes to (-)-menthol is the Takasago process. It involves two key steps, the isomerization of (+)-citronellal to (+)-isopulegol with an aqueous $ZnBr_2$ catalyst, and its hydrogenation to (-)-menthol (Scheme 1, route A) [1]. A greener alternative is the substitution of homogeneous methodologies with cleaner heterogeneous approaches. The use of bifunctional solid catalysts may even simplify this synthesis leading to one-pot procedure (route B). Unfortunately, although several active and selective heterogeneous catalysts for the one-pot synthesis of menthols from citronellal have been reported the diastereoselectivity in the (±)-menthol isomer was generally lower than that with homogeneous catalysts (52–76% *vs* 94%). Very recently we reported fluoride-based materials as a new porous catalysts family in which the surface area and pore size can be tuned accordingly to the preparation route [2]. In the light of the above information we present in this study the diastereoselective one-pot synthesis of (±)-menthol using an ionic gold supported on a porous metal fluoride catalyst.

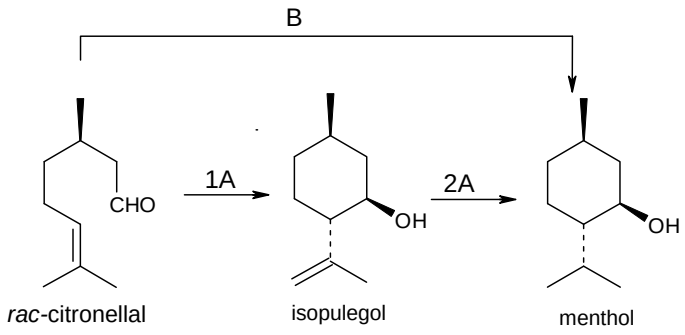

Scheme 1. The synthesis of menthol from citronellal in two stepts (route 1A+2A) and in one-pot (route B)

Experimental

Mesoporous MgF_2 supports with surface area of 276 m^2/g and pore size of 24 Å were prepared using a reported procedure and used as support [2]. The ionic gold-supported on MgF_2 catalysts were synthesized as reported elsewhere by deposition of Au via impregnation with tetrachloroauric acid. Au-x denoted the activation temperature. The obtained samples were characterized by ICP-AES, XRD, EXAFS, XPS, TG-DTA, DR-UV-Vis and cyclic voltammetry. Activity tests were carried out in pressurized reactors as described in Ref. [3].

Results and discussion

As evidenced by ICP-AES, a complete impregnation of the gold compound on the mesoporous MgF_2 co-catalyst was achieved without any loss of gold and the final concentration was 4.0 wt% Au. Because tetrachloroauric acid is not stable in water, chloride

ions become partially substituted by hydroxyl groups resulting in an acidic impregnation solution. Thus, the surface of the magnesium fluoride becomes protonated and positively charged. Therefore, the negatively charged chloride-containing gold complexes should strongly adsorb on the positively charged support surface resulting in immobilized ionic gold nanostructures, as EXAFS shown.

$$[AuCl_{4-i}OH_i]^- + MgF_2 \longrightarrow [AuCl_{3-i}OH_{i+1}]^- / MgF_2 \quad (i = 0\text{-}3)$$

Their thermal activation at 100ºC preserve the Au^{3+} species while at 150ºC a reduction of Au^{3+} to Au^{+} or even to metallic species takes place. Different techniques used for the characterization of the prepared samples confirm these suppositions. However, the catalytic tests demonstrated the catalytic active species are Au^{3+}. In the presence of the molecular hydrogen it is slightly reduced to Au^{+} species that is non-active for the hydrogenation step. An interesting feature of these catalysts is the easy re-oxidation capacity of the Au^{+} species to Au^{3+} by their simple exposure to air atmosphere. This capacity was also demonstrated by electrochemical studies. Based on these structural features we have demonstrated that one-pot synthesis of menthols is possible with selectivities of 92.5% for almost total conversion with a preserved ds of (±)-menthol: (±)-neo-menthol = 87.8 : 12.2. The identified catalytic cycle is given in Scheme 2.

Table 1. The catalytic performances of Au/MgF_2 [a]

Sample	X[%]	$S_{isopulegols}$[%]	$S_{menthols}$[%]
MgF_2[b]	95.0	87.0	-
Au-100	99.0	57.0	43.0
Au-150	0.5	0	0
Au-100[c]	99.0	39.2	60.8
Au-100[d]	99.0	7.5	92.5

[a] Reaction conditions: 100 mg catalyst, 1.0 mL (860 mg) citronellal, 5 mL toluene, 80°C, 15 atm H2, 22 h. [b] The cyclization of citronellal to isopulegol: 100 mg catalyst, 1.0 mL citronellal, 5 mL toluene, 80°C, 6 h. [c] The second catalytic charge. [d] The third catalytic charge.

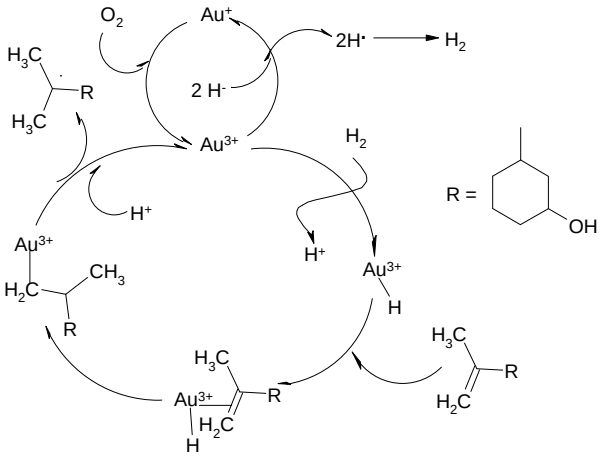

Scheme 2. Catalytic cycle for the one-pot synthesis of menthol

Conclusions

In conclusion, we have shown the bi-functional Au^{3+}/MgF_2 mesoporous catalyst is able to catalyze, for the first time, the diastereoselective one-pot heterogeneous synthesis of (±)-menthol. These results also propose a route for the preparation of ionic noble metals on mesoporous fluoride supports as bi-functional catalysts.

Acknowledgements: This work was financially supported by CNCSIS (PN II TE 91/2010 project).

References

[1]. G. S. Clark, *Menthol*, *Perfumer Flavorist*, **1998**, 25, 33
[2]. S. M. Coman, P. Patil, S. Wuttke, E. Kemnitz, *Chem. Commun*., **2009**, 460–462
[3]. A. Negoi, S. Wuttke, E. Kemnitz, D. Macovei, V. I. Parvulescu, S. M. Coman, *Angew. Chem. Int. Ed*., **2010**, 49, 1–6

Benzylation of benzene with benzyl alcohol on zeolite catalysts

N. Candu, M. Tudorache, S.M. Coman, V.I. Parvulescu
Department of Organic Chemistry, Biochemistry and Catalysis, Faculty of Chemistry, University of Bucharest, Bdul Regina Elisabeta 4-12, Bucharest 030016, Romania, vasile.parvulescu@g.unibuc.ro

Introduction

Friedel-Crafts alkylation is a very important reaction of organic chemistry that is used for the production of a large variety of chemicals for a wide range of industrial segments. An important chemical compound obtained through the benzylation of benzene is diphenylmethane (DPM) (Scheme 1). DPM and its derivatives are industrially important compounds used as pharmaceutical intermediates [1] and fine chemicals [2]. In the fragrance industry diphenylmethane has been used as both a fixative and a scenting soap, as a synergist in some insecticides and as a plastisizer for dyes [3]. The identification of a zeolite catalyst for this step may then provide solutions for similar reactions.

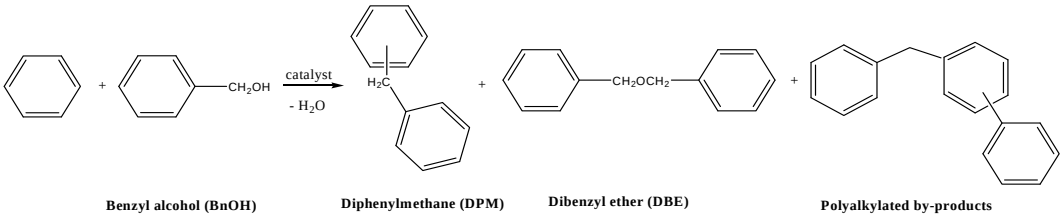

Scheme 1**.** Friedel–Crafts benzylation of benzene with benzyl alcohol.

Experimental

Commercial zeolites with different structures and chemical compositions were purchased from different companies (H-Beta zeolites: PQ25 (Si/Al=10.0) and PQ75 (Si/Al=3.0) Mordenites: HSZ 600 (Si/Al=35.8) and CBV 20A(Si/Al=10.8)). They have been characterized using nitrogen adsorption-desorption isotherms, NH_3-TPD, Py-FT-IR and dynamic light scattering experiments (DLS). The benzylation reactions were carried out in free solvent conditions using three reaction methodologies: (A)- adding all benzyl alcohol at the beginning of the reaction, (B)- by dropwise addition of benzyl alcohol (1-2 drops/min for 4 hours) and (C)-under continuous flow conditions (with different: molar ratio of B/BnOH: 1/1, 5/1, 10/1; flow: 0.1, 0.2 and 0.3mL/min and temperatures: 373K and 423K). In a typical procedure, the catalyst (0.12- 0.60 g) was mixed with 40 mmol of benzene and 40 mmol of BnOH. All reactions were carried out at 323-423K for 5 min-6 h under vigorous stirring (1400rpm).

Results and discussion

While some differences were observed among the surface areas (PQ25= 465m^2/g; PQ75=534m^2/g; HSZ 600=438m^2/g and CBV 20A=362m^2/g), depending both on the Si/Al ratios and the type of zeolite, the pore volume of these materials is very close (PQ25= 0.19mL/g and PQ75=0.18mL/g; HSZ 600=0.18mL/g and CBV 20A=0.16mL/g), that is in a very good concordance with the typical high external surface area of beta zeolites.

Following the methodology A the etherification of benzyl alcohol to DBE is faster than the benzylation of benzene DPM. On the other hand, the variation of the selectivity to DPM (from 9.1 to 30.9) as a function of the reaction temperature and time suggests that the generated DBE acts as an alkylating agent [4]. With methodology B, an apparent high excess of benzene into the reaction medium is induced and the etherification reaction may be confined. The use of flow methodology (C) brings several advantages as, for example, an improved heat and mass transfer and a precise control over reaction conditions. Consequently, important improvements of the chemical reaction in terms of yield, selectivity and reproducibility were achieved. Under optimal conditions following the route (B), selectivities of 77% in DPM were achieved for a conversion of BnOH of 58% in 4h of reaction at 353 K. The flow procedure (C) appeared however to be more advantageous. Thus a selectivity of almost 90% of DPM, for a conversion of 99.2% of BnOH was obtained. It has to be pointed out that the investigated catalytic system has also some practical advantages such as: (i) availability and low costs of the catalysts; (ii) simple and practical experimental set-up; (iii) easier purification of the final product due to the lower content of by-products. The catalytic efficiency combined with practical advantages of the catalytic experimental set-up and the "green" elements of the reaction itself make this process appealing even in the commercial stage. Table 1 compiles results obtained with all three reaction methodologies.

Table 1 Benzylation of benzene with benzyl alcohol at 373K over zeolite PQ25.

Methodology	C_{BnOH} (%)	S_{DPM} (%)	By-products (%)	
			DBE	Polyalkylated benzene
A	72.6	18.7	77.9	3.4
B	57.9	77.0	17.2	5.8
C	20	24.8	75.2	1.7
A*	96.8	56.7	43.3	0.2
C*	99.2	88.9	9.4	1.7

Reaction conditions: 3.56 mL of benzene; 4.16 mL of BnOH; 600 mg of catalyst PQ25; reaction time = 4h; *Molar ratio B/BnOH=10/1: 35.6 mL of benzene; 4.16 mL of BnOH; 600 mg of catalyst.

Among the investigated catalysts the zeolite beta PQ25 was the most effective. Actually, the performances of the catalysts followed the order PQ25 > PQ75 > HSZ600 > CBV20A. This order accounts of several structural and textural factors: number and strength of the acid sites, exposed surface, particle size. Recycling tests showed that the catalysts kept the activity and selectivity to DPM at least for four reaction cycles.

Conclusions

This catalytic study demonstrated that the benzylation of benzene can be carried out in "green" advantageous conditions even by using a less reactive alkylating agent as BnOH and with commercial catalysts as Beta zeolites.

Acknowledgements: This work was financially supported by CNCSIS (PN II TE 91/2010 project).

References

[1]T.W. Bastock, J.H. Clark, Speciality Chemicals, Elsevier, London, 1991.
[2] B.M. Khadilkar, S.D. Borkar, Chem. Technol. Biotechnol. 71 (1998) 209–212.
[3] D. Yin, C. Li, L. Tao, N. Yu, S. Hu, D. Yin, J. Mol. Catal. A: Chem. 245 (2006) 260–265..
[5] N. Candu, M. Florea, S.M. Coman, V.I. Parvulescu, Appl. Catal. A: General 393 (2011) 206–214.

A study of the effect of electron donating and electron withdrawing groups on the catalytic performance of V-MIL-47

Karen Leus[1], Matthias Vandichel[2], Yingya Liu[1] ,Guy B. Marin[3], Michel Waroquier[2],Veronique Van Speybroeck[2] and Pascal Van Der Voort[1]

1 Center for Ordered Materials, Organometallics and Catalysis, Department of Inorganic and Physical Chemistry, Ghent University, Belgium
2 Center for Molecular Modeling, Ghent University, Belgium
3 Laboratory for Chemical Technology, Ghent University, Belgium
Pascal.vandervoort@ugent.be

Introduction

Metal Organic Frameworks (MOFs) are crystalline porous solids composed of a three-dimensional network of metal ions held in place by multidentate organic molecules. In recent years, MOFs have received considerable attention as potentially valuable materials for gas storage and catalysis. Until now, most of the studies on the catalytic activity of MOFs are focused on structures that contain coordinative unsaturated metal sites, as it is often believed that the coordinative saturated MOFs will not be catalytically active. In this contribution we will discuss the catalytic performance of a completely saturated Metal Organic Framework, V-MIL-47 [1], in the oxidation of cyclohexene [2]. Furthermore the synthesis of the amine and nitro functionalized MIL-47 will be discussed and the catalytic performance of these MIL-47 analogues with extra electron donating or withdrawing groups will be compared to the conventional MIL-47 in the oxidation of cyclohexene. Moreover a catalytic cycle, based on molecular modeling on the V-MIL-47 will be presented.

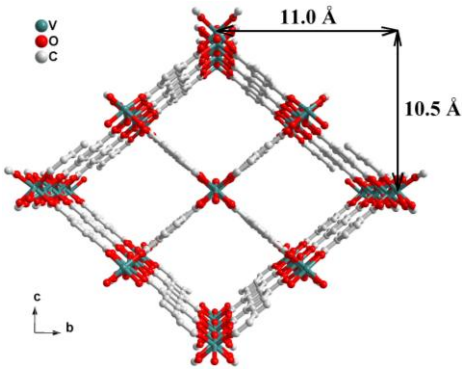

Experimental

MIL-47 was synthesized according to a route described in literature [1]. Also the synthesis of the amine functionalized MIL-47 and the oxidation of the amine group towards the nitro group was based on a procedure described in literature [3,4].
For the catalytic tests, a 100 ml round bottom flask was charged with 30 ml of chloroform used as solvent, 5 ml of cyclohexene and 6.2 ml of 1,2,4-trichlorobenzene (used as internal standard). We have used 2 oxidants, namely tert-butylhydroperoxide (TBHP) in water and TBHP in decane. The substrate/oxidant ratio was 1/2. The reaction mixture was stirred during a required time and at a temperature of 50 degrees under an inert argon atmosphere. Aliquots were gradually taken out of the mixture, diluted with ethylacetate and subsequently analyzed by GC. After a catalytic run, the catalyst was recovered by a simple filtration on a combined nylon-membrane filter, washed with acetone and vacuum dried overnight. The filtrate was analyzed by XRF to determine the leached vanadium.
All systems have also been modelled on the B3LYP/6-311+g(3df,2p) level of theory to calculate the reaction kinetics.

Results and discussion

In Figure 1, the total cyclohexene conversion and detailed product distribution in the cyclohexene oxidation with TBHP in water for MIL-47 is shown. As can be seen from this figure, MIL-47 shows a remarkable activity for the conversion of cyclohexene which is comparable to the homogeneous catalyst $VO(acac)_2$ having the same loading of vanadium. Heterogeneity and stability tests have been performed indicating that the use of TBHP in decane as oxidant enhances the stability of the catalyst after successive runs. Moreover, XRF analysis of the filtrate after catalysis, has clearly shown that the leaching of V can be neglected when TBHP in decane is used as oxidant.

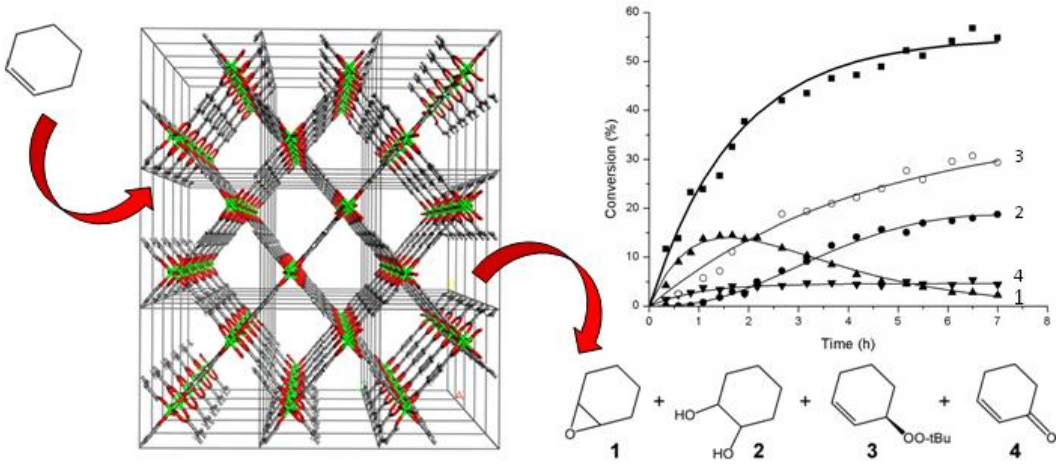

Figure: The catalytic performance of MIL-47 in the oxidation of cyclohexene with TBHP in water as oxidant (numbers1-4 represent the yield of each product)

Theoretical calculations on the structurally similar homogeneous catalyst $VO(acac)_2$ have revealed that the succesful epoxidation is accompanied by a linker exchange with TBHP. A similar mobility of the terephthalic linkers is required to explain the high catalytic activity of the saturated vanadium center in MIL-47. Furthermore, a profound study of the effect of extra electron donating or withdrawing groups on the catalytic performance will be discussed in detail in comparison to the MIL-47.

Conclusions

MIL-47 shows a remarkable catalytic activity in the oxidation of cyclohexene. Furthermore, the use of TBHP in decane as oxidant reduces the leaching and enhances the stability of the catalyst. Moreover, initial theoretical calculations have shown that a linker has to fold away to explain the high catalytic activity of MIL-47.

Acknowledgements

This research is co-funded by the Ghent University, GOA grant nr. 01G00710 and Methusalem grant nr. 01M00409, BELSPO in the frame of IAP 6/27 and the European Research Council (FP7(2007-2013) ERC grant nr. 240483).

References

[1] Barthelet K, Marrot J., Riou D., Férey G., Angewandte Chemie International Edition 41 (2002) 281.
[2] Leus K., Muylaert I., Vandichel M., Marin G. B., Waroquier M.,Van Speybroeck V., Van Der Voort P., Chemical Communications 46 (2010) 5085.
[3] Ahnfeldt T., Gunzelmann D., Loiseau T., Hirsemann D., Senker J., Férey G., Stock N., Inorganic Chemistry 48 (2009), 3057-3064.
[4] Rajender Reddy K., Uma Maheswari C., Venkateshwar M., Lakshmi Kantam M., Advanced Synthesis and Catalysis 351 (2009) 93.

Acylation of *p*-xylene over Zeolites and MOFs

D. Procházková, L. Kurfiřtová, J. Pavlatová, N. Žilková and J. Čejka
J. Heyrovský Institute of Physical Chemistry, Academy of Sciences of the Czech Republic, v.v.i., Dolejškova 3, CZ-182 23, Prague 8 Czech Republic, dana.prochazkova@jh-inst.cas.cz

Introduction

The Friedel-Crafts acylations of aromatic compounds are important reactions for the production of intermediates of fine chemicals. Traditional homogeneous Friedel-Crafts catalysts like $AlCl_3$, BF_3 and H_2SO_4 involve several problems like difficulty in separation and recovery, disposal of spent catalyst, corrosion, high toxicity, moisture sensitivity and undesirable reactions. The replacement of the homogeneous catalysts by heterogeneous can overcome these problems whereas the most challenging group of tested materials is zeolites [1,2]. Metal organic frameworks have attracted a great deal of attention in the past decade. These coordination polymers connecting together metal ions with organic linkers combine properties of organic and inorganic porous materials. MOFs are promising materials in size-, shape- and enantio-selective catalysis.

This work is aimed to study the acylation of *p*-xylene with acid anhydrides and acyl chlorides over zeolites and MOFs. The effect of the acylating agent, the structure of catalyst and the Si/Al ratio of zeolites on the course of the reaction was tested. In addition, the effect of the amount of the catalyst, the molar ratio of substrate/acylating agent on the conversion and selectivity in *p*-xylene acylation was studied.

Experimental

Acylation of *p*-xylene was carried out in multi-experiment work station StarFish. Acylation experiments were performed at atmospheric pressure and temperature 130 °C. Zeolites (Mordenite, Ferrierite, Beta, ZSM-5, SSZ-35 and USY (0.2 and 0.6 g cat.)) with different Si/Al ratios and MOFs (Cu-BTC, Fe-BTC and MIL100(Cr) (0.2 g cat.)) were used. Benzoyl chloride, hexanoyl chloride, propionic anhydride and isobutyric anhydride were used as acylating agents. The course of the acylation reaction was monitored by gas chromatography and mass spectroscopy.

Results and discussion

The highest conversions of acylating agent were achieved over large pore zeolites Beta and USY with all tested acyl chlorides and acid anhydrides. Conversion of benzoyl chloride decreased in the order: USY 79.8 % > Beta 50.8 % > Mordenite 43.9 % > ZSM-5 37.5 % > SSZ-35 22.4 % > Ferrierite 15.8 % (Fig. 1).

Selectivities to monoacylated *p*-xylene over USY zeolite were following: benzoyl chloride 90.5 % > propionic anhydride 78.0 % > hexanoyl chloride 67.2 % > isobutyric anhydride 33.1 % (at conversion of acylating agent 40 %). It was found that for acylation of *p*-xylene with propionic anhydride the optimum concentration of active sites contains zeolite Beta with Si/Al ratio 25 while the highest isobutyric anhydride conversion was achieved over zeolite Beta with Si/Al ratio 19.

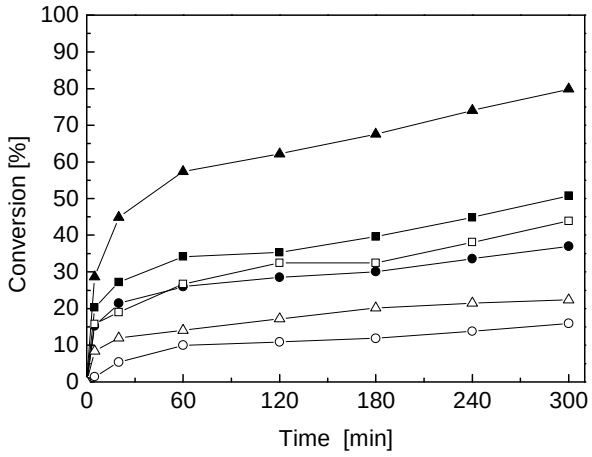

Figure 1. Acylation of *p*-xylene with benzoyl chloride: ■ Beta, ▲ USY, ● ZSM-5, □ Mordenite, ○ Ferrierite, Δ SSZ-35.

MOFs materials were found to be effective catalysts in *p*-xylene acylation. Benzoyl chloride conversions decreased in the order: Fe-BTC 100 % > USY 46.1 % > Cu-BTC 39.6 % > Beta 33.4 % > MIL100(Cr) 25.2 %. It was found that conversion of benzoyl chloride over Fe-BTC, Cu-BTC and MIL100(Cr) increased with increasing amount of catalyst. Conversion of benzoyl chloride increased with decreasing concentration of acylating agent over all tested MOFs.

Acknowledgements

Authors thank to Grant Agency of the Czech Republic for financial support (104/07/0383, 203/08/H032). The support of the EU project MACADEMIA is also highly appreciated (228862).

References

[1] Sartori, G., Maggi, R., Use of solid catalysts in Friedel-Crafts Acylation Reactions, Chem. Rev, 106 (2006) 1077-1104

[2] Bejblová M., Procházková D., Čejka J., Acylation reactions over zeolites and mesoporous Catalysts, ChemSusChem, 2 (2009) 486-499

The sulfonation of mesoporous phenolic resins and their catalytic activity as acid solid catalyst in esterification reactions

Ilke Muylaert,[a] Els De Canck,[a] Jeremy Spileers,[b] An Verberckmoes,[a,b] Pascal Van Der Voort[a]

[a]*Ghent University, Center for Ordered Materials, Organometallics and Catalysis, Krijgslaan 281-S3, 9000 Ghent, Belgium,* [b]*Faculty of Applied Engineering Sciences, University College Ghent, Schoonmeersstraat 52, 9000 Ghent, Belgium, Pascal.Vandervoort@UGent.be,*

Introduction

In recent years, the development of ordered mesoporous polymers – a new class of mesoporous materials – has attracted increasingly attention since these materials combine the large surface areas and porosity of mesoporous materials with the characteristics of organic polymers. In the field of catalysis, these materials are nowadays explored as straightforward heterogeneous support for different types of catalytic reactions. [1,2] An important advantage of phenol/formaldehyde resins is the very high mechanical and hydrothermal stability, especially in comparison with the relative unstable silica based mesoporous materials. [3]

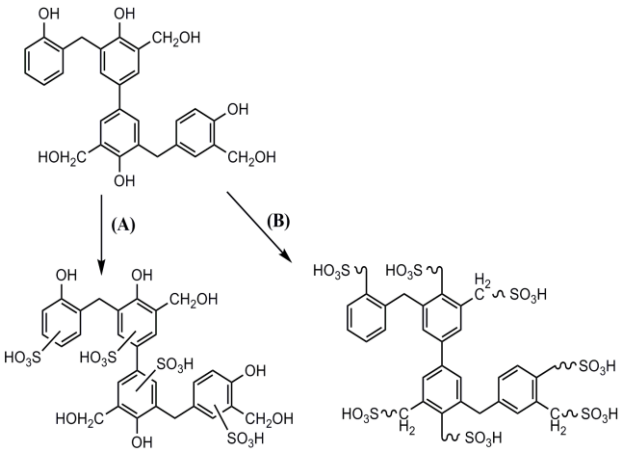

In this study, highly ordered mesoporous phenolic resins are discussed as acid catalyst in the esterification of propanol with acetic acid. The polymers are sulfonated using two different sulfonation routes: (a) by direct sulfonation of the aromatic rings and (b) by grafting sulfonic acid precursors on the hydroxyl groups. These acid solid catalysts are investigated for their catalytic activity in esterification reactions.

Figuur 1 - Sulfonation of mesoporous phenolic resins: (a) via the aromatic ring and (b) via the hydroxyl groups

Experimental

Ordered mesoporous phenolic resins are synthesized as reported by Zhang et al. [4] The polymers are sulfonated by different procedures (table 1):
Via the hydroxylgroups with grafting of SO_3H-silane precursors on the surface:

- insert 2: mercaptopropyltrimethoxysilane and oxidation of the propyl group to sulfonic acid group
- insert 3: 2-(4-chlorosulfonylphenyl)ethyltri-methoxysilane.

Via the aromatic ring by stirring the mesoporous solid in:

- insert 4: 2.5M H_2SO_4 solution
- insert 5: 2.5M H_2SO_4 solution with triflic acid anhydride
- insert 6: chlorosulfonic acid in dichloromethane

Via the aromatic ring by a gas phase reaction:

- insert 7: with fuming sulphuric acid

Insert 8 is a commercial available acid resin (Amberlyst-16) as a reference catalyst.

Results and discussion

The mesoporous resins exhibit large surface areas of more than 500 m²/g, large pore volumes (0,5 cm³/g) and narrow pore size distributions (6 nm). The acidity is determined by an acid-base titration and catalysts with acidities ranging from 0.2 to 2 mmol H^+/g are synthesized (table 1).

Table 1 – Overview of the acidity and the catalytic activity of the different catalysts
[a] Acidity (mmol H^+/g),
[b] Propanol conversion (%) after three hours reaction time

	Catalyst	Ac.[a]	Conv.[b]
1 P/F resin	Blanco	0.02	16
2 - Hydroxyl	Pr-SO_3H	0.23	9
3 - Hydroxyl	Ph-SO_3H	0.71	97
4 - Aromatic ring	H_2SO_4	0.24	24
5 - Aromatic ring	H_2SO_4/Tf_2O	0.59	51
6 - Aromatic ring	$ClSO_3H$	1.31	60
7 - Aromatic ring	Fum. H_2SO_4	1.90	98
8 Reference	Amberlyst-16	4.20	91

Figuur 2 – Propanol conversion in function of time with (a) FDU-15-SO_3H (insert 7) and (b) amberlyst-16 (insert 8)
Propanol (30 mmol), acetic acid (100 mmol) and toluene (30 mmol, internal standard) were refluxed in a two-necked round bottom flask under vigorous stirring under argon atmosphere at 90°C. Subsequently, 25 mg of the dried catalyst was added. The propanol conversion was followed by sampling 0.1 ml of the reaction medium at several times. The sample was immediately diluted with 0.5 ml acetonitrile and injected in the gas chromatograph.

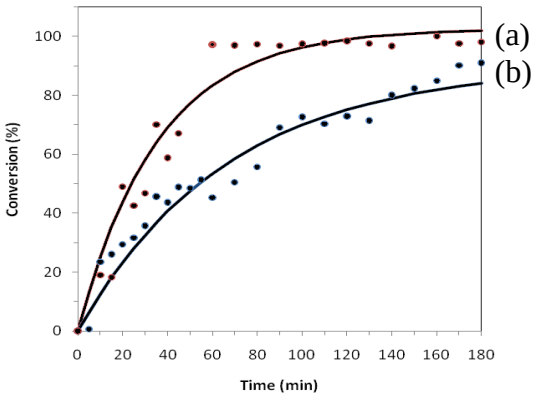

The acid catalysts are evaluated for their catalytic activity in the esterification of acetic acid with propanol. Table 1 gives an overview of the propanol conversion after three hours. The catalytic tests were performed with the same catalyst mass. Figure 2 shows the conversion curve of propanol in function of time of the sulfonated resin with the highest acidity (insert 7) and the commercial resin Amberlyst-16 (insert 8). Although, the acidity per gram is half of the commercial catalyts, the initial reaction rate for the sulfonated FDU-15 is significantly higher compared to Amberlyst-16. Moreover, the FDU-15-SO_3H catalyst reaches total propanol conversion after 60 minutes already. These preliminary results show that this straightforward acid catalyst has excellent acidic properties and is promising for other types of acid catalyzed esterification reactions.

References

[1] Meng Y., Gu D., Zang F., Shi Y., Yang H., Li Z., Yu C., Tu B., Zhao D., *Angew. Chem. Int. Ed.* **2005**, 44, 7053-7059.
[2] Xing R., Liu N., Liu Y., Wu H., Jiang Y., Chen L., He M., Wu P., Adv. Funct. Mater., **2007**, 17, 2455-2461
[3] Muylaert I., Borgers M., Bruneel E., Schaubroeck J., Verpoort F., Van Der Voort P., *Chem. Comm.* **2008**, 37, 4475-4477.
[4] Gao P., Wang A., Wang X., Zhang A., *Catal. Lett*. **2008**, 125, 289-295

Acidic and Catalytic Properties of Mesoporous SBA-15 Aluminosilicates Synthesized by pH-adjusting Method

A. Ungureanu[1], B. Dragoi[1], D. Meloni[2], V. Hulea[3], V. Solinas[2], E. Dumitriu[1]
[1]*Technical University "Gh. Asachi", Faculty of Chemical Engineering and Environmental Protection, 70A D. Mangeron, Iasi, Romania*
[2]*Università di Cagliari, Dipartimento di Scienze Chimiche, Complesso Universitario Monserrato, s.s. 554 Bivio Sestu, 09042 Monserrato (CA), Italy*
[3]*Institut Charles Gerhardt, UMR 5253, CNRS-UM2-ENSCM-UM1, Laboratoire de Matériaux Avancés pour la Catalyse et la Santé, 8 rue de l'Ecole Normale, 34 296 Cedex 5, France*
Corresponding author: vasile.hulea@enscm.fr

Introduction

The successful synthesis of SBA-15-type ordered mesoporous silicas overcome the main limitations of MCM-41 (i.e. thermal and hydrothermal stability) and opened up many opportunities for new applications, particularly as catalysts. Among various metal-doped SBA-15 silicas, Al-containing SBA-15 has great potential in moderate acid-catalyzed reactions (e.g. alkylation). Therefore, efforts have been made to introduce Al and to create Brönsted acidity in the neutral silica framework of SBA-15 by various synthetic strategies, which include direct synthesis and post-synthesis grafting. However, as compared to these conventional methods, the two-step 'pH adjusting method' is more convenient to get higher amounts of tetrahedral aluminium onto SBA-15 and thus an enhanced number of Brönsted acid sites [1,2]. Within this context, we use ammonia adsorption microcalorimetry to study the effect of Si/Al ratio on the acidic properties of Al-SBA-15 synthesized by the 'pH adjusting method' in relation to their catalytic properties in the *tert*-butylation of phenol.

Experimental

Al-SBA-15 samples (**AS-*X***, *X* = Si/Al in gel) were prepared by a modified 'pH-adjusting method' [1] using $Al(NO_3)_2 \cdot 9H_2O$ as aluminium source. The calcined solids were systematically characterized by ICP-AES to assess Si/Al atomic ratio and by low-angle XRD, N_2 physisorption at -196 ^oC and ^{27}Al MAS NMR to investigate the structural and textural features as well as the coordination of Al atoms. Acidic properties were studied by volumetric ammonia adsorption/readsorption measurements at 80 ^oC and by heat flow microcalorimetry [3]. The catalytic tests were performed in the liquid-phase alkylation of phenol (PhOH) with *tert*-butyl alcohol (TBA) at 70 ^oC [4].

Results and discussion

The XRD patterns exhibit three well-resolved peaks indexed as the (100), (110) and (200) reflections associated with the *p6mm* hexagonal symmetry typical of SBA-15 materials. The samples display N_2 adsorption/desorption isotherms of type IV assigned to 2-D hexagonal mesostructures with cylindrical pores. As shown in Table 1, the specific surface area (S_{BET}) and pore volume (V_{pore}) vary with the Si/Al ratio. The pore size (D_{meso}) decreases as more aluminium is grafted on the SBA-15 surface, in line with the increase in pore thickness (T_{pore}).

Table 1. Structural, textural and acidic properties of Al-SBA-15 materials

Sample	ICP	XRD		N_2 adsorption/desorption			NH_3 ads. microcalorimetry		Catalysis
	Si/Al	d_{100} (nm)	T_{pore} (nm)	S_{BET} (m^2/g)	V_{pore} (cm^3/g)	D_{meso} (nm)	$V_{tot\ 0.2\ torr}$ (μmol/g)	$V_{irr\ 0.2\ torr}$ (μmol/g)	TOF (h^{-1})
AS-*100*	130	8.9	0.7	345	1.25	9.6	204	76	6.39
AS-*50*	71.0	8.6	0.9	360	1.15	9.0	285	133	5.80
AS-*20*	24.7	8.8	1.9	380	1.10	8.2	421	188	5.73
AS-*10*	11.7	8.6	2.1	400	1.08	7.8	520	280	4.76
AS-*5*	5.2	8.6	2.8	420	0.90	7.2	650	295	3.73

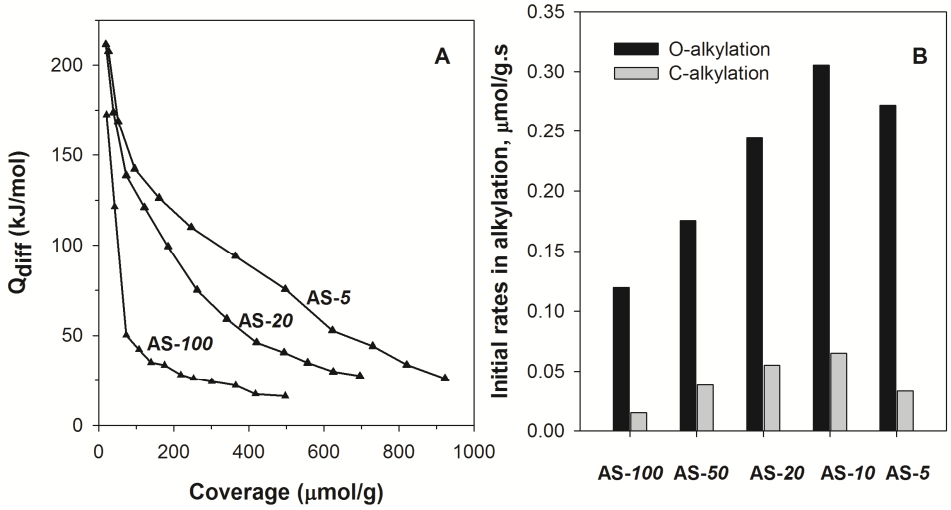

Figure 1. A. Differential heat of ammonia adsorption onto Al-SBA-15 samples;
B. Initial reaction rates in the O- and C-alkylation of PhOH with TBA

^{27}Al MAS NMR data pointed out that calcined Al-SBA-15 samples contain more tetrahedral aluminium (T_{Al}) than octahedral (O_{Al}) for Si/Al = 100-10, whereas AS-*5* sample contains larger amounts of O_{Al} and even pentahedral Al (P_{Al}). Moreover, T_{Al}/O_{Al} ratio diminished with the increase in the Al content, suggesting a similar variation of the Brönsted/Lewis acid sites ratio. However, as observed from the equilibrium NH_3 adsorption/readsorption measurements and the profiles of differential adsorption heat (Fig.1A), the samples containing more grafted Al show an improved acidity in terms of the number and strength of the acid sites. Thus, the total number of acid sites (volume of adsorbed NH_3, $V_{tot\ 0.2\ torr}$) as well as the number of strong acid sites (volume of irreversible adsorbed NH_3, $V_{irr\ 0.2\ torr}$), increase with the decrease in Si/Al ratio (Table 1). The alkylation of PhOH with TBA over Al-SBA-15 results in two different classes of products: O-alkylated products (*tert*-butylphenylether: TBPE) and C-alkylated products (2- and 4-*tert*-butylphenol: TBP and 2, 4-di-*tert*-butylphenol). As shown in Fig.1B, the initial reaction rates in O- and C-alkylation increase with the decrease in Si/Al ratio from 100 to 10 and then decrease for AS-*5*, despite its higher acidity. Nevertheless, TOF number decreased as Si/Al ratio decreases. Interesting, for all catalysts, TBPE is the main product in the early stages of the alkylation reactions, as already reported for large-pore zeolites [4]. The 4-TBP/2-TBP ratio was 1±0.1 at all conversion values.

Conclusions

Mesoporous Al-SBA-15 was successfully synthesized by the 'pH-adjusting method' which allowed grafting of large amounts of Al atoms on the siliceous SBA-15 framework. Structural and textural analyses indicated ordered hexagonal mesoporous structures for all samples. In line with ^{27}Al MAS NMR data, ammonia adsorption microcalorimetry indicated an improved number and strength of the acid sites for the samples containing more aluminium, in good agreement with the catalytic activity for the alkylation of phenol with *tert*-butyl alcohol.

Acknowledgements

B. Dragoi acknowledges the project PERFORM-ERA "Postdoctoral Performance for Integration in the European Research Area" (ID-57649), financed by the European Social Fund and the Romanian Government.

References

[1] Wu, S., Han, Y., Zou, Y.C., Song, J.W., Zhao, L., Di, Y., Liu, S.Z., Xiao, F.S., Chem. Mater., 16 (2004), 486-492.
[2] Gallo, J.M.R., Bisio, C., Gatti, G., Marchese, L., Pastore, H.O., Langmuir, 26 (2010), 5791–5800.
[3] Ungureanu, A., Thang, H.V., Trong On, D., Dumitriu, E., Kaliaguine, S., J. Therm. Anal. Calorim., 87 (2007), 417-422.
[4] Dumitriu, E., Hulea, V., J. Catal., 218 (2003), 249-257.

Synergistic effects of encapsulated phthalocyanine complexes in MIL-101 for the selective aerobic oxidation of tetralin

Emanuel Kockrick, Tristan Lescouet, Evgeny V. Kudrik, Alexander B. Sorokin and David Farrusseng
IRCELYON, Université Lyon I, CNRS, 2 av. Albert Einstein, F-69626 Villeurbanne, France.
E-mail: david.farrusseng@ircelyon.univ-lyon1.fr

Introduction

Over the last decade, metal–organic frameworks (MOFs) have been introduced as a new class of heterogeneous catalyst systems. Rapid progress is being made in developing MOF-based catalysts for selective oxidation of hydrocarbons. One approach consists in designing MOFs that possess metallic clusters with catalytic centers. Corma *et al.* have investigated Cu-pymo and Co-ZIF-9, in which the clusters are responsible for the selective oxidation of tetralin in air. Another approach resides in using MOFs as a host matrix to support the catalyst. MIL-101, which exhibits a 3D pore system with calibrated cavities of 2.9 nm and 3.4 nm, presents a very promising pore structure for the development of supported metallic or oxide complexes as "ship-in-a-bottle" catalysts. Metal phthalocyanine complexes (MPc) exhibit outstanding performance as oxidation catalysts. Unfortunately, MPc usually self-assemble to oligomer structures in solution through π stacking, which strongly limits their catalytic applications in homogeneous processes.

The objective of this work is to encapsulate large MPc in cavities of MIL-101 for the selective oxidation of tetralin into 1-tetralone, a diesel fuel additive and an intermediate for the synthesis of agricultural chemicals. To the best of our knowledge, this is the first report on the synergistic effect of the confinement of molecular catalysts in porous MOFs.

Experimental

A catalytic screening of different unsupported metal phthalocyanine catalysts in aerobic tetralin oxidation has enabled the identification of two different perfluorinated complexes ($MPcF_{16}$, M = Fe, Ru) and the bulky dimer, $(FePc^tBu_4)_2N$, which were selected for encapsulation. This reaction was performed in parallel batch reactors at 8 bar of O_2 at 90 °C with a substrate-to-MPc molar ratio of 36 000 : 1. The products were analyzed by GC and GC-MS. The TONs of the molecular catalysts follow the order $(FePc^tBu_4)_2N$ > $RuPcF_{16}$ > $FePcF_{16}$. Interestingly, similar selectivities toward 1-tetralone were obtained for the three molecular complexes.

The MPc–MOF composite materials were prepared by wet infiltration of the deep blue-colored MPc solutions into Cr–MIL-101 with a maximal theoretical complex loading inside the MOF of 9 wt%. The actual complex loading for the perfluorinated complexes inside the MIL-101 was determined by ICP-OES measurements to be 2.1 wt% and 3.6 wt% for $FePcF_{16}$ and $RuPcF_{16}$, corresponding to approximately 0.8 and 1.2 complexes per large pore respectively. X-Ray powder diffraction and N_2 physisorption measurements demonstrate the stability of MIL-101 host materials after the encapsulation process, since similar diffraction patterns and isotherm shapes were obtained. As expected, the specific surface area and pore volume decrease for complex-containing MOF systems. For $RuPcF_{16}$@MIL-101, the total pore volume decreases by 16 % with respect to pure MIL-101, which is more than the weight

loading of 3.6 wt%. This clearly shows that the complexes are incorporated into the porous structure and thus reduce the pore volume by preventing the N_2 from entering the cavities. For the bulky $(FePc^tBu_4)_2N$@MIL-101, the total pore volume decreases by only 5%, which corresponds to the weight gain of 5.2 wt% after loading. This indicates that the voluminous $(FePc^tBu_4)_2N$ complex is not incorporated into the mesoporous structure of the MIL-101. The homogeneous distribution of different iron and ruthenium complexes inside the MIL-101 support was verified by EDS analysis.

Results and discussion

The encapsulated perfluorinated complexes were tested in similar conditions with a tetralin-to-complex molar ratio of 147 000 : 1 for $FePcF_{16}$@MIL-101 and 92 000 : 1 for $RuPcF_{16}$@MIL-101, respectively. Note that pure MIL-101 shows no catalytic activity. $FePcF_{16}$@MIL-101 and $RuPcF_{16}$@MIL-101 catalysts show very high TONs (Fig. 1). The turnover number of $FePcF_{16}$@MIL-101 was 48 200 after 24 h, almost eight times higher than for the homogeneous $FePcF_{16}$ catalyst (TON = 6300). Significantly, the $FePcF_{16}$@MIL-101 catalyst provided a higher selectivity (up to 80 %) toward the desired 1-tetralone compared to the homogeneous $FePcF_{16}$ (68 %) at similar conversion. The higher activity for encapsulated complexes has previously been explained by the preclusion of the dimerization process by π stacking that is typically observed for homogeneous catalysts. Previously published activities of up to 3000 TON d^{-1} are, however, significantly lower than those determined in the present study. To the best of our knowledge, this is the highest catalytic activity ever reported for homo- and heterogeneous tetralin oxidations. In contrast, a limited conversion of up to 4 % was obtained for the $(FePc^tBu_4)_2N$@MIL-101 catalyst. This is consistent with the hypothesis that $(FePc^tBu_4)_2N$ is not encapsulated within the mesoporous structure of the MIL-101.

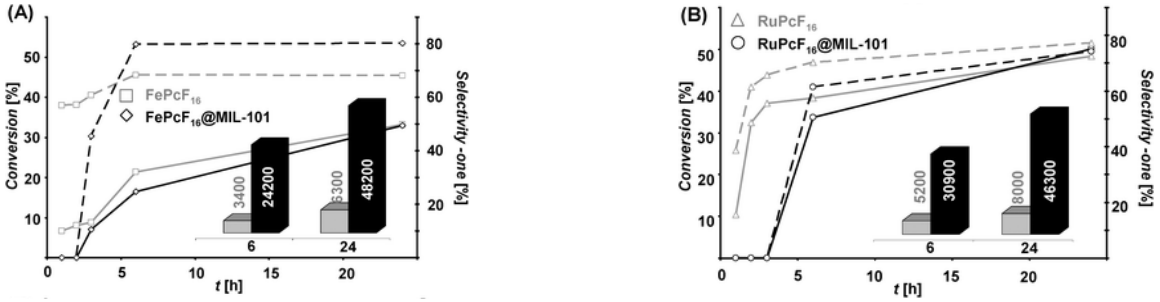

Fig. 1 Tetralin conversion (solid line) and selectivity toward 1-tetralone (dashed line) of homogeneous $FePcF_{16}$ and $RuPcF_{16}$ complexes (grey) and $FePcF_{16}$@MIL-101 (A) and $RuPcF_{16}$@MIL-101 (B) (black)

Conclusions

In summary, this study demonstrates that the encapsulation of MPc in MIL-101 allows an activity increase of approximately one order of magnitude. This increase in activity may arise from the dispersion of the molecular complexes as isolated monomers in the nanopore cavities and/or from the confinement effects provided by the host porous structure. In contrast, the $(FePc^tBu_4)_2N$ dimer, which is too large to penetrate into the porous structure, does not show this synergistic effect.

Acknowledgements

We thank the ANR for financial support (ANR-08-BLANC-0183-01).

Evidence for Polyoxometalates Encapsulation in the Mesocavities of MIL-101(Cr) and its Excellent Performance as Catalyst

J. Juan-Alcañiz, E. Ramos-Fernández, J. Gascon and F. Kapteijn
Catalysis Engineering – Dept. of Chemical Engineering, Delft University of Technology
Julianalaan 136, 2628 BL Delft, The Netherlands
J.JuanAlcaniz@tudelft.nl

Introduction

Metal Organic Frameworks (MOFs) are nowadays at the upfront of materials research. In recent years, the combination of organic and inorganic subunits in fully crystalline porous materials has given rise to thousands of MOF structures with a vast topological richness.
Notwithstanding that impressive progress has been made during the last decade, heterogeneous catalysis using MOFs is still in an immature stage [1]. The absence of functionalities (other than open metal or weak functional organic sites like amines) and their relative low thermal and chemical stability is in most of these structures to a large extent limiting their catalytic applicability [2]. Robust structures like MILs and ZIFs reveal improved thermal and chemical stabilities without precedents for this new class of materials. In addition, MTN and sodalite topologies offer tremendous possibilities in catalysis for the direct encapsulation of active guest molecules.
In this work, a new strategy has been developed for the direct encapsulation of polyoxometalates (POMs) in MOFs. The presence of quasi-spherical cages yields to a suitable immobilization of large active species (*i.e.* Keggin heteropoly-acids) where leaching is avoid [3]. Indeed, MIL-101 built up from supertetrahedra (ST) building units, resulting in two types of mesoporous cages accessible through 12 Å (medium cavities) and 15 Å (large cages), appears an excellent host for one of the most attractive polyoxometalates, phosphotungstic acid (PTA ~ 14 Å).

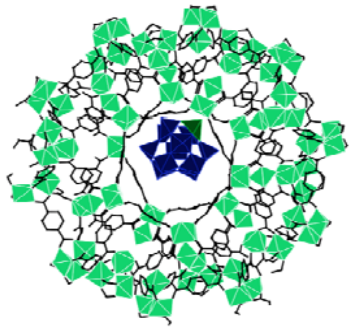

Figure 1. MIL-101 cavity with PTA encapsulated

Experimental

Following a novel approach, polyoxometalates are added to the synthesis mixture, and exposed to high temperature and pressure conditions during the hydrothermal synthesis. Two different routes of MIL-101 synthesis have been used to study the effect of the pH on the stability of the polyoxometalate. PTA-MIL-101 resulting solids have been characterized by different techniques like N_2 adsorption, TGA, vibrational spectroscopies, XRD, NMR and Elemental Analysis. The catalytic performance has been tested in the Knoevenagel condensation reaction. The mechanism has been studied by kinetic analysis and ATR-FTIR spectroscopy.

Results and discussion

The addition of PTA to MIL-101 synthesis mixture yields the direct encapsulation of POMs of different nature. Vibrational spectroscopies prove the presence of lacunary sites in the case of HF synthesis (not possible to observe specific PTA vibrations) while using TMAOH as mineralizing agent, the softer conditions stabilize the PTA during encapsulation.

In comparison with samples prepared following traditional impregnation routes, the encapsulated catalysts show an outstanding performance in C-C bond formation reactions involving cyano substrates like in the Knoevenagel condensation. Spectroscopic and kinetic evidences show that in contrast to the orthodox base catalyzed Knoevenagel mechanism, in the case of this hybrid catalyst the reaction proceeds via activation of the methylene compound and not via activation of the aldehyde reactant.

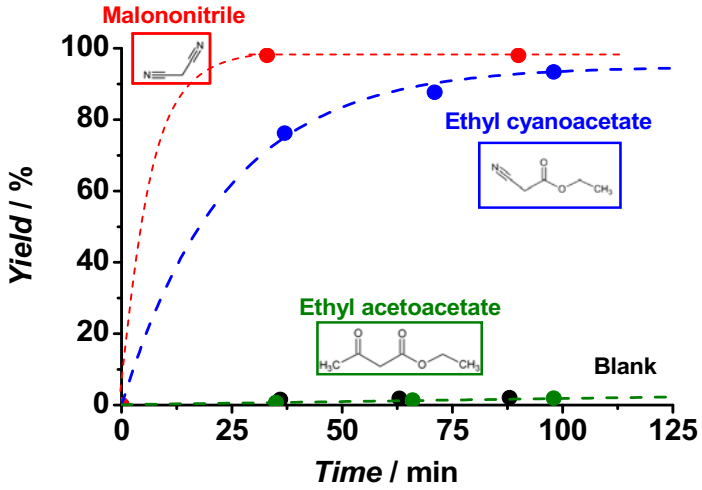

Figure 2. Knoevenagel condensation reaction of (8 mmol) Benzaldehyde and (7 mmol) three different active hydrogen components using 0.5g of PTA-MIL-101(Cr) and Toluene (5 mL) as solvent at 65°C. (Red) Malononitrile; (Blue) Ethyl cyanoacetate; (Green) Ethyl acetoacetate; (Black) Blank of the reaction (the same for all reactants).

Conclusions

We have demonstrated the successful encapsulation of POMs in the supercages of MIL-101. This new solid catalyst shows a stunning performance in different Knoevenagel condensations. The reaction mechanism proceeds via activation of the methylene compound.

Acknowledgements

The Delft University of Technology is gratefully acknowledged for financial support. The Department of Materials Science and Engineering of Delft University of Technology is acknowledged for the XRD analyses.

References

[1] A. Corma, H. García, and F.X. Llabrés I Xamena, Chemical Reviews 110 (2010) 4606-4655
[2] S.T. Meek, J.A. Greathouse, and M.D. Allendorf, Advanced Materials 23 (2010) 249-267
[3] J. Juan-Alcaniz, E.V. Ramos-Fernandez, U. Lafont, J. Gascon, and F. Kapteijn, Journal of Catalysis 269 (2010) 229-241

Metal organic frameworks with zeolitic topologies as catalysts for mild oxidation

Patryk Florczak, Kamila Kędzierska, Stanisław Kowalak
Faculty of Chemistry, A. Mickiewicz University, Poland,
patrykf84@o2.pl

Introduction

Metal organic frameworks (MOF) are the enormously growing group of coordination polymers (CPs) with crystalline, ordered, porous structure. They are family of the molecular sieves consisting of organic segments and coordinatively linked metal cations. The ZIF (zeolitic imidazolate framework) is a type of MOF materials showing the same or similar topology as conventional zeolites. Exceptionally high surface area of some MOF makes them very promising materials for storage and separation of gases. They can be also used as matrices for sensors, optical and microelectronic devices. Despite lower thermal stability than that of inorganic zeolites they are also considered potential catalysts. The catalytic active sites can be attributed to metal cations or to functional groups attached to organic segments. It is also possible to introduce active species into their inner voids (e.g. by encapsulation). The following work is focused on preparation of MOF molecular sieves containing Cu, V or Zn and examination of their catalytic activity in a mild oxidation of cyclohexene and 2,3,6-trimethylphenol (TMP) with tert-butyl hydroperoxide (TBHPO) as an oxidant.

Experimental

Presented MOF materials were prepared according to the published recipes with some modifications. The samples were characterized by means of XRD, FTIR, UV-vis, adsorption measurement.
Synthesis of ZIF-90 [1]. The mixture of aqueous solutions of imidazole and $NaHCO_3$ were heated and treated with solution of $CuSO_4$. After 5 h heating the colored precipitate of product was filtered and washed with water and then dried.
Synthesis of $Cu(INA)_2$ [2]. The mixture of copper acetate and isonicotinic acid were ground in ball mill. The progress in solvent-free reaction was reflected in color change (from violet to blue). Then sample was heated to 200 °C, and finally washed with water and dried.
Synthesis of MIL-47 [3]. Mixture of aqueous solutions of VCl_3, terephthalic acid and HF was subjected to hydrothermal crystallization in autoclave at 200°C for 4 days. The product was washed with DMF and $CHCl_3$.
Synthesis ZIF-8 [4]. Zinc nitrate and methylimidazole were dissolved in DMF and heated at 100°C. Then triethylamine was admitted to hot solution and heating was continued at 140°C for several hours. The resulted brown product was washed with DMF, $CHCl_3$ and MeOH.
Catalytic tests. The oxidation of cyclohexene (CH) and trimethylphenol (TMP) with TBHPO as oxidant and acetonitrile as mixing solvent was conducted in closed vials under static conditions at 60°C. The same amounts of catalysts were added to the mixtures. The blank experiment without any catalyst was carried out too. The reaction products were analyzed by means of G.C.

Results and discussion

The XRD patterns of ZIF-90, ZIF-8, MIL-47 were very much alike those presented in literature [3, 4]. Only XRD pattern of $Cu(INA)_2$ was different than literature data [2]. The IR

spectra of MIL-47 show typical bands of the carboxylate group (from BDC ligand) at 1631-1571 cm^{-1} and at 1441-1371 cm^{-1} from the asymmetric and symmetric vibration, respectively. The bands at 1040 cm^{-1} assigned to vibrations of the pyridine ring were seen for the sample $Cu(INA)_2$. Imidazoles as constituent parts of ZIF-90 and ZIF-8(methylimidazole) were reflected in bands at 1591 cm^{-1}, 1450 cm^{-1}, 1303cm^{-1}, 991 cm^{-1} and 740 cm^{-1}. The samples showed considerable catalytic activity (Fig. 1) for cyclohexene oxidation (except for ZIF-8). The CH reaction products (Fig. 2) contained: di(2-cyclohexenyl)-ether, 2-cyclohexenone, 2-cyclo-hexenone-1-ol, 1-(tert-butyl peroxy)-2-cyclohexene, cyclohexene oxide and cyclohexane-1,2-diol. Peroxide was predominant product in reactions catalyzed by Cu bearing samples, while alcohol prevailed for V containing MIL-47. Ether predominated in blank reaction test.

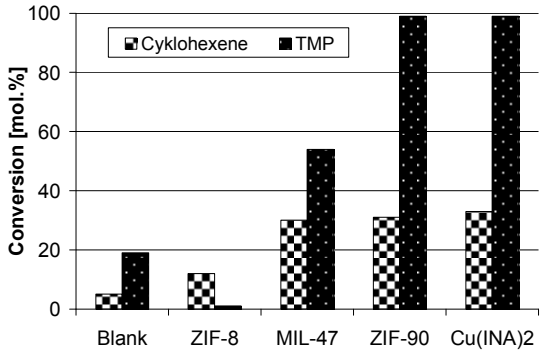

Fig. 1. Conversion of CH and TMP at $^{o}60$

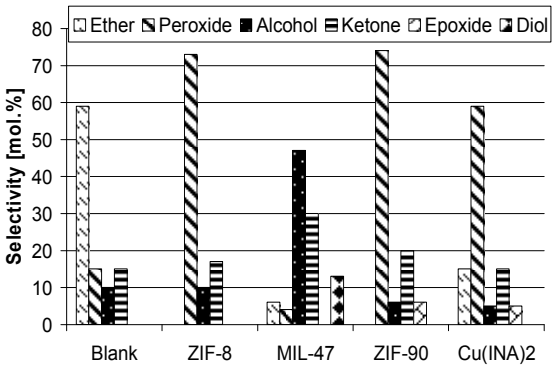

Fig. 2. Selectivity in CH oxidation

ZIF-90 and $Cu(INA)_2$ showed high activity for of TMP oxidation, although selectivity to trimethylbenzoquinone (TMBQ) was low (~10%). Products of TMP condensation (e.g. $C_{18}H_{22}O_2$) were identified and markedly contributed in product mixtures. Sample MIL-47 show much lower activity and even less selectivity to TMBQ. ZIF-8 again appeared inactive. Conversion in blank experiment was ~ 20% and selectivity to TMBQ 2%.

Conclusions

The MOF samples containing Cu cations (ZIF-90 with sodalite topology and $Cu(INA)_2$) show considerable catalytic activity in mild oxidation reactions. The sample MIL-47 with vanadium cations also shows a noticeable activity, whereas the Zn bearing material (ZIF-8) is practically inactive. The results clearly indicate a crucial role of metal cations in the MOF structure for catalytic activity and selectivity of these materials.

Acknowledgements

P. Florczak appreciates the financial support from grant Nr N N204 020639

References

[1] Masciocchi, N., Bruni, S., Cariati, E., Cariati, F., Galli, S., Sironi, A., Extended Polymorphism in Copper(II) Imidazolate Polymers: A Spectroscopic and XRPD Structural Study, Inorganic Chemistry, 40 (2001), 5897-5905

[2] Pichon, A., Lazuen-Garay, A., James. S., Solvent-free synthesis of a microporous metal–organic framework, Crystal Engineering Communications, 8 (2006), 211–214

[3] Barthelet, K.., Marrot, J., Riou, D., Férey. G., A Breathing Hybrid Organic - Inorganic Solid with Very Large Pores and High Magnetic Characteristics, Angewandte Chemie International Edition, 41 (2002), 281-284

[4] Ordonez, M., J. Balkus Jr. K., Ferraris, J., Musselman, I., Molecular sieving realized with ZIF-8/Matrimid® mixed-matrix membranes, Journal of Membrane Science, 361 (2010), 28-37

Oxidative dehydrogenation of C_2-C_4 hydrocarbons over Fe-ZSM-5 zeolites in the presence of N_2O

Jolanta Kowalska-Kuś, Krystyna Nowińska
Faculty of Chemistry, Adam Mickiewicz University, Poznań, Poland
E-mail:jolakow@amu.edu.pl

Introduction

Oxidative dehydrogenation (ODH) of light paraffins is a viable alternative to conventional pyrolysis methods of olefin production, particularly if their numerous drawbacks are regarded. The most important advantages of ODH process are: lower reaction temperature (400°C) and lack of thermodynamic limitation. Olefins, obtained in this process, are not available in the natural row materials, while the demand for them, as semi-finished products in organic industry, is very high. Therefore, a great effort of chemical industry and research groups is focused on searching for new ways of receiving these useful products [1]. The iron modified ZSM-5 zeolites showed promising results in oxidative dehydrogenation process in the presence of nitrous oxide as an oxidant [2].

Experimental

ZSM-5 zeolites (Süd Chemie), were modified with iron (III) cations by means of ionic exchange procedure from aqueous solution of $Fe(NO_3)_3 \cdot 9H_2O$ with following calcination at 600°C or 900°C for 2 hours. Number of iron introduced into ZSM-5 zeolites was estimated on the basis of ICP-OES measurements. The catalytic tests for C_2-C_4 hydrocarbons oxydehydrogenation with N_2O as an oxidant, were performed in continuous flow reactor at 400°C under atmospheric pressure, with WHSV=4500 ml/h/g_{cat} and contact time of 0.8 s. Prior to oxidative experiments, the catalysts were pretreated in helium flow at 450°C. Substrates: hydrocarbon and N_2O were diluted with helium (molar ratio of hydrocarbon: nitrous oxide: helium = 1 : 1.5 : 12.5). The products were analyzed using on-line GC, equipped with TCD detector, and in case of C_4 hydrocarbons (n-butane and isobutane) ODH, also with FID detector. The acidity of studied catalysts was estimated by means of ammonia TPD and FT-IR spectra of adsorbed pyridine. FT-IR spectroscopy of adsorbed NO as molecular probe as well as H_2-TPR measurements were used for assessment of nature of catalytically active iron species.

Results and discussion

Fe-ZSM-5/N_2O catalytic system, very efficient for benzene to phenol oxidation [3] appeared very promising in ODH reaction of light paraffins. N_2O decomposes over active iron complexes and forms adsorbed monoatomic oxygen species, that are able to oxidize hydrocarbon molecules. The lifetime of monoatomic oxygen species depends on the nature and distribution of iron complexes located inside zeolites channels. In turn, the formation of active iron complexes depends considerably on various properties of zeolite matrices such as Si/Al ratio, amount of iron introduced into zeolite, temperature of calcination and in a consequence the acidity of zeolite. Considering the great importance of above parameters in oxidative activity of Fe-ZSM-5 system used for benzene hydroxylation, we have employed the catalysts of different iron concentration calcined at temperature 600°C or 900°C for

hydrocarbons ODH reaction. The oxidative activity changed distinctly with length of carbon chain and the highest conversion was obtained for C_4 hydrocarbons. It resulted from the lowest value of C-H bond energy in C_4 alkanes molecules, compared to that in C_2 and C_3 hydrocarbons and finally, the lowest energy of hydrogen removal. Lower activity of isobutene oxidation in comparison to n-butane results from geometric limitation. Against expectation, the temperature of calcination did not change the activity of alkanes considerably. Nevertheless, the temperature of catalysts calcination affected markedly the product distribution, especially for hydrocarbons with longer carbon chain (C_3-C_4). Generally, the reaction of oxidative dehydrogenation was predominant over catalysts calcined at 900°C (Fig. 1). Selectivity towards olefins over these catalysts was even two or three times higher than that over catalysts activated at 600°C. Only in case of isobutane the predominant product was CO_2, what additionally confirmed that oxidation of isobutane occurred on the external surface of zeolites. It looked as if acidity of catalysts was responsible for these changes. Catalysts calcined at 600°C and 900°C contained the same amount of iron, but they differed considerably in acidity. Results of ammonia TPD evidence much lower total acidity of high temperature treated samples, while the FT-IR spectra of adsorbed pyridine suggest a removal of strong protonic sites with calcination. Partial elimination of Bronsted centers could be responsible for an increase in olefin selectivity. The nature of iron complexes was discussed on the grounds of FT-IR spectra of adsorbed NO molecule probe and H_2-TPR measurements. Adsorption of NO on Fe-ZSM-5 zeolites resulted in an appearance of three strong bands located at 1630, 1880 and 2133 cm^{-1}. First two bands were visible in spectra of Fe-ZSM-5 catalysts calcined at both temperatures (600°C or 900°C) and were attributed to different nitrozyl structures adsorbed on Fe^{2+} species. The band at 2123 cm^{-1} was assigned to NO^+ group adsorbed on Bronsted acidic sites. H_2-TPR measurements additionally confirmed the presence of Fe^{2+} species in Fe-ZSM-5 zeolites.

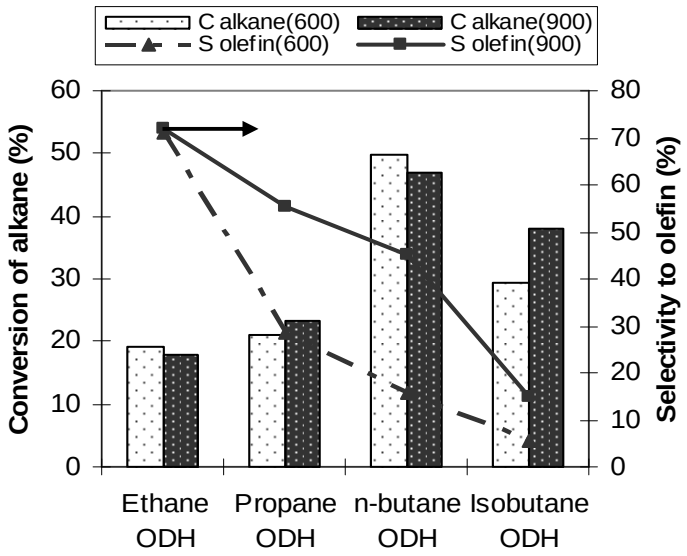

Fig. 1. Catalytic activity of Fe-ZSM-5 (calcined at 600 or 900 °C) in C_2-C_4 ODH reaction

Conclusions

1. FT-IR spectra of adsorbed NO show that thermal treatment already at 600°C results in autoreduction of Fe^{3+} ions located in extra-framework positions
2. Isolated iron species containing of Fe^{2+} ions show a great importance for hydrocarbons oxydehydrogenation
3. Acidic centers are indispensable for reagent activation, however, the presence of strong protonic sites leads the ODH reaction towards by-products formation.

References

[1] López Nieto, J. M., Topics Catal., 41 (2006), 3-15
[2] Held, A., Kowalska, J., Nowińska, K., Appl. Catal. B: Environ., 64 (2006), 201-208
[3] Panov, G.I., Uriarte, A.K., Rodkim, M.A., Sobolev, V. I., Catal. Today, 41 (1998), 365-385

One-step synthesis of methyl isobutyl ketone over Pd-containing zeolite MFI

M.A. Nikitina, V.V. Ordomsky, I.I. Ivanova
Lomonosov Moscow State University, Department of Chemistry, Moscow, Russia,
MariaNikitina88@gmail.com

Introduction

Methyl isobutyl ketone (MIBK) is commercially produced by a three-step process, including acetone condensation, diacetone alcohol dehydration and mesityl oxide (MO) dehydrogenation. The first two stages have thermodynamic limitations, which lead to relatively low yield of the target product. Therefore, one-step synthesis of MIBK over heterogeneous catalysts is a highly desired alternative to a traditional scheme. Pd-containing zeolites are among the most promising heterogeneous catalysts which can be used in this process [1]. The main drawbacks of these catalysts are connected with rapid catalyst deactivation and comparatively short lifetime, which can be associated with acetone and mesityl oxide condensation into heavy products blocking the active sites of the catalyst. The addition of different metal oxides to Pd/zeolite can promote faster hydrogenation of MO and prevent its further condensation with acetone and formation of carbonaceous deposits deactivating the catalyst.
The aim of this paper was to investigate the effect of various metal oxides (MeO_x) on the catalytic behavior of Pd/H-MFI catalyst in one–step synthesis of MIBK.

Experimental

MeO_x/H-MFI systems were obtained by impregnation of zeolites NH_4^+-MFI (Si/Al=25, 40, 140) with aqueous solutions of corresponding metal salts. Samples were dried at 100°C for 12 h and calcined under airflow at 500 - 600°C for 6 h. Ti, Sn, Ce, Zr, Fe, Cr, Mo and Ba oxides were chosen as modifiers. The content of metal in the samples was 0.3 wt.% for Ti, Sn, Ce, Zr, Fe, Cr, Mo and 2.5 wt% for BaO. For the preparation of Pd-containing catalysts the samples were further impregnated with aqueous solutions of Pd chloride to obtain 0.1 wt.% for Pd in each sample. The catalyst were dried and calcined under airflow at 500°C for 6 h
All the catalysts were characterized using low temperature N_2 adsorption, IR-spectroscopy, TG, TPD-NH_3, TPD-CO_2 and XPS techniques. The catalytic activity of the samples was tested in acetone hydro conversion under 30 atm and at 150-170°C. The weight hourly space velocity (WHSV) was varied from 1.7 to 4.7g/g*h. The reaction products were analyzed on line by GC analysis using Crystal 2000M chromatograph, equipped with 30 m Carbowax capillary column.

Results and discussion

Characterization of the catalysts prepared by XPS confirmed the presence of the following oxides BaO, TiO_2, CeO_2, ZrO_2, Cr_2O_3, Fe_2O_3, SnO in the samples. The analysis of FTIR and N_2 adsorption data suggested that no significant changes in the catalyst structure and porosity took place upon the catalyst modification with various oxides. The acidic properties of Pd/MeO_x/H-MFI catalysts also did not show significant differences.
The catalytic data obtained over various samples were compared with the parent Pd/H-MFI system as shown in Fig. 1. Basing on the results obtained all the metal oxides used for catalysts modification can be divided into two groups. The first group of metal oxides (CeO_2, Fe_2O_3, Cr_2O_3, SnO) leads to significant decrease of MIBK yields and fast catalyst

deactivation. The most tremendous changes were observed in the case Pd-Sn/H-MFI catalyst, which was not active at all in MIBK synthesis. On the contrary, the second group of metals (BaO, TiO_2, ZrO_2) leads to some increase of catalytic activity or resistance of catalyst to deactivation. The best results were obtained over Pd-Ti/H-MFI and Pd-Ba/H-MFI.

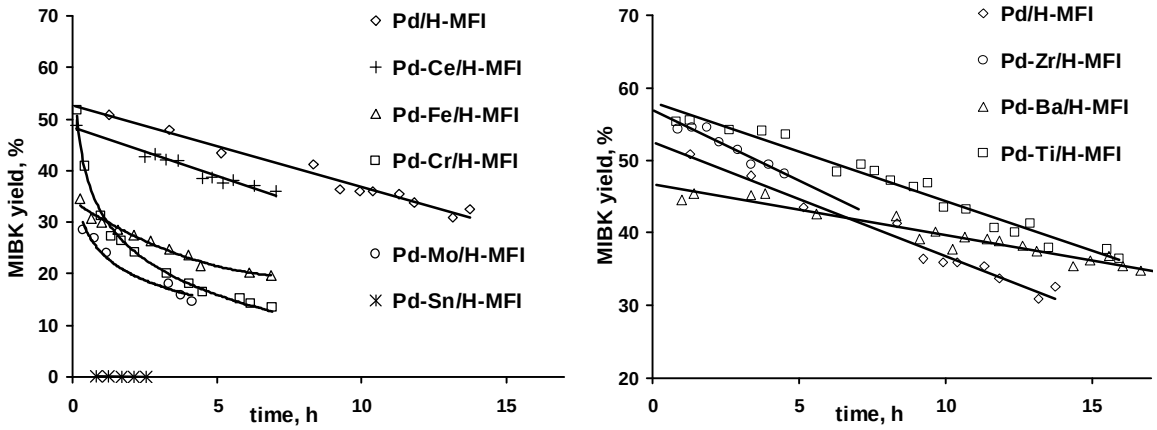

Figure 1. Acetone conversion into MIBK over $Pd/MeO_x/H$-MFI catalysts (T=170^oC, p=30 atm, H_2/Ac=0.6, WHSV=3,2 g/g*h).

The results obtained can be accounted for by the strong metal support interactions between Pd and catalyst surface modified by various metal oxides [2]. These interactions may lead either to the decrease or to the increase of electron density on palladium and therefore affect MO hydrogenation. To check this hypothesis the best and the worth catalysts were studied in toluene hydrogenation. The results pointed that while Pd-Ti/H-MFI demonstrated extremely high activity, Pd-Sn/H-MFI did not show any toluene hydrogenation. This observation confirmed that addition of small amounts of metal oxide promoters may strongly affect the state of Pd and therefore its hydrogenation properties, which governs catalyst activity and stability in MIBK synthesis.
In the case of Pd-Ba/H-MFI, the highest stability to deactivation could be also due to other reasons, such as different mechanism of acetone condensation, involving basic pathway over BaO basic active sites.

Conclusions

The deactivation of Pd/H-MFI in the one-step synthesis of MIBK can be reduced by addition of metal oxide promoters, capable to enhance hydrogenation function of the catalyst. The best catalytic performance in terms of activity and stability was observed on the catalyst modified with TiO_2. Modification of acid-base properties by introducing of basic BaO leads to the creation of additional centers of condensation, which also increases the stability of the catalyst in the MIBK process.

References

[1] Chen P. Y., Chu S. J., Lin W. C., Wu K. C., Yang C. L., The Synthesis of Methyl Isobutyl Ketone over Palladium Supported Zeolites. Studies in Surface Science and Catalysis, 83 (1994), 481-488.
[2] Coq B., Figueras F., Bimetallic palladium catalysts: influence of the co-metal on the catalyst performance, Journal of Molecular Catalysis A: Chemical, 173 (2001), 117-134.

Enantioselective hydrogenation of ethyl pyruvate on supported platinum systems: optimisation of reaction conditions through factorial design

V. Montes, J. Hidalgo-Carrillo, M.A. Aramendía, A. Marinas, J.M. Marinas, F.J. Urbano**.**
*Facultad de Ciencias, Universidad de Córdoba, Campus de Rabanales, Edificio Marie Curie, 14014-Córdoba***.** alberto.marinas@uco.es

Introduction

Enantioselective hydrogenations of prochiral substrates are interesting processes in Pharmaceutical Industry. One of the methods to carry out such processes through heterogeneous catalysis consists in the application of a metal hydrogenation catalyst together with a strongly adsorbed chiral molecule which induces chirality to the process (the so-called chiral modifier).

There are three main systems of this type: i) nickel modified by tartaric acid for chiral hydrogenation of beta-ketoesters; ii) palladium modified by cinchona alkaloids for hydrogenation of C=C activated bonds; iii) platinum modified by cinchona alkaloids for enantioselective hydrogenations of alpha-ketoesters.

There are different features influencing the catalytic performance of the resulting system. Some of them are common to hydrogenation processes (support, metal precursor, solvent, metal particle size) but there is an additional feature to be considered: the need for the adsorption of the chiral modifier in the immediate vicinity of the substrate in a specific manner [1-5]. In this sense, a typical chiral modifier should consist of the following parts:

1. Flat aromatic ring (π conjugated system) for anchoring onto the Pt surface.
2. Stereogenic center(s) responsible for enantiodiferentiation.
3. Heteroatom to interact with the substrate through hydrogen-bonding. It is typically a nitrogen atom though Baiker et al. showed that it could also consist in a hydroxyl group [3].

To make the system even more complicated, the use of some aromatic compounds as additives can also improve the results [4].

In the present piece of research, enantioselective hydrogenation of ethyl pyruvate is performed on platinum-based systems modified by cinchonidine (CD). Catalytic performance is discussed in terms of platinum precursor, support (USY or MCM-41) and solvent. The effect of the use of a chiral additive (4-Hydroxy-D-Phenylglycine, 4OHDPG) to the reaction medium is also studied. A first screening allowed us to select a catalyst and a solvent. Further improvement of catalytic performance was carried out through factorial design (using hydrogen pressure, concentration of chiral modifier –cinchonidine- and additive –4OHDPG- as the variables).

Experimental

Different platinum-based systems, in a weight nominal content of 5% were synthesized through impregnation using acetyl acetonate (1) and cloroplatinic acid (2) as the platinum precursor. Supports were commercially available USY zeolites (CBV780 (1) and CBV300 (2) from Zeolyst International) and MCM-41 (3), Re. 643653 from Aldrich.

Catalyst nomenclature includes a prefix indicating the support and a suffix referring to the platinum precursor. Therefore, for instance, system 2.1. was obtained through impregnation of platinum acetylacetonate on CBV300.

Prior to their use, the systems were activated at 400ºC under hydrogen. Standard reaction conditions were as follows: 20 mL solvent, 20 mg catalyst, 2 mg cinchonidine, 200 μL ethyl pyruvate, 20ºC.

As usual, enantiomeric excess (e.e.) is expressed using the formula e.e.= (R-S)/(R+S)

Results and discussion

A first screening was carried out at a hydrogen pressure of 1 bar. Results are shown in Figure 1. As can be seen, the highest enantiomeric excess to (R)-ethyl lactate (57% e.e. at 66% conversion) was achieved using 1.1. system (i.e. USY CBV780 zeolite and platinum acetyl acetonate as the precursor) in acetic acid. These conditions were then used for further improvement through factorial design. Figure 2, is an example of the positive effect of 4OHDPG on e.e. values at low cinchonidine contents despite the null e.e. values obtained when 4OHDPG alone was used as the chiral modifier.

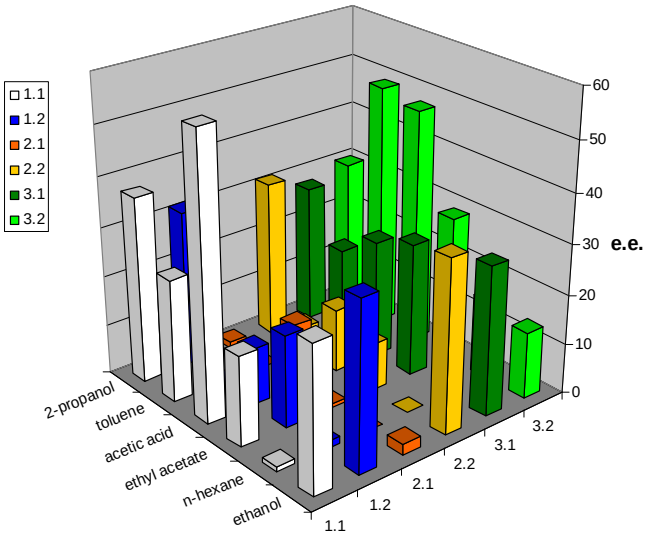

Figure 1. Preliminary screening of catalysts and solvents for enantioselective hydrogenation of ethyl pyruvate under standard conditions (see text)

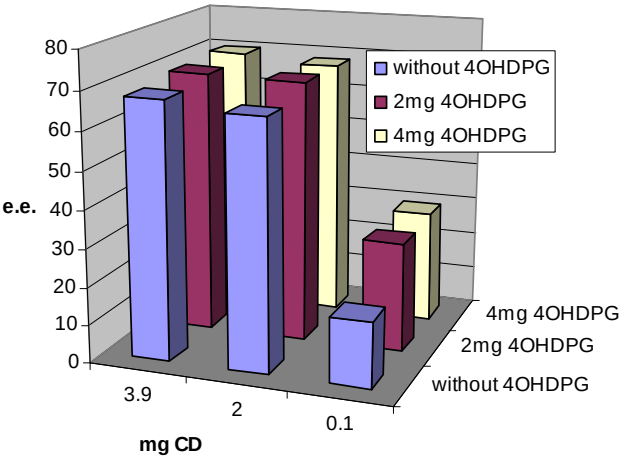

Figure 2. Results found for catalyst 1.1. for a hydrogen pressure of 5 bar. Effect of the use of 4-hydroxy-D-Phenylglycine (4OHDPG) as the additive. CD denotes cinchonidine.

Conclusions

Factorial design has proven an interesting tool in order to optimize experimental conditions in enantioselective hydrogenations. Despite the null e.e. obtained with 4-hydroxy-phenylglycine, the addition of such a chemical to the reaction medium leads to a substantial increase in e.e. for low cinchonidine contents.

Acknowledgements

MICINN (projects CTQ2008/01330 and CTQ2010/18126), Consejería de Educación y Ciencia de la Junta de Andalucía (Projects P07-FQM-02695, P08-FQM-3931 and P09-FQM-4781) and FEDER funds are gratefully acknowledged.

References

[1] Baiker, A., Journal of Molecular Catalysis A, 115 (1997), 473-393.
[2] Hoxha, F., Schimmoeller, B., Cakl, Z., Urakawa, A., Mallat, T., Pratsinis, S.E., Baiker, A., Journal of Catalysis 271 (2010), 115–124.
[3] Marinas, A., Mallat, T., Baiker, A., Journal of Catalysis, 221 (2004), 666–669.
[4] Tálas, E., Margitfalvi, J.L., Catalysis Communications, 9 (2008), 984–989.
[5] Blaser, H.U., Jalett, H.P., Wiehl, J., Journal of Molecular Catalysis, 68 (1991), 215-222.

Chemoselective Alkylation of Aromatics with Benzyl Alcohol over Mesoporous ZSM-5 with Enhanced Mesoporosity

Hailian Jin, Mohd Bismillah Ansari, Yong-Hwan Mo and Sang-Eon Park*
Laboratory of Nano-Green Catalysis and Nano Center for Fine Chemical Fusion Technology, Department of Chemistry, Inha University, Incheon, 402-751, South Korea, corresponding:separk@inha.ac.kr

Introduction

Alkylation of aromatics by zeolites is one of commercial reaction process to produce important alkyl aromatics in large scale. However, zeolites with small diffusion pore size gave limitation for large molecules, which led to development of catalyst with large molecular dimensions [1].

Many trials have been devoted to obtain zeolite single crystals with uniform mesopore in order to take advantages of both mesoporous and microporous materials [2]. Currently, the supramolecular soft template method is immensely adopted because it preferably lead cooperative self-assembly of framework building blocks such as zeolites to form periodic mesoporous solids. T. Bein reviewed the self-assembly strategies with zeolites which can be attached to pre-treated substrates via electrostatic interaction [3]. This inspired us to utilize such interaction to synthesize highly crystalline mesoporous zeolite with the developed intracrystalline mesopores, because anionic character on the surface of zeolite would enable to interact with cationic surfactants to give a birth of the mesoporosity inside of the zeolite crystals. Recently, we reported the new synthetic method for mesoporous MFI zeolites with enhanced mesoporosity by microwave induced assembly between the sulfonic acid functionalized zeolite nanoparticles and counter cationic surfactant. Sulfonic acid group as negative charge enhancer to interact with cationic mesoporous template boosted surface of zeolite crystals through the ionic interactions. [4].

The catalytic performance of enhanced accessibility due to mesoporosity and acidity were demonstrated in the alkylation of benzene, toluene and mesitylene with benzyl alcohol as alkylating agents. The effect of mole ratios of aromatic with benzyl alcohol and reaction time were also studied.

Experimental

Synthesis of Hierarchical mesoporous ZSM-5

The mesoporous ZSM-5 were synthesized as follow: ZSM-5 nano zeolites were prepared from a clear solution with the following molar composition: $1Al_2O_3$: $60SiO_2$: 11.5TPAOH: $1500H_2O$. The precursor solution was pre-crystallized and followed by functionalization with MPTES under MW. H_2O_2 (30% in water) was added to oxidize thiol group for obtaining sulfonic acid funtionalized zeolite nanoparticles. The resultant solution was added to CTAB solution and stirred several hours, then move to MW (165 ℃ for 1.5 h) as [Meso-ZSM-5(SO_3H-CTAB)-MW], whereas in hydrothermal (HT) method the vessel was maintained at 165 ℃ for 3 days as ZSM-5 (SO_3H-CTAB)-HT. Microporous ZSM-5 [ZSM-5 (HT)] was synthesized with the same molar composition without surfactant by HT method.

Alkylation of aromatics with various alcohols

Prior to the catalytic experiments each zeolite was activated at 450 ℃ for 90 min and then cooled down in a desiccator. The alkylation reactions were carried out with aromatic, alcohol and Catalysts in a 25 ml single-necked flask, stirred 15-120 min at 100 ℃. The mole ratio of aromatic with benzyl alcohol was verified as 1:2, 1:1, 2:1, 3:1, and 4:1.

Results and discussion

Meso-ZSM-5(SO_3H-CTAB)-MW was unique in the sense that they contained both the interconnected micropores and mesopores inside of single crystals (XRD&TEM). It exhibited much larger uniform mesoporosity than those of Meso-ZSM-5(CTAB)-MW, ZSM-5 (SO_3H-CTAB)-HT, and ZSM-5 (HT) (BET).

The influence of mesoporosity and its acidity in the mesoporous ZSM-5 was investigated by the alkylation of mesitylene with benzyl alcohol (BA) as test reaction (Table 1). The Meso ZSM-5 (SO_3H-CTAB)-MW gave not only better conversion but also 2 times higher chemoselectivity of benzylated mesitylene (2-benzyl-1,3,5-trimethylbenzene, 9.6 x 6.8 Å) than the others. Whereas the conversion of benzyl alcohol over Meso ZSM-5 (CTAB)-MW, ZSM-5 (SO_3H-CTAB)-HT and ZSM-5 (HT) were pretty high but mostly converted to self alkylated product B. This significant difference in catalytic activity and selectivity was resulted from the existence of acidity inside of mesopores, which definitely allowed the benzylation in mesopores. These results were well matched with the FTIR investigation of DTBPy adsorption as discussed (not shown). In alkylation of benzene and toluene similar result with that of mesitylene were observed.

Table 1. Alkylation of mesitylene with benzyl alcohol over various MFI zeolites.

Catalyst	Conversion (%)		Product distribution (%)		
	Mesitylene	BA	A	B	Others
Meso ZSM-5 (SO_3H-CTAB)-MW	32.2	99.3	60.2	18.4	21.4
Meso ZSM-5 (CTAB)-MW	19.5	91.8	31.8	40.1	28.1
ZSM-5 (SO_3H-CTAB)-HT	2.8	46.3	23.3	61.9	14.8
ZSM-5 (HT)	4.8	13.4	14.5	63.2	22.3

* Reaction condition: Substrate / BA / Dodecane = 16 : 8 : 1; Catalyst = 0.05 g; 100 ℃; 60 min. A: 2-benzyl-1,3,5-trimethylbenzene; B: Dibenzyl ether.

Conclusions

The Meso ZSM-5 (SO_3H-CTAB)-MW synthesized through the microwave induced assembly between the anionic functionalized zeolite nanoparticles and alkyltrimethylammonium cationic surfactants showed much better catalytic activity and chemoselectivity of monoalkylated product than those of Meso ZSM-5 (CTAB)-MW, ZSM-5 (SO_3H-CTAB)-HT and ZSM-5 (HT) due to enhaced mesoporosity and acidity.

Acknowledgements

This work was supported by National Research Foundation of Korea (NRF) grant funded by the Korea government (MEST) (2009-0083073).

References

[1] Beken, S., Dejaegere, E., Tehrani, K., Paul, J., Jacobs, P., Baron, G., and Denayer, J., Alkylation of deactivated aromatic compounds on zeolites. Adsorption, deactivation and selectivity effects in the alkylation of bromobenzene and toluene with bifunctional alkylating agents, Journal of Catalysis, 235 (2005), 128-138

[2] Groen, J., Zhu, W., Brouwer, S., Huynink, S., Kapteijn, F., Moulijn, J., and Pérez-Ramírez, J., Direct Demonstration of Enhanced Diffusion in Mesoporous ZSM-5 Zeolite Obtained via Controlled Desilication, Journal of American Chemistry Society, 129 (2006), 355-360

[3] Bein, T., Zeolitic Host–Guest Interactions and Building Blocks for the Self-Assembly of Complex Materials, MRS Bulletin, 30 (2005), 713-720

[4] Jin, H., Kim, K., Ansari, M., and Park, S., Mesoporous MFI Zeolites by Microwave Induced Assembly between Sulfonic acid Functionalized MFI Zeolite Nanoparticles and Alkyltrimethylammonium Cationic Surfactants, Chemical communications, Submitted (2010)

Asymmetric organocatalytic michael reaction of nitroalkens into trans-chalcone with mesoporous silica having trans-1,2-diaminocyclohexane

Eun-Young Jeong, Cheang-Rae Lim and Sang-Eon Park*
Laboratory of Nano-Green Catalysis and Nano Center for Fine Chemical Fusion Technology, Department of Chemistry, Inha University, Incheon, 402-751, South Korea, corresponding:separk@inha.ac.kr

Introduction

The C-C bond formation reactions is an important are in the modern pharmaceuticals and organic synthesis.[1] Recently, heterogeneous asymmetric catalysis have attracted much attention in recent years, owing to the easy recovery and separation of the catalyst from the reaction system. Most of synthetic methods for heterogeneous catalysts were grafting or immobilization of homogeneous catalyst onto the solid supports.
Trans-1,2-Diaminocyclohexane(DACH) ligand and L-proline have been enormously used as chiral ligands in several catalytic transformation under homogenous conditions. [2-3] Our group also prepared l-proline functionalized mesoporous silica was synthesized under acidic condition using a poly(ethylene oxide)-poly(propylene oxide)-poly(ethylene oxide) triblock copolymer template ($EO_{20}PO_{70}EO_{20}$, Pluronic P-123, BASF).[4] Furthermore, we successfully directly synthesized trans-1,2 diaminocyclohexane functionalized mesoporous silica by using microwave method. The direct functionalization of chiral ligand into the framework of mesoporous materials is expected to be useful for the heterogeneous asymmetric catalysis. So, we adopt the direct synthesis of chiral ligand functionalized mesoporous silica by using thermal and microwave irradiation. Then, chiral ligand functionalized mesoporous silicas were applied to enantioselective asymmetric catalytic reactions.

Experimental

1) Synthesis of trans-1,2-diaminocyclohexane precursor
The (1S,2S)-(+)-1,2-Diaminocyclohexane (46 mmol) were added to the (3-chloropropyl)triethoxysilane (23 mmol). The resulting solution was stirred at 80 ℃ for 18 hours. The resulting mixture was rinsed with freshly distilled pentane. The solvent was pumped off from the filtrate. The yellowish solution was distilled.

2) Synthesis of trans-1,2-diaminocyclohexane(DACH) functionalized mesoporous silica
Trans-1,2-diaminocyclohexane (DACH) functionalized mesoporous silica were prepared by DACH precusor and sodium metasilicate with Pluronic P123 (EO20PO70EO20, Aldrich) and c-HCl. The mixture was aged and heated under microwave irradiation (300 W, 100%, Milestone) or thermal method. Trans-1,2-diaminocyclohexane precursor to SiO2 molar ratios in the initial synthesis mixture were 5%, 7.5% and 10% .

Results and discussion

XRD patterns of chiral DMS-n (n=5, 7.5 ,10) are presented in Fig. 1a. The XRD patterns of all samples exhibit three well-resolved diffraction peaks (d_{100}, d_{110} and d_{200}), which can be assigned to the mesostructure of hexagonal space group symmetry P6mm. The N2 adsorption–desorption isotherms of 1,2-diaminocyclohexane ligand functionalized

functionalized mesoporous silica (chiral DMS-n) are shown in Fig. 1b. The samples had the type IV isotherm of hysteresis loop with H1-type which was characteristic for highly ordered two-dimensional hexagonal mesostructured with uniform cylindrical channels. Also, two step desorption branch were appeared in the plugged hexagonal templated silica due to the pore blocking. And it was evidenced in the isotherms in Fig. 1b. For asymmetric catalytic application, 'plugged' pore could provide confinement effect.

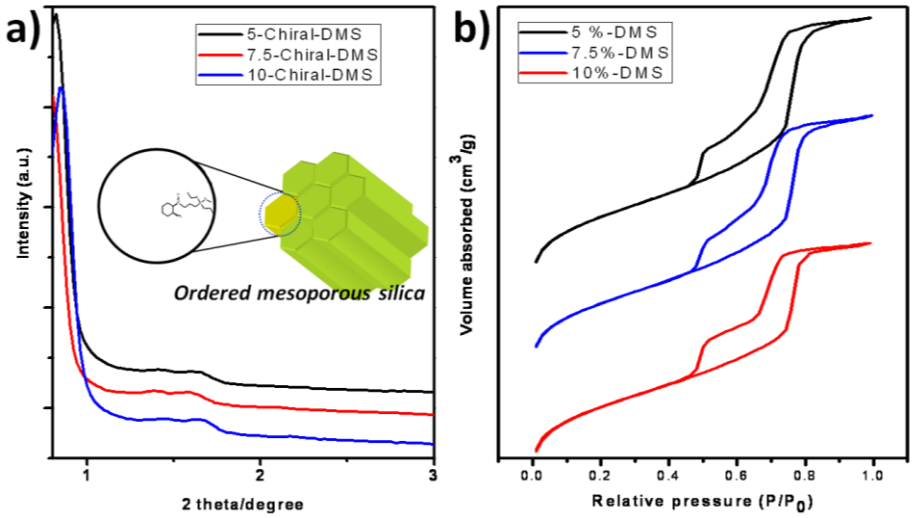

Figure 1. Powder XRD patterns (a) and nitrogen adsorption-desorption isotherms (b) for samples of trans-1,2 diaminocyclohexane functionalized mesoporous silica (chiral DMS-n)

Conclusions

Trans-1,2 diaminocyclohexane functionalized mesoporous silica (chiral DMS-n) has been directly synthesized. The catalysts having short channel with plugs in the pore structure showed outstanding catalytic activity as well as chirality enhancement in the enantioselective michael reaction.

Acknowledgements

This work was supported by the Korea Science and Engineering Foundation (KOSEF) and funded by Korea government (MOST) (Project number: 2009-0083525).

References

[1] Merino, P., Tejero, T., Organocatalyzed Asymmetric α-Aminoxylation of Aldehydes and Ketones—An Efficient Access to Enantiomerically Pure α-Hydroxycarbonyl Compounds, Diols, and Even Amino Alcohols, Angewandte Chemie International Edition, 43 (2004), 2995-2997

[2] Jiang, D., Gao, J., Li, J., Yang, Q., Li, C., Structural control of mesoporous ethane-silicas with trans-(1R,2R)-diaminocyclohexane in the pore and asymmetric catalysis, Microporous and Mesoporous Materials**,** 113 (2008), 385-392.

[3] Jiang, D., Gao, J., Yang, J., Su, W., Yang, Q., Li, C., Mesoporous ethane-silicas functionalized with trans-(1R,2R)-diaminocyclohexane: Relation between structure and catalytic properties in asymmetric transfer hydrogenation, Microporous and Mesoporous Materials**,** 105 (2007), 204-210

[4] Adi Prasetyanto, E., Lee, S.-C., Jeong, S.-M., Park, S.-E., Chiral enhancement in diethyl malonate addition by morphosynthesized l-proline mesoporous silica, Chemical Communications,105 (2008)**,**1995-1997

Synthesis of metalloporphyrin bridged periodic mesoporous organosilica as a heterogeneous catalyst for aerobic Baeyer-Villiger oxidation

Eun-Young Jeong, Sang-Eon Park*
Laboratory of Nano-Green Catalysis and Nano Center for Fine Chemical Fusion Technology, Department of Chemistry, Inha University, Incheon, 402-751, South Korea, corresponding:separk@inha.ac.kr

Introduction

Among the various ordered mesoporous materials, periodic mesoporous organosilicas (PMOs) has been considered as one of attractive OMSs. This periodic mesoporous organosilicas are an unique type of ordered mesoporous silica in which organic moieties are integrated onto the silica framework entirely or randomly to form hybrid organic–inorganic materials. The most important characteristic of PMOs are that they can incorporate various organo functionalities into inorganic frameworks to form organic– inorganic hybrid materials of which diverse organofunctionalities offer broad application. [1] The organic moieties of PMOs mainly rely on various silsesquioxanes of such as disilanes, trisilanes, and tetrasilanes with different organic bridging groups. Their syntheses were started at the end of the twentieth century with three independent groups of S. Inagaki, G. A. Ozin and A. Stein. Organosilane precursors in the form of trisilanes and tetrasilanes were rarely used. Our group prepared melamine bridged PMOs with high reproducibility by co-condensation using N2,N4,N6-tris(3-(triethoxysilyl) propyl)-1,3,5-triazine-2,4,6-triamine (TBTS) and sodium metasilicate in the presence of P123 (P123, $EO_{20}PO_{70}EO_{20}$) at a highly acidic concentration.[2] Also there are one reports on porphyrin in PMO materials from our group.[3] Herein, we would like to present several types of porphyrin-bridged periodic mesoporous organosilica, which will be useful for Baeyer-Villiger oxidation. The obtained results demonstrate that Fe-TCPP-PMO is a promising and efficient catalyst for the Baeyer-Villiger oxidation of ketones to esters using O_2 as the oxidant.

Experimental

1) Synthesis of M-TCPP-silsesquioxane (M=Cu, Fe, Sn and Free)
3-aminopropyltriethoxysilane, M-tetrakis(4-carboxyphenyl)porphyrin (M-TCPP) and dicyclohexyl carbodiimide were suspended in 50 ml of tetrahydrofuran (THF). The mixture was refluxed overnight under nitrogen atmosphere. After cooling down to room temperature, the product was washed with petroleum ether.

2) Synthesis of M-tetrakis(4-carboxyphenyl)porphyrin bridged periodic mesoporous silica
M-TCPP-tetrasilanes linked in the PMO were synthesized by the self-assembly of M-TCPP-tetrasilanes (prepared in our laboratory) together with TEOS as a surplus silica source and cetyltrimethylammonium bromide (CTABr). Then, the synthesized M-TCPP-PMOs were used to catalyze the Baeyer-Villiger oxidation with molecular oxygen as the oxidant.

Results and discussion

Table 1. Physicochemical properties for M-TCPP-PMO

Sample	*TEOS/M-TCPP-tetrasilane*	*N_2 adsorption-desorption analysis*			*X-ray diffraction*			*UV-Vis spectroscopy*
		Surface area (m^2/g)	*Pore diameter (nm)*	*Total pore volume ($cm^3 g^{-1}$)*	*d_{100} (nm)*	*a_0 (nm)*	*Wall thickness (nm)*	*Soret band*
Fe-TCPP-PMO-10	*90:10*	*871*	*2.07*	*0.80*	*3.8*	*4.42*	*2.35*	**409**
Fe-TCPP-PMO-20	*80:20*	*530*	*1.94*	*0.71*	*4.03*	*4.69*	*2.75*	**410**
Cu-TCPP-PMO-10	*90:10*	**1087**	**2.47**	**0.91**	**4.01**	**4.62**	**2.20**	**416**
Cu-TCPP-PMO-20	*80:20*	**859**	**1.97**	**0.60**	**4.06**	**4.72**	**2.76**	**417**
Sn-TCPP-PMO-10	*90:10*	*450*	*1.67*	*0.34*	**4.3**	**5.00**	**3.33**	**420**
Sn-TCPP-PMO-20	*80:20*	*350*	*1.62*	*0.28*	**4.6**	**5.35**	**3.71**	**419**

The synthesis of M-TCPP-PMOs from TEOS and M-TCPP-tetrasilanes were described in Scheme 1. The synthetic conditions, the pore sizes, cell unit parameters, and the pore volume of these mesoporous materials are summerized in Table 1.

In the table 1, when the M-TCPP tetra silane content increases from 10 wt % to 20 wt%, the pore diameters curves decrease. But the wall thickness increases. The tendency of mesopore shrinkage with increasing M-TCPP tetra silane loading is also exhibited by changes in the surface area and total pore volume, which indicate worse mesostructural features with higher loading of M-TCPP groups. Also, M-TCPP unit bridged into mesoporous silica was checked by UV-DR spectroscopy.

Conclusions

M-TCPP bridged periodic mesoporous organosilica has been successfully synthesized by microwave heating or thermal method. The catalysts having short channel in the pore structure showed outstanding catalytic activity of Baeyer-Villiger oxidation as well as chirality enhancement in the enantioselective Michael reaction and diethyl malonate addition.

Acknowledgements

This work was supported by the Korea Science and Engineering Foundation (KOSEF) and funded by Korea government (MOST) (Project number: 2009-0083525).

References

[1] Hatton, B., Landskron, K., Whitnall, W., Perovic, D., Ozin, G. A., Past, Present, and Future of Periodic Mesoporous OrganosilicasThe PMOs, Acc. Chem. Res, 38 (2005), 305-312

[2] Prasetyanto, E. A., Ansari, M. B., Min, B.-H., Park, S.-E., Melamine tri-silsesquioxane bridged periodic mesoporous organosilica as an efficient metal-free catalyst for CO2 activation, Catalysis Today, 158 (2010), 252-257

[3] Jeong, E.-Y., Burri, A., Lee, S.-Y., Park, S.-E., Synthesis and catalytic behavior of tetrakis(4-carboxyphenyl) porphyrin-periodic mesoporous organosilica, Journal of materials chemistry, 20 (2010), 10869-10875

Synthesis and characterization of Au supported on carbonaceous materials-based catalysts for the selective oxidation of glycerol

Sonia Gil*, Miriam Marchena, Amaya Romero[1], José Luís Valverde
*Facultad de Ciencias Químicas / Escuela Técnica Agrícola[1], Departamento de Ingeniería Química, Universidad de Castilla-La Mancha, 13071 Ciudad Real, Spain. *E-mail address: sonia.gil@uclm.es.*

Introduction

Carbonaceous supports, typically activated carbon, are widely used in heterogeneous catalysis due to their specific properties, such as resistance to acid/basic media, possibility of controlling porosity and surface chemistry and easy recovery of the metal [1]. The discovery of novel carbon nanostructures has led to an important increase in works related to their catalytic applications. Carbon nanofibers (CNF) are characterized by high aspect ratio bodies with enhanced mechanical strength and surface areas in the range 10-200 m^2 g^{-1}. They present a large amount of edges in the lattice and basal regions, providing increased metal-support interactions, and lower mass transfer constraints associated with their mesoporous character, in comparison with microporous activated carbons. Consequently, CNF have been proposed as potential catalyst supports although, there is still a dearth of studies dealing with their use in oxidation reactions. In the present work, we report the preparation and characterization of Au supported on three different types of carbon nanofibers ((CNF-Platelet (CNF-P), CNF-Fishbone (CNF-F) and CNF-Ribbon (CNF-R)), and its application on the liquid phase selective oxidation of glycerol, giving rise to many compounds [2]. Actually, the majority of these products are produced using non-environmentally stoichiometric oxidation processes or low productivity fermentation processes. So, replacement of these processes by friendly environmentally and low cost processes, such as the use of cheap oxidizing agents with the use of heterogeneous catalysts will be a step forwards.

Experimental

The three different types of CNF supports were prepared by the catalytic decomposition of ethylene over Ni supported on silica, at different temperatures, 723, 873 and 1023 K [3], and demineralised using HF to remove the parent catalyst particles. The metal function (Au) was introduced on the support by two different techniques: impregnation (-IMP) and sol-gold using THPC as oxidizing agent (-SGT). Both supports and catalysts were characterized by the following techniques: N_2 adsorption-desorption, X-ray diffraction (XRD), transmission electron microscopy (TEM), Raman spectroscopy, temperature programmed oxidation (TPO), temperature programmed desorption (TPD) and temperature programmed reduction (TPR). Catalytic activity measurements were carried out with oxygen under pressure to 5 bar, 333 K, 300 ml of a 0.3 M glycerol solution, glycerol/Au = 3500 mol/mol, 1000 rpm and NaOH/glycerol = 2 mol/mol.

Results and discussion

The physicochemical properties of the supports have been described in detail elsewhere [4]. After the incorporation of the metallic phase (Au), it was evaluated the reduction capacity of the catalysts by temperature programmed reduction (TPR), setting the reduction temperature of 623 K as a suitable temperature to carry out the activation of the catalysts before the reaction step, which ensures a complete reduction of the metallic phase without affecting the structural properties of the supports. The diffraction patterns of X-rays showed a major peak at $2\theta \approx 26°$, corresponding to the (002) diffraction plane of graphite, as well as, four small peaks at $2\theta \approx 38º$, 44º, 64º and 77º corresponding to the (111), (200), (220) y (311) planes of metallic gold respectively. These small peaks are representative of small gold particles, as observed from TEM analysis. The average particle size based on the area, obtained by TEM

micrographs are shown in Table 1. As observed, Au particles deposited by the sol-gold method had an smaller average size than those synthesized by impregnation, which favored the catalytic activity as will be discussed below.

Table 1. Physicochemical properties of the Au catalysts.

	Au/CNF-P -IMP	Au/CNF-P -SGT	Au/CNF-F -IMP	Au/CNF-F -SGT	Au/CNF-R -IMP	Au/CNF-R -SGT
Au loading (% w/w)	1.4	1.0	1.4	0.8	1.1	0.6
TPR $T_{máx}$ (K)	600	639	630	645	634	656
TPR-H_2 consumption (µmol g_{Au}^{-1}) (experimental/theorical)	16.4/0.72	12.5/0.53	12.6/0.71	9.1/0.41	11.4/0.57	8.5/0.32
$\bar{d}_s$ (nm)	27.1	24.2	25.5	22.2	19.2	13.2
BET surface area (m^2g^{-1})	135	147	98	118	94	104
Total pore volume (cm^3g^{-1})	0.038	0.043	0.030	0,032	0.026	0.029

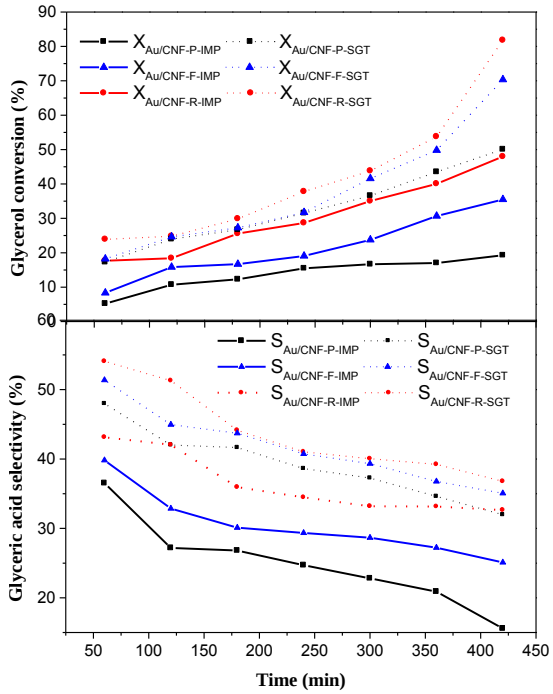

Catalytic results, Fig. 1, show the increased conversion of glycerol with time, thus obtaining the following order of activity Au/CNF-R-SGT > Au/CNF-F-SGT > Au/CNF-P-SGT > Au/CNF-R-IMP > Au/CNF-F-IMP > Au/CNF-P-IMP. These catalytic results can be explained taking into account the nature of the different carbonaceous supports. Thus, the most crystalline material (CNF-R) promoted a strong anchoring of small, thin and faceted Au particles, which facilitated the proton abstraction from glycerol, increasing its catalytic conversion. On the other hand, Au particle size, closely linked to the preparation method of the catalyst, is another parameter that had significant influence on the catalytic activity in the glycerol oxidation. According to results listed in Table 1 and Fig. 1, both conversion and selectivity increased with decreasing gold particle sizes.

Figure 1. Conversion of glycerol and selectivity to glyceric acid as a function of time-on-stream.

Conclusions

The crystalline nature of the carbon support has a strong influence on the way in which the Au metal particles were anchored to the support. At higher support crystallinity, the smaller Au Au particle sizes were obtained and, as consequence, the higher activity and selectivity in the liquid-phase oxidation of glycerol were noted.

References

[1] Serp, P., Corrias, M., Kalck, P., Carbon nanotubes and nanofibers in catalysis, Appl. Catal. A 253 (2003) 337-358.

[2] Demirel-Gülen, S., Lucas, M., Claus, P., Liquid phase oxidation of glycerol over carbon supported gold catalysts, Catal. Today 102 (2005) 166-172.

[3] Park, C., Keane, M.A., Catalyst support effects in the growth of structured carbon from the decomposition of ethylene over nickel, J. Catal. 221 (2004) 386-399.

[4] Jiménez, V., Nieto-Márquez, A., Díaz, J.A., Romero, R., Sánchez, P., Valverde, J.L., Romero, A., Pilot plant study of the influence of the operating conditions in the production of carbon nanofibers, Ind. Eng. Chem. Res. 48 (2009) 8407-8417.

Gas – phase hydrogenation of 2 – tert – butylphenol over Ni – based catalysts

José Antonio Díaz[a*], Rebeca Díaz[a], José Luis Valverde[a], Amaya Romero[b].
Departamento de Ingeniería Química, Facultad de Ciencias Químicas, Universidad de Castilla – la Mancha, Campus Universitario s/n, 13071 Ciudad Real (Spain)[a]. Facultad de Ciencias Químicas, Escuela Técnica Agrícola[b].
[*]*E-mail adress: joseantonio.diaz@uclm.es*

Introduction

Hydrogenation of tert – butylphenols, like 2- and 4 – tert – butylphenol, produces a mixture of *cis*- and *trans*- isomers of 2- and 4 – tert – butylcyclohexanol, respectively. These alkylcyclohexanols are used in fragrance and perfumery industry. In both cases, the *cis*-isomer is more demanded [1]. Stereoelectivity plays an important role in these reactions, because both isomers and the corresponding cyclohexanone are produced. This factor and activity of the hydrogenation could be influenced by many variables: pH of the medium, reaction temperature, pressure, and type of catalyst used.

All studies about hydrogenation of 2 – tert – butylphenol are carried out in the liquid phase, over nickel, palladium and ruthenium – based catalysts. The liquid – phase reaction places restrictions on temperature and pressure and therefore the equipment is more complicated. The catalyst must be separated from the products, creating additional complications [2]. The gas – phase hydrogenation could be a promising alternative. For this reaction, carbonaceous materials could be interesting supports because of their special properties (high mechanical strength, chemical inertness, and the can be used both in acidic and basic solutions. It is relatively easy to use combustion for recovery of the precious metal after deactivation of the catalyst [3].

In the present work, influence of catalyst support in gas – phase hydrogentation of 2 – tert – butylphenol were studied. Nickel – based catalysts were prepared by impregnation method. Herringbone carbon nanofibers (CNF), activated carbon (AC), graphite (G) and γ – alumina (AL) were used as catalyst support. For the best of our knowledge no report on gas – phase hydrogenation of 2 – tert – butylphenol is given in the literature.

Experimental

Catalysts were prepared by impregnation method with a solution of $Ni(NO_3)_2{\cdot}6H_2O$. Metal loading were approximately 12%. The suspension was filtered, washed with deionised water and dried at 383 K for 24 hours. N_2 adsorption – desorption method (BET), X – ray diffraction (DRX), temperature – programmed reduction (TPR), acid – base titration and transmission electron microscopy (TEM) were used for catalysts and supports characterization. Catalytic tests were realized in a Microactivity reactor. Initially, catalyst loading (30 mg) was reduced at 400ºC with hydrogen. 2-TBP hydrogenation experiments were carried out at 250 ºC and atmospheric pressure.

Results and discussion

Table 1 shows the main characterisation results of catalysts. TPR profiles revealed that completely reduction of nickel particles were achieved at 673K. This fact is confirmed by XRD patterns, that showed three peaks at 44.4º, 51.9º and 76.3º corresponding to the (1 1 1), (2 0 0) and (2 2 0) planes of metallic nickel for all catalysts. The average particle size based on the area, by counting from TEM micrographs, are shown in Table 1. As it observed, average particle size changed as function of support properties and porosity.

Table 1. Summary of characterisation data of catalysts used.

	CNF-12,3VI	AC-10,9VI	AL-11,7VI	G-11,9VI
Ni loading (%w/w)	12.3	10.9	11.7	11.9
BET Surface area (m^2/g)	56.78	265.36	125.20	8.56
Pore volume (cm^3/g)	0.245	0.192	0.245	0.053
TPR – T_{max} (K)	566	553	558	584
TPR – H_2 consummed (mmol/g) (exp/the)	0.749/0.314	0.226/0.278	0.315/0.299	0.408/0.304
d_s (nm)	73.48	42.62	49.58	29.46

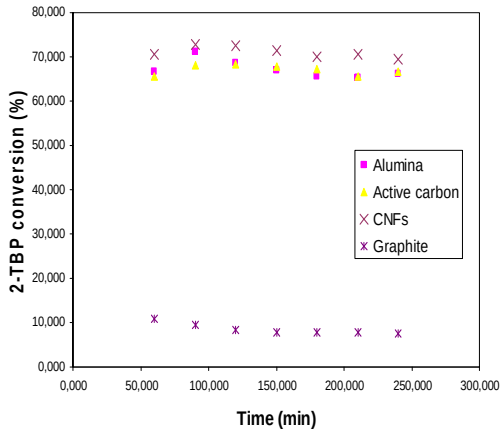

Figure 1 shows results on catalytic experiments. Catalytic activity order was CNF > AL > AC > G, which confirmed that catalysts prepared with higher particle size presented higher catalytic activity.

Figure 1. 2-TBP conversion vs time for all catalysts.

Conclusions

Particle size plays an important role in gas – phase hydrogenation of 2 – tert – butylphenol. Ni/CNFs-12,3VI shows the largest metal particles and consecuently the most catalytic activity. Use of different catalyst supports doesn´t affect selectivity to 2 – tert – butylcyclohexanol.

References

[1] B. Silberova, L. Červeny. R. Kinetics and Cat. Letters 67 (1999), 29.
[2] A. Kalantar, H. Backman, J. H. Carucci, T. Salmi, D. Murzin. J. Catal. 227 (2004), 60.
[3] E. Ochoa – Fernández, D. Chen, Z. Yu, B. Tøtdal, M. Rønning, A. Holmen. Catal. Today 102 – 103 (2005), 45.

Acidic and catalytic properties of hierarchical zeolites and hybrid ordered mesoporous materials assembled from MFI protozeolitic units

D.P. Serrano[a,c], R.A. García[b], G. Vicente[a], M. Linares[a], D. Procházková[d] and J. Čejka[d]

[a] *Chemical and Energy Technology Department,* [b] *Chemical and Environmental Technology Department, Rey Juan Carlos University,* [c] *IMDEA Energy Institute, Móstoles, Madrid, Spain,* [d] *J. Heyrovský Institute of Physical Chemistry, Academy of Sciences of the Czech Republic, Prague.* rafael.garcia@urjc.es

Introduction

Zeolites are well known crystalline microporous materials widely used as heterogeneous catalysts and adsorbents in a variety of fields, like oil refining, petrochemistry and in the Fine Chemical industry. However, as a result of their small pore size, significant drawbacks are associated to them in applications involving large compounds. The synthetic effort for developing materials with large and well defined pores resulted in the successful synthesis of ordered mesoporous materials [1]. Unfortunately, the amorphous walls of these materials were not able to match the stability, acid strength and catalytic activity typically associated to crystalline zeolites. Accordingly, in recent years, much research work and great attention have been devoted to overcome the limitations of both types of materials by trying to combine the advantages of zeolites and benefits from ordered mesoporous materials. This is the case of hierarchical zeolites [2] and hybrid ordered mesoporous zeolitic materials [3], both of them employed in the present work, performing the 1,2-epoxyoctane isomerisation and anisole acylation, as catalytic tests, being compared with both conventional Al-MCM-41 and nanocrystalline ZSM-5 zeolite.

Experimental

Hierarchical zeolites (h-ZSM-5) were prepared by crystallization of zeolitic precursors that previously were silanized by treatment with phenylaminopropyltrimethoxysilane (PHAPTMS), following a procedure earlier reported [2]. Two samples have been prepared varying the amount of PHAPTMS. The synthesis of the hybrid sample (HZM) was based on the assembling of MFI precursors around CTAB micelles [3]. The reference samples were prepared according to procedures previously published [1,4]. All samples were characterized by conventional techniques. The acidic properties of the materials under study were extensively investigated by adsorption-desorption of different base probe molecules. The liquid phase rearrangement and acylation experiments were carried out in stirred batch autoclave and in a 250 ml three-necked batch reactor, respectively.

Results and discussion

The textural and acidic properties of the MFI zeolite-based materials are summarized in Table 1. Argon adsorption measurements confirmed the presence of a secondary porosity, and also significant modifications are observed in the nature of the acid sites in hierarchical ZSM-5. Hybrid HZM material possesses larger concentration of Lewis and Brønsted acid sites than Al-MCM-41. The variation of these properties has a strong effect on its catalytic activity in the different reactions, such as 1,2-epoxide rearrangement and anisole acylation. Thus, Figure 1.a shows the evolution of the epoxide conversion along the reaction time obtained with the different acidic catalysts studied.

Table 1. Physicochemical properties of the samples.

	S_{BET} (m^2/g)	S_{EXT}[a] (m^2/g)	T_{max}[b] (ºC)	Acid sites[b] (mmol/g)	Si/Al[c]	c_L[d] (mmol/g)	c_B[d] (mmol/g)
ZSM-5 (0%)	431	78	357	0.4259	31	0.09	0.26
h-ZSM-5 (5%)	524	261	349	0.3660	32	0.17	0.15
h-ZSM-5 (12%)	696	456	329	0.3303	34	0.23	0.11
Al-MCM-41	893	893	258	0.2012	28	0.14	0.02
HZM	976	956	259	0.2671	29	0.15	0.05

[a]$S_{EXT}= S_{BET}- S_{\mu PORE,}$ [b]NH_3-TPD, [c] ICP, [d]pyridine-adsorption FTIR

While a significant improvement is obtained in the case of the hierarchical zeolites compared to standard ZSM-5, the highest conversion corresponds with the HZM sample. Remarkable differences are observed between the catalysts in terms of product distribution (Figure 1.b). Octanal and octenols were the main products obtained over the hierarchical zeolites while heavy products are also formed by aldol condensation in the case of ordered mesoporous solids. Accordingly, considering both activity and selectivity, the best performance is exhibited by hierarchical zeolites since they combine a strong acidity, possessing both Lewis and Brosted acid sites, with the absence of steric and diffusional limitations.

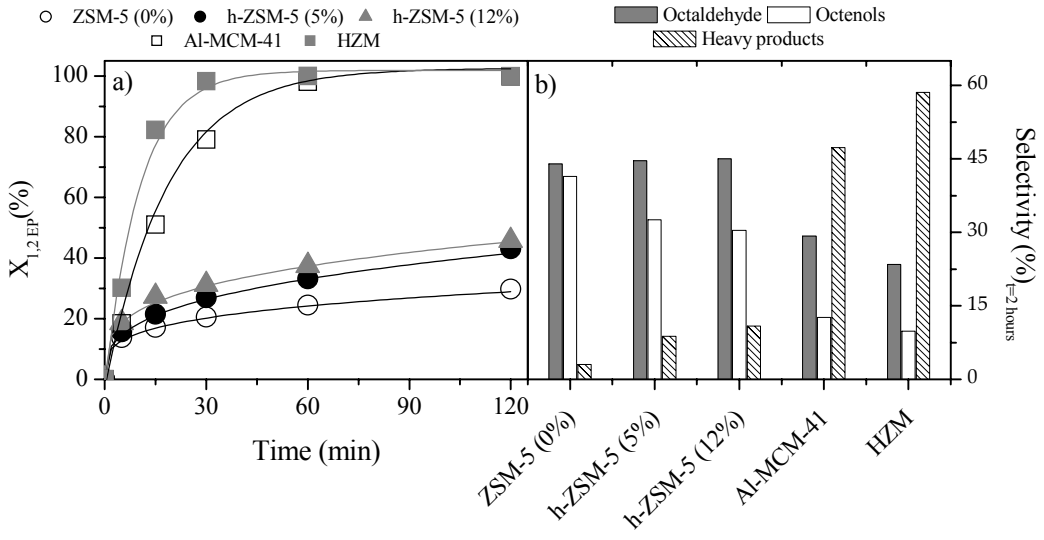

Figure 1. 1,2-epoxyoctane catalytic rearrangement: a) time evolution of conversion, b) product distribution for 2 h reaction time.

Acknowledgements

The financial support of the Spanish government (CTQ2005-09078/PPQ, CTQ2008-05909/PPQ) is gratefully acknowledged.

References

[1] A. Matsumoto, H. Chen, K. Tsutsumi, M. Grun, K. Unger, Micropor. Mesopor. Mater. 32 (3) (1999) 55.
[2] D.P. Serrano, J. Aguado, J.M. Escola, J.M. Rodriguez, A. Peral, Chem. Mater. 18 (2006) 2462.
[3] D.P. Serrano, R.A. Garcia, D. Otero, Appl. Catal. A 359 (2009) 69.
[4] R. van Grieken, J.L. Sotelo, J.L. Menendez and J.A. Melero Micropor. Mesopor. Mater. 39 (2000), 135.

Heterometallic Porphyrin-MOF [Zn_2(ZnCuTCPP)$(bpy)_{1.5}$] (HP-MOF) and its Application into Catalytic Oxidation

Seung-Yeop Lee, Eun-Young Jeong and Sang-Eon Park*
Laboratory of Nano-Green Catalysis and Nano Center for Fine Chemical Fusion Technology, Department of Chemistry, Inha University, Incheon, 402-751, South Korea, corresponding:separk@inha.ac.kr

Introduction

MOFs (Metal-Organic Frameworks) are crystalline structures consisting of transition metal ions and chelating organic ligands. In recent era MOF have been widely used in area of selective gas adsorption, gas storage, separation and catalysis. The utilization of MOF in catalysis is very limited as most MOF frameworks are based on Zn metal ion which is feebly active in catalysis. Recently MOFs are utilized in catalysis as supports for immobilization of metal nanoparticles, however use of such MOF is prone to nanoparticle leaching problem and deactivation of catalyst. [1] In order to overcome this limitation heterometallic MOF with active catalytic centres was synthesized by modification of SBU (Secondary Building Unit) with metalloporphyrins which can posses a catalytically active metal ion inside the polypyrrole unit and Zinc metal in coordination framework. Heterometallic poryphrin MOF [Zn_2(ZnCuTCPP)$(bpy)_{1.5}$] (HP-MOF) was synthesized by PPF-4 through treatment with copper solution. The morphology and structure of HP-MOF and PPF-4 were similar and posses paddle-wheel type morphology as depicted by X-ray diffraction. [2] The catalytic properties of HP-MOF were investigated in ethyl benzene and styrene oxidation reactions and catalytic results were compared with that of PPF-4.

Experimental

Synthesis of Porphyrin paddle-wheel framework (PPF)-4

tetrakis(4-carboxylphenyl)porphyrin (prepared in our laboratory) (0.38 mmol), zinc nitrate hexahydrate (0.76 mmol), and 4,4′-bipyridine (0.38 mmol) were added to N,N′-dimethylformamide (DMF, 25 mL) in a vial. The mixture was tightly capped and consequently strirred to ensure homogeneity and heated to 100 °C for 24 h. Then the mixture was cooled to room temperature. Purple flat square crystals were precipitated, filtered and washed by DMF.

Synthesis of HP-MOF

PPF-4 was added to solution of methanol of copper(II) nitrate trihydrate (0.1 M) and stirring at room temperature for 24 hours. After filtered and washed by fresh methanol, the crystal was evacuated by vacuum oven for 24 hours at room temperature.

Results and discussion

XRD patterns of as-synthesized PPF-4, evacuated PPF-4 and evacuated HP-MOF are presented in Fig. 1a. The XRD sample of as-sythesized PPF-4 showed Sharp diffraction peak similar to those reported earlier. After evacuation of PPF-4, a change in XRD pattern was observed. The XRD pattern of HP-MOF is similar to the evacuated PPF-4 depicting same paddle like structure. Optical microscopy revealed HP-MOF square type (Fig. 1b).

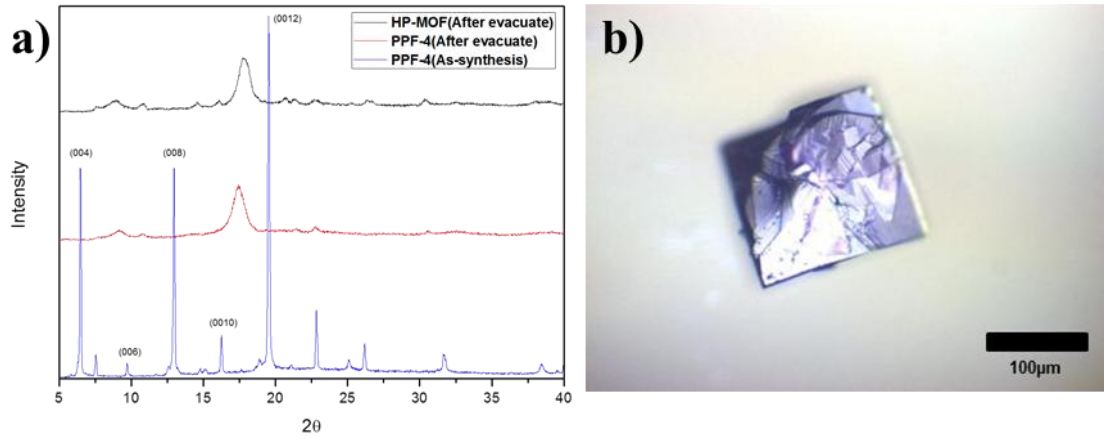

Figure 1. Powder XRD patterns of PPF-4, HP-MOF (a) and Image of HP-MOF by optical microscope (b)

The influence of copper ion in HP-MOF was investigated in oxidation of ethyl benzene and compared with that of PPF-4. The conversion in case of HP-MOF was higher with similar selectivity to that of PPF-4 which is due to existence of active metal centre Cu^{2+}

Table 1. Oxidation of Ethylbenzene with TBHP over PPF-4 and HP-MOF.

Catalyst	Conversion (%)	Product distribution (%)			
		A	B	C	Others
PPF-4	1.67	33.01	42.09	13.43	11.46
HP-MOF	25.12	29.70	40.95	13.76	15.59

* Reaction condition: Substrate : oxidant = 1 : 1, solvent = 3ml, Catalyst = 0.05g; 50℃; 6hours. A: benzaldehyde, B: acetophenone, C: (oxybis(ethane-1,1-diyl))dibenzene.

Conclusions

The HP-MOF synthesized show similar XRD pattern to that of PPF-4 concluding paddle wheel like structural arrangement. Due to the existence of active metal centre Cu^{2+} high conversion in ethyl benzene oxidation were observed compared to that of PPF-4 in.

Acknowledgements

This work was supported by the Korea Science and Engineering Foundation (KOSEF) and funded by Korea government (MOST) (Project number: 2009-0083525).

References

[1] Gao, S.; Zhao, N.; Shu, M.; Che, S., Palladium nanoparticles supported on MOF-5: A highly active catalyst for a ligand- and copper-free Sonogashira coupling reaction, Applied Catalysis A: General, 338 (2010), 196-201

[2] Choi, E.-Y.; Barron, P. M.; Novotny, R. W.; Son, H.-T.; Hu, C.; Choe, W., Pillared Porphyrin Homologous Series: Intergrowth in Metal−Organic Frameworks, Inorganic Chemistry, 48 (2008), 426-428

Preparation and utilization of bifunctional catalyst based on layered double hydroxides for benzylacetone preparation

Iva Paterová[1], Eliška Vyskočilová[1], Petr Svačina[1], Lenka Tůmová[1], Libor Červený[1], František Kovanda[2]
[1]*Department of Organic Technology, Institute of Chemical Technology Prague, Technicka 5, 166 28 Prague 6, Czech Republic; Iva.Paterova@vscht.cz*
[2]*Department of Solid Materials, Institute of Chemical Technology Prague, Technicka 5, 166 28 Prague 6, Czech Republic*

Introduction

Benzylacetone, commercially desired fragrance, is usually being prepared in two steps; aldol condensation of benzaldehyde with acetone and in the following hydrogenation of benzylidenacetone. For the catalysis of aldol condensation hydroxides are used almost exclusively. But due to the escalating demands for cleaner, more environmentally acceptable technology, the efforts exist to find heterogeneous catalysts that would allow easier handling, product separation and the reuse. Hydrotalcite and their synthetic structural analogues are described as quite promising catalysts [1] for the synthesis of chemical specialties. Their use for aldol condensation of benzaldehyde with acetone is described in several works [2], [3], [4], [5].
This study consists of 2 parts. The first part is focused on two step preparation of benzylacetone using hydrotalcite as a catalyst for aldol condensation of benzaldehyde with acetone.
The second part will deal with preparation of benzylacetone using bifunctional hydrotalcite catalysts. Based on results obtained from aldol condensation using hydrotalcite catalysts, these catalysts will be modified by precious metals (Pd or Pt) and used for "one-pot" aldol condensation and hydrogenation of benzaldehyde with acetone. In the following reaction conditions of this "one-pot" synthesis will be optimized.

Experimental

Hydrotalcites were prepared by coprecipitation method using nitrates solutions $Al(NO_3)_3.H_2O$ and $Mg(NO_3)_3.6H_2O$ at constant pH of 10 ± 0.1 and at 348 K. Obtained hydrotalcite was dried at 378 K for at least 12 hours. The activation process consists of hydrotalcite calcination at 773 K for 6-8 h and subsequent rehydration. Both steps were performed under nitrogen atmosphere. The phase composition of hydrotalcite was determined by X-ray powder diffraction (XRD). The exact ratio of Mg / Al in prepared hydrotalcite was calculated from the contents of Mg and Al in the samples determined by atomic absorption spectrometry (AAS).
Aldol condensation was carried out with prepared hydrotalcites at temperatures from 323 K to 336 K using different solvents. Hydrogenation was conducted under constant hydrogen pressure in a stainless steel autoclave with the volume of 300 ml. Ni supported catalysts were used for hydrogenation. The samples obtained from kinetic experiments were analyzed using gas chromatograph Shimadzu GC2010 Plus.

Results and discussion

Aldol condensation of benzaldehyde with acetone was tested with a series of hydrotalcites prepared with different ratios of Mg / Al in the range 2-5. In this work the best results were

achieved with a ratio Mg / Al equals 2 and 3, for which almost the same reaction courses were observed. Similar results were described by Rao [3] and Campanati [5]. Optimization of aldol condensation conditions was carried out. Increasing the reaction temperature from 323 K to reflux temperature (336 K) had, as expected, a positive effect on the reaction rate. The influence of used solvent was also studied. Different solvents such as n-heptane, toluene, acetone and isopropyl alcohol, were chosen for testing. The best result, almost 98 % conversion of benzaldehyde after 3.5 h of the reaction, was achieved using isopropyl alcohol.
For benzylideneacetone hydrogenation, the second step of the benzylacetone synthesis, optimal reaction conditions (temperature, hydrogen pressure) and the most suitable nickel supported catalyst were searched for. The influence of temperature and hydrogen pressure was monitored in the range from 333 K to 373 K respectively from 2 to 5 MPa.

Conclusions

The hydrotalcite series of various Mg/Al ratios was prepared. The most active hydrotalcites are the ones with Mg/Al ratio equal 2 and 3. Optimal reaction conditions of studied aldol condensation are the temperature of 336 K using isopropyl alcohol as a solvent. For the second step of benzylacetone preparation, the suitable Ni supported catalyst and the optimal reaction conditions were also found, the temperature of 353 K and hydrogen pressure of 5 MPa. Subsequently, obtained results will be utilized for research focused on “one-pot” reaction with the use of bifunctional hydrotalcites.

Acknowledgements

The financial support from the Ministry of Education, Youth and Sports of the Czech Republic by the research project # MSM 604 613 73 01 is gratefully acknowledged.

References

[1] Kunde L. B., Gade S. M., Kalyani V. S., Gupte S. P.: Catal. Commun. 10(14), 1881 (2009).
[2] Guida A., Lhouty M. H., Tichit D., Figueras F., Geneste P.: Appl. Catal. A 164, 251 (1997).
[3] Rao K. K., Gravelle M., Valente J. S., Figueras F.: J. Catal. 173(1), 115 (1998).
[4] Lopéz J., Valente J. S., Clacens J.-M., Figueras F.: J. Catal. 208(1), 30 (2002).
[5] Campanati M., Franceschini S., Piccolo O., Vaccari A., Ziemanis A.: Catal. Commun. 5, 145 (2004).
[6] Abello S., Vijaya-Shankar D., Perez-Ramirez J.: Appl. Catal. A 342(1-2) 119 (2008).

Cinnamyl alcohol preparation using Meerwein-Ponndorf-Verley reduction

Eliška Leitmannová – Vyskočilová, Dana Irglová, Iva Paterová, Libor Červený
Institute of Chemical Technology, Department of Organic Technology, Technicka 5, Prague, Czech Republic, leitmane@vscht.cz

Introduction

Cinnamyl alcohol is desired compound used in the perfume chemistry [1]. It can be found in almost all perfumed cosmetic product, for example perfumes, shampoos, soaps and of course detergents. From available cinnamaldehyde can be prepared by selective hydrogenation on metal supported catalysts or by Meerwein-Ponndorf-Verley (MPV) reduction.
MPV reductions are reactions catalyzed by metal oxides (Al, Ti, Zr, B) with surface basicity or Lewis acidity. The hydrogen donors are secondary alcohols - propan-2-ol, butan-2-ol, pentan-2-ol etc. In homogeneous arrangement the catalyst can be for example aluminiumisopropoxide, boron triethoxide [2], aluminiumacetoxydiisobutylane [3]. As heterogeneous catalysts for MPV reductions pure zirconium oxide or doped with boron was used for example [4,5]. Another interesting catalyst used was zirconium-1-propoxide or aluminium-1-propoxide anchored on silica, mesoporous sieves or zeolites [5,6]. In this work we would like to present another heterogeneous catalysts used for MPV preparation of cinnamyl alcohol.

Experimental

Heterogeneous catalysts for MPV reduction were prepared using the instructions given in the literature [5]. Used reduction catalysts are given in the Table 1. As a comparison experiment the MPV reduction using aluminiumisopropoxide was realized. Conditions used for the experiments were following: distillation apparatus, reflux, atmospheric pressure. Amount of catalyst is also given in the Table 1.

Table 1. Catalysts and catalyst amount used in the MPV reduction of cinnamaldehyde.

Catalyst	Catalyst amount wt. ratio catalyst : substrate	Reaction conditions
Aluminiumisopropoxide	1:15; 1:20; 1:30	reflux 101 kPa propane-2-ol
Si-MCM-41	1:15	
Zr-MCM-41	1:15	
Ti-MCM-41	1:15	
TS-1	1:15	

Results and discussion

The MPV reduction was carried out with aluminiumisopropoxide to determine the undesired product in the reaction mixture and for comparison the “modern” zeolite catalyst with usual catalyst. Aluminiumispropoxide is not the catalyst for industrial use due to many disadvantages. In the reaction mixture two undesired reactions take place – formation of hemiacetal of cinnamyl adehyde with propane-2-ol and autocondenzation of two molecules of cinnamaldehyde. These undesired products were detected using all chosen catalyst.
From the chosen heterogeneous catalysts the highest selectivity to desired cinnamyl alcohol showed the Zr-MCM-41. Si-MCM-41 and TS-1 had no activity in the desired reaction and

only the undesired hemiacetal was formed. TS-1 was inactive probably due to the small pores of the material. Using Ti-MCM-41 small amount of desired alcohol was prepared and higher amount of catalyst should be necessary.

Conclusions

Heterogeneous catalysts for Meerwein-Ponndorf-Verley reduction were tested in the preparation of cinnamyl alcohol, desired fragrance. The influence of the catalyst amount was tested using aluminiumisopropoxide, the catalyst showing the highest yield of desired fragrance was chosen. Mesoporous sieve doped with zirconia was the most active from the row of tested siliceous catalyst, TS-1 and MCM-41 were inactive.

Acknowledgements

The financial support from the Ministry of Education, Youth and Sports of the Czech Republic by the research project MSM 604 613 73 01 is gratefully acknowledged.

References

[1] Arctander, S.: Perfume and Flavor Chemicals II., part 1, Montclair, New Jersey, 1969.
[2] Uysal, B., Buyuktas, B. S.: Chemical Papers 64 (2010) 123 – 126.
[3] Cha J. S., Yi J. E.: J Incl Phenom Macrocycl Chem 65 (2009) 15 – 23.
[4] Urbano F. J., Aramendía M. A., Marinas A., Marinas J. M.: Journal of Catalyst 268 (2009) 79 – 88.
[5] Liu S. H., Jaenicke S., Chuah G. K.:Journal of Catalysis 206 (2002) 321 – 330.
[6] Yongzhong Z., Jaenicke S., Chuah G. K.: Journal of Catalysis 218 (2003) 396 – 404.

Glucose oxidation using silica- and alumina-supported gold nano-particles

K. Odrozek[1], B. Gaweł[2], G. Øye[2], T. Didriksen[3], M. Stöcker[3], J. Mrowiec-Białoń[1,4*]
[1]*Department of Chemical Engineering, Silesian University of Technology, Gliwice, Poland*
[2] *Norwegian University of Science and Technology Trondheim, Norway;*
[3] *SINTEF, Materials and Chemistry, Oslo, Norway;*[4]*Institute of Chemical Engineering Polish Academy of Sciences, Gliwice, Poland; jmrowiec@polsl.pl*

Introduction

In this work we compare catalytic properties of gold nano-particles (NPs) supported on functionalized mesoporous silicas and aluminas in the reaction of glucose oxidation to gluconic acid using oxygen or hydrogen peroxide as oxidants. Relationships between the composition of supports/size of gold NPs and catalytic activity were investigated.

Experimental

Nano-sized gold was deposited on alumina and silica modified supports. Samples 1 and 2 were obtained by mixing suitable amount of aluminum nitrate, cerium chloride or zirconyl chlorate, boehmite nano-powder and water. The obtained paste was shaped, dried at 150^{o}C and finally calcined at 500^{o}C. Sample 3 was obtained by a phase separation method using polyethylene oxide and aluminum nitrate. The gold precursor was deposited on the supports by the incipient wetness impregnation method and reduced with $NaBH_4$. All materials contained 0.5 wt. % of gold. Samples 4-6 are based on the SBA-15 materials and they were obtained in a multistage procedure. First, silica SBA-15 materials were synthesized [1], next they were modified with alumina followed by amine- or thiol- groups functionalization. Finally, gold nano-particles (1 wt. %) were deposited using two methods: i) *in situ* reduction of $HAuCl_4$ with $NaBH_4$ (samples 4 and 5) and ii) colloidal-deposition (sample 6) [2]. For sample 4 additional reduction with H_2 followed by calcination at 500^{o}C were applied. The catalytic properties and their stability were tested in the reaction of glucose oxidation to gluconic acid using H_2O_2 or oxygen as oxidants. The products were analysed by HPLC.

Results and discussion

The structural properties of the samples are listed in Table 1.

Table 1. Texture properties of the samples

No.	Catalyst	S_{BET} (m^2g^{-1})	V_p (cm^3g^{-1})	d_m (nm)	d_{Au} (nm)
1	Al5Ce0.5Au	108	0.27	9.5	ca. 5
2	Al5Zr0.5Au	127	0.28	8.4	ca. 5
3	Al0.5Au	187	0.43	6.7	ca. 5
4	SiNH5Al1Au(R)	573	1.11	7.8	n.a.
5	SiNH10Al1Au	n.a.	n.a.	n.a.	ca. 5
6	Si10AlSH1Au	260	0.33	6.3	ca. 10

S_{BET} – specific surface area, V_p – mesopore volume, d_m – average pore diameters, d_{Au} – average size of gold nano-particles; n.a. - not available yet

SBA-15-based materials had larger specific surface areas than the modified alumina supports. The pore sizes and the specific volumes were similar (exception sample 4). The average size

of gold NPs was ca. 5 nm with the exception of the sample 6 prepared by the colloidal-deposition method (ca. 10 nm). The gold content determined by ICP analysis was 0.83 wt% for the samples with a nominal content 1 wt%.
All samples were active in the glucose oxidation (Fig. 1) using H_2O_2 (molar ratio H_2O_2 to glucose was 1:1). Almost 95% of conversions and the highest reaction rate were obtained for amine modified SBA-15 materials (samples 4 and 5). A strong relationship between the size of Au NP and the activity was observed in the glucose oxidation by oxygen (Fig. 1). The catalyst with 10 nm gold nano-particles was inactive in this reaction (sample 6). Samples 1-5 showed good activities but the reaction rates were smaller by one order of magnitude than in the case of H_2O_2. The selectivity towards gluconic acid formation was almost 100%; ca. 1 % of by products were detected by the HPLC method. Overall, all catalysts showed better stabilities in the presence of H_2O_2. A small decrease of conversion was observed in subsequent cycles. This relationship is well seen for sample 4 (Fig. 2).

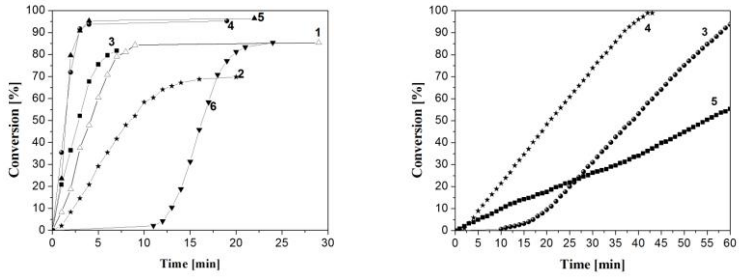

Figure 1. Glucose conversion for Au-catalysts using H_2O_2 (left) and O_2 (right) as the oxidant (numbers correspond to the sample numbers mentioned in Table 1).

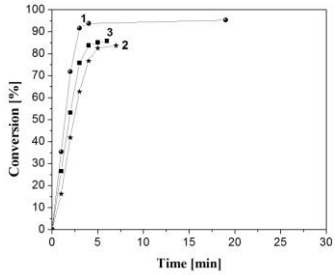

Figure 2. Glucose conversion for sample 4 during three catalytic cycles.

Conclusions

It was found that gold NPs supported on alumina and silica functionalized materials are active in glucose oxidation to gluconic acid. A strong relationship between size of NPs and activity was found.

Acknowledgements

This work was supported by the Polish-Norwegian Research Found project No PNRF-109-A I-1/07

References

[1] Zhao, D. Feng, J., Huo, Q., Fredrickson, G.H., Chmelka, B.F., Stucky, G.D., J. Amer, Chem. Soc., **120** (1998), 6024.
[2] Biella, S., Porta, F., Prati, L., Rossi, M., Catal. Lett. **90** (2003) 23.

Preparation and utilization of perillyl acetate

Štekrová M., Dudková-Paterová I., Leitmannová-Vyskočilová E. and Červený L.
Institute of Chemical Technology, Department of Organic Technology, Technická 5, 166 28 Prague 6, Czech Republic, E-mail: Martina.Stekrova@vscht.cz

Introduction

Perillyl acetate is a fragrance that has been suggested for use in perfumery, e.g. in the modification of certain essential oils (Bergamot, etc.) [1]. The starting material for preparation of perillyl acetate can be β-pinenoxide [2,3]. The simplest way of the preparation of perillyl acetate is generally the reaction of β-pinenoxide with acetanhydride in dichlormethane as a solvent and montmorillonite K-10 as an acid catalyst [3]. The use of perillyl acetate is not only in perfume chemistry but also as a starting material for the preparation of some other valuable chemical specialities. The most interesting product usually prepared from perillyl acetate is perillyl alcohol, due to its antimicrobial and antineoplastic activity [2]. Perillyl alcohol could serve as an initial substance for the preparation of very valuable fragrance called Mayol. The main aim of this work was to find the most effective way for the perillyl acetate preparation from β-pinenoxide. The reaction conditions, especially the catalyst will be optimized. The prepared perillyl acetate will be saponificated to prepare perillyl alcohol (optimal way would be chosen) and the last step will be the hydrogenation of perillyl alcohol to Mayol.

Experimental

Preparation of perillyl acetate

In the typical experiment 2 g of β-pinenoxide and 10 g of acetanhydride were added into the flask and acid catalyst was then slowly dosed. Homogenous catalyst was added dropwise into the reaction mixture in amount of 2 g (100 wt.% to β-pinenoxide) or heterogenous catalyst was added in amount of 0.4 g (20 wt.% to β-pinenoxide).

Saponification of perillyl acetate

The saponification of perillyl acetate was carried out by two methods from the literature [2,4].
1) The obtained perillyl acetate and 30 % water solution of sodium hydroxide [4] were put into the flask and then the heating started. The reaction was proceeded under the mild boil (408 K) for 3 hours. After that the top layer was separated and distilled.
2) Perillyl acetate, water, methanol and anhydrous sodium carbonate [2] were mixed in the flask and the reaction mixture was stirred at room temperature for 13 hours. Finally the extraction and purification of perillyl alcohol was carried out.

Hydrogenation of perillyl alcohol

Perillyl alcohol (2.4 g), nickel catalyst NiSAT 320 RS (0.24 g) and isopropyl alcohol (80 ml) were introduced into the stainless steel autoclave Parr 4843 (volume 150 ml). The reaction conditions were: temperature 353 K and pressure 10 MPa.

Results and discussion

Preparation of perillyl acetate

The study of perillyl acetate formation from β-pinenoxide was carried out. The optimal catalyst able to open both of the rings (epoxidic as same as carbonic) of initial β-pinenoxide

was searched. Opening of only epoxidic ring leads to the undesired myrtenyl acetate. Desired product was perillyl acetate and its isomers. Boric acid, phosphoric acid, acetic acid and citric acid were tested from homogeneous catalysts and zeolite USY (CVB 720), Strong Solid Acid, montmorillonite K-10 [3] and γ-alumina were tested from heterogeneous catalysts. From the results using homogenous and heterogenous catalyst the optimal conditions for perillyl acetate formation were found: 1 : 5 : 1 ratio β-pinenoxide : acetanhydride : acetic acid, 323 K, 2 h.

Saponification of perillyl acetate

As it was mentioned above two saponification processes were adopted from the literature. Thanks to shorter reaction time and final treatment of the product, the saponification through the water solution of sodium hydroxide was chosen.

Hydrogenation of perillyl alcohol

The last step in the perillyl acetate utilization is the following hydrogenation of obtained perillyl alcohol to Mayol. The reaction was carried out using a nickel catalyst NiSAT 320 RS under the conditions mentioned in the experimental part. After 6 h the composition of the reaction mixture was 94.6 % (54.1 % *cis*-isomer and 40.5 % *trans*-isomer) of Mayol and 2.4 % of dihydroperillyl alcohol.

Conclusions

The preparation of perillyl acetate from β-pinenoxide was carried out, followed by its converting to perillyl alcohol and to the desired fragrance Mayol. The best results for the perillyl acetate preparation were obtained using acetic acid (1 : 1 to β-pinenoxide) as a catalyst, 323 K and acetanhydride ratio (1 : 5 β-pinenoxide : acetanhydride). The achieved yield of perillyl acetate was 78.7 %. Myrtenyl acetate, which was undesirable reaction product, was present in the reaction mixture in amount of 4 %, but the mixture was successfully distilled. The yield of perillyl acetate after separation steps was: 67 % of perillyl acetate with purity 98 %.

Perillyl alcohol was prepared by saponification followed by distillation. The yield of perillyl alcohol was 94.4 % at 100 % conversion of perillyl acetate**.** Finally the Maoyl was prepared. The yield of this desired fragrance was 47.7 % calculated on the initial β-pinenoxide.

Acknowledgements

This work was carried out with financial support of the Grant Agency of the Czech Republic (grant No. 203/08/H032-1) and the Ministry of Education, Youth and Sports of the Czech Republic by the research project # MSM 604 613 73 0.

References

[1] Arctander, S.: Perfume and Flavor Chemicals II., part 1, Montclair, New Jersey, 1969.

[2] Chastain D. E., Mody N., Majetich G.: US 5994598 (1999), CAN 132:3478.

[3] Tatarova L. E., Korchagina D. V., Volcho K. P., Salakhutdinov N. F., Barkhash V. A.: Russian Journal of Organic Chemistry, 39 (2003), 1147-1153.

[4] Ansari H. R., Fido P. E.: GB 1508602 (1974), CAN 84:122072.

Aldol condensation using zeolites

Sarah Becharová, Eliška Vyskočilová-Leitmannová, Libor Červený
Department of Organic Technology, Institute of Chemical Technology Prague, Technická 5,166 28 Prague 6, Czech Republic; E-mail: Sarah.Becharova@vscht.cz

Introduction

Aldol condensation is very often used in many organic syntheses of fine chemicals and drugs. It is a carbon-carbon bond forming reaction generally carried out to form larger molecules at mild temperatures. This condensation is a reaction between two molecules of aldehyde or ketone in different combinations. One molecule becomes nucleophile and the other electrophile. This reaction can be catalyzed by basic or acidic catalysts. Basic catalysis is preferred due to the using acidic catalysts undesirable polymers should be formed, the reaction time is longer and the conversion is not so high. This work deals with the aldol condensation using zeolites as catalysts. The use of zeolites with basic properties in catalysis was reported a long time ago [1,2] and the interest in these materials is recently increasing. Basic zeolites are obtained by substitution of proton located in ion exchange sites by alkaline metals or organic molecules. Exchanged ion affect the basicity of zeolite, for example for alkaline metals exchanged in zeolites oxygen basicity increase in order Li<Na<K<Rb<Cs [3,4]. Frequently a hydrogenation of the product of aldol condensation is needed, so recently the research leads to form bifunctional catalyst for "one-pot" synthesis, which means aldol condensation and following hydrogenation in the same reactor.
One of the most interesting applications of bifunctional catalysts is synthesis of methyl-isobutyl ketone (MIBK) from acetone. In work [5] zeolites NaX and CsX were impregnated by Pt, best conversion and selection was reached with Pt/NaX.

Experimental

The starting materials are sodium form of faujasite zeolites with two different Si/Al molar ratios. The first is zeolite X (Si/Al=1.5) and the other zeolite Y (Si/Al=2.5). At first as an exchanged ion cesium is studied the next step would be alkylammonium cations. The exchange of cations was done by different methods. One of the methods was exchange of sodium ions by NH^{4+} and then by cesium. Impregnation of zeolites by metals (Pd, Pt) was performed as is described in literature [7].
Aldol condensation of aldehydes and ketones was chosen as a model reaction for study of activity and selectivity of prepared zeolites. As a first reaction a self-condensation of propanal was studied. Reaction was realized in autoclave, reaction temperature was 100 °C. As a second reaction an attractive condensation of benzaldehyde and acetone was chosen.

Results and discussion

The amount of exchanged ions and ratio of Si/Al was measured by XRF. Crystallinity of zeolites was monitored by XRD. Structure of zeolites was not determined.
If self-condensation of propanal was performed under normal pressure, zeolite catalyzed only oxidation to propionic acid. Reaction in an autoclave using catalyst NaX leads to desirable product (2-methylpent-2-enal) the conversion was 19 % after 3 hours.
Reaction of benzaldehyde and acetone was realized using these zeolites: NaX, NaY, CsX, HY. Maximal concentration of desired products (benzylideneacetone and 4-hydroxy-4-phenylpropanone) was reached with zeolite HY.

Conclusions

Zeolites were prepared by various methods. They were tested using two model reactions. One of them was self-condensation of propanal, where the highest yield of desired product was reached with NaX catalyst. The second one was condensation benzaldehyde with acetone, the highest yield of desired products was obtained with zeolite HY. Impregnated zeolites will be used for one-pot reaction of benzaldehyde and acetone followed by hydrogenation leading to desired fragrance benzylacetone.

Acknowledgements

The authors would like to thank Grant Agency of Czech Republic (Grant no. 203/08/H032-1) for financial support and to the Ministry of Education, Youth and Sports (grant No. MSM 6046137301).

References

[1] P.B. Venuto, P.S. Landis, Adv. Catal. 18 (1968) 331.
[2] Y.Ono, Stud. Surf. Sci. Catal. 5 (1980) 19.
[3] U.D. Joshi, S.S. Tamhankar, V.V. Joshi, C.V. Rode, V.P. Shiralkar, Appl. Catal. A: Gen. 239 (2003) 209.
[4] L. Martins, D. Cardoso, Quim. Nova 29 (2006) 358.
[5] Huang T. J., Haag W.O., USA patent 4,339,606 (1982).
[6] Corma A., García H., Leyva A., Primo A., Appl. Cat. A (2003) 41-49.
[7] Bejblová M., *Thesis*, VŠCHT Praha, 2005.

Metathesis catalyzed by methyltrioxorhenium

Radka Zdeňková, Eliška Vyskočilová - Leitmannová, Libor Červený
Department of Organic Technology, Institute of Chemical Technology Prague, Technická 5, 166 28 Prague 6, Czech Republic; E-mail: Radka.Zdenkova@vscht.cz

Introduction

Metathesis of olefins [1] is applied in many industrial processes. This reaction is used for the synthesis of some basic compounds, as well as for the preparation of polymers specialities. Metathesis can be catalyzed by methyltrioxorhenium (MTO) [2]. Attractivity of this catalyst is mainly in the using metathesis of olefinic compounds with heteroatoms. MTO is homogenous catalyst, but its heterogenized form is preferred for this reaction [3]. Immobilization of organometallic complexes is realized by their anchorage on the insoluble support material. The main advantages of heterogenized catalyst are easy separation from the reaction mixture and possibility of reuse. MTO immobilization may be realized, for example, by using silicate or alumosilicate materials.

Experimental

Before metathesis MTO was immobilized on the support, e.g. alumosilicate - siral 40 (1 g). Dichloromethane was used as a solvent (9 ml). Immobilization was realized using Schlenk technique to avoid contact of used materials (especially MTO) with air humidity. In the first step, the support was dried (for 5 hours at the temperature of 723 K under nitrogen atmosphere). After that, the support was directly modified in the reaction flask (for 3 hours at 393 K, and pressure of 133.3 Pa). In the second step MTO was dissolved in dichlormethane. The suspension of MTO and support was stirred for 1 hour. After that the substrate was added in the molar ratio substrate : MTO 6 : 1. Several linear α-olefins (pent-1-ene, hex-1-ene, oct-1-ene) were used for metathesis. Reaction was carried out at the room temperature.

Results and discussion

Metathesis was performed using the three substrates (pent-1-ene, hex-1-ene and oct-1-ene). After 24 hours conversion of pent-1-ene was 87 %, conversion of hex-1-ene was 67 % and the conversion of oct-1-ene was 64 %. At 50% of substrate conversion, the yield of product of the pent-1-ene metathesis (oct-4-ene) was 34 %. In the case of hex-1-ene, the yield of product (dec-5-ene) was 27 % and in the case of oct-1-ene it achieved (tetradec-7-ene) 30 %.

Conclusions

Heterogenized MTO was tested as catalyst for olefin metathesis. The reaction conditions were optimized. Both the high conversion (87 %) and the high yield of product (34 %, at 50 % conversion substrate) was achieved by using pent-1-ene as a substrate.

Acknowledgements

This work was carried out with financial support of the Grant Agency of the Czech Republic (grant No. 203/08/H032-1) and the Ministry of Education of the Czech Republic (6046137301).

References

[1] Mol, J.C., J. Mol. Catal., 65 (1991), 145-162.

[2] Herrmann, W.A.; Wagner, W.; Flessner, U.N.; Volkhardt, U.; Komber, H. Angew. Chem., Int. Ed. Engl. 30 (1991), 1636.

[3] Kühn, F.E., Scherbaum, A., Herrmann, W. A. J., Organomet. Chem. 689 (2004), 4149-4164.

Immersion calorimetry as a tool to evaluate the catalytic performance of titanosilicate materials in the epoxidation of cyclohexene

Jarian Vernimmen[a], Matteo Guidotti[b], Joaquin Silvestre-Albero[c], Erika O. Jardim[c], Myrjam Mertens[d], Oleg I. Lebedev[e,f], Gustaaf Van Tendeloo[f], Rinaldo Psaro[b], Francisco Rodríguez-Reinoso[c], Vera Meynen[a], Pegie Cool[a]

[a]*Laboratory of Adsorption and Catalysis, University of Antwerp, Universiteitsplein 1, B-2610 Wilrijk, Belgium; jarian.vernimmen@ua.ac.be.*

[b]*CNR-Istituto di Scienze e Tecnologie Molecolari, via G. Venezian 21, 20133 Milano, Italy.*

[c]*Laboratorio de Materiales Avanzados, Universidad de Alicante, Ctra. San Vicente s/n, E-03690 Alicante, Spain.*

[d]*Flemish Institute for Technological Research (VITO N.V.), Boeretang 200, B-2400 Mol, Belgium.*

[e]*CRISMAT, UMR 6508, CNRS-ENSICAEN, 6 Bd Marechal Juin, 14050 Caen, France.*

[f]*EMAT, University of Antwerp, Groenenborgerlaan 171, B-2020 Antwerpen, Belgium.*

Introduction

Nanoporous titanosilicates often find application as redox catalysts at both benchmark and industrial scale. The classical example of a successful titanosilicate is titanium-silicalite-1 (TS-1), which is very efficient in catalyzing oxidation processes with H_2O_2 as oxidant. Also purely mesoporous materials, such as Ti-SBA-15 and Ti-MCM-41, and combined micro- and mesoporous structures, e.g. Ti-MMM-1 [1] and MTS-9 [2], can be useful catalysts in certain reactions. In order to correlate the catalytic activities of materials with its structural properties, it is important that (i) the structural characterization is executed thoroughly and (ii) the surface chemistry, more specifically the interactions of the reactants with the active sites of the catalyst, is taken into account. An excellent technique to study the interaction of molecules with a solid surface is immersion calorimetry, in which the heat/enthalpy of immersion is a measure for the degree of interaction. However, reports in which catalytic testing is combined with immersion calorimetry are very scarce. Moreover, to the best of our knowledge, there is no literature available that explicitly combines the catalytic conversion of a specific molecule with immersion calorimetry of the same molecule.

In this work, we report for the first time the combined use of immersion calorimetry and a catalytic test reaction for the comparative evaluation of different Ti-containing siliceous catalysts [3]. The catalytic results for the epoxidation of cyclohexene are correlated with the heat of immersion of cyclohexene for the different catalysts, namely TS-1, Ti-containing MCM-41 (obtained by grafting a Ti(IV) inorganic precursor) and three types of combined zeolitic/mesoporous materials (SBA-TS-15-pH 1; SBA-TS-15-pH 13; meso-TSM) (Fig. 1). The goal is to demonstrate that immersion calorimetry can be a very useful extra tool for the interpretation of catalytic test results.

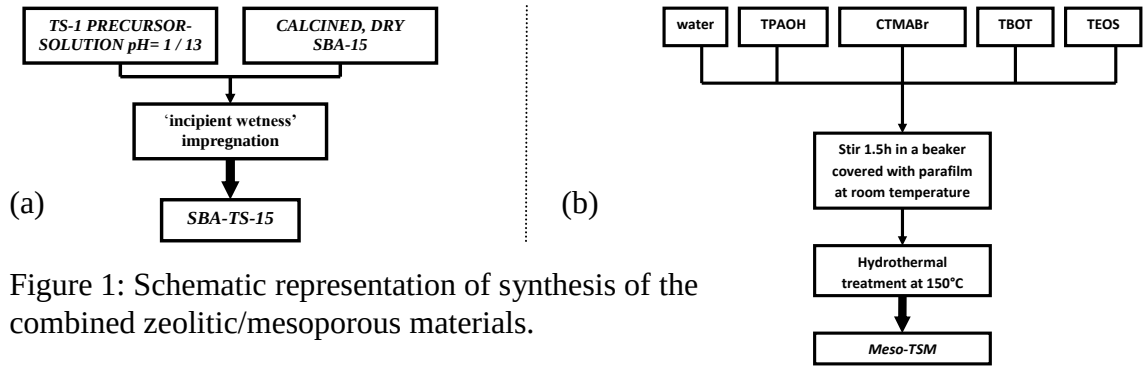

Figure 1: Schematic representation of synthesis of the combined zeolitic/mesoporous materials.

Results and discussion

The structural characteristics of the different titanosilicates are listed in Table 1.

Table 1. Structural characteristics of the different catalysts.

	N_2-sorption					XRD	EPMA
	BET ($m^2.g^{-1}$)	Vμ ($mL.g^{-1}$)	Vtot ($mL.g^{-1}$)	Rads (nm)	isotherm type	MFI zeolite profile	% Ti
TS-1	360	0.11	0.33	-	I	yes	4.1
MCM-41 support	1450	0.00	0.80	1.0	IV	-	-
Ti-MCM-41	1330	0.00	0.99	1.1	IV	-	1.4
SBA-15 support	827	0.15	0.99	3.6	IV	-	-
SBA-TS-15-pH 1	406	0.05	0.42	3.2	IV	no	0.9
SBA-TS-15-pH 13	457	0.08	0.48	3.4	IV	no	1.3
meso-TSM	786	0.00	0.79	1.5	IV	yes	1.2

The catalytic test results point out that the divergent structural properties of the titanosilicates have a large influence, resulting in the following order of catalytic activity: Ti-MCM-41 >> meso-TSM >> SBA-TS-15-pH 1 ≥ SBA-TS-15-pH 13 > TS-1 ≈ 0. Immersion calorimetry in pure cyclohexene shows that the order of interaction between cyclohexene and the catalysts' surface is Ti-MCM-41 > meso-TSM > SBA-TS-15-pH 1 > SBA-TS-15-pH 13 > TS-1. This order completely coincides with the order of the catalytic activity in the epoxidation reaction, catalyzed by the different titanosilicates.

Conclusions

We demonstrated for the very first time that the combination of catalytic testing and immersion calorimetry, when using the same molecule, can lead to important insights into the influence of the different titanosilicates on its catalytic behaviour. Immersion calorimetry can hence be used as an auxiliary characterization tool for a better understanding of the interaction between the solid catalyst and the substrate. More specifically, immersion calorimetry with cyclohexene can be applied as a screening tool for the catalytic epoxidation of cyclohexene. Nevertheless, it should be kept in mind that immersion calorimetry can only serve as an adequate screening tool (with a straightforward interpretation) for catalysts, when the adsorption of the molecules used as immersion liquid is the rate-determining step in the catalytic reaction.

Acknowledgements

J. Vernimmen thanks the Fund for Scientific Research-Flanders (FWO-Vlaanderen) for financial support. The Concerted Research Project (CRP, GOA-project) sponsored by the Special Fund for Research at the University of Antwerp is acknowledged. The networks of Excellence (EU-FP6), INSIDE-POReS and IDECAT, are gratefully acknowledged. R. Psaro and M. Guidotti acknowledge financial support from the European Community's 7th Framework Programme through the Marie Curie Initial Training Network NANO-HOST, (Grant Agreement no. 215193) and from the Italian Ministry of Education, University and Research through the Project "ItalNanoNet" (prot. no. RBPR05JH2P).

References

[1] R.H.P.R. Poladi, C.C. Landry, Micropor. Mesopor. Mater., 52 (2002), 11-18

[2] X. Meng, D. Li, X. Yang, Y. Yu, S. Wu, Y. Han, Q. Yang, D. Jinag, F.-S. Xiao, J. Phys. Chem. B, 107 (2003), 8972-8980

[3] J. Vernimmen, M. Guidotti, J. Silvestre-Albero, E.O. Jardim, M. Mertens, O.I. Lebedev, G. Van Tendeloo, R. Psaro, F. Rodríguez-Reinoso, V. Meynen, P. Cool, Langmuir, accepted

Asymetric reduction of imines using immobilized chiral catalyst

I. Lusticka[a], O. Kysilka[b], L. Cerveny[a], P. Kocovsky[b*]

[a]*Department of Organic Technology, Institute of Chemical Technology - Prague, Technicka 5, 166 28 Prague 6, Czech Republic*

[b]*WestChem, Department of Chemistry, University of Glasgow, Joseph Black Building, G12 8QQ, Glasgow, United Kingdom*
[*]*email: pavelk@chem.gla.ac.uk*

Introduction

Asymmetric reduction of imines represents one of the most efficient methods for the preparation of chiral amines (Fig. 1). This reduction can be catalyzed by a chiral catalyst derived form N-methylvaline formamide [1].

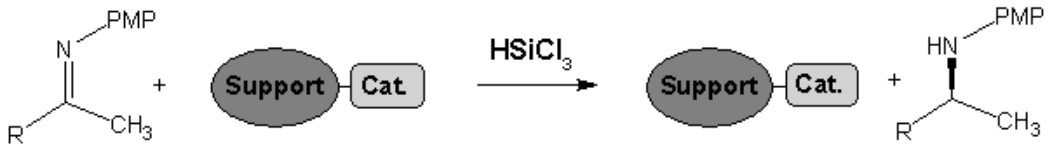

Figure 1: Reaction scheme of asymmetric reduction

In recent decades the immobilization of homogeneous catalysts has become very popular. The main disadvantage of homogeneous catalysis (no-reuse of the catalyst) may be eliminated by immobilization [2], owing to this immobilization catalyst could be readily separated and used again.

Experimental

N-methylvaniline-derivated formamide was used as a catalyst. Mesoporous inorganic molecule sieves MCM-41 and SBA-15 were used as supporting materials. Chiral catalyst was prepared by a multistep synthesis. Immobilizations were carried out under the inert atmosphere of Ar. Reductions of imines were carried out on a laboratory scale in the presence of immobilezed catalyst and trichlorosilane in the toluene.
Elementar analysis, BET analysis, ^{1}H NMR, ^{13}C NMR and HPLC chiral column was used for quantification and qualification of these products.

Results and discussion

In the first part of the study malic acid chloride (Fig. 2) was prepared as a catalyst precursor in several steps.

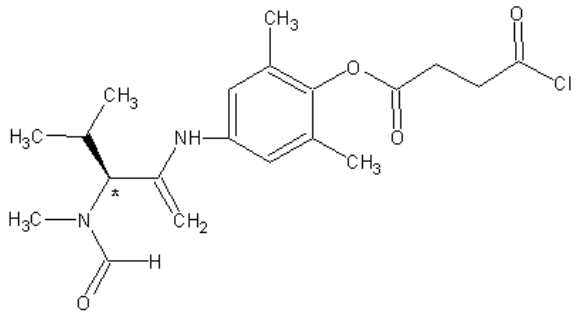

Figure 2: Scheme of the chiral catalyst

The catalyst was immobilized on the mesoporous molecular sieves (MCM-41 and SBA-15) by the covalent bonding. MCM-41 was prepared by hydrotermal synthesis [3] (Surface area 1034 m^2/g). Immobilized amount of the catalysts was approximately 0.90 mmol/g. The rest of hydroxyl groups on the carrier surface were capped by acetylchloride in the presence of pyridine in anhydrous THF. Immobilized catalyst was used for the asymmetric reduction of imines. Experiments were carried out under folloving conditions: trichlorsilane was added to a suspension of imine and the catalyst in anhydrous toluene. The reaction mixture was stirred overnight at room temperature under an argon atmosphere. After the work up the product was obtained in hight yeld (87%). The immobilized catalyst was separated and could be reused.

Conclusions

An efficient way for asymetric reduction of imines with trichlorosilane using the chiral catalyst immobilized on inorganic mesoporous sieves has been divided.
The catalyst was sucessfully anchored to a solid support (mesoporous molecular sieves), the immobilized amount was 0.9 mmol/g.
Asymetric reduction of imines in the presence of trichlorsilane and immobilized chiral catalyst has been observed.

Acknowledgements

This work was carried out with the financial support from the Grant Agency of the Czech Republic (203/08/H032-1) and the Ministry of Education of the Czech Republic (6046137301).

References

[1] Malkov, A. V., Vrankova, K., Stoncius, S., Kocovsky, P., J. Org. Chem., 74 (2009), 5839 - 5849
[2] Malkov, A. V., Figlus M., Kocovsky, P., J. Org. Chem., 73 (2008), 3985 - 3995
[3] Kresge, C. T., Leonowicz, M. E., Roth, W. J., Vartuli, J. C., Beck, J. S., Nature, 359 (1992), 710

Novel basic catalysts based on porous coordination polymers with MIL-101 structure

Martin Hartmann, Marcus Fischer

Erlangen Catalysis Resource Center, Friedrich-Alexander-Universität Erlangen-Nürnberg, Egerlandstr. 3, 91058 Erlangen, Germany, Martin.Hartmann@ecrc.uni-erlangen.de

Introduction

Metal-organic framework (MOF) materials have been explored for applications in heterogeneous catalysis in recent years. In addition to the use of MOFs as supports for the deposition of highly dispersed metal particles, the incorporation of active centers such coordinatively unsaturated metal sites and the functionalization of the organic linkers with acidic or basic groups seems to be most promising. In our contribution, different MOFs carrying amino groups at their organic linkers [1,2] were synthesized and tested in the Knoevenagel condensation, a convenient test reaction for evaluation of the catalytic activity of basic materials.

Experimental Section

Fe-MIL-101-NH_2 and Al-MIL-101-NH_2 were synthesized from 2-aminoterephthalic acid and $FeCl_3 \cdot 6\ H_2O$ or $AlCl_3 \cdot 6\ H_2O$, respectively, in DMF at 110 °C. For comparison, CAU-1 was synthesized under solvothermal conditions from 2-aminoterephthalic acid and $AlCl_3 \cdot 6\ H_2O$ in methanol at 125 °C as reported by Stock et al. [2]. The obtained materials were activated by soxhlet extraction with Ethanol and characterized by powder X-ray diffraction, nitrogen adsorption at 77 K (Figure 1), NMR and FT-IR spectroscopy (Figure 2). The catalytic tests were carried out in batch reactors employing toluene as solvent under inert atmosphere. At regular intervals small aliquots were withdrawn and analyzed by gas chromatography.

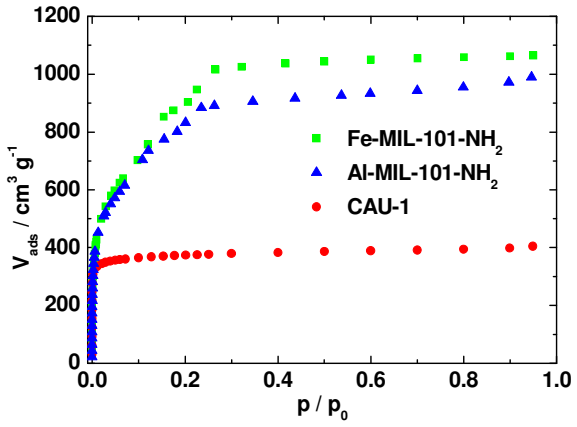

Figure 1: N_2-adsorption isotherms of the three MOFs employed in this study.

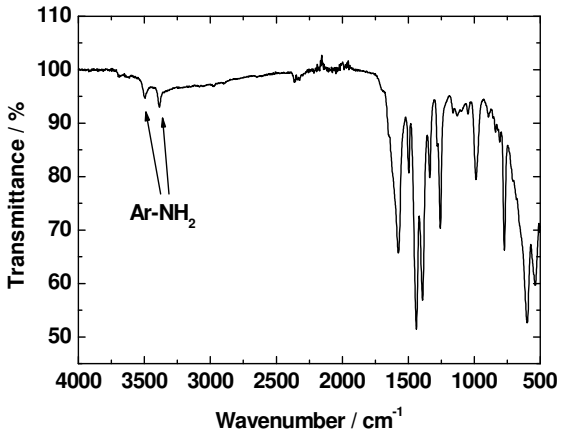

Figure 2: FT-IR spectrum of activated Al-MIL-101-NH_2.

Results and Discussion

The three MOFs (Fe-MIL-101-NH_2 (A_{BET} = 3438 m^2g^{-1}), Al-MIL-101-NH_2 (A_{BET} = 3031 m^2g^{-1}) and (CAU-1 [2] (A_{BET} = 1492 m^2g^{-1})) compared in this study are active catalysts in the Knoevenagel condensation of benzaldehyde with malononitrile and with ethyl cyanoacetate yielding benzylidenemalononitrile (BzMN) and ethyl α-cyanocinnamate (EtCC), respectively, as the only detected products. Due to the very small pore windows of CAU-1 (0.3 to 0.4 nm) the Knoevenagel condensation proceeds much slower over this catalyst in comparison to the amino-MIL-101 derivatives, which possess open pore windows of up to 1.6 nm and reach a conversion of more than 90 % within three hours (Figure 3). These different behaviors suggest that pore diffusion of the product or even of the educts is strongly limited or actually impossible in the case of CAU-1 and thus the catalytic transformation primarily takes place at the outer surface of the crystallites. Although the unfunctionalized Fe-MIL-101 also catalyzes the reaction to some extent, the presence of amino groups drastically accelerates the formation of EtCC as shown in figure 4.

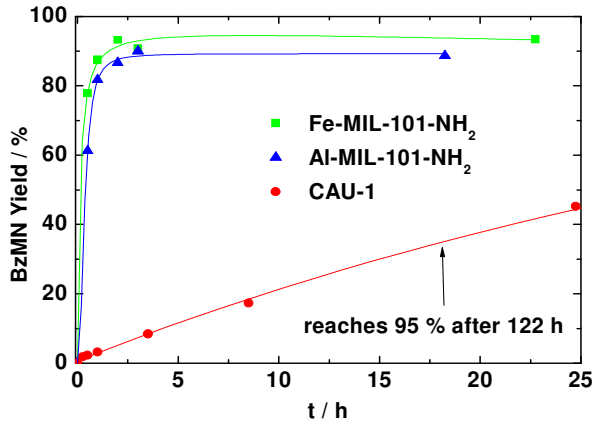

Figure 3: Comparison of the catalytic activity of catalysts with different pore sizes in the Knoevenagel condensation of benzaldehyde with malononitrile.

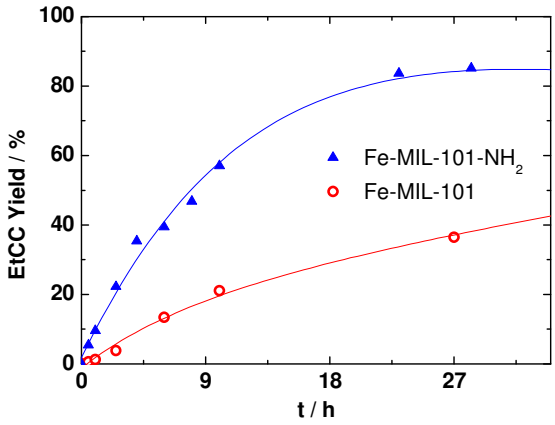

Figure 4: Comparison of the catalytic activity of Fe-MIL-101-NH_2 and Fe-MIL-101 in the Knoevenagel condensation of benzaldehyde with ethyl cyanoacetate.

In additional experiments, we confirmed by removal of the solid catalysts after a conversion of 30 %, that there is no leaching of catalytically active species into the liquid phase. Details of experiments concerning the recyclability of the solid catalysts will be shown in the paper.

References

[1] S. Bauer, C. Serre, T. Devic, P. Horajada, J. Marrot, G. Férey and N. Stock; *Inorg. Chem.*; **2008**; *47 (17)*; 7568-7576.
[2] T. Ahnfeldt, N. Guillou, D. Gunzelmann, I. Margiolaki, T. Loiseau, G. Férey, J. Senker and N. Stock; *Angew. Chem. Int. Ed.*; **2009**; *48 (28)*; 5163-5166.

Chiral periodic mesoporous organosilicas synthesized by a facile one-pot approach.

R. A. García, R. van Grieken, V. Morales, J. A Villajos

Chemical and Environmental Technology Department, Rey Juan Carlos University, Móstoles, Madrid, Spain. victoria.morales@urjc.es

Introduction

Chiral periodic mesoporous organosilicates have been recently developed as a variety of periodic mesoporous oganosiliceous materials (PMOs) [1,2]. Insertion of chirality inside the PMOs constitutes a breakthrough for potential applications mainly as suitable catalysts for the asymmetric synthesis. Hence, the development of novel heterogeneous chiral ligands that could effectively induce asymmetry might be crucial not only in organic synthesis, but it could allow the preparation of new valuable materials for applications in areas such as adsorption, chromatography, optical device, sensors, etc. As best, at least two steps are needed for accomplishing the chiral PMOs. Previously, the organic synthesis of the usually non-commercial chiral bis-organosilane is performed following different reaction steps and further purification, with the subsequent assemblage of the chiral precursor around the templating micelles [3]. This tedious drawback is circumvented by the procedure that we outline herein, in which a new, easy and unprecedented one-pot approach to the synthesis of chiral PMOs SBA-15-like material was accomplished, based on a tartrate derivative chiral precursor and a non-chiral bis-organosilane [4].

Experimental

Once the chiral tartrate derivative employed as chiral precursor, protected L-(+)-dimethyl tartrate (DMT), is mixed with the (N-methyl-3-aminopropyl)-trimethoxysilane under the conditions needed for synthesizing a SBA-15-like framework material, a transamidation reaction takes place, leading to the bis-silylated chiral precursor. Besides, the presence of the silica source employed, tetraethylortosilicate or 1,2-bis(triethoxysilylethane) and the copolymer surfactant Pluronic 123 type triblock copolymer provide the mesoscopic ordering to the final material, following the procedure earlier reported [4]. Therefore, during the in-situ transamidation reaction the hydrolysis of the chiral and non-chiral bis-organosilane silica precursors and the condensation of these latter species around the micelles coming from the structure-directing agent are readily accomplished leading to a chiral PMO material.

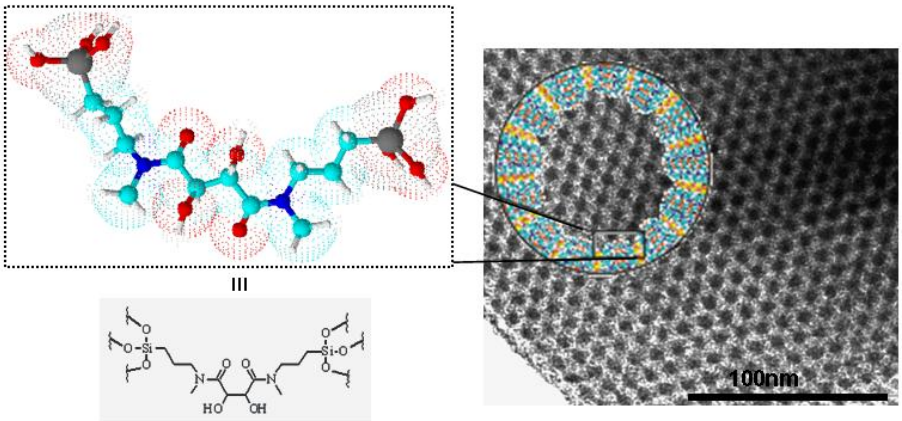

Figure 1. TEM image of chiral PMO SBA-15 type material synthesized by a one-pot approach.

Results and discussion

The synthesis of chiral PMO SBA-15 type materials with different silica sources by an easy one-pot methodology has been studied. Furthermore these chiral periodic mesoporous solid materials with an incorporation as high as 50% molar of dimethyl tartrate derivative chiral auxiliary precursor (Sharpless ligand) have been synthesized, without any sensitive decline of the textural properties referred to the materials ordering. Likewise FTIR and NMR solid state techniques (Figure 2) confirm the chiral ligands coordination environments in the three dimensional structure of the mesoporous material prepared. Knowledge of the detailed molecular architecture, including surfactant interactions and the surfactant's spatial distribution within the framework, enable the rational design and synthesis of novel chiral PMO materials with the desirable and tunable properties.

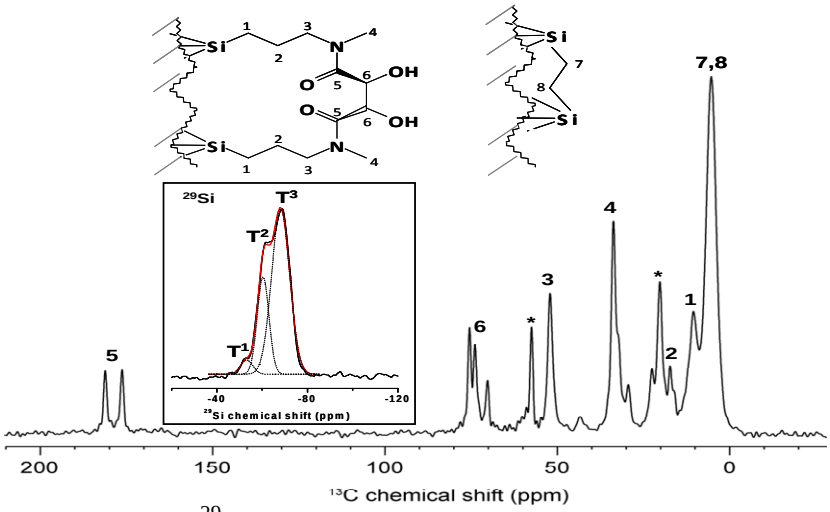

Figure 2. ^{13}C CP-MAS and ^{29}Si CP-MAS solid state NMR spectrum of the chiral PMO sample with a ratio BTSE: DMT 50:50.

The thioanisole asymmetric oxidation reaction has been used to validate and compared the heterogeneously synthesized catalysts activity, achieving enantiomeric excess (ee) and yield to sulfoxide up to 40 and 75%, respectively, being significative the influence of the organosilica framework nature on the catalytic behaviour. Key to the widespread application of the one step approach enclosed in this work is the various chiral auxiliaries that could be immobilized following this methodology and, more importantly, its simplicity, because the quiral bis-silane formation, the incorporation of the chiral functional moieties and the formation of the mesoporous material occur in a single synthetic step. This approach would mean a higher overall throughput than the more tedious procedures previously reported, in which the organic chiral precursor has to previously prepared, separated and purified and subsequently added in a second-step to the inorganic support synthesis media.

Acknowledgements

The financial support of the Spanish government (CTQ2008-05909/PPQ) is gratefully acknowledged.

References

[1] T. Asefa, M.J. MacLachlan, N. Coombs, G. A. Ozin, Nature.1999, 402, 867.
[2] C. Baleizao, B. Gigante, D. Das, M. Álvaro, H. Garcia, A. Corma, Chem. Commun, 2003, 1860.
[3] R.A. García, R. Van Grieken, J. Iglesias, V. Morales, D. Gordillo, Chem. Mater. 2008, 20, 2964.
[4] R.A. García, R. Van Grieken, J. Iglesias, V. Morales, N. Villajos. J. Catal. 2010, 274, 221.

Catalytic activity of Co_3O_4 nanoparticles supported on aluminosilicate materials

A. Pineda, A. M. Balu, J. M. Campelo, D. Luna, R. Luque, J. M. Marinas, A. A. Romero
Departamento de Química Orgánica, Universidad de Córdoba, Campus de Rabanales, Edificio Marie Curie (C-3), Ctra Nnal IV, Km 396, E-14014 Córdoba, Spain,
e-mail: q62alsor@uco.es

Introduction

Transition metal nanoparticles (TMNPs) have recently attracted a great deal of interest in our aim to develop readily available and cheaper as well as more efficient catalysts as alternatives to the traditional widely employed noble metal catalysts in a wide range of catalytic reactions [1]. Their stabilisation onto supports via alternative methodologies including microwave irradiation (MWI), ultrasounds (US) and ball-milling (BM) are some of the most appealing approaches for NPs control and stabilisation to the design of well dispersed, small size nanomaterials with enhanced catalytic applications [2]. Cobalt oxide nanoparticles have been used in selective oxidation processes including CO and VOCs oxidation. Herein, we report the preparation of supported cobalt oxide nanoparticles on Al-SBA-15 and their application in the microwave-assisted selective oxidation of benzyl alcohol to benzaldehyde using hydrogen peroxide as green oxidant.

Experimental

Al-SBA-15 (Si/Al 20 ratio) were prepared according with a previously reported method by Bonardet et al. [3] using Pluronics P_{123} as template. Materials with a 0.5 wt.% Co loading were subsequently prepared by three different methods, namely wet impregnation (CoAlWI) and microwave irradiation (CoAlMW, followed a previously reported protocol by our group [4]) as well as a novel ball-milling approach (CoAlBM) in which the support and the cobalt precursor [$Co(NO_3)_3$] were grinded together in a chamber using 10 mm stainless steel balls for 10 minutes at 500 rpm. All prepared materials were calcined at 773 K during 4 hours. Samples were characterized using techniques including X-Ray diffraction (XRD), Nitrogen physisorption, Elemental Analysis, X-Ray Photoelectron Spectroscopy (XPS) and UV-vis.

Results and discussion

Figure 1 depicts the structure of the supported cobalt nanoparticles on Al-SBA-15. According to the diffraction lines in the materials, the structure could be indexed to the JCPDS 9-418 card, corresponding to the Co_3O_4 phase. Table 1 shows the conversion obtained in short time

of reaction for all the materials are very similar, in the range of 40-45%, with high selectivities to benzylaldehyde.

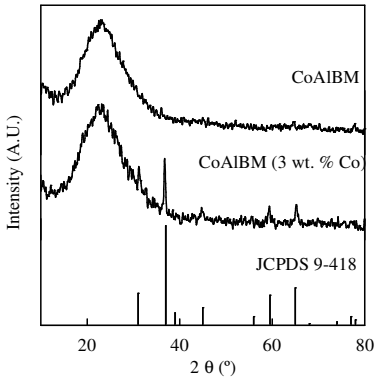

Figure 1 XRD patterns of CoAlBM y CoAlBM (3 wt.%), showing the presence of Co_3O_4 according to the JCPDS 9-418 card.

Table 1. Activities and selectivities to benzaldehyde of cobalt nanoparticles supported on Al-SBA-15 in the microwave assited oxidation of benzyl alcohol to benzaldehide with hydrogen peroxide as green oxidant[a].

Materials	Substrate	Product	Conversion (mol%)	$S_{benzaldehyde}$ (mol%)
Al-SBA-15	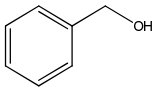	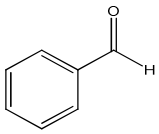	16	> 99
CoAlBM			42.5	97
CoAlMW			38	89
CoAlWI			41.4	> 99

[a] Reaction conditions: 0.05 g catalyst, 2 mmol benzyl alcohol, 0.3 mL H_2O_2 50% (v/v), 2 mL acetonitrile, microwave irradiation, 300W, reaction time, 5 minutes.

Conclusions

Cobalt nanoparticles supported on Al-SBA-15 have been synthesized by three different methods. Catalytic activities of the ball-milling synthesized material in the microwave-assisted oxidation of benzyl alcohol to benzaldehyde were comparable to those obtained by the others two well established methods, which offers an interesting, simple and efficient alternative to conventional methods for the preparation of supported nanoparticles.

Acknowledgements

The authors greatly acknowledge funds from Ministerio de Ciencia e Innovación (Projects CTQ2010-18126, CTQ2008-01330, AT2009-0031) and Consejería de Educación y Ciencia de la Junta de Andalucia (FQM-191 and P07-FQM-02695), cofinanced with FEDER funds.

References

[1] Astruc, D., Transition-metal nanoparticles in catalysis: from historical background to state in the art, Nanoparticles and catalysis, Ed. D. Astruc, 2008, Wiley-VCH, Weinheim, Germany, 1-48.
[2] Campelo, J.M., Luna, D., Luque, R., Marinas, J.M., Romero, A.A., *ChemSusChem.*, 2 (2009), 17-34.
[3] Jarry, B., Launay, F., Nogier, J.P., Montouilluot, V., Gengembre, L., Bonardet, J.L., Appl. Catal. A, 309 (2006), 177-186.
[4] Balu, A.M., Pineda, A., Yoshida, K., Campelo, J.M., Gai, P.L., Luque, R., Romero, A.A., Chem. Commun., 46 (2010), 7825-7827.

Activity of Zr-SBA-15 materials in the Friedel-Crafts acylation of anisole with benzoyl chloride

M. D. Gracia, E. Losada, J. M. Campelo, D. Luna, R. Luque, J. M. Marinas, A. A. Romero

Departamento de Química Orgánica, Universidad de Córdoba, Campus de Rabanales, Edificio Marie Curie (C-3), Ctra Nnal IV$_a$, Km 396, E-14014 Córdoba, Spain.
Email-qo1capej@uco.es

Introduction

Friedel-Crafts acylation of aromatic compounds is one of the most important methods for the production of aromatic ketones, which are key intermediates in the production of fine chemicals, pharmaceuticals and agrochemicals [1, 2]. Acylation of aromatics have traditionally been performed using homogeneous mineral acids including $AlCl_3$, $FeCl_3$, $ZnCl_2$ and HF. Such conventional catalysts have inherent problems such as corrosivity, toxicity and effluent disposal. Hence, the homogeneous catalytic process needs to be replaced by a more effective, heterogeneous catalytic method from the view point of environmental friendliness, ease of separation of products and ease of regeneration of catalyst.

Herein, we report the direct preparation of Zr-SBA-15 materials via sol-gel hydrothermal synthesis and their activity in the acylation of anisole with benzoyl chloride.

Experimental

Materials were synthesized following a previously reported protocol by our group [3] using $ZrONO_3$ .x H_2O as Zr precursor. Samples were denoted as Zr-X where X stands for the Si/Zr ratio in the synthesis gel (e.g. Si/Zr 40, 20, 10 and 5). Well structured Zr-SBA-15 materials with high surface areas and narrow pore size distributions were obtained. Materials were characterized by pyridine (PY) and 2,6-dimethyl pyridine (DMPY) adsorption, X-Ray Diffraction (XRD), Transmission Electron Microscopy (TEM), Thermal Analysis (TG/DTA), Diffuse Reflectance Infrared Fourier Transform Spectroscopy (DRIFTS), and N_2 adsorption.

The activity of the solid acids was also investigated in the Friedel-Crafts acylation of anisole with benzoyl chloride. Reactions were carried out under microwave irradiation and compared to those under conventional heating.

Results and discussion

Results obtained in the liquid-phase acylation of anisole with benzoyl chloride under conventional heating are summarised in Table 1. Selectivities were, in all the cases, almost quantitative (>93%) to the formation of p-methoxidiphenilmethanone (F4) [the difference to 100 % corresponds to o-methoxidiphenilmethanone (F2)]. All materials exhibited good activities in the reaction after 24 h under conventional heating, with the exception of Zr-40. The catalytic activity in the materials was found to increase with an increase in the zirconium content. In addition, the catalytic activity increase for Zr-10 and Zr-5 was related with the increase of the density of acid sites. The catalysts were also found to be relatively reusable under the investigated reaction conditions upon regeneration (1 h in air, 600ºC).

Table 1. Time of reaction, total conversion (X_T,), selectivity (S_{F4}) and surface acidity, measured by PY and DMPY titration (μmol probe molecule per g of catalyst and μmol probe molecule per m^2 at 300ºC) of Zr-SBA-15 in the acylation of anisole with benzoyl chloride under conventional heating (140ºC, 10 mL anisole, 1 mL benzoyl chloride, 0.1 g catalyst).

Catalyst	Time (h)	X_T (mol%)	S_{F4} (mol%)	PY (μmol g^{-1})	PY (μmol m^{-2})	DMPY (μmol g^{-1})	DMPY (μmol m^{-2})
Zr-40	24	45.3	93.7	82	0.09	26	0.03
Zr-20	24	60.7	93.0	128	0.15	65	0.08
Zr-10	24	76.2	94.1	146	0.19	76	0.10
Zr-5	24	80.5	93.0	66	0.11	62	0.10
ZrO_2	24	3.4	96.0	20	0.20	-	-

Reactions were also conducted under microwave irradiation where the effect of parameters including time of reaction, microwave power and quantity of catalyst were investigated. Optimised reaction conditions (2.5 mL anisole, 0.25 mL benzoyl chloride, 300W, 0.075 g catalyst-3 times more as compared to conventional heating-) provided comparable and even superior conversion values to those achieved under conventional heating after 24 h (Table 2). Zr-5 was also found to be the most active material with conversion values over 96% in 30 minutes.

Table 2. Total conversion (X_T) and selectivity (S_{F4}) of the Zr-SBA-15 materials in the acylation of anisole with benzoyl chloride under microwave irradiation (300 W, 30 min, 2.5 mL anisole, 0.25 mL benzoyl chloride, 0.075g catalyst).

Catalysts	X_T (mol%)	S_{F4} (mol%)	$T_{máx}$ (ºC)
Zr-40	35.3	91.3	150
Zr-20	68.8	92.7	157
Zr-10	90.9	92.6	159
Zr-5	96.4	93.2	152
ZrO_2	7.1	94.8	155

Conclusions

Zr-SBA-15 materials were found to be active, selective and reusable in the Friedel-Crafts acylation of anisole with benzoyl chloride. Zr-5 was also found to be the most active material in the investigated reaction both under conventional heating and microwave irradiation conditions.

Acknowledgements

The authors greatly acknowledge funds from Ministerio de Ciencia e Innovación (Projects CTQ2008-01330/BQU and CTQ2010-18126) and Junta de Andalucía (FQM-191 and P09-FQM-4781), cofinanced with FEDER funds.

References

[1] Bond, G., Gardner, J.A., Mccabe, R.W., Shorrock, D.J., J. Mol. Catal. A Chem., 278(2007), 1.
[2] Kantam, M.L., Ranganath, K.V.S., Sateesh, M., Kumar, K.B.S., Choudary, B.M., J. Mol. Catal. A Chem. 225 (2005), 15.
[3] Gracia, M. J., Losada, E., Luque, R., Campelo, J. M., Luna, D., Marinas, J. M., Romero, A.A., Appl. Catal. A 349 (2008), 148.

Friedel-Crafts alkylation of anisole with benzyl alcohol. Microporous vs mesoporous materials.

E. Losada, M. D. Gracia, J. M. Campelo, D. Luna, R. Luque, J. M. Marinas, A. A. Romero

Departamento de Química Orgánica, Universidad de Córdoba, Campus de Rabanales, Edificio Marie Curie (C-3), Ctra Nnal IV$_a$, Km 396, E-14014 Córdoba, Spain.
Email-qo1capej@uco.es

Introduction

Friedel-Crafts alkylations are important types of reactions in organic chemistry [1]. The liquid phase benzylation of aromatic compounds by benzyl alcohol is of significance for the production of diphenylmethane and substituted diphenylmethanes, which are key industrial compounds used as pharmaceutical intermediates and fine chemicals. Zeolites (including H-ZSM-5 and H-Y) are solid acid catalysts which have received a great deal of attention due to their strong acidity and regular porous structure with excellent stability [2]. Recently, ordered mesoporous silica materials such as MCM-41 and SBA-15 were comparatively proved to be of considerable interest because of their regular pore array with uniform and tunable mesopore diameter (2.0–3.0 nm) as compared to zeolites as well as high surface area and pore volume. In this work, the surface properties and catalytic activities of micro- and mesoporous materials have been compared in the alkylation of anisole with benzyl alcohol.

Experimental

Friedel-Crafts alkylations were performed under conventional heating in a multipoint reactor (Carrousel Reaction Station^{TM}, Radleys Discovery Technologies) at 140ºC for 24 h. Samples were periodically withdrawn from the reaction mixture and reaction products were separated and analyzed by gas chromatography (GC). Al- and Ga-SBA-15 materials employed in this study (Ga-20-A and Al-20-A, with a Si/Ga or Si/Al ratio of 20) were previously reported by our group [3]. A conventional Al-MCM-41 material with Si/Al 20 ratio and a range of zeolites (ZSM-5, MOR, BEA and HY) with different SiO_2/Al_2O_3 ratios (included in brackets in Tables 1 and 2) were also characterised and tested in the alkylation reaction.

Results and discussion

Textural and acid properties of the investigated micro- and mesoporous materials are summarised in Table 1. Materials exhibited high surface areas and typical pore diameters of zeolites and mesoporous MCM-41 and SBA-15. The activity of the materials was then investigated in the alkylation of anisole with benzyl alcohol (Table 2). Al-20-A exhibited quantitative conversion of starting material with complete selectivity to monoalkylated products (2-methoxybenzophenone and 4-methoxybenzophenone) after 30 min reaction. Comparatively, mesoporous Al-MCM-41 and Al-SBA-15 gave high conversions at 30 min of reaction (Table 3) probably due to their comparatively high Brönsted acidities. Interestingly, highly acidic zeolites provided different activities depending on acid distribution and pore sizes. Small to medium pore size zeolites (H-ZSM-5) exhibited poor activities in the

alkylation at short reaction times, while larger pore zeolites (H-BEA Si/Al 75 and zeolite-Y Si/Al 60) gave excellent conversions after 30 minutes of reaction (Table 2).

Table 1. Textural properties and surface acidity [measured by pyridine (PY) and 2,6-dimethyl pyridine (DMPY) titration (μmol probe molecule per g of catalyst at 300ºC)] of a range of micro- and mesoporous materials.

Materials (SiO_2/Al_2O_3 ratios)	Pore structure	S_{BET} (m^2/g^{-1})	D_{BJH} (nm)	PY, 300ºC (μmol g^{-1})	DMPY, 300ºC (μmol g^{-1})
H-Y (60)	3D; 7.4 Å	720	0.7	49	27
H-BEA (75)	3D; 7.5x5.7 Å	680	0.8	158	84
ZSM-5 (50)	3D; 5.4x5.6 Å	425	0.6	203	41
H-MOR (5)	1D; 7.4 Å	562	0.5	61	35
Ga-20-A	-	902	4.9	127	28
Al-20-A	-	900	6.7	171	98
Al-MCM-41 (Si/Al 20)	-	943	2.5	124	65

Table 2. Activities [total conversion (Xt, mol%)] and selectivities to 2--methoxybenzophenone (S_{F2}, mol%) of different acidic micro- and mesoporous materials in the liquid-phase alkylation of anisole with benzyl alcohol.

Materials	0.5 h		6 h	
	X_t (mol%)	S_{F2} (mol%)[a]	X_t (mol%)	S_{F2} (mol%)[a]
H-Y (60)	87	51.1	96.1	54.9
H-BEA (75)	53.5	47.4	85	52.4
ZSM-5 (50)	5.6	48.7	20	51.8
H-MOR (5)	49.9	54.1	97.9	53.8
Ga-20-A	20.6	54.6	81.7	53.1
Al-20-A	82.8	54.3	100	52.9
Al-MCM-41 (Si/Al 20)	82.8	54.5	100	53.3

[a]The difference to 100 corresponds to 4-methoxybenzophenone

Conclusions

Mesoporous Al-SBA-15 and Al-MCM-41, with a higher contribution of Brönsted acid sites, were highly active and selective to monoalkylated products (2- and 4-methoxybenzophenone). Comparably, small to large pore zeolites exhibited high activities in the alkylation at short reaction times, except for H-ZSM-5 (50). The interesting difference in activity between the materials could be correlated with the different pore sizes and acidities of the materials.

Acknowledgments

The authors greatly acknowledge funds from Ministerio de Ciencia e Innovación (Projects CTQ2008-01330/BQU and CTQ2010-18126) and Junta de Andalucía (FQM-191 and P09-FQM-4781), cofinanced with FEDER funds.

References

[1] G.A. Olah, Friedel-Crafts Chemistry, Wiley, New York, 1973.
[2] Ch. Baerlocher, L.B. McCusker, D.H. Olson, in: Atlas of Zeolite Structure Types, sixth ed., Elsevier, 2007. ‹www.iza-online.org›.
[3] Gracia, M. J., Losada, E., Luque, R., Campelo, J. M., Luna, D., Marinas, J. M., Romero, A.A., Appl. Catal. A 349 (2008), 148.

Selectivity in Sorption and Hydrogenation of FAMEs and Triglycerides on MFI Zeolites.

An Philippaerts[1], Sabine Paulussen[1], Stuart Turner[2], Gustaaf Van Tendeloo[2], Pierre Jacobs[1], Bert Sels[1*]
[1]*Center of Surface Chemistry and Catalysis, K.U. Leuven, Heverlee, Belgium*
[2]*EMAT, University of Antwerp, Antwerpen, Belgium*
[*]*bert.sels@biw.kuleuven.be*

Introduction

Catalytic hydrogenation of vegetable oils is a well-known process in food industry to make the oil more resistant against air autoxidation and/or to obtain fats with a certain melting profile[1]. Unfortunately, hydrogenated edible oils have negative health impact, due to the *cis/trans* isomerization of the double bond, occurring in parallel with hydrogenation[2].
One aim of the present research is to investigate the fundamental basis for selective removal of *trans*-isomers from a hydrogenated oil sample via sorptive and size exclusion phenomena. It is known that zeolites act as molecular sieves, excluding the access of molecules with a diameter too large to enter the pores. The idea is to find a zeolite with a pore structure that is able to distinguish the linear *trans* chain from the bended *cis* chain. Next, the zeolites were loaded with Pt and tested in the selective hydrogenation of a mixture of methyl oleate (*cis* isomer) and methyl elaidate (*trans* isomer) (Fig. 1). Finally, the concepts found in the hydrogenation of FAMEs were extrapolated to the level of triglycerides.

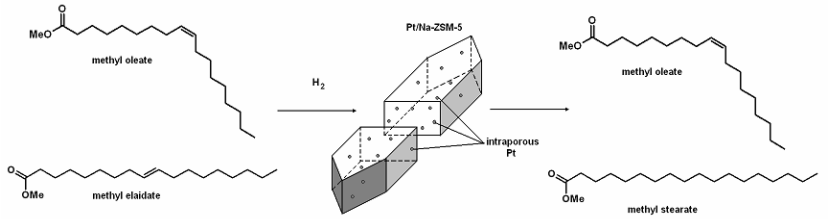

Figure 1. Selective removal of *trans*-fatty acid isomer in presence of the *cis* isomer by shape selective hydrogenation over Pt on ZSM-5 zeolite.

Experimental

Zeolites were purchased from Zeolyst or synthesized according to a published procedure[3]. Pt was introduced in the different supports via three different techniques, *viz.* incipient wetness impregnation (IWI), ion-exchange (IE) and competitive ion-exchange (CIE). Pt loaded catalysts are activated by a successive calcination and reduction, under flowing O_2 and H_2, respectively. Catalyst samples were characterized by SEM, TEM, electron tomography, XPS, XRD, CO-chemisorption and UV-vis. Room temperature chromatographic adsorption experiments were conducted in the HPLC mode. Hydrogenation of equimolecular mixtures of methyl oleate (MO) and methyl elaidate (ME) as well as pure triglycerides (OOO, EEE, SOO, LLL, LnLnLn) and vegetable oils were carried out in batch autoclaves at 65 °C, 60 bar H_2 and 500 rpm. The FAMEs were analyzed with GC, whereas triglycerides were analyzed with RP-HPLC.

Results and discussion

Different zeolite topologies were tested in order to find a pore system that is able to distinguish between the linear *trans* chain and the bended *cis* chain. ZSM-5 zeolite (MFI topology) appears the best choice: the quasi-linear *trans* isomer is sorbed more preferably. This preference was further investigated in relation to various compositional parameters, the

Si/Al ratio of the zeolite matrix being the most important one. Loading the ZSM-5 zeolite with Pt clusters within the crystal matrix allows the selective hydrogenation of the *trans*-isomer, while leaving the *cis*-isomer almost unreacted. Obviously, the location of Pt is very critical. Only the Pt particles in the zeolite matrix will selectively hydrogenate the *trans* isomer[4]. Various synthesis procedures with varying compositions and heat pretreatment were investigated to locate Pt well dispersed within the zeolite matrix, as will be demonstrated with scanning and transmission electron microscopic images (with tomography). Besides the position of the Pt clusters, the zeolite particle size is another important parameter to selectively hydrogenate the *trans*-FAME isomer.

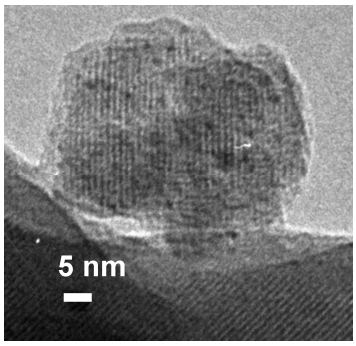

Figure 2. HR-TEM image of 0.5 wt% Pt/ZSM-5 containing small Pt nanoclusters.

Next, some of the Pt/ZSM-5 catalysts were tested in the hydrogenation of pure triglycerides and vegetable oils. Also in the hydrogenation of model triglycerides a preference of *trans* over *cis* hydrogenation is observed. Moreover, the chain on the central position of the glycerol backbone is preferably reduced, and points to pore mouth adsorption in *tuning fork* conformation[5]. The catalytic data show that some shape-selective Pt/ZSM-5 catalysts are capable of hydrogenating common soybean oils into stable (devoid of C18:3), essentially *trans*-free, fats with extraordinary plasticity, very useful for high-nutritive bakery shortenings[6].

Conclusions

In this work the concept of shape-selectivity is applied in the hydrogenation of FAMEs and triglycerides. Because of their smaller diameter, *trans* isomers are faster hydrogenated than *cis* isomers[4]. Moreover a second type of shape-selectivity was found in the hydrogenation of triglycerides: because of the regioselective property of Pt/ZSM-5, central unsaturated fatty acids are hydrogenated faster, resulting in an enrichment of intermediately reduced triglycerides[5]. The melting characteristics of this unique fat composition perfectly match those of commercial bakery shortenings, however, with the important advantage of having only traces of *trans* fatty acids[6].

Acknowledgements

A.P. acknowledges the F.WO.-Vlaanderen (Research Foundation – Flanders) for a doctoral fellowhip. The authors acknowledge the Flemisch government for a long term sponsoring (Methusalem, CASAS). We are grateful to BELSPO for an IAP-PAI network

References

[1] H.B.W. Patterson in "Hydrogenation of Fats and Oils: Theory and Practice, AOCS press, 1994
[2] Mozaffarian, D., Katan, M., Ascherio, A., Stampfer, M., Willett, W. *N. Engl. J. Med.* (2006) 354, 1601
[3] Sano, T., Wakabayashi, S., Oumi, Y., Uozumi, T., *Micropor. Mesopor. Mater.* (2001) 46, 67
[4] Philippaerts, A., Paulussen, S., Turner, O.I., Van Tendeloo, G., Poelman, H., Bulut, M., De Clippel, F., Smeets, P., Sels, B. Jacobs, P., *J. Catal.* (2010) 270, 172
[5] Philippaerts, A., Paulussen, S., Breesch, A., Turner, S., Lebedev, O.I., Van Tendeloo, G., Sels, B., Jacobs, P., Angew. Chem. Int. Ed. (2011), accepted
[6] Philippaerts, A., Breesch, A., De Cremer, G., Kayaert, P., Hofkens, J., Van den Mooter, G., Jacobs, P., Sels, B. (submitted).

Heterogeneously Catalyzed Epoxidation of Unsaturated Fatty Acid Methyl Esters with Hydrogen Peroxide

N. Wilde [a], *C. Worch* [a], *W. Suprun* [a], *R. Gläser* [a]

nicole.wilde@uni-leipzig.de

[a] *Institute of Chemical Technology, Universität Leipzig, 04103 Leipzig, Germany*

Introduction

Epoxidized fatty acid esters and their derivatives are attractive renewable feedstocks for a broad range of large-scale industrial syntheses of chemicals and intermediates such as components for plastics or lubricants, cosmetics or pharmaceuticals [1-2]. In view of the principles of green chemistry, homogeneously and heterogeneously catalyzed epoxidations are the preferred alternatives to conventional stoichometric conversions, typically based on peracids as epoxidizing agents. In several recent studies, catalytic epoxidations were reported using organic hydroperoxides, such as *tert*-butyl- or cumene hydroperoxide [3-5]. However, hydrogen peroxide would be an economically and environmentally largely preferred oxidant.
The present work was, thus, devoted to investigating the potential of heterogeneously catalyzed epoxidation of C-18 unsaturated fatty acid methyl ester (FAMEs) with H_2O_2 as the sole oxidant.

Experimental

Supported metal catalysts, e.g., Ti, Mo or W on SiO_2, Al_2O_3 or MCM-41, as well as an industrial titanium silicalite-1 (TS-1) were used for the heterogeneous catalyzed epoxidation of FAME with H_2O_2 in the liquid phase. The metal-containing catalysts as obtained from co-condensation or wet impregnation of the supports were characterized by different physico-chemical methods including XRD, XPS, N_2-sorption, NH_3-TPD and H_2-TPR.
Catalytic tests were carried out batchwise under mild conditions in the liquid phase at ambient pressure (323 K, CH_3CN solvent, molar ratio H_2O_2 : FAME = 5 : 1, catalyst mass = 150 mg).

Results and Discussion

The results show that the catalytic activity and epoxide selectivity strongly depend on the nature of the catalytically active components as well as of the support (Figure 1).

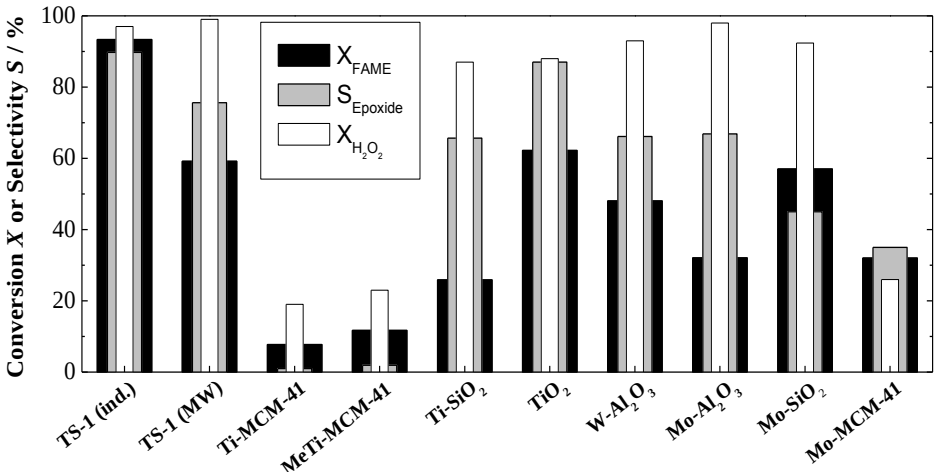

Figure 1: Conversion of methyloleate, H_2O_2 and epoxide selectivity over different catalysts in acetonitrile at 323 K after 24 h.

The most promising results with almost complete FAME conversion and an epoxide selectivity up to 90 % are achieved over the industrial TS-1 catalysts. These results were achieved after optimizing the particle size of the catalyst, the reaction temperature, solvent and molar ratio H_2O_2 : FAME. In particular, acetonitril as a dipolar but aprotic solvent appears to be the most suitable choice (Figure 2). As seen from the H_2O_2 conversion (Figure 1, 2) and in view of the 5-fold acess of H_2O_2 over the reactant FAME, a large part of the H_2O_2 is decomposed without beeing utilized for the epoxitation reaction.
Studies on the catalyst reusability show that the activity is steadily reduced and accompanied by an increase of epoxide selectivity in three consecutive runs (Figure 3). However, calcination of the TS-1 catalyst at 673 K in air completely restores both initial activity and selectivity.

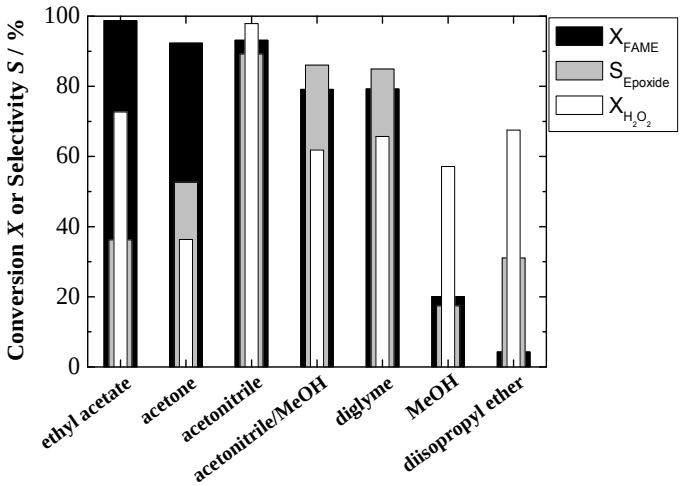

Figure 2: Conversion of methyloleate, H_2O_2 and epoxide selectivity over TS-1 in different solvents at 323 K after 24 h.

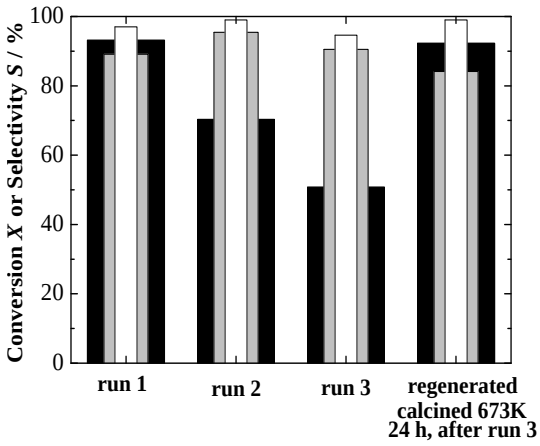

Figure 3: Reusability and regeneration of TS-1 for the epoxidation of methyloleate at 323 K after 24 h.

As shown in Figure 4, TS-1 is an active and selective catalysts even for the epoxidation of rapseed oil methyl ester, i.e., biodiesel. The initial conversion occurs with a only slightly lower rate than with FAME as the reactant, while the epoxide selectivity reached after 24 h is comparable. These results show that the heterogeneously catalyzed epoxidation can be achieved with H_2O_2 as the only oxidizing agent using unsaturated esters derived from renewable raw material without additional purification.

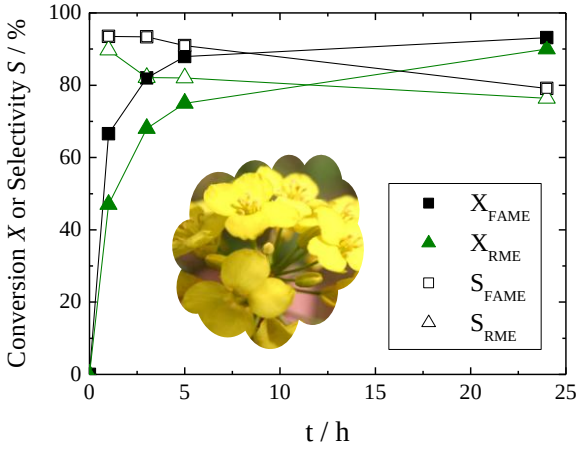

Figure 4: Methyloleate (FAME) and RME conversion and epoxide selectivity over TS-1 at 323 K.

References

[1] M.A. Camblor, A. Corma, P. Esteve, A. Martinez, S. Valencia, Chem. Commun. (1997) 795.
[2] A. Campanella, E. Rustoy, A. Baldessari, M.A. Baltanas, Biores. Technol. 101 (2010) 245.
[3] P.T. Anastas, J.C.Warner, "Green Chemistry- Theory and Practice", Oxford University Press, New York, 1998.
[4] M. Guidotti, N. Ravasio, R. Psaro, E. Gianotti, S. Coluccia, J. Mol. Catal. A: Chem. 250 (2006) 218.
[5] M. Guidotti, R. Psaro, N. Ravasio, M. Sgobba, E. Gianotti, S. Grinberg, Catal. Lett. 122 (2008) 53.

Mesoporous Titania as Catalysts Support for Fine-Chemical Synthesis

N. Linares[a], S. Hartmann[b], A. Galarneau[b], P. Barbaro[a*]

[a] *Istituto di Chimica dei Composti Organo Metallici – Consiglio Nazionale delle Ricerche (ICCOM-CNR), Via Madonna del Piano 10, 50019 Sesto Fiorentino, Italy. E-mail: pierluigi.barbaro@iccom.cnr.it*
[b] *Institut Charles Gerhardt Montpellier, UMR 5253 CNRS/UM2/ENSCM/UM1, ENSCM, 8 rue de l'Ecole Normale, 34296 Montpellier Cedex 5, France.*

Introduction

Highly selective chemical processes are required for the production of fine chemicals. In spite of the higher Turnover Frequencies (TOFs) and enantioselectivities in asymmetric synthesis provided by homogeneous catalysts, industry clearly prefers the heterogeneous ones because of their easier recovery and recycling after use and limited loss and agglomeration of metal [1]. Nowadays a great number of oxide materials have been used as supports for homogeneous single-site catalysts and quasi-homogeneous metal nanoparticles. Among others, titania is a very versatile material with a wide range of different applications including catalysis and photocatalysis. Furthermore, the strong metal-support interaction phenomenon makes this material an excellent choice for the preparation of highly selective hydrogenation catalysts after Pd deposition [2].
Here, we report the synthesis of different mesoporous titania materials and their use as supports for the selective synthesis of fine-chemicals under mild conditions.

Experimental

Highly homogeneous titanate nanotubes (Fig.1c) were prepared by hydrothermal treatment of anatase-TiO_2 powders [3a]. Mesoporous TiO_2 xerogels were synthesized by stirring at 60°C a mixture of $Ti(O_nBut)_4$, ethanol, HCl, aqueous solution of urea. The resulting gel was aged and dried in a Petri dish for 7 days at 25°C, and then treated with water under reflux. Meso-/macroporous TiO_2 monoliths were prepared using a modified Konishi [3b] method. All titania supports were calcined at 350°C under air. Pd nanoparticles (NPs) were prepared by the incipient wetness technique. The impregnation of $Pd(NO_3)_2$ as metal precursor followed by reduction with H_2 at room temperature produce the supported nanoparticles. The catalysts were tested in hydrogenation reactions using pro-chiral substrates such as, methyl benzoylformate (MBF) and methyl 2-acetamidoacrylate (MAA).

Results and discussion

The mesoporous nature of the supports was studied by N_2 sorption isotherms at 77K and TEM (Fig. 1). TiO_2 xerogels feature pore diameter of 7 nm formed by an aggregation of 8 nm nanoparticles, specific surface area of 195 m^2/g, pore volume of 0.27 mL/g. TiO_2 monoliths feature pore diameter of 4.5-6.5 nm, specific surface area of 130-220 m^2/g, pore volume of 0.18 mL/g, and a homogeneous network of macropores adjustable between 0.3 and 3 μm (Fig. 1e). Titanate nanotubes feature internal diameter of 5.4 nm (Fig. 1d) and developed a specific surface

area of 230 m^2/g. For all materials, a slight decrease in surface area and pore size occurs after Pd NPs deposition. XRD patterns of TiO_2 xerogels and monoliths show characteristic peaks of anatase-type crystalline TiO_2 (Fig. 1b), while the nanotubes present peaks of $Na_xH_{2-x}Ti_3O_7$ titanate structures. After Pd NPs deposition, a weak shoulder appears at $2\theta = 40^o$ corresponding to the (111) plane of Pd(0). TEM images of Pd/titanate nanotubes show Pd-NPs with an average size of 3 nm (Fig. 1d). Hydrogenation of MBF and MAA with Pd-NPs (molar ratio catalyst/substrate = 1/250) supported on the titania supports give quantitative conversions at 25°C after 2 h of reaction with bubbling H_2 in aqueous media and negligible leaching of Pd.

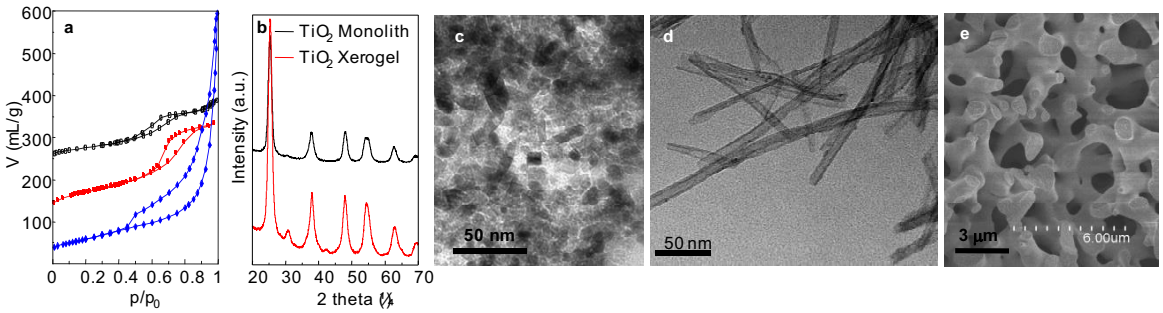

Fig. 1. a) N_2 sorption isotherms of titanate nanotubes (blue), (upset of 100) TiO_2 xerogel (red) and (upset of 200) TiO_2 monolith (black), b) XRD patterns of TiO_2 xerogel (red) and monolith (black), TEM images of (c) TiO_2 xerogel and (d) Pd-titanate nanotubes, e) SEM picture of TiO_2 monolith.

Conclusions

Different Pd-TiO_2 catalysts have been synthesized and tested in hydrogenation reactions in aqueous media. The mesoporous TiO_2 xerogels and monoliths possess an adequate morphology for their use in flow conditions. Further works will be performed to test these catalysts in flow reactions for hydrogenation.

Acknowledgements

The authors thank the European Community's Seventh Framework Programme through the Marie Curie Initial Training Network NANO-HOST, (Grant Agreement no. 215193).

References

[1] P. Barbaro, V. Dal Santo, F. Liguori, *Dalton Trans.*, 39 (2010) 8391-8402.

[2] (a) M.A. Aramendía, J.C. Colmenares, A. Marinas, J.M. Marinas, J.M. Moreno, J.A. Navío and F.J. Urbano, *Catal. Today*, 128 (2007) 235-244. (b) P. Weerachawanasak, P. Prasethdam, M. Arai, J. Panpranot, *J. Mol. Catal. A*, 279 (2008) 133-139.

[3] (a) K-P. Yu, W-Y. Yu, M-C. Kuo, Y-C. Liou, S-H. Chien, *Appl. Catal. B*, 84 (2008) 112-118. (b) J. Konishi, K. Fujita, K. Nakanishi, K. Hirao, K. Morisato, S. Miyazaki, M. Ohira, *J. Chromatogr. A*, 1216 (2009) 7375–7383.

Strained Surface Siloxanes as Source of Synthetically Important Radicals

Antony J. Ward, Rebecca A. Lesic, Viktoria Fabos, Anthony F. Masters and Thomas Maschmeyer*

*Laboratory of Advanced Catalysis for Sustainability, School of Chemistry, The University of Sydney, NSW 2006 Australia, *E-mail: th.maschmeyer@chem.usyd.edu.au*

Introduction

In catalysis, SiO_2 is widely used as an inert support, although it has been shown to catalyse a variety of reactions, some by photolysis.[1] So-called "reactive silica" for catalytic applications can be generated by thermal and chemical treatment of silica.[2-4] A common theme in much of this work has been the intermediacy of "strained siloxane bridges", frequently suggested to be part of a Si_3O_3 ring. There have been few, if any, attempts to examine chemical models of the structures of these defects and surface sites, and to probe their chemical reactivities, and those of SiO_2-supported metal catalysts.

Experimental

Preparation of silsesquioxanes: The cyclohexyl-substituted silsesquioxanes, *a*6*b*0 and *a*7*b*3, were prepared following the procedure outlined by Pescarmona *et al.* [5]

Preparation of PMA in hexane: The selected silica source (0.0400 g) and methyl acrylate (8 mL) were heated under reflux in hexane (30 mL) for 24 h. The reaction mixture was cooled to room temperature and the hexane removed *in vacuo* to afford poly(methyl acrylate) as a highly viscous gel.

Preparation of PMA in sc-CO_2: In a typical example, pre-treated silica (0.0975g) and methyl acrylate (18 mL) were placed in a Parr reactor. The reactor was pressurised with CO_2 (32 bar) and heated in order to achieve $scCO_2$ conditions (76 bar, 210 ºC). After 1 h under sc conditions the reactor was cooled to room temperature and the CO_2 vented. Poly(methyl acrylate) was obtained as a pale yellow, highly tacky polymer.

Results and discussion

The data obtained for the polymerisation of methyl acrylate in $scCO_2$ at 210 ºC are shown in Table 1. After 1 h, when using silica calcined at 600 ºC prior to use (denoted $SiO_{2(600)}$), the poly(methyl acrylate) (PMA) was obtained in 85% yield and possessed a near theoretical PDI of 1.3. When the same silica was exposed to the atmosphere for 3 months prior to use, a yield of PMA was obtained which was only slightly above the baseline yield with a PDI of 5.9 (Entry 3).

Table 1. Polymerisation data of methylacrylate in $scCO_2$ using silica initiators[a]

Entry	Catalyst	Time (h)	Yield (%)[b]	M_n [e]	PDI
1	-	1	22	800	5.1
2	$SiO_{2(600)}$	1	85	12000	1.3
3	$SiO_{2(600)}$[c]	1	35	1700	5.9
4	$SiO_{2(600)}$[d]	1	81	11000	1.5
5	$SiO_{2(300)}$	1	63	10000	4.3
6	$SiO_{2(850)}$	1	59	5400	5.2

[a] Reaction conditions: $scCO_2$ at 76 bar and 210 ºC, [b] Yields were determined by integration of the ^1H NMR spectra of the reaction mixtures. [c] Silica that was calcined at 600 ºC then exposed to the atmosphere at room temperature for 3 months. [d] Silica used in entry 4, but re-calcined at 600 ºC prior to use. [e] Number-average molecular weight.

However, when the same silica was re-calcined at 600 ºC, the originally observed activity was re-established (Entry 4). Investigations into the activity of the silica revealed that silica calcined at 300 ºC or 850 ºC showed significant decreases in yield and polymer quality (Entries 5 and 6). Use of radical traps revealed the polymerisation was free-radical in nature.

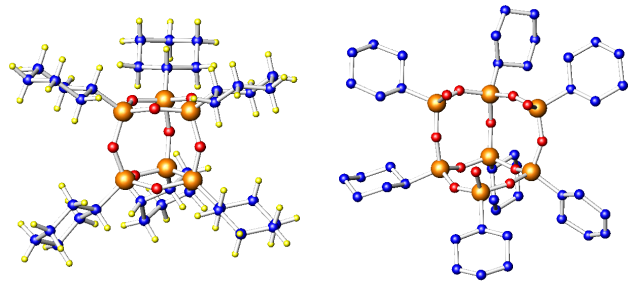

Figure 1. The silsesquioxanes *a6b*0 (left) and *a7b*3 (right).

As a means of probing the reactivity of Si_3O_3 rings, we have studied two cyclohexyl-substituted silsesquioxanes: the fully-condensed *a6b*0, [$(cySi)_6O_9$], which contains Si_3O_3 rings; and, the incompletely condensed *a7b*3, [$(cySi)_7O_9(OH)_3$], which has no Si_3O_3 rings (Fig. 1). When used as initiators for the polymerisation of methyl acrylate (hexane, 70 ºC with similar solvation properties to sc-CO_2) *a6b*0 achieved a 53% yield of PMA with a PDI of 3.9. When the *a7b*3 was used, no polymerisation above the baseline yield was obtained. This result reveals the importance of the strained Si_3O_3 rings for the generation of radicals to initiate the polymerisation reaction.

In order to provide the requisite energy for the reactions of silsesquioxane defect analogues with small molecules, and identify the reaction products, we have examined the reactions of silsesquioxanes with small molecules by Atmospheric Pressure Chemical Ionisation (APCI) and Collision Induced Decomposition (CID) mass spectroscopy. The product distribution obtained from the mass spectrometer induced reaction of *a6b*0 with methyl acrylate is shown in Fig. 2. Under the same conditions no products are observed when *a7b*3 was used. In addition, many other small molecules (such as CH_3OH, $CHCl_3$, CH_2Cl_2, CH_3CN and NH_4^+) have been found to react with both *a6b*0 and *a7b*3 under similar conditions.

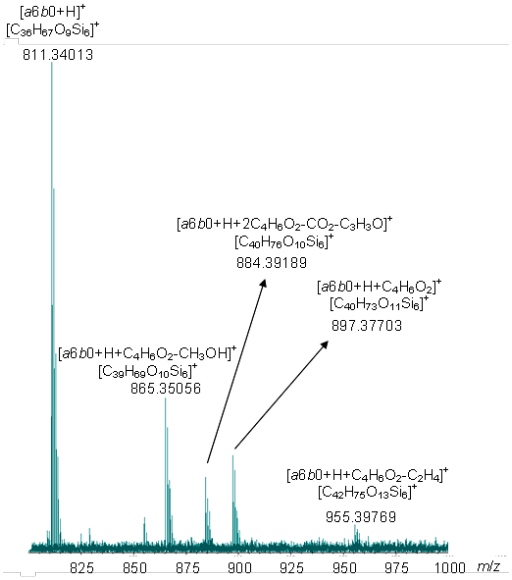

Figure 2. APCI mass spectrum of the reaction of *a6b*0 and methyl acrylate

Conclusions

Silica calcined at 600 ºC has been shown to be an active initiator for the polymerisation of methyl acrylate in scCO_2 and hexane. Examination of the same reaction using silsesquioxanes has revealed the importance of the highly strained Si_3O_3 rings for the generation of radicals to initiate the polymerisation.

References

[1] Y. Inaki, H. Yoshida, K. Kimura, S. Inagaki, Y. Fukushima, T. Hattori, *Phys. Chem. Chem. Phys.* 2 (2000) 5293-5297.

[2] C. Morterra, M.J.D. Low, *Ann. New York Acad. Sci.* 220 (1973) 133-244.

[3] V.A. Radzig, in: G. Pacchioni, L. Skuja, D.L. Griscom (Eds.), *Defects in SiO_2 and Related Dielectrics: Science and Technology*, Kluwer, Dordrecht, 2000, pp. 339-370.

[4] M.J.D. Low, *J. Catal.* 103 (1987) 496-501.

[5] Pescarmona, P.P.; van der Waal, J.C.; Maschmeyer, T. *Eur. J. Inorg. Chem.* (2004) 978-983.

Synthesis of [Al]-SSZ-60 and its catalytic properties in alkylation of biphenyl

H.Naiki,[1] K.Komura,[1] and Y.Sugi*[1,2]
[1] *Department of Materials and Technology, Faculty of Engineering, Gifu University, Gifu 501-1193, Japan. e-mail: ysugi@gifu-u.ac.jp*
[2] *Nagoya Industrial Science Research Institute, Nagoya 464-0819, Japan.*

Introduction

The alkylation of poly nuclear aromatics, such as biphenyl (BP) and naphthalene (NP), is important proves to elucidate the catalytic potential of microporous environment of zeolite. We previously found the steric restriction of the transition states of the products is a key for the shape-selective formation of the least bulky products, such as 4,4'-dialkylbiphenyl (4,4'-DABP) and 2,6-dialkylnaphthalene (2,6-DAN) [1]. Highly selective formation of these isomers occurs by the fitting of the transition state with the channels, where are controlled by size of zeolite channels and alkylating agents. We are interesting in catalytic properties of SSZ-60 with SSY topology was first found by Shevron group, which has one dimensional corrugated channels with 12-MR pore entrances. In this paper, we studied the establishment of synthetic conditions, and applied for the alkylation of BP.

Experimental

Cis- and *trans*-*N*-ethyl-*N*-(3,3,5-trimethylcyclohexyl)pyrrolidine was prepared by the reductive amination of 3,3,5-trimethylcyclohexanone with pyrrolidine over 5% Pd on Charcoal (Kawaken Finechemical, Tokyo, Japan) in the presence of MS-5A at 80 and 150 °C, respectively. *Cis*- and *trans*-*N*-ethyl-*N*-(3,3,5-trimethylcyclohexyl)pyrrolidinium hydroxide (R^+OH) were prepared with ethyl iodide, and converted to hydroxide by DIAION SANUP. The gel with the ratio: SiO_2 (Carb-o-sil M5) 1: NaOH 0.08 : R^+OH 0.2 : NaB_4O_7 : 0.01 : H_2O 42.0 was heated at 160°C with stirring according to the literatures [2].

The isopropylation of BP over SSZ-60 was carried out according to the previous papers, and analyzed by Shimadzu GC-18A equipped with Ultra-1 capillary columns.

Results and discussion

Synthesis of Al-SSZ-60. R^+OH (*cis*/*trans* = 4/96 and 96/4) did not yield SSZ-60 phase even by heating 5 days. However, the heating of gel containing R^+OH (*cis*/*trans* = 53/47) appeared weak SSZ-60 phase, although XRD intensity was weak (Fig. 1). The seeding of the poorly crystallized samples enhanced the crystallinity of [B]-SSZ-60, however, products with the

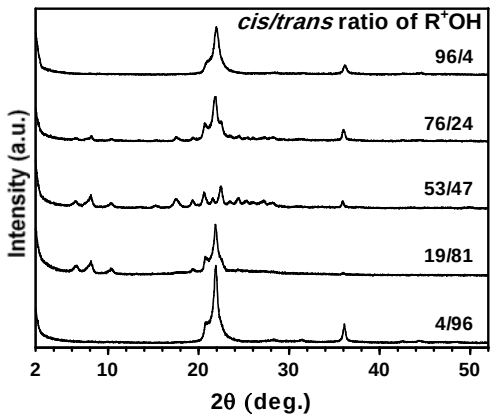

Fig. 1. Effects of *cis*/*trans* ratio of R^+OH on formation of [B]-SSZ-60

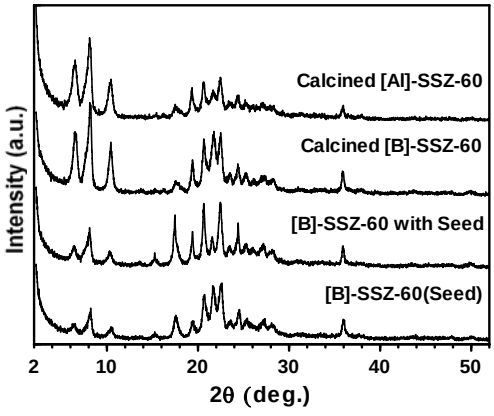

Fig. 2. [B]- and [Al]-SSZ-60 tuned up of the synthesis with seeding

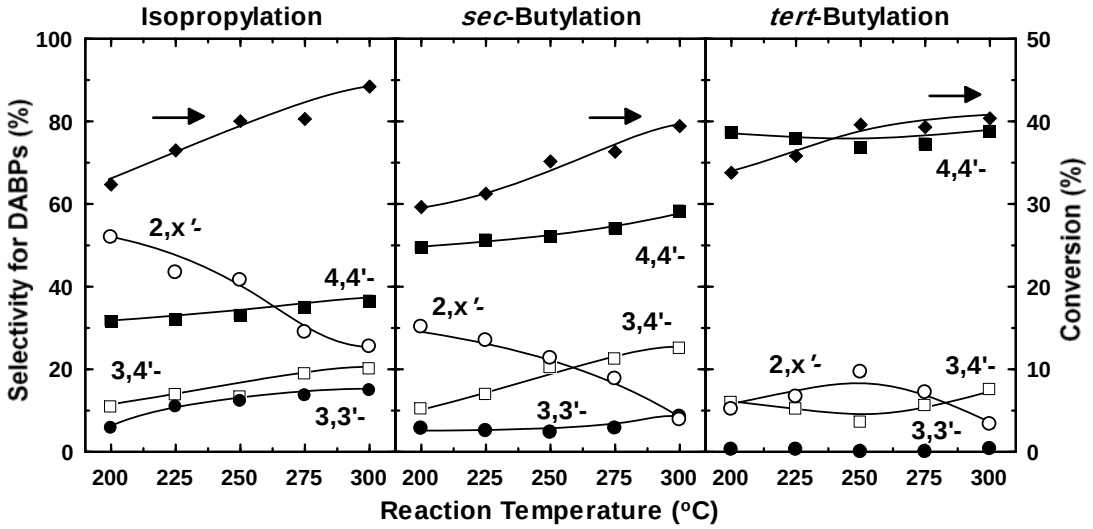

Fig. 3. The effects of the reaction temperature on the alkylation of BP over [Al]-SSZ-60. Reaction conditions: BP, 25 mmol; [Al]-SSZ-60 (SiO_2/Al_2O_3 = 163), 0.135 g; 0.8 MPa propene; 0.4 MPa 1-butene and 2-methylpropene; and period: 4 h.

high intensity could not be obtained (Fig. 2). The final [Al]-SSZ-60 has 62 m^2/g of surface area and 0.09 mL/g of pore volume (0.11 mL/g in the literature [2]). Thus obtained [B]-SSZ-60 was aluminated with aluminum nitrate yielding [Al]-SSZ-60 with SiO_2/Al_2O_3 = 176). Al^{3+} species are tetrahedrally coordinated in the framework from ^{27}Al-NMR spectra.

The alkylation of BP. The selectivity for 4,4'-diisopropylbiphenyl (4,4'-DIPB) was less than 30% in the range of 200-300°C. However, the selectivities for 4,4'-di-*sec*-butylbiphenyl (4,4'-DSBB) and 4,4'-di-*tert*-butylbiphenyl (4,4'-DTBB) were enhanced by the use of bulky alkylating agent: 1-butene and 2-methylpropene: 50-60% in sec-butylation using 1-butene and 70-80% in *tert*-butylation using 2-methylpropene. These levels of the selectivities for 4,4'-dialkylbiphenyl were in the similar level of results over SSZ-53 and SSZ-42 [3]. These results shows the channels of SSZ-60 is too wide for the selective formation of 4,4'-DIPB. SSZ-60 can not prevent the transition states of bulky DIPB isomers by the steric restriction of corrugated channels. However, the bulky alkylating agents increase the size of the transition state, particularly for bulky 2- and 3-substituted isomers, and restrict the formation of bulky products because of the exclusion from the channels. These results indicate that the selectivities of the least bulky isomers are determined by the exclusion of bulky transition states. The fitting of the transition state is essential for the high selectivities.

Conclusion

[Al]-SSZ-60 was synthesized through [B]-SSZ-60 by the use of a 1:1mixture of *cis* and *trans*-*N*-ethyl-*N*-(3,3,5-trimethylcyclohexyl)pyrrolidinium hydroxide (R^+OH) as SDA. The seeding of poorly crystallized samples enhanced the crystallinity of [B]-SSZ-60.

The selectivities for 4,4'-DIPB was 30 – 40% in the isopropylation of BP: the channels are too loose for the selective formation of 4,4'-DIPB. However, alkylation of BP was enhanced by the use of bulky alkylating agent; however, the bulky alkylating agents restrict the formation of bulky products because of the exclusion of bulky 2- and 3-substituted isomers, from the channels. These results indicate that fitting of the transition state is essential for the high selectivities.

References

[1] Y. Sugi, *et a1*., J. Jpn. Petrol. Inst., 53 (2010) 263; J. Chin. Chem. Soc., 57 (2010) 1.
[2] (a) A. Burton, S. Elomari, Chem. Commun., (2004) 2618. (b) S. Emori, EP1419105B1.
[3] Y. Sugi, *et al*., Bull. Chem. Soc. Jpn., 80 (2007) 2232.

Pd nanoparticle-doped mesoporous silicates for the selective aerobic oxidation of allylic alcohols

Chris M. A. Parlett [(a)], Adam F. Lee [(a)(*)], Karen Wilson, [(a)] Steve Wainwright, [(b)] and Duncan W. Bruce [(b)]
(a) School of Chemistry, Cardiff University, Cardiff, CF10 3AT, UK (b) Department of Chemistry, University of York, York, YO10 5DD, UK (*) e-mail: leeaf@cardiff.ac.uk

Introduction

The selective oxidation of allylic alcohols is of interest to the pharmaceutical and fine chemical industries as it can lead to valuable intermediates. Conventional methods using stoichiometric reagents (chromates or permanganates) is undesirable, as large quantities of waste are produced, resulting in low atom efficiency and a high *E*-factor. A "greener" alternative is heterogeneous catalysis. Palladium nanoparticles are known to be active catalysts for the selective oxidation of alcohols [1]. Supporting these on high surface area (350 m^2 g^{-1}) mesoporous alumina significantly increases activity when compared to equivalent low surface area supports [2], which is due to the increasing oxide character of the nanoparticles, a consequence of higher metal dispersions, which is enhanced with decreasing loadings. Here the aim is to investigate whether this trend is observed for several of mesoporous silica supports and one commercial non porous silica support. Mesoporous silicas [3,4] have higher surface areas, up to 700-1000 m^2 g^{-1}, larger pore diameters (up to 30 nm) compared to their alumina counterparts [5] and allow the synthesised of a range of pore networks which could prove to be beneficial.

Experimental

Mesoporous SBA-15/16 and KIT-6 supports were prepared using the methods of Stucky [3] and Ryoo respectively [4]. Commercial non-porous silica (Sigma Aldrich), with an average surface area of 200 m^2 g^{-1}, was used as a benchmark. Pd was deposited via the wet incipient wetness technique from a $[Pd(NH_3)_4](NO_3)_2$ precursor. Impregnated samples were subsequently calcined at 500 °C for 2 h in air prior to reduction at 400 °C for 2 h under flowing hydrogen (10 cm^3min^{-1}). Catalytic activity and selectivity was assessed in the liquid phase selective aerobic oxidation of allylic alcohols at 90 °C in stirred batch reactors.

Results and Discussion

Low angle XRD and TEM (Fig. 1) confirmed the pore networks remained intact following palladium impregnation. Porosimetry indicated a slight decrease in pore volume and surface area for the mesoporous supports, although pore diameter was unaffected. XPS revealed an inverse dependence of oxide content on bulk metal loading for all silicas, with surface oxide favoured over higher surface area and interconnected mesopore supports.

The influence of mass transport limitations was assessed across each support. For mesoporous supports reactant diffusion improved with pore interconnectivity, in the order of KIT-6>SBA-16>SBA-15. Comparing the catalysts under non-mass transfer limited conditions, allowed further insight into the active species. Initial rates, normalised to both surface Pd and surface PdO (Fig. 2), reveal that activity does not simply increase with Pd dispersion, and that Pd metal is not the active site. In contrast, normalising initial rates to surface PdO concentration, reveals oxide as the surface species responsible for selective oxidation. In accordance with

this observation, oxygen addition during reactions enhances the desired pathway by stabilising PdO towards in-situ reduction.

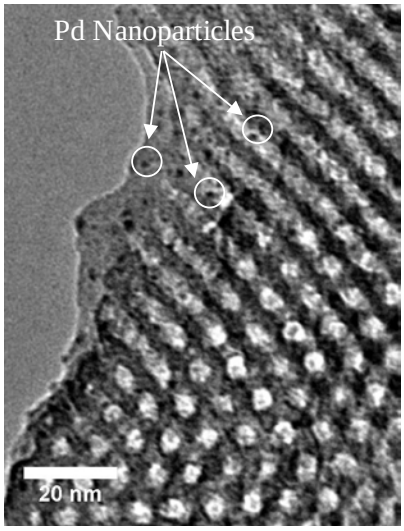

Figure 1 – TEM image of Pd impregnated SBA-15 (Pd nanoparticles less than 2nm circled).

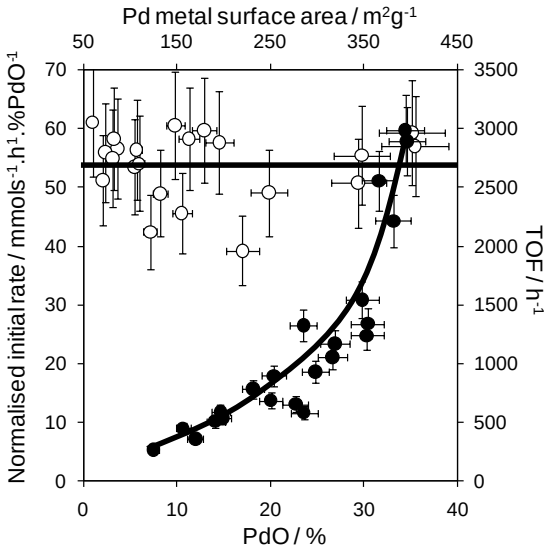

Figure 2 – Catalyst activity normalised to PdO (primary axis) and Pd surface area (secondary axis)

Conclusion

Silica supported Palladium nanoparticles show high activity for the selective oxidation of allylic alcohols. Activity significantly increases with support surface area, mesopore interconnectivity, and *decreasing* metal loading, providing strong evidence that highly oxidised Pd nanoparticles are the active site responsible for allylic alcohol oxidation [2].

Acknowledgements

We thank the ESPRC for studentship support (CMAP) and a Leadership Fellowship (AFL).

References

1. Vinod, C. P., Wilson, K. & Lee, A. F. Recent advances in the heterogeneously catalysed aerobic selective oxidation of alcohols, Journal of Chemical Technology & Biotechnology. 86 (2011), 161-171
2. Hackett, S. F. J., Brydson, R. M., Gass, M. H., Havery, I., Newman, A. D., Wilson, K. & Lee, A. F. High-Activity, Single Site Mesoporous Pd/Al_2O_3 Catalysts for Selective Aerobic Oxidation of Allylic Alcohols, Angewandte Chemie International Edition. 46 (2007), 8593-8596
3. Zhao, D., Huo, Q., Feng, J., Chmelka, B. F. & Stucky, G. D. Nonionic Triblock and Star Diblock Copolymer and Oligomeric Surfactant Syntheses of Highly Ordered, Hydrothermally Stable, Mesoporous Silica Structures, Journal of the American Chemical Society, 120 (1998), 6024-6036
4. Kim, T-W., Kleitz, F., Paul, B. & Ryoo, R. MCM-48-like Large Mesoporous Silicas with Tailored Pore Structure: Facile Synthesis Domain in a Ternary Triblock Copolymer-Butanol-Water System, Journal of the American Chemical Society, 127 (2005), 7601-7610
5. Vaudry, F., Khodabandeh, S. & Davis, M. E. Synthesis of Pure Alumina Mesoporous Materials, Chemistry of Materials, 7 (1996), 1451-1464

MnS-1 as a selective catalyst for the solvent-free oxidation of alkyl aromatics to aromatic ketones with molecular oxygen

S. Cecowski[1], N. Novak Tušar[1], S.C. Laha[2], V. Kaučič[1], Roger Gläser[3]
[1]*Nationa Institute of Chemistry, Hajdrihova 19, 1000 Ljubljana, Slovenia*
[2]*SABIC Research & Technology Pvt. Ltd., Manjusar, Vadodara 391775, Gujarat, India*
[3]*Institute of Chemical Technology, Universität Leipzig, Linnéstr. 3, 04103 Leipzig, Germany*
natasa.novak@ki.si

Introduction

Porous silicates are used as catalytic supports in chemical reactions [1,2]. Incorporation of transition metals into their framework generates catalytically active sites. In recent years, manganese (III)-containing porous catalysts have received considerable attention as catalysts for the selective oxidation of hydrocarbons using molecular oxygen (air) as the oxidant [2,3]. In order to obtain environmentally benign catalyst, this is an important feature together with the mild and solvent-free conditions in the liquid phase. Among the attractive conversions is the selective oxidation of alkyl aromatics in benzylic position to the corresponding aromatic ketones. The synthesis of these ketones via Friedel–Crafts acylation of aromatics or conversion of aromatics with stoichiometric oxidants like $KMnO_4$ leads to the formation of hazardous waste in large amounts. Therefore, the use of solid catalysts which are selective, use molecular oxygen as the terminal oxidant and allow application of solvent-free conditions would provide an environmentally friendly and economically attractive alternative. Here, we report, for the first time, on the successful direct oxidation of alkyl aromatics in benzylic position to the corresponding aromatic ketones by molecular oxygen in the presence of microporous Mn silicalite-1 (MnS-1).

Experimental

Highly crystalline MnS-1 (crystals with 1 μm in size) was prepared by hydrothermal synthesis as described in the literature [4] using tetrapropylammonium hydroxide instead of tetraethylammonium hydroxide as a template. The local environment of Mn was characterized using X-ray absorption spectroscopy (EXAFS - Extended X-Ray Absorption Fine Structure and XANES - X-Ray Absorption Near Edge Structure). The catalytic experiments were carried out in the liquid phase under stirring in a stainless-steel high-pressure batch reactor (HR100, Berghof) equipped with a sampling tube with a sintered metal frit (pores < 0.5 μm) [5]. Liquid samples were collected at different reaction times (1 and 6 h) or, after cooling and depressurizing the reactor. The samples were analyzed by capillary gas chromatography using a flame ionization detector (chromatograph: Agilent 5890 Series II, column: INNOWAX (J&W), 60 m x 0.32 mm x 0.5 μm). Product identification was achieved by authentic samples and by GC-MS.

Results and discussion

Extended X-ray Absorption Fine Structure (EXAFS) analyses of the Mn K edge absorption spectra of MnS-1 revealed manganese cations coordinated to two oxygen atoms at a distance of 1.93 Å and one oxygen atom at a longer distance of 2.15 Å in the first coordination sphere. The short distance of 1.93 Å is consistent with the average tetrahedral Mn^{+3}-O distance of

1.93(4) Å as expected for an isomorphous substitution within the silicate framework. Additionally, in the second coordination sphere at the distance of 3.52 Å a presence of Si atoms is indicated. According to X-Ray Absorption Near Edge Structure (XANES) studies, the average oxidation number of Mn is 2.75±0.05 ($n(Mn^{2+})/n(Mn^{3+}) \cong 25\%/75\%$).

Ethylbenzene, 4-methylethylbenzene and diphenlymethane were converted with very high to excellent selectivity for the corresponding aromatic ketone over the manganese-containing nanoporous silica catalyst MnS-1. With diphenylmethane as the substrate the conversion is much lower probably due to the larger molecular diameter of diphenylmethane. (Table 1).

Table 1. Results of the selective oxidation of alkyl aromatics with molecular oxygen over [Mn]S-1.[a]

Substrate	Catalyst	Conv./%	*TOF*/ h^{-1}	Product selectivity/mol%	
				Ketone	Others[b]
Ethylbenzene	MnS-1	33	106	87	13
4-Methylethylbenzene	MnS-1	54	173	87	13
Diphenylmethane	MnS-1	4	12	100	-

[a] Reaction conditions: n(substrate) = 50 mmol, n(1,4-dichlorobenzene) = 5.0 mmol (0.74 g, internal standard), m(catalyst) = 0.25 g; p_{O_2} = 10 bar; T = 110 °C; t = 6 h. [b] Mixture of 1-(R)ethanol and R-carboxylic acid [R = phenyl and 4-methylphenyl].

Conclusions

In summary, the oxidation of various alkyl aromatics in benzylic position to the corresponding aromatic ketones can be successfully achieved in high selectivity over the microporous Mn-containing silicalite-1 using molecular oxygen as the terminal and single oxidant under mild, solvent-free liquid-phase conditions. The presence of isolated Mn^{3+}-species in a hydrophobic environment on the catalyst surface favours high conversion rates.

Acknowledgements

Funding from the European Commission (NoE INSIDE-POReS, contract no. NMP3-CT-2004-500895) and the Slovenian Research Agency (program P1-0021) and access to synchrotron ELETTRA, Trieste, Italy (research project 2006600) are acknowledged.

References

[1] Corma, A., García, H., Lewis acids as catalysts in oxidation reactions: From homogeneous to heterogeneous systems, Chem. Rev., 102 (2002) 3837-3892.
[1] Novak Tušar, N., Jank, S., Gläser, R., Manganese-Containing Porous Silicates: Synthesis, Structural Properties and Catalytic Applications, ChemCatChem, 3 (2011) 254-269.
[3] Thomas, J.M., Raja, R., Innovations in oxidation catalysis leading to a sustainable society, Catal. Today, 117 (2006) 22-31.
[4] Novak Tušar, N., Zabukovec Logar, N., Arčon, I., Thibault-Starzyk, F., Ristić, A., Rajić, N., Kaučič, V., Manganese-Containing Silica-Based Microporous Molecular Sieve MnS-1: Synthesis and Characterization, Chem. Mater. 15 (2003) 4745-4750.
[5] Laha, S.C., Gläser, R., Characterization and catalytic performance of [Cr]MCM-41 and [Cr]MCM-48 prepared by either classical or microwave heating, Microporous Mesoporous Mater. 99 (2007) 159-166.

Al (III) and Ce (IV) Incorporation into Helical Mesoporous Silica

A.I. Carrillo,[a*] E. Serrano,[a] M.D. Gracia,[b] R. Luque,[b] J. García Martínez[a*].
[a]*Molecular Nanotechnology Lab, Inorganic Chemistry Dpt., University of Alicante, Aptdo. 99 – E-03080 Alicante (Spain),*[b]*Organic Chemistry Dpt., Universidad de Córdoba, Campus de Rabanales, Edif. Marie Curie, E-14014, Córdoba (Spain). E-mail: ada.carrillo@ua.es*

Introduction

Mesoporous silica materials have attracted a great deal of interest owing to their promising properties and uses. [1,2] Such materials are designed and assembled in controlled ways with the aim to achieve specific pore sizes and/or shapes. Among them, helically structured materials have been the subject of numerous studies due to their potential in applications including chiral selective separation/recognition and catalysis. [3] However, silica-based mesostructured materials are intrinsically catalytically inactive due to the lack of active sites on their structure. With the aim to overcome this limitation, herein we describe a simple methodology to isomorphically incorporate Al and Ce in mesostrutured silica helicoidal materials to prepare highly active and stable catalysts with acid and redox properties.

Experimental

In a typical synthesis, 0.4 g cetyltrimethylammonium bromide (C_{16}TAB) as surfactact was dissolved in 100 mL of aqueous ammonia solution (30 wt %). 2.0 mL TEOS and different quantities of $AlCl_3 \cdot 6H_2O$ or $Ce(NO_3)_3 \cdot 6H_2O$ were then added and the mixture reacted at 40ºC for 3 h under stirring (600 rpm), followed by aging at 100ºC for 24 h in an autoclave. Upon cooling, the solid product was washed, filtered off, and air dried overnight. The surfactant was removed by calcination at 550ºC for 8 h (2ºC min^{-1}) under air. Samples were denoted as Al- or Ce-HMM. Two different Si/Al (190 and 95) and Si/Ce ratios (1000 and 500) were prepared. A pure MCM-41 sample was also synthesized for comparative purposes.

Results and discussion

N_2 adsorption isotherms of the calcined Al- and Ce-HMM materials (Si/Al 95 and Si/Ce 500) are depicted in Figure 2a. These isotherms are type IV, which is characterisctic of mesoporous materials. TEM images of sample Al-HMM (Si/Al= 95) also show the helical morphology is preserved at low quantities of metal into the silica framework.

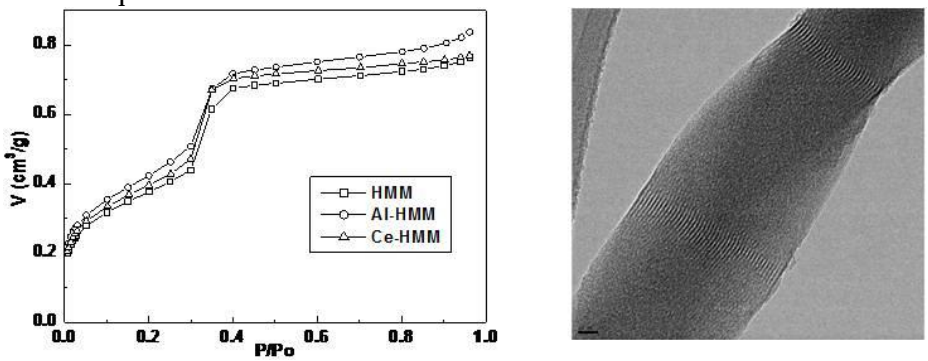

Figure 1. Adsorption isotherms Al-HMM and Ce-HMM (Si/M 95 or 500 ratio) as compared to siliceous HMM (Left). Representative TEM image of helical Al-HMM sample (Si/Al 95, equivalent to 1 wt% of Al) (Right).

The catalytic properties of Al- and Ce-HMM were subsequently investigated in two test reactions under microwave irradiation, namely the oxathioketalisation of cyclohexanone with 2-mercaptoethanol (Scheme 1) and the oxidation of cyclohexene with *tert*-butil hydroperoxide (TBHP). Results included in Figure 2 show both materials were active and very selective in the investigated reactions, being also highly reusable under the chosen reaction conditions. Activities were remarkably superior to those of similar Al- and Ce-MCM-41 materials prepared using conventional methodologies, demonstrating the effect of the metals on the helical mesostructures.

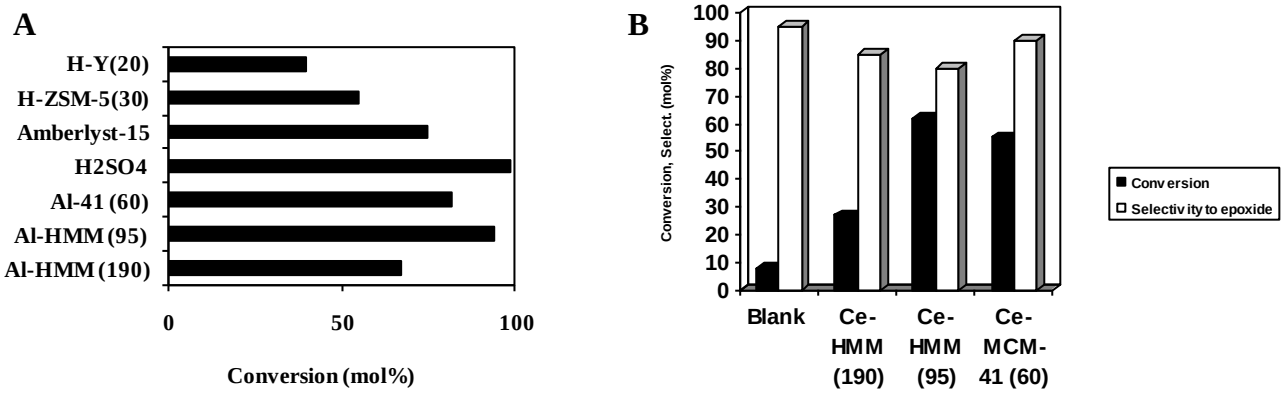

Figure 2. A) Activities of Al-HMM (Si/Al 95 and 190 ratios) materials compared to related acid catalysts in the oxathioketalisation of cyclohexanone with 2-mercaptoethanol (Reaction conditions: 5 mmol cyclohexanone, 10 mmol 2-mercaptoethanol, 0.05 g catalyst, microwaves, 300 W, 2 min, 70ºC (maximum temperature achieved). B) Activities of Ce-HMM materials in the oxidation of cyclohexene with TBHP (Reaction conditions 2 mmol cyclohexene, 4 mmol TBHP, 0.1 g catalyst, microwaves, 200 W, 30 min, 100-120ºC).

Conclusions

Alluminium or Cerium incorporated helical mesoporous materials have been succesfully prepared by direct synthesis. Aluminium metal has been incorporated into a silica matrix with different coordinations whereas cerium metal is preferently tetrahedrally coordinated. Helical morphology is preserved until Si/Al ratios of 95 (1 wt% aluminium) or Si/Ce ratios of 500 (1 wt% Cerium) without altering the helical morphology of the materials.

Acknowledgements

E.S. acknowledges financial support from Spanish MICINN through the Juan de la Cierva Program (ref. JCI–2008–2165). The authors thank Dr. Cristina Almansa Carrascosa, for assistance with the Transmission Electron Microscopy, and the Department of Applied Physics of the University of Alicante, especially Dr. Carlos Untiedt, for their continuous support. RL gratefully acknowledges MICINN for the concession of a Ramon y Cajal contract (ref. RYC-2009-04199).

References

[1] (a) E.F. Christabel, D. Khushalani, S. Mann, Chem. Commun., (2001), 2028-2029. (b) J. Garcia-Martinez, Tomorrow's Chemistry Today, ed. B. Pignataro, Wiley-VCH, Weinheim, (2007).
[2] (a) T. Gier, X. Bu, P. Feng, G.D. Stucky, Nature, 395 (1998), 154-157. (b) D. Bradshaw, T.J. Prior, E.J. Cussen, J.B. Claridge, M.J. Rosseinsky, J. Am. Chem. Soc. 126 (2004), 6106-6114. (c) A.E. Rowan, R.J.M. Nolte, Angew. Chem. Int. Ed. 37 (1998), 63-68.
[3] L. Zhang, S. Qiao, Y. Jin, L. Cheng, Z. Yan, G.Q. Lu, Adv. Funct. Mater. 18 (2008), 3834.

Chemicals from biomass: acid zeolites as catalysts for the one-pot synthesis of long chain alkyl acetals of 5-hydroxymethyl furfural derivatives with potential surfactant applications

Karen S. Arias, Onofre Casanova, María José Climent, Avelino Corma, Sara Iborra
Instituto de Tecnología Química (UPV-CSIC). Universidad Politécnica de Valencia
Avenida de los Naranjos s/n, 46022 Valencia (Spain). Siborra@itq.upv.es

Introduction

5-Hydroxymethyl furfural (HMF) is a basic nonpetroleum chemical readily accessible from renewable resources, such as acid catalyzed dehydration of fructose.[1,2] HMF has a high potential industrial demand since it is a versatile molecule which can be converted into several derivatives with multiple applications, e.g. pharmaceuticals, antifungals, and polymer precursors.[3] Besides it is considered as a novel scaffold for pharmacologically active compounds.[4] For valorizing biomass, we have prepared HMF derivatives with potential nonionic surfactants applications in the presence of solid acid catalysts. In a first step the acetalization-etherification reaction of HMF with methanol was performed using zeolites as catalysts and then it could be transformed into long chain alkyl acetals by means of a transacetalization reaction. Finally the results of one *pot* reaction involving the etherification–acetalization and transacetalization with long chain fatty alcohols will be compared.

Experimental

A solution of HMF (1 g) in 20 mL of methanol was magnetically stirred and heated at 65 ºC in the presence of a previously activated Beta zeolite (0.4 g), during 6 h to obtain dimethyl acetal ether **1**. The transacetalization of **1** with octanol was carried out using zeolites as catalysts with a molar ratio **1**/octanol of 1/2 at 40 ºC during 2.5 h. To remove the methanol a Dean-Stark instrument with a stream of nitrogen was used. At the end of the reaction the catalyst was filtered and washed with CH_2Cl_2, and the organic solution was analyzed by ^1H NMR spectroscopy (300MHz Varian VXR-400S) and GC-MS (Hewlet-Packard 5988 A).

Results and discussion

The direct acetalization reaction of HMF with octanol was first carried in the presence of different acid zeolites as catalysts. However in all cases very poor selectivity to 5-hydroxymethyl dioctyl acetal was obtained due to the existence of a competitive HMF dimerisation through the hydroxymethyl group. Then we propose an alternative route to obtain potential surfactant molecules based on HMF dialkyl acetal derivatives bearing the hydroxymethyl group protected as methyl ether. The process involves as first step the acetalization-etherification reaction of HMF with methanol (pathway A Scheme 1) and then the transacetalization of the dimethyl acetal with fatty alcohols (pathway B, Scheme 1)

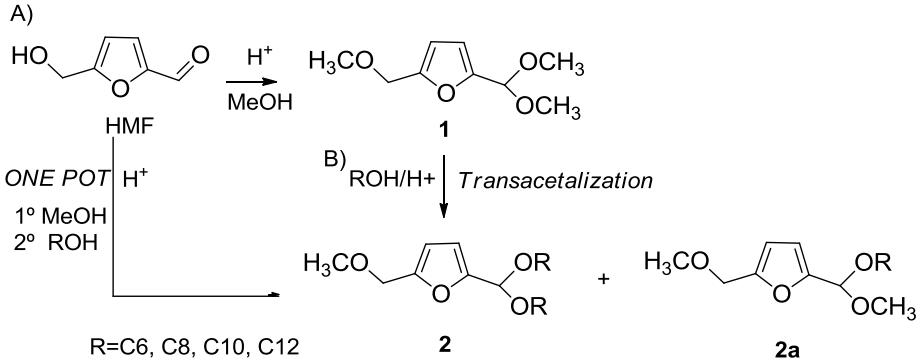

Good yield of **1** (98 %) are obtained when HMF was reacted with methanol in the presence of Beta zeolite (Si/Al=12) at moderate temperature. The transacetalization of **1** with long chain alcohols was carried out using a series of molecular sieves with different pore and topologies (see Table 1).

Table 1. Results of transacetalization reaction of dimethyl acetal ether **1** with n-octanol

Catalyst	Brönsted Acidity		Si/Al	Conv. (%)	Yield (%)			Selectivity (%)
	150ºC	250ºC		**1**	**2**	**2a**	Others	**2**
PTSA	-	-	-	96	39	32	25	40
MCM-41	19,5	5	12	100	82	16	2	**82**
Mordenite	67,4	54,3	10	100	76	22	2	**73**
ZSM-5	42,9	24,5	15	80	52	27	1	65
Beta	42,6	27,1	12	99	96	2	1	**97**
Y	114	94,4	3	96	69	24	3	**72**

Reaction conditions: **1**/OctOH=0.5, T^a=40ºC, N_2, 2.5 wt% of catalyst respect to **1**, 2.5 h. Acidity measures were carried out by adsorption-desorption of pyridine by IR spectroscopy.

For the transacetalization of **1** with octanol, Beta zeolite results the most active and selective catalyst followed by MCM-41 and Mordenite. The lower activity of HY zeolite, which possesses the highest amount of acid sites with higher strength, could be attributed to a deactivation of the catalyst caused by the high hydrophilic character of this material which produces a strong adsorption of the reactants and intermediate species. The study of the influence of the Si/Al ratio was performed on a series of Beta zeolite, and reveals that samples with Si/Al ratio between 27-50, exhibits high activity for the transacetalization reaction which was related with the adsorption properties of the catalyst surface. When the transacetalization of **1** was carried out using different alcohols such as hexanol, decanol and dodecanol good yields (95-98 %) and selectivities to the corresponding acetal (95-98 %) were obtained after 6 h. The Beta zeolite (Si/Al=12) could be reused up to three consecutive cycles without loss of activity. Finally, the preparation of dialkyl acetal methyl ether **2** was performed in one pot process starting from HMF and methanol. Thus when the yield of dimethyl acetal ether **1** was 98 % the methanol was removed and the fatty alcohol was added to the reactor. Yields of 97-99 % and selectivities to the corresponding dialkyl acetal of 97-98 % were obtained after 4-7 h.

Conclusions

Beta zeolite is a recyclable catalyst able to carry out the acetalization-etherification of HMF with methanol followed by transacetalization with fatty alcohols to produce HMF derivatives with potential surfactant properties. The whole process can be performed in one-pot process achieving excellent yields of the dialkyl acetal derivatives. For transacetalization reaction adsorption properties of the catalyst surface are as important as the concentration of active acid sites.

References

[1] J. N. Chheda, G W. Huber, J A Dumesic Angew. Chem. Int. (2007), 46, 7164.
[2] A. Corma, S. Iborra, A. Velty, Chemical Reviews (2007), 107(6), 2411-2502.
[3] C. Moreau, M. N. Belgacem, A. Gandini Topics in Catal. (2004) 27, (1-4).
[4] P. Gupta, S.K. Singh, A. Pathak, B. Kundu, Tetrahedron 58 (2002) 10469

Mesoporous aluminosilicates as efficient and reusable catalysts for chemoselective formation of 1,5-benzothiazepines

María José Climent, A. Corma, Sara Iborra, Anna F. Lopez, Laura Martin
Instituto de Tecnología Química (UPV-CSIC). Universidad Politécnica de Valencia
Avenida de los Naranjos s/n, 46022 Valencia (Spain)
Mjcliol@qim.upv.es

Introduction

Synthesis of benzothiazepines constitute an important area of research due to a large number of 1,5-benzothiazepines exhibits a variety of pharmaceutical activities, such as, muscle relaxant, inhibitor HIV-integrase, anticonvulsant, antibiotics[1] and in cardiovascular treatments and Alzheimer's disease.[2]Commonly, 1,5-benzothiazepines are prepared by reacting *o*-aminothiophenol with ketones, α,β-unsaturated carbonyl compounds and β-haloketones in the presence of acid or basic homogeneous catalysts.[3] However examples in literature about the synthesis of 1,5-benzothiazepines using heterogeneous catalysts are scarce. Thus, exchanged Y zeolites (CeY, LaY, NaY, HY), Mordenite and Montmorillonite KSF,[4] Al_2O_3,[5] have been used as catalysts giving the corresponding g1,5-benzothiazepine with good to moderate yields although in all cases, high amount of catalyst was required. In this work we have performed the synthesis of 2,3-dihydro-1,5-benzothiazepines starting from *o*-aminothiophenol and chalcone using micro and mesoporous aluminosilicates as acid catalysts (Scheme 1).

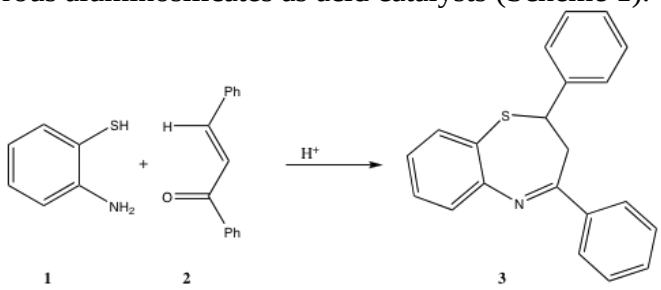

Scheme 1. Synthesis of 2,3-dihydro-1,5-benzothiazepine from chalcone and o-aminothiophenol

Experimental

Mordenite and HY zeolites in their acid form were commercial samples (PQ Corporation). ITQ-2 zeolite and MCM-41 were prepared according to references [7] and [8] respectively. Acidity measurements were carried out by adsorption-desorption of pyridine by IR spectroscopy.

A mixture of 2-aminothiophenol (1,2 mmol), chalcone (1 mmol) and 8 mL of toluene was magnetically stirred and heated at desired temperature. Then, the catalyst was added (15 wt% respect to the total mass of reagents). At the end of the reaction the catalyst was filtered and washed with CH_2Cl_2, and the organic solution was analyzed by ^{1}H NMR spectroscopy (300MHz Varian VXR-400S) and GC-MS (Hewlet-Packard 5988 A).

Results and Discussion

The synthesis of 2,3-dihydro-1,5-benzothiazepines (**3**) from o-aminothiophenol (1) and 1,3-diphenyl-2-propenone (2) was carried out in the presence of a large-pore tridirectional (HY) and monodirectional (Mordenite) zeolites, a delaminated ITQ-2 zeolite and a mesoporous aluminosilicate (MCM-41). The results showed that the

activity follows the order of MCM-41~ITQ-2>HY~Mordenite> MCM-41-Si.
The highest activity showed by MCM-41, despite their lower relative acidity respect to microporous materials, was attributed to its higher pore size which allows for fast diffusion of reagents and/or products along with the presence of a high concentration of silanol groups on the surface, which are also involved in catalytic activity. Optimization of Si/Al ratio of the MCM-41, showed that MCM-41 with Si/Al ratio of 12 was the most active and selective catalyst. Moreover, it could be reused four cycles without appreciable lost of activity. Finally, MCM-41 was used as acid catalyst for the synthesis of different 1,5-benzothiazepines with excellent success achieving yields between 80-90 % within 2-3 h.

Table 1. Results of the synthesis of 1,5-benzothiazepine using different heterogeneous acid catalysts

Catalyst	Si/ Al	Area (m^2/g)	A.B.[b] 250ºC	A.B.[b] 350ºC	Conv. (%)	Yield(%) **3**	Select.(%) **3**
Mordenite	12	507	54	29	86	86	100
HY	5	750	110	58	87	85	100
ITQ-2	12	573	30	20	80	80	100
MCM-41	12	1100	5	4	99[a]	99[a]	100
MCM-41 Si	-	-	1	0	63	29	47

Reaction conditions: Molar ratio **2**:**1**= 1,2, 15%wt catalyst, toluene refluxed during 5h. [a] 2h of reaction. [b] Acidity(μmol Py/g catalyst) calculated using extinction coefficient [6].

Conclusions

The mesoporous aluminosilicate MCM-41 gives higher catalytic activity and selectivity than microporous materials in the synthesis of 2,3-dihydro-1,5-benzothiazepines. This fact can be explained by the larger pore, which avoids diffusional restrictions. The study of the influence of the Si/Al ratio of MCM-41 catalyst showed that the number of acid sites is the fundamental factor to control the catalytic activity under these reaction conditions. The MCM-41 catalyst with Si/Al=12 was the optimum and could be reused during four consecutive cycles without loss of activity. Finally, excellent yields of substituted benzothiazepines were obtained using this catalyst.

References

[1](a) Bariwal, B., Upadhyay, K.D., Manvar, A.T., Trivedi, J.C., Singh, J.S., Jain, K.S., Shah, A.K., 1,5-Benzothiazepine, a versatile pharmacophore: A review, Eur. J. Med. Chem., 43 (2008) 2279-2290 (b) Zhang, P., Wang, L.Z., Wu, H.S., Ming Lan, J., Li Yuan, Xiang, W.Y., Synthesis and biological evaluation of a novel series of 1,5-benzothiazepine derivatives as potential antimicrobial agents, Eur. J. Med. Chem., 44 (2009) 2815-2821

[2] Birks, J., Alzheimer Demen.,2 (2006) 580.

[3](a) Pant, S., Singhal, B., Upreti, M., Pant, U., Syntheses of 1,5-Benzothiazepines. Part 20. Syntheses of 8-Substituted-2,5-dihydro-2-(4-N-dimethylaminophenyl)-4-(4-methoxyphenyl)-1,5-benzothiazepines, Molecules, 3 (1998) 159-163 (b) Upreti, M., Pant, S., Dandia, A., Pant, U.C., Indian J. Chem. 36B (1997) 1181 (c) Patel, V.M., Desai, K.R., Indian J. Chem. 43B (2004) 199.

[4] (a) Arya, K., Dandia, A., Bioorg. Med. Chem. Lett. 18 (2008) 114- (b) Dandia, A., Sati, M., Loupy, A., Green Chem. 4 (2002) 599.

[5] Hekmastshoar, R., Sadjadi, S., Shiri, S., Heravi, M.M., Beheshtiha, Y.S., Synth. Comm., 39 (2009) 2549.

[6] Emeis, C.A., J. Catal., 141 (1993) 347.

[7] Corma, A., Fornes, V., Pergher, S.B., Maesen, Th.L.M., Buglass, J.G., Nature 376 (1998) 353.

[8] Corma, A., Fornes, V., Navarro, M.T., Perez-Pariente, J., J. Catal., 148 (1994) 569.

Mesoporous 1,3,5-benzene tribenzoate (BTB) based MOFs and their application in gas storage and catalysis

Georg Nickerl[(a)], Kristina Gedrich[(a)], Nicole Klein[(a)], Maja Heitbaum[(b)], Andreas Notzon[(b)], Ulrich Stoeck[(a)], Irena Senkovska[(a)], Frank Glorius[(b)], Stefan Kaskel[(a)*]
[(a)] Department of Inorganic Chemistry, Dresden University of Technology, Bergstrasse 66, 01069 Dresden, Germany; [(b)] Organisch-Chemisches Institut, Westfälische Wilhelms-Universität Münster, Corrensstrasse 40, 48149 Münster, Germany
[*]Stefan.Kaskel@chemie.tu-dresden.de

Metal-Organic Frameworks (MOFs), a new class of porous materials built from metal atoms or clusters (nodes) interlinked by multifunctional organic ligands (linkers) have attracted considerable interest due to their outstanding characteristics such as high specific surface areas and large pore volumes in conjunction with high crystallinity. Up to now numerous MOFs have been synthesized and characterized with different objectives among them catalytic and gas storage applications.[1-4] 1,3,5-Benzene tribenzoate (BTB) has turned out to be a versatile linker for construction of Metal-Organic Frameworks with large pores.[5-7]

Here, we report the synthesis and crystal structures of new Metal-Organic Frameworks obtained by using 1,3,5-benzene tribenzoic acid or chiral substituted analogues of it, as well as their characterization and application in enantioselective catalysis and gas adsorption.

DUT-6 (DUT = Dresden University of Technology), $Zn_4O(2,6\text{-NDC})(BTB)_{4/3}$ (NDC = naphthalene dicarboxylate), is a mesoporous MOF containing two types of linkers: the trifunctional BTB and bifunktional 2,6-NDC.[8] The octahedral secondary building unit is built by a Zn_4O-cluster and six bridging carboxylate groups. Four of the six carboxylate groups of $Zn_4O(COO)_6$ unit are derived from the BTB linker surrounding the cluster in a square arrangement to give a (3,4)-connected net with Pt_3O_4-topology, while two additional 2,6-NDC linkers occupy the residual octahedral sites and further crosslink the network. The resulting framework exhibits uniform mesopores of 25-30 Å in diameter. It has shown to be a leading benchmark material for gas storage applications, especially with regard to hydrogen (5.64 wt.% at 50 bar), methane (230 mg g^{-1} at 100 bar) and *n*- butane (1.1 g g^{-1}) uptake (Figure 1).

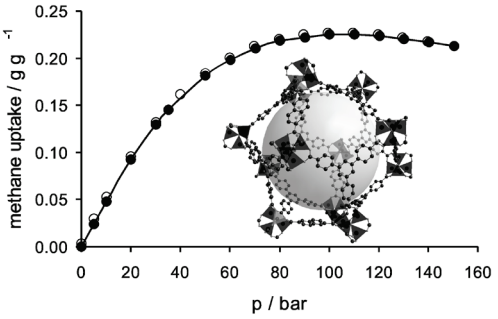

Figure 1: Methane (25°C) high pressure excess adsorption (●) and desorption (○) isotherm of DUT-6.

DUT-9, $Ni_5O_2(BTB)_2$, possesses a new framework topology and is formed by BTB linkers and Ni_5O_2 clusters, which is a novelty in MOF chemistry.[9] Supercritical drying of the as synthesized DUT-9 followed by additional activation results in a material having a high concentration of open metal sites per cluster, large pores (up to 25 Å in diameter) and remarkable adsorption properties (pore volume: 2.18 cm^3g^{-1}, hydrogen uptake: 5.85 wt.% at 40 bar, methane uptake: 219 mg g^{-1} at 100 bar).

Within the context of prospective catalytical applications, the development of new MOF catalysts plays a key role. A new approach to the synthesis of chiral Metal-Organic Frameworks was developed by modifying the BTB linker with chiral and enantiomerically pure oxazolidinone subunits (H_3ChirBTB-n).[10] Conversion of the substituted BTB linkers with zinc nitrate yields the chiral MOFs Zn_3(ChirBTB-1)$_2$ and Zn_3(ChirBTB-2)$_2$ (Figure 2). Zn_3(ChirBTB-1)$_2$ consists of a dinuclear zinc paddlewheel unit that is surrounded by four

modified BTB linkers. The resulting framework has a twisted boracites (tbo) topology and exhibits three different types of pores including a larger pore, approximately 33.7 Å in diameter, with accessible zinc sites pointing towards the center of the pore. Despite using the same reaction conditions for Zn_3(ChirBTB-2)$_2$ as for Zn_3(ChirBTB-1)$_2$ a totally different structure was obtained. Zn_3(ChirBTB-2)$_2$ is built by trinuclear zinc units being interconnected by the modified BTB linkers to give a 3D framework with channels being 18 Å wide.

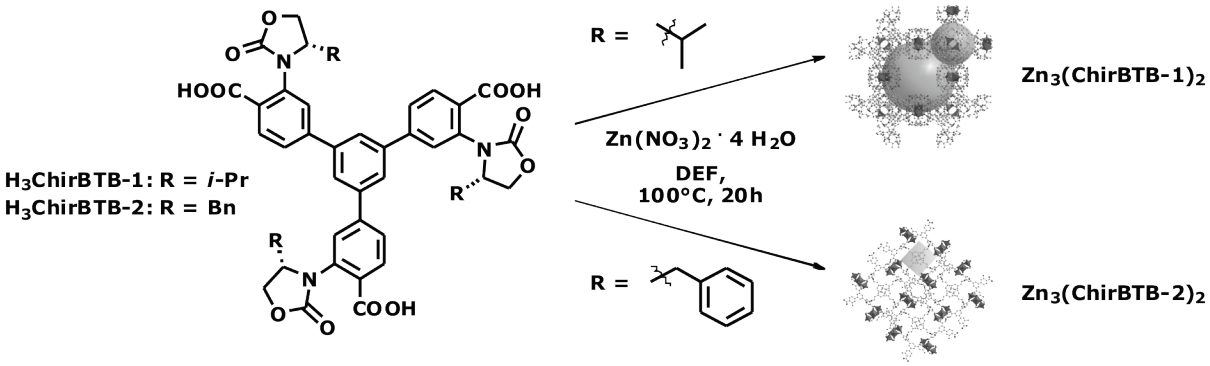

Figure 2: Synthesis and crystal structures of Zn_3(ChirBTB-n)$_2$.

Zn_3(ChirBTB-1)$_2$ and Zn_3(ChirBTB-2)$_2$ were tested in Mukaiyama Aldol reactions since the pores of these materials are accessible even for large molecules, and thus the Lewis acidic metal sites can be used for the catalytic conversion of organic substrates. Zn_3(ChirBTB-1)$_2$shows a high conversion rate for the reaction of aromatic aldehydes with 1-methoxy-1-(trimethylsiloxy)-2-methyl-1-propene outperforming other mesoporous MOFs like MIL-101 and MOF-177 as well as the homogeneous analogue zinc nitrate. The ChirBTB-MOFs also show an enantioselective catalytic behavior, e.g., the reaction of napthaldehyde with 1-methoxy-1-(trimethylsiloxy)-2-methyl-1-propene at room temperature in the presence of Zn_3(ChirBTB-1)$_2$ gives the Aldol product with an *ee* value of 40 %.

[1] Senkovska, I.; Kaskel, S.; Solvent-induced pore-size adjustment in the metal-organic framework [Mg_3(ndc)$_3$(dmf)$_4$] (ndc = naphthalenedicarboxylate), Eur. J. Inorg. Chem., 22 (2006) 4564-4569.
[2] Sabo, M.; Henschel, A.; Fröde, H.; Klemm, E; Kaskel, S.; Solution infiltration of palladium into MOF-5: synthesis, physisorption and catalytic properties, J. Mater. Chem, 17(2007), 3827-3832.
[3] Henschel, A.; Gedrich, K.; Kraehnert, R.; Kaskel, S.; Catalytic properties of MIL-101 , Chem. Commun., 35 (2008), 4192-4194.
[4] Senkovska, I.; Hoffmann, F.; Fröba, M.; Getzschmann, J.; Böhlmann, W.; Kaskel, S.; New highly porous aluminum based metal-organic frameworks: Al(OH)(ndc) (ndc = 2,6-naphthalene dicarboxylate) and Al(OH)(bpdc) (bpdc = 4,4'-biphenyl dicarboxylate), Microporous Mesoporous Mater., 122 (2009), 93-98.
[5] Chen, B.; Eddaoudi, M.; Hyde, S.T.; O'Keeffe, M.; Yaghi, O.M.; Interwoven metal-organic framework on a periodic minimal surface with extra-large pores, Science, 291 (2001), 1021-1023.
[6] Chae, H.K.; Siberio-Perez, D.Y.; Kim, J.; Go, Y.B.; Eddaoudi, M.; Matzger, A.J.; O'Keeffe, M.; Yaghi, O.M.; A route to high surface area, porosity and inclusion of large molecules in crystals, Nature, 427 (2004), 523-527.
[7] Koh, K.; Wong-Foy, A.G.; Matzger, A.J.; A crystalline mesoporous coordination copolymer with high microporosity, Angew. Chem. Int. Ed., 47 (2008), 677-680.
[8] Klein, N.; Senkovska, I.; Gedrich, K.; Stoeck, U.; Henschel, A.; Mueller, U.; Kaskel, S.; A Mesoporous Metal-Organic Framework, Angew. Chem. Int. Ed., 48 (2009), 9954-9957.
[9] Gedrich, K.; Senkovska, I.; Klein, N.; Stoeck, U.; Henschel, A.; Lohe, M. R.; Baburin, I. A.; Mueller, U.; Kaskel, S.; A Highly Porous Metal-Organic Framework with Open Nickel Sites, Angew. Chem. Int. Ed., 49 (2010), 8489-8492.
[10] Gedrich, K.; Heitbaum, M.; Notzon, A.; Senkovska, I.; Fröhlich, R.; Getzschmann, J.; Mueller, U.; Glorius, F.; Kaskel, S.; A Family of Chiral Metal–Organic Frameworks, Chem. Eur. J., (2011), DOI: 10.1002/chem.201002568.

Gold Nanoparticles on Nanometric Ce and Ti Oxides catalyze the N-Monoalkylation of Amines with Alcohols through a One-pot Process

A.Corma*, J. Navas, María J. Sabater

*Instituto de Tecnología Química UPV-CSIC, Universidad Politécnica de Valencia, Consejo Superior de Investigaciones Científicas, Avenida Los Naranjos s/n, 46022, Valencia, Spain; Tel: 34 96 3877800, Fax: 34 96 3877809, e-mail: acorma@itq.upv.es

Introduction

Amines, which are versatile intermediates in organic synthesis and important structural elements in natural products and therapeutic drugs, are synthesized through a sequential transformation in the same pot using gold nanoparticles supported on oxides (CeO_2, TiO_2, etc). In particular, these gold-based catalytic systems efficiently catalyze the N-monoalkylation of amines with alcohols to give secondary amines in the absence of solvents, based on the hydrogen transfer methodology [1]. In this case and similar to other transition metals, gold hydride complexes containing an Au-H structure are the plausible key intermediates in this gold catalyzed transformation [2].

Experimental

- Catalysts Au(1%wt),Ru(1%wt)-CeO_2, Au-$Ga_3Al_3O_9$ 1.5%wt, Au-TiO_2 1.5%wt and Au-CeO_2 1.75%wt were prepared according to literature procedures [3].
-Catalytic reactions: 1 mmol of aniline, 1mL of benzyl alcohol and catalyst (from 0.5 to 0.82 mol %) were placed in a 2mL reaction vessel. The resulting mixture was vigorously stirred at 180^{o}C under a nitrogen atmosphere (1 bar). The reaction was monitored by GC using n-dodecane as external standard.

Results and discussion

In this reaction an alcohol is oxidized to the corresponding aldehyde giving a metal hydride intermediate. The aldehyde formed in situ reacts with a primary amine to give an imine, which is hydrogenated by the metal hydrides formed on the metal surface to give the desired secondary amine and hence closing the catalytic cycle (Scheme 1).

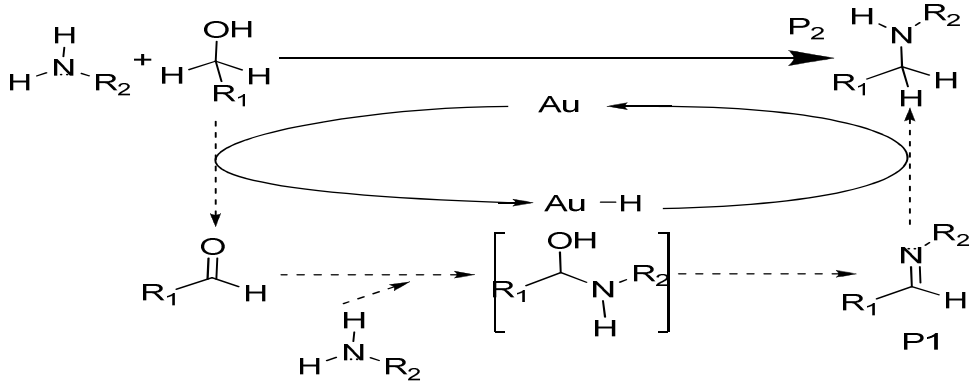

Scheme 1. Schematic representation of the N-monoalkylation of amines with alcohols catalyzed by gold.

The results obtained with different gold supported catalysts are listed in Table 1.

Table 1. Results obtained using different gold catalyst. [a]

Entry	Catalyst	t (h)	Conv. (%)	Yield (%)		
				P1	P2	others
1	Au-TiO_2 1.5%wt, 0.82%mol	5	100	5	85	10
2	Au-CeO_2 1.73% wt, 0.66%mol	5	100	6	90	4
3	Au(1%wt),Ru(1%wt)-CeO_2, 0.5%mol	5.5	83	50	23	10
4	Au-$Ga_3Al_3O_9$ 1.5%wt, 0.5%mol	5.5	100	53	15	32
5[b)]	Au/CeO_2 1.73% wt, 0.35%mol	6.5	88	3	85	<1

a) Reaction conditions: 1mmol aniline, catalyst (0.5-0.82 mmol %), 1 mL of benzyl alcohol, 180ºC, 1 bar N_2. b) equimolar amounts of aniline and alcohol, no solvent.

Results in table 1 show that Au-TiO_2 and Au-CeO_2 are the best catalysts since both efficiently catalyze the cascade reaction in a relatively short period of time and high selectivity values towards the secondary amine are obtained.

Conclusions

Gold nanoparticles supported on nanometric oxide particles (CeO_2, and TiO_2) efficiently catalyze the N-alkylation of amines with alcohols under hydrogen transfer conditions to afford secondary amines. The process is clean (water is formed as the only by-product) and selective to the desired secondary amine. The reaction gives good yields of monoalkylated amine in the absence of solvent, and avoids the use of hydrogen and pressurized systems, hence providing an efficient and clean alternative to the synthesis of amines.

Acknowledgements

We thank Consolider-Ingenio 2010 (project MULTICAT), Spanish MICINN (Project MAT2006-14274-C02-01), Generalitat Valenciana (Project PROMETEO/2008/130) for financial support. J.N expresses his gratitude to the Consejo Superior de Investigaciones Científicas for a JAE fellowship.

References

[1] Guillena, C.; Ramon, D.J.; Yus, M.; *Chem. Rev.*, 110 2010**,** 3, 1611–1641.
[2]Abad, A.; Corma, A.; Concepcion, P.; García H.; Angew. Chem., 44 (2005),26, 4066 –4069.
[3] a) Sreethawong, T.; Sukjit, D.; Ouraipryvan, P.; Catalysis Letters**,** 38(2010), 3-4**,** 160-170.**, b)** Otero, C.; Delgado, M.; Montouillout, V.; Massiot D.; Z. Anorg. Allg. Chem., 631 (2005), 2121. , **c)** Grirrane, A., Corma, A., Garcia H, Journal of Catalysis, 264 (2009) 138–144, **d)** Carrettin, S., Guzman, J., Corma, A., Angew. Chem., 44 (2005), 14, 2242-2245.

Catalytic pyrolysis of lignin for the production of high added value chemicals and fuels

K. Kalogiannis, S. Stefanidis, A. A. Lappas
CERTH/CPERI, P.O. Box 361, GR-57001 Thermi-Thessaloniki, Greece
M. Stöcker* (Michael.Stocker@sintef.no), L. Hannevold and Aud I. Spjelkavik
SINTEF Materials and Chemistry, P.O.Box 124 Blindern, N-0314 Oslo, Norway
F. Öhman
INNVENTIA AB, Box 5604, SE-11486 Stockholm, Sweden

Introduction

Lignin is used mainly as an energy source in pulp mills. In this work we investigate the upgrading of lignin through a catalytic pyrolysis process. The classical thermal pyrolysis of lignin has been widely studied in the literature, however, crucial problems like limited yields of specific chemicals and bio-oil stability, acidity, and fractionation are unresolved. The use of heterogeneous catalysts in the biomass pyrolysis for the production of high added value bio-chemicals such as phenols and bio-fuels has received strong attention during the recent years [1]. Limited information is however available on the production mechanism of specific compounds (like phenols) from catalytic lignin pyrolysis [2]. This work focused on heterogeneous catalytic pyrolysis of various types of lignin for the production of high added value chemicals (such as phenols and aromatics) and fuels that could be used as co-feeds for petroleum streams in existing refining processes.

Experimental

Bench scale pyrolysis unit

The thermal and catalytic lignin pyrolysis experiments were performed on a bench scale fixed bed reactor. The reactor operated at 500°C using 1.5 g of lignin and 0.7 g of catalyst. Details of the experimental set up and the procedures are given elsewhere [1]. In this work, the physical and chemical characterization of the liquid product (bio-oil) was very important. This type of characterization was carried out by routine analysis (water content, elemental analysis: GC-FID) and advanced characterization techniques using GC-MS and 2DGC-TOFMS.

Lignin samples

Three lignin samples supplied by Innventia were used in this study. One from Softwood and two from Hardwood named Softwood, Hardwood-1 and Hardwood-3, respectively. All lignins were characterized at CPERI and Innventia. The elemental analysis of the lignins is presented in Table 1.

Table 1. Elemental analysis of lignins on a moisture and ash free basis

Sample name	Elemental analysis (wt.- %), dry basis				Ash (wt.- %)	Moisture (wt.- %)
	C	H	O	S		
Softwood	63.68	5.52	28.34	1.89	0.58	32.8
Hardwood-1	59.35	5.48	30.15	2.25	2.77	38.9
Hardwood-3	62.90	6.23	28.45	2.23	0.19	30.52

Catalyst samples

Both commercial (Zeol.1 = MFI, Zeol.2 = MOR and Zeol.3 = BEA) and novel mesoporous catalysts (Al-MCM-41 and Al-SBA-15) synthesized by SINTEF were examined in this work.

Strongly acidic commercial zeolites were tested along with mesoporous materials of mild acidity. The Si/Al ratios varied between 16 and 48, while surface areas were in the range of 120 to 1200 m^2/g.

Results and discussion

In the first stage of this work we carried out lignin thermal pyrolysis using a softwood and two hardwood lignins (Hardwood-1 and Hardwood-3). Softwood lignin produced a bio-oil with 30.7 wt.-% yield on biomass and oxygen of 25 wt.-% in the organic phase. The hardwood lignins showed yields of 29 and 41 wt.-% on biomass with oxygen contents of 33 and 22 wt.-% in the organic phase, respectively. It was clear that Hardwood-3 yielded more and a higher quality biooil, with less material available for coke formation. Hardwood-1 on the other hand was more difficult to deoxygenate. All three lignin types were catalytically pyrolysed with Zeol.1 to study their deoxygenation potential. The bio-oil oxygen content was further reduced along with the bio-oil yield. In all cases the use of heterogeneous catalysts resulted in the increase of aromatic compounds and the reduction of heavy components. For the purposes of this study two types of catalysts were evaluated: commercial zeolites and synthesized mesoporous catalysts. The data from all the tests were compared so that a mapping of both the commercial and the novel mesoporous catalysts could be used as a tool for the evaluation of the catalysts' performance. All catalysts were tested with Hardwood-1. From the commercial catalysts, Zeol.1 and Zeol.3 had the best performance. Mesoporous catalysts produced a wide range of different bio-oils depending on the Si/Al ratio. The Al rich systems seemed to be the best suited material for biomass pyrolysis. The higher deoxygenation was achieved with the Al-MCM-41(1) producing a bio-oil with an oxygen content of about 17 wt.-%. The Al-MCM-41(3) yielded more phenols.

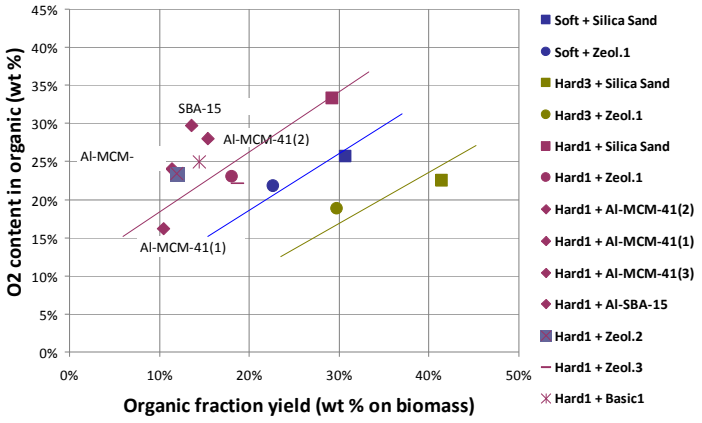

Conclusions

Catalytic pyrolysis of lignin proved to be a very interesting and promising process for the production of fuels and chemicals. The quality and the yield of the bio-oil depend on the lignin and catalyst type. Reduction of the oxygen content of bio-oil with catalysts was achieved at the expense of the organic fraction yield. Zeol.1 and Zeol.3 yielded the best bio-oil quality. The mesoporous catalysts produced a variety of bio-oils, with focus on either aromatic hydrocarbons or phenols.

Acknowledgements

This project has received funding from EU's Framework Programme 7 (FP7) under the Grant Agreement No. NMP2-LA-2009-228589 (AFORE).

References

[1]. Antonakou, E., Lappas, A., Nilsen, M.H., Bouzga, A., Stöcker, M., Evaluation of various types of Al-MCM-41 materials as catalysts in biomass pyrolysis for the production of bio-fuels and chemicals, Fuel, 85 (2006), 2202-2212.

[2]. Stöcker, M, Biofuels and biomass-to-liquid fuels in the biorefinery: Catalytic conversion of lignocellulosic biomass using porous materials, Angew. Chem. Int. Ed., 47 (2008), 9200-9211.

Catalytic sulphonated PVA membranes for the synthesis of isoborneol from camphene

A. Machado[a], J.E. Castanheiro[b], J. Vital[a]*, A.M. Ramos[a], M.H. Casimiro[a], J.V. Pinto[c]
a: REQUIMTE/CQFB, FCT, Universidade Nova de Lisboa, Caparica, Portugal, jmv@dq.fct.unl.pt
b: CQE, Departamento de Química, Universidade de Évora, Évora, Portugal
c: Departamento de Ciência dos Materiais and Cenimat/I3N, FCT, Universidade Nova de Lisboa, Caparica, Portugal

Introduction

Monoterpenes are widely used in the pharmaceutical, cosmetic and food industry as active components of drugs and ingredients for artificial flavors and fragrances [1]. Camphene is an attractive raw material employed for the synthetic manufacturing of isoborneol and borneol that are used in the formulation of soaps, cosmetic perfumes and medicines as well as in the industrial production of camphor, which is used as an odorant/flavorant in pharmaceutical, household and industrial products [2]. Traditionally, strong mineral acids, e.g. sulphuric acid, are used for the hydration of camphene [1], leading to environmental problems and economical inconveniences due to effluent disposal. These problems can be overcome by the use of solid acid catalysts, such as zeolites and heteropolyacids which have been used for the hydration of camphene [3]. In this work, sulphonated polymeric membranes have been prepared, consisting in poly(vinyl alcohol) crosslinked with succinic acid and used for the selective synthesis of isoborneol from camphene.

Experimental

PVA (Aldrich, average molecular weight: 935000) was dissolved in water at 80ºC, during 24 h. Aqueous 10 wt.% PVA solutions were mixed with succinic acid (5 wt. %) and different loadings of sulphoacetic acid (10, 20 and 30 wt. %) and vigorously stirred at room temperature for 24 h. The solutions were poured and cast on a Teflon plate and allowed to dry at 60ºC during 24 h. In order to complete the esterification reaction, the dried membranes were heated at 120ºC, during 24 h under vacuum. The membranes were characterized by FTIR/ATR, AFM, SEM and Temperature Programmed Pyrolysis. Textural characterization, as well as swelling degree, water contact angle and acidity was also evaluated. The membranes were used as catalysts in the hydration reactions of camphene.

Results and discussion

Figure 1 shows the FTIR spectra of PVAx membranes, where x stands for 10, 20 and 30 wt. % loading of sulphoacetic acid. The bands around 1180 and 1040 cm-1 appearing in the sulphonated membranes, usually assigned to the O=S=O asymmetric and symmetric vibrations are a strong indication of the presence of sulphonic acid groups in the polymeric matrix.

Figure 2 shows the conversion profiles for the three membranes tested, where it can be seen that higher loadings of sulphonic groups leads to higher conversions. The selectivity torwards isoborneol was also higher for the PVA membrane with 30 wt. % of sulphoacetic acid (92 %).

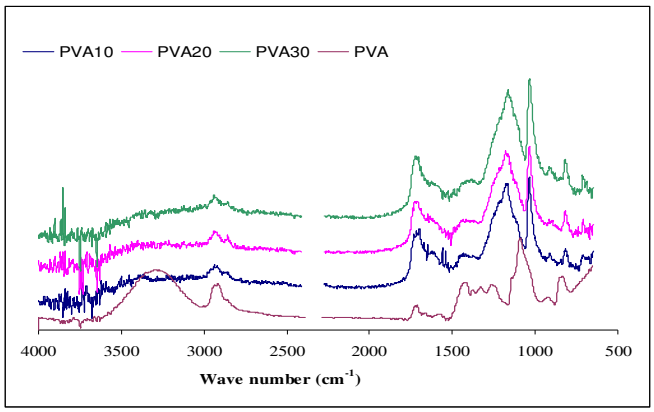

Figure 1. FTIR spectra of PVA10, PVA20, PVA30 and PVA.

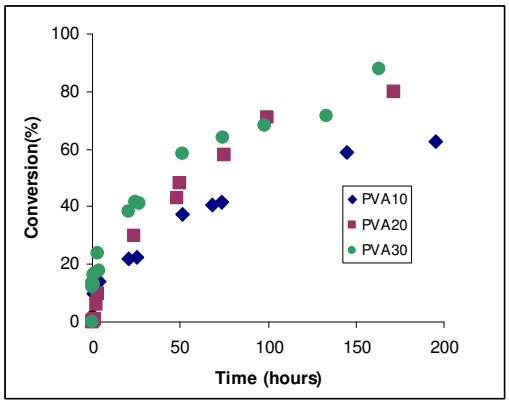

Figure 2. Conversion profiles of camphene to isoborneol.

Conclusions

PVA membranes were successfully sulphonated with sulphoacetic acid and have shown to be active catalysts in the hydration of camphene to synthesize isoborneol with high selectivities. Higher loadings of sulphonic acid groups lead to higher conversions and selectivities.

Acknowledgements

A. Machado acknowledges the Fundação para a Ciência e a Tecnologia for a doctoral grant SFRH/BD/27324/2006.

References

[1] Rocha, K.A., Kozhevnikov I.V., Gusevskaya, E.V., Hydration and acetoxylation of camphene catalyzed by heteropoly acid, Journal of Molecular Catalysis A: Chemical, 192 (2003), 129-134.
[2] Lana, E.J.L., Rocha, K.A., Kozhevnikov, I.V., Gusevskaya, E.V., One-pot synthesis of diisobornyl ether from camphene using heteropoly acid catalysts, Journal of Molecular Catalysis A: Chemical, 243 (2006), 258–263.
[3] Castanheiro, J.E., Machado, A., Fonseca, I.M., Ramos, A.M., Vital, J., Bifunctional catalytic PVA membranes for the direct synthesis of camphor from camphene, Studies in Surface Science and Catalysis, 162 (2006), 673-680.

Gold (III) stabilized over ionic liquid grafted in MCM-41 for highly efficient three-component coupling reactions

Luis F. Bobadilla[a], José A. Odriozola[a], Teresa Blasco[b]
[a] *Universidad de Sevilla-ICMSE, Av. Américo Vespucio, 49, 41092 Sevilla (Spain)*
[b] *Instituto de Tecnología Química UPV-CSIC, Av. de los Naranjos, s/n, 46071 Valencia (Spain)*
bobadilla@icmse.csic.es

Introduction

Propargylamines are versatile synthetic intermediates in organic synthesis and are also important structural elements in natural products and therapeutic drugs molecules [1]. These compounds can be synthesized through C-H activation by catalytic coupling of alkyne, aldehyde and amine (A^3 coupling), where water is the only theoretical by-product [2]. Homogeneous catalyst has been proposed for this reaction, among them cationic gold species show the highest catalytic activity [3]. However, besides the potential limitations of homogeneous catalysis for achieving a sustainable catalytic process, the rapid reduction of cationic gold species into inactive metallic atoms is unavoidable when gold salts activate alkynes/alkenes [4, 5]. Heterogeneous catalyst may therefore be an attractive solution to this problem. Since previous literature reports, using gold salts/complexes as catalysts, indicate that Au(III) and Au(I) could be the active species [3], we have prepared gold catalysts dispersed in a ionic liquid (IL) grafted MCM-41 in which partially charged and electron-deficient gold atoms are stabilized.

Experimental

The ionic liquid 1-(tryethoxy-silylpropyl)-3-methyimidazolium chloride was previously prepared and further "grafted" on MCM-41 with a solution of $AuCl_3$ in acetonitrile. A reference catalyst was also prepared by impregnating the MCM-41 support with the gold solution. Evidences for the grafting process were obtained by elemental analysis (ICP-AES and CHN) and ^{29}Si-NMR.

In the general procedure for the three-component coupling reaction, the desired amount of supported gold catalyst was added to a mixture of benzaldehyde (1,0 mmol), piperidine (1,2 mmol) and phenylacetylene (1,3 mmol), without solvent, and with *n*-octane as an internal standard. The A^3 coupling was performed in a closed glass reactor (2.0 mL, SUPELCO) with rapid stirring (1000 rpm) at 80ºC in air for 12 h. The product mixtures were cooled to room temperature and washed with acetonitrile. Aldehyde conversion was determined through GC analysis of the remaining liquid upon catalyst separation.

Results and discussion

Elemental analysis (3,016% N, 12,080% C and 2,344% H) of the functionalized gold catalyst gives a C/N = 4,95 molar ratio, suggesting the grafting of the ionic liquid (C/N=6.5) involving the lost of one of more ethoxy groups. Indeed, the ^{29}Si MAS NMR spectrum of the MCM-41 after grafting shows a decrease on the signal of the Q^3 silanol groups and the appearance of three low field peaks corresponding to T^3 (R-Si(OSi)$_3$), T^2 (R-Si(OSi)$_2$(OR')) and T^1 R-Si(OSi) (OR')$_3$ species. The measured gold amount, 2,098%, is quite close to the target value and accounts for ca. 10 IL molecules per gold atom.

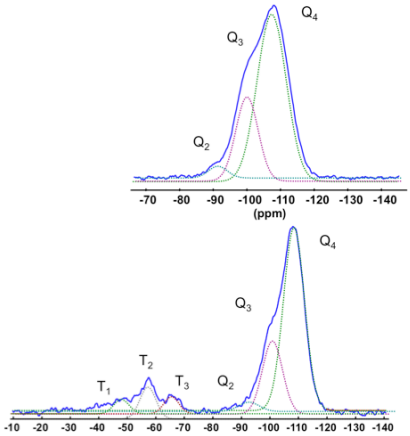

Figure 1. ^{29}Si-NMR MCM-41 (up) and MCM-41 functionalized (down)

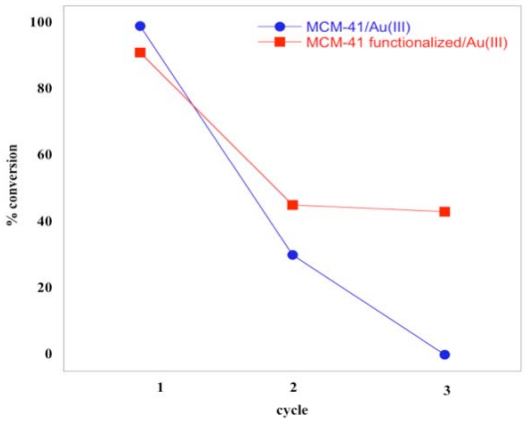

Figure 2. Cycles of conversion in the two catalyst

Figure 2 shows the conversion after three reaction cycles for the prepared catalysts. Although the activity decreases due to gold leaching the functionalized catalyst performs better after three reaction cycles since gold (III) species interact with the ionic liquid allowing its stabilization. Therefore, functionalizing the support with IL opens a path for the preparation of gold(III) heterogeneous catalyst for the three-component coupling reaction.

Acknowledgements

Luis F. Bobadilla thanks the Junta de Andalucía for his Ph.D. fellowship.

References

1. G.C. Bond and D.T. Thompson, Cat. Rev. Sci. Eng., 1999. **41**: p. 319.
2. I. Naota, H. Takaya, and S.I. Murahashi, Chem. Rev., 1998. **98**: p. 2599.
3. C. Wei and C.-J. Li, J. Am. Chem. Soc., 2003. **125**: p. 9584.
4. Corma, A., Cat. Rev. Sci. Eng., 2004. **46**: p. 369.
5. X. Zhang and A. Corma, Chem. Commun., 2007. **3080**.

Surface selective silylation of MCM-41 with trimethylsilyltriflate: quantitative characterization and catalytic application

Hara, Kenji [1]; Akahane, Saiko [1, 2]; Wiench, Jerzy W [3]; Pruski, Marek [3, 4]; Lin, Victor S.-Y[3, 4]; Fukuoka, Atsushi [1]
[1] *Catalysis Research Center, Hokkaido University, Japan.* [2] *Department of Chemistry, Faculty of Science, Hokkaido University, Japan.* [3] *U.S. DOE Ames Laboratory, United States.* [4] *Department of Chemistry, Iowa State University, United States, fukuoka@cat.hokudai.ac.jp*

Introduction

Mesoporous silica has been widely used as a support material for heterogeneous catalysts due to its high surface area and regular pore structure. However, discrimination between its internal surface and external surface has significance in some applications. In this study, we demonstrate that selective modification of the external surface of mesoporous silica MCM-41 can be achieved using trimethylsilyltrifluromethansulfonate ($Me_3SiOSO_2CF_3$, TMSOTf). In the application of the silylated mesoporous silica in Cu-catalyzed phenol polymerization, $Cu(OAc)_2$ supported on the externally silylated MCM-41 exhibits higher catalytic activity than the corresponding Cu/MCM-41 catalyst without silylation.

Experimental

Modification of the entire silica surface was conducted by heating a mixture of MCM-41 (1.0 g) and TMSOTf (2.8 mL, 16 mmol) in anhydrous toluene (6.7 mL) at 353 K for 16 h under argon to afford TMS-MCM-TMS (Figure 2a). The corresponding sample with selective slilylation of the external surface, denoted as TMS-MCM (Figure 2b), was prerapred by a reaction of as-synthesized MCM (1.0 g, containing surfactant) and TMSOTf (0.32 mL, 1.7 mmol). After the silylation with TMSOTf, the surfactant was extracted with EtOH-conc. HCl solution (93:7, v/v) at 373 K twice for 20 h.

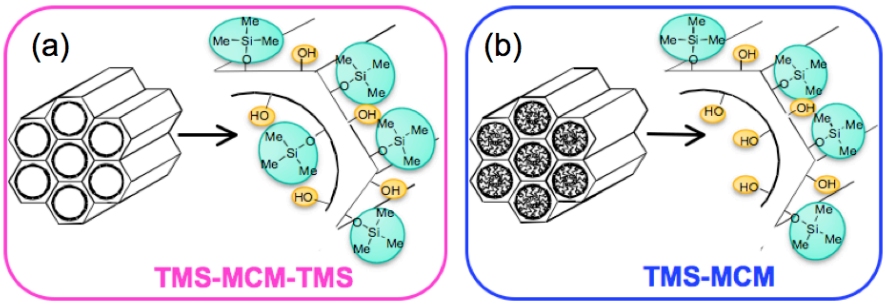

Figure 1. Schematic drawing of (a) TMS-MCM-TMS and (b) TMS-MCM.

The Cu-catalyzed polymerization of 1,6-dimethylphenol was carried out using catalysts Cu/MCM and Cu/TMS-MCM, prepared from MCM-41 and TMS-MCM, respectively. Into a solution of $Cu(OAc)_2 \cdot H_2O$ (39 mg) in acetonitrile (40 mL), mesoporous silica (MCM-41 or

TMS-MCM, 0.24 g) was added during gentle stirring. The concentrations of supported Cu were estimated at 1.1 wt% for Cu/MCM and 0.78 wt% for Cu/TMS-MCM. The catalytic polymerization reaction was performed using 1,6-dimethylphenol (0.3 mmol) and pyridine (0.1 mL) in toluene (0.5 mL) under oxygen atmosphere at 298 K, in the presence of equivalent relative amounts of Cu sites in (1,6-dimethylphenol/Cu = 50).

Results and discussion

The nitrogen adsorption experiment (Table 1) indicated that TMS-MCM-TMS has decreased BET surface area, decreased primary mesopore diameter and increased pore wall thickness compared to MCM-41. The same analyses showed almost no difference between TMS-MCM and MCM-41, which is consistent with selective external sylilation of TMS-MCM.

Table 1. Textural Parameters of Modified Mesoporous Silicas.

Sample	BET surface area (m^2 g^{-1})	Primary mesopore volume (cc g^{-1})	Primary mesopore diameter (nm)	Pore wall thickness (nm)
TMS-MCM-TMS	850 ± 60	0.43 ± 0.03	3.5 ± 0.1	1.3 ± 0.1
TMS-MCM	1020 ± 80	0.75 ± 0.06	4.1 ± 0.1	0.8 ± 0.1
MCM-41	1080 ± 80	0.75 ± 0.07	4.0 ± 0.1	0.8 ± 0.1

As an application of the MCM-41 silylated selectively on the external surface, Cu-catalyzed polymerization of 1,6-dimethylphenol was investigated. $Cu(OAc)_2$ was supported on TMS-MCM and MCM to obtain Cu-supported mesoporous silica catalysts, Cu/MCM and Cu/TMS-MCM, respectively. Cu/TMS-MCM afforded a higher polymer product distribution than Cu/MCM. The higher molecular weight distributions can be attributed to the polymerization enhanced by the Cu species on the internal pore, where mass transfer limitation is likely to result in higher concentration of the polymer in the internal mesopore.
Quantitative analyses of the modified mesoporous silica were conducted by use of the recently developed solid-state ^{29}Si NMR will be also presented.

Conclusions

The surface silanol groups on mesoporous silica MCM-41 were silylated with trimethylsilyltrifluromethansulfonate (TMSOTf) to afford the selective silylation on the external surface. In the application of the silylated mesoporous silica in Cu-catalyzed phenol polymerization, $Cu(OAc)_2$ supported on the externally silylated MCM-41 exhibits higher catalytic activity than the corresponding Cu/MCM-41 catalyst without silylation.

Alkyllactates and Lactic Acid Prepared From Sugars Using Silica-Carbon Composite Materials

Filip de Clippel[a], Michiel Dusselier[a], Li Peng[a], Roosje Ooms[a], Lars Giebeler[b], Steffen Oswald[b], Paolo Pescarmona[a], Pierre A. Jacobs[a] and Bert F. Sels[*,a]

Center for Surface Chemistry and Catalysis, Katholieke Universiteit Leuven, Kasteelpark Arenberg 23, 3001 Heverlee,Belgium. Fax: +32 16 321998; Tel: +32 16 321610;
** Bert.sels@biw.kuleuven.be*

Introduction

Recently we presented a new class of carbon silica materials (CSM) with tunable bimodal porosity obtained by the synthesis of nano-sized graphitic crystallites inside the mesopores of a silica template [1]. Its porosity characteristics are readily controlled by the pyrolysis conditions and the amount of carbon precursor. These porous materials can be tuned from microporous over biporous to mesoporous composites. Past research by molecular probing techniques already demonstrated the shape selective properties of CSMs [1].
Here we report the use of this CSM composite in the valorisation of common sugar molecules. Lactic acid has the potential to become a green, very large volume and commodity-chemical intermediate as it can be produced from renewable carbohydrates. Both lactic acid and its ester derivatives are of major economic importance. Lactic acid is abundant in food processing and a key intermediate in the production of bio-degradable plastics. Alkyllactates are common in the pharmaceutical and cosmetic industry and highly anticipated as benign green solvent. Both can be catalytically produced from triose molecules e.g. dihydroxyaceton (DHA) by a two step pathway reaction involving both Lewis acid (LA) and Brønsted acid (BA) sites (Figure 1) [2]. Moreover an additonal retro-aldol reaction allows their synthesis straight from common sugars molecules e.g. sucrose [3]. The hybrid CSM allows for the independent introduction and tuning of these functionalities in order to optimize the synthesis of lactic acid or its ester derivative from DHA and straight from the sugar.

Experimental

Sn-Si-MCM-41 is prepared by the modified Stöber procedure and consequent grafting with anhydrous $SnCl_4$. After drying and calcination of the catalyst the pores are filled with a furfurylacohol carbon precursor solution by incipient wetness impregnation. Heating in He at 423 K initiates in situ polymerisation of the carbon. Further increase of the temperature up to 1173 K results in the final Sn-Si-CSM product. A selection of Sn-Si-CSM samples is treated in O_2 at various temperatures (373-773 K) for 8 hours. Catalytic conversion of trioses is performed for 6 hours in ethanol or water solvent at 363 K and 383 K respectively while hexoses are converted in methanol at 428 and 463 K for 20 and 6 hours respectively.

Results and discussion

Conversion of DHA in ethanol solvent demonstrates an increase of the ethyllactate (ELA) yield after addition of a carbon component from 26 % (Sn-MCM-41) up to 88 % at the highest carbon loading. Post synhesis oxidation of the CSM catalyst further enhances the ELA yield up to 100 %. Qualitative and quantitative analysis of the surface oxygen groups in the carbon fraction is performed using TPD, P-NMR and XPS. It shows the amount of oxygen

can be controlled by the pyrolysis temperature, the amount of carbon deposited into the silica pores and the oxidation treatment. It is well known surface oxygen groups are related to weak BA. As such a correlation between the amount of BA sites and the activity of the catalyst was demonstrated. Moreover all Sn-Si-CSM catalysts remain highly selective (95 %) towards the ELA product due to the absence of strong BA. Recycling experiments show no significant decrease in activity. Similar trends were observed in water solvent and lactic acid yields of 100% are obtained.

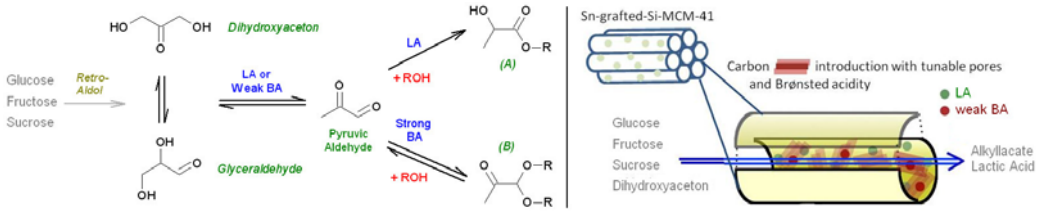

Figure 1: Reaction scheme of the conversion of mono- and disaccharides towards added-value alkyllactates

Finally Sn-Si-CSM catalysts are tested in the conversion straight from common sugars. As dehydratation of sugars is catalysed by BA and results in unwanted side products, subtle tuning of the balance between LA and BA is required. A maximal methyllactate yield of 41% is obtained at 428 K.

Conclusions

A new Silica-Composite material is presented with adjustable porosity. The hybrid nature allows for selective functionalisation and independent tuning of the catalytic sites on the silica and carbon component. This was demonstrated to be especially usefull in a one-pot multifunctional approach such as the conversion of sugars to lactates.

Acknowledgements

Special thanks are given to the Belgian Science Policy, the grant associated with its 'Interuniversity Attraction Poles' (IAP) program made this Ph.D. research topic possible. Also the 'Fond Wetenschappelijk Onderzoek' is greatfully acknowledged for its support.

References

[1] de Clippel F., Harkiolakis A., Ke X., Vosch T., Van Tendeloo G., Baron G.V., Jacobs P.A., Denayer J.F.M., Sels B.F., Molecular sieve properties of mesoporous silica with intraporous nanocarbon, Chemical Communications, 46 (2010), 928-930.
[2] Janssen K.P.F., Paul J.S., Sels B.F., Jacobs P.A., Glyoxylase biomimics: zeolite catalyzed conversion of trioses, Studies in Surface Science and Catalysis, 170B (2007), 1222-1227.
[3] Holm M.S., Saravanamurugan S., Taarning E., Conversion of Sugars to Lactic Acid Derivatives Using Heterogeneous Zeotype Catalysts, Science, 328 (2010), 602-605.
[4] de Clippel F., Dusselier M., Peng L., Ooms R., Giebeler L., Oswald S., Pescarmona P., Jacobs P.A., Sels B., Alkyl Lactate and Lactic Acid Prepared From Sugars Using Carbon-Silica Composite Materials, Journal of the American Chemical Society, *submitted.*

[V,Al]-ITQ-18: The novel delaminated catalyst obtained from [V,Al]-Nu-6(1) zeolite.

Mendelssolm K. de Pietre[1], Marco A. Fraga[2] and Heloise O. Pastore[1*]
[1]*Instituto de Química, Universidade Estadual de Campinas, Rua Monteiro Lobato 270, Campinas-SP, Brasil, CEP 13084-971,* [*]*gpmmm@iqm.unicamp.br*
[2]*Instituto Nacional de Tecnologia, Avenida Venezuela, 82. CEP:20081-312.*

Introduction

A new class of porous materials allowing the access of large molecules to the internal zeolitic area while maintaining the acidic sites found in zeolites are the layered materials that can be delaminated.[1] It is possible to obtain single or packs of layers with a certain degree of size selectivity, where the active sites are accessible from the external surface, as observed in ITQ-18, from delamination of Nu-6(1)[1].

Experimental

The synthesis gel of [V,Al]-Nu-6(1) was prepared with the following molar composition: SiO_2: xAl_2O_3: $yVOSO_4$: 0.14R: zNaOH: $33H_2O$ (R=4,4'-bipyridine). The synthesis of the layered precursor follows that in the literature.[1] The [V,Al]-Nu-6(1) prepared was suspended in a aqueous solution of cetyltrimethylammoniumbromide (CTABr) and tetraethylammonium hydroxide (TEAOH) and refluxed for 66 h. After that, the slurry was placed in an ultrasound bath (50W, 40 kHz) for 1 h. Half of the slurry was washed, dried and calcined at 640ºC, generating the [V,Al]-ITQ-18(B). Concentrated HCl was added to the other half until pH<2.0. It was washed, dried and calcined at 640ºC, generating the [V,Al]-ITQ-18(A). Catalytic experiments were performed under nitrogen in a micro reactor. Xylose (30 mg), powdered catalyst (20 mg) and a solvent mixture (W/T) comprising H_2O (0.5 mL) and toluene (1.0 mL) were poured into the reactor. The mixture was heated at 140ºC and stirred for 1h. The samples were characterized by: X-ray diffraction (Shimadzu XRD 7000, CuKa, 30 mA, 40 kV), UV-Vis spectroscopy (UV-Vis-Nir Cary 50), ^{29}Si- ^{27}Al- and ^{51}V-MAS-NMR (Bruker Avance 400+) and surface area (Micromeritics, ASAP 2020). The products in the aqueous and organic phases were quantified using HPLC (Alliance).

Results and discussion

X-ray diffraction (Fig 1A) confirms the formation of the layered precursor, [V,Al]-Nu-6(1).[1] The swollen material presented a peak at $2\theta = 2.3^{o}$ (≈ 4.0 nm) indicative that CTA^+ is intercalated in the precursor, causing turbostratic effects as observed by the broadening of the peaks and their diminished intensity. After ultrasound treatment and acid treatment, no structural differences in relation to the swollen material were observed. The alkaline- and acid-treated materials were calcined generating the [V,Al]-ITQ-18(B) for alkaline- and [V,Al]-ITQ-18(A) for acid-treated samples. The specific BET surface area confirms the success of the delamination: the Nu-6(2) zeolite presents S_{BET}=70 m^2/g and S_{micro}=43 m^2/g, while the delaminated sample, values of S_{BET} =852 m^2/g and S_{micro}=14 m^2/g were found. ^{29}Si-MAS-NMR (Fig 1B) shows the presence of Q_4 sites typical of three-dimensional structure. Differently, for delaminated samples, the presence of Q_3 and Q_2 sites is observed, typical of single sheets found in delaminated structures.[1] In the ^{27}Al-MAS-NMR spectra of delaminated samples (not shown) tetrahedral Al sites, responsible for strong Bronsted acid sites were observed. In accordance with UV-Vis spectra (Fig. 1D) that presents bands attributed to tetrahedral V^{5+} species with different distortion degrees (at 215, 270 and 335 nm)[2] the ^{51}V-MAS-NMR (Fig 1C) spectra shows the presence of tetrahedral vanadium species with signals at -570 and -625 ppm.[2] For [V,Al]-ITQ-18(B), the only signal observed

is the one due to tetrahedral species (-625 ppm) while for [V,Al]-ITQ-18(A) sample two new signals appear at -507 and -520 ppm, along with a new UV-vis band at 400 nm (Fig 1D); these signals can be assigned to extraframework octahedral vanadium species. The extraframework situation of this V species was easily confirmed by after ion-exchange with NH_4Cl followed by calcination: the procedure made the band to disappear. Finally, the advantages of the delaminated materials in catalytic reactions are clearly observed in the xylose dehydration, Fig 1E. The best conversions and selectivies to furfural were achieved for delaminated samples indicating that xylose molecules have an easier access to the active acid sites of the delaminated samples in relation to Nu-6(2) zeolite. The extraframework species present in [V,Al]-ITQ-18(A) have strong influence in the reaction since conversion and selectivity decreased after their removal by ion-exchange with NH_4Cl.

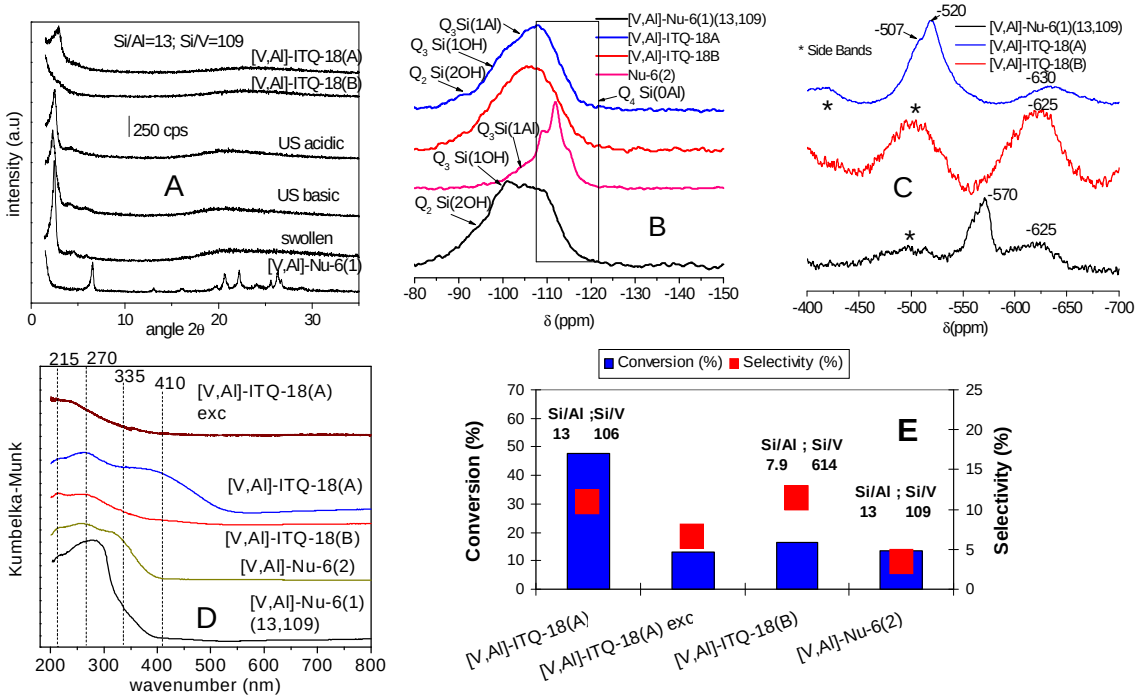

Figure 1: (A) X-ray patterns of [V,Al]-ITQ-18 synthesis; (B) ^{29}Si-MAS-NMR, (C) ^{51}V-MAS-NMR , (D) UV-Vis spectra and (E) Xylose conversion and Furfural selectivity after 1h, at 140 ^{o}C.

Conclusions

The delamination process was successfully performed and both vanadium and aluminium are incorporated into the framework. The delamination performed in alkaline media caused the extraction of framework V atoms that were reprecipitated upon addition of acid to extraframework octahedral sites that can be easily ion exchanged. The material prepared under alkaline conditions presented tetrahedral vanadium species only. The delaminated materials are more active and selective to furfural in the xylose dehydration than the corresponding zeolite.

Acknowledgments

The authors thank the Fundação de Amparo à Pesquisa no Estado de São Paulo (FAPESP) and Conselho Nacional de Desenvolvimento Científico e Tecnológico (CNPQ) for financial support and fellowships, respectively.

References

[1] A. Corma; V. Fornés; U. Díaz, *Chem. Commun.*, **2001**, 2642–2643

[2] S. Dzwigaj Curr. *Opin. Solid State Mater. Sci.*, **2003,** 7, 461.

Selective oxidation of tetralin over Cr-containing mesoporous catalysts

Adrienn Bangó*, János Halász
Department of Applied and Environmental Chemistry, University of Szeged, Rerrich tér 1, H-6720 Szeged, Hungary; adriennbango@gmail.com

Introduction

Oxidation is one of the most fundamental transformations in organic chemistry. Important intermediates for fine chemical production can be prepared by direct hydroxylation or selective oxidation of condensed cyclic hydrocarbons, such as naphthalene, tetralin or decalin [1]. Selective oxidation of tetralin produces mainly 1-tetralone, that is keto-hydronaphthalene used as a reactive intermediate. It can be converted to compounds of industrial importance, including dyes, pharmaceuticals and agrochemicals [2]. 1-Tetralone is important commercially as the starting material for 1-naphthol manufacture [3].
Oxidation of condensed aromatics with H_2O_2 was studied over ZSM-5, MCM-41 and SBA-15 catalysts modified byTi, Fe, Cr and V. In the presence of mesoporous catalysts significant activity and selectivity could be observed, the optimal yield was found over Cr-MCM-41 [4]. The use of aqueous H_2O_2 in the oxidation of organic substrates is very attractive from the point of view of synthetic organic chemistry, since aqueous H_2O_2 is an environmentally clean and easy to handle reagent [5].
The aim of present work is to clarify the details of the oxidation of condensed tetralin by H_2O_2 over Cr-MCM-41 and Cr-SBA-15 catalysts, and to find the optimal conditions for production of 1-tetralone (or 1-tetralole).

Experimental

MCM-41 materials were synthesized of the literature procedure [6]. Cr-MCM-41 samples were synthesized like for Si-MCM-41 sample, but $Cr(NO_3)_3 \cdot 9H_2O$ (1; 5 %, Aldrich) was added to the solution of C_{16}TMABr, water and ethanol. The SBA-15 synthesis was carried out by Zhao's method [7]. For incorporation of Cr, either distilled water solution of $Cr(NO_3)_3$ (1 and 5 %) was added to the starting mixture.
The catalyst samples were characterized by XRD, N_2 adsorption and TEM. The oxidation of tetralin was carried out at 50 ^oC for 5 hours in a continuous mixed glass reactor The reaction mixtures were prepared with molar ratio of tetralin to oxidant (H_2O_2) = 1:1 and 1:5 in acetonitrile as solvent. The H_2O_2 concentration was determined by titration with $KMnO_4$. The GC analysis was carried out using a *Shimadzu GC2010* equipment with *Supelco SPB624* column.

Results and discussion

On the data of XRD patterns and TEM pictures is clearly evident the mesoporous nature of our synthesized catalyst. The X-ray diffractograms were recorded at low diffraction angles for the calcined Cr-MCM-41 and Cr-SBA-15 samples. Sharp reflection lines in the 2θ ~2° were observed (Fig.1). The TEM picture shows the hexagonal structure of the SBA-15 and MCM-41 (Fig 2).
The conversion data can be seen on Fig. 3. At the given conditions the MCM-41 sample exhibits the highest conversion, while in the presence of SBA-15 only ~ 5 % conversion can be reached. The selectivities are depicted on Fig. 4. Over Cr-MCM-41 (5 %) the main products are the tetralone and the tetralol, the selectivity for these two components is close to 70 %.

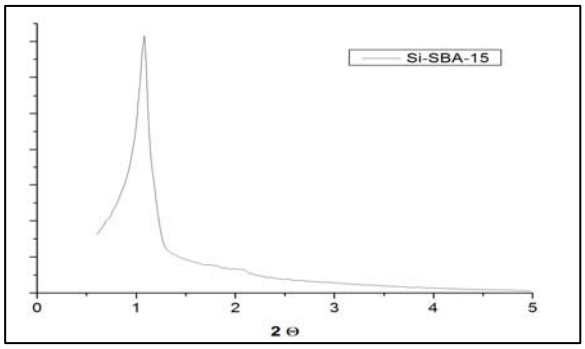

Figure 1. XRD pattern of Cr-SBA-15

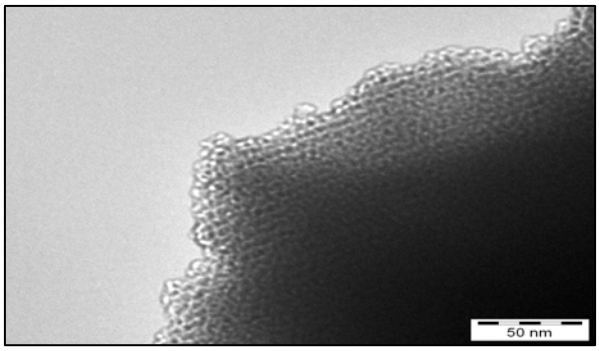

Figure 2. TEM images of Cr-SBA-15

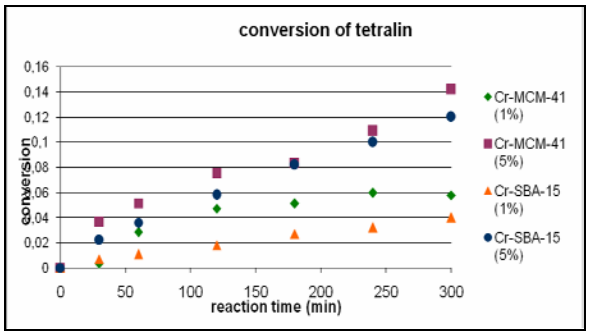

Figure 3. Conversion of tetralin over Cr-MCM-41 and Cr-SBA-15

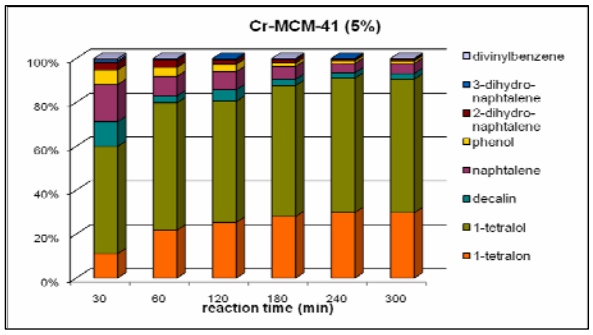

Figure 4. Selectivity of products in the oxidation of tetralin over Cr-MCM-41 (5%)

Over Cr-SBA-15(2) broader spectrum of product can be observed (see Fig. 9 and 10), however, the selectivity for the desired compounds also high. Two important facts can be appointed: (i) the conversion is relatively high and (ii) the chromium release is not taking place. It means that the catalyst is stable and reusable.

Conclusions

In the case of the synthesized Cr-containing mesoporous catalysts, the MCM-41 exhibits the highest conversion, while using SBA-15, the conversion depends on the preparation method. Considering the selectivity in the oxidation of tetralin, the formation of 1-tetralone and 1-tetralol with relatively high yield could be reached in acetonitrile over MCM-41, however chromium leaching was observed. Over Cr-SBA-15 prepared by isomorphous substitution the 1-tetralone/tetralol yield is slightly lower than that of MCM-41, however no chromium extraction can be detected, so this catalyst is reusable and the leaving Cr^{3+} or Cr^{6+} do not contaminate the product or the environment.

References

[1] R.A. Shaik, G. Chandrasekar, K. Biswas, J.S. Choi, W.J. Son, S.Y. Jeiong, W.S. Ahn, Catal. Today, 132 (2008) 52.
[2] A. Covarrubias-Zuniga, F. Cantu, L.A. Maldonado, J. Org. Chem. 63 (2008) 2918.
[3] J.D. Chen, R.A. Sheldon, J. Catal. 153 (1995) 1.
[4] A. Bangó, J. Halász, React. Kinet. Catal. Lett., 96 (2009) 413.
[5] W.R. Sanderson, Pure Appl. Chem. 72 (2000) 1289–1304.
[6] M. Grün, I. Lauer, K.K. Unger, Adv.Mater., 9 (1997) 254.
[7] Zhao D., Feng J., Huo Q., Melosh N., Frederickson G.H., Chmelka B.F., Stucky G.D., Science 279 (1998) 548.

Hydrogenation of light unsaturated nitriles over Pt and Rh nanoparticles supported on mesoporous materials

Adrienn Bangó, János Halász and István Hannus*

Department of Applied and Environmental Chemistry, University of Szeged
Rerrich tér 1, H-6720 Szeged, Hungary; hannus@chem.u-szeged.hu

Introduction

The chemoselective hydrogenation of unsaturated carbonyl or nitrile compounds is basic process in the synthesis of important fine chemicals. The unsaturated amines are most valuable products in the reaction of nitriles, however, the selective hydrogenation of –CN group in the presence of C=C bond is a difficult task [1]. These reactions can be achieved over supported noble metals, however, there are several factors affected on the activity and selectivity. These are the metal, support, size and shape of the particles, preparation, activation, etc. Pt, Rh nanoparticles supported on MCM41 or SBA15 mesoporous materials could be active and selective in the hydrogenation of unsaturated nitriles. Pt and Rh nanoparticles can be prepared by alcohol reduction of the proper salt in the presence of PVP [poly(vinyl-pyrrolidone)] [2,3].

In this work we prepared different Pt and Rh catalysts supported on SBA15 and MCM41 mesoporous structures and tested them in the hydrogenation of light α,β-unsaturated nitriles (acrylonitrile: AN, methacrylonitrile: MAN and crotonitrile: CN).

Experimental

For synthesis of Pt nanoparticles PVP was sonicated in ethylene glycol (EG), and K_2PtCl_4 dissolved in distilled water was dropped into the PVP solution slowly. In synthesis of Rh nanoparticles $RhCl_3$ was dissolved in water and it was added to a stirred solution of PVP in EG at 190 °C.

For preparation of supported catalysts, calculated amount (0.1, 1.0 or 2.0 w/w%) of Pt, Rh or Pt,Rh (bimetallic) nanoparticle solution was mixed in ethanol and pure siliceous SBA15 or MCM41 was added and the suspension was sonicated.

The nanoparticles were characterized by XRD and TEM and the supported samples were analyzed by TEM and nitrogen adsorption.

Acrylonitrile hydrogenation was monitored using a reaction cell that permitted IR measurements of the gas phase as well as the catalyst surface that was pressed in a wafer and inserted in the reactor. IR spectroscopy is an excellent tool for analyzing different unsaturated nitriles [4].

The hydrogenation of nitriles was carried out in the temperature range of 20-50 ^oC in a laboratory batch reactor with flowing hydrogen at atmospheric pressure using acetone as solvent. For each experiment 1 cm^3 reactant (AN, MAN or CN) and 100 mg catalyst was added into 50 cm^3 solvent, and the reaction was followed by five hours. The GC analysis was carried out using a Shimadzu GC2010 equipment with a Supelco SPB-PUFA column.

Results and discussion

Fig. 1 shows the TEM images of Pt (Fig. 1/A) and Rh (Fig. 1/B) nanoparticles. The particles are dominantly cubic, while the particle size distribution is quite uniform. We found that the average particle size of Pt nanocrystals is 3-4 nm, while the average size of the discrete Rh particles is about 7-8 nm.

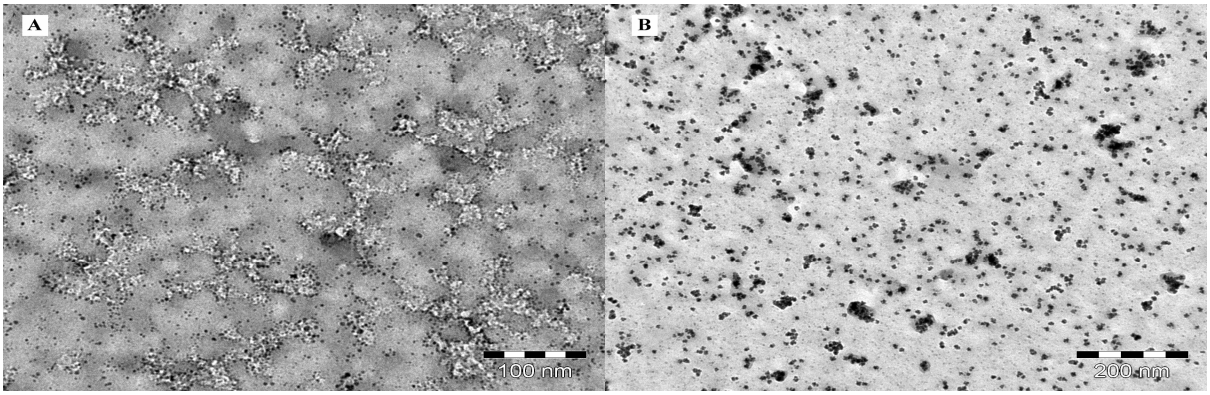

Figure 1: TEM images of Pt (A) and Rh (B) nanoparticles

In the hydrogenation of AN in the presence of Pt/SBA15 the formation of allylamine as intermediate and propylamine (PA) could be detected. Unexpectedly amount of propionitrile could be observed, while it would be the main product of hydrogenation of C=C bond. However, all of the components mentioned reacted further to form di- and tri-PA.

Over Rh/SBA15 formation of propionitrile was observed indicating the activity of this catalyst in the hydrogenation of C=C bond.

In the hydrogenation of MAN over Pt/SBA-15, the formation of methallylamine (max. selectivity 20 % at 1 h reaction time) and isobutylamine (25 % at 4 h) was higher than the similar products in the reaction of AN. Formation of higher amines also took place with total hydrogenation into isobutene. Over Rh/SBA-15 both butyronitrile (max. 27 % at 3 h) and isobutylamine (~ 20 % at 4 h) formed.

The kinetic curves of CN hydrogenation can be seen on Fig. 2. The conversion of CN is close to 100 % at 5 h. The selectivities have similar features but higher values for the valuable products than that of AN or MAN.

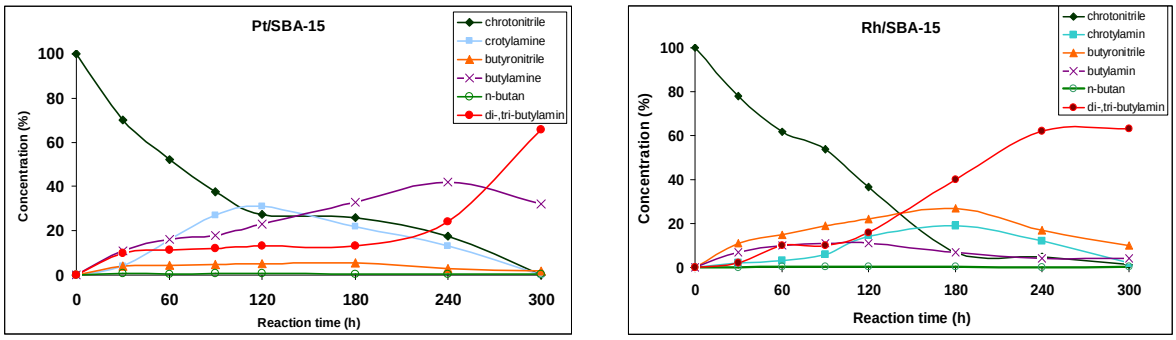

Figure 2: Typical reaction profiles of crotonitrile hydrogenation in butanol at 50 °C, Pt/SBA-15, Rh/SBA15

Conclusion

The nanoparticle containing Pt/SBA15 and Rh/SBA15 catalyst are active in the hydrogenation of light unsaturated nitriles, the reactions are different over the catalysts system, which is a proper starting point to the optimization for production the desired compounds.

References

1. P. Kukula and K. Koprivova: J. Catal., 234 (2005) 161.
2. M.E. Grass, R.M. Rioux and G.A. Somorjai: Catal. Lett., 128 (2009) 1.
3. J.R. Renzas, Y. Zhang, W. Huang and G.A. Somorjai: Catal. Lett. 132 (2009) 317.
4. A. Béres, Z, Kónya, I. Hannus, Á. Molnár and I. Kiricsi: Appl. Catal. A: Gen., 146 (1996) 331.

Post-functionalization of IRMOF-3 with Chiral "Pincer" Transition Metal Complexes. New Recyclable Enantioselective Catalysts on Hydrogenation of Alkenes.

A. Arnanz, C. del Pozo-Ochoa, G. Villaverde-Cantizano, M. Iglesias and F. Sánchez
Instituto de Quimica Orgánica (CSIC). Juan de la Cierva, 3 28006 Madrid. Spain.
Instituto de Ciencia de Materiales de Madrid (CSIC). Sor Juana Inés de la Cruz, 3 28049 Cantoblanco (Madrid). Spain.

Introduction

Metal-organic frameworks (MOFs) are porous, crystalline materials that are attractive for applications in gas adsorption,[1] separations,[2] and catalysis[3] because of their chemical tunability, high porosities, and good thermal stability.[4] Unfortunately, some of the most promising materials are limited because of instability with respect to moisture. Stabilizing these MOFs against ambient humidity would make these porous materials more suitable for specialized and industrial applications. The post-synthetic modification (PSM) approach, which has become an important tool in developing diverse systems with extended functionally and introducing new physical and chemical properties into MOFs,[5] offers an opportunity to address this challenge.

Results and discussion

Amine-containing MOFs can readily undergo PSM to form imine-functionalized MOFs.[6] This work presents the effect of PSM on isoreticular metal-organic framework (IRMOFs-3). IRMOFs-3 is a cubic framework comprised of Zn_4O clusters and 2-amino-1,4-benzenedicarboxylate (NH_2-BDC). In this work we have prepared new catalysts by post-derivatization of an IRMOF-3 through their amine group by reaction with a series of chiral precursors, obtained from 2-bromomethyl-6-hydroxymethylpyridine by reaction with a chiral amine and oxidation to aldehyde.

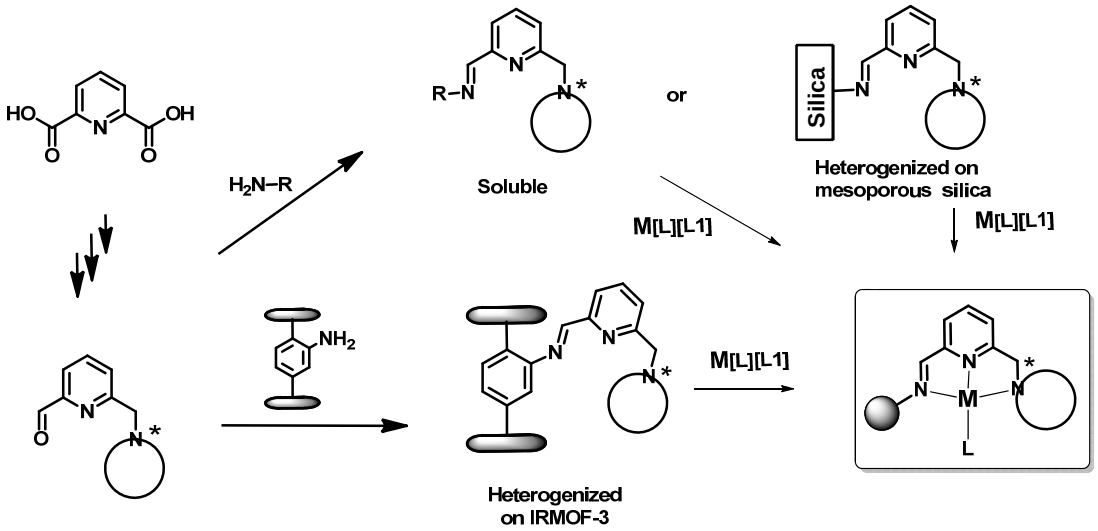

Scheme 1. Synthesis of new catalytic materials: soluble, heterogenized on a silica matrix and heterogenized on IRMOF-3 support.

In a previous step we have prepared soluble organometallic complexes with imine-pyridine-amine ligands for use in homogeneous media and grafted complexes on MCM-41 mesoporous silicas optimazing the reaction conditions.

For preparation of functionalized IRMOF-3, a sample of freshly prepared porous material, thoroughly washed with chloroform to remove occluded DMF solvent and dried under "vacuo", was contacted at room temperature with a chloroform solution of an amine-aldehyde, to form an imine group which causes a color change from cream to light or deep yellow (depending on the loading of aldehyde). The color change is accompanied by a new UV–Vis absorption band at 450 nm and a new ^{13}C NMR band at 167 ppm due to the C = N, which are indicative of the formation of the corresponding imine, as similar founded in soluble ligands synthetized previously. The final step to prepare the new complex-containing material, IRMOF-3-[M], consisted in reacting a suitable complex precursor ($PdCl(cod)_2$, $[Rh(cod)(thf)_2]PF_6$) with the imine-modified material.

The new heterogenized complexes, IRMOF-3-[M] were compared with the reference soluble complexes and with the heterogenized catalysts over MCM-41 mesoporous silica matrices. Preliminary studies on the catalytic activity of the aminopyridineimino- IRMOF-3-Rh and Pd complexes show that are active catalysts for hydrogenation and cyclopropanation of test alkenes with an activity similar to that observed for the corresponding soluble systems used as reference. The enantioselectivity observed forhydrogenation of substrates as diethyl itaconate is marginal and increases with increasing steric hindrance around of double bond. The catalysts are easily recovered from the reaction by simple filtration and reused in several successive reactions.

Conclusions

A novel catalysts has been prepared by modification of a amine-containing metal organic framework (IRMOF-3) with coordinative unsaturated transition metal complexes based on a post-synthesis strategy. The resulting heterogeneous IRMOF-3-[M] catalyst exhibits catalytic activity which has emulated the catalytic properties of homogeneous transition metal catalysis, moreover the supported catalysts could be recycled several times by simple isolation for filtration or centrifugation without lost of catalytic performances.

Acknowledgements

We thank the Dirección General de Investigación Científica y Técnica of Spain (Project MAT2006-14274-C02-02, Consolider-Ingenio 2010-(CSD-0050-MULTICAT) for financial support.

References

[1] Murray, L. J.; Dinca, M.; Long, J. R. Chem. Soc. Rev. 38 (2009**),** 1294– 1314.
[2] Li, J.-R.; Kuppler, R. J.; Zhou, H.-C. Chem. Soc. Rev. 38 (2009**),** 1477– 1504.
[3].(a) Lee, J. Y.; Farha, O. K.; Roberts, J.; Scheidt, K. A.; Nguyen, S. B. T.; Hupp, J. T. Chem. Soc. Rev. 38 (2009**),** 1450–1459; (b) Ma, L.; Abney, C.; Lin, W. Chem. Soc. Rev. 38 (2009**),** 1248–1256.
[4] Long, J. R.; Yaghi, O. M. Chem. Soc. Rev. 38 (2009**),** 1213–1214.
[5] Wang, Z.; Cohen, S. M. Chem. Soc. Rev. 38 (2009**),** 1315–1329
[6] X. Zhang, F. X. Llabrés i Xamena, A. Corma, J. Catal. 265 (2009), 155 – 160.

Zeolites: An efficient catalyst for the synthesis of coumarin derivatives

Abbas Teimouri[1], Alireza Najafi Chermahini[2]
1. Faculty of science, Payame Noor University (PNU), Isfahan, P.O.Box: 81395-671, Iran
Email: a_teimouri@pnu.ac.ir
2. Department of Chemistry, Faculty of science, Yasouj university, Yasouj, Iran

Abstract

A simple highly versatile and efficient synthesis of various Synthesis of coumarins from phenols and ethyl acetoacetate using zeolite as a catalyst in ethanol at moderate temperature. Short reaction times and milder conditions, easy work-up and purification of products by non-chromatographic methods. The catalyst can be recovered for the subsequent reactions and reused without any appreciable loss of efficiency.

Keywords: Zeolite, Green synthesis, coumarin.

Introduction

Coumarins, are one of the most important compounds of natural product and in synthetic organic chemistry. The synthesis of coumarins and their derivatives has attracted considerable attention from organic and medicinal chemists for many years as a large number of natural products contain this heterocyclic nucleus. They are widely used as additives in food, perfumes, cosmetics [1], pharmaceuticals and optical brighteners [2]. Coumarin derivatives also find applications in pharmaceutical, fragrance and agrochemical industries [3].

Coumarin and its derivatives can be synthesized by various methods, Pechmann reaction is the most widely used method for the preparation of substituted coumarins since it proceeds from condensation of phenols with beta-ketonic esters in the presence of a variety of acidic condensing agents. Substituted coumarins can be prepared by using various reagents such as H_2SO_4, $POCl_3$ [4], $AlCl_3$, $FeCl_3$, HCl, $TiCl_4$, $ZnCl_2$, Heteropolyacids [5], trifluoro acetic acid [6], clays [7], solid acid catalysts [8], Zr solid acid catalysts [9], ionic liquids [10]. However, these reagents are required in excess and their corrosive nature makes them difficult to handle, and formation of several side products is a problem.

As a part of our continuing effort towards the development of useful synthetic methodologies [11]. Herein, we report the Synthesis of coumarins from phenols and ethyl acetoacetate using zeolite as a catalyst in ethanol under reflux.

2. Experimental

All reagents were purchased from Merck and Aldrich and used without further purification. Products were characterized by spectroscopy data (IR, FTIR, ^{1}H NMR and ^{13}C NMR spectra), elemental analysis (CHN) and melting points.

ZSM-5 Zeolite was synthesized according to the procedure described earlier. The solid phase obtained was filtered, washed with distilled water several times, dried at 120 °C and then calcined at 550 °C. And followed by ion exchange with NH_4NO_3 solution (three times), the acid hydrogen form of the compound is prepared by transferring the oven-dried compound to a tube furnace. Heat the ammonium zeolite for 3 hours to ensure the thermal decomposition of NH_4^+ ions. [12].

3. Results and discussion

In the reaction between phenols and ethyl acetoacetate, (scheme 1) to minimize the formation of byproducts and to achieve good yield of the desired product, the reaction is optimized by varying the amount of catalyst, we found ethanol and 25 mg of zeolite catalyst an efficient reaction medium in terms of reaction time as well as yield.

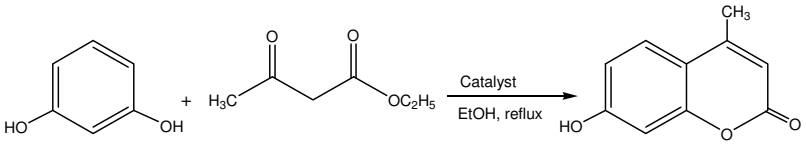

Scheme 1. Schematic synthesis of coumarins

4. Conclusions

In conclusion, a one-pot, mild, efficient, and environmentally benign protocol has been developed for the synthesis of, quinoline derivatives catalyzed by zeolites in high yields. Compared to previously reported methods, Moreover, the mild reaction conditions, easy work-up, clean reaction profiles, lower catalyst loading and cost efficiency render this approach as an interesting alternative to the existing methods.

References

[1] Kennedy, O., Thornes, R.D., Coumarins: Biology, Applications and Mode of Action, Wiley and Sons, Chichester, 1997.
[2] Zahradnik, M., The Production and Application of Fluorescent Brightening Agents, Wiley and Sons, 1990.
[3] Gunnewegh, E.A., Hoefnagel, A.J., van Bekkum, H., J. Mol. Catal. A: Chem. 100 (1995) 87.
[4] Ahmed, S.Z., Desai, R.D. Proc. Ind. Acad. Sci. 5A (1937) 277.
[5] Heravi, M. M., Sadjadi, S., Oskooie, H. A., Hekmat Shoar, R., Bamoharram, F. F., Catalysis Communications 9 (2008) 470–474.
[6] Woods, L.L., Sapp, J., J. Org. Chem. 27 (1962) 3703.
[7] Biswas, G.K., Basu, K., Barua, A.K., Bhattacharya, P., Ind. J. Chem. 31B (1992) 628.
[8] Hoefnagel, A.J., Gunnewegh, E.A., Downing, R.S., Bekkum, H.V., J. Chem. Soc. Chem. Commun. (1995) 225.
[9] a) Reddy, Benjaram M., Patil, Meghshyam K., Lakshmanan, Pandian., Journal of Molecular Catalysis A: Chemical 256 (2006) 290–294.
b) Tyagi, Beena., Mishra, Manish K., Jasra, Raksh V., Journal of Molecular Catalysis A: Chemical 286 (2008) 41–46.
[10] a) Potdar, Mahesh K., Mohile, Swapnil S., Salunkhe, Manikrao M., Tetrahedron Letters 42 (2001) 9285–9287. b) Singh, V., Kaur, S., Sapehiyia, V., Singh, J., Kad, G.L., Catalysis Communications 6 (2005) 57–60.
[11] a) Dabbagh, H. A., Teimouri, A., Najafi Chermahini, A., Journal of Applied Catalysis B: Environmental. 76 (2007) 24. b) Teimouri, A., Najafi Chermahini, A., Momenbeik, F., Zarei, A., Dalirnasab, Z., Ghaedi, A., Journal of Heterocyclic Chemistry 47 (2010) 913.
[12] a) Argauer, R. J., Landolt, G. R., *US Patent No. 3 702 886*, 1972. b) Dwyer, J., Chemistry and Industry, 2, April (1984) 258-26. c) Guth, J. L., Non-ConventionalCrystalline Microporous Solids, in Zeolite Microporous Solids: Synthesis, Structure, and Reactivity, Kluwer Academic, The Netherlands, 1992, 49. d) Choudhary, V. R., Panjala, D., Banerjee, S., Applied Catalysis A: General 231 (2002) 243–251.

Separations

FEZA 2011

Multi-Component Adsorption of Heavy Metal Ions from Aqueous Solutions onto Nano-Structured Calcium Silicate

Martin Klimsa[1], Giancarlo Barassi[1], Thomas Borrmann[1], Joachim Kinkel[2]
[1]*Victoria University of Wellington, New Zealand, martin.klimsa@vuw.co.nz*
[2]*Georg-Simon-Ohm Hochschule Nuernberg, Germany*

Introduction

A novel sorbent material, nano-structured calcium silicate (NCaSil), for removing toxic metal ions from industrial, communal or agricultural wastewaters has been investigated. NCaSil comprises nano-sized calcium silicate platelets 5-10 nm thick and up to 300 nm across[1]. These self-assemble into particles of approximately 1-5 µm in size with a three-dimensional open framework "gypsum desert rose" structure which significantly distinguishes NCaSil from other amorphous silicates. The material has a high porosity and pore volume accommodating up to 500-700 g oil 100 g^{-1} silicate (ASTM Oil Absorption test D281) and a high and readily accessible surface area of up to 700 m^2 g^{-1}(see Figure 1); both of these features are controllable during the synthesis. The surface of the nano-sized platelets contains both silanol (Si-OH) groups and Ca^{2+} ions which collectively provide bonding sites for the adsorption of ions and functionalisation of the NCaSil by various species of ions [2].

The kinetics and equilibrium data of the up-take of Cu^{2+}, Fe^{2+} and Pb^{2+} as single, binary and ternary component systems have been conducted. The Langmuir and Freundlich isotherm models were applied and from the kinetic studies, various rate and thermodynamic parameters were evaluated.

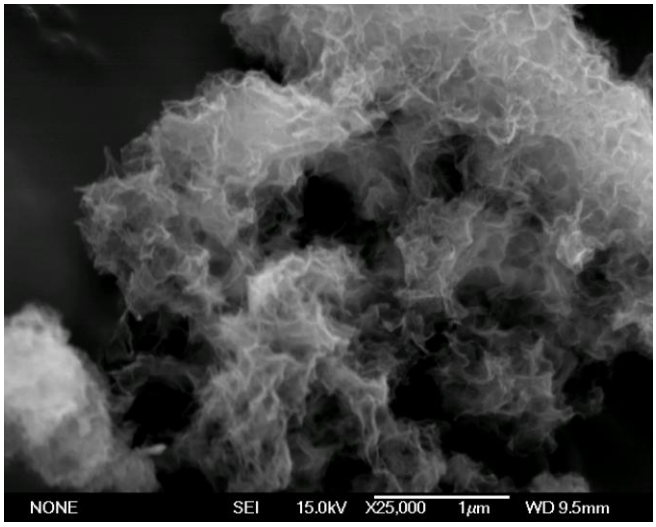

Figure 1: SEM image of NCaSil showing its porous microstructure.

Experimental procedure

Batch sorption studies were performed to obtain both rate and equilibrium data. Different temperatures and metal ion concentrations were employed to obtain isotherm parameters. Known amounts of NCaSil were added to the metal containing solutions and the temperature

was adjusted. 24 hours was chosen as the contact time to establish the reaction equilibrium based on preliminary experiments. After filtering the solutions the remaining concentrations of Cu^{2+}, Fe^{2+} and Pb^{2+} were determined using atomic adsorption spectroscopy (AAS).

To investigate the kinetic data a known mass of NCaSil was added to a metal containing solution and samples were taken at certain times (usually 9 samples were collected in the first hour of an experiment) and the metal ion concentration remaining in solution was measured again by AAS.

For the characterisation of starting and recovered materials scanning electron microscopy (SEM), dispersive X-ray spectra analysis (EDS) and X-ray diffraction spectroscopy (XRD) were used.

Results and discussion

First results show that NCaSil is able to adsorb divalent metal ions out of aqueous solutions as shown in Figure 2.

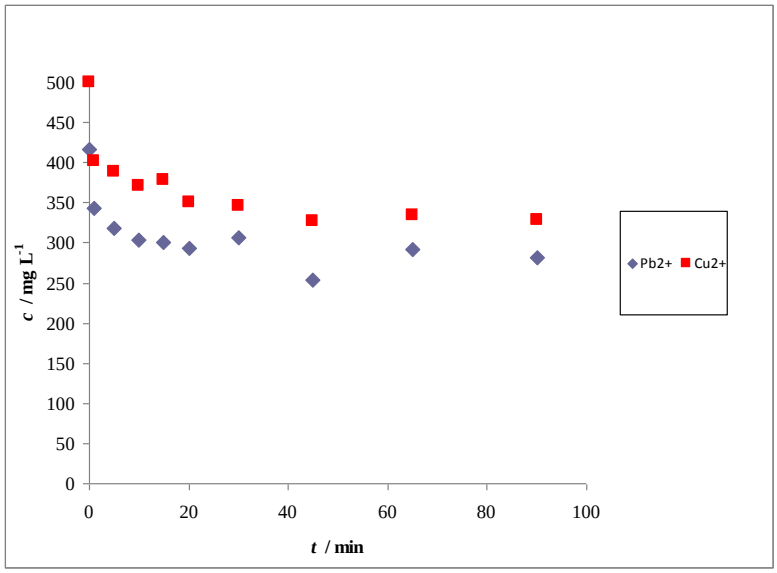

Figure 2: Binary component sorption of Cu^{2+} and Pb^{2+} using 1 g L^{-1} NCaSil at room temperature

XRD and EDS analyses approximate that the silicate promotes formation of minerals and metal salt(s) depending on the as source materials. In the case of $CuSO_4 \cdot 5H_2O$ as a source, Brochantite starts to grow on the surface of NCaSil. This process means that the adsorbed metal ions are transformed into salts that are stable in solution and can be removed to obtain water purification and minerals that can be processed to recover the metals.

References

[1] McFarlane, A.J., The Synthesis and Characterisation of Nano-Structured Calcium Silicate, PhD Thesis in School of Chemical and Physical Sciences. 2007, Victoria University of Wellington: Wellington.

[2] Cairns, M. J., Borrmann, T., Hoell, W. H.; Johnston, J. H. A study of the uptake of copper ions by nanostructured calcium silicate, Microporous and Mesoporous Materials, 95 (2006), 126–134.

Preparation of Silicalite Pervaporation Membrane for Concentrating Ethanol from Ethanol-water mixture

Hideyuki Negishi, Toru Ikegami and Keiji Sakaki
National Institute of Advanced Industrial Science and Technology (AIST),
h-negishi@aist.go.jp

Introduction

Silicalite membranes with high alcohol permselectivity are expected for use in the continuous separation/concentration process of bio-ethanol and bio-butanol which are produced from the fermentation broth [1-3]. Pervaporation (PV), which employs ethanol-permselective silicalite membranes, is a promising approach for refining low-concentration bio-ethanol solutions as an alternative to distillation [4]. We also reported the preparation of the tubular silicalite membranes [5]. Highly efficient membrane with high reproducibility is required for utilization.
In this study, we investigated the reproducibility of silicalite membranes and the membrane separation performance for concentrating ethanol from ethanol/water mixture by PV.

Experimental

Silicalite membranes on a tubular porous stainless steel support were prepared by hydrothermal synthesis with an electrophoretic deposition as a seeding. This is a general secondary growth method. Seeding conditions, composition of synthetic gel and temperature conditions of hydrothermal synthesis were also the same with those of our previous report [5]. Controlling the aging temperature of synthetic gel was studied. The aging conditions were controlled at specific temperature in the range of 25 to 30°C for 3 h 20 min to 3 h 40 min; i.e., at 25°C for 3 h 40 min. Pervaporation separation of ethanol from 5wt% ethanol-water mixture was measured at 30°C and 60°C.

Results and discussion

Membrane separation performance of the prepared silicalite membranes is shown in Fig. 1. This is the result of PV of the ethanol from the ethanol/water mixture at 30°C. Solid symbols denote the performance of the membranes by the hydrothermal synthetic gel aged at room temperature for 3 h 20 min. Here, the room temperature means 18 to 28°C. Therefore, it is thought that the temperature during aging maybe changed. In these cases, the membrane performance varied greatly.
On the other hand, open symbols denote the performance of the membranes by the hydrothermal synthetic gel whose aging temperature and time was controlled precisely. Here,

aging temperatures were within the 25 to 30°C, and the variation of temperature during aging was controlled within 1K. In these cases, separation factor showed at least 50. It means permeated ethanol was concentrated from 5 wt% to at least 72 wt% at 30°C. This suggested that the fabrication reproducibility of the silicalite separation membrane improved remarkably. The average of total flux showed about 0.4 kg/m^{2}h at 30°C. Furthermore, by the membranes prepared on these strict conditions, flux also increased as separation factor improved.

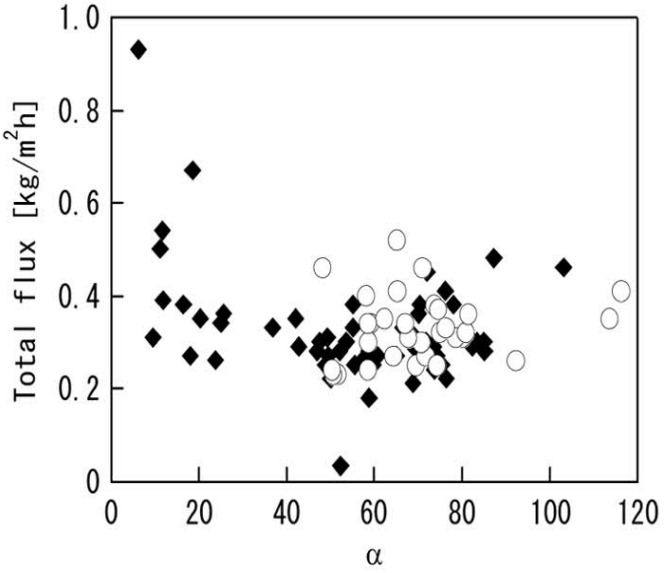

Fig. 1 Ethanol pervaporation performance of silicalite membrane from 5wt% ethanol/water mixture at 30°C
◆: Aging conditions of hydrothermal synthesis gel at room temperature (18 to 28°C with no temperature controlled),
○: Aging conditions of hydrothermal synthesis gel controlled strictly at 25 to 30°C and the variation was within 1K.

Conclusions

By controlling the aging conditions of hydrothermal synthetic gel strictly, especially, to prevent variation of the aging temperature of the gel, silicalite membranes of high membrane separation performance were able to be produced with sufficient reproductively.

Acknowledgements

This work was supported by the New Energy and Industrial Technology Development Organization (NEDO) of Japan.

References

[1] T. Ikegami, D. Kitamoto, H. Negishi, K. Haraya, H. Matsuda, Y. Nitanai, N. Koura, T. Sano, and H. Yanagishita, *J. Chem. Technol. Biotechnol.*, **78**, 1006-1010 (2003).
[2] D. J. O'Brien, L. H. Roth and A. J. McAloon, *J. Memb. Sci.*, **166**, 105-111 (2000).
[3] H. Negishi, T. Ikegami and K. Sakaki, *Chem. Lett.*, **39**, 1312-1314 (2010).
[4] T. Ikegami, T. Morita, S. Nakayama, H. Negishi, D. Kitamoto, K. Sakaki, Y. Oumi, T. Sano, K. Haraya and H. Yanagishita, *J. Chem. Technol. Biotechnol.*, **84**, 1172-1177 (2009).
[5] H. Negishi, M. Okamoto, T. Imura, D. Kitamoto, T. Ikegami, Y. Idemoto, N. Koura, T. Sano and H. Yanagishita, *J. Am. Ceram. Soc.*, **89**, 124-130 (2006).

Variable-temperature FT-IR studies on the thermodynamics of CO, N_2 and CO_2 adsorption on zeolite H-Beta

Montserrat Rodríguez Delgado and Carlos Otero Areán
Department of Chemistry, University of the Balearic Islands, E-07122 Palma de Mallorca, Spain. E-mail address: montserrat.rodriguez@uib.es

Introduction

Current concern about the increasing level of carbon dioxide in the atmosphere is propelling research on reversible CO_2 adsorbents capable of separating CO_2 from flue gases (mainly N_2) of coal fired power stations; a process directly involved in carbon capture and storage (or sequestration), CCS [1,2]. Current technology for CCS related to energy production uses mainly alkanolamine solutions, but, besides being energy-intensive and expensive, that technology can pose environmental hazards derived from accidental spills and from waste processing; hence the convenience to search for cheaper and safer CO_2 adsorbents. Among them, porous solids such as porous carbons, metal-organic frameworks and zeolites constitute a main line of research [3].

Experimental

We report on an IR spectroscopic and thermodynamic study of CO, N_2 and CO_2 adsorption on the zeolite H-Beta. For that purpose, we used variable-temperature IR (VTIR) spectroscopy. The IR cell used allows to perform in situ sample activation (degassing) followed by gas dosing and recording IR spectra while simultaneously measuring temperature and gas equilibrium pressure inside the closed cell. The VTIR method [4] is a convenient experimental approach to determine not only the IR spectroscopic features of adsorbed species, but also the corresponding values of standard adsorption enthalpy, ΔH^0, and entropy, ΔS^0, through the equation:

$$\ln[A/(A_M - A)p] = (-\Delta H^0/RT) + (\Delta S^0/R) \quad (1)$$

where A is the (integrated) IR absorbance measured at a known equilibrium temperature, T, and pressure, p, while A_M stands for maximum absorbance (at full coverage).

Results and discussion

Representative IR spectra of CO_2 adsorbed on H-Beta (Si:Al = 20:1) are shown in Fig. 1. The blank IR spectrum of H-Beta (bold spectrum) shows IR absorption bands at 3737 and at 3615 cm^{-1} assigned to isolated silanol groups and to Brønsted acid hydroxyl groups (Al–O(H)Si groups), respectively. Upon interaction of the zeolite with adsorbed carbon dioxide the band at 3615 cm^{-1} decreases to an extent that is a function of temperature. Simultaneously, a new and much broader band corresponding to Brønsted-acid OH species interacting with CO_2 appears, showing a maximum at about 3460 cm^{-1}. In the low temperature regime, a small perturbation of the free silanol band at 3737 cm^{-1} was also observed; the intensity of this band was found to decrease (as a function of temperature) as a result of interaction of free silanols with adsorbed CO_2. In the CO_2 IR spectroscopic region (Fig. 1b), the main feature observed is a distinctive band at 2348 cm^{-1}, which grows when temperature is decreased. This band corresponds to the CO_2 asymmetric stretching vibration (ν_3 mode) perturbed by interaction

with the zeolite Brønsted acid OH groups. The weak band at 2283 cm^{-1} comes from the ν_3 mode of $^{13}CO_2$ (natural abundance about 1%) and it is of no concern here. From the whole series of VTIR spectra recorded, and by using integrated intensity of the IR absorption bands corresponding to the ν_3 mode (2348 cm^{-1}) the van't Hoff plot depicted in Fig. 1 (inset) was obtained, applying Eq. (1). From that linear plot, the corresponding values of standard adsorption enthalpy and entropy resulted in ΔH^0 = -33(±1) kJ mol^{-1} and ΔS^0 = -146(±10) J mol^{-1} K^{-1}. Within experimental error, the same values were obtained from the corresponding van't Hoff plot obtained using integrated intensity of the IR absorption bands at 3460 cm^{-1}.

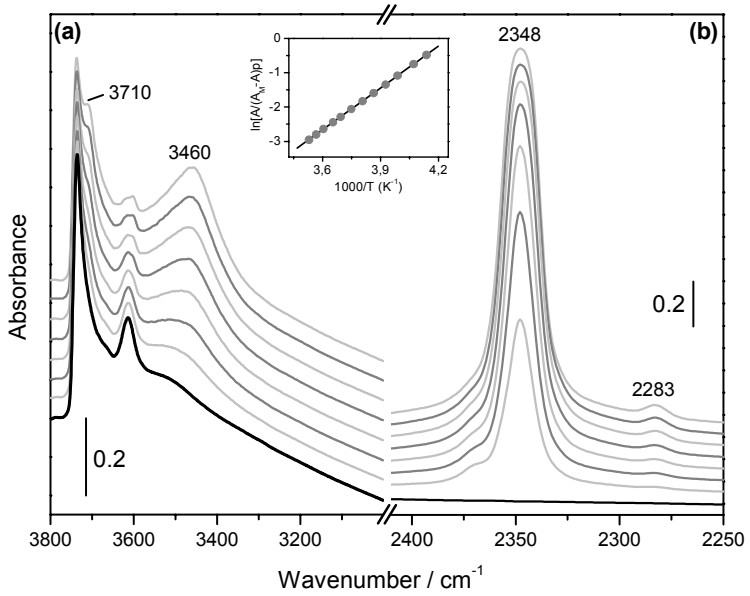

Figure 1. Representative variable temperature IR spectra of CO_2 adsorbed on H-Beta: (a) O–H stretching region, and (b) $\nu_3(CO_2)$ stretching region. Blank zeolite spectrum shown in black. From top to bottom, temperature goes from 180 to 253 K, and equilibrium pressure from 0.12 to 1.42 mbar. Inset shows the van't Hoff plot for CO_2 adsorbed on H-Beta; data obtained from the $\nu_3(CO_2)$ stretching band at 2348 cm^{-1}.

Interaction of carbon monoxide and dinitrogen with the zeolite Brønsted acid sites was found to involve an enthalpy change of -27 and -19 kJ mol^{-1}, respectively; the corresponding entropy change was -150 and -140 J mol^{-1} K^{-1}. The whole set of results will be analysed and discussed in the context of gas separation and carbon capture and sequestration using zeolites.

References

[1] Stern, N., *The Economics of Climate Change: The Stern Review*, Cambridge University Press, Cambridge, UK, 2006.

[2] Pachauri, R. K., Reisinger, A. (Eds.), *IPCC Fourth Assessment Report: Climate Change* 2007, IPCC (http://www.ipcc.ch/), 2007.

[3] D'Alessandro, D. M., Smit, B., Long, J. R., Carbon dioxide capture: prospects for new materials, Angewandte Chemie International Edition, 49 (2010), 6058-6082.

[4] Garrone, E., Otero Areán, C., Variable temperature infrared spectroscopy: A convenient tool for studying the thermodynamics of weak solid-gas interactions, Chemical Society Reviews, 34 (2005), 846-857.

Sorption of Cu(II) onto a Nano-structured Calcium Silicate Hydrate

Giancarlo Barassi[1], Martin Klimsa[1], Thomas Borrmann[1], Joachim Kinkel[2]
1.- Victoria University of Wellington, New Zealand, giancarlo.barassi@vuw.ac.nz
2.- Georg-Simon-Ohm-Hochschule Nürnberg, Germany

Introduction

Nano-structured Calcium Silicate (NCaSil) is a proprietary material of Victoria University [1], which has been found to have multiple uses such as sorption of metal ions. The material consists of a backbone structure of tetrahedral silica and hydrated calcium ions. This gives rise to platelets stacked semi-randomly which may aggregate forming particles of a few micrometres in size (approx. 1-100 μm) with a high surface area typically in the order of 300-700 m^2 g^{-1} as shown in Fig. 1. The surface chemistry grants the possibility to adsorb Cu^{2+} ions by a combined mechanism of ion exchange with Ca^{2+} ions on the surface and precipitation as insoluble hydroxide salts due to the presence of hydroxyl groups.

Experimental

NCaSil synthesis was achieved via precipitation of dissolved silica with calcium ions at alkaline pH. The material was filtered and washed with water and ethanol and stored at 110°C. Sorption kinetic experiments were carried out at 293 K contacting under stirring in a flask 1.00 g of NCaSil with 1.00 L of a 1000 mg L^{-1} $CuSO_4$ solution. Samples were taken at different time intervals and purified by filtration. The content of copper in solution was measured by atomic absorption spectroscopy.

Results and discussion

The sorption of Cu^{2+} onto NCaSil occurred in a fast manner reaching the equilibrium after 200 min with a loading capacity of 581 mg g^{-1} as shown in Fig. 2. The high R^2 value of 0.9999 obtained by fitting Ho's pseudo second order model [2] to the experimental data suggests that the sorption follows pseudo-second order kinetic. Kinetic parameters were obtained from this model such as: the kinetic rate constant k (1.67×10^{-4} g mg^{-1} min^{-1}), initial sorption rate h (56.5 mg g^{-1} min^{-1}) and the amount adsorbed at the equilibrium q_e (581 mg g^{-1}). A mechanism that explains a second order sorption process has not yet been elucidated, but the increment in the release of calcium ions in the presence of copper ions and the availability of hydroxyl groups on the surface of the material suggests that it could be an ion exchange combined with precipitation as insoluble hydroxide salts. During the realization of the kinetic experiment the solution color changed after 6 hours from blue to greenish, which can be attributed to the formation of a mineral phase over the sorbent. Crystals ranging from 1 μm to 5 μm are shown in Fig. 1 with and even composition of Cu, O and S for all crystals as shown by an EDS map. Further analysis by powder-XRD showed that the pattern displayed in Fig. 1 corresponded to brochantite $Cu_4(SO_4)(OH)_6$, which is consistent with

studies by Cairns et al. [3] where atacamite was formed when copper chloride was used under similar experimental conditions.

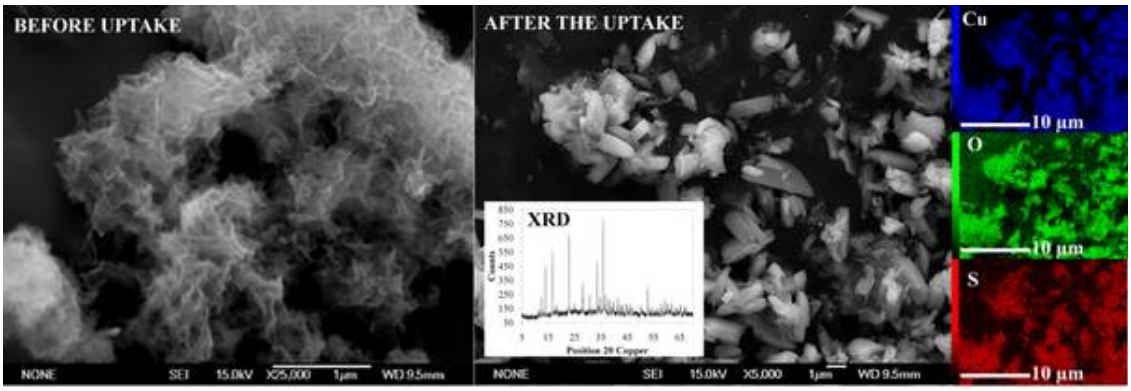

Figure 1. SEM micrograph of NCaSil before the uptake. SEM micrograph, EDS map and powder-XRD difractogram of brochantite crystals after the uptake.

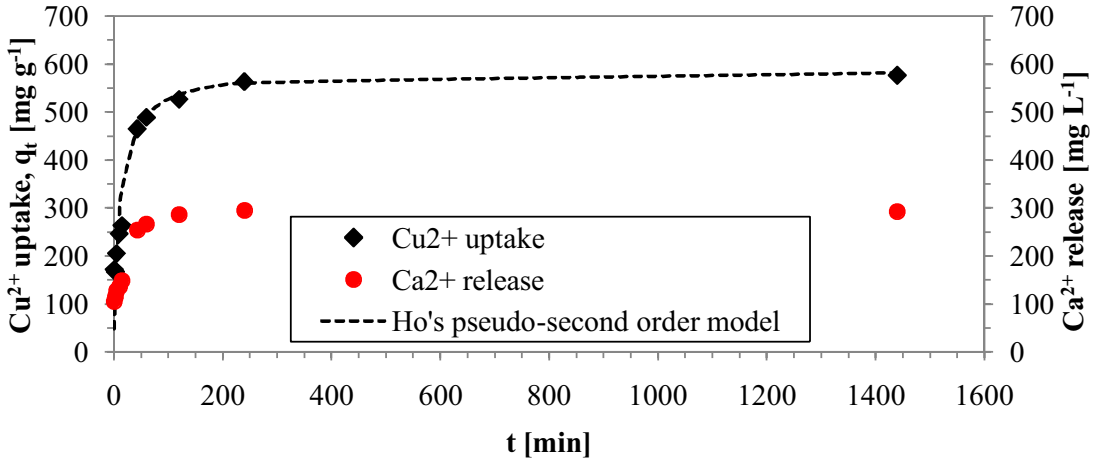

Figure 2. Cu^{2+} uptake and Ca^{2+} release at 293 K.

Conclusions

NCaSil is suitable as sorbent for Cu^{2+} ions presenting a fast kinetic and high uptake capacity. Brochantite was formed under the studied conditions granting the possibility of treating waste water effluents containing copper ions and generating a reusable product.

Acknowledgements

The author would like to acknowledge *Corporación Nacional de Investigación Científica y Tenológica* (CONICYT, Chile) and Victoria University of Wellington (VUW, New Zealand) for CONICYT-VUW 2009 PhD scholarship.

References

[1] J.H. Johnston, A.J. McFarlane, T. Borrmann, Nano-structured Calcium Silicate, Patent Application, New Zealand (2006), 537747, PCT Application PCT/NZ2006/000003.

[2] Ho, Y.S.,G. McKay, Pseudo-second order model for sorption processes. Process Biochemistry, 34 (1999), 451-465.

[3] Cairns, M.J., Borrmann T., Höll, W.H., Johnston, J.H., A study of the uptake of copper ions by a nanostructured calcium silicate, Microporous and Mesoporous Materials, 95 (2006), 126-134.

Synthesis of titanosilicates at a mild condition and post-treatment for selectivity enhancement

Young-Hun Kim*, Jongwon Jeon**
**Department of Environmental Engineering, Andong National University, Andong, Korea,*
***Department of Applied Chemistry, Andong National University, Andong, Korea*
Email of corresponding author: youngkim@andong.ac.kr

Introduction

Sodium titanosilicate was developed by Anthony and co-workers in 1993. The material is a framework structure with cavities and tunnels. Titanosilicate is known as a selective adsorbent for Cs-137, Sr-90 and actinides from a liquid nuclear waste in the presence of salts, organic compounds including detergent and complexing agents. Titanosilicates have attracted a lot of attention during last decades for its synthetic methods and applications. Nuclear waste which is generated from nuclear industries including nuclear power plants and development of nuclear weapons has been an environmental concern. Safe and economical disposal of the waste is required. Liquid nuclear waste contains some highly soluble radionuclides such as Cs-137 and Sr-90. Hydrothermal synthesis of crystalline titanosilicate needs a very high temperature in a sealed vessel for several days. A modified method, which allows synthesis of titanosilicate at mild condition, was developed by authors. The titanosilicate synthesized at the mild condition showed relatively high sorption capacity for several cations including Cs, Sr, Pb, Cu, and Cd. The modified method has advantages over previous hydrothermal methods with closed vessel and long time incubation at high temperature. In current study, a post-treatment was conducted with the titanosilicate prepared from the modified methods and tested for selectivity for target radionuclides.

Experimental

Na- and K-type titanosilicate was synthesized by the modified method which allows synthesis at a mild condition and large amount of production. Na-titanocilicate was prepared from titanium isopropoxide, tetraethylorthosilicate, and sodium hydroxide. K-titanosilicate was synthesized from a similar reaction condition of Na-titanosilicate except potassium hydroxide instead of sodium hydroxide. The synthesized titanosilicate was acid washed to make H-type titanosilicate at variable pH. The concentration of nitric acid was ranged from 1M to 0.0025M. Prepared titanosilicate (0.5g) was mixed with 20 mL of each acid solution for 2 hours. The acid washed titanosilicate was rinsed with deionized water, filtered, and dried at 40℃ for 2 hours. The acid washed titanosilicate was tested for the structural properties through XRD and sorption properties including selectivity for cesium. Sorption test was conducted in two steps. A preliminary sorption test was conducted to observe the selectivity of each titanosilicate and sorption isotherm was obtained through a series of sorption experiments.

Results and discussion

The XRD pattern of Na-titanosilicate after and before acid washing was obtained as shown in Fig. 1. Based on the structural characteristics of titanosilicate, it is found that a sodium titanium silicate phase of composition Na2TiSiO5 (STOS) was gradually disappeared as the concentration of acid getting high but TS showed no change. Sorption experiments showed that sorption capacity for Ca and Sr was decreased after acid washing while the capacity for Cs was not changed. This indicates that the selectivity for Cs was increased and the selectivity for Ca and Sr was decreased. It should note that Cs, a monovalent cation was one of the most challengeable targets to be removed through ion-exchange, especially in the presence of divalent cations such as Ca, Fe, Mg. Same experiments with K-titanosilicate

showed different results. The sorption capacity of Cs was not changed while the sorption capacity for Ca and Sr slightly increased. This indicates that the sorption selectivity of K-titanosilicate was affected by a post-treatment, acid washing.

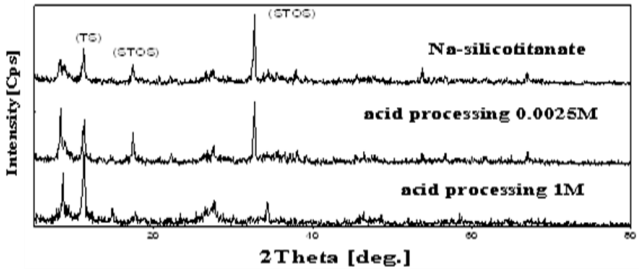

Fig 1. XRD pattern of Na-titanosilicate acid washed.

Table 1. Removal ratio of cations by the acid washed Na-titanosilicate.

Acid Concentration	Removal ratio (%)		
	Cs	Ca	Sr
1M	99.13	9.21	4.35
0.5M	98.99	10.27	5.41
0.1M	99.08	95.89	99.43
0.025M	98.46	98.79	99.50
0.0025M	99.83	69.84	93.76

Conclusions

Current study showed that a modified hydrothermal synthetic method could produce a large amount of titanosilicate and a post-treatment could change the structural property of the sorbent and this could lead to sorption capacity and selectivity for the radionuclies from aqueous phase.

Acknowledgements

This study was financially supported by National Research Foundation of Korea (NRF) of the Korean Ministry of Education, Science, and Technology (Grant Number: M20706000036-07M0600-03610).

References

[1] Clearfield, A., Tripathi, A., Medevedev, D., In situ type study hydrothermally prepared titanates and silicotitanates, J. MATER. SCI., 41(2006), 1325-1333

[2] Elizabeth, A, B., Abraham, C., Titanium silicates, $M_3HTi_4O_4(SiO_4)_3 * 4H_2O$ ($M = Na^+, K^+$), with three-dimensional tunnel structures for the selective removal of strontium and cesium from wastewater solutions, Microporous materials, 11(1997), 65-75

[3] Nyman, M., Bonhomme, F., Maxwell, R, S., Nenoff, T, M., First Rb silicotitanate phase and Its K-structural analogue: new members of the SNL-A family (*Cc*-$A_2TiSi_6O_{15}$; A) K, Rb, Cs), Chem. Mater, 13(2001), 4603-4611

[4] Celestian, A, J., Parise, J, B., Smith, R, I., Toby, B, H., Clearfield, A., Role of the hydroxyl-water hydrogen-bond network in structural transitions and selectivity toward cesium in $Cs_{0.38}(D_{1.08}H_{0.54})SiTi_2O_7 \cdot (D_{0.86}H_{0.14})_2O$ crystalline silicotitanate, Inorg. Chem., 46(2007), 1081-1098

[5] Celestian, A, J., Kubicki, J, D., Hanson J., Clearfield, A., Parise, J, B., The mechanism responsible for extraordinary Cs ion selectivity in crystalline silicotitanate, J. Am. Chem. SOC., 130(2008), 11689-11694

Olefin Paraffin separation turned on its head. Selective adsorption and separation of short chain paraffins via gate opening effects in the Metal Organic Framework ZIF-7

Canan Gücüyener, Johan van den Bergh, Jorge Gascon* and Freek Kapteijn.
Catalysis Engineering, Chemical Engineering Department, Delft University of Technology, Julianalaan 136, 2628 BL, Delft, The Netherlands
j.gascon@tudelft.nl

Introduction

During the last decade, Metal Organic Frameworks (MOFs) have earned themselves a great deal of attention in the field of nano-structured materials. Among the various proposed applications, the use of MOFs as selective adsorbents in gas separation processes seems to be most promising on a short/mid term.[1] Indeed, some features of MOFs make them behave as unusual adsorbents with the potential of overcoming classical separation problems of the chemical industry, i.e. short chain olefin/paraffin separation or natural gas upgrading.

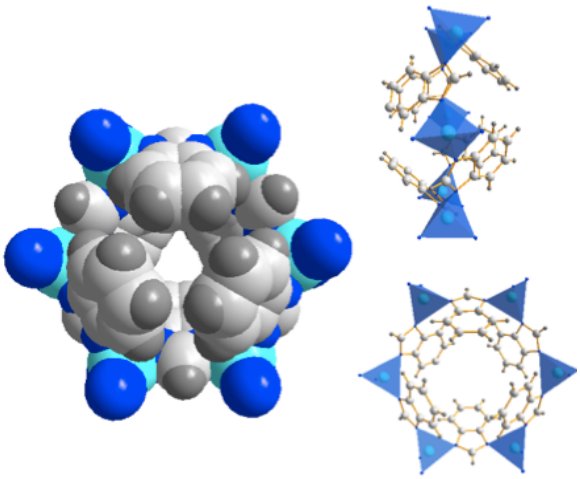

Figure 1.- Main cavity of ZIF-7 (left) together with the lateral (top-right) and front (bottom-right) view of the six membered ring (6MR) pore opening. Zn clusters are represented as polyhedra.

In this work we report the unusual paraffin selectivity of the metal organic framework ZIF-7 [2] (Figure 1) in the adsorptive separation of ethane/ethylene [3] and propane/propylene mixtures together with a rigorous performance assessment in which adsorption, desorption and diffusion limitations are discussed. Although a few materials showing higher olefin uptakes during single component adsorption had been reported before, to the best of our knowledge, this is the first study showing such behaviour for mixtures.

Experimental

A series of ZIF-7 crystals with different morphologies has been synthesized and characterized by means of X-ray diffraction, thermo-gravimetric analysis, *in situ* DRIFT, nitrogen adsorption and SEM. Single component adsorption isotherms together with breakthrough separation experiments were used to assess the separation performance of the adsorbents.

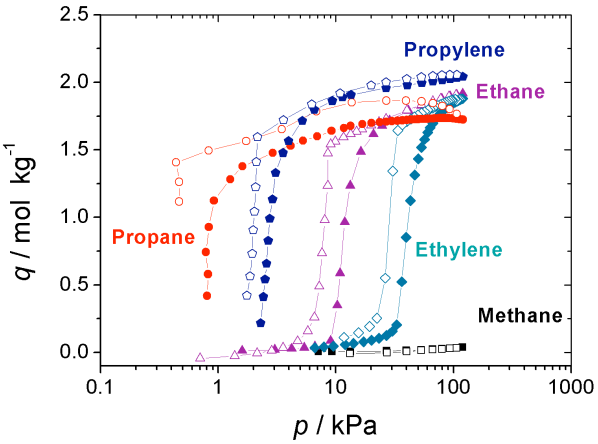

Figure 2.- Adsorption (closed symbols) - Desorption (open symbols) isotherms of several hydrocarbons on ZIF-7 powder at 25 °C.

Results and discussion

Figure 2 shows the adsorption isotherms of several light hydrocarbons on the ZIF-7 framework at 25 °C. Since the crystallographic pore opening of ZIF-7 is 0.3 nm, the observed type-IV isotherms can only be understood in terms of a change in the conformation of the benzimidazole (BIM) linker. The interaction between the adsorbate and the BIM linker strongly affects the adsorption process, resulting in a gate-opening effect. Specific threshold pressures control the uptake and release of individual molecules, unlocking the openings to the ZIF-7 cavities. This creates a pressure window in which paraffins adsorb while olefins do not.

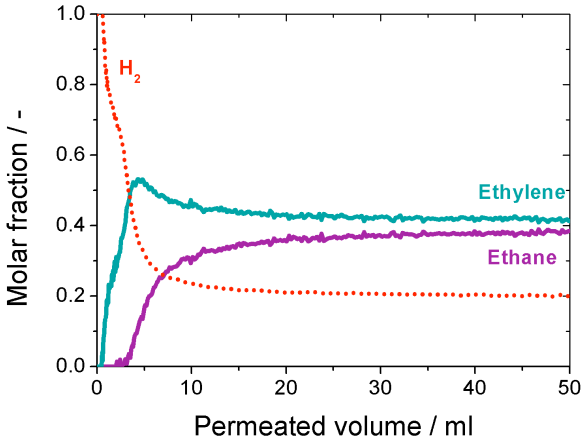

Figure 3.- Breakthrough profile (molar fraction at the exit of the column vs. permeated volume) obtained for an equimolar mixture of C_2H_4 and C_2H_6 on a column packed with ZIF-7 pellets at 25 °C and 1 bar. H_2, contributing the 20% of the mixture flow, is added to monitor the dead volume of the breakthrough setup (F_{C2H6}=F_{C2H4}=4 ml(STP)/min).

We assessed the performance of ZIF-7 for the separation of olefin/paraffin mixtures: binary adsorption was studied in terms of breakthrough experiments. Figure 3 shows the separation performance for an ethane/ethylene/hydrogen mixture (40: 40: 20) over a ZIF-7 column. From the beginning of the experiment ethylene free of ethane is eluted. After a certain point, the paraffin keeps adsorbing but already some breaks through. It is noted that even though at the used partial pressure of ethylene was enough as to *open* the structure, the ZIF-7 adsorbent shows remarkable ethane selectivity. In the case of propane/propylene mixtures, both diffusion and gate opening effects rule the separation, enabling to tune the selectivity of the adsorbent simply by adjusting the separation temperature.

Conclusions

The first example of a microporous material displaying selective adsorption of paraffins over olefins is presented. The interaction between the adsorbates and the benzene rings in the narrow ZIF-7 windows appear to dominate the adsorption process, inducing a ‘gate opening’ effect and enabling the selective discrimination between molecules of very similar sizes, but different shapes. This gate-opening effect can be utilized in the separation of mixtures, resulting in an inverse adsorption selectivity for the paraffin.

References

[1] J.R. Li et al. Chem. Soc. Rev., 38 (2009) 1477-1504.
[2] K.S. Park, et al J. Am. Chem. Soc., 132 (2010) 17704-17706.
[3] Gucuyener et al. J. Am. Chem. Soc., 132 (2010) 17704-17706.

DD3R: Challenge with the synthesis, great potential for the separation of small hydrocarbons

Canan Gücüyener*, Johan van den Bergh, Alberto Martinez Joaristi, Jorge Gascon, Freek Kapteijn
Catalysis Engineering, Chemical Engineering Department, Delft University of Technology, Julianalaan 136, 2628 BL, Delft, The Netherlands
*Corresponding author, +31(0)152782108, e-mail: c.gucuyener@tudelft.nl,

Introduction

DDR belongs to the porosils, and further to zeosils due to its channel-like pore geometry and 8MR windows [1]. These 8MR windows enable only small molecules to penetrate, making the use of DDR crystals conceivable in separation applications. However, the reproducibility of the DD3R synthesis is still a challenge. The challenge results from the possible side product formation: synthesis of competitive phases like D1H (DOH) and Sigma-2 (SGT) may also occur. The parallel formation of these by-products do not just decrease the purity of product, they can also attach on the surface of the synthesis containers, acting as a seed for further synthesis and hindering future syntheses of DD3R. In this work, next to an assessment of the different synthetic methods proposed in the literature, where we pay special attention to the possible cleaning methods that avoid "memory effects" in the synthesis vessels, we explore the potential of this zeolite, in the adsorptive separation of small hydrocarbons: propylene from propane and the enantiomeric separation of cis/trans 2-butene isomers.

Experimental

Different synthesis routes adapted from the literature [2-4] were followed in order to assess their reproducibility. These routes are named as Method 1, 2 and 3 as given in Figure 1.

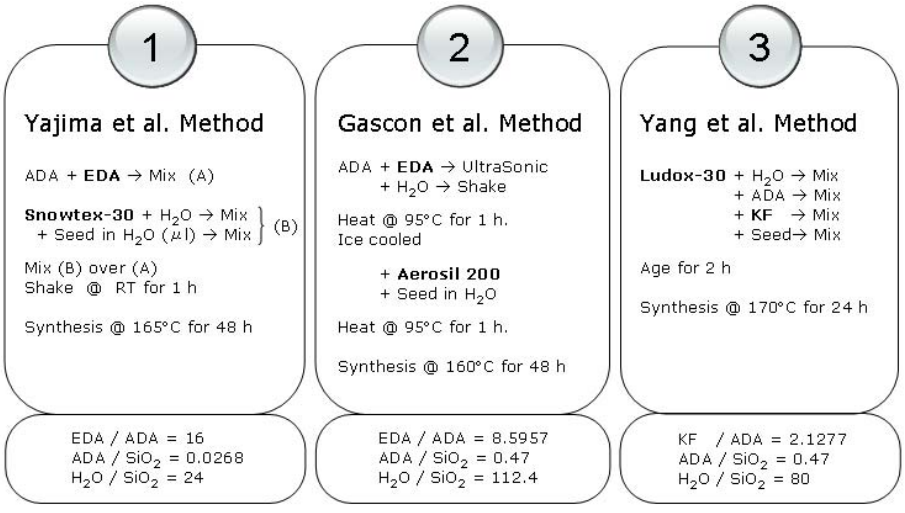

where EDA and ADA stands for ethylenediamine and adamantine amine, respectively.

Figure 1. Different DD3R synthesis routes proposed in the literature.

Characterization of the samples was carried out by XRD, SEM, nitrogen adsorption, TGA and NMR. The performance of the adsorbent in the separation of propylene from propane and in the separation of butene isomers was studied in packed columns by means of breakthrough experiments and by single component adsorption.

Results and discussion

Reproducibility of the materials obtained by three methods differs quite from each other. Representative XRD patterns of the powders are given in Figure 2. In general, it is concluded that the addition of KF as the mobilizing agent instead of ethylenediamine, stabilizes the formation of pure phase DD3R, while hindering the growth of Sigma-2 (SGT).

When it comes to the separation performance, results revealed DD3R as a very effective molecular sieve for the separation or purification of propane–propylene mixtures and for the separation of cis/trans 2-butene isomers (Figure 3)

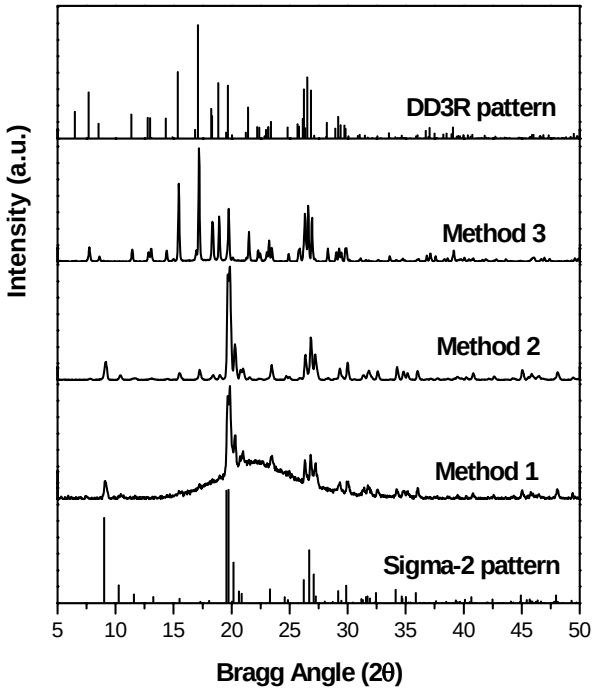

Figure 2. XRD patterns of the powders obtained by different synthesis methods.

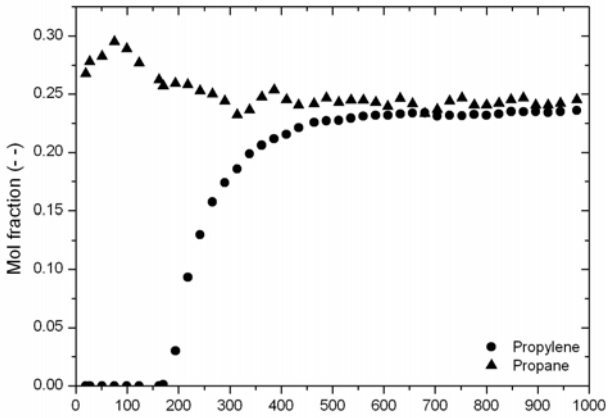

Figure 3. Propane-propylene breakthrough curves at 353 K, W_{DD3R} = 0.57 g, $F_{C3H6} = F_{C3H8}$ = 2 ml/min (STP), F_{He} = 4 ml/min (STP)

Conclusions

Assessment of three different synthetic methods has been made. Using the fluoride route 100% reproducibility in the synthesis of DD3R has been established. Unlike other zeolites, fluoride synthesis for porosils are less known and thus the effects of fluoride addition to the synthesis is also studied. The great potential of DD3R as shape selective adsorbent has been shown in the separation of the geometric 2-butene isomers and in the separation of propylene from propane.

Acknowledgements

The research leading to these results has received funding from the European Community's Seventh Framework Programme through the Collaborative Project NEXT-GTL, under agreement n° 229183

References

[1] H. Gies, B. Marler, and U. Werthmann, Molecular Sieves: Science and Technology 1 (1998) 35-64.
[2] J. Gascon, W. Blom, A. van Miltenburg, A. Ferreira, R. Berger, and F. Kapteijn, Microporous and Mesoporous Materials 115 (2008) 585-593.
[3] K. Yajima, and K. Nakayama, US2009/0011926 A1, 2009.
[4] Q.L. Yang, S.L. Zhong, and X. Lin, Chinese Journal of Inorganic Chemistry 25 (2009) 191-194.

PSA process for CO_2/N_2 separation in real condition on an ultramicroporous MOF (SIM-1)

Sonia Aguado and David Farrusseng

IRCELYON, Institut de Recherches sur la Catalyse et l'Environnement de Lyon, Université Lyon 1, CNRS F-69626 Villeurbanne, France, E-mail: sonia.aguado@ircelyon.univ-lyon1.fr

Zeolite Imidazole Frameworks (ZIFs) are a new subclass of porous metal-organic frameworks in which divalent metal cations are linked by imidazolate anions into tetrahedral frameworks that frequently possess a zeolite topology. Several of them exhibit large cavity (>10 Å) and good chemical and thermal stability, a combination of properties rarely to be found among other porous MOF materials.[1] In this work, we present a new imidazolate based MOF, the SIM-1.[2] SIM-1 is isostructural to ZIF-8 (SOD) and consists of Zn_4 tetrahedra linked by carboxylimidazolate (Fig. 1). The functional ligand confers enhanced adsorption properties to SIM-1 compared to those obtained with ZIF-8. The permanent porosity of guest-free (activated) SIM-1 is confirmed by gas adsorption measurements. The type-I isotherm observed for N_2 adsorption at 77 K indicates the microporosity of SIM-1. The BET surface area is 500 $m^2 \cdot g^{-1}$.

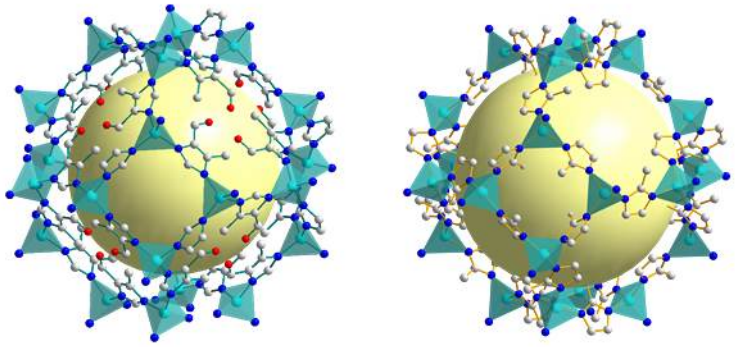

Figure 1. Schematic drawing of the frameworks of SIM-1 and ZIF-8.

Metal-Organic Frameworks are new promising materials with potential industrial applications for CO_2 selective adsorption. MOF receive an enormous attention form the scientific community due to the large pore volume and surface area achieved with this kind of materials. However, highly porous materials are not necessarily interesting for separation applications, since gas-solid interactions are mainly diluted on large cavities. In this sense, materials with low-moderate porosity are more interesting since they maximize wall-adsorbate interactions. The effect of confinement and the introduction of specific adsorption sites (induced by the surface chemistry) are linked variables that should be optimised.

Pressure Swing Adsorption (PSA) processes are of special interest because of their intrinsic eco-compatibility and flexibility. Adsorbents candidate to be implemented in PSA processes have to satisfy several requisites: (1) high CO_2/N_2 selectivity, (2) high CO_2 specific capacity, (3) high regenerability (e.g. high working capacity) by moderate depressurisation, (4) fast interparticle diffusion, (5) chemical and physical stability, (6) low cost per unit volume, (vii) reasonable packing density to avoid oversized vessels.

The adsorption of CO_2 and N_2 gas were examined at 303 K. CO_2 uptake at 5 bar is five times higher than that of N_2, suggesting a stronger interaction between the framework and the CO_2 molecules. This behaviour led us to examine the separation of CO_2 from N_2. we will show breakthrough curves at real conditions (gas composition and humidity) that prove high adsorption capacity, complete selectivity, and complete regenerability of the material. [3]

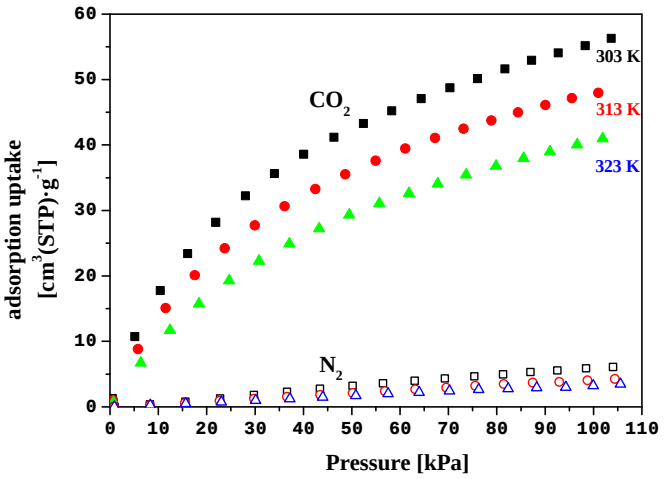

Figure 2. CO_2 and N_2 adsorption isotherms of SIM-1 at 303-323 K..

References

[1] R. Banerjee, A. Phan, B. Wang, C. Knobler, H. Furukawa, M. O'Keeffe, O. Yaghi, *Science*, **2008**, *319*, 939.
[2] D. Farrusseng, S. Aguado, J. Canivet. FR09/04488, **2009**.
[3] Patent pending

Catalytic conversion of alcohols in packed bed zeolite membrane reactor

D.A. Fedosov[1], A.V. Smirnov[1], E.E. Knyazeva[1], I.I. Ivanova[1], L.I. Trusov[2]
[1)] *Lomonosov Moscow State University, Department of Chemistry, Moscow, Russia, dfedosov@phys.chem.msu.ru*
[2)] *ASPECT Association, Moscow, Russia*

Introduction

Combination of two most important steps of chemical processes, such as reaction and product separation, in one technological unit can be efficiently realized in membrane reactors. There are a lot of commercially important reactions, where membranes can be applied for the improvement of process parameters. Zeolite membranes are among the most promising materials for the application in catalytic membrane reactors due to their high permeabilities and inherent selectivity based on the molecular filtration and adsorption properties [1]; moreover zeolites are stable at relatively high temperatures in organic media. In this work we focused at membrane-assisted catalytic dehydration of alcohols, namely propanol-2 to propylene and butanediol-1,4 (BDO) to tetrahydrofurane (THF), over alumina and Amberlyst as standard catalysts. The main disadvantage of these catalysts is fast deactivation in the presence of water, which is adsorbed on acidic sites. NaA zeolite membranes were selected for water removal from the reaction zone which could be an efficient way to maintain catalytic activity.

Experimental

Zeolite membranes were prepared by in situ crystallization of zeolite NaA on a flexible metal-ceramic support [2]. Separation parameters of this material towards water/organic components of reaction mixture were determined before catalytic runs in membrane reactor. Water-organic mixtures were passed through the cell with two flat NaA zeolite membranes under the conditions close to operating in dehydration processes: temperature 100 °C, feed rate 2-7 $g*h^{-1}$, evacuation of permeate side to 1 mbar. Permeate was collected in the traps cooled with liquid nitrogen and analyzed by GC. Dehydration of alcohols was carried out in the reactor of the similar construction, packed with catalyst. Amberlyst-15 and γ-Al_2O_3 were used as catalysts. The conditions of the experiments are listed in Table 1.

Table 1. Operating conditions.

Process	Catalyst	Temperature (°C)	WHSV (h^{-1})	Permeate pressure (mbar)
Propanol-2 dehydration	Amberlyst-15	105	1.5	1
	γ-Al_2O_3	220, 240	1.5	1
BDO to THF	Amberlyst-15	105	3.35	1

To compare membrane mode and conventional catalytic process both reactions were run under the same conditions in packed bed reactor (PBR), which was transformed from packed bed membrane reactor (PBMR) by means of replacement of membranes by impermeable inert walls.

Results and discussion

NaA zeolite membranes demonstrated high separation efficiency towards water-organic mixtures; the data are presented in Table 2.

Table 2. Separation factor of membranes

Target mixture	Water content in the feed, wt.%	Separation factor α
Water/Propanol-2	12	2860
Water/BDO	6	>10000
Water/THF	5	>10000

It was shown that the separation factor increases with the increase of the size and the hydrophobicity of organic molecules in aqueous solutions. It corresponds to the decrease of surface coverage with organic component and also more complete realization of the molecular filtration transport through membrane.

The role of NaA membranes in PBMR was to decrease partial pressure of water directly in the reaction zone. Water negatively affects the catalyst activity due to the strong interaction with the active sites, therefore lower partial pressure of water in reactor could shift adsorption equilibrium leading to higher reagent conversion. The experimental results presented on Fig. 1 revealed significant increase of the catalytic activity in the case of membrane mode in comparison with conventional continuous flow catalytic reactor mode over γ-Al_2O_3 and Amberlyst catalysts. Twofold increase of conversion was reached for gas phase propanol-2 dehydration. In the case of liquid-phase THF synthesis application of membranes led to slower catalyst deactivation and the increase of BDO conversion by 10%.

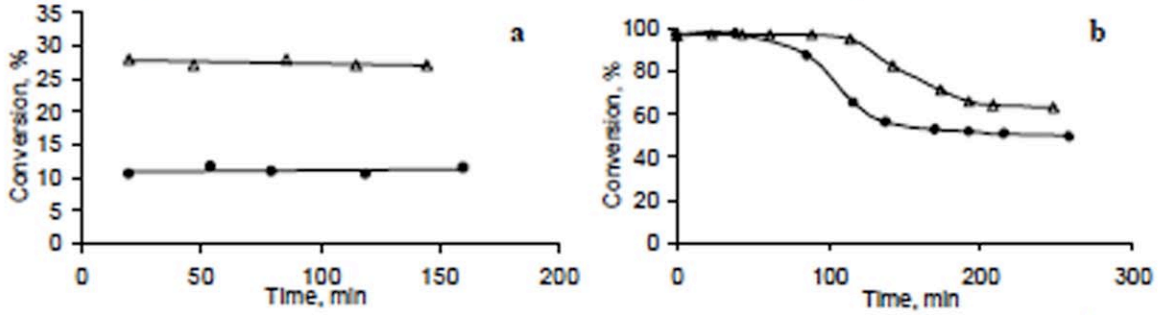

Figure 1. Conversion of propanol-2 over γ-Al_2O_3 at T = 220°C, WHSV 1.5 h^{-1} (a) and butanediol-1,4 over Amberlyst-15 at T = 105°C, WHSV 3.35 h^{-1} (b) in PBMR mode (Δ) and PBR mode (•).

In the case of propanol-2 dehydration over Amberlyst-15 at 105°C the conversion reached 72% instead of 33% in PBR mode.

Conclusions

NaA zeolite membranes were found to be selective and thermally stable during water removal from water-organic mixtures. These membranes were successfully integrated with PBR, allowed to increase the catalytic activity and enhance the product yield in catalytic alcohol dehydration due to shifting of adsorption equilibrium.

References

[1] J. Coronas, J. Santamaría, Catalysis Today 51 (1999), 377-389.
[2] I.I. Ivanova, L.I. Trusov, E.E. Knyazeva, V.P. Fedotov, M.A. Nikitina, I.V. Dobryakova, A.V. Smirnov, D.A. Fedosov, Patent RU 2322390, 2006.

Influence of Intermetallic diffusion barrier on Pd Membrane

Mohammad Hossein Sayyar[3,*]; Milad Rasouli[1,3]; Sahar Chitsazan[1,3]; Nakisa Yaghobi
[1] *Islamic Azad University, South Tehran Branch, Tehran, Iran*
[2] *Department of Petrochemical, Iran Polymer and Petrochemical Institute, Tehran, Iran*
[3] *Pars Coating Technology Co., P.O.Box: 14155/3499, Tehran, Iran*
** sayyar@parscoating.com*

Introduction

To reduce intermetallic diffusion between the metal support and the Pd layer, and thereby improving the stability of the Pd/PSS composite membrane, Ma et al. [1] used a controlled in-situ oxidation of the porous stainless steel prior to plating to produce an oxide layer to act as a diffusion barrier between the Pd and the PSS [2]. The objective of this research is to investigate the effects of temperature on the formation of the intermetallic diffusion barrier layer by the controlled in-situ oxidation method for Pd/PSS membrane.

Experimental

Porous 316L stainless steel supports were purchased from Mott Metallurgical Corporation (0.2 μm grade) and Fuji Filter Company (0.5 μm grade). Two of the support tubes were then oxidized in furnace in the presence of air at 400, 600 and 800 $^{\circ}$C for 2 h, with heating and cooling rates of 3 $^{\circ}$Cmin^{-1}. The furnace was purchased from ELITE THERMAL SYSTEM model TSH12/50/300-2416CG. The oxidation layer formed acts as a diffusion barrier between the PSS substrate and the Pd catalyst. The substrate was then activated by pre-seeding with finely divided Pd nuclei. Procedure for Pd coating.
The composition of the Pd plating solution is given in Table 1. The hydrazine (reducing agent) was added just prior to plating. The plating solution was renewed every 90 to 120 minutes. After deposition was completed the membrane was left to cool to room temperature and dried. After each drying, the weight and helium flux were measured. The weight gains before and after the plating were used to determine the thickness of the membrane.

Table 1 Chemical composition of the plating solution.

Chemicals	Pd bath
$Pd(NH_3)_4Cl_2.H_2O$ (g/l)	4-6
$Na_2EDTA.2H_2O$ (g/l)	40-80
NH_4OH (28%) (ml/l)	190-400
H_2NNH_2 (1M) (ml/l)	5-10
Polyoxyalkylene alkyl ether (ml/l)	0.1-0.5
pH	10-11
Temperature (^{o}C)	60

Results and discussion

Figure 1. shows the SEM pictures of a typical grade 0.2 μm grade Mott PSS after oxidation in 400^{o}C, 600^{o}C, and 800^{o}C.

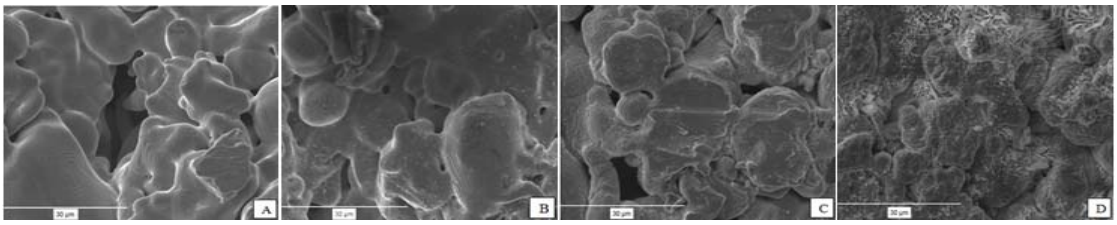

Figure 1. (A) supports after cleaning (B) oxidized at 400°C; (C) oxidized at 600°C; (D) oxidized at 800°C.

Figure 2. shows the change of the properties of the 0.5 μm grade Fuji Filter PSS tubes following oxidation of the cleaned tubes. The oxygen peaks confirm the formation of oxide layers on the supports. It was observed that the amount of oxygen on the support increased with higher oxidation temperatures, indicating a thicker oxide layer. As the oxidation temperature was increased, the weight gain increased indicating the formation of more oxide at higher temperatures. The formation of greater quantities of oxide gave a higher resistance to the He permeation.

Table 2. Percent weight gain and He flux change after oxidation for Mott PSS supports

Tube	Oxidation (°C)	Δm (%)	Thickness (μm)	He Flux, J (cm^3/cm^2min)
1	20	0	0	701
2	400	0.035	--	700
3	600	0.78	0.2-0.3	565
4	800	4.69	1-6	27

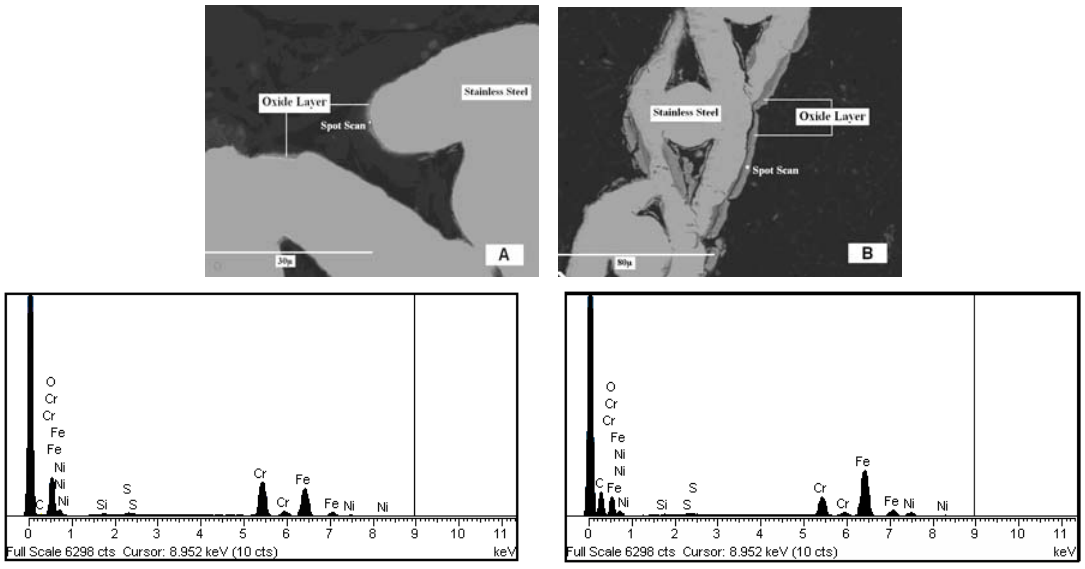

Figure 2. Cross section oxide of the layer of the Fuji PSS supports and EDS spot scans after oxidation on oxide layer at (A) 600°C, and (B) 800°C.

Among the oxides that can be formed with the elements of stainless steel, Cr_2O_3 is the most stable due to its low Gibbs free energy, the low diffusion rates of elements in the oxide scale, and its high chemical stability under a H_2 atmosphere. The SEM micrograph of the sample oxidized at 800˚C showed a thicker dark region with a very nonuniform thickness was observed. It could also be observed that the surface of this oxide layer was very crumbly. The thickness of the dark region varied from 1 to 6 μm from spot to spot since the oxide layer was

relatively thick. After Pd coating, the final thicknesses of the dense Pd membrane were 23-27 μm on 0.2 μm grade Mott supports and 32-35 μm on 0.5 μm grade Fuji plate supports.

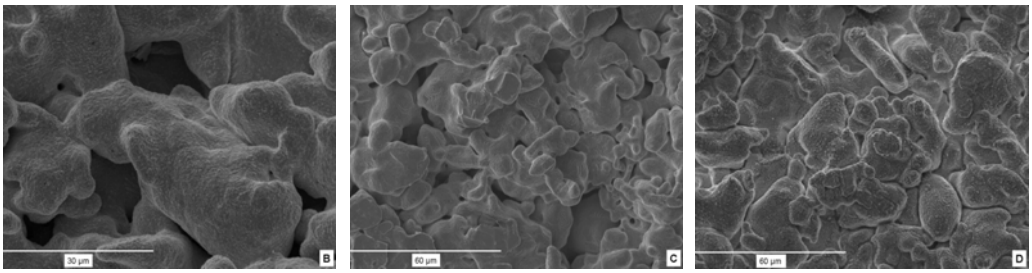

Figure 3. SEM photographs of: B - after 13.5 hr plating; C - after 15 hr; and D - after 24 hr

Conclusions

Oxidation process was carry out in diffrent temprature. It was observed that the amount of oxygen on the support increased 10 times with higher oxidation temperatures indicating a thicker oxide layer. Sample oxidized at 800˚C showed a thicker dark region with a very nonuniform thickness. It was also observed that the surface of this oxide layerwas crumbly. The thickness of the dark oxide region varied from 1 to 6 μm from spot to spot. Therefore, it is the most desirable oxide phase for use as a barrier layer to intermetallic diffusion. Membranes produced by this method have been shown to be stable for over 6000 h in the Temprature of 800^{o}C.

References

[1] US Patent 6152987, “Hydrogen gas-extraction module and method of fabrication”
[2] P.P. Mardllovich, Y. She, Y.H. Ma., “Stabillity of hydrogen flux through Pd/porous stainess steel compsite membranes” Proc.Fifth Int. Conf . Inorg . Membr 1 (1998) 246

Influence of structural properties of original mesoporous LTA zeolite generated by using organosilane surfactant on their ion-exchange behaviour

S. Devautour-Vinot [a *], F. Marchandeau[a], B. Prélot [a], E. Gérardin [a], J. Zajac [a], J-M. Douillard [a], Ryong Ryoo[b,c].

[a] *Institut Charles Gerhardt Montpellier UMR 5253 CNRS-UM2, C. C. 1503, Place Eugène Bataillon, 34095 Montpellier cedex 5, FRANCE*

[b] *Department of Chemistry, KAIST, Daejeon 305-701, Korea*

[c] *Graduate School of Nanoscience and Technology (WCU), KAIST, Daejeon 305-701, Korea*

**email: devaut@lpmc.univ-montp2.fr*

Introduction

There is an increasing concern with respect to contamination of aqueous ecosystems. Sorption processes are very attractive for water treatment applications. The removal of heavy metal cations can be explored using efficient technological solution based on innovative materials. The high cation-exchange capacity of zeolites offers an efficient separation base. In this context, mesoporous LTA zeolites were synthesized in order to overcome usual diffusion problems due to the microporosity. The objective of this work was to study the cation-adsorption of mesoporous LTA zeolites, including homoionic cations as Ca^{2+} and Sr^{2+}. The solution depletion procedure was used to date. The heat effects were measured by titration microcalorimetry. Dielectric Relaxation spectroscopy based on the Thermally Stimulated Currents (TSC) technique was also employed to determine both the distribution of the cation among the different crystallographic sites and their de-trapping energy ΔE. The TSC data were correlated with the ion adsorption capacities.

Experimental

Materials. LTA zeolite containing mesoporosity was hydrothermally synthesized with using 3-(trimethoxysilyl)propylhexadecyldimethyl ammonium chloride as a mesopore-generating organosilane surfactant (OSS). Different loadings of OSS was added into a conventional zeolite synthesis mixture containing sodium hydroxide, sodium metasilicate nonahydrate, sodium aluminate and distilled water.

Adsorption capacity and microcalorimetry. Measurements were carried out using the usual batch procedure at free pH in water for Ca^{2+} and Sr^{2+} cations, starting with the homoionic sodium form of the mesoporous LTA. The concentrations in the aqueous phase were monitored by using an ionic chromatography analyzer (Shimadzu HPLC) equipped with a conductivity detector. The Ca^{2+} and Sr^{2+} content in the exchanged LTA was checked by using ICP-AES. The heat effects were evaluated from titration microcalorimetry with successive additions of aliquots of cations, step-by step along the isotherm.

Dielectric Relaxation Spectroscopy. The Thermally Stimulated Currents (TSC) technique (Setaram apparatus) was used to evaluate the electrical properties of the different anhydrous LTA samples. With porous aluminosilicates compounds [1], the TSC signal is ascribed to the dielectric relaxation of the extra-framework cations, regarded as a cation hopping. The resulting data were analyzed by considering a distribution of the de-trapping energy $G(\Delta E)$, characterizing the nature of the relaxing ion and its environment.

Results and discussion

Figures 1a and 1b illustrate the evolution of the depolarization current with temperature, as recorded from TSC experiments for the anhydrous Na and Ca mesoporous LTA, respectively.

The Sr LTA (not shown here) exhibits similar behaviors than Ca LTA. The position and the shape of the TSC peaks depend on the cation nature, as well as on the mesoporosity loading of the LTA. These tendencies are reported in figure 2 in terms of the distribution function of the cation de-trapping energy. As reported for microporous zeolites, the Na form of the LTA exhibits a less energetic dielectric signal than the Ca form [2]. This suggests that the exchange of Na by Ca ions is favored. In addition, the Na LTA dielectric response is very sensitive to the mesoporosity loading of the solid: with the percent of OSS, we observe an increase of the Na de-trapping energy and a less homogenous distribution of the Na ions among the different crystallographic sites of the LTA. On the opposite, the distribution functions of the Ca LTA are similar, whatever the OSS loading.

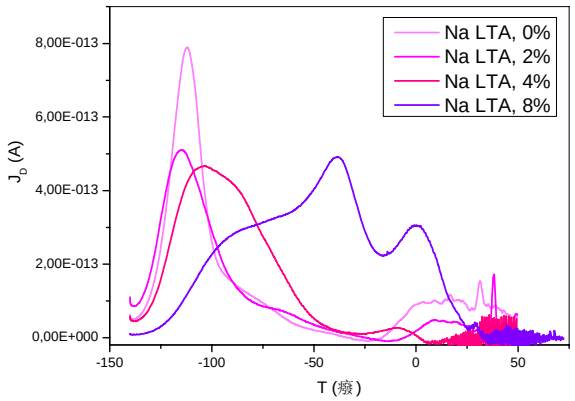

Figure 1a. Evolution of the depolarisation current with temperature, for anhydrous Na LTA, where % represents the OSS weigh percent of precursors.

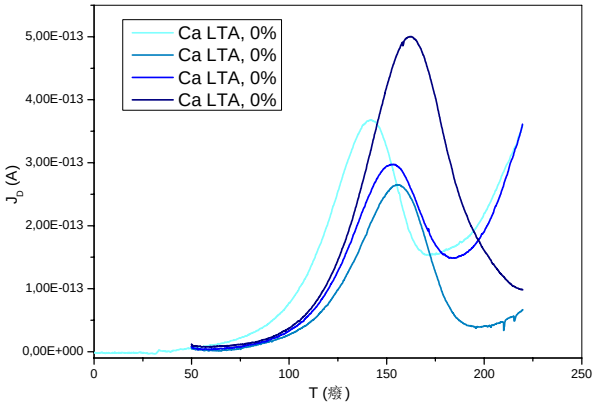

Figure 1b. Evolution of the depolarisation current with temperature, for anhydrous Ca LTA, where % represents the OSS weigh percent of precursors.

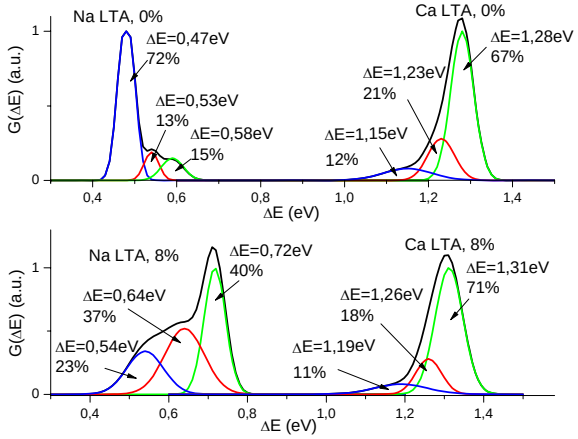

Figure 2. Distribution functions of the de-trapping energy for Na LTA and Ca LTA with 0 and 8 % of OSS.

The evolutions of the cation distributions among the crystallographic sites and the cation de-trapping energy, i.e. the cation/LTA interaction energy, are further discussed in the light of molecular simulation calculations data.

Acknowledgements

The authors greatly acknowledge the financial support of this work by the French ANR within the CILSAMES project (ANR-07-JCJC-0044) and the GNR PARIS 1115 (Physico-chimie des Actinides et des radioéléments aux interfaces et en solution).

References

[1] S. Devautour *et al.*, *J. Phys. Chem. B* **105**, 9157 (2001)
[2] J.M. Kalogeras *et al.*,, *Cryst. Res. Technol.* **31**, 693 (1996)

Application of Pd and Cu-supported SBA-15 in the adsorption of benzothiophene

E. Vilarrasa[1], D.C.S. Azevedo[2], P. Braos-García[1], R. Moreno-Tost[1], A. Infantes-Molina[3], C. L. Cavalcante Jr.[2], A. Jiménez-López[1] and E. Rodríguez-Castellón[1].
[1]*Departamento de Química Inorgánica (Unidad Asociada al ICP-CSIC), Facultad de Ciencias, Universidad de Málaga, 29071, Málaga, Spain.*
[2]*Department of Chemical Engineering, Universidade Federal do Ceará, Campus do Pici, bl. 709, 60455-760, Fortaleza, Brazil.*
3Instituto de Catálisis y Petroleoquímica, CSIC, Cantoblanco, 28049 Madrid, Spain.

Introduction

Aromatic sulfur compounds, such as benzothiophene (BT) and its derivatives, are noticeably refractory to hydrodesulfurization (HDS) processes. In order to meet the increasingly strict environmental requirements, selective physisorption may be a feasible option to lowering the sulfur content of the outlet streams of current HDS units. Yang and co-workers have reported an extensive work on the preparation of adsorbents, especially zeolites, containing transition metals. Copper(I) and palladium(II) have demonstrated to be the most selective towards sulfur compounds as compared to other aromatic species present in fossil fuels [1]. Since BT and its derivatives are bulky molecules, mesoporous matrices, such as MCM-41 and SBA-15, have been recently proposed for their adsorption [2]. The present work reports adsorption/desorption studies of benzothiophene (BT) on SBA-15 loaded with $PdCl_2$ and CuCl by in situ FTIR.

Experimental

The SBA-15 was prepared as described elsewhere [3], and the impregnated samples were prepared following a similar procedure as that reported by the group of Yang [4]. The adsorbents were characterized by N_2 adsorption isotherms, TEM, X-ray diffraction and X-ray photoelectron spectroscopy (XPS). The prepared samples and the pristine SBA-15 were then subjected to adsorption at 20 $^{\circ}$C of BT vapors (carried by He at 150 mL min^{-1}), followed by desorption under the same helium flux at distinct temperatures. DRIFT spectra of the adsorbents (under adsorption/desorption) were recorded in situ. To assess adsorptive capacity for DBT, 100 mg of adsorbent was put in contact with organic solutions (500 ppm in hexane) of BT or DBT inside sealed vials. The vials were kept in a thermostat bath at 25 ºC for 72 h, after which the liquid-phase composition was determined by gas chromatography provided with a flame ionization detector. Normalised adsorbed phase concentrations (μmol of S m^{-2} of adsorbent) were calculated by mass balances.

Results and discussion

The incorporated metals were well dispersed as nanoparticles on the mesoporous channels of SBA-15, under different oxidation states. All the N_2 adsorption-desorption isotherms at 77 K are typical of mesoporous silica (Figure 1). The surface areas decreased significantly for samples with incorporated metals (469, 186 and 109 m^2 g^{-1} for SBA-15, $PdCl_2$SBA-15 and CuClSBA-15, respectively), although hexagonal arrangement and average pore size remained approximately unaltered. To investigate the oxidation states of palladium present on the surface of the solid, the Pd 3*d* spectral region of this element in XPS was examined. Two distinct peaks and their doublets (Pd $3d_{5/2}$ and Pd $3d_{3/2}$) may be decomposed, which evidences that more than one oxidation state of the metal is present on the surface. A low intensity

contribution centred at 335.8 eV was ascribed to metallic palladium, and the main contribution at 337.5 eV was ascribed to the presence of palladium oxychloride. In the case of CuClSBA-15 sample, the Cu 2p core level signal shows the simultaneous presence of Cu(I) and Cu(II).

The incorporation of metals effectively increased the retention of the adsorbent towards the sulfur compound and the FTIR results were analysed in the light of the textural parameters and surface characteristics. The incorporation of palladium slightly enhances the adsorption of BT, but in the case of CuClSBA-15 sample, the adsorption of BT is strongly enhanced mainly due to the interaction between Cu(I) and BT. This adsorption capacity is much higher than that observed by Wang et al. [1,4].

FT-IR absorbance spectra collected in operando with a DRIFT cell for the adsorption of BT vapours at 20 ºC confirm that stronger binding energies develop (with respect to the non-impregnated SBA-15).

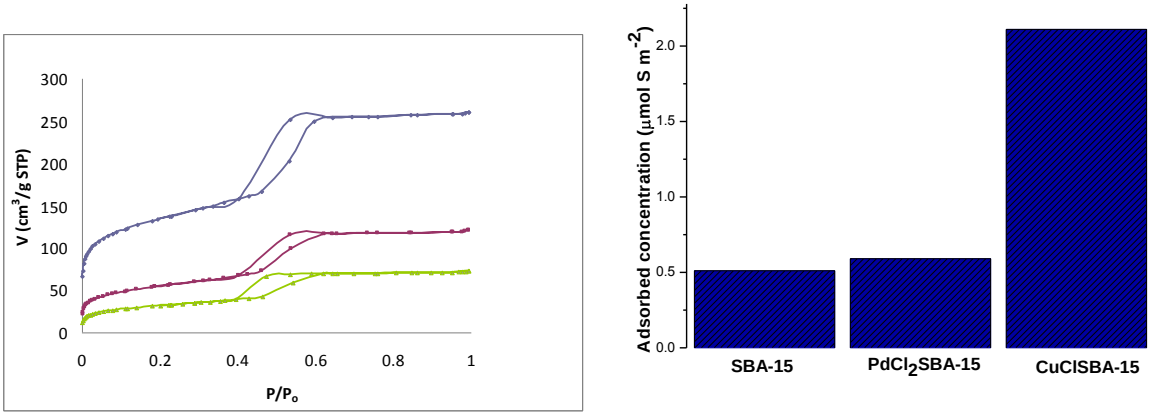

Figure 1. N_2 adsorption-desorption isotherms at 77 K for SBA-1 (blue), $PdCl_2$SBA-15 (magenta) and CuClSBA-15 (green), and adsorbed sulfur (μmol of S/g) from BT organic solutions (C_0 = 500 ppm; 100 mg of adsorbent in 20 mL of solution) at 25 ºC for the adsorbent under study.

Acknowledgements

We acknowledge the support from the Ministry of Science and Innovation (MICINN, Spain) through the project MAT2009-10481, the Regional Government (JA) through the Excellence Proiect (P06-FQM-01661 and P07FQM-5070) and FEDER funds. A.I.M. thanks to the MICINN, Spain, for a Juan de la Cierva contract, and R.M.T. thanks to the MICINN, Spain for a Ramón y Cajal contract. We also acknowledge a grant from the Brazilian Ministry of Education, project CAPES/MECD 084/05.

References

[1] Y. Wang, F. H. Yang, R. T. Yang, J. M. Heinzel and A. D. Nickens, *Ind. Eng. Chem. Res.*, 45 (2006) 7649.

[2] E. Vilarrasa-Gacía, A. Infantes.Molina, R. Moreno-Tost, E, Rodríguez-Castellón, A. Jiménez-López, C.L. Cavalcante Jr. and D.C.S. Azevedo, Energy Fuels 24 (2010) 3436.

[3] M. Gómez-Cazalilla, J.M. Mérida-Robles, A. Gurbani, E. Rodríguez-Castellón and A. Jiménez-López, J. Solid State Chem. 180 (2007) 1130.

[4] Y. Wang, R. T. Yang and J. M. Heinzel, *Chem. Eng. Sci.*, 63 (2008) 356.

High flux ZSM-5 membrane in advanced oxidation reactor for treating endocrine disrupting compounds

Wai Kit CHAN, King Lun YEUNG*
*Department of Chemical and Biomolecular Engineering, The Hong Kong University of Science and Technology, Clear Water Bay, Kowloon, Hong Kong, PR China, kekit@ust.hk, kespain@ust.hk**

Introduction

Endocrine disrupting compounds affect human hormonal system and they are difficult to be treated by conventional water treatment process. Those low-level but potent pollutants could be treated by the advanced oxidation reactor effectively. Inorganic zeolite membrane is selected for separating those EDCs in the reactor. ZSM-5 zeolite is widely used in many industrial applications such as purification, separation and catalysis etc. ZSM-5 is very hydrophilic comparable to other high silica zeolite which make itself a good candidate on water separation. However, the water permeation flux is far from satisfaction because the convention preparation method (using organic template) would reduce the hydrophilicity and from thermal cracks. In this work, template-free method [1] is introduced which made ZSM-5 membrane much thinner (1.5 μm) and defects-free. By combining the ozone oxidation, the performance of the reactor [2] could be greatly enhanced in terms of overall carbon removal.

Experimental

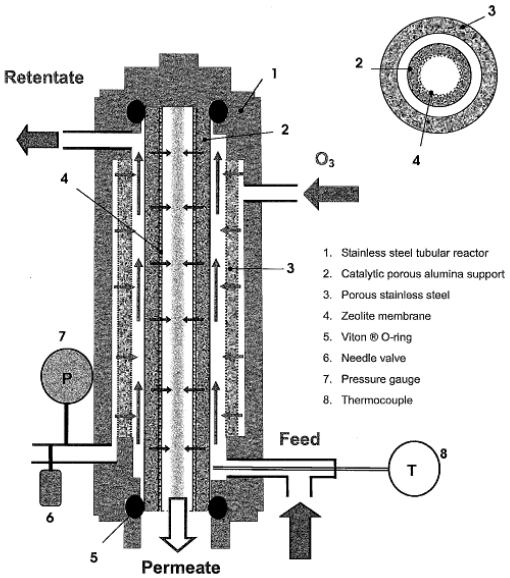

Diagram 1. Schematic diagram of the reactor [3]

Table 1. Experiment parameters for treating organics pollutant

O_3 concentration	100 ppm
Gas feed rate	20 ml/min
Temperature	25℃
Vacuum pressure	<0.7 Torr
Membrane Surface Area	0.001414 m^2
Pollutant source	Potassium Hydrogen Phthalate (KHP)
Source concentration	250 ppmC
Feed rate	Vary for different residence time

Ozone and water was fed continually to the system. Retentate and Permeate would be collected and sent for TOC and UPLC analysis. Water feed rate could be varied in order to obtain an appropriate residence time.

Results and discussion

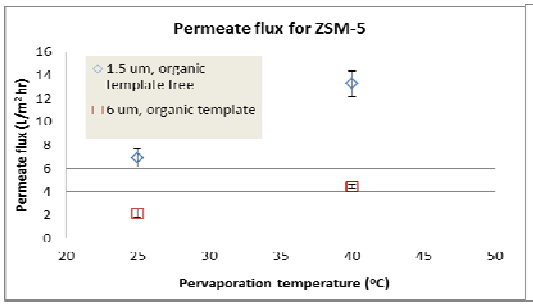

Figure 1. Comparison of flux between 1.5 µm and 6 µm ZSM-5

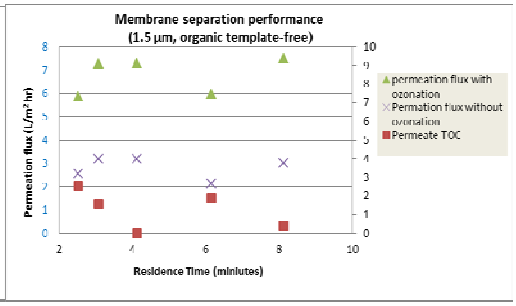

Figure 2. Permeation flux and permeate quality at different residence time.

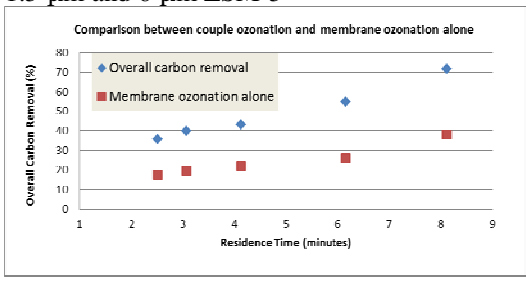

Figure 3. Reactor performance at different residence time

From figure 1, the water permeation flux for 1.5 µm ZSM-5 is obviously much higher than that of 6 µm. By combining ozonation and membrane pervaporation, the overall carbon removal rate could be greatly enhanced by over than 80% which also permeating clean water which contain 1.27 $\pm$ 1 ppmC TOC. Together with ozonation, the permeation flux increased due to the reduction on membrane fouling.

Conclusions

By using organic template-free method, a thinner but highly selective ZSM-5 membrane could be synthesized. Because of the high permeation flux, the performance of the advanced oxidation reactor could be enhanced.

Acknowledgements

The authors gratefully acknowledge financial supports from the Hong Kong Innovation and Technoloy Fund.

References

[1] Re Lai, George R. Gavalas, ZSM-5 membrane synthesis with organic-free mixture, Division of Chemistry and Chemical Engineering, California Institute of Technology, Pasadena, CA 91125, USA

[2] Samuel Heng, King Lun Yeung, Malik Djafer, Jean-Christophe Schrotter, A novel membrane reactor for ozone water treatment, Journal of membrane Science 289 (2007) 67-75

[3] Samuel Heng, Catalytic Membrane Reactor for Water and Wastewater Treatment, A thesis submitted to The Hong Kong University of Science and Technology

Selective CO_2 Separation of an Elastic Layer-structured MOF with a Sorption Column

SONG, Chi[a]; ITOH Tsutomu[b]; KONDO, Atsushi[c]; KAJIRO, Hiroshi[d]; OHBA, Tomonori[a]; KANEKO Katsumi[b]; KANOH Hirofumi[a]
Chiba Univ.[a], Shinshu Univ.[b], Tokyo Univ. Agricul. Technol.[c], Nippon Steel Corp.[d]
kanoh@pchem2.s.chiba-u.ac.jp

Introduction

Elastic layer-structured metal organic frameworks (ELMs) having flexible two-dimensional structure show a gate phenomenon in sorption/desorption of simple gas molecules. The gate phenomenon is accompanied by expansion/shrinkage of the layers. The gas sorption/desorption is not based on a physical adsorption, but on a chemical reaction, which is a clathrate formation with high cooperativity. The cooperative clathrate formation could be analyzed thermodynamically.[1-4]

The gate phenomenon shows advantages in separation of CO_2 from mixed gases and in storage of CH_4 owing to easy release of absorbed molecules. Choice of the combination of building blocks such as metals, ligands or counter ions brings about specific sorption properties for various gas molecules. Particularly, ELM-11, $[Cu(bpy)_2(BF_4)_2]n$ (bpy = 4.4'-bypyridine), is one of the most promising candidate for materials to selectively separate CO_2, because ELM-11 shows the gate phenomenon in CO_2 sorption dependent on pressure and temperature. It will enable us to separate CO_2 efficiently by changing pressure or temperature easily.

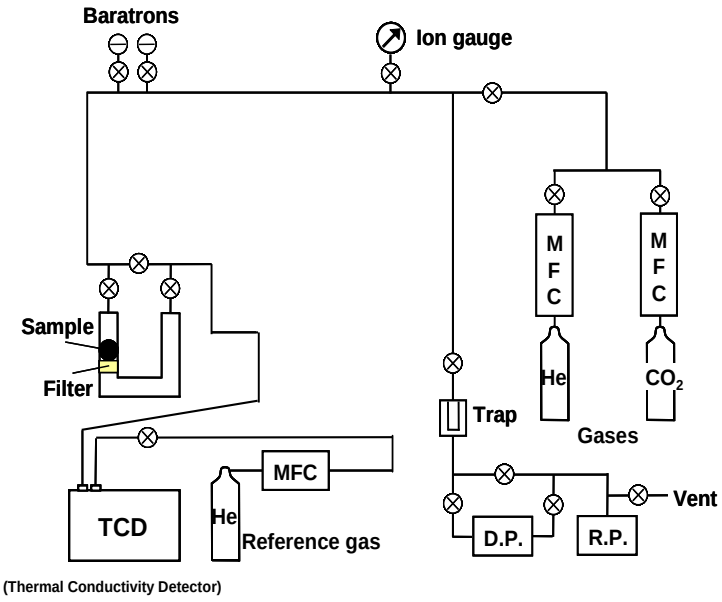

Figure 1 Diagram of an experimental line for a CO_2 sorption column.

Experimental

ELM-11 was prepared as a powder sample according to a modified method for that reported before.[5] The flow method was used for CO_2 separation with a column of ELM-11. CO_2 concentration was determined mainly with a thermal conductivity detector (TCD) and

partly a Q-MASS detector. The used sorption line is briefly described in Figure 1. Sorption behaviors of mixed gases of He/CO_2, N_2/CO_2, and CH_4/CO_2 on the ELM-11 column were examined at 258, 273, and 298 K. Sorption isotherms of CO_2 on ELM-11 in different systems were obtained using different partial pressure of CO_2 in the mixed gases.

Results and discussion

Filled circles in Figure 2 indicate the sorption isotherm of CO_2 as a pure component by a static sorption method at 273 K. The sorption does not occur below P = 280 Torr, but the isotherm shows abrupt and vertical sorption: This is the gate phenomenon, which is accompanied by the expansion of the layer distance of ELM-11. The sorption reaches a saturated amount above P = 350 Torr easily.

Also another sorption isotherm of CO_2 on ELM-11, which is obtained using mixed gases of CH_4/CO_2 with different partial pressures of CO_2, are shown with open circles in Figure 2. The gate phenomenon on CO_2 sorption was definitely found under the coexistence of CH_4, although a gate-opening pressure shifted to the higher pressure or a more modest uprise in the sorption curve was observed, which are most likely to arise from the dynamic sorption behaviors. The lowered sorbed amount of CO_2 on ELM-11 should be not because of the effect of the coexisting CH4 but because of the dynamic condition. Thus, very highly selective sorption of CO_2 was accomplished using the ELM-11 column.

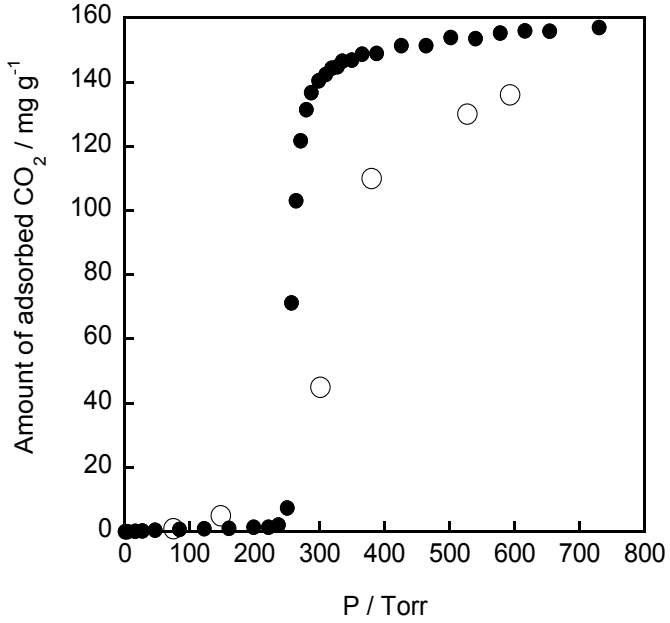

Figure 2 CO_2 sorption isotherms of ELM-11 at 273 K.
○: column method using mixed gases of CH_4 / CO_2
●: static method using a pure CO_2.

References

[1] A. Kondo, H. Noguchi, S. Ohnishi, H. Kajiro, A. Tohdoh, Y. Hattori, W.-C. Xu, H. Tanaka, H. Kanoh, K. Kaneko, *Nano Lett.*, **2006**, 6, 2581.
[2] H. Kanoh, A. Kondo, H. Noguchi, H. Kajiro, A. Tohdoh, Y. Hattori, W.-C. Xu, M. Inoue, T. Sugiura, K. Morita, H. Tanaka, T. Ohba, K. Kaneko, *J. Colloid Interface SCi.*, **2009**, 334, 1.
[3] H. Kajiro, A. Kondo, K. Kaneko, and H. Kanoh, *Int. J. Mol. Sci.*, **2010**, 11, 3803.
[4] A. Kondo, A. Chinen, H. Kajiro, T. Nakagawa, K. Kato, M. Takata, Y. Hattori, F. Okino, T. Ohba, K. Kaneko, H. Kanoh, *Chem. Eur. J.*, **2009**, 15, 7549.
[5] A. J. Blake, S. J. Hill, P. Hubberstey, W. S. Li, *J. Chem. Soc., Dalton Trans.* **1997**, 913-914.

MODELING THE REGENERATION OF A SILICALITE COLUMN SATURATED WITH LIQUID ETHANOL BY AIR PURGE

J.A. Delgado, M. A. Uguina, J.L. Sotelo, V.I. Águeda, P. Gómez, V. Hernández
Departamento de Ingeniería Química, Facultad de Químicas, Universidad Complutense de Madrid, Av. Complutense s/n, 28040 Madrid. E-mail: jadeldob@quim.ucm.es

Introduction

Alcohol production by fermentation of renewable resources, such as biomass, is becoming an interesting method for producing bioethanol, which can be used as fuel by mixing it with gasoline, or like an additive to increase the octane number. The conventional technology for producing ethanol by fermentation is based in the use of distillation in order to separate the ethanol from the fermentation mixture (with a concentration that usually lies between 4 and 10 %w/w, [1]), which requires a high consumption of energy [2]. Using this technology, up to 42 MJ/L of ethanol can be required, while the energy obtained with the combustion of one liter of ethanol only produces 23.5 MJ. Therefore, several alternatives have been proposed, including ethanol extraction with supercritical carbon dioxide, solvent extraction, adsorption-based processes and pervaporation. Among these alternatives, adsorption-based processes are very promising in order to reduce the energy requirement for this separation. Pitt et al. [1] proposed a adsorption-desorption cyclic process for recovering ethanol from fermentation broths based on the selective sorption of ethanol on solid sorbents, such as polymeric resins and hydrophobic zeolites. This process includes two steps: (1) an ethanol adsorption step, by feeding the aqueous solution from the fermentation broth, and (2) a regeneration step by desorption using hot air. From preliminary design calculations, it was determined that is possible to concentrate an 8 % w/w ethanol-water mixture up to 99 % w/w, using two adsorption stages in series, with a total energy consumption of 3.8 MJ/L of product. However, although these results were very promising, they were obtained from a very simplified model, without taking into account the adsorption-desorption kinetics.

The objective of this work is the development of a kinetic model for simulating the regeneration step of an adsorption-desorption cyclic process for producing fuel grade ethanol, using air purge. The regeneration starts when the total concentration of ethanol in the bed (including the interstitial liquid and the adsorbed phase) is higher than 99.5 % w/w. In order to validate the model, a series of regeneration experiments have been performed at different temperatures, using air to dry a bed of silicalite pellets initially saturated with liquid ethanol. For each experiment, the ethanol weight and the bed temperature were recorded. Some unknown parameters of the model have been estimated by regressing the experimental data, and the experimental curves have been compared with those predicted by the model.

Experimental

The experimental setup consists on an aluminum column (10 cm length, 1.5 cm diameter) loaded with the adsorbent (silicalite Zeosorb T-4722), resting on an analytical balance, which registers the column weight with time. The bed is covered with a spiral-wound electrical resistance to heat the column. An autonomous temperature logger

(with batteries) registers the bed temperature with time. The bed is connected to a gas supply with a Teflon tube. The resistance wires and the Teflon tube are long and thin enough not to affect the measured weight significantly.

Results and discussion

The model employed is based on mass, energy and momentum balances. In order to describe the ethanol desorption, it is assumed that the total amount of ethanol retained in the bed is divided into two zones. The first zone includes the macropores in the silicalite pellets. In this zone, the ethanol is not bound to the adsorbent, so its vapour pressure it is equal to the saturation pressure of pure ethanol. The second zone includes the silicalite micropores, where the ethanol is bound to the adsorbent. In this zone, the ethanol vapour pressure is lower than the saturation pressure, and it is estimated from the adsorption isotherm. The ethanol adsorption isotherm has been measured experimentally and it has been included in the kinetic model. Figures 1 and 2 show a comparison between the experimental weight and temperature curves and the theoretical ones obtained with the model for an air flowrate of 660 ml/min.

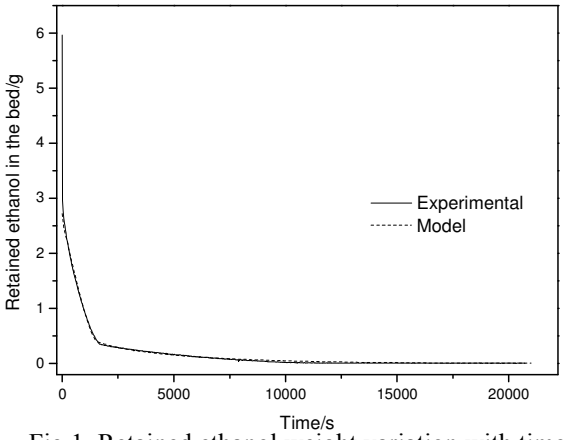

Fig.1. Retained ethanol weight variation with time.

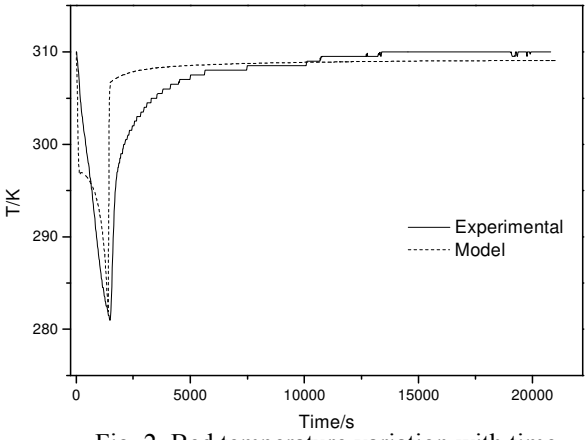

Fig. 2. Bed temperature variation with time.

It is observed that the model reproduces the experimental results satisfactorily, especially the slope change in the ethanol weight curve. In the macroporous zone, the process is controlled by the unbound ethanol evaporation, where the driving force is practically constant and equal to the difference between saturation pressure and partial pressure of the ethanol in the gas, so the weight decreases almost linearly. The theoretical concentration profiles obtained from the model show that the change in slope occurs when the unbound ethanol evaporates completely.

Acknowledgements

The authors appreciate the Education and Science Ministery's economical help (ProyectoCTQ2009-08838)

References

[1] Pitt, W.W.; Haag, G.L.; Lee, D.D., Biotechnology and Bioengineering, XXV, 123 (1983).

[2] Sircar, S. Patente EEUU 5030775 (1991)

Adsorption and diffusion of nitrogen, methane and carbon dioxide in microwave synthesized ETS-4

V.I. Águeda, J.A. Delgado, M.A. Uguina, E. Doutel, V. Hernández
Department of Chemical Engineering, Faculty of Chemistry, Complutense University of Madrid, 28040 Madrid. E-mail: viam@quim.ucm.es

Introduction

The separation of nitrogen from methane is becoming increasingly important in the natural gas industry for natural gas recovery and enhanced oil recovery. Natural gases that contain significant amounts of nitrogen need to be upgraded in order to meet the pipeline quality for minimum heating value specifications (typically < 4% inerts according to US pipeline specifications) [1,2]. The separation of carbon dioxide from methane is also important in the processing of natural gas obtained from coalseam and landfill gases because it reduces the energy content. Carbon dioxide must be removed prior to low temperature processing for NGL recovery. Generally, pipeline specifications for natural gas require a carbon dioxide concentration below 2-3%. The removal of nitrogen and carbon dioxide from natural gas by pressure swing adsorption (PSA) is an interesting alternative due to its low energy requirements and low capital investment costs. For this separation, it is desirable to use an adsorbent selective to carbon dioxide and nitrogen, to obtain methane as the purified product. The selectivity can be based on differences in the equilibrium or kinetics of adsorption, or both. Therefore, the corresponding adsorption and diffusion parameters must be known to design the separation equipment. Titanosilicate ETS-4 is a material with kinetic and equilibrium selectivity to nitrogen and carbon dioxide in their mixtures with methane, because it possesses a small pore network, the size of which may be tuned (reduced) by calcination [2]. In a previous work, we measured the adsorption and diffusion parameters of nitrogen and methane on ETS-4 synthesized by microwave heating [3]. However, the precise mechanism of separation in ETS-4 is complex, being determined in part by the material's framework composition, and the content and type of extra-framework cations. The objective of this work is to measure the adsorption and diffusion parameters of nitrogen, methane, and also of carbon dioxide, on ETS-4 (both in Na and Sr forms) synthesized by microwave heating with different framework composition and cation content than in our previous work. It must be noted that it is very difficult to find information about the diffusion parameters of carbon dioxide in ETS-4 in the literature.

Experimental

Na-ETS-4 has been synthesized following the method proposed by Coutinho et al. [4], but with a different composition of the precursor gel: 8,5 H_2O_2 : 2 TiO_2 : 11,33 SiO_2 : 16 NaOH : 761 H_2O.The synthesized NaETS4 had a Ti/Si ratio of 0.4, and a Na content of 13.4% w/w. Sr-ETS-4 was obtained by mixing Na-ETS-4 crystals with $SrCl_2 \cdot 6H_2O$, resulting in a material with a cation content of 0.9% w/w of Na and 20.4% w/w of Sr. The adsorption and diffusion parameters are estimated by modeling the experimental pulse responses obtained by injecting small amounts of the adsorbing gases in a stream of carrier gas (helium or nitrogen), passing through a bed of adsorbent with controlled temperature. The outlet of the bed is connected to a thermal conductivity detector, where the pulse responses are recorded.

Results and discussion

Figures 1 and 2 show pulse responses with beds loaded with 1 g of NaETS4 and 1 g of SrETS4 at 298 K, respectively. The curves have been fitted with a theoretical model

describing the mass balance in the system [3], assuming a linear adsorption isotherm. The effect of void volume is considered by simulating the pulse responses of helium as tracer and nitrogen as carrier. The theoretical responses obtained by fitting the adsorption and diffusion parameters (adsorption equilibrium Henry's law constant, and diffusion time constant = diffusivity/particle radius^2) are also included in Figure 1. The pulses of carbon dioxide have been obtained after deactivating the irreversible adsorption sites due to the chemisorption of carbon dioxide on the extra-framework cations.

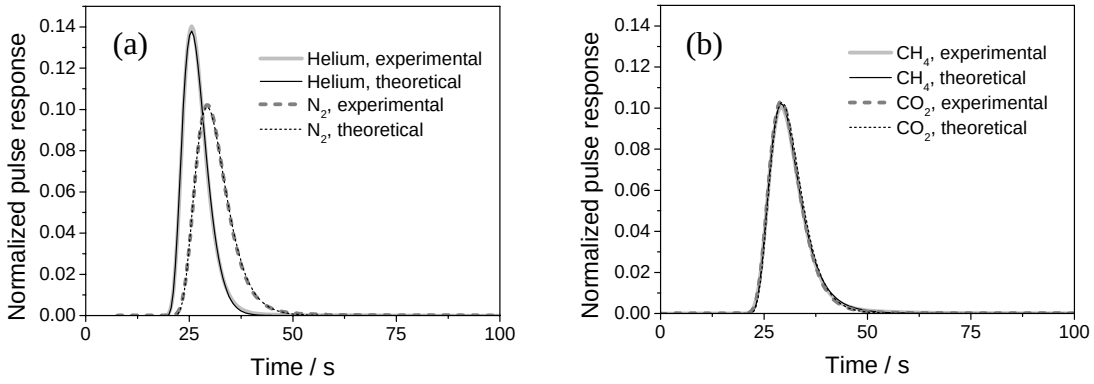

Figure 1. Pulse responses in NaETS4 (a) Pulse responses of helium (in nitrogen) and nitrogen. (b) Pulse responses of methane and carbon dioxide (very similar, overlapped).

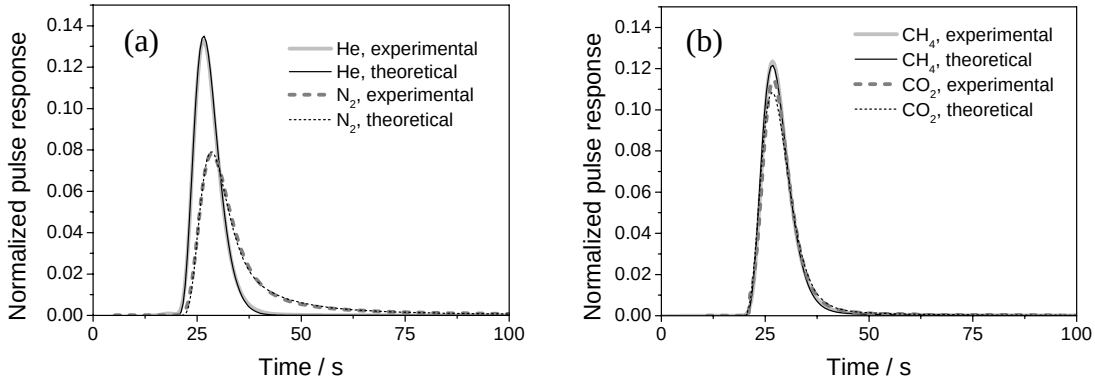

Figure 2. Pulse responses in SrETS4 (a) Pulse responses of helium (in nitrogen) and nitrogen. (b) Pulse responses of methane and carbon dioxide (similar, overlapped)

It is observed that the pulses of nitrogen, methane and carbon dioxide in NaETS4 are rather similar, indicating the low selectivity to nitrogen and carbon dioxide of this material. The differences are more noticeable in SrETS4, due to its smaller pore size. The nitrogen pulse is lower and wider in SrETS4 than in NaETS4, due to a strong increase of its adsorption equilibrium constant, and a strong reduction in the diffusivity. The methane pulse is sharper in SrETS4 (more similar to the one of helium), indicating a lower selectivity to methane, coming from both a lower adsorption equilibrium constant and a lower diffusivity. The carbon dioxide pulse in SrETS4 is lower and wider than the one of methane, due to the higher diffusivity of carbon dioxide in this material.

References

[1] Jayaraman, A.; Hernández-Maldonado, A. J.; Yang, R. T.; Chinn, D.; Munson, C. L.; Mohr, D. H. Chem. Engng. Sci. 2004, 59, 2407.
[2] Engelhard Corporation, Adsorption Processes for Natural Gas Treatment, A Technology Update, www.engelhard.com, 2005.
[3] Delgado, J.A.; Uguina, M.A., Agueda, V.I.; Garcıa-Sanz, A., Langmuir 24 (2008) 6107.
[4] Coutinho, D.; Losilla, J. A.; Balkus, K. J. Jr. Micropor. Mesopor. Mater. 90 (2006) 229.

Binary mixture adsorption of dimethylcarbonate and methanol on various zeolites

Y. Oumi[a], H. Ueda[b], M. Miyamoto[c], S. Uemiya[c], T. Inuzuka[a], T. Sano[b]
aDivision of Instrument Analysis, Life Science Research Center, Gifu University, Yanagido 1-1, Gifu 501-1193, Japan, oumi@gifu-u.ac.jp
b Department of Applied Chemistry, Graduate School of Engineering, Hiroshima University, Kagamiyama 1-4-1, Higashi-Hiroshima 739-8527, Japan
c Department of Materials Science and Technology, Gifu University, 1-1 Yanagido Gifu 501-1193, Japan

Introduction

Polycarbonate resins are widely used in the manufacturing of thermoplastic materials due to suitable mechanical and optical properties, and synthesized by a reaction between bisphenol A and phosgene. To replace harmful phosgene, alternative processes have been proposed by many researchers in the view of the so-called 'sustainable society' and 'green chemistry'[1]. Especially, the synthesis route through diphenyl carbonate (DPC) obtained by a reaction DMC and phenol as starting source has attracted considerable attention as one of the green processes [2]. But the conversion rate of DMC to DPC is very low because of small equilibrium constant. In order to increase the conversion rate, therefore, the removal of methanol (MeOH) obtained as by-product is needed form the reaction system.

In order to clarify the potential of adsorptive separation of MeOH from a binary mixture of MeOH/DMC on zeolite, we investigated the adsorption behaviors of MeOH and DMC on various zeolites.

Experimental

The single component and binary mixture adsorption experiments of MeOH and DMC vapors on the zeolites with various pore size and Si/Al ratios were carried out at 10 ~ 60 °C by a Belsorp 18 and a FMS-BG adsorption apparatus (Bel Japan Inc.), respectively. Prior to adsorption measurements, the powdered zeolites (ca. 0.3 ~ 1.0 g) were evacuated at 400°C for 10 h. The binary mixture adsorption experiments of DMC and MeOH vapors were performed by combining volumetric and gravimetric methods. The DMC/MeOH ratio in the initial mixed vapor was varied from 100/0 to 0/100.

Results and discussion

At first, the single component adsorption isotherms of pure MeOH and DMC vapors on the siliceous zeolites with different pore sizes and Si/Al ratios were measured using a conventional volumetric method. As shown in Fig.1 and Table 1, the amount of MeOH and DMC adsorbed increased with an increase in the pore diameter of siliceous zeolites (Runs 1~4). With a decrease of Si/ Al ratio, the amount of MeOH adsorbed increased, whereas the amount of DMC decreased (Runs 3, 5, 6). Namely, the amounts of MeOH and DMC adsorbed were strongly dependent on the pore size and Si/Al ratio of used zeolite. The ideal separation MeOH/DMC ratio was calculated using each adsorbed amount at P/Ps ratio of 0.5. The MeOH/DMC ratio increased with a decrease of the pore size and Si/Al ratio. This result suggests that the smaller pore size and Si/Al ratio are better for the adsorptive separation of MEOH/DMC system. Therefore, MeOH and DMC single adsorption measurements were performed using LTA type zeolite with 8-membered rings and Si/Al ratio of 1 (Run 7). As expected, the MeOH/DMC ratio was higher, indicating that LTA type zeolite has the high potential for the adsorptive separation of MeOH/DMC system.

For the adsorption separation of binary mixture using zeolite, the understanding of adsorption behaviors of each component of MeOH and DMC in the binary mixture on zeolite is needed. Therefore, the influence of the MeOH/DMC ratio in the initial mixed vapor was investigated by combining volumetric and gravimetric methods [3]. The dosing ratio of each vapor was varied from 100/0 to 0/100. Fig. 2 shows the relationship between the mole fraction of MeOH in the initial mixture and the mole fraction of MeOH adsorbed on LTA. From a comparison of the mole fraction of MeOH in the adsorbed phase with the initial composition of binary mixture, it became clear that the mole fraction of MeOH adsorbed was strongly dependent on the equilibrium pressure, indicating more selective adsorption of MeOH on LTA on higher equilibrium pressure.

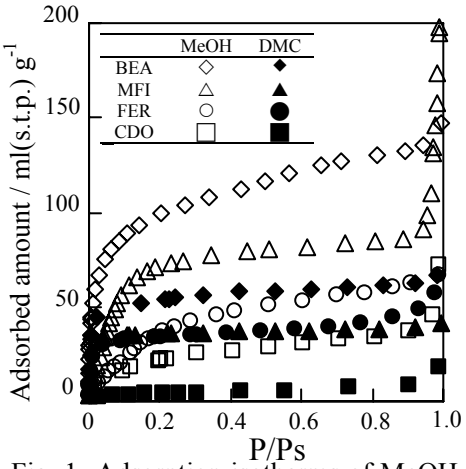

Fig. 1 Adsorption isotherms of MeOH and DMC on various siliceous zeolites at 25ºC.

Conclusions

The single component and binary mixture adsorption behaviors of MeOH and DMC were investigated. It was found from the single component adsorption experiments that the MeOH and DMC adsorption are strongly influenced by the pore size and Si/Al ratio. From the above results, it was suggested that a LTA type zeolite is effective for adsorptive separation. It was also found from the binary mixture adsorption experiments that more selective adsorption of MeOH on LTA takes place under the higher equilibrium pressure.

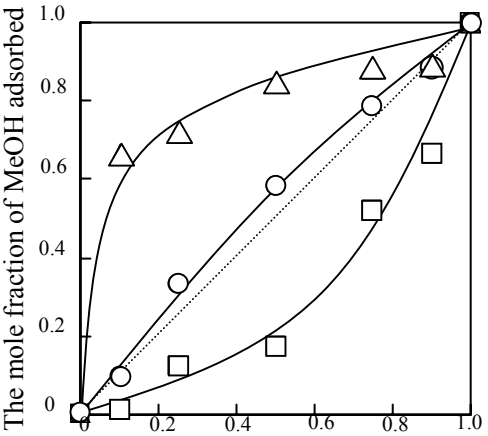

Fig. 2 Relationship between the mole fraction of MeOH in the initial mixture of DMC and MeOH and the mole fraction of MeOH adsorbed on LTA zeolites.
Equilibrium pressure : □: 0.1 kPa, ○: 1 kPa, △: 3 kPa.

References

[1] Keller, N., Rebmann, G., Keller, V., Catalysts, mechanisms and industrial processes for the dimethylcarbonate synthesis, Journal of Molecular Catalysis A: Chemical, 317 (2010), 1-18.

[2] Rivetti, F., Enichem, Continuous process for the preparation of phenyl methyl carbonate, US Patent 5,705,673 (1998).

[3] Oumi, Y., Miyajima, A., Miyamoto, J., Sano, T., Binary mixture adsorption of water and ethanol on silicalite, Studies in Surface Science and Catalysis, 142 (2002), 1595-1602

Table 1. Amounts of MeOH and DMC adsorbed on various zeolites. (P/Ps=0.5, 25ºC)

Run	Code	Channel structure	Si/Al ratio	BET surface area /m^2g^{-1}	Pore volume /cm^3g^{-1}	MeOH adsorbed /ml(s.t.p)g^{-1}	DMC adsorbed /ml(s.t.p)g^{-1}	MeOH /DMC
1	BEA	12, 12	∞	584	0.25	116.8	58.5	2.0
2	MFI	10, 10	∞	406	0.18	80.1	36.9	2.2
3	FER	10, 8	∞	360	0.14	50.2	36.8	1.4
4	CDO	8, 8	∞	141	0.06	28.8	5.5	5.2
5	FER	10, 8	90	320	0.14	55.2	34.2	1.6
6	FER	10, 8	10	273	0.11	73.6	4.8	15.3
7	LTA	8	1	-	-	125.8	2.7	46.6

Hydrogen adsorption onto exchanged zeolites A and Y

Redouane. MELOUKI, Youcef. BOUCHEFFA.
U.E.R Chimie Appliquée, E.M.P, BP 17 Bordj El-Bahri 16111, Alger, Algérie.
Melouki.redouane@gmail.com

Introduction

Industrialization generated an improvement of living conditions, which involved increase consumption energy. The most problem in the 21st century is the exhaution of fossil energy sources and the environment impacts due to hydrocarbons consumption [1]. Hydrogen is a credible alternative as a new energy source; the main obstacle of its uses is having a safety and effective method for mastered storage [2, 3]. There are four storages approaches: liquid form, gas compressed, hydrides metal and by adsorption in porous materials ways. The first two storage modes are currently the most used, but their performances do not satisfy the technical criteria required in terms of safety and output. Recent researches are focused on the adsorption into porous solid for storage [4]. Several porous solids are candidates, activated carbon [5], nanostructures carbon [6], MOFs (metal-organic frameworks) [7] and zeolites [8]. In the present work, we have studied hydrogen adsorption factors on zeolite type NaA with various calcic exchange ratios and on HY exchanged zeolite with silver. Our experimental work will be carried out at -196°C and relative pressures about 1 bar.

Experimental

The aim of this work is to examine A and Y zeolites hydrogen adsorbed capacity at the nitrogen liquid temperature (-196C), under atmospheric pressure and exchange effect of calcium and silver respectively. Five exchanges ratios of A zeolite: 0, 33, 44, 57 and 74 %, respectively noted A0, A33, A44, A57 and A74. Thus, four exchange ratios of Y zeolite: 0, 10, 50 and 98, respectively noted Y0, Y10, Y50 and Y98. Firstly, we determined textural properties versus exchange nature with nitrogen adsorption at -196°C using a surface analyzer (Quantachrome Nova 3200e) apparatus. After activation (300°C, dynamic vacuum 10^{-3} bar), the sample is cooled down till -196°C. Thereafter, hydrogen is injected per amounts up to 1 bar. Quantities adsorbed are measured using a thermobalance (Setaram MTB 10^{-8}).

Results and discussion

We observe that the exchange affects the microporous structure of zeolites. The dimensions and the valences of the compensation cations modulate the adsorbent internal porosity. According to IUPAC classification, the obtained hydrogen adsorption isotherms curves for all zeolites are type I. The largest mass adsorbed is equivalent to 1.16 and 1.05 % recorded respectively as A57 and Y0 (Fig. 1). By checking with Langmuir model, it can be observed that physical absorption is prevalent. The exchange ratio influences the beginning adsorption rate. Also, the increasing in the calcic exchange ratio improves the initial adsorption rate, following the adsorbed quantities involving. On the other hand, in Y zeolite, the initial rate decreases with silver exchange ratio (Fig. 2).

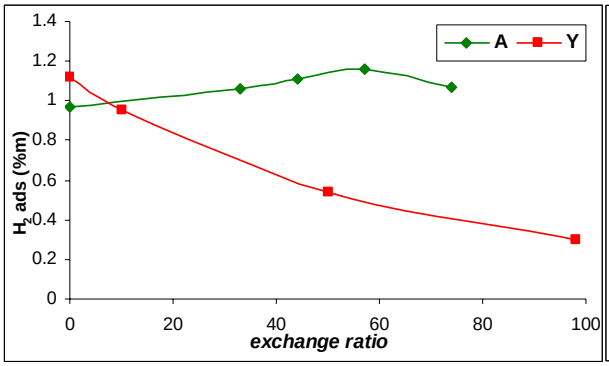

Figure 1. %m adsorbed hydrogen according to exchange ratio.

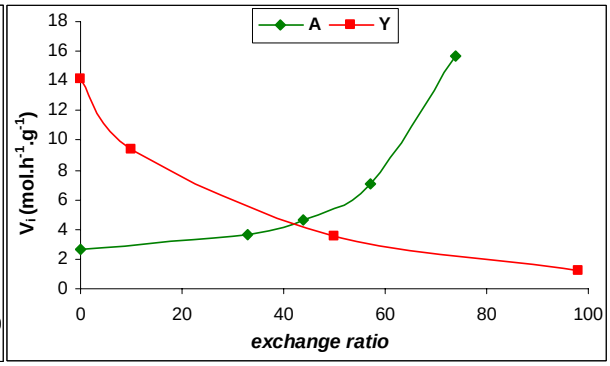

Figure 2. Hydrogen adsorption initial rate according to exchange ratio

Conclusions

The obtained adsorption isotherms curves show that hydrogen adsorption on A and Y zeolites is a physical way. The comparison between hydrogen adsorbed quantities on both zeolites types shows the effect of the electrostatic field. This last comes with the difference in zeolites atoms electronegativity and the compensation cation. In general, the high electronegativity of the compensation cations prevents the hydrogen adsorption. The micropores presence in an adsorbent increases considerably its adsorption capacity. Calcic exchange in A zeolite supports the hydrogen adsorption as well as the adsorption initial rate. In Y zeolite, silver exchange decreases hydrogen adsorbed quantities and adsorption initial rate.

References

[1] H. W. Langmi and G. S. McGrady, Non-hydride systems of the main group elements as hydrogen storage materials, Coordination Chemistry Reviews, 251 (2007), 925-935.
[2] T. Klinger, Géopolitique de l'énergie, Studyrama perspectives, 2008.
[3] H. W. Langmi, A. Walton, M. Al-Mamouri, S. R. Johnson, D. Book, J.D. Speight, P.P. Edwards, I. Gameson, P. A. Anderson and I.R. Harris, Hydrogen adsorption in zeolites A, X, Y and RHO, J. Alloys and Compounds, 356-357 (2003), 710-715.
[4] S. M. Luzan, H. Jung, H. Chun and A.V. Talyzin, Hydrogen storage in Co-and Zn-based metal-organic frameworks at ambient temperature, International journal of hydrogen energy 34(2009) pp.9754-9759.
[5] B. Weinberger and F. D. Lamari, High pressure cryo-storage of hydrogen by adsorption at 77 K and up to 50 MPa, International journal of hydrogen energy 34 (2009), 3058-3064.
[6] P. Benard and R. Chahine, Storage of hydrogen by physisorption on carbon and nanostructured materials, Scripta Materialia 56 (2007), 803-808.
[7] S. M. Luzan and A.V. Talyzin, Hydrogen adsorption in Pt catalyst/MOF-5 materials, Microporous and Mesoporous Materials 135 (2010), 201-205.
[8] G. T. Palomino, M.R. L. Carayol and C. O. Arean, Thermodynamics of hydrogen adsorption on the zeolite Ca-Y, Catalysis Today 138 (2008), 249-252.

Second-Harmonic Imaging of Guest Behaviour in Zeolites

Monique A. van der Veen,[1,2] Thierry Verbiest,[2] Dirk E. De Vos[1]
1 Center for Surface Chemistry and Catalysis, K.U.Leuven, Kasteelpark 23, box 2461, 3001 Leuven, Belgium
2 Molecular Electronics and Photonics, Department of Chemistry,K.U.Leuven, Celestijnenlaan 200D, box 2425, 3001 Leuven, Belgium
monique.vanderveen@biw.kuleuven.be

Introduction

In our 3-D macroscopic world we always enter tubular systems, such as tunnels and corridors, face-first. In the microscopic zeolite world something similar curiously seems to happen as well. Often bifunctional molecules enter zeolite pores with one functional group first, which leads to dipolar molecular chains. The technique that allowed this observation was second-harmonic generation or frequency doubling, since it is extremely sensitive to symmetry breaking like dipolar order. This stimulated effort in synthesizing guest molecule-zeolite assemblies to provide efficient frequency doubling materials.[1]

A few years ago we started to use SHG not as an aim in itself, but as an analytical tool to study guest behaviour in zeolites. As SHG is an optical effect that is forbidden in liquids, it is ideally suited to spectroscopically study zeolites in the liquid phase. We used it to follow adsorption and diffusion processes on zeolitic materials in the liquid phase in real-time.[2]

Recently we expanded our approach to second-harmonic generation microscopy (SHGM). SHGM has mainly emerged in the last decade for the visualization of biological systems, but has hardly been used so far in materials science. Herein we present the first SHGM studies on microporous materials. A study of *p*-nitroaniline in SAPO-5 crystals reveals that the tool can be used to map the organization of guest molecules. The study revealed the extent of the cooperative behaviour of PNA in SAPO-5.[3] For ZSM-5 crystals it is shown that the organization of the guest molecules can be used to determine the crystallographic orientation of the different intergrown crystal parts.[4] The extent of dipolar chains in ZSM-5 moreover pointed towards a specific diffusion behaviour which has been further unravelled *in situ* with SHGM in the liquid phase.

Experimental

All microscopy images were taken with an enhanced CCD camera (Hamamatsu) on a wide-field microscope coupled to a femto-second Ti-sapphire laser in transmission geometry. By using appropriate filters, the set-up can be used to record both two-photon fluorescence (2PF) images and SHG images. With a polarizer and a half-wave plate in the incident laser beam, we were able to record polarization patterns for each position on the image. The liquid phase experiments were performed in a Ludin Chamber from Life Imaging Services.

Results and discussion

Micrometre sized crystals of zeolite ZSM-5 are known to have an intergrown structure which can easily be seen via polarized light microscopy as an hourglass structure inside the crystal.[5] Via polarized SHG microscopy on ZSM-5 crystals filled with PNA, we discerned two polarization patterns (see Figure 1). The four lobe pattern corresponds to a zigzag

orientation of the PNA molecules, thus PNA in the zigzag pores, while the two lobe pattern corresponds to straight chains of PNA, thus PNA in the straight pores. That way we could unravel that the ramp protruding from hexagonal face is in fact 90° rotated with respect to the hexagonal facet (see Figure 1). This way, we could also unravel how the different pyramidal parts of the hourglass structure were oriented with respect to each other. In fact, we could only visualize the pores directly accessible from the outer surface (only there dipole chains are formed) when these were parallel with the sample plane of the SHG-microscope.[4] These symmetry requirements of SHG add extra discrimination, such that only certain pores are visualized each time. This makes SHG-microscopy a powerful tool for revealing structural details of zeolites. Playing with the right probe molecule per zeolite should allow such a study for a large group of zeolites.

Figure 1

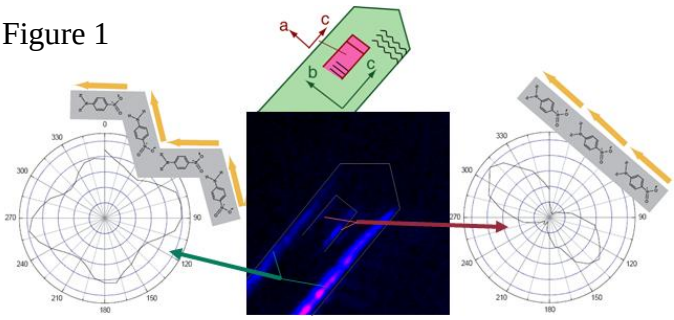

As can be seen in Figure 1, SHG is generated only in the areas close to the crystal edges. This indicates disruption of the dipole chains due to diffusion of PNA from one pore type to the other as PNA diffuses deeper into the crystal. We studied this behaviour in more detail by following the adsorption and diffusion of a series of molecules in ZSM-5 crystals *in situ* in the liquid phase with the SHG-microscope.

With SHGM we studied the organization of PNA in SAPO-5 crystals (AFI). From the polarized SHG-image we determined a how the PNA molecules were aligned with the pore direction, thus providing us with maps of the orientation of PNA. In AFI type materials PNA can coexist in two different phases. A phase separation that can already take place within a single AFI pore.[6] However, it was unknown whether the interactions between PNA chains in adjacent pores would also induce a spatial matching beyond one dimension? Our SHG-maps provided direct evidence that domain formation extends not only in one, but in three dimensions.[3]

Conclusions

SHGM is a powerful tool to map the organization and follow the diffusion of guest molecules, and via probe molecules to obtain crystallographic information.

Acknowledgements

M.A.v.d.V. is a postdoctoral fellow of FWO (Belgium). We thank K.U. Leuven (CASAS Methusalem, GOA and INPAC grants), IAP project 6/27 (Belgium) and Strep FP6 CarbonChip.

References

[1] a) Cox et al. Chem. Mater., 2 (1990), 609. b) Marlow et al. J. Phys. Chem., 97 (1993), 11289. c) Kim et al. Adv. Mater.; 19 (2007), 260.

[2] a) van der Veen et al. Langmuir, 25(2009), 4256. b) van der Veen et al. ChemPhysChem, 11(2010), 870.

[3] van der Veen et al. Phys. Chem. Chem. Phys., 12 (201) 10688.

[4] van der Veen et al. J. Am. Chem. Soc., 132 (2010), 6630.

[5] Weidenthaler et al. J. Phys. Chem., 98 (1994) 12687.

[6] Leike and Marlow, Zeolites, 16 (1996) 65.

Adsorption of polar volatile organic compounds on polymer-derived carbon supported on mesoporous alumina and silica

Piotr Kuśtrowski, Rafał Janus, Barbara Dudek, Zofia Piwowarska

Faculty of Chemistry, Jagiellonian University, Ingardena 3, 30-060 Kraków, Poland, kustrows@chemia.uj.edu.pl

Introduction

Volatile Organic Compounds (VOCs) have been recognized as hazardous polutants discharged into the atmosphere because of their negative influence on human health, role in smog formation and statospheric ozone destruction [1]. Carcinogenic and mutagenic properties of VOCs resulted in an appearence of rigid acts regulating their permissible concentration in indoor air and industry exhaust gases. Many different methods of the VOCs' removal are known and used on a large scale; e.g. catalytic and thermal oxidation, cryogenic condensation, biofiltration and gas permeation. Nevertheless, adsorption seems to be the most effective, technically non-complicated, cheapest and environmentally friendly technique of the VOCs elimination. Moreover, adsorption is non-destructive method which enables recovery of adsorbate.
The most common adsorbents of VOCs are activated carbons based on carbonized biomass, coal or waste polymers, but their microporosity causes diffusion limitations. In this work we present a new approach to the synthesis of polymer-derived adsorbents. We have extended an accessible surface of carbon by the deposition of polyacrylonitrile (PAN) layers on mesoporous alumina or silica supports followed by thermal activation.

Experimental

Organic-silica composite materials with the various intended PAN/support mass ratios (0.1, 0.2, 0.4, 0.6, 0.8, 1.2, 1.6 and 2.0) were synthesized by radical polymerization of acrylonitrile in the aqueous slurry of an inorganic support (mesoporous Al_2O_3 or SiO_2). The polymer/support mass ratios were controlled by using required acrylonitrile amounts [2]. The obtained PAN/support hybrid materials were dried and subsequently carbonized in a tubular oven at 350°C with an isothermal period of 4 h. The precursors and calcined PAN/support samples were analyzed by thermogravimetric method. The textural parameters of the calcined materials were determined by low-temperature adsorption of nitrogen. The morphology was studied using a scanning electron microscope. The surface chemical composition was investigated by means of the following spectroscopic techniques: DRIFT, UV-vis-DRS and XPS. The carbonized composites were tested as adsorbents of methyl-ethyl ketone (MEK) vapor. This compound was chosen as a model molecule representing a wide range of compounds classified as VOCs.

Results and discussion

The deposition of polyacrylonitrile followed by carbonization resulted in a gradual decrease in surface area and total pore volume of the applied support. This fact confirms the successful coating of the whole surface with carbonaceous species. The coating effectiveness was determined by thermogravimetric (TG) analyses in flowing air. The TG measurements in the inert atmosphere revealed that only part of PAN mass is lost at the carbonization temperature equal 350°C. It was found by DRIFT that carbonization at this temperature caused

transformation of the polymer into so called “ladder form” of PAN [2]. The adsorption capacities of the silica supports strongly increased after the deposition of a small amount of PAN-based carbonaceous species. On the other hand, deposition of higher PAN amounts caused a continuous decrease in the MEK adsorption because of the reduction of accessible surface and pore volume. The isotherms of N_2 adsorption of the pure support and carbonizates and the sorption capacities for chosen series PAN/MCM-41 are displayed in Fig.1.

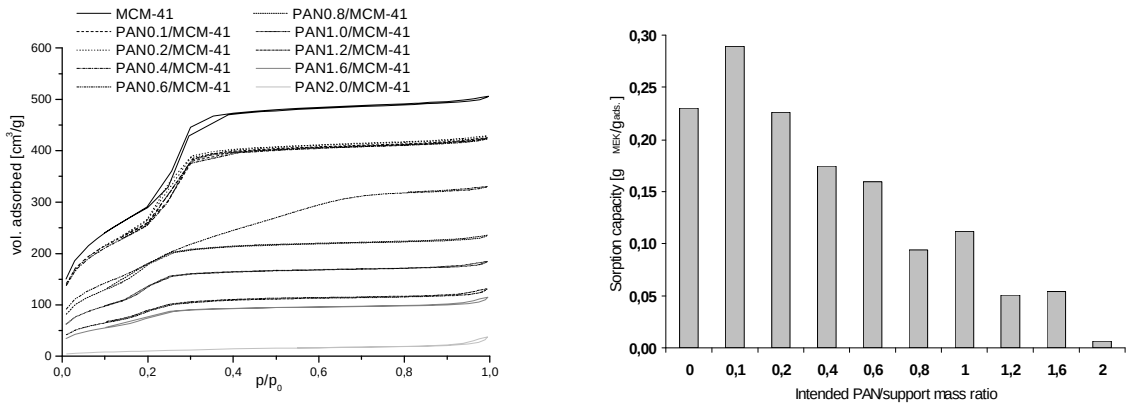

Figure 1. The low-temperature N_2 adsorption isotherms (left-hand) and MEK sorption capacities (right-hand) for a MCM-41-based series of nanocomposites

Conclusions

An introduction of polymer reduced the surface area and pore volume of porous silica and alumina. The TG measurements exhibited that the effectiveness of PAN deposition depended on the nature of a support and a PAN/support ratio (the higher intended ratio, the lower coating effectiveness). The carbonization of hybrid PAN/support materials at 350°C caused forming the unsaturated ladder form of PAN, which showed a high potential in adsorption of polar organic compounds. The PAN/support samples with the lowest carbon loading displayed the highest sorption capacities, higher than the parent support, and appeared to be promising materials for commercial applications to VOCs removal.

Acknowledgements

This work was supported by the Polish Ministry of Science and Higher Education under the grant no. N N507 553238. Rafał Janus wishes to thank the Foundation for Polish Science MPD Programme co-financed by the EU European Regional Development Fund for the financial support.

References

[1] Dawson, H.E., McAlary, T., A Compilation of Statistics for VOCs from Post-1990 Indoor Air Concentration Studies in North American Residences Unaffected by Subsurface Vapor Intrusion, Ground Water Monitoring and Remediation, 29 (2009), 60-69

[2] Kuśtrowski, P., Janus, R., Kochanowski, A., Chmielarz, L., Dudek, B., Piwowarska, Z., Michalik, M., Adsorption properties of carbonized polyacrylonitrile deposited on γ-alumina and silica gel by precipitation polymerization, Materials Research Bulletin, 45 (2010), 787-793

The use of diffusion cell dynamics for diagnostics of silicalite-1 membranes

Arlette Zikanova[a], Vlastimil Fila[b], Pavel Hrabanek[a], Bohumil Bernauer[b], Libor Brabec[a], Ivan Jirka[a], Milan Kocirik[a]

[a]*J. Heyrovský Institute of Physical Chemistry of the ASCR, v.v.i.; Dolejškova 2155/3, 18223 Prague 8, Czech Republic, milan.kocirik@jh-inst.cas.cz*
[b]*Institute of Chemical Technology Prague, Technická 5, 16628 Prague 6 Dejvice, Czech Republic*

Introduction

Principal requirements on diagnostics of zeolite gas separation membranes are (i) to estimate parasitic penetrants flows through defective (non-zeolitic) pores and (ii) to estimate texture parameters of defective pores. Thus, there is a need in availability of rapid and reliable diagnostic technique with the capability to meet the above requirements. The appropriate experimental technique to fulfill this task appeared to be measuring of dynamic responses of a semi-open diffusion cell with a binary testing mixture of penetrants.

Experimental

The method is exemplified in this work on composite silicalite-1 membranes synthesized on asymmetric α-alumina porous discs prepared in our laboratory. The zeolite layer synthesis occurred from clear solutions. This operation was facultatively repeated several times. The calcination of the membrane proceeded in air flow using heating programs with maximum temperature T_{max} between 330 and 550°C. The membrane was characterized by SEM (combined with HF etching), XPS and UV-VIS spectroscopy and elemental analysis. The dynamic tests were performed in the diffusion cell with open upstream compartment which was separated from the closed one by the tested membrane. The cell was operated at 30°C and closed compartment was stirred. The binary gas mixture used was CH_4-N_2. Prior to non-stationary single component permeation consisted upstream flow and content of closed compartment of the same gas (CH_4 or N_2). The dynamic run was started with injection of a small amount of the corresponding gas into the closed compartment. The dynamic response was represented by gauge pressure $\Delta p_{CH4}(t)$ (and $\Delta p_{N2}(t)$) in the closed compartment. The corresponding normed responses were defined as:

$$M(t) = \Delta p_{CH4}(t) / \Delta p^{0}_{CH4} \quad (1), \quad P(t) = \Delta p_{N2}(t) / \Delta p^{0}_{N2} \quad (2), \quad X(t) = \Delta p_{\Sigma}(t) / x^{0}_{CH4} . p_a \quad (3)$$

superscript *0* denotes the initial value. In experiments with binary species the system was as a rule initially in the same condition as the single component experiment with N_2. The dynamic run was started with a stepwise change in feed composition from pure N_2 to a mixture N_2 + CH_4. During this experiment there was recorded the normed response $X(t)$:

where $\Delta p_{\Sigma}(t)$, x^0_{CH4} and p_a stand for total gauge pressure in closed compartment, step change in molar fraction of CH_4 in the feed and ambient pressure, respectively. Texture parameters of the defective pores were evaluated by the comparison of measured responses with those simulated by the model given below. As a rule also the response $x_{CH4}(t) / x^0_{CH4}$ was evaluated based on GC analysis of the gas in the closed compartment.

Mathematical model

The mathematical model of the system involves mass balance equations for cell compartments and constitutive and mass balance equations for the penetrants in zeolitic layer, in porous system of the support and in defective pores. The non-stationary diffusion of penetrants in continuous zeolitic matrix is described by Generalized Maxwell Stefan (GMS) formalisms and transport in the support and in defective pores is described by Dusty Gas Model (DGM).

Results and Discussion

The $X(t)$ response represented for all the calcined membranes a curve $X(t) \geq 0$ with $X(0) = 0$, $X(t) \rightarrow 0$ for $t \rightarrow 0$. The curve is characterized by a maximum X_{max} (t_{max}) and a width Δt at $X = X_{max}/2$. A development of the X(t) responses in dependence on calcination temperature T_{max} together with the results of responses simulation and the results of silicalite-1 crystals and layers etching [1,2] and results of XPS and UV-VIS analysis [3] showed that for heating programs with $T_{max} \geq 400°C$ all the membrane porous system (micropores + defective pores) percolates. For program with $T_{max} \cong 400°C$ the value X_{max} attains for a given membrane its maximum value but there are still organic residues in the defective pores. As T_{max}, increases X_{max} decreases to its limiting value in high temperature region which is reached at $T_{max} \cong 480°C$. The dynamic responses measured for such membranes characterize the defective pores free of template residue and the texture parameters evaluated are the true characteristics of the membrane synthesis method used.

Acknowledgements

The financial support by The Grant Agency of the AS CR via grant KAN 400720701 and IAA 400400909 is gratefully acknowledged.

References

[1] L. Brabec, M. Kocirik, Silicalite-1 polycrystalline layers and crystal twins: Morphology and grain boundaries, Materials Chemistry and Physics, 102 (2007) 67-74.
[2] L. Brabec, M. Kocirik, Silicalite-1 crystals etched with hydrofluoric acid dissolved in water or acetone, Journal of Physical Chemistry C, 114 (2010) 13685-13694.
[3] I. Jirka, P. Sazama, A. Zikanova, P. Hrabanek, M. Kocirik, Low temperature removal of templates from high-silica ZSM-5. Catalytic effect of zeolitic framework, Microporous and Mesoporous Materials 137 (2011) 8-17.

Effect of air humidity on the removal of carbon tetrachloride from air using Cu-BTC Metal-Organic Frameworks

Ana Martín-Calvo[1], Elena García-Pérez[1], Almudena García-Sánchez[2], Rocío Bueno-Pérez[1], Said Hamad[1], and Sofia Calero[1]*

*[1]Department of Physical, Chemical, and Natural Systems, University Pablo de Olavide, Ctra. Utrera km. 1. 41013 Seville, Spain. [2] Process & Energy Laboratory, Delft University of Technology, Leeghwaterstraat 44, 2628CA Delft, The Netherlands. Corresponding author S. Calero (*scalero@upo.es)

Introduction

Carbon tetrachloride was originally synthesized in 1839. In the early 20th century, it had extensive applications as dry cleaning solvent, lava lamps, fire extinguishers, refrigerants, and pesticides. Some years later, it was proved that the exposure to carbon tetrachloride had several adverse health effects. In addition, carbon tetrachloride plays a role in ozone depletion and in the greenhouse effect. For all these reasons, carbon tetrachloride was phased out in the 2nd Montreal Protocol's revision in 1992. Unfortunately, this molecule remains involved in several industrial processes either due to the lack of suitable replacements or due to it generation as undesirable by-products, so still today we find significant concentrations of this component on air.

Recently we demonstrated that adsorption selectivity in favour of carbon tetrachloride can be further enhanced by selective blockage of the Cu-BTC framework [1]. This short communication is to date the only work that analyzes the capacity of Cu-BTC to separate carbon tetrachloride from air. The aim of this work is to cover the gap with an extensive simulation study, which provides a detailed analysis on the adsorption, diffusion, and separation of carbon tetrachloride from dry and humid air, using Cu-BTC.

Methods

In this work we use Monte Carlo and Molecular Dynamics simulations to study adsorption and diffusion of oxygen, nitrogen, argon, and carbon tetrachloride molecules as pure components and mixtures in Cu-BTC. The adsorption selectivity of carbon tetrachloride is analyzed for air with relative humidity ranging from 0 to 100%. Firstly, we provide accurate sets of Lennard-Jones parameters that we fitted to reproduce the experimental vapor-liquid equilibrium curves of all molecules under study. Secondly we discuss the preferential sites of adsorption and the adsorption selectivity obtained for the different systems at room temperature. The differences observed on the self-diffusion of carbon tetrachloride in Cu-BTC as pure component and as part of a multi-component mixture are also discussed.

Results and discussion

In order to analyze the effect with water as competing molecule we performed simulations in a range of different air models, with relative humidities spanning from 0% (0% of water vapor at 298 K and 10^5 Pa) to 100% (4% of water vapor at 298 K and 10^5 Pa).

The results obtained show a preferential adsorption of carbon tetrachloride over water, oxygen, nitrogen and argon molecules for all percentages of air relative humidity. Although the selectivity values are always in favor of carbon tetrachloride we observe different trends depending on the air relative humidity. The average occupation profiles in Cu-BTC obtained for water and carbon tetrachloride during the adsorption of the five-component mixture illustrate the large affinity of water for the metal center in Cu-BTC and the subsequent adsorption of these molecules in the windows and octahedral cages (Figure 1)

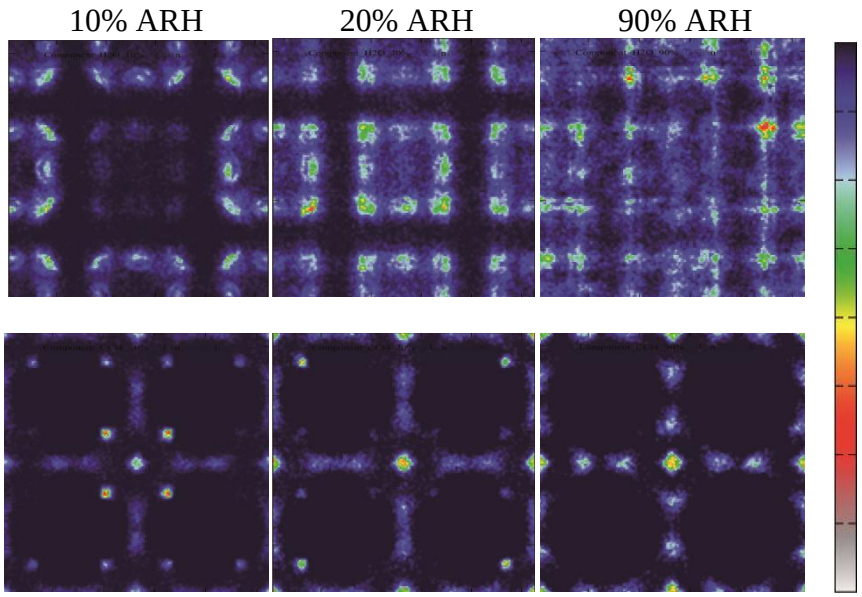

Figure 1. Average occupation profiles of water (top) and carbon tetrachloride (bottom) in Cu-BTC at 298 K. The profiles were obtained from the molecular simulations of five-component mixtures of carbon tetrachloride in air with relative humidity 10% (left), 20% (medium), and 90% (right). The same color gradation (from dark blue to white) is employed in all figures, although the total number of molecules present in the unit cell is different for each calculation.

Conclusions

According to our results, this material shows extremely high adsorption selectivity in favor of carbon tetrachloride. We demonstrate that this selectivity can be further enhanced in humid air. Our simulations results for five component mixtures involving humid air revealed diffusion values for carbon tetrachloride up to three orders of magnitude larger than those obtained in dry air [2].

Acknowledgements

This work is supported by the Spanish MCINN (CTQ2010-16077) and by the Junta de Andalucía (P07-FQM-02595).

References

[1] Calero, S., Martín-Calvo, A., Hamad, S., and Garcia-Perez, E. *Chemical Communications*, **47**, 508-510, 2011
[2] Martín-Calvo, A., García-Pérez, E., García-Sanchez, A., Bueno-Pérez, R., Hamad, S., and Calero, S., *Physical Chemistry Chemical Physics*, 2011 (submited)

TGA investigation of propene adsorption over Ag- and Cu- exchanged X zeolites

Fouad Benaliouche[a], Youcef Boucheffa[a], Philip Ayrault[b], Samuel Mignard[b] and Patrick Magnoux[b]
[a]*EMP,UER de Chimie Appliquée, BP 17 Bordj El-Bahri, 16111, Algiers, Algeria, benaliouche.fouad@gmail.com*
[b]*Laboratoire de Catalyse en Chimie Organique, 40 Avenue du Recteur Pineau, 86022 Poitiers, France*

Introduction

The industrial separation of olefin from olefin/paraffin mixtures, such as propene/propane and ethylene/ethane by cryogenic distillation has been used for over 70 years [1]. Although this separation process is efficient, it is the most energy consuming distillation in both the chemical and petrochemical industries [2]. The adsorption using the π-complexation sorbents is a good alternative to olefin/paraffins separation process. Transition metals containing zeolites, such as Ag and Cu, present a particular geometrical and chemical selectivity for olefins. These metals may form a strong but reversible bond with the olefin molecules allowing to their recovery via either a pressure or temperature change [3]. An important problem found during the adsorption process is olefin polymerisation, which is due to the acidity of the adsorbent and can induce a loss of the adsorption capacity [4-6]. The aim of the present study is to evaluate the acidity effect on the adsorption of propene over various Ag- and Cu- exchanged X zeolites. The effect of fractional surface coverage, the nature and the strength of the propene adsorption will be discussed.

Experimental section

The parent material used for this study is NaX zeolite (SiO_2/Al_2O_3 = 3, Na_2O/H_2O = 0.025 and Na_2O/SiO_2 = 1.2) prepared following the procedure reported in our previous study [6]. Prior to modification, the NaX zeolite is treated with NaCl in order to bring the Al/Na ratio to equilibrium. The modification of NaX zeolite is achieved by following the conventional ion-exchange technique (liquid phase ion exchange) to obtain Ag- and Cu- exchanged forms. Ionic exchange is carried out in various aqueous solutions containing the appropriate amount of $AgNO_3$ or $CuCl_2$ (supplied by Merck). The ion exchange procedure is repeated several times to ensure that the desired level of ion exchange is obtained. Thus, zeolites with different metal loadings ranging from low to high exchange are obtained. The detailed exchange procedures are well described in our previous work [6]. The exchange degrees are determined by elemental analysis following standard procedures. Phase purity of the exchanged zeolites is examined by PANalytical-X'Pert PRO diffractometer. The powder X-ray diffraction (XRD) patterns are collected over a 2θ range of 3-50° using Cu-Kα radiation (λ = 1.54060 Å). The porosity of all samples is measured by adsorption and desorption of nitrogen at -196 °C using a Micromeritics ASAP 2010 surface analyzer. For FTIR spectroscopy of pyridine adsorption, the measurements are performed on a Nicolet Magna 750 spectrometer equipped with a vacuum cell. Adsorption of propene is studied using a Setaram microbalance at 273, 291, 323 and 423 K under a pressure range of 0-97 kPa.

Results and discussion

An example of the propene adsorption–desorption isotherms of NaX zeolite and its Ag-exchanged forms measured at 273 and 423 K are shown in Fig. 1-a, and b. The results show

that all Ag-exchanged zeolites exhibit a type I isotherm characteristics without any change in shape, and that the adsorption capacity decreases noticeably with an increase of Ag exchange degree.

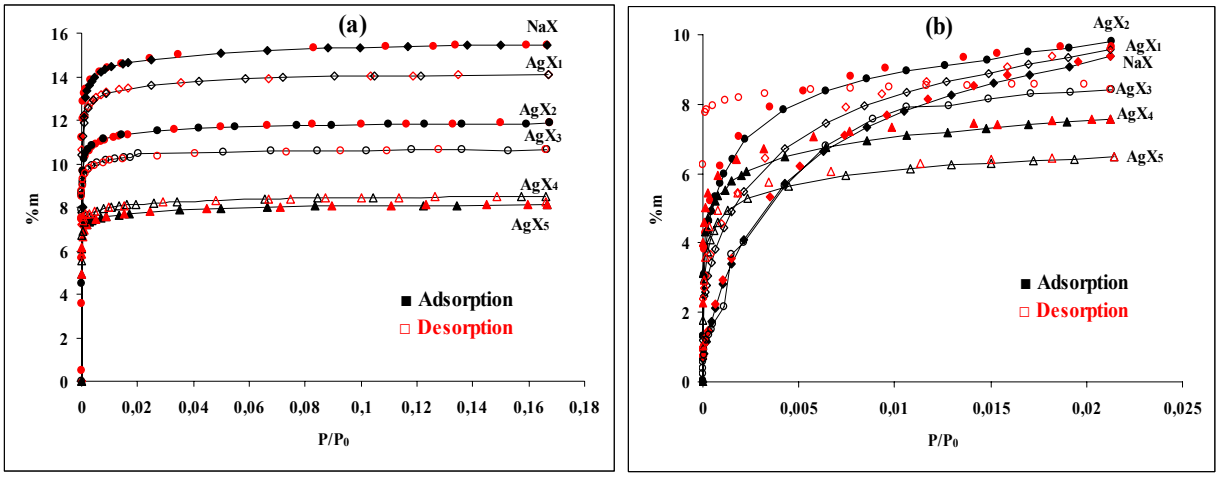

Figure 1. Weight increase of Ag- exchanged X zeolite vs. partial pressure of propene at 273 K (a), and 423 K (b).

When the temperature increases to 423 K, an hysteresis loops is visible on each adsorption-desorption isotherm. In this case, the propene molecules are strongly held and the desorption becomes difficult. Nearly the same evolution of the propene adsorption is observed for Cu-exchange (isotherms not shown). All these behaviors could be related to the oligomeric species formation. The fast oligomerization reaction of propene on the Ag- and Cu exchanged zeolites is catalyzed by the relatively high concentration of Brønsted and Lewis acid sites as estimated by IR spectroscopy [6].

Conclusion

Our results show that starting from 323 K, a formation of oligomeric compounds (coke deposition) takes place by polymerization of propene on the Ag- and Cu- exchanged X zeolites. The oligomeric compounds formation is related to the Brønsted and Lewis acid sites, which are estimated by IR spectroscopy. In addition, we show that the ion exchange carried out with copper and silver is effective for the propene retention via π-complexation and particularly at high exchange degree.

References

[1] Keller, G. E., Marcinkowsky, A. E., Verma, S. K., Wiliamson, K. D., In Separation and Purification Technology, Li, N. N., Calo, J. M., Eds.; Marcel Dekker, NY, 1992, p. 59.
[2] Safarik, D. J., Eldridge, R. B., Olefin/Paraffin Separations by Re- active Absorption, Industrial & Engineering Chemistry Research, 37 (1998), 2571-2581.
[3] Yang, R. T., Adsorbents: fundamentals and applications; Wiley-Interscience, 2003.
[4] Delahay, G., Coq, B., in: Guisnet, M., Gilson, J.-P., Eds.; Zeolites for Cleaner Technologies, Catalytic Science Series, Imperial College Press, London, 2002, vol. 3 p. 345.
[5] Boucheffa, Y., Thomazeau, C., Cartraud, P., Magnoux, P., Guisnet, M., Jullian, S., Formation of Carbonaceous Compounds from Propene and Isobutene over a 5A Zeolite. Influence of Temperature on their Compositions and Locations, Industrial & Engineering Chemistry Research, 36 (1997), 3198-3204.
[6] Benaliouche, F., Boucheffa, Y., Ayrault, P., Mignard, S., Magnoux, P., NH_3-TPD and FTIR spectroscopy of pyridine adsorption studies for characterization of Ag-and Cu-exchanged X zeolites, Microporous & Mesoporous Materials, 111 (2008), 80-88.

Improved amine-functionalized hexagonal mesoporous silica for CO_2 adsorption

G. Calleja, R. Sanz, A. Arencibia, E. S. Sanz-Pérez
Department of Chemical and Energy Technology, ESCET
Universidad Rey Juan Carlos, C/ Tulipán s/n, 28933 Móstoles, Madrid, Spain.
guillermo.calleja@urjc.es

Introduction

Among the technological strategies developed to reduce CO_2 emissions, gas phase adsorption over mesostructured materials stands out as a noteworthy technique. The functionalization of these materials with organic molecules containing amino groups gives as a result less toxic and corrosive adsorbents with easier regeneration processes than liquid absorbents [1].

In this work, hexagonal mesoporous silica (HMS) has been synthesized by using a primary alkylamine as a template. By varying the carbon chain length of this template, analogous mesostructured materials with different textural properties have been obtained. All of them have been functionalized by grafting with a diethylenetriamine-ending organosilane (DT) and by wet impregnation with an organic polymer, polyethyleneimine (PEI), to check their CO_2 adsorption capacity.

Experimental

HMS samples were synthesized by using tetraethylorthosilicate (TEOS) as the silica source, and a single alkylamine such as octylamine (8N), decylamine (10N) and dodecylamine (12N) as a structure directing agent. After hydrolysis, to obtain the silica framework, solids were filtered and calcined at 550 ºC. The obtained materials were denoted as HMS-*x*, where *x* represents the number of carbon atoms in the alkylamine molecule (*x* = 8, 10, or 12).

Grafting functionalization with DT (diethylene-triamine-trimethoxysilane) was performed under reflux in toluene. Grafted samples were named as HMS-*x*-DT. A wet impregnation procedure, following the original method from Song and co-workers [2] was performed to obtain PEI functionalized samples, named HMS-*x*-PEI (y), where *y* represents the PEI weight percentage in the final adsorbent material. Prepared samples were characterized by X-ray diffraction, H, C, N elemental analysis, and N_2 adsorption/desorption isotherms at 77 K. Pure CO_2 adsorption/desorption isotherms performed at 45 ºC in the range 0.1-6 bar.

Results and discussion

Table 1 summarizes the textural properties, nitrogen content and CO_2 adsorption capacity obtained for the siliceous supports (HMS-8, 10 and 12) as well as for the HMS-12 functionalized samples. Silica samples exhibit a wider pore size when using longer surfactant molecules, since larger micelles in solution are formed, as observed. As seen in Table 1, pore diameter and pore volume values vary from 1.46 nm and 0.72 cm^3/g for HMS-8 up to

2.09 nm and 0.96 cm^3/g for HMS-12. CO_2 adsorption capacity of these samples is quite low in the pressure range studied, showing an isotherm behaviour typically associated to a physisorption process.

HMS-12 functionalized samples are representative of the functionalized samples general behaviour. A remarkable decrease of their textural properties is observed, showing a high incorporation of organic molecules into their pores. Nitrogen content for DT grafted sample is 7.6 wt %, while values for PEI impregnated materials range from 9.5 to 19.0 wt %. CO_2 adsorption isotherms have been carried out in the same conditions corresponding to the exhaust combustion gases at coal-fired thermal power stations: 45 ºC and 0.15 atm. The obtained adsorbents present chemisorption-like CO_2 isotherms, with a higher adsorption capacity for increasing nitrogen content. DT grafted sample adsorption capacity is 58.5 mg CO_2/g, and PEI impregnated samples present values from ca. 60 to 80 mg CO_2/g ads. However, adsorption efficiency of these materials reaches its maximum value (0.24 mol CO_2/ mol N) for HMS-12-DT, in which organic chains are covalently bonded to the silica surface.

Similarly, HMS-8 and 10 have also been functionalized with DT and PEI (50). For PEI (50) impregnated materials, CO_2 adsorption capacity showed no significant differences. However, samples grafted with DT presented adsorption values dependent on the textural properties of the starting HMS support: for wider pores, higher adsorption capacities were registered.

Table 1. Textural properties, N content and CO_2 adsorption capacity measured at 45 ºC of siliceous and functionalized HMS mesoporous materials.

Sample	S_{BET} (m^2/g)	D_P (nm)	V_P (cm^3/g)	N (wt. %)	mg CO_2/g ads.		mol CO_2/mol N	
					0.15 atm	4.5 atm	0.15 atm	4.5 atm
HMS-8	1056	1.46	0.72	-	2.8	47.8	-	-
HMS-10	918	2.04	0.72	-	2.6	48.2	-	-
HMS-12	1181	2.09	0.96	-	2.5	50.6	-	-
HMS-12-DT	39	1.30	0.10	7.6	58.5	89.9	0.24	0.38
HMS-12-PEI (30)	52	-	0.13	9.5	58.0	88.6	0.19	0.30
HMS-12-PEI (50)	27	-	0.08	14.0	68.4	88.1	0.16	0.20
HMS-12-PEI (70)	2	-	<0.01	19.0	82.2	95.1	0.14	0.16

Conclusions

Functionalization by either grafting or impregnation produces highly loaded materials. As the nitrogen content of the sample increases, a higher CO_2 adsorption capacity is obtained, being HMS-12-PEI (70) the best result, with a CO_2 uptake up to 82.2 mg CO_2/g ads at 0.15 atm and 45 ºC, i.e., in similar conditions than the exhaust fumes of coal-fired power stations.

References

[1] DOE/OS-FE, Carbon sequestration. State of Science, Office of Science and Office of Fossil Energy, US Department of Energy, Washington, DC, 1999.

[2] Xu, X., Song, C., Andrésen, J.M., Miller, B.G., Scaroni, A.W., Novel polyethylenimine-modified mesoporous molecular sieve of MCM-41 type as high-capacity adsorbent for CO_2 capture, Energy Fuels, 16 (2002), 1463–1469.

Isotherm constructions from the nanoscale FTIR understanding of gas adsorption on microporous: CO adsorbed on NaY zeolite as a case study

Olivier CAIRON
*UPPA-UFR S&T BP1155, 64013 Pau France. * olivier.cairon@univ-pau.fr*

Introduction

Cationic zeolites' applications in the separation processes mainly concern gas/solid adsorption based on the zeolites' selective adsorption properties resulting from two key parameters: their pore size selectivity and their affinity for guest molecules. Gas separation performances of alkali-exchanged zeolites used as industrial sorbents are firstly assessed through their affinity and their retention capacities for each gas component; both being determined thanks to the experimental adsorption isotherms determined by gravimetric, volumetric or calorimetric experiments [1]. In spite of the very informative insights that can be deduced from, these approaches are limited to a global or macroscopic description of the cationic zeolites' properties. Addressing a molecular understanding of the role that cations play towards each gas regarding selectivity and adsorption capacities is a challenge that might open promising routes for further developments of new zeolite-like materials with improved performances.
On the other hand, IR spectroscopy of small probe molecules is one of the more informative techniques for describing at the molecular level how gas adsorption on cationic zeolites occurs. After recalling some of the main IR insights from our recent studies devoted to CO adsorbed on NaY [2, 3], the purpose of this communication is to present the method we developed allowing us to construct microporous-like isotherm with respect to our previous FTIR insights of CO adsorption on NaY Faujasite.

Experimental

IR spectra of progressive CO adsorption (80K) on a self-supporting thin pellet of NaY zeolite (Union Carbide, Si/Al ~ 2.5, m= 5.4 mg) have been recorded as previously described [2, 3]. The CO molecules that were stepwise introduced in the cell from a control volume by doses ranged from 0.4 to 40 μmol induce a progressive increasing of equilibrium pressure (P_{CO}) that was recorded for each IR spectrum. Curve fitting of IR spectra was achieved thanks to the Omnic Peak Resolve® software. More details on the peak fitting procedure and its meaningful regarding the as-formed CO adsorbed species are provided and discussed hereafter.

Results and discussion

CO adsorption on dehydrated NaY Faujasite occurs only on Na^+ cations populating the SII positions in the large α-cages. From recent IR insights, we demonstrated that progressive CO adsorption results from the completion of the cationic coordination vacancies of these SII Na^+ cations [2, 3]. As a result, mono and di-carbonyls adsorbed species - $Na^+(CO)$ and $Na^+(CO)_2$ or M, D - are evidenced through their individual vibrating νCO positions around 2171 and 2163 cm^{-1}, respectively. Moreover, thorough analysis of the IR spectra outlines that mono-and di-carbonyls' formation are of CO pressure dependence. For instance, whilst M formation is favoured at low pressure (P_{CO} = 0.7 Pa), D are progressively formed either 'directly' or resulting from mono- to di-carbonyls conversion. According to these results, it can be put forward that each of recorded IR spectra can be meaningful fitted using two individual mono- and di-carbonyls peaks as components. Fig. 1 illustrates the above curve fitting purpose for different sets of CO pressure and highlights how the line shape of spectra is affected with respect to the sum of the two M and D components.

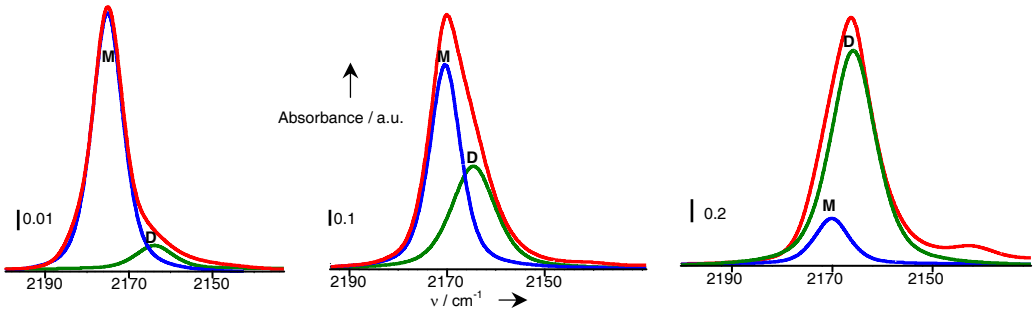

Figure 1: IR spectra curve fitting based on mono (M) and di-carbonyls (D) peaks components for various PCO sets (PCO = 0.4, 2.2 and 5 Pa, from the left to the right part).

The above curve fitting procedure was applied to all spectra recorded for PCO ranging from 0 to 20 Pa. Then, areas (integrated intensities) of M and D peak components were calculated and reported versus their corresponding PCO, Fig. 2 (left scale). The concentration profiles of each of the M and D species are thus reported. At very low CO amounts, M species predominate and their conversion to D species begins for PCO > 1.2 Pa (the M profile declines). Concomitantly, D formation slightly appears for low CO amounts and predominates at higher CO pressure (PCO > 2.5 Pa) till a plateau is reached.

The M and D area calculations combined with the Bee-Lambert law are used hereafter for adsorbed CO concentration determination. Based on our previous quantitative procedure [4], it requires however some assumptions to be made that will be discussed at the presentation. As a result, the as-calculated number of adsorbed CO molecules is reported, Fig. 2, right scale. Thus, it can be clearly outlined that from a qualitative point of view, the CO concentration profile matches well with those of microporous isotherms of Type I, according to the IUPAC classification. Moreover, from a quantitative point of view, the NaY micropores are fulfilled with around 80 CO molecules per unit cell (u.c) as indicated by the plateau shape for high CO pressure. Considering that theoretically 32 Na^+ cations per unit cell are populating SII sites and that only D species are formed according IR features, our quantitative calculations match well these theoretical data.

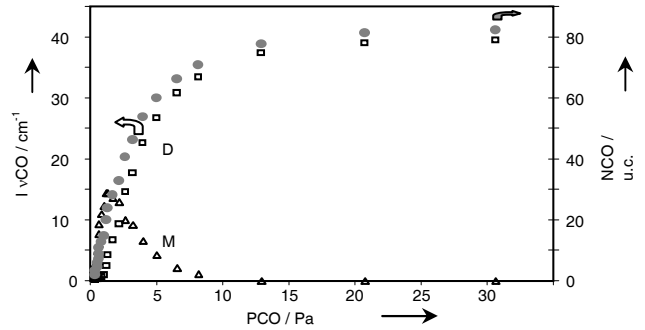

Figure 2: The M and D concentration profiles versus equilibrium PCO (left part).As-calculated concentration of adsorbed CO molecules (full circles, right part)

Conclusions

Our interpretation of IR spectra relies upon curve fitting to extract individual gas isotherms. This bottom-up approach should provide a better understanding of gas adsorption performances of cationic zeolites towards their chemical composition.

References

[1] Keller, J. U., Staudt, R., Gas Adsorption Equilibria, (2005), Springer Science
[2] Cairon, O.; Loustaunau, A., J. Phys. Chem. C, 112 (2008), 18493-18501
[3] Cairon, O., Phys.Chem.Chem.Phys., 12 (2010), 14217-14226
[4] Cairon, O.; Chevreau, T., J. Chem. Soc., Faraday Trans., 94 (1998), 323-330

Highly oriented neutral and cation-free $AlPO_4$ LTA: from seed crystal monolayer to molecular sieve membrane

A. Huang, and J. Caro

Leibniz University Hannover, Institute for Physical Chemistry and Electrochemistry, Germany
Email; aisheng.huang@pci.uni-hannover.de

Introduction

Zeolites with their uniform pore structure and high thermal stability are widely used in the chemical industry as catalyst, ion exchanger and adsorbent. [1] Apart from the use of zeolites as powders, supported zeolite layers are of interest for many potential applications. It is well recognized that control of the microstructures of the zeolite layers, such as grain orientation and grain boundaries, play an important role in their performances. [2-4] Oriented zeolite layers exhibit superior performances compared to randomly oriented ones. Highly oriented zeolite layers have been prepared by both direct in-situ growth and secondary growth. For secondary growth of oriented zeolite layers, a highly oriented monolayer of zeolite seeds is helpful. Much effort has been made to assemble zeolite crystals as oriented seed monolayer, including physical adsorption chemical bonding. [5, 6]

Recently, we have developed a novel neutral and cation-free aluminophosphate ($AlPO_4$) LTA molecular sieve membrane with hydrogen permselectivity. [7] In combination with ultrasonication, herein we report a simple, effective and versatile strategy to prepare a highly oriented $AlPO_4$ LTA monolayer through the use of polyethyleneimine (PEI) as an interlayer, which can attach seed crystals as hydrogen-bonding mediator. [8, 9] After the attachment of oriented seed crystals, hydrothermal secondary growth follows to prepare an oriented $AlPO_4$ LTA membrane. It can be expected a highly oriented $AlPO_4$ LTA molecular sieve membrane will show superior separation performances compared to a randomly oriented one.

Experimental

A highly oriented $AlPO_4$ LTA seeds monolayer was prepared by ultrasonication using PEI as mediator among the $AlPO_4$ LTA crystals and the substrate. The close packing is attributed to a certain degree of surface migration by repeated bond breaking (by ultrasonication) and bond formation (by PEI) between the $AlPO_4$ LTA microcrystals and the alumina support. The oriented $AlPO_4$ LTA molecular sieve membrane on porous Al_2O_3 support was prepared through secondary growth of the oriented $AlPO_4$ LTA monolayer at 200 ºC for 5 h as reported previously. [7]

Results and discussion

Figure 1a and b show a highly oriented $AlPO_4$ LTA monolayer and molecular sieve membrane formed on the porous Al_2O_3, respectively. For separation of single and binary mixtures at 200 ºC (Figure 2), the oriented $AlPO_4$ LTA membrane showed a higher H_2 selectivity than a random $AlPO_4$ LTA membrane.

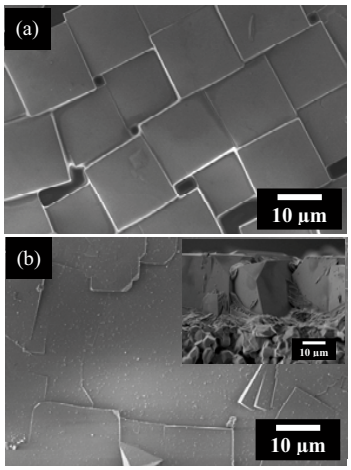

Figure 1

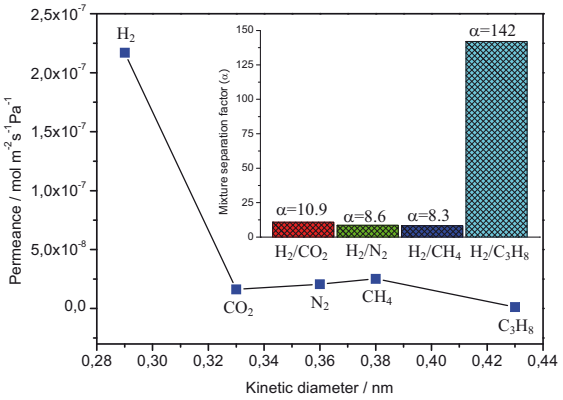

Figure 2

Conclusions

Through the use of PEI as a hydrogen-bonding interlayer in combination with ultrasonication, we have developed a simple, effective and versatile strategy to assemble highly oriented $AlPO_4$ LTA monolayers on non-porous and porous substrates. After secondary growth, the former oriented monolayer grew into a well-intergrown oriented membrane layer with a preferential (h00) orientation. For permeation of single gas and separation of binary mixtures, the porous Al_2O_3-supported oriented $AlPO_4$ LTA membrane showed a higher H_2 selectivity than a random $AlPO_4$ LTA membrane since the oriented growth could minimize the defect density and the transport pathways through the grain boundaries.

Acknowledgements

Financially supported by DFG (Ca147/11-3), as a part of the European joint research project "International Research Group: Diffusion in Zeolites" of DFG, CNRS and EPSRC.

References

[1] M. E. Davis, *Nature* **2002**, *417*, 813
[2] G. A. Ozin, A. Kuperman, A. Stein, *Angew. Chem. Int Ed. Engl.* **1989**, *28*, 359.
[3] Z. Lai, G. Bonilla, I. Diaz, J. Nery, K. Sujaoti, M. A. Amat, E. Kokkoli, O. Terasaki, R. W. Thompson, M. Tsapatsis, D. G. Vlachos, *Science*, **2003**, *300*, 456.
[4] M. A. Snyder, M. Tsapatsis, *Angew. Chem. Int. Ed.* **2007**, *46*, 7560.
[5] Y. Liu, Y. Li, W. Yang, *J. Am. Chem. Soc.* **2010**, *132*, 1768.
[6] A. Kulak, Y. Lee, Y. S. Park, K. B. Yoon, *Angew. Chem. Int. Ed.* **2000**, *39*, 950.
[7] A. Huang, F. Liang, F. Steinbach, T. M. Gesing, J. Caro, *J. Am. Chem. Soc.* **2010**, *132*, 2140.
[8] R. Ranjan, M. Tsapatsis, *Chem. Mater.* **2009**, *21*, 4920.
[9] K. B. Yoon, *Acc. Chem. Res.* **2007**, *40*, 29.

Characterization of Zeolite 5A by Ethylene and Ethane Adsorption

Masoud Mofarahi ,Seyyed Milad Salehi
Chemical Engineering Department,Persian Gulf University,Bushehr,IRAN
Corresponding author: Mofarahi@pgu.ac.ir, Fax:+98771 4540376

Abstract

Olefin/paraffin separations are one of the most important separations in the refining and petrochemical industries that currently are done by complicated or energy intensive processes. Because of the worldwide increasing demand and cost of energy sources, adsorption processes are becoming strong competitors for conventional separation processes in the chemical and petrochemical industries. Pure and multicomponent adsorption data are necessary information for designing a separation process on the basis of adsorption. However, with the presentation of new industrial adsorbents, it seems to be necessary to determine their properties for separation systems. In this work, pure and binary equilibrium data of the ethylene and ethane on a zeolite 5A (provided by Zeochem Co.) at various temperature (283 K , 303 K and 323 K) and pressure range 0 to 9 bar by volumetric method were presented. The total amount of binary gas mixture was directly measured by experiment for ethylene/ethane system, and the amount of each species adsorbed was predicted by thermodynamics modeling. Such data have never been previously published. Vacancy solution theory (VST) is usually used for pure component data (Table 1) correlation as well as mixture adsorption isotherm prediction (Table 2). Application of this theory to correlate pure data and predict binary gas adsorption in ethylene/ethane system was investigated. An optimization program was applied to correlate pure adsorption isotherms and obtained parameters were used to predict equilibrium binary gas mixture (Figure 1). As a result of thermodynamics modeling, adsorption selectivity was predicted by VST model and the results reconfirm that zeolite 5A has a good selectivity for separation of ethylene and ethane from each other (Figure 2). Comparison of the results from the experiments and the thermodynamics modeling gave a good agreement.

Table **1**. Regression Results for Pure Ethane Adsorption on Zeolite 5A

(Temperature(K	$n_1^{s,\infty}(\frac{mol}{kg})$	$b_1(\frac{m}{kg})$	Λ_{1v}	Λ_{v1}	%AAD
283	2.43	0.1742	1.847	0.5412	10.45
303	2.35	0.1191	2.686	0.4286	6.85
323	2.12	0.0516	2.152	0.3291	3.96

Table 2. Comparison of Predictions Error of Models for Different C_2H_4/C_2H_6 mixtures

	Ethylene 20%			Ethylene 50%			Ethylene 80%		
Model	**K 283**	**K 303**	**K 323**	**K 283**	**K 303**	**K 323**	**K 283**	**K 303**	**K 323**
VST	6.21	4.51	4.78	5.62	3.86	4.31	4.46	6.38	5.43

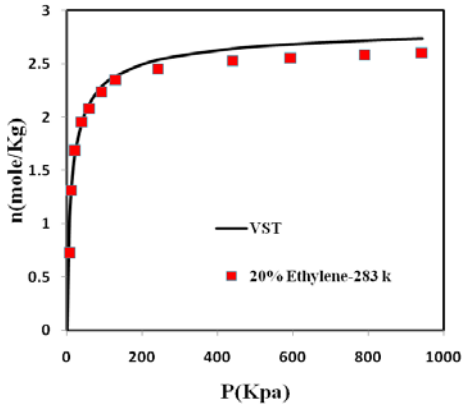

Figure 1. Experimental total amount of adsorption isotherms for C_2H_4/C_2H_6 20:80 mixture at 283 K prediction by VST model.

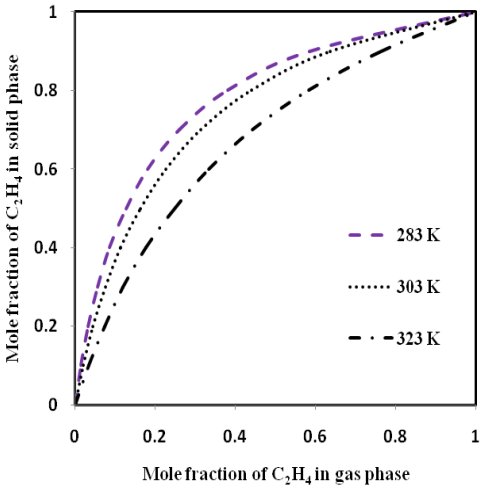

Figure 2. Predicted adsorbed phase versus gas phase composition at 800 kPa.

Pure and Multicomponent Equilibrium Adsorption Isotherms of Carbon Dioxide, Nitrogen and Oxygen over Zeolite 13X

Masoud Mofarahi ,Seyyed Masoud Sayah
Chemical Engineering Department,Persian Gulf University,Bushehr,IRAN
Corresponding author: Mofarahi@pgu.ac.ir, Fax:+98771 4540376

Abstract

In this work, pure, binary and ternary equilibrium data of the carbon dioxide, nitrogen and oxygen over a zeolite 13X (provided by Zeochem Co.) were measured and evaluated by ideal adsorbed solution theory. The measurements were conduced on the basis volumetric method at temperatures of 283, 303, and 323 Kelvin and at pressure to 950KPa. The ideal adsorbed solution theory (IAST) model based on Langmuir equation and langmuir-Freundlich equation provides a powerful framework to predict multicomponent gas adsorption particularly for systems species of similar chemical structure. The IAST model as a correlative tool is analyzed and demonstrated by applying it to all a set of single, binary and ternary data for the CO2/N2/O2 adsorption system. Amount of adsorption of each components are obtained in the mixture as well as selectivity from thermodynamic prediction. The prediction of IAST model to binary and ternary data indicates a very good agreement.

Apparatus and Procedure

The adsorption apparatus shown in Figure 1 is based on the static volumetric method. There are an adsorption cell and a loading cell. Used were 1/8 in. tubes and 1/8 in. valves to minimize dead volume as much as possible. The adsorption cell, loading cell, and dead volumes were measured using helium gas. The total amount of gas introduced and recovered in the system was determined by appropriate pressure, temperature, and volume measurements. The temperature in each cell was measured by K-type thermocouple operated within (0.01 K accuracy); the pressure was measured with a pressure transducer. Temperatures and pressures were recorded at constant time intervals with a recorder (Logoscreen 50, Jumo Co.). During measurement, adsorption cell was immersed in a water bath (MC 12, Julabo Tech.) maintained at ± 0.02 K via a refrigeration circulator. Prior to each isotherm measurement, zelolite 13X particles were regenerated in an oven overnight (300 °C for 6 h) under a vacuum of less than 0.05 mbar.

Isotherm of pure adsorption

Adsorption isotherms of pure carbon dioxide, nitrogen and oxygen measured at three temperatures (283,303 and 343) K are plotted in Figures 2,3 and 4 and are in Figure 2. The adsorption isotherm data were correlated by Langmuir models.

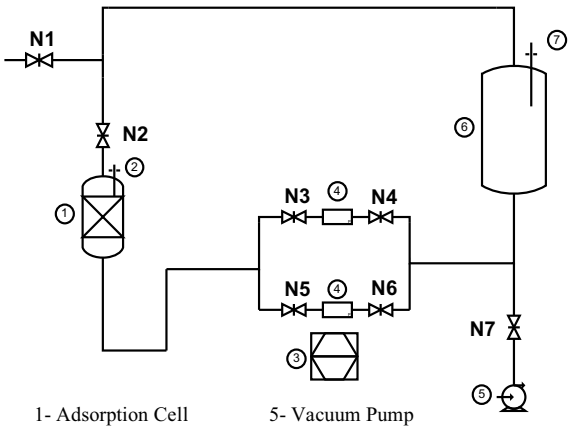

1- Adsorption Cell
2- Thermocouple
3- Recorder
4- Pressure Transducer
5- Vacuum Pump
6- Reservoir
7- RTD

Figure1. Schematic diagram of the adsorption apparatus

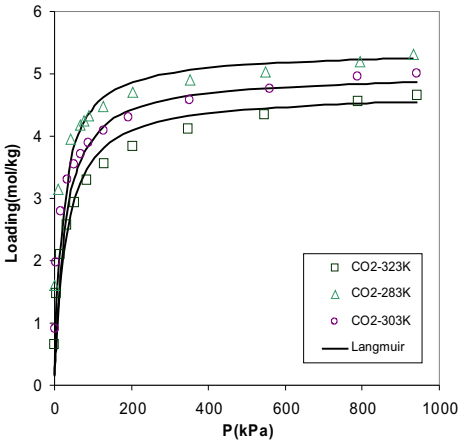

Figure2. Experimental adsorption isotherms of CO_2 over Zeolite 13x and regression by Langmuir.

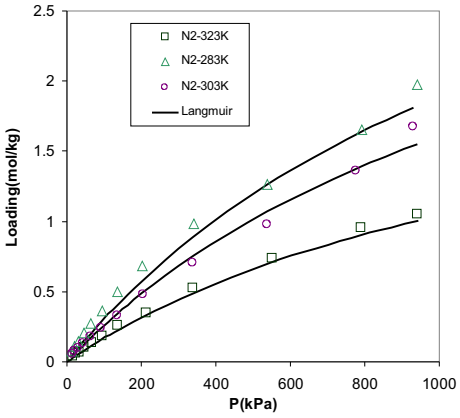

Figure 3. Experimental adsorption isotherms of N_2 over Zeolite 13x and regression by Langmuir.

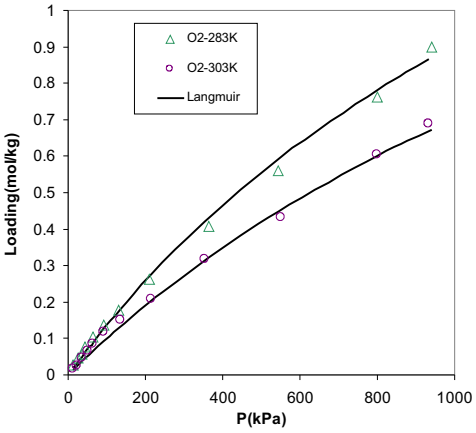

Figure 4. Experimental adsorption isotherms of O_2 over Zeolite 13x and regression by Langmuir

.

Packing density of adsorbates inside the micropores of zeolites. Studies by nitrogen postadsorption

J.M. Guil, R. Guil-López[#], J.A. Perdigón-Melón[#]
Instituto "Rocasolano", CSIC. Serrano, 119, 28006-Madrid (Spain)
J.M.Guil@iqfr.csic.es

Introduction

We have been working along years on the assessment of the microporous network of zeolites of new synthesis and PILCs based on studies of the adsorption of organic molecules of different size and shape, mainly by adsorption microcalorimetry (see, for instance, refs. 1). A certain number of known zeolites and various adsorbates were used. It was shown that the packing density (d_{pck}= $n_{\mu p}/V_{\mu p}$, adsorbate uptake/micropore volume) of each probe molecule depends on the size and shape of channels and cavities of the zeolite. The values for toluene were high and somewhat dependent on zeolite texture whereas those for *n*-hexane ranged from near the molar liquid density to much lower values in zeolites of narrow micropores. In the case of mesitylene, the packing density inside those zeolites where mesitylene can penetrate was in the order of one third of its liquid density. So, a fraction of the micropore space has to be empty. The aim of this work is to prove the existence and determine the volume of those voids by means of nitrogen post-adsorption experiments (77 K) performed after controlled partial filling of the micropores.

Experimental

A large number of zeolites (Beta, SSZ-26, mordenite, SSZ-24, ZSM-11, ZSM-12, ferrierite) have been studied. Toluene, *m*-xylene, *o*-xylene, *n*-hexane, mesitylene were used as pre-adsorbates.

Results and discussion

The amount of each adsorbate that fills up the micropores was determined from the differential calorimetric isotherms, n^{ads}-q^{st} (Fig.1). A second (readsorption) isotherm was used to calculate de amount that remains irreversibly adsorbed, n_{irr}, (Fig.1). The later amount was also determined from volumetric isotherms (Fig.2).

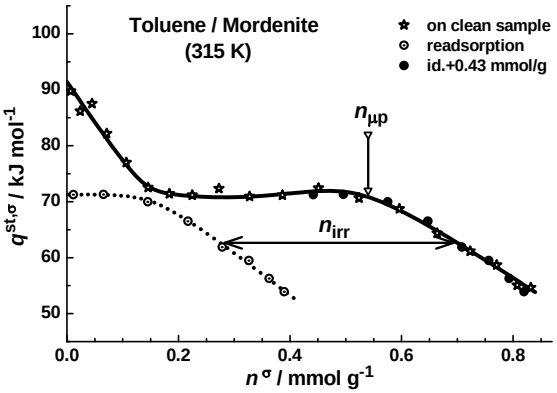

Fig. 1. Differential calorimetric isotherms of toluene adsorption on mordenite.

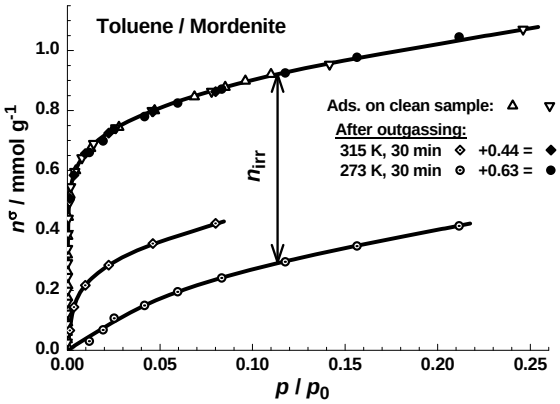

Fig. 2. Volumetric isotherms of toluene adsorption on mordenite.

Adsorption of nitrogen (77 K) on the sample with different controlled amounts of pre-adsorbate, n_{irr}, gave the amount of nitrogen, $n_{acc}(N_2)$, that

[#] Present addresses: RGL. I.de Catálisis y Petroleoquímica, CSIC, Madrid, Spain. JAPM, Universidad de Alcalá de Henares, Spain.

was adsorbed on voids, in between adsorbate molecules (Fig.3). From this quantity, the volume accessible to nitrogen, V_{acc}, was calculated. Plots of V_{acc} vs n_{irr} allowed us to calculate the "true" packing density of adsorbates, d_{pck}, inside the zeolite micropores (Fig.4):

$$V_{acc}(N_2) = V_{\mu p} \text{ ("t" method)} - (1/d_{pck}) \cdot n_{irr}$$

But in fact, more information is readily obtained from these data.

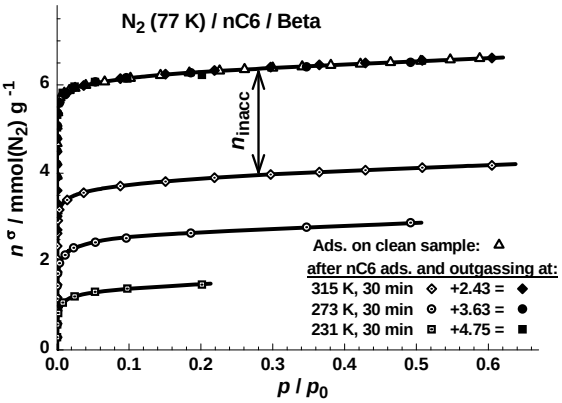

Fig. 3. Nitrogen isotherms on β-zeolite with different n-hexane pre-adsorbed amounts.

Results for nitrogen adsorption on β-zeolite after *n*-hexane and toluene pre-adsorption are presented in Fig.4.a. Values of packing density of toluene and *n*-hexane inside the micropores, calculated from the large initial linear part (Fig.4a), are well above their liquid densities: 13.1 and 10.9 mmol/cm^3, compared to 9.11 and 7.49 mmol/cm^3, respectively. The wide channels and cavities of this zeolite allow a "free" closest packing of adsorbates to occur. It is the confinement inside the micropores what makes it possible to measure the void space between pre-adsorbate molecules; that cannot be done in the bulk liquid although, certainly, empty space exist. When micropores are nearly full, the volume accessible to nitrogen decreases, probably due to diffusion restrictions.

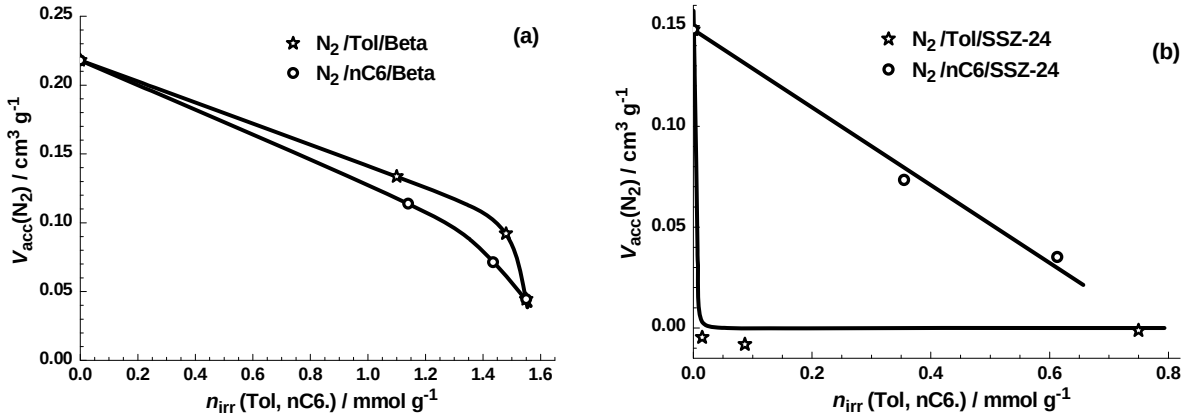

Fig. 4. Volume accessible to nitrogen *vs* irreversible amount of pre-adsorbate: a) β-zeolite; b) SSZ-24

The case of SSZ-24 is another interesting example. It has only unidirectional wide channels. The packing density of *n*-hexane calculated from nitrogen post-adsorption experiments (Fig.4b), 5.18 mmol/cm^3, is similar to that obtained from *n*-hexane adsorption, 4.86 mmol/cm^3. With toluene, however, a small amount adsorbed is enough to block the entrance to nitrogen. A tilted position of toluene molecules - maximum interaction with micropore walls - can be visualised.
Information of interest is obtained for other zeolites and the potential of this methodology is so established.

Acknowledgements

Authors acknowledge the financial support from the Ministry of Science and Innovation, Spain (Project FIS2010-15502) and Madrid Autonomous Community (Project CM P2009/ESP-1691).

References

[1] a) J.M. Guil, R. Guil-López, J.A. Perdigón-Melón, A. Corma. "Determining the topology of zeolites by adsorption microcalorimetry of organic molecules ". *Micropor. Mesopor. Mat.*, 22 (1998) 269. b) A. Corma, A. Chica, J.M. Guil, F.J. Llopis, G. Mabilon, J.A. Perdigón-Melón, S. Valencia. "Determination of the pore topology of zeolite IM-5 by means of catalytic test reactions and hydrocarbon adsorption measurements". *J. Catal.* 189 (2000) 382.

Study of the adsorption of sterols by mesoporous material MCM-41, modified by organosilanes

E.V. Borodina[1], O.O. Krizhanovskaya[1], S.I. Karpov[1], V.F. Selemenev[1], F. Roessner[2]
[1] *Department of analytical chemistry, Voronezh State University, University Square 1, 394054 Voronezh, Russia*
[2] *Department of industrial Chemistry 2, Carl v. Ossietzky University, Ammerlaender Heerstreet 114 -118, D-26111 Oldenburg, Germany*
evborodina@gmail.com

Introduction

Conventional materials applied in separation science and chromatography are unstructured materials, with their pore volume represented by a disordered narrowing and widening maze. This sorbent structure gives rise to uncertainty of residence time of molecules in the pore maze, increasing the time of establishing sorbent - sorbate equilibrium [1]. To avoid the disadvantages and increase the separation and extraction efficiency, a structured material with uniform pores and homogeneous distribution over the surface can be used. The development of ordered-mesoporous materials has been done to eliminate these drawbacks of amorphous silica [2]. In the last decade the grafted organosilanes materials arose on the basis of matrix with ordered mesopores material based on MCM-41 structure [3, 4]. The surface modification can be achieved by covalent attachment. The high surface area allows grafting a high amount of modifier. These materials are widely used in various fields of science and technology, such as chromatography [1], sorption [5] and catalysis.

In this work, the surface modification of mesoporous MCM-41 by organosilanes and the adsorption of sterols on MCM-41 mesoporous material were studied.

Experimental

MCM-41 (Sued Chemie Company, Germany) was used as an inorganic matrix for the grafting. The different types of modifer, containing alkylchain were used as a modifier. Alkyl grafted MCM-41 samples were prepared by the addition of alkylsilane to a suspension containing calcinated MCM-41 at 540 °C. The mixture was refluxed for 24 - 36 hours then the products were washed with methanol and n-hexane, and dried at 60°C for 4 hours. Diffuse reflectance infrared fourier transform spectra (DRIFT) were recorded on a Bruker Equinox 55 for a wavenumber range of 400 - 4000 cm^{-1} with a resolution of 4 cm^{-1}. Samples were prepared by mixing the test sample with KBr (Merck, Germany) at a ratio of 1 : 4. The typical sorption procedure includes a placing the grafted sample of MCM-41 into a SPE column and conditioned with about 5 ml of n-hexane, followed by the elution of solution with biologically active substance. The fractions of eluate were taken every minute to check the analyzer performance at regular interval during the sorption process. The GC-FID method was used for the control of quantity of substances in every fraction.

Results and discussion

From the data obtained from DRIFT, the control of grafting layer and analysis of intermolecular interactions between the atoms of the attached modifier can be done. Figure 1 shows the DRIFT spectra of MCM-41 and grafted samples recorded at room temperature in

the range of 4000 – 1400 cm^{-1}. The appearance of the bands at 1475, 1490 (δ_{C-H} groups in the CH_2 and CH_3) [26], 2854, 2892, 2956 and 3021 cm^{-1} (ν_{C-H} groups in the CH_2 and CH_3) confirms the successful modification of the mesoporous material.

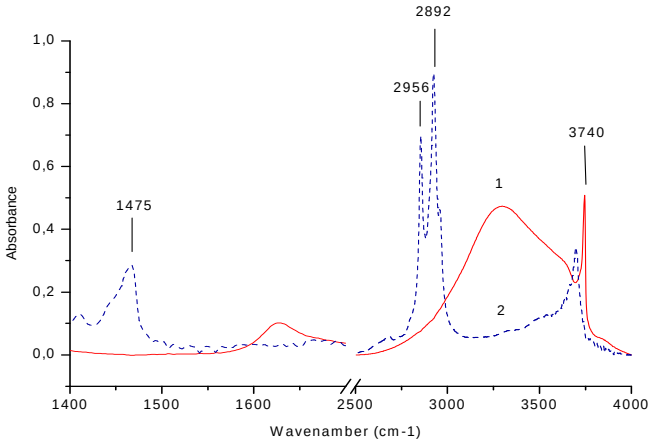

Figure 1. DRIFT spectra of initial MCM-41 (1) and grafted by octadecylsilane MCM-41 (2) recordered at 25 °C

The silicon surface modified by aliphatic silane (alkylcoverage) can reduce the possibility of water adsorption and it follows, the adsorption capacity of alkyl modified MCM-41 samples under the chosen conditions is higher in comparison with initial MCM-41. It can be explained by: 1) steric hindrance effect of remaining after modification free silanol grous by attached alkylsilanes; 2) higher affinity of nonpolar alkylated mesoporous material to hydrophobic substanses.

Conclusions

The sorption of sterols on the alkyl modified MCM-41 samples was studied. The ordered mesoporous material MCM-41, modified with alkylsilane, shows promise as a high surface area adsorbent for effective and rapid extraction of biologically active substances, such as sterols.

Acknowledgements

This work was supported by Russian Ministry of Science and Education and the German Academic Exchange Service (DAAD) under the program «Mikhail Lomonosov 2010/2011».

References

[1] Yu.V. Patrushev, V.N. Sidelnikov, M.K. Kovalev, M.S. Mel'gunov, Capillary Gas Chromatographic Column with a Porous Layer Based on a Mesoporous Material, Rus J Phys Chem A 82 (2008) 1202 - 1209.
[2] J. S. Beck, J. C. VartUli, W. J. Roth, M. E. Leonowicz, T. Kresge, K. D. Schmitt, C. T-W. Chu, D. H. Olson, E. W. Sheppard, S. B. McCullen, J. B. Higgins, J. L. Schlenkert, A new family of mesoporous molecular sieves prepared with liquid crystal templates, J Am Chem Soc 114 (1992) 10834 10843.
[3] K. Kailasam, A. Fels, K. Müller Octadecyl grafted MCM-41 silica spheres using trifuctionalsilane precursors – preparation and characterization, Microporous and Mesoporous materials 117 (2009) 136 – 147
[4] S. Chiarakorn, T. Areerob, N. Grisdanurak Influence of functional silanes on hydrophobicity of MCM-41 synthesized from rice husk, Science and technology advanced materials 8 (2007) 110 - 115
[5] A. J. O'Connor, A. Hokura, J. Kisler, S. Shimazu, G. W. Stevens, Y. Komatsu Amino acid adsorption onto silica molecular sieves, Separation and purification technology, 48 (2006) 197 - 201

Potential of metal-modified MFI zeolite membranes and role of the support

Julius Motuzas[1*], Martin Drobek[1], Eric Louradour[2], Nadine Del Bianco[2] and Anne Julbe[1]
1-Institut Européen des Membranes (UMR 5635 CNRS), Université Montpellier 2, CC47, Place Eugène Bataillon, 34095 Montpellier Cedex 5, France. Julius.Motuzas@iemm.univ-montp2.fr
2- Céramiques Techniques Industrielles (CTI SA), 382, Avenue du Moulinas, 30340 Salindres, France

Introduction

Zeolites are attractive membrane materials because of their calibrated pore size and their large range of possible modifications. Modifications can be useful for occluding non-zeolite pores or decreasing zeolite channel size, modifying surface polarity, organo- or hydrophilicity, adsorption and catalytic properties. Various additives (Fe, B, Ge, V, Ti, carbon, noble metals, metal-organic or organic molecules…) can be inserted in zeolite membranes by either *in-situ* or post-synthetic methods. The additive location (extra- or intra-framework, intra- or inter-crystals) drastically impacts the final membrane properties and performance. When *in-situ* methods are used, the zeolite network formation is strongly impacted by the type and quantity of additive within the mother sol. A number of modified zeolite membranes have already been evaluated for separations or reactions in either liquid or gas phase. The synthesis procedure impacts on the nature, distribution and location of modifying species, and on the associated membrane performance. In this work the direct insertion of several types of additives into MFI membrane structure will be reported, as well as their impact of the membrane properties and performance. Different types of commercial alumina supports will be considered for membrane growth, as membrane performance may be also impacted by the support on which they are grown.

Experimental

The standard mother sol composition was typically: $1SiO_2$: 0.4TPAOH : $19.5H_2O$: $4C_2H_5OH$. TEOS was used as a silica precursor. Several additives (*Add*) such as $Al(C_3H_7O)_3$, $FeC_6H_5O_7$, H_3BO_3, NH_4VO_3 or $Ni(NO_3)_2$ have been considered and integrated in the mother sol in order to prepare modified MFI membranes on α-Al_2O_3 commercial supports with 100-200 nm pore sizes. Supports were provided by CTI SA, ATECH, Inocermic or Pall-Exekia. A microwave oven (Milestone ETHOS 1600) was used for preparing the seeds, as described in [1]. Membranes were formed by secondary growth (classical or MW heating), observed by FE-SEM (Hitachi 4500) and their microstructure was analysed by XRD (PANalytical X'Pert Pro). Membrane quality and performances were compared through single gas permeance measurements.

Results and discussions

Representative micrographs of the modified-membranes prepared under MW heating are shown in Figure 1. The additives such as Al, Fe, B or V inhibit membrane growth for both microwave and conventional heating methods. The formation of the membranes was hardly operated at temperature $\leq$160°C when the molar ratio Si/*Add* was below 100. A similar tendency was already observed in

the case of Ti additive [2], although microwave-assisted heating could potentially modify the reaction pathways. Single gas permeance studies were useful to compare the membrane quality and define the synthesis parameters (mother sol formulation, heating method, temperature and duration) yielding optimum thickness and crystal preferential orientation. The role of additives for modifying the membrane permeance, selectivity and reactivity will be reported.

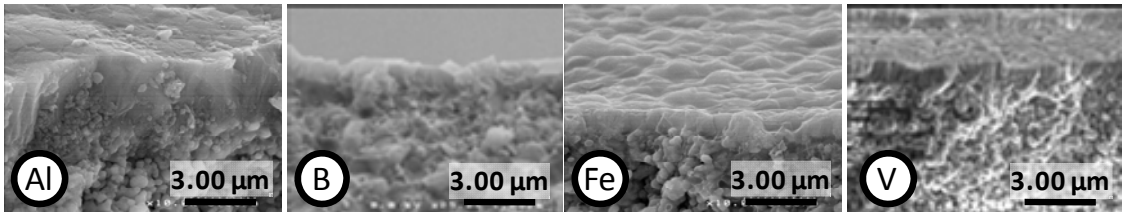

Figure 1. SEM observations of modified-MFI membranes (the additive is reported on each micrographs) prepared at 160°C by microwave heating (2.5h, 400 W).

The type of porous alumina support used for growing the membranes was also found to be a key parameter influencing membrane growth and performance. For example, differences in the order of gas permeance (e.g. He and N_2) at room temperature and in the permeance profiles vs. temperature were evidenced, depending on the support provider. Further work is currently in progress to understand these results.

Conclusions

The influence of several additives on the formation and performance of MFI membranes was studied in the present work. As expected membrane formation was strongly disturbed by the presence of additives in the mother sol and optimum synthesis conditions were determined. The role of additives for modifying the membrane performance and properties was discussed. The influence of the alumina support provider was also evidenced by comparing namely He and N_2 single gas permeances at room temperature and the evolution of permeance profiles vs. temperature. The results of this study will help selecting the most promising couples "MFI-additive(s)" / "support(s)" for further modification or direct application of MFI zeolite membranes, in either fluid separations or catalytic reactors.

Acknowledgements

Part of research leading to these results has received funding from French FUI, the region of Languedoc-Roussillon and OSEO Innovation, under grant agreement N° 092906408 EJ N°5728 (MEGA project).

References

[1] Motuzas, J., Julbe, A., Noble R.D., Van der Lee, A., Beresnevicius, Z.J., Rapid synthesis of oriented silicalite-1 membranes by microwave-assisted hydrothermal treatment, Microporous and Mesoporous Materials, 92 (2006), 259-269.
[2] Motuzas, J., Mikutaviciute, R., Gerardin, E., Julbe, A., Controlled growth thin and uniform TS-1 membranes by MW-assisted heating, Microporous and Mesoporous Materials, 128 (2010), 136-143.

Selective adsorption of phenolic compounds onto SBA-15 mesoporous molecular sieve

Camelia Luchian[1], Marius Niculaua[2], Valeriu V. Cotea[2], Nicolae Bilba[1], Aurelia Vasile[1]
[1] *The "Al. I. Cuza" University, Faculty of Chemistry, Laboratory of Materials Chemistry, 11 Carol I Bd., 700506 Iasi, Romania*
[2]*The University of Agricultural Sciences and Veterinary Medicine, 3, Mihail Sadoveanu Alley, Iaşi, 700490, Romania*
Kamelia_luchian@yahoo.com

Introduction

The quality of a wine depends on its numerous constituents, the presence/absence and amount of a given compound playing a considerable role. Phenolic compounds contribute markedly to the color, flavor, bitterness and astringency of the final product. Browning of wines is a result of an auto-oxidation process due to presence of oxygen (the initiator of the process), polyphenols (the oxidable mater) and of certain metal ions, Fe^{2+}/Fe^{3+}, Cu^{2+} (as activators of the process). The retention of some phenolic compounds by means of an adsorbent is the method frequently used for eliminating this phenomenon.
Silica SBA-15 exhibit pore sizes from 5 to 30 nm, wall thicknesses of 3.1–6.4 nm and BET surface areas from 630 to 1040m^2/g. The silanol groups (Si–OH), always present, are responsible for the adsorption of organic molecules. These OH groups are mainly placed on the SBA-15 internal surface that represents the main contribution to the total surface area of the porous material. Up to our knowledge, there are no scientific reports on the application of the mesoporous SBA-15 material in oenology.
The aim of this study is to investigate the potential use of a mesoporous material SBA-15 as adsorbent for the polyphenols from a Cabernet Sauvignon wine originated from Romania .

Experimental

The purely siliceous molecular sieve SBA-15 was synthesized hydrothermally in acidic media via a hydrogen bonding (S^0H^+) (X^-I^+) templating route according to a procedure reported earlier, with some modifications [1]. The typical gel molar composition was 1TEOS:0,017P123:5,95HCl:194H_2O. Fig.1 shows the SAXRD pattern of the calcined silica SBA-15 used as adsorbent. The diffractogram presents three clear peaks which are characteristic of 2-D hexagonally ordered structure (P6nm symmetry) namely the (100), (110), (200) crystal planes and the corresponding d_{hkl} spacings of 9.007, 5.1905 and 4.5502nm.
Fig.2 shows the nitrogen adsorption-desorption isotherm at -196^{0}C and the pore size distribution curve calculated with BJH formula from the adsorption isotherm. The structural parameters of calcined mesoporous silica-SBA-15 are summarized in Table 1.
We used a HPLC method to separate and quantify in a very short time a number of 18 phenolic compounds [2].
The chromatograms of methanolic extract of phenols removed from SBA-15 are shows in Fig. 3.

Table 1. Structural parameters derived from XRPD data and nitrogen physisorption

Sample	d_{100} spacing (nm)	a_0 (nm)	S_{BET} (m^2/g)	D_{BJH} (nm)	Total pore volume (cm^3/g)	Wall thickness (nm)
Si-SBA-15 (calcined)	9.007	10.40	774	6.62	0.942	3.78

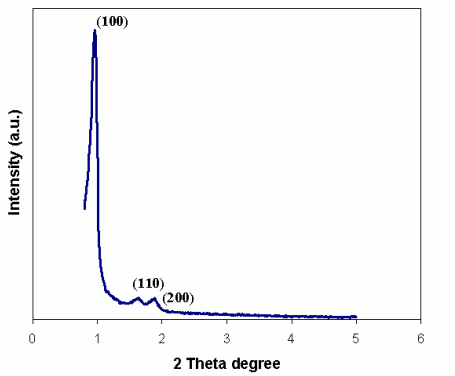

Fig.1. Small-angle XRPD pattern of Si-SBA-15

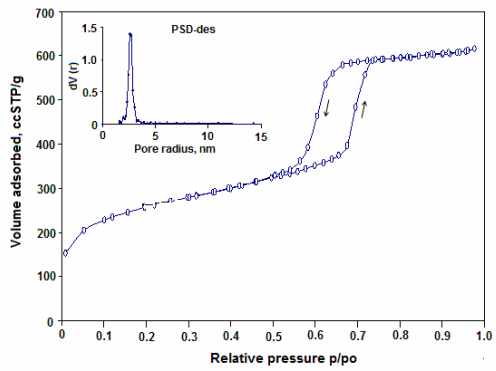

Fig.2. The N_2 adsorption – desorption isotherm at -196^{0}C of silica-SBA-15. Inset: the pore size distribution (PSD)

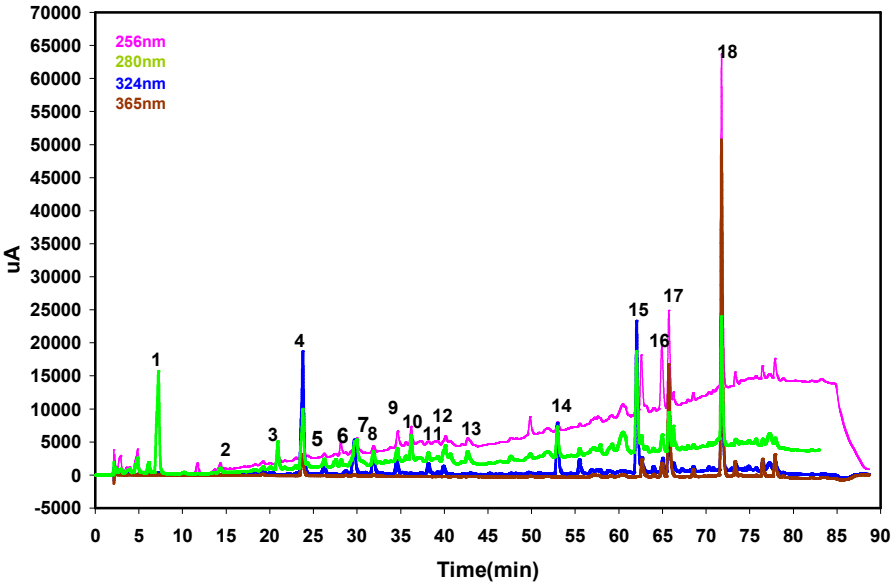

Fig. 3. The chromatogram of methanolic extract of polyphenols adsorbed onto SBA-15: 1-gallic acid; 2-protocatechuic acid; 3-para-hydroxybenzoic acid; 4-gentisic acid; 5-meta-hydroxybenzoic acid; 6-vanillic acid; 7-catechin; 8-caffeic acid; 9-clorogenic acid; 10-syringic acid;11-para-coumaric acid; 12-epicatechin; 13-salicylic acid ;14- sinapic acid; 15-trans-resveratrol; 16-rutin trihydrate; 17-cis-resveratrol; 18-quercitin

Conclusions

The results show that SBA-15 material has a selective action on the phenolic compounds, retaining specific molecules in a larger quantity, due to its structure. Quercitine, cis- and trans-resveratrol is the phenolic compounds adsorbed in the largest quantities.

References

[1] Zhao, D., Feng, L., Huo, Q., Melosh, N., Fredrickson, G.H., Chmelka, B.F., Stucky, G.D., Triblock copolymer syntheses of mesoporous silica with periodic 50 to 300 angstrom pores. Science (Washington D.C.), 279(1998), 548-552

[2] Castellari, M., Sartini, E., Fabiani, A., Arfelli, G., Amati, A., Analysis of wine phenolics by high-performance liquid chromatography using a monolithic type column, J. Chromatography, A 973(2002), 221–227

Selective adsorption of a pollutant (Mesosulfuron) on modified mesoporous silicas

Adeline TROUVE, Sabine VALANGE, Isabelle BATONNEAU-GENER and Samuel MIGNARD
LACCO (UMR650)3, Université de Poitiers, 40 av. du Recteur Pineau, 86022 PoitiersCedex
Samuel.mignard@univ-poitiers.fr

Introduction

The removal of a pesticide such as methyl-mesosulfuron from water is a major challenge to human health. One difficulty is that these molecules are often very large and their diffusion (and hence their adsorption) are difficult into zeolites. In addition, water molecules are preferentially adsorbed compared to organic pollutant. Mesoporous silicas with larger pore sizes should enable a better adsorption of these molecules. However, mesoporous silicas exhibit a high density of silanols groups which exhibit a large affinity for water molecules.
In this work, the adsorption of methyl-mesosulfuron was then been studied in a batch reactor using four MCM-41-type mesoporous silicas exhibiting various silanols concentrations obtained by the grafting of various chemical groups such as $Si(CH_3)_3$, NH_2 or phenyl.

Experimental

Methyl-mesosulfuron is an herbicide used in the cultivation of wheat. It has a 3-dimensional structure whose geometry can be inscribed in a cylinder of diameter 9.87 Å and 11.97 Å in length. These dimensions fall into the category of large molecules for adsorption in zeolites. The pKa of methyl-Mesosulfuron is 4.35 and that the proton of the sulfonimide function is the most acidic. The acid form R-NH, function sulfonimide of methyl Mesosulfuron predominates at acidic pH values below the pKa which greatly reduces the solubility of the contaminant (see below).

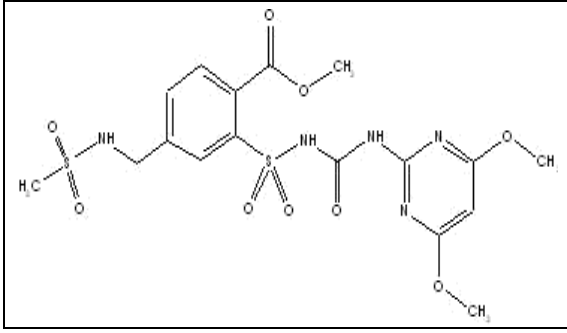

Formula : $C_{17}H_{21}N_5O_9S_2$
Molecular weight : 503,55g.mol^{-1}
Melting point : 195,4°C
Solubility in water :
pH = 5 : 7,24 mg.L^{-1}, 20°C
pH = 7 : 483 mg.L^{-1}, 20°C
pH = 9 : 15.390 mg.L^{-1}, 20°C
pKa = 4,35 at 20°C

The experiments were performed at 25 ° C using 40 mg of solid in 20 mL of solution at 100 mg.L^{-1} placed in closed vials of 30 mL and mechanically stirred for 24 hours. Note that the low solubility of the pollutant in water at acidic pH does not do the research for a pH less than or equal to pKa. So, the experiments were then carried out at pH = 7.2 close to natural conditions [1-2].

Results and discussion

The density of silanols was determined from the adsorption isotherms of nitrogen and water. From these isotherms, we calculated the surface of the material (A_{BET}) and the amount of water adsorbed as a monolayer (N_{mono}). Assuming that a single water molecule is adsorbed by the silanol SiOH group, the density of silanol groups is calculated as follows :

$$\text{Density of silanols by nm}^2 = (N_{mono} \times N_A) / (A_{BET} \times 10^{18}) \text{ (where } N_A \text{ is Avogadro number)}$$

The hydrophobicity of a solid can be directly related to the density of silanols groups. Indeed, the higher the density of silanols, the higher the number of water molecules adsorbed that disadvantage the adsorption of organic molecules. In other words, the higher the density of silanols, the lower the hydrophobicity. To evaluate the effect of the hydrophobicity, the adsorption of methyl-mesosulfuron was then performed. The results are listed in Table 1.

Table 1 : density of silanols and capacity of adsorption of methyl-mesosulfuron

Catalyst	Density of silanols (SiOH per nm²)	Adsorption capacity of mesosulfuron ($mg.g^{-1}$)
MCM-41-$Si(CH_3)_3$	2.0	2.6
MCM-41-Phényl	3.6	5.4
MCM-41	5.3	1.3
MCM-41-NH_2	6.3	3.2

The adsorption capacities in methyl-mesosulfuron do not appear to depend on the hydrophobicity of the solid. Indeed, the amount of methyl-mesosulfuronadsorbed by MCM-41-$Si(CH_3)_3$ was lower than for silica MCM-41-NH_2 and MCM-41-Phenyl but higher than for silica MCM-41. The adsorption in MCM-41 can easily be explained by the presence of silanol groups inside the channels allowing the retention of the species R-NH by hydrogen bonds. However, silica modified by phenyl groups MCM-41-Ph appears to be the best adsorbent. The amount of silanols groups of this solid (3.6 $SiOH.nm^{-2}$) is lower than that of silica MCM-41 (5.3 $SiOH.nm^{-2}$). In this case, interactions with the silanols groups only cannot explain the adsorption of methyl-mesosulfuron and another kind of interactions improving the adsorption of this pollutant should be involved. These favorable interactions resulting from the presence of phenyl groups could be due to π-π stacking, phenomenon occurring between the pollutant molecule and the grafted aromatic ring of MCM-41.

Conclusions

The adsorption of methyl-mesosulfuron was then been studied using four MCM-41-type mesoporous silicas exhibiting various silanols concentrations obtained by the grafting of various chemical groups such as $Si(CH_3)_3$, NH_2 or phenyl. It has been shown that the adsorbed form is the acidic one and the interactions with the adsorbent are hydrogen bonds. Furthermore, the elimination of organic pollutant does not necessarily require hydrophobic solids to improve adsorption capacities. The addition of specific groups is essential in order to induce specific interactions with the pollutant.

References

[1] M. Khalid, G. Joly, A. Renaud, P. Magnoux, Ind. Eng. Chem. Res. 43 (2004) 5275
[2] B. Koubaissy, Thesis University of Poitiers (France) November 2007, p.89

CO_2-adsorption at room temperature over PtKL catalysts modified by rare earths cations

J. Álvarez-Rodríguez[a,b], A. Guerrero-Ruiz[a], I. Rodríguez-Ramos[b], A. Arcoya[b]
[a] *Departamento de Química Inorgánica y Química Técnica, C/ Senda del Rey nº9, 28040 Facultad de Ciencias, UNED, Madrid, Spain.*
[b] *Instituto de Catálisis y Petroleoquímica, CSIC, C/ Marie Curie nº 2, 28049 Madrid, Spain.*
jalvarez@ccia.uned.es

Introduction

Nowadays it is a matter of fact that the World is in a Global Warming stage for most of the scientific community, probably due to the increase of the atmospheric concentration of greenhouse gases (GHG), at least in part of anthropologic origin. So, intensive works have been done to develop technologies that reduce the production of GHG, or to minimize its impact. By the way, a recent reported elaborated by an expert Group of the Intergovernmental Panel on Climate Change have been published dedicated to the available technologies for Carbon dioxide Capture and Storage (CCS) [1] to prevent the fatal goal of 450 ppm of CO_2, which is identified as a critical point that could be reached in a close date [2]. In this area adsorption processes are potentially one of the most effective, and realistic, technical solution to moderate the continuous increase of carbon dioxide atmospheric presence. With this purpose recent papers [3 and there in] on ion exchanged zeolites such as, BETA, X, Y, ZSM-5 or FER, reported that carbon dioxide adsorption capacities were significantly altered due to the 1) the acid-basic properties of zeolites; 2) the polarizing power of the exchanged cations; and, 3) the effective pore size of zeolite employed. Although a number of works about CO_2 adsorption on zeolites have been published, no systematic researches on the CO_2-adsorption over rare earth modified zeolites have been reported. Since CO_2 is a molecule with a quadrupole moment, the presence of rare earths as countercations in the KL zeolite can produce important changes in the CO_2 adsorption-desorption processes over this zeolite, and with that aim we have begun this work. Moreover, in order to facilitate subsequent desorption-reaction procedures with a chemical transformation of CO_2 into valuable products; Pt was included in the formulation of these samples.

Experimental

Different portions of the Pt KL-zeolite were ion exchanged with aqueous solutions of the corresponding nitrates of La, Ce, Pr, Nd or Sm as described elsewhere [4]. CO_2 adsorption experiments were performed in a conventional volumetric system at 300K, after outgassing the samples at 623K. Every gas pulse of a controlled sequence ones were registered both initial pressure and stabilized pressure twice times, fresh and after outgas at 623K, and then adequate units of CO_2-uptake of irreversible and reversible, respectively, were plotted in order to get the double isotherm of every sample. Temperature Programmed Desorption (TPD) of

CO_2 measurements were performed in a quartz vessel fitted with a glass apparatus, connected to a mass spectrometer (Baltzers, QMG 421), directly attached to the vacuum system. Selected m/z ions were registered simultaneously to a signal of a thermocouple K-type placed close to the sample. For each experiment, a sample placed in the quartz bulb was contacted with 150 Torr of CO_2 during 30 min, outgassed and stabilized under high vacuum at room temperature, before they were heated up to 900 K at 10 K min^{-1}, with a continuous analysis of evolved gases by MS. FTIR-spectra of self-supported wafers was registered by a Nicolet 5ZDX spectrometer, after pretreatment of reduction, contacted with CO_2 and outgas at RT.

Table 1. Resume of adsorption measurements of CO_2 for the samples at 300K

Sample	Total adsorption (μmoles CO_2/g sample)	Reversible adsorption (μmoles CO_2/g sample)	Irreversible adsorption (μmoles CO_2/g sample)
PtKL	138	134	4
PtLaKL	139	99	40
PtCeKL	316	300	16
PtPrKL	249	203	46
PtNdKL	236	158	78
PtSmKL	344	249	95

Results and discussion

As summarize Table 1, the CO_2 adsorption capability of all the samples containing rare earths is larger than that of Pt/KL sample. The type and strength of the surface adsorption sites of the samples was determined from the TPD profiles of CO_2 which evidence two principal zones of desorption temperatures, as previously reported [5]. The first one at higher temperatures (>500K) which may be related to structural carbonates (H), and a second zone at lower temperatures where desorption process resemble to the one reported for surface basic sites (L). These TPD profiles let classify the samples attending to H/L ratio as: type I (H/L>1) for PtKL; type II (H/L≈1) for PtPrKL, PtNdKL and PtSmKL; and type III (H/L<1) for PtCeKL and PtLaKL. Both, the number of adsorption sites and their strength may be discussed in term of the polarizing power of the countercations and their location in the zeolite framework.

References

[1] Metz, B.;Davidson, O.; de Coninck, H. C.; Loos, M.; Meyer, L.A. (Eds.), IPCC, 2005: IPCC Special Report on Carbon Dioxide Capture and Storage, Cambridge University Press, Cambridge, United Kingdom and New York, NY, USA, 442 pp. (http://www.ipcc.ch/pdf/special-reports/srccs/srccs_wholereport.pdf)

[2] Online Trends: A compendium of Data on Global Change: Atmospheric Carbon Dioxide and Carbon Isotope Records (http://cdiac.ornl.gov/trends/co2/contents.htm)

[3] Seung-Tae Y., Jun K., Wha-Seung A., CO2 adsorption over ion-exchanged zeolite beta with alkali and alkaline earth metal ions, Microporous and Mesoporous Materials, 135 (2010) 90-94.

[4] Álvarez-Rodríguez, J., Guerrero-Ruiz, A., Rodríguez-Ramos, I., Arcoya, A., Selective hydrogenation of citral over Pt/KL type catalysts doped with Sr, La, Nd and Sm, Applied Catalysis A (Under Revision)

[5] Sato, S., Takahashi, R., Kobune, M., Gotoh H., Basic properties of rare earth oxides, Applied Catalysis A: General, 356 (2009) 57-63.

Permeation and separation properties of TS-1 membrane for hydrocarbon mixtures

Dũng Tiến Công[1], Vlastimil Fíla[1], Pavel Hrabánek[2], Bohumil Bernauer[1]
[1]*Department of Inorganic Technology, ICT Prague, Technická 5, 166 28 Prague*
[2]*J. Heyrovský Institute of Physical Chemistry of the ASCR, Dolejškova 2155/3, 182 23 Prague*
(congt@vscht.cz or Vlastimil.Fila@vscht.cz)

Introduction

Titanium silicalite (TS-1) is well known to be an efficient catalyst for several selective oxidation reactions: selective oxidation of alcohols [1], epoxidation of alkenes [2], hydroxylation of aromatics [3] etc. Its zeolite structure is composed of straight (0.54 x 0.56 nm) and sinusoidal (0.51 x 0.54 nm) channels perpendicularly crossing each other to form intersection. Therefore, on the other hand, TS-1 zeolite is potential candidate for applying as zeolite membrane and membrane reactor.

Aims of this study were (i) to develop a procedure for defect-free titano-silicate (TS-1) membrane synthesis, (ii) to study the properties of these membranes in light hydrocarbons separation.

Experimental

Two TS-1 membranes with different Si/Ti ratios were synthesized on stainless steel support by secondary growth method. The support was covered by a seed layer formed by *in situ* seeding step. The TS-1 membrane layers were synthesized on seeded stainless steel support by crystallization step. This step was repeated until as-synthesized membrane was impermeable for N_2 before the template removing step. The template removal was carried out at 480^0C for 24 hours with the heating and cooling rate of 0.5^0C/min.

The membrane was mounted inside the stainless steel cell and sealed with silicone O-ring. The feed composition and flow rates were controlled by mass flow controllers. Pressures at feed and permeate sides of the membrane were adjusted with pressure regulators. Single component and equimolar binary mixture permeation was studied according to Wicke-Kallenbach method using helium as sweep gas. Gas chromatograph equipped with TCD and FID detector was used to analyze the composition of permeate and retentate streams.

Results and discussion

Two titanium silicalite-1 membranes with Si/Ti ratio of 100 (M1) and 25 (M2) were prepared on stainless steel support. As-synthesized membranes were characterized by XRD, SEM, FT-IR and UV-VIS methods and the results show that TS-1 layers were successfully prepared. Titanium atoms were isomorphously substituted in the zeolite framework and no anatas-like oxide species were detected.

The results of single gas permeation show that the surface diffusion is the main transport mechanism of hydrocarbons. CH_4 flux continuously decreases with increasing of temperature in the range of 25°C - 175°C, while C_2H_6, C_3H_8 and n-C_4H_{10} flux curves as a function of temperature have the maxima (fig. 1). The maximum position shifts to higher temperature with number of carbons in hydrocarbons in following order: $CH_4 < C_2H_6 < C_3H_8 <$ n-C_4H_{10}

The results of the binary mixture separation experiments show that there is a correlation between amount of titanium in the zeolite framework and the ability of TS-1 membranes to separate hydrocarbons from CH_4. The separation factor increases with titanium content incorporated in the zeolite framework. With increasing temperature, the competitive absorption becomes less important and leads to lower separation factor. In the range of

measured temperature generally the separation factors are in the order of n-C_4H_{10}/CH_4> C_3H_8/CH_4> C_2H_6/CH_4 (fig.1). Comparison with literature data is shown in Table 1.

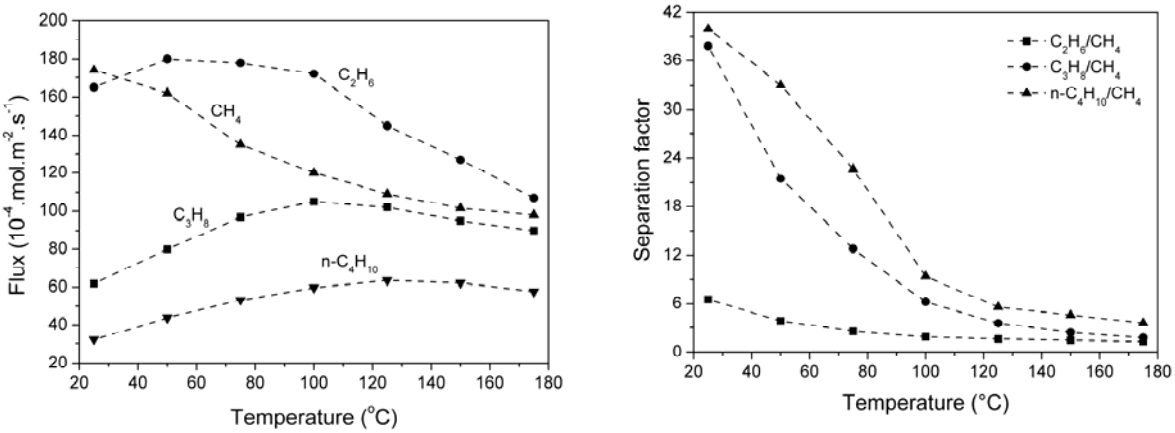

Fig. 1. Fluxes of single hydrocarbons and separation factors for binary mixtures at 101 kPa for membrane M2.

Table 1: Comparison of binary mixture separation using MFI membranes

Membrane	Experimental conditions	Separation factor			Flux (mmol.m^{-2}.s^{-1})			References
		C_2/C_1	C_3/C_1	n-C_4/C_1	C_2	C_3	n-C_4	
TS-1/SS[a] (Si/Ti=100)	300 K; 101 kPa; W-K	9.3	24.5	19.5	15.5	6.5	2	This work
TS-1/SS (Si/Ti=25)		6.5	37.8	40	15.1	6.2	2.7	
S-1[b]/Al_2O_3	298 K; W-K	-	-	16.7	-	-	1.9	[4]
S-1/SS	300 K; 101 kPa; W-K	7	-	-	15	-	-	[5]
ZSM-5 / α-Al_2O_3 (Si/Al=270)	348 K; W-K[c]	-	-	11.3	-	-	0.22	[6]
S-1/α-Al_2O_3 [d]	298 K; 100 kPa; W-K	-	-	102	-	-	0.32	[7]

[a]stainless steel; [b]silicalite-1; [c]P_{feed}= 2 bar; $P_{permeate}$= 1 bar; [d]membrane P180 in the reference

Conclusions

TS-1 membranes with different Si/Ti ratio were successfully prepared on the stainless steel support. The membrane with Si/Ti ratio of 25 showed higher selectivity for separating n-C_4H_{10}/CH_4, C_3H_8/CH_4, C_2H_6/CH_4 mixtures. The maximum separation factor of 40 was obtained for n-C_4H_{10}/CH_4 at room temperature.

Acknowledgement

The financial support for this research by Grant Agency of ASCR via Grants No IAA400400909, by Ministry of Education, Youth and Sports via grant MSM 6046137301 is gratefully acknowledged.

References

[1] C.N. A. Esposito, F. Buonomo, US Patent 4,480, 135 (1984).
[2] M.G. Clerici, G. Bellussi, U. Romano, J. Catal., 129 (1991) 159-167.
[3] A.J.H.P. van der Pol, A.J. Verduyn, J.H.C. van Hooff, Appl. Catal., A, 92 (1992) 113-130.
[4] Z.A.E.P. Vroon, K. Keizer, M.J. Gilde, H. Verweij, A.J. Burggraaf, J. Membr. Sci., 113 (1996) 293-300
[5] L.J.P. van den Broeke, W.J.W. Bakker, F. Kapteijn, J.A. Moulijn, AlChE J., 46 (1999) 976-985.
[6] S. Wohlrab, T. Meyer, M. Stöhr, C. Hecker, U. Lubenau, A. Oßmann, J. Membr. Sci., 369 (2011) 96-104.
[7] K. Keizer, A.J. Burggraaf, Z.A.E.P. Vroon, H. Verweij, J. Membr. Sci., 147 (1998) 159-172.

A comparative study for arsenic behavior sorption in zeolites applying cyclic voltammetry

[1]M. Luna Quiroz, [1,*]R.M. Luna Sánchez, [2] J. Aguilar Pliego,[2] R. Rodriguez Trejo
[1]*Depto. Energía,UAM-A, Av. San Pablo 180, México, D.F., 02200, México*
[2]*Depto.Ciencias Básicas, UAM-A, Av. San Pablo 180, México, D.F., 02200, México*
*rmls@correo.azc.uam.mx

Introduction

The presence of arsenic in groundwater or surface water exceeds permissible concentrations at the global level. Conventional chemical treatments such as the filtration, ion exchange, absorption on activated alumina and reverse osmosis among others [1] they have shown efficacy but high operating costs, which makes them unattractive. Then, there is need to employ other procedures for the elimination of toxic metals. The use of the zeolites has been a good proposal since long ago, because these have properties of ion exchange, charge selectivity and structure, as well as stability at high temperatures, which are insoluble in solvents organic meaning, have greater resistance to experimental conditions [2]. For this reason, there is a continued interest in characterizing the zeolite using conventional electrochemical techniques in combination with structural chemistry [3]. Therefore the objectives of this study are characterize and identify arsenic behavior through the cyclic voltammetry technique using carbon paste electrode modified with synthetic zeolites exchanged with cobalt, as well as establish optimal conditions for which detect the presence of arsenic contained in electrolyte support.

Experimental

The work was developed with a synthetic zeolite type A, from the company Union Carbide Corporation. All reagents used as graphite powder (Alfa Aesar), silicone oil (Sigma Aldrich), $NaNO_3$ (Sigma Aldrich), Co $(NO_3)_2.6H_2O$ (Sigma Aldrich), $Na_2HAsO_47H_2O$ (Sigma Aldrich), $NaAsO_2$ (Sigma Aldrich) were analytical reagent grade. Solutions 0.01 M $NaNO_3$ arsenic (arsenite and arsenate) were used as electrolyte support and their concentrations varied from 0.2 to 0.5 ppm. Also solutions 1.63 mM Co to pre-concentrate the zeolite were prepared. The electrochemical analyses consisted of cyclic voltammetry, where an EG and G PARC 263 potentiostat coupled to a PC with the M270 software was used to impose the electrochemical signal and measure the voltammetric response. An electrochemical cell was fitted with three ports: one for the working electrode (carbon paste electrode, CPE–graphite-electroactive species), another for the counter electrode (graphite bar, Alfa Aesar, Johnson Matthey 99.9995%) and the last for the reference electrode ($Hg/Hg_2SO_4/K_2SO_4$ (sat), SSE (E =0.615 V/SHE)). The working electrode was prepared by mixing 0.8 g natural graphite powder (Alfa Aesar, 2–15 Am, 99.9995%), 0.2 of the electroactive species (Zeolite A) and silicone oil in an agate mortar to a homogeneous paste. The quantity of silicone oil (Sigma, q =0.96 g/mL, m =200 cS) employed depended on the zeolite type. Once the paste was ready, it was introduced into a 7 cm-long, 0.2-cm interior polyethylene syringe. A platinum wire, welded to a copper wire, was used as the electrical contact. To prepare the paste, the zeolite A was dried in a furnace for 24 hours after; it was mixed with the oil and the carbon powder in an agate mortar. Once the working electrode and the solutions (Cobalt and Arsenic) were ready, the electrode was place into the solution of cobalt for 15 minutes, after; it was removed from this and washed with distillate water then placed in the other solution (contained arsenite

or arsenate) for five minutes. After this time, the voltammogram was developed. When the experiment finished, the exposed surface from the working electrode was removed and washed with distillate water.

Results and discussion

The aim of the present work is to establish the oxidation and reduction processes for the arsenic species. Cyclic voltammetry was applied to the samples in order to analyze the electrochemically behavior of arsenic sorption into zeolites A. For this study, all voltammograms were traced in the anodic directions, initiating the sweep potential from the OCP value ((Open Circuit Potential vs. SSE). The anodic and cathodic potential limits were set at 1.0 V vs. SSE for each case. The sweep velocity was 20 mVs^{-1}.

Figure 1 contains the typical voltammetric response of each arsenic solution (different charge) for 0.5 ppm arsenite and arsenate concentration, in an independently solution. It can be noted in the figure that there is a different behavior because there are distinct arsenic species in the solution. Peak showing arsenite, differs markedly of arsenate. Such oxidation peak is probably due to the arsenite capacity to oxidize into arsenate. In arsenate species this does not happen since it is in its maximum oxidation state. However, the behavior of arsenate shows a slight oxidation at low values of potential (approximately 300 mV), which can be associated with the cobalt contained in zeolite, which is in a state 2+ and could be oxidizing a fraction to cobalt 3+.

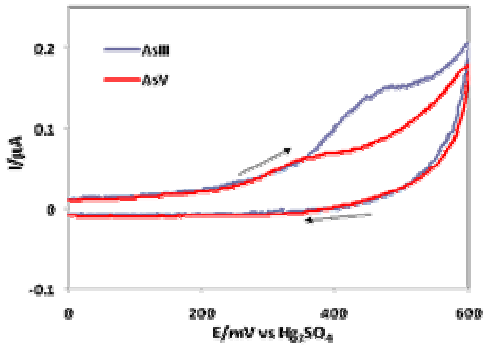

Figure 1. Typical cyclic voltammograms obtained for electroactive specie (zeolite A)-CPE in a pre-concentrated cobalt solution (1.63 mM Co). The sweep potential was initiated from the OCP. v = 20 mVs-1.

Conclusions

The results shown the feasibility to extract arsenic contained in groundwater applying the voltammetry technique as a first approximation. Cobalt plays an important role during the pre-concentration otherwise the arsenic species could not be adsorbed.

References

[1] Xu, Y., Nakajima, T., Ohki, A., Adsorption and removal of arsenic (V) from drinking water by aluminum-loaded Shirasu-zeolite, Journal of Hazardous Materials, B92 (2002), 275-287
[2] Walkarius, A., Zeolite-Modified solid carbon paste electrodes, Journal Solid State Electrochemistry, 7 (2003), 671-677
[3] Walkarius, A, Zeolite-Modified Electrodes: Analytical Applications and Prospects, Electroanalysis, 8 11 (1996), 971-986.

Adsorption of the Ethane and Ethylene on Natural Mordenite and Mordenite exchanged with K^+

Diana Vargas Hernández, Rosario Hernández Huesca and María Ana Pérez Cruz
Facultad de Ciencias Químicas, Benemérita Universidad Autónoma de Puebla, México
rosario.hernandez@fcquim.buap.mx

Introduction

The separation of light hydrocarbon mixtures with very low relative volatility as ethane/ethylene of (1.5) using cryogenic distillation is a very expensive process [1].Therefore it is necessary to develop new technologies that offer a viable alternative for their separation. Selective adsorption is a potential alternative method, which is based on the specific interaction between the olefin and chemically modified adsorbents [2]. Adsorption studies of pure hydrocarbons using microporous adsorbents, such as the Mexican natural zeolite type Mordenite (ZNT) can be suitable for this purpose and can be modified by ion exchanged for provide active sites that enhance the selective adsorption. Therefore the main objective of this work is to study the effect of K^+ concentration in the ZNT sample for study the adsorption ethane (C_2H_6) and ethylene (C_2H_4) at different temperatures and establish which of the studied samples is the most suitable C_2H_6-C_2H_4 mixtures separation.

Experimental

The natural Mordenite ZNT was extracted from the Tamaulipas state in Mexico. This sample was modified for exchange with 0.5 M of KCl solution. The exchanged samples were dried at room temperature during 24 hours, the K^+, Na^+, Ca^{2+}quantity was determined by the atomics emission technique, using an emission spectrophotometer Varian 1450. The gas adsorption equilibrium isotherms were measured in a high vacuum volumetric system, totally made of Pyrex glass and equipped with grease free values. Before equilibrium measurements, all samples were first activated in situ at 400 °C in an oven up to a residual pressure of <1 x 10^{-2} Torr and kept for 3 h at these conditions. After sample dehydration, the temperature was decreased to the desired point and the sample was allowed to stabilize for at least 1.5 h before the beginning of the measurements. The C_2H_6 and C_2H_4 adsorption isotherms on three samples at different temperatures were fitted by the Dual-Langmiur model, eq 1.

$$a = a_{m,1}\frac{K_1P}{1+K_1P} + a_{m,2}\frac{K_2P}{1+K_2P} \quad (1)$$

Result and discussion

The composition of exchanged samples are shown in Table 1, the data showthat Na^+ y Ca^{2+} were partially replaced by K^+, obtained: ZNT-K1.5 and ZNT-K1.8. Fig. 1 shows C_2H_6 and C_2H_4 adsorption isotherms on ZNT at different temperatures these isotherms are of type I (BDDT classification). This means that the molecules of both hydrocarbons were able to penetrate the microporous structure of the adsorbent.

Table 1. Chemical Composition (weigh %)

Muestra	CaO	K_2O	Na_2O
ZNT	1.75	0.49	1.63
ZNT-K1.5	0.11	1.50	0.41
ZNT-K1.8	0.24	1.80	0.71

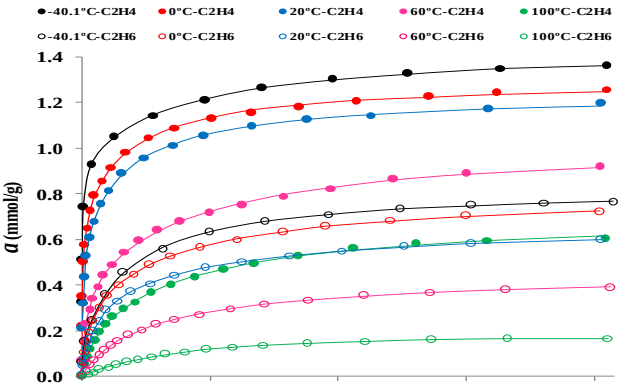

Figure 1. Adsorption isotherms for C_2H_4 and C_2H_6 on ZNT at different temperatures.

The interaction of C_2H_4 was stronger than of C_2H_6 with ZNT because probably the specific interaction between active centers (cations) of the zeolite with the π bond of the ethylene.
The goal of introducing big cation such as K^+ (1.33 Å) onto the crystal structure of the ZNT sample was reduced the diffusion for C_2H_6 without affecting the diffusion for C_2H_4 and the effect in adsorption of gases both. The equilibrium isotherms on ZNT-K1.5 and ZNT-K1.8 shown that the adsorption behavior was similar that observed in the ZNT sample. However it can be seen that the adsorbed amounts of both hydrocarbons on the exchanged samples are lower than those on the ZNT sample could be due to the decrease of the micropore accessibility and basicity of the Mordenite with a larger content of K^+ cations. The diminution of ethylene adsorbed in the exchanged samples can be due the diminution of the K^+ ion electronegativity.
The data in Table 2 show that the fitting parameters of dual Langmuir equation, values of equilibrium constants (K_1 and K_2) for the C_2H_6 y C_2H_4 at 20 ºC in the three samples studied (observed the same tendency for all temperatures studied). The value of equilibrium constants decreased in the order ZNT>ZNT-K1.5>ZNT-K1.8, confirming, that degree of adsorbate–adsorbent interaction decreases with increasing of K^+ in the samples. The value of equilibrium constants K_1 and K_2 is smaller for ethane with respect to ethylene; this confirms the interaction of ZNT sample is greater for ethylene.
The result established for the ZNT sample the selectivity is encourage with increasing of the temperature and is the most suitable for separating mixtures of C_2H_6 and C_2H_4 at high temperatures, for example, 100ºC. At low temperatures or close to environment the selectivity increased with the content of K^+, the ZNT-K1.8 sample is most suitable for the separation (Table 3).

Table 2. Values of Dual-Langmiur Constantes.

	ZNT		ZNT-K1.5		ZNT-K1.8	
	K_1	K_2	K_1	K_2	K_1	K_2
C_2H_4	0.6854	0.0246	0.2506	0.0187	0.0879	0.0104
C_2H_6	0.0960	0.0082	0.0541	0.0076	0.0448	0.0057

Table 3. Percentages of selectivity of ethylene.

Temperatura ºC	ZNT	ZNT-K1.5	ZNT-K1.8
-40.1	64	72	73
0	64	70	73
20	67	68	71
60	70	67	70
100	78	69	73

Conclusions

The natural mordenite (ZNT) showed a high adsorptioncapacity for both hydrocarbons, but certain selectivity toward ethylene, because of specific interactions of the ethylene molecules with cationic adsorption centers the πorbitals of this olefin.
With base on the results it is possible to suppose that if there was contacted a C_2H_6-C_2H_4 mixture with the studied samples, ethylene would selective adsorbed due to interaction strong of π bond with the adsorbent and pure C_2H_6 is obtained to adsorber exit, while the C_2H_4 could be recovered of adsorbent by regeneration process. This process of separation could take place even at room temperature.

Acknowledgements

The authors thank the Consejo Nacional de Ciencia y Tecnología (CONACYT, México) for financial support via a scholarship (No. 219821).

References

[1]Yang, R. T. *Gas separation by Adsorption Processes*; Butterworth Publishers: Boston, 1987.
[2] Yang, R. T. In *Gas Separation by Adsorption Processes*; Imperial College Press and World Scientific Publishers: River Edge, NJ, 1997; Vol. 1, Chapter 1.

Calcium-impregnated MCM-48: creation of basic sites

Fernando J. Quites and Heloise O. Pastore

Institute of Chemistry, University of Campinas, Rua Monteiro Lobato, 270, Cidade Universitaria Zeferino Vaz, Campinas, 13084-971, Brazil
gpmmm@iqm.unicamp.br

Introduction

MCM-48 is the cubic *Ia*3*d* member of the M41S mesoporous silica family, its 3D interpenetrating bicontinuous networks of channels provides more favorable mass transfer in the catalytic reactions than MCM-41 with a 1D hexagonal pore system [1]. Pure silica MCM-48 possesses a neutral framework, which limits its applications as a catalyst. To construct the catalytic sites on the surface of mesoporous silica is an effective method to modify the nature of the silica framework by the incorporation of heteroatoms [2] or by impregnation of transition metal species [3] in a post-synthesis process. In this study, the creation of basic sites (CaO) was performed by wet impregnation using $Ca(NO_3)_2$ as the source of calcium ions. The materials produced were characterized by X-ray diffraction (XRD), low-temperature nitrogen adsorption; elemental analysis and Fourier transform infrared (FT-IR) spectroscopy.

Experimental

MCM-48 mesoporous molecular sieves were prepared by hydrothermal synthesis as described by Froba *et. al.* [3]. Calcium-impregnated MCM-48 samples prepared by the isovolumetric impregnation were designated as xCaO-MCM-48, where x represents the mass percentage of CaO loaded on MCM-48. In a typical synthesis, MCM-48 was impregnated with a $Ca(NO_3)_3$ aqueous solution at room temperature for 4 h, then the solvent was eliminated in a rotovapor, and finally the sample was calcined in air at 550 °C for 6 h.

Results and discussion

Figure 1 shows the powder X-ray diffraction patterns of samples prepared in this work. The XRD pattern of the MCM-48 (Fig. 1a) exhibits a sharp d_{211} Bragg reflection, a weak d_{220} shoulder and several unresolved peaks between 3º and 5º 2θ which confirms the presence of a *Ia3d* bicontinuous cubic phase. The XRD patterns of samples prepared from it did not change significantly after impregnation/calcination of Ca-MCM-48. The peak intensity, however, decreased slightly, and the peaks with higher *hkl* indices, i.e., (420) and (332), almost completely disappeared in the diffractograms of samples with larger content of CaO (see Fig. 1d). The observed decrease of the XRD peak intensity is probably due to the pore filling by the impregnated oxide. Disappearance of higher *hkl* peaks may be due to the lower structural order of MCM-48 after of impregnation of calcium oxide.

The N_2 adsorption-desorption isotherms at 77 K for the original MCM-48 and CaO-MCM-48 samples are shown in Fig. 2. The N_2 adsorption isotherm of the pristine MCM-48 is a typical type IV adsorption isotherm characteristic of mesoporous material. Although for the xCaO-MCM-48 materials had also presented type IV adsorption isotherms, a significant decrease in the surface areas and pore volumes was observed, probably due to significant pore filling with CaO (Table 1).

The FTIR spectra of xCaO-MCM-48 materials (not shown) presented absorption bands at 1500-1400 cm^{-1} related with $\delta(CO_3^{2-})$ vibrations. Peaks were observed also in the spectra of ^{13}C MAS-RMN at 160 ppm associated with chemical shift of CO_3^{2-} groups.

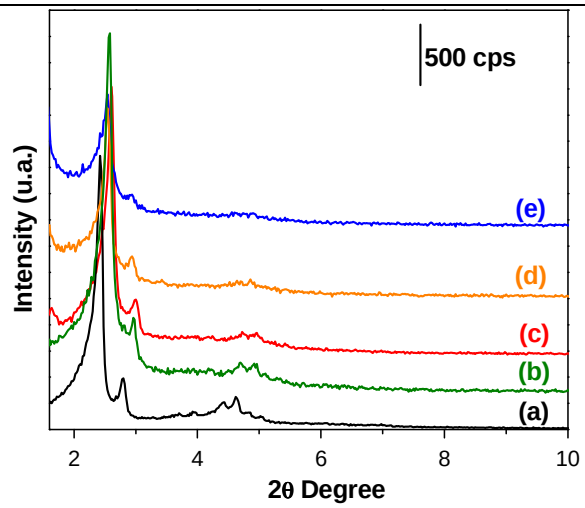

Figure 1. XRD patterns of (a) MCM-48, (b) 5CaO-MCM-48, (c) 10CaO-MCM-48, (d) 17CaO-MCM-48 and (e) 25CaO-MCM-48.

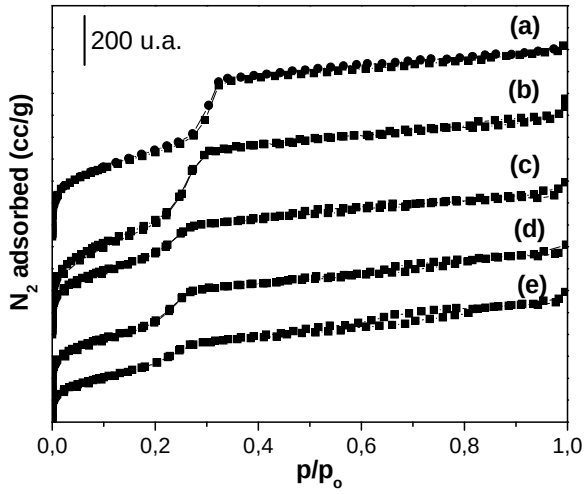

Figure 2. Nitrogen adsorption-desorption isotherms of (a) MCM-48, and xCaO-MCM-48 with x= (b) 5, (c) 10, (d) 17 and (e) 25.

Table 1. Porosity properties of MCM-48 and xCaO-MCM-48 samples

x	d_{211}* /nm	a_o* /nm	S_{BET}/m2.g^{-1}	V_P/cm^3.g^{-1}	D_P/nm
0	3.67	8.98	1794	1.450	3.5
5	3.45	8.46	1321	0.968	3.3
10	3.41	8.36	1126	0.968	3.4
17	3.48	8.52	854	0.829	3.4
25	3.51	8.89	459	0.344	3.3

*Calculated by XRD.

Conclusions

Using the wet impregnation technique calcium nitrate was introduced into the mesopores of MCM-48 silica. In a sequential combination of drying and calcination procedures, CaO were synthesized within the pore system of this molecular sieve. N_2 adsorption/desorption measurements still revealed mesoporosity on the host/guest compounds although a reduction of the total BET surface area and the pore radius occurs, both being indications of a decoration/coating of the inner surface of the silica walls. The presence of basic sites was verified by ^{13}C MAS-RMN and FTIR spectroscopy, showing that the materials produced in this work can be good candidates for application on adsorption of acid gases as well as on heterogeneous catalysis.

Acknowledgements

The authors are grateful to Fundação de Amparo à Pesquisa no Estado de São Paulo (FAPESP) for financial support to this work and to Conselho Nacional de Desenvolvimento Científico e Tecnológico (CNPq) for fellowships.

References

[1] Kim, J. M., Kim, S. K., Ryoo, R. Synthesis of MCM-48 single crystals Chemical Communications (1998) 259-260.

[2] Zhan, W., Guo, Y., Wang, Y., Liu, X., Guo, Y., Wang, Y, Zhang, Z., Lu, G. Synthesis of Lanthanum-Doped MCM-48 Molecular Sieves and Its Catalytic Performance for the Oxidation of Styrene Journal Physical Chemistry B, 111 (2007) 12103-12110.

[3]Köhna, R., Fröba, M. Nanoparticles of 3d transition metal oxides in mesoporous MCM-48 silica host structures: Synthesis and characterization Catalysis Today, 68 (2001) 227–236.

SAPO-34 mixed matrix membranes based on PIM-1 and polyimides polymers: role of molecular sieve surface properties and morphology

M.G. Buonomenna,[1] G. Golemme,[1,4]* P.M. Budd,[2] C.R. Mason,[2] L. Starannikova,[3] N. Belov,[3] Yu. P. Yampolskii[3]

[1]*Dipartimento di Ingegneria Chimica e dei Materiali, Università della Calabria; and Consorzio INSTM; Via Pietro Bucci 45A, I-87030 Rende (CS), Italy* *ggolemme@unical.it*,
[2] *Organic Materials Innovation Centre, School of Chemistry, The University of Manchester, Manchester M13 9PL, UK.*
[3]*A.V. Topchiev Institute of Petrochemical Synthesis, Russian Academy of Sciences, 29 Leninsky Prospect, 119991, Moscow, Russia*
[4]*ITM-CNR, Istituto per la Tecnologia delle Membrane; Via Pietro Bucci 17C, I-87030 Rende (CS), Italy.*

Introduction

SAPO-34 (CHA) membranes have been reported to be effective for CO_2/CH_4 separations due to the pore size of 0.38 nm of the molecular sieve, equal to the kinetic diameter of the CH_4 molecule. Mixed matrix membranes (MMMs) are one of the most promising solutions to improve the separation performance of polymers [1]. A key research issue in the fabrication of defect-free MMMs is the adhesion of the polymer on the molecular sieve [2]. The detachment from the filler is the major problem when using glassy polymers. This work describes the preparation and characterization of different MMMs based on SAPO-34 functionalised with different groups according to the chemical nature of the hosting polymers: i.e. $(CH_2)_2Ph$ and $(CH_2)_3NH_2$ for PIM-1 and PI84 polymers, respectively. The factors leading to high aspect ratio SAPO-34 crystals are currently investigated.

Experimental

The synthesis of SAPO-34 crystals has been carried out by using the tetraethylammonium ion and dipropylamine as structure-directing agents, and methylene blue as a crystal growth inhibitor. The effect of different variables on the morphology of SAPO-34 crystals has been investigated: aging time, hydrothermal treatment time and temperature. Suspensions of SAPO-34 in polymer solutions were poured on leveled glass and the solvent was let to evaporate. The residual solvent of the MMMs was removed in a vacuum oven. The morphology of the membranes was observed by scanning electron microscopy (ESEM FEG QUANTA 200) at 0.2/30 kV. Sample specimens were freeze-fractured in liquid nitrogen to guarantee a sharp brittle fracture.

Results and discussion

In Fig. 1 the SEM pictures of the synthesized SAPO-34 crystals are shown. The morphology of the crystals ranges from cubic to platelet like with aspect ratio from 1.2 to 16.

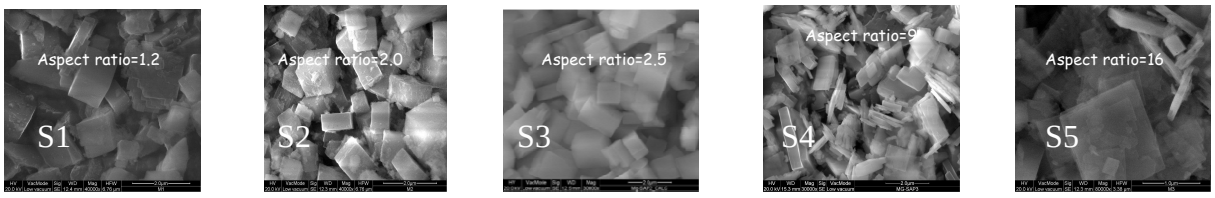

Figure 1. SEM analysis of SAPO-34 crystals synthesized varying the aging time and the duration of the hydrotermal treatment**.**

In Figure 2 the cross section of PIM-1/ SAPO-34$(CH_2)_2Ph$ and PI84/SAPO-34$(CH_2)_3NH_2$ membranes prepared by using crystals S3 are reported. In both cases a homogeneous

dispersion and a good adhesion between the crystals and the two different polymeric matrices have been obtained.

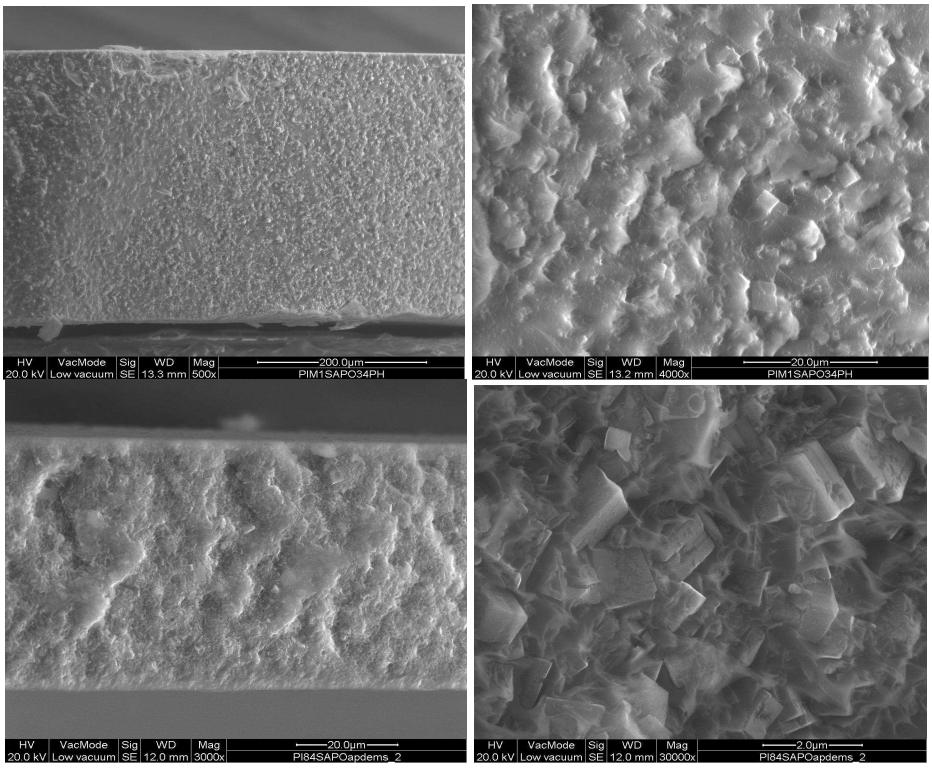

Figure 2. SEM analysis of the cross section of the MMMs PIM-1/ SAPO-34$(CH_2)_2Ph$ (top) and PI84/SAPO-34$(CH_2)_3NH_2$ (bottom) membranes

In this presentation the gas transport properties of the new MMMs and the effect of the aspect ratio of the functionalized SAPO-34 crystals will be discussed.

Acknowledgements
The work leading to these results has received funding from the European Community's Seventh Framework Programme (FP7/2007-2013) under grant agreement no. NMP3-SL-2009-228631, project DoubleNanoMem. We are grateful to Dr. Orazio Russo of Micromeritics Italia for his helpful support.

References

[1] T.S. Chung, L.Y. Jiang, Y. Li, S. Kulprathipanja, Prog. Polym. Sci. 32 (2007) 483-507.
[2] R. Mahajian, R. Burns, M. Schaeffer, W.J. Koros, Journal of Applied Polymer Science 86 (2001) 881-890.

Efficient CO_2 and CH_4 adsorption and separation utilizing the open metal sites of the CPO-27 coordination polymers

Pascal D. C. Dietzel, Falk Schuricht, Kari Anne Andreassen, Richard Blom
SINTEF Materials and Chemistry, Oslo, Norway, pascal.dietzel@sintef.no

Introduction

Coordination polymers containing accessible coordination sites, also called open metal sites or coordinatively unsaturated metal sites, are extremely interesting for application in gas adsorption and separation. This is due to the large interaction energy between the exposed coordination site of the metal cation in the coordination polymer and the sorbate molecule, which usually is significantly larger than at more shielded adsorption sites. An electron donating molecule might even form a coordination bond with the cation which can be assumed to be stronger than the interaction to a sorbate molecule without free electron pairs. In addition, the heat of adsorption may vary in a large energy range as a function of the type of metal cation and sorbate. These differences can be exploited in removal of one or more strongly adsorbing components from mixtures. Materials with a large number of exposed metal sites may consequently be eminently usable in separation processes, like the removal of carbon dioxide from mixtures with methane usually necessary during the processing of natural gas. The CPO-27-M coordination polymers contain a high concentration of open metal sites and are known for a number of divalent cations (M = Mg^{2+}, Mn^{2+}, Co^{2+}, Ni^{2+}, Zn^{2+}). We herein present our comparative study of the CO_2 and CH_4 adsorption and selective CO_2/CH_4 separation in this series of interesting compounds.

Experimental

Single component sorption isotherms of CO_2 and CH_4 were collected for CPO-27-M with M = Mg^{2+}, Mn^{2+}, Co^{2+}, Ni^{2+} in the temperature range 278-473 K and at pressure up to 50 and 100 bar, for CO_2 and CH_4, respectively. The isosteric heat of adsorption for both gases was calculated as a function of loading using at least three isotherms at different temperature.
Breakthrough measurements were performed in the temperature range of 303-353 K and at pressures between 1 and 10 bar using a 10/90 CO_2/CH_4 mixture.
Powder X-ray diffraction experiments of CPO-27-Ni and Co exposed to CO_2 were performed using synchrotron radiation at the ESRF.

Results and discussion

The CPO-27-M coordination polymers are based on a fairly rigid framework which resembles a honeycomb. After removal of the solvent, in "activated" state, they contain a significant number of exposed metal sites (6.4-6.6 mmol g^{-1} and 8.2 mmol g^{-1} for CPO-27-Ni/Co/Mn and CPO-27-Mg, respectively) which are accessible from within the pores of ~12 Å diameter.
All of the members of the CPO-27 series have a significant capacity for adsorption of methane and carbon dioxide (Figure 1) [1-4]. This is reflected in the unusually high initial isosteric heats of adsorption which are in the range of 30-43 kJ mol^{-1} for the first molecule of CO_2 adsorbed and 18-20 kJ mol^{-1} for CH_4 for the various members of the series. Crystal structure determinations have shown that the open metal site is indeed the primary adsorption

site for CO_2 and CH_4 [1, 2]. After full occupation of the first adsorption site, the heat of adsorption of CO_2 drops to ~25 kJ mol^{-1}, which is more usual for coordination polymers without accessible sites.
The difference in heats of adsorption of CO_2 and CH_4 results in significant preferential adsorption of the stronger adsorbing carbon dioxide. Quantitative removal of CO_2 from mixtures with N_2 or CH_4 has recently been reported for CPO-27-Ni and Mg, respectively [4, 5]. A comparison which also includes the Mn and Co compound reveals quantitative removal of the carbon dioxide from 10/90 mixtures with methane in all cases. Significant adsorption capacities, depending on the temperature, are observed, with the maximum adsorption capacity mainly being determined by the formula weight of the respective compound. Because CPO-27-Mg is ca. 22% lighter than the other members of the series and it has the largest isosteric heat of adsorption for CO_2, it also has the largest adsorption capacity. However, the crystal structure and adsorption capacity of the magnesium compound are degraded drastically if water is added to the gas feed. Application of the CPO-27-Mg compound must therefore be limited to dry gas mixtures. On the other hand, CPO-27-Ni remains largely unaffected – both structurally and in separation ability – by the presence of trace amounts of water.

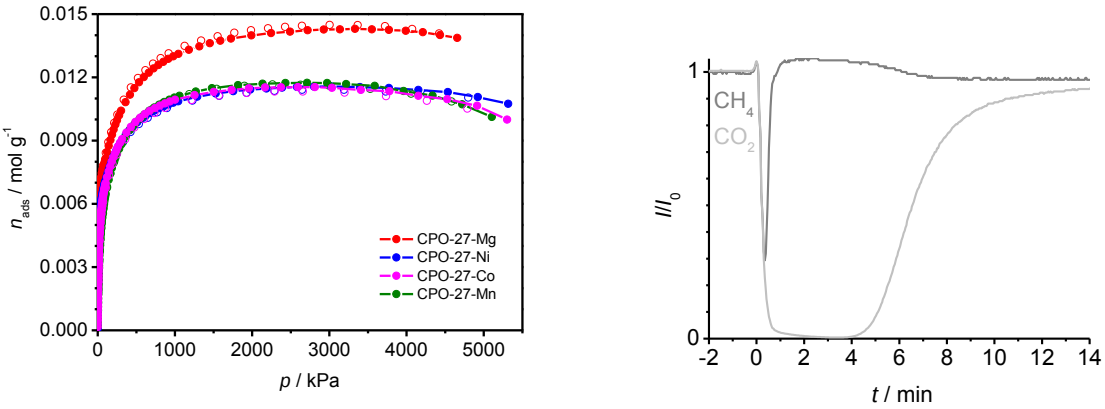

Figure 1. High capacity for CO_2 adsorption in the CPO-27 series (left, at 298 K) and exemplary breakthrough curve showing almost complete removal of carbon dioxide from mixture with methane (right, at 323 K and 1 bar).

Conclusions

All CPO-27-M compounds show a significant ability to separate CO_2 from CH_4 at ambient temperatures. CPO-27-Ni is the only of the compounds which can be handled in ambient atmosphere after synthesis without severe consequences on the adsorption properties. It may therefore be the best suited material of the series for application, even though its adsorption capacity is significantly smaller than that of CPO-27-Mg, the material in the series with the highest capacity for CO_2 adsorption.

References

[1] P. D. C. Dietzel, R. E. Johnsen, H. Fjellvåg, S. Bordiga, E. Groppo, S. Chavan, and R. Blom, Chem. Commun. 2008, 5125-5127.
[2] H. Wu, W. Zhou and T. Yildirim, J. Am. Chem. Soc. 2009, 131, 4995-5000.
[3] S. R. Caskey, A. G. Wong-Foy and A. J. Matzger, J. Am. Chem. Soc. 2008, 130, 10870-10871.
[4] P. D. C. Dietzel, V. Besikiotis and R. Blom, J. Mater. Chem. 2009, 19, 7362-7370.
[5] D. Britt, H. Furukawa, B. Wang, T. G. Glover and O. M. Yaghi, Proc. Nat. Acad. Sci. 2009, 106, 20637-20640.

Influence of Germanium in the propane/propylene separation performance using ITQ-29 zeolite as adsorbent

Miguel Palomino, Avelino Corma, José Luis Jordá, Fernando Rey and Susana Valencia
Instituto de Tecnología Química (UPV-CSIC). Av. de los Naranjos s/n. 46022 Valencia. Spain
miparo@itq.upv.es

Introduction

Separation of propane/propylene mixtures is usually carried out by cryogenic distillation and this is a highly energetically demanding procedure [1]. The high investment required and the operation costs associated to this distillation process have motivated the search of alternatives for the separation of mixtures comprised by olefins and paraffins. It is in this context where zeolites appear as selective adsorbent materials able to perform this type of separations [2]. The high thermal and chemical stability of zeolites makes them suitable materials for their use in adsorption and separation processes in a wide range of temperatures and operation conditions.
Conventional zeolite A (LTA) with a Si/Al ratio of one is widely used as adsorbent and in separation processes, however, it is not appropriated for carrying out processes involving the presence of olefins since they oligomerize in the acidic sites of the zeolite. Therefore, the availability of having this material in its purely siliceous form (ITQ-29 zeolite) and, consequently, with no acidity in the structure, opens new possibilities for hydrocarbon separations involving olefins [3]. In this work, we have studied the propane/propylene separation using ITQ-29 zeolite as adsorbent and how the presence of Ge in the structure influences the separation performance.

Experimental

Zeolite ITQ-29 was synthesized with two different compositions. One of them was prepared as pure silica and named as Si-ITQ-29, and the other was synthesized with a Si/Ge ratio of 2 and named as Ge-ITQ-29. The samples obtained were submitted to characterization prior to the hydrocarbon adsorption measurements. The kinetic adsorption experiments were done using a gravimetric instrument (IGA, "Intelligent gravimetric Analyzer") from Hiden Isochema, employing samples previously outgassed under vacuum at 400ºC. The adsorption kinetics of propane and propylene were determined at 25ºC and 30 kPa.

Results and discussion

The XRD patterns obtained for ITQ-29 zeolites indicated that they were consistent with the LTA structure and characterization by means of N_2 and Ar adsorption as well as SEM confirmed the high crystallinity of the samples. The composition and the pore apertures obtained from the refinement of the XRD data are shown in Table 1. It can be observed that Ge-ITQ-29 possesses a nearly circular pore aperture, whereas Si-ITQ-29 zeolite has one of the dimensions being slightly smaller.

Table 1. Composition and pore apertures of ITQ-29 zeolites.

Zeolite	Si/Ge	Pore aperture (Å)
Si-ITQ-29	∞	4.13 × 4.37
Ge-ITQ-29	2	4.21 × 4.29

The results obtained for the propane and propylene kinetic adsorption experiments using Si-ITQ-29 as adsorbent are shown in Fig. 1a. It is clearly evidenced there that diffusion of propane is much slower than that of propylene giving a ratio of the diffusion coefficients of propylene vs. propane higher than 90 and, therefore, allowing a kinetic separation process based on the differences in the diffusion rates of both components.

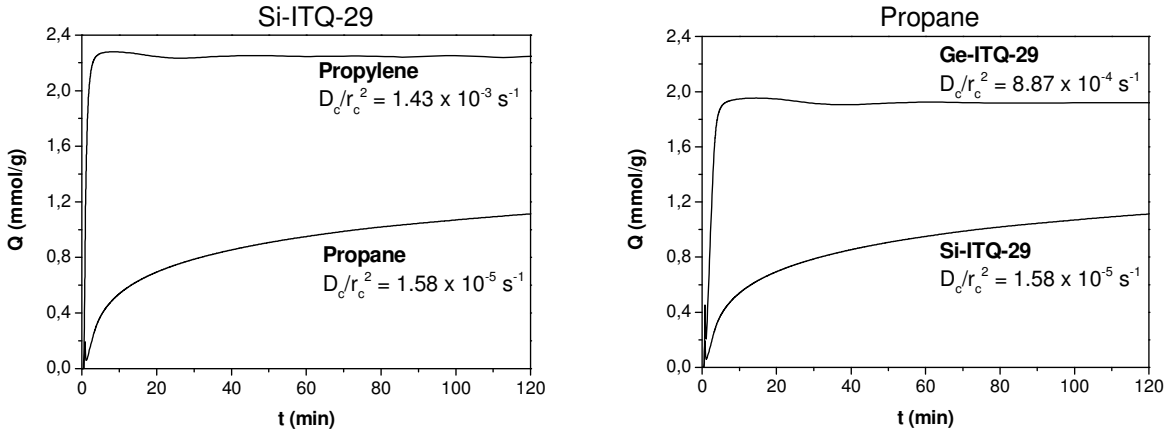

(a) *(b)*

Figure 1. Kinetic measurements of propane and propylene adsorption on Si-ITQ-29 zeolite at 25ºC and 30 kPa (a), and comparison of propane adsorption on Si-ITQ-29 and Ge-ITQ-29 zeolites (b).

On the other side, the results obtained when using Ge-ITQ-29 zeolite as adsorbent are very similar to those of Si-ITQ-29 in the case of propylene but, surprisingly, adsorption of propane is much faster (Fig. 1b). This is a consequence of the small difference in the shape of the pores that yields to a slightly larger length of the pore aperture in one of the dimensions in the case of incorporating Ge into the zeolite framework. As a result, the propane/propylene separation ability of Ge-ITQ-29 zeolite is not as good as that of Si-ITQ-29.

Conclusions

From the results obtained in this work, we can conclude that Si-ITQ-29 allows the propane/propylene kinetic separation and that changes in the chemical composition of the zeolite by incorporation of Ge produce small differences in the pore aperture dimensions that greatly influence the propane diffusion rate. This results in a different propane/propylene separation performance of Si-ITQ-29 and Ge-ITQ-29.

Acknowledgements

Financial support by Spanish and regional institutions is gratefully acknowledged (MAT2009-14528-C02-01, PAID-06-08:3279 and GV/2009/066). M. P. thanks CSIC for a JAE doctoral fellowship.

References

[1] D.J. Safarik, R.B. Eldridge, *Industrial & Engineering Chemistry Research* 37 (1998) 2571-2581.
[2] R.M. Barrer, in *Zeolite and Clay Minerals as Sorbents and Molecular Sieves*, Academic Press, London (1978).
[3] A. Corma, F. Rey, J. Rius, M.J. Sabater, S. Valencia. Nature 431 (2004) 287-290.

Advanced technological applications

FEZA 2011

In vitro controlled - release of nanobiomaterials based on captopril.

Iuliana Florentina Alexa, Maria Ignat, Valeriu Sunel, Eveline Popovici
Department of Materials Chemistry, Al. I. Cuza University, Bvd. Carol I, No. 11, 700506, Iasi, Romania, alexaiulianaflorentina@yahoo.com

Introduction

Nowadays, nanomaterials are applied in many biomedical fields, such as clinical diagnosis, drug delivery, *in vitro* and *in vivo* fluorescent markers [1]. This study is based on the development of the synthesized drug delivery systems that are composed of successfully captopril loaded nanoparticles as LDH, MCM-41 and SBA-15 materials. Among the studied drug delivery systems, silica-based materials having a well defined structure and surface properties appear to be promising candidates. The purpose of this study is to obtain drug delivery systems with high efficiency in therapeutic treatment. As captopril has been delivered, the remained drug-support does not affect in any way the body. On the contrary, it is dissolved, degraded and easily removed from the body [2, 3].

Experimental

As it is known, captopril is a drug that blocks the formation of angiotensin in the kidneys resulting in vasodilatation, being used for the treatment of hypertension and some types of congestive heart failure. In the experiment, the drug loading is carried out by a simple impregnation method. This way, LDH, SBA-15, and MCM-41 were involved as porous nanomaterials to be impregnated. Then, the obtained systems were tested in the drug release process realized in synthetic stomach media (PBS). Comparing with a release process from the pharmaceutical formulations of this drug, the captopril-loaded LDH, SBA-15, and MCM-41 can be considered more efficient controlled drug delivery systems.

The obtained materials were analyzed by N_2 sorption, UV-Vis DR, SEM and FTIR Spectroscopy. Also using the Kärber method, in a pharmacodynamic laboratory, the toxicity of the synthesized materials, with and without loaded drug, was determined. In Table 1 we listed the toxicity values and the textural properties of our materials.

Table 1

Sample	DL50, mg/Kg body	Surface area, m^2/g	Pore volume, cm3/g	Pore radius, nm
$CapH_2$	6590	-	-	-
LDH	7410	195.47	0.395	3.17
LDH- $CapH_2$	7315	16.17	0.048	1.93
MCM-41	7260	1024.2	0.743	1.87
MCM-41- $CapH_2$	7485	801.5	0.387	1.18
SBA-15	7410	862.13	0.927	3.79
SBA-15- $CapH_2$	7522	599.34	0.806	3.54

Results and discussion

The drug delivery properties of captopril-loaded materials have been investigated by captopril release in the simulated gastrointestinal and intestinal fluids. Fig. 1 shows the release profiles of LDH-CapH_2, SBA-15-CapH_2 and MCM-41-CapH_2 in solutions at pH value of 7.4. The BET surface areas and the total pore volumes decreased upon loading with captopril indicating that the drug was introduced inside the channels of the porous matrices and the mesoporous structure remained as the drug was loaded. Due to a higher surface area, MCM-41-CapH_2 has the largest amount of the loaded drug (29.90 wt %), while SBA-15-CapH_2 exhibits a percentage of 22.61 % loaded drug. The loaded amount is proportional to the specific surface area of the material (the same trend can be observed for the LDH-CapH_2 sample).

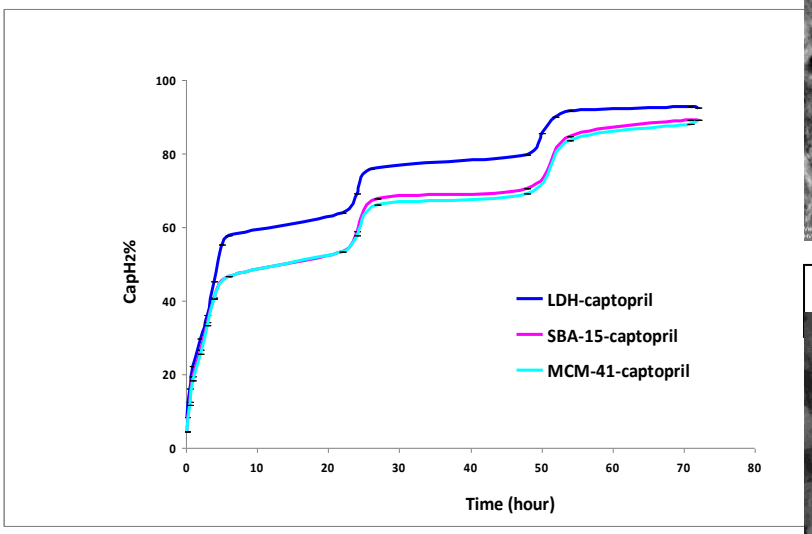

Fig.1. Controlled - release of captopril in PBS media

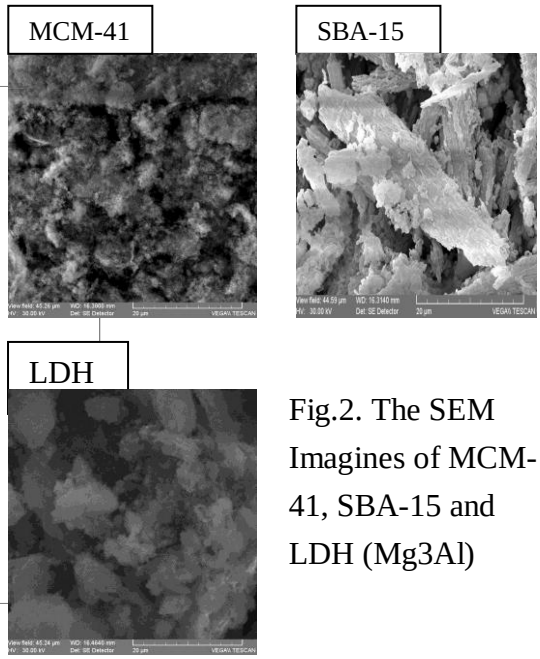

Fig.2. The SEM Imagines of MCM-41, SBA-15 and LDH (Mg3Al)

Conclusions

The delivery profiles showed that the captopril release rates could be controlled by managing the textural properties and morphology of the mesoporous silica, i.e. SBA-15 and MCM-41. This way, a well-controlled and economical system for CapH_2 delivery could be achieved by adjusting appropriate surface areas, pore sizes and suitable morphologies of these materials.

In order to demonstrate that the synthesized materials are perfect drug delivery systems, in the near future we plan to do a large number of pharmacological tests in rats and analysis of macrophages from mousses.

Acknowledgements

This study was supported by POSDRU/88/1.5/S/47646 project, funded by European Social Fund, POSDRU 2007-2013

References

[1] A.L. Doadrio, E.M.B. Sousa, J.C. Doadrio, J. Pe´rez Pariente, I.Izquierdo-Barba, M. Vallet-Regı, J. Control. Release, 97 (2004), 125
[2] F. Cavani, F. Trifiro, A.Vaccari, Catal. Today 11 (1991), 173-301
[3] P. Torchilin, Nat. Rev. Drug Discov., 4 (2005), 145 – 160

Sulfur pigments with zeolite L matrices, the novel ultramarine analogs

Aldona Jankowska[1], Natalia Koperska[1], Stanisław Hoffmann[2], Janina Goslar[2], Stanisław Kowalak[1]
[1] *Faculty of Chemistry, A. Mickiewicz University, Poznań, Poland,*
[2] *Institute of Molecular Physics, Polish Academy of Sciences, Poznań, Poland*
aljan@amu.edu.pl

Introduction

The natural (lazurite) and synthetic ultramarine are aluminosilicate sodalites containing sodium oligosulfide (mostly NaS_3) molecules (chromophores) encapsulated inside β-cages. It has been found that analogs of ultramarine can be prepared from zeolites, mostly from those containing sodalite units in their crystalline structure (e.g. LTA, FAU, SOD) [1]. Not only sodium but another alkali cations were used for syntheses as well as zeolite structures containing different than β-cages. It seemed that encapsulation of sulfur anion-radicals into small ε-cages in erionite or cancrinite [2] resulted in more pronounced population of smaller S_2^- anion radicals (compared to S_3^-).
The following study is devoted to preparation of sulfur pigments with zeolite L which allows to benefit small cancrinite (ε) cages forming the LTL structure and exclusive presence of potassium cations. The results of earlier works indicated that the attempts to replace sodium for potassium in close vicinity of anion-radicals during thermal pigment synthesis was not very efficient [3]. The use of zeolite L provides a chance to prepare the pigments with sulfur chromophores accompanied by potassium cations, encapsulated in small voids (ε -cages).

Experimental

Zeolites L were prepared by hydrothermal crystallization of the initial gel containing K_2O-Al_2O_3-SiO_2-H_2O [4], without any sodium cations. The pigments were prepared by mixing and grinding zeolite L with sulfur (20 wt.%) and K_2CO_3 or Na_2CO_3 regarding various Me_2/S ratio. The mixtures were heated in covered crucibles for two hours in range 500 – 800°C. The products were washed with distilled water and dried. The characterization comprised XRD, UV-vis, ESR and Raman spectroscopy

Results and discussion

The resulted samples indicate much less intense coloration than those prepared from zeolite A [1]. The contribution of blue chromophore is low or negligible (particularly in samples with Na). The yellow or ochre colors prevail in Na bearing samples (Table). Typical electronic spectra are given in Fig. 1. The Raman spectra indicate limited contribution of anion-radicals S_3^- and S_2^-. The prevailing yellow (~400nm) chromophores are oligosulfides (e.g. S_6^{2-}). Samples prepared from low and medium alkaline mixtures with K_2CO_3 and sulfur maintain the LTL structure after heating at all applied temperatures, whereas the alkali rich samples undergo transformation towards kaliophilite upon heating at 650 and 800°C. The low or medium contribution of sodium (Na_2CO_3) in preparation mixtures did not affect the structure of parent zeolites neither at 500° nor at 650°C. The sample prepared at 650°C from mixture with Na/S = 0.6 show poor (LTL) crystallinity, while the samples obtained from sodium rich mixtures (Na/S = 1.0) show appearance of SOD structure. A contribution of S_3^- radical (UV-vis band at ~600nm) in the latter is much more pronounced that in samples with preserved LTL structure. All the Na bearing mixtures become amorphous upon thermal treatment at

800°C, but they still show intense coloration. The ESR spectra of selected samples under study indicate noticeable differences compared with signals of sulfur radicals (S_3^-) encapsulated in sodalite cages of conventional ultramarine. The lines are very narrow even at room temperature which suggests very rigid entrapment of the radicals inside the ε-cages.

Table 1. Properties of pigments prepared under indicated conditions

K_2/S	T (°C)	Color	Struct.
0.2	500	L. cel.	LTL
0.6	500	P. cel.	LTL
1.0	500	P. cel.	LTL
0.2	650	white	LTL
0.6	650	White	LTL
1	650	Green	Kal.+un.
0.2	800	White	LTL
0.6	800	Cel.	LTL[#]
1	800	L. cel.	Kal.

Na_2/S	T (°C)	color	Struct.
0.2	500	White	LTL
0.6	500	Yellow	LTL
1	500	Yellow	LTL
0.2	650	White	LTL
0.6	650	Ochre	LTL[#]
1	650	Ochre	SOD[#]
0.2	800	Ochre	Am.
0.6	800	Yellow	Am.
1	800	Ochre	Am.

[#]-poor crystallinity, Kal.-kaliophilite, Am.-amorphous, un.-unknown, cel.-celadon, L-light, P-pale

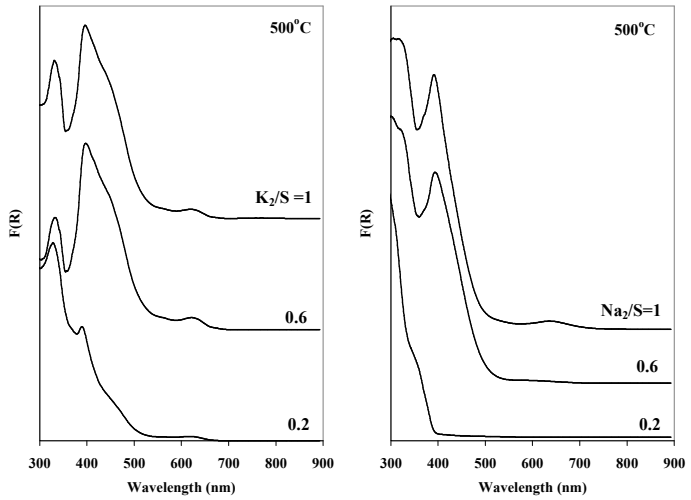

Figure 1. Typical electronic spectra of samples prepared at 500°C with K or Na cations.

Conclusions

The sulfur pigments obtained from zeolite K-L, sulfur and K_2CO_3 contain limited number of sulfur anion-radicals, and oligosulfides are prevailing chromophores. Admixture of sodium to initial mixture affect noticeably a coloration of the products and influences the direction of thermal structure transformation. The original LTL structure is maintained for the samples obtained from the mixtures with low and medium alkalinity, particularly heated at lower temperatures. Samples prepared with K transfer to kaliophilite under severe conditions, while those with Na undergo amorphization of form sodalite. The recorded ESR spectra illustrate different confinement and surrounding of S_3^- within ε-cages than that in conventional ultramarine.

Acknowledgements

A. Jankowska appreciates the financial support from grant No. N N204 20154.

References

[1] Kowalak S., Jankowska A., *Inorganic sulfur pigments based on nanoporous materials*, Ordered Porous Solids, ch. 22 p. 591, Valtchev V., Mintova S., Tsapatsis M. (Ed.) Elsevier (2009).
[2] Kowalak S., Jankowska A., Zeidler S., Więckowski A.B., J. Solid State Chem. 180 (2007) 1119–1124.
[3] Hoffmann S.K., Goslar J., Lijewski S., Jankowska A., Kowalak S., Micr. Mes. Mat. 127 (2010) 205–212.
[4] Robson H., Lillerund K.P., Verified syntheses of zeolitic materials, Second Revised Ed. (2001).

Experimental characterization and technical evaluation on zeolites in different sized sorption thermal energy storage systems

A. Laß-Seyoum[1], D. Borozdenko[1], T. Friedrich[1], M. Blicker[2], T. Langhof[2]
[1]*ZeoSys GmbH, Falkenberger Straße 40, 13088 Berlin, Germany*
[2]*Fraunhofer Institut Grenzflächen- und Bioverfahrenstechnik, Nobelstrasse 12, 70569 Stuttgart, Germany*

Introduction

Currently three types of thermal energy storage principles are known: sensible, latent and thermo-chemical thermal energy storage.

The studies reported here are focused exclusively on closed sorption thermo-chemical storage system. The possibility of long-term storage with minimal thermal losses and a high energy storage density are the main advantages of this system compared with sensible and latent thermal storage principles. While some research and development activities have been executed in the past [1- 3], more advanced sorption materials and system configurations are still needed for efficient thermal storage at higher temperatures, particularly in the range of 120 – 250 °C to have a significant potential for industrial applications.

The main objective of the studies presented here is to characterize and evaluate different synthetic zeolites in sorption energy storage system and to find out the influence of up-scaling the system on the thermodynamic behavior of the materials.

Experimental

Experimental characterizations were performed on a wide range of zeolites with different chemical composition, geometry, pore and particle size (with or without binding materials) using static adsorption under vacuum followed by thermo-gravimetric differential scanning (TG-DSC) dynamic desorption methods.

In addition to µg scale investigations, a laboratory set-up capable of simulating the dynamics and processes of a closed sorption thermal energy storage system was used to measure the temperature distributions in the storage system, adsorption capacities, energy densities, power, pressure gradient and hydrothermal stability. Technical evaluations have also been carried out in different sized test systems, in order to find out the influence of up-scaling from lab-scale (V = 1.5 L) to semi-technical (V = 12 L and 50 L) and technical storage systems (V = 1 m^3) on the performance of the sorption materials.

Results and discussion

For each of the investigated storage materials six adsorption/desorption cycles have been carried out. Through static adsorption performed under vacuum (10.5 mbar, relative humidity 33 %, 25 g zeolite), about 18 - 32 % of water was adsorbed and equilibrium was reached within 2 weeks. Further investigations on a specific zeolite using dynamical adsorption/desorption method show results confirming those obtained from static adsorption with different equilibrium conditions.

Under specific test conditions ($T_{condenser/vaporizer}$ = 10 °C/30 °C, p = 0,1 - 2 mbar, $T_{desorption}$ = 200 °C) in lab-scaled and semi-technical test systems, a maximum temperature ranging from about 125 °C to 145 °C has been achieved.

Conclusions

Several experimental characterizations on different Zeolites have been carried out using different thermo analytical methods in order to achieve pre-selection of optimal sorption zeolites out of a very broad spectrum of materials.

From tests carried out in 1.5 liter lab-scale test rig it was possible to get detailed thermodynamic characteristic features of the pre-selected zeolites. The technical evaluation in larger scale (15 L and 50 L semi-technical as well as 1 m³ technical systems) reveal quite satisfactory results, even though clear scaling effects were observed. Further technical evaluation and performance verification tests in a 1 m³ technical system will be done in the near future by integrating the system with combined heat and power (CHP) plant for higher charging temperatures up to 200 °C.

Acknowledgements

The authors gratefully acknowledge the financial support of the European Commission Framework Programme under grant agreement FP7-SME-2007-1-222116.

References

[1] Bayerisches Zentrum für Angewandte Energieforschung ZAE (www.zae-bayern.de)
[2] Fraunhofer-Institut für Solare Energiesysteme ISE (www.ise.Fraunhofer.de)
[3] H. Stach , J. Mugele, J. Jänchen and E. Weiler, "Influence of Cycle Temperatures on the Thermochemical Heat Storage Densities in the Systems Water/Microporous and Water/Mesoporous Adsorbents", Adsorption 11 (2005) 393 - 404.

Metal-organic framework single crystals as photoactive matrices for the generation of metallic microstructures

Rob Ameloot,[1] Maarten B. J. Roeffaers,[2] Gert De Cremer,[1] Frederik Vermoortele,[1] Johan Hofkens,[2] Bert F. Sels,[1] and Dirk E. De Vos[1]*
[1] *Department of Microbial and Molecular Systems, Center for Surface Chemistry and Catalysis, K.U.Leuven, Kasteelpark Arenberg 23, B-3001 Leuven (Belgium)*
[2] *Department of Chemistry, K.U.Leuven, Celestijnenlaan 200F, B-3001 Leuven (Belgium)*
Email: Dirk.DeVos@biw.kuleuven.be

Introduction

Lithographic patterning techniques have evolved into tremendously powerful tools for creating metallic features. However, current techniques are best suited for patterning two-dimensional structures. The lack of efficient processes to create three-dimensional structures sparked considerable interest in the development of nonconventional lithographic techniques. Here we present how a photoactive matrix can be used for deposition of metallic features in three dimensions by localized photoreduction [1].

Results and discussion

The photoactive material used is MOF-5, a metal-organic framework (MOF) material. MOFs are microporous crystalline materials built up from nodes of metal ions connected by organic linkers. Recently, photocatalytic activity has been observed in a number of MOFs based on transition metal ions and carboxylate linkers [2-4]. In the case of MOF-5, the crystal lattice is built up from Zn_4O nodes, in which a central oxygen atom is connected to four Zn atoms, linked together by terephthalate ligands. Since the coordination sphere of each node contains twelve carboxylate oxygen atoms, resulting in Zn_4O_{13} clusters, the photoactivity of MOF-5 is explained by zinc oxide quantum dot behavior [5-6].

Direct-writing of metallic silver patterns inside single MOF-5 crystals was performed as depicted in Fig. 1A. The crystal is placed on a microscope cover glass, which acts as the transparent floor of a liquid sample holder to which a 10 mM ethanolic silver nitrate solution was added. The beam of a pulsed 780 nm laser is focused through the objective of an inverted microscope on a plane buried between 10 and 60 μm inside the crystal. Pattern generation is achieved by moving the sample using a computer controlled piezoelectric stage, thus positioning the laser focal point according to the pixel coordinates of a digitized image. At each position the laser stops for a predetermined activation time, thereby irradiating the photocatalytically active MOF-5 matrix and thus triggering the local reduction of Ag^+ ions which results in a metallic silver dot. To illustrate the patterning capability of the presented method, the word “KULeuven” was encoded as a two-dimensional 22 × 22 pixel quick-response code (QR code) (Fig. 1B) and written inside a MOF-5 crystal (Fig. 1C). For an activation time of 250 ms per pixel, the digitized image is reproduced as a 60 × 60 μm^2 pattern of well-defined dark dots of 700 to 800 nm across. The dimensions of these activated spots decrease with irradiation time.

Figure 2 shows two identical QR-codes written in planes spaced 10 μm apart. A side view, obtained by tipping over the crystal, illustrates the strict confinement of the metallic regions to their respective image planes. The dimension of the activated spots in the Z direction is about 2.5 μm.

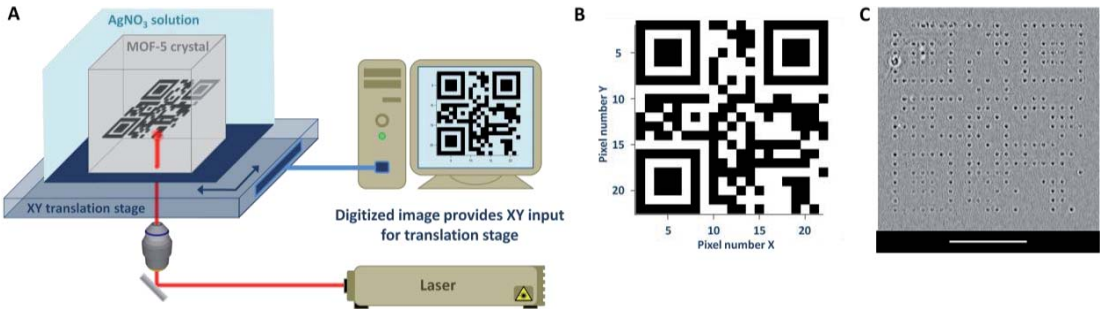

Figure 1. A) Schematic representation of the setup. B) Template image of the 22 × 22 pixel QR-code encoding the word "KULeuven". C) Transmission optical micrograph of the pattern depicted in (B) written in a single MOF-5 crystal. Scale bar: 25 μm.

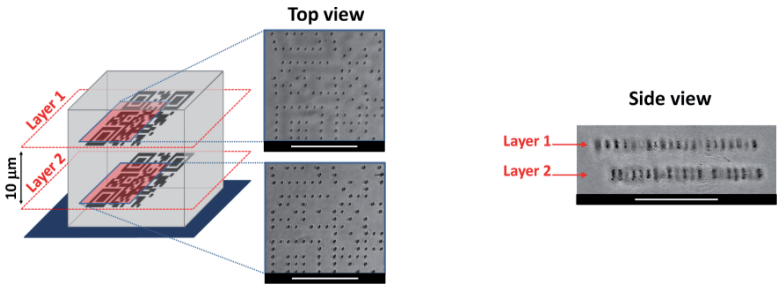

Figure 2. Top and side views of two QR-codes in planes spaced 10 μm apart. Scale bars: 25 μm.

Conclusions

In summary, we demonstrated a laser direct-write process to generate three-dimensional metallic features by using a highly porous, photocatalytically active MOF as a single crystal matrix. The resulting metallodielectric structures might find application in optics and microelectronics.

Acknowledgements

The authors are grateful to the Belgian Federal Government for support in IAP project 6/27 and to FWO Vlaanderen for project funding G.0453.09 and support for R.A., M.B.J.R and G.D.

References

[1] Ameloot, R., Roeffaers, M. B. J., De Cremer, G., Vermoortele, F., Hofkens, J., Sels, B. F., De Vos, D. E., Metal-organic framework single crystals as photoactive matrices for the generation of metallic microstructures, Advanced Materials, (2011), in press

[2] Gascon, J., Hernandez-Alonso, M. D., Almeida, A. R., van Klink, G. P. M., Kapteijn, F., Mul, G. Isoreticular MOFs as Efficient Photocatalysts with Tunable Band Gap: An Operando FTIR Study of the Photoinduced Oxidation of Propylene, Chemsuschem, 1 (2008), 981-983

[3] Dan-Hardi, M., Serre, C., Frot, T., Rozes, L., Maurin, G., Sanchez, C., Ferey, G. A New Photoactive Crystalline Highly Porous Titanium(IV) Dicarboxylate, Journal of the American Chemical Society, 131 (2009), 10857-10859

[4] Silva, C. G., Luz, I., Llabres i Xamena, F. X., Corma, A., Garcia, H., Water Stable Zr-Benzenedicarboxylate Metal-Organic Frameworks as Photocatalysts for Hydrogen Generation, Chemistry-A European Journal, 16 (2010), 11133-11138

[5] Xamena, F., Corma, A. & Garcia, H. Applications for metal-organic frameworks (MOFs) as quantum dot semiconductors, Journal of Physical Chemistry C, 111 (2007), 80-85

[6] Bordiga, S., Lamberti, C., Ricchiardi, G., Regli, L., Bonino, F., Damin, A., Lillerud, K. P., Bjorgen, M., Zecchina, A, Electronic and vibrational properties of a MOF-5 metal-organic framework: ZnO quantum dot behaviour, Chemical Communications, (2004), 2300-2301

Detection of radiation damage on natural zeolite using cathodoluminescence

Hirotsugu Nishido
Research Institute of Natural Science, Okayama University of Science
nishido@rins.ous.ac.jp

Introduction

Cathodoluminescence (CL), the light emission induced by electron irradiation, has been widely applied in mineralogical and petrological investigations, especially for carbonate and silica minerals. The nature of the luminescent centers for a CL emission results from an intrinsic (lattice defects) and/or extrinsic (impurities) properties of the crystal. CL method enables observation of trace element distribution and defects in the lattice, which often cannot be detected with other techniques. Although the CL measurements of a number of geological materials have been reported by many investigators, no CL data on zeolite minerals has emerged up to the present. A new system of a cathodoluminescence scanning electron microscopy (CL-SEM) achieved the CL spectral measurements of natural zeolites with high sensitive at various temperatures. In this study, CL emission caused by radiation damage was first confirmed from bikitaite, which is a rare natural zeolite occurring as an alteration product of spodumene in lithium-rich pegmatite dikes at Bikita, Fort Victoria, Zimbabwe.

Experimental

Crystal fragments of bikitaite were selected for CL measurements after carbon-coating on polished surfaces. Color CL images were captured using a cold-cathode microscope (Luminoscope: Nuclide ELM-3R), consisting of an optical microscope, an electron gun, and a cooled charge-coupled device (CCD) camera (Nikon). SEM-CL analysis was conducted using an SEM (JEOL: JSM-5410) combined with a grating monochromator (Oxford: Mono CL2) to measure CL spectra ranging from 300 to 800 nm in 1 nm steps with a temperature controlled stage. The CL intensity emitted from the samples was collected using a retractable parabolic mirror collector coated with Al (collecting efficiency 75 %). The collected CL was dispersed by the grating monochromator, which had the following characteristics: 1200 grooves/mm, a focal length of 0.3 m, F of 4.2, limit of resolution of 0.5 nm, and slit width of 4 mm at the inlet and outlet. The dispersed CL was collected by a photocounting method using a photomultiplier tube (Hamamatsu: R2228) and converted to digital data. CL spectra and CL images are obtained employing a new system of CL-SEM, which comprises a SEM (Jeol JSM-5400) combined with an integral grating monochromator (Oxford Mono CL2) with high sensitive and high spatial resolution over the wide wavelength range of 300 nm ~ 800 nm. High magnification CL image can be obtained using SEM-CL system in a scanning mode linked to SEM.

Results and discussion

Bikitaite shows a bright thin emission band as CL halo along the outer surface and in the cracks (Fig. 1). Its spectrum has a broad peak centered at 460 ~ 470 nm in blue region. No activator of impurity elements can be assigned to the emission center, but structural defect should be a candidate for this center based on a width of the spectral peak. By considering its occurrence in pegmatite, the blue CL of bikitaite might be assigned to structural defects as observed in the quartz and feldspar with radiation-induced damage closely associated with natural radionuclide minerals. Therefore, the alpha particles from radioactive pegmatite solution containing radioactive elements such as U and Th during formation process can cause structural defects (e.g. oxygen deficient center) in the lattice of bikitaite. It leads to an energy loss process of specific ionization along the track of a charged particle, suggesting luminescence halo as a thin band along the surface and in the cracks of the bikitaite grain. This analysis provides valuable applications to geodosimetry and geochronology, e.g., estimating leakage of nuclear waste from geologic disposal facility and dating of sedimentary zeolites coexisted with natural radionuclide.

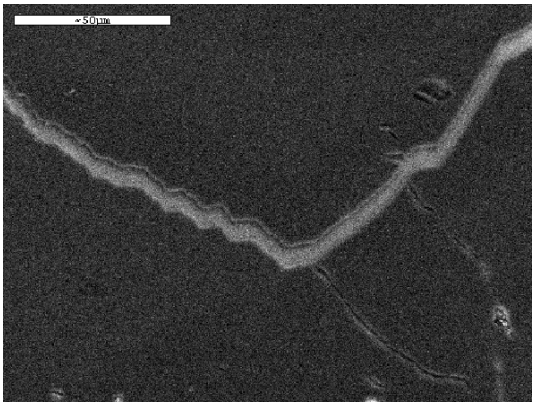

Figure 1 CL image of radiation damage (CL halo) in the crack of Bikitaite. Scale bar: 50 μm

Removal of Toxic Heavy Metals from Water by Magnetic Mesoporous Nanosorbents

Xinqing Chen[1], Tsz Nok Ng[1], Manuel Arruebo[2] and King Lun Yeung[1]

[1]Department of Chemical and Biomolecular Engineering,
Hong Kong University of Science and Technology, Hong Kong, P.R. CHINA and
[2]Aragon Nanoscience Institute(INA), University of Zaragoza, 50009 Zaragoza, Spain
Corresponding author: kekyeung@ust.hk

Introduction

There is a growing interest in the use of magnetic porous sorbents for the removal of heavy metals [1-2] and organic pollutants including oils, dyes and volatile organic compounds from aqueous systems. Mesoporous MCM-41 has the advantage of enormous surface area and large easily accessible pores that are amenable to chemical modifications. This work reports a magnetic sorbent based on MCM-41 for the selective adsorption of chromium oxyanions which is commonly found in the waste effluents from electroplating, metallurgical, tannery and textile industries [3]. The selective adsorption of CrO_4^{2-} at near neutral pH was achieved by the magnetic mesoporous sorbent after chemical modification. Single and binary components adsorptions were carried out for CrO_4^{2-} and Cu^{2+}, and the effects of pH and metal concentrations were investigated and modelled. Simulated polluted water was also investigated using tap, river and mountain run-off waters.

Experimental

A colloidal suspension of magnetic Fe_3O_4 nanoparticles was prepared by sonochemical method from a synthesis solution with molar composition of 3.2 $FeCl_3$: 1.6 $FeCl_2$: CTABr: 39 NH_4OH: 2300 H_2O. Twenty milliliters of magnetic colloid was added to a solution of 1 CTABr: 292 NH_4OH: 2773 H_2O under vigorous mixing. The magnetic iron oxide nanoparticles were incorporated within the MCM-41 matrix with the addition of TEOS in the mixture according to prior methods [4], aminopropyls were grafted on the pores of the magnetic MCM-41 from 3-aminopropyltrimethoxysilane by reflux and the resulting *NH_2-magMCM-41* was converted to Fe^{3+}-*magMCM-41* by overnight adsorption of Fe^{3+} from a 50 mM $FeCl_3$ in 2-propanol.

Results and discussion

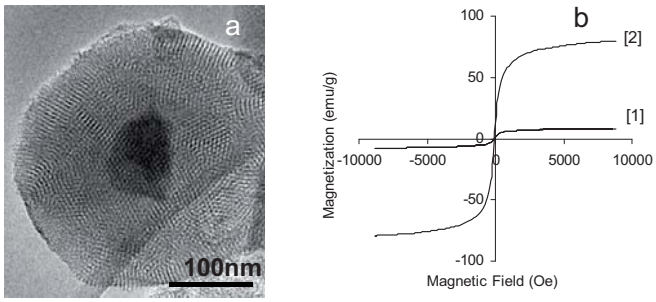

Figure 1(a) TEM picture of nanometer-sized *magMCM-41* and (b) the magnetic properties of *magMCM*-41 [1] and magnetic iron oxide nanoparticles [2]

The embedded cluster of iron oxide nanoparticles and the magnetic ordered mesopores of MCM-41 are clearly seen from the TEM picture of *magMCM-41* in Fig. 1a. The iron oxide nanoparticles display superparamagnetic behavior and have a magnetic moment of 80.0 emu.g^{-1} at 10000 Oe, while the *magMCM-41* exhibits a magnetic moment of 8.30 emu.g^{-1} at 10000 Oe with a diamagnetic contribution from SiO_2 as shown by the room temperature magnetization isotherms in Fig. 1b. Table 1 represents the characterization information of these materials.

Table 1. Physical, chemical and adsorption properties of MCM-41 adsorbents.

Adsorbent	BET surface area (m^2/g)	Pore size (nm)	Aminopropyls (mmole/g)	Fe^{3+} (mmole/g)	Adsorption capacity (mmole/g)	
					chromium	copper
MCM-41	1001	3.17	0	0	0	0
NH_2-MCM-41	750	2.86	2.8	0	1.8	0.9
magMCM-41	800	3.20	0	0	0	0
Magnetic Fe^{3+}*-magMCM-41*	585	2.78	2.7	1.3	1.5	0

The adsorption and separation studies of magnetic nanosorbent (Fe^{3+}-*magMCM-41*) were performed on equimolar CrO_4^{2-} and Cu^{2+} solutions. The nanosorbent adsorbed only chromium (i.e., 1.3 ± 0.2 mmole.g^{-1}) over the entire pH range of the study (from 2 to 5). The distribution coefficient K_d of chromium oxyanions on the magnetic nanosorbent was measured to be 112,000 from distilled water at pH5 compared to 30000 from mountain run-off water at the same pH which showed the remove percentage of chromium from mountain run-off water is more than 97%.

Conclusions

This work shows that it is possible to prepare magnetic nanosorbents of superb selectivity, large capacity and high magnetization by embedding magnetic iron oxide nanoparticles in the matrix of mesoporous MCM-41 particles. Deliberate modification of the pore channel with suitable organic and inorganic moieties creates surface sites for selective adsorptions. The high magnetization of the sorbents means that it could be separated and recovered using magnetic field and allow possibility of resource recovery for recycle and reuse.

Acknowledgements

The authors gratefully acknowledge the financial support from the Hong Kong Research Grant Council (605009).

References

[1] Yavuz, C. T.; Mayo, J. T.; Yu, W. W.; Prakash, A.; Falkner, J. C.; Yean, S.; Cong, L.; Shipley, H. J.; Kan, A.; Tomson, M.; Natelson, D.; Colvin, V. L. Low-field magnetic separation of monodisperse Fe_3O_4 nanocrystals. *Science* **2006**, *314*, 964-967.

[2] Oliveira, L. C. A.; Petkowicz, D. I.; Smaniotto, A.; Pergher, S. B. C. Magnetic zeolites: a new adsorbent for removal of metallic contaminants from water. *Water Res.* **2004,** *38,* 3699-3704.

[3] Barnhart, J. Occurrences, uses, and properties of chromium. *J. Regul. Toxicol. Pharm.* 1997, 26, S3–S7.

[4] Ho, K.Y.; McKay, G.; Yeung K.L. Selective adsorbents from ordered mesoporous silica. Langmuir 2003, 19, 3019-3024.

Double-layered Zeolite-Nafion Composite Membrane for Self-humidifying Micro Fuel Cell

Wei HAN, Chun Tung CHEUNG, Ho Yee POON & King Lun YEUNG *
Department of Chemical and Biomolecular Engineering, The Hong Kong University of Science and Technology, Clear Water Bay, Kowloon, Hong Kong, P.R. China
** Corresponding author: kekyeung@ust.hk*

Introduction

External humidification equipment is often necessary for proton exchange membrane fuel cell (PEMFC) because Nafion as the most common electrolyte membrane presents sharply-decreased proton conductivity under low membrane hydration, which complicates the system design and operation, and lowers the overall energy efficiency [1]. Many attempts have been made to achieve the operation without humidification via different self-humidifying electrolyte membranes including Pt-zirconium phosphate hydrate (ZrP)-Nafion [2], Pt-SiO_2-Nafion [3], Pt-clay-Nafion [4] and Pt-NaY-Nafion [1]. Recently we developed a new concept of self-humidifying membrane: confined zeolite-Nafion composite membrane [5]. The fuel cell with confined HZSM-5-Nafion composite membrane can deliver power density of 572 mW/cm^2 at 50^oC without humidification and tolerate high temperature operation under dry conditions. Here we prepared double-layered zeolite-Nafion composite membranes in order to further improve cell performance.

Experimental

Silicalite-1 and HZSM-5 films with different thickness were grown on micro-structured stainless steel mesh (SSM) via hydrothermal process. Confined zeolite-Nafion composite membranes were prepared by casting Nafion resin suspension in water and 1,2-propanediol into SSM with zeolite films, followed by hot-pressing between two pieces of porous stainless steels with Pt/C catalyst layers at 130^oC under 10 MPa pressure for 3 min to prepare membrane-electrode assembly.

Results and discussion

Figure 1 shows clearly the double-layered structure of SSM with HZSM-5-silicalite-1 film. Thicknesses of HZSM-5 and silicalite-1 films are 5 and 7 micrometers, respectively. EDX result verifies ultra-low Si/Al ratio (12.4) of HZSM-5 film, which benefits proton transport through HZSM-5 film. Figure 2 presents MPD vs. Temp. curves of the fuel cell with different electrolyte membranes without humidification. The fuel cell with double-layered HZSM-5(5μm)-silicalite-1(7μm)-Nafion gives much higher performances compared to other fuel cells from 25^oC to 100^oC. It outputs the highest performance at 50^oC and still gives a high OCV of 0.94 V at 100^oC, whereas OCV of the fuel cell with single-layered HZSM-5(7μm)-Nafion decreased obviously from 0.94 V at 50^oC to 0.64 V at 100^oC.

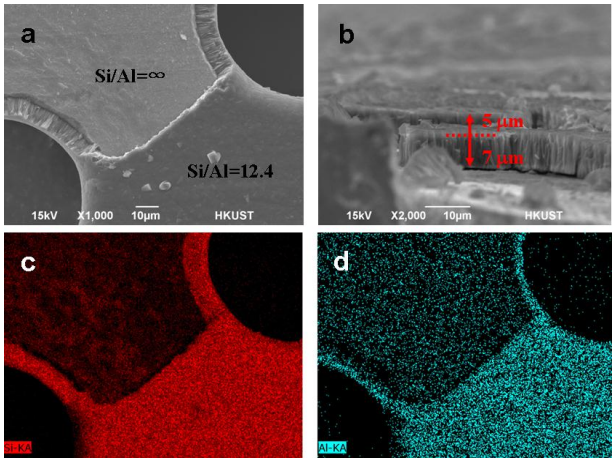

Figure 1. (a, b) SEM and (c, d) EDX mapping images of SSM with HZSM-5-silicalite-1 film

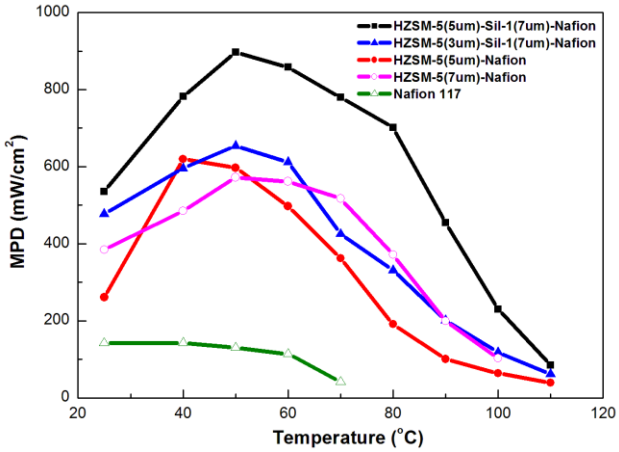

Figure 2. MPD comparison of the fuel cells with different electrolyte membranes at different operation temperature without humidification (H_2 and O_2 flow rate: 10 ml/min)

Conclusions

Confined HZSM-5-silicalite-1-Nafion composite membranes are prepared and applied as electrolyte membranes of self-humidifying fuel cell. Compared to HZSM-5-Nafion, double-layered zeolites improved remarkably OCV and MPD values of the fuel cell, which can be attributed to better balance between water-remaining ability and fuel crossover.

Acknowledgements

The authors gratefully acknowledge financial supports from the Hong Kong Research Grant Council and Innovation & Technology Fund.

References

[1] Son, D.H., Sharma, R.K., Shul, Y.G., Kim, H., Preparation of Pt/zeolite-Nafion composite membranes for self-humidifying polymer electrolyte fuel cells, Journal of Power Sources, 165 (2007), 733-738

[2] Lee, H.K., Kim, J.I., Park, J.H., Lee, T.H., A study on self-humidifying PEMFC using Pt-ZrP-Nafion composite membrane, Electrochimica Acta, 50 (2004), 761-768

[3] Wang, L., Xing, D.M., Liu, Y.H., Cai, Y.H., Shao, Z.G., Zhai, Y.F., Zhong, H.X., Yi, B.L., Zhang, H.M., Pt/SiO_2 catalyst as an addition to Nafion/PTFE self-humidifying composite membrane, Journal of Power Sources, 161 (2006) 61-67

[4] Zhang, W., Li, M.K.S., Yue, P.L., Gao, P., Exfoliated Pt-clay/Nafion nanocomposite membrane for self-humidifying polymer electrolyte fuel cells, Langmuir, 24 (2008) 2663-2670

[5] Han, W., Yeung, K.L., Confined zeolite-Nafion composite membrane for self-humidifying micro fuel cell, Chemical Communications, Submitted.

Synthesis of Nanoporous Co_3O_4 for VOC gas Sensors Applications

Nguyen Hoa,[a] Sherif A El-Safty*[a,b]
[(a)]*National Institute for Materials Science, Exploratory Materials Research Laboratory for Energy and Environment, 1-2-1 Sengen, Tsukuba, Ibaraki, 305-0047, Japan.*
[(b)] *Graduate School for Science and Engineering, Waseda University, 3-4-1 Okubo, Shinjuku-ku, Tokyo 169-8555, Japan.*
Email: Sherif.elsafty@nims.go.jp; Sherif@aoni.waseda.jp

Introduction

Air pollution due to the presence of volatile organic compounds (VOCs), such as benzene, acetone, and toluene, are very dangerous because of their toxicity and extreme flammability. For instance, breathing low levels of benzene can cause drowsiness, dizziness, rapid heart rate, headaches, tremors, confusion, and unconsciousness. Therefore the development of gas sensors for early detection of flammable and/or toxic gases is necessary.

Among materials used for gas sensors applications, cobalts oxide (Co_3O_4), a p-type semiconductor having a direct band gap of ~2 eV is one of the most interesting prospects due to its high response. For instance, Zhang et al. reported on the use of Co_3O_4 loaded on SnO_2 for ethanol and acetone detection. Patil et al. reported that Co_3O_4 nanorods showed high sensitivity and fast response to CO. Using the nanoporous Co_3O_4 for gas sensor applications is one of the key factors to improve the sensor performance.

In this work, we introduce the synthesis and use of high crystalline nanoporous Co_3O_4 for effective acetone, benzene and ethanol gas sensors application. The nanoporous Co_3O_4 are synthesized via a facile hydrothermal method, using cobalt chloride and urea as precursors. This simple synthesis method allows fabricating large yield of products with different morphologies and meets the growing demand for mass production of nanostructured materials required in gas sensor technology. The gas-sensing properties of synthesized nanorods are investigated to volatile organic compounds (VOCs). The nanoporous Co_3O_4 have been found to be effective in the detection of acetone. In addition, the effects of carrier gases (reference) on the sensing properties of Co_3O_4 are also studied to clarify the sensing mechanisms of sensors.

Experimental

The nanostructured Co_3O_4 was fabricated by hydrothermal method. In typical synthesis, 0.01 mol $CoCl_2.6H_2O$ and different amount of urea were dissolved in 50 ml distilled water to obtain a clear solution. Thereafter, the solution was transferred into a Teflon-lined autoclave of 100 ml in volume for hydrothermal process at temperature of 180^oC for 16 hr. After cooling down to room temperature, the pink precipitate was collected and rinsed several times with distilled water and ethanol before being dried at 45^oC. Finally, the nanoporous Co_3O_4 were formed as black powders by calcining pink product at 500^oC in air for 8 hr.

The sensors were fabricated using thick film techniques. The gas sensing properties of nanoporous Co_3O_4 were tested to acetone, benzene, and ethanol. The desired concentration of test gases (VOCs) was introduced into the sensing chamber for 5 min then switched to dry air for recovery. The sensor response is defined as S=100×(R-Ro)/Ro (in the case resistance increases). R and Ro is sensor resistance in the present of test gas and carrier gas, respectively.

Results and discussion

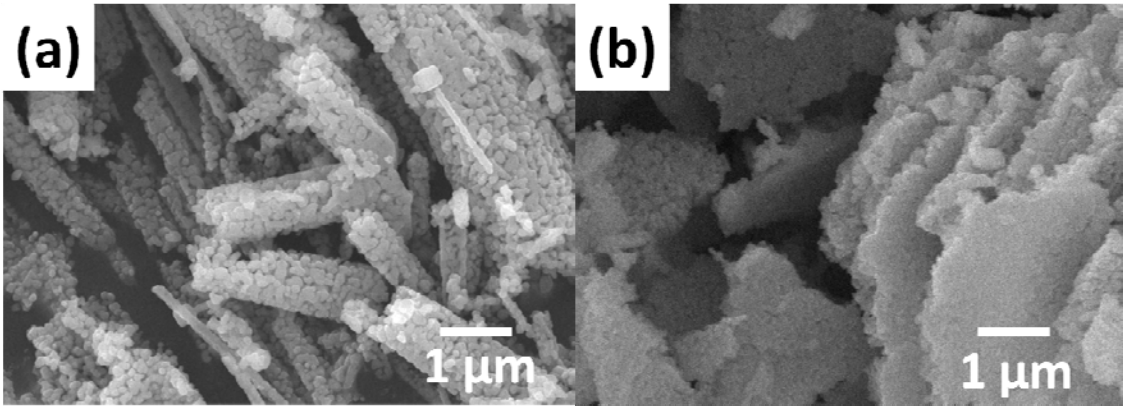

Fig. 1. FESEM images of nanoporous Co_3O_4 fabricated using different amount of urea: (a) 0.02 mol, (b) 0.04 mol.

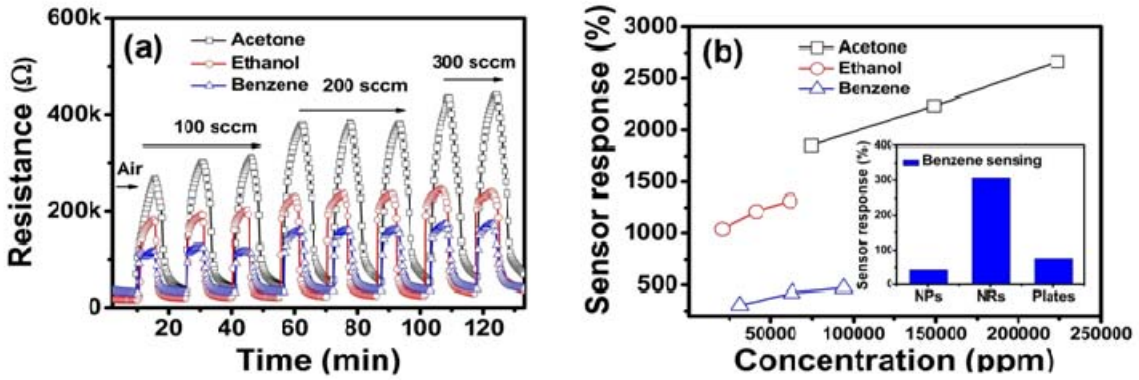

Fig. 2. (a) the change in sensor resistance upon exposure to different concentration of Acetone, Ethanol, Benzene. (b) Sensor response as a function of gases concentration; ((b)-inset) the response to benzene of nanoparticles (NPs), meso-macro porous nanorods (NRs) and porous plates (plates).

Conclusions

Large yields of crystalline nanoporous Co_3O_4 have been successfully synthesized using the hydrothermal method, and without using any surfactants or structure-directing agents for gas sensor applications. The fabrication fulfills the growing demand for a simple, low-cost, mass-producted and controllable synthesis of nanoporous Co_3O_4 for thick-film gas sensors technology. The synthesized nanoporous Co_3O_4 were found to be effective in the detection of acetone, benzene, and ethanol. It has good stability, high sensitivity, and fast response and recovery time.

Acknowledgements

We acknowledge the Japan Society for the Promotion of Science (JSPS) for financial support (Grant No/ P09606).

References

[1] Pearton S. J.; Ren F.; Wang Y. L.; Chu B.H.; Chen K.H.; Chang C.Y.; Lim W.; Lin J.; Norton D.P.; Prog. Mater. Sci., 2010, 55, 1-59.
[2] Patil L. A.; Shinde M. D.; Bari A. R.; Deo V.V., Sens. Actuators B 2009, 143, 270-277.

Organic Dyes Removal from Water by Mesopore Cage Adsorbents

Sherif A. El-Safty[1,2]*, Md. Rabiul Awual[1], M. Khodary[1]
[1] *National Institute for Materials Science (NIMS), 1-2-1 Sengen, Tsukuba-shi, Ibaraki-ken 305-0047, Japan.* [2] *Graduate School for Science and Engineering, Waseda University, 3-4-1 Okubo, Shinjuku-ku, Tokyo 169-8555, Japan. E-Mail: sherif.elsafty@nims.go.jp and sherif@aoni.waseda.jp*

Introduction

Recently, nanoscience and nanotechnology have gained considerable public interest due to the needs and applications of nanomaterials in all areas of human endeavor, including industry, agriculture, business, medicine, and public health [1]. Dyes are group of substances applied widely in industries, including textile preparation and pharmaceutical development [2]. The release of dyes without purification can pollute the environment [3]. Several methods have been proposed for dyes removal but adsorption by solid adsorbents shows promise and the most attractive and efficient methods for purification and separation of trace organic contaminants.

We present a simple pathway synthesis of cubically ordered mesocage *Im3m* aluminosilica membranes (disc-like monoliths measuring 1.2 mm in width and ~12 mm in length). The casting of microemulsion liquid crystalline phases of triblock copolymer F108 ($EO_{141}PO_{44}EO_{141}$) surfactant assists significantly in the fabrication of well-defined mesostructures with condensed and rigid disc-like membranes. Functional acid sites, multidirectional (3D) pore connectivity, high-aluminum content, and ordering structures of aluminosilica adsorbents exhibit efficient removal of organic dyes such as N'-disalicylidene-4,5-diamino-6-hydroxy-2-mercaptopyrimidine (H_2DSPy), to a maximum of 100% within a short period from aqueous solution. However, this approach permits easy-to-use removal assays of organic compounds, and portable and reusable chemical adsorbents without any mesostructural damage even under rigorous chemical treatment for a number of reuse/cycles (Scheme 1).

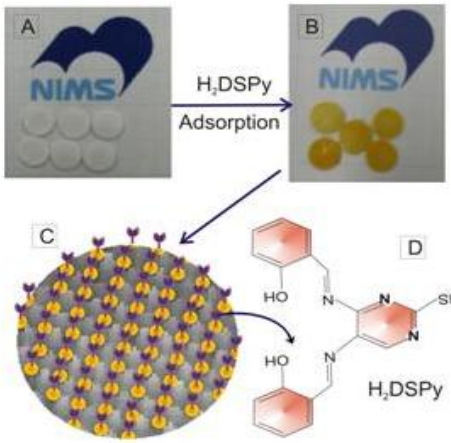

Scheme 1. Aluminosilica adsorbents before (A) after (B) the adsorption of H_2DSPy dye (D) inside the mesocage cavity and onto pore surfaces of 3D cubic Pm3n structures (C) 3D TEM image and was recorded with disc-like monolithic adsorbents.

Experimental

Synthesis of mesopore case adsorbents and H_2DSPy dye

Synthesis process of cubic Im3m aluminosilica monoliths (i.e., disc-like membrane), such as at the Si/Al ratio of 9.0 (mole/mole) and at F108/ Tetramethylorthosilicate (TMOS) ratio of 0.8 (w/w), the precursor solution was stirred for 30 min to form a homogenous sol-gel solution. “Disc-like” membranes were gently dried at room temperature for 2 h and subsequently allowed to stand in a tightly closed ingot for 1 day to complete the drying process. Organic moieties were removed by calcination at 550 °C under air for 5 h.

The H_2DSPy dye was prepared by dissolving 25 mmol (2.372 gm) of 4,5-diamino-6-hydroxy-2-mercaptopyrimidine in 20 ml of DMF and stirred for 3 h. After that 50 mmol (6.106 ml) of salicylaldehyde was mixed in 150 ml of ethanol. The 4,5-diamino-6-hydroxy-2-mercaptopyrimidine solution was added to the salicylaldehyde solution and refluxed for 2 h.

The yellow precipitate was filtered and washed with small amount of ethanol and then dried at 60 ^{o}C. The purity of the (H_2DSPy) dye product was analyzed by CHNS elemental analyses.

Results and discussion

Characterization of cage cubic Im3m aluminosilica disc-like monoliths

The characterization of mesopore cage adsorbents were performed by using several instruments such as X-ray diffraction (XRD) patterns, N_2 adsorption isotherms, NMR spectra, HRTEM images. N_2 adsorption isotherms (Fig. 1*)* of aluminosilica disc-like monoliths were consistent with those of cage mesoporous materials [4]. Adsorption branches significantly shifted toward a lower relative pressure (P/P_o) with the increase in aluminum content. Cage aluminosilica monoliths observed the appreciable textural parameters of specific surface area (S_{BET}), mesopore volume (Vp), and tunable pore diameters of 8.9–10 nm. Increase in the spherical cavity of aluminosilicas may be attributed to the instability of aluminum in the framework of disc-like monoliths.

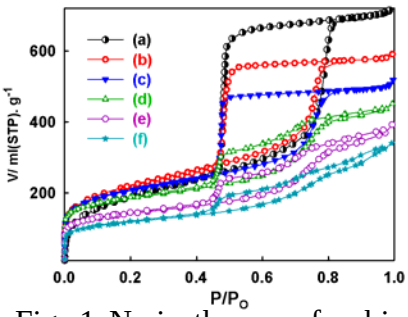

Fig. 1 N_2 isotherms of cubic Im3m aluminosilica disc-like monoliths with Si/Al ratios of 19 (a), 9.0 (b), 4.0 (c), 2.33 (d), 1.5 (e) and 1 (f).

Removal of H_2DSPy dye onto monolithic adsorbents

The successful design of condensed and rigid (disc-like) monoliths with active acid sites, multidirectional (3D) pore connectivity, well-defined cage cavities, and mechanical stability is promising for easy-to-use adsorbents for H_2DSPy dye within a short period. In this study, we performed a series of batch contact-time experiments to define and evaluate systematically the suitable conditions of H_2DSPy dye adsorption on the mesocage adsorbents. Concentration of adsorbate solutes was continuously detected and monitored using UV–vis absorption at 369 nm as a function of time (Fig. 2) and under specific conditions (i.e., temperature, shaking rate, and adsorbate concentration). Scheme 1B shows that the uniformity of pore surface not only leads to a facile accessibility of H_2DSPy dye to the cavity sites but likewise increases the homogeneous transport and diffusion of dye molecules to the binding sites of nano-adsorbent surfaces.

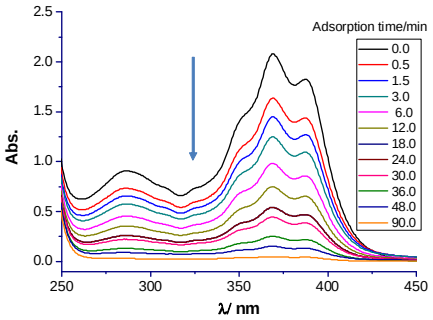

Fig. 2 Time sequence of decrease in adsorption of [0.5 mmol L^{-1}] H_2DSPy using 0.3 gm cubic Im3m disc-like aluminosilica monoliths at 40 ^{o}C.

Conclusions

The fabricated cubic Im3m mesocages with uniform entrance and large cavity pores of aluminosilicates as highly promising candidates for the colorimetric monitoring of organic dyes in an aqueous solution. The adsorbents are reversible, reusable for a number of reuse/cycles, and able to use long time without any noticeable deterioration.

References

[1] El-Safty, S. A., Prabhakaran, D., Kiyozumi, Y., Mizukami, F., Nanoscale membrane strips for benign sensing of Hg^{II} ions: A route to commercial waste treatments, Advanced Functional Materials, 18 (2008) 1739-1750.
[2] Bechtold, T., Ali, A. M., Mussak, R., Natural dyes for textile dyeing: A comparison of methods to assess the quality of Canadian golden rod plant material, Dyes and Pigments, 75 (2007) 287-293.
[3] Alaton, I. A., Gursoy, B. H., Schmidt, J. E., Advanced oxidation of acid and reactive dyes: Effect of Fenton treatment on aerobic, anoxic and anaerobic processes, Dyes and Pigments 78 (2008) 117-130.
[4] El-Safty, S., Shahat, A., Ogawa, K., Hanaoka, T., Highly ordered, thermally/hydrothermally stable cubic Ia3d aluminosilica monoliths with low silica in frameworks, Micro. Meso. Mater., 138 (2011) 51–62.

Design of Metal Organic Frameworks (MOF) for the Encapsulation, Transport and Release of Biological Molecules: a QSAR approach and Experiments

Cédric Gaudin[1], Emilie Ivanoff[1,3], Denise Cuhna[2], Patricia Horcajada[2], Christian Serre[2], Sabine Devautour-Vinot[1], Gwénaël Chevé[3], Aziz Yasri[3], Olivier Loget[3], Guillaume Maurin[1].
[1]*Institut Charles Gerhardt Montpellier, UMR 5253 CNRS, Université Montpellier 2, France*
[2]*Institut Lavoisier, Université de Versailles St Quentin, Versailles, France*
[3]*Oribase Pharma, Montpellier, France*
guillaume.maurin@univ-montp2.fr

Introduction

Metal Organic Framework materials (MOF) are among the most promising materials for use in processes such as gas-adsorption, storage, separation and catalysis [1]. A new and exciting application for MOFs lies in the area of drug-delivery [2], where the MOF would act as a host material to encapsulate, transport and further release the drug at the target site. Until now, polymeric or mesoporous silica have been proposed for this task, and their use allows one to avoid several problems, such as degradation, high protein-binding, barrier crossing, low solubility/stability in biological media. However, these materials do not possess the structural and chemical versatility of the MOF structures, which would allow the fine-tuning of these properties and thus the optimization of the framework for the encapsulation and release of a given drug molecule. This project exploits computational techniques in tandem with experiments to first design the required features of MOF materials for optimizing their encapsulation properties. Experiments were first realized by incorporating caffeine, an amphiphilic model drug (liporeductor) into the flexible functionalized iron terephthalate MIL-88B MOFs. Quantitative Structure Activity Relationships (QSAR), which has already been proven to be successful in the design of novel drug molecules has been further used to correlate the drug encapsulation rate to the properties of the MOF systems.

Methodology

The QSAR establishes quantitative relationships between a target property, here the drug encapsulation rate, and appropriate descriptors that characterize the MOFs. The QSAR modeling workflow can be divided into three major steps: (*i*) analysis of data (calculation and selection of molecular descriptors), (*ii*) model building, and (*iii*) model validation. Molecular descriptors encode the feature of the materials, and correspond to chemical, electronic and physical descriptions of the materials. Molecular descriptors were calculated using the MOE package [3]. The non-informative descriptors that contain only small variation across the data set were then rejected. The best subset of molecular descriptors was further selected using (a) genetic algorithms and (b) forward-selection procedure, implemented both in the Weka [4] code. QSAR models were built using the multi-linear regression (MLR), which relates property of the MOF with the selected descriptors. Models were described with two statistical parameters, the coefficient of cross-validation Q^2 and the root mean square error *RMSE* value. The predictability and robustness of the models were verified using a cross-validation with leave-one-out (LOO) and *Y*-scrambling methods [5]. In this last test, the dependent-variable vector, *Y*-vector, is randomly shuffled, and new QSAR random models were developed.

Results and discussion

Prior to the computational effort, experimental data were collected on a library of 10 iron terephthalates MIL-88B bearing different functional groups on the aromatic ring and their caffeine encapsulation rate. 296 molecular descriptors were calculated for each MIL-88B. QSAR model was further built using a set of two descriptors. A LOO cross validation

procedure was performed. Results showed that the validation accuracy expressed as Q^2 equals 0.71 and the estimation error of the model *RMSE is* 2.1. *Y*-randomization was carried out, and no significant random models were retrieved, proving the robustness of our QSAR model (figure 1).

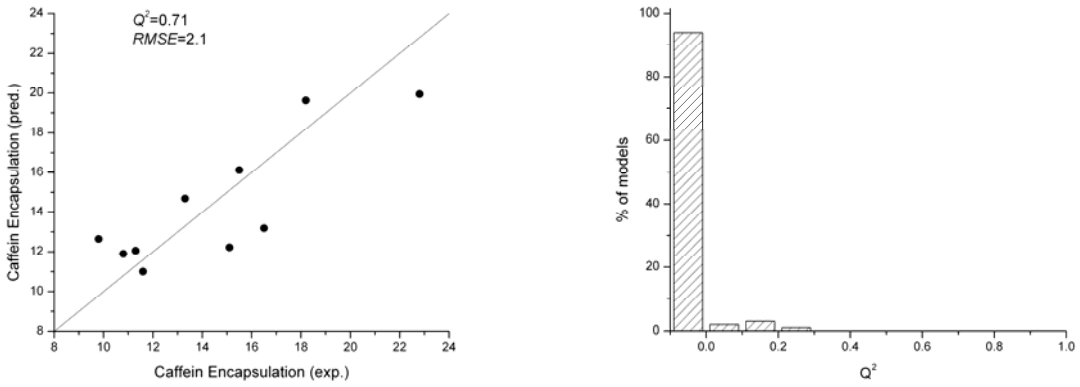

(a) *(b)*

Figure 1: The validation of the QSAR model using LOO cross-validation (a) and Y-scrambling (b). (a) Plot of experimental versus predicted caffeine encapsulation of our QSAR model. (b) Validation plot based on 100 random models, represented by their prediction performance Q^2.

As mentioned above, the so-obtained model involves two descriptors: lip_don and vsurf_wp1 corresponding to the number of hydrogen donor groups and the volume delimited by the polar functions respectively, both present on the organic part of the MOFs. Consistent with this observation, the functionalized MIL-88B forms that lead to the highest encapsulation rate contain either amino or hydroxyl grafted functions and a large volume delimited by the polar functions.

Conclusions

This complete investigation allowed the prediction of the most optimal chemical features of the flexible MIL-88B materials for combining both an efficient uptake of a model biomolecule, i.e. caffeine. A further step will consist of validating this conclusion by the synthesis of novel functionalized MIL-88B forms that contain more polar functions grafted on the organic linker. This additional data will further help us to refine the QSAR models. Future work will concentrate on probing the influence of the topology of such nanovector on the encapsulation rate obtained for caffeine or other hydrophilic/hydrophobic drugs, by considering a large variety of rigid MOFs.

Acknowledgements

The project is funded by an EU project ERC-2007-209241-"BioMOFs" and by the Region Languedoc-Roussillon.

References

[1] G. Férey, *Chem. Soc. Revs.*, 37, 191-214 **(2008)**
[2] P. Horcajada *et al*., *Nature Mater.*, 7, 172-178 (**2010**)
[3] Molecular Operationg Environment Chemical Computing Group: Montreal, Canada. http://www.chemcomp.com/
[4] I.H. Witten, E. Frank, *Data Mining: Practical Machine Learning Tools and Techniques with Java Implementations*; Morgan Kaufman: San Francisco (**2000**)
[5] S. a. E. L Wold, *Statistical Validation of QSAR Results. In Chemometrics Methods in Molecular Design*, VCH: Weinheim, 309−318 (**1995**)

High-throughput characterization of porous materials with *infra*SORB

P. Wollmann[(a)], M. Leistner[(b)], O. Throl[(a)], W. Grählert[(b)], F. Dreisbach[(c)], and S. Kaskel[(a)(b)*]
[(a)] *Dresden University of Technology, Department of Inorganic Chemistry*
[(b)] *Fraunhofer Institute for Material and Beam Technology,Department CVD/thin film techn.*
[(c)] *Rubotherm GmbH, Bochum/Germany*
[*] *Stefan.kaskel@chemie.tu-dresden.de*

Introduction

The discovery of novel porous materials is an essential element in the development of materials for energy and gas storage, emission reduction and carbon dioxide separation. High-throughput screening is nowadays an established tool for product control of known materials, the discovery of novel materials [1] and catalyst characterization [2], some automated synthesis techniques are commercially available. The discovery of novel porous frameworks like zeolites [3, 4] focuses on automated X-ray diffraction and the identification of new phases [5]. However, structural analysis from powder patterns is still a bottle neck in the discovery of new materials.

Together with new fields of application for porous materials, a special need for a fast high-throughput adsorption characterization tool arises in laboratories and industry. Today, volumetric and gravimetric instruments (for determining porosity) available on the market offer a lower number of multiple ports and the measurement often takes several hours. Thus, the intention was to develop a simple tool with a multiple sample interface. The room-temperature operated *infraSORB* instrument is based on adsorption heat detection for rapid screening of specific surface area and porosity [6]. It allows the fast screening of 12 samples within 5 minutes. Beside the investigation of new materials the instrument can also be used for product control. The advantages of the setup are an enormous time benefit in connection with an easy-to-use interface and a sufficient accuracy. Measurements and applications of the *infra**SORB*** instrument on different porous materials (zeolites, activated carbon, MOFs) will be presented.

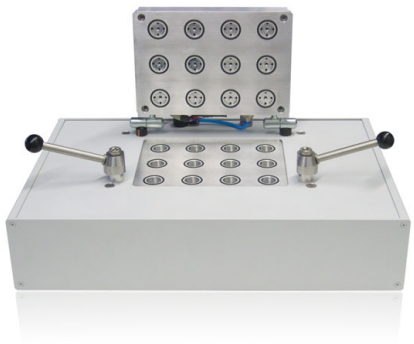

*infra**SORB** instrument with 12-port interface*

Experimental

Table 1. measurement characteristics.

sensor type	micropyrometer
adsorptive gas	room temperature adsorption (i.e. butane, CO_2)

purge gas	nitrogen
measurement duration	< 5 minutes
recorded signal	V(t), temperature depended

The recorded voltage signal is analyzed by an automated software algorithm, thereby the last step is a time-based integration. Mass values are included in the processed data to avoid influences on the result. Hence, the correlation of overall adsorption capacity and surface area to the relation of signal to gram is determined.

Results and discussion

For instrument characterization activated carbons were used as adsorbents due to their broad surface range. Butane was chosen adsorptive gas (non-polar, fits to activated carbon). Figure 1 show the results of the correlation of the integrated signal to surface area values.

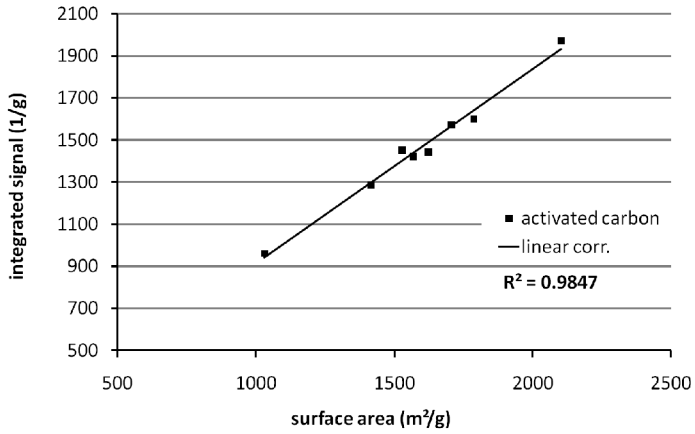

Figure 1. Correlation of integrated signal and surface area.

Furthermore, the basic idea was proved by correlation of integrated signal to gravimetrically determined butane capacities (data not shown), resulted in a quality factor (R^2) above 0.98.

References

[1] McFarland, E.W., Weinberg, W.H., *Combinatorial approaches to materials discovery*, Trends in Biotechnology, 17 (1999), 107-115

[2] Thomson, S., Hoffmann, C., Ruthe, S., Schmidt, H.-W., Schüth, F., *The development of a high-throughput reactor for the catalytic screening of three phase reactions*, Applied Catalysis A: Genreal, 220 (2001), 253-264

[3] Jiang, J., Yu, J., Corma, A., *Extra-Large Pore Zeolithes: Bridging the gap between Micro and Mesoporous structures*, Angew. Chem. Int. Ed. 49 (2010), 3120.

[4] Cundy, C.S., Cox, P.A., *The hydrothermal synthesis of zeolithes: History and development from the earliest days to the present time*, Chem. Rev., 103 (2003), 663.

[5] Stock, N., Hilbrandt, N., Choi, K., Bein, T., *High-throughput strategies for the hydrothermal synthesis of zeolithes and related materials*, Studies in Surface Science and Catalysis, 135 (2001), 550-557

[6] Kaskel, S., Wollmann, P., Leistner M., *Method and Device for determining the adsorption of a gas on materials*, patent, DE 2009-102009031764 / WO 2010-DE756

Photocatalytic CO_2 Activation into CH_4 over Titania Dispersed Materials – Catalyst Screening and Mechanistic Evaluation

Chieh-Chao Yang[a], Jarian Vernimmen[b], Bart van der Linden[c], Vera Meynen[b], Pegie Cool[b], Guido Mul[a]

[a] *PhotoCatalytic Synthesis Group, IMPACT Institute, University of Twente*
[b] *Laboratory of Adsorption and Catalysis, University of Antwerp*
[c] *Catalysis Engineering, Chemical Engineering Department , Delft University of Technology*

email: c.yang@utwente.nl

Introduction

Artificial photosynthesis is a promising technology for energy-to-fuel conversion, and to diminish emissions of the greenhouse gas CO_2. Different semiconductors, porous materials with isolated metal centers, and Ti-nanotubes were tested for activity in the target reaction.[1-3]. Usually methane is observed as the main product in gas phase conditions. However, it is difficult to compare activity data reported in the literature, since usually activity is determined under different experimental conditions. In this presentation we will present a screening facility allowing a fair comparison of various catalytic formulations. Furthermore, we will evaluate the role of possible intermediates in the formation of methane over the most active catalyst, Ti-SBA-15.

Experimental

All the illumination experiments were carried out in a combinatorial photoreactor system, consisting of a set of multi-batch reactors connected to a compact gas chromatograph, equipped with a fully automated sampling program. The set-up enables photocatalyst screening up to 12 catalysts, quick analysis (within 80 sec) of each reactor, and a fair comparison of activity. The applied catalytic activity testing system is shown in Fig. 1.

Figure 1. Combinatorial photoreactors applied for gas phase CO_2 reduction.

In this study, we conducted illumination tests with various starting gas compositions (CO, CO_2, H_2O or H_2). Other possible byproducts of CO_2 reduction, such as CH_3OH, C_2H_2, C_2H_4 and C_2H_6, were also used as initial reactants, in order to demonstrate if any further conversion of these species leads to CH_4.

Results and discussion

A first screening of catalyst formulations indicated that titania dispersed over SBA-15 (Ti-SBA-15) showed the highest production rate of CH_4 in a mixture of CO_2 and H_2O, as compared to other titania based catalysts, and in addition also C_2 products were found. Over this catalyst, the highest rate of CH_4 and C_2 formation was observed in a mixture of CO and

H_2O, followed by CO and H_2, CO_2 and H_2O, and the lowest rate was obtained in CO_2 and H_2. The results are displayed in Fig. 2.

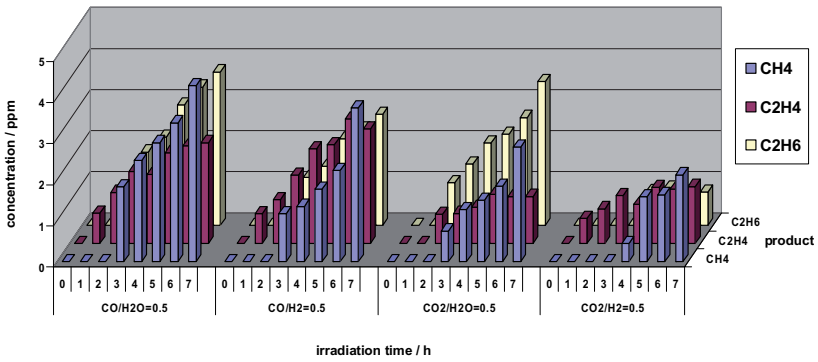

Figure 2. Product distribution of Ti-SBA-15 in various conditions after 7h-illumination.

Oxidation of alkanes and alkenes into CO_2 was also observed during photo-illumination. However, the presence of H_2O suppresses this backward reaction, resulting in enhanced CH_4 formation. The results will be discussed in relation to mechanistic propositions described in the literature, including CO hydrogenation [4], and a possible role of carbonaceous deposits [5]. Also possible reasons for the back reaction of hydrocarbons with photoactivated H_2O will be addressed.

Conclusions

The highest production of CH_4 was obtained over a Ti-SBA-15 catalyst, and in particular starting from a mixture of CO and H_2O. H_2 activation is not as efficient as water activation over Ti-SBA-15.

Acknowledgements

This work was supported by ACTS (NWO, the Netherlands), in the framework of an NSC-NWO project (Project Number NSC-97-2911-I-002-002).

References

[1] M. Anpo, H. Yamashita, K. Ikeue, Y. Fujii, S.G. Zhang, Y. Ichihashi, D.R. Park, Y. Suzuki, K. Koyano, T. Tatsumi, Photocatalytic reduction of CO_2 with H_2O on Ti-MCM-41 and Ti-MCM-48 mesoporous zeolite catalysts, Catalysis Today, 44 (1998) 327-332.

[2] I.H. Tseng, J.C.S. Wu, H.Y. Chou, Effects of sol-gel procedures on the photocatalysis of Cu/TiO_2 in CO_2 photoreduction, Journal of Catalysis, 221 (2004) 432-440.

[3] O.K. Varghese, M. Paulose, T.J. LaTempa, C.A. Grimes, High-Rate Solar Photocatalytic Conversion of CO_2 and Water Vapor to Hydrocarbon Fuels, Nano Letters, 9 (2009) 731-737.

[4] F. Saladin, L. Forss, I. Kamber, Photosynthesis of CH_4 at a TiO_2 surface from gaseous H_2O and CO_2, Journal of the Chemical Society-Chemical Communications, (1995) 533-534.

[5] H. Yamashita, A. Shiga, S. Kawasaki, Y. Ichihashi, S. Ehara, M. Anpo, Photocatalytic synthesis of CH_4 and CH_3OH from CO_2 and H_2O on highly dispersed active titanium-oxide catalysts, Energy Conversion and Management, 36 (1995) 617-620.

Multufunctional Materials with Tailored Properties, Tuneable Reactivity and Compatibility for Gas Sensing Application

S. Thomas,[1] Ph. Bazin,[1] D. Robbes,[2] V. de Waele,[3] S. Mintova[1]

[1]*Laboratoire Catalyse et Spectrochimie (LCS), ENSICAEN, Université de Caen-CNRS, 6 Bd. Maréchal Juin, 14050 Caen, France*
[2]*GREYC UMR 6072, ENSICAEN, Université de Caen, CNRS, 6 Bd. Maréchal Juin, 14050 Caen, France*
[3]*Laboratoire de Spectrochimie Infrarouge et Raman (LASIR), CNRS, Universite de Lille I, 59655 Villeneuve d'Ascq Cedex, France*

Introduction

The combination of micro-to-meso-porosity with semiconductivity in the new materials opens up more applications such as electronic and optoelectronic devices, electrocatalysis, electroanalysis and sensors. The completely controlled structures of the porous materials make them attractive as true shape-selective compounds. Besides, a number of novel applications depend not only on the control of pore structure and intra-porous chemistry, but also on the ability to control the external morphology and surface properties, for example in thin films and layers for separations or in the design of sensor devices. In the case of highly reactive chemical sensors, the incorporation of different metals is expected not only to change their hydrophilicity but also to lead to formation of chemical sensors with enhance selective towards gases such as CO, NO_x, O_2, etc.

Metal clusters confined in porous materials have been extensively studied, however, the size control and location of the clusters seem to be difficult especially when the porous nanoparticles are store in suspensions. The dimension of internal voids in the microporous compounds is in the range of 5-12 Å, which is expected to be the upper limit of size of the clusters that can be stabilized in the hosts without crystalline destruction. Besides, the metal clusters of nanometer sizes above the limit of the pores of the microporous host can only be localized at the surfaces.

The aim of this work is to develop a synthetic strategies for generation of structurally defined, functionalized microporous crystals (LTL, BEA and GIS-type zeolites) with metal and semiconductor (Pt, Pd, Cu, CdS) clusters for further assembly in thin films for sensor application. The metal-containing zeolite based sensors are exposed to different analytes such as alcohols, CO, alkenes and water. The focus is on enhancement of reactivity and selectivity of the chemical sensors toward CO in the presence of hydrocarbons and water and vice versa.

Experimental

Stable coating suspensions of discrete nanosized zeolites (GIS, LTL, BEA) from colloidal precursor suspensions under hydrothermal synthesis conditions are prepared. The crystalline samples were loaded with Pt, Pd, Cd and Cu by ion exchange treatment. The metal clusters in the nanosized zeolites are formed by radiolysis of the suspensions using the gamma ray emitted from a ^{60}Co panoramic source. Finally, the stabilized metal containing nanoparticles

are assembled in mono-to-multi-layered films by chemical binding and spin-patterned-deposition on sensors devices (QCM) and silicon wafers.

Results and Discussion

The stability and crystalline structure of metal containing nanosized zeolites before and after gamma irradiation are confirmed with DLS and XRD measurements. It is found that the particle size distribution in the suspensions did not change at ambient conditions for more than a year; a monomodal particle size distribution for the GIS, LTL, BEA- type zeolite crystals in the suspensions with a mean diameter smaller than 80 nm is revealed.

The coating suspensions of metal containing zeolites were deposited in thin films on QCM and silicon wafers. The structural features of the films prior exposing to various gases are studied by GI-XRD, SEM and ellipsometry. The Bragg peaks of both the zeolites and the metal clusters are present; the measurements at different penetration depths reveal that the clusters are homogeneously distributed along the film thickness and have size smaller than 1.8 nm.

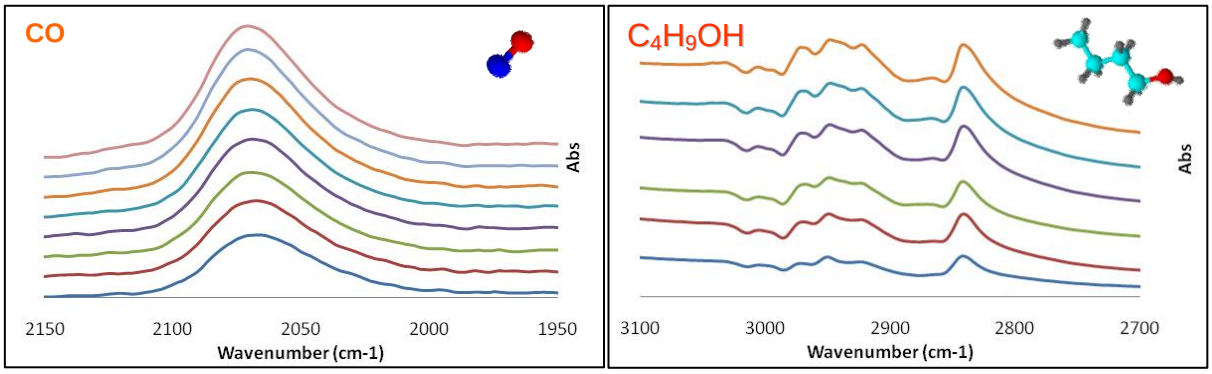

Figure 1. Simultaneous sensing of CO (3 -100 ppm) and C_4H_9OH (0.1-1.0%) in the presence of water on Pt-Beta film: high selectivity at low concentration, fast response, and reversibility.

The thin films deposited on the sensor devices are exposed to different concentrations of gases. The sensing response and reversibility of the sensors toward single gas or a mixture in the presence of water are investigated at 25, 50 and 75 °C at various low concentrations. As can be seen (Figure 1), the metal-containing films are sensitive to low concentrations of CO and hyrocarbons, moreover the presence of hydrocarbons does not change the sensitivity of the films towards CO and vice versa. The saturation for each concentration of CO and hydrocarbons takes less than a minute, which is a function of the thickness of the films, size of the zeolite and location of the metal clusters. The adsorption or co-adsorption isotherms were modelled by Langmuir equation, and heats of adsorption were calculated.

The microporous crystals with nanometer dimensions, variable pore architecture and chemical composition (hydrophilic/hydrophobic) containing metal clusters (Pt, Pd, Cu, CdS) demonstrated enhanced sensitivity for different analytes ($C_nH_{2n+1}OH$, C_nH_{2n+2}, CO, CH_3CN). The sensor selectivity towards alcohol and alkenes in the presence of CO is increased, while the presence of water does not influence on the sensing behaviour. The improved transport properties of the self-organized materials with nanosized dimensions and preferred crystal orientation are bringing a large improvement in their sensing performance.

Hierarchical nanostructured carbon with multimodal porosity as cathode catalyst support in proton exchange membrane fuel cell

Min-Sik Kim, Jong Ho Kim, Min Young Song, Dae Soo Yang, and Jong-Sung Yu*

Department of Advanced Materials Chemistry, Korea University, 208 Seochang, Jochiwon, ChungNam 339-700, Republic of Korea. E-mail: jsyu212@korea.ac.kr

Ordered hierarchical nanostructured carbon (OHNC) with ordered macroporous array interconnected with mesopores or another hierarchical nanostructured carbon (HNC) with hollow macroporous core/mesoporous shell (HCMS) were investigated as cathode catalyst supports in PEMFC. The unique structural characteristics such as large surface area and mesopore volume enable the HNCs to support high loading (i.e., 60 wt%) Pt nanoparticles with small particle size along with uniform particle dispersion. In addition, interconnected macropores-mesopores of the HNCs facilitate fast mass transport. Compared with commercial Vulcan XC carbon-supported high Pt loading catalyst, the HNCs-supported ones have demonstrated considerably improved catalytic activity toward oxygen reduction reaction and markedly enhanced PEMFC polarization performance, which is mainly contributable to fantastic support effect from the HNCs.

Introduction

Materials with multimodal pore size distribution have attracted considerable attention since they combine the benefits of high surface area micro- or mesoporosity with easily accessible diffusion pathway in macroporous networks. Different pore regimes created in a body can often provide their respective advantages unique to the corresponding porosity in the material. Recently, significant progress has been made in the synthesis of ordered meso- and macroporus carbons with nanometer precision for many fundamental and technological interests [1]. Rapidly expanding research efforts in this field have proceeded further to produce more complex hierarchical porous carbons.

Although proton exchange membrane fuel cell (PEMFC) has attracted much attention as future energy sources [2,3], one of the main challenges identified for its commericalization is the decrease of Pt usage in the catalyst layer. Catalyst support technology has been proved as an important and efficient approach to enhance the utilization of the platinum [4-7], and carbon black Vulcan XC-72 (VC) frequently used as a catalyst support for low temperature fuel cells [8]. In this work, ordered hierarchical nanostructured carbons (HNCs) with multimodal porosity were explored as a catalyst support for Pt catalyst nanoparticles in proton exchange membrane fuel cell (PEMFC).

Experimental

Ordered hierarchical nanostructured carbon (OHNC) was synthesized using ordered hierarchical nanostructured silica as sacrificial template [4]. Hollow core-mesoporous carbon (HCMSC) was also fabricated thorough nanocasting method of silica core-mesoporous shell silica template [6]. Furfuryl alcohol (FFA) was used as carbon precursor for both cases. Carbon-supported Pt nanoparticle catalysts were prepared by homogenous deposition method along with a microwave-assisted polyol process. For estimation of the electrochemical active surface area of Pt in various carbon-supported Pt catalysts, a three-electrode electrochemical cell (i.e., half-cell) was employed, and cyclic voltammetric (CV) measurements were conducted in 0.5 M H_2SO_4 at room temperature with a scan rate of 25 mV/s. For evaluation of catalytic activities toward oxygen reduction reaction (ORR) and cell polarization performance of supported Pt catalysts, single cells were constructed. Membrane electrode assembly (MEA)

with area of 6.25 cm^2 was employed to construct a single cell, which had been fabricated by hot-pressing a pretreated Nafion 112 (DuPont) sandwiched by the anode and cathode.

Results and discussion

In this study, OHNC with ordered macroporous array interconnected with mesopores and HCMS were investigated as cathode catalyst supports in PEMFC. The unique structural characteristics such as large surface area and mesopore volume enable the HNCs to support high loading (i.e., 60 wt%) Pt nanoparticles with small particle size along with uniform particle dispersion. All the supported Pt catalysts exhibit the characteristics of the Pt face-centered cubic structure. The average particle sizes were calculated from the broadening of the Pt (220) reflection as about 5.0 nm for the VC-supported Pt (60 wt%), 3.3 nm for the OHNC-supported Pt (60 wt%) and 3.1 nm for the HCMSC-supported Pt (60 wt%) using a Debye-Scherrer equation.

Electrochemical active surface area were calculated as 65 m^2/g and 68 m^2/g for Pt in the OHNC-supported Pt (60 wt%) and HCMSC-supported Pt (60 %) nanoparticles catalysts, respectively, which are much larger than that (36 m^2/g) for Pt in Pt (60 wt%)/VC, implying better utilization efficiency of Pt/HNC due to smaller Pt nanoparticles, better dispersion, and more efficient mass transport networks around the Pt nanoparticles supported on the HNCs than on the VC. Larger Pt electrochemical active surface area is expected to provide the HNC-supported Pt catalyst with higher ORR activity and improved fuel cell performance. In addition, interconnected macropores-mesopores of the HNCs facilitate fast mass transport. Compared with VC-supported high Pt loading catalyst, the HNC-supported ones have demonstrated considerably improved catalytic activity toward ORR and markedly enhanced PEMFC polarization performance, which is mainly contributable to fantastic support effect from the HNCs. Furthermore, the HNC-supported high metal loading Pt catalysts (i.e., 40 or 60 wt%) outperform the HNC-supported low metal loading Pt catalyst (i.e., 20 wt%) even at a low catalyst loading of 0.2 mg Pt/cm^2, which represents a significant breakthrough in fuel cell technology because the fabricating cost of the supported noble metal catalyst and the system weight can be reduced greatly due to the considerable decrease in the required amount of catalyst support while high fuel cell performance can be still achieved through the usage of unique catalyst support HNCs.

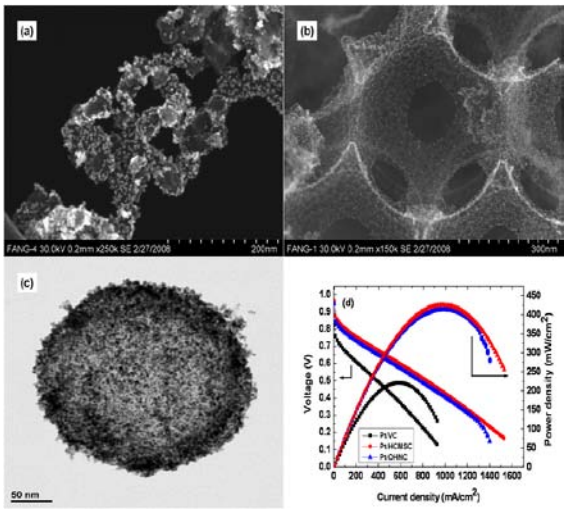

Fig.1 SEM and TEM images for Pt(60wt%)/VC (a), Pt(60wt%)/OHNC (b), Pt(60wt%)/HCMSC (c), and PEMFC polarization and power plots for the various supported Pt cathode catalysts.

References

[1] G.S. Chai, I. S. Shin and J.-S. Yu, Adv. Mater., 16 (2004) 2057.
[2] B. Fang, J. H. Kim and J.-S. Yu, Electrochem. Commun., 10 (2008) 659.
[3] J. H. Kim and J.-S. Yu, Phys. Chem. Chem. Phys. 12(2010) 15301.
[4] B. Fang, J. H. Kim, M. S. Kim and J.-S. Yu, Chem. Mater., 21 (2009) 789.
[5] B. Fang, J. H. Kim, M. S. Kim, M. W. Kim and J.-S. Yu, Phys. Chem. Chem. Phys., 11(2009)1380.
[6] B. Fang, J. H. Kim, C. G. Lee and J.-S. Yu, J. Phys. Chem. C, 112 (2008) 639.
[7] J. H. Kim, B. Fang, M.-S Kim, S. B. Yoon, T. -S. Bae, and J.-S. Yu, Electrochim. Acta, 55(2010), 7628.
[8] K. Kinoshita, Electrochemical Oxygen Technology, John Wiley & Sons, New York, 1992.

Zeolites and Related Mesoporous Materials for Multi-talented Environmental Solutions.

C. Perego, R. Bagatin, M. Tagliabue, R. Vignola.
eni S.p.A., Research Center for Unconventional Energies, v. G. Fauser 4, 28100, Novara, ITALY.
E-mail: carlo.perego@eni.com

Despite of over 25 years of intensive technological effort, sub-surface environment cleanup still remains a challenge. Traditional technologies have succeeded in reducing immediate threats of contaminated sites, while their ability to get further quality water improvements have been severely hampered by site-to-site variability, contaminant properties and inadequate design/implementation of remediation systems. Undoubted difficulties have been met in presence of heavy contaminations and within this framework, reliable and economical methodologies are still sought. Biological treatments are suitable mainly when few contaminants are present or low contaminant concentration allows microbial activities. In more complex situations, physical-chemical treatments are preferred. Among them, adsorption technologies are considered simple and effective for water treatment: the challenge is finding adsorbents able to operate in situations involving natural interfering species (*e.g.* humic substances or inorganic ions). Nanomaterials and membranes could provide a technological breakthrough in this field. Ideal adsorbents should have excellent adsorptive capacity, fast adsorption/desorption kinetics, long service life and stability under operating conditions. Activated Carbons (ACs) are typical ones. Unfortunately, ACs suffers of fire risk, pore clogging, hygroscopicity and lack of regenerability when used for the removal of Volatile Organic Compounds (VOCs).
Zeolites and related mesoporous materials have been investigated as alternative adsorbents because of their high adsorption capacity, reliable desorption performances and excellent chemical stability. In this paper we describe their use as versatile materials for environmental protection: natural zeolites for removal of heavy metals by ion exchange, hydrophobic zeolites in case of organic/oil contamination and silica-alumina mesoporous materials in case of massive organic/oil contamination. Finally, zeolite membranes are proposed for situations where use of adsorbents is improper (*i.e.* in presence of very high concentrations of mixed organic contaminants).
Natural zeolites for environmental applications are still gaining interests mainly due to their properties and significant worldwide occurrence. Specifically, their ion-exchange capacity for cations (*i.e.* ammonium and heavy metal) has been largely demonstrated.
Recently, natural zeolites and their modified forms have also been reported for removal of anions and organics from water systems. One of the purposes of this paper is updating recent research results on inorganic cation adsorption using natural zeolites as well as on modified zeolites for removal of anions and organic compounds. Application of synthetic (hydrophobic) zeolites for groundwater treatment deserves a special attention. Traditionally, remediation is performed using Pump & Treat (P&T) technology, involving extraction (*pump*) and the aboveground treatment (*treat*) of the groundwater before its re-injection. This technology needs adsorbents characterised by very fast adsorption/desorption kinetics. Use of Permeable Reactive Barriers (PRBs) represents a further innovative approach: the remediation is operated directly on the groundwater without the need of pumping on the ground. Adsorbent employed should have both high permeability and ability to front interfering effects able to reduce process efficiency. Hydrophobic zeolites have been proposed in both methodologies, as improvement to Granular Activated Carbons (GACs) exploiting both their high kinetics and selectivity. Furthermore, metal-doped zeolites have been claimed as

catalysts for organic contaminant decomposition in PRBs (*e.g.* halogenated compunds). We describe performances and advantages of using zeolites in field trials in both P&T and PRB applications: results have been obtained in gasoline refuelling stations (P&T) and in a coastal petrol refinery (PRB) respectively [1–3]. Successful experiences with zeolites have demonstrated their excellent adsorption capacity, inertness toward high molecular weight substances (*e.g.* humic acids) and inorganic cations, structure stability after prolonged immersion in water and finally, complete regenerability by simple thermal treatments. It has to be pointed out that advantage of using the same zeolite lot in subsequent cycles compensates the higher costs of these adsorbents with respect to conventional ones (*e.g.* GACs). On the other hand, zeolites, due to their structural limits, underperform in situations where huge hydrocarbon concentrations, dispersed oil and different types of heavy metals are present at the same time (*e.g.* produced waters from oil extraction). Recent works have shown that mesoporous materials can have larger adsorption capacity, good selectivity and improved recoverability for the removal of toxic compounds from aqueous solutions. The preparation of silica-based adsorbents has generated considerable interest due to their unique large specific surface area, regular pore structure and modified surface properties. Moreover, they can also be regenerated for many times after saturation. Mesoporous Silica-Alumina adsorbents (MSA) have been tested at eni laboratories for the removal of large amounts of organic compounds, (benzene and toluene at concentrations higher than 200 ppm) and dispersed oil. The need of contemporary removal of heavy metals, often present as cations and anions, and organic compounds has stimulated the synthesis of functionalised mesoporous silica, originating families of adsorbents specific for toxic cations or anions. Functional groups are anchored on the surface or inside the pores of the mesoporous silica. As a result, the adsorption capacity is partially influenced by metal-ligand concentrations. In general, removal of very high concentrations of contaminants can not be managed by adsorption. In this case, membrane separation systems could be the most practical choice.

Characterizations and applications of zeolite membranes have been extensively investigated since the mid of 1990s, owing to their potential molecular sieving action, controlled host–guest interactions and high thermal and chemical stability. The advantages of inorganic membranes compared with organic ones mainly refer to possibilities of high pressure application, steam cleaning and back flushing to remove fouling. The uniformity of zeolite micropore size is a key factor in comparison with amorphous membranes, where control of pore size distribution is difficult. There are a number of factors which control the separation properties of zeolite membranes: pore size, Si/Al-ratio and type of counter ions are among the most important. Furthermore, morphology, size and arrangement of zeolite crystals in a layer strongly affect permeation and separation characteristics, so that zeolite membrane technology, although very promising, presents difficulty in commercial diffusion.

As a conclusion, experiences presented and results obtained demonstrate that zeolites and related mesoporous materials could provide effective solutions for environmental remediation with particular reference to complex situations.

References

[1] R. Vignola, U. Cova, F. Fabiani, G. Grillo, R. Sbardellati, R. Sisto, Removal of MTBE and Hydrocarbons from Groundwater Using Specific Zeolites in Full-scale Pump & Treat and Demonstrative Permeable Reactive Barrier, Proceedings of the 4th International FEZA Conference, Paris, France (2008).

[2] R. Vignola, G. Grillo, R. Sisto, G. Capotorti, P. Cesti, M. Molinari, Synthetic Zeolites as Sorbent Material for Permeable Reactive Barriers at Industrially Contaminated Sites, Proceedings of the International Symposium on Permeable Reactive Barriers, Belfast, Northern Ireland (2004).

[3] R. Vignola, R. Bagatin, A. De Folly D'Auris, C. Flego, E. Previde Massara, M. Nalli, R. Sisto, Zeolite Performance and Longevity in a Permeable Reactive Barriers: one Year of Field Experience in a Refinery's Groundwater: Part 1 : the Performance, Micropor. Mesopor. Mater. (in press).

Adsorption of 2-methylbenzoic acid onto MCM-41 materials: a kinetic study

Daniela Aiello*, Ilaria Mirabelli, Flaviano Testa, Rosario Aiello

*Department of Chemical Engineering and Materials, CR-INSTM, 87036 Arcavacata di Rende (CS), Italy; *corresponding.author@email: daniela.aiello@unical.it*

Introduction

MCM-41 type mesoporous material is a candidate as low cost unconventional adsorbent in technological fields where sorptive performances are required, besides the common adsorbents such as activated carbon, perlite, silica gel, etc. [1-2]. For practical applications of adsorption such as process design and control, it is important to study the mechanism of adsorption, to describe the adsorption kinetics and finally to suggest a model. Until now, kinetic models have been described adsorption processes on materials such as activated carbon. Mesostructured materials with periodic surface and porous properties are particularly suitable in order to confirm the effectiveness of such models.
In this work, long-range ordered MCM-41 mesoporous material has been used as adsorbent for 2-methylbenzoic acid, chosen as model molecule. The sorption kinetics were described using the pseudo-first-order and pseudo-second-order equations already reported in the literature [3-4].

Experimental

MCM-41 was prepared using a procedure described elsewhere [5]. Batch adsorption experiments were performed at room temperature using polyethylene bottles containing organic solutions (2-methylbenzoic acid in ethanol) and the adsorbent (MCM-41 powder) by soaking procedure. The initial solution concentrations of 2-methylbenzoic acid in ethanol were in the range of $C_0 = 4 \times 10^3 \div 20 \times 10^3$ mg L^{-1}. After the adsorption step, at appropriate time intervals (5 min ÷ 24 h), the liquid was separated from solid phase by centrifugation. The concentrations of the 2-methylbenzoic acid in solution were determined by UV-VIS spectrophotometer by monitoring the absorbance changes at the wavelength of maximum absorbance (231 nm).

Results and discussion

MCM-41 material exhibits a unidirectional pore system composed of well-defined hexagonal pore structure. It is characterized by a type IV isotherm, with BET surface area of 1034 m^2g^{-1}, an average BJH pore diameter of 3.1 nm and pore volume of 1.1 m^3g^{-1}. Fig. 1 shows the amounts of adsorbed 2-methylbenzoic acid, *q(t)*, onto MCM-41 material *vs* time obtained from solutions with different initial concentrations. It was observed that the amount of acid adsorbed increases with the increase of its initial concentration in solution. Moreover, for longer times an equilibrium state was reached. Two sorption kinetic equations, the pseudo-first-order (1) and pseudo-second-order (2), were used in this work in order to describe the experimental data:

$$\frac{dq}{dt} = k_1(q_e - q(t)) \qquad (1) \qquad\qquad \frac{dq}{dt} = k_2(q_e - q(t))^2 \qquad (2)$$

where *t* is the contact time [min], *dq/dt* is the rate of adsorption, *q(t)* and q_e are the sorption capacities [mg/g] at time *t* and at the equilibrium state, $(q_e\text{-}q(t))$ represents the driving force of the adsorption process, k_1 and k_2 are the kinetic constant.

Both kinetic models assume that the "rate of adsorption on the surface" is the limiting state determining the overall rate of the adsorption process in the non-stationary state.
As a consequence, *dq/dt* is related to the coverage surface fraction $\theta_t=q(t)/q_{max}$, defined as the ratio between the amount of molecules adsorbed and the maximum adsorption capacity.

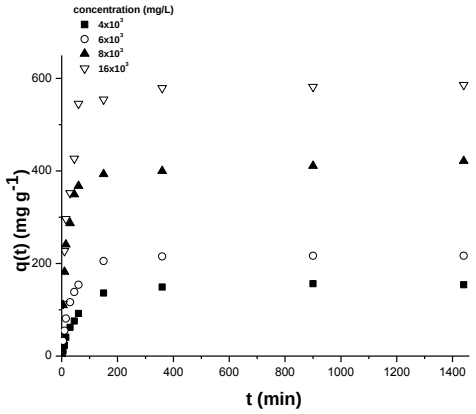

Fig. 1 *q(t) vs t* at various initial concentrations C_0

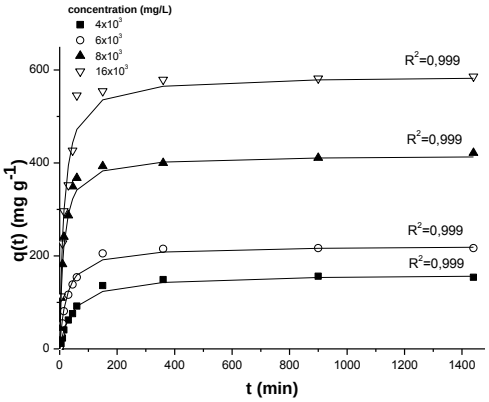

Fig. 2 Pseudo-second-order kinetic model

Pseudo-first-order kinetic model (results not reported) shows a good fit with the experimental data only for low amounts of the 2-methylbenzoic acid adsorbed, obtained at low initial concentrations and corresponding to a low coverage surface fraction $\theta_e=q_e/q_{max}$.
The pseudo-second-order kinetic equation (Fig. 2) shows the best fit for all coverage surface fractions obtained, at all initial concentrations of 2-methylbenzoic acid solutions investigated. In the pseudo-second-order model, the weight attributed to the coverage surface fraction is higher with respect to the pseudo-first-order. In fact:

$$(q_e-q(t))\propto(\theta_e-\theta_t) \text{ and } (q_e-q(t))^2\propto(\theta_e-\theta_t)^2$$

For this reason, for low values of θ_e both models show a good fit, while at high θ_e only the pseudo-second-order model better describes the adsorption process. It has been possible to estimate the maximum theoretical amount of sorbate (q_{max}) on the surface of MCM-41 material determining the concentration of OH groups/nm^2. In fact, the silanol groups act as sites of adsorption through hydrogen bonds with carboxylic functions of 2-methylbenzoic acid. For C_0= 6 x 10^3 mg L^{-1}, a value of θ_e= 0.45 is found and R^2 are 0.986 and 0.999 for pseudo-first-order and pseudo-second-order, respectively. For C_0= 8 x 10^3 mg L^{-1}, θ_e= 0.86 is found and R^2 for pseudo-first-order is 0.948.

Conclusions

Adsorption processes of 2-methylbenzoic acid on MCM-41 materials have been analyzed using kinetic models of pseudo-first and pseudo-second-order. The best fit are obtained with the pseudo-second-order model with the adsorption rate proportional to the driving force square of the process $(\theta_e-\theta_t)^2$.

References

[1] P.J. Branton et al., *Chem. Commun*., (1993), 1257;
[2] E.W. Shin et al., *Environ. Sci. Technol.*, 38, (2004), 912;
[3] S. Lagergren, *Svenska VetenskaPsad Handl.*, 24, (1898), 1;
[4] Y.S. Ho, *Process. Biochem.*, 34, (1999), 451;
[5] Kumar D. et al., *Colloids Surface A*, 109, (2001), 187.

Encoding silver exchanged zeolites by 3D photoactivation

Gert De Cremer,[1] Eduardo Coutiño-Gonzalez,[2] Maarten B.J. Roeffaers,[2] Dirk E. De Vos,[1] Johan Hofkens,[2] Tom Vosch,[2] Bert F. Sels[1]
[1] *Microbial and Molecular systems, Katholieke Universiteit Leuven, Belgium, gert.decremer@biw.kuleuven.be*
[2] *Department of Chemistry, Katholieke Universiteit Leuven, Belgium*

Introduction

Encoded microcarriers are a key element in multiplex (bio)assays in which multiple independent reactions are investigated in the same solution, and in high throughput split-and-mix synthesis methods for creating large libraries of compounds from a set of common building blocks.[1] In a typical multiplex assay, each target is attached to a host particle with a specific 'barcode'. Generally this code is determined by the incorporation of different fluorescent tags in specific concentration ratios (optical encoding), and thus only a limited amount of unique codes is available. While these strategies rely on encoding of microcarriers in advance of the experiment (fixed encoding), a more flexible approach where the encoding occurs during the assay (active encoding) was recently worked out, based on spatial selective photobleaching.[2] Here we introduce a new strategy for active encoding of microcarriers based on photo-induced formation of fluorescent silver cluster in a zeolite host, yielding codes with a positive contrast and an improved photostability compared to the photobleaching method. Photoactivation by UV-irradiation of silver-exchanged zeolites, resulting in the formation of emissive silver clusters, was demonstrated before by our group.[3] However, the spatial resolution of photoactivation was extremely poor due to the large contribution of unlocalized scatter light on the overall photoactivation. By using a 2-photon excitation source for photoactivation, these scattering effects could be minimized yielding unprecedented 3D resolutions.[4]

Experimental

Large zeolite Na-A crystals (± 20 µm) were synthesized according to the Charnell procedure. Subsequently the Na-counterions were exchanged for K-ions followed by a partial exchange of K^+ for Ag^+, resulting in large Ag,K-A zeolites with a silver loading of ± 8wt%.
On these crystals 3D photoactivation was performed by 2-photon excitation using a femtosecond pulsed 780 nm Mai Tai (Spectra Physics) laser, in combination with an inverted fluorescence confocal microscope (Olympys IX-70). Patterns were written inside the crystals by positioning the crystals via a 3D piezo-stage with respect to the laser beam. An exposure time of about 250 ms at a laser power of about 400 kW/cm^2 is sufficient to create a bright fluorescent spot with diffraction-limited size inside the crystal.
After photoactivation, the patterns were imaged with the same setup, but at reduced laser power, to avoid further photoactivation during imaging. The fluorescence was collected on a Perkin Elmer APD detector.

Results and discussion

Figure 1 shows some examples of photoactivated patterns inside an individual zeolite crystal. For instance, in panel b, the image of a lion is activated. Even the fine details of the image, such as the curly tail and the tongue of the lion, are well resolved, yielding a realistic replication of the original template on a scale of 17 µm by 17 µm. By controlling the photoactivation time, different intensity levels can even be obtained within one image,

allowing the creation of grey-scale images. This is illustrated in Figure 1d, where an intensity profile along the white dashed line of Figure 1b is shown (black curve), together with the corresponding profile of the template image in Figure 1c (red curve). The tongue of the lion, which is grey in the template image, indeed exhibits about half the fluorescence intensity as the surrounding activated regions. To illustrate the data-storage or encoding possibilities of this material, the text 'Katholieke Universiteit Leuven' was encoded according to the QR-code system and written inside an individual 20-µm-sized zeolite particle (Fig. 1e). In Figure 1g, a zoom of an individual activated spot from the image in panel e is shown, together with its corresponding 2D Gaussian fit (coloured contour plot), showing the actual writing resolution of about 250nm in the *xy*-plane. The obtainable z-resolution is about 1 µm, allowing the activation of several well-resolved layers of codes on top of each other inside an individual zeolite crystal. Moreover, photostability studies show that the activated fluorescent patterns are about 2 orders of magnitude more photostable than organic dyes loaded in zeolites.

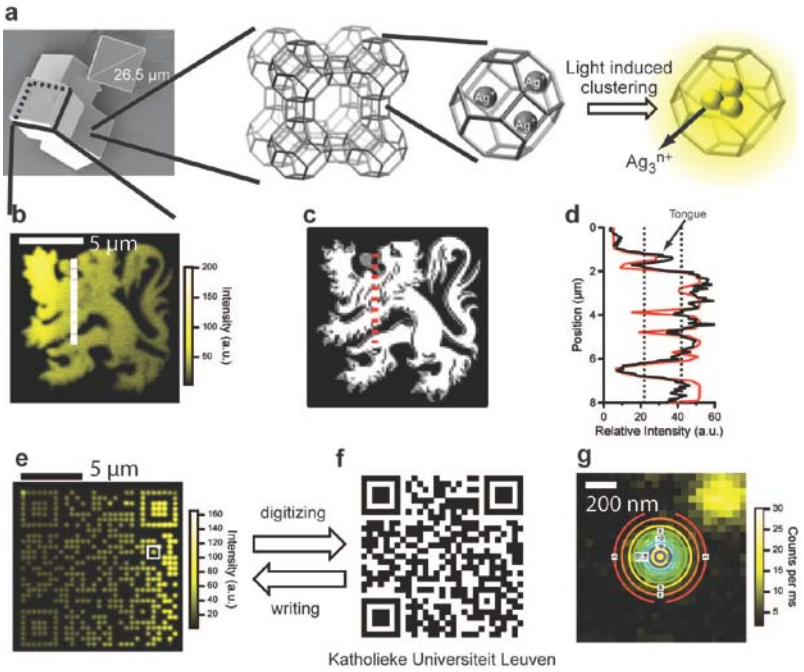

Figure 1: Photoactivation of fluorescent patterns in individual zeolites by 2-photon excitation.

Acknowledgements

We are grateful to prof. V. Valtchev for the synthesis of the large zeolite A particles. Furthermore we thank financial support from FWO, IDECAT and the Flemish government

References

[1] K. Braeckmans *et al*,**Nature Reviews Drug Discovery** 2002, 1, 447.
[2] K. Braeckmans *et al*, **Nature Materials** 2003, 2, 169.
[3] G. De Cremer *et al*, **Angewandte Chemie-International Edition** 2008, 47, 2813.
[4] G. De Cremer *et al*, **Advanced Materials**, 2010, 22, 957.

Polyamide fibers with α-tocopheryl acetate encapsulated into zeolite Y

Rubio, C.[a], Liédana, N.[a], Pérez, E.[a], Piera, E.[b], Caballero, M. A.[b], Coronas, J.[a], Téllez, C.[a]
[a] *Chemical Engineering Department and Nanoscience Institute of Aragon. Universidad de Zaragoza, 50018 Zaragoza, Spain. ctellez@unizar.es*
[b]*Research and Development Department. Nurel S.A., 50016 Zaragoza, Spain*

Introduction

Nowadays it is necessary a development and innovation of high value-added materials in order to compete in textile industry. In this context, microencapsulation technology is a growing area in this field. Vitamin E (α-tocopheryl acetate) is considered an excellent ally of beauty and health thanks to its capability of capturing and deactivating free radicals.
Zeolite Y is used as an encapsulation material for several reasons related to its microporous, adsorption capacity and crystalline structure [1, 2]. Compared to polymers, inorganic materials generally exhibit much higher stability regarding solvent, pressure, and temperature, and porous materials are used to prolong the action of the additive.

Experimental

The optimized encapsulation process of vitamin E into zeolite Y and the special fibers consists of four stages [3]. The first one activates the zeolite surface and pores introducing zeolite Y in a stove at 250 ºC for 24 hours. Then, the encapsulation, where the α-tocopheryl acetate and the zeolite Y (3:1, wt/wt) are mixed under vigorous stirring at 110 ºC for 24 hours. The third step is the post-treatment stages: these include drying in a stove at 80 ºC for approximately 12 hours and subsequent grinding and micronization to a particle size of approximately 1-2 μm. Finally, the zeolite microcapsules are supplied to the industrial spinning process to obtain the special polyamide-6 fibers [4].
To extract the α-tocopheryl acetate encapsulated in zeolite microcapsules liquid-liquid extraction in autoclave has been used while for extraction from the special fibers the method was liquid-liquid extraction using a condenser.

Results and discussion

The presence of α-tocopheryl acetate in the created zeolite microcapsules is determined by means of infra-red spectroscopy. The analyses of the different samples show the main representative peaks of the α-tocopheryl acetate as well as the main peaks corresponding to zeolite Y (Figure 1).

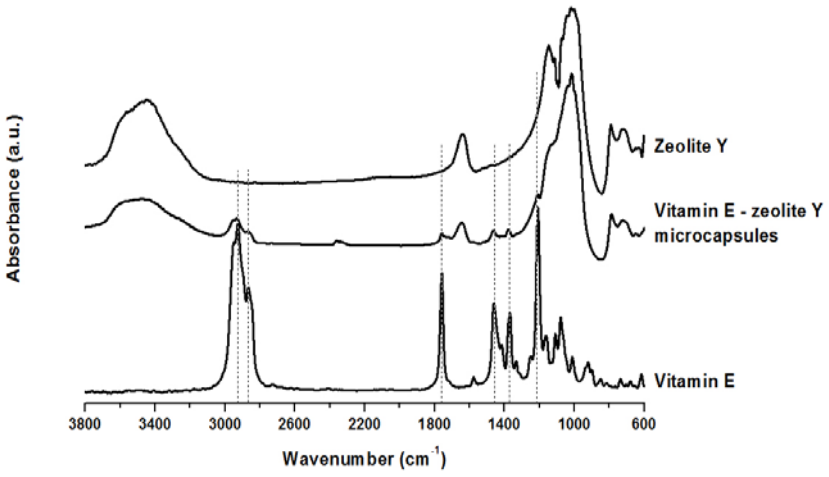

Figure 1. Infra-red spectra of vitamin E-zeolite Y microcapsules and standards of vitamin E and zeolite Y.

In order to quantify the amount of α-tocopheryl-acetate present in the vitamin E-zeolite Y microcapsules thermogravimetric analyses have been used. Two main weight losses have been observed, the first one corresponds to weight loss of water (12.2%) and the second one corresponds to the loss of encapsulated α-tocopheryl acetate (20.4%).
By means of high performance liquid chromatography has been possible to quantify the amount of vitamin E extracted from both vitamin E-zeolite Y microcapsules and the resulting special fibers. The yield of the liquid-liquid extractions increases with the temperature, so the best result is achieved with a liquid-liquid extraction in autoclave at 130 ºC.
Figure 2 shows SEM images of a fiber without zeolite and a fiber with zeolite. The fiber without zeolite presents TiO_2 spherical particles used as white pigment with a size of approximately 200 nm. The fiber with zeolite Y microcapsules presents these TiO_2 particles and particles of 1-2 μm which aspect correspond to zeolite Y and EDX analysis identified the presence of silicon and aluminium.

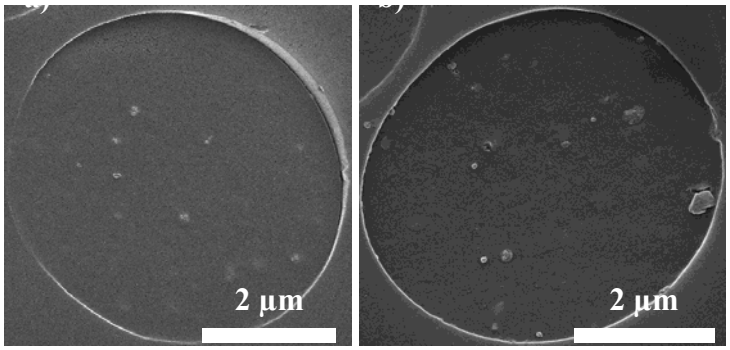

Figure 2. SEM images of a fiber without zeolite (a) and with zeolite Y microcapsules (b)

The introduction of the zeolite microcapsules in the fiber does not affect significantly its mechanical properties. Fabrics knitted with vitamin E-zeolite Y microcapsule yarns state a significant presence of vitamin E even after 100 washing machine cycles.

Conclusions

A useful and simple encapsulation methodology has been developed, optimized and characterized to obtain vitamin E-zeolite Y microcapsules, which are used to fabricate special textile polyamide fibers, with beneficial properties due to presence of α-tocopheryl-acetate and gave rise to commercial products (NOVAREL®).

Acknowledgements
Financial support from the Spanish Ministry of Science and Innovation (TRA2009_0049) is acknowledged.

References

[1] Muñoz-Pallares, J., Corma, A., Primo, J., Primo-Yufera, E., Zeolites as pheromone dispensers, Journal of Agricultural and Food Chemistry, 49 (2001), 4801-4807
[2] Horcajada, P., Marquez-Alvarez, C., Ramila, A., Perez-Pariente, J., Vallet-Regi, M., Controlled release of Ibuprofen from dealuminated faujasites, Solid State Sciences, 8 (2006), 1459-1465
[3] Pérez, E., Martín, L., Rubio, C., Urieta, J. S., Piera, E., Caballero, M. A., Téllez, C., Coronas, J., Encapsulation of α-tocopheryl acetate into zeolite Y for textile application, Industrial & Engineering Chemistry Research, 49 (2010), 8495-8500
[4] Caballero, M. A., Zagalaz, P., Segura, S. J., Piera, M. E., Pérez, E., Téllez, C., Coronas, J., Process for the additivation of synthetic fibres, artificial fibres and polymers with special properties, (2008). Patent numbers: EP1923423-A1, US2008128941-A1, CN101225556-A, KR20080043729-A, TW200837228-A

Inclusion of antioxidants in MCM-41: physico-chemical properties and activity

P. Iliade[1], L. Gastaldi[2], E. Ugazio[2], S. Sapino[2], M.E. Carlotti[2], S. Coluccia[1], G. Berlier[1]
[1] *Dipartimento di Chimica I.F.M. and NIS Centre of Excellence, Università degli Studi di Torino, Via P. Giuria 7, 10125 Torino, Italy.* patrizia.iliade@unito.it
[2] *Dipartimento di Scienza e Tecnologia del Farmaco, Università degli Studi di Torino, Via P. Giuria 9, 10125 Torino, Italy*

Introduction

Oxidative stress has been one of the most widely studied biochemical processes and is the consequence of an imbalance between pro- and antioxidant species. The former essentially concerns highly reactive oxygen or nitrogen species (ROS or RNS) that can lead to the oxidation of lipids, proteins or nucleic acids and contribute to the cellular dysfunction. To avoid oxidative stress, cells are equipped with two major antioxidant defense systems. The first concerns enzymes which catalyze ROS or RNS degradation, while the second involves antioxidants like vitamins A, C, E and glutathione, which act by redox reactions [1]. Flavonoids have recently attracted a great interest as potential reducing agents, hydrogen-donating antioxidants and singlet oxygen quenchers; in some cases metal chelating properties have been proposed [2].
Quercetin, in particular, satisfies all the proposed criteria for effective radical scavenging, since the o-dihydroxy-structure in the central ring confers higher stability to the radical form and participates in electronic delocalization [3]. The therapeutic usefulness of these potential benefits is, however, limited by the unfavourable physico-chemical properties of this compounds, especially its very poor water solubility and its low thermal and photostability. A recently proposed approach to protect the antioxidants from photodegradation and to improve their solubility in pharmaceutical formulations is based on the inclusion in supramolecular structures (phospholipids, cyclodextrins, etc.). The resulting systems should also allow a gradual release of the antioxidant for topical treatments [4].
In this work, we have studied the inclusion of quercetin in an inorganic host, mesoporous silica (MCM-41), which has been chosen for the well known properties: high surface area, ordered porosity allowing the diffusion of bulky molecules, thermal stability, biocompatibility [5] and possibility to tune the hydrophilic character by surface functionalization. For comparison, the same approach has been followed to stabilize Trolox®, a water-soluble analog of vitamin E often employed as a benchmark for its antioxidant activity.

Experimental Section

Different procedures were followed to prepare antioxidant/MCM-41 hybrid materials: impregnation from water, methanol, water/ethanol solutions, or kneading method employing acetone as volatile solvent. The antioxidant/silica weight ratio was varied and the hydrophilic/hydrophobic character of MCM-41 was tuned by *in vacuo* thermal treatments or surface functionalization with n-octyl groups.
The resulting hybrid materials were characterized by XRD, gas-volumetric analysis, DSC, TGA, and FTIR spectroscopy. UV-Vis spectroscopy and HPLC analysis were employed to measure the antioxidant loading. *In vitro* release was studied by evaluating the diffusion through an artificial membrane in aqueous solution, in gel and in O/W emulsion. The same media were employed to perform photodegradation runs with an UVB lamp. Radical scavenging activity was investigated by DPPH assay.

Results and Discussion

Figure 1 reports some representative results about the inclusion of quercetin within the pores of MCM-41. Gas volumetric analysis (left panel) shows a consistent decrease in surface area

and in pores volume and dimension with respect to bare MCM-41. The low angle XRD patterns of the same materials (right panel) display the typical peaks of a hexagonal network of mesopores (P6mm), testifying that the long range order is preserved after quercetin inclusion. The shift towards higher 2θ values indicates a decrease of *d* spacing, suggesting the presence of quercetin molecules within the pores. The interaction between the antioxidants and the silica surface was studied by FTIR spectroscopy, indicating that both quercetin and Trolox® interact with surface silanol Si-OH groups by hydrogen bonding, through the aromatic ring and the carbonyl/carboxyl groups.

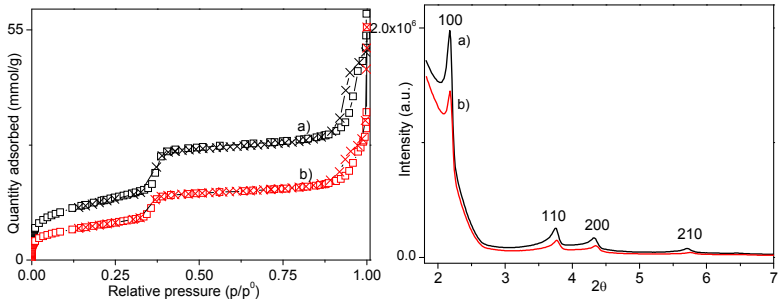

Figure 1. Left) Nitrogen adsorption/desorption isotherms and right) powder XRD patterns of a) MCM-41 and b) 1:4 quercetin/MCM-41 complex prepared by kneading method.

In vitro tests showed a slower release of quercetin and Trolox® after inclusion in the MCM-41 matrix, in agreement with an increase of photostability under UVB irradiation; a certain radical scavenging activity was observed for the hybrids. Significant differences were remarked among the many prepared and tested samples, suggesting that the results can be optimized by modifying the inclusion procedure and the antioxidant loading. In particular, it was noted that the optimal preparative conditions for quercetin and Trolox® are different, suggesting an important role of the hydrophilic/hydrophobic interaction with the silica surface. The functionalization of MCM-41 with n-octyl groups, to favour the hydrophobic interaction with quercetin, did not result in better performance in terms of activity and photostability, suggesting the importance of Si-OH groups in stabilizing the organic molecules within the pores.

Conclusions

The inclusion of antioxidants within the pores of MCM-41 was studied. The improvement in photostability and antiradical activity could be rationalized in terms of the hydrophilic/hydrophobic interaction with the silica surface. Further work is in progress to improve the performances of the hybrid materials.

References

[1] Sies H., Strategies of antioxidant defense, Eur. J. Biochem., 215 (1993), 213–219

[2] Ohshima, H., Yoshie, Y., Auriol, S., Gilibert, I., Antioxidant and pro-oxidant actions of flavonoids: Effects on DNA damage induced by nitric oxide, peroxynitrite and nitroxyl anion, Free Radic. Biol. Med., 25 (1998), 1057-1065

[3] Calabro, M.L., Tommasini, S., Donato, P., Raneri, D., Stancanelli, R., Ficarra, P., Ficarra, R., Costa, C., Catania, S., Rustichelli, C., Gamberini, G., Effects of alpha and beta-cyclodextrin complexation on the physico-chemical properties and antioxidant activity of some 3-hydroxyflavones, J. Pharm. Biomed. Anal., 35 (2004), 365–377

[4] Sapino, S., Carlotti, M.E., Cavalli, R., Trotta, M., Trotta, F., Vione, D., Effect of alkyl-gamma-cyclodextrins on the stability of retinol, J. Incl. Phenom. Macrocycl. Chem., 57 (2007), 451-455

[5] Gianotti, E., Bertolino, C.A., Benzi, C., Nicotra, G., Caputo, G., Castino, R., Isidoro, C., Coluccia, S., Photoactive hybrid nanomaterials: indocyanine immobilized in mesoporous MCM-41 for "in-cell" bioimaging, ACS Appl. Mater. Inter., 1 (2009), 678-687.

The progression of Metal-Organic Frameworks – From academic research to industrial production and applications

Dr. Manuela Gaab, Dr. Natalia Trukhan, Dr. Stefan Maurer, Dr. Ulrich Müller
BASF SE, Ludwigshafen, Germany

Introduction

For decades researchers in industry have developed and studied synthetic microporous materials like zeolites. Applications in adsorption, refinery, petrochemistry and more recently emission control have given rise to an annual demand of more than 1.5 million metric tons in total. More recently, in parallel to academic research, metal-organic frameworks (MOFs) have been industrially investigated. Due to the high porosity of these new compounds some fields in application might overlap with those zeolites have conventionally been used for.

Prerequisits for industrial processing

Emphasis is put on the manufacture of light weight and simple-to-process aluminium-based MOFs developed by BASF. The typical synthetic process can include the different steps of preparation as well as recycling of the solvent and further processing of the dried powder into shaped material.

Issues of prime importance for production scale-up are an appropriate space-time-yield (STY) (kg of MOF per m^3 of reaction mixture per day) and product work-up

leading to the desired properties. On industrial scale, e.g. spray drying can be used to prepare MOF powder yielding the desired porosity and morphology of the particles.

MOF production at BASF

Based on these findings, the synthesis procedure for one of BASF's MOFs (Basolite A520) has already been optimized to allow for organic solvent-free preparation. Basolite A520 e.g. can be synthesized in a water-based route that has already led to ton-scale production. Thereby the Al-MOF is industrially produced *via* both an economic and environmentally-friendly process. This reliable access together with their adsorption and gas storage properties paves the way to the broad application of MOFs. The latter is moreover driven by the current global megatrends that require innovative applications by using high potential materials.

Inclusion of dye molecules within MgAPO-5

Raquel García[a], Virginia Martínez-Martínez[b], Cecilia Corcóstegui[b], Iñigo López-Arbeloa[b], Joaquín Pérez-Pariente[a]

a) Instituto de Catálisis y Petroleoquímica (CSIC), C/Marie Curie 2, 28049, Cantoblanco, Madrid, Spain; b) Departamento de Química Física, Universidad del País Vasco, UPV/EHU, Apartado 644, 48080 Bilbao, Spain. rgs@icp.csic.es

Introduction

The encapsulation of dyes into nanostructured ordered systems is a good strategy to provide new functional materials with interesting optical, chemical and electrical properties [1]. In this regard, zeolites and zeotypes are very interesting as host materials due to the open nature of their framework with a well-defined internal structure made of uniform cages, cavities, or channels. In particular, microporous materials containing linear channels running through hexagonal microcrystals allow the formation of highly monomeric and anisotropic oriented dye systems [2]. In this work, we have studied the inclusion directly during crystallization of the dye Pironine Y (PY; Figure 1) within MgAPO-5 (AFI structure-type material).

Experimental

Gels of composition: *x* MgO: 1 P_2O_5: (1-*x*/2) Al_2O_3: *y* Triethylamine (TEA): *z* PY: 300-310 H_2O, where *x*, *y* and *z* where varied according to Table 1.The gels were heated at 180ºC for 24h under static conditions. The materials were characterized by XRD, TGA, CHN analysis and confocal fluorescence microscopy.

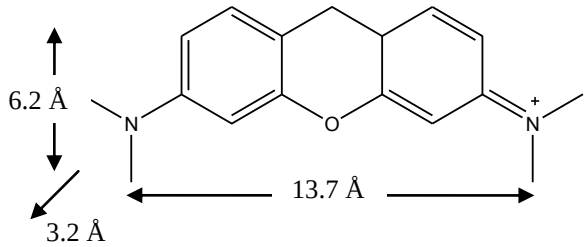

Figure 1. Molecule of Pironine Y

Results and discussion

Initially, magnesium aluminophosphate materials were prepared using triethylamine (TEA) as structure directing agent (SDA) in synthesis gels with a high water concentration in order to favor the crystallization of big crystals, suitable for study by microscopy. Competitive crystallization with MgAPO-34 (CHA structure-type) was observed under the initial synthesis conditions (C-1, Table 1) as triethylamine can direct the synthesis of both AFI and chabazite structures. Decreasing of the SDA content (C-2) or the magnesium content (C-3) drives the products of crystallization to pure AFI topology. Therefore, these conditions were chosen for the incorporation of the dye during synthesis, experiments C-4 and C-5 in Table 1. In the presence of the dye, slightly pink prismatic crystals of MgAlPO-5 were obtained as the main product of crystallization with similar crystal size to those obtained for the preparations in the absence of dye molecules.

The proof of the incorporation of the dye in crystals of the different samples was assessed by fluorescence microscopy (Figure 2). Incorporation of the dye within AFI structure is only possible if the dye molecules are aligned with their long axis along the channel direction (pore dimensions: 7.3 x 7.3 Å). Since the transition dipole moment of the PY dye is also parallel to the long axis of the molecule, the encapsulated molecules will only show fluorescence in the direction of the alignment and no fluorescence will be observed in other directions. This would not be possible for dyes adsorbed on the external surface.

Table 1. Gel compositions and products of selected experiments: *x* MgO: 1 P_2O_5: (1-*x*/2) Al_2O_3: *y* TEA: *z* pyronine Y: 300-310 H_2O. All the gels were heated at 180ºC for 24h.

Experiment	x	y	z	Product
C-1	0.2	1.5	0	AFI+CHA
C-2	0.2	0.75	0	AFI
C-3	0.1	1.5	0	AFI
C-4	0.2	0.75	0.008	AFI
C-5	0.1	1.5	0.008	AFI

Analysis of crystals of sample C-4 and C-5 shows that the fluorescence is not homogeneous along the particles but concentrated on the center of the crystals and decreases towards the ends. This has been previously observed for a related system [3] and suggests that the dye molecules are preferentially incorporated during the early stages of crystallization and are gradually replaced by SDA molecules as the crystallization proceeds. Emission spectra of the crystals show a maximum at about 545 nm, slightly different to the data measured for an ethanolic solution of the dye (565 nm).

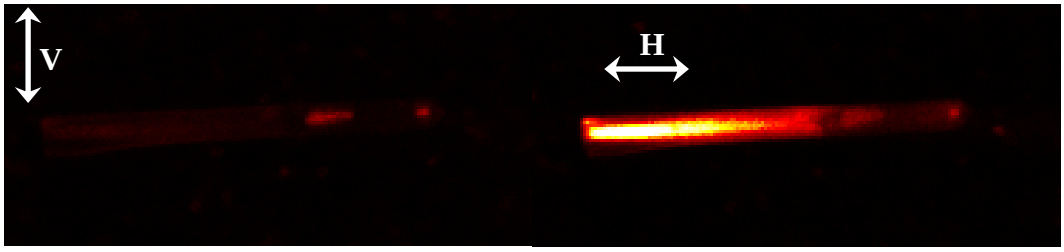

Figure 2. Fluorescence images of a crystal fragment of sample C-4.

Conclusions

Pironine Y can be encapsulated within MgAPO-5 crystals directly during crystallization of the material. The dye molecules are mainly incorporated along the direction of the AFI channels, which coincides with the main axis of the prismatic crystals. The distribution of the dye molecules along the zeotype crystals suggests some competition between the dye and the amine during crystallization and evidences that the dye is mainly incorporated during the nucleation stage.

Acknowledgements

We are thankful for the financial support of the Spanish Ministry of Science and Innovation MICINN, Project MAT-2009-13569.

References

[1] Owaga, M., Kuroda, K., Chem. Rev., 95 (1995) 399.
[2] Gfeller, N., Calzaferri, G., J. Phys. Chem. B, 101 (1997) 1396.
[3] Weiβ, Ö, Loerke, J., Wüstefeld,U., Marlow, F., Schüth, F., Journal of Solid State Chemistry, 167 (2002) 302.

Cisplatin-loaded Folic Acid Functionalized Mesoporous Silica Selectively Enters and Kills Folate Receptor Expressing Cancer Cells

Luigi Pasqua[a*] Catia Morelli[b], Pamela Maris[b], Diego Sisci[b], Enrico Perrotta[c], Ida Perrotta[c], Carlo Versace[d], Flaviano Testa[a].
[a]*Department of Chemical Engineering and Materials,* [b]*Pharmaco- Biology Department;*
[c]*Ecology Department;* [d]*Physics Department; University of Calabria, Via P. Bucci 87036 Rende (CS) Italy.*
**Corresponding author: l.pasqua@unical.it.*

Introduction

Folic acid, shows a great promise as a tumour-homing agent in the preparation of devices for drug targeting to cancer cells. This essential vitamin has a high affinity for FR (Folate Receptors), which can actively internalize bound folates and folate conjugated compounds via receptor-mediated endocytosis. Furthermore, FR are over-expressed by several kinds of cancer cells. Thus folate conjugation to anti-cancer drugs will improve drug selectivity and decrease negative side effects. Bifunctional hybrid mesoporous silica potentially useful for drug targeting has been synthesized starting from neutral surfactant-templated mesoporous silica and covalently coupling folic acid preferentially on the external surface of the particles [1]. In this report non functionalized mesoporous silica nanoparticles MSNs and folic acid (FOL) grafted MSNs (MSN-FOL) are tested towards cellular internalization. Finally, cisplatin (Cp) loaded MSN-FOL, were tested on cancerous FR-positive (HeLa), cancerous FR-negative or normal FR-negative (HEK293) cells.

Experimental

The molar composition of the synthesis mixtures investigated was: 1 SiO_2-0.52 decane - 0.324 Triton X-100-126.2 H_2O the resulting material was named MSN_{surf}.
After 3-aminopropyltriethoxysilane functionalization the so-obtained mesoporous silica nanospheres, named, MSN-AP and were functionalized with folic acid according a procedure reported in reference [1] to obtain MSN-FOL. For Fluorescence labelling of MSN**,** Fluorescein isothiocyanate (FITC,) was added to the above reported procedure to obtain MSN-AP and the product MSN-FITC was obtained. MSN-FITC-FOL preparation was carried out according the procedure presented above for MSN-FOL using MSN-FITC instead of MSN-AP as starting material. For MSN-FOL-Cp preparation, 120 mg of Cisplatin (Cp, Sigma) (CAUTION: Cp is a mutagenic and carcinogenic agent) were dissolved in 6 ml of DMF and MSN-FOL were suspended in the Cp solution and stirred for 24 hours. The material were characterized by X-Ray powder diffraction, N_2 adsorption-desorption porosimetry, FT-IR MAS-NMR, SEM, TEM and DLS. Endocytic mechanisms in the selected cancerous FR-positive (HeLa), cancerous FR-negative or normal FR-negative (HEK293) were examined by TEM.

Results and discussion

TEM observations have been carried out on the differently functionalized nanoparticles at various time points to evaluate if specific endocytic pathways are activated depending on the nature of MSNs surface functionalization. Interestingly, MSN never entered HeLa (Figure 1a), neither other cancerous (T47D, MCF-7 and SKBR3) and normal (HEK293) cell lines,

indicating that non functionalized particles are inert and do not interact with the biological systems. To investigate if the cellular uptake could be ascribed to electrostatic interactions between the protonated aminopropyl (AP) groups bound to the MSN surface and the negatively charged cell membranes, MSN-AP particles were tested. The results showed that AP groups do not significantly affect cellular uptake (Figure 1b). A highly specific, receptor mediated, cellular internalization of MSN-FOL, occurs exclusively in folate receptor (FR) expressing cells (Figure 1c). Furthermore, once inside, the particles localize in endosomal cavities and are expulsed from the cell mostly in a 48 h time period. Finally, to assess if MSN-FOL could represent a reliable tool for drug targeting purposes, we loaded the particles with the chemotherapeutic drug cisplatin, and tested the obtained MSN-FOL-Cp on FR over-expressing HeLa cells and on normal FR negative HEK293 cells.

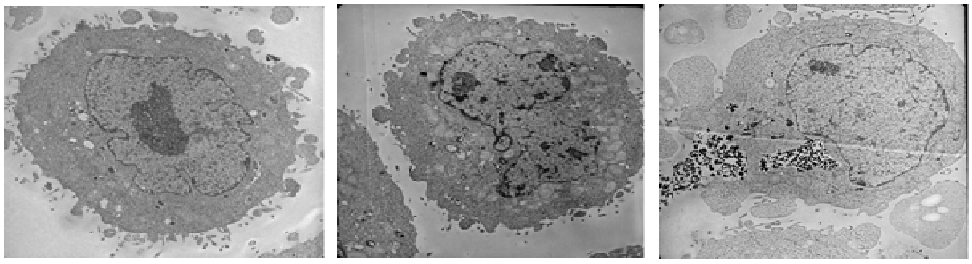

a) b) c)

Figure 1. Tem micrographs of FR expressing HeLa cells treated with a)MSN, b)MSN-AP c) MSN-FOL.

A strong growth arrest was observed after 2-3 days in MSN-FOL-Cp treated HeLa cells, if compared to the less dramatic growth retardation caused by comparable amounts of free Cp, while MSN-FOL did not affect cell proliferation. On the contrary, FR-negative HEK293 cells, showed no difference between the growth inhibition observed in MSN-FOL-Cp and free Cp treated samples, with respect to control and MSN-FOL samples.

Conclusions

In conclusion, our mesoporous silica nanoparticles represent a great potential for localized drug release since they are able to be internalized into FR over-expressing tumour cells, where they are retained without showing any toxic effect, being mostly exocytosed within 48h. MSN-FOL-Cp are able to induce growth arrest exclusively in FR-expressing cells, demonstrating that the folic acid function is the activator in the cellular uptake process. Interestingly cellular uptake does not occur unless opportunely functionalized.

Acknowledgements

Financial support has been provided by: PRIN 2007 (Progetti di Ricerca di Interesse Nazionale) - Prot. 2007N9A3A4_002), AIRC (Associazione Italiana Ricerca Cancro) grants, MIUR Ex 60% – 2009.

References

[1] L. Pasqua, F. Testa, R. Aiello, S. Cundari and J. B. Nagy, Preparation of bifunctional hybrid mesoporous silica potentially useful for drug targeting Microporous and Mesoporous Materials 103 (2007), 166-173.

Drug delivery based on mesoporous silica: A functioning device tested in vivo

P. Behrens,[1] N. Ehlert,[1] R. Lensing,[2] A. Bleich,[3] P.P. Müller,[4] T. Lenarz,[2] M. Stieve[2]
[1] *Institute for Inorganic Chemistry, Leibniz University Hannover, Germany; Peter.Behrens@acb.uni-hannover.de*
[2] *Institute for Laboratory Animal Science and Central Animal Facility, Hannover Medical School, Germany*
[3] *Institute of Inorganic Chemistry, Leibniz University Hannover, Germany*
[4] *Helmholtz Center for Infection Research, Braunschweig, Germany*

Introduction

Mesoporous silica is currently being investigated for a variety of biomedical applications, especially for the delivery of drugs and biomolecules as enzymes or DNA. In order to further advance the use of mesoporous silica as a novel biomaterial, in addition to simple laboratory experiments determining release kinetics and to in vitro tests using cell cultures, animal experiments have to be performed. For applications aimed at being using in the body, mesoporous silica has to prepared in a suitable form. Currently, the focus is on mesoporous silica nanoparticles (MSNPs), although the potential hemolytic effect on red blood cells has to be dealt with. Another suitable form are mesoporous silica films. We have explored such films, deposited on a standard implant material (Bioverit®II, a mica-glass ceramic) [1-6].
Here, we report on the efficacy of a thin mesoporous film on a Bioverit®II middle ear implant as a drug delivery system for the local release of an antibiotic. After having optimized the loading of the films, studied their release kinetics, investigated their biocompatibility in cell cultures and their antibacterial action in bacterial cultures [4], we have performed in vivo experiments in rabbits. The results show that even from a thin film enough antibiotic is released to effectively combat an intentionally placed middle ear infection.

Experimental

Bioverit®II specimen were coated with a nanoporous silica layer by dip-coating or spray-coating and were then calcined. These materials were functionalized by a grafting step to obtain sulfonic acid groups on the surface. At a pH of 4, these are deprotonated and negatively charged whereas the antibiotic used, ciprofloxacin, is positively charged. Thus, the amount of ciprofloxacin which can be loaded into the pores is increased substantially due to electrostatic interactions. The time-dependent release of ciprofloxacin was determined with UV-vis photometry. The antibacterial efficacy of the drug-loaded nanoporous films was tested in bacteria cultures of *Pseudomonas aeruginosa* (strain PAO1) a bacterium which can cause chronic middle ear infections. The general biocompatibility of the materials was demonstrated in cell culture experiments with fibroblasts [4]. Animal experiments were carried out with female New Zealand White rabbits. Bioverit®II implants were spray-coated and calcined to establish mesoporous silica films which were then sulfonate-modified. Two types of prostheses were implanted, the control group (n=7) receiving implants without the antibiotic. The study group (n=7) obtained ciprofloxacin-loaded implants. Animals of both groups were euthanized at the latest 1 week after infection [6]. The animal study was conducted in accordance with the German law for animal protection and with the European Communities Council Directive 86/609/EEC for the protection of animals used for experimental purposes.

All experiments were approved by the Local Institutional Animal Care and Research Advisory committee and permitted by the local government (Ref.: 33.9-42502-04-09/1734).

Results and discussion

Mesoporous silica films can be produced on Bioverit®II specimen with thicknesses ranging from 40 to 150 nm. For flat samples, dip-coating was used, the irregular formed prostheses were coated by a spraying procedure. After calcination, such films showed only a minor ciprofloxacin uptake. The loading could be improved nearly ten-fold (to about 2 mg cm^{-2} of the macroscopic surface) by functionalizing the surface with sulfonic acid groups. Attempts to prolong the drug release over an extended time period by adding further silane coatings were successful, but resulted in compromised biocompatibility. Loaded and unloaded sulfonate-functionalized mesoporous films, however, showed excellent biocompatibility and strong antibacterial action in vitro [4].
For the in vivo experiments, middle ears of rabbits were intentionally infected with *Ps. aeruginosa* and implants were placed using an established operation procedure [7]. Various parameters checking the clinical condition clearly showed that the animals of the study group were in better clinical condition than those of the control group. Necropsy showed that all the animals in the control group had developed an abscess in the middle ear, whereas only one animal of the study group presented pus. The microbiological examination confirmed the almost complete elimination of bacteria in this group, as tested on middle ear and implant irrigations as well as on swap samples of the middle ear [6].

Conclusions

The animal experiments clearly showed the high efficacy of the mesoporous silica-based drug release system presented here. This work therefore represents the first example of a functioning biomedical device based on mesoporous silica which has been successfully tested in vivo.

Acknowledgements
This work was supported by the DFG within the SFB 599 „Sustainable bioresorbable and permanent implants based on metallic and ceramic materials" (TPD1).

References
[1] Turck, C., Brandes, G., Krueger, I., Behrens, P. Lenarz, Th., Stieve, M., Histological Evaluation of Novel Ossicular Chain Replacement Prostheses: An Animal Study in Rabbits. Acta Oto-Laryngol. 127 (2007) 801-808
[2] Vogt, J.C., Brandes, G., Krueger, I., Behrens, P., Nolte, I., Lenarz, T., Stieve, M. A comparison of different nanostructured biomaterials in subcutaneous tissue. J. Mater. Sci. Mater. Med. 19 (2008) 2629-2636
[3] Vogt, J.C., Brandes, G., Ehlert, N., Behrens, P., Nolte, I., Mueller, P.P., Lenarz, T., Stieve, M. Free Bioverit® II implants coated with a nanoporous silica layer in a mouse ear model – a histological study. J. Biomater. Appl. 24 (2009) 175-191
[4] Ehlert, *N.*, Badar, M., Christel, A., Lohmeier, S.J., Luessenhop, T., Stieve, M., Lenarz, T., Mueller, P.P., Behrens, P., Mesoporous Silica Coatings for Controlled Release of the Antibiotic Ciprofloxacin from Implants J. Mater. Chem. 21 (2011) 752-760
[5] Ehlert, N., Hoffmann , A., Luessenhop, T., Gross, G., Mueller, P.P., Stieve, M., Lenarz, T., Behrens, P., Amino-modified silica surfaces efficiently immobilize bone morphogenetic protein 2 (BMP2) for medical purposes. Acta Biomater. (2011), online version: doi:10.1016/j.actbio.2010.12.028
[6] Lensing, R., Bleich, A., Smoczek, A., Glage, S., Behrens, P., Ehlert, N., Müller, P.P., Lenarz, Th., Stieve, M., Efficacy of mesoporous silica coating as antibiotic delivery system on middle ear prostheses in rabbits, in prep.
[7] Stieve, M., Hedrich, H., Battmer, R.D., Behrens, P., Müller, P.P., Lenarz, Th., Experimental middle ear surgery in rabbits: a new approach for reconstructing the ossicular chain, Laboratory animal, 43 (2009) 198-204

In vitro evaluation of surface-modified silica nanoparticles for the delivery of camptothecin

Carlos Muniesa,[†] Sonia Miranda,[‡] Yolanda Fernández,[‡] Manuel Quesada,[†] Jorge Ruiz,[‡] Simó Schwartz Jr,[‡] Avelino Corma,[†] Ibane Abasolo,[‡] Pablo Botella[†]
[†]*Instituto de Tecnología Química (UPV-CSIC), Av. Los Naranjos s/n, 46022 Valencia, Spain;* [‡]*CIBBIM-Nanomedicina and Networking Biomedical Research Center on Bioengineering, Biomaterials and Nanomedicine (CIBER-BBN), Hospital Universitari Vall d'Hebron, Universitat Autònoma de Barcelona, Passeig Vall d'Hebron 119-129, 08035 Barcelona, Spain.*

Introduction

20(S)-camptothecin (CPT), has shown significant antitumor activity in a broad spectrum of human malignancies [1]. Unfortunately, its clinical application is hampered by a poor pharmaceutical profile, with extreme aqueous insolubility, low stability and severe systemic toxicities [2]. Therefore, the development of controlled delivery strategies could lead to significant advantages in the clinical use of this drug. At this point, mesoporous silica nanoparticles have found application for intracellular delivery and release of CPT in *in vitro* [3] and *in vivo* [4] studies. However, such release does not depend on a specific intracellular stimulus, but on the molecular diffusion through the pores, resulting in premature release of the drug in biological fluids. In this study, we report a novel and robust delivery platform for CPT based in amorphous silica nanoparticles (SNPs) that transport the drug covalently linked (ester bond) at the 20-OH position. The surface of these SNPs has been modified with trihydroxysilylpropyl carboxylate groups, which are ionized at physiological pH, thus, provoking electrostatic repulsion and improving colloidal stability in aqueous medium. This CPT covalently linked to SNP was subjected to biological validation by *in vitro* studies, showing cell internalization and cytotoxic activity over several cancer cell lines.

Experimental

SNP materials with CPT (SNP-CPT) or with CPT and Cy5.5 (SNP-CPT-Cy5.5) were prepared according to [5]. The main characteristics of these materials are listed in Table 1. Nanoparticles have been characterized by DLS, TEM, XRD, BET, ^{13}C-MAS-NMR, UV-Vis and elemental analysis. Release test for every sample were carried out both in PBS and human plasma and CPT was quantified on HPLC systems with a C-18 reverse phase column. Internalization of nanoparticles in HeLa cells after incubation with SNP-CPT-Cy5.5 (750 μg/mL) and Lysotracker Green was analyzed by confocal microscopy using excitation peaks at 488/633 nm and emission at 522/693 nm for Lysotracker and Cy5.5, respectively. *In vitro* activity of SNP-CPT or free CPT was tested by MTT assay (72 h) over 4 cell lines: HeLa (cervix carcinoma), U87MG (glioblastoma), HCT-116 (colon cancer) and HT-29.Fluc (colon cancer), with final doses ranging from 0.025 to 2.5 μg/mL (in CPT equivalents).

Table 1. Main characteristics of materials tested in the present work.

Sample	CPT Loading (wt%)	Cy5.5 Loading (wt%)	Particle Size (nm)
SNP-CPT	7.5	---	147.7 ± 59.9
SNP-CPT-Cy5.5	4.7	0.3	102.2 ± 31.0

Results and discussion

SNP-CPT material showed great stability in biological fluids (PBS, plasma) and very low premature release of CPT before reaching the target cells. Confocal microscope images of SNP-CPT-Cy5.5 in HeLa cells demonstrated that the Cy5.5 red fluorescence completely

overlapped with the green fluorescence of Lysotracker (Figure 1), indicating that nanoparticles were internalized by endocytosis [6]. The sub-micron size of the nanoparticle aggregates would probably favor the clathrin mediated internalization process. Additionally, the negative surface charge would also help nanoparticles to escape from the endolysosomes and enter the cytosolic compartment, where they would release their cargo [7]. Table 2 shows that SNP-CPT induces cell death at slightly higher concentration than the free drug in the four lines tested. This is probably due to uncompleted hydrolysis of the ester linking by intracellular esterases. Sensitivity to CPT and SNP-CPT varies among cell lines, HT-29 being the most sensitive.

Figure 1. Internalization of SNP-CPT-Cy5.5 in HeLa cells. Confocal images were obtained for Lysotracker (a) and SNP-CPT-Cy5.5 (b), and merged afterwards to demonstrate that nanoparticles are allocated inside acidic organelles (c).

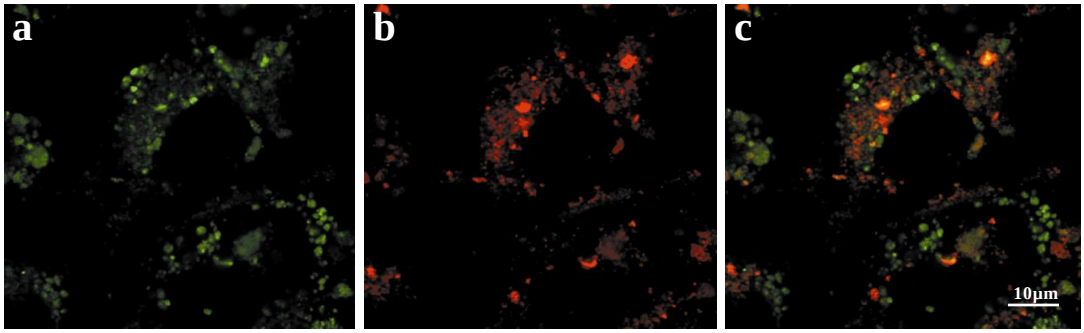

Table 2. IC_{50} values (MTT assay) for CPT and SNP-CPT in different cancer cell lines.

Cell Line	CPT[a]	SNP-CPT[a]
HeLa	0.008 ± 0.003	0.014 ± 0.006
HT-29.Fluc	0.002 ± 0.001	0.006 ± 0.002
U87-MG	0.061 ± 0.024	0.144 ± 0.035
HCT-116	0.039 ± 0.012	0.120 ± 0.011

[(a)]Each value indicates the mean ± SEM (µg/mL) of three to five experiments

Conclusions

We present a novel system for delivery of CPT into cancer cells based in very small and stable surface-modified silica nanoparticles. SNP-CPT internalization by endocytic pathway leads to efficient growth inhibition and cell death. This is a promising platform for CPT biological delivery that can be used to improve drug efficiency.

Acknowledgements

This work was supported by projects MAT2006-14274-C02-01 and PI080771.

References

[1] Venditto, V. J.; Simanek, E. E. *Mol. Pharm.* 7 (2010), 307-349.
[2] Gottlieb, J. A.; Guarino, A. M.; Call, J. B.; Oliverio, V. T.; Block, J. B. *Cancer Chemother. Rep.* 54 (1970), 461-470.
[3] Lu, J.; Liong, M.; Zink, J. I.; Tamanoi, F. *Small* 3 (2007), 1341-1346.
[4] Lu, J.; Liong, M.; Li, Z.; Zink, J. I.; Tamanoi, F. Small 6 (2010), 1794-1805.
[5] Fernández, Y.; Muniesa, C.; Miranda, S.; Quesada, M.; Ruiz, J.; Schwartz Jr, S.; Corma, A.; Abasolo, I.; Botella, P. *Submitted to ACS Nano*.
[6] He, Q.; Zhang, Z.; Gao, Y.; Shi, J.; Li, Y. *Small* 5 (2009), 2722-2729.
[7] Slowing, I.; Trewyn, B. G.; Lin, V. S. *J. Am. Chem. Soc.* 128 (2006), 14792-14793.

Functional bio-gated silica mesoporous supports for controlled delivery applications

Andrea Bernardos, Estela Climent, Laura Mondragón, Elena Aznar, M. Dolores Marcos, Félix Sancenón, Pedro Amorós, Ramón Martínez-Máñez.
Instituto de Reconocimiento Molecular y Desarrollo Tecnológico, Centro Mixto Universidad Politécnica de Valencia - Universidad de Valencia.
CIBER de Bioingeniería, Biomateriales y Nanomedicina (CIBER-BBN)
Universidad Politécnica de Valencia. Camino de Vera s/n 46022, Valencia (España).
E-mail: mmarcos@qim.upv.es

Introduction

Recently, the emergence of biotechnology research has generated great interest in developing new systems to improve not only the pharmacological and therapeutic properties of drugs but also diagnostic methodologies right at the forefront of nanomedicine.
Gated silica mesoporous nanoparticles offer a fresh approach for biomedical applications as they can incorporate a large variety of "gates" that can control on command the delivery of the entrapped guest. Molecular gates can be defined as nanoscopic molecular, supramolecular or macromolecular-based systems that allow mass transport to be triggered by target stimuli. [1] Thus, the external surface of a nanoscopic mesoporous support is functionalized with suitable molecules that upon an external stimulus, the gate is "opened" and allows the release of the previously entrapped cargo in the pores (See Scheme 1). The silica mesoporous supports (SMPS) that are used as starting material show unique features, such as stable mesoporous structure and large surface areas (up to 1200 m2/g). Additionally, the size of the particles (nanometric/micrometric) and the pore size (2-10 nm) can be selected depending on the final application and the characteristics of the loaded cargo.

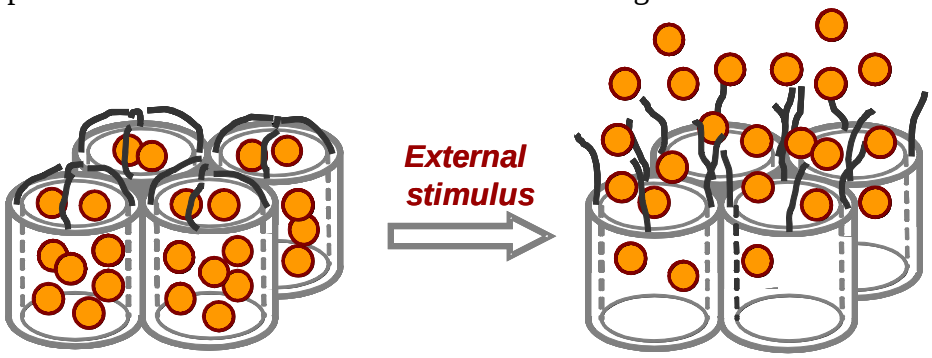

Scheme 1. Scheme of gated mesoporous support.

Results and discussion

Bearing in mind these ideas, we have developed a gated SMPS using antigen-antibody interactions, triggered in the presence of the analyte sulfathiazole.[2] In this approach, the external surface of a suitable SMPS is first functionalized with a hapten and then the mesopores are capped with a certain antibody that shows good affinity and selectivity towards the anchored hapten via suitable interaction through the two binding IgG regions of the former. The presence in the solution of the corresponding complementary antigen to the antibody (sulfathiazole) induced the uncapping of the pores and release of the entrapped guest.

Also inspired by functional entities that perform active tasks in living organisms, we have demonstrated the development of DNA capped SMPS.[3] In this approach, the external surface of a suitable SMPS is first functionalized with an amine derivative and then the mesopores are capped with a certain DNA fragment that shows an unspecific interaction with the protonated amino groups. In presence of the complementary DNA sequence, the delivery of the entrapped guest was observed. The uncapping process is very selective and DNA sequences differing in just one pair were unable to open the gate.

Finally, our group has also demonstrated that the attachment of a commercially available hydrolyzed starch derivative Glucidex 47 as gatekeeper on the surface of silica mesoporous supports provided a suitable method for the design of mesoporous systems that were able to deliver entrapped guests by a biocontrolled uncapping using amylase.[4] Thus, when the pores where capped with the starch derivative, the presence of the enzyme induces cargo release from the hybrid material. In addition, this material was tested for the controlled release in intracellular media using HeLa and LLC-PK1 cells. These experiences showed an internalization of nanoparticles via endocitosis process and the delivery of dye by degradation of the starch by the lysosomal enzymes. Furthemore, when the hybrid material was loaded with the cytotoxic agent doxorrubicine the material internalization induced a decrease in cell viability due to molecular gate degradation by enzymes. This was the first example of enzyme-induced in-cell delivery using capped mesoporous silica nanoparticles.

Conclusions

The possibility of using different biological host-guest pairs opens a wide range of possibilities in the development of target-induced delivery from capped-SMPS that can be used as a new paradigm for signalling/diagnosis applications using the selective delivery of a dye. In addition, we have demonstrated that the use of gated silica mesoporous supports as bio-controlled drug delivery vehicles is a promising area in the field of biomedical applications.

Acknowledgements

The authors wish to express their gratitude to the Spanish Government (Projects MAT2009-14564-C04) and the Generalitat Valencia (Projects PROMETEO/2009/016) for support. A.B. is grateful to the Universidad Politécnica de Valencia for an FPI grant. E.C. is grateful to the Spanish Ministerio de Ciencia e Innovación for a FPU grant.

References

[1] Aznar, E., Sancenón, F., Martínez-Máñez, R., Controlled release using mesoporous materials containing gate-like scaffoldings, Expert Opinion on drug delivery, 6 (2009), 643-655
[2] Climent, E., Bernardos, A., Martínez-Máñez, R., Maquieira, A., Marcos, M.D., Pastor, N., Puchades, R., Sancenón, F., Soto, J., Amorós, P., Controlled Delivery Systems Using Antibody-Capped Mesoporous Nanocontainers, Journal of the American Chemical Society, 131 (2009), 14075-14080
[3] Climent, E., Martínez-Máñez, R., Sancenón, F., Marcos, M.D., Soto, J., Maquieira, A., Amorós, P., Controlled Delivery Systems Using Oligonucleotide-Capped Mesoporous Silica Nanoparticles, Angewandte Chemie International Edition, 49 (2010), 7281-7283
[4] Bernardos, A., Mondragón, L., Aznar, E., Marcos, M.D., Martínez-Máñez, R., Sancenón, F., Soto, J., Barat, J.M., Pérez-Payá, E., Guillem, C., Amorós, P., Enzyme-Responsive Intracellular Controlled Release Using Nanometric Silica Mesoporous Supports Capped with “Saccharides”, ACS Nano, 4 (2011), 6353 – 6368

Effect of pH on the mesopore structure and Al incorporation of disorder mesoporous materials

G.Gonzalez [a],[*], V.Sazo[b], M.E. Gomes[a]
[a]*Lab Materiales, Centro. Ing.Materiales y Nanotecnologia, Instituto Venezolano de Investigaciones Cientificas.*
[b] *Escuela de Quimica, Fac. Ciencias,Centro de Catálisis,Petróleo y Petroquímica, Universidad Central de Venezuela, Caracas 1020-A, Venezuela*
**[a]Corresponding author: Fax:58-212 5041418 and e-mail:gemagonz@ivic.gob.ve; gemagonz@gmail.com*

Introduction

In the present work a detailed study of the effect of pH, in the range of 0 to 4.5, over the mesostructure of a disordered mesoporos material has been carried out. Also, the effect of hydrolysis on the Al incorporation at the different pH, was studied varying the order of addition of the aluminum salt, before and after hydrolysis. The materials were characterized by SEM, TEM, ICP and N_2 adsorption. Catalytic activity of 1-butene was performed . The materials showed a disordered mesostructure for all the pH range studied. A continuous increase in pore diameter and decrease in particle size with pH increase was observed. Al incorporation was favoured as pH increased; the highest incorporation was obtained at pH 4.5. An important effect of hydrolysis on Al incorporation was manifested on the location of the metal. Hydrolysis also had an effect on the distribution and strength of the acid sites. The materials that showed the highest skeletal isomerization selectivity were those synthesized at pH 4.5, with Al incorporated after hydrolysis.

Experimental

Nonilfenolpolietoxilado was used as surfactant. Tetraethoxysilane (TEOS), Aldrich and $Al(NO_3)_3$. $9H_2O$ from Fischer were used as silica and aluminium sources. The disordered mesoporos materials (SMIVIC) were synthesized with the following procedure, but modifying the pH of the synthesis gel from 0 to 4.5. The surfactant was dissolved in de-ionized water under continuous agitation for 12h at room temperature, acid solution of HCl (12 M) was added till pH cero was reached. TEOS was added under continuous agitation. Al incorporation was performed by adding a certain amount of $Al(NO_3)_3$. $9H_2O$ to the synthesis gel before TEOS hydrolysis (BH) or after TEOS hydrolysis (AH), to obtain a Si/Al ratio =30. The variation of pH (0-4.5) was carried out 1h after the silica hydrolysis began with NH_4OH solution. Hydrothermal synthesis was performed under continuous stirring for 48h at 363K in a closed bottle immerses into a thermostatic bath. The solid products obtained were filtered, thoroughly washed with distilled water and dried at 333K for 48h. Calcination was carried out at 793K for 10h under an air flux with a heating rate of 1K/min to remove the template.

Results and discussion

Fig. 1 shows the dramatic change of particle morphology by SEM for the different pH used. The formation of macropores and the reduction of particle size as pH increases can be observed.. There are several parameters that influence the hydrolysis and condensation reactions: activity of metal alkoxide, water/alkoxide ratio, solution pH, temperature and nature of the solvent and additive [1]. The microstructure and surface chemistry of materials are very sensitive to variation of these parameters. Fig. 2 show the N_2 adsorption isotherms and BJH pore size distribution of the materials synthesized at the different pH without The pore size distribution calculated by BJH model for each material is presented on the right hand side. The isotherms are type IV, except for pH 0 that shows a characteristic

supramicroporous isotherm. The pore size and pore volume increase with the increase in pH The incorporation of Al narrows and flattens up the desorption branches, becoming parallel to the adsorption branches similar to a H4 type, suggesting the presence of solids consisting of aggregates or agglomerates of particles forming slit shape pores with uniform shape. As pH is increased the condensation rate increases while the hydrolysis rate decreases [1]. However in the range of pH below 4, hydrolysis of TEOS is still high compared to its condensation rate. In this environment the Al species can interact with the surfactant through weak electrostatic interactions and this interaction will change the final location of the Al species if the process takes place before or after hydrolysis.

Conclusions

The variation of pH has a strong influence in the mesostructure. Increase pH increases pore volume, pore diameter and surface area. The particle size decreases with increase in pH, especially for pH 4.5. Increase pH also favors Al incorporation.
The hydrolysis condition determines the distribution of structural Aluminum in the materials.

References

[1] T C.J.Brinker and G.W.Scherrer, Sol-Gel Science, Academic Press, London, 1990,pp. 97-234

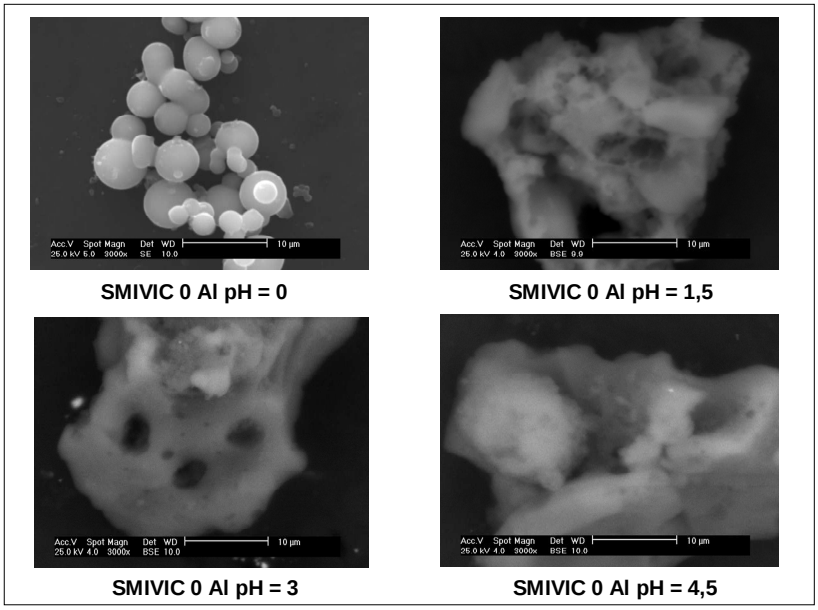

Fig. 1 SEM images of the materials synthesized at different pH

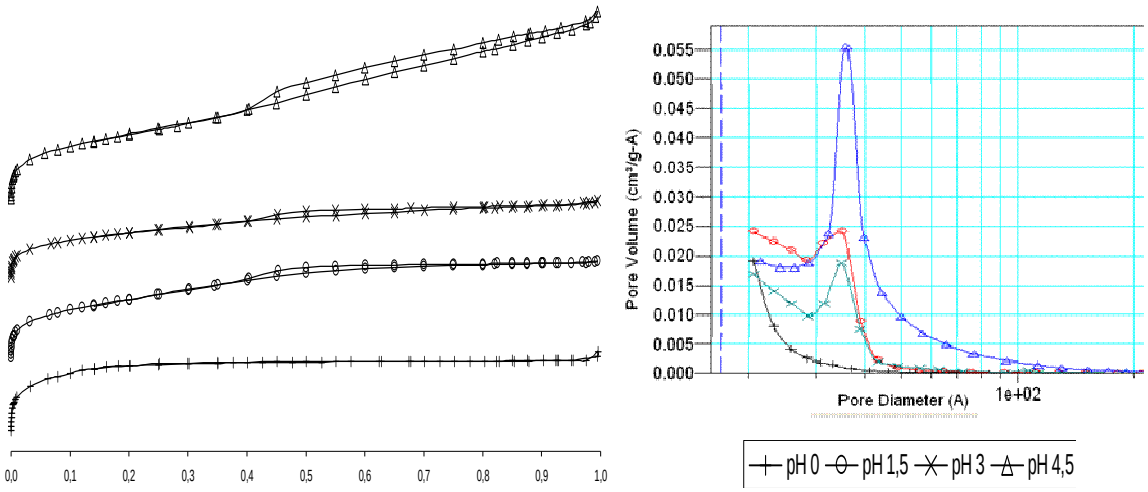

Fig. 2 N_2 adsorption isotherms of the materials synthesized at different pH

Recent Research Reports

FEZA 2011

Molecular Dynamics Simulation of Water in IFR and TON Zeosils

Yu. G. Bushuev*, G. Sastre
**Ivanovo State University of Chemistry and Technology, Ivanovo, Russia, yuriyb2005@gmail.com*
Instituto de Tecnologia Quimica, UPV – CSIC, Valencia, Spain

Introduction

We investigated "spring" and "bumper" behavior [1] of pure silica zeolites (zeosils) using computer simulation methods. These phenomena were observed and studied experimentally in pressure intrusion – extrusion water processes for ITQ-4 (IFR) [2] and TON [3] zeosils. Our goal was shedding light on the molecular mechanism of the phenomena.

Method

Molecular dynamics (MD) simulations of water – zeolite systems were carried out with the GULP code [4]. We have chosen earlier proposed BS force field [5] for calculation of zeolite energy, with flexible modification of SPC water potential [6], and specially optimized potential for silanol groups. The simulation cells consisted from 1×1×2 unit cells of ITQ-4 (ca. 18.6× 13.4×15.3 Å, N = 64 SiO_2, V=3700 Å^3) and 1×1×4 unit cells of TON (ca. 13.9× 17.3× 20.2Å, N=96 SiO_2, V= 4830 Å^3). Water molecules are loaded only in one channel of simulation cells with periodic boundary conditions. All crystallographic cell parameters and atomic positions were varied during the MD simulations. The Ewald summation was used to evaluate Coulombic energy. MD calculations were performed as *NPT* canonical ensemble at P=0.0 Pa and T=300 K, using the leapfrog algorithm for the integration of the equations of motion. A time step of 1 fs was used in all the MD runs. Each system was allowed to relax and equilibrate for 100 ps of MD simulation.

Results and discussion

Firstly, we investigated relative energetic stability of defectless ITQ-4 (IFR) and TON zeosils at different water loading (N) with respect to dry zeosils (N=0) and pure water. Results of calculations are presented in Fig. 1. The main difference between systems is a region of stability for water molecules which is observed at $20<N<30$ in the case of IFR zeosil. Hydrophobicity of both zeolites decreased under external intrusion pressure, but only IFR zeosil became hydrophilic. This observation explains the "spring" behavior of TON zeosil in intrusion – extrusion water experiments. Several Q_3 structural defects were found experimentally in calcined IFR (ca. 1.8 per u.c.) and their amount increases significantly with hydrostatic pressure (ca. 3 per u.c.). At the next stage of our investigation we calculated energies of IFR at different defect site distributions and water loading. We created silanol defect sites based on NMR data.

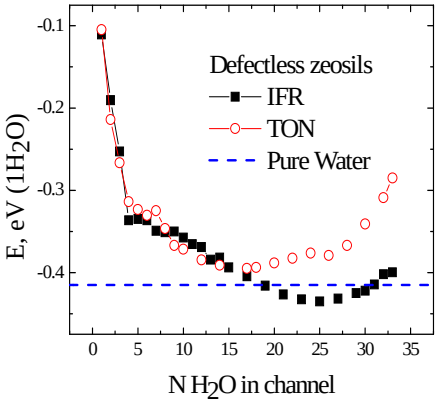

Figure 1. Energy of water in zeosils

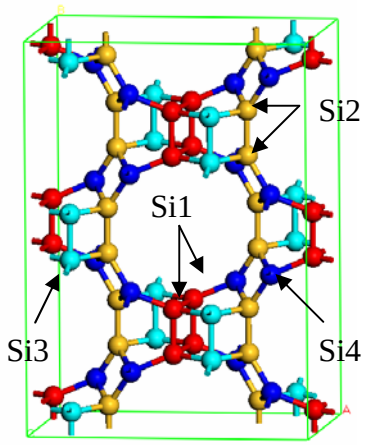

Figure 2. 1×2×1 unit cell of IFR

We considered: 1Si1-1Si1, 1Si1-1Si4, 1Si3-1Si3, 2Si4-2Si2-2Si1 defect sites, where the first digit is number of Si atoms with attached OH groups. Nomenclature of topologically different silicon atoms is presented in Fig. 2. Silanol nests were created by eliminating one Si atom and terminating broken bonds.

We found that in all cases the region of energetic stability becomes wider. In the case of 1Si1-1Si1 and 2Si4-2Si2-2Si1 the curves are under pure water energy straight line (except very small and large loading) as depicted in Fig. 3. Internal view on IFR channel is presented in Fig. 4. We analyzed shapes of water clusters depending on loading.

Computer simulations show that TON zeosil should have “spring” behavior because it is hydrophobic at any loading, but IFR zeosil should be a “bumper” in water intrusion-extrusion processes due to its hydrophilic behaviour at high loading and formation of silanol defects.

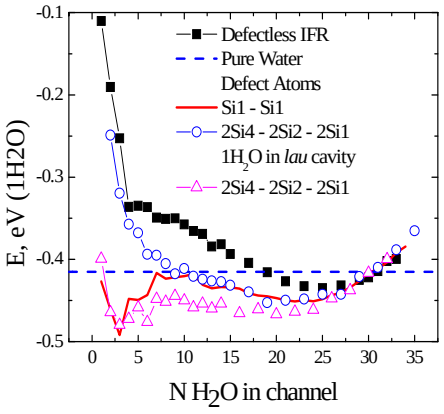

Figure 3. Energy of water in IFR.

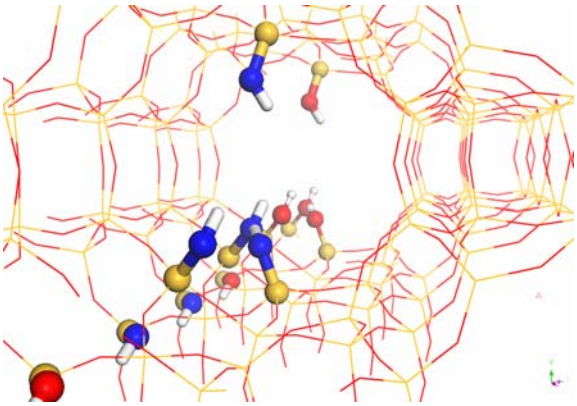

Figure 4. 2Si4 - 2Si2 – 2Si1 defect positions.

References

[1] Eroshenko, V. A.; Fadeev, A. Y. *Colloid J.* **1995**, *57*, 446.
[2] Saada, M.A.; Rigolet, S.; Paillaud, J.-L.; Bats, N.; Soulard, M.; Patarin, J. *J. Phys. Chem. C* **2010,** *114* (26), 11650.
[3] Tzanis, L.; Trzpit, M.; Soulard, M.; Patarin, J. *Micropor. Mesopor. Mater.*, **2011**, In Press.
[4] Gale, J. D.; Rohl, A. L. *Mol. Simul.* **2003**, *29*, 291.
[5] Bushuev, Yu. G.; Sastre, G. *J. Phys. Chem. C* **2009**, *113*, 10877.
[6] Bushuev, Yu. G.; Sastre, G. *Micropor. Mesopor. Mater.* **2010**, 129, 42.

Influence of Intermetallic diffusion barrier on Pd Membrane

Mohammad Hossein Sayyar[3,*]; Milad Rasouli[1,3]; Sahar Chitsazan[1,3]; Nakisa Yaghobi
[1] *Islamic Azad University, South Tehran Branch, Tehran, Iran*
[2] *Department of Petrochemical, Iran Polymer and Petrochemical Institute, Tehran, Iran*
[3] *Pars Coating Technology Co., P.O.Box: 14155/3499, Tehran, Iran*
** sayyar@parscoating.com*

Introduction

To reduce intermetallic diffusion between the metal support and the Pd layer, and thereby improving the stability of the Pd/PSS composite membrane, Ma et al. [1] used a controlled in-situ oxidation of the porous stainless steel prior to plating to produce an oxide layer to act as a diffusion barrier between the Pd and the PSS [2]. The objective of this research is to investigate the effects of temperature on the formation of the intermetallic diffusion barrier layer by the controlled in-situ oxidation method for Pd/PSS membrane.

Experimental

Porous 316L stainless steel supports were purchased from Mott Metallurgical Corporation (0.2 µm grade) and Fuji Filter Company (0.5 µm grade). Two of the support tubes were then oxidized in furnace in the presence of air at 400, 600 and 800 $^{\circ}$C for 2 h, with heating and cooling rates of 3 $^{\circ}$Cmin^{-1}. The furnace was purchased from ELITE THERMAL SYSTEM model TSH12/50/300-2416CG. The oxidation layer formed acts as a diffusion barrier between the PSS substrate and the Pd catalyst. The substrate was then activated by pre-seeding with finely divided Pd nuclei. Procedure for Pd coating.
The composition of the Pd plating solution is given in Table 1. The hydrazine (reducing agent) was added just prior to plating. The plating solution was renewed every 90 to 120 minutes. After deposition was completed the membrane was left to cool to room temperature and dried. After each drying, the weight and helium flux were measured. The weight gains before and after the plating were used to determine the thickness of the membrane.

Table 1 Chemical composition of the plating solution.

Chemicals	Pd bath
$Pd(NH_3)_4Cl_2.H_2O$ (g/l)	4-6
$Na_2EDTA.2H_2O$ (g/l)	40-80
NH_4OH (28%) (ml/l)	190-400
H_2NNH_2 (1M) (ml/l)	5-10
Polyoxyalkylene alkyl ether (ml/l)	0.1-0.5
pH	10-11
Temperature (^{o}C)	60

Results and discussion

Figure 1. shows the SEM pictures of a typical grade 0.2 µm grade Mott PSS after oxidation in 400^{o}C, 600^{o}C, and 800^{o}C.

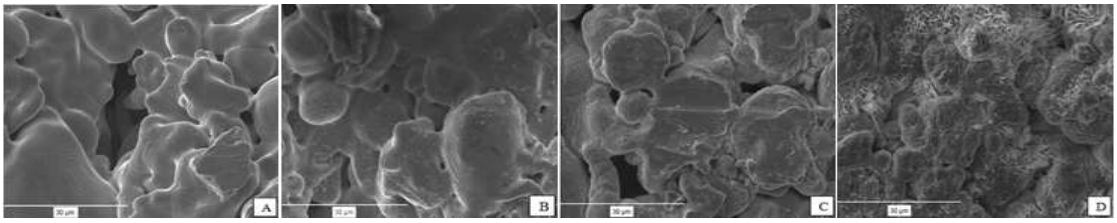

Figure 1. (A) supports after cleaning (B) oxidized at 400°C; (C) oxidized at 600°C; (D) oxidized at 800°C.

Figure 2. shows the change of the properties of the 0.5 µm grade Fuji Filter PSS tubes following oxidation of the cleaned tubes. The oxygen peaks confirm the formation of oxide layers on the supports. It was observed that the amount of oxygen on the support increased with higher oxidation temperatures, indicating a thicker oxide layer. As the oxidation temperature was increased, the weight gain increased indicating the formation of more oxide at higher temperatures. The formation of greater quantities of oxide gave a higher resistance to the He permeation.

Table 2. Percent weight gain and He flux change after oxidation for Mott PSS supports

Tube	Oxidation (°C)	Δm (%)	Thickness (µm)	He Flux, J (cm^3/cm^2min)
1	20	0	0	701
2	400	0.035	--	700
3	600	0.78	0.2-0.3	565
4	800	4.69	1-6	27

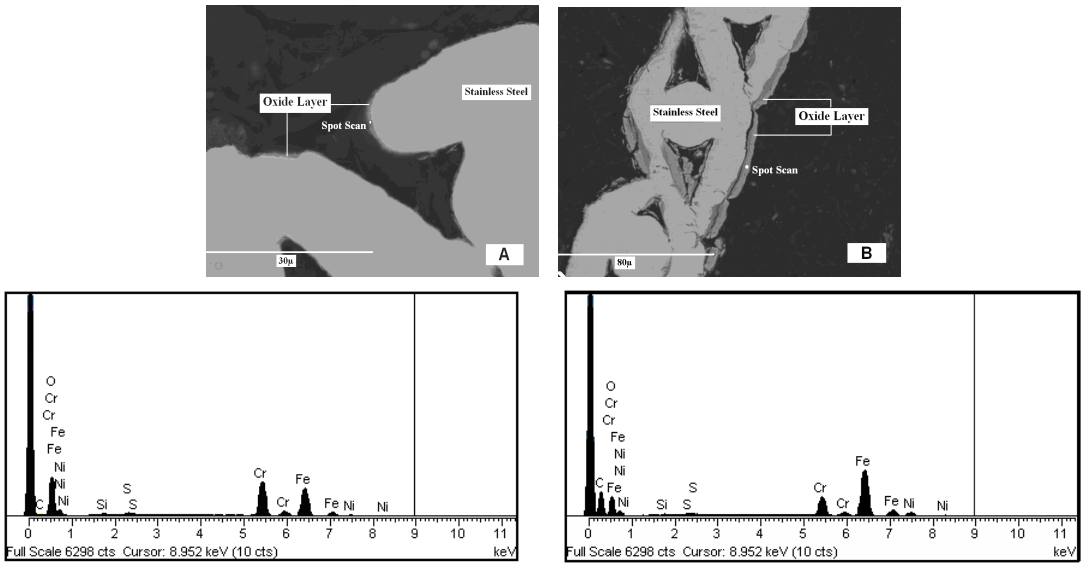

Figure 2. Cross section oxide of the layer of the Fuji PSS supports and EDS spot scans after oxidation on oxide layer at (A) 600°C, and (B) 800°C.

Among the oxides that can be formed with the elements of stainless steel, Cr_2O_3 is the most stable due to its low Gibbs free energy, the low diffusion rates of elements in the oxide scale, and its high chemical stability under a H_2 atmosphere. The SEM micrograph of the sample oxidized at 800˚C showed a thicker dark region with a very nonuniform thickness was observed. It could also be observed that the surface of this oxide layer was very crumbly. The thickness of the dark region varied from 1 to 6 µm from spot to spot since the oxide layer was

relatively thick. After Pd coating, the final thicknesses of the dense Pd membrane were 23-27 µm on 0.2 µm grade Mott supports and 32-35 µm on 0.5 µm grade Fuji plate supports.

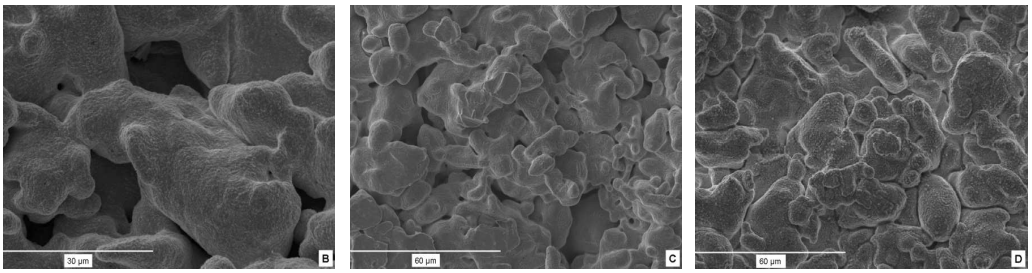

Figure 3. SEM photographs of: B - after 13.5 hr plating; C - after 15 hr; and D - after 24 hr

Conclusions

Oxidation process was carry out in diffrent temprature. It was observed that the amount of oxygen on the support increased 10 times with higher oxidation temperatures indicating a thicker oxide layer. Sample oxidized at 800˚C showed a thicker dark region with a very nonuniform thickness. It was also observed that the surface of this oxide layerwas crumbly. The thickness of the dark oxide region varied from 1 to 6 µm from spot to spot. Therefore, it is the most desirable oxide phase for use as a barrier layer to intermetallic diffusion. Membranes produced by this method have been shown to be stable for over 6000 h in the Temprature of 800^{o}C.

References

[1] US Patent 6152987, “Hydrogen gas-extraction module and method of fabrication”
[2] P.P. Mardllovich, Y. She, Y.H. Ma., “Stabillity of hydrogen flux through Pd/porous stainess steel compsite membranes” Proc.Fifth Int. Conf . Inorg . Membr 1 (1998) 246

Zeolite research at the chemistry department, Addis Ababa University

Wondimagegne Mamo, Negash Getachew, Ignacio J. Villar-Garcia, Yonas Chebude, Isabel Diaz
Chemistry Department, Addis Ababa University, P.O. BOX 1176, Addis Ababa, Ethiopia.
Instituto de Catálisis y Petroleoquímica, CSIC, Madrid, Spain. idiaz@icp.csic.es

Abstract

Ethiopia holds vast natural deposits of zeolites which are mostly unexploited. The Chemistry Department of Addis Ababa University (AAU), in collaboration with the Earth Sciences Department, is initiating research projects and postgraduate programs that can create scientific knowledge on zeolite research and provide with an expertise hub, i.e. qualified personnel, scientific knowledge, technology development for the country. The close collaboration with the Ministry of Mines of Ethiopia is helping in the discovery, identification and characterization of new natural zeolite deposits in the country. Preliminary studies have discovered abundant resources of Philipsite and Clinoptilolite, the latter being a potential catalyst. Furthermore, natural zeolites could be very useful as additives for the local cement and plastic industries and could be paramount in the purification of potable water. The Chemistry Department of AAU has several research lines currently in progress that would benefit as well from the use of zeolites and other porous materials. We are undertaking projects to implement the use of zeolites, both synthetic and natural, in the catalytic conversion of biomass or vegetable materials of natural occurrence in Ethiopia.

Results

Figure 1 collects the research projects currently running in the laboratories of the chemistry department at AAU.

1) Modified Zeolites 2) Vernonia oil 3) Ionic liquids 4) Furfural

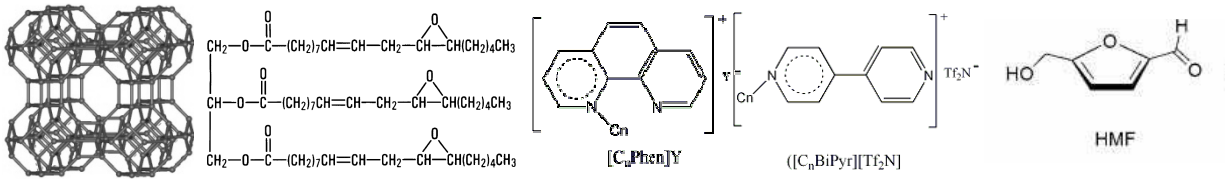

1) Modified Zeolites: We intend to survey the potential use of these natural zeolites in the catalytic process of biomass. In most of the cases with natural zeolites, a previous modification of the zeolite is required in order to achieve a desired acidity. On the other hand, we have started encapsulating some transition metal, and rare earth complexes in the zeolite cavities. These materials could find application for water purification. More specifically, the encapsulation of rare earth complexes in the zeolite cavities will be tested in the elimination of fluorine from potable water. Fluorine contamination is leading to major health problems especially in the Rift Valley area in Ethiopia.

2) Vernonia Oil: Vernonia galamensis is a native plant that grows in the low land areas of Ethiopia, whose seeds contain a significant concentration (approx 40%) of naturally epoxidised triglyceride oils. Among other alternatives to oil derived chemicals, sugar fatty acid esters, synthesised from renewable resources such as carbohydrates, have found broad applications in the food industry, cosmetics, detergents and medical supplies. Our group is investigating biosynthetic routes for the production of sugar fatty acid esters using vernonia oil derivatives and endemic sugars such as cassava starch as starting materials. These products will constitute a new class of naturally epoxydized surfactans with the potential to be used also as starting materials in the synthesis of biodegradable polymers offering an environmentally benign alternative to petroleum based products. The enzymatic esterification of sugars in ionic liquids has been investigated and the results show that the enzyme is highly active in the ionic liquid media. In order to improve enzyme stability enzymes supported on mesoporous materials are also being tested with promising results.

3) Ionic liquids: Ionic liquids are salts that are liquid below 100°C. They exhibit unique properties, including non volatility (no atmospheric emissions) that makes them suitable and advantageous solvents for applications as diverse as catalysis, nanoparticle synthesis and electropolymerization. Current research in our laboratories concentrates in the development of new families of ionic liquids based on 1, 10-phenanthrolinium and 4-4-bipyridinium cations. These ionic liquids exhibit excellent solubilities for metal compounds. The excellent coordination ability of the 4,4-bipyridinium cation is expected to enhance the solubility of glucose in the ionic liquid media and therefore, they are potential solvents/active additives for the heterogeneous catalytic processes involving biomass: the derivatisation of vernonia oil and the synthesis of HMF from glucose.

4) Furural: Among the many biomass-derived chemicals, two major key compounds, furfural and 5-hydroxymethylfurfural, readily available through dehydration of xylose and fructose, respectively, are suitable starting materials for the preparation of further monomer units required for polymer applications. The conclusion of these early experiments in the synthesis of 5-hydroxymethylfurfural predict that among the commercially available zeolites Mordenite, with a channel like structure, yields better balance between activity and selectivity than Zeolite Y, with a cage type of structure. Along with the porosity, Si/Al ratio has to be moderate in the range of 11 to 30, and some degree of hydrophobicity is desirable in order to prevent the re-adsorption of the products and further re-hydration leading to levulinic and formic acid [1-5]. In our group we are investigating the use of ionic liquids as reaction solvents in the presence of zeolites as catalysts. We will present our preliminary results on the synthesis of HMF using Zeolite Y with different Si/Al ratio, at various temperatures, and in the presence of commercial ionic liquids with and without co-solvents. Variations in the extraction methods will be presented as well.

Acknowledgements

The Spanish Cooperation Agency for Development, AECID, is acknowledged for the financial support (C/030766/10). The authors also acknowledge Addis Ababa University and CSIC for institutional support.

References

[1] C. Moreau, R. Durand, C. Pourcheron, S. Razigade, Industrial Crops and Products 3 (1994) 85-90

[2] C. Moreau, R. Durand, S. Razigade, J. Duhamet, P. Faugeras, P. Rivalier, P. Ros, G. Avignon, Applied Catalysis A: General 145 (1996) 211-224

[3] C. Moreau, R. Durand, F. Alies, M. Cotillon, T. Frutz, M.A. Theoleyreet, Industrial Crops and Products 11 (2000) 237–242

[4] C. Lansalot-Matras, C. Moreau, Catalysis Communications 4 (2003) 517–520

[5] C. Moreau, A. Finiels, L. Vanoyeet, Journal of Molecular Catalysis A: Chemical 253 (2006) 165

Where are all the Vanadium MOFs?

Fabian Carson*, Wei Wan, Yifeng Yun, Xiaodong Zou*
Berzelii Center EXSELENT on Porous Materials and Inorganic and Structural Chemistry, Department of Materials and Environmental Chemistry, Stockholm University, SE-106 91 Stockholm, Sweden
** fabian.carson@mmk.su.se, xzou@mmk.su.se*

Introduction

Metal-Organic Frameworks (MOFs) have received tremendous attention during the last decade since the publications of MOF-5[1] and HKUST-1[2] in 1999. These two MOFs contain Zn tetramers and Cu paddlewheels, respectively, as metal nodes, which continue to be popular in MOF synthesis, despite their instability in air and water[3]. However, Férey's group has done much work on the use of trivalent metals in MOFs, such as Fe^{3+} and Cr^{3+}, which tend to be more stable[4,5]. In particular, they have synthesised various vanadium MOFs, for example MIL-47[6]. Our aim was to synthesise new vanadium MOFs. This has led to the discovery of two new interrelated vanadium-containing MOFs, MIL-88(V) and MIL-101(V).

Experimental

The vanadium MOFs, MIL-88(V) and MIL-101(V) were synthesised solvothermally using VCl_3 and terephthalic acid as the metal and ligand sources, respectively. The resulting green powders were separated from the mother liquor by centrifugation and dried at room temperature. The samples were studied by powder X-ray diffraction (PXRD) and transmission electron microscopy (TEM). N_2 sorption isotherm was performed on a MIL-101(V) sample.

Results and discussion

The powder X-ray diffraction (PXRD) patterns in Fig. 1 are similar to those of MIL-88B(Cr)[7] and MIL-101(Cr)[5], respectively, showing that we have synthesised the vanadium analogues of MIL-88(V) and MIL-101(V). The PXRD pattern of MIL-88(V) (Fig. 1a) gives a hexagonal unit cell of a = 10.62 Å, c = 19.21 Å, which is close to that of MIL-88B(Cr) (a = 11.05 Å, c = 18.99 Å). The PXRD pattern of MIL-101(V) (Fig. 2b) shows that the sample contains MIL-88(V) as an impurity. We are currently working on obtaining pure MIL-101(V).

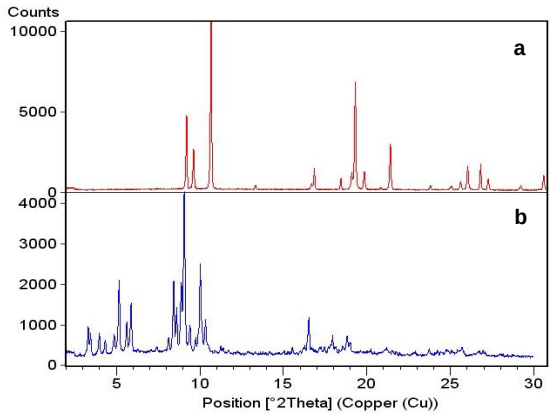

Figure 1. PXRD pattern of (a) MIL-88(V) and (b) MIL-101(V).

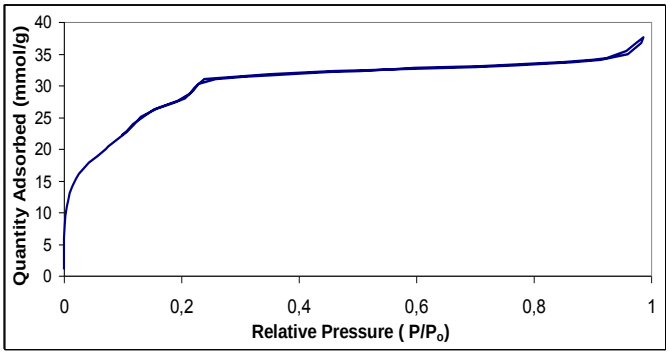

Figure 2. The N_2 sorption isotherm on a MIL-101(V) sample.

The MIL-88(V) crystals (0.5 × 0.5 × 2.5 μm) are too small for single crystal diffraction (Fig. 3). Therefore, the unit cell parameters were determined from a tilt series of electron diffraction (ED) patterns (2) to be a = b = 10.1 Å, *c* = 18.6 Å, α = β = 90° and γ = 120°, similar to those obtained from PXRD.

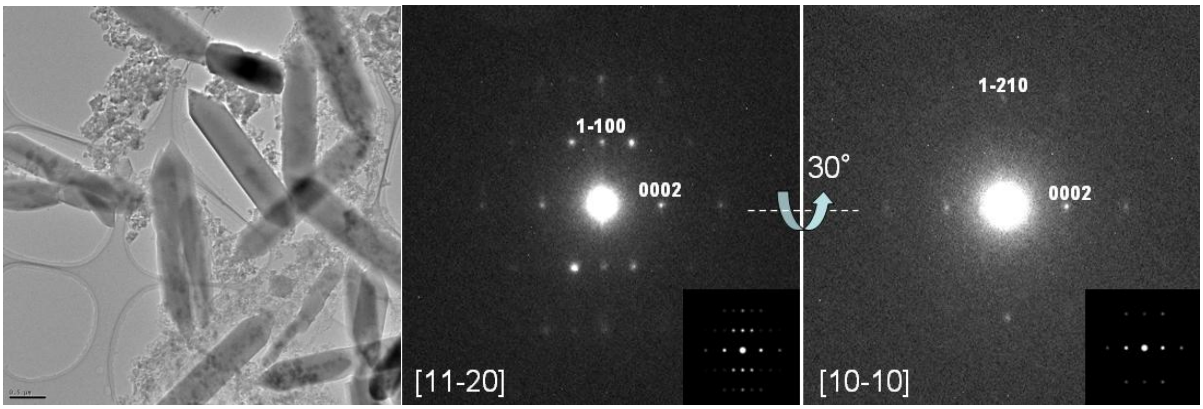

Figure 3. TEM image and electron diffraction patterns of MIL-88(V). The two ED patterns are tilted along the horizontal ***c***-axis by 30°. Insets are the simulated ED patterns.

The N_2 sorption isotherm of MIL-101(V) is shown in Fig. 2. The calculated BET surface area from this isotherm is 2300 m^2/g. However, to correctly characterise the material, it will be necessary to attain pure MIL-101(V).

Early investigations indicate a phase transition from MIL-88(V) to MIL-101(V) with increased synthesis times, indicating that MIL-88(V) is a kinetic product. We are currently trying to better understand this phase transition.

Conclusions

We have synthesised and partially characterised two new vanadium analogues of MIL-88 and MIL-101; MIL-88(V) and MIL-101(V). Further characterisation of these materials is in progress.

Acknowledgements

This project is supported by the Swedish Research Council (VR) and the Swedish Governmental Agency for Innovation Systems (VINNOVA) through the Berzelii Center EXSELENT. Wei Wan is supported by a post doctoral grant from the Carl-Trygger Foundation.

References

[1] Li, H., Eddaoudi, M., O'Keeffe, M., Yaghi, O. M., Nature, 402 (1999), 276-279.
[2] Chui, S. S. Y., Lo, S. M. F., Charmant, J. P. H., Orpen, A. G., Williams, I. D., Science, 283 (1999), 1148-1150.
[3] Low, J. J., Benin A. I., Jakubczak P., Abrahamian J. F., Faheem S. A., Willis R. R., J. Am. Chem. Soc. 131 (2009), 15834-15842.
[4] Serre, C., Millange, F., Surblé, S., Férey, G., Angew. Chem. Int. Ed. 43 (2004), 6285-6289.
[5] Férey, G., Mellot-Draznieks, C., Serre, C., Millange, F., Dutour, J., Surblé, S., Margiolaki, I., Science, 309 (2005), 2040-2042.
[6] Barthelet, K., Marrot, J., Riou, D., Férey, G., Angew. Chem. Int. Ed., 41 (2002), 281-284.
[7] Surblé, S., Serre, C., Mellot-Draznieks, C., Millange, F., Férey, G., Chem. Comm., 3 (2006), 284-286.

Synthesis of Faujasite with Nanometric Crystals

Thiago F. Chaves[*]; Heloise O. Pastore[**]; Dilson Cardoso[*]

[*]*Federal University of São Carlos – Catalysis Laboratory - São Carlos – SP, Brazil.*

[**]*Universidade Estadual de Campinas – UNICAMP, Campinas – SP, Brazil.*

dilson@ufscar.br

Introduction

Reducing the size of zeolite crystals from the micrometric scale to the nanometer scale has produced significant changes in the properties of these materials. For example, the use of zeolites formed by nanocrystals gives rise to significant improvements in traditional applications, as for instance catalysis and separation. The ratio of external to internal number of atoms grows rapidly with decreasing particle size, increasing the external surface area [1]. Moreover, smaller crystals have a larger amount of exposed pores, reflecting lower internal diffusion limitations when compared to micrometric-sized zeolite crystals [2]. Considering the growing importance of zeolite nanocrystals in catalysis, this work investigates the synthesis conditions to obtain a FAU zeolite with nanocrystals without using an organic template.

Experimental

A typical molar composition containing the following ratio: 5.5 Na_2O : 1.0 Al_2O_3 : 10 SiO_2 : 180 H_2O, was used to synthesize the faujasite zeolite. The reagents used in the synthesis were Aerosil 380 (Evonik), sodium aluminate (Riedel de Haën – 54% Al_2O_3 : 41% Na_2O : 5% H_2O), sodium hydroxide (Quimis) and deionized water (Riedel de Haën - 54% Al_2O_3: 41% Na_2O: 5% H_2O), (Quimis). The reaction mixture formed was transferred to a Teflon-lined stainless steel autoclave and kept in an oven at 100 °C for 6 h. After this time elapsed, the solid obtained was washed several times until the pH reached 8 and then dried at 60 °C. The samples were characterized by X-ray Diffraction (XRD), Nitrogen Physisorption, Transmission Electron Microscopy (TEM), Energy Dispersive Spectroscopy (EDS) and Nuclear Magnetic Resonance (NMR) of ^{29}Si.

Results and discussion

The alkalinity effect on the product properties was checked, changing the number of Na_2O moles in the synthesis gel. This modification was performed by adding sodium hydroxide in quantities to achieve a Na_2O/Al_2O_3 molar ratio of 5.5, 6.5, 7.5 and 8.5. The hydrothermal treatment time was of 6 hours at 100 °C. Figure 1 shows the diffraction patterns for the different samples. Increasing the amount of Na_2O in the synthesis mixture decreased the intensity of the diffraction peaks. The results of nitrogen physisorption show that the micropore volume and the samples' external surface area decrease with the increasing amount of Na_2O. The sample Y-B5.5, showed an external area of 39 m^2/g and a micropore volume of 0.27 cm^3/g. Comparatively, the sample Y-B8.5 showed an external surface area of 27 m^2/g and micropore volume of 0.06 cm^3/g, showing that the material is not yet well structured. This may be related to an increased alkalinity in the reaction mixture for the samples with high contents of Na_2O, thereby favoring a higher dissolution of the zeolite. To decrease crystal size and improve the micropore volume, the reaction mixture was subjected to additional aging, therefore favoring the formation of a greater number of crystallization nuclei. For this, the sample with the Na_2O/Al_2O_3 ratio of 8.5 was chosen, shown in Figure 1, it was the one that formed the worst diffraction pattern of the FAU structure. Aging was performed at 25 ° C for 24, 48 or 72 h.

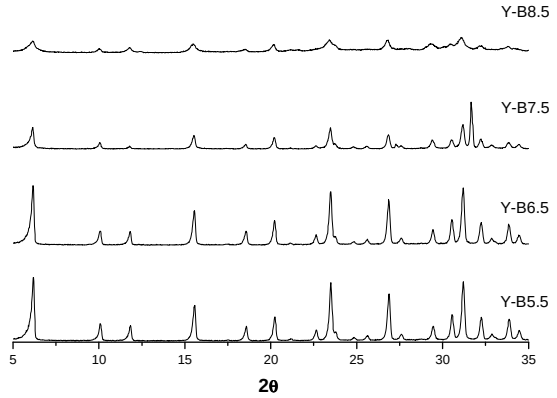

Figure 1. XRD of the samples synthesized with different Na_2O/Al_2O_3 ratios.

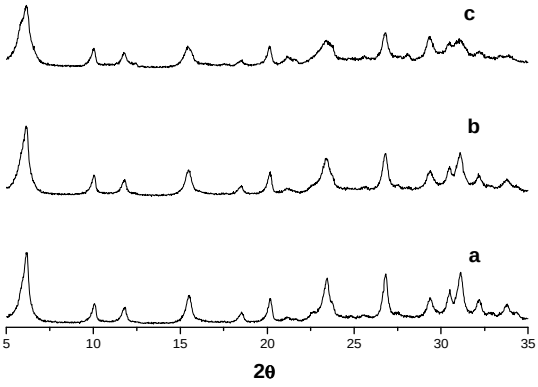

Figure 2. XRD of the samples synthesized with different aging times: 24 (a), 48 (b) and 72 h (c).

The diffraction patterns (Figure 2) of the three samples with aging exhibit the characteristic peaks of FAU. The sample aged for 72 h has a micropore volume of 0.23 cm^3/g and external surface area of 115 m^2/g, respectively. The TEM results show that this zeolite has aggregates smaller than 100 nm, hence Figure 3 shows the crystal planes for the plane (111), showing that this zeolite is well crystallized. The NMR spectrum of ^{29}Si shows the different chemical environments of Si atoms, the Si/Al ratio obtained from the NMR peak areas is of 1.46, close to that obtained by EDS (Figure 4).

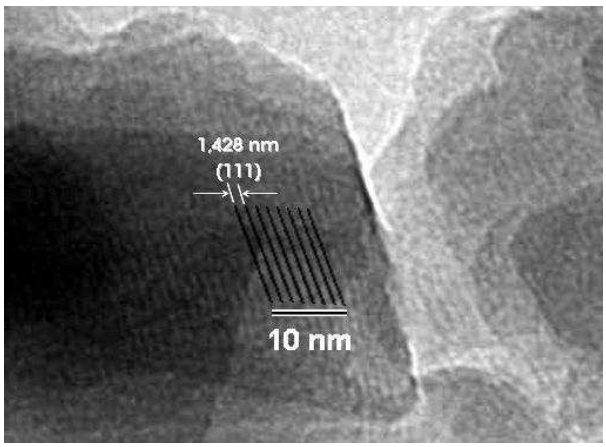

Figure 3. TEM sample aged for 72 h.

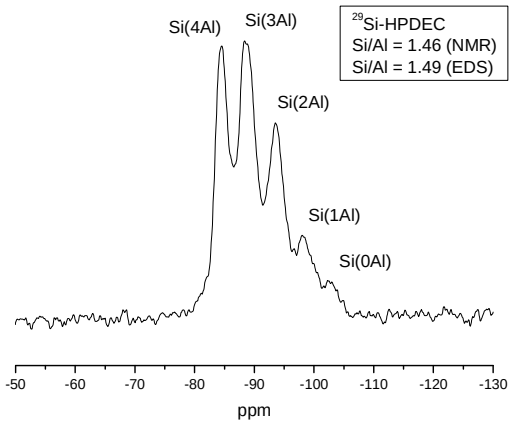

Figure 4. NMR of ^{29}Si-HPDEC of the sample aged for 72 h.

Conclusions

It was possible to synthesize nanometric crystals with the FAU structure, without requiring organic templates, with high external surface areas. Due to this material's presumably lower diffusion limitations, it can potentially be used as catalysts or adsorbents.

Acknowledgements

CNPq - National Council for Scientific and Technological Development and FAPESP - Foundation for Research in the State of São Paulo.

References

[1] L. Tosheva, V.P. Valtchev, Chem. Mater. 17 (2005) 2494-2513.

[2] P.M. Lima, T. Garetto, C.L. Cavalcante Jr., D. Cardoso, Catal. Today (2011), doi: 10.1016/j.cattod.2011.02.031 (in press).

Low-temperature investigation of the zeolite paulingite

Bieniok A.[1], Göttig P.[2] and Brendel U.[2]
[1]*University of Salzburg, Materials Engineering & Physics, Hellbrunnerstr.34, 5020-Salzburg, Austria, anna.bieniok@sbg.ac.at*
[2]*University of Salzburg, Molecular Biology, Billrothstr.11, 5020 Salzburg, Austria*

Introduction

Paulingite is one of the most interesting natural zeolites due to its complex framework structure and its large unit cell volume. It occurs as colorless, transparent rhombic dodecahedra {110} in vugs of basaltic rocks. The size of the crystals varies between several µm to mm. Only nine occurrences of paulingite are known worldwide, four of them from the USA and five from Europe. In the majority of cases the samples are K, Ca- paulingites with Si/Al ratios around 3 [1]. The general formula is $(K_2, Ca, Na_2, Ba)_{x/8}[Si_{672-x}Al_xO_{1344}] \cdot n\ H_2O$ with $432 < n < 700$. Paulingite crystallizes in the cubic space group Im3m. Depending on the cation filling, the cell constant for fully hydrated paulingite varies between 35.030 Å (paulingite-K) and 35.240 Å (paulingite-K,Ca) [2]. The complex framework structure builds up a 3-dimensional channel system with eight-ring openings (framework type code PAU; <100> **8** 3.6 x 3.6***). Seven different polyhedral cage types can be distinguished in the framework, among others the α-cage, known from zeolite A, and the double-eight ring D8R [3]. Thermogravimetric analyses have shown that the dehydration of paulingite occurs in several steps and that the structure breaks down above 523 K [4]. After water loss of approximately 75% a partly dehydrated structure exists at 373 K with a reduced cell constant of 33.88 Å [5]. The flexible structure responds to dehydration at higher temperatures with a cell volume reduction of about 10% and a transformation to a low-symmetry phase in space group I-43m. The subject of the present study is the behavior of the framework structure at low temperature conditions.

Experimental

A transparent single crystal of paulingite-Ca, K from Ritter, Grant County, Oregon, USA, was used for the diffraction experiments. The 150 µm size crystal is a fragment of a rhombic dodecahedron. The composition of this Ca-rich sample is $Ca_{59}K_{36}Na_{14}Ba_2[Si_{499}Al_{173}O_{1344}] \cdot 550\ H_2O$ [1]. The diffraction measurements were performed using a micro-focus X-ray rotating anode source with CuKα-radiation and optimized X-ray optics combined with an image plate detector with 345 mm diameter. The sample was cooled in a dry flow of N_2 and rates of 120 K/h. Data sets were collected at 296 K, 283 K, 263 K, 225 K, 150 K and 100 K. The maximum resolution of the data sets is 1.55 Å. Data processing and refinement of the structure model were performed with CCP4 programs [6] and Shelxl [7].

Results and discussion

The cell constant of hydrated paulingite at room temperature (296 K) is 35.113(4) Å. After cooling in dry N_2 to 100 K, a_0 decreases to 34.245(5) Å, corresponding to a unit cell contraction of 7.2% . Fig. 1 shows the values of the cell constants at different temperatures. From geometric structure simulations it is known that the compression of the PAU framework to a cell with lattice constants smaller than 33.6 Å is only possible if the inversion center and the diagonal 2-fold axes are disregarded [8]. Therefore, space group I-43m was chosen for the refinement of the LT-structure. Using isotropic displacement factors, convergence was achieved with R1=0.0895 and a GoF of 1.2. The structure of paulingite at 100 K comprises

tetrahedrally compressed α-cages and elliptically distorted eight-rings. The deformation resembles the distortion observed in the partly dehydrated, high-temperature form of paulingite.

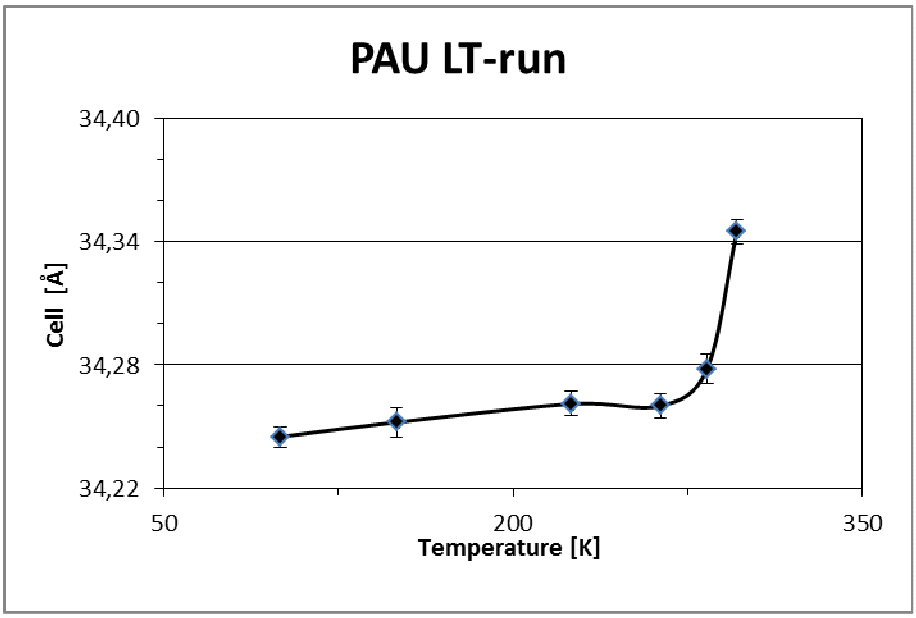

Figure 1. Cell constants [Å] of paulingite at low temperatures [K].

However, the decrease of the unit cell volume is in both cases predominantly caused by dehydration and is not a solely thermally induced effect. This interpretation is supported by the measurement of paulingite in a flow of dry nitrogen at 296 K. The cell volume drops from 35.113(4) Å to 34.345(6) Å, which means a volume reduction of 6.6% as a response to the lower humidity of the environment and the immediate dehydration. It is the loss of water molecules that causes the flexible framework structure of paulingite to collapse and to adapt its cell volume to the remaining water molecules and cations filling the pores of the framework.

Conclusions

The investigation demonstrates not only the low-temperature behavior of paulingite but also the sensitivity of collapsible zeolite structures to humidity and environmental conditions.

References

[1] Tschernich, R.W., Wise, W., Paulingite: variations in composition, American Mineralogist 67 (1982) 799-803
[2] Passaglia, E., Gualtieri, A.F., Marchi, E., The crystal chemistry of paulingite, European Journal of Mineralogy 13 (2001), 113-119
[3] Bieniok, A., Joswig, W., Baur, W.H., A study of paulingites: pore filling by cations and water molecules, Neues Jahrbuch für Mineralogie - Abhandlungen 171/2 (1996) 119-134
[4] Lengauer, C.L., Giester, G., Tillmanns, E., Mineralogical characterization of paulingite from Vinarická Hora, Czech Republic, Mineralogical Magazine 61 (1997) 591-606
[5] Bieniok, A., Crystal structure of partly dehydrated paulingite, in Colella, C. and Mumpton, F.A., eds.: Natural Zeolites for the Third Millenium, (2000) 53-60
[6] Collaborative Computational Project, Number 4, The CCP4 Suite: Programs for Protein Crystallography, Acta Crystallographica D50 (1994) 760-763
[7] Sheldrick, G.M., A short history of SHELX, Acta Crystallographica A64 (2008) 112-122
[8] Bieniok, A., The dehydration of the zeolite paulingite, Neues Jahrbuch für Mineralogie – Monatshefte 11 (1997) 498-504

Molecular Dynamics Simulation of Water in IFR and TON Zeosils

Yu. G. Bushuev*, G. Sastre
**Ivanovo State University of Chemistry and Technology, Ivanovo, Russia, yuriyb2005@gmail.com*
Instituto de Tecnologia Quimica, UPV – CSIC, Valencia, Spain

Introduction

We investigated "spring" and "bumper" behavior [1] of pure silica zeolites (zeosils) using computer simulation methods. These phenomena were observed and studied experimentally in pressure intrusion – extrusion water processes for ITQ-4 (IFR) [2] and TON [3] zeosils. Our goal was shedding light on the molecular mechanism of the phenomena.

Method

Molecular dynamics (MD) simulations of water – zeolite systems were carried out with the GULP code [4]. We have chosen earlier proposed BS force field [5] for calculation of zeolite energy, with flexible modification of SPC water potential [6], and specially optimized potential for silanol groups. The simulation cells consisted from 1×1×2 unit cells of ITQ-4 (ca. 18.6× 13.4×15.3 Å, N = 64 SiO_2, V=3700 Å^3) and 1×1×4 unit cells of TON (ca. 13.9× 17.3× 20.2Å, N=96 SiO_2, V= 4830 Å^3). Water molecules are loaded only in one channel of simulation cells with periodic boundary conditions. All crystallographic cell parameters and atomic positions were varied during the MD simulations. The Ewald summation was used to evaluate Coulombic energy. MD calculations were performed as *NPT* canonical ensemble at P=0.0 Pa and T=300 K, using the leapfrog algorithm for the integration of the equations of motion. A time step of 1 fs was used in all the MD runs. Each system was allowed to relax and equilibrate for 100 ps of MD simulation.

Results and discussion

Firstly, we investigated relative energetic stability of defectless ITQ-4 (IFR) and TON zeosils at different water loading (N) with respect to dry zeosils (N=0) and pure water. Results of calculations are presented in Fig. 1. The main difference between systems is a region of stability for water molecules which is observed at $20<N<30$ in the case of IFR zeosil. Hydrophobicity of both zeolites decreased under external intrusion pressure, but only IFR zeosil became hydrophilic. This observation explains the "spring" behavior of TON zeosil in intrusion – extrusion water experiments. Several Q_3 structural defects were found experimentally in calcined IFR (ca. 1.8 per u.c.) and their amount increases significantly with hydrostatic pressure (ca. 3 per u.c.). At the next stage of our investigation we calculated energies of IFR at different defect site distributions and water loading. We created silanol defect sites based on NMR data.

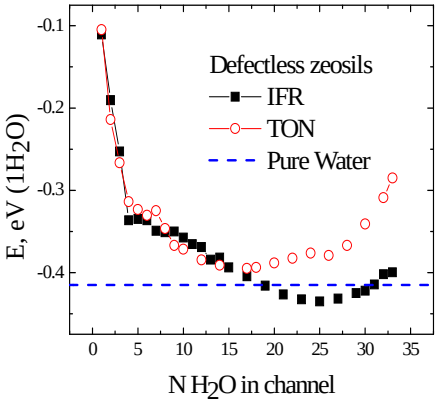

Figure 1. Energy of water in zeosils

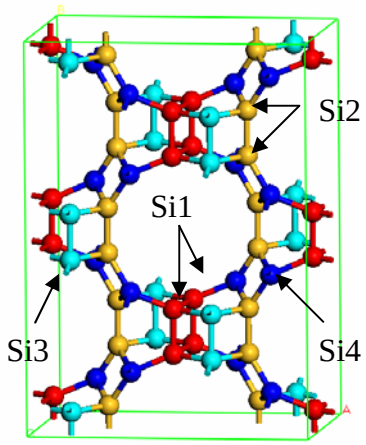

Figure 2. 1×2×1 unit cell of IFR

We considered: 1Si1-1Si1, 1Si1-1Si4, 1Si3-1Si3, 2Si4-2Si2-2Si1 defect sites, where the first digit is number of Si atoms with attached OH groups. Nomenclature of topologically different silicon atoms is presented in Fig. 2. Silanol nests were created by eliminating one Si atom and terminating broken bonds.

We found that in all cases the region of energetic stability becomes wider. In the case of 1Si1-1Si1 and 2Si4-2Si2-2Si1 the curves are under pure water energy straight line (except very small and large loading) as depicted in Fig. 3. Internal view on IFR channel is presented in Fig. 4. We analyzed shapes of water clusters depending on loading.

Computer simulations show that TON zeosil should have “spring” behavior because it is hydrophobic at any loading, but IFR zeosil should be a “bumper” in water intrusion-extrusion processes due to its hydrophilic behaviour at high loading and formation of silanol defects.

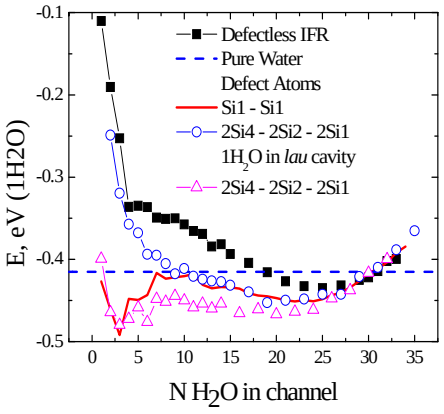

Figure 3. Energy of water in IFR.

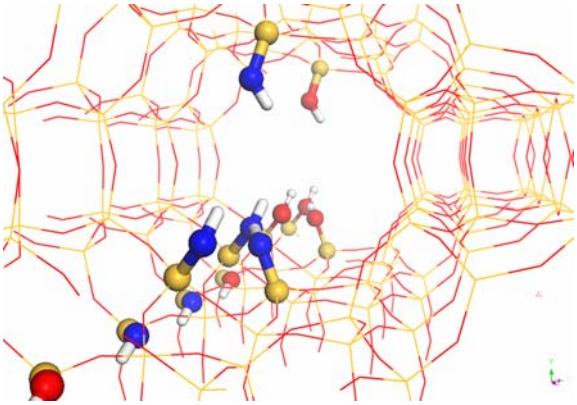

Figure 4. 2Si4 - 2Si2 – 2Si1 defect positions.

References

[1] Eroshenko, V. A.; Fadeev, A. Y. *Colloid J.* **1995**, *57*, 446.
[2] Saada, M.A.; Rigolet, S.; Paillaud, J.-L.; Bats, N.; Soulard, M.; Patarin, J. *J. Phys. Chem. C* **2010,** *114* (26), 11650.
[3] Tzanis, L.; Trzpit, M.; Soulard, M.; Patarin, J. *Micropor. Mesopor. Mater.*, **2011**, In Press.
[4] Gale, J. D.; Rohl, A. L. *Mol. Simul.* **2003**, *29*, 291.
[5] Bushuev, Yu. G.; Sastre, G. *J. Phys. Chem. C* **2009**, *113*, 10877.
[6] Bushuev, Yu. G.; Sastre, G. *Micropor. Mesopor. Mater.* **2010**, 129, 42.

Density functional study of the Al distribution effects on the double proton transfer mechanisms upon 4,4'-bipyridine adsorption on H-ZSM-5

M. Castellà-Ventura[1], Y. Akacem[2], E. Kassab[1]
[1] *Laboratoire de Chimie Théorique, Université Pierre et Marie Curie, 75252, Paris, France, ek@lct.jussieu.fr*
[2] *Laboratoire de Modélisation Moléculaire, Faculté de Chimie, Alger, Algérie*

Introduction

The present theoretical study is the extension of our previous work reported on the double proton transfer reaction between 4,4'-bipyridine ligand (44BPY) and Brønsted acid sites of H-ZSM-5 simulated by a two ten-membered ring cluster (2-10T) with two particular distributions adapted to the concerted mechanism, leading to the formation of the diprotonated dication $44BPYH_2^{2+}$ [1]. This dication was observed by Raman spectrometry upon adsorption of 44BPY inside H-ZSM-5 [2]. In our study, extensive cluster density functional theory (DFT) calculations have been carried out on six other Al distributions in order to gain an understanding of the influence of the Al distribution on the different mechanisms (concerted and consecutive) of the double proton transfer from H-ZSM-5 to 44BPY. The energetic, structural and vibrational properties of the adsorption complexes involved in the proton transfer reaction have been characterized.

Theoretical model

The zeolite straight channel is simulated by two ten-membered ring clusters, arranged in parallel way. Each ring is composed of nine Si atoms and one Al atom. Six Al distributions (Al1, Al1'), (Al1, Al2'), (Al1, Al3'), (Al1, Al4'), (Al1, Al5'), and (Al1, A6') are considered in our study (Fig. 1). Taking into account of the location of the protons associated with the Al atoms, 24 (Al, H) configurations may be generated. Among them, 8 (Al, H) configurations have been chosen. 44BPY is initially positioned perpendicularly to the 10T rings, and its molecular centre is fixed on the cluster straight channel axis during the geometry optimization. For all Al configurations, the structures of the adsorption complexes have been optimized, their adsorption energies have been calculated, the minimum energy pathways for proton transfer have been characterized, and the vibrational frequencies of adsorbed 44BPY have been analyzed.
All calculations have been carried out with the DFT method at the B3LYP/6-31+G* level.

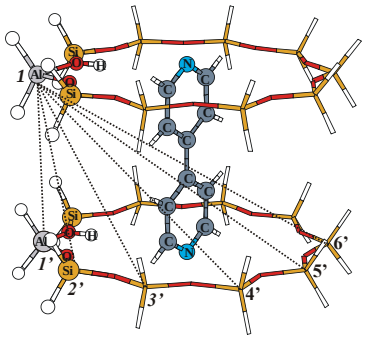

Figure 1. Schematic representations of 44BPY in the straight channel of H-ZSM-5

Results and discussion

For the double proton transfer from H-ZSM-5 to 44BPY, two mechanisms according to the Al distribution have been proposed: a concerted mechanism in which both protons are simultaneously transferred [1], and a consecutive mechanism in which the transfer of the two protons takes place successively.
Only for the two (Al1, Al6') and (Al1, Al5') distributions in which the two acidic protons are the farthest from each other, the double proton transfer may occur through a concerted mechanism. The related potential energy surface shows only one minimum corresponding to the formation of the bidentate ion-pair complex $44BPYH_2^{2+}/Z^{2-}$.
For the six other Al configurations, the double proton transfer reaction likely occurs via a consecutive mechanism. The potential energy surface has two minima corresponding to the formation of the monodentate $44BPYH^{+}/Z^{-}$ and bidentate ion-pair $44BPYH_2^{2+}/Z^{2-}$ complexes. In the first step, only one proton is transferred, giving the monodentate complex $44BPYH^{+}/Z^{-}$. The calculated adsorption energies for the six monodentate complexes are slightly sensitive to the Al distribution. On the other hand, in the second step, the transfer of the second acidic proton leading to the formation of the bidentate complex $44BPYH_2^{2+}/Z^{2-}$ depends on the Al distribution. For the (Al1, Al1'), (Al1, Al2') and (Al1, Al3') distributions, the bidentate complexes are less stable than the corresponding monodentate complexes, whereas it is the opposite for (Al1, Al4'), (Al1, Al5'), and (Al1, Al6') distributions. The height barriers of the energy paths connecting two minima corresponding to mono- and bidentate complexes strongly depend on the Al distribution (Fig. 2).

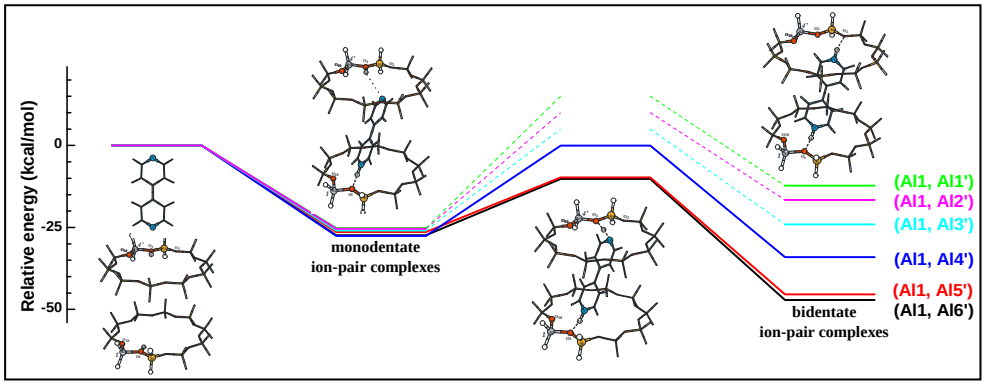

Figure 2. Energy diagram for the double proton transfer via the consecutive mechanism

The calculated vibrational frequencies and frequency shifts of 44BPY adsorbed as mono- or diprotonated species are in good agreement with available experimental data. It was found that most of them are insensitive to the Al distribution.

Conclusions

The proton transfer reactions upon adsorption of 44BPY on H-ZSM-5 were investigated by DFT calculations at the B3LYP/6-31+G* level using a 2-10T cluster. Our results provide new insights on the nature of the species formed upon adsorption, and clearly show that the formation of the mono- or bidentate ion-pair complexes are governed by the Al distribution.

References

[1] Kassab, E., Castellà-Ventura, M., Akacem, Y., J. Phys. Chem. C, 113 (2009) 20388-20395
[2] Moissette, A, Batonneau, Y., Brémard, C., J. Am. Chem. Soc., 123 (2001) 12325-12334

TRANSLATIONAL AND ROTATIONAL MOBILITY OF METHANOL-d_4 IN NaX(1.3) ZEOLITE: A DEUTERON NMR INVESTIGATION

Z.T. Lalowicz[1], G. Stoch[1], A. Birczyński[1], M. Punkkinen[2], E. Ylinen[2], K. Góra-Marek[3], J. Datka[3]
[1]*H. Niewodniczański Institute of Nuclear Physics PAS, Kraków, Poland*
[2]*Wihuri Physical Laboratory, Department of Physics, University of Turku, Turku, Finland*
[3]*Department of Chemistry, JagellonianUniversity, Kraków, Poland*
Zdzislaw.Lalowicz@ifj.edu.pl

Introduction

Mobility of organic molecules in cages of zeolites has drawn a lot of attention [1]. It was well established that adsorption behaviour of methanol in faujasites was mainly determined by methanol-cation interaction. In that context o lot of attention was devoted to the migration of cations and the concentration dependence of methanol self-diffusivity [2,3]. Molecular mobility, both diffusivity and reorientation, is determined by the forces between the organic molecules and the zeolite complex framework. The forces may range from weak van der Waals interaction, electrostatic interaction with extra-framework cations to strong hydrogen bonding. Analysis of the deuteron NMR spectra at a wide range of temperatures provides information on the distribution of species, on the nature of binding sites, and about the symmetry of rotation of the sorbed molecules [4]. Temperature dependence of the relaxation rate allows to estimate the strength of interactions and to follow their evolution.

Experimental and discussion

We apply deuteron NMR spectroscopy to determine rotational mobility of CD_3OD molecules (172 molecules per uc) in NaX(1.3) zeolite. Low temperature spectra disclose several components related to well specified rotational modes for various possible locations. Two localized methanol configurations may be pointed out, based on the schemes proposed in previous papers [2,3]. First one considers a bonding to cation with some possible interaction of deuteriums with framework oxygens in the neighborhood (a parallel to the cage wall confuguration). In the second one the methanol OD is involved in the hydrogen bond to the framework oxygen and CD_3 remains rather free in the space (a perpendicular to the cage wall configuration). We attribute labels relating methyl and hydroxyl groups to their

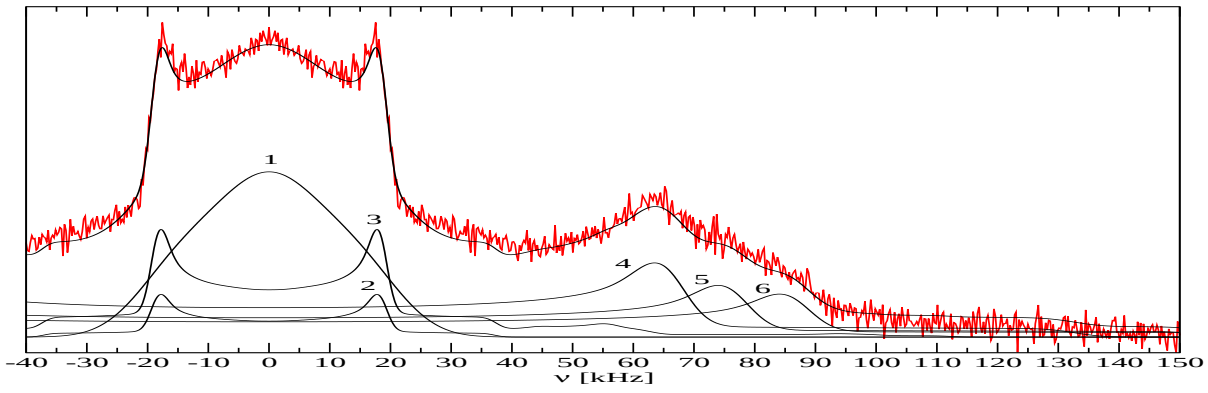

Figure 1. Deuteron NMR spectrum of CD_3OD in NaX at 30.3K. Components: 1-pagoda, 2-three-fold rotation of CD_3I, 3-threefold tunneling of CD_3II, 4, 5 and 6-Pake's doublets.

The spectrum in Fig.1 exhibits diverse mobility of deuterons even at 30.3K. The component 1, called pagoda here, represents the case of two-fold jumps of tunneling CD_3II. That is the case for about 50% of them, the remaining undergo rotational tunneling about C_3 axis and contribute to the component 3 calculated according to [5]. Component 2 reprents a fraction (4%) of CD_3I still rotating at 30.3K, while remaining ones contribute to Pake's doublet 4, i.e. are immobilized. Two more doublets, 5 and 6, also from motionless deuterons, are attributed to ODI and ODII, respectively. Temperature dependence of their contributions provides information on the mobility evolution in the adsorbate system. The fraction of tunnelling CD_3 decays with increasing temperature, and at about 50K all CD_3II (37.5% of the total signal) contribute to the pagoda. The rigid components decay in parallel to a 12% plateau at about 100K, attributed to still motionless deuterons of ODII. The threefold rotation component grows accordingly to plateau at 50% at about 80K, coming from CD_3I and ODI. Above 167.5K all components narrow significantly to a sum of Gaussian spectra with width decreasing on temperature.

Complex relaxation processes of methanol molecules at two configurations, characterized by three time constants at low temperature, were analysed in terms of a distribution of interactions. On increasing temperature there is a phase transition at 167.5K, and strongly localized molecules may diffuse. Spectra indicate isotropic reorientation of methanol molecules above the phase transition and indeed there are just two time constants in the relaxation. Both exhibit the same temperature dependence, but there is about one order (exactly 3^{-2}) of magnitude difference in relaxation rates as the quadrupole coupling constant of CD_3 deuterons is 1/3 of that for OD due to fast internal rotation. Molecules move on cage walls first and then at 250K diffusion across cages leads to a dramatic change in the temperature dependence of the relaxation rate. That feature appears to be common for a number of molecules.

Conclusion

A picture of methanol molecules mobility, diversified due to their different location, obtained by deuteron NMR adds new features, particularly at low tempeartures, to those obtained by other methods. Some data need more detailed analysis and interpretation. Among these are values of the quadrupole coupling constant. These values are 177kHz, 205kHz and 232kHz for immobile deuteron doublets 4, 5 and 6, respectively. These are expected to reflect a strength and length of chemical bonds.

Acknowledgements

This project was generously supported during 2010-2013 by the Ministry of Science and Education, Poland, Grant no N N202 127 939.

References

[1] Schantz, D. F., Lobo, R.F., Guest-host interaction in zeolites as studied by NMR spectroscopy: implications in synthesis, catalysis and separations, Topics in Catalysis, 9 (1999), 1-11
[2] Maurin, G., Plant, D.F., Henn, F., Bell, R.G., Cation migration upon adsorption of methanol in NaY and NaX faujasite systems: a molecular dynamics approach, J. Phys. Chem., B 110 (2006), 18447-18454
[3] Nanok, T., Vasenkov, S., Keil, F.J., Fritzsche, S., Molecular dynamics symulation study of the concentration dependence of the self-diffusivity of methanol in NaX zeolite, Microporous and Mesoporous Mater., 127 (2010), 176-181
[4] Lalowicz, Z.T., Stoch, G., Birczyński, A., Punkkinen, M., Krzystyniak, M., Góra-Marek, K., Datka, J., Dynamics of hydroxyl deuterons and bonded water molecules in NaDY(0.8) zeolite as studied by means of deuteron NMR spectroscopy and relaxation, Solid State Nucl. Magn. Reson. 37, (2010) , 91-100
[5] Lalowicz, Z.T., Werner, U., Müller-Warmuth, W., Rotational tunnelling of CD_3 groups in molecular crystals as studied by NMR spectra, Z. Naturforsch. 43a (1988), 219-227

Identification of preferred Al sites in industrial ZSM-5 catalyst

Alexander Cepak, Wolfgang Schmidt, Claudia Weidenthaler
Max-Planck-Institut für Kohlenforschung, Mülheim an der Ruhr, Germany,
weidenthaler@kofo.mpg.de

Introduction

Aluminium sites in zeolite frameworks cause negative framework charges that are compensated by cations or protons. They are thus the origin of activity of acidic zeolite catalysts. The distribution of aluminum within a given zeolite is thus crucial for the catalytic performance of a given zeolite. Next to pore diameters and pore geometry, local enrichment or homogeneous distribution of aluminum sites may strongly affect reaction kinetics and catalyst deactivation characteristics. The question whether preferred aluminum sites exist is an issue of an ongoing discussion [1], especially for high silica zeolites. In the present contribution, different strategies have been followed to identify aluminum sites in industrially used ZSM-5 zeolite via crystallographic evaluation of powder diffraction data. These included direct assessment of aluminum positions by neutron diffraction, indirect identification of aluminum sites by location of extra-framework cations, and electron density analysis of fully dealuminated ZSM-5.

Experimental

The ZSM-5 material (SM-27) was provided by AlSi Penta GmbH. Ion exchanges have been performed three times at 75°C in either 0.5 M K_2SO_4, $Cu(NO_3)_2*3H_2O$, or $Zn(NO_3)_2*6H_2O$ salt solutions for 20 min. Sodium exchange was performed similarly in 0.1 M NaOH solution. The products were washed with hot de-ionized water and dried at 50°C in air. XRD measurements of dehydrated zeolite powders in sealed capillaries were performed on a STADI P diffractometer in Debye-Scherrer geometry using a curved primary germanium monochromator. Neutron diffraction experiments on dehydrated samples in sealed vanadium containers have been performed at the D2B beamline at ILL in Grenoble. For Rietveld refinements Fullprof and Topas software packages have been used whereas GFourier has been used for difference Fourier analyses.

Results and discussion

Direct identification of aluminum within the zeolite framework is impossible with XRD data since aluminum and silicon cannot be distinguished. Even though silicon and aluminum have slightly different scattering cross sections, also for neutron diffraction data, direct identification of specific aluminum sites turned out to be difficult, if not impossible. As the consequence, aluminum sites had to be identified indirectly via location of extra-framework cations. These cations serve as counter ions that balance the negative framework charges due to the presence of aluminum within the zeolite framework. Provided that the aluminum sites are homogeneously dispersed within the zeolite crystallite (no zoning) and that the concentration of aluminum is not too high, extra-framework cations can been assumed to be relatively isolated. In that case, one can assume that extra-framework cations will be located in the proximity of the negative framework charges, and thus in the proximity of the

aluminum sites. For this purpose, different cations (K^+, Cu^{2+}, Zn^{2+}) have been exchanged on extra-framework positions in SM-27, an industrial zeolite that is known to have a homogeneous aluminum distribution. The positions of these cations have been located by Rietveld refinements and difference-Fourier analyses from X-ray and neutron diffraction data. From the refinement of the occupancy factor of the cation positions and the evaluation of the distance of the cation to the framework oxygen atoms, several cation positions have been confirmed. From the analysis of the neighboring oxygen atoms to these cations, potential aluminum positions have been deduced. T-positions with a certain probability to be occupied by aluminum in the investigated ZSM-5 zeolite are illustrated in Figure 1 [2].

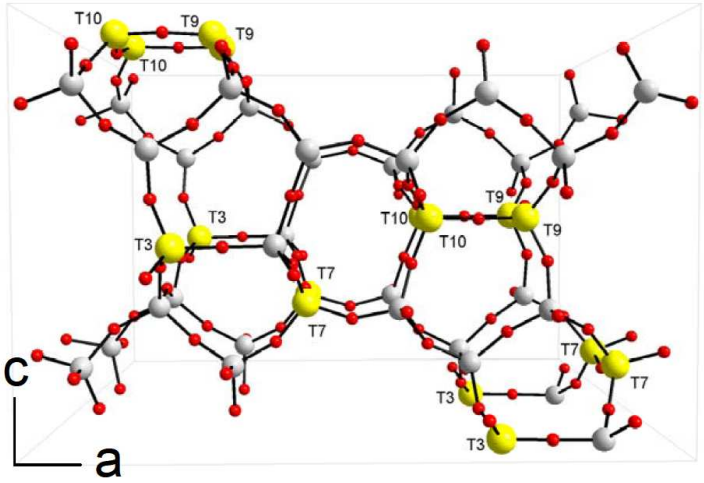

Figure 1. Potential Al positions in AlSi Penta ZSM-5 SM-27.

As can be seen, four T-positions have been identified. One could pose the question whether these positions are indeed all occupied by aluminum. A critical review of the data will be given together with a thorough discussion on the reliability of the data, the methods, and the strategies used.

Acknowledgements

The authors thank Hermann Gies for helpful discussion and a very fruitful co-operation.

References

[1] S. Sklenak, J. Dedecek, C. Li, B. Wichterlová ,V. Gábová , M. Sierka, J. Sauer, Phys. Chem. Chem. Phys., 2009, 11, 1237–1247.

[2] A. Cepak, Dissertation, Ruhr-Universität Bochum, 2010.

Comparison of IMF and MFI frameworks in the copper-zeolite catalyzed NH_3-SCR reaction

Peter N. R. Vennestrøm,[a,b] Marie Grill,[a] Arkady Kustov,[a] Patricia Concepcion,[b] Saray García, [b] Avelino Corma*,[b]

[a] R&D Division, Haldor Topsøe A/S, Nymøllevej 55, DK-2800 Kgs. Lyngby, Denmark
[b] Instituto de Tecnología Química, UPV, Av. Naranjos s/n, E-46022 Valencia, Spain
**E-mail: acorma@itq.upv.es*

Introduction

The selective catalytic reduction (SCR) of NO_x using NH_3 over transition metal containing zeolites is considered the most promising technology to reduce NO_x emissions from diesel vehicles.[1] Cu and Fe-zeolites catalyst are the most used. Copper containing zeolites are of special interest because of their low-temperature SCR-activity compared to e.g. iron containing zeolites. One of the major drawbacks of copper systems is the fast deactivation during operating conditions primarily because of dealumination [2] and copper migration [3] This study concentrates on the influence of the framework on the stability of the SCR catalyst by comparing the IMF type framework, in which framework-Al are expected to be more stable, with the traditional MFI type framework.

Experimental

IM-5 (IMF framework) was synthesized to produce similar Si/Al ratios (11) and similar crystal sizes (0.1-0.3 μm) as in a commercially available ZSM-5 (MFI framework). The zeolites were ion exchanged with copper acetate solutions of varying molarity to obtain different Cu/Al ratios (see Table 1).
Catalytic tests were carried out in a reactant gas composition of 500 ppm NO, 530 ppm NH_3, 10 % O_2, and 5 % H_2O, balanced with N_2 to a total flow rate of 300 NmL/min. Prior to measurements the samples (40 mg) were treated in the reaction mixture for 1 h at 550 °C.
A simulated aging of the samples were performed by heating the samples in an diesel exhaust stream containing ca. 10 % H_2O and 7 % O_2 at 750 °C for 16 hours.

Results and discussion

Copper zeolite catalysts with three similar copper loads were prepared (see Table 1). In the fresh state IMF and MFI type catalysts behave very similar (see Figure 1 and Figure 2) indicating that the framework has little influence on the catalyst performance in the fresh state. At medium and high copper loads a maximum low temperature conversion is obtained. At the same time with increasing copper loads the NO conversion drops at higher temperatures because of the competing ammonia oxidation reaction (see Figure 2).

Table 1. Overview of fresh and aged samples, copper load and the BET surface area

Catalyst	Framework	Cu wt. %	Cu/Al	S_{BET} (m^2/g)	
				Fresh	Aged
Cu(0.29)-IM-5	IMF	2.28	0.29	390	323
Cu(0.43)-IM-5	IMF	3.35	0.43	368	258
Cu(0.62)-IM-5	IMF	4.81	0.62	353	220
Cu(0.28)-ZSM5	MFI	2.20	0.28	453	241

Cu(0.44)-ZSM5	MFI	3.37	0.44	366	215
Cu(0.62)-ZSM5	MFI	4.68	0.62	350	259

After simulated aging the surface area drops for all systems. The smallest relative decrease is seen for samples with the IMF structure containing low to medium amounts of copper. In Figure 1 and 2 the conversion of NO at 225 and 450°C is shown for all catalysts before and after aging. It is noticeable that the low temperature activity drops drastically after ageing for all catalysts and that an increasing copper load slightly improves the performance. In all cases, the Cu-IMF catalyst outperforms the Cu-MFI type when similar copper loads are compared after aging. One of the reasons for this behavior appears to be the increased stability of Al in the framework of IMF compared to MFI-type zeolites.

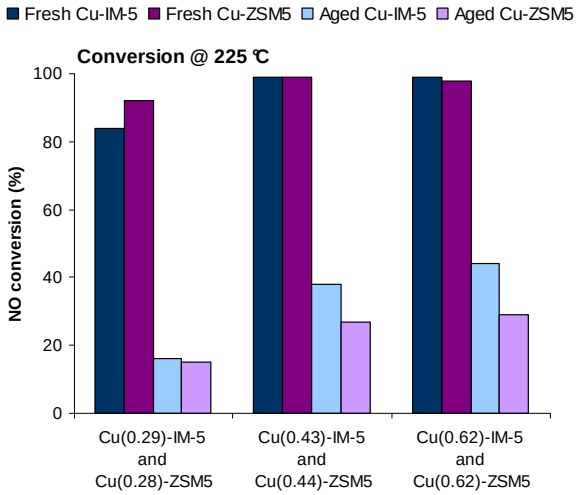

Figure 1 Comparison of conversion of NO at 225 °C with NH_3 over the different catalyst (fresh and aged)

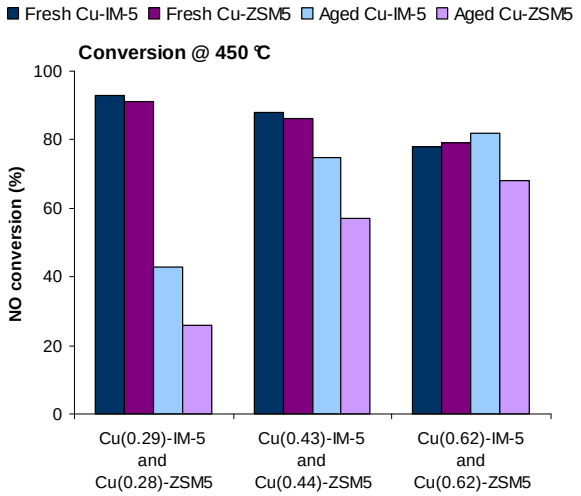

Figure 2 Comparison of conversion of NO at 450 °C with NH_3 over the different catalyst (fresh and aged)

It is known that deactivation of 10-member ring frameworks is more pronounced compared to other framework types.[5] Therefore the comparison between IMF and MFI frameworks gives the opportunity to investigate the deactivation mechanism and determine the influence of framework stability and copper species on catalyst deactivation under realistic conditions. For this purpose XRD, NH_3-TPD, ^{28}Al- and ^{29}Si-MAS-NMR and adsorption of different probe molecules monitored by FTIR have been used and results are going to be presented.

Conclusions

In the fresh state Cu-IMF and Cu-MFI-type catalysts appear to perform very similar, which indicates little influence of framework type between three dimensional 10-member-ring frameworks in the NH_3-SCR reaction. After simulated aging the Cu-IMF type catalyst outperform the Cu-MFI type for similar Cu-loadings The role of framework and copper species stability was elucidated for the two systems. In all cases deactivation is more severe at low temperatures.

References

[1] Brandenberger, S., Kröcher, O., Tissler, A., Althoff R., Chem. Rev., 50 (2008), 492-531
[2] Grinsted, R. A., Jen, H.-W., Montreuil, C. N. Rokosz, M. J., Shelef, M., Zeolites, 13 (1993), 602-606
[3] Park, J.-H., Park, H. J., Baik, J. H. Nam, I.-S., Shin, C.-H., Lee, J.-H., Cho, B. K. Oh, S. H., J. Catal., 240 (2006), 47-57
[4] Corma, A., Martíınez-Triguero, J., Valencia, S., Benazzi, E., Lacombe, S., J. Catal., 206 (2002), 125-133
[5] Fickel, D. W., D'Addio, E., Lauterbach, J. A., Lobo, R. F., Appl. Catal. B, 102 (2011), 441-448

FAU zeolites in the alkylation of industrial fractions of isobutane and olefins

Rishat R. Shiriiazdanov, Vladimir K. Smirnov, Artur R. Davletshin
Ufa State Petroleum Technical University, petroleum9@bk.ru
«CATACHEM Company», Ltd.
Institute of Petroleum Refining and Petrochemistry

Introduction

Alkylation of isobutane by olefins, practically the only process which allows yields high-quality component of gasoline, the percentage of involvement which in the fuel is limited only by existing production resources.
Modern alkylation process implemented in the industry with the use of liquid acid catalysts (sulfuric and hydrofluoric acids), but has a number of known environmental and economic drawbacks, which led to the need to find new effective catalytic systems of alkylation of isobutane by olefins. Therefore, the 70 years XX century began development to the creation of heterogeneous alkylation catalysts, which were invited in large number of different options. In the course of many years research it was found that the most promising heterogeneous catalysts of the alkylation of isobutane by olefins are:

- catalytic system containing zeolites modified with noble or transition metals;
- catalytic systems containing zeolite - faujasite type in rare-earth form.

Based on these catalytic systems, and were made attempts to implement in the industry the alkylation technology in the USSR (processes ATK Grozny research institute) and abroad (a process AlkyClean - Companies ABB Lummus Global, Albemarle Catalysts, and Neste Oil, a process ExSact - Company Exelus, Alkylene process - Company UOP LLC), but, unfortunately, has been implemented on pilot and pilot tests only.
Analysis of the process development of solid-acid alkylation showed that the creation of effective heterogeneous catalysts lies in the use of zeolites, mainly faujasite type (structure type FAU) [1].

Experimental

In collaborative studies on the development of zeolite-containing alkylation catalyst held Department of Technology of Oil and Gas USPTU, CATACHEM Company and the Division of Fuel Institute of Petroleum Refining and Petrochemistry were synthesized and investigated catalytic systems based on zeolite type Y. Acidic characteristics of zeolite Y - the density of acid sites, their availability and distribution of the force - have been optimized by means of a post-synthetic methods (decationization, dealumination and ion exchange).
The starting material for the preparation of a series of samples № 1-3 using zeolite NaY obtained from solutions of sodium silicate, ammonium sulphate and alkali, having 100% crystallinity, molar ratio of SiO_2/Al_2O_3 = 5,2, the content of Na_2O = 13,1% wt. The starting material for the preparation of a series of samples № 4-6 used zeolite NaY produced by Catalysts and Chemicals Industries Co. Ltd, (Japan), which has 100% crystallinity, molar ratio of SiO_2/Al_2O_3 = 5,0, the content of Na_2O = 13,3% wt. To obtain of samples of the series used the sample № 7 HNa-USY-2 – low-alkaline high-silica zeolite Y produced by Ishimbay specialized chemical plant of catalysts with the ratio of SiO_2/Al_2O_3 = 9,1, the content of Na_2O = 1,99% wt.

Results and discussion

Prepared 23 samples of zeolite Y, with different chemical composition (sodium, calcium, and lanthanum), the ratio of SiO_2/Al_2O_3 in the structure and degree of crystallinity, which provides them different acidic characteristics and, therefore, indicators of activity and selectivity in the alkylation. By the nature of the modified zeolite, a process modification, chemical composition and ratio SiO_2/Al_2O_3 samples are grouped into 7 series:

- series number 1 and number 2 - samples of zeolite Y, have different degrees of exchange on the sodium cations, different ratio SiO_2/Al_2O_3 in the structure;
- series № 3, 4 and number 7 - samples of low-and high-silicon zeolite Y, have different degrees of exchange on cations of ammonium, calcium, and lanthanum;
- series number 5 and number 6 - sample of comparison – low-silica zeolite Y, have different degrees of exchange on the cations sodium, calcium, and lanthanum.

Based on the modified zeolites prepared 23 samples alumina and zirconium silicate zeolite catalysts.

Conclusions

As a result of revealed studies found that the greatest interest is ultrastable (high-silicon) Y in polycation-decationated form (HCaLa-USY/Si-O-Zr) with a binder based on zirconium silicate obtained by the sol-gel method. Use as a binder - zirconium silicate in the synthesis of catalyst leads to reduced of formation of condensation products C_{9+} by enhancing the cracking reactions and by increase the yield of fractions of C_5-C_7, which also allows to extend the lifetime of the catalyst, while maintaining rates at a high level.

Acknowledgements

Rishat R. Shiriiazdanov thanks the company Haldor Topsoe A/S
for providing personalized grant

References

[1] Gerzeliev I.M., Tsodikov M.V., and Khadzhiev S.N. New routes for manufacturing of isoparaffins as environmentally friendly, high-octane components of motor gasoline, Petroleum Chemistry, 2009, Vol. 49, 1.

A comparative study of high pressure storage of hydrogen and methane in microporous materials

A. Gil[a], S.A. Korili[a], M.A. Vicente[b], R. Trujillano[b] A. Vallone[c], A.A. García Blanco[c], K. Sapag[c]

[a] *Departamento de Química Aplicada, Universidad Pública de Navarra, 31006 Pamplona, Spain (Antonio Gil: andoni@unavarra.es)*
[b] *GIR-QUESCAT, Departamento de Química Inorgánica, Universidad de Salamanca, Plaza de la Merced S/N, 37008 Salamanca, Spain*
[c] *Instituto de Física Aplicada CONICET-UNSL, Chacabuco 917, San Luis, Argentina*

Introduction

The development of materials with high capacity for fuel gas storage, gas capture or purification and separation processes are of great interest in recent years. One of the key parameters that control the gas adsorption and separation capacities is the presence of micropores. Carbon materials, metal-organic framework (MOF) materials and zeolites are materials that have been proved to be efficient for these applications [1].

The aim of this work is the development and design of suitable adsorbents for gas storage systems. Various microporous materials, selected considering the chemical composition and the structural properties, have been applied in this study for hydrogen and methane storage at high pressure. Equilibrium adsorption data have been also analysed using isotherm models, in order to investigate the adsorbate-adsorbent interaction.

Experimental

The materials used in this work were an activated carbon (MAXSORB, Kansai Coke and Chemicals), three MOFs (Basolite C300, Basolite Z1200 and Basolite A100, Aldrich), an alumina-pillared clay [2] and three zeolites (Fluka).

Nitrogen, hydrogen, carbon dioxide and methane low pressure physisorption experiments were performed on two static volumetric analysers, a Micromeritics ASAP 2010 and a Quantachrome Autosorb 1. Hydrogen and methane high pressure physisorption experiments were performed on another volumetric apparatus, VTI Corporation model HPVA 100. All samples were previously degassed for 24 h at 473 K at a pressure lower than 0.133 Pa.

Results and discussion

The textural properties of the solids have been derived from the results of nitrogen and carbon dioxide adsorption at 77 and at 273 K. Representative results are summarized in Table 1. From these properties, it is clear that all materials can be considered as microporous solids.

Table 1. Textural properties derived from nitrogen and carbon dioxide adsorption at 77 and 273 K.

Materials	S_{Lang} (m^2/g)	Vp (cm^3/g)	$V\mu pN_2$ (cm^3/g)	$V\mu pCO_2$ (cm^3/g)	S_{ext} (m^2/g)
Basolite A100	856	0.915	0.285	0.568	97
Basolite Z1200	1870	0.685	0.643	0.367	12
MS-5A	597	0.249	0.212	0.199	14
MS-10A	557	0.339	0.189	0.225	33
MS-13X	691	0.353	0.240	0.252	25
Al-PILC	271	0.133	0.093	0.097	17

The hydrogen and methane adsorption isotherms, shown in Figure 1, are of type I in the BDDT classification [3], indicative of a physisorption process. To establish whether the gas uptake mechanism is in fact an adsorption process, the effect of the nitrogen microporous volumes on the gas volume uptake has been studied. According to the results of the present work, both hydrogen and methane uptake are related to the microporosity of the materials [2]. Several isotherm equations [4] have been used to describe the experimental adsorption results. From this study a strong degree of heterogeneity for the adsorption of hydrogen has been obtained.

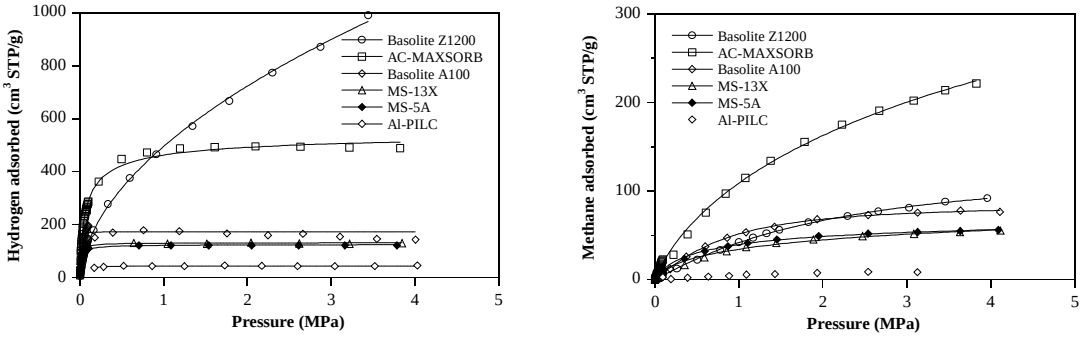

Figure 1.- Experimental (symbols) and model (lines) isotherms for the adsorption of hydrogen at 77 K and methane at 298 K.

Acknowledgments

This work was supported by the Spanish Ministry of Science and Innovation (MICINN) and the European Regional Development Fund (FEDER) through projects MAT2007-66439-C02 and MAT2010-21177-C02.

References

[1] Yang, R.T., in Adsorbents: fundamentals and application, John Wiley & Sons, Inc., Hoboken New Jersey, (2003).
[2] Gil, A., Trujillano, R., Vicente, M.A., Korili, S.A., Hydrogen adsorption by microporous materials based on alumina-pillared clays, International Journal of Hydrogen Energy, 34 (2009), 8611-8615.
[3] Gregg, S.J., Sing, K.S.W., in Adsorption, surface area and porosity, Academic Press, London, (1991).
[4] Do, D.D., in Adsorption analysis: equilibria and kinetics, Imperial College Press, London, (1998).

Adsorption of fuel-based pollutants into high silica zeolite Y: An experimental and computational study

Chiara Bisio[1], Ilaria Braschi[1,2], Giorgio Gatti[1], Vittoria Sacchetto[1], Maurizio Cossi[1], Leonardo Marchese[1]

[1] Interdisciplinary Nano-SiSTeMI Centre, Department of Advanced Science and Technologies, University of Eastern Piedmont A. Avogadro, Alessandria (Italy); [2] Department of Agroenvironmental Science and Technologies, University of Bologna, Bologna (Italy). Corresponding author's email address: ilaria.braschi@unibo.it

Introduction

Fuel-based pollutants are commonly present in soil and ground water coming from areas where refinery plants and gas stations are located. To restrict downward movement of contaminants, physical barriers made of a continuous synthetic layer of low permeability materials constructed as the base of a land cell can be used [1,2]. The information needed to properly scale these barriers includes the nature and strength of interactions between pollutants and barrier fillers. Also the adsorption selectivity of filler in the presence of a number of pollutants is believed very important to foresee the real behaviour of these chemicals always present as a complex mixture.

In this study the adsorption of chemicals representative of fuel-based pollutant families (both single molecules and binary contaminant mixtures) on high silica zeolite Y (a material commonly used to built sorbent barrier) has been studied by FTIR spectroscopy and augmented by models and *ab initio* calculations.

Experimental

n-Hexane, toluene, 1,2-dichloroethane, and methyl *tert*-buthyl ether were selected as representative of hydrocarbons, aromatics, halogenated and oxygenated compounds family, respectively.

The adsorption of pollutants has been studied in high silica zeolite Y (200 SiO_2/Al_2O_3), HSZ-Y, on the basis of its high hydrophobicity and pore dimension large enough to let enter the selected molecules. The host/guest interactions between zeolite surface and model molecules were followed by FTIR spectroscopy by contacting vapours of single pollutants with zeolite self-supporting pellets outgassed at room temperature. Experiments were performed by using special cells connected to high vacuum lines allowing *in-situ* adsorption/desorption experiments. Binary mixtures of model molecules were in addition adsorbed on HSZ-Y to study the relative affinity and interactions of each pollutant with the sorbent phase. The arrangement of pollutants included in a Y zeolite cage has been optimized at the DFT level with the hybrid functional B3LYP and a double-zeta basis set. Harmonic vibrational spectra were calculated to facilitate the assignment of absorptions in experimental infrared spectra.

Results and discussion

The infrared spectrum of HSZ-Y shows a spectral region (3743-3730 cm^{-1}) were the absorption of isolated silanols located at the external surfaces of crystal and in internal defects of zeolite cage takes place. Upon adsorption of pollutants, isolated silanols stretching modes are shifted to 3230, 3596, 3620, 3700 cm^{-1} in the presence of methyl *tert*-buthyl ether, toluene, 1,2-dichloroethane, and *n*-hexane, respectively. This downward shift suggests the formation of H-bonded complexes of different strength between silanols and organic pollutant in the order: methyl *tert*-buthyl ether >> toluene > 1,2-dichloroethane > *n*-hexane. In addition, changes in some stretching modes of aliphatic and aromatic CH_3, CH_2, and CH groups of adsorbed pollutants indicate the contribution of Van der Waals interactions with zeolite

framework whose strength is in the order: 1,2-dichloroethane >> *n*-hexane >> methyl *tert*-buthyl ether > toluene. The DFT structure of methyl *tert*-buthyl ether computed into zeolite cage is represented in Figure 1A. All interactions are reversible at room temperature: as a matter of fact pollutant/silanols complexes are not stable upon progressive reduction of the pollutant pressure.

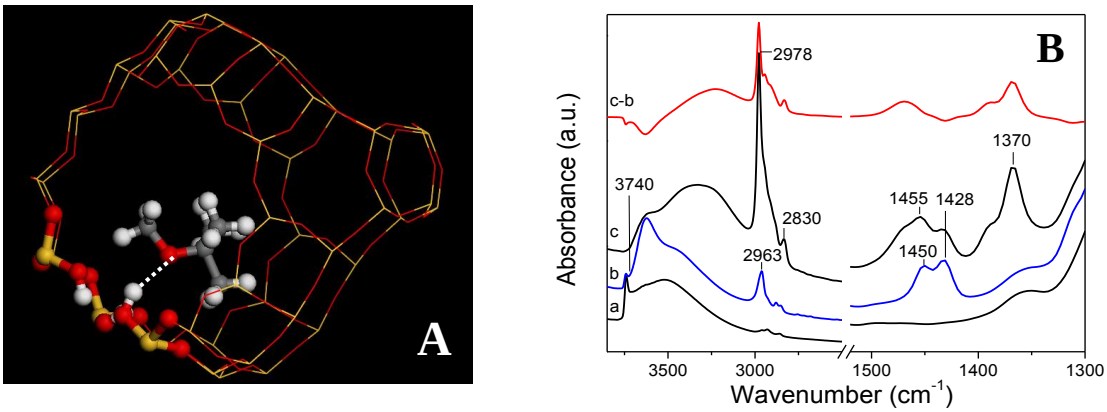

Figure 1A): DFT structure of one molecule of *methyl* tert-buthyl ether H-bonded to a silanol inside a zeolite Y cage; B): FTIR spectra of Y zeolite (SiO_2/Al_2O_3= 200) after dehydration at rt (a), after adsorption of 15 mbar of 1,2-dichloroethane (b) and subsequent adsorption of 20 mbar methyl *tert*-buthyl ether (c). "c-b" curve results from the subtraction of spectrum b from spectrum c.

As far as the adsorption of binary mixture is concerned, methyl *tert*-buthyl ether shows the best affinity for zeolite Y silanols and displaces all the other pollutants previously H-bonded (In Figure 1B, the adsorption of 1,2-dichloroethane and methyl *tert*-buthyl ether is reported as a representative example).
As expected, methyl *tert*-buthyl ether is also able to remove water molecules from zeolite adsorption sites owing to its higher Lewis base character. The competitive interactions among all classes of model pollutants with HSZ-Y were studied by FTIR spectroscopy in the presence and absence of hydration water, and information concerning formation of H-bonding and Van der Waals interactions with zeolite framework were collected aiming to understand the behaviour of sorbent phase upon real working conditions.

Conclusions

High silica zeolite Y shows an adsorption selectivity which is the highest for methyl *tert*-buthyl ether, followed by toluene, 1,2-dichloroethane and *n*-hexane. The concentration of silanols in HSZ-Y available for H-bonding interactions is drastically reduced by the presence of methyl *tert*-buthyl ether which is often found in soils contaminated with fuel-based pollutants. The non-polar portion of HSZ-Y – i.e. the siloxane fraction - which is the vast majority of the network, remains available for Van der Waals interactions with the less polar pollutants as hydrocarbons and aromatic compounds.

Acknowledgements

Research co-funded by Research Center for Non-Conventional Energy, Istituto eni Donegani – Environmental Technologies.

References

[1] Bowman, R.S., Applications of surfactant-modified zeolites to environmental remediation, Micropor. Mesopor. Mater. 61 (2003) 43–56; [2] Vignola, R., Cova, U., Fagiani, F., Grillo, G., Molinari, M., Sbardellati, R., Sisto, R. (2008) Zeolites and Related Materials: Trends, Targets and Challenger. *SSSC* (A. Gedeon, P. Massiani, F. Babonneau Eds.) 174, 573-576.

Permeance and selectivity of helium and hydrogen in nanocomposite MFI-alumina hollow fibre for tritium processes

O. Borisevich[1], D. Demange[1*], T. Parracho[1#], M. Pera-Titus[2], C.-H. Nicolas[2]

[1] *Karlsruhe Institute of Technology, Institute for Technical Physics, Tritium Laboratory Karlsruhe, Germany*
[2] *University of Lyon, Institut de Recherches sur la Catalyse et l'Environnement de Lyon (IRCELYON), France*
[#] *present address Universidade Tecnica de Lisboa, Portugal*
* Corresponding author: david.demange@kit.edu

Introduction

Energy production using nuclear fusion is an attractive alternative to the present fission power plants. The most favourable fusion reaction is the one between deuterium and tritium (hydrogen isotope mass 2 and 3). However, special requirements for fuel handling and processing have to be considered due to the radioactive properties of tritium. A closed loop is necessary to recover and reuse the unburned fraction of tritium and efficient detritiation systems (for glove-boxes and rooms) have to be implemented as well.
Many tritium processes (detritiation systems, tritium extraction from breeder blanket [1]) rely on adsorption/desorption using zeolite packed beds, to remove from a tritiated stream tritiated water or molecular tritium at room and cryogenic temperature, respectively. As an alternative, the Tritium Laboratory Karlsruhe (TLK) has recently proposed the use of zeolite membranes as pre-concentration step that would avoid immobilisation of tritium, and ensure simple and fully continuous operation without cryogenic temperatures or temperature cycles [2].
Based on a literature study, some promising types of zeolite membranes were identified and several multistage membrane processes were simulated [3]. Since the literature data for such applications is scarce, sometimes disagree concerning temperature behaviour of permeance, and vary with membrane types and production, a dedicated experimental study has been started at TLK. This paper presents the firsts results obtained on MFI-alumina hollow fibre and single gases permeation experiments using helium and hydrogen (replacing tritium).

Experimental

The nanocomposite MFI-alumina hollow fibre used in the present study is prepared by IRCELYON via pore-plugging synthesis on porous asymmetric 15 cm-long support with o.d. 1.65 mm and i.d. 1.44 mm. The surface area of the membrane is 4.97 cm^2, the equivalent thickness of zeolite layer is less than 1 μm. Detailed description could be found in [4]. It is immobilized on the supporting alumina perforated tube using a home-made glaze. Finally it is assembled in the stainless steel module and sealed with cylindrical graphite o-ring. At first the hollow fibre is conditioned by heating at 400°C under vacuum during 6 h to remove some adsorbed species from the pores. Then the leak tightness of the membrane is checked by measurement of permeance at different Δp in the range 100-500 mbar. The experiment is carried out in the dead-end mode. The gas is fed inside the hollow fibre, and the permeate flow is measured at steady-state condition by mass flow controller, while the retentate outlet is closed. The pressure difference across the membrane is kept constant at about 500 mbar using two pressure sensors at both the feed and permeates sides. The module is thermostated in a high temperature cylindrical oven from room temperature up to 400°C.

Results and discussion

The experimental results obtained in the present work are displayed in Figure 1. The single gas permeance is calculated from the measured permeate flow rate, the pressure difference, and geometrical membrane data with precision of ± 2%. The permeance of hydrogen decreases significantly with temperature, from 1.3 µm/m²· s ·Pa at room temperature to 0.78 µm / m^2·s·Pa at 400°C, while for helium this decrease is negligible. Thus the sorption-surface diffusion mechanism is applicable to our results. At the same time the ideal selectivity (determined as the ratio of permeances for single gas experiments) decreases as well, from 2.2 at room temperature to 1.5 at 400°C. From the other hand the permeation level still remains high enough to make these nanocomposite MFI-alumina hollow fibres that make them attractive for application in a pre-concentration stage in the breeder blanket.

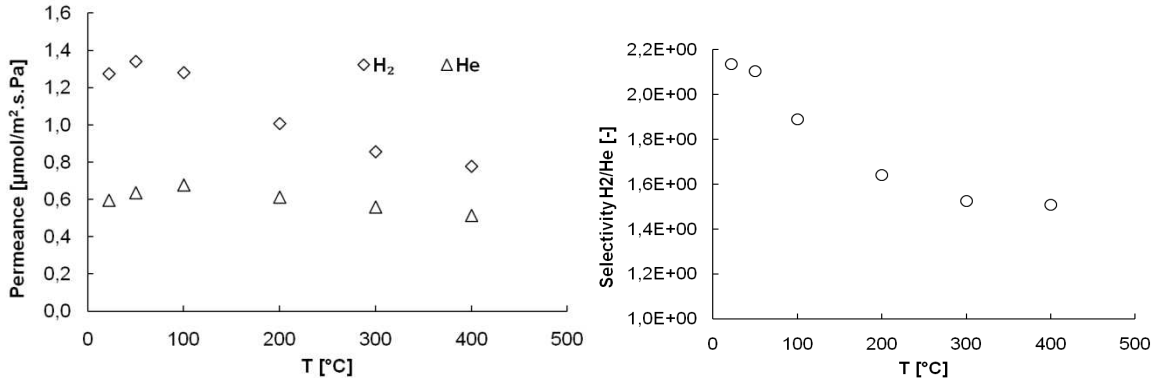

Figure 1: Single gas permeance (on the left) and ideal selectivity (on the right) for hydrogen and helium in nanocomposite MFI-alumina hollow fibre as a function of temperature

Conclusions

The experimental study of zeolite membranes for tritium processes has started. It is shown that such membranes are highly permeable for components of mixture encountered in fuel cycle of fusion machines. This makes them attractive for further investigations in this field since several applications could be envisaged.

Acknowledgements

This work has been financially supported by the Energy Centre and the Fusion Program of the Karlsruhe Institute of Technology.

References

[1] Ricapito I., Chiampichetti A., Agostini P., Benamati G., Tritium processing systems for the helium cooled pebble bed test blanket module, Fusion Engineering and Design 83 (2008), 1461–1465.
[2] Demange D., Stämmler S., Kind M., A new combination of membranes and membrane reactors for improved tritium management in breeder blanket of fusion machines, Fusion Engineering and Design, 2011, (in Press, doi:10.1016/j.fusengdes.2010.12.083).
[3] Stämmler S., Demange D., Kind M., Potential use of zeolite membranes for separation and recovery of tritium produced in the breeder-blanket of fusion machine, Proceeding of 5th International Zeolite Membrane Meeting, May 23-26, 2010 Loutraki, Greece.
[4] Pera-Titus, M., Alshebani, A., Nicolas, C.-H., Roumégoux, J.-P., Miachon, S., Dalmon, J.-A., Nanocomposite MFI-Alumina Membranes: High-Flux Hollow Fibers for CO2 Capture from Internal Combustion Vehicles, Industrial and Engineering Chemistry Research 48 (2009) 9215-9223.

Identification of preferred Al sites in industrial ZSM-5 catalyst

Alexander Cepak, Wolfgang Schmidt, Claudia Weidenthaler
Max-Planck-Institut für Kohlenforschung, Mülheim an der Ruhr, Germany,
weidenthaler@kofo.mpg.de

Introduction

Aluminium sites in zeolite frameworks cause negative framework charges that are compensated by cations or protons. They are thus the origin of activity of acidic zeolite catalysts. The distribution of aluminum within a given zeolite is thus crucial for the catalytic performance of a given zeolite. Next to pore diameters and pore geometry, local enrichment or homogeneous distribution of aluminum sites may strongly affect reaction kinetics and catalyst deactivation characteristics. The question whether preferred aluminum sites exist is an issue of an ongoing discussion [1], especially for high silica zeolites. In the present contribution, different strategies have been followed to identify aluminum sites in industrially used ZSM-5 zeolite via crystallographic evaluation of powder diffraction data. These included direct assessment of aluminum positions by neutron diffraction, indirect identification of aluminum sites by location of extra-framework cations, and electron density analysis of fully dealuminated ZSM-5.

Experimental

The ZSM-5 material (SM-27) was provided by AlSi Penta GmbH. Ion exchanges have been performed three times at 75°C in either 0.5 M K_2SO_4, $Cu(NO_3)_2*3H_2O$, or $Zn(NO_3)_2*6H_2O$ salt solutions for 20 min. Sodium exchange was performed similarly in 0.1 M NaOH solution. The products were washed with hot de-ionized water and dried at 50°C in air. XRD measurements of dehydrated zeolite powders in sealed capillaries were performed on a STADI P diffractometer in Debye-Scherrer geometry using a curved primary germanium monochromator. Neutron diffraction experiments on dehydrated samples in sealed vanadium containers have been performed at the D2B beamline at ILL in Grenoble. For Rietveld refinements Fullprof and Topas software packages have been used whereas GFourier has been used for difference Fourier analyses.

Results and discussion

Direct identification of aluminum within the zeolite framework is impossible with XRD data since aluminum and silicon cannot be distinguished. Even though silicon and aluminum have slightly different scattering cross sections, also for neutron diffraction data, direct identification of specific aluminum sites turned out to be difficult, if not impossible. As the consequence, aluminum sites had to be identified indirectly via location of extra-framework cations. These cations serve as counter ions that balance the negative framework charges due to the presence of aluminum within the zeolite framework. Provided that the aluminum sites are homogeneously dispersed within the zeolite crystallite (no zoning) and that the concentration of aluminum is not too high, extra-framework cations can been assumed to be relatively isolated. In that case, one can assume that extra-framework cations will be located in the proximity of the negative framework charges, and thus in the proximity of the

aluminum sites. For this purpose, different cations (K^+, Cu^{2+}, Zn^{2+}) have been exchanged on extra-framework positions in SM-27, an industrial zeolite that is known to have a homogeneous aluminum distribution. The positions of these cations have been located by Rietveld refinements and difference-Fourier analyses from X-ray and neutron diffraction data. From the refinement of the occupancy factor of the cation positions and the evaluation of the distance of the cation to the framework oxygen atoms, several cation positions have been confirmed. From the analysis of the neighboring oxygen atoms to these cations, potential aluminum positions have been deduced. T-positions with a certain probability to be occupied by aluminum in the investigated ZSM-5 zeolite are illustrated in Figure 1 [2].

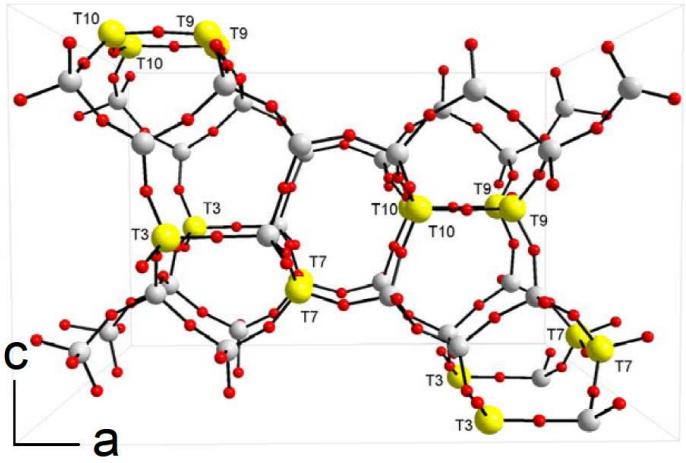

Figure 1. Potential Al positions in AlSi Penta ZSM-5 SM-27.

As can be seen, four T-positions have been identified. One could pose the question whether these positions are indeed all occupied by aluminum. A critical review of the data will be given together with a thorough discussion on the reliability of the data, the methods, and the strategies used.

Acknowledgements

The authors thank Hermann Gies for helpful discussion and a very fruitful co-operation.

References

[1] S. Sklenak, J. Dedecek, C. Li, B. Wichterlová ,V. Gábová , M. Sierka, J. Sauer, Phys. Chem. Chem. Phys., 2009, 11, 1237–1247.

[2] A. Cepak, Dissertation, Ruhr-Universität Bochum, 2010.

Structure Determination of Germanates by Combining XRPD, TEM and IR-Spectroscopy

A. Ken Inge,[1,2] Tom Willhammar,[1,2] Christian Baerlocher,[3] Lynne B. McCusker[3] and Xiaodong Zou[*,1,2]
[1]*Berzelii Center EXSELENT on Porous Materials, Stockholm University, Sweden*
[2]*Inorganic and Structural Chemistry, Department of Materials and Environmental Chemistry, Stockholm University, Sweden*
[3]*Laboratory of Crystallography, ETH Zurich, Switzerland*
[*]*xzou@mmk.su.se*

Introduction

Open-framework germanates are of particular interest for their ability to form structures with extra-large pores (>18-membered rings). These very open-frameworks are often built of composite building units (CBUs) with combinations of GeO_4 tetrahedra, GeO_5 trigonal bipyramids and GeO_6 octahedra (Figure 1). One example is the $Ge_{10}(O,OH)_{27\text{-}28}$ cluster (Ge_{10}) in phases such as SU-61 [1], a framework with 26-ring channels analogous to those of MCM-41. As with zeolites, many germanate phases have a tendency to form crystals too small for structure determination by single crystal X-ray diffraction (XRD) even on a synchrotron source. Due to their large unit cell volumes, structure determination from X-ray powder diffraction (XRPD) can be complicated by the large number of severely overlapping of reflections. Beam damage is an issue when subjecting germanate crystals to extensive transmission electron microscopy (TEM) studies, although selected area electron diffraction (SAED) can be more easily obtained on beam sensitive samples than high resolution imaging. Each of these three techniques were applied separately in unsuccessful attempts to solve the structure of a novel germanate, SU-66. Through a combination of IR spectroscopy, SAED and XRPD, we have finally obtained a reasonable framework structure for SU-66.

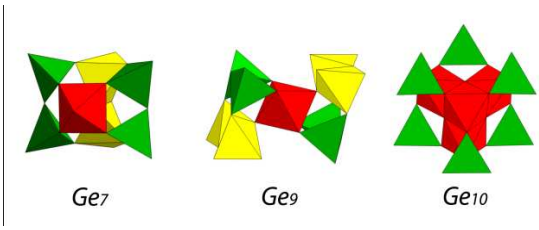

Figure 1. CBUs commonly found in germanates including the $Ge_7(O,OH,F)_{19}$ (Ge_7), $Ge_9(O,OH,F)_{26}$ (Ge_9) and $Ge_{10}(O,OH)_{28}$ (Ge_{10}) clusters.

Experimental

The IR spectra of 14 germanate compounds with various CBUs were recorded. The spectra revealed bands characteristic to the CBUs found in the frameworks. The IR spectrum of SU-66 was recorded and compared to the spectra of known structures for CBU identification.

Unit cell parameters and reflection conditions of SU-66 were determined from both XRPD and SAED data. The XRPD pattern, unit cell parameters, space group and CBU were input into FOX [2] for structure determination using real-space methods. The resulting structure was then used as a model file for Superflip [3], where the initial phases were allowed to vary by up to 20% [4].

Results and discussion

Crystallographic parameters obtained by both XRPD and SAED (Figure 2a) indicate that SU-66 has a space group and unit cell (*Pmcm*, a = 31.60 Å, b = 18.66 Å, c = 14.96 Å) related to that of the known structure SU-61 (*Cmcm*, a = 34.48 Å, b = 19.88 Å, c = 14.86 Å), which is built of Ge_{10} clusters. IR results (Figure 2b) also indicated the presence of Ge_{10} clusters in SU-66. The positions and orientations of Ge_{10} clusters in the asymmetric unit were found by FOX. The structure from FOX was used to define the initial phases for charge-flipping in Superflip to obtain a structure with more reasonable atomic positions.

SU-66 has a framework with two Ge_{10} clusters in the asymmetric unit. Half of the clusters are in an arrangement similar to that found in SU-61, while the other half are rotated. The structure contains 12-, 18- and 26-ring channels along [001] and 8-ring channels along [010]. Half of the 8-rings and 26-rings in SU-61 are replaced by 12-rings and 18-rings, respectively, in SU-66 (Figure 2c). The final framework contains 53 symmetrically independent atoms (17 Ge-atoms), and is therefore one of the more complicated frameworks solved from XRPD data.

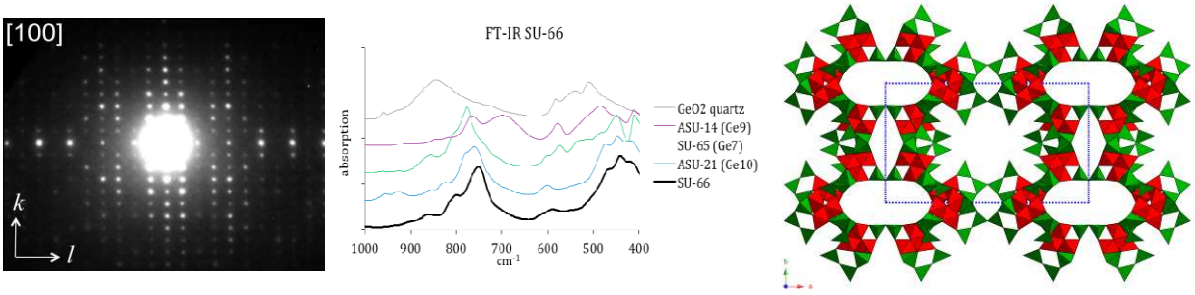

(a) (b) (c)

Figure 2. (a) SAED of SU-66 along [100]. (b) IR spectrum of SU-66 compared with those of various known germanates. (c) The structure of SU-66 obtained after performing FOX, Superflip, and some early refinement with XRS [5].

Conclusions

We have determined the building unit of SU-66 by IR spectroscopy, its unit cell parameters and space group by XRPD and TEM, and consistently obtained a reasonable structure using real-space methods from XRPD data. The combination of these techniques has been shown to be powerful for structure determination of complicated polycrystalline phases.

Acknowledgements

We thank Dr. Dan Xie, Ms. Dubravka Šišak and Mr. Jürgen Grässlin for the valuable discussions regarding XRPD and TEM. This project is supported by the Swedish Governmental Agency for Innovation Systems (VINNOVA), the Swedish Research Council (VR) and Göran Gustafsson Foundation.

References

[1] Christensen, K. *et al.*, *J. Am. Chem. Soc.*, 130 (**2008**), 3758-3759.
[2] Favre-Nicolin, V & Cerny, R., J. Appl. Cryst., 35, (**2002**), 734-743.
[3] Palatinus, L. & Chapuis, G., *J. Appl. Cryst.* 40, (**2007**), 786-790.
[4] McCusker, L., Baerlocher, C., Sisak, D., private communication, manuscript in preparation.
[5] Baerlocher, C., Hepp, A., *XRS-82*, (**1982**).

Overview of processes using zeolite at the Tritium Laboratory Karlsruhe

D. Demange*, N. Bekris, U. Besserer, T.L. Le, F. Kramer, A. Parracho#, R. Wagner

Karlsruhe Institute of Technology, Institute for Technical Physics, Tritium Laboratory Karlsruhe, Postfach 3640, D-76021 Karlsruhe, Germany
 # present address: Culham Centre for Fusion Energy (JET), OX14 3DB, OXON, England
** Corresponding author: david.demange@kit.edu*

Introduction

Nuclear fusion using mixtures of deuterium and tritium is proposed as alternative to the present fission power plants. Since tritium is radioactive and expensive, special requirements for fuel handling and processing have to be considered. The Tritium Laboratory Karlsruhe (TLK), which is a world-wide unique semi-technical facility, operates several processes relying on molecular sieve beds (MSB) containing zeolite material.

Detritiation systems using zeolite and AMOR facility for MSB regeneration

Under routine operation as TLK infrastructure [1], the individual tritium retention systems connected to each glove box and the central tritium retention system are recovering residual tritium from primary and secondary containments before the detritiated gases are released into the environment (Fig. 1, left). Both processes rely on the same principle: i) tritium (HT) oxidation on CuO or other Pd- or Pt- based catalysts, ii) tritiated water (HTO with tritium at ppm level) adsorption at room temperature on MSB containing 15 kg of a 4A/13X zeolite mixture. This allows handling and processing significant amounts of tritium while minimising the tritium releases.

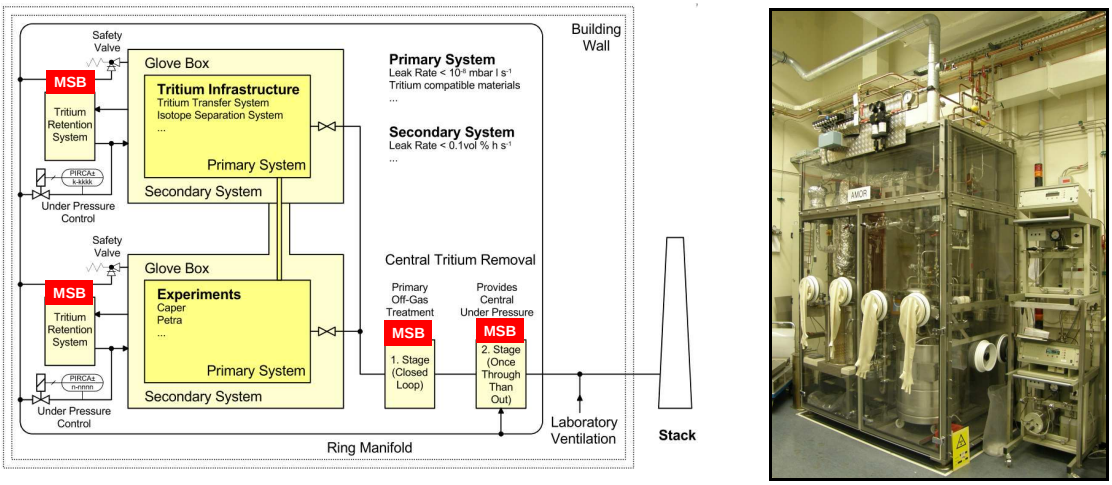

Figure 1: Schematic layout of the TLK tritium confinement (on the left) and picture of the AMOR facility for MSB regeneration (on the right).

The MSB regeneration is performed in the AMOR facility [2] (Fig. 1, right) using dry N_2 re-circulated in a closed loop at about 10 m^3/h. Heating is achieved by i) pre-heating the gas, ii) a heating mantle, and iii) the in-bed integrated heater. The regeneration procedure is performed isothermally at 300°C and lasts for about 48 h to dry the MSB down to residual water less than 1% in weight. The desorbed tritiated water is collected as liquid using a condenser. Typically a batch corresponds to 1- 2 kg of water containing tritium between 10^9 - 10^{12} Bq/kg.

This water was so far considered as waste and therefore transferred for later treatment to the central waste department. However, the recent commissioning of a new water detritiation system [3] will allow tritiated water reprocessing so that the TLK tritium cycle will be fully closed.

Handling and processing highly tritiated water

In contrast to the large amounts of HTO of intermediate and low activity routinely produced in tritium facilities, highly tritiated water (HTW) up to stoichiometric DTO (5×10^{16} Bq/kg) is much more difficult to manage. Among the potential techniques to recover tritium from it, the use of a catalytic palladium membrane reactor (PERMCAT) has been proposed. The experimental demonstration at small scale but with relevant tritium levels is in progress [4]. Firstly, HTW is produced oxidising gaseous tritium, processed with a PERMCAT reactor, and afterwards the detritiated water containing residual tritium amounts is collected in a small MSB containing about 100 g of zeolite 5A. The MSB is used here for sampling purpose: after disconnecting it from the process, it is placed inside a sensitive calorimeter to measure the residual tritium content in order to finally determine the PERMCAT detritiation efficiency. In a later stage, this collected tritiated water is desorbed from the MSB for a second run on PERMCAT prior to its final handling in the liquid form. Such operation, i.e. MSB regeneration followed by PERMCAT, would be typically the best method to be used in any future fusion machines for the detritiation of HTW. During the MSB regeneration, the control of the water desorption rate process is required to ensure optimal tritium recovery efficiency.

Conclusions

Since it ensures safe and simple operation, MSB containing zeolite are widely used in tritium handling facilities. For glove box and atmosphere detritiation, oxidation of tritium followed by a drying step into zeolite packed beds was demonstrated to be very efficient and reliable. Reconditioning the MSB allows reusing them close to their nominal performances and significantly reduces the operation costs. The R&D activities (experiments and simulations) are now focusing on the regeneration (desorption) step. This is particularly important for MSB in the detritiation systems with respect to possible memory effects, and for MSB containing highly tritiated water that should be detritiated continuously in the vapour phase.

Acknowledgements

This work was supported by the European Communities under the contract of Association between EURATOM and Karlsruhe Institute of Technology. The views and opinions expressed herein do not necessarily reflect those of the European Commission.

References

[1] Besserer, U., Dörr, L., Glugla, M., Tritium confinement, retention, and releases at the tritium laboratory Karlsruhe, Fusion Science and Technology 54 (2008) 160

[2] Hutter, E., Adami, D., Besserer, U., Penzhorn, R.D., AMOR facility: regeneration of molecular sieve beds used for the retention of tritium at the tritium laboratory Karlsruhe, Fusion Technology (1996) 1189 - Proceedings of the 19th SOFT, Lisbon, Portugal.

[3] Cristescu, I. et al., Commissioning of water detritiation and cryogenic distillation systems at TLK in view of ITER design, Fusion Engineering and Design 82 (2007) 2126
[4] Demange, D. et al., CAPER modifications and first experimental results on highly tritiated water processing with PERMCAT at the Tritium Laboratory Karlsruhe, Proceedings of the 9th ICTST, Nara, Japan, 2010 – to appear in Fusion Science and Technology.

Ethanolysis of vegetable oil using mesoporous SBA-15

M.C.G. Albuquerque(*), S. A. Quintella, R.M.A. Saboya and C.L. Cavalcante Jr.
Universidade Federal do Ceará – UFC, Departamento de Engenharia Química
Campus do Pici, Bl. 709, 60455-760 Fortaleza, CE, Brazil
(*)Corresponding author: monica@gpsa.ufc.br

Introduction

The most common process for biodiesel production consists in a transesterification reaction in which a triglycerides source (vegetable oil or animal fat) reacts to a short chain alcohol (usually methanol) in catalyst presence. Since ethanol is largely obtained in Brazil from renewable sources (mostly sugarcane) it might be advantageous to replace methanol in the transesterification reaction for biodiesel production. This study presents the use of a lanthanum SBA-15 catalyst in vegetable oil transesterification using ethanol. The catalyst has lanthanum oxide as active phase inserted into the SBA-15 framework by isomorphous substitution.

Experimental

The SBA-15 modified with lanthanum was synthesized by hydrothermal method using Pluronic P123, tetraethyl orthosilicate, hydrated lanthanum chloride, HCl and distilled water. The mixture was stirred for 22 h at a temperature of 333 K. The resulting gel was submitted to hydrothermal treatment at a temperature of 373 K for 48 h. After filtration and calcination, the samples were characterized through X-ray diffraction (DRX), N_2 adsorption and desorption isotherms at 77 K, and scanning electron microscopy (SEM). The transesterification reaction was carried out at inert atmosphere using 1000 rpm agitation using molar ratio of ethanol and oil of 20:1. When the oil and ethanol mixture reached the desired temperature, 343 K, the catalyst was inserted to the reaction mixture using a catalyst/oil mass ratio of 0.01. Samples of 5 mL were taken after 6h, filtered under vacuum to extract the catalyst from the reaction mixture.

Results and discussion

The diffractograms and SEM micrographs of the original SBA-15 and the lanthanum modified SBA-15 are shown in Figs. 1 and 2, respectively. The textural properties are shown in Table 1.

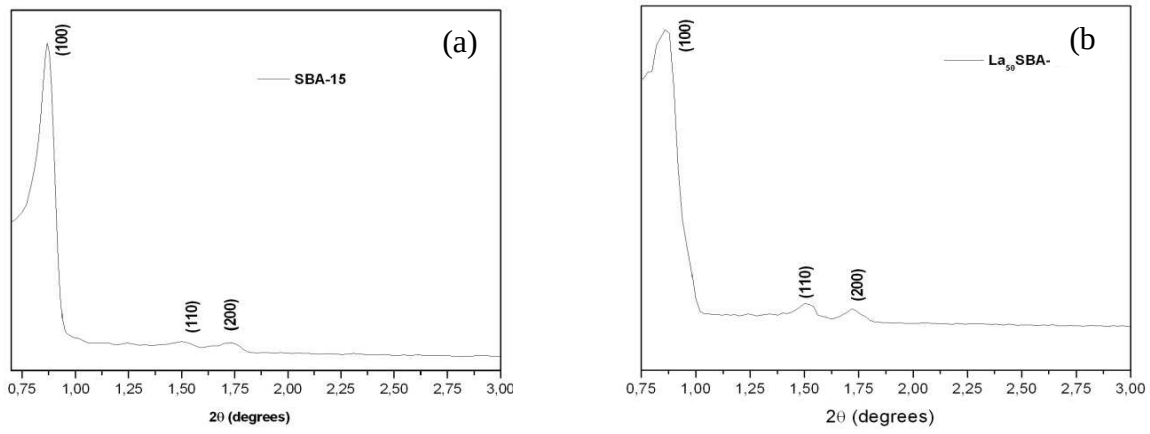

Figure 1. Diffractograms of SBA-15 samples. (a) original ; (b) lanthanum modified.

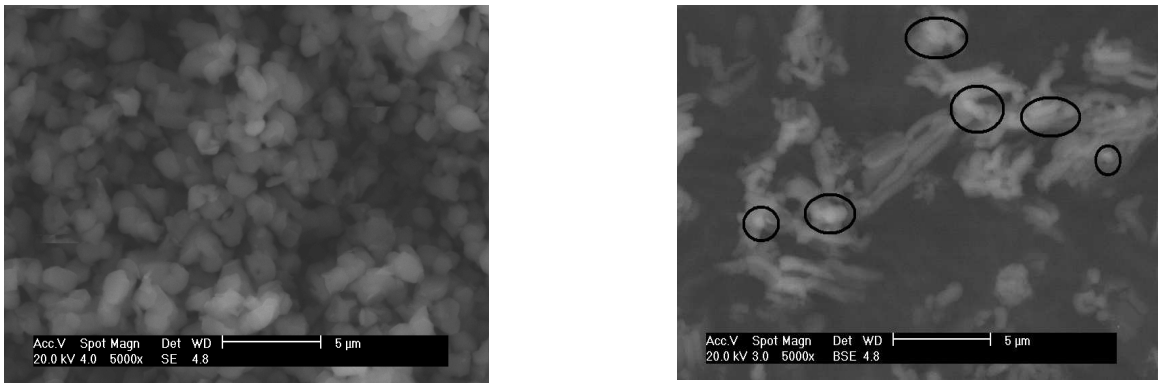

Figure 2. SEM micrographs of SBA-15 samples. (a) original ; (b) lanthanum modified

Table 1. Textural characterization of SBA-15 samples.

Sample	D_p(nm)	V_p(cm^3g^{-1})	S_{BET}(m^2g^{-1})
SBA-15	4.33	0.95	931.3
Lanthanum SBA-15	7.29	1.09	735.2

The calculated value of the conversion of soybean oil with ethanol using lanthanum modified SBA-15 as catalyst in the transesterification reaction was 80% v/v, which is comparable to previously reported values (see Table 2). The classical homogenous process catalyzed by KOH is reported using ethanol as transesterificant agent with conversions as high as 96%v/v, however the downstream separation of the products (ester/glycerin phases) is rather difficult if compared to heterogeneous systems.

Table 2. Comparison of conversion to biodiesel with previously reported values.

Oil/Alcohol	Alcohol/Oil molar ratio	Catalyst	Catalyst/oil mass ratio	Temp. (K)	Time (h)	Conv. (%vv)	Ref.
Soybean/EtOH	20	La_{50}SBA15	0.01	343	6	80.0	This study
Soybean/EtOH	18.8	homogeneous (KOH)	0.01	n.a.	4	96.0	1
Soybean/MeOH	21	Ca_3La oxide	0.05	331	3	94.3	2

Acknowledgements
The authors acknowledge financial support provided by CNPq – Conselho Nacional de Desenvolvimento Científico e Tecnológico.

References

[1] Barbosa, D.C., Serra, T.M., Meneghetti, S.M.P., Meneghetti, M.R., Biodiesel production by ethanolysis of mixed castor and soybean oils, Fuel 89 (2010) 3791-3794.
[2] Yan, S., Kim, M., Salley, S.O., Simon Ng, K.Y., Oil transesterification over calcium oxides modified with lanthanum, Appl. Catal. A-Gen. 360 (2009) 163-170.

Comparison of IMF and MFI frameworks in the copper-zeolite catalyzed NH_3-SCR reaction

Peter N. R. Vennestrøm,[a,b] Marie Grill,[a] Arkady Kustov,[a] Patricia Concepcion,[b] Avelino Corma*,[b]

[a] R&D Division, Haldor Topsøe A/S, Nymøllevej 55, DK-2800 Kgs. Lyngby, Denmark
[b] Instituto de Tecnología Química, UPV, Av. Naranjos s/n, E-46022 Valencia, Spain
**E-mail: acorma@itq.upv.es*

Introduction

The selective catalytic reduction (SCR) of NO_x using NH_3 over transition metal containing zeolites is considered the most promising technology to reduce NO_x emissions from diesel vehicles.[1] Cu and Fe-zeolites catalyst are the most used. Copper containing zeolites are of special interest because of their low-temperature SCR-activity compared to e.g. iron containing zeolites. One of the major drawbacks of copper systems is the fast deactivation during operating conditions primarily because of dealumination [2] and copper migration [3] This study concentrates on the influence of the framework on the stability of the SCR catalyst by comparing the IMF type framework, in which framework-Al are expected to be more stable, with the traditional MFI type framework.

Experimental

IM-5 (IMF framework) was synthesized to produce similar Si/Al ratios (11) and similar crystal sizes (0.1-0.3 μm) as in a commercially available ZSM-5 (MFI framework). The zeolites were ion exchanged with copper acetate solutions of varying molarity to obtain different Cu/Al ratios (see Table 1).
Catalytic tests were carried out in a reactant gas composition of 500 ppm NO, 530 ppm NH_3, 10 % O_2, and 5 % H_2O, balanced with N_2 to a total flow rate of 300 NmL/min. Prior to measurements the samples (40 mg) were treated in the reaction mixture for 1 h at 550 °C.
A simulated aging of the samples were performed by heating the samples in an diesel exhaust stream containing ca. 10 % H_2O and 7 % O_2 at 750 °C for 16 hours.

Results and discussion

Copper zeolite catalysts with three similar copper loads were prepared (see Table 1). In the fresh state IMF and MFI type catalysts behave very similar (see Figure 1 and Figure 2) indicating that the framework has little influence on the catalyst performance in the fresh state. At medium and high copper loads a maximum low temperature conversion is obtained. At the same time with increasing copper loads the NO conversion drops at higher temperatures because of the competing ammonia oxidation reaction (see Figure 2).

Table 1. Overview of fresh and aged samples, copper load and the BET surface area

Catalyst	Framework	Cu wt. %	Cu/Al	S_{BET} (m^2/g)	
				Fresh	Aged
Cu(0.29)-IM-5	IMF	2.28	0.29	390	323
Cu(0.43)-IM-5	IMF	3.35	0.43	368	258
Cu(0.62)-IM-5	IMF	4.81	0.62	353	220
Cu(0.28)-ZSM5	MFI	2.20	0.28	453	241
Cu(0.44)-ZSM5	MFI	3.37	0.44	366	215
Cu(0.62)-ZSM5	MFI	4.68	0.62	350	259

After simulated aging the surface area drops for all systems. The smallest relative decrease is seen for samples with the IMF structure containing low to medium amounts of copper. In Figure 1 and 2 the conversion of NO at 225 and 450°C is shown for all catalysts before and after aging. It is noticeable that the low temperature activity drops drastically after ageing for all catalysts and that an increasing copper load slightly improves the performance. In all cases, the Cu-IMF catalyst outperforms the Cu-MFI type when similar copper loads are compared after aging. One of the reasons for this behavior appears to be the increased stability of Al in the framework of IMF compared to MFI-type zeolites.

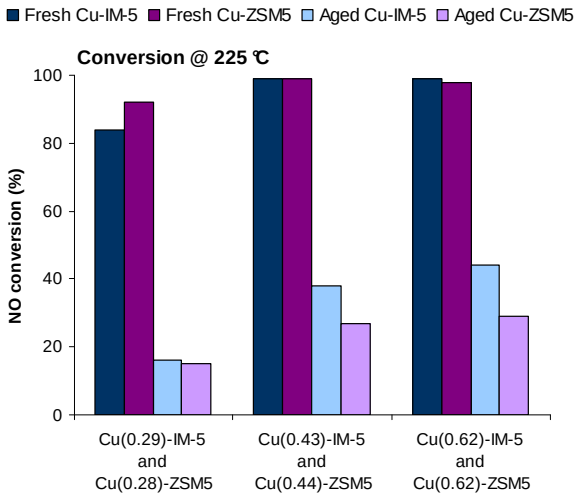

Figure 1 Comparison of conversion of NO at 225 °C with NH_3 over the different catalyst (fresh and aged)

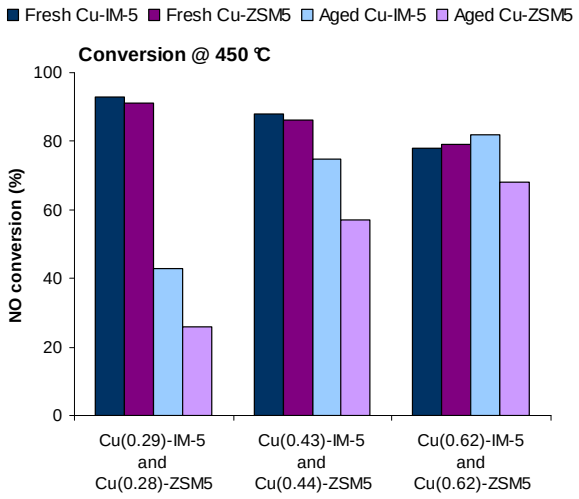

Figure 2 Comparison of conversion of NO at 450 °C with NH_3 over the different catalyst (fresh and aged)

It is known that deactivation of 10-member ring frameworks is more pronounced compared to other framework types.[5] Therefore the comparison between IMF and MFI frameworks gives the opportunity to investigate the deactivation mechanism and determine the influence of framework stability and copper species on catalyst deactivation under realistic conditions. For this purpose XRD, NH_3-TPD, ^{28}Al- and ^{29}Si-MAS-NMR and adsorption of different probe molecules monitored by FTIR have been used and results are going to be presented.

Conclusions

In the fresh state Cu-IMF and Cu-MFI-type catalysts appear to perform very similar, which indicates little influence of framework type between three dimensional 10-member-ring frameworks in the NH_3-SCR reaction. After simulated aging the Cu-IMF type catalyst outperform the Cu-MFI type for similar Cu-loadings The role of framework and copper species stability was elucidated for the two systems. In all cases deactivation is more severe at low temperatures.

References

[1] Brandenberger, S., Kröcher, O., Tissler, A., Althoff R., Chem. Rev., 50 (2008), 492-531
[2] Grinsted, R. A., Jen, H.-W., Montreuil, C. N. Rokosz, M. J., Shelef, M., Zeolites, 13 (1993), 602-606
[3] Park, J.-H., Park, H. J., Baik, J. H. Nam, I.-S., Shin, C.-H., Lee, J.-H., Cho, B. K. Oh, S. H., J. Catal., 240 (2006), 47-57
[4] Corma, A., Martíınez-Triguero, J., Valencia, S., Benazzi, E., Lacombe, S., J. Catal., 206 (2002), 125-133
[5] Fickel, D. W., D'Addio, E., Lauterbach, J. A., Lobo, R. F., Appl. Catal. B, 102 (2011), 441-448

Adsorption of fuel-based pollutants into high silica zeolite Y: An experimental and computational study

Chiara Bisio[1], Ilaria Braschi[1,2], Giorgio Gatti[1], Vittoria Sacchetto[1], Maurizio Cossi[1], Leonardo Marchese[1]

[1] Interdisciplinary Nano-SiSTeMI Centre, Department of Advanced Science and Technologies, University of Eastern Piedmont A. Avogadro, Alessandria (Italy); [2] Department of Agroenvironmental Science and Technologies, University of Bologna, Bologna (Italy). Corresponding author's email address: ilaria.braschi@unibo.it

Introduction

Fuel-based pollutants are commonly present in soil and ground water coming from areas where refinery plants and gas stations are located. To restrict downward movement of contaminants, physical barriers made of a continuous synthetic layer of low permeability materials constructed as the base of a land cell can be used [1,2]. The information needed to properly scale these barriers includes the nature and strength of interactions between pollutants and barrier fillers. Also the adsorption selectivity of filler in the presence of a number of pollutants is believed very important to foresee the real behaviour of these chemicals always present as a complex mixture.

In this study the adsorption of chemicals representative of fuel-based pollutant families (both single molecules and binary contaminant mixtures) on high silica zeolite Y (a material commonly used to built sorbent barrier) has been studied by FTIR spectroscopy and augmented by models and *ab initio* calculations.

Experimental

n-Hexane, toluene, 1,2-dichloroethane, and methyl *tert*-buthyl ether were selected as representative of hydrocarbons, aromatics, halogenated and oxygenated compounds family, respectively.

The adsorption of pollutants has been studied in high silica zeolite Y (200 SiO_2/Al_2O_3), HSZ-Y, on the basis of its high hydrophobicity and pore dimension large enough to let enter the selected molecules. The host/guest interactions between zeolite surface and model molecules were followed by FTIR spectroscopy by contacting vapours of single pollutants with zeolite self-supporting pellets outgassed at room temperature. Experiments were performed by using special cells connected to high vacuum lines allowing *in-situ* adsorption/desorption experiments. Binary mixtures of model molecules were in addition adsorbed on HSZ-Y to study the relative affinity and interactions of each pollutant with the sorbent phase. The arrangement of pollutants included in a Y zeolite cage has been optimized at the DFT level with the hybrid functional B3LYP and a double-zeta basis set. Harmonic vibrational spectra were calculated to facilitate the assignment of absorptions in experimental infrared spectra.

Results and discussion

The infrared spectrum of HSZ-Y shows a spectral region (3743-3730 cm^{-1}) were the absorption of isolated silanols located at the external surfaces of crystal and in internal defects of zeolite cage takes place. Upon adsorption of pollutants, isolated silanols stretching modes are shifted to 3230, 3596, 3620, 3700 cm^{-1} in the presence of methyl *tert*-buthyl ether, toluene, 1,2-dichloroethane, and *n*-hexane, respectively. This downward shift suggests the formation of H-bonded complexes of different strength between silanols and organic pollutant in the order: methyl *tert*-buthyl ether >> toluene > 1,2-dichloroethane > *n*-hexane. In addition, changes in some stretching modes of aliphatic and aromatic CH_3, CH_2, and CH groups of adsorbed pollutants indicate the contribution of Van der Waals interactions with zeolite

framework whose strength is in the order: 1,2-dichloroethane >> *n*-hexane >> methyl *tert*-buthyl ether > toluene. The DFT structure of methyl *tert*-buthyl ether computed into zeolite cage is represented in Figure 1A. All interactions are reversible at room temperature: as a matter of fact pollutant/silanols complexes are not stable upon progressive reduction of the pollutant pressure.

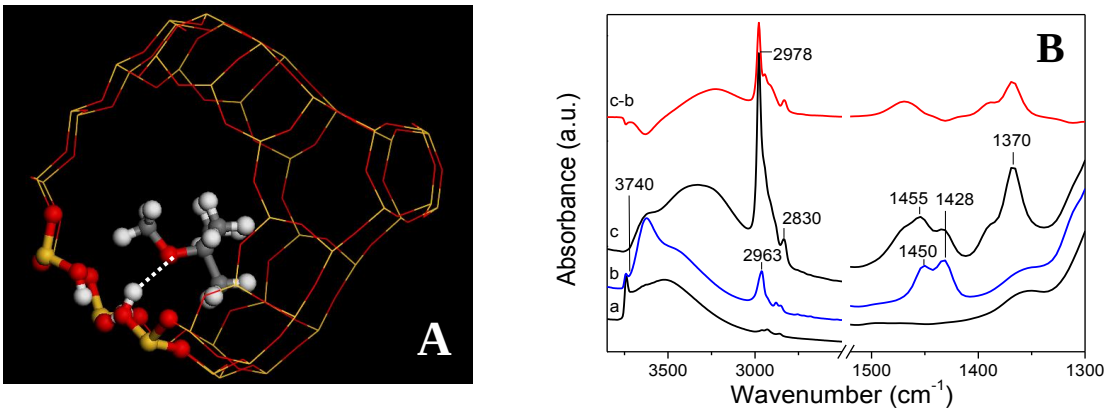

Figure 1A): DFT structure of one molecule of *methyl* tert-buthyl ether H-bonded to a silanol inside a zeolite Y cage; B): FTIR spectra of Y zeolite (SiO_2/Al_2O_3= 200) after dehydration at rt (a), after adsorption of 15 mbar of 1,2-dichloroethane (b) and subsequent adsorption of 20 mbar methyl *tert*-buthyl ether (c). "c-b" curve results from the subtraction of spectrum b from spectrum c.

As far as the adsorption of binary mixture is concerned, methyl *tert*-buthyl ether shows the best affinity for zeolite Y silanols and displaces all the other pollutants previously H-bonded (In Figure 1B, the adsorption of 1,2-dichloroethane and methyl *tert*-buthyl ether is reported as a representative example).
As expected, methyl *tert*-buthyl ether is also able to remove water molecules from zeolite adsorption sites owing to its higher Lewis base character. The competitive interactions among all classes of model pollutants with HSZ-Y were studied by FTIR spectroscopy in the presence and absence of hydration water, and information concerning formation of H-bonding and Van der Waals interactions with zeolite framework were collected aiming to understand the behaviour of sorbent phase upon real working conditions.

Conclusions

High silica zeolite Y shows an adsorption selectivity which is the highest for methyl *tert*-buthyl ether, followed by toluene, 1,2-dichloroethane and *n*-hexane. The concentration of silanols in HSZ-Y available for H-bonding interactions is drastically reduced by the presence of methyl *tert*-buthyl ether which is often found in soils contaminated with fuel-based pollutants. The non-polar portion of HSZ-Y – i.e. the siloxane fraction - which is the vast majority of the network, remains available for Van der Waals interactions with the less polar pollutants as hydrocarbons and aromatic compounds.

Acknowledgements

Research co-funded by Research Center for Non-Conventional Energy, Istituto eni Donegani – Environmental Technologies.

References

[1] Bowman, R.S., Applications of surfactant-modified zeolites to environmental remediation, Micropor. Mesopor. Mater. 61 (2003) 43–56; [2] Vignola, R., Cova, U., Fagiani, F., Grillo, G., Molinari, M., Sbardellati, R., Sisto, R. (2008) Zeolites and Related Materials: Trends, Targets and Challenger. *SSSC* (A. Gedeon, P. Massiani, F. Babonneau Eds.) 174, 573-576.

Synthesis of mullite and Cu / or Fe mullite and their catalytic activity in wet peroxide oxidation of phenol

Iva Buljan[a], Cleo Kosanović[b], Karolina Maduna Valkaj[c], Ozren Wittine[c], Stanka Zrnčević[c]
[a]*R. Boskovic Institute, Bijenicka 54, Zagreb, Croatia*
[b]*Meteorological and hydrological Service, Gric 3, Zagreb, Croatia*
[c]*Faculty of Chemical Engineering and Technology, University of Zagreb, Marulicev trg 19, Zagreb, Croatia*
ibuljan@irb.hr

Introduction

Due to their open framework, zeolites are metastable materials, which can be transformed into non-zeolite crystalline aluminosilicates above a certain temperature [1-2]. Since many of the synthetic zeolites have compositions close to those of aluminosilicate-based ceramics, their thermal treatment may result in the formation of ceramic materials, such as mullite. [3]. The need of temperature stable catalysts with selective characteristics induced the synthesis of metal incorporated mullite. The improved new catalysts are designed for the wet oxidation of phenol solutions that are found to be one of the most important representative of organic pollutants and are toxic even at low concentration [4].

Experimental

Zeolite A was synthesised by a known synthesis procedure [5]. Ion exchange of the original Na^+ ions from the starting zeolite precursor with NH_4^+ ions was carried out by previously described procedure [6]. The resulting NH_4A was then partial exchanged with Cu /Fe from copper nitrate or iron chloride solution, respectively. Post synthesis thermal induced transformations of ammonium, iron and copper form of zeolite A at the appropriate temperature (1273K) and time (3h) in a controlled-temperature chamber furnace yield into a mixture of mullite and amorphous SiO_2 in the first case, Fe-mullite and amorphous SiO_2 in the second case and to Cu-mullite and SiO_2 in the third case. Alkaline treatment of the resulting powder mixtures in 2MNaOH solution resulted to pure mullite, Fe-mullite and Cu-mullite phases after the dissolution of the entire crystal content of amorphous SiO_2.
The final products were characterized by Fourier Transform Infra Red spectroscopy, X-ray diffraction and Scanning electron microscopy.
The evaluation of their catalytic performances for the wet hydrogen peroxide oxidation of phenol was carried out in a stainless steel Parr reactor in batch operation mode under the conditions of the experiments listed in Table 1.

Table 1. Experimental conditions for the estimation of catalytic activity

Catalyst	Temperature(K)	Pressure(kPa)	c*phenol*(moldm^{-3})	cH_2O_2(moldm^{-3})
m_{CAT}=0.1gdm^{-3}	353	100	0.01	0.1
of mullite				
Fe-mullite				
Cu-mullite				

Results and discussion

Figure 1. presents the conversion of phenol as a function of the time over mullite, Cu-mullite and Fe-mullite under the same conditions of the experiment. The highest decrease in phenol concentration showed Fe-mullite catalyst.

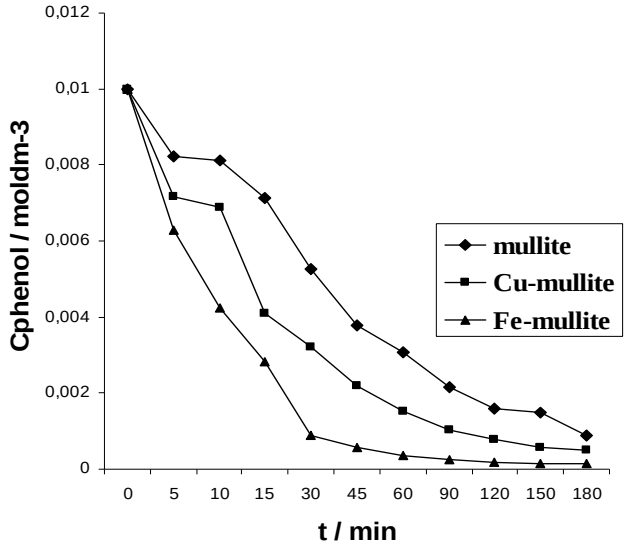

Figure 1. Phenol oxidation over mullite, Cu-mullite and Fe-mullite

Conclusions

The present study reports on the catalytic oxidation of phenol on Cu / or Fe exchanged mullite catalyst. Incorporating specific cations (Cu, Fe) into mullite has been found to be a useful technique for improving catalytic properties as it is obtained from the results on the catalytic oxidation of phenol.

Acknowledgements

The authors thank the Ministry of Science of the Republic of Croatia for financial support.

References

[1] Subramanian, M.A., Corbin, D.R., Chowdhry, U., Better ceramic substrates through zeolites, Bulletin of Material Science., 16 (1993), 665-678
[2] Dell'Agli, G., Ferone, C., Mascolo, M.C.,Pansini, M., Thermal transformation of Ba-exchanged A and X zeolites into monoclinic celsian, Solid State Ionics 127 (2000), 309-317
[3] Kosanović, C., Subotić, B., Invariability of the particulate properties during the thermal treatment of potassium-exchanged zeolite A: evidence for "amorphous crystals", Microporous Materials, 12 (1997), 261-266
[4] Catrinescu, C., Teodosiu, C., Macoveanu, M., Miehe-Brendl!e, J., Le Dred, R., Catalytic wet peroxide oxidation of phenol over Fe-exchanged pillared beidellite, Water Research, 37 (2003), 1154–1160
[5] Thompson R.W. , Franklin K.C., Verified Syntheses of Zeolitic Materials, H. Robson (ed.) Second Revised Edition, Elsevier Science, Amsterdam (2001), 179-180
[6] Kosanović, C., Čižmek, A., Subotić, B., Šmit, I., Stubičar, M., Tonejc, A., Mechanochemistry of zeolites: Part 4, Influence of cations on the rate of amorphization of zeolite A by ball milling, Zeolites, 15 (1995), 632-636

Permeance and selectivity of helium and hydrogen in nanocomposite MFI-alumina hollow fibre for tritium processes

O. Borisevich[1], D. Demange[1*], T. Parracho[1#], M. Pera-Titus[2], C.-H. Nicolas[2]

[1] *Karlsruhe Institute of Technology, Institute for Technical Physics, Tritium Laboratory Karlsruhe, Germany*
[2] *University of Lyon, Institut de Recherches sur la Catalyse et l'Environnement de Lyon (IRCELYON), France*
[#] *present address Universidade Tecnica de Lisboa, Portugal*
* Corresponding author: david.demange@kit.edu

Introduction

Energy production using nuclear fusion is an attractive alternative to the present fission power plants. The most favourable fusion reaction is the one between deuterium and tritium (hydrogen isotope mass 2 and 3). However, special requirements for fuel handling and processing have to be considered due to the radioactive properties of tritium. A closed loop is necessary to recover and reuse the unburned fraction of tritium and efficient detritiation systems (for glove-boxes and rooms) have to be implemented as well.
Many tritium processes (detritiation systems, tritium extraction from breeder blanket [1]) rely on adsorption/desorption using zeolite packed beds, to remove from a tritiated stream tritiated water or molecular tritium at room and cryogenic temperature, respectively. As an alternative, the Tritium Laboratory Karlsruhe (TLK) has recently proposed the use of zeolite membranes as pre-concentration step that would avoid immobilisation of tritium, and ensure simple and fully continuous operation without cryogenic temperatures or temperature cycles [2].
Based on a literature study, some promising types of zeolite membranes were identified and several multistage membrane processes were simulated [3]. Since the literature data for such applications is scarce, sometimes disagree concerning temperature behaviour of permeance, and vary with membrane types and production, a dedicated experimental study has been started at TLK. This paper presents the firsts results obtained on MFI-alumina hollow fibre and single gases permeation experiments using helium and hydrogen (replacing tritium).

Experimental

The nanocomposite MFI-alumina hollow fibre used in the present study is prepared by IRCELYON via pore-plugging synthesis on porous asymmetric 15 cm-long support with o.d. 1.65 mm and i.d. 1.44 mm. The surface area of the membrane is 4.97 cm^2, the equivalent thickness of zeolite layer is less than 1 μm. Detailed description could be found in [4]. It is immobilized on the supporting alumina perforated tube using a home-made glaze. Finally it is assembled in the stainless steel module and sealed with cylindrical graphite o-ring. At first the hollow fibre is conditioned by heating at 400°C under vacuum during 6 h to remove some adsorbed species from the pores. Then the leak tightness of the membrane is checked by measurement of permeance at different Δp in the range 100-500 mbar. The experiment is carried out in the dead-end mode. The gas is fed inside the hollow fibre, and the permeate flow is measured at steady-state condition by mass flow controller, while the retentate outlet is closed. The pressure difference across the membrane is kept constant at about 500 mbar using two pressure sensors at both the feed and permeates sides. The module is thermostated in a high temperature cylindrical oven from room temperature up to 400°C.

Results and discussion

The experimental results obtained in the present work are displayed in Figure 1. The single gas permeance is calculated from the measured permeate flow rate, the pressure difference, and geometrical membrane data with precision of ± 2%. The permeance of hydrogen decreases significantly with temperature, from 1.3 µm/m²· s ·Pa at room temperature to 0.78 µm / m^2·s·Pa at 400°C, while for helium this decrease is negligible. Thus the sorption-surface diffusion mechanism is applicable to our results. At the same time the ideal selectivity (determined as the ratio of permeances for single gas experiments) decreases as well, from 2.2 at room temperature to 1.5 at 400°C. From the other hand the permeation level still remains high enough to make these nanocomposite MFI-alumina hollow fibres that make them attractive for application in a pre-concentration stage in the breeder blanket.

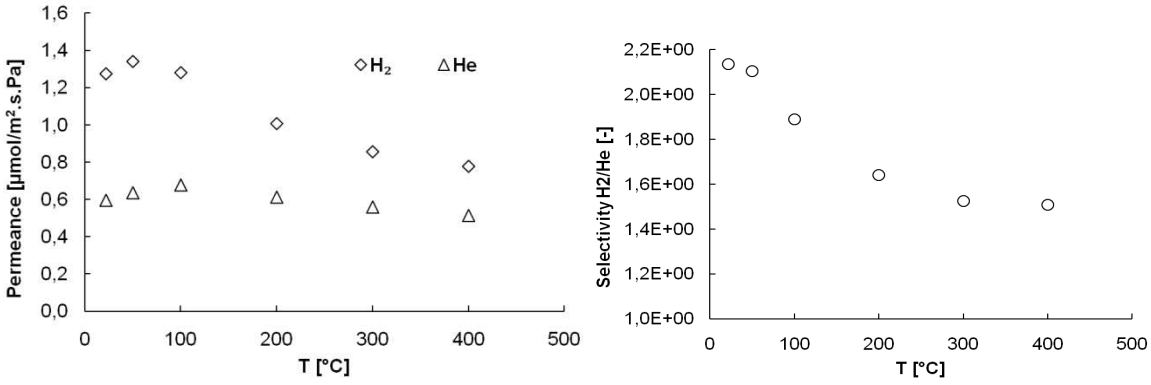

Figure 1: Single gas permeance (on the left) and ideal selectivity (on the right) for hydrogen and helium in nanocomposite MFI-alumina hollow fibre as a function of temperature

Conclusions

The experimental study of zeolite membranes for tritium processes has started. It is shown that such membranes are highly permeable for components of mixture encountered in fuel cycle of fusion machines. This makes them attractive for further investigations in this field since several applications could be envisaged.

Acknowledgements

This work has been financially supported by the Energy Centre and the Fusion Program of the Karlsruhe Institute of Technology.

References

[1] Ricapito I., Chiampichetti A., Agostini P., Benamati G., Tritium processing systems for the helium cooled pebble bed test blanket module, Fusion Engineering and Design 83 (2008), 1461–1465.
[2] Demange D., Stämmler S., Kind M., A new combination of membranes and membrane reactors for improved tritium management in breeder blanket of fusion machines, Fusion Engineering and Design, 2011, (in Press, doi:10.1016/j.fusengdes.2010.12.083).
[3] Stämmler S., Demange D., Kind M., Potential use of zeolite membranes for separation and recovery of tritium produced in the breeder-blanket of fusion machine, Proceeding of 5th International Zeolite Membrane Meeting, May 23-26, 2010 Loutraki, Greece.
[4] Pera-Titus, M., Alshebani, A., Nicolas, C.-H., Roumégoux, J.-P., Miachon, S., Dalmon, J.-A., Nanocomposite MFI-Alumina Membranes: High-Flux Hollow Fibers for CO2 Capture from Internal Combustion Vehicles, Industrial and Engineering Chemistry Research 48 (2009) 9215-9223.

Synthesis of Faujasite with Nanometric Crystals

Thiago F. Chaves[*]; Heloise O. Pastore[**]; Dilson Cardoso[*]

[*]*Federal University of São Carlos – Catalysis Laboratory - São Carlos – SP, Brazil.*

[**]*Universidade Estadual de Campinas – UNICAMP, Campinas – SP, Brazil.*

dilson@ufscar.br

Introduction

Reducing the size of zeolite crystals from the micrometric scale to the nanometer scale has produced significant changes in the properties of these materials. For example, the use of zeolites formed by nanocrystals gives rise to significant improvements in traditional applications, as for instance catalysis and separation. The ratio of external to internal number of atoms grows rapidly with decreasing particle size, increasing the external surface area [1]. Moreover, smaller crystals have a larger amount of exposed pores, reflecting lower internal diffusion limitations when compared to micrometric-sized zeolite crystals [2]. Considering the growing importance of zeolite nanocrystals in catalysis, this work investigates the synthesis conditions to obtain a FAU zeolite with nanocrystals without using an organic template.

Experimental

A typical molar composition containing the following ratio: 5.5 Na_2O : 1.0 Al_2O_3 : 10 SiO_2 : 180 H_2O, was used to synthesize the faujasite zeolite. The reagents used in the synthesis were Aerosil 380 (Evonik), sodium aluminate (Riedel de Haën – 54% Al_2O_3 : 41% Na_2O : 5% H_2O), sodium hydroxide (Quimis) and deionized water (Riedel de Haën - 54% Al_2O_3: 41% Na_2O: 5% H_2O), (Quimis). The reaction mixture formed was transferred to a Teflon-lined stainless steel autoclave and kept in an oven at 100 °C for 6 h. After this time elapsed, the solid obtained was washed several times until the pH reached 8 and then dried at 60 °C. The samples were characterized by X-ray Diffraction (XRD), Nitrogen Physisorption, Transmission Electron Microscopy (TEM), Energy Dispersive Spectroscopy (EDS) and Nuclear Magnetic Resonance (NMR) of ^{29}Si.

Results and discussion

The alkalinity effect on the product properties was checked, changing the number of Na_2O moles in the synthesis gel. This modification was performed by adding sodium hydroxide in quantities to achieve a Na_2O/Al_2O_3 molar ratio of 5.5, 6.5, 7.5 and 8.5. The hydrothermal treatment time was of 6 hours at 100 °C. Figure 1 shows the diffraction patterns for the different samples. Increasing the amount of Na_2O in the synthesis mixture decreased the intensity of the diffraction peaks. The results of nitrogen physisorption show that the micropore volume and the samples' external surface area decrease with the increasing amount of Na_2O. The sample Y-B5.5, showed an external area of 39 m^2/g and a micropore volume of 0.27 cm^3/g. Comparatively, the sample Y-B8.5 showed an external surface area of 27 m^2/g and micropore volume of 0.06 cm^3/g, showing that the material is not yet well structured. This may be related to an increased alkalinity in the reaction mixture for the samples with high contents of Na_2O, thereby favoring a higher dissolution of the zeolite. To decrease crystal size and improve the micropore volume, the reaction mixture was subjected to additional aging, therefore favoring the formation of a greater number of crystallization nuclei. For this, the sample with the Na_2O/Al_2O_3 ratio of 8.5 was chosen, shown in Figure 1, it was the one that formed the worst diffraction pattern of the FAU structure. Aging was performed at 25 ° C for 24, 48 or 72 h.

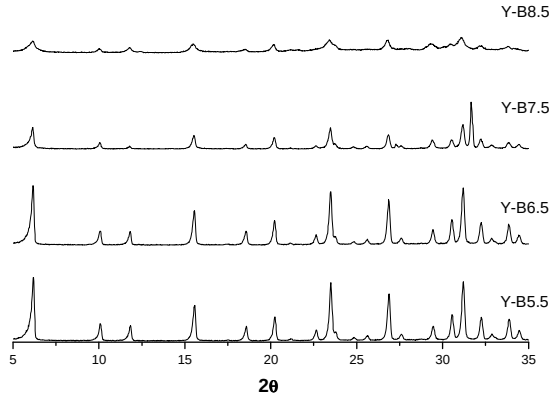

Figure 1. XRD of the samples synthesized with different Na_2O/Al_2O_3 ratios.

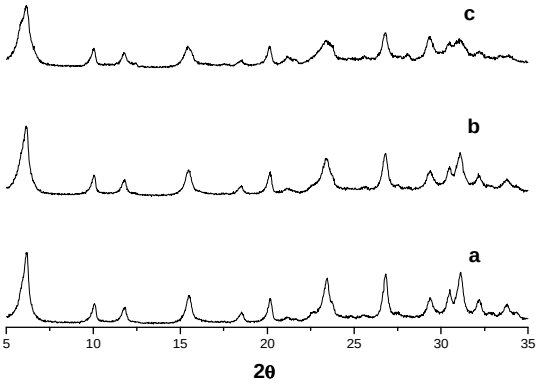

Figure 2. XRD of the samples synthesized with different aging times: 24 (a), 48 (b) and 72 h (c).

The diffraction patterns (Figure 2) of the three samples with aging exhibit the characteristic peaks of FAU. The sample aged for 72 h has a micropore volume of 0.23 cm^3/g and external surface area of 115 m^2/g, respectively. The TEM results show that this zeolite has aggregates smaller than 100 nm, hence Figure 3 shows the crystal planes for the plane (111), showing that this zeolite is well crystallized. The NMR spectrum of ^{29}Si shows the different chemical environments of Si atoms, the Si/Al ratio obtained from the NMR peak areas is of 1.46, close to that obtained by EDS (Figure 4).

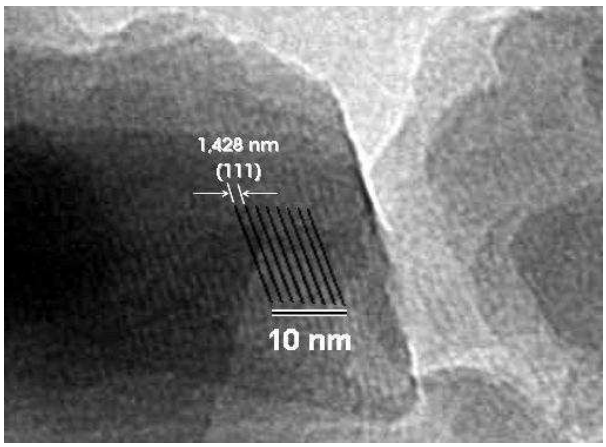

Figure 3. TEM sample aged for 72 h.

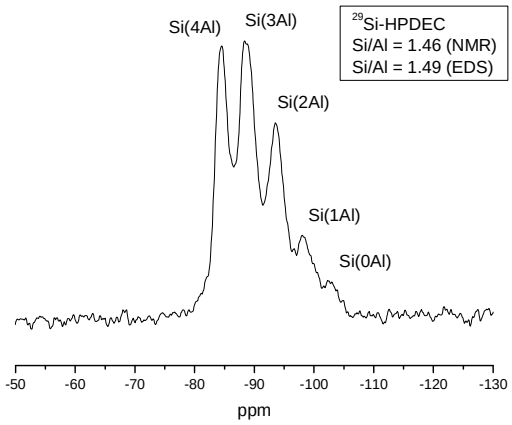

Figure 4. NMR of ^{29}Si-HPDEC of the sample aged for 72 h.

Conclusions

It was possible to synthesize nanometric crystals with the FAU structure, without requiring organic templates, with high external surface areas. Due to this material's presumably lower diffusion limitations, it can potentially be used as catalysts or adsorbents.

Acknowledgements

CNPq - National Council for Scientific and Technological Development and FAPESP - Foundation for Research in the State of São Paulo.

References

[1] L. Tosheva, V.P. Valtchev, Chem. Mater. 17 (2005) 2494-2513.

[2] P.M. Lima, T. Garetto, C.L. Cavalcante Jr., D. Cardoso, Catal. Today (2011), doi: 10.1016/j.cattod.2011.02.031 (in press).

Controlling the selectivity of lignin conversion into phenols and aromatic molecules over zeolites

Ekaterina Troussard[1, 2], Zhiqiang Ma[1], Jeroen A. van Bokhoven[1, 2]
[1]*Institute for Chemical and Bioengineering, ETH Zurich, Wolfgang-Pauli-Str. 10, 8093 Zurich, Switzerland*
[2]*Laboratory for Catalysis and Sustainable Chemistry, Paul Scherrer Institute, 5232 Villigen, Switzerland, jeroen.vanbokhoven@chem.ethz.ch*

Introduction

Lignin is a highly oxygenated polymer consisting of phenolic compounds. It has long been recognized as a potential feedstock for producing fine chemicals and fuels and fast pyrolysis is one of the most effective methods for its transformation, although the formation of coke and gases (mainly CO_2, CO, and CH_4) is unfavorable, and must be avoided [1]. Therefore, catalysis is essential to improve this process. We show that the yield of desired liquid products can be maximized using zeolites as catalyst. The pore size and topology and Si/Al ratio had great influence on the product distribution.

Experimental

Commercial zeolites H-ZSM5 (Zeochem, Switzerland) with Si/Al = 13, 25, 50, and 200 and laboratory synthesized silicalite were calcined in air at 550 ^{o}C for 5 h prior to pyrolysis. Alkaline lignin (TCI Europe) had C:H:O:S:N composition as 48:5:36:2.8:0.2 by weight. Before pyrolysis, lignin and catalysts were physically mixed, grinded and sieved (< 200 mesh, 75 μm). The samples were accurately weighted and introduced into the reactor with loose quartz wool packing.

Fast pyrolysis experiments were conducted using a platinum coil pyrolyzer 5150 (CDS Analytical, USA). The probe was a computer controlled resistively heated element which held an open ended quartz reactor. During pyrolysis, the products were brought by a helium carrier gas stream through a 300 ^{o}C heated transfer line and analyzed online with an Agilent 7890A gas chromatograph system. The system was equipped with 3 channels: HP5 column with Agilent 5975C mass spectrometer detector for condensable organic compounds, Plot/Q and mol sieve columns with TCD for separation of non-condensable C_1-C_2 and permanent gases. The yield of solid left after pyrolysis was determined gravimetrically. The yields of non-condensable gases (CO, CO_2, CH_4, C_2H_6) were quantified by calibration of GC with standard gas/He mixtures, (Messer AG, Switzerland). The yield of liquids was assumed to be the remaining difference. The products in the liquid phase were classified into several categories according to their functionalities: non-aromatic esters, ketons, aldehydes, furans, acids; nonaromatic hydrocarbons; aromatic hydrocarbons; aromatic hydrocarbon alkoxy; phenols; phenols alkoxy; and unidentified compounds.

Results and discussion

The conditions of lignin fast pyrolysis, such as temperature, heating rate, reaction time, and sample weight were optimized over lignin without catalysts. The target maximum yield of 40 wt % liquid was achieved at 650 ^{o}C, 20 ^{o}C/ms, 20 s and sample weight of 1.5 mg. These conditions were chosen for further study.

Figure 1 shows (a) the conversion of lignin and (b) the selectivity to phenol alkoxy species in the liquid fraction for different Si/Al ratios and different catalyst loadings. Compared to pure lignin pyrolysis (catalyst loading 0%), the conversion of lignin slightly

decreased. Increasing catalyst loading led to significant increase of lignin conversion. Depending on the zeolite it reached 60-70% conversion. However the composition of the catalyst did not influence the conversion of lignin. For example, silicalite revealed similar behavior as acid zeolites. We believe that acid centers of the zeolite do not participate in lignin breaking up, which corresponds to the fact that such polymeric compounds as lignin cannot penetrate zeolite pore structure and thus cannot reach acid sites of ZSM-5 located in channel intersections. It is well known that lignin pyrolysis follows a radical reaction pathway; first lignin depolymerizes to generate a significant amount of radical species, which undergo repolymerization to form coke [2]. The fact that with participation of zeolite (Fig. 1a) less coke is being formed suggests that zeolite prevents this repolymerization, probably stabilizing highly active radical species which can enter the pores.

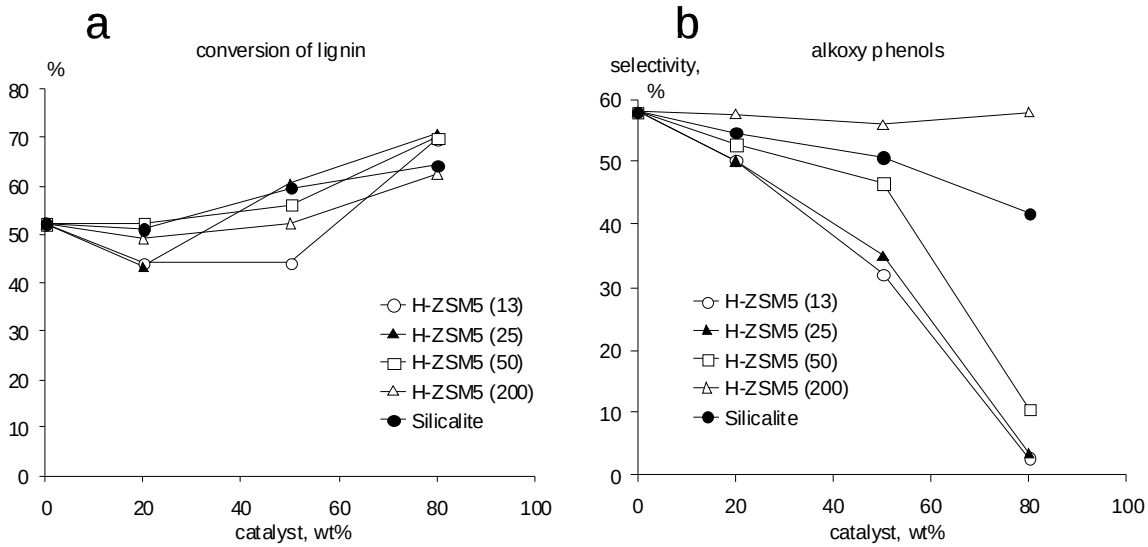

Fig. 1. Conversion of lignin (a) and selectivity to alkoxy phenolic compounds in the liquid fraction (b) as a function of catalyst loading and catalyst composition.

Nevertheless, the acidity of ZSM-5 plays an important role in the composition of the liquid fraction. Without catalyst, alkoxy phenolic species are the main products of pyrolysis: they are the building units of the lignin polymer and thus primary reaction products. With the increase of catalyst content, they were converted into phenols and aromatic hydrocarbons (not shown). Such reactions happen over acid sites of zeolite. Thus the amount and nature of active sites is very important for product composition. Fig. 1b shows that highly acid zeolites shift the selectivity from alkoxy phenolic compounds to aromatics such as benzene and toluene. These findings give us an important key on how to tune the products of lignin fast pyrolysis, by choosing the right catalyst to adsorb and convert primary products of lignin breaking to useful chemicals.

Conclusions

Acid zeolites play a dual role in fast pyrolysis of lignin. The porous structure of zeolite captures the initial products of lignin pyrolysis: oxygenated aromatics (alkoxy phenols). This prevents their repolymerization and coke formation. The application of zeolites of different acidity allows transforming those initial products to aromatics by dealkoxylation and dehydroxylation.

[1] T.P. Vispute, H. Zhang, A. Sanna, R. Xiao, G.W. Huber, *Science*, 330 (2010) 1222
[2] C. A. Mullen and A. A. Boateng, *Fuel Process. Technol.*, (2010) 91:1446-1458

Synthesis of mullite and Cu / or Fe mullite and their catalytic activity in wet peroxide oxidation of phenol

Iva Buljan[a], Cleo Kosanović[b], Karolina Maduna Valkaj[c], Ozren Wittine[c], Stanka Zrnčević[c]
[a]*R. Boskovic Institute, Bijenicka 54, Zagreb, Croatia*
[b]*Meteorological and hydrological Service, Gric 3, Zagreb, Croatia*
[c]*Faculty of Chemical Engineering and Technology, University of Zagreb, Marulicev trg 19, Zagreb, Croatia*
ibuljan@irb.hr

Introduction

Due to their open framework, zeolites are metastable materials, which can be transformed into non-zeolite crystalline aluminosilicates above a certain temperature [1-2]. Since many of the synthetic zeolites have compositions close to those of aluminosilicate-based ceramics, their thermal treatment may result in the formation of ceramic materials, such as mullite. [3]. The need of temperature stable catalysts with selective characteristics induced the synthesis of metal incorporated mullite. The improved new catalysts are designed for the wet oxidation of phenol solutions that are found to be one of the most important representative of organic pollutants and are toxic even at low concentration [4].

Experimental

Zeolite A was synthesised by a known synthesis procedure [5]. Ion exchange of the original Na^+ ions from the starting zeolite precursor with NH_4^+ ions was carried out by previously described procedure [6]. The resulting NH_4A was then partial exchanged with Cu /Fe from copper nitrate or iron chloride solution, respectively. Post synthesis thermal induced transformations of ammonium, iron and copper form of zeolite A at the appropriate temperature (1273K) and time (3h) in a controlled-temperature chamber furnace yield into a mixture of mullite and amorphous SiO_2 in the first case, Fe-mullite and amorphous SiO_2 in the second case and to Cu-mullite and SiO_2 in the third case. Alkaline treatment of the resulting powder mixtures in 2MNaOH solution resulted to pure mullite, Fe-mullite and Cu-mullite phases after the dissolution of the entire crystal content of amorphous SiO_2.
The final products were characterized by Fourier Transform Infra Red spectroscopy, X-ray diffraction and Scanning electron microscopy.
The evaluation of their catalytic performances for the wet hydrogen peroxide oxidation of phenol was carried out in a stainless steel Parr reactor in batch operation mode under the conditions of the experiments listed in Table 1.

Table 1. Experimental conditions for the estimation of catalytic activity

Catalyst	Temperature(K)	Pressure(kPa)	c*phenol*(moldm^{-3})	cH_2O_2(moldm^{-3})
m_{CAT}=0.1gdm^{-3}	353	100	0.01	0.1
of mullite				
Fe-mullite				
Cu-mullite				

Results and discussion

Figure 1. presents the conversion of phenol as a function of the time over mullite, Cu-mullite and Fe-mullite under the same conditions of the experiment. The highest decrease in phenol concentration showed Fe-mullite catalyst.

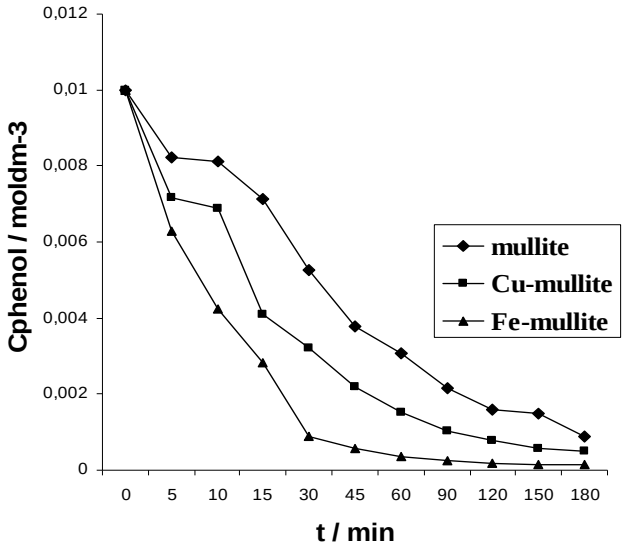

Figure 1. Phenol oxidation over mullite, Cu-mullite and Fe-mullite

Conclusions

The present study reports on the catalytic oxidation of phenol on Cu / or Fe exchanged mullite catalyst. Incorporating specific cations (Cu, Fe) into mullite has been found to be a useful technique for improving catalytic properties as it is obtained from the results on the catalytic oxidation of phenol.

Acknowledgements

The authors thank the Ministry of Science of the Republic of Croatia for financial support.

References

[1] Subramanian, M.A., Corbin, D.R., Chowdhry, U., Better ceramic substrates through zeolites, Bulletin of Material Science., 16 (1993), 665-678
[2] Dell'Agli, G., Ferone, C., Mascolo, M.C.,Pansini, M., Thermal transformation of Ba-exchanged A and X zeolites into monoclinic celsian, Solid State Ionics 127 (2000), 309-317
[3] Kosanović, C., Subotić, B., Invariability of the particulate properties during the thermal treatment of potassium-exchanged zeolite A: evidence for "amorphous crystals", Microporous Materials, 12 (1997), 261-266
[4] Catrinescu, C., Teodosiu, C., Macoveanu, M., Miehe-Brendl!e, J., Le Dred, R., Catalytic wet peroxide oxidation of phenol over Fe-exchanged pillared beidellite, Water Research, 37 (2003), 1154–1160
[5] Thompson R.W. , Franklin K.C., Verified Syntheses of Zeolitic Materials, H. Robson (ed.) Second Revised Edition, Elsevier Science, Amsterdam (2001), 179-180
[6] Kosanović, C., Čižmek, A., Subotić, B., Šmit, I., Stubičar, M., Tonejc, A., Mechanochemistry of zeolites: Part 4, Influence of cations on the rate of amorphization of zeolite A by ball milling, Zeolites, 15 (1995), 632-636

Controlling the selectivity of lignin conversion into phenols and aromatic molecules over zeolites

Ekaterina Troussard[1, 2], Zhiqiang Ma[1], Jeroen A. van Bokhoven[1, 2]
[1]*Institute for Chemical and Bioengineering, ETH Zurich, Wolfgang-Pauli-Str. 10, 8093 Zurich, Switzerland*
[2]*Laboratory for Catalysis and Sustainable Chemistry, Paul Scherrer Institute, 5232 Villigen, Switzerland, jeroen.vanbokhoven@chem.ethz.ch*

Introduction

Lignin is a highly oxygenated polymer consisting of phenolic compounds. It has long been recognized as a potential feedstock for producing fine chemicals and fuels and fast pyrolysis is one of the most effective methods for its transformation, although the formation of coke and gases (mainly CO_2, CO, and CH_4) is unfavorable, and must be avoided [1]. Therefore, catalysis is essential to improve this process. We show that the yield of desired liquid products can be maximized using zeolites as catalyst. The pore size and topology and Si/Al ratio had great influence on the product distribution.

Experimental

Commercial zeolites H-ZSM5 (Zeochem, Switzerland) with Si/Al = 13, 25, 50, and 200 and laboratory synthesized silicalite were calcined in air at 550 ^{o}C for 5 h prior to pyrolysis. Alkaline lignin (TCI Europe) had C:H:O:S:N composition as 48:5:36:2.8:0.2 by weight. Before pyrolysis, lignin and catalysts were physically mixed, grinded and sieved (< 200 mesh, 75 μm). The samples were accurately weighted and introduced into the reactor with loose quartz wool packing.

Fast pyrolysis experiments were conducted using a platinum coil pyrolyzer 5150 (CDS Analytical, USA). The probe was a computer controlled resistively heated element which held an open ended quartz reactor. During pyrolysis, the products were brought by a helium carrier gas stream through a 300 ^{o}C heated transfer line and analyzed online with an Agilent 7890A gas chromatograph system. The system was equipped with 3 channels: HP5 column with Agilent 5975C mass spectrometer detector for condensable organic compounds, Plot/Q and mol sieve columns with TCD for separation of non-condensable C_1-C_2 and permanent gases. The yield of solid left after pyrolysis was determined gravimetrically. The yields of non-condensable gases (CO, CO_2, CH_4, C_2H_6) were quantified by calibration of GC with standard gas/He mixtures, (Messer AG, Switzerland). The yield of liquids was assumed to be the remaining difference. The products in the liquid phase were classified into several categories according to their functionalities: non-aromatic esters, ketons, aldehydes, furans, acids; nonaromatic hydrocarbons; aromatic hydrocarbons; aromatic hydrocarbon alkoxy; phenols; phenols alkoxy; and unidentified compounds.

Results and discussion

The conditions of lignin fast pyrolysis, such as temperature, heating rate, reaction time, and sample weight were optimized over lignin without catalysts. The target maximum yield of 40 wt % liquid was achieved at 650 ^{o}C, 20 ^{o}C/ms, 20 s and sample weight of 1.5 mg. These conditions were chosen for further study.

Figure 1 shows (a) the conversion of lignin and (b) the selectivity to phenol alkoxy species in the liquid fraction for different Si/Al ratios and different catalyst loadings. Compared to pure lignin pyrolysis (catalyst loading 0%), the conversion of lignin slightly

decreased. Increasing catalyst loading led to significant increase of lignin conversion. Depending on the zeolite it reached 60-70% conversion. However the composition of the catalyst did not influence the conversion of lignin. For example, silicalite revealed similar behavior as acid zeolites. We believe that acid centers of the zeolite do not participate in lignin breaking up, which corresponds to the fact that such polymeric compounds as lignin cannot penetrate zeolite pore structure and thus cannot reach acid sites of ZSM-5 located in channel intersections. It is well known that lignin pyrolysis follows a radical reaction pathway; first lignin depolymerizes to generate a significant amount of radical species, which undergo repolymerization to form coke [2]. The fact that with participation of zeolite (Fig. 1a) less coke is being formed suggests that zeolite prevents this repolymerization, probably stabilizing highly active radical species which can enter the pores.

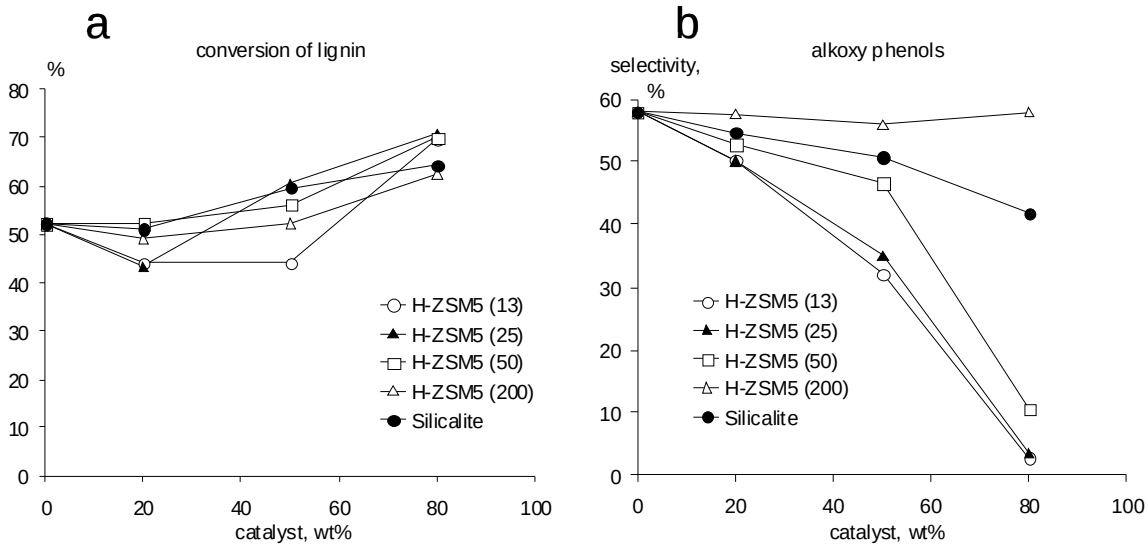

Fig. 1. Conversion of lignin (a) and selectivity to alkoxy phenolic compounds in the liquid fraction (b) as a function of catalyst loading and catalyst composition.

Nevertheless, the acidity of ZSM-5 plays an important role in the composition of the liquid fraction. Without catalyst, alkoxy phenolic species are the main products of pyrolysis: they are the building units of the lignin polymer and thus primary reaction products. With the increase of catalyst content, they were converted into phenols and aromatic hydrocarbons (not shown). Such reactions happen over acid sites of zeolite. Thus the amount and nature of active sites is very important for product composition. Fig. 1b shows that highly acid zeolites shift the selectivity from alkoxy phenolic compounds to aromatics such as benzene and toluene. These findings give us an important key on how to tune the products of lignin fast pyrolysis, by choosing the right catalyst to adsorb and convert primary products of lignin breaking to useful chemicals.

Conclusions

Acid zeolites play a dual role in fast pyrolysis of lignin. The porous structure of zeolite captures the initial products of lignin pyrolysis: oxygenated aromatics (alkoxy phenols). This prevents their repolymerization and coke formation. The application of zeolites of different acidity allows transforming those initial products to aromatics by dealkoxylation and dehydroxylation.

[1] T.P. Vispute, H. Zhang, A. Sanna, R. Xiao, G.W. Huber, *Science*, 330 (2010) 1222
[2] C. A. Mullen and A. A. Boateng, *Fuel Process. Technol.*, (2010) 91:1446-1458

Mesoporous HZSM-5 Zeolite for Adsorption of Pharmaceutically Active Compounds from Aqueous Solutions.

Vladislav Rac[1], Vesna Rakić[1], Vera Dondur[2], Aline Auroux[3]
[1]*Faculty of Agriculture, Department of Chemistry, University of Belgrade, 11000 Belgrade, Serbia;* [2]*Faculty of Physical Chemistry, University of Belgrade, 11000 Belgrade, Serbia;* [3]*Institut de Recherches sur la Catalyse et l'Environnement de Lyon (IRCELYON), UMR 5256 CNRS/Université Lyon1, 2 av. Albert Einstein, 69626 Villeurbanne Cedex, France.*
Corresponding author: aline.auroux@ircelyon.univ-lyon1.fr

Introduction

Nowadays, the presence of pharmaceutically active compounds as pollutants in the aquatic environment is considered a relevant and very important topic [1]. Pharmaceuticals have physiological effects on humans and animals in very low concentrations. Today, we are aware that certain discarded pharmaceuticals can persist in the environment and make their way back to us either via the food chain or via drinking water. Some members of eminent prescription-drug groups are ubiquitous in natural aquatic systems, since they are polar molecules and hence soluble in water [1]. Therefore, their detection, the investigation of their effects and discovery of versatile possibilities to remove them from the environment impose challenges for researchers.
Recently, mesoporous zeolites, obtained by desilication procedures, have attracted attention since they express improved ability as carriers for large active species [2, 3]. In this work, we report results concerning adsorption of salicylic acid, a non-steroidal anti-inflammatory drug – diclofenac Na, a β blocker – atenolol and phenol from aqueous solution, using mesoporous HZSM-5 zeolite.

Experimental

Mesopore formation in HZSM-5 zeolite (Zeolyst, Si/Al = 26) has been done through silicone extraction by sodium hydroxide (0.2 M), using procedure reported in reference 2. The surface areas, pore volumes and pore sizes were measured by nitrogen adsorption at 78 K on a Micromeritics 2010 apparatus, after pre-treatment at 673 K during 4 hours. XRD measurements, performed on a Bruker D5005 powder diffractometer scanning from 2° to 80° (2θ) at a rate of 0.02° s^{-1} using a Cu Kα radiation, have proven that MFI structure has been preserved after desilication procedure. Salycylic acid (SA), diclofenac-Na (DFK), atenolol (ATL) and phenol (PH) have been purchased from Sigma, Aldrich, pharmaceutical company "Galenika", Belgrade, Serbia and Fluka, respectively). The adsorption was studied at 303 K, equilibrium adsorbate concentrations were determined by Shimadzu UV-1650PC spectrophotometer. In parallel experiments performed under the same conditions, the heats evolved as a result of adsorption were measured by titration microcalorimetry (Titrys from Setaram). In order to estimate the population and strength of acid sites, ammonia adsorption (done at 423 K) on both parent and mesoporous zeolite has been studied by means of microcalorimetry. These experiments gave evidence that desilication procedure did not influence importantly the acidity of ZSM-5 zeolite.

Results and discussion

Desilication of parent HZSM-5 (Si/Al = 26) resulted in development of mesoporosity; which is evident from the profiles of isotherms of low-temperature nitrogen adsorption, presented in Figure 1 (left). Table 1 summarizes the textural properties of both zeolites.

Table 1. Textural properties of parent and mesoropous HZSM-5 zeolite.

HZSM-5 zeolite	V_{pore} [cm^3 g^{-1}], at P/Po = 0.98	V_{micro} [cm^3 g^{-1}], t-plot method	S_{meso} [m^2 g^{-1}], t-plot method	S_{BET} [m^2 g^{-1}], BET method
Parent	0.24	0.14	64	365
Mesoporous	0.45	0.14	173	470

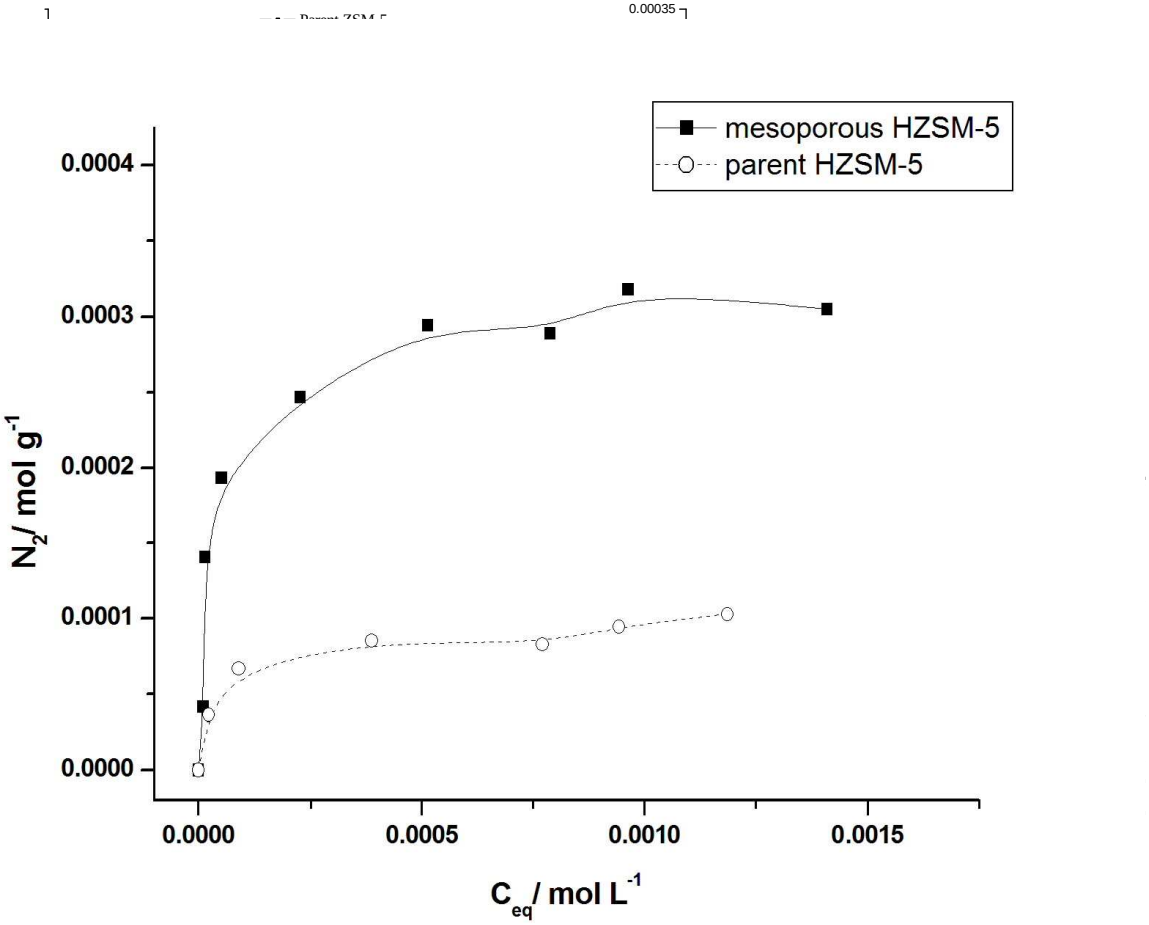

The results obtained in this work show that desilication procedure improves mesoporosity in MFI type zeolites what offers possibility to use these materials as effective adsorbents for pollutants of water. Mesoporous ZSM-5 zeolite shows improved capacities for adsorption of atenolol and diclofenac-Na from aqueous solutions. From the results obtained in this work, it can be inferred that improved mesoporosity and increased free volume inside the zeolite structure are the most important for adsorption capabilities of mesoporous zeolites toward pharmaceutically active compounds.

References

[1] Khetan, S.K., Collins, T.J., Human pharmaceuticals in the aquatic environment: a challenge to green chemistry. Chem. Rev. 107 (2007), 2319–2364.
[2] Mitchell, S., Pérez-Ramírez, J., Mesoporous zeolites as enzyme carriers: Synthesis, characterization, and application in biocatalysis, Cat. Today 168 (2011) 28-37.
[3] Verboekend, D., Pérez-Ramírez, J., Desilication mechanism revisited: Highly mesoporous all-silica zeolites enabled through pore-directing sgents, Chem. Eur. J. 17 (2011) 1137 – 1147.
[4] Damjanovic, Lj., Rakic, V., Rac, V., Stosic, D., Auroux, A., The investigation of phenol removal from aqueous solutions by zeolites as solid adsorbents, Journal of Hazardous Materials 184 (2010) 477–484.

Influence of Intermetallic diffusion barrier on Pd Membrane

Mohammad Hossein Sayyar[3,*]; Milad Rasouli[1,3]; Sahar Chitsazan[1,3]; Nakisa Yaghobi
[1] *Islamic Azad University, South Tehran Branch, Tehran, Iran*
[2] *Department of Petrochemical, Iran Polymer and Petrochemical Institute, Tehran, Iran*
[3] *Pars Coating Technology Co., P.O.Box: 14155/3499, Tehran, Iran*
** sayyar@parscoating.com*

Introduction

To reduce intermetallic diffusion between the metal support and the Pd layer, and thereby improving the stability of the Pd/PSS composite membrane, Ma et al. [1] used a controlled in-situ oxidation of the porous stainless steel prior to plating to produce an oxide layer to act as a diffusion barrier between the Pd and the PSS [2]. The objective of this research is to investigate the effects of temperature on the formation of the intermetallic diffusion barrier layer by the controlled in-situ oxidation method for Pd/PSS membrane.

Experimental

Porous 316L stainless steel supports were purchased from Mott Metallurgical Corporation (0.2 µm grade) and Fuji Filter Company (0.5 µm grade). Two of the support tubes were then oxidized in furnace in the presence of air at 400, 600 and 800 $^{\circ}$C for 2 h, with heating and cooling rates of 3 $^{\circ}$Cmin^{-1}. The furnace was purchased from ELITE THERMAL SYSTEM model TSH12/50/300-2416CG. The oxidation layer formed acts as a diffusion barrier between the PSS substrate and the Pd catalyst. The substrate was then activated by pre-seeding with finely divided Pd nuclei. Procedure for Pd coating.
The composition of the Pd plating solution is given in Table 1. The hydrazine (reducing agent) was added just prior to plating. The plating solution was renewed every 90 to 120 minutes. After deposition was completed the membrane was left to cool to room temperature and dried. After each drying, the weight and helium flux were measured. The weight gains before and after the plating were used to determine the thickness of the membrane.

Table 1 Chemical composition of the plating solution.

Chemicals	Pd bath
$Pd(NH_3)_4Cl_2.H_2O$ (g/l)	4-6
$Na_2EDTA.2H_2O$ (g/l)	40-80
NH_4OH (28%) (ml/l)	190-400
H_2NNH_2 (1M) (ml/l)	5-10
Polyoxyalkylene alkyl ether (ml/l)	0.1-0.5
pH	10-11
Temperature (^{o}C)	60

Results and discussion

Figure 1. shows the SEM pictures of a typical grade 0.2 µm grade Mott PSS after oxidation in 400^{o}C, 600^{o}C, and 800^{o}C.

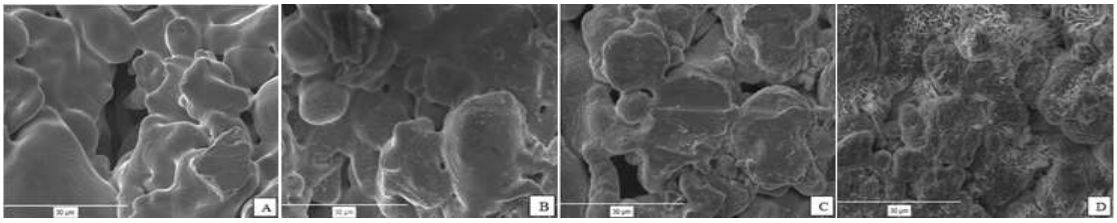

Figure 1. (A) supports after cleaning (B) oxidized at 400°C; (C) oxidized at 600°C; (D) oxidized at 800°C.

Figure 2. shows the change of the properties of the 0.5 µm grade Fuji Filter PSS tubes following oxidation of the cleaned tubes. The oxygen peaks confirm the formation of oxide layers on the supports. It was observed that the amount of oxygen on the support increased with higher oxidation temperatures, indicating a thicker oxide layer. As the oxidation temperature was increased, the weight gain increased indicating the formation of more oxide at higher temperatures. The formation of greater quantities of oxide gave a higher resistance to the He permeation.

Table 2. Percent weight gain and He flux change after oxidation for Mott PSS supports

Tube	Oxidation (°C)	Δm (%)	Thickness (µm)	He Flux, J (cm^3/cm^2min)
1	20	0	0	701
2	400	0.035	--	700
3	600	0.78	0.2-0.3	565
4	800	4.69	1-6	27

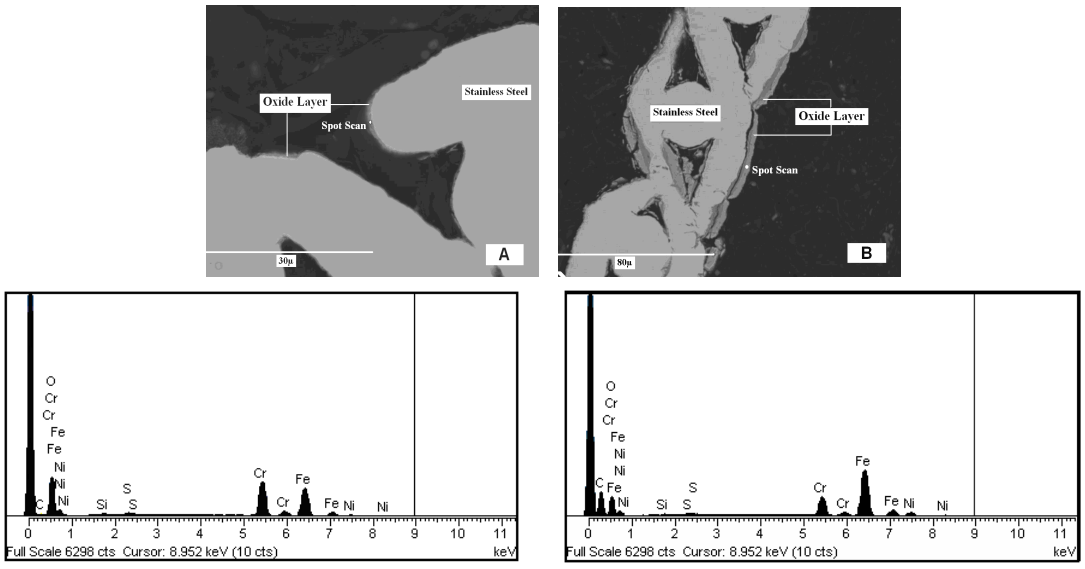

Figure 2. Cross section oxide of the layer of the Fuji PSS supports and EDS spot scans after oxidation on oxide layer at (A) 600°C, and (B) 800°C.

Among the oxides that can be formed with the elements of stainless steel, Cr_2O_3 is the most stable due to its low Gibbs free energy, the low diffusion rates of elements in the oxide scale, and its high chemical stability under a H_2 atmosphere. The SEM micrograph of the sample oxidized at 800˚C showed a thicker dark region with a very nonuniform thickness was observed. It could also be observed that the surface of this oxide layer was very crumbly. The thickness of the dark region varied from 1 to 6 µm from spot to spot since the oxide layer was

relatively thick. After Pd coating, the final thicknesses of the dense Pd membrane were 23-27 µm on 0.2 µm grade Mott supports and 32-35 µm on 0.5 µm grade Fuji plate supports.

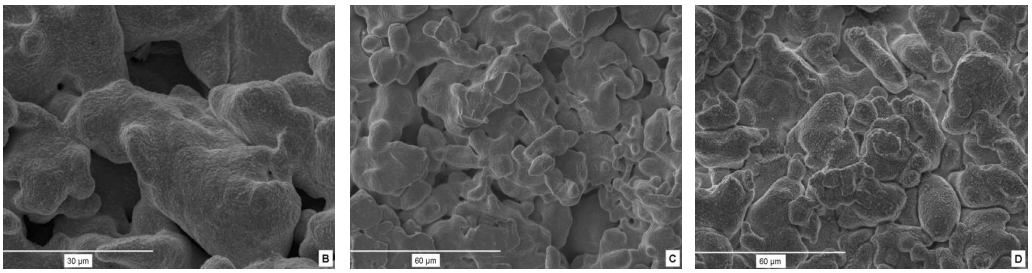

Figure 3. SEM photographs of: B - after 13.5 hr plating; C - after 15 hr; and D - after 24 hr

Conclusions

Oxidation process was carry out in diffrent temprature. It was observed that the amount of oxygen on the support increased 10 times with higher oxidation temperatures indicating a thicker oxide layer. Sample oxidized at 800˚C showed a thicker dark region with a very nonuniform thickness. It was also observed that the surface of this oxide layerwas crumbly. The thickness of the dark oxide region varied from 1 to 6 µm from spot to spot. Therefore, it is the most desirable oxide phase for use as a barrier layer to intermetallic diffusion. Membranes produced by this method have been shown to be stable for over 6000 h in the Temprature of 800^{o}C.

References

[1] US Patent 6152987, “Hydrogen gas-extraction module and method of fabrication”
[2] P.P. Mardllovich, Y. She, Y.H. Ma., “Stabillity of hydrogen flux through Pd/porous stainess steel compsite membranes” Proc.Fifth Int. Conf . Inorg . Membr 1 (1998) 246

Narrowed pore size distribution of thermally stable mesostructured aluminas

L. López-Pérez, H.J. Heeres and I. Melián-Cabrera*

*Chemical Reaction Engineering, University of Groningen, Nijenborgh 4, 9747 AG Groningen The Netherlands. *i.v.melian.cabrera@rug.nl*

Introduction

Aluminas are key materials in catalysis. They serve as a support for many applications. One of the most important is perhaps for hydrotreatment catalysts, as γ-alumina. This type of materials has shown excellent performance when hosting NiMo or CoMo; they are low cost and recyclable. The preparation is based on the precipitation leading to materials with BET surface areas up to 300 m^2/g with pore volumes of 0.8-1.0 cm^3/g [1]. The porosity comes from the interparticles void space of the microcrystalline aggregates. The pore dimension lies in the high mesopore region, and importantly, a wide pore size distribution is typically obtained. It would be desirable to narrow this distribution of pores and, if possible, shifting it into the lower mesopore region. This can be done by using surfactants during the hydrolysis in a similar fashion as reported for MCM-41 silicas. However, our case is more complex since the hydrolysis of aluminum salts is much faster than silicon. This challenge has been addressed extensively and partly solved by using Aluminum alcoxides and various types of anionic, cationic or non-ionic surfactants as structure-directing agents.

Bagshaw and Pinnavaia [2] reported a I^oS^o type mesoporous alumina material with unprecedented textural features having BET surface areas ranging between 425-535 m^2/g. Considerable research was undertaken afterwards including more insight on non-ionic surfactants by means of adding acid catalysts or employing anionic or cationic surfactants. It can be noted beyond doubt that small changes in the synthesis conditions have a big impact on the mesophase formation. The topic has been reviewed by Márquez-Alvarez et al [3] covering a thorough analysis of the synthetic aspects known. Until recently, the materials reported were indeed mesoporous but not having an ordered pores arrangement. Niesz et al. [4] were the first to synthesize mesoporous aluminas with an ordered pore arrangement. The trick was performing a HCl catalyzed hydrolysis of aluminum tri-*tert*-butoxide using Pluronic P123 in ethanol with a controlled amount of water. Although the material showed well organized pores as evidenced by TEM, the textural data manifested a wide pore size distribution and a lack of closure in the high p/po region of the isotherm, i.e. mostly extraparticle pores. This challenged us on making a new material with ideally a narrow distribution of pores in relatively bigger particles that allows having interparticle pores more defined.

In this paper we have developed new synthetic aspects arriving to materials with much narrower pore size distribution in the low mesopore region. This was achieved by proper selecting the Al source, the solvent (must be similar to the alkoxide to avoid exchange reaction with the alkoxide) and carefully controlling the evaporation and drying rate.

Experimental

The synthesis protocol is based on the sol-gel chemistry in acid medium using HCl with a non-ionic surfactant (Pluronic P123) [3]. Several modifications to this method were thoroughly investigated covering the use of aluminium tri-sec-butoxide as Al source; two types of alcohols, namely absolute ethanol and sec-butyl alcohol as well as the critical ageing and drying protocol.

The molar composition of the final gel of this study was: 1 Al^{3+}: 0.017 Pluronic P123 : 30 2-C_4H_9OH : 6 H_2O : 1.8 HCl.

Results and discussion

The quality of the ordering for the hybrid mesophases was evaluated by SAXS as well as by the steepness of the capillary filling in the N_2 physisorption isotherms. Table 1 summarizes the results obtained (not shown) where several parameters were investigated: alcohol type, temperature, and evaporation protocol. It must be noted that the temperature corresponds to hydrolysis as well as for the drying steps; therefore, the total synthesis time varies among samples. It was found that a highly ordered alumina mesophase can be obtained under strictly defined conditions (dark area in table) using sec-butyl alcohol and drying under dry-N_2 at 60 ^oC after an ageing isothermal period. We believe that at these conditions a good compromise between the rates of hydrolysis and condensation of the Al-oxides retaining the block copolymer is achieved. This material showed a 2D hexagonal ordering with a defined 100 reflection centered at 1.44 degrees (a_0=69.7 Å). The excellent textural properties were manifested by an intense PSD located 41 Å due to the sharp capillary condensation in narrow interparticle mesopores. The latter is due to the isotherm closure; the material possesses a BET of 411 m^2/g with 0.58 cm^3/g. This PSD is much narrower (and having smaller pores) than for a commercial γ-alumina and prior art [4].

Table 1. Crystalline ordering of the calcined mesophases. Shading code: black is highly ordered, vertical to a partly ordered material while the dotted region is when an amorphous material was found.

	Ethanol		**sec-butyl alcohol**	
Temp. (K)	Stove furnace	N_2 aided evaporation	Stove furnace	N_2 aided evaporation
313				
333				
353	g.e.	g.e.		

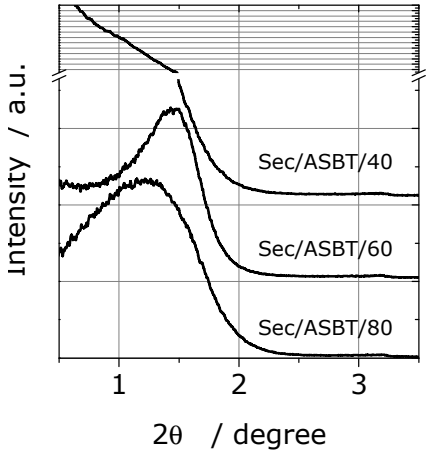

Figure 1. SAXS patterns for calcined samples that were synthesized and dried in sec-butyl alcohol at 40, 60 and 80 ^oC.

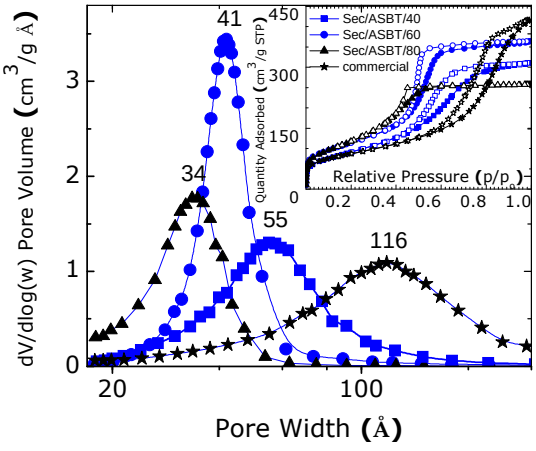

Figure 2. Pore size distributions for the mesophases prepared under sec-butyl alcohol under N_2 flow. Inset: full isotherms.

References

[1] C. Misra, Industrial Alumina Chemicals: ACS Monograph 184, Washington DC, 1986.
[2] S.A. Bagashaw, T.J. Pinnavaia, T. J. Angew. Chem., Int. Ed. Engl. 1996, 35, 1102.
[3] C. Márquez-Alvarez, et. al. Catal. Rev. 2008, 50, 222.
[4] K. Niesz, P. Yang and G. A. Somorjai. Chem. Commun. (2005)1986-1987.

Synthesis and catalytic application of DDR-type zeolite with trivalent heteroatoms

Masato Yoshioka, Toshiyuki Yokoi, Hiroyuki Imai and Takashi Tatsumi*
Chemical Resources Laboratory, Tokyo Institute of Technology, Yokohama, Japan,
**ttasumi@cat.res.titech.ac.jp*

Introduction

Zeolites have been utilized in many industrial technologies, including gas adsorption, ion exchange, separation and catalysis because of their unique porosity and high surface area. Recently, 8-membered ring (8-MR) zeolites and zeotype materials have attracted much attention in expectation of selective catalysis based on their small pores. For example, **CHA**-zeotype materials such as SSZ-13 and SAPO-34 showed a catalytic activity for methanol to olefins (MTO) reaction to selectively provide ethene and propene, which are important chemicals for the polymer industry. Recently, we reported that **RTH**-zeotype materials such as [Al,B]-RUB-13 and [Al,B]-TTZ-1 showed a high selectivity for propylene in the MTO reaction [1]. Although, besides these structures, a variety of 8-MR zeolites with different structures have been synthesized, the studies on the compositional variations leading to their catalytic applications of other 8-MR zeolites have been rather limited.

DDR-type zeolite, which was discovered at 1987, consists of *mtn* cages as composite building unit with the openings of 8-MR and has two-dimensional channels with aperture size of 0.36 x 0.44 nm [2]. **DDR**-type zeolites have been synthesized in the presence of several organic nitrogen compounds such as 1-adamantanamine, quinuclidinium hydroxide, *N*-methyltropinium iodide as organic structure-directing agent (OSDA) [3]. However, the incorporation of heteroatoms into the framework and catalytic application have not been fully investigated.

In this study, we report the synthesis of **DDR**-type zeolite with trivalent heteroatoms. The catalytic performance of thus prepared zeolites in the MTO reaction was also assessed.

Experimental

The metallosilicates with a **DDR** topology ([M]-ZSM-58, M = Al and Ga) were synthesized according to the original recipe of ZSM-58 with modifications [2]. In typical synthesis of [Al]-ZSM-58, aluminum sulfate and *N*-methyltropinium iodide (MTI) were added to an aqueous solution containing NaOH with stirring. Fumed silica was added to the mixture. The molar composition of the reaction mixture was 1.0 SiO_2 : 0.025 $Al_2(SO_4)_3$: 0.033 NaOH : 0.25 MTI : 40 H_2O. Thus prepared mother gel was crystallized in an oven at 160^oC for 7 days with tumbling at 40 rpm. The solid product was recovered by filtration, washing with distilled water and drying overnight at 100^oC. In the synthesis of [Ga]-ZSM-58, $Ga(NO_3)_3 \cdot n\ H_2O$ (n = 7-9, Wako) was used as Ga source.

The conversion from sodium-type into proton-type zeolites was conducted by repeated ion exchange with 2 M ammonium nitrate solution and subsequent calcination at 550^{o}C for 6 h. Thus prepared acid-type zeolites were used as catalysts for the MTO reaction.

The MTO reaction, which gives methane (C1), ethane (C2), ethene (C2=), propane (C3), propene (C3=), C4-C6 hydrocarbons and dimethyl ether (DME) as products, was carried out in a fixed bed reactor. The selectivities of the products were calculated on the carbon numbers basis. The reaction was performed at 375^{o}C at a W/F of 17-34 g h mol^{-1}. Typically, 100 mg catalyst was centered at a quartz reactor in a furnace and 5 % methanol diluted with helium was used as reactant. The weight hourly space velocity (WHSV) of methanol was 0.5-1.0 h^{-1}. The catalyst was calcined prior to the reaction at 500^{o}C for 1 h, and then the reactor was cooled to the reaction temperatures.

Results and discussion

XRD measurements showed that [Al]-ZSM-58 with the atomic ratios of Si/Al ranging from 18 to 25 were crystallized. The products with the Si/Al ratios of 29 to 73 were a mixture of the **DDR**-phase and unknown phase. Similarly, in the case of gallium, [Ga]-ZSM-58 with the Si/Ga ratio of 17 was obtained, while high silica products with Si/Ga ratios of 35 to 81 were a mixture of **DDR**-phase and unknown phase. The SEM images revealed that the products with the **DDR**-phase were cubic crystals about 50-150 nm in size irrespective of the kind and/or the amount of heteroatoms.

The ^{27}Al MAS NMR spectrum of [Al]-ZSM-58 with the Si/Al ratio of 18 exhibited a sharp peak at 58 ppm, which is assigned to tetrahedrally coordinated Al in the framework. In addition, a small peak at 0 ppm, which is assigned to octahedrally coordinated Al was observed. The ^{71}Ga MAS NMR spectrum of [Ga]-ZSM-58 with the Si/Ga ratio of 17 exhibited a broad peak at 170 ppm, which assigned to tetrahedrally coordinated Ga in the framework. No marked peak at 0 ppm assigned to octahedrally coordinated gallium was observed.

The MTO reaction were conducted over [Al]-ZSM-58 with the Si/Al ratio of 18 and [Ga]-ZSM-58 with the Si/Ga ratio of 17. In the case of [Al]-ZSM-58, the conversion of methanol kept 100% until the time on stream of 360 min, and the main product was constantly propene with the selectivity of 42%. In the case of [Ga]-ZSM-58, the conversion was drastically decreased from 98% to 58% at the time on stream of 250 min. Although the main product was propene with the selectivity of 50% in initial stage, the formation of dimethyl ether (DME) was observed at the time on stream of 150 min.

Conclusions

Aluminosilicate and gallosilicate with **DDR** topology were successfully synthesized by the hydrothermal synthesis method in the presence of *N*-methyltropinium iodideas OSDA. **DDR**-type aluminosilicate exhibited a long catalyst life with the selectivity to propene of over 40 % kept in the MTO reaction.

References

[1] T. Yokoi, M. Yoshioka, H. Imai and T. Tatsumi, Angew. Chem. Inter. Ed. 48 (2009) 9884,

[2] E. W. Valyocsik, U. S Patent 4,698,217 (1987)

[3] D. H. Olson, M. A. Camblor, L. A. Villaescusa, G. H. Kuehl, Microporous Mesoporous Mater. 67 (2004) 27.

Fig. 1 Selectivity and conversion of MTO reaction over [Al]-ZSM-58 (top) and [Ga]-ZSM-58 (bottom)

Multi–Ammonium Surfactants Directing the Formation of MFI Zeolite Nanosheets

Woojin Park, Kyungsu Na and Ryong Ryoo*
[1]*Center for Functional Nanomaterials, Dept. of Chemistry,*
[2]*Graduate School of Nanoscience and Technology (WCU),*
*KAIST, Daejeon 305–701, Korea. *E–mail: rryoo@kaist.ac.kr*

Introduction

Hierarchically microporous–mesoporous architectures built with zeolitic crystalline frameworks (hierarchical zeolites) have attracted great attention in zeolite science due to the advantage of facile diffusion *via* mesopores. The zeolite mesopores are known to be generated through a post–synthetic demetallization treatment, or using a mesopore–generating agent during the synthesis process. Our laboratory has developed a synthetic approach using surfactants that are functionalized with zeolite structure–directing groups.[1] In the synthesis approach, the surfactant head group acts as a structure–directing agent for crystalline MFI zeolite framework while a large number of surfactant molecules are self–assembled into a lamellar mesophase due to the hydrophobic interaction between tails. The zeolite–structure–directing function and the resultant zeolite morphologies are markedly affected by the number of ammonium groups, the length of spacers between ammonium groups, the surfactant alkyl tail, and also other short alkyl groups. This analysis has been discussed in this presentation.

Experimental

Surfactants were synthesized in the laboratory.[2–4] These surfactants were used as structure–directing agents instead of tetrapropylammonium, which is commonly used in the conventional synthesis of MFI zeolite. Tetraeothoxylsilane, fumed silica or water glass was used as the silica source. Sodium aluminate or aluminum sulfate was the Al source. Zeolite synthesis was performed in an autoclave that was tumbled in an oven at 150°C. The products were characterized by powder XRD, TEM, SEM, and nitrogen adsorption.

Results and discussion

A hexagonally ordered mesoporous aluminosilicate material without framework crystallinity, similar to MCM–41, was generated within 1 h when hydrothermal synthesis was performed with $C_{22}H_{45}$–$N^+(CH_3)_2$–C_6H_{12}–$N^+(CH_3)_2$–C_6H_{13} (designated as $C_{22-6}N_2Me$). With increasing the reaction time, this mesophase transformed consecutively to a lamellar mesophase without crystallinity, unilamellar MFI zeolite, and finally multilamellar MFI zeolite, as shown in Scheme 1.[2,3] The rates of the transformations depended on the details of the synthesis conditions, such as silica sources, counter anions of surfactants (OH^- or Br^-), sodium content, and pH.[3] The thickness of the individual zeolite nanosheets was 2 nm, independent of the synthesis conditions and the lamellar packing order. The structural transformation from unilamellar to multilamellar was a thermodynamically–favored spontaneous process, which takes place through dissolution–recrystallization under a highly basic condition like the Ostwald ripening process. This process can be retarded by decreasing the pH of the synthesis gel and/or reducing the length of the surfactant tail. Through the delicate control of such variables, the unilamellar MFI

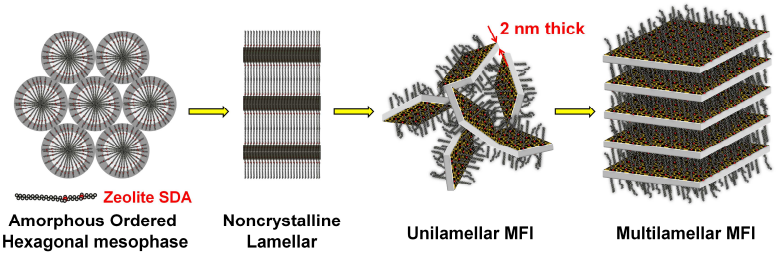

Scheme 1. Schematic diagram showing a consecutive structural transformation upon excessive hydrothermal aging.

zeolite having a high surface area and total pore volume (660 m^2g^{-1} and 1.0 cm^3g^{-1}) could be synthesized even under Na^+–rich conditions using an inexpensive silica source like water glass. The high surface area and pore volume, as compared with 400 m^2g^{-1} and 0.2 cm^3g^{-1} of bulk MFI zeolite, is due to the mesopores between adjacent zeolite nanosheets.

The effects of the number of ammonium groups, spacer length, hydrophobic tail length, and alkyl moiety in the surfactants with the schematic formula of *tail*–$N^+(CH_3)_2$–{*spacer*–$N^+(R)_2$}$_{n-1}$–C_6H_{13} ($C_{t-s}N_nR$) were investigated in the synthesis of MFI zeolite nanosheets.[4] The *n* number was varied over 1 ~ 4. The *tail* was selected among linear alkyl chains (–C_tH_{2t+1}, t = 6 ~ 22). The *spacer* was an alkylene bridge (–C_sH_{2s}–, s = 3, 6 and 8). *R* was alkyl groups (–C_xH_{2x+1}, x = 1 ~ 4). MFI zeolite nanosheets were obtained in the range of n = 2 ~ 4. The thickness of the nanosheets increased with *n* in this range (Figure 1). However, for n = 1, crystalline zeolite was never obtained. When the spacer length, *s*, was 6 and 8, MFI nanosheets were obtained. In the case of a short spacer with s = 3, the surfactant was decomposed into a small amine that led to the generation of bulk MFI zeolite. The surfactant tail for the generation of the zeolite nanosheet should be as long as –$C_{10}H_{19}$. In addition, the *R* group at the terminal ammonium should be –CH_3 or –C_2H_5 to direct the MFI structure. In the case of –C_3H_7 group, only a non–zeolitic silicate product was obtained.

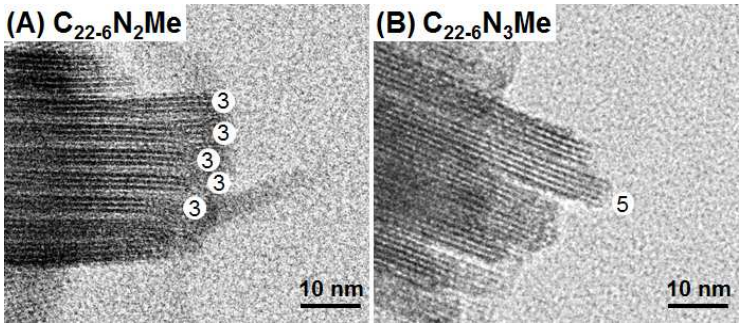

Figure 1. Effects of ammonium numbers in the structure–directing surfactants on the formation of MFI zeolite nanosheets.

Conclusions

The formation of the MFI zeolite nanosheets is due to the self–assembly of surfactant molecules into a lamellar mesophase while the surfactant head groups functions as a MFI zeolite structure–directing agent. At least two suitable ammonium groups are necessary in the head group, for the generation of the zeolite. The nanosheet thickness can be precisely controlled by the number of ammonium groups. Among the ammonium groups, the one directly attached to the surfactant alkyl tail, does not seem to directly function as the zeolite porogen. Nevertheless, it is necessary as a part of the surfactant configuration for zeolite structure generation. This information will be useful for synthesis of other zeolite–structure–directing surfactants that may lead to various types of nanomorphic zeolites with various framework structures, such as ordered mesoporous materials with a microporous zeolite framework in the future.

Acknowledgements

This work was supported by the National Honor Scientist Program and World Class University Program of the Ministry of Education, Science and Technology in Korea.

References

[1] Choi et al. Nature 461 (2009), 246–250
[2] Na et al. Journal of the American Chemical Society 132 (2010), 4169–4177
[3] Na et al. Chemistry of Materials 23 (2011), 1273–1279
[4] Park et al. manuscript in preparation for submission to Chemistry of Materials (2011)

MOF's Characterisation with innovative volumetric/calorimetric techniques

Emmanuel Wirth, Rémi André, Pierre Le Parlouër, Application Laboratory
SETARAM Instrumentation, 7 rue de l'Oratoire, 69300 Caluire, France
wirth@setaram.com

Metal-organic frameworks (MOFs) offer an advantage over classical other porous materials (activated carbon, zeolithes) because their properties can be tailored due to the vast available choices of metal clusters and organic linkers. Nowadays these structure are foreseen to multiple applications in gas adsorption, like hydrogen storage, selective adsorption of CO2 against CH4, CO2 against H2,…

The gas sorption Sievert's technique has proven to have many advantages over the other techniques for the evaluation of the ad/ab-sorbed amount of gas by the materials in a wide range of temperature and pressure. In addition, there is a total freedom in the size and shape of the sample holder in the volumetric technique, enabling the coupling of techniques and in-situ measurements of various chemical and physical parameters. X-rays and neutrons diffractomers, mass spectrometers, calorimeters have already been successfully tested and allow to have simultaneous PCT isotherms and kinetic measurement with structural, gas composition or thermodynamic data.

The thermodynamic of the adsorption is essential for the practical application and among all the enthalpy of adsorption (or desorption) is a key parameters.

Practically there are two ways to determine this enthalpy. The first one is an indirect method, where the enthalpy is derived from adsorption isotherms at different temperatures. The second one is a direct method, where the enthalpy is measured via calorimetric technique. The biggest disadvantage of this technique is that it gives a result per mole of solid sample and not per mole of gas. Recently the combination of manometric technique (to quantify the amount of hydrogen absorbed/released) and calorimetry was successful to overcome this issue and the direct measurement of enthalpy of formation per mole of gas was reported [1-3].

The paper will present some new results on combinations of calorimetric and volumetric technique, especially on Cu-BTC, selected as an example of Metal Organic Framework that is available commercially. It will give an overview of the state-of-the art possibility of combined analysis together with the Sievert's technique

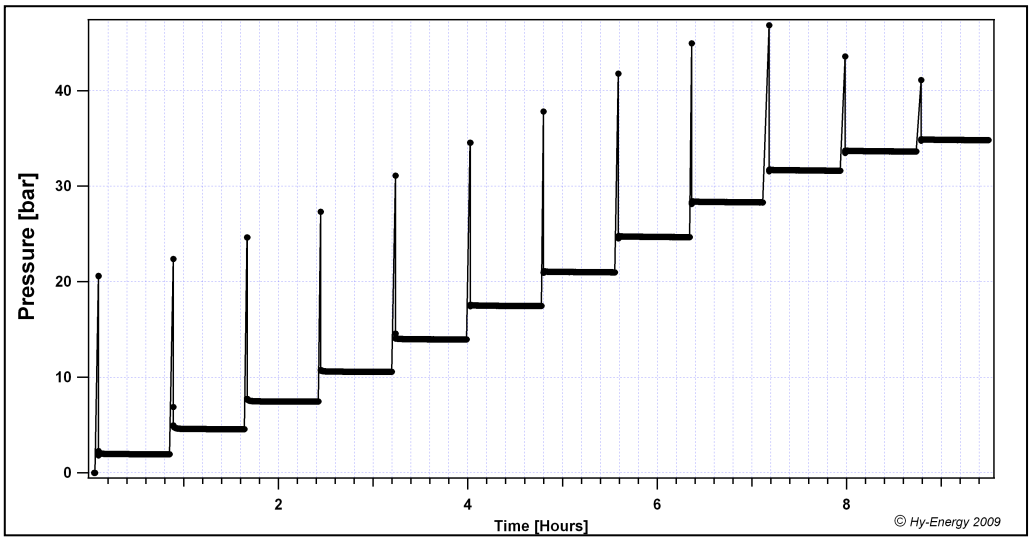

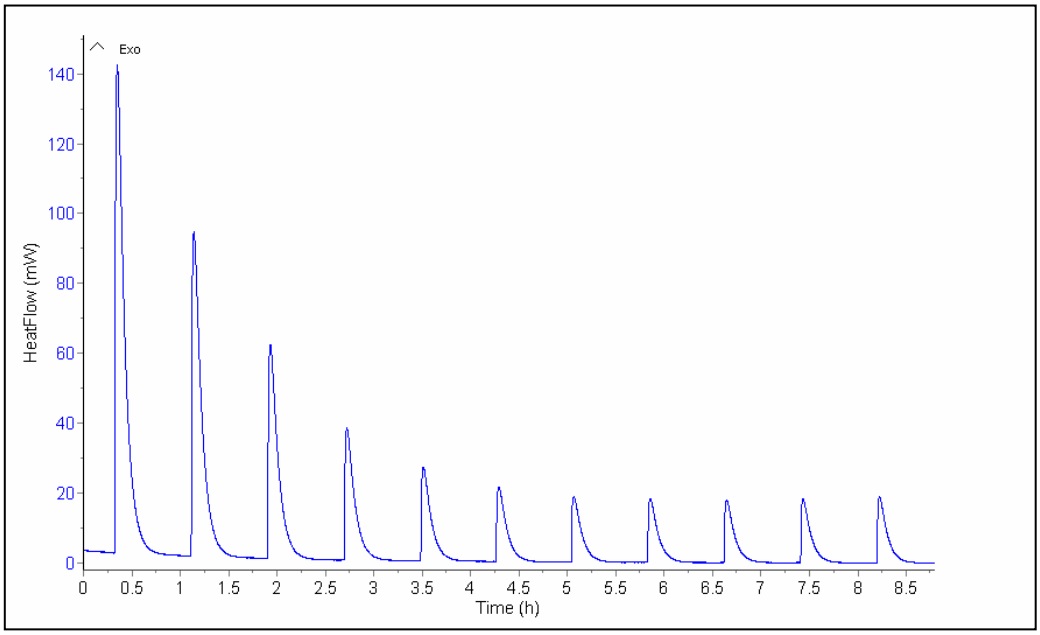

Up: Pressure versus time during the experiment of CO2 adsorption. At the beginning of each aliquot, the step is the measurement of the pressure in the manifold.

Down: Heat Flow signal versus time obtained on the calorimeter. The exothermic peaks correspond to the successive doses.

References:

1. C. Milanese et al., IJHE, 35 (2010) 1285 – 1295.

2. R. André, E. Wirth, P. le Parlouër, Proceedings of the 7th Heat Flow Calorimetry Conference. (2010).

3. C. Milanese et al., IJHE, accepted for publication.

INDEX OF AUTHORS

FEZA 2011

A

A Bieniok RRR-06-Mon-209 1036
A. Aleksandrov Hristiyan RRR-21-Wed-210 1067
A. Bonk Fabio SC-P-115-Wed-052 421
Abasolo Ibane TA-P-024-Wed-200 1015
Abasov Safa PE-P-012-Mon-120 661
Abellán Gonzalo TA-O-05 191
Aboul-Gheit Ahmed PE-P-058-Wed-134 752
Abu Rabi-Stankovic Andjela SM-P-030-Wed-178 942
Afonina Elena FC-O-06 149
Aguado Sonia NM-P-007-Mon-070 471
Aguado Jose PE-P-041-Wed-117 718
Aguado José SC-P-066-Wed-004 325
Aguado Sonia SM-P-008-Mon-177 897
Agueda V. Ismael PE-P-044-Wed-120 724
Agueda Mate Vicente Ismael SM-P-015-Mon-184 912
Agueda Mate Vicente Ismael SM-P-016-Mon-185 914
Aguilar Pliego Julia NM-P-039-Wed-075 534
Aguilar-Pliego Julia SC-P-107-Wed-044 405
Aguilar-Pliego Julia SM-P-036-Wed-184 954
Ahn John SM-O-10 177
Ahnfeldt Tim NM-O-05 99
Aiello Rosario NM-P-023-Mon-086 503
Aiello Daniela TA-O-02 185
Aiello Daniela TA-P-016-Wed-192 999
Aiello Rosario TA-P-016-Wed-192 999
Akacem Y. RRR-22-Wed-211 1069
Akahane Saiko FC-P-049-Wed-164 867
Akinyeye Richard SC-P-108-Wed-045 407
Alayon Evalyn Mae C. SC-O-07 51
Albela Belén NM-P-049-Wed-085 554
Albela Belén SC-O-15 67
Alegria Elisabete PE-P-027-Mon-135 690
Aleksandrov Hristiyan NM-P-026-Mon-089 509
Alexa Iuliana Florentina TA-P-001-Mon-191 969
Aliyev Agadadash Th-P-003-Mon-094 573
Ali-Zadeh Gulya Th-P-003-Mon-094 573
Al-Khattaf S. SM-O-10 177
Almarza Noe G. SC-P-057-Mon-057 307
Aloise Alfredo FC-O-04 145
Aloise Alfredo SC-P-063-Wed-001 319

Alonso-Escobar C. SC-O-13 63
Al-Othman Zeid NM-P-052-Wed-088 560
Al-Resayes Saud I NM-P-052-Wed-088 560
Al-Rubaye Rana NM-P-035-Wed-071 526
Alvarez Alba SC-P-048-Mon-048 291
Álvarez-Rodríguez Jesus SM-P-034-Wed-182 950
Álvaro-Muñoz Teresa NM-P-036-Wed-072 528
Al-Yassir N. SM-O-10 177
Ambroj Diego NM-P-037-Wed-073 530
Ameloot Rob FC-O-07 151
Ameloot Rob TA-P-004-Mon-194 975
Amenitsch Heinz SC-P-080-Mon-063 353
Amorós Pedro SC-P-017-Mon-017 229
Amorós Pedro SC-P-018-Mon-018 231
Amorós Pedro TA-P-025-Wed-201 1017
Amoureux Jean-Paul SC-O-12 61
Anderson Michael NM-P-022-Mon-085 501
Anderson Paul A. SC-O-23 83
Andrade Marta PE-P-027-Mon-135 690
André Gilles Th-P-035-Wed-109 637
André Rémi RRR-36-Wed-225 1093
Andreassen Kari Anne SM-P-040-Wed-188 962
Anglerot Didier PE-P-043-Wed-119 722
Ansari Mohd Bismillah FC-P-014-Mon-156 797
Antoine Gédéon SC-P-104-Wed-041 399
Aprea P. SC-P-125-Wed-220 441
Aprile Carmela FC-O-03 143
Aquino Cindy FC-O-05 147
Aramendía María A. FC-P-013-Mon-155 795
Aranda Pilar SC-P-078-Wed-016 349
Aranovich Ilia PE-P-035-Wed-111 706
Arcoya Adolfo SM-P-034-Wed-182 950
Arencibia Amaya SM-P-024-Wed-172 930
Arias Karen FC-P-042-Wed-157 853
Arletti Rossella SC-P-112-Wed-049 415
Armandi Marco SC-P-093-Wed-030 379
Armendáriz Herrera Héctor SC-P-132-Wed-223 454
Armstrong Jennifer SC-P-008-Mon-008 215
Arnanz A. FC-P-054-Wed-169 877
Arnold Gilles SC-O-01 39
Arribas Maria A. PE-O-03 127
Arruebo Manuel TA-P-006-Mon-196 979

Atanes Evangelina SC-P-110-Wed-047 411
Attfield Martin NM-P-022-Mon-085 501
Auroux Aline SM-O-09 175
Awadallah Ahmed PE-P-058-Wed-134 752
Awual Md. Rabiul TA-P-009-Mon-199 985
Aydemir Buğçe PE-P-017-Mon-125 671
Ayrault Philip SM-P-023-Wed-171 928
Azaïs Thierry TA-O-02 185
Azevedo Diana C. S. SM-P-012-Mon-181 906
Aznar Elena TA-P-025-Wed-201 1017

B

B. J. Roeffaers Maarten TA-P-004-Mon-194 975
B. Mccusker Lynne RRR-17-Wed-206 1058
B. Mccusker Lynne RRR-20-Wed-209 1065
B.Nagy Jànos SC-P-063-Wed-001 319
B.Nagy Janos TA-P-022-Wed-198 1011
Baba Toshihide PE-P-003-Mon-111 645
Babaluo Ali Akbar SC-P-113-Wed-050 417
Babonneau Florence SC-P-046-Mon-046 287
Babonneau Florence TA-O-02 185
Bac Nurcan NM-P-013-Mon-076 483
Baccile Niki SC-P-046-Mon-046 287
Baerlocher Christian RRR-17-Wed-206 1058
Baerlocher Christian RRR-20-Wed-209 1065
Bagatin Roberto TA-P-015-Wed-191 997
Baino Francesco SC-P-105-Wed-042 401
Baklanov Mikhail SC-P-056-Mon-056 305
Balanzat Emmanuel NM-O-08 105
Balci Suna SC-P-127-Wed-064 445
Balikci Filiz SC-P-131-Wed-221 452
Balu Alina M. FC-P-031-Wed-146 831
Banares Miguel SC-P-106-Wed-043 403
Bangó Adrienn FC-P-052-Wed-167 873
Bangó Adrienn FC-P-053-Wed-168 875
Bankovic Predrag SM-P-030-Wed-178 942
Bao Huixin FC-O-01 139
Bao Xinhe NM-P-028-Mon-091 513
Barassi Giancarlo SM-P-001- Mon-170 883
Barassi Giancarlo SM-P-004-Mon-173 889

Barbaro Pierluigi FC-P-036-Wed-151 841
Barbera Katia PE-P-036-Wed-112 708
Barbier Jacques Jr. PE-P-029-Mon-137 694
Barczak Mariusz SC-P-030-Mon-030 255
Barczak Mariusz Th-P-033-Wed-107 633
Bartolomeu Rui SC-P-098-Wed-035 389
Batalha Nuno PE-O-05 131
Bats Nicolas NM-O-04 97
Bats Nicolas NM-P-007-Mon-070 471
Bats Nicolas SC-P-070-Wed-008 333
Bats Nicolas Th-P-004-Mon-095 575
Bautista L. Fernando NM-P-041-Wed-077 538
Bayati Behruz SC-P-113-Wed-050 417
Bazer-Bachi Delphine NM-O-04 97
Bazer-Bachi Delphine Th-P-004-Mon-095 575
Bazin Philippe PE-O-02 125
Bazin Phillip TA-P-013-Mon-203 993
Bazzano Francesca SM-O-08 173
Bazzarelli F. SM-O-07 171
Beale Andrew PE-O-01 123
Beato Pablo PE-P-036-Wed-112 708
Becharová Sarah FC-P-025-Mon-167 819
Behrens Peter TA-P-023-Wed-199 1013
Bein Thomas NM-P-006-Mon-069 469
Bein Thomas SC-P-080-Mon-063 353
Bein Thomas TA-O-03 187
Bekris N. RRR-24-Wed-213 1073
Belen Albela SC-P-104-Wed-041 399
Belin Thomas PE-P-029-Mon-137 694
Bellat Jean Pierre SM-O-11 179
Bellussi Giuseppe SM-O-08 173
Belopukhov Evgeny PE-P-014-Mon-122 665
Belov N. SM-P-039-Wed-187 960
Beltrán Daniel SC-P-017-Mon-017 229
Beltrán Daniel SC-P-018-Mon-018 231
Belver Carolina SC-P-078-Wed-016 349
Belyi Alexander PE-P-014-Mon-122 665
Ben Tayeb Karima PE-P-026-Mon-134 688
Benabdallah Rachida SC-P-112-Wed-049 415
Benaliouche Fouad SM-P-023-Wed-171 928
Benamor Taissire SC-P-005-Mon-005 209
Bengueddach Abdelkader SC-P-112-Wed-049 415

Bentrup Ursula ... SC-P-044-Mon-044 ... 283
Bergeret Gerard ... NM-P-007-Mon-070 ... 471
Berhault Gilles ... SC-P-126-Wed-063 ... 443
Berlier Gloria ... TA-P-019-Wed-195 ... 1005
Bernardo P. ... SM-O-07 ... 171
Bernardos Andrea ... TA-P-025-Wed-201 ... 1017
Bernauer Bohumil ... SC-P-024-Mon-024 ... 243
Bernauer Bohumil ... SM-P-021-Mon-190 ... 924
Bernauer Bohumil ... SM-P-035-Wed-183 ... 952
Bértolo Raquel ... SC-P-098-Wed-035 ... 389
Besserer U. ... RRR-24-Wed-213 ... 1073
Bhawe Yashodhan ... SC-P-032-Mon-032 ... 259
Bilba Nicolae ... SM-P-032-Wed-180 ... 946
Bion Nicolas ... PE-P-029-Mon-137 ... 694
Birczyński A. ... RRR-28-Wed-217 ... 1079
Birczynski Artur ... SC-P-083-Wed-020 ... 359
Birsa Čelič Tadeja ... NM-O-06 ... 101
Birsa Čelič Tadeja ... SC-P-060-Mon-060 ... 313
Birsa Čelič Tadeja ... SC-P-065-Wed-003 ... 323
Bisio C. ... NM-O-03 ... 95
Bisio Chiara ... RRR-14-Mon-217 ... 1052
Blanco Carmen ... NM-P-017-Mon-080 ... 491
Blanco Rosa M ... NM-P-034-Wed-070 ... 524
Blasco T. ... SC-P-122-Wed-059 ... 435
Blasco T. ... SC-P-123-Wed-060 ... 437
Blasco T. ... SC-P-124-Wed-061 ... 439
Blasco Teresa ... FC-P-048-Wed-163 ... 865
Bleich Andre ... TA-P-023-Wed-199 ... 1013
Bleken Francesca ... PE-P-021-Mon-129 ... 679
Bleken Francesca ... PE-P-036-Wed-112 ... 708
Bleken Francesca ... Th-P-029-Wed-103 ... 625
Blicker Mike ... TA-P-003-Mon-193 ... 973
Blom Richard ... SM-P-040-Wed-188 ... 962
Bobadilla Luis F. ... FC-P-048-Wed-163 ... 865
Bogaerts Thomas ... Th-P-024-Wed-098 ... 615
Boix Alicia ... PE-P-059-Wed-135 ... 754
Bonelli Barbara ... NM-P-045-Wed-081 ... 546
Bonelli Barbara ... SC-P-093-Wed-030 ... 379
Bonneviot Laurent ... NM-P-049-Wed-085 ... 554
Bonneviot Laurent ... SC-O-15 ... 67
Bonnier Fabien ... Th-P-004-Mon-095 ... 575
Bordiga Silvia ... PE-P-036-Wed-112 ... 708

Borisevich O. RRR-15-Mon-218 1054
Borodina E. V. NM-P-031-Wed-067 518
Borodina Elena SM-P-030-Wed-178 942
Boronat Mercedes NM-P-042-Wed-078 540
Borowski Piotr Th-P-033-Wed-107 633
Borozdenko Dmitry TA-P-003-Mon-193 973
Borrmann Thomas SM-P-001- Mon-170 883
Borrmann Thomas SM-P-004-Mon-173 889
Botas J. Ángel NM-P-029-Wed-065 514
Botas J. Ángel PE-P-034-Mon-142 704
Botella Pablo TA-O-04 189
Botella Pablo TA-P-024-Wed-200 1015
Botková Šárka PE-P-038-Wed-114 712
Bottinelli Emanuela NM-P-025-Mon-088 507
Boucheffa Youcef SM-P-018-Mon-187 918
Boucheffa Youcef SM-P-023-Wed-171 928
Bouchiba N. RRR-18-Wed-207 1060
Boukoberine Yamina SC-P-128-Wed-204 447
Boulhout Mohammed NM-P-047-Wed-083 550
Boutin Anne Th-P-030-Wed-104 627
Bozejewicz Witold NM-P-010-Mon-073 477
Brabec Libor SC-P-024-Mon-024 243
Brabec Libor SM-P-021-Mon-190 924
Bracco S. NM-O-03 95
Braos-García Pilar SM-P-012-Mon-181 906
Braschi Ilaria RRR-14-Mon-217 1052
Bremard Claude Th-P-012-Mon-103 591
Brémard Claude SC-O-06 49
Brikgi María SC-P-071-Wed-009 335
Briones Laura PE-P-041-Wed-117 718
Broccia Patrizia SM-O-08 173
Broclawik Ewa Th-P-005-Mon-096 577
Bronić Josip RRR-01-Mon-219 1025
Bronić Josip SC-P-067-Wed-005 327
Bronić Josip Th-P-018-Wed-092 603
Bruce Duncan W FC-P-039-Wed-154 847
Brunel Daniel NM-O-07 103
Buchwalter Paulin SC-P-058-Mon-058 309
Budd P. M. SM-O-07 171
Budd P.M. SM-P-039-Wed-187 960
Bueno-Perez Rocio Th-P-020-Wed-094 607
Bueno-Pérez Rocío SM-P-022-Wed-170 926

Bulanek Roman SC-P-042-Mon-042 279
Bulánek Roman PE-P-038-Wed-114 712
Buljan Iva RRR-27-Wed-216 1077
Bulut Metin SC-P-041-Mon-041 277
Buonomenna M. G. SM-O-07 171
Buonomenna M.G. SM-P-039-Wed-187 960
Butler Keith Th-O-06 119
Bux Helge SM-O-05 167

C

Caballero Miguel Angel TA-P-018-Wed-194 1003
Caballero-Rivero Estefanía Th-P-019-Wed-093 605
Cacciaguerra Thomas SC-P-050-Mon-050 295
Cadours Renaud PE-P-004-Mon-112 647
Cairon Olivier SM-P-025-Wed-173 932
Caldarelli S. NM-O-03 95
Calefi Paulo Sergio NM-P-011-Mon-074 479
Calero Sofia SM-P-022-Wed-170 926
Calero Sofia Th-O-03 113
Calero Sofia Th-P-002-Mon-093 571
Calero Sofía Th-P-019-Wed-093 605
Calero Sofia Th-P-020-Wed-094 607
Calero Sofía Th-P-023-Wed-097 613
Caliskan Sevket SC-P-086-Wed-026 365
Caliskan Sevket SC-P-087-Wed-024 367
Calleja Guilermo NM-P-029-Wed-065 514
Calleja Guillermo SM-P-024-Wed-172 930
Calvo Rogelio PE-P-041-Wed-117 718
Cambra Alberto SC-P-110-Wed-047 411
Campelo Juan M. FC-P-031-Wed-146 831
Campelo Juan Manuel FC-P-032-Wed-147 833
Campelo Juan Manuel FC-P-033-Wed-148 835
Candu Natalia FC-P-003-Mon-145 775
Cantín A. SC-P-122-Wed-059 435
Cantín A. SC-P-124-Wed-061 439
Čapek Libor PE-P-038-Wed-114 712
Capela Sandra PE-P-047-Wed-123 730
Caputo D. SC-P-125-Wed-220 441
Caputo Giuseppe NM-P-025-Mon-088 507
Carati Angela SM-O-08 173

Cardoso Dilson RRR-05-Mon-208 1034
Carey Thomas SC-O-23 83
Carlotti Maria Eugenia TA-P-019-Wed-195 1005
Carmona María Ángeles PE-P-013-Mon-121 663
Carniato F. NM-O-03 95
Caro Jürgen SM-O-05 167
Caro Jürgen SM-P-026-Wed-174 934
Carpentier Kevin PE-P-032-Mon-140 700
Carrillo Adela I. NM-P-046-Wed-082 548
Carrillo Isabel SC-P-110-Wed-047 411
Carrillo-Cabrera Wilder SC-P-052-Mon-052 299
Carrillo Gómez Adela Isabel FC-P-041-Wed-156 851
Carrillo Gómez Adela Isabel SC-O-17 71
Carrillo Gómez Adela Isabel SC-P-088-Wed-025 369
Carson Fabian RRR-04-Mon-207 1032
Carvalho Ana Paula NM-P-030-Wed-066 516
Carvalho Ana Paula PE-P-027-Mon-135 690
Carvalho Diego SC-P-033-Mon-033 261
Carvalho Kele SC-P-072-Wed-010 337
Casado Clara NM-P-032-Wed-068 520
Casado Clara NM-P-037-Wed-073 530
Casale Sandra SC-O-15 67
Casale Sandra SC-P-098-Wed-035 389
Casimiro Maria FC-P-047-Wed-162 863
Castanheiro José FC-P-047-Wed-162 863
Castellà-Ventura M. RRR-22-Wed-211 1069
Castillo Juan Manuell Th-O-03 113
Castillo Sanchez Juan Manuel Th-P-034-Wed-108 635
Castillón-Barrasa Felipe NM-P-053-Wed-089 562
Caullet Philippe SC-P-070-Wed-008 333
Cavalcante Jr. Celio L. SM-P-012-Mon-181 906
Cecowski Saša FC-P-040-Wed-155 849
Čejka Jiří FC-P-005-Mon-147 779
Čejka Jiří FC-P-019-Mon-161 807
Čejka Jiří SC-O-19 75
Čejka Jiří SC-P-002-Mon-002 203
Čejka Jiří SC-P-013-Mon-013 223
Čejka Jiří SC-P-016-Mon-016 227
Čendak Tomaž SC-P-060-Mon-060 313
Centeno Miguel Angel NM-P-002-Mon-065 461
Centi Gabriele FC-O-04 145
Cepak Alexander RRR-16-Wed-205 1056

Červený Libor FC-P-021-Mon-163 811
Červený Libor FC-P-022-Mon-164 813
Červený Libor FC-P-024-Mon-166 817
Červený Libor FC-P-025-Mon-167 819
Červený Libor FC-P-026-Mon-168 821
Červený Libor FC-P-028-Wed-143 825
Cestari Alexandre NM-P-012-Mon-175 481
Cesteros Yolanda PE-P-046-Wed-122 728
Cesteros Yolanda SC-P-053-Mon-053 301
Chaisuwan Thanyalak SC-P-099-Wed-036 391
Chal Robin SC-P-050-Mon-050 295
Chalupka Karolina PE-P-037-Wed-113 710
Chalupka Karolina SC-P-106-Wed-043 403
Chan Wai Kit SM-P-013-Mon-182 908
Chang Jong San SC-P-075-Wed-013 343
Chaplais Gérald SC-P-076-Wed-014 345
Chaves Thiago F. RRR-05-Mon-208 1034
Chávez-Rivas Fernando NM-P-053-Wed-089 562
Che Michel SC-P-106-Wed-043 403
Chebude Yonas RRR-03-Mon-206 1030
Chen Xinqing SC-P-020-Mon-020 235
Chen Xinqing TA-P-006-Mon-196 979
Chernyavsky Valery Th-P-021-Wed-095 609
Cheung Chun Tung TA-P-007-Mon-197 981
Chevé Gwénael TA-P-010-Mon-200 987
Chica Antonio PE-P-063-Wed-139 762
Chiesa Mario SC-P-045-Mon-045 285
Chiesa Mario SC-P-062-Mon-062 317
Chitsazan Sahar RRR-30-Wed-219 1083
Chitsazan Sahar SM-P-010-Mon-179 901
Chizallet Céline Th-P-004-Mon-095 575
Chlubná Pavla SC-O-19 75
Chlubná Pavla SC-P-013-Mon-013 223
Chmelik Christian SM-O-05 167
Cho Kanghee NM-P-016-Mon-079 489
Christel Gervais SC-P-046-Mon-046 287
Čičmanec Pavel PE-P-038-Wed-114 712
Ciftci Aysegul PE-P-006-Mon-114 651
Çiğdem Güldür PE-P-065-Wed-141 765
Ciuffi Katia NM-P-011-Mon-074 479
Ciuffi Katia NM-P-012-Mon-175 481
Climent Maria José FC-P-042-Wed-157 853

Climent Maria José FC-P-043-Wed-158 855
Climent Estela TA-P-025-Wed-201 1017
Coasne Benoit SC-P-077-Wed-015 347
Colella C. SC-P-125-Wed-220 441
Coleto Inés PE-P-013-Mon-121 663
Coluccia Salvatore NM-P-025-Mon-088 507
Coluccia Salvatore TA-P-019-Wed-195 1005
Coman Simona M. FC-P-002-Mon-144 773
Coman Simona M. FC-P-003-Mon-145 775
Combariza Aldo F. Th-P-011-Mon-102 589
Combariza Aldo F. Th-P-015-Mon-106 597
Concepción Patricia PE-O-03 127
Concepción Patricia RRR-11-Mon-214 1046
Cong Dung Tien SM-P-035-Wed-183 952
Constantin Cristian Th-P-034-Wed-108 635
Cool Pegie FC-P-027-Mon-169 823
Cool Pegie NM-P-020-Mon-083 497
Cool Pegie NM-P-027-Mon-090 511
Cool Pegie SC-P-062-Mon-062 317
Cool Pegie TA-P-012-Mon-202 991
Cool Pegie Th-P-017-Mon-108 601
Coq Bernard PE-P-004-Mon-112 647
Coq Bernard PE-P-043-Wed-119 722
Corà Furio Th-O-01 109
Corcóstegui Cecilia TA-P-021-Wed-197 1009
Corma A. PE-P-066-Wed-142 767
Corma A. SC-P-090-Wed-027 373
Corma Avelino FC-P-042-Wed-157 853
Corma Avelino FC-P-043-Wed-158 855
Corma Avelino FC-P-045-Wed-160 859
Corma Avelino NM-O-07 103
Corma Avelino NM-P-021-Mon-084 499
Corma Avelino NM-P-024-Mon-087 505
Corma Avelino NM-P-042-Wed-078 540
Corma Avelino NM-P-051-Wed-087 558
Corma Avelino PE-P-052-Wed-128 740
Corma Avelino PE-P-061-Wed-137 758
Corma Avelino RRR-11-Mon-214 1046
Corma Avelino SC-P-119-Wed-056 429
Corma Avelino SM-P-041-Wed-189 964
Corma Avelino TA-O-04 189
Corma Avelino TA-P-024-Wed-200 1015

Corma Avelino Th-P-011-Mon-102 589
Coronado Eugenio TA-O-05 191
Coronado Juan M. PE-P-057-Wed-133 750
Coronas Joaquin NM-P-032-Wed-068 520
Coronas Joaquín NM-P-037-Wed-073 530
Coronas Joaquín SC-P-094-Wed-031 381
Coronas Joaquín SM-O-02 161
Coronas Joaquín TA-P-018-Wed-194 1003
Cossi Maurizio RRR-14-Mon-217 1052
Cotea Valeriu V. SM-P-032-Wed-180 946
Cotman Magda PE-P-042-Wed-118 720
Coudert François-Xavier Th-P-030-Wed-104 627
Coudert François-Xavier Th-P-031-Wed-105 629
Coudert François-Xavier Th-P-032-Wed-106 631
Coulomb Jean - Paul Th-P-035-Wed-109 637
Coutino-Gonzalez Eduardo TA-P-017-Wed-193 1001
Cravillon Janosch SM-O-05 167
Cretescu Igor PE-P-053-W-128 742
Cubillas Pablo NM-P-022-Mon-085 501
Cucinotta F. NM-O-03 95

D

Da Costa Patrick PE-P-047-Wed-123 730
Da Costa Patrick SC-P-098-Wed-035 389
Da Costa-Serra Javier Francisco PE-P-063-Wed-139 762
Dąbrowski Andrzej SC-P-030-Mon-030 255
Dakovic Aleksandra SM-O-09 175
Daou Jean SC-O-01 39
Dari D. SC-P-122-Wed-059 435
Dari D. SC-P-124-Wed-061 439
Das Tapan PE-P-002-Mon-110 643
Dath J.P. PE-P-001-Mon-109 641
Datka Jerzy RRR-10-Mon-213 1044
Datka J. RRR-28-Wed-217 1079
Datka Jerzy SC-P-049-Mon-049 293
Datka Jerzy SC-P-083-Wed-020 359
Datka Jerzy Th-P-005-Mon-096 577
Daturi Marco PE-O-02 125
Daturi Marco SC-P-075-Wed-013 343
Davis Mark SC-P-032-Mon-032 259

Davletshin Artur R. RRR-12-Mon-215 1048
De Canck Els FC-P-006-Mon-148 781
De Canck Els NM-P-004-Mon-067 465
De Canck Els NM-P-009-Mon-072 475
De Clippel Filip FC-P-050-Wed-165 869
De Cremer Gert TA-P-004-Mon-194 975
De Cremer Gert TA-P-017-Wed-193 1001
De Faria Emerson NM-P-011-Mon-074 479
De Jong Krijn P. PE-O-04 129
De Jong Krijn P. SC-P-041-Mon-041 277
De Jongh Petra E. PE-O-04 129
De Jongh Petra E. SC-P-041-Mon-041 277
De La Osa Ana Raquel PE-P-031-Mon-139 698
De La Peña Víctor A. PE-P-057-Wed-133 750
De La Torre Olalla PE-P-061-Wed-137 758
De Luca Pierantonio SC-P-063-Wed-001 319
De Lucas Antonio PE-P-031-Mon-139 698
De Ménorval Louis-Charles SC-P-062-Mon-062 317
De Rivas Beatriz PE-O-07 135
De Souza E Silva Juliana SC-P-055-Mon-055 303
De Sterck Bart Th-P-025-Wed-099 617
De Toni Marta Th-P-031-Wed-105 629
De Toni Marta Th-P-032-Wed-106 631
De Vos Dirk FC-O-07 151
De Vos Dirk SM-P-019-Mon-188 920
De Vos Dirk TA-P-017-Wed-193 1001
De Waele Vincent TA-P-013-Mon-203 993
De Wispelaere Kristof Th-P-025-Wed-099 617
De Wispelaere Kristof Th-P-028-Wed-102 623
Decolatti Hernán PE-P-048-Wed-124 732
Decolatti Hernán PE-P-059-Wed-135 754
Dedecek Jiri SC-P-051-Mon-051 297
Dedecek Jiri SC-P-102-Wed-039 397
Degirmenci Volkan SC-O-14 65
Deka Upakul PE-O-01 123
Del Bianco Nadine SC-P-084-Wed-021 361
Del Bianco Nadine SM-P-031-Wed-179 944
Del Pozo-Ochoa C. FC-P-054-Wed-169 877
Delevoye Laurent SC-O-12 61
Delgado Dobladez José Antonio SM-P-015-Mon-184 912
Delgado Dobladez José Antonio SM-P-016-Mon-185 914
Demange D. RRR-15-Mon-218 1054

Demange D. RRR-24-Wed-213 1073
Demirci Selami NM-P-013-Mon-076 483
Dendooven Jolien SC-P-056-Mon-056 305
Dennenwaldt Teresa SC-P-080-Mon-063 353
Derewinski Miroslaw SC-P-121-Wed-058 433
Detavernier Christophe SC-P-056-Mon-056 305
Devautour-Vinot Sabine SM-P-011-Mon-180 904
Devautour-Vinot Sabine TA-P-010-Mon-200 987
Devic Thomas NM-P-038-Wed-074 532
Devic Thomas Th-P-013-Mon-104 593
Devos Dirk NM-P-028-Mon-091 513
D'haen Jan SC-P-056-Mon-056 305
Di Renzo Francesco SC-P-112-Wed-049 415
Diaz U. SC-P-090-Wed-027 373
Diaz Urbano NM-O-07 103
Diaz Urbano NM-P-021-Mon-084 499
Díaz Urbano NM-P-024-Mon-087 505
Diaz Isabel NM-O-08 105
Diaz Isabel NM-P-034-Wed-070 524
Díaz Isabel NM-P-036-Wed-072 528
Diaz Isabel SC-O-23 83
Díaz Isabel RRR-03-Mon-206 1030
Díaz-García Manuel SC-P-107-Wed-044 405
Díaz López José Antonio FC-P-018-Mon-160 805
Díaz Moreno Rebeca FC-P-018-Mon-160 805
Díaz-Maroto Javier PE-P-031-Mon-139 698
Didriksen Terje FC-P-023-Mon-165 815
Dietzel Pascal D. C. SM-P-040-Wed-188 962
Dimitrov Momtchil PE-P-015-Mon-123 667
Dimitrov Momtchil PE-P-016-Mon-124 669
Dimitrov Ljubomir SC-P-091-Wed-028 375
Döblinger Markus SC-P-080-Mon-063 353
Dodin Mathias SC-P-070-Wed-008 333
Dogu Gulsen PE-P-006-Mon-114 651
Doğu Timur PE-P-017-Mon-125 671
Dohmen Christian TA-O-03 187
Dolbecq Anne Th-O-02 111
Doménech Antonio SC-O-21 79
Doménech-Carbó María Teresa SC-O-21 79
Dörfler Thilo SC-P-080-Mon-063 353
Dorset Douglas SC-P-002-Mon-002 203
Douillard Jean-Marc SM-P-011-Mon-180 904

Doutel Erica SM-P-016-Mon-185 914
Dragoi Brandusa FC-P-007-Mon-149 783
Drahokoupil Jan SC-P-024-Mon-024 243
Dreisbach Frieder TA-P-011-Mon-201 989
Drozdek Marek NM-P-020-Mon-083 497
Drobek Martin SC-P-084-Wed-021 361
Drobek Martin SM-P-031-Wed-179 944
Dubbeldam David Th-P-020-Wed-094 607
Dudek Barbara NM-P-020-Mon-083 497
Dudek Barbara SM-P-020-Mon-189 922
Dudková-Paterová Iva FC-P-024-Mon-166 817
Dumitriu Emil FC-P-007-Mon-149 783
Dupuy Benoit PE-P-025-Mon-133 686
Durand Robert PE-P-004-Mon-112 647
Durand Véronique SC-P-084-Wed-021 361
Düren Tina Th-P-008-Mon-099 583
Dusselier Michiel FC-P-050-Wed-165 869
Dzierzak Joanna FC-O-02 141
Dzitko Jakub NM-P-010-Mon-073 477
Dzwigaj Stanislaw PE-P-037-Wed-113 710
Dzwigaj Stanislaw SC-P-093-Wed-030 379
Dzwigaj Stanislaw SC-P-106-Wed-043 403

E

E. De Vos Dirk TA-P-004-Mon-194 975
Edwards Peter SC-P-047-Mon-047 289
Eggink Emma Th-P-002-Mon-093 571
Ehlert Nina TA-P-023-Wed-199 1013
Eilertsen Einar SC-O-18 73
Eilertsen Einar André SC-P-019-Mon-019 233
El Fallah Jaafar NM-O-08 105
El Fallah Jaafar NM-P-036-Wed-072 528
El Haskouri Jamal SC-P-017-Mon-017 229
El Haskouri Jamal SC-P-018-Mon-018 231
Elizalde Gonzales Maria P. SC-P-044-Mon-044 283
Eller Zoltán PE-P-022-Mon-130 681
El-Masry Mohamed PE-P-058-Wed-134 752
El-Safty Sherif TA-O-07 195
El-Safty Sherif TA-P-008-Mon-198 983
El-Safty Sherif TA-P-009-Mon-199 985

Enferadi KerenkanAmir SC-P-113-Wed-050 417
Escola Jose PE-P-041-Wed-117 718
Esquivel Dolores NM-P-009-Mon-072 475
Esquivel Dolores PE-P-013-Mon-121 663

F

F. Madeira Filipa SC-P-038-Mon-038 271
F. Sels Bert TA-P-004-Mon-194 975
Fabos Viktoria FC-P-037-Wed-152 843
Fairen-Jimenez David Th-P-008-Mon-099 583
Fajula Francois PE-O-04 129
Fajula François PE-P-007-Mon-1151 653
Fajula François SC-P-041-Mon-041 277
Fajula Francois SC-P-096-Wed-033 385
Fajula Francois Th-P-013-Mon-104 593
Fang Lin NM-P-049-Wed-085 554
Farrusseng David FC-P-008-Mon-150 785
Farrusseng David NM-O-04 97
Farrusseng David NM-P-007-Mon-070 471
Farrusseng David SM-P-008-Mon-177 897
Fattakhova-Rohlfing Dina NM-P-006-Mon-069 469
Fattakhova-Rohlfing Dina NM-P-014-Mon-077 485
Fatullayeva Sevda PE-P-012-Mon-120 661
Fatullayeva Sevda Th-P-003-Mon-094 573
Faye Delphine SC-O-01 39
Feckl Johann M. NM-P-006-Mon-069 469
Fedosov Daniil SM-P-009-Mon-178 899
Feldhoff Armin SM-O-05 167
Fenando Chávez-Rivas SC-P-089-Wed-026 371
Ferdov Stanislav NM-P-040-Wed-076 536
Ferey Gerard Th-P-013-Mon-104 593
Férey Gérard NM-P-001-Mon-064 459
Férey Gérard SC-P-075-Wed-013 343
Fernandes Auguste PE-P-047-Wed-123 730
Fernandes Auguste SC-P-098-Wed-035 389
Fernandez Christian NM-P-045-Wed-081 546
Fernandez Christian SC-P-097-Wed-034 387
Fernandez Eduardo PE-P-041-Wed-117 718
Fernandez Eduardo TA-O-04 189
Fernandez Lorenzo SC-P-018-Mon-018 231

Fernandez Yolanda TA-P-024-Wed-200 1015
Fernández-Martínez Francisco SC-P-110-Wed-047 411
Ferreira Ana Paula PE-P-047-Wed-123 730
Ferreira Breno NM-P-011-Mon-074 479
Fila Vlastimil SC-P-024-Mon-024 243
Fila Vlastimil SM-P-021-Mon-190 924
Fila Vlastimil SM-P-035-Wed-183 952
Filinchuk Yaroslav SM-O-01 159
Fimia Antonio TA-O-04 189
Finiels Annie PE-O-04 129
Finiels Annie PE-P-007-Mon-1151 653
Fiol Bibiloni Gabriel SC-P-026-Mon-026 247
Fiorilli Sonia SC-P-105-Wed-042 401
Fischer Marcus FC-P-029-Wed-144 827
Fjellvaag Helmer PE-P-021-Mon-129 679
Floquet Nicole Th-P-035-Wed-109 637
Florczak Patryk FC-P-010-Mon-152 789
Florek-Milewska Justyna SC-P-085-Wed-022 363
Folliet Nicolas SC-P-046-Mon-046 287
Folliet Nicolas TA-O-02 185
Franch Cristina PE-P-052-Wed-128 740
Friedrich Heiner PE-O-04 129
Friedrich Heiner SC-P-041-Mon-041 277
Friedrich Thomas TA-P-003-Mon-193 973
Fripiat José SC-P-132-Wed-223 454
Fritzsche Siegfried SM-O-05 167
Frolich Karel SC-P-042-Mon-042 279
Frydova Eva SC-P-042-Mon-042 279
Fuchs Alain Th-P-030-Wed-104 627
Fuchs Alain Th-P-031-Wed-105 629
Fuchs Alain Th-P-032-Wed-106 631
Fujimoto Ayumi SC-P-012-Mon-012 221
Fujiwara Saori SC-P-059-Mon-059 311
Fukuoka Atsushi FC-P-049-Wed-164 867
Furumoto Yoshiyasu PE-P-005-Mon-113 649

G

G. Bell Robert RRR-23-Wed-212 1071
G. Bushuev Yu. RRR-07-Mon-210 1038
Gaab Manuela TA-P-020-Wed-196 1007
Gaberova Lucia SC-O-08 53
Gabova Vendula SC-P-051-Mon-051 297
Gabrovšek Roman SC-P-064-Wed-022 321
Galarneau Ann FC-P-036-Wed-151 841
Galarneau Anne SC-P-077-Wed-015 347
Gallardo Alberto SC-P-057-Mon-057 307
Galve Alejandro SC-P-094-Wed-031 381
Gambarotta Enrico Francesco SM-O-08 173
Gao Feifei SC-O-15 67
Gao Xionghou SC-P-010-Mon-010 219
Garcia Alicia PE-P-041-Wed-117 718
García Hermenegildo TA-O-05 191
García Rafael A. FC-P-019-Mon-161 807
García Rafael A. FC-P-030-Wed-145 829
García Raquel TA-P-021-Wed-197 1009
García Teresa NM-P-024-Mon-087 505
García Blanco A.A. RRR-13-Mon-216 1050
Garcia-Martinez Javier NM-P-046-Wed-082 548
García-Martínez Javier FC-P-041-Wed-156 851
García-Martínez Javier SC-O-17 71
García-Martínez Javier SC-P-088-Wed-025 369
García-Montalbán Luz Th-P-019-Wed-093 605
Garcia-Perez Elena Th-O-03 113
García-Pérez Elena SM-P-022-Wed-170 926
García-Pérez Elena Th-P-023-Wed-097 613
García-Sánchez Almudena SM-P-022-Wed-170 926
Garcia Sanchez Almudena Th-P-002-Mon-093 571
García-Trenco Andrés PE-P-055-Wed-131 746
Garforth Arthur NM-P-035-Wed-071 526
Gargiulo N. SC-P-125-Wed-220 441
Garrone Edoardo NM-P-045-Wed-081 546
Garrone Edoardo SC-P-093-Wed-030 379
Gascon Jorge FC-P-009-Mon-151 787
Gascon Jorge SM-O-01 159
Gascon Jorge SM-O-02 161
Gascon Jorge SM-P-006-Mon-175 893
Gascon Jorge SM-P-007-Mon-176 895

Gastaldi Lucia TA-P-019-Wed-195 1005
Gatta Diego Th-P-022-Wed-096 611
Gatti Giorgio RRR-14-Mon-217 1052
Gaudin Cédric TA-P-010-Mon-200 987
Gaweł B. FC-P-023-Mon-165 815
Ge Qinqin SM-O-04 165
Geboers Jan PE-O-06 133
Geboers Jan PE-P-032-Mon-140 700
Gedrich Kristina FC-P-044-Wed-159 857
Gener Isabelle SM-P-033-Wed-181 948
Gerardin Corine NM-P-015-Mon-078 487
Gérardin Corine SC-P-050-Mon-050 295
Gérardin Emilie SM-P-011-Mon-180 904
Gerds A. RRR-09-Mon-212 1042
Getachew Negash RRR-03-Mon-206 1030
Ghorbel Abdelhamid PE-P-064-Wed-140 764
Ghorbel Abdelhamid SC-P-126-Wed-063 443
Ghysels An Th-P-028-Wed-102 623
Giacalone Francesco FC-O-03 143
Gianotti Enrica NM-P-021-Mon-084 499
Gianotti Enrica NM-P-025-Mon-088 507
Gianotti Enrica SC-P-045-Mon-045 285
Giebeler Lars FC-P-050-Wed-165 869
Gies Hermann NM-P-028-Mon-091 513
Gies Hermann SC-P-069-Wed-007 331
Gil A. RRR-13-Mon-216 1050
Gil Antonio NM-P-012-Mon-175 481
Gil Barbara NM-P-038-Wed-074 532
Gil Villarino Sonia FC-P-017-Mon-159 803
Giordano Girolamo FC-O-04 145
Giordano G. SC-P-090-Wed-027 373
Gläser Roger FC-P-035-Wed-150 839
Gläser Roger FC-P-040-Wed-155 849
Gläser Roger PE-P-033-Mon-141 702
Glorius Frank FC-P-044-Wed-159 857
Gobechiya Elena SC-P-021-Mon-021 237
Gobechiya Elena SM-O-01 159
Gobin Oliver SM-O-10 177
Golemme G. SM-O-07 171
Golemme G. SM-P-039-Wed-187 960
Göltl Florian Th-O-04 115
Golubeva Olga SC-P-022-Mon-022 239

Golubina Elena PE-P-050-Wed-126 736
Gomes M.E. TA-P-026-Wed-202 1019
Gomes Maria Elena SC-P-118-Wed-055 425
Gómez Diego A. Th-P-015-Mon-106 597
Gómez Diego A. Th-P-016-Mon-107 599
Gómez Gema PE-P-034-Mon-142 704
Gómez Juan Pedro PE-P-054-Wed-130 744
Gomez Pilar PE-P-044-Wed-120 724
Gómez Pilar SM-P-015-Mon-184 912
Gómez-Hortigüela Luis Th-O-01 109
Gommes Cedric J. SC-P-041-Mon-041 277
Gonçalves Alexandre SC-P-072-Wed-010 337
Gonzalez Beatriz NM-P-034-Wed-070 524
González Fernando NM-P-017-Mon-080 491
Gonzalez Gema SC-P-118-Wed-055 427
Gonzalez Gema TA-P-026-Wed-202 1019
González Jorge NM-P-051-Wed-087 558
González María Dolores PE-P-046-Wed-122 728
Goossens Steven PE-O-06 133
Gora-Marek Kinga SC-P-083-Wed-020 359
Góra-Marek Kinga RRR-10-Mon-213 1044
Góra-Marek K. RRR-28-Wed-217 1079
Góra-Marek Kinga SC-O-20 77
Gorgojo Patricia SC-P-094-Wed-031 381
Goslar Janina TA-P-002-Mon-192 971
Goupil Jean-Michel NM-O-08 105
Goupil Jean-Michel SC-P-074-Wed-012 341
Grabowski Sandra SC-P-069-Wed-007 331
Gracia Maria Dolores FC-P-032-Wed-147 833
Gracia Maria Dolores FC-P-033-Wed-148 835
Gracia María Dolores FC-P-041-Wed-156 851
Graetsch Heribert SC-P-076-Wed-014 345
Grählert Wulf TA-P-011-Mon-201 989
Grams Jacek SC-P-101-Wed-038 395
Granato Teresa NM-P-023-Mon-086 503
Grecco Saulo SC-P-031-Mon-031 257
Grecco Saulo SC-P-033-Mon-033 261
Grecco Saulo SC-P-072-Wed-010 337
Gref Ruxandra SC-P-075-Wed-013 343
Grill Marie RRR-11-Mon-214 1046
Gruenert Wolfgang FC-O-06 149
Grüner Daniel SC-P-052-Mon-052 299

Gruttadauria Michelangelo FC-O-03 143
Grzechowiak Jolanta SC-P-101-Wed-038 395
Grzechowiak R. Jolanta SC-P-092-Wed-029 377
Gualtieri A. F. SC-P-125-Wed-220 441
Gucuyener Canan SM-P-006-Mon-175 893
Gücüyener Canan SM-P-007-Mon-176 895
Guenneau Flavien TA-O-02 185
Guerrero-Ruiz Antonio SM-P-034-Wed-182 950
Guidotti Matteo FC-P-027-Mon-169 823
Guil Jose M. SC-P-057-Mon-057 307
Guil Jose M. SM-P-029-Wed-177 940
Guilera G. SC-O-13 63
Guillem Carmen SC-P-018-Mon-018 231
Guillon Emmanuelle PE-P-045-Wed-121 726
Guil-Lopez Rut SM-P-029-Wed-177 940
Guncheva Maya PE-P-015-Mon-123 667
Guncheva Maya PE-P-016-Mon-124 669
Guo Qiaoxia SC-P-010-Mon-010 219
Gushikem Yoshitaka SC-P-055-Mon-055 303
Gutierrez Laura PE-P-048-Wed-124 732
Gutierrez Laura PE-P-059-Wed-135 754
Gutierrez Mirella SC-P-107-Wed-044 405
Gutiérrez Arzaluz Mirella NM-P-039-Wed-075 534
Gutierrez-Ortiz Jose Ignacio PE-O-07 135
Gutiérrez-Sevillano Juan José Th-P-019-Wed-093 605
Guzmán Castillo M. Lourdes SC-P-132-Wed-223 454

H

Ha Jeong-Myeong SC-O-18 73
Hadt Ryan G. PE-P-011-Mon-119 659
Hafner Jürgen Th-O-04 115
Halász János FC-P-052-Wed-167 873
Halász János FC-P-053-Wed-168 875
Halász János PE-P-062-Wed-138 760
Hamad Said SM-P-022-Wed-170 926
Hamad Said Th-P-019-Wed-093 605
Hamada Boudjemaa SC-P-128-Wed-204 447
Hamidi Fatiha SC-P-112-Wed-049 415
Han Wei TA-P-007-Mon-197 981
Hancsók Jenö PE-P-022-Mon-130 681

Hannevold L. FC-P-046-Wed-161 861
Hannus István FC-P-053-Wed-168 875
Haouas Mohamed NM-P-001-Mon-064 459
Haouas Mohamed SC-O-09 55
Haouas Mohamed SC-P-019-Mon-019 233
Hara Kenji FC-P-049-Wed-164 867
Harada Yasumitsu PE-P-005-Mon-113 649
Hartmann Martin FC-O-01 139
Hartmann Martin FC-P-029-Wed-144 827
Hartmann Sarah FC-P-036-Wed-151 841
Hayden Oliver NM-P-006-Mon-069 469
Hazar Guesmi Th-P-026-Wed-100 619
He Ming Yuan NM-P-049-Wed-085 554
Heinrich Frances SC-P-069-Wed-007 331
Heitbaum Maja FC-P-044-Wed-159 857
Held Agnieszka PE-P-023-Mon-131 683
Hemelsoet Karen Th-P-025-Wed-099 617
Hemelsoet Karen Th-P-028-Wed-102 623
Henriques Carlos PE-P-047-Wed-123 730
Henriques Carlos SC-P-098-Wed-035 389
Hensen Emiel SC-O-14 65
Hensen Emiel Th-P-009-Mon-100 585
Hernández Verónica SM-P-015-Mon-184 912
Hernández Verónica SM-P-016-Mon-185 914
Hernández Beltrán Francisco SC-P-132-Wed-223 454
Hernandez Huesca Rosario SM-P-037-Wed-185 956
Hernández-Rodríguez M. SC-P-122-Wed-059 435
Hernández-Rodríguez M. SC-P-123-Wed-060 437
Herrera-Pérez Gabriel SC-P-107-Wed-044 405
Herskowitz M. SC-P-129-Wed-110 448
Hertz Audrey SC-P-084-Wed-021 361
Heylen Steven PE-P-010-Mon-118 657
Hidalgo-Carrillo Jesús FC-P-013-Mon-155 795
Hoa Nguyen TA-P-008-Mon-198 983
Hoffmann Stanislaw TA-P-002-Mon-192 971
Hofkens Johan TA-P-004-Mon-194 975
Hofkens Johan TA-P-017-Wed-193 1001
Honda Koutaro SC-P-012-Mon-012 221
Hong Suk Bong SC-O-08 53
Hong Suk Bong SC-P-097-Wed-034 387
Hong Suk Bong Th-P-001-Mon-092 569
Horcajada Patricia SC-P-075-Wed-013 343

Horcajada Patricia TA-P-010-Mon-200 987
Horcajada Patricia Th-P-013-Mon-104 593
Horňáček Michal PE-P-060-Wed-163 756
Horňáček Michal SC-P-120-Wed-057 431
Hossein Mohammad RRR-30-Wed-219 1083
Hould Nathan SC-O-02 41
Houthoofd Kristof FC-O-08 153
Houthoofd Kristof NM-P-027-Mon-090 511
Howe Russell SC-P-061-Mon-061 315
Hrabanek Pavel SC-P-024-Mon-024 243
Hrabanek Pavel SM-P-021-Mon-190 924
Hrabanek Pavel SM-P-035-Wed-183 952
Hrenovic Jasna SC-P-001-Mon-001 201
Huang Aisheng SM-P-026-Wed-174 934
Huang Yining SC-P-130-Wed-222 450
Hudec Pavol PE-P-060-Wed-163 756
Hudec Pavol SC-P-120-Wed-057 431
Huguet Edouard PE-P-004-Mon-112 647
Hulea Vasile FC-P-007-Mon-149 783
Hulea Vasile PE-O-04 129
Hulea Vasile PE-P-004-Mon-112 647
Hulea Vasile PE-P-007-Mon-1151 653
Hulea Vasile PE-P-043-Wed-119 722
Hums Eric SC-P-108-Wed-045 407
Hungría Ana B. SC-P-017-Mon-017 229
Hureau Matthieu SC-O-06 49
Hureau Matthieu Th-P-012-Mon-103 591
Hwang Sonjong SC-O-18 73
Hwang Young Kyu SC-P-075-Wed-013 343

I

Ibarra Salvador SC-P-132-Wed-223 454
Iborra Sara FC-P-042-Wed-157 853
Iborra Sara FC-P-043-Wed-158 855
Ide Yusuke FC-P-001-Mon-143 771
Ide Yusuke SC-P-009-Mon-009 217
Ide Yusuke SC-P-012-Mon-012 221
Iglesias M. FC-P-054-Wed-169 877
Iglesias José NM-P-041-Wed-077 538
Ignat Maria TA-P-001-Mon-191 969

Ikeda Takuji PE-P-051-Wed-127 738
Ikegami Toru SM-P-002-Mon-171 885
Iliade Patrizia TA-P-019-Wed-195 1005
Imai Hiroyuki FC-O-09 155
Imai Hiroyuki RRR-33-Wed-223 1088
Imai Hiroyuki SC-O-22 81
Imai Hiroyuki SC-P-038-Mon-038 271
Imai Hiroyuki SC-P-039-Mon-039 273
Impéror-Clerc Marianne SC-P-046-Mon-046 287
In Martin NM-P-015-Mon-078 487
Inagaki Satoshi PE-P-028-Mon-136 692
Infantes Molina Antonia SM-P-012-Mon-181 906
Inocente Rodríguez-Iznaga SC-P-089-Wed-026 371
Inuzuka Toshiyasu SM-P-017-Mon-186 916
Irglová Dana FC-P-022-Mon-164 813
Isaeva Vera FC-O-06 149
Itabashi Keiji SC-P-040-Mon-040 275
Itakura Masaya SC-P-009-Mon-009 217
Itoh Tsutomu SM-P-014-Mon-183 910
Ivanoff Emilie TA-P-010-Mon-200 987
Ivanova Irina FC-P-012-Mon-154 793
Ivanova Svetlana NM-P-002-Mon-065 461
Ivanova Irina PE-P-035-Wed-111 706
Ivanova Irina SC-P-096-Wed-033 385
Ivanova Irina SM-P-009-Mon-178 899
Iwamoto Masakazu SC-P-036-Mon-036 267
Iwase Yasuyoshi PE-P-003-Mon-111 645

J

J. Quites Fernando SM-P-038-Wed-186 958
Jacobs Pierre FC-P-034-Wed-149 837
Jacobs Pierre A. FC-P-050-Wed-165 869
Jacobs Pierre PE-O-06 133
Jacobs Pierre PE-P-001-Mon-109 641
Jacobs Pierre PE-P-032-Mon-140 700
Janiszewska Ewa SC-P-025-Mon-025 245
Jankowska Aldona TA-P-002-Mon-192 971
Janousch Markus PE-P-024-Mon-132 684
Jansen J. C. SM-O-07 171
Janus Rafal NM-P-020-Mon-083 497

Janus Rafal SM-P-020-Mon-189 922
Jardim Erika FC-P-027-Mon-169 823
Jaroszewska Karolina SC-P-092-Wed-029 377
Jaroszewska Karolina SC-P-101-Wed-038 395
Jastrabik Lubomir Th-P-006-Mon-097 579
Jeandel Xavier PE-O-02 125
Jentys Andreas PE-P-024-Mon-132 684
Jentys Andreas SM-O-10 177
Jeon Jongwon SM-P-005-Mon-174 891
Jeong Eun-Young FC-P-015-Mon-157 799
Jeong Eun-Young FC-P-016-Mon-158 801
Jeong Eun-Young FC-P-020-Mon162 809
Jerome Christine NM-P-015-Mon-078 487
Jiménez Vicente NM-P-019-Mon-082 495
Jiménez López Antonio SM-P-012-Mon-181 906
Jiménez-Sanchidrián César NM-P-009-Mon-072 475
Jiménez-Sanchidrián César PE-P-013-Mon-121 663
Jin Hailian FC-P-014-Mon-156 797
Jin Won Seo SC-P-056-Mon-056 305
Jirka Ivan SC-P-024-Mon-024 243
Jirka Ivan SM-P-021-Mon-190 924
Jo Changbum NM-P-016-Mon-079 489
Jo Changbum SC-P-034-Mon-034 263
Joeri Denayer SM-O-06 169
Jordá J. L. SC-P-122-Wed-059 435
Jordá J. L. SC-P-123-Wed-060 437
Jordá J. L. SC-P-124-Wed-061 439
Jordá José Luis SM-P-041-Wed-189 964
Jordá José Luis TA-O-05 191
Jorík Vladimír PE-P-060-Wed-163 756
Jothimurugesan Kandaswamy PE-P-002-Mon-110 643
Jovanovic Dusan SM-P-030-Wed-178 942
Jovanovic Mina SM-O-09 175
Jovanovic Mina Th-P-027-Wed-101 621
Jović-Joviić Nataša SM-P-030-Wed-178 942
Jozwiak Wojciech PE-P-037-Wed-113 710
Juan-Alcaniz Jana FC-P-009-Mon-151 787
Juan-Alcaniz Jana SM-O-01 159
Julbe Anne SC-P-084-Wed-021 361
Julbe Anne SM-P-031-Wed-179 944
Julien Cousin Saint Remi SM-O-06 169
Jung Jinhwan NM-P-016-Mon-079 489

K

K. De Pietre Mendelssolm FC-P-051-Wed-166 871
Kagawa Noriko FC-P-001-Mon-143 771
Kajiro Hiroshi SM-P-014-Mon-183 910
Kalogiannis K. FC-P-046-Wed-161 861
Kalvachev Y. SC-P-091-Wed-028 375
Kamegawa Tahkashi NM-P-008-Mon-071 473
Kamimura Yoshihiro SC-P-040-Mon-040 275
Kaneko Katsumi SM-P-014-Mon-183 910
Kanellopoulos Nick NM-P-050-Wed-086 556
Kanoh Hirofumi SM-P-014-Mon-183 910
Kapteijn Freek FC-P-009-Mon-151 787
Kapteijn Freek SM-O-01 159
Kapteijn Freek SM-O-02 161
Kapteijn Freek SM-P-006-Mon-175 893
Kapteijn Freek SM-P-007-Mon-176 895
Kapustin Gennadii FC-O-06 149
Karanikolos Georgios NM-P-050-Wed-086 556
Karbowiak Thomas SM-O-11 179
Kärger Jörg SC-P-062-Mon-062 317
Kärger Jörg SM-O-05 167
Károly Zoltán SC-P-117-Wed-054 425
Karpov Sergey SM-P-030-Wed-178 942
Kasian Nataliia FC-O-08 153
Kaskel S. RRR-09-Mon-212 1042
Kaskel Stefan FC-P-044-Wed-159 857
Kaskel Stefan TA-P-011-Mon-201 989
Kassab E. RRR-22-Wed-211 1069
Katada Naonobu SC-P-004-Mon-004 207
Katada Naonobu Th-P-001-Mon-092 569
Katovic Andrea NM-P-023-Mon-086 503
Katz Alexander SC-O-18 73
Kaučič Venčeslav FC-P-040-Wed-155 849
Kaučič Venčeslav NM-O-06 101
Kaučič Venčeslav NM-P-048-Wed-084 552
Kaučič Venčeslav PE-P-042-Wed-118 720
Kaučič Venčeslav SC-P-060-Mon-060 313
Kaučič Venčeslav SC-P-064-Wed-022 321
Kaučič Venčeslav SC-P-065-Wed-003 323
Kaučič Venčeslav SC-P-114-Wed-051 419
Kawahara Takahito Th-P-007-Mon-098 581

Kawase Takashi NM-P-003-Mon-066 463
Kędzierska Kamila FC-P-010-Mon-152 789
Keilbach Andreas SC-P-080-Mon-063 353
Keita Bineta Th-O-02 111
Kemnitz Erhard FC-P-002-Mon-144 773
Ken Inge A. RRR-17-Wed-206 1058
Kenmogne Régine PE-O-04 129
Kenmogne Régine SC-P-041-Mon-041 277
Kharitonov Aleksandr Th-P-021-Wed-095 609
Khatib Sheima J. SC-P-057-Mon-057 307
Khitev Yuri SC-P-096-Wed-033 385
KhodaryMohamed TA-P-009-Mon-199 985
Khuong-Trung Thuy Th-P-013-Mon-104 593
Kibby Charles PE-P-002-Mon-110 643
Kikuchi Eiichi SC-P-079-Wed-017 351
Kiliç Emre PE-P-049-Wed-125 734
Kilos Beata SC-P-032-Mon-032 259
Kim Jeongnam NM-P-016-Mon-079 489
Kim Jung Ho NM-P-033-Wed-069 522
Kim Seong-Su PE-P-056-Wed-132 748
Kim Seong-Su PE-P-056-Wed-132 748
Kim Seong Su SC-P-066-Wed-004 325
Kim Young-Hun SM-P-005-Mon-174 891
Kim Jung Ho TA-P-014-Mon-204 995
Kinkel Joachim SM-P-001- Mon-170 883
Kinkel Joachim SM-P-004-Mon-173 889
Kirschhock Christine FC-O-08 153
Kirschhock Christine PE-P-010-Mon-118 657
Kirschhock Christine SC-P-021-Mon-021 237
Kirschhock Christine SC-P-034-Mon-034 263
Kirschhock Christine SM-O-01 159
Kirschhock Christine E.a. SC-O-04 45
Kiryanov Dmitriy PE-P-014-Mon-122 665
Kjelstrup Signe Th-O-03 113
Klein Nicole FC-P-044-Wed-159 857
Kleymenov Evgeny SC-O-07 51
Klimova Tatiana PE-P-018-Mon-126 673
Klimsa Martin SM-P-001- Mon-170 883
Klimsa Martin SM-P-004-Mon-173 889
Klupp Taylor Robin N. FC-O-01 139
Knyazeva Elena PE-P-035-Wed-111 706
Knyazeva Elena SM-P-009-Mon-178 899

Kochkar Hafedh SC-P-126-Wed-063 443
Kocirik Milan SC-P-024-Mon-024 243
Kocirik Milan SM-P-021-Mon-190 924
Kockrick Emanuel FC-P-008-Mon-150 785
Kocovský Pavel FC-P-028-Wed-143 825
Köhn Ralf SC-P-080-Mon-063 353
Kolb Ute SC-P-095-Wed-032 383
Kollár Márton PE-P-022-Mon-130 681
Kollár Márton SC-P-117-Wed-054 425
Kolvenbach Robin SM-O-10 177
Kolyagin Yuri SC-P-096-Wed-033 385
Komatsu Takayuki PE-P-051-Wed-127 738
Komura Kenichi FC-P-038-Wed-153 845
Kondo Junko FC-O-09 155
Kondo Junko N. SC-O-22 81
Kondo Junko N. SC-P-039-Mon-039 273
Kondo Atsushi SM-P-014-Mon-183 910
Konno Hiroki SC-P-059-Mon-059 311
Konno Hiroki Th-P-007-Mon-098 581
Konnov Stanislav PE-P-035-Wed-111 706
Koperska Natalia TA-P-002-Mon-192 971
Koranyi Tamas FC-O-08 153
Korhonen Satu PE-O-01 123
Korili Sofia NM-P-012-Mon-175 481
Korilia S.a. RRR-13-Mon-216 1050
Kosanović Cleo RRR-27-Wed-216 1077
Kotova D.I. NM-P-031-Wed-067 518
Koudelkova Eva SC-P-042-Mon-042 279
Kovanda František FC-P-021-Mon-163 811
Kowalak Stanisław FC-P-010-Mon-152 789
Kowalak Stanislaw NM-P-005-Mon-068 467
Kowalak Stanislaw NM-P-010-Mon-073 477
Kowalak Stanislaw SC-P-025-Mon-025 245
Kowalak Stanislaw TA-P-002-Mon-192 971
Kowalska-Kuś Jolanta FC-P-011-Mon-153 791
Kowalska-Kuś Jolanta PE-P-023-Mon-131 683
Koyama To-Ru PE-P-003-Mon-111 645
Kozlova Ludmila FC-O-06 149
Kozyra Pawel Th-P-005-Mon-096 577
Kramer F. RRR-24-Wed-213 1073
Kramer Herman J.m. Th-P-034-Wed-108 635
Krizhanovskaya Oksana SM-P-030-Wed-178 942

Krstic Jugoslav SM-P-030-Wed-178 942
Ksibi Zouhaier PE-P-064-Wed-140 764
Kubota Yoshihiro PE-P-028-Mon-136 692
Kubota Yoshihiro PE-P-028-Mon-136 692
Kubů Martin SC-O-19 75
Kubů Martin SC-P-016-Mon-016 227
Kudrik Evgeny FC-P-008-Mon-150 785
Kullmann Simon FC-O-01 139
Kumar Narendra SC-P-120-Wed-057 431
Kun Zhang SC-P-104-Wed-041 399
Kurfirtova Lenka FC-P-005-Mon-147 779
Kustov Leonid FC-O-06 149
Kustov Arkady RRR-11-Mon-214 1046
Kustova Marina PE-P-036-Wed-112 708
Kustrowski Piotr NM-P-020-Mon-083 497
Kustrowski Piotr SC-P-049-Mon-049 293
Kustrowski Piotr SM-P-020-Mon-189 922
Kysilka O. FC-P-028-Wed-143 825

L

Lacarriere Antoine PE-P-007-Mon-1151 653
Lacroix-Desmazes Patrick NM-P-015-Mon-078 487
Lafon Olivier SC-O-12 61
Laforge Sebastien PE-P-025-Mon-133 686
Laforge Sebastien PE-P-026-Mon-134 688
Laforge Sébastien PE-P-045-Wed-121 726
Laha Subhash Chandra FC-P-040-Wed-155 849
Lai Zhiping SC-P-003-Mon-003 205
Lalowicz Z.t. RRR-28-Wed-217 1079
Lalowicz Zdzislaw SC-P-083-Wed-020 359
Landau M.V. SC-P-129-Wed-110 448
Langhof Timo TA-P-003-Mon-193 973
Lanzafame Paola FC-O-04 145
Lappas A. A. FC-P-046-Wed-161 861
Larrea Angel NM-P-032-Wed-068 520
Lass-Seyoum Asnakech TA-P-003-Mon-193 973
Latorre Julio SC-P-018-Mon-018 231
Laurent Bonneviot SC-P-104-Wed-041 399
Laurent Guillaume TA-O-02 185
Lauridant Natacha SC-O-01 39

Lavrencic Štangar Urška SC-P-114-Wed-051 419
Layrac Geraldine NM-P-015-Mon-078 487
Lázár Károly SC-P-117-Wed-054 425
Lazare Sandrine Th-P-004-Mon-095 575
Lazarova Tzvetomila PE-P-015-Mon-123 667
Le T.I. RRR-24-Wed-213 1073
Le Parlouër Pierre RRR-36-Wed-225 1093
Lecocq Vincent NM-O-04 97
Lecocq Vincent Th-P-004-Mon-095 575
Lee Adam F FC-P-039-Wed-154 847
Lee Jun Kyu Th-P-001-Mon-092 569
Lee Seung-Yeop FC-P-020-Mon162 809
Leistner Matthias TA-P-011-Mon-201 989
Leithall Rebecca SC-P-045-Mon-045 285
Leitmannová – Vyskočilová Eliška FC-P-021-Mon-163 811
Leitmannová – Vyskočilová Eliška FC-P-022-Mon-164 813
Leitmannová – Vyskočilová Eliška FC-P-025-Mon-167 819
Leitmannová – Vyskočilová Eliška FC-P-026-Mon-168 821
Leitmannová-Vyskočilová Eliška FC-P-024-Mon-166 817
Lemaire Arnaud NM-P-044-Wed-080 544
Lemberton Jean-Louis PE-O-05 131
Lemos Francisco PE-O-05 131
Lemos Francisco PE-P-045-Wed-121 726
Lenarz Thomas TA-P-023-Wed-199 1013
Lensing Rebecca TA-P-023-Wed-199 1013
León Adela NM-P-042-Wed-078 540
Lercher Johannes PE-P-024-Mon-132 684
Lercher Johannes SM-O-10 177
Leroi Catherine PE-P-004-Mon-112 647
Leroi Catherine PE-P-043-Wed-119 722
Lescouet Tristan FC-P-008-Mon-150 785
Lesic Rebecca FC-P-037-Wed-152 843
Leus Karen FC-P-004-Mon-146 777
Leus Karen Th-P-014-Mon-105 595
Levy Alan SC-P-045-Mon-045 285
Lewandowska Anna SC-P-106-Wed-043 403
Lewis Dewi Th-O-06 119
Lezanska Maria SC-P-073-Wed-011 339
Li Jiyang SC-P-006-Mon-006 211
Li Yanshuo SM-O-05 167
Li Xu SC-P-006-Mon-006 211
Li Yu NM-O-02 93

Li Yu NM-P-044-Wed-080 544
Liédana Nuria TA-P-018-Wed-194 1003
Lillerud Karl Petter PE-P-036-Wed-112 708
Lillerud Karl Petter SC-P-019-Mon-019 233
Lillerud Karl Petter Th-P-010-Mon-101 587
Lim Cheang-Rae FC-P-015-Mon-157 799
Lim Ivy Hwee SC-P-109-Wed-046 409
Lin Victor FC-P-049-Wed-164 867
Linares Carlos Felipe SC-P-035-Mon-035 265
Linares Carlos Felipe SC-P-071-Wed-009 335
Linares María FC-P-019-Mon-161 807
Linares Noemi NM-P-046-Wed-082 548
Linares Perez Noemi FC-P-036-Wed-151 841
Liotta Leonarda FC-O-03 143
Littlefield Benjamin SC-P-007-Mon-007 213
Liu Ming SC-P-039-Mon-039 273
Liu Xiaolong SC-O-03 43
Liu Yingya FC-P-004-Mon-146 777
Liu Yujing NM-P-006-Mon-069 469
Liu Zhong-Min NM-P-044-Wed-080 544
Liu Ying-Ya Th-P-014-Mon-105 595
Liu Yu SC-P-032-Mon-032 259
Llabrés I Xamena Francesc X. NM-P-042-Wed-078 540
Llewellyn Philip SC-O-08 53
Llewellyn Philip SC-P-075-Wed-013 343
Llewellyn Philippe Th-P-035-Wed-109 637
Llopis Francisco J. NM-P-051-Wed-087 558
Llusar Rosa SC-P-088-Wed-025 369
Llusar Rosa SC-P-088-Wed-025 369
Lobanov Maxim PE-P-050-Wed-126 736
Lobo Alan Th-O-06 119
Lobo Raul SC-O-02 41
Loiseau Thierry NM-P-001-Mon-064 459
Lokteva Ekaterina PE-P-050-Wed-126 736
Lónyi Ferenc PE-P-048-Wed-124 732
Lónyi Ferenc PE-P-059-Wed-135 754
López Ana FC-P-043-Wed-158 855
López María Isabel PE-P-013-Mon-121 663
López-Arbeloa Fernando Th-O-01 109
López-Arbeloa Iñigo TA-P-021-Wed-197 1009
Lopez-Fonseca Ruben PE-O-07 135
Lopez-Ram-De-Viu Pilar NM-P-032-Wed-068 520

Lorgouilloux Yannick ... SC-O-04 ... 45
Lorgouilloux Yannick ... SC-P-070-Wed-008 ... 333
Losada Elia ... FC-P-032-Wed-147 ... 833
Losada Elia ... FC-P-033-Wed-148 ... 835
Louradour Eric ... SC-P-084-Wed-021 ... 361
Louradour Eric ... SM-P-031-Wed-179 ... 944
Luaces S ... TA-O-06 ... 193
Luchian Camelia Elena ... SM-P-032-Wed-180 ... 946
Luck Francis ... PE-P-007-Mon-1151 ... 653
Lugo Eder ... PE-P-040-Wed-116 ... 716
Lugo-Medina Eder ... NM-P-053-Wed-089 ... 562
Łukarska Małgorzata ... NM-P-005-Mon-068 ... 467
Luna Diego ... FC-P-031-Wed-146 ... 831
Luna Diego ... FC-P-032-Wed-147 ... 833
Luna Diego ... FC-P-033-Wed-148 ... 835
Luna Sánchez Rosa María ... SM-P-036-Wed-184 ... 954
Lunin Valery ... PE-P-050-Wed-126 ... 736
Luque Priscy ... PE-P-040-Wed-116 ... 716
Luque Rafael ... FC-P-031-Wed-146 ... 831
Luque Rafael ... FC-P-032-Wed-147 ... 833
Luque Rafael ... FC-P-033-Wed-148 ... 835
Luque Rafael ... FC-P-041-Wed-156 ... 851
Luštická Ivana ... FC-P-028-Wed-143 ... 825
Luz Ignacio ... NM-P-042-Wed-078 ... 540

M

M. Moura Hipassia ... SC-P-115-Wed-052 ... 421
M. Stevens Sam ... RRR-19-Wed-208 ... 1063
Ma Zhiqiang ... RRR-26-Wed-215 ... 1075
Ma Hao ... SC-P-105-Wed-042 ... 401
Macario Anastasia ... FC-O-04 ... 145
Macario Anastasia ... SC-P-090-Wed-027 ... 373
Machado Angela ... FC-P-047-Wed-162 ... 863
Machoke Albert ... SC-P-068-Wed-006 ... 329
Madrigal Roque F. ... TA-O-04 ... 189
Maduna Valkaj Karolina ... RRR-27-Wed-216 ... 1077
Madzivire Godfrey ... SC-P-108-Wed-045 ... 407
Maes Bert ... NM-P-027-Mon-090 ... 511
Magnoux Patrick ... PE-O-05 ... 131
Magnoux Patrick ... PE-P-025-Mon-133 ... 686

Magnoux Patrick PE-P-029-Mon-137 694
Magnoux Patrick PE-P-045-Wed-121 726
Magnoux Patrick SM-P-023-Wed-171 928
Magusin Pieter SC-O-14 65
Mahingsupan Nuntiya SC-P-099-Wed-036 391
Maier Sarah PE-P-024-Mon-132 684
Makowski Wacław SC-O-10 57
Makowski Waclaw SC-P-077-Wed-015 347
Malek Andre SC-P-032-Mon-032 259
Malfatti Luca SC-P-046-Mon-046 287
Mali Gregor NM-O-06 101
Mali Gregor NM-P-048-Wed-084 552
Mali Gregor SC-P-060-Mon-060 313
Mallada R TA-O-06 193
Malola Sami Th-P-029-Wed-103 625
Malpartida Irene PE-O-02 125
Mamo Wondimagegne RRR-03-Mon-206 1030
Mandlmeier Benjamin NM-P-006-Mon-069 469
Mandlmeier Benjamin SC-P-080-Mon-063 353
Manjón-Sanz Alicia SC-P-081-Wed-018 355
Manko Maria SC-P-077-Wed-015 347
Marchandeau Franck SM-P-011-Mon-180 904
Marchena Miriam FC-P-017-Mon-159 803
Marchese L. NM-O-03 95
Marchese Leonardo RRR-14-Mon-217 1052
Marcos Maria Dolores TA-P-025-Wed-201 1017
Marichal Claire SC-P-070-Wed-008 333
Marie Olivier PE-O-02 125
Marie-Anne Springel-Huet SC-P-104-Wed-041 399
Marin Guy B. FC-P-004-Mon-146 777
Marin Guy B. PE-P-053-Wed-129 742
Marinas Alberto FC-P-013-Mon-155 795
Marinas Jose M FC-P-031-Wed-146 831
Marinas José María FC-P-013-Mon-155 795
Marinas Jose Maria FC-P-032-Wed-147 833
Marinas Jose Maria FC-P-033-Wed-148 835
Maris Pamela TA-P-022-Wed-198 1011
Marler Bernd SC-P-076-Wed-014 345
Maroneze Camila SC-P-055-Mon-055 303
Marquez-Alvarez Carlos SC-P-107-Wed-044 405
Márquez-Álvarez Carlos NM-P-036-Wed-072 528
Marszalek Bartosz NM-P-038-Wed-074 532

Martens Johan FC-O-03 143
Martens Johan FC-O-08 153
Martens Johan NM-P-027-Mon-090 511
Martens Johan SC-P-021-Mon-021 237
Martens Johan SC-P-034-Mon-034 263
Martens Johan SC-P-056-Mon-056 305
Martens Johan A PE-P-010-Mon-118 657
Martens Johan A. SC-O-04 45
Martí Laura FC-P-043-Wed-158 855
Martí-Gastaldo Carlos TA-O-05 191
Martín Juan PE-P-034-Mon-142 704
Martín-Calvo Ana SM-P-022-Wed-170 926
Martín-Calvo Ana Th-P-019-Wed-093 605
Martínez Agustín PE-O-03 127
Martínez Agustín PE-P-055-Wed-131 746
Martínez Carlos SC-P-071-Wed-009 335
Martinez Blanes Jose Maria NM-P-002-Mon-065 461
Martinez Joaristi Alberto SM-P-007-Mon-176 895
Martinez-Joaristi Alberto SM-O-01 159
Martinez-Joaristi Alberto SM-O-02 161
Martínez-Máñez Ramón TA-P-025-Wed-201 1017
Martínez-Martínez Virginia TA-P-021-Wed-197 1009
Martínez-Triguero Joaquín SC-P-119Wed-056 429
Martins Angela NM-P-030-Wed-066 516
Martins Angela PE-P-027-Mon-135 690
Martins João PE-P-045-Wed-121 726
Martins Leandro SC-P-028-Mon-028 251
Martins Leandro SC-P-029-Mon-029 253
Martos Carmen NM-P-029-Wed-065 514
Masalska Aleksandra SC-P-092-Wed-029 377
Masalska Aleksandra SC-P-101-Wed-038 395
Maschmeyer Thomas FC-O-05 147
Maschmeyer Thomas FC-P-037-Wed-152 843
Mason C. R. SM-O-07 171
Mason C.R. SM-P-039-Wed-187 960
Massiani Pascale SC-P-093-Wed-030 379
Masters Anthony FC-O-05 147
Masters Anthony FC-P-037-Wed-152 843
Masuda Takao SC-P-059-Mon-059 311
Masuda Takao Th-P-007-Mon-098 581
Matejkova Martina SC-P-024-Mon-024 243
Matsukata Masahiko SC-P-079-Wed-017 351

Maučec Darja PE-P-042-Wed-118 720
Maupin Irène PE-P-029-Mon-137 694
Maurelli Sara SC-P-045-Mon-045 285
Maurer Stefan TA-P-020-Wed-196 1007
Maurin Guillaume TA-P-010-Mon-200 987
Maury Sylvie PE-P-026-Mon-134 688
Mavrodinova Vessela NM-O-08 105
Mayerová Jana PE-P-038-Wed-114 712
Mayoral Alvaro NM-P-032-Wed-068 520
Mayoral Álvaro NM-P-037-Wed-073 530
Mayoral Álvaro SC-O-23 83
Mazaj Matjaž NM-O-06 101
Mazaj Matjaž NM-P-048-Wed-084 552
Mazaj Matjaž SC-P-064-Wed-022 321
Mazali Italo SC-P-055-Mon-055 303
Mcgarrity Erin Th-P-002-Mon-093 571
Mckinlay Alistair C. TA-O-01 183
Medina Francisco PE-P-064-Wed-140 764
Mejidova Solmaz Th-P-003-Mon-094 573
Melero Juan A. NM-P-041-Wed-077 538
Mellot-Draznieks Caroline Th-O-02 111
Meloni Daniela FC-P-007-Mon-149 783
Melouki Redouane SM-P-018-Mon-187 918
Meng Xiangju SC-O-05 47
Mengual J. PE-P-066-Wed-142 767
Mentré Olivier SC-O-12 61
Mercan Derya SC-P-131-Wed-221 452
Merino Estíbaliz NM-O-07 103
Merkling Patrick Jacques Th-P-020-Wed-094 607
Mertens Myrjam SC-P-062-Mon-062 317
Mertens Myrjam Th-P-017-Mon-108 601
Metzger A. SC-P-129-Wed-110 448
Meynen Vera FC-P-027-Mon-169 823
Meynen Vera NM-P-027-Mon-090 511
Meynen Vera SC-P-062-Mon-062 317
Meynen Vera TA-P-012-Mon-202 991
Meynen Vera Th-P-017-Mon-108 601
Michaux Florentin SC-P-046-Mon-046 287
Mignard Samuel SM-P-023-Wed-171 928
Mignard Samuel SM-P-033-Wed-181 948
Miguel P.J. PE-P-066-Wed-142 767
Mihályi R. Magdolna PE-P-059-Wed-135 754

Mijoin Jérôme PE-P-029-Mon-137 694
Miletto Ivana NM-P-025-Mon-088 507
Milina Maria SC-P-027-Mon-027 249
Miller Stuart R. NM-P-018-Mon-081 493
Millini Roberto SC-P-082-Wed-019 357
Millini Roberto SM-O-08 173
Millot Yannick SC-P-093-Wed-030 379
Millot Yannick SC-P-106-Wed-043 403
Milutinovic-Nikolic Aleksandra SM-P-030-Wed-178 942
Ming-Yuan He SC-P-104-Wed-041 399
Minoux Delphine PE-P-001-Mon-109 641
Minoux Delphine SC-P-050-Mon-050 295
Mintova Svetlana SC-P-074-Wed-012 341
Mintova Svetlana TA-P-013-Mon-203 993
Mirabelli Ilaria TA-P-016-Wed-192 999
Miranda Sonia TA-P-024-Wed-200 1015
Miró Eduardo PE-P-048-Wed-124 732
Mitchell Sharon SC-P-027-Mon-027 249
Mitchell Sharon SC-P-116-Wed-053 423
Mitoraj Mariusz Th-P-005-Mon-096 577
Mitsova Lyubomira PE-P-015-Mon-123 667
Miyaji Akimitsu PE-P-003-Mon-111 645
Miyamoto Manabu SM-P-017-Mon-186 916
Mizuno Shun SC-O-22 81
Mlekodaj Kinga SC-O-10 57
Mo Yong-Hwan FC-P-014-Mon-156 797
Mofarahi Masoud SM-P-027-Wed-175 936
Mofarahi Masoud SM-P-028-Wed-176 938
Moggach Stephen A. Th-P-008-Mon-099 583
Moh Pak NM-P-022-Mon-085 501
Mohamad El Eter SC-P-104-Wed-041 399
Mohammed Boulhout SM-O-03 163
Moissette Alain SC-O-06 49
Moissette Alain Th-P-012-Mon-103 591
Moizan Virginie NM-P-007-Mon-070 471
Mojović Zorica SM-P-030-Wed-178 942
Moliner Manuel NM-P-051-Wed-087 558
Moliner-Marin Manuel SC-P-032-Mon-032 259
Mondragón Laura TA-P-025-Wed-201 1017
Montagne Lionel SC-O-12 61
Montanari Erica SC-P-082-Wed-019 357
Monteiro Rita NM-P-030-Wed-066 516

Monteiro Rita PE-P-027-Mon-135 690
Montes Vicente FC-P-013-Mon-155 795
Montes De C. Consuelo SC-P-037-Mon-07 269
Montoya Noemí SC-O-21 79
Mora Manuel PE-P-013-Mon-121 663
Moragues Alaina SC-P-017-Mon-017 229
Morales Gabriel NM-P-041-Wed-077 538
Morales José Manuel SC-P-017-Mon-017 229
Morales Victoria FC-P-030-Wed-145 829
Morelli Catia TA-P-022-Wed-198 1011
Moreno Ines SC-O-16 69
Moreno-Tost Ramón SM-P-012-Mon-181 906
Mores Davide Th-P-028-Wed-102 623
Mori Kohsuke NM-P-008-Mon-071 473
Mori Kohsuke PE-P-009-Mon-117 655
Morisset Sophie PE-O-05 131
Morris Russell E. TA-O-01 183
Mortera Renato SC-P-105-Wed-042 401
Motokura Ken PE-P-003-Mon-111 645
Motuzas Julius SC-P-084-Wed-021 361
Motuzas Julius SM-P-031-Wed-179 944
Moulin Beatrice SC-O-08 53
Mowat John P. S. NM-P-018-Mon-081 493
Mrowiec-Białoń Julita FC-P-023-Mon-165 815
Mueller Peter P. TA-P-023-Wed-199 1013
Mugica Álvarez Violeta NM-P-039-Wed-075 534
Mugnaioli Enrico SC-P-095-Wed-032 383
Mul Guido TA-P-012-Mon-202 991
Müller Ulrich NM-P-028-Mon-091 513
Müller Ulrich TA-P-020-Wed-196 1007
Munakata Hajime PE-P-003-Mon-111 645
Muniesa Carlos TA-O-04 189
Muniesa Carlos TA-P-024-Wed-200 1015
Murzin Dmitry Yu. SC-P-120-Wed-057 431
Musyoka Nicholas SC-P-108-Wed-045 407
Muylaert Ilke FC-P-006-Mon-148 781

N

N. Vayssilov Georgi RRR-21-Wed-210 1067
Na Kyungsu NM-P-016-Mon-079 489
Na Kyungsu RRR-35-Mon-223 1091
Nachtegaal Maarten SC-O-07 51
Nachtigall Petr SC-O-19 75
Nagiev Tofik PE-P-039-Wed-115 714
Nagieva Inara PE-P-039-Wed-115 714
Naiki Hiroaki FC-P-038-Wed-153 845
Najafi Alireza FC-P-055-Wed-190 879
Nakai Kazuyuki SC-P-079-Wed-017 351
Nakasaka Yuta SC-P-059-Mon-059 311
Nakasaka Yuta Th-P-007-Mon-098 581
Nam In-Sik SC-O-08 53
Naono Hiromitsu SC-P-079-Wed-017 351
Nassar Eduardo NM-P-011-Mon-074 479
Navarro María Teresa PE-P-063-Wed-139 762
Navarro M. T. SC-P-122-Wed-059 435
Navarro M. T. SC-P-124-Wed-061 439
Navas Javier FC-P-045-Wed-160 859
Negishi Hideyuki SM-P-002-Mon-171 885
Negoi Alina FC-P-002-Mon-144 773
Neimark Alexander Th-P-030-Wed-104 627
Nesterenko Nikolay PE-P-001-Mon-109 641
Ng Tsz Nok SC-P-020-Mon-020 235
Ng Tsz Nok SM-P-013-Mon-182 908
Ng Tsz Nok TA-P-006-Mon-196 979
Ng Tsz Nok TA-P-007-Mon-197 981
Nickerl Georg FC-P-044-Wed-159 857
Nicolas C.-H. RRR-15-Mon-218 1054
Niculaua Marius SM-P-032-Wed-180 946
Nieto-Draghi Carlos NM-P-007-Mon-070 471
Nigra Michael SC-O-18 73
Nihtjanova D. SC-P-091-Wed-028 375
Nikitina Maria FC-P-012-Mon-154 793
Nikolaeva Elena SC-P-022-Mon-022 239
Nishido Hirotsugu TA-P-005-Mon-195 977
Niwa Miki SC-P-004-Mon-004 207
Niwa Miki Th-P-001-Mon-092 569
Nomura Kondo Junko SC-P-038-Mon-038 271
Nossov Andreï TA-O-02 185

Notzon Andreas FC-P-044-Wed-159 857
Nouno Kazuma Th-P-001-Mon-092 569
Nouroozi Fatemeh PE-P-033-Mon-141 702
Novak Tušar Nataša FC-P-040-Wed-155 849
Novak Tušar Nataša PE-P-042-Wed-118 720
Novak Tušar Nataša SC-P-114-Wed-051 419
Nowińska Krystyna FC-P-011-Mon-153 791
Nowińska Krystyna PE-P-023-Mon-131 683

O

O. Pastore Heloise FC-P-051-Wed-166 871
O. Pastore Heloise SC-P-115-Wed-052 421
O. Pastore Heloise SM-P-038-Wed-186 958
Obradovic Bojana Th-P-027-Wed-101 621
O'brien Matthew PE-P-021-Mon-129 679
Ocanto Freddy SC-P-071-Wed-009 335
Ocanto Uzcategui Freddy William SC-P-035-Mon-035 265
Ochoa Cristina PE-P-057-Wed-133 750
Odriozola José Antonio FC-P-048-Wed-163 865
Odriozola Jose Antonio NM-P-002-Mon-065 461
Odriozola Jose Antonio NM-P-002-Mon-065 461
Odrozek Klaudia FC-P-023-Mon-165 815
Ogino Isao SC-O-18 73
Ohba Tomonori SM-P-014-Mon-183 910
Öhman F. FC-P-046-Wed-161 861
Okada Shusuke NM-P-008-Mon-071 473
Okubo Tatsuya SC-P-040-Mon-040 275
Okumura Kazu SC-P-004-Mon-004 207
Oleynikov Peter SC-P-100-Wed-37 393
Olivas Amelia PE-P-040-Wed-116 716
Olivo Roberto NM-P-023-Mon-086 503
Olsbye Unni PE-P-021-Mon-129 679
Olsbye Unni PE-P-036-Wed-112 708
Olsbye Unni Th-P-010-Mon-101 587
Onida Barbara SC-P-105-Wed-042 401
Ooms Roosje FC-P-050-Wed-165 869
Ordomsky Vitaly FC-P-012-Mon-154 793
Orhun Onder SC-P-086-Wed-026 365
Orhun Onder SC-P-087-Wed-024 367
Ortega Ilida TA-O-04 189

Ortiz Belen NM-P-017-Mon-080 491
Osmundsen Christian Mårup SC-P-023-Mon-023 241
Oswald Steffen FC-P-050-Wed-165 869
Oszust-Cieniuch Monika SC-P-030-Mon-030 255
Otero Arean Carlos SC-P-026-Mon-026 247
Otero Arean Carlos SM-P-003-Mon-172 887
Otero Areán Carlos SC-P-015-Mon-015 225
Otorozhenko Tatyana PE-P-050-Wed-126 736
Oumi Yasunori SM-P-017-Mon-186 916
Oye Gisle FC-P-023-Mon-165 815
Ozawa Kenichi PE-P-051-Wed-127 738

P

P Göttig RRR-06-Mon-209 1036
Paillaud Jean-Louis SC-P-070-Wed-008 333
Paixão Viviana NM-P-030-Wed-066 516
Palčić Ana RRR-01-Mon-219 1025
Palčić Ana SC-P-067-Wed-005 327
Palomares Antonio Eduardo PE-P-052-Wed-128 740
Palomino Miguel SC-P-119-Wed-056 429
Palomino Miguel SM-P-041-Wed-189 964
Palomino Cabello Carlos SC-P-015-Mon-015 225
Palumbo Luisa SC-P-102-Wed-039 397
Pan Yichang SC-P-003-Mon-003 205
Panov Gennady Th-P-021-Wed-095 609
Paranthaman Selvarengan Th-P-032-Wed-106 631
Park Dongho PE-P-056-Wed-132 748
Park Jin Sol NM-P-033-Wed-069 522
Park Min Bum SC-P-097-Wed-034 387
Park Sang-Eon FC-P-014-Mon-156 797
Park Sang-Eon FC-P-015-Mon-157 799
Park Sang-Eon FC-P-016-Mon-158 801
Park Sang-Eon FC-P-020-Mon162 809
Park Woojin RRR-35-Mon-223 1091
Parlett Christopher M A. FC-P-039-Wed-154 847
Parracho A. RRR-24-Wed-213 1073
Parracho T. RRR-15-Mon-218 1054
Parsons Simon Th-P-008-Mon-099 583
Parvulescu Vasile I. FC-P-002-Mon-144 773
Parvulescu Vasile I. FC-P-003-Mon-145 775

Pasqua Luigi TA-P-022-Wed-198 1011
Passos Aline SC-P-028-Mon-028 251
Pastore Heloise FC-O-05 147
Pastore Heloise O. RRR-05-Mon-208 1034
Pastravanu (Coromelci) Cristina PE-P-053-W-128 742
Patarin Joël SC-O-01 39
Patarin Joël SC-P-076-Wed-014 345
Patarin Joël RRR-02-Mon-205 1027
Paterová Iva FC-P-021-Mon-163 811
Paterová Iva FC-P-022-Mon-164 813
Paul G. NM-O-03 95
Paul Webley SM-O-06 169
Paula De Cuhna Denise TA-P-010-Mon-200 987
Paulin Christian SM-O-11 179
Paulussen Sabine FC-P-034-Wed-149 837
Pavlatova Jana FC-P-005-Mon-147 779
Pearce Gordon M. NM-P-018-Mon-081 493
Peng Li FC-P-050-Wed-165 869
Peral Angel PE-P-041-Wed-117 718
Peral Angel SC-O-16 69
Peral Angel SC-P-066-Wed-004 325
Peral I SC-O-13 63
Perathoneer Siglinda FC-O-04 145
Pera-Titus Marc NM-P-007-Mon-070 471
Pera-Titus M. RRR-15-Mon-218 1054
Perdigón Ana C. NM-P-017-Mon-080 491
Perdigon-Melon Jose A. SM-P-029-Wed-177 940
Perego Carlo TA-P-015-Wed-191 997
Pereira Joana PE-P-047-Wed-123 730
Pereira Murilo SC-P-055-Mon-055 303
Pérez Eduardo TA-P-018-Wed-194 1003
Pérez Joaquin SC-P-107-Wed-044 405
Pérez Óscar PE-P-018-Mon-126 673
Pérez-Cabero Mónica SC-P-018-Mon-018 231
Perez Cruz Maria Ana SM-P-037-Wed-185 956
Pérez-Pariente Joaquín TA-P-021-Wed-197 1009
Pérez-Pariente Joaquín Th-O-01 109
Perez-Ramirez Javier SC-P-027-Mon-027 249
Pérez-Ramírez Javier SC-P-116-Wed-053 423
Pérez Romo Patricia SC-P-132-Wed-223 454
Perez Velez Roxana SC-P-044-Mon-044 283
Perrotta Enrico TA-P-022-Wed-198 1011

Perrotta Ida TA-P-022-Wed-198 1011
Pescarmona Paolo FC-O-03 143
Pescarmona Paolo FC-P-050-Wed-165 869
Pesquera Carmen NM-P-017-Mon-080 491
Peters Andreas PE-P-033-Mon-141 702
Petkov Petko NM-P-026-Mon-089 509
Petranovskii Vitalii NM-P-053-Wed-089 562
Petrik Leslie SC-P-108-Wed-045 407
Philippaerts An FC-P-034-Wed-149 837
Philippaerts An PE-O-06 133
Picone Lorena SC-O-08 53
Piera Elena TA-P-018-Wed-194 1003
Pietrzyk Piotr SC-P-073-Wed-011 339
Pilatos Georgios NM-P-050-Wed-086 556
Pilorz Karol Th-P-033-Wed-107 633
Pina M.O TA-O-06 193
Pinard Ludovic PE-O-05 131
Pinard Ludovic PE-P-026-Mon-134 688
Pineda Antonio FC-P-031-Wed-146 831
Pinel Catherine NM-O-04 97
Pinnavaia Thomas J. PE-P-056-Wed-132 748
Pinnavaia Thomas J. SC-P-066-Wed-004 325
Pintar Albin PE-P-042-Wed-118 720
Pinto Joana FC-P-047-Wed-162 863
Pires Joao SC-P-057-Mon-057 307
Pirutko Larisa Th-P-021-Wed-095 609
Piumetti Marco SC-P-093-Wed-030 379
Piwowarska Zofia NM-P-020-Mon-083 497
Piwowarska Zofia SM-P-020-Mon-189 922
Pizarro Patricia PE-P-034-Mon-142 704
Pizarro Patricia SC-O-16 69
Pölczmann György PE-P-022-Mon-130 681
Pollesel Paolo SM-O-08 173
Poly Evelyne NM-O-07 103
Pombeiro Armando PE-P-027-Mon-135 690
Ponomareva Olga PE-P-035-Wed-111 706
Ponomoreva Olga SC-P-096-Wed-033 385
Poon Ho Yee TA-P-007-Mon-197 981
Popovici Evelini PE-P-053-W-128 742
Popovici Evelini TA-P-001-Mon-191 969
Portilla M. Teresa NM-P-051-Wed-087 558
Pouzar Miloslav PE-P-038-Wed-114 712

Prélot Bénédicte SM-P-011-Mon-180 904
Prince Julia PE-P-056-Wed-132 748
Prochazkova Dana FC-P-005-Mon-147 779
Procházková Dana FC-P-019-Mon-161 807
Pruski Marek FC-P-049-Wed-164 867
Psaro Rinaldo FC-P-027-Mon-169 823
Pulcinelli Sandra SC-P-029-Mon-029 253
Pulinthanathu Sree Sreeprasanth SC-P-056-Mon-056 305
Pullumbi Pluton Th-P-031-Wed-105 629
Punkkinen M. RRR-28-Wed-217 1079

Q

Qin Zhengxing SC-P-010-Mon-010 219
Qiu Shi-Lun SC-P-076-Wed-014 345
Quesada Manuel TA-O-04 189
Quesada Manuel TA-P-024-Wed-200 1015
Quoineaud Anne-Agathe Th-P-004-Mon-095 575

R

R. Mihályi Magdolna SC-P-117-Wed-054 425
R. Mihályi Magdolna PE-P-022-Mon-130 681
Rafael Zamorano-Ulloa SC-P-089-Wed-026 371
Ragon Florence NM-P-038-Wed-074 532
Raja Robert FC-O-02 141
Raja Robert SC-P-045-Mon-045 285
Rajic Nevenka SC-P-001-Mon-001 201
Rajic Nevenka SM-O-09 175
Rajic Nevenka Th-P-027-Wed-101 621
Rakic Vesna RRR-29-Wed-218 1081
Rakic Vesna SM-O-09 175
Ramirez-Cuesta Timmy SC-O-24 86
Ramôa Ribeiro Fernando PE-O-05 131
Ramôa Ribeiro Fernando PE-P-045-Wed-121 726
Ramón Daniel SC-P-017-Mon-017 229
Ramos Ana FC-P-047-Wed-162 863
Ramos-Fernandez Enrique FC-P-009-Mon-151 787
Ramsahye Naseem Th-P-013-Mon-104 593
Rangel Maria SC-P-031-Mon-031 257

Rangel Maria SC-P-033-Mon-033 261
Rangus Mojca NM-O-06 101
Rangus Mojca NM-P-048-Wed-084 552
Rangus Mojca SC-P-060-Mon-060 313
Rangus Mojca SC-P-064-Wed-022 321
Rangus Mojca SC-P-065-Wed-003 323
Ranjeet Singh SM-O-06 169
Rasouli Milad RRR-30-Wed-219 1083
Rasouli Milad SM-P-010-Mon-179 901
Rathousky Jiri NM-P-006-Mon-069 469
Rathousky Jiri NM-P-014-Mon-077 485
Raúl Sanz SM-P-024-Wed-172 930
Ravon Ugo SC-O-03 43
Rayon Alegria Rebeca NM-P-039-Wed-075 534
Rea Thomas SC-O-18 73
Reboul Julien NM-P-015-Mon-078 487
Recnik Aleksander SC-P-001-Mon-001 201
Reinsch Helge NM-O-05 99
Ren Nan Th-P-018-Wed-092 603
Renz Michael PE-P-061-Wed-137 758
Rey Fernando NM-P-051-Wed-087 558
Rey Fernando PE-P-063-Wed-139 762
Rey Fernando SC-P-119-Wed-056 429
Rey F. SC-P-122-Wed-059 435
Rey F. SC-P-123-Wed-060 437
Rey F. SC-P-124-Wed-061 439
Rey Fernando SM-P-041-Wed-189 964
Reyes Dorys SC-P-071-Wed-009 335
Ribas Íñigo PE-P-054-Wed-130 744
Ribeiro Filipa PE-P-047-Wed-123 730
Ribeiro Filipa SC-P-098-Wed-035 389
Ribera Antonio TA-O-05 191
Richard Frederic PE-P-025-Mon-133 686
Rico Elena NM-P-012-Mon-175 481
Rives Vicente NM-P-012-Mon-175 481
Rives Vicente SC-P-048-Mon-048 291
Rizzo Caterina SM-O-08 173
Robbes Diddier TA-P-013-Mon-203 993
Robin Julien PE-P-007-Mon-1151 653
Rocha João NM-P-030-Wed-066 516
Rodriguez Araceli PE-P-044-Wed-120 724
Rodríguez Castellón Enrique SM-P-012-Mon-181 906

Rodriguez Delgado Montserrat SC-P-026-Mon-026 247
Rodriguez Delgado Montserrat SM-P-003-Mon-172 887
Rodríguez-Iznaga Inocente NM-P-053-Wed-089 562
Rodríguez-Ramos Inmaculada SM-P-034-Wed-182 950
Rodriguez-Reinoso Francisco FC-P-027-Mon-169 823
Rodriguez-Reinoso Francisco NM-P-027-Mon-090 511
Rodriguez-Trejo Rosa SM-P-036-Wed-184 954
Roeffaers Maarten TA-P-017-Wed-193 1001
Roessner Frank SM-P-030-Wed-178 942
Rojas Tomas SC-P-071-Wed-009 335
Roldán Rafael PE-P-013-Mon-121 663
Roldán Rafael PE-P-054-Wed-130 744
Romanos Georgios NM-P-050-Wed-086 556
Romero Antonio FC-P-031-Wed-146 831
Romero Antonio Angel FC-P-032-Wed-147 833
Romero Antonio Angel FC-P-033-Wed-148 835
Romero Amaya NM-P-019-Mon-082 495
Romero Amaya PE-P-031-Mon-139 698
Romero Izquierdo Amaya FC-P-017-Mon-159 803
Romero Izquierdo Amaya FC-P-018-Mon-160 805
Romero Pilar NM-P-032-Wed-068 520
Romero Sarria Francisca NM-P-002-Mon-065 461
Romero-Salguero Francisco José NM-P-009-Mon-072 475
Romero-Salguero Francisco José PE-P-013-Mon-121 663
Rosa Marinalva SC-P-029-Mon-029 253
Rossetti Ilenia SC-P-093-Wed-030 379
Roth Wieslaw SC-O-19 75
Roth Wieslaw SC-P-002-Mon-002 203
Ruaux Valérie SC-P-074-Wed-012 341
Rubio Cesar TA-P-018-Wed-194 1003
Ruiz Jorge TA-P-024-Wed-200 1015
Ruiz José Rafael PE-P-013-Mon-121 663
Ruiz-Hitzky Eduardo SC-P-078-Wed-016 349
Rydz Michal PE-P-019-Mon-127 675
Ryoo Ryong NM-P-016-Mon-079 489
Ryoo Ryong RRR-35-Mon-223 1091
Ryoo Ryong SC-P-034-Mon-034 263
Ryoo Ryong SM-P-011-Mon-180 904
Ryzhikov Andrey PE-P-043-Wed-119 722

S

Saavedra Ana NM-P-017-Mon-080 491
Sabater María José FC-P-045-Wed-160 859
Sabater M. José SC-P-119-Wed-056 429
Sacchetto Vittoria RRR-14-Mon-217 1052
Sadakane Masahiro FC-P-001-Mon-143 771
Sadakane Masahiro PE-P-005-Mon-113 649
Sadakane Masahiro SC-P-009-Mon-009 217
Sadakane Masahiro SC-P-012-Mon-012 221
Sadowska Karolina RRR-10-Mon-213 1044
Sadowska Karolina SC-P-049-Mon-049 293
Sahin Fikrettin NM-P-013-Mon-076 483
Sakaki Keiji SM-P-002-Mon-171 885
Salagre Pilar PE-P-046-Wed-122 728
Salagre Pilar SC-P-053-Mon-053 301
Salehi Seyyed Milad SM-P-027-Wed-175 936
Salmi Tapio SC-P-120-Wed-057 431
Salmones José NM-P-056-Wed-090 564
Sampedro Carmen PE-O-07 135
Sancenón Felix TA-P-025-Wed-201 1017
Sánchez F. FC-P-054-Wed-169 877
Sánchez Paula NM-P-019-Mon-082 495
Sánchez Paula PE-P-031-Mon-139 698
Sanchez Motta Tatiana SC-P-053-Mon-053 301
Sánchez-Sánchez Manuel SC-P-081-Wed-018 355
Sánchez Valente Jaime SC-P-132-Wed-223 454
Sánchez-Vázquez Rebeca NM-P-041-Wed-077 538
Sankar Gopinathan SC-P-111-Wed-048 413
Sano Tsuneji FC-P-001-Mon-143 771
Sano Tsuneji PE-P-005-Mon-113 649
Sano Tsuneji SC-P-009-Mon-009 217
Sano Tsuneji SC-P-012-Mon-012 221
Sano Tsuneji SM-P-017-Mon-186 916
Santamaria J. TA-O-06 193
Santilli Celso SC-P-028-Mon-028 251
Santilli Celso SC-P-029-Mon-029 253
Sanz Eloy SM-P-024-Wed-172 930
Sanz Raul SC-O-16 69
Sapag K. RRR-13-Mon-216 1050
Sapino Simona TA-P-019-Wed-195 1005
Sartbaeva Asel SC-P-047-Mon-047 289

Sartbaeva Asel Th-P-022-Wed-096 611
Sarv Priit SC-P-121-Wed-058 433
Sastre Enrique NM-P-036-Wed-072 528
Sastre Enrique SC-P-081-Wed-018 355
Sastre Enrique SC-P-107-Wed-044 405
Sastre G. SC-P-123-Wed-060 437
Sastre G. RRR-07-Mon-210 1038
Sastre German Th-P-011-Mon-102 589
Sastre German Th-P-015-Mon-106 597
Sastre German Th-P-016-Mon-107 599
Savonnet Marie NM-O-04 97
Saxton Robert PE-P-002-Mon-110 643
Sayah Seyyed Masoud SM-P-028-Wed-176 938
Sayyar Mohammad Hossein SM-P-010-Mon-179 901
Sazama Petr SC-P-051-Mon-051 297
Sazama Petr SC-P-102-Wed-039 397
Sazo Virginia SC-P-118-Wed-055 427
Sazo V. TA-P-026-Wed-202 1019
Schaack Bernd Bastian SC-P-109-Wed-046 409
Schaffert David TA-O-03 187
Schlossbauer Axel TA-O-03 187
Schmidt F. RRR-09-Mon-212 1042
Schmidt Wolfgang RRR-16-Wed-205 1056
Schmidt Wolfgang SC-O-11 59
Schnell Sondre Th-O-03 113
Schoonheydt Robert A. PE-P-011-Mon-119 659
Schrader Wolfgang SC-P-109-Wed-046 409
Schuricht Falk SM-P-040-Wed-188 962
Schuster Jörg SC-P-080-Mon-063 353
Schüth Ferdi SC-P-109-Wed-046 409
Schwartz Jr. Simo TA-P-024-Wed-200 1015
Schwieger Wilhelm SC-P-068-Wed-006 329
Schwingenschlögl Udo RRR-08-Mon-213 1040
Sebastian Victor NM-P-032-Wed-068 520
Sekine Yasushi SC-P-079-Wed-017 351
Selemenev V.F. NM-P-031-Wed-067 518
Selemenev Vladimir SM-P-030-Wed-178 942
Sels Bert FC-P-034-Wed-149 837
Sels Bert PE-O-06 133
Sels Bert PE-P-032-Mon-140 700
Sels Bert PE-P-032-Mon-140 700
Sels Bert TA-P-017-Wed-193 1001

Sels Bert F. FC-P-050-Wed-165 869
Sels Bert F. PE-P-011-Mon-119 659
Selvam Thangaraj SC-P-068-Wed-006 329
Senkovska Irena FC-P-044-Wed-159 857
Sergi Pietro SC-P-063-Wed-001 319
Serra-Crespo Pablo SM-O-01 159
Serra-Crespo Pablo SM-O-02 161
Serrano David P. FC-P-019-Mon-161 807
Serrano David P. PE-P-034-Mon-142 704
Serrano David PE-P-041-Wed-117 718
Serrano David P. PE-P-057-Wed-133 750
Serrano David P. SC-O-16 69
Serrano David SC-P-066-Wed-004 325
Serrano Elena SC-P-088-Wed-025 369
Serrano Elena NM-P-046-Wed-082 548
Serrano Elena FC-P-041-Wed-156 851
Serre Christian NM-P-038-Wed-074 532
Serre Christian SC-P-075-Wed-013 343
Serre Christian TA-P-010-Mon-200 987
Serre Christian Th-P-013-Mon-104 593
Sezgi Naime Asli PE-P-017-Mon-125 671
Shamzhy Mariya SC-O-19 75
Shamzhy Mariya SC-P-013-Mon-013 223
Shao Jia SM-O-04 165
Shao Lang SC-P-006-Mon-006 211
Shein O SC-P-129-Wed-110 448
Shen Baojian SC-P-010-Mon-010 219
Shepherd Ashley SC-P-061-Mon-061 315
Shetti Vasudev SC-P-045-Mon-045 285
Shibata Shohei SC-P-012-Mon-012 221
Shimojima Atsushi SC-P-040-Mon-040 275
Shin Jiho Th-P-001-Mon-092 569
Shiriiazdanov Rishat R. RRR-12-Mon-215 1048
Shrestha Kanu Sapna RRR-23-Wed-212 1071
Shutkina Olga PE-P-035-Wed-111 706
Shvets Olekseiy SC-O-19 75
Shvets Oleksiy SC-P-013-Mon-013 223
Sidor Jolanta SC-P-049-Mon-049 293
Silva Telma PE-P-027-Mon-135 690
Silva Edilene SC-P-031-Mon-031 257
Silva Edilene SC-P-033-Mon-033 261
Silva Edilene Da SC-P-072-Wed-010 337

Silvestre-Albero Ana NM-P-027-Mon-090 511
Silvestre-Albero Joaquin FC-P-027-Mon-169 823
Simancas R. SC-P-122-Wed-059 435
Simancas R. SC-P-124-Wed-061 439
Simon-Masseron Angélique RRR-02-Mon-205 1027
Simon-Masseron Angélique SC-P-076-Wed-014 345
Sisci Diego TA-P-022-Wed-198 1011
Skistad Wegard PE-P-036-Wed-112 708
Sklenak Stepan Th-O-05 115
Slater Ben Th-O-06 119
Smeekens Sylvia PE-P-010-Mon-118 657
Smeets Pieter J. PE-P-011-Mon-119 659
Smeulders Geert NM-P-027-Mon-090 511
Smiešková Agata PE-P-060-Wed-163 756
Smiešková Agáta SC-P-120-Wed-057 431
Smirnov Andrey SM-P-009-Mon-178 899
Smirnov Vladimir K. RRR-12-Mon-215 1048
Smith Andy SC-P-111-Wed-048 413
Smolikov Mikhail PE-P-014-Mon-122 665
Sobalik Zdeněk SC-P-051-Mon-051 297
Sobalik Zdeněk Th-O-05 117
Sobalík Zdeněk PE-P-030-Mon-138 696
Sobczak Izabela PE-P-019-Mon-127 675
Solinas Vicenzo FC-P-007-Mon-149 783
Solomakha Vladimir SC-P-013-Mon-013 223
Solomon Edward I. PE-P-011-Mon-119 659
Solsona Benjamin SC-P-018-Mon-018 231
Solt Hanna PE-P-048-Wed-124 732
Song Chi SM-P-014-Mon-183 910
Song Min Young NM-P-033-Wed-069 522
Song Min Young TA-P-014-Mon-204 995
Sorokin Alexander FC-P-008-Mon-150 785
Sorribes Iván SC-P-088-Wed-025 369
Sotelo Jose Luis PE-P-044-Wed-120 724
Sotelo Sancho José Luis SM-P-015-Mon-184 912
Soulard Michel SC-O-01 39
Soyer Emmanuel Th-P-004-Mon-095 575
Spileers Jeremy FC-P-006-Mon-148 781
Spjelkavik A.i. FC-P-046-Wed-161 861
St. Petkov Petko RRR-21-Wed-210 1067
Ståhl Kenny SC-P-023-Mon-023 241
Starannikova L. SM-P-039-Wed-187 960

Starikov Roman PE-P-012-Mon-120 661
Starokon Evgeny Th-P-021-Wed-095 609
Stawicka Katarzyna PE-P-020-Mon-128 677
Stefanidis S. FC-P-046-Wed-161 861
Štekrová Martina FC-P-024-Mon-166 817
Stieve Martin TA-P-023-Wed-199 1013
Stoch G. RRR-28-Wed-217 1079
Stoch Grzegorz SC-P-083-Wed-020 359
Stock Norbert NM-O-05 99
Stock Norbert NM-P-018-Mon-081 493
Stöcker M. FC-P-046-Wed-161 861
Stoeck Ulrich FC-P-044-Wed-159 857
Stoecker Michael FC-P-023-Mon-165 815
Stojakovic Djordje SC-P-001-Mon-001 201
Strauss Mathias SC-P-055-Mon-055 303
Struelens Pieter PE-P-001-Mon-109 641
Su Bao-Lian NM-O-02 93
Su Bao-Lian NM-P-043-Wed-079 542
Su Bao-Lian NM-P-044-Wed-080 544
Su Jie SC-P-052-Mon-052 299
Suborić Boris Th-P-018-Wed-092 603
Subotić Boris SC-P-067-Wed-005 327
Subotić Boris RRR-01-Mon-219 1025
Sugi Yoshihiro FC-P-038-Wed-153 845
Sunel Valeriu TA-P-001-Mon-191 969
Suprun Wladimir FC-P-035-Wed-150 839
Svačina Petr FC-P-021-Mon-163 811
Svelle Stian PE-P-036-Wed-112 708
Svelle Stian Th-P-029-Wed-103 625
Swang Ole Th-P-010-Mon-101 587
Swang Ole Th-P-029-Wed-103 625
Swiercynski Dariusz PE-P-007-Mon-1151 653
Szeifert Johann M. NM-P-006-Mon-069 469
Szyja Bartek Th-P-009-Mon-100 585

T

Taarning Esben SC-P-023-Mon-023 241
Tabor Edyta PE-P-030-Mon-138 696
Taborda Farlán SC-P-037-Mon-07 269
Taborda Farlán SC-P-100-Wed-37 393
Tagiyev Dilgam PE-P-012-Mon-120 661
Tagiyev Dilgam Th-P-003-Mon-094 573
Tagliabue Marco SM-O-08 173
Tagliabue Marco TA-P-015-Wed-191 997
Tago Teruoki SC-P-059-Mon-059 311
Tago Teruoki Th-P-007-Mon-098 581
Takechi Kazuyoshi PE-P-028-Mon-136 692
Tarasenko Alexander Th-P-006-Mon-097 579
Tasbihi Minoo SC-P-114-Wed-051 419
Tatsumi Takashi FC-O-09 155
Tatsumi Takashi NM-P-028-Mon-091 513
Tatsumi Takashi RRR-33-Wed-223 1088
Tatsumi Takashi SC-O-22 81
Tatsumi Takashi SC-P-038-Mon-038 271
Tatsumi Takashi SC-P-039-Mon-039 273
Taulelle Francis NM-P-001-Mon-064 459
Taulelle Francis SC-O-09 55
Taulelle Francis SC-P-019-Mon-019 233
Tawbi Khouloud RRR-02-Mon-205 1027
Tecimer Aylin SC-P-127-Wed-064 445
Teimouri Abbas FC-P-055-Wed-190 879
Téllez Carlos NM-P-037-Wed-073 530
Téllez Carlos SC-P-094-Wed-031 381
Téllez Carlos SM-O-02 161
Téllez Carlos TA-P-018-Wed-194 1003
Temi Domenico Mirko FC-O-04 145
Temst Kristiaan SC-P-056-Mon-056 305
Testa Flaviano NM-P-023-Mon-086 503
Testa Flaviano TA-O-02 185
Testa Flaviano TA-P-016-Wed-192 999
Testa Flaviano TA-P-022-Wed-198 1011
Thomas Sébastien TA-P-013-Mon-203 993
Thommes Matthias SC-P-116-Wed-053 423
Throl Oliver TA-P-011-Mon-201 989
Thybaut Joris W. PE-P-053-Wed-129 742
Tichit Didier PE-P-043-Wed-119 722

Tielens Frederik SC-P-043-Mon-043 281
Tielens Frederik SC-P-106-Wed-043 403
Titelman L. SC-P-129-Wed-110 448
Tkachenko Olga FC-O-06 149
Toch Kenneth PE-P-053-Wed-129 742
Tom Remy SM-O-06 169
Tomiyama Takuya SC-P-004-Mon-004 207
Torrealba Francys SC-P-035-Mon-035 265
Torres Rodríguez Miguel NM-P-039-Wed-075 534
Tortajada Marta SC-P-017-Mon-017 229
Trébosc Julien SC-O-12 61
Trejda Maciej PE-P-020-Mon-128 677
Trejda Maciej SC-P-043-Mon-043 281
Trens Philippe PE-P-043-Wed-119 722
Trens Philippe Th-P-013-Mon-104 593
Tricot Grégory SC-O-12 61
Triguero Carlos Th-P-030-Wed-104 627
Triki Mohamed PE-P-064-Wed-140 764
Tromp Moniek PE-O-06 133
Troussard Ekaterina RRR-26-Wed-215 1075
Trouve Adeline SM-P-033-Wed-181 948
Trujillano R. RRR-13-Mon-216 1050
Trujillano Raquel NM-P-011-Mon-074 479
Trujillano Raquel NM-P-012-Mon-175 481
Trujillano Raquel SC-P-048-Mon-048 291
Trukhan Natalia TA-P-020-Wed-196 1007
Trusov Lev SM-P-009-Mon-178 899
Tsoncheva Tanya PE-P-015-Mon-123 667
Tsunoji Nao PE-P-005-Mon-113 649
Tudorache Madalina FC-P-002-Mon-144 773
Tudorache Madalina FC-P-003-Mon-145 775
Tuel Alain SC-O-03 43
Tuğba Çelik PE-P-065-Wed-141 765
Tůmová Lenka FC-P-021-Mon-163 811
Turakulova Anara PE-P-050-Wed-126 736
Turner Stuart FC-P-034-Wed-149 837
Turner Stuart PE-O-06 133
Turnes Palomino Gemma SC-P-015-Mon-015 225
Tvarůžková Zdeňka PE-P-030-Mon-138 696
Tvarůžková Zdeňka SC-P-102-Wed-039 397
Tylus Włodzimierz SC-P-092-Wed-029 377
Tzompantzi Francisco PE-P-056-Wed-132 748

U

U Brendel RRR-06-Mon-209 1036
Ueda Kohtaro SC-P-079-Wed-017 351
Ueda Hitoshi SM-P-017-Mon-186 916
Uemiya Shigeyuki SM-P-017-Mon-186 916
Ugazio Elena TA-P-019-Wed-195 1005
Uguina Zamorano María Angeles SM-P-015-Mon-184 912
Uguina Zamorano María Angeles SM-P-016-Mon-185 914
Ungureanu Adrian FC-P-007-Mon-149 783
Urbano Francisco José FC-P-013-Mon-155 795
Urbina De Navarro Caribay SC-P-035-Mon-035 265
Urbina De Navarro Caribay SC-P-071-Wed-009 335
Urbiztondo M TA-O-06 193
Uriel Santiago NM-P-032-Wed-068 520
Urquieta-González Ernesto SC-P-031-Mon-031 257
Urquieta-González Ernesto SC-P-033-Mon-033 261
Urquieta-Gonzalez Ernesto Antonio SC-P-072-Wed-010 337
Ustaoglu Zeynep NM-P-013-Mon-076 483

V

V. Peskov Maxim RRR-08-Mon-213 1040
Valencia Diego PE-P-018-Mon-126 673
Valencia Susana SC-P-119-Wed-056 429
Valencia Susana SM-P-041-Wed-189 964
Valente Jaime S. PE-P-056-Wed-132 748
Vallone A. RRR-13-Mon-216 1050
Valtchev V. SC-P-091-Wed-028 375
Valtchev Valentin NM-O-08 105
Valtchev Valentin RRR-21-Wed-210 1067
Valtech Valentin NM-P-036-Wed-072 528
Valverde José Luis NM-P-019-Mon-082 495
Valverde José Luis PE-P-031-Mon-139 698
Valverde Palomino José Luis FC-P-017-Mon-159 803
Valverde Palomino José Luis FC-P-018-Mon-160 805
Valyon József PE-P-022-Mon-130 681
Valyon József PE-P-059-Wed-135 754
Valyon József SC-P-117-Wed-054 425
Van Bokhoven Jeroen PE-P-024-Mon-132 684
Van Bokhoven Jeroen A. RRR-26-Wed-215 1075

Van Bokhoven Jeroen A. SC-O-07 51
Van De Voorde Ben FC-O-07 151
Van De Vyver Stijn PE-P-032-Mon-140 700
Van Den Bergh Johan SM-P-006-Mon-175 893
Van Den Bergh Johan SM-P-007-Mon-176 895
Van Der Linden Bart TA-P-012-Mon-202 991
Van Der Mynsbrugge Jeroen Th-P-025-Wed-099 617
Van Der Veen Monique SM-P-019-Mon-188 920
Van Der Voort Pascal FC-P-004-Mon-146 777
Van Der Voort Pascal FC-P-006-Mon-148 781
Van Der Voort Pascal NM-P-004-Mon-067 465
Van Der Voort Pascal NM-P-009-Mon-072 475
Van Der Voort Pascal Th-P-014-Mon-105 595
Van Der Voort Pascal Th-P-024-Wed-098 615
Van Donk Sander PE-O-04 129
Van Donk Sander SC-P-041-Mon-041 277
Van Donk Sander SC-P-050-Mon-050 295
Van Doorslaer Sabine SC-P-062-Mon-062 317
Van Grieken Rafael FC-P-030-Wed-145 829
Van Oers Cynthia J. Th-P-017-Mon-108 601
Van Santen Rutger Th-P-009-Mon-100 585
Van Speybroeck Veronique FC-P-004-Mon-146 777
Van Speybroeck Veronique Th-P-014-Mon-105 595
Van Speybroeck Veronique Th-P-024-Wed-098 615
Van Speybroeck Veronique Th-P-025-Wed-099 617
Van Speybroeck Veronique Th-P-028-Wed-102 623
Van Tendeloo Gustaaf FC-P-027-Mon-169 823
Van Tendeloo Gustaaf FC-P-034-Wed-149 837
Van Tendeloo Gustaaf NM-P-027-Mon-090 511
Van Tendeloo Guastaaf NM-P-044-Wed-080 544
Van Tendeloo Gustaaf PE-O-06 133
Van Tendeloo Gustaaf SC-P-062-Mon-062 317
Van Tendeloo Guastaaf NM-O-02 93
Van Tendeloo Leen SC-P-021-Mon-021 237
Vanbutsele Gina FC-O-08 153
Vandichel Matthias FC-P-004-Mon-146 777
Vandichel Matthias Th-P-014-Mon-105 595
Vandichel Matthias Th-P-024-Wed-098 615
Vanelderen Pieter PE-P-011-Mon-119 659
Vantomme André SC-P-056-Mon-056 305
Vargas Hernandez Diana SM-P-037-Wed-185 956
Varisli Dilek PE-P-006-Mon-114 651

Varyani Lavni RRR-23-Wed-212 1071
Vasile Aurelia SM-P-032-Wed-180 946
Vasilyeva Svetlana NM-P-031-Wed-067 518
Vause Kevin NM-P-043-Wed-079 542
Vayssilov Georgi NM-P-026-Mon-089 509
Vela Maria Mercedes SC-P-110-Wed-047 411
Velamazán N. SC-P-122-Wed-059 435
Velamazán N. SC-P-124-Wed-061 439
Velty Alexandra NM-P-024-Mon-087 505
Vennestrøm Peter N.r RRR-11-Mon-214 1046
Verberckmoes An FC-P-006-Mon-148 781
Verbiest Thierry SM-P-019-Mon-188 920
Verboekend Danny SC-P-027-Mon-027 249
Verheyen Elke FC-O-08 153
Verheyen Elke SC-P-034-Mon-034 263
Vermisoglou Eleni NM-P-050-Wed-086 556
Vermoortele Frederik FC-O-07 151
Vermoortele Frederik TA-P-004-Mon-194 975
Vernimmen Jarian FC-P-027-Mon-169 823
Vernimmen Jarian SC-P-062-Mon-062 317
Vernimmen Jarian TA-P-012-Mon-202 991
Versace Carlo TA-P-022-Wed-198 1011
Vezin Herve PE-P-026-Mon-134 688
Vezin Hervé SC-O-06 49
Vicente Aurélie SC-P-097-Wed-034 387
Vicente Aurelie NM-P-045-Wed-081 546
Vicente Gemma FC-P-019-Mon-161 807
Vicente Miguel Angel NM-P-011-Mon-074 479
Vicente Miguel Angel NM-P-012-Mon-175 481
Vicente M.A. RRR-13-Mon-216 1050
Vidal J. A. SC-P-123-Wed-060 437
Vidal-Moya J.A. SC-P-122-Wed-059 435
Vidal-Moya J. A. SC-P-124-Wed-061 439
Vignola Rodolfo TA-P-015-Wed-191 997
Vilarrasa-Garcia Enrique SM-P-012-Mon-181 906
Villajos Jose A. FC-P-030-Wed-145 829
Villajos José A. NM-P-029-Wed-065 514
Villar-García Ignacio J. RRR-03-Mon-206 1030
Villaverde-Cantizano G. FC-P-054-Wed-169 877
Vimont Alexandre SC-O-08 53
Vimont Alexandre SC-P-075-Wed-013 343
Vispe Eugenio NM-P-032-Wed-068 520

Vispe Eugenio NM-P-037-Wed-073 530
Vital Joaquim FC-P-047-Wed-162 863
Vitale-Brovarone Chiara SC-P-105-Wed-042 401
Vitalii Petranovskii SC-P-089-Wed-026 371
Vlugt Thijs Th-P-002-Mon-093 571
Vlugt Thijs J.H. Th-O-03 113
Vlugt Thijs J.H. Th-P-034-Wed-108 635
Volkringer Christophe NM-P-001-Mon-064 459
Vosch Tom TA-P-017-Wed-193 1001
Vuono Danilo SC-P-063-Wed-001 319

W

Wach Anna NM-P-020-Mon-083 497
Wach Anna SC-P-049-Mon-049 293
Wagner Ernst TA-O-03 187
Wagner R. RRR-24-Wed-213 1073
Wainwright Steve FC-P-039-Wed-154 847
Wan Wei RRR-04-Mon-207 1032
Wan Wei SC-P-052-Mon-052 299
Wang Baojie SC-P-010-Mon-010 219
Wang Lixia PE-P-051-Wed-127 738
Wang Yanyan SC-P-006-Mon-006 211
Wang Zhengyang SC-P-052-Mon-052 299
Wang Zhengbao SM-O-04 165
Warad Ismail NM-P-052-Wed-088 560
Ward Antony FC-P-037-Wed-152 843
Warnant Jerome NM-P-015-Mon-078 487
Waroquier Michel FC-P-004-Mon-146 777
Waroquier Michel Th-P-014-Mon-105 595
Waroquier Michel Th-P-024-Wed-098 615
Waroquier Michel Th-P-025-Wed-099 617
Waroquier Michel Th-P-028-Wed-102 623
Warrender Stewart SC-O-08 53
Watanabe Kentaro PE-P-009-Mon-117 655
Weckhuysen Bert PE-O-01 123
Weckhuysen Bert PE-P-021-Mon-129 679
Weckhuysen Bert Th-P-028-Wed-102 623
Wei Ying-Yu NM-P-044-Wed-080 544
Weidenthaler Claudia RRR-16-Wed-205 1056
Weller Mark SC-P-007-Mon-007 213

Weller Mark SC-P-008-Mon-008 215
Wells Stephen Anthony Th-P-022-Wed-096 611
Wharmby Michael T. NM-P-018-Mon-081 493
Wharmby Michael T. Th-P-008-Mon-099 583
Wheatley Paul S. TA-O-01 183
Wichterlova Blanka SC-P-051-Mon-051 297
Wichterlova Blanka SC-P-102-Wed-039 397
Wiebcke Michael SM-O-05 167
Wiench Jerzy FC-P-049-Wed-164 867
Wilde Nicole FC-P-035-Wed-150 839
Willhammar Tom RRR-17-Wed-206 1058
Willhammar Tom SC-P-037-Mon-07 269
Willhammar Tom SC-P-100-Wed-37 393
Williams Edward SC-P-008-Mon-008 215
Wilson Karen FC-P-039-Wed-154 847
Wirth Emmanuel RRR-36-Wed-225 1093
Wittine Ozren RRR-27-Wed-216 1077
Woertink Julia S. PE-P-011-Mon-119 659
Wojtaszek Anna SC-P-043-Mon-043 281
Wollmann Philipp TA-P-011-Mon-201 989
Wong Ka-Lun SC-P-074-Wed-012 341
Wongkasemjit Sujitra SC-P-099-Wed-036 391
Worch Christian FC-P-035-Wed-150 839
Wragg David PE-P-021-Mon-129 679
Wright Paul SC-O-08 53
Wright Paul A. NM-P-018-Mon-081 493
Wright Paul A. Th-P-008-Mon-099 583
Wu Junbiao SC-P-006-Mon-006 211
Wu Lei SC-P-076-Wed-014 345
Wu Leilei SC-O-14 65
Wu Peng NM-P-049-Wed-085 554
Wuttke Stefan FC-P-002-Mon-144 773

X

Xiao Feng-Shou NM-O-01 91
Xiao Fengshou NM-P-028-Mon-091 513
Xie Dan RRR-20-Wed-209 1065
Xiong Yanliang SC-O-04 45
Xue Ming SC-P-076-Wed-014 345
Xuereb David FC-O-02 141

Y

Yaghobi Nakisa RRR-30-Wed-219 1083
Yaghobi Nakisa SM-P-010-Mon-179 901
Yamashita Hiromi NM-P-008-Mon-071 473
Yamashita Hiromi PE-P-009-Mon-117 655
Yamazaki Hiroshi FC-O-09 155
Yampolskii Y. SM-P-039-Wed-187 960
Yan Yushan SM-O-04 165
Yang Chieh-Chao TA-P-012-Mon-202 991
Yang Dae Soo TA-P-014-Mon-204 995
Yang Yongxing PE-P-057-Wed-133 750
Yang Xiao-Yu NM-O-02 93
Yang Xiao-Yu NM-P-043-Wed-079 542
Yang Xiao-Yu NM-P-044-Wed-080 544
Yaremov Pavel SC-P-013-Mon-013 223
Yashiki Ayako SC-P-012-Mon-012 221
Yasri Aziz TA-P-010-Mon-200 987
Yeung King Lun SC-P-020-Mon-020 235
Yeung King Lun SM-P-013-Mon-182 908
Yeung King Lun TA-P-006-Mon-196 979
Yeung King Lun TA-P-007-Mon-197 981
Yilmaz Bilge NM-P-028-Mon-091 513
Yilmaz Selahattin PE-P-049-Wed-125 734
Ylinen E. RRR-28-Wed-217 1079
Yokoi Toshiyuki FC-O-09 155
Yokoi Toshiyuki RRR-33-Wed-223 1088
Yokoi Toshiyuki SC-O-22 81
Yokoi Toshiyuki SC-P-038-Mon-038 271
Yokoi Toshiyuki SC-P-039-Mon-039 273
Yoshida Masayuki SC-P-079-Wed-017 351
Yoshioka Masato RRR-33-Wed-223 1088

Yoshioka Masato SC-P-039-Mon-039 273
Yoshitake Hideaki NM-P-003-Mon-066 463
Yot Pascal Th-P-013-Mon-104 593
Younes Bouizi SC-P-104-Wed-041 399
Yu Jihong SC-P-006-Mon-006 211
Yu Jong-Sung NM-P-033-Wed-069 522
Yu Jong-Sung TA-P-014-Mon-204 995
Yun Yifeng RRR-04-Mon-207 1032
Yun Yifeng SC-P-052-Mon-052 299

Z

Zabukovec Logar Nataša NM-P-048-Wed-084 552
Zabukovec Logar Nataša SC-P-060-Mon-060 313
Zabukovec Logar Nataša SC-P-064-Wed-022 321
Zabukovec Logar Nataša SC-P-065-Wed-003 323
Zajac Jureck SM-P-011-Mon-180 904
Zalucka Joanna Th-P-005-Mon-096 577
Zanardi Stefano SC-P-082-Wed-019 357
Zanzottera Cristina NM-P-045-Wed-081 546
Závěta Karel PE-P-030-Mon-138 696
Zdeňková Radka FC-P-026-Mon-168 821
Zečević Jovana PE-O-04 129
Zečević Jovana SC-P-041-Mon-041 277
Zhang Lu SC-P-130-Wed-222 450
Zhiryakova Diana PE-P-015-Mon-123 667
Zhiryakova Diana PE-P-016-Mon-124 669
Zhou Zhou FC-O-01 139
Zhu Guang-Shan SC-P-076-Wed-014 345
Zikanova Arlette SC-P-024-Mon-024 243
Zikanova Arlette SM-P-021-Mon-190 924
Zilkova Nadezda FC-P-005-Mon-147 779
Žilková Nadežda SC-P-016-Mon-016 227
Ziolek Maria PE-P-019-Mon-127 675
Ziolek Maria PE-P-020-Mon-128 677
Ziolek Maria SC-P-043-Mon-043 281
Ziolek Maria SC-P-085-Wed-022 363
Zokaie Mahsa Th-P-010-Mon-101 587
Zones Stacey SC-O-18 73
Zornoza Beatriz SM-O-02 161
Zou Xiaodong RRR-04-Mon-207 1032

Zou Xiaodong RRR-17-Wed-206 1058
Zou Xiaodong SC-P-052-Mon-052 299
Zou Xiaodong SC-P-100-Wed-37 393
Zou Xiaodong SC-P-037-Mon-07 269
ZrnčevićStanka RRR-27-Wed-216 1077
Zukal Arnošt PE-P-038-Wed-114 712
Zunic Marija SM-P-030-Wed-178 942
Zunkovic Emanuela SC-P-064-Wed-022 321
Zywert Anna NM-P-005-Mon-068 467

PLATINUM

GOBIERNO DE ESPAÑA · MINISTERIO DE CIENCIA E INNOVACIÓN

TOTAL

GRACE Davison

PID Eng&Tech
www.pidengtech.com

ExxonMobil

bp

Abelló Linde

BRUKER

micromeritics®
The Science and Technology of Small Particles™

GENERALITAT VALENCIANA

REPSOL

GOLD

ZEOLYST INTERNATIONAL

SILVER

SECAT
Sociedad Española de Catálisis

UNIVERSITAT POLITÈCNICA DE VALÈNCIA

ITQ Valencia · CSIC · CEMEX · Escuela Técnica Superior Ingenieros Industriales Valencia
Cátedra CEMEX-Sostenibilidad

JM Johnson Matthey Catalysts

amtech
high throughput technology

PRAXAIR

Universitat d'Alacant
Universidad de Alicante

PANalytical

SETARAM Instrumentation
KEP Technologies

SÜD-CHEMIE
CREATING PERFORMANCE TECHNOLOGY

Quantachrome INSTRUMENTS

UBE
UBE INDUSTRIES,LTD.

SACHEM
mission. critical. chemistry.

NanoMEGAS
Advanced Tools for electron diffraction

vidra FOC
FABRICACIÓN DE APARATOS DE VIDRIO Y SUMINISTROS GENERALES DE LABORATORIOS

HALDOR TOPSOE
CATALYSING YOUR BUSINESS

CECA
ARKEMA GROUP

COLLABORATORS

RSC Publishing

EXHIBITORS

TECNOVAC
TECNOLOGÍA DE VACÍO S.L.

BEL JAPAN, INC.
Specialist in Adsorption

amtech
high throughput technology

BRUKER

bonsai
ADVANCED TECHNOLOGIES

IBERFLUID instruments

Quantachrome INSTRUMENTS

Teknokroma
Professionally Friendly

SACHEM
mission. critical. chemistry.

Hiden Isochema
Advancing Sorption Analysis